

12th INTERNATIONAL CONFERENCE ON THE STABILITY
OF SHIPS AND OCEAN VEHICLES



STAB2015

UNIVERSITY OF STRATHCLYDE,
GLASGOW, 19-24 JUNE 2015

PROCEEDINGS

Volume 1



STAB2015

**12th INTERNATIONAL CONFERENCE ON THE
STABILITY OF SHIPS AND OCEAN VEHICLES**

JUNE 14-19, 2015

GLASGOW, SCOTLAND

PROCEEDINGS

Edited by

STAB2015 Secretariat

The Department of Naval Architecture and Marine Engineering

University of Strathclyde

Published and distributed by:

STAB2015 Secretariat
Department of Naval Architecture and Marine Engineering
University of Strathclyde
Henry Dyer Building, 100 Montrose Street
Glasgow, G4 0LZ, UK

Telephone: +44 (0)141 548 4094

TABLE OF CONTENTS

PREFACE	i
STAB/STAB2015 COMMITTEES	v
STAB2015 SPONSORS	vi
KEYNOTE ADDRESS	1
Safety & Stability through Innovation in Cruise Ship Design	3
Harri Kulovaara, Royal Caribbean International	
Design for Safety and Stability	15
Henning Luhmann, MEYER WERFT	
Stability Barrier Management for Large Passenger Ships	23
Dr Tor Svensen, DNVGL	
Offshore Caring - Safety Management	37
Professor Chengi Kuo, for Keppel Singapore	
Direct Assessment Will Require Accreditation – What this Means	49
Dr Arthur Reed, ONRG	
A Classification Society Perspective for Ship Stability	79
Prof. Fai Cheng, LR	
Ship Stability in Practice	81
Ross Ballantyne, Sea-Transport Solutions	
ClassNK Activities Related to Stability in Collaboration with NAPA	89
Taise Takamoto, ClassNK and Jun Furustam, NAPA Ltd	
Ship stability, Dynamics and Safety: Status and Perspectives	97
Dr. Gabriele Bulian, University of Trieste	
Session 2-Work shop 1 Plenary (Veterans of Stability)	143
Contributions from the Class of 1975	145
Chengi Kuo	

Session 3-Work shop 2 Plenary (SRDC).....	157
Ship Stability & Safety in Intact Condition through Operational Measures.....	159
Igor Bačkalov, Gabriele Bulian, Anders Rosén, Vladimir Shigunov, Nikolaos Themelis	
Ship Stability & Safety in Damage Condition through Operational Measures	173
Evangelos Boulougouris, Jakub Cichowicz, Andrzej Jasionowski, Dimitris Konovessis	
Session 5.1 – 2nd GENERATION IS	181
A Numerical Study for Level 1 Second Generation Intact Stability Criteria	183
Arman Ariffin, Shuhaimi Mansor, Jean-Marc Laurens	
Study on the Second Generation Intact Stability Criteria of Broaching Failure Mode	195
Peiyuan Feng, Sheming Fan, Xiaojian Liu	
CALCOQUE: a Fully 3D Ship Hydrostatic Solver	203
François Grinnaert, Jean-Yves Billard, Jean-Marc Laurens	
Session 5.2 – DAMAGE STABILITY	213
A New Approach for the Water- on- Deck- Problem of RoRo- Passenger Ships	215
Stefan Krueger, Oussama Nafouti, Christian Mains	
The Impact of the Inflow Momentum on the Transient Roll Response of a Damaged Ship.....	227
Teemu Manderbacka, Pekka Ruponen	
Safety of Ships in Icing Conditions.....	239
Lech Kobylinski	
Session 5.3 – DYNAMIC STABILITY.....	249

An Investigation of a Safety Level in Terms of Excessive Acceleration in Rough Seas.....251

Yoshitaka Ogawa

Application of IMO Second Generation Intact Stability Criteria for Dead Ship Condition to Small Fishing Vessels.....261

Francisco Mata-Álvarez-Santullano, Luis Pérez-Rojas

Investigation of the Intact Stability Accident of the Multipurpose Vessel MS ROSEBURG271

Adele Lübcke

Session 6 – EMSA III PLENARY WORKSHOP281

Risk Acceptance and Cost-Benefit Criteria Applied in the Maritime Industry in Comparison with Other Transport Modes and Industries283

John Spouge, Rolf Skjong, Odd Olufsen

Probabilistic Assessment of Survivability in Case of Grounding: Development and Testing of a Direct Non-Zonal Approach293

Gabriele Bulian, Daniel Lindroth, Pekka Ruponen, George Zaraphonitis

Damage Stability Requirements for Passenger Ships – Collision Risk-Based Cost-Benefit Assessment.....307

Rainer Hamann, Odd Olufsen, Henning Luhmann, Apostolos Papanikolaou, Eleftheria Eliopoulou, Dracos Vassalos

Session 7.1 – 2nd GENERATION IS317

An Investigation into the Factors Affecting Probabilistic Criterion for Surf-Riding319

Naoya Umeda, Toru Ihara, Satoshi Usada

Numerical Prediction of Parametric Roll Resonance in Oblique Waves..331

Naoya Umeda, Naoki Fujita, Ayumi Morimoto, Masahiro Sakai, Daisuke Terada, Akihiko Matsuda,

Numerical Simulation of the Ship Roll Damping341

Min Gu, Jiang Lu, Shuxia Bu, Chengsheng Wu, Gengyao Qiu,

Investigation of the Applicability of the IMO Second Generation Intact Stability Criteria to Fishing Vessels	349
Marcos Miguez González, Vicente Díaz Casás, Luis Pérez Rojas, Daniel Pena Agras, Fernando Junco Ocampo,	
Session 7.2 – DAMAGE STABILITY	361
A Concept about Strengthening of Ship Side Structures Verified by Quasi-Static Collision Experiments	363
Schöttelndreyer Martin, Lehmann Eike	
A Numerical and Experimental Analysis of the Dynamic Water Propagation in Ship-Like Structures.....	373
Oliver Lorkowski, Florian Kluwe, Hendrik Dankowski	
Dynamic Extension of a Numerical Flooding Simulation in the Time-Domain	383
Hendrik Dankowski, Stefan Kruger	
URANS Simulations for a Flooded Ship in Calm Water and Regular Beam Waves	393
Hamid Sadat-Hosseini, Dong-Hwan Kim, Pablo Carrica, Shin Hyung Rhee, Frederick Stern,	
Session 7.3 – DYNAMIC STABILITY	409
Modified Dynamic Stability Criteria for Offshore Vessel	411
Govinder Singh, Chopra	
On Aerodynamic Roll Damping	425
Carl-Johan Söder, Erik Ovegård, Anders Rosén	
SPH Simulation of Ship Behaviour in Severe Water Shipping Situations	433
Kouki Kawamura, Hirotada Hashimoto, Akihiko Matsuda, Daisuke Terada,	
A Reassessment of Wind Speeds used for Intact Stability Analysis.....	441
Peter Hayes, Warren Smith, Martin Renilson, Stuart Cannon	
Session 8.1 – 2nd GENERATION IS	451

On the Application of the 2nd Generation Intact Stability Criteria to Ro-Pax Vessels and Container Vessels.....453

Stefan Krueger, Hannes Hatecke, Paola Gualeni, Luca Di Donato

A Study on Applicability of CFD Approach for Predicting Ship Parametric Rolling465

Yao-hua Zhou, Ning Ma, Jiang Lu, Xie-chong Gu

Estimation of Ship Roll Damping – a Comparison of the Decay and the Harmonic Excited Roll Motion Technique for a Post Panamax Container Ship.....475

Sven Handschel, Dag-Frederik Feder, Moustafa Abdel-Maksoud

Assessing the Stability of Ships under the Effect of Realistic Wave Groups489

Panayiotis A. Anastopoulos, Kostas J. Spyrou

Session 8.2 – DAMAGE STABILITY499

Roll Damping Assessment of Intact and Damaged Ship by CFD and EFD Methods.....501

Ermina Begovic, Alexander H. Day, Atilla Incecik, Simone Mancini, Domenica Pizzirusso

Investigation of the Impact of the Amended S-Factor Formulation on ROPAX Ships513

Sotiris Skoupas

Stability Upgrade of a Typical Philippine Ferry.....521

Dracos Vassalos, Sokratis Stoumpos, Evangelos Boulougouris

The Evolution of the Formulae for Estimating the Longitudinal Extent of Damage for the Hull of a Small Ship of the Translational Mode.....529

O.O. Kanifolskyi

Parametric Rolling of Tumblehome Hulls using CFD Tools.....535

Alistair Galbraith, Evangelos Boulougouris

Session 8.3 – DYNAMIC STABILITY545

Influence of Rudder Emersion on Ship Broaching Prediction.....	547
Liwei Yu, Ning Ma, Xiechong Gu	
Offshore Inclining Test.....	557
Mauro Costa de Oliveira, Rodrigo Augusto Barreira, Ivan Neves Porci�ncula	
Lifecycle Aspects of Stability – Beyond Pure Technical Thinking	575
Henrique M. Gaspar, Per Olaf Brett, Ali Ebrahimi, Andre Keane	
An Experimental Study on the Characteristics of Vertical Acceleration on Small High Speed Craft in Head Waves.....	587
Toru Katayama, Ryosuke Amano	
Session 9.1 – 2nd GENERATION IS	599
An Approach to Assess the Excessive Acceleration based on Defining Roll Amplitude by Weather Criterion Formula with Modified Applicability Range	601
Rudolf Borisov, Alexander Luzyanin, Michael Kuteynikov, Vladimir Samoylov	
A Simplified Simulation Model for a Ship Steering in Regular Waves.....	613
Xiechong Gu, Ning Ma, Jing Xu, Dongjian Zhu	
Prediction of Wave-Induced Surge Force Using Overset Grid RANS Solver	623
Hirotada Hashimoto, Shota Yoneda, Yusuke Tahara, Eiichi Kobayashi	
Session 9.2 – DAMAGE STABILITY	633
Life-Cycle Risk (Damage Stability) Management of Passenger Ships	635
Dracos Vassalos, Yu Bi	
Free- Running Model Tests of a Damaged Ship in Head and Following Seas	643
Taegu Lim, Jeonghwa Seo, Sung Taek Park, Shin Hyung, Rhee	
Main Contributing Factors to the Stability Accidents in the Spanish Fishing Fleet.....	653
Francisco Mata-�lvarez-Santullano	

Session 9.3 – EXTREME BEHAVIOUR	661
A Time-Efficient Approach for Nonlinear Hydrostatic and Froude-Krylov Forces for Parametric Roll Assessment in Irregular Seas	663
Claudio A. Rodríguez, Marcelo A. S. Neves, Julio César F. Polo	
Non-Stationary Ship Motion Analysis Using Discrete Wavelet Transform	673
Toshio, ISEKI	
A Study on the Effect of Parametric Rolling on Added Resistance in Regular Head Seas	681
Jiang Lu, Min Gu, Naoya Umeda	
Session 10.1 – 2nd GENERATION IS	689
A Study on Roll Damping Time Domain Estimation for Non Periodic Motion	691
Toru KATAYAMA, Jun UMEDA	
Investigation of the 2nd Generation of Intact Stability Criteria in Parametric Rolling and Pure Loss of Stability	701
Haipeng Liu, Osman Turan, Evangelos Boulougouris	
Requirements for Computational Methods to be Used for the IMO Second Generation Intact Stability Criteria.....	711
William Peters, Vadim Belenky, Sotirios Chouliaras, Kostas Spyrou	
Session 10.2 – NAVAL SHIP STABILITY	723
Analytical Study of the Capsize Probability of a Frigate.....	725
Fre´de´ric Le Pivert, Abdelkader Tizaoui, Radjesvarane Alexandre, Jean-Yves Billard	
Aerodynamics Loads on a Heeled Ship.....	735
Romain LUQUET, Pierre VONIER, Andrew PRIOR, Jean-François LEGUEN	
Validation of Time Domain Panel Codes for Prediction of Large Amplitude Motions of Ships	745
Erik Verboom, Frans van Walree	

Session 10.3 – EXTREME BEHAVIOUR	755
Surf-Riding in Multi-Chromatic Seas: “High-Runs” and the Role of Instantaneous Celerity	757
Nikos Themelis, Kostas J. Spyrou, Vadim Belenky	
Stability and Roll Motion of a Ship with an Air Circulating Tank in Its Bottom	769
Ikko Watanabe, Satowa Ibata, Seijiro Miyake, Yoshiho Ikeda	
A Study on the Effects of Bilge Keels on Roll Damping Coefficient.....	775
Yue Gu, Sandy Day, Evangelos Boulougouris	
Session 11.1 – RISK-BASED STABILITY	785
Some Remarks on Stochastic Dynamic Analysis of Nonlinear Ship Rolling in Random Seas	787
Wei Chai, Arvid Naess, Bernt J. Leira	
Risk Analysis of a Stability Failure for the Dead Ship Condition.....	799
Tomasz Hinz	
Application of the Envelope Peaks over Threshold (EPOT) Method for Probabilistic Assessment of Dynamic Stability	809
Bradley Campbell, Vadim Belenky, Vladas Pipiras	
Split-Time Method for Estimation of Probability of Capsizing Caused by Pure Loss of Stability	821
Vadim Belenky, Kenneth Weems, Woei-Min Lin	
Session 11.2 – NAVAL SHIP STABILITY	841
Beyond the Wall	843
Richard Dunworth	
Exploration of the Probabilities of Extreme Roll of Naval Vessels.....	855
Douglas Perrault	
Comparative Stability Analysis of a Frigate According to the Different Navy Rules in Waves.....	869

Emre Kahramanoğlu, Hüseyin Yılmaz, Burak Yıldız

Towing Test and Motion Analysis of a Motion-Controlled Ship - Based on an Application of Skyhook Theory.....879

Jialin Han, Teruo Maeda, Takeshi Kinoshita, Daisuke Kitazawa

Session 11.3 – EXTREME BEHAVIOUR889

Statistical Uncertainty of Ship Motion Data891

Vadim Belenky, Vladas Pipiras, Kenneth Weems

An Investigation into the Capsizing Accident of a Pusher Tug Boat.....903

Harukuni Taguchi, Tomihiro Haraguchi, Makiko Minami, Hidetaka Houtani

Rapid Ship Motion Simulations for Investigating Rare Stability Failures in Irregular Seas911

Kenneth Weems, Vadim Belenky

Dynamic Instability of Taut Mooring Lines Subjected to Parametric Excitation923

Aijun Wang, Hezhen Yang, Nigel Barltrop, Shan Huang

Session 12.1 – DAMAGE STABILITY929

Flow Model for Flooding Simulation of a Damaged Ship.....931

Gyeong Joong Lee

An Overview of Warships Damage Data from 1967 to 2013.....953

Andrea Ungaro, Paola Gualeni

Advanced Damaged Stability Assessment for Surface Combatants.....967

Evangelos Boulougouris, Stuart Winnie, Apostolos Papanikolaou

Dynamic Stability Assessment of Naval Ships in Early-Stage Design.....979

Heather A. Tomaszek, Christopher C. Bassler

Session 12.2 – DECISION SUPPORT962

Prediction of Survivability for Decision Support in Ship Flooding Emergency962

Pekka Ruponen, Daniel Lindroth, Petri Pennanen

Crew Comfort Investigation for Vertical and Lateral Responses of a Container Ship.....999

Ferdi Çakıcı, Burak Yıldız, Ahmet Dursun Alkan

Novel Statistical prediction on parametric roll resonance by using onboard monitoring data for officers.....1007

Daisuke Terada, Hirotada Hashimoto, Akihiko Matsuda

Target Ship Design and Features of Navigation for Motion Stabilization and High Propulsion in Strong Storms and Icing.....1017

Vasily N. Khramushin

Session 12.3 – INSTABILITY OTHER THAN ROLL MOTION1027

Prediction of Parametric Rolling of Ships in Single Frequency Regular and Group Waves1029

Shukai Liu, Apostolos Papanikolaou

Probabilistic Response of Mathieu Equation Excited by Correlated Parametric Excitation.....1041

Mustafa A. Mohamad, Themistoklis P. Sapsis

Coupled Simulation of Nonlinear Ship Motions and Free Surface Tanks1049

Jose Luis Cercos-Pita, Gabriele Bulian, Luis Pérez-Rojas, Alberto Francescutto

Modelling Sailing Yachts Course Instabilities Considering Sail Shape Deformations1063

Emmanouil Angelou, Kostas J. Spyrou

Session 13.1 – STABILITY IN ASTERN SEAS1075

Coherent Phase-Space Structures Governing Surge Dynamics in Astern Seas1077

Ioannis Kontolefas, Kostas J. Spyrou

Toward a Split-Time Method for Estimation of Probability of Surf-Riding in Irregular Seas.....1087

Vadim Belenky, Kenneth Weems, Kostas Spyrou

The Effect of Ship Speed, Heading Angle and Wave Steepness on the Likelihood of Broaching-To in Astern Quartering Seas.....1103

Pepijn de Jong, Martin. R. Renilson, Frans van Walree

Session 13.2 – LIQUEFACTION.....1115

Computation of Pressures in Inverse Problem in Hydrodynamics of Potential Flow.....1117

Ivan Gankevich, Alexander Degtyarev

Potential Assessment of Cargo Liquefaction Based on an UBC3D-PLM Model.....1123

Lei Ju, Dracos Vassalos

Coupled Granular Material and Vessel Motion in Regular Beam Seas..1133

Christos C. Spandonidis, Kostas J. Spyrou

Session 13.3 – EXTREME BEHAVIOUR1143

Numerical Simulation of Ship Parametric Roll Motion in Regular Waves Using Consistent Strip Theory in Time Domain.....1145

Shan Ma, Rui Wang, Wenyang Duan, Jie Zhang

Validation of Statistical Extrapolation Methods for Large Motion Prediction.....1157

Timothy Smith, Aurore Zuzick

Coupled Hydro – Aero – Elastic Analysis of a Multi – Purpose Floating Structure for Offshore Wind and Wave Energy Sources Exploitation...1171

Thomas P., Mazarakos, Dimitrios N., Konispoliatis, Dimitris I., Manolas, Spyros A., Mavrakos, Spyros G., Voutsinas

Session 14 – 40 Years of Stability1183

SOTA on Damage Stability of Cruise Ships – Evidence and Conjecture1185

Dracos Vassalos

SOTA on Dynamic stability of ships Design and Operation.....1197

Jan Otto de Kat

SOTA on Intact Stability Criteria of Ships – Past, Present and Future
.....1199

Alberto Francescutto

PREFACE

Dear delegates, colleagues and friends

1975 – 2015: the best 40 years of stability!

Welcome to Glasgow, the cradle of modern Naval Architecture and shipbuilding, the place where all came together to shine for over a century and shape our profession. Now the sound of bells and horns and clutter is all but gone but the spirit leaves on, if not in the few surviving yards in the Clyde, certainly in the classrooms at the Department of Naval Architecture, Ocean and Marine Engineering (NAOME) at the University of Strathclyde where such legacy still moulds, inspires and guides the young minds that flock the classrooms every year from around the world.

With artefacts on human endeavours at sea dated as far back as 6500 B.C., it is mind boggling to think that it was not until 250 B.C. when the first recorded steps to establish the foundation of Naval Architecture, floatability and stability, were made by Archimedes. It is even more astonishing that practical pertinence and function of these two very basic principles remained dormant for nearly two millennia after this (probably lack of recorded history), before the first attempts to convey the meaning of stability to men of practice took place in the 18th century by Hoste and Bouguer. Regulations, especially addressing accidents that involve water ingress and flooding, were introduced even much later. Notably, the first specific criterion on residual static stability standards was introduced at the 1960 SOLAS (Safety Of Life At Sea) Convention. This “tortoise” pace of developments gave way to the steepest learning curve in the history of Naval Architecture with the introduction of the probabilistic damage stability rules in SOLAS 1974 as an alternative to the deterministic requirements. Prompting and motivating the adoption of a more rational approach to stability and survivability, this necessitated the development of appropriate methods, tools and techniques capable of meaningfully addressing the physical phenomena involved. The UK Department of Transport sought help from NAOME in understanding the underlying concepts. This was the start of a close collaboration between UK Government and NAOME that is going strong to this day. With funding from the UK Government and industry NAOME established a strong international group on the stability of ships and ocean vehicles that served as one of the incubators for the development of the modern subject of ship stability. This, in turn, attracted similarly-minded scholars and industry leaders from around the globe to lay the foundations for international collaboration on the subject and to STAB 1975 – the first Conference on the Stability of Ships and Ocean Vehicles. Within 40 years, this new impetus has climaxed to the “zero tolerance” concept of Safe Return to Port for damaged passenger ships and to the Second Generation Intact Stability Criteria, all goal-based, all performance-inspired, using first-principles tools with strong scientific foundation to guide the way forward.

What is most impressive is that irrespective of these astonishing developments and despite unrelenting effort institutionally, country-wide and world scale the field remains relevant and of high focus, combining deep scientific basis with practical and ethical concerns stemming from a continually changing industry and society. Stability represents a prime driver for naval architects whilst the form and consequences of intact and damage stability regulations remain at the forefront of interest at IMO. Many ship stability problems remain “unsolved” as manifested by unacceptable loss in human lives in accidents that continue to happen too frequently for comfort. With rising societal regard for human life and the environment and with technology driving innovation in complex and safety-critical ship concepts, such as the giants of the cruise ships being built today, the subject will remain a central focus for as long as there is human activity at sea. Some of the younger members of our small fraternity will have the opportunity to reflect on this, 40 years on!

Organising a large Conference as most of you will know is not a mean task. But, we have been blessed with a superb Local Organising Committee whose help, advice and support made all the difference. We would like to express our gratitude to Dr Evangelos Boulougouris, Caroline McLellan and Lin Lin who have given their all to the Conference with admirable dedication, inspiration and zest. A vote of thanks goes to all our colleagues at NAOME and all the students who offered enthusiastically and unreservedly their support in all the vast array of preparatory work leading to the Conference.

We are indebted, of course, to the international Standing Committee for entrusting this prestigious Conference to the University of Strathclyde and NAOME, especially so to the current Chair, Professor Alberto Francescutto. The help, advice and support received by everyone are gratefully acknowledged.

This is also a good opportunity to express our gratitude and thanks to all the delegates of the STAB 2015 Conference, the keynote speakers, the authors, reviewers and presenters. Special thanks goes to the University of Strathclyde and NAOME for their support and to the City Council and Tourist Board of Glasgow for being so forthcoming and helpful. Last, but not least, the STAB 2015 sponsors: Lloyds Register of Shipping, Royal Caribbean Cruise Lines, DNVGL, ONR Global, Class NK, Keppel Offshore and Marine and Sea Transport Solutions. Their support is gratefully appreciated.

The past forty years have been challenging but rewarding and enjoyable. We have attended the STAB Conferences and Workshops in many parts of the world and were impressed by the enthusiasm for the subject by the participants, old and new, and the great effort expended by the organisers to provide a nurturing and stimulating environment. The most treasured experience of all has been the opportunity to meet similarly-minded people and to develop long-lasting friendships. We hope you will find STAB 2015 would offer the same environment to you.

We do not expect to be attending STAB 2015 but stability is now in our blood and we will continue to give our support to the subject and share our experience with our younger colleagues. We know the subject is in good hands and we wish everyone success.

Professors Chengi Kuo and Dracos Vassalos
Chairmen, STAB 2015
Department of Naval Architecture, Ocean and Marine Engineering
The University of Strathclyde
Glasgow, Scotland, UK
June 2015

This page is intentionally left blank

STAB INTERNATIONAL STANDING COMMITTEE

Professor Alberto Francescutto (Chairman)	University of Trieste, Italy
Dr. Vadim Belenky	David Taylor Model Basin, USA
Hendrik Bruhns	Herbert-ABS, USA
Professor Alexander Degtyarev	University of St. Petersburg, Russia
Dr. De Kat, Jan	ABS, Denmark
Professor Marcelo Neves	Federal University of Rio de Janeiro, Brazil
Professor Apostolos Papanikolaou	National Technical University of Athens, Greece
Professor Luis Perez-Rojas	University of Madrid, Spain
Professor Konstantinos Spyrou	National Technical University of Athens, Greece
Dr. Naoya Umeda	Osaka University, Japan
Professor Dracos Vassalos	University of Strathclyde, United Kingdom
Dr. Frans van Walree	Maritime Research Institute, Netherlands

STAB2015 LOCAL ORGANISING COMMITTEE

Professor Dracos Vassalos (Chair)	University of Strathclyde, NAOME
Professor Chengi Kuo (Chair)	University of Strathclyde, NAOME
Professor Sandy Day	University of Strathclyde, NAOME
Professor Osman Turan	University of Strathclyde, NAOME
Professor Panagiotis Kaklis	University of Strathclyde, NAOME
Dr Evangelos Boulougouris	University of Strathclyde, NAOME
Dr Cantekin Tuzcu	Maritime and Coastguard Agency
Dr Dimitris Konovessis	Nanyang Technological University
Dr Andrzej Jasionowski	Safety at Sea Brookes Bell
Dr Luis Guarin	Safety at Sea Brookes Bell
Carolyn McLellan	University of Strathclyde, NAOME
Pamela Leckenby	University of Strathclyde, NAOME
Lin Lin	University of Strathclyde, NAOME
Renyou yang	University of Strathclyde, NAOME

STAB2015 SPONSORS

Lloyd's Register

DNV-GL

Royal Caribbean International

Office of Naval Research-Global

Keppel Corporation

Class NK

Sea-Transport Solutions



KEYNOTE ADDRESS

Safety & Stability through Innovation in Cruise Ship Design

Harri Kulovaara, Royal Caribbean International

This page is intentionally left blank



Safety & Stability through Innovation in Cruise Ship Design

Harri Kulovaara, *Executive Vice President, Maritime and Newbuildings,
Design and Technology, RCCL* HarriKulovaara@rccl.com

ABSTRACT

The guests see one aspect of the operations, which may be the size of the vessel, the features of a restaurant, comfortable staterooms or the amazing architecture of the vessel. But what they do not necessarily see is everything behind this, making it work. Still, it is always there. It is about culture, it is about focus, it is about continuous improvement and it is about working together with the best minds; above all, it is about competence and knowledge – people!

Elevating the expectations, setting the goals and being true to them – every newbuilding project at Royal Caribbean Cruises starts by setting goals towards improving the guest experience. The same process that has created innovative vessels on the guest side has also been applied to the technical side. The result is the most technologically advanced cruise vessels in the world today with the highest levels of stability and safety, a strong focus on the environment and continual energy efficiency improvements.

Keywords: *cruise ship design, safety and innovation, safety culture, life-cycle stability and safety*

1. INTRODUCTION¹

The organisation of Royal Caribbean Cruises Ltd is built around a fleet of 44 cruise vessels, operated by 7 strong brands. The combined capacity of the existing fleet is about 102,000 berths. In addition to that, 8 vessels are on order, boosting the capacity further by 10 per cent during the next few years. The itineraries include more than 480 destinations worldwide. A fleet of innovative and trendsetting vessels is turned into a winning concept by over 60,000 dedicated employees involved in all kinds of different tasks both ashore and onboard – from the chairman, to the naval architects designing the vessels, to the

cabin stewards ensuring that the guests get a good night's sleep in a tidy stateroom.

2. DESIGN TRENDS

Economies of scale have driven the development towards larger and larger cruise vessels. A large vessel opens up new possibilities. When Project Genesis was initiated, eventually resulting in the Oasis class, the design team looked at the advantages of many different sizes, from 150,000 to 250,000 GT. They decided to go for a record-breaking 220,000 GT design. The size was not a means in itself; they just needed an outstanding product, taking the guests' vacation experience to the next level. A large vessel offers more real estate and extended width, allowing new architectural possibilities. It became possible to open up the ship even more and create a substantially wider promenade, which again was regarded as a giant leap.

Compiled by Par-Henrik Sjoström based on discussions with the author and additional interviews with Kevin Douglas, Janne Lietzen, Mika Heiskanen, Clayton Van Welter, and Thomas McKenney



A driving thought throughout the development of Genesis was the concept of neighborhoods – to offer distinct and separate areas for people with different lifestyles, needs and priorities. Step by step over two years of systematic development work the Genesis solution grew up and the contract was signed in February 2006. Now the "MkII"-version of the successful Oasis-class is being built, with delivery of the Harmony of the Seas scheduled for 2016. At about the same time the third vessel of the Quantum-class, Ovation of the Seas, will be handed over. Although somewhat smaller than the Oasis-class, the Quantum-class is said to be the most technologically advanced cruise vessel design in the world. By taking all of the latest collective knowledge and experience across the company and industry, Royal Caribbean has further developed holistic safety and stability elements. For example, the size of Oasis class provided the opportunity to improve the design from the safety perspective as well.

The development towards improved safety on cruise vessels has been driven by the industry. In many cases new, innovative vessel designs have been challenging the existing regulations. As old rules are often not applicable to new designs, the ship designers push the envelope, challenging existing "truths". The result is that new technology is utilized in a much larger extension than before in all areas, including safety. It is no exaggeration to state that the cruise vessel design of today provides a better and safer platform for the operators. Beyond safety, the cruise vessel of today is also more environmentally friendly and fuel efficient. These improvements have been – and continue to be – possible due to hundreds of ongoing initiatives that target not only meeting current rules and regulations, but going above and beyond them.

However, Royal Caribbean and the cruise industry have come a long, and occasionally rocky, way before reaching the status as a major player in the multi-billion dollar vacation

market. The first purpose-built cruise vessel, designed for leisure cruises in warm waters, was developed in the late 1960s. It originated from a Norwegian project for the expanding Caribbean cruise market. It also materialized the dream of Edwin W Stephan, a multi-talented American visionary, who first came up with the idea of a cruise line operating a fleet of high-class, purpose-built new buildings instead of old ocean liners, which were common in those days.

In 1968 Edwin W Stephan travelled to Oslo to meet with Norwegian owners. He presented his idea and got the support of I M Skaugen and Anders Wilhelmsen. Together with a third partner, Gotaas-Larsen, they established Royal Caribbean Cruise Line A/S in 1969, and the rest is history. Edwin W Stephan was the cruise line's president from 1969 to 1996, when he became vice chairman of the board of directors. At various times he had served as general manager, CEO, president and vice chairman.

Edwin W Stephan had a vision and was extremely focused on materializing it. This pioneering spirit has been present in the company ever since. It began with a total of three sister vessels being ordered from Wärtsilä Helsinki shipyard. It is said that it was a bargain for the owner, as the shipyard was desperately searching for a way to enter the cruise market.

These references could not have been better ones. The vessels to be named Song of Norway, Nordic Prince and Sun Viking are still today regarded as exceptionally innovative in their technical design and layout. Introducing many interesting features, the Song of Norway drew much attention. The vessel had a large pool deck and was the first ship in the world designed specifically for warm-weather cruising. It is not an understatement to say that she revolutionized the cruise industry, as previous ships were usually built with far less open space on deck.



Edwin W Stephan's vision also included what was to become a distinctive feature on Royal Caribbean's ships – the glass-walled cocktail lounge cantilevered from the funnel. Had he not been quite headstrong this might not have been the case today. When he first told the naval architects he wanted something like the Space Needle in Seattle, they were skeptical. A rival cruise line even predicted such a construction would shake right off the funnel.

The 18,000 GT Song of Norway made her maiden voyage from Miami on November 7, 1970 and became an instant success. She also made most of the existing cruise fleet feel old fashioned overnight. The Song of Norway was a purpose-built cruise ship, while the bulk of the cruise fleet was formed by former ocean liners, built in the 1950s, made obsolete on their original routes by the booming transcontinental air traffic.

The development since Song of Norway has been amazing. The Song of Norway class was followed by the twice as big Song of America in 1982. Just five years later the 73,192 GT Sovereign of the Seas entered service. Under Richard Fain's leadership and vision, who became the cruise line's Chairman and CEO in 1988, the culture of innovation and transformational ship design continued. Royal Caribbean has taken a place in the forefront of cruise ship development, introducing a row of trendsetting vessels, each generation with new features, of which many have been adapted by the whole industry.

Perhaps the most transformational and influential ship in the entire cruise industry is the 137,276 GT Post-Panamax cruise vessel Voyager of the Seas, originally known as Project Eagle. Delivered in 1999 by Kvaerner Masa-Yards in Turku, Finland (which after several changes of ownerships is now working under the name Meyer Turku), Voyager of the Seas became the lead vessel of the Voyager class, totalling five ships.

In 1995 Project Eagle took a new course when Harri Kulovaara joined Royal Caribbean. His experience from innovative ship design work in the ferry company Silja Line influenced the project in a positive manner, which in that stage more resembled a much larger version of the Sovereign class than something really ground breaking.

A unique feature was the huge horizontal atrium Royal Promenade, which was for the first time introduced on a cruise vessel. The "prototype" for the Royal Promenade can still be seen onboard Silja Line's cruise ferries Silja Serenade and Silja Symphony, built in 1990 and 1991.

The Voyager class marked a real turning point for Royal Caribbean, placing the company in a league of its own with respect to creativity and new innovations.

One such innovation was introducing the first ice rink at sea, another entertainment medium that further solidified Royal Caribbean's place at the forefront of cruise entertainment. Its integration into the ship design, placed amidships on the neutral axis with minimum motions, further emphasized the focus on safety, not just for guests, but also for the crew.

Voyager of the Seas was regarded as a unique cruise vessel that mixed elements from the US cruise industry and Scandinavian ferry technology. But there was more to come. Probably the most amazing floating structure built so far is the Oasis class, a record-breaker in almost every aspect. Project Genesis was the largest commercial shipbuilding design effort ever undertaken, breaking totally new ground. The vessels were built with a larger Royal Promenade than the Voyager class and the updated Freedom class. The width of the vessel enables two parallel superstructures between which is a park with over 12,000 living plants and trees, Central Park, and the Boardwalk, inspired by Atlantic City.



The latest class of Royal Caribbean ships, the Quantum class, is not only a technological masterpiece; it once more introduces new experiences for the guests. A unique feature is North Star, an observation capsule, which is telescopically lifted to a height of 90 metres. Even the inside cabins have a view as they are fitted with an 82 inch video wall, serving as a virtual balcony with real-time images of the sea, offering the same view as the outside cabins.

After the turn of the millennium the trend towards a lower average age of cruise passengers has accelerated. A new market is formed by families travelling with children. The latest generations of cruise vessels are designed to fit the expectations of a much more heterogeneous market than 45 years ago when the Song of Norway-class was delivered. Now there are cruise passengers of all ages and with many different social backgrounds.

Today Royal Caribbean Cruises is the second largest cruise company in the world. The cruise industry has evolved from a niche to a major player in the vacation market. As it all started in the Caribbean, this area has maintained its position as the most important cruise market in the world. However, the Caribbean has become a mature market. The growth has moved to Europe and during the last years there are huge growth expectations for the Far East with China as the driving force.

Key features for the cruise industry of today are very high guest satisfaction and great value for money. As a product on the vacation market a cruise is superior. Innovation has been driving the experience and service level far above what you can expect ashore. The convenience of a cruise is outstanding: a high-standard floating hotel, providing excellent service and entertainment, moves along with the guest and offers interesting new destinations almost every day along the cruise.

The cruise industry is about a never-ending quest to provide the best vacation to the guests.

It is driven by consumer demands while economies of scale provide cost advantages and opportunities. Royal Caribbean has been in the business since the beginning of the modern era of the cruise industry. The lesson learnt during the past decades is that there is no shortcut to success. There is no silver bullet; it is all about culture and process. The success is built upon an innovative mind-set and the cornerstones for Royal Caribbean's activities are guest experience, environment, energy efficiency, and most importantly safety.

Everyone is asking: 'what is the one thing going on?' The answer is that there are several hundreds of initiatives going on. It is not just one thing, it is a mass of things, it is a way of thinking, a process.

3. SAFETY IS THE CORE

In the same way Royal Caribbean is pushing the cruise vessel architecture to its limit the company is driving the technical design, always with highest priority on the extremely important sectors of safety and environment. The foundation of the cruise industry is to ensure the safety of the guests in all conditions, including possible emergency situations.

Safety is indeed the core of all activities within the company. The guests shall feel the safety culture onboard and feel that they are well taken care of – even if something exceptional would occur. Knowing this, everything is set for an enjoyable and relaxing holiday onboard.

In general, safety is no doubt the most important issue at sea, no matter what kind of vessel we are talking about. On a cruise vessel, with several thousand passengers and crew onboard, it is absolutely crucial. The policy of Royal Caribbean has, for decades, been a proactive one – to take safety to a limit far above and beyond compliance. The vessel should remain floating as a priority and new



technology and design tools have contributed to great progress, driving better and safer rules for damage stability. Ultimately it is about just that. If the design cannot withstand extensive damage, the game is over when an accident occurs – as was the case with the Titanic in 1912.

Safety is a complex and vast field, containing much more than built-in damage stability requirements. Redundancy, for example, is essential in the modern way of thinking, where the ship should be the safe haven even if a serious accident should occur.

Royal Caribbean has pioneered redundancy. In 1995 the so called half ship concept was implemented with the Vision class, based upon separate engine rooms mainly for fire division. In practice this means, that in case of an engine room fire the vessel would still have capacity left to generate enough power not only for propulsion, but also for all the vital functions in the hotel part of the ship.

In 1999 double hulls in engine rooms and two totally independent engine rooms were introduced in the Voyager class to reduce the risks of flooding of these vital spaces if the hull would be penetrated by grounding or collision. Since 2007 Royal Caribbean has built its ships by the principles of Safe Return to Port along with enhanced guest comfort requirements. In 2013, additional divisions were included between engine rooms to improve damage stability in addition to building them within the double hull. Extensive 3D-topographic simulations have been completed to verify configurations, along with consequence studies and safe return to port simulations.

Royal Caribbean has been pioneering many other sectors for enhanced safety and security as well. In an early stage the company took a robust approach towards the adoption of paperless navigation, including an internal approval process above and beyond that of regulation. An enhanced bridge layout, focusing on human-centred design, was

introduced with the Voyager class. The utilization of electronic mustering systems was taken to the next level in the Oasis class, leveraging this technology to further enhance evacuation and accountability.

An essential part of safety is also good manoeuvrability. Manoeuvring calculations, simulations and model tests have been incorporated both onboard and in shore-based training. The result is that every new generation of vessels has presented improved manoeuvrability, regardless of size. There are also innovative utilization practices for dynamic positioning systems within operation.

Project Eagle, resulting in the Voyager class, is a good example of ground breaking thinking regarding safety. The dramatic increase in size was driven by experience, also leading to giant leaps in safety. The alternative design principle was extensively used for the development of the horizontal atrium, the Royal Promenade. Such a large space as the Royal Promenade presented a real challenge for fire safety, not only for the designers, but also for the shipyard and the classification society.

In the Voyager-class, double engine rooms and advanced safety simulations were also adapted. The advanced integrated navigation systems, originally developed for demanding navigation of large cruise ferries in narrow archipelago fairways, soon found their way to Royal Caribbean's cruise vessels. Equipment and ergonomics of the bridge on Voyager of the Seas was state-of-the-art, and probably the most advanced on a cruise vessel at the time.

The Oasis of the Seas was the first ship designed with a known safety level, based upon the Risk-Based Design methodology. For crisis management an Onboard Decision Support System was adopted.

Technology made it possible to take such huge leaps in ship design without compromising safety. It had become possible



to simulate virtually everything on a cruise vessel during the very early phases of design: strength, stability, logistics, passenger flows, evacuation routes, damage stability, obstructed views in the theatre, manoeuvring in port, etc. It was now also possible to visualize the interiors of the vessel during the early stages. Simulation technology made it possible to design vessels that are progressive in all areas regarding customer satisfaction, operational advantages, energy efficiency and overall safety.

A main goal during the project was to design a vessel with improved levels of safety. The latest technology was utilized in all areas. The large number of passengers provided an opportunity to improve new evacuation routines and routes, including on-line registering of passengers at assembly stations.

Computational fluid dynamics calculations were used for optimizing the hull and its details. This process improved detail design and eventually created substantial energy savings. The machinery solution was adapted from Voyager and Freedom with two totally independent engine rooms and doubled systems.

The Solstice and Oasis class did in advance fulfil the principles of the coming regulations for “safe return to port”. In addition, the design of both classes helped shape the Safe Return to Port regulations by being used as examples during detailed analyses. Based upon a Casualty Threshold concept, where this defines the amount of damage the vessel is able to sustain and still safely return to port, a large 3D-computer model was created, including all channels, valves, cables and components. Numerous simulations took place, testing what would happen if a section was lost, analysing optimal routing for cables, etc. Part of the tools and the technology was developed exclusively for the Oasis-class and used for the first time to a greater extent.

Mainly due to the increased size of Oasis, there was a requirement to develop novel concepts in multiple areas including life-saving. Without compromising the design and safety of the vessel, several innovative designs were developed including optimized evacuation of the 8,500 passengers and crew, the largest lifeboats installed on a ship so far with a capacity of 370 persons each, and a large Marine Evacuation System (MES) for 450 persons each, designed for boarding through chutes.

Due to the configuration and novel design an alternative design process was extensively applied, including extensive fire simulations as per SOLAS Alternative Design and Arrangements. Alternative means of fire division was carried through in the form of roller shutters, enabling longitudinal and transversal fire breaks.

Royal Caribbean also pioneered a feature called the Safety Command Centre on the Solstice and Oasis class. Since the 1990s Royal Caribbean vessels were equipped with a safety desk on the bridge, evolving into the separate space on Celebrity Solstice in 2008 and Oasis of the Seas in 2009.

If a serious accident occurred the Safety Command Centre is manned, acting as a centre for resource allocation. Command, communication, evacuation and incident management all have dedicated resources that are specialized. The true power of the space is the potential to leverage the allocated resources through design and technology. Committing to a larger footprint allows objective-oriented teams to focus on their work stream. The team leader supports the command more effectively due to optimal span of control, thereby having a more ideal number of responsibilities and resources to manage.

This concept was further developed on the Quantum-class by dividing the Safety Command Centre into three pods. On the port side is the Evacuation & Command Pod, on the



starboard side the Incident Pod and amidships the Command Pod.

4. SAFETY LIFECYCLE

The philosophy of Royal Caribbean is that safety is not only about how a newbuilding is designed but also concerning virtually everything that takes place over the life cycle of the vessel. One important issue is how to train the ship operators and how to set the standards for the operations. The operators have to know exactly which tools are provided to monitor the stability in operations and also how to understand them. They have to understand a possible damage situation in a very complex manner, using the technological tools provided.

Training is essential in the safety lifecycle. The operational standards and levels of training are enhanced to fit for purpose and rigorous technology qualification. The company has a safety culture program that stresses the necessity of efficient emergency response procedures and training.

Royal Caribbean talks about the safety lifecycle of a ship, containing four phases: Ship Design (Design and NB phase), Strategic Stability Management (operational life cycle), Operational Stability Management (per voyage) and Emergency Stability Management (emergency situations).

The design of the ship is setting the bar. Over the life cycle of the ship several modifications are done. They can either impact the construction negatively or positively. With deeper knowledge of the vessel it is possible during a refit to enhance the stability by applying new types of watertight doors, adding ducktails, removing weight up high or splitting tanks. Through this process it is possible to improve the vessel stability, despite the fact that the original design has been modified. If no measures are taken, the ship will gain weight and the stability will be impacted.

Already in the design and newbuilding phase there is greater collaboration between partners such as the Cruise Ship Safety Forum (CSSF), the world's leading shipbuilders and designers, academic institutions, authorities, technology suppliers and the Cruise Lines International Association (CLIA).

The CSSF has become a very active unit, where the majority of cruise lines, shipyards and classifications societies are represented. The forum is collectively working on several topics and has been pushing the envelope in a positive manner. Developing thoughts and giving recommendations to cruise lines, shipyards and even to the International Maritime Organization (IMO).

In the design phase the regulations are to a great extent providing the basis. But it is of course, as in the case of Royal Caribbean, possible to go above and beyond that.

The stability, and hence the safety of the vessel, does not remain unchanged through the entire operational life cycle. It is therefore important that it is constantly monitored to make sure that the vessel lives up to the initial design aspects and elements. This is called Strategic Stability Management. It starts with stability analytics that utilizes a shore-side stability analytics program for tracking and trending fleet stability parameters.

This process also includes a deadweight management system to better optimize both hull efficiency and stability. The potential exists for more robust policies and procedures, which can result in positive change with minimal cost.

Operational Safety Management is how a vessel is operated during each voyage. It is about how all the technological tools are applied and used to determine the stability and loading conditions. It includes control of water tight doors and deadweight management.



For example watertight door exemptions have been objectively assessed in an effort to strategically reduce opening times and thereby increase vessel survivability. These experiences are encouraging. Going beyond the requirements laid out by Class and authorities on two different ship classes, watertight door opening hours have been reduced from 40 to 80 percent.

Emergency Stability Management aims to prepare the operators for a critical situation. The key is training – it has to be the best training with the best procedures if the ship is damaged.

Royal Caribbean is also a step ahead in this field. For example, SOLAS has mandated fire and life boat drills on a weekly and monthly basis. But SOLAS has not mandated any damage control drills. Royal Caribbean started mandating damage control drills a couple of years ago on a few ships and now they have adapted the practice fleet-wide. Their ships do not only have fire drills and lifeboat drills, but they also have proposed through IMO that damage control drills be completed on a regular basis. For all RCCL brands there is a monthly damage control drill frequency in policy. The two newbuildings of Quantum class have also been delivered with Damage Control Plans updated to incorporate Damage Response.

The life cycle of a cruise vessel is like a journey itself. The trick is to make sure that all the competence and knowledge is transferred in a meaningful manner to the operators via training and tools. When new knowledge and new competence is found, there becomes ways to improve existing ships with relatively small modifications.

An important issue is the impact of Stability Management on Safety. Compliance serves as the clear baseline for safety while the actual ship design sets the bar. Stability management systems and procedures for a vessel in operation can raise, maintain or lower that bar.

Royal Caribbean continues towards enhanced Stability Management. Based upon a holistic approach, linking Strategic, Operational, and Emergency Stability Management, the aim is to ensure better understanding of existing ships as well as the impacts of lightship growth and reduction of stability.

The measures taken should initiate actions to improve both physical changes and operational practices. These measures will increase knowledge and understanding of specific ships, creating possibilities to develop even more efficient training processes and procedures to reduce risk of progressive flooding. An important part of the follow-up process is benchmarking and sharing best practices with the industry through the CSSF and to develop an industry-wide approach.

There are several issues on the agenda: Damage Control Response Plans (along with stability computers), damage consequences, decision identification and simulation support tool, attained index live on bridge based on watertight door status and linking/improving communication between the Engine Control Room and Safety Command Centre. The vision is to provide a further benchmark in the passenger ship and maritime industry, not just for cruise ships.

The CSSF continues working very actively on these improvements and even developed papers and practices for IMO, with recommendations such as damage control drills.

5. PROBABILISTIC DAMAGE STABILITY

When designing the Oasis- and Solstice-class vessels Royal Caribbean made a decision to utilize the probabilistic damage stability requirements ahead of time for safety. At that time the deterministic calculation model was still in use, calculating if the ship survives damage to any two of its compartments.



The probabilistic damage calculation methods were developed more than 10 years ago, supported by an ever increasing level of computing power.

The index required by SOLAS for the Oasis of the Seas is approximately 0.88. This means that Oasis could survive 88 per cent of the defined damage situations deriving from accident statistics without losing the ship. The actual calculated index for Oasis of the Seas, the attained index, is 0.91. When calculated in the project stage, Royal Caribbean was already informed that due to the simulations made they had a reason to believe the actual capability of the ship was much better. The simulations indicated that Oasis of the Seas could actually survive 98 per cent of all damages.

By then it had become clear that the calculation methods, which are demanded by SOLAS are conservative thus giving a very conservative view of the ship safety level. Since then a lot of work and research has been completed by the company and its associates that has verified that the presented calculations for the Oasis of the Seas were correct.

We feel strongly that the cruise ship industry, academia and regulators now urgently need to start focusing on improving the calculation methods to better indicate the true safety levels of a vessel. The rules are simplified and give a very conservative estimate of the situation. For example, longitudinal bulkheads in engine rooms protect better against raking side damage, but do not impact the attained index (meaning you don't get credit for it). This is why designing to a standard above the rules is desired, especially in areas that the rules do not directly address. Royal Caribbean is also working towards improving safety in this field. Simulations are used to enable a much higher standard of safety to the ships, making these simulations exceptionally important.

The use of the simulations allows us to better understand the likely consequences for

the myriad of different damage scenarios. With that knowledge the ship's operating team can be trained and educated so that they are more likely guided to a successful outcome in the event of progressive flooding.

Once more, this reiterates the need to go beyond the current rules while also identifying the conservative nature of the simplifications made in the rule calculations. Simulations are critical for training and understanding. These findings will be shared with the industry and the ship designers so that they collectively, as an industry, can work towards better regulations.

We have always had a gut feeling that the actual safety levels of our cruise ships exceeded the results of the calculated methods. The simplified calculation method does not give credit to the actual built-in safety. The probabilistic regulations have been very important; they have helped us to improve the safety of ships. However, through simulations and model scale work we have found out that they give a conservative look and now we hope that the industry starts really working on putting down research in order to get even better results in this respect to redefine the regulations.

Today there is a wide spread opinion in the industry that it is necessary to further enhance the probabilistic damage stability regulations to more accurately reflect the actual improved safety levels. Having all this information, it is asked if the probabilistic method really does advance safety. There is a great opportunity to advance and improve safety, along with more realistic regulations, by looking for long-term solutions and benchmarking cruise industry practices to all passenger vessels and the maritime industry as a whole. Continuing research on the entire life-cycle and on existing ships as well as further development of advisory, support and training tools is critical for the success of continual improvement in safety and specifically damage stability for all vessels.



6. THE FUTURE AND NEED FOR INNOVATION

The tremendous success behind cruising is the sum of a number of factors, such as high service, innovative ships offering many activities and experiences for the guests, a pristine environment, interesting destinations and cost effective operations.

Effective operations through economies of scale have enabled large scale cruising. In the early days it was a vacation form for the wealthy. Today cruising is available for a large spectrum of consumers in a large number of countries.

Future trends in cruise ship design and operations show a continuing growth in the average ship size as larger vessels replace smaller aging vessels. Still, it is unlikely that the maximum size will increase significantly in the foreseeable future compared to the largest vessels of today. When talking about the super large ships, like the Oasis class, we believe that it will be some time before going beyond that size. The reason for the ultra large size of these vessels is, to a great extent, architectural, they were designed wide enough to really be opened up in the centre.

Future development is to a great extent a question about features, activities, experiences onboard and the ability to deliver unique destinations. The designers will continue to develop novelty in architectural design solutions, such as open spaces, large atriums and indoor-outdoor areas. Every new generation of Royal Caribbean's ships have more new attractions and features. The guests want even more diversification regarding activities, features and options onboard. As a target group on the market, families become more and more important, which has to be taken into consideration even more when designing new ships.

The cruise vessels of today reflect the design trends in the land-based leisure industry.

This is especially true regarding restaurants onboard. Cruise ships are cutting edge on the culinary side today, offering many different choices and specialty restaurants. The trends of dining ashore are also the trends of dining on cruise ships.

Furthermore, there is still a focus on smaller ships, which are being designed to satisfy niche markets and deliver smaller and more remote destinations.

The focus will remain strong on safety. Regarding the environment, it will most likely become even stronger. For example, focus will be on advanced emission purification systems, both regarding water and air, as well as improved efficiencies with focus on alternative fuels.

Again, technology is the enabler in every respect. Technology and computing power is helping to design ships in a totally different manner than has been possible before. It is also enabling them to be operated in a totally different manner than in the past.

The design loop for all of the learnings across guest experience, energy, safety is a continuous cycle for newbuilds and the existing fleet, taking lessons learned from each and applying them to the other. For ships that can't be changed from a design perspective, operational aspects are emphasized to better understand the current state of the vessel. All of the challenges that currently face our current and future fleet are very complex and require a structured and innovative process to make continual advancements and improvements. The end result will hopefully be a buried success for safety, as the types of situations that are being protected against are never desired. It is important that complacency is avoided and that innovation is the driver that keeps us moving forward in the direction of continuous improvement.

7. INNOVATION IS THE DRIVER



Designing and operating a fleet of cruise vessels demands a holistic view from every perspective. Key factors during cruise operations, such as guest experience, impacts on the sensitive marine environment, energy efficiency and safety do not live a life of their own, as they are all tightly connected to each other.

It is of utmost importance to understand that one thing does not rule out another. In modern cruise ship design and operation they support each other, from the launching of a newbuilding project to recycling at the end of the life cycle. Technology has become an integral part of design and ship features. Royal Caribbean Cruises has, during all of its existence, been known to be an innovator in the industry. The company has by designing and building ten generations of innovative cruise ships, become trendsetters. This has been made possible by a specific culture, set of values and capabilities and a way of working with the greatest minds of the industry. There is a constant drive to make innovation part of the culture to make it everyone's responsibility and everyone's desire. Sustainability of innovation comes from culture.

The company has strong in-house leadership that collaborates with the best expertise available to nurture innovative solutions. Without this knowledge and experience it would be impossible to innovate. The cornerstone for the approach towards safety is a rigorous risk assessment process and risk centrality, utilizing state of the art technical and design technology. It is a never-ending loop of continuous improvement and feedback. There is always something that can be done better. Royal Caribbean works with the experts in the damage stability field to build better competence and better tools, improving processes and sharing this knowledge with the shipping industry.

This vast competence is applied in every new and existing ship in the Royal Caribbean fleet, aiming at safer designs and safer

operation of existing ships. Technology and tools have been, and will continue to be, a tremendous player in this work.

The goal of continuous improvement in all areas is a journey, and we as an industry are part of driving the technology and tools that facilitate achieving this goal. A successful journey or outcome can be characterized using the simple formula of adding a restless desire, ambition, technology and tools, and the best competence in the industry.

Safety is not just for Royal Caribbean, but the industry as one unified body. There should be no competition when it comes to safety. Sharing and developing passion with others, as we are doing within the CSSF, remains a primary focus for us. Our presence at this Stability Conference exemplifies our willingness to share this point with all the key players.

8. CONCLUDING REMARKS

We will finish this keynote address by using two quotes:

“There is no such thing as perfect Safety, but there is perfect dedication to continuous improvement and Safety, and Royal Caribbean is fully committed to both of them.”

(Richard Fain – Chairman and CEO, RCCL)

“We are constantly working together in order to learn from the operational procedures, how we can apply better thinking, better training and better technical tools into that. We always think about how the use of advanced technology can help the crews to operate the ships more efficiently with less impact on the environment and with the highest possible safety standards.”

(Harri Kulovaara – EVP Maritime and Newbuildings, RCCL)

This page is intentionally left blank

KEYNOTE ADDRESS

Design for Safety and Stability

Henning Luhmann, MEYER WERFT

This page is intentionally left blank



Design for Safety and Stability

Henning Luhmann, *MEYER WERFT* henning.luhmann@meyerwerft.de

Jörg Pöttgen, *MEYER WERFT* joerg.poettgen@meyerwerft.de

ABSTRACT

Safety and stability are two key aspects for the successful design of ships while keeping the balance between efficiency and performance of the ship. In the past the main drivers for safety improvements have been catastrophic accidents but a change of mind is needed to enhance safety and stability within the given envelope of design constraints. This can only be achieved when beside comprehensive calculation tools basic design methods will be developed and used in the daily design work. A method to predict the attained subdivision index has been developed and has been shown here as an example for a simplified design method.

Keywords: *design, safety, cruise ships, stability index*

1. INTRODUCTION

The design of complex ships, like cruise ships, is an everlasting quest to find the right balance between the performance of the ship, for cruise ships this is the satisfaction of the guests on board, efficiency of operation and safety and environmental protection. Obviously the compliance with rules and regulations are the basis for each design, but the development of technologies and new design ideas challenging the application of regulations.

2. DESIGN TO SAFETY

Shipbuilding and design of ships has a very long tradition and is mainly built on experience. Main drivers for design changes towards a safer ship have been in the past mainly accidents or near-accidents and experiences of the designers as well as operational feedback. Very popular examples are the capsizing of the VASA, the sinking of TITANIC or the foundering of ESTONIA. In the past such kind of accidents also influenced the rule making process and based on the IMO rules the current state-of-the-art has been defined.

Merchant ships are designed, built and operated to be part of an enterprise to generate profit. This main objective together with the challenge to find the right balance with rules and regulations is usually the motivation not to design to safety but to squeeze the rules and their interpretation to the limits and maximizing the profit for shipbuilder and operator. By maximising the nominal capacity of a ship and designing the ship for the date of delivery only by ignoring the life time of the ship and the operational needs the strategy for design will fail on the long run. A change of mind is needed for the whole industry to maximize the safety within the given envelope in close cooperation with the operator and for the life-time of the ship.

Another important factor for the design process is the available time. Decisions influencing the global safety of a ship, like the watertight subdivision, are defined at an very early stage of design and needs to be kept unchanged until delivery. Hence, the methods you may apply to determine the safety needs to be fast and robust. Complex tools like parametric optimizations may be used from time to time to expand the level of experience but they are un-

suitable for the daily design work. The industrialization of outcome of research projects is very important to take new technologies into use, but it also worth to reconsider experiences and knowledge from the old days.

3. STABILITY RELATED TOPICS FOR DESIGNERS

There are many different topics which may influence the stability or general safety of a ship which needs to be considered during the design. The following figure illustrates a possible accident scenario.

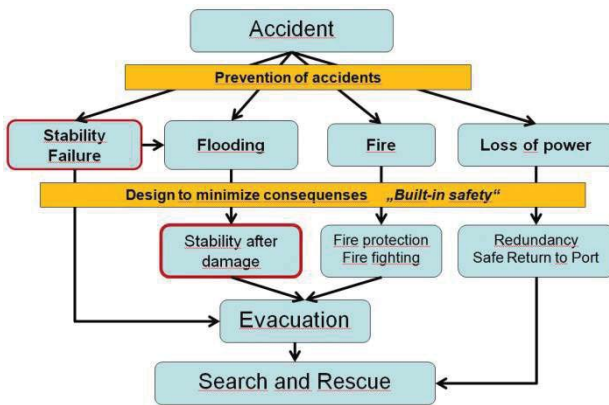


Figure 1 Accident Scenario

Although the best way to improve the safety is the prevention of any accident the focus of most of the designers and researchers is the mitigation of any accident. In particular the extensive discussion about stability after flooding during the recent years, which is still ongoing, is leading somehow in the wrong direction.

In the daily work of ship designs some basic elements like a accurate estimation of light weight and centre of gravity is much more important than a fancy flooding simulation. Proper weight and COG estimations together with the reasonable account for future growth and service based loading conditions form the basis for the hull form and thus the stability behaviour of the ship during its life time. The constant verification of weight and intact stability, including dynamic stability behaviour,

ensures that the ship will meet the requirements from the regulations as well as for the performance.

The detailed investigation for stability after flooding is the second focus during the design. To find the best subdivision is again a huge iterative process to align the different demands of space requirements, operability and survivability after damage. Also other safety rules, like escape routes are challenging parameters in this process.

As explained before this needs to take place within a very short time frame and the following presentation of a method to judge on the damage stability capabilities for different hull forms in an easy way is a good example how modern first-principle tools together with basic knowledge can be combined to form a powerful design tool.

During the development of a new hull form it was recognized, that the normally used hard points for the hull form designer will not reflect all different demands a hull form has to fulfil. Therefore an algorithm has been developed to compare different hull forms under special interest of the demands of the damage stability calculation.

4. DESIGN OF A NEW HULL FORM

During the design process different hull forms are developed to find the best for the given design. Hard points for the hull designer are defined to reflect any constraints, which are the following:

- Geometry
 - Lpp
 - Bmax
 - Design draught
- Hydrostatics
 - Minimum KM on design draught
 - LCB
 - Displacement



A new kind of hard point has been searched for the hull designer that guarantees the same level of the attained index.

4.1 The Stability Energy Index

The fundamental idea was formulated by RAHOLA already in 1923. He invented the stability energy of a vessel which was used for the stability rating of different vessels. Based on these principles the following algorithm was developed.

Contributing Factors

The area under the righting lever arm curve is calculated from the upright to a certain range of heel. This area is been called E_{phi} .

To reflect the influence of the damage stability calculation E_{phi} is only calculated for the design draught of a vessel but for all three draughts relevant for the calculation of the attained subdivision index:

- Light service draught (D_l)
- Deepest subdivision draught (D_s)
- Partial subdivision draught (D_p)

Basic Calculations

A variation of different hull forms with the same KG on the different draughts is calculated according the above mentioned principles. The watertight subdivision for the calculation of the attained index has been the same for all four hull forms.

The below diagram show the resulting attained index in comparison with the computed area under the GZ-curve from upright to 22° of list.

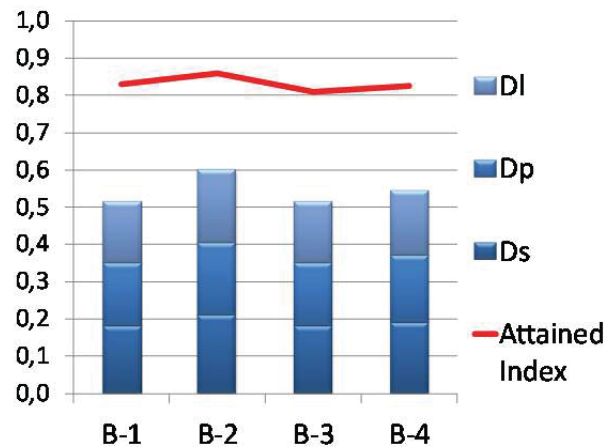


Figure 1 Area under the GZ curve compared with the Attained Index A_i

As the ship is not floating on the three initial draughts after damage anymore, an additional draught has been considered to reflect the situation of the vessel after flooding. This ‘over’ draught (D_o) is the deepest subdivision draught D_s plus 40% of the difference between D_s and D_l . In addition a weight factor 0.5 for D_l is used to adjust for the minor influence of this draught. Figure 2 show the improvement driven by these decisions.

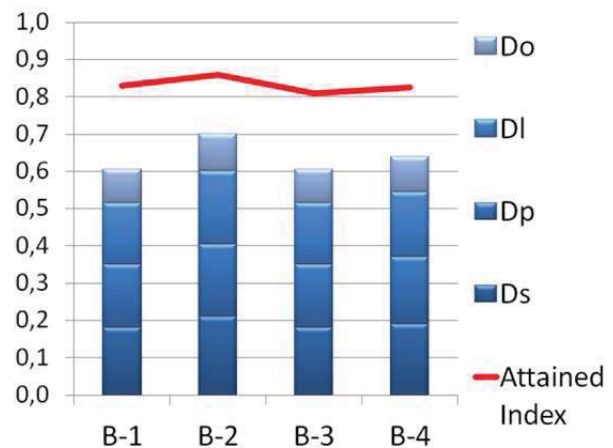


Figure 2 Area under the GZ curve compared with the Attained Index A_i with an additional draught D_o

Calculation Rule for the Stability Energy Index

Based on the findings an easy algorithm for the hull form designer has been developed to verify if his hull form will reach the Stability Energy

Index and to calculate the Required Stability Energy Index as a hard point for the hull for designer based on a given Attained Index reached in the damage stability calculation

The hull form designer will get the draughts D_l , D_p , D_s and D_o with their corresponding KG values. For each draught the corresponding area under the GZ curve has to be calculated from 0° to 22° list and summed up according the following formulae.

$$SE_{phi} = 0.5 \times E_{phi-l} + E_{phi-p} + E_{phi-s} + E_{phi-o}$$

with :

$$\begin{aligned} E_{phi-l} &= E_{phi}(D_l; KG_l; 0^\circ - 22^\circ) \\ E_{phi-p} &= E_{phi}(D_p; KG_p; 0^\circ - 22^\circ) \\ E_{phi-s} &= E_{phi}(D_s; KG_s; 0^\circ - 22^\circ) \\ E_{phi-o} &= E_{phi}(D_o; KG_o; 0^\circ - 22^\circ) \end{aligned} \quad [1]$$

Stability Energy Index versus given Attained Index

Based on further calculations a simple calculation rule for SE_{phi} at a given Attained Index could be derived statistically.

$$SE_{phi}(RAI) = 2 \times RAI - se_{ship} \quad [2]$$

with: RAI = Required Attained Index and
 se_{ship} = correction factor for different ships [approx. $0.96-1.06^1$]

The following diagram shows the results by using the above introduced formula. For the same KGs and watertight subdivision the attained index has been calculated as well as the SE_{phi} indicated as the Real SE_{phi} in the diagram. A very good correlation has been found and with this prove this method has been used during parametric optimizations of hull forms resulting in the optimum compromise between hydrodynamic performance, space requirements and sufficient stability after flooding.

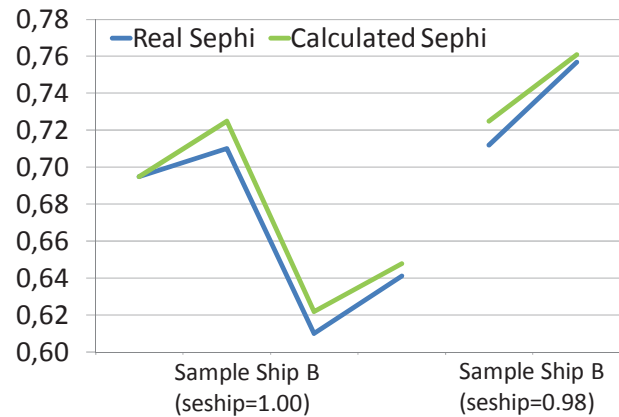


Figure 3 congruence between the real and the calculated SE_{phi}

5. EXAMPLE DESIGN TO SAFETY

One other example for design to safety is the arrangement of watertight doors in a passenger ship. The space below the bulkhead deck is subdivided into watertight compartments and on cruise ships, each square meter is used for the accommodation of the crew and technical spaces like workshops and laundries or storage areas. Each of the watertight compartments requires two means of escape, one of them needs to be a vertical stair or escape leading to the embarkation deck, the second one is usually a watertight door leading into the adjacent compartment.

If operational needs are not considered in the right way at an early design stage the purpose of the spaces may cause that watertight doors are required to be open during normal service and not only as an emergency escape. Typical examples are the laundry and the connected linen stores. In the past laundry and linen stores have been located in adjacent watertight compartments, but recent designs have shown that this can also be placed on top of each other. With this vertical flow the watertight doors may be kept closed during normal operation and this really increases the safety level.

¹ To be further investigated



6. RISK MANAGEMENT AND FUTURE CHALLENGES

The safety related design process requires a high degree of transparency and close cooperation between the stake holders. Not only shipyard and operator are required to cooperate, also the regulatory bodies, like flag administration and classification societies, and technical experts need to be part of the team.

This approach has a number of positive effects. One is of course that the design is of outstanding quality, usually with a proven higher safety level than required by the rules and regulations, on the other hand the lack of knowledge about the special challenges for large cruise ships can be communicated in a better way to a wider audience.

A basic challenge however remains new designs and also new rules and regulations improve the safety of new ships significantly in a continuous way, however it takes about 30 to 40 years to get a whole fleet renewal. The question how to upgrade the safety of the existing fleet is one of the major tasks for the industry and the regulatory bodies in the coming years. Otherwise the gap in safety level between old and new ships will become unacceptable. The introduction and quantification of active safety measures may be one possible way to solve this problem.

7. CONCLUSIONS

Ship design always focus on safety and stability, however instead of interpreting given rules and regulations to their limits a change of mind is needed to maximize safety within the given design constraints. A proper holistic approach based on close cooperation between regulators, designers and operators is the way ahead, while using highly sophisticated calculation tools together with experience and traditional simple design methods to avoid the repetition of mistakes which have happened in the past. A method has been shown how this combination

of modern tools with old experiences can be used in the daily design process.

This page is intentionally left blank

KEYNOTE ADDRESS

Stability Barrier Management for Large Passenger Ships

Dr Tor Svensen, DNVGL

This page is intentionally left blank



Stability Barrier Management for Large Passenger Ships

Tobias King, *DNV GL*, tobias.king@dnvgl.com

Clayton Van Welter, *Royal Caribbean Cruises, Ltd.*, cvanwelter@rccl.com

Tor E. Svensen, *DNV GL*, tor.e.svensen@dnvgl.com

ABSTRACT

This paper deals with major accident risk related to stability on large passenger ships. The main scope of work is to investigate the impact stability related risk has on the total risk picture, and introduce barrier management as an approach to control stability related risk. The paper also addresses some main elements in stability management, highlights critical barriers and presents a case study on how stability barrier management may function in practise.

Keywords: *Stability barrier management, barrier management, stability management, safety management, passenger ships, cruise ships, bowtie*

1. MAJOR ACCIDENT RISK FOR PASSENGER VESSELS

Several definitions of major accident exist, as described by DNV GL and the Norwegian Ship-owners Association in the report “Good Practices - Barrier Management in Operation for the Rig Industry” [1]. Although somewhat different, they all have in common that they refer to large scale consequences, in terms of impact on life, property and the environment. They also indicate that the consequences may be immediate or delayed, suggesting that there is a potential for escalation. Further, major accidents are complicated by nature and hard to predict. They involve a complex risk picture,

multi-linear chain of events, failure in several safety features, and with a potential for uncontrolled escalation.

Accidents related to ship damage stability have been shown to be a major risk contributor for passenger ships through the joint industry project Risk Acceptance Criteria and Risk-Based Damage Stability [2] and the Goal-Based Damage Stability project (GOALDS) [3] where annual accident frequencies for passenger ships were determined based on the IHS Fairplay. To increase the accuracy, the data was filtered according to several criteria and the following accident categories were selected for analysis: Collision, contact, grounding, (also designated wrecked/stranded) and fire/explosion

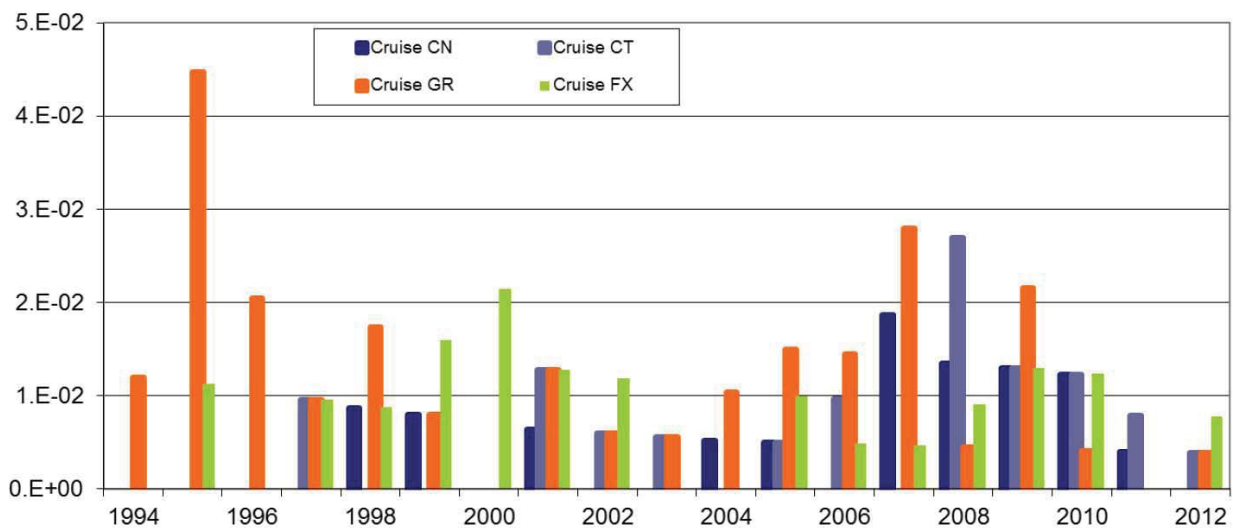


Figure 1: Annual accident frequencies for passenger ships (excluding ropax) [2] [3]

Explanation to figure:

- CN: Collision
- CT: Contact
- GR: Grounding (incl. Wrecked/Stranded)
- FX: Fire/explosion

The accident frequency statistics show that the main risk contributors for cruise ships are stability related. From 2000 to 2012, there were a total of 59 cruise ship casualties related to grounding, contact and collision and 21 to fire.

The events in the accident statistics above are all initial events considered to be serious, and could lead to a major accident with significant loss of life. For major accidents such as capsizing or sinking the risk is uncertain - we are still dependent on our perceptions to determine the risk. Exposure to some risk is unavoidable when operating a large passenger vessel in a seaway and it is not feasible for the industry to contemplate building and operating risk-free ships. The alternative would be a passenger ship never leaving port. The purpose of managing major accident risks is therefore not to eliminate the risk itself but to understand and control it so that risk can be managed in the most effective way.

2. INTRODUCTION TO BARRIER MANAGEMENT

The purpose of the barrier management approach to safety is to take into account the low frequency and high consequence major accidents by addressing the complexity of these scenarios. If a risk analysis predicts a major accident to occur once in a hundred years, it is hard to tell whether this happens tomorrow, in fifty years or in a hundred. Consequently, management of major accident risk requires good systems, which captures this complexity and reduces uncertainty. This is the main objective, or rationale, behind barrier management[1].

2.1 Bowties – the Foundation for Barrier Management

A common way to illustrate barriers is by James Reason's Swiss Cheese Model [4]:

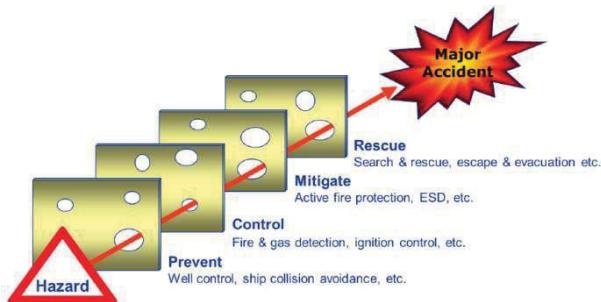


Figure 2: Swiss cheese model

As revealed by its name, the Swiss Cheese model illustrates an event sequence in which barriers are presented as cheese slices. The holes in the cheese slices represent barrier failure. Throughout the lifetime of a ship, holes in this model are expected to constantly move and change sizes depending on a multitude of causes, such as type of operation, condition of the ship, crew competence, to name but a few. For a major accident to happen, holes in the Swiss Cheese Model need to align, allowing for an accident trajectory.

Safety barriers are defined by making bowties, as has been defined by DNV GL and the Norwegian Shipowner's Association [1] to consist of the following elements:

- Hazard/Threat: Potential for human injury, damage to the environment, damage to property, or a combination of these (ISO 13702).
- Hazardous event: Incident which occurs when a hazard is realised (NORSOK Z-013; ISO 13702).
- Barriers: Barriers refer to measures established with an explicit purpose to (1) prevent a hazard from being realised, or (2) to mitigate the effects of a hazardous event.

A simplified presentation of the elements in the bowtie diagram is as follows:

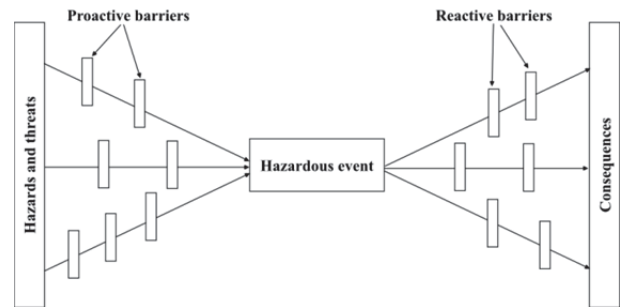


Figure 3: Simplified bowtie diagram [5]

An example for stability could be a ship sailing in a busy waterway in heavy fog (threat) leading to collision (hazardous event) that may lead, in turn, directly to loss of life (consequences).

The bowtie tool is flexible and standards vary between different companies depending on their needs and what the bowtie structure is used for. As an example, bowties for accident analysis may differ from bowties used to define barriers in a safety management system or bowties used for the purpose of regulatory development. DNV GL typically uses major accidents as defined in chapter 1 as hazardous events in the centre of the bowties [1]. Examples of such hazardous events are fire/explosion, capsizing, collision/grounding, loss of power generation, loss of propulsion/manoeuvring, terrorism and pollution to air/sea.

These hazardous events are selected to best capture the complexity of major accidents. The bowties are naturally interlinked, meaning that the same incident may be a hazardous event, consequence or a threat depending on how the operator decides to set up the bowtie. Likewise, the same incident may be a threat in one bowtie, and a consequence in another. As an example, a collision may lead to fire/explosion, capsizing, loss of power generation or pollution to sea. Likewise loss of power generation may lead to collision.

From a safety management perspective, the purpose of the bowtie is to define barriers that are the foundation of the management system.



The only way to control a major accident risk is by controlling the integrity of the barriers at all times. By spotting degradation of a barrier at an early stage, one can take necessary action before an accident trajectory opens in the Swiss cheese model. Further, there is a need to have a process in place that continuously analyses the barriers for improvement potential, either by strengthening the existing barriers or adding new ones.

Using the bowtie structure as a basis for barrier management also contributes to the understanding of major accident risk. If one understands the bowtie, one will also improve the understanding of the complexity of accident risk and the purpose of the different safety functions. For every item that is sorted and managed under a barrier, be it e.g., a job in a maintenance system, a procedure or a rule, the function and purpose of the item is self-explanatory - the bow-tie structure explains *why* the item is there. Likewise, the bowtie structure explains *how* we manage our barriers. A certain barrier is managed by the totalities of items beneath it in the structure. As the complexity of the passenger ship industry develops, the bowtie concept may be useful for handling a novel design, which requires a different approach to managing safety barriers than what is stipulated through regulation and conventional design processes, which more often than not lack structure and rationale.

2.2 Moving Beyond Compliance

Given the severe consequences of a major accident on a large passenger vessel, it is the opinion of the authors that a compliance-based safety culture is not sufficient. History has proven that the current international structure for rules and regulations cannot keep up with the pace in which the industry is developing. The aftermath of the Estonia and the Herald of Free Enterprise accidents are two examples where update of international regulations first came as a consequence of a major accident.

Weaknesses in safety barriers must be addressed before an accident happens and this is one of the main purposes of a barrier management system. By systematically seeking improvements to barriers, the target goes from being in compliance to continuous improvement.

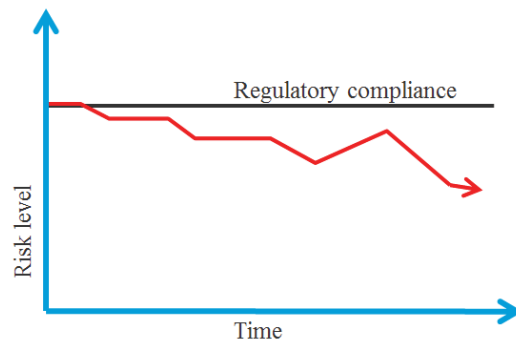


Figure 4: Targeting continuous improvement vs targeting compliance

Some operators of large passenger ships have taken steps beyond compliance on some aspects relating to stability. Examples are cruise ships designed to withstand more than three compartment damage, double skin at the engine room region of cruise ships, larger GM than the required value for compliance, enhanced damage response procedures, shore side training in damage control, increased drill frequencies, etc.

The next step for such companies could be to introduce a barrier management system that systemizes these initiatives and ensures that the improvements continue. However, simply placing a modern approach upon aging foundations will lead to increased long-term workload, frustration and a general hesitation towards acceptance of the modern approach. The transformation must not be done by adding work, but rather by working smarter, and it must be seen and understood as a means of delivering higher value.



3. STABILITY BARRIER MANAGEMENT

In 2012 Royal Caribbean Cruises Ltd and DNV GL worked together in defining a framework for enhanced stability management [6]. The focus on stability has continued and can be seen in the light of the following trends:

- Increasing size of passenger ships, which both increases the severity of the worst case consequences and increases the complexity of barriers related to e.g. evacuation.
- Manning and training. Finding competent crew is an increasing challenge, which makes training ever more important.
- Workload onboard ships.

- Operation in new areas and continual shifts in deployment strategy.
- New operators entering the market with little passenger ship experience.
- Ship revitalization projects and conversions whose scope impacts stability.
- Complexity of new approaches to ship stability: shift from deterministic to probabilistic stability regulations
- Increased level of automation.

3.1 Stability Bowties

The following bowtie for Capsizing was created as a prototype by DNV GL in 2014:

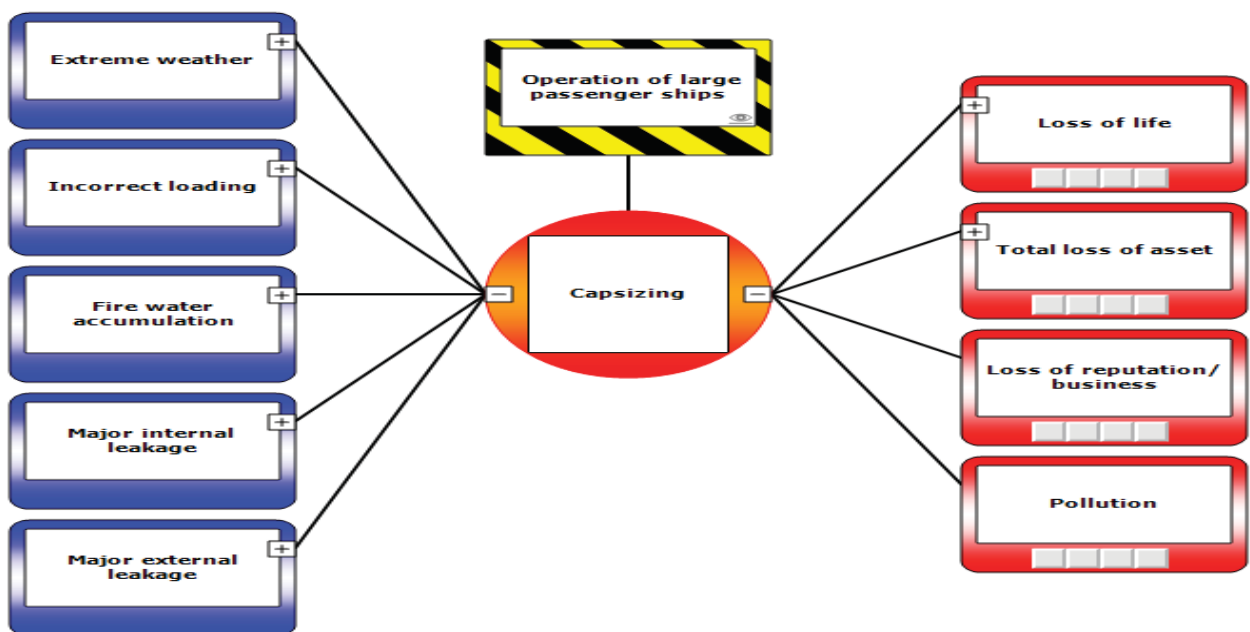


Figure 5: High level bowtie diagram, only showing threats and consequences.

To account for the complexity of the major accident, the bowtie diagram can be broken down into a number of elements. The following

example is for the sub-function Detect Leakage.

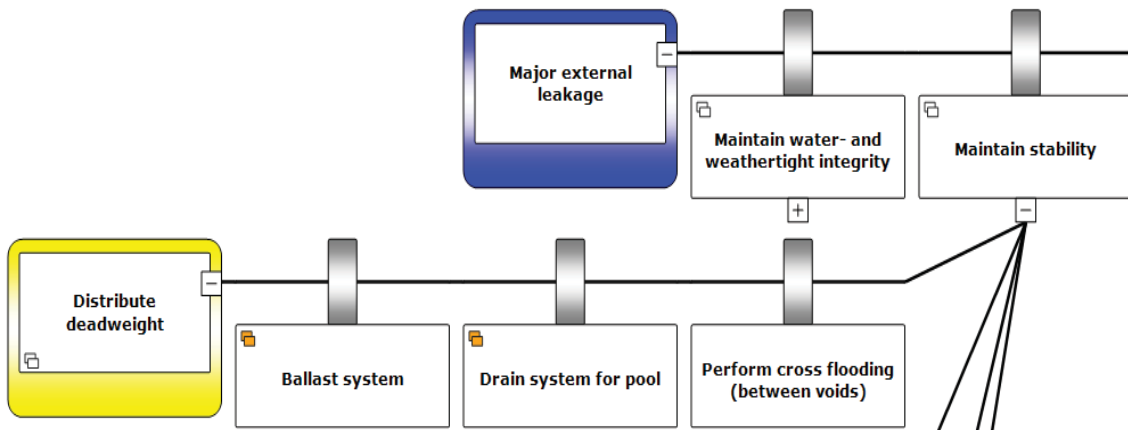


Figure 6: Elements in bowtie diagram

The bowtie diagram will typically consist of dozens of different barrier elements that all need to be considered in the barrier management system. While the full detail bowtie serves its purpose for designing the barrier management system and barrier analysis, it may be beneficial to simplify it for the purpose of day-to-day management. In the following example, four preventive barriers against capsizing have been designed for use in a stability barrier management system.

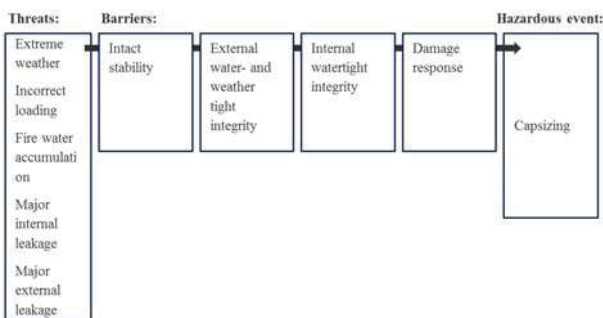


Figure 7: Example of preventive barriers against capsizing, for use in a stability management system.

Besides the four barriers above, there are several other barriers that may be relevant for stability barrier management. A bowtie with Collision/Grounding as the Hazardous Event is interesting with regards to the accident statistics, which highlights this as the major risk contributor for passenger vessels. The

Collision/grounding and Capsizing bowties would be interlinked, as they can be seen as threats/causes and consequences for each other (collision can be a cause for capsizing, and capsizing a consequence in collision). In the bowtie above, collision/grounding is included in the threat “Major external leakage”. Having Collision/grounding and Capsizing as hazardous events in separate bowties, will allow for a better risk presentation as it will capture the other threats for capsizing and the other consequences of collision/grounding.

The following main areas are seeing the most attention in the industry:

- Barriers related to Navigation, i.e preventing collision/grounding/contact.
- Watertight doors, which is a part of the barrier Internal Watertight Integrity, i.e preventing capsizing or sinking.
- Damage response: Detection, assessment and mitigation of a damage.

And as with most barriers, the challenges with ensuring the integrity are all related to people, processes and technical systems.

Navigation is an important barrier as it is far most to the left in the accident scenario described above. Controlling this barrier and preventing an accident from happening in an early stage is of course preferable to mitigation after e.g., grounding. At the same time it is a complicated barrier, involving management of people, processes and advanced systems. There have been significant investments into



navigation systems and training over the last years, but still the shipping industry as a whole has not seen a reduction of navigational accidents.

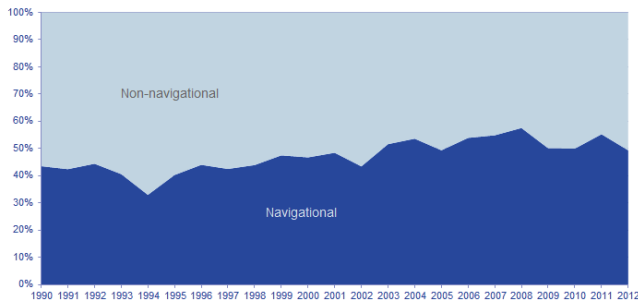


Figure 8: Distribution of navigational vs non-navigational accidents, 1990-2012 (All vessels, excluding fishing and miscellaneous categories). Source: IHS Fairplay

Watertight doors are a critical system for maintaining internal watertight integrity of the ship. The watertight doors stand out from other watertight bulkhead penetrations because of the following:

- The size of the opening. The bilge systems on dry side of the bulkhead may handle small leaks but not the flow rate through an open watertight door.
- The possibility that the door is open at the time of the accident and will depend on the combination people, processes and technical systems in order to be closed.
- The water tight doors may frequently be in use and thereby over time be prone to failure.

Watertight doors are used as a case study in chapter 4.

3.2 Main Elements of Stability Barrier Management

The total robustness of a safety barrier can be seen as the sum of the inherent robustness, which is latent in the ship design and the robustness, which needs to be managed during operation. Therefore, the ship design sets the bar and the operation of the vessel can be seen

as the ability to keep the bar as close to the design intent. Having said this, interventional or active measures (e.g., counterballast post damage, use of inflatable devices, active foam, etc.), may with time and technological innovation change this norm. This is outlined further in the following.

The operational part can further be broken down into strategic, operational and emergency stability management [6]

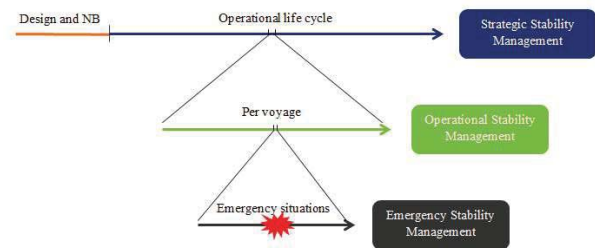


Figure 9: Main Elements of Stability Management

- Ship design and new building: The management process ensuring that the ship is designed and built with an inherent level of safety and sufficient margins as a result of current regulation and a company's safety culture, addressing aspects such as layout constraints, number of bulkheads, tank arrangement, steel weight, centre of gravity, WTD arrangement and deck openings.
- Strategic stability management - operational life cycle perspective: shore side barrier management processes that ensure fleet-wide control over barriers, continuous improvement and allows for long term planning of stability enhancing measures based on data and operator feedback.
- Operational stability management - per voyage perspective: On board barrier management processes that control barriers and react to important factors and parameters to ensure that the voyage is safe, efficient, in compliance and according to company policy. The operational level of stability management is strongly linked to strategic management



and is a key predictor for effective strategic management.

- Emergency stability management – emergency situations: Both on board and shore side emergency response procedures that give a structured and clear response to ensure full barrier integrity and thereby preventing loss of stability.

The inherent robustness in passenger ship design with regards to stability has developed significantly in the last decade, in particular with the transition from deterministic to probabilistic rules for stability. In addition some ship owners have introduced own standards, such as designing ships with double skin.

However, for the industry as a whole, it is the claim of the authors that the traditionally design focused culture for stability management must be shifted to one where the operation is seen as integral player to maintaining barrier integrity. Examples on how stability management in operations can be improved have been demonstrated by Royal Caribbean Cruises Ltd who since 2012 have enhanced their damage response procedures, increased the shore side training on damage control, introduced data tracking of opening hours of watertight doors and increased damage response drill frequencies [6] to name but a few of the many initiatives.

4. CASE STUDY: WATERTIGHT DOORS

In this chapter we are using a barrier defined as Internal Watertight Integrity and the sub-function Watertight Doors as an example on how barrier management may function in practice. The chapter exemplifies how the barrier can be managed by cooperation between the shore side and ship side of an organization.

The following figure shows how watertight doors can be represented as a sub-function in a simplified bowtie.

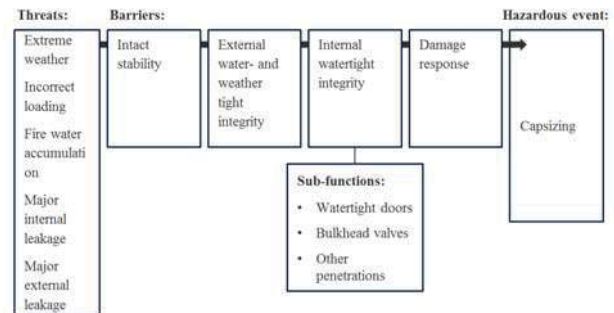


Figure 10: Simplified bowtie, including internal watertight integrity and watertight doors.

With a barrier management system, the operator knows why watertight doors are important, knows the condition and takes necessary action to ensure maximum integrity to the safety barrier. A person with knowledge about the bowtie structure will also know why watertight doors are important, so the chapter focuses on how a company could know the condition of the watertight doors and take necessary action.

While watertight doors are chosen as an example in this paper, it is important to highlight the need for also managing the other sub-functions in the barrier to ensure that there are no holes in the Swiss cheese. Time and resources should be distributed according to the importance of the sub-functions, and with the bowtie as a basis there are possibilities to do a risk calculation for each barrier, which can be used as input for concentrating resources to the most critical areas.

Besides being an important function, watertight doors are interesting as an example for the following reasons:

- It is possible to measure data which may be available via the watertight door control system or the VDR. Further, the data can be aggregated to ship class and fleet level and be used for analytics. This is already



being done by some operators. There is also a possibility of live data streaming of this data from ship to shore and provide shore side with a live feed on the status of the barrier.

- There is a certain degree of complexity to the watertight doors as a sub-function. It has elements related to the people, processes and technical systems.
- Watertight doors must be managed in all elements of stability management: Design, strategic, operational and emergency. It thereby also requires active participation from both ship side and shore side.

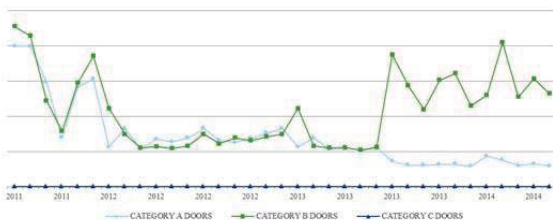


Figure 11: Example: Trending of opening hours for watertight doors

4.1 Ship side barrier management, watertight doors

Ship side will perform a barrier analysis for their ship, and their input for determining the status of the watertight doors will typically be the following:

- Tests and inspections
- Maintenance
- Drills
- Data monitoring of opening hours of the ship's watertight doors over time. This data may be measured against pre-defined targets.
- Partners or third party inspections, typically class, port state control or maker of systems. Ideally the partners report in the same barrier management structure as the operator.
- The 'last barrier analysis'. How has the status progressed since last time?

A combination of colour coding and pre-defined acceptance criteria is a common method for reporting the status.

Based on the barrier assessment, the officers will perform the following actions:

- Report the status of the safety barriers to shore side for further analysis in a ship class and fleet perspective
- If needed, perform any necessary action on the ship's watertight doors. These actions may be related to people, processes or technical systems.

4.2 Shore side barrier management, watertight doors

Shore side personnel will perform a barrier analysis for the fleet and for different ship classes. The barrier structure will be identical as the on-board analysis, but the perspective and number of units will differ. Their input for determining the status of the watertight doors will typically be the following:

- Barrier analysis for individual ships, reported by each ship. Are the reported deficiencies systematic in their nature, or is it a one-off?
- Maintenance records aggregated to fleet level
- Data monitoring of opening hours of the fleet's watertight doors over time. This data may be measured against pre-defined targets.
- Partners or third party inspections, typically class, port state control or maker of systems.
- The last barrier analysis. How has the status progressed over time?

Based on the barrier assessment, the shore side personnel may perform actions toward the ships related to people, processes or the technical systems. They may take immediate action against individual ships if needed, but the main task of the shore side management is to provide instructions, guidance and training



to enable the ship's crew and officers to manage the watertight doors in operation and emergency situations.

Another important task of shore side management is to assess the confidence of the barrier assessment, asking if enough information is available in order to confidently set a status on a barrier, or if more sources of information are needed. This may for instance lead to changes in maintenance/test/inspection intervals for watertight doors or setting up systems for tracking and trending opening hours. Likewise, the acceptance criteria for the barrier assessment should be reviewed at regular intervals; this is where both shore side and ship side has the opportunity of raising the bar by setting new targets and thereby ensuring continuous improvement and concentrate resources on the most critical elements.

Shore side management will also be responsible for bringing relevant findings from the barrier analysis to the design phase, ensuring that the next generations of passenger ships are modified to strengthen the barrier. If a flooding situation occurs and one or more watertight doors are open, the survivability of the ship is most likely significantly reduced as expressed by the attained index A calculated in accordance with SOLAS. The designers must find solutions to reach an equivalent level of safety. In such a setting, input from strategic and operational stability management may be valuable, as has already been proven by some operators. By tracking and trending opening hours of watertight doors, one can pinpoint which doors have the biggest effect on survivability and the operation, and redesign accordingly.

5. CONCLUSIONS

Collision or grounding leading to water ingress and capsizing or sinking have been shown to be a major risk contributor for passenger ships. Given the severe consequences of a major accident on a large

passenger vessel, it is the opinion of the authors that a compliance based safety culture is not sufficient. Moving beyond compliance means explicitly addressing risks and risk mitigation.

The introduction of barrier management can be an effective way of systemizing both prevention and mitigation in order to reduce risk and ensure continuous improvement. Barrier management must address people, processes and technological systems. Whilst the ship is designed and built with an inherent level of safety, it is necessary to address the important elements of stability in holistic view and over time. Watertight doors represent a good example of barrier management addressing all elements of stability management: Design, strategic, operational and emergency.

Proper stability management addressing all four phases of stability management using a barrier management system will in the opinion of the authors contribute to reducing the risk of large scale accidents involving major loss of life.

6. ACKNOWLEDGMENTS

The authors would like to thank Tom Allan, Ole Christian Astrup, Kevin Douglas, Helge Hermundsgård, Andrzej Jasionowski, Harri Kulovaara, Odd Olufsen, Trond Schiestad, Dracos Vassalos and Anne Marie Wahlstrøm for their valuable input which has been essential for writing this paper.

7. REFERENCES

- S. Øie, A. M. Wahlstrøm, H. Fløtaker and S. Rørkjær, "Good Practices - Barrier Management in Operation for the Rig Industry," DNV GL, 2014.

DNV GL, "DNV GL Report No. PP092633/1-



1/1, Risk level and Acceptance Criteria for Passenger Ships. First interim report, part 1: Risk level of current fleet.," Høvik, Norway.

SLF 55/INF.9, "The GOAL based Damage Stability project (GOALDS) – Development of a new risk-based damage stability requirement for passenger ships," IMO, 2012.

J. Reason, "Managing the Risks of Organizational Accidents," Burlington: Ashgate Publishing Company, 1997.

O. C. Astrup, A. M. Wahlstrøm and T. King, "A Framework Addressing Major Accident Risk in the Maritime Industry," DNV GL, 2015.

C. Van Weter and T. King, "Proposed Best Practices in Stability Management," RCCL, DNV, 2012.

This page is intentionally left blank

KEYNOTE ADDRESS

Offshore Caring - Safety Management

Professor Chengi Kuo, for Keppel Singapore

This page is intentionally left blank



Offshore Caring - Safety Management

Chengi, Kuo, *Department of naval architecture, ocean and marine engineering*

University of Strathclyde, Glasgow, chengi.kuo@strath.ac.uk

ABSTRACT

The paper is concerned with integrating the management of caring and safety in an offshore project in order that a pro-active method would be available. It is aimed at minimising any adverse effects of the project activities on the environment. After introducing the background, a brief review of safety management is performed before examining the influences of major disasters. Major disasters relating to Piper Alpha and Deepwater Horizon are discussed. Treatments of environmental impact are considered before proposing the Offshore Caring-Safety Management (OCSM) approach. The main conclusion is that pro-active attitude will assist in caring the environment and be safer while minimising reactive thinking.

Keywords: *Caring and safety management, hazard, risk, offshore*

1. INTRODUCTION

In the early days of offshore hydrocarbon exploration and exploitation, the safety of offshore installations was addressed by following the experience ship safety approach. This is not surprising as searching and producing of oil was taking a new step in going from onshore operations to working in the waters. In practice, this was not a direct adaptation as there were some key differences, such as ships float and used mainly for transportation while offshore installations were attached to the ground and did work. As offshore hydrocarbon activities progressed from shallow waters to deep waters, the drilling and production were being done by “rigs” under the names of jack ups, semi submersibles and FPSO (Floating Production Storage Offloading) vessels, see for example Rendal (2010). Little attention was paid to the adverse effects of these activities. The paper will highlight treatment of ship safety, influence of offshore disasters, consider how environmental impact is being tackled and examine possible approaches before proposing

the Offshore Caring -Safety Management (OCSM) approach for offshore application.

2. HIGHLIGHT OF SHIP SAFETY MANAGEMENT

The treatment of ship safety is based on evolutionary approach which makes minor changes to existing regulations using the lessons learnt from failures or accidents which have occurred in practical operations. Once the failure information is examined and analysed, the recommended agreed decisions would be responded by the relevant authorities and the practical implementation is achieved using fresh prescriptive regulations. It should be noted that this regulatory approach assumes that safety is absolute and this is a fundamental weakness which will be discussed later.

Significant changes have been made in ship safety when major disasters occurred and most influential ones include:



- Sinking of passenger ship Titanic, leading to SOLAS (Safety Of Life At Sea) regulations, IMO (2004).
- Capsizing of Ro Ro ferry the Herald of Free Enterprise, DTp (1987)
- Grounding of Exxon Valdis in Alaska leading to OPA 90 (Oil Pollution Act) which require tankers to have double hull if the operators plan to ship oil into USA, US Coast Guard (1990).

In the light of these disasters, many research studies have been performed by operators, classification societies, industry and academics. The more important maritime ones involve greater use of risk based methods, Vassalos (2009), Formal Safety Assessment (FSA), IMO (1996) and Goal Based Standard (GBS), IMO (2004). These methods are focused on ship safety and have had little direct influence on offshore oil and gas operations.

In recent years great attention is being paid to safety management that is putting greater emphasis on management, see Kuo (1998) for details on various aspects of maritime safety management.

3. APPROACH TO OFFSHORE SAFETY

In the early days of offshore hydrocarbon exploration and exploitation, the safety of offshore installations was addressed by following the experience ship safety approach. This is not surprising as searching and producing of oil was taking a new step in going from onshore operations to working in the waters. In practice, this was not a direct adaptation as there were some key differences, such as ships float and used mainly for transportation while offshore installations were attached to the ground and did work. As offshore hydrocarbon activities progressed from shallow waters to deep waters, the drilling and production were being done by Mobile

Offshore Drilling Unit (MODU) that include semi - submersibles and later FPSOs.

Deficiencies were noted in applying ship approach but no significant changes made until the explosion of jacket structure Piper Alpha in the North Sea in 1988, HSE (1990). More recently explosion and fire of semi-submersible Deepwater Horizon and followed by oil spillage from the Macondo well in the Gulf of Mexico in 2010, US Coast Guard (2012). Further discussion of their impact will be summarised in the next two sections.

4. IMPACT OF PIPER ALPHA DISASTER IN 1988

In spite of incompatibilities the adapted ship safety approach it was continued to be used with minor modifications. It was only the major disaster of Piper Alpha in the North Sea and subsequent Public Inquiry of Lord Cullen that enabled the introduction of alternative approach, see HSE (1992). The Cullen report made 106 recommendations and the most significant being the approach based on the goal setting concept which is applied in other industries such as nuclear power industry. The offshore hydrocarbon industry adopted the name safety case approach. The principal aim was to make the operator think about safety and share responsibility for safety. In the practical implementation of the safety case approach, the operator defines the safety goal to be achieved and how the goal will be met to a national authority, in the UK it is Health and Safety Executive (HSE). HSE accepts the safety case but do not give its approval. To verify the operator is doing what has been written in the report, the HSE inspectors will make regular inspection visits and they can stop the installation's production if they find the operators are not doing what has been given in the submitted report.

The most significant outcomes of using the safety case approach have been to change the operator's safety attitude and culture and have

great responsibility. Although the safety case approach has been in existence for nearly 27 years there is scope for improvement when the environmental impact is taken into account.

5. EFFECT OF DEEPWATER HORIZON DISASTER IN 2010

The Deepwater Horizon was a MODU working in the Macondo field off the coast of Louisiana in the Gulf of Mexico. The operator was BP and the main contractors were Transocean and Halliburton who had various responsibilities. The former owned and operated the MODU and the latter on drilling activities.

There was a blow out at the wellhead and the equipment known as BOP (Blow Out Preventer) did not stop the surging oil and gas. A major explosion and fire occurred on Deepwater Horizon in April 2010 leading to death to 11 of 126 people working on board. Oil was spilling into ocean to a record quantity until July 2010 before the well was re-capped.



Figure.1 Explosion and fire of Deepwater Horizon

The effect of the explosion and oil spillage shock the oil and gas industry as well as the nation. As oil spillage continued, event was on top of America's media agenda and a number of committees were set up or re-organised to investigate this incident, a key one is given by

National Commission (2012). A good discussion of the event can be found in the book by Sutton (2014). The outcome of the major oil spillage is more regulations that require the operators to implement a SEMS (Safety and Environmental Management System) program, see Sutton (2014) for a summary of key steps involved.

There are many reasons for this failure and the main reason is understood to be the failures of the management in the wider sense. These range from pressure to minimise cost though ineffective communication arrangement to sound decision making.

6. ADDRESSING OFFSHORE ENVIRONMENTAL IMPACT

The methods of addressing environmental impact are at present based on prescriptive regulatory principle and the level of their implementation depend on the countries having the rights to the continental shelves. There are two popular methods used in both the maritime and offshore industries. One method focuses on controlling pollution and discharges by regulations. The other covers broader scope and comes under the name of Environmental Impact Assessment (EIA). These will now be briefly considered

a) Pollution related regulations

Similar to the use of prescriptive regulations to address safety, there are now well-established prescriptive regulations for dealing with pollution. The high profile ones are concerned with oil pollution caused by crude oil tankers, e.g. MARPOL, IMO (2006) and Oil Pollution Act 1990, OPA 90 (1990) and US Coast Guard (1990). There are also regulations concerned with other types of pollution, e.g. discharges into the atmosphere. In the offshore hydrocarbon activities, for example, there are regulations associated with disposal of drilling cuttings, flaring of gas and decommissioning of offshore installations.



The merits and drawbacks concerning the use of these regulations for addressing environmental impact are basically the same as those outlined for safety. The exception is that there are more maritime safety experience and data than what are available to address offshore environmental impacts. This in turn can be difficult in devising balanced EI regulations.

b) EIA and its usage

With growing interest in environmental issues in the past four decades and recognition that all development activities need to achieve sustainability, fresh legislations have been formulated in attempt to reach a proper balance between industrial developments and their effects on the environment. The outcome has been that large projects have to perform an EIA, e.g. a new building and how it will affect the environment.

An EIA assesses the possible positive or negative impacts a proposed project may have on the environment that include physical, social and economic effects. The EIA use is particularly valuable to decision makers regarding the viability of the project. The EIA process can be represented by a flow diagram with blocks such as project background, identifying key impacts, evaluating their significance, consulting the public, communicating findings in the form of environmental statements and decision making. There has been extensive work in EIA and further information can be found for examples in Therivel & Morris (2009) and Glasson et al (2009).

For oil and gas activities in the UKCS, DECC (2014) gives information including a concise summary on the EIA legislations, guidance on how to meet the requirements and the aspects needing interaction with the UK Department of Energy and Climate Change (DECC). In general it is DECC which considers environmental impact and when safety issues arise, the UK Health and Safety Executive would be involved.

7. POSSIBLE OPTIONS FORWARD

Main possible options forward for integrating offshore environmental impact with safety management include:

a) Introducing more stringent regulations

Since prescriptive regulatory approach has played a very important role and it is continually being applied, the authorities can introduce more stringent regulations to control the EI of offshore hydrocarbon activities. The key merit of this option is that it can show to the public that “something has been firmly done”. The main drawback is that EI, like safety, is not an absolute entity. It is most unlikely that this option would not be fully effective. In addition all weaknesses of prescriptive regulatory approach would be present, see Kuo (2007).

b) Performing an EIA

Introduce EIA to offshore hydrocarbon activities would enable many aspects of environmental impact to be examined more fully. The key merits include: EI would receive full attention at an early stage and effort to minimise its effects could be incorporated; the process would assist in educating everyone on how EI can be treated. The main drawback is that existing EIA covers a huge number of factors ranging from economic and political to social and culture that technological aspects receive limited attention. For this reason EIA, in the existing form, may be too “global” for interface with safety management and this in turn leads to the danger for EI and safety management being treated separately. Other drawbacks include: difficulties in obtaining reliable input data for the assessment, time needed to do an EIA for an offshore activity and the need to train more people in applying EIA methodology from an engineering stand point.

c) Preparing an environmental impact case

The safety management of offshore installations in UKCS has evolved from implementing prescriptive regulatory approach to using safety case concept, and it is possible to ask the operators to prepare an Environmental Impact Case in a similar way to a safety case.

The main merit is that environmental impact would be given focused attention like safety and this ensures that the various critical issues are examined more closely and in greater depth. This in turn would increase greater awareness of potential adverse effects of specific operations on the offshore environment. The main drawback is the danger that safety management and EI could go by different routes due to many different angles the issues can be addressed and this is undesirable as it is only when they are considered together that the true benefits can be achieved. Other drawbacks include: duplication of effort and conflict between the two entities.

8. WHICH WAY FORWARD?

It can be seen from the previous section that all the options have merits and drawbacks. For these reasons, none of three methods, in the present form, would justify the development efforts in integrating environment impact with safety management. Furthermore, to reduce environmental impact tends to be a responsive mind set.

For an approach that can take into account the integration of safety management and impact on the offshore environment, there is a need to explore fresh and innovative treatments. In addition, the successful approach must meet, as best as possible, the following criteria:

- Be pro-active in addressing offshore environment
- Can take into account non-absolute nature of safety and caring

- The role of human action, attitude, behaviour must be transparent
- Able to integrate caring management and safety management
- Would be usable in practical situations

9. PROPOSING AN OCSM APPROACH

The approach is called Offshore Caring - Safety Management (OSCM) and it is developed from the use of the Generic Management System Circuit (GMSC) unit to generate a standard safety case, Kuo (2007). The basic GMSC unit is made up of two principal parts as shown in Figure 2. One is a common management system circuit and the other is a specific process scheme. In present form, would justify the development efforts in integrating environment impact with safety management. Furthermore, to reduce environmental impact tends to be a responsive mind set.

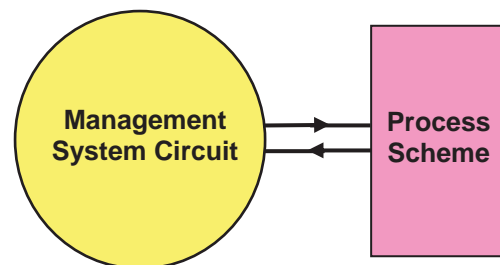


Figure 2 Basic unit of Generic Management System Circuit (GSMC)

The management system circuit has five elements. It begins by defining the goals and performance criteria before organising resources and activities to ensure the goals can be met. The process scheme is then implemented. The results obtained are measured against the performance criteria before reviewing the feedback and lessons learnt as well as documenting the experience gained. These five elements are placed on a revolving circuit so as to ensure improvement is continuous and iteration is introduced via feedback from the review element to the define element.

The process scheme can take any form depending on the situation in question. For the caring- safety management method the two schemes are caring and safety, see Figure 3.

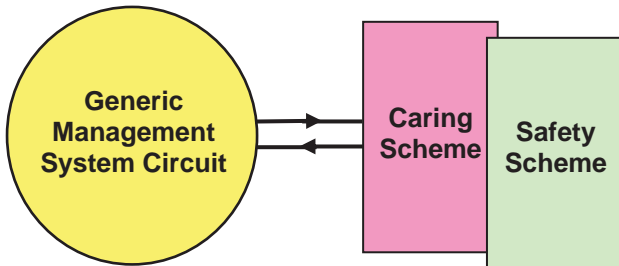


Figure 3 GMSC with caring and safety schemes

The scheme has four main steps of: identifying hazards, assess the risk level of the hazards, reduce the intolerable risk levels of hazards and prepare for emergencies. The resulting arrangement for GMSC for safety and environmental impact is shown in Figure 4.

The next section highlights how caring is integrated with safety management.

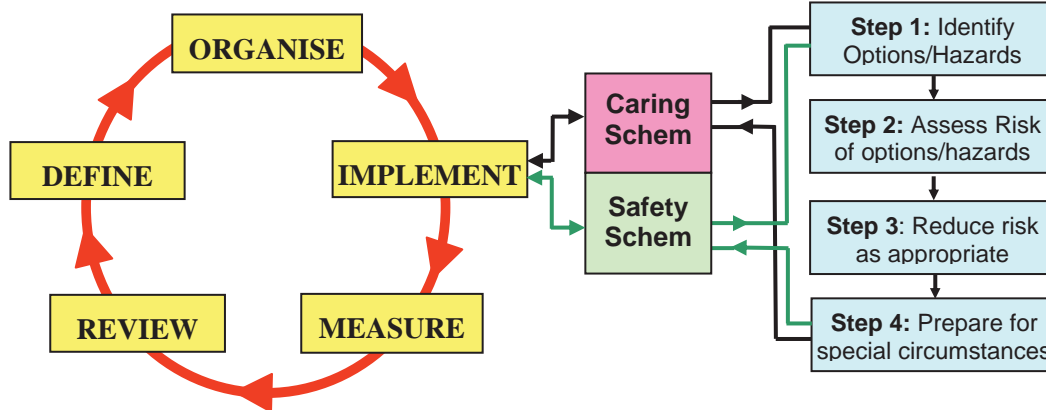


Figure 4 Sketch showing GMSC for caring – safety schemes

10. INTEGRATING CARING AND SAFETY MANAGEMENT

There are five main elements in the GMSC

Element 1: DEFINE

There are two tasks to be performed in this element.

- Define the goals for caring and safety.
- Define a set of performance criteria that involve technological and human factors

Element 2: ORGANISE

A number of activities are involved and include for example

- Planning and scheduling of activities
- Identify sources of information

Element 3: IMPLEMENT

This element is concerned with the implementation of the caring-safety scheme. This scheme involves identify options, opportunities and hazards. Their risk levels are then assessed and reduced as appropriate. This is followed by preparing for special situations and generation of results.

Element 4: MEASURE

The results obtained should be measured against the performance criteria defined in Element 1.

Element 5: REVIEW

Following from the previous elements the review would cover analysis of the lessons learnt, exploring scope for improvement and

benchmarking. On completion of review information would be feedback to Element 1 for further iteration if required.

A mind map for OCSM approach is given in Figure 5.

combined caring and safety management approach. Caring task can be implemented at concept and initial design phases of a product's life cycle. This would lead to savings in time and costs.

- The roles of education and training

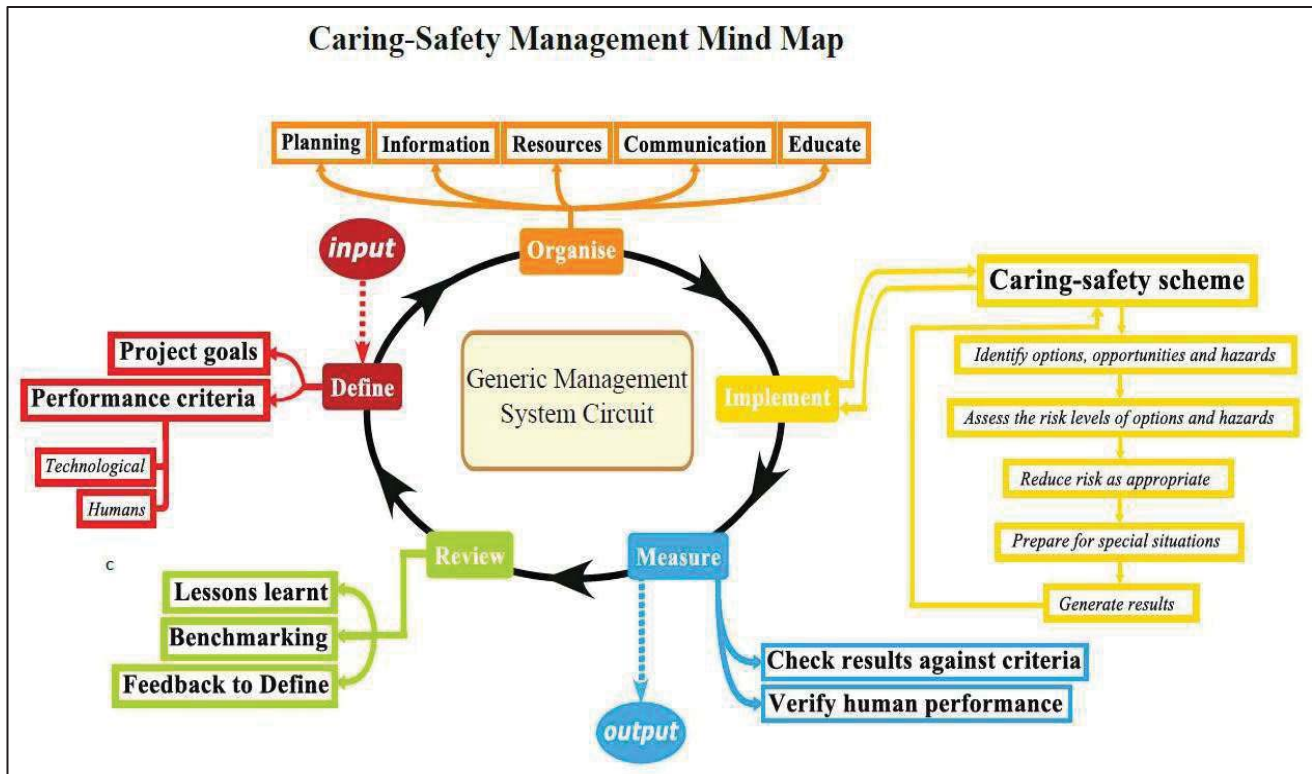


Figure.5 A mind map of an Offshore Caring-Safety Management approach

11. DISCUSSION

The following items deserve brief discussion.

- Integrating caring and safety

Safety is generally treated as a single entity and with demands to prevent pollution from offshore operations the efforts are devoted to minimising environmental impact. This means a responsive attitude is adopted. There is a need to change the way we think by integrating caring with safety. Caring is a pro-active response. There a number of ways in achieving the integration and this can be done through a

When a new procedure or working practice is being introduced in many activities it is quite common to hear people express opinions like: "We need to give the staff or team training". The word education is never mentioned. One would question why this is the case? There are many reasons and some examples include: They associate training with doing something practical; they think education is going to school, college or university; they have given little thought about the roles of education and training. Education and training have many similarities but also differences. A key difference is on the emphasis. Education focuses on achieving competence and involves developing and changing attitudes and behaviours of those concerned. Training



concentrates on improving a person's efficiency in doing a specific tasks, see Kuo (1998).

In practice, education and training go together. E & T has a dual role of generating a positive safety culture & enhancing capability. Indeed, training alone has several serious weaknesses. The key ones include: no insight into the task being trained to do; lack of ability to correct minor deviation from routine.

12. CONCLUSIONS

There are three main conclusions to be draw:

Firstly, caring and safety are non- absolute entities in that there are no right or wrong answer to a situation so long as the goals are met and a generic management system is needed to ensure consistent and effective solutions are obtained in its usage.

Secondly, there is a tendency to put emphasis on reducing environment impact which is a responsive approach and it would be better to use a pro-active approach via integrating caring management with safety management.

Thirdly, successful practical application of technological advances require the active support of a positive caring and safety culture coupled continuing focused efforts in education and training.

13. ACKNOWLEDGEMENTS

I wish to thank the following for their valuable help in the preparation of this paper: Saishuai Dai, Shan Huang and Oleg Sukovoy.

14. REFERENCE

- DECC, 2014, "Environmental legislation", Website of UK Department of Energy and Climate Change.
- DTp, 1987, "MV Herald of Free Enterprise-Fatal Accident Investigation (The Sheen report).", HMSO Report of Court No.8074, UK Department of Transport.
- Glasson, J, et all, 2009, "Introduction to environmental impact assessment", SPON Press, London, 1999
- HSE, 1990, "The Public Inquiry into the Piper Alpha disaster (The Cullen report)", HSMO Cm1310.
- HSE, 1992, "A Guide to Offshore Installation (Safety Case) Regulations", UK Health and Safety Executive, HMSO, L30. 110E. ISBN: 9-280141-83-X.
- IMO, 1995, "Formal Safety Assessment (FSA)" Submitted by the UK Government to the 65th Session of IMO's Maritime Safety Committee, Agenda Item24.
- IMO, 2006, "MARPOL (Marine Pollution regulations)", International Maritime Organisation Publication IC520C. ISBN: 9-280142-16-X 200.
- IMO, 2004, "Goal based standards (GBS)". Submitted by the IMO council (89) to the 79th Session of IMO's Maritime Safety Committee.
- IMO, 2004, "SOLAS (Safety Of Life At Sea)" International Maritime Organisation Publication ID 1110E, ISBN: 9-280141-83-X.
- Kuo, C 1998 "Managing ship safety", LLP Ltd, ISBN: 1 85978 841 6.



Kuo, C, 2007, "Safety management and its maritime application", The Nautical Institute, ISBN: 1 870077 83 0.

National commission, 2011, "National commission on BP Deepwater Horizon oil spill and offshore drilling", Report for President.

Randall, R, 2010, "Elements of Ocean engineering", SNAME publication, ISBN: 978-0-939773-77-0.

Sutton, I, 2014, "Offshore safety management", Elsevier 2014, ISBN: 978-0-323-26206-4.

Therivel, R & Morris, P, 2009, "Methods of environmental impact assessment", Routledge-Taylor & Francis Group, London.

US Coast Guard, 1990, "Oil Pollution Act 90", US Coast Guard, Washington DC.

Vassalos, D, 2009, "Risk-based ship design", Springer 2009. ISBN: 978-3-540-89041-6.

This page is intentionally left blank

KEYNOTE ADDRESS

Direct Assessment Will Require Accreditation – What this Means

Dr Arthur Reed, ONRG

This page is intentionally left blank



Direct Assessment Will Require Accreditation—What This Means

Arthur M. Reed, *Carderock Division, Naval Surface Warfare Center (NSWCCD)*,
arthur.reed@navy.mil

Aurore V. Zuzick, *Carderock Division, Naval Surface Warfare Center (NSWCCD)*,
aurore.zuzick@navy.mil

ABSTRACT

With the advent of the second-generation intact stability criteria, IMO has initiated a two-tier performance-based stability assessment process for unconventional hulls. If the design fails the first tier evaluations, it progresses to the second tier, where direct assessment criteria are applied. The design is considered satisfactory if the direct assessment criteria are passed. If these criteria are not passed, operator guidance is needed to provide vessel operators with the information needed to safely operate the vessel in dangerous conditions. Ship motion simulation tools are needed to apply the direct assessment criteria and generate operator guidance, if necessary.

A framework is presented for certification that simulation tools used for direct assessment of stability failures and generation of operator guidance are sufficiently accurate for these purposes. Based on US Navy experience, guidance is provided on the Verification, Validation and Accreditation (VV&A) process, structure, and participation, and acceptance criteria are given for both quantitative and qualitative accreditation approaches. Accreditation acceptance criteria are tailorable to ship-specific VV&A efforts, particularly with regards to definition of critical motions and physical limits.

Keywords: *Verification, Validation and Accreditation; VV&A; Formal VV&A*

1 INTRODUCTION

For commercial vessels, the classical intact stability criteria is based on the work of Rahola (1939) and is incorporated in the International Code on Intact Stability, the 2008 IS Code (MSC 85/26/Add.1¹). Similar criteria for naval vessels is provided by Sarchin & Goldberg (1962) and codified in the NATO Naval Ship Code

(NATO, 2007a,b) and by a US Navy Design Data Sheet (Rosborough, 2007). These criteria are prescriptive—that is they are a set of criteria, defined based on empirical data, which are *assumed* to ensure that a vessel meeting the criteria will have adequate static stability. The history of development and the background of the IMO criteria are described by Kobylinski & Kastner (2003); a summary of the origin of these criteria is also available in chapter 3 of the Explanatory Notes to the International Code on Intact Stability (MSC.1/Circ.1281).

The deficiency of these prescriptive ap-

¹References to IMO documents such as “MSC 85/26/Add.1” appear in the list of references with an “IMO” prefix, i.e. as: IMO MSC 85/26/Add.1. As there is no ambiguity in the names of the IMO citations, the year will be omitted from the citations.



proaches is that their adequacy is contingent upon vessels and their modes of operation lying within the “design space” of the vessels that define the empirical data used to derive the criteria. However, the design space is not necessarily well defined and modern vessels are more and more tending to lie outside of the traditional design space—the classical intact stability criteria do not apply to these latter vessels.

Beginning in the early 2000’s efforts were initiated to develop performance based stability criteria for commercial vessels with the re-establishment of the intact-stability working group by IMO’s Subcommittee on Stability and Load Lines and on Fishing Vessels Safety (SLF) (cf. Francescutto, 2004, 2007). Over time, the terminology to describe the new intact stability criteria evolved from “performance based” to “next generation” to “2nd generation,” the terminology in use today. This entire evolution is described in the introduction to Peters, *et al.* (2011).

The SLF Working Group decided that the second-generation intact stability criteria should be performance-based and address three modes of stability failure (SLF 48/21, paragraph 4.18):

- *Restoring arm variation* problems, such as parametric roll and pure loss of stability;
- *Stability under dead ship condition*, as defined by SOLAS regulation II-1/3-8; and
- *Maneuvering related problems in waves*, such as surf-riding and broaching-to.

Ultimately, a fourth mode of stability failure was added:

- *Excessive accelerations*.

The deliberations of the Working Group led to the formulation of the framework for the second generation intact stability criteria, which is described in SLF 50/4/4 and was discussed at the 50th session of SLF in May 2007. The key elements of this framework were the distinction between parametric criteria (the 2008 IS Code) and performance-based criteria, and between probabilistic and deterministic criteria. Special attention was paid to probabilistic criteria; the existence of the *problem of rarity* was recognized for the first time and a definition was offered. Also,

due to the rarity of stability failures, the evaluation of the probability of failure with numerical tools was recognized as a significant challenge.

“Second-generation intact-stability criteria” are based on a multi-tiered assessment approach: for a given ship design, each stability-failure mode is evaluated using two levels of vulnerability assessment. The two tiers or levels of vulnerability assessment criteria are characterized by different levels of accuracy and computational effort, with the first level being simpler and more conservative than the second.

A ship which fails to comply with the first level is assessed by the second-level criteria. In a case of unacceptable results, the vessel must then be examined by means of a direct assessment procedure based on tools and methodologies corresponding to the best state-of-the-art prediction methods in the field of ship-capsizing prediction. This third-level criteria should be as close to the physics of capsizing as practically possible.

The framework and the concept of vulnerability criteria were first introduced in Belenky, *et al.* (2008a). The state-of-the-art in the assessment of vulnerability is presented in detail in Peters, *et al.* (2011). Criteria for pure loss of stability, parametric roll, and surf riding and broaching were codified in February of this year in SDC 2-WP.4 Annexes 1, 2 and 3, respectively.

Direct assessment procedures for stability failure are intended to employ the most advanced technology available, yet be sufficiently practical so as to be uniformly applied, verified, validated, and approved using currently available infrastructure. Ship motions in waves, used for assessment on stability performance, can be reproduced by means of numerical simulations or model tests (SLF 55/3/11). The process of approval, which we will call accreditation will be the major focus of the remainder of this paper.

The structure of this paper will consist of a definition of Verification, Validation and Accreditation (VV&A), a description of the VV&A process, and accreditation criteria. The VV&A process will be subdivided into the process structure, documentation, specific intended uses,



and a description of Verification and Validation (V&V). The acceptance criteria will be split between quantitative and qualitative criteria, where quantitative is the more rigorous and thus more difficult.

2 DEFINITION OF VV&A

If decisions regarding the design and construction of ships, each costing hundreds of millions of dollars, if not a few billion dollars (in the case of naval vessels), are going to be made based on the stability predictions of a simulation tool, there must be a reasonable assurance that the tool provides acceptably accurate results. The process by which a tool may be determined to be sufficiently accurate is known as verification, validation and accreditation.

Quoting from a US Navy VV&A presentation, “Verification, Validation, and Accreditation are three interrelated but distinct processes that gather and evaluate evidence to determine, based on the simulation’s intended use, the simulation’s capabilities, limitations, and performance relative to the real-world objects it simulates.” Beck, *et al.* (1996), AIAA (1998), DoD (1998, 2003, 2007, 2012), McCue, *et al.* (2008), ASME (2009), and Reed (2009) provide different, although consistent, definitions of the three components of VV&A. The U.S. DoD definitions for these three terms are provided below, each followed by a practical commentary relevant to computational tools for predicting dynamic stability.

1. Verification—the process of determining that a model or simulation implementation accurately represents the developer’s conceptual description and specification, i.e., does the code accurately implement the theory that is proposed to model the problem at hand?

2. Validation—the process of determining the degree to which a model or simulation is an accurate representation of the real world from the perspective of the intended uses of the model or simulation, i.e., does the theory and the code that implements the theory accurately model the relevant physical problem of interest?

3. Accreditation—the official determination that a model or simulation, . . . is acceptable for use for a specific purpose, i.e., is the theory and the code that implements it adequate for modeling the physics relevant to a specific platform? In other words, are the theory and code relevant to the type of vessel and failure mode for which it is being accredited?

2.1 Verification

Experience with attempting to verify ship-dynamics software has been that the documentation for many hydrodynamic codes, particularly the theoretical basis, is neither complete nor rigorous enough for the verification process to be separated from the validation process. Under these circumstances, when one finds that the computations do not adequately model the physical reality, one is left to ponder whether the code is not accurately modeling the intended physics or whether the intended physics are not adequate for the problem. In this case, the dilemma becomes: should one attempt to debug the code or should one abandon use of the code because its underlying physics model is not adequate? Attempting to resolve this dilemma can be expensive, in terms of both time and money.

Another issue related to verification of software is the actual quality of the code and the documentation of the code itself. Often the coding does not follow any consistent standard and there is often insufficient guidance to link the actual code back to its theoretical basis.

As for the actual verification of the code, this is best done by means of unit tests, where each module and block of modules is exercised against known or expected solutions. When properly constructed, these unit tests will not only test the module against normal execution, but also against unexpected or unanticipated inputs, to determine if the code handles error exceptions correctly via error traps or error returns. Many codes are not designed robustly enough so as to deal with anomalous inputs—they expect that the input will always be correct and that all modules output that is input to other modules provide correct input. Rationally, this is a rather



naïve assumption.

2.2 Validation

Validation commences with a series of Elemental Tests (or comparisons to model data), which provide insight into a simulation's ability to capture the overall physics of the ship motions in waves problem. Elemental tests consider such quantities as roll decays, calm water turning circles, calm water zig-zag maneuvers, turning circles in regular waves, and acceleration from rest in calm water. The results of the elemental tests provide evidence that the computational tool is capturing the physics of the problem of a ship maneuvering in waves. They also provide confidence that the quantitative comparison results obtained with available model data may be assumed characteristic of the code and applicable for similar conditions for which model data is not available.

It is reasonable to assume that if a predictive tool is capable of predicting responses in extreme seas, it should be capable of making reasonable predictions of motions in moderate seas. The motions problem in small and moderate seas can be characterized as the seakeeping problem. In the seakeeping problem, the ship's control system should have no difficulty in maintaining the ordered speed and heading—on the average the vessel will maintain a constant heading at a constant speed. These are the standard assumptions of seakeeping theory.

Thus, as a first order validation, the computational tool should be capable of reproducing the single significant amplitude motions that are measured during a model test in moderate seas, where we interpret the term motions in a most liberal way as motions, velocities and/or accelerations—this can also be considered an Elemental Test. This liberal interpretation is necessitated by the fact that, depending on how the experiment is run, it can be very difficult to measure linear (as opposed to rotational) displacements. The major challenge here is that experimental data is required, and the experimental data must be of sufficient duration in irregular seas to have sufficiently small confidence bands

for the comparisons to be meaningful (*cf.* ITTC, 2011, Sect. 5; 2014, Sect. 5). The Acceptance Criteria section to follow will discuss some possible statistical means of comparison.

In order to accommodate the validation of simulations for predicting motions in extreme seas and stability failures, situations must be examined that are not easily characterized using techniques that are routinely used for seakeeping validation. Nonlinear dynamics methods appear to show significant promise. There are two aspects of nonlinear dynamics that appear to apply to validation. The first is *nonlinear time-series analysis* and the second is *bifurcation analysis*, these methods are discussed in detail in Reed (2009), summarized here. A third issue is that of *the problem of rarity*, which is also briefly discussed below.

Nonlinear Time-Series Analysis—In nonlinear time-series analysis (*cf.* Kantz & Schreiber, 2004), the same time-series analysis is applied to motions measured on a physical model (or ship) and to simulations of the same vessel, in the same environment, as observed during the measurements. The results of the two sets of analysis are compared to each other, often graphically, to determine whether they have produced similar results.

McCue, *et al.* (2008) provides examples of nonlinear time-series analysis, applied as it might be for validation of simulations. Both qualitative and quantitative metrics that may apply were examined. Some qualitative measures include: reconstructed attractors, correlation integrals, recurrence plots, and Poincaré sampling; possible quantitative measures are: correlation dimension, Lyapunov exponent comparison, system entropy, and approximations to the equations of motion (EoM).

While nonlinear time-series analysis techniques can easily illustrate differences between measurements and predictions, there is still much to be investigated. The range of time-series analysis techniques, which may be applicable to dynamic-stability failure prediction certainly has not been exhausted. However, these comparisons are at best qualitative; quantitative



methods, particularly for physical understanding and for comparing experimental and computed results, are needed. Bifurcation analysis techniques may provide this necessary additional insight.

Bifurcation Analysis—There are at least four bifurcations that have been observed in ship dynamics which could be used to analyze whether or not a dynamic-stability code is producing the correct dynamic behavior: Fold bifurcation (Spyrou, 1997; Belenky & Sevastianov, 2007: Sect. 4.5.2 for roll, Sect. 6.5.6 for yaw; Francescutto, *et al.*, 1994), Flip bifurcation (Spyrou, 1997; Belenky & Sevastianov, 2007: Sect. 4.5.3 for roll, Sect. 6.5.6 for yaw), Hopf bifurcation (Spyrou, 1996; Belenky & Sevastianov, 2007: Sect. 6.5.2; Kan, 1990a,b), and Homoclinic bifurcation (Belenky & Sevastianov, 2007: Sect. 6.3.5). Bifurcation analysis (Spyrou, *et al.*, 2009) would appear to be appropriate for application to the lateral-plane aspects of dynamic stability.

The Problem of Rarity—Another issue for the VV&A of simulations for dynamic stability is the “problem of rarity,” where the time between events is long compared to the wave period (Belenky, *et al.*, 2008a,b). Large numbers of realizations may be required to observe dynamic stability failures, either in a simulation or experimentally.

Even if these events are observed, direct comparison between realizations is difficult due to the stochastic nature of the failure event. One method that may help to resolve this problem is the use of deterministic critical-wave groups. This would enable direct comparison of realizations, while also capturing the worst-case conditions of the stochastic environment necessary to assess the ship’s stability performance. Themelis & Spyrou (2007, 2008) demonstrated the production of deterministic critical-wave groups using simulation tools, and Clauss (2008) and others have done so experimentally.

2.3 Accreditation

Accreditation is the process by which a computational tool is certified as being sufficiently accurate and thus acceptable for use in a particular case for a particular vessel of class of vessels. In the IMO context, this would be a vessel of a particular size and proportions, which will have a particular mode of operation. In practice this would also be tied to a particular mode of stability failure, and would be defined as a particular Specific Intended Use (SIU).

As much of the rest of this paper will be focused on accreditation, accreditation will not be discussed further here except to state that accreditation can be thought of as validation with acceptance criteria. Depending on the druthers of the Flag Administration, accreditation may require more model data than validation, but this is a detail—albeit a potentially expensive one, that does not affect the process.

3 DESCRIPTION OF THE VV&A PROCESS

The VV&A in the process leading to accreditation by a Flag Administration must be a formal process with structure that is prescribed. The process and structure that will be described is that employed by the US Navy (Navy, 1999, 2002, 2004, 2005). However, some commentary will be provided as to how this process might be modified without compromising the integrity of the process.

3.1 Accreditation Responsibilities and Organizations

This structure includes the identification of an Accreditation Authority (AA) and the establishment of three panels: the Accreditation Review Panel (ARP), the Simulation Control Panel (SCP) and the Modeling and Simulation PropONENT (MSP). There are four documents that are produced during this formal process: an Accreditation Plan (AP), a Verification and Validation (V&V) Plan, a V&V Report, and an Accreditation Report. The first three of these are produced by the MSP under the guidance of the



SCP, and the latter is produced by the SCP. All of the VV&A efforts are centered about a statement or set of statements that define what the vessel is that will be assessed, its mode of operation and the stability failures that are considered critical for this type of vessel—these are the Specific Intended Uses. Finally, the process includes verification and validation of the modeling and simulation (M&S) tool.

The AA is the individual representing the Flag Administration who will actually accredit the modeling and simulation tool for use with a particular specific intended use (SIU). The ARP is the panel which recommends to the AA whether or not he should accredit the simulation tool. The group in the middle of this process is the SCP who guide the VV&A process, providing guidance to the MSP review the MSP products and prepare a report based on the resulting simulations for the ARP. The SCP is composed of the individuals who will actually perform most of the work, preparing plans, running the simulations, and preparing the V&V report.

The following material based on “Best Practices Guide for Verification, Validation, and Accreditation of Legacy Modeling and Simulation” (Navy, 2005), describes the role and responsibilities of the AA, ARP, SCP and MSP.

Accreditation Authority—The AA is the senior management level individual directly responsible to approve the use of an M&S capability for a particular application or set of applications. The AA will:

- a. Resource the VV&A effort
- b. Develop the accreditation process
- c. Establish the ARP, approve the chairman and its charter
- d. Designate models and/or simulations for VV&A
- e. Approve the M&S Accreditation Plan
- f. Accredit the models and/or simulations (Approve/Disapprove/Resolve ARP M&S accreditation recommendations and assessment reports)
- g. Maintain and disseminate gathered VV&A information

Accreditation Review Panel—The ARP is composed of AA representatives and Subject

Matter Experts (SMEs) as needed, and the ARP will include a Flag Administration representative(s). The Flag Administration will reconvene the ARP for each M&S milestone effort and should allow tailoring of approaches and participants to the specific models and simulations under consideration. The AA or his designated representative chairs the ARP. The ARP will:

- a. Develop M&S Accreditation Plans with MSP assistance
- b. Establish Simulation Control Panels (SCPs) (Report all resource requirements for VV&A activities to the AA prior to execution of tasking)
- c. Approve the V&V Assessment Report
- d. Review V&V information
- e. Prepare the Accreditation Recommendation Letters

The ARP Chair shall:

- a. Approve the SCP Charter, establish the SCP, designate the Chair, and approve SCP membership
- b. Coordinate development of the Accreditation Plan for the designated M&S
- c. Oversee SCP activities
- d. Approve the VV&A Assessment Report

Simulation Control Panel—The SCP(s) should consist of technical SMEs from the relevant Flag Administration and supporting organizations. The SCP is not a permanent body. An SCP will be chartered for each model or simulation designated for accreditation. The SCP chairman is designated by and reports directly to the ARP chairman. The SCP will:

- a. Provide guidelines for V&V Plan development to the MSP
- b. Approve the V&V Plan
- c. Guide the gathering of V&V information
- d. Provide guidelines for the V&V Report to the MSP
- e. Approve the V&V Report
- f. Prepare the Accreditation Report and deliver it to the ARP

M&S Proponent—An MSP is a developer, maintainer, modifier, or user of a model or simulation designated for VV&A. The MSP will:



- a. Provide a Point of Contact (POC) to the ARP Chairman
- b. Assist the ARP in drafting the M&S Accreditation Plan
- c. Develop a Configuration Management (CM) Plan for the M&S
- d. Develop a V&V Plan and deliver to the SCP
- e. Execute the V&V Plan upon approval by the SCP
- f. Develop the V&V Report and deliver to the SCP, along with supporting documentation
- g. Assist the SCP in determining model capabilities versus requirements
- h. Provide VV&A Status to the Flag Administration M&S

With the assistance of the MSP, the SCP will identify model test data that is appropriate for use in the VV&A process and also define the acceptance criteria that the MSP will use in its comparison of computed results to experimental results. There are two substantial challenges related to this, the first and potentially most expensive of these will be identifying sufficient data of acceptable quality for use in the validation effort. As identified in ITTC (2011, Sect. 5; 2014, Sect. 5), this is not something that can be done with a single run of a model in a single sea state. It is conceivable that 10's of runs will be required at each speed and heading in each relevant sea state. If sufficient data is not available, the confidence intervals for the results will be so large as to render the comparisons meaningless.

The second challenge is that of deciding what constitutes an acceptable comparison between experimental results and simulations. This is an area in which there is substantial experience and in which there is significant guidance—see the last section of this paper.

An issue that is often overlooked in the VV&A process is Configuration Management (CM). Because software is seldom static—it tends to change over time. If software changes after it has been accredited, there is no assurance that it is still capable of simulating what it was accredited for correctly. Thus, the necessity of a Configuration Management Plan; the development of a CM Plan is one of the MSP's

responsibilities. Although a CM Plan does not contribute directly to the VV&A of a M&S tool, its proper development and implementation assures that the M&S can and will remain accredited over time, quoting from Navy (1999) “A strong CM plan is one of the critical ingredients in ensuring the continued credibility of models and simulations.”

The process outlined above has three panels performing the work of the VV&A. This is intended to isolate the panel recommending whether or not the simulation tool should be accredited or not, the ARP, from the individuals performing the computations, the MSP. If it is not felt that this level of isolation is required, then the process can be simplified by eliminating the SCP. The functions of the SCP would need to be distributed between the ARP and the MSP. As it is unlikely that the AA will have the expertise to make an informed judgment as to the adequacy of an M&S tool, there will need to be an independent panel of subject matter experts between the AA and the MSP, who can advise and make recommendations to the AA. By definition the MSP is not composed of independent individuals, they are experts on the M&S tool being evaluated.

3.2 Formal Accreditation Process

It should be noted that the Flag Administration formal accreditation process for M&S VV&A includes three phases: *designation*, *execution*, and *accreditation*. Preceding these three phases is a *designation process*. The *designation process* and *designation phase* are separate activities. The designation process is that process that leads to the selection and formal designation of M&S for accreditation. The designation phase is the initial activity that takes place after the selected model or simulation has been identified for accreditation.

Designation Process

The purpose of M&S VV&A designation is for the user and the owner/developer to agree that the model or simulation selected is capable of satisfying the specified need and that



there are sufficient resources to complete accreditation. Each Flag Administration will have specific variations on designating M&S—these guidelines are intended to provide a basic understanding. An external organization, such as a classification society or consulting group, identifies the need to accredit a model or simulation and requests accreditation from the Flag Administration.

The Flag Administration should ensure that an “M&S Accreditation Designation Request Form” be completed and submitted to that Flag Administration. This form will provide the information that is necessary to process the designation request.

Figure 1 provides a process flow diagram for the formal accreditation process, showing the designation, execution, and accreditation phases and their interactions with the Accreditation Authority, Accreditation Review Panel, Simulation Control Panel, and the Modeling and Simulations Proponent. A description of the phases follows.

Designation Phase

During the designation phase, the AA establishes the ARP. The ARP establishes the SCP and documents information from the preceding designation process in an Accreditation Plan. This document will consist of a description of the M&S, an overview of its intended use, M&S requirements and acceptability criteria, the V&V techniques to be used, and the AA’s Plan of Action and Milestones (POA&M) for the accreditation effort.

The designation phase is completed when the Accreditation Plan receives AA approval.

Execution Phase

The execution phase of the V&V process begins with the development of the V&V Plan. The plan should contain the specific qualitative and/or quantitative testing requirements to satisfy the acceptance criteria of the accreditation plan. The SCP provides V&V Plan guidelines to the MSP. These guidelines should consist of an outline, schedule for the execution phase,

and clarification of any questions regarding the accreditation plan requirements. V&V Plans may vary greatly based upon previous V&V efforts, the complexity of simulation functionality, length of usage, scope of intended use, and M&S application requirements.

Once the V&V Plan is approved by the SCP, the MSP is tasked with executing that plan. According to the length and complexity of the required V&V, the SCP may have one or more In-Progress Reviews to ensure that the schedule and product development is progressing according to schedule. Prior to completion of V&V testing, the SCP should provide the MSP with guidance for the V&V Report. This guidance should include an outline, inputs on desired formats of information, and distribution formats. When all required V&V efforts and documentation are complete, the MSP provides a final V&V Report to the SCP for evaluation and approval.

The V&V Report should summarize all V&V efforts in accordance with the requirements set forth in the V&V Plan. The SCP can decide to approve the V&V Report with or without modification. As the V&V Report is a critical document in the accreditation process, modification to the report might be necessary to clarify V&V results or to correct deficiencies. Once the V&V Report is approved, the SCP must prepare an Accreditation Report.

The Accreditation Report summarizes the overall V&V execution, provides an assessment of the demonstrated functionality’s support of the specific intended use, and makes a recommendation to the ARP for action on the results. This recommendation could be any one of the following:

- a. The model or simulation can be used as is for the specific intended use
- b. The model or simulation can be used for the specific intended use with recommended modifications
- c. The model or simulation requires additional V&V to be considered suitable for accreditation
- d. The model or simulation should not be used

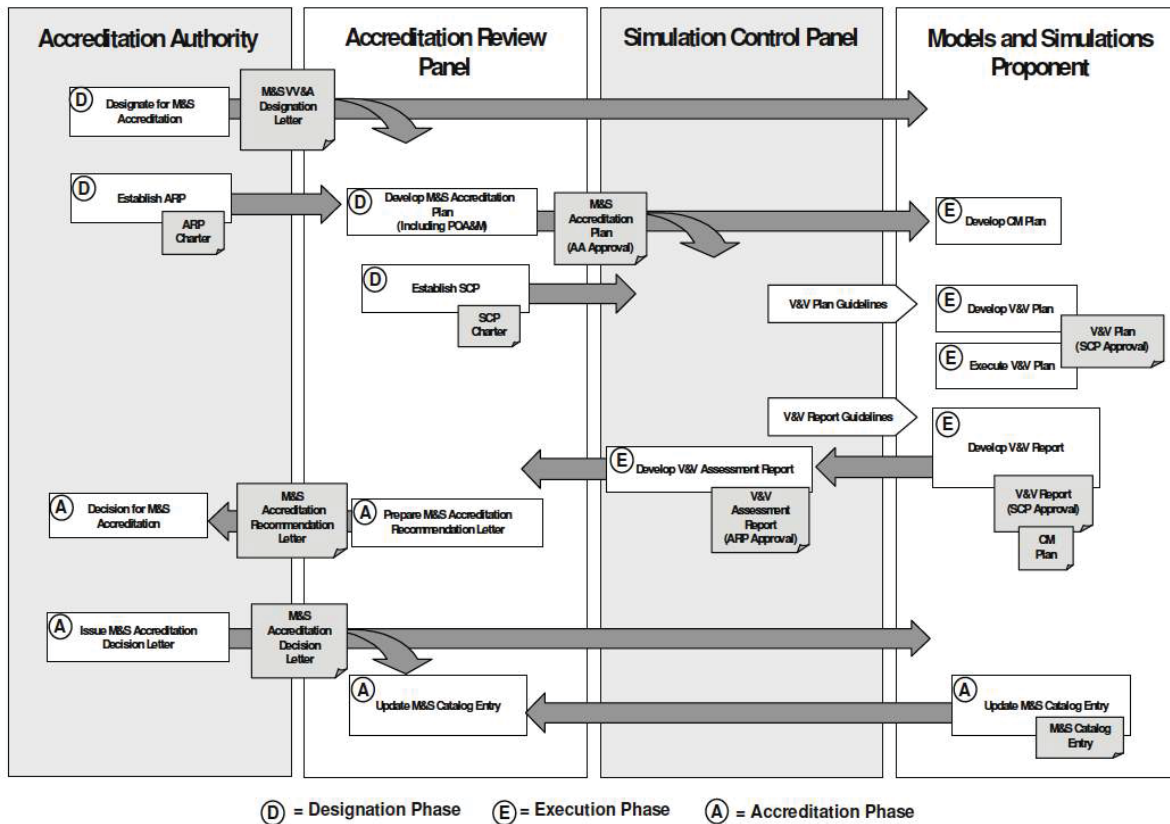


Fig. 1 M&S VV&A Process (Navy, 2005)

for the specific intended use

A major challenge of the VV&A process for a dynamic stability code is that of determining acceptable V&V techniques. The DoD VV&A Recommended Practices Guide provides information and guidance on many V&V techniques and statistical methods. However, they do not seem to be tailored to dealing with the predictions from stochastic processes. Thus the section on Acceptance Criteria that follows.

Accreditation Phase

Upon completion of the Accreditation Report, the ARP evaluates the report for consistency, correctness, and completeness. Once the ARP is satisfied that the V&V information provided meets the stated accreditation requirements, the ARP prepares an M&S Accreditation Recommendation Letter.

This recommendation provides all the M&S information required to support accreditation, such as version and intended use. The

AA can approve the recommendation, deny the recommendation, or request additional information. Upon approval by the AA, an M&S Accreditation Decision Letter is sent to the MSP and the ARP. The SCP is dissolved at this time. If the recommendation is denied or if additional information is required, the AA should provide written notification to the ARP and MSP. The SCP may be retained if the ARP decides that further V&V is required for accreditation.

The accreditation remains in effect as long as the intended use or limitations/assumptions of the model or simulation do not change, or until revoked by the AA. If the functionality or the intended use of the model or simulation defined in the M&S Accreditation Decision Letter change, the AA must submit the model or simulation for re-accreditation.

Governing Principles of Accreditation

One governing principal of the accreditation process is to leverage from other VV&A



effort of the Flag Administration (and other Flag Administrations) to the greatest degree possible. Therefore the group seeking accreditation should strive to capture and use other VV&A efforts performed by the Flag Administration. The group seeking accreditation at a minimum should request information about existing VV&A from the applicable Flag Administration(s) and should invite representatives from the Flag Administration to participate in the ARP and/or SCP of the new accreditation effort.

Another governing principle of this process is to place authority in M&S matters consistent with the accountability for the proper use of M&S. M&S is accredited for a specific purpose or a specific use. This specific use or specific purpose drive M&S requirements, which have to be demonstrated by proper V&V techniques before the M&S can be accredited. M&S requirements should be levied on the MSP by the Accreditation Authority. M&S requirements should be imposed on the Flag Administration by IMO.

3.3 Documentation

There are four core documents that are produced during the VV&A process. They are the Accreditation Plan, the V&V Plan, the V&V Report and the Accreditation Report. These documents are produced over time, used at different times by different groups. Thus they must all be complete and independent. As much of the information included in each document is common, it should be shared for consistency and efficiency.

The following material describes the four core reports, it is based on information extracted from: Department of Defense Standard Practice: Documentation of Verification, Validation, and Accreditation (VV&A) for Models and Simulations (DoD, 2012).

The *Accreditation Plan* focuses on: defining the criteria to be used during the accreditation assessment; defining the methodology to conduct the accreditation assessment; defining the resources needed to perform the accredita-

tion assessment; and identifying issues associated with performing the accreditation assessment.

The *V&V Plan* focuses on defining the methodology for scoping the V&V effort to the application and the acceptability criteria; defining the V&V tasks that will produce information to support the accreditation assessment; defining the resources needed to perform the V&V; and identifying issues associated with performing the V&V.

The *V&V Report* focuses on documenting the results of the V&V tasks; documenting M&S assumptions, capabilities, limitations, risks, and impacts; identifying unresolved issues associated with V&V implementation; and documenting lessons learned during V&V.

The *Accreditation Report* focuses on documenting the results of the accreditation assessment; documenting the recommendations in support of the accreditation decision; and documenting lessons learned during accreditation.

Table 1, from DoD (2012), shows the outlines of the four core VV&A documents. The appendices of DoD (2012) provide detailed templates for these four documents.

3.4 Specific Intended Uses

SIUs are the statements that define the scope of the problem or simulation that is to be modeled, and for which the M&S will be accredited. In the context of direct assessment under second-generation intact stability, this will need to include a definition of the vessel for which the M&S tool is to be accredited—accreditation for small fishing vessels may well not apply to a RO/PAX vessel; as well as the mode of stability failure that is anticipated to be an issue. There can, and in fact would likely be multiple SIUs for the same VV&A activity.

The SIUs are used to determine what needs to be characterized and analyzed from the perspective of the V&V process. This is accomplished by the development of a *Requirements Flow-Down Table*. In the Requirements Flow-Down Table, each SIU is decomposed in to several high level requirements (HLRs),



Table 1 Outlines of four core VV&A documents, report sections in *italic* text are common and shared across all four documents. (DoD, 2012)

Accreditation Plan	V&V Plan	V&V Report	Accreditation Report
Executive Summary	Executive Summary	Executive Summary	Executive Summary
1 <i>Problem Statement</i>	1 <i>Problem Statement</i>	1 <i>Problem Statement</i>	1 <i>Problem Statement</i>
2 <i>M&S Requirements and Acceptability Criteria</i>	2 <i>M&S Requirements and Acceptability Criteria</i>	2 <i>M&S Requirements and Acceptability Criteria</i>	2 <i>M&S Requirements and Acceptability Criteria</i>
3 <i>M&S Assumptions, Capabilities, Limitations & Risks/Impacts</i>	3 <i>M&S Assumptions, Capabilities, Limitations & Risks/Impacts</i>	3 <i>M&S Assumptions, Capabilities, Limitations & Risks/Impacts</i>	3 <i>M&S Assumptions, Capabilities, Limitations & Risks/Impacts</i>
4 Accreditation Methodology	4 V&V Methodology	4 V&V Task Analysis	4 Accreditation Assessment
5 Accreditation Issues	5 V&V Issues	5 V&V Recommendations	5 Accreditation Recommendations
6 <i>Key Participants</i>	6 <i>Key Participants</i>	6 <i>Key Participants</i>	6 <i>Key Participants</i>
7 Planned Accreditation Resources	7 Planned V&V Resources	7 Actual V&V Resources Expended	7 Actual Accreditation Resources Expended
		8 V&V Lessons Learned	8 Accreditation Lessons Learned
Suggested Appendices A <i>M&S Description</i> B <i>M&S Requirements Traceability Matrix</i> C <i>Basis of Comparison</i> D <i>References</i> E <i>Acronyms</i> F <i>Glossary</i> G Accreditation Programmatic H Distribution List	Suggested Appendices A <i>M&S Description</i> B <i>M&S Requirements Traceability Matrix</i> C <i>Basis of Comparison</i> D <i>References</i> E <i>Acronyms</i> F <i>Glossary</i> G V&V Programmatic H Distribution List I Accreditation Plan	Suggested Appendices A <i>M&S Description</i> B <i>M&S Requirements Traceability Matrix</i> C <i>Basis of Comparison</i> D <i>References</i> E <i>Acronyms</i> F <i>Glossary</i> G V&V Programmatic H Distribution List I V&V Plan J Test Information	Suggested Appendices A <i>M&S Description</i> B <i>M&S Requirements Traceability Matrix</i> C <i>Basis of Comparison</i> D <i>References</i> E <i>Acronyms</i> F <i>Glossary</i> G Accreditation Programmatic H Distribution List I Accreditation Plan J V&V Report

which characterize important aspects of the SIU. The HLRs are each further mapped into several detailed-functional requirements (DFRs). A comparison metric and acceptance criteria are then identified for each DFR.

The SUIs are used to determine what needs to be characterized and analyzed from the perspective of the V&V process. This is accomplished by the development of a Requirements Flow-Down Table. In the Requirements Flow-Down Table, each SIU is decomposed in to several high level requirements (HLRs), which characterize important aspects of the SIU. The HLRs are each further mapped into several detailed-functional requirements (DFRs). A

comparison metric and an acceptance criterion are identified for each DFR. Additional clarification is provided by the definition of the comparison metrics and their associated acceptance criteria. High-level requirements reflect the technical specifications provided by SME-opinion. Detailed-functional requirements provide additional specifications as necessary to more fully-describe each HLR. Requirements Flow-Down Tables are useful tools in high-level assessment of the appropriateness of the proposed accreditation criteria as well as required components of the Accreditation Plan (DoD, 2012).

To clarify this, an example of an SIU and its accompanying Requirements Flow-Down Table,



Table 2, are provided. The prototype SIU is:

“The XYZ simulation tool will be used to generate operator guidance polar plots for all applicable speeds and headings against pure loss of stability for RO/PAX vessels in the 11,000–13,000 t displacement range, lengths of 130–150 m, and with beam-to-draft ratios of 4.5 to 5.5. These polar plots will enable the vessel operators to avoid situations where pure loss of stability could be an intact stability issue. The information used to generate the operator guidance polar plots will be developed using numerical data generated by the XYZ simulation tool.”

4 VALIDATION APPROACH AND ACCEPTANCE CRITERIA

Following are proposed validation acceptance criteria, which could be applied when seeking accreditation for a numerical simulation tool to be used for direct assessment of stability failure. Two types of accreditation are examined: *Quantitative Accreditation* and *Qualitative Accreditation*. *Quantitative Accreditation* is achieved only if the simulation tool successfully passes all elemental tests and quantitative validation criteria. *Qualitative Accreditation* results from quantified measures of simulation tool accuracy being assessed as “good enough” and is only achieved if the tool passes all elemental tests. For the purpose of this discussion, we treat each type of accreditation as a separate SIU.

The code accreditation is based on comparison to non-rare and rare model-scale data representative of the conditions the vessel would be expected to operate in. It is generally considered that model-scale data captures the relevant physics and scale effects can be accounted for through accepted scaling laws. Utilizing data from multiple scales of models will help to demonstrate the validity of this assumption. Correlation with full-scale trials data will occur prior to certification of the Quantitative Accreditation. Model-scale motion data are collected for a set speed, relative wave heading, and seaway using a model that matches the geometry and anticipated mass properties of the full-scale ship.

Validation is accomplished by comparing statistical properties calculated from model test and simulation data sets for a given speed-heading-seaway combination; these properties are known as condition statistics. Methods for calculating a desired condition statistic from the available data vary depending on the lengths of the motion time histories.

In the case of scale-model test data, run lengths are limited by the size of experimental facilities and statistical properties are calculated from a series of repeated shorter runs. Multiple runs are collected for each speed-heading-seaway combination to form an ensemble of data. The ensemble of data provides enough exposure time (data samples) to accurately represent the statistics of the ship motion at the given speed-heading-seaway combination. Multiple simulation realizations are made at the model-scale test conditions to generate an ensemble of simulation data with the same number of runs and exposure time as the model test.

Non-rare motions will be compared using the motion standard deviation and its uncertainty interval. Rare motions will be compared using the 90th percentile of peak amplitudes and its uncertainty interval. Rather than compare statistically-extrapolated motions for rare motion comparison, the proposed acceptance criteria utilize the most rare motion characteristics of the available model test data which are considered repeatable and not subject to significant variation due to sampling.



Table 2 Example Requirements Flow-Down Table.

High Level Requirements	Detailed Functional Requirement	Comparison Metric	Acceptance Criteria	
HLR 1.a Simulation must demonstrate good correlation to model data for ship responses to elemental tests to suggest that underlying physics are sound.	DFR 1.a.1 Simulation must demonstrate the ability to successfully predict critical motion values in a large number of Quantitative Accreditation conditions for which model test data is available for comparison.	CM 1.a.1 Check-list of quantifiable metrics defining “reasonable” correlation for elemental tests used to inform SME opinion	AC 1.a ARP will vote using SME opinion informed by elemental test comparisons whether to assess subsequent acceptance criteria.	
	DFR 1.a.2 Collective SME judgment shall ultimately decide whether or not this requirement is met (regardless of the code’s ability to meet the suggested quantifiable metrics).	CM 1.a.2 SME opinion/judgment		
HLR 1.b The simulation and model-scale data must show consistently good correlation ranging from the more simple conditions to the more complex conditions. Good correlation must be demonstrated for the range of operational, environmental, and loading conditions defined in the Quantitative Accreditation scope for which comparison model data are available.	DFR 1.b.1 Parameters which characterize the ship’s operating condition relative to the seaway, and identify the corresponding critical motion, must be assessed.	CM 1.b.1 Mean values, μ , of achieved speed and heading	AC 1.b.1 Differences between mean achieved speed and mean heading for each validation condition must be less than specified amounts.	
	DFR 1.b.2 All comparisons must take into account all known sources of uncertainty (sampling, instrument, condition, etc.).	CM 1.b.2 90% uncertainty intervals on the each parameter (model and simulation)		AC 1.b.2 The 90% confidence intervals on each parameter value (and A90%) for a given motion and condition must overlap in order to suggest that the underlying populations (model and simulation) may be the same.
	DFR 1.b.3 Parameters that are used to define Quantitative Accreditation polar plots risk values and lifetime risk calculation must be assessed. If direct validation of these quantities is not achievable, a sufficient substitute quantity shall instead be assessed. (rare motion metrics)	CM 1.b.3 The 90th percentile of peak amplitudes, A90%, of motions (in lieu of exceedance rates of physical limit thresholds which are not expected to be available for validation)		
	DFR 1.b.4 Parameters that are used to evaluate the Quantitative Accreditation system health must be assessed. (non-rare motion metrics)	CM 1.b.4 Mean standard deviation, σ , of motions		



Table 2 (Cont'd) Example Requirements Flow-Down Table.

High Level Requirements	Detailed Functional Requirement	Comparison Metric	Acceptance Criteria
HLR 1.c Necessary accuracy of the simulation shall be influenced by an appropriate balance between technical excellence and judiciousness	DFR 1.c Thoughtful engineering judgment shall be applied in the determination of permissible differences between simulation and model test results.	CM 1.c Margin applied to observed sample parameter values (defined in CM 1.b.2 and CM 1.b.3)	AC 1.c The observed values of compared sampled parameters may be deemed acceptable if the difference between the values is less than a specified amount. (margin)
HLR 1.d The safety of the ship and sailor must be prioritized and reflected in the criteria established for validation.	DFR 1.d.1 Reasonable conservatism on the part of the simulation solution should be endorsed to promote the overall safety of the sailor.	CM 1.d.1 Margin applied to observed sample parameter values (defined in CM 1.b.2 and CM 1.b.3)	AC 1.d.1 The margin allowed by AC 1.c shall be increased by 50% in the case of over-prediction on the part of the simulation to allow for additional conservatism on the part of the simulation. (additional conservative margin)
	DFR 1.d.2 Determination of simulation tool success must only be reached using reasonably high-fidelity validation data sets.	CM 1.d.2 Combined uncertainty in the comparison, calculated as a function of the 90% uncertainty intervals (CM 1.b.2) on both data sets, model and simulation	AC 1.d.2 Successful validation comparisons for both rare and non-rare motions (and A90%) may only be accepted if the combined uncertainty in both data sets is sufficiently small.
HLR 1.e Simulation must be deemed usable for conditions within the current scope of the Quantitative Accreditation for which comparison model test data is not available.	DFR 1.e.1 Simulation must demonstrate the ability to successfully produce critical motion values in a large number of Quantitative Accreditation conditions for which model test data is available for comparison.	CM 1.e.1 Number of conditions which successfully pass the following criteria: AC.1.b.1 through AC 1.d.	AC 1.e 70% of Quantitative Accreditation conditions for which model data are available for comparison must pass criteria (AC 1.a through AC 1.d) for 100% of critical motion parameter values. (rare and non-rare motion assessments calculated independently)



4.1 Elemental Tests

Elemental tests (or comparisons to model data) provide insight into the code's ability to capture the overall physics of the ship motion problem. They also provide confidence that the quantitative comparison results obtained with available model data may be assumed characteristic of the code and applicable for similar conditions for which model data is not available. The results of the elemental tests provide evidence to the ARP to inform their final decision making. Subject matter experts on the SCP will provide the ARP with general guidelines about the comparisons; this guidance will include both qualitative and quantitative characteristics of good correlation.

The code will simulate the following elemental tests in support of validation:

- Roll decays
- Zig-zag maneuvers
- Calm water turning circles
- Turning circles in regular waves
- Acceleration from rest tests
- Generation of response amplitude operators (RAO) for comparison with model data (if available)
- Integrity values

Standard maneuvering and seakeeping analyses of the time histories will be performed on the code and model data time histories in order to provide comparison quantities for SCP guidance. Integrity values will be plotted on polar and surface plots to investigate the code's ability to capture the ship's capsize boundary. An integrity value is a ratio between the number of runs which did not include a dynamic stability event divided by the total number of runs examined. This metric allows for comparisons between model test and simulation in which the ship response is highly sensitive to initial conditions. Since the initial conditions under which each model test was performed cannot be known precisely, a range of simulations is performed in an attempt to cover the range of possibilities.

This elemental test is included on the list above to specifically address the known dynamic stability concerns associated with a ship operating in stern quartering seas. Characterization

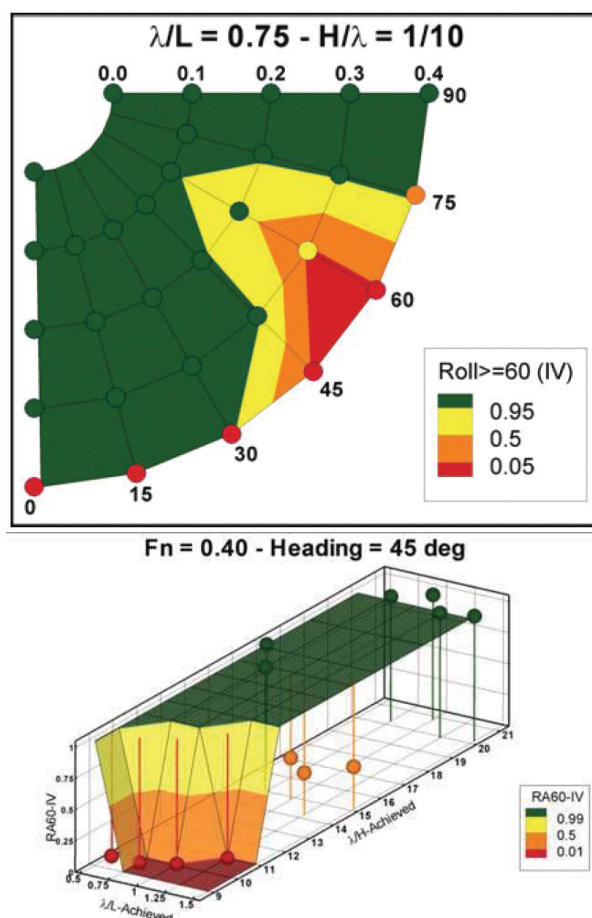


Fig. 2 Notional Integrity Value Polar Plot (top) and Surface Plot (bottom)

of the ship's response in these conditions from irregular seas model data is challenging, so integrity value plots (using regular waves model test results) provide the necessary additional insight into the code's ability to capture this aspect of the physics. Figure 2 shows an example of integrity value surface and polar plots.

4.2 Quantitative Validation

Beyond successful demonstration that the general ship motion physics are captured by the code, it will be assessed for its suitability for each of the specific intended uses. These assessments are quantitative in nature, although ARP opinion will ultimately be included in all final accreditation recommendations. Following are recommended quantitative acceptance criteria for Quantitative Accreditation and Qualitative Accreditation.



Definitions

The acceptance criteria described in this section for Quantitative Accreditation utilize statistical quantities and their uncertainty intervals calculated for a single motion and condition (speed, heading, wave height, wave period); these quantities are referred to as condition statistics.

Scale-model tests are characterized by multiple repeated runs of short run lengths. For each comparison to model data, an equivalent number of runs and run durations will be performed by the code. The condition statistics will be calculated from the model data time histories and the code time histories in the same manner. The condition statistic varies by SIU and rare or non-rare motion. The statistical quantities examined are: condition standard deviation (non-rare motion), condition 90th percentile amplitude (rare motions), and condition mean.

Mean values of speed and heading are used to compare the results of achieved speed and heading in a seaway. Standard deviation values are used to compare non-rare motion responses. 90th percentile of peaks values are used to compare rare motion ship responses. Direct assessment of very rare ship motions is typically prohibited by the limitations of available model test data, and this condition statistic was selected as the peak amplitude threshold for comparison because analysis has suggested that it is the highest motion magnitude (most rare quantity) that is statistically stable for typical model data sets. Higher percentiles of the peaks showed great variation in repeated simulations, suggesting that statistical sampling combined with the non-linear system led to instability in the values above the 90th percentile provides the analysis used to determine this threshold. Figure 3 illustrates relationship between peak distributions and percentiles of peaks for two data sets.

Uncertainty associated with the value of the condition statistic (mean, standard deviation, or percentile) is captured by intervals applied about the condition statistic. The size of these intervals is influenced by sampling statistics, instrumentation uncertainties, and variations in the condi-

tions under which the model was tested.

Uncertainty due to statistical sampling is captured by a confidence interval. The confidence interval is a conventional mathematical quantity which NIST (2014) defines as a range of values which is likely to contain the population parameter of interest. Its purpose is to account for the possible difference between a discrete value derived from limited population samples from the underlying population value. The level of confidence associated with the interval defines its length and corresponds to the probability that the sampled value and intervals encompass the true population value. When defined relative to a mean value and assuming a large sample size, the confidence interval is defined as

$$CI_{\mu} = z_{1-\alpha/2} \frac{\sigma}{\sqrt{N}}$$

where σ is the sample standard deviation, N is the number of samples, α is the desired significance level (corresponds to confidence level), and z is the two-tailed Gaussian distribution factor with significance level, α . The upper and lower bounds of the confidence intervals applied to the sample mean are defined as

$$\mu_{\text{sample}} \pm CI_{\mu}$$

where μ_{sample} is the sample mean. Belenky, *et al.* (2013) provides an extension of this theory to calculate the confidence interval on the ensemble mean standard deviation value from a set of time histories of ship motions for one parameter and one condition. Calculation of the confidence interval for a quantile or percentile is a standard statistical process, which utilizes the binomial distribution.

It should be noted that the terms “confidence” and “uncertainty” are often used interchangeably. This document uses the term uncertainty to include all sources of uncertainty. The confidence level is 90-percent for comparisons involving confidence intervals. Figure 4 shows the relationship between the condition statistic value, intervals and uncertainty limits used in motion comparisons.

The difference between condition statistics

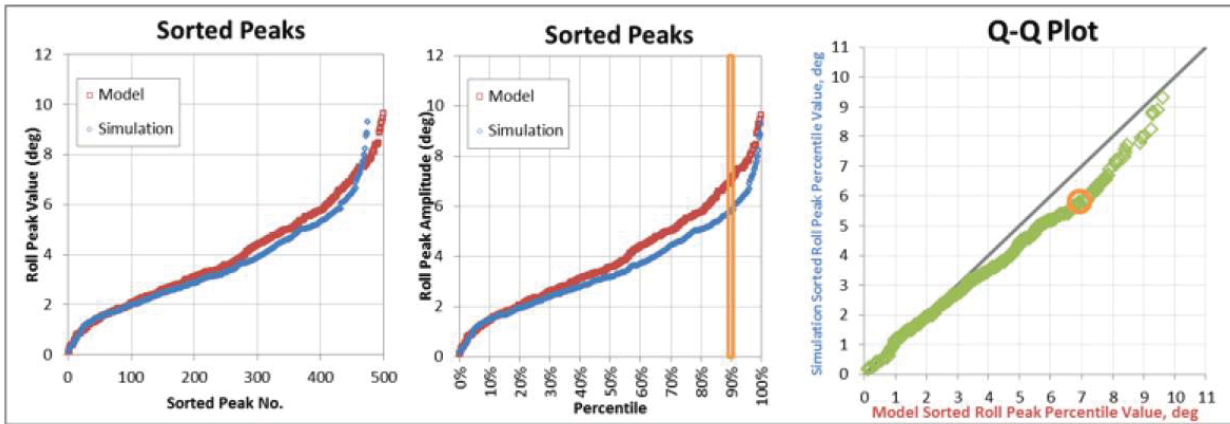


Fig. 3 Sorted Peak Amplitudes for Two Data Sets [by number (left), by percentile (center), percentiles plotted against one another (right)]

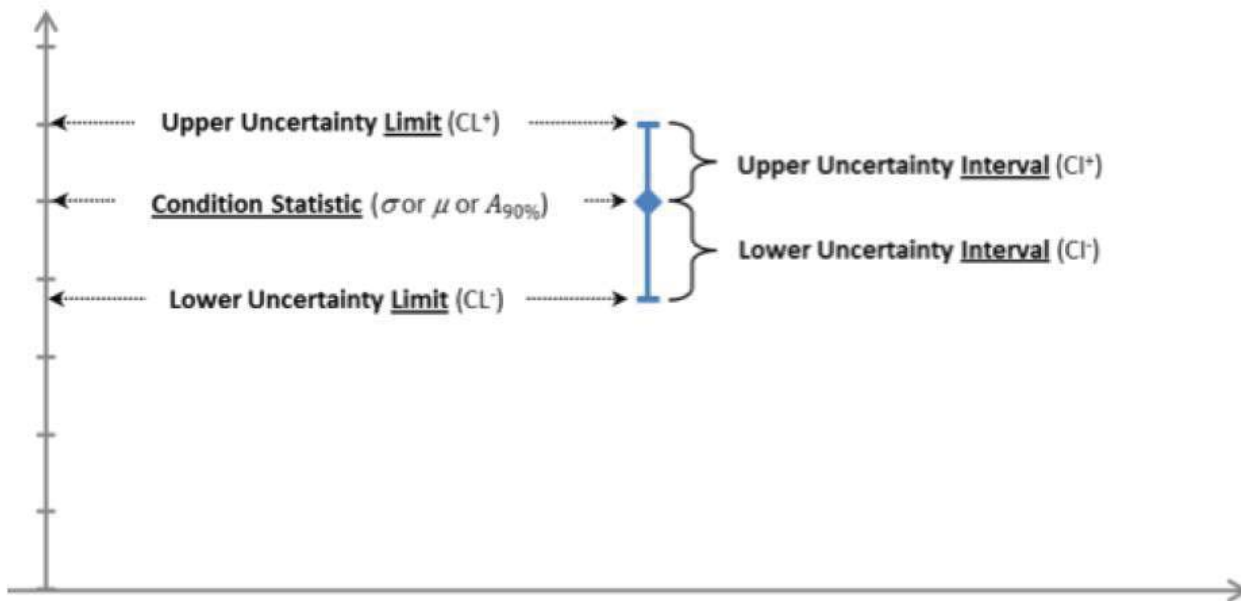


Fig. 4 Metric Nomenclature (condition statistic, interval, and limit)

is the primary metric used for quantitative validation and is defined as the model test value subtracted from the simulation value. A positive value is associated with simulation over-prediction, and a negative value denotes simulation under-prediction. This concept is certainly not new to the field of validation, but its use is often associated with largely deterministic processes. The use of the difference between data sets as a foundation for validation acceptance criteria is consistent with industry practice. (*cf.* Oberkampf & Barone, 2006; AIAA, 1998; ASME, 2009; Eça & Hoekstra, 2012).

Both Oberkampf & Barone (2006) and ASME (2009) refer to this quantity as the error between model and experimental results, noting that the experimental results are only an estimated measure of the “true” parameter value.

The confidence interval on the difference between condition statistic values of a model and simulation result can be formulated as a function of the confidence intervals on each set. The confidence interval on the difference between mean values is defined as

$$CI_{\Delta\mu} = z_{1-\alpha/2} \sqrt{\frac{\sigma_1^2}{N_1} + \frac{\sigma_2^2}{N_2}} \quad (1)$$



where the subscripts 1 and 2 distinguish between data sets.

Additional sources of uncertainty may be applicable to the sample value, including uncertainty due to instrumentation limitations and uncertainty due to variability of the conditions under which the data was generated. Combined uncertainty intervals constructed from multiple sources of uncertainty are typically the root sum of squared intervals calculated separately for each source. While confidence intervals (based only on sampling characteristics) are symmetric, combined uncertainty intervals may be asymmetric.

To compare two data sets with equal number of samples (i.e. $N_1 = N_2$) and symmetric confidence intervals, (1) can be rearranged and described in terms of the confidence intervals associated with each data set value as

$$CI_{\Delta\mu} = z_{1-\alpha/2} \sqrt{\left(\frac{CI_{\mu,1}}{z_{1-\alpha*/2}}\right)^2 + \left(\frac{CI_{\mu,2}}{z_{1-\alpha*/2}}\right)^2} \quad (2)$$

where α^* refers to the level of significance associated with the sample intervals and α refers to the level of significance associated with the uncertainty in the difference.

Equation (2) lends itself to a definition of the combined uncertainty (e.g. statistical, instrument, etc.) in the difference between samples which is agnostic to the methods used to define the combined uncertainty intervals associated with each data set, assuming the uncertainties of each set are Gaussian distributed. Further, (2) can be adapted to account for asymmetric intervals by distinguishing between the upper and lower intervals associated with each set.

For validation purposes, consider the definition of the difference (simulation minus benchmark) to compare two ensemble mean standard deviation quantities. Given combined uncertainty intervals associated with each data set of significance level α^* , the upper and lower combined uncertainty intervals on the difference

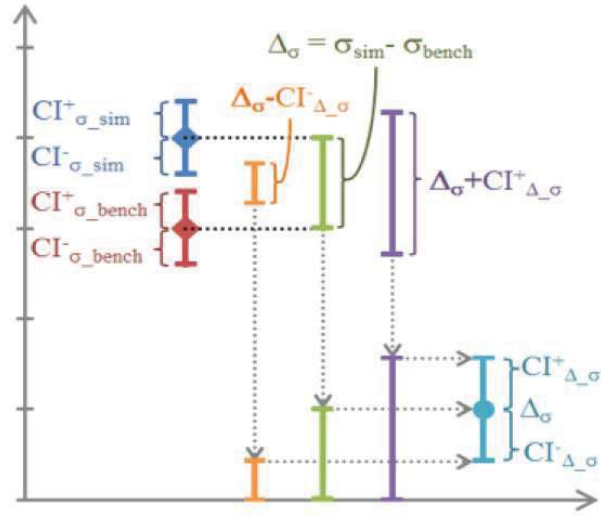


Fig. 5 Uncertainty Intervals On Two Data Sets and On the Difference Between Data Sets

can be calculated as

$$CI_{\Delta} = z_{1-\alpha/2} \sqrt{\left(\frac{CI_{\text{bench}}^-}{z_{1-\alpha*/2}}\right)^2 + \left(\frac{CI_{\text{sim}}^+}{z_{1-\alpha*/2}}\right)^2}$$

and

$$CI_{\Delta} = z_{1-\alpha/2} \sqrt{\left(\frac{CI_{\text{bench}}^+}{z_{1-\alpha*/2}}\right)^2 + \left(\frac{CI_{\text{sim}}^-}{z_{1-\alpha*/2}}\right)^2}$$

where the subscripts “bench” and “sim” refer to the benchmark (or model test) and simulation data sets, respectively. Figure 5 illustrates the relationships between the uncertainty intervals on both data sets and the uncertainty interval on the difference. The formulation of the confidence interval on the difference based on the confidence intervals on both samples is applicable to comparisons of mean, standard deviation, and amplitude percentile quantities.

The combined uncertainty intervals surrounding a difference between simulation and benchmark statistics enclose the region within which the “true” difference between populations is found. The level of confidence associated with interval calculations corresponds to the probability that the true difference is within the interval limit. For a 90-percent level of confidence, there is a 90-percent probability that the difference between the simulation and benchmark re-



sults is between the lower and the upper interval extents.

Positive values denote a simulation value which is greater than the benchmark (over-prediction) while negative values denote under-prediction. A zero-crossing of an interval denotes the possibility that there is no difference between the underlying. It should be noted, however, that the confidence level associated with the interval does not equal the probability that the difference is zero. In fact, there is equal likelihood that the true difference falls anywhere else within the interval extents.

As noted above, when the uncertainty interval on the difference crosses zero, there may be no difference between the two populations. A zero-crossing of difference intervals is most analogous to an overlap of uncertainty intervals associated with two data sets. Note, however, that zero-crossing is a more “strict” measure of similitude than interval overlap. For the same level of significance, it is mathematically possible for the intervals to slightly overlap without the corresponding interval on the difference crossing through zero.

A particularly useful attribute of the difference between statistics is its ability to convey information about the simulation’s accuracy for a given parameter across a range of conditions. This utility forms the foundation of acceptance criteria for quantitative validation.

4.3 Quantitative Accreditation (Acceptance Criteria)

The Quantitative Accreditation acceptance criteria are a tiered series of *channel*, *condition*, and *code* criteria. An evaluation of each critical motion is made to assess a speed-heading-seaway condition. The *channel criteria* are applied to the statistical properties calculated from model test and simulation time histories. The *condition criteria* are applied to the results of the *channel criteria* for each unique environmental and operational condition combination within the validation data domain space. Finally, the *code criteria* are applied to the results from the *condition criteria* to determine the final accred-

itation outcomes. The code acceptance is based on passing over 70-percent of the conditions.

Figures 6 and 7 provide an overview of acceptance criteria for Quantitative Accreditation of non-rare motions and rare motions, respectively.

Channel Criteria

Condition statistics (standard deviation and 90th percentile values) calculated from model and simulation time histories are used (with their associated uncertainty intervals) to assess the code’s ability to provide the required non-rare and rare motion ship response. The motions listed in Figures 6 and 7 are considered “critical channels” for assessment of intact stability-related motions. Channel criteria are defined relative to a physical limit value for each motion. Physical limit definitions may be tailored to address ship-specific hull and machinery requirements. Yaw and yaw rate physical limits are defined relative to the definition of a broach.

Condition statistics and uncertainty intervals for both model and simulation data sets are calculated for a single motion and condition from the respective sets of time histories of the motion. The difference between condition statistics (including uncertainty) is then calculating from the results of both data sets

Ordered values of ship speed and heading identify the ship’s operational environment for each condition. The average (mean) achieved values of speed and heading resulting from the ordered values and the ship’s response to the seaway influence the ship’s motions response. Condition mean values are determined from time histories of both simulation and model tests and are represented by the variable, μ .

The channel criteria are applied to the critical motions as four tests (referred to as Four Box criteria) which result in a “pass,” “fail,” or “null” conclusion. Figure 8 illustrates the relationship between the Four Box criteria and the determination of the motion comparison for both non-rare and rare channel criteria. Figure 9 shows an example (roll standard deviation) of the relationship between condition statistic difference

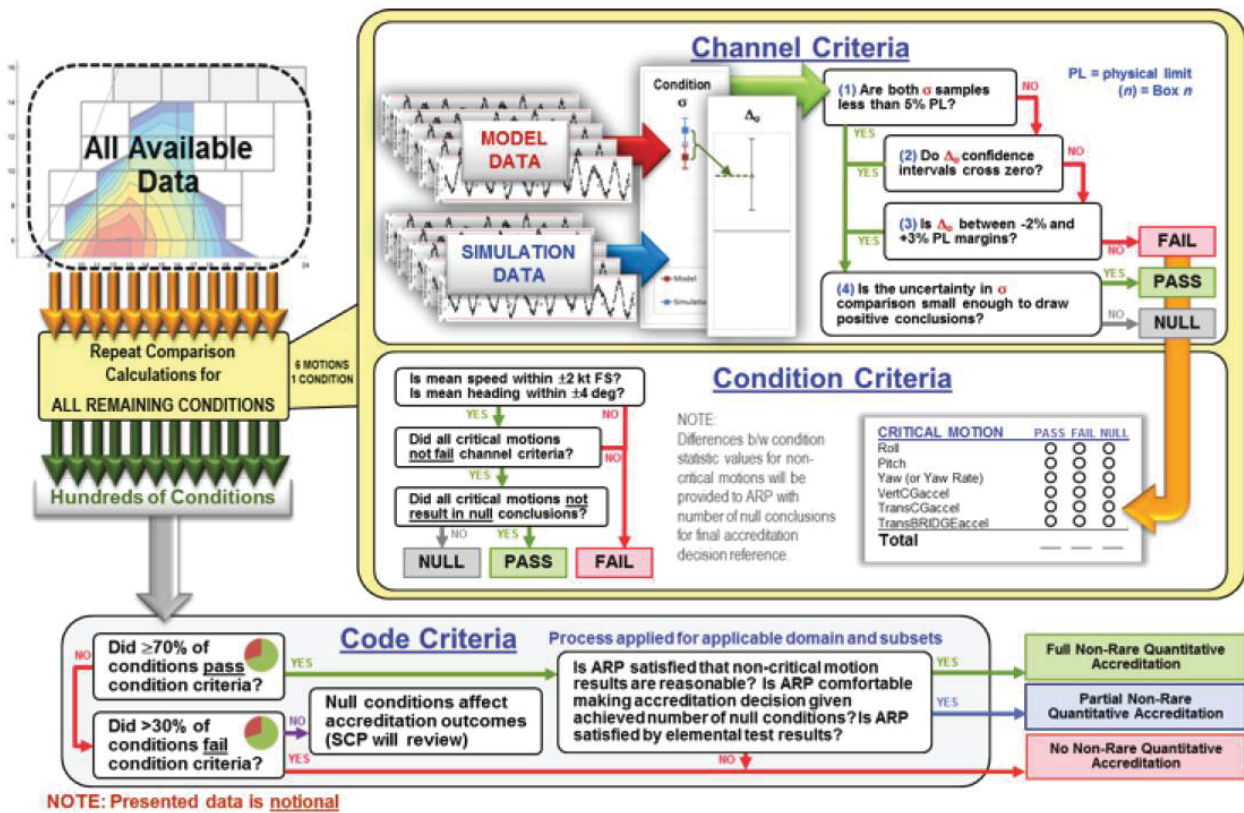


Fig. 6 Acceptance Criteria for Quantitative Accreditation Support (Non-Rare Motions)

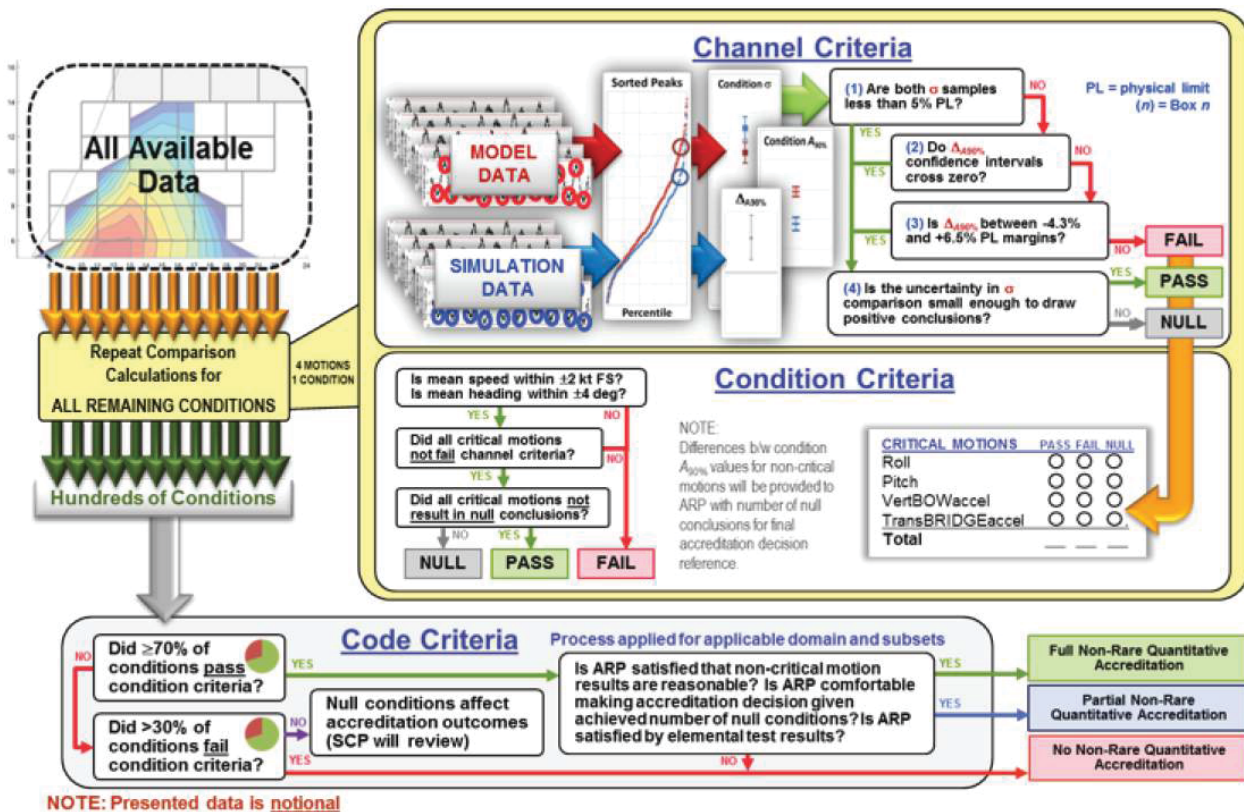


Fig. 7 Acceptance Criteria for Quantitative Accreditation Support (Rare Motions)

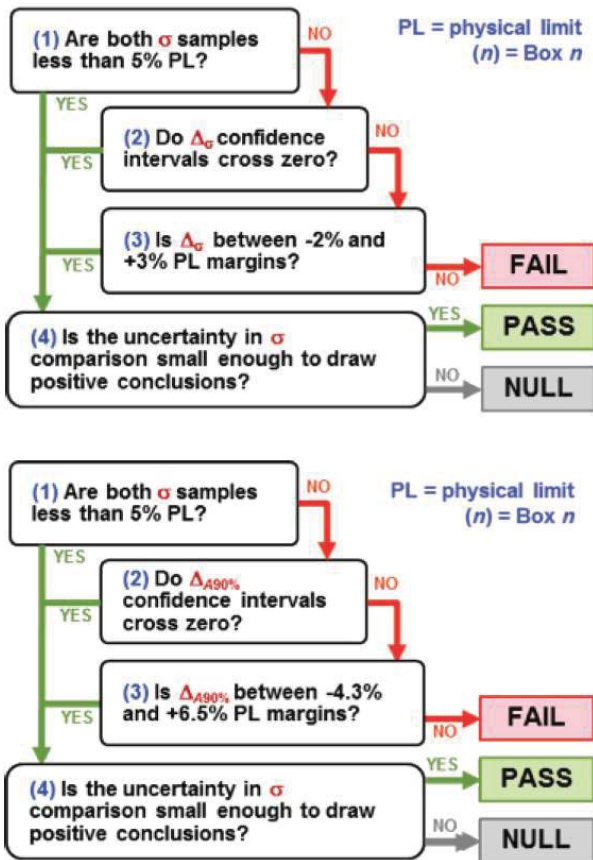


Fig. 8 Overview of Channel Criteria for Quantitative Accreditation for Non-Rare (top) and Rare (bottom) Motions

values and the four-box channel criteria.

Box 1: Very Small Motions

The Box 1 criterion is met if both the model and simulation condition σ -values are less than 5-percent of the physical limit. Passing the Box 1 criterion indicates that the motions are sufficiently small to pose no significant risk to ship operations.

Box 2: Zero Crossing of the Difference Uncertainty Interval

The Box 2 criterion is met if the uncertainty intervals about the difference between condition statistics passes through zero. Demonstration of a zero-crossing indicates a non-negligible statistical probability that the two condition statistics (model and simulation) may come from the same distribution and may be statistically the same (i.e. zero difference).

Box 3: Samples Within Margins

The Box 3 criterion is met if the model and simulation condition statistics differ by a permissibly small amount, or margin. The sample margins are conservatively biased; greater differences are allowed for over-prediction than for under-prediction. The margin values for non-rare motion comparisons are 3-percent of the physical limit for simulation over-prediction and 2-percent of the physical limit for simulation under-prediction. The margin values for rare motion comparisons are 6.5-percent of the physical limit for simulation over-prediction and 4.3-percent of the physical limit for simulation under-prediction. The margin values applied to the condition 90th percentile values are the non-rare motion margins multiplied by 2.15. This factor is based on the relationship between standard deviation and the 90th percentile of peaks for the Rayleigh distribution. Passing the Box 3 criterion addresses cases where the uncertainty intervals are small, but the condition statistic values are sufficiently similar to one another for practical purposes.

Box 4: Limitations on Uncertainty

The Box 4 criterion is met if the overall uncertainty in a comparison is less than a specified amount based on statistical Type II error (accepting what should be rejected due to too much uncertainty). The following equation presents the simplified numerical criterion for this test in terms of the confidence intervals on each data set.

$$\sqrt{(CI_{\sigma_{\text{model}}})^2 + (CI_{\sigma_{\text{code}}})^2} < 5\% \text{ of the physical limit}$$

Note that the characteristic interval length for each data set should be taken as the average of the upper and lower intervals if the intervals are asymmetric.

Failure of the Box 4 criterion does not signify a deficiency on the part of the simulation. Rather, failure of the Box 4 criterion denotes a comparison of poor quality from which no positive conclusions may be drawn.

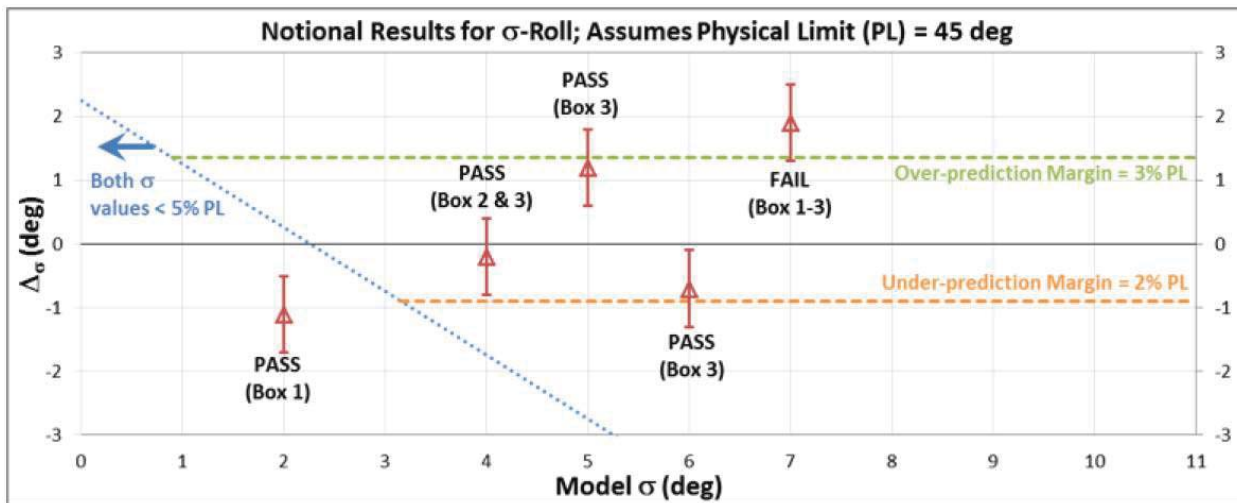


Fig. 9 Illustration of Channel Criteria for Quantitative Accreditation

Condition Criteria

Three outcomes are possible for the condition criteria: “pass,” “fail,” and “null.” The condition criteria are passed if the differences between mean speed and heading are permissibly small and 100-percent of the critical channels pass the channel criteria. The condition criteria are failed if the mean speed or heading differences are excessively large or one or more channels within a condition fail the channel criteria. The condition criteria results in a null conclusion if all of the following criteria are met: 1) mean speed and heading differences are permissibly small, 2) no motions fail the channel criteria, and 3) one or more motions result in a null conclusion of the channel criteria. Figure 10 illustrates the relationship between the condition criteria and the possible outcomes.

The simulation must demonstrate the ability to sufficiently model the mean speed and heading of the condition. The condition mean achieved model and simulation values of speed over ground and heading must fall within 2 knots full-scale and 4 degrees, respectively. Note that these limits should be tailored (based on ship speed and natural pitch and roll periods) to limit permissible deviation from wave encounter frequency.

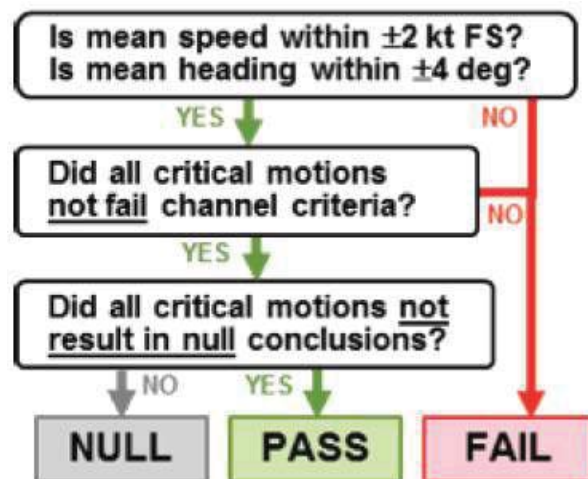


Fig. 10 Condition Criteria for Quantitative Accreditation (Rare and Non-Rare Motions)

Code Criteria

The code will pass the quantitative criteria for either rare or non-rare motions if at least 70-percent of conditions pass the respective quantitative condition criteria. The code will fail the code criteria for either rare or non-rare motions if more than 30-percent of the conditions fail the respective quantitative condition criteria. Otherwise, further review by the SCP is required due to the influence of null conditions on pass/fail outcomes. Further, the ARP must be satisfied with the percentage and locations within the domain space of non-null conditions ultimately available for the code comparison. Table 3 summarizes the quantitative code criteria, which are



applied separately for rare and non-rare results.

The ARP must also be satisfied by the accuracy reports for the non-critical rare and non-rare motions (not included in the channel comparisons). A description of the accuracy reports calculated for these channels is given below in the Qualitative Accreditation section.

The 70-percent criterion will be applied, and accreditation recommendations determined by the ARP, for non-rare motions across the following domain spaces:

- Across domain space
- Across defined operational conditions (speed and heading combinations)
- Across defined environmental conditions (wave height and period combinations)

4.4 Qualitative Accreditation

Qualitative Accreditation recommendations for the code's ability to simulate non-rare and rare motions is accomplished by generating accuracy reports (indicating differences between simulation and model results) for each channel across the relevant domain spaces, following the methodology presented in Zuzick, *et al.* (2014). Figures 11 and 12 provide an overview of the non-rare motion and rare motion, respectively, Quantitative Accreditation validation process. Statistical properties and the differences between these values are calculated from model test and simulation time histories. These values are calculated for each motion and unique environmental and operational condition combination within the validation data domain space. Finally, measures of overall accuracy are calculated from the observed difference values and provided to the ARP in the accuracy report.

The main difference between Qualitative and Quantitative Accreditation is the result of the effort. While Quantitative Accreditation provides "pass", "fail", or "null" outcomes to comparisons, Quantitative Accreditation provides statements about the simulation tool's accuracy (e.g. "The simulation over-predicts roll by 1.5 degrees across the validation domain."). These quantified measures of accuracy are contained

in accuracy reports and can be used to establish margins on simulation results for ship-specific operator guidance generation.

Accuracy Reports

Qualitative Accreditation results in quantified measures of accuracy of critical and non-critical rare and non-rare motions results produced by the simulation tool across the domain and for subsets of the domain. For Qualitative Accreditation accuracy reporting, the 90-, 95- and 99-percent confidence intervals will each be calculated on the difference. The condition statistics examined through accuracy reports are standard deviation (for non-rare motions), 90th-percentile of amplitude peak (for rare motions), and mean values (for achieved speed and heading).

In addition to calculating the difference between condition statistics, the percent difference between values (difference divided by the model data condition statistic) will be calculated for each motion and condition. Within the maneuvering and seakeeping simulation community, a 20-percent difference (or smaller) is a generally-accepted measure of good correlation of standard deviation. The ARP will be provided with the percentage of channels compared whose percent difference was less than or equal to 20-percent as an additional measure of the code's overall accuracy.

To quantify the code's overall ability to capture rare and non-rare motions, generalized accuracy reports will be generated for each motion using the differences (and associated uncertainties) between the code and model test condition statistics over a range of conditions.

Figure 13 provides a notional representation of a non-rare and rare motion accuracy report for one mode of motion. Each accuracy report will contain the following quantities:

- Arithmetic mean of the difference (including arithmetic means of upper and lower uncertainty limits)
- Weighted mean of the difference (including weighted means of upper and lower uncertainty limits)



Table 3 Quantitative Code Criteria

PASS	FAIL	NULL	Comment
70%	N/A	N/A	Code Passes
N/A	> 30%	N/A	Code Fails
< 70%	< 30%	> 0%	Further examination of null conditions

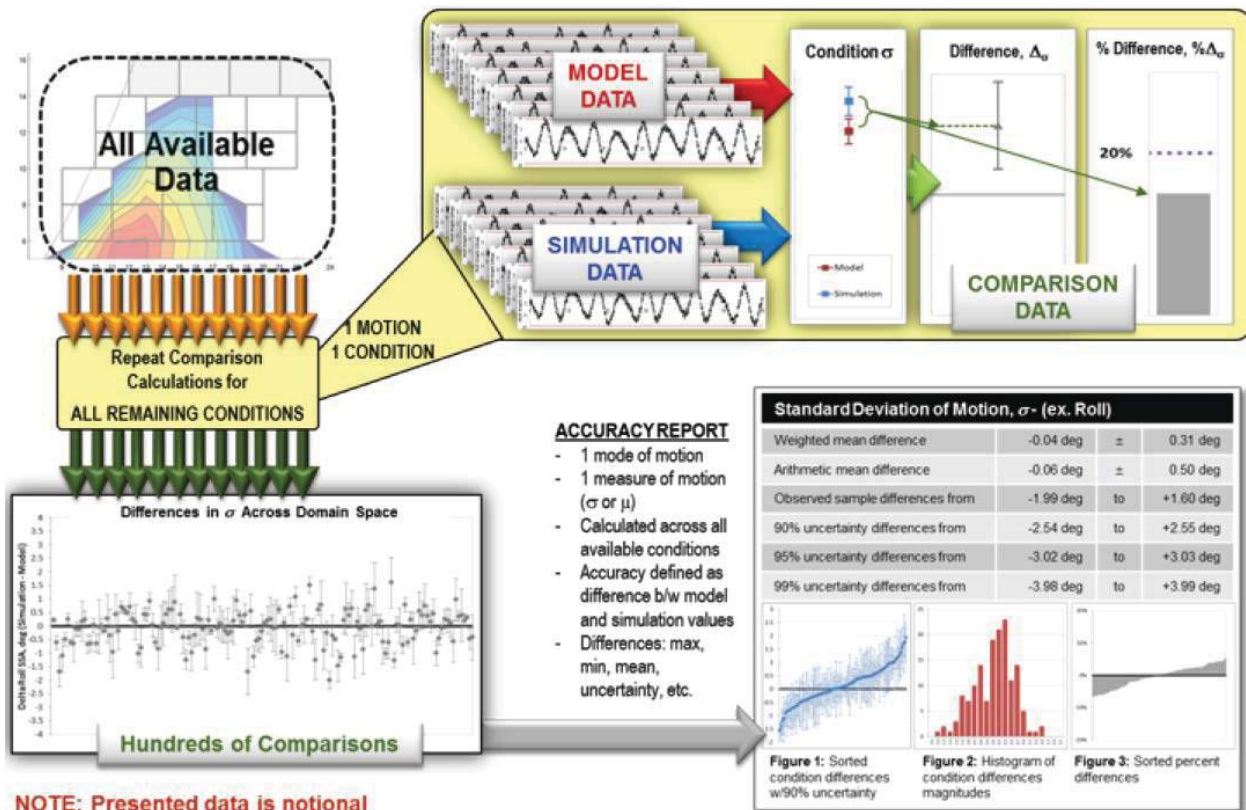


Fig. 11 Acceptance Criteria (Accuracy Reports) for Qualitative Accreditation Support (Non-Rare Motions)

– Weighting of each comparison condition is determined by the inverse of the combined length of the uncertainty intervals

- Range of observed sample differences
- Range of observed upper and lower uncertainty limits for 90%, 95%, and 99% confidence intervals
- Plot of sample differences (including 90-percent uncertainty limits) sorted from smallest to largest sample differences
- Histogram of sample difference magnitudes
- Quantile-quantile plot of motion peak amplitudes showing all conditions in the domain

A non-rare and rare motion accuracy report will be generated for each motion using individual comparison results from conditions categorized by several domain spaces. Quantified measures of accuracy will be calculated for each motion for the following domains:

- Across domain space
- Across defined operational conditions (speed and heading combinations)
- Across defined environmental conditions (wave height and period combinations)

5 CONCLUSIONS

With the advent of the second-generation intact stability criteria, IMO has initiated a two-tier

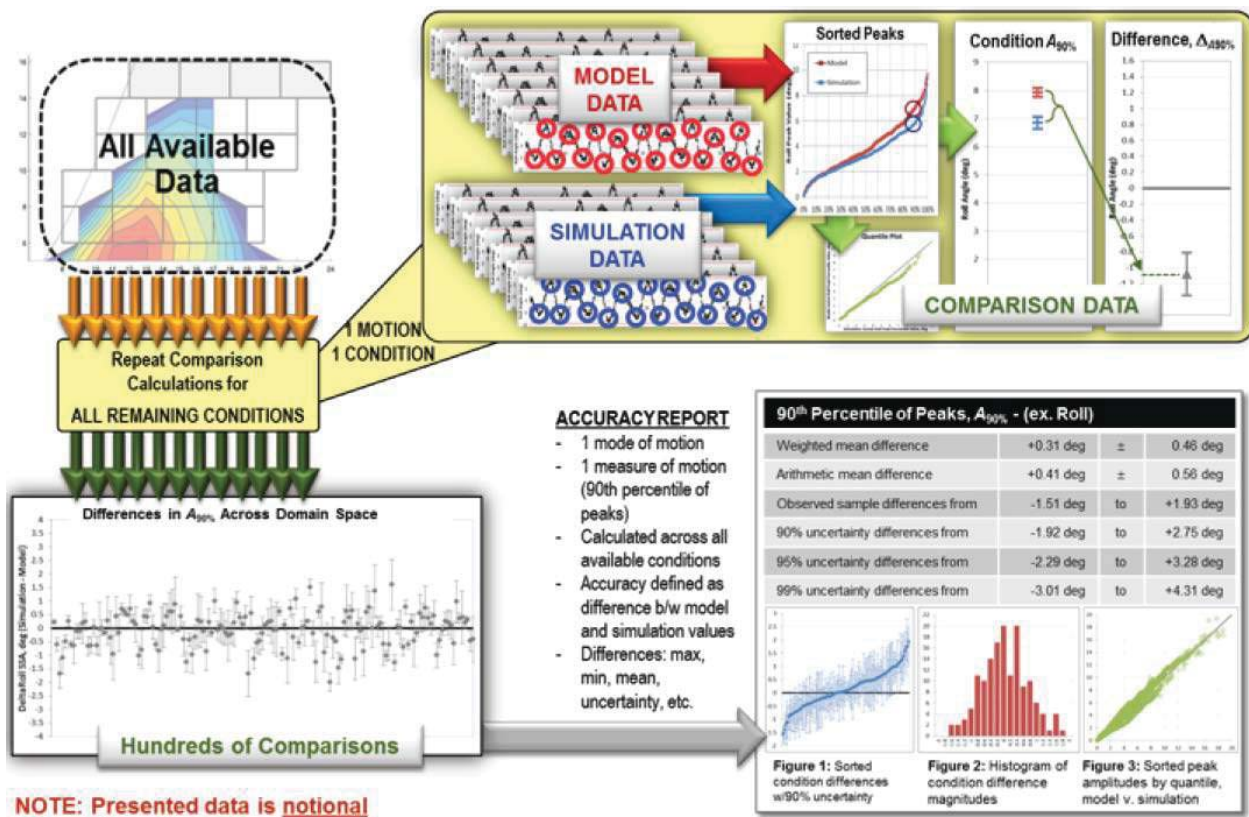


Fig. 12 Acceptance Criteria (Accuracy Reports) for Qualitative Accreditation Support (Rare Motions)

performance-based stability assessment process for unconventional hulls with a risk of intact stability failure. The first tier has two levels where simplified physics-based algorithms are used to assess a design. If the design fails the first level test, which is very simple but quite conservative, the design is then assessed using the second level criteria. The second level test is also simple, but it is more involved and less conservative than the first level method. If the design fails these first tier evaluations, it then progresses to the second tier, where direct assessment criteria are applied.

The design is considered satisfactory if the direct assessment criteria are passed. If these criteria are not passed, operator guidance is needed to provide vessel operators with the information needed to safely operate the vessel in dangerous conditions. Ship motion simulation tools are needed to apply the direct assessment criteria and generate operator guidance, if necessary.

A framework is presented for certification

that simulation tools used for direct assessment of stability failures and generation of operator guidance are sufficiently accurate for these purposes. Based on US Navy experience, guidance is provided on the VV&A process, structure, and participation, and acceptance criteria are given for both quantitative and qualitative accreditation approaches. Accreditation acceptance criteria are tailorable to ship-specific VV&A efforts, particularly with regards to definition of critical motions and physical limits.

ACKNOWLEDGMENTS

The authors wish to express their appreciation to Philip Alman of NAVSEA, and David Drazen, Christopher Kent, Joel Park and Timothy Smith of DTMB for their many hours of discussion and contributions relating to acceptance criteria. We would also like to thank Vadim Belenky, William Belknap and Brad Campbell of DTMB for their discussions on the VV&A process—from both a Navy and IMO perspective, during

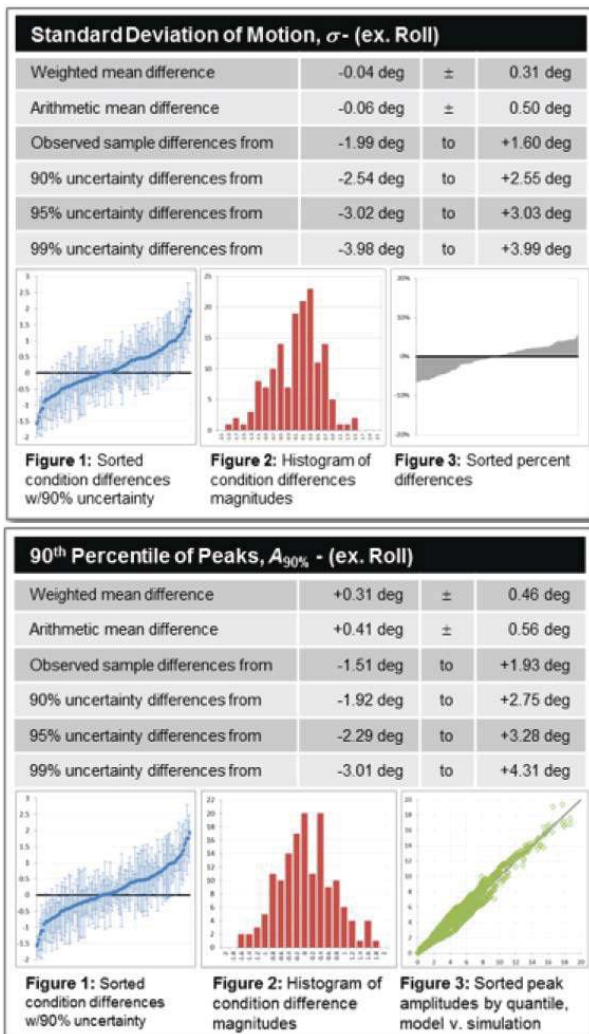


Fig. 13 Notional Non-Rare (top) and Rare (bottom) Motion Accuracy Report for Roll (NOTE: Data presented is notional)

the preparation of this paper. Finally, we would like to thank Joe Gorski of DTMB for his thorough review of the paper.

REFERENCES

AIAA (1998) Guide for the Verification and Validation of Computational Fluid Dynamics Simulations. AIAA G-077-1998 Guide, Reston, VA: American Institute of Aeronautics and Astronautics, viii+19 p.

ASME (2009) V&V 20-2009, Standard for Verification and Validation in Computational Fluid Dynamics and Heat Transfer. New York, NY: American Society of Mechanical

Engineers, x+87 p.

Beck, R. F., A. M. Reed & E. P. Rood (1996) Application of modern numerical methods in marine hydrodynamics. *Trans. SNAME*, 104:519–37, Jersey City, NJ.

Belenky, V., J. O. de Kat & N. Umeda (2008a) Towards Performance-Based Criteria for Intact Stability. *Marine Tech.*, 45(2):101–123.

Belenky, V., V. Pipiras, C. Kent, M. Hughes, B. Campbell, T. Smith (2013) On the Statistical Uncertainties of Time-domain-based Assessment of Stability Failures: Confidence Interval for the Mean and Variance of a Time Series. *Proc. 13th Int'l Ship Stability Workshop*, Brest, France, 8 p.

Belenky, V. L. & N. B. Sevastianov (2007) *Stability and Safety of Ships: Risk of Capsizing* (2nd ed.). SNAME, Jersey City, NJ, xx+435 p.

Belenky, V., K. M. Weems, W-M. Lin (2008b) Numerical Procedure for Evaluation of Capsizing Probability with Split Time Method, *Proc. 27th Symp. Naval Hydro.*, Seoul, Korea, 25 p.

Clauss, G. (2008) The Taming of the Shrew: Tailoring Freak Wave Sequences for Seakeeping Tests. *J. Ship Res.*, 52(3):194–226.

DoD (1998) DoD Modeling and Simulation (M&S) Glossary. DoD 5000.59-M, U. S. Department of Defense, 175 p.

DoD (2003) DoD Modeling and Simulation (M&S) Verification, Validation, and Accreditation (VV&A). DoD Instruction 5000.61, U. S. Department of Defense, 10 p.

DoD (2007) DoD Modeling and Simulation (M&S) Management. DoD Directive 5000.59, U. S. Department of Defense, 7 p.

DoD (2012) Department of Defense, USD (AT&L) MIL-STD-3022 w/Change 1: Department of Defense Standard Practice: Documentation of Verification, Validation, and Accreditation (VV&A) for Models and Simulations, 55 p.



- Eça, L. & M. Hoekstra (2012) Verification and Validation for Marine Applications of CFD, Gothenburg, Sweden: *Proc. 29th Symp Naval Hydro*.
- Francescutto, A. (2004) Intact Ship Stability—The Way Ahead. *Marine Tech.*, 41:31–37.
- Francescutto, A. (2007) Intact Stability of Ships—Recent Developments and Trends. *Proc. 10th Int'l Symp. Practical Design of Ships and Other Floating Struct (PRADS '07)*. Houston, TX, Vol. 1, pp. 487–496.
- Francescutto, A., G. Contento & R. Penna (1994) Experimental Evidence of Strong Nonlinear Effects in the Rolling Motion of a Destroyer in Beam Seas. *Proc. 5th Int'l Conference of Stability of Ships & Ocean Vehicles (STAB 94)*, Florida Institute of Technology, Melbourne, FL, Vol. 1, 13 p.
- IMO MSC 85/26/Add.1 (2008) International Code on Intact Stability, 2008 (2008 IS Code). London, 96 p
- IMO MSC.1/Circ.1281 (2008) Explanatory Notes to the International Code on Intact Stability, 2008, London, 30 p.
- IMO SDC 2-WP.4 (2015) Development of Second Generation Intact Stability Criteria, Development of Amendments to Part B of the 2008 IS Code on Towing, Lifting and Anchor Handling Operations, Report of the working group (Part 1), London, UK, 48 p.
- IMO SLF 48/21 (2005) Report to Maritime Safety Committee, London, UK, 65 p.
- IMO SLF 50/4/4 (2007) Framework for the Development of New Generation Criteria for Intact Stability, submitted by Japan, the Netherlands and the United States, London, UK, 6 p.
- IMO SLF 55/3/11 (2013) Development of second generation intact stability criteria, comparison study of draft level 2 vulnerability criteria for stability under dead ship condition. Submitted by Italy and Japan. London, UK, 4 p.
- ITTC (2011) The Specialist Committee on Stability in Waves: Final Report and Recommendations to the 26th ITTC. *Proc. 26th ITTC*, Rio de Janeiro, Brazil, 36 p.
- ITTC (2014) The Committee on Stability in Waves: Final Report and Recommendations to the 27th ITTC. *Proc. 27th ITTC*, Copenhagen, Denmark, 67 p.
- Kan, M. (1990a) Surging of large-amplitude and surf-riding of ships in following seas. *Naval Arch. & Ocean Engin.*, 28:49–62.
- Kan, M. (1990b) A Guideline to Avoid the Dangerous Surf-riding. *Proc. 4th Int'l Conf. Stability of Ships & Ocean Vehicles*, University Federico II of Naples, Naples, Italy, pp. 90–97.
- Kantz, H. & T. Schreiber (2004) *Nonlinear time series analysis*. Cambridge University Press, Cambridge, UK, xvi+369 p.
- Kobylinski, L. K. & S. Kastner (2003) *Stability and Safety of Ships: Regulation and Operation*. Elsevier, Amsterdam, 454 p.
- McCue, L. S., W. R. Story & A. M. Reed (2008) Nonlinear Dynamics Applied to the Validation of Computational Methods. *Proc. 27th Symp. on Naval Hydro*, Seoul, South Korea., 10 p.
- NATO (2007a) Buoyancy, Stability and Controlability. Chapter III of Naval Ship Code, NATO Naval Armaments Group, Maritime Capability Group 6, Specialist Team on Naval Ship Safety and Classification, Allied Naval Engineering Publication ANEP-77, vii+121 p.
- NATO (2007b) Guidance on NSC Chapter III Buoyancy and Stability, Part B: Application. Chapter 3, Guide to the Naval Ship Code, NATO Naval Armaments Group, Maritime Capability Group 6, Specialist Team on Naval Ship Safety and Classification, 91 p.
- Navy (1999) SECNAV Instruction 5200.40: Verification, Validation, and Accreditation (VV&A) of Models and Simulations, 21 p.
- Navy (2002) SECNAV Instruction 5200.38A: Department of the Navy Modeling and Simulation Management, 8 p.
- Navy (2004) Department of the Navy, Model-



- ing and Simulation Verification, Validation, and Accreditation Implementation Handbook, Volume I, VV&A Framework, 39 p.
- Navy (2005) Approved Navy Modeling and Simulation Standard: Best Practices Guide for Verification, Validation, and Accreditation of Legacy Modeling and Simulation. Navy Modeling and Simulation Standards Project, 48 p.
- NIST (2014) National Institute of Standards and Technology, "NIST/SEMATECH e-Handbook of Statistical Methods," [Online]. Available: <http://www.itl.nist.gov/div898/handbook/>. [Accessed 1/2/2014]
- Oberkampf, W. L., & M. F. Barone (2006) Measures of agreement between computation and experiment: Validation metrics. *J. Comp. Physics*, 217, 5–36.
- Peters, W., V. Belenky, C. Bassler, K. Spyrou, N. Umeda, G. Bulian, B. Altmayer (2011) The Second Generation Intact Stability Criteria: An Overview of Development. *Trans. SNAME*, 119:225–264.
- Rahola, J. (1939) The judging of the stability of ships and the determination of the minimum amount of stability especially considering the vessel navigating Finnish waters. PhD Thesis, Technical University of Finland, Helsinki, viii+232 p.
- Reed, A. M. (2009) A Naval Perspective on Ship Stability. *Proc. 10th Int'l Conf. Stability of Ships & Ocean Vehicles (STAB '09)*, St. Petersburg, Russia, pp. 21–44.
- Rosborough, J. M. (2007) Stability and buoyancy of U.S. Naval surface ships. Design Data Sheet DDS 079-1, Version: 2.01, 30 Jan 2008, Carderock Division, Naval Surface Warfare Center Report NSWCCD-20-TR-2007/05, 107 p.
- Sarchin, T. H. & L. L. Goldberg (1962) Stability and buoyancy criteria for U. S. Naval surface ships. *Trans. SNAME*, 72:418–58.
- Spyrou, K. J. (1996) Dynamic Instability in Quartering Seas: The Behavior of a Ship During Broaching. *J. Ship Res.*, 40(1):46–59.
- Spyrou, K. J. (1997) Dynamic Instability in Quartering Seas—Part III: Nonlinear Effectson Periodic Motions. *J. Ship Res.*, 41(3):210–223.
- Spyrou, K. J., K. M. Weems & V. Belenky (2009) Patterns of Surf-Riding and Broaching-to Captured by Advanced Hydrodynamic Modelling. *Proc. 10th Int'l Conf. Stability of Ships and Ocean Vehicles (STAB 09)*, St. Petersburg, Russia, 15 p.
- Themelis, N. & K. J. Spyrou (2007) Probabilistic Assessment of Ship Stability. *Trans. SNAME*, 117:181–206.
- Themelis, N. & K. J. Spyrou (2008) Probabilistic Assessment of Ship Stability Based on the Concept of Critical Wave Groups. *Proc. 10th Int'l Ship Stability Workshop*, Daejeon, S. Korea, 11 p.
- Zuzick, A. V., A. M. Reed, W. F. Belknap & B. L. Campbell (2014) Applicability of the Difference Between Population Statistics as an Acceptance Criteria Metric for Seakeeping Validation. *Proc. 14th Int'l Ship Stability Workshop*, Kuala Lumpur, Indonesia, 9 p.

KEYNOTE ADDRESS

A Classification Society Perspective for Ship Stability

Prof. Fai Cheng, LR

This page is intentionally left blank

KEYNOTE ADDRESS

Ship Stability in Practice

Ross Ballantyne, Sea-Transport Solutions

This page is intentionally left blank



Ship Stability in Practice

Ross Ballantyne/Stuart Ballantyne, *Sea-Transport Solutions*

ABSTRACT

Designing outside the box but inside the rules – a challenge for any Naval Architect. Modern ship designs are advancing at a faster pace than what the regulators can capture within a code of rules and guidelines.

Ship stability, in particular, is an aspect of naval architecture where a framework of prescriptive rules makes it difficult in practice to achieve an economically and operationally viable solution for unique ship designs.

This paper draws from the experience of an established international marine design firm and brings to attention various issues that are emerging as designs evolve, whilst proposing a way forward for establishing a foundation for practical safe stability assessments in the maritime sector and for future developments on the subject.

1. INTRODUCTION

Ship to Shore. Sea Transport Solutions (STS) CEO, Stuart Ballantyne, fascinated with ship design, left his job at sea as a navigator/deck officer after 7 years and returned to Glasgow to start studying for a career change in Ship Design. It was this foundation of seagoing experience at an early stage where practical, out of the box thinking ship design solutions were established with the Australian Marine Design Firm in 1976. A family based company where employees are a mixture of both Naval Architects and Seafarers, has proven to be a recipe for success with a series of Award Winning designs. This combination of theoretical and practical know-how has provided connections and close working relationships with the maritime regulators for on-going advice and direction for developing and refining the codes of practical ship design. With more and more regulating authorities and their college graduate personnel coming onto the maritime scene, ship stability has always been cause for great debate between

designers, operators and authorities. This paper endeavours to briefly highlight the problems, issues, gaps and interactions with ship stability rules in practice.

2. DAMAGE STABILITY LEGISLATION

Queensland, Australia, which is home to over 9,000 commercial vessels and around 260,000 recreational vessels, is a good place to set the scene of the where the maritime industry is globally. For it is here where decisions on ship selection were always bottom line driven. It is also where the STS design firm was established.

The Queensland Maritime regulators at the time were restructuring the Australian Domestic Code into a “Uniform Shipping Laws Code”, which was strongly influenced by unions and the GRT and NRT based



code was changed to a length basis, but not fairly. Stability rules were also tightened and this meant that operators of a 36 metre charter vessel had to have extra crew for fewer passengers. The operators came looking for a solution to reduce the crew back to original manning size and increase the passenger numbers, but there was to only be one immediate answer: a catamaran.

Catamarans in those days had a poor reputation for sea handling, so it was in the tank test facilities in Strathclyde where a series of tests with symmetric and partial asymmetric catamaran hulls with bulbous bows was carried out.



Figure 1 - Shangri La 20m Catamaran, hull centrelines toe out, asymmetric hulls with bulbs. Strathclyde Ph D. Student Apostolis Tsanticos standing in photo.

As ex seafarers, the company established a series of minimum tunnel clearances forward and amidships to avoid slamming loads. 20 years later these became compulsory in class rules.

STS also worked with Lloyds Register (LR) as the guinea pig in the establishment of the Special Service Craft (SSC) rules which had been purchased from the Russians. These very

sensible rules were first principles based, instead of the old empirical rules, which allowed room to minimise the weight with high tensile steel hulls and aluminium superstructured catamarans and sensibly attack the subdivision requirement rules.

Like most coastal regions, Australia is home to a number of Landing Craft designs which consistently capsize with loss of lives and cargoes as per the below table. A combination of a shallow deck immersion (typically 4-5 degrees in a stern trim configuration) and a bit of movement of deck cargo, a vessel is upside down within 3 to 5 seconds.

Australia			
•"M.V. Keppel Trader"	16m	1996	Capsized on voyage from Darwin – 1 killed
•"M.V. Tasma"	35m	1991	Capsized on voyage from Cairns to Karumba - no-one killed
•"M.V. Thuppen"	20m	1988	Capsized circa Townsville-Magnetic Island 1 killed,
•"M.V. Piera"	50m	1992	Ex qld en route to Lihir PNG circa, capsized, Master and Engineer killed, vessel lost
•"M.V. Shellbourne Bay"	20m	1994	Capsized in Thursday Island Harbour (twice !!) Smooth waters, rudder heeling moment causing deck-edge immersion. No-one killed. Trucks on board
•"M.V. Narapi"	25m	1992	Capsized in Horne island – cargo shifted- no subdivision, then sank - not located
•"M.V. Major Dundee"	30m	1993	Truck fell of legs and moved transversely during voyage in partially smooth waters, vessel then had deck edge immersion and promptly capsized, Airlie beach, no-one killed.
•"M.V. Hinchinbrook Island"	16m	2000	Capsized near Cardwell, Queensland. Partially smooth waters – 1 killed. Manslaughter charges now against owner and surveyor.
PNG			
•"M.V. Sir Garrick"	32m	1982	Capsized Kerema Gulf- master killed
•"M.V. Pakori"	25m	1993	Sank at Kikori through stern flooding - no one killed
Solomon Islands			
•"M.V. Vula"	30m	1987	Capsized killing 20 passengers. The Government then introduced a ban prohibiting landing craft to carry passengers.
•"M.V. Bulamakow"	40m	1991	Capsized on a cargo run, crew killed.
Fiji			
M.V. Adi Ywaitui	40m	2006	Capsized killing 1 crew member

Table 1 - Capsized Landing Craft

STS addressed this lack of stability with side buoyancy, whilst at the same time also addressing the Landing Craft's poor performance in head seas by designing a ship shape high bow, ultimately leading to the development and patent of the "Stern Landing Vessel" (SLV). The SLV, in other words, is a back to front landing craft which there are now 24 in operation and several currently under construction.



Figure 2 - SLV on the beach

Part of the hull design also incorporated a 'V hull' shape which birthed the first "no ballast" bulk carrier the "MV Deepwater" in 1990.



Figure 3 – SLV "MV Deepwater"

The company clashed heavily with the Australian Maritime Safety Authority (AMSA) regulators who said these well-deck novel designs were not compliant with the definition of "Freeboard Deck" -the uppermost continuous deck. AMSA were insisting on freeing ports from the well deck which is impossible with toxic cargoes such as lead zinc, or any other cargo for that instance. The design of these small bulk carriers was so to withstand total swamping in any loaded condition, however this common sense was only accepted after lengthy discussions and

model test experiments. A well deck configuration is far more robust in a heavy seaway.

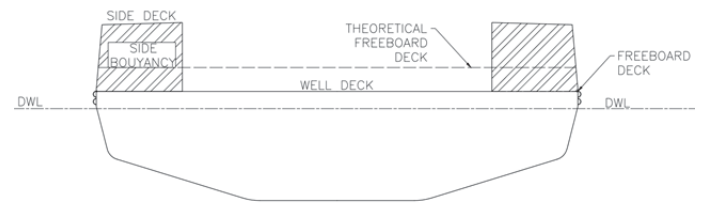


Figure 4 - Well Deck, Flat Deck and 'effective' deck level

3. RESILIENCE

In the case of the small 5300dwt self-discharging bulk carrier, *MV Wunma*, with a well deck configuration, she was abandoned fully loaded in a cyclone in the Gulf of Carpentaria in November 2007. This is the ultimate test for any ship and generally bulk carriers would be overwhelmed in such a situation.

Despite some very bad press at the time, the vessel survived intact, with no loss of life or injuries or pollution and, under her own power, entered the port of Weipa 3 days later. The Australian Government, spent AU\$6m on a marine court of enquiry. With no injuries, pollution or damages, this was an enquiry into being nearly pregnant! As a result of this incident and the press coverage of an unsinkable ship, STS secured a contract for a 14,000dwt SLV from the Middle East.





Figure 5 - MV Wunma, with a well deck configuration

4. FORWARD THINKING

The fact that 99% of all clients are after a vessel which makes a profit, ship designers often have to think outside the box. In the case of a client who was after an SLV with a 10 vehicle 65 tonne deck load within a very limited space of time, a second-hand 30 metre length, narrow-beamed, 15 knot small patrol boat with a 3 tonne deck load was purchased and converted.



Figure 6 - LARA V, before alteration.

Without touching the vessel's engineering or electrical system, gull wings either side of the vessel were fabricated and attached. With buoyancy of the added shape equal to the weight added including a 5 metre SLV stern section, the vessel ended up carrying the required 65 tonnes as well as gaining another knot in speed.



Figure 7 - LARA V, after alteration.

The *Lara V* alteration of course caused concern with the regulators at the time who insisted this could not be done. The vessel however was compliant in all aspects of ship design but not all stability criteria at the time, with one example, the requirement to have the GZ_{max} occur after 20° heeling angle. With this new trimaran hull configuration, this obsolete rule could not be met. The regulators could not see the 'intent' of the rules and although the stability criteria on face value had not passed 100%, the vessel's significant increase in stability safety was surprisingly not an easy argument, but ultimately an argument that was won. Basically it was taking the exceptionally low GM and raising it considerably with the aid of a trimaran shape that was really the core solution. The commercial risk was taken by our design office and had a happy ending technically, operationally and commercially.

5. GRT ISSUES

When addressing the problems of the South Pacific nations, numerous capsizes were occurring predominantly with vessels



that were under 500GRT. It was conclusive that the bottom dollar ship selection of vessels below 500GRT was to escape from an “IMO convention vessel benchmark”, at which point the extra expense it incurs. The unfortunate part of this is that the resultant sub 500GRT vessels are only 40-45m in waterline length and the predominant trade winds generate a wave height and frequency only suitable for a minimum 60m L_{WL} vessel, instead these small waterline vessels fall into the troughs of the oncoming waves. Survivors of these tragedies such as the, Rabaul Queen, reported that “three large waves overcame the vessel” prior to capsize. The local regulators then finger-pointed to passenger overloading, where in fact the water on deck captured within the bulwarks is believed to be the major offending contribution to the capsize and loss of 142 lives. Marine operators have continued to push for the 500GRT benchmark to be replaced with 60m L_{WL} without success.

The Dutch Naval Architect, Ernst Vossnack, also concluded that the pursuit of a lower GRT by eliminating forecastle and aftercastle buoyancy was the primary reason for the capsize of small Mediterranean 999GRT and 1499grt vessels in heavy weather, where their dynamic stability reserves were overwhelmed by the harsh reality of big waves.

This issue of GRT should be seriously addressed with the IMO to avoid further loss of life with naval architects creating ships that are fundamentally unseaworthy. It appears IMO are no longer interested in Safety of Life at Sea and have for the last decade, in this author’s opinion, had a myopic view on environmental

issues and very little or no interest in the ongoing capsizes of landing craft and the demise of sub paragraph GRT vessels.

6. ASSESSING UNCONVENTIONAL SHIPS

Addressing the major problems of worldwide transshipping (restrictions of a 2m wave height and 20 knot wind speeds and transportable moisture limits (TML)), the Floating Harbour Transhipper (FHT) was developed. This innovation incorporates exports of bulk commodities from remote small shallow draft harbours with shallow draft SLV’s to an FHT which has a wet dock to offload these small feeder barges.

Two interlinked vessels, one loading, one discharging creates its own problems, but stability in the end was not one of them. The ‘ship within a ship’ concept was beyond standard ship stability criteria, so a series of model test basin experiments were required to evaluate safety of the vessels at sea, which for now, have satisfied the local marine regulators.

Model test facilities are a great tool for assessing ship safety and stability, but unfortunately access to these resources are not always available in a timely manner or at bargain prices. Computational fluid dynamics (CFD) software is becoming more powerful, so perhaps one day the regulatory bodies may embrace the results of these tools with greater confidence, thereby allowing for a greater quantity of unique vessel designs to be designed, assessed and built.



Ross Ballantyne/ Stuart Ballantyne

Figure 8 - Floating Harbour Transhipper
(FHT)

7. CONCLUDING REMARKS

So how does a Design Office focus on out-of-the-box practical solutions deal with stability regulations during the design phase: problems, issues, gaps, interactions, recommendations?

As a ship design company that have expanded into owning and operating ports and vessels, we prefer to find experienced ex mariners with current seagoing qualifications in amongst the regulators. This is getting more difficult and with this difficulty comes frustration, as the pure academic regulator will hide not only in the prescriptiveness of the regulations as opposed to the intent, but sometimes his or her own misguided interpretation of the regulations.

We would encourage the regulators to employ seafarers who do not only have deepsea experience, but rather more importantly have sea time on smaller, modern coastal vessels.

Innovation has a long way to go with commercial vessels and there is a strong future for the industry if we do not constrain the thinking.

KEYNOTE ADDRESS

**ClassNK Activities Related to Stability in Collaboration
with NAPA**

Taise Takamoto, ClassNK and Jun Furustam, NAPA Ltd

This page is intentionally left blank



ClassNK Activities Related to Stability in Collaboration with NAPA

Mitsuhiko Kidogawa, *General Manager of Hull Department, ClassNK* kidogawa@classnk.or.jp

Taise Takamoto, *Manager of Hull Department, ClassNK* takamoto@classnk.or.jp

Jan Furustam, *Product Manager, Naval Architecture, NAPA Ltd.* jan.furustam@napa.fi

ABSTRACT

ClassNK has developed an application called “ClassNK Manager” in collaboration with NAPA Group. The application is designed to support ship designers carry out stability calculation based on NAPA 3D model and create the relevant booklets in compliance with statutory rules. The primary objective of the cooperation is to assist the naval architect in performing regulatory engineering calculations in a way that makes designs safer and makes the classification process faster.

Keywords: *Stability Booklet, Application, ClassNK, NAPA*

1. INTRODUCTION

Designing market competitive ships in a short period of time with minimal resources is a demanding task in the current situation of shipbuilding industry. In order to add higher values to new building ships, more detailed studies are required in the design phase while design conditions.

Regarding statutory rules, regulations are becoming more complicated, e.g. SOLAS 2009, and they require accurate treatment of 3D geometries. Therefore, there is also a strong need of 3D systems from the viewpoints of statutory calculations and class approval.

For classification societies, it is important to support shipyards. ClassNK has been developing an application called “ClassNK Manager” based on the NAPA 3D model for stability calculation collaborating with NAPA group.

2. HISTORY OF COLLABORATION BETWEEN CLASSNK AND NAPA

ClassNK began using NAPA System in 2005. In order to improve customer service, from 2008, ClassNK started to collaborate with NAPA group to develop a new concept application which assist designer to prepare the stability booklet in accordance with rules. The fundamentals of the project lied in designing the application to be so user friendly that no specific training would be needed.

From 2011, ClassNK also start to collaborate with NAPA group to develop the interface system to achieve Data Linkage between the ClassNK software for Harmonised CSR and NAPA Steel using the NAPA 3D model.

Furthermore, ClassNK and NAPA group developed “ClassNK-NAPA Green” which helps owners and operators better monitor and optimize the efficiency of vessel operations.



In 2014, ClassNK acquired NAPA in order to ensure that innovation in software benefits the entire maritime industry and make new innovations available to everyone.

3. OUTLINE OF THE APPLICATION

The developed application, “ClassNK Manager”, is based on the NAPA Manager concept which comprises a framework for modelling a work process on top of the NAPA 3D model bringing the accuracy and efficiency of the ship design package into an easy-to-use and practical form. The NAPA Manager concept is widely used in the design work at world’s leading shipyards and design consultancies.

The key function of ClassNK Manager associated with stability is outlined below.

2.1 Intact Stability

The GM limit curve in accordance with 2008 IS Code can be created easily. The output of calculation results related to the Stability Information and Loading Manual for approval can be issued easily with a good and useful format. In general, very short time will be available to make the Stability Information and Loading Manual loaded onboard, because those cannot be made without the result of inclining experiment or lightweight measurement and they should be prepared to comply with the convention rule before the ship’s delivery. This tool will be useful to issue these documents within a short period of time.

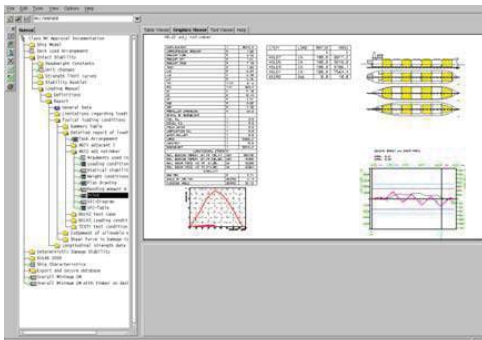


Figure 1 Loading Condition View

GM limit curve in accordance with 2008 IS Code can be created easily. The output of calculation results related to the Stability Information and Loading Manual for approval can be issued easily with a good and useful format. In general, very short time will be available to make the Stability Information and Loading Manual loaded onboard, because those cannot be made without the result of inclining experiment or lightweight measurement and they should be prepared to comply with the convention rule before the ship’s delivery. This tool will be useful to issue these documents within a short period of time.

When timber deck cargoes are loaded, the buoyancy of the timber deck cargo can be taken into account in accordance with Paragraph 3.5.3 “Calculation of stability curves for ships carrying timber deck cargoes” in 2008 IS Code. The shape of timber deck cargo can be easily defined and used to calculate stability taking the reserve buoyancy of the timber deck cargo into account. The alternative stability criteria for timber deck cargo can be selected for each loading condition for stability calculation.

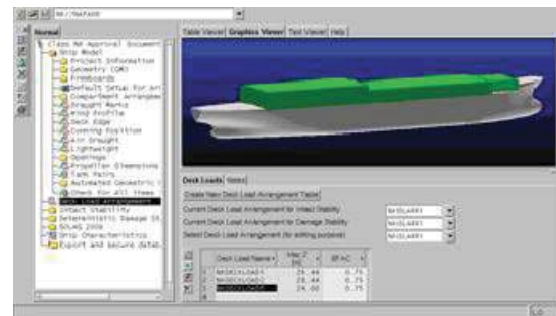


Figure 2 Input of Timber Deck Cargo

2.2 Damage Stability

The calculation results of Deterministic Damage Stability can be printed in a good and useful format easily. The permeability of the flooded compartments can be easily defined in



accordance with the convention rules, and the damage cases can be generated.

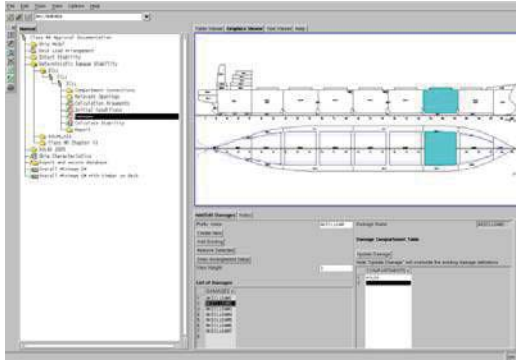


Figure 3 Input of ICLL Damage Case

2.3 2009 SOLAS Damage Stability

Probabilistic damage stability regulated in SOLAS II-1, Part B-1 and double bottom damage stability regulated in SOLAS II-1, Part B-2 can be calculated in accordance with the requirements. Zone damages can be created automatically based on the subdivision table defined by the user.

The buoyancy of timber deck cargo can be justifiably credited in damage stability calculations required by SOLAS II-1, when the integrity of the lashed timber deck cargo complies with the provisions of Chapters 3 and 4 of the CODE OF SAFE PRACTICE FOR SHIPS CARRYING TIMBER DECK CARGOES, 1991 (Resolution A.715(17)).

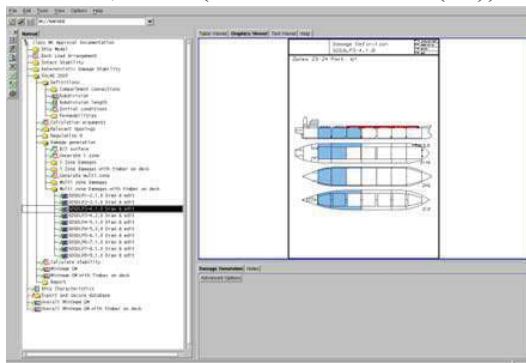


Figure 4 SOLAS 2009 multi-zone Damage

2.4 Creation of Grain Loading Booklet

Grain Heeling Moment can be calculated in accordance with International Grain Code by easy input. The output of calculation related Grain Loading Booklet for approval can be issued easily with a good and useful format in accordance with International Grain Code. In general, very short time will be available to make the Grain Loading Booklet loaded onboard, because those cannot be made without the result of inclining experiment or lightweight measurement and they should be prepared to comply with the convention rule before the ship's delivery. This tool will be useful to issue Grain Loading Booklet within a short period of time.

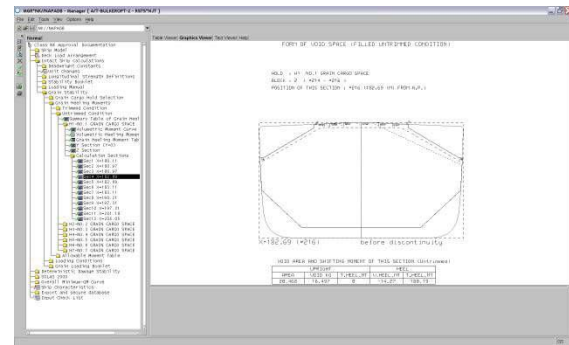


Figure 5 Creation of Grain Loading Booklet

2.5 Compliance Check of Statutory requirements

New loading conditions are often created by the owner's request before ship's delivery. However, the compliance of statutory requirements for these conditions are not checked at designed stage.

We created the function which is used for easy checking of the compliance of stability requirements for new loading conditions. After creating new loading conditions, the end-users can find the compliance of stability requirements visually.



Figure 6 Compliance check of intact stability

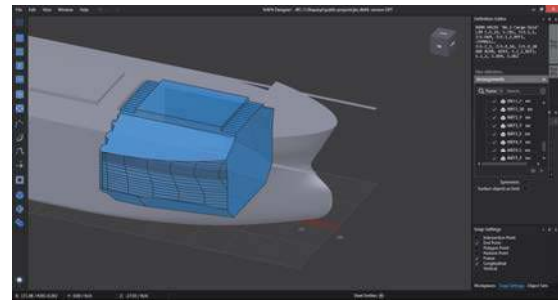


Figure 7 NAPA Designer offers intuitive tools for modelling

4. CONTINUOUS IMPROVEMENT OF THE CLASSIFICATION PROCESS

The further development of the application is aligned to making the classification process between the naval architect and the approving body as smooth as possible. Key elements in realizing these requirements are,

- Understanding the ship design process and the needs of the different stakeholders involved in the shipbuilding project
- Implementing new features through a market driven approach when designing the user experience to ensure that the tools provided fit the need of the user community as a whole
- Ensuring that the engineering methods comply with the existing domain of rules and modern computation models
- Serving naval architecture in practice

While the application today covers the needed regulatory domain, creation of the geometry model has so far been assumed to be pre-existing. With the exception of some domain specific modelling for objects such as down flooding openings, deck edges the product model is assumed to be existing prior to using the application. Current development is ongoing for making the creation of the geometry model easier and faster by creating a new workflow for the statutory compliance domain using the NAPA Designer.

The loading computer of the vessel is based on the same data as used in basic design of the vessel. Analogically to stability calculations for basic design, classification work is needed for the loading computer. Today, the loading computer is often created from scratch in the detail design stage of the vessel and is based on the final ('as built') calculations done at the delivery stage of the vessel. As the relevant information is already available in a standard format hosted by the product model of the vessel, the creation of the loading computer can be made significantly more efficient than it currently is using a single product model of the vessel.

The mission of both the cooperating companies is to provide excellent tools and services to the marine industry in the field of regulatory analysis of ships. The development of the tools and services is tightly connected with changing rules and new methodologies constantly developing in the IMO and in research globally, for example second generation intact stability criteria and amendments to the SOLAS Chapter II – 1 Subdivision and Damage Stability Regulation to name a few.

5. CONCLUSIONS

Ship design is getting into higher levels year by year while the design cycle is getting shorter and requirements such as statutory rules and design conditions are getting more complicated. In this circumstance, the



enhancement of efficiency of ship design and its approval have becoming more important.

ClassNK and NAPA group have developed “ClassNK Manager” based on the NAPA System. The application will support ship designers to carry out stability calculations based on NAPA 3D model in accordance with statutory rules.

“ClassNK Manager” is integrated into “Statutory Compliance Manager” in order to contribute to improve efficiency of ship design and to speed the classification approval process.

Authors expect that “Statutory Compliance Manager” will contribute to enhance the efficiency of stability calculation in accordance with the complicated statutory rules.

6. REFERENCES

- K. Mizutani, 2005, “Application of NAPA Manager to Ship Initial Design, Proceedings”, Conference Paper, ICCAS.
- N. Ueda and S. Takeda, 2007, “Integrated 3D Design Environment for Early Design Stage, Proceedings”, Conference Paper, ICCAS.
- T. Takamoto, 2010, “Development of 3D model based application for creating stability documents supporting statutory rules”, Conference Paper, INMARCO.
- M. Kidogawa, T. Takamoto, J. Furustam and T. Masui, 2011, “3D model based User-Friendly & Practical application for creating stability documents supporting statutory rules”, Conference Paper, ICCAS.

This page is intentionally left blank

KEYNOTE ADDRESS

Ship Stability, Dynamics and Safety: Status and Perspectives

Dr. Gabriele Bulian, University of Trieste

This page is intentionally left blank



Ship Stability, Dynamics and Safety: Status and Perspectives

Igor Bačkalov, *University of Belgrade, Serbia*, ibackalov@mas.bg.ac.rs

Gabriele Bulian, *University of Trieste, Italy*, gbulian@units.it

Jakub Cichowicz, *Brookes Bell LLP, Scotland (UK)*, jakub.cichowicz@brookesbell.com

Eleftheria Eliopoulou, *National Technical University of Athens, Greece*, eli@deslab.ntua.gr

Dimitris Konovessis, *Nanyang Technological University, Singapore*, dkonovessis@ntu.edu.sg

Jean-François Leguen, *DGA Hydrodynamics, France*, jean-francois.leguen@intradef.gouv.fr

Anders Rosén, *KTH Royal Institute of Technology, Sweden*, aro@kth.se

Nikolaos Themelis, *National Technical University of Athens, Greece*, nthemelis@naval.ntua.gr

ABSTRACT

With the aim of analysing the current status and possible future perspectives of research in the field of ship stability, dynamics and safety, this paper deals with an extensive review of the research work presented at the International Conferences on Stability of Ships and Ocean Vehicles (STAB Conferences) and the International Ship Stability Workshops (ISSW) held during the period 2009-2014. The reviewed material is organised in different sections, corresponding to a set of identified main typical focal macro-topics of research. On the basis of the reviewed material, consolidated research topics are highlighted together with emerging topics, and ideas for possible future research and its needs and focus are provided. Discussion is also provided regarding the link between research and educational aspects.

Keywords: *ship stability; ship dynamics; ship safety; STAB; ISSW; review*

1. INTRODUCTION

Ship stability is undoubtedly a subject of paramount importance in the field of Naval Architecture, its fundamentals having wider implications for the design and operation of ships and floating units. Moreover, “stability” is a concept which, in Naval Architecture, has a very wide meaning, embracing ship stability fundamentals with ship dynamics and ultimately ship safety. In this respect, research in the field has received considerable attention within the whole maritime community, resulting in the contemporary evolution of the

subject to the integrated notion of “ship stability, dynamics and safety” as it is being currently appreciated.

Although, due to its wide implications for the design, regulatory development and operation of ships, the subject receives attention in almost all the Naval Architecture scientific forums, the series of the International Conferences on Stability of Ships and Ocean Vehicles (STAB Conferences) and the International Ship Stability Workshops (ISSW) are certainly the venues where expertise and contemporary developments tend to be



collected and thoroughly debated. Therefore, a review of the status and perspectives of research and contemporary developments in “ship stability, dynamics and safety”, the subject of this paper, can certainly be considered as representative of the field when based on work presented in these series of international conferences and workshops. Following these considerations, herein a review has been carried out considering the series of the International Conferences on Stability of Ships and Ocean Vehicles (STAB Conferences) and the International Ship Stability Workshops (ISSW) organised during the period 2009-2014. This period was chosen since some of the contributions from earlier events have been reported in the “Contemporary Ideas on Ship Stability” series of two books [1.1, 1.11], in special issues of International Shipbuilding Progress [1.4, 1.9] and in some issues of Marine Technology [1.3, 1.5, 1.6]. It should be noted, however, that the work carried out in this review is to a very large extent exhaustive of the research included in the two STAB and four ISSW events covered in the review period (2009-2014), as compared to the selective earlier reporting, and this approach is in line with some reviews carried out in the past regarding single STAB events [1.2, 1.7, 1.8, 1.10]. For completeness of the review, some linked references presented elsewhere have also been included.

In order to provide an organised review, firstly, a set of main typical focal macro-topics of research related to the subject of ship stability, dynamics and safety have been identified. The paper has been organised in a series of sections corresponding to such topics, namely:

- Intact stability
- Damage stability
- Stability for specific types of vessels and floating objects (fishing vessels, naval vessels, inland vessels, other types of vessels and floating objects)
- Roll damping & anti-rolling devices, CFD for ship stability, and modelling of granular materials

- Ship stability in operation
- Modelling of environment

As a result, for each topic, a structured review is herein provided of the research carried out, organised in the appropriate sub-topics constituting the macro-topic covered in each section of the paper. The review is then followed by an elaboration of ideas for possible future research and its needs and focus.

Furthermore, the additional topic of “education” is also considered. In this context, some considerations are provided on aspects related to the transferring of present evolution of knowledge in the field of ship stability, dynamics and safety, to future Naval Architects during their university education.

2. INTACT STABILITY

Nonlinear ship dynamics in intact condition is one of the fundamental research topics when dealing with ship safety. Indeed, when comfort or operability are of concern, linear (or weakly nonlinear) approaches are typically sufficient. Instead, when the goal is to address the safety of the vessel in adverse weather conditions, large amplitude motions (particularly roll) are to be taken into account, with the consequent need of properly accounting for, and modelling of, (often strongly) nonlinear effects. In the past, nonlinear ship dynamics was often considered as an almost purely-research topic. However, with the increase of the computing capabilities and the advances of the research, this topic has transferred knowledge and tools also to the design and operation of vessels, as well as to the regulatory framework.

In the period of time considered in this review, an important topic has grown and has attracted attention, i.e. the IMO development of so-called “Second Generation Intact Stability Criteria (SGISC)”. In this framework, a specific set of failure modes associated with potentially dangerous dynamic stability phenomena in waves are considered, namely:



parametric roll, pure loss of stability, surf-riding and broaching and excessive accelerations. Such failure modes are strictly connected with nonlinear phenomena. As such, criteria aimed at guaranteeing sufficient safety with respect to these failure modes, need to embed the main features of the underlying nonlinear dynamics. Furthermore, the 3+1 tiers structure of SGISC allows accommodating methodologies at different levels of sophistication, from simple approaches up to the use of more complex nonlinear ship motions time domain tools. The development of SGISC has therefore represented a direct or indirect attractor for a significant amount of papers investigating the dynamics of the various failure modes and/or presenting possible methodologies for addressing such failure modes at design (or operational) stage.

With regard to SGISC, continuously updating overviews of development and general discussions have been provided over time [2.1, 2.2, 2.3, 2.23 2.62, 2.81, 2.85], showing the evolution of the framework. The more advanced status of development has been achieved, so far, with respect to Level 1 and Level 2 vulnerability criteria for the various failure modes. In this respect, in the observed time period, proposals have been put forward for addressing parametric roll [2.24, 2.37, 2.38], pure loss of stability [2.24], surf riding and broaching [2.25, 2.37], dead-ship condition [2.38], and excessive accelerations [2.40]. Also, test applications, sample calculations and consistency checks of the available Level 1&2 proposals have been presented [2.84, 2.101]. Some specific experiments have also been carried out to validate the mathematical models proposed for being implemented in Level 1 and Level 2 criteria [2.39, 2.59, 2.94], and importance was also given to a designers-oriented clarification of the underlying dynamics of surf-riding [2.92]. A more specific attention is yet to be given to the topic of regulatory application of direct stability assessment and associated development of operational guidance, although the interest is growing over time. A specific general

discussion on tools and methodologies for regulatory direct stability assessment was presented in [2.64], while a discussion on the development of appropriate ship-specific operational guidance for increasing ship safety was given in [2.26]. Direct assessment procedures for surf-riding and broaching assessment have been proposed in [2.25].

In parallel to the implementation of concepts and methods from nonlinear dynamics into design through SGISC, research has of course progressed on fundamental aspects of nonlinear ship motions. In the following, an attempt is made to report the identified contributions by dividing them according to failure modes considered by SGISC. However, this sharp separation, although pragmatic, is clearly an oversimplified scheme for categorizing stability-related research in the field on nonlinear dynamics in intact condition. A number of contributions indeed span among different failure modes, or touches diverse topics. Therefore, other subjects will also be considered in the following.

The first nonlinear phenomenon to be addressed is surely parametric roll. Indeed, among various potentially dangerous dynamic stability phenomena in waves, parametric roll has clearly gathered the majority of the attention. Specific benchmark studies have been organised in order to assess the prediction capabilities of existing simulations tools [2.18, 2.47]. An evolution in addressing the phenomenon could clearly be noticed. Indeed, while in the past parametric roll was mostly studied by means of 1-DOF uncoupled roll models, more recent research has clearly shifted towards the use of more advanced mathematical models, where more degrees of freedom are taken into account, at different levels of sophistication. The 1-DOF modelling, with roll restoring variations calculated assuming quasi-static heave and pitch, can nowadays be considered as a consolidated tool for sufficiently simple applications at the (early) design stage. Such model has also been



used, explicitly or implicitly, in developing parametric roll Level 1 & Level 2 vulnerability criteria in the framework of SGISC. For more advanced applications, models with more DOFs have been developed and used, i.e. 3-DOF [2.10, 2.12, 2.35, 2.66, 2.67, 2.97], 4-DOF [2.12], 6-DOF [2.11, 2.50, 2.67, 2.72]. With the increase in the complexity of the simulation tools, also the computational effort tends to increase. In view of this, simple indications for identifying potentially dangerous conditions of speed/heading have been presented in [2.11], with the intention of providing means for reducing the computational efforts in determining the inception and amplitude of parametric roll. Regarding the convergence of modelling techniques, it is to be noted that still there exists a significant variety of modelling when more than 1-DOF is considered: single time scale vs double (slow-manoeuving and fast-seakeeping) time scale, consideration of memory effects or constant hydrodynamic coefficients, modelling details of damping, modelling of manoeuvring forces, etc. From the point of view of the peculiar nonlinear characteristics of parametric rolling, detailed studies have been carried out in some cases. The extent and shape of instability regions in regular waves, as well as the amplitude of roll within the instability regions was numerically studied in [2.10] through time domain simulations of a 3-DOF model, while a semi-analytical approach based on direct application of Floquet theory was used in [2.16] for the identification of instability regions in longitudinal regular waves. Results from such studies also relate with the observation that parametric roll can have a non-monotonic relation between amplitude of forcing and amplitude of roll motion [2.15, 2.51]. Although the majority of studies regarding parametric roll have dealt with conventional vessels, some studies have also been presented for unconventional hull forms, such as trimarans [2.13, 2.16]. Some attention has also been given to roll reduction means, intended to mitigate parametrically excited roll, such as passive anti-rolling tanks [2.34, 2.77] and

active rudder stabilization [2.67, 2.90]. In the context of parametric roll, it is also worth mentioning the book in [2.82], where different authors have dealt with some of the mentioned topics, and also with other aspects of parametric roll resonance.

Studies on the dynamics of loss of stability have, instead, been more limited in number. In [2.36] a probabilistic approach was presented for dealing with pure loss of stability in irregular longitudinal waves. Comparisons between experimental results and numerical simulations have been instead reported in [2.39, 2.94].

In parallel to the already mentioned contributions regarding the development of SGISC, additional fundamental research studies have also been carried out with respect to surf-riding and broaching. In [2.5], a 6-DOF blended code (LAMP) was used to study the ship behaviour in following/quartering waves and an approach based on continuation analysis was also implemented which allows tracing equilibria and periodic motions. With the same goal, a continuation analysis approach was also used in [2.75]. A detailed investigation of yaw motion and low-speed-broaching in following/quartering waves was instead presented in [2.9], where rudder control was used in order to reduce undesired yaw motions. In [2.76] an approach based on an extended Melnikov method was presented for improving the semi-analytical determination of the (second) surf-riding threshold. While most of the studies are based on regular waves, research progressed also on two open points: the issue of providing a proper definition of surf-riding in case of irregular waves and the problem of providing proper tools for the identification of surf-riding occurrence from simulated time series. To this end, ideas and proposals have been provided in [2.39, 2.74, 2.91, 2.102].

Fundamental aspects of nonlinear roll dynamics in beam waves have also been subject of specific investigation, also in this



case in parallel to the already mentioned contributions specifically targeting SGISC. In [2.68] the inception of sub-harmonic roll motion was studied experimentally and also numerically with 1-DOF and 6-DOF models in the particular cases of bi-chromatic waves. Sub-harmonic motions in irregular beam waves have been experimentally observed and numerically simulated in [2.89]. In [2.73] the Melnikov method was used for determining the critical wave forcing leading to capsize using a 1-DOF approach, while in [2.41] the extended Melnikov method was used for the same purpose considering a 3-DOF mathematical model. An interesting and uncommon set of experiments and comparison with numerical simulations (1-DOF and 4-DOF) of roll motion in irregular beam waves and fluctuating wind have been carried out and reported in [2.59]. In [2.4] the beam sea condition was instead addressed from a more regulatory perspective, by proposing a procedure combining model tests and numerical simulations for the determination of a Weather Criterion GM limit curve.

A notable amount of research efforts was also observed regarding the development, tuning and use of blended codes for the simulation of large amplitude ship motions and manoeuvring in waves. Herein, the wording blended (or hybrid) codes is intended to identify advanced systems-based tools having the necessary characteristics for efficient time domain simulation of nonlinear large amplitude ship motions in waves. Due to the high level of semi-empiricism which is present in such codes, a variety of blended codes exist, in a variety of different “flavours”. However, in general, blended codes are typically embedding (or at least are expected to embed) nonlinear rigid body dynamics, Froude-Krylov pressure calculation on the instantaneous wetted surface of the hull, radiation and diffraction effects based on linear (or partially nonlinear) hydrodynamics, and, when necessary, appropriate models for manoeuvring forces, steering means, propulsors, mooring lines, wind effects, etc. Such codes can also be

considered, in most cases, as suitable tools for direct stability assessment in the framework of SGISC. In this respect, some general considerations have been provided in [2.70] regarding the characteristics of codes intended to be used for direct stability assessment in the framework of SGISC. In [2.86] an approximate technique was presented for speeding up the calculation of Froude-Krylov forces in blended codes. In [2.17] a blended 6-DOF code for the simulation of ship motions and manoeuvring in waves was presented, designed to determine, in addition to ship motions, also instantaneous loads on the vessel, and discussion was provided regarding the difficulties involved in creating a consistent and still numerically efficient model. A methodology was presented in [2.32] for improving the capabilities of the 6-DOF blended code FREDYN of taking into account water on deck by improving the estimation of the free surface elevation around the vessel. In [2.33] the main theoretical aspects at the basis of the development of the 6-DOF blended code TEMPEST have been described, and some comparison between numerically computed and experimentally measured forces have been reported. A detailed description of the modelling of hull lift and cross flow drag forces used in TEMPEST, together with some sample calculations, has been presented in [2.54]. The blended code NLOAD3D was used in [2.69] and an interesting conceptual link with EEDI related issues has been provided together with a series of useful information regarding the process of software tuning. In [2.71] simulations in following quartering long crested irregular waves were carried out using the blended code LAIDYN in conditions characterised by strong narrowing of the spectrum due to Doppler effect, leading to large rolling, and simulations in following quartering waves were also carried out in [2.100] using a two-time-scales mathematical model. In [2.14] the blended code NLOAD3D was used for the simulation of parametrically excited rolling motion in irregular sea, and a methodology, based on the use of coherence function, has been proposed for trying to discriminate between



parametrically excited roll and 1:1 direct roll resonance on the basis of the analysis of time histories from numerical simulation. Such methodology has later been used also in [2.52]. Other examples of use of blended 6-DOF codes can be found in, e.g.: [2.12] (NMRIW, phenomenon: parametric roll), [2.5] (LAMP, phenomenon: surf-riding & broaching), [2.68] (SHIXDOF, phenomenon: nonlinear roll in beam sea), [2.79] (phenomena: parametric roll, surf-riding and broaching).

With the increased possibility of using advanced nonlinear ship motions simulation tools for the assessment of safety in intact condition, and with the foreseeable possibility that such tool can be used within the approval process (e.g. through Direct Assessment in SGISC, or through SOLAS provisions for alternative design) or for defining ship-specific operational guidance, the issue of a proper validation has become of significant practical importance. However, the validation process (or actually, the verification, validation and accreditation process) of such complex, usually modular and partially semi-empirical, tools is not a straightforward task. This is especially true when considering strongly nonlinear behaviours (coexisting solutions, strong dependence on initial conditions, possibility of chaotic motions, etc.) and/or nonlinear motions in irregular waves (convergence of statistical estimates, non-Gaussian distributions, etc.). Proposal of general procedures and/or frameworks for the validation of modular codes for the purpose of large amplitude ship motions simulation have been described in [2.7, 2.42], while attention to metrics and acceptance criteria was given in [2.63, 2.65, 2.93]. Connected with the process of validation, is also the problem of uncertainty assessment/propagation in experiments and simulations, and of sensitivity analysis. Such topics have, unfortunately, received limited attention in the field of nonlinear ship dynamics. In this context, an uncertainty propagation study in case of simplified mathematical models for parametric roll was carried out in [2.53] and a sensitivity analysis

was carried out in [2.35] with respect to damping coefficient in a 3-DOF nonlinear mathematical model for parametric roll prediction.

In addition to the above, other specific topics related with nonlinear ship dynamics in intact condition have been addressed by a more limited number of contributions. Measurement and modelling of forces due to deck in water was the subject of the study in [2.6]. The use of artificial neural networks, as physics-free adaptable models, has received some attention as a tool for the very short term prediction of motions [2.78] and for parameter identification in physics-based mathematical models [2.8]. A database of experimental results from (semi-)captive model tests carried out on a fishing vessel in following waves has been described in [2.96], with the intention of providing reference data for the tuning of blended 6-DOF codes. Experimental equipment and techniques for ship motions tests in following waves, targeting specifically the case of small models were described in [2.95]. In [2.87], the problem of yaw instability of a turret moored FSRU in waves was addressed experimentally and numerically.

Ship intact stability has been well studied within a deterministic context, due to the nonlinear character that spans the extreme ship motions, especially the rolling motion, which could jeopardize ship safety. Nevertheless, the weather environment a ship operates is actually a random field. At the same time uncertainty covers other operational parameters. Therefore, a issue that stability researchers had to consider was the incorporation of random sea and wind in the nonlinear ship motion problem, something that it is not straightforward due to the nonlinear relation between excitation and response. Moreover, the next step was the integration of the associated hazards into a risk-based framework. Studies related to the abovementioned context are reviewed in the following.



Using numerical simulations to predict extreme events is often a popular choice to directly attack to the problem, however there are some issues related with the statistical treatment of the results, the, hopefully, rare character of capsize events and the respective validation of the models and methods of prediction. In [2.29] the “Envelope Peaks over Threshold” (EPOT) was used, comprised by a statistical extrapolation, allowing explicit account of influence of nonlinearity of GZ curve on roll distribution. From a similar viewpoint in [2.56] the EPOT method was used, combined with the FREDYN code, in order to produce the targeted Generalised Pareto Distribution. The authors suggest that the EPOT method requires the least number of simulations for reliable results of a rare event. A discussion on the EPOT method can also be found in [2.80]. Moreover direct counting and Poisson distribution fitting techniques have been examined in [2.43]. In this context, dangerous wave conditions that produce rare events through hydrodynamic simulations were defined. In addition, direct counting was used in [2.91] for the statistical analysis of surf-riding realisations observed as high-runs. A high-run was defined as the time segment in which ship’s speed is maintained higher than her expected one, and mean time durations of high-runs were calculated. An approach to generate the distribution of extreme values of parametric roll was presented in [2.44], by using a Design Load Generator (DLG), a process to approximate the extreme value distribution of a Gaussian random variable. Moreover, in [2.48] several alternatives were examined for the modelling the distribution of parametric roll including a Gram-Charlier series, the Pearson type IV distribution, and an approximation based on a moving average. It is also worth mentioning that probabilistic methods for the assessment of parametric rolling can also be found in some of the contributions in [2.82].

As mentioned before, the problem of rarity represents a challenge to be addressed. One possible method to deal with it is the statistical

extrapolation. In such method one aims to use data where the targeted event (e.g. a specified, large, roll amplitude) has not occurred and then appropriately extrapolate the data for carrying out predicting regarding the target event. In [2.99], features of the modelling of the tail of the distribution of peaks as a Generalized Pareto Distribution (GPD), which can be derived from the Generalized Extreme Value distribution, have been examined. The key issue of this method is the appropriate selection of the threshold limit. Moreover, in [2.98] a multi-tier validation study for the statistical extrapolation method based on the Generalised Pareto Distribution was presented. The comparison was carried out considering the “true” values derived from numerical simulations by a direct counting method. The determination of confidence intervals for estimates of mean and variance from a time series, taking into account the correlation structure of the process, was examined in [2.88], with particular emphasis on simulations of roll motion. Another approach to the rarity issue of capsize is the so-called split time method [2.80]. For example, in [2.45] the split-time method for the evaluation of the time-dependent probability of broaching-to has been implemented, describing the development of a simple model of nonlinear surging and surf-riding response in following irregular seas. Furthermore, in [2.83], the split-time method has been utilised for the evaluation of the probability of capsizing for the case of variation of righting arm in waves, as in case of pure loss of stability. The threshold in roll angle was fixed and then the critical roll rate at the instant of up-crossing was calculated. On the other hand, the problem of nonlinearity has been attempted to be treated by the piece-wise method. In [2.19], capsizing has been considered as a sequence of two random events, up-crossing through a certain threshold and capsizing after up-crossing. A critical roll rate was introduced as a stochastic process defined at any instant of time. From a similar viewpoint, in [2.20], the capsizing probability of a Ro-Pax in dead-ship condition has been calculated by using the piece-wise linear



approach, and the correlation between winds and waves on the capsizing probability has been examined.

The concept of wave groups has been also utilised as they can constitute the critical wave episodes for the assessment of dynamic stability. In [2.22] experiments were described which have been performed in a model basin to generate groups of large-amplitude waves in irregular seas. Generation of asymmetric wave groups is the first step in the development of an experimental test technique that ensures a model will be exposed to multiple realistic extreme wave events. Furthermore, in [2.27], a method using wave groups to evaluate ship response in heavy seas was presented. Wave groups critical to ship response were defined, separating the complexity of the nonlinear dynamics of ship response from the complexities of a probabilistic description for the response. Finally, in [2.57] a comparison of two different methodologies for the calculation of exceedance rates utilising the same seakeeping code for the modelling of ship motion was presented. The first method refers to the critical wave groups approach and the second to direct Monte Carlo simulations. A discussion on the method of critical wave groups can also be found in [2.80].

Using stochastic differential equations represents another approach for the probabilistic treatment of nonlinear rolling motion. However closed-form solutions cannot always be derived in manageable form. In [2.21], new equations were derived governing the joint, response-excitation, pdf of roll motion, roll velocity and excitation, without any simplifying assumptions concerning the correlation and probabilistic structure of the excitation. Furthermore, in [2.61], the probabilistic characteristics of the long-time steady-state response of a half oscillator, subject to a coloured, asymptotically stationary, Gaussian or non-Gaussian (cubic Gaussian) excitation, are derived by means of the Response-Excitation theory. On the other hand, in [2.46], Gaussian and non-Gaussian

response of nonlinear ship rolling in random beam waves has been studied by moment equations. An automatic neglect tool was developed to handle the complex and untraceable higher order cumulant neglect method and capture the non-Gaussian effect of the nonlinear rolling phenomena. The developed tool was also used in [2.58], where dynamical systems forced by filtered Gaussian coloured noise were studied using Gaussian and non-Gaussian cumulant neglect methods, and, numerically, using the path integral method.

Finally, as mentioned previously, risk-based frameworks for the assessment of intact stability have been developed. For example, in [2.28], inland container vessel rolling due to the influence of beam gusting winds was investigated, and a critical analysis was given of the requirements of the European Directive for Technical Requirements for Inland Waterway Vessels. In [2.60], an overview and a critical analysis of the regulations for river-sea ships were given, and some of the existing regulations were evaluated from the probabilistic point of view. Moreover, in [2.30] a discussion was provided on the tolerable risk associated with the loss of a naval vessel due to the weather conditions. A review of tolerable risk and potential methodologies for calculating an annual probability of loss of the vessel using time domain simulations and statistics of observed weather conditions aboard naval ships was also presented. On the other hand, in [2.31], different intact dynamic stability methodologies that can be employed to naval ship design addressing dynamic stability in such a way as to minimize technical and safety risks in an economical manner have been discussed. Finally, in [2.55], a proper risk analysis and management framework was presented that can be brought into the process of stability control of naval ships by quantifying uncertainties, identifying and calculating consequences, and by developing status metrics that are based on risk-based calculations.



Based on the observed status, some directions could be suggested for future research. In case of research in the field of SGISC, two topics are likely to become of significant importance and require further research: direct stability assessment on one side, and associated development of ship-specific operational guidance on the other side. These two topics require development: of appropriate mathematical models, of verification, validation and accreditation procedures, and of appropriate application guidance. So far, most of the available experience regarding ship dynamics is based on the use of linear seakeeping tools, which are however not typically intended for being used in a regulatory framework. Bringing nonlinear time domain simulations of ship motions into the regulatory framework is going to be a challenging activity. With respect to parametric roll, nowadays it seems that the fundamental aspects of such phenomenon in regular longitudinal waves are quite well established. However, research is still needed in following/bow quartering waves and in irregular waves. In case of parametric roll in irregular waves, research is still necessary on more accurate estimations of the inception threshold, and on how to effectively model and handle the strong non-Gaussianity of the motion. In case of loss of stability in following waves, not much research efforts have been noticed in the analysed period. However, research would be useful regarding loss of stability in following waves, particularly in terms of characterization of roll motion in irregular sea. In case of surf-riding and broaching, two main topics could benefit from further research, namely: control/mitigation of the phenomenon, and description/definition of the phenomenon in irregular sea. In case of roll dynamics in dead-ship condition, it seems that a lack of information is present regarding the vessel behaviour in non-beam waves, since the beam-sea case is often considered as a reference condition for experiments and simulations. As a result, additional research on the topic of nonlinear rolling in quartering waves (where direct excitation and parametric

excitation combine) would be useful. For all these phenomena, and, in addition, for the increasingly important topic of assessment of ship motions and manoeuvring in adverse weather conditions, blended 6-DOF codes will likely show their usefulness. However, for a proper application of such tools, it would be useful to more thoroughly investigate uncertainty and error propagation, and to perform sensitivity analyses. Indeed, estimation of confidence on predictions, and identification of the most sensible parameters could help in identifying those blocks of the experimental/simulation chain where efforts are to be put to reduce uncertainty. In this respect, it is expectable that, roll damping modelling will play a key role. These aspects seem to have been given limited attention so far. Regarding the modelling of environment, in practice, most of the reviewed research has been carried out considering either regular waves or irregular long crested waves. Short crested irregular waves have been very seldom considered. This is understandable in case of experiments, due to intrinsic limitations of most facilities. However, this also reflects in most of the presented numerical investigations, since they are often compared with experimental data. As a result, information associated with short crested waves is rarely available. Also, detailed information associated with nonlinear ship motions in sea states characterised by non-idealised, more realistic sea spectra are largely missing. It is therefore useful that additional research efforts are put in the experimental and numerical assessment of nonlinear ship motions in more realistic sea conditions. This also means improving, when necessary, the modelling of wind actions, in addition to the modelling of action of waves. With reference to probabilistic approaches in intact stability, possible forthcoming studies could be envisioned. For example, one concerns the incorporation of CFD models into probabilistic methods and how the massive incurred computational cost could be appropriately decreased. Thus, the utilisation of critical realistic wave groups could be introduced in such assessments. On the other



hand, the work related with statistical extrapolation could pave the way in order to properly minimise the required data for the prediction of rare events within reasonable confidence intervals, keeping in mind that these models should appropriately reproduce the governing physics of the targeted problem. Furthermore, stochastic differential mathematical models that capture the nonlinear behaviour of rolling motions is also another worthwhile direction, however it should be reminded that up to now only primitive models of rolling motion have been used, thus questioning the practicality of this approach when advanced models are needed. Finally, one of the goals of the research in the field of nonlinear ship dynamics should always be to better understand the complex phenomena associated with the motions of a vessel at sea. However, in addition to this, one of the goals should also be to eventually transfer knowledge and tools from the level of research to the level of application (design/operation). According to the observed status of research and development, this goal is definitely achievable.

3. DAMAGE STABILITY

The subject of damage stability has arguably been in the forefront of developments relating to stability and safety research for the period of the last 30 years, with concerted large-scale initiatives taking place involving the research community, regulatory authorities and industry. During the review period considered in this paper research on damage stability has evolved in a number of diverse but interrelated directions, including direct simulations of motions in the damaged condition, research on the prediction of ship behaviour following progressive flooding and on experimental techniques, development of rules and regulations, probabilistic and risk-based methods and frameworks, integration of damage stability into ship design, research on safe return to port as well as on the importance of active operational measures for damage

mitigation and containment, and last but not least, accident investigations.

A number of studies for validation of codes for the direct simulation of ship motions in the damaged condition, including in most cases experimental validation, were carried out during the review period.

Numerical simulations and benchmarking against data from physical experiments of a generic RoPax ship have been performed, investigating how parametric variations can lead to establishing of survival limits outside which capsizing will not occur or certainly occur and addressing ship's survival as a time-independent problem, [3.16]. In order to validate a dynamical model accounting for coupling in ship motions and floodwater dynamics (coupling of flooding module with MARIN's software FREDYN), model tests were carried out on a generic destroyer model (1:40) with floodable internal compartments, [3.19]. The study reported in [3.20] focused on the validation of results of numerical simulations using the software tool (Shipsurv) which calculates motions, internal loads and survivability of damaged naval ships in seaways. Validation results for flooding case of a barge and cross-flooding case of a RoPax ship as reported during ITTC benchmark study were also presented. Numerical and scale model tests of a damaged cruise vessel were presented in [3.21]. Simulations and model tests were performed in calm seas and in regular and irregular waves whereas experiments were conducted at MOERI's ocean engineering basin. The numerical studies were performed with use of a quasi-dynamic CFD code. In [3.22] an application of the DoE (Design of Experiments) methodology in building a model for transient flooding was presented, which was tested through physical experiments on a model of damaged ship section (PRR02) subjected to 6-DOF forced oscillations. In [3.29] a methodology for coupling of a seakeeping solver (PROTEUS3) with a volume-of-fluid (VOF) solver was presented in assessing the behaviour of a



damaged ship in waves. Flooding and internal water dynamics was simulated by the VOF solver, while the seakeeping solver addressed the external fluid-structure interaction. Numerical simulations were then compared with experiments (originating from ITTC tests) in case of a Ro-Ro ferry in regular beam waves. The presence of floodwater onboard a vessel was simulated within the LAIDYN software using the lump-mass method [3.30]. The time varying mass of floodwater was pre-calculated through the NAPA Flooding Simulation tool in calm water. An example application for a passenger vessel was considered in the simulations carried out in calm water and in irregular waves. In [3.36] an investigation on the time to capsize for a RoPax vessel (M.S. Estonia) using both physical model experiments and computer based time domain simulations was presented. The computer model also included a two-dimensional multi-model sloshing model, composed by a non-linear near-resonance pendulum model and an acceleration ratio model at non-resonance used for calculating the transverse centre of gravity of ingresses water in the damaged compartment and on car deck. In [3.37] a study on the evaluation of the performance of cross-flooding arrangements using Computational Fluid Dynamics (CFD) was reported. Computations for a simple arrangement including scaling effects were first carried out with model experiments performed for the validation of the computational results. Comparisons with the factors evaluated by the IMO simplified regression formulae were carried out. Computations for a complex arrangement was also carried out and compared with results from existing studies. A flooding extent prediction decision-support method including the intermediate phases of flooding was presented in [3.38]. The simplified, but reasonably accurate, algorithm was evaluated on the basis of test cases featuring comparisons to experimental data and time accurate flooding simulation results. In [3.39] simulation results addressing the probability to capsize and the flooding of ships in collision damages were presented. The results were discussed in the

context of the IMO regulatory concept for orderly abandonment for damaged passenger ships (in addition to the safe return to port regulatory provisions). Timely identification of the damage and the enhancement of survivability requirements were suggested as rational measures for improved survivability and safety of people onboard passenger ships. In [3.40] a numerical model for progressive flooding simulation was presented. The model utilises a direct approach in which the flow between the compartments is computed based on the Bernoulli equation and the current pressure heads at each intermediate step. The implemented approach makes use of graph theory in modelling the flooding paths. The developed method was validated by investigating the accident of the S.S. Heraklion occurred in 1966 and the results of the simulation method were compared with model tests of a barge performed at the Helsinki University of Technology in 2006. In [3.41] a CFD study for the flooding process of a fully constrained damaged compartment was presented, which was then extended to the flooding scenario of a damaged cruiser in calm water with 6-DOF motions. In [3.59], the Stability in Waves Committee of the 27th ITTC reported their investigation on how to deal with the ship inertia contributions due to floodwater mass from three points of view: (1) floodwater domain, (2) floodwater inertia itself, (3) floodwater entering the ship. The Committee suggested three criteria for accounting on floodwater dynamics in damage stability.

In many cases, progressive flooding is the determinant factor of ship capsizing or sinking. A number of investigations and research initiatives were reported on the subject of progressive flooding, including verification through experiments. In [3.5], the application of the pressure-correction technique for analysis of progressive flooding in a damaged large passenger ship was studied through a case study focusing on the efficient convergence of the pressure-correction iterations. In addition, a simple method for estimation of increased



flooding due to waves and implementation of pumping and closing of open doors into the pressure-correction equation were discussed. A numerical method capable of describing the progressive flooding of ships, accounting for complex subdivision arrangements, was presented in [3.6]. Numerical results were shown for the progressive flooding of the ITTC box-shaped barge. Comparison was made with experimental results aiming at validating the numerical simulation method and conclusions are drawn. In [3.7] the flooding phenomena with emphasis on transient and progressive flooding stages of damaged Ro-Ro ships were analysed and recommendations were proposed for an alternative assessment of the flooding process.

Research has also been reported on the use of experimental data for damage stability and survivability performance verification. A direct link of the s-factor with the time to capsize was discussed in [3.4] showing how to utilise experimental data from 30-minute test runs for the s-factor based on longer duration of tests. In [3.11] a series of experiments performed in calm water and in waves in order to study the motions and flooding process of a damaged cruise vessel were reported. The in-waves effects of inflow and outflow through opening and internal water motion were investigated in [3.12]. In [3.59] the work carried out by “The Stability in Waves” Committee of the 27th ITTC was presented, concerning the investigation of the significance of scale effects related to air pressure on flooding model tests under atmospheric conditions. Particular attention was given to effects associated with trapped air. The results were employed to update ITTC model test procedure for damage stability experiments.

Research on probabilistic and risk-based methods for the development of rules and regulations, and comparisons between different regulatory provisions has received great attention during the review period. A review and historical background of damage stability regulations with respect to Ro-Ro passenger

ships was presented in [3.14]. Some vulnerabilities of the probabilistic framework based on HARDER EU-funded project were highlighted in terms of specific modes of flooding and modes of loss typical to RoPax ships (low residual freeboard, flooding to car deck and presence of long-lower holds). The EU-funded project GOALDS was presented in [3.15] which is considered as the next step forward following HARDER project. Inconsistencies in predicting survivability of large and small passenger vessels, issues related to accumulation of water on deck (RoPax) and omission of grounding in the probabilistic framework were pointed out in this particular research work. In [3.24] issues related to evaluating probability of collision and subsequent hull breach leading to flooding of internal spaces of the ship were addressed. From this perspective, discussion focused on aspects of models used in evaluating risk from ship to ship collision. A comparison on the survivability assessment between SOLAS’s s-factor and Static Equivalent Method (SEM) was presented in [3.17] by two case studies of a RoPax ship *Polonia* and a box-shaped barge, identifying large discrepancies between SOLAS and SEM. In [3.18], middle-sized RoPax vessels were considered and comparisons were carried out regarding the level of safety achieved by SOLAS 2009 compliant vessels and ships compliant with SOLAS 90+SA (Stockholm Agreement). To this end limiting GM curves were compared. Limiting GM was also sought by means of model test. In [3.23] concepts related to capsize band were addressed and simple regression models were presented allowing for linking probability of capsize with sea state. In [3.25], a probabilistic model was presented for grounding damage characteristics (separately for full, non-full and all vessels) based on an updated accidents database proposed by the EU-funded GOALDS project. Also, an analysis was reported regarding the probability of breaching double bottom shells designed in marginal compliance with SOLAS Reg. 9 requirements. In [3.26] the importance of wave statistics in the survivability assessment



through “s-factor” within SOLAS2009 was assessed. The concept of “critical significant wave height” was discussed with particular attention to its dispersion for a given set of residual stability parameters as well as the importance of considering the “operational wave profile” of the vessel for obtaining more appropriate measures of survivability. The IMO work on SOLAS2009 requirements in the context of RoPax vessels was analysed in [3.27]. Open issues in SOLAS2009 regarding the accounting for water on deck were reported. The need for specific requirements for RoPax vessels, which could be vulnerable to fast capsize in case of water accumulated on large undivided spaces was also discussed there. A historical overview regarding SOLAS regulations associated with watertight doors and discussed whether this regulatory treatment is still appropriate for passenger ships of the future was provided in [3.28].

Research on the development of probabilistic and risk-based methods for new regulatory and design frameworks extending the capabilities of current provisions was also a focal area during the review period. In [3.31], the sequence of ship collision, flooding and loss of stability within given time has been investigated on the basis of an interdisciplinary calculation procedure. The method looked at the interaction between structural and damage stability computations and has been used to study the significance of various parameters, such as significant wave height and size of damage. A direct comparison of probabilistic and deterministic regulatory frameworks for damage stability on a selection of Ro-Ro passenger vessels of various sizes has been undertaken in [3.32]. Both numerical and analytical performance-based assessment methods were utilised, highlighting inherent inconsistency in each framework. The study constituted an attempt to present state-of-the-art methodology for damage stability assessment appropriate even for non-standard designs. In [3.34], the development of an alternative formulation for the assessment of the survivability of a damaged ship in waves

was presented. The authors discussed briefly concerns related to the current survivability model and present the process of development that led to the re-engineered formulation. The proposed formula based on simple and rational model accounted well for size of the ship and floodwater dynamics. In [3.35], established numerical methods for the measurement of performance-based survivability have been utilized and used as benchmark against available analytical methods in an attempt to define a rational requirement for the level of survivability. Survivability analysis results on representative cruise and Ro-Pax ships were related to design and operational parameters with a view to define and quantify the relationships between damage survivability characteristics following a collision and time available for evacuation with potential outcomes in terms of people potentially at risk. In [3.42], a new methodology for probabilistic bottom damage stability requirements following grounding has been developed, which takes into account also the probability of safe beaching. The analysis of the probability of safe beaching was based on historical data (indicating about 80%) and a specifically developed methodology, also indicating large values. An alternative formulation for the probability of a compartment flooding following grounding (the p factor) based on the GOALDS database on grounding damage was proposed in [3.43]. To this end, original GOALDS formulations for the probability density functions of damage characteristics, which employed rational functions, were substituted by alternative ones based on exponential or triangular distributions, and this made it possible to arrive at a closed form for the p factor. In [3.47] the results of a study about the influence of the longitudinal subdivision in the lower cargo hold of a Ro-Pax vessel on the attained subdivision index calculated according to MSC.216(82) were presented.

Developments on the use, implications and application of probabilistic and risk-based frameworks for design and operational



purposes also received attention. A way forward for establishing a stronger foundation to safety assurance in the maritime sector and for future developments on the subject of damage stability of passenger ships was proposed in [3.48]. In [3.49], the implications of the GOALDS revision of the regulatory requirements for the damage stability of passenger ships upon ship design were investigated. In particular, the study addressed impact of differences between the SOLAS 2009 and GOALDS formulations of the s -factor. In [3.52], the impact of the SOLAS 2009 formulation on the design and operational characteristics of ROPAX vessels was investigated. An in-depth review of the adopted formulation were analysed and applied within a multi-objective optimisation procedure developed and tested on RoPax ships. The practical design implications of SOLAS 2009 were discussed from a shipyard perspective in [3.54], where attention was given to the problem of rules' interpretation on the attained A-indices and the consequent perception of the safety level, and attention was also given to the importance of a true safety culture during the design phase. In [3.62] a historical overview of regulatory framework from HARDER project up to SOLAS 2009 was given. The research work proposed a re-assessment of existing large passenger vessels, with retrospective application for vessels with attained index A significantly lower than the required index R. Furthermore, some interesting considerations were provided regarding the impact of the new regulations on the safety level of certain types of vessels. The safety level of pre-SOLAS90 and SOLAS90 vessels was examined in [3.60]. In this study, SOLAS2009 vessels were assumed to have the same safety level with vessels complying with the deterministic SOLAS90 standards. The study focussed on Cruise ships and RoPax vessels of 1,000GT and above. Casualties and associated data regarding fatalities were extracted from IHSF database. Potential Loss of Life (PLL) values were calculated for both categories. F-N curves were also determined and assessed against the ALARP region.

A final area of developments of probabilistic and risk-based methods can be found in the development and testing of contemporary approaches for advanced tools for risk-based assessment. A systematic approach in constructing risk models using Bayesian Networks was presented in [3.3]. An approach also based on Bayes Networks was presented in [3.53], where a risk model for assessing risk associated with the occurrence of a collision accident was described. In [3.33] a data mining framework for ship safety management was presented. The approach utilised Bayesian Networks as a risk modelling technique, and provides means for systematic extraction of information stored in available data. Particular emphasis was placed on the integration of aspects of damage stability into such a framework for an overall management of ship lifecycle safety. The Goal Based Design, as an alternative to Risk-Based Design, was discussed in [3.9]. A case study was presented in order to demonstrate integration and advantages of Goal Based Design within the design process. In [3.10] the SAFEDOR design platform, a stand-alone multi-disciplinary design tool, was presented. In addition to the feature of regular optimisation platforms, the tool brought in an innovative functionality allowing for capturing the dynamics of the design process. As a result, incremental improvements through design optimisation became a secondary purpose of the platform, while the primary one was design from scratch towards trade-offs and cost-effective concepts. Experimental tests and numerical studies, carried out in relation to the progress of flooding, were described in [3.51] in the framework of FLOODSTAND project. A new approach to flooding simulation for onboard use has been developed. The authors discussed application of stochastic modelling to ship capsizes and uncertainties related to the "time-to-capsize" have been analysed. In [3.55] a benchmarking study addressing survivability assessment of a small RoPax ship was performed according to three different probabilistic frameworks – SOLAS 2009, GOALDS and SLF 55. The results showed that



all three regulations results in comparable values of A-index and that there was considerable room for cost-effective design solutions resulting in attained safety levels well above the requirements for damage stability. In [3.56] the notion of vulnerability was used to present a concept of emergency response and crisis management in flooding casualties. Based on real catastrophic accidents (e.g. M.S. Estonia) they discussed inherent vulnerabilities in ship design and operation. This led to the concept of vulnerability management (identification, screening, reducing, mitigation and emergency responses).

Implications of contemporary issues such as safe return to port and the need for operational and emergency response measures has received great attention during the review period. A classification society's perspective on the Safe Return to Port requirements was discussed in [3.13], addressing residual operability of safety-critical systems onboard passenger vessels. The philosophy that the "ship is its best lifeboat" was highlighted by referring to potential issues relating to interpretation of the regulations, presenting relevant information to the master and its harmonization with the damage stability framework. In [3.50] the survivability assessment of damaged ships with respect to the coupled effects of structural degradation and damage stability in the context of the Safe Return to Port (SRtP) framework for passenger ship safety was assessed. The survivability was evaluated in the time domain with varying wave loads. An approach to safety in damaged condition for RoPax vessels was described in [3.61], embracing the full spectrum of measures (regulatory, design, operational and emergency response). A thorough and detailed discussion was presented regarding possible means and methodologies for the increase of safety of the vessels, using an holistic perspective, going from design to operation and, if necessary, emergency response.

Accident investigations are intended to determine the main and root cause of an

incident, to identify possible unsafe conditions and recommend actions to mitigate or ideally eliminate similar cases in the future. In this context, the capsizing of a 12,000 DWT bulk carrier which suffered heavy storm weather, when sailing in South-West Black Sea, was presented in [3.1]. The analysis focused on the circumstances of the accident as well as the sequence of events leading to loss of stability, capsizing and sinking. The catastrophic loss of Ro-Ro passenger ship M.S. Estonia who sank rapidly between Estonia and Finland was presented in [3.2]. The analysis focused on the use of a combined simulation and model test approach for analysing ship's sinking sequence. An accident investigation of the dredger Rozgwiazda which capsized and sank while being towed was discussed in [3.44]. The reason of the capsizing was sea water inflow to one hold and locker through opening of the hawse hole which had not been closed and properly secured on departure. The study presented most probable sequence of events and was accompanied with stability calculations performed for each major stage. In [3.46] the results of the accident investigation for S.S. Heraklion was presented including the reconstruction of the accident data available from a variety of original investigation reports, ship files and legal evidence. Ship's loading and post-damage behaviour was re-investigated and the flooding/ sinking of the ship were simulated in time domain. The same accident was investigated in [3.45]. The loss sequence was studied with use of an advanced numerical method. The study revealed interesting aspects of the earlier phase of the accident (before and during the flooding of the main garage deck). In [3.58], the capsizing of the French pre-dreadnought Bouvet during World War One (WWI) was investigated. The aim was to clarify hypotheses associated with the accident and to test modern tools against the well documented event. For that purpose both numerical computations and experiments were carried out. The investigation pointed to the presence of longitudinal bulkheads which, in case of breach in the compartment, allow off-centre flooding to induce a large heel angle and



the correctness of a recommendation for the installation of cross-flooding ducts, which was not followed during construction.

Following the review of the current status of research on the topics relating to damage stability as addressed above, some insight and suggestions can be provided for directions future research could take.

Regarding the assessment of damage stability, direct simulations of the flooding process is a topic which will continue to receive attention. Benchmarking studies of the various codes developed is still required as well as research on progressive flooding and the development of experimental techniques and procedures. Research on the development of simplified methods suitable for design and regulatory purposes, e.g. p-factors and s-factors, would eventually evolve to the development of integrated methods, for example, to include treatment of consequences from collision and grounding incidents. With the increase of computational capabilities, and with the dissemination of information for in-house development of tools for dynamic flooding simulations, it seems there is space for advances in this respect, moving little by little the use simulations from research to design, or some detailed aspects of design. Also, it is worth noticing that the introduction of SOLAS 2009, and subsequent current research, has changed the perspective regarding damage stability assessment from a design and a regulatory perspective.

On the associated topic of development of rules for damage stability, the research of project HARDER and other initiatives worldwide, lead to the introduction of SOLAS 2009 and subsequent developments at IMO. Recent developments in project GOALDS and projects led by EMSA will lead the way for possible future regulatory developments. Research has progressed regarding the possibility of improving the s-factor. Furthermore, research is ongoing regarding the introduction of a probabilistic regulatory framework dealing

with grounding damages. It is therefore likely that some attention will be given, in the near-medium future, to this topic. Furthermore, the introduction of the requirements for safe return to port by IMO, is directing additional research focus in the area of post-damage availability of essential ship systems.

The development of probabilistic and risk-based methods for damage stability and safety has received considerable attention. Risk assessment is extensively used for rule development purposes, cost-effectiveness analysis and the proposal of adequate safety thresholds. Simplified tools are developed for capturing the time-domain behaviour of the ship by means of simplified formulae (simplified time-to-capsize approaches). Different approaches are used for risk analysis, for example, fault and event trees, Bayesian networks, etc. There is a variety of research issues still to be adequately addressed, namely the availability and representativeness of the selected accident datasets used, integration of considerations of the effects of the human element, research on formal data mining methods to achieve proper filtering and clustering of the dataset used, the integration of simplified probabilistic models of the flooding process within current practice in developing risk models, the consideration of the full chain of events starting from pro-active measures aiming to reduce the frequency of collision or grounding incidents occurring, to the direct association with structural degradation leading to flooding and the assessment of mitigating the consequences of flooding, the treatment of uncertainties in the data used and uncertainty propagation within the chain of events considered, and finally, the assumptions made and parameters considered in developing representative frameworks for cost-effectiveness assessment which should include costs and benefits expected from the reduction of the frequency and consequences of the accidents to the society and the environment.

The area of design implications due to advancements in damage stability research is



set to receive considerable attention in the future. Current contributions relate to the development of design concepts and methodologies and multi-objective and multi-criteria optimisation techniques. This trend is to continue developing, particularly as research on design parameterisation and concept development and their integration within contemporary design practices. Associated areas of research which will definitely play a significant role are developments in post-damage availability of essential ship systems, and the consideration of active design and operational measures for accident prevention and mitigation of consequences.

Finally, regarding accident investigation, even though being pro-active is the appropriate approach for ensuring safety, it is a fact that, unfortunately, accidents still happen and will likely still happen in the future. Therefore best use should be made of the process of learning from accidents, for increasing the level of safety of the relevant engineering field in general, and the field ship stability in this particular context. Accidents data can therefore provide valuable information for software development, application and for a better understanding of the physical phenomena. The research carried out in this area during the reporting period, highlights the further need for use of advanced scientific methods for accident investigations. In addition, further efforts should be spent in promoting a better reporting of stability-related data (loading conditions, damage characteristics, openings, etc.) in all those accidents reports associated with stability-related accidents. Such data are indeed very important for a technical assessment of the accident and, possibly, for having at disposal quantitative information for historical data analysis.

4. STABILITY FOR SPECIFIC TYPES OF VESSELS AND FLOATING OBJECTS

4.1 Fishing Vessels

From the stability point of view, fishing vessels may be treated as special due to a number of design features related to their operational requirements. Fishing vessels are also specific because of a well-known regulatory paradox: despite the fact that fishing is recognized as one of the most hazardous occupations, the major international regulations addressing various aspects of stability and safety are not mandatory for this type of ships.

The problem is particularly evident in case of small fishing vessels whose length does not exceed 24 m. A group of papers dealing with practical measures on how to tackle the safety of such vessels could be distinguished. The safety of small fishing vessels is the subject of [4.1.10] where the Safety Recommendations for decked fishing vessels of less than 12 metres in length and undecked fishing vessels, jointly developed by IMO, ILO and FAO, have been presented. In [4.1.4] a government-supported educational and advisory program was presented, that does not directly deal with the stability, but primarily addresses the safety-related habits of the crew (the Safest Catch program). On the other hand, the contribution [4.1.7] presented a cost-efficient iOS-based solution (an app) SCraMP, that supplies the fishing boat crew with a “safety index” (calculated upon measured roll, heave and pitch motions), roll period and metacentric height and warns of risks associated with large amplitude motions.

Another group of papers concerns the model tests performed either to investigate the accidents of fishing vessels or to gain a better insight into dynamic behaviour of vessels in seaway. The results of investigations into three accidents that occurred in Spanish waters were given in [4.1.1]. Again, the stability of the



small vessels is addressed: all the examined ships (two purse seiners that capsized in following/quartering waves and a trawler that capsized in – most probably – beam seas) were below 24 m in length. The paper deals with a number of practical aspects of model testing. Experimental analysis of foundering of two Japanese fishing vessels was the subject of [4.1.9]. A purse seiner capsized in head waves and foundered due to a combination of improper loading and inadequate drainage of green water from the exposed deck. The examined stern trawler sank in matter of minutes in adverse weather conditions, after flooding of the engine room through watertight doors that were supposed to be closed. Both accidents pointed out the importance of proper stability management that seems to be often lacking on fishing vessels.

Model experiments are also used to validate mathematical models and numerical tools used in simulation of fishing vessel dynamics. In [4.1.3, 4.1.5] experiments with both physical and numerical models were used in order to test the decision-support system, based on artificial neural networks (ANN), that warns the skipper of the parametric roll resonance risk. Further research on this topic was presented in [4.1.8], where model tests were used for validation of a mathematical model that was later used in training of ANN for parametric roll prediction. The contribution in [4.1.6] reported on an in-depth research campaign, that made use of both model tests and sea trials carried out on a 23 m long trawler in order to validate a numerical simulator, developed within the scope of the study with an ultimate goal to gain understanding of the small fishing vessels behaviour in extreme seas.

In some papers, fishing vessels were not of the primary concern of the research carried out but were used in case studies or as sample ships. In [4.1.2] several capsizing accidents associated with freak waves were investigated, three of which involved fishing vessels.

Based on the reported papers it may be concluded that, presently, the research advances towards short- and mid-term solutions that would enable crew to gain an insight into dynamic behaviour of the vessel and take a more active role in risk avoidance. Small craft (below 24 m in length) were in the focus of the most of the studies. If some trend can be established, it appears that the research in this area moves away from the studies done in the past which mostly dealt with, conditionally speaking, a long-term approach to the safety of fishing vessels (e.g. development of the regulations).

It also seems that not many studies focus on specific design and operational features that pose a source of hazards for fishing vessels safety. In that respect, the dynamics of a vessel in case of the fishing gear malfunction or the loss of a paravane could be interesting topics. Similarly, the risks associated with the operation in ice conditions have not received any attention in the reviewed period. In past, some studies concerned with the effects of water trapped on deck were presented as well; it seems that this topic is not exhausted either. Finally, another valuable research direction was already reported in the section dedicated to the Nonlinear Dynamics: the stability of fishing vessels in light of the present framework of the Second Generation of Intact Stability Criteria [4.1.11].

4.2 Naval Vessels

Naval ships can also be considered as a special type of ships. At STAB 2009, Arthur Reed gave a keynote [4.2.1] about a naval perspective on ship stability and wrote: “A navy has the same concerns relative to stability failures that all ship owners, designers and operators have. The significant differences arise from the fact that a navy is not governed by IMO regulations ; that the naval vessel is often much more costly than a commercial vessel; and that the naval vessel may not have the luxury of avoiding dangerous weather



conditions when performing its missions, while a commercial vessel may be able to choose an alternate route. In addition to these differences, a navy often has access to more research and development funds to investigate these issues than the commercial builder and operator". Since this date there was a naval session during every STAB or ISSW. About four papers were presented each year, with the exception of ISWW2011 when there was no naval session, but nevertheless still some papers were presented addressing naval vessels.

As mentioned in [4.2.1], naval ships are governed by different rules than commercial vessel. Many regulations for naval vessels (e.g. those from United States, United Kingdom, Canada, Australia and France) are coming from the original studies of Sarchin and Goldberg in 1962, as mentioned in [4.2.9]. Suggested criteria were based on the experience of two destroyers who sank during COBRA typhoon in December 1944. The two mentioned papers demonstrated the need for improvements in stability assessment methodologies, connected with the appearance of modern hull forms and the need for a higher level of safety. Several navies work on this subject by participating to the NSWG (Naval Stability Standards Working Group). The methodology described in [4.2.9] was based on two main parts: determination ship hydrostatics, on one side, and estimation of probability of capsizing through direct simulation, on the other side. Then an analysis was carried to find a correlation between the two, concluding that parameters related to GZ curve are more correlated with the simulated probability of capsize than form parameters, and that stronger results are obtained when considering GZ curves in waves. The last step for such an analysis would be to define a "tolerable risk level", and a justified choice for it was discussed in [4.2.8]. From setting the tolerable risk level, it could then be possible to set the corresponding limiting values of the stability parameters. Such a methodology is defined in [4.2.10] as "rules based on probabilistic dynamic approaches". Furthermore, in [4.2.10], other possible

approaches for rule-development are also described, that can be employed to naval ship design and that address dynamic stability in such a way as to minimize technical and safety risks in an economical manner, namely: empirically based rules, direct probabilistic assessment and relative probabilistic assessment. A global view of risk assessment method for naval ship design is presented in [4.2.18]. After a definition of risk (the etymology of the word "risk" is complex and, among various possible origins, it includes also a link with the concept of collision with rocks at sea) the paper introduces the Naval Ship Code (NSC) prepared by NATO with the objective to provide rules for naval ship design. Similarly to the process undergone at IMO, also NATO has followed the "Goal Based Standards" (GBS) approach, but taking into account the specific aspects associated with naval ships. In [4.2.19] an approach is described which is meant to include risk into the overall weight and stability control process, taking into account the uncertainty in weights and position of centre of gravity. Within this framework, it is proposed to add error bands on ship KG values, and to add multiple (colour coded) KG limit curves associated with known consequences (e.g. increase of heeling angles, margin line immersion, etc.).

Studies performed on a series of French frigates have been reported in [4.2.20, 4.2.26]. In [4.2.20] parameters related with the GZ curve are correlated to annual probability to capsize calculated by direct simulations using FREDYN. In [4.2.26], instead, results from direct simulations are compared with approaches based on simplified mathematical modelling. In this context, Melnikov method and measurement of the erosion of the attraction basin are used as tools for the analysis.

Dedicated numerical codes for simulation of ships in severe sea states are nowadays used for, and in some cases are necessary for quantifying the level of safety of naval vessels in intact condition. The US Navy has embarked



upon the development of a new blended (hybrid) computational tool, named TEMPEST, for simulating the nonlinear response of a ship in severe sea states, and the theoretical background of TEMPEST has been described in [4.2.15]. Another numerical code which has been used for investigating large amplitude motions for naval ship is FREDYN, developed by the CRNAV. With reference to FREDYN, in [4.2.13] an improvement of the code was described which was aimed at introducing the possibility of taking into account water on deck in an efficient way. Model experiments have been used to validate the code. A more comprehensive validation study of the code against experimental data is also presented in [4.2.21]. The validation was carried out by deterministically reproducing ship motions in experimentally measured wave trains. Also the progressive flooding module of FREDYN has been subject to validation, as reported in [4.2.14]. In particular, in [4.2.14] the simulation methodology was described (fluid considered with horizontal free surface at each time step and Bernoulli equation used for determining the flow through compartments), and simulations have been compared with dedicated model experiments. FREDYN was also used in [4.2.27], where results from a large number of direct simulations have been analysed using different techniques, and attention was given on how to report the outcomes using relatively simple and easily understandable visual indications.

As for commercial ships, operator guidance and training using shiphandling simulators are more and more used by navies and have encouraging potential for the future, as mentioned in [4.2.17]. Indeed, according to [4.2.17], the use of simulators for training in heavy weather can compensate the fact that mariners historically receive minimal initial formation on the topic of shiphandling in heavy weather (mostly relying on mentoring and hands on experience), and the fact that, in many present cases, the time actually spent at sea may represent a smaller portion of the mariner's career in comparison with the past.

In [4.2.16], a description was given regarding the interfacing of a state-of-the-art bridge simulator with the state-of-the-art numerical code FREDYN for the evaluation in real time of ship motions. A series of Naval Operator Ship Handling Workshops were held at the Royal Netherlands Naval College bridge simulator facility considering different simulation scenarios, and the feedback from different officers of the watch was clearly positive. Essential and desirable additional improvements for the simulator have also been identified.

An important subtype of naval ships is represented by landing craft. These ships are relatively small and they could be subject to stability-related problems, in particular due to the open vehicles deck. Moreover, as pointed out in [4.2.12], these ships present different characteristics compared with those more standard warships around which naval stability standards have been originally designed. As a result of this difference, specific rules for landing craft have to be designed, and progress made by Royal Navy in this direction have been described in [4.2.12] in accordance with the performance requirements of the Naval Ship Code. Similarly, a study by the Royal Australian Navy regarding motions and stability of landing craft was presented in [4.2.24]. Ship motions were investigated with and without water on deck using FREDYN. Also, the authors stressed the importance of a proper prediction of the roll damping, which is a critical factor for properly predicting ship motions and, for landing craft, it cannot be determined by usual tools. In [4.2.11] an example of instrumentation installed on a French mine hunter was described. The system was intended to help the crew in checking the stability of the ship, by using a traditional loads calculator but also a sea states estimator and a roll period measurement.

The tumblehome special naval ship hull form proposed by ONR has been the subject of several investigations. Although it constitutes a typology of scarce interest for commercial



shipping, this special hull form has been proposed, in some cases, to validate the IMO Second Generation Intact Stability Criteria, due to its possible vulnerability to certain failure modes. For the ONR tumblehome vessel, parametric roll was investigated in [4.2.25], while dead-ship condition was investigated in [4.2.22, 4.2.29]. For these papers, the approach was the same: development of numerical tools, comparison with Second Generation Intact Stability Criteria and, finally, determination of safe zone (KG and/or speed) and suggestion of improvement on numerical codes. CFD calculations, system-based prediction methods and experiments have been instead presented in [4.2.6]. Then, in [4.2.28] the tumblehome hull form was used to present an approach where few CFD calculations are carried out in order to tune a manoeuvrability model. Use of the ONR tumblehome hull form for addressing the following sea condition can be found in [4.2.7, 4.2.30].

Also in damaged condition approaches are used for naval ships which are different in comparison with commercial vessels. In [4.2.5] a very useful database of Polish naval ship accidents was referenced. A simplified approach was also proposed for the on board estimation of the time to sink due to flooding. This approach was validated against model test and indications were given regarding the need of tuning of permeability. Although there could be debate on whether historical damage data from commercial ships can also be used for naval ships, in [4.2.3] data from the HARDER database have been used to derive deterministic damage extent for naval vessels. The proposed solution was to set the deterministic damage extent that naval ships should be capable of withstanding on the basis of the 50th, 80th and 95th percentile of damage extents as obtained from the available historical data, depending on a specified category of damage severity (limited/moderate/severe). In [4.2.32] the determination of the optimum number of watertight compartments was instead addressed from an original cost-benefit analysis point of view. The more usual approach for intact

stability analysis, based on comparison of rule's criteria with the risk evaluated by a direct time domain numerical code, has been used in [4.2.2] but for the more complex case of a damaged ship. The evaluation of ship performance was based on the use of an innovative index, referred to as the Relative Damage Loss Index (RDLI). In the contributions [4.2.4, 4.2.31] an interesting experience on the evolution of rules was proposed. As mentioned before, most of naval rules came from Sarchin & Goldberg studies in 1962. This is the case of Royal Navy rules, and in particular for damage stability criteria. One criterion in particular includes a dynamic allowance for heave and roll in waves. This aspect is taken into account by the so-called V-lines criterion. In [4.2.4, 4.2.31] an alternative methodology was proposed where numerical estimation of motions in waves was used in order to possibly extend the original approach to vessels of different type compared with those used by Sarchin and Goldberg.

With the exception of the previously mentioned Polish naval ships accident database, well documented naval ship accidents are rarely published. One very old event, namely the dramatic capsizing of the pre dreadnought ironclad *Bouvet* during World War One, has however been reported and discussed in [4.2.33].

In the considered review period, only one paper [4.2.23] was dedicated to submarines. In particular, the contribution in [4.2.23] dealt with the very special topic of Mathieu instability of surfacing submarines.

Some comments can then be provided regarding possible topics for further research. Behaviour of submarines, including the surfacing time, seems to be a complex problem which has unfortunately not very much been investigated (or published). Therefore, further published analysis on this topic would be welcome. Then, as naval rules are based on quite old standards based on old hull forms, work is required in order to check if some



modifications are needed in order to take into account new hull form (including, for instance, tumblehome vessels or even multihulls). In this context, it would also be worth to collect and critically re-analyse the justification which was originally given for existing (old) rules. In the process of updating stability regulations, there is a need for determining the tolerable risk associated with rules, and to this aim it would be preferable to use advanced numerical codes. In this context, existing general codes could therefore need to be improved or adapted in order to deal with the particular features of naval ships. With respect to nonlinear ship motions in waves, one important mode of stability failure for naval ships is broaching. Research in this domain is therefore needed for naval ships, which could be required to safely operate at high speed in very severe sea states.

4.3 Inland Vessels

Although research in the field of inland navigation is active within various conferences and journals, the safety and stability of inland vessels has so far not received much attention in the STAB conferences and workshops. In recent years, only two papers dealing with the stability of inland vessels were presented in STAB/ISSW events. In [4.3.1] a probabilistic safety assessment of inland container vessels exposed to gusting beam wind was presented (see [4.3.2] also). A review and a probabilistic analysis of the ship stability regulations intended for the river-sea ships was given in [4.3.3].

What makes inland vessels special from the stability point of view? Even though the wind-generated waves, due to a limited fetch, could be disregarded in the analysis of dynamic stability of ships in inland waterways, there are other, quite specific environmental loads and potential hazards that ought to be taken into account. The strong, gusting winds, in particular in combination with other heeling moments and effects may induce both partial and total stability failures. On the other hand,

shallow-water sectors and periods of low water levels may cause grounding and contact. Some typical features of inland vessels, such as exceptionally low freeboards (some rules allow navigation with practically no freeboard) and carriage of non-fixed containers, are particularly important from the stability viewpoint. The river-sea navigation implies basically inland vessels (with few modifications) that operate in the coastal maritime stretches. Clearly, in such cases, the stability in waves should be assessed as well, having in mind the specific form and design features of river-sea ships.

Focusing on Europe only, perhaps the most important task of the future research is the improvement and harmonization of stability regulations. Both intact and damage stability rules intended for inland vessels are deterministic. In addition, the regulations imposed by the Directive 2006/87/EC (stemming from the Rhine Commission rules and valid on most of the waterways of European Union) are merely static stability requirements. Moreover, unlike in maritime transport, there is no common set of safety rules applicable to inland ships worldwide.

To carry out the aforementioned task efficiently, proper mathematical modelling of safety phenomena typical for inland vessels is required. Recent accidents on inland waterways in Europe warn against the oversimplified treatment of stability. The understanding and accurate modelling of weather phenomena (wind in particular) is of equal importance.

The notion of risk in inland navigation is a challenging topic too. Besides human casualties, environmental damage, loss of cargo and ship damage, accidents in inland navigation often yield an additional consequence: the suspension of navigation due to the waterway blockage. For instance, the tanker Waldhof that capsized in intact condition disrupted the navigation on the Rhine for 32 days in 2011, causing financial loss that amounted to EUR 50 million.



Finally, it is interesting to point out that the first practical implementation of the probabilistic approach to intact stability was realized in innovative rules for river-sea navigation, applied in Belgium and France. This seems to be a very promising track.

4.4 Other Types of Vessels and Floating Objects

Some contributions have also addressed some specific topics related with floating offshore structures. From a geometrical point of view, floating offshore structures are often characterised by shapes which are not elongated, as in the case of conventional vessels. This marked three-dimensionality can require reconsideration of, and/or elaboration on, concepts and calculation techniques for static stability and dynamics which are instead well consolidated for the case of conventional vessels. Contributions concerning static stability of floating offshore structures can be found in [4.4.2, 4.4.4, 4.4.13], where the issue of a proper calculation of the calm water righting lever for floating structures of generic shape has been discussed. More specifically, the potential energy of the floating structure was used in [4.4.2, 4.4.4, 4.4.13] as a fundamental tool to directly or indirectly determine the most critical ship restoring, and calculation methodologies have been proposed. Floating offshore structures have also been addressed from the point of view of nonlinear dynamics, since their shape and their possible mooring configurations can lead to the inception of ship motions governed by nonlinear phenomena. The behaviour of a long vertical cylindrical structure, representative of a spar platform, has been numerically investigated in [4.4.8] by means of an analytical nonlinear 3-DOF (heave/roll/pitch) mathematical model, indicating the potential occurrence of sub-harmonic roll motions for certain wave periods and height in regular waves. A long vertical cylindrical structure (mono-column), with different mooring configurations, has later been studied

experimentally and numerically in [4.4.14]. Sub-harmonic motions (pitch and roll) have been observed, both in regular and in irregular waves, with different response patterns depending on the mooring arrangement. Still remaining in the field of nonlinear motions, in [4.4.9] large amplitude sub-harmonic yaw motions have been observed, both experimentally and by using a 7-DOF nonlinear mathematical model, in regular waves for a system comprising a TLWP (Tension Leg Wellhead Platform) connected to a nearby moored FPSO (Floating Production Storage and Offloading vessel). The study presented in [4.4.1] was instead more related with design and rules assessment, presenting an analysis of the effect of uncertainty of some parameters (most notably the position of centre of gravity) on the overall assessment of static stability criteria for an FPSO.

Nonlinear ship dynamics in the particular case of multi-hull vessels has also been considered. Roll restoring variations and parametric roll in case of trimaran vessels have been addressed experimentally in [4.4.6], by measuring roll restoring in waves and identifying conditions of occurrence of parametrically excited roll motion. The topic of parametric roll for a trimaran vessel was also investigated in [4.4.7], where instability regions and roll response curves were experimentally determined and compared with predictions based on a 1-DOF mathematical model. Another type of multi-hull, a semi-SWATH, was considered in [4.4.11] in case of following waves. In the study, a 3-DOF (heave/pitch/surge) mathematical model was developed and used to investigate the occurrence of the phenomenon of bow-diving and to assess the possibility of its reduction through active or fixed fin stabilizers.

Phenomena specifically relevant to mono-hull high-speed craft have also been subject of some contributions. In [4.4.12], the roll restoring moment of a planning craft operating at planning speeds was investigated experimentally and by means of two different



mathematical models. In [4.4.19] an experimental investigation has been reported regarding the occurrence of the spinout phenomenon for a radio controlled high-speed craft model.

Furthermore, specific aspects of other special vessels/units have been addressed. A discussion has been provided in [4.4.12] regarding operational aspects and specific static stability issues of float on/float off (FLO/FLO) heavy-lift semi-submersible vessels during the de-ballasting phases. In [4.4.15] a numerical study was presented regarding second order forces for a series of variants of a semi-submersible floating structure. The second order drift roll moment was investigated because it was considered relevant to the observed possible occurrence, for this type of floating objects, of steady heel angles in head sea. In [4.4.18] the same phenomenon was investigated experimentally by considering three configurations of a semi-submersible (bare hull, with vertical barriers, and with sponge damping layers) in head waves. A weathervane turret moored floating storage and regasification unit (FSRU) was instead the subject of the study presented in [4.4.16]. The study provided an experimental investigation on the behaviour of yaw motion in regular and irregular waves, identifying regions of wave periods associated with the inception of yaw motions with large non-zero mean. Such regions have been linked with regions of instability of low-frequency yaw under second order forces, and numerical/analytical calculations have been carried out to predict such regions. Interestingly, the observed behaviour shows similarities with yaw instability during towing operations as presented in [4.4.17, 4.4.21].

Sailing yachts have been considered in [4.4.5]. The effects of size on the stability and safety of very large sailing yachts have been discussed from a design perspective, also in view of a reported series of wind tunnel experiments addressing wind heeling moment.

In addition to floating objects, also helicopters and Wing-In-Ground (WIG) craft have been given some attention. In [4.4.3], a study has been presented on anti-capsizing floatation devices fitted on a helicopter. Two technical solutions have been considered, and results of static stability calculations and capsizing model tests in irregular waves have been presented to assess the effectiveness of the solutions. The topic of WIG craft has instead been addressed in [4.4.20], where the take-off phase of a WIG craft has been numerically studied by means of a 3-DOF mathematical model (surge/heave/pitch).

Particular static and dynamic characteristics of floating offshore structures undoubtedly represent an opportunity for continuous research. However, the observed quantity of contributions within STAB/ISSW indicates that this opportunity seems not to have been fully exploited in the observed period of time, and possibility for improvements is clearly available. The strong three-dimensionality of (most) floating offshore structures represents a challenge for research on the development of new specific approaches or for the extension of tools and concepts originally developed for static and dynamic analysis of conventional ships. In fact such concepts/tools/methodologies of analysis often embed, implicitly or explicitly, assumptions and/or simplifications based on the elongated shape of conventional vessels, and can therefore become unsuitable if naively used. Moreover, the frequent presence of mooring lines in the configuration/operation of offshore floating structures add a further degree of complexity (also for ship-shaped floating objects) which is typically not considered for conventional freely floating vessels. Multi-bodies interaction, with associated increased system complexity, is another distinctive feature of offshore applications which is not considered in the typical analysis of freely floating/free running vessels. These general aspects, combined with the reported evidence of specific stability-related issues pertinent to floating offshore structures, provide sufficient



ground to suggest an increase of interest and efforts on this topic in the future. It should also be considered that floating offshore structures are, typically, high-budget designs. As a result, high-end technologies, tools and concepts can be more easily accommodated within the design flow compared with conventional vessels. This aspect could be seen as a facilitator in the process of transferring research outcomes to practice.

Somewhat similarly to offshore floating structures, multihull vessels would also be worth additional attention in the future, with the aim of addressing stability-related design aspects and developing and/or improving specific models for prediction of ship motions and manoeuvring in waves, which can better take into account the hydrodynamic interaction between hulls.

High-speed craft are also associated with specific technical issues and specific dynamic phenomena. High-speed craft have been traditionally handled, mostly, outside STAB/ISSW framework. However, the high speed of such vessels has consequences on many stability-related aspects: stability is no longer governed by hydrostatics and hydrodynamics plays a fundamental role also in calm water, damage stability safety is governed by damage dimensions not in line with conventional low-speed vessels, dynamic phenomena occurring on high-speed craft are often so specific that they cannot be observed in conventional low-speed vessels, methodologies for ship motions and manoeuvring in waves for high-speed craft require significant re-thinking and re-modelling compared with those used for low-speed conventional vessels, etc. . Therefore, it seems there could be justification for trying, in the future, to increase the attention on this topic from the perspective of stability and (nonlinear) dynamics also within STAB/ISSW.

In general, what is clear from the analysis of the available STAB/ISSW literature on special types of vessels/floating objects, within

the considered time period, is that, as expected, peculiarities of the design eventually reflect on peculiarities of associated issues and phenomena. This fact should therefore be seen, and exploited, as an opportunity stimulating curiosity, research and development.

5. ROLL DAMPING & ANTI-ROLLING DEVICES, CFD FOR SHIP STABILITY, AND MODELLING OF GRANULAR MATERIALS

An accurate prediction of roll motion is of fundamental importance when ship safety is assessed. In case of an intact ship, the accuracy in the prediction of roll motion is, for a large set of dynamic phenomena, strongly dependent on the accuracy in the prediction of roll damping. In parallel to this, the fact that roll damping is, for conventional ships, governed by viscous effects, makes accurate roll damping prediction a very difficult task. Roll damping estimation and modelling have therefore represented important topics of research in the field of ship stability. In the considered review period, the subject of roll damping has been addressed from different perspectives and using different approaches.

The most commonly used approach for the estimation of roll damping has been in the past, and still is, based on semi-empirical methods. In this context, a simplified version of the well-known Ikeda's method was presented in [5.5], where regression formulae, derived from systematic application of original Ikeda's method, were proposed for the estimation of the various roll damping components. The approach has also been implemented within the framework of IMO Second Generation Intact Stability Criteria. In [5.4], following application examples, warnings have been given regarding the application of Ikeda's method to vessels with characteristics not in line with the original sample used for the development of the method. Proposals for improvements in estimation of bilge keel roll



damping in case of shallow draught vessels, large rolling amplitude and non-uniform flow can be found in [5.10], while proposals for improvement of bilge keels roll damping modelling within time domain simulations have been presented in [5.18, 5.34]. The issue of proper modelling of roll damping in time domain simulations, in particular in case of large amplitude roll motions, has also been addressed in [5.9]. In [5.9] it was proposed to use different roll damping models at different rolling amplitudes, i.e. for regions assumed to be associated with substantially different physical phenomena (e.g. bilge keels or deck in water/out of water). The necessity of improvements in the modelling of bilge keels effects was also claimed and discussed in [5.16], with particular attention to the application in time domain simulation of large amplitude ship motions in waves, with or without forward speed.

Although semi-empirical methods still remain a reference tool for the prediction of roll damping, in the considered review period a significant number of studies have been presented where CFD techniques have been used with the intention of analysing roll damping (herein the short wording “CFD” is intended to refer to computational fluid dynamics techniques aimed at solving Navier-Stokes equations including viscous effects). In [5.17], forced roll motions (1-DOF - fixed roll axis) in calm water and beam waves have been simulated with CFDSHIP-IOWA. Large amplitude rolling motions up to 35deg and forward speed have been considered, with attention given to forces acting on bilge keels. CFD simulations using the commercial code Fluent have been used in [5.33] to study possible interaction effects between bilge keels plates. Such effects were considered to be the possible source of disagreement between experimental results and semi-empirical predictions based on Ikeda’s method for a vessel with round cross sections fitted with bilge keels. Comparisons between experiments, semi-empirical predictions based on Ikeda’s method, and CFD simulations using Fluent,

have also been reported in [5.38] in the study of shallow water effects on roll damping for 2D sections. 1-DOF roll decay and forced roll motion of DTMB5415 have been simulated in [5.39] using the code SURF, and an analysis of flow field and pressure distributions with and without bilge keels has been reported. The same hull form was also used in [5.26], where roll decays (see also [5.15]) and forced roll motions have been simulated using the commercial code Fluent. This study also showed some forced roll simulations which are reported to have been carried out at full scale. A numerical study on roll damping, with simulations reported to have been carried out at full scale using the commercial code STAR-CCM+, was presented in [5.31] for a twin-screw RoPax ship, allowed to rotate around a fixed axis through sliding meshes. The influence of roll amplitude (up to 35deg), ship speed, vertical position of the roll axis, presence of bilge keels (with possible emergence/re-entrance) and presence of rudder have been thoroughly investigated, and comparisons have been reported with semi-empirical predictions based on methods of Ikeda and of Blume. The influence of degrees of freedom (sway/heave/roll) left free in roll decay has been addressed in [5.19]. Numerical simulations have been carried out using the solver ICARE for DTMB5512 at model scale, and then compared with experiments. Results confirmed a known characteristic, i.e. the fact that roll decays with prescribed fixed axis are often not representative of the actual ship behaviour, due to lack of coupling of roll with, mainly, sway, which should then be left free.

For practical limitations, the large majority of data regarding roll damping are available from model scale experiments. CFD techniques have been used in some cases to try predicting full scale roll damping, although corresponding validation is typically missing. However, in [5.30] a unique set of results have been presented regarding roll decays with forward speed carried out at full scale (through rudder action) for a modern Panamax Pure Car and Truck Carrier (PCTC). Full scale data were



then compared with experimental results at model scale and with predictions based on Ikeda's method. For the extraction of full scale roll damping coefficients, a method of analysis of full scale roll decays was also presented combining the classical 1-DOF model with a polynomial function aimed at removing low-frequency experimental disturbances. Different analysis methods for determining roll damping from roll-decay experiments have also been discussed in [5.11, 5.19, 5.20].

Anti-rolling tanks have also been given attention in a series of contributions, and they have been studied using analytical methods or by means of CFD approaches. In this latter case, preference was given to meshless methods such as MPS (Moving Particle Semi-implicit) and SPH (Smoothed Particle Hydrodynamics), thanks to their capabilities of handling violent sloshing flows which often occur in free surface anti-rolling tanks. An analytical model for a (passive/active) U-tube anti-rolling tank has been coupled in [5.12] with a nonlinear 3-DOF model (roll/heave/pitch) for parametric roll assessment. In [5.27], MPS has been used to simulate 2D flow and resulting forces in a U-tube tank and in a rectangular free surface tank, coupling the tank with a 1-DOF roll model for parametric roll, and comparing simulations with experiments. In [5.1], SPH has been used to simulate 2D flow and resulting forces in a free surface rectangular tank, free to rotate around a fixed axis, and forced by a sliding mass (an archetypal 1-DOF mechanical model for roll motion). Experimental results with fluids having different viscosity have been compared with simulations. The SPH approach has later been extended to 3D simulations, taking advantage of parallelization on graphical processing units (GPUs), see [5.28].

As an active anti-rolling means, rudder-roll stabilization has also been considered. The use of active rudder-roll stabilization to mitigate parametric rolling has been studied in [5.21] with a blended 6-DOF code (in 6-DOF and in 3-DOF configuration), and in [5.36] with a 4-

DOF model. In [5.23], instead, an unusual active anti-rolling device, based on a controlled wing assumed to be placed beneath the hull, has been proposed and studied numerically. An extensive control-oriented review of the development of, and challenges associated with, some active anti-rolling means (fin stabilizers, rudder, gyrostabilisers) can be found in [5.32].

As described above, an increasing application of CFD techniques has been observed in the fields of roll damping prediction and anti-rolling tanks performance assessment. CFD techniques have increasingly been used also for more general purposes in various additional contributions. Direct CFD simulation of free running ship motions in waves are still a too time consuming task for systematic application. However, a series of contributions combining simulations using CFDShip-Iowa, experiments and systems-based simulations for the ONR Tumblehome, have shown that, on one side, CFD techniques are becoming a reliable surrogate for model experiments and, on the basis of this, CFD simulation can be used as reference data for tuning more classical system-based approaches. For example, in [5.3] free running and semi-captive conditions in waves have been considered, giving attention to following waves, and to the occurrence of surf-riding, broaching and periodic motions. Semi-captive conditions have also been addressed in [5.6] for the HTC container vessel in bow and head waves. Further, in [5.13] ship motions and manoeuvring in calm water and in waves (turning circle and zig-zag) have been considered and a 4-DOF system-based model has been tuned making use of CFD results. A similar approach was also used in [5.22], considering manoeuvrability in following waves (straight running, course keeping, zig-zag) (see also [5.35]).

CFD techniques have been used not only for the case of intact vessel, but also for the case of damaged vessel. In this case, together with the inherent complexity in simulating the



fluid within the ship internal layout, one of the most challenging difficulties is the simulation of the fluid motion considering both internal and external hydrodynamics. In [5.2] a volume-of-fluid (VOF) approach was used, among other applications (dam break and tank sloshing), to simulate the progressive flooding of a compartment. The free flooding of a compartment, as well as the flooding of a freely floating 2D box and an internal sloshing problem, have been addressed in [5.7] by means of a 3D parallel SPH approach. The commercial code Fluent was instead used in [5.8] to simulate the progressive flooding due to side damage, and the consequent motions, of a freely floating 3D barge. Air compressibility was taken into account and dynamic meshing was used. CFD simulations of flooding process in calm water (with and without ship motions), roll decays (intact & damaged condition) and motions in regular beam waves (intact and damage), have been carried out in [5.25] with CFDSHIP-IOWA for the SSRC cruiser. In the simulations 6-DOF have been considered, and results have been compared with experimental data. Roll decays in damaged condition have also been simulated in [5.15] assessing also the influence of free or fixed sway. A mixed (blended) computational approach has instead been used in [5.14] to simulate ship roll motion in beam waves. In the proposed approach, external hydrodynamics has been addressed by the blended 6-DOF code PROTEUS3, while internal flooding has been addressed by means of a VOF approach. In [5.24], the SURF code has been used to simulate the flow behaviour through cross-flooding arrangements, and outcomes have been compared with experiments and with IMO guidelines as given in MSC.245(83).

An important aspect to be borne in mind when addressing ship stability, dynamics and safety, is that not all the cargoes onboard can be categorised as single rigid blocks, or as standard fluid cargoes. This is the case of granular materials, which are made of a huge number of interactive constituent small bodies, with their own specific behaviour and specific

interaction characteristics, depending on the material. As a result, granular materials behave differently from both a single rigid body and from a Newtonian fluid. As such, they pose risk to the safety of the vessel, and require special treatment in simulations. In this respect, contributions have been given in [5.29] regarding the direct simulation of granular materials (see also [5.37] for an extension of the analysis). In [5.29, 5.37], different available simulation approaches have been described and a soft sphere molecular dynamics approach was eventually detailed and used in a series of example calculations.

Considering the observed status of the research in the addressed topics, it is eventually possible to provide some comments and suggestions for possible directions of future research.

Roll damping is clearly a fundamental subject in the field of ship motions and stability. Indeed, an inaccurate prediction of roll damping can render useless even the most accurate ship motions model, if this is intended for roll motion prediction and ship safety assessment. Despite this is a very well known situation, it is evident that semi-empirical methodologies, i.e. the type of methods which are more likely to have a more widespread use, are still today showing difficulties in providing predictions systematically agreeing with experimental data. It is therefore of utmost importance that such methodologies are improved and/or updated, in order to give to designers and researchers, more precise, and still fast and easy to use, tools for roll damping prediction. Accurate predictions of roll damping are not only relevant when direct ship motions simulations are carried out. They are also relevant when roll damping becomes a factor within intact stability regulations (as it is the case, for instance, of the Weather Criterion and in some methodologies within the Second Generation Intact Stability Criteria). In this context imprecise roll damping estimations can lead, eventually, to uneven levels of safety for vessels complying with the criteria. More



accurate prediction tools could also promote a virtuous design practice aimed at increasing the ship roll damping. Improvement of roll damping estimation should also be pursued at the level of modelling. While the concept of amplitude/frequency dependent linear equivalent roll damping as a substitute for nonlinear roll damping is suitable for frequency domain approaches, this is not the case when time domain large amplitude simulations are to be carried out. In this case, reliable time domain models need to be used. There is space, in this context, for improving present modelling of roll damping moment (which is mostly based on a nonlinear roll damping depending on roll velocity) in order to better account for phenomena occurring at large rolling amplitudes. Also, efforts should be spent in improving the modelling of roll damping when the ship is at forward speed and when the vessel is free running in waves, and in order to better understand to what extent information from roll decays in calm water can be considered appropriate for large amplitude ship motions in waves. Such type of improvements would largely benefit the accuracy of prediction of blended large amplitude ship motions codes. Scale effects in roll damping represent another topic which would benefit from further elaboration. Full scale experiments have been limited, and considering the associated difficulties, this is understandable. However, examples have been shown that carrying out full scale experiments is feasible not only for naval ships, but also for civil vessels. Additional, possibly systematic (e.g. at sea trials), efforts in this respect could therefore be recommended, with the aim of considering cargo, and possibly passenger, vessels. Together with the improvement in the predictions of roll damping, also prediction method for rolling period should be improved. Indeed, the rolling period represents a key aspect governing the dynamics of the vessel. Inaccurate predictions of such quantity inevitably lead to imprecise dynamic simulations. Since the added mass/inertia affecting the actual roll period is typically well predicted by nowadays standard linear

seakeeping codes, it means that efforts should be spent in improving the methodologies for predicting dry radii of inertia.

Direct CFD approaches have gained increasing attention, especially thanks to the more widespread availability of suitable computational resources. Although some research has been carried out on using CFD approaches for directly simulating the motions of an intact free running ship in waves, the associated computational time is still prohibitive. However, such tools can be used in a virtuous combination with existing systems-based approaches (which are typical of blended ship motions codes). Useful research could therefore be directed into a more extensive validation of CFD tools, and on the use of such tools for tuning, or developing, appropriate, simpler and faster, mathematical models. This could typically include roll damping from decays, manoeuvring forces, forces due to appendages, wind effects, etc. Some use of direct CFD computations has been reported also for the damaged ship condition. Also in this context complete direct simulations are still prohibitively time consuming. However, similarly to the case of intact vessels, direct CFD simulations could be used to better tune semi-empirical progressive flooding tools (e.g. tuning of discharge coefficients). CFD approaches, in both intact and damaged condition, after proper validation, could be used not only for tuning, but also for producing surrogate (with respect to experiments) validation data for checking more simplified, semi-empirical, approaches.

With reference to anti-rolling devices, contributions have been provided for different types of system. Anti-rolling tanks (U-tube and free surface) continue, as in the past, to be a topic of interest. Additional interest was given to rudder-roll stabilization. With the increased availability of computational resources, anti-rolling tanks could be targeted for more in depth studies on the, possibly nonlinear, characteristics of the coupled tank-ship system. This could help in providing better tools at the



design stage, and better information to the masters for operating vessels with such devices. Also, interest should be given to understanding whether, for passive devices, present knowledge and calculation and experimentation capabilities could allow to take such systems into account within intact stability regulations dealing with ship dynamics. Going to rudder-roll stabilization, the observed interest could benefit from a virtuous link with the field of controls, combining existing knowledge in such field, with more advanced dynamical models typical of the field of ship stability. In terms of active systems, it would be beneficial to dedicate more efforts to the modelling and assessment of active anti-rolling tanks, especially in case of large amplitude nonlinear motions.

A limited number of contributions have been provided on the interesting emerging topic of granular materials, which is relevant to certain types of cargo. Being such materials different from a perfectly solid or a perfectly Newtonian fluid cargo, a better understanding is necessary regarding the impact of granular cargoes in dynamic conditions. Also, this topic of research could be linked with the issues associated with the inception of liquefaction. Considering the limited availability of research in this specific context, the interest and complexity of the phenomenon, and its importance for the safety of certain types of vessels, it is expectable, and desirable, that further experimental and numerical studies will be carried out in the future.

6. SHIP STABILITY IN OPERATION

Enhancing the stability of ships during their operation could be a challenging task considering the uncertainty that spans the various operational parameters such as the weather and loading conditions as well as the human reactions in critical situations. On the other hand, the large amplitude response of a ship in random seas and the various instabilities that may appear have been well

studied, while probabilistic methods and numerical simulation tools have been already incorporated in the design process. Moreover, it should not be disregarded that operational guidance is also considered as an important element in the second generation intact stability criteria. However, stability failures, either affecting ship's safety or cargo's integrity still occurring, and thus, it becomes obvious how all the knowledge gained from the above fields could be appropriately utilised in the operation of a ship.

One of the available methods is through the operational guidance to ship's master based on numerical simulation tools. A respective study was presented in [6.1], where polar diagrams of maximum acceptable significant wave height versus the seaway period and wave direction for different speeds and load cases were shown for the cases of excessive motions and accelerations for containerships in heavy seaways. In [6.8, 6.12] another approach was considered where stability limits for pure loss of stability and parametric rolling were derived from GM variation spectra calculated from stability variation RAO's and arbitrary seaway spectra based on linear response theory. The approach was evaluated in comparison to real stability incidents and time-domain simulations, and the importance of proper representation of the wave environment was highlighted.

From another viewpoint, one could take advantage of the direct measurements of ship motions in order to predict, and subsequently advice on stability in order to avoid possible forthcoming undesiring events. In [6.6], an approach for assessing parametric roll resonance based on roll motion time series was presented. The approach utilized the time varying autoregressive modelling procedure and parametric roll was detected by studying the characteristic roots of the time varying autoregressive operator. Additionally, in [6.14] an alternative autoregressive modelling procedure for parametric roll detection based on time series analysis was examined in order



to decrease the required computational cost. In this case, an exponential autoregressive modelling procedure was applied. On the other hand, in [6.10] it was demonstrated that influential parameters of the encountered wave pattern, such as peak frequency and amplitude, can be detected through the monitoring of heave and pitch motions, which were considered as signals with time-dependent spectral content. In [6.9] an application was described for implementation in mobile phones and similar devices. Utilizing built-in accelerometers and gyroscopes, the application can provide low budget operators, like fishermen, with ship motion recordings, information about natural roll period and GM, and a safety index reflecting the severity of the motions.

In a similar manner, on-board tools can be utilised in order to optimise, in real time stability and provide the appropriate guidance to the crew. In [6.7] a 1-DOF simulation model was proposed as a candidate to use for generation of real time on-board guidance in terms of parametric rolling. Typical results were in the form of polar plots of roll amplitudes that could be presented to the crew to indicate dangerous zones with respect to parametric rolling. Furthermore in [6.13] a description was given of the practical implementation methodology of an artificial neural network (ANN) system for parametric roll prediction, which can be integrated in a fishing vessel for onboard stability guidance. A 1-DOF mathematical rolling model was used instead of expensive and time consuming towing tank tests for the training of the ANN.

On-board safety assessments can significantly enhance operational guidance to the crew also in critical conditions. From the viewpoint of damage stability, the contribution in [6.4] highlighted the challenges in real-time simulations of complex physical processes and/or evaluation of random scenarios by presenting real flooding scenarios leading to significant loss of life. The importance of time

in crises management and consequences mitigation was therefore illustrated.

Various methodologies have been presented for the accurate prediction of sea conditions. In [6.5] a method for on-board sea state estimation was explored and validated. Based on the wave buoy analogy the method builds on comparison between measured and calculated ship motion response spectra and minimization of the error to obtain the parameters of a sea state spectrum formulation. Besides, in [6.11] computational issues associated with the identification process of the wave spectrum on the basis of indirect dynamic measurements of oscillation motion of the dynamic object in a seaway were examined, specifically the parametric identification based on the adaptive model that can be carried out in the on-board intelligent system.

Providing the right information to the crew will not ensure safe operation if crew's training in critical weather conditions is not sufficient. A discussion was offered in [6.3] on the growing trend of turning to new technologies in heavy weather ship-handling training, which complements the traditional education relying on mentoring and experience. The importance of fidelity (virtual reality) in simulators was mentioned, in terms of real time 6-DOF large amplitude motions. This issue was also discussed in [6.2] where a benchmark study for the coupling between a bridge simulator with a nonlinear blended sea-keeping code (FREDYN) was presented. The incorporation of advanced numerical tools in bridge simulator could enhance the training of the heavy weather ship-handling.

Operational guidance has revealed, without doubt, its importance in preventing ship accidents associated with stability failures. Polar plots based on extensive time-domain simulations for all sea states and loading conditions stand as one of the strategies, so the validation and the capability of the numerical tools to capture the related phenomena are necessary. Real time on-board guidance based



on the measurement of ship motions is also a promising direction but the implemented mathematical modelling can adequately and promptly predict the forthcoming events keeping in mind the short time window that is available after the initiation of an instability. The techniques of artificial neural network could help on this direction. Besides, safety assessments aiming at the capturing of the basic stability failures could improve route planning given that the prevailing weather conditions could be sufficiently predicted. Last, but not least, crew performance in safety critical conditions should be enhanced, either by utilising crisis management on-board tools or by training in advanced bridge simulators capable of reproducing extreme ship response in rough weather.

7. MODELLING OF ENVIRONMENT

A proper modelling of the environment (typically waves and, in some cases, wind) is fundamental in obtaining accurate estimations of ship motions. Therefore, the modelling of the environment plays a crucial role in the evaluation of ship safety. In this context, in [7.1], analytical expressions of typical sea spectra used in Naval Architecture were analysed, showing that, with proper renormalization, such shapes can be approximated by families of functions usually used for describing probability density functions. The topic of extreme (freak) waves has instead been the subject of investigation in [7.2], where non-Gaussian behaviours in case of generation of short crested waves were reported, and a series of accidents are reviewed in view of the possible occurrence of freak waves, considering weather forecasting/hindcasting information. The experimental modelling of extreme waves was investigated in [7.4], where different approaches were described for experimental modelling of extreme waves and nonlinear effects on wave crests distributions have been investigated, showing that, for a given sea state steepness, the directional wave spreading

reduces the probability of occurrence of extreme wave crest heights. A direct specific link between environmental modelling and nonlinear ship motions assessment was instead provided in [7.3]. In [7.3], idealised spectra and spectra coming from forecasting/hindcasting were both used together with simplified semi-analytical spectral methods for assessing risk of pure loss of stability and parametric rolling, showing that spectral representation can have a significant influence on the final assessment.

Considering the mentioned importance of environment modelling for ship motions predictions, it is evident that future developments in this context should aim at guaranteeing that more realistic environmental models are used in the field of ship stability. Although detailed information on realistic environment are nowadays potentially available (thanks to wave measurements through buoys and/or wave radars, numerical wind&waves forecasting/hindcasting tools, etc.), their use within the ship stability framework is still limited and requires developments and/or transferring of information from other fields. The availability of area specific probabilistic models of directional sea and associated wind spectra could provide an important resource for improving the accuracy of ship safety assessment compared with the presently common use of standard reference environmental conditions. Also, virtuous links could be created between nonlinear ship motions assessment tools and onboard measurement of environmental conditions (wind and waves), in order to provide accurate and relevant real-time measures of ship safety.

8. EDUCATION

Beyond doubt, four decades of ship stability conferences and workshops brought numerous scientific achievements and considerably increased the level of knowledge and the understanding of phenomena related to the ship safety in real operational conditions. Even if



limited to a much shorter time window, the present paper clearly demonstrates this fact. From the educational point of view, the question is, however, to what extent this “newly” acquired knowledge can be/is actually transferred to the present generations of undergraduate naval architecture students, or, more importantly, to what extent this knowledge is supposed to be transferred.

Although the concept of the university education varies across the globe, the objective of the engineering studies is principally the same: to nurture an individual capable of coping with daily tasks and challenges of a particular engineering field. From the naval architecture perspective, the question arises whether this goal is still attainable with the present state of teaching on ship stability, based on classical, mostly deterministic approach that was common in the past. Maintaining its historic role as one of the most important generators of progress, the maritime trade keeps on evolving. New ships, unconventional in terms of size, hull form and powering represent the milestones in this evolutionary process. With new ships, however, new safety and stability problems emerge, while some old problems resurface in a different form. There is a possibility that, if the educational process does not evolve as well, we may end up in educating the engineers of yesterday that are to be struggling with the challenges of tomorrow.

There are some warning signs already. A recent conversation with a young naval architect, employed in a shipyard of a considerable size, who stated that “the ship stability is solved” and that “the seakeeping is the next big thing”, indicated that there is a false impression on what ship stability is in the first place. It is reasonable to assume that the organization of the educational practice was one of the factors that contributed to this misleading image.

So, what is the ship stability about? The idea that the metacentric height represents the stability of a vessel sufficiently well was

gradually superseded by the understanding that the characteristics of the righting arm provide a better insight into the problem, which ultimately led to the founding of the statistical criteria. Further progress resulted in the stability criteria based on the assessment of static and dynamic heel of the ships exposed to external loads, including the “severe wind and rolling criterion” better known as the Weather Criterion. Forty-year history of STAB conferences and workshops was instrumental in shaping the contemporary notion of stability as dynamics of ships (and other floating structures) exposed to the environmental loads (waves, wind and current) where (nonlinear) roll is not the only motion of interest. As a result, modern notion of ship stability in intact condition has become a subject closely related to seakeeping and manoeuvring, whereby the term “intact ship stability” is often used to refer to “large amplitude ship motions and manoeuvring in waves”. The associated phenomena are dealt with methods “borrowed” from nonlinear dynamics and/or are analysed in a probabilistic manner. Of course, the “basic” ship stability problems have not vanished in the meantime. According to some statistics a considerable number of stability failures of small container vessels happen in port, i.e. in calm water conditions.

The assessment of stability in damaged condition evolved from the deterministic approach to a probabilistic one, through at the times turbulent process, triggered by a series of catastrophic accidents involving large number of fatalities. In addition, the knowledge gained through model experiments and numerical simulations performed over the years revealed the importance of flooding dynamics (progressive flooding, sloshing in internal flooded compartments, water accumulation on deck, etc.).

Within the academic community, there is a dilemma whether (and to what extent) these developments are addressed in the classrooms, at least at the undergraduate / M.Sc. level. Therefore, herein, an effort is made to identify



the factors that could hamper the implementation of contemporary concepts of ship stability in the teaching process. Is there a need for an additional, “advanced” course on ship stability and what are the obstacles to the introduction of such a course?

In order to efficiently carry out an “advanced” course on ship stability, a number of conditions are to be met. Due to the fact that it deals with genuinely nonlinear phenomena, ship stability has an inherent “deficiency”: it is complex. The students should be familiar with a list of topics, some of which fall out of the scope of the traditional undergraduate naval architecture courses. Regarding the standard naval architecture subjects, in addition to the knowledge of intact and damage stability in calm water, the comprehension of seakeeping and manoeuvring, beyond the basic level, would be necessary as well. Other desirable “skills” include the understanding of fundamental probability concepts, statistical analysis and stochastic processes. A brief survey of the curricula of several European universities revealed that the courses on probability and statistics are more often than not elective ones and, as such, sometimes in collision with other, equally important engineering subjects. The use of methods of nonlinear dynamics in ship stability problems has become widely accepted. Nonlinear dynamics, however, is normally taught at the postgraduate level. As a result, does it mean that one should obtain a Ph.D. in order to become a “stability engineer”?

The limited availability of appropriate literature is also evident. The available books on the subject either deal with the basic problems of static and dynamic stability in calm water, suitable for introductory courses on ship buoyancy and stability, or discuss much more advanced topics, better fitting for the postgraduate level. Finding an appropriate balance between these two extremes presents a considerable challenge for the lecturer. It should be added, however, that some books that could be used in the ship stability

education of young naval architects were authored by well known researchers within the stability field [8.2, 8.3, 8.4]. Furthermore, the Contemporary ideas on ship stability series [8.1, 8.5] could also be considered as reference material for providing students with a modern approach to ship stability-related issues.

The problem is, however, that although we may refer to such a course as to an advanced one in comparison to the present programs (which inevitably generates a sense that it could be an “elective” subject intended for those that are more research-inclined) the topics discussed are either becoming or have already become a part of everyday engineering practice. Such is the case with, e.g. present probabilistic damage stability regulations; while the floodable lengths curve was a straightforward and an easily understandable tool, that could be incorporated without difficulty in the students’ exercises, the current probabilistic rules are not effortlessly explained (let alone applied in the classroom) whereby the lack of sufficient previously-acquired knowledge of the probability concepts is just a part of the problem. The application of the methodologies embedded in present proposals for “Second Generation Intact Stability Criteria” requires the knowledge of a considerable amount of all the aforementioned subjects. Some experiences indicate that this could be the next “bottleneck” of the engineering practice. Given that the naval architect’s work is guided by the regulatory regime, it sounds reasonable to reiterate the dilemma whether future engineers will be appropriately “armed” under present state of undergraduate education. Without a proper understanding of theoretical foundations of present and future stability criteria, the increase of ship safety may not be proportional to the evident rise of the level of knowledge.

How to introduce these new topics efficiently, without producing a sense of saturation with the ship stability issues and also having in mind that the available time is limited? From the pedagogical point of view,



the evident complexity of the contemporary ship stability topics underlines the need for a “wise” approach to the teacher-student interaction. Such an approach, if based on the understanding of modern perception, may capitalize on the present day tools. The importance of the experimental work can never be overestimated, but it should be noted that complex phenomena are not easily reproduced when resources are limited. Video recordings of successful experiments (nowadays available more than ever) may seem to be a feasible alternative. Indeed, the effect of visually-aided lessons on students’ attention is undisputed. Some believe, however, that the extensive use of videos may oversimplify the teaching process and limit (or even replace) the ability of abstract thinking, very much needed in engineering disciplines. That said, we should be reminded that teaching is about the development of: conceptual understanding; engineering design skills including creativity and judgment; personal and interpersonal skills such as communication and team work; abilities to identify own limitations; active approach to continuous learning throughout lifetime, etc.

The topic is far from being exhausted. The intention herein is merely to put the observed issues on the table and hopefully initiate a wide-ranging discussion on the matter. There isn’t a more competent forum to start such a debate than the STAB conference. In relation to that, the following should be noted. The ship stability as an academic discipline may considerably benefit from an inherent quality of the ship stability as a scientific field: it has a distinct international dimension. In the end, this contribution is an example of collaboration at the international level. International cooperation in the education, including exchange of students and lecturers (i.e. the experts in various areas) cannot solve the problem, but could be a good step towards the understanding of its proportions. Within the framework of the Stability Research & Development Committee several activities in that direction have been already facilitated.

9. FINAL REMARKS

In this paper, a review has been presented of recent developments and elaborated on ideas for future directions on the subject of ship stability, dynamics and safety. The added-value for such an undertaking is explained by the need of a clear and structured overview of past research and results available, before proceeding with future research and the directions and focus it should take.

It is hoped that this work will be useful to both young and experienced researchers in providing a concise reference of the research undertaken in the past six years, and in driving forward with improvements in our knowledge of ship stability and ship dynamics, and on how to improve ship safety through new, innovative and more efficient concepts. This work could be stimulating for identifying lines of research, having a more immediate evidence of the efforts spent in the considered period by many different researchers and institutions.

As a final suggestion, it could be recommended that this massive review exercise is carried out on a regular basis by covering a shorter period than the six years covered herein. A suggestion is that future similar contributions could be done covering the period between two subsequent STAB conferences, in a way that there is some overlap between subsequent reviews. In this way, this effort can become systematic and would provide the means for continuous monitoring of research on the subject of ship stability, dynamics and safety.

10. ACKNOWLEDGMENTS

This collaborative effort has been undertaken by a group of members of the “Stability R&D Committee” (www.shipstab.org/stability-r-d-committee-srdc/). The authors would like to express their sincere thanks to the organisers of the 12th International Conference on Stability of Ships



and Ocean Vehicles (STAB 2015, Glasgow, UK) for the opportunity given to present this work.

11. REFERENCES

Due to the resulting large number of reviewed papers, for the benefit of the reader, the list of references is presented in accordance with the section of the paper each reference has been reviewed in. A limited number of papers appear in more than one sub-list.

Introduction

- 1.1 Vassalos, D., Hamamoto, M., Papanikolaou, A., Molyneux, D., (Editors), 2000, "Contemporary Ideas on Ship Stability", Elsevier, Oxford.
- 1.2 Belenky, V.L., 2001, "Seventh international conference on the stability of ships and ocean vehicles (STAB' 2000) - A review", Marine Technology, Vol. 38, No. 1, pp. 1-8.
- 1.3 Marine Technology, 2003, Sixth International Stability Workshop Papers Reviewed by the SNAME Stability Panel SD-3, in Vol. 40, No. 3.
- 1.4 International Shipbuilding Progress, 2004, Special issue: Selected Papers from the 8th International Conference on Stability of Ships and Ocean Vehicles (STAB 2003), Vol. 51, No. 2/3.
- 1.5 Marine Technology, 2004, Sixth International Stability Workshop Papers Reviewed by the SNAME Stability Panel SD-3, in Vol. 41, No. 1.
- 1.6 Marine Technology, 2004, Sixth International Stability Workshop Papers Reviewed by the SNAME Stability Panel SD-3, in Vol. 41, No. 2.
- 1.7 Pérez Rojas, L., Fernández Gutiérrez, D., "Sobre la Estabilidad de Buques y Vehículos Oceánicos. Una visión de la Conferencia "STAB 2003" ", Ingegneria Naval, Junio 2004, pp. 101-110.
- 1.8 Pérez Rojas, L.P., Belenky, V.L., 2005, "A review of the 8th International Conference on the Stability of Ship and Ocean Vehicles (STAB 2003)", Marine Technology, Vol. 42, No. 1, pp. 21-30.
- 1.9 International Shipbuilding Progress, 2007, Special issue: Selected Papers from the 9th International Conference on Stability of Ships and Ocean Vehicles (STAB 2006), Vol. 54, No. 4.
- 1.10 Neves, M.A.S., Belenky, V., 2008, "A review of the ninth international conference on the stability of ships and ocean vehicles (STAB 2006)", Marine Technology, Vol.45, No. 3, pp. 147-156.
- 1.11 Neves, M.A.S., Belenky, V., de Kat, J.O., Spyrou, K., Umeda, N., (Editors), 2011, "Contemporary Ideas on Ship Stability and Capsizing in Waves", Springer, Dordrecht, Heidelberg, London, New York.

Intact Stability

- 2.1 Kobyliński, L., 2009, "Future Generation Stability Criteria – Prospects and Possibilities", Proc. STAB2009, pp.101-110.
- 2.2 Bassler, C. C., Belenky, V., Bulian, G., Francescutto, A., Spyrou, K., Umeda, N., 2009, "A Review of Available Methods for Application to Second Level Vulnerability Criteria", Proc. STAB2009, pp. 111-128.
- 2.3 Belenky, V., Bassler, C.C., Spyrou, K., 2009, "Dynamic Stability Assessment in Early-Stage Ship Design", Proc. STAB2009, pp.141-153.

- 2.4 Larsson, A., Ribbe, G., Routi, A.-L., 2009, "A Procedure for Determining a GM Limit Curve Based on an Alternative Model Test and Numerical Simulations", Proc. STAB2009, pp. 181-189.
- 2.5 Spyrou, K., Weems, K., Belenky, V., 2009, "Patterns of Surf-Riding and Broaching-To captured by Advanced Hydrodynamic Modelling", Proc. STAB2009, pp.331-345.
- 2.6 Grochowalski, S., 2009, "Investigation of The Hydrodynamic Forces Generated on Submerged Part of a Deck During Ship Large Motions In Waves", Proc. STAB2009, pp. 399-408.
- 2.7 Grochowalski, S., Jankowski, J., 2009, "Validation Methodology for Simulation Software of Ship Behaviour in Extreme Seas", Proc. STAB2009, pp. 409-420.
- 2.8 Xing, Z., McCue, L., 2009, "Parameter Identification for Two Nonlinear Models of Ship Rolling Using Neural Networks", Proc. STAB2009, pp. 421-428.
- 2.9 Maki, A., Umeda, N., 2009, "Bifurcation and Chaos in Yaw Motion of a Ship at Lower Speed in Waves and its Prevention Using Optimal Control", Proc. STAB2009, pp. 429-440.
- 2.10 Neves, M.A.S., Vivanco, J.E.M., Rodríguez, C.A., 2009, "Nonlinear Dynamics on Parametric Rolling of Ships in Head Seas", Proc. STAB2009, pp. 509-520.
- 2.11 Shigunov, V., El Moctar, O., Rathje, H., 2009, "Conditions of Parametric Rolling", Proc. STAB2009, pp. 521-532.
- 2.12 Ogawa, Y., 2009, "A Study on Numerical Modelling for the Parametric Rolling", Proc. STAB2009, pp. 533-540.
- 2.13 Katayama, T., Taniguchi, T., Umeda, N., 2009, "An Experimental Study on Parametric Rolling of A High Speed Trimaran In Head Sea", Proc. STAB2009, pp. 541-548.
- 2.14 Hong, S.Y., Yu, H.C., Kim, S., Sung, H.G., 2009, "Investigation of Parametric Roll of a Container Ship in Irregular Seas by Numerical Simulation", Proc. STAB2009, pp. 549-558.
- 2.15 Spanos, D., Papanikolaou, A., 2009, "On the Decay and Disappearance of Parametric Roll of Ships in Steep Head Waves", Proc. STAB2009, pp. 559-566.
- 2.16 Bulian, G., Francescutto, A., Fucile, F., 2009, "Numerical and Experimental Investigation on the Parametric Rolling of a Trimaran Ship in Longitudinal Regular Waves", Proc. STAB2009, pp. 567-582.
- 2.17 Sutulo, S., Guedes Soares, C., 2009, "Computation of Hydrodynamic Loads on a Ship Manoeuvring In Regular Waves", Proc. STAB2009, pp. 609-620.
- 2.18 Spanos, D., Papanikolaou, A., 2009, "Benchmark Study on Numerical Simulation Methods for the Prediction of Parametric Roll of Ships in Waves", Proc. STAB2009, pp. 627-635.
- 2.19 Belenky, V., Reed, A.M., Weems, K.M., 2009. "Probability of Capsizing in Beam Seas with Piecewise Linear Stochastic GZ Curve", Proc. STAB 2009, pp. 637-650.
- 2.20 Ogawa, Y., 2009, "A Study for the Effect of Correlation between Winds and Waves on the Capsizing Probability under Dead Ship Condition", Proc. STAB 2009, pp. 651-660.
- 2.21 Athanassoulis, G., Tsantili, I., Sapsis, T., 2009, "New Equations for the Probabilistic Prediction of Ship Roll Motion in a Realistic Stochastic Seaway", Proc. STAB 2009, pp. 661-672.
- 2.22 Bassler, C., Dipper, M., Lang, G., 2009, "Formation of Large-Amplitude Wave Groups in an Experimental Model Basin", Proc. STAB 2009, pp. 673-686.
- 2.23 Francescutto, A., Umeda, N., 2010, "Current Status of New Generation Intact Stability Criteria Development", Proc. ISSW2010, pp.1-5.
- 2.24 Peters, W. S., Belenky, V., Bassler, C. C., 2010, "On Vulnerability Criteria for Righting Lever Variations in Waves", Proc. ISSW2010, pp. 6-16.
- 2.25 Umeda, N., Yamamura, S., 2010, "Designing New Generation Intact Stability Criteria on Broaching Associated with Surf-Riding", Proc. ISSW2010, pp. 17-25.
- 2.26 Shigunov, V., El Moctar, O., Rathje, H., 2010, "Research towards Goal-Based Standards for Container Shipping", Proc. ISSW2010, pp. 26-31.



- 2.27 Bassler, C., Belenky, V., Dipper, M., 2010, "Application of Wave Groups to Assess Ship Response in Irregular Seas", Proc. ISSW2010, pp. 58-66.
- 2.28 Hofman, M., Bačkalov, I., 2010, "Risk-Based Analysis of Inland Vessel Stability", Proc. ISSW2010, pp. 67-72.
- 2.29 Campbell, B., Belenky, V., 2010, "Assessment of Short-Term Risk with Monte-Carlo Method", Proc. ISSW2010, pp. 85-92.
- 2.30 Peters, A., 2010, "Tolerable Capsize Risk of a Naval Vessel", Proc. ISSW2010, pp. 93-107.
- 2.31 Alman, P., 2010, "Approaches for Evaluating Dynamic Stability in Design", Proc. ISSW2010, pp. 121-128.
- 2.32 Carette, N. F. A. J., Walree, F. van, 2010, "Calculation method to include water on deck effects", Proc. ISSW2010, pp. 166-172.
- 2.33 Belknap, W.F., Reed, A.M., "TEMPEST — A New Computationally Efficient Dynamic Stability Prediction Tool", Proc. ISSW2010, pp. 185-197.
- 2.34 Neves, M.A.S., Rodriguez, C.A., Vivanco, J.E.M., Villagómez Rosales, J.C., Agarwal, R., 2010, "Integrity Diagrams of the Ship/U-Tank System Undergoing Parametric Rolling", Proc. ISSW2010, pp. 288-294.
- 2.35 Hashimoto, H., Umeda, N., 2010, "A study on Quantitative Prediction of Parametric Roll in Regular Waves", Proc. ISSW2010, pp. 295-301.
- 2.36 Bulian, G., 2010, "Checking vulnerability to pure loss of stability in long crested following waves: a probabilistic approach", Ocean Engineering, Vol. 37, pp. 1007-1026.
- 2.37 Peters, W.S., Belenky, V., Bassler, C.C., Spyrou, K., 2011, "On Vulnerability Criteria for Parametric Roll and Surf-riding", Proc. ISSW2011, pp.1-6.
- 2.38 Bulian, G., Francescutto, A., 2011, "Considerations on Parametric Roll and Dead Ship Conditions for the Development of Second Generation Intact Stability Criteria", Proc. ISSW2011, pp. 7-18.
- 2.39 Umeda, N., Izawa, S., Sano, H., Kubo, H., Yamane K., Matsuda, A., 2011, "Validation Attempts on Draft New Generation Intact Stability Criteria", Proc. ISSW2011, pp. 19-26.
- 2.40 Shigunov, V., Rathje, H., El Moctar, O., Altmayer, B., 2011, "On the Consideration of Lateral Accelerations in Ship Design Rules", Proc. ISSW2011, pp. 27-35.
- 2.41 Wu, W., McCue, L., 2011, "Melnikov's Method Applied to a Multi-DOF Ship Model", Proc. ISSW2011, pp. 73-78.
- 2.42 Belknap, W.F., Smith, T.C., Campbell, B.L., 2011, "Addressing Challenges in the Validation of Dynamic Stability Simulation Tools", Proc. ISSW2011, pp. 81-89.
- 2.43 Leadbetter, M., Rychlik, I., Stambaugh, K., 2011, "Estimating Dynamic Stability Event Probabilities from Simulation and Wave Modeling Methods", Proc. ISSW2011, pp. 147-154.
- 2.44 Kim, D., Troesch, A., 2011, "Stochastic Wave Inputs for Extreme Roll in Near Head Seas", Proc. ISSW2011, pp. 155-161.
- 2.45 Belenky, V., Spyrou, K., Weems, K., 2011, "Split-Time Methods for Surf-Riding and Broaching-To", Proc. ISSW2011, pp. 163-168.
- 2.46 Su, Z., Falzarano, J., 2011, "Gaussian and Non-Gaussian Response of Ship Rolling in Random Beam Waves", Proc. ISSW2011, pp. 189-193.
- 2.47 Reed, A.M., 2011, "26th ITTC Parametric Roll Benchmark Study", Proc. ISSW2011, pp. 195-204.
- 2.48 Belenky, V., Weems, K., 2011, "On the Distribution of Parametric Roll", Proc. ISSW2011, pp. 205-212.
- 2.49 Míguez González, M., López Peña, F., Díaz Casás, V., Neves, M.A.S., 2011, "Large Amplitude Roll Motion Forecasting through an Artificial Neural Network System", Proc. ISSW2011, pp. 219-224.
- 2.50 Song, K.H., Kim, Y., 2011, "Quantitative Analysis of Parametric Roll and Operational Guidance", Proc. ISSW2011, pp. 225-232.
- 2.51 Schreuder, M., 2011, "Parameter Study of Numerical Simulation of Parametric Rolling of Ships", Proc. ISSW2011, pp. 233-240.
- 2.52 Hong, S.H., Nam, B.W., Yu, H.-C., Kim, S., 2011, "Investigation of Susceptibility of Parametric Roll in Regular and Irregular Waves", Proc. ISSW2011, pp. 241-248.
- 2.53 Wu, W., Bulian, G., McCue, L., 2011, "Uncertainty Analysis for Parametric Roll Using Non-intrusive Polynomial Chaos", Proc. ISSW2011, pp. 249-255.
- 2.54 Hughes, M.J., Kopp, P.J., Miller, R.W., "Modelling of Hull Lift and Cross Flow Drag Forces in Large Waves in a Computationally Efficient Dynamic Stability Prediction Tool", Proc. ISSW2011, pp. 331-339.
- 2.55 Tellet, D., 2011, "Incorporating Risk into Naval Ship Weight and Stability Control", Proc. ISSW2011, pp. 369-374.
- 2.56 Ypma, E., Harmsen, E., 2012, "Development of a New Methodology to Predict the Capsize Risk of Ships", Proc. STAB2012, pp.1-10.
- 2.57 Shigunov, V., Themelis, N., Spyrou, K., 2012, "Critical wave groups vs. direct Monte-Carlo simulations for typical stability failure modes of a containership", Proc. STAB2012, pp. 11-21.
- 2.58 Falzarano, J., Su, Z., Jamnongpipatkul, A., 2012 "Application of Stochastic Dynamical System to Nonlinear Ship Rolling Problems", Proc. STAB2012, pp. 21-29.
- 2.59 Kubo, T., Umeda, N., Izawa, S., Matsuda, A., "Total Stability Failure Probability of a Ship in Irregular Beam Wind and Waves: Model Experiment and Numerical Simulation", Proc. STAB2012, pp. 39-46.
- 2.60 Bačkalov, I., 2012, "A Probabilistic Analysis of Stability Regulations for River-Sea Ships", Proc. STAB2012, pp. 67-78.
- 2.61 Athanassoulis, G., Tsantili, I., Kapelonis, Z., 2012, "Steady State Probabilistic Response of a Half Oscillator Under Colored, Gaussian or non-Gaussian Excitation", Proc. STAB2012, pp. 79-90.
- 2.62 Kobylinski, L., 2012, "Stability Criteria - 50 Years of Experience and Future Prospects", Proc. STAB2012, pp. 91-100.
- 2.63 Smith, T., 2012, "Approaches to Ship Motion Simulation Acceptance Criteria", Proc. STAB2012, pp. 101-114.
- 2.64 Peters, W.S., Belenky, V.B., Reed, A.M., 2012, "On Regulatory Framework of Direct Stability Assessment", Proc. STAB2012, pp.115-128.
- 2.65 Cooper, M., McCue, L., 2012, "Effectiveness of Chaotic System Measures for the Validation of Ship Dynamics Simulations", Proc. STAB2012, pp. 363-372.
- 2.66 Hashimoto, H., Umeda, N., 2012, "Validation of a Numerical Simulation Model for Parametric Rolling Prediction Using a PCTC", Proc. STAB2012, pp. 141-149.
- 2.67 Yu, L., Ma, N., Gu, X., 2012, "Study on Parametric Roll and Its Rudder Stabilization Based on Unified Seakeeping and Maneuvering Model", Proc. STAB2012, pp. 159-169.
- 2.68 Bulian, G., Sinibaldi, M., Francescutto, A., 2012, "Roll Motion of a Ship with Low Metacentric Height in Bichromatic Beam Waves", Proc. STAB2012, pp. 187-200.
- 2.69 Kim, S., Sung, Y.J., 2012, "Numerical Simulations of Maneuvering and Dynamic Stability of a Containership in Waves", Proc. STAB2012, pp. 215-225.
- 2.70 Belknap, W.F., Reed, A.M., Hughes, M.J., 2012, "Model Characteristics and Validation Approach for a Simulation Tool Supporting Direct Stability Assessment", Proc. STAB2012, pp. 227-242.
- 2.71 Matusiak, J., Stigler, C., 2012, "Ship Roll Motion in Irregular Waves During a Turning Circle Maneuver", Proc. STAB2012, pp. 291-297.
- 2.72 Breu, D., Holden, C., Fossen, T., 2012, "Stability of Ships in Parametric Roll Resonance Under Time-Varying Heading and Speed", Proc. STAB2012, pp. 305-313.
- 2.73 Fan, J., Zhu, R., Miao, G., Huang, X., 2012, "The Unstable Boundary of Large Amplitude Rolling of a Ship in Waves", Proc. STAB2012, pp. 315-321.
- 2.74 Spyrou, K., Belenky, V., Themelis, N., Weems, K., 2012, "Conditions for Surf-riding in an Irregular Seaway", Proc. STAB2012, pp. 323-336.
- 2.75 Tigkas, J., Spyrou, K., 2012, "Continuation Analysis of Surf-riding and Periodic Responses of a Ship in Steep



- Quarterming Seas”, *Proc. STAB2012*, pp. 337-349.
- 2.76 Wu, W., Spyrou, K., 2012, “Technical Note: Prediction of the Threshold of Global Surf-Riding by an Extended Melnikov Method”, *Proc. STAB2012*, pp. 441-445.
- 2.77 Hashimoto, H., Ito, Y., Kawakami, N., Sueyoshi, M., 2010, “Numerical Simulation Method for Coupling of Tank Fluid and Ship Roll Motions”, *Proc. STAB2012*, pp. 477-485.
- 2.78 Míguez González, M., Díaz Casás, V., López Peña, F., Pérez Rojas, L., 2012, “Experimental Parametric Roll Resonance Characterization of a Stern Trawler in Head Seas”, *Proc. STAB2012*, pp. 625-634.
- 2.79 Pagès, A., Maisonneuve, J.-J., Wandji, C., Corrigan, P., Vincent, B., 2012, “Small Fishing Vessels Study and Modelling for the Improvement of the Behaviour in Extreme Seas”, *Proc. STAB2012*, pp. 643-653.
- 2.80 Belenky, V., Weems, K., Bassler, C. C., Dipper, M., Campbell, B., Spyrou, K. J., 2012, “Approaches to rare events in stochastic dynamics of ships”, *Probabilistic Engineering Mechanics*, Vol. 28, pp. 30-38.
- 2.81 Peters, W., Belenky, V., Bassler, C., Spyrou, K., Umeda, N., Bulian, G., Altmayer, B., 2012, “The Second Generation Intact Stability Criteria: An Overview of Development”, *Trans. SNAME*, Vol. 119 (2011), pp. 225-264.
- 2.82 Fossen, T.I., Nijmeijer, H., (Editors) 2012, “Parametric Resonance in dynamical systems”, contributing authors: Belenky, V., Blanke, M., Breu, D., A., Bulian, G., Feng, L., Fey, R.H.B., Fossen, T.H., Francescutto, A., Galeazzi, R., Hashimoto, H., Holden, C., Huss, M., Jensen, J.J., Kraaij, C.S., Mallon, N.J., Neves, M.A.S., Nijmeijer, H., Palmquist, M., Pettersen, K.Y., Poulsen, N.K., Pena-Ramirez, Rodriguez, C.A., Rosen, A., Sogawa, Y., Tsukamoto, I., Umeda, N., Weems, K., - Springer
- 2.83 Belenky, V., Weems, K., Pipiras, V., 2013, “Split-time Method for Calculation of Probability of Capsizing Due to Pure Loss of Stability”, *Proc. ISSW2013*, pp.70-78.
- 2.84 Wandji, C., Corrigan, P., 2013, “Sample Application of Second Generation IMO Intact Stability Vulnerability Criteria as Updated during SLF 55”, *Proc. ISSW2013*, pp. 121-129.
- 2.85 Umeda, N., 2013, “Current Status of Second Generation Intact Stability Criteria Development and Some Recent Efforts”, *Proc. ISSW2013*, pp. 138-157.
- 2.86 Weems, K., Wundrow, D., 2013, “Hybrid Models for Fast Time-Domain Simulation of Stability Failures in Irregular Waves With Volume-Based Calculations for Froude-Krylov and Hydrostatic Forces”, *Proc. ISSW2013*, pp. 130-137.
- 2.87 Cho, S.K., S., H.G., Hong, S.Y., Kim, Y.H., 2013, “Study of the Stability of Turret moored Floating Body”, *Proc. ISSW2013*, pp.199-206.
- 2.88 Belenky, V., Pipiras, V., Kent, C., Hughes, M., Campbell, B., Smith, T., 2013, “On the Statistical Uncertainties of Time-domain-based Assessment of Stability Failures: Confidence Interval for the Mean and Variance of Time Series”, *Proc. ISSW2013*, pp. 251-258.
- 2.89 Bulian, G., Francescutto, A., 2013, “Second Generation Intact Stability Criteria: on the validation of codes for direct stability assessment in the framework of an example application”, *Polish Maritime Research*, No.4/2013, pp. 52-61.
- 2.90 Söder, C.-J., Rosén, A., Ovegård, E., Kutteneuler, J., Huss, M., 2013, “Parametric roll mitigation using rudder control”, *Journal of Marine Science and Technology*, Vol. 18, pp. 395-403.
- 2.91 Spyrou, K., Themelis, S., Kontolefas, L., 2014, “What is Surf-Riding in Irregular Seas?”, *Proc. ISSW2014*, pp. 12-18.
- 2.92 Peters, W.S., Belenky, V., Spyrou, K., 2014, “Regulatory Use of Nonlinear Dynamics: an Overview”, *Proc. ISSW2014*, pp.28-35.
- 2.93 Zuzick, A.V., Reed, A.M., Belknap, W.F., Campbell, B.L., 2014, “Applicability of the Difference between Population Statistics as an Acceptance Criteria Metric for Seakeeping Validation”, *Proc. ISSW2014*, pp. 36-43.
- 2.94 Umeda, N., Kawaida, D., Ito, Y., Tsutsumi, Y., Matsuda, A., Terada, D., 2014, “Remarks on Experimental Validation Procedures for Numerical Intact Stability Assessment with Latest Examples”, *Proc. ISSW2014*, pp. 77-83.
- 2.95 Nakamura, M., Yoshimura, Y., Shiken, D., 2014, “Model Experiments in Following and Quarterming Seas using a Small Size Ship Model”, *Proc. ISSW2014*, pp. 85-92.
- 2.96 Horel, B., Guillermin, P.-E., Rousset, J.-M., Alessandrini, B., 2014, “Experimental Database for Surf-Riding and Broaching-to Quantification based on Captive Model Tests in Waves”, *Proc. ISSW2014*, pp. 94-104.
- 2.97 Lu, J., Gu, M., Umeda, N., 2014, “Experimental and Numerical Study on Predicting Method of Parametric Rolling in Regular Head Seas”, *Proc. ISSW2014*, pp.117-125.
- 2.98 Smith, T., 2014, “Example of Validation of Statistical Extrapolation”, *Proc. ISSW2014*, pp. 140-143.
- 2.99 Campbell, B., Belenky, V., Pipiras, V., 2014, “On the Application of the Generalized Pareto Distribution for Statistical Extrapolation in the Assessment of Dynamic Stability in Irregular Waves”, *Proc. ISSW2014*, pp. 149-156.
- 2.100 Yu, L., Ma, N., Gu, X., 2014, “Numerical Investigation into Ship Stability Failure Events in Quarterming Seas Based on Time Domain Weakly Nonlinear Unified Model”, *Proc. ISSW2014*, pp. 229-235.
- 2.101 González, M.M., Casás, V.D., Pérez-Rojas, L., Ocampo, F.J., Pena, D., 2014, “Application of Second Generation IMO Intact Stability Criteria to Medium – Sized Fishing Vessels”, *Proc. ISSW2014*, pp. 269-277.
- 2.102 Spyrou, K.J., Belenky, V., Themelis, N., Weems, K., 2013, “Detection of surf-riding behavior of ships in irregular seas”, *Nonlinear Dynamics*, Vol. 78, 2014, pp. 649-667
- ### Damage Stability
- 3.1 Kishev, R., Rakitin, V., Kirilova, S., 2009, “Analysis of the Capsize and Loss of a 12000 Dwt Bulk Carrier”, *Proc. STAB2009*, pp. 191-198.
- 3.2 Källström, C., Allenström, B., Ottosson P., 2009, “Analysis of the Sinking Sequence of MV Estonia Using a Combined Simulation and Model Test Approach”, *Proc. STAB2009*, pp. 199-208.
- 3.3 Vassalos, D., Cai, W., Konovessis, D., 2009, “Data Mining of Marine Accident/Incident Database for use in Risk-Based Ship Design”, *Proc. STAB2009*, pp. 209-218.
- 3.4 Pawłowski, M., 2009, “Developing the S Factor”, *Proc. STAB2009*, pp. 245-252.
- 3.5 Ruponen, P., 2009, “On the Application of Pressure-Correction Method for Simulation of Progressive Flooding”, *Proc. STAB2009*, pp. 271-279.
- 3.6 Santos, T.A., Dupla, P., Soares C.G., 2009, “Numerical Simulation of the Progressive Flooding of a Box-Shaped Barge”, *Proc. STAB2009*, pp. 281-294.
- 3.7 Mallat, C.K., Rousset, J.M., Ferrant P., 2009, “On Factors Affecting the Transient and Progressive Flooding Stages of Damaged Ro-Ro Vessels”, *Proc. STAB2009*, pp. 295-305.
- 3.8 Cichowicz, J., Vassalos, D., Logan J., 2009, “Probabilistic Assessment of Post-Casualty Availability of Ship Systems”, *Proc. STAB2009*, pp. 453-462.
- 3.9 Tsakalakis, N., Vassalos, D., Puisa R., 2009, “Goal-Based Ship Subdivision and Layout”, *Proc. STAB2009*, pp. 687-696.
- 3.10 Puisa, R., Vassalos, D., Guarín L., 2009, “Design for Safety with Minimum Life-Cycle Cost”, *Proc. STAB2009*, pp. 697-706.
- 3.11 Lee, D., Choi, J., Kang, H.J., 2009, “Improvement of Survivability by Behaviour Simulation of a Damaged Ship”, *Proc. STAB2009*, pp. 741-746.
- 3.12 Cho, S.K., Sung, H.G., Nam, B.W., Hong, S.Y., Kim K.S., 2009, “Experimental Study on Flooding of a Cruiser in Waves”, *Proc. STAB2009*, pp. 747-753.
- 3.13 Dodman, J., 2010, “Going Forward with Safer Return to Port”, *Proc. ISSW2010*, pp. 32-37.
- 3.14 Scott, A.L., 2010, “Damage Stability of Ro-Pax Ships with Water on Deck”, *Proc. ISSW2010*, pp. 38-45.
- 3.15 Papanikolaou, A., Mains, C., Russas, S., Szalek, R., Tsakalakis, N., Vassalos, D., Zaphronitis, G., 2010,



- “GOALDS – Goal Based Damage Stability”, Proc. ISSW2010, pp. 46-57.
- 3.16 Spanos, D., Papanikolaou, A., 2010, “On the Time-Dependent Survivability of RoPax Ships”, Proc. ISSW2010, pp. 143-147.
- 3.17 Pawlowski, M., 2010, “Comparison of s-Factor According to SOLAS and SEM for Ro-Pax Vessels”, Proc. ISSW2010, pp. 148-152.
- 3.18 Ogawa, Y., Takeda, S., 2010, “A Study on the Damage Stability Requirements for Ro-Ro Passenger Ships”, Proc. ISSW2010, pp. 153-158.
- 3.19 Ypma, E.L., Turner, T., 2010, “An Approach to the Validation of Ship Flooding Simulation Models”, Proc. ISSW2010, pp. 173-184.
- 3.20 Corrigan, P., Arias, A., 2010, “Flooding Simulations of ITTC and SAFEDOR Benchmark Test Cases using CRV Shippers Software”, Proc. ISSW2010, pp. 238-245.
- 3.21 Cho, S.K., Sung, H.G., Hong, S.Y., Nam, B.W., Kim, Y.S., 2010, “Study on the Motions and Flooding Process of a Damaged Ship in Waves”, Proc. ISSW2010, pp. 246-254.
- 3.22 Khaddaj-Mallat, C., Rousset, J.M., Alessandrini, B., Delhommeau, G., 2010, “An Application of the DOE Methodology in Damage Survivability”, Proc. ISSW2010, pp. 255-261.
- 3.23 Tsakalakis, N., Cichowicz, J., Vassalos, D., 2010, “The Capsize Band Concept Revisited”, Proc. ISSW2010, pp. 262-271.
- 3.24 Mermiris, G., Vassalos, D., 2010, “Damage Stability Making Sense”, Proc. ISSW2010, pp. 302-309.
- 3.25 Papanikolaou, A., Bulian, G., Mains, C., 2011, “GOALDS – Goal Based Damaged Stability: Collision and Grounding Damages”, Proc. ISSW2011, pp. 37-44.
- 3.26 Spanos, D., Papanikolaou, A., 2011, “Considerations on the Survivability Assessment of Damaged Ships”, Proc. ISSW2011, pp. 45-52.
- 3.27 Scott, A., 2011, “IMO Developments on RoPax Safety”, Proc. ISSW2011, pp. 53-56.
- 3.28 Pearson, J., 2011, “Impact of Watertight Door Regulations on Ship Survivability”, Proc. ISSW2011, pp. 57-59.
- 3.29 Gao, Z., Gao, Q., Vassalos, D., 2011, “Numerical Study of Damaged Ship Motion in Waves”, Proc. ISSW2011, pp. 257-261.
- 3.30 Manderbacka, T.L., Matusiak, J.E., Ruponen, P., 2011, “Ship Motions Caused by Time-Varying Extra Mass on Board”, Proc. ISSW2011, pp. 263-269.
- 3.31 Schreuder, M., 2011, “A Method for Assessment of the Survival Time of a Ship after Collision”, Proc. ISSW2011, pp. 375-390.
- 3.32 Tsakalakis, N., Puisa, R., Mohamed, K., Vassalos, D., Tuzcu, C., 2011, “A Performance-Based Survivability Assessment of Regulatory Frameworks”, Proc. ISSW2011, pp. 391-397.
- 3.33 Cai, W., Konovessis, D., Vassalos, D., 2011, “Integration of Damage Stability into a Risk Management Framework”, Proc. ISSW2011, pp. 399-404.
- 3.34 Cichowicz, J., Tsakalakis, N., Vassalos, D., Jasionowski, A., 2011, “Survivability of Passenger Vessels – Re-engineering of the S-Factor”, Proc. ISSW2011, pp. 405-414.
- 3.35 Tsakalakis, N., Konovessis, K., Vassalos, D., 2011, “Defining Rational Damage Stability Requirements”, Proc. ISSW2011, pp. 415-420.
- 3.36 Ran, H., Rask, I., Janson, C. E., 2012, “Damaged Ro-Pax Vessel Time to Capsize”, Proc. STAB2012, pp. 373-379.
- 3.37 Ohashi, K., Ogawa, Y., Shiraishi, K., 2012, “Study on the Evaluation for Performance of the Cross Flooding Arrangements by means of the Computational Fluid Dynamics”, Proc. STAB2012, pp. 381-389.
- 3.38 Ruponen, P., Larmela, M., Pennane, P., 2012, “Flooding Prediction Onboard a Damaged Ship”, Proc. STAB2012, pp. 391-400.
- 3.39 Spanos, D., Papanikolaou, A., 2012, “Time Dependent Survivability against Flooding of Passenger Ships in Collision Damages”, Proc. STAB2012, pp. 401-409.
- 3.40 Dankowski, H., 2012, “An Explicit Progressive Flooding Simulation Method”, Proc. STAB2012, pp. 411-423.
- 3.41 Sadat-Hosseini, H., Kim, D. H., Lee, S. K., Rhee, S. H., Carrica, P., Stern, F., Rhee, K. P., 2012, “CFD and EFD Study of Damaged Ship Stability in Calm Water and Regular Waves”, Proc. STAB2012, pp. 425-452.
- 3.42 Shiraishi, K., Ogawa, Y., 2012, “A Study for the Harmonised Probabilistic Approach for Damage Stability Taking Account of the Difference Between Collision and Grounding”, Proc. STAB2012, pp. 453-460.
- 3.43 Pawlowski, M., Glowacka, D., 2012, “Developing the p-Factor for Grounding”, Proc. STAB2012, pp. 461-470.
- 3.44 Szoza, Z., 2012, “Capsizing and Sinking of the Dredger Rozgwiazda”, Proc. STAB2012, pp. 735-741.
- 3.45 Kruger, S., Dankowski, H., Teuscher, C., 2012, “Numerical Investigations of the Capsizing Sequence of SS HERAKLION”, Proc. STAB2012, pp. 743-753.
- 3.46 Papanikolaou, A., Boulougouris, E., Sklaventis, A., 2012, “Investigation into the Sinking of the RO-RO Passenger Ferry S.S HERAKLION”, Proc. STAB2012, pp. 755-766.
- 3.47 Junco, F., Marcote, J. M., Dia, V. and Miguez, M., 2012, “Influence of Lower Cargo Deck Longitudinal Subdivision of SOLAS 90/2004 on Ro-Pax Vessels over Attained Damage Stability Indices as 2006 Amendments SOLAS per MSC 216(82)”, Proc. STAB2012, pp. 767-773.
- 3.48 Vassalos, D., 2012, “Damage Stability of Passenger Ships – Notions and Truths”, Proc. STAB2012, pp. 775-789.
- 3.49 Puisa, R., Zagorski, P., Vassalos, D., 2012, “Effect of Revised Damage Survivability Formulation upon Ship Design”, Proc. STAB2012, pp. 791-806.
- 3.50 Kwon, S., Chen, Q., Mermiris, G., Vassalos, D., 2012, “Coupling of Progressive Structural Failure and Loss of Stability in the Safe Return to Port Framework”, Proc. STAB2012, pp. 807-818.
- 3.51 Jalonen, R., Ruponen, P., Jasionowski, A., Maurier, P., Kajosaari, M., Papanikolaou, A., 2012, “FLOODSTAND – Overview of Achievements”, Proc. STAB2012, pp. 819-829.
- 3.52 Zaraphonitis, G., Skoupas, S., Papanikolaou, A., Cardinale, M., 2012, “Multiobjective Optimisation of ROPAX Ships Considering the SOLAS 2009 and GOALDS Damage Stability Formulations”, Proc. STAB2012, pp. 831-840.
- 3.53 Montewka, J., Goerlandt, F., Ehlers, S., Hinz, T., Kujala, P., 2013, “A risk framework for maritime transportation systems”, Proc. ISSW2013, pp. 58-69.
- 3.54 Lemoine, L., Mahé, F., Morisset, N., Bertin, R., 2013, “Interpretation and Design Implications of Probabilistic Damage Stability Regulation”, Proc. ISSW2013, pp. 214-227.
- 3.55 Zaraphonitis, G., Papanikolaou, A., Roussou, C., Kanelopoulou, A., 2013, “Comparative Study of Damage Stability Regulations and Their Impact on the Design and Safety of Modern RoPax Ships”, Proc. ISSW2013, pp. 235-242.
- 3.56 Vassalos, D., Jasionowski, A., 2013, “Emergency Response in Ship Flooding Casualties”, Proc. ISSW2013, pp. 259-263.
- 3.57 Lee, G.J., Walree, F. van, Reed, A.M., Peters, A., Gualeni, P., Katayama, T., Duan, W.Y., 2014, “Air Pressure Scale Effects during Damage Model Tests”, Proc. ISSW2014, pp. 105-109.
- 3.58 Billard, J.Y., Grinnaert, F., Delumeau, I., Vonier, P., Creismeas, P., Leguen, J.F., Ferreiro, L.D., 2014, “Forensic Study of BOUVET Capsizing”, Proc. ISSW2014, pp. 110-116.
- 3.59 Lee, G.J., Reed, A.M., Van Walree, F., Peters, A., Gualeni, P., Katayama, T., Duan, W., 2014, “The Inertia Contributions due to Floodwater Mass”, Proc. ISSW2014, pp. 199-203.
- 3.60 Yuzui, T., Ogawa, Y., 2014, “Consideration of Risk Level in Terms of Damage Stability of Old Ship”, Proc. ISSW2014, pp. 278-285.
- 3.61 Vassalos, D., Boulougouris, E., Guarin, L., Jasionowski, A., Garner, J., 2014, “Regulatory, Design, Operational and Emergency Response Measures for Improving the Damage Survivability of Existing RoPax”, Proc. ISSW2014, pp. 292-300.
- 3.62 Tagg, R., 2014, “Comparison of Survivability between



- SOLAS 90/95 and SOLAS 2009 Ships - A Retrospective View 10 Years on from Project HARDER”, Proc. ISSW2014, 8 pp.
- Stability for Specific Types of Vessels and Floating Objects**
- Fishing Vessels**
- 4.1.1 Marón, A., Carrillo, E., Prieto, M.E., Gutiérrez, C., Carmona, J.C., Miguel, F., 2009, “Investigation on the Causes of Fishing Vessel Capsizes by Means of Model Tests. The CEHIPAR Experience”, Proc. STAB 2009, pp. 219-228.
- 4.1.2 Waseda, T., Kinoshita, T., 2010, “Freak waves and capsizing accidents”, Proc. ISSW 2010, pp. 79-84.
- 4.1.3 Míguez González, M., López Peña, F., Díaz Casás, V., Neves, M.A.S., 2011, “Large Amplitude Roll Motion Forecasting through an Artificial Neural Network System”, Proc. ISSW 2011, pp. 219-224.
- 4.1.4 McKay, G., Krgovich, J., Howe, B., 2012, “The Safest Catch Program – Fishermen Taking Ownership of Safety”, Proc. STAB 2012, pp. 635-642.
- 4.1.5 Míguez González, M., Díaz Casás, V., López Peña, F., Pérez Rojas, L., 2012, Experimental Parametric Roll Resonance Characterization of a Stern Trawler in Head Seas, Proc. STAB 2012, pp. 625-634.
- 4.1.6 Pagès, A., Maisonneuve, J.-J., Wandji, C., Corrigan, P., Vincent, B., “Small Fishing Vessels Study and Modelling for the Improvement of the Behaviour in Extreme Seas”, Proc. STAB 2012, pp. 643-653.
- 4.1.7 McCue, L., 2012, “Putting Vessel Motion Research into the Hands of Operators”, Proc. STAB 2012, pp. 679-687.
- 4.1.8 Míguez González, M., Díaz Casás, V., López Peña, F., Pérez Rojas, L., 2013, “Experimental Analysis of Roll Damping in Small Fishing Vessels for Large Amplitude Roll Forecasting”, Proc. ISSW 2013, pp. 95-103.
- 4.1.9 Taguchi, H., Matsuda, A., Shoji, K., 2013, “Experimental Investigations into Accidents of Two Japanese Fishing Vessels”, Proc. ISSW 2013, pp. 104-111.
- 4.1.10 Gudmundsson, A., 2013, “The FAO/ILO/IMO Safety Recommendations for Decked Fishing Vessels of Less than 12 metres in Length and Undecked Fishing Vessels – a major milestone to improve safety for small fishing vessels”, Proc. ISSW 2013, pp. 112-120.
- 4.1.11 González, M.M., Casás, V.D., Pérez-Rojas, L., Ocampo, F.J., Pena, D., 2014, “Application of Second Generation IMO Intact Stability Criteria to Medium – Sized Fishing Vessels”, Proc. ISSW2014, pp. 269-277.
- Naval Vessels**
- 4.2.1 Reed, A.M., 2009, “A Naval Perspective on Ship Stability”, Proc. STAB2009, pp. 21-44.
- 4.2.2 Peters, A. J., Wing, D., 2009, “Stability Evaluation and Performance Based Criteria Development for Damaged Naval Vessels”, Proc. STAB2009, pp. 155-170.
- 4.2.3 Smith, D., Heywood, M., 2009, “Accidental Damage Templates (ADTS). A Basis for the Future of Naval Ship Safety Certification?”, Proc. STAB2009, pp. 229-234.
- 4.2.4 Heywood, M., Smith, D., 2009, “Application of Dynamic V-Lines to Naval Vessels”, Proc. STAB2009, pp. 235-244.
- 4.2.5 Mironiuk, W., 2009, “The Research on the Flooding Time and Stability Parameter of the Warship after Compartments Damage”, Proc. STAB2009, pp. 253-260.
- 4.2.6 Sadat-Hosseini, H., Carrica, P., Stern, F., Umeda, N., Hashimoto, H., Yamamura, S., Matsuda, A., “Comparison CFD and System-Based Methods and EFD for Surf-Riding, Periodic Motion, and Broaching of ONR Tumblehome”, Proc. STAB2009, pp. 317-329.
- 4.2.7 Maki, A., Umeda, N., 2009, “Bifurcation and Chaos in Yaw Motion of a Ship at Lower Speed in Waves and its Prevention Using Optimal Control”, Proc. STAB2009, pp. 429-440.
- 4.2.8 Peters, A., 2010, “Tolerable Capsize Risk of a Naval Vessel”, Proc. ISSW2010, pp. 93-107.
- 4.2.9 Perrault, D., Hughes, T., Marshall S., 2010, “Developing a Shared Vision for Naval Stability Assessment”, Proc. ISSW2010, pp. 115-120
- 4.2.10 Alman, P.R., 2010, “Approaches for Evaluating Dynamic Stability in Design”, Proc. ISSW2010, pp. 121-128.
- 4.2.11 Leguen, J.-F., Caqueneau, C., Mogenicato, E., Dupau, T., Régnier, E., Vonier, P., Dispa, H., Lorin, F., 2010, “Operator Guidance for French Mine Hunters”, Proc. ISSW2010, pp. 129-133.
- 4.2.12 Atkins, J., Marshall, S., 2010, Noel-Johnson, N., 2010, “Landing Craft Stability Standard”, Proc. ISSW2010, pp. 134-142.
- 4.2.13 Carette, N.F.A.J., van Walree, F., 2010, “Calculation Method to Include Water on Deck Effects”, Proc. ISSW2010, pp. 166-172.
- 4.2.14 Ypma, E., Turner, T., 2010, “An Approach to the Validation of Ship Flooding Simulation Models”, Proc. ISSW2010, pp. 173-184.
- 4.2.15 Belknap, W.F., Reed, A.M., 2010, “TEMPEST – A New Computationally Efficient Dynamic Stability Prediction Tool”, Proc. ISSW2010, pp. 185-197.
- 4.2.16 Marshall, S., 2010, “Heavy Weather Ship-Handling Bridge Simulation”, Proc. ISSW2010, pp. 198-201.
- 4.2.17 Van Buskirk, L.J., Alman, P.R., McTigue, J.J., 2010, “Further Perspectives on Operator Guidance and Training for Heavy Weather Shiphandling”, Proc. ISSW2010, pp. 202-208.
- 4.2.18 Alman, P.R., 2011, “Thoughts on Integrating Stability into Risk Based Methods for Naval Ship Design”, Proc. ISSW2011, pp. 359-368.
- 4.2.19 Tellet, D., 2011, “Incorporating Risk into Naval Ship Weight and Stability Control”, Proc. ISSW2011, pp. 369-374.
- 4.2.20 Beaupty, B., Stachelhausen, N., Billard, J.-Y., Mogenicato, E., Vonier, P., Leguen, J.-F., 2012, “Operability of French Naval Ships over 50 Years”, Proc. STAB2012, pp. 575-581.
- 4.2.21 Walree, F. van, 2012, “Development and Validation of a Time Domain Seakeeping Code for a Destroyer Hull Form Operating in Extreme Sea States”, Proc. STAB2012, pp. 583-591.
- 4.2.22 Gu, M., Lu, J., Wang T., 2012, “An Investigation on Stability under Dead Ship Condition of a Tumblehome Hull”, Proc. STAB2012, pp. 593-598.
- 4.2.23 Karlinskiy, S., Efimov, A., 2012, “Mathieu Instability of Surfacing Submarine”, Proc. STAB2012, pp. 599-605.
- 4.2.24 Hayes, P., Smith, W., Renilson, M., Cannon, S., 2012, “Naval Landing Craft Stability – Simulation of Extreme Roll Motions and Shipping of Water into the Well Deck”, Proc. STAB2012, pp. 607-616.
- 4.2.25 Lu, J., Gu, M., 2012, “An Investigation on Parametric Rolling of a Tumblehome Hull”, Proc. STAB2012, pp. 617-623.
- 4.2.26 Brodu, A., Mauger, E., Billard, J.-Y., 2013, “Comparison of Global Technique and Direct Evaluation of Capsizing Probability on French Frigates”, Proc. ISSW20013, pp. 158-164.
- 4.2.27 Perrault, D., 2013, “Examination of the Probability Results for Extreme Roll of Naval Vessels”, Proc. ISSW20013, pp. 178-184.
- 4.2.28 Araki, M., Sadat-Hosseini, H., Sanada, Y., Umeda, N., Stern, F., 2013, “System Identification using CFD Captive and Free Running Tests in Severe Stern Waves”, Proc. ISSW2013, pp. 165-177.
- 4.2.29 Gu, M., Lu, J., Wang, T., 2013, “Experimental and Numerical Study on Stability under Dead Ship Condition of a Tumblehome Hull”, Proc. ISSW2013, pp. 192-198.
- 4.2.30 Spyrou, K., Themelis, S., Kontolefas, L., 2014, “What is Surf-Riding in Irregular Seas?”, Proc. ISSW2014, pp. 12-18.
- 4.2.31 Peters, A., Goddard, R., Dawson, N., 2014, “A New Approach to the Derivation of V-Line Criteria for a Range of Naval Vessels”, Proc. ISSW2014, pp. 58-66.
- 4.2.32 Marshall, S., Goddard, R., Horner, D., Randles, I., 2014, “Small Combatant Accidental Damage Extents”, Proc. ISSW2014, pp. 67-74
- 4.2.33 Billard, J.-Y., Grinaert, F., Delumeau, I., Vonier, P.,



- Creismeas, P., Leguen, J.-F., Ferreiro, L.D., 2014, "Forensic Study of BOUVET Capsizing", *Proc. ISSW2014*, pp. 110-116.
- Inland Vessels**
- 4.3.1 Hofman, M., Bačkalov, I., 2010, "Risk-Based Analysis of Inland Vessel Stability", *Proc. ISSW2010*, pp. 67-72.
- 4.3.2 Bačkalov, I., Kalajdžić, M., Hofman, M., 2010, Inland vessel rolling due to severe beam wind: a step towards a realistic model, *Probabilistic Engineering Mechanics*, Vol. 25, No. 1, pp. 18-25.
- 4.3.3 Bačkalov, I., 2012, "A probabilistic analysis of stability regulations for river-sea ships", *Proc. STAB2012*, pp. 67-77.
- Other types of vessels and floating objects**
- 4.4.1 Vasconcellos, J. M., Guimaraes, N., 2009, "Risk Evaluation in Floating Offshore Structures", *Proc. STAB2009*, pp. 53-64
- 4.4.2 Santen, J. van, 2009, "The Use of Energy Build up to Identify the Most Critical Heeling Axis Direction for Stability Calculations for Floating Offshore Structures", *Proc. STAB2009*, pp. 65-76
- 4.4.3 Delorme, L., Denante, M., Santucci, P., De-Gelas, A., 2009, "New Floation Devices to Avoid Helicopters' Total Inversion After Capsize", *Proc. STAB2009*, pp. 77-86
- 4.4.4 Breuer, J. A., Sjölund, K.-G., 2009, "Steepest Descent Method. Resolving an Old Problem", *Proc. STAB2009*, pp. 87-99.
- 4.4.5 Deakin, B., 2009, "Stability Regulation of Very Large Sailing Yachts", *Proc. STAB2009*, pp. 171-180.
- 4.4.6 Katayama, T., Taniguchi, T., Umeda, N., 2009, "An Experimental Study on Parametric Rolling of A High Speed Trimaran In Head Sea", *Proc. STAB2009*, pp. 541-548.
- 4.4.7 Bulian, G., Francescutto, A., Fucile, F., 2009, "Numerical and Experimental Investigation on the Parametric Rolling of a Trimaran Ship in Longitudinal Regular Waves", *Proc. STAB2009*, pp. 567-582.
- 4.4.8 Rodriguez, C.A., Neves, M.A.S., 2012, "Investigation on parametrically excited motions of Spar platforms in waves", *Proc. STAB2012*, pp. 509-517.
- 4.4.9 Rivera, L.A., Neves, M.A.S., Cruz, R.E., Esperança, P.d.T., 2012, "A study on unstable motions of a tension leg platform in close proximity to a large FPSO", *Proc. STAB2012*, pp. 519-532
- 4.4.10 Judge, C.Q., 2012, "Dynamic Transverse Stability for High Speed Craft", *Proc. STAB2012*, pp. 545-556.
- 4.4.11 Maimun, A., Rahimuddin, Abdul Ghani, M.P., Muhammad, A.H., 2012, "Bow Diving of Semi-Swath Vessel in Following Seas and Fins Stabilizer Effect", *Proc. STAB2012*, pp. 557-568.
- 4.4.12 Handler, P., Jarecki, V., Bruhns, H., 2012, "FLO/FLO Heavy Lift Critical Stability Phases", *Proc. STAB2012*, pp. 569-574.
- 4.4.13 Santen, J. van, 2013, "Problems met in stability calculations of offshore rigs and how to deal with them", *Proc. ISSW2013*, pp. 9-17.
- 4.4.14 Polo, J.C., Rodríguez, C., Neves, M.A.S., 2013, "Experimental and Numerical Investigation on the Stability in Waves of a Mono-column Platform", *Proc. ISSW2013*, pp. 18-27.
- 4.4.15 Hong, S.Y., Nam, B.W., Kim, N.W., Cho, Y.S., 2013, "Investigation of Nonlinear Roll Motion Characteristics of a Shallow Draft Semi-submersible", *Proc. ISSW2013*, pp. 28-35.
- 4.4.16 Cho, S.K., Sung, H.G., Hong, S.Y., Kim, Y.H., 2013, "Study of the Stability of Turret moored Floating Body", *Proc. ISSW2013*, pp. 199-206.
- 4.4.17 Fitriadhy, A., Yasukawa, H., Koh, K.K., 2013, "Course stability of a ship towing system in wind", *Ocean Engineering*, Vol. 64, pp. 135-145.
- 4.4.18 Kim, N.W., Nam, B.W., Choi, Y.M., Hong, S.Y., 2014, "An Experimental Investigation on Reduction of List Angle of a Semi-submersible Platform in Head Sea", *Proc. ISSW2014*, pp. 157-164.
- 4.4.19 Katayama, T., Ohashi, S., 2014, "A Study on Spinout Phenomena of Planing Craft in High Speed Turning with Radio Control Small Model", *Proc. ISSW2014*, pp. 249-253.
- 4.4.20 Rahimuddin, Maimun, A., Mobassher Tofa, M., Jamei, S., Tarmizi, 2014, "Stability Analysis of a Wing in Ground Effect Craft", *Proc. ISSW2014*, 8 pp.
- 4.4.21 Sinibaldi, M., Bulian, G., 2014, "Towing simulation in wind through a nonlinear 4-DOF model: Bifurcation analysis and occurrence of fishtailing", *Ocean Engineering*, Vol. 88, pp. 366-392.
- Roll Damping & Anti-rolling Devices, CFD for Ship Stability, and Modelling of Granular Materials**
- 5.1 Pérez-Rojas, L., Bulian, G., Botia-Vera, E., Cercos-Pita, J.L., Souto-Iglesias, A., Delorme, L., 2009, "A Combined Experimental and SPH Approach to Sloshing and Ship Roll Motions", *Proc. STAB2009*, pp. 261-270.
- 5.2 Gao, Z., Vassalos, D., Gao, Q., 2009, "A Multiphase CFD Method For Prediction Of Floodwater Dynamics", *Proc. STAB2009*, pp. 307-316.
- 5.3 Sadat-Hosseini, H., Carrica, P., Stern, F., Umeda, N., Hashimoto, H., Yamamura, S., Matsuda, A., 2009, "Comparison CFD and System-Based Methods and EFD for Surf-Riding, Periodic Motion, and Broaching of ONR Tumblehome", *Proc. STAB2009*, pp. 317-329.
- 5.4 Bassler, C.C., Reed, A.M., 2009, "An Analysis of the Bilge Keel Roll Damping Component Model", *Proc. STAB2009*, pp. 369-385.
- 5.5 Kawahara, Y., Maekawa, K., Ikeda, Y., 2009, "A Simple Prediction Formula of Roll Damping of Conventional Cargo Ships on the Basis of Ikeda's Method and Its Limitation", *Proc. STAB2009*, pp. 387-398.
- 5.6 Gao, Q., Vassalos, D., 2009, "Simulation of Wave Effect on Ship Hydrodynamics by RANSE", *Proc. STAB2009*, pp. 591-596.
- 5.7 Shen, L., Vassalos, D., 2009, "Applications of 3D Parallel SPH for Sloshing and Flooding", *Proc. STAB2009*, pp. 723-732.
- 5.8 Strasser, C., Jasionowski, A., Vassalos, D., 2009, "Calculation of the Time-to-Flood of A Box-Shaped Barge by Using CFD", *Proc. STAB2009*, pp. 733-733.
- 5.9 Bassler, C.C., Reed, A.M., Brown, A.J., 2010, "A Method to Model Large Amplitude Ship Roll Damping", *Proc. ISSW2010*, pp. 217-224.
- 5.10 Katayama, T., Yoshioka, Y., Kakinoki, T., Ikeda, Y., 2010, "Some Topics for Estimation of Bilge-Keel Component of Roll Damping", *Proc. ISSW2010*, pp. 225-230.
- 5.11 Pawlowski, M., 2010, "Approximation of the Non-Linear Roll Damping", *Proc. ISSW2010*, pp. 231-237.
- 5.12 Neves, M.A.S., Rodríguez, C.A., Vivanco, J.E.M., Villagómez Rosales, J.C., Agarwal, R., 2010, "Integrity Diagrams of the Ship/U-Tank System Undergoing Parametric Rolling", *Proc. ISSW2010*, pp. 288-294.
- 5.13 Sadat-Hossenli, H., Araki, M., Umeda, N., Sano, M., Yeo, D.J., Toda, Y., Carrica, P.M., Stern, F., 2011, "CFD, System-Based, and EFD Preliminary Investigation Of ONR Tumblehome Instability and Capsizes with Evaluation of the Mathematical Model", *Proc. ISSW2011*, pp. 135-145.
- 5.14 Gao, Z., Gao, Q., Vassalos, D., 2011, "Numerical Study of Damaged Ship Motion in Waves", *Proc. ISSW2011*, pp. 257-261.
- 5.15 Gao, G., Vassalos, D., 2011, "Numerical Study of the Roll Decay of Intact and Damaged Ships", *Proc. ISSW2011*, pp. 277-282.
- 5.16 Greeley, D.S., 2001, "Some Results from a New Time-Domain Bilge Keel Force Model", *Proc. ISSW2011*, pp. 283-289.
- 5.17 Bassler, C., Miller, R., Reed, A., Brown, A., "Considerations for Bilge Keel Force Models in Potential Flow Simulations of Ship Maneuvering in Waves", *Proc. ISSW2011*, pp. 291-307.
- 5.18 Katayama, T., Yoshioka, Y., Kakinoki, T., Miyamoto, S., 2001, "A Study on Estimation Method of Bilge-Keel



- Component of Roll Damping for Time Domain Simulation", Proc. ISSW2011, pp. 309-315.
- 5.19 Hua, M.T., Régnier, E., Mélice, M., Leguen, J.-F., 2011, "Approximation of Roll Damping by a Second Order Oscillator for Experiments at Different Scales and Numerical Calculations", Proc. ISSW2011, pp. 317-323.
- 5.20 Lewandowski, E.M., 2011, "Comparison of Some Analysis Methods for Ship Roll Decay Data", Proc. ISSW2011, pp. 325-330.
- 5.21 Yu, L., Ma, N., Gu, X., 2012, "Study on Parametric Roll and Its Rudder Stabilization Based on Unified Seakeeping and Maneuvering Model", Proc. STAB2012, pp. 159-169.
- 5.22 Araki, M., Sadat-Hosseini, H., Sanada, Y., Umeda, N., Stern, F., 2012, "Study of System-based Mathematical Model Using System Identification Technique with Experimental, CFD, and System-Based Free Running Trials in Following Waves", Proc. STAB2012, pp. 171-185.
- 5.23 Belibassakis, K.A., Politis, G.K., 2012, "Roll Stabilization by Vertical Thrust-Producing Flapping Wings Using Active Pitch Control", Proc. STAB2012, pp. 201-213.
- 5.24 Ohashi, K., Ogawa, Y., Shiraiishi, K., 2012, "Study on the Evaluation for Performance of the Cross-Flooding Arrangements by means of the Computational Fluid Dynamics", Proc. STAB2012, pp. 381-389.
- 5.25 Sadat-Hosseini, H., Kim, D.H., Lee, S.K., Rhee, S.H., Carrica, P., Stern, F., Rhee, K.-P., 2012, "CFD and EFD Study of Damaged Ship Stability in Calm Water and Regular Waves", Proc. STAB2012, pp. 425-452.
- 5.26 Gao, Q., Vassalos, D., 2012, "The Numerical Study of Hydrodynamic Coefficients by RANS", Proc. STAB2012, pp. 471-476.
- 5.27 Hashimoto, H., Ito, Y., Kawakami, N., Sueyoshi, M., 2012, "Numerical Simulation Method for Coupling of Tank Fluid and Ship Roll Motions", Proc. STAB2012, pp. 477-485.
- 5.28 Pérez-Rojas, L., Cercós-Pita, J.L., "3D GPU SPH Analysis of Coupled Sloshing and Roll Motion", Proc. STAB2012, pp. 487-496.
- 5.29 Spandonidis, C.C., Spyrou, K.J., 2012, "Use of Granular Material Dynamics Simulation for the Study of Cargo Shift of Ships", Proc. STAB2012, pp. 497-507.
- 5.30 Söder, C.-J., Rosén, A., Werner, S., Huss, M., Kutteneuler, J., 2012, "Assessment of Ship Roll Damping through Full Scale and Model Scale Experiments and Semi-Empirical Methods", Proc. STAB2012, pp. 877-886.
- 5.31 Handschel, S., Köllisch, N., Abdel-Maksoud, M., 2012, "Roll Damping of Twin-Screw Vessels: Comparison of RANSE with Established Methods", Proc. STAB2012, pp. 887-898.
- 5.32 Perez, T., Blanke, M., 2012, "Ship Roll Damping Control", Annual Reviews in Control, Vol. 36, pp. 129-147.
- 5.33 Miyake, T., Ikeda, Y., 2013, "A Study on Roll Damping of Bilge Keels for New Non-Ballast Ship with Rounder Cross Section", Proc. ISSW2013, pp. 36-43.
- 5.34 Katayama, T., Umeda, J., Hashimoto, H., Yildiz, B., 2013, "A Study on Roll Damping Estimation for Non Periodic Motion", Proc. ISSW2013, pp. 44-49.
- 5.35 Araki, M., Sadat-Hosseini, H., Sanada, Y., Umeda, N., Stern, F., 2013, "System Identification Using CFD Captive and Free Running Tests in Severe Stern Waves", Proc. ISSW2013, pp. 165-177.
- 5.36 Söder, C.-J., Rosén, A., Ovegård, E., Kutteneuler, J., Huss, M., 2013, "Parametric roll mitigation using rudder control", Journal of Marine Science and Technology, Vol. 18, pp. 395-403.
- 5.37 Spandonidis, C.C., Spyrou, K.J., 2013, "Micro-scale modeling of excited granular ship cargos: A numerical approach", Ocean Engineering, Vol. 74, pp. 22-36.
- 5.38 Katayama, T., Yildiz, B., Umeda, J., 2014, "Numerical Estimation and Validation of Shallow Draft Effect on Roll Damping", Proc. ISSW2014, pp. 204-209.
- 5.39 Araki, M., Ohashi, K., Hirata, N., 2014, "An Analysis of Bilge Keel Effects using RANS with Overset Grids Method", Proc. ISSW2014, pp. 216-228.
- 6.1 Shigunov, V., 2009, "Operational Guidance for Prevention of Container Loss", Proc. STAB2009, pp. 473-482.
- 6.2 Marshall, S., 2010, "Heavy Weather Ship-Handling Bridge Simulation", Proc. ISSW2010, pp. 198-201.
- 6.3 Buskirk, L.J. van, Alman, P.R., McTigue, J.J., 2010, "Further Perspectives on Operator Guidance and Training for Heavy Weather Shiphandling", Proc. ISSW2010, pp. 202-208.
- 6.4 Jasonowski, A., 2010, "Decision Support for Crisis Management and Emergency Response", Proc. ISSW2010, pp. 209-216.
- 6.5 Nielsen, U., Stredulinsky, D.C., 2011, "Onboard Sea State Estimation Based on Measured Ship Motions", Proc. ISSW2011, pp. 61-67.
- 6.6 Terada, D., Matsuda, A., 2011, "Onboard Analysis of Ship Stability Based on Time-Varying Autoregressive Modeling Procedure", Proc. ISSW2011, pp. 69-74.
- 6.7 Song, K.H., Kim, Y., 2011, "Quantitative Analysis of Parametric Roll and Operational Guidance", Proc. ISSW2011, pp. 225-232.
- 6.8 Ovegård, E., Rosén, A., Palmquist, M., Huss, M., 2012, "Operational Guidance with Respect to Pure Loss of Stability and Parametric Rolling", Proc. STAB2012, pp. 655-668.
- 6.9 McCue, L., 2012, "Putting Vessel Motion Research into the Hands of Operators", Proc. STAB2012, pp. 679-687.
- 6.10 Enshaei, H., Birmingham, R., 2012, "Monitoring of Dynamic Stability via Ship's Motion Responses", Proc. STAB2012, pp. 707-718.
- 6.11 Degtyarev, A., Busko, I., Nechaev, Y., 2012, "System Identification for Wave Measurements Using Ship as a Buoy", Proc. STAB2012, pp. 725-734.
- 6.12 Rosén, A., Björnsson, L., Palmquist, M., Ovegård, E., 2013, "On the Influence of Sea State Idealizations and Wave Directionality in Dynamic Stability Assessments", Proc. ISSW2013, pp. 50-57.
- 6.13 González, M.M., Casás, V.D., Peña, F.L., Rojas, L.P., 2013, "Experimental Analysis of Roll Damping in Small Fishing Vessels for Large Amplitude Roll Forecasting", Proc. ISSW2013, pp. 95-103.
- 6.14 Terada, D., Matsuda, A., 2013, "Onboard Evaluation of the Transverse Stability for Officers", Proc. ISSW2013, pp. 207-213.

Modelling of Environment

- 7.1 Pawłowski, M., 2009, "Sea Spectra Revisited", Proc. STAB2009, pp. 463-472.
- 7.2 Waseda, T., Kinoshita, T., 2010, "Freak Waves and Capsizing Accidents", Proc. ISSW2010, pp. 79-84.
- 7.3 Rosén, A., Björnsson, L., 2013, "On the influence of sea state idealizations and wave directionality in dynamic stability assessments", Proc. ISSW2013, pp. 50-57.
- 7.4 Hennig, J., Walree, F. van, 2014, "Modelling of Extreme Waves Related to Stability Research", Proc. ISSW2014, pp. 210-215.

Education

- 8.1 Vassalos, D., Hamamoto, M., Papanikolaou, A., Molyneux, D., (Editors), 2000, "Contemporary Ideas on Ship Stability", Elsevier, Oxford.
- 8.2 Kobylinski, L.K., Kastner, S., 2003, "Stability and Safety of Ships, Volume I: Regulation and Operation", Elsevier, Oxford.
- 8.3 Pawłowski, M., 2004, "Subdivision and damage stability of ships", Euro-MTEC Series, Technical University of Gdansk.
- 8.4 Belenky, V.L., Sevastianov, N.B., 2007, "Stability and Safety of Ships: Risk of Capsizing", The Society of Naval Architect and Marine Engineers.
- 8.5 Neves, M.A.S., Belenky, V., de Kat, J.O., Spyrou, K., Umeda, N., (Editors), 2011, "Contemporary Ideas on Ship Stability and Capsizing in Waves", Springer, Dordrecht, Heidelberg, London, New York.

Ship Stability in Operation



Description of abbreviations used in the list of references:

Proc. STAB2009 – Proceeding of 10th International Conference on Stability of Ships and Ocean Vehicles, 22-26 June 2009, St. Petersburg, Russia

Proc. ISSW2010 - Proceeding of 11th International Ship Stability Workshop, 21-23 June 2010, Wageningen, The Netherlands

Proc. ISSW2011 - Proceeding of 12th International Ship Stability Workshop, 12-15 June 2011, Washington D.C., USA

Proc. STAB2012 - Proceeding of 11th International Conference on the Stability of Ships and Ocean Vehicles, 23-28 September 2012, Athens, Greece

Proc. ISSW2013 - Proceeding of 13th International Ship Stability Workshop, 23-26 September 2013, Brest, France

Proc. ISSW2014 - Proceeding of 14th International Ship Stability Workshop, 29 September - 01 October 2014, Kuala Lumpur, Malaysia

This page is intentionally left blank

Session 2–Workshop 1 Plenary (Veterans of Stability)

Contributions from the Class of 1975

This page is intentionally left blank



STAB 2015, GLASGOW

14-19 JUNE 2015

CONTRIBUTIONS FROM THE CLASS OF 1975



Representatives of the Class of 1975

- 1 Chengi Kuo**
(University of Strathclyde)

- 2 Hartmut Hormann**
(Formerly of Germanischer Lloyd)

- 3 Anthony Morrall**
(BMT Group)

- 4 John Martin**
(Formerly of University of Edinburgh)

- 5 Allan Gilfillan**
(Formerly of Maritime Coastguard Agency)

- 6 Alan Graham**
(Formerly of YARD Limited)

- 7 Sigi Kastner**
(Formerly of University of Bremen)



Contributions

1. Chengi Kuo (University of Strathclyde)

Reasons for organising the first conference in 1975

I met Mr Harry Bird of UK Board of Trade in 1968 and he was the UK representative at IMCO (Inter-governmental Maritime Consultative Organisation). He told me at IMCO most countries were supported by senior academics and in UK no one was interested in ship stability. Would I be interested in helping him. I said yes and became involved in devising criteria for assessing computer programs for calculating ship stability. Later I got to know various delegates to IMCO which became IMO. In 1972 I won a major research contract for three years to explore how theoretical methods can be incorporated into assessing ship stability. As we came near to the end of the contract, we wanted to share our work with people working on ship stability. The idea of having an international conference was our choice.

Aspects of particular personal interest in the 1975 Conference

There were a number of items of interest:

a) Static stability: Most of the interests were on static or quasi-static ship stability. The area under the GZ curve got a lot of debate. Generally it was about the quantities of areas up to certain angle of heel. It did not seem logical.

b) Theoretical solutions: Our team's attempts to introduce some theoretical solutions were not receiving much enthusiasm. The feedbacks we received were that the stage had not been reached for complicated equations; few understood the equations.

c) Ocean vehicles: Little special attention

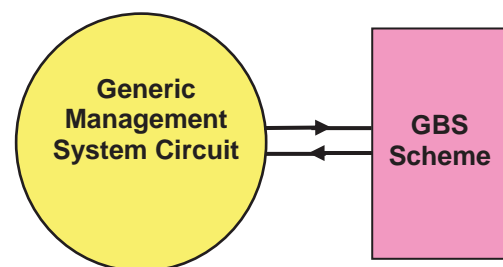
was given to the stability of ocean vehicles. These vehicles were shape and responses to ships, yet modified ship stability rules were in use. For example, semisubmersibles were being used for exploring drilling in the North Sea.

d) Meeting people: It was a valuable experience in meeting some of the people whose studies we were familiar with, and since it was the first biggish marine international conference to be held in Glasgow we were very well supported by the Glasgow City Council and the University.

Research priorities for the next 10-20 years

I would like to see more emphasis put on fundamental issues and their links to present approaches. Two examples are given here:

a) Non absolute nature of safety: Safety is dominated by personal perceptions as can be illustrated by two persons trying to cross a busy road. One thinks it is unsafe and the other thinks it is safe. Both of them are correct because judgement of safe or not safe is based on personal perception. By accepting safety is non absolute, a management system would be needed to address safety issues. The regulatory efforts such as FSA (Formal Safety Assessment) and GBS (Goal Based Standard) assume safety is absolute. It is necessary to link them to management systems if they are to yield consistent results such as the sketch for GBS.



b) Influence of human factors: Considerable advances have been made in technological aspects of safety but insufficient



efforts are being made to ensure improved methods are available for addressing human factors. For example, when defining a project goal and performance criteria both technological and human criteria should be included. The latter will ensure features such as human attitudes and behaviour are measured. By having this facility it may help in reducing maritime accidents

2. **Hartmut Hormann** (Formerly of Germanischer Lloyd)

Reasons for attending the first conference in 1975

It was something thrilling, this Stability Conference at Strathclyde University! I then was exactly 10 years within my professional life, in hindsight still a youngster, though I did not feel so at the time. – From the onset of my employment with GERMANISCHER LLOYD I had been dealing with intact and damage stability problems, including lots of routine work in approving respective design features and the stability booklets required to be put on board – and used there.

Stability was only one of my areas of activities, but my then boss decided I should attend the Conference. I was particularly pleased to be there together with my admired teacher Prof Kurt Wendel. – Again in hindsight this experience has played its part in developing my lifelong interest in stability; as my career developed, of course, dealing with stability problems represented less and less of my time; in later years it felt like a relief from daily pressures, once I had the chance to engage in a true technical stability issue.

In a classification society one is automatically at a hinge or joint between R&D, regulatory requirements, and on-board application. I treasured this position and I had lots of opportunities to work with researchers on one side, in regulatory bodies (chiefly IMO, where I had the privilege to chair the STAB-

Subcommittee for six years), and on the other end to learn about all the related practical problems on board.

Aspects of particular personal interest in the 1975 Conference

I am supposed to think back to the 1975 Conference and I would offer just a few and certainly non-representative thoughts. For the majority of the attendees here today it might sound strange that then the accuracy of cross curves of stability was still a problem. Less strange, because it went on for many years if not for decades, is the fact that the Rahola-criteria in essence were the only tool which could be applied in practice. (It was not called so, but the stability values given in both international and national recommendations for application on board were simple derivatives of Rahola's findings).

In 1975 the profession had just begun to apply the mathematics ruling ship motions, and the capacity of computers – rather still “electric calculation machines” at the time – was a problem with respect to the volume of data needed to adequately define the hull forms. We then remembered still the time, when another German professor, Georg Weinblum, had managed to describe ship lines by mathematical functions. (Prof Weinblum had just passed away in 1974).

In listening to the presentations at the conference, I got confirmed, what I roughly knew before: the scientists had made significant progress in understanding ship motions and their repercussions on the risk of capsizing; however, I could clearly see that there was a big gap between their results and an application in practice. Since then the profession has gone a long way.

Quite naturally, having spent almost my entire professional life in a classification society (with a short intermission at a yard), my main interest concerning stability focussed on the practicability of what research brought



about. The two areas towards which the mentioned gap had to be closed were, and are still, to formulate the regulations defining sufficient stability and to see to it that these requirements can be applied in on-board practice.

Research priorities for the next 10-20 years

And these sentences bring me to formulate my expectations for work to be done has the safety factor to be chosen to avoid a ship capsizing with a sufficiently high probability. I know, the discussion of this issue has not only technical aspects, it has also to take into account the acceptance of accident rates by the general public – not an easy task! The other area to be addressed is the big field of human errors; there are multiple “opportunities” to individually fail in assessing the actual stability while the ship is in service and to draw the right conclusions.

I am retired since 13 years now, and I have not any longer really followed the developments in my former profession, but I am reasonably sure that these aspects need attention also in future.

3. Anthony Morrall (BMT Group)

Reasons for attending the first conference in 1975

My reasons for attending the first conference in 1975 can be traced back to the UK’s Holland Martin Committee Inquiry into Trawler Safety following the loss of three trawlers in 1968 in which a total of 58 crew members died, with just one survivor. My Director at this time was James Paffett, a member of this Committee, and he asked me to assist the UK Department of Transport with the drafting of new fishing vessel safety regulations, following the recommendations of the Inquiry. My first task was to help with the technical aspects through the “Freeboard

Committee”, now renamed as the Fishing Industry Safety Group (FISG), which led to the introduction of the UK’s *Fishing Vessels (Safety Provisions) Rules 1975*. This new legislation introduced IMO’s (IMCO’s) intact stability criteria A168 for the first time and was one of recommendations of the Holland Martin Inquiry, which influenced subsequent UK legislation on maritime safety.

My role as a technical advisor to the Department of Transport continued for many years and in addition I attended numerous IMO meetings on fishing vessel safety as well as the Torremolinos International Convention for the Safety of Fishing Vessels in 1977. Prior to attending the first International Conference on Stability of Ships and Ocean Vehicles in 1975 I had therefore become heavily involved in fishing vessel stability and safety, although this was additional to my other responsibilities at the NPL Ship Division.

My paper at the first conference reported on an experimental and analytical investigation of capsizing of a side trawler in irregular beam seas. The results of this investigation gave an indication of the conditions in which capsize would occur. A time-domain analysis using an analogue simulator program was employed to model capsize and this approach was considered “a realistic proposition, providing roll damping coefficients for the ship, rather than for the model were used”. The question of adequate safety for these vessels was more problematical, but the best criterion for survival was considered to be through “a simplified dynamic approach”, “without forgetting good seamanship”.

My interest in fishing vessel stability and safety continued long after the first conference and over the years I have been responsible for several experimental investigations into the losses of fishing vessel, such as the Gaul, Trident, and Solway Harvester. I was also involved in model experiments and computer flooding simulations investigating the sudden and catastrophic capsizing of the passenger/car



ferries the Herald of Free Enterprise and the European Gateway and the sail-training ship Marques.

Aspects of particular personal interest in the 1975 Conference

I found the first conference rather daunting even though many of the delegates were known to me at the time, particularly Prof Chengi Kuo and the late Harry Bird, Prof. Yucel Odabasi and Bill Cleary. Subsequently, many others became known to me through my work on stability, such as Professors Paulling and Mоторo, or through IMO stability working groups with distinguished delegates such as Dorin, Dudziak, Kastner, Kobylinski, Kure, Rakhmanin, Takahashi, and Tsuchiya etc., all of whom attended the first conference.

Looking back on this conference many of the papers were attempting to produce a better understanding of specific aspects of stability, including dynamic considerations in irregular seas, as well as considering ways in which future stability criteria might be addressed. All of the presentations reinforced the need for further research on this topic in order to progress the state-of-the-art. This has become the lasting legacy of the first conference, thanks mainly to the efforts of Prof Kuo and the support given to him by Harry Bird and others. All subsequent work and progress made on intact stability criteria can therefore in my view be traced back to the first conference in 1975.

The most interesting aspect of the conference was the enthusiasm expressed by most of the delegates not only to understand the physics of all the phenomena related to ship stability in a seaway, but to question the status quo, and to consider how future stability criteria might include dynamic aspects. The phenomena of parametric rolling and the Mathieu instability are of course not new; for example the stability variations experienced by a ship moving in longitudinal waves have been studied by a number of eminent people in the

past e.g.: Froude (1861), Kempf (1938), Graff & Heckscher (1941) and Pauling (1959, 1961, 1974, 2001), but at the conference these and other phenomena were being reconsidered, in the context of intact stability criteria and ship safety.

Research priorities for the next 10-20 years

Since the first conference in 1975 significant progress has been made in the field of ship stability, not only at subsequent conferences but at IMO. For example, IMO has undertaken the development of so-called "Second Generation Intact Stability Criteria" (SGISC) with the intention of providing a new set of rules covering the different phenomena. This development is in recognition of the fact that traditional intact stability criteria does not adequately address all intact stability phenomena and cannot give any indication of safety margins in any sea state except still water. However, despite its limitations IMO's stability criteria A167 and A168, which are based on a statistical analysis of casualty data, have proven very effective since their introduction in 1968; this is mainly because of their relation to hull form geometry and obvious physical meaning to naval architects and ship's officers.

The intact stability phenomena of particular interest include Parametric Rolling, Broaching, and Dead Ship etc. However, despite of the progress made, accurate prediction of extreme motion leading to capsizing from these phenomena remains outstanding. More accurate modelling of the physics, including non-linear roll damping, rudder action, and the effect of stabilisers is therefore needed before these new criteria can provide reliable and practical guidance to designers and ship operators. A container ship after experiencing parametric rolling is shown in the picture.



At the moment the prediction of these stability phenomena remain a challenging task. The new generation of intact stability criteria may therefore only be able to provide an approximate guide for these phenomena, unless advances are made in the modelling. Although intact stability phenomena have been known for some time a database of incidents has to my knowledge, not been compiled. This would have allowed a risk assessment to have been made on these phenomena.

Most of IMO's work on the Second Generation Intact Stability Criteria has been supported by theoretical calculations and model tests, but very little emphasis appears to have been given to providing guidance to the master for avoiding dangerous situations. In contrast, MSC Circular 1329 for High Speed Craft provides guidance to the master for avoiding dangerous situations in following seas.

The survival of a vessel in heavy sea as a result of extreme motions, and of roll in particular, is one of the most fundamental requirements considered by a naval architect when designing a ship. New design and operational criteria for all intact stability phenomena will ultimately depend upon more accurate modelling of the physics involved, as well as making use of advanced simulation and virtual reality techniques. Education is also needed to improve the general understanding of the safety implications of extreme dynamic behaviour and how this relates to design and operational considerations. Guidance to masters for avoiding dangerous situations for vessel most at risk, perhaps by the use of simulators, should also be a higher priority than at present.

In summary, my views on the current and future developments of new intact stability criteria are as follows:

i. Despite recent progress there is still some way to go before the Second Generation Intact Stability Criteria are introduced as regulatory design tools with more advanced guidance for avoiding dangerous situations.

ii. Future stability criteria must undoubtedly take into account all physical phenomena likely to occur during a vessel's service. The advancement of this aim through more advanced modelling and realistic simulation should be the main emphasis for stability and safety over the next decade.

iii. The prediction of capsize for all physical phenomena with an acceptable degree of certainty is an extremely difficult task; these phenomena are non-linear and extremely rare events of seakeeping behaviour that can be affected by both rudder and fin stabiliser action.

iv. Future intact stability criteria and the related safety of ships in critical sea conditions should ideally be quantified in terms of risk or loss or of exceeding certain bounds of motion, as a result of environmental forces.

v. The above approach is more appropriate to the seakeeping assessment of a ship's likely behaviour, and this approach could also help establish broad margins of safety.

vi. The emphasis of any new stability and safety research should be on ship design and operational criteria for all intact stability phenomena, including excessive roll motion and accelerations.

4. **John Martin** (Formerly of University of Edinburgh, Department of Mathematics)

Reasons for attending the first conference in 1975



At the time of the 1975 conference, I had recently become involved with the Strathclyde Ship Stability Group through my former research supervisor, the late Professor Fritz Ursell. My role was to help out with mathematical matters, such as advising them on their forays into the stability theory of differential equations and dynamical systems. I subsequently participated in workshops for naval architects and regulators to help them understand these ideas. I also undertook some personal research in nonlinear aspects of wave-body interactions such as the steady tilting of semi-submersibles in regular waves – a problem flagged at the 1975 conference. My involvement in ship stability work ceased during the 1980's so I am very far from up-to-date with more recent developments.

Aspects of particular personal interest in the 1975 Conference

As an applied mathematician, with experience in the linear theory of water waves and floating bodies, my overwhelming impression at the conference was that the real issues of ship stability and capsize far exceeded the scope of small amplitude approximations or perturbation expansions; it was fully nonlinear, involving large, highly nonlinear waves and extreme motions, whether leading to capsize or survival. This, therefore, called into question much of the classical modelling, whether deterministic or statistical, based on small amplitudes and superposition of various effects. It appeared that physical understanding of capsize mechanisms was limited at quite a basic qualitative level, with questions being raised such as: what forces are critical in the “ultimate half roll”; is coupling important e.g. between roll and yaw; is parametric resonance significant – a long list!

Systems of nonlinear differential equations were proposed, largely of the kind obtained in linear theory with additional hypothesised nonlinearities, and some of their qualitative predictions compared with observations of full scale events or model tank experiments. With

many of these systems there seemed to be a huge problem with proliferation of parameters and near impossibility of measuring most of them. Indeed, even some of the most basic parameters in the linear theory (damping, added mass, etc) are only really defined in time-harmonic situations where they are frequency-dependent and really represent history effects in the time domain (i.e. needing integro-differential equations).

Wrapping all this up into usable stability criteria was the final challenge; something which, like the GZ curve, can be measured or calculated and simple criteria applied. There is a paradox here: that the better a theoretical model replicates the physics (even going to the “ideal” of a full numerical simulation) the more it replicates the difficulties of identifying dangerous situations, key parameters and stability criteria. High quality simulation may be useful as a cheaper alternative to tank testing (maybe offering the possibility of basing regulations on survival testing in defined “dangerous” conditions), but it does not lead to simple quantifiable criteria based on system parameters. Ironically this requires a simplification of the full physics – one which reliably captures all the key effects (if such a simplification actually exists).

Towards the end of the conference, there was optimism that the large body of work on stability for differential equations (phase space analysis and Lyapunov theory in particular) would translate directly to ship stability and deliver the required criteria. These theories, however, were mostly “local”, i.e. giving conditions for an equilibrium position or some other particular solution to be stable to sufficiently small perturbations. I could not see how the forces leading to capsize could be regarded as “sufficiently small”! The mathematicians only demand existence of a Lyapunov function for local stability; it needn't be a particularly efficient one, often leading to unrealistically harsh stability conditions. The real challenge is the “global” problem of defining and using practical stability



boundaries (in whatever parameter space is found relevant), not over-pessimistic and expressed in terms which can be measured and applied for actual vessels.

Research priorities for the next 10-20 years

Most, if not all, of the above qualms were discussed in some form or other at the 1975 conference which did a wonderful job of agenda setting. Given that I ceased to work in ship stability during the 1980's, I would not presume to set any newer agenda for the next 10-20 years. However, it will be extremely interesting to discover what has been achieved on these matters in the past 40 years, which of the original agenda items are still open and relevant, and what new priorities have emerged.

5. Allan Gilfillan (Formerly of Maritime Coastguard Agency)

Reasons for attending the first conference in 1975

In 1975 I was still involved in the investigations in the loss of the trawler Gaul in February 1974. As you know the Gaul was lost in a very heavy storm off the north of Norway – the only clue being a lifebelt washed ashore in a Norwegian Fjord. The Gaul and her sister vessels had recently been acquired by Hellyer Brothers as part of their purchase of Ranger Fishing from P&O, and the owners were concerned for safety of the ships which they had bought. In the absence of any clues all we could do was to carry out a review of their stability and the impact that various fittings might have had on the safe operation of the vessels. Various scenarios for the loss were postulated, but it was not possible to agree on the most likely cause. After the Formal Inquiry had made its judgement, the Department of Transport (or whatever name it went under at that time) arranged for a series of model tests to be carried out at NMI and made the Gaul data

available for academic study – but I can't remember whether the results from these studies were available in time for the stability conference – my copy of the proceedings was lodged in YARD's library.

Aspects of particular personal interest in the 1975 Conference

I think that I found most of the papers at the 1975 Conference interesting – but can't really remember many details. After 1975, my role in the company changed to a more general project management and administrative functions and this lasted until I retired from YARD/BAeSYSTEMS in 1999. This undoubtedly explains my loss of memory.

Research priorities for the next 10-20 years

Since 1975 a lot of work has been done both experimentally and through simulations to better understand flooding and stability in a dynamic domain, rather than the classical static approach taken previously. I don't believe it is feasible, or cost effective, to undertake these detailed simulations to every ship design and the challenge to the academic community is to turn the results into a practical set of rules which can be applied by naval architects working in ship design offices. After I retired I participated in using the results from the "Derbyshire" investigations into an amendment to the load line rules on hatch loading. One further point concerns probabilistic damage stability, which as you know involves calculating an "Attained index" of survivability against a "required index". (incidentally, when I worked in John Browns, I gathered the data for your exercise for the Swedish Authorities on the probabilistic stability of the "Kungsholm") I have long thought that the whole probabilistic method needs to be turned round so that the historic damage probability data is used to define the lengths and penetration at various locations along the length of the vessel which any ship design has to survive.



6. Alan Graham (Formerly of YARD Limited)

Reasons for attending the first conference in 1975

My keen interest in stability matters really began when I joined the Marine Division of the Department of Trade and Industry, (now the Maritime Coastguard Agency), in 1968.

Within a few days of joining the Department, I was invited to attend a meeting in London at the headquarters of the Inter-Governmental Consultative Organisation (IMCO) that is the present-day Inter-Governmental Organisation (IMO). The meeting was composed of a special group experienced in ship stability matters and were representative of the major maritime nations. The group had been commissioned by the Sub-Committee on Subdivision, Stability and Load Lines to investigate the manner in which Part B, Chapter II of SOLAS, (the regulations governing the minimum standards of subdivision and stability for passenger ships), might be improved. These anachronistic regulations were to be replaced by regulations based upon the concept of the probability of survival. This change was long overdue since they had barely been changed since the 1920's. From that time onwards, until my retirement from full time employment, a great proportion of my work was to attend IMO sessions as a member of that group. In the latter years, I became Chairman of the group.

Aspects of particular personal interest in the 1975 Conference

When I was invited to attend the STAB 75 conference in Glasgow, it gave me an opportunity to gauge what progress had been made in the research efforts in developing reliable stability criteria. As I recall, the majority of the papers presented at STAB 75 related to intact stability, rather than residual stability after assumed damage. However, effective subdivision regulations need to be

underpinned by reliable intact stability criteria to be meaningful, so I was anxious to learn what research effort was being made at that time.

I had the rather optimistic impression that within a reasonably short timeframe such criteria might be developed, enabling them to be introduced into safety regulations. I did not appreciate how difficult a task it would prove to be.

Research priorities for the next 10-20 years

Safety regulations were becoming increasingly risk-based. Regulations of a highly deterministic nature will be phased out. Future research will take account of this.

Human behaviour in an emergency may significantly exacerbate a potentially hazardous situation. Regulations in the future will need to take care of this to discourage the use of an 'active' device in an emergency situation, where the use of a 'passive' device would be preferable.

There is a strong possibility that passenger ships carrying very large numbers may, in the future, be required to remain afloat for a minimum time after assumed damage. Clearly, urgent research is required if such a 'time to stay afloat' criterion is ever to become a reality.

Now that a revised text for the outdated Part B, Chapter II of SOLAS has been approved, I would like to see a similar procedure adopted - initially for cargo ships and later to other ship types, including high speed craft and multi-hulls. At each stage, extensive research effort would be needed.

7. Sigi Kastner (Formerly of University of Bremen)

Reasons for attending the first conference in 1975



I attended the conference because it offered an opportunity to meet other researchers who were working on ship stability from other organisations. It also enabled me to publish a paper at the conference.

Aspects of particular personal interest in the 1975 Conference

Personally, I found it very interesting to meet colleagues from other countries working in the same field of ship design and research on the improvement of ship safety at sea.

I remember discussions at and after STAB 1975 on whether further Conferences should be organized by IMO. However, it was decided that solely scientific bodies and not governments should organize the STAB Conferences. It turned out to be a big success: Since then, every three years the next STAB has been organized in another part of the world.

Research priorities for the next 10-20 years

Future emphases should be placed on problems of the environmental impact of fuel consumption and type of fuel, considering the growing number of large container ships and passenger vessels. However, safety with respect to the particular ship type, the human factor in ship operation, connection of ship and harbour, and modern computer technology, will play an important role further on.

This page is intentionally left blank

Session 3– Workshop 2 Plenary (SRDC)

**Ship Stability & Safety in Intact Condition through
Operational Measures**

**Ship Stability & Safety in Damage Condition through
Operational Measures**

This page is intentionally left blank



Ship Stability & Safety in Intact Condition through Operational Measures

Igor Bačkalov, *University of Belgrade, Serbia*, ibackalov@mas.bg.ac.rs

Gabriele Bulian, *University of Trieste, Italy*, gbulian@units.it

Anders Rosén, *KTH Royal Institute of Technology, Sweden*, aro@kth.se

Vladimir Shigunov, *DNV GL, Germany*, vladimir.shigunov@dnvgl.com

Nikolaos Themelis, *National Technical University of Athens, Greece*, nthemelis@naval.ntua.gr

ABSTRACT

Guaranteeing a sufficient level of safety from the point of view of stability is typically considered to be a matter of design. However, it is impossible to ensure safety only by design measures, and operational measures can then represent a complementary tool for efficiently and cost-effectively increasing the overall safety of the vessel. Time could therefore be coming for systematically considering operational measures as a recognised and normed integral part of a holistic approach to ship safety from the point of view of stability. In this respect, the scope of this paper is to identify open challenges and to provide, in general, food for thoughts for stimulating a discussion on the topic of operational measures, with specific attention to the intact ship condition. The aim of the discussion should be to provide ground for further proceeding towards the goal of implementing a virtuous integrated approach to ship stability safety which gives due credit to effective and robust operational risk control options.

Keywords: *ship stability; ship dynamics; ship safety; operational measures; intact condition*

1. INTRODUCTION

Guaranteeing a sufficient level of safety from the point of view of stability is typically considered to be a matter of design. It is indeed often assumed that the required level of safety is to be guaranteed by implementing proper passive measures at the design stage, in the form of design characteristics (hull shape, subdivision, systems redundancy, etc.) and in the form of limitations on the acceptable loading conditions.

The matter of safety-by-design, both in intact and damaged condition, has been, and of course still is on top of the agenda, especially regarding the rule-making process. However, it is impossible to ensure safety only by design measures, and design rules implicitly assume a

certain level of knowledge, skills, experience and prudence of ship masters and crew. These human factors, which are commonly referred to as “good/prudent seamanship”, represent, therefore, a crucial aspect in determining the ship level of safety. The skills of existing officers are however challenged by rapid development of unconventional ship types and shipping solutions. In some dangerous, or potentially dangerous, operational situations, it can therefore be a great challenge for the ship officers to take the most appropriate decisions for reducing the risk level. Such situations can be effectively addressed by operational measures aimed at providing a decision support for the crew. The implementation of operational risk control options can represent a valid tool for efficiently and cost-effectively increasing the overall level of safety of the



vessel, both in intact and in damaged condition, also in those cases for which design variations would not be cost-effective. This is typically the case with issues associated with dangerous dynamic stability phenomena in intact condition.

In fact, looking at numerous accidents reports it can be easily understood that several accidents could have been avoided, or at least mitigated, by implementing appropriate operational countermeasures. Depending on the case, such operational risk control options could be aimed at the prevention of the occurrence of the accident (measures aimed at the reduction of accident frequency/likelihood) or at the mitigation of its consequences.

Although operational measures become effective during the actual life at sea of the vessel, the combination of planning and implementation of such measures involves both the design and the operation phases of the vessel. It is therefore needed to properly “design operational safety measures”, both for intact and for damaged condition. Indeed, operational measures are expected to be of different nature and to follow different approaches when considering an intact condition (a “normal state” of the vessel) and a damaged condition (an “abnormal state” of the vessel).

As a result, guaranteeing safety through operational measures is linked with various aspects of the vessel (hull shape, ship handling, subdivision, cargo handling, systems design, etc. etc.), with different phases of the vessel’s life (from concept design to actual operation at sea), and with different stakeholders (ship officers, ship owner, cargo owner, shipyards & designers, class, administration).

It can therefore be understood that the concept of “ship stability & safety through operational measures” embraces a variety of conceptual, theoretical, technical, regulatory and educational challenges, with consequent opportunities for research and development.

The combination of passive design measures, with active operational measures, can therefore represent a virtuous holistic approach for increasing, in a cost-effective way, the overall level of safety of the vessel, and this concept is further elaborated in this paper with specific attention to the intact condition.

Present intact stability IMO/SOLAS regulations and class rules are mostly “design oriented” and based on an implicit “passive safety” concept. In this context, operational aspects are given a limited attention, often in the form of qualitative, more than quantitative, indications. As a result, operational measures aimed at increasing the overall safety level of the vessel are put in place by ship owners and operators on the basis of a mostly voluntary, and not harmonised, approach.

This situation, where operational safety measures are neither facilitated nor sufficiently normed by the regulators, does not promote the implementation of approaches aimed at increasing safety through proper and cost-effective operational measures. The eventual result is a lack of promotion of holistic approaches to safety, with consequent missing of opportunities for a potential increase of the fleet safety level.

An example of what the shipping system is possibly missing in terms of potential increase of safety can be found by looking at the experience from a European PCTC operator. In such case, the occurrence of large amplitude motions, associated with phenomena driven by variations of restoring in waves, have been significantly decreased by implementing a holistic pro-active framework including a chain of activities: design optimization to ascertain ships’ hull forms which are sufficiently robust for their intended service (using extensive numerical simulations and model experiments); continuous recording of ship motions and wave measurements with associated analysis and follow up (particularly in case of occurrence of dangerous events); education of all officers (with particular reference to the dangerous



phenomena the vessel can be prone to); and onboard installation of operational guidance systems. As can be noticed, such activities embrace all the phases of the life of the vessel, and are targeting the vessel design, the vessel operation, and the education of the crew. The implementation of such a risk management framework was eventually successful, leading to a reduction of parametric rolling events to a very low rate (of the order of about one per five ship-years for the latest generation of vessels).

There are therefore many opportunities for research and development associated with the idea of giving a more systematic and quantifiable importance to operational measures. At the same time, however, there are also numerous challenges. Some ideas regarding opportunities and challenges have been collected in the following, where the discussion is split in three sections, namely: design, regulatory and classification aspects; tools and methodologies; implementation in operation. However, a sharp separation proved to be very difficult since several of the given considerations are actually conceptually spanning more than one, and in some cases, all the three sections. As a result, some topics appear in more than one section taking, however, a different flavour depending on the perspective they are looked from.

2. DESIGN, REGULATORY AND CLASSIFICATION ASPECTS

Presently, ship stability safety in intact condition is normed by “design oriented” IMO/SOLAS regulations or class rules. The design approach is typically aimed at verifying specific loading conditions and at determining limitations in terms of acceptable KG values, to guarantee a “sufficient static roll restoring” according to specific requirements. Fulfilment of such requirements is implicitly assumed to guarantee a “sufficient level of safety”.

Some general indications are given by regulations regarding the risk involved in

having too large static restoring, since this can lead to excessive accelerations. However, such indications do not typically translate into quantitative limitations on GM. Some quantitative indications regarding too large metacentric heights can be applied in the preparation of the cargo securing manual, for those vessels for which this relevant.

The main weakness of such approach is that the criteria used for the determination of acceptable/unacceptable loading conditions are mostly semi-empirical in nature, and do not provide explicit information regarding the possibly dangerous phenomena a vessel could be prone to in a specific loading condition. Furthermore, in some cases, existing regulations do not sufficiently or properly cover certain dangerous phenomena, which are typically associated with large amplitude ship motions under the action of wind and waves.

As a result of this situation, it might happen that a vessel may undergo crew injuries or cargo loss or damage in heavy sea despite fulfilling existing regulations. Conversely, it might happen that a vessel, marginally complying with existing regulations, still has a sufficient level of safety potentially allowing for a further increase of payload and, thus, profitability. In addition to this, the strongly semi-empirical and statistical nature of present regulations does not provide the master with any information regarding the expected behaviour of the vessel at sea. The lack of information, in turn, can lead the master to take wrong decisions in case of a dangerous situation (e.g. selecting speed and/or heading in facing harsh environmental conditions). Also, the present regulatory framework is not designed for incorporating active operational measures as a means for guaranteeing the required level of safety in certain specific, potentially dangerous, conditions.

The mentioned limitations in the prevailing regulatory framework have recently been tackled, conceptually, in the development of the IMO Second Generation Intact Stability



Criteria (SGISC). Indeed, in the framework of SGISC, specific criteria are developed for specific dangerous stability phenomena in waves. This allows identifying, at the design stage, the type of phenomena the particular vessel is prone to. The identification of such phenomena becomes clear with the determination of the governing criteria, and associated failure mode, in the definition of acceptable/unacceptable loading conditions. It is worth noting that, because these criteria are based on a dynamic approach, the usual concept of “limiting GM” is, in principle, abandoned, and this can potentially lead to problems on how to treat this situation from an approval (Administration, or Class on behalf of the Administration) perspective.

In addition, the framework of SGISC allows guaranteeing, in principle, a sufficient level of safety by means of a combination of design requirements and of properly developed ship-specific operational guidance. Alternatively, it is also possible, in principle, to approve the vessel, in the specific loading condition, subject to the fulfilment of some specific operational limitations. “Operational limitations” are herein intended as limitations on the overall operability of the vessel in specific loading conditions (e.g. operations allowed only in certain geographical areas/sheltered waters, or up to a certain significant wave height). On the other hand, ship-specific “operational guidance” is intended as a detailed recommendation to the master on how to handle the vessel, in a specific environmental condition, to reduce the likelihood of inception of “stability failures” to an acceptable level.

It can therefore be seen that the envisioned framework of SGISC gives significant importance to ship-specific operational measures (operational guidance, or operational limitations). Actually, the framework of the SGISC can be seen as shift of paradigm, going from the current situation where ships are regarded as safe when designed and loaded in accordance with the current stability criteria

assuming they are just operated on the basis of generic good seamanship, to a situation where ships would be designed considering the possibility of also developing ship-specific operational guidance contributing at keeping the likelihood of stability failures below an acceptable limit. The present target date for addressing “guidelines for direct stability assessment” and “requirements for development of ship specific operational guidance” within SGISC has been set to 2017. The SGISC framework is then supposed to be initially implemented as non-mandatory regulations through the 2008 IS Code, and a possible mandatory application is therefore likely far away in time. Under such a situation, a series of questions arise. To what extent will these new voluntary criteria actually be used if they are not forced by a mandatory framework? How many shipping companies/shipowners will dedicate resources to fulfill these criteria if they are non-mandatory? Will the owners/designers be interested in a pro-active verification of non-mandatory criteria, in view of a possible future mandatory application, or in view of having a better understanding of the dynamic characteristics of the vessel? Will this lead to a wider, more informed, introduction of operational-oriented measures? And how could operational measures be used to increase the safety of some of existing ships that obviously would benefit from stability and safety improvements, but which will not be affected by the new criteria?

However, irrespective of the specific regulatory framework, it is clear that efforts should be spent, in general, to introduce operational measures in the design process, as viable and accepted risk control options. Indeed, implementing operational measures can represent a cost-effective way for increasing safety and, also, competitiveness. An example in this respect can be found in case of inland navigation, where suspension of navigation is sometime introduced in case of too harsh weather conditions (typically wind). In some cases, navigational limitations based on weather conditions are also introduced, on a



local basis, for sea-going vessels (to avoid, e.g., port entrance problems). However, a vessel able to operate safely in such harsh conditions could become more competitive, if the cost-effectiveness analysis indicates so. Similar considerations could also apply to vessels operating in sheltered waters, on specific routes, etc.

Implementing such an approach is not free from technical and regulatory challenges, which, at this moment, have not really been sufficiently addressed. As a result, several questions are open and more are likely to come.

Operational limitations could be introduced by changing the reference environmental conditions for the evaluation of intact stability criteria, when this is feasible according to the structure and background of the criterion (this is doable, for instance, at Level 2 vulnerability assessment in the framework of SGISC). The vessel should then be approved with such limitations noted. Operational aspects are presently under responsibility of the Administrations. In presence of operational limitation, it could be necessary for the master to demonstrate the compliance of the planned travel (loading condition, route and associated weather forecasts) before leaving the port, and such plan should be approved by the Administration. It is worth noting at this stage that operational limitations are well-known in rules for classification of vessels for combined river-sea or sea-river navigation, and therefore some experience could be gathered from that context. In the same context, approaches have also been developed in order to allow the operation of inland vessels (with few modifications) in the coastal maritime stretches up to a certain, pre-computed, significant wave height. It is however evident that having this procedure in place for a large number of sea-going vessels would require significant procedural efforts.

In case of development of ship-specific operational guidance, three main possible means can be envisaged for providing such

guidance to the master: pre-computation at the design stage, real-time computations on board during operation, real-time computations onshore during operation. In addition, a combination of these three approaches could also be considered as an option. Each of these approaches presents pros and cons from the technical and the regulatory perspective, which so far have not yet been deeply investigated.

From a regulatory perspective, one fundamental issue is the definition of the type software, and associated underlying mathematical model, which can be accepted for preparing ship-specific operational guidance. This aspect has to do with the verification, validation and accreditation process, which should be expected to eventually end up in an approval. At this moment, different options are on the table regarding possibly applicable mathematical models, ranging from simplified 1-DOF models intended for being used for single specific failure modes, up to 6-DOF hybrid tools simulating a vessel free running in wind and waves. Of course this wide spectrum of possibilities needs to be standardised to obtain a uniform application of the regulations.

Regarding how to prepare ship-specific operational guidance, on the one hand, one could be tempted to think that a large number of pre-computations should be carried at the design phase. Results of such computations should then be processed in order to give information to the master on how to safely handle the vessel in dangerous environmental conditions. Such information could then be provided in terms of, e.g. polar diagrams (or any other type of relevant representation) reporting some measure of stability failure. On one side, an advantage of such pre-computed operational guidance is that they could be approved, likely by the Class on behalf of the Administration, already in the design stage. On the other side, however, this could be a difficult approach, for a series of reasons. The first problem is the large number of computations to be carried out, because the set of scenarios to be checked could become huge: different



loading conditions, different wave conditions (separating at least swell and wind waves, considering different significant wave heights and characteristics spectral periods), different wind conditions (in terms of mean wind, gustiness spectrum, relative direction with respect to waves), different wave headings, different ship speeds, etc. All these combinations would eventually lead to a very large matrix of simulation scenarios. Another issue to be taken into account when considering the preparation of pre-computed ship-specific operational guidance has to do with the modelling of the environment. Indeed, although typical spectral models can be introduced in the pre-computation phase for both wind and waves, it is also known that the actual environmental conditions can differ significantly from the idealised models. As a result, wind and wave spectra encountered at sea will not correspond, in general, to the ones assumed in the pre-computations. How to use, then, data obtained from pre-computations in such cases? And how to “approve” an instrument, with associated methodology, intended for carrying out this inference? Connected to this, there is also another open question: what level of approximation can be accepted in the representation of the actual environment through simplified idealised parameterised models (with a reduced number of parameters), while still keeping the ability of reasonably identifying the possibility of occurrence of dangerous situations? In short, how much can the description of the environment be simplified, while still keeping a sufficiently accurate prediction of ship motions for identifying dangerous scenarios?

If, alternatively, ship-specific operational guidance would be designed to be potentially based on real-time calculations using the environmental conditions locally encountered by the vessel, this approach could ideally solve some of the issues associated with pre-computations at the design stage. At the same time, the real-time approach would lead to several challenges from the point of view of the approval process, depending on how the

computations are carried out. Indeed, real-time computations could be carried out, in general, onboard or onshore. These two alternatives are associated with different levels of available computational resources and information. As a result, a real-time system based onboard (characterised by limited computational resources and limited data access due to satellite bandwidth limitations) would likely be significantly different from a real-time system based onshore (where computational resources and data access are no longer an issue). Such difference in the system would reflect, on one side, on the type of tools and methodologies which can be applicable. On the other side, such difference in the computational system and associated approaches would also reflect in differences in the approval process.

Another issue to be addressed is the definition of “stability failure” for a proper integration within a regulatory framework. When speaking about operation, there could be different types of “failures” with escalating levels of severity, ranging from passengers’ severe discomfort, to cargo shifting/loss/collapsing, up to ship capsizing. Such types of failures are typically defined by appropriate limits of angles (usually roll, but also pitch) and/or accelerations. In addition, it could be necessary to provide specific “failure conditions” for different types of vessels and/or different types of cargo onboard. For instance, in case of cargo vessels, “failure conditions” need to be defined to avoid the occurrence of cargo shift, cargo loss, or possible cargo collapsing, taking into account the specific vessel, transported cargo and associated lashing arrangement. Then, the most critical mode of cargo failure will depend on the specific case. For instance, in case of inland navigation, the sliding, with possible loss, of non-secured containers can become the governing cargo-related failure condition, while this is typically not the case for sea-going vessels which transport secured containers.

A further challenge for a proper application of ship-specific operational guidance is



associated with a sufficiently accurate determination of the parameters of the actual ship loading conditions, which are relevant for dynamic stability computations. From the perspective of “classical” intact stability criteria, a check of the compliance of the loading condition can be carried out by knowing the position of the (solid) centre of gravity and free surface effects (e.g. by tanks’ sounding). Accurate knowledge of these parameters is already a challenge, and in many occasions the crew only has an estimation (in some cases a rough estimation) of the actual loading condition. This is a typical case for, e.g., container vessels, where the loading condition cannot be accurately determined using only the declared containers’ weight (the situation will however improve by the introduction of the mandatory weighting of containers expected in 2016). In case of methodologies intended to determine the dynamic behaviour of the vessel at sea, in addition to the knowledge of KG/GM, it is necessary to know also the characteristic vessel periods (particularly roll period). An inaccurate evaluation of the roll period (or, equivalently, of the roll inertia) can lead to inaccuracies in the application of ship-specific operational guidance. It is therefore a challenge, from a regulatory perspective, to put in place uniform procedures which can guarantee that the guidance to the master is provided on the basis of accurate enough input data for the underlying computational tool.

A challenge which is also likely to be faced in the approval process, is associated with the uncertainty in the estimation of the parameters (e.g. roll damping, radii of inertia, wind coefficients, etc.) for carrying out the simulations aimed at providing ship-specific operational guidance. Indeed, many of the parameters used in the simulations will be affected by some level of uncertainty. Such uncertainty will then propagate to the final results, which, then, will also be uncertain. Therefore, the challenge for the approval process will be how to address this inherent level of uncertainty.

Another interesting aspect which is likely necessary to be properly taken into account in respect to the development and approval of ship-specific operational guidance is the use of active means for motion reduction (typically roll). When assessing present intact stability criteria, it is typical to neglect the effect of active anti-rolling means. However, neglecting active means when preparing ship-specific operational guidance can produce misleading guidance. A typical example is represented by active anti-rolling fins for certain vessels (e.g. cruise ships). Such anti-rolling devices tend to have a significant beneficial effect on roll motion at sufficiently high forward ship speed. Neglecting the additional damping effect of anti-rolling fins could lead to issuing operational recommendations to the master which are not properly exploiting the increase of forward speed (and thus damping) as a risk control option. Of course, taking into account active anti-rolling devices (e.g. stabilizing fins, anti-rolling tanks, etc.) introduces further complexity in the mathematical modelling which is to be used for developing operational guidance.

Another global challenge from a design and regulatory perspective is associated with the decision on when/how to accept a ship-specific operational guidance, instead of requiring a design modification or flagging the considered loading condition as “not seagoing”. Indeed, there will be a region of high “safety level” where the vessel, in the considered loading condition, will comply without additional requirements. There will likely be a region of low “safety level” where the vessel, in the considered loading condition, will not comply at all. As a result, the loading condition will either be considered as “unacceptable” or design modifications will be required to increase the passive safety. However, there will be an intermediate region where it will be possible to ensure the required safety level by providing ship-specific operational guidance. How to measure the “safety level” and where to put the “boundaries” is a significant



challenge from the technical and from the rule-development/approval perspectives.

Furthermore, in all these considerations, it was implicitly assumed that, given “ideally perfect operational guidance”, the crew would respond appropriately by following them. The reality, however, is clearly fuzzier. Ship-specific operational guidance cannot be perfect for different reasons: approximation of the underlying mathematical modelling, inaccurate knowledge of environmental conditions, inaccurate knowledge of loading condition, etc. On top of this, the human factor becomes crucial, because, when dealing with operational guidance, the type of risk control option is active, and no longer passive, and typically, in intact condition, it could require human intervention (unless an automatic system is introduced). However, the human action is intrinsically uncertain, and the question arises of whether and how to take this uncertainty into account for the approval of procedures and tools for ship-specific operational guidance.

3. TOOLS AND METHODOLOGIES

To guarantee safety through operational measures, it is necessary to be able to predict large amplitude ship motions under the action of wind and waves. This requires using tools which are able to address nonlinear ship motions, and classical linear seakeeping tools are, in general, not appropriate for this purpose.

Simulation tools addressing nonlinear ship motions are, in the vast majority of cases, based on time-domain simulations. This makes the required computational time a challenging problem. In order for such tools to be viable in the framework of providing ship-specific operational guidance to the master it is therefore necessary to have at disposal tools which are fast enough, as well as application methodologies which reduces the required time for the computation of motions and subsequent provision/development of the operational guidance to an acceptable level. The acceptability level with respect to

computational time depends on whether the tools and procedures are to be used in the design phase or in the operation phase.

As already said, in fact, three main categories of approaches can be envisioned for ship-specific operational guidance: pre-computation at the design stage, real-time computations on board during operation, and real-time computations onshore during operation. Different types of mathematical models can better suit different approaches. Indeed, tools and methods at various levels of detail can be utilised for nonlinear ship motions assessment.

Nowadays, the highest level of simulation complexity which is still compatible with the need for extensive series of simulations is represented by hybrid 6-DOF tools simulating the vessel freely manoeuvring in waves. The typically required computational time makes these tools more suitable for an application within a procedure targeting the design phase. However, under proper design of the methodology, they could also be implemented in a framework based on onshore real-time calculations using forecast weather data. In this moment, these tools are hardly applicable for real-time approaches using locally measured wind and sea conditions (e.g. through anemometers and wave radars, or using vessel motions to infer the sea spectrum). Nevertheless, such tools could ideally be implemented in frameworks intended for deterministic prediction of ship motions in a short time-horizon (of the order of minutes), provided the associated methodologies would prove to be robust enough and the prediction time-horizon would prove to be long enough to allow the actual implementation of some risk control option.

At reduced level of complexity there are several possible approaches, based on nonlinear models, typically with a reduced number of degrees of freedom. Such models are much faster, and therefore, in principle, more appealing, especially if the aim is the implementation of real-time, or near real-time



approaches. However, the reduction in the model complexity is often achieved by targeting the model to certain specific failure modes (e.g. resonant roll, variations of stability in waves, manoeuvring-related problems such as surf-riding and broaching). As a result, such models should be used very carefully, with a clear understanding of the modelling limitations. Indeed, such specific dynamical models, targeted to specific failure modes, typically provide wrong operational indications if misused, i.e. if used outside their region of applicability.

Irrespective of the used dynamical model for the prediction of ship motions and/or for the identification of potentially dangerous conditions, there are a series of common challenges impacting tools and methodologies.

A challenge which was already anticipated in the previous section has to do with the description of the environment (wind and waves). Indeed, it is known that the actual environmental conditions can differ significantly from the idealised simplified and parameterised spectral models which are commonly used for simulation purposes. Sea and wind spectra encountered in operation shows larger shape variability than that which can be modelled by superimposing the classical two wave systems: wind waves (with spreading) and swell (with or without spreading). Also, more than two systems can coexist, with a significant potential variability in terms of relative direction. In this respect the question then arises of whether and, if so, to what extent, the differences between the actual environment and the parameterised simplified environmental conditions actually impact the capability of providing relevant operational guidance. In addition to this, questions are also open regarding the impact, on the relevance of the prediction, of introducing or neglecting nonlinear effects such as a nonlinear description of the wave field, breaking waves, rogue waves, etc.

With respect to environmental modelling, it is also necessary to bear in mind some other

aspects. First of all, not all mathematical models are capable of taking into account multi-directional waves. This is the typical case for some 1-DOF models which were developed only for the long-crested sea case. As a result, environmental modelling limitations can be implicitly introduced by the used mathematical model, and the consequent impact on the prediction capabilities should be assessed. Furthermore, practical limitations exist regarding the modelling of the environment, depending on whether the operational guidance are developed through pre-computations at design stage, or whether the operational guidance are linked with real-time computations in operation. Indeed, taking into account the actual variability of the environmental conditions in a framework based on pre-computations at design stage is likely to be not viable due to the corresponding too large matrix of simulation scenarios. As a result, in such a framework, simplifications in terms of number of parameters for the modelling of the environment are necessary. Alternatively, calculations should be carried out on reduced sets of scenarios, assuming the other scenarios to be “safe” (e.g. avoiding unnecessary calculations in small significant wave heights). On the other hand, in a framework based on real-time computations, the actual environment could be exactly taken into account, at least in principle, provided that the information regarding wind and waves spectra are available (from measurement or forecast) and provided the tool and the procedure for issuing the guidance is able to appropriately use such information. There are also special situations where getting information regarding the environmental conditions can be difficult. It is the case, for instance, of inland navigation, where microclimate effects can be difficult to be captured in a real-time framework based on weather forecast.

An important point to be taken into account when considering tools and procedures to be used for operational guidance, is the fact that the framework, in general, has to be based on a probabilistic approach where the likelihood of an intact stability failure is typically required to



be at acceptable probability levels, which can be very low. This means that failure events to be “discovered” (and for which guidance should be issued) can become rare events. This poses significant challenges in terms of procedure for assessing the risk level of a specific scenario. Indeed, direct Monte Carlo approaches require a large number of realizations to be able to quantify the likelihood of occurrence of rare events with sufficient accuracy. In some cases a direct Monte Carlo approach can become unfeasible, without introducing some more advanced calculation procedures. Procedures have been proposed making use of split-time approaches, wave-groups approaches, approaches based on first-order reliability methods, or approaches relying on extrapolation based on significant wave height. In most cases such approaches were proposed for the use in a design-level pre-computation framework, but potential could exist for their use also in a real-time calculation framework. In some cases such approaches have been designed for application in a route-optimization framework. In such case, translating them to an operational-guidance framework could be mostly a matter of computational speed.

Another important aspect to be taken into account when generating operational guidance relates to the manoeuvring behaviour of the vessel in wind and waves. In numerous mathematical models the (average) ship speed and the (average) heading angle are kept fixed. Although this is a useful assumption for assessing the behaviour of the vessel in the nominally defined conditions, such an approach misses a series of important characteristics. First of all this approach does not take into account the effect of active rudder control. There are phenomena, such as broaching, where the modelling of the rudder control has a significant effect on the outcomes of the assessment. Other phenomena which are not considered by constant (average) speed models are the involuntary speed reduction and the ship ability to keep the commanded course. These phenomena can make some combinations of speed and course not realistic

because they would be practically not achievable by the vessel. Furthermore, neglecting speed variations can miss the speed reduction in high groups in head sea, as well as the typical prolonged staying of the vessel on the wave crest in following waves due to asymmetric surging, and this can influence certain phenomena (e.g. parametric roll, pure loss of stability, surf-riding and broaching). Whether taking into account all these aspects is something to be done directly by the ship motions simulation model, or whether this can be done by intermediate approaches mixing different mathematical models, is, presently, a matter of investigation. A matter of investigation is also the understanding of the extent to which the mentioned modelling aspects are affecting the issuing of operational guidance.

A further matter connected with tools and methodologies for operational guidance is the definition of “stability failure”, because such definition cannot be considered to be totally independent of the tool used for the computations. The definition of “stability failure” needs to be consistent with, and needs to properly account for, the capabilities and limitations of the tool which will eventually be used for the evaluation of the ship behaviour. For instance, while a 6-DOF tool is able to provide the full kinematics of the vessel, the same cannot be said, in general, for models with reduced number of degrees of freedom (e.g. 1-DOF models). In this latter case additional assumptions and approximations need to be introduced to try taking into account the missing degrees of freedom, when this is needed. This eventually reflects in the overall capability and accuracy of different tools to take into account stability failures associated with, e.g., accelerations. Such situation needs therefore to be properly accounted for when defining the “failure conditions” to be used.

Other types of less conventional approaches have been proposed, or can be envisaged, for issuing operational guidance in a real-time framework, where use is made of specifically designed and trained Artificial Neural



Networks (ANN). Although such approach is appealing, thanks to the associated computational speed and adaptability, some challenges for its use are evident. The model needs to be properly and extensively trained at the design stage (with possible update during the operation), through appropriate simulations. In addition, and connected with the training phase, attention must be paid to the use of ANN outside the training range, since such approaches typically lack extrapolation capabilities.

When considering approaches for a real-time calculation framework, two options have been mentioned: onboard computations and onshore computations (through an onshore support team). These two approaches significantly differ in terms of availability of computational resources and expertise of users, and this, in turn, reflects on the fact that significantly different models and/or procedures are expected to be used in the two cases. In case computations are carried out onboard, fast and simple models are expected to be employed, whereas more complex and computationally intensive models can be used for calculations carried out onshore. The same is valid for the calculation procedures to be used. Indeed, even fast simulation models can result in slow computations if the application procedure requires too many calculations for the available resources. In case calculations are carried out onboard, such procedures shall therefore be fast and simple (possibly based on simplified nonlinear frequency domain approaches). On the other hand calculation procedures based onshore can benefit, and therefore be allowed to require, significantly larger computational resources.

Formulating ship specific operational guidance is hence a trade-off between accuracy and simulation time, and also between accuracy in the ship dynamics modelling and the accuracy in the sea state representation. In his context, on one extreme there are 6-DOF simulation tools having the potential for providing a higher level of accuracy, which is however paid at the cost of the increased

simulation time. On the other extreme, simplified frequency domain methods exist, for example, for the determination of stability limits for parametric rolling and pure loss of stability from estimated spectra of GM variation, which are determined from GM variation transfer functions and wave spectra according to linear response theory. Such methods require very small computational effort, making them applicable for real-time computations. However the reduced computation time is paid by the likely reduction in the prediction accuracy. Where the optimum trade-off is positioned is a matter, on the one hand, of goals and, on the other hand, of technological and theoretical evolutions. This means that the optimum trade-off is something moving with time, experience and research & development.

4. IMPLEMENTATION IN OPERATION

The onboard implementation of means for providing operational guidance to the master is, evidently, the final goal. It is also evident, from the discussion so far, that a series of technological challenges are associated with the actual implementation of such a system. While some of such challenges are of general nature, some others, again, depend on how operational guidance is assumed to be provided: on the basis of pre-calculations at design stage, on the basis of real-time onboard calculations, on the basis of real-time onshore calculations, or a mixture of the three. Challenges associated with theoretical and technological aspects, however, are only one part of the picture. Aspects associated with ergonomics (human factors) are also important for a successful implementation of an onboard operational guidance system, which, in essence, is (part of) a decision support system. Indeed, in a system development phase, the attention is typically focussed on calculation methods. However, moving from such phase to the later phase of the implementation, clearly requires taking the matter of interaction with crew in due account.



Two fundamental aspects are directly linked with onboard implementation: loading condition on one side, and prevailing weather conditions on the other side. Indeed, irrespective of how the operational guidance is actually determined (pre-calculations or real-time calculations), for an onboard implementation, it is clearly necessary for the system to know the present (or future, in case of forecasts) loading condition and the present (or future, in case of forecasts) weather conditions. It is therefore necessary that an actual onboard implementation will be able to get information regarding the loading condition and weather conditions.

Regarding the loading condition, the starting point is evidently the loading condition as known (estimated) at the departure, combined with the sounding of the tanks during the voyage (or an estimation of consumptions), and/or combined with the information on loaded/unloaded cargo weights in case this is relevant to the vessel operation. However, such an approach is limited with respect to two aspects. First, it gives an estimation of the actual loading condition which can be affected by uncertainty. Second, typically, it does not give information regarding the inertia, which needs therefore to be estimated, introducing, again, uncertainty. In order to provide accurate operational guidance, it is therefore necessary to try implementing approaches which can increase the accuracy in the knowledge of the relevant mechanical characteristics of the vessel. For instance, to increase the accuracy in the knowledge of GM, it could be envisaged to systematically perform some kind of simplified inclining test at the departure, something which some vessels/operators are already doing. Alternatively, methods could be devised for carrying out an approximate GM determination while at sea. Clearly, appropriate approaches should also be implemented in order to have also a sufficiently accurate knowledge of the trim and displacement. To this end, the common procedure of direct reading of draught marks in port can be supplemented by, e.g., approaches making use of data from automatic

draught measuring systems which, following proper processing, could be used to provide a real-time estimation of trim and displacement during navigation (at least in time windows of sufficiently mild weather conditions). However, the knowledge of GM, for a given trim and displacement, is not sufficient for predictions addressing ship dynamics for safety purposes. In such case the rolling period (or rolling inertia) is one of the parameters which need to be properly known. To this end it could be envisaged to implement procedures for systematically carrying out small roll decays, at least at the departure, for estimating the roll period. Alternatively, real-time monitoring systems could be used to estimate the natural roll period of the vessel during operation. Other parameters could also be necessary such as, e.g., the pitch inertia. For the determination of the pitch inertia, real-time monitoring of the pitch motion, possibly linked with knowledge of local weather conditions, could be of help. Of course, none of these approaches can be considered more than an estimation of the actual quantity of interest. However, trying to increase the accuracy of the estimation represents a means for increasing the accuracy of the overall decision support system.

Once the actual loading condition is assumed to be known with a sufficient accuracy, the other big challenge is the knowledge of the weather conditions, i.e. wind and waves (and possibly current). Two main approaches can be implemented onboard in this respect: use of forecast data, or use of data from real-time measurements. A combination of the two can also be envisaged, where, for instance, forecast data could be corrected by an analysis of systematic comparison of forecast and actual measurements. In general, however, the type of measuring system could be tied to the type of procedure which is used for issuing the operational guidance. Indeed, guidance based on pre-computations could in principle make use of real-time estimation/measurements of weather conditions. However, a challenge in this case is faced: how to use pre-computed data in nominal weather conditions for issuing guidance associated with the presently



measured ones? Such challenge actually occurs also with forecast data, whenever the forecasted weather condition does not (sufficiently) match any one in the set of those originally used in pre-calculations. Real-time measurement, as well as forecasted data, can be used, instead, at least in principle, without difficulties, whenever sufficiently fast algorithms are used for the issuing of operational guidance. However, this requires algorithms able to account for the complexity of the environment (directional sea spectra, wind spectrum, etc.). On the other hand, real-time monitoring is typically of no use if operational guidance approaches are based on relatively slow computations (onboard, but more likely onshore). In such case the only viable option for issuing operational guidance based on motions statistics is the use of forecast data. Alternatively, deterministic short-time horizon (of the order of minutes) guidance could be potentially based on real-time measurements. In this case, however, wave radars should be used.

Also connected with the monitoring of weather conditions, it is worth mentioning a relevant fact, providing some associated brief considerations. Presently, the IMO MSC.1/Circ.1228, which basically represents the prototype of ship-independent (i.e. generic) operational guidance, assumes that a monitoring of the weather conditions based on observations by the crew is sufficient. The question, then, is whether this assumption can be considered valid for a modern ship-specific operational guidance system. It is indeed known that the level of accuracy of visual observations is limited, and the example case of (basically impossible) estimation of weather conditions by visual observations at night should serve as a sufficient example to show the limitation of the approach. Therefore, considering that the accuracy of the predictions of ship motions is typically limited by the element of the prediction chain with the higher combination of inaccuracy and sensitivity coefficient, it is very likely that environmental conditions estimated on the basis of visual observations cannot be considered compatible

with a robust ship-specific operational guidance system.

The other mentioned challenge for a practical successful onboard implementation is associated with human factors and, in details, with the relation between the system and the crew. One important aspect to be taken into account is the usability and understanding by the crew of the information given by the support system. In this respect it is important that the post-processing of the data is made with the aim of providing immediately and clearly understandable information regarding the potential danger level of the conditions. Polar diagrams (speed and course for the present weather scenario) are a typical way of presenting results based on the analysis of, for instance, some statistical quantity relevant to the ship safety (e.g. expected mean roll amplitude, or maximum roll amplitude for a given nominal exposure time, or similar data regarding the acceleration, or quantities associated with cargo failure). Guidance information, based on the processing of such data, should be provided using appropriate colour coding for immediate understanding, and the parsimonious use of audio alarms could also be considered. Similar polar representations can also be used to report regions of speed and course leading to specific problems (e.g. parametric roll, pure loss of stability, manoeuvring and course keeping problems, etc.).

With reference to the interaction of the system with the crew, it is also important to be sure that the system is accurate enough (and not, for instance, too conservative) for the crew to rely on it when taking decisions. Experience has shown that the trust of the crew in operational guidance and decision support information is very much dependent on how well the information corresponds to their own experience of the operational situation.

Another important aspect for a successful holistic approach to safety through operational measures is associated with the training/education of the crew. The crew is



indeed likely to take in low consideration guidance information received from a system that is not sufficiently well understood in terms of underlying theoretical and/or technical background. Also, not all crews are fully aware of the more complex stability failure modes. Enhancing the crew education and awareness is hence of utmost importance. Such education should consider general stability aspects as well as certain aspects regarding the specific vulnerabilities of their ships. As an example, just informing crews about the outcomes of SGISC Level 2 assessment for their particular ship, would already imply a significant safety improvement compared to the current situation, since it would give a better awareness of the susceptibility of the vessel to different phenomena in a transparent way. Part of the process of education could also be based on follow up from accidents, or near-accidents. In this case, the recording, and following analysis together with the crew, of the actual weather conditions and ship motions at the moment of the (near-)accident, could prove being of great help and impact.

Furthermore, education and training of crew could also be enhanced by increasing the use of virtual reality simulators embedding also operational guidance systems. This would have two main benefits. On the one side it could help the crew in familiarising with the operational guidance system. On the other side, it could help in improving and updating the operational guidance system on the basis of the experience made during the virtual simulations and on the basis of the feedback gathered from the users.

5. FINAL REMARKS

Although the overall ship safety in intact condition is the result of a combination of design and operational measures, operational safety measures are presently neither facilitated nor sufficiently normed by the regulators. This situation does not promote the implementation of approaches aimed at increasing safety through proper and cost-effective operational

measures. At the same time, however, clear and large potentialities exist for increasing the fleet safety level by properly combining passive design measures with active operational risk control options. It seems, therefore, that time could be coming for systematically considering operational measures as a recognised and normed integral part of a holistic approach to ship safety from the point of view of stability. However, several challenges are to be faced, requiring efforts from the point of view of research & development and from the point of view of the rule-making process. In this context, the scope of this paper has been to identify such open challenges and to provide, in general, food for thoughts for stimulating a discussion on this topic, with specific attention to the intact condition. The aim of the discussion should be to provide ground for further proceeding towards the goal of implementing a virtuous integrated approach to ship stability safety which gives due credit to effective and robust operational risk control options.

6. ACKNOWLEDGEMENTS

This collaborative effort has been undertaken by a group of members of the “Stability R&D Committee” (www.shipstab.org/stability-r-d-committee-srdc/). The authors would like to express their sincere thanks to the organisers of the 12th International Conference on Stability of Ships and Ocean Vehicles (STAB 2015, Glasgow, UK) for the opportunity given to present this work.

7. REFERENCES

Bačkalov, I., Bulian, G., Cichowicz, J., Eliopoulou, E., Konovessis, D., Leguen, J.-F., Rosén, A., Themelis, N., 2015, “Ship stability, dynamics and safety: status and perspectives”, Proc. 12th International Conference on the Stability of Ships and Ocean Vehicles (STAB2015), 14-19 June 2015, Glasgow, Scotland, UK



Ship Stability & Safety in Damage Condition through Operational Measures

Evangelos Boulougouris, *University of Strathclyde, UK*, evangelos.boulougouris@strath.ac.uk

Jakub Cichowicz, *Brookes Bell, UK*, jakub.cichowicz@brookesbell.com

Andrzej Jasionowski, *Brookes Bell, Singapore*, andrzej.jasionowski@brookesbell.com

Dimitris Konovessis, *Nanyang Technological University, Singapore*, dkonovessis@ntu.edu.sg

ABSTRACT

Guaranteeing a sufficient level of safety from the point of view of stability is typically considered to be a matter of design. However, it is impossible to ensure safety only by design measures, and operational measures can then represent a complementary tool for efficiently and cost-effectively increasing the overall safety of the vessel. Time could therefore be coming for systematically considering operational measures as a recognised and normed integral part of a holistic approach to ship safety from the point of view of stability. In this respect, the scope of this paper is to identify open challenges and to provide, in general, food for thought for stimulating a discussion on the topic of operational measures, with specific attention to the damaged ship condition. The aim of the discussion should be to provide ground for further proceeding towards the goal of implementing a virtuous integrated approach to ship stability safety which gives due credit to effective and robust operational risk control options.

Keywords: *ship stability; ship dynamics; ship safety; operational measures; damaged condition.*

1. INTRODUCTION

Required levels of safety with respect to damage ship stability are typically guaranteed by the consideration and evaluation of the effectiveness of proper passive measures at the design stage against applicable regulatory provisions. These measures are in the form of potential design alternatives (hull shape, subdivision, systems redundancy and availability, etc.) and for acceptable loading conditions.

Concerted research and development efforts in the period of the last 20 or so years have mobilised the international maritime community to research on the theoretical understanding of the flooding process and to focus and act on the development of new probabilistic rules for damage stability for all ship types, new ship designs extending and

challenging known design limitations, and the Safe Return to Port (SRtP) regulations. Risk-based approaches and cost-effectiveness considerations have been extensively used in this process. A major finding is that the overall level of safety of a ship can only be guaranteed when considering passive design measures in conjunction with active operational measures, in a holistic, balanced and cost-effective manner.

The concepts of time to flood and time to evacuate and how they interrelate are fundamental notions in determining safety thresholds with respect to ship stability and flooding. In principle, vulnerability to flooding relates to the cumulative probability for time to capsize within a given time in the operational environment of the vessel, accounting either for all statistical damages or for a given damage scenario. This also provides the key input for



vulnerability monitoring, which in turn offers all the essential information for damage control and emergency response.

There are therefore many further opportunities for research and development associated with the idea of giving a more systematic and quantifiable importance to operational measures. At the same time, however, there are also numerous challenges. Some ideas regarding opportunities and challenges have been collected in the following, where the discussion is split in three sections, namely: operational guidance and procedures; systems availability post-damage; active measures for damage containment. In this paper, we provide elaborations on open challenges and food for thought for stimulating a discussion on the topic of operational measures, with specific attention to the damaged ship condition.

2. OPERATIONAL GUIDANCE AND PROCEDURES

Technological advances in computing hardware over the last decades have facilitated solution of many problems in ever decreasing amount of time. However, the progress in technical calculus, involving modelling based on the fundamental physical laws, has been just as significant, and despite the availability of ever greater processing power, many cases of numerical approximations to reality remain impractical to compute. It is for this reason that advanced prognosis have only had limited success in proliferating the field of instantaneous decision support.

Although highly advanced computerised safety management systems (SMS), have found accelerated support, their advisory functionality are mostly limited to detection only, with more sophisticated prognosis and advisory capabilities remaining at prototyping and development stages.

Such prototype simulation approaches available for use in prognosis comprise a range of phenomena such as (a) ship response to flooding progression, modelled through various but direct solution to conservation of momentum laws, or through quasi-static iterative approximations, (b) structural stress evolution under flooding, (c) the mustering process, (d) fire and smoke spread, and possibly many other.

Some of the reasons inhibiting their more wide use for decision support arise due to a series of practical problems in addition to sheer computational effort, such as the following:

- Each of these processes may vary at any instant of time due to changing conditions.
- The input is subject to considerable uncertainty.
- For any set of input information the outcome is random due to computational and modelling uncertainties as well as due to random nature of environmental or process conditions themselves.
- Each may be seriously influenced by decision choices.

The nature as well as inseparable combination of these engineering challenges imply that the projection functionality would need to be iterated for a range of uncertain conditions of either of the scenarios occurring as well as for a range of decision options, so that the best choice can be identified with controllable degree of confidence. This, in turn, implies that the computational task of scenario projection in real time in support of decision making will likely remain a serious challenge, as most of these analyses require substantial amount of processing time, at present accounted in hours.

Vulnerability Log, or VLog for short, has been proposed to be the functionality to inform the crew at all times on the instantaneous



vulnerability to flooding of the vessel, considering its actual loading conditions, the environmental conditions and the actual watertight integrity architecture (Jasionowski, A, 2011). The vulnerability is proposed to be measured in terms of the probability that a vessel might capsize within given time when subject to any feasible flooding scenario. Figure 1 demonstrates the distribution of vulnerability logged on a demonstration ship.

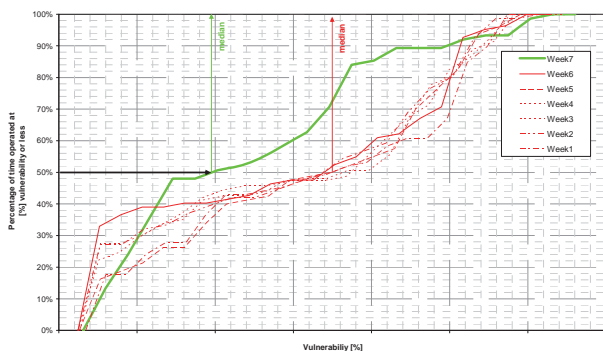


Figure 1: Distribution of vulnerability logged on a demonstration ship. The actual vulnerability values are undisclosed. The impact of the awareness of the crew on the day-to-day management of watertight integrity, and hence crew and ship preparedness, can be seen in Week 7, when explanation and training on use of VLog had been given

Since until a casualty occurs it is impossible to anticipate any specifics of a flooding case a ship might suffer and therefore let the crew prepare for it, it seems plausible that instead the crew is made aware of the range of such flooding specifics together with projected impact these can have on the ship state. The crew would be able to infer the criticality of the situation evolving immediately, based on their own awareness, and hence decide instinctively of the best possible actions to follow. Ship vulnerability to flooding will naturally vary significantly from a flooding case to a flooding case, and subject to what condition the vessel operates at, at which environment and what is the watertight integrity status. All these must, therefore, be considered.

The framework for vulnerability assessment given in the source (Jasionowski, A, Vassalos,

D, 2006) can serve as a very informative model for use in the context of decision making. It reflects fundamentals of physical processes governing ship stability in waves and explicitly acknowledges uncertainty of such predictions by exploiting probability theory.

Therefore, further research efforts should be expanded to establish and verify practicalities of the principles of the proposed functionality, as well as to assess impact of all engineering approximations that are used in application of the proposed model. Many such aspects should be considered, with key focus on uncertainty in the widest sense, pertaining to its both aleatory as well as epistemic types. Example impact of treatment of actual tank loads in assessing stability, effects of damage character, relative importance of transient flooding stages, accuracy of physical experimentation used as basis data, or simple elements such as effect of computational speed on functionality of the whole proposition, or ergonomics of the conveying techniques used. The prime objective is to find solution acceptable for wider industrial application.

3. SYSTEMS AVAILABILITY POST-ACCIDENT

Formally, the safe return to port regulations adopted at 82nd session of MSC and subsequent amendments to SOLAS are not linked to damage stability and although it makes little sense to speculate about the reasons behind the separation, the formal disengagement by IMO seem to be utterly intentional. Nevertheless, the separation does not undermine the strong and authentic interrelation between the damage stability framework and SRtP, at least in part of the latter referring to flooding casualties (in short: all SRtP-compliant vessels need to demonstrate that their safety-critical systems remain operational outside the casualty area following single-compartment flooding). That is, SRtP capability is to be demonstrated for specific subset of all possible flooding scenarios.



As a matter of fact, it is the way the subset of flooding scenarios is being defined that prevents harmonisation of SRtP with damage stability framework. The SRtP subset is deterministic while the damage stability calculations draw from probabilistic domain (Cichowicz, J, Vassalos, D, Logan, J, 2009, Dodman, J., 2010). Notwithstanding the lack of harmonisation the SRtP is an important concept that transposes concept of survivability from that of the hull to that of the ship. In essence, the SRtP require the assessment to be performed on system models embedded within the vessel arrangement including both WT subdivision and A-class boundaries. Such modelling and evaluation philosophy was adopted during the development of iSys – an FMEA and SRtP-compliance assessment tool.

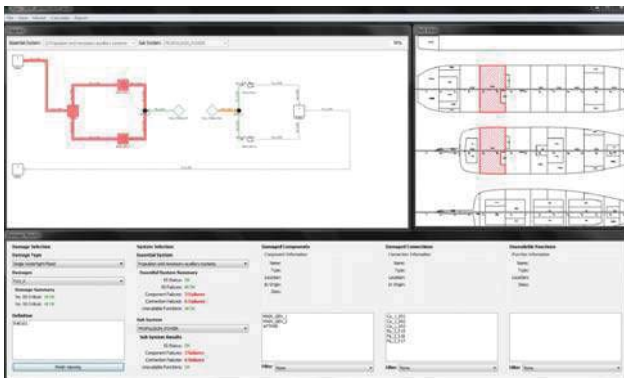


Figure 2: The iSys package allows for rapid modelling of complex systems embedded in ship's arrangement. The tool allows for assessing post-casualty availability of the systems and is capable of generating recommendations for restoring functionality

The most difficult aspect of post-casualty availability assessment derives from complexity of interconnected system models with time needed for evaluation by traditional calculators linked exponentially to the model size. Furthermore, as experience shows identification of design flaws in typical onboard plant requires high-resolution models able to capture fine details of the functionality. The design principles of ship systems are robust and backed by long experience hence in principle the onboard system are equally robust

and have acceptable level of built-in redundancy. Yet, the complex system often suffer from well-hidden deficiencies resulting in serious vulnerabilities to even minor flooding or fire accidents (as observed during some quite-recent incidents on cruise ships). The problem of such concealed vulnerabilities is particularly important for passenger ships (ever-growing in capacity and sailing to the most remote corners of the oceans) and the off-shore production plants (where again the isolation and accessibility of remote assistance becomes a serious issue).

Finally, the concept of post-casualty availability has an additional flavour in the context of active means of reducing a risk of rapid capsize. In particular, although the project GOALDS demonstrated clearly that accuracy of survivability assessment can be greatly improved by adopting the rational and design-friendly s-factor formulation. This allows for safer designs and cheaper designs but still the “mythical” requirements for the required index R to be equal to 1 remains commercially unattainable without use of active stability-enhancing devices. These, in turn would have to comply with “enhanced” (probabilistic) SRtP requirements. This highlights how strong the link between damage stability and systems' availability is.

4. ACTIVE MEASURES FOR DAMAGE CONTAINMENT

Traditionally, in order to reduce the severity of the consequences of a flooding event, we have been relying on passive risk control measures, for example, enhanced internal watertight subdivision arrangements. This has received considerable focus and research over the last 30 years, and it seems that we may have reached a stage that no further vulnerability enhancements may be expected from passive design measures.

In this respect, there are measures that may reduce the severity of consequences of a



flooding event, measures of operational nature and/or active measures and as such less amenable to statutory verification unless an alternative method is applied.

Therefore, new measures for risk reduction (operational and in emergencies) should be considered in addition to design (passive) measures. What needs to be demonstrated and justified is the level of risk reduction and a way to account for it, the latter by adopting a formal process and taking requisite steps to institutionalise it. IMO Circular 1455 on Alternatives and Equivalents offers the means but we still have to overcome the philosophical and practical problems of “summing up” risk reduction from design and operational means.

For risk control measure in damage stability the rules are focusing on design solutions, normally referred to as passive measures (category 1 measures) shown in Figure 3 (Vassalos, D, 2013). Operational/active measures (category 2 measures) whilst abundant in SOLAS Ch. II-2 (e.g. damage control), have not been validated to the same level of rigour as category 1 measures. Finally, measures/systems focusing on emergency response (category 3 measures), such as Decision Support Systems for Crisis Management, Evacuation, LSA, Escape and Rescue, whilst fuelling debates on being effective risk control measures or not, the cost-effectiveness of their risk reduction potential has never been measured nor verified.

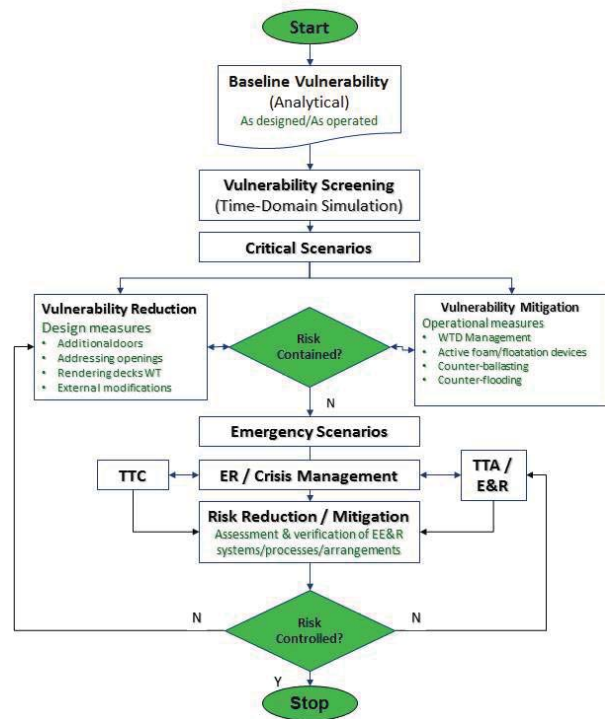


Figure 3: Vulnerability Management

It is also evident that survivability following a serious incident such as hull breach due to collision or grounding, resulting in water ingress, is still relatively low. Deriving from the foregoing, the following arguments may be put forward:

- Design (passive) measures are saturated. Hence, any such measures to improve damage stability severely erode the ship earning potential and are being resisted by industry.
- Traditionally, the industry is averse to operational (active) measures and it takes perseverance and nurturing to change this norm.
- Up until recently, there was no legislative instrument to assign credit for safety improvement by active means. It is IMO Circular 1455 that opened the door to such innovation.
- Key industry stakeholders are keen to explore this route.

Inspired by these considerations, a system that can be fitted to new or retrofitted to existing RoPax in order to reduce the



likelihood of capsizing/sinking and further water ingress following a major incident / accident (Vassalos, D, 2015). The proposed system utilises standard units comprising containers of polyurethane foaming agents, pumps and piping, distributed to safety-critical ship compartments and delivered through dedicated nozzles either directly into the compartment or in a flexible membrane, which is pre-inflated in an emergency and then filled under pressure. The system is able to withstand the ingress water pressure and provides a void filling mechanism to reduce flooding and thus enhance the buoyancy and stability of the vessel. The use of the system is under the full control of the crew, with a decision support system available to help the ship officers decide where and when the system will act as well as inform them of the ensuing effect. The system complies with identified requirements for the timely delivery of the foam in the damaged compartments to prevent progressive flooding and stability loss.

The foam itself meets all the environmental and health criteria, it is not toxic to humans and its release does not pose any danger to the people onboard or the environment. The system is illustrated in Figure 4.

Key characteristics of the system include:

Modular/Standardised design:

- System of (standard) parts
- Raw foam stored in sealed containers
- Dedicated pump per container
- Piping system running along the centre of the vessel
- Nozzles located in each of the primary spaces.

Non-intrusive:

- Optimum location in vessel – “void”, “out of the way” spaces.

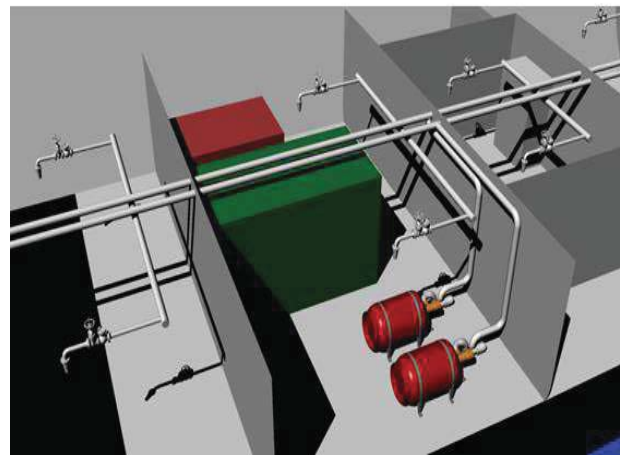
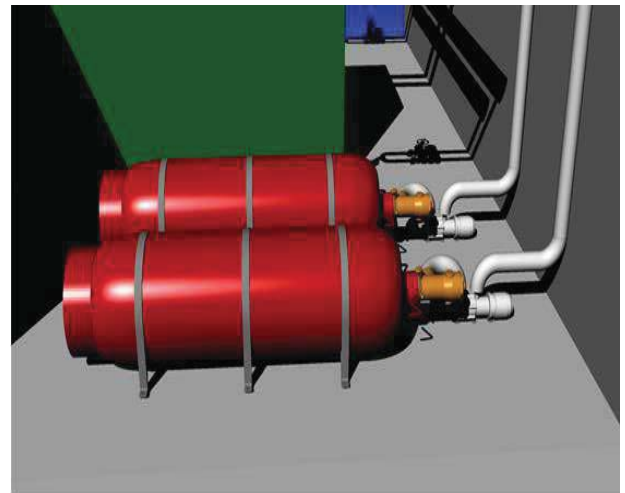


Figure 4: Damage Stability Recovery System (DSRS)

5. FINAL REMARKS

In this paper, we provided some elaborations on the current state-of-affairs with regards to operational measures relating to damage stability and safety. The aim is to stimulate discussion and provide ground for further proceeding towards the goal of implementing a virtuous integrated approach to ship stability safety which gives due credit to effective and robust operational risk control options.



6. ACKNOWLEDGEMENTS

This collaborative effort has been undertaken by members of the “Stability R&D Committee” (www.shipstab.org/stability-r-d-committee-srdc/). The authors would like to express their sincere thanks to the organisers of the 12th International Conference on Stability of Ships and Ocean Vehicles (STAB 2015, Glasgow, UK) for the opportunity given to present this work.

7. REFERENCES

Jasionwoski, A., 2011, “Decision Support for Ship Flooding Crisis Management”, Ocean Engineering, Volume 38, pp. 1568–1581.

Jasionwoski, A., Vassalos, D., 2006, “Conceptualising Risk”, Proceedings of the 9th International Conference on Stability of Ships and Ocean Vehicles (STAB 2006), Rio de Janeiro, Brazil.

Cichowicz, J., Vassalos, D., Logan, J., 2009, “Probabilistic Assessment of Post-Casualty Availability of Ship Systems”, Proceedings of the 10th International Conference on Stability of Ships and Ocean Vehicles (STAB 2009), St. Petersburg, Russia.

Dodman, J., 2010, “Going Forward with Safe Return to Port”, Proceedings of the 11th International Ship Stability Workshop, Wageningen, The Netherlands.

Vassalos, D: “Emergency Response in Flooding Casualties”, 13th International Ship Stability Workshop, Brest, France, 21-26 September 2013.

Vassalos, D: “Life-Cycle Vulnerability Management of RoRo Passenger Ships”, Damaged Ship III, RINA International Conference, London, UK, March 2015.

This page is intentionally left blank

Session 5.1 – 2nd GENERATION INTACT STABILITY

A Numerical Study for Level 1 Second Generation Intact Stability Criteria

Study on the Second Generation Intact Stability Criteria of Broaching Failure Mode

CALCOQUE: a Fully 3D Ship Hydrostatic Solver

This page is intentionally left blank



A Numerical Study for Level 1 Second Generation Intact Stability Criteria

Arman Ariffin, *ENSTA Bretagne, LBMS EA 4325, Brest, France*

arman.ariffin@ensta-bretagne.org

Shuhaimi Mansor, *Faculty of Mechanical Engineering, University Teknologi Malaysia, Malaysia*

shuhaimi@mail.fkm.utm.my

Jean-Marc Laurens, *ENSTA Bretagne, LBMS EA 4325, Brest, France*

jean-marc.laurens@ensta-bretagne.fr

ABSTRACT

During the last International Ship Stability Workshop held in Brest last September, several questions were raised concerning the existing IMO intact stability rules and the new proposed regulations. The lower level (level 1) criteria are conservative but should be easily implemented in stability codes. In this particular study it was investigated if and how an existing and extensively used commercial computer code, in the present case GHS©, could handle level 1 criteria. For simple and realistic cases it was found that a relatively small angle of trim can cause the capsizing of the vessel. These clearly unsafe examples indicate that the existing rules are insufficient. The new intact stability rules aim to deal with failure modes generally associated with extreme weather conditions such as parametric rolling, broaching or pure loss of stability in astern waves but they may also prevent capsizing due to environmental loading. Some of the difficulties encountered with the computation are presented to assess the extent of the necessary development. Finally an illustrative example is presented to verify whether the existing and future regulations can prevent certain obviously dangerous situations.

Keywords: *second generation intact stability, weather criterion, GZ curve*

1. INTRODUCTION

Intact stability is a basic requirement to minimise the risk of the capsizing of vessels. It is a guideline for the ship designer, ship operator and classification society to design, build and commission the ship before it starts its service life at sea. A comprehensive background study of intact stability development was written by Kuo & Welaya (Welaya & Kuo, 1981). Their paper "A review of intact stability research and criteria", stated

that the first righting arm curve was proposed by Reedin 1868, but the application was presented by Denny in 1887. In addition, in 1935, Pierrottet tried to rationally establish the forces which tend to capsize a ship and proposed a limiting angle at which the dynamic level of the ship must be equal to or greater than the sum of work done by the inclining moments. However, Pierrottet's proposal was too restrictive in the design process and it was not accepted.



Kuo and Welaya also mentioned the famous doctoral thesis written by Jaakko Rahola in 1939. Rohola's thesis evoked widespread interest throughout the world at that time because it was the first comprehensive study and proposed method to evaluate the intact stability which did not require complex calculations.

The First International Conference for ship stability which was held at the University of Strathclyde in 1975, Tsuchiya presented a new method for treating the stability of fishing vessels (Tsuchiya, 1975). He introduced a list of coefficient to define the weather stability criteria. He disregarded the idea of a stability assessment using simple geometrical stability standards such as metacentric height and freeboard, or the shape of the righting arm curve. He proposed a number of factors which, in his opinion, are crucial. He introduced a certain coefficient which should be calculated and plotted on a diagram as a function of metacentric height and the freeboard for every stability assessment. He concluded that his proposed method should be confirmed by a comparison with actual data on fishing boat activities and empirical stability standards.

The first generation intact stability criteria was originally codified at IMO in 1993 as a set of recommendations in Res A.749(18) by taking into account the former Res.A.167 (ES.IV) ("Recommendation on intact stability of passenger and cargo ships under 100 meters in length" which contained statistical criteria, heeling due to passenger crowding, and heeling due to high speed turning, 1968) and Res A.562.(14) ("Recommendation on a severe wind and rolling criterion (Weather Criterion) for the intact stability of passenger and cargo ships of 24 meters in length and over," 1985). These criteria were codified in the 2008 IS Code and became effective as part of both SOLAS and the International Load Line Convention in 2010 in IMO Res MSC.269(85) and MSC.207(85) (Peters et al., 2012).

The actual work to review IS Code 2008 was highlighted during the 48th session of the

SLF in Sept. 2005 (IMO, 2005). The work group decided to address three modes of stability failure:

- a. Restoring arm variation.
- b. Stability under dead ship condition.
- c. Manoeuvring-related problems in waves.

There are two conferences that address the development of second generation intact stability criteria. These are the International Conference on Stability of Ship Ocean Vehicles (STAB) and the International Ship Stability Workshop (ISSW). An experimental evaluation of weather criteria was carried out at the National Maritime Research Institute, in Japan. They conducted a wind tunnel test with wind speeds varying from 5m/s to 15 m/s. The results showed some differences compared to the current estimation. For example the wind heeling moment depended on the heel angle and the centre of drift force was higher than half draft (Ishida, Taguchi, & Sawada, 2006). The experimental validation procedures for numerical intact stability assessment with the latest examples was presented by Umeda and his research members in 2014 (Umeda et al., 2014). They equipped the seakeeping and manoeuvring basin of the National Research Institute of Fisheries Engineering in Japan with a wind blower to examine dead ship stability assessment.

A review of available methods for application to second level vulnerability criteria was presented at STAB 2009 (Bassler, Belenky, Bulian, Spyrou, & Umeda, 2009). They concluded that the choice of environmental conditions for vulnerability criteria is at least as important as the criteria themselves. A test application of second generation IMO intact stability criteria on a large sample of ships was presented during STAB 2012. Additional work remains to be carried out to determine a possible standard for the criteria and environment conditions before finalising the second generation intact stability criteria (Wandji & Corrigan, 2012).



During the ISSW 2013, Umeda presented the current status of the development of second generation intact stability criteria and some recent efforts (Umeda, 2013). The discussion covered the five failure modes: pure loss of stability, parametric rolling, broaching, harmonic resonance under dead ship condition and excessive acceleration.

2. BACKGROUND OF IS CODE 2008

The Intact Stability Code 2008 is the document in force. The code is based on the best "state-of-the-art" concept (IMO, 2008). It was developed based on the contribution of design and engineering principles and experience gained from operating ships. In conjunction with the rapid development of modern naval architecture technology, the IS Code will not remain unchanged. It must be re-evaluated and revised as necessary with the contribution of the IMO Committees all around the globe (IMO, 2008).

The IS Code 2008 is divided into 2 parts. Part A consists of the mandatory criteria and Part B contains the recommendation for certain types of ships and additional guidelines. As stated in Part A, the IS Code applies to marine vehicles of 24 metres in length and more. Paragraph 2.2 of Part A lists the criteria regarding the righting arm curve properties and Paragraph 2.3 describes the severe wind and rolling criteria (weather criterion).

The IS Code 2008 Part A 2.2 sets four requirements for righting arm (GZ) curve properties (Grinnaert and Laurens 2013):

- a. Area under the righting lever curve,
 - i. not less than 0.055 meter-radian up to a 30° heel angle.
 - ii. not less than 0.09 meter-radians up to a 40° heel angle, or downflooding angle.

- iii. not less than 0.03 meter-radians from a 30° to 40° heel angle or between 30° to the downflooding angle.

- b. The righting lever GZ shall be at least 0.2m for a heel angle greater than 30°.

- c. The maximum righting lever shall occur at a heel angle not less than 25°.

- d. The initial GM shall not be less than 0.15 meters.

The additional requirement for passenger ships is stated in Part A, Paragraph 3.1. It states that:

- a. The angle of heel due to passenger crowding shall not be more than 10°.
- b. A minimum weight of 75kg for each passenger and the distribution of luggage shall be approved by the Administration.
- c. The centre of gravity for a passenger standing upright is 1 m and for a seated passenger 0.3 m above the seat.

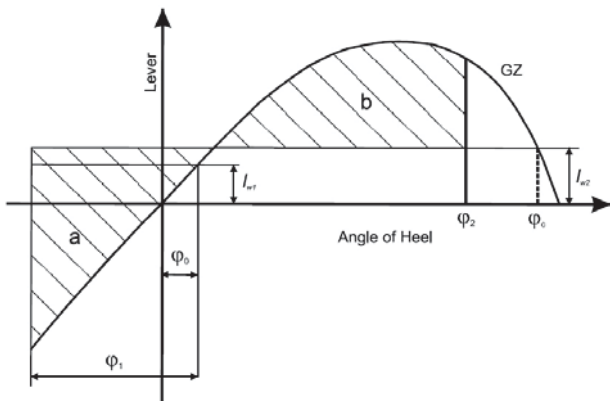
The IS Code 2008 Part A 2.3 concerns the weather criterion. The ship must be able to withstand the combined effects of beam wind and rolling at the same time. The conditions are:

- a. the ship is subjected to a steady wind pressure acting perpendicular to the ship's centreline which results in a steady wind heeling lever (lw_1).
- b. from the resultant angle of equilibrium (φ_0), the ship is assumed to present an angle of roll (φ_1) to windward due to wave action. The angle of heel under action of steady wind (φ_0) should not exceed 16° or 80% of the angle of deck edge immersion, whichever is less.

- c. the ship is then subjected to a gust wind pressure which results in a gust wind heeling lever (lw_2); and under these circumstances, area b shall be equal to or greater than area a , as indicated in Figure 1:

The heeling lever shall be calculated using formula:

$$l_{w1} = \frac{P \cdot A \cdot Z}{1000 \cdot g \cdot \Delta} \quad (1)$$



$$l_{w2} = 1.5 l_{w1} \quad (2)$$

Figure 1 Severe wind and rolling

where lw_1 = steady wind heeling angle, lw_2 = gust wind heeling lever, P = wind pressure of 504 Pa, A = projected lateral area (m^2), Z = vertical distance from the centre of A to the centre of the underwater lateral area or approximately to a point at one half of the mean draught (m), Δ = displacement (t) and g = gravitational acceleration of 9.81 m/s^2 .

Part 3.1 of the IS Code 2008 only concerns passenger ships. Passenger ships have to also pass the criteria of Part 2.2 and 2.3. The heeling angle on account of turning should not exceed 10° , when calculated using the following formula:

$$M_R = 0.200 * \frac{V_0^3}{1.778} * \Delta * (KG - \frac{d}{2}) \quad (2)$$

where: M_R = heeling moment (kNm), v_0 = service speed (m/s), V_{WL} = length of ship at waterline (m), Δ = displacement (tons), d = mean draught (m), KG = height of centre of gravity above baseline (m).

The centrifugal force F_c is equal to $\Delta V_0^2/2R$ where R is the radius of gyration. The smaller R , the higher F_c . But the formula proposed in the code is $R = 5L_{wl}$ which is the maximum value R can take according to manoeuvring code (Veritas, 2011). The formula is therefore not conservative.

3. DEVELOPMENT OF A SECOND GENERATION IS CODE

The Sub-Committee on Stability and Load Lines and on Fishing Vessels Safety 48th Session IMO (2005) emphasized the requirement of revising the current IS Code. The importance of the work on the comprehensive review of the current IS Code 2008 would significantly affect the design and ultimately enhance the safety of ships (Mata-Álvarez-Santullano & Souto-Iglesias, 2014).

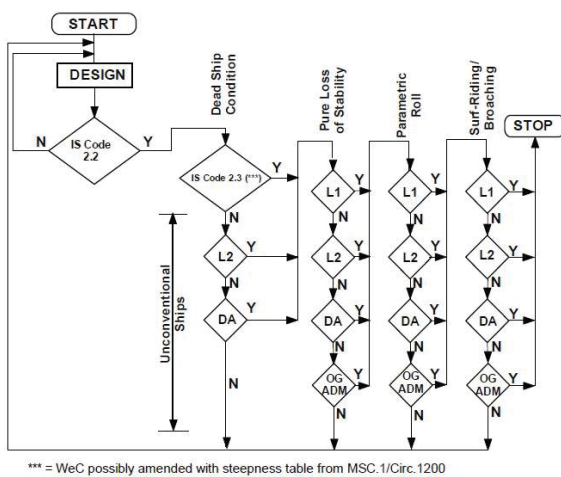
Intact Stability is a crucial criterion that concerns most of naval architects in the design stage. The current Intact Stability (IS) Code 2008 is in force. Except for the weather criterion the IS Code 2008 only concerns the hydrostatics of the ship. It does not cover the seakeeping behaviour of the ship and first and foremost, it always considers a ship with negligible trim angle. In head seas, the ship can take some significant angle of trim which may affect the righting arm. Van Santen, 2009 also presents an example of a vessel capsizing because of the small angle of trim. For the enhancement and improvement of intact stability criteria, the International Maritime Organisation (IMO) introduced the new generation intact stability criteria in 2008 (Francescutto, 2007).

Figure 2 presents the procedure to apply to the second generation intact stability rule.



Once the basic criteria described in Section 2 have been satisfied, each failure mode is verified to satisfaction at the most conservative level.

The development of the second generation intact stability criteria focuses on five dynamical stability failure modes. Performing such a complete calculation of time-dependent dynamical phenomena would require well-trained engineers as well as advanced tools (IMO, 2013a). The aim of level 1 is to devise a simple computational method, but the criteria are very conservative. Level 2 criteria are more realistic since wave shape is taken into account but the computation remains static. Level 3 involves seakeeping simulations.



*** = WeC possibly amended with steepness table from MSC.1/Circ.1200

Figure 2 Structure of Second Generation Intact Stability Criteria IMO (2008)

The formula used in this paper is based on SDC1/INF.8 (IMO, 2013b). 1. Parametric rolling stability failure criteria mode as stated in SDC/1 INF.8 Annex 1 (submitted by correspondence group). 2. Pure loss of stability failure mode as stated in SDC/1 INF.8 Annex 2 (submitted by correspondence group). 3. Dead ship stability failure mode as stated in SDC/1 INF.8 Annex 16 (submitted by Italy and Japan). 4. Broaching stability failure mode as stated in SDC/1 INF.8 Annex 15 (submitted by United States and Japan).

3.1 Dead Ship Condition for Level 1

Based on SDC/1 INF.8 Annex 16, for level 1 vulnerability criteria for the dead ship stability failure mode, a ship is considered not to be vulnerable to the dead ship stability failure mode if:

$$b \geq a \quad (3)$$

where a and b should be calculated according to the "Severe wind and rolling criterion (weather criterion)" in Part A – 2.3 of the Code12, and substituting the steepness factor s in Table 2.3.4-4 in Part A – 2.3, by the steepness factor s specified in Table 4.5.1 in MSC.1/Circ.1200.

3.2 Pure Loss of Stability for Level 1

Based on SDC/1 INF.8 Annex 2, for level 1 vulnerability criteria for the pure loss of stability failure mode, a ship is considered not to be vulnerable to the pure loss of stability failure mode if:

$$GM_{\min} > R_{PLA} \quad (4)$$

where $R_{PLA} = [\min(1,83 d (Fn)^2, 0.05)]m$ and GM_{\min} = the minimum value of the metacentric height [on level trim and without taking free surface effects into consideration] as a longitudinal wave passes the ship calculated as provided in 2.10.2.2 (ref SDC/1 INF.8 Annex 2),or

$$GM_{\min} = KB + I_L/V - KG \quad (5)$$

$$\text{only if } [(V_D - V)/A_w (D-d)] \geq 1.0 \quad (6)$$

d = draft corresponding to the loading condition under consideration; I_L = moment of inertia of the waterplane at the draft d_L ;

$$d_L = d - \delta d_L \quad (7)$$

KB = height of the vertical centre of buoyancy corresponding to the loading condition under consideration; KG = height of

the vertical centre of gravity corresponding to the loading condition under consideration; V = volume of displacement corresponding to the loading condition under consideration;

$$[\delta d_L = \min(d - 0.25d_{full}, (L \cdot S_W / 2))] \quad (8)$$

$S_W = 0.0334$, D = Depth, V_D = volume of displacement at waterline equal to D , A_W = waterplane area of the draft equal to d .

3.3 Parametric Rolling for Level 1

Based on SDC/1 INF.8 Annex 1 for level 1 vulnerability criteria for the parametric rolling failure mode, a ship is considered not to be vulnerable to the parametric roll failure mode if:

$$\Delta GM / GM > R_{PR} \quad (9)$$

$$\Delta GM = (I_H - I_L) / 2V \quad (10)$$

where ΔGM = amplitude of the variation of the metacentric height when a longitudinal wave passes the ship, GM = metacentric height, $R_{PR} = 0.5$, I_H = moment inertia of the waterplane at the draft d_H , I_L = moment inertia of the waterplane at the draft d_L , and V = volume of displacement corresponding to the loading condition under consideration.

3.4 Surf-riding/Broaching for Level 1

Based on SDC/1 INF.8 Annex 15 for level 1 vulnerability criterion for the surf-riding (Spyrou, Themelis, & Kontolefas, 2013)/broaching stability failure mode, a ship is considered not to be vulnerable to the broaching stability failure mode if:

$$F_n < 0.3 \text{ or } L_{BP} > 200\text{m} \quad (11)$$

where $F_n = V_{max} / (L_{BP} \cdot g)^{0.5}$, V_{max} = maximum service speed in calm water (m/s), L_{BP} = the length between perpendicular (m), and g = gravitational acceleration (m/s).

4. PROPOSAL FOR EXPERIMENTAL WORK ON WEATHER CRITERIA

The highest level criterion for the second generation intact stability code is the direct stability assessment using a time-domain numerical simulation. The tools should be validated by experimental results. The guideline of direct stability assessment was produced at the initiative of the United States and Japan as in SDC1/INF.8 in Annex 27(IMO, 2013b).

Recent experiments carried out by Umeda and his research members (Umeda et al., 2014) presented during the ISSW 2014 provide examples of comparisons between model experiments and numerical simulations for stability under dead ship condition and for pure loss of stability in astern waves. The experiment using a model 1/70 CEHIPAR2792 vessel was conducted in a seakeeping and manoeuvring basin. A wind blower consisting of axial flow fans and controlled by inverters with a v/f control law was used to provide the wind input. The experimental setup is shown in Figure 3 and 4. They concluded that for the dead ship condition, an adequate selection of representative wind velocities generated by wind fans is crucial and for the pure loss of stability, an accurate Fourier transform and the reverse transformation of incident irregular waves are important.

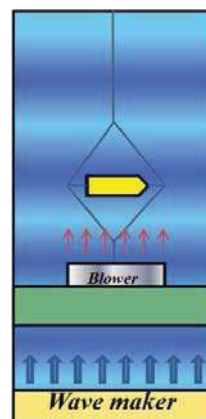


Figure 3 Overview of experimental setup (Umeda et al., 2014).

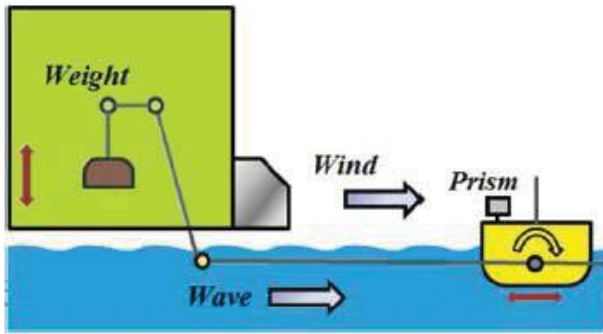


Figure 4 Lateral view of experimental setup (Umeda et al., 2014).

An experimental study will be carried out at the Low-Speed Wind Tunnel of the Aeronautics Laboratory at the University Teknologi Malaysia in 2016. The aim of the study is to validate the weather criterion in the IS Code 2008 using the wind tunnel results. For the dead ship condition, the study will consist of two layered vulnerability criteria and a ship is requested to comply with at least one of them. This is because the use of expensive numerical simulations for a direct assessment should be minimised in order to realise a feasible application of the new scheme. It is also essential that the numerical simulations used for the direct assessment should be validated by physical model experiments (Kubo, Umeda, Izawa, & Matsuda, 2012).

4.1 Wind Tunnel Specifications

This wind tunnel has a test section of 2 m (width) x 1.5 m (height) x 5.8 m (length). The maximum test velocity is 80m/s (160 knots or 288 km/h). The wind tunnel has a flow uniformity of less than 0.15%, a temperature uniformity of less than 0.2°C, a flow angularity uniformity of less than 0.15° and a turbulence level of less than 0.06% (Mansor, 2008).

The wind tunnel is equipped with a six component balance for load measurements. The balance is a pyramid type with the virtual balance moment at the centre of the test section. The balance has the capacity to measure the aerodynamic forces and moments in 3-D. The aerodynamic loads can be tested as a function

of the various wind directions by rotating the model using the turntable. The accuracy of the balance is within 0.04% based on 1 standard deviation. The maximum load range is $\pm 1200\text{N}$ for axial and side loads. It also has the capacity to measure surface pressure using electronic pressure scanners. The balance load range for the wind tunnel is presented in Table 1.

5. STABILITY EVALUATION

A naval ship is used for the stability calculation. The ship is a patrol vessel (Ariffin, 2014) with a cruising speed of 12 knots, and a maximum speed of 22 knots. Its overall length is 91.1 metres, the design draft is 3.4 metres and the maximum draft is 3.6 metres for a displacement of 1800 tons. Finally the vessel's block coefficient, C_b , is 0.448 and the prismatic coefficient, C_p , is 0.695.

The body plan of the ship is shown in Figure 4.

Load Component and Accuracy	Type of balance		
	External	Semi-span	Internal
Axial force, F_x (N)	± 1200	± 900	± 182
Side force, F_y (N)	± 1200	± 900	± 356
Normal force, F_z (N)	± 1200	± 4500	± 445
Roll moment, M_x (Nm)	± 450	± 1362	± 7
Pitch moment, M_y (Nm)	± 450	± 250	± 62
Yaw moment, M_z (Nm)	± 450	± 450	± 50
Primary accuracy, % (based on ± 1 standard deviation)	0.04	0.04	<0.10

Table 1 Balance load range (Noor & Mansor, 2013)

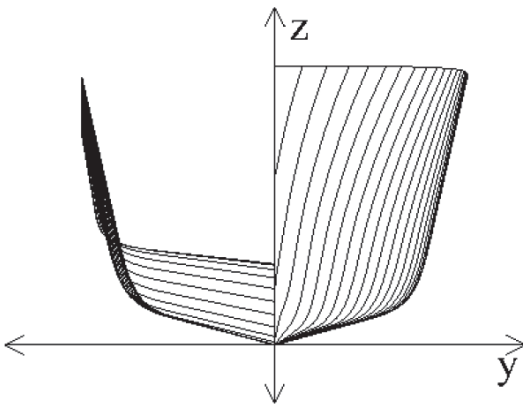


Figure 4 Body plan of the vessel

The level calculations in the present paper are based on a formula in SDC 1/INF.8. Only criteria for level 1 were verified. The results were obtained using the GHS software for the level 1 verification of pure loss of stability and parametric rolling. The VCG for the vessel was varied from 3.0 to 7.0 meters for analysis purposes. Direct calculation was used for the dead ship condition and the surf-riding/broaching.

5.1 Dead Ship Condition for Level 1

Based on SDC/1 INF.8 Annex 16, proposed by Italy and Japan, the steepness factor, s in Part A – 2.3 Table 2.3.4-4 was changed to the steepness factor s in Table 4.5.1 in MSC.1/Circ.1200. In GHS, the steepness factor is defined by $s = 0.0992364 + 0.0058416T - 0.0011127T^2 + 0.0000331T^3$ with $0.035 \leq s \leq 0.1$. Table 4.5.1 in MSC.1/Circ.1200 is the extension of Table 2.3.4.4. The graft of steepness factor, s vs roll period, T in Table 4.5.1 can be computed with the 5th order polynomial $s = 0.016 + 0.0385T - 0.0058T^2 + 0.0003T^3 - 0.000009T^4 + 0.00000009T^5$ with $0.02 \leq s \leq 0.1$.

The vessel passed the level 1 dead ship condition using the proposed amended criteria.

5.2 Pure Loss of Stability for Level 1

As in SDC/1 INF.8 Annex 2, the GM_{min} is calculated based on a range of VCG from 3 to 7m. The result shows that the change of VCG will affect the GM_{min} significantly. With the

increment of VCG, the max VCG to pass the IS Code 2008 is 5.46 m and the max. VCG to pass the level 1 pure loss of stability is 6.6 m. The result is shown in Figure 5.

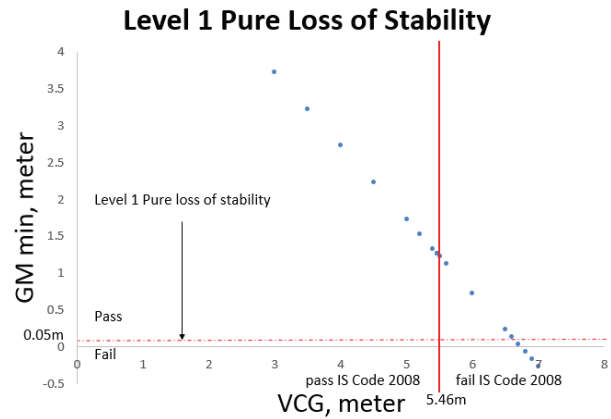


Figure 5 Result of Level 1 Pure loss of stability

It appears that the level 1 pure loss of stability criterion is less restrictive than the existing IS Code 2008 for conventional ships.

5.3 Parametric Rolling for Level 1

The $\Delta GM/GM$ is calculated based on a range of VCG from 3 to 7 m in SDC/1 INF.8 Annex 1. The result shows that the change of VCG affects the $\Delta GM/GM$ significantly. With the increment of VCG, the max VCG to pass the IS Code 2008 is 5.46 m and the max. VCG to pass the level 1 pure loss of stability is 5.56 m. The results are shown in Figure 6.

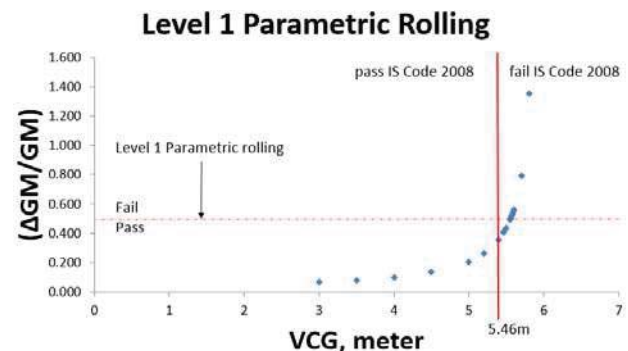


Figure 6 Result of Level 1 Parametric rolling

In this case, the level 1 parametric rolling criterion is less restrictive than the IS Code 2008.

5.4 Surf-riding/Broaching for Level 1

In SDC/1 INF.8 Annex 12, proposed by United States and Japan, the criterion is based on ship dimension and maximum speed. The vessel is tested with various speeds. The results show that the maximum speed (22 knots) is vulnerable to broaching and the cruising speed (12 knots) is not vulnerable to broaching. The results are shown in Figure 7. The maximum speed at which the ship is not vulnerable to broaching is 17.4 knots.

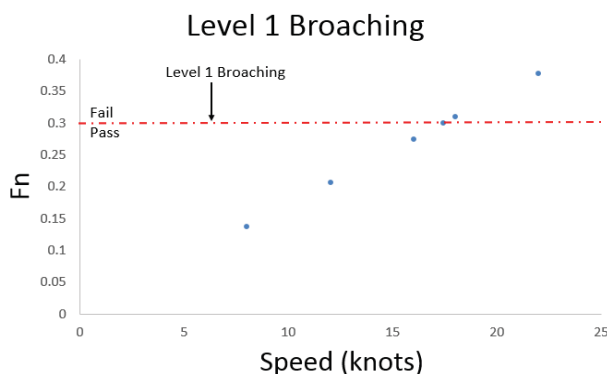


Figure 7 Result of Level 1 Broaching

6. DISCUSSION

The patrol boat whose body plan is presented in Figure 4, passes the level 1 criteria for the dead ship condition, the pure loss of stability and the parametric rolling. But it failed to meet the criteria for broaching at maximum speed.

The GHS© code can currently handle the level 1 verification for pure loss of stability, and parametric rolling. The level 1 verification for broaching does not require GHS© output. The level 1 verification for dead ship condition requires a change of the wave steepness value, s whereas the current code has a range of $0.035 \leq s \leq 0.1$ but the proposed change for level 1 broaching required a range of $0.02 \leq s \leq 0.1$.

7. CONCLUSIONS

This paper presents the results for a naval ship for a level 1 verification based on a proposed change of second generation intact

stability criteria as outlined in the current state of development by the International Maritime Organisation (IMO).

The vessel which already complied with the existing IS Code 2008, easily passes the level 1 criteria for pure loss of stability and parametric rolling but does not meet the broaching criterion at maximum speed.

The dead ship condition is based on weather criteria and there is no proposed change to the current regulations except for the wave steepness value. The wind tunnel experimental facility will be used to investigate the possibility of proposing some new or amended rules for the weather criterion.

8. ACKNOWLEDGEMENT

The authors would like to acknowledge the support of the Government of Malaysia, the Government of the French Republic and the Direction des Constructions Navales (DCNS).

9. REFERENCES

- Ariffin, A. (2014). Air Flow and Superstructure Interaction on a Model of a Naval Ship. Master Thesis, Universiti Teknologi Malaysia.
- Bassler, C. C., Belenky, V., Bulian, G., Spyrou, K. J., & Umeda, N. (2009). A Review of Available Methods for Application to Second Level Vulnerability Criteria. In *International Conference on Stability of Ships and Ocean Vehicles* (pp. 111–128).
- Francescutto, A. (2007). The Intact Ship Stability Code: Present Status and Future. In *Proceedings of the 2nd International Conference on Marine Research and Transportation*, Naples, Italy, Session A (pp. 199–208).
- IMO. (2005). SLF 48/21 Report to the Maritime Safety Committee.



- IMO. (2008). International Code of Intact Stability.
- IMO. (2013a). SDC 1/5/1 - Development of Second Generation Intact Stability Criteria. Remarks on the Development of the Second Generation Intact Stability Criteria Submitted by Germany.
- IMO. (2013b). SDC 1/INF.8 - Development of Second Generation Intact Stability Criteria.
- Ishida, S., Taguchi, H., & Sawada, H. (2006). Evaluation of the Weather Criterion by Experiments and its Effect to the Design of a RoPax Ferry. International Conference on Stability of Ships and Ocean Vehicles, 9–16.
- Kubo, T., Umeda, N., Izawa, S., & Matsuda, A. (2012). Total Stability Failure Probability of a Ship in Irregular Beam Wind and Waves: Model Experiment and Numerical Simulation. In 11th International Conference on Stability of Ships and Ocean Vehicles.
- Laurens, J.-M., & François, G. (2013). Stabilité Du Navire: Théorie, Réglementation, Méthodes De Calcul (Cours Et Exercices Corrigés). Ellipses, Paris.
- Mansor, S. (2008). Low Speed Wind Tunnel Univeristi Teknologi Malaysia.
- Mata-Álvarez-Santullano, F., & Souto-Iglesias, A. (2014). Stability, Safety and Operability of Small Fishing Vessels. Ocean Engineering, 79, 81–91. doi:10.1016/j.oceaneng.2014.01.011
- Noor, A. M., & Mansor, S. (2013). Measuring Aerodynamic Characteristics Using High Performance Low Speed Wind Tunnel at Universiti Teknologi Malaysia. Journal of Applied Mechanical Engineering, 03(01), 1–7. doi:10.4172/2168-9873.1000132
- Peters, W. M., Belenky, V. M., Bassler, C. M., Spyrou, K. M., Umeda, N. M., Bulian, G. V., & Altmayer, B. V. (2012). The Second Generation Intact Stability Criteria: An Overview of Development. Transactions - The Society of Naval Architects and Marine Engineers, 119(225-264).
- Spyrou, K. J., Themelis, N., & Kontolefas, I. (2013). What is Surf-Riding in Irregular Seas? In International Conference on Marine Safety and Environment.
- Tsuchiya, T. (1975). An Approach for Treating the Stability of Fishing Boats. In International Conference on Stability of Ships and Ocean Vehicles.
- Umeda, N. (2013). Current Status of Second Generation Intact Stability Criteria Development and Some Recent Efforts. In International Ship Stability Workshop.
- Umeda, N., Daichi Kawaida, Ito, Y., Tsutsumi, Y., Matsuda, A., & Daisuke Terada. (2014). Remarks on Experimental Validation Procedures for Numerical Intact Stability Assessment with Latest Examples. In International Ship Stability Workshop (pp. 77–84).
- Van Santen, J. (2009). The Use of Energy Build Up to Identify the Most Critical Heeling Axis Direction for Stability Calculation for Floaring Offshore Structures. In 10th International Conference on Stability of Ship and Ocean Vehicles (pp. 65–76).
- Veritas, B. (2011). Rules for the Classification of Steel Ship.
- Wandji, C., & Corrigan, P. (2012). Test Application of Second Generation IMO Intact Stability Criteria on a Large Sample Ships. In International Conference on Stability of Ships and Ocean Vehicles (pp. 129–139).



Welaya, Y., & Kuo, C. (1981). A Review of
Intact Ship Stability Research and
Criteria. Ocean Engineering, 8, 65–84.

This page is intentionally left blank



Study on the Second Generation Intact Stability Criteria of Broaching Failure Mode

Peiyuan Feng, *Marine Design & Research Institute of China (MARIC)*, pyfeng23@163.com

Sheming Fan, *Marine Design & Research Institute of China (MARIC)*, fan_sm@maric.com.cn

Xiaojian Liu, *Marine Design & Research Institute of China (MARIC)*, cz_liu_xj@sina.com

ABSTRACT

This paper evaluates the vulnerability of sample ships to the broaching stability failure mode according to the current proposal submitted to IMO's Subcommittee on Ship Design and Construction (SDC). Sensitivity analysis is performed to study the influence of input parameters on the assessment result. Sample calculations are then performed and the results are analyzed with an emphasis on the appropriateness of the current proposal. Consequently, some comments concerning the potential impact of the broaching stability criteria on ship design is proposed.

Keywords: *surf-riding, broaching, stability assessment, sample calculations, ship design*

1. INTRODUCTION

The International Maritime Organization (IMO) is currently working on the second generation intact stability criteria of five failure modes to ensure the safety of ships in waves more effectively. Broaching is among the five and is considered to be the most complicated one due to its highly nonlinear and chaotic nature. Broaching occurs when a ship cannot keep a constant course despite the maximum steering effort typically in following and quartering waves. Surf-riding is usually regarded as the prerequisite of broaching, which occurs when a ship is captured by the wave approaching from the stern that accelerates the ship to the wave celerity. Small-size high-speed ships such as fishing vessels are most vulnerable to this stability failure mode.

To investigate the mechanism behind this hazardous phenomenon, significant theoretical and experimental efforts have been made by researchers in the recent decades (Umeda et al., 1999, Spyrou, 2001, Umeda &

Vassalos, 1996, Hashimoto et al., 2004, Hashimoto & Stern, 2007, Maki et al., 2010), which form a good foundation for the development of broaching stability assessment criteria.

According to IMO, a three-tiered approach is applied for assessing the five stability failure modes. Level 1 is meant to be simple and conservative, whose purpose is to distinguish ships that are clearly not vulnerable. If found vulnerable, the ship is then required for Level 2 evaluation which is less conservative. The method adopted for Level 2 evaluation is meant to be based on simplified physics and involve calculations with reduced computational efforts. If the ship is found vulnerable again, direct stability assessment using the most advanced state-of-the-art technology has to be performed.

The current proposal from U.S. and Japan (SDC 2/INF.X, 2014) follows the three-tiered framework: Level 1 evaluation only needs the ship length and speed information; Level 2 evaluation is based on a simplified surf-riding



model, the probability of surf-riding occurrence in irregular seaway is chosen as the criteria for assessment; Level 3 direct stability assessment procedures are still under discussion, the draft guidelines can be found in SDC1/INF.8 (2013).

This study focuses on the Level 2 evaluation. The main purpose is to analyze and verify the current proposal through sensitivity analysis and sample calculations. Concerns towards the appropriateness of the Level 2 criteria such as the threshold value are raised. Consequently, the potential impact of the broaching stability criteria on ship design is discussed.

This study can help designers better understand the second generation intact stability criteria of broaching failure mode and the establishing of the regulation.

2. CURRENT BROACHING STABILITY FAILURE ASSESSMENT PROPOSAL

The following introduction of the current proposal to assess the Level 1 and Level 2 broaching stability failure mode is based on the contents of Annex 32 and Annex 35 in SDC 2/INF.X (2014).

2.1 Level 1 Vulnerability Criteria

A ship is considered not to be vulnerable to the broaching stability failure mode if:

$$L > 200m \quad \text{or} \quad Fn > 0.3 \quad (1)$$

where, $Fn = V_s / \sqrt{Lg}$ is the Froude number; V_s is ship service speed in calm water; L is the length of ship.

If the ship fails to pass Level 1 criteria, Level 2 assessment is needed.

2.2 Level 2 Vulnerability Criteria

For a ship to pass Level 2 assessment, it is required that:

$$C < R_{SR} \quad (2)$$

where, C represents the probability of surf-riding occurrence; R_{SR} is the standard value. Two opinions exist for the value of R_{SR} , with $1e-4$ by Japan and $5e-3$ by U.S.

C is estimated by:

$$C = \sum_{H_s} \sum_{T_z} \left(W2(H_s, T_z) \frac{\sum_{i=1}^{N_\lambda} \sum_{j=1}^{N_a} W_{ij} C2_{ij}}{\sum_{i=1}^{N_\lambda} \sum_{j=1}^{N_a} W_{ij}} \right) \quad (3)$$

where, $W2(H_s, T_z)$ is the weighting factor of short-term sea state according to long-term wave statistics; H_s is the significant wave height; T_z is the zero-crossing wave period; W_{ij} is a statistical weight of a wave with steepness $s_j = (H/\lambda)_j$ varying from 0.03 to 0.15; and wave length to ship length ratio $r_i = (\lambda/L)_i$ varying from 1.0 to 3.0. Details concerning these factors are specified in SDC 2/INF.X (2014).

$C2_{ij}$ is the key element which represents whether surf-riding/broaching occurs for each wave case, which is defined as follows:

$$C2_{ij} = \begin{cases} 1 & \text{if } Fn > Fn_{cr}(r_j, s_i) \\ 0 & \text{if } Fn \leq Fn_{cr}(r_j, s_i) \end{cases} \quad (4)$$

where, $Fn_{cr} = u_{cr} / \sqrt{Lg}$ is the critical Froude number corresponding to the threshold of surf-riding (surf-riding occurs under any initial condition); u_{cr} is the critical ship speed determined by solving the following equation:

$$T_e(u_{cr}; n_{cr}) - R(u_{cr}) = 0 \quad (5)$$



where, $R(u)$ is the calm water resistance of the ship approximated by N^{th} order polynomial:

$$R(u) \approx \sum_{i=0}^N r_i u^i = r_0 + r_1 u + r_2 u^2 + \dots \quad (6)$$

$T_e(u_{cr}; n_{cr})$ is the propulsor thrust in calm water:

$$T_e(u_{cr}; n_{cr}) = (1 - t_p) \rho n_{cr}^2 D_p^4 K_T(J) \quad (7)$$

$$K_T(J) \approx \sum_{i=0}^N \kappa_i J^i = \kappa_0 + \kappa_1 J + \kappa_2 J^2 + \dots \quad (8)$$

where, n_{cr} is number of propeller revolutions corresponding to the threshold of surf-riding, which is estimated based on Melnikov method by solving the following equation:

$$2\pi \frac{T_e(c_w; n_{cr}) - R(c_w)}{f} = \sum_{i=1}^N \sum_{j=1}^i C_{ij} (-2)^j I_j \quad (9)$$

where,

$$C_{ij} = \frac{c_i}{fk^j} \left\{ \frac{i!}{j!(i-j)!} \right\} \frac{(fk)^{j/2}}{(m+m_x)^{j/2}} c_w^{i-j} \quad (10)$$

$$c_i = -\frac{(1-t_p)(1-w_p)^i \rho \kappa_i}{n^{i-2} D_p^{i-4}} + r_i \quad (11)$$

$$I_j = 2\sqrt{\pi} \Gamma\left(\frac{j+1}{2}\right) / \Gamma\left(\frac{j+2}{2}\right) \quad (12)$$

$$\Gamma(N) = (N-1)! \quad (13)$$

$$\Gamma\left(N + \frac{1}{2}\right) = (2N-1)!! \frac{\sqrt{\pi}}{2^N} \quad (14)$$

In the above equations, c_w is the wave celerity; k is the wave number; t_p is the thrust deduction factor; w_p is the wake fraction; D_p is the propeller diameter.

The amplitude of wave surging force f in equation (9) is calculated as:

$$f = \rho g k \frac{H}{2} \sqrt{F_C^2 + F_S^2} \quad (15)$$

where,

$$F_C = \sum_{i=1}^{N_s} S(x_i) \exp\{-0.5kd(x_i)\} \sin kx_i \Delta x_i \quad (16)$$

$$F_S = \sum_{i=1}^{N_s} S(x_i) \exp\{-0.5kd(x_i)\} \cos kx_i \Delta x_i \quad (17)$$

where, $d(x_i)$ and $S(x_i)$ are the draft and the submerged area of the ship at station i in calm water, respectively.

3 SENSITIVITY ANALYSIS

Level 2 assessment involves many parameters which might be hard to obtain at the early design stage. Usually, empirical formula and/or model experiment results are used as the initial estimation. Therefore, it is meaningful to perform the sensitivity analysis to evaluate the influence of input parameter variation on the assessment result.

A purse seiner ($L_{PP}=42.5\text{m}$, $B=7.8\text{m}$, $d=3.2\text{m}$, $C_B=0.6721$) is chosen as the target ship for the sensitivity analysis. The service speed of the ship is 6.5m/s ($Fn=0.32$), therefore the ship cannot pass Level 1 assessment.

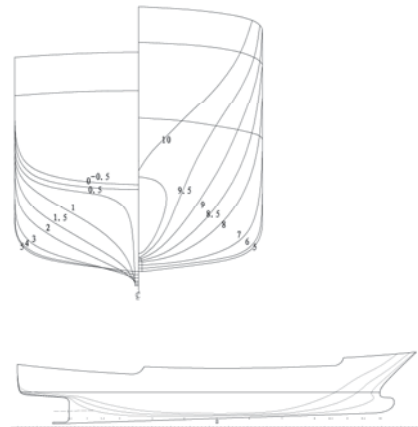


Figure 1 Lines of the purse seiner.

3.1 Influence of Resistance Estimation

Two aspects are studied, one is the influence of the order of polynomials for resistance curve approximation, and the other is the influence of resistance estimation error. The propeller thrust coefficients are approximated by 2nd order polynomials.

Figure 2 demonstrates the influence of order of polynomials for curve fitting. As can be seen, the curve fitting results in low and middle speed region ($Fn < 0.35$) have small differences. However, the differences increase between $N_{Fit}=3$ and $N_{Fit}=4$ or 5 in the high speed region.

The results are listed in Table 1. As expected, there is a 29.5% difference of C value between $N_{Fit}=3$ and $N_{Fit}=5$. Therefore, proper choice of the order of polynomials for resistance curve fitting is important for the assessment.

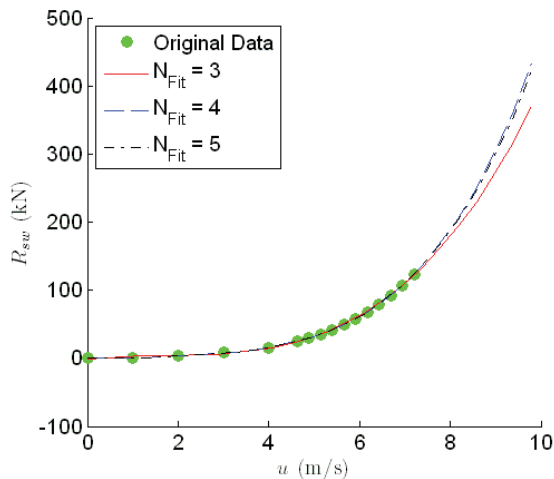


Figure 2 Resistance curve approximation.

The influence of estimation error is also listed in Table 1. According to the results, if there is 1% uncertainty in the estimated data, there will be about 1% difference in the attained C value. Moreover, with the increase of estimation uncertainty, the differences in

the attained C values grow rapidly. Typically, if there is 5% uncertainty in the resistance estimation, which is quite likely in terms of RANS based CFD computations, the resulting difference in the attained C value can be up to 16%.

However, it should be pointed out that the lack of data in high speed region (Fn around 0.45) may have some influence on the obtained result, which implies that accurate estimation of ship resistance at high speeds is also important.

Table 1 Resistance Estimation Influence

Case	Uncertainty (%)	N_{Fit}	C	ΔC (%)
1	0	5	1.90E-02	
2	0	4	1.82E-02	4.2
3	0	3	2.46E-02	29.5
4	1	5	1.88E-02	1.1
5	3	5	1.79E-02	6.0
6	5	5	1.59E-02	16.3

3.2 Influence of Propulsion Estimation

Similar studies are performed to investigate the influence of propulsion input data uncertainty, where the resistance curve is approximated by 5th order polynomials.

Figure 3 demonstrates the influence of order of polynomials for K_T curve approximation, and very small differences can be noticed. As shown by the results listed in Table 2, this will cause roughly 2% difference in the attained C value. Moreover, it is demonstrated that the result is not very sensitive to the K_T coefficient estimation error. If the uncertainty is within 2%, the final difference can be kept within 1%.

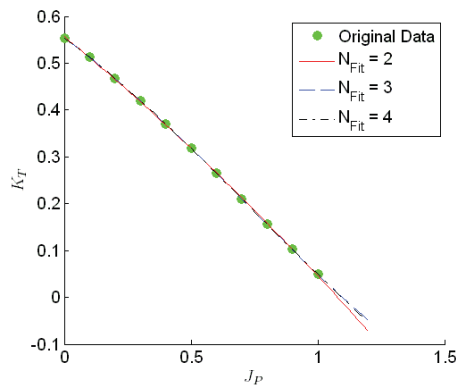


Figure 3 Thrust coefficient approximation.

Table 2 Propulsion Estimation Influence

Case	Uncertainty (%)	N_{Fit}	C	ΔC (%)
1	0.0	2	1.90E-02	
2	0.0	3	1.94E-02	2.1
3	0.0	4	1.94E-02	2.1
4	1.0	2	1.91E-02	0.5
5	1.5	2	1.90E-02	0.2
6	2.0	2	1.91E-02	0.7

Table 3 Influence of w_P and t_P Estimation

Case	w_P	t_P	C	ΔC (%)
1	0.287	0.287	1.90E-02	
2	0.316	0.287	1.84E-02	3.2
3	0.258	0.287	1.94E-02	2.1
4	0.287	0.316	1.88E-02	1.1
5	0.287	0.258	1.92E-02	1.1

The influence of w_P and t_P are also studied by varying them either 10% larger or smaller. The results are listed in Table 3. As can be seen, both parameters have small influence on the final C value. Comparatively speaking, the result is more sensitive to w_P than t_P .

3.3 Influence of Wave Force Calculation

As pointed out by Japan (SDC 2/INF.X, 2014), the wave-induced surge force could often be over-estimated because only the Froude-Krylov component is considered in

current procedure. Japan thus proposed an empirical correction factor for the diffraction effect as follows:

$$f = \mu_x \rho g k \frac{H}{2} \sqrt{F_C^2 + F_S^2} \quad (18)$$

$$\mu_x = \begin{cases} 1.46C_b - 0.05 & C_m < 0.86 \\ (5.76 - 5C_m)C_b - 0.05 & 0.86 < C_m < 0.94 \\ 1.06C_b - 0.05 & C_m \geq 0.94 \end{cases} \quad (19)$$

where, μ_x is the empirical correction factor; C_m is the midship section coefficient.

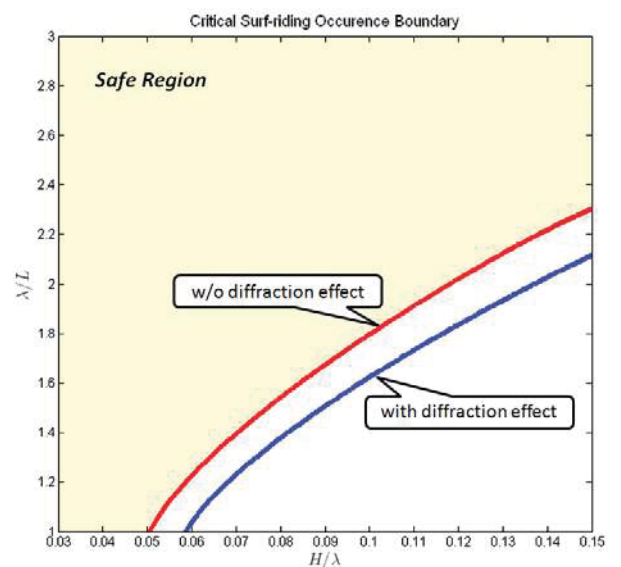


Figure 4 Surf-riding occurrence boundary.

The change of critical surf-riding boundary after correcting for the diffraction effect is illustrated in Figure 4, where the safe region corresponds to $C_{2ij}=0$. As can be seen, the safe region is increased, and correspondingly, the attained C value decreases from 1.90E-02 to 9.40E-03, which is 50.5% smaller. Therefore, the wave force calculation has significant influence on the assessment. Investigations on more accurate wave force estimation methods are crucial in subsequent researches.



4 SAMPLE CALCULATIONS

Based on the sensitivity analysis result, sample calculations are performed to 10 ships. The calm water resistance curve and the propeller thrust coefficient are approximated by the 5th and 2nd order polynomials, respectively. The correction for the diffraction effect is not considered since it has not yet been included in the standard procedure. The results of the sample calculations are analyzed to verify the appropriateness of the current proposal.

4.1 Sample Ships

The main particulars of the 10 sample ships are listed in Table 4.

Table 4 Main Particulars of Sample Ships

NO.	Ship Type	F_n	L_{PP} (m)	B (m)	d (m)	C_B
1	Purse Seiner	0.320	42.5	7.8	3.2	0.6721
2	Purse Seiner	0.285	43.0	8.5	3.7	0.8011
3	Purse Seiner	0.268	54.0	10.0	4.1	0.7396
4	Fishing Boat	0.364	29.5	6.0	1.8	0.4796
5	Fishing Boat	0.290	41.0	7.0	2.8	0.5800
6	Traffic Boat	0.496	16.0	6.0	1.8	0.5277
7	Traffic Boat	0.553	19.5	5.0	1.4	0.4925
8	Gillnet Boat	0.332	27.1	5.4	2.0	0.5610
9	Trawler	0.316	36.8	7.2	2.8	0.5850
10	Crab Boat	0.285	39.0	6.6	2.7	0.5940

Fishing boats and small-size high-speed boats are chosen intentionally because they are most vulnerable to the broaching stability failure. Moreover, the Froude numbers of the sample ships are around 0.3, with four below 0.3 and six over 0.3. However, none of the ship length is over 200m.

The offset data, calm water resistances and propeller open water data of the sample ships are provided by the design institutes, while w_p and t_p are estimated by:

$$w_p = C_B/3 + 0.063 \quad (20)$$

$$t_p = w_p \quad (21)$$

4.2 Assessment Results

The results are shown in Table 5. Four ships can pass the Level 1 assessment because their Froude numbers are below 0.3. When it comes to Level 2 assessment, the setting of the standard value R_{SR} plays an important role. If $R_{SR} = 1e-4$, only two of the four remaining ships (NO.2 and NO.3) can further pass Level 2 assessment while inconsistency occurs to NO.5 and NO.10, even when the diffraction effect is included (NO.5- μ_x and NO.10- μ_x); however, if $R_{SR} = 5e-3$, all the four remaining ships can further pass Level 2 assessment, and the consistency can be guaranteed.

Since Level 2 assessment is meant to be less conservative than Level 1 assessment, the occurrence of inconsistency should be avoided. Therefore, based on the current sample calculation results, $R_{SR} = 5e-3$ seems to be a more proper standard value.

Table 5 Assessment Results

NO.	Level 1	Level 2		
		C	Conclusion	
			$R_{SR}=1e-4$	$R_{SR}=5e-3$
1	Fail	1.90E-02	Fail	Fail
2	Pass	0.00E+00	Pass	Pass
3	Pass	0.00E+00	Pass	Pass
4	Fail	3.26E-01	Fail	Fail
5	Pass	3.40E-03	Fail	Pass
5- μ_x		5.43E-04	Fail	Pass
6	Fail	9.68E-01	Fail	Fail
7	Fail	1.00E+00	Fail	Fail
8	Fail	1.11E-01	Fail	Fail
9	Fail	1.97E-02	Fail	Fail
10	Pass	1.70E-03	Fail	Pass
10- μ_x		3.30E-04	Fail	Pass

4.3 Impact on Ship Design

Some insights concerning the potential impact of the broaching stability criteria on ship design can be obtained through further investigation into the sample ship calculation results.

Taking the NO.10 crab boat as the example, the F_n — C relation curve is shown in Figure 5. As can be seen, the slope of the curve around $F_n=0.3$ is very steep, which implies that a slight change of F_n will cause a significant change in the attained C . Therefore, a slight increase of ship length or decrease of ship speed might be helpful for meeting the criteria requirement.

Furthermore, we can see from Table 4 and 5 that NO.6 and NO.7 traffic boats are most vulnerable to the broaching stability failure mode due to their small lengths. The same situation might happen to most ships with small lengths and thus high Froude numbers. If the second generation intact stability criteria come into force, the existing small-size high-speed ships may have to increase their lengths in order to comply with the regulation. Otherwise, they can only operate under much slower speeds, which do not seem to be very feasible for these task-oriented vessels.

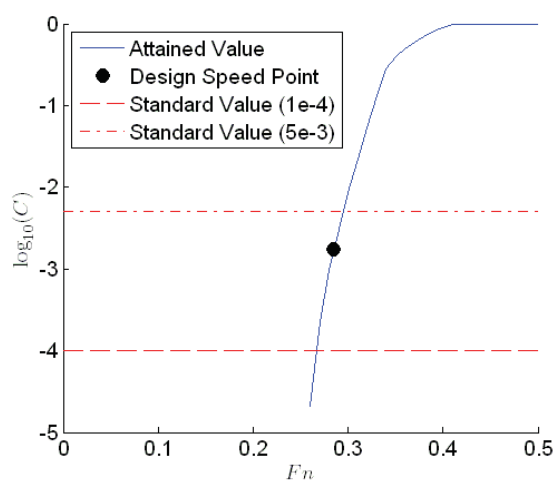


Figure 5 F_n — C relation curve.

5 CONCLUSIONS

This study tries to identify the most crucial parameters of the broaching stability criteria assessment through sensitivity analysis, and to verify the current proposal based on sample calculations. The main conclusions are summarized as follows:

- 1) Resistance estimation accuracy has big influence on the attained index value C . Calm water resistance estimation at high ship speeds is important for curve fitting. The result is also quite sensitive to the uncertainty level of resistance estimation. A 5% uncertainty in the resistance data may cause a significant difference on the attained C value. However, prediction of resistance at large Froude numbers is very difficult and error prone. CFD results for Froude numbers over 0.4 are considered to be unreliable, so the estimation of the resistance at high speeds should be studied.
- 2) The result of attained C value is not very sensitive to the K_T coefficient estimation error, so as the wake fraction w_P and thrust deduction coefficient t_P . The results seem to justify the use of rough approximations for the propeller thrust coefficient as well as w_P and t_P in the initial design stage.
- 3) The wave force calculation has significant influence on the assessment result. The attained C value can be halved if the diffraction effect is taken into account through an empirical correction model. Further studies on this aspect are crucial and definitely necessary.
- 4) Based on the sample calculation results, $R_{SR} = 5e-3$ seems to be a more proper standard value than $R_{SR} = 1e-4$. To better justify the choice of the standard value, more sample calculations that cover a wider range of ship types are preferable.



6. REFERENCES

- Hashimoto, M. and Stern, F., 2007, "An Application of CFD for Advanced Broaching Prediction", Proceedings of the Japan Society of Naval Architects and Ocean Engineers, Vol. 5E, pp. 51-52.
- Hashimoto, M., Umeda, N. and Matsuda, A., 2004, "Importance of Several Nonlinear Factors on Broaching Prediction", Journal of Marine Science and Technology, Vol. 9, pp. 80-93.
- Maki, A., Umeda, N. et al., 2010, "Analytical Formulae for Predicting the Surf-riding Threshold for a Ship in Following Seas", Journal of Marine Science and Technology, Vol. 15, pp. 218-229.
- SDC 1/INF.8, 2013, "Development of Second Generation Intact Stability Criteria", Subcommittee on Ship Design and Construction, 1st session, Agenda item 5, Annex 27.
- SDC 2/INF.X, 2014, "Development of Second Generation Intact Stability Criteria", Subcommittee on Ship Design and Construction, 2nd session, Agenda item 5, Annex 32.
- Spyrou, K. J., 2001, "Exact Analytical Solutions for Asymmetric Surging and Surf-riding", Proceedings of the 5th International Workshop on Stability and Operational Safety of Ships, University of Trieste, pp. 4.4.1-3.
- Umeda, N. and Vassalos, D., 1996, "Non-linear Periodic Motions of a Ship Running in Following and Quartering Seas", Journal of the Society of Naval Architects of Japan, Vol. 179, pp. 89-101.
- Umeda, N., Matsuda, A. et al., 1999, "Stability Assessment for Intact Ships in the Light of Model Experiments", Journal of Marine Science and Technology, Vol. 4, pp. 16-26.



Calcoque: a Fully 3D Ship Hydrostatic Solver

François Grinnaert, *French Naval Academy Research Institute*, francois.grinnaert@ecole-navale.fr

Jean-Yves Billard, *French Naval Academy Research Institute*, jean-yves.billard@ecole-navale.fr

Jean-Marc Laurens, *ENSTA Bretagne*, Jean-Marc.LAURENS@ensta-bretagne.fr

ABSTRACT

Calcoque is a 3D hydrostatic computer code developed at the French Naval Academy. It computes equilibrium, stability and bending moment. A matrix algorithm transforms the classical representation of the ship by stations into a volume mesh made of tetrahedrons, prisms and hexahedrons, which can have large dimensions without degradation of the numerical result. At present the codes can handle the existing IMO intact stability criteria. It can also compute damage stability. The software code has a geometric equilibrium algorithm compatible with a strong coupling between the heel and trim. The balance position is determined on calm water and on static waves with two or three degrees of freedom. These characteristics make the code fully compatible with the second generation intact stability criteria. After some particularities of the code are presented, the paper shows a sample of computation applied to the pure loss of stability failure mode.

Keywords: *Equilibrium, algorithm, volume mesh, second generation intact stability criteria, pure loss of stability*

1. INTRODUCTION

Calcoque is a 3D hydrostatic computer code developed at the French Naval Academy for academic and research use. It computes equilibrium, stability (intact and damage) and bending moment and can handle the existing IMO intact stability criteria. It uses an unusual 3D volume method for hydrostatic computations based on meshes made of tetrahedrons, prisms and hexahedrons.

The goal of this study is to use this 3D hydrostatic volume method to compute first and second level pure loss of stability criteria for a passenger ship. These criteria are extracted from IMO second generation intact stability regulation currently under development and validation (Bassler, et al., 2009, Francescutto, et. al., 2010, Wandji, et al., 2012). In order to avoid any assumption about the height of the centre of gravity, the criteria

are evaluated through KG_{\max} curves they generate.

This paper presents the 3D hydrostatic volume method and its application on pure loss of stability criteria.

2. VOLUME HYDROSTATIC COMPUTATION

The hydrostatic solver consists of three main algorithms. The first one transforms a classical representation of the ship by sections into a volume mesh. The second algorithm is cutting the volume mesh by a plane, generating two volume sub-meshes (one on each side of the plane) and a surface mesh at the intersection. The third one searches the balance position of the ship on calm water and on static waves with three degrees of freedom (sinkage, heel, trim) or two degrees of freedom (fixed heel). These algorithms are partially described

in a handbook (Grinnaert & Laurens, 2013) but have never been introduced in open literature. They are described below.

2.1 Generation of Volume Mesh

The ship is designed with stations, which are a list of (Y, Z) points with the same longitudinal coordinate X. Stations must be ordered from aft to forward. They are symmetrical, defined on port side only. The first point of each station is on the ship's centreline (Y=0). Vertical coordinate of the points are increasing ($Z_{i+1} > Z_i$).

Lines defined by the user connect some points of stations in order to represent the main edges of the hull. A line starts at any station and ends at any other one located forward. It has a unique point on each station it intersects and cannot miss out any station. Two lines can intersect only at a station point.

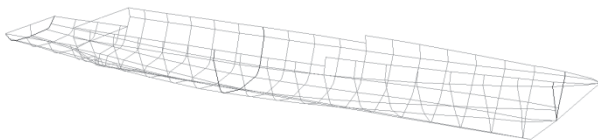


Figure 1 Stations and lines of an offshore patrol vessel.

Stations and lines (Figure 1) are used to generate a volume mesh of the ship through a "matrix" algorithm which builds the N-1 strips defined by the N stations. For each strip between stations indexed i and i+1, the process is organized in two steps.

First step. The first step consists of the generation of a matrix defining the links between all the points of the station i and all the points of station i+1. Let us consider a strip defined by a aft station with 5 points (port side only) and a forward station with 4 points. Let us consider 3 user lines. The first one links point 1 of the rear station to point 1 of the forward station (keel line). The second links point 2 (rear) to point 3 (forward). The third links point 5 (rear) to point 4 (forward). The

strip and its links can be represented by Figure 2 (stations in black, lines in grey).

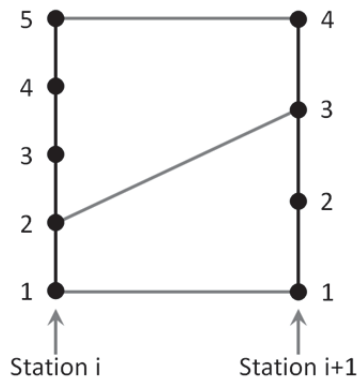


Figure 2 Strip defined by two stations and three lines.

Thus, a link matrix is defined with 5 rows associated with the 5 points of the rear station, and 4 columns associated with the 4 points of the forward station. The three user lines are represented in this matrix by three black dots in the appropriate cells (Figure 3).

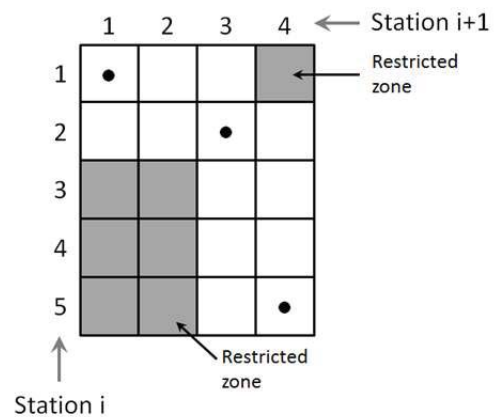


Figure 3 Link matrix associated with the strip.

Each link in the matrix defines two restricted zones which are the upper right cells and the lower left cells. This avoids considering a line which crosses another. In the current sample, the restricted zones defined by the second link (2-3) appear in grey in Figure 3. Both other links (1-1 and 5-4) define no restricted zone.

Thus, the matrix filled with user links is automatically completed with other links by going from the upper left corner to the lower right corner without missing out any cells

while passing by all cells associated with user links. Diagonal path is favoured (link 1-1 to link 2-2). If not possible, the path is horizontal (2-2 to 2-3) or vertical (3-4 to 4-4). These added links are grey dots in the left part of Figure 4. They can be added on the strip diagram (right).

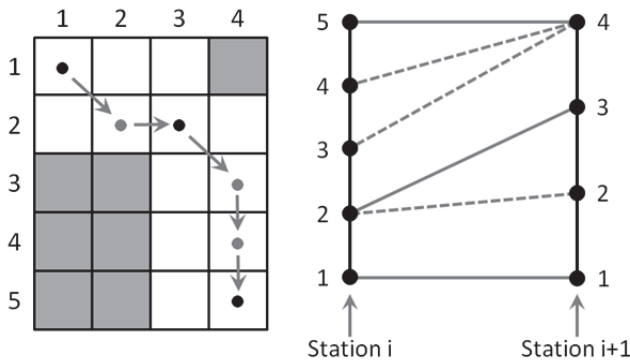


Figure 4 Completed link matrix (left) and associated strip diagram (right).

Second step. The second step consists of the generation of the volume and surface meshes defined by the completed link matrix. A diagonal path (1-1 to 2-2 and 2-3 to 3-4) generates a tetragon on each side of the hull and a hexahedron which connects both together. A horizontal path (2-2 to 2-3) generates a triangle on each side of the hull and a prism, whose bases are on the forward station. A vertical path (3-4 to 4-4 and 4-4 to 4-5) also generates two triangles and one prism, but their bases are on the rear station. The surface mesh associated with the current sample is shown in Figure 5.

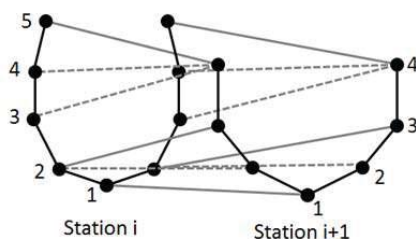


Figure 5 3D wireframe view of the strip and its surface mesh.

Flat volumes should be eliminated (same Z coordinate of the points). Some volumes may be simplified: in the sample, the first

hexahedron is a prism because the Y coordinate of the first point of each station is null.

The volume mesh of the entire ship is created by concatenating all strips (Figure 6). The volume mesh may be corrected to represent the real hull. It may be cut at the watertight deck and the void spaces (bow thruster tunnel, water inlets, flooded rooms for damage stability ...) may be extracted. Both operations need a routine which cuts the mesh by a plane, described below. Volume meshes of appendages and propellers may be added.

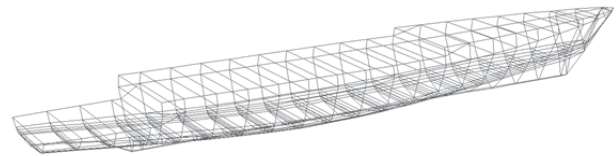


Figure 6 Wireframe view of the volume mesh of an offshore patrol vessel.

2.2 Cutting the Volume Mesh by a Plane

Cutting a volume mesh by a plane is necessary to define the waterplane. It also permits to extract some volumes from the hull (void spaces or flooded rooms) and to define volume meshes of the compartments and surface meshes of the decks. The volume mesh is made of prisms and hexahedrons. The former can be divided in three tetrahedrons and the latter in two prisms or six tetrahedrons. The cutting routine of prisms and hexahedrons only handles simple cases: volume entirely on one side or the other of the plane, a face contained in the plane or face “parallel” to the plane. In other cases, the volume being cut is previously decomposed into three or six tetrahedrons. Each point of the tetrahedron can be located on one side of the plane, included in the plane, or on the other side. Then, we have $3^4=81$ possibilities. However, the order of points having no importance (unlike the necessary orientation of the vertices of a surface mesh) the number of possibilities is reduced to 15 and may be simplified to 8 (see Table 1).

Case	Topology
A	No point on the upper side 1 tetrahedron on the lower side 1 intersecting triangle if 3 points in the plane
B	No point on the lower side 1 tetrahedron on the upper side
C	2 points on the upper side 2 points on the lower side 1 prism on the upper side 1 prism on the lower side 1 intersecting tetragon
D	1 point on the upper side 3 points on the lower side 1 tetrahedron on the upper side 1 prism on the lower side 1 intersecting triangle
E	3 points on the upper side 1 point on the lower side 1 prism on the upper side 1 tetrahedron on the lower side 1 intersecting triangle
F	1 point on the upper side 1 point in the plane 2 points on the lower side 1 tetrahedron on the upper side 1 tetrahedron on the lower side 1 intersecting triangle
G	2 points on the upper side 1 point in the plane 1 point on the lower side 1 tetrahedron on the upper side 1 tetrahedron on the lower side 1 intersecting triangle
H	1 point on the upper side 2 points in the plane 1 point on the lower side 1 tetrahedron on the upper side 1 tetrahedron on the lower side 1 intersecting triangle

Table 1 Cut cases of a tetrahedron with a plane.

2.3 Research of the Balance Position

The research algorithm for the balance position is partially presented in a handbook (Grinnaert & Laurens, 2013). A second method has since been implemented in the Calcoque software.

Definition of the Balance Position. The three degrees of freedom are sinkage (e , metre), heel (φ , radian) and trim (θ , radian). Sinkage

replaces draught which has no sense while heel approaches 90 degrees. Sinkage is defined as the algebraic distance between a ship fixed point Q (coordinates $L_{PP}/2, 0, Z$ of the reference waterline $10H$) and its projected point P on the calm water waterplane (even for computation on static waves). See Figure 7.

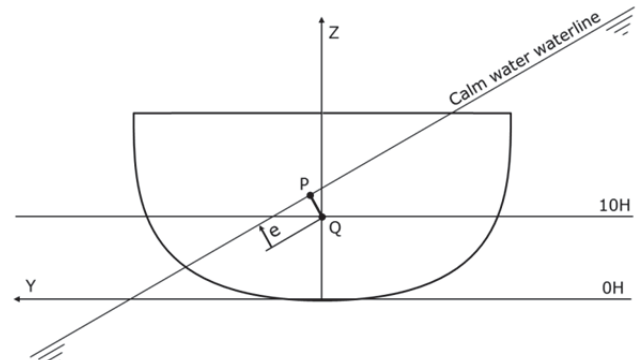


Figure 7 Sinkage.

Balance is achieved if the three following conditions are met:

$$\varepsilon_V = \nabla_0 - \nabla = 0 \quad (1.1)$$

$$\varepsilon_x = 0 \quad (1.2)$$

$$\varepsilon_y = 0 \quad (1.3)$$

With:

∇ Computed displacement volume (m^3)

∇_0 Ship displacement volume (m^3)

ε_V Volume gap (m^3)

ε_x Longitudinal gap (m, defined below)

ε_y Transverse gap (m, defined below)

Heel can be free (research of the balance position) or fixed (GZ curve computation). In that case, the third condition is ignored and the transverse gap ε_y is the righting arm lever GZ.

Inclined Ship Planes. ε_x and ε_y gaps are respectively the algebraic longitudinal and transverse distances between the centre of gravity (G) and the Earth vertical through the centre of buoyancy (B). Two “inclined ship planes” are defined to compute these gaps. Their line of intersection is the Earth vertical whose director vector is \mathbf{n}_1 .

The transverse plane of inclined ship also contains vector \mathbf{n}_2 defined as:

$$\mathbf{n}_2 = \frac{\mathbf{n}_1 \wedge \mathbf{X}}{\|\mathbf{n}_1 \wedge \mathbf{X}\|} \quad (2)$$

The longitudinal plane of inclined ship contains \mathbf{n}_1 and \mathbf{n}_3 vectors with:

$$\mathbf{n}_3 = \mathbf{n}_2 \wedge \mathbf{n}_1 \quad (3)$$

In the ship fixed coordinates system, the three vectors are:

$$\begin{aligned} n_{1,x} &= -\sin \theta \\ n_{1,y} &= -\sin \varphi \cos \theta \\ n_{1,z} &= \cos \varphi \cos \theta \end{aligned} \quad (4.1)$$

$$\begin{aligned} n_{2,x} &= 0 \\ n_{2,y} &= \cos \varphi \\ n_{2,z} &= \sin \varphi \end{aligned} \quad (4.2)$$

$$\begin{aligned} n_{3,x} &= \cos \theta \\ n_{3,y} &= -\sin \varphi \sin \theta \\ n_{3,z} &= \cos \varphi \sin \theta \end{aligned} \quad (4.3)$$

Thus, ε_x and ε_y gaps are respectively the algebraic distances between G and the transverse and longitudinal planes of the inclined ship. They are computed as follows:

$$\varepsilon_x = \mathbf{BG} \cdot \mathbf{n}_3 \quad (5.1)$$

$$\varepsilon_y = \mathbf{GZ} = \mathbf{BG} \cdot \mathbf{n}_2 \quad (5.2)$$

Gaps and planes are shown in Figure 8.

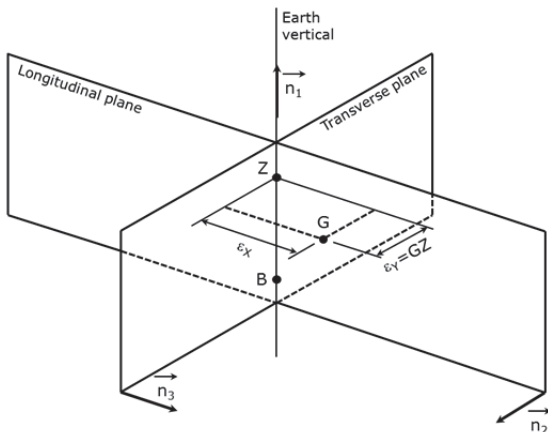


Figure 8 Gaps and inclined ship planes.

This expression of the longitudinal gap is more accurate than the simplified strip method proposed by the SLF 52/INF.2 (annex 6) which consists in:

$$LCB = LCG \quad (6)$$

Hydrostatic computation on calm water.

The waterplane, depending on sinkage (e), heel (φ) and trim (θ), is defined with a point P (see Figure 7) and the vector \mathbf{n}_1 with:

$$\mathbf{QP} = e \cdot \mathbf{n}_1 \quad (7)$$

When searching for the balance position, the displacement volume (∇) and its centre (B) are computed by cutting the watertight volume mesh by the waterplane.

Hydrostatic computation on waves. Watertight volume is previously divided in strips by cutting with transverse planes. SLF 52/INF.2 (annex 6) recommends at least 20 strips. In each strip, the following are defined (see Figure 9):

- Plane P₁: strip's rear plane.
- Plane P₂: strip's forward plane.
- Line D₃: through point P with director vector \mathbf{n}_3 (longitudinal line included in the calm waterplane).
- Point I₁: intersection of P₁ and D₃.
- Point I₂: intersection of P₂ and D₃.

Three points (A, B and C) define the strip's local waterplane. They are defined as follows (see Figure 9):

$$\mathbf{OA} = \mathbf{OI}_1 + \mathbf{n}_2 + z_1 \cdot \mathbf{n}_1 \quad (8.1)$$

$$\mathbf{OB} = \mathbf{OI}_1 - \mathbf{n}_2 + z_1 \cdot \mathbf{n}_1 \quad (8.2)$$

$$\mathbf{OC} = \mathbf{OI}_2 + z_2 \cdot \mathbf{n}_1 \quad (8.3)$$

With:

$$z_1 = \frac{h}{2} \cos(k \cdot x_1 + \Phi) \quad (9.1)$$

$$z_2 = \frac{h}{2} \cos(k \cdot x_2 + \Phi) \quad (9.2)$$

$$\Phi \in [0, 2\pi[$$

- h Wave height (m)
- k Wave number (m^{-1})
- x_1 Longitudinal position of the rear plane of the strip
- x_2 Longitudinal position of the forward plane of the strip

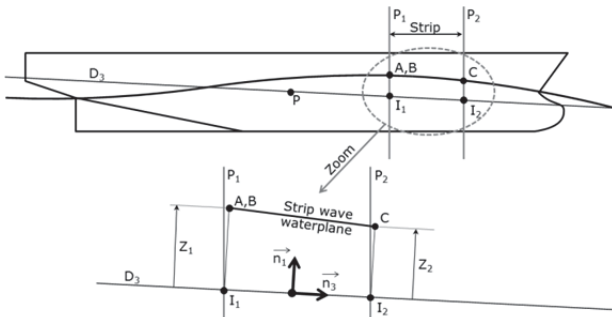


Figure 9 Strip wave waterplane.

Balance - First Method. The process is iterative. At each step, three gaps (two if fixed heel) are computed as explained above. Sinkage, heel and trim are corrected as follows before being used in the next step:

$$e_{i+1} = e_i + \frac{\varepsilon_{\nabla}}{A_{WP}} \quad (10.1)$$

$$\varphi_{i+1} = \varphi_i + \frac{\varepsilon_y}{|GM_T|} \quad (10.2)$$

$$\theta_{i+1} = \theta_i + \frac{\varepsilon_x}{|GM_L|} \quad (10.3)$$

With:

- e_i sinkage at step i (m)
- e_{i+1} sinkage at step $i+1$ (m)
- φ_i heel at step i (rad)
- φ_{i+1} heel at step $i+1$ (rad)
- θ_i trim at step i (rad)
- θ_{i+1} trim at step $i+1$ (rad)

Absolute values of the metacentric heights permit to let the process diverge in case of transverse or longitudinal instability. At first step, the waterplane area (A_{WP}) and metacentric heights (GM_T , GM_L) may be calculated with the hydrostatic table or by direct computation on the waterplane surface mesh, which must be

projected on an Earth-horizontal plane in case of computation on waves. At next steps, they are computed as follows:

$$A_{WP} = \frac{\nabla_{i+1} - \nabla_i}{e_{i+1} - e_i} \quad (11.1)$$

$$GM_T = \frac{\varepsilon_{y,i+1} - \varepsilon_{y,i}}{\varphi_{i+1} - \varphi_i} \quad (11.2)$$

$$GM_L = \frac{\varepsilon_{x,i+1} - \varepsilon_{x,i}}{\theta_{i+1} - \theta_i} \quad (11.3)$$

When the three gaps (ε_{∇} , ε_{φ} , ε_{θ}) are small enough, the balance position is considered reached. This method is compatible with a strong coupling between the heel and trim (unconventional floating structures). However, it is fragile if the coupling between the trim and sinkage is strong because the corrections of trim and sinkage may conflict.

Balance - Second Method. This method is also iterative and has been developed after the publication of the handbook (Grinnaert & Laurens, 2013). Before the iterative process, an initial hydrostatic computation gives the three gaps for initial values of e , θ and φ . At each step of the iterative process, three hydrostatic computations (two if fixed heel) are performed. They permit to evaluate separately the influence of a small increment of sinkage, heel and trim on the values of the three gaps. These computations are listed in Table 2.

	Input data			Output data		
1	$e + \varepsilon_e$	θ	φ	$\varepsilon_{\nabla e}$	$\varepsilon_{x e}$	$\varepsilon_{y e}$
2	e	$\theta + \varepsilon_{\theta}$	φ	$\varepsilon_{\nabla \theta}$	$\varepsilon_{x \theta}$	$\varepsilon_{y \theta}$
3	e	θ	$\varphi + \varepsilon_{\varphi}$	$\varepsilon_{\nabla \varphi}$	$\varepsilon_{x \varphi}$	$\varepsilon_{y \varphi}$

Table 2 Hydrostatic computations.

With:

- ε_e $d_{full}/100$ small sinkage increment
- ε_{θ} 0.1 degree small trim increment
- ε_e 1.0 degree small heel increment
- d_{full} (m) full loaded ship draught

Then, still in the same iteration, the following system of three equations with three unknowns (2×2 if fixed heel) is solved:



$$\begin{pmatrix} \frac{\varepsilon_{\nabla e} - \varepsilon_{\nabla}}{\varepsilon_e} & \frac{\varepsilon_{\nabla \theta} - \varepsilon_{\nabla}}{\varepsilon_{\theta}} & \frac{\varepsilon_{\nabla \varphi} - \varepsilon_{\nabla}}{\varepsilon_{\varphi}} \\ \frac{\varepsilon_{xe} - \varepsilon_x}{\varepsilon_e} & \frac{\varepsilon_{x\theta} - \varepsilon_x}{\varepsilon_{\theta}} & \frac{\varepsilon_{x\varphi} - \varepsilon_x}{\varepsilon_{\varphi}} \\ \frac{\varepsilon_{ye} - \varepsilon_y}{\varepsilon_e} & \frac{\varepsilon_{y\theta} - \varepsilon_y}{\varepsilon_{\theta}} & \frac{\varepsilon_{y\varphi} - \varepsilon_y}{\varepsilon_{\varphi}} \end{pmatrix} \times \begin{pmatrix} de \\ d\theta \\ d\varphi \end{pmatrix} = \begin{pmatrix} -\varepsilon_{\nabla} \\ -\varepsilon_x \\ -\varepsilon_y \end{pmatrix}$$

Unknowns are de , $d\theta$ and $d\varphi$, which are increments of sinkage, trim and heel to be added at current values to cancel the gaps. The second and third terms of the diagonal are respectively the longitudinal and transverse metacentric heights. Their sign may be used to detect instability and invert the sign of the trim and heel increments.

At the end of the iteration, a last hydrostatic computation is done using corrected values of sinkage, trim and heel. If the three gaps are small enough, the balance position is considered reached.

This second method is as suitable as the first for a strong coupling between the heel and trim. It is more robust in case of strong coupling between the trim and sinkage. The number of iterations is very small (1 or 2, see Table 3) but the number of hydrostatic computations is similar. If n is the number of iterations, the number of hydrostatic computations is $3n + 1$ if the heel is fixed and $4n + 1$ if it's free.

Comparison of Methods. Table 3 shows the GZ computed for a 13,000-ton ferry (length 160 m) using both methods. It also shows numbers of iterations and hydrostatic computations to reach each balance position with fixed heel. The maximum allowed gaps are 1 m^3 in volume and 1 millimetre for ε_x . The maximum difference between both GZ is lower than 0.02 millimetres.

Heel (deg.)	First method			Second method		
	GZ (m)	Nb. iter.	Nb. calc.	GZ (m)	Nb. iter.	Nb. calc.
0	0.000	8	8	0.000	2	7
1	0.042	6	6	0.042	1	4
2	0.085	7	7	0.085	1	4
3	0.130	11	11	0.130	1	4
4	0.176	7	7	0.176	1	4
5	0.224	7	7	0.224	1	4
10	0.484	8	8	0.484	2	7
15	0.774	8	8	0.774	2	7
20	1.103	8	8	1.103	2	7
25	1.441	7	7	1.441	2	7
30	1.737	8	8	1.737	2	7
35	1.984	5	5	1.984	2	7
40	2.179	5	5	2.179	2	7
45	2.252	6	6	2.252	2	7
50	2.189	6	6	2.189	2	7
	Sum	107		Sum		90

Table 3 Comparison of both balance methods.

Transverse metacentric height computation. The transverse metacentric height is computed using two first points of the GZ curve (0 and 1 degree).

$$GM_T = \left(\frac{dGZ}{d\varphi} \right)_{\varphi=0} \quad (13)$$

In the case of the hydrostatic computation on waves, the inertia of the projected waterplane is not used as recommended in the simplified strip method proposed by the IMO (see SLF 52/INF.2 annex 6).

3. APPLICATION TO THE PURE LOSS OF STABILITY FAILURE MODE

3.1 Goal and Ship Presentation

The volume method is applied to compute the first and the second level of pure loss of stability criteria for a ferry whose characteristics are shown in Table 4. These criteria are extracted from second generation intact stability criteria, which are currently under development and validation at the IMO.

They are thoroughly presented by Umeda (2013). Two methods are proposed for the level one criterion. The first method considers a parallel waterplane with lowest draught (d_L). The second method consists in minimum GM_T computation on a static sinusoidal wave which has the same length as the ship. Both methods are tested. No assumption of centre of gravity position is made. KG_{max} curves are computed for several displacements with zero trim. Two watertight volumes are considered, respectively limited at 14 m and 9 m above base line. Their meshes include appendages. Void spaces are truncated (bow thruster's tunnel and retractable stabilizers' housings).

Length overall	L_{OA}	175 m
Length between perpendiculars	L_{PP}	160 m
Breadth	B	24 m
Full load displacement	Δ	13147 tons
Draught	d_{full}	6.00 m
Froude number @ 25 knots	Fn	0.325

Table 4 Ship main characteristics.

3.2 Watertight volume limited at 14 m

KG_{max} curves for the first and the second level of pure loss of stability criteria are shown in Figure 10.

First level. Both methods proposed for the first level give significantly different results. The first is quite more conservative than the second. The curve associated with first method has a hook at a draught of 5.67 m, which is the consequence of a loss of inertia on the parallel waterplane due to the stabilizers housings (see dark grey waterplane in Figure 11). Using the theoretical hull would mask this phenomenon.

Recommendation: Regulation should specify the hull to use (real or bare). It should be noted that the simplified strip method proposed by the SLF 52/INF.2 annex 6 is not compatible with a real hull. This simplified method has been used by Wandji and Corrigan to apply the second generation criteria on a large sample of ships (Wandji, et al., 2012).

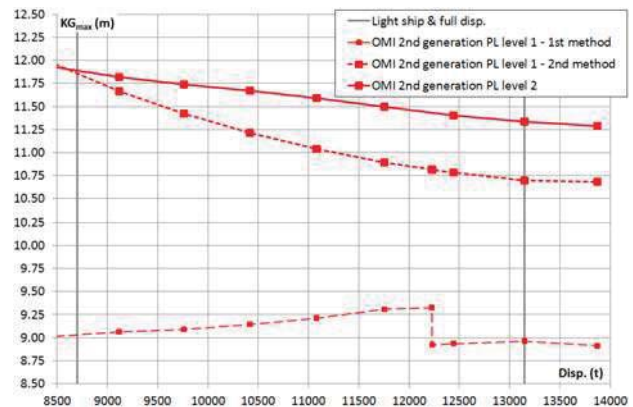


Figure 10 KG_{max} curves associated with 1st and 2nd level pure loss of stability criteria.



Figure 11 Parallel waterplanes for $d=6.00$ m (light grey) and $d_L=3.33$ m (dark grey).

Second level. We observe that the second level criterion is less conservative than both first level methods (except for one point below light ship displacement).

Comparison with first generation criteria. KG_{max} curves associated with first and second generation criteria are compared in Figure 12. We observe that the pure stability loss criteria do not introduce a higher requirement for this ship. The existing ship will comply with the new regulation but the architect will need to compute the second level criterion to prove it.

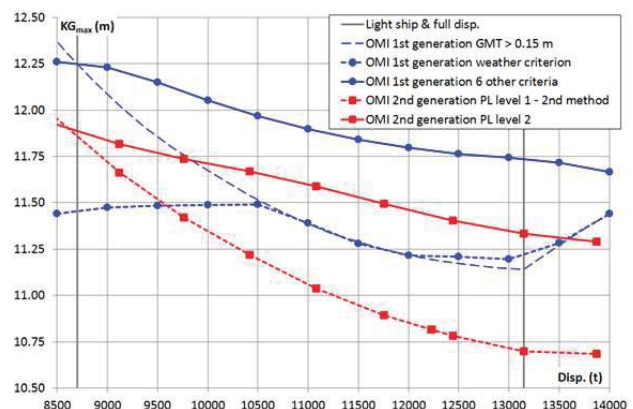


Figure 12 Comparison of 1st and 2nd generation criteria KG_{max} curves.

3.3 Influence of watertight deck height

The watertight deck is lowered from 14 to 9 metres.

First level. Lowering the watertight deck has normally no influence on the first level criterion which considers only metacentric height (hence small inclinations). For the first method (parallel waterplane at lowest draught), this is evident. For the second method (GM computation on wave), the wave crest should pass over the watertight deck, reducing the waterplane and its inertia. This situation does not occur with the watertight deck at 9 m (free-board at full load is 3 m, to be compared with wave half-height which is 2.67 m). However, it appears at a draught over 6 m if the watertight deck is lowered at 8 m (in this case the ship does not comply with the current regulation). See KG_{max} curves in Figure 13.

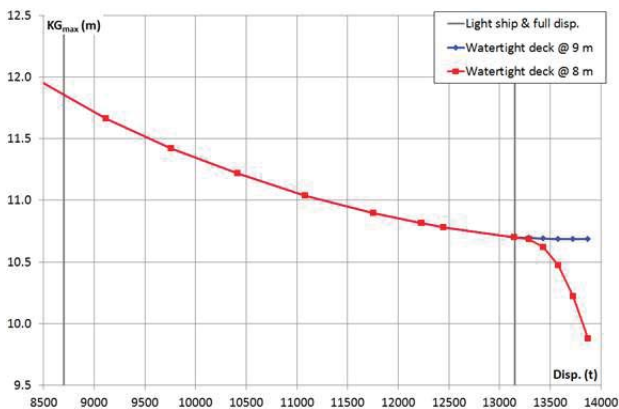


Figure 13 KG_{max} curves for 1st level criterion (2nd method) for watertight deck at 9 and 8 m.

The situation for the last point of the curve “Watertight deck @ 8 m” in Figure 13 ($d=6.25$ m) is shown in Figure 14. The waterplane is truncated on a quarter of its length. This situation should not occur in reality because the wave crest should not flood the garage deck even if its volume is considered as not watertight.

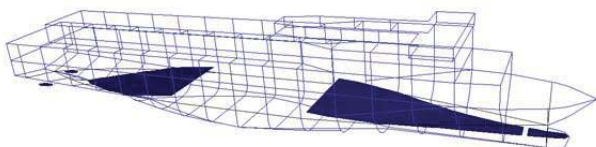


Figure 14 Truncated waterplane.

Recommendation: Regulation should specify the watertight volume to use. French military regulation (IG6018A) considers two different watertight volumes. The “bulkhead deck” is its upper limit which is tight to prolonged immersion. This watertight volume is considered in damage stability. In this sample, this deck should be the garage deck at 8 or 9 m above baseline. The “weather deck” is the upper limit which is tight to non-prolonged immersion. It may be the bulkhead deck or above. The increased watertight volume associated with this deck is considered in intact stability. In this sample, this deck should be located at 14 m above baseline (first passenger deck).

Second level. KG_{max} curves associated with the second level criterion for the lowered watertight volume height are shown in Figure 15. They are compared to those associated with the first level (independent from the watertight volume height) and those associated with the first generation criteria recalculated for the same watertight volume. As before, we observe that the pure loss of stability criteria do not introduce any additional requirement compared to first generation criteria. However, we note that the second level criterion is more demanding than the first level criterion calculated by the second method (GM computation on wave). This is a paradoxical situation.

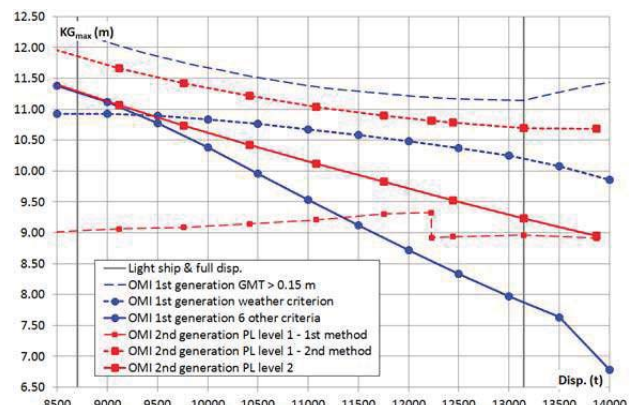


Figure 15 KG_{max} curves for a watertight volume limited at 9 m.

Figure 16 compares the KG_{max} curves associated with pure loss of stability criteria first and second level computed for both watertight decks located at 9 m and 14 m from baseline.

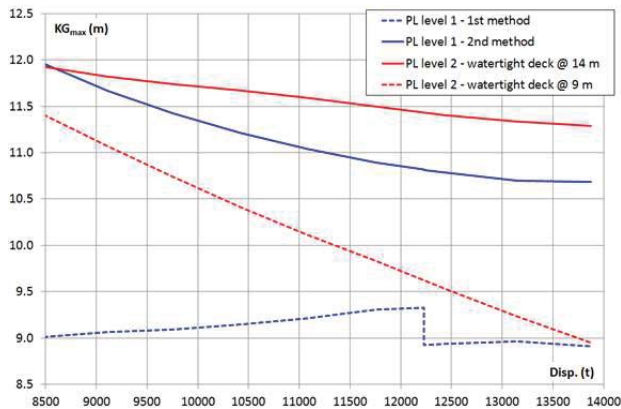


Figure 16 Influence of the watertight volume height on pure loss of stability KG_{max} curves.

4. CONCLUSION

The 3D hydrostatic volume code implemented in the Calcoque software is fully compatible with the first and second level pure loss of stability criteria. It can handle the real hull of the ship, with its appendages and void spaces. Use of this code to compute KG_{max} curves of a passenger ship showed:

- New requirements regarding pure loss of stability criteria are similar to those of the first generation criteria.
- The importance of a rigorous definition of the watertight volume to be considered (real or bare hull, upper limit).
- A paradoxical situation when the watertight deck is lowered (first level requires more than second level).

The study should be continued with other civilian and military ships of different geometries and extended to parametric roll, whose hydrostatic computations are similar to those of pure loss of stability.

5. REFERENCES

- Bassler, C., Belenky, V., Bulian, G., Francescutto, A., Spyrou, K., Umeda, N., "A Review of Available Methods for Application to Second Level Vulnerability Criteria", Proceedings of the 10th International Conference on Stability of Ships and Ocean Vehicles, pp. 111-128, 2009.
- Direction Générale de l'Armement, "Stabilité des bâtiments de surfaces de la Marine Nationale", IG6018A, 1999, Restricted diffusion.
- Francescutto, A., Umeda, N., "Current Status of New Generation Intact Stability Criteria Development", Proceedings of the 11th International Ship Stability Workshop, pp 1-5, 2010.
- Grinnaert, F., Laurens, J.-M., Stabilité du navire – Théorie, réglementation, méthodes de calcul – Cours et exercices corrigés, ISBN 978-2-7298-80644, Ellipses, 2013.
- SLF 52/INF.2, "Information collected by the intersectional Correspondence Group on Intact Stability", Submitted by USA, IMO, London, 2009.
- Umeda, N., "Current Status of Second Generation Intact Stability Criteria Development and Some Recent Efforts", Proceedings of the 13th International Ship Stability Workshop, pp 138-157, 2013.
- Wandji, C., Corrigan, P., "Test Application of Second Generation IMO Intact Stability Criteria on a Large Sample of Ships", Proceedings of the 11th International Conference on the Stability of Ships and Ocean Vehicles, pp 129-139, 2012.

Session 5.2 – DAMAGE STABILITY

**A New Approach for the Water - On - Deck - Problem of
RoRo - Passenger Ships**

**The Impact of the Inflow Momentum on the Transient Roll Response
of a Damaged Ship**

Safety of Ships in Icing Conditions

This page is intentionally left blank



A New Approach for the Water - On - Deck - Problem of RoRo - Passenger Ships

Stefan Krueger, Oussama Nafouti *Hamburg University of Technology, Germany*

Christian Mains *DNV GL Hamburg, Germany*

ABSTRACT

Since the ESTONIA accident in 1994, the so called water on deck problem for RoRo-Passenger Ships has been subject to many investigations. Being the central part of the Stockholm-Agreement (MSC Circ.1891 and EU directive), the water on deck problem was included in the damage stability calculations in addition to SOLAS 74/90 II-1/8. Although some of the assumptions are not physical sound, it is obvious that the safety level of RoRo- Passenger Ships has significantly been improved by including the water on deck problem in the safety regime. Unfortunately, the SOLAS 2009 does not explicitly address this problem, and there have been indications that the present safety level of the SOLAS 2009 seems not to cover the Stockholm Agreement for most of the smaller RoRo- Passenger Ships/ Ferries. However, when accidents of ships are analysed where water on the vehicle deck plays the dominating role, one finds that in most cases the problem is more related to intact stability. This is due to the fact that the involved ships were not damaged below the waterline, and this does especially hold for all problems related to firefighting on the vehicle deck.

Therefore we tried to formulate the water on deck problem as an intact stability criterion. In a first step, the stability limiting amount of water on deck needs to be determined. Then, in a second step, righting levers for the intact condition including this amount of water on deck can be computed, and some defined intact stability criteria can be applied. When determining the amount of water on deck which shall be used as design value, it is useful to analyse the relevant accidents. As a matter of fact, the ships accumulated water on deck due to various reasons, and the crew continued their operation until the situation became irreversible. They were not aware that they had run into a dangerous situation. This led to the idea to use the alteration of the roll period with water on deck as a suitable design criterion) and as an indicator for dangerous situation which easily can be measured by the crew). Consequently, we performed numerical roll decay tests with several RoRo-Passenger ships, where we varied the amount of water on deck. As an interesting result, we found that when increasing the amount of water on deck, the roll period first increases slightly and then changes drastically with a steep gradient. As a good rule of thumb we found that when the roll period doubles, a significant amount of water has accumulated on deck, but the ship still has a significant remaining stability margin against capsizing. Thus we used this approach to come to a reasonable design value for the minimum amount of water to be considered on deck. We also found a significant influence from centre casings on the amount of water on deck, which has to be considered. The proposed stability criteria have to be complied with for the intact condition including a dedicated amount of water on deck. These loading conditions were defined in such a way that all ships which are fully compliant to Stockholm Agreement do also fulfil our new approach, which is quite robust.

Keywords: *RoRo-Passenger Vessel, Water on Deck Problem, GM required curves, safety level.*



1. INTRODUCTION

One of the critical design characteristics of RoRo-Passenger Vessels is the large vehicle deck. In case of water ingress into the vehicle deck, the water is flowing freely on the deck and substantial heeling moments can be built up. If the amount of accumulated water on such a vehicle deck is increasing up to a critical value, the (initial) stability of the ship is going to vanish and the ship rapidly capsizes or takes a substantial heeling angle which extends the evacuation time significantly. Due to the nature of capsizing, accidents with water on deck often lead to a large number of casualties that might be reduced if one can set up a simple rule for crew and officers when the amount of accumulated water would become dangerous. Water may accumulate on deck due to opened vehicle compartments (Heraklion, Estonia), or by faulty operations (Herald of Free Enterprise, Jan Hewliusz) or due to firefighting measures (Al SALAM BOCCACIO). The ESTONIA disaster has made the water on deck problem obvious, and after this accident the damage stability regulations for RoRo-Passenger ships operating in European waters have been updated by explicitly taking into account accumulated water on deck. These regulations are known as “Stockholm-Agreement”. The basic design philosophy behind this stability standard is to reduce the amount of possible floodwater on the vehicle deck by sufficient residual freeboard between the vehicle deck and the damaged waterline. If this criterion cannot be complied with, the stability of the ship must be increased in such a way that the ship can withstand the assumed amount of floodwater which led to an increase vehicle deck for post ESTONIA RoRo-Passenger ship designs. Despite the fact that the physical background of the Stockholm- Agreement was subject to many discussions in the past, there is no doubt that the application of this regulation to RoRo- Passenger vessels has significantly improved the overall safety level of this ship type.

When the stability code for Passenger Vessels was updated with the enforcement of the SOLAS 2009, the damage stability regime for Passenger Vessels became a probabilistic one. In SOLAS 2009, water on deck is not explicitly addressed, but the Stockholm Agreement remains in force for all RoRo-Passenger vessels calling a European Port. As the Stockholm- Agreement is a local stability standard only, there are many discussions and research projects dealing with the question if in the framework of the SOLAS 2009 the Stockholm- Agreement is still needed or not. The results were quite controversial: Some researches came to the conclusion that the SOLAS 2009 would provide a higher safety level compared to the Stockholm- Agreement, and others pointed out that there might be still a deficiency even in the new SOALS 2009. As a consequence of this discussion, a modification of the s-factor of the SOLAS 2009 for RoRo-Passenger ships has been suggested during the last SDC- session at IMO with a future option to skip the Stockholm agreement. It is still an option (and presently under discussion) to modify the required index R of the SOLAS 2009. However this poses the difficulty that a modified R-index would also affect all vessels designed according to the SPS code, as the SPS code refers to the SOLAS 2009. In fact, the situation is quite complex. To come to possible solutions, the following two questions need to be answered:

- Is there still a need for considering water on deck for RoRo-Passenger vessels even in the frame work of the SOLAS 2009?
- If the first question is answered with “yes”, which possible options exist to improve the design of RoRo passenger ships?

Consequently, the present paper will deal with these two questions.

2. STABILITY OVERVIEW

In this chapter, we will discuss the influence of the existing different regulations on the design of RoRo-Passenger ships. This is necessary to understand if there is a need for the explicit treatment of water on deck or not.

2.1 Before 2009

Before 2009, the situation was quite clear: A RoRo- Passenger ship had to fulfil SOLAS 74/90 II-1/8 (deterministic approach) including permissible floodable lengths. If the ship was operated in Europe, it had also to fulfil Stockholm- Agreement, where the full compliance was obtained if the ship was designed for a significant wave height of 4m. Depending on the number of passengers, the ship had to withstand one or two compartment flooding. The damage length was defined as $0.03L+3m$, and the penetration depth was maximum $B/5$. The ship had to survive all possible damages within the prescribed damage extents. Due to the deterministic nature of the stability standard, not all possible damages could be included. Otherwise it would not have been possible to design a ship. Krueger and Dankowski [1] have analysed the amount of damages covered by the SOLAS 74/90 II-1/8, depending on the ship length L (see Fig. 1, green curve).

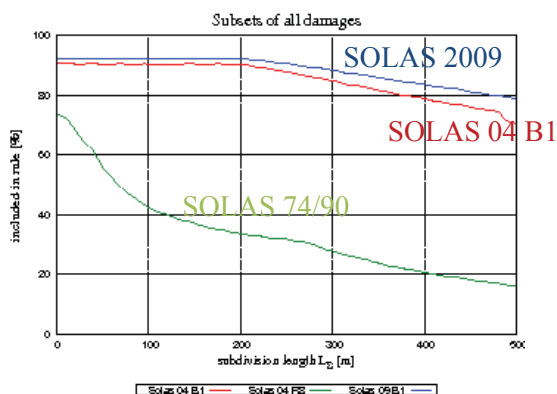


Figure 1: Percentage of possible damages covered by several damage stability standards. Green: SOLAS 74/90 II-1/8, 2- Compartment-Flooding.

If we assume that the HARDER- statistics represents all possible damages (100%), we can obtain from Monte- Carlo- Simulations the percentage of damages which are covered by e.g. SOLAS 74/90 II-1/8. Fig. 1 shows that for a 200m RoRo-Passenger ship, only abt. 35% of all possible damages are included, but the ship has to survive them all. Due to this circumstance, the ship has a hidden safety reserve, because it is well possible that the ship survives damages which are not in the scope of SOLAS 74/90 II-1/8. Despite these considerations, the situation was in principle quite clear for the designer, but there remained the following practical difficulties:

- The floodable length calculation was challenging when the ship was equipped with a long lower hold.
- The safety philosophy targeted on sufficient residual freeboard, at the same time it was not allowed to submerge the Margin Line. This made double hull designs/side casings (on the vehicle deck) not attractive, and the increased residual freeboard resulted in increased VCGs and all the related problems.

But as already pointed out, the overall safety level seemed to be sufficient.

2.2 Since 2009

The SOLAS 2009 has put forward a probabilistic damage stability assessment. As a consequence, more possible damages have to be investigated (blue curve in Fig. 1) compared to the previous deterministic standard, but not all of these damages have to be survived. The amount of damages which has to be survived strongly depends on the number of passengers on board, and slightly on the ship length (exactly: The required R- index). Now the number of passengers on board determines the safety level of the ship. It is well known that if a ship is only designed according to probabilistic principles, designs may be created

where a minor damage can lead to the total loss of the ship. Therefore, the SOLAS 2009 also contains a deterministic addendum which prohibits such designs. The damage assumptions of this deterministic addendum have been taken from SOLAS 74/90 II-1/8, but with a reduced maximum penetration of B/10 instead of B/5. If the ship has less than 400 persons, one compartment damage is assumed. This requirement must also be fulfilled by each ship complying with SOLAS 2009. If the ship shall operate in European waters, the Stockholm- Agreement must be additionally applied which results in B/5 damage penetration and the additional water on deck. This makes the design consideration more complicated and reduces the designer's flexibility. In the following we will discuss the problem further.

If we look at the SOLAS 2009 only, we have to fulfil two requirements: The probabilistic part and the deterministic addendum. The safety level of the probabilistic part strongly depends on the number of passengers, the deterministic part does not (except for the decision of one or two compartment flooding). It is now of utmost importance to understand which of the two elements of the SOLAS 2009 is the governing stability criterion: If the number of passengers is sufficiently high, the probabilistic part determines the safety level. On the other hand, if the number of passengers is small enough, the deterministic part of the SOLAS 2009 determines the stability. From some sample calculations we have made [1], one can roughly say that this number of passengers is about 1500. That means that for all RoRo-Passenger-Vessels with about 1500 or less passengers, the stability limit of the SOLAS 2009 is defined by the deterministic addendum (SOLAS 74/90 II-1/8, but B/10 penetration).

If such a design now needs to comply with the Stockholm- Agreement, the situation becomes at least challenging as this standard prescribes to survive all B/5 damages according to SOLAS 74/90 II-1/8. In such a

case, the safety of the ship is determined by the Stockholm- Agreement. In [1] we have developed a method to quantify the difference of the absolute safety levels of different damage stability standards, as an example see Fig. 2. Concerning the ship design this simply means that if a RoRo-Passenger ship with about 1500 Pax or less shall be designed to operate in European Waters, the designer simply needs to fulfil the Stockholm- Agreement. The SOLAS 2009 is then also fulfilled, maybe with small design changes.

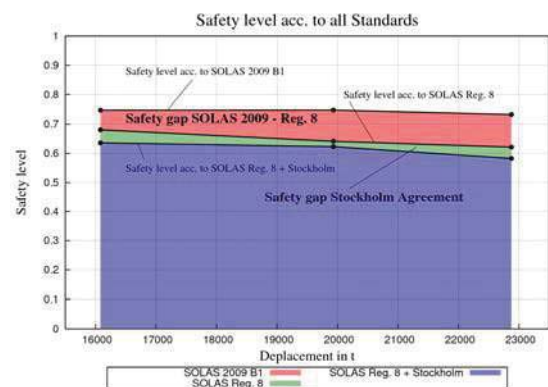


Figure 2: Determination of safety levels of different damage stability standards. Here: 1500 Pax, 200m RoPax with B/10 Lower Hold [1].

It has been in principle understood that there remains a problem in the SOLAS 2009 with passenger ships carrying a smaller number of passengers. This holds for all passenger vessels. Consequently there are ongoing discussions to possibly modify the R- index for smaller number of passengers. But the difficulty remains that all SPS ships might also be affected by such a modification.

On the other hand it became obvious that at least a rough treatment of the large vehicle decks of RoRo-Passenger should be included in the damage stability. A modification of the s- factor has been suggested, where the required righting lever h and the range of positive righting levers have been increased. However, one needs to remember that the s- factor is determined from a power of $1/4$, and thus small alterations of the required values are not effective. It is therefore questionable whether



this approach is a full compensation of the water on deck problem.

From all these findings, we can draw the following conclusions:

- There seems to be a necessity to improve the R- index for passenger ships with smaller number of passengers. This problem affects all passenger ships.
- It is not yet clear whether the modification of the s- factor is sufficient. This problem affects only RoRo- passenger ships.

What makes a solution extremely challenging is that both conclusions are coupled together: It may turn out that if a possible future R-value is conservative enough, there may be no need to explicitly include water on deck in the damage stability assessment. On the other hand one has to remember that a critical amount water on deck leads to a rapid capsize of the ship, and it is not certain in how far this failure mode is still in the scope of a possibly revised SOLAS 2009. Therefore, according to the opinion of the authors it makes sense to look for alternative possibilities to include a possible rapid capsize scenario due to a critical amount of water on deck in a stability regime. This could also help to separate problems which are only related to RoRo-Passenger ships from problems which are relevant for all types of passenger vessels.

2.3 General considerations

When we deal with the water ingress on a RoRo-Passenger ship vehicle deck, we automatically consider it as a damage stability problem. But is that really true? As a matter of fact, the bulkhead deck is the upper limit of the water tight subdivision, and all watertight bulkheads must be extended to this deck (with an exception of moveable bow ramps). Above the vehicle deck, the ship is typically weathertight, and it needs to be weathertight to fulfil the intact stability requirements. From a pure damage stability point of view, the

accumulation of water on deck could simply be avoided by arranging freeing ports, but then, the ship cannot fulfil the intact stability requirements. Consequently, the ingress of water on a vehicle deck means water ingress above the watertight subdivision on the freeboard deck (which is the bulkhead deck for a RoRo-Passenger vessel). Regardless how the water has entered into the vehicle compartment, we put forward the argument that we can formally treat water on the freeboard deck as a green water problem on the freeboard deck. This becomes more obvious if we take into account one event which can lead to a substantial accumulation of water on the vehicle deck, namely firefighting. In these cases (like AL SALAM BOCACCIO) the ship did not have a structural damage which lead to a water ingress. Although in other cases water entered on the vehicle deck due to structural damages (ESTONIA and HERAKLION), these damages were always above the watertight subdivision, affecting a weathertight superstructure. The same holds for the accidents of JAN HEWELIUSZ and HERALD OF FREE ENTERPRISE. These ships did also not experience a damage of the watertight subdivision. The same holds for the RoRo-Ferry investigated by Ikeda et. Al. during model experiments, where water was allowed to enter the vehicle deck through the open bow door [6]. The only exemption known to the authors is the EUROPEAN GATEWAY accident. This ship experienced a damage below the bulkhead deck. A large heel during an intermediate stage of flooding occurred, which resulted in progressive flooding of the vehicle deck and finally the ship capsized. This is indeed a typical damage stability accident, and the failure is well covered by the existing damage stability regime.

From these findings we can conclude that most of the accidents where water ingress on the vehicle deck played a major role are actually accidents where the ship did not formally experience damage to the watertight subdivision, but water entered on the freeboard deck of an intact ship. Due to the unique design



boundary condition of RoRo-Passenger vessels, no freeing ports can be arranged on the freeboard deck to allow the water to leave the deck. Consequently, this circumstance allows water to accumulate on the freeboard deck which is a potential threat to the safety of the ship. This situation is unique for RoRo-Passenger vessels, and needs according to our opinion a unique treatment. From these findings, the following arguments can be put forward:

- Due to the fact that most accidents with water on deck happened in an intact ship condition with respect to the watertight subdivision, this problem should be regulated by the intact stability regulations.
- Due to the unique design boundary condition of RoRo-Passenger vessels, the problem must be dealt with only for this specific ship type.

If once the argument is put forward to formulate an intact stability criterion for RoRo-Passenger ships, this has also the advantage that the water on deck problem can be completely decoupled from the current developments of the damage stability code.

With the above mentioned findings it becomes clear that there is always the risk that a critical amount of water may enter the vehicle deck on an intact RoRo-Passenger ship and will accumulate there. Consequently, a RoRo-passenger vessel must have the ability to withstand a certain amount of water on the vehicle in the intact condition. If this is once put forward, the following questions have to be answered:

- How much floodwater shall be assumed on the vehicle deck?
- How shall the stability requirements be validated?

If the first point has successfully been treated, the stability requirements could then simply be solved by taking into account the

stability reduction due to the free surface of the floodwater in the vehicle deck.

These questions will be answered in the following sections.

3. AMOUNT OF DESIGN WATER ON DECK

The first step of a possible intact stability criterion covering water on the vehicle deck must be the determination of a reasonable amount of water which is to be assumed on the vehicle deck. The Stockholm-Agreement relates this amount of floodwater to the residual freeboard to the bulkhead deck. The design philosophy behind this approach is that any water ingress into the vehicle compartment should be avoided as far as possible. This approach neglects the fact water ingress due to firefighting is independent from the position of vehicle deck. The same holds for the development of the so called “static equivalent method” (SEM), which was developed by Vassalos [2] as an improvement of the Stockholm-Agreement. To cover also the firefighting problem, an alternative approach needs to be developed.

In this context it helps to analyse the most important accidents where water on deck played a major role. All these accidents followed a comparable scheme: Due to different circumstances, water entered on the vehicle deck and started to accumulate there. The crew was not aware of the fact that the situation became dangerous, and they continued their operation. When the amount of water increased to a critical value, the crew detected that there was something wrong, but then it was already too late: The ship experienced a large heel, all the water on deck flew to one side and the situation was irreversible. Consequently, a criterion for a critical amount of water on deck shall try to avoid that the stability situation leads to an irreversible condition. The irreversibility of such conditions lies in the fact that the water

which has been accumulated in a quasi upright condition suddenly flows to one side when the initial stability becomes small or even negative. This circumstance has brought up the idea to analyse the roll period with water on deck. This can be done by a numerical roll decay test. We have used the nonlinear time domain seakeeping code E4ROLLS [3] to perform such calculations. Nafouti [4] has used this technique to analyse the alteration of the roll period of several RoRo-Passenger vessels where he has systematically varied the amount of water on deck. In the computations, the water on the vehicle deck is modelled by shallow water equations according to Glimm's method [5] and it is allowed to flow freely on the vehicle deck. The method is also able to take into account the blockage of the flow due to a centre casing. The roll motion can be initiated by a non-zero roll speed at the upright condition. From the computed time series, the roll period can be determined.

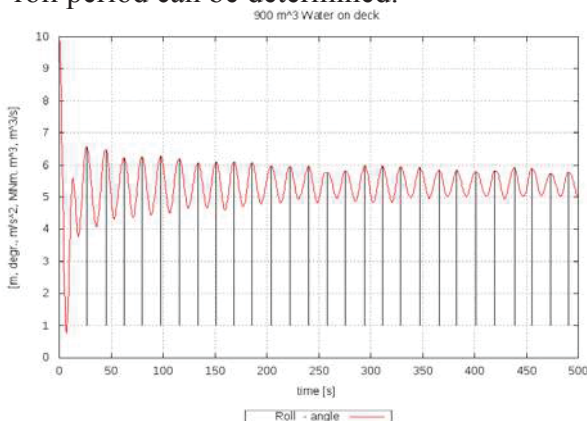


Fig. 3: Numerical roll decay test with 900m³ water on deck of the RoPax Ferry EMSA2 [4],[1].

The principle is shown in Fig. 3. The figure shows the time plot of the roll angle of the RoPax- Ferry EMSA2 [1] with 900m³ water on the vehicle deck. When the roll motion is excited by an initial disturbance, the ship gradually oscillates around the final static equilibrium. The roll period with water on deck can then simply be determined by counting the peaks. When the amount of water on deck is systematically varied, the alteration of the roll period can be determined as a function of the amount of water on deck. This has been done

for twelve different RoRo-Passenger ship configurations. In the beginning, a centre casing was not considered. The results were quite interesting, and two of them are presented in figures 4 and 5.

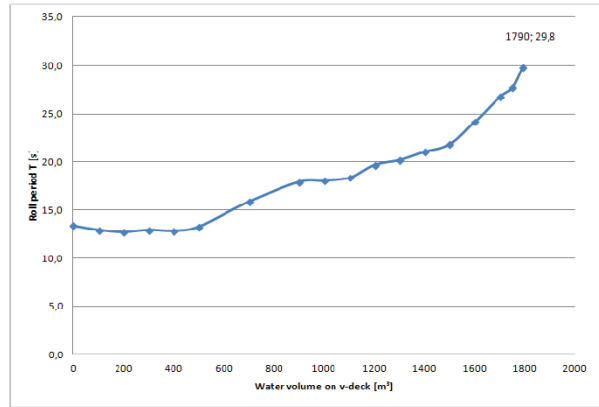


Figure 4: Alteration of the roll period as a function of the amount of water on the vehicle deck for the RoPax EMSA1 [1].

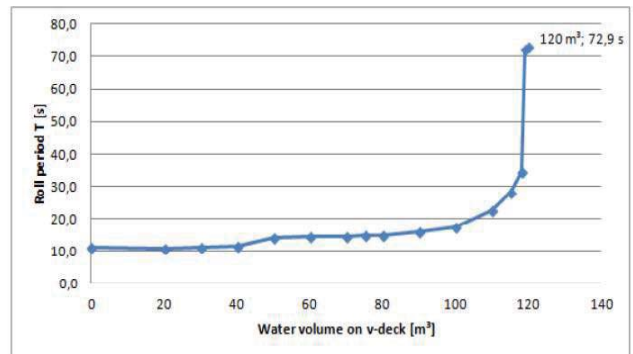


Figure 5: Alteration of the roll period as a function of the amount of water on deck, for the RoPax EMSA2.

The figures show the development of the roll period of two RoRo-Passenger vessels as a function of the water volume on deck. This has been increased until the ship reached a large heel of 30 Degree or more during the computation. This critical volume is also indicated in the figures. For smaller volumes the results show that the roll period changes slightly, and the gradient of the curve becomes steeper towards the final capsizes. This can be nicely observed in Fig. 4. This general trend was found for all ships analysed. Fig. 4 leads to the idea that a doubling of the roll period due to



the influence of water on deck can be taken as a first idea to determine the minimum amount of water on deck the ship has to withstand: There is still a good safety margin from the doubling of the roll period to the final capsizing, and a substantial amount of water is required to actually double the roll period. Therefore we have chosen the doubling of the roll period in a numerical roll decay test to determine an amount of water which could be used for the stability evaluation in a later step (such change of the roll period can also be observed by officers and crew). We have checked this relation for other RoRo-Passenger ship designs and came to similar conclusions.

But this criterion alone is not sufficient: If for example a wide double hull would be fitted onto the vehicle deck, it will not be possible to double the roll period with reasonable amounts of water on deck. Therefore, we need a second criterion which limits the design amount of water on deck in case a doubling of the roll period cannot be achieved. From our investigations (with indeed a limited number of designs) it seemed to be most promising to limit the amount of water on deck to 6% of the total displacement. This gave the best agreement with the numerical computations. Then it finally boils down to the following procedure to determine the design amount of water on deck:

Determine the amount of water on deck which leads to a doubling of the roll period.

Determine 6% of the total displacement and take the smaller value of both evaluations.

A special consideration is required for centre casings: A centre casing has no influence on the hydrostatics of the floodwater, but it prohibits the free flow on the vehicle deck. Consequently, a larger amount of water is required to double the roll period when a centre casing is fitted. From a safety point of view, this is correct, because according to the authors' opinion, the centre casing bears an additional risk: If the water accumulates on a

vehicle deck with a centre casing, the floodwater dynamics lead to a less severe alteration of the ship's motion, and the crew has reduced chances to detect that the situation is potentially dangerous. According to our basic assumptions this means that more water on the deck will be accumulated as without a centre casing. When the ship then begins to list, all the floodwater flows irreversibly to one side and the centre casing becomes irrelevant. Consequently, long centre casings could make the situation potentially more dangerous, and this would require a larger amount of water on deck to be considered during the design. Such behaviour is exactly demonstrated by the computations of the numerical roll decay tests. But this means that also the limiting value of the amount of water on deck needs to be corrected for the presence of a centre casing. We have performed all calculations for configurations with and without centre casing, and the length of the casings was systematically varied [4]. From the comparison of the different numerical results we suggest the following relation for the minimum amount of water which should be considered on the vehicle deck:

$$V (T=2T_0) [\%] = 6 [\%] + 3.75 (L_{\text{Casing}}/L_{\text{Deck}}) [\%]$$

Here, V is the design volume of water on deck as percentage of the total displacement, L_{Casing} denotes the overall length of the centre casing and L_{Deck} is the length of the vehicle deck. However, one needs to take into account that due to the limited number of designs we have analyzed, this relationship may be seen as a first rough guess.

This design amount of water on deck is now used to carry out calculations of the static lever arm curves.

4. STABILITY CRITERIA

The design amount of water on the vehicle deck which has been determined by a.m.

procedure is now used to carry out computations of the static righting lever. The volume is kept constant and the ship (including the water) is allowed to trim freely. The principal shape of such a righting lever curve is shown in Fig. 6.

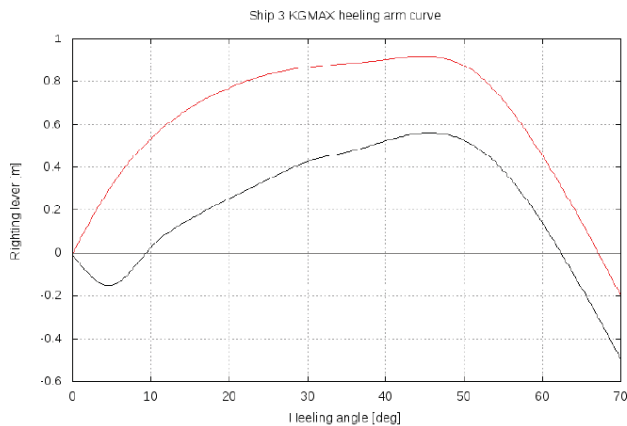


Figure 6: Righting lever curves of the intact condition (red) and with the design volume of water on deck (black) according to section 4.

Figure 6 shows the comparison of the righting lever curve for the intact condition (red) and the remaining stability when the design amount of water on deck is applied. For this particular righting lever curve stability criteria need to be developed. These criteria should be close to criteria which are already in use. They should be of the following type:

- The static equilibrium should be limited to a certain value (taking into account limitations for possible evacuation).
- The negative area under the righting lever curve should be limited in relation to the positive residual area under the righting lever curve to avoid capsizing when the ship swings over to the other side.
- There should be a requirement for the maximum lever and for the area below the righting lever curve.

These kinds of criteria are principally known from other IMO- instruments. The question is now to find reasonable minimum values.

One possible approach to set up the limiting values is that the safety level of a RoRo-Passenger ship according to the newly proposed criterion shall be equivalent to the existing safety level. For most of the ships we have analyzed, the safety level was determined by the Stockholm- Agreement. Only the two ships EMSA1 and EMSA2 did not comply with the Stockholm Agreement. For our investigations, they were additionally fitted with a double hull on the vehicle deck until they were compliant with the Stockholm Agreement. All our ships were then evaluated by the described procedure. If all Stockholm Agreement - compliant ships should pass the newly developed criterion, the following stability values need to be obtained including the design amount of water on the vehicle deck:

- The static heel should be limited to 12 Degree.
- The area under the righting lever curve from the equilibrium to the angle of no return or possible progressive flooding must be three times larger compared to the (negative) area under the righting lever curve from 0 to the equilibrium.
- The maximum righting lever should be 0.2m or more.
- The area under the righting lever curve from the equilibrium to 30 Degree should be 55mmrad or more.

These are reasonable values which are close to those used by the Intact Stability Code 2008. According to our investigations, a RoRo-passenger ship which fulfils these requirements including the design amount of water on the vehicle deck has an equivalent level of safety with respect to water ingress on the vehicle deck as a ship which fulfils the Stockholm-Agreement damage stability standard. Therefore our approach seems to offer a reasonable alternative to cover water on vehicle decks by keeping the existing safety level without the necessity of including this problem in the damage stability regulations.



5. SHIPS INVESTIGATED

The following table summarizes the most important data of the RoRo- Passenger ships. Design alternatives of the basic designs were created by adding additional double hulls and/or center casings of different lengths.

S hip	L	P ax	Lower Hold	Doub.H ull
1	8 0	3 00	No	No
2	2 00	6 00	Yes	No
3	1 50	6 00	No	No
4	1 60	1 600	No	No
5	1 15	6 50	No	Yes
6	1 65	1 500	No	No

The ships 3,4,5 and 6 fulfill the Stockholm-Agreement Standard, the Ships 1 and 2 did not. In our investigations they were made with the Stockholm- Agreement by fitting a double hull on the vehicle deck.

6. CONCLUSIONS

An alternative method was presented which covers the effect of entrapped water in the vehicle deck of a RoRo- Passenger ship on the stability. In contrary to the existing stability standards, our method treats the problem as an intact stability problem. This is justified by the fact that in the relevant accidents, no damage below the bulkhead deck occurred. Further, the newly proposed method covers water

accumulation due to fire fighting. As a first step of the analysis, a design amount of water on the vehicle deck needs to be determined. This can be obtained by the calculation of the roll period, and the design water volume is reached when the roll period takes twice its initial value. If this cannot be achieved, the design water volume is limited. A centre casing is accounted for by an increased design water volume. Static lever arm curves can be calculated including this amount of water on deck, and stability criteria have been proposed which ensure a lever of safety which is equivalent to the Stockholm Agreement. The method is in principle straight forward and quite simple. But it should be further developed: Instead of performing numerical roll decay tests, it could also be possible to establish a relation between hydrostatic parameters of the righting lever curve including water on deck and the resulting roll period, although this might be challenging for the centre casings. And the proposed criteria need further evaluation due to the fact that we investigated a limited number of designs only.

7. ACKNOWLEDGEMENTS

Part of this research has been funded by the German Federal Ministry of Economics and Energy in the framework of the research project LESSEO. Without this funding, this project would not have been possible.

8. REFERENCES

- Valanto, P., Krüger, S., Dankowski, H.: Research for the Parameters of the Damage Stability Calculation including the Calculation of Water on Deck of Ro-Ro Passenger Vessels for the amendment of the Directives, 2003/25/EC and 98/18/EC. HSVA- Report No. 1669, Hamburg, 2009
- Vassalos, D. et al: SEM- Static Equivalent Method- Background and Application. The Ship Stability Research Centre, University



of Strahclyde, Glasgow, UK, June 2000.

Kröger, P.: Simulation der Rollbewegung von Schiffen im Seegang. Report 473, Hamburg University of Technology, Hamburg, Germany, February 1987.

Nafouti, O.: Development of an Intact Stability Criterion for RoRo-Passenger Ships against Capsizing due to Trapped Water on Vehicle Deck. Hamburg University of Technology, Report A-55. June 2014

Glimm, J.: Solutions in the Large for Nonlinear Hyperbolic Systems of Equations. Commun. Pure Appl. Math, 18:697-715,1965

Shimizu, N., Roby, K., Ikeda, Y.: An experimental study on Flooding into the Car Deck of a RORO Ferry through Damaged Bow Door. J. Kansai N.A., Japan, No. 225, March 1996

This page is intentionally left blank



The Impact of the Inflow Momentum on the Transient Roll Response of a Damaged Ship

Teemu Manderbacka, *Aalto University, School of Engineering, Department of Applied Mechanics*

teemu.manderbacka@aalto.fi

Pekka Ruponen, *Napa Ltd* pekka.ruponen@napa.fi

ABSTRACT

Dynamics of an abrupt flooding case are studied by comparing fully dynamic and quasi-static flooding simulation methods. Transient asymmetric flooding is traditionally modelled by dividing the compartment into smaller parts with bulkheads representing different obstructions in the flooded compartment. The implications of this assumption are studied by varying the size of the opening on the dividing bulkhead. The importance of the inflooding jet to the response is shown. The jet i.e. the inflooding momentum flux is modelled as force acting on the lumped mass. When the flooded compartment does not have significant obstructions it is important to account for the inflooding momentum flux.

Keywords: *damage stability; dynamic simulation; transient flooding*

1. INTRODUCTION

Collision or grounding can cause a large opening on the ship hull. An abrupt flooding may lead to ship capsizing at the intermediate stages of flooding (*Spouge, 1985*). The roll response to an abrupt flooding is a complex problem. The geometry of the flooded compartment and the damage affect the flooding. The flooding process consists of the inflow, floodwater motions and its progression (*Khaddaj-Mallat et al., 2011*). These, in turn, are all affected by the ship motions. The ship response and the flooding process are coupled.

The inflow phenomenon is governed by the inflooding jet. The obstructions in the flooded compartment affect the propagation floodwater and the ship response (*de Kat and van't Veer, 2001; Ikeda et al., 2003*). As shown for example in the experiments of *Manderbacka et al., (2015b)*. In the beginning of the flooding a dam-breaking type jet ingress the damaged compartment. When the opening is relatively

large, the jet can push floodwater to the opposite side of the opening. As the jet meets the opposite wall in the compartment a water run-up on the wall takes place. This run-up creates a breaking wave on the wall. The jet is partly reflected from the wall and can create a reflected wave propagating back towards the opening side. As a consequence, the sloshing of the floodwater is created.

The inflow jet had been observed to play an important role in case of an undivided compartment. The ship can roll to the opposite side of the damage. In this case, the opening can be lifted above the sea surface and the inflow can be stopped (*Ikeda and Ma, 2000; Ikeda and Kamo, 2001*). The inflooding jet can be slowed down in case of a compartment with obstructions. In these cases, a quasi-static modelling of the flooding may be sufficient. The transient asymmetric flooding of symmetrical compartments has traditionally been modelled by dividing the compartment into smaller parts with bulkheads representing



different obstructions e.g. the main engines in the flooded compartment, Santos *et al.* (2002) and Ruponen *et al.* (2009). If the size of the connecting opening between the parts is large, the dynamics of the floodwater may still be significant. In this paper the implications of this assumption are studied by varying the size of the opening on the dividing bulkhead.

This work aims to study the impact of the inflow momentum on the roll response for different damaged compartment layouts. Here a calculation method described in Manderbacka *et al.*, (2015a) based on the lumped mass motions is applied (Spanos and Papanikolaou, 2001; Jasionowski, 2001; Valanto, 2008) The ship and flooded water motions are fully coupled and simulated in the time domain. The rate of change of the momentum due to the inflooding water (inflow momentum) is accounted for.

The impact of the inflow momentum is studied for different damaged compartment layouts for an abrupt large flooding. The response to transient flooding is simulated for undivided and divided compartments. The divided compartments have non-watertight divisions allowing but limiting the cross-flooding. A systematic variation of flooded space arrangements is realized. Size of the damage and internal opening in the divided compartment are varied. The limits of the flooded compartment geometry (size and divisions) where the inflow momentum should be accounted for and where the quasi-static simulation is sufficient are studied.

2. METHODS

Ship motions are modelled as a rigid 6 d.o.f motions. Hydrostatic forces acting on the ship hull are integrated over the actual wetted surface. Hull surface is presented with triangular panels.

Radiation forces are divided on the added mass and potential damping parts. The added

mass and damping matrices are assumed to be constant, they are pre-calculated for the ship with the potential theory based strip method code (Frank 1967).

All the equations of motion are written in the ship fixed coordinate system \mathbf{xyz} , which is fixed to the intact ship center of gravity *cog*. Ship angular position is expressed in modified Euler angles. The inertial \mathbf{XYZ} and ship fixed coordinate system and its orientation is shown in Figure 1.

Flooded water is modelled in each flooded room as a lumped mass concentrated on its center of gravity. The floodwater surface is assumed to stay plane but is free to move (Jasionowski, 2001; Spanos and Papanikolaou, 2001; Valanto, 2008). Position of the lumped mass in ship fixed coordinate system \mathbf{r}_i is a function of the lumped mass m_i and the angle of the free surface ϕ_i Figure 2. The flow through the opening is modelled with the hydraulic model based on Bernoulli equation (Dillingham, 1981; Ruponen, 2007). In/outflow jet i.e. the inflow momentum flux is accounted for as a force acting on the lumped mass (Manderbacka 2015a). Energy dissipation in the motion of the floodwater due to the viscous effects is modelled as a friction force acting on the lumped mass (Manderbacka *et al.*, 2014).

Equations of motion for the ship and the lumped mass are combined into one system with $6 + n$ d.o.f, where n is number of flooded rooms. Position of the ship and floodwater are solved time integration applying fourth order Runge-Kutta scheme. Simulations performed with the presented method are denoted as **sim**. The impact of the inflow momentum on the roll response was studied by simulating the cases also without accounting for it. The simulations where the inflow momentum flux is eliminated are denoted as **sim no fdm**.

In order to compare different methods of predicting the ship response to an abrupt flooding quasi-static flooding simulation was also performed. In addition to the dynamic

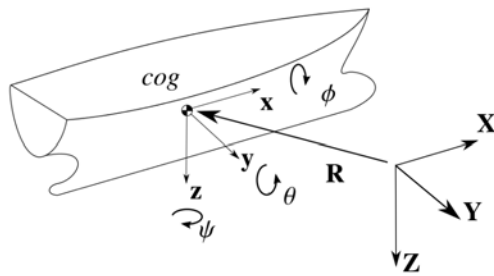


Figure 1. Ship coordinate system.

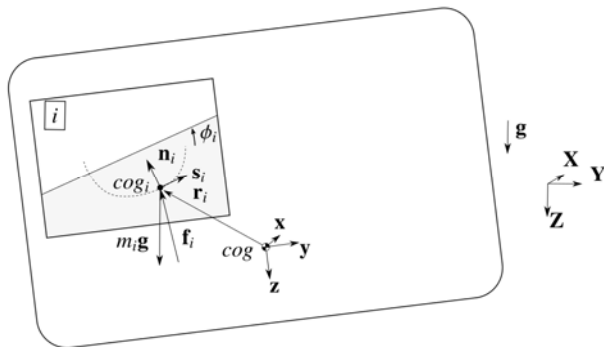


Figure 2. Model for the motions of the lumped mass with a moving free surface (Manderbacka et al., 2015a).

simulation described above (where the flooded water sloshing is simulated by a lumped mass with a moving free surface method) the ship response was simulated with NAPA software quasi-static flooding simulation (Ruponen et al., 2007). Quasi-static NAPA simulations are denoted as **NAPASTa**. One degree of freedom model, where the roll motion is modelled is added to NAPA quasi-static flooding simulation. This model is denoted as **NAPAdyn**, where the linear equation of roll motion is solved. Linear roll damping is applied. Draft and trim are treated as quasi-static.

2.1 Validation

The lumped mass with a free moving surface method was validated against the measurement data (Manderbacka et al., 2015a). Transient flooding of the Box shaped barge model was measured by (Manderbacka et al., 2015b). The same model was used for the ITTC benchmark study on the progressive

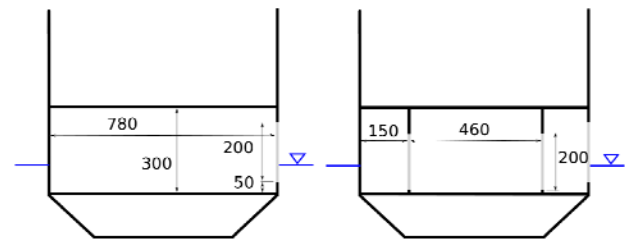


Figure 3. Box shape barge flooded undivided compartment (on left) and divided compartment (on right).

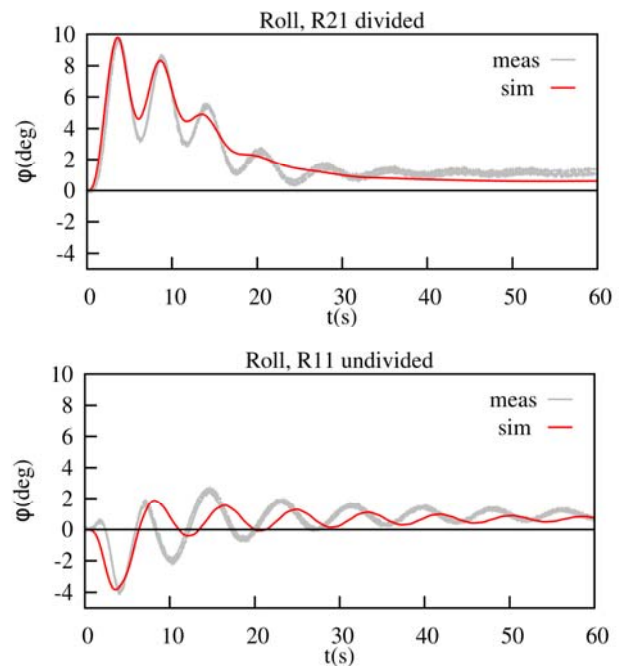


Figure 4. Measured and simulated roll response to abrupt flooding of Box shaped barge. Undivided compartment (above) and divided compartment (below) (Manderbacka et al., 2015a).

flooding (van Walree and Papanikolaou, 2007). Load case and damage opening was modified compared to the progressive flooding tests. Two different compartments were flooded separately, undivided and divided compartment Figure 3. Both compartments were of same size. The divided compartment had two longitudinal bulkheads with narrow and tall openings (20 mm wide and 200 mm high). The breach on the starboard side was 200 mm x 200 mm square opening. In the measurements for the undivided compartment, the model experiences largest roll on the opposite side of the breach, on portside, while for the divided compartment flooding the

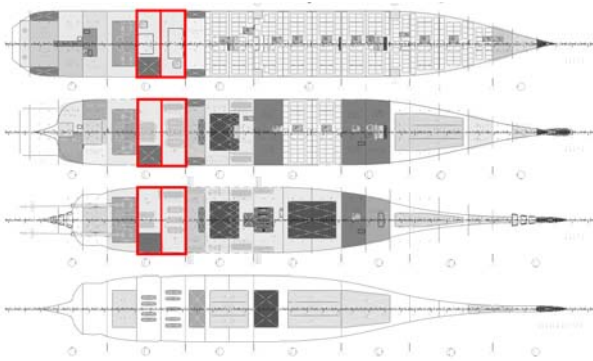


Figure 5. Ship general arrangement and engine room compartments.

model rolled on the breach side, on starboard. The maximum roll angles are well predicted by the presented simulation method Figure 4.

3. CASE STUDY

Case study was performed on the Floodstand Concept Ship A. The ship is a Post Panamax cruise ship with size of 125 000 GT. It is designed for world-wide cruises with capacity of total 5600 persons on board. The design of the vessel shall fulfil relevant international rules and regulations (*Kujanpää and Routi, 2009*). Main particulars of intact Concept Ship A are presented in Table 1. In this flooding case study engine rooms 1 and 2 are flooded, Figure 5. Hull is presented by 6508 triangular panels, Figure 6. Water density in the simulations was 1025.0 kg/m^3 and gravitational acceleration 9.807 m/s^2 .

Table 1: Ship main particulars.

Length L_{oa}	327.0 m
Length L_{pp}	300.7 m
Breadth B	37.4 m
Draft T	8.1 m
Displacement Δ	63823 t
Initial stability GM_0	1.9 m
Height of CoG KG	19.2 m
Roll radius of gyration	
$k_{xx} (= 0.42B)$	15.708 m
Pitch and yaw radii of gyration	
$k_{yy} = k_{zz} (= 0.26L_{pp})$	78.182 m
Roll natural period T_ϕ	26.2 s
Roll damping factor ξ	0.027

3.1 Damage Case

The layout of the damaged compartments is simplified. Compartments are prismatic tanks with permeability of 1.0 each. The locations of the center of the compartment bottom and compartment dimensions are listed in Table 2. The engine blocks are not included in the compartments in the simulations. Instead the obstructing effect of the engine blocks is modelled by a non-watertight longitudinal bulkhead in the middle.

External hull breach height ranged over the height of the compartment. Four different breach widths L_B are introduced. The breach width for the biggest breach is equal to the compartment length $L_B=L_R$. Then the breach width is reduced to half $L_B=L_R/2$, then $L_B=L_R/4$ and finally smallest breach width $L_B=L_R/8$ is used. The breach is located on the starboard side. The simulation is performed in calm water. Initially ship is at even keel. The hull breach is introduced in the beginning of the simulation. Hull breach is presented as a line opening shown in Figure 6.

The undivided compartment cases were simulated with above mentioned four different breach widths. In addition to the undivided cases, simulations were performed for divided engine room compartments, Figure 7. The engine room compartments were divided by a non-watertight longitudinal bulkhead. The opening height on the longitudinal bulkhead was equal to the compartment height. The opening width L_O was varied. Four different opening widths were used; largest opening width was equal to the compartment length $L_O=L_R$, then $L_O=L_R/2$, $L_O=L_R/4$ and the smallest opening width was $L_O=L_R/8$ of the compartment length. Largest opening on the bulkhead corresponds to the undivided compartment case. The difference in the simulation in comparison to the undivided case is that the engine room compartment is divided into two spaces with an opening between the starboard and portside space ranging over the entire compartment height and length.

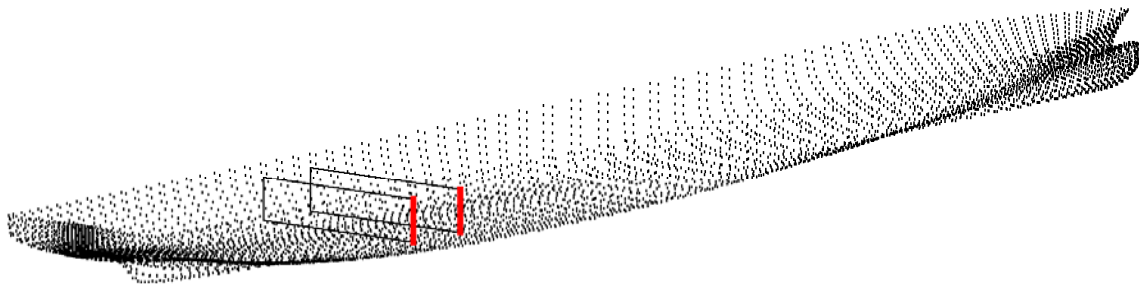


Figure 6. Hull panels. 6508 triangular panels and a 2D representation of the flooded engine room compartments with breach on starboard side.

Altogether 16 different configurations of the flooded compartments with four different breach and four different opening widths were simulated Figure 7. Breach and the opening had discharge coefficient $C_d=0.6$. The case $L_O=L_R$, where the divided compartment had the largest opening, was also simulated with the discharge coefficient value $C_d=1.0$.

Table 2. Flooded compartments.

compartment 1, engine room closer to aft		
x1, from aft PP	70.115	m
y1, from CL	0.0	m
z1, bottom height from keel	3.2	m
room 1 length	13.65	m
room 1 breadth	37.4	m
room 1 height	8.4	m
compartment 2, engine room closer to bow		
x2, from aft PP	83.89	m
y2, from CL	0.0	m
z2, bottom height from keel	3.2	m
room 2 length	13.9	m
room 2 breadth	37.4	m
room 2 height	8.4	m

Table 3. Damage opening.

breach to room 1		
discharge coeff. C_d	0.6	
opening height	8.4	m
breach to room 2		
discharge coeff. C_d	0.6	
opening height	8.4	m

4. RESULTS

4.1 Undivided Compartment

Total floodwater volume in the undivided compartments is calculated with simulation where the inflow is taken into account, **sim** in Figure 8. and without taking the inflow momentum into account with presented simulation method and with NAPA quasi-static flooding simulation, **sim no fdm** and **NAPasta** in Figure 8. The compartment is symmetrical and the ship initial metacentric height stays positive in flooded case so no roll motion occurs when in-flooding momentum is not taken into account. Total floodwater volume is simulated with NAPA until the equilibrium stage is reached.

With simulations accounting for the inflow momentum, the ship experiences roll on the portside i.e. the opposite side of the damage. At biggest opening, the ship experiences smallest transient roll (approx. 6 degrees) The transient roll is increased when the opening size is reduced to half (approx. 8 degrees). Highest transient roll (approx. 9 degrees) is experienced at the opening width 1/4 of room length, Figure 9.

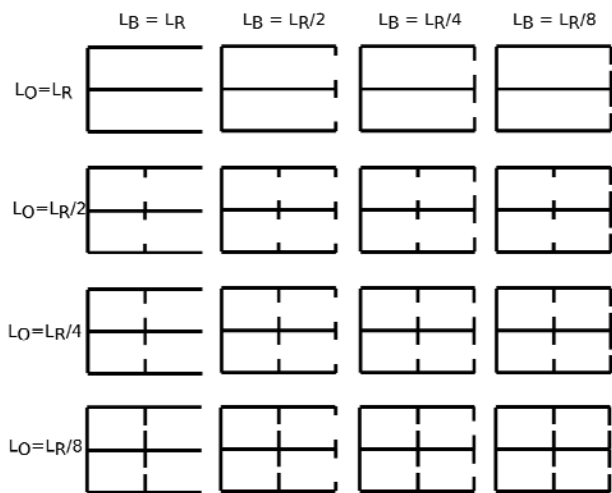


Figure 7. Configurations of flooded compartments (viewed from above) at different breach L_B and opening L_O widths. Breach is on the starboard side.

The maximum floodwater volume is attained fastest with the biggest opening, around 15 seconds after the damage. The time to attain the maximum floodwater volume is roughly doubled always when the opening size is halved.

The transversal y position (positive towards starboard) of the floodwater center of gravity is shown in Figure 10. With the biggest opening the motion of the floodwater center of gravity is more limited due to bigger volume than in case of smaller openings.

4.2 Divided Compartment

The biggest roll in case of the undivided compartment flooding was reached when the breach width was one fourth of the compartment length. Here both engine compartments are divided in the middle by the longitudinal non-watertight bulkhead. Four different opening widths were introduced to the dividing longitudinal bulkhead in the center line. Opening width was varied from compartment length to one eighth of the compartment length. The biggest opening corresponds to a situation where the whole longitudinal bulkhead is open i.e. the division

into two rooms in this case is virtual. This case is simulated with two different discharge coefficient values, one for no pressure loss $C_d=1.0$ and the other with same discharge coefficient as in the breach $C_d=0.6$. Other opening widths were simulated with the discharge coefficient $C_d = 0.6$, the same value

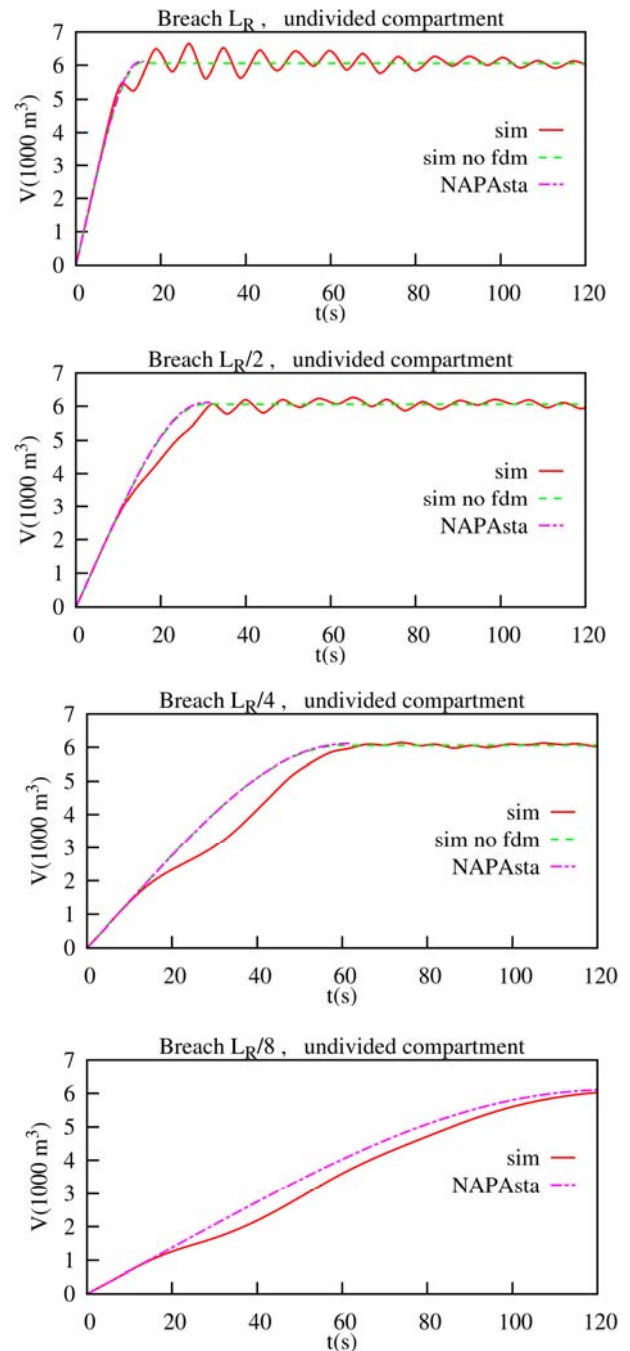


Figure 8. Total floodwater volume. Undivided compartment flooding case at four different breach widths.

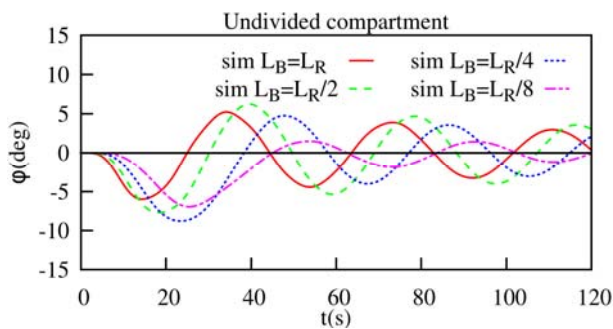


Figure 9. Roll in the undivided compartment flooding case at four different breach widths.

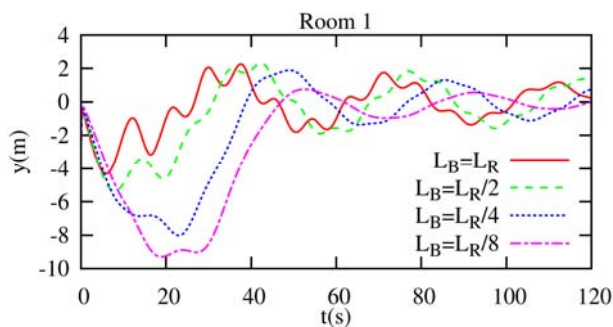


Figure 10. Transversal position of the floodwater center of gravity with different breach widths.

was used for the breach. These cases with breach width $L_B=L_R/4$ were simulated with presented simulation method including **sim** the inflow momentum flux, without the impact of the inflow momentum flux **sim no fdm** and with NAPA quasi-static and dynamic roll motion models, **NAPasta** and **NAPAdyn**, respectively. The total floodwater volume for these cases is shown in Figure 11 and roll response in Figure 12. When the opening width of the dividing bulkhead is biggest the results between the methods vary the most. At biggest opening $L_O=L_R$ with the discharge coefficient $C_d=1.0$ the result of the simulation with undivided compartment is also shown in the figures of volume and roll time histories. In this case the presented simulation method with inflow momentum flux predicts approximately 5 degree roll on the opposite side of the damage. The simulation with undivided compartment predicts even bigger roll angle. The flooding is also slower with **sim** calculation due to the roll on the opposite side of the damage.

When the opening width is reduced the presented simulation method predicts the first roll on the damage side. Reducing the opening width increases the roll angle on the damage side with all the simulation methods. When the opening width is smallest $L_O=L_R/8$ the results between different methods correspond quite well to each other. Results of the fully quasi-static simulation **NAPasta** differ the most from the other methods.

4.3 First Maximum Roll Angle

A summary of the first maximum roll angle for four different breach widths is shown as a function of the opening width in Figure 13. The opening width L_O is made proportional to the breach width L_B . In most of the cases ship experiences the first roll angle on the damage side. In fact the quasi-static simulations and the simulations where the inflow momentum flux is not accounted for predict the first roll on the damage side in all cases. The dynamic simulation for divided compartments with the inflow momentum flux accounted for predict first maximum roll on the opposite side or close to zero when the opening is four times wider than the breach. When the opening width is reduced, the first roll on the damage side increases and its value predicted by all the methods gets closer.

The case where the opening reached over the whole compartment was calculated as one undivided compartment. The simulations with undivided compartment predict the first roll on the opposite side of the damage at all breach widths Figure 9. When the breach side is reduced the simulation **sim** with divided compartment gets closer to the results of the undivided compartment simulations Figure 13.

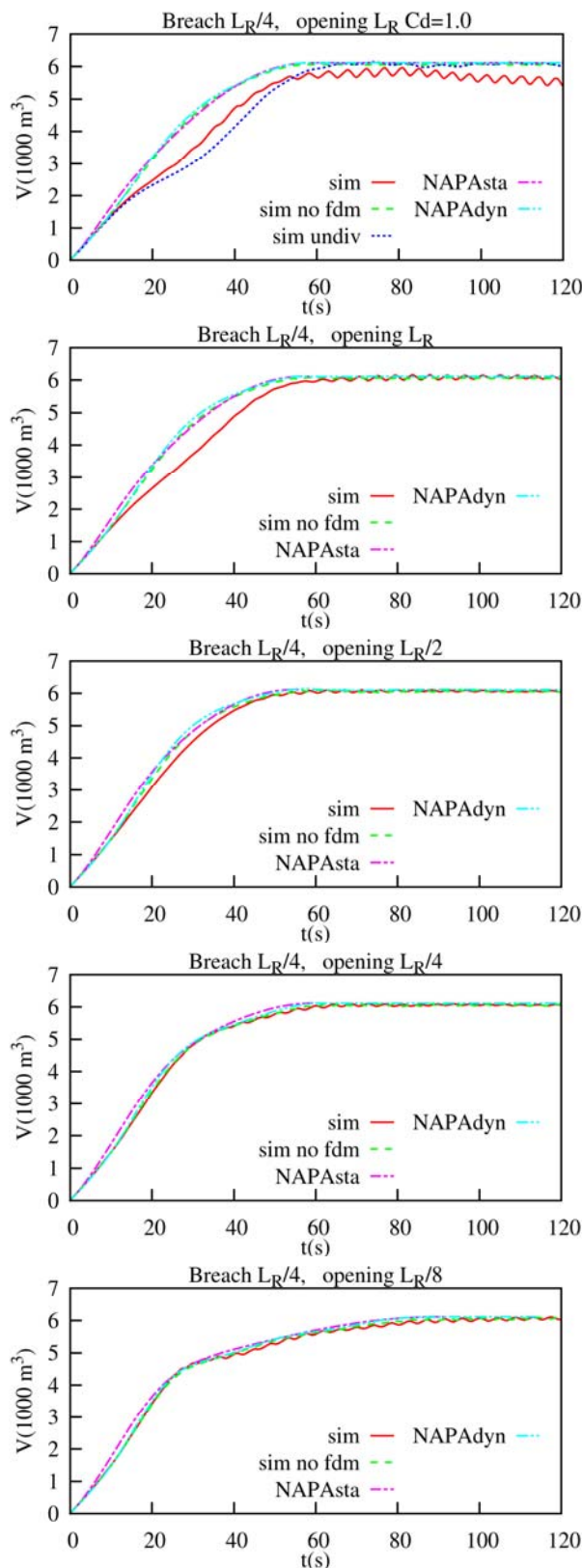


Figure 11. Total floodwater volume. Divided compartment with five different bulkhead openings. . Breach width is $L_R/4$.

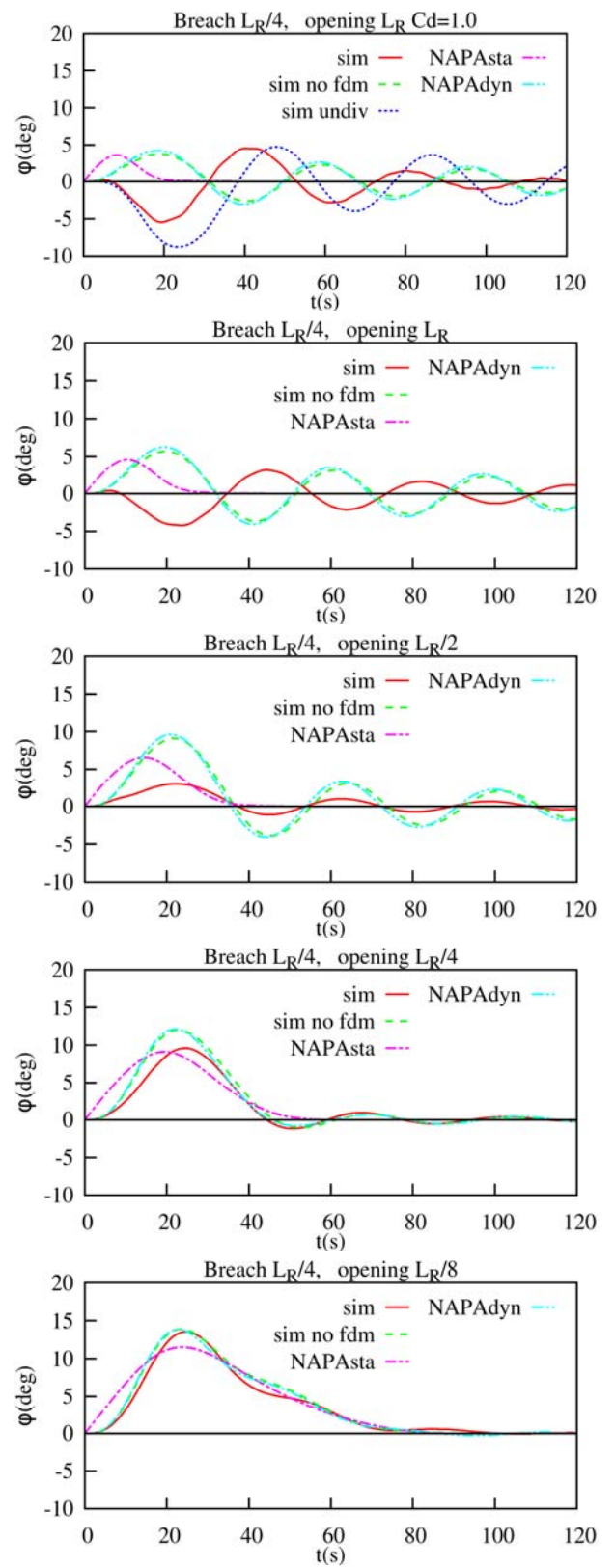


Figure 12. Roll motion. Divided compartment with five different bulkhead openings. Breach width is $L_R/4$.

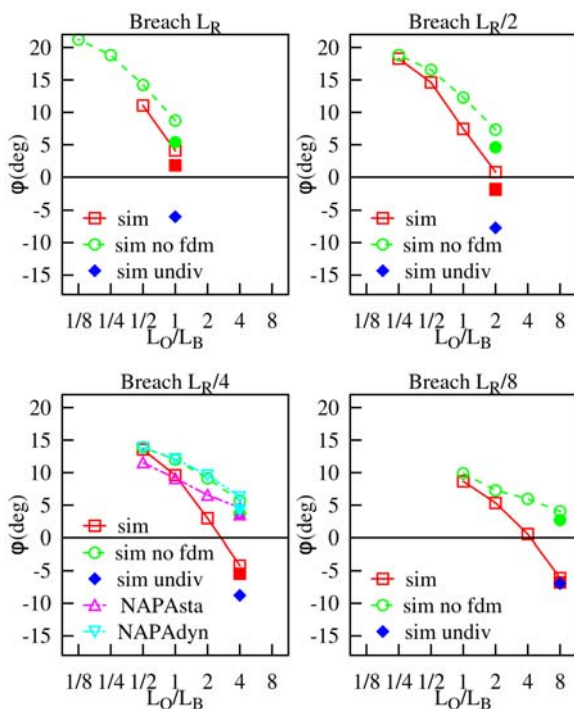


Figure 13. First roll angle for different breach widths as a function of opening width per breach width. Filled red square and filled green circle are **sim** and **sim no fdm** with opening $C_d=1.0$.

5. DISCUSSION

For divided compartments, where the opening on the dividing wall is small, all the methods give quite similar results. The flooding is asymmetric and the cross flooding is slow. The water motion inside the smaller compartment does not affect the roll response and it is sufficient to simulate the flooding with a quasi-static simulation method. When the width of the opening on the dividing longitudinal bulkhead is increased, the results between the methods start to deviate from each other. Different methods do not even agree on the direction of the initial roll angle. The inflooding water can be pushed fast on the opposite side of the breach when the compartment is undivided or the opening on the dividing bulkhead is sufficiently wide. In this case the quasi-static methods or calculation, which do not account for the inflooding momentum flux and thus are not

modelling the inflooding jet, cannot predict the initial roll on the opposite side.

6. CONCLUSIONS

Abrupt flooding cases to an undivided compartment with four different breach sizes and flooding cases to divided compartment at one breach size were simulated with four different methods; Dynamic flooding simulation with lumped mass method with a moving free surface with and without the inflow momentum flux and a totally quasi-static simulation and quasi-static simulation with one degree of freedom were applied.

Presented case and simulations give insight to the significance of the assumptions when predicting the transient flooding response. The importance of the inflooding jet to the response is shown. When the opening on the dividing bulkhead is small compared to the breach, i.e. the obstructions in the compartment are significant, the assumption of quasi-static simulation is sufficient. Conversely, the bigger the opening is on the bulkhead compared to the breach i.e. there are not significant obstructions in the compartment, accounting for the inflow momentum flux becomes more important.

7. ACKNOWLEDGMENTS

Aalto University, School of Engineering and City of Turku, MERIDIEM Maritime Innovation Hub are greatly appreciated for the financial support.

8. REFERENCES

- de Kat, J. O., van't Veer, R., 2001. Mechanisms and physics leading to the capsizing of damaged ships. In: Proceedings of the 5th International Ship Stability Workshop. Trieste, Italy.
- Dillingham, J., 1981. Motion studies of a



- vessel with water on deck. Marine Technology 18 (1), 38–50.
- Frank, W., 1967. Oscillation of cylinders in or below the free surface of deep fluids. Tech. Rep. 2375, Naval Ship Research and Development Center, Washington, DC.
- Ikeda, Y., Kamo, T., 2001. Effects of transient motion in intermediate stages of flooding on the final condition of a damaged PCC. In: Proceedings of the 5th International Ship Stability Workshop. Trieste, Italy.
- Ikeda, Y., Ma, Y., 2000. An experimental study on large roll motion in intermediate stage of flooding due to sudden ingress water. In: Proceedings of the 7th International Conference on Stability of Ships and Ocean Vehicles. Launceston, Australia, 270–285.
- Ikeda, Y., Shimoda, S., Takeuchi, Y., 2003. Experimental studies on transient motion and time to sink of a damaged large passenger ship. In: Proceedings of the 8th International Conference on Stability of Ships and Ocean Vehicles. Madrid, Spain, pp. 243–252.
- Jasionowski, A., 2001. An integrated approach to damage ship survivability assessment. Ph.D. thesis, University of Strathclyde.
- Khaddaj-Mallat, C., Rousset, J.-M., Ferrant, P., 2011. The transient and progressive flooding stages of damaged ro-ro vessels: A systematic review of entailed factors. Journal of Offshore Mechanics and Arctic Engineering, 133 (3).
- Kujanpää, J., Routi, A.-L., 2009. WP1: Concept Ship Design A. Tech. Rep. Deliverable 1.1a, STX Europe, Finland, FLOODSTAND, EU FP7.
- Manderbacka, T., Mikkola, T., Ruponen, P., Matusiak, J. E., 2015a. Transient response of a ship to an abrupt flooding accounting for the momentum flux. Accepted for publication in J. of Fluids and Structures, June 2, 2015.
- Manderbacka, T., Ruponen, P., Kulovesi, J., Matusiak, J. E., 2015b. Model experiments of the transient response to flooding of the box shaped barge. Accepted for publication in J. of Fluids and Structures, June 2, 2015.
- Manderbacka, T. L., Jacob, V., Carriot, T., Mikkola, T., Matusiak, J. E., 2014. Sloshing forces on a tank with two compartments, application of the pendulum model and CFD. In: Proceedings of the ASME 2014 33rd International Conference on Ocean, Offshore and Arctic Engineering. San Francisco, California, USA.
- Ruponen, P., 2007. Progressive flooding of a damaged passenger ship. Ph.D. thesis, Helsinki University of Technology, Ship Laboratory.
- Ruponen, P., Metsä, A., Ridgewell, C., Mustonen, P., 2009. Flooding Simulation as a Practical Design Tool, Schifstechnik – Ship Technology Research, Vol. 56, 3-12.
- Ruponen, P., Sundell, T., Larmela, M., 2007. Validation of a simulation method for progressive flooding. International Shipbuilding Progress 54 (4), 305–321.
- Santos, T. A., Winkle, I. E., Guedes Soares, C., 2002. Time domain modelling of the transient asymmetric flooding of ro-ro ships. Ocean Engineering 29 (6), 667–688.
- Spanos, D., Papanikolaou, A., 2001. On the stability of fishing vessels with trapped water on deck. Ship Technology Research-Schiffstechnik 48, 124–133.
- Spouge, J. R., 1985. The Technical Investigation of the Sinking of the Ro-Ro Ferry European Gateway. Transactions of RINA 127, 49–72.
- Valanto, P., 2008. Research study on the



sinking sequence and evacuation of the MV
Estonia - final report. Tech. Rep. 1663,
HSVA, Hamburg, Germany.

This page is intentionally left blank



Safety of Ships in Icing Conditions

Lech Kobylinski, *Foundation for Safety of Navigation and Environment Protection, Poland*

lechk@portilawa.com

ABSTRACT

Icing of the above water part of ship poses serious hazard to stability. Icing may occur in high latitudes but also sometimes in other sea routes in adverse weather conditions. Present stability requirement as, for example, in 2008 IS Code, include certain provisions related to icing, but they seem to be inadequate, in particular in view of opening northern sea routes and trends to exploit arctic waters where possibility of icing and its effect on stability must be seriously considered. In the paper physical phenomena related to formation of icing and available data on amount of icing in various areas are considered. Possibility of application of risk analysis to the effect of icing on stability is also discussed

Keywords: *safety of ships, icing, risk analysis*

1. INTRODUCTION

Few years ago within a project sponsored by the Polish Committee for Scientific Research the group of ten experts was assembled consisting of seven ship masters having at least 20 years of service at sea on different types of ships, two scientist involved in stability matters and one experienced naval architects having wide experience in designing different types of ships. The group was charged with the task of assessing the importance of different hazards to stability for different types of ships. The Delphic method was used and the game was arranged. The game did show that the group of experts attached rather high priority (index 4 of the range 0 to 5) to hazard of icing in particular to fishing vessels and smaller passenger ships.

One of the masters having served many years on board passenger ships, produced photos of severe icing that happened during one particular voyage in North Atlantic. One of those photos reproduced below shows how serious threat to stability icing may pose.

At the same time about 300 stability accidents, the data on which were collected from many various sources, including IMO data bank, [IMO 1985] and book of Aksiutin and Blagoveschensky [1975] were analysed and it was discovered that in about 26 cases from the above number of accidents icing was considered as a main cause of capsizing.



Fig.1. Severe icing on m/s Stefan Batory in North Atlantic. (Courtesy of Captain H.Majek)

It is also difficult to imagine, that icing may cause capsizing of ships even in Black Sea, where two fishing vessels capsized because of severe icing in 2002 [Sukhanov et al 2003]. It is clear, that icing is creating severe hazard to stability and must be taken into consideration for ships operating in the areas where icing may occur.

2. STRUCTURAL MODEL OF ICE ACCRETION

Usual way of taking into account the effect of ice accretion on stability is based on very simple and deterministic structural model. It is assumed that certain amount of additional mass of accrued ice is taken on board. The centre of gravity of the ice is assumed to be in the centre of this mass. Because the mass of accrued ice usually is smaller than 10 per cent of the mass of the ship, simplified method of calculation of the new metacentric height and stability levers curve may be used. This is shown in the attached sketch (fig. 2)

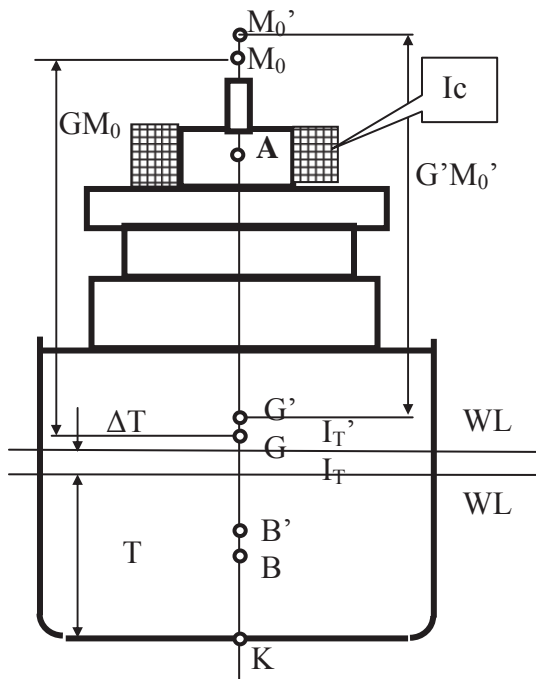


Fig.2. Structural model of the effect of ice accretion

New metacentric height could be calculated by the formula:

$$G'M_0' = GM_0 + \frac{m}{\rho \nabla + m} \left(T + \frac{\Delta T}{2} - KA - GM_0 \right)$$

Because when ice is accrued always:

$$KA > T + \frac{\Delta T}{2} - GM_0$$

then the new metacentric height would be always smaller than the original one without icing.

New stability levers could be calculated with the formula (Fig.3):

$$GZ = BN - KG' \sin \varphi$$

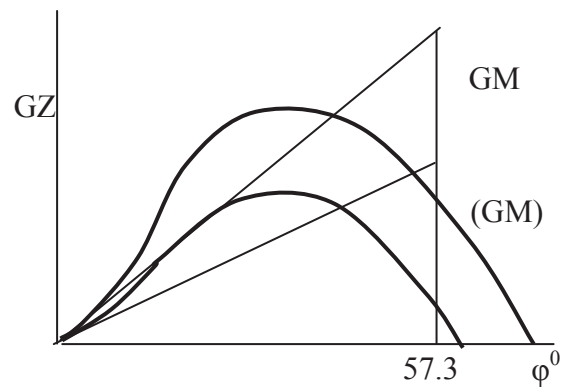


Fig. 3. Reduction of stability levers with icing

Accrued ice will also affect ship motion characteristics in rough sea, particularly rolling periods and deck wetness characteristics but these factors are rarely taken into account when considering problem of icing. The main problem is, however, proper estimation of the mass and centre of gravity of the accrued ice.

3. PHYSICS OF ICE ACCRETION

The physics of ice accretion is very complex and unpredictable phenomenon. Ice accretion depends on many factors as for example on:

- Temperature of air



- Temperature of the upper layer of water
- Wind velocity and direction
- Sea surface condition (waves, current etc)
- Ship speed, course in relation to wind and waves
- Ship characteristics (freeboard, deck and superstructures arrangement, ship motions etc)

Ice may accumulate basically in three different ways

- Freezing rain or drizzle cause thin layer of ice distributed almost evenly over decks, superstructures and rigging including high positioned objects like masts, antennas etc. Layer of accumulated ice increases quite slow, therefore dangerous increase of the position of centre of gravity occurs only when the ship is long time exposed to those effects. Generally this way of accumulating ice is not very dangerous for the ship.
- The second way of accumulating ice occurs when the temperature is at least 9⁰ C less than the temperature of water. Freezing fog in contact with cold metal creates thin layer of ice. This usually is close to the waterline and is not very dangerous to the ship.
- The third way of icing is most dangerous. This type of ice accretion occurs when the temperature of air is very low and there is stormy wind and waves. In such situation sprays of water freeze in contact with the hull, decks, superstructures and rigging. It is less likely that sprays are cause icing higher above the water, however. But if at the same time there is heavy freezing rain, then large amount of ice may accumulate high above the water. This is the most dangerous case. The photo in fig. 1 shows how large amount of ice may accumulate on board The photo shows ice

accrued on the deck of m.s Stefan Batory in North Atlantic.

In some publications information could be found that at very low air temperatures (below – 180C) this type of ice accretion is not present, because water sprays freeze in air and do not stick to the ship construction. Other observations do not agree with this, however. Four Russian fishing vessels capsized in Bering Sea in 1965 at temperatures between – 200 and -220 C. On “Norilsk” ship heavy icing was observed at temperature -280 C [Aksiutin 1975].

Usually icing does not occur at temperatures of water above +60, but in some cases icing was observed even at water temperature +80C.

The third type of icing occurs most often and when in conjunction with freezing rain is most dangerous. According to data collected by Borisenko [Aksiutin 1986], who analysed about 2000 cases of icing on ships of Russian fleet, frequency of different kinds of icing was as shown in the table 1.

Table 1. Frequency of different types of icing (percent)

	Sprays	Sprays plus rain	Snow	Fog, rain drizzle
Northern hemisphere	89.9	6.4	1.1	2.7
Southern hemisphere	50.0	41.0		9.0

Obviously heavy icing occurs usually only in certain areas. Chart where heavy icing may be expected is included in the IMO IS Code [IMO 2008]. The other chart showing areas in North Atlantic and North Pacific Oceans is reproduced in fig. 4. [Sechrist et al 1989]. However there are known incidents where heavy icing occurred in other areas, even in Black Sea.



For example extreme icing was observed on two Russian fishing vessels in Black Sea on 9th December 2002. Both ships capsized and foundered. Synoptic situation at that time was as follows: because of suddenly changing air circulation over eastern part of Black Sea, layer of cold air came over this part and air temperature drops down from +10°C to -18°C in 24 hours. Strong wind of about 35 m/s velocity called “Bora” occurred. Icing on both vessels started fast increasing and as all attempts to remove it failed, it was not possible to save the vessels [Sukhanov et al 2003]. According to data provided by Aksiutin (1986) heavy icing may be expected in periods and areas as shown in the table 2.

Northern Atlantic Ocean	15 Dec-15 April
Barents Sea	1 Jan - 15 March
Baltic Sea	15 Dec-
Baffin Sea	1 Dec-31 March
New Foundland area	1 Jan - 15 March
Bering Sea and Okhock Sea	1 Dec- 29 Feb
Japan Sea	1 Dec- 29 Feb
North-West Pacific Ocean	15 Dec-31 March
Karsk and , Laptiev Sea	15 June -15 Nov
Chukock Sea	15 June -15 Nov
East Siberian Sea	15 June -15 Nov

As icing depends on air temperature and wind velocity some data were published showing how fast layer of ice accumulates with increasing wind velocity and decreasing temperature. The diagram showing icing dependence on air temperature and wind velocity developed in Japan is reproduced in fig. 5 [Sawada 1962].

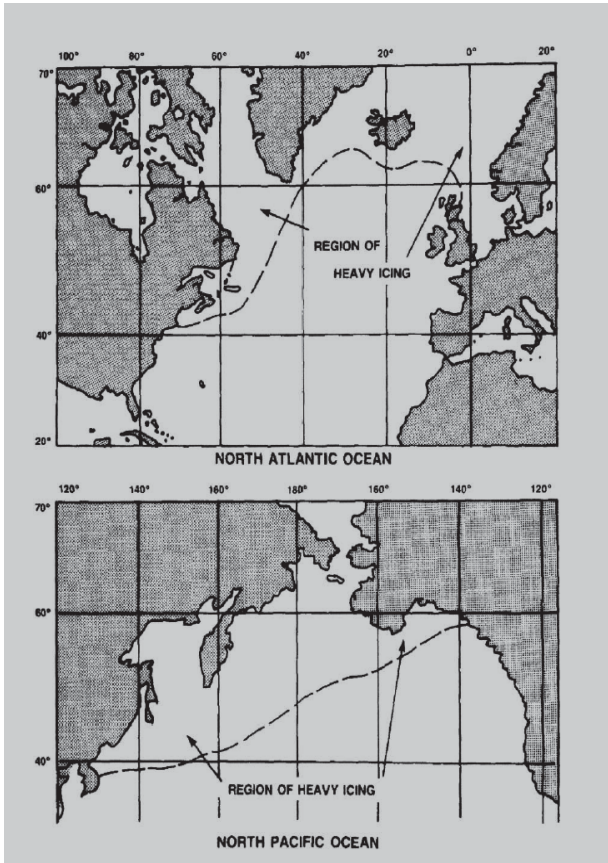


Fig. 4. Chart of areas where icing may be expected [Sechrist et al 1989].

Table 2. Areas and periods where heavy icing may be expected [Aksiutin 1975]

Area	Period
North-west Atlantic Ocean,	15 Dec-15 March
Norway and Greenland Sea	15 Dec-31 March

Similar diagrams were developed by Overland et al [1986] and also by the US Navy [1988]. Rate of ice accretion depends on the water and air temperature and on the wind velocity. According to Mertins [1968] who on the basis of 4000 observations in North Atlantic area, with the temperature of water 0°C and air temperature -6°C discovered that the ice accumulation may be 7 to 14cm in 24 hours.

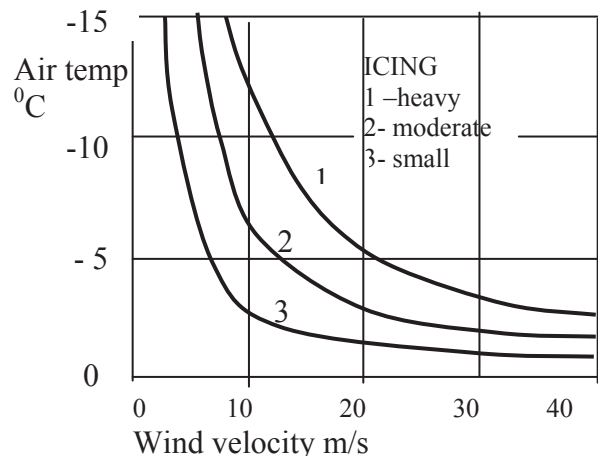


Fig.5. Icing dependence on air temperature and wind velocity. [Sawada 1962]

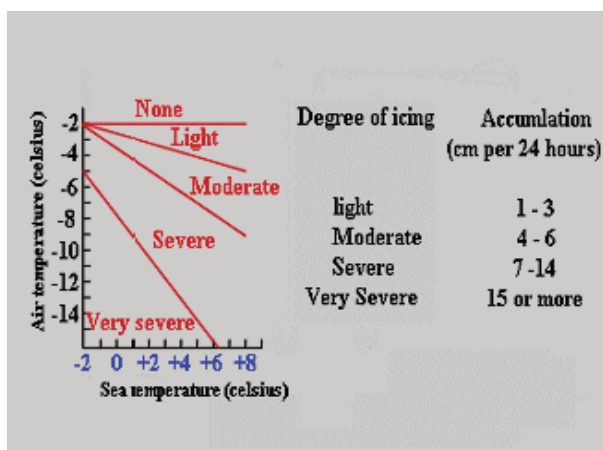


Fig 6. Nomogram for estimation of icing in North Atlantic for wind force 9-10⁰B [Mertins 1968]

Mertins [1968] produced also diagrams for prediction of icing in relation on air and water temperatures and on wind force. One of these diagrams for wind force 9 -100B is reproduced in fig.6.

4. CURRENT CRITERIA OF ICING

Problem of icing is considered currently in several IMO instruments, for example in the IS Code, Polar Code, Torremolinos Protocol and in some other documents. The requirements and recommendations included there are not repeated here; they may be easily found in those documents, in particular in the 2008 IS Code, Chapter 6 and Annex 2 [IMO 2009] and they are not very different in other IMO documents.

The basic requirements for fishing vessels consist of specification of certain amount of accrued ice on exposed surfaces of weather decks and on projected lateral areas on each side of the vessel above the waterplane.

In most IMO instruments the recommended amount of accrued ice is:

- 30 kg/m² of open weather decks, and gangways;

- 7.5 kg/m² for projected lateral area of each side of the vessel above the water plane.

In several national recommendations different values of accrued ice per square meter of open decks and projected lateral areas are recommended, but in general those values are not very different from the above.

In mid-eighties of the last century at the time when first edition of the IS Code was considered at IMO, many delegations pointed out that the above values are underestimated because 30 kg/m² practically means 3 cm thick layer of ice. After discussion, however, it was decided that adoption of higher values in certain regions was left to the decision of national Administrations.

Aksyutin and Blagoveschensky [1975] pointed out that thickness of layer of ice as recommended in the IS Code was widely different from values observed in different regions. In 1000 observed cases of icing they analysed, thickness of accrued ice was greater than recommended by IS Code for fishing vessels:

- In Baltic Sea by 76%
- In Bering Sea by 71%
- In Okhock and Japan Sea by 60%

The actual mass of accrued ice exceeded the mass calculated according to the recommendation of IS Code

- In Barents Sea by 270%
- In Okhock Sea by 200%
- In Bering Sea by 360%
- In Baltic Sea by 1000%

According to the same observations calculated position of the centre of gravity of accrued ice was usually 20 to 60 % higher than calculated according to IS Code recommendation which had important effect on stability characteristics of the vessel. There are many similar data available showing that ice accretion in certain conditions may be much larger than recommended by IS Code. This was duly noticed by the IMO Subcommittee, however finally it was decided to leave the



decision in respect of the amount of accrued ice in hands of the national administrations.

5. OPERATIONAL FACTORS

Safety of ships in situations where icing occurs depends greatly on operational factors, first of all on possibility to remove accrued ice. In several IMO recommendations in this respect included, for example, in the IS Code, there is operational guidance on how to behave in situations when icing occurs, on how to prepare the vessel and what kind of equipment for removal of accumulated ice should be on board. Such operational guidance is essential for safety of the vessel but in real life quite often in cannot be observed.

Removal of excessive ice accumulating very fast in in bad weather, particularly if the vessel is weathering against the wind, cannot be accomplished because access to the forward part of the ship is too dangerous. Moreover in modern ships the number of crew members who could be employed in this work is much

smaller than it was in older times. This particularly applies to small container ships and ships carrying deck load of timber. In fishing vessels having low freeboard in stormy weather deck is constantly flooded by the waves and if covered with ice, slippery. Therefore access there is risky. According to current requirements in relation to icing, assessment of safety in icing condition was left to the judgement of national Administrations. The requirements concerning values of accrued ice as, for example in the IS Code, seem to be roughly applicable to icing at comparatively mild weather conditions. There is nowhere, however, guidance on how to perform risk analysis for ships sailing in areas where heavy icing might occur.

6. EVENT TREE AND FAULT TREE FOR DANGEROUS ICING

Branches of event tree and fault tree for dangerous icing are shown in figs 7 and 8.

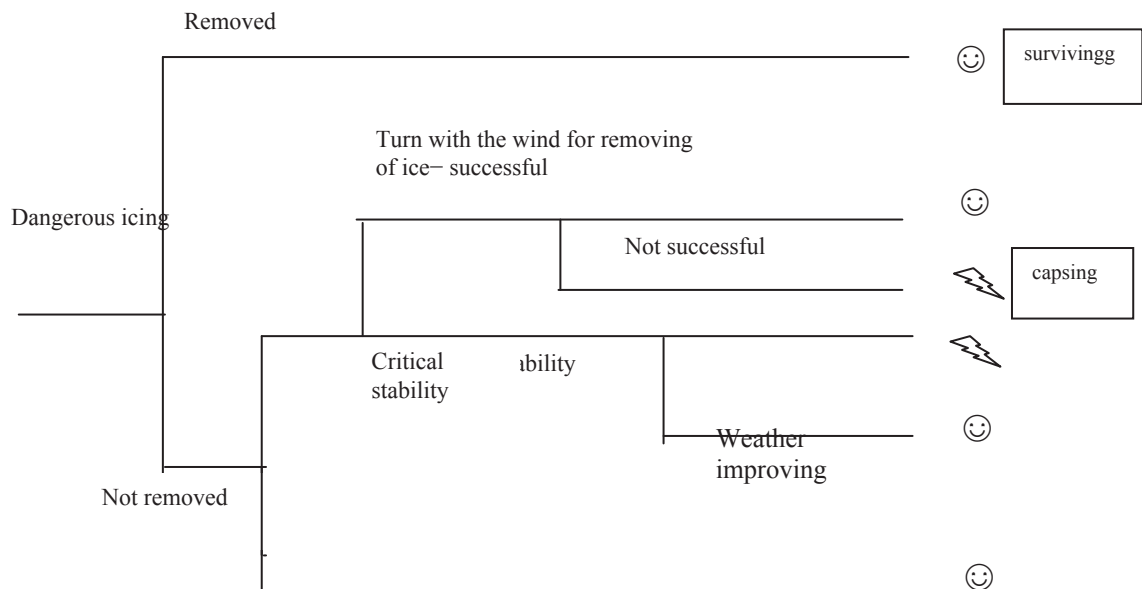


Fig.7. Branch of event tree for heavy icing

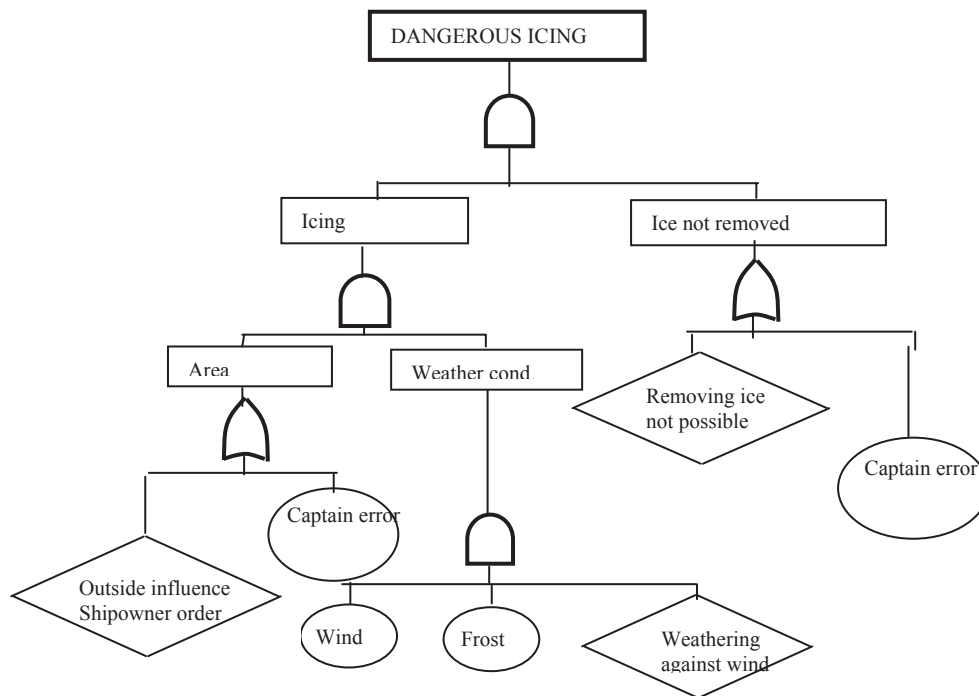


Fig.8. Branch of fault tree for dangerous icing

They may help national Administrations when performing risk analysis in order to assess safety of a ship intended to operate in areas where heavy icing might occur. Risk analysis should include scenarios that may cause loss of stability and in all cases reduction of metacentric height and stability levers due to ice accumulated should be taken into account.

In the risk analysis scenarios of ship motions in areas where icing is possible should apart from hazards from icing take into account hazards from wind and waves. Scenarios where human error is taken into account should be also considered. Ice accumulated should be removed as fast as possible. However it is not always possible. As mentioned above there are many situations when ice removal is risky or not possible at all. For example, if in stormy weather ship is weathering against the wind and ice is accumulated in the front part of the ship, manoeuvre to turn the ship with the wind in order to make access to front part possible is too dangerous. This is taken into account in fault tree shown in fig. 8.

Obviously two factors should be present if icing would be possible: firstly vessel should operate in area where icing is possible and

secondly weather conditions must be such, that formation of icing may occur. Both factors are taken into account in the fault tree shown in fig. 8. The situation that the vessel would be in the area where icing occurs depends on the route, therefore on the decision of shipowner but it may depend on the decision of the master who ignored danger and decided not to avoid area where icing may occur.

The difficult part of the risk analysis is attribution of probabilities to particular events in the fault tree and assessment of the probability of top event which is dangerous icing. Probably the only method would be assessment by experts having enough experience in operating ships in areas where icing occurs. In the example shown in fig. 9 probabilities were taken as example values. In the exercise performed that was mentioned in the introduction and where Delphic method was used the conclusion was that the probability of dangerous icing that may lead to capsizing was of the order of 10^{-7} (hourly) or 10^{-3} (ship and year). It seems, however, that this probability is underestimated and based mainly on the experience of one ship master who served on large passenger ship operating on North Atlantic route.

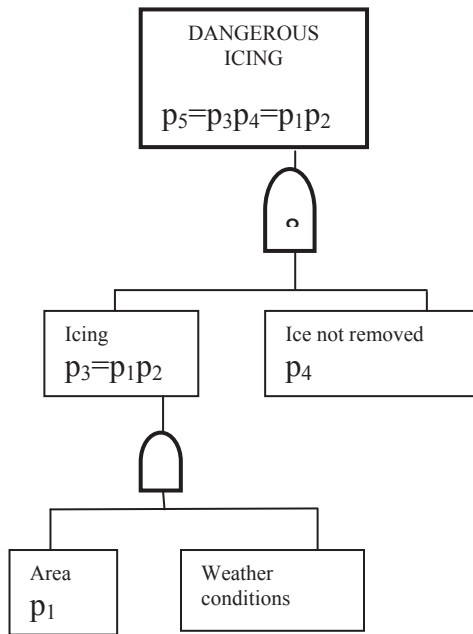


Fig. 9. Simplified fault tree for calculation of probabilities

Estimation of the probabilities in the fault tree in order to assess the top event probability is rather difficult and probably should be made by experts having sufficient experience of navigating in areas where icing might occur. It is doubtful if general accessible data on icing in areas in question are available, although national Administrations may have their own data. However with expanding navigation in arctic routes international recommendations are certainly needed.

7. CONCLUSIONS AND RISK CONTROL OPTIONS

From the point of view calculation of stability characteristics in icing condition poses no problems. For the majority of ships navigating around the world hazard of icing does not exist at all or may appear with such small probability that it is not taken into account. It is essential, however, for ships navigating in northern or southern seas, especially important for fishing vessels. For those vessels risk control options should be considered. Those options include preventive options as well as mitigation options. (Fig.10).

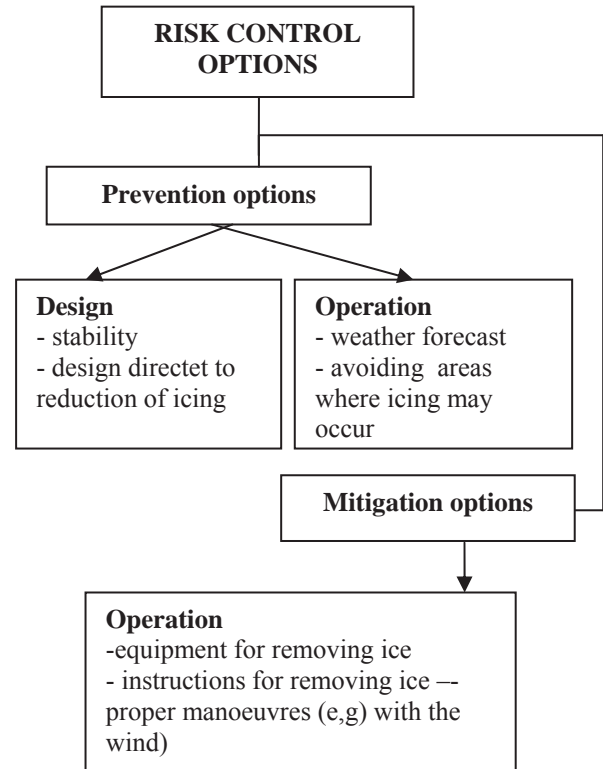


Fig. 10 Risk control options

Prevention options are mainly related to ship design including stability and suitable design of decks and superstructures intended to reduce possibility of accumulation of ice. Mitigation options are related to the possibility of removing ice and safe manoeuvring in stormy weather.

Current requirements of the IS Code related to icing include mostly recommendations and guidance for skippers of fishing vessels for ensuring survival of icing that may be valid also for other types of ships. However recommended values of ice accretion seem to be underestimated. Risk analysis performed should allow adoption of more diversified values of ice accretion in different areas. Also it may allow to take into considerations risk control options

8. REFERENCES

- Aksyutin, L.R (1986): Fighting casualties of sea-going ships due to loss of stability. Sudostroyenye, Leningrad



- Aksyutin, L.R., Blagoveschensky S.N. (1975):
Avarii sudov ot potery ostoichivosti.
Sudostroyenye, Leningrad (in Russian)
- IMO (1985): Analysis of intact stability
casualty records. Submitted by Poland.
Documents SLF 30/4/4/ and SLF /38
- IMO (2009): International Code on Intact
Stability, 2008. London
- Mertins H.O. (1968): Icing on fishing vessels
due to spray. Maritime Observations, Vol.
38, No. 221, London
- Overland J. E., Pease C.H., Preisendorfer R.
W. Comisky A. L. (1986): Prediction of
vessel icing. Journal of climate and
Applied Meteorology. , Vol 25 pp. 1793-
1806
- Savada T. (1962): Icing on ships and its
forecasting. Japan Society of Snow and
Ice, Vol 24, Tokyo
- Sukhanov S.I., Panov V. V., Lavrenov I. V.
(2003): Extreme ship's icing in the Black
Sea. Arctic and Atlantic Research Institute ,
Russia
- Sechrist F.S., Fett R.W., Perryman D.C. (1989)
Forecast handbook for the Arctic. Chapter
10: Icing. Naval Environmental Prediction
Research Facility. Technical Report TR89-
12
- U.S. Navy (1988): Cold weather handbook for
surface ships. OPNAV P-03C-01-89. Chief
of Naval Operations, Washington DC

This page is intentionally left blank

Session 5.3 – DYNAMIC STABILITY

**An Investigation of a Safety Level in Terms of Excessive Acceleration
in Rough Seas**

**Application of IMO Second Generation Intact Stability Criteria for
Dead Ship Condition to Small Fishing Vessels**

**Investigation of the Intact Stability Accident of the Multipurpose
Vessel MS ROSEBURG**

This page is intentionally left blank



An Investigation of a Safety Level in Terms of Excessive Acceleration in Rough Seas

Yoshitaka Ogawa, *National Maritime Research Institute, Japan* ogawa@nmri.go.jp

ABSTRACT

A probability of occurrence of lateral acceleration owing to the rolling motion was evaluated to investigate a safety level for a prevention of the situation that excessive acceleration occurs. Firstly, sea state in the sea area of excessive acceleration accident was examined by means of hindcast wave data. Through the comparison of the long term prediction of lateral acceleration, the correlation between loading condition, sea state and long term probability was examined. It is clarified that threshold probability of excessive lateral acceleration depends on loading condition and sea state. Consequently, the safety level of excessive lateral acceleration was discussed.

Keywords: *new generation intact stability criteria, lateral acceleration, container vessel, long term prediction*

1. INTRODUCTION

Currently, the construction of a reliable methodology for estimating a capsizing probability is an urgent issue for the proper provision of the safety because the International Maritime Organization (IMO) started to develop the new-generation intact stability criteria for five major capsizing modes, which contains the stability under excessive acceleration, dead ship conditions, parametric rolling, broaching and pure loss of stability with performance based approaches.

With regard to the excessive acceleration, accidents of ballast loading container vessels due to excessive acceleration were the trigger for the new-generation intact stability criteria. In accordance with the casualty report of CHICAGO EXPRESS (Federal Bureau of Maritime Casualty Investigation of Germany, 2009), a very serious marine casualty occurred on board the 8749 TEU2 container vessel CHICAGO EXPRESS in the morning on 24 September 2008.

The vessel navigated in South China Sea from Hong Kong to Ningbo following instructions to shipping from the local port authority because of the approaching Typhoon "HAGUPIT". After reaching the open sea, the CHICAGO EXPRESS encountered heavy winds and swell from a south-easterly direction; this exposed the vessel to rolling motions of up to approximately 32 degrees. The vessel was suddenly hit by a particularly violent wave coming from starboard just as she rolled to starboard. Following that, the CHICAGO EXPRESS keeled over severely several times, at which the inclinometer registered a maximum roll angle of 44 degrees for an estimated period of 10 seconds.

It is remarkable that requirement for the prevention of excessive lateral acceleration has the possibility to restrict GM and to be the opposite side of ensuring sufficient stability because current large vessel generally has sufficient GM to ensure the adequate safety for damage stability. On the other hand, if the ship has sufficient (or excessive) stability, large rolling angles can occur which then result in large lateral accelerations and cargo damage.



Typically, this situation occurs if the encounter frequency of the waves is in resonance to the natural roll frequency of the ship. This means that all types of ship have certain possibility to meet large acceleration. This also means that it is rational to prevent such a phenomenon that occurs frequently not only by the design criteria but also by the operational guidance or limitation.

Therefore, it is important to assess the probability of occurrence of excessive lateral acceleration and to provide the adequate information for adequate safety and operation.

Based on the background, first, a database of world wave and wind is constructed by means of the hindcast data, which can provide worldwide wind and wave data synchronized in space and time. Sea state in the sea area where accident of excessive acceleration occurred was examined by the comparison of a probability of occurrence of wave height. It is found that sea state in the sea area of accident was not necessarily severe compared with that of North Atlantic and North Pacific. This indicates that large lateral acceleration can occur in other sea areas.

Second, the correlation between realistic loading condition, sea state and probability of occurrence was examined by computation of the long term prediction of lateral acceleration. It is clarified that threshold probability of excessive lateral acceleration depends on the combination of loading condition and sea state. It is also clarified that excessive lateral acceleration occurs in a relatively high probability owing to the roll resonance. Finally, the safety level of excessive lateral acceleration is discussed.

2. CONSIDERATION OF SEA STATE AT THE SEA AREA OF ACCIDENT OWING TO EXCESSIVE ACCELERATION

2.1 Source Data of Wave and Wind

For the examination of correlation between winds and waves, it is preferable that wind data synchronizes with wave data in space and time. Based on this background, the wave and wind statistics are composed by the wave hindcast data. The present hindcasting data is computed by means of the third generation wave hindcasting model of Global Climate by Japan Weather Association (JWA3G model). Grid point value (GPV) of sea winds, provided by the Meteorological Agency of Japan, is used as an input of this model. Significant wave height, wave period and peak direction of waves, mean wind speed and wind direction are computed. These are composed by lattice of 2.5 degree interval (all area from 70 degrees of North latitude to 70 degrees of South latitude). In the present study, data of the 10-year span from January 1997 to December 2006 are used.

The third generation wave hindcasting models basically adopt not conservative methods such as SMB (Sverdrup, Munk and Bretschneider) method or PNJ (Pierson, Neumann and James) method (e.g. British Maritime Technology Limited, 1985) but the spectral method, which is the mainstream of the ocean waves forecasting/hindcasting model. In a spectral method, individual growth and attenuation of each component wave was computed. Prior to the application, the validity of numerical computation of JWA3G model was verified (Japan Weather Association, 1993) through the numerical simulation in accordance with the SWAMP (Sea Wave Modeling Project) method (The SWAMP group, 1985), which is constructed as a verification method of the numerical computation of ocean wave in the world meteorological community.

2.2 Spatial Distribution of Wave Height

Figures 1 to 5 show the contour of average of significant wave height in annual and four seasons. It is found that wave in Southeast Asia is relatively calmer than that in North Pacific because wave of Southeast Asia is affected by weather from South Pole to the south Indian Ocean. On the other hand, it is also found that wave height in South China Sea is relatively higher than that in around South China Sea. It is remarkable in autumn and winter owing to low pressure and typhoon. It is clarified that these findings are consistent with existing findings.

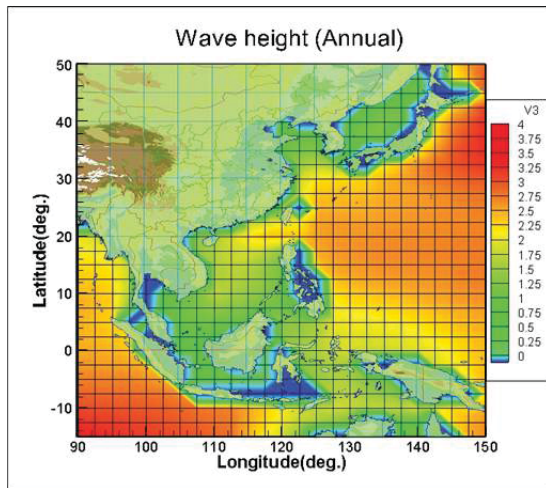


Figure 1 Contour of average of significant wave height (annual).

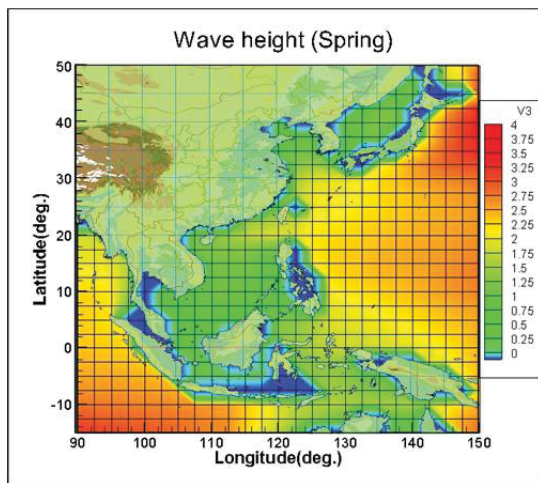


Figure 2 Contour of average of significant wave height (spring: March - May).

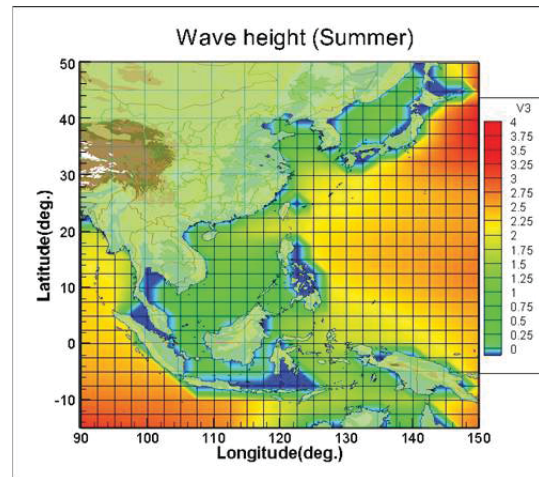


Figure 3 Contour of average of wave height (summer: June - August).

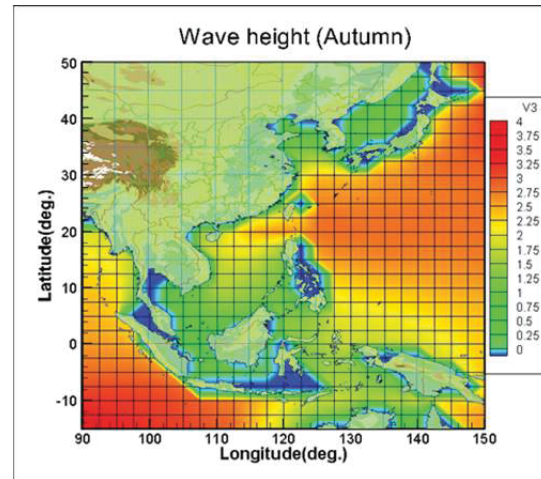


Figure 4 Contour of average of significant wave height (autumn: September - November).

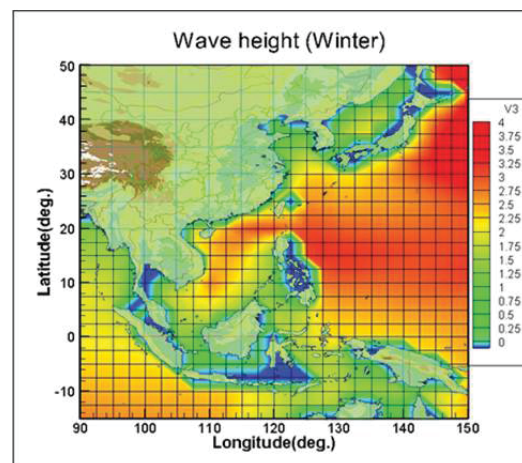


Figure 5 Contour of average of wave height (winter: December - February).



2.3 Statistical Characteristic of Wave Height

Probability of exceedance of wave height is evaluated based on the statistical analysis of wave and wind data. For the comparison of wave height between South China Sea, North Pacific and North Atlantic, the sea area in statistical analysis shown in Figure 6 is defined.

It is found that wave in South China Sea is relatively calmer than that in North Pacific and North Atlantic because wave of Southeast Asia is affected by weather from South Pole to the south Indian Ocean. On the other hand, in autumn, severe sea state in the area close to Hong Kong is similar to that in North Pacific and North Atlantic owing to typhoon in low pressure.

It is found that occurrence probability of sever sea state in North Atlantic and North Pacific is about 10 or 10² times higher than that in South China Sea. This means that large acceleration can occur in other sea area such as North Atlantic and North Pacific. Therefore, it is rational that long term prediction for the determination of safety level of lateral acceleration should be evaluated based on the long term probability in North Atlantic or North Pacific.

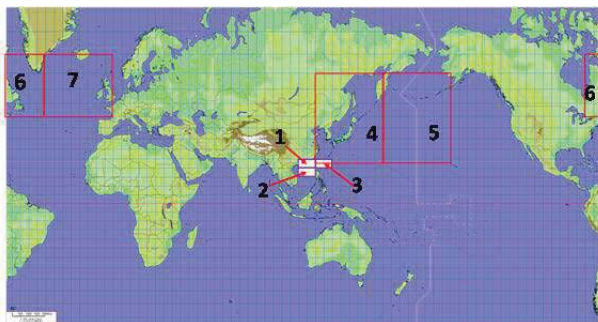
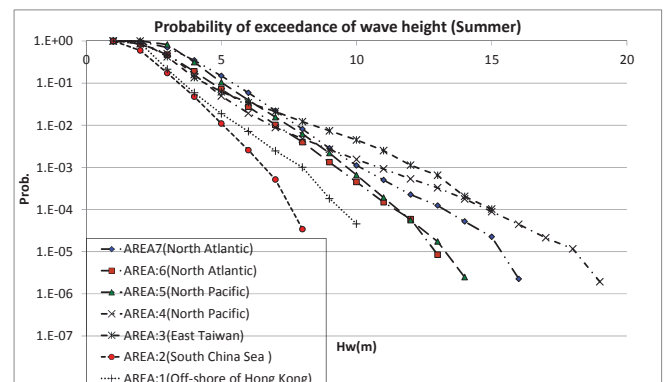
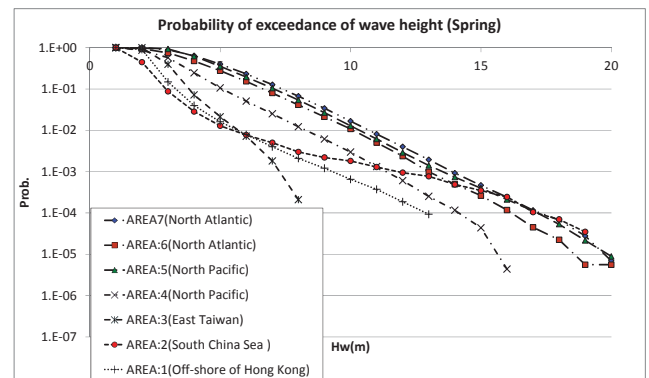
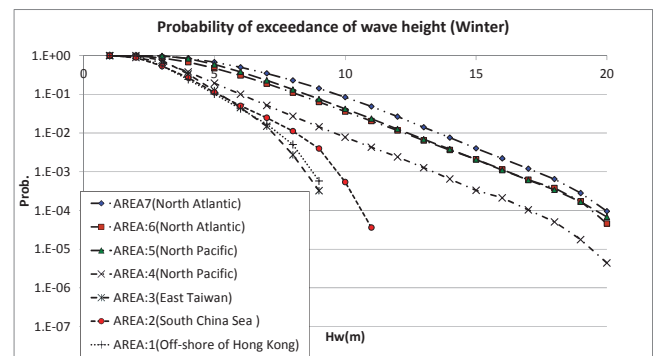
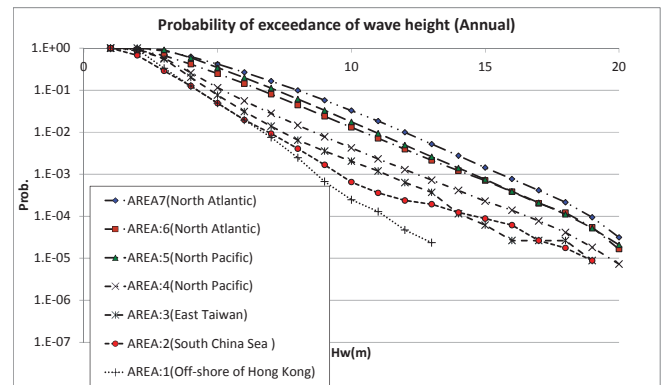


Figure 6 The sea area as the object of the present study



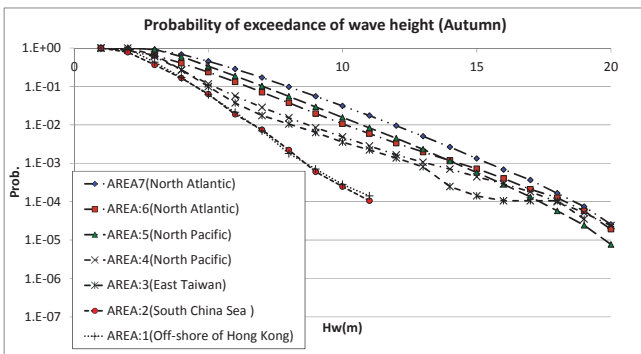


Figure 7 Probability of exceedance of wave height.

3. EVALUATION OF OCCURRENCE OF PROBABILITY OF EXCESSIVE ACCELERATION

3.1 Computation of Long term Probability

Short term and long term probability of lateral acceleration is computed based on the superposition of linear response amplitude operator (Price, W. G. and Bishop, R.E.D., 1974). Container ship and crude tanker were used for object ships in the present study. Table 1 indicates loading conditions of object ships. Loading conditions of them were assumed based on the loading manual of the same ship type.

Response amplitude operator of ship motion and acceleration was computed by means of linear strip method (NSM). ISSC Spectrum was used as a wave spectrum. Cosine square distribution was assumed as a wave directional spectrum. Ship speed in the computation was assumed as 3 knots.

Scatter diagrams of wave height and wave period in North Atlantic, North Pacific and South China Sea were made by means of hindcast data. Tables 2, 3 and 4 show these scatter diagrams. Area of North Atlantic, North Pacific and South China Sea corresponds to areas, which is shown in Figure 4, respectively.

Table 1 Loading conditions of object ships in the present study.

Ship type	Lpp (m)	Loading condition	draught (m)	GM (m)
Container ship	283.8	Full	14.0	1.0
		Partial	11.0	5.0
		Ballast	8.8	7.0
Crude tanker	307.0	Full	19.5	12.0
		Ballast	8.0	28.0

3.2 Short Term Probability of Lateral Acceleration

Standard deviation of lateral acceleration at bridge as a function of mean wave period is shown in Figures 8 to 12. It is found that standard deviation becomes larger in the case of large GM. In the accident of CHICAGO EXPRESS (Federal Bureau of Maritime Casualty Investigation of Germany, 2009), significant wave height and acceleration in the bridge were estimated to be 7.5m and 1G ($=9.8\text{m/s}^2$). In the case of ballast condition of object container ship, it is found that maximum acceleration exceeds 1G when wave height exceeds about 8m.

With regard to the object ships in the present study, it is important to examine long term probability of ballast condition because having sufficient stability could induce large rolling angles and resulting in large lateral accelerations.

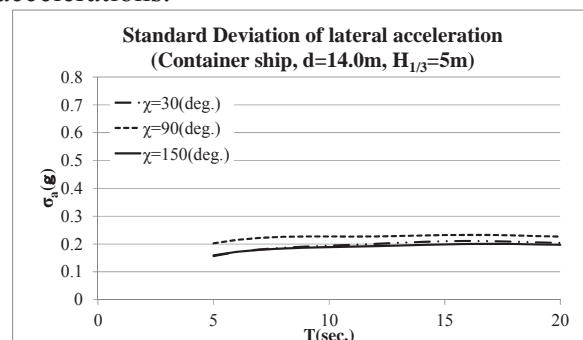


Figure 8 Standard deviation of lateral acceleration at bridge (Container ship, Full loading).

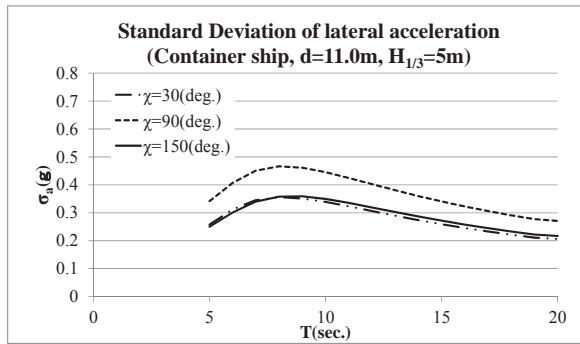


Figure 9 Standard deviation of lateral acceleration at bridge (Container ship, Partial condition).

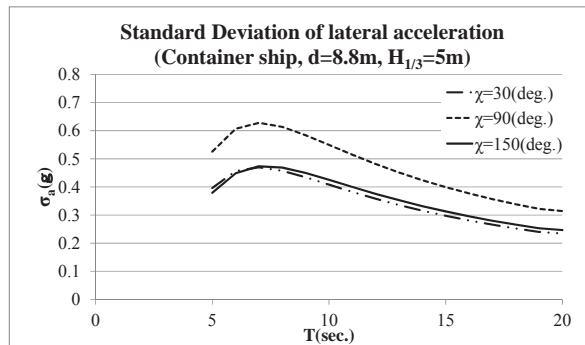


Figure 10 Standard deviation of lateral acceleration at bridge (Container ship, Ballast condition).

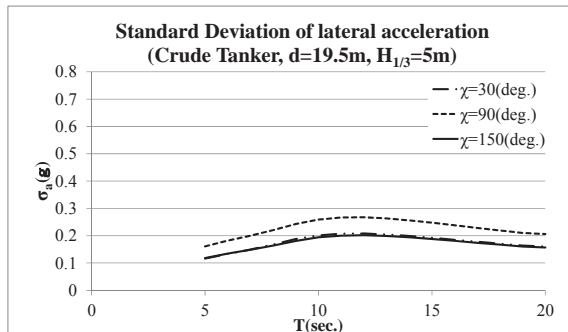


Figure 11 Standard deviation of lateral acceleration at bridge (Crude tanker, Full loading).

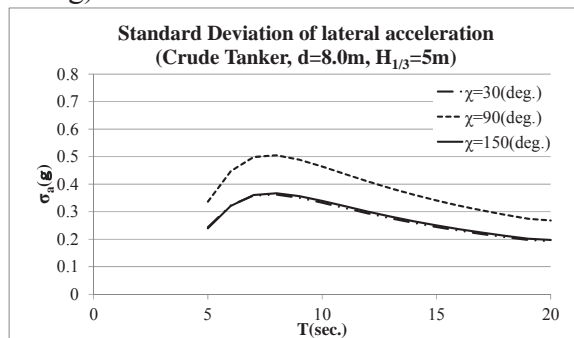


Figure 12 Standard deviation of lateral acceleration at bridge (Crude tanker, Ballast condition).

3.3 Long Term Probability of Lateral Acceleration

Figures from 13 to 15 show long term prediction of lateral acceleration of container ship using wave scatter diagram of North Atlantic, North Pacific and South China Sea, respectively. Figures from 16 to 18 show long term prediction of lateral acceleration at bridge of crude tanker.

It is found that long term probability in beam seas is higher than that in other wave direction because large lateral acceleration is caused by the rolling resonance. In the present computation, long term probability of 1G corresponds to about from $10^{2.5}$ to $10^{1.5}$ in beam seas. It is clarified that large acceleration can occur with high probability because large lateral acceleration is caused by the rolling resonance.

Figure 19 and Figure 20 show long term prediction of rolling of container ship and crude tanker, respectively. It is found that probability of occurrence of rolling corresponds to about from 25 to 30 at the same probability of acceleration of 1G. This is the same level as that in the casualty report of CHICAGO EXPRESS (Federal Bureau of Maritime Casualty Investigation of Germany, 2009).

It is clarified that probability of excessive lateral acceleration largely depends on the loading condition. It is also clarified that excessive lateral acceleration occurs in a relatively high probability owing to the roll resonance. This means that all types of ship have certain possibility to meet large acceleration. Therefore, it is basically difficult to exclude all risk of excessive lateral acceleration only based on the design criteria. It is essential to prevent such a phenomenon that occurs frequently by the combination of design criteria and operational limitation.



Table 2 Scatter diagram of wave height and wave period (South China Sea).

number of data																				
average(Hw)=																				
average(Hp)=																				
T(sec.)																				
Hw(m)	-5	6	7	8	9	10	11	12	13	14	15	16	17	18	19	20				
20	0.0E+00																			
19	0.0E+00	2.9E-06	2.9E-06	0.0E+00	0.0E+00	0.0E+00	0.0E+00	0.0E+00	0.0E+00											
18	0.0E+00	2.9E-06	2.9E-06	0.0E+00	0.0E+00	0.0E+00	0.0E+00	0.0E+00	0.0E+00											
17	0.0E+00	2.9E-06	0.0E+00																	
16	0.0E+00	8.8E-06	2.9E-06	0.0E+00																
15	0.0E+00	0.0E+00	0.0E+00	0.0E+00	0.0E+00	2.9E-06	1.2E-05	5.8E-06	0.0E+00											
14	0.0E+00	0.0E+00	0.0E+00	0.0E+00	0.0E+00	5.8E-06	1.8E-05	2.9E-06	0.0E+00	0.0E+00	2.9E-06	0.0E+00	0.0E+00	0.0E+00	0.0E+00	0.0E+00				
13	0.0E+00	0.0E+00	0.0E+00	0.0E+00	0.0E+00	4.4E-05	4.8E-05	1.6E-05	2.9E-06	2.9E-06	0.0E+00	0.0E+00	0.0E+00	0.0E+00	0.0E+00	0.0E+00				
12	0.0E+00	0.0E+00	0.0E+00	0.0E+00	0.0E+00	8.0E-05	1.9E-05	8.8E-06	2.9E-06	0.0E+00										
11	0.0E+00	0.0E+00	0.0E+00	0.0E+00	4.4E-05	1.7E-04	2.7E-05	5.8E-06	0.0E+00	0.0E+00	2.9E-06	0.0E+00	0.0E+00	0.0E+00	0.0E+00	0.0E+00				
10	0.0E+00	0.0E+00	0.0E+00	0.0E+00	1.3E-04	2.2E-04	3.1E-05	2.4E-05	5.8E-06	0.0E+00	2.9E-06	0.0E+00	0.0E+00	2.9E-06	0.0E+00	0.0E+00				
9	0.0E+00	0.0E+00	0.0E+00	1.9E-05	5.3E-04	3.4E-04	4.5E-05	1.8E-05	1.2E-05	2.9E-06	5.8E-06	0.0E+00	6.8E-06	2.9E-06	0.0E+00	0.0E+00				
8	0.0E+00	0.0E+00	0.0E+00	2.4E-04	1.8E-03	2.6E-04	5.6E-05	1.2E-05	2.9E-06	5.8E-06	3.9E-06	0.0E+00	1.3E-05	7.8E-06	0.0E+00	0.0E+00				
7	0.0E+00	0.0E+00	5.8E-06	1.9E-03	3.6E-03	2.6E-04	5.1E-05	2.3E-05	5.8E-06	9.7E-06	8.8E-06	1.4E-05	2.3E-05	0.0E+00	0.0E+00	0.0E+00				
6	0.0E+00	0.0E+00	3.1E-04	8.9E-03	3.3E-03	3.6E-04	1.2E-04	3.4E-05	1.6E-05	1.3E-05	1.9E-05	1.6E-05	0.0E+00	0.0E+00	0.0E+00	0.0E+00				
5	0.0E+00	5.0E-05	1.0E-02	2.0E-02	2.9E-03	8.9E-04	4.1E-04	1.3E-04	1.1E-04	4.6E-05	1.3E-05	2.6E-05	2.4E-05	0.0E+00	0.0E+00	0.0E+00				
4	5.8E-06	3.5E-03	4.7E-02	3.0E-02	7.6E-03	2.6E-03	1.1E-03	4.9E-04	2.4E-04	1.3E-04	3.1E-05	5.8E-06	0.0E+00	0.0E+00	0.0E+00	0.0E+00				
3	1.6E-03	4.8E-02	9.1E-02	6.3E-02	2.4E-02	9.7E-03	2.4E-03	5.7E-04	4.6E-04	1.5E-04	6.8E-06	2.9E-06	0.0E+00	0.0E+00	0.0E+00	0.0E+00				
2	4.1E-02	1.1E-01	1.5E-01	1.2E-01	4.0E-02	1.2E-02	2.3E-03	5.5E-04	2.7E-04	1.1E-04	0.0E+00	0.0E+00	0.0E+00	0.0E+00	0.0E+00	0.0E+00				
1	4.8E-02	4.5E-02	2.3E-02	1.1E-02	2.9E-03	6.3E-04	3.5E-04	1.8E-05	0.0E+00											

Table 3 Scatter diagram of wave height and wave period (North Atlantic).

number of data																				
average(Hw)=																				
average(Hp)=																				
T(sec.)																				
Hw(m)	-5	6	7	8	9	10	11	12	13	14	15	16	17	18	19	20				
20	0.0E+00	9.1E-06	1.4E-05	8.7E-07	0.0E+00	0.0E+00	0.0E+00	0.0E+00	0.0E+00	0.0E+00										
19	0.0E+00	0.0E+00	0.0E+00	0.0E+00	0.0E+00	0.0E+00	1.2E-06	1.8E-05	2.9E-05	1.2E-06	0.0E+00	0.0E+00	0.0E+00	0.0E+00	0.0E+00	0.0E+00				
18	0.0E+00	0.0E+00	0.0E+00	0.0E+00	0.0E+00	0.0E+00	7.6E-06	5.1E-05	3.5E-05	5.8E-07	0.0E+00	0.0E+00	0.0E+00	0.0E+00	0.0E+00	0.0E+00				
17	0.0E+00	0.0E+00	0.0E+00	0.0E+00	0.0E+00	2.9E-07	1.9E-05	8.9E-05	2.9E-05	5.8E-07	0.0E+00	0.0E+00	0.0E+00	0.0E+00	0.0E+00	0.0E+00				
16	0.0E+00	0.0E+00	0.0E+00	0.0E+00	0.0E+00	2.0E-06	6.8E-05	1.7E-04	2.8E-05	8.7E-07	0.0E+00	5.8E-07	0.0E+00	0.0E+00	0.0E+00	0.0E+00				
15	0.0E+00	0.0E+00	0.0E+00	0.0E+00	0.0E+00	6.1E-06	2.6E-04	2.0E-04	2.4E-05	2.6E-06	0.0E+00	0.0E+00	0.0E+00	0.0E+00	0.0E+00	0.0E+00				
14	0.0E+00	0.0E+00	0.0E+00	0.0E+00	0.0E+00	4.7E-05	6.4E-04	2.1E-04	2.0E-05	2.9E-06	0.0E+00	0.0E+00	0.0E+00	0.0E+00	0.0E+00	0.0E+00				
13	0.0E+00	0.0E+00	0.0E+00	0.0E+00	5.0E-06	2.4E-04	1.2E-03	1.8E-04	2.1E-05	2.0E-06	8.7E-07	0.0E+00	0.0E+00	0.0E+00	0.0E+00	0.0E+00				
12	0.0E+00	0.0E+00	0.0E+00	0.0E+00	2.7E-05	1.2E-03	1.9E-03	1.8E-04	2.1E-05	4.1E-06	1.2E-06	0.0E+00	0.0E+00	0.0E+00	0.0E+00	0.0E+00				
11	0.0E+00	0.0E+00	0.0E+00	1.8E-06	2.5E-04	3.4E-03	1.9E-03	1.7E-04	2.2E-05	6.4E-06	8.7E-07	0.0E+00	0.0E+00	0.0E+00	0.0E+00	0.0E+00				
10	0.0E+00	0.0E+00	0.0E+00	2.8E-05	1.7E-03	6.6E-03	1.6E-03	1.8E-04	3.7E-05	1.1E-05	1.7E-06	0.0E+00	0.0E+00	0.0E+00	0.0E+00	0.0E+00				
9	0.0E+00	0.0E+00	0.0E+00	3.2E-04	7.2E-03	8.6E-03	1.5E-03	2.4E-04	7.2E-05	1.7E-05	1.5E-06	0.0E+00	0.0E+00	0.0E+00	0.0E+00	0.0E+00				
8	0.0E+00	0.0E+00	1.1E-05	2.6E-03	1.8E-02	8.1E-03	1.5E-03	4.7E-04	2.0E-04	2.6E-05	1.7E-06	0.0E+00	0.0E+00	0.0E+00	0.0E+00	0.0E+00				
7	0.0E+00	0.0E+00	2.8E-04	1.4E-02	2.6E-02	6.6E-03	2.2E-03	1.1E-03	2.3E-04	4.7E-05	1.1E-05	3.5E-06	0.0E+00	0.0E+00	0.0E+00	0.0E+00				
6	0.0E+00	3.7E-05	3.0E-03	4.1E-02	2.4E-02	7.5E-03	5.3E-03	1.3E-03	2.8E-04	8.4E-05	1.8E-05	6.4E-06	0.0E+00	0.0E+00	0.0E+00	0.0E+00				
5	1.5E-06	7.1E-04	2.2E-02	5.4E-02	2.4E-02	1.8E-02	7.2E-03	1.1E-03	2.5E-04	7.3E-05	1.4E-05	3.5E-06	1.2E-06	2.9E-07	2.9E-07	0.0E+00				
4	1.3E-04	8.5E-03	4.9E-02	5.9E-02	4.5E-02	2.2E-02	5.1E-03	6.7E-04	1.5E-04	7.1E-05	1.5E-05	3.5E-06	2.3E-06	2.9E-07	5.8E-07	1.5E-06				
3	4.2E-03	3.8E-02	6.6E-02	8.1E-02	4.2E-02	1.0E-02	2.0E-03	4.5E-04	1.4E-04	6.0E-05	9.3E-06	5.2E-06	2.0E-06	2.9E-07	0.0E+00	0.0E+00				
2	2.7E-02	4.4E-02	5.8E-02	3.8E-02	9.2E-03	2.5E-03	8.5E-04	2.4E-04	8.6E-05	4.0E-05	9.9E-06	5.6E-06	0.0E+00	0.0E+00	0.0E+00	0.0E+00				
1	3.0E-02	9.8E-03	6.5E-03	4.5E-03	2.2E-03	1.2E-03	6.2E-04	1.5E-04	7.3E-05	3.4E-05	6.7E-06	1.2E-06	0.0E+00	0.0E+00	0.0E+00	0.0E+00				

Table 4 Scatter diagram of wave height and wave period (North Pacific).

number of data																				
average(Hw)=																				
average(Hp)=																				
T(sec.)																				
Hw(m)	-5	6	7	8	9	10	11	12	13	14	15	16	17	18	19	20				
20	0.0E+00	3.5E-06	9.1E-06	1.2E-06	0.0E+00	1.6E-07	0.0E+00	0.0E+00	0.0E+00	0.0E+00										
19	0.0E+00	0.0E+00	0.0E+00	0.0E+00	0.0E+00	0.0E+00	2.6E-07	1.1E-05	8.2E-06	1.7E-06	1.6E-07	0.0E+00	0.0E+00	0.0E+00	0.0E+00	0.0E+00				
18	0.0E+00	0.0E+00	0.0E+00	0.0E+00	0.0E+00	0.0E+00	3.1E-06	2.2E-05	1.1E-05	3.5E-06	4.2E-07	1.6E-07	0.0E+00	0.0E+00	0.0E+00	0.0E+00				
17	0.0E+00	0.0E+00	0.0E+00	0.0E+00	0.0E+00	2.6E-07	9.9E-06	4.0E-05	1.4E-05	2.9E-06	4.2E-07	0.0E+00	0.0E+00	0.0E+00	0.0E+00	0.0E+00				
16	0.0E+00	0.0E+00	0.0E+00	0.0E+00	0.0E+00	0.0E+00	3.5E-05	7.5E-05	9.9E-06	1.0E-06	1.6E-07	1.6E-07	0.0E+00	0.0E+00	0.0E+00	0.0E+00				
15	0.0E+00	0.0E+00	0.0E+00	0.0E+00	0.0E+00	4.0E-06	1.1E-04	9.3E-05	1.2E-05	4.2E-06	6.4E-07	0.0E+00	1.6E-07	0.0E+00	0.0E+00	0.0E+00				
14	0.0E+00	0.0E+00	0.0E+00	0.0E+00	1.6E-07	2.5E-05	2.7E-04	1.1E-04	1.3E-05	3.8E-06	1.2E-06	1.6E-07	0.0E+00	0.0E+00	0.0E+00	0.0E+00				
13	0.0E+00	0.0E+00	0.0E+00	0.0E+00	1.9E-06	1.1E-04	5.2E-04	1.0E-04	1.3E-05	4.2E-06	1.2E-06	1.6E-07	0.0E+00	0.0E+00	0.0E+00	0.0E+00				
12	0.0E+00	0.0E+00	0.0E+00	0.0E+00	1.6E-05	5.1E-04	8.1E-04	9.8E-05	1.3E-05	3.5E-06	9.0E-07	1.3E-06	1.6E-07	0.0E+00	0.0E+00	0.0E+00				
11	0.0E+00	0.0E+00	0.0E+00	8.4E-07	1.5E-04	1.5E-03	9.6E-04	9.3E-05	1.7E-05	4.8E-06	2.2E-06	1.4E-06	8.4E-07	0.0E+00	0.0E+00	0.0E+00				
10	0.0E+00	0.0E+00	0.0E+00	1.4E-05	8.9E-04	3.1E-03	8.9E-04	9.6E-05	2.0E-05	1.1E-05	3.6E-06	1.6E-06	1.0E-06	5.2E-07	0.0E+00	0.0E+00				
9	0.0E+00	0.0E+00	0.0E+00	2.0E-04	3.9E-03	4.4E-03	8.4E-04	1.3E-04	4.3E-05	1.8E-05	6.2E-06	3.0E-06	1.1E-06	0.0E+00	0.0E+00	0.0E+00				
8	0.0E+00	0.0E+00	9.0E-06	1.7E-03	9.9E-03	4.6E-03	8.9E-04	2.6E-04	1.5E-04	5.0E-05	1.3E-05	7.4E-06	2.3E-06	0.0E+00	0.0E+00	0.0E+00				
7	0.0E+00	0.0E+00	1.9E-04	8.8E-03	1.6E-02	4.5E-03	1.4E-03	7.2E-04	2.8E-04	1.1E-04	2.7E-05	8.1E-06	1.5E-06	0.0E+00	0.0E+00	0.0E+00				
6	0.0E+00	1.7E-05	2.2E-03	2.6E-02	1.7E-02	5.4E-03	4.3E-03	1.5E-03	4.5E-04	1.4E-04	3.0E-05	5.8E-06	1.0E-06	2.6E-07	0.0E+00	0.0E+0				

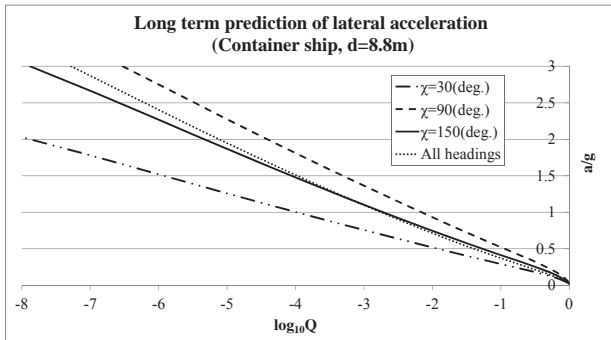


Figure 13 Long term prediction of lateral acceleration at bridge of container ship (Ballast condition, wave scatter diagram: South China Sea).

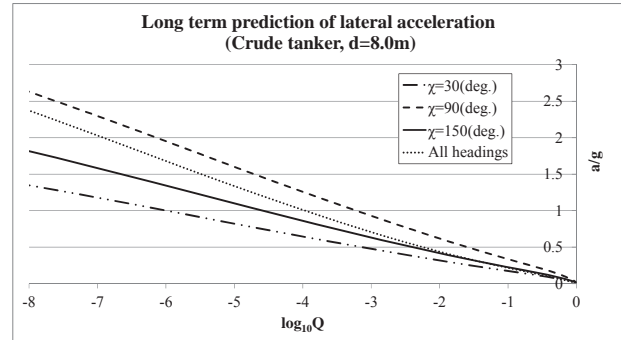


Figure 16 Long term prediction of lateral acceleration at bridge of crude tanker (Ballast condition, wave scatter diagram: South China Sea).

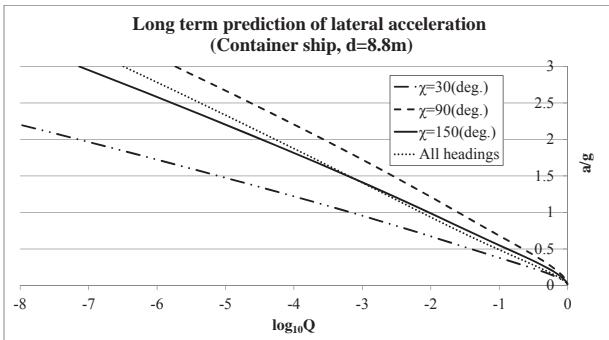


Figure 14 Long term prediction of lateral acceleration at bridge of container ship (Ballast condition, wave scatter diagram: North Atlantic).

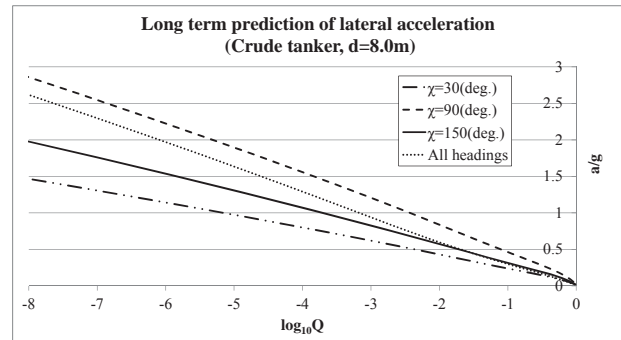


Figure 17 Long term prediction of lateral acceleration at bridge of crude tanker (Ballast condition, wave scatter diagram: North Atlantic).

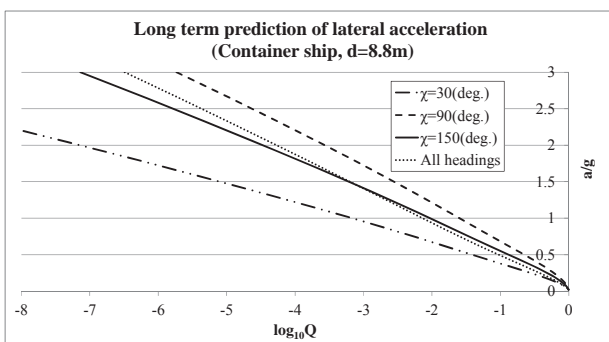


Figure 15 Long term prediction of lateral acceleration at bridge of container ship (Ballast condition, wave scatter diagram: North Pacific).

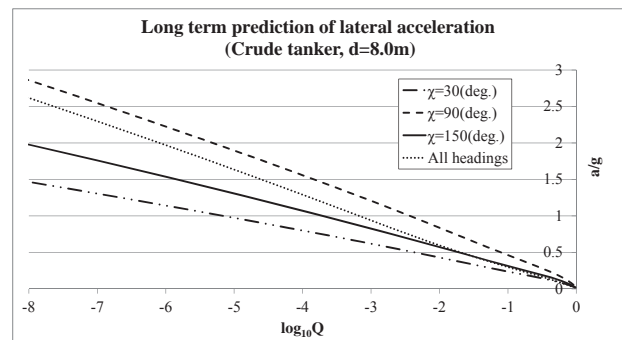


Figure 18 Long term prediction of lateral acceleration at bridge of crude tanker (Ballast condition, wave scatter diagram: North Pacific).

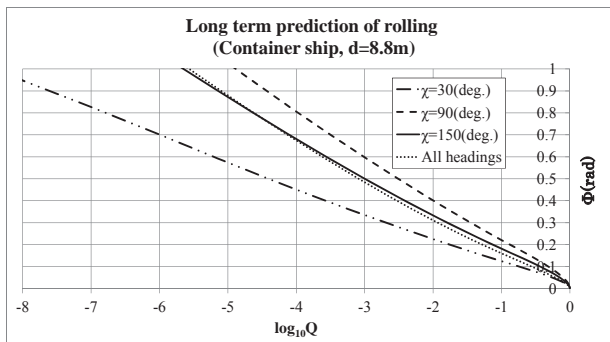


Figure 19 Long term prediction of rolling of container ship (Ballast condition, wave scatter diagram: South China Sea).

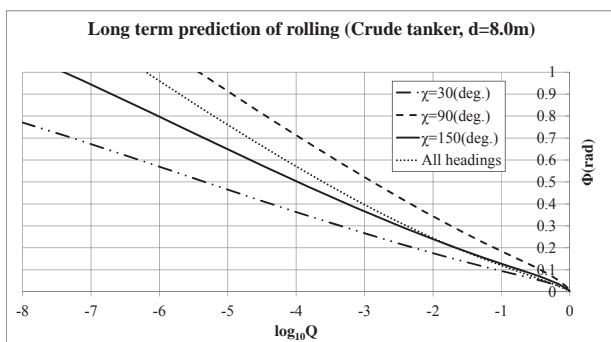


Figure 20 Long term prediction of rolling of crude tanker (Ballast condition, wave scatter diagram: South China Sea).

4. CONCLUSIONS

For the assessment of the correlation between loading condition, sea state and probability of occurrence of lateral acceleration, the short term and long term probability of lateral acceleration was computed. Conclusions are as follows:

1) Sea state in North Atlantic and North Pacific is severer than that in South China Sea although wave becomes severer in the area close to Hong Kong.

2) Lateral acceleration of the object ships in this study becomes larger in the ballast condition.

3) Excessive lateral acceleration occurs in a relatively high probability owing to the roll resonance.

4) It is rational to prevent such a phenomenon that occurs frequently not only by the design criteria but also by the operational guidance or limitation.

5. ACKNOWLEDGMENTS

The present study was carried out in cooperation with the Japan Ship Technology Research Association through the Japanese project for the stability safety in the fiscal year of 2014 that is supported by the Nippon Foundation.

6. REFERENCES

- Federal Bureau of Maritime Casualty Investigation of Germany, 2009, "Fatal accident on board the CMV CHICAGO EXPRESS during Typhoon "HAGUPIT" 24 September 2008 off the coast of Hong Kong", Investigation Report 510/08.
- British Maritime Technology Limited, 1985, "Global Wave Statistics".
- Price, W. G. and Bishop, R.E.D., 1974, "Probabilistic Theory of Ship Dynamics", London: Chapman and Hall Ltd.
- The SWAMP group, 1985, "Ocean wave modelling", Plenum Press.
- Japan Weather Association, 1993, "Research and development of the ocean-waves prediction model and waves information service system by means of a spherical-surface coordinate system".

This page is intentionally left blank



Application of IMO Second Generation Intact Stability Criteria for Dead Ship Condition to Small Fishing Vessels

Francisco Mata-Álvarez-Santullano, *Maritime Accident and Incident Investigations Standing
Commission, Government of Spain*, fmata@fomento.es

Luis Pérez-Rojas, *ETSIN UPM, Madrid, Spain*. luis.perezrojas@upm.es

ABSTRACT

This work analyses the applicability of the Second Generation Intact Stability Criteria (SGISC) to small fishing vessels. The stability performance of a set of ten small fishing vessels in dead ship condition is analysed in relation with the degree of fulfilment of the same vessels of the IMO Weather Criterion. The results obtained show that the vessels which present better stability regarding the SGISC in general show less stability margin under the IMO Weather Criterion. These inconsistencies suggest that SGISC in dead ship condition could require further development for its application to small fishing vessels.

Keywords: *Second generation intact stability criteria, dead ship condition, small vessel, fishing vessel, weather criterion*

1. INTRODUCTION

It is widely recognized that the current stability framework can be improved, being necessary to explore new approaches to develop new intact stability criteria which could capture the complexity of the dynamics experienced by seagoing vessels. The IMO Sub-Committee on Stability and Load Lines and Fishing Vessels at its 45th meeting in 2002 (SLF 45) established a working group with the long-term aim to redefine the Intact Stability Code according to a performance standards approach (Francescutto, 2004). In its current status, the Second Generation Intact Stability Criteria (SGISC) framework contemplates five failure modes: Pure loss of stability, parametric roll, surf-riding / broaching, dead-ship condition; and excessive accelerations. This SGISC is intended to substitute or at least complement to some extent the current stability framework. Regarding the current status of the SGISC in dead ship condition, the IMO

weather criterion is proposed to be the 1st tier criterion for the dead ship condition. The 2nd tier criterion is based on the calculation of the probability of capsizing in certain conditions. Therefore, homogeneity in the trends observed by the application of both stability standards to the same vessels would be expectable.

Focusing in the application of the SGISC for dead ship condition to small fishing vessels, the authors have undertaken a research to study the influence of a specific fishing effort control regulations on the accident rates of part of the Spanish fishing fleet (Mata-Álvarez-Santullano and Souto-Iglesias, 2014, 2012). In the course of this investigation the stability performance in rough weather of ten small fishing vessels under IMO weather criterion and SGISC for dead ship condition was studied.

The current work presents the results of this part of the investigation: the comparison of the stability performance of ten small fishing



vessels under these two mentioned stability criteria.

2. VESSELS STUDIED

Ten small fishing vessels have been studied. They are grouped in two sets: five fishing vessels which were lost in stability

related accidents, and the five vessels which were decommissioned for building the lost ones. These two sets of vessels are referred to as “lost vessels” and “predecessors”, and are given the codes F1 to F5 and P1 to P5, respectively. The ten vessels are presented in Table 1.

Boat	SFFR ¹ code	Gear type	Year of build	Length overall (m)	Tonna ge (GT)	Notes
F1	25057	Seines	2001	17	34.18	Lost vessel
F2	24593	Hook and lines	1999	16.02	29.97	Lost vessel
F3	24391	Seines	1999	18	44.83	Lost vessel
F4	24358	Gilnets / entangling nets	1999	20.5	87.03	Lost vessel
F5	24199	Seines	1999	19.4	59.01	Lost vessel
P1	16060	Seines	1989	15	17.11	Predecessor to 25057
P2	11830	Hook and lines	1963	11.3	5.86	Predecessor to 24593
P3	5969	Seines	1978	14.1	28.7	Predecessor to 24391
P4	251	Gilnets / entangling nets	1983	16	47	Predecessor to 24358
P5	5154	Seines	1959	15.75	29	Predecessor to 24199

Table 1 Fishing vessel case studies

¹ SFFR: Spanish fishing fleet register



The ships in this table are referred to using the SFFR code. The European equivalent to such code is obtained adding to it the country code (ESP). This database may be accessed at <http://ec.europa.eu/fisheries/fleet/index.cfm?lg=en>.

Images of the ten vessels are included in Figure 1.

Vessels	Lost vessel	Predecessor
F1-P1		
F2-P2		No photography available
F3-P3		
F4-P4		

F5-P5



Figure 1. Images of the ten vessels studied

It has not been possible to obtain precise information about all predecessors, for the following reasons:

- Some documents are missing in the ship file or there is not ship file in the Spanish Maritime Administration, as some vessels are quite old.
- Some documents were not compulsory by the regulation that was in force when some of the predecessors were built (e.g. hullform plan, stability book...)
- The shipyards where some boats were built do not exist nowadays or do not keep files of those boats.

Due to these reasons, not all the main dimensions and characteristics of these are available. Some of them have been estimated according to the following procedures:

- Hullforms were obtained by affine transformation of known similar fishing vessels. The vessels from which the studied ones were obtained had similar dimensions, the same type of fishing gear, hull material, and hull type (stern and bow). When possible, ships built in close years and from the same areas of operation were chosen.

- Unknown main dimensions were estimated by linear regression of databases of fishing vessels, similar in size, type of fishing gear, year of built, hull material and area of operation.

For each of the ten fishing studied a characteristic loading condition is established. Each vessel has been studied in one loading condition only, chosen from the information available, normally the full load condition. In the case of vessels for which no stability booklets were available (most predecessors) a loading condition close to the full load is estimated, with the best information available.

3. METHODOLOGY FOR THE ANALYSES

The Weather Criterion is one of general provisions of the IMO 2008 Intact Stability Code. This criterion was originally developed to guarantee the safety against capsizing for a ship losing all propulsive and steering power in severe wind and waves, which is known as a dead ship condition. This criterion is well known and explanatory notes have been developed by IMO explaining the fundamentals behind the criterion (IMO, 2008), the underlying physical laws and the implicit assumptions.

A graphical representation of this criterion is shown in Figure 2.

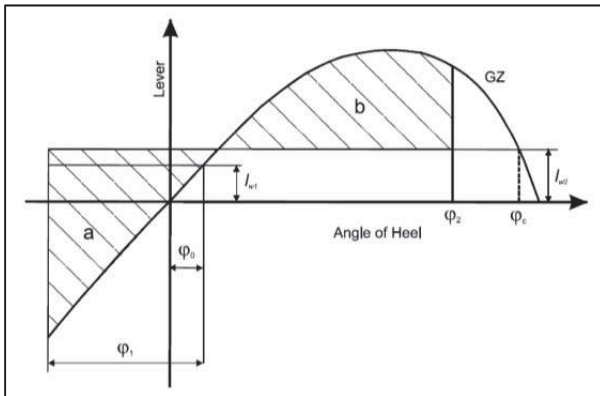


Figure 2 Graphical representation of the weather criterion

The basic principle of the weather criterion is an energy balance between the beam wind heeling and righting moments with a roll motion taken into account. The underlying physical ideas behind the criterion are:

- The ship is assumed to be heeled under the action of a steady beam wind providing a constant, heel independent, heeling moment;
- In addition, the ship is assumed to roll (mainly due to the action of waves) around the equilibrium angle under the action of constant beam wind with amplitude determined according to the criterion.
- When the ship is at the maximum heel to the windward side, a gust occurs leading to a wind heeling moment that is 50% higher than the heeling moment due to the steady wind.
- The ship is required to have sufficient dynamic stability to survive the considered scenario. This will occur if 'b' (Figure 2) is larger than 'a'. Otherwise the vessel will reach the capsizing angle.

It is worth to mention that, under the Spanish regulations, Weather Criterion is not required to be complied with if the area below the stability curve up to a heel angle of 30° is over 0.065 rad x m.

The Weather Criterion is based on partially semi-empirical approaches. To overcome the inherent limitations to this criterion, a Second Generation Intact Stability Criteria (SGISC) for dead ship condition is under development by IMO. Some authors (Bulian and Francescutto, 2006) have proposed a methodology to assess the ship vulnerability to the failure mode "dead ship condition". Under this approach vulnerability is assessed by estimating the short term probability of capsizing by calculating the roll motion under the combined action of stochastic wind and waves. This is the basis of the methodology agreed by the IMO SLF sub-committee for the 2nd tier vulnerability criteria for the dead ship condition (IMO, 2013).

In this paper the probability of capsizing is estimated following the methodology by Bulian and Francescutto with some modifications which are explained hereinafter. Most of the text and formulae included in this section is taken directly from these references. This section is not intended to be a thorough description of the methodology, and further details and explanations may be found in the referenced documents by Bulian and Francescutto (Bulian and Francescutto, 2006, 2004) and IMO.

3.1 Roll model

The objective of this analysis is obtaining a short-term capsize index C_s by means of a simplified calculation methodology which takes into account the roll dynamics in given environmental conditions. The roll motion of the ship can be described by the following 1-dof non-linear model:

$$(J_{xx} + J_{add}) \cdot \ddot{\varphi} + D(\dot{\varphi}) + \Delta \cdot \overline{GZ}(\varphi) = M_{wind,tot}(\varphi, t) + M_{waves}(t) \quad (1)$$

where

- J_{xx} is the ship dry moment of inertia
- J_{add} is the added moment of inertia

- $D(\phi')$ is the general damping moment
- Δ is the ship displacement
- $GZ(\phi)$ is the restoring lever
- $M_{wind,tot(\phi,t)}$ is the total instantaneous moment due to wind taking
- $M_{waves(t)}$ is the total instantaneous moment due to waves

For simplicity, a linear roll damping model is chosen, therefore $D(\phi') = 2 \cdot \mu \cdot \phi'$, with

$$\mu = k \cdot \sqrt{(J_{xx} + J_{add}) \cdot GM \cdot \Delta} \quad (2)$$

where GM is the transversal metacentric height and k a non-dimensional damping coefficient. Following Tello et al. (Tello et al., 2011) the coefficient k may be taken constant for fishing vessels similar to the studied, equal to 0.12.

The spectrum of wave moment is estimated according to the methodology by Bulian and Francescutto. Under this assumption, the excitation moment due to waves M_{waves} is assumed to be a Gaussian process, whose spectrum, $SM_{waves(\omega)}$ is estimated from the sea wave slope spectrum $S_{\alpha\alpha}(\omega)$:

$$S_{M_{waves}}(w) = (\Delta \cdot \overline{GM} \cdot f_{r,waves}(w))^2 \cdot S_{\alpha\alpha}(w) \quad (3)$$

Where $f_{r,waves(\omega)}$ is the effective wave slope function and the spectrum of the wave slope $S_{\alpha\alpha}$ is to be calculated as

$$S_{\alpha\alpha}(w) = \frac{\omega^4}{g^2} \cdot S_{zz}(w) \quad (4)$$

3.2 Wave moment spectrum

Spectrum of wave moment has been obtained by two different methods:

1. Moment of waves is directly computed by state-of-the-art linear seakeeping software that calculates wave loads and vessel motions in regular waves, on the basis of three dimensional potential theory. To avoid problems associated with roll-sway-yaw coupling in the 1-dof roll model only Froude-Krylov moments are considered for the calculations.

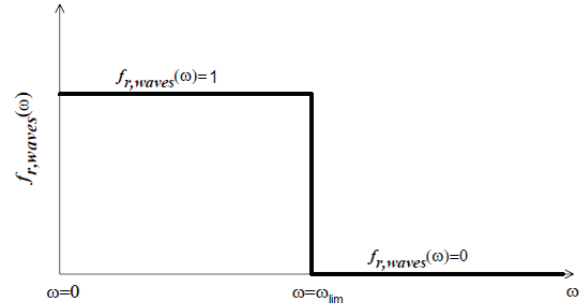


Figure 3 Simplified effective wave slope function

2. A very simplified form for $f_{r,waves(w)}$ is used (Figure 3): a step function that takes value 1 for frequencies lower than w_{lim} , and takes value 0 for values higher than w_{lim} , being w_{lim} the frequency corresponding to a wave having a length equal to one half of the ship breadth:

$$w_{lim} = \sqrt{\frac{2\pi \cdot g}{B/2}} \quad (1)$$

3.3 Roll spectrum

Assuming wind and waves moments to be Gaussian processes, locally uncorrelated, the spectrum of the total roll moment can be computed as the sum of the non-dimensional wind and waves moment spectra.

$$S_m(w) = S_{\delta m_{wind}}(w) + S_{m_{waves}}(w) \quad (6)$$

The final roll spectrum $S_x(\omega)$ can be obtained as follows:

$$S_x(w) = \frac{w_0^4 S_m(w)}{[w_e^2(\varphi_s) - w^2]^2 + [2 \cdot \mu \cdot w]^2} \quad (7)$$



Where ϕ_s is the static equilibrium heel angle under the action of the static wind with velocity V_w and ω_e is the modified roll natural frequency close to the equilibrium angle ϕ_s , given by the equation

$$w_e = w_0 \cdot \sqrt{\frac{GM_{res}(\phi_s)}{GM}} \quad (8)$$

Where $GM_{res}(\phi_s)$ is the derivative of the righting lever curve at ϕ_s .

The linear roll damping model chosen allows us to compute directly the spectrum as all terms in the right side of the above equation are known.

3.4 Capsize index and mean capsize time

The capsizing event is defined as the up-crossing of a certain “equivalent area virtual capsize” angle. In order to take into account the actual shape of the righting lever, two virtual capsize angles to leeward and windward are defined, in such a way that the area under the actual residual righting lever and under the linearized residual righting lever are the same. Such “equivalent area” virtual capsize angles are to be calculated by equations 9 and 10.

$$\text{windward:} \quad \varphi_{cap,EA-} = \varphi_s - \sqrt{\frac{-2}{GM_{res}(\varphi_s)} \cdot \int_{\varphi_{cap,-}}^{\varphi_s} GZ_{res}(\xi) d\xi} \quad (9)$$

$$\text{leeward:} \quad \varphi_{cap,EA+} = \varphi_s + \sqrt{\frac{-2}{GM_{res}(\varphi_s)} \cdot \int_{\varphi_s}^{\varphi_{cap,+}} GZ_{res}(\xi) d\xi} \quad (10)$$

$$\left\{ \begin{array}{l} CI = 1 - \exp(-\lambda_{EA} \cdot T_{exp}) \quad (11) \\ T_{cap} = 1/\lambda_{EA} \quad (12) \\ \lambda_{EA} = \frac{1}{T_{z,Cs}} \cdot \left[\exp\left(-\frac{1}{2 \cdot RI_{EA+}^2}\right) + \exp\left(-\frac{1}{2 \cdot RI_{EA-}^2}\right) \right] \quad (13) \end{array} \right.$$

$$\left\{ \begin{array}{l} RI_{EA+} = \frac{\sigma_{Cs}}{\Delta\varphi_{res,EA+}}; \Delta\varphi_{res,EA+} = \varphi_{cap,EA+} - \varphi_s \quad (14) \\ RI_{EA-} = \frac{\sigma_{Cs}}{\Delta\varphi_{res,EA-}}; \Delta\varphi_{res,EA-} = \varphi_s - \varphi_{cap,EA-} \quad (15) \end{array} \right.$$

Where $GZ\varphi = GZ(\varphi) \cdot I_{wind,tot}$ and $I_{wind,tot}$ is the heeling moment lever due to the action of the mean wind.

From this point, the mean capsize time T_{cap} and the capsize index CI can be estimated. These magnitudes are given by the expressions in equations 11 and 12.

The exposure time T_{exp} is taken equal to 3600 s, and the quantities σ_{Cs} and $T_{z,Cs}$ are to be determined:

$$\left\{ \begin{array}{l} \sigma_{Cs} = \sqrt{m_0} \quad (16) \\ T_{z,Cs} = 2 \cdot \pi \cdot \sqrt{\frac{m_0}{m_2}} \quad (17) \end{array} \right.$$

For a more complete description of the methodology and the process to obtain CI and T_{cap} , the work under development by IMO (IMO, 2013) should be consulted.

3.5 Conditions of the analysis

For the ten vessels studied, T_{cap} and CI have been calculated in two sea states defined by the significant wave height and modal wave period according to the standardized scale adopted by NATO (Military Agency for Standardization, NATO, 1983). For all vessels, SSN4 and SSN5 have been studied, corresponding to significant wave heights of 1.88m and 3.25m with modal periods of 8.8s and 9.7 s respectively. The Bretschneider wave spectrum and exposure time of 1 hour have been considered.

4. RESULTS

4.1 Weather Criterion

Table 2 presents the degree of compliance of the ten vessels studied with the Weather Criterion. Only two vessels (F1 and F2) fail to comply with the criterion, although it must be remarked that none of the case studies had to comply with Weather Criterion, as in all cases the area under the GZ curve up to 30° is larger than 0.065 m.rad.

Vessel	b / a (%)	Heel angle due to steady wind moment (deg)
F1	15.1	9.8
F2	63.2	6.3
F3	143.1	7.1
F4	348.0	5.1
F5	125.6	5.9
P1	147.7	6.6
P2	193.4	5.9
P3	293.0	3.0
P4	306.9	3.4
P5	337.2	1.7

Table 2 Summary of the weather criterion results for the ten vessels studied

4.2 SGISC. Vulnerability in dead ship condition

For the ten vessels studied, Capsize Index (CI) and Mean Capsize Time (T_{cap}) have been obtained according to the methodology explained previously. Results of the analyses are presented in tables 3 to 6.

SSN4 – wave moment calculated by linear seakeeping program

Vessel	Static heel angle ($^\circ$)	CI	T_{cap} (hours)
F1	0.8	5.33E-04	1875
F2	0.6	3.96E-07	2526427
F3	0.7	8.07E-08	12393879
F4	0.5	8.11E-12	1.23E+11
F5	0.6	5.43E-05	18407
P1	0.8	4.14E-03	241
P2	0.6	1.59E-05	63087
P3	0.3	8.06E-09	124132802
P4	0.4	5.60E-10	1.78E+09
P5	0.2	1.46E-07	6847793

Table 3 CI and T_{cap} in SSN4. Wave moment calculated by linear seakeeping program

SSN5 – wave moment calculated by linear seakeeping program

Vessel	Static heel angle ($^\circ$)	CI	T_{cap} (hours)
F1	1.7	0.898827	0.44
F2	1.3	0.060066	16.14
F3	1.5	0.034321	28.63
F4	1.1	0.000404	2477.51
F5	1.3	0.498709	1.45
P1	1.6	0.986700	0.23
P2	1.2	0.271029	3.16
P3	0.6	0.008210	121.30
P4	0.7	0.002221	449.67
P5	0.4	0.030468	32.32

Table 4 CI and T_{cap} in SSN5. Wave moment calculated by linear seakeeping program

**SSN4 – wave moment calculated by
simplified effective wave slope function**

Vessel	Static heel angle (°)	CI	T _{cap} (hours)
F1	0.8	0.012652	78.5
F2	0.6	0.000141	7105.5
F3	0.7	0.000098	10170.0
F4	0.5	0.000002	464736.8
F5	0.6	0.011733	84.7
P1	0.8	0.075432	12.8
P2	0.6	0.007261	137.2
P3	0.3	0.001136	879.9
P4	0.4	0.000049	20328.1
P5	0.2	0.019307	51.3

Table 5 CI and T_{cap} in SSN4. Wave moment calculated by simplified effective wave slope function

**SSN5 – wave moment calculated by
simplified effective wave slope function**

Vessel	Static heel angle (°)	CI	T _{cap} (hours)
F1	1.7	1.00	0.119
F2	1.3	0.5790	1.155
F3	1.5	0.5464	1.265
F4	1.1	0.1099	8.586
F5	1.3	0.9992	0.140
P1	1.6	1	0.060
P2	1.2	0.9949	0.189
P3	0.6	0.8766	0.478
P4	0.7	0.3702	2.163
P5	0.4	0.9997	0.125

Table 6 CI and T_{cap} in SSN5. Wave moment calculated by simplified effective wave slope function

5. RESULTS ANALYSIS

Regarding the Weather Criterion, it is interesting that, while under the Spanish stability regulations in force, Weather Criterion was not required to be checked for F1 and F2, these two vessels failed to pass it.

It is to be noted a very low b/a ratio of about 15% for F1. When comparing the lost vessels with their predecessors, it can be seen that, in general, predecessors have more margin with respect to the criterion limits. Except F4, all the lost vessels have lower b/a ratio than any of the predecessors. Regarding the heel angle due to steady wind, in all cases predecessors have lower values, which is indicative of better stability.

The main result of the SGISC analysis is that in general predecessors present worst stability in dead ship condition, except for the pair F3-P3 and F5-P5, for which the trend is not so clear.

One outcome observed looking at tables 3 to 6 is that in general higher CI's are obtained when using the simplified effective wave slope function for estimating the wave moments than the CIs obtained using the linear seakeeping Froude-Krylov roll moments. This is an expectable result, as in general the simplified effective wave slope function reaches higher values in the frequency calculation domain than the effective wave slope estimated by the seakeeping program.

The comparisons between F3-P3 and F5-P5 provide different results depending on which roll moment calculation method is chosen. For instance, comparing vessels F3 and P3 in SSN5, if roll moment is obtained by linear seakeeping calculations, P3 results to have lower CI (that is to say, better stability performance). On the contrary, if the wave roll moment is estimated by the simplified effective wave slope, F3 results with better stability. This suggests that in some cases the simplified effective wave slope may not provide the needed accuracy at estimating wave roll moment for the intended regulatory use.

Except for the pairs of vessels F3-P3 and F5-P5, in general, the lost vessels seem to



have better behaviour in dead ship condition than the predecessors.

According to the results obtained, it seems the two methods used for comparing the stability in rough weather (IMO standard Weather Criterion, and 2nd Generation Stability Criteria dead ship condition) does not correlate. While according to Weather Criterion predecessors show in general better performance, in dead ship condition the lost vessels tend to have smaller capsize indexes.

6. CONCLUSIONS

The analysis conducted has not thrown consistent results in regards to pointing to the lost vessels as less secure from the point of view of these rough weather criteria.

Considering the variability in the results obtained, it is guessed that further validation work might be needed for ensuring that Second generation intact stability criteria (SGISC) in dead ship condition is providing a robust methodology to quantitatively determine capsizing probabilities for regulatory purposes. The large sensibility of short term capsize index CI and capsize time T_{cap} formulation to small input parameters variations may indicate that further validation is needed in order to ensure the methodology it suitable for early design stability assessment or regulatory purposes, as in design stages many vessel parameters are still uncertain or may have a large variability which would affect the values of CI and T_{cap} .

At this stage, this methodology is believed to provide good guidance at design stages when comparing different design options or comparing vessels.

7. REFERENCES

Bulian, G., Francescutto, A., 2004, "A simplified modular approach for the

prediction of the roll motion due to the combined action of wind and waves", Proceedings of The Institution of Mechanical Engineers Part M-journal of Engineering for The Maritime Environment 218, 189–212. doi:10.1243/1475090041737958

Bulian, G., Francescutto, A., 2006, "Safety and operability of fishing vessels in beam and longitudinal waves", International Journal of Small Craft Technology.

Francescutto, A., 2004, "Intact Ship Stability: The Way Ahead", Marine Technology Vol. 41, pp. 31–37.

IMO, 2008. Circular MSC.1/Circ.1281. Explanatory notes to the international code on intact stability, 2008.

IMO, 2013. Development of second generation intact stability criteria. Vulnerability assessment for dead-ship stability failure mode. Submitted by Italy and Japan (No. SC 1/INF.6), Sub-committee on ship design and construction. International Maritime Organization, London.

Mata-Álvarez-Santullano, F., Souto-Iglesias, A., 2012, "Fishing effort control policies and ship stability: Analysis of a string of accidents in Spain in the period 2004–2007". Marine Policy, Vol. 40, pp. 10–17. doi:10.1016/j.marpol.2012.12.027

Mata-Álvarez-Santullano, F., Souto-Iglesias, A., 2014, "Stability, safety and operability of small fishing vessels", Ocean Engineering Vol. 79, pp. 81–91. doi:10.1016/j.oceaneng.2014.01.011

Military Agency for Standarization, NATO, 1983, "Standardized wave and wind environments and shipboard reporting of sea conditions (No. 4194)", STANAG.

Tello, M., Ribeiro e Silva, S., Guedes Soares, C., 2011, "Seakeeping performance of fishing vessels in irregular waves", Ocean Engineering Vol. 38, pp. 763–773. doi:10.1016/j.oceaneng.2010.12.020

Investigation of the Intact Stability Accident of the Multipurpose Vessel MS ROSEBURG

Adele Lübcke, *Institute of Ship Design and Ship Safety, Hamburg University of Technology*

adele.luebcke@tu-harburg.de

German Federal Bureau of Maritime Casualty Investigation (Hamburg)

ABSTRACT

This paper presents the results of the accident of the multipurpose vessel MS ROSEBURG. On the voyage from Riga to Barrow Haven the ship was laden with timber cargo on the deck and in the hold. In the Bay of Kiel the ship was caught by a gust of wind and reached a heeling angle of 10 to 15 degrees. The deck cargo began to slip and lashing straps for cargo securing broke. The ship reached a heeling angle of 40 degrees. About 75 percent of the deck cargo was lost. Afterwards the ship rested at a stable equilibrium.

Keywords: *Intact Stability; Ship Accident; Accident Investigation; Ship Safety; MS ROSEBURG*

1. INTRODUCTION

The investigation of accidents is useful to better understand the casualty roots. In this paper the accident of MS ROSEBURG is investigated which happened in an intact condition of the vessel. Hence conclusions can be made, whether the applicable intact stability criteria are sufficient.

MS ROSEBURG was built in 1990 as a combined freighter for timber and grain cargo. On the relevant voyage the vessel was laden with timber cargo in the hold and on deck and a few cable reels in the hold. The ship started in Riga on the evening of 02 November 2013. Three days later, on 05 November 2013, MS ROSEBURG reached the Bay of Kiel, where the accident occurred.

The sequence of events leading to the accident is reconstructed by the witness statements. The crew of the vessel, the harbour police and the company for the recovery of the timber cargo were asked to

comment on the accident. According to this the accident happens as follows:



Figure 1 Consequences of the accident

At five o'clock the captain asked for the permission of anchoring to perform small repairs. Shortly afterwards the ship began to heel and reached a heeling angle of 10 to 15 degree caused by a gust of wind. As a result of the heeling angle and the related accelerations the timber cargo on deck slipped and the load securing failed. Hence the ship reached a heeling angle of 40 degree and the

main part of timber cargo on deck went overboard. Following the stability of MS ROSEBURG was increased and the vessel reached a stable position of equilibrium. In Figure 1 the consequences of the accident are shown. People were not injured in the accident.

In this paper the questions will be answered, which stability condition resulted in the accident and why it occurred in the Bay of Kiel. Therefore, the paper begins with the presentation of MS ROSEBURG and the according calculation model. Afterwards the documents of the loading condition are analysed checking the consistency. In addition it is analysed why the voyage from Riga to the Bay of Kiel was without an accident. This is done by the calculation of the accelerations of the deck cargo taking into account realistic environmental conditions during the voyage. Finally the process of the accident and all related information are summarized in the conclusion.

All calculations are executed within the ship design environment E4 which is developed by the Institute of Ship Design and Ship Safety at the Hamburg University of Technology and partners.

2. SHIP AND CALCULATION MODEL

2.1 MS ROSEBURG

The multipurpose vessel MS ROSEBURG was originally built in 1990 as MV BALTIC BORG by the shipyard FERUS SMIT BV Hoogezand as Hull No. 257. The call sign of the vessel is V2PS2. MS ROSEBURG is classified at Lloyd's Register in Rotterdam. The ship is designed for timber and grain cargo with a maximum permissible deadweight of 3005 t. A side view of the vessel is presented in figure 2. At the time of the accident, the ship was registered in St.

John's, Canada. In table 1 the main dimensions of MS ROSEBURG can be found.

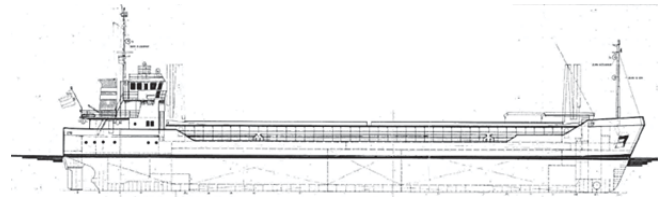


Figure 2 Side view of MS ROSEBURG

Length over all	78.00 m
Breadth	12.50 m
Draft at summer freeboard	4.95 m
Depth to main deck	6.60 m

Table 1 Main dimension of MS ROSEBURG

According to the stability booklet the safety requirements of the Intact Stability Code are applied. In the following investigation these rules are considered for the evaluation of the stability condition in the different loading conditions which means:

- $GM_0 \geq 0.15$ m
- $h(30^\circ) \geq 0.20$ m
- h_{\max} at $\varphi \geq 25^\circ$
- $\text{Area}(0^\circ, 30^\circ) \geq 0.055$ m·rad
- $\text{Area}(0^\circ, 40^\circ) \geq 0.090$ m·rad
- $\text{Area}(30^\circ, 40^\circ) \geq 0.030$ m·rad
- Weather Criteria

2.2 Calculation Model

The calculation model of MS ROSEBURG is presented in figure 3. For the investigation the buoyancy body is composed of the forecastle (green) and the stern geometry (red) up to the height of 8.8 m which corresponds to the height of the hatch cover (blue). The sheer strake is not taken into account as a part of the buoyancy body. Furthermore the deckhouse is not modelled due to the fact that it is only relevant at a

heeling angle of more than 45 degrees which did not occur during the accident.

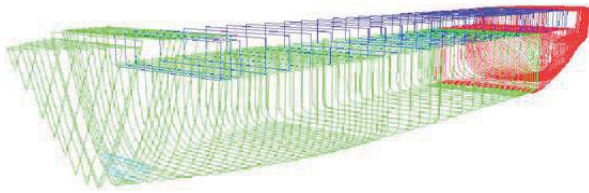


Figure 3 Calculation model

To control the calculation model, a comparison of a standard loading condition of the stability booklet ("Timber length packages Departure") is made between the given and calculated hydrostatic characteristics and the weight distribution. The values of the weight, the draft, the stability etc. are approximately similar. The comparison is shown in table 2 in detail. Therefore it can be assumed that the calculation model represents the real behaviour of MS ROSEBURG.

	Calc.		Stab. Booklet	
Displacement	4037.0	t	4037.070	t
Draft at AP	4.923	m	4.928	m
Draft at FP	4.949	m	4.950	m
LCG from AP	39.742	m	39.739	m
VCG a. BL	4.922	m	4.931	m
GM ₀	0.449	m	0.454	m
GG'	0.030	m	0.038	m

Table 2 Comparison of the calculated and given values

3. THE DECISIVE VOYAGE

On the second of November 2013 MS ROSEBURG was laden with timber cargo and cable reels and left the port of Riga at 20.00 o'clock. The destination of the voyage was the harbour of Barrow Haven, UK. On the fifth of November 2013, the vessel reached the Bay of Kiel where the accident occurred. The track of the vessel is displayed in figure 4.

Following the documents of the loading conditions of the voyage are analysed at the departure and the arrival time. The stability condition must be significantly changed at the Bay of Kiel. Otherwise the accidents would already take place during the voyage.



Figure 4 AIS Data of MS ROSEBURG

3.1 Departure Condition

Based on the documentation of the on board computer, the ship has an deadweight of 2886 t with a draft of 5.00 m forward, 4.90 m aft and a mean draft of 4.95 m. Furthermore, the lever arm curve is calculated which is presented in figure 5.



Figure 5 Lever arm curve during the departure time

From this, it can be said, the deadweight and the draft do not exceed the maximum values. Also the intact stability criteria are fulfilled by this loading condition.

It was recognized that the printout from the on board computer has a discrepancy

regarding the cargo on deck. The timber packages on deck are specified with a volume of 609 m³, but without a mass and a centre of gravity. From further documents it is clear that the mass of the hold cargo must include the mass of the timber packages on the hatch covers/ on deck.

Therefore, a new calculation is performed with a corrected centre of gravity for the load of the timber cargo on deck. It is assumed that the mass of the cargo is 1845 t in the hold and 300 t on deck. This corresponds to the loading condition of comparison from the stability booklet. As a result the initial stability of the ship is reduced from 0.891 m to 0.412 m, also the lever arm for greater heeling angles. In figure 6 the lever arm curve with a corrected centre of gravity is presented. In this case MS ROSEBURG do not comply the applicable intact stability criteria.



Figure 6 Lever arm curve during the departure time with corrected centre of gravity

3.2 Arrival Condition according to Shipping Company

Furthermore the shipping company created an additional loading condition, which must describe the loading condition at arrival time in the Bay of Kiel. This document was ensured by an inspector at the office of the shipping company.

In comparison to the corrected on board document (departure condition, corrected) the information about the mass of the cargo load and the water ballast differ partly. The total mass of the timber cargo is 2555 t in this case, which is 323 t greater than the given value of the on board computer with 2232 t. Looking at the mass of the timber cargo in hold the values are practically equal. But the mass of the decks cargo is increased by 323 t in case of the information by the shipping company. Additionally the mass of the ballast water is reduced from previous 563 t (departure condition, corrected) to 250 t. Therefore the double bottom tanks are empty. Figure 7 shows the regarding lever arm curve. In this condition MS ROSEBURG has a significant reduced stability based on the additional weight on deck and the missing water ballast in the double bottom tanks.

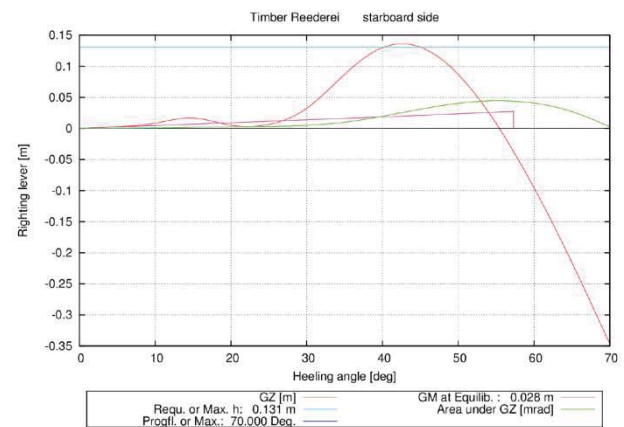


Figure 7 Lever arm curve according to shipping company

It has to be mentioned the draft with 4.90 m forward, 5.18 m aft and a mean draft of 5.04 m exceeds the limit of 4.95 m. Accordingly the vessel is formally overloaded. In this condition the intact stability criteria are not fulfilled. From this it is not clear, why the shipping company did not noticed that the stability condition is insufficient.

3.3 Consideration about the Cargo Plan

Due to the disagreement about the timber cargo (difference of 323 t) further documents and information are analysed to find the true loading condition during the voyage. In figure 8 the cargo plan of MS ROSEBURG can be found. From this it can be said that there are no deviations between the data of the on board computer and the cargo plan. The mass of the cargo on deck is also included in the mass of the cargo in hold which does not represent the centre of gravity correctly.

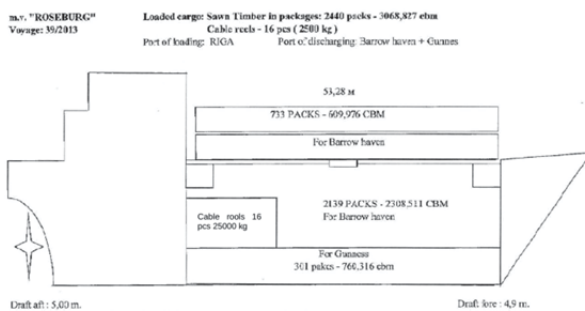


Figure 8 Cargo Plan

The company, which recovered the lost timber packages, specifies the cargo with 700 packages of timber. According to evidence up to 75 percent of the on deck cargo went overboard. Thereby the total number of timber packages on deck can be calculated with a result of at least 933 packages. The cargo plan gives a value of only 733 timber packages. Hence the information of the cargo plan and the printout of the on board computer are doubtful.

Furthermore timber packages with a mass of around 750 to 800 t were recovered from the water. Taking into account wet wood has a 1.7 times major mass density than dry wood, the loss of cargo is determined to 440 to 470 t. This corresponds to the loss of 75 percent deck cargo. Hence the cargo on deck is assumed to 587 to 626 t. The range of the calculated deck cargo fits to the given value by the shipping company.

But how is the difference of the deck cargo between the information of the on board

document and the shipping company explainable? Firstly, it was established that the loading condition at departure time does not include a mass of a deck cargo but a volume with 609 m³ of timber packages. Hence the assumption is made the mass of this cargo is considered in the value of the cargo in hold. However this hypothesis seems to be incorrect. Such a volume is approximately equivalent to a mass of 300 t which corresponds to the difference between the cargo plan and the information of the shipping company. From this and the above considerations it follows immediately that the printout of the on board computer does not include the mass of the deck cargo with the given volume of 609 m³.

3.4 Most Likely Loading Condition at Departure Time

Following from the previous considerations the cargo on deck was not correctly declared regarding the mass and the centre of gravity in the printout of the on board computer. Hence the loading condition at departure time is corrected in accordance to the previous investigations. This loading condition is considered to be the most likely loading condition at departure time in Riga. In figure 9 the corrected lever arm curve is presented.



Figure 9 Lever arm curve at departure time in Riga with corrected centre of gravity and cargo load

The corrections take into account the centre of gravity of the timber cargo on deck and the missing mass. The additional deck cargo is estimated with 320 t. This value is calculated from the difference between the information s of the timber cargo from the on board computer and the shipping company. The centre of gravity is assumed with the value of the loading condition of comparison of the stability booklet.

In consideration of this the deadweight is determined to 3206 t in the loading condition on departure from Riga. Thus the maximum value of 3005 t is exceeded. Furthermore the intact stability criteria are not complied.

3.5 Summary of the Loading Condition during the Voyage

From the analysis of the documents and all information MS ROSEBURG is overloaded at departure. At this time it is not possible that some ballast water tanks were empty because that results in a stability condition according to the lever arm curve in figure 7 which is with high probability the accident condition. Based on the departure loading case the accident condition is produced by draining the ballast water tanks. Consequently it is most likely that the accident at the Bay of Kiel was a result of the intention to comply with the load lines because the maximum draft was checked before entering the Kiel Canal. Otherwise the accident would have happened much earlier during the voyage. In section 4 the assumption of the loading conditions is investigated in detail.

4. ANALYSIS OF THE ROLL MOTION AND THE HEELING MOMENTS

Following, dynamic investigations of the roll motion and the heeling moments are made for the validation of the stability condition at accident time. Furthermore it is

check whether the vessel could have achieved the Bay of Kiel in the most likely loading condition without any loss of cargo and further stability problems.

4.1 Accident Condition

At the accident time it is assumed that MS ROSEBURG has the stability condition according to the loading condition of the shipping company. In figure 7 the related lever arm is already presented. It shows the vessel has an equilibrium position at zero degree without a resulting moment. But small heeling moments result in a roll motion around the equilibrium position. Thereby there is a limit for the moment which has the effect that the vessel has the new equilibrium position of approximately 25 degree.

For the investigation the roll motion is calculated for defined heeling moments acting on the vessel in still water. The heeling moment M_{heel} is determined by the shift of the transverse centre of gravity dy_G which is incrementally increased. Thereby the calculation is made for the determination of the maximum roll angle φ_{max} the static angle of the equilibrium φ_{stat} and the maximum transverse acceleration a_y on deck during the roll motion. In table 3 the results are summarized.

dy_G [mm]	M_{heel} [mt]	φ_{max} [°]	φ_{stat} [°]	a_y [m/s ²]
1	4	9.5	3.8	1.6
2	8	10.7	5.1	1.8
3	12	12.1	5.9	2.0
4	16	13.6	6.6	2.2
5	20	15.4	7.0	2.5
6	24	19.0	7.8	3.2
7	28	28.2	8.4	4.5
8	32	29.5	9.0	5.0
9	36	30.4	9.8	5.1
10	40	31.1	25.5	5.3
11	44	31.8	25.8	5.5

Table 3 Results of the calculation of the roll motion for different heeling moments

The results correspond to the previous assumptions. Small heeling moments cause small static and maximum heeling angles and moderate accelerations in transverse direction. From a heeling moment of 28 mt (see table 3, printed in bold type) the ship reached a maximum heeling angle of 28 degree because the first stability level is passed. The equilibrium position is found at a heeling angle of 8.4 degree providing the cargo on deck does not slip. In figure 10 the roll angle is shown in time domain. The related maximum acceleration is 4.5 m/s².

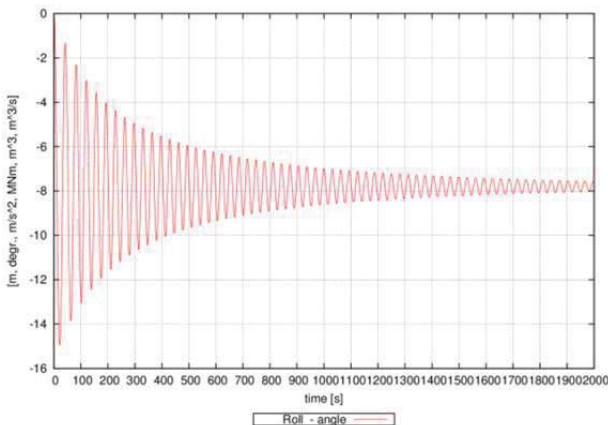


Figure 10 Roll angle for a heeling moment of 28 mt

In case of a heeling moment of 40 mt (see table 3, printed in bold type) the equilibrium position is at a heeling angle of 25 degree, but the transverse acceleration is slightly larger in comparison to the previous calculation. In figure 11 the heeling angle in time can be found. Hence it is assumed the lashings of the timber packages on deck fail not later than in case of a resulting acceleration of 4 to 5 m/s². But it is also possible the cargo securing breaks down earlier because from the described sequence of events leading to the accident the heeling angle is 10 to 15 degree caused by the gust of wind. With high probability it can be assumed that the acceleration of 4.5 m/s² is sufficient to trigger the failure of the load securing. Hence the

value is used for the following calculation in section 4.2.

According to the calculations the accident takes place in the assumed stability condition (loading condition of the shipping company) as a result of a heeling moment of 28 mt. Using equation 1 the wind speed can be calculated for a given heeling moment. The wind lateral area A_{lat} is determined with 600 m² and a wind lever z_w of 6.5 m. The density of air ρ_{air} is 1.226 kg/m³. Thereby the influence of waves and others is not taken into account.

$$M_{heel} = \frac{1}{2} \cdot \rho_{air} \cdot v_w^2 \cdot A_{lat} \cdot z_w \quad (1)$$

The assumed heeling moment of 28 mt corresponds to a wind speed of 10.7 m/s which is equivalent to 5.5 Beaufort. In addition the calculation is made for a heeling moment of 40 mt which is caused by a wind speed of 12.8 m/s or 6.0 Beaufort.

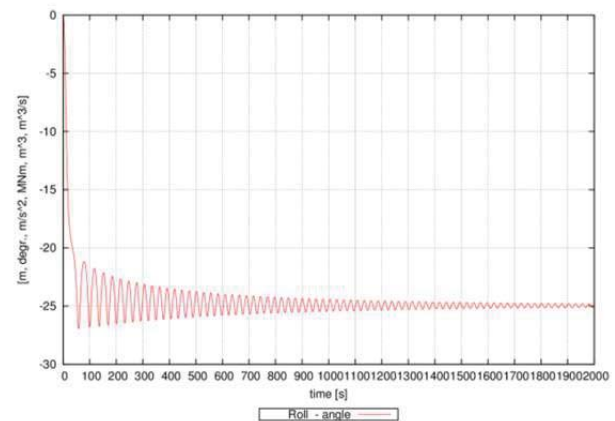


Figure 11 Roll angle for a heeling moment of 40 mt

The information about the weather condition is given by the German Weather service, which based on measurements and observations of surrounding stations. At the accident time the significant wave height is specified with 0.5 m and wind strength of 4 to 5 Beaufort, in gusts 6 to 7 Beaufort. Following it can be said the wind heeling moment caused the accident with a high probability of occurring.

The investigation confirms the accident progresses in this stability condition. Furthermore it is clear the voyage of MS ROSEBURG would not occur without a critical incident in this loading condition.

4.2 Most Likely Loading Condition at Departure Time

In addition the most likely loading condition at departure time has to be investigated to prove that the voyage would happen without a loss of cargo. Therefore a polar diagram is calculated which presents the significant wave height for the transverse acceleration of 4.5 m/s^2 in real sea condition. This acceleration is determined from the previous considerations which have to occur to cause the loss of the cargo on deck during the voyage. In figure 12 the polar diagram is exemplarily shown for a wave period of 7.5 s and 8.5 s. The sea condition is generated by a JONSWAP-spectrum.

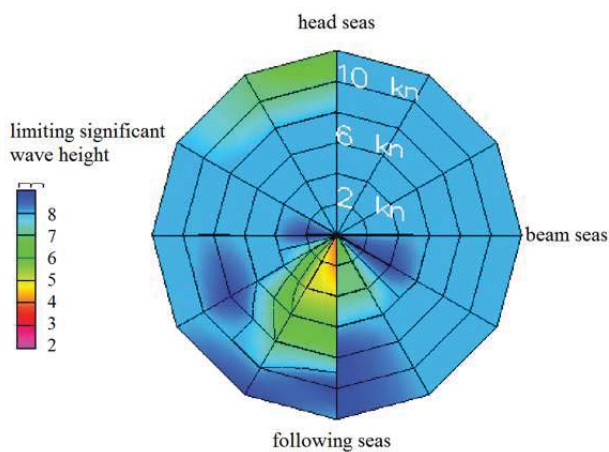


Figure 12 Polar diagram for a wave period of 7.5 s (left) and 8.5 s (right)

The significant wave height has to be not less than 5.0 m to cause a loss of cargo on deck. That is not occurred with high probability. The sea state and weather information confirm this assumption. Hence the vessel has started the voyage with ballast

water which corresponds to the reconstructed loading condition. Otherwise the accident would have happened during the voyage.

5. CONCLUSIONS

The paper presents the intact stability accident of MS ROSEBURG. Therefore the investigations are carried out based on the documents found by the competent authorities during the recovery of the lost cargo of the vessel, the description of the weather conditions and the given evidence.

MS ROSEBURG left the port of Riga with a sufficient stability but without the compliance of the established intact stability criteria. Also the permitted deadweight was exceeded caused by the timber load and additional ballast water to have a sufficient stability. The analysis of the roll motion in natural seaway shows the voyage could take place without a loss of cargo in this loading condition.

As a result of the presented investigation the ballast water was pumped out in the Bay of Kiel. Hence the maximum draft was complied, but the stability of the vessel was reduced significantly. Consequently a small gust of wind caused the accident of MS ROSEBURG.

Such an investigation of an intact stability accident shows that the existing intact stability criteria are sufficient. The compliance of the applicable regulations would have avoided this accident.

6. ACKNOWLEDGMENTS

The author would like to thank for the support of the German Federal Bureau of Maritime Casualty Investigation (Hamburg) and the permission to use the information of MS ROSEBURG.



7. REFERENCES

Bundesamt für Schifffahrt und Hydrografie.
Unpublished, 2013.

German Federal Bureau of Maritime Casualty
Investigation(Hamburg)Untersuchungsber
icht. 342/13, 2013.

German Weather Service. Unpublished, 2013.

Wasserschutzpolizei Kiel. Unpublished, 2013.

This page is intentionally left blank

Session 6 – EMSA III WORKSHOP

Risk Acceptance and Cost-Benefit Criteria Applied in the Maritime Industry in Comparison with Other Transport Modes and Industries

**Probabilistic Assessment of Survivability in Case of Grounding:
Development and Testing of a Direct Non-Zonal Approach**

Damage Stability Requirements for Passenger Ships – Collision Risk-Based Cost-Benefit Assessment

This page is intentionally left blank



Risk Acceptance and Cost-Benefit Criteria Applied in the Maritime Industry in Comparison with Other Transport Modes and Industries

John Spouge, *DNV GL* john.spouge@dnvgl.com

Rolf Skjong, *DNV GL* rolf.skjong@dnvgl.com

Odd Olufsen, *DNV GL* odd.olufsen@dnvgl.com

ABSTRACT

This paper identifies the risk acceptance and cost-benefit criteria of various transport modes and industries, and compares them with those currently applied to the maritime industry.

The current maritime criteria are in general within the range of criteria used in other industries and transport modes, and in most cases in line with good practice elsewhere, so far as this can be determined. In the light of this, the paper considers whether there are any opportunities for improvements of the maritime criteria.

Keywords: *Risk Criteria, Cost-Benefit, Transport*

1. INTRODUCTION

This paper presents results from the third study commissioned by the European Maritime Safety Agency (EMSA) related to the damage stability of passenger ships. The study aims at further investigating the damage stability in a formal safety assessment (FSA) framework in order to cover the knowledge gaps that have been identified after the finalisation of the previous EMSA studies and the GOALDS project. Part of this study focussed on risk acceptance and cost-benefit criteria (DNV GL 2015), and that work is summarised in the present paper.

The objectives of this work were to identify the risk acceptance and cost-benefit criteria of various transport modes and industries, and to compare them with those currently applied to the maritime industry (IMO 2013).

The following transport modes and industries were reviewed:

- Aviation transport (EASA 2013, ICAO 2001, EUROCONTROL 2001, DfT 2007).
- Road transport (SafetyNet 2009a, 2009b, DoT 2013, ACDS 1991, Diernhofer et al 2010, PIARC 2012).
- Rail transport (European Commission 2012, RSSB 2009, LU 2012).
- Nuclear industry (ICRP 1997, EURATOM 1996).
- Onshore process (HSE 2001, BEVI 2004, Duijm 2009, HKPD 2011).
- Offshore oil & gas (ISO 2000).
- Healthcare (USEPA 2010).

The review concentrated on criteria for risks of fatalities, but it also covered criteria for risks of injuries and ill health.



2. DECISION-MAKING IN THE MARITIME INDUSTRY

When designing, managing or regulating ships, decisions sometimes have to be made about questions such as:

- Does the ship have adequate safety to be approved for operation?
- Are restrictions or other safety measures necessary to reduce its risks?
- How much risk reduction is required?
- What level of safety should be achieved by new rules?

To answer questions such as these, the decision-maker must decide when the ship or the maritime operation is safe enough, i.e. when the risks are so low that further safety measures are not necessary. Risk criteria are intended to guide this decision-making process in a systematic way.

In a quantitative risk assessment (QRA), risk criteria can be used to translate numerical risk estimates (e.g. 10⁻⁷ per year) into value judgements (e.g. “negligible risk”) which can be set against other value judgements (e.g. “beneficial transport of goods”) in a decision-making process, and presented to the public to justify a decision.

Risk criteria are also useful where risks are to be compared or ranked. Such comparisons are sometimes complicated by the multi-dimensional nature of risk, e.g. rare high-consequence accidents may be exchanged for more likely low-consequence ones. Risk criteria can help the ranking of such options.

Risk assessment is often a qualitative process, based on expert judgement. In this case, risk criteria may be qualitative standards that help decide whether further action is needed.

The risks of accidents on a ship are not the only consideration when making decisions about safety standards. Operational, economic, social, political and environmental factors may

be important too. As a result, decisions about safety levels on ships are complex judgements, which cannot be reduced to simple rules or criteria. Nevertheless, it is possible to provide guidance on some of the most critical risk issues, and this is what risk criteria attempt to do.

3. TERMINOLOGY

The term “risk criteria” is defined by ISO (2009) as “terms of reference against which the significance of a risk is evaluated”. Despite the existence of this standard term, different industries use varying terminology for this concept, as shown in Table 1.

Table 1. Terminology Equivalent to Risk Criteria in Different Industries

INDUSTRY	TERMINOLOGY
Aviation transport	Target level of safety
Road transport	Safety targets
Road transport of dangerous goods	Risk criteria
Rail transport	Risk acceptance criteria (RAC)
Nuclear industry	Dose limits
Onshore process industry	Risk criteria
Maritime industry	Risk evaluation criteria

The current guidelines on FSA (IMO 2013) define “risk evaluation criteria” as the term to describe “criteria used to evaluate the acceptability/tolerability of risk”. Despite this, the annex containing the criteria also uses the terms “risk criteria” and “risk acceptance criteria”. It might therefore be appropriate to follow ISO by standardising on the term “risk criteria”. However, the term “risk acceptance criteria” could be considered clearer for people unfamiliar with the ISO definition, and its abbreviation (RAC) is also useful.

It is generally considered impractical to divide risks simply into “acceptable” and

“unacceptable”. In reality, there is a spectrum, in which higher risks need more stringent control. Risk criteria therefore typically divide the risk spectrum into regions, each calling for different types of response and usually give qualitative terms to each. The different terms used by decision-makers can be sorted into the following groups:

Unacceptable/ Intolerable/ <i>De manifestis</i>	Highest risk
Tolerable/ Risk reduction desirable/ ALARP/ALARA	Intermediate risk
Acceptable/ Negligible/ <i>De minimis</i>	Lowest risk

In this paper, the terms within each group are treated as interchangeable.

4. TYPES OF RISK CRITERIA

Risks can be measured in many ways, and for every metric that can be used to describe a risk, there are corresponding risk criteria. In this paper the following types of risk criteria are distinguished:

- Risk matrix criteria – evaluating the regions on a matrix of accident frequency (or probability) and consequence (or severity) – e.g. Figure 1.

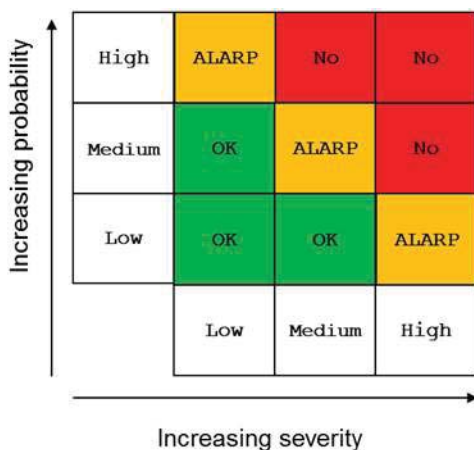


Figure 1 Example Risk Matrix Criteria

- Individual risk criteria – evaluating the risk of death to an individual – e.g. Figure 2.

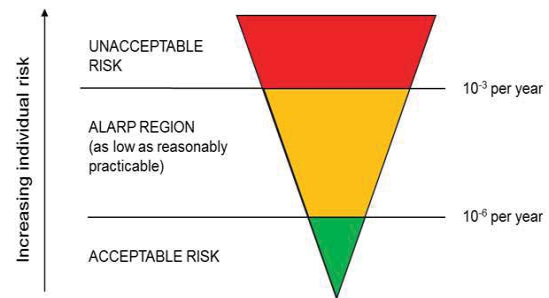


Figure 2 Example Individual Risk Criteria

- Societal risk criteria - evaluating the risk of death to the whole exposed population. These often apply to frequency-fatality (FN) curves – e.g. Figure 3.

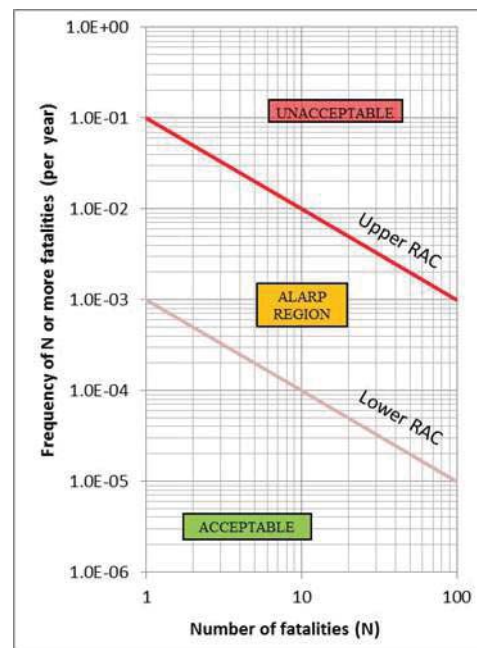


Figure 3 Example Societal Risk Criteria

- Cost-benefit criteria - evaluating the cost of risk reduction measures in a cost-benefit analysis (CBA). Although these do not evaluate the significance of risks directly, and hence are not strictly risk criteria at all, they do evaluate the need for risk reduction, and are closely connected to risk criteria.



Table 2. Application of Types of Risk Criteria in Different Industries

INDUSTRY	RISK MATRIX	INDIVIDUAL RISK	SOCIETAL RISK	ALARP/COST-BENEFIT
Aircraft design (EASA)	√			
Air Traffic Management (EUROCONTROL)		√		
Airports (UK)		√		
Road transport (EU MS)		√	√	√
Road transport of DG (ACDS)		√	√	√
Road transport of DG (Switzerland)			√	√
Road tunnels (Austria)		√		
Rail transport (ERA)		√	√	
Rail transport/LU (UK)		√	√	√
Nuclear (ICRP)		√		√
Onshore process (UK)		√		√
Onshore process (Netherlands)		√	√	√
Onshore process (Flanders)		√	√	
Onshore process (France)	√			√
Offshore (ISO)	√			
Healthcare				√
Maritime		√	√	√

Table 2 shows the metrics that are used for risk criteria in various transport modes and industries. Many industries make use of individual and societal risk criteria, and cost-benefit or qualitative criteria defining when risks are as low as reasonably practicable (ALARP). Risk matrix criteria are also widely used, but the table shows only those industries using them as their primary metric for decision-making on risk.

5. PRINCIPLES FOR RISK CRITERIA

Most risk criteria have developed through a process of expert judgement and political compromise. Nevertheless, it is worthwhile to consider the fundamental principles that could be used to develop and justify risk criteria.

The following principles have been suggested in different industries, but have been expressed here in a way that would be valid for any activity that involves risks of accidents:

1. Justification of activity – the risks of

the activity should be justified by its benefits (in terms of people transported, value of leisure activities, jobs etc) for the society as a whole.

2. Optimisation of protection – the risks should be minimised by appropriate safety measures, taking account of their benefits (in terms of risk reduction) and costs, and also of established good practice.

3. Equity – the risks should not be unduly concentrated on particular individuals or communities.

4. Aversion to catastrophes – the risks of major accidents (involving multiple-fatalities, high cost or widespread impacts) should be a small proportion of the total.

5. Proportionality – the detail in the risk assessment should be proportionate to the level of risk, and negligible risks should be exempted from detailed assessment.

6. Continuous improvement – overall risks should not increase, and preferably should reduce.

Table 3 indicates where these principles are applied in other transport modes and industries.



Table 3. Application of Principles for Risk Criteria in Different Industries

INDUSTRY	JUSTIFICATION OF ACTIVITY	OPTIMISATION OF PROTECTION	EQUITY	AVERSION TO CATASTROPHES	PROPORTIONALITY	CONTINUOUS IMPROVEMENT
Aircraft design (EASA)				√		
ATM (EUROCONTROL)						√
Airports (UK)		√	√		√	
Road transport (EU MS)		√				√
Road transport (USA, Norway)		√				
Road transport of DG (ACDS)	√	√	√	√	√	
Road transport of DG (Switz)		√		√	√	
Road tunnels (Austria)		√		√	√	
Rail transport (ERA)			√			√
Rail transport (UK)		√	√			√
Nuclear (ICRP)	√	√	√			
Onshore process (UK)		√	√		√	
Onshore process (Netherlands)		√	√	√		
Onshore process (Flanders)			√	√		
Onshore process (France)		√		√	√	
Onshore process (HK)		√	√	√	√	
Offshore oil & gas		√	√			
Healthcare		√				
Maritime	√	√	√	√	√	

The current maritime criteria (IMO 2013) apply all the principles except continuous improvement. The only enhancement that might be considered, based on the principles used in other industries, might therefore be to include an element to ensure continuous improvement. This could, for example, consist of a requirement that fatality risks or total loss rates in the maritime fleet as a whole, or in the fleets of specific ship types, should decline at a rate no less than that achieved over the previous decade.

6. INDIVIDUAL RISK CRITERIA

Individual risk criteria are intended to ensure that individual people are not exposed to excessive risk. This implements the equity principle, giving all individuals the same protection. Individual risk criteria can also

define a negligible risk level, below which further risk reduction is not required. This implements the proportionality principle, allowing simpler assessment for smaller risks.

Individual risks are relatively easy to calculate in a risk analysis, and most approaches to risk criteria include limits on individual risks, so they are sometimes seen as the most important type of risk criteria. However, modern risk assessment practice is typically to use individual risk criteria as outer limits on a process that tries to make the risks ALARP, and therefore cost-benefit criteria (or qualitative equivalents) are usually more important. Furthermore, experience suggests that most ships would comply with standard individual risk criteria. However, individual risk criteria are still important when demonstrating to the public, who may distrust cost-benefit calculations, that acceptable safety levels have been achieved.



Table 4. Individual Risk Criteria in Different Industries

INDUSTRY	MAXIMUM INDIVIDUAL RISK (per year)	NEGLIGIBLE INDIVIDUAL RISK (per year)
Airports (UK)	10^{-4} (public)	10^{-5}
Road transport of DG (ACDS)	10^{-3} (workers), 10^{-4} (public)	10^{-6}
Rail transport (ERA)	Various FWSI per pass km	-
Rail transport (UK)	1.038 FWI per 10^8 pass km	-
London Underground	10^{-3} (workers), 10^{-4} (public)	10^{-6}
Nuclear (ICRP)	10^{-3} (workers), 10^{-4} (public)	-
Onshore process (UK)	10^{-3} (workers), 10^{-4} (public)	10^{-6}
Onshore process (Netherlands)	10^{-6} (public LSIR)	-
Onshore process (Flanders)	10^{-5} (public LSIR)	10^{-7}
Onshore process (HK)	10^{-5} (public LSIR)	-
Offshore oil & gas (UK)	10^{-3} (workers)	-
Maritime	10^{-3} (crew), 10^{-4} (passengers)	10^{-6}

Table 4 shows the individual risk criteria that are in use in other transport modes and industries. In the UK the individual risk criteria from HSE (2001) are used in all industries, and these are also used in the maritime industry criteria. When the values of the criteria are different, this partly reflects the different approaches to ALARP in the national legal systems. In the rail industry, individual risk criteria are expressed as fatalities and weighted serious injuries (FWSI) per passenger km, which cannot be compared to the other metrics

7. SOCIETAL RISK CRITERIA

Societal risk criteria are intended to limit the risks from the ship to the society as a whole, and to local communities who may be affected by it. One purpose is to implement the equity principle, giving all communities the same protection. Societal risk criteria can also define a negligible risk level, below which further risk reduction is not required. This implements the proportionality principle, allowing simpler assessment for smaller risks. Societal risk criteria expressed as FN curves can also implement the principle of aversion to catastrophes.

Societal risk criteria are particularly important for transport activities, which spread their risks over a constantly changing population of passengers and people near to their ports. Compared to fixed installations, this tends to produce relatively high societal risks despite relatively low individual risks.

Societal risk criteria are also important where there is potential for catastrophic accidents. These are a particular concern for passenger ships and liquefied gas carriers, which have the potential to affect large numbers of people in a single accident, although the likelihood is very low.

Table 5 shows the societal risk criteria that are in use in other transport modes and industries. It shows both the maximum and negligible criteria for FN curves, and the applicable range of fatalities (N). Some of the criteria depend on tunnel or road length (L) in km. The table also shows fatality rate criteria where used.

Despite their attractiveness, there are many theoretical and practical challenges in understanding and using FN criteria, especially when comparing activities with different societal benefits (such as ships whose size or cargo is much larger than average).



Table 5. Societal Risk Criteria in Different Industries

INDUSTRY	RANGE	MAXIMUM FN (per year)	NEGLIGIBLE FN (per year)	FATALITY RATE (per year)
Road transport of DG (ACDS)	≥ 1	$0.1/N$	$10^{-4}/N$	-
Road transport of DG (NL)	≥ 10	$10^{-2}L/N^2$	-	-
Road tunnels (Austria)	≥ 10	-	$0.1L^{0.5}/N^2$	10^{-3} per tunnel year
Road tunnels (Czech Republic)	1 - 1000	$0.1/N$	$10^{-4}/N$	-
Road tunnels (Denmark)	≥ 1	$0.4/N^2$	$0.004/N^2$	-
Road tunnels (France)	-	-	-	10^{-3} per tunnel year
Road tunnels (Germany)	10 - 1000	-	$0.01L/N^2$	6.2×10^{-3} per tunnel km per year
Road tunnels (Italy)	≥ 1	$0.1/N$	$10^{-3}/N$	-
Rail transport (ERA)	-	-	-	Value per train km for each MS
Rail transport (UK)	-	-	-	1.9×10^{-7} per train km
Onshore process (Netherlands)	≥ 10	$10^{-3}/N^2$	-	-
Onshore process (Flanders)	10 - 1000	$10^{-2}/N^2$	-	-
Onshore process (HK)	1 - 1000	$10^{-3}/N$	$10^{-5}/N$	-
Maritime (tanker)	≥ 1	$0.02/N$	$2 \times 10^{-4}/N$	
Maritime (dry cargo)	≥ 1	$0.01/N$	$10^{-4}/N$	
Maritime (passenger ro/ro)	≥ 1	$0.1/N$	$0.001/N$	

As a result, there are at present no widely accepted societal risk criteria, and FN criteria that have been developed are often not used in practice, or are treated as guidelines that indicate where risk reduction might be cost-effective. Because cost-benefit criteria make use of integrated measures of fatality risk, some authorities consider these automatically take account of quantifiable societal risks. Societal concerns, including concern about catastrophe risks, are better addressed through qualitative decision making rather than embedded in the risk criteria.

The current maritime criteria are unusual in having a consistent methodology to take account of societal benefit (Norway 2000). They may therefore be considered more advanced than the criteria in other industries. Nevertheless, given the difficulties with societal risk criteria, it is recommended that they are treated as guidelines rather than rigid rules. If exceeded, they indicate opportunities

for risk reduction, and should not be considered to demonstrate that risks are unacceptable.

8. COST-BENEFIT CRITERIA

Cost-benefit criteria define the point at which the benefits of a risk reduction measure just outweigh its costs. This implements the principle of optimisation of protection. By systematically evaluating a range of measures, it is possible to show whether the risks are ALARP.

One of the most important issues in a cost-benefit analysis (CBA) of safety measures is the value assigned to reductions in fatality risks. The critical parameter is the “value of preventing a fatality” (VPF). It should be emphasised that this does not refer to any individual fatality, but to a small change in risk to many lives, equivalent to a single statistical fatality. The VPF is an input to the CBA, but it



is often very critical to the evaluation of safety measures.

Several types of cost-benefit criteria are in use:

- Cost of averting a fatality (CAF) - the cost of a measure divided by the expected number of fatalities averted. A measure is normally recommended if its CAF is less than the VPF. Hence the VPF can be seen as a type of cost-benefit criterion.
- Cost per quality-adjusted life year (QALY) - the cost of a measure divided by the life-years saved, standardised to equivalent years of healthy life. This is similar to the VPF but refers to health risks.
- Net present value (NPV) - the difference between the discounted benefits and the discounted costs of a measure. A measure is normally recommended if its NPV is positive.
- Benefit/cost ratio (BCR) - the discounted benefits of a measure divided by the discounted costs. A measure is normally recommended if its BCR is greater than 1.
- Internal rate of return (IRR) - the discount rate that makes the discounted benefits of a measure equal to the discounted costs, and hence would make its NPV equal to zero. A measure is recommended if its IRR is greater than the usual discount rate.

The VPF can be set through techniques such as:

- Human capital approaches. These estimate the VPF in terms of the future economic output that is lost when a person is killed.
- Willingness to pay (WTP) approaches. These estimate the amount that people in society would be prepared to pay to avoid a statistical fatality.
- Life quality approaches. These are based on social indicators of quality of life that reflect life expectancy and gross domestic product (GDP). By relating the costs of a measure to the GDP and the risk benefits to life expectancy, it is possible to identify the point at which further safety measures

have a negative overall impact on the quality of life.

Table 6 shows the cost-benefit criteria that are in use in other transport modes and industries. Some industries do not use CBA at all. Some countries, notably the UK, have standardised on VPFs across all industries and transport modes. Others vary because of differences in national income and the VPF setting technique used.

The VPF of \$3m in the maritime criteria (IMO 2013) was derived from 1998 statistics. New calculations in the present study (DNV GL 2015) indicate an appropriate VPF would be approximately \$7m. This uses the life quality approach, based on 2012 GDP data and updated life expectancies and fractions of time in economic activity, with the results averaged over all OECD members.

The maritime criteria are unique in taking account of injuries by adjusting the criterion for studies that do not model injury costs explicitly. It would be clearer to value injury risks separately following approaches in the road and nuclear industries. For sensitivity tests, a range of VPF from \$4m to \$8m is considered appropriate.

The maritime criteria are also unique in distinguishing gross and net costs of averting a fatality (GCAF and NCAF). The need for this arises because decisions on risk reduction measures can sometimes be sensitive to the inclusion of non-fatality economic benefits. The two separate criteria make clear whether this is so, but because both are compared to the same criterion, GCAF appears redundant since NCAF is always lower. However, GCAF is simpler to calculate, and NCAF sometimes becomes negative, which has no clear meaning. The distinction is logical but somewhat confusing. Other industries address this issue by using the criterion of NPV instead, and it may be possible to do the same in future developments of the maritime criteria.



Table 6. Cost-Benefit Criteria in Different Industries

INDUSTRY	CRITERIA USED	VPF (Original units)	VPF (\$m 2012)
Airports (UK)	Qualitative	-	-
Road transport (EU MS)	NPV, BCR and IRR	€0.056 to 2.1m	\$0.1m to \$4.3m
Road transport (UK)	NPV, BCR	£1.7m	\$2.8m
Road transport (USA)	NPV	\$9.1m	\$9.1m
Road transport (Norway)	NPV	NOK26.5m	\$4.5m
Road transport of DG (ACDS)	CAF	£2m	\$5.3m
Road tunnels (Austria and others)	Qualitative	-	-
Rail transport (UK)	NPV	£1.7m	\$2.8m
London Underground	Qualitative	-	-
Nuclear (UK)	NPV	£1.7m	\$2.8m
Onshore process (UK)	Qualitative	-	-
Onshore process (Netherlands)	Qualitative	-	-
Onshore process (France/HK)	Qualitative	-	-
Offshore oil & gas	CAF	Various	Various
Healthcare (USA)	NPV	\$7.4m	\$7.4m
Healthcare (WHO/UK/Spain)	Cost per QALY	-	-
Maritime	GCAF and NCAF	\$3m	\$4m to \$8m

9. CONCLUSIONS

The overall conclusion from the review of risk criteria used in different industries and transport modes is that each application differs in terms of the types of criteria used, the principles for their development, and the specific values adopted. In some countries, the same approaches are used in different industries and transport modes, but overall the pattern is one of difference rather than commonality.

The current maritime criteria are in general within the range of criteria used in other industries and transport modes, and in most cases are in line with good practice elsewhere, so far as this can be determined. Only a few minor improvements have been suggested.

10. REFERENCES

- Transport of Dangerous Substances”, Health and Safety Commission, Advisory Committee on Dangerous Substances, HMSO.
- ACDS (1991), “Major Hazard Aspects of the
- BEVI (2004), “Decree on External Safety of Installations”, Ministry of Housing, Physical Planning and Environment.
- DfT (2007), “Control of Development in Airport Public Safety Zones”, DfT Circular 01/2010, Department for Transport, London.
- DoT (2013), “Guidance on Treatment of the Economic Value of a Statistical Life in US Department of Transportation Analyses”, Department of Transportation, Washington.
- Diernhofer, F., Kohl, B. & Hörhan, R. (2010), “New Austrian Guideline for the Transport of Dangerous Goods through Road Tunnels”, 5th International Conference on Tunnel Safety and Ventilation, Graz.
- DNV GL (2015), “Risk Acceptance Criteria



- and Risk Based Damage Stability. Final Report, part 1: Risk Acceptance Criteria”, Report EMSA/OP/10/2013 for European Maritime Safety Agency.
- Duijm, N.J. (2009), “Acceptance Criteria in Denmark and the EU”, Danish Ministry of the Environment, project 1269.
- EASA (2013), “Certification Specifications and Acceptable Means of Compliance for Large Aeroplanes (CS-25)”, (Annex to ED Decision 2013/010/R) European Aviation Safety Agency, Amendment 13, June 2013.
- EURATOM (1996), “Basic Safety Standards for the Protection of the Health of Workers and the General Public against the Dangers Arising from Ionising Radiation”, Directive 96/26/EURATOM, Council of the European Union.
- EUROCONTROL (2001), “Risk Assessment and Mitigation in ATM”, Eurocontrol Safety Regulatory Requirement ESARR4, April 2001.
- European Commission (2012), “Decision 2012/226/EU of the European Commission of 23 April 2012 on the second set of common safety targets as regards the rail system”.
- HKPD (2011), “Hong Kong Planning Standards and Guidelines, Chapter 12 : Miscellaneous Planning Standards and Guidelines”, Planning Department, The Government of Hong Kong Special Administrative Region.
- HSE (2001), “Reducing Risks, Protecting People. HSE’s Decision-Making Process”, Health & Safety Executive, HSE Books.
- ICAO (2001), “Air Traffic Services”, Annex 11 to the Convention on International Civil Aviation, 13th edition, International Civil Aviation Organization, Montreal, Canada.
- ICRP (1977), “Recommendations of the ICRP”, International Commission on Radiological Protection, Publication 26.
- IMO (2013), “Revised Guidelines for Formal Safety Assessment (FSA) for Use in the IMO Rule-Making Process”, MSC-MEPC.2/Circ.12, International Maritime Organization.
- ISO (2000), “Petroleum and natural gas industries - Offshore production installations - Guidelines on tools and techniques for hazard identification and risk assessment”, International Standard ISO 17776:2000.
- ISO (2009), “Risk Management - Vocabulary”, Guide 73:2009, International Organization for Standardization.
- LU (2012), “London Underground Safety Certificate and Safety Authorisation Document”, v2, January 2012.
- Norway (2000), “Formal Safety Assessment: Decision Parameters Including Risk Acceptance Criteria”, MSC 72/16, International Maritime Organization.
- PIARC (2012), “Current Practice for Risk Evaluation for Road Tunnels”, World Road Association.
- RSSB (2009), “Railway Strategic Safety Plan 2009-2014”, Rail Safety & Standards Board, London.
- Safety Net (2009a), “Quantitative Road Safety Targets”, European Commission Directorate-General Transport and Energy.
- Safety Net (2009b), “Cost-benefit analysis”, European Commission Directorate-General Transport and Energy.
- USEPA (2010), “Guidelines for Preparing Economic Analysis”, US Environmental Protection Agency.



Probabilistic Assessment of Survivability in Case of Grounding: Development and Testing of a Direct Non-Zonal Approach

Gabriele Bulian, *University of Trieste*, gbulian@units.it

Daniel Lindroth, *NAPA Ltd*, daniel.lindroth@napa.fi

Pekka Ruponen, *NAPA Ltd*, pekka.ruponen@napa.fi

George Zaraphonitis, *National Technical University of Athens*, zar@deslab.ntua.gr

ABSTRACT

This paper presents the results of ongoing research efforts aimed at the theoretical development and practical implementation of a probabilistic framework for regulatory assessment of ship survivability following grounding accidents, with particular attention to passenger vessels. In the envisioned framework, the probabilities of flooding of a compartment, or a group of compartments, i.e. the so-called “p-factors”, are determined using a flexible and easily updatable direct non-zonal approach. The assessment of the conditional ship survivability, on the other hand, is based on the SOLAS “s-factor”. The general framework is described, together with implementation details in the specific case of bottom grounding. Testing results, carried out using a specifically developed software tool, are also reported.

Keywords: *ship stability; grounding; p-factors; non-zonal approach; bottom damage*

1. INTRODUCTION

Past and more recent accidents have shown that grounding can potentially have catastrophic consequences. This is particularly true when speaking of passenger vessels, for which the risk to be accounted for is the potential loss of lives. Express Samina in 2000, Sea Diamond in 2007, Princess of the Stars in 2008 and Costa Concordia in 2012, are some examples of such accidents.

From a regulatory point of view, present SOLAS damage stability regulations for passenger and (dry) cargo vessels (IMO, 2014a) address ship survivability following a flooding due to collision in a probabilistic framework, with some additional deterministic requirement on top of the basic probabilistic

ones. The underlying distributions of damage characteristics were originally developed in the framework of the EU-funded HARDER project (Lützen, 2002), and have then been adapted as a result of discussion at IMO (IMO, 2003a,b, 2004a, 2005).

On the other hand, SOLAS regulations for passenger and cargo ships do not specifically address the case of grounding damages within the probabilistic framework. Safety with respect to bottom grounding is instead addressed deterministically through Chapter II-1 - Regulation 9 “Double bottoms in passenger ships and cargo ships other than tankers”. Regulation 9 (IMO, 2014a), which was developed using historical data of grounding damages (IMO, 2004b), sets minimum double bottom requirements and specifies



deterministic bottom grounding damage characteristics to be used for survivability assessment in case of vessels with unusual bottom arrangements. An analysis of the effectiveness of the deterministic requirements in Reg.9 in light of the statistics of grounding damage characteristics collected in the GOALDS project can be found in (IMO, 2012; Papanikolaou et al., 2011).

It should also be reminded that SOLAS Reg.9 only deals with grounding damages assumed to penetrate the vessel vertically, from the ship bottom (i.e. bottom grounding damages). However, as both historical data and more recent accidents show, grounding damages can also result in breaches on the side of the vessel, extending partially or totally above the double bottom. Side damages can also be the result of the contact with fixed or floating objects. However, such type of damages is presently not considered by Reg.9.

Therefore, a lack of harmonization exists in present SOLAS regulations, between the applied probabilistic framework for collision-related survivability, and the applied deterministic framework for bottom grounding-related survivability. Such situation could benefit from a harmonization towards a fully probabilistic framework for both collision and grounding damages. Indeed, with particular reference to stability-related regulations, the present evolution of knowledge and practice regarding rule-development, taking into account risk-assessment, indicates that the more rational way to address the problem of survivability following an accident is by trying to develop a regulatory framework based on probabilistic concepts. Probabilistic frameworks, in addition of being more strictly related with reality, also allow more design flexibility, which, instead, is in some cases impaired by deterministic prescriptions. Moreover, in the grounding framework, it would also be necessary to introduce damages occurring on the side of the vessel, in addition to bottom damages.

In order to develop a probabilistic framework for survivability assessment in damaged condition, two elements are needed. Firstly, it is necessary to specify an appropriate geometrical and probabilistic model for the damage shape, position and extent. Secondly, it is necessary to have at disposal a means for assessing the conditional ship survivability following a damage. With a view towards a harmonization with existing SOLAS damage stability regulations dealing with collision accidents, these two elements can be used to determine, respectively, the so-called “p-factors” (i.e. the probability of flooding a compartment, or group of compartments) and the consequent “s-factors”.

In present SOLAS regulations, “p-factors” for collision damages can be calculated by means of analytical formulae which have been derived starting from the underlying distributions of damage characteristics (Lützen, 2002). Following the “zonification” process, such formulae are applied to ships having compartments of generic shape. However, this is just an approximation, and the formulae are strictly valid only for box-shaped vessels having box-shaped compartments.

Studies carried out within the GOALDS project (Bulian & Francescutto, 2010) indicated that, in case of bottom grounding, the development of analytical, or semi-analytical, “p-factors”, although it was technically possible, would have been hardly applicable to realistic ships and subdivision layouts. To overcome this difficulty, it was therefore suggested to address the determination of “p-factors” using a direct approach, based Monte Carlo generation of breaches, starting from the underlying probabilistic model.

In the past, a direct approach for the determination of “p-factors”, in case of collision damages, was also explored by Koelman (2005). In this study, a methodology based on direct deterministic integration of the underlying probability density functions of damage characteristics was used. Moreover, a



direct, non-analytical determination of the probability of flooding of (group of) compartments, starting from the underlying distributions of damage characteristics, is implicit in the alternative assessment of accidental oil outflow performance or of double hull and double bottom requirements within MARPOL (IMO, 2003c, 2014b). For MARPOL oil outflow assessment, a direct approach of the Monte Carlo type was used by Kehren, & Krüger (2007) for the determination of the probabilities of damaging a compartment (or group of compartments) following bottom damages. Furthermore, Kehren, & Krüger (2007) also correctly pointed out that the same philosophy could have been used also for survivability assessment.

It is therefore the scope of this paper to present the results of ongoing research efforts aimed at the theoretical development and practical implementation of a probabilistic framework for regulatory assessment of ship survivability following grounding accidents, with particular attention to the case of passenger vessels. In the envisioned framework, “p-factors” are determined using a flexible and easily updatable direct non-zonal approach, while the assessment of the conditional ship survivability is based on the SOLAS “s-factor”. In the following, the general framework is described. Although the framework has been developed for both bottom and side grounding damages, and it could be extended to collision damages (and also to, e.g., accidental oil outflow performance), herein implementation details are given only for the specific case of bottom grounding. An example testing application, carried out using a specifically developed software tool, is also reported.

2. OUTLINE OF THE APPROACH

Scope of the assessment is to determine an attained subdivision index, which is meant to be representative of the survivability of the vessel following a bottom grounding accident

leading to hull breach. Furthermore, in order to allow a possible harmonization with existing regulations, the approach is designed to be formally in line with present SOLAS probabilistic assessment of survivability following a collision accident (hereinafter, briefly, SOLAS2009).

Considering bottom grounding damages, an attained subdivision index $A_{GR,B}$ is defined in line with SOLAS2009, considering three calculation draughts d_s (deepest subdivision draught), d_p (partial subdivision draught) and d_l (light service draught), as follows:

$$A_{GR,B} = 0.4A_{GR,B,s} + 0.4A_{GR,B,p} + 0.2A_{GR,B,l} \quad (1)$$

Each partial index is given by the summation of contributions from all damage cases taken into consideration:

$$A_{GR,B,c} = \sum_{i_c} p_{i_c} \cdot s_{i_c} \quad \text{with } c = s, p, l \quad (2)$$

where i_c represents each compartment or group of compartments under consideration, p_{i_c} accounts for the probability that only the compartment or group of compartments under consideration may be flooded, and s_{i_c} accounts for the probability of survival after flooding the compartment or group of compartments under consideration.

In the considered methodology, the “s-factors” are assumed to be determined in accordance with the GZ-based methodology in SOLAS2009. On the other hand, factors p_{i_c} are determined by means of a direct, non-zonal approach. In this approach, on the basis of the probabilistic model for the damage characteristics, a sufficiently large number of breaches, each one with an associated probability of occurrence, are generated by a Monte Carlo procedure. For each breach, the corresponding compartments which become open to the sea are identified. Then, all

breaches leading to the flooding of the same compartment, or group of compartments, are grouped into what are commonly referred to as “damage cases”, and the probability contributions of each breach in each “damage case” are summed up to obtain estimates of p_{ic} . “Non-contact cases” are disregarded and the remaining “p-factors” are renormalized in such a way that they sum up to unity. This renormalization is assumed to be acceptable as long as the fraction of generated non-contact breaches is small enough, which is achievable by a careful definition of the probabilistic model of the considered damage (Bulian & Francescutto, 2012).

It is to be noted that the described direct procedure leads to an automatic determination of damage cases. Also, this fully automatic procedure does not need the preliminary “zonification” process, which is instead required when using analytical “p-factors”, as in case of SOLAS2009. For such reason, this procedure can be referred to as “non-zonal”. Furthermore, this procedure does not have any limitation regarding the actual shape of the compartments. Since the outcome from this procedure is affected by sampling uncertainty, the number of generated breaches must be large enough to achieve an acceptable convergence of the attained subdivision index. The general logic of the proposed direct non-zonal approach is shown in Figure 1.

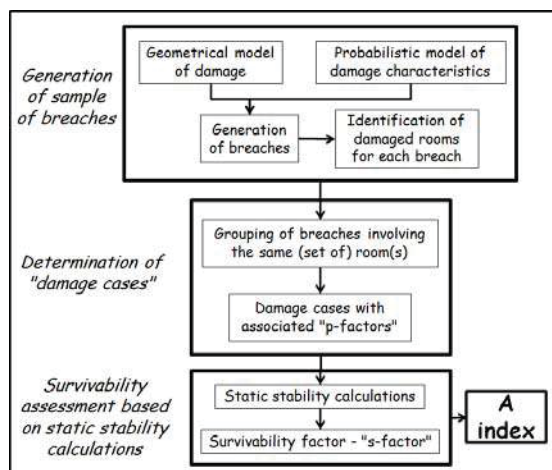


Figure 1: General logic of the proposed direct non-zonal approach for damaged ship survivability assessment.

It should be highlighted that the proposed approach is a simplified one, intended to be in line with the SOLAS2009 framework. In particular, the approach is simplified in terms of survivability assessment (“s-factors”), which is assumed to be performed on the basis of a GZ-based static stability assessment. In case survivability is to be assessed by means of more advanced tools, such as time domain dynamic flooding simulations, then a survivability assessment should be carried out for each individual breach, and grouping in terms of “damage cases” is no longer possible. This latter approach, which was followed in the past by, e.g., Vassalos et al. (2008) (for grounding and collision) and by Spanos & Papanikolaou (2014) (for collision), is, however, much more time consuming, and more challenging to be applied in a regulatory framework. Furthermore, in case of dynamic flooding simulations, probabilistic models of damage characteristics which are specifically intended for such purpose should be used.

It is also worth noticing that, for consistency with SOLAS2009, the attained subdivision index in (1), which is then expected to be compared with a properly defined required subdivision index R , has been defined using three draughts. However, specifying requirements of the type $A \geq R$, provided separately for each draught, would allow removing the well-known arbitrariness in the identification of the limiting GM curve. Indeed, specifying requirements of the type $A \geq R$ for each draught, would lead to a unique identification of the limiting GM for each ship draught.

In principle, different “p-factors” should be calculated for each of the three draughts (subdivision, partial and lightest draught). However, since the generation of the damage cases might be quite time consuming, particularly in case a very large number of hull breaches is to be generated, it was decided at this stage to generate the damage cases and calculate the corresponding “p-factors” only for the deepest subdivision draught d_s , and use the

same “p-factors” and damage cases also for the partial subdivision draught d_p and the light service draught d_l . The methodology, however, can also be applied, without any problem, by considering draught dependent “p-factors”.

3. GEOMETRICAL CHARACTERISATION OF DAMAGE

In order to apply the described direct non-zonal approach, it is first necessary to provide a clearly defined, unambiguous geometrical model for the type of damage to be considered. Herein, bottom damages, i.e. damages penetrating the bottom of the vessel in vertical direction, are considered. Such type of damages is conventionally referred to as “type B00”. A sketch of this type of damages is shown in Figure 2, while a detailed representation of the damage geometry, and defining parameters, is shown in Figure 3. In Figure 3 and in the following, the ship-fixed coordinate system is assumed to be right handed.

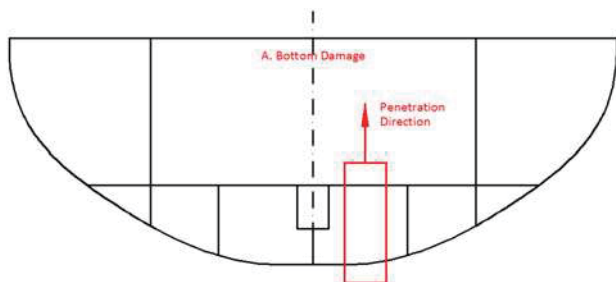


Figure 2: Sketch of bottom damage.

The damage is assumed to be box-shaped. Moreover, the damage is assumed to be a “potential damage”, i.e. a damage which can also partially extend, in some cases, outside the vessel. There are some main reasons for the selection of a box as shape of the damage. The first reason is that significantly more complex modelling could not have been supported by the limited available information from accidents. Then, a box-shaped damage has favourable geometrical characteristics from the computational perspective. Finally, a box-shaped damage is more conservative, from the

point of view of stability assessment, compared with other possible typical choices, such as, e.g. triangular or parabolic penetrations. With reference to Figure 3, the defining parameters for a damage of type B00 are:

- Longitudinal position of forward end of damage: X_F [m];
- Transversal dimensionless position of centre of measured damage: $\eta_{dam} = Y_{dam} / b(X_F, z^*)$ [-];
- Longitudinal extent of potential damage, i.e. potential damage length: $L_{x,p}$ [m];
- Transversal extent of potential damage, i.e. potential damage width: $L_{y,p}$ [m];
- Vertical extent of potential damage, i.e. potential damage penetration: $L_{z,p}$ [m];
- Vertical position to be used for the transversal positioning of damage: z^* [m];

In the definition of η_{dam} , the quantity Y_{dam} [m] is the dimensional transversal position of the centre of the measured damage (not to be confused with the transversal position of the centre of potential damage, $Y_{dam,p}$ [m]). The quantity $b(X_F, z^*)$ [m] is the breadth of the vessel at a longitudinal position corresponding to the forward end of damage, X_F , and vertical position z^* . For the positioning of the damage, given the characterising variables, it is necessary that the software tool is able to determine the intersection between the section at X_F and a waterplane at $z = z^*$. Defining $y_{SB}(X_F, z^*)$ and $y_{PS}(X_F, z^*)$ as, respectively, the coordinates of the starboard and portside limits of $b(X_F, z^*)$, the quantity Y_{dam} is determined as:

$$\begin{cases} Y_{dam} = y_c(X_F, z^*) + \eta_{dam} \cdot b(X_F, z^*) \\ y_c(X_F, z^*) = \frac{y_{PS}(X_F, z^*) + y_{SB}(X_F, z^*)}{2} \\ b(X_F, z^*) = y_{PS}(X_F, z^*) - y_{SB}(X_F, z^*) \end{cases} \quad (3)$$

On the other hand, the quantity $Y_{dam,p}$ is defined as:

$$\begin{cases} Y_{dam,p} = Y_{dam} + \\ + \frac{\text{sign}(\delta)}{2} \cdot \max\{(L_{y,p} - L_{y,lim}) ; 0\} \\ \text{where} \\ \delta = Y_{dam} - y_c(X_F, z^*) \\ L_{y,lim} = \min \left\{ \begin{array}{l} 2 \cdot (y_{PS}(X_F, z^*) - Y_{dam}) ; \\ 2 \cdot (Y_{dam} - y_{SB}(X_F, z^*)) \end{array} \right\} \end{cases} \quad (4)$$

Note: $\text{sign}(\delta < 0) = -1$; $\text{sign}(\delta = 0) = 0$;
 $\text{sign}(\delta > 0) = 1$

If an intersection with the hull at $x = X_F$ and $z = z^*$ is not obtained, as could happen, for instance, for X_F in the very forward or very aft part of the vessel, and for small values of z^* , then $y_{SB}(X_F, z^*)$ and $y_{PS}(X_F, z^*)$ are to be set equal to 0. In case multiple intersections are found, then $y_{PS}(X_F, z^*)$ is set as the maximum y-coordinate among the intersections, and $y_{SB}(X_F, z^*)$ is set as the minimum y-coordinate among the intersections, in such a way that $b(X_F, z^*)$ represents the maximum breadth at $x = X_F$ and $z = z^*$.

The above mentioned geometrical characterisation (in particular the transversal positioning of the damage) has been devised with the intention of reducing the occurrence of “non-contact damages”, i.e. generated damages which, eventually, do not get in contact with the hull of the vessel.

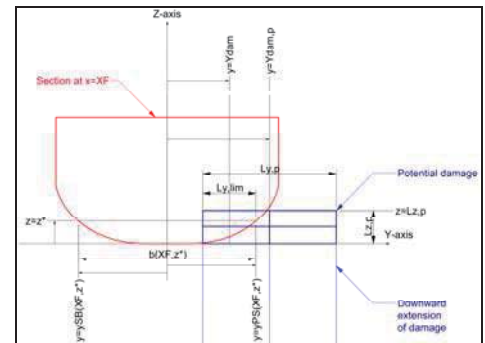
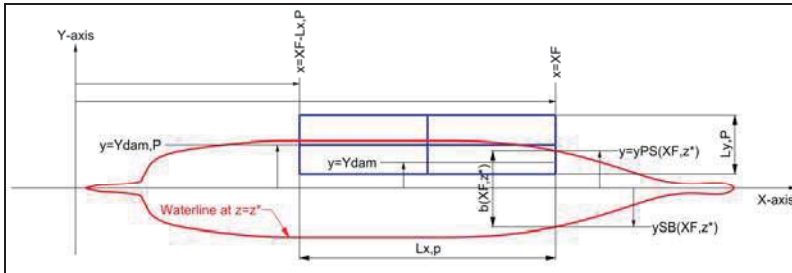


Figure 3: Geometrical parameters characterising bottom damages (type B00).

4. PROBABILISTIC MODEL OF DAMAGE CHARACTERISTICS

In order to develop a probabilistic model for the damage, it is necessary to introduce a probabilistic characterisation for the variables,

described in the previous section, which are used to specify the generic breach.

The primary interest of this study is to provide a methodology suitable, in particular, for the survivability assessment of passenger vessels. To this end, herein reference is made to the distribution of bottom damage characteristics as determined in the GOALDS



project for the category of non-full vessels (Bulian & Francescutto, 2011; Papanikolaou et al., 2011). Such distributions have been derived from the analysis of the GOALDS database of grounding damage characteristics. It is to be noted that, in case of accidents resulting in multiple breaches, as it is common in case of grounding, the damage characteristics as analysed in GOALDS refer to an “equivalent damage” (Papanikolaou et al., 2011; IMO, 2012). An “equivalent damage” is a single box-shaped breach which is meant to represent, only for the purpose of static stability calculations, the region of the vessel actually damaged by multiple breaches.

The considered distributions are reported analytically in Table 1-Table 5. Graphical representations of the corresponding cumulative distributions are reported in Figure 4- Figure 8. Damages are assumed to be generated such that the forward end of the damage, X_F , is distributed between X_{MIN} and $X_{MAX} = X_{MIN} + L_{ship}$. For application to real vessels, and in order to reduce the fraction of non-contact cases, it is suggested, at this stage, to set X_{MIN} and X_{MAX} at the extremities of the freeboard length of the vessel as specified by the International Convention on Load Lines (IMO, 2014c). For simplicity of notation, in specifying the distribution for X_F (see Table 1), it is assumed that $X_{MIN} = 0$. In addition, for simplicity of notation, in specifying the distribution for the damage penetration (see Table 5), the vertical position of the ship bottom is assumed to be at $z_{bottom} = 0$. It is also noted that, while in GOALDS the distribution of Y_{dam} (see Table 2) was assumed to be uniform in $[-B/2, B/2]$ (with B the ship breadth), herein the ship breadth B is substituted by the local ship breadth $b(X_F, z^*)$, and Y_{dam} is assumed to be uniformly distributed, according to the local breadth, in $[-b(X_F, z^*)/2, b(X_F, z^*)/2]$. Moreover, in the actual generation of the damages, the vertical position for the transversal positioning of damage, i.e. z^* , is assumed to coincide with the top of the potential damage box, i.e. $z^* = z_{bottom} + L_{z,p}$.

All damage characteristics are assumed to be independent random variables. In the framework of a regulatory assessment this is considered to be an acceptable approximation, although it can lead, with low probability, to the occurrence of damage boxes with high aspect ratios. It is however easy to introduce limitations in this respect, if deemed necessary.

Table 1: Distribution of dimensionless longitudinal position of forward end of damage.

Dimensionless longitudinal position of forward end of damage $\xi_{F,dam} = X_F / L_{ship}, \xi_{F,dam} \in [0,1]$	
<i>CDF</i> (x)	$\alpha_1 \cdot x + (1 - \alpha_1) \cdot x^{\alpha_2}$
<i>PDF</i> (x)	$\alpha_1 + \alpha_2 \cdot (1 - \alpha_1) \cdot x^{(\alpha_2 - 1)}$
α_1	0.325
α_2	3.104
Note: here X_F is intended to be measured starting with $X_F = 0$ at X_{MIN} , and $L_{ship} = X_{MAX} - X_{MIN}$.	

Table 2: Distribution of dimensionless transversal position of centre of measured damage.

Dimensionless transversal position of centre of measured damage $\eta_{dam} = Y_{dam} / b(X_F, z^*), \eta_{dam} \in [-0.5, 0.5]$	
<i>CDF</i> (x)	$x + 0.5$
<i>PDF</i> (x)	1
Note: ship centreplane is assumed to be at $y = 0$	



Table 3: Distribution of dimensionless longitudinal extent of potential damage (potential damage length).

Dimensionless potential damage length $\lambda_{x,p} = L_{x,p} / L_{ship}$, $\lambda_{x,p} \in [0,1]$	
$CDF(x)$	$\frac{\alpha_1 \cdot x^2 + \alpha_2 \cdot x}{x + (\alpha_1 + \alpha_2 - 1)}$
$PDF(x)$	$\frac{\alpha_1 \cdot x^2 + (\alpha_1 + \alpha_2 - 1) \cdot (2 \cdot \alpha_1 \cdot x + \alpha_2)}{[x + (\alpha_1 + \alpha_2 - 1)]^2}$
α_1	0.231
α_2	0.845

Table 4: Distribution of dimensionless transversal extent of potential damage (potential damage width).

Dimensionless potential damage width $\lambda_{y,p} = L_{y,p} / B$, $\lambda_{y,p} \in [0,1]$	
$CDF(x)$	$\frac{\alpha_1 \cdot x^2 + \alpha_2 \cdot x}{x + (\alpha_1 + \alpha_2 - 1)}$
$PDF(x)$	$\frac{\alpha_1 \cdot x^2 + (\alpha_1 + \alpha_2 - 1) \cdot (2 \cdot \alpha_1 \cdot x + \alpha_2)}{[x + (\alpha_1 + \alpha_2 - 1)]^2}$
α_1	0.110
α_2	0.926

Table 5: Distribution of dimensional vertical extent of potential damage (potential damage penetration), measured from baseline. Ship-size-dependent model.

Dimensional potential damage penetration $L_{z,p}$ [m] , $L_{z,p} \in [0, L_{z,p,max}]$	
$CDF(x)$	$\frac{\alpha_1 \cdot x}{x + L_{z,p,max} \cdot (\alpha_1 - 1)}$
$PDF(x)$	$\frac{L_{z,p,max} \cdot \alpha_1 \cdot (\alpha_1 - 1)}{[x + L_{z,p,max} \cdot (\alpha_1 - 1)]^2}$
Parameters	$\alpha_1 = 1.170$; $\alpha_B = 0.636$; $k_{MB} = 0.503$; $L_{z,p,max}(B) = \min\{k_{MB} \cdot B^{\alpha_B}, T\}$ with B in [m]
Note: this is the distribution of the damage penetration measured from the bottom, fixing the vertical position of the bottom, conventionally, at $z_{bottom} = 0$	

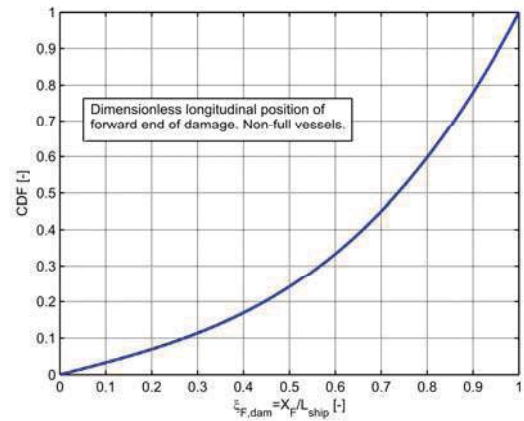


Figure 4: Plot of cumulative distribution dimensionless longitudinal position of forward end of damage.

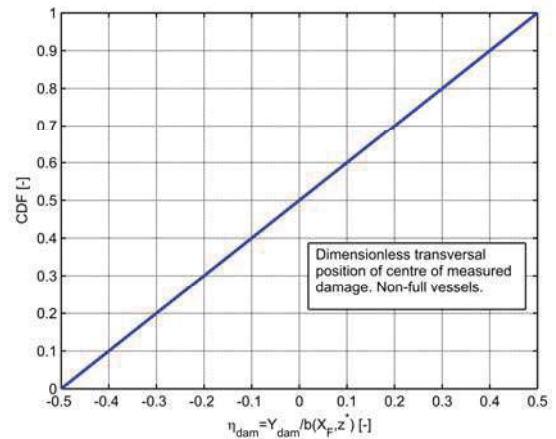


Figure 5: Plot of cumulative distribution of dimensionless transversal position of centre of measured damage.

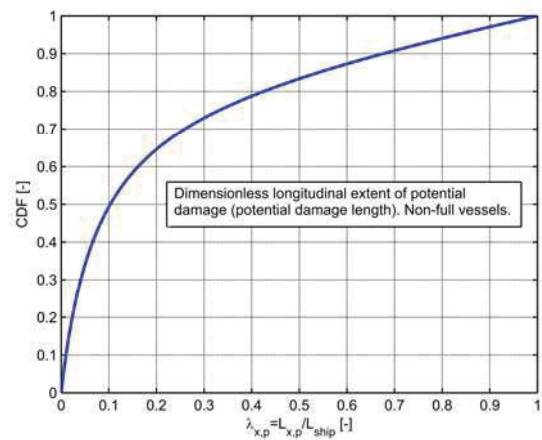


Figure 6: Plot of cumulative distribution of dimensionless longitudinal extent of potential damage (potential damage length).

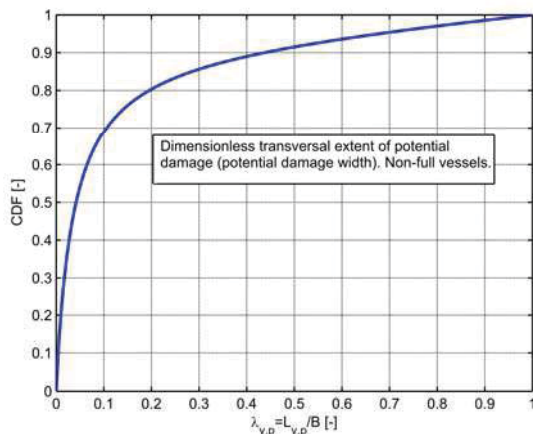


Figure 7: Plot of cumulative distribution of dimensionless transversal extent of potential damage (potential damage width).

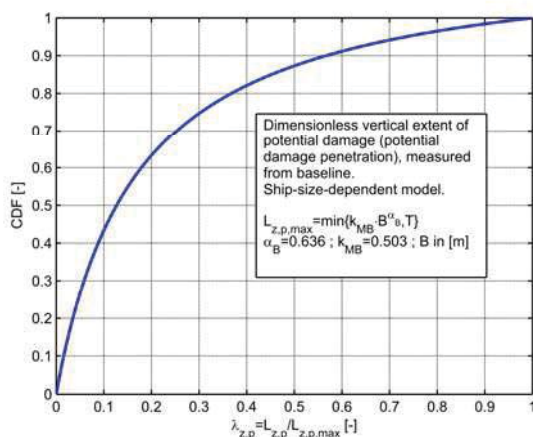


Figure 8: Plot of cumulative distribution of dimensional vertical extent of potential damage (potential damage penetration), measured from baseline. Ship-size-dependent model.

5. IMPLEMENTATION AND EXAMPLE RESULTS

The described approach has been implemented in a dedicated software tool within the NAPA software environment. A series of successful initial verification cross-checks of the NAPA tool have been carried out regarding the generation of damages and the determination of “p-factors” using an in-house tool available at University of Trieste. The developed tool within the NAPA software environment was designed to be easy to use for

practical application purposes, still retaining a sufficient flexibility for research applications. With reference to practical (design) applications, the developed tool allows a user, in a fully automated way, to generate breaches, to determine damage cases and associated “p-factors” and, eventually, to calculate the attained subdivision index. Furthermore, batch processing is possible, in order to more easily handle repeated or multiple calculations. Presently the tool allows to handle bottom damages (“type B00”), as well as side grounding damages (“type S00”). This latter type of damage is however not discussed in this paper.

Herein the developed approach has been applied through the NAPA tool on a simplified example case. The scope of the example calculations was, firstly, to provide a reference example for comparative purposes, and, secondly, to assess the typical level of dispersion which can be expected for the A-index when applying the described procedure.

To this end, a notional vessel was developed which is simple enough for software verification purposes, and which can be easily and freely reproduced. The considered test vessel is a barge having a box-shaped hull and box-shaped internal compartments. The main characteristics of the barge are reported in Table 6, while a view of the general arrangement is shown in Figure 9.

Table 6: Main characteristics of the test barge.

Length	100m	d_s	4.0m
Breadth	16m	d_p	3.6m
Total height	10m	d_l	3.0m
Assumed number of passengers	750	Height of double bottom	1.6m

The barge has a total length of 100m (starting from $x = -4m$ up to $x = 96m$), a breadth of 16m and a total height of 10m. The barge has a double bottom with height equal to 1.6m. A horizontal deck (the bulkhead deck) is



positioned 6m above the ship bottom. The deepest subdivision draught is set to 4m, while the light draught is set to 3m, this leading to a partial subdivision draught according to SOLAS of 3.6m. A series of transversal bulkheads are fitted, which extend from the ship bottom up to the bulkhead deck. The transversal bulkheads are uniformly spaced at a distance of 10m from each other, leading to a total of 10 zones. With the exception of the extreme aft and forward zones, the double bottom is longitudinally subdivided, leading to central compartments of 6m in width and wing compartments of 5m in width on each side. In the extreme aft and forward zones the double bottom extends from side to side. Eventually, this leads to a total of 26 rooms in the double bottom, 10 rooms immediately above the double bottom and a single room above the deck up to the maximum height, summing up to a total of 37 rooms.

Each room in the double bottom is associated with an unprotected opening, which becomes relevant in the s-factor calculation whenever the associated compartment belong

to the considered damage case. Such openings are meant to represent overflow vents, and are modelled in NAPA as one-way connections from the associated double bottom room to the uppermost room. Unprotected openings are all vertically positioned at 7.5m above the ship bottom, and longitudinally positioned at the centre of the associated room. For the central double bottom rooms, and for double bottom rooms extending from side to side, the opening is also transversally positioned at the centre of the room, which coincides with the ship centreline. On the other hand, for wing compartments, the openings are positioned at 0.5m from the ship side, i.e. at $y = 7.5m$ or $y = -7.5m$, for port or starboard side double bottom wing compartments, respectively. Unprotected openings are reported in Figure 9 as small red squares. It is worth recalling that unprotected openings have an effect on the attained subdivision index, through the s-factor, since the \overline{GZ} curve contributes in the s-factor calculation until the relevant openings (if any) are immersed.

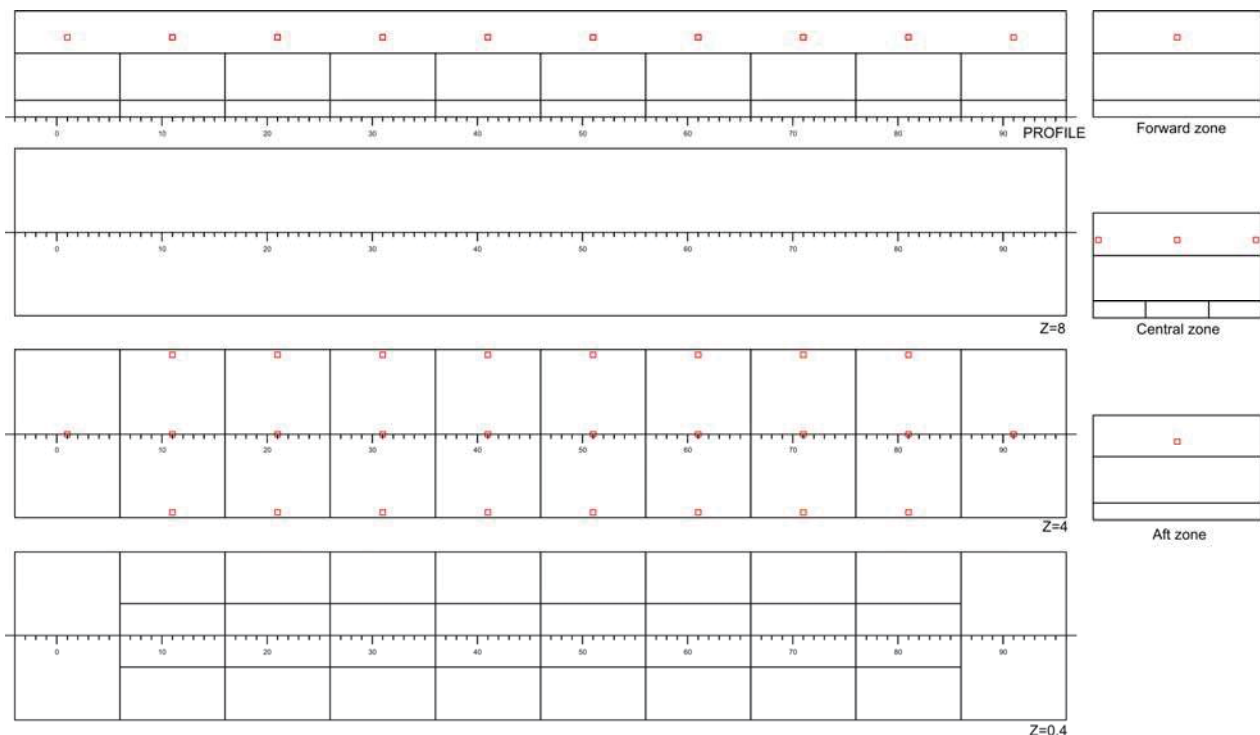


Figure 9: Layout of the test barge. Red squares marks the position of one way unprotected openings.

For the considered test vessel, the attained subdivision index $A_{GR,B}$ has been calculated according to (1). Damages have been generated considering a length of the ship equal to the overall length of the barge ($X_{MIN} = -4m$, $X_{MAX} = 96m$, $L_{ship} = 100m$ - See Table 1 and Table 3). An increasing number of generated breaches have been considered, namely: 10^3 , 10^4 and 10^5 . For each case, a series of 20 different repetitions have been run, and for each repetition the index $A_{GR,B}$ has been determined.

In the determination of $A_{GR,B}$, the “s-factor” has been calculated according to SOLAS Regulation 7-2 (IMO, 2014a), considering only the final stage of flooding. Heeling moments due to passengers on one side and due to wind have been considered in the determination of the “s-factor”. On the other hand, considering the absence of information for this simplified test case, the moment due to the launching of survival craft has been neglected. For the sake of the present testing, the same metacentric height, $GM = 2.0m$, has been used for the three calculation draughts.

Results from the described example calculations are shown in Figure 10. Black squares represent the attained subdivision index $A_{GR,B}$ as obtained from each single repetition, for the different numbers of generated breaches. Superimposed, the curve of the average index among the available repetitions is also reported. Around the average index, an approximate simplified Gaussian confidence band is shown, which extend for $\pm 2\sigma_A$, with σ_A being the standard deviation of $A_{GR,B}$ as estimated from the available repetitions, for each number of breaches. This band is to be interpreted as a simplified approximate region within which the outcome from a single run will lie, with approximately 95% probability. If the A-index is averaged among different repetitions, the confidence band for the averaged index decreases by the square root of the number of repetitions.

From a practical point of view, the results in Figure 10 provide indications regarding the number of breaches to be used in order to obtain a given accuracy for $A_{GR,B}$. Alternatively, they provide information regarding the confidence in the estimated A-index. For instance, when 10^4 breaches are used for the example case, σ_A is estimated as $1.65 \cdot 10^{-3}$. This means that, if a single repetition is considered, then, with approximately 95% confidence, the true attained index is in an interval of $\pm 3.30 \cdot 10^{-3}$ around the obtained $A_{GR,B}$. In case the index is obtained by averaging, e.g., five repetitions, then the expected 95% confidence interval around the obtained average reduces to $\pm 3.30 \cdot 10^{-3} / \sqrt{5} = \pm 1.48 \cdot 10^{-3}$. From the perspective of practical applications, the obtained results indicate that calculations based on the generation of 10^4 breaches can be considered to provide an acceptable level of accuracy, particularly when using multiple repetitions. It can therefore be preliminary suggested to carry out a series of five repetitions, with 10^4 breaches for each repetition.

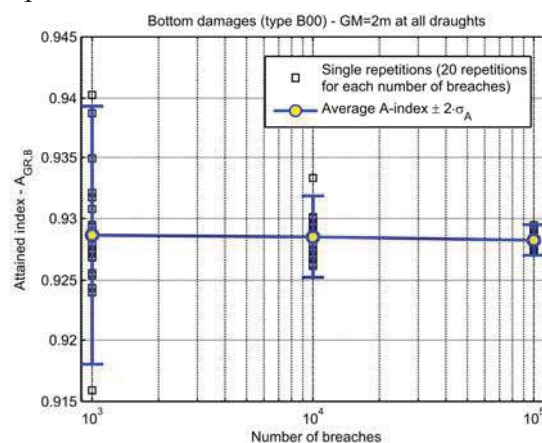


Figure 10: Example calculations for $A_{GR,B}$.

6. FINAL REMARKS

In this paper, a probabilistic approach has been presented for the regulatory assessment of damaged ship survivability following a grounding accident. The presented approach is flexible and easily updatable. Furthermore, the essence of the described approach was



designed to be in line with existing SOLAS2009 probabilistic regulations dealing with survivability following a collision. As a result, this potentially allows for a harmonization within the existing SOLAS framework.

The main difference between the described approach and present SOLAS2009 regulations resides in the way the “p-factors” are determined.

Indeed, SOLAS2009 uses analytical expressions for the determination of “p-factors”. Such expressions have been developed, and are strictly valid, only in case of box-shaped vessels with orthogonal subdivision, which is clearly not the case for most real vessels. Their practical application to real vessels is hence approximate, and it requires, in addition, the so-called “zonification” of the vessel, combined with explanatory notes aimed at specifying how to address compartments having complex (non-box-shaped) layouts. Furthermore, the analytical expressions for the determination of “p-factors” are strongly tied with the underlying distributions for the assumed damage characteristics, which do not appear explicitly in the regulations. As a result, although the “zonal approach” is fast and practical, it is inherently approximate and difficult to update. While its application in case of collision has been considered sufficiently accurate, the same cannot be said in case of damages due to grounding.

To take a step forward with respect to the present situation, the approach presented herein is based on the idea of determining the “p-factors” using a direct non-zonal approach. In such an approach, as a first step, the geometrical model of the damage is clearly described. Then, appropriate distributions are specified for the damage characteristics. These two elements lead to a fully characterised, transparent and easily updatable probabilistic model for the position and extent of the damage. This explicit model is then used to

generate a sufficiently large number of breaches on the vessel. Collecting breaches leading to the same set of damaged compartments allow to automatically determine what are commonly called “damage cases” together with their associated “p-factors” (probability of occurrence). The occurrence of non-contact cases is addressed by proper renormalization of “p-factors”. Combining the obtained “p-factors” with the “s-factor” calculated, for instance, according to SOLAS, for each “damage case”, and for each calculation draught, it is eventually possible to arrive at an attained survivability index. This index is intended to represent the survivability of the vessel following a grounding accident. The number of generated breaches needs to be large enough to achieve sufficient convergence of the attained index.

Once the geometrical model of the damage is clearly and properly described, hopefully limited explanatory notes regarding the application of the methodology are necessary, and the methodology is able to handle any compartment shape. Moreover, this approach can be easily updated in terms of underlying geometrical damage model and associated probability distributions, since no explicit analytical expressions, which in the general case cannot be obtained without essential simplifications, are to be developed for the determination of “p-factors”. When new, or better, probabilistic damage models, or new, or better, probability distributions for the characteristics of existing damage types become available, they can simply substitute the existing ones in the calculation code, together with the generation procedure for the breaches (if this is needs to be modified). The software tool and its underlying logic (which is actually very simple) remain exactly the same. Such flexibility and ease of update can be exploited in a number of ways: periodic update of the regulations, alternative design assessment taking into account structural effects, ship-specific damage models, model tuning based on direct structural calculations, specific damage models for implementation



into dynamic flooding simulations, just to mention a few possibilities.

In this paper, an example has been reported for the case of bottom grounding damages. However, the same procedure and software tool can be used, and have been developed, also for the case of grounding damages to the side of the vessel, extending partially or totally above the double bottom. In addition, the same procedure and software tool could be applied also to the case of collision, provided some updates are introduced in the current SOLAS framework. It is also important to note that this procedure is not totally new for the IMO regulatory framework. In fact, a procedure very close to the one reported herein, is already at the basis of the alternative assessment of accidental oil outflow performance or of double hull and double bottom requirements within MARPOL. As a result, almost the same software tool and logic could be applied also to such cases.

Preliminary testing of the described framework have shown that the number of breaches to be generated in order to achieve a sufficient convergence of the attained subdivision index is reasonable enough to render the approach practical for engineering purposes.

7. ACKNOWLEDGEMENTS

The financial support from the European Maritime Safety Agency (EMSA), in the framework of project EMSA/OP/10/2013 “Study assessing the acceptable and practicable risk level of passenger ships related to damage stability”, is acknowledged. The information and views set out in this paper are those of the authors and do not necessarily reflect the official opinion of EMSA.

8. REFERENCES

- Bulian, G., Francescutto, A., 2010, “Probability of flooding due to grounding damage using a p-factor formulation”, GOALDS Project
- Bulian, G., Francescutto, A., 2011, “Probabilistic modelling of grounding damage characteristics”, GOALDS Project
- Bulian, G., Francescutto, A., 2012, “Bottom damages: possible ways to reduce the occurrence and/or influence of non-contact cases in view of practical applications”, GOALDS Project
- IMO, 2003a, “SLF46/3/3 - Final recommendations from the research project HARDER”, Submitted by Norway and the United Kingdom, 6 June
- IMO, 2003b, “SLF46/INF.5 - Evaluation of Required Subdivision Index R for Passenger and Dry Cargo Ships - Report from the research project HARDER”, Submitted by Norway and the United Kingdom, 6 June
- IMO, 2003c, “MEPC.110(49) - Revised Interim Guidelines for the Approval of Alternative Methods of Design and Construction of Oil Tankers under Regulation 13F(5) of Annex I of MARPOL 73/78”, Adopted on 18 July
- IMO, 2004a, “SLF47/INF.4 - Bottom damage statistics for draft regulation 9”, Submitted by Germany and Norway, London, UK, 9 June
- IMO, 2004b, “SLF47/17 - Report to the Maritime Safety Committee”, 27 September
- IMO, 2005, “MSC80/3/5 - Report of the Intersessional Working Group on Subdivision and Damage Stability (SDS)”, 21 January 2005



- IMO, 2006, “MSC.216(82) - Adoption of Amendments to the International Convention for the Safety Of Life At Sea, 1974, as amended”, 8 December
- IMO, 2012, “SLF55/INF.7 - The GOAL based Damage Stability project (GOALDS) – Derivation of updated probability distributions of collision and grounding damage characteristics for passenger ships”, Submitted by Denmark and the United Kingdom, 14 December
- IMO, 2014a, “International Convention for the Safety of Life at Sea (SOLAS)”
- IMO, 2014b, “International Convention for the Prevention of Pollution from Ships, 1973, as modified by the Protocol of 1978 - Annex I”
- IMO, 2014c, “International Convention on Load Lines, 1966, as amended by the 1988 Protocol by res. MSC.143(77) in 2003”
- Kehren, F.-I., Krüger S., 2007, “Development of a Probabilistic Methodology for Damage Stability Regarding Bottom Damages”, Proc. 10th International Symposium on Practical Design of Ships and Other Floating Structures (PRADS2007), Houston, Texas, USA
- Koelman, H.J., 2005, “On the procedure for the determination of the probability of collision damage”, International Shipbuilding Progress, Vol. 52, pp. 129–148
- Lützen, M., 2002, “Damage Distributions”, HARDER Document 2-22-D-2001-01-4 (version:4 , date: 2002-07-29). See also Lützen, M., 2001, “Ship Collision Damage”, PhD thesis, Department of Mechanical Engineering, Maritime Engineering, Technical University of Denmark, Lyngby
- Papanikolaou, A., Bulian, G., Mains, C., 2011, “GOALDS – Goal Based Damaged Stability: Collision and Grounding Damages”, Proc. 12th International Ship Stability Workshop, 12-15 June, pp. 37-44
- Spanos, D., Papanikolaou, A., 2014, “On the time for the abandonment of flooded passenger ships due to collision damages”, Journal of Marine Science and Technology, Vol. 19, pp. 327–337
- Vassalos, D., Jasionowski, A., Guarin, L., 2008, “Risk-Based Design: a Bridge too Far?”, Proc. 6th Osaka Colloquium on Seakeeping and Stability of Ships, 26-29 March, Osaka, Japan, pp. 201-212



Damage Stability Requirements for Passenger Ships – Collision Risk based Cost Benefit Assessment

Rainer Hamann, DNV GL Rainer.Hamann@dnvgl.com

Odd Olufsen, DNV GL Odd.Olufsen@dnvgl.com

Henning Luhmann, Meyer Werft Henning.Luhmann@meyerwerft.de

Apostolos Papanikolaou, National Technical University Athens papa@deslab.ntua.gr

Eleftheria Eliopoulou, National Technical University Athens eli@deslab.ntua.gr

Dracos Vassalos, University of Strathclyde d.vassalos@strath.ac.uk

ABSTRACT

Currently built passenger ships have to comply with SOLAS 2009 probabilistic damage stability requirements. There are, however, serious concerns regarding the sufficiency of these requirements with respect to the Required Subdivision Index R, which should properly account for the risk of People On Board (POB) and ship's inherent survivability in case of loss of her watertight integrity. In recent years extensive research on determining the appropriate level of R using risk-based methods has been carried out. The urgency of the matter was reinforced by the quite recent *Costa Concordia* (2012) accident, even though this accident was not related to a collision event. This paper outlines the objectives, the methodology of work and first results of the ongoing studies funded by EMSA (EMSA III project) focusing on risk-based damage stability requirements for passenger ships. In compliance with IMO Formal Safety Assessment process a collision risk model is further developed based on the results of EU GOALDS project and a new required index shall be suggested by means of cost-benefit assessment. The updated collision risk model uses information from the most recent analysis of casualty reports of databases considering the period 1990 to 2012.

Keywords: Collision, Risk Model, Damage Stability, Passenger Ship Safety, Formal Safety Assessment, Cost Benefit Analysis

1. INTRODUCTION

In January 2009 the SOLAS 90 deterministic damage stability requirements for passenger ships were replaced by the new harmonised SOLAS 2009 probabilistic requirements, which were to a great extent based on research work of the HARDER project. However, that time when IMO Sub-Committee SLF was in the process of developing SOLAS 2009, it was mandated by IMO Marine Safety Committee *not to raise the safety level*. At that time this was considered satisfactory, except for the Ro-Ro cargo and

car carriers ships in general, for which the required survivability level was significantly raised. Therefore, for the majority of ship types, including the passenger ships, the required damage stability index (R-Index) was adjusted to represent *on average* the safety level of a representative sample of ships of the particular ship type with satisfactory survivability regarding the likely collision damages. A review of related developments can be found in Papanikolaou and Eliopoulou (2008).



Since then, extensive research on determining the appropriate level of R using risk-based methods has been carried out in particular in the projects funded by EMSA, e.g. EMSA study on specific damage stability parameters of Ro-Pax vessels (2011) and the partially EU funded project GOALDS (Papanikolaou et al., 2013). One of the key contributions of GOALDS (2009 – 2012) was the *risk-based* derivation of a *new damage stability requirement* for passenger ships, which was supported by conducting a series of concept design studies for sample RoPax and cruise ships, including their formal optimisation with respect to technical, economic and safety (risk) criteria. Key results of this project were submitted to IMO for consideration in the rule-making process (SLF 55/INF.7, SLF 55/INF.8, SLF 55/INF.9) and were positively reviewed by IMO FSA expert group (MSC 93/6/3, 2013).

Despite of all the above research efforts there were still some unanswered questions and the objectives of the EMSA III study are to cover the specific knowledge gaps that were identified after the finalisation of the previous EMSA projects and GOALDS. These knowledge gaps are the effect of (open left) watertight doors, the consideration of grounding and raking damages the in damage stability evaluation as well as the consolidation of the collision risk model. This paper is focusing on the consolidated collision risk model.

The EMSA III study uses a risk-based cost-benefit assessment for derivation of new damage stability requirements. In context of IMO rule making procedures this process is specified in the Guidelines for Formal Safety Assessment (FSA, MSC-MEPC.2/Circ.12 2013). In risk-based cost-benefit assessment the impact of risk reducing measures in relation to their costs and monetary benefits (Cost of Averting a Fatality, CAF) is quantitatively compared to well specified thresholds (value of preventing a fatality). These thresholds are

accepted by regulator and in accordance with the FSA Guidelines, and were based on a Life Quality approach. Therefore, this assessment requires the development of a risk model and a cost model for the aspect under consideration.

The focus of the work outlined in this paper is on damage stability requirements as covered by current regulations of SOLAS 2009. Accordingly, the collision risk model is particularly developed for this purpose and consequences focus on damage stability related casualties (fatalities due to sinking).

2. FLEET ATRISK

The risk model developed in section 0 was quantified using initial accident frequencies that were calculated determining accidents and fleet at risk for a sample complying with the characteristics specified already in GOALDS project:

- Ship types: cruise, passenger ships, Ro-Pax and RoPaxRail;
- $GT \geq 1,000$ – most ships below $GT 1,000$ operate on non-international voyages;
- ≥ 80 m length (LOA) - most ships below 80 m in length operate on non-international voyages;
- Built ≥ 1982 ;
- Accidents in the period 1994-01-01 and 2012-12-31;
- IACS class at time of accident – to reduce the potential effect of under reporting;
- IACS class for determination of ship years;



- Froude No. ≤ 0.5 – to eliminate High Speed Craft (HSC) from the study.

For the further analysis two basic ship categories were considered and the different samples merged accordingly:

- Cruise, comprising cruise and passenger ships with accommodation for more than 12 passengers in cabins;
- RoPax, comprising Ro-Pax and Ro-Pax-Rail vessel with accommodation for more than 12 passengers.

The development of fleet size in terms of ship years for both categories and the period 1994 to 2012 is shown in

Figure 1. For the samples the number of ship years was 3,290 for Cruise and 6,738 for RoPax.

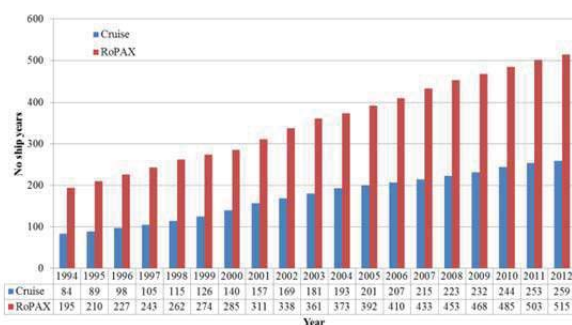


Figure 1 Fleet size per year for ship categories Cruise and RoPax

3. COLLISION CASUALTIES

Initial raw casualty data were retrieved from the IHS Fairplay database. The particular records were inserted in the newly developed database allowing for more detailed statistical investigation. Before inserted records were

reviewed and enhanced by additional information to the extent available; the data in hand were re-analysed and post-processed in the way to produce input to the pre-developed collision risk model.

All captured accidents occurred during the ship's operational phase and were assigned to one of the predefined main incident categories according to the last “accidental event”. Regarding the definition of each accident event, the relevant IMO descriptions were adopted (MSC/Circ.953, 2000).

In the post 2000 period, a total of 67 serious collision events occurred involving IACS classed Cruise and RoPax ships, see **Table 1**.

Focusing on Cruise ships, 17 accidents were assigned as collision events (**Table 1**); the vast majority of them; 88% (15 accidents out of 17) occurred in terminal areas. Heavy weather conditions were reported in 7 cases, good weather in 2 cases whereas there was no weather report concerning the remaining accidents.

In 43% of the collision accidents, the Cruise vessel was the struck one. In cases where the Cruise ship was the struck one, striking ships are: another Cruise ship (2 cases), a barge (1 case), a Chemical/Oil Tanker (1 case), a Bulk Carrier (1 case) and a Containership (1 case). Finally, no ship total loss and no fatalities were reported within the study period.

Regarding RoPax ships, in total 50 serious collision events occurred involving IACS classed RoPax ships, ref. Table 1. About 57% of the particular collision events occurred in Terminal areas, 39% in limited waters and 2% in Open Sea during en-route operation. Heavy weather conditions were reported in 9 cases, good weather in 3 cases, under poor visibility in 5 cases, under freezing conditions in 2 cases whereas there was no weather report concerning the remaining accidents.

In 58% of the collision accidents, the RoPax ship was the struck vessel. In cases where the RoPax ship was the struck one, striking ships are: another RoPax ship (9 cases), a Ro-Ro Cargo ship (3 cases), a General Cargo (3 cases), a Bulk Carrier (2 cases), a Chemical/Oil Tanker (1 case), a Containership (1 case), a tug (1 case) and a Fishing vessel (1 case). Finally, no ship total loss and no fatalities were reported within the study period.

Time Period			
1994 - 2012		2000 - 2012	
No of casualties ¹	1/ship year ²	No of casualties ¹	1/ship year ³
Cruise			
19	5.78E-03	17	6.36E-03
RoPax			
52	7.72E-03	50	9.38E-03

Table 1: Number of casualties for ship categories Cruise and RoPax as well as related initial accident frequencies for periods 1994 to 2012 and 2000 to 2012

Table 2 presents the calculated frequencies used for input to the collision risk model. The previous analysis carried out in GOALDS project started with year 1994 and therefore the focus for collecting and investigating casualty reports was put on the period 1994 to 2012. For the current analysis the time period covers year 2000 to 2012 due to higher annual accident frequencies compared to 1994 to 2000. Anyway, the same constrains with GOALDS project are adopted as described in the previous section.

4. COLLISION RISK MODEL

The collision risk model in EMSA III project was developed on basis of the risk

¹ serious cases, IACS ships at the time of incident
² Calculated considering IACS classed ships and the selection criteria specified: 3290 ship years
³ Calculated considering IACS classed ships and the selection criteria specified: 2673 ship years

model developed for GOALDS incorporating newly available information. Starting point for the risk model was the high-level collision event sequence considering main influences on the development of consequences (**Figure 2**), i.e. considering whether the ship was struck or striking (initiator), the location of the accident (operational area), the possibility of water ingress and in case of water ingress the possibility of sinking including the velocity.

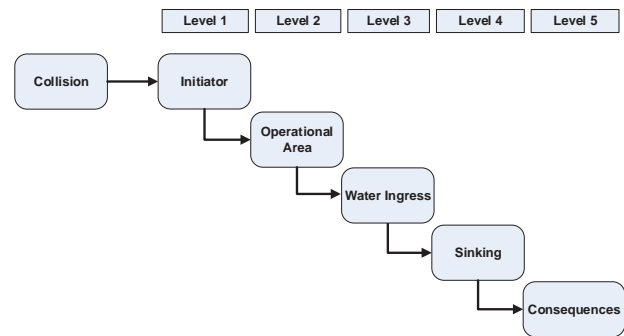


Figure 2 High-level event sequence for collision casualties of passenger ship

The developed collision risk model is shown in Figure 7 for the example of ship type Cruise. The main differences to the GOALDS collision risk models are:

- Merging scenarios “en route” and “limited waters” because in both branches the same dependent probabilities were used;
- Reduced fatality rate for sinking in terminal area of 5% considering the effects of limited water depth and good SAR;
- Estimate dependent probabilities for the events “initiator”, “operational area” and “water ingress” on basis of a sample received by merging the reports for Cruise and RoPax.

Initial accident frequencies are summarised in Table 2 above. Dependent probabilities for initiator (struck/striking), operational area (terminal/limited waters-en route) and water

ingress were estimated on basis of the casualty reports collected for the period 1994 to 2013. As this risk model is dedicated to damage stability the probability of sinking was estimated on basis of SOLAS 2009 damage stability requirements. Hence, the probability of sinking is equal to 1-A.

For consider the uncertainty in the initial accident frequencies, the dependent probabilities as well as the consequences with respect to Person On Board distributions were estimated for the nodes in the risk model and risk was calculated in terms of PLL by means of Monte Carlo simulation. Distributions were estimated on basis of the confidence intervals that were calculated using the approach suggested by Engelhardt (1994). **Figure 3** shows exemplarily the used log-normal distribution for a Cruise ship being struck

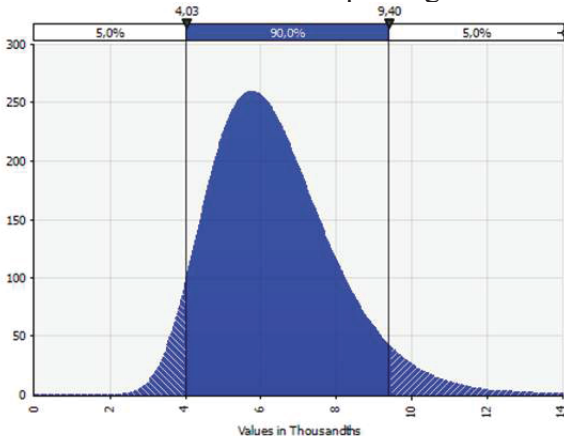


Figure 3 Log-normal distribution for Cruise ship being struck with 90% confidence interval.

The collision risk for Cruise ships and RoPax were calculated considering typical occupancy rates. For Cruise ships the occupancy rate was 90%, i.e. 90% of certified passenger and crew capacity. For RoPax three different occupancy rates for passengers were defined approximating seasonal variation of people on board over the year:

- 100% for 12.5% of the year (high season);

- 75% for 25% of the year (medium season); and,
- 50% for 62.5% of the year (low season).

Number of crew was kept constant using nominal value.

Table 2 summarises the collision risk in terms of PLL for six reference ships. These collision risk values were calculated for the damage stability index attained for the original design.

Table 2 Collision risk in terms of Potential Loss of Lives (mean values) calculated for ship types considered in cost benefit analysis

Ship type and size	PLL (fatalities per ship year)	Number of Persons (POB)
large cruise	6.32E-02	6730
small cruise	9.67E-03	478
ropax baltic	1.04E-01	3280
ropax Med	6.80E-02	1700
ropax ferry	2.95E-02	625
double end	2.71E-02	610

As shown, risk in terms of PLL increased with number of persons on board which is quite obvious because the risk model considers the ship size only via the attained index and corresponding POB when estimating the probability of sinking.

5. COST-BENEFIT ANALYSIS

The main objective of the cost-benefit assessment (CBA) is the evaluation of risk control options with respect to their economic impact, i.e. compare related costs with monetary threshold CAF (Cost of Averting a Fatality). The basic assumption for design work was to keep the business model and the transport task constant during the design variations. In particular the defined capacities

like number of cabins, lane metres and deadweight, operational profiles with regard to speed and turnaround times, as well as specific demands for the ship, e.g. restrictions of main dimensions, have been preserved.

For the different design variants a cost-benefit calculation has been done, based on the same method as applied in GOALDS. For all cost elements only the change compared to the reference design has been calculated.

All values are calculated on 2014 levels and the life-cycle costs are assessed using a discount factor of 5% over the 30 year lifetime of the ship.

The change of three main cost elements has been evaluated in the cost benefit analysis (CBA):

- Change of production costs, for structure, outfitting and equipment, including also design costs and other costs such as insurance, financing etc.;
- Change of operational costs, mainly the change of fuel costs due to modified main dimensions or hull form;
- Change of revenue – theoretical revenues arising from the design modification were not investigated since the transportation task / business model of the owner was kept constant; therefore only the change of scrap value due to the reduced probability of total loss (sinking of ship) due to an increase of A was calculated.

The future fuel price development is connected to a high degree of uncertainty; the fuel costs may, however, have significant influence on the cost effectiveness of the risk control options. In order to achieve comparable results, the same approach as in the GOALDS project has been used where the development of fuel prices is based on the estimations of the Annual Energy Outlook 2012 prepared by the

U.S. Energy Information Administration (EIA), as shown in the following graph (**Figure 4**).

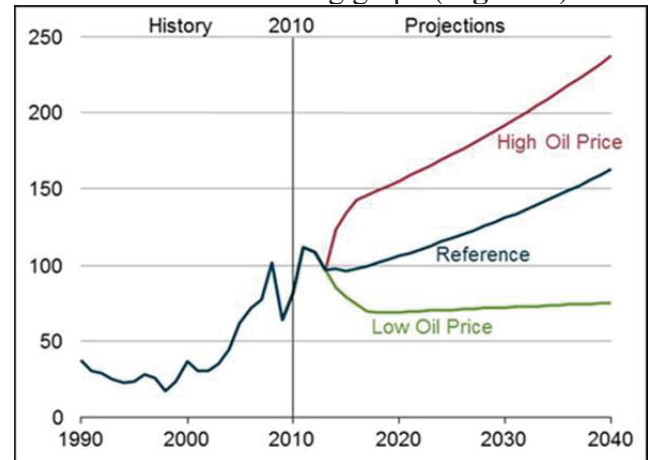


Figure 4 Average annual oil prices for the three scenarios 'low', 'reference' and 'high', 1990-2035⁴ (2010 US\$ per bbl)

In respect to the coming environmental regulations and the use of low sulphur fuels, a fuel mix has been defined for the life time of each of the sample ships. For each design variant a calculation of the annual fuel consumption has been made based on the given operational profile which considers different percentages of port time, as well as the distribution of different operational speeds.

As the business model is kept constant, e.g. the same number of cabins or amount of deadweight and cargo capacity, the only change in the revenue is calculated based on small variations of the business model and on the reduced probability of total loss due to the changed attained index A.

This small contribution to the revenue is based on the GOALDS investigations, in which published newbuilding and scrapping prices from IHS Fairplay database have been analysed to achieve a coarse relation between ship size and the price for design and construction.

Secondary effects costs which may be faced by the operator or the society following a large

⁴ Remarkably with respect to the volatility of prices: early 2015 oil prices are well below the 2010 predicted Low Price Level

accident has not been accounted for due to limited available data.

6. NEW PASSENGER SHIP DESIGNS

New designs of six passenger ships have been developed to form the basis for the optimization and benchmark for the subdivision index, as well as for grounding and the effect of open water tight doors.

All designs comply with the current statutory rules and regulations, e.g. SOLAS 2009 including ‘Safe Return to Port’ where applicable. Some of the RoPax designs also comply with the EU directive for RoRo passenger ships, known as Stockholm Agreement.

The designs have been selected in close cooperation between the designers and ship operators in such a way that the world fleet will be well represented and as a complement to the designs investigated in GOALDS. **Figure 5** shows a plot of the actual world fleet of XY ships in terms of length and person on board, and the sample ships. The main characteristics of the sample ships are summarised in **Table 3**.

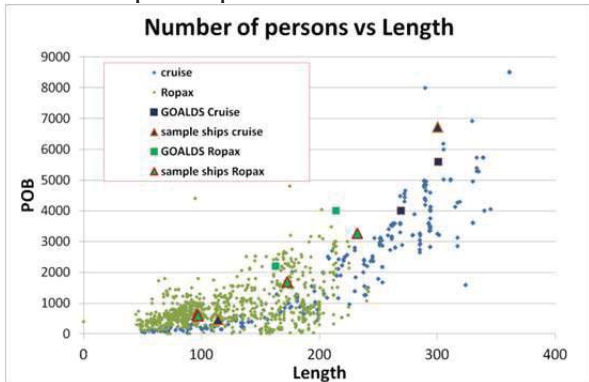


Figure 5 Selection of sample ships with regard to length and POB (RoPax and Cruise)

For all ships a number of risk control options have been executed mainly due to the moderate variation of breadth and freeboard as well as changes to the internal watertight subdivision. The focus was laid on practical feasible design variations which results in a

workable ship but with highest increase of the attained subdivision index according to SOLAS 2009. For the RoPax designs the new defined s-factor has been used, while the Stockholm Agreement has not been considered. Also the effect of any large lower hold has been investigated for two of the RoPax sample ships, as cargo capacity is the main design target and source of revenue for some ferry routes.

To allow an effective design the new defined CAF limits of 4 to 8 mill USD have been converted for each of the sample ships into graphs showing the maximum allowable costs to stay with the limits of cost effectiveness (Figure 6 shows the results for ‘large Cruise’). The 5% and 95% confidence intervals are also shown.

Table 3 Overview of sample ships

Type	Length (m)	GT	Number of persons
Large cruise	294.6	153400	6730
Small cruise	113.7	11800	478
Baltic RoPax	232.0	60000	3280
Med RoPax	172.4	43000	1700
Small cruise	113.7	11800	478
Small RoPax	95.5	7900	625
Double ender	96.8	6245	610

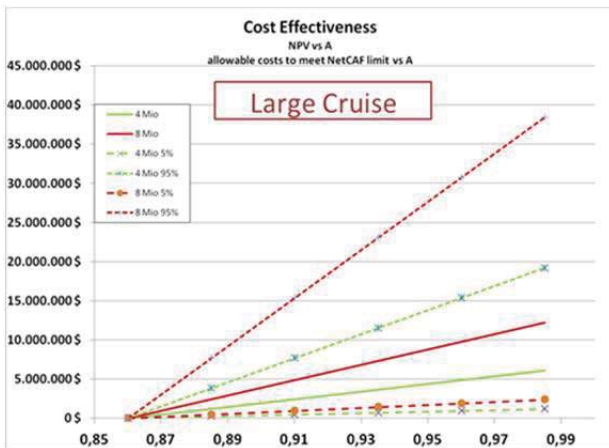


Figure 6 Diagram of cost effectiveness for large cruise ship

As explained in section 5 the costs and possible benefits for each Risk Control Option will be determined. Costs spread over the lifetime of the vessel will be transferred to a Net Present Value, i.e. future costs are transferred to a reference year (2014) using interest rate.

As seen in the risk model in Figure 7 the level of Attained Index (A) is directly used parameter in the risk model indicating whether the ship will sink or not. For an improvement in A there is a corresponding reduction in Potential Loss of Lives. This is what can be directly plotted in the Figure 6 to visualise whether the investigated RCO is within CAF limits of 4 or 8 mill USD. Additionally, corresponding confidence intervals are plotted allowing consideration of uncertainty in the risk model.

The results of the investigation of the sample ships will be used in the further work of this project to suggest a new level of R

7. SUMMARY AND CONCLUSIONS

The FSA on cruise ships demonstrated impressively that collision and grounding accidents are major risk contributors in particular due to water ingress leading to loss of stability.

The determination of an appropriate level of required damage stability (R-Index) for passenger ships has been a matter of extensive research. For instance the project GOALDS dealt with the quantification of damage stability related risk and identification of design options for mitigating the risk of collision and grounding accidents. However, despite of all research efforts some issues related to damage stability remain. One of the current key topics in this context is related to the update of damage stability requirements.

In IMO FSA Guidelines the ALARP process is recommended for determining new requirements respectively updating them. This process focuses on making the risk “as low as reasonable practical”, which comprises the development of a risk model for quantifying risk reduction and performing cost-benefit assessment. By cost-benefit assessment the economic impact of risk mitigating measures is evaluated by means of monetary thresholds.

In this paper the investigations focusing on a reduction of damage stability related risk, and following the procedures of the IMO FSA Guidelines were described, i.e. development of the risk model and design modification followed by cost-benefit assessment. The purpose was to be able to recommend the level of the required index R covering collision damages. An updated risk model has been developed which was further used in the cost-benefit assessment of six sample ships (two cruise and four RoPax ships). These sample ships were representative for the world fleet with respect to size, capacity and type. For each sample ship a number of risk control options have been executed mainly due to the moderate variation of breadth and freeboard as well as changes to the internal watertight subdivision. The work focused on obtaining practical feasible design variations with highest possible level of attained index A according to SOLAS 2009.

For each design modification a cost-benefit assessment has been carried out giving the



related Cost of Averting a Fatality (CAF). For modified designs where a CAF value less than the threshold of 4 and 8 mill USD is found the corresponding attained index A is taken into consideration for suggesting the level of R. The work carried out so far provided design variations with increased damage stability and in compliance with set CAF threshold, i.e. cost-beneficial designs.

8. ACKNOWLEDGEMENTS

The authors would like to express gratitude to EMSA for providing funding to the study.

The information and views set out in this paper are those of the authors and do not necessarily reflect the official opinion of EMSA.

9. REFERENCES

- Engelhardt, M.E., 1994: Events in Time: Basic Analysis of Poisson Data. Idaho National Engineering Laboratory, Idaho 83415.
- MSC-MEPC.2/Circ.12, 2013: Revised Guidelines for Formal Safety Assessment (FSA) for Use in the IMO Rule-Making Process. IMO London, 2007.
- MSC 93/6/3, 2013: Report of the intersessional meeting of the Experts Group on Formal Safety Assessment (FSA). Submitted by IMO Secretariat, IMO London.
- MSC/Circ.953, 2000: Reports on marine casualties and incidents. Revised harmonized reporting procedures - Reports required under SOLAS regulation I/21 and MARPOL 73/78 articles 8 and 12, December 2000, IMO London.
- Papanikolaou, A., Hamann, R., Lee, B-S, Mains, C., Olufsen, O, Tvedt, E., Vassalos, D., Zaraphonitis, G., 2013: GOALDS - Goal Based Damage Stability of Passenger Ships, Transactions of the 2013 Annual Conference of the Society of Naval Architect and Marine Engineers (SNAME), Seattle.
- Papanikolaou, A., Eliopoulou, E., 2008: On the Development of the New Harmonised Damage Stability Regulations for Dry Cargo and Passenger Ships, Journal of Reliability Engineering and System Safety (RESS), Elsevier Science, Vol. 93, 1305-1316.
- SLF 55/INF.7, 2012: The GOAL based Damage Stability project (GOALDS) – Derivation of updated probability distributions of collision and grounding damage characteristics for passenger ships. Submitted by Denmark and United Kingdom, IMO London.
- SLF 55/INF.8, 2012: The GOAL based Damage Stability project (GOALDS) - Derivation of updated probability of survival for passenger ships. Submitted by Denmark and United Kingdom, IMO London.
- SLF 55/INF.9, 2012: The GOAL based Damage Stability project (GOALDS) – Development of a new risk-based damage stability requirement for passenger ships based on Cost-Benefit Assessment. Submitted by Denmark and United Kingdom, IMO London.
- U.S. Energy Information Administration, 2012: Annual Energy Outlook – 2012

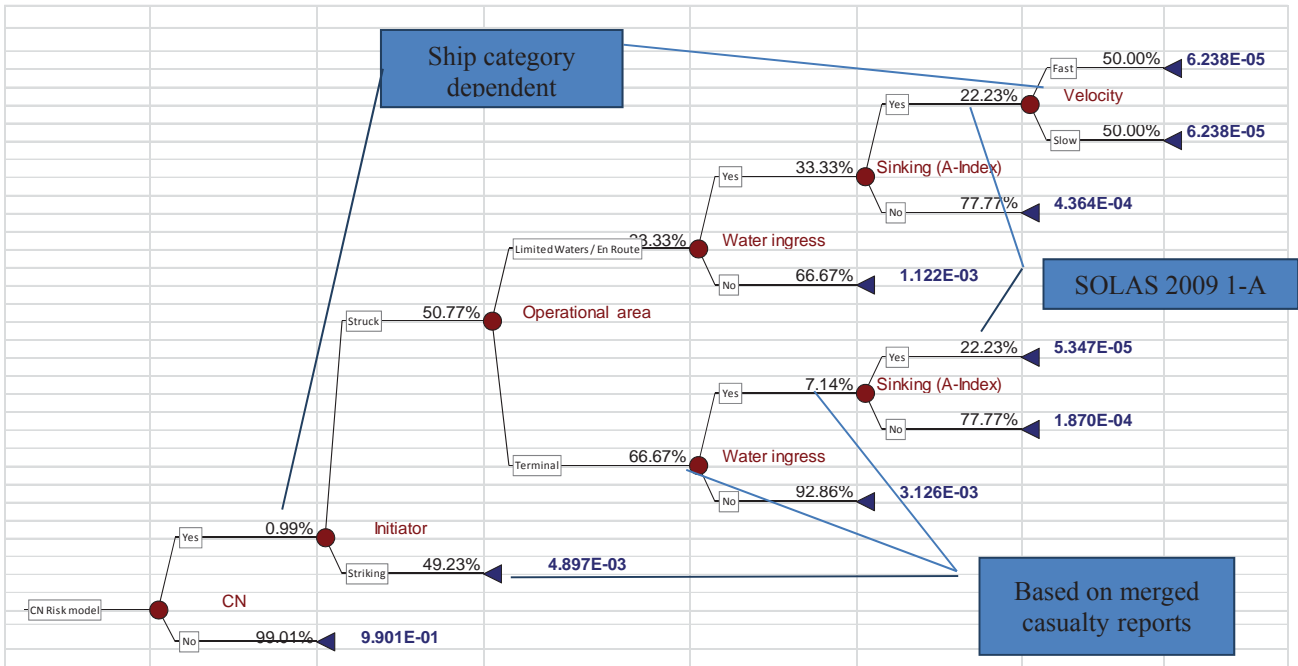


Figure 7 CN risk model for cruise ship

Table 4: Main particulars of ship designs optimised

No	Type	Length bp	Breadth	Draught	Gross Tonnage	Number of Persons
		m	m	m	tonnes	
1	large cruise	300.00	40.80	8.75	153400	6730
2	small cruise	113.70	30.00	5.30	11800	478
3	PoPax Baltic	232.00	29.00	7.20	60000	3280
4	RoPax Med	172.40	31.00	6.60	43000	1700
5	RoPax ferry	95.95	20.20	4.90	7900	625
6	RoPax double end	96.80	17.60	4.00	6245	600

Session 7.1 – 2nd GENERATION INTACT STABILITY

An Investigation into the Factors Affecting Probabilistic Criterion for Surf-Riding

Numerical Prediction of Parametric Roll Resonance in Oblique Waves

Numerical Simulation of the Ship Roll Damping

Investigation of the Applicability of the IMO Second Generation Intact Stability Criteria to Fishing Vessels

This page is intentionally left blank



An Investigation into the Factors Affecting Probabilistic Criterion for Surf-Riding

Naoya Umeda, *Osaka University* umeda@naoe.eng.osaka-u.ac.jp

Toru Ihara, *Osaka University* ihara-t2ac@mlit.go.jp

Satoshi Usada, *Osaka University* satoshi_usada@naoe.eng.osaka-u.ac.jp

ABSTRACT

The second generation intact stability criteria for broaching are now under development. In this process, several elements should be investigated with nonlinear ship dynamics and stochastic theories for regulatory application. First, the effect of diffraction effects on surf-riding probability was investigated so that the effect is essential for reasonable operational limitation. Second, the effect of estimation of calm-water resistance was examined so that reasonably good fitting of resistance curve is proposed. Third, the effect of different stochastic wave theories was also investigated. These results could provide a base of discussion at the IMO.

Keywords: *Broaching, diffraction effect, IMO, Second generation intact stability criteria, stochastic wave theory*

1. INTRODUCTION

When surf-riding occurs, a ship occasionally suffers broaching, which could result in capsizing. Therefore, the International Maritime Organisation (IMO) circulated its operational guidance for preventing surf-riding (IMO, 1995) and drafted its design criteria for surf-riding (Japan, 2014) as a part of the second generation intact stability criteria. These operational and design requirements are based on global bifurcation analyses, i.e. phase plane analysis and the Melnikov analysis, because surf-riding can be regarded as a global bifurcation of uncoupled surge motion in regular following waves.

Although these approaches were well validated with model experiments, some additional elements should be developed for regulatory criteria. Firstly wave-induced surge force, which induces surf-riding, should be accurately estimated. Secondly, ship calm-water resistance, which could prevent surf-riding, should be practically modelled. Thirdly, a gap between the global bifurcation of periodically excited system and realistic irregular waves should be resolved. Finally the relationship be-

tween the surf-riding and capsizing should be established for proper use of direct stability assessment in future. Thus, this paper attempts to provide some guides for these elements for establishing operational and design criteria, following outline of the draft surf-riding criteria at the IMO.

2. OUTLINE OF PROBABILISTIC SURF-RIDING CRITERION

2.1 Surf-riding threshold in regular waves

The draft criterion utilises calculation of surf-riding probability for a given ship in the North Atlantic or its operational area. Firstly, the surf-riding threshold in various regular waves is systematically calculated with the wave-induced surge force, calm-water ship resistance, propeller thrust and displacement. Here the Melnikov analysis is used to determine the bifurcation point where a trajectory starting from one unstable surf-riding equilibrium point coincides with a trajectory from another unstable surf-riding threshold. This means that such trajectory is definitely a periodic orbit but its period is infinite

because reaching an unstable equilibrium requires infinite time. Thus this bifurcation point can be regarded as a border between periodic states and the equilibrium which is surf-riding. In this analysis, this bifurcation point is straightforwardly calculated by solving a nonlinear equation without time domain simulation. The Melnikov analysis is applied to this issue by Kan (1990) with linear calm-water resistance model and then Spyrou (2006) proposed to use cubic calm-water modelling. The formula used here allows us to use any order polynomial fitting of ship resistance, which was well validated in model experiments (Maki et al., 2010).

2.2 Surf-riding probability in irregular waves

In the draft criterion, the given ship is judged as vulnerable to broaching if the surf-riding probability in the North Atlantic is larger

than the acceptable level. The surf-riding probability is calculated by integrating the probability density of local wave height and wavelength in which operational speed is above the surf-riding threshold as obtained in the section 2.1. This procedure appeared in Umeda (1990) is based on the assumption that irregular waves can be divided into a train of many local waves having different heights and lengths because surf-riding occurs only with one local wave. Indirect validation of this procedure in the light of the Monte Carlo simulation for pitch motion can be found in Umeda et al. (2011). The probability density of local waves can be calculated by Longuet-Higgins's works (1983) or equivalent, assuming that ocean waves are narrow-banded process. Their validation results used the field observation by Goda (2000). Furthermore, by using a wave scattering diagram and the results obtained so far, surf-riding probability for a certain water area can be calculated.

3. DIFFRACTION EFFECT ON SURF-RIDING

3.1 Wave-induced surge force

Surf-riding means that a ship runs with a wave. Thus the encounter frequency is zero. For predicting surf-riding, it is essential to accurately predict wave-induced surge forces at zero encounter frequency. If we could ignore disturbance due to a ship, the Froude-Krylov force, which can be easily calculated, could be sufficient. Many comparisons between model experiments and the Froude-Krylov prediction, however, indicate that the Froude-Krylov approach significantly overestimates the experiment (e.g. Ito et al., 2014). An example is shown in Figure 1.

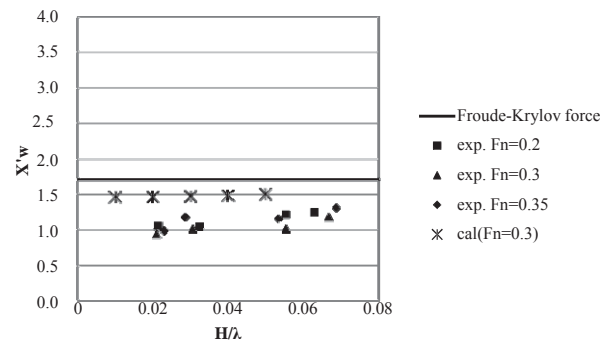


Figure 1 Wave-induced surge force for the ITTC A1 containership with the wavelength to ship length ratio of 1 for different wave steepnesses, H/λ , and the Froude numbers, F_n . Here the wave-induced surge force is normalised with the product of ship weight and wave steepness. (Y. Ito, et al., 2014).

These results indicate that the measured wave-induced surge force is almost linear so that this discrepancy cannot be explained with wave nonlinearity. Thus Umeda (1984) and Ito et al. (2014) applied a thin ship theory and a slender body theory, respectively. Here diffraction effect, i.e. change of wave-making resistance due to periodic change of incident wave profile, is theoretically calculated because the three-dimensional wave pattern due to an oscillatory

point source at the zero encounter frequency tends to that due to the Kelvin source. The strength of source distribution can be determined with the hull surface condition with water particle velocity due to waves taken into account. As shown in Figure 1, this diffraction effects explain the discrepancy between the model experiment and the Froude-Krylov prediction to some extent. More quantitative agreement can be achieved with the CFD simulation (Sadat-Hosseini et al., 2011.)

3.2 Diffraction effect on surf-riding probability

It was already published that diffraction effect on surf-riding threshold in regular waves is indispensable to avoid inconsistency between

the IMO operational guidance and the draft criteria (Umeda et al., 2011). The critical nominal Froude number for surf-riding estimated with the Froude-Krylov force on its own could be smaller than 0.3, which is requirement of the IMO operational guidance, while that with the measured wave force is larger than 0.3.

As a next step, it is necessary to quantify the diffraction effect on surf-riding probability as the final output of the draft criterion. The comparisons of surf-riding probability with and without diffraction force are conducted as shown in Figures 2-7. The subject ships used here are two containerships, a pure car carrier (PCC), a RoRO ship and two hypothetical war ships. Their principal particulars are shown in Table 1.

Table 1 Principal particulars of the subject ships

	C11 container-ship	ITTC A1 container-ship	RoRo	PCC	ONR- flare	ONR-tumblehome
Length : $L_{BP(m)}$	262.0	150.0	187.7	192.0	154.0	154.0
Breadth: $B(m)$	40.0	27.2	24.5	32.26	18.78	18.78
Mean Draught: $d(m)$	11.5	8.5	6.9	8.18	5.494	5.494
Block coefficient: C_b	0.560	0.667	N/A	0.537	0.536	0.536
Metacentric height: $GM(m)$	0.56	0.739	1.00	1.25	0.755	2.07

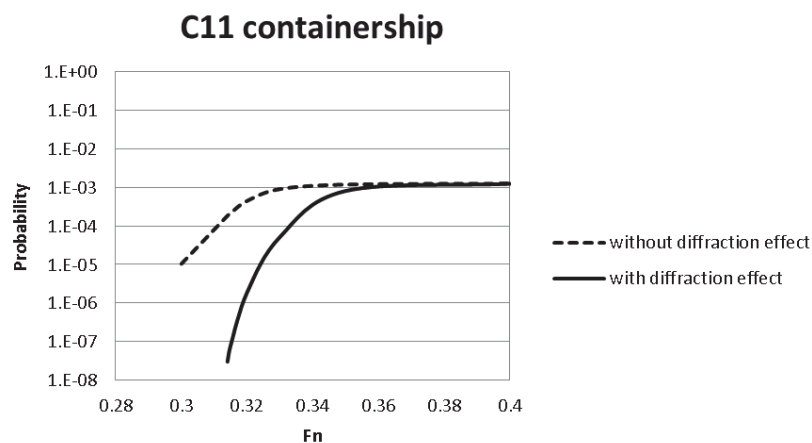


Figure 2 Surf-riding probability for the modified C11 containership with and without diffraction effect.

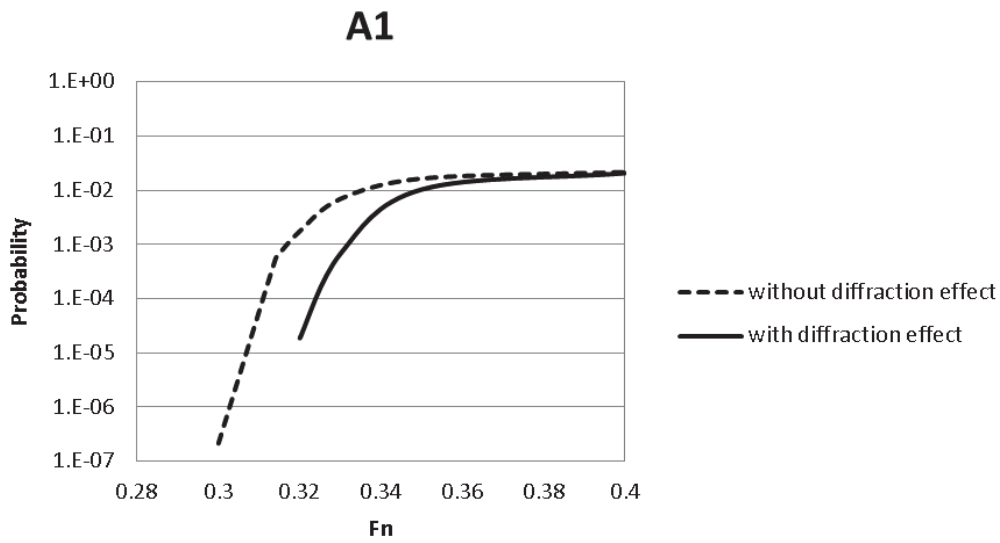


Figure 3 Surf-riding probability for the ITTC A1 containership with and without diffraction effect.

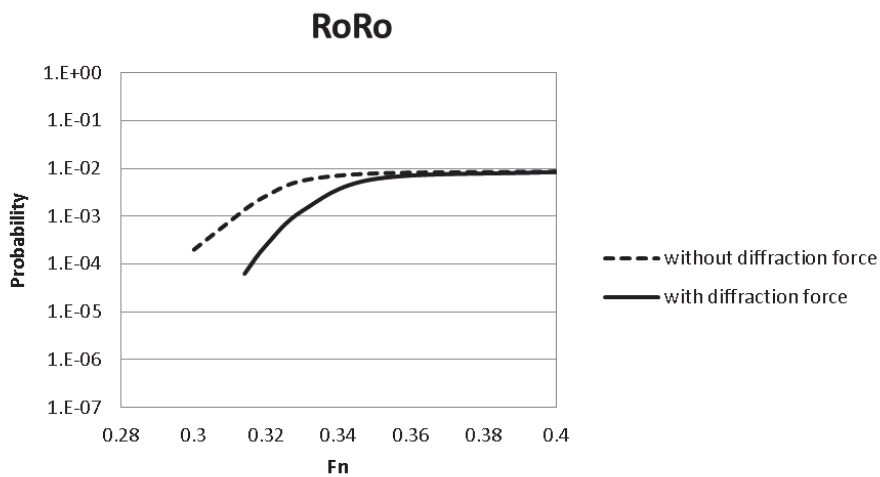


Figure 4 Surf-riding probability for a RoRo ship with and without diffraction effect.

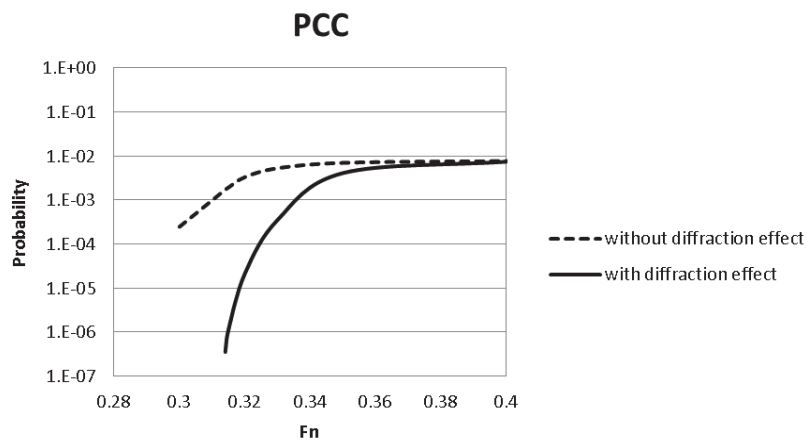


Figure 5 Surf-riding probability for a car carrier with and without diffraction effect.

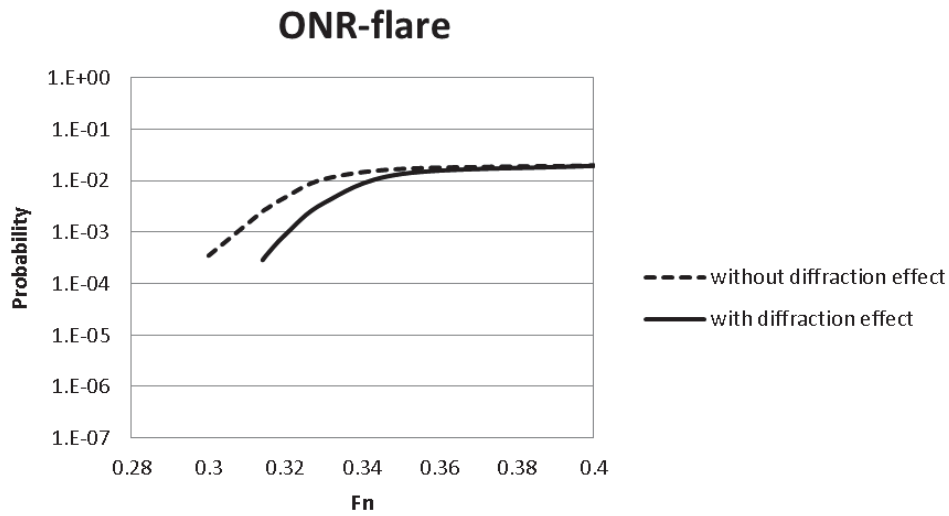


Figure 6 Surf-riding probability for the ONR flare topside vessel with and without diffraction effect.

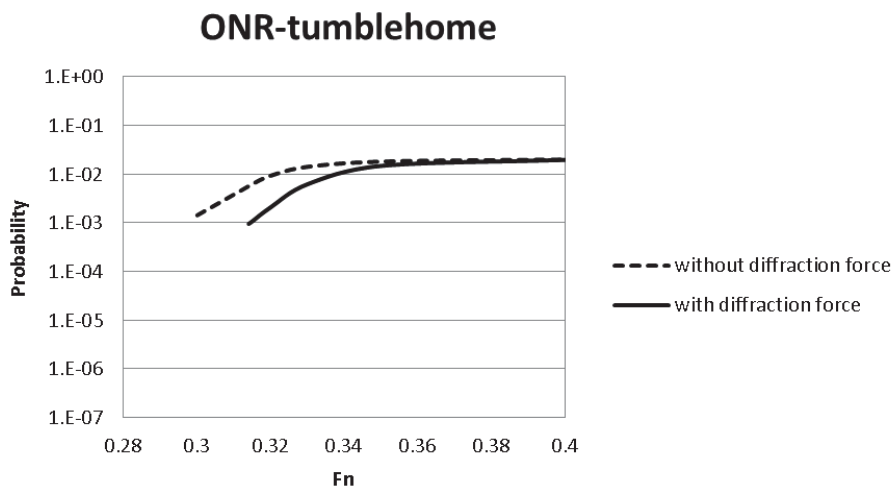


Figure 7 Surf-riding probability for the ONR tumblehome topside vessel with and without diffraction effect.

These comparisons demonstrate that surf-riding probability without diffraction effect is significantly larger than that with diffraction effect. As a result, for avoiding inconsistency with the operational requirement, the acceptable probability level is 10^{-4} with diffraction force and 5×10^{-3} without diffraction effect (Japan, 2015).

Then a question could arise: this difference in acceptable probability is crucial or not. It can be quantify with Equation (1).

$$P(T) = 1 - (1 - p)^{T/T_e} \quad (1)$$

where P : probability of surf-riding within the time interval of T , p : conditional probability of surf-riding when the ship meets a wave and T_e : average of encounter wave period. By using Equation (1), the time interval of non-surf-riding, T_s , can be calculated with Equation (2).

$$T_s = T_e \log(1 - p) / \log(1 - P) \quad (2)$$

Thus, if we assume $T_e = 10$ s and the confidence level of 5 per cent, $p = 10^{-4}$ and 5×10^{-3} could result in $T_s = 1.4$ hours and 1.7 minutes,

respectively. This result clearly indicates that an estimation without diffraction effect is not practical.

4. EFFECT OF CALM-WATER RESISTANCE SAMPLING ON SURF-RIDING

Other than the wave-induced surge force, calm-water ship resistance is an important factor for estimating surf-riding. Prediction of calm-water ship resistance itself is rather a routine for naval architects for guaranteeing ship speed and for complying with the EEDI (Energy Efficiency Design Index) requirement. Model test for these purposes, however, is not always executed for a given ship design. Thus, it is appropriate to allow the use of speed/power trial. In this case we should examine whether the estimation with only limited number of ship speed is sufficient or not. For providing an answer for this question, the authors attempt to verify the use of speed/power trial in place of model test.

For the sample ships in this paper, we already completed model tests in calm-water up to the Froude number of 0.6. Firstly all available test

data was fitted with a quintic curve. Secondly, to simulate speed/power trial we sampled three conditions, i.e. service speed, maximum service speed and maximum speed, from the model test data. We assumed here that the service speed corresponds to 85 per cent of the MCR (Maximum Continuous Rating), the maximum service speed does 100 per cent of the MCR and the maximum speed does 110 per cent of the MCR. Then the speed/resistance curve is fitted with a quadratic model, which requires three unknown parameters.

Figures 8 and 9 show examples of comparisons of fitted calm-water resistances. As a whole, quintic modelling with all experimental data is quite satisfactory. For the ONR tumblehome topside vessel as shown in Figure 8, the sampled speeds coincides with wave celerity range for wavelength to ship length ratio from 1.0 to 1.2 so that quadratic modelling well agrees with the quintic modelling for higher speed range. For the PCC, the sampled speeds are slower but the agreement with the quintic modelling is not so unsatisfactory. This might be because quadratic modelling, which has only one trough, is more robust than cubic modelling or higher order polynomial modelling.

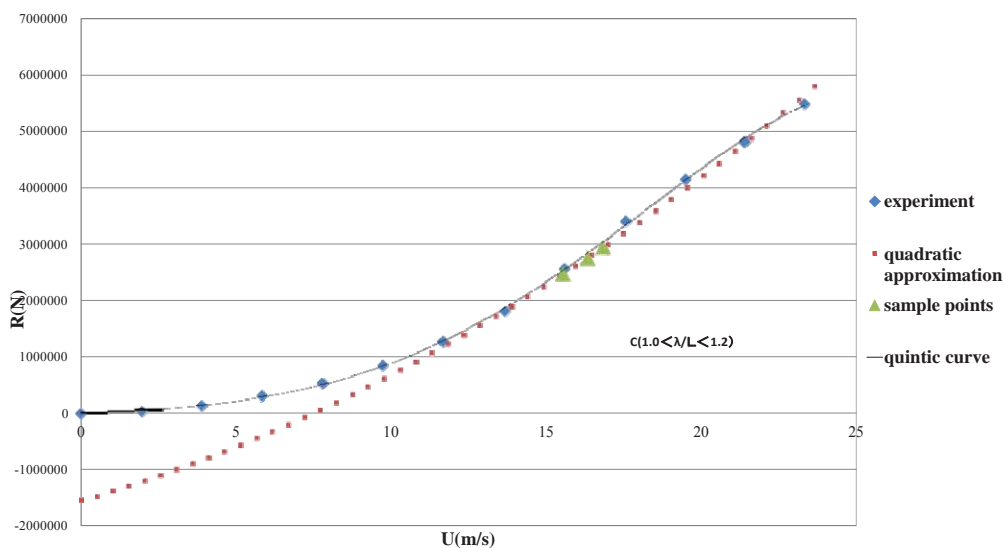


Figure 8 Calm-water resistance of the ONR tumblehome topside vessel

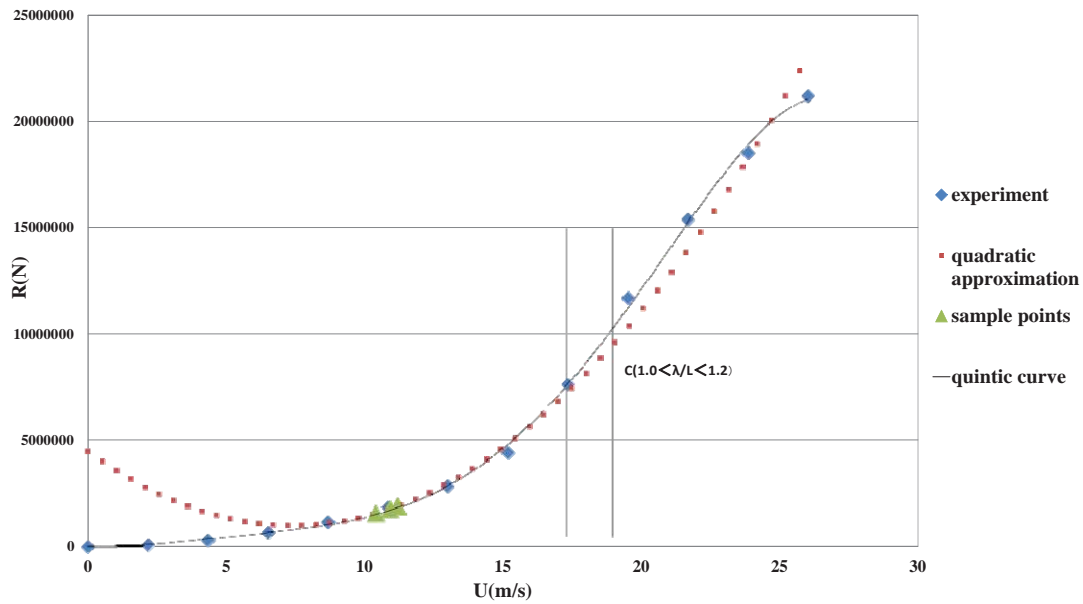


Figure 9 Calm-water resistance of the PCC

Furthermore, surf-riding probabilities of the sample ships are calculated with different calm-water modelling. The results shown in Figures 10-15 demonstrate that surf-riding probabilities with three speed sampling well agree with those with full range sampling. This could be because good agreement of calm-water resistance in the wave celerity range for wavelength to ship length ratio from 1.0 to 1.2, which is responsible for surf-riding prediction.

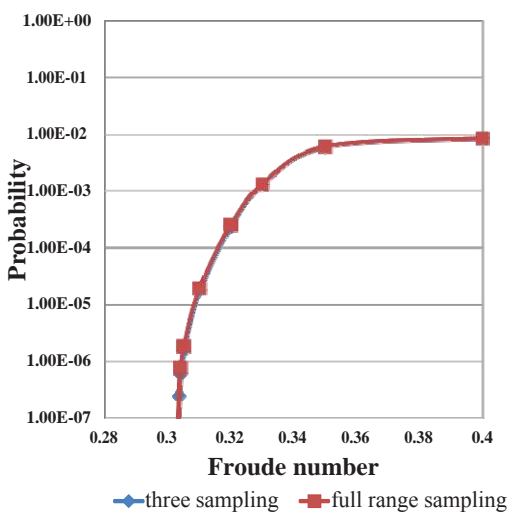


Figure 10 Effect of calm-water resistance modelling on surf-riding probability of the RoRo ship

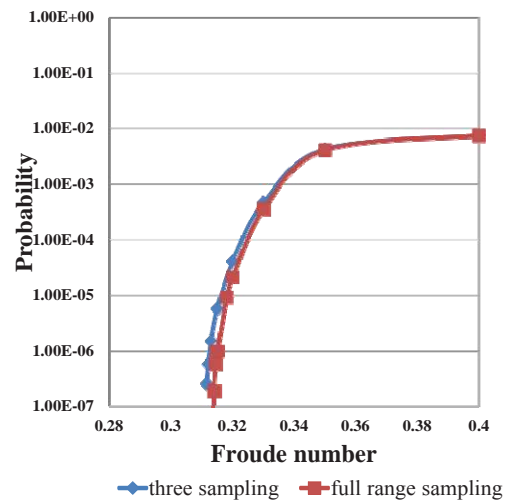


Figure 11 Effect of calm-water resistance modelling on surf-riding probability of the PCC

5. EFFECT OF STOCHASTIC WAVE THEORIE

In the draft criterion, it is necessary to calculate the joint probability density function of wave height and wavelength in a stationary seaway specified as a wave spectrum with Longuet-Higgins's work (1983) or equivalent. In 1957 Longuet-Higgins derived the formula by using the joint probability density of amplitude and phase of wave envelope. Here the relationship between the local wave period,

T , and wave envelope phase, ϕ , was simplified as

$$T = 2\pi / (\bar{\sigma} + \dot{\phi}) \quad (3)$$

$$\approx T_{01} (1 - \dot{\phi} / \bar{\sigma}) \quad (4)$$

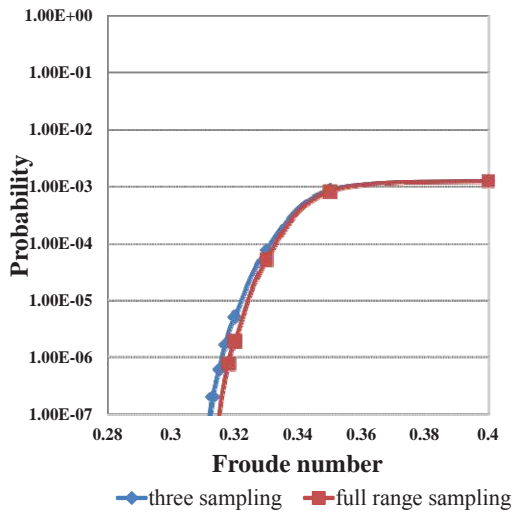


Figure 12 Effect of calm-water resistance modelling on surf-riding probability of the C11 class containership

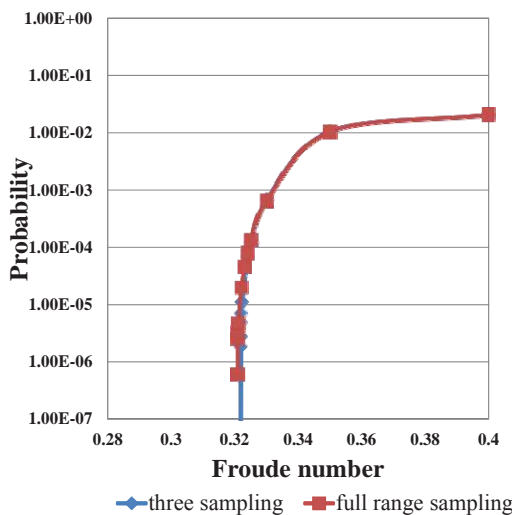


Figure 13 Effect of calm-water resistance modelling on surf-riding probability of the ITTC A1 containership

was pointed out that this formula cannot explain the physically observed fact that short local waves have smaller wave local height. Then, in 1983, Longuet-Higgins revised his own formula with more precise relationship between the local wave period and wave envelope phase, i.e. Equation (3) in place of Equation (4). As a result, he resolved the drawback of his original formula.

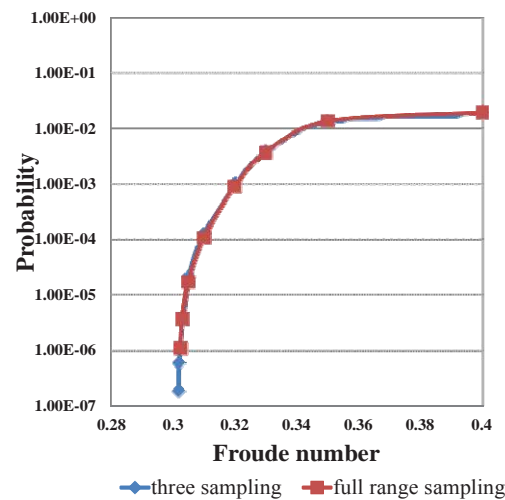


Figure 14 Effect of calm-water resistance modelling on surf-riding probability of the ONR flare topside vessel

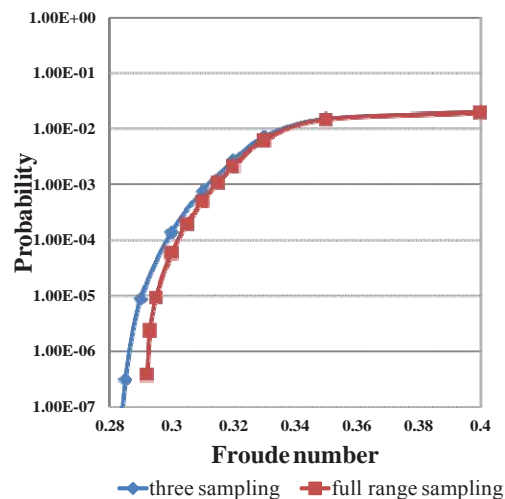


Figure 15 Effect of calm-water resistance modelling on surf-riding probability of the ONR tumblehome topside vessel

where T_{01} is the mean wave period, σ is the mean wave circular frequency and a dot indicates differentiation with time. Later on it

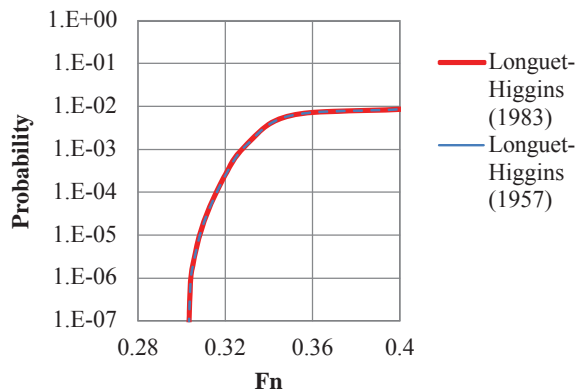


Figure 16 Effect of the wave probability formulae on surf-riding probability of the RoRo ship

It is indispensable for practical application of them to quantify effect of these two different formulae on surf-riding probability. Thus the authors executed comparison studies using the subject ships. The result shown in figure 16 as an example indicates the difference in surf-riding probability is negligibly small. This could be partly because the subject ships are longer so that they do not respond to smaller waves. Thus it can be presumed that at least the use of the formula in Longuet-Higgins (1983) is recommended although a similar study using a smaller ship is desirable.

6. RELATIONSHIPS WITH BROACHING

If a ship does not comply with the draft criterion for surf-riding, it is expected that her safety against capsizing due to surf-riding/broaching is examined with the direct stability assessment, in which failure probability in irregular seaways is directly estimated with a numerical time-domain simulation. This is because surf-riding is only a prerequisite for broaching or capsizing.

For verifying this approach, the authors calculate also probability of capsizing due to broaching in the North Atlantic. The calculation method used here was proposed and

validated with the Monte Carlo simulation by Umeda et al. (2007). The failure probability is calculated by integrating the probability density of local wave height and wavelength on the region in which capsizing due to broaching occurs in systematic time domain simulation using a coupled surge-sway-yaw-roll model with an autopilot in periodic waves. Here capsizing is defined as the roll angle of 90 degrees or over and the rudder gain is 1.

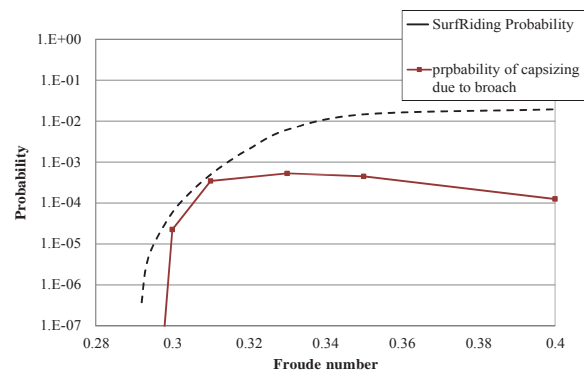


Figure 17 Comparisons between surf-riding probability and probability of capsizing due to broaching for the ONR tumblehome topside vessel.

The results shown in Figure 17 indicate that the probability of capsizing due to broaching is smaller than the surf-riding probability. Thus we can conclude that the draft criterion for surf-riding guarantees safety against capsizing due to broaching. It is noteworthy here that in critical speed range around the Froude number of 0.3 the difference between the two is rather small. This means that the safety margin is not so large.

7. CONCLUSIONS

For reasonably evaluating surf-riding probability to be used for design and operational criteria, diffraction effect on wave-induced surge force is indispensable, calm-water resistance can be modelled with model tests covering the Froude number up to 0.6 or standard speed/power trials and choice of stochastic wave theory is not crucial. The evaluated surf-riding probability is a conserva-



tive index for capsizing due to broach.

8. ACKNOWLEDGEMENTS

This work was supported by JSPS (Japan Society for Promotion of Science) KAKENHI Grant Number 24360355 and 15H02327. It was partly carried out as a research activity of Goal-based Stability Criteria Project of Japan Ship Technology Research Association in the fiscal year of 2013, funded by the Nippon Foundation. The authors appreciate Mr. William Peters from United States Coast Guard and Dr. Vadim Belenky from David Taylor Model Basin for their useful discussion.

9. REFERENCES

- Goda Y., 2000, "Random seas and design of maritime structures", Advanced Series on Ocean Engineering, Vol. 15. World Scientific Pub Co Inc, Singapore.
- IMO, 1995, "Guidance to the Master for Avoiding Dangerous Situations in Following and Quartering Seas, MSC/Circ. 707.
- Ito, Y., N. Umeda and H. Kubo, 2014, "Hydrodynamic Aspects on Vulnerability Criteria for Surf-Riding of Ships", Jurnal Teknologi, Vol. 66, No. 2, pp. 127-132.
- Japan, 2014, "Information collected by the Correspondence Group on Intact Stability", IMO, SDC 2/INF.10.
- Kan, M. 1990, "A Guideline to Avoid the Dangerous Surf-riding", Proceedings of the 4th International Conference on Stability of Ships and Ocean Vehicles, University Federico II of Naples (Naples), pp.90-97.
- Longuet-Higgins, M.S., 1983, "On the joint distribution of wave periods and amplitudes in a random wave field", Proc. Roy., Soc. ³²⁸
- London, Ser. A, Vol. 389, pp. 241-258.
- Longuet-Higgins, M.S., 1957, "The statistical analysis of a random, moving surface", Phil. Trans. Roy., Soc. London, Ser. A (966), Vol. 249, pp. 321-387.
- Maki, A., N. Umeda, M. Renilson and T. Ueta, 2010, "Analytical Formulae for Predicting the Surf-Riding Threshold for a Ship in Following Seas", Journal of Marine Science and Technology, Vol.,15, No.3, pp.218-229.
- Sadat-Hosseini, H., P. Carrica, F. Stern, N. Umeda et al., 2011, "CFD, system-based and EFD study of ship dynamic instability events: Surf-riding, periodic motion, and broaching", Ocean Engineering, Vol. 38, pp. 88-110.
- Spyrou, K.J., 2006, "Asymmetric Surging of Ships in Following Seas and its Repercussion for Safety", Nonlinear Dynamics, Vol.43, pp.149-172.
- Umeda, N., 1984, "Resistance Variation and Surf-riding of a Fishing Boat in Following Sea", Bulletin of National Research Institute of Fisheries Engineering, No. 5, pp. 185-205.
- Umeda, N., 1990, "Probabilistic Study on Surf-riding of a Ship in Irregular Following Seas", Proceedings of the 4th International Conference on Stability of Ships and Ocean Vehicle, Naples, pp.336-343.
- Umeda, N., Shuto, M. and Maki, A., 2007, "Theoretical Prediction of Broaching Probability for a Ship in Irregular Astern Seas", Proceedings of the 9th International Ship Stability Workshop, Hamburg, pp. 1.5.1-1.5.7.
- Umeda, N., S. Izawa, H. Sano, H. Kubo and K. Yamane, 2011, "Validation Attempts on Draft New Generation Intact Stability Criteria", Proceedings of the 12th



International Ship Stability Workshop,
Washington D.C., pp.19-26.

Umeda N., Yamamura S., Matsuda, A., Maki,
A. and Hashimoto, H., 2008, “Model
Experiments on Extreme Motions of a
Wave-Piercing Tumblehome Vessel in
Following and Quartering Waves”, Journal
of the Japan Society of Naval Architects
and Ocean Engineers ,Vol. 8, pp. 123-
129.

This page is intentionally left blank



Numerical Prediction of Parametric Roll Resonance in Oblique Waves

Naoya Umeda, *Osaka University* umeda@naoe.eng.osaka-u.ac.jp

Naoki Fujita, *Osaka University* naoki_fujita-0210@i.softbank.jp

Ayumi Morimoto, *Osaka University* cubx1520@gmail.com

Masahiro Sakai, *Osaka University* masahiro_sakai@naoe.eng.osaka-u.ac.jp

Daisuke Terada, *National Research Institute of Fisheries Engineering*, dterada@fra.affrc.go.jp

Akihiko Matsuda, *National Research Institute of Fisheries Engineering*, amatsuda@fra.affrc.go.jp

ABSTRACT

Numerical prediction of parametric roll in head and following waves has been intensively investigated so that requirements for reasonably good prediction are almost revealed. On the other hand, prediction of parametric roll in oblique waves has not yet been sufficiently established. This is because coupling with sway and yaw motions are unavoidable. Since parametric roll for actual ships occurs with very low forward velocity, even accurate prediction of lee ways in waves is not so easy. Therefore, in this study, the authors present a numerical model of parametric roll in oblique waves with low-speed manoeuvring forces taken into account. Then the numerical prediction was compared with newly executed free-running model experiments of a hypothetical ship. Its results demonstrate the present model shows reasonably good agreement with the experiment. This information could be used for identifying minimum requirements for good prediction of parametric roll in oblique waves.

Keywords: *parametric rolling, IMO, Second generation intact stability criteria, direct stability assessment, operational guidance*

1. INTRODUCTION

Although danger of parametric rolling had been well known among scientists (e.g. Watanabe, 1934), the accident of a C11 class post Panamax containership (France, 2003) induced extensive studies on this phenomenon. As a result, several numerical models for parametric rolling were developed and some of them were well validated with model experiments in head and following waves (Reed, 2011). These models deal with coupled heave-pitch-roll motions by using simultaneous nonlinear differential equations and the hydrodynamic coefficients used in the equations are calculated with potential theories

and empirical viscos force estimation. Time dependence of roll restoring coefficient, including coupling from other modes and diffraction moment depending on heel angle, is indispensable.

Based on such progress in research for parametric rolling, at the International Maritime Organisation (IMO), stability criteria for preventing parametric roll is now under development (Umeda, 2013). They consist of three layers: the first and second layers use simplified estimation of occurrence and magnitude of parametric roll in head and following waves with averaging method applied to uncoupled roll model with restoring variation; the third layer means direct use of numerical simulation in time domain of

coupled roll model in irregular waves. For the latter case, the numerical models mentioned before could be used. It is noteworthy here that the third layer requires not only calculation in head and following waves but also in oblique waves. This is because we have to evaluate safety for all ship courses. For oblique waves, validation efforts for existing numerical models Sanchez & Nayfeh, 1990; Neves & Valerio, 2000) were not sufficient so far partly because a model experiment requires a seakeeping and manoeuvring basin and partly because coupling with manoeuvring motion including rudder actions are unavoidable.

Based on this understanding, the authors attempted to validate a numerical simulation model taking low-speed manoeuvring model in oblique waves with a newly executed model experiment in a seakeeping and manoeuvring basin. This numerical model is an extension of the model published in Hashimoto and Umeda (2011) for head and following waves, which were well validated with model experiments of containerships and a car carrier in the towing tank of Osaka University. The ship used in this paper is a typical ship having large flare and transom stern, i.e. a hypothetical ship known as the ONR flare topside vessel, of which hull form is open for public. At this stage comparisons in regular oblique waves are ready to be published. Comparisons in irregular oblique waves are a task for future. In this paper, details of the numerical model are described for facilitating development of the guidelines for the direct assessment at the IMO.

2. NUMERICAL MODEL FOR PARAMETRIC ROLL IN OBLIQUE WAVES

2.1 Coordinate systems and equations of coupled motions

The coordinate systems used here are shown in Figure 1. The space-fixed coordinate system is $O_1-\xi\eta\zeta$, the coordinate system

moving with a constant speed of U and course of χ is O_2-XYZ and the body-fixed coordinate system is $G-xyz$. Here we assume that a wave propagates in the direction of $O_1\xi$ axis. The ship oscillates around the O_2-XYZ . G indicates the centre of ship mass and O_1G_0 indicates initial depth of centre of ship mass. The ship motions around the O_2-XYZ are denoted by x_i : surge ($i=1$), sway ($i=2$), heave ($i=3$), roll ($i=4$), pitch ($i=5$) and yaw ($i=6$).

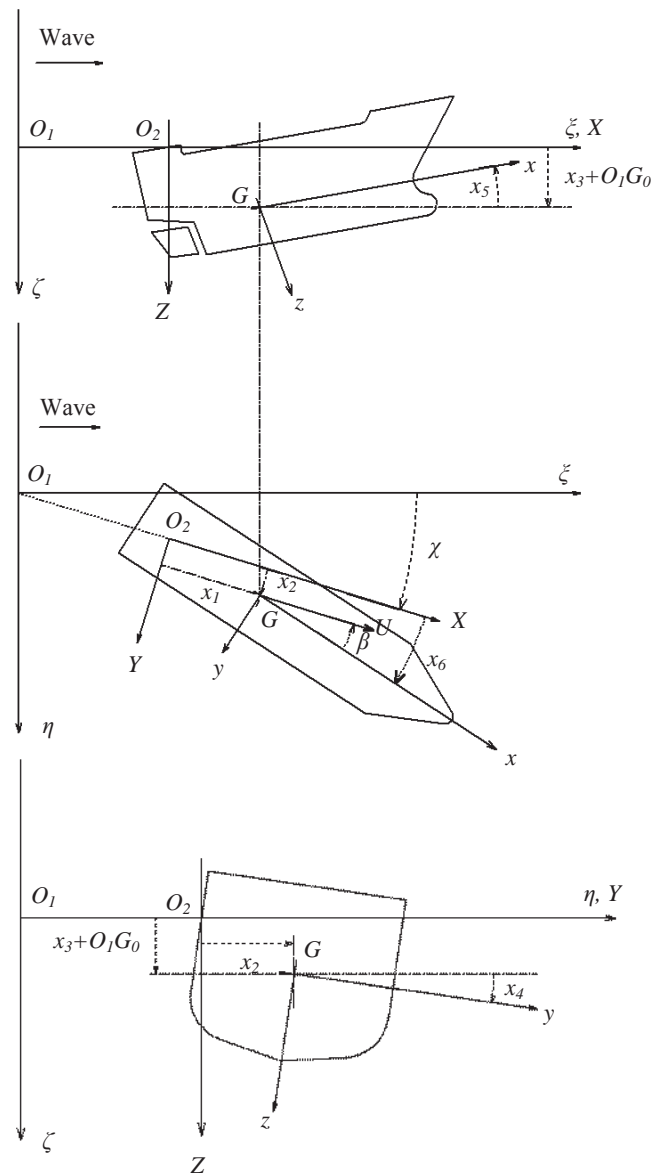


Figure 1 Coordinate systems

The coupled sway-heave-roll-pitch-yaw motions are modelled as follows:



$$\begin{cases} m\ddot{x}_2 = F_2(x_2, x_3, x_4, x_5, x_6, \dot{x}_2, \dot{x}_3, \dot{x}_4, \dot{x}_5, \dot{x}_6, \ddot{x}_2, \ddot{x}_3, \ddot{x}_4, \ddot{x}_5, \ddot{x}_6, t) \\ m\ddot{x}_3 = F_3(x_2, x_3, x_4, x_5, x_6, \dot{x}_2, \dot{x}_3, \dot{x}_4, \dot{x}_5, \dot{x}_6, \ddot{x}_2, \ddot{x}_3, \ddot{x}_4, \ddot{x}_5, \ddot{x}_6, t) \\ I_{xx}\ddot{x}_4 = F_4(x_2, x_3, x_4, x_5, x_6, \dot{x}_2, \dot{x}_3, \dot{x}_4, \dot{x}_5, \dot{x}_6, \ddot{x}_2, \ddot{x}_3, \ddot{x}_4, \ddot{x}_5, \ddot{x}_6, t) \\ I_{yy}\ddot{x}_5 = F_5(x_2, x_3, x_4, x_5, x_6, \dot{x}_2, \dot{x}_3, \dot{x}_4, \dot{x}_5, \dot{x}_6, \ddot{x}_2, \ddot{x}_3, \ddot{x}_4, \ddot{x}_5, \ddot{x}_6, t) \\ I_{zz}\ddot{x}_6 = F_6(x_2, x_3, x_4, x_5, x_6, \dot{x}_2, \dot{x}_3, \dot{x}_4, \dot{x}_5, \dot{x}_6, \ddot{x}_2, \ddot{x}_3, \ddot{x}_4, \ddot{x}_5, \ddot{x}_6, t) \end{cases} \quad (1)$$

where m : ship mass, I_{xx} : moment of inertia of ship mass in roll, I_{yy} : moment of inertia of ship mass in pitch, I_{zz} : moment of inertia of ship mass in yaw, t : time and F_j : force or moment in the j direction. A dot denotes differentiation with time. Here we assume that the surge motion x_1 is zero, for avoiding estimation of added mass, so that the ship runs with a constant velocity and a straight course. The forces are modelled with Equation (2).

$$F_j = F_j^R + F_j^B + F_j^{FK} + F_j^D + F_j^{EG} + F_j^{MLS} + F_j^{DEL} \quad (2)$$

where the superscript R indicates the radiation component, B the component due to hydrostatic pressure, FK the component due to incident wave pressure, D the diffraction component, EG component due to gravity, MLS the hull force due to manoeuvring motion and DEL the force due to rudder action.

2.2 Buoyancy and Froude-Krylov Forces

If we assume incident waves are sinusoidal, their profile, ζ_w , and wave pressure, p , are given by Equations (3-4).

$$\zeta_w = \zeta_a \cos\left(\frac{\omega_k^2}{g}\xi - \omega_k t\right) \quad (3)$$

$$p = \rho g \zeta_a \exp\left(-\frac{\omega_k^2}{g}(\zeta - \zeta_w)\right) \cos\left(\frac{\omega_k^2}{g}\xi - \omega_k t\right) \quad (4)$$

where ρ : water density, ζ_a : wave amplitude, g : gravitational acceleration, ω_k : wave circular frequency and t : time. Here water pressure is adjusted to be zero at the wave surface

although this is a higher order correction under the assumption of small wave steepness.

Then submerged hull surface, S_H , can be determined with Equation (5).

$$S_H = S_H(\zeta_G, \zeta_w, x_3, x_4, x_5) \quad (5)$$

By integrating the water pressure on the wetted hull surface, the buoyancy, F_j^B , and Froude-Krylov forces, F_j^{FK} , can be calculated as follows:

$$F_j^B = \rho g \int_L dx \int_{S_H} -\zeta n_j ds \quad (6)$$

$$F_j^{FK} = -\int_L \int_{S_H} p n_j ds dx \quad (7)$$

where L indicates the range of hull in x direction. The gravitational force, F_3^{EG} , in the vertical direction are given by

$$F_3^{EG} = mg \quad (8)$$

2.3 Radiation and Diffraction Forces

The radiation force, F_i^R , can be calculated as follows:

$$F_i^R = \sum_{j=2}^6 (-A_{ij}(x_4)\ddot{x}_j - B_{ij}(x_4)\dot{x}_j - C_{ij}(x_4)x_j) \quad (9)$$

where the added mass, A_{ij} , the wave damping coefficient, B_{ij} , and the restoring coefficient, C_{ij} , are given by

$$A_{22} = \int_L A_{H22} dx, \quad A_{23} = \int_L A_{H23} dx, \quad A_{24} = \int_L A_{H24} dx$$

$$A_{25} = -\int_L x A_{H23} dx, \quad A_{26} = \int_L x A_{H22} dx$$

$$A_{32} = \int_L A_{H32} dx, \quad A_{33} = \int_L A_{H33} dx, \quad A_{34} = \int_L A_{H34} dx$$

$$A_{35} = -\int_L x A_{H33} dx, \quad A_{36} = \int_L x A_{H32} dx$$

$$A_{42} = \int_L A_{H42} dx, \quad A_{43} = \int_L A_{H43} dx$$



$$A_{45} = -\int_L xA_{H43}dx, A_{46} = \int_L xA_{H42}dx$$

$$A_{52} = -\int_L xA_{H32}dx, A_{53} = -\int_L xA_{H33}dx$$

$$A_{54} = -\int_L xA_{H34}dx$$

$$A_{55} = \int_L x^2 A_{H33}dx, A_{56} = -\int_L x^2 A_{H32}dx$$

$$A_{62} = \int_L xA_{H22}dx, A_{63} = \int_L xA_{H23}dx, A_{64} = \int_L xA_{H24}dx$$

$$A_{65} = -\int_L x^2 A_{H23}dx, A_{66} = \int_L x^2 A_{H22}dx$$

$$B_{22} = \int_L B_{H22}dx, B_{23} = \int_L B_{H23}dx, B_{24} = \int_L B_{H24}dx$$

$$B_{25} = -\int_L xB_{H23}dx + U \int_L A_{H23}dx$$

$$B_{26} = \int_L xB_{H22}dx - U \int_L A_{H22}dx$$

$$B_{32} = \int_L B_{H32}dx, B_{33} = \int_L B_{H33}dx, B_{34} = \int_L B_{H34}dx$$

$$B_{35} = -\int_L xB_{H33}dx + U \int_L A_{H33}dx$$

$$B_{36} = \int_L xB_{H32}dx - U \int_L A_{H32}dx$$

$$B_{42} = \int_L B_{H42}dx, B_{43} = \int_L B_{H43}dx,$$

$$B_{45} = -\int_L xB_{H43}dx + U \int_L A_{H43}dx$$

$$B_{46} = \int_L xB_{H42}dx - U \int_L A_{H42}dx$$

$$B_{52} = -\int_L xB_{H32}dx - U \int_L A_{H32}dx$$

$$B_{53} = -\int_L xB_{H33}dx - U \int_L A_{H33}dx$$

$$B_{54} = -\int_L xB_{H34}dx - U \int_L A_{H34}dx$$

$$B_{55} = \int_L x^2 B_{H33}dx, B_{56} = -\int_L x^2 B_{H32}dx + U \int_L xA_{H32}dx$$

$$B_{62} = \int_L xB_{H22}dx - U \int_L A_{H22}dx$$

$$B_{63} = \int_L xB_{H23}dx + U \int_L A_{H23}dx$$

$$B_{64} = \int_L xB_{H24}dx + U \int_L A_{H24}dx$$

$$B_{65} = -\int_L x^2 B_{H23}dx, B_{66} = \int_L x^2 B_{H22}dx$$

$$C_{25} = U \int_L B_{H23}dx, C_{26} = -U \int_L B_{H22}dx$$

$$C_{35} = U \int_L B_{H33}dx$$

$$C_{45} = U \int_L B_{H43}dx$$

$$C_{46} = -U \int_L B_{H24}dx$$

$$C_{55} = -U \int_L xB_{H33}dx - U^2 \int_L A_{H33}dx$$

$$C_{56} = U \int_L xB_{H32}dx + U^2 \int_L A_{H32}dx$$

$$C_{65} = U \int_L xB_{H23}dx + U^2 \int_L A_{H23}dx$$

$$C_{66} = -U \int_L xB_{H22}dx - U^2 \int_L A_{H22}dx$$

$$A_{Hij} - i \frac{B_{Hij}}{\omega} = -\rho \int_{S_H} \varphi_j n_i ds$$

Here φ_j and n_i are the velocity potential of two-dimensional flow with hull and linear free surface condition and normal vector to the hull surface. The added mass and damping in roll are estimated as follows:

$$I_{xx} + A_{44} = W \cdot GM \left(\frac{T_\phi}{2\pi} \right)^2 \quad (10)$$

$$B_{44} \dot{x}_4 = \alpha \dot{x}_4 + \beta |\dot{x}_4| \dot{x}_4 + \gamma \dot{x}_4^3 \quad (11)$$

The α , β , γ and T_ϕ can be estimated with roll decay test of a ship model.

The diffraction force, F_j^D , can be calculated as follows (Salvesen et al., 1970):

$$F_j^D = \zeta_a F_{kj}^D(x_4) \cos(-\omega_e t - \varepsilon_{kj}^D(x_4)) \quad (12)$$

where

$$F_{kj}^D = |E_{kj}^D|$$



$$\varepsilon_{kj}^D = \arg E_{kj}^D$$

$$E_{kj}^D = \frac{\rho g \zeta_a}{i\omega} \int_L \int_{S_H} (i\omega_k - U \frac{\partial}{\partial x}) \varphi_D n_j ds$$

$$\omega_e = \omega_k - (\omega_k^2 / g) U \cos \chi$$

And φ_D is the diffraction velocity potential of two-dimensional flow with hull and linear free surface condition in incident waves.

2.4 Manoeuvring Forces

Since parametric roll occurs at low speed, it is desirable to estimate manoeuvring forces with a mathematical model suitable for such situation where ship forward velocity is comparable to ship lateral velocity (Umeda & Yamakoshi, 1989). The hull manoeuvring forces, F_i^{MLS} , can be estimated as the sum of linear lift components, Y_L and N_L , and nonlinear cross-flow drag components, Y_C and N_C , as follows:

$$F_2^{MLS} = Y_C + Y_L$$

$$F_6^{MLS} = N_C + N_L \quad (13)$$

where

$$Y_C = \frac{1}{2} \rho \int_{-L/2}^{L/2} d \cdot C_D |v + rx| (v + rx) dx$$

$$N_C = \frac{1}{2} \rho \int_{-L/2}^{L/2} d \cdot C_D |v + rx| (v + rx) x dx$$

$$Y_L = Y_v v + Y_r r$$

$$N_L = N_v v + N_r r$$

$$u = (U + \dot{x}_1) \cos x_6 + \dot{x}_2 \sin x_6$$

$$v = -(U + \dot{x}_1) \sin x_6 + \dot{x}_2 \cos x_6$$

$$r = \dot{x}_6$$

$$Y_v = \left(\frac{1}{2} \rho L_{pp} d \cdot u \right) \cdot Y_v'$$

$$N_v = \left(\frac{1}{2} \rho L_{pp}^2 d \cdot u \right) \cdot N_v'$$

$$Y_r = \left(\frac{1}{2} \rho L_{pp}^2 d \cdot u \right) \cdot Y_r'$$

$$N_r = \left(\frac{1}{2} \rho L_{pp}^3 d \cdot u \right) \cdot N_r'$$

Here u and v are the surge and sway velocity defined with the body-fixed coordinate system G-xyz, respectively. C_D is the cross-flow drag coefficient when the ship is laterally towed.

The rudder-induced forces, F_i^{DEL} , are calculated as follows:

$$F_2^{DEL} = -(1 + a_H) \frac{1}{2} \rho A_R u_R^2 f_\alpha \delta$$

$$F_6^{DEL} = -(x_R + a_H x_H) \frac{1}{2} \rho A_R u_R^2 f_\alpha \delta \quad (14)$$

where

$$\delta = -K_p x_6$$

$$u_R = \varepsilon u_p \sqrt{1 + \frac{8K_T}{\pi J^2}}$$

$$u_p = (1 - w_p) U$$

$$J = \frac{u_p}{nD_p}$$

$$K_T = aJ^2 + bJ + c$$

$$u_R = \varepsilon u_p \sqrt{1 + \frac{8}{\pi} \left(a + \frac{b}{J} + \frac{c}{J^2} \right)}$$

$$= \varepsilon u_p \sqrt{1 + \frac{8}{\pi} \left(a + \frac{bnD}{u_p} + \frac{cn^2 D^2}{u_p^2} \right)}$$

$$= \varepsilon u_p \sqrt{u_p^2 + \frac{8}{\pi} (a u_p^2 + bnD u_p + cn^2 D^2)}$$

Here δ : rudder angle, a_H : the interaction factor for rudder force between hull and rudder, x_H : the longitudinal position of rudder force due to

interaction between hull and rudder, x_R : the longitudinal rudder position, A_R : the rudder area, f_{α} : the hydrodynamic rudder lift slope, K_p : the rudder gain, n : the propeller revolution number, D_p : the propeller diameter, K_T : the rudder gain, ε : the wake ratio between propeller and rudder. The flow straightening effect is ignored.

The system parameters for manoeuvring forces and moments, such as C_D and Y_v , can be estimated with captive model experiment of a ship. In this paper, we used the coefficients measured in the circular motion tests of the C11 class post Panamax containership, whose hull form is similar to the ONR flare topside vessel.

3. MODEL EXPERIMENTS

For validating a numerical model for parametric rolling in oblique waves, experiments using a 1/48.8 scaled model of the 154m-long ONR flare topside vessel were executed at the seakeeping and manoeuvring basin of National Research Institute of Fisheries Engineering, based on the ITTC recommended procedure on intact stability model test (ITTC, 2008). The ship was propelled with an electric motor and two propellers and steered with two rudders. The propeller RPM was controlled to be a constant and the auto pilot was used with the rudder gain of 1.0. The roll, pitch and yaw angles were measured by a fibre optical gyroscope.

Table 1 Principal Particulars of the ONR Flare topside vessel

Length : L_{pp}	154.0 [m]	3.158 [m]
Breadth : B	19.65 [m]	0.403 [m]
Depth : D	15.2 [m]	0.312 [m]
Draught : d	5.753 [m]	0.118 [m]
Displacement : W	9733 [ton]	83.93 [kg]
Longitudinal position of center of buoyancy from the midship : LCB	6.45 [m] aft	0.132 [m] aft
Radius of gyration in pitch : K_{yy}/L_{pp}	0.272	0.272
Block coefficient : C_b	0.536	0.536
Metacentric height : GM	0.8095 [m]	0.0166 [m]
Natural roll period : T_{ϕ}	21.11[s]	3.023 [s]

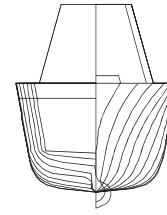


Figure 2 Body plan of the the ONR Flare topside vessel

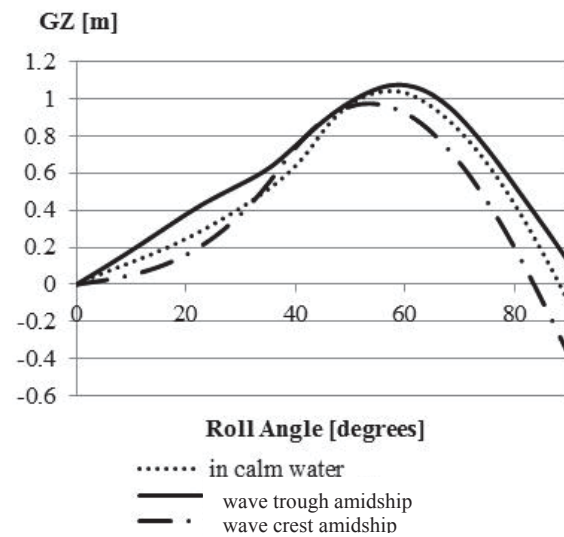


Figure 3 GZ variations of the ONR flare topside vessel in longitudinal waves whose wavelength to ship length ratio is 1.25 and the wave steepness is 0.03.

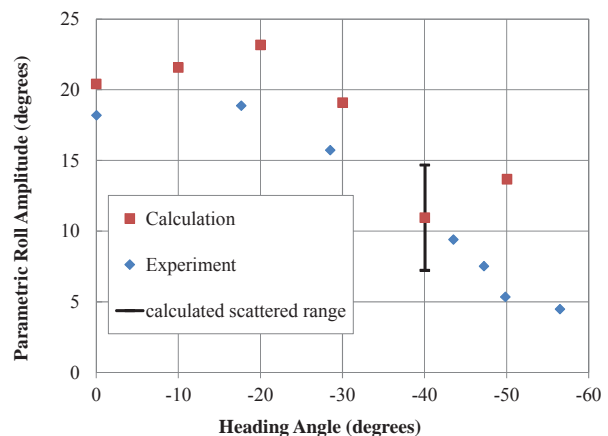


Figure 4 Steady amplitude of parametric roll in oblique waves.



The principal particulars and body plan of the subject ship are shown in Table 1 and Figure 2, respectively.

The experiment shown here is executed for regular astern waves. The wavelength to ship length ratio is 1.25 and the wave steepness is 0.03. Under this wave condition, the GZ curve of this vessel definitely changes due to longitudinal waves as shown in Figure 3. The auto pilot course ranges from 0 degrees from the wave direction to 70 degrees but no parametric roll occurred for the auto pilot course of 70 degrees. The propeller RPS is set to be 72, which corresponds to the Froude number of 0.05 in calm water. In addition, speed trials, roll decay tests and propeller open test were executed for this ship model.

4. RESULTS AND DISCUSSION

The numerical results are compared with the experimental results as shown in Figure 4. Here the steady amplitude for each condition is plotted. An example of numerical runs is shown in Figure 5. In this case the roll motion is settled to a steady periodic state. The roll period is twice the pitch period, and is nearly equal to the ship natural roll period. Thus this can be judged as a typical parametric rolling. Similarly, in the auto pilot course of -30 degrees the steady periodic state was simulated as shown in Figure 6. However, in case of the auto pilot course of -40 degrees as shown in Figure 7, the calculated roll angle does not settled to a periodic state. Similar complicate response was reported by Hashimoto & Umeda (2004) with an uncoupled roll model with parametric and direct excitation. Thus this could be a future task with nonlinear dynamics.

The calculated values slightly overestimate the measured values. Good agreement between the two can be found at the heading angle of 0 degrees but some discrepancies can be found in case of oblique waves. The heading angle is rather different from the specified autopilot course. This could indicate that steady wave

forces and manoeuvring forces could have some roles.

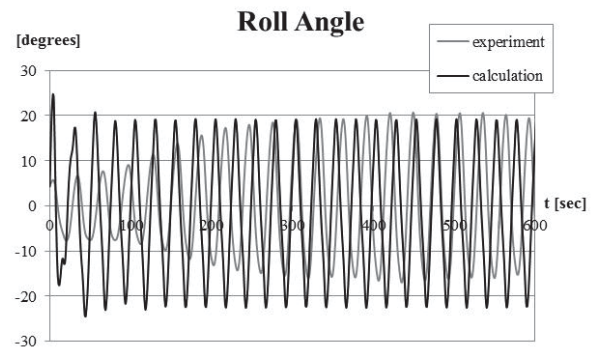


Figure 5 Time series of roll and pitch angles with the auto pilot course of -10 degrees.

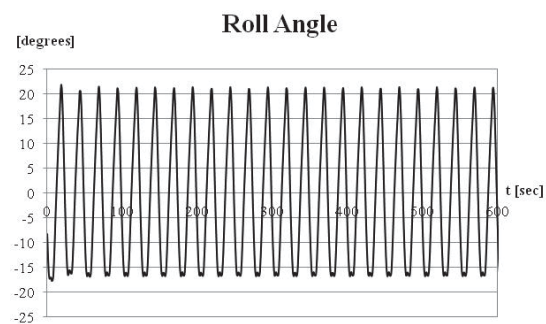


Figure 6 Time series of roll angle with the auto pilot course of -30 degrees.

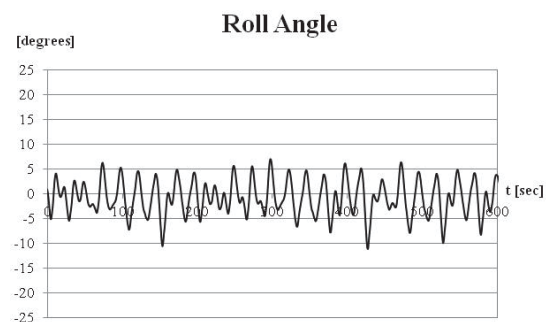


Figure 7 Time series of roll angle with the auto pilot course of -40 degrees.

The largest roll amplitude occurs at the heading angle different from head waves both



in experiment and calculation. However, when the heading angle further increases, the roll amplitude decreases. This is due to the shift of encounter frequency together with the reduction of roll restoring variation.

5. CONCLUSIONS

Parametric roll in regular oblique waves was realised in free-running model experiments. The 5 degrees-of-freedom numerical model slightly overestimates the experimental results. The numerical model used here includes nonlinear Froude-Krylov components, radiation / diffraction components as functions of roll angle and manoeuvring forces. The roll amplitude decreases with the increasing heading angle but the largest roll occurs with non-head waves. Non periodic roll response was found in one case of numerical simulation. Following this preliminary validation, wider validation studies in oblique waves will be executed with different ships and different wave heading in the near future.

6. ACKNOWLEDGEMENTS

This work was supported by JSPS (Japan Society for Promotion of Science) KAKENHI Grant Number 24360355 and 15H02327. It was partly carried out as a research activity of Goal-based Stability Criteria Project of Japan Ship Technology Research Association in the fiscal year of 2013, funded by the Nippon Foundation. The authors thank Prof. H. Hashimoto, Mses. F. Yoshiyama and N. Yamashita for their effective assistance during the work described here.

7. REFERENCES

- France, W.N., Levadou, M., Treacle, T.W. et al., 2003, "An Investigation of Head-Sea Parametric Roll and Its Influence on Container Lashing System", Marine Technology, 40(1), pp.1-19.
- Hashimoto, H. and N. Umeda, 2004, "Nonlinear analysis of parametric rolling in longitudinal and quartering seas with realistic modeling of roll-restoring moment", Journal of Marine Science and Technology, Vol. 9, pp. 117-126.
- Hashimoto, H. and Umeda, N., 2010, "A Study on Qualitative Prediction of Parametric Roll in Regular Head Wave", Proceedings of the 10th International Ship Stability Workshop, Wageningen, pp.295-301.
- ITTC, 2008: Recommended Procedures, Model Tests on Intact Stability, 7.5-02-07-04.
- Neves, M.A.S. and Valerio, L. 2000, "Parametric Resonance in Waves of Arbitrary Heading", Proceedings of the 7th International Conference on Stability and Operational Safety of Ships and Ocean Vehicles, Launceston, B, pp. 680-687.
- Reed, A.M., 2011, "26th ITTC Parametric Roll Benchmark Study", Proceedings of the 12th International Ship Stability Workshop, Washington D.C., pp. 195-204.
- Salvesen, N., Tuck, E.O. and O. Faltinsen, 1970, "Ship Motions and Sea Loads", Transaction of the Society of Naval Architects and Marine Engineers.
- Sanchez, N.E. and Nayfeh, A.H. 1990, "Rolling of Biased Ships in Quartering Seas", Proceedings of the 18th Symposium on Naval Hydrodynamics, Michigan.
- Umeda, N. and Y. Yamakoshi, 1989, "Hydrodynamic Forces Acting on a Longitudinally Non-symmetric Ship Under Manoeuvring at Low Speed", Journal of the Kansai Society of Naval Architects, No. 211, 127-137, (in Japanese.)
- Umeda, N. 2013, "Current Status of Second Generation Intact Stability Criteria", Proceedings of the 13th International Ship Stability Workshop, Brest, pp. 138-157.



Watanabe, Y., 1934, “On the Dynamical Properties of the Transverse Instability of a Ship due to Pitching”, Journal of the Society of Naval Architects, Vol. 53, pp. 51-70 (in Japanese)

This page is intentionally left blank



Numerical Simulation of the Ship Roll Damping

Min Gu, *China Ship Scientific Research Center, Wuxi, China* gumin702@163.com

Jiang Lu, *China Ship Scientific Research Center, Wuxi, China* lujiang1980@aliyun.com

Shuxia Bu, *China Ship Scientific Research Center, Wuxi, China* bushuxia8@163.com

Chengsheng Wu, *China Ship Scientific Research Center, Wuxi, China* cswu@163.com

Gengyao Qiu, *China Ship Scientific Research Center, Wuxi, China* xiaogeng502@163.com

ABSTRACT

The roll damping is a critical hydrodynamic coefficient for predicting roll motion. In this paper, the forced roll motion of a 2-dimensional ship section and free roll motion of a 3-dimensional hull are simulated based on the RANS model in calm water. For the forced rolling, firstly, the influences of different calculation parameters are investigated through the methods of orthogonal design and variance analysis. Then the simulations about different roll amplitudes are carried out based on the selected parameters. For the free rolling, the free decay experiments and numerical simulations are performed. These calculated results are agreed well with experimental data, which validate the presented method can yield satisfactory results for roll damping coefficients.

Keywords: *roll damping; RANS; forced rolling; free rolling*

1. INTRODUCTION

The roll damping is a critical hydrodynamic coefficient for predicting roll motion, such as parametric rolling and stability under dead ship condition. The roll damping coefficient should be predicted with high accuracy. The vulnerability criteria are under development by the International Organization (IMO) of the second generation of intact stability criteria, in which the roll damping have been calculated by Ikeda's (1977, 1978, 1979, 2000, 2004) simplified method. These formulas can be used quite well for the conventional ship, but the predicted results are sometimes conservative or underestimated for unconventional ships (Japan, 2011a, Japan, 2011b, Sweden, 2011). This is because the roll damping is strongly nonlinear, which has some direct relationships with fluid viscosity and flow characteristics, such as the flow separation and vortex shedding. So the experience or semi-experience formulas can't

take the full consideration of different characteristics for different objects. The calculated results of most traditional ships by Ikeda's method can fit experimental data well at the same order magnitude. However, if the size is outside the application range of Ikeda's method, or for the large amplitude roll motion in some phenomena, such as parametric rolling, the accuracy will be low in these conditions, which limit the scope of application of Ikeda's method.

The corresponding group of IMO proposed that the roll damping could be calculated by roll decay / forced roll test or CFD (United States & Japan, 2014). Although the model tests can predict the roll damping very well, but it is costly and time-consuming as well as most of experimental data are limited to a certain frequency range and particular geometry, which is impossible for the large-scale



expansion of the application (Blok & Aalbers, 1991, Haddara & Bass, 1988).

The influence of viscosity should be considered during the calculation of roll damping. The CFD numerical simulation can consider different objects and its characteristic, which can also reduce the cost. With the development of CFD technology, the turbulent models have been improved, such as RANS model, discrete vortex method. In addition, the fine structure of the flow field can also be analyzed by CFD, so CFD could be widely used to predict roll damping. Forced roll method and free decay method are two main methods for calculation of the roll damping.

K.B.Salui et al. (2000), Ronald et al. (2002), Miller&Stern (2002), Salui & Vassalos (2003), Frederick Jaouen et al.(2011) simulated forced roll motions for different kinds of ship or two-dimensional ship sections using the RANS model. Wilson et al. (2006) predicted the roll decay of a DTMB Model 5512 hull based on the RANS technique. Miller et al. (2008) conducted roll decay and forced roll simulations using DTMB Model 5415 based on the RANS approach. Sun kyun Lee et al. (2011) performed CFD simulations for the roll damping of a damaged passenger ship by solving RANS equations. These results are in good agreement with the experimental data. The above analysis proved that the roll damping coefficients can be accurately solved using RANS approach.

In this paper, firstly the forced motions of two dimensional ship section of Series 60 based on the orthogonal design and variance analysis are carried out, in which different calculation parameters for roll damping are analyzed. Secondly, the free motions of a three dimensional 4250TEU containership have been simulated. The comparisons between the computed results and the experimental results proved that the roll damping can be predicted by RANS-based method. These can provide

technical support for the development of second generation intact stability criteria.

2. FORCED ROLLING

For the forced roll motion, the section of Series 60 is chosen, as experimental tests on its forced roll have been conducted by Ikeda (Ikeda et al. 1977). The same principles are used in the simulations, as shown in table 1. During the calculation, the roll center is located in the intersection between waterline and mid-perpendicular. The formula (1) is used for the roll motion. Then formula (2) is used to get the dynamic moment. Finally, formulas (3) are used to get the roll damping coefficients and non-dimensional coefficients.

Table 1 Principal particulars of S.S.5.

Section	<i>B</i>	<i>T</i>	<i>KG</i>
S.S.5	0.237m	0.096m	0.096m

Where *B* is the width of model; *T* is the draught; *KG* is the vertical height of center of gravity.

$$\phi = \phi_0 \sin(\alpha t) \quad (1)$$

$$M_d(t) = \iint_s (\tau_{y,z} - \tau_z y) ds + \iint_s p_d (n_z y - n_y z) ds \quad (2)$$

$$B_{44} = \frac{MR}{\omega \phi_0} \Rightarrow \hat{B}_{44} = \frac{B_{44}}{\rho \nabla B^2} \sqrt{\frac{B}{2g}} \quad (3)$$

Where ϕ_0 is the initial roll amplitude, ε is the initial phase, τ is the shear stress on the surface of the hull, p_d is the dynamic pressure on the surface of the hull, M_d is the instant roll moment at the maximum rolling angular velocity, ∇ is the volume for the model.



Table 2 Calculation conditions

Cases	$\hat{\omega}$	ϕ_0 (rad)
1	0.58	0.1
2	0.58	0.15
3	0.58	0.175

The calculation conditions are shown in table 2. Where $\hat{\omega} = \omega\sqrt{B/2g}$, ω is the frequency of rolling. We can see that the non-dimensional frequency ($\hat{\omega}$) is equal to 0.58, and the initial roll amplitudes are 0.1rad, 0.15rad, 0.175rad, 0.22rad respectively.

2.1 Orthogonal design

The simulation results can be affected by different parameters, such as the mesh quantity, mesh quality(y^+), turbulent mode, boundary condition and discretization method. In order to find out the best combination of these parameters, we choose the initial roll amplitude $\phi_0 = 0.175\text{rad}$ to analyze these influencing factors based on the orthogonal design and variance analysis. According to the previous studies, the values of y^+ are always very small during the forced roll motion, especially for ships with bilge keels, so the enhance wall function is used, in which y^+ is approximately 1. The discretization method is SIMPLE which has a wide application. Finally, we focus our attentions on the following factors: mesh quantity, turbulent model and boundary condition.

The ship section is 16m, so we chose a circular section as the calculating domain, whose diameter is approximately 12.5 times of the model's width ($D \approx 12.5B$), and the boundary conditions including 3 parts: (1) the upper boundary of the circular domain; (2) the bottom boundary of circular domain; (3) the section surface, as shown in figure 1.

For the part of mesh quantity, we choose 10 thousands mesh as a benchmark. Three

different kinds of mesh quantities are 10 thousands, 20 thousands and 40 thousands based on the geometric proportion increasing and decreasing design, as shown in figure 2. The selection of turbulent model should consider the practicality and efficiency. In this paper, we studied standard $k-\omega$ model (s $k-\omega$), SST $k-\omega$ and RNG $k-\epsilon$. The boundary conditions are all walls, all velocity-inlet, the bottom boundary of circular domains wall and the upper boundary of circular domains pressure-outlet, respectively.

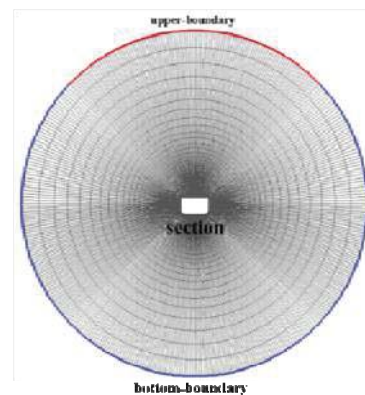


Fig.1 The boundary conditions

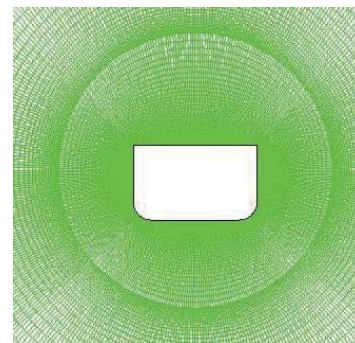


Fig.2 The part of the calculating domain (mesh quantity=40 thousands)

According to above analysis, we can get the table of factors and levels, as shown in table 3. The orthogonal layout and the two columns interaction layout $L_{27}(3^{13})$ are selected after considering the columns and degrees (Wei & Wu, 2013), and the layout is shown in table 4, in which the 9,10,12,13 are blank columns (error columns).

Table 3 Factors and levels



Level	Factor			2	A2: 20t	B2: s k- ω	C2: 2 vel
	A:Mesh quantity	B:Mesh quality	C:Boundary condition				
3	A3: 40t	B3: RNG k- ϵ	C3: 1wall+1pre				
1	A1: 10t	B1: sst k- ω	C1: 2 walls				

Table 4 Top design of the calculation program

Factor	A	B	(A×B) ₁	(A×B) ₂	C	(A×C) ₁	(A×C) ₂	(B×C) ₁	(B×C) ₂
Num	1	2	3	4	5	6	7	8	9 10 11 12 13

2.2 Variance analysis

The numerical simulations for the combination of different parameters have been conducted based on RANS model. The VOF method is used for the free surface modeling. The pressure-correction algorithm of SIMPLE type is used for the pressure-velocity coupling. The modified HRIC is used for the discretization of VOF equation, and the dynamic mesh technique is used by UDF. The non-dimensional roll damping coefficients can be got by formula (3). We selected several y^+ values from two calculating cases, and the results show that the enhanced wall function was appropriate, as shown in figure 3.

The non-dimensional coefficients were got for different computational schemes. Then the

significance of the test was investigated through the table of variance analysis, as shown in table 5. During the variance analysis, the relative errors between simulation results and experimental results were adopted as the analyze benchmark.

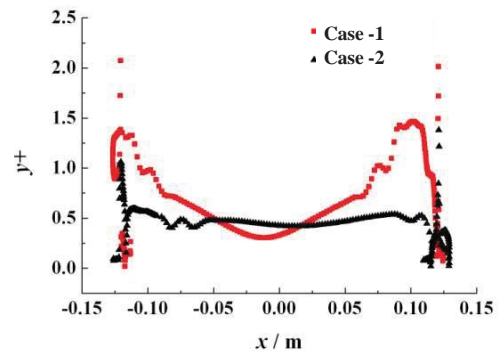


Fig. 3 The value of y^+

Table 5 Variance analysis

Soruce of variation	Quadratic sum-S	Degree of freedom-f	Mean square-V	F	Significance	F_a
A	0.61	2	0.30	10.64	**	$F_{0.05}(2,12)=3.89$
B	0.47	2	0.23	8.18	**	
C	0.34	2	0.17	5.86	*	$F_{0.01}(2,12)=6.93$
A×B	0.52	4	0.13	4.52	*	
A×C	0.17	4	0.04	1.45		$F_{0.05}(4,12)=3.26$
B×C	2.12	4	0.53	18.50	**	
e	0.61	2	0.30			$F_{0.01}(4,12)=5.41$



The values of F showed that the factor B×C (the interaction between turbulent model and boundary condition), the factor A (mesh quantity) and the factor B (turbulent model) have large influence on the results. The factor A×B (the interaction between mesh quantity and turbulent model) and the factor C (boundary condition) also have effects on the results, but the effects are not obvious compared with the above three factors.

The collocation table of B and C was listed to seek the best combination, as shown in table 6. The results showed that the combination of B1 and C1, B1 and C2 were both available. However, we find that the combination of B1 and C1 was easier to convergence and the computational process was more stable during the calculation, so we choose the combination of B1 and C1 as the best combination.

Table 6 The match of B and C

	B1	B2	B3
C1	0.33	1.76	1.23
C2	1.35	2.79	2.26
C3	0.25	1.69	1.16

Statistical hypothesis: the influence of controlled and control factors on results have no significant difference.

This hypothesis can be proved by formula (4). The results showed that the factors are significant differences, which meanings other factors which have not been taken into consideration have little effect on the results during our numerical simulation. Therefore the appropriate turbulent model and boundary condition as well as the mesh quantity can get good results on forced roll simulations. We should note that the enhanced wall function is adopted during the calculation. Otherwise, the results were not consistent with the actual situation. This means the mesh quality (y^+) has the most important effect on the results. The current results can only be adopted on the premise of the guarantee of y^+ .

$$F = \frac{\sum S / \sum f}{S_e / f_e} = 8.18 > \begin{cases} F_{0.01}(18,8) = 5.41 \\ F_{0.05}(18,8) = 3.17 \end{cases} \quad (4)$$

From the above analysis we see that: on the guarantee of y^+ , the design of A2 (40 thousands mesh), B1 (SST k- ω), C1 (all boundary conditions are walls) is the best combination.

2.3 The calculation results and analysis

Based on the above combination, more research about other conditions were conducted, and the results are shown in figure 4. This figure shows a comparison between the numerical simulation results and experimental results, we can see that the results are in good accordance with the experimental results, so the combination is feasible.

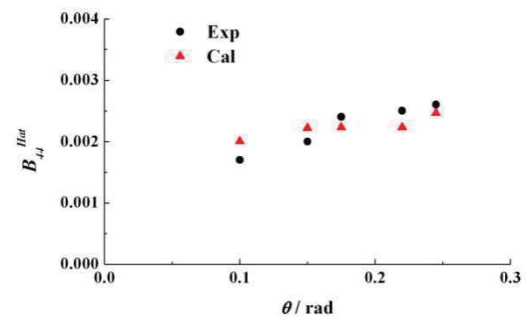


Fig.4 The non-dimensional damping coefficients for different roll amplitudes

3. THE FREE ROLLING

For the free roll decay motion, the object is a 4250TEU containership due to the availability of experimental data for validation. The free roll decay simulations were performed based on the unsteady RANS model and compared to experimental data.

3.1 Experiment

The principal particulars and body plan of this containership are shown in table 7 and figure 5, respectively. Roll decay experiments were performed with a 1/62.97 scaled model at the seakeeping basin (length: 69m, breadth: 46m, height: 4m) of CSSRC (China Ship Scientific Research Center), as shown in figure 6. The initial roll angle was 25 degrees in calm water.



Fig.6 The ship model in free decay test

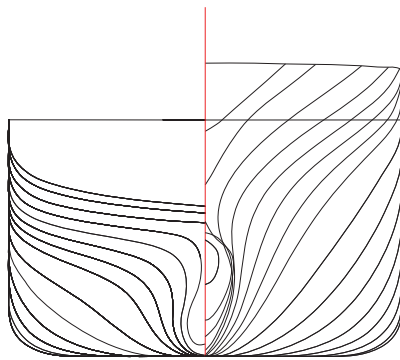


Fig. 5 Lines of 4250TEU containership

Table 7 Principal particulars of the 4250TEU Containership

Items	Ship	Model
Length: L	251.88m	4.0m
Draft: T	12.6m	0.2m
Breadth: B	32.2m	0.511m
Depth: D	19.3m	0.3065m
GM	1.62m	0.0257m
T_{φ}	21.19s	2.7s
K_{vv}	0.3L	0.3L

3.2 Simulation

In this paper, the simulations of roll decay at 25 degrees initial roll angle in calm water were performed. During the simulation, the VOF method is used for the free surface modeling. A pressure-correction algorithm of SIMPLE type is used for the pressure-velocity coupling. The SST $k-\omega$ model is incorporated for turbulence modeling. The solution domain is formed in two parts: the first part (S1) moves with the body, and the second part (S2) is fixed, as shown in figure 7. For the purpose of wave absorption, two artificial damping zones were located at the second part (S2), which is far away from the hull.

3.3 Comparison

The results of numerical simulations of roll decay histories were compared with the experimental results, as shown in figure 8. It shows that the period agrees well with the experimental data with the growth of the time. However, the amplitude of CFD becomes a little larger than the experiment. The future calculations are needed to verify these phenomena.

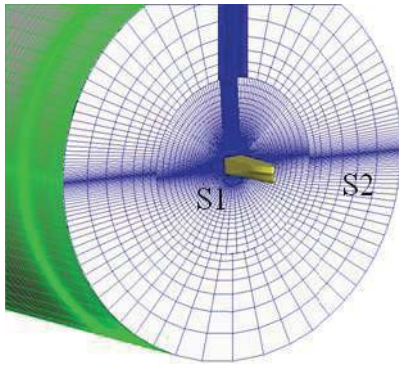


Fig. 7 The solution domain in free decay

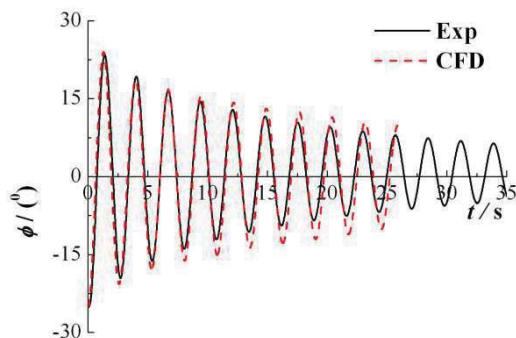


Fig. 8 The comparison of experimental results and numerical simulation of free decay

4. CONCLUSIONS

As a result of experimental and numerical study on roll damping by the forced rolling with two dimensional ship sections of Series 60 and by the free rolling with a 3-dimensional hull based on the RANS model, the following remarks are noted:

- 1) For the forced motion, an applicable results of roll damping can be got based on the combination of enhance wall function, SST $k-\omega$ model, the wall boundary conditions as well as the appropriate mesh quantity.
- 2) For the free roll motion, the roll motion of a 3-dimensional hull based on the RANS model in calm water was simulated, and the results were in reasonable agreement with the experimental results.

3) Both the forced rolling and free rolling based on RANS approach have the abilities to predict the roll damping.

4) More works should be made in future to improve calculating accuracy of roll damping, especially for free roll motion condition.

5. ACKNOWLEDGEMENTS

This research is supported by Ministry of Industry and Information Technology of China (No. [2012] 533). The authors sincerely thank the above organization.

6. REFERENCES

- Blok, J.J. and Aalbers. A.B., 1991, "Roll Damping Due to Lift Effects on High Speed Monohulls", FAST'91.
- Frederick Jaouen, Arjen Koop, Guilherme Vaz, 2011, "Predicting Roll Added Mass and Damping of a Ship Hull Section Using CFD", Proceedings of the ASME 2011 30th International conference on ocean, offshore and arctic engineering, Netherlands.
- Haddara, M.R. BASS, D.W., 1988, "Non-linear Models of Ship Roll Damping", International Shipbuilding Progress, 35/401, pp. 5-24.
- Japan, 2011a, "Interim Verification and Validation Report on Simplified Roll Damping", IMO SLF 54/INF 12, Annex 7.
- Japan, 2011b, "Additional Validation Data on Simplified Roll Damping Estimation for Vulnerability Criteria on Parametric Rolling", IMO SLF 54/INF 12, Annex 11.
- K.B.Salui and D.Vassalos, 2003, "A RANS Based Technique to Compute Forced Rolling Responses in Three-Dimensional Flows", Computational Fluid Dynamic Technology in Ship Hydrodynamic, UK, pp. 13-18.



- K.B.Salui, Tanmay Sarkar and Dracos Vassalos, 2000, "An Improved Method for Determining Hydrodynamic Coefficients in Roll Motion Using CFD Techniques", Ship Technology Research, Vol. 47, pp.161-174.
- Robert Wilson and Fred Stern, 2002, "Unsteady RANS Simulation of a Surface Combatant with Roll Motion", 24th Symposium on Naval Hydrodynamics Fukuoka, Japan.
- Miller, R., W. Gorski J.J., and Fry, D.J. 2002, "Viscous Roll Predictions of a Circular Cylinder with Bilge Keels", 24th Symposium on Naval Hydrodynamics Fukuoka, Japan.
- Miller, R., W. Bassler C.C., et al. 2008, "Viscous Roll Predictions for Naval Surface Ships Appended with Bilge Keels using URANS", 27th Symposium on Naval Hydrodynamics, Seoul, Korea.
- Sungkyun Lee, Ji-Myoung You, 2011, "Free Roll Decay Study of a Damaged Ship for CFD Validation", Proceedings of the ASME 2011 30th International conference on ocean, offshore and arctic engineering, Netherlands.
- Sweden, 2011, "Evaluation of Ikeda's simplified method for prediction of roll damping", IMO SLF 54/3/6.
- United States and Japan, 2014, "Draft Guidelines of Direct Stability Assessment Procedures as a Part of the Second Generation Intact Stability Criteria, IMO SDC1/INF.8, Annex 27.
- Wei Ze, Wu Chengsheng, Ni Yang, 2013, "Optimum Hydrodynamic Design of Helical Strake on Spar Platforms Based on Orthogonal Design and CFD Method", Journal of Ship Mechanics, Vol. 17, PP. 1133-1139.
- Wilson, R.V. and Fred Stern, 2002, "Unsteady RANS Simulation of a Surface Combatant with Roll Motion", 24th Symposium on Naval Hydrodynamics Fukuoka, Japan.
- Wilson, R.V., Carrica, P.M., and Stern, F, 2006, "Unsteady RANS method for ship motions with application to roll for a surface combatant", Computers and Fluids, Vol. 35(5), pp. 501-524.
- Yoshiho Ikeda, Yoji Himeno and Norio Tanaka, 1977, "On Eddy Making Component of Roll Damping Force on Naked Hull", Journal of the society of Naval Architects of Japan. Vol. 142.
- Yoshiho Ikeda, Yoji Himeno and Norio Tanaka, 1978, "Components of Roll Damping of Ship at Forward Speed", Journal of the society of Naval Architects of Japan, Vol. 143.
- Yoshiho Ikeda, Yoji Himeno and Norio Tanaka, 1979, "On Roll Damping Force of Ship-Effect of Hull Surface Pressure Created by Bilge Keels", Journal of the society of Naval Architects of Japan, Vol. 165
- Yoshiho Ikeda and Katayama, T., 2000, "Roll Damping Prediction Method for a High-Speed Planning Craft", Proceedings of the 7th International Conference of Ships and Ocean Vehicles (STAB'2000), Vol. 2, PP. 532-541.
- Yoshiho Ikeda, 2004, "Prediction Methods of Roll Damping of Ships and Their Application to Determine Optimum Stabilization Devices", Marine Technology.



Investigation of the Applicability of the IMO Second Generation Intact Stability Criteria to Fishing Vessels

Marcos Míguez González, *GII, University of A Coruña, Spain* mmiguez@udc.es

Vicente Díaz Casás, *GII, University of A Coruña, Spain* vdiaz@udc.es

Luis Pérez Rojas, *Model Basin, ETSIN, Technical University of Madrid* luis.perezrojas@upm.es

Daniel Pena Agras, *GII, University of A Coruña, Spain* dpagras@udc.es

Fernando Junco Ocampo, *GII, University of A Coruña, Spain* fjunco@udc.es

ABSTRACT

In this work, the vulnerability of seven fishing vessels of mid and small size, representative of the Spanish fleet, to some of the failure modes covered by the IMO Second Generation Intact Stability Criteria, has been studied. The latest draft proposals for Level 1 and 2 checks for parametric roll, pure loss of stability and dead-ship condition, as presented in the IMO SDC 1 (2013), have been applied to the aforementioned sample vessels. The results are commented, and some notes regarding the applicability of this criteria as a design tool are also included.

Keywords: *Second generation intact stability criteria, parametric roll, pure loss of stability, dead ship condition, fishing vessels stability*

1. INTRODUCTION

The Second Generation Intact Stability Criteria have been under development by the IMO SLF Sub-Committee for the last ten years, beginning in the 48th session of the SLF (Peters *et al.*, 2011). The main aim of these criteria is to increase the ship safety by quantifying its tendency to experiencing one of the so called failure modes. These are basically dynamic instabilities derived from the interaction while sailing between the ship and the waves and wind, and which are not covered by the traditional intact stability requirements. These failure modes include five phenomena: parametric roll resonance, loss of stability in stern waves, broaching, dead-ship condition and excessive accelerations.

The structure of the criteria is the same for all the aforementioned failure modes. They

follow a three level arrangement: the Level 1 represents the easiest method of evaluation, and also the most conservative one. If the vessel fails to comply with Level 1, a Level 2 check has to be carried out, where a more detailed evaluation, also more complicated, is proposed. Finally, if the vessel is also found to be vulnerable under Level 2 criteria, a direct assessment has to be done, where stability operational guidelines have to be developed from the detailed analysis of more realistic sailing situations.

Regarding the development of the criteria, their current status can be found in the report of the Correspondence Group on Intact Stability to the SDC 1. Parametric roll and loss of stability draft criteria have been already agreed and draft explanatory notes developed, broaching and dead-ship condition draft criteria and explanatory notes are also available and



excessive acceleration criteria are still under discussion (IMO SDC 1/5/3, 2013).

Second generation intact stability criteria are mainly focused on cargo and passenger ships; although some fishing vessels have been considered in the different applicability analysis of the criteria (three vessels in IMO SLF55/Inf.15 (2012a) and IMO SDC 1/Inf.8 (2013) and two in IMO SLF55/Inf.15 (2012b)), they're very few compared to the rest of the typologies.

The fleet of fishing vessels is the largest worldwide. Moreover, the fishing activity is known for being one of the most dangerous industrial activities in many countries, such as Spain (MIT, 2014), U.K. (Roberts, 2010) or the U.S. (BLS, 2013).

Most of the effort spent on increasing the safety of fishing vessels has been directed at improving the crew training in the fields of static stability (cargo stowage, post-construction modifications, overloading and reduction in freeboard) and ship operation (flooding prevention) (Míguez-González *et al.*, 2012a). In fact, fishing vessel stability criteria, with the exception of the IMO Weather Criterion (which is not mandatory for all of them), are based on static stability principles. However, dynamical instabilities (parametric roll, loss of stability, broaching, dead ship condition) are also known to affect fishing vessels and to be the possible cause of many accidents (Mata-Alvarez-Santullano & Souto-Iglesias, 2014). And neither of them are analysed during the vessel design process or included within crew training programs.

Related to this fact, and in addition to their possible implementation as mandatory requirements, the application of second generation intact stability criteria as complementary design tools, could lead to very important increases in the safety of this type of vessels. So, the main objective of this work is to evaluate the suitability of the proposed second generation intact stability criteria to

fishing vessels, and their application as a design tool to improve their safety levels from the dynamic stability point of view.

In order to do this, the draft second generation intact stability criteria proposed in IMO SDC 1/Inf.8 (2013), including parametric roll, pure loss of stability and dead-ship condition failure modes, have been applied to a sample of seven fishing vessels. These are representative of the different typologies present on the Spanish fleet of mid-sized fishing vessels, including trawlers, longliners and purse seiners, with lengths ranging from 20 to 70 meters. From the obtained results, the vulnerability of the different vessels to the aforementioned failure modes and the suitability of these draft criteria as a first stage design tool have been analysed.

2. TEST VESSELS

One of the main characteristics of the fishing vessel fleet is its vast heterogeneity; the arrangement of the different ships depends on the used fishing gear, on tradition and regional factors or on regulatory issues. This fact makes it very difficult to analyse fishing vessels as a whole. In our case, the mid-sized Spanish fishing fleet, which is the largest in Europe in terms of tonnage, has been selected (EU Commission, 2014). From this, we focused on the vessels of more than 20 m long (usually operating in open seas), which in the Spanish case, are more than 1400 units (MAGRAMA, 2013).

The selected ships try to cover all the main typologies present on the aforementioned fleet, and two medium sized stern trawlers (named Trawler 1 and 2), one large stern trawler (Large Trawler), one longliner (Longliner), one medium size purse seiner (Purse Seiner) and one large tuna purse seiner (Tuna Purse Seiner), were chosen. Experimental head sea data of the Trawler 2, is available in Míguez-González *et al.* (2012b).



Table 1: Vessel characteristics (1).

Vessel	L_{PP} (m)	B (m)	d (m)
Trawler 1	25.70	8.50	3.25
Trawler 2	29.00	8.00	3.30
Large Trawler	60.60	12.50	4.60
Longliner	24.00	8.20	3.20
Purse Seiner	21.00	7.00	2.70
Tuna Purse Seiner	67.60	14.00	4.80
TS Trawler (d ₁)	22.00	6.90	2.30
TS Trawler (d ₂)	22.00	6.90	2.46

Table 2: Vessel characteristics (2).

Vessel	L_{PP}/B	B/D	D/d	C_b	C_m
Trawler 1	3.02	1.51	1.73	0.56	0.85
Trawler 2	3.63	1.38	1.76	0.57	0.86
Large Trawler	4.85	1.63	1.66	0.54	0.88
Longliner	2.93	1.41	1.81	0.68	0.90
Purse Seiner	3.00	2.19	1.19	0.67	0.89
Tuna Purse Seiner	4.83	1.54	1.90	0.53	0.93
TS Trawler (d ₁)	3.19	2.06	1.46	0.47	0.74
TS Trawler (d ₂)	3.19	2.06	1.36	0.48	0.75

Table 3: Vessel characteristics (3).

Vessel	A_L (m ²)	Z (m)	ϕ_{fl} (deg)
Trawler 1	145	4.47	64.3
Trawler 2	162	4.38	65.4
Large Trawler	415	5.57	53.6
Longliner	120	4.09	68.6
Purse Seiner	83	3.50	54.3
Tuna Purse Seiner	361	7.60	69.1
TS Trawler (d ₁)	95	3.37	57.2
TS Trawler (d ₂)	91	3.37	57.2

Moreover, and for comparison purposes, a typical U.K. beam trawler (named TS Trawler), which has been broadly studied (Neves & Rodríguez, 2006), has also been selected.

The main characteristics of the analysed vessels are included in Tables 1 and 2. In Table 3, some of the parameters needed for the evaluation of the IMO Weather Criterion are presented, where A_L is the projected lateral area over the waterline, Z is the distance from the centre of A_L to the half of the mean draft and ϕ_{fl} is the first downflooding angle.

Table 4: Tested Conditions.

Vessel	F_n	d (m)	GM_T (m)	ω_0 (rad/s)
Trawler 1 LC1	0.32	3.25	0.653	0.692
Trawler 1 LC2	0.32	3.25	0.350	0.507
Trawler 2	0.31	3.30	0.350	0.539
Large Trawler	0.31	4.60	0.350	0.345
Longliner LC1	0.34	3.20	0.495	0.625
Longliner LC2	0.34	3.20	0.350	0.526
Purse Seiner	0.36	2.70	0.350	0.616
Tuna Purse Seiner LC1	0.34	4.80	0.916	0.498
Tuna Purse Seiner LC2	0.34	4.80	0.350	0.308
TS Trawler LC1	0.32	2.30	0.730	0.902
TS Trawler LC2	<u>0.32</u>	<u>2.46</u>	<u>0.436</u>	<u>0.697</u>

Regarding the tested loading conditions, in all cases the design draft has been selected; in the case of the TS Trawler, two different drafts, for which experimental data are available (Paffet, 1976), have been chosen. When the real GM was available for the selected draft, that was the applied value; in addition, another condition with the minimum GM according to the Torremolinos Protocol (350 mm), was also defined for these cases. When no data was available, the minimum GM of 350 mm was selected.

The natural roll frequency for all cases was computed by using a roll radius of gyration (including added inertia) of $0.43 \cdot B$, estimated from the experimental data in Míguez-González *et al.* (2012b). In all cases, no bilge keels were considered ($A_{BK} = 0$), and the design speed was chosen to compute the reference ship speed (V_{PR}).

3. CRITERIA DESCRIPTION

In this work, the vulnerability of the selected vessels to parametric roll, pure loss of stability and dead-ship condition failure modes have been analysed by applying the proposals contained in the different annexes of IMO SDC 1/Inf.8 (2013). Parametric roll criteria and their explanatory notes are contained in Annexes 1 and 3; pure loss of stability criteria and their explanatory notes in Annexes 2 and 4; and



dead-ship condition criteria in Annex 16. The draft explanatory notes of dead-ship condition are included in IMO SDC 1/Inf.6 (2013).

3.1 Parametric roll

The phenomenon of parametric roll is generated by the variation of the roll restoring term due to the wave passing along the hull. Its effects are more intense in longitudinal waves, when the wave encounter frequency approximates the double of the ship roll natural frequency. Under these conditions, roll motion can reach very large amplitudes.

The parametric roll vulnerability criteria are divided into two levels, both based on the analysis of the GM variation in longitudinal waves. In the Level 1, the GM in calm water is compared to the amplitude of GM variation (ΔGM) in a longitudinal wave of wavelength equal to ship length and a constant steepness of $S_W = 0.0167$. The ship is considered vulnerable if:

$$\frac{\Delta GM}{GM} > R_{PR} \quad (1)$$

Where R_{PR} represents roll linear damping, that may be taken as 0.5 or a value dependant on bilge keel area and midship coefficient.

The Level 2 presents two checks. The first one is similar to that of Level 1, but computations have to be made for a set of 16 waves, with different lengths and steepness's, and the results of each wave case have to be weighted and summed up. Moreover, an additional requirement that takes into account the vessel forward speed has to be also considered. According to this first check, the ship will be considered vulnerable if:

$$C1 = \sum_{i=1}^N W_i C_i > R_{PRO} \quad (2)$$

Where R_{PRO} is 0.06 or 0.1, W_i is the wave case weight and C_i is a coefficient equal to 1 if the ship is vulnerable under GM and speed checks, and 0 if not. GM vulnerability checks are the same as those of the first level criterion, but computed for each of the wave parameters. The ship is considered as vulnerable if:

$$GM(H_i, \lambda_i) < 0 \quad (3)$$

$$\frac{\Delta GM(H_i, \lambda_i)}{GM(H_i, \lambda_i)} > R_{PR} \quad (4)$$

The speed requirement consists on comparing the design speed of the ship (V_D) and a reference speed for parametric roll appearance (V_{PRi}), which depends on the metacentric height on waves and calm water, on wave conditions and on natural roll period. Although not specified in the rules, for a ship with two very different sailing conditions (such as trawlers), it could be important, in order to accurately evaluate this requirement, to take into account the two possible sailing speeds. In any case, the ship is considered vulnerable if:

$$V_{PRi} < V_D \quad (5)$$

If the ship is found to be vulnerable under the first check, a second check has to be done. This has a similar structure to the previous one; the ship will be considered vulnerable if:

$$C2 = \sum_{i=1}^N W_i C_i > R_{PR1} \quad (6)$$



In this case, W_i is again the wave case weight (which are obtained from a wave scatter diagram with 306 wave cases) and C_i is a coefficient equal to 1 if the roll motion of the ship, computed by using an uncoupled equation of roll motion, is over 25 degrees, and 0 if it is not.

3.2 Pure loss of stability

The reduction of the transverse stability of the ship, when it sails in stern seas and wave crest persists for a long time near amidships, is the cause of this failure mode. In waves of wavelength similar to ship length, and in low stability conditions, it could lead to large roll and even capsizing.

Pure loss of stability criteria are only of application to ships of length of more than 24 m and speeds of Froude over 0.2, 0.26 or 0.31 (to be decided), and are also divided into two levels. Level 1 is similar to that of the parametric roll failure mode, and consists on evaluating the minimum GM (GM_{min}) when a wave of wavelength equal to ship length and a constant steepness of $S_w = 0.0334$ passes the ship. The vessel would be considered as vulnerable if:

$$GM_{min} < R_{PLA} \quad (7)$$

where R_{PLA} is the minimum value between 0.05 m and a speed and draft dependant factor.

The second level check consists of three criteria (CR_j), computed for two possible set of waves (16 or 306 cases).

$$CR_{j=1,3} = \sum_{i=1}^N W_i C_j \quad (8)$$

Each CR_j is obtained by weighting the coefficients C_{ji} , which are evaluated for each wave condition; $C1_i$ is equal to 1 if the angle of vanishing stability (ϕ_v) is over 30 degrees or the angle of steady heel in waves (ϕ_s) is over 15 or 20 degrees; $C2_i$ is equal to 1 if the maximum loll angle (ϕ_{loll}) is over 25 degrees; and $C3_i$ is equal to 1 if the maximum GZ value is under $8 \cdot (H / \lambda) \cdot d \cdot Fn^2$.

So, the ship is considered vulnerable if:

$$\max(CR_1, CR_2, CR_3) > R_{PLO} \quad (9)$$

Where R_{PLO} is 0.06 for the first set of waves and 0.15 if the second option is adopted.

3.3 Dead-ship condition

The dead ship condition of a ship takes place when all of its machinery becomes out of operation, disabling its propulsive and manoeuvring capabilities. Under these conditions, the vessel may be affected by severe beam wind and waves, not being able to escape this dangerous situation. The objective of the dead ship stability criteria, is to ensure that the ship is able to withstand the effect of the aforementioned beam excitations for a given amount of time.

As in the case of the previous two failure modes, they are divided into two levels. The Level 1 check corresponds to the well-known IMO Weather Criterion (Severe Wind and Rolling Criterion), included in the IMO 2008 Intact Stability Code, but with a modification on the wave steepness's for large draft vessels.

The Level 2 assessment proposes a probabilistic approach for evaluating the vessel vulnerability to the analysed failure mode. The procedure consists on determining the long term vulnerability of the ship by computing the coefficient C ; if it is under the reference value

of 10^{-3} , the ship is considered as non-vulnerable.

To obtain this long term coefficient, a short term vulnerability index C_S is computed for different wave and wind conditions, characterized by the significant wave height (H_s), the zero crossing period (T_z) and the wind speed (U_w). Once computed, the C index is obtained as a weighted average of the C_S values:

$$C = \sum_{H_s} \sum_{T_z} (W(H_s, T_z) \cdot C_S(H_s, T_z, U_w)) \quad (10)$$

The short term environmental conditions, together with the probability weighting factors ($W(H_s, T_z)$), are obtained by applying the North Atlantic scatter diagram (IACS Recommendation 34), although other wave cases may be accepted.

The short term vulnerability index is obtained by considering the ship as a 1 d.o.f. linear system which rolls under the action of beam irregular waves and gusty winds, which spectra are obtained from the corresponding short term wave characteristics (H_s, T_z). After obtaining some parameters from the residual righting lever curve under the effect of steady wind moment, the roll standard deviation and zero crossing frequency corresponding to the wave and wind moment spectra are obtained by solving the roll equation in frequency domain.

The short term vulnerability index represents the probability of capsizing in the analysed conditions in a given exposure time (3600 s in this case), and is computed from the vessel roll characteristics defined above and two virtual capsizing angles, obtained by equalling the area under the residual righting lever curves and a linearized (in the equilibrium heel angle due to steady wind), residual righting lever curve.

In the method draft explanatory notes (IMO SDC 1/Inf.6, 2013), in addition to the

description of the applied methodology, a procedure for computing the effective wave slope coefficient and an alternative methodology for computing the C_S index are also included. Moreover, a method for estimating the necessary roll damping coefficients is presented, based on the least squares fitting of the equivalent linear roll damping coefficient obtained by the Ikeda method for different roll amplitudes.

4. RESULTS AND DISCUSSION

In this section, the results obtained from the application of parametric roll, pure loss of stability and dead-ship condition criteria are presented and commented. The ones corresponding to the first two failure modes, have been already presented in Míguez-González et al. (2014), where draft requirements described in IMO SLF 55/WP.3 (2013) for parametric roll, loss of stability and broaching, were applied to the same sample vessels.

4.1 Parametric roll

In this case, Level 1 and Level 2 first check have been carried out. The Level 1 results are shown in Table 5, where ΔGM is the GM variation on the specified waves and ΔGM_{alt} is the alternative GM variation in waves computed considering the waterplane inertias at drafts d_h and d_l . The Level 2 first check results are shown in Table 6. There, ΔGM_{max} is the maximum GM variation for all the 16 wave cases, GM_{avg} is the corresponding average GM for that wave case and V_{PR} is the reference ship speed for resonance in that conditions.

According to the results, all ships, excepting the Large Trawler and the Tuna Purse Seiner in the low GM condition, pass Level 1 check.



Table 5: Parametric roll. Level 1 results.

Vessel	ΔGM (m)	ΔGM_{alt} (m)	$\Delta GM/GM$	Level 1
Trawler 1 LC1	0.090	0.164	0.251	Pass
Trawler 1 LC2	0.090	0.164	0.468	Pass
Trawler 2	0.102	0.133	0.379	Pass
Large Trawler	0.109	0.251	0.718	Fail
Longliner LC1	0.051	0.062	0.126	Pass
Longliner LC2	0.051	0.062	0.178	Pass
Purse Seiner	0.035	0.046	0.130	Pass
Tuna Purse Seiner LC1	0.154	0.295	0.322	Pass
Tuna Purse Seiner LC2	0.153	0.295	0.843	Fail
TS Trawler LC1	0.095	0.205	0.281	Pass
TS Trawler LC2	0.107	0.181	0.414	Pass

Table 6: Parametric roll. Level 2 results. 1st
check.

Vessel	ΔGM_{max} (m)	GM_{avg} (m)	ΔGM_{max} / GM_{avg}	V_{PR} (m/s)	Level 2
Trawler 1 LC1	0.075	0.650	0.115	1.186	Pass
Trawler 1 LC2	0.073	0.347	0.211	2.040	Pass
Trawler 2	0.085	0.353	0.241	0.728	Pass
Large Trawler	0.104	0.360	0.287	1.707	Pass
Longliner LC1	0.044	0.495	0.089	1.110	Pass
Longliner LC2	0.045	0.349	0.128	0.935	Pass
Purse Seiner	0.034	0.352	0.097	1.171	Pass
Tuna Purse Seiner LC1	0.152	0.895	0.169	2.090	Pass
Tuna Purse Seiner LC2	0.152	0.330	0.460	3.069	Pass
TS Trawler LC1	0.090	0.719	0.125	1.019	Pass
TS Trawler LC2	0.100	0.444	0.225	0.473	Pass

Regarding Level 2 check, all ships pass the criteria for all wave cases ($CI = 0$). The criteria, for these vessels, are consistent, as no vessel is found to be non-vulnerable under Level 1 and vulnerable under Level 2.

In Míguez-González et al. (2014) and references therein, these results were analysed and compared to experimental data present in the literature, in order to analyse the suitability of the criteria to these small vessels. In the cases of the Trawler 2 and the TS Trawler, small variation of GM in waves has been

obtained. So, both of them have been considered as non-vulnerable, while experimental data have shown their large tendency to developing parametric roll. However, the small wave heights and probabilities (weighting factors, which represent a small probability for the ship facing them in real sailing), associated with the waves of small wavelength that correspond to these ships length, is the cause of this consideration. Moreover, the results obtained for the Tuna Purse Seiner were also compared to experimental data available, showing a good consistency.

From the different typologies of vessels studied, it can be seen that those ships with larger bow flares and hanging sterns, such as trawlers and the tuna purse seiner, are the most vulnerable to this failure modes, presenting the largest GM variations from all the sample.

4.2 Pure loss of stability

Pure loss of stability criteria are of application to all the sample ships, as their speeds are, in all cases, equal or over $Fn = 0.31$. Level 1 and Level 2 (Option A, 16 reference wave cases) checks have been carried out. The results of the Level 1 check are presented in Table 7, where GM_{min} is the minimum GM as the specified wave passes the ship, and GM_{min_alt} is the alternative minimum GM computed considering the waterplane inertia at draft d_L . The Level 2 results are presented in Table 8, where GZ_{max} is the minimum smallest GZ curve maximum for all the 16 wave cases, ϕ_v , ϕ_s and ϕ_{loll} are respectively the vanishing stability, the steady heel and the loll angles for that condition and R_{PL3} is the vulnerability limit for the presented GZ_{max} .

As can be seen, the largest vessels (Large Trawler and Tuna Purse Seiner in the two loading conditions), together with the TS Trawler in the low GM condition, are found to be vulnerable under Level 1 check.



Table 7: Pure loss of stability. Level 1 results.

Vessel	GM_{min} (m)	GM_{min_alt} (m)	Level 1
Trawler 1 LC1	0.452	0.488	Pass
Trawler 1 LC2	0.148	0.184	Pass
Trawler 2	0.172	0.075	Pass
Large Trawler	0.193	-0.147	Fail
Longliner LC1	0.391	0.342	Pass
Longliner LC2	0.246	0.197	Pass
Purse Seiner	0.276	0.231	Pass
Tuna Purse Seiner LC1	0.626	0.028	Fail
Tuna Purse Seiner LC2	0.060	-0.540	Fail
TS Trawler LC1	0.520	0.105	Pass
TS Trawler LC2	<u>0.271</u>	<u>-0.113</u>	Fail

Table 8: Pure loss of stability. Level 2 results.
Option A.

Vessel	GZ_{max} (m)	ϕ_v (deg)	ϕ_s (deg)	ϕ_{roll} (deg)	R_{PL3}	Level 2
Trawler 1 LC1	0.422	90	0	0	0.084	Pass
Trawler 1 LC2	0.199	70	0	0	0.085	Pass
Trawler 2	0.746	125	0	0	0.075	Pass
Large Trawler	0.187	51	0	0	0.115	Pass
Longliner LC1	0.392	82	0	0	0.088	Pass
Longliner LC2	0.293	73	0	0	0.089	Pass
Purse Seiner	0.269	78	0	0	0.086	Pass
Tuna Purse Seiner LC1	0.995	111	0	0	0.148	Pass
Tuna Purse Seiner LC2	0.451	95	0	0	0.136	Pass
TS Trawler LC1	0.254	70	0	0	0.056	Pass
TS Trawler LC2	0.144	58	0	0	0.060	Pass

Regarding Level 2 check, all vessels were found to be non-vulnerable (all criteria were fulfilled in all wave cases), and criteria are consistent for this set of vessels.

Like in the case of parametric roll failure mode, in Míguez-González et al. (2014) and references therein, the obtained results were compared with available experimental data. Regarding both the TS Trawler and the Tuna Purse Seiner, a large tendency to capsizing in stern seas has been described, showing a good agreement between the vulnerability analysis and the towing tank test data. In the case of the

Trawler 2, and although some reduction of stability in stern seas has been shown in the literature, no capsizing occurred in any of the tested conditions. So, results seem to be consistent also for this vessel. Again, the vessels with larger bow flares and hanging sterns (trawlers and tuna purse seiner), are shown to be more vulnerable than the others.

4.3 Dead-ship condition

As have been already mentioned, the Level 1 and Level 2 dead-ship condition checks have been carried out. In Table 9, the intact stability characteristics of the different vessels are shown (all GM values are over the minimum, as shown in Table 4). As it can be seen, there are two vessels, the Trawler 1 and the TS Trawler in the low GM conditions, which do not fulfil the minimum requirements stated by the Torremolinos Protocol.

Regarding the Level 1 check, in Table 10 the obtained results are presented. There, ϕ_0 is the angle of equilibrium under the steady wind heel lever, ϕ_1 is the windward roll angle and ϕ_2 is the minimum between the downflooding angle and 50 degrees. a and b are the areas under the GZ and wind heeling lever curves stated in the IMO Weather Criterion. It can be appreciated that all ships, with the exception of the TS Trawler, but including the Trawler 1 in the low GM condition (LC2), pass the Level 1 check.

In Table 11, the results of the Level 2 check are presented. In there, ϕ_{Smax} is the maximum steady heel angle for all the wave conditions tested, $\sigma_{\phi Smax}$ is the maximum roll standard deviation, $T_{Z\phi max}$ is the maximum roll zero crossing period and C , is the long term probability failure index.



Table 9: Intact stability results.

Vessel	Area 0-30 (m.rad)	Area 0-40 (m.rad)	Area 30-40 (m.rad)	Max. GZ (m)	Max. GZ Angle (deg)
Trawler 1 LC1	0.0833	0.1506	0.0673	0.489	47.3
Trawler 1 LC2	0.0426	0.0795	0.0369	0.271	44.5
Trawler 2	0.0560	0.1093	0.0532	0.863	75.5
Large Trawler	0.0642	0.1189	0.0547	0.321	35.5
Longliner LC1	0.0759	0.1434	0.0675	0.461	45.0
Longliner LC2	0.0565	0.1095	0.0530	0.360	43.6
Purse Seiner	0.0550	0.0960	0.0435	0.301	45.8
Tuna Purse Seiner LC1	0.1282	0.2366	0.1084	1.079	64.5
Tuna Purse Seiner LC2	0.0550	0.1036	0.0515	0.575	60.0
TS Trawler LC1	0.078	0.1277	0.0497	0.304	41.4
TS Trawler LC2	0.0507	0.0850	0.0341	0.203	37.7

Table 10: Dead ship condition. Level 1 results.

Vessel	ϕ_0 (deg)	ϕ_1 (deg)	ϕ_2 (deg)	b (m.rad)	a (m.rad)	Level 1
Trawler 1 LC1	7.4	24.2	50	0.1396	0.0743	Pass
Trawler 1 LC2	15.3	21.5	50	0.0432	0.0392	Pass
Trawler 2	12.6	22.8	50	0.1029	0.0474	Pass
Large Trawler	9.4	12.4	50	0.0919	0.0166	Pass
Longliner LC1	6.6	25.7	50	0.1549	0.0651	Pass
Longliner LC2	9.2	23.9	50	0.1059	0.0447	Pass
Purse Seiner	8.8	25.5	50	0.0855	0.0489	Pass
Tuna Purse Seiner LC1	3.6	17.3	50	0.3114	0.0505	Pass
Tuna Purse Seiner LC2	9.5	13.4	50	0.1148	0.0172	Pass
TS Trawler LC1	8.3	23.4	50	0.0672	0.0777	Fail
TS Trawler LC2	12.2	22.6	50	0.025	0.0507	Fail

The roll damping coefficients of the different vessels, were obtained from the experimental data of a stern trawler with no bilge keels (Trawler 2), described in Míguez-González *et al.* (2013).

It can be seen that all the small vessels (with the exception of the Trawler 2), fail the Level 2 criteria.

Table 11: Dead ship condition. Level 2 results. No Bilge Keels.

Vessel	ϕ_{Smax} (deg)	$\sigma_{\phi max}$ (deg)	$T_{z\phi max}$ (s)	C	Level 2
Trawler 1 LC1	18.0	10.1	10.7	2.38E-03	Fail
Trawler 1 LC2	32.0	12.4	11.8	2.97E-03	Fail
Trawler 2	25.0	11.7	9.4	4.60E-04	Pass
Large Trawler	18.0	11.3	14.0	1.46E-05	Pass
Longliner LC1	14.0	12.5	9.8	1.28E-02	Fail
Longliner LC2	19.0	14.6	10.2	9.24E-03	Fail
Purse Seiner	19.0	13.5	9.4	2.02E-02	Fail
Tuna Purse Seiner LC1	8.0	9.0	13.5	5.53E-05	Pass
Tuna Purse Seiner LC2	20.0	11.1	18.2	3.02E-07	Pass
TS Trawler LC1	24.0	12.1	12.5	1.11E-02	Fail
TS Trawler LC2	34.0	20.1	16.6	1.60E-02	Fail

Table 12: Dead ship condition. Level 2 results. Bilge keel effect included.

Vessel	ϕ_{Smax} (deg)	$\sigma_{\phi max}$ (deg)	$T_{z\phi max}$ (s)	C	Level 2
Trawler 1 LC1	18.0	8.9	11.0	4.37E-04	Pass
Trawler 1 LC2	32.0	11.1	12.0	9.91E-04	Pass
Trawler 2	25.0	10.5	9.5	8.61E-05	Pass
Large Trawler	18.0	10.1	14.1	1.58E-06	Pass
Longliner LC1	14.0	10.9	9.9	3.20E-03	Fail
Longliner LC2	19.0	12.9	10.3	2.43E-03	Fail
Purse Seiner	19.0	11.9	9.5	5.94E-03	Fail
Tuna Purse Seiner LC1	8.0	7.9	13.6	3.84E-06	Pass
Tuna Purse Seiner LC2	20.0	9.9	18.3	1.59E-08	Pass
TS Trawler LC1	24.0	10.7	13.1	3.12E-03	Fail
TS Trawler LC2	34.0	17.9	17.2	5.44E-03	Fail

In order to investigate the influence of the damping coefficients on the obtained results, a new computation including a 40 % increase in damping was carried out. This increase could reflect the effect of bilge keels (Chun *et al.*, 2001), which are installed in all of these vessels in the reality.



In this new case (Table 12), the Trawler 1 is found to be non-vulnerable in all conditions, while the small vessels are again found vulnerable. However, a very significant decrease of the probability index (C) is shown.

In all cases, a very high tendency to capsizing could be seen in the small vessels, while larger vessels seem to be safer from the dead-ship condition point of view. Regarding the consistency of the criteria, and considering the large effect of roll damping, the only relevant ship for analysis is that of Trawler 2, as experimental data of roll damping were available. According to it, criteria seem to be consistent. However, further analysis is necessary applying realistic values of damping coefficients.

5. CONCLUSIONS

In this work, the application of the draft second generation intact stability criteria for parametric roll, pure loss of stability and dead-ship condition, as presented in IMO SDC 1/5/3 to a sample of seven vessels representative of the Spanish fishing fleet, has been done. The objective of this study was to analyse their applicability to this fleet, in order to use them as a design tool to reduce the high number of accidents due to dynamic stability issues which usually affect this type of ships.

In order to do this, Level 1 and Level 2 checks were carried out for the three failure modes mentioned above, checking the consistency of the criteria and analysing the results to determine their suitability to a fleet to which, in principle, they were not focused to.

Regarding the pure loss of stability failure, a very good agreement between the results and available experimental data has been found, showing a very good consistence of the criteria.

In the case of parametric roll resonance, some discrepancies, mainly due to the environmental conditions under consideration

in the criteria, have been found, especially for the small ships.

Finally, from the analysis of the dead-ship failure mode, it has been observed that small ships fail Level 2 criteria after passing Level 1, which shows some inconsistency of the criteria; however, and considering the observed large sensibility of the Level 2 check to the roll damping, a more precise estimation of the damping coefficients is needed to make a conclusion on this matter.

In any case, the proposed methodology look like a set of simple and easy to use set of tools that could be straightforwardly applied during the design stage, to analyse the vulnerability of the studied vessels to those failure modes.

6. ACKNOWLEDGEMENTS

The present work was supported by the Spanish Ministry of Economy and Competitiveness A-TEMPO contract with EDF funding.

7. REFERENCES

- BLS, 2013, "National Census of Fatal Occupational Injuries in 2013 (Preliminary Results)", News Release of the Bureau of Labor Statistics, U.S. Dept. of Labor, US.
- Chun, H. H., Chun, S. H., & Kim, S. Y., 2001, "Roll damping characteristics of a small fishing vessel with a central wing", Ocean Engineering, Vol. 28(12), pp. 1601-1619.
- EU Commission, 2014, Facts and figures on the Common Fisheries Policy – Basic statistical data – 2014 Edition, Publications Office of the EU, Luxembourg.
- IMO SDC 1/5/3, 2013, "Development of Second Generation Intact Stability Criteria. Rpt. of the correspondence group on Intact Stability. Submitted by Japan", London.



- IMO SDC 1/Inf.6, 2013, “Vulnerability assessment for dead-ship stability failure mode. Submitted by Italy and Japan”, London.
- IMO SDC 1/Inf.8, 2013, “Information Collected by the Correspondence Group on Intact Stability. Submitted by Japan, Annex 7, Sample calculation results of draft vulnerability criteria for parametric rolling, pure loss of stability and excessive accelerations”, London.
- IMO SLF 55/Inf.15, 2012a, “Information Collected by the Correspondence Group on Intact Stability. Submitted by Japan. Annex 6, Application and comments of vulnerability criteria on a large ship sample”, London.
- IMO SLF 55/Inf.15, 2012b, “Information Collected by the Correspondence Group on Intact Stability. Submitted by Japan, Annex 22, Sample calculations for vulnerability criteria on pure loss of stability, Level 2”, London.
- IMO SLF 55/WP.3, 2013, “Report of the Working Group (Part 1)”, London.
- MAGRAMA, 2013, Estadísticas pesqueras: Flota pesquera de pesca marítima. Número de buques pesqueros y eslora media, por tipo de pesca y caladero, MAGRAMA, Madrid.
- Mata-Álvarez-Santullano, F., Souto-Iglesias, A., 2014, “Stability, safety and operability of small fishing vessels”, Ocean Engineering, vol. 79, 81–91.
- Míguez-González, M., Díaz-Casás, V., Pérez-Rojas, L., Junco, F., Pena, D., 2014, “Application of Second Generation IMO Intact Stability Criteria to Medium–Sized Fishing Vessels”, Proceedings of the 2014 International Ship Stability Workshop, Kuala Lumpur.
- Míguez-González, M., Díaz-Casás, V., Lopez-Peña, F., Pérez-Rojas, L., 2013, “Experimental analysis of roll damping in small fishing vessels for large amplitude roll forecasting”, Proceedings of the 13th Int. Ship Stability Workshop, Brest.
- Míguez-González, M., Caamaño-Sobrino, P., Tedín-Álvarez, R., Díaz-Casás, V., Martínez-López, A., López-Peña, F., 2012a, “Fishing vessel stability assessment system”, Ocean Engineering, vol.41, 67-78.
- Míguez-González, M., Díaz-Casás, V., Lopez-Peña, F., Pérez-Rojas, L., 2012b, “Experimental parametric roll resonance characterization of a stern trawler in head seas”, Proceedings of the 11th International Conference on the Stability of Ships and Ocean Vehicles, Athens.
- MIT, 2014, Estadística de Accidentes de Trabajo, Ministerio de Empleo y Seguridad Social, Madrid.
- Neves, M. A. S., Rodríguez, C. A., 2006, “On unstable ship motions resulting from strong non-linear coupling”, Ocean Engineering, Vol. 33, pp. 1853-1883.
- Paffett, J.A.H., 1976, Experiments with a model of MFV Trident and an alternative round-stern design, National Maritime Institute (NMI), UK.
- Peters, W., Belenky, V. Bassler, C., Spyrou, K., Umeda, N., Bulian, G., Altmayer, B., 2011, “The second generation intact stability criteria: an overview of development”, Transactions of the Society of Naval Architects and Marine Engineers, 119, 225-264.
- Roberts, S. E., 2010, “Britain's most hazardous occupation: Commercial fishing”, Accident Analysis & Prevention, vol. 42(1), p.44-49.

This page is intentionally left blank

Session 7.2 – DAMAGE STABILITY

**A Concept about Strengthening of Ship Side Structures Verified by
Quasi-Static Collision Experiments**

**A Numerical and Experimental Analysis of the Dynamic Water
Propagation in Ship-Like Structures**

**Dynamic Extension of a Numerical Flooding Simulation in the Time-
Domain**

**URANS Simulations for a Flooded Ship in Calm Water and Regular
Beam Waves**

This page is intentionally left blank



A Concept about Strengthening of Ship Side Structures Verified by Quasi-Static Collision Experiments

Schöttelndreyer, Martin, *Institute for Ship Structural Design and Analysis of TUHH,*

martin.schoettelndreyer@tuhh.de

Lehmann, Eike, *Institute for Ship Structural Design and Analysis of TUHH,*

lehmann@tuhh.de

ABSTRACT

The present work is dealing with the question, how to improve local parts of ship constructions to increase the safety of life at sea as well as environmental protection. Local parts which have to be strengthened are on the one hand selected parts of ship side structures and they are on the other hand constructions to protect tanks filled with highly explosive or flammable liquids like LNG. The strengthening is achieved by filling void spaces with granulate material. To investigate their effects on the failure mechanism, several quasi-static and large-scaled experiments were conducted on the test facility of TUHH.

KEYWORDS: *collision-test, side structure, strengthening, granulate material*

1. INTRODUCTION

This paper is based on a research work carried out in a collaborative joint research project. The project ELKOS started in 2009 and was finished in 2013. ELKOS stands for: „Improving collision safety by integrating effects of structural arrangements in damage stability calculations“. The scope of the project was divided in three sub-projects:

- validating collision calculations by large scale experiments using design variants of side structures
- development of a method to predict the damage stability of ship designs on the basis of the collision mechanics close to reality
- development of collision-mechanical analysis method for double-hull alternatives to identify damage calculation parameters

The superior research objective was to develop a method that allows adequate consideration of structural arrangements which significantly increase collision safety in damage stability calculations for new products. TUHH was engaged in this project with its institutes „Ship Structural Design and Analysis“- responsible for the first sub-project and „Ship Design and Ship Safety“- responsible for the second sub-project. The experimental structures were built at the German shipyard Flensburger Schiffbau-Gesellschaft (FSG) which was the industrial partner and also responsible for the third sub-project.

The Institute of Ship Design and Ship Safety determined the statistical distribution of the collision energy with a Monte-Carlo-Simulation. With this method the probability of the double hull failure of specific side structure constructions was predicted. The determined probability of the double hull failure



corresponds well with the regulation of the SOLAS 2009 B1. For side structures which increase the collision resistance significantly the probability of the double hull failure was determined and could have been integrated in the damage calculation in form of a probability distribution. Thus the damage calculation index according to SOLAS 2009 B1 could be calculated. Thereby it was found that a side structure being locally improved to increase the collision resistance has a marginal influence on the leakage safety index. The reason therefore is based on the fact that the improved structures only prevent leakage of compartments for low-energy-collisions. The statistical part for low-energy-collision appears rarely for the examined RoRo-ferry. For that reason an economic benefit according to SOLAS 2009 B1 could not be realized. Finally the results show that it is not advantageous in respect of the leakage safety index to shift the inner hull towards the outer hull by realizing an equivalent absorption of energy regarding the SOLAS 2009 B1. For more details see Krüger et al. (2014).

However, the authors like to mention that in reality a lot of sailors lost their lives due to collisions in coastal areas. In the period of the years 2002-2012 sixty-six ship collisions were registered by the German Federal Bureau of Maritime Casualty Investigation (BSU). Most of them happened in the Kiel-Canal (12 cases), Port of Hamburg (10 cases), river Elbe (6 cases), river Weser (4 cases) and Kiel (3 cases). Thereby three sailors lost their lives in the Kiel-Canal and one sailor on the river Elbe. Furthermore the society's attitude towards environmental protection has changed severely during the last decades. The demand for safer transports of chemicals and fuels especially in coastal areas has become a very important matter with high priority. Thereby it is justified that also low-energy-collisions have to be investigated to prevent human lives and to avoid environmental damage.

In addition to this fact the authors note that the safety level of cars due to crash according

to the European New Car Assessment Programme (EURO NCAP) is done for velocities of 29 km/h for side pole and 50 km/h for side mobile barrier and frontal impacts. Generating a speed range out of the EURO NCAP crash tests with an upper and a lower bound by taking a Cayenne (Porsche) and a Mini (BMW Group) the range of 13-27% can be determined. This range covers 3.2-5.5 kn regarding a large container ship (187 625 tdw, $v_{\max}=24.3$ kn) and the range 2.9-4.9 kn for a smaller container ship (11 500 tdw, $v_{\max}=18.3$ kn). However, structural improvements for higher safety are restricted by physical bound. Up to this bound engineers have the possibility to work preventively and to evaluate this work. Furthermore, the authors present the results of the first sub-project for a reinforced side structure.

After several disasters of tank ships causing enormous environmental pollution due to oil spills, new IMO construction requirements for oil tankers had been established. These requirements are addressed to all tank ships ordered after 6 July 1993 had to be built with a double hull or an alternative design. The possibility of an alternative design poses a new challenge on engineers.

One obvious disadvantage of all presented structures is that they are very expensive in manufacturing and owners have to modify the common and approved structure. This leads to an additional risk in operation for example fatigue.

The idea of filling foamed material or concrete in void spaces of ship side structures is not new. The already realised designs served as additional safety in case of flooding regarding the hydrostatic of ships. At the beginning of the 20th century the double bottoms of lifeboats were filled with cork and in 1994/1995 the void spaces of the ferry SIER were packed with blocks of EPS, see Kulzep (2001). The first design of a 171.8 m long ship for the transport of radioactive waste was published in Hutchison (1987). This design was

provided with blocks of urethane with a density of 101.9 kg/m^3 to increase the safety in case of a collision. Collision experiments with side structures equipped with filling material are not known.

The only known experiment related to collision experiments is published in Nagasawa et al. (1981) who investigated ship structures which struck a bridge pier. The aim was to protect the bridge pier. Therefore a composite-type consisting of outer hull and polyurethane filled inside and a grid-composite type also packed with polyurethane were investigated in collision experiments with a rigid bow model. Next to the already mentioned collision experiments in the Netherlands one grounding experiment was conducted, see Kulzep (2001). A double bottom structure was packed also with blocks of polystyrol with a density of 22 kg/m^3 and driven against a synthetic rock in a real grounding experiment.

Finally, a current draft International Code of Safety for Ships using Gases or other Low flashpoint Fuels (IGF Code) by IMO shows certain parallels to the construction requirements for tank ships in the future. In case of an external damage caused by collision the suggested regulation 5.3.4 demands that the fuel storage tanks shall be placed as close as possible to the centreline. Minimum is the lesser of $B/5$ and 11.5 m from the ship side at right angles to the centreline at the level of summer load line. In the IGF Code an alternative design is also in the discussion and moves a strengthened side structure in the focus of engineering.

Concluding all presented concepts one major disadvantage is that the steel-core or the filling material will make inspections for class renewal in periodical time difficult. For an alternative design to protect e.g. LNG storage tanks a potential filling material must be easy to remove and to refill after inspection.

2. EXPERIMENTAL CONDITIONS

2.1 Test model of the side structure

In two collision tests the protective effects of the investigated granulate material could have been determined. Hence a conventional side structure derived by a RoRo-vessel (designed and built on the German shipyard FSG) was scaled approximately 1:3 except the stiffeners and the frames. The conventional side structure was used for both experiments, except of minor modifications in applying different kinds of collar plates.

The complete test model has a length over all of 5788 mm, a breadth of 3490 mm and a height of 900 mm as presented in Figure 1. The investigated area within the surrounding support-constructions measured a length of 3400 mm and a breadth of 2260 mm. The wall thickness of the four web frames amounts to 5 mm and the two shell plates amount to 4 mm. The frames of the side structure consist of eight bulb profiles HP 140x7.

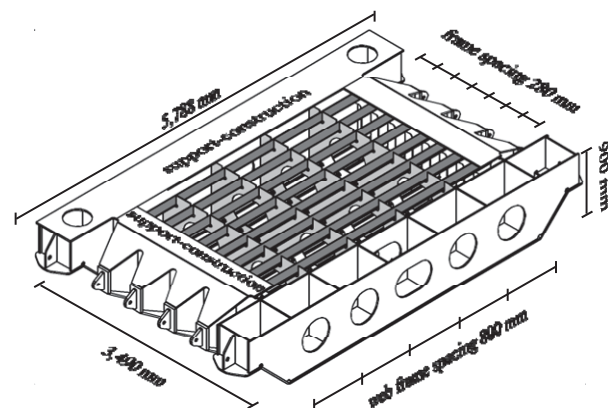


Figure 1 Side structure without shell plate

Both collision tests were enforced with a cylindrical rigid bulbous bow. The construction measured a diameter of 813 mm and a length over all of 1700 mm. The collision angle was 90° . With a collision speed of 0.2 mm/sec the whole test procedure is quasi-static, see Tautz et al. (2010).

2.2 Granulate material

For the determination of the granulate material following aspects were considered: Environmental harmless, hydrolyse and heat resistance as well as less mass density. The choice of an eligible material enables inspections of the structure.

Hence the filled side structure was equipped with multicellular hollow spheres made out of glass which exhibit the specification of Table 1.

Table 1 Specification of glass multicellular hollow spheres

grain size distribution	>2.0 mm
bulk density	190-250 kg/m ³
grain density	380-480 kg/m ³

This mineral material has the following useful characteristics: fire-proof, good thermal insulation, heat resistant up to ca. 900 °, hydrophobic, acoustical absorption, high adhesion, environmental friendly production and 100% recyclable. It is very light for granulate material, has good characteristics under compressive load and is easy to remove/refill with the use of an industrial hover.

2.3 Test plant and configuration

Both collision tests are carried out on the existing test-plant of the Institute of Ship Structural Design and Analysis of TUHH, see Figure 2.

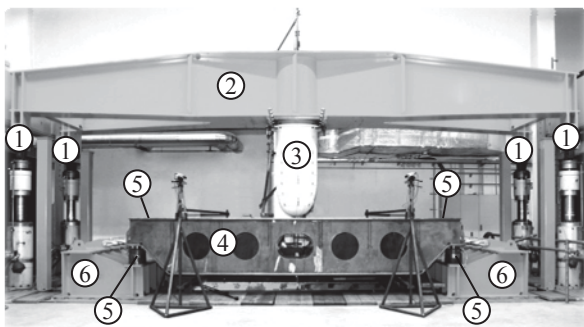


Figure 2 Test plant and configuration

Collision forces are applied by four hydraulic cylinders (1) which are connected with a cross-beam (2). The test model of the bulbous bow (3) is located underneath the middle of the cross-beam and is driven against the side structure (4).

Collision forces are measured at the hydraulic cylinders as well as at the pressure load cells (5) between side structure and support (6). The hydraulic cylinders are limited to 400 mm regarding the maximum range of displacement. Thus larger displacements are implemented by using appropriate interim pieces between the bulbous bow and the cross-beam.

2.4 Experimental results

In Figure 3 the measured results of both experiments are compared with each other. The measured results of the collision test with the conventional side structure are represented by the grey curve and the results of the collision test with the filled side structure by the black graph.

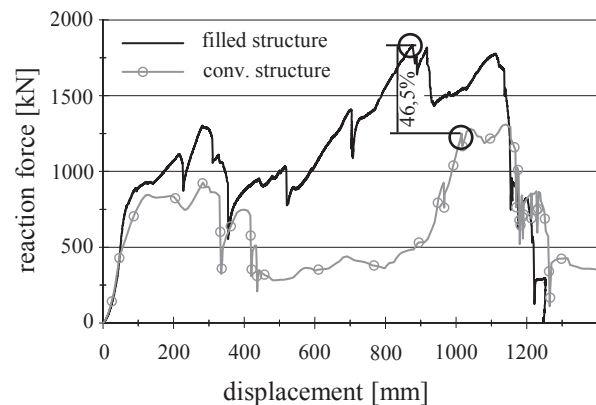


Figure 3 Measured reaction forces

The meaningful characteristics of the reaction forces are described in Schöttelndreyer et al. (2013). The cracks in the inner shell occur at the two marked points in Figure 3 and are chosen for comparison of the absorbed energy plotted in Figure 4. In total a significant increase of the reaction force of 46.5 % was achieved by the side structure filled with multicellular glass hollow spheres.

The integration of the reaction forces in Figure 3 leads to the absorbed energies of the side structures. The filled side structure has got the ability to absorb 70.5% more energy than the conventional side structure at the time of the inner hull failure.

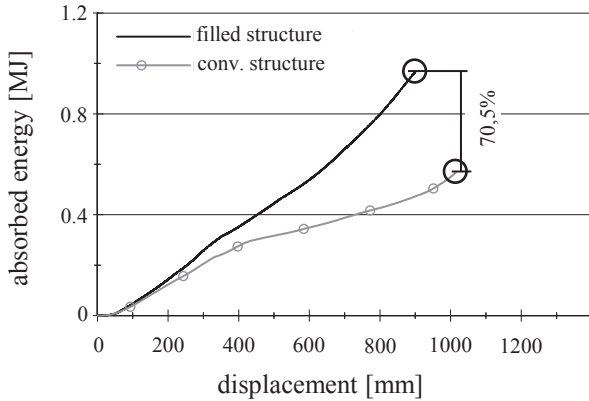


Figure 4 Absorbed energies of conventional and filled side structure

This significant enhancement of absorbed energy is generated by two effects. The primary effect is the compression and the collapse of the multicellular glass hollow spheres. At the beginning the material exhibits a crushable behaviour. Under high compression the material changes its constitutional characteristics and becomes a hard mass with a nearly incompressible behaviour. The secondary effect is the transfer of the reaction force to the inner hull construction which arises from the constitutional change of the multicellular glass hollow spheres of the primary effect.

3. VERIFICATION OF SIMULATION

The properties of the steel structure were determined by numerous specimen in the form of tensile tests in accordance to the Norm DIN EN ISO 6892-1 (2009) and the choice of one numerical optimization tool as well as one validated power law hardening approach, see Schöttelndreyer (2015). For highly non-linear simulations a failure criteria must be determined which deletes finite elements by reaching e.g. a critical rupture strain. The criteria developed by Scharrer et al. (2002) in

charge for the German classification society Germanischer Lloyd (since 2013: DNV GL) is quite simple in appliance and generates good results in simulations for ship collisions which was confirmed within the project ELKOS. The critical rupture strain ε_c represents the first principal strain and can be calculated for the uniaxial stress state by equation (1)

$$\varepsilon_c = 0.079 + 0.76 \frac{t}{l_e} \quad (1)$$

and for the biaxial stress state by equation (2).

$$\varepsilon_c = 0.056 + 0.54 \frac{t}{l_e} \quad (2)$$

The parameters t and l_e describe the shell thickness and the element length. To determine the properties of the multicellular glass hollow spheres several different tests had to be accomplished. The deviatoric perfect plastic yield function for the chosen material “Soil and Foam” developed by Krieg (1972) is given in equation (3):

$$\Phi = J_2 - \left(a_0 + a_1 \cdot p + a_2 \cdot p^2 \right) \quad (3)$$

The parameter J_2 is the second invariant of the stress deviator and the constants a_0 , a_1 , a_2 characterise the deviatoric plane and must be calculated. The hydrostatic pressure p can be evaluated with the principal stresses measured in triaxial compression tests in accordance to the Norm DIN 18137 – 2 (2011) known in the geotechnical engineering to predict the behaviour of soils. The volumetric part of the yield function as well as the plastical deformability was achieved by using uniaxial compression tests. Further details are published in Schöttelndreyer et al. (2013).

3.1 Comparison between Experiment and Simulation

For all collision simulations the programme LS-DYNA version 971/ R6.1.0 is used. Therefore the geometry of the side structure was simplified. The stiffeners of the outer and inner hull are modelled with beam elements in order to avoid geometric disturbances for solid elements. They only have a different breadth but the same height and cross section like the bulb profiles. With this modification the granulate material could be modelled with five blocks of solid elements using a mapped mesh.

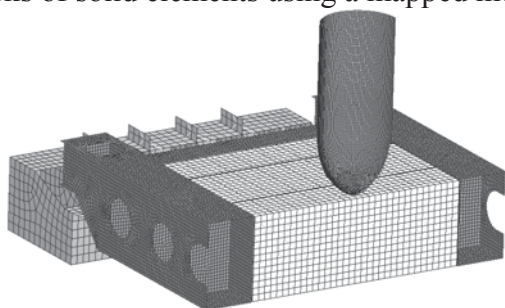


Figure 5 Half of the FE-model without outer shell

The outer and inner shell are modelled with four-noded quadrilateral shell elements using five integration points through their thickness and their critical rupture strain which is calculated by equation (2). Caused by the different scale rates for the stiffeners (more than 1:2), the equation (1) cannot be used for the test model of the side structure. In Schöttelndreyer et al. (2013) a critical rupture strain was determined by simulations. In Figure 6 the reaction forces of the experiment and the appendant simulation are presented.

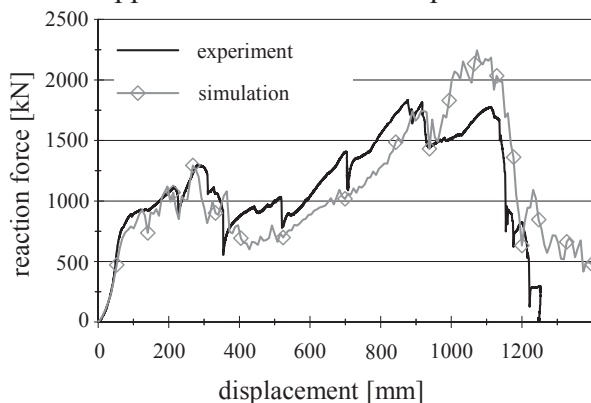


Figure 6 Comparison of the reaction forces

The simulation underestimates the reaction force with 5%. The displacement is 1% deeper as measured in the experiment when the first crack in the inner shell occurs. Only the failure of the frames is overestimated at a displacement between 1000 mm and 1200 mm.

Thus a transfer to real structures is justified and delivers furthermore conservative results.

4. NUMERICAL EXAMPLE OF USE

On 3rd of Mai 2013 a collision occurred between the ferries NILS HOLGERSSON and URD in the port of Lübeck-Travemünde. During a turning-manoeuve the NILS HOLGERSSON struck the parallel middle body of the URD which was fastened to the pier. This collision leads to the structural damage of the URD above and underwater and to a minor damage of the bow structure. The damage of both vessels is shown in Figure 7.



Figure 7 Collision between the ferries NILS HOLGERSSON and URD in the port of Travemünde

Using the experience of this accident, the benefit of the granulate material in a real ship structure is quite simple to investigate. The dissipated energies as well as the ship motions are not difficult to calculate. Almost the whole kinetic energy of the NILS HOLGERSSON is dissipated by the structure of the URD. The kinetic energy can be determined with the known equation (4).

$$E_{kin} = \frac{1}{2} \Delta v^2 \quad (4)$$

The required data like displacement Δ , draft, trim of the NILS HOLGERSSON are published in the report of the Bundesstelle für Seeunfalluntersuchung (2013). All the other values like AIS-data, geometry of the NILS HOLGERSSON, main frame as well as several photos of the damage of the URD were given by diverse institutions.

The struck ferry URD was built in 1981 on the Italian shipyard Nuovi Cantieri Apuania. In 2001 the ship was extended with a 20.25 m long mid-part-section which was struck. She has got a length and a breadth over all of 171.05 m and 20.82 m and a maximal depth of 5.43 m. The design of the main frame with all characteristic dimensions is presented in Figure 8.

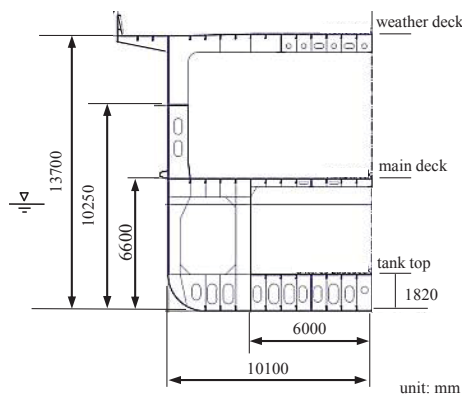


Figure 8 Main frame of the URD

The frame spacing and the arrangement of web plates are plotted in Figure 9 and amounts 750 mm and 1500/2250 mm.

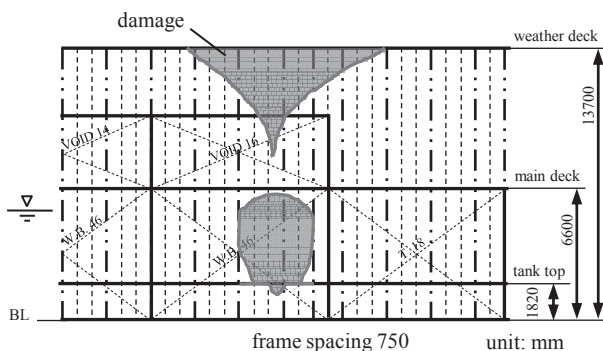


Figure 9 Side view (10100 mm) of the modelled section with the projected damage of the URD

The striking ferry NILS HOLGERSSON was built in 2001 on the German shipyard SSW Fähr-und Spezialschiffbau GmbH. She has got a length and a breadth over all of 190.77 m and 35.87 m and a maximal depth of 6.20 m. She struck the URD with a displacement of 20500 t in a collision angle of 82° with a speed of 6.52 kn. Caused by the minor damage her bow structure is discretised as a rigid part.

To confirm the benefit of the multicellular glass hollow spheres in the structure of the URD a FE-model validated by Martens (2014) is taken and modified analogical to the filled side structure model of the experiment. The size of the four-noded quadrilateral shell elements of the outer and inner shells amounts to 100 mm. In the model of Martens (2014) the stiffeners of the conventional structure are modelled as L- profiles with nearly the same section modulus like the original bulb profiles. Therefore the rupture strain is calculated by equation (2). Comparative simulations of the conventional structure with shell elements and beam elements for the stiffeners deliver comparable results. The rupture strain for the beam elements is determined by equation (1). The blocks of solid elements to describe the behaviour of the multicellular glass hollow spheres range from baseline to main deck and from inner hull (6000 mm) to outer hull (10100 mm), see Figure 8. The movement of the model is prohibited in all translational directions at mid ship and only in longitudinal direction of the ship at the two ends of the section. The rigid bow structure of the NILS HOLGERSSON is driven against the structure of the URD with the above mentioned velocity of 6.52 nm at the beginning of the simulation.

4.1 Benefit of the multicellular glass hollow spheres

For the evaluation of this analysis the calculated energies are separated in one part which is absorbed by the steel structure above the water surface and one part which is absorbed by the steel structure beneath the

water surface. In order to realise further analysis of the filled structure, the granulate material is separated in addition. In Figure 10 the black curves represent the energies of the conventional structure and the grey curves of the filled structure.

Before the outer shell fails there is no benefit to observe in Figure 10. The outer shell

primary effect. In addition 28 MJ are dissipated of the steel structure beneath the water surface. The steel structure beneath the water surface of the conventional side structure exhibits the absorption of 17 MJ at a penetration of 6.5 m. That demonstrates 11 MJ less than the structure of the filled model. This 11 MJ are dissipated because the collapsed multicellular glass hollow spheres also change their constitutional

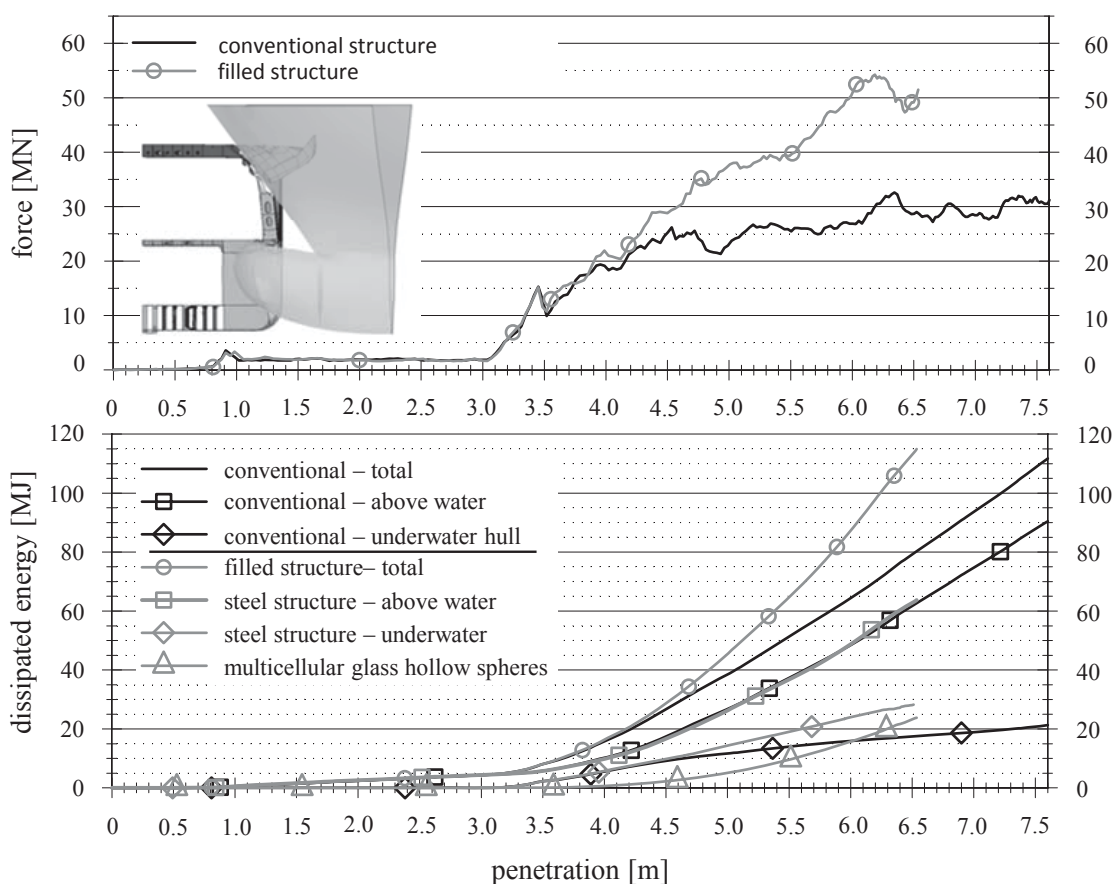


Figure 10 Results of simulation of the conventional and the filled side structure

fails in both simulations at a penetration of 3.5 m with almost the same energy level. At a penetration of 4.0 m the multicellular glass hollow spheres start to act.

The energy absorption of the underwater hull increases significant at a penetration of 4.5 m. Also in these simulations the two mentioned effects of the multicellular glass hollow spheres are confirmed. At the maximal penetration of 6.5 m in the simulation of the filled side structure the multicellular glass hollow spheres absorbed 24 MJ which is the

characteristics and become incompressible in a real ship structure. This behaviour enables the transfer of the collision force to a large area of the inner hull construction with its stiffeners and web frames. The stiffeners and web frames deflect the collision force to the main deck and tank top as well as to the bulkheads.

Using multicellular glass hollow spheres in the structure of the URD shows that the rupture of the inner hull could have been avoided and therefore the flooding of the investigated compartment would have been prevented.

4.2 Additional benefit of the multicellular glass hollow spheres

The determined benefit leads to the following question: What is the advantage for owners?

First at all they can protect their sailors/goods with a strengthened ship structure and prevent environmental damage for low-energy-collision. In reality owners are still in a hard competition. Therefore they normally tend to comply with the existing regulations. If the regulations give benefits for safer and strengthened ships in future, owners will modify the structure of their existing ships or order new ships which will increase safety at sea.

Regarding the already introduced draft IGF Code with an estimated allowance of alternative designs, owners will have a justification for reducing the distance (less than B/5) between storage tanks and ship side which might increase the loading capacity of their cargo holds.

This advantage can be illustrated with a simulation where the inner hull of the ferry URD is shifted, see Figure 11.

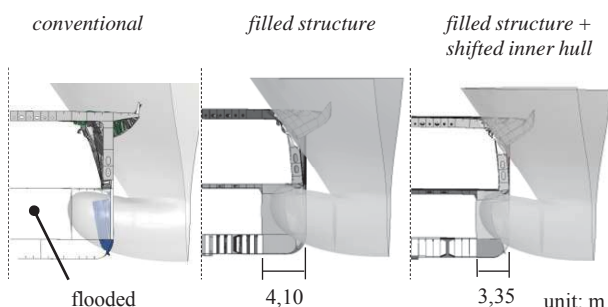


Figure 11 Failure mode of the conventional, filled and filled structure with shifted inner hull

Her double bottom construction is designed with longitudinal stiffeners with a spacing of 750 mm. In this simulation the inner hull of the URD is shifted one stiffener towards the outer shell and the void is filled with multicellular glass hollow spheres. Also with

this arrangement the flooding of the compartment could have been avoided.

5. CONCLUSIONS

This paper presents a simple but extremely effective concept to strengthen ship side structure. The concept with a granulate material inside of void spaces enables inspections without complications in a periodical time. Therefore a conventional side structure and a side structure equipped with multicellular glass hollow spheres enhanced with a rigid bulbous bow were conducted. The results showed that the filled side structure absorbed 70.5% more energy than the conventional one. With the knowledge of the experiments and the appendant and validated simulations the protecting effects of the granulate materials can be transferred to real ship structures.

Therefore one collision scenario is chosen which happened on the German maritime waterways in Lübeck-Travemünde. Without regarding the SOLAS 2009 B1 the concept enables the possibility to strengthen the side structure according to the conventional design on the one hand and on the other hand to reduce the distance of inner hull and outer shell to get larger cargo holds which generates an economic benefit for the owners.

This gives designers more possibilities for modification of existing ships e.g. to protect a LNG power unit as well as for the general structure arrangement of new ships. This concept does not touch the conventional and approved construction and owners do not take an additional risk by using a new strengthened ship construction.

6. ACKNOWLEDGMENTS

The work was performed within the research Project ELKOS, funded by German Federal Ministry of Economics and Technology (BMWi) carrying the project no. 03SX284B.



The authors are responsible for the content of this paper and wish to thank those who supported this project. The authors' gratitude is particularly addressed to the German shipyard Flensburger Schiffbau-Gesellschaft which delivered the cross-beam, the two supports for the test-plant and the test models.

7. REFERENCES

- Bundesstelle für Seeunfalluntersuchung, 2013, "Kollision der Ro/Pax-Fähre NILS HOLGERSSON mit der Ro/Pax-Fähre URD im Hafen von Lübeck-Travemünde am 3. Mai 2012", (Untersuchungsbericht 154/12)
- DIN 18137-2, 2011, "Soil, investigation and testing – Determination of shear strength – Part 2: Triaxial test", Berlin, Beuth Verlag GmbH.
- DIN EN ISO 6892-1, 2009, "Metallic materials - Tensile testing – Part 1: Method of test at room temperature", Berlin, Beuth Verlag GmbH
- Hutchison, B.L., Laible, D.H., Kristensen, D.H. and Jagannathan, S., 1987, "Conceptual design and probabilistic safety assessment for a nuclear waste transport and emplacement ship". SNAME Transactions, Vol. 95, pp.283-317
- Kulzep, A., 2001, "Verhalten von ausgeschäumten Schiffsstrukturen bei Kollisionen und Grundberührungen", Diss., Hamburg University of Technology TUHH, Hamburg
- Krieg, R.D., 1972, "A simple constitutive description for cellular concrete", (Report - SC-DR-72-0883)
- Krüger, S., Dankowski, H., 2014, "Integration von strukturellen Maßnahmen zur Verbesserung der Kollisionssicherheit von RoRo-Fahrgastschiffen in die Leckstabilitätsberechnung", (Report – BMWI -03SX284A)
- Nagasawa, H.; Masaaki, T., 1981; "A study on the Collapse of Ship Structure in Collision with Bridge Piers". In: Naval Architecture and Ocean Engineering, VOL. 19, p. 102-116
- Scharrer, M. ; Zhang, L. ; Egge, E. D. ; Jamarillo, D., 2002, "Wettbewerbsvorteile durch informationstechnisch unterstützte Produktsimulation im Schiffbau- WIPS" Technical Report MTK0614 Kollisionsberechnungen in schiffbaulichen Entwurfssystemen, Germanischer Lloyd, Hamburg
- Schöttelndreyer, M. ; Tautz, I. ; Fricke, W. ; Lehmann, E., 2013, "Side structure filled with multicellular glass hollow spheres in a quasi-static collision test". In: Collision and Grounding of Ships and Offshore Structures - Proc. of the 6th International Conference on Collision and Grounding of Ships and Offshore Structures (ICCGS), pp. 101-108
- Schöttelndreyer, M., 2015, „Füllstoffe in der Konstruktion: Ein Konzept zur Verstärkung von Schiffsseitenhüllen“, Diss., Hamburg University of Technology TUHH , published prospectively in 2015, Hamburg
- Tautz, I., Schöttelndreyer, M., Fricke, W., Lehmann, E., 2010, „Experimental investigations on collision behaviour of bow structures“, In: Proc. of 5th International Conference on Collision and Grounding of Ships, Espoo, pp. 179-183
- Martens, I., 2014, „Konstruktive Aspekte beim Entwurf von Bugwülsten zur Verbesserung des Energieaufnahmevermögens bei Schiffskollisionen“, Diss., Hamburg University of Technology TUHH , Hamburg



A Numerical and Experimental Analysis of the Dynamic Water Propagation in Ship-Like Structures

Oliver Lorkowski, *Flensburger Schiffbau-Gesellschaft mbH & Co. KG*, lorkowski@fsg-ship.de

Florian Kluwe, *Flensburger Schiffbau-Gesellschaft mbH & Co. KG*, kluwe@fsg-ship.de

Hendrik Dankowski, *Hamburg University of Technology*, dankowski@tu-harburg.de

ABSTRACT

Current damage stability rules for ships are based on the evaluation of a ship's residual stability in the final flooding stage. Up to the stage of this report, the dynamic water propagation within the inner subdivision as well as intermediate flooding stages and their influence on the resulting stability are considered on a very basic level in the damage stability regulations and may thus lead to an inappropriate evaluation of the safety level in damaged condition.

The investigation of accidents like the one of the Estonia or the European Gateway reveals that intermediate stages of flooding and the dynamic flooding sequence result in significant fluid shifting moments which have a major influence on the dependent stability of damaged ships. Consequently, the critical intermediate stages should be considered when evaluating designs with large cargo decks like RoRo vessels, RoPax vessels and car carriers.

Within this report, an enhanced numerical flooding calculation method is validated by a series of model tests with the aim to investigate its capabilities and limitations and to improve the understanding of a ship's time dependent damage stability. The model tests haven been carried out with a ship-like test body which comprises a typical subdivision. In this respect, emphasis has been given on the evaluation of critical intermediate stages of flooding which are characterised by large roll angles and roll velocities.

By the end of this report, the results of the model test campaign and the calculation method are compared and discussed in the context of the observed influencing factors on the flooding process to evaluate its' prediction accuracy for intermediate stages of flooding.

Keywords: *intermediate stages of flooding, ship design, damage stability*

1. INTRODUCTION

The recent introduction of the harmonized, probabilistic damage stability regulations in 2009 [SOLAS II-I, Part B-1] let to a new assessment of the damage stability of RoPax and Pax vessels where the time dependent evaluation of the ships damage stability has

become more important. This damage stability regulation requires for passenger ships the evaluation of intermediate stages of flooding with respect to the maximum righting lever, its range, cross flooding time and the equilibrium heel angle. The damage stability assessment of contemporary RoPax and Pax vessels may comprise several hundred leak cases, so that



the evaluation of these intermediate stages of flooding can be very time consuming if carried out by use of the available methods.

Furthermore, the results of the first study of the European Maritime Safety Agency (EMSA) has indicated, that the attained safety level of RoPax vessels can be significantly lower according to the harmonized damage stability regulations (SOLAS 2009) in comparison to the old deterministic damage stability regulations (SOLAS 90) in combination with the Stockholm agreement (EC-Directive 2003/25/EC).

This is due to the fact that the SOLAS 2009 regulations do not require considering accumulated water on vehicle decks for the stability assessment (compare Valanto, 2009).

For this reason, a research project called LESSEO had been introduced in 2011 with the aim to develop new calculation methods for the evaluation of a ship's time dependent damage stability and to propose a new approach for assessment large free surfaces on vehicle decks within the current regulation frame work.

This report focuses on the validation of a quasi-static calculation method which has been developed by Dankowski 2013 to evaluate a ship's time dependent damage stability. This calculation method has already applied for accident investigations (e.g. in Krueger et al. 2012, Dankowski 2013) and its' basic functionality has been tested with the model test results of (Ruponen 2007). In the investigations of this report, emphasis has been given on the validation by damage scenarios with initial flooding prevention. These damage scenarios are of particular interest with respect to their intermediate stages of flooding and are derived from a model test campaign with a test body, which has been conducted within the LESSEO research project. The comparison between measured and calculated results illustrates the potential and limitations of the calculation method and enhances the

understanding of such complex flooding scenarios.

The following sections give a brief overview about the theoretical background of the calculation method and the conducted the model test campaign. Within the validation section, the model test results are described and compared to results from the calculation method.

At the end of this report, a summary of results of the validation is given and put into the context of further research and possible areas of improvement.

2. NUMERICAL METHOD

This section comprises a brief overview about the theoretical background of the quasi-static calculation method. For further reading please refer to Krüger et al. 2012, Dankowski 2013, Dankowski 2012, Dankowski & Krüger 2012, Dankowski et al. 2014.

Within the quasi-static approach, the sinking sequence is estimated by a finite number of consecutive quasi-static changes of the floating position. The floating position in the respective time step is determined under equilibrium condition of the hydrostatic and gravity forces. These forces change within the flooding process due to the propagation of water volumes through internal and external openings. The water volume within a compartment is determined via the integral of the inflow and outflow fluxes (mass balance). The governing equation for the determination of the fluxes is the Bernoulli equation, formulated for a streamline between the points a and b:

$$dz = \frac{p_a - p_b}{\rho g} + \frac{u_a^2 - u_b^2}{2g} + z_a - z_b - \varphi_{ab} \quad (1)$$

The term φ_{ab} accounts for energy dissipation along the stream line which is



mainly caused by the jet expansion behind the opening (Dankowski 2013). This energy loss is assumed to be proportional to a semi-empirical discharge coefficient C_d , which reduces the flux velocity u :

$$u = C_d \cdot \sqrt{2g \cdot dz} \quad (2)$$

The discharge coefficient has been determined from outflow experiments for the applied opening types in the model test campaign (compare Dankowski et al. 2014) and depends on the shape and size of the discharge opening. The applicability of such determined model scale discharge coefficients to full-scale ships has been investigated e.g. in (Stening 2010), (Ruponen, 2010) and (Ikeda et al. 2004). The results of the FLOODSTAND research project in (Stening 2010) indicate that full-scale openings show larger discharge coefficients than corresponding model-scale openings. Anyhow, full-scale measurements in (Ruponen 2010) have revealed that the general course of the flooding sequence can be predicted with satisfactory accuracy even if a rough estimation for the discharge coefficient is used in the calculation method.

From the given brief overview about the theoretical background, the following assumptions can be summarized for the quasi-static calculation method:

- The flooding process is assumed to be sufficiently slow e.g. as a consequence of small
- leaks and large compartments so that the change in the ship's floating position can be regarded as quasi-static
- Water propagation is exclusively driven by the static pressure differences at the openings.

- Besides the energy loss at the openings, no further energy loss is accounted for. Thus, frictional losses e.g. due to wall friction, flow separation, circulation or wave breaking are assumed to play a minor role in the flooding process.
- The free surface of the water is assumed to be flat so that no waves or sloshing forces are accounted for.

3. MODEL TEST CAMPAIGN

The model test campaign of the LESSEO research project comprises roll damping experiments for the determination of the effective roll damping coefficients, inclining experiments for the determination of the vertical centre of gravity, outflow experiments for the determination of the empirical discharge coefficients and sinking experiments with symmetrical and asymmetrical subdivision. While a brief overview about the model test campaign has already been given in Dankowski et al. 2014 this section summarises the main particulars of the developed test body. The main dimensions of the test body are given in Table 1:

Length over all	2.02	m
Breadth	0.42	m
Depth	0.42	m
Draft	0.20	m
Displacement	159	k g
Vertical Centre of Gravity	0.178	m

Table 1: Main dimensions of the test body

The test body is depicted in Figure 1.

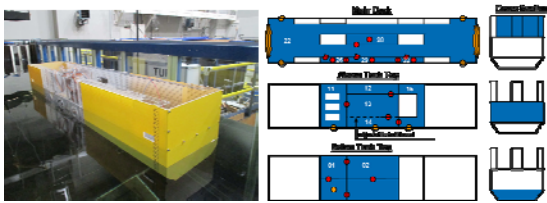


Figure 1: Test body 1

The test body consists of three parts: A yellow coloured aft body, a transparent mid ship section and a yellow coloured fore body (compare left hand side of Figure 1). The floodable compartments are located in the mid ship section. The internal subdivision is shown on the left hand side of Figure 1 and has been derived from contemporary RoRo and RoPax ships. The main deck (compartment 22) e.g. represents a typical vehicle deck with centre and side casing, compartment 11 represents an engine room compartment and compartment 15 has been derived from a void space around a bunker tank compartment. Compartment 14 comprises an adjustable bulkhead which can be located at the position B/5, 2B/5 or B/2. The test body can be flooded through 10 external openings: One at the bottom of compartment 1, three at the side of the compartments 11, 14, 15, four freeing ports and a stern and bow door in compartment 22 (compare left hand side of Figure 1). The external openings are either closed or dynamically opened by pulling a plug. Furthermore, the test body is equipped with 18 internal openings which are either open or statically closed by a tape to generate the respective leak case.

4. MEASUREMENT DEVICES

Within the test campaign, the following quantities have been measured:

- Angular velocities and longitudinal accelerations in 3D (ship fixed coordinates),
- Translation and rotation on of the test body in 3D (earth fixed coordinates),

- Filling level in the flooded compartments (ship fixed coordinates)
- Pressure in the double bottom compartment.

The measurement devices are located in the fore and aftbody and are powered by three Lithium-Polymer rechargeable battery packs. The accumulated, measured data are transferred via a local WiFi connection the data processor, which is located next to the test facility. Through the chosen measurement device set-up it is ensured that the test body's motion is not influenced by any cable connections. Anyhow, some uncertainty considerations with respect to applied measurement devices have to be taken into account when evaluating the measured signal. The uncertainty of the measured signal depends on the measurement device and is given in this case for the 95% confidence interval.

The angular velocities and longitudinal accelerations are measured by an inertial measurement unit (IMU), which is placed in the forward compartment of the test body. The uncertainty of the measured values is $\pm 1E-3$ rad/s for the angular velocities and $\pm 1E-2$ m/s² for the accelerations. The angles and translations are measured by a stereo camera system. These magnitudes are measured with an uncertainty of $1E-3$ deg and $1E-4$ m respectively. The filling levels are measured via resistive wave probes. The uncertainty of the filling level has been determined to ± 1 mm. In this respect it is worth to mention that these sensors are sensible to the environmental conditions such as tank water quality, gas content of the water, ambient temperature and manufacturing imperfections on the wire distance of surface quality. Thus, these factors have to be taken into account within the calibration of these sensors to obtain a sufficient accuracy of the measure signal. The pressure of the double bottom compartments is measured by two piezo resistive pressure transducers. The uncertainty of the measured signal is ± 0.2 mbar.



More details about the measurement devices are given in (Dankowski et al. 2014) and (Pick 2009).

5. VALIDATION

For the validation of the quasi-static calculation method, test cases with initial flooding obstruction e.g. through longitudinal bulkheads, engine casings and girders have been selected to quantify their influence on the course of flooding. Within the following evaluation, emphasis has been given on the evaluation of the roll angle, since this quantity is also of interest of the evaluation of the intermediate flood stages within the current damage stability regulation framework. At the following leak cases, the test body has been tested at its' design condition (compare Table 1).

5.1 Leak Case 1

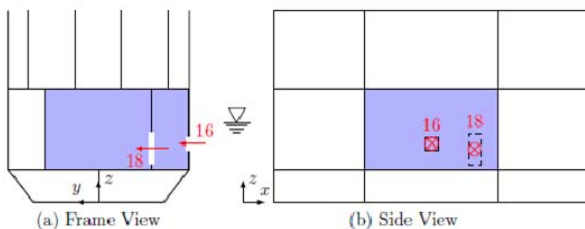


Figure 2: Side damage and long. bulkhead at B/5 with door opening

The first leak case presented here is a damage scenario with initial flooding prevention through a longitudinal bulkhead. The leak case is shown in Figure 2. The model is flooded through a side damage opening (16) and a door opening (18) in the longitudinal bulkhead at B/5. The initial flooding prevention is caused by the longitudinal offset of these two openings.

The measured roll motion and filling level is shown in Figure 3. The filling level sensor 27 is located in compartment 14 close to the shell, sensor 28 is located in compartment 13 at mid ships. The plug has been pulled at time

instant 0s. After opening the leak, the test body starts rolling to starboard after 1s at a nearly constant roll velocity of 9 deg/s. The water propagation in the compartment is characterized by an inhomogeneous water distribution, caused by the jet and spray in compartment 14.

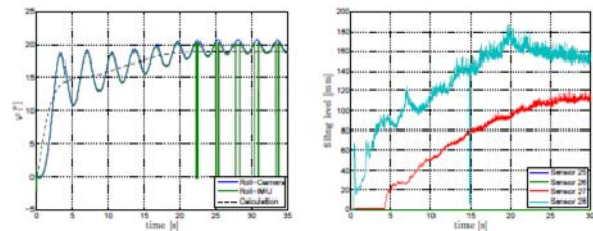


Figure 3: Roll motion (left) and filling level (right) of leak case 1.



Figure 4: Video sequence at time steps 3s, 6s and 20s for leak case 1.

This fact is also visible in the difference of the filling level signals for sensor 28 and 27 in Figure 3. After about 3s, the inner side of the leak opening becomes submerged so that the incoming water flux starts to decrease continuously as a consequence of the rising hydrostatic pressure in the compartment (compare Figure 4 at 3s).

The change in the water flux causes a lower roll velocity so that the test body starts to decelerate. Due to the inertia of the test body, an overshoot angle of 18 deg is reached after 3.5s. From the comparison with the static righting lever curves including fluid shifting moments shown in Figure 5 follows, that the dynamic roll angle is about twice as high as it would be in the ideal static case with an equal filling level distribution (compare curve for 20% average filling level).

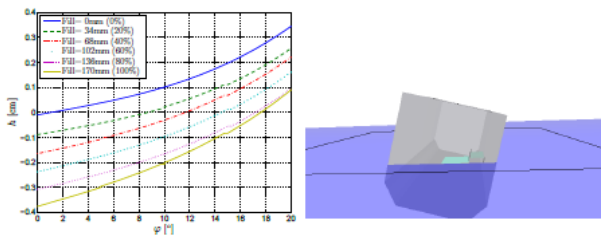


Figure 5: Static righting lever curve (left) and level difference in the compartments 13&14 at 3s (right)

Since the restoring and inclining moments are at this angle not in equilibrium, the vessel starts to roll back to port side. This dynamic process induces a natural roll motion to the test body of about 4 deg amplitude. After about 6s, the inner opening (18) becomes completely immersed and the water level raises quasi-static within the two compartments (see Figure 4 at 6s). At the time instant of 20s, the test body reaches its final floating condition at an average roll angle of 19 deg. The two compartments are almost completely flooded (compare time instant 20s in Figure 4).

From Figure 3 follows, that the basic effect of the initial flooding prevention is the increased roll velocity and large overshoot angle at the beginning of the flooding process. The increased roll velocity is in general well represented by the quasi-static method, as the comparison in Figure 3 illustrates. The quasi-static method shows also a change in the roll velocity where the inner side of leak opening becomes immersed, but the induced roll motion including its overshoot angle cannot be resolved. The magnitude of the roll velocity has been slightly underestimated by the calculation method which is assumed to be caused by the more inhomogeneous water distribution at the model test and the inertia of the model. Furthermore, the course of the measured and calculated roll motion reveals that the immersion of the leak opening results also in a balancing process of the water levels at the longitudinal bulkhead. At the previous time steps, the water level had been significant higher in the wink tank compartment due to the larger pressure difference at the leak opening

(compare Figure 5 (right) and Figure 4 at 3s). As the mass flux through the leak opening decreases, the pressure difference at the longitudinal bulkhead is sufficient to raise the water level up to the values of the wink tank compartment. This balancing of the water levels equalizes the whole flooding process so that roll velocity decreases further between the time instants 5-8s. Finally, both the numerical model and test body reach their final floating position after about 20s. The comparison of the final calculated and measured roll angle indicates that calculated value is slightly lower. This fact is assumed to be related to the accuracy of the determined vertical centre of gravity. The vertical centre of gravity had been determined from an inclining experiment and turns out to be slightly underestimated for the considered leak case.

5.2 Leak Case 2

This leak case has been selected according to the findings from the European Gateway accident in 1974 (compare Dankowski 2013). A principal sketch of the involved compartments is shown in Figure 6.

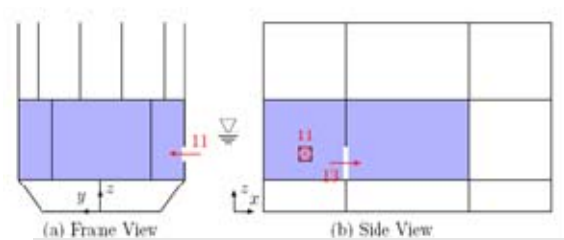


Figure 6: Side damage in the auxiliary engine room compartment and open bulkhead door

The test body is flooded through a small side damage in the auxiliary engine room compartment (11) and progressive flooding is taking place through the door openings in the transversal and longitudinal bulkheads. The measured roll angle and filling level are shown in Figure 7. Level sensor 25 had not been connected during this leak case. Level sensor 26 is located in the auxiliary engine room compartment at starboard, near the leak, sensor 27 is located in the forward compartment close



to the bulkhead door and sensor 28 is located in the starboard wing compartment. The plug has been again pulled at time instant 0s. The test body comprises a slight initial heel to portside.

After the leak had been opened, the water starts to flow to portside as a consequence of the initial heel angle. This process induces a corresponding roll motion to the test body. After about 2s, the water level in front of the engine box has increased significantly so that a roll motion is initiated towards the opposite direction, which is characterized by a sudden shift of the water volume to starboard (compare time instant 2s in Figure 7 and Figure 8) and results in a roll velocity of 3 deg/s. After about 5s, the test body reaches an intermediated flood stage at a roll angle of 10 deg.

At this time instant, the inner side of the

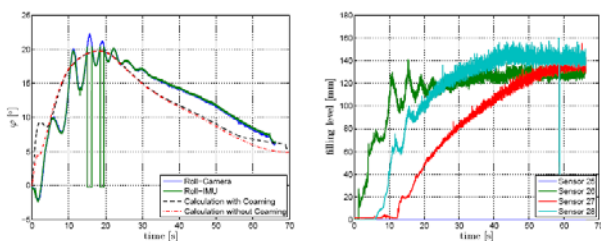


Figure 7: Roll motion (left) and filling level (right) of leak case 2.



Figure 8: Video screen shots of compartment 11 at 1s, 2s und 17s.

leak opening becomes fully immersed so that the mass flux, driven by the pressure head difference in and outside the compartment, is reduced. While the inclining moment through the free water surface remains nearly constant at this time step, the additional water volume causes a reduction of the test body's vertical centre of gravity, similar to the effect of a ballast water tank, which gives in turn a reduction of the roll motion at time instant 5-7s.

After 7s flooding time, the opening in the transverse bulkhead becomes immersed and progressive flooding is taking place in the forward compartments (compare time step 7s in Figure 9 and filling level sensor 27 in Figure 7).



Figure 9: Video screen shots of compartment 12,13 and 14 at 6s, 15s and 30s.

This flooding process yields to a more asymmetric water distribution within the test body and increases the roll angle up 20 deg after 15s. The test body's motion at the time instants up to 20s is characterized by an oscillatory roll motion which is assumed to be caused by the sudden immersion and emergence of the door opening in the transverse bulkhead and the inertia of the model. At time instant 20s, the door opening in the longitudinal bulkhead at portside becomes immersed so that the portside wing compartment is flooded correspondingly. This flooding process reduces the roll moment and induces consequently a slow up righting movement of the test body. The up righting process takes about 40s and is assumed to be influenced by the fluid damping within the compartments. This thesis is also supported by the fact that induced roll motion declines rapidly after time step 20s. After about 65s, the test body reaches its' final equilibrium position at a roll angle of 7 deg.

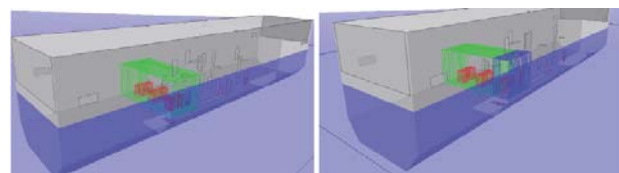


Figure 10: Numerical model without coaming (left) and with coaming (right).

The numerical model has been tested with two configurations, shown in Figure 10. The first configuration considers the compartmentation according to the general



arrangement of the test body. The engine casings are modelled as void spaces to cover their displacement effect.

In the second configuration, additional openings with coamings have been added at the starboard engine box to account for the corresponding water accumulation within the first time instants. A similar modelling strategy had been applied at the accident investigation of the European Gateway (compare Dankowski 2013). The comparison of the measured and calculated roll motion in Figure 7 indicates that the course of flooding has been predicted by both numerical models with a satisfactory accuracy since the up righting and rolling characteristic is very similar. However, the intermediate roll angle at time instant 15s is slightly underestimated which is assumed to be also related to the a difference the vertical centre of gravity (compare also roll angle differences at the final floating condition). In terms of the initial heel angle, it had been observed that an initial heel to portside cannot be correctly covered by the quasi-static method, since this heel angle would also result in a final heel angle to portside (at 65s).

The effect of the coaming and thus initial flooding prevention of the engine box can be identified from the comparison of the two calculated roll motion curves: The initial flooding prevention increase the intermediate roll angle but does not affect the course of flooding in the later time steps. Nevertheless, if it is considered, that the intermediate measured roll angle at time instant 5s comprises a dynamic contribution due to the inertia of the test body, the degree of flooding prevention is well represented by the second numerical model (with coaming).

Finally, the comparison between measured and calculated roll motion indicates, that the up righting process after 20s is significantly slower at the model test than predicted by the numerical calculation. This fact confirms the previous made assumption that up righting process is possibly influenced by the fluid

damping of the water e.g. at the longitudinal bulkheads which may have a similar effect as nozzle plates of passive roll damping tank.

6. CONCLUSIONS

The results for above presented leak cases indicate that the course of flooding is well represented by the calculated values of the quasi-static calculation method. Thus, the comparison between the estimated and measured flooding process allows drawing the conclusion that the quasi-static water propagation proves to be the main driver for the flooding of enclosed spaces. Further effects such as additional energy dissipation or the dynamic elevation of the free surface are of minor importance for the considered leak cases. Furthermore, the results of leak case with initial flooding prevention at the engine boxes indicate, that such dynamic water accumulation can be modelled with sufficient accuracy by introducing some virtual coamings at the engine casing. This finding is also in line with accident investigation of the European Gateway in Dankowski 2013.

Nevertheless, the comparison between measured and calculated flooding sequence indicates also an area of improvement with respect to the consideration of water and body dynamics.

These quantities may not be disregarded for cases where the vessels exact motion is of interest. Such cases may comprise a dynamic immersion of non water tight openings which can lead to the progressive flooding of further compartments. The body dynamics could be approximated by dynamic model to solve the corresponding equation of motion. This dynamic model could be connected to the quasi-static method to increase its' prediction accuracy in terms of the roll angle magnitude.

With respect to the evaluation of the full-scale time dependent damage stability of ships, it has to be mentioned that the accuracy of the



prognosis depends on the available input data and the level of detail of the numerical model. Chadi et al. 2009 have summarised possible influencing factors on the time dependent damage stability such as scale effects on the fluid flow, geometric similarity (e.g. permeability of the compartments, representation the buoyancy body and weight items, consideration of internal structures etc.) as well as the consideration of the time dependent structural integrity of openings such as windows, doors etc. The presented quasi-static calculation method can account for most of these factors but requires in turn a sufficient accuracy of the input values (e.g. pressure height of collapsing windows, discharge coefficients etc.) which are sometimes not available. Thus, the numerical model may compromise in the level of detail and the respective input data is often subject to assumptions. However, the accident investigations of Dankowski 2013 and full-scale measurements Ruponen 2010 indicate, that the general course of flooding of full-scale ships is well represented by the quasi-static method, even if assumptions regarding the discharge coefficient or time-dependent openings are made.

Summarising the findings above, the quasi-static calculation method is in the view of the authors an appropriate tool for the estimation of a ship's time dependent damage stability and can enhance the identification of critical intermediate stages of flooding.

7. ACKNOWLEDGMENTS

Special thanks go to the Federal Ministry of Economics and Technology (BMWi) for funding and supporting this research project.

Furthermore, special thanks go to the Institute of Mechanics and Ocean Technology for providing the towing tank and work shop facilities. In particular, the authors would like to thank Marc-André Pick (Hamburg University of Technology), who supported this

research with his ideas, thoughts and expertise regarding the measurement device setup, the integration into the model and the data processing. Finally, the authors would like to thank Prof. Andrés Cura Hochbaum (TU Berlin) for supporting us with the motion exciter.

8. REFERENCES

- Chadi, Khaddaj-Mallat, Jean Marc Rousset, & Pierre, Ferrant. 2009. On factors affecting the transient and progressive flooding stages of damaged Ro-Ro vessels. In: Proceedings of 10th International Ship Stability Workshop. Ecole Centrale de Nantes, equipe hydrodynamique et genie oceanique, laboratoire de mecanique des fluides.
- Dankowski, H. 2012 (September). An Explicit Progressive Flooding Simulation Method. In: Spyrou, K. J., Themelis, N., & Papanikolaou, A. D. (eds), 11th International Conference on the Stability of Ships and Ocean Vehicles.
- Dankowski, H. 2013 (August). A Fast and Explicit Method for the Simulation of Flooding and Sinkage Scenarios on Ships. Ph.D. Thesis, Hamburg University of Technology, Institute of Ship Design and Ship Safety. ISBN 978-3-89220-668-2.
- Dankowski, H., & Krüger, S. 2012 (June). A Fast, Direct Approach for the Simulation of Damage Scenarios in the Time Domain. In: 11th International Marine Design Conference. University of Strathclyde, Glasgow, UK.
- Dankowski, H., Lorkowski O. Kluwe F. 2014. An Experimental Study on Progressive and Dynamic Damage Stability Scenarios. In: Proceedings of the ASME 2014 33rd International Conference on Ocean, Offshore and Arctic Engineering,



OMAE2014, June 8-13, San Francisco,
USA.

Ikeda, Y., Ishida, S., Katayama, T., & Takeuchi, Y. 2004. Experimental and Numerical Studies on Roll Motion of a Damaged Large Passenger Ship in Intermediate Stages of Flooding. In: Proceedings of the 7th International Ship Stability Workshop.

Krüger, S., Dankowski, H., & Teuscher, C. 2012. Numerical Investigations of the Capsizing Sequence of SS HERAKLION. In: Proceedings of the 11th International Conference on Stability of Ships and Ocean Vehicles.

Pick, M., A. 2009 (September). Ein Beitrag zur numerischen und experimentellen Untersuchung extremer Schiffsbewegungen. Ph.D. Thesis, Hamburg University of Technology, Institute of Mechanics and Ocean Dynamics. ISBN 978-3-18-333911-2.

Ruponen, Pekka. 2007. Progressive Flooding of a Damaged Passenger Ship. Ph.D. thesis, Helsinki University of Technology.

Ruponen, Pekka, Kurvinen, P., Saisto, I., & Harras, J. 2010. Experimental and Numerical Study on Progressive Flooding in Full-Scale. In: RINA Transactions 2010 Part A - International Journal of Maritime Engineering. RINA. Stening, Mikael. 2010. Pressure losses and flow velocities in flow through manholes and cross-ducts. In: FLOODSTAND project. Floodstand Deliverable, no. D2.3. Aalto University (TKK).

Valanto, P. 2009 (July). Research for the Parameters of the Damage Stability Rules including the Calculation of Water on Deck of Ro-Ro Passenger Vessels for the amendment of the Directives 2003/25/EC and 98/18/EC. Final Report 1663. European Maritime Safety Agency (EMSA).



Dynamic Extension of a Numerical Flooding Simulation in the Time-Domain

Hendrik Dankowski, dankowski@tu-harburg.de

Stefan Krüger, krueger@tu-harburg.de

Institute of Ship Design and Ship Safety, Hamburg University of Technology

ABSTRACT

A fast and explicit numerical flooding simulation has already been validated with the help of results from model tests and successfully applied to the investigation of several severe ship accidents like the one of the Costa Concordia. The progressive flooding method in the time-domain computes the flux between the compartments based on the Bernoulli equation combined with a quasi-static approach for the evaluation of the current floating position.

The numerical method is now extended to take into account the effects of the dynamic motion of the vessel during the flooding. As it has been observed by recent model tests, the dynamic motion of the vessel might play an important role for the flooding process especially during the initial transient phase after the damage occurred. To take this into account, the hydrostatic evaluation during each time step is replaced by an integration of the equation of motions in the time-domain.

The extended method will be validated with results from the model tests to demonstrate the influence of the dynamic motion of the vessel on the flooding process. In addition, the new model test campaign of various flooding cases are described. The enhanced method allows to give an in-depth view on the dynamic propagation of the flood water after a damage to the watertight integrity of a ship occurred. Effects like the acceleration or delay of the flooding by the dynamic motion of the vessel itself are investigated. In addition, the dynamic extension is compared with the results obtained from the quasi-static approach to demonstrate the applicability of both methods.

The extension of the already very powerful numerical flooding method will not only better resolve the initial phase of flooding. It will also accelerate the existing method, since the search for a new hydrostatic equilibrium is replaced by fewer volumetric calculations for the integration of the equation of motions. Applications of such a fast numerical flooding simulation in the time-domain are complex accident investigations and next generation damage stability tools to be used on-board for decision support. A reliable and fast prediction of the flooding sequence after a damage occurred assist the crew to decide whether an evacuation of the vessel is required or not.

Keywords: *Progressive Flooding; Sinking; Dynamic Flooding; Ship Design; Accident Investigation; Ship Safety*

1. INTRODUCTION

In the past, a numerical flooding simulation has been developed and presented in sev-

eral publications (Dankowski, 2012; Dankowski and Dilger, 2013; Dankowski, 2013; Dankowski et al., 2014). To further extend and validate the method, a research project called LESSEO has

been initiated. Within this project, a model test campaign has been conducted and the numerical methods to compute the time-dependent damage stability of ships were extended or newly developed.

First results of this research project were presented in Lorkowski et al. (2014). Additional test cases and new results are also given in Lorkowski et al. (2015). The focus of this paper is on the dynamic extension of the numerical flooding simulation. The underlying physical model is described together with the validation on two test cases from the model test campaign.

The numerical methods are implemented in the ship design environment E4, a first-principal ship design software used and developed at our institute together with partners from the German shipbuilding industry. In doing so, direct access to the whole ship data model and already implemented computational algorithms like hydrostatic evaluations is granted.

2. NUMERICAL METHODS

First, the quasi-static method is summarized. A more detailed description including validation test cases can be found in Dankowski and Krüger (2012; 2013). Second, the dynamic extension of this method is described, which takes into account the dynamic movement of the ship and its influence on the flooding process. This is accomplished by the solution of the non-linear differential equation of motions of the vessel.

2.1 Quasi-Static Method

The quasi-static method has been developed to estimate the time dependent damage stability of ships. It is assumed that most flooding incidents are mainly driven by the relatively slow progressive flooding of the ship and dynamic effects can be neglected. Its focus is on the fast and accurate computation of different scenarios to investigate full scale accidents. Several accident investigations have already been

successfully performed, while the last investigation was on the accident of the Costa Concordia (Dankowski et al., 2014).

The method is in general capable to consider time dependent openings by a pressure height criterion and defined closure/opening times for watertight doors. Furthermore, an air compression model according to Boyles law has been implemented to account the effect of trapped air within the compartments.

The floodwater ingress and the spreading of the floodwater inside the vessel are computed by a hydraulic model for the water fluxes. For each time step, the new distribution of the floodwater inside the complex inner subdivision of the ship is computed and a new floating equilibrium position is determined based on the new resulting hydrostatic moments caused by the floodwater.

Details of the method will roughly be sketched in the following. The pressure head differences at the openings lead to a water in- or egress to the watertight integrity of the ship or between two inner compartments:

$$dz = \frac{p_a - p_b}{\rho g} + \frac{u_a^2 - u_b^2}{2g} + z_a - z_b, \quad (1)$$

$$u = \sqrt{2g \cdot dz}. \quad (2)$$

By integrating the velocity u over the area of the opening, the volume flux is determined assuming a perpendicular flow direction to the opening. Any dissipative losses are taken into account by a semi-empirical discharge coefficient C_d :

$$\frac{\partial V}{\partial t} = Q = \int_A \mathbf{u} \cdot d\mathbf{A} = \int_A \mathbf{u} \cdot \mathbf{n} dA. \quad (3)$$

The solution of this integral becomes more complicated if the opening is large and of arbitrary shape and orientation. Therefore, larger openings are discretized in smaller, elementary parts for which an analytical solution of the volume flux can be determined.

The connection of all compartments by openings can be modelled by directed graphs.

Each compartment is represented by a node and the openings are the corresponding edges.

2.2 Dynamic Flooding Simulation

Especially during the initial phase of flooding, the dynamic motion of the ship can have a significant influence on the flooding process. Larger roll oscillations are also observed during the model tests. To better study the influence of the dynamic motions of the vessel, the existing flooding model is extended by means of the numerical solution of a non-linear ordinary differential equation of motions of all six degrees of freedom. The general structure of this equation with \mathbf{x} as the state vector writes as follows:

$$\mathbf{M} \cdot \ddot{\mathbf{x}} + \mathbf{B} \cdot \dot{\mathbf{x}} + \mathbf{C} \cdot \mathbf{x} = \mathbf{F} \quad (4)$$

where \mathbf{M} is the generalized mass matrix including added masses, \mathbf{B} is the damping matrix and \mathbf{C} is the stiffness matrix together with the external forces \mathbf{F} as the right hand side. All of the components of this equation are strongly non-linear, since these depend on the changing mass properties of the vessel by the ingressing flood water and the right hand side is evaluated by a direct computation of the hydrostatic properties for the current floating position.

Since the focus on this method is on a first study of the influence of the dynamic motions on the flooding process and to even improve the computational runtime of the method, the following simplification is applied: The damping matrix is assumed to be a percentage of the mass matrix, as so for the hydrodynamic masses.

On the other hand, the stiffness matrix is directly derived from the current hydrostatic stiffness matrix and no linearization is done here. The external forces on the right hand side are defined by the resulting hydrostatic forces due to gravitation and buoyancy for the current mass properties and the floating condition at each time step.

During the flooding process, it is supposed that especially the changing mass distribution

has a large impact on the motions. The current fluid masses in the different compartments are known at each time step, such that these can be compiled to update the mass matrix concurrently.

In practice, this is done by initially computing the overall mass matrix of dry and wet (filling in tanks and the flood water) components from the current loading condition, then subtracting again the wet part at the beginning and by updating the current wet part of the mass matrix from the distribution of the flood water at each time step.

The numerical solution of the differential equation is performed by the adaptive 4-5th order Runge-Kutta method by Fehlberg (1969). Due to the fact that the search for a new hydrostatic equilibrium is now replaced by the numerical efficient integration of the differential equation, less costly hydrostatic evaluations are required and the computational runtime is significantly reduced. In addition, it is in most cases sufficient to update the mass matrix only at each outer time step and not in between the Runge-Kutta steps, which further reduces the required computational effort.

This model will be compared to the test cases to identify if it is appropriate to compute such physical problems with this numerical method. The validation will also be used to identify important effects which play an important role in this scope to further improve the model.

3. MODEL TESTS

Before coming to the results from the validation, the model test setup will briefly be described. Further details can be found in Lorkowski et al. (2014; 2015).

The model is shown in Figure 1 together with its main dimensions in Table 2. The whole model is build out of acrylic glass. Around one third of the model around the mid section can be flooded including the main deck. Most of the measurement equipment is located in the aft and



Figure 1 The inclined model in the test basin after flooding

fore part of the model below the main deck.

Table 1 Main Dimensions of the Model

Length over all	L	2.02 m
Breadth	B	0.42 m
Depth	D	0.42 m
Draught	T	0.18 m
Displacement	Δ	144 kg

The following quantities are measured during the model test campaign:

1. Filling levels in the flooded compartments
2. Model's motions in six degrees of freedom
3. Air pressure in the double bottom

The measurement setup has been developed at the Institute of Mechanics and Ocean Technology of the Hamburg University of Technology. In the following, a brief overview about the measurement setup is given. Further details about the measurement setup are given in Lorkowski et al. (2014); Pick (2008).

3.1 Filling Levels

The filling levels in the flooded compartments are measured by filling level sensors. The physical principle of these sensors is based on Ohm's law: The water changes the electrical resistance and thus the voltage between the wires. The change in voltage is proportional to the fill-

ing level. The relationship between voltage and filling is derived from the calibration of the sensors (see also Figure 2). The data of each filling level sensor is stored continuously on its own memory card with 228 Hz and written to a file. Through this procedure, it is ensured that the filling level data is at any time step synchronously with the other measurement devices.



Figure 2 The level sensors during calibration

Furthermore, the water level in the compartments is recorded by three high speed cameras. These cameras are capable to capture the filling level of the flooded compartment with a rate up to 240 frames per second. The video data of the cameras is used to verify the measured filling levels of the filling level sensors and to provide some background information on the flooding process.

3.2 Motion Tracking

The vessel's motion is measured by a combination of an inertial measurement unit (IMU) with an optical stereo camera system. The data of both measurement devices is combined via a Kalman filter to obtain the overall highest accuracy in terms of acceleration, velocity and altitude in all six degrees of freedom. The accuracy for the translational degrees of freedom is less than 0.1 mm and for the rotational degrees of freedom less than 0.01 degree (Pick, 2008).

3.3 Inner Subdivision

The subdivision of the model is shown in Figure 3. The subdivision of the mid ship section has been designed according to a typical subdivision layout of a RoRo vessel. The floodable compartments are indicated by the light blue color.

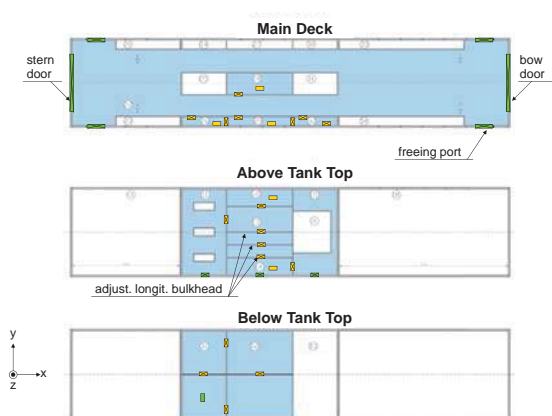


Figure 3 General arrangement sketch of the test body

In horizontal direction, the model consists of the main and the tank top deck. In longitudinal direction, the model is subdivided through the side and center casing on the main deck, the center line girder in the double bottom and the two longitudinal bulkheads above the tank top. The longitudinal bulkhead at starboard can be adjusted to the positions $0.2 B$, $0.35 B$ and $0.5 B$.

The compartment in the aft of the mid section above the tank represents a typical engine room compartment. The displacement of the engines has been considered through three watertight boxes. The C-shaped fore compartment is similar to a typical bunker tank compartment. The large cargo hold compartment above the main deck comprises a closeable bow and stern door and four freeing ports. Every floodable compartment is equipped with an air pipe to avoid incomplete flooding events as a result of compressed air pockets.

3.4 Openings

The four different geometric shapes of the openings has been derived from typical openings on board of ships such as stair cases, bulkhead doors, man holes, holes for pipes in the double bottom etc.

The openings are indicated by the colored boxes in Figure 3: Openings through bulkheads are marked with a crossed box, openings in decks are marked with a blank box. The external openings are indicated by the green color, internal openings are indicated by the yellow color.

The model can be flooded through ten external openings: One in the bottom below tank top, three side openings above tank top, two doors and four freeing ports on the main deck.

The external bottom and side openings are located below the water surface and can be opened by pulling a plug, which is connected to a thin rope. The surface of the plug has been manipulated with fabric-tape, to ensure satisfactory sealing characteristics. Compared to other sealing materials such as rubber or foam, the chosen material offers the advantage that the surface of the plug can be accurately adjusted to the opening dimensions by adding very thin layers of tape. In addition, some grease were applied to further improve the sealing. This procedure allows to keep the required pulling force to a minimum to avoid any induced side or roll motion of the vessel while opening the plug.

3.5 Motion Exciter

The model can be excited via a motion exciter, which has initially been developed by Otten (2008). The original exciter were newly constructed for the model tests and is shown in Figure 4.

The motion exciter consists of two masses, which are driven by an electrical motor. The masses rotate about the vertical axis in contrary direction and at the same speed. Depending on the orientation of the motion exciter, the masses

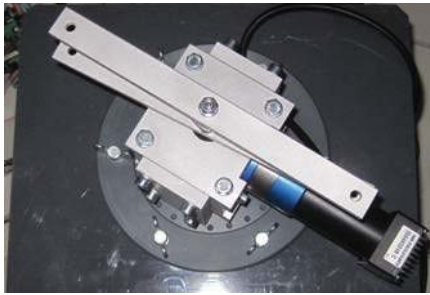


Figure 4 The top view of the used motion exciter

overlap either in longitudinal or transverse direction in such a way that a roll or pitch moment is induced to the model. The frequency of the motion exciter can be varied by adjusting the voltage of the electric motor via an transformer.

4. THE INVESTIGATED TEST CASES

From the comprehensive model test campaign two test case are selected to compare the measured results with the computed values from the quasi-static method and the dynamic flooding computation.

The validation test cases are selected to have a significant dynamic roll motion, where only the average mean values can be reproduced by the quasi-static method. Both cases have a symmetric layout but result in a final equilibrium heeling angle of around 5 degrees, while heeling angles up to 20 degrees occur during the intermediate stages of flooding.

The following computational setup for the two test cases are used:

Table 2 Computational setup in full scale

Testcase		A	B	
Outer time step	dt	0.5	0.5	s
Damping factor	f_B	2	5	%
Initial roll velocity	$\dot{\varphi}_0$	-0.4	0.5	°/s
Initial stability	\overline{GM}	0.52	0.51	m

The computations are performed in full scale with a model scale of $\lambda = 100$ resulting for ex-

ample in a time step of $dt = 0.05$ s in model scale. The typical computational time for one of the model test cases, which lasted around 100 seconds, is approximately 3-5 seconds.

4.1 Damage Case A

The setup of the first test case is shown in Figure 5. The model is flooded through a side damage below the water line. The water further spreads to the other side through a longitudinal bulkhead and from the center through a door to the compartment located further aft in model.

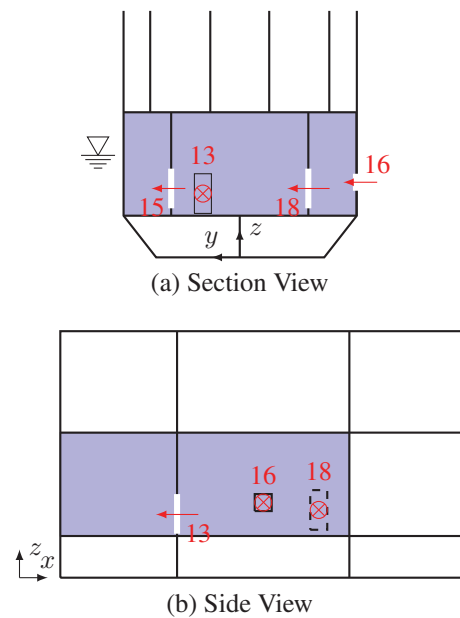


Figure 5 Setup Case A

The roll angle of the model observed during the model tests together with the computed ones are shown in the plot in Figure 6.

Since the water is first prevented by the longitudinal bulkhead, the roll angle increases very fast at the beginning. After around one second, this increase slows down before the maximum roll angle of a little more than 20 degrees is reached after 20 seconds. After this point, the model uprights again before it comes to rest at around 5 degrees of heel.

Even though the damage case has a symmetric layout, the final equilibrium is not upright. This can be explained by the fact, that the final

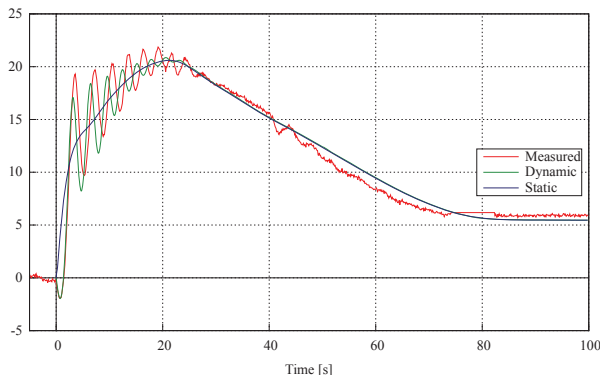


Figure 6 Case A: Roll motion measured and computed

equilibrium would not be stable at an heel angle of zero, but the model finds its new and stable equilibrium at around 5 degrees.

The motion of the vessel highly oscillates at the beginning until the maximum heel angle is reached. After this point, the flooding slows down, the motion is highly damped by the additional flood water and the progressive flooding phase continues.

The quasi-static computation can only predict the mean average motion of the vessel. However, this general mean motion is quite well reproduced.

The results obtained from the dynamic flooding method match all phases of flooding of this test case very well. At the start, the initial small roll velocity leads first to a small angle to port side before the very unsteady phase follows. Even though, only a very simplified damping model is assumed, the computed motion matches quite well with the measured one. This can be explained by the fact that most of the damping simply comes from the additional flood water.

4.2 Damage Case B

The layout of the second test case is more simple as shown in Figure 7. Only one compartment is flooded through a side damage. This compartment is of C-shape kind if looking from

above. This shape leads to a quite complex flooding behaviour since the small channel at the front prevents an immediate symmetric flooding of the whole compartment.

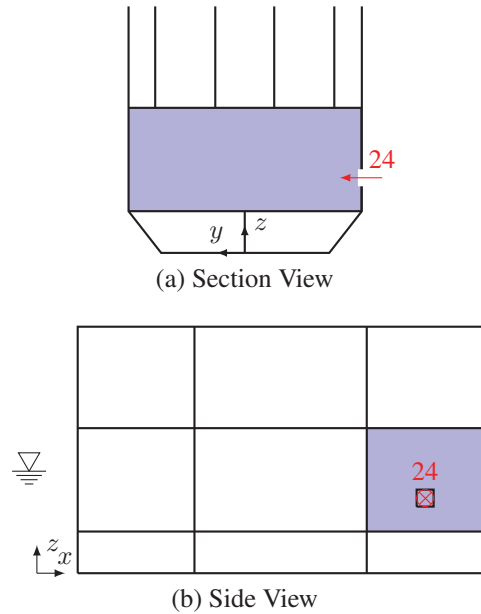


Figure 7 Setup Case B

To better illustrate the complex and irregular flooding, two snapshots from the video taken during the model test is shown in Figure 8. The camera is located in front of the flooded compartment and looks to the aft in direction of the leak.



(a) After around 2 seconds



(b) After around 4 seconds

Figure 8 Case B: Snapshots from the flooding

It can be depicted from the snapshots that at the beginning the incoming water jet hits the wall opposite to the leak and the water propagates with an uneven and irregular surface further through the channel to the other side.

The measured roll angle is compared to the values obtained from the numerical methods as shown in Figure 9.

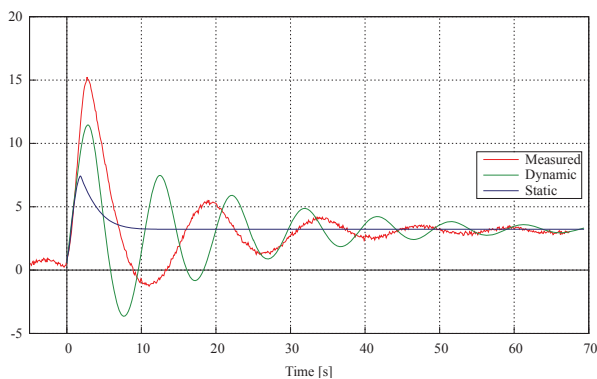


Figure 9 Case B: Roll motion measured and computed

First, the heel angle increases quite fast to around 15 degrees. A strongly damped roll oscillation follows before the model comes to rest at around 3.5 degrees. The final equilibrium is again not at zero degrees, because the initial stability would not be sufficient.

The quasi-static method finds the same final equilibrium but it reaches this point after only 10 seconds. The measured time and the time computed with the dynamic method is around 5 times larger.

The roll oscillation and the movement of the model is again quite well reproduced by the dynamic simulation. However, the damping which is observed during the model is higher and more non-linear. The roll period is faster stretched compared to the computed values. But the general dynamic motion behaviour is also shown by the numerical method, since around the same maximum heel angle is reached and also the overall flooding time is very similar.

5. CONCLUSIONS AND OUTLOOK

An existing powerful flooding simulation method has been successfully extended by a dynamic model. This does not only reproduces the real flooding behaviour better, it is also more efficient by means that the computational time is reduced.

The dynamic extension has been validated with the help of two model tests of a large test campaign. The results and the comparison from these tests are very valuable, since it allows to better understand such complex flooding phenomena.

The dynamic motions computed with the new dynamic model matches quite well the observed behaviour during the model tests. This could be further improved by a more complex and better computation of the real damping forces and the added masses.

The numerical flooding simulation is improved by its applicability and its performance, which is a very important step to bring such systems also on board of ships. Only an appropriate accurate and sufficient fast numerical method to compute the dynamic flooding behaviour of ships in the time domain would help and assist the crew on board to make the correct decision after a severe damage to watertight integrity of the ship happened.

A further extension to include also the influence of waves is possible, but several accidents in the past have shown that many of these accidents mainly caused by a damage to the hull followed by flooding happened in calm water. Vessels like the Costa Concordia or the Express Samina suffered an underwater damage in coastal regions at a moderate or quiet sea state.

In addition, the extended method could also be used to re-evaluate already investigated accidents or to apply it to new accident investigations to learn from these and to improve the overall safety of ships.

6. ACKNOWLEDGMENT

Special thanks go to the Federal Ministry of Economics and Technology (BMW) for funding and supporting this research project. In addition, special thanks go to our partner in this research project, the Flensburger Shipyard. Furthermore, thanks go to the Institute of Mechanics and Ocean Technology for providing the towing tank and work shop facilities. In particular, the authors would like to thank Marc-André Pick, who supported this research with his ideas, thoughts and expertise regarding the measurement device setup, the integration into the model and the data processing.

7. REFERENCES

- The ASME 2014 33rd International Conference on Ocean, Offshore and Arctic Engineering, number 33, San Francisco, California, USA, 6 2014. ASME, ASME. geplant.
- H. Dankowski. An Explicit Progressive Flooding Simulation Method. In K. J. Spyrou, N. Themelis, and A. D. Papanikolaou, editors, 11th International Conference on the Stability of Ships and Ocean Vehicles, Athens, Greece, 9 2012.
- H. Dankowski. A Fast and Explicit Method for the Simulation of Flooding and Sinkage Scenarios on Ships. Ph.D. Thesis, Hamburg University of Technology, Institute of Ship Design and Ship Safety, 8 2013. URL <http://doku.b.tu-harburg.de/volltexte/2013/1222/>. ISBN 978-3-89220-668-2.
- H. Dankowski and H. Dilger. Investigation of the Mighty Servant 3 Accident by a Progressive Flooding Method. In Proceedings of the ASME 2013 32nd International Conference on Ocean, Offshore and Arctic Engineering, number ISBN 978-0-7918-4492-2, Nantes, France, 7 2013. ASME, ASME.
- H. Dankowski and S. Krüger. A Fast, Direct Approach for the Simulation of Damage Scenarios in the Time Domain. In 11th International Marine Design Conference, Glasgow, UK, 6 2012. University of Strathclyde.
- H. Dankowski and S. Krüger. Progressive Flooding Assessment of the Intermediate Damage Cases as an Extension of a Monte-Carlo based Damage Stability Method. In Chang-Sup Lee and Suak HoVan, editors, 12th International Symposium on Practical Design of Ships and Other Floating Structures, number ISBN 978-89-950016-0-8, Changwon City, Gyeongnam Province, Korea, October 2013. The Society of Naval Architects of Korea.
- H. Dankowski, P. Russell, and S. Krüger. New Insights into the Flooding Sequence of the Costa Concordia Accident. In Proceedings of the ASME 2014 33rd International Conference on Ocean, Offshore and Arctic Engineering ASM (2014). geplant.
- Erwin Fehlberg. Low-order classical Runge-Kutta formulas with step size control and their application to some heat transfer problems. NASA Technical Report 315, NASA, 1969.
- O. Lorkowski, H. Dankowski, and F. Kluwe. An Experimental Study on Progressive and Dynamic Damage Stability Scenarios. In Proceedings of the ASME 2014 33rd International Conference on Ocean, Offshore and Arctic Engineering ASM (2014). geplant.
- O. Lorkowski, F. Kluwe, and H. Dankowski. A Numerical and Experimental Analysis of the Dynamic Water propagation in Ship-Like Structures. In K. J. Spyrou, N. Themelis, and A. D. Papanikolaou, editors, 12th International Conference on the Stability of Ships and Ocean Vehicles, Athens, Greece, 9 2015.
- N. Otten. Rolldämpfung von Schiffsmodellen mit und ohne Schlingerkiel. Diploma thesis, TU Berlin, 2008.
- Marc-André Pick. Ein Beitrag zur numerischen und experimentellen Untersuchung extremer Schiffsbewegungen. Dissertation, Technische Universität Hamburg-Harburg, Denickestr. 22, 21071 Hamburg, Oct 2008.

This page is intentionally left blank



URANS Simulations for a Flooded Ship in Calm Water and Regular Beam Waves

Hamid Sadat-Hosseini, *IIHR – Hydrosience & Engineering*, hamid-sadathosseini@uiowa.edu

Dong-Hwan Kim, *IIHR – Hydrosience & Engineering*, donghwan-kim@uiowa.edu

Pablo Carrica, *IIHR – Hydrosience & Engineering*, pablo-carrica@uiowa.edu

Shin Hyung Rhee, *Seoul National University Towing Tank*, shr@snu.ac.kr

Frederick Stern, *IIHR – Hydrosience & Engineering*, frederick-stern@uiowa.edu

ABSTRACT

CFD simulations are conducted for zero-speed damaged passenger ship SSRC in calm water and waves with 6DOF motions including flooding procedure in calm water, roll decay in calm water and motions in regular beam waves for various wavelengths. The simulations model the 6DOF soft spring experimental mount, the one- and two-room flooding compartment configurations, including both intact and damaged conditions. For flooding and roll decay, simulations show ability predict the trend of increases in roll period and damping due to flooding, as reported in ITTC (2002). The damping magnitudes were often under-predicted with large errors while the roll period and compartment water height were well predicted. Two-room compartment simulation showed three times larger damping than one-room compartment cases whereas the roll period was similar for both conditions. For wave cases, all motions show primarily 1st order response, except for parametric roll condition which shows large $\frac{1}{2}$ harmonic response for the intact ship. The 2nd order responses are small for both damaged and intact ship. The larger roll period and damping for the damaged ship shift the peak of responses to smaller wave frequency and reduce the amplitude of responses. The average error is often large for 1st order intact ship pitch and damaged ship surge and pitch and for most $\frac{1}{2}$ and 2nd order responses. Large errors could be partially due to the complex mounting system in the experiment. Overall, current CFD results show better predictions than those reported for potential flow solvers even though the computational cost is larger.

Keywords: *CFD, Damage Ship Stability, Calm Water, Beam Waves*

1. INTRODUCTION

Safety is of high priority in ship design but poorly understood and often in conflict other important requirements such as powering, seakeeping and maneuvering. To meet new energy efficiency IMO guidelines requires a reduction in the main engine output. However, lowering output may result in diminished seakeeping and maneuvering performance. Finalization of the guidelines for minimum power requirement is in progress. Intact/damaged and static/dynamic stability are all major concerns.

Damaged dynamic stability is most complex and been research focus as summarized by the last several ITTC Stability in Waves Committee and Specialist Committee Reports. Flooding process, floodwater dynamics and ship motions are studied. Passenger and ferry ships are specified as benchmarks for experimental and simulation studies. For the zero-speed calm water damaged condition, the roll period and damping are larger than for the damaged condition. Increasing KG showed larger roll period and smaller damping and increasing floodwater height showed both larger roll period and damping. Tests for regular and



irregular waves indicated second harmonic roll motion and capsizing, respectively. Recent focus is on time to flood and safe return to port and survival boundaries in irregular waves.

Potential flow methods are the common numerical approach to study the damaged ship stability (Papanikolaou et al., 2000; Palazzi and De Kat, 2004). The 6DOF damaged ship motions in waves are solved by various strip theory or panel based methods. The viscous effects are treated by semi-empirical approaches. The inflow and outflow of water through the openings is computed by the Bernoulli based equations including orifice, sluice gate and weir equations. The non-linear sloshing effect inside the compartment is often neglected, and the internal water surface is assumed to be either horizontal or a freely movable plane. The capability of potential flow methods for a damaged passenger ship (PRR1) with zero-speed was evaluated in 23rd ITTC Specialist Committee on Prediction Methods of Extreme Ship Motions and Capsizing using several benchmark experimental data for free roll decay in calm water, motion in regular waves and survivability boundaries in irregular waves (ITTC, 2002). The potential flow predictions were only assessed for motions and not evaluated for floodwater height. The results from several potential flow tools showed overestimation of the damped roll frequency ($E=-22\%D$) and underestimation of logarithmic roll damping coefficient ($E=62\%D$) for roll decay, scattered results for regular waves with large over prediction for roll frequency ($E=-15\%D$) and amplitude ($E=-91\%D$), and only qualitative agreement with experimental data in irregular waves. Note that the comparison errors were not given in ITTC report and calculated by authors as $E=(D-S)\%D$ between the experimental data (D) and simulation (S) values.

The CFD study of the damaged ship is performed for very limited cases. Few studies only used CFD to predict the dynamic effect of floodwater and then coupled with the potential flow solvers for ship motion prediction (Strasser et al., 2009; Gao et al., 2013).

Therefore, the accuracy of the predicted motions was still associated with the level of nonlinearity implemented in the potential flow solver. The complete physics-based CFD simulations are conducted only for the ship in calm water with semi-captive condition. Gao and Vassalos (2011) demonstrated the capability of CFD prediction for roll decay prediction of a damaged ship for initial angle $\pm 5^\circ$. The simulations were conducted for 1DOF and 2DOF conditions with free roll motion w/ or w/o sway motion. Gao et al. (2011) validated motions and floodwater heights for 3DOF damaged barge in calm water free to heave, roll and pitch. The time history of roll motion showed quite large error ($E\sim 200\%D$) during the initial part of the flooding procedure while it is predicted well after the compartment is fully flooded. Additionally, the heave and pitch motions were well predicted with $E<5\%D$. The trends of computed floodwater heights were generally consistent with the experimental measurements. However, there were differences between numerical simulation and experiment which could not be quantified.

Herein, the capabilities of physics-based CFD simulations are assessed for zero-speed ship flooding and roll decay in calm water and regular beam waves with 6DOF motions using the experimental data provided by Lee et al. (2015). The simulations model the soft spring experimental mount, the one- and two-room flooding compartment configurations, including both intact and damaged conditions. The errors are evaluated for floodwater and motions using the experimental data. The level of the errors is compared with that from previous potential flow studies and the cost and benefit for the current approach is described.

2. EXPERIMENTAL VALIDATION DATA

2.1 Facility, model, mount, measurement systems

The tests are conducted in the Seoul National University (SNU) towing tank, which



is 110 m long, 8 m wide and 3.5 m deep. A 1:82.75 scale, L=3.0 m geosim of the SSRC passenger ship is used for the experiments. Model-scale geometric parameters are summarized in Table 1. The model is appended with a compartment installed at the mid-ship as shown in Fig. 1a. The compartment is divided by a side wall into two rooms connected through a small hole, so that there is a cross-flooding between the rooms. Both compartment rooms have ventilation holes on their roof to have atmosphere pressure inside the rooms during flooding. The flooding occurs through a gate located on the starboard side of the compartment. The compartment layout is shown in Fig. 1b.

Table 1 The main particulars of SSRC

Description	Particulars
Ship Model	
Length between perpendiculars [m]	3
Beam (B/L) [-]	0.143
Draft (T/L) [-]	0.034
Damage length [m]	0.150
LCG/L [-]	0.520
KG/L [-]	0.032
Radius of gyration along x-axis [-]	0.053 (0.0501*)
Radius of gyration along y-axis [-]	0.250
Radius of gyration along z-axis [-]	0.250
Heave and pitch frequency	1.003 Hz
Roll frequency	0.487 Hz
Damaged Compartment	
Number of Rooms	Two
Compartment shape	Box
Ventilation hole	Yes
Opening door shape	Rectangular
Opening door length	0.0727
Opening door height	0.061

*adjusted k_{xx}

In the experiments, the ship was located in the mid-tank, free to all degree of motions. For wave cases, the aft and fore of the model were attached to the stationary carriage using four springs to compensate the drift motion of the ship in the experiment. All springs were initially installed to be parallel and close to the free surface. A simple mass-spring measurement showed that the spring force has linear behavior within the range of possible spring length during the experiment. The

effective spring stiffness is shown to be 5.946 N/m and the spring forces are off by 6.8148 N from the one estimated by $F=kx$. For flooding of the compartment, its gate was opened using an air cylinder that pulled up the gate in the vertical direction. The opening time was approximately 0.09 second in model scale and it was confirmed that the induced roll motion due to the opening mechanism was negligible.

Table 2 The EFD and CFD test matrix for SSRC

Type	ϕ_i (deg)	# of comp. room	sea condition	validation variables
Flooding	0.0	-	Calm water	$\phi, \zeta_{A,B,C}$
Intact roll decay	-13.7	-	Calm water	ϕ
	-20.5	-		
	-15.6	1		
Damaged roll decay	15.9	1	Calm water	ϕ
	-25.5	1		$\phi, \zeta_{A,B,C}$
	26.7	1		ϕ
	-28.6	2		$\phi, \zeta_{A,B,C,D,E}$
Intact beam waves*	-	2	$\lambda/L=0.52, 1.17, 1.99, 2.20, 2.42$	$x, y, z, \phi, \theta, \psi, \zeta_{A,B,C,D,E}$
	-	2	$H/\lambda=1/60, 1/100$	$\zeta_{A,B,C,D,E}$
Damaged beam waves*	-	2	$\lambda/L=0.52, 1.17, 1.99, 2.20, 2.42$	$x, y, z, \phi, \theta, \psi, \zeta_{A,B,C,D,E}$
	-	2	$H/\lambda=1/60, 1/100$	$\zeta_{A,B,C,D,E}$

*CFD simulations in waves are only conducted for $H/l=1/60$.

Two measurement systems were used for the experiments: flooding water and ship motion measurement systems. The height of the flooding water was measured by five capacitance type wave probes at locations A, B, C, D, E in the compartment (ζ_i ; $i=A,B,C,D,E$) as shown in Fig. 1b. The 6DOF motion responses ($x, y, z, \phi, \theta, \psi$) were measured with a combination of the accelerometers and inertial measurement unit (IMU). The IMU was mainly used for the roll motion measurement in the free roll decay test. The accelerometers were used to obtain 6DOF motion responses from the test results in regular waves. From the measured accelerations, the 6DOF motion responses of the model were obtained using the strap-down method. It should be noted that the accelerations were first filtered using band-pass filtering in Matlab and then numerically

ship model is still free to all modes of motion. The spring forces for all 6DOF were computed in earth coordinate system and then transformed to ship-fixed coordinate system with origin at the center of gravity (G) to be considered in the equations of motion. The spring moments in ship-fixed coordinate were calculated by cross product of the moments' arm and forces described in ship-fixed coordinate.

The displacement of each spring was found in earth coordinate system based on the position of the two ends of that spring. For spring i , one end is attached to the ship at point P_i and another is attached to the carriage at point C_i . The location of P_i changes during simulation as it is located on the ship. The location of P_i in earth coordinate system was found based on:

$$r_{P_i} = r_G + R \cdot d_{P_i} \quad (1)$$

Here, r_{P_i} and d_{P_i} are the displacement vector of P_i in earth and ship coordinate system, r_G is the displacement vector of G in earth coordinate system, and R is the rotational matrix from ship to earth coordinate system.

The force for the i^{th} spring attached to the ship at point P_i and the carriage at C_i was calculated as follows:

$$F_i = \frac{r_{C_i} - r_{P_i}}{|r_{C_i} - r_{P_i}|} \cdot f(r_{C_i} - r_{P_i}) \quad (2)$$

where, F_i is the force vector in earth coordinate system and f is the spring force function which is dependent on the spring displacement. In this study, the formula found from experiment is used.

The total spring induced forces in earth coordinate system (F) are sum of the forces induced by each spring as shown in Eq. (3). Then the total forces were transformed into ship coordinate system (Eq. (4)).

$$F = \sum_{i=1}^4 F_i \quad (3)$$

$$F' = R^{-1} \cdot F \quad (4)$$

where F' is the total spring induced forces in ship coordinate system.

For the spring moments, each spring force was transformed to ship coordinate system first and then the moment induced by each spring was calculated by cross product of the moments' arm and forces:

$$F'_i = R^{-1} \cdot F_i \quad (5)$$

$$M'_i = (r_{C_i} - r_{P_i}) \times F'_i \quad (6)$$

$$M' = \sum_{i=1}^4 M'_i \quad (7)$$

After calculating the spring forces and moments in ship-fixed coordinates, they were added to the total forces and moments applied on the right hand side of the equations of motion. The total forces and moments are the fluid forces and moments integrated at each time step not only on the ship hull but also inside the flooded compartment. This means that the change of the ship mass and/or center of gravity due to the flooding are already included in the integrated forces and moments. Therefore, there's no need to modify the ship mass, moment of inertia or center of the gravity unlike the traditional methods. In the traditional methods, the flooded compartments are treated often as an additional weight to the ship. The added weight then changes the center of gravity and moments of inertia of the ship and consequently the equations of motion have to be solved for the ship with the new properties.

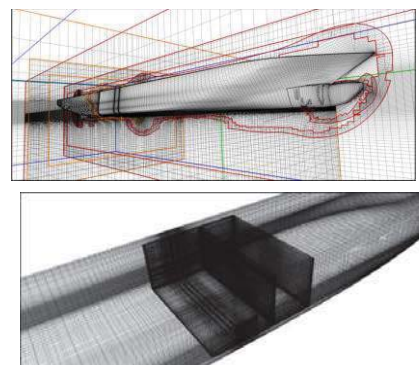


Figure 2 Grid topology for damaged SSRC and compartment.



3.2 Domain, boundary conditions, grids, conditions, and analysis method

The computational domain extends from $-1.5 < x < 1.5$, $-1.2 < y < 1.2$, $-1 < z < 0.25$ for roll decay and flooding procedure simulation and $-1.5 < x < 1.5$, $-2 < y < 1$, $-1 < z < 0.25$ for regular wave simulations of intact/damaged SSRC in dimensionless coordinates based on ship length. The ship axis is aligned with x with the bow at $x=0$ and the stern at $x=1$. The y axis is positive to starboard with z pointing upward. The free surface at rest lies at $z=0$.

Several types of boundary condition are used in this CFD study. The far field boundary conditions are imposed on the top and bottom of background. The no-slip condition is applied on the solid surfaces on the hull or inside the compartment. On the sides, the zero gradient boundary condition is applied. For calm water simulation, the inlet and exit boundary conditions are used for inlet and outlet of the domain. For waves, the inlet and outlet boundary conditions are calculated from the linear potential flow solution of waves.

Table 3 CFD and EFD comparison of roll motion for calm water cases

Type	ϕ_i	EFD/CFD	f_d			δ			α			$\bar{\phi}$	ϕ_m			Ave.
			f_d^p	f_d^s	Ave.	δ^p	δ^s	Ave.	α^p	α^s	Ave.		ϕ_m^p	ϕ_m^s	Ave.	
Flooding		EFD	0.452	0.439	0.446	0.083	0.201	0.142	0.037	0.088	0.063	-2.489	0.93	0.81	0.87	
		CFD	0.436	0.433	0.435	0.042	0.122	0.082	0.018	0.053	0.036	-2.472	2.68	2.58	2.63	
		E%D	3.54	1.37	2.47	49.40	39.30	42.25	51.35	39.77	43.20	0.68	-188.17	-218.52	-202.30	65.78
Intact Roll Decay	-13.7	EFD	0.489	0.488	0.489	0.181	0.193	0.187	0.089	0.094	0.092	0	8.24	9.25	8.75	
		CFD	0.486	0.487	0.487	0.120	0.096	0.108	0.058	0.057	0.058	0	9.14	9.1	9.12	
		E%D	0.61	0.20	0.41	33.70	50.26	42.25	34.83	39.36	37.16	0.00	-10.92	1.62	-4.29	19.04
	-20.5	EFD	0.493	0.492	0.493	0.267	0.241	0.254	0.132	0.119	0.126	0	12.48	11.81	12.15	
		CFD	0.490	0.488	0.489	0.242	0.187	0.215	0.119	0.091	0.105	0	13.18	11.73	12.46	
		E%D	0.61	0.81	0.71	9.36	22.41	15.55	9.85	23.53	16.33	0.00	-5.61	0.68	-2.55	8.16
Ave. E%D		0.61	0.51	0.56	21.53	36.33	28.90	22.34	31.45	26.75	0.00	8.27	1.15	110.19	13.60	
Damaged Roll Decay	-15.7	EFD	0.438	0.441	0.440	0.391	0.159	0.275	0.171	0.070	0.121	-2.897	5.74	10.39	8.07	
		CFD	0.444	0.442	0.443	0.255	0.128	0.192	0.114	0.057	0.086	-2.480	7.17	11.01	9.09	
		E%D	-1.37	-0.23	-0.80	34.78	19.50	30.36	33.33	18.57	29.05	14.39	-24.91	-5.97	-12.71	17.13
	15.9	EFD	0.438	0.437	0.438	0.336	0.193	0.265	0.147	0.084	0.116	-2.628	7.68	14.29	10.99	
		CFD	0.445	0.445	0.445	0.241	0.170	0.206	0.107	0.076	0.092	-2.354	8.08	13.93	11.01	
		E%D	-1.60	-1.83	-1.71	28.27	11.92	22.31	27.21	9.52	20.78	10.43	-5.21	2.52	-0.18	11.04
	-25.5	EFD	0.444	0.440	0.442	0.385	0.188	0.287	0.171	0.083	0.127	-2.932	11.07	14.61	12.84	
		CFD	0.432	0.444	0.438	0.363	0.233	0.298	0.157	0.103	0.130	-2.351	11.07	16.61	13.84	
		E%D	2.70	-0.91	0.90	5.71	-23.94	-4.01	8.19	-24.10	-2.36	19.82	0.00	-13.69	-7.79	11.07
	26.7	EFD	0.443	0.444	0.444	0.356	0.268	0.312	0.157	0.119	0.138	-2.474	9.87	17.24	13.56	
		CFD	0.445	0.431	0.438	0.285	0.164	0.225	0.127	0.071	0.099	-2.373	9.96	13.61	11.79	
		E%D	-0.45	2.93	1.24	19.94	38.81	28.04	19.11	40.34	28.26	4.08	-0.91	21.06	13.06	16.46
-28.6	EFD	0.434	0.432	0.433	0.542	0.183	0.363	0.235	0.079	0.157	-5.843	8.04	17.37	12.71		
	CFD	0.402	0.416	0.409	0.439	0.184	0.312	0.176	0.077	0.127	-4.995	9.66	16.95	13.31		
	E%D	7.37	3.70	5.54	19.00	-0.55	14.07	25.11	2.53	19.43	14.51	-20.15	2.42	-4.72	10.67	
Ave. E%D		2.70	1.92	2.04	21.54	18.94	19.76	22.59	19.01	19.97	12.65	10.24	9.13	7.69	13.28	

Table 4 CFD and EFD comparison of water height inside the compartment for calm water cases

Type	ϕ_i	EFD/CFD	ζ_A		ζ_B		ζ_C		ζ_D		ζ_E		Ave. $\bar{\zeta}_i$	Ave. f_{ζ}	Ave.
			$\bar{\zeta}_A$	f_{ζ_A}	$\bar{\zeta}_B$	f_{ζ_B}	$\bar{\zeta}_C$	f_{ζ_C}	$\bar{\zeta}_D$	f_{ζ_D}	$\bar{\zeta}_E$	f_{ζ_E}			
Flooding	0	EFD	0.080	0.465	0.071	0.441	0.064	0.465	no comp. #2		no comp. #2				
		CFD	0.078	0.444	0.071	0.435	0.064	0.424	no comp. #2		no comp. #2				
		E%D	2.55	4.47	0.81	1.33	-0.39	8.74	no comp. #2		no comp. #2		1.25	4.85	3.05
Damaged Roll Decay	-25.5	EFD	0.073	0.428	0.064	N/A	0.055	0.437	no comp. #2		no comp. #2				
		CFD	0.074	0.415	0.068	N/A	0.063	0.430	no comp. #2		no comp. #2				
		E%D	-1.89	2.96	-6.49		-13.44	1.62	no comp. #2		no comp. #2		7.27	1.53	4.40
	-28.6	EFD	0.089	0.446	0.062	N/A	0.059	0.426	0.089	0.440	0.077	N/A			
		CFD	0.086	0.402	0.072	N/A	0.061	0.419	0.083	0.413	0.075	N/A			
		E%D	3.67	9.99	-16.27		-4.47	1.44	6.62	6.14	2.46		6.70	3.51	5.11

The computational grids are overset, with independent grids assembled together to generate the total grid. The grid includes the ship hull boundary layer, compartment room 1 and 2, ventilation hole, connection grids, refinements, and background. The boundary layer grids are small enough ($y^+ < 1$) to capture the boundary layer. Because the ship hull is symmetric respect to center-plane, the grid for one side of the ship was generated and then mirrored respect to center-plane. Two Cartesian grids are used for the inside of the rooms 1 and 2 of the compartment. Two connection grids are also used; one at the opening door located between the two rooms and another one located at the compartment door. A circular cylinder grid was designed for ventilation hole. Cartesian grids are used for several refinements around the ship. In addition, a Cartesian grid for background is used to impose the far-field boundary conditions. The grid size ranges from 2.4M to 28.5M depending on the damage/intact and calm water/wave conditions of the simulations. For calm water cases, the grid size is 6.3M for the intact ship and 19.8M and 28.5M for the damaged ship with one- and two-room compartment, respectively. For wave cases, the grid size for the intact ship is 7.09M-12.2M, finer for short wave cases. The grid size for the damaged ship is within 24.1M-27.1M grid points. For verification study, a fine grid with 19.9M and a coarse grid with 2.4M points are generated from the medium grid with 7.09M points using refinement/coarsen ratio of $\sqrt{2}$. The details of grid system for damaged SSRC with the two-room compartment are shown in Fig. 2.

For the coarse grid (2.4M), 32 CPUs have been employed in parallel running for 72 hours wall clock time with computational cost of 2300 CPUh. The computational cost increases with the increase of the grid size reaching to 97000 CPUh for the finest grid (28.5 M) as it requires 288 CPUs running for about 14 days. Compared to the presumably negligible computational cost for potential flow solvers, the computational cost for current CFD study is

large but it is a complete physics-based method which can be used for much more complex conditions compared to potential flow.

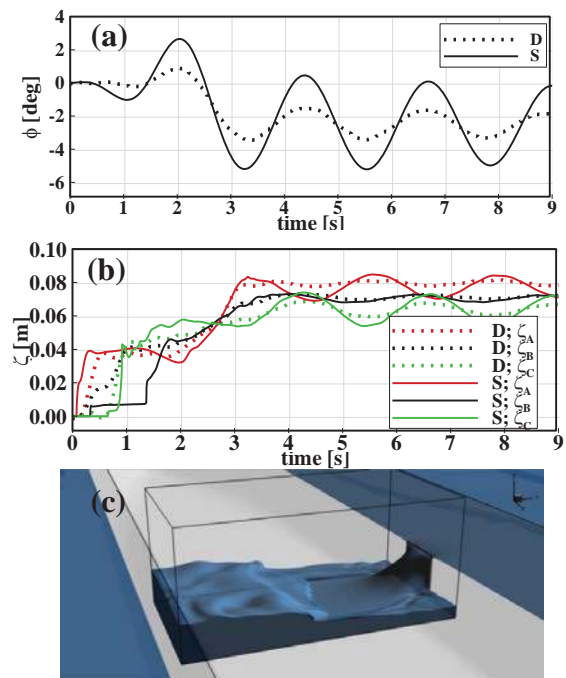


Figure 3 Flooding procedure for damaged SSRC in calm water: (a) roll; (b) floodwater height; (c) a snap shot of the predicted compartment flooding

The simulations are carried out in calm water and in waves, as shown in Table 2. The simulations are performed for the ship at zero Fr and free to all motions. For calm water, the flooding and intact/damaged roll decay cases with all different initial roll angles are simulated. For beam waves, the intact/damaged ship simulations are conducted only for the largest wave slope ($H/\lambda=1/60$) for $\lambda/L=0.52, 1.17, 1.99, 2.2, 2.42$. For all CFD simulations, k_{xx} value is adjusted to $0.0501L$ (see Table 1), found from preliminary roll decay simulation compared with the experimental data. It should be noted that experimental setup usually has difficulties to fix k_{xx} of the model to the desired value.

The validation variables are motions and water height as listed in Table 2. For flooding and roll decay, validation study is also conducted for the roll decay variables including mean roll angle (ϕ_{mk}), damping frequency (f_{dk}), logarithmic decrement (δ_k) and linear damping coefficient (α_k), and their averages over k roll



cycles ($\phi_m, f_d, \delta, \alpha$), following roll decay analysis method described in Irvine et al. (2013). Harmonic analysis are conducted for the cases in beam waves.

4. VERIFICATION STUDY

Iterative U_I and grid U_G and time U_T size uncertainties were evaluated following Stern et al. (2001) and Xing and Stern (2010) for the intact configuration regular beam waves $\lambda=2.4L$ and $H/\lambda=1/60$ conditions. The verification variables included the 1st harmonic amplitude of 6DOF motions ($x_1, y_1, z_1, \phi_1, \theta_1, \psi_1$) and corresponding phases ($x_{\epsilon 1}, y_{\epsilon 1}, z_{\epsilon 1}, \phi_{\epsilon 1}, \theta_{\epsilon 1}, \psi_{\epsilon 1}$).

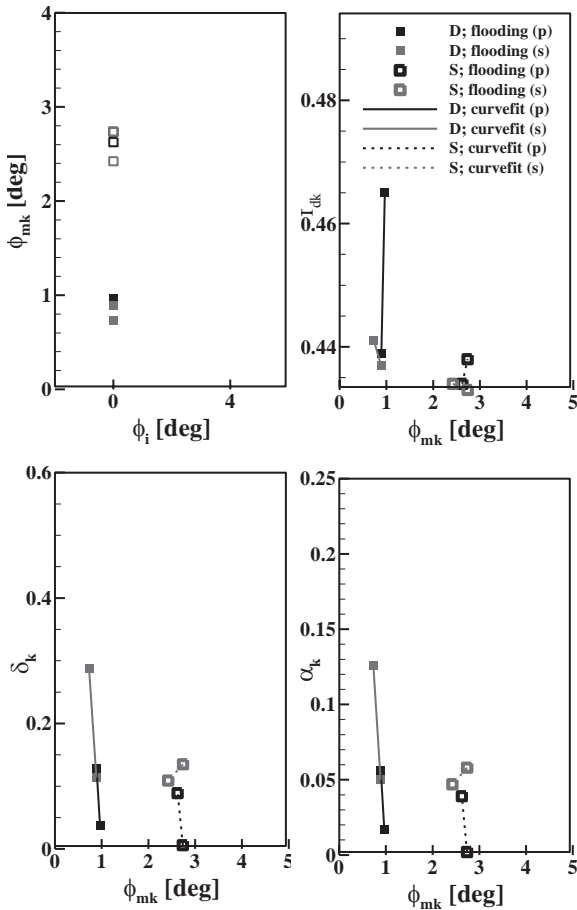


Figure 4 Variation of ϕ_{mk} with respect to ϕ_i and $f_{dk}, \delta_k, \alpha_k$ with respect to ϕ_{mk} for flooding

The verification study showed $U_I < 2\% S_1$ for both 1st harmonic amplitudes and phases with average values 0.75 and 1.22, respectively. The largest U_I was for surge and heave motions i.e.

x_1, z_1 and $x_{\epsilon 1}, z_{\epsilon 1}$. U_G/U_T were mostly MC and OC with small/large P values thus far from asymptotic range with average values 1.28/0.18 and 9.64/3.49 for amplitudes and phases, respectively. Similar to U_I , the largest U_G/U_T were for surge and heave motions. Average U_{SN} is 1.05 and 8.30 for amplitudes and phases, respectively. Further studies are needed for improved convergence and flooded conditions.

5. FLOODING

Fig. 3 shows a comparison of the experimental and computational roll and flooded compartment wave elevations along with a snap shot of the predicted compartment flooding.

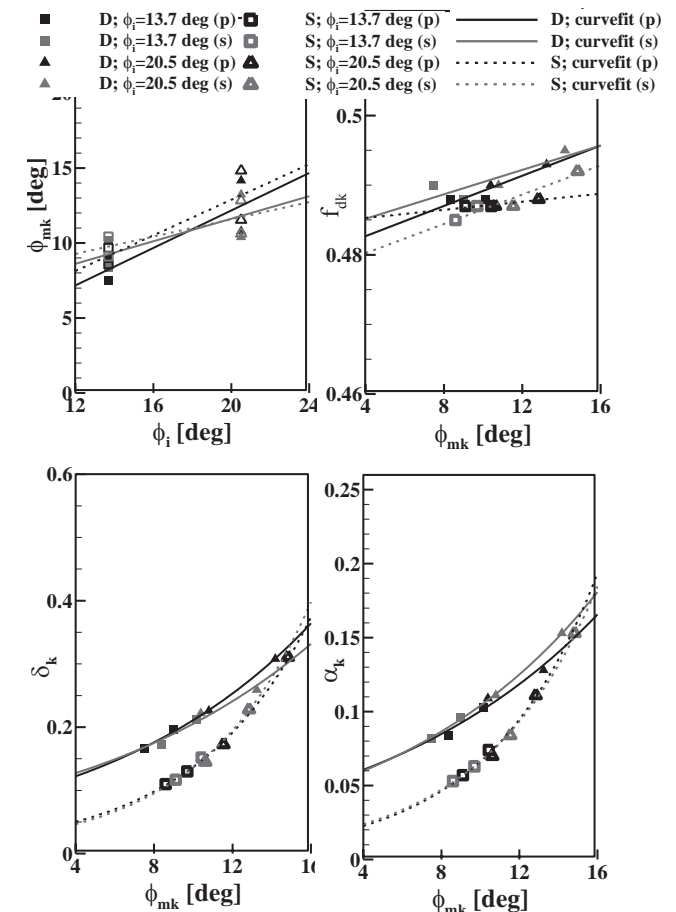


Figure 5 Variation of ϕ_{mk} with respect to ϕ_i and $f_{dk}, \delta_k, \alpha_k$ with respect to ϕ_{mk} for intact roll decay

Fig. 4 shows comparison of the experimental and computational ϕ_{mk} vs. initial roll angle (ϕ_i) and f_{dk}, δ_k and α_k vs. ϕ_{mk} .



Values are shown for both the port and starboard sides since the damaged roll response is asymmetric.

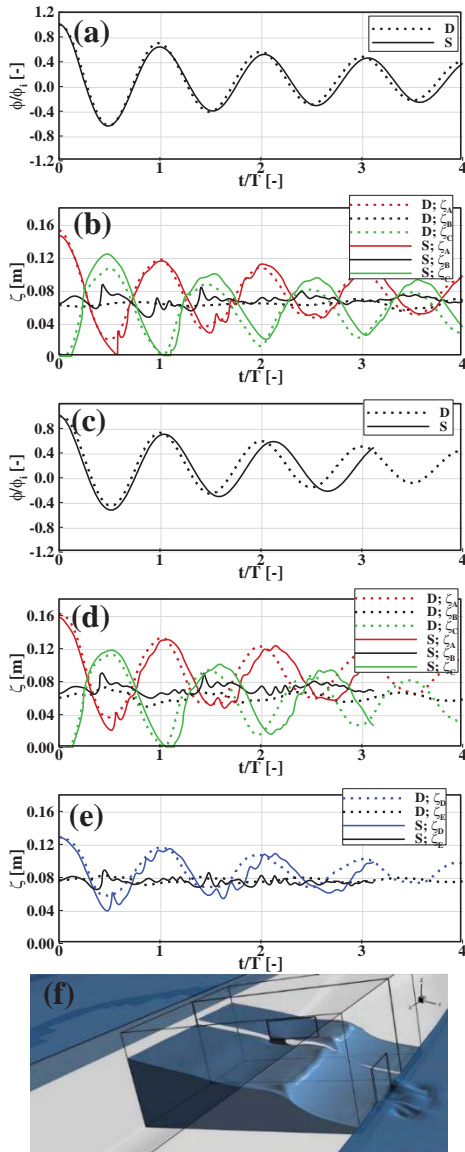


Figure 6 Results for damaged roll decay: (a) roll for $\phi_i = -25.5^\circ$; (b) floodwater height for $\phi_i = -25.5^\circ$; (c) roll for $\phi_i = -28.6^\circ$; (d) floodwater height in room #1 for $\phi_i = -28.6^\circ$; (e) floodwater height in room #2 for $\phi_i = -28.6^\circ$; (f) a snap shot of the predicted two-room compartment flooding

Table 3 and 4 summarizes the values and comparison error for the validation variables which are averaged over roll cycles. For f_d , CFD shows similar values for the intact and damaged side (~ 0.43) while EFD shows slightly larger value for the intact side. The error for f_d is 3.5%D for the intact side and 1.37%D for the damaged side, showing that CFD can predict the damaged ship roll

frequency quite well unlike the potential flow tools (ITTC, 2002). CFD results also show good agreement for heel angle $E < 1\%D$, and compartment wave elevation frequency/mean $E < 9\%/3\%D$, but the linear damping are under predicted by $E = 43\%D$ and consequently mean roll angle are predicted three times larger than EFD. The damped roll frequency is about 10% less than the one available for the intact ship roll decay, due to the lower GM value. Fig. 3c snap shot of the flooding compartment shows water entry with sloshing. The sloshing frequency is close to the damped roll frequency as shown in Table 4.

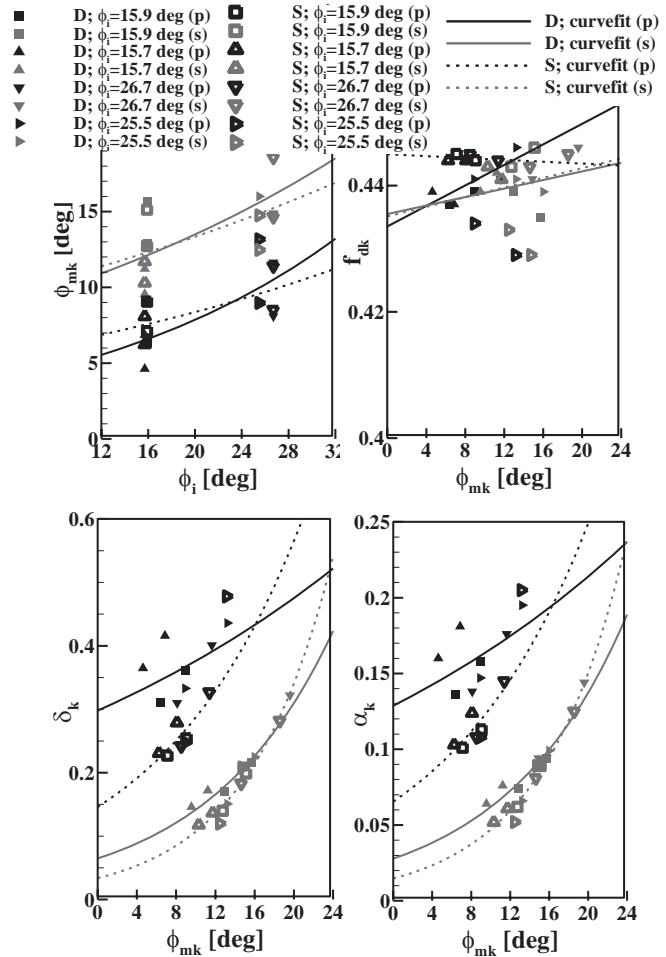


Figure 7 Variation of ϕ_{mk} with respect to ϕ_i and $f_{dk}, \delta_k, \alpha_k$ with respect to ϕ_{mk} for damaged roll decay

6. INTACT AND DAMAGED ROLL DECAY

Fig. 5 shows the comparison of the experimental and computational intact condition roll decay ϕ_{mk} vs. ϕ_i and f_{dk}, δ_k and



α_k vs. ϕ_{mk} . f_{dk} changes slightly during roll decay confirming that the restoring moment of the ship is fairly linear. The damped roll frequency is close to roll natural frequency (see Table 1) and about 10% larger than the damped roll frequency in flooding, as explained earlier. Table 3 summarize the values and errors for the validation variables. For f_d , E is <1%D for both intact roll decay cases, showing very good agreement with the experimental data. The E

values for linear damping is about 37%D for the intact case with smaller initial roll angle ϕ_i while the error decreases to 16%D for the case with larger ϕ_i . Nonetheless, the results show close agreement with the experimental data as the error for ϕ_m is 4% for the case with smaller ϕ_i , dropping to 2.5% for the case with larger ϕ_i . The simulations display strong roll, sway and yaw coupling for which validation data is not available.

Table 5 CFD and EFD comparison of 1/2, 1st and 2nd harmonic amplitudes for intact SSRC in beam waves with $H/\lambda=1/60$

λ/L	0.52			1.17			1.99			2.2			2.42			Ave E%D	
	EFD	CFD	E%D	EFD	CFD	E%D	EFD	CFD	E%D	EFD	CFD	E%D	EFD	CFD	E%D		
1st	x/A	0.030	0.034	-13	0.021	0.029	-42	0.017	0.010	39	0.025	0.016	35	0.013	0.015	-14	29
	y/A	0.533	0.525	1	0.673	0.843	-25	1.253	0.864	31	1.349	0.935	31	0.994	0.965	3	18
	z/A	0.936	1.530	-63	1.030	1.081	-5	0.853	0.893	-5	0.772	0.987	-28	0.728	0.978	-34	27
	ϕ/Ak	0.121	0.201	-66	0.548	0.354	35	4.786	4.720	1	6.297	5.543	12	5.643	5.038	11	25
	θ/Ak	0.022	0.011	49	0.007	0.030	-306	0.049	0.016	67	0.074	0.014	82	0.063	0.014	78	116
	Ψ/Ak	0.005	0.005	-1	0.009	0.019	-101	0.029	0.047	-61	0.046	0.056	-21	0.034	0.050	-48	46
	Avg. E%D			32			86			34			35			31	44
2nd	x/A	0.002	0.000	92	0.001	0.000	77	0.004	0.021	-458	0.011	0.000	95	0.008	0.000	95	163
	y/A	0.003	0.011	-225	0.006	0.012	-121	0.027	0.057	-111	0.119	0.009	92	0.109	0.006	94	129
	z/A	0.001	0.024	-3895	0.007	0.010	-47	0.201	0.059	71	0.150	0.017	89	0.168	0.006	96	840
	ϕ/Ak	0.003	0.027	-846	0.018	0.017	2	0.045	0.102	-128	0.027	0.057	-110	0.114	0.073	36	224
	θ/Ak	0.000	0.002	-1300	0.002	0.000	94	0.016	0.011	32	0.015	0.002	89	0.007	0.004	41	311
	Ψ/Ak	0.001	0.000	92	0.001	0.000	71	0.010	0.009	11	0.009	0.001	94	0.002	0.001	16	57
	Avg. E%D			1075			69			135			95			63	287
1/2	x/A	0.032	0.010	67	0.013	0.001	91	0.005	0.001	86	0.012	0.000	97	0.005	0.002	53	79
	y/A	5.602	0.565	90	0.004	0.036	-785	0.007	0.007	0	0.012	0.033	-178	0.117	0.007	94	229
	z/A	0.599	0.047	92	0.022	0.020	9	0.029	0.005	83	0.100	0.015	85	0.053	0.008	84	71
	ϕ/Ak	5.777	7.186	-24	0.007	0.148	-2016	0.044	0.184	-319	0.056	0.092	-64	0.719	0.073	90	503
	θ/Ak	0.069	0.002	97	0.007	0.002	75	0.002	0.001	48	0.010	0.000	96	0.009	0.001	91	81
	Ψ/Ak	0.058	0.044	23	0.001	0.005	-327	0.002	0.009	-475	0.003	0.002	50	0.002	0.004	-96	194
	Avg. E%D			66			550			169			95			85	193
Avg. E%D			391			235			113			75			60	175	

Table 6 CFD and EFD comparison of 1/2, 1st and 2nd harmonic amplitudes for damaged SSRC in beam waves with $H/\lambda=1/60$

λ/L	0.52			1.17			1.99			2.2			2.42			Ave E%D	
	EFD	CFD	E%D	EFD	CFD	E%D	EFD	CFD	E%D	EFD	CFD	E%D	EFD	CFD	E%D		
1st	x/A	0.027	0.040	-49	0.022	0.023	-7	0.015	0.021	-40	0.011	0.017	-55	0.004	0.015	-298	90
	y/A	0.399	0.646	-62	0.573	0.832	-45	0.731	0.852	-17	1.017	0.903	11	1.094	1.053	4	28
	z/A	1.069	1.416	-32	0.966	1.016	-5	0.856	1.032	-21	0.810	1.088	-34	0.859	1.085	-26	24
	ϕ/Ak	0.140	0.288	-106	0.391	0.572	-46	2.033	1.092	46	4.520	4.388	3	5.539	5.162	7	42
	θ/Ak	0.025	0.033	-31	0.013	0.021	-60	0.013	0.021	-66	0.045	0.013	71	0.065	0.008	87	63
	Ψ/Ak	0.010	0.010	-3	0.009	0.009	-1	0.019	0.022	-15	0.029	0.042	-45	0.038	0.053	-40	21
	Avg. E%D			47			27			34			37			77	44
2nd	x/A	0.005	0.000	93	0.002	0.001	65	0.009	0.002	75	0.003	0.000	91	0.007	0.001	91	83
	y/A	0.004	0.004	10	0.011	0.019	-73	0.049	0.059	-20	0.070	0.018	75	0.119	0.005	96	55
	z/A	0.009	0.013	-36	0.011	0.017	-49	0.126	0.008	94	0.176	0.023	87	0.229	0.054	76	68
	ϕ/Ak	0.000	0.038	-9263	0.015	0.109	-603	0.066	0.083	-26	0.276	0.161	42	0.036	0.253	-603	2107
	θ/Ak	0.001	0.000	35	0.000	0.003	-809	0.000	0.000	-49	0.013	0.001	89	0.007	0.002	71	211
	Ψ/Ak	0.000	0.000	-35	0.001	0.002	-24	0.004	0.003	23	0.014	0.000	97	0.004	0.004	1	36
	Avg. E%D			1579			271			48			80			156	427
1/2	x/A	0.034	0.001	97	0.021	0.001	96	0.009	0.012	-29	0.002	0.000	78	0.003	0.001	78	76
	y/A	0.505	0.016	97	0.053	0.046	13	0.035	0.065	-84	0.070	0.085	-22	0.006	0.016	-188	81
	z/A	0.116	0.045	61	0.064	0.038	40	0.030	0.018	40	0.066	0.035	48	0.063	0.013	80	54
	ϕ/Ak	0.558	0.245	56	0.126	0.699	-456	0.143	0.425	-196	0.326	0.491	-51	0.027	0.301	-1019	356
	θ/Ak	0.008	0.001	86	0.004	0.002	40	0.004	0.000	89	0.007	0.001	79	0.002	0.001	23	63
	Ψ/Ak	0.010	0.000	98	0.005	0.009	-72	0.002	0.024	-1391	0.004	0.005	-10	0.002	0.018	-665	447
	Avg. E%D			82			120			305			48			342	179
Avg. E%D			569			139			129			55			192	217	



Fig. 6 shows the comparison of the experimental and computational damaged condition roll decay and two compartment wave elevations along with a snap shot of the predicted two compartment flooding. The roll decay and floodwater height time histories show good agreement between the experimental data and CFD.

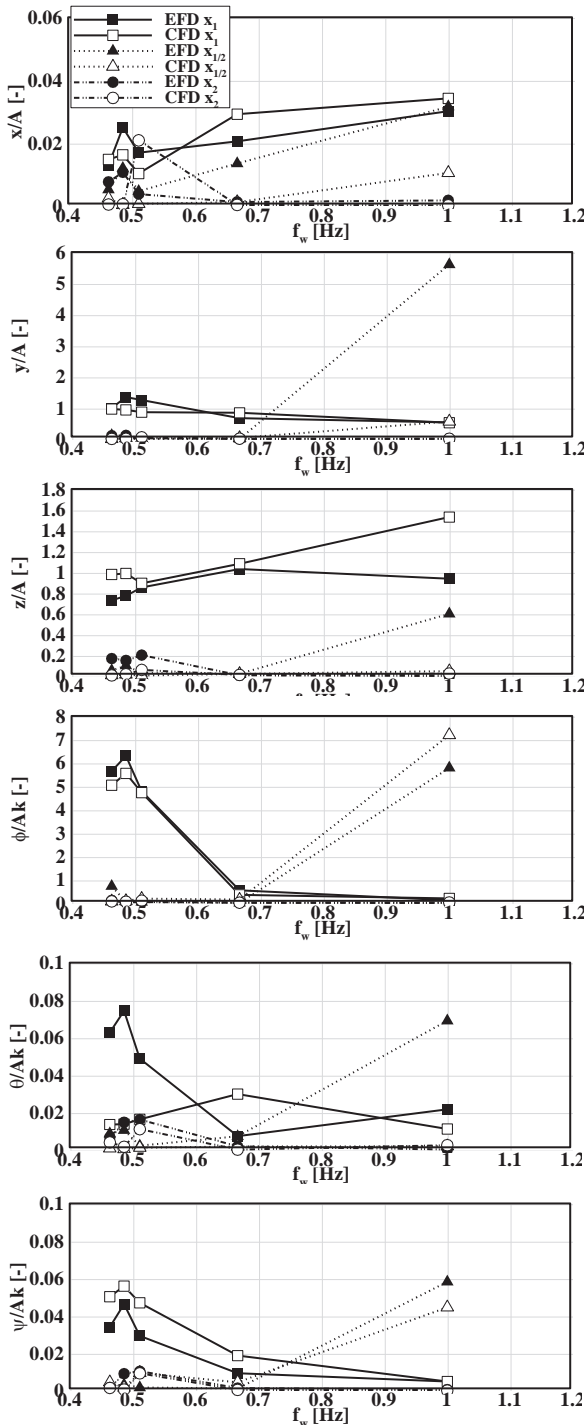


Figure 8 RAO of intact ship motions in beam waves with $H/\lambda=1/60$ for different wave frequency

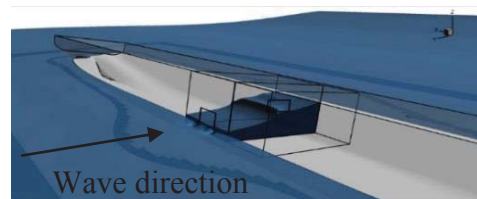
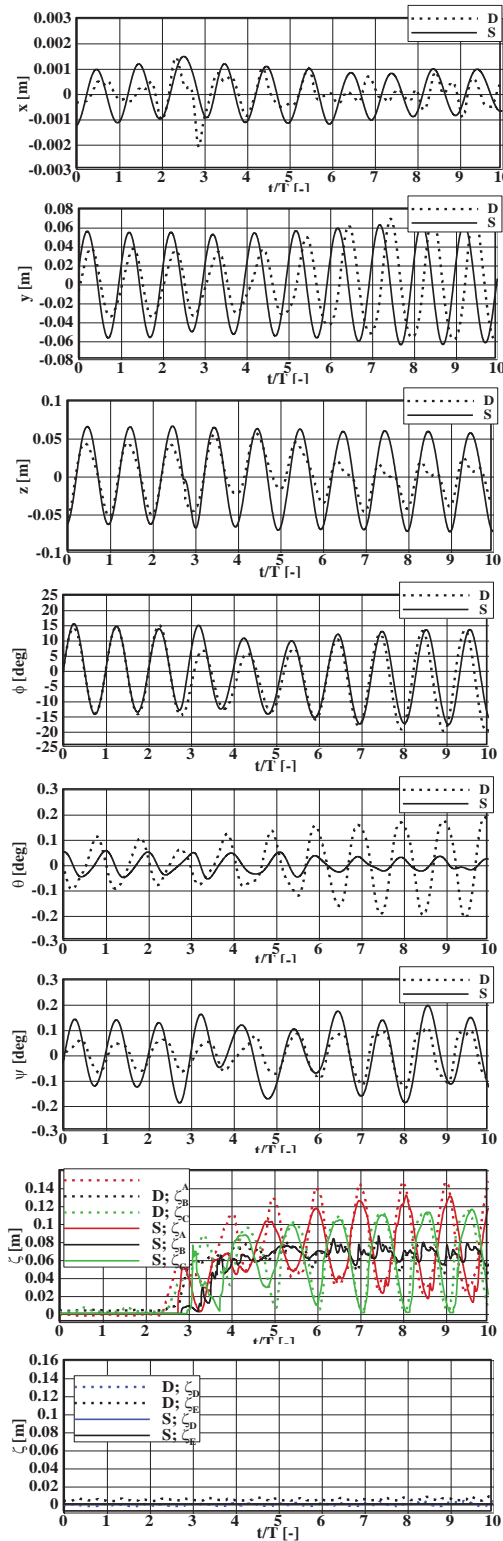


Figure 9 Time history of damaged ship motions in beam waves with $\lambda=2.42L$ and $H/\lambda=1/60$



Fig. 7 shows the comparison of the experimental and computational damaged condition roll decay ϕ_{mk} vs. ϕ_i and f_{dk} , δ_k and α_k vs. ϕ_{mk} . The experiments and simulations show scatter for the roll decay variables compared to the intact condition. The values are more scattered for portside. Tables 3 and 4 summarize the values and errors for the validation variables. Similarly as for flooding (and intact roll decay) the error for f_d is quite small for all damaged roll decay cases. The error is <2% for the cases with one-room compartment and <6% for the case with two-room compartment, showing much better prediction for current CFD studies compared to the potential flow studies ($E \sim 22\% D$), reported in ITTC (2002). α is mostly under predicted for current CFD simulations, same as for potential flow studies. However, the error values are within 2.4-29%D which is less than those reported for potential flow studies ($E \sim 62\% D$). The current results also show $E=10.7-17\% D$ for ϕ_m , $E=1.4-10\% D$ for wave frequency and $E=1.9-16\% D$ for mean wave elevation. Overall, the simulations are in both qualitative and quantitative agreement with the experiments. The simulations display strong roll, sway and yaw coupling for which validation data is not available. Fig. 6f snap shot of the two compartment flooding shows water entry with sloshing. The sloshing frequency is close to the damped roll frequency as shown in Table 4.

Comparison of the intact and damaged roll decay shows the damped roll frequency is 10%/11% smaller and damping is 15%/45% larger for the damaged ship with one/two -room compartment, which follows the stated trends in ITTC Stability in Waves Committee report (2002). Since the water height in both rooms are quite same, it was expected to have similar effect on the damped roll frequency for both one- and two-room compartment cases. However, the flooding water acts as an anti-rolling tank and damps the roll motion more quickly for the case with larger volume of flooded water. Additionally, the results showed average heel angle of -2.7

deg for one-room compartment and -5.84 deg for two-room compartment cases. The heel angle for one room compartment cases are comparable with the one for the flooding (-2.5 deg).

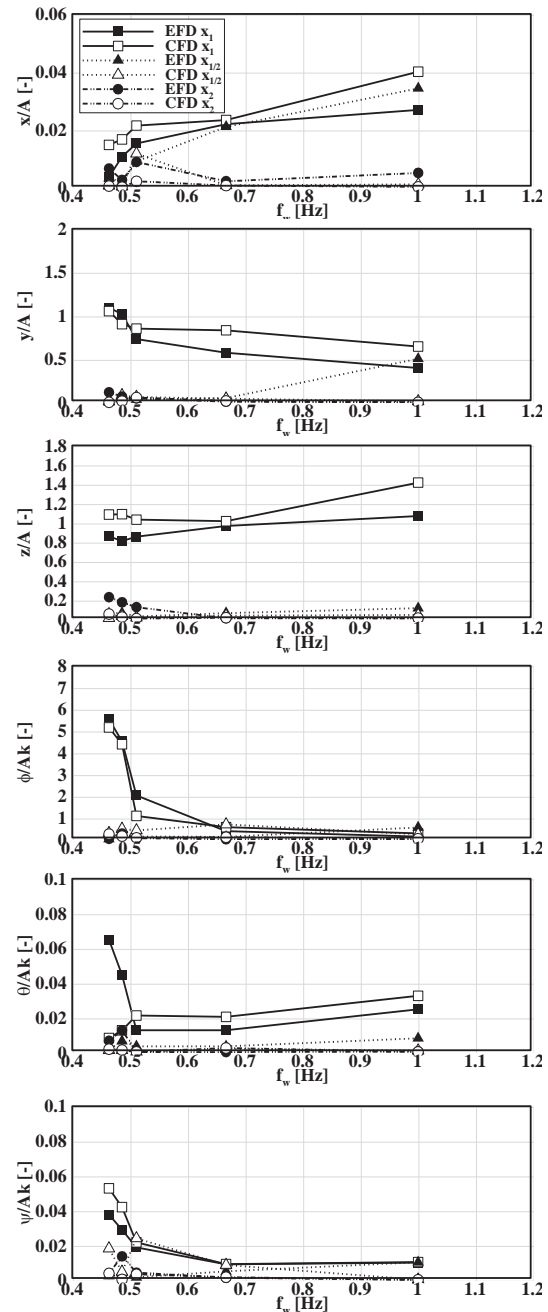


Figure 10 RAO of damaged ship motions in beam waves with $H/\lambda=1/60$ for different wave frequency



7. INTACT AND DAMAGED BEAM WAVES

Fig. 8 shows the comparison of the experimental and computational intact beam waves 6DOF 1st order (RAO), $\frac{1}{2}$ and 2nd order responses. Table 5 summarizes the validation variable and E values. All motions show primarily 1st order response, except for parametric roll condition which shows large $\frac{1}{2}$ harmonic response. The peak for roll, sway and yaw responses are at same wave frequency showing strong roll, sway and yaw coupling. The 1st order response for sway, roll and yaw is near the roll resonance condition while their large $\frac{1}{2}$ harmonic response is where the wave frequency is nearly twice of the roll frequency.

The heave 1st order response is quite large $z/A=1.0$, causing 1st order response for pitch and surge in beam waves due to surge, heave and pitch coupling. The 2nd order responses are small. The E value for 1st order responses is often larger for pitch motion with maximum error for $\lambda/L=1.17$, as the EFD value is surprisingly too small for that wavelength condition. Overall, the averaged errors for 1st order responses are quite similar for different wavelength conditions ($E\sim 31-35\%D$) without considering $\lambda/L=1.17$ test case. For $\frac{1}{2}$ and 2nd order responses, the average errors are 63-135% D and 66-169% D , respectively, excluding the large errors often shown for $\lambda/L=0.52$ and 1.17. Large E values could be due to the complex mounting system in the experiment. Nonetheless, the simulations are in both qualitative and quantitative agreement with the experiments.

Fig 9 shows the comparison of the experimental and computational damaged ship beam waves roll and flooded compartment wave elevations along with a snap shot of the predicted compartment flooding. Fig. 10 shows the comparison of the experimental and computational damaged beam waves 6DOF 1st order (RAO), $\frac{1}{2}$ and 2nd order responses. Table 6 and 7 summarizes the validation variable E

values. All motions show primarily 1st order response. Similarly as for the intact condition, the peaks for roll, sway and yaw responses are located at same wave frequency. Parametric roll ($\frac{1}{2}$ harmonic response) is not shown. The 2nd order responses are small. The average E value for 1st harmonic responses is within 27-77% D for different wavelength conditions. Among all motions, the largest errors are often for surge and pitch motions. Even though the average error for 1st harmonic roll amplitude for all the wavelength cases ($E=42\%D$) is quite large, it is still much smaller than the value report for potential flow studies in ITTC report ($E\sim 91\%D$) since the viscous effects are more accurately predicted. Similarly as for the intact condition, $\frac{1}{2}$ and 2nd order variables show larger errors. Large error values could be due to the complex mounting system in the experiment. As shown in Table 7, the mean value of the compartment water height is well predicted with $E<6.5\%D$ while $\frac{1}{2}$, 1st and 2nd harmonic amplitudes of the compartment water height show large errors. Nonetheless, the water heights are in both qualitative and quantitative agreement with the experiments, as shown in Fig. 9.

Comparing the intact and damaged ship shows that larger roll damping for the damaged ship reduces the amplitude of 1st order responses. Additionally, the peak for 1st order responses for the damaged ship (roll resonance) occurs at smaller wave frequency (longer wavelength) confirming larger roll period for the damaged ship. Similarly, the peak for $\frac{1}{2}$ order responses (parametric roll) should occur at longer wavelength due to flooding and thus more simulations between $\lambda/L=0.52$ and 1.17 are required to resolve the peak for $\frac{1}{2}$ order responses. Unlike the beam wave results for damaged passenger Ro-Ro ship reported in 23rd ITTC report (2002), 2nd order responses were small for SSRC damaged ship.



Table 7 CFD and EFD comparison of water height inside the compartment for beam wave cases

Type	λ/L	EFD/CFD	ζ_A				ζ_B				ζ_C				Ave.	Ave.	Ave.	Ave.	Ave.
			$\bar{\zeta}_A$	ζ_{A1}	ζ_{A2}	$\zeta_{A1/2}$	$\bar{\zeta}_B$	ζ_{B1}	ζ_{B2}	$\zeta_{B1/2}$	$\bar{\zeta}_C$	ζ_{C1}	ζ_{C2}	$\zeta_{C1/2}$	$\bar{\zeta}$	ζ_1	ζ_2	$\zeta_{1/2}$	
Damaged beam waves	0.52	EFD	0.079	0.017	0.007	0.005	0.069	0.002	0.006	0.001	0.065	0.016	0.006	0.007					
		CFD	0.076	0.023	0.008	0.002	0.069	0.002	0.009	0.000	0.067	0.022	0.008	0.002					
		E%D	3.05	-34.74	-10.63	63.96	-0.31	-64.75	-50.07	62.16	-3.22	-39.41	-24.89	63.71	2.20	46.30	28.53	63.28	35.08
	2.20	EFD	0.077	0.050	0.003	0.007	0.067	0.002	0.005	0.000	0.060	0.052	0.007	0.006					
		CFD	0.086	0.047	0.008	0.005	0.069	0.006	0.002	0.001	0.063	0.051	0.007	0.005					
		E%D	-10.45	4.28	-189.37	26.95	-4.06	-261.22	61.63	-53.63	-5.08	3.41	6.34	29.23	6.53	89.63	85.78	36.60	54.64
	2.42	EFD	0.074	0.055	0.002	0.003	0.066	0.004	0.006	0.000	0.064	0.057	0.008	0.004					
		CFD	0.078	0.060	0.009	0.000	0.066	0.011	0.004	0.001	0.067	0.056	0.011	0.001					
		E%D	-5.38	-8.35	-377.56	92.59	-0.31	-189.50	38.89	-119.14	-4.55	1.93	-36.41	82.16	3.41	66.59	150.95	97.96	79.73

8. CONCLUSIONS AND FUTURE RESEARCH

URANS capabilities are assessed for zero-speed ship flooding using experimental validation data for flooding and roll decay in calm water and regular beam waves at zero speed.

For flooding and roll decay, the simulations show the ability to predict the trend of increases in roll period and damping due to flooding, as reported in ITTC (2002). The damping magnitudes were often under-predicted similar to potential flow studies reported in ITTC (2002). However, the errors are smaller for current CFD studies ($E < 43\%D$) compared to those reported for potential flow ($E \sim 62\%D$) even though the computational cost is larger. The damped roll frequency and floodwater heights were well predicted with $E < 5.5\%D$ and $E < 7\%D$, respectively. Therefore, CFD could predict the hydrodynamic added moment of inertia due to the flooding unlike the potential flow as reported in ITTC (2002). Two-room compartment simulation showed three times larger damping than one-room compartment cases whereas the roll period was similar for both conditions. The simulations display strong roll, sway and yaw coupling for which validation data is not available. The compartment showed sloshing with a frequency close to the damped roll frequency for all calm water cases.

For the beam wave cases, all motions show primarily 1st order response, except for the parametric roll condition which shows large $\frac{1}{2}$ harmonic response for the intact ship. The 2nd order responses are small for both the damaged and intact ship, unlike ITTC (2002). The average error for 1st order responses is 44%D with large errors for the intact ship pitch motion and damaged ship surge and pitch motions. The results show that the average error for 1st harmonic roll amplitude ($E = 42\%D$) is much smaller than that for potential flow studies in ITTC (2002) ($E \sim 91\%D$) since the viscous effects are more accurately predicted. $\frac{1}{2}$ and 2nd order variables show also large errors. Large error values could be due to the complex mounting system in the experiment. The compartment water height mean value was predicted very well ($E < 6.5\%D$) while $\frac{1}{2}$, 1st and 2nd order water height amplitude show large errors. The trend of responses against the wave frequency is similar for sway, roll and yaw motions and also for surge, heave and pitch motions due to the strong coupling between them. For the damaged ship, the larger roll period and damping shift the peak of responses to smaller wave frequency and also reduce the amplitude of responses.

In future, the damaged ship behavior in beam waves approaching the ship from the intact side will be studied. Additionally, damaged stability for the self-propelled free running ship in following or head waves will be investigated.

9. ACKNOWLEDGEMENTS

The research was sponsored by the US Office of Naval Research (ONR) grant 000141-41-04-6-5 and ONR Global as part of the Naval International Cooperative Opportunities in Science and Technology Program (NICOP) under the supervisions of Drs. Ki-Han Kim and Woei-Min Lin. The CFD simulations were conducted utilizing DoD HPC.

10. REFERENCES

- Gao, Q., Vassalos, D., 2011, Numerical study of the roll decay of intact and damaged ships. In: 12th STAB workshop, Washington, US.
- Gao, Z., Gao, Q., Vassalos, D., 2011, Numerical simulation of flooding of a damaged ship, Ocean Engineering, Volume 38, Issues 14–15, Pages 1649–1662.
- Gao, Z., Gao, Q., Vassalos, D., 2013, Numerical study of damaged ship flooding in beam seas. Ocean Eng. 61, 77-87.
- Huang J., Carrica P., Stern F., 2008, „Semi-coupled air/water immersed boundary approach for curvilinear dynamic overset grids with application to ship hydrodynamics,, International Journal Numerical Methods Fluids, Vol. 58, pp. 591-624.
- Irvine, M., Longo, J., Stern, F., 2013, Forward Speed Calm Water Roll Decay for Surface Combatant 5415: Global and Local Flow Measurements, Journal of Ship Research, Vol. 57, 2013.
- ITTC, 2002, The Specialist Committee on Prediction of Extreme Ship Motions and Capsizing, Proceedings of 23rd International Towing Tank Conference, Venice, 2002.
- Lee S., You J.M, Lee H.H., Lim T., Park S.T., Seo J., Rhee S.H., and Rhee K.P., 2015, Experimental Study on the Six Degree-of-Freedom Motions of a Damaged Ship Floating in Regular Waves, IEEE Journal of Oceanic Engineering, DOI:10.1109/JOE.2015.2390751.
- Lee S., You J.M, Lee H.H., Lim T., Rhee S.H., and Rhee K.P., 2012, Preliminary Tests of a Damaged Ship for CFD Validation, International Journal of Naval Architecture and Ocean Engineering, Vol. 4, No. 2, pp.172-181.
- Lim, T., Seo, J., Park, S.T., Rhee, S.H., 2014, Experimental Study on the Safe-Return-to-Port of a Damaged Ship in Head Seas, 30th SNH, Hobart, Australia.
- Palazzi, L., De Kat, J. O., (2004). “Model experiments and simulations of a damaged ship with air flow taken into account”, Marine Technology, 41 (1), 38-44.
- Papanikolaou, A., Zaraphonitis, G., Spanos, D., Boulougouris, E., Eliopoulou, E., (2000). “Investigation into the capsizing of damaged Ro- Ro passenger ships in waves”, Proc. of the 7th Intl Conf on Stability of Ships and Ocean Vehicles, STAB2000, Tasmania, pp. 351-362.
- Stern, F., Wilson, R. V., Coleman, H. W., and Paterson, E. G., 2001, Comprehensive Approach to Verification and Validation of CFD Simulations—Part 1: Methodology and Procedures, ASME J. Fluids Eng., 123(4), pp. 793–802.
- Strasser, C., Jasionowski, A., Vassalos, D., 2009, Calculation of the time-to-flood of a box shaped barge by using CFD. In: 10th STAB conference, St. Petersburg, Russia.
- Xing, T. and Stern, F., 2010, Factors of Safety for Richardson Extrapolation, ASME Journal of fluids engineering, Vol. 132, No. 6, DOI: 061403.

This page is intentionally left blank

Session 7.3 – DYNAMIC STABILITY

Modified Dynamic Stability Criteria for Offshore Vessel

On Aerodynamic Roll Damping

SPH Simulation of Ship Behaviour in Severe Water Shipping Situations

A Reassessment of Wind Speeds Used for Intact Stability Analysis

This page is intentionally left blank



Modified Dynamic Stability Criteria for Offshore Vessels

Govinder Singh, Chopra, *Director, SeaTech Solutions International (S) Pte Ltd*

info@seatechsolutions.com

ABSTRACT

Stability has always been the biggest concern of vessels owners, operators and naval architects. Stability defines the safety and operability of a vessel, and for any activities to take place, these two points have to be fulfilled. The stability of offshore vessels has become an issue with the trend of increasing roles and unpredictable operations that one offshore vessel has throughout its lifespan.

This paper attempts to provide a ship designer's perspective on the stability issues based on our own experience and suggests a modified dynamic stability criteria more suitable for these offshore vessel operations.

KEYWORDS: *Stability of offshore vessels; Offshore operating environment; Crane operations; Towing; Anchor handling.*

1. INTRODUCTION

There is a well-known Chinese saying “Water can support the ship and it can also capsize it”. Every vessel is capable of capsizing; the only question is under which conditions. The International Maritime Organization’s (IMO) Maritime Safety Committee agreed in principle that “*ships are to be designed and constructed for a specific design life to be safe and environmentally friendly, when properly operated and maintained under specified operating and environmental conditions, in intact and specified damaged conditions throughout their life*” (IMO, 2009).

The IMO Criteria for stability has been developed for commercial vessels and has proven to be reasonably safe. How relevant is this criteria for other types of vessels such as offshore support vessels or workboats?

The number of Offshore Support Vessels (OSV) has increased over the years (see Fig 1). To date, approximately 30 per cent of world’s oil and gas production comes from offshore. As the search for oil moves to deeper waters the challenges increase and the operating sea conditions get harsher. As a result, offshore vessels have evolved to keep pace with the ever changing demands. Today offshore vessels support a variety of duties e.g. for search and rescue, diving support, well intervention, maintenance support, hotel service etc.; either as specialist vessels or as multi-purpose vessels. Further, offshore vessels are no more limited for oil and gas industry; we see increasing use in industries such as offshore wind farms and deep sea mining.

1.1 Offshore Support Vessels Operations

There are many differences between OSVs and commercial vessels, in terms of their operating profiles, operating environment vulnerability and the risks faced. The roles of



OSVs are more diverse as compared to commercial vessels, e.g. transportation of goods and personnel, towing; diving support, search and rescue, well intervention, oceanographic surveys and deep sea mining etc (see Table 1). Unlike commercial vessels which are primarily used to carry cargo or passengers from one port to another, OSVs are built as workboats and they carry out different operations, as and when required to support the offshore industry. The duties these vessels may be asked to perform are unpredictable.

	Offshore Vessels / Workboats	Commercial Vessels
Types of Vessels	-Tugs -AHTS (Anchor Handling Towing Vessels) -PSV (Platform Supply Vessels) -DSV (Diving Support Vessels) -Survey -Well intervention -Fire fighting vessel -Deep sea mining	-Bulk carriers -Container ships -Tankers -Ocean liners -Cargo ships -Passenger Ships
Size	Length < 100m	Length > 100m
Characteristics	-Power horses -Very manoeuvrable -GM approx. 1m -Lower freeboards -Higher vulnerability to capsize -Unpredictable operations	-Optimised power for sailing -Do not require high manoeuvrability -GM > 2m -High freeboards -Predictable operations
Modes of Operation	-Sailing -Standby -Harbour -DP (Dynamic Positioning) -Anchor handling -Towing -Crane operations -Deck Cargo -Fire fighting	-To carry cargo, or passengers from point A to point B -Sailing -Harbour

Operating Environment	-Wind – 35 knots -Currents – 1.5 knots -Waves – 6m -Not only when sailing, but also when stationary as in DP.	-Commercial vessels can reduce speed or change course. -Operators will try to avoid seasons where the conditions of the sea are harsh; some operators may have a fixed operating months where they can predict the sea conditions
	-As activity moved further and further offshore, harsher operating sea conditions.	

Table 1: Main difference of OSVs and Commercial Vessels

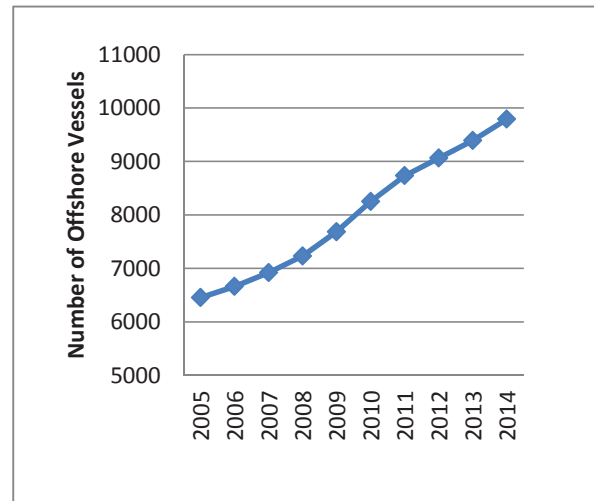


Fig 1: Number of offshore vessels by year (Clarkson Service Limited 2015)

1.2 Operating Environment

As operations move further offshore, the greater the environmental uncertainties, hence, the larger the number of safety factors that need to be applied to achieve a target level of structural adequacy and reliability. (Paik and Thayamballi 2007) The OSV is required to operate and work in this harsh environment. Anchor handling operations, Towing, Crane Operations etc. need to be carried out under these conditions. Most OSVs are required to remain in a particular position in Dynamic Positioning mode over a long period of time to



support the offshore operations. For example a Diving Support Vessel (DSV) which supports diving operations need to have its position unchanged as the lives of the divers are dependent on the vessel. Therefore, unlike commercial vessels which can choose to make a detour to avoid extreme weathers, OSVs need to withstand harsh weather conditions while remaining stationary at a particular position.

1.3 Stability for Operations

As the OSV is a different form of vessel, and the operating conditions are different, the relevance of the IMO stability criteria to such operations is studied and a possible modified criterion is proposed which may more realistically take into consideration the operations as well as the operating conditions under which OSVs need to operate.

Designers know how to make ships safer but safety always comes at a cost. In practice, therefore, there is a compromise between safety and the economies of operations, and the vessel is designed to regulatory minima, because that gives the most economical solution with acceptable safety. Traditionally, regulations and stability information booklets provide limited safety guidance to the master of the ship but they do give the operator the full confidence to go to sea in the false belief that the ship is safe. It may not be safe though, particularly if it is a small vessel in big seas, and would depend on how the vessel is operated in these conditions. For OSVs which may have unpredictable operating conditions, it becomes crucial to develop a limiting envelope together with practical methods of assessing the level of safety of a ship in the range of sea states in which a ship might remain safe from capsize. Regulators have the greatest responsibility but sometimes they may be intimidated by industrial, commercial and political pressures. We should use what we learn to improve safety for all, by developing

simple formulae which may offer operators means of safety assessment.

2. EVOLUTION OF IMO STABILITY REQUIREMENTS

The first IMCO (IMO) Resolutions concerning stability criteria were adopted in 1968 by Assembly resolutions A167(ES.IV) for passenger and cargo ships under 100 meters in length and in A.168(ES.IV) for fishing vessels, the Resolutions are based on the analysis of statistical data on casualties and on ships considered safe from the point of view of stability. (Kobylinski and Kastner 2003)

Recognising that the stability criteria may not be “rational” since resolution A.167 was applicable only to small ships (length of not more than 100 meters), the committee decided to develop a “weather criteria” requirement for the situation where the ship is exposed to beam wind when rolling on the wave hence aiming to improve safety against capsize. Weather criterion was then introduced and adopted by resolutions A.562(14) for passenger and cargo vessels and A.685(17) for fishing vessels and its application was not limited to ships under 100 meters in length.

In dead ship condition with severe wind and corresponding roll, the ship must comply with the “weather criterion”. The main scope of this criterion is to determine the ability of a ship to withstand severe wind and rolling from a beam sea by comparing heeling and righting moments.

However the criterion is for dead ship and still not related to the wind force that the ship may encounter, in service, while operating.

Intact Stability (IS) Code, a harmonisation of the existing stability requirements and weather criterion, was initially adopted in 1993 by resolution A.749(18). Current version of the IS Code 2008 was adopted about 15 years later by resolution MSC.267(85). IS Code preserved



basic stability criteria, statistical as well as weather criterion virtually unchanged. The basic statistical criteria and weather criteria were now made compulsory by way of reference in the SOLAS Convention to part A of the IS Code 2008.

Recognising the fact that the design and normal operation of offshore supply vessels are different compared to conventional cargo ships, IMO came up with “Guidelines for the Design and Construction of Offshore Supply Vessels”, A.469(XII) adopted on November 1981 and superseded by Res.MSC.235(82). For offshore vessels, the same criteria used for merchant vessels have been passed on. Classification society have prescribed criteria for certain operating modes of OSV such as: towing; fire fighting; anchor handling; and crane operations.

In February 2015, the sub-committee for Ship Design and Construction (SDC) agreed on draft amendments pertaining to vessels that engage in anchor handling operations (SDC-2 2015). These changes to part B of the International Code on Intact Stability, 2008 (2008 IS Code) are slated for submission to MSC 95 for approval. Vulnerability criteria and standards (level 1 and 2) related to ‘parametric roll, pure loss or stability and surf-riding / broaching; and to ice accretion in timber deck cargo’ were some of the other amendments the sub-committee has agreed in principle to draft.

A correspondence group has been set up to assist with these amendments concerning towing and lifting operations. They are expected to report their findings to the next session of SDC.

3. LIMITATIONS OF PRESENT STABILITY CRITERIA

Regardless of the particular situation being evaluated, however, the conventional approach to stability evaluation still remains valid. The

goal is to ensure that there is sufficient righting energy along with adequate freeboard to the downflooding points.

The criteria included currently in the IS Code is a design criteria, addressed mainly to ship designers. However, it is well known that about 80% of all casualties at sea are due to operational factors and the human factor. Resolution A.167(ES.IV) in the preamble acknowledges this, stressing the importance of good seamanship. It is to be noted that many stability casualties still happen every year, and most of these with small ships. Such accidents may not create strong reaction or public opinion as the casualties with large ships do.

Casualties for Merchant Vessels have been reducing significantly over the last 5 years. However, the casualties for OSVs do not show a similar decrease (see Fig 2).

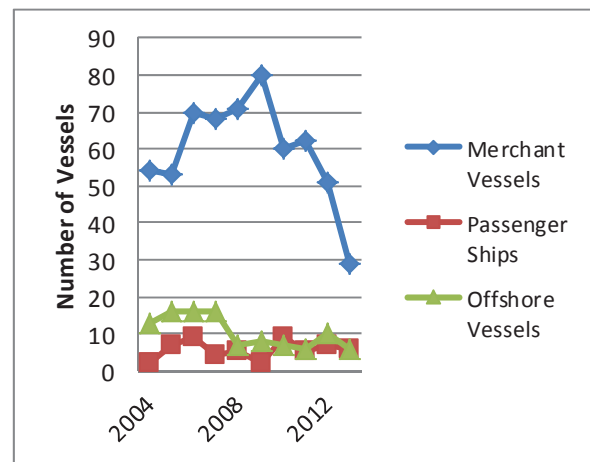


Fig 2: Losses & Casualties of Merchant Vessels, Passenger Ships & Offshore Vessels (Clarkson Services Limited 2015)

At its core, the afloat stability of the vessel is a function of:

- Adequate buoyancy and stability of the hull form;
- Preventing water from ingress into the buoyant body
- Limiting the movement of any water which does manage to enter the buoyant body



Based on the geometry and hull form, the vessels stability characteristics get fixed at the design stage, such as KM, KN etc. Each hull form being unique, the stability characteristics will be different, however for a given set of fixed dimensions, there is little room for designers to drastically improve these stability characteristics.

3.1 Watertight Integrity

The other major aspect of capsizing is the watertight integrity.

3.1.1 External Watertight Integrity

As noted earlier, one of the most important parts of ensuring adequate stability involves providing external watertight and weathertight integrity so that the hull boundary remains effective in providing buoyant force and righting energy. This is most often expressed as the location of the downflooding points into the hull. (Rousseau and Breuer, 2007)

3.1.2 Downflooding Point

“Downflooding point” is the point at which water could enter the hull envelope which was providing buoyancy and stability. From an external integrity standpoint, it is important to note that intact stability is an expression of an intermittent phenomenon, so that the vessel is presumed to incline under the effect of the environment and then return upright when that effect is removed. This has implications for the types of closures that can be considered to eliminate downflooding.

There are generally two types of downflooding points assumed in the calculation of stability: unprotected openings and weathertight openings. Openings which may be closed watertight may be ignored as downflooding points, but the types of these are limited.

3.1.3 Unprotected Openings

The most common unprotected opening is the ventilator, since provision of air to combustion machinery is necessary for operations. The possibility exists that in certain conditions, however, some of the unprotected openings may be closed such as during the preparation for severe storm or for the duration of the tow and when the hull is unmanned and not in an operational condition

Unprotected openings are important in both intact and damage stability, since water can enter the hull even during intermittent immersion of the opening.

3.1.4 Weathertight Openings

Providing weathertight closures on openings into the buoyant envelope removes them from consideration in intact stability because they are assumed to be effective in preventing the ingress of water during intermittent immersion.

There are two facts to remember regarding such closures, however: they must be manually or automatically engaged to be effective, and they will not prevent water ingress if they remain submerged, under water pressure.

In order that engagement is assured, a closure must either be automatically closing (like a ball or float check closure on a tank vent pipe) or must be specifically closed as part of a procedure such activating a screw-down ventilator closure during storm preparation.

Since they serve such a vital role in maintaining the external boundaries, it is important that closures are periodically inspected and are maintained in proper working condition.



When it is possible for an opening to be submerged for long periods, as in the case of openings below the final damage waterline, it is necessary to provide positive closure and maximum degree of confidence of the effectiveness of the closing means in preventing entry of water when subject to the same pressure head of water as the surrounding structure. In general, this involves bolted manholes or positive closing valves which are as effective as the surrounding boundary. These openings are therefore excluded from the list of downflooding points in all analyses of stability.

Penetrations in the shell for wire rope have been accepted based on a dual “pinch valve” assembly, which fails in the closed position and can be tested with applied pressure. In addition to such testing during construction of the unit, proper inspection and maintenance is also critical to ensure that the valve materials are not worn and rendered ineffective.

Ventilation closures are specifically excluded from consideration as watertight, due to the typically large size of ventilation openings and the concern over the provision of a truly watertight seal to the appropriate pressure head.

No less important than the ability to keep water outside of the buoyant envelope is the ability to limit the extent to which it can progress in the event that damage has occurred. The subdivision of a floating vessel is the means by which the final inclination or parallel sinkage is limited, which in turn helps keep the downflooding openings above the waterline, after damage.

3.1.5 Automatic Closing Openings

All tank vents and overflows are required to have automatic closures, not just the ones which might be subject to intermittent immersion.

3.2 Dynamic Positioning (DP) Mode

The present stability criteria have not dealt with such conditions of operations which take place with simultaneous wind, waves and currents. The “weather criteria” considers a dead ship or a stationary ship. However, all offshore vessels operations are carried out often under harsh sea conditions. In the DP mode, the reaction or forces from the thrusters to counter the environmental forces/moments resulting in heeling moments needed to be added in the “weather criteria”, along with crane operations. In actual operations, “worst” downflooding point may need to be considered.

4. LIMITING ENVELOPE

For safe operations, a limiting envelope could be provided for the operator’s guidance.

4.1 Limiting KG

The limiting KG is the maximum KG complying with prescribed and applicable set of criteria at a given draft.

4.2 Limiting Heel

This is another useful guidance for operators. The heel cycle needs to be less than the angle of which water may flood the vessel through opening left without weathertight closures.

4.3 Limiting Sea Conditions during Different Modes of Operations

Perhaps, this is the most critical guidance for the operator - limiting sea conditions i.e. the wind, wave, and current limitations.

5. CASE STUDIES

Stability investigations were carried out on existing designs of offshore vessels, in order to have a better perception of the limitations of the present stability criteria as applied to offshore vessels and then identify areas where the criteria may be modified to take better account of the actual operations.

The types of vessels investigated were as follows (see Tables 2-5):

1. Anchor Handling Tugs / Supply Vessels (AHTS) – 3 Nos.
2. Tugs – 3 Nos.
3. Platform Supply Vessels (PSV) – 3 Nos.
4. Diving Support Vessels (DSV) – 3 Nos.

Table 2: Dimensions of three unique AHTS

AHTS			
	AHTS1	AHTS2	AHTS3
Length B.P.	44.4m	63.1m	62.5m
Beam (Mld)	12.6m	14.8m	17.0m
Depth (Mld)	5.5m	6.5m	8.5m
Design Draft	4.5m	4.8m	6m
Bollard Pull	50MT	80MT	130MT

Table 3: Dimensions of three unique Tugs

TUG			
	Tug1	Tug2	Tug3
Length B.P.	25.5m	25.2m	27.0m
Beam (Mld)	10.5m	9.5m	12.0m
Depth (Mld)	4.5m	5.0m	5.3m
Design Draft	3.0m	4.0m	4.5m
Bollard Pull	35MT	40MT	50MT

Table 4: Dimensions of three unique PSV

PSV			
	PSV1	PSV2	PSV3
Length B.P.	73.6m	48.2m	57.4m
Beam (Mld)	17.0m	12.6m	18.0m
Depth (Mld)	8.0m	5.0m	5.0m
Design Draft	6.3m	3.5m	2.5m

Table 5: Dimensions of three unique DSV

DSV			
	DSV1	DSV2	DSV3
Length B.P.	55.0m	55.2m	83.4m
Beam (Mld)	13.3m	13.8m	18.2m
Depth (Mld)	5.0m	5.0m	7.8m
Design Draft	4m	3.6m	4.2m

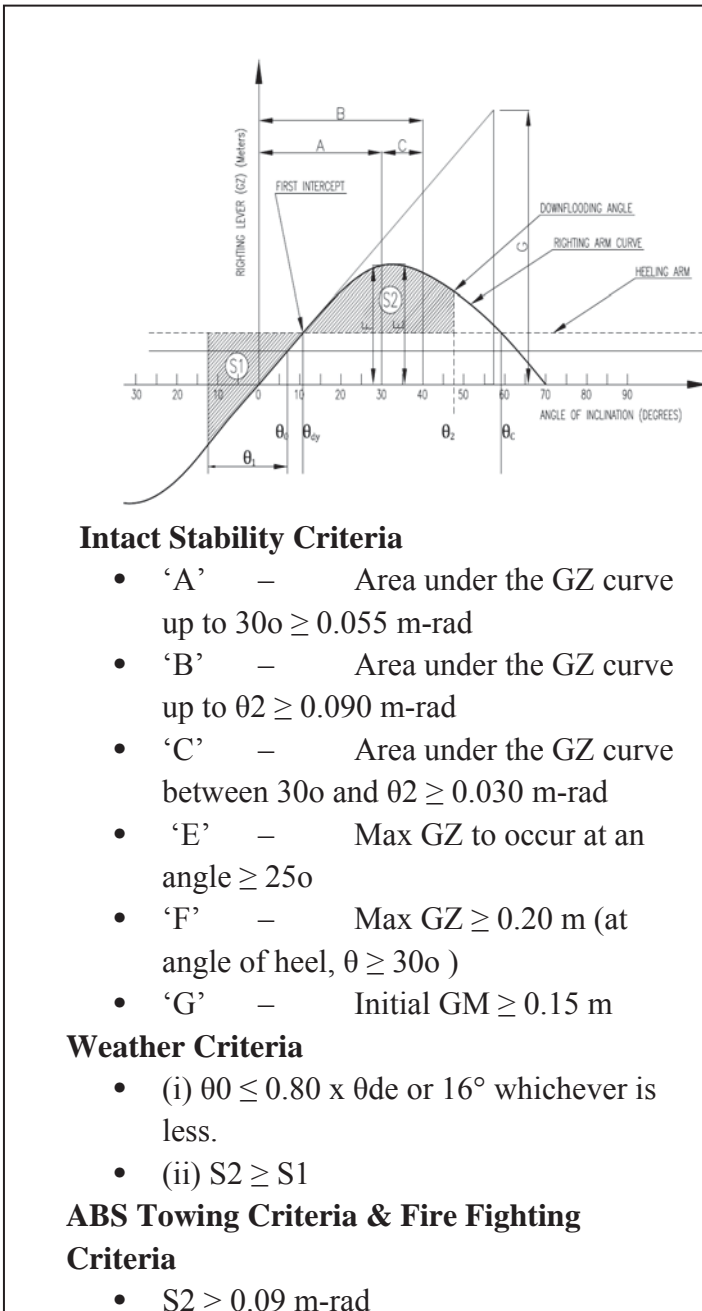


Fig 3: Intact Stability, Weather, Towing and Fire Fighting Criterion

5.1 Dominant Criteria

Limiting KG values were calculated under different draft conditions for all the criteria as defined in Figs 3-4.

1. Intact stability criteria (Fig 3)
2. Weather criteria (Fig 3)
3. Towing & Fire fighting criteria (Fig 3)
4. Crane criteria (Fig 4)

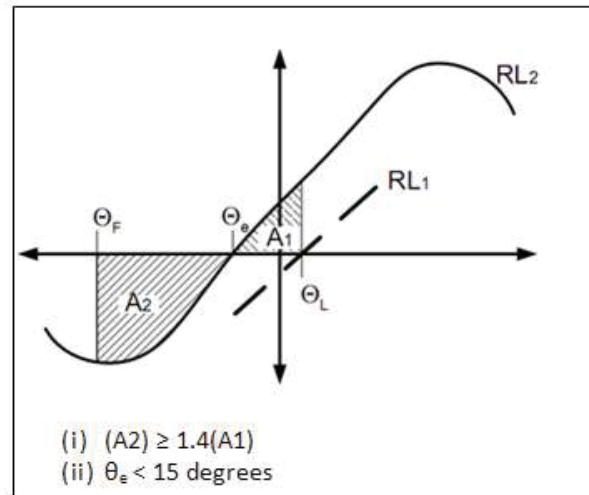


Fig 4: Stability with loss of Crane load

Investigations revealed a certain pattern in the criteria which was most dominating at different draft loading conditions (see Table 6).

Table 6: Dominant criteria under four different loading conditions

	Dominant Criteria			
	AHTS	TUG	PSV	DSV
Light Draft	Weather	Towing	Weather	Weather
Light Draft - Mid Operating Draft	Towing	Towing	Weather	Crane
Mid operating draft - Normal operating draft	Towing	Towing	Max 92° angle	Crane
Normal operating - Max draft	Max 92° angle	Max 92° angle	Max 92° angle	Max 92° angle



5.2 Operational Stability

Offshore vessels provide support for the offshore industry and perform these operations under harsh sea conditions.

A series of operations to deploy and retrieve anchors for oil rigs or floating platform is called anchor handling. The AHTS should be equipped with high bollard pull, stern roller and high handling capacity winches on board.

Two accidents have already been reported in the history of this industry, and these operations are indeed considered hazardous.

The reduction of dynamic transverse stability of anchor handling vessels due to the additional overturning moment induced by the lifting anchor load is to be considered (Gunu and Moon, 2012). Along with this the wind and wave forces can lead the vessel into capsize situation.

The present criteria provides for downflooding from unprotected openings which are normally the Engine Room Ventilator openings/louvers as it is assumed all other openings can be closed weathertight and will so be closed. However in offshore vessels

and tugs, this is not the case. There may be other openings such as steering gear compartments ventilators or sometimes even doors to accommodation spaces may not be closed tight. We would rightly term this as bad seamanship or mishandling, but this makes the ship more vulnerable to capsizing. A case is made for considering such downflooding points which are not considered in the present criteria and these are termed as “worst” downflooding points.

Limiting KG curves were plotted (Fig 6 to 9) during operations for each type of vessel and for the following cases:

1. Without wind
2. With wind
3. With wind and “worst” downflooding (DF) point (see Fig 5)
4. With wind, “worst” downflooding (DF) point and aft trim 1% L

In cases of the DSV Crane Operations, the classification society Det Norske Veritas (DNV) requirement already considers the effect of wind during crane operations. However as the DSV operations are in DP mode, the additional heeling moment of the thrusters must be considered. This also has a significant impact on reducing the limiting KG (see Fig 9)

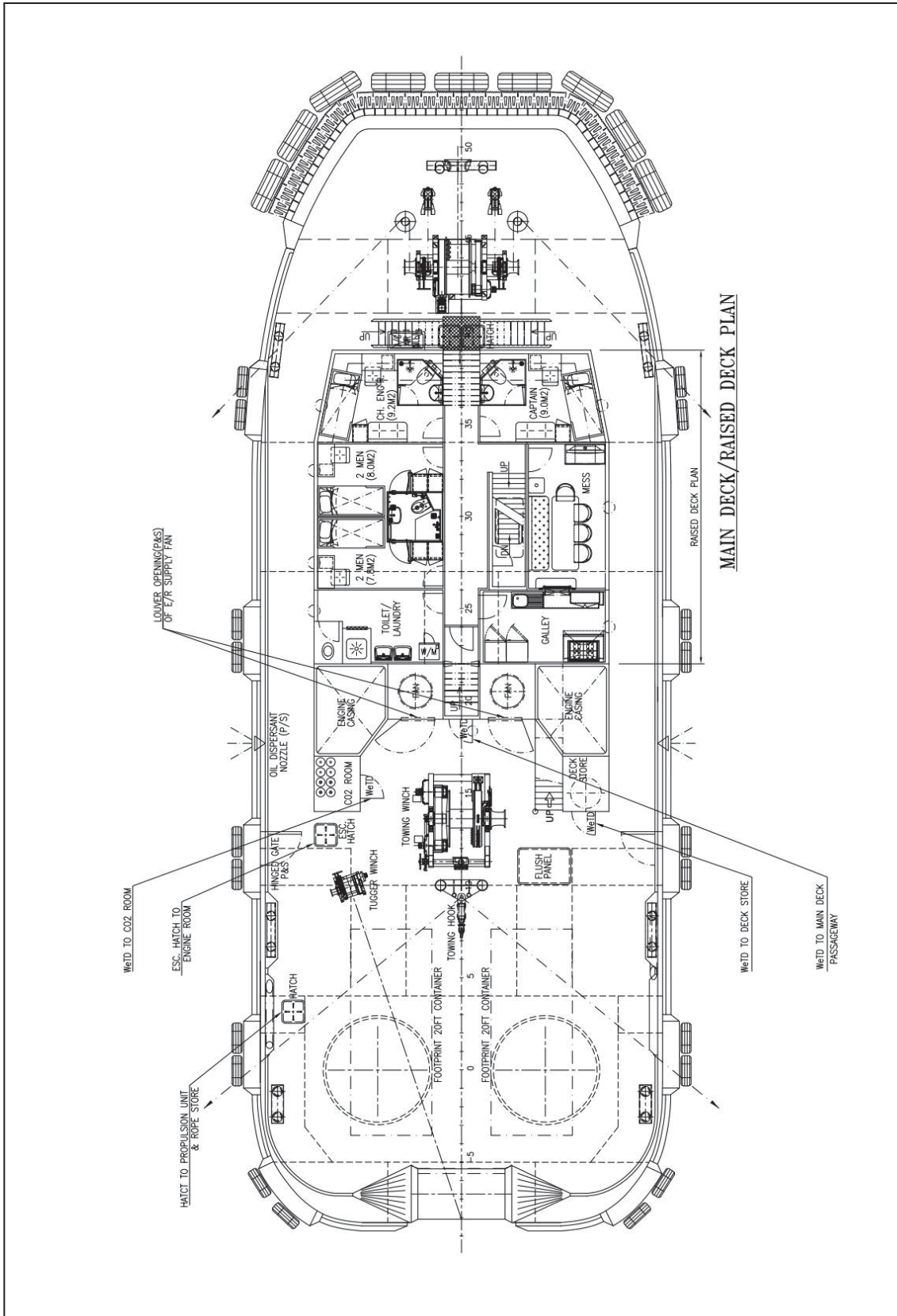


Fig 5: Downflooding Points

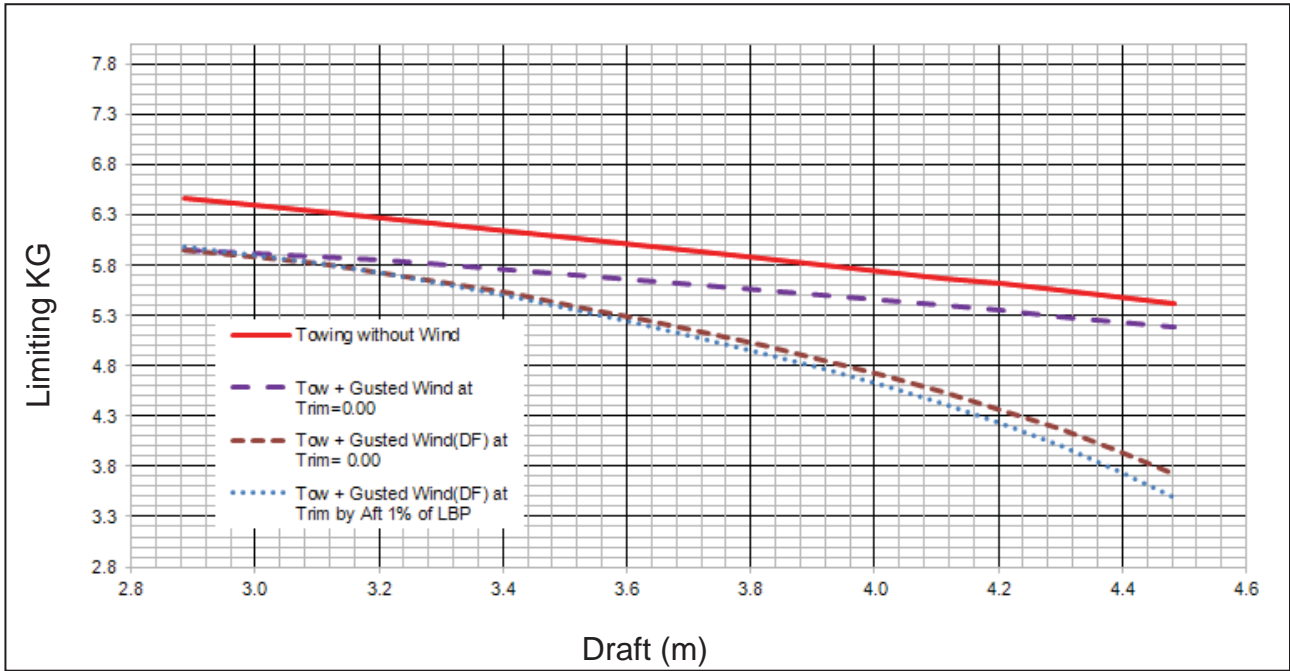


Fig 6: AHTS – Limiting KG

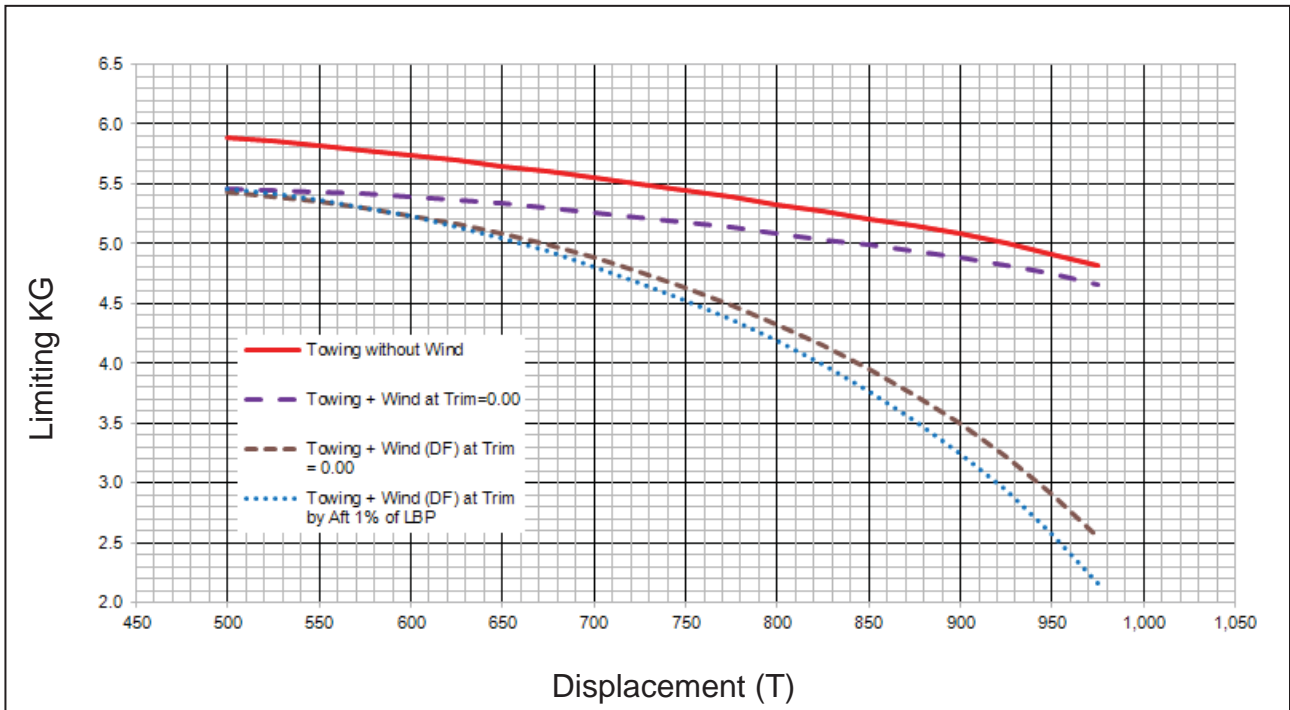


Fig 7: Tug – Limiting KG

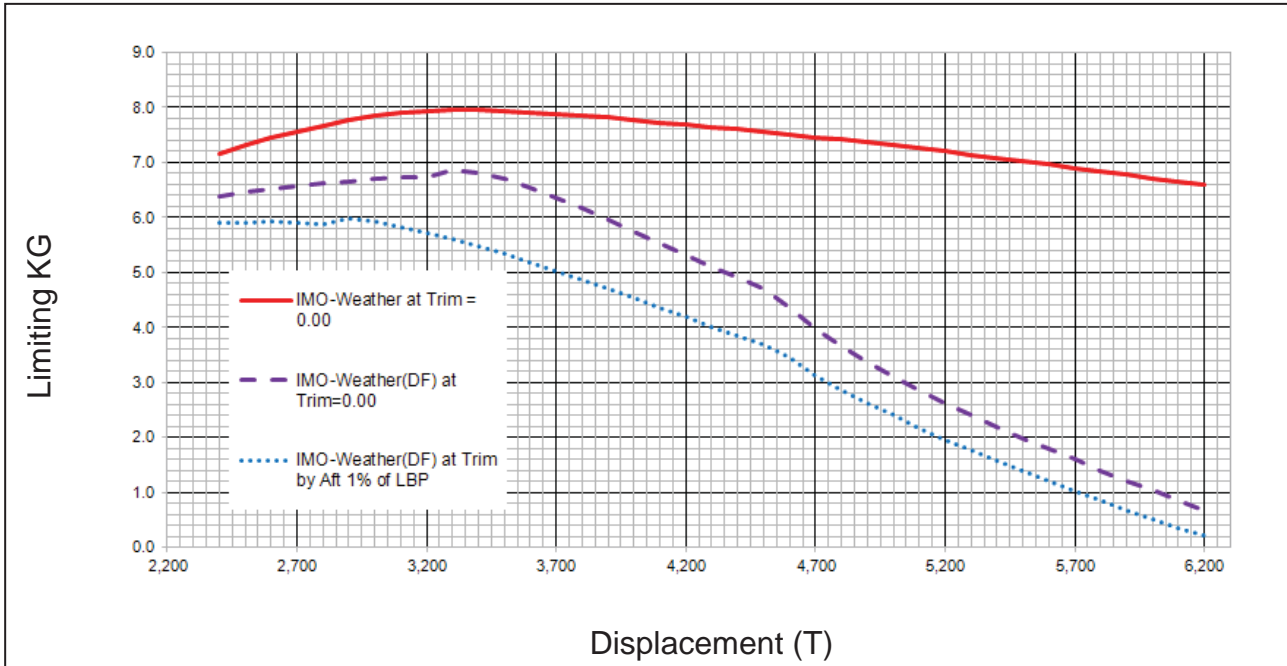


Fig 8: PSV – Limiting KG

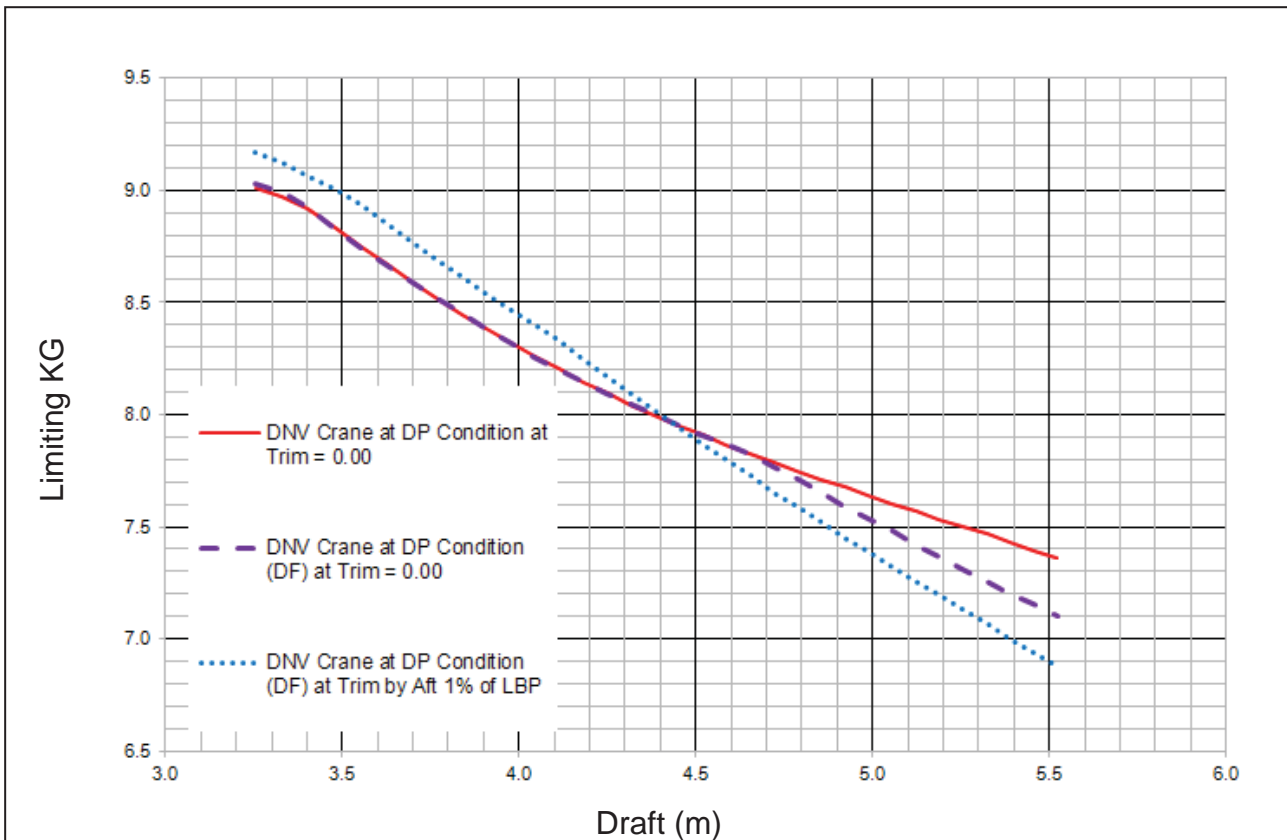


Fig 9: DSV – Limiting KG



There is a significant impact of downflooding point and aft trim on the reduction in the limiting KG. (Shown in Table 7)

Table 7: Percentage Reduction in Limiting KG

Type of Vessel	Lower Downflooding Point	With Aft Trim
AHTS	28%	4%
TUG	44%	7%
PSV	89%	7%
DSV	7%	3%

6. CONCLUSION

From the results of the case studies, there appears a strong case for modifying the existing criteria to include the following:

- Wind, wave and current forces superimposed on the existing criteria for towing, anchor handling, fire fighting operations etc.
- More fail safe means to ensure external watertight integrity
- Effect of worst downflooding point to be considered coupled with the effect of aft trim
- Effect of thruster forces to be considered as additional heeling moments during DP mode.

Presently, stability is a shared responsibility (see Table 8).

Table 8: Roles and Responsibilities (Rohr, 2003)

	Responsible	Accountable	Consulted	Informed
Design for Stability	Principal Naval Architect	Design Firm	Regulatory / Vessel Operations	Owner
Produce for Stability	Building Yard	Owner's Agent	Regulatory / Vessel Operations Master	Vessel Operations / Owner
Operate for Stability	Load Planner / Crew	Ship Master	Vessel Operations	Vessel Operations / Owner

A gradual shift of mindset is required from this shared responsibility for stability. Stability is the **sole** responsibility of the operator. It is

the responsibility of the designer, regulatory bodies and other stakeholders to provide accurate and limiting envelope for operations and provide simple user friendly guidance to the operator.

Additionally, the operators deserve quality and intense training not only in “basic stability” but in “operations stability”.

For operators guidance in decision making, easy to use stability advisory tools (software) should be made available with built-in limits from the limiting envelope.

Further detailed research would be required to analyse further existing designs with inputs from operators on their operational requirements and finally provide a basis to develop a modified stability criteria for offshore vessels.

7. REFERENCES

- Clarkson Services Limited, 2015, World Fleet Register Online – Timeseries.
- IMO, 1967, “Report of the Sub-Committee on Subdivision and Stability”. STAB VII/11.
- IMO, 1984, “Intact Stability, Report of the ad hoc working group”, SLF29/WP.7.
- IMO, 1985, “Analysis of intact stability casualty records”. Submitted by Poland. SLF
- IMO, 2002, “Guidelines for Formal Safety Assessment (FSA) for use in the IMO rulemaking process”, MSC/Circ.1023; MEPC/Circ.392.
- IMO, 2009, Report of the Maritime Safety Committee on its eighty-sixth session.
- IMO, 2015, Sub-Committee on Ship Design



and Construction (SDC), 2nd Session,
16-20 February 2015.

Gunnu G.R.S., and Moon, T., 2012, “Stability Assessment of Anchor Handling Vessel during Operation Considering Wind Loads and Wave Induced Roll Motions”, Proceedings of the Twenty-second (2012) International Offshore and Polar Engineering Conference, Centre for Ships and Ocean Structures, Norwegian University of Science and Technology, Norway

Kobylinski, L., and Kastner, S., 2003, “Safety and Stability of Ships”, Vol. 1, Elsevier.

Paik, J.K. and Thayamballi, A.K., 2007, “Ship-Shaped Offshore Installations: Design, Building and Operations”, Chapter 4 – Environmental Phenomena and Application to Design, Cambridge University Press

Rohr, J., 2003, “Stability Management for DP Platform Supply Vessels”, Dynamic Positioning Committee, Dynamic Positioning Conference Paper, Houston, Texas.

Rousseau J.H., and Breuer, J.A., 2007, “Developments in Watertight Integrity on Floating Offshore Installations”, ABS Technical Papers 2007, Offshore Technology Conference Vol. Houston, Texas.



On Aerodynamic Roll Damping

Carl-Johan Söder, *Wallenius Marine AB & KTH Royal Institute of Technology*, cjsoder@kth.se

Erik Ovegård, *Seaware AB & KTH Royal Institute of Technology*, ovegard@kth.se

Anders Rosén, *KTH Royal Institute of Technology*, aro@kth.se

ABSTRACT

In this paper an approach for estimating aerodynamic roll damping is formulated. The approach utilizes wind tunnel tests and the concept of effective levers to relate roll induced apparent wind to a damping moment. Evaluation of the approach on a typical PCTC demonstrates that the aerodynamic damping in certain conditions can be of similar magnitude as the hydrodynamic damping when the weather is rough. The importance of considering this component in the formulation of operational guidance with respect to parametric roll is highlighted using analysis of a real incident and simplistic simulations.

Keywords: *Roll damping, Parametric roll, Roll decay, Wind damping, Aerodynamic damping, Wind tunnel tests*

1. INTRODUCTION

In November 25 2011, a Panamax Pure Car and Truck Carrier (PCTC), was passing south of a heavy low pressure in the North Atlantic outside of Newfoundland. Wind speeds over 22 m/s were measured onboard and a combined significant wave height of about 5 meter was registered. The vessel was traveling in bow waves and the speed was reduced to about 10 knots to avoid bow slamming. A recorded roll motion sequence from this day is given in Figure 1. The wind came initially in from the same direction as the waves and gave the vessel a static wind list of some 3 degrees to starboard. The roll motion was limited. As the vessel was passing the low pressure the wind rapidly shifted in direction and dropped in speed. As a consequence, the wind list diminished and shortly afterwards the vessel started to roll heavily. During this sequence the course was kept un-changed while the apparent wind direction went from at the bow to straight heading. Minutes later the Master decided to alter the course to port to regain the bow wind

effect. After the rolling diminished the vessel was listing to port due to the new apparent wind direction.

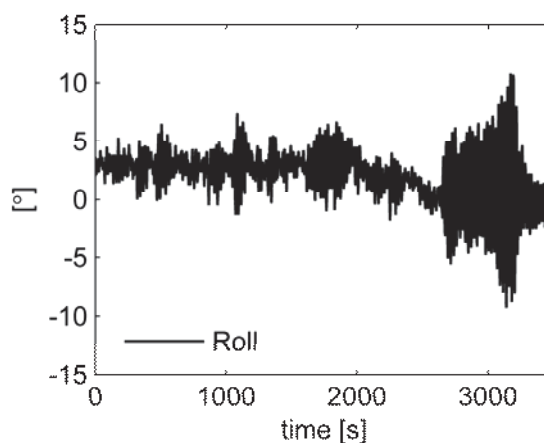


Figure 1: Heavy rolling event in the North Atlantic with a Pure Car and Truck Carrier. Initially small roll angles were experienced onboard but as the wind shifted the wind list diminishes and large roll angles were developed.

When the rolling occurred the vessel was pitching heavily with a period of half the roll

period, which indicates that this was a typical case of parametric roll. In case of parametric resonance the roll damping is decisive for the roll amplitude. As long as the damping is sufficiently high the parametric excitation will not result in any amplified roll motions, while if the damping is too low large roll angles can develop rapidly.

Captains of PCTC's generally prefer bow wind in rough weather as the wind is claimed to have a "stabilizing effect" on the roll motions. The here described event gives credibility to this claim and indicates that the changing aerodynamic damping during the turn of first the wind then the ship, had a significant influence on the development of parametric roll.

Today, roll decay model tests are considered the most accurate way to estimate the roll damping for a certain ship (IMO 2006). Due to associated costs, model tests are however normally limited to a few, often hypothetical design load cases. Alternatively, semi-empirical methods such Ikeda (1978) may be used to estimate the damping. In common for both these approaches is that they only consider the hydrodynamic damping. In Söder et al. (2012) it was discussed whether the wind could make any significant contribution to the total damping. Otherwise, very limited work has been done on aerodynamic roll damping.

In this paper an approach for estimating the aerodynamic roll damping is formulated. The approach is applied on m/v Fidelio, a PCTC similar to the one in the event 2011. The significance of aerodynamic damping is assessed relative to the hydrodynamic damping and the importance of considering this component in operational guidance is discussed.

2. AERODYNAMIC DAMPING

An approach for estimating the aerodynamic roll damping is here developed based on similar principles as used to estimate the hydrodynamic lift induced damping in Ikeda (1978).

As illustrated in figure 2 the air flow past the vessel, the apparent wind, V_a and ψ , is determined by the ship speed V_s , the true wind speed V_t and the true wind direction γ . Aerodynamic drag D_A is generated in the flow direction and if ψ differs from zero, an aerodynamic lift force L_A is induced perpendicular to the flow. The sum of the projected transversal components of D_A and L_A decides the transversal force Y . The centre of effort of this force is typically some distance zY above the centre of gravity. A heeling moment is hereby generated that is fairly constant if the ship and wind speeds are steady.

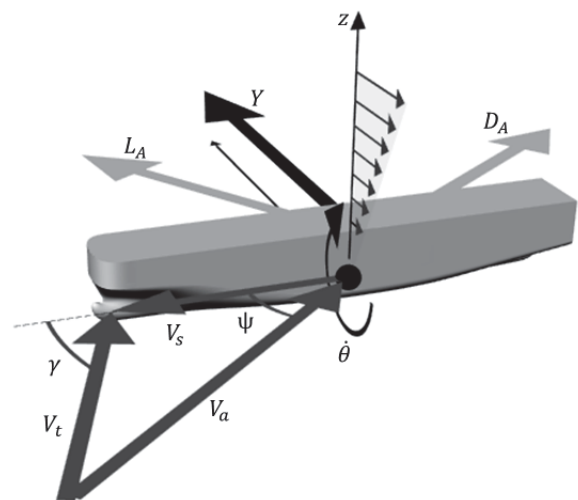


Figure 2: Illustration of velocity and force components that are decisive for the generation of aerodynamic roll damping.

If the vessel is rolling the roll velocity $\dot{\theta}$ induces a transversal velocity field, linearly increasing from the centre of roll, that also contributes to the apparent wind. This results in variations in heeling moment over the roll cycle which can be interpreted as aerodynamic roll damping,



$$B_A \dot{\theta} = (Y_{\dot{\theta}}(V_{a\dot{\theta}}, \psi_{\dot{\theta}}) - Y(V_a, \psi)) z_Y. \quad (1)$$

where $Y_{\dot{\theta}}$ is the transversal force including the apparent wind effect from the roll induced velocity field

$$V_{a\dot{\theta}} = \sqrt{(V_S + V_t \cos \gamma)^2 + (V_t \sin \gamma + \dot{\theta} z_v)^2} \quad (2)$$

$$\psi_{\dot{\theta}} = \tan^{-1} \left(\frac{V_t \sin \gamma + \dot{\theta} z_v}{V_S + V_t \cos \gamma} \right) \quad (3)$$

The lever z_Y is here estimated as half the distance from the centre of roll to the bridge deck while z_v is estimated as $z_v = 4/3 z_Y$ based on the concept of effective levers similarly as in Ikeda (1978). These estimations are obviously rough and should be assessed in future work.

3. EVALUATION

The methodology is evaluated on m/v Fidelio which is a modern Panamax PCTC, built in 2011 with cargo capacity of 8000 cars. A picture of the vessel is seen in figure 3 with main particulars according to table 1.



Figure 3: M/v Fidelio, a Pure Car and Truck Carrier

Table 1: Main particulars of m/v Fidelio in the design load condition

Length	[m]	220
Beam	[m]	32.3
Draft	[m]	9.5
GM	[m]	1.1
Displacement	[m ³]	41000
Air draft	[m]	40

The hydrodynamic roll damping was estimated using towing tank model tests in Söder et al. (2012). The tests were performed at SSPA in Sweden with a 1:30 scaled model and the results are shown in figure 4 for non-dimensional linear equivalent damping at 5° roll angle.

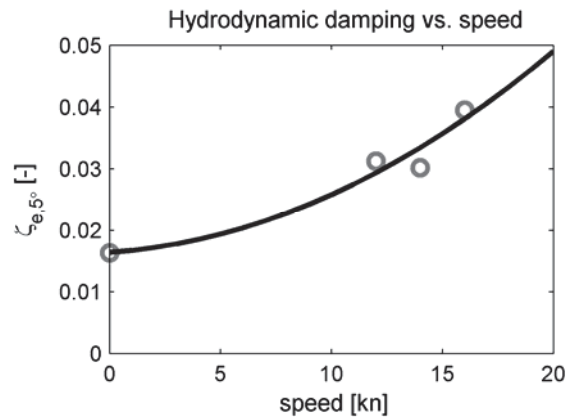


Figure 4: Non-dimensional linear equivalent hydrodynamic roll damping at 5° roll angle vs. speed.

The aerodynamic forces are determined using static wind tunnel tests with a 1:100 scaled model pictured in figure 5.

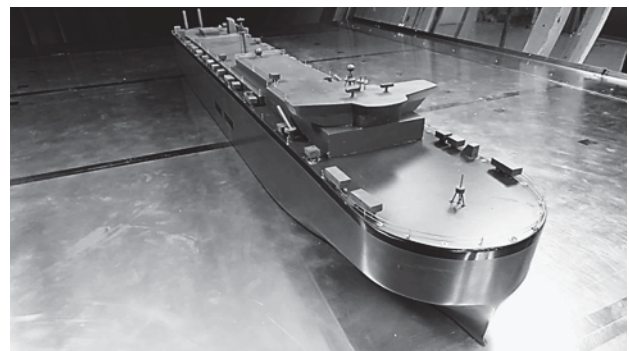


Figure 5: Wind tunnel model of PCTC Fidelio

The tests were performed at STARCS in Sweden. A closed circuit low speed tunnel was used with a test section measuring \varnothing 3.6m x 7 m. The measured transversal lift coefficient C_Y as function of ψ is given in figure 6, relating to the transversal force Y as



$$C_Y(\psi) = \frac{Y}{\frac{1}{2}\rho AV_a^2 A_S} \quad (4)$$

where ρ is the air density and A_S is the reference area which here is set to the projected side area of the vessel. The tests were performed in Reynolds numbers in the order of $5 \cdot 10^6$. A sensitivity study showed a slight increase of lift with Reynolds number which indicates that the force coefficients in full scale, with a Reynolds number up to 100 times higher could be somewhat higher.

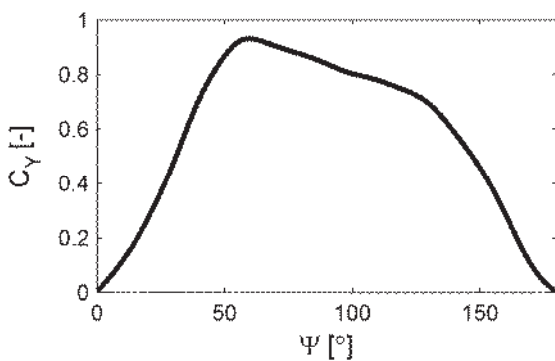


Figure 6: Non-dimensional transversal force coefficient as function of apparent wind angle for PCTC Fidelio.

Figure 7 shows the resulting aerodynamic roll damping for the design load condition at vessel speeds from 0-20kn, true wind directions 0-360° and a true wind speed of 20m/s.

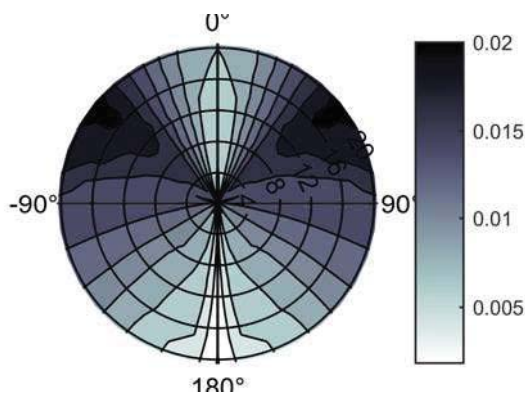


Figure 7: Predicted aerodynamic roll damping at 20m/s true wind speed as function of true wind direction and speed of the vessel.

The aerodynamic damping is practically linear with the roll velocity. At zero ship speed the damping reaches its maximum in bow wind, at a true wind direction of around 35°. At 20kn ship speed the maximum damping is found around 50° true wind direction. That is because the apparent wind direction is decisive and for the given condition a true wind direction of 50° corresponds to an apparent wind direction close to 35°.

The damping increases fairly linearly with the apparent wind speed as a consequence of that the wind pressure increase with the square of the apparent wind speed while the angle of attack ψ_θ decreases with the apparent wind speed (equation 3). As a consequence, when the true wind is strong the ship speed dependence is modest.

In figure 8 the ratio between aerodynamic and hydrodynamic damping is shown for different ship speeds and headings for the design load case and a true wind speed of 20m/s.

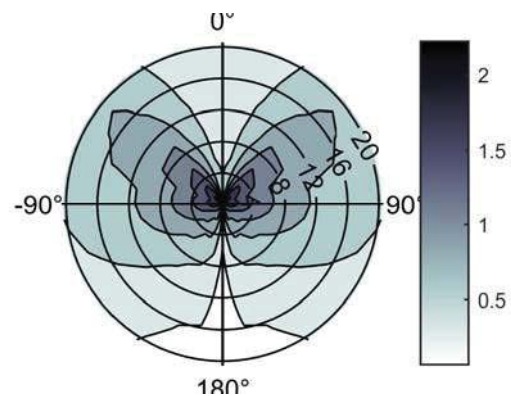


Figure 8: The ratio between aerodynamic damping and hydrodynamic damping for different ship speeds and headings at a true wind speed of 20m/s.

Notably, at bow winds and reduced ship speed the aerodynamic damping is of similar magnitude as the hydrodynamic damping. This implies that the typical roll amplitudes in those conditions will be reduced by half, which



supports the Captains preference for bow wind in rough weather to gain a “stabilizing effect”.

In figure 9 time series of roll, speed, heading, true wind angle (TWA) and true wind speed (TWS) from the event in 2011 are plotted. The lowest diagram is the aerodynamic damping estimated based on the presented approach. As seen the decreased wind speed and shift in direction causes a sudden drop in aerodynamic damping and after that the vessel starts to roll heavily. There appears to be a strong correlation between the reduction of roll damping and initiation of large roll motions.

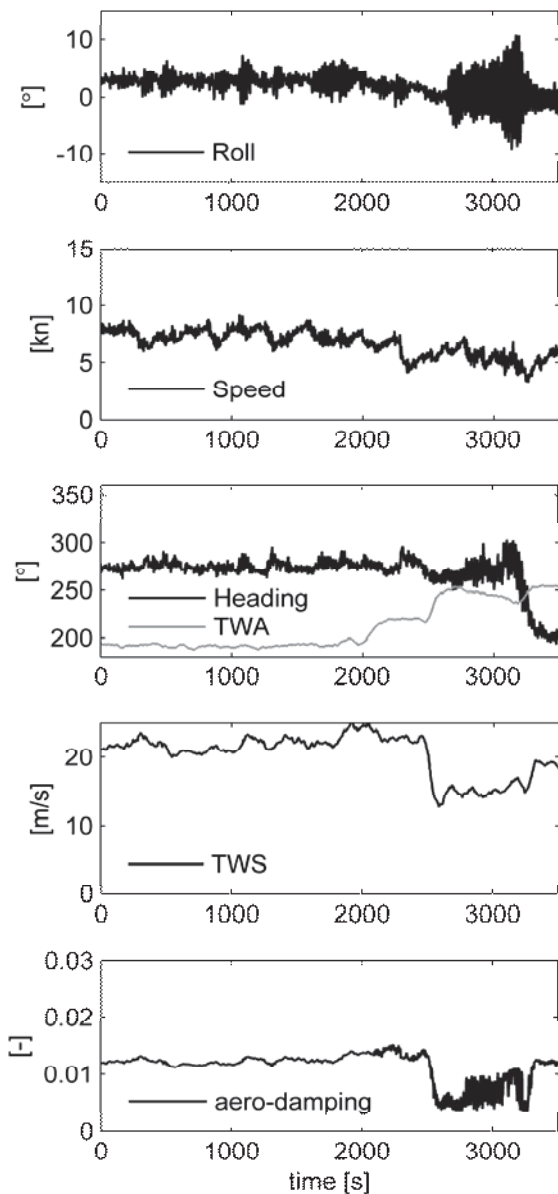


Figure 9: Time series of Fidelio’s roll motions, speed, heading, true wind angle (TWA), true wind speed (TWS) and estimated aerodynamic damping from the event in 2011.

4. OPERATIONAL GUIDANCE

The effect of considering or not considering the aerodynamic roll damping in the formulation of operational guidance with respect to parametric rolling, will here be studied in a simplistic manner using the Parametric Roll Failure Index (PRFI) introduced in Ovegård et al (2012). According to Dunwoody (1989a) the GM-variation in waves produces an effect analogous to a roll damping reduction. Based on this the PRFI was in Ovegård et al (2012) formulated as

$$PRFI = E[\zeta^*]/\zeta \quad (6)$$

where ζ is the linear roll damping expressed as a fraction of the critical damping, while $E[\zeta^*]$ is the expected value of the GM-variation related roll damping reduction. $E[\zeta^*]$ is calculated according to Dunwoody (1989b) based on the GM-variation spectrum, which in turn is calculated from the wave spectrum and the GM-variation transfer function. Theoretically parametric roll will occur in conditions where there is a 2:1 relation between the GM-variation and roll natural frequencies and where the GM-variation related roll damping reduction is larger than the actual roll damping, i.e. where $PRFI > 1$. In Ovegård et al (2012) it was however concluded that $PRFI = 4$ is a more appropriate limit to be used in operational guidance.

Two cases are here studied. The first is a hypothetical case with Fidelio in design load condition, with a ship speed of between 0 and 12 knots, a true wind speed of 20 m/s, and a sea state with a significant wave height of 5m and a mean period of 8s represented by a Jonswap wave spectrum with the shape factor set to 3.3. The two diagrams in Figure 10 could be advisory plots presented to the ship crew in



these conditions, with wind and waves coming from 0°. The grey zones indicate ship speeds and headings where $PRFI \geq 4$, which hence should be considered unsafe with respect to parametric rolling. In the upper diagram the aerodynamic roll damping is included while only the hydrodynamic damping is taken into account in the lower diagram. As seen the aerodynamic damping has a large influence in these conditions and the crew is advised very differently depending on if the aerodynamic effects are considered or not.

The second case represents the incident in 2011 described in the introduction. The ship speed is here between 6 and 10 knots and the true wind speed is 19 m/s. The sea state is based on analysis of weather data from the ECMWF Wave Atmospheric Model with a significant wind wave height of 5.14 m, a mean wind wave period of 9.81s, a significant swell height of 3.76 m and a mean swell period of 12.0 s. The wind waves are modeled as a Jonswap spectrum and the swell as an Ochi3 spectrum, both with shape parameters of 3.3 (Michel 1999). Figure 11 shows the corresponding advisory plots, with and without aerodynamic roll damping. As seen the difference between the unsafe zones is not as large as in the previous hypothetical case. Nevertheless, the circle that marks the approximate speed and heading during the incident is just at the boundary of the unsafe zone in the case with aerodynamic damping representing the conditions before the wind shift, while it is well inside the unsafe zone in the case without aerodynamic damping representing the conditions after the wind shift when the vessel started rolling.

5. CONCLUSIONS

Captains of PCTC's generally prefer bow wind in rough weather as the wind is claimed to have a "stabilizing effect" on the roll motions. This paper presents a simple approach for estimating the aerodynamic damping of volume carriers. The approach utilizes the

concept of effective levers to relate roll induced transversal velocity to relative wind variations which causes angle of attack and wind pressure variations that generates a damping moment.

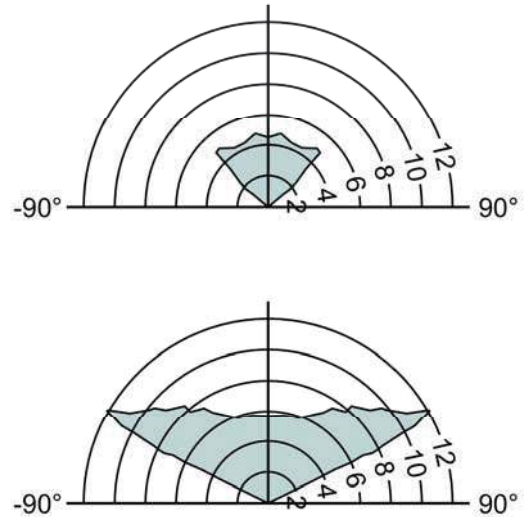


Figure 10: Advisory plots regarding parametric rolling with $PRFI \geq 4$ in the grey zones for Fidelio in design load condition, ship speed between 0 and 12 knots, true wind 20m/s, significant wave height 5m, mean period of 8s, wind and waves coming from 0°, with (top) and without (bottom) aerodynamic roll damping.

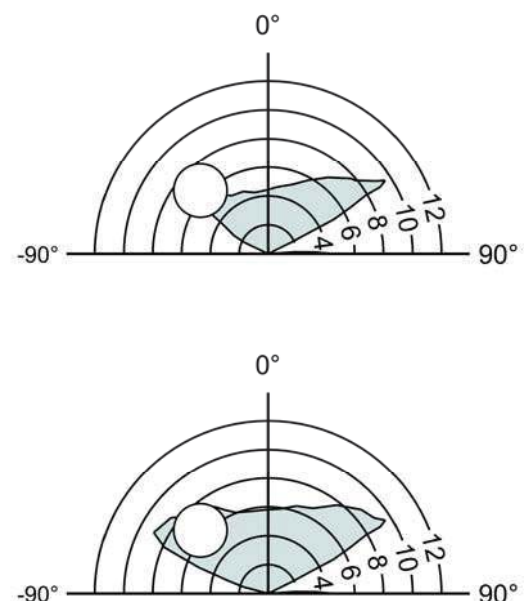




Figure 11: Advisory plots regarding parametric rolling with $PRFI \geq 4$ in the grey zones in conditions corresponding to the incident in 2011, with (top) and without (bottom) aerodynamic roll damping representing before and after the wind shift. Head wind is set to 0° .

Evaluation of the approach on a typical PCTC demonstrates that the damping can be considerable in rough weather. For the considered vessel the largest damping is generated at apparent wind angles at the bow. For that heading combined with reduced speed the magnitude of the aerodynamic damping is actually in parity with the hydrodynamic damping. This means that ordinary roll motions will be reduced by half which well supports the captains' preferences for bow wind angles in rough weather.

Critical roll events of PCTC's are normally related to parametric excitation and in case of parametric resonance the roll damping is the limiting factor. For operational guidance systems providing in-situ ship-specific decision support a proper consideration of aerodynamic damping will increase the operability of the vessels. When creating, or validating, a decision support system for roll motions the wind damping is an important component to avoid unnecessary warnings to the crew and unnecessary cost for the owner or operator.

Future work should aim at assessing the effective levers that are used to couple roll velocity to an equivalent (mean) transversal velocity and a subsequent angle of attack and induced lift of the superstructure. These levers have a large influence on the results and were estimated using rough assumptions for this work.

6. ACKNOWLEDGMENTS

This research has been financially supported by the Swedish Mercantile Marine Foundation (Stiftelsen Sveriges Sjömanshus) and the Swedish Maritime Administration

(Sjöfartsverket) which are both gratefully acknowledged.

7. REFERENCES

- Dunwoody A.B., 1989a, "Roll of a Ship in Astern Seas –Response to GM Fluctuations", Jour. of Ship Research, 33(4), pp. 284-290.
- Dunwoody A.B., 1989b, "Roll of a Ship in Astern Seas – Metacentric Height Spectra", Jour. of Ship Research, 33(3), pp. 221-228.
- IMO 2006, Interim Guidelines For Alternative Assessment Of The Weather Criterion, MSC.1/Circ.1200.
- Ikeda, Y., Himeno, Y. & Tanaka, N., 1978, "Components of roll damping of ship at forward speed", Journal of the Society of Naval Architects of Japan, Vol. 143.
- Michel W.H, 1999, "Sea Spectra Revisited", Marine Technology, Vol 36, No. 4, Winter, pp. 211-227.
- Ovegård E., Rosén A., Palmquist M., Huss M., 2012, "Operational Guidance with Respect to Pure Loss of Stability and Parametric Rolling", 11th Intl Conf on the Stability of Ships and Ocean Vehicles (STAB 2012), Greece.
- Soder C-J., Rosén A., Werner S., Huss M. & Kutenkeuler J., 2012, "Assessment of Ship Roll Damping Through Full Scale and Model Scale Experiments and Semi-Empirical Methods", 11th Intl Conf on the Stability of Ships and Ocean Vehicles (STAB 2012), Greece.

This page is intentionally left blank



SPH Simulation of Ship Behaviour in Severe Water-Shipping Situations

Kouki Kawamura, *National Maritime Research Institute*, kawamura@nmri.go.jp

Hirotsada Hashimoto, *Kobe University*, hashimoto@port.kobe-u.ac.jp

Akihiko Matsuda, *National Research Institute of Fisheries Engineering*, amatsuda@fra.affrc.go.jp

Daisuke Terada, *National Research Institute of Fisheries Engineering*, dterada@fra.affrc.go.jp

ABSTRACT

Fishing vessels, having relatively small freeboard, are prone to suffer water-shipping in severe sea state. The water impact and the accumulated water effect could make fishing vessels be unstable and capsize in the worst situation. Therefore to secure the safety of fishing vessel under water-shipping condition is important, but it is not easy to numerically predict the water behaviour/influence associated with the violent water-shipping where the water impact, the large free-surface deformation, and the strong coupling with the ship motion appear compositely. In this paper, SPH simulation using GPU is performed to predict the 6DoF ship motion in water-shipping situations. Then the prediction accuracy of the SPH method is investigated through comparisons with dedicated captive and free-motion tests.

Keywords: *Water-shipping, SPH, 6DoF motion, Experiment, GPU*

1. INTRODUCTION

Since most of Japanese fishing vessels have relatively small freeboard to increase the efficiency of fishery operation/fishery regulation using gross tonnage, they occasionally suffer water-shipping in severe sea state. The shipped water is easily accumulated on deck because of the existence of large bulwark, so the water-shipping event has potential danger resulting in large heeling/capsizing in the worst situation. Since there have been many accident reports in which fishing vessels capsized due to most likely the water-shipping, there is a strong demand to develop a numerical simulation method for ship dynamic behaviours when suffering serious water-shipping. However, water-shipping problems contain several difficulties; how to deal highly nonlinear free-surface flows

and their impacts and to estimate the coupling effect with ship motions. Therefore, advanced numerical approaches are required for the quantitative assessment of ship stability/safety against the severe water-shipping. Analytical approaches are very limited for this event because the nonlinear free-surface flows are to be dealt, and CFD (Computational Fluid Dynamics) has good ability to overcome the difficulties. Among CFDs, mesh-based CFD is well developed and evaluated so far but still have difficulties/complexity to precisely capture the largely-deformed free surface flows with the fragmentation and the reconnection, and particle methods have an advantage in terms of the capturing of non-diffusive nonlinear free-surface flows.

In this paper, the SPH (Smoothed Particle Hydrodynamics) method, which is a truly mesh-free CFD and is fully Lagrangian method, is applied to a water-shipping problem. In order



to investigate the applicability of the SPH method, a captive model test in steep waves is firstly conducted to observe the water on deck situation and to measure the hydrodynamic force acting on the ship model in water-shiping condition. Then the SPH result is compared with the experiment to confirm the prediction accuracy. Secondly ship motion measurement in steep wave trains is executed for the same ship model. Then a SPH simulation of 6DoF (Degrees of Freedom) motions, including the water-shiping event in in regular steep waves, is executed and compared with the measurement. Through the comparisons with the captive and free-motion tests, it is demonstrated that the SPH method provides a promising result for realizing the quantitative safety assessment of fishing vessels in severe water-shiping condition.

2. NUMERICAL METHOD

SPH

The SPH method derives from astrophysical field and was developed by Monaghan (1994) for free-surface flows of weak-compressible fluid. The SPH governing equations dealing with compressible fluids are shown in Eqs.1-2. The momentum conservation equation can be written in SPH notation as Eq.3 and the viscous term Π_{ij} is calculated using the artificial viscosity proposed by Monaghan (1992) given as Eqs.4-5. The pressure of weakly compressible fluid is determined by solving an equation of state expressed as Eq.6 (Monagan and Kos, 1999). The quintic form kernel (Wendland, 1995), Eq.7, is used as the SPH interpolator. Time forwarding is explicit for all equations, so the SPH method is suitable for parallel computing using GPU (Graphics Processing Unit). Further explanation and references can be found in literatures, e.g. SPHysics user guid by Gesteira et al. (2010).

$$\frac{D\rho}{Dt} + \rho \nabla \cdot \mathbf{u} = 0 \quad (1)$$

$$\frac{D\mathbf{u}}{Dt} = -\frac{1}{\rho} \nabla P + \mathbf{g} + \Theta \quad (2)$$

$$\frac{d\mathbf{u}}{dt} = -\sum_j m_j \left(\frac{P_j^2}{\rho_j^2} + \frac{P_i^2}{\rho_i^2} + \Pi_{ij} \right) \nabla_i W_{ij} + \mathbf{g} \quad (3)$$

$$\Pi_{ij} = \begin{cases} \frac{-\alpha c \mu_{ij}}{\rho} & u_{ij} r_{ij} < 0 \\ 0 & u_{ij} r_{ij} > 0 \end{cases} \quad (4)$$

$$\mu_{ij} = \frac{h u_{ij} r_{ij}}{r_{ij}^2 + (0.01h^2)^2} \quad (5)$$

$$P = \frac{c_0^2 \rho_0}{7} \left[\left(\frac{\rho}{\rho_0} \right)^7 - 1 \right] \quad (6)$$

$$W(r, h) = \frac{21}{16\pi h^3} \left(1 - \frac{q}{2} \right)^4 (2q + 1) \quad (7)$$

$$0 \leq q (= r/h) \leq 2$$

SPH solver

An open source code of DualSPHysics (<http://dual.sphysics.org/>) that combines CUDA and OpenMP, based on the SPH method is used. DualSPHysics can utilise GPUs for arithmetic processing, so that over 3,000 threads parallelization can be performed on CUDA platform. Because of difficulties in implementation of several algorithms into GPU-based code, the basic SPH algorithms, not the latest ones, are available in the current DualSPHysics code. However DualSPHysics can deal with much large number of particles as compared to the ParallelSPH code, so that the global analysis of ship motions, incident waves and their interactions as well as the local water-shiping phenomenon can be solved in the same framework.

In this study, TeslaC2050 developed for GPU computing and GTXITAN done for gaming are used. The numerical models and conditions used for the SPH simulation are shown in Table 1. The reduced speed of sound is used to avoid the excessive CPU load and is decided not to exceed the certain Mach number. The variable time step is determined to satisfy the CFL (Courant-Friedrichs-Lewy) condition in each step.

Table 1 Numerical condition

Time step marching	Verlet
Viscosity parameter: α	0.08
Kernel compact support: $2h$ [m]	0.225
Speed of sound: C [m/s]	26.7
Particle distance: dx [m]	0.075
CFL number	0.3

3. MODEL EXPERIMENT

In order to investigate the applicability/accuracy of the SPH method for water-shipping problems, a model experiment for validation is conducted. The model ship is an 80 tonnage Japanese purse seiner because she could suffer the water-shipping in stormy wave condition due to the relatively small freeboard. As a first step towards quantitative safety assessment of the fishing vessel against the water on deck, a simplified ship model, in which the ship profile along the centre line is uniformly projected in width direction, is used as shown in Fig.1. The principal dimension of the model is shown in Table 2. The heights of freeboard and forecastle, L/B , and L/D are set to keep the original value of the subject fishing vessel. For the simplicity, the bulwark is neglected in this study.

With use of the simplified ship model, a captive test and free-motion measurement are conducted to validate the SPH simulation using a GPU.

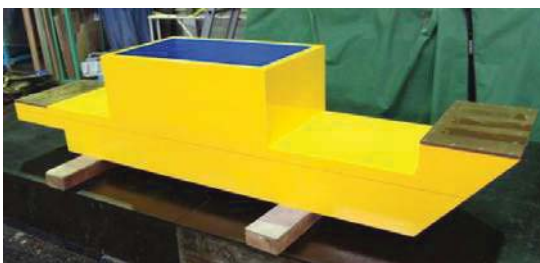


Figure 1 Simplified purse-seiner model

Table 2 Particulars of the model

Length : L_{OA} [m]	1.6
Breadth : B [m]	0.33
Depth : D [m]	0.126
Draught: d [m]	0.12
mass : M [kg]	55.2
Metacentric height: GM [m]	0.00922
Gyro radius in roll: k_{xx}/B	0.40
Gyro radius in pitch: k_{yy}/L	0.30
Gyro radius in yaw: k_{zz}/L	0.30

Captive test

A captive model experiment is conducted at the towing tank of Osaka University. The ship model is fixed in 6 degrees of freedom, and hydrodynamic forces of surge, sway, roll and yaw are measured by a dynamometer located at the centre of ship gravity. Regular wave trains are generated by a plunger-type wave generator. The wave condition used in the captive test is shown in Table 3. The encounter angle to the incident waves is set to be zero (following wave) and sixty (stern quartering wave) degrees.

Table 3 Wave condition

λ [m]	H [m]	H/λ	λ/L
1.75	0.1575	0.090	1.094

Free-motion test

Ship motion measurement is conducted at the seakeeping and manoeuvring basin of National Maritime Research Institute of Fisheries Engineering. The ship model is completely free in the experiment and all the 6 DoF component of surge, sway, heave, roll, pitch, and yaw are measured by an on-board optical gyro scope and a total station system, and are stored in an on-board computer. The instantaneous position of the centre of ship gravity in the earth-fixed coordinate system can be measured by the total station system. (Umeda et al., 2014) The total station system uses two prisms attached to the ship model with the different position. The theodolite

emits light to the prisms and measures the phases of lights reflected by the prisms, so the instantaneous position of each prism in the earth-fixed coordinate can be calculated. By combining the positions of the two prisms and roll, yaw, and pitch angles measured by the gyro scope, instantaneous position of the centre of ship gravity can be determined. The prisms and the theodolite used in the experiment are shown in Fig.2.

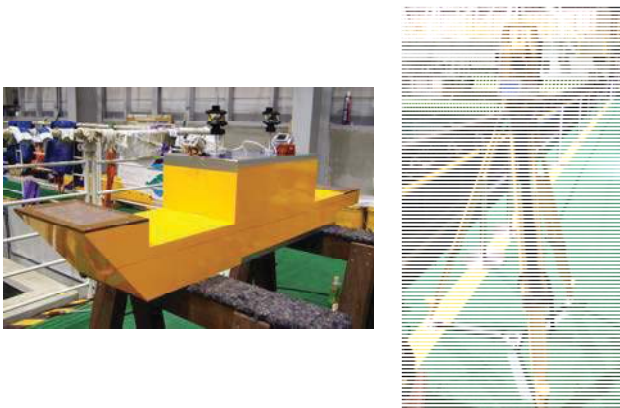


Figure 2 Two prisms (left) and theodolite (right)

Regular steep waves are generated by a plunger-type wave generator and the tested wave condition is shown in Table 4. The initial encounter angle to the wave is 0 degrees (following wave). Firstly a vertical motion is excited by wave-ship interaction and a lateral motion is also excited after a while, and then the fully combined 6 DoF motion is excited. During the measurement, the shipping water on both the fore and aft upper decks is recorded by a water-proof camera of GoPro hero3.

Table 4 Wave condition

λ [m]	H [m]	H/λ	λ/L
1.75	0.1945	0.111	1.094

4. RESULTS AND DISCUSSION

Numerical simulations using the DualSPHysics code are performed for the same conditions as the captive test and free-motion measurement to discuss the applicability/accuracy of the SPH method in the prediction of 6 DoF motions under water-

shipping situations. Regular waves are generated by a flap-type wave generator realized by imposing the moving wall boundary condition.

Captive test

In the simulation of captive test, different sizes of numerical wave tanks are used depending on the encounter angle to reduce CPU costs as shown in Table 5. The comparisons of hydrodynamic force acting on the ship between the experiment and the SPH simulation are shown in Figs.3-4. Here $t=0$ means the time when a wave crest is passing the centre of ship gravity. Figs.5-6 show the water-shiping situation.

Table 5 Numerical wave tank

Encounter angle [deg]	Length [m]	Width [m]	Depth [m]
0.0	7.5	1.5	1.2
	No. of fluid particles [million]	No. of wall particles [million]	Total No. of particles [million]
	12.30	1.37	13.67
Encounter angle [deg]	Length [m]	Width [m]	Depth [m]
-60.0	7.5	3.0	1.2
	No. of fluid particles [million]	No. of wall particles [million]	Total No. of particles [million]
	25.18	1.76	26.94

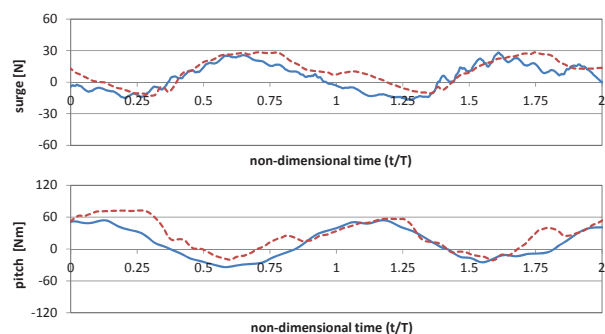


Figure 3 Comparison of wave-induced surge force and pitch moment ($\chi=0\text{deg}$)

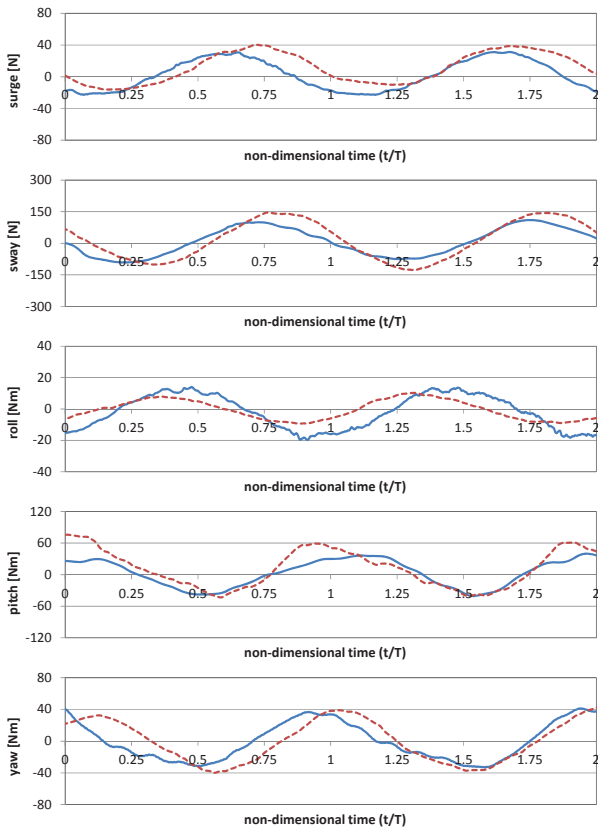


Figure 4 Comparison of wave-induced surge force and pitch moment ($\chi=60\text{deg}$)

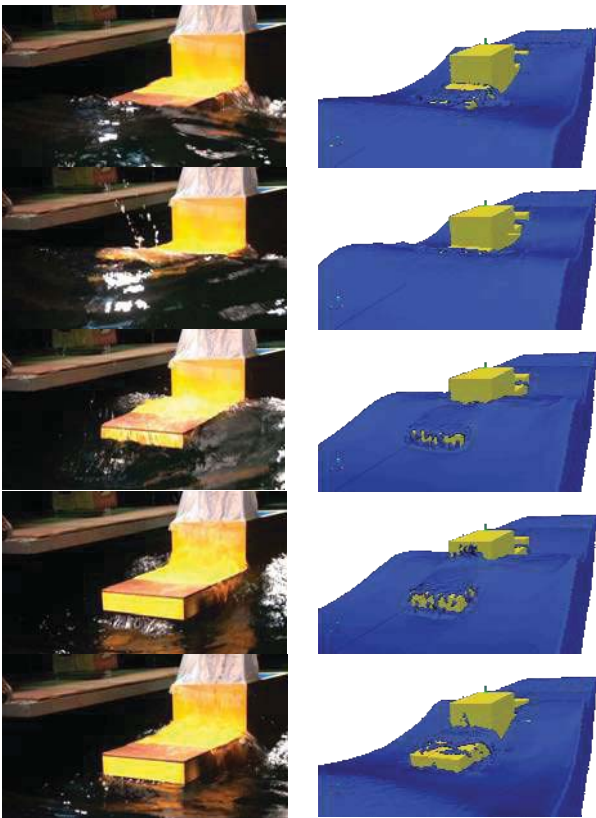


Figure 5 Comparison of water-shipping situation ($\chi=0\text{deg}$)

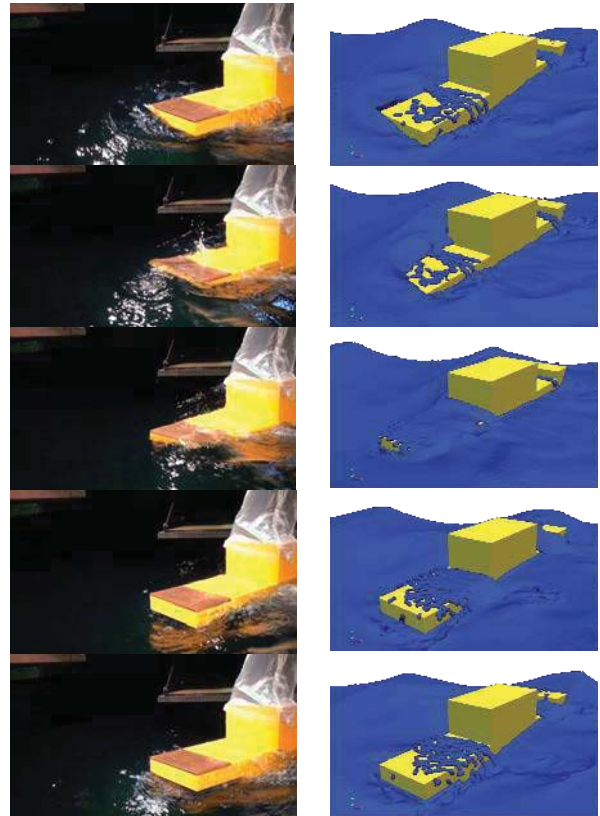


Figure 6 Comparison of water-shipping situation ($\chi=-60\text{deg}$)

In case of the encounter angle of 0 degrees, the hydrodynamic force in heave and pitch becomes vertically asymmetric. This phenomenon can be explained that the water impact to the superstructure push the ship forward as well as the steady drift force in surge and the accumulated water on the aft deck induce the bow-up moment in pitch, under severe water-shipping situation. The SPH method can capture this experimentally confirmed trend. In case of the encounter angle of 60 degrees, the asymmetric pitch disappears because the water on deck happens not only on the aft deck but also on the fore deck. The amplitude of wave-induced yaw moment is well predicted by the SPH simulation but there is certain phase shift, and the prediction accuracy is not so satisfactory in sway and roll. This discrepancy might be improved by increasing the number of fluid particles, which equals to increase the spatial resolution, because the pressure assessment for thin layer of shipping water requires a certain number of particles in vertical direction.



4.2 Free-motion test

The SPH simulation with the same condition of the ship motion measurement is executed. The size of numerical tank, the numbers of fluid and wall particles are shown in Table 6, respectively. Numerical test is performed with the initial angles of -3 degrees and 60 degrees for the comparison of transient and steady motions, respectively. The comparisons of the x- and y-positions, heave, roll, pitch and yaw motions between the model experiment and the SPH simulation are shown in Figs.7-8.

Table 6 Numerical wave tank

Length [m]	Width [m]	Depth [m]
10.0	3.0	0.5
No. of fluid particles [million]	No. of wall particles [million]	Total No. of particles [million]
23.22	1.34	24.56

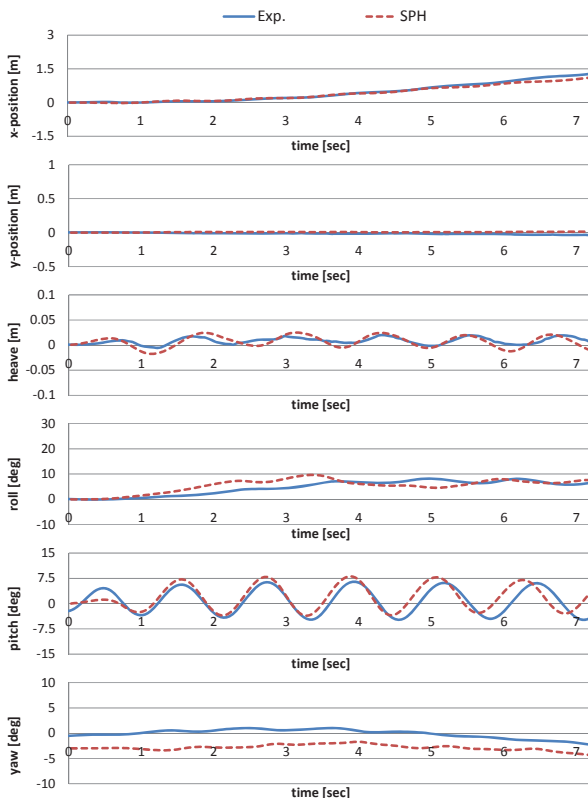


Figure 7 Comparison of transient motion in following waves

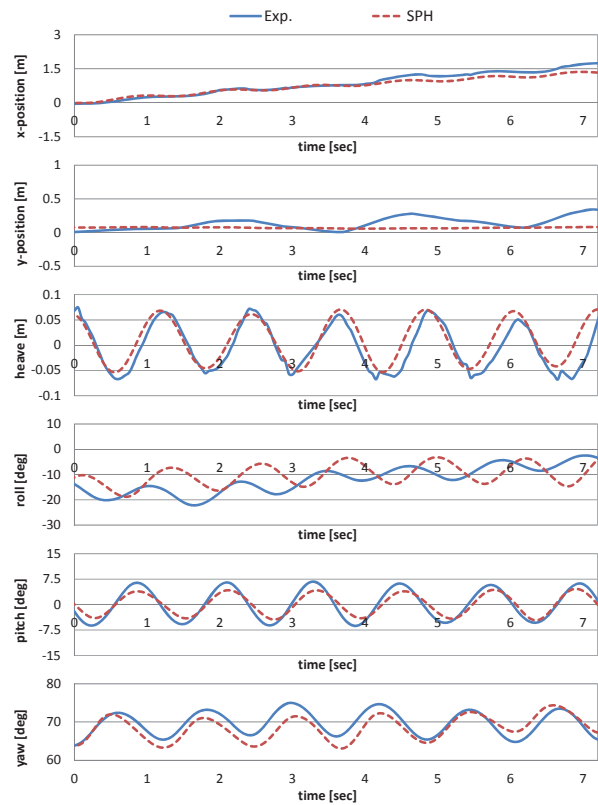


Figure 8 Comparison of steady periodic motion in stern quartering waves

Both in the experimental and numerical results for a transient motion, the lateral motions are almost negligible because of the small encounter angle, except for the heeling due to accumulated water on deck. The drift in longitudinal-direction (surge), heave and pitch motions are dominant in this situation, and the SPH well reproduces the experimental result. In case of a periodic steady state, the SPH result agrees with the experimental one qualitatively in all the 6 DoF motions. The agreement in sway and roll motions are slightly worse than other 4 motions, as presumed from Fig.4. The numerical simulation of the ship motion in steep waves shows the consistent result with the captive test results. To summarize, the prediction accuracy of the ship behaviour in severe water-shiping condition is reasonable and acceptable for practical uses.

Comparisons of the ship behaviour and the shipping water situation on the aft deck are shown in Figs.9-10 and Figs.11-12, respectively. In the experimental result of the



transient motion, severe water-shipping on the aft deck happens and hits the vertical wall of the superstructure with the significant water splashing. The SPH result well reproduces the ship-wave interaction with the violent shipping water flows in following seas. In the periodic steady state, the water-shipping happens much less compared to the transient motion both in the experiment and the simulation. Regarding the water on deck situation, the experimental result is more violent in the transient motion and the amount of the water on deck is larger in the steady state than the SPH results. For the first discrepancy, it might be because that water flows tend to over-damp due to the energy dissipation when the artificial viscosity is used. For the second discrepancy, the predicted amplitude of pitch moment is smaller than the experiment as shown in Fig.8, so the amount of water on deck becomes smaller because the water-shipping mainly happens when the ship stern is going down.

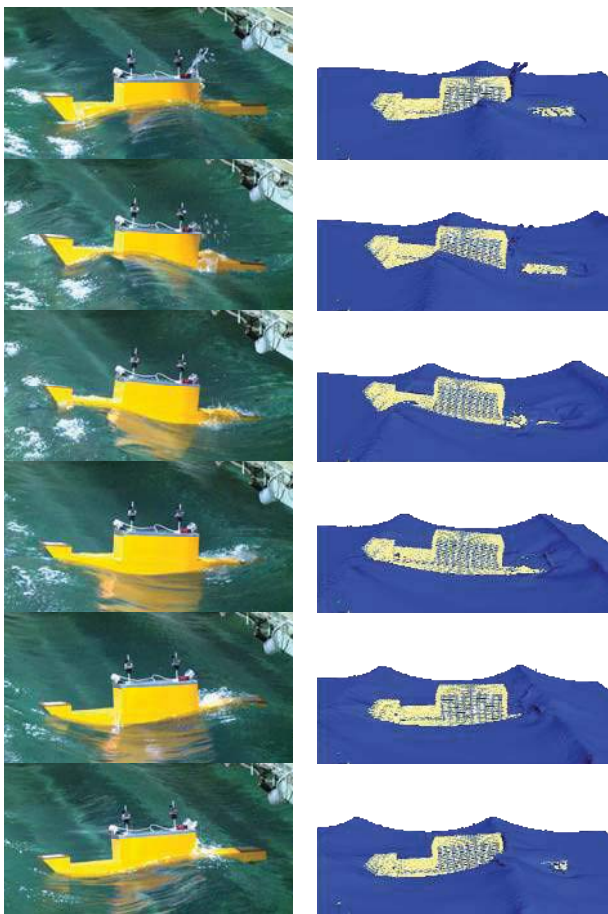


Figure 9 Comparison of ship transient motion

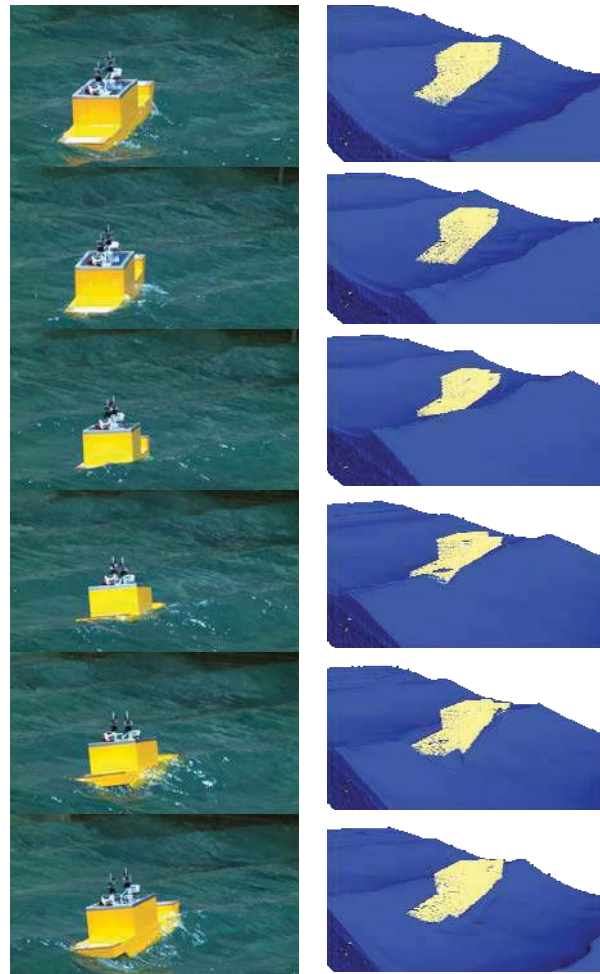


Figure 10 Comparison of ship steady motion

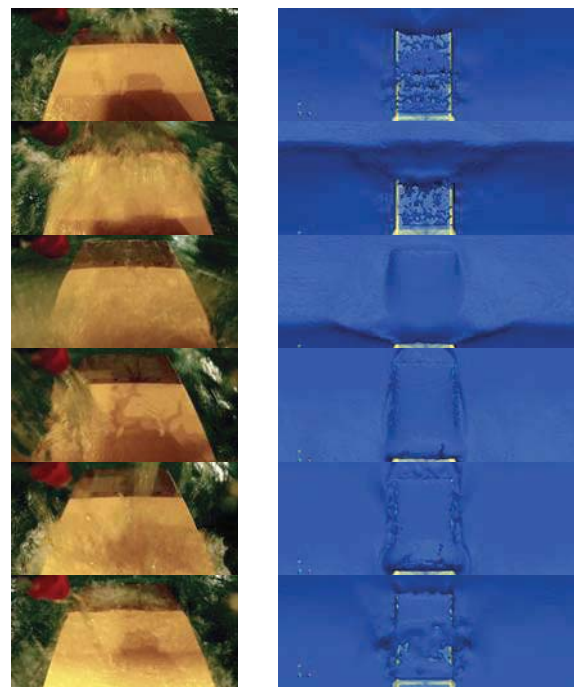


Figure 11 Comparison of shipping water on the aft deck in transient state

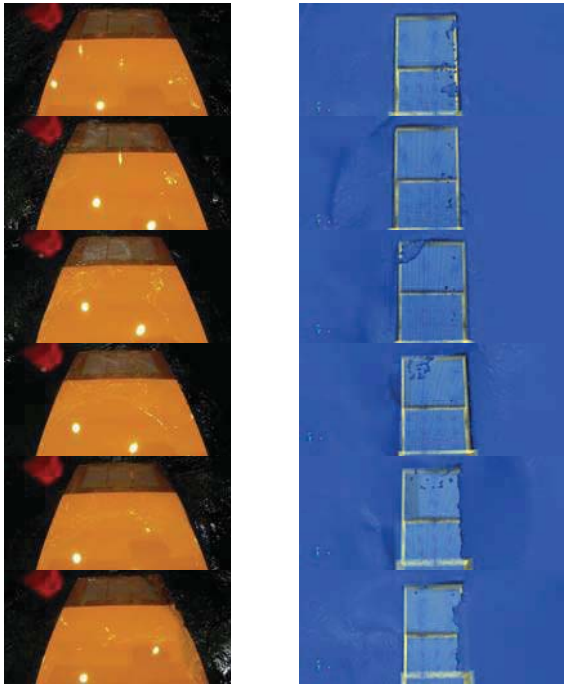


Figure 12 Comparison of shipping water on the aft deck in steady state

5. CONCLUSIONS

SPH simulation using GPU is performed to predict the 6DoF ship motion in water-shiping condition. The applicability and the prediction accuracy are investigated through comparisons with dedicated captive and free-motion tests in very steep waves using a simplified model of a fishing vessel. The calculated wave-induced hydrodynamic force agrees with the captive test qualitatively and the SPH method well reproduces the ship dynamic behaviour, in severe water-shiping situations. From the comparison results, it is demonstrated that the SPH simulation using GPU has good potential for the quantitative safety assessment of fishing vessels in water-shiping situation. Similar investigation using more realistic 3-D hull geometries is expected as a next step.

6. ACKNOWLEDGMENTS

This work was supported by JSPS KAKENHI Grant Number 26630454.

7. REFERENCES

- Gesteira, M.G., Rogers, B.D., Dalrymple, R.A., Crespo, A.J.C. and Narayanaswamy, M., 2010, "User Guide for the SPHysics code", <https://wiki.manchester.ac.uk/sphysics/index.php/Documentation>
- Monaghan, J.J., 1992, "Smoothed particle hydrodynamics", *Annual Rev. Astron. Appl.*, 30: pp. 543-574.
- Monaghan, J.J., 1994, "Simulating free surface flows with SPH", *Journal Computational Physics*, 110: pp. 543-574.
- Monaghan, J.J. and Kos, A., 1999, "Solitary waves on a Cretan beach", *J. Wtrwy. Port, Coastal and Ocean Eng.*, 125: pp. 145-154.
- Umeda, N., Furukawa, T., Matsuda, A. and Usada, S., 2014, "Rudder Normal Force during Broaching of a Ship in Stern Quartering Waves", *Proceedings of the 30th Symposium on Naval Hydrodynamics*, Tasmania.
- Wendland, H., 1995, "Piecewise polynomial, positive definite and compactly supported radial functions of minimal degree", *Advances in Computational Mathematics*, 4(1): pp. 389-396.
- ## 8. NOMENCLATURES
- | | |
|--------------|------------------|
| ρ | density |
| t | time |
| \mathbf{u} | velocity vector |
| P | pressure |
| \mathbf{g} | gravity vector |
| Θ | diffusion term |
| m | mass |
| W | weight function |
| α | tuning parameter |
| c | speed of sound |
| \mathbf{r} | position vector |
| λ | wave length |
| H | wave height |



A Reassessment of Wind Speeds used for Intact Stability Analysis

Peter Hayes, *DNPS, Department of Defence, Australia*, peter.hayes5@defence.gov.au

Warren Smith, *University of New South Wales Canberra, Australia*, w.smith@adfa.edu.au

Martin Renilson, *Higher College of Technology, UAE*, martin.renilson@hct.ac.ae

and *Australian Maritime College, Australia*, m.renilson@amc.edu.au

Stuart Cannon, *DSTO, Department of Defence, Australia*, stuart.cannon@dsto.defence.gov.au

The views expressed in this paper are those of the authors and not necessarily endorsed by the Department of Defence, Australia.

ABSTRACT

The intact stability of maritime surface vessels (ships, boats, landing craft, *etc.*) should be as-sessed for the most extreme environment that they are designed for or limited to operate in: namely the nominal and gust wind speeds and associated wave height and wave frequency profile.

The IMO and naval weather criteria apply to ocean going vessels but each use different wind speeds. The IMO criterion uses a single nominal wind speed (26 ms^{-1}) and a small gust factor ($\sqrt{1.5} = 1.225$) for all assessed vessels, irrespective of operational environment or expectations. The naval weather criteria uses different gust wind speeds for different operational expectations, with most significantly higher than the IMO gust wind speed. Yet these criteria are intended to assess the suitability of vessels for essentially similar operational expectations.

This paper revisits the basis of the wind speeds used for stability analysis. A range of standard-ized wind speeds for different types of operational service is proposed.

Keywords: *Stability, Wind Speed,*

NOMENCLATURE

t	time interval, in sec
V_{avg}	average or nominal wind speed at 10 m height, in ms^{-1}
V_{gust}	gust wind speed at 10 m height, in ms^{-1}
V_z	wind speed at height z , in ms^{-1}
V_{ref}	reference wind speed at height z_{ref} , in ms^{-1}
WSR_{600}	wind speed ratio based on an average over 600 seconds (10 minutes)

WSR_{3600}	wind speed ratio based on an average over 3600 seconds (1 hour)
z	height above the surface, in m
z_{ref}	reference height, in m
α	exponent

1. INTRODUCTION

Ship stability knowledge and practise has developed over the centuries much as other branches of engineering have, starting with trial and error, progressing to rules of thumb and then, relatively recently, introducing and de-



veloping analysis based on more rigorous application of scientific principles. Unlike other branches of engineering such as structural analysis, the ‘science’ of ship stability has not progressed much beyond the beginnings of scientific principles. Empirical relationships and heuristic information are heavily relied upon in developing criteria. In the main only still water characteristics are used to assess transverse stability in extreme environments. The use of seakeeping and manoeuvring characteristics in an extreme seaway to simulate and predict ship behaviour, such as broaching, that could lead to capsize has only in recent decades been actively explored.

Existing stability criteria are based on the still water characteristics of the vessel, incorporating various factors to account for operation in severe environments. Some, such as the basic IMO criteria, require nominated characteristics of the righting arm curve, including minimum areas under the GZ curve and minimum GM values. These were based on early work, such as that of Rahola (1939). This type of criteria that have been derived empirically are strictly only valid for the data set and the environments used in their derivation. However these criteria have been extended to many vessel types and sizes not in the original data set, and to environments markedly different than those original environments.

Weather criteria have been introduced in more recent decades that attempt to include the effects of wind and waves as overturning forces to be resisted. In these criteria, wave effects are usually introduced to the still-water righting moment curve by a ‘roll-back’ angle. Wind effects are introduced by a wind heeling moment/lever function, generally based on the up-right wind heeling moment.

There are a number of different factors that contribute to a stability criterion, wind speed being one. Especially important are the hidden factors and cause/effect mechanisms that drive how the criteria actually works (e.g. different wind/heel relationships, how much of the

buoyant structure is considered, roll back from nominal or gust equilibrium). The easiest example is probably the area ratio (refer to Figure 1): the naval criteria (DDS079, 1975) uses a \cos^2 relationship for the wind moment/lever with ship heel, requiring $A1/A2 \geq 1.40$, whereas the IMO criterion (IMO2008, 2009) uses a constant wind moment/lever relationship, requiring $A1/A2 \geq 1.00$.

The IMO wind speed (and wave age part of the roll back formulation) are intended to be an "average" between the height of a tornado (high winds, young, steep developing seas) and the aftermath (lower winds, more fully developed seas). So the criterion coefficients somehow relate this average environment to both the height of the tornado and the environment in its aftermath. What is actually being modelled here has become clouded, with wind speed used as a tuning factor.

Adopted in this paper is the premise that inputs (especially wind and wave effects) should be treated in as rigorous and realistic a manner as possible and then any criterion relationship coefficients tuned to give results that match experimental and real life data. This approach has the following advantages:

- Inputs can be investigated generally in isolation without hidden factors clouding results, allowing for better treatments over time.
- Criteria can be developed from established engineering principles largely independent of the inputs. Over time this could allow for better criteria to be developed.
- Inputs can be varied to allow for different environments in a logical and transparent manner.

The treatment of wind, particularly developing a standardised set of wind speeds for stability analyses, is the subject of this paper.



2. WIND CHARACTERISTICS

2.1 Wind Velocity Profile

The average or nominal wind does not have the same wind speed at all heights above the earth surface. Near the surface, friction and surface roughness affect the strength or speed of the wind. This is the ‘constant shear’ region, which extends to about 100 m above the surface. Within this region the variation in wind speed over the ocean is commonly approximated by (e.g. McTaggart and Savage, 1994, EM 1110-2-1100, 2002):

$$V_z = V_{ref} \left(\frac{z}{z_{ref}} \right)^\alpha \quad (1)$$

The value of α varies from 0.1 to 0.4 depending on surface roughness. McTaggart and Savage (1994) reported that α varies from 0.12 to 0.14 for stormy ocean conditions. A common value for α is 0.13 ($\approx 1/7.5$).

The international meteorological community has standardized on reporting wind speeds at a 10 m height above the surface. Historically, this height was not always used and measurements of opportunity, such as ship’s anemometers, could be at any height. When comparing wind speeds from different sources, conversion to a common baseline height (10 m) using equation (1) may be necessary.

2.2 Wind Gusts

The long term average wind speed is used in wave growth models and is usually the nominal wind speed reported by the local weather bureau. In Australia, and generally internationally, the 10-minute maximum sustained wind speed average, at 10 meters height, is used as the nominal wind speed.

The spatial distribution of packets of wind blowing in a particular direction with a rela-

tively constant wind speed is seemingly random in nature. A time history at a particular point will provide various statistics about the wind, such as the average and standard deviations of wind speed and direction, and so on. Unlike ocean waves, which can be viewed in an analogous manner, the wind statistics can quickly change, and there is a need to take statistics over limited time intervals. Durst (1960) established a relationship for gust wind speeds for different durations based on analysis of winds over open and flat terrain.

For a 1-hour (3600-seconds) average maximum sustained wind speed, the Durst wind speed ratio for winds of smaller duration is given by (EM 1110-2-1100 2002):

$$WSR_{3600}(t) = 1.277 + 0.296 \tanh \left(0.9 \log_{10} \left(\frac{45}{t} \right) \right) \quad (2)$$

If the wind speed ratio for a different return period, say 10-minutes (600-seconds), is calculated, it is a simple matter to obtain the wind speed ratio relative to that new return period:

$$WSR_{600}(t) = \frac{WSR_{3600}(t)}{WSR_{3600}(600)} \quad (3)$$

The wind speed ratios based on 1-hour, 10-minute and 1-minute average maximum sustained wind speeds are plotted in Figure 1. The gust ratio for a 5-sec gust duration when com-

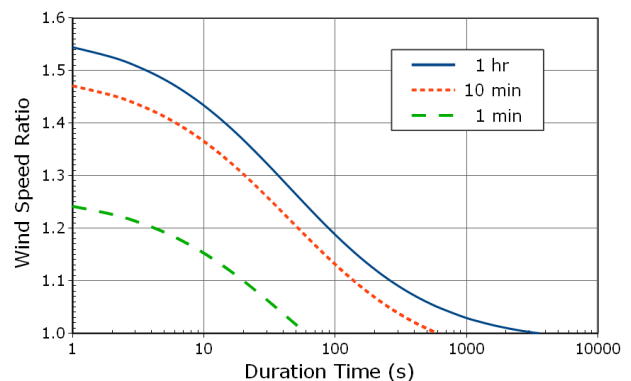


Figure 1 Wind speed ratio for 1 hour, 10 minute and 1 minute averaging periods

pared to the 10-min average is 1.4122, very close to $\sqrt{2} = 1.4142$.

In more recent years there have been many studies of wind gustiness, especially in hurricanes, each arriving at different gust factors. One example is the gust model developed by the Engineering Sciences Data Unit, ESDU. Vickery and Skerlj (2005) presented data indicating that the ESDU gust model, using a roughness of 0.03m, gave the best fit to available data, though the Durst model also gave a fit close to this preferred ESDU model. Limited data indicated that gust factors at sea are a little lower than over land by an average factor of 0.95, Vickery and Skerlj (2005). A later analysis by Vickery et al. (2007) presented a comparison of the ESDU gust model to available data, this time based on a 1-minute nominal period, reproduced as Figure 2. Overlaid on this figure (dashed line) is the Durst model for 1-minute nominal wind speeds. The Durst model appears to give better predictions for gusts longer than 3 seconds. Also, converting to 10-minute nominal winds would result in 15-20% higher gust factors.

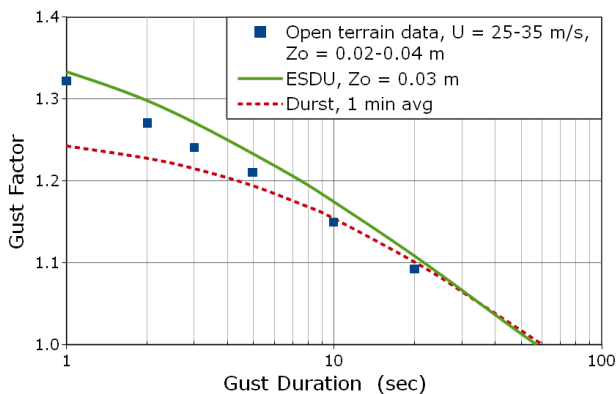


Figure 2 Comparison of the ESDU model to gust data, adapted from Vickery et al. (2007)

The ESDU model is somewhat complicated to apply, whereas the Durst model is relatively simple. Noting that the two give fairly similar results and that the Durst model dates from the 1960s when wind speeds for stability analysis

were selected, the Durst model is adopted for this paper.

2.3 Tropical Cyclone Scales

There are a number of schemes for categorising the severity of tropical cyclones. A summary of the various scales used throughout the world as given by Tropical Cyclone Scales (2013) is:

- Atlantic Ocean and East Pacific Ocean - characterised by the United States developed Saffir-Simpson Hurricane Scale, which is based on 1-minute maximum sustained wind speeds.
- West Pacific Ocean, Northern Hemisphere monitored by the Japan Meteorological Agency's Regional Specialized Meteorological Centre (RSMC). The typhoon intensity scale is based on 10-minute maximum sustained wind speed.
- North Indian Ocean - monitored by the India Meteorological Department's Regional Specialized Meteorological Centre in New Delhi, India. The cyclonic storm scale is based on a 3-minute averaging period to determine sustained wind speeds.
- South-Western Indian Ocean - monitored by Météo-France which runs the Regional Specialized Meteorological Centre in La Reunion. The tropical cyclone scale is based on a 10-minute average maximum sustained winds.
- South Pacific Ocean and South-Eastern Indian Ocean - monitored by either the Australian Bureau of Meteorology and/or the Regional Specialized Meteorological Centre in Nadi, Fiji. Both warning centres use the Australian tropical cyclone intensity scale, which is based on 10-minute maximum sustained wind speed combined with estimated maximum wind gusts, which are a further 30-40% stronger.

It can be seen that there are a number of different scales used to characterise tropical cyclones, potentially making comparisons erroneous.



Table 1 Beaufort wind scale, adapted from Tropical Cyclone Scales (2010)

Beaufort	Description	Wind				Tropical Cyclone Scales		
		Upper Wind Speed		Potential 5 sec Gust		US	Japan	AU
		Knots	m/s	Knots	m/s			
6	Strong Breeze	27	13.9	38	19.6	Tropical Depression	Tropical Depression	Tropical Depression
7	Near Gale	33	17.0	47	24.0			
8	Gale	40	20.6	56	29.1	Tropical Storm	Tropical Storm	Cat 1 Tropical Cyclone
9	Strong Gale	47	24.2	66	34.1			
10	Storm	55	28.3	78	40.0			
11	Violent Storm	63	32.4	89	45.8	Cat 1 Hurricane	Severe Tropical Storm	Cat 2 Tropical Cyclone
12	Hurricane	71	36.5	100	51.6			
13		80	41.2	113	58.1	Cat 2 Hurricane	Typhoon	Cat 3 Severe Tropical Cyclone
14		89	45.8	126	64.7	Cat 3 Hurricane		
15		99	50.9	140	71.9			
16		109	56.1	154	79.2	Cat 4 Hurricane	Cat 4 Severe Tropical Cyclone	
17		118	60.7	167	85.7			
+						Cat 5 Hurricane	Cat 5 Severe Tropical Cyclone	

The Beaufort wind scale is used to categorize wind speed and, in the absence of reliable instrumentation, is often used to report wind speed. Wind speeds used in the Beaufort scale reflect the standard 10-minute average at 10-metres height. The Beaufort Scale is typically defined to Beaufort 12. It was extended to Beaufort 17 in 1944, intended for special cases, such as tropical cyclones (Met Office, 2010).

The tropical cyclone scales of interest are the US Saffir-Simpson scale and the Japanese scale, as they have been influential on wind speed selection used in stability analyses, and, for the authors, the Australian tropical cyclone scale. These tropical cyclone scales have been compared to the Beaufort scale in Table 1, using the Durst relationship to convert US 1-minute sustained wind speed to 10-minute sus-

tained wind speeds. This illustrates the differences between the tropical cyclone scales. Of note is that the US hurricane categories start at Beaufort 11 and the Japanese typhoon category (which is subdivided for internal use) starts at Beaufort 12.

3. WIND SPEEDS

3.1 IMO

The IMO uses a wind speed of 26 ms⁻¹ (50.5 knots) as the nominal wind speed in its weather criterion, with a gust factor (GF) of 1.225 ($\sqrt{1.5}$) to give a gust wind speed of 31.8 ms⁻¹ (61.9 knots). The nominal wind speed is equivalent to a mid Beaufort 10 wind. Noting

that the gust heeling lever governs the weather criterion, using the 5-second gust factor of 1.412 equates the IMO gust wind of 31.8 ms⁻¹ to a nominal wind speed of 22.5 ms⁻¹ (43.8 knots), which is mid Beaufort 9. For vessels expected to avoid the worst weather and that can use weather routing to do so, mid Beaufort 9 represents fairly severe weather - but it is certainly not the worst that could be encountered. Not all vessels, whether or not they are using weather routing, can successfully avoid the worst weather.

According to Yamagata (1959), the selection of 26 ms⁻¹ was an average between the maximum winds of a tropical cyclone (called a typhoon by the Japanese) and the more steady winds in the immediate aftermath. This also made allowance for wave age—waves tend to be younger and therefore steeper in short duration winds compared to the more fully developed waves that occur with time. However, an examination of the actual data presented, especially Table III of Yamagata (1959) (adapted as Table 2 here), would suggest a higher value.

Table 2 Nominal wind environments, adapted from Yamagata (1959)

Event	Avg Trailing Wind Speed (ms ⁻¹)	Max Wind Speed At Centre (ms ⁻¹)	Application
Barometric Gradient	10		Smooth waters
Front	15		Inshore
Low	15	32	Offshore
Typhoon	20	50	Ocean going

Comparing Table 1 with Table 2, the maximum wind speeds of Table 2 could possibly be gust wind speeds. The question then is what gust ratio to apply.

Yamagata (1959) provided data, reproduced as Figure 3 here, that showed gust factors ranged from 1.0 to 1.7 with an average of 1.23 ($\approx \sqrt{1.5}$). At higher wind speeds, above about

30 ms⁻¹, the maximum gust factor was 1.3. The average value was adopted, taken as $\sqrt{1.5}$ (= 1.225).

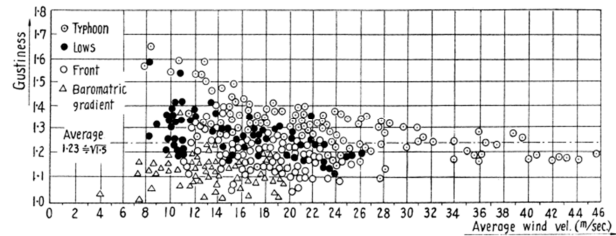


Figure 3 Wind gustiness, from Yamagata (1959)

The variation of wind speed with location from the peak of a tropical cyclone through to the trailing wind was simplified (Yamagata, 1959). This simplification was similar to Figure 4 (the bottom line is the Yamagata simplification, apparently using the data from Table 2, though how this was effected is not immediately apparent). The maximum wind speed adopted was about 32 ms⁻¹. From Table 2, this is the maximum wind velocity for a low pressure system. If the value of 50 ms⁻¹ from Table 2 is taken as a gust wind speed, using a gust factor of 1.225 (the gust factor assumed by the Japanese) gives a nominal wind speed of 40.8 ms⁻¹. Alternatively, using a gust factor of 1.412 (the gust factor from Durst) gives a nominal wind speed of 35.4 ms⁻¹. Neither matches the 32 ms⁻¹ that was used.

Taking the data of Table 2 as the intended values, a number of different analyses can be performed. Assuming that the typhoon maximum wind speed is a gust wind speed and the gust factor of 1.225 applies, the average and gust wind speeds of the central or tropical cyclone zone should have been calculated as:

$$\begin{aligned}
 V_{avg} &= \frac{\left(\frac{50}{1.225} + 20 \right)}{2} \\
 &= 30.4 \text{ ms}^{-1} \\
 V_{gust} &= 1.225 \times 30.4 \\
 &= 37.2 \text{ ms}^{-1}
 \end{aligned}
 \tag{4}$$



If the 5-second gust factor of 1.412 was used instead, the respective wind speeds would be:

$$\begin{aligned}
 V_{avg} &= \frac{\left(\frac{50}{1.412} + 20\right)}{2} \\
 &= 27.7 \text{ ms}^{-1} \\
 V_{gust} &= 1.412 \times 30.4 \\
 &= 39.1 \text{ ms}^{-1}
 \end{aligned}
 \tag{5}$$

This second result is close to the top of Beaufort 10 (nominal to 28.3 ms⁻¹, gusts to approximately 40.0 ms⁻¹). This suggests that Beaufort 10 is a more realistic wind definition for vessels intended for unlimited operation at sea, though still avoiding centres of severe tropical disturbance.

Figure 4 shows the result when applying different gust factors (GF) to the specified maximum wind speed at the centre of a typhoon of 50.0 ms⁻¹.

Applying the same method and the 5-second gust factor of 1.412, the respective wind speeds for a low pressure system would be:

$$\begin{aligned}
 V_{avg} &= \frac{\left(\frac{32}{1.412} + 15\right)}{2} \\
 &= 18.8 \text{ ms}^{-1} \\
 V_{gust} &= 1.412 \times 18.8 \\
 &= 26.5 \text{ ms}^{-1}
 \end{aligned}
 \tag{6}$$

This last result is the middle of Beaufort 8 (nominal to 20.6 ms⁻¹, gusts to approximately 29.1 ms⁻¹). This suggests that Beaufort 8 is more appropriate for vessels that must avoid the worst weather. Such vessels would need ready access to refuge.

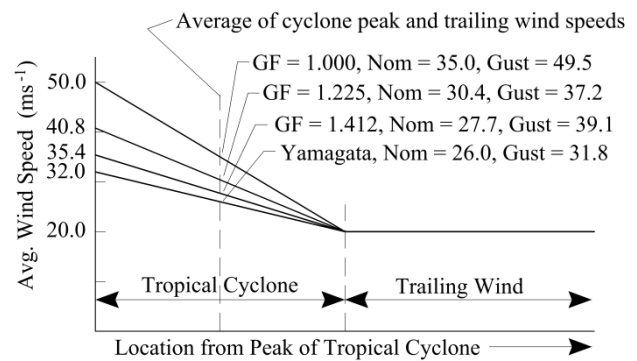


Figure 4 Simplified typhoon wind velocity, adapted from Yamagata (1959)

3.2 Naval

There is no actual historical evidence available for the development of the naval criteria wind speeds. The likely rationale for their selection can be deduced once the different tropical cyclone scales employed by different authorities are considered.

The defining event for formulating USN intact stability, Typhoon Cobra in 1944 (also known as Halsey's Typhoon), was described as Force 12 with average winds 50 to 75 knots and gusts as high as 120 knots. Brown and Deybach (1998) reported that the USN identified 100 knots as a reasonable wind velocity for ship survival in tropical storms. DDS 079-1 (1975) specified wind speeds for various service categories as:

- Ocean and Coastwise:
 - 100 knots - Ships which must be expected to weather the full force of tropical cyclones.
 - 80 knots - Ships which will be expected to avoid centres of tropical disturbance; and
- Coastwise:
 - 60 knots - Vessels which will be recalled to protected anchorages if winds over Force 8 are expected.

A number of observations can be made about the USN categories:

- 100 knots is the 5-second gust speed for Beaufort 12. It seems reasonable to assume that, for this service category, a gust



factor of about 1.5, rounded to a neat result, was applied to a nominal wind of Beaufort 12.

- 80 knots is close to the 5-second gust speed for Beaufort 10 - refer to Table 1. Under the US system, this is the strongest Beaufort wind not categorized as a hurricane and 80 knots applies to ships expected to avoid centres of tropical disturbance. It seems reasonable to assume that, for this service category, a gust factor of about 1.5, rounded to a neat result, was applied to a nominal wind of Beaufort 10.
- Beaufort 8 has a nominal wind speed to 40 knots. 60 knots is 1.5 times the nominal wind speed. It seems reasonable to assume that a gust factor of about 1.5, rounded to a neat result, was applied.
- The USN categories are essentially for ocean voyaging ships (100 and 80 knots wind speed) and for limited range vessels (60 knots) able to return easily to shelter. The latter category could include ship's boats which would not operate in severe environments and which could return to the parent ship.

3.3 NSCV

The Australian National Standard for Commercial Vessels (NSCV, 2002) defined environments deemed suitable for domestic operations. The wind environments were presented as Beaufort wind speeds and gust pressures, with a formula to convert pressures to equivalent wind speeds. Using this formula revealed a wide range of gust factors, ranging from 1.3 for the ocean going categories to 1.76 for a protected waters category.

In the Australian context, it is desirable to use the NSCV categories where possible as most vessels available commercially in Australia would have been assessed against the NSCV. This can best be done by matching gusting wind pressures, which are used for analysis in the NSCV.

4. STANDARD WIND SPEEDS

The reanalysis of the original Japanese data presented in Yamagata (1959), the interpretation of the naval wind speeds presented in DDS 079-1 (1975) and inclusion of the NSCV categories strongly suggest the wind speeds defined in Table 3 for a range of service categories should apply. The wind speeds prescribed are nominal or average wind speeds. A gust factor of around 1.4 is recommended to derive the gust or design wind speed typically used in quasi-static analyses. This would most easily be arranged by doubling the nominal wind heeling moment (equivalent to a gust factor of $\sqrt{2} = 1.414$).

This paper developed the wind speeds recommended for offshore and ocean-going vessels. Table 3 also presents recommended wind speeds for operation of limited duration offshore (coastal) and in more protected areas. These were developed by Hayes (2014) and are appropriate for the Australian context. Other jurisdictions will possibly need to vary from these suggestions to suit local conditions.

Associated wave heights have been shown in Table 3 for completeness. They were derived from basic wind/wave relationships (Hayes, 2014) and are not intended to be definitive.

It is useful to define a number of service categories for the purposes of setting the environments (and any other pertinent parameters) applicable to the intended uses of a vessel. A vessel intended to stay in position except in the most severe weather should clearly be assessed using a more severe environment to that for a vessel intended to coastal hop only when suitable weather presents itself. The service categories, once defined, would be applied to most vessels, selecting the most appropriate category for the intended service of the vessel. This allows for clear definitions that can be applied and understood across the fleet.



Table 3 Suggested standard environments

Service Category	Wind					Sig. Wave Height m	NSCV Equivalent ⁴		
	Nominal Speed ¹			Pressure ²			Category	Pressure Pa	Sig Wave Ht m
	B'fort	Kts	m/s	Nominal Pa	Gust ³ Pa				
Ocean Unlimited	12	71	37	987	1974	14.0	None		
Ocean Limited	10	55	28	592	1184	9.5	None		
Offshore	8	40	21	313	626	6.0	A / B	600	>6
Coastal	7	33	17	213	426	4.5	C	450	4.5
Inshore	6	27	14	143	285	2.5	D	360	2.5
Smooth Waters	6	27	14	143	285	0.6	E	300	0.6

- Notes: 1. 10-minute average at 10 metres.
2. Based on flat plate, 500 Pa at 26 m/s.
3. Gust pressures 2 times the nominal pressure.
4. Data from NSCV (2002)

Suggested descriptions of the service categories are presented in Table 4. Note that in the naval context, a safe haven can include the parent ship and that the size of the environment and

range from the safe haven, not geographical limits, are the important parameters. This could also apply in the commercial context.

Table 4 Suggested service categories

Service	Description	Weather & Sea Characteristics	Survival & Rescue Infrastructure
Ocean Unlimited	Fully independent operation at sea, able to hold station in all but extreme conditions, able to resume duties after conditions abate.	Severe tropical cyclone or equivalent, extreme winds and extreme seas.	Early rescue not likely. Probable extended period in survival mode.
Ocean Limited	Independent operations at sea, avoiding centres of severe tropical disturbance, able to resume duties when conditions abate.	Storm force weather or equivalent. Very high winds and very high seas.	Early rescue not likely. Probable extended period in survival mode.
Offshore	Independent operation within 200 nautical miles or 12 hours at cruising speed (whichever is less) of a safe haven. Return to safe haven if winds likely to exceed Beaufort 8.	Gale force weather and very rough seas.	Survival in moderate conditions or early location likely and within helicopter range for rescue.
Coastal	Restricted operations within 4 hours travel at cruising speed of a safe haven.	Near gale force weather and rough seas.	Survival in benign conditions or early rescue.
Inshore	Operates within specified geographical limits defined as 'partially smooth' or within 2 hours travel at cruising speed of a safe haven in an equivalent environment.	Strong winds and moderate seas.	Rescue facilities and/or shoreline nearby.
Smooth Waters	Operates within specified geographical limits defined as 'smooth' or within 1 hour travel at cruising speed of a safe haven in an equivalent environment.	Strong winds and operates only in small waves.	Rescue facilities and/or shoreline nearby.



The suggested service categories would apply to a majority of cases. Special purpose vessels, intended for very specific roles, environments and survival probabilities, could require very specific operational profiles and environments to be defined.

5. CONCLUSIONS

Reiterating, inputs to stability criteria (especially wind and wave effects) should be treated in as rigorous and realistic a manner as possible. Any criterion relationship coefficients should then be developed such that the results of applying the criteria match experimental and real life data – i.e. they are realistic predictors of safe vessels for the intended extreme environment.

A standardised set of wind speeds for stability analyses would mean that the use of wind speed becomes more transparent, with less opportunity to cloud how it shapes the criteria coefficients. How the criteria would then be developed to accommodate these standardised wind speeds is a different question to be answered by more research.

Wind speeds appropriate for general stability analyses have been developed and defined in terms of different service categories. Adopting these, or similar, wind speeds and service categories allows for stability analyses appropriate to the actual use of and operational limitations of different vessels and is encouraged.

6. REFERENCES

- Brown, A.J. and Deybach, F., 1998. Towards a Rational Intact Stability Criteria for Naval Ships, Naval Engineers Journal, 110 (1), pp. 65–77.
- DDS 079-1, 1975. Stability and Buoyancy of U.S. Naval Surface Ships. United States, Department of the Navy, Naval Ship Engineering Centre.
- Durst, C. S., “Wind Speed Over Short Periods of Time,” Meteorological Magazine, 89, 181-187, 1960.
- EM 1110-2-1100, 2002. Coastal Engineering Manual – Part II – Chapter 2: Meteorology and Wave Climate, US Army Corps of Engineers.
- Hayes, P., 2014, Naval Landing Craft Stability, Masters Thesis, University of New South Wales, Australia.
- McTaggart, K. and Savage, M., 1994. Wind Heeling Loads on a Naval Frigate, 5th International Conference on Stability of Ships and Ocean Vehicles, Melbourne, Florida, USA
- Met Office, 2010. National Meteorological Library and Archive Fact Sheet 6 The Beaufort Scale, URL: <http://www.metoffice.gov.uk/corporate/library>
- NSCV, 2002. National Standard for Commercial Vessels (NSCV), URL: <http://www.amsa.gov.au/domestic/standards/>
- Rahola, J. 1939, The Judging of the Stability of Ships and the Determination of the Minimum Amount of Stability, Ph.D. Thesis, The University of Finland, Helsinki, Finland.
- Tropical Cyclone Scales, 2013. Wikipedia article, URL: http://en.wikipedia.org/wiki/Tropical_cyclone_scales
- Vickery, P.J., Masters, F.J., Powell, M.D. and Wadhers, D., 2007. Hurricane Hazard Modelling: The Past, Present and Future, 12th International Conference on Wind Engineering, Cairns, Australia.
- Vickery, P.J. and Skerlj, P.F., 2005. Hurricane Gust Factors Revisited, Journal of Structural Engineering, pp. 825–837.
- Yamagata, M. (1959). Standard of Stability Adopted in Japan, Transactions Royal Institution of Naval Architects 101: 27. 417.

Session 8.1 – 2nd GENERATION INTACT STABILITY

**On the Application of the 2nd Generation Intact Stability Criteria to
Ro-Pax Vessels and Container Vessels**

**A Study on Applicability of CFD Approach for Predicting Ship
Parametric Rolling**

**Estimation of Ship Roll Damping – a Comparison of the Decay and the
Harmonic Excited Roll Motion Technique for a Post Panamax
Container Ship**

**Assessing the Stability of Ships under the Effect of Realistic Wave
Groups**

This page is intentionally left blank



On the application of the 2nd Generation Intact Stability Criteria to Ro-Pax and Container Vessels

Stefan Krueger, Hannes Hatecke

Hamburg University of Technology, Germany

Paola Gualeni, Luca Di Donato

University of Genoa, Italy

ABSTRACT

A new set of intact stability criteria is under development at IMO with the aim to address the stability failures of a ship in a seaway. These criteria are structured in a three level approach. The first two levels consist of calculations characterized by different levels of accuracy. The third level is named “direct assessment” and typically a numerical tool for hydrodynamics calculations is envisaged for the assessment. However, at present no criteria or procedures have been developed for this third level.

In the various scenarios of modern merchant ships, Ro Ro-Passenger vessels represent a very interesting field of investigation for intact stability vulnerability assessment especially for the righting lever variations in waves. For the specific stability failures of parametric roll and pure loss of stability, in the present paper, we apply the 2nd Generation of Intact Stability Criteria to some typical Ro Ro-Passenger ferries and results are presented in terms of computed curves of minimum required GM. We have also carried out a direct assessment of the stability using the “Insufficient Stability Event Index” (ISEI- concept) and compared the obtained GMReq – curves.

This comprehensive investigation has the purpose to assess the reliability of the newly proposed criteria as technically consistent and harmonized safety rules.

To this aim the investigation domain has been enhanced to the cargo ships field, in particular considering three selected containerships that have suffered serious accidents in a heavy seaway.

Keywords: *Intact stability failure modes, direct assessment, GM required curves, safety level.*

1. INTRODUCTION

In the latest years, under the specific agenda item named “second-generation intact-stability criteria,” IMO has been active on the development of vulnerability criteria for the assessment of ship behaviour in a seaway. The importance of this issues is already pointed out in the Preamble of the Intact Stability code (2008): “It was recognized that in view of a

wide variety of types, sizes of ships and their operating and environmental conditions, problems of safety against accidents related to stability have generally not yet been solved. In particular, the safety of a ship in a seaway involves complex hydrodynamic phenomena which up to now have not been fully investigated and understood”



Among the failure modes recognised by the IMO are:

- Pure loss of stability
- Parametric roll
- Dead ship condition in beam seas
- Surf-riding and broaching-to

Only the first two are faced in the present investigation, in the specific field of Ro-Pax ships. For a larger perspective on the subject, also three Container vessels' behaviour has been analysed.

If a ship is susceptible to a stability failure that is neither explicitly nor properly covered by the existing intact stability regulations, the ship is regarded as an "unconventional ship" in terms of that particular stability failure mode.

"Second-generation intact-stability criteria" are based on a multi-tiered assessment approach: for a given ship design, each stability failure mode is evaluated relying on two levels of vulnerability assessment, characterized by different levels of accuracy and computational effort.

A ship which fails to comply with the first level is assessed at the second-level criteria. In turn, if unacceptable results are found again, the vessel must then be examined by means of a direct assessment procedure based on tools and methodologies corresponding to the best state-of-the-art prediction methods in the field of ship-capsizing prediction. This third-level criteria should be as close to the physics of capsizing as practically possible.

Direct assessment procedures for stability failure are intended to employ the most advanced technology available, and to be sufficiently practical to be uniformly applied, verified, validated, and approved using currently available infrastructure. Ship motions in waves, used for assessment on stability performance, can be reproduced by means of numerical simulations or model tests.

Where model tests have the disadvantage that investigations in short crested, irregular seas are hardly possible.

Calculations performed in the current work are structured in three phases.

First, all the ships are judged with the mandatory intact stability regulation (IS Code, 2008), in order to define the safety level at present. Then a direct assessment is performed by means of non-linear time domain, computations, able to compute the so called "insufficient stability event index" (ISEI). A more thorough description of ISEI is given in the next paragraphs. Following the above mentioned calculations, GMReq sets of values are obtained from both the IS code criteria (usually for Ro-Pax corresponds to the Weather Criterion) and the direct assessment method. A gap, in terms of GMReq, between the two approaches is the obtained result, as it could be expected.

At this point the Second Generation Intact Stability Criteria are introduced to complete the outline of the situation.

The aim of this work is to show how suitably the new stability requirements apply in addressing parametric roll and pure loss problems, filling the range between the mandatory and the numerically simulated stability safety level. In the following the structure of the new criteria is explained, as well as a description of the direct assessment methodology. Finally, results for the case studies are presented and properly discussed.

2. 2ND GENERATION INTACT STABILITY CRITERIA

In this work the IMO document used for the calculations is the SDC 1 Inf. 8 with the updates of the SDC/ISCG of the latest months. All the amendments have been implemented in the ship design software package E4 of the



Hamburg University of Technology, developed in Fortran90 language.

In the following the first two levels of vulnerability criteria, for the specific failure modes of Parametric roll and Pure Loss of stability, are briefly explained.

2.1 Level 1 Vulnerability Criteria

The first level consists of simple formulae based on the ship hydrostatics and regards the GM sensitiveness to waterline variation due to wave profile. In fact, as an effect of a wave passing the ship, the lever arm as well as the metacentric height will face a change due to the modification of the water plane area and the immersed volume distribution, considering the ship to be balanced in sinkage and trim. It is recognized that most of the times the worse situation in terms of stability is represented by the wave crest situated amidships.

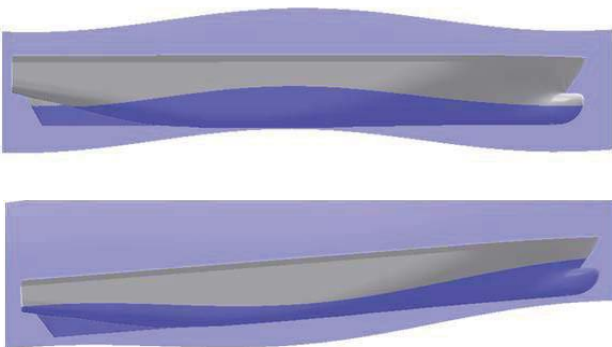


Figure 1: Wave with the length of the ship with crest and trough located at amidships.

Parametric Roll: A ship is vulnerable to parametric roll, according to level 1, if the ratio between the amplitude of the GM variation in waves and the GM in still water is less than a certain value. The formula reads as follows:

$$\frac{\Delta GM}{GM} \leq R_{PR}$$

Where R_{pr} is taken as 0.5 or as a value function of the midship section coefficient C_m and the bilge keel area, whichever is the less.

Longitudinal sinusoidal waves with a length λ and steepness Sw of 0.0167 are taken for the calculation of the ΔGM . The wave crest is centred at the longitudinal centre of gravity at each 0.1 forward and aft thereof.

Pure loss of stability: For cases with speed corresponding to Froude number of significantly high values (in the draft proposal threshold value for example 0.31), a ship is considered potentially dangerous to this phenomenon. In such case the criterion reads as follows:

$$GM_{MIN} > R_{PLA}$$

GM_{MIN} is the minimum value of the metacentric height as a longitudinal wave passes the ship. It has been observed that the most critical situation is quite often presenting the wave crest in the surrounding of the amidships longitudinal position. R_{PLA} is defined as: $\min(1.83 d (Fn)^2, 0.05)$, with d the draft of the loading condition under consideration. The wave length considered to compute the GM is the same of the ship length and the steepness in this case is 0.0334 (the double of the one applied for parametric roll).

2.2 Level 2 Vulnerability Criteria

The compliance with the first level is in principle always possible provided that the sufficient (usually high) level of stability (for example in terms of GM) is met. One of the reasons for that could be also the conservative approach of the described formulae (i.e. the high safety margin implied). To this regard it is worth mentioning that a very high GM value might imply also some shortcomings and recently at IMO attention has also been given to the issue of excessive accelerations. It should also be mentioned that unrealistically high values of GM pose a severe burden to the design of the ship.



Therefore for both parametric roll and pure loss more complex formulations are needed in order to get a more realistic stability level. The way to gain this target consists basically of developing an averaged assessment on a larger set of environment conditions. For the purpose of this paper a series of longitudinal sinusoidal waves (proposed as an option in the draft rule text) from a length λ of 22m to 630m are used for the computation of a weighted average.

Parametric Roll: The first check the ship has to pass requires that the weighted average among all the wave cases is less than a certain value RPR (in our case 0.1).

$$\frac{\Delta GM(H_i, \lambda_i)}{GM(H_i, \lambda_i)} < R_{PR}$$

At the same time it is also requested that:

$$V_{PRI} < V_D$$

Therefore, besides that check on GM also the design speed V_D of the ship shall not exceed the resonance speed V_{PRI} .

Moreover, if this check is not overcome, the roll motion has to be assessed in head and following seas for a range of operational speeds. Different options are possible for this computation: a numerical transient solution, an analytical steady state solution or a numerical steady state solution. In this work the second option has been attempted using the updated formula of the working group when the 5th degree polynomial fitting of the righting lever curve was not precise enough. No satisfactory results have been obtained with this approach, therefore we considered the first check as the only possible requirement in the evaluation of the GM required curves. It should in this context be mentioned that if the criteria will be

made mandatory, it must be guaranteed that they are numerically stable.

Pure loss of stability: The same wave cases, with double of the steepness are applied for this second level. Three criteria have to be assessed, addressing the issues of a limit for the vanishing stability angle, for the maximum loll angle and for the maximum value of the righting arm. For the angle parameters we applied the proposed standards of 30 degrees, 25 degrees respectively. The standard value for the criterion addressing the maximum righting arm is expressed as a function of wave steepness, F_n , and ship draft.

3. DIRECT ASSESSMENT

As already mentioned, if the ship is found to be vulnerable under the first two levels (or more realistically, if the GM_{Req} in order to comply with is too high), a direct assessment is required, possibly related with the quantification of a capsizing risk. No rules are actually available for this procedure, therefore the numerical tool E4ROLLS, developed by Söding Kroeger and Petey provided by the Hamburg University of Technology, has been applied. With this tool, the 6-DOF motion of the ship is computed in an irregular short-crested seaways. While heave, pitch, sway and yaw are computed by means of strip theory in the frequency domain, roll and surge, due to their nonlinear nature, are determined in the time domain.

For the roll motion the following equation has been used (Kröger 1987):

$$\ddot{\varphi} = \frac{M_{wind} + M_{sy} + M_{wave} + M_{tank} - M_d - m(g - \ddot{\zeta})h_s}{I_{xx} - I_{xz}(\psi \sin \varphi + \vartheta \cos \varphi)} + \frac{I_{xz}[(\vartheta + \vartheta \varphi^2) \sin \varphi - (\psi + \psi \varphi^2) \cos \varphi]}{I_{xx} - I_{xz}(\psi \sin \varphi + \vartheta \cos \varphi)}$$

here M_{wind} , M_{sy} , M_{wave} and M_{tank} are the moments due to wind, sway, waves and fluid in tanks respectively. The damping is



considered in M_d and the restoring moment in the term h_s , representing the restoring arm in the seaway according to the Grim's concept of the equivalent wave modified by Söding. I_{xx} and I_{xz} are the moments of inertia around the longitudinal axis and the product of inertia, respectively, calculated for the actual mass distribution, introduced for the yaw moment influence. As a result of the calculations, a polar plot produced by a computation can be represented for example in figure 2. The diagram is characterized by representative wave length (and period as well), different speed on each circle, different encounter angles and wave height (coloured). All calculations are carried out for short crested irregular seas. The limiting significant wave height which identifies a situation as dangerous derives either from the Blume criterion or from a maximum roll angle of 50 degrees, whichever is the less:

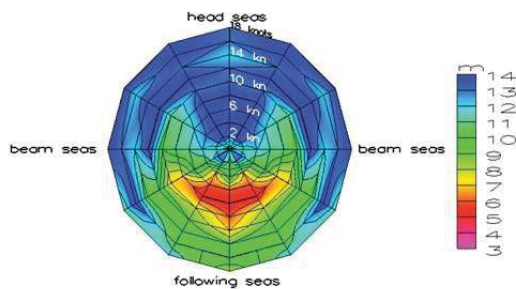


Figure 2: Polar Plot for a single significant wave period Each colour represents the limiting significant wave height.

To determine if the loading condition under analysis is safe or not, the direct assessment makes use of the ISEI concept. The Insufficient Stability Event Index, developed by Krueger and Kluwe, gives a failure index in terms of long term prediction:

$$ISEI = \int_{T_1=0}^{\infty} \int_{H_{1/3}}^{\infty} \int_{\mu=-\pi}^{\pi} \int_{v_s}^{v_{max}} p_{sea}(H_{1/3}, T_1) \cdot p_{dang}(H_{1/3}, T_1, \mu, v_s) \cdot dv_s \cdot d\mu \cdot dH_{1/3} \cdot dT_1$$

Here p_{sea} represents the environmental context by means of a two dimensional probability density function for a sea-state characterized by significant height $H_{1/3}$ and period T_1 , whereas p_{dang} denotes the probability that the stability condition under consideration is dangerous in the current seastate, using the two failure criteria mentioned before.

p_{sea} is taken from the North Atlantic Area according to the Global Seaway Statistics by Söding.

The limit between the safe and the unsafe situation is defined by the threshold value of the index $1 \cdot 10^{-3}$. Six wave periods are typically used for each calculation which should be arranged around the period representing a wave length corresponding to ship length.

4. APPLICATION CASES

For the investigation, four Ro-Pax of significantly different geometry are analysed. For each ship the main dimensions are shown below.

RoPax 1

Lpp [m]	171
B [m]	27
T [m]	6.6
V [kn]	23

Table 1: Main dimensions of RoPax1

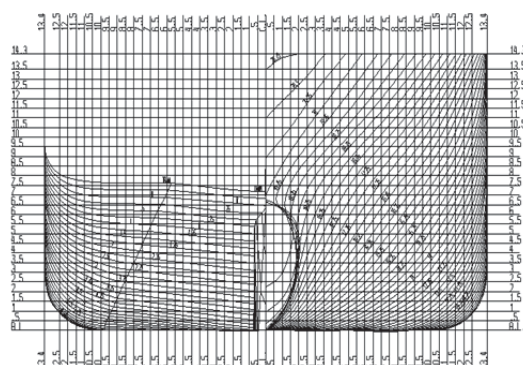


Figure 3: Body plan of the RoPax1



RoPax 2

Lpp [m]	186
B [m]	30
T [m]	7.8
V [kn]	25

Table 2: Main dimensions of RoPax2

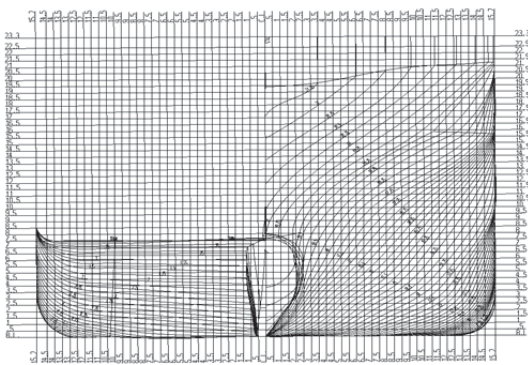


Figure 4: Bodyplan of the RoPax 2

RoPax 3

Lpp [m]	110
B [m]	15
T [m]	6
V [kn]	25

Table 3: Main dimensions of RoPax3

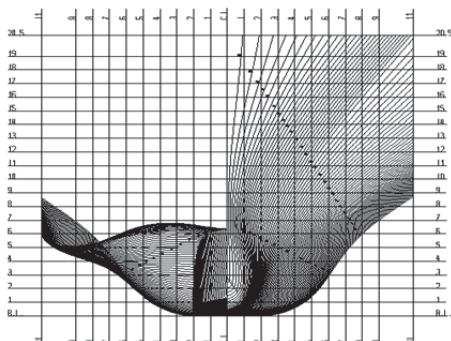


Figure 5: Body plan of the RoPax 3

RoPax 4

Lpp [m]	156
B [m]	19
T [m]	6.86
V [kn]	17
GM accident [m]	1.691

Table 4: Main dimensions of RoPax4

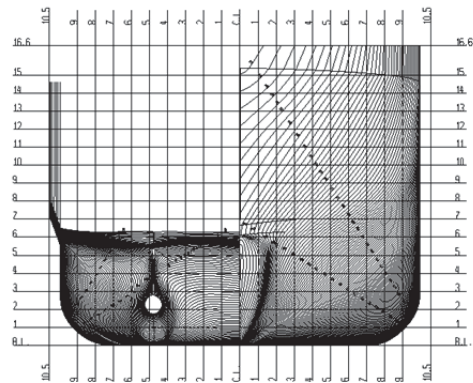


Figure 6: Bodyplan of RoPax4

This last Ropax4 ship has a geometry which has experienced a capsizing due to the dynamic phenomena studied by the new criteria. It has been analysed in order to check if the two levels of parametric roll and pure loss of stability recognize a stability problem at the loading condition of the accident.

5. CALCULATIONS AND RESULTS

General procedure

As mentioned before, three calculation phases are covered to obtain all the final results useful for the comparison purposes, aim of this paper:

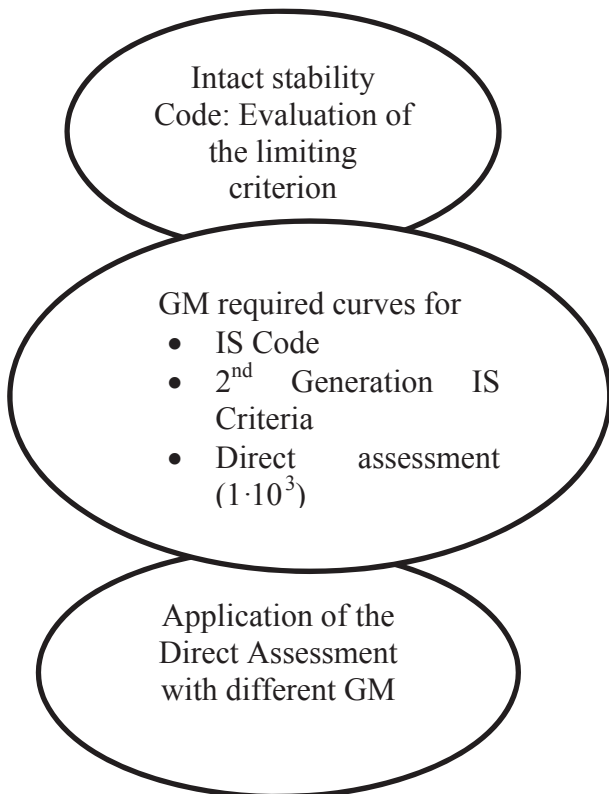


Figure 7: Procedure adopted

As a general comment, it is worth mentioning that usually the limiting GM for a RoRo passenger ferry, neglecting the damage condition, is represented by the weather criterion. With E4ROLLS this GMReq- value is compared with the results obtained by the ISEI concept. Beyond the level 1 of Parametric Roll and Pure Loss of Stability, very conservative, the level 2 is the one in charge to smoothly converge to the direct assessment GM requirements.

RoPax 1

As already mentioned, at first the limiting GM curve with reference to IS Code has been identified. At the design draft this ferry fulfils the weather criterion, with a GM of 0.8m. At this loading condition the direct assessment has been applied, showing an insufficient stability in following seas. This is evident from the polar plot representation and quantitatively by the ISEI value higher than the 10-3.

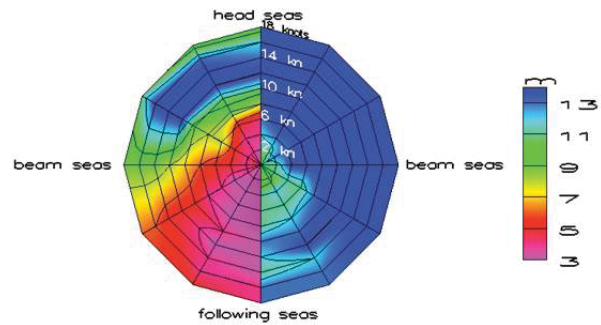


Figure 8 Two polar plots for limiting capsizing wave height for a wave length of 172m. Left: GM=0.8m Right: GM=1.9m

After few iterations, a value of ISEI of $1 \cdot 10^{-3}$ is found at a GM of 1.9m, more than one meter increment compared to the present regulations. In figure 8 results are reported for calculations performed at both GM values (GM= 0.8 m left, GM= 1.9 m right). It can be observed that the ship faces already several problems in following seas with wave heights of 3m for the GM required by the weather criterion (0.8m). From a direct assessment, there isn't any sharp boundary between a parametric roll and a pure loss of stability failure; each dangerous situation is often a combination of both. The GMReq curves read as follows:

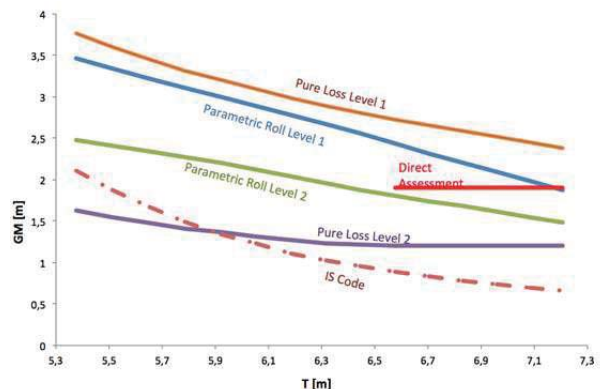


Figure 9 : GM_{Req} curves for the RoPax 1

In figure 9, results derived by the direct assessment are represented by straight horizontal line, as an extrapolation of the calculation carried out at draft 6.6 m and GM= 1.9 m. The second levels of parametric roll and pure loss of stability criteria seem to work properly in the range of the GM limiting values,



between the IS Code and the Direct Assessment curves. For the design draft of 6.6m, the first levels requires a GM up to three meters, not so high considering the conservative approach of these two criteria. For the second level it is evident that the limiting criterion is the one relevant to the parametric roll, in this case very close to the direct assessment requirements.

RoPax 2

The second Ro-Pax, larger in size than the first one, requires a GM of 1.1m at the design draft in accordance with the weather criterion. Applying the direct assessment, E4ROLLS shows again more the need of more than one meter increment between the IS Code requirement and the GM corresponding to the ISEI of 1·10-3. The results with the two different GM values are reported in figure 10.

Curve trends in figure 11 for RoPax2 represent nearly the same behaviour of RoPax1. It is possible again to identify the conservative nature of levels 1 criteria and, as far as level 2 is concerned, the strong difference in terms of GM requirements between pure loss and parametric roll criteria.

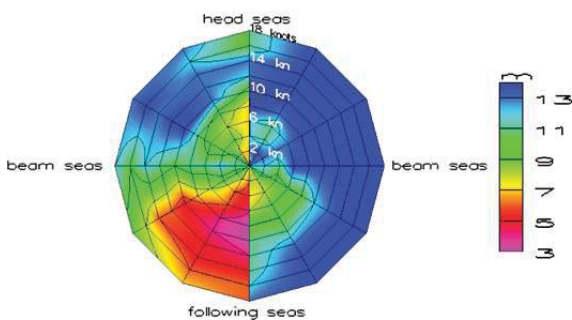


Figure 10: Two polar plots for limiting capsizing wave height for a wave length of 172m. Left: GM=1.1m Right: GM=2.179m

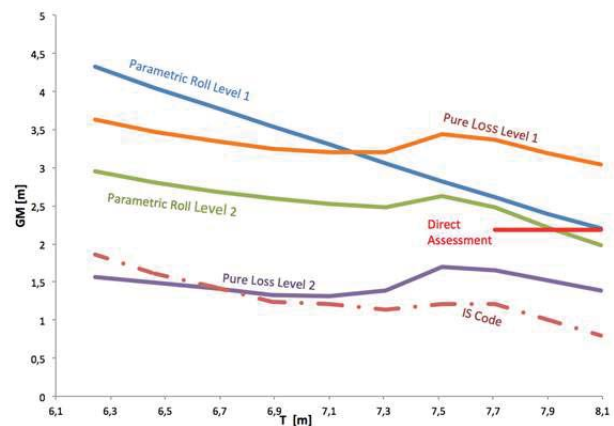


Figure 11: GM req curves for the RoPax 2

RoPax 3

This high speed ferry was designed to meet the ISEI- standard. The limiting GM resulting from the IS Code therefore corresponds more or less to the one computed by the direct assessment i.e. 3.2m. The second level assessments requires values identifying even lower curves. On the other hand, the first levels are extremely conservative, leading to 5-7 m of required GM. Compared to the other two examples, it can be observed an inversion of the level 2 between parametric roll and pure loss of stability; the last one for high drafts requires more stability. As the righting lever curve of this particular ship strongly deviates from the linear representation by GM (fig 12), the example clearly shows that the proposed criteria have problems to cope with such kind of ships.

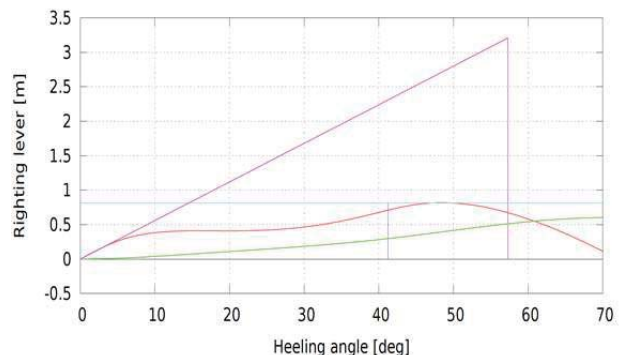


Figure 12: GZ curve for RoPax3

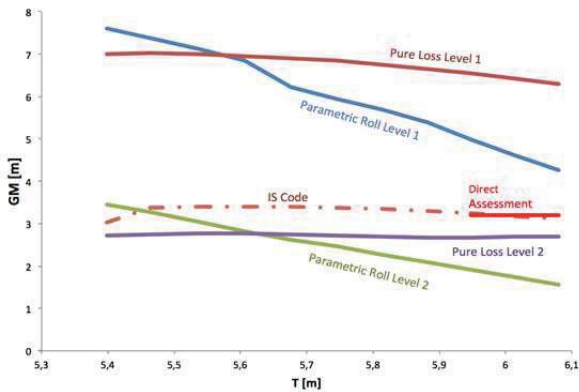


Figure 13: GM required curves for the RoPax 3
RoPax 4

As introduced before, for this ferry the conditions of the accident have been reproduced in the direct assessment computational tool, in order to analyse if the 2nd generation criteria could have prevented that situation. The ship was sailing at a draft of 6.86m with a GM of 1.691m; the direct assessment has been already applied by Kluwe and Krueger resulting in a required metacentric height of 1.89m to fulfil the usual ISEI of 10-3. Considering only the level 2, it is evident for a range of realistic drafts, that criteria show GM results differing (in positive and negative gap) of nearly 0.2 from the IS Code requirements. Actually, a not negligible detail is to be mentioned, i.e. the ship was sailing with a threshold GM value (exactly on the IS Code curve). At the same time, it appears how the criterion for the second level-parametric roll for that draft requires a lower GM value in comparison with the one at the time of the accident (fig.14).

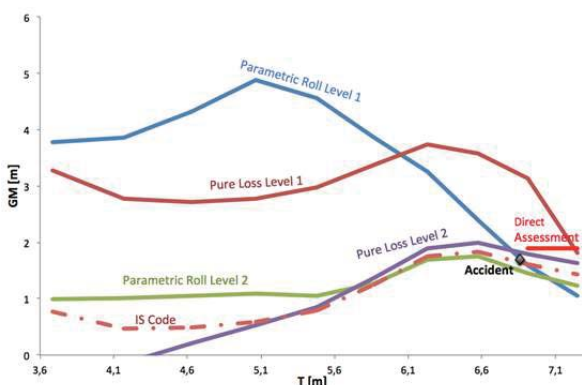


Figure 14: GM required curves for the RoPax 4

Further Cases

So far only problems related to minimum stability requirements have been addressed. It is well known anyway, that an excessive stability can produce problems as well, resulting in excessive accelerations. In figures 11-13-14-15, the level 1 criteria point out a possible problem of this kind, with GM required up sometimes to 7 or 8 meters. Therefore to conclude this investigation, three Container ships are analysed. All these three examples have experienced problems of excessive acceleration as a consequence of sailing with high GM in ballast condition. In the following, the computed curves for the new criteria are presented.

Container 1

This ship was sailing with 8.1 m of draft with a GM of 7.712 m. The limiting criterion for low drafts in this case is the maximum GZ arm position at 25°. The condition of the accident lies in the middle of parametric roll and pure loss limiting curves derived from level 1, leaving space for discussion about the excessive stability requirements (fig. 15).

Container 2

For this ship the accident occurred at a draft of 5.59m and a GM of 4.52m. From the curves, it appears that the accident condition is moderately above any present and future rules (fig.16).

Container 3

The ship experienced the accident at a draft of 5.72m and a GM of 5.67. In this example the accident condition is well above the level 1 criteria for both parametric roll and pure loss of stability (fig. 17).

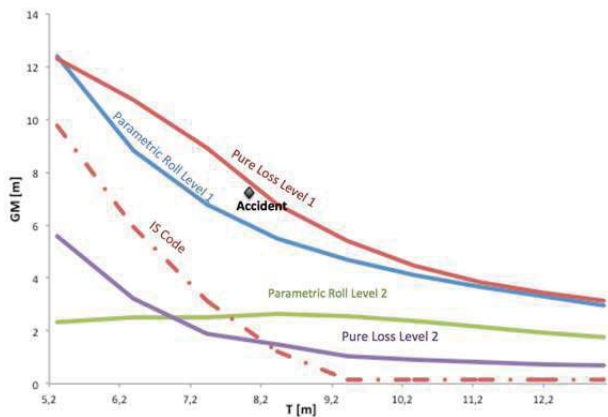


Figure 15: GM required curves for the Container 1

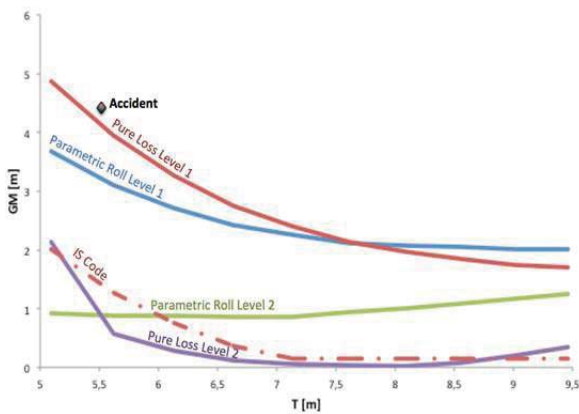


Figure 16: GM required curves for the Container 2

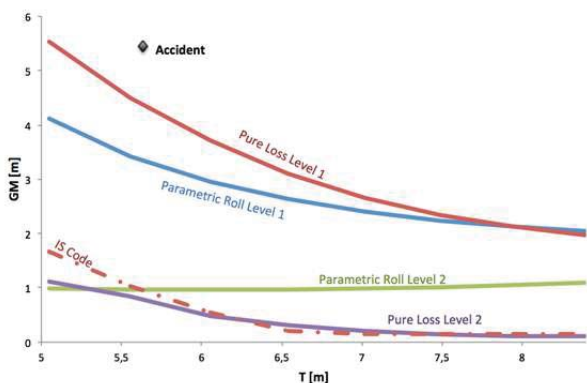


Figure 17: GM required curves for the Container 3

4. CONCLUSIONS

The second generation intact stability criteria, as at present proposed in draft by IMO,

have been applied to a selected set of ships for the specific stability failure modes of parametric roll and loss of stability in waves.

In particular the interest has been focused on the Ro-Ro passenger ship typology and four vessels have been investigated.

Nevertheless, some other special cases have been analysed as well, for the discussion of possible shortcomings due to excessive accelerations. With this purpose, the attention has shifted to the field of containers ships referring to three ships that suffered serious incident.

For the above mentioned ships, comprehensive calculations have been carried out, starting from the present Intact Stability Code requirements, addressing the two lower vulnerability levels up to the direct assessment approach. For this final level, a specified tool is not described by the IMO draft rules text and, for the purpose of this paper, a computational tool available at Hamburg University of Technology has been applied.

Results shows a rather satisfactory consistency among the different assessment levels that has been ascertained by means of the minimum GM curves for a range of drafts.

However, criteria show some difficulties to cope with ships where the righting lever curve strongly deviates from the linear representation by the initial GM. This is a consequence of the approach the criteria are based on. This deficiency clearly points out the necessity for establishing a direct assessment.

An important issue is represented by the high level of GM required in some occasions to comply with the second generation intact stability criteria: From the analysis of the accidents reports it appears how in any case this has not prevented the ship to suffer stability failures in waves, with the further negative implication of high accelerations. This



finding also points out the necessity for establishing a direct assessment. Hamburg,

5. REFERENCES

Blume, P., (1987) "Development of new Stability criteria for Dry Cargo Vessels".
In Proc. PRADS, Vol.3

Grim, O., (1961). "Beitrag zu dem Problem der Sicherheit des Schiffes im Seegang". Schiff und Hafen, 61(8)

Hatecke, Krueger (2013), "The Impact of the second generation intact stability criteria on RoRo-Ship Design" . Proceedings for PRADS2013

Kluwe, F., (2009) "Development of a minimum stability criterion to prevent large amplitude roll motions in following seas " . PhD Thesis, Hamburg

Krueger S., Kluwe F. (2010) "Development of threshold values minimum stability criterion based of full scale accidents "

IMO SDC 1/INF.8 (2013) Information collected by the Correspondence Group on Intact Stability regarding the second generation intact stability criteria development. Submitted by Japan 13 November 2013.

IMO SDC 1 /Annex XX Draft explanatory notes on the vulnerability of ships to the parametric rolling stability failure mode. Working version for sample calculation in the correspondence group established at the SDC 1

Soeding, H., and Tonguc, E., (1986). "computing capsizing frequencies in a seaway". In Proc. STAB, Vol. 2

Kröger, P. (1987) : "Simulation der Rollbewegung von Schiffen im Seegang. Report 473, TU Hamburg-Harburg,

This page is intentionally left blank



A Study on Applicability of CFD Approach for Predicting Ship Parametric Rolling

Yao-hua, Zhou, *School of Naval Architecture, Ocean and Civil Engineering, Shanghai Jiao Tong University, Shanghai 200240, China, E-mail: yhzhou@ccs.org.cn*

Ning, Ma, *State Key Laboratory of Ocean Engineering, Shanghai Jiao Tong University, Shanghai 200240, China, E-mail: ningma@sjtu.edu.cn*

Jiang, Lu, *China Ship Scientific Research Center, Wuxi 214082, China*

Xie-chong, Gu, *State Key Laboratory of Ocean Engineering, Shanghai Jiao Tong University, Shanghai 200240, China*

ABSTRACT

New criteria for Parametric Rolling (PR) are considered in the development of 2nd generation intact stability criterion, by the International Maritime Organization (IMO). As it is well known, estimation methods of the roll damping affect the prediction of parametric rolling significantly, and most estimation approaches for roll damping are based on experiment data or Ikeda's empirical formula. When the new criteria are applied in the design stage of ship, the accuracy of estimation approach for roll damping will be a key aspect of the validity of prediction. In this research, a hybrid method is proposed that 3D CFD approach is utilized to calculate the roll damping, while potential theory method is adopted for predicting parametric rolling motion. Furthermore, direct simulation is also investigated for PR of containership based on CFD approach. Comparative study is carried out for these two methods and potential method whose roll damping is estimated by simplified Ikeda's method and experimental data. According to the results, the CFD approach could achieve satisfactory agreements with the experiment for both roll damping and roll amplitude of PR. Therefore, CFD approach may be suitable to be utilized for PR analysis especially at the early design stage when lack of experiment data.

Keywords: *Parametric rolling; Roll damping; CFD;*

1. INTRODUCTION

Due to the lack of experiment data in the initial design stage, the roll damping is usually obtained by semi-empirical method such as simplified Ikeda's method, so the prediction of PR will be doubtful, because the roll damping has not yet been determined. Considering the significant effect of roll damping on parametric rolling, the estimation method of roll damping needs further investigation.

Fully nonlinear CFD approach could be a good choice for this purpose, and it is preferable to directly obtain the roll damping by CFD approach for numerical prediction model of PR. In this study, a hybrid method is developed based on 3D CFD approach and potential method. The parametric rolling is simulated and validated for containership C11. Good agreement has been achieved. Furthermore, numerical study also has been

carried out to investigate the applicability of direct CFD prediction for parametric rolling.

2. HYBRID METHOD FOR PREDICTING PARAMETRIC ROLLING

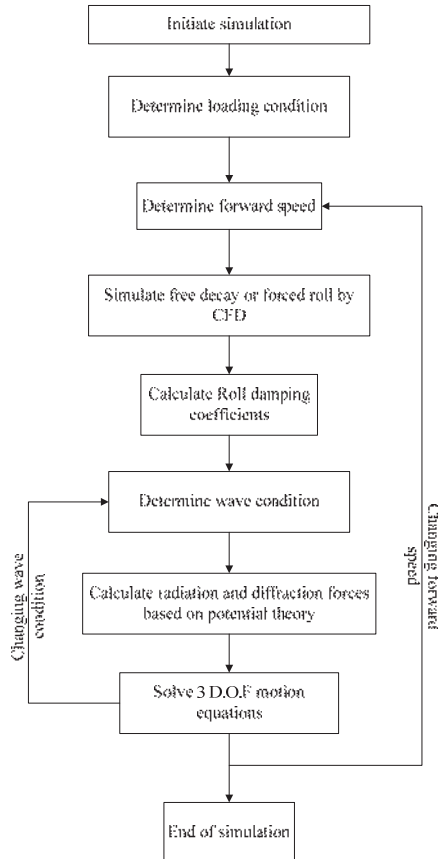


Figure 1 Conceptual scheme of hybrid method for assessment

The hybrid method is developed based on non-linear 3D CFD approach and 3D potential method. CFD approach is utilized for calculation of roll damping and potential method is adopted for calculation of radiation and diffraction forces. The method follows process shown in Figure 1.

2.1 Numerical models

The hybrid method adopts a 3 D.O.F weakly nonlinear model (roll, heave and pitch) for the simulation of ship motion. Such kind of models that considering the time delay effect

and nonlinearity of Froude-Krylov forces has been successfully applied for the simulation of parametric rolling (Turan, 2008, Chang, 2008.). Motion equations are shown in Eqn (1) (Zhou, 2010).

$$\begin{aligned}
 & (M + \mu_{33})\ddot{\eta}_3 + \int_0^t K_{33}(t-\tau)\dot{\eta}_3 d\tau + \mu_{35}\ddot{\eta}_5 \\
 & + b_{35}\dot{\eta}_5 + \int_0^t K_{35}(t-\tau)\dot{\eta}_5 d\tau = F_3^{IS} + F_3^D - Mg \\
 & (I_{xx} + \mu_{44})\ddot{\eta}_4 + \int_0^t K_{44}(t-\tau)\dot{\eta}_4 d\tau \\
 & = F_4^{IS} + F_4^D + F_4^V \\
 & (I_{yy} + \mu_{55})\ddot{\eta}_5 + \int_0^t K_{55}(t-\tau)\dot{\eta}_5 d\tau + c_{55}\eta_5 \\
 & + \mu_{53}\ddot{\eta}_3 + b_{53}\dot{\eta}_3 + \int_0^t K_{53}(t-\tau)\dot{\eta}_3 d\tau = F_5^{IS} + F_5^D
 \end{aligned} \quad (1)$$

Where F^{IS} is the composition force of Froude-Krylov force and restore force which are calculated based 3D pressure integration method for the instantaneous wetted hull; diffraction forces F^D are predicted by 3D frequency domain potential method; radiation forces are calculated based on impulse response theory in the motion equation to considering the memory effect (as shown in Eqn (2)).

$$K_{jk}(\tau) = \frac{2}{\pi} \int_0^\infty (B_{jk}(\omega_e) - b_{jk}) \cos \omega_e \tau d\omega_e \quad (2)$$

Where $B_{jk}(\omega_e)$ is wave making damping that calculated by frequency domain potential theory method. μ_{jk} is added mass or moment of inertia, which is calculated for mean wetted surface by solving boundary problem.

F_4^V is moment due to roll damping, and is simplified as shown in Eqn (3).

$$F_4^V = -(A \cdot \dot{\eta}_4 + C \cdot \dot{\eta}_4^3) \quad (3)$$

Where A and C are roll damping coefficients that calculated by CFD approach.

The Roll damping coefficients are calculated based on motion or moment data of numerical simulations for free decay or forced roll of scaled model. The simulation is carried out by 3D RANSE solver ISIS-CFD (Deng, 2010). This flow solver uses the incompressible unsteady Reynolds-averaged

Navier Stokes equations (RANSE), which is based on the finite volume method to build the spatial discretization of the transport equations. The face-based method is generalized to three-dimensional unstructured meshes for which non-overlapping control volumes are bounded by an arbitrary number of constitutive faces. The flow solver deals with multi-phase flows and moving grids.

2.2 Validation and Discussions

The well-known Container ship C11 (Lu, 2011) is utilized for numerical simulation to validate the hybrid method.

2.2.1 Estimation of roll damping by CFD simulation

First, four ship models of different types are utilized for validating numerical simulation method, including S175, 3100TEU container ship, Warship and Concept Trimaran. S175 is a public experimental model, without bilge keel or rudder. 3100TEU is commercial ship that still in service, with bilge keels and rudder installed in the model. The experiments of these container ships are conducted by Shanghai Jiao Tong University. Warship is a model of combatant published by RINA (RINA, 1980), and installed with bilge keels, rudders and stabilizer fins. The Concept Trimaran is a Concept ship for research purposes that developed by Harbin Engineering University (Zhou, 2010). Table 1 shows the principal dimensions of the four models. Figure 2 shows the model of 3100TEU.

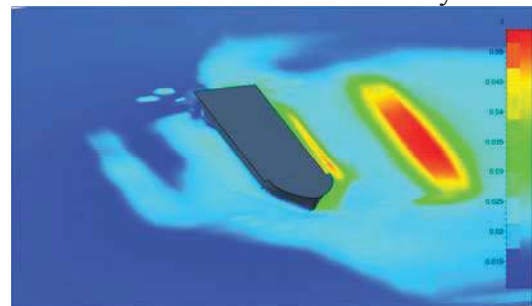


Figure 2 the model of 3100TEU container ship

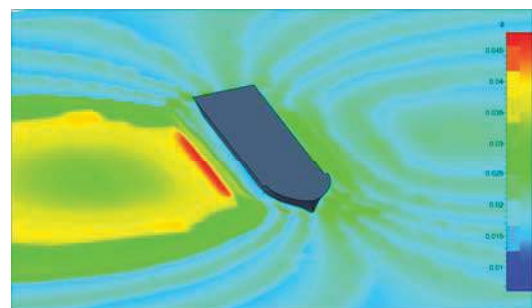
Table.1 Principal Dimensions

		S175	3100TEU	Warship
Length L_{pp}	(m)	3.034	3.120	6.000
Breadth B	(m)	0.440	0.469	0.654
Draft T	(m)	0.165	0.173	0.204
GM	(m)	0.017	0.013	0.028
		Trimaran		
Length L_{WL} (main hull)	(m)	3.120		
Breadth B_{WL} (main hull)	(m)	0.240		
Draft T (main hull)	(m)	0.116		
GM	(m)	0.140		

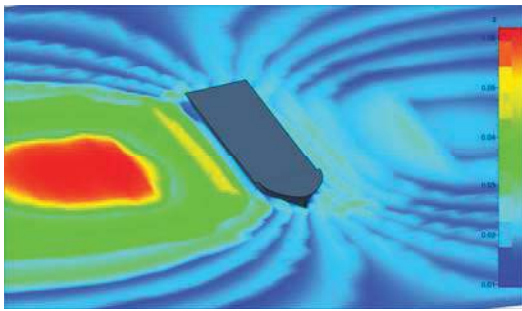
All of the predictions are procured on 0.79~1.2M grid. Figure 3 shows the free surface around 3100TEU model in free decay test simulation. The generation and propagation of wave trough and crest in wide area due to radiation could be observed obviously.



(a) T=8.1s



(b) T=8.7s

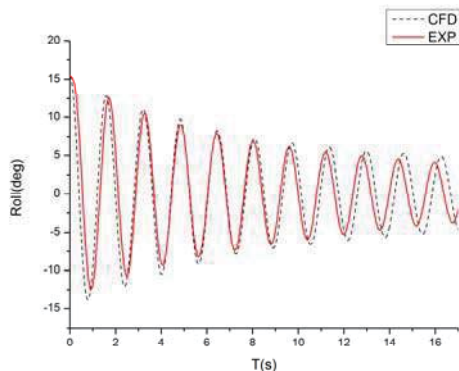


(c) T=9.0s

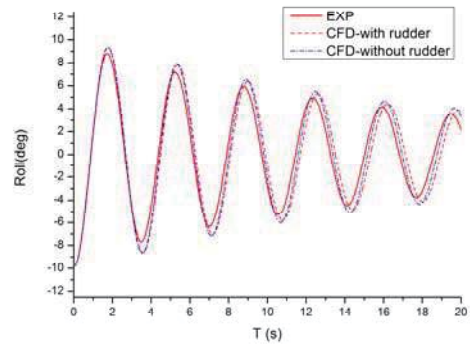
Figure 3 Free surface height around 3100TEU model

Figure 4 shows the roll decay curves of S175 and 3100TEU, including the comparisons between the experimental data and simulations. Figure 5 shows the CFD simulation results of Warship and Trimaran.

As shown in Figure 4 and Table 2(a), good accuracy could be achieved for the natural roll period. Moreover, with the increase in the number of rolling cycles, errors of the time history due to cumulative error are inevitable. By fitting the extinction curve, it could be found that, the CFD method is able to ensure the simulation of roll damping to achieve a satisfactory accuracy, even if there are certain errors for the amplitude and phase of roll. The comparisons of B_{44} and 2μ show that (Table 2(b)), the CFD method proposed by this study could achieve good agreement for the simulation of free decay in calm water at zero velocity, and the errors are acceptable.

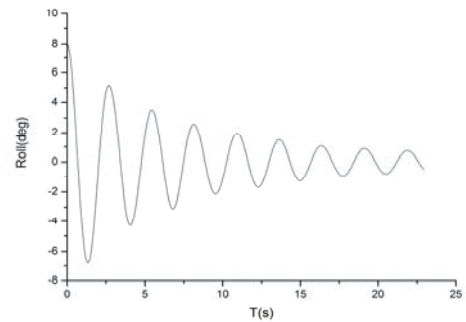


(a) S175

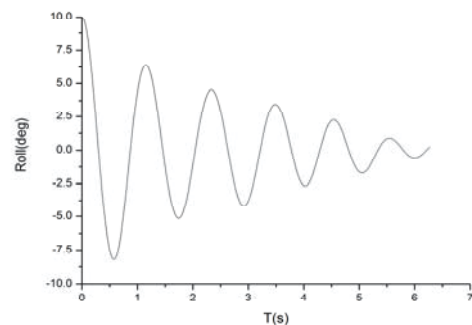


(b) 3100TEU

Figure 4 The time histories of free rolling of S175 and 3100TEU ($F_n=0$)



(a) Warship



(b) Trimaran

Figure 5 the time histories of free rolling of Warship and Trimaran ($F_n=0$)

Table 2 (a) The natural roll periods T_{roll}

		CFD (s)	EXP (s)
S175		1.635	1.600
3100TEU	with rudder	3.610	3.600
	no rudder	3.570	
Warship		2.735	2.66



Trimaran	1.108	1.100
----------	-------	-------

Table 2 (b) The extinction/damping coefficients

	\hat{B}_{44} (0~15degs) / 2μ	CFD	EXP
S175	\hat{B}_{44}	4.34E-4~3.59E-3	4.86E-4~4.25E-3
3100TEU	\hat{B}_{44} (with rudder)	2.03E-3~8.13E-3	2.27E-3~7.32E-3
	\hat{B}_{44} (no rudder)	2.05E-3~6.10E-3	
Warship	2μ	0.0878	0.094
Trimaran	2μ	0.117	0.123

For the estimation of roll damping for C11, the scale of CFD simulation is taken as the same scale of model test. All of the predictions are procured on 1.44M grid (as shown in Figure 6).

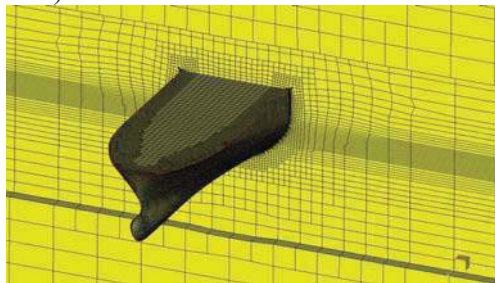


Figure 6 Meshes of typical section of C11

For blind simulation of parametric rolling, the initial heel angle or forced roll amplitude is difficult to determine for estimation of roll damping. Therefore, these two values are taken as 20 degrees for both CFD simulations. Figure 7 and Figure 8 show the simulations of forced roll and free decay at $F_n=0.0, 0.05$ and 0.1 . Then roll damping coefficients A and C are estimated for further parametric rolling prediction.

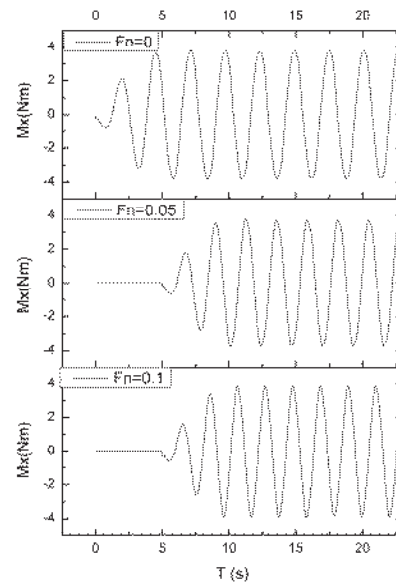


Figure 7 Time history of roll moment for forced roll simulation of C11

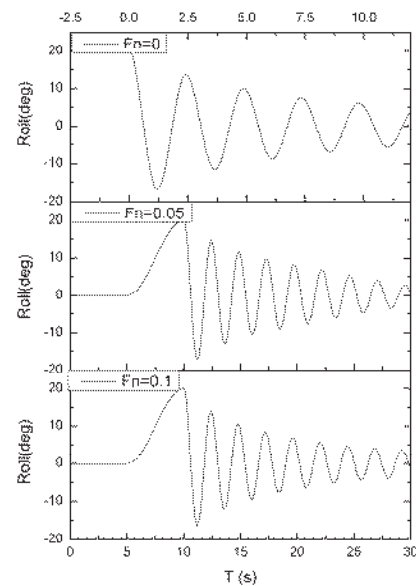


Figure 8 Time history of free decay simulation of C11

Table 3 The damping coefficients of C11 (full scale)

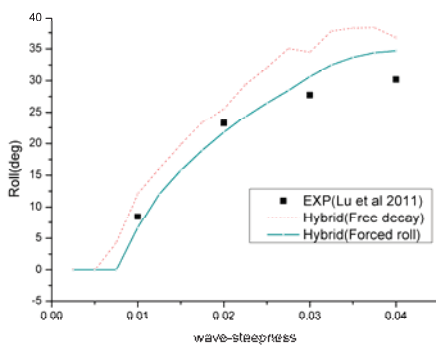
	F_n	A	C
Free decay	0.0	3.68E+08	5.59E+10
	0.05	2.82E+08	4.28E+10



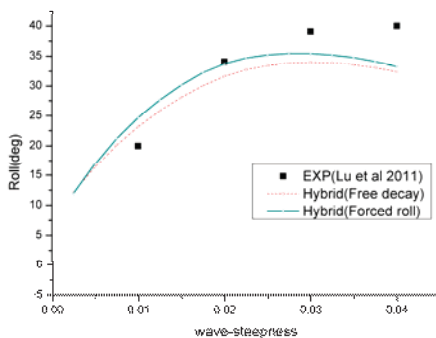
	0.1	2.53E+08	8.25E+10
	0.0	6.22E+08	6.92E+10
Forced roll	0.05	3.18E+08	2.99E+10
	0.1	2.60E+08	3.63E+10

2.2.2 Validation and analysis of parametric rolling results

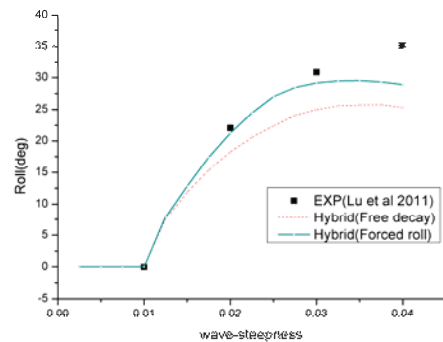
Figure 9 shows the predictions of parametric rolling for C11 by hybrid method. Two options of estimating roll damping coefficients were compared with experiment data. According to prediction results, the hybrid method (with forced roll damping) could successfully predict parametric roll for different speeds and wave-steepness. For cases those amplitudes around and less than 27~33 degrees could achieve satisfactory accuracy.



a) $F_n=0.0$



b) $F_n=0.05$



c) $F_n=0.1$

Figure 9 Roll amplitudes prediction for PR

The initial heel angle or forced roll amplitude plays an important role on obtaining the roll damping characteristic such as equivalent damping coefficients (Hashimoto, 2010). In this study, the initial heel angle and forced roll amplitude are both taken as 20 degrees for estimation of roll damping coefficients. Thus, the agreement is not good for cases with large amplitudes. Therefore, how to determine the initial heel angle or forced roll amplitude for blind simulation of PR by hybrid method still needs further study in the future. These values could be taken as 20 degrees temporarily to be consistent with IMO's Level 2 criteria.

According to the present results of C11, it is appropriate to adopt the hybrid method (forced roll), and this method could bring great advantage in the initial design stage especially in the lack of experiment data for a new design.

3. STUDY ON APPLICABILITY OF DIRECT CFD METHOD FOR PREDICTING PARAMETRIC ROLLING

In order to improve the forecasting precision of PR for optimal design, in theory the best way is to carry out good simulation for encountered wave surface accounting the action of ship, highly nonlinear restoring forces and hydrodynamic forces, and large roll-heave-

pitch resonance. Different from traditional potential methods, fully nonlinear CFD approach could be a good choice for state of the art method for this purpose. Thus, it is also necessary to carry out comparative study for hybrid method with “state of the art” methods such as 3D direct CFD approach.

The direct CFD prediction method utilizes the same RANS solver as in the estimation of roll damping. Most of parameter settings and mesh generation also follow the same principles. All of the predictions are procured on 2.77M grid. As shown in Figure 10, cylindrical computational domain is created with sliding grid for simulating near field flow of ship.

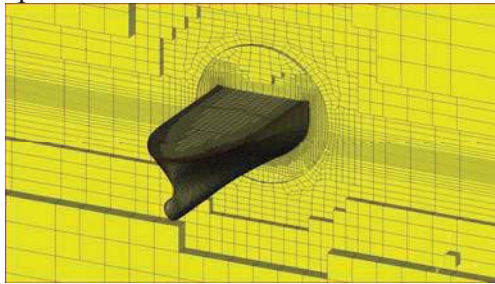
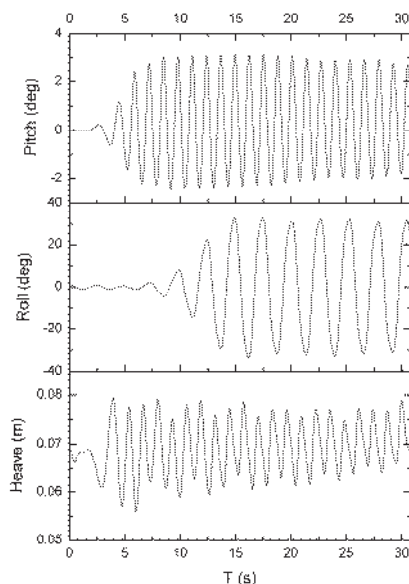
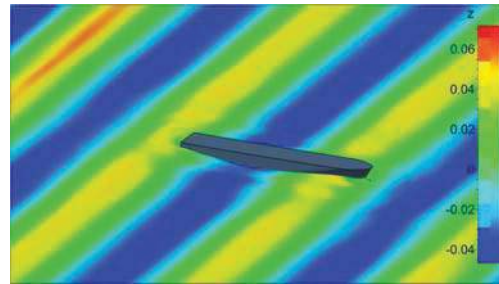


Figure 10 Refined meshes of typical section of C11

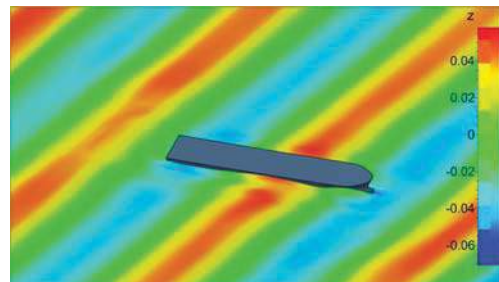
3 D.O.F motions (roll, pitch and heave) are free for simulation of PR. Sway and yaw are limited and neglected.



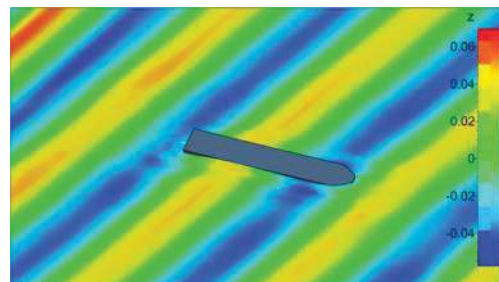
a) Time history of motion responses



b) Simulation of PR (t=16.704s)



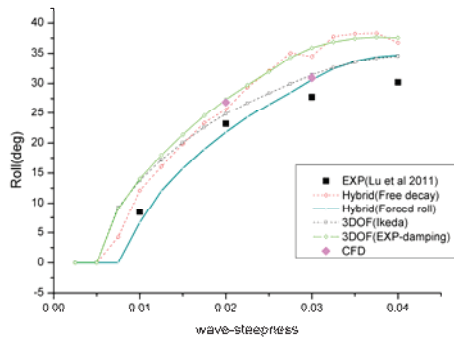
c) Simulation of PR (t=17.052s)



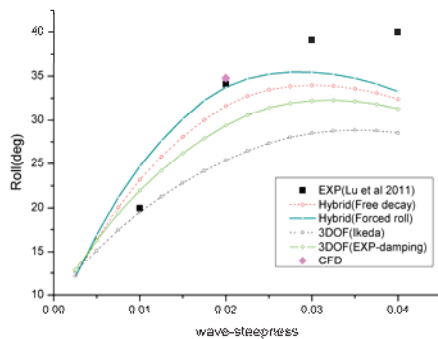
d) Simulation of PR (t=17.4s)

Figure 11 Simulations of Parametric Rolling (Fn=0, wave-steepness 0.03)

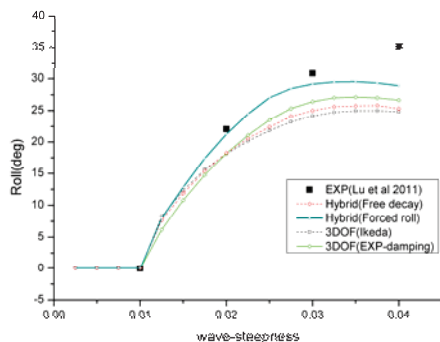
Figure 11 shows the time histories of motion responses and interactions between fluid field and ship at Fn=0. Figure 12 shows the comparisons of roll amplitudes predicted by different methods, including Hybrid method, direct CFD method and potential theory method whose roll damping is estimated by simplified Ikeda’s method and experimental data (3 D.O.F(Ikeda) and 3 D.O.F(EXP-damping)).



a) $F_n=0.0$



b) $F_n=0.05$



c) $F_n=0.1$

Figure 12 Comparisons of roll amplitudes for
PR

In Figure 12, results show the influence of four estimating methods of roll damping on PR amplitudes. Roll amplitudes of hybrid method (Free decay) is very close to 3 D.O.F (EXP-damping), It indicates roll damping estimated by free decay based on CFD simulation achieved good accuracy for prediction of PR,

and can be a good option to replace free decay tests which are currently carried out in initial design stage.

On the whole, Hybrid method and direct CFD prediction method could achieve good accuracy for prediction of PR. These two methods are considered to be more appropriate as options for numerical models of direct stability assessment of PR.

4. CONCLUSIONS

The research results show that, the CFD approach has good applicability in simulating parametric rolling, and has positive significance for the development of direct stability assessment criteria of PR. Overall, hybrid method needs less computational resource, and is more suitable for engineering application comparing to direct CFD method. It is suggested to pay enough attentions to the application of CFD approach in the study and development of guideline of direct stability assessment criteria in the future.

5. ACKNOWLEDGMENTS

This work was supported by Ministry of Industry and Information Technology of the People's Republic of China No. [2012]533, and the Chinese Government Key Research Project KSHIP-II Project (Knowledge-based Ship Design Hyper-Integrated Platform) No.201335.

6. REFERENCES

- G.B. Deng, P. Queutey, M. Visonneau. Seakeeping Prediction for a Container Ship with RANS Computation [C]. The 9th International Conference on Hydrodynamics, 2010.
- Hirotsada Hashimoto, Naoya Umeda. A study on Quantitative Prediction of Parametric



Roll in Regular Waves [C]. Proceedings of the 11th International Ship Stability Workshop, 2010.

Jiang Lu, Naoya Umeda, Kun Ma, Predicting parametric rolling in irregular head seas with added resistance taken into account [J]. Journal of Marine Science and Technology, (2011) 16:462–471.

Osman Turan, Zafer Ayaz. Parametric rolling behaviour of azimuthing propulsion-driven ships [J]. Ocean Engineering 35 (2008) 1339-1356.

RINA. Wave Induced Motions and Loads on a Model Warship [R]. 1980.

Yong-quan Chang, Fan Ju. et al. Analysis of ship parametric rolling in head sea [J]. Chinese Journal of Hydrodynamics, Vol.23, No.2, 2008 (in Chinese).

Yao-hua Zhou. The Prediction of Roll Damping and Nonlinear Motion of Trimaran [D]. Harbin Engineering University, 2010(in Chinese).

This page is intentionally left blank



Estimation of Ship Roll Damping - a Comparison of the Decay and the Harmonic Excited Roll Motion Technique for a Post Panamax Container Ship

Sven Handschel, *TU Hamburg-Harburg*, sven.handschel@tuhh.de

Dag-Frederik Feder, *TU Hamburg-Harburg*, dag.feder@tuhh.de

Moustafa Abdel-Maksoud, *TU Hamburg-Harburg*, m.abdel-maksoud@tuhh.de

ABSTRACT

The decay motion as well as the harmonic excited roll motion are established techniques to estimate roll damping for ships. This paper compares the advantages and disadvantages of both techniques and focuses on their applicability. Different analysis methods for both techniques to determine the nonlinear roll damping moment are investigated with the aim of developing an exact estimation approach without additional filtering, curve fitting and offset manipulation of the recorded time series. Damping coefficients of both techniques are compared for available experiments of the benchmarking post panamax container ship model Duisburg Test Case (DTC). Reasons for deviations are investigated, and the influence of an accurate estimation of the current nonlinear hydrostatic moment will be shown. In this context, the experimental estimation is more convenient than an additional calculation. A method for the determination of the nonlinear hydrostatic moment during a harmonic excited roll motion test is presented. Different approximations of roll damping based on series expansion are investigated. Disadvantages of a widely used approach are discussed based on the results.

Keywords: *roll damping, decay technique, harmonic excited roll motion technique*

1. INTRODUCTION

Boundary element methods (BEM) based on the potential theory can, in most cases, simulate ship motions with sufficient accuracy. They are accurate enough for many applications, and compared to finite volume methods (FVM), they are computationally efficient. Ship motions are mainly damped by the generation of surface waves which radiate from the ship. This is not valid for the roll motion. The roll motion is influenced by additional damping effects which cannot be predicted by BEMs. To consider these effects,

roll damping is often estimated separately. Hence different techniques exist. Common techniques are (I) the roll decay (see e.g. Spouge, 1988), (II) the harmonic excited roll motion (called HERM, see Sugai et al., 1963, Blume, 1979 and Handschel et al., 2014a) and (III) the harmonic forced roll motion (Bassler et al., 2010 and Handschel et al. 2014b), see also Figure 1. Techniques (I) and (II) estimate the roll damping moment from the roll angle recording. In technique (III) the roll moment is directly determined on a fixed predefined roll axis.



Applicability of the techniques: Table 1 shows a comparison of the properties of all three techniques. Only with the decay (I) and the harmonic excited roll motion technique (II) does the ship roll with a natural free motion axis. In fact, the fixed roll axis of technique (III) and the direct determination of the moment enable an easy validation process for numerical simulation methods (see also Handschel et al., 2014b), but the natural motion coupling of the degrees of freedom is suppressed. In this paper, technique (III) will not be further investigated.

Table 1 Advantages and disadvantages of techniques to estimate roll damping

* less/small *** high/large	(I)	(II)	(III)
Real motion coupling	yes	yes	no
Steady roll motion	no	possible	possible
Large roll amplitudes	*	***	***
Forward speed	*	***	***
Time and cost	*	**	***

In contrast to the harmonic excited roll motion technique (II), no roll damping for large roll amplitudes and forward velocities can be estimated by the decay technique (I). Large forward velocities are associated with large damping moments. The high roll damping

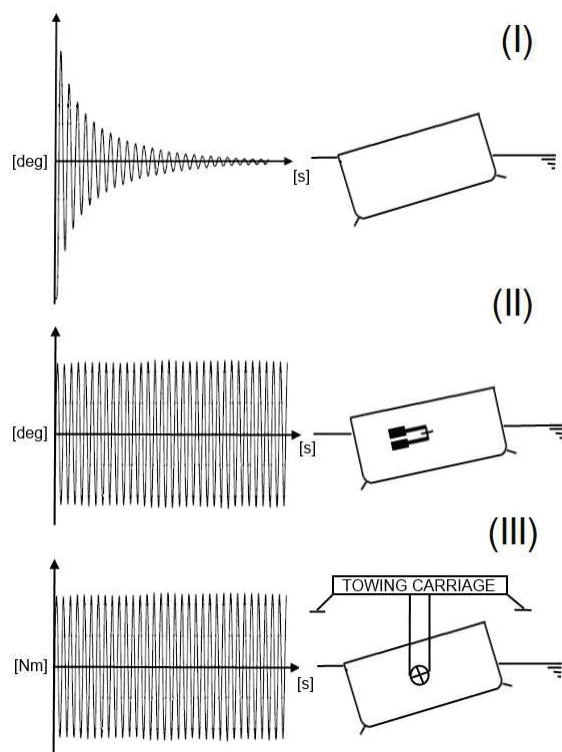


Figure 1 Techniques to estimate roll damping

prevents the realisation of sufficient numbers of roll periods with the decay technique, which are necessary to analyse roll damping with high accuracy. Nevertheless, the decay technique is a low cost technique and does not require much towing tank testing time.

Post panamax container ship: In the present paper model tests are included for the post panamax container ship Duisburg Test Case (DTC, Table 2, see el Moctar et al., 2012). The model is equipped with bilge keels, a propeller and a full spade rudder. The bilge keels are separated in five parts with a breadth of $0.008 B_{WL}$. Especially the huge bow flare area as well as the transom stern is typical for this type of ship. The model tests were carried out for DTC with a full scale length of $L_{WL} = 361m$ in full loading condition at Hamburg ship model basin (HSVA, Schumacher, 2010). A scale factor of 59.467 is applied.

Table 2 Main dimensions Duisburg Test Case (DTC) for full loading and ballast condition – scale factor 1:59.467

	full loading	ballast
L_{WL}	6.0691 m	5.9391 m
B_{WL}	0.8576 m	0.8576 m
D	0.2354 m	0.2018 m
KG	0.3992 m	0.235 m
C_B	0.6544	0.6288
∇	$0.7887 m^3$	$0.6496 m^3$
i_{xx}	$0.3967 B_{WL}$	$0.3801 B_{WL}$
i_{yy}, i_{zz}	$0.2447 L_{WL}$	$0.2713 L_{WL}$

The paper presents results for both measurement techniques (I) and (II). Three different analysis methods based on a one degree of freedom, namely the roll motion equation, are investigated. The focus is set on identifying a method which determines roll damping without additional filtering and curve fitting. The analysis methods should also work with typical measurement offsets which could be observed in the available roll angle

¹ It is assumed that the prior filtering of the signals with a measurement amplifier is weak.

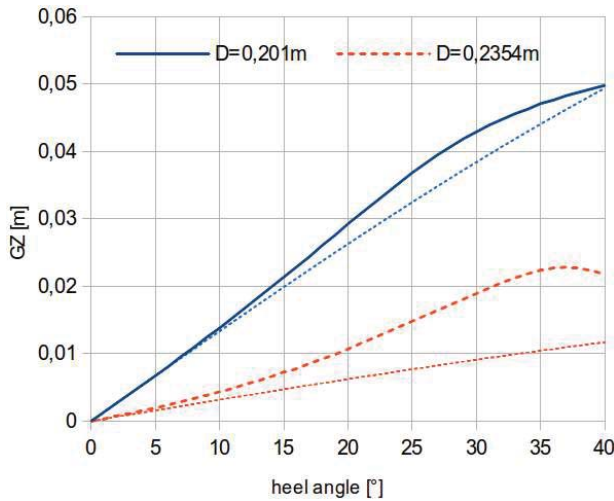


Figure 2 GZ curve DTC: full loading (red) and ballast condition (blue) / dotted line: linearization of hydrostatic moment

measurements. Furthermore, it will be shown that a comparison of the results for both techniques depends on an exact determination of the hydrostatic moment. For the application in ship motion simulations, damping coefficients are usually formulated as a linear, quadratic or as a cubic function of the roll velocity. The applicability of these approximations will be discussed. It will be shown that each approach can lead to certain deviations.

2. ROLL MOTION OF SHIPS

2.1 Equation of Roll Motion

Considering one degree of freedom, the roll equation can be formulated based on Newton's second law. The coefficients of the inertia moment of the ship M_φ , damping moment N_φ , restoring moment S_φ and the external moment F_φ are usually formulated with a balance between the rigid body moments and external moments:

$$M_\varphi \frac{\partial^2 \varphi}{\partial t^2} + N_\varphi \frac{\partial \varphi}{\partial t} + S_\varphi \varphi = F_\varphi(t). \quad (1)$$

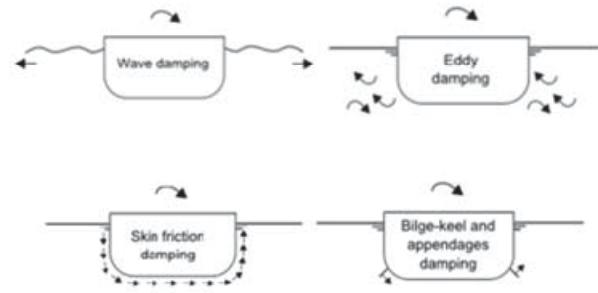


Figure 3 Separation of roll damping phenomena

The $GZ(\varphi_{heel})$ -curve, the change of the lever arm over the heel angle, characterises the hydrostatic moment

$$S_\varphi(\varphi) = \frac{g\Delta GZ(\varphi)}{\varphi}. \quad (2)$$

It can be determined by static or dynamic measurements (see Section 4). Figure 2 includes the $GZ(\varphi_{heel})$ -curves for both load cases.

The undamped natural frequency of the ship can be described by the ratio of the hydrostatic and inertia moment coefficients:

$$\omega_0 = \sqrt{\frac{S_\varphi}{M_\varphi}}. \quad (3)$$

From this equation, the total inertia, the sum of the ship inertia and the virtual inertia due to the acceleration of the fluid, can be determined exactly at the undamped natural frequency by

$$M_\varphi = \frac{g\Delta GZ(\varphi)}{\omega_0^2 \varphi}. \quad (4)$$

2.2 Roll Damping

The roll damping moment N_φ is generated by wave radiation, vortex generation and the lift and friction on the hull (see Himeno, 1981 and

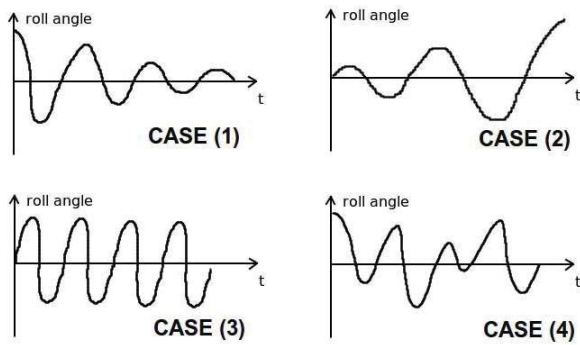


Figure 4 Rolling of ships in irregular waves

Figure 3²). In addition, ship appendages can have a noticeable effect on roll damping.

For the consideration of the total roll damping, additional damping terms are embedded in BEM simulation methods. These were usually estimated by the decay (I) or harmonic excited roll motion (HERM, II) technique via experiments or numerical simulations (see Sarkar, 2000, Salui, 2004, Rööös, 2009, el Moctar et al., 2010, Gao et al., 2010, Handschel et al., 2012a).

Using an energy approach over one period,

$$E_E = 4 \int_0^{\varphi_a} N_{\varphi} \dot{\varphi} d\varphi = \pi N_{\varphi} \omega \varphi_a^2, \quad (5)$$

the damping moment can be expressed as an equivalent damping coefficient N_{φ} which depends on the roll frequency ω and the roll amplitude assuming harmonic behaviour $\varphi = \varphi_a \sin(\omega t)$. The equivalent non-

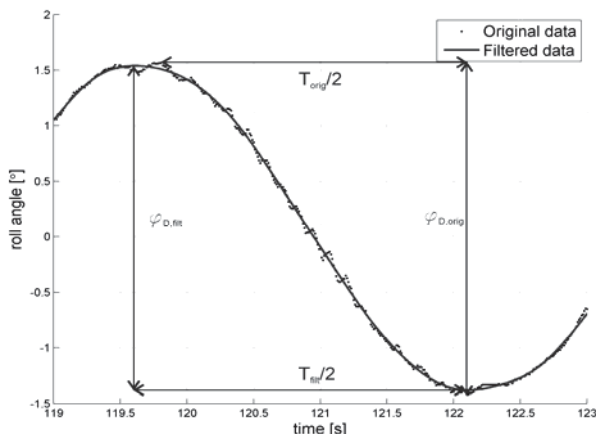


Figure 5 Comparison unfiltered and filtered signal

dimensional roll damping coefficient B_{φ} is formulated according to the ITTC as

$$B_{\varphi}(\varphi_a) = \frac{N_{\varphi}(\varphi_a)}{\rho \nabla B_{WL}^2} \sqrt{\frac{B_{WL}}{2g}}. \quad (6)$$

2.3 Roll Motion in Irregular Waves

The rolling of ships in irregular waves can be divided in four scenarios, see Figure 4: a roll motion with (1) a decreasing roll amplitude, (2) an increasing roll amplitude, (3) a constant roll amplitude and (4) an alternation of increasing and decreasing amplitudes. The variation of the roll amplitude depends mainly on the wave period and wave height.

A problem of the discussed techniques is that each of them considers only one of four scenarios. The decay motion (I) corresponds to the first case, HERMs (II) to case (3).

3. ESTIMATION OF ROLL DAMPING

3.1 Roll Decay Motion

Roll decay measurements are straight forward and can be easily realised. The ship is excited once and decayed to the rest position. The measured time series of the roll angle are analysed to estimate roll damping. Carried out in towing tanks, they are less expensive than other techniques.

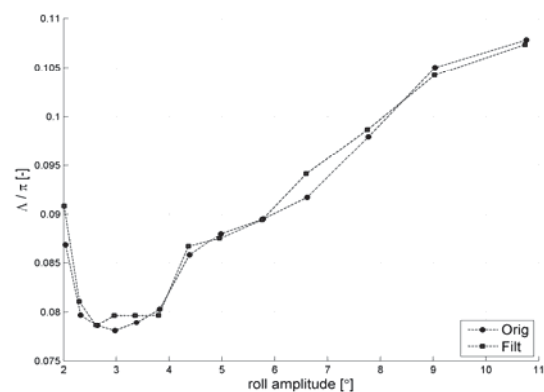


Figure 6 Comparison unfiltered and filtered results for logarithmic decrement – full loading condition, Fn=0.10

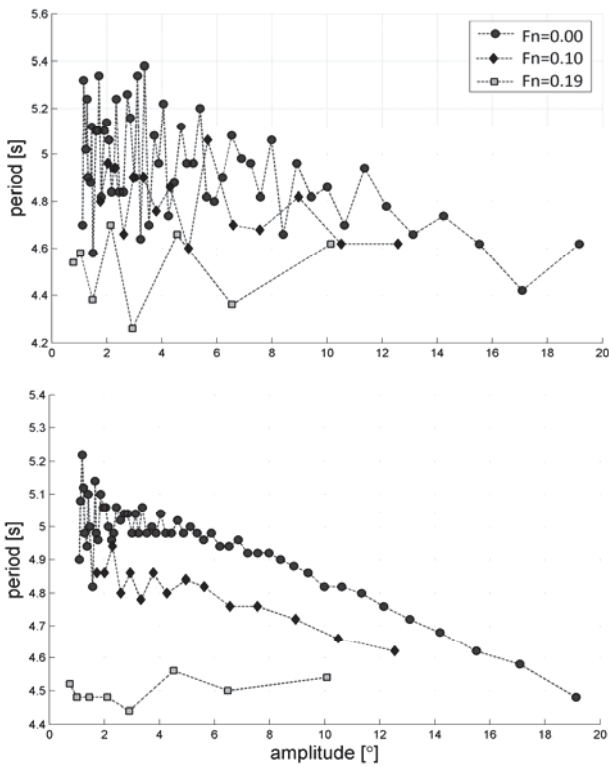


Figure 7 Comparison unfiltered (upper diagram) and filtered resonance roll period for full loading condition

Three methods (A, B and C) are investigated for the (D)ecay technique. Methods based on the logarithmic roll decrement (D.A) and energy conservation (D.B and D.C) are analysed. The roll motion occurs in the damped natural frequency

$$\omega_D = \omega_0 \sqrt{1 - \left(\frac{N_{\phi e}}{2\omega_0 M_\phi} \right)^2} \quad (7)$$

which is evaluated for every half period. The influence of low-pass filtering is investigated. The measurement window in Figure 5 shows an example of the filter application. The influence of noise on determining double amplitudes ϕ_D is not significant for the presented results, see Figure 6. Improvements can mainly be observed for determining the roll period $T = 2\pi / \omega_D$ from peak to peak (Figure 7).

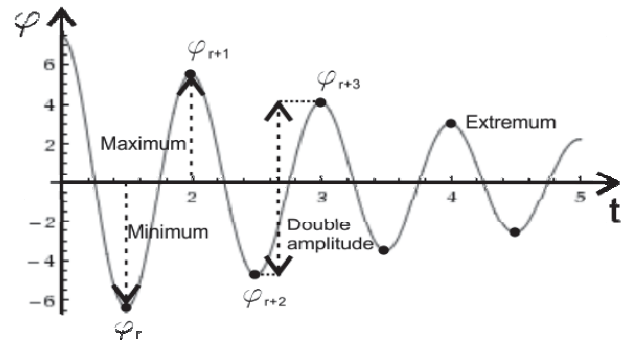


Figure 8 Decay test

Method (D.A): Four variations of the logarithmic decrement method

$$\Lambda = \frac{1}{j} \ln \frac{|\varphi(t)|}{|\varphi(t + j \frac{2\pi}{\omega})|} \quad (8)$$

are tested: with all extrema, only maxima or minima as well as double amplitudes, see Figure 8. Only the application of double amplitudes compensates for possible measurement offsets. The damping coefficient is defined as

$$N_{\phi e}(\varphi_a) = \frac{M_\phi \omega_D(\varphi_a)}{\pi} \ln \left(\frac{|\varphi_r - \varphi_{r+1}|}{|\varphi_{r+2} - \varphi_{r+3}|} \right) \quad (9)$$

for

$$\varphi_a = \left(\frac{|\varphi_r - \varphi_{r+1}| + |\varphi_{r+2} - \varphi_{r+3}|}{4} \right) \quad (10)$$

Method (D.B): The ‘Froude’-energy method (see Spouge, 1988) is based on the energy conservation of the dissipated energy E_E and the – hydrostatic – potential energy $E_{D.B}$ in the roll maximum ($\dot{\phi} = 0$):

$$E_{D.B} = g\Delta \int_{\varphi_D}^{\varphi_{D+1}} GZ(\varphi) d\varphi \quad (11)$$

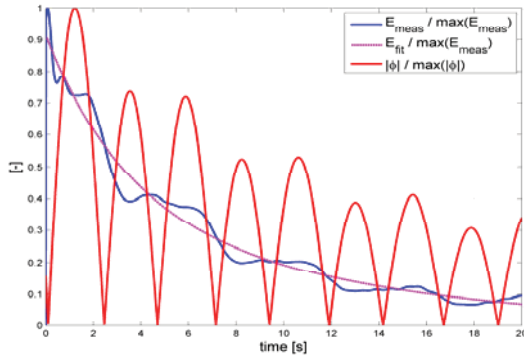


Figure 9 Curve fit (dotted, pink) of energy function (blue), Eq. (13) – full loading condition, $F_n=0.10$

Instead of using only extrema, it is more useful to formulate the method for double amplitudes φ_D to compensate for possible measurement offsets. Both energy formulations are equated ($E_E = E_{D,B}$), which results to

$$N_\varphi(\varphi_a) = \frac{E_{D,B}}{\pi\omega_D\varphi_a^2}. \quad (12)$$

Method (D.C): This method (see Roberts, 1985 and Spouge, 1988) is also based on energy conservation, but for the sum of potential and kinetic energy. Instead of using an integral term as method (D.B), Roberts recommends a differential term to estimate the energy loss rate $dE_{D,C}/dt$. The energy equation is given by:

$$E_{D,C}(t) = \frac{1}{2}\dot{\varphi}^2 + \frac{1}{2}\omega_D^2\varphi^2. \quad (13)$$

In contrast to Spouge, 1988, who fitted the function $E_{D,C}$ by a cubic spline curve, in this investigation exponential functions are used, see Figure 9. The roll damping follows to

$$N_\varphi(\varphi_a) = -M_\varphi \left(\frac{dE_{D,C}}{dt} \right) / E_{D,C}. \quad (14)$$

Applicability of method (A), (B) and (C): The methods presented can be used in the resonance frequency ω_D and for ships with linear or nonlinear righting arm curves. Table 3

shows an overview of advantages and disadvantages of each analysis method in the case of a decay motion. The focus was set on three points: (i) if a filtering of the roll angle time series is required, (ii) if a curve fitting is necessary for the analysis method and (iii) if a measurement offset of the roll angle leads to deviations of the results. The information given in Table 3 has been verified in a comparative study for an analytical decay function in the Appendix, Figure 17.

Unfortunately, with all methods, the time series have to be filtered³ to achieve satisfied results. Double amplitudes compensate for deviations due to measurement offsets in methods (D.A) and (D.B). Method (D.C) is able to estimate roll damping for larger amplitudes based on a curve fitting of the energy. It has to be mentioned that an approximation by curve fitting is a compromise between exactness and the possibility to estimate roll damping over a wider range of roll amplitudes.

Table 3 Advantages and disadvantages of the presented analysis methods for technique (I)

	(D.A) ⁴	(D.B)	(D.C)
Filter required	yes	yes	yes
Curve fit required	no	no	yes
Sensitive to measurement offset	weak	weak	yes
# of peaks at start for which no result of N_φ can be estimated	2	2	0

3.2 Harmonic Excited Roll Motion

The (H)armonic roll motion corresponds to the third scenario (constant amplitude) of the roll motion in irregular waves, see Figure 4. The motion is excited by two contrary rotating weights (Blume, 1979) or by flying wheels

³ Butterworth lowpass filter 8th-order with cutoff frequency $\omega_C = 5\omega_D$.

⁴ Logarithmic roll decrement method with double amplitudes.



(Sugai et al., 1963). Three different analysis methods are known which are independent from the roll resonance frequency. Details can be found in Handschel et al., 2014a.

The methods are all based on energy conservation over one roll period, see Eq. (5). The maximum roll amplitude, the peak, occurs at the frequency (see also Spouge, 1988)

$$\omega_p = \omega_0 \sqrt{1 - \frac{1}{2} \left(\frac{N_{\varphi e}}{\omega_0 M_\varphi} \right)^2} \quad (15)$$

for harmonic motion with sinusoidal excitation.

Method (H.A): The roll angle

$$\varphi(t) = \varphi_a \sin(\omega t + \mathcal{G}) \quad (16)$$

is *phase-shifted* by \mathcal{G} with respect to the initiated roll moment, see Figure 10,

$$F_\varphi(t) = F_{\varphi,a} \sin(\omega t). \quad (17)$$

The work done by the exciting moment in one roll period is

$$E_{H.A} = \int_0^T F_\varphi \dot{\varphi} dt = F_{\varphi,a} \varphi_a \pi \sin \mathcal{G}. \quad (18)$$

The dissipated damping energy and the work done by the exciting moment over one roll period should be the same. With the relation $E_E = E_{H.A}$ the equivalent roll damping can be calculated by:

$$N_\varphi(\varphi_a) = \frac{F_{\varphi,a} \sin \mathcal{G}}{\omega \varphi_a}. \quad (19)$$

Method (H.B): The roll moment and roll angle span a closed trajectory in phase-space, a Lissajous curve (Figure 10). The area inside the

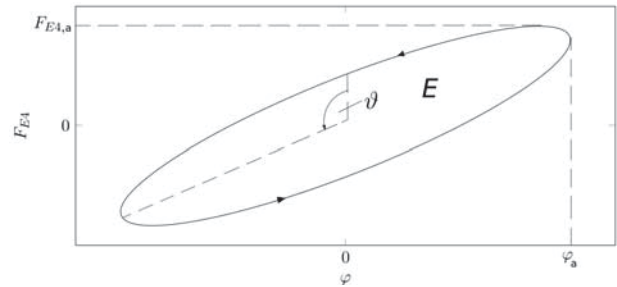


Figure 10 phase plot of the roll moment (here F_{EA}) and the excited roll angle, Lissajous curve trajectory is the energy which dissipates over a roll period

$$E_{H.B} = \int_{-\frac{\pi}{\omega}}^{\frac{\pi}{\omega}} F_\varphi d\varphi \quad (20)$$

$$N_\varphi(\varphi_a) = \frac{E_B}{\pi \omega \varphi_a^2}. \quad (21)$$

Method (H.C): The analysis with the Fourier transform is based on the condition that only the damping moment is phase-shifted by 90° to the roll angle. A Fourier polynomial approximates the roll moment:

$$F_\varphi(t) = \sum_{k=1}^{\infty} \begin{pmatrix} C_{A,k} \\ C_{B,k} \end{pmatrix} \cdot \begin{pmatrix} \sin(k\omega t) \\ \cos(k\omega t) \end{pmatrix}, \quad (22)$$

which will be inserted in Equation (20).

$$E_{H.C} = \int_{-\frac{\pi}{\omega}}^{\frac{\pi}{\omega}} \sum_{k=1}^{\infty} \begin{pmatrix} C_{A,k} \\ C_{B,k} \end{pmatrix} \cdot \begin{pmatrix} \sin(k\omega t) \\ \cos(k\omega t) \end{pmatrix} d\varphi \quad (23)$$

$$E_{H.C} = \pi \varphi_a C_{B,1} \Rightarrow N_\varphi(\varphi_a) = \frac{C_{B,1}}{\omega \varphi_a} \quad (24)$$

Applicability of method (A), (B) and (C): The methods presented can be used for all frequencies ω and for ships with linear or nonlinear curves of righting arm. Table 4 shows an overview of advantages and disadvantages of each analysis method in the



case of a harmonic roll motion with constant roll amplitude. As an example a comparison of the non-dimensional damping coefficient for an

analytical test case is given in Table 5 of the Appendix. It can be summarised that all three methods are very robust. A low-pass filter was not used for the presented case. Correct results can be obtained by method (H.A) for $\mathcal{G} \rightarrow n\pi (n \in \mathbb{Z})$ when high sampling rate can be achieved. If the signal is overlapped by a strong background noise or has a low sampling rate, method (H.C) is recommended due to the robustness of the Fourier transform approach.

Table 4 Advantages and disadvantages of the presented analysis methods for technique (II)

	(H.A)	(H.B)	(H.C)
Filter required/used	no	no	no
Curve fit required	no	no	no
Sensitive to Measurement offset	weak	weak	weak
Sensitive to $\mathcal{G} \rightarrow n\pi (n \in \mathbb{Z})$	yes	no	no

3.3 Comparison of both techniques

For a comparison of both techniques

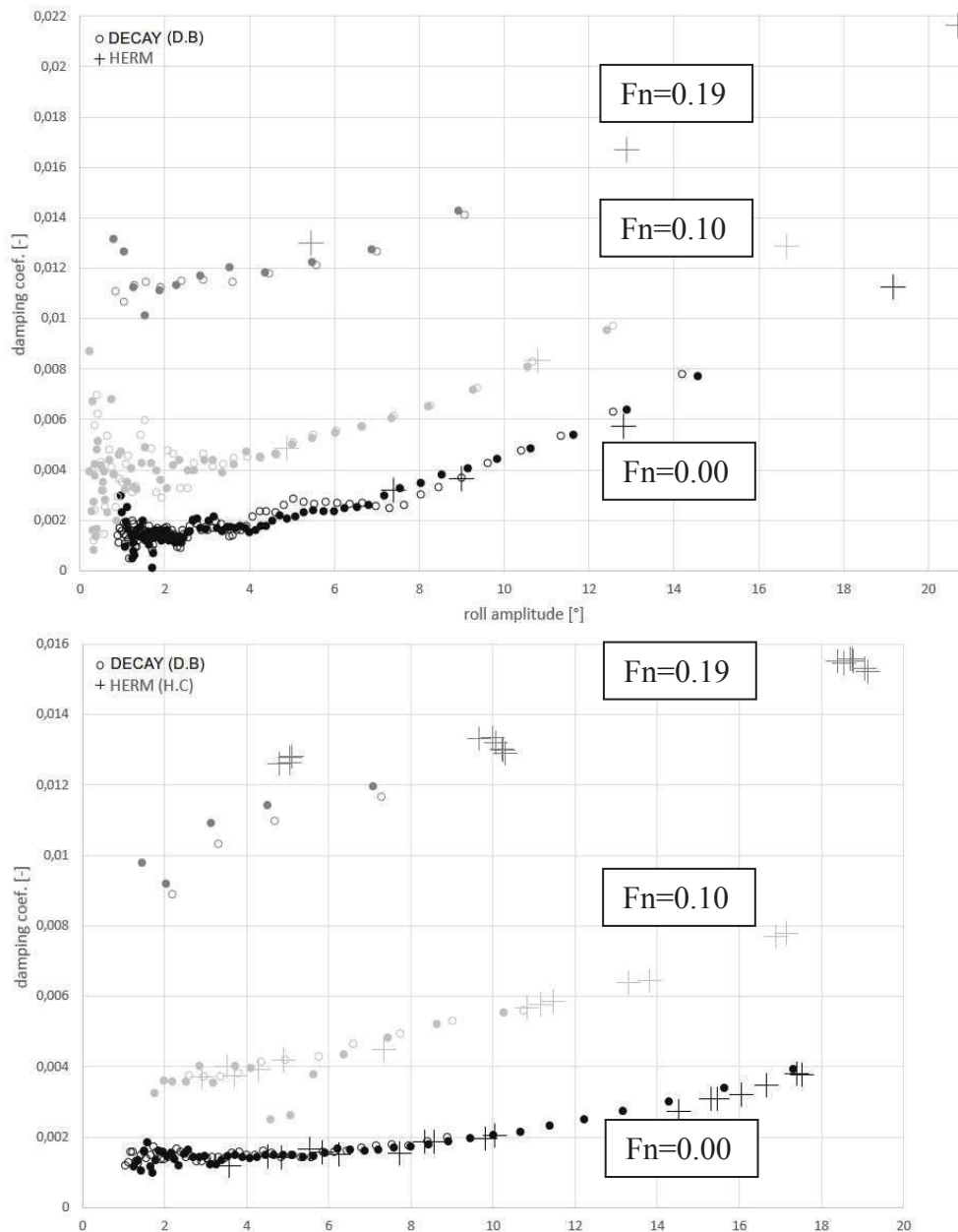


Figure 11 and 12 Comparison of data points with technique I (D.B) and technique II (H.C) for ballast (upper figure) and full loading condition (lower figure) - Fn=0.00 (black), Fn=0.10 (light grey), Fn=0.19 (grey)



methods (D.B) and (H.C) are selected. The decay measurement results have partially an offset. For this reason method (D.C) cannot be applied. To compare both experimental results, the non-dimensional formulation B_{φ} (see Eq. 6) is chosen. Compared to technique (II) where the moment is forced and known, a moment for technique (I) must be calculated. Therefore, besides the time series of the roll angle, the estimation of the roll inertia or roll hydrostatic moment is necessary to calculate the damping moment. In the present roll resonance frequency ω_D , the inertia and hydrostatic moment are equal. Because of the complexity in estimating the roll inertia moment, it is recommended to estimate the hydrostatic moment. Method (D.B) is based on this recommendation. The results for ballast and full loading conditions at Froude numbers 0.00, 0.10 and 0.19 are presented in Figures 11 and 12.

Deviations between both techniques (I) and (II) are mainly based on the different approaches to estimate damping and their realisation or uncertainties of the model tests and analysis errors.

- Deviations can be based on the different approaches. Technique (I) is similar to scenario case (1), technique (II) similar to case (3). These deviations cannot be prevented and are physically-based.
- Technique (II) is carried out with a steering rudder which holds the model on course in the narrow towing tank. Unfortunately, the influence of the rudder was not investigated. It should be expected that the rudder has an influence on the roll motion.
- To estimate roll damping by the decay technique (I), the righting arm curve has to be determined with high accuracy. To prevent deviations due to uncertainties of additional model tests or computations, it is recommended to determine the hydrostatic moment

based on the existing decay or HERM measurements. Different aspects can influence the GZ-values compared to computational estimated values, e.g. the manufacturing accuracy of the model as well as the correct model setup due to large scale factors. Unfortunately, an effective approach to estimate the hydrostatic roll moment based on HERM model tests was developed after carrying out the tests with the DTC, see Section 4. For this reason, GZ-values can be evaluated for only a few roll amplitudes, see Figure 14.

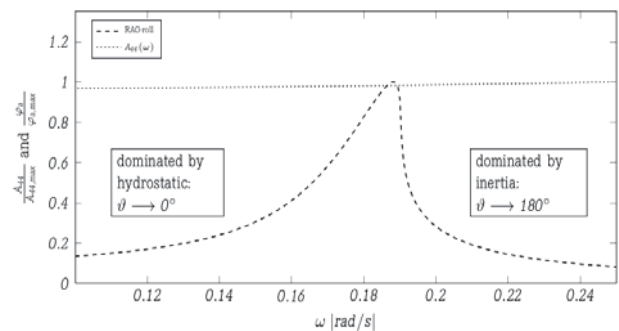


Figure 13 Sample Response Amplitude Operator (RAO) for the roll motion and virtual added inertia

4. DYNAMIC ESTIMATION OF HYDROSTATIC ROLL MOMENT

Two experimental techniques can be applied to estimate the lever arm GZ:

- A *static* technique – inclining tests with different weights and distances.
- A *dynamic* technique using HERM measurements.

Nearly all roll amplitudes occur twice: once in the frequency range dominated by the hydrostatic moment (ω_1) and once in the frequency range dominated by the inertia moment (ω_2), see Fig. 13 and Handschel et al., 2014a.

If the virtual added inertias of both frequencies are equated, this results to

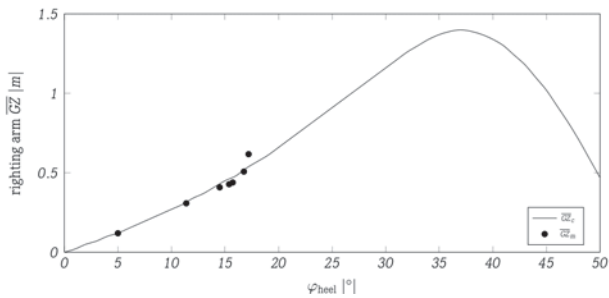


Figure 14 Estimation of the righting arms based on measurement results and calculated GZ-values (full scale)

$$\overline{GZ}(\varphi_a) = \frac{\omega_1^2 X - c_\alpha \omega_2^2 F_{\varphi,a} \cos \vartheta_1}{g\Delta(\omega_1^2 - c_\alpha \omega_2^2)} \quad (25)$$

with

$$X = F_{\varphi,a} \cos \vartheta_2 - (c_\alpha - 1)\varphi_a \omega_2^2 i_{xx}^2 \Delta \quad (26)$$

and $c_\alpha = A_{\varphi,2} / A_{\varphi,1}$ the ratio of both virtual added inertia. If the virtual added inertia is equal for both frequencies, Equation (25) simplifies to

$$\overline{GZ}(\varphi_a) = \frac{\omega_1^2 F_{\varphi,a} \cos \vartheta_2 - \omega_2^2 F_{\varphi,a} \cos \vartheta_1}{g\Delta(\omega_1^2 - \omega_2^2)} \quad (27)$$

Figure 14 shows the differences between calculated GZ-values and measured values. Differences are up to 7% in the present case, see Handschel et al., 2014a.

5. IMPLEMENTATION OF ESTIMATED DAMPING MOMENTS IN SHIP MOTION SIMULATIONS

5.1 Frequency Domain

Although results of both techniques look similar, the estimation with the HERM (II) technique is recommended. In frequency

domain, the roll motion is also simulated as a steady-state harmonic motion, scenario case (3), see Figure 4.

5.2 Time Domain – Series Expansion

Regardless of which technique is selected to estimate roll damping, usually a polynomial expansion of the roll velocity with linear, quadratic or cubic terms is used to approximate roll damping over various roll amplitudes (Spouge, 1988 and 26th ITTC, 2011).

$$N_\varphi \dot{\varphi} = N_{\varphi 1} \dot{\varphi} + N_{\varphi 2} \dot{\varphi}^2 + N_{\varphi 3} \dot{\varphi}^3 \quad (28)$$

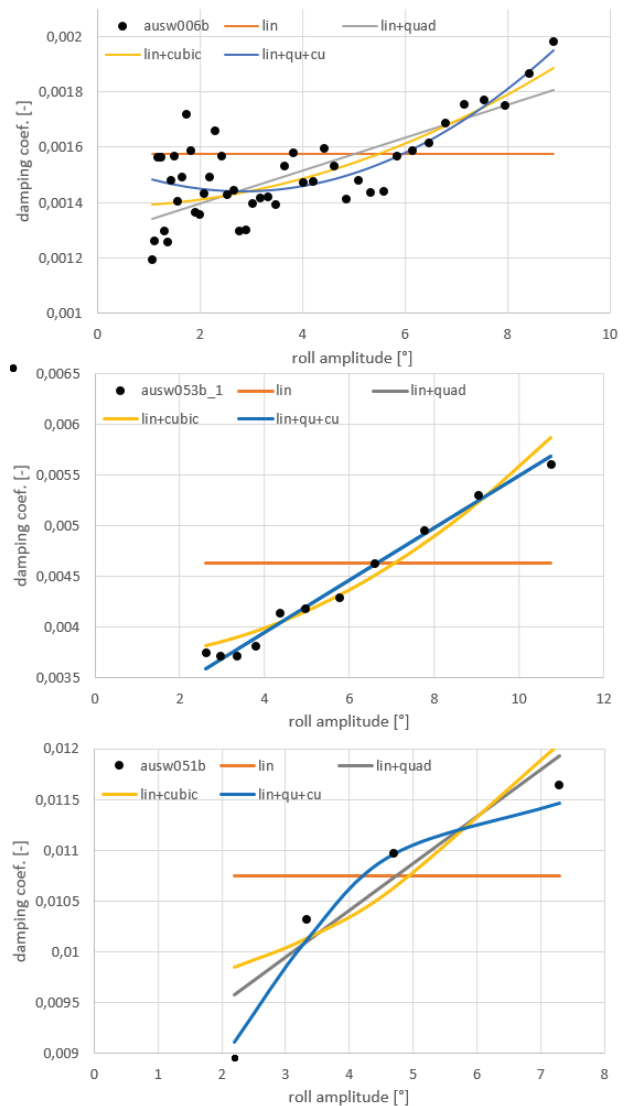


Figure 16 Different polynomials for data points of decay measurements with $F_n=0.00$ (upper), 0.10 and 0.19 (lowest)



A widely used approach is that different combinations of order of the polynomial expansions are included directly in the analysis methods (D) and (H), see Figure 15 - upper chart.

As an example, results for the full loading condition of the container ship DTC are fitted to a

- *linear:*

$$N_{\varphi} \dot{\varphi} = N_{\varphi_0} \dot{\varphi},$$

- *linear+quadratic:*

$$N_{\varphi} \dot{\varphi} = N_{\varphi_1} \dot{\varphi} + N_{\varphi_2} \dot{\varphi} |\dot{\varphi}|,$$

- *linear+cubic:*

$$N_{\varphi} \dot{\varphi} = N_{\varphi_1} \dot{\varphi} + N_{\varphi_3} \dot{\varphi}^3$$

- and *linear+quadratic+cubic:*

$$N_{\varphi} \dot{\varphi} = N_{\varphi_1} \dot{\varphi} + N_{\varphi_2} \dot{\varphi} |\dot{\varphi}| + N_{\varphi_3} \dot{\varphi}^3$$

function, see Figure 16. It can be clearly seen for the investigated ship that for each Froude number a different polynomial fits more suitable to the estimated equivalent damping coefficients (data points). For the smallest Froude number $Fn=0.00$, a linear+cubic polynomial seems to be the best choice. The damping results for a Froude number of 0.10 can be fitted with a linear+quadratic approach, whereas the largest Froude number 0.19 needs at least a linear+quadratic+cubic polynomial for the estimated data points. The selection of the right polynomial is different for every case and cannot be generalized at least for the presented model. Furthermore, extrapolations should be omitted.

It is recommended to select an approximation by series expansion or interpolation after the analysis of the time series, see Figure 15 – lower chart. A control plot helps to identify mismatches. Data points can be summarised and averaged before an approximation. This also leads to discrete

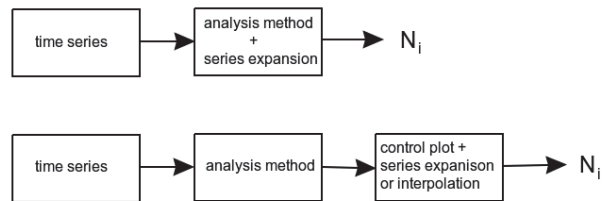


Figure 15 Flow chart of roll damping estimation from time series – general procedure (upper picture), recommended procedure (lower)

distances between data points for a correct approximation.

6. CONCLUSIONS

Different analysis methods for the decay (I) and harmonic excited roll motion (HERM, II) techniques are compared. The focus is set on the accurate estimation of roll damping without additional low-pass filtering and curve fitting. Recommended analysis methods are identified regarding the sensitivity of measurement offsets. These methods are:

- for the *decay technique*: method (D.B), based on the determination of the potential energy in the roll maximum ($\dot{\varphi} = 0$)
- and for the *HERM technique*: method (H.C), based on the determination of the first Fourier coefficient in phase with the roll velocity.

All analysis methods consider non-linear GZ curves of the ship geometry. For a comparison of the damping results for both techniques, a correct estimation of the hydrostatic moment is needed. Therefore, a possibility of using the dynamic test results to estimate the GZ curve during HERM measurements is presented.

Series expansions are often used for time domain simulations to approximate equivalent damping results. The form of series expansion should not be generalized over all Froude numbers, at least for the presented test case.



7. ACKNOWLEDGEMENT

The project was funded by the German Federal Ministry of Economics and Technology under the aegis of the BMWi-project “Best-Rolldämpfung” within the framework program “Schiffahrt und Meerestechnik für das 21. Jahrhundert”. The authors would like to thank the cooperation partners in the project: University Duisburg-Essen, Potsdam Model Basin and the DNV-GL. The authors thank also the HSVA for the support during the evaluation of the test results.

8. REFERENCES

- 26th ITTC, Specialist Committee on Stability in Waves, 2011, “Recommended Procedures – Numerical Estimation of Roll Damping”, International Towing Tank Conference, URL January 2015: <http://itcc.sname.org>.
- Bassler, C.C., Reed, A.M. and Brown, A.J., 2010, “Characterization of Energy Dissipation Phenomena for Large Amplitude Ship Roll Motions”, Proceedings of the 29th American Towing Tank Conference, Annapolis, MD, USA.
- Blume, P., 1979, “Experimentelle Bestimmung von Koeffizienten der wirksamen Rolldämpfung und ihrer Anwendung zur Abschätzung extremer Rollwinkel”, Ship Technology Research / Schiffstechnik, Vol. 26, pp. 3-23 (in German).
- el Moctar, B., Shigunov, V. and Zorn, T., 2012, “Duisburg Test Case: Post-Panamax Containership for Benchmarking”, Ship Technology Research / Schiffstechnik, Vol. 59/3.
- el Moctar, B., Kaufmann, J., Ley, J., Oberhagemann, J., Shigunov, V. and Zorn, T., 2010, “Prediction of ship resistance and ship motion using RANSE”, A Workshop on Numerical Ship Hydrodynamics, Proceedings, Vol. II, Gothenburg, Sweden.
- Gao, Q., Jin, W. and Vassalos, D., 2010, “Simulation of Roll Decay by RANS Approach”, A Workshop on Numerical Ship Hydrodynamics, Proceedings, Vol. II, Gothenburg, Sweden.
- Handschel, S., Köllisch, N., Soproni, J.P. and Abdel-Maksoud, M., 2012a, “A Numerical Method for the Estimation of Ship Roll Damping for Large Amplitudes”, 29th Symposium on Naval Hydrodynamics, Gothenburg, Sweden.
- Handschel, S. and Abdel-Maksoud, M., 2014a, “Improvement of the Harmonic Excited Roll Motion Technique for Estimating Roll Damping”, Ship Technology Research / Schiffstechnik, Vol. 61/3, pp. 116-130.
- Handschel, S., Fröhlich, M., and Abdel-Maksoud, M., 2014b, “Experimental and Numerical Investigation of Ship Roll Damping by Applying the Harmonic Forced Roll Motion Technique”, 30th Symposium on Naval Hydrodynamics, Hobart, Tasmania, Australia.
- Himeno, Y., 1981, “Prediction of Ship Roll Damping – State of the Art”, Report at Univ. of Michigan – Nav. Arch. And Mar. ENgr., USA.
- Roberts, J.B., 1985, “Estimation of Nonlinear Ship Roll Damping from Free-Decay Data”, Journal of Ship Research, Vol. 29/2, pp. 127-138.
- Röös, B., 2009, “Numerische Untersuchung der Rolldämpfung”, Diploma Thesis, University Duisburg-Essen (in German).
- Salui, K.B., 2004, “A RANS Based Prediction Method of Ship Roll Damping Moment”, University Research Presentation Day, University of Glasgow and Strathclyde.
- Sarkar, T. and Vassalos, D., 2000, “A RANS-



based technique for simulation of the flow near a rolling cylinder at the free surface”, Journal of Marine Science and Technology, Vol. 5.

Spouge, J.R., 1988, “Non-Linear Analysis of Large Rolling Experiments”, Int. Shipbuild. Progr., Vol. 35/403, pp. 271-320.

Schumacher, A., 2010, “Rolldämpfungsversuche mit dem Modell eines großen Containerschiffes – Teilvorhaben Mat-Roll”, Report at Hamburgische Schiffbau-Versuchsanstalt (HSVA), Germany (in German).

Sugai, K. and Yamanouchi, Y., 1963, “A Study on the Rolling Characteristics of Ship by Forced Oscillation Model Experiments”, Journal of Society of Naval Architects of Japan, pp. 54-66 (in Japanese).

9. APPENDIX

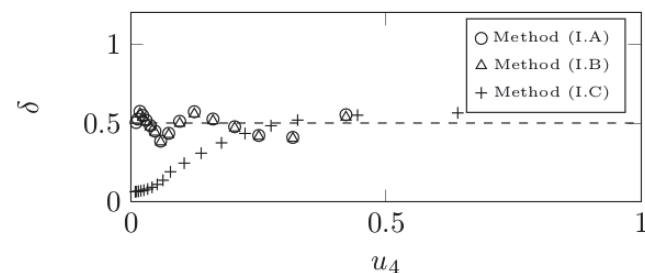
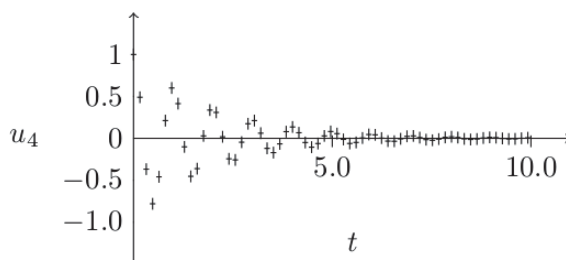
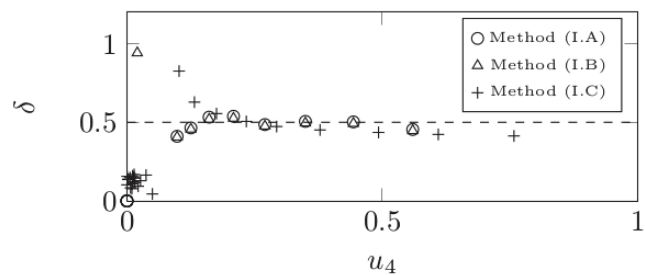
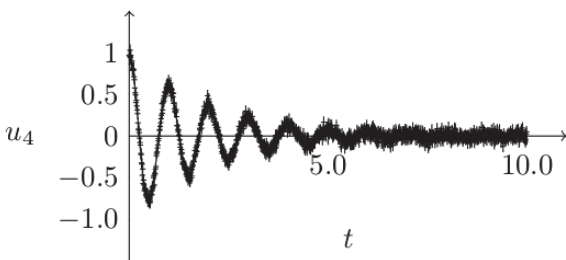
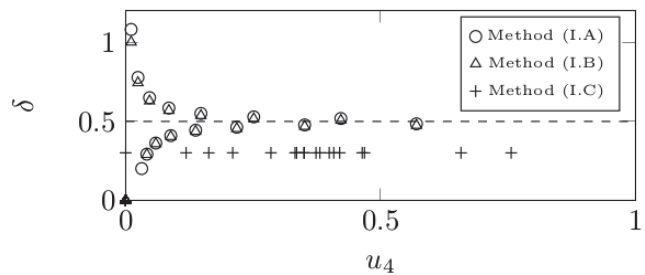
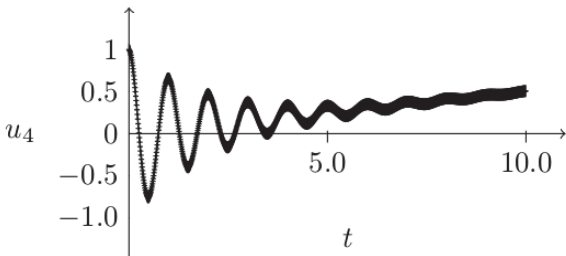
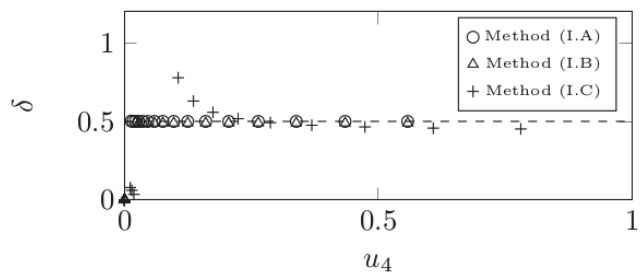
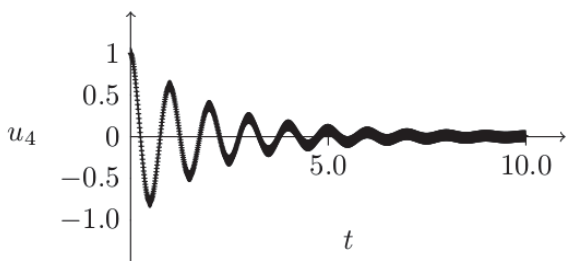




Figure 17 Comparison of methods (D.A), (D.B) and (D.C) – D is labelled as I in the legends, left column: signal, right column: damping value, dotted line: target damping value – an undisturbed signal (first picture), signal with white Gaussian noise (second), signal with a large offset (third) and a signal with a lower sampling rate (fourth)

Table 5 Comparison of methods (H.A), (H.B) and (H.C) – target damping value is 0.5 – for an undisturbed signal, signal with white Gaussian noise, signal with a large offset and a signal with a lower sampling rate

	(H.A)	(H.B)	(H.C)
<i>Undisturbed signal</i>	0.49820	0.50076	0.50103
<i>White Gaussian noise</i>	0.59482	0.49009	0.49160
<i>Large offset</i>	0.52570	0.50076	0.50127
<i>Lower sampling rate</i>	0.32717	0.46653	0.48473



Assessing the Stability of Ships under the Effect of Realistic Wave Groups

Panayiotis A. Anastopoulos, *Department of Naval Architecture and Marine Engineering, National
Technical University of Athens, Greece, panasto@central.ntua.gr*

Kostas J. Spyrou, *Department of Naval Architecture and Marine Engineering, National Technical
University of Athens, Greece, k.spyrou@central.ntua.gr*

ABSTRACT

Ship propensity for stability failure in random beam seas is addressed. A novel method based on the systematic construction of realistic wave groups is proposed. Derived waveforms are sequences of varying heights and periods with high probability of occurrence. To demonstrate the approach, stability analysis is performed on a modern container vessel using an uncoupled equation of roll motion. The effects of height and period variations on the system's transient response and on the integrity of its safe basin are discussed against the context of a "regular sea" investigation.

Keywords: *irregular seas, wave groups, transient capsizing, safe basin erosion, integrity curves, Karhunen-Loève theorem*

1. INTRODUCTION

The study of large amplitude ship motions in a stochastic sea is one of the most challenging computational tasks in naval architecture. On the one hand, advanced methods of nonlinear dynamics are indispensable for yielding insights into the mechanisms of capsizing. At the same time, however, such methods have not been so practical for providing estimates of capsizing tendency, especially when employing computationally expensive numerical techniques. This is compounded by the fact that, for quantitative accuracy in dynamic stability predictions, detailed hydrodynamic modelling is highly desirable. For rare phenomena like capsizing, the efficiency of long-time simulations on heavy models is disputed since most of the time is idly expended on simulating innocuous ship-wave encounters. This has motivated the development of a number of techniques for directly extracting those time intervals when hazardous wave episodes occur.

A relevant phenomenon, often observed in wind-generated seas, is wave grouping. Wave groups are sequences of high waves with periods varying within a potentially small range (Masson & Chandler, 1993, Ochi, 1998). Notably, the occurrence of dangerous wave group events, leading to motion augmentation, does not necessarily imply exceptionally high waves. Resonant phenomena, often "felt" in the first few cycles of wave group excitation, are crucial for the integrity of a marine system. The manifestation of ship instability under the effect of wave groups was the objective of three recent studies, reviewed, in brief, next.

Reaping the benefits coming from the separation of dynamics from randomness, the "critical wave groups" approach disassembles the problem in a deterministic and a probabilistic part (Themelis & Spyrou, 2007). In the former, critical combinations of heights, periods and run lengths, related to regular wave groups that incur unacceptably large dynamic



response, are identified. The critical, in terms of ship stability, waveforms represent basically thresholds, defined by regular wave trains. Statistical analysis of the seaway is included in the probabilistic part of the approach. The propensity for ship stability failure is quantified by calculating the probability of encountering any train higher than the determined critical threshold.

A statistical approach for the prediction of extreme parametric roll responses was presented in the study of Kim & Troesch (2013). The method is based on the assumption that the fluctuation of instantaneous GM is a Gaussian random process. The “Design Loads Generator” was employed to generate an ensemble of irregular wave groups, associated with the extreme value distribution of a surrogate process, representing time-varying metacentric height groups (Kim, 2012). The derived wave trains, realized as a lower bound of the “true” excitation, were, eventually, utilized as input to a high fidelity hydrodynamic system for simulating the actual nonlinear response of a C11 containership.

Malara et al. (2014) proposed an approach for the estimation of the maximum roll angle, induced by spectrum compatible wave group excitation. Representation of the load process in the vicinity of an exceptionally high wave was formulated within the context of the “Quasi-Determinism” theory (Boccotti, 2000). The approach is asymptotically valid in the limit of infinitely high waves and its use is possibly suitable for heights at least twice the significant wave height of the considered sea state (Boccotti, 2000).

In the following section, a new, spectrum compatible, method of wave group loads is proposed. The method expands upon Themelis & Spyrou (2007) on the one hand, by considering realistic wave group profiles; and on Malara et al. (2014) by removing the “extreme waves” assumption imposed by the theory of Quasi-Determinism. The objective is an in-depth investigation of the effects of short

duration irregular seaways on the transient response and engineering integrity of a modern container vessel.

2. MODELLING OF WAVE GROUP LOADS

9.1 Stochastic treatment of wave successions

The assumption of height sequences which fulfil the Markov property has been employed with remarkable success in a number of studies for the derivation of wave groupiness measures (Kimura, 1980, Battjes & van Vledder, 1984, Longuet-Higgins, 1984). On the other hand, the application of straightforward spectral techniques, targeting the statistical elaboration of wave period groupings, is full of inherent limitations.

Recently, an extended Markov-chain model, allowing for cross-correlations between successive heights and periods, was proposed (Anastopoulos et al., 2014). A computational method, based on envelope analysis in conjunction with the theory of copula distributions, produced explicit formulas for the transition probabilities of the process. The joint expectations of consecutive heights h_i and periods t_i were expressed by the following set of coupled equations:

$$\bar{h}_i = \int_0^{\infty} h_i f_{H_i|H_{i-1}, T_{i-1}}(h_i|h_{i-1}, t_{i-1}) dh_i \quad (1a)$$

$$\bar{t}_i = \int_0^{\infty} t_i f_{T_i|H_{i-1}, T_{i-1}}(t_i|h_{i-1}, t_{i-1}) dt_i \quad (1b)$$

where H and T are the height and period random variables at time step i , with state variables h and t , respectively. The “most expected” wave sequence can iteratively be constructed using equations (1a)-(1b). The whole waveform becomes explicitly dependent



on the wave occupying the centre of the group if the key characteristics of the highest wave are selected as initial conditions for the iteration process.

2.1 Estimating transition kernels via Monte Carlo simulations

Comprehensive description of the analysis associated with the theoretical estimation of the transition kernels, given by equations (1a) and (1b), can be found in Anastopoulos et al. (2014). In this study, a JONSWAP spectrum (Hasselmann et al., 1973), with peak period $T_p = 13.6s$ and significant wave height $H_s = 10m$, was considered in order to simulate time series of water surface elevation. The main idea is to arrange the generated data in the following vector sets and proceed to regression analysis.

$$\mathbf{A} = \begin{bmatrix} h_i \\ h_{i-1} \\ t_{i-1} \end{bmatrix}, \quad \mathbf{B} = \begin{bmatrix} t_i \\ h_{i-1} \\ t_{i-1} \end{bmatrix} \quad (2)$$

Then, the transition mechanisms can be expressed through a best-model-fit method. Figure 1 explains the concept of a “correlation surface”, which fits data of vector \mathbf{A} . In the same figure, the (h_i-t_i) plane corresponds to the total population of joint height-period realizations. The smoothened bivariate height and joint height-period distributions for successive waves are also provided.

2.2 The Karhunen-Loève representation

The Karhunen-Loève theorem is employed in order to construct continuous-time analogues of wave sequences, related to the predictions of the Markov-chain model described before (Karhunen, 1947, Loève, 1978). The main advantage of the specific approach over the traditional Fourier series representation is that it ensures the minimum total mean-square error resulting out of its truncation. In other words,

all the information provided by the auto-covariance function of the original process, can efficiently be integrated within the few waves of a group sequence. The theorem states that the water surface displacement η admits the following decomposition:

$$\eta(x,t) = \sum_{n=0}^{\infty} a_n f_n(x,t), \quad -T < t < T \quad (3)$$

In the case of a Gaussian random process, the coefficients, a_n ($n = 0,1,\dots$), are random independent variables. An efficient computational procedure for the basis functions f_n is described in Sclavounos (2012).

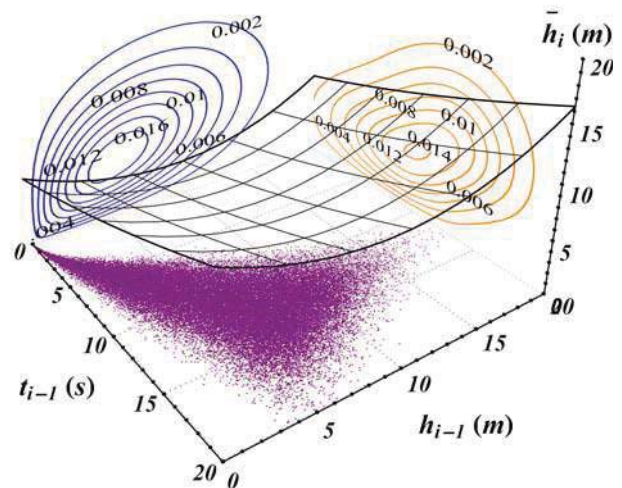


Figure 1: Correlation surface for the prediction of the “most expected” wave heights.

Spectrum compatible wave loads can directly be constructed if appropriate geometric constraints are imposed on equation (3). The key is to formulate a well-defined interpolation problem for the values of water surface displacement at time instants when crests, troughs and zero-crossings occur. To this end, the truncation of the series expansion (3) should be explicitly dependent on the number of waves j participating in the group formation. In this case, the space-time expansion of the original process η is reformulated as:



$$\eta(x, t) = \sum_{n=0}^{6j} a_n f_n(x, t), \quad -T < t < T \quad (4)$$

The Markov-chain/Karhunen-Loève (MC-KL) model was employed to generate the family of irregular wave groups, shown in Figure 2. The derived waveforms are comprised of $j = 5$ waves and correspond to the same central wave period T_c . The root-mean-square value (H_{rms}) of the simulated sea state heights was the assumed threshold that individual wave heights should exceed. As demonstrated, groups of different durations arise when changing the value of the central wave height H_c . Furthermore, the convergence rate of the approach is tested in Figure 3. The vertical axis denotes the absolute relative error with respect to the estimation of the spectral variance; and the horizontal axis, the corresponding number of stochastic components kept in equation (3). Considering a run length of $j = 5$ waves would result in a small truncation error of approximately 2%.

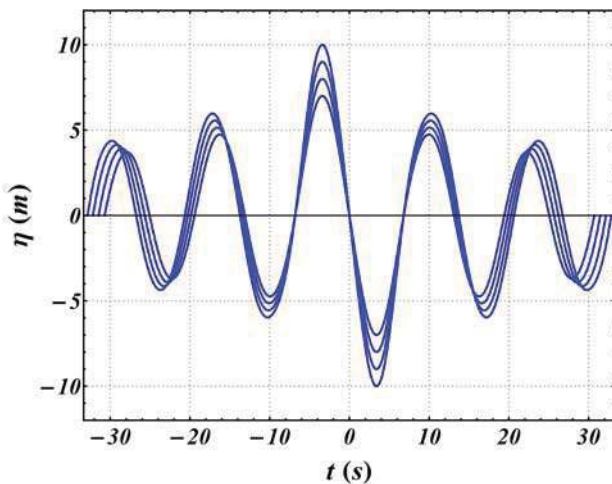


Figure 2: Wave groups of increasing $H_c = 14\text{m}$, 16m , 18m and 20m . $T_c = T_p$.

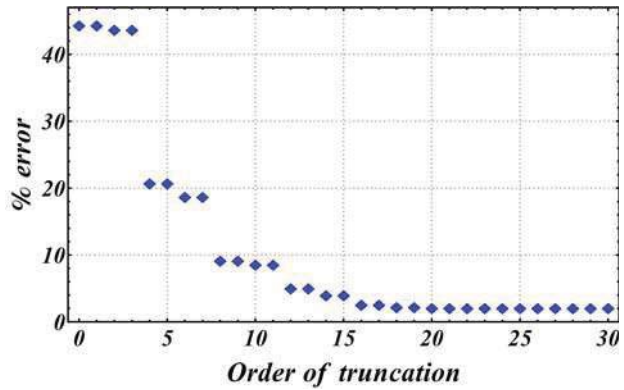


Figure 3: Error in spectral variance for various truncation orders.

2.3 Roll motion in long-crested irregular wave groups

A 4800 TEU panamax containership was selected for a preliminary application of the method. The main particulars and the considered loading condition are shown in Table 1. No information about the existence of bilge keels was provided; thus, the bare hull of the ship, shown in Figure 4, was only considered.

Table1: Ship main particulars

Displacement (Δ)	68199	Tons
Length between perpendiculars (L_{BP})	238.35	m
Breadth (B)	37.30	m
Draught (T)	11.52	m
Depth (D)	19.60	m
Service speed (V_s)	21	kn
Metacentric height (GM)	2.85	m
Natural period (T_0)	15.25	s

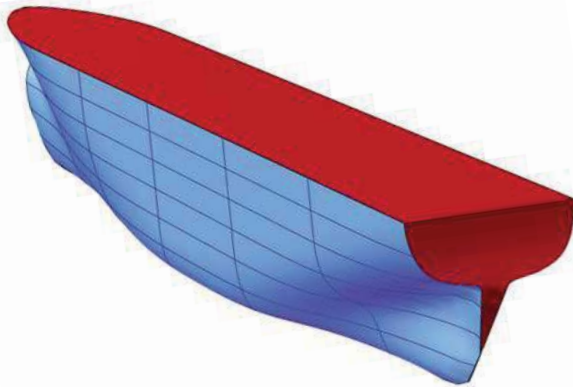


Figure 4: The hull of the containership modelled with *Mathematica*®.

In the presence of long incident waves, ship motion is studied under the Froude-Krylov assumption. In this case, the following uncoupled equation, written in terms of the relative roll angle ϕ , is employed:

$$(I_{44} + A_{44})\ddot{\phi} + D(\dot{\phi}) + \Delta GZ(\phi) = M_{wave}(t) \quad (5)$$

where I_{44} and A_{44} are the roll moment of inertia and the added moment, respectively. Customary quadratic damping moment D is assumed:

$$D(\dot{\phi}) = B_1\dot{\phi} + B_2\dot{\phi}|\dot{\phi}| \quad (6)$$

The damping coefficients were calculated according to the hydrodynamic component moment analysis, described in Ikeda et al. (1978). To the GZ -curve was fitted a 9th degree polynomial. The wave induced moment was modelled as (Wright & Marshfield, 1980):

$$M_{wave}(t) = -I_{44}\ddot{\alpha}(t) \quad (7)$$

with α being the instantaneous wave slope at the middle of the ship.

3. TRANSIENT CAPSIZE DIAGRAMS

The “transient capsize diagram” is a plot of wave period against the steepness ratio associated with critical, from ship dynamics perspective, roll angles (Rainey & Thompson, 1991). Ship motion in real seas is inherently transient and the use of steady-state analysis can be only indicative (Spyrou & Thompson, 2000). Below we shall extend the idea of the transient capsize using the MC-KL model in order to identify thresholds of unsafe behaviour under the “most expected” wave group loads. This can offer a rational treatment to problem of quantifying low-probability wave encounters.

Calculating transient capsize diagrams in the case of regular wave groups is a straightforward procedure, commonly advocated in the literature. On the other hand, analysis of the system’s transient response in irregular seas can turn into a complicated task, mostly due to the lack of necessary definitions. The appropriate selection of wave group characteristics, to be labelled on the stability diagram, is the greatest concern in the specific approach. In order to provide satisfactory answers to this issue, separation of height from period variations was attempted. Transient capsize diagrams were eventually calculated for the three cases shown in Table 2.

Table 2: Wave group case studies

Case	Description
01	<i>Regular wave groups</i>
02	<i>Regular wave groups with varying heights</i>
03	<i>MC-KL wave groups</i>

The construction algorithm of wave sequences related to Case 02 is based on simple manipulations of the MC-KL model. Firstly, joint height-period successions were calculated according to the original formulation of the method. Cross-correlations between consecutive heights and periods were fully



considered. In the end, however, the predicted periods were discarded and the derived height sequences were associated with constant periods. The Karhunen-Loève theorem was applied again to construct continuous counterparts.

In all three cases of Table 2 the produced wave groups were comprised of $j = 5$ individual waves with heights greater than H_{rms} . Moreover, without loss of generality, zero initial conditions at the moment of encounter were assumed. According to the Weather Criterion ship capsizes was considered the exceedance of the down-flooding angle $\varphi_f = 40$ degrees.

3.1 The effect of height variations

In Figure 5 the transient capsizes diagrams of Cases 01 and 02 are superimposed. The “mean wave steepness” curve, denoted by H_m/λ , was calculated from the average wave height H_m of groupings derived for Case 02. The steepness ratio of the respective highest wave is given by the H_c/λ - curve. The horizontal axis is the non-dimensional wave period T with respect to the ship natural period T_0 .

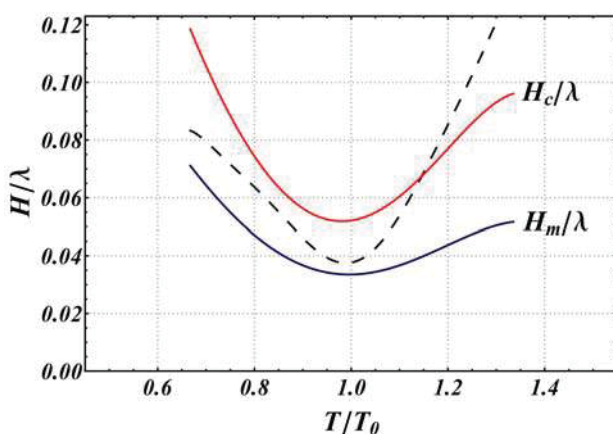


Figure 5: Transient capsizes diagrams for Cases 01 (dashed line) and 02 (solid lines).

Figure 5 reveals the existence of three regions with qualitatively different stability features. In region A ($T/T_0 \leq 0.85$) the critical steepness

ratio of the regular wave trains was found very close to that of the maximum wave, calculated in Case 02. Rapid exceedance of φ_f was encountered, in both cases, within the first three wave cycles. In region B ($0.85 < T/T_0 \leq 1.10$), which is the region of resonant response, the two methods are totally equivalent. Since j was constantly fixed, the produced wave groups were of exactly the same duration. Moreover, height variations were found to have little influence on the performance of the vessel considering that the mean critical steepness H_m/λ was approximately the same for both methods. Stability failure was experienced after the third wave cycle. Finally, in region C ($T/T_0 > 1.10$) the two methods exhibit substantial discrepancies. The key finding is that roll motion is build-up during the developing stage of non-periodic wave groups. The position of the highest wave plays a crucial role for the manifestation of instability, leading to moderate critical steepness predictions.

3.2 The effects of period variations

In the same spirit, the transient capsizes diagrams of Cases 01 and 03 are shown in Figure 6. The period of the highest wave of a single run is T_c . In Figure 7 critical wave groups of Case 03 are represented in terms of the average period (T_{avg}) and shortest period (T_{min}) in a non-dimensional form with respect to T_c .

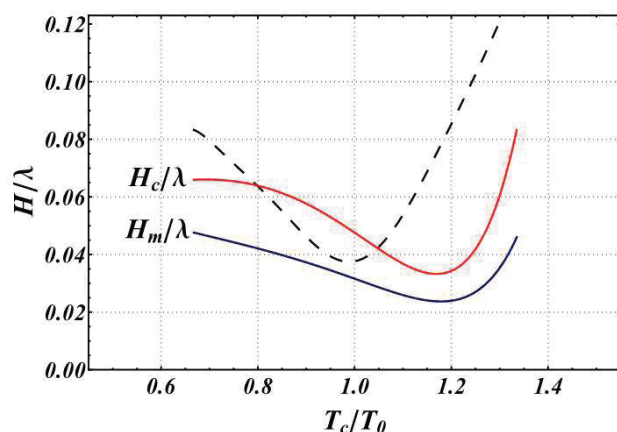


Figure 6: Transient capsizes diagram for Cases 01 (dashed line) and 03 (solid lines).

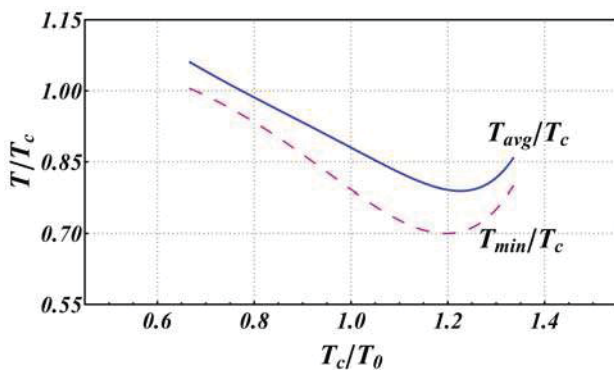


Figure 7: Period variations for Case 03; solid line: T_{avg}/T_c , dashed line: T_{min}/T_c .

Figure 6 indicates that modelling of realistic period successions results in a wider instability area, shifted to the region of long waves. In a typical MC-KL wave group the highest wave is surrounded by two waves with only slightly different periods. This fact, also reported in the experimental study of Su (1986), implies an “almost regular” waveform in the vicinity of the high central wave. In Figure 7 such phenomena are mostly associated with region A. However, motion augmentation is still possible in regions B and C if estimated periods vary within a sufficiently small range.

In Figure 8 short time histories of simulated roll motion are displayed. Ship responses that exceed plot boundaries are related to capsizing events, included in Figures 5 and 6. Dashed, thin and thick lines denote Cases 01, 02 and 03, respectively. The upper panel is associated with region A, where quick violation of the capsizing criterion is experienced in all case studies. In region B resonant phenomena dominate resulting in dangerous build-up of roll motion (middle panel). Finally, in region C, exceptionally high regular wave trains led to immediate capsizing (bottom panel). On the other hand, Cases 02 and 03 produced progressively increasing roll amplitudes.

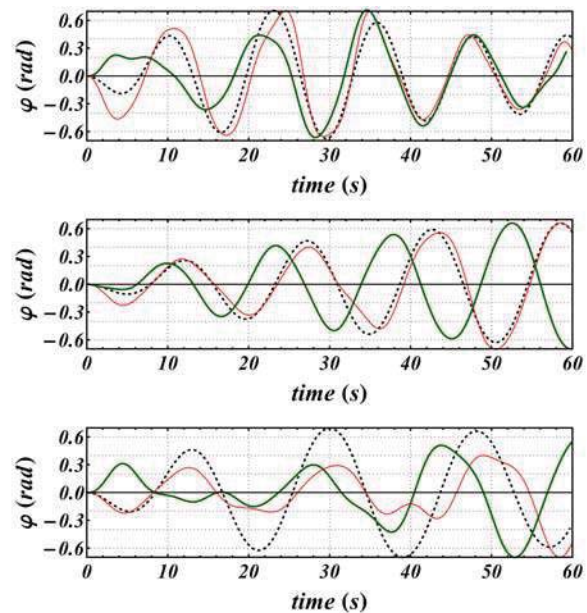


Figure 8: Roll response time-histories; upper panel: $T_c/T_0 = 0.789$, middle panel: $T_c/T_0 = 1.049$, lower panel: $T_c/T_0 = 1.246$.

4. SAFE BASIN EROSION AND INTEGRITY CURVES

In this section the non-linear response of the system is investigated up to the limiting angle of vanishing stability $\varphi_v = 66$ degrees. Basins of attraction are constructed after repeated simulations of ship motion with different initial conditions. The short duration of wave group excitation allows for a considerable reduction of the computational burden. In the study of Thompson (1989) rapid erosion and stratification of the safe basin was observed to take place under small variations of the wave parameters. The same logic is applied below using the MC-KL approach.

In Figure 9 the “integrity curves” of the vessel are illustrated. The probability of capsizing is quantified by the ratio of the actual safe basin area over the estimated area in free decay. The horizontal axis is the non-dimensional central wave height H_c with respect to Airy breaking limit H_0 . Analysis was performed for a fixed central wave period $T_c =$



T_p . Rapid loss of engineering integrity is observed when modelling successions of realistic wave periods.

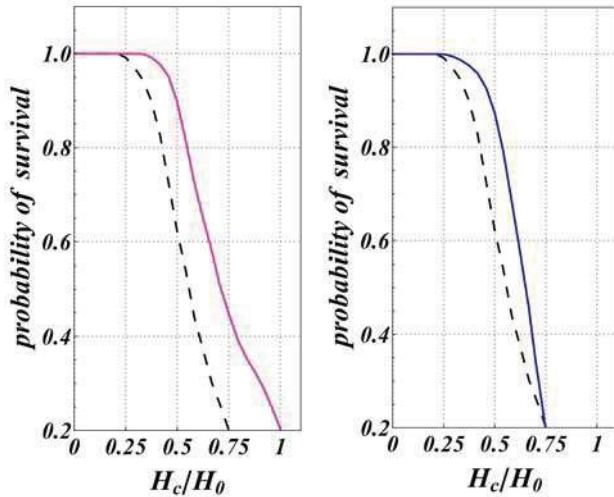


Figure 9: Integrity curves; left panel: Cases 01 (dashed line) & 02 (solid line); right panel: Cases 01 (dashed line) & 03 (solid line).

Basins of attraction, indicating 10% and 40% loss of the originally safe area appear in Figure 10. The graphs correspond to a 400x400 grid of initial conditions. Black colour implies initial conditions that led to quick capsize, practically within the first wave cycle. Purple and blue regions indicate capsizing during the second and third wave cycles, respectively. Safe regions remained uncoloured. In the case of regular group excitation, striations arise close to the basin boundary. At later stages of the erosion process these striations expand rapidly to the internal of the initially safe basin. On the other hand, for Cases 02 and 03 the basins start to erode “from within”. In most cases capsizing is experienced when encountering the highest wave of the train.

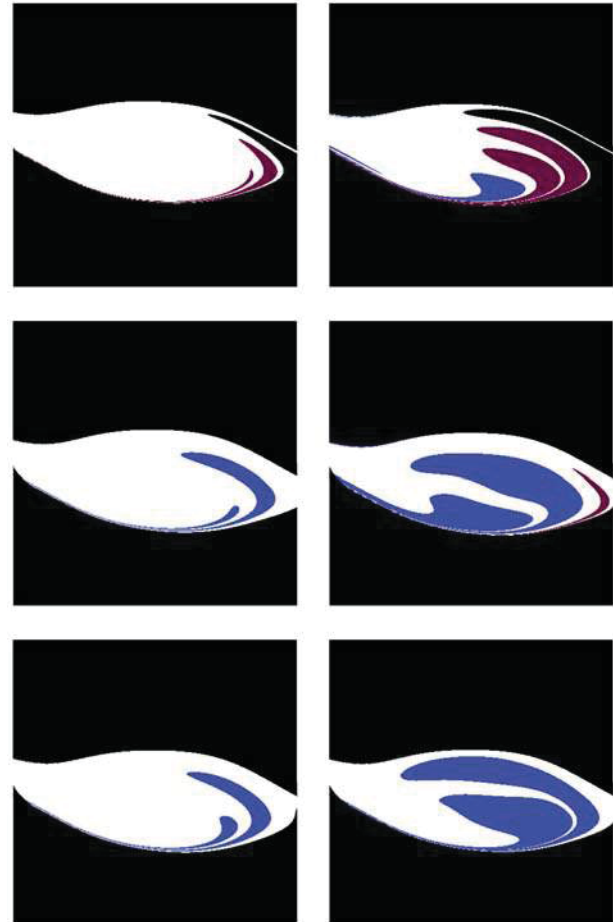


Figure 10: Transient basin erosion. Left column: 10% integrity loss; right column: 40% integrity loss; from top to bottom: Cases 01, 02, 03.

5. CONCLUSIONS

A new model for the systematic construction of spectrum-compatible wave group loads was presented. The effects of wave grouping phenomena on the performance of a modern containership were investigated. Stability analysis was performed in terms of transient capsize diagrams. The idea was to simulate wave induced moments with high probability of occurrence and study separately the effects of height from period variations within the group formations. The results indicate that realistic wave groups yield a wide instability region, yet shifted with respect to the regular case. In some cases, lower capsize



thresholds were defined by wave successions of gradually increasing heights rather than common regular trains. Finally, the concept of quantifying safe operational conditions through integrity curves was discussed. The conclusion is that the sudden erosion of the safe basin caused by irregular wave group excitation is a qualitatively different process from the typical regular approach.

6. ACKNOWLEDGMENTS

This work has been supported by the Greek General Secretariat of Research and Technology under the General Program "ARISTEIA I" (contract reference number GSRT-252).

7. REFERENCES

- Anastopoulos, P.A., Spyrou, K.J., Bassler, C.C., and Belenky, V., 2014, "Towards an improved critical wave groups method for the assessment of large ship motions in irregular seas", Proceedings of the 7th International Computational Stochastic Mechanics Conference, Santorini, Greece (to be published).
- Battjes, J.A., and van Vledder, G.P., 1984, "Verification of Kimura's theory for wave group statistics", Proceedings of the 19th International Coastal Engineering Conference, ASCE, Houston, TX, pp. 642-648.
- Boccotti, P., 2000, "Wave Mechanics for Ocean Engineering", Elsevier, Oxford, England, ISBN: 978-0-444-50380-0.
- Hasselmann, K. et al, 1973, "Measurements of wind-wave growth and swell decay during the Joint North Sea Wave Project (JONSWAP)", Deutschen Hydrographischen Zeitschrift, A.12, pp. 1-95.
- Ikeda, Y., Himeno, Y., and Tanaka, N., 1978, "A prediction method for ship roll damping", Report No. 00405 of Department of Naval Architecture, University of Osaka Prefecture.
- Karhunen, K., 1947, "Über lineare Methoden in der Wahrscheinlichkeitsrechnung", Annales Academiæ Scientiarum Fennicæ. Ser. A. I. Math.-Phys., Vol. 37, pp. 1-79.
- Kim, D-H., 2012, "Design loads generator: Estimation of extreme environmental loadings for ship and offshore applications", PhD thesis, The University of Michigan.
- Kim, D-H., and Troesch, A.W., 2013, "Statistical estimation of extreme roll response in short crested irregular head seas", SNAME Transactions.
- Kimura, A., 1980, "Statistical properties of random wave groups", Proceedings of the 17th International Coastal Engineering Conference, ASCE, Sydney, Australia, pp. 2955-2973.
- Loève, M., 1978, "Probability theory", Vol. II, 4th ed., Graduate Texts in Mathematics, Springer-Verlag, London, England, ISBN: 0-387-90262-7.
- Longuet-Higgins, M.S., 1984, "Statistical properties of wave groups in a random sea state", Philosophical Transactions of the Royal Society of London A, Vol. 312(1521), pp. 219-250.
- Malara, G., Spanos, P.D., and Arena, F., 2014, "Maximum roll angle estimation of a ship in confused sea waves via a quasi-deterministic approach", Elsevier Probabilistic Engineering Mechanics, Vol. 35, pp. 75-81.
- Masson, D., and Chandler, P., 1993, "Wave groups: A closer look at spectral methods", Elsevier Coastal Engineering, Vol. 20(3-4), pp. 249-275.



- Ochi, M., 1998, "Ocean Waves: The Stochastic Approach", Cambridge University Press, Cambridge, England, ISBN: 978-0-521-01767-1.
- Rainey, R.C.T., and Thompson J.M.T., 1991, "The transient capsize diagram – a new method of quantifying stability in waves", Journal of Ship Research, Vol. 35(1), pp. 58-62.
- Sclavounos, P.D., 2012, "Karhunen-Loève representation of stochastic ocean waves", Proceedings of Royal Society of London A, Vol. 468(2145), pp. 2574-2594.
- Spyrou, K.J., and Thompson, J.M.T., 2000, "The nonlinear dynamics of ship motions: a field overview and some recent developments", Philosophical Transactions of the Royal Society A, Vol. 358 (1771), pp. 1735-1760.
- Su, M.Y., 1986, "Extreme wave group in storm seas near coastal water", Proceedings of the 20th International Coastal Engineering Conference, ASCE, Taipei, Taiwan, pp. 767-779.
- Themelis, N., and Spyrou, K.J., 2007, "Probabilistic Assessment of Ship Stability", SNAME Transactions, Vol. 115, pp. 181-206.
- Thompson, J.M.T., 1989, "Chaotic phenomena triggering the escape from a potential well", Proceedings of Royal Society of London A, Vol. 421(1861), pp. 195-225.
- Wright, J.H.G., and Marshfield, W.B., 1980, "Ship roll response and capsize behaviour in beam seas", RINA Transactions, Vol. 122, pp. 129-148.

Session 8.2 – DAMAGE STABILITY

**Roll Damping Assessment of Intact and Damaged Ship by CFD and EFD
Methods**

**Investigation of the Impact of the Amended S-Factor Formulation on
ROPAX Ships**

**The Evolution of the Formulae for Estimating the Longitudinal Extent
of Damage for the Hull of a Small Ship of the Translational Mode**

Parametric Rolling of Tumblehome Hulls using CFD Tools

This page is intentionally left blank



Roll Damping Assessment of Intact and Damaged Ship by CFD and EFD Methods

Ermina Begovic, *University of Naples Federico II*, begovic@unina.it

Alexander H. Day, *University of Strathclyde, Glasgow*, sandy.day@strath.ac.uk

Atilla Incecik, *University of Strathclyde, Glasgow*, atilla.incecik@strath.ac.uk

Simone Mancini, *University of Naples Federico II*, simone.mancini@unina.it

Domenica Pizzirusso, *postgraduate student EniCorporate University*, albairpina@libero.it

ABSTRACT

This paper presents an assessment of the roll damping of DTMB 5415 naval ship model in both intact and two compartments symmetric damaged scenarios. An experimental assessment of roll decay is performed at zero speed at different initial heel angles at the University of Strathclyde, Glasgow. Reported experimental results are decay curves, natural frequency and period of roll for intact and damaged ship. CFD calculations are performed by *CDApco StarCCM+* software investigating the accuracy and efficiency of the numerical approach. In the numerical procedure the sensitivity analysis on mesh refinement for damaged ship was performed. Furthermore, a sensitivity analysis on time step and turbulence models was performed for the intact ship. Numerical results are plotted against experimental to verify the precision of the numerical simulations. Obtained numerical results are shown to be reasonably accurate although the calculation time still precludes the use of CFD analysis as a standard design procedure.

Keywords: *DTMB 5415 navy ship, intact ship, damaged ship, CFD, EFD, roll decay*

1. INTRODUCTION

Although most vessel responses can be calculated with acceptable accuracy by potential theories in the frequency domain, this is more difficult for roll response due to the viscous damping effects which are not negligible in roll. Roll damping plays an important role in the vessel seakeeping, which is the basis for the precise prediction of vessel motions in waves. The most common approach adopted is based on the Ikeda (1976) empirical method in which the equivalent total damping coefficient is calculated as a sum of potential, friction, eddy-making, appendages and lift contributions. The roll damping coefficient can be also be obtained through a ship model roll

decay tank test but there is evident lack of this approach in typical design procedures.

Very recently use of CFD methods in calculating roll damping has become possible due to developments in computing power. Numerical simulation based on CFD offers the advantage of considering viscous flow, although calculations are still very time consuming and experience of the modeling of this phenomenon is still very limited. A major problem in roll decay simulation, common to any problem of transient ship motion, is the necessity of special computational techniques such as deforming mesh, moving mesh and grid interface.



One of the first CFD assessments of roll decay is by Wilson (2006) who performed simulations for a bare hull and bilge-keel-appended surface combatant model (referred as DTMB 5512) using the software *CFDSHIP-IOWA*. Roll decay simulations are performed for three cases: the bare hull at $Fr = 0.138$ and 0.28 and the hull with bilge keels at $Fr = 0.138$. Comparisons of EFD and CFD damping coefficients for the low speed case with bilge keels showed very small differences, generally less than 0.4%, while comparisons for the bare hull cases at both speeds showed larger differences for damping coefficients (up to 20%) even though the difference in time histories for the roll motion showed reasonable agreement (<4.5%).

Yang *et al.* (2012) presented simulation performed using the commercial software package *Fluent* of roll decay for the same vessel, DTMB 5512, with initial heel angles: 5, 10 and 15 degrees at $Fr = 0.28$. The authors reported very good results in terms of damping coefficient and two examples of decay curve but no details on the method and calculation procedure are given. Yang *et al.* (2013) performed numerical simulations of free decay and forced rolling at various forward speeds and amplitudes for DTMB 5512 and S60 hulls to predict ship roll damping, using a RANS solver using a dynamic mesh technique. The influences of forward speed, roll amplitude and frequency on the ship roll damping are evaluated. The authors report the difference between numerical and experimental results as 1.3 to 2.5%.

Handsichel *et al.* (2012) applied RANS simulations to calculate roll damping coefficients of a RoPax vessel in full scale. The influence of the roll amplitude up to 35 degrees, three ship speeds, the vertical position of the roll axis, and the interaction between the bilge keels and the ship hull are analysed. Detailed validation data for a RoPax ship was not available but authors compared the numerical results with Ikeda's method. Avalos *et al.* (2014) investigated a roll decay test of the

middle section of an FPSO with bilge keels by the numerical solution of the incompressible two-dimensional Navier–Stokes equations. The simulations indicated the strong influence of the bilge radius on the damping coefficient of the FPSO section. Very good results were generally obtained for cases with bilge keels, although sometimes the agreement for the oscillation period was not so good in the case with the larger bilge keel. The worst results in terms of damping and oscillation period were obtained for the section without bilge keels. The authors highlighted that the numerical simulation confirmed the occurrence of the so-called damping coefficient saturation: i.e. the phenomenon in which the damping coefficient does not increase with amplitude as predicted by conventional quadratic theory.

Gao & Vassalos (2011) presented results of numerical simulations of roll decay of DTMB 5415 with bilge keel in both intact and damage conditions by RANS. The comparison shows that the agreements between calculation and model test are acceptable with slightly larger period and smaller damping obtained from the calculation. Gao *et al.* (2013) presented an integrated numerical method that couples a seakeeping solver based on the potential flow theory and a Navier–Stokes (NS) solver with the volume of fluid (VOF), developed to study the behaviour of a damaged ship in beam seas. The integrated method was used to simulate the roll decay of a damaged Ro–Ro ferry and the ferry's motion in regular beam seas. Validation against experimental data showed that the proposed method can yield satisfactory results with acceptable computational costs.

This work continues the stream of investigation on the applicability of CFD methods for roll damping determination. The commercial software *CD Adapco StarCCM+* is used for roll decay simulation of an intact and damaged bare hull DTMB 5415 model, tested by authors at the University of Strathclyde.



2. MODEL DTMB 5415 GEOMETRY AND DATA

2.1 DTMB 5415

Roll damping was studied for the well-known benchmark naval hull form DTMB 5415, constructed in fibreglass as 1/51 scale model used in experimental campaign in Begovic et al. (2013). The main particulars of the DTMB 5415 model are given in Table 1.

Table 1. Main Particulars DTMB 5415

Particulars	Ship	Model 51
L_{OA} (m)	153.300	3.0
L_{PP} (m)	142.200	2.788
B_{WL} (m)	19.082	0.374
B_{OA} (m)	20.540	0.403
D (m)	12.470	0.244
T (m)	6.150	0.120
V (m ³)	8424.4	0.0635
Δ (t, kg)	8635	63.5
C_B	0.505	0.505
C_P	0.616	0.616
C_M	0.815	0.815
KM (m)	9.493	0.186
KG (m)	7.555	0.148
GM (m)	1.938	0.038
LCG (m)	70.137	1.375
$k_{xx-WATER}$ (m)	6.932	0.136
k_{yy-AIR} (m)	36.802	0.696
k_{zz-AIR} (m)	36.802	0.696

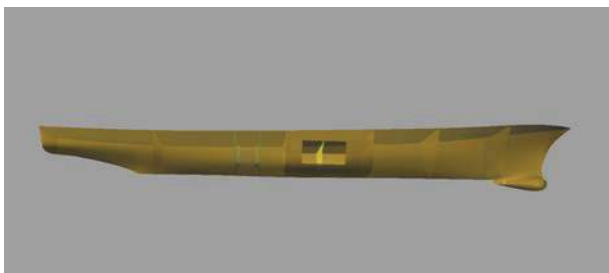


Figure 1 DTMB 5415

The internal geometry of the 1:51 model was identical to that presented by Lee *et al.* (2012). The model has been fitted with the 5 watertight bulkheads located as shown in Figure 1. The damage opening shown in Fig. 2 leads to two compartment (3 and 4) symmetric flooding. The flooded length extended from $x_1 = 65.66$ m (ship scale) to $x_2 = 90.02$ m, corresponding to 17% of the length between perpendiculars. This extension seemed reasonable for a destroyer type of ship, as it is expected that this type of ships have to preserve all functionality with two compartments damage. Both compartments were fitted with the small tube to assure the air-flow during tests, visible on the port side of model at Fig.2.



Figure 2 Damage opening of DTMB 5415

The exact amount of flooded water is determined from hydrostatic calculations, i.e. for the measured immersion and trim angle, the displaced volume was found. All characteristics of damaged ship are reported in Table 2.



Table 2. Damaged case principal characteristics

Particulars	SHIP	MODEL
$L_{\text{flooded compartments}}$ (m)	24.36	0.478
B_{WL} (m)	19.458	0.382
T_{mean} (m)	7.41	0.145
Trim [+ aft] (deg)	-0.656	-0.656
Δ (t)	11273.8	0.083
Mass of flooded water (t/kg)	2638.9	0.019
LCG (m)	71.622	1.404
KM (m)	9.427	0.185
KG (m)	6.654	0.130
GM (m)	2.773	0.054

2.2 Experimental results for intact ship

The tests have been performed at the Kelvin Hydrodynamics Lab, University of Strathclyde. The model motion has been tracked using a Qualisys optical system at frequency of 137.36 Hz. In Figure 3, four decay cases are reported for the bare hull intact ship, with different initial heel angles of: 4.00, 13.43, 19.38 and 28.00 deg.

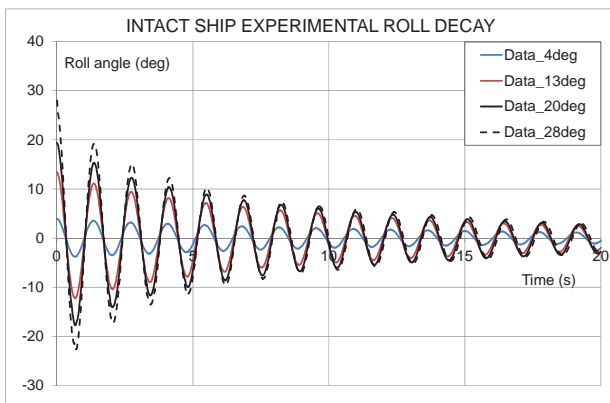


Figure 3 Roll decays of intact DTMB 5415

Results of simple analysis of roll damping coefficient for all tested decays according to ITTC (2011) nomenclature and standard logarithmic decay are natural period and damping coefficients: linear α and quadratic β , reported in Table 3. The trends of measured decays reported in Fig.3 indicate very small damping for small initial heel: in 15 roll cycles

the roll amplitude decreased from initial 4.0 deg heel to 1.1 degree. It can be further noted that the 20 and 13 deg decay curves converge for amplitudes lower than 5 degrees indicating that the roll damping mechanism at large amplitude heel angles is different to that at small angles and that the damping formulations proposed by Fernandes & Oliveira (2009) and Bessler (2010) are suitable for both small and large angles.

2.3 Experimental results for damaged ship

For the damaged ship only cases with initial amplitudes higher than 10 deg have been considered due to the much higher damping of the damaged ship with respect to the intact case. Two cases with initial amplitudes of 13.5 and 19.1 deg are given in Figure 4. It can be noted that in 10 cycles the roll amplitude is reduced to 1deg. It can be further noted from Figs. 3 and 4 that the natural period of the damaged ship (1.518s) is significantly higher than that of the intact ship (1.368s).

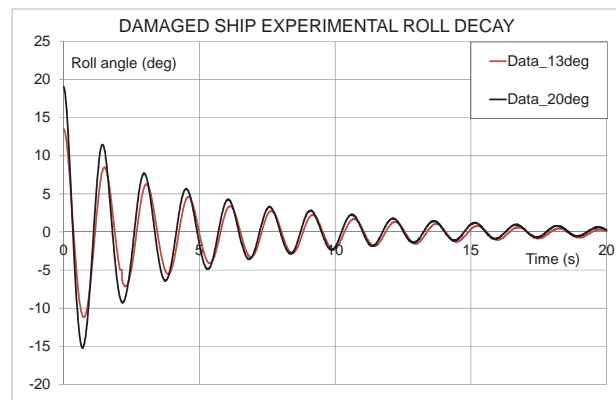


Figure 4 Roll decays of damaged DTMB 5415

Table 3. Roll decay analysis summary

	Intact	Damaged
ω_4 (1/rad)	4.593	4.135
T_4 (s)	1.368	1.518
α (1/s)	0.0604	0.1358
β (1/rad)	0.1237	0.2628



From Table 3 it can be seen that the damaged ship exhibits a higher natural roll period as well as much higher linear and quadratic damping coefficients α and β than those for the intact ship. This difference is mainly due to the flood water dynamics, inside and outside the compartment, generating some waves and some vortices. It can be noted that both linear and quadratic damping coefficients have increased by more than double.

3. NUMERICAL SET UP

In this work the commercial software *CD Adapco StarCCM+ V.8.04* has been used for the calculations of roll decay curves. It is well known that the accuracy of CFD results and the calculation time strongly depends on the type of the mesh and number of cells used, and therefore meshing is optimized for the “most challenging” case, i.e. damaged ship with 19.1 deg initial heel. In present work, a moving mesh and grid interface have been used for modelling the roll decay phenomenon. For the interaction between the moving body and the free surface a Chimera grid or overset mesh technique is used. To solve the time-marching equations, an implicit solver has been used to find the field of all hydrodynamic unknown quantities, in conjunction with an iterative solver to solve each time step. The software uses a *Semi Implicit Method for Pressure Linked Equations* to conjugate pressure field and velocity field, and an *Algebraic Multi-Grid* solver to accelerate the convergence of the solution.

The free surface is modelled with the two phase volume of fluid technique (*VoF*). A segregated flow solver approach is used for all simulations. The Reynolds stress problem is solved by means of $k-\varepsilon$ turbulence model.

3.1 Mesh generation and sensitivity analysis

A trimmed mesh of hexahedral type is used, shown in Fig. 5. In order to optimize the

discretization of each region and to avoid large computational costs, the region around the hull is finer than the far field regions.

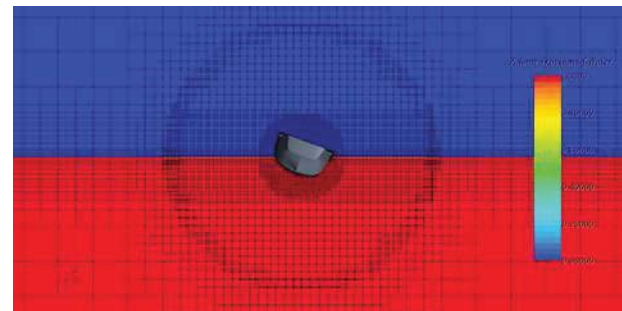
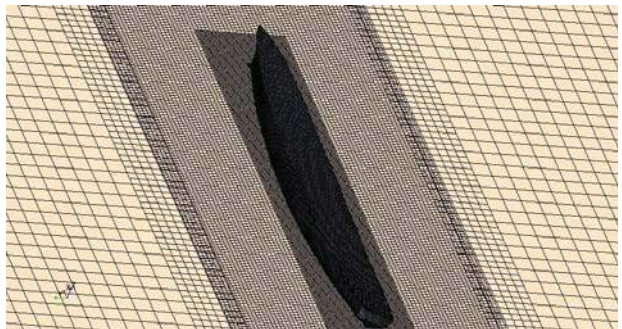
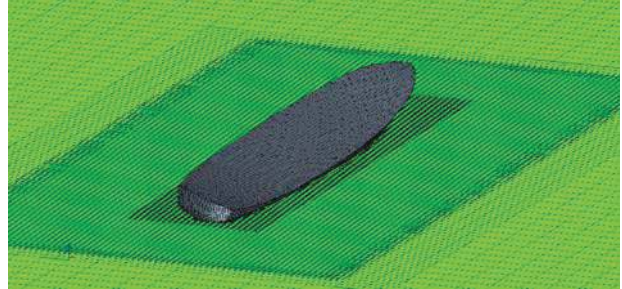


Figure 5 Hexahedral trimmed mesh

The mesh shown in Fig.5 is the result of the sensitivity analysis performed with two trimmed meshes and two hybrid meshes (polyhedral and trimmed) running 5 seconds of model roll decay simulation. A summary of cell numbers and CPU time for 32 processors is given in Table 4. The obtained roll decay histories are shown in Fig.6 indicating that the Hybrid_1 mesh gives completely incorrect results, and it was thus stopped after 3 seconds. It can be noted how the refinement of the free surface VoF (Hybrid_1 vs. all others) in the range of the complete hull model height (not only the “seakeeping” free surface) yields significant improvement in roll decay



simulation. From Fig.6 very small difference can be noted between Trim_2 and Hybrid_2 meshes in quality of results while the computational time is extremely prohibitive for the Hybrid_2 case.

Table 4. Mesh sensitivity analysis summary

Grid Type	No. Cells	CPU Time
	$\times 10^6$	(h)
Hybrid_1	1.194	90
Trim_1	0.709	40
Trim_2	1.476	90
Hybrid_2	2.590	192

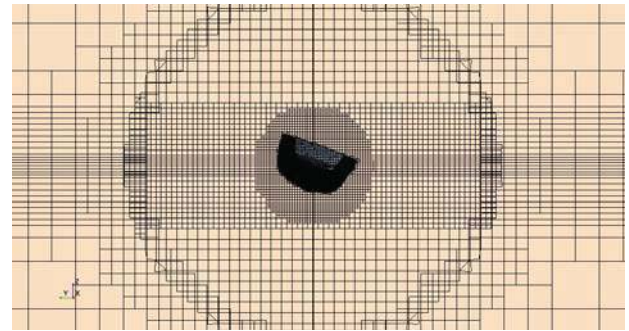


Figure 5c Mesh Trim_2

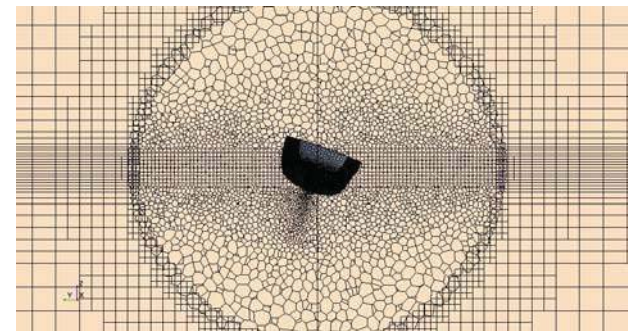


Figure 5d Mesh Hybrid_2

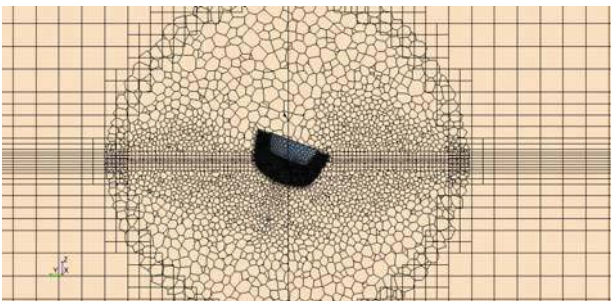


Figure 5a Mesh Hybrid_1

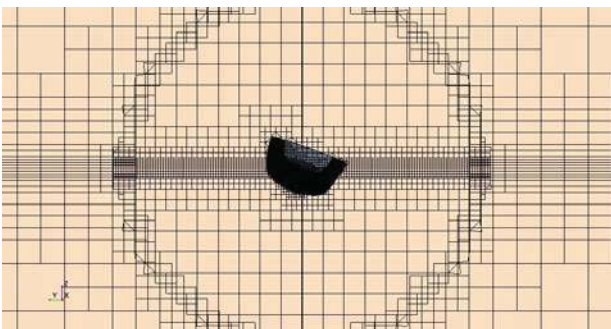


Figure 5b Mesh Trim_1

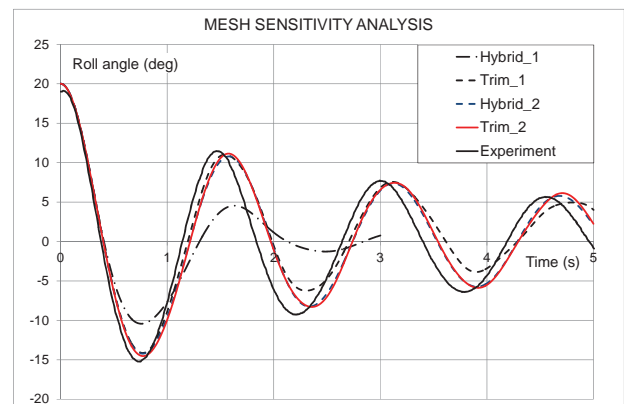


Figure 6. Mesh sensitivity results

3.2 Boundary Conditions and solver settings

All the boundaries, as defined in the numerical set up, are shown in Fig. 7.

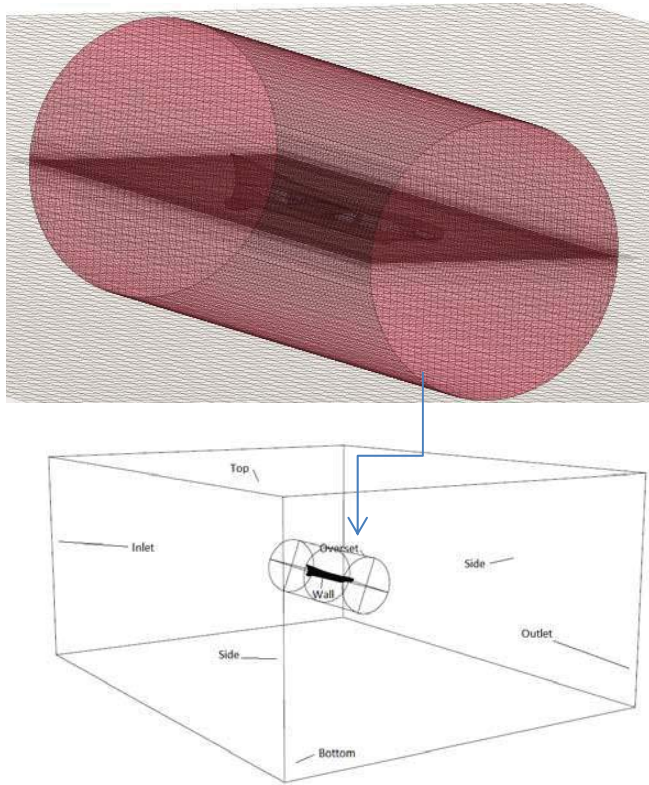


Figure 7 Domain and Boundary representation

The conditions applied to each of them are summarised in Table 5. For each simulation, the hull is heeled at the initial angle of the roll decay curve. The origin of the coordinate system is at the model CG. For the intact case the calculations have been performed with $k-\epsilon$ and $k-\omega$ turbulence models. All properties of the numerical solver are reported in Table 6.

Table 5 Boundary conditions summary

Inlet	Velocity inlet condition
Outlet	Velocity inlet condition
Bottom/Top	Velocity inlet condition
Sides	Pressure outlet
Hull	Wall with no-slip condition
Symmetry plane	Not existing
Overset	Boundary Interface

Once all the boundary conditions have been imposed, the last step is defining the numerical set up. The ITTC “Practical Guidelines for Ship CFD Applications” recommendation for

time step choice for periodic phenomena such as roll decay and vortex shedding is at least $1/100$ of phenomenon period. The measured roll period varies from 1.37 to 1.52 seconds resulting in recommended minimum of 0.015s. Sensitivity analysis has been performed for time steps equal to 0.002s and 0.001s. The simulations have been performed for intact ship at 19.43 deg initial heel and results are given in Fig. 8.

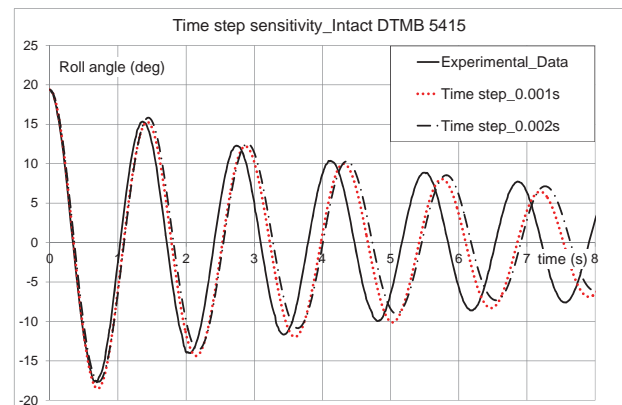


Figure 8 Time step sensitivity

Although the initial step of 0.002s is one order of magnitude lower than ITTC recommended time step, it can be seen that the simulation results are not stable with this time step. Both: decay curve and roll period are improved in simulation with 0.001s time step. Trying lower time step has been considered too expensive in terms of calculations costs.

Results of simulations with $k-\epsilon$ and $k-\omega$ turbulence models are given in Fig. 9. Numerical results are within 1% difference although it is not possible to appreciate the difference between two numerical curves.

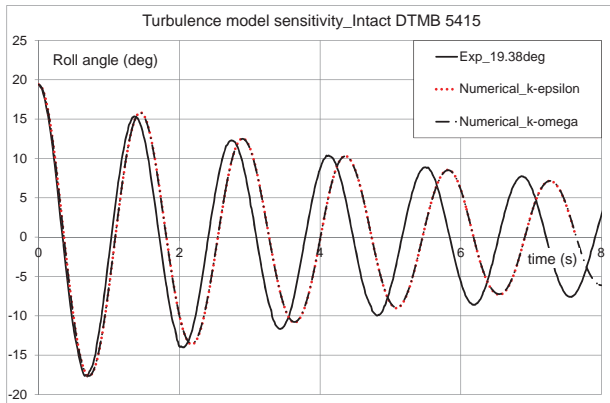


Figure 9 Turbulence models sensitivity

Final numerical set up used for the simulations is reported in Table 6.

Table 6 Solver settings summary

Convection Term	2 nd order
Temporal Discretization	2 nd order
Time-step (s)	0.001
Iteration per time step	12
Turbulence Model	k- ϵ / k- ω

4. NUMERICAL RESULTS

4.1 Intact ship

The final simulations for the intact ship have been performed for 4.00 and 28.00 degrees initial heel. The larger angle represents a limit for mesh functionality. The lower angle gives the part of extinction curve common to all experimental decays reported in Fig. 3, where none of the simulations arrived due to the necessary computing time. The mesh scene is given in Fig. 10 for both simulations. The total number of cells is 1.24M. The calculation time depends on the turbulence model and the initial heel angle; for the k- ϵ model using 32 processors, 1s of simulation takes about 13 hours for 4.00 deg and about 8 hours for 28.00 deg initial heel.

Results compared with the experimental data are given in Figs. 11 and 12.

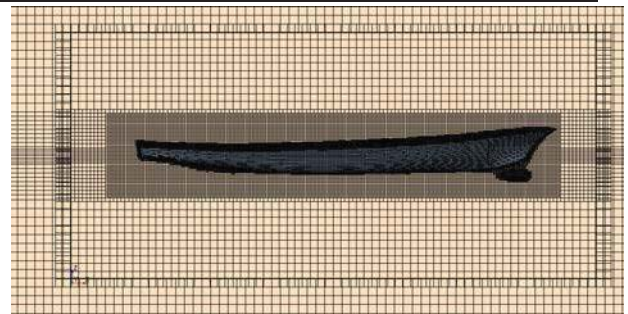


Figure 10 Mesh Scene for Intact model

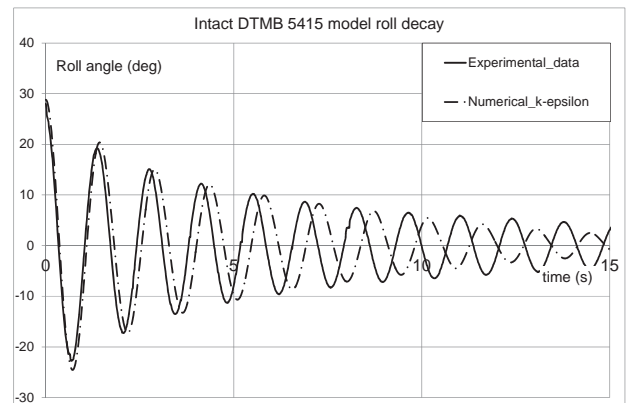


Figure 11 Comparison of experimental and numerical results

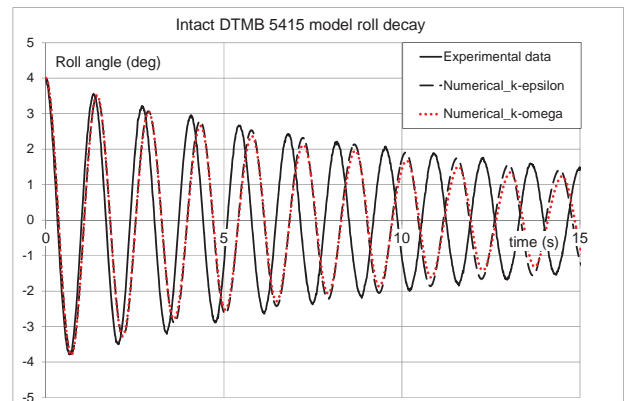


Figure 12 Comparison of numerical and experimental results

In both simulations a good trend of magnitude of decay curves with higher roll period can be observed. Roll oscillation period in all simulations is 1.443 seconds, and does not show dependence on roll angle. With respect to experimental result of 1.369s, this gives a difference of 5.4%.



4.2 Damaged ship

The final simulation for the damaged ship is performed for 15 seconds model time. Details of the mesh in the flooded compartments is shown in Fig. 12. The numerical roll decay curve compared with the experimental data for the damaged ship is given in Fig. 13.

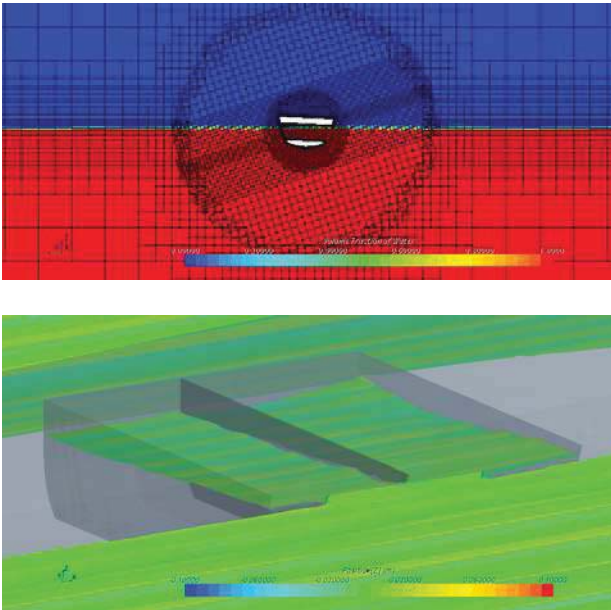


Figure 12 Damage detail

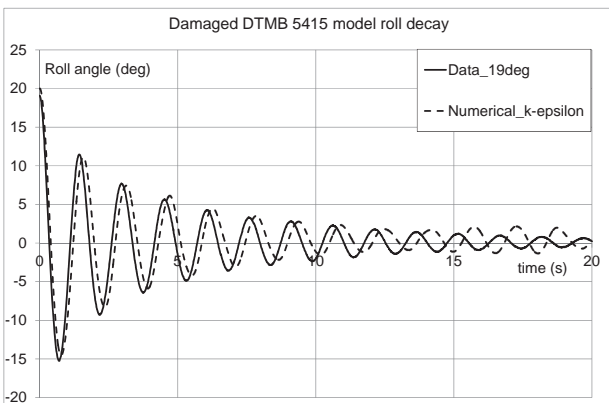


Figure 13 Numerical vs Experimental Roll Decay

It can be seen that oscillation period of numerical results 1.56 s is longer than of experimental, 1.518s, leading to the difference of 2.8%.

4.3 Damping coefficients comparison

Assessment of damping coefficients in experimental procedure generally is done analysing more than five decay curves. Results presented in Table 4 are calculated for 10 decays, including large and small initial angles. Due to required CPU time, it is not possible to use the same number of decays within numerical procedure; therefore the comparison of damping coefficients is done for two numerical cases vs. respective experimental results. Decay coefficient analysis is given in Fig. 14.

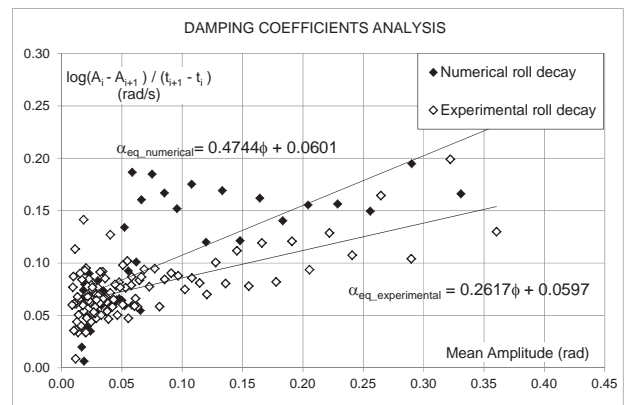


Figure 14 Damping coefficient determination

The linear coefficient α obtained for numerical and experimental results can be considered equal (0.0601 vs. 0.0597). The quadratic coefficient β is obtained by multiplying the angular coefficient of trend line by $0.75 \cdot \pi / \omega$. The values obtained are 0.243 and 0.124 for numerical and experimental results, respectively. Looking at the numerical data in Figs. 11 and 14, two problems for simulation at very high initial heel are evident. The first one is the higher predicted damping, which depends upon calculation settings (mesh, time step, solver, etc). The second problem, which presents a serious challenge, is that the time required for simulation to arrive at small angles is too long and without this part of the extinction curve the damping coefficient prediction will not be realistic.



5. CONCLUSIONS

This work focuses on the use of commercial software *CD Adapco StarCCM+* RANS solver for the analysis of roll damping properties of the bare hull naval ship DTMB 5415.

Roll damping is considered through the roll decay curve prediction, which is the beginning for any further analysis of roll damping coefficients and it is directly compared with the decay curves obtained from experiments performed by the authors. Experimental results concern intact and damaged ship behaviour in free roll decay starting from different angles ranging from 4 to 28 degrees and damaged ship data can be added to Gothenburg CFD workshop (2010).

Mesh sensitivity in numerical simulations is optimised for the damaged ship case considering hexahedral trimmed and hybrid meshes with different refinements, sizes and shapes. The trimmed mesh is chosen as it has the same accuracy of fine hybrid but significantly lower computational time. Obtained numerical results have reasonable damping coefficient prediction but the period of oscillations differ from experiments by up to 4%. These results are in line with those presented by Gao (2011, 2013) and Avalos (2014). It has to be commented that numerical predictions are highly determined by the quality rather than the quantity of the mesh

The serious challenge for the use of CFD method for damping prediction lies in the extremely high computational time required. Without considering the time necessary for the mesh generation, the calculation time of 5-6 days on 32 computers is impractical for common design practice. However there is great potential to use these simulations to generate damping coefficients numerically for flooded compartments of different geometry and to use these results to improve those semi-empirical formulae typically used in design practice, such as those based on experiments by Katayama (2009).

6. ACKNOWLEDGMENTS

The authors gratefully acknowledge the availability of 32 processors at Calculation Centre SCoPE, University of Naples and thanks to SCoPE academic staff for the given support.

7. REFERENCES

- Avalos, G. O.G., Wanderley J. B.V., Fernandes A.C., Oliveira, A.C, 2014, "Roll damping decay of a FPSO with bilge keel", *Ocean Engineering* 87 , pp. 111– 120
- Begovic, E., Mortola, G., Incecik, A., and Day, A.H., 2013, "Experimental assessment of intact and damaged ship motions in head, beam and quartering seas", *Ocean Engineering*, 72, pp. 209 - 226.
- Fernandes A.C., Oliveira A.C., 2009, The roll damping assessment via decay model testing (new ideas about an old subject), *J.Marine Science Application* (2009), 8:144-150,
- Gao, Z., Gao, Q., Vassalos, D., 2013, "Numerical study of damaged ship flooding in beam seas", *Ocean Engineering* 61 , pp. 77 – 87.
- Gao, Q., Vassalos, D., 2011, "Numerical study of the roll decay of intact and damaged ships", Proceedings of the 12th International Ship Stability Workshop, Washington D.C., pp. 277–282.
- Katayama T., Kotaki M., Katsui T., Matsuda A., 2009, "A Study on Roll Motion Estimation of Fishing Vessels with Water on Deck", *Journal of the Japan Society of Naval Architects and Ocean Engineers*, Vol.9, pp.115-125 (in Japanese)
- Lee Y., Chan H.S, Pu Y., Incecik A., Dow R.S., 2012, "Global Wave Loads on a Damaged Ship", *Ships and Offshore Structures* 7(3),



pp. 237-268

Lewandowsky E.M., 2004, “The Dynamics of Marine Craft: Maneuvering and Seakeeping”, World Scientific Publishing Co. Pte Ltd, Advanced Series on Ocean Engineering, Vol. 22

Sadat-Hosseini H., Kim D.H, Lee S.K, Rhee S.H., Carrica P., Stern F., Rhee K.P., 2012, “CFD and EFD Study of Damaged Stability in Calm Water and Regular Waves”, Proceedings of the 11th International Conference on the Stability of the Ships and Ocean Vehicles, Greece, pp. 425 – 452

Wilson, R.,V., Carrica, P.M., Stern F., 2006, “Unsteady RANS method for ship motions with application to roll for a surface combatant”, *Computers & Fluids* 35, pp. 501–524

Yang, B., Wang, Z.C., Wu, M., 2012, “Numerical Simulation of Naval Ship’s Roll Damping Based on CFD”, *Procedia Engineering* 37, pp. 14 – 18

Yang, C. L., Zhu, R.C., Miao G.P., Fan J., 2013, “Numerical simulation of rolling for 3-D ship with forward speed and nonlinear damping analysis”, *Journal of Hydrodynamics*, 25(1), pp. 148-155

ITTC Recommended Procedures and Guidelines., 2011, “Practical Guidelines for Ship CFD Applications”, 7.5-03-02-03

This page is intentionally left blank



Investigation of the Impact of the Amended S-Factor Formulation on ROPAX Ships

Sotiris Skoupas, *Lloyd's Register (LR)* sotiris.skoupas@lr.org

ABSTRACT

The adoption of the probabilistic framework in the 2009 Amendments to SOLAS, was a major change against the deterministic approach used for the damage stability assessment of passenger and dry cargo ships. Over the last years, a number of serious concerns have been raised regarding the survivability of SOLAS 2009 ships in comparison with the requirements of Stockholm Agreement (Directive 2003/25/EC). A number of studies and discussions exist along the marine industry and IMO of how the water on deck effect could be incorporated under the SOLAS regulations. Recently, the SDC Sub-Committee at its first session has agreed in principle to the proposed amendments to SOLAS chapter II-1, including the survivability assessment of ROPAX ships. The main objective of this paper is to investigate the impact of the revised s-factor formulation on existing designs.

Keywords: *damaged ship stability, ROPAX ship, probabilistic assessment*

1. INTRODUCTION

The 2009 amendments to SOLAS and the adoption of the harmonized probabilistic damage stability regulations for dry cargo and passenger ships (SOLAS 2009), was a significant step towards a more rational approach for the assessment of ship's survivability after damage. The EU-funded research project HARDER (1999-2003) investigated all elements of the existing approach and proposed new formulations for the damage and survival probabilities and for the maximum acceptable risk level (minimum safety requirements) taking into consideration enhanced probabilistic data. The final recommendations submitted to SLF 46 and the new harmonized regulations adopted by Marine Safety Committee on May 2005 (Resolution MSC.194(80)) and entered into force on 1 January 2009.

Since the harmonised probabilistic damage stability regulations became mandatory there is a continuous process in the international and national maritime regulatory bodies of developing amendments to SOLAS chapter II-1 and of the associated explanatory notes (resolution MSC.281(85)). A number of regulations have been identified as needing for improvement as realised over the years that the new SOLAS could not cater for the expeditious developments in the design of large passenger ships. Moreover, concerns were expressed by EU member states and the Maritime Safety Agency (EMSA), regarding the safety equivalence between SOLAS 2009 and the provisions of Stockholm Agreement (Directive 2003/25/EC) for RoRo passenger ships. It is noted that SOLAS 2009 was not aiming to include water-on-deck (WoD) effects on RoPax ships because the Stockholm Agreement was not part of the SOLAS 90 standard then in force [Papanikolaou, 2013].



Last year IMO SDC Sub-Committee at its first session (SDC 1) has agreed in principle to the proposed amendments to SOLAS chapter II-1, including a revised formulation for the survivability assessment of ROPAX ships. This paper aims to identify the impact of the revised s-factor formulation on existing designs.

2. REGULATORY FRAMEWORK

2.1 The current s-factor formulation

The s-factor represents the probability of survival after flooding a compartment or group of compartments after collision damage and its current formulation as found in SOLAS II-1 Reg.7-2 is based on the concept of critical significant wave height H_{Scrit} , as derived from the original HARDER project:

$$H_{Scrit} = 4 \frac{\max(GZ, 0.12)}{0.12} \frac{\max(Range, 16)}{16} = 4s^4 \quad (1)$$

In order to account transient capsize phenomena in the calculation of the survival probability and prevent asymmetric flooding, a factor K is applied to the final stage of flooding as a function of the final heeling angle at the equilibrium θ_e ($K = 1$ if $\theta_e \leq 7^\circ$, 0 if $\theta_e \geq 15^\circ$ and $[(15 - \theta_e)/(15 - 7)]^{1/2}$ elsewhere).

Therefore, the s-factor at the final stage of flooding is determined as:

$$S_{final} = K \left[\frac{GZ_{max}}{0.12} \frac{Range}{16} \right]^{1/4} \quad (2)$$

where:

$$GZ_{max} \leq 0.12m \text{ and } Range \leq 16^\circ$$

For passenger ships, SOLAS 2009 requires the calculation of s_{mom} at the final equilibrium, which is the survival probability considering the maximum transverse moment at the

damaged condition resulted by the wind force and the evacuation of the ship (passengers movement to one side and lifeboats lurching). In addition, for passenger ships only, where the intermediate stages of flooding may be critical, it is required the calculation of the ship's survival probability ($s_{intermediate}$) before the final equilibrium is reached. Where cross-flooding fittings are required, the time for equalization shall not exceed 10 min. When the heel angle at any intermediate stage exceeds 15° the value of $s_{intermediate}$ is zero. In any other case it is calculated as follow:

$$S_{intermediate} = \left[\frac{GZ_{max}}{0.05} \frac{Range}{7} \right]^{1/4} \quad (3)$$

where:

$$GZ_{max} \leq 0.05m, Range \leq 7^\circ$$

The s-factor for any damage case is then obtained from the formula:

$$s = \text{minimum}\{s_{intermediate}, S_{final} \cdot s_{mom}\} \quad (4)$$

The value of s-factor is also depending on the floatability of the ship at the final equilibrium and the immersion of critical points like horizontal evacuation routes, vertical escapes, control stations, etc. The immersion of any of the critical points result $s=0$.

2.2 The Stockholm Agreement

The Stockholm Agreement (SA) applies to RoRo passenger ships operating on regular scheduled voyages or visiting designated ports in North West Europe and Baltic Sea. The requirements of SA aim to increase ship's safety by accounting the risk of accumulation of water on the RoRo deck; water on deck (WoD) effect. The regulatory framework is based on a deterministic approach having as



main parameters the residual freeboard (F_B) in the way of damage and the sea state, by means of significant wave height (H_s). The ship shall meet the survival criteria as described in SOLAS 90 Ch.II-1 Reg.8 paragraphs 2.3 to 2.3.4 when a hypothetical amount of water accumulated on the RoRo deck. If $F_B \geq 2.0\text{m}$ no water is assumed while if $F_B \leq 0.3\text{m}$ the height (h_w) of water on deck is taken as $h_w = 0.5\text{m}$. Intermediate heights of water are obtained by linear interpolation. With respect to the sea conditions, if the significant wave height in the voyage area is $H_s \leq 1.5\text{m}$ then no water is assumed to be accumulated on the RoRo deck due to damage while if $H_s \geq 4.0\text{m}$ the height of the water is based on the residual freeboard and calculated as above. Intermediate values are determined by linear interpolation. It is noted that, as an alternative to the above compliance with SA requirements can be demonstrated by carrying out model tests based on the specific method described in Directive 2003/25/EC.

2.3 The amended s-factor formulation

The SDC sub-committee at its first session on January 2014 finalized the draft amendments to SOLAS Ch. II-1 based on the report of the working group at SLF55 and of the correspondence group (SDC 1/WP.5/Add.1). According to the agreed amendments the survival probability for ROPAX ships is calculated using the formula:

$$S_{final} = K \left[\frac{GZ_{max}}{TGZ_{max}} \frac{Range}{TRange} \right]^{1/4} \quad (5)$$

where:

$$GZ_{max} \leq TGZ_{max} \text{ and } Range \leq TRange$$

$$TGZ_{max} = 0.20\text{m} \text{ and } TRange = 20^\circ$$

for each damage case that involves a RoRo space,

or

$$TGZ_{max} = 0.12\text{m} \text{ and } TRange = 16^\circ \text{ otherwise}$$

3. APPLICATION OF THE AMENDED FORMULATION

Two existing ROPAX designs are used in order to investigate the impact of the amended survival probability on the stability characteristics, with respect to the attained subdivision index (A), and damage stability requirements, in terms of the minimum required intact metacentric height (GM). It is noted that for both ships the requirements of Reg.7 were more onerous than those of Reg.8 and Reg.9 when either the existing or the amended s-factor formula was used. All ships have been designed according to SOLAS 2009 and SA stability requirements.

3.1 Ship 1

The first ship is a large sized RoRo passenger day/night ferry which can accommodate 1900 passengers, is fitted with one lower hold and is divided into 18 watertight zones along the subdivision length of 200.8m.

In total 1146 damaged conditions are investigated for the three intact draughts (light, partial and deepest) with the damages to extend up to four zones. At 840 cases, at least one RoRo space is involved in the damage scenario Figure 1. For the most of them the vessel has sufficient GZ and Range in order to achieve $s=1$ or not enough stability and/or floatability leading to $s=0$ when both the existing and the revised s-factor formulation is considered.

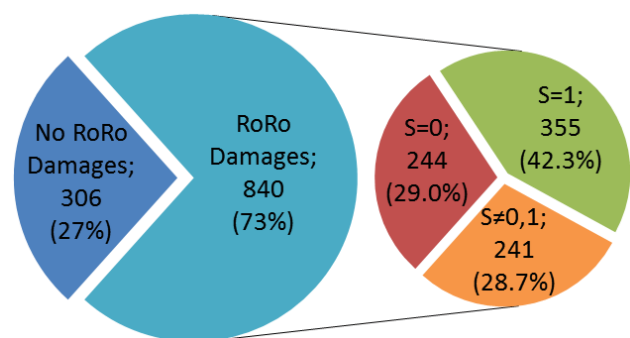


Figure 1: Damaged conditions studied, Ship 1

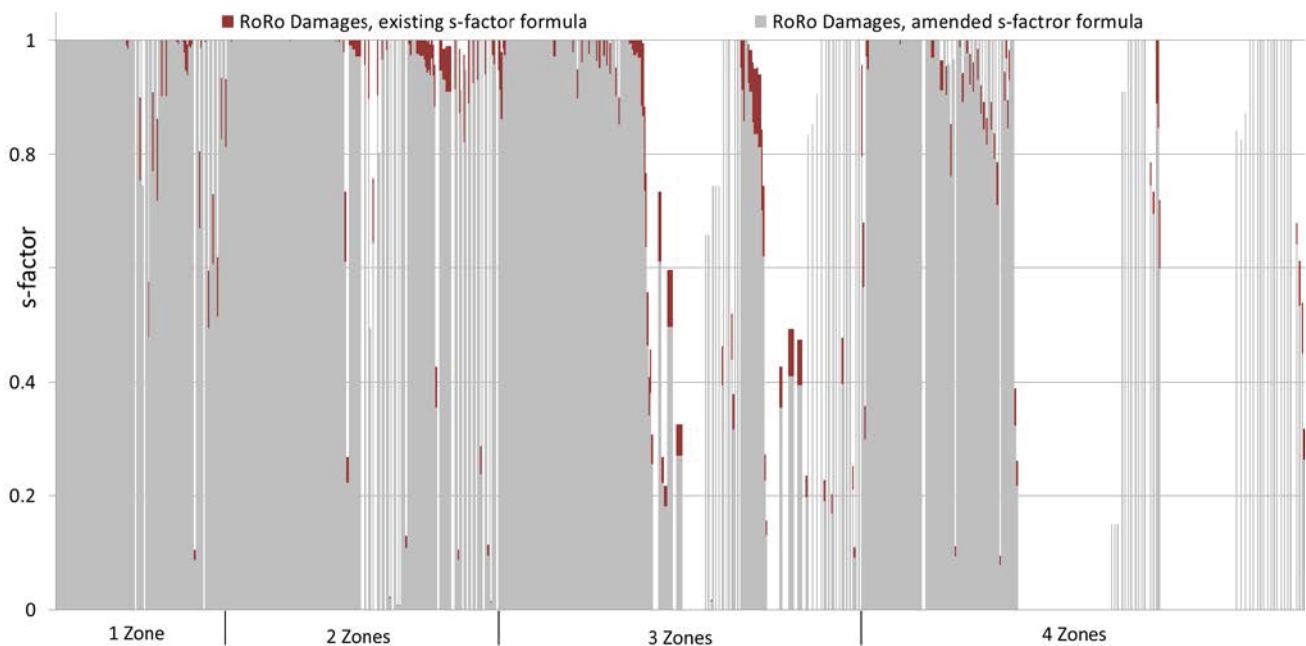


Figure 2: Survival probability of RoRo damages based on the existing and amended formula, Ship 1

For the rest 355 cases a mean reduction 8.7% occurred in the survival probability. If all 840 cases where a RoRo space is involved are accounted then the mean reduction to the s-factor is 2.5%. The Figure 2 shows the differences in the s-factor values for all damages where a RoRo space is involved when the existing and amended formula is used. It is also noted that for 88 or 10% of these cases the survival probability was one when calculated with the existing formula but reduced after the Equation 3 is used.

The required subdivision index according to SOLAS II-1 Reg.6, is $R=0.79108$. The calculations show that when the revised s-factor formulation is used, the attained index is reduced per 1.6%, decreased from $A=0.79164$ to $A^*=0.77915$, where A and A^* are the attained subdivision index according to the existing and amended Reg.7, respectively. As can be seen from Table 1, the minimum GM values need to be increased per 7cm in order the vessel to achieve compliance with Reg.6. For the calculation of the new GM, the values at partial (DP) and deepest subdivision draught (DS) equally increased while the GM value at the light service draught (DL) remained constant.

According to the approved stability information, the ship complies with the requirements of Stockholm Agreement (WoD) for a significant wave height of 4.0m at the light, partial and deepest draughts when the metacentric height values are at least those shown on the Table 1. It can be seen that the amended s-factor formulation for ROPAX ships, which leads to more onerous requirements, is able to draw up the water on deck effect, in terms of minimum required GM.

Table 1: Minimum required GM values, Ship 1

	Existing s-factor	Amended s-factor	WoD
Initial Condition	GM (m)	GM _S (m)	GM _W (m)
DL 5.10m, TR-0.3m	5.180	5.180	2.440
DP 6.00m	1.760	1.830	1.850
DS 6.60m	1.760	1.830	1.850
A	0.79164	0.79169	-
R	0.79108		-

3.2 Ship 2

The second ship is a large sized RoRo passenger day ferry with the capability to accommodate 300 passengers and transport vehicles on the main and upper garage decks and in one lower hold. The subdivision length of 211.9m is divided into 18 watertight zones while the required subdivision index is lower in comparison with the first ship ($R=0.70036$) because of the significantly smaller number of passengers.

The total number of the damage conditions investigated for the light, partial and deepest draughts was 1353 assuming the ship damaged up to four zones. As can be seen on Figure 3, the 81% of the examined cases involve a RoRo space. More than half of them did not have sufficient stability or enough floatability and result a zero survival probability regardless of the formulation used. On the other hand, 18% of them result $s=1$ based on both the existing and revised s-factor formula. For the rest 262 cases a mean reduction of 10.2% occurred in the s-factor values. If all 1098 cases involving a RoRo space are considered, then the mean reduction to the s-factor is 2.4%. It is also noted that 79 or 7% of the cases with a damaged RoRo space had a unitary probability of survival when calculated with the existing

formula but reduced after the amended formula used.

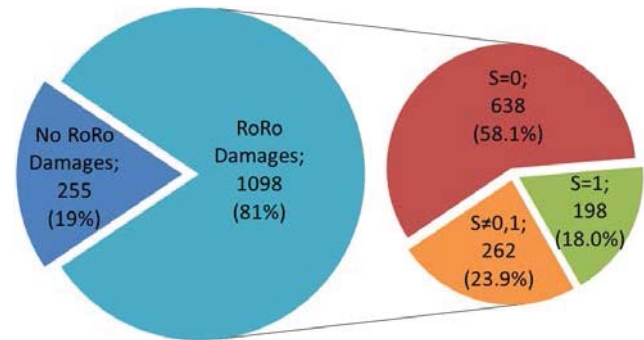


Figure 4: Damaged conditions studied, Ship 2

The impact of the amended s-factor formulation on the survival probabilities for all damages involving a RoRo space can be seen on Figure 4. The subdivision index of the ship has been reduced from $A=0.70245$ to $A^*=0.68265$ or 2.8%, where A and A^* are the attained subdivision indices according to the existing and the amended s-factor formulation, respectively. In order the vessel to achieve $A=R$ the intact GM values need to be increased per 11cm equally for both the partial (DP) and deepest subdivision conditions (DS). As per the first ship, the GM value corresponding to the light service condition (DL) remains constant (Table 2).

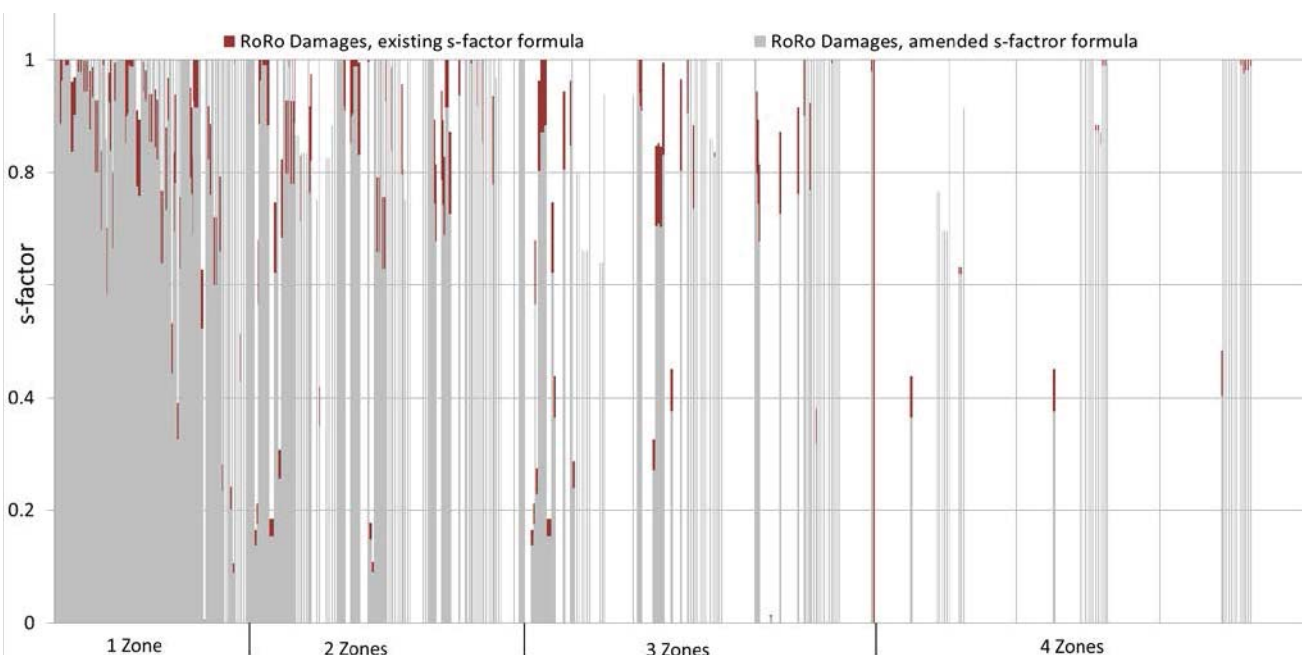


Figure 3: Survival probability of RoRo damages based on the existing and amended formula, Ship 2



Table 2: Minimum required GM values, Ship 2

	Existing s-factor	Amended s-factor	WoD
Initial Condition	GM (m)	GM _S (m)	GM _W (m)
DL 5.01m, TR-0.2m	4.610	4.610	2.141
DP 5.79m	1.500	1.610	1.611
DS 6.30m	1.900	2.010	2.024
A	0.70245	0.70213	-
R	0.70036		-

4. CONCLUSIONS

Following many discussions within the maritime community, last year the SDC subcommittee finalised the draft amendments to SOLAS Ch.II-1. A brief study for the effect of the amended survival probability for ROPAX ships has been presented in this paper.

The results show that, with respect to the requirements of Stockholm Agreement, the amended SOLAS Ch.II-1 was able, in terms of minimum required GM, to draw up the water on deck effect for the vessels under investigation. On the other hand, and due to the nature of the probabilistic approach, it is recognised that it is difficult to figure out possible critical damage cases and identify potential vulnerabilities in design with regard to damage cases involve a RoRo space. It is important to note that as the number of the vessels investigated is rather small the generalisation of the above outcomes is not possible.

5. ACKNOWLEDGMENTS

The author(s) acknowledge the support of Lloyd's Register Strategic Research & Technology Policy.

Lloyd's Register Group Limited, its affiliates and subsidiaries and their respective officers, employees or agents are, individually and collectively, referred to in this clause as the 'Lloyd's Register'. Lloyd's Register assumes no responsibility and shall not be liable to any person for any loss, damage or expense caused by reliance on the information or advice in this document or howsoever provided, unless that person has signed a contract with the relevant Lloyd's Register entity for the provision of this information or advice and in that case any responsibility or liability is exclusively on the terms and conditions set out in that contract.

6. REFERENCES

- EU, Directive 2003/25/EC of the European Parliament and the Council of 14 April 2003 on Specific Stability Requirements for Ro-Ro Passenger Ships, Official Journal of the European Union, May 2003
- HARDER, 1999-2003, "Harmonisation of Rules and Design Rationale". EC funded project, DG XIIBRITE.
- HSVA, 2009, "Research for the Parameters of the Damage Stability Rules including the Calculation of Water on Deck of Ro-Ro Passenger Vessels, for the amendment of the Directives 2003/25/EC and 98/18/EC", Final Report Part I-II, funded by EMSA, July 2009, <http://www.emsa.europa.eu>.
- Papanikolaou, A., Bulian, G. and Mains, C., 2011, "GOALDS – Goal Based Ship Stability: Collision and Grounding Damages", Proceedings of the 12th International Ship Stability Workshop, Washington D.C.
- Papanikolaou, A. (ed.), Guedes Soares, C., Jasionowski, A., Jensen, J., Mc George, D., Papanikolaou, A., Poylio, E., Sames, P., Skjong, R., Skovbakke-Juhl, J. and Vassalos, D. "Risk-based Ship Design – Methods, Tools and Applications"



SPRINGER, ISBN 978-3-540-89041-6,
February 2009.

Papanikolaou, A., Hamann, R., Lee, B.S.,
Mains, C., Olufsen, O., Tvedt, E., Vassalos,
D. and Zaraphonitis, G., "GOALDS - Goal
Based Damage Stability of Passenger
Ships" Proc. 2013 Annual Meeting & Expo
& Ship Production Symposium - SNAME,
Washington D.C., 6-8 November 2013.

IMO MSC 80/24, 80/24/Add.1, "Report of the
Maritime Safety Committee on its Eightieth
Session", May 2005.

IMO SDC 1/7, 1/7/Add.1, "Revision of
SOLAS Chapter II-1 Subdivision and
Damage Stability Regulations", Report of
the SDS Correspondence Group, Submitted
by the United Kingdom, October 2013.

IMO SDC 1/WP.5/Add.1., "Revision of
SOLAS Chapter II-1 Subdivision and
Damage Stability Regulations,
"Development of Guidelines on Safe
Return to Port for Passenger Ships, Any
other Business, Report of the Stability
Working Group", January 2014.

IMO SLF 46/INF.6, "Development of Revised
SOLAS Chapter II-1 Parts A, B and B-1,
Development of generalized s-factor", Final
recommendations from the research project
HARDER, Submitted by Norway and the
United Kingdom, June 2003.

IMO SLF 55/8/2. "Revision of SOLAS
Chapter II-1 Subdivision and Damage
Stability Regulations", Report of the SDS
Correspondence Group, Submitted by the
United Kingdom, November 2012.

Jasionowski, A. "Study of the specific damage
stability parameters of Ro-Ro passenger
ships according to SOLAS 2009 including
water on deck calculation", Project No.
EMSA/OP/08/2009, Ship Stability
Research Centre (SSRC), Final Report,
November 2011.

Zaraphonitis, G., Skoupas, S., Papanikolaou,
A., Cardinale, M. "Multi-Objective
Optimization of RoPax Ships Considering
the SOALS 2009 and GOALDS
Damage Stability Formulations",
Proc. 11th International Conference
on Stability of Ships and Ocean
Vehicles (STAB2012), Athens, 23-28
September 2012.

This page is intentionally left blank



Stability Upgrade of a Typical Philippine Ferry

Dracos Vassalos, Sokratis Stoumpos, Evangelos Boulougouris

Naval Architecture, Ocean and Marine Engineering, University of Strathclyde, Glasgow G4 0LZ, Scotland

ABSTRACT

The waterborne transport in the Philippines has been a sensitive subject amplified by the lack of rules and regulations to restrict ship-owners profit-driven decisions, leading to overloading, with significant impact on ship stability. Most of the Tier-II vessels are using solid ballast to balance trim and increase static stability at the expense of freeboard. To improve matters whilst facilitating the currently adopted process, solutions are required that offer additional buoyancy with increased stability. To this end, a solution is proposed here through the addition of sponsons, providing the required level of intact stability and residual floatability/stability, using a typical Ro-Pax. In this paper, a case study is presented to demonstrate the validity of the proposed solution.

Keywords: damage stability, freeboard, load line, conversion, sponsons

1. INTRODUCTION

In the Philippines, it has become common practice to overload passenger ferries with additional people carried, leading to a significantly low freeboard, below the ICLL'66 levels. This increases the risk for the people on-board. In order to keep in operation the vessels concerned without compromising safety severely, an immediate solution is required. One of the obvious solutions identified is the addition of buoyancy by increasing the volume of the hull with sponsons. There are three categories of ships used in the region, namely: old vessels about to be withdrawn from service; the second-hand IMO Tier-II compliant ships (with solid ballast); and the new-built IMO Tier-III compliant vessels (IMO, 2015). This paper focuses on the second category and a case study of the stability upgrade process, using an existing Ro-Pax as a basis, which has already undergone modifications involving the addition of partial decks and other items, aiming at increasing her payload. The extent of modification required to restore vessel floatability and residual stability to satisfactory levels is indicative of

the level of risk of these vessels and of the need to take action.

2. CURRENT SITUATION

There are currently approximately 7,000 islands in the Philippines. They are served by ferries providing vital links for trade, communities and tourism. Nearly a billion ferry passenger journeys were conducted in 2013 in South East Asia, according to INTERFERRY. The reason for the concern being raised about domestic ferries is the thousands of lives lost at sea on a yearly basis because of the level of risk inherent in these vessels and the ignorance of people on how unsafe they really are. An overview of the situation is given by the Worldwide Ferry Safety Association reported over the last 14 years, 163 accidents leading to 17,000 fatalities (from which 50% occurred in China, Philippines, Indonesia and Bangladesh) were recorded. This contradicts with IMO's aim to continuously improve the safety of ships and reduce to acceptable levels the risk to people on board. The latter is the main reason why the regulations in this area must come in line with

the rest of the international shipping (Adamson, 2015).

2.1 Operational Issues

The major issues of the IMO Tier-II compliant vessels used in this area derives from the wish of ship-owners to increase the capacity of their vessels without considering the limiting criteria set at the design stage. The conversion commences as soon as the vessels are bought in order to increase the passenger carrying capacity with the addition of decks. This results to a change of the longitudinal and vertical distribution of weights and therefore solid ballast (concrete in most cases) is added to adjust the trim and improve the upright static stability. This results in an additional increase of the draught, leading to an increased displacement and resistance but most importantly to a significantly reduced freeboard, impacting the reserved buoyancy and the damage stability of the vessel. The extent of this problem is of such magnitude that demands drastic measures and one such measure is proposed here, as described next.

3. CONCEPT DESCRIPTION

The additional structural parts that are considered for the enhancement of buoyancy and stability are sponsons located at each side of the vessel with a ducktail formation at the aft end. Both modifications will affect buoyancy as well as hydrodynamic properties, which with proper consideration could lead to an increase of the propulsive efficiency and, potentially, to a reduction of fuel consumption or to an increase of service speed. The geometry of these appendages is illustrated in figures 1 and 2. Such a solution will allow the removal of the solid ballast. The resulting hull form has sufficient stability as indicated in the following.

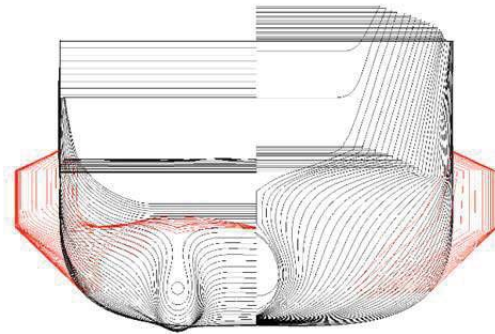


Figure 1 Sponsons with ducktail fitted on the existing hull.

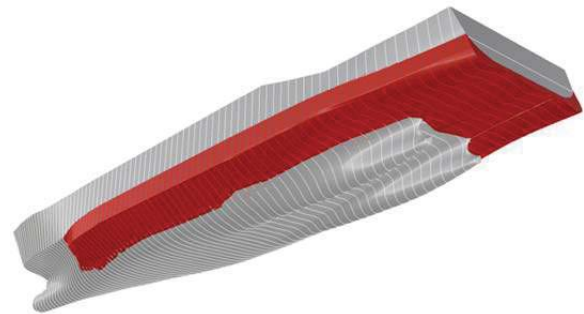


Figure 2 Body plan view of upgraded vessel.

4. REGULATORY FRAMEWORK

4.1 Intact stability

For the present case study the regulations of IMO IS Code 2008 concerning the intact stability of passenger ferry ships (IMO, 2008) is used. Full load departure condition is used.

4.2 Damage stability

Regarding damage stability, an investigation is carried out to assess whether the design will comply with the stability requirements of Regulation 8, Chapter II-1 of SOLAS 1974, SOLAS 88 Amended / II-1 / Reg. 8, for Ships Constructed from 29-4-1990 to 1-10-1994 (IMO, 1988).



The damage case particulars (size) are determined in accordance with the extent of damage in SOLAS 1974. Thus, the worst case 1-compartment damage scenario is considered, involving the engine room and the RoRo deck flooded in full-loaded departure.

5. CASE STUDY

For the calculations performed, a second-hand Ro-Pax ship operating in the Philippines that complies with IMO Tier-II was selected as sample for the comparison before/after the upgrade proposed in this paper.

5.1 Existing ship

This vessel has undergone a number of modifications, as described next:

- 1) Reinforcements to the freeboard deck to accommodate the new stowage layout and installation/relocation of new fixed cargo securing device;
- 2) Re-plating of the opening of the upper deck (mid-portion in way of ramp) to accommodate additional passengers. Installation of additional side structures P/S. Installation of additional comfort rooms between frames 15-25 P/S. Cropping out dining tables (inside and outside) and replacement with double bed bunks. Cropping out of seats between frames 90-100 and replacement with double bed bunks;
- 3) "A Deck" was extended from frame 30 going aft and relocation of inflatable life raft. The conversion of the open space in passenger area was made by installing double bed bunks as well as addition of new cabins on both sides of the vessel. Passenger walkways were created from frame 10-60 P/S along with a passenger ramp (aft) P/S.
- 4) The navigation bridge deck was extended aftwards from frame 72 to frame 30 and tables and chairs were installed as well as re-installation of lifeboat and davits.
- 5) Solid ballast was added in the double bottom at the fore end (in Void No. 3 & Void No. 4 to reduce the trim to acceptable levels and reduce the vertical centre of gravity.

5.2 Upgraded ship

The proposed upgrades according to the present proposal are as follows:

- 1) Removal of the solid ballast from the double bottom.
- 2) Installation of sponsons. Both the added buoyancy and their structural weight were taken into account
- 3) Extension of the sponsons to the aft end in order to form a ducktail, helping the adjustment of the trim, the increase of buoyancy and stability.

5.3 Ship particulars

The main vessel's particulars before and after the proposed changes are illustrated in table 1 below:

Table 1
Ship's particulars

	Existing Ship	Upgraded Ship
Length (O.A.)	86.90 m	86.90 m
Length (P.P.)	74.00 m	74.00 m
Breadth (mld)	14.00 m	17.18 m
Depth (mld)	10.20/5.50 m	10.20/5.50 m
Draught (designed)	4.35 m	4.02 m
Main engine	3,500 x 2 PS	3,500 x 2 PS



	Existing Ship	Upgraded Ship
Speed (trial max)	15 knots (average)	>15 knots (average)
Passenger Capacity	516 P	516 P
Crew	53 P	53 P
Container Capacity	30 units – 10 ft. van	30 units – 10 ft. van

As seen in table 1, the increase of breadth resulted in draught reduction. The number of passengers is the same for both cases, which is an attractive feature for the ship-owner.

5.4 Lightship calculations of the upgraded ship

The authors examined a number of different sponson sizes before deciding on the configuration presented here. The lightship weight is acquired from the existing stability booklet and the data from the inclined experiment performed following the initial conversion of the sample vessel.

Table 2
Lightship calculations

	Mass (t)	LCG (m)	LCG MOM (tm)	VCG (m)	VCG MOM (tm)
Lightship	1805.72	-5.89	-10632.1	7.16	12936.2
Permanent Ballast Void No.3	-53.00	19.37	-1026.61	2.08	-110.24
Permanent Ballast Void No.4	-38.31	14.98	-573.88	0.74	-28.35
Sponsons	76	-12.72	-966.72	3.67	278.92
Total	1881.72	-6.164	-11599	7.023	13215

5.5 Stability analysis

The initial ship hullform was modelled in Maxsurf[®] (Bentley, 2014) and the resulting

hydrostatics properties were compared with the original, showing only minor differences. Following this, the geometry of the sponsons was attended to and the resulting hull form was analysed.

The results indicate that the intact stability of the vessel following the installation of sponsons is improved. However, due to the removal of the permanent ballast from the forward part of the vessel, the trim increases. On the other hand, the damage stability of the vessel is significantly improved with the volume acquired from the sponsons contributing to the buoyancy, especially at the aft end. The increased waterplane area leads to an increase of the metacentric height, resulting to compliance with all the required stability regulations. The data for intact and damage stability at the full load condition are shown in table 3.

Table 3
Intact full load condition calculations

	Existing Ship	Upgraded Ship
Draught amidships, m	4.348	4.021
Displacement, t	2739	2723
Volume (displaced) m ³	2671.87	2656.95
Trim (+ve by stern), m	0.434	0.592
LCB from amidsh.(+ve aft), m	3.492	4.462
LCF from amidsh.(+ve aft), m	7.282	8.468
KG fluid m	6.207	6.293
GMt corrected m	0.939	4.372
Immersion (TPc) tonne/cm	9.060	10.769

As seen in table 3, the displacement for the upgraded ship is reduced as the weight of the sponsons is smaller than the weight of the solid ballast removed. The trim shows a minor increase but the draught amidships reduces. Noticeable changes are the increase of the TPC and the shift of LCF and LCB towards the aft end. There is, obviously, a marked improvement in GM.



In table 4 below the respective results are presented for damage of the engine room at full load condition according to Regulation 8, Chapter II-1 of SOLAS 1974, SOLAS 88 Amended / II-1 / Reg. 8, for Ships Constructed from 29-4-1990 to 1-10-1994 (IMO, 1988):

Table 4
Damage full load calculations

	Existing Ship	Upgraded Ship
Draught Amidships, m	5.264	4.712
Displacement, t	2739	2723
Volume (displaced), m ³	2671.888	2656.948
Trim (+ve by stern), m	0.688	0.627
LCB from amidsh.(+ve aft), m	3.501	4.463
LCF from amidsh.(+ve aft), m	5.852	7.752
KG fluid, m	6.207	6.293
GMt corrected, m	0.768	3.662
Immersion (TPc), tonne/cm	7.533	8.870

In the intact stability calculations performed, both designs comply with the regulations. However, the damage stability of the existing vessel fails to comply with the SOLAS requirements. The results from the upgraded vessel are promising seen on table 5 below albeit an extensive modification. A major impact on the margin line and deck line can be observed.

Table 5
Damage freeboard

Key points	Existing ship	Upgraded ship
	Freeboard, m	Freeboard, m
Margin Line (freeboard pos = -24.03 m)	0.013	0.584
Deck Edge (freeboard pos = -24.03 m)	0.089	0.66
DF point Vent. Head 1	5.698	6.235
DF point Vent. Head 2	5.698	6.235

Table 5 presents a comparison of the damage stability results for both vessels. It is clear that the upgraded vessel meets the criteria

whilst the existing fails to comply with. This is also apparent comparing figures 3 and 4.

Figure 3: GZ curve existing ship

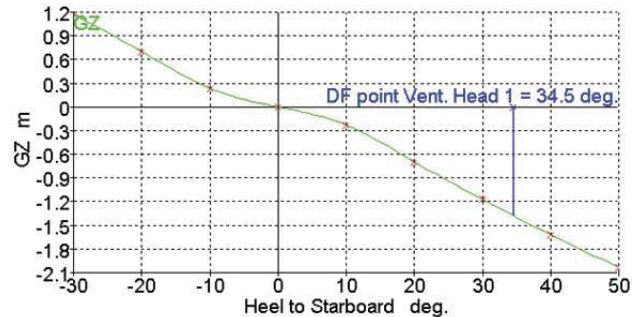
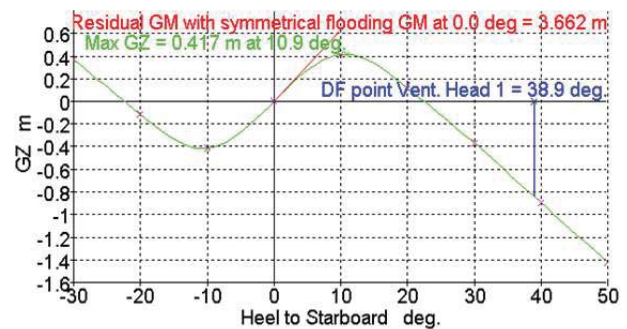


Figure 4: GZ curve upgraded ship



The results demonstrate that the existing ship loses stability in the scenario considered, which involves one-compartment damage. In a real scenario the existing ship will capsize almost instantly following one-compartment damage.

In contrast to the existing ship, the upgraded vessel has a range of positive stability of about 20 degrees. This meets the minimum requirements of damage stability set by SOLAS, namely angle at equilibrium post damage area under the GZ curve as well as residual GM as seen in Tables 5, 6 and 7.

Table 6
Residual freeboard criteria

Criteria	Value	Units	Actual	Status
Heel angle at equilibrium for unsymmetrical flooding - Equil based	7.0	deg	0.0	Pass
Margin line immersion - Equil based	0.000	m	0.584	Pass



Table 7
Damage stability criteria

Criteria	Value	Units	Actual	Status
Range of residual positive stability	15.0	deg	22.4	Pass
Area under residual GZ curve	0.8594	m.deg	5.7613	Pass
Maximum residual GZ (method 2 - manual calc.)	0.100	m	0.417	Pass
Maximum GZ (intermediate stages)	0.050	m	0.417	Pass
Range of positive stability (intermediate stages)	7.0	deg	22.4	Pass
Residual GM with symmetrical flooding	0.050	m	3.662	Pass

6. CONCLUDING REMARKS

From the results presented in this paper the following conclusions may be drawn:

The condition of the existing fleet as represented by the sample ship examined herein is unacceptable, as the vessel has no stability in case of damage. The present study shows that a medium cost conversion could provide a basic level of safety. Similar solutions have been used in Europe to upgrade existing ships in the late 80s and 90s.

Regarding the intact stability of the existing ship, it is clear that the conversion process leading to increased capacity focuses on satisfying stability and freeboard requirements for intact ships and as such it meets pertinent requirements. This is encouraging, as the process adopted, meets the requirements laid down by the Philippine Administration.

For the damage stability, equally interesting and worth noting is that freeboard requirements are also satisfied for the converted ship, even though the Philippines Merchant Marine Rules and Regulations (PMMRR) are not explicit enough when it comes to damaged ships. However, the ship has no damage stability whatsoever and this is the heart of the whole problem.

On the contrary, for the upgraded ship following the addition of sponsons the vessel intact stability has been further enhanced, meeting the requisite criteria with considerable margin.

Regarding damage stability, the addition of sponsons and ducktail bring the required effect on damage stability, perhaps with some further adjustment on the trim still required, which will be easily achieved with a more in-depth study following due optimization process. The size of the sponsons is indicative of the degree of non-compliance and the perilous situation resulting from the conversion process of the RoRo tonnage imported in Philippines and then converted to increase carrying capacity.

The key problem leading to this situation is lack of damage stability regulations in PMMRR, which should be attended to with immediate effect to apply to all existing and any newly imported or constructed ships.

Sponsons are not a panacea. They provide the additional buoyancy required for the sought out increase in payload whilst providing the platform to meet damage stability requirements as apply in international regulations. Should this solution proved to be infeasible due to financial or other reasons there are alternative solutions that could be considered. However, leaving the current fleet in the situation that it currently is, is not an option that should be accommodated any longer.

7. REFERENCES

- Adamson, L. (2015). Domestic Ferry Safety in S.E. Asia [Recorded by IMO Podcast].
- Bentley. (2014). Maxsurf Suite Enterprise.
- IMO. (1988). *SOLAS 88 Amended / II-1*.
- IMO. (2008). *IS CODE 2008 Annex II RES. MSC.267(85)*.
- IMO. (2015). *Enhancement of Safety of Passenger Ships Engaged in Domestic Services in Philippines*. Manila and Cebu: IMO.



8. APPENDIX I

NOMENCLATURE

Units	The metric system is used
Shell plating	The shell plate thickness used in the calculations
Keel	The thickness of the keel plate
Draught	The draught T used in the calculations is measured from the baseline at $L_{pp}/2$.
Base Line	The base line of the ship is the upper side of the keel plate
DISP	Tabulated displacements are measured on the outside of the shell plating
AP	Aft Perpendicular
FP	Forward Perpendicular
L_{pp}	Length between perpendiculars
KMT	Transverse metacentric height at zero angle of heel measured from the baseline
LCB	Longitudinal position of centre of buoyancy measured from midship
LCF	Longitudinal position of centre of floatation measured from midship
TPC	Tonnes Per Centimetre. i.e., weight which when added or subtracted will change the draught by one centimetre.
MCT	Longitudinal moment required to change trim by one centimetre
T	Draught amidships, measured from the upper side of the keel plate at $L_{pp}/2$.
T_{aft}	Moulded draught measured at AP
T_{fwd}	Moulded draught measured at FP

TRIM TRIM aft is positive when t_{aft} is larger than t_{fwd} i.e. the ship has an aft trim; TRIM is negative when t_{fwd} is larger than t_{aft} i.e. the ship has a forward trim.

This page is intentionally left blank



The Evolution of the Formula for Estimating the Longitudinal Extent of Damage for the Hull of a Small Ship of the Transitional Mode

[O.O.] [Kanifolskyi], [Odessa National Maritime University], [Ukraine]

SUMMARY

Old and new requirements of the High Speed Craft Code, and the methods of some researchers for calculating the damage length for a ship's hull, are considered in this article. Damage occurs more often in small vessels than in large vessels. Collisions between ships and ship's grounding are two of the main reasons for the loss of ships. The damage to the vessel is determined, for the worst case scenario. Long and narrow damage ("raking"), which absorbs the kinetic energy of the vessel, is the worst case scenario. Small high speed craft were selected for analysis. This article describes the requirements of the High Speed Craft Code related to high-speed vessels. Small vessels of the transitional mode are a category of high-speed vessels, as operated at relative velocities $1 \leq Fr_V \leq 3$, where $Fr_V = \frac{v}{\sqrt[3]{V}}$ - the Froude number based on volume. The formula for calculating the length of the possible damage of hull should take into account data on the material, the thickness of the plating, the width of the damage, the vessel's speed and its displacement. This paper proposes a comparative analysis of the size of the possible length of the hull damage, which has been calculated using different methods. The formula for calculating damages is proposed for small high speed vessels, but is possible to use this formula to other types of ships.

1. INTRODUCTION

Ships of the transitional mode belong to the category of high-speed vessels, because they are operated at relative velocities $1 \leq Fr_V \leq 3$. In the High Speed Craft Code 1994 [1]: "High speed craft" is defined as a craft capable of maximum speed (m/s) equal to or exceeding: $v_{max} \geq 3,7V^{0,1667}$, where V is the displacement corresponding to the design waterline (m^3). After the transformation of the Froude number, velocity is $v = 3,13Fr_V^{0,1667}$. From this inequality and the equation, it can be concluded that the vessel is at high speed at $Fr_V \geq 1,18$. The term "small" ship of the transitional mode is defined in article [2] and in accordance with the data of this work such vessels have lengths less than 40 m and a displacement less than 190 t. These data were

obtained on the basis of the requirements of the strength of the vessel, vertical accelerations, the optimal relative dimensions of the high-speed vessel and the comparison of two energies: the energy of the moving ship and the energy of the sea wave. The causes of the loss of ships remain steady over the years [3]. In this paper, several types of the collisions are considered: collisions between ships and the ship's grounding. These are the two main causes of loss of ships; accounting for 10.3% and 33.1% of annual losses respectively. For small ships, the probability of damage is three times more, than for large ships. It is necessary to consider the data and methods, which are offered by different researchers, for calculation of the length of the possible damage of the hull of small high speed ship, as a result of collisions with an undersea object.



2. THE DATA ON POSSIBLE EXTENT OF DAMAGE

One of the variants in calculating the extent of damage was offered by W. Hovgaard [4]. He noted that the length of damage, caused by blast of the torpedo, ranges from 8 to 17 m. The average length of the damage is taken as 11 m. According to the IMO data the average length of damage is: for vessels less than 70 m. - 2.5 m; for vessels (70-108 m.) - 6.2 m; for vessels (109-131 m.) - 7.8 m; for vessels (132-145 m.) - 9.5 m; for vessels with a length over 145 m. - 11.8 m. This information does not take into account the speed of the vessel [5].

The HSC Code [1] proposes a possible length of bottom or side damage equal to 10% of the length of the vessel, L , or $3m + 0,03L$, or 11 meters, whichever is the least. For a large passenger vessel (category "B" craft), which, after the flooding of one compartment retains the capability to navigate safely, there is a requirement to increase the possible length of the bottom damage by 50%, in the case of damage to the bow of the vessel.

This Code [1] defines two types of vessels. These categories are listed below in a short form. "Category A craft" is high-speed passenger craft operating on a route with high probability of the evacuation at any points of the route all passengers and crew. They can be rescued with the time to prevent persons in survival craft from exposure causing hypothermia or 4 hours and carrying not more than 450 passengers. "Category B craft" is any high-speed passenger craft other than a category "A" craft.

The length of the damage, according to the formula $l_d = 3m + 0,03L$, for a vessel with length 145 m, is equal to 7.4 m. This value corresponds to the Hovgaard's assumptions. Information about the speed of the ship, hull material, thickness of the plating and the width of the damage is absent in these data.

Some of the accidents which occurred with the high-speed vessels have shown that damage equal to 10% of the length of the ship did not give a good picture of the damage. The paper [6] demonstrated more probability of full length damage, for craft with length about 60 m, than for craft with length about 30 m. In this paper, the researchers took into account the material of the hull, the speed of the ship and others parameters. The proposals for predicting the extent of the damage to the hull in a collision with an underwater object have been developed. It is noted that the main difficulty in the theoretical analysis of the probable collision is the choice of scenario for the events. It is shown that the length of the relative damage for high-speed vessels is several times greater than for conventional vessels.

Some variants of the characteristics of possible damage are described below [6]. The long and narrow damage ("raking") is driven by the kinetic energy of the ship. The wide damage after collision with a rock is driven by the kinetic energy of the ship also. After this type of damage the ship may be lifted vertically. Side damage will occur after incorrect maneuvering. The driving energies for this damage process are the wind and the waves. The greatest length of the damage will be in the first variant. In this paper, a formula for determining the length of possible damage, which includes the kinetic energy of the vessel and the "raking" force, is proposed, but this proposition does not contain practical guidance for calculating the length of the damage based on different hull materials, plating thickness and damage width.

In the HSC Code [7] there is a new assumption about the possible length of the side damage equal to $l_d = 0,75V^{1/3}$ or $(3 \text{ m} + 0,225V^{1/3})$, or 11 m, whichever is the least. V - volume of displacement corresponding to the design waterline (m^3). The main difference between new and old rules is the use in calculating formulas of volume of displacement instead of the length.



Any part of the hull is considered to be vulnerable to raking damage if it's in contact with the water at speed in smooth water and it also lies below two planes which are perpendicular to the craft middle line plane and at heights as shown in figure 1.

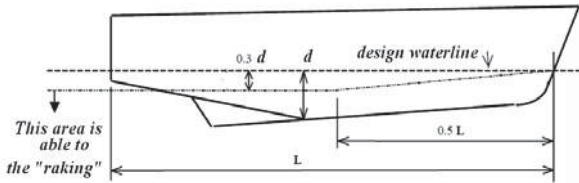


Figure 1. The area vulnerable to “raking”.

Two different longitudinal extents are considered. The first is 55% of the length, measured from the forward point of the underwater volume. The second is a percentage of the length, applied anywhere in the length of the craft, equal to 35%. For craft with length less than 50 m the extent equal to $(L/2 + 10) \%$. In areas not vulnerable to “raking”, the damage must be taken to be the same as for the sides.

V.U.Minorsky, in work [8], suggests that the length of the damage can be calculated by the formula, $l_d = a\sqrt{dE}$, a - the coefficient of the local strength of the damaged vessel, dE - the energy of the collision. These calculations using this formula are based on the collision with two ships. In an accident that occurs due to contact with an underwater object and ship, calculations with these formulas are difficult.

3. THE METHOD FOR CALCULATING THE LENGTH OF POSSIBLE DAMAGE FOR THE HULL OF A HIGH-SPEED VESSEL

The force of the resistance of the hull material can be written as:

$$R = E \frac{l_d}{L} bt \quad (1)$$

where E - Young's modulus, kN/m^2 ; b - the width of the damage, m ; t - the thickness

of the plating, m ; l_d - the length of the damage, m .

The kinetic energy of the vessel is equal to the work of the resistance of the hull's material, at the part of the vessel.

$$\frac{mv^2}{2} = Rl_d \quad (2)$$

Some ship's hull can not be damaged, after collision, but it is better to consider a more dangerous case, with damage. The case of cutting the plating of the vessel, without the effect of frames, has more dangerous, because it would lead to greater damage length.

In these calculations it is assumed that the engine is stopped and the speed of the vessel at the end of the process equals to zero. A variant of the collision is contact with an underwater object, “raking”.

$$l_d = \sqrt{\frac{mv^2 L}{2Ebt}} \quad (3)$$

where m - the mass of the ship, t ; v - the speed, m/sec ; L - the length of the ship, m .

For example, the calculation of the possible length of the damage of high-speed vessel, with relative speed $F_{rV} = \frac{v}{\sqrt{g^3 V}} = 1.6$, the width of

the damage is 0,01 m; length of ship 40 and 60 m were made, Figure 2 (formula).

The results of calculations by different methods are presented, Figure 2.

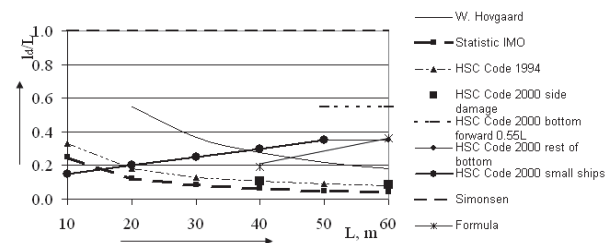


Figure 2. The relative length of the damage $l = \frac{l_d}{L}$ and the ship length.

The proposed scheme, for calculating the length of the damage, can be applied to vessels of various designs: with a double bottom and without it. Vessels may have restrictions



navigation area, and may not have [9]. Proposed formula makes it possible to determine the length of damage to ships with different materials and different Froude number based on volume. The following tables show the calculations for the vessel, which has steel, aluminum alloy or wood hull. The athwartships girth of damage are 7 m [10], $0,2v^{1/3}$ [7] и 0.01 m. The last value corresponds approximately to the average thickness of the shell plating of the ship and in the case of landing on an underwater obstacle, which has the same width; this obstacle will be damaged rather than the vessel's hull. For example, the calculations of possible length of the damage for vessel with length 60 m, at the relative speeds 1.6 and 3, with different hull's materials (steel, aluminium alloy, wood) were made, figures 3 and 4.

$Fr_V = 1.6$		Material		
		steel	alum. alloy	wood
The athwartships girth of damage is 7 m	m	0,8	1,1	2,1
	$i = \frac{L_d}{L}$	0,01	0,02	0,04
The athwartships girth of damage is $0,2v^{1/3}$ m	m	1,6	2,2	4,2
	$i = \frac{L_d}{L}$	0,03	0,04	0,07
The athwartships girth of damage is 0,01 m	m	21,7	29,1	56,1
	$i = \frac{L_d}{L}$	0,36	0,48	0,94

Figure 3. The length of the damage,

$$Fr_V = \frac{v}{\sqrt{g^3 \sqrt{V}}} = 1.6 .$$

$Fr_V = 3$		Material		
		steel	alum. alloy	wood
The athwartships girth of damage is 7 m	m	1,53	2,1	4,0
	$i = \frac{L_d}{L}$	0,03	0,03	0,07
The athwartships girth of damage is $0,2v^{1/3}$ m	m	3,0	4,1	7,9
	$i = \frac{L_d}{L}$	0,05	0,07	0,13
The athwartships girth of damage is 0,01 m	m	40,6	54,2	60
	$i = \frac{L_d}{L}$	0,68	0,9	1,0

Figure 4. The length of the damage,

$$Fr_V = \frac{v}{\sqrt{g^3 \sqrt{V}}} = 3 .$$

The formula (3) can be used for small high speed vessels, but is possible to use this formula to other types of ships.

4. CONCLUSIONS

The length of damage significantly depends on the hull's material and the width of the damage. For a high speed vessel collision with an underwater object is the most probable. The formula for calculating the length of the possible damage, that takes into account data on the material, the thickness of the plating and the width of the damage, can give more accurate data on the extent of the damage. Until now, such a differentiated method for the determination of the extent of the ship's hull damage have not been used.

5. REFERENCES

- “International Code of Safety for High-Speed Craft, 1994” International Maritime Organisation, London.
- Kanifolskyi O.O. The term "high-speed small craft of the coastal navigation". Bulletin of the Odessa National Maritime University. - Odessa: ONMU, 2010. - № 29. - P. 17-25
- Aleksandrov M.N. Safety of life at sea. – L.: Shipbuilding, 1983 – 208 p.
- Hovgaard W. Structural design of warship. – M., 1947 – 367 p.
- Volkov B.N. The study of the flooding of the ships, with the help of the theory of probability. L.: Shipbuilding, 1963.
- Cerup Simonsen. Det Norske Veritas “Raking Damage to High Speed Craft: Proposal for the High Speed Code”. Conference RINA “High speed craft”, 2004.
- “International Code of Safety for High-Speed Craft, 2000” International Maritime Organisation, London.
- Minorsky V.U. Eine Studie über Schiffscollisionen mit Bezug auf schiffbauliche Schutzmaßnahmen für Kernenergieantriebsanlagen /



V. U. Minorsky // Schiff und Hafen.- 1960.-
№2.- P. 21.

MSC 71/7/1. Revision of the HSC Code. -3 p.

Germanischer Lloyd. High Speed Craft. Rules
for Classification and Construction. -
Humburg: Gebrüder Braasch, 1996.-300 p.

This page is intentionally left blank



Parametric Rolling of the Tumblehome Hull using CFD

Alistair Galbraith, *University of Strathclyde*, alistair.galbraith.2013@uni.strath.ac.uk

Evangelos Boulougouris, *University of Strathclyde*, evangelos.boulougouris@strath.ac.uk

ABSTRACT

Parametric rolling is one of the five failure modes introduced by the draft amendments to IMO's 2008 IS Code. The aim of this paper is to study the use of CFD for the detection of parametric rolling. The ONR Tumblehome model 5613 was utilised and the simulation was set up using an overset mesh to allow motions to all 6 degrees of freedom. The results were validated against results presented from previous research. A number of different simulations were run and the results are presented and discussed herein.

Keywords: *parametric rolling, tumblehome hull, computational fluid dynamics*

1. INTRODUCTION

The tumblehome hulls main feature is the inward sloping freeboard. This is where the ships beam is wider at the waterline and becomes narrower towards the deck. This is in contrast to conventional flared and wall-sided hull designs.

The design was used heavily in warship design for the French and Russian navies in the early 20th century, the most notable being the Russian cruiser Aurora. However due to the hulls disadvantage in stability compared to other vessels, the hull design was eventually discontinued from mainstream vessels.

However with recent developments and a greater knowledge of ship stability and behaviour in certain sea environments, the Tumblehome Hull has returned to development in the form of a Naval Combatant.

The main reason for its return to service is due to its stealth capability and its wave-piercing bow. Though there has been a huge development of ship behaviour in different sea-types, for stability it has been noted that the Tumblehome is still at a disadvantage (Hashimoto, 2009).

2. BACKGROUND

2.1 Stability Issues

As the Tumblehome hull heels over, the waterplane area decreases resulting in the metacentric height decreasing. Therefore, though the GZ curve increases initially with heel angle, it very quickly begins to decrease reaching the angle of vanishing stability. Additionally with a lower metacentric height, the righting arm will be smaller, taking it longer for the hull to recover to its upright position (Hashimoto, 2009).

2.2 Parametric Rolling

A symmetrical ship moving in head seas is expected to have pitch, heave and surge motions according to the linear theory, but no roll. However due to non-linear effects, roll motions can occur at certain encounter frequencies due to a combination of external and internal factors. This phenomenon is called "auto parametrically excited motion" or "parametric motion" in short to indicate that the motion is the result the periodic variation of certain parameters of the oscillating system



rather than the outcome of a time-varying external force (France, 2001). Once this roll motion has commenced, it can grow to large amplitudes (see Figure 1) and in extreme cases, may result in the loss of the vessel.

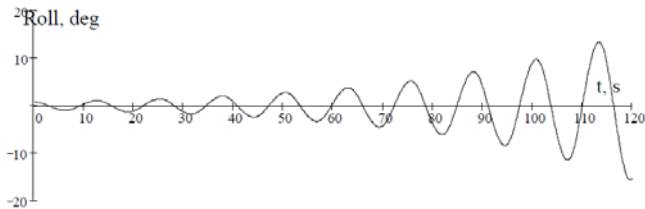


Figure 1. Parametric roll resonance (ABS, 2004)

Due to the restoring force of the tumblehome being smaller than comparable ships, it is therefore more susceptible to parametric rolling.

2.3 Criteria for Parametric Rolling

For Parametric Rolling to occur, the following conditions should be satisfied with the ship moving in pure head or following long-crested seas (France, 2001):

- The wave encounter period is approximately one-half the ships natural roll period
- The wave length is in the order of ship's length (0.8 to 2 times of LBP)
- The wave damping is below a certain threshold
- The wave height is above a certain threshold level

As the wave moves along the ship, the mean GM is smaller than conventional hullforms. Due to the relationship $\omega_n = \sqrt{(\Delta * GM / (I + A))}$, the effective natural frequency for parametric rolling to occur is smaller. Therefore the ship will encounter parametric rolling at low forward speeds. This is important, as roll damping is smaller at slower forward speeds, therefore the best course of action to avoid the phenomenon is to increase speed (McCue, 2007).

The IMO Second Generation Intact Stability criteria are developed in order to take into account stability failures that are not sufficiently covered in the 2008 Intact Stability code. The second generation criteria assess the vulnerability of the ship to parametric rolling as well as pure loss of stability on the wave crest, excessive accelerations, dead ship condition and Surfing and broaching (Kruger, 2013).

There are various levels to investigate if a ship is vulnerable to parametric rolling resulting in a loss of stability. The Level 1 criterion is a conservative approach and involves a relatively simple calculation that the ship has to meet to show it is not vulnerable to the parametric rolling stability failure mode. It involves the variation of GM as the wave moves along the ship. If the criterion is not met in level 1, the ship in question should then be subjected to a more detailed assessment where it is required to meet the criteria for Level 2 criteria (Liu, 2014). If the ship fails to satisfy these criteria, then methods for the direct assessment of the stability of the vessels should be applied (Level 3).

2.4 Computer Fluid Dynamics (CFD)

Computational Fluid Dynamics approach can be a very useful tool for the study of the parametric rolling susceptibility of ships and a valid direct stability assessment (Level 3) method (Hosseini, 2011; IMO-SDC 2/INF.7, 2014). The software Star-CCM+ (CD-Adapco, 2015) was the tool used in the present study. The domain definition is shown in Figure 2.

It has had a positive response and is accredited for its ease of use by clients from across the industry. It has a user-friendly interface due to the automation of many functions and has many features that enable the program to tackle problems with complex shapes, such as the Tumblehome hull with its inward shaped bow.



It is capable of modelling Eulerian Multiphase, required for the interaction of the fluids air and water due to waves. It is also capable of simulating fifth order waves that are more representative of a real-life wave-pattern (CD-Adapco, 2015).

2.5 Overset mesh

In order to allow the ship to roll while encountering head waves, an overset mesh was required (see Figure 2).

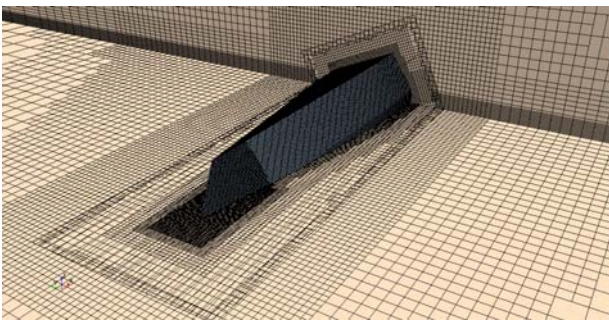


Figure 2. Rotated Overset Mesh

The domain (see Figure 3), where the simulation would take place was split in two; the fixed background was fixed and contained the freesurface and the overset containing the ship and was able to move as required in 6DOF. Both these meshes were able to interact allowing realistic waves and ship movements.

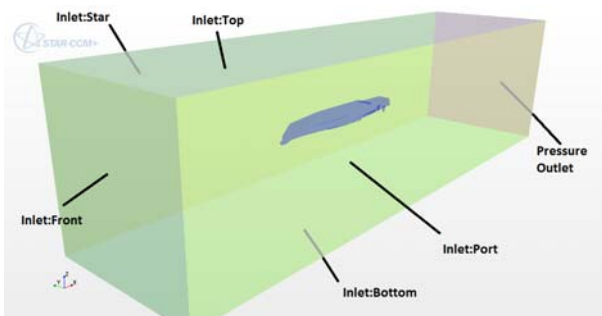


Figure 3. Domain definition

2.6 ONR Tumblehome model

The model used for the study was the ONR Tumblehome Hull model 5613 that was

developed by Naval Surface Warfare Center, Carderock Division (NSWCCD) for ONR. (Bishop, 2005, Bassler, 2007)

The model used was based off the hull DDG-51, which is approximately half the size of the DDG-1000 Zumwalt Class. The tumblehome freeboard is angled inward 10 degrees from the vertical (Bishop, 2005).

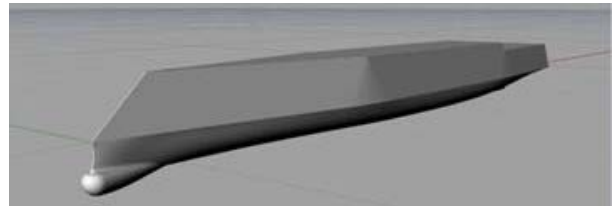


Figure 4. ONR Tumblehome Model without Bilge Keels

The dimensions used for the ONR Tumblehome hull are given in Table 1. For the

Table 1. Main Particulars of ship and model

	Full-Scale (15C, SW)		1/32 Model-Scale (20C, FW)	
	m	ft	cm	in
Lpp	154	505	481	15.8 ft (189.6 in)
Beam	18.8	61.7	58.8	1.93 ft (23.2 in)
L/B	8.2	8.2	8.2	8.2
Max. Depth	14.5	47.6	45.3	1.49 ft (17.8 in)
Max. Freeboard	9.00	29.5	28.1	0.92 ft (11.1 in)
Draft	5.50	18.0	17.2	0.56 ft (6.77 in)
Displacement	8790 tonnes	8650 LT	261 kg	575 Lbs
LCB (aft of FP)	79.6	261	249	8.16 ft
VCB (above BL)	3.26	10.7	10.2	0.33 ft (4.01 in)
KM _T	9.74	32.0	30.4	1.00 ft (12.0 in)

simulation, the 1/32 model scale was utilised.

For the numerical simulations, the bilge keels were removed as can be seen in Figure 4. This was because they would produce a damping force that would prevent the occurrence of parametric rolling and it will also increase the meshing requirements around them.

3. METHODOLOGY

3.1 Initial assessment

The full scale model was imported into the Maxsurf Stability software, (Bentley, 2014) where the position of the centre of gravity was



inputted along with the parameters of the wave. The program was used in order to calculate the change in GM as the wave passes by the hullform. This change in GM (ΔGM) was used for the calculation of the Level 1 Vulnerability Criteria for Parametric Rolling. A ship was considered not to be vulnerable to the parametric rolling stability failure mode if (IMO SDC 2/WP.4, 2014):

$$(\Delta GM)/GM \leq R_{pr} \quad (1)$$

The result was $(\Delta GM)/GM=0.37$ and $R_{pr}=0.17$, demonstrating the tumblehome hull without its bilge keels is failing the first criteria, making that the ship vulnerable to parametric rolling.

3.2 Simulation Setup

The simulation was run using an allocated 36 cores over two cycles taking approximately 48.3 hrs for a simulation time of 70 seconds. Therefore 1738.8 CPU hrs were required with each of the 35,000 iterations taking 2.98 minutes per iteration to complete. The ARCHIE-WeSt state-of-the art High Performance Computer was used for the runs (ARCHIE-WeSt, 2015) The hardware used includes Dell C6100 servers with Dual Intel Xeon X5650 2.66 GHz CPU's (6 cores each), having a RAM of 48 GB, linked by 4xQDR Infiniband Interconnect.

In total about 5 million cells were required to build up the simulation with 1.8 million cells required for the background domain and 2.9 million cells for the overset mesh. The file size was 2GB.

3.3 Wave Conditions and Ship's speed

The conditions used in the simulation were known to result in parametric rolling. They were set up as follows; the full scale wave encounter frequency was 0.8 rad/s, 4.6 rad/s in model scale. The waveheight in full scale of was 7.5m and 0.234m in model scale. The full

scale wavelength was 154m, which resulted in 4.8125m in model scale. Finally, the Froude Number was 0.106.

3.4 Initiating roll

Due to the ship travelling in headwaves, rolling will not occur unless there is an initiating event. Two methods were used to initiate the roll motions of the ship. The first method involved the ship positioned in its upright position with an initial angular velocity of 0.1 rad/s exerted onto the model.

The second method again involved the ship in its upright position but involved a small shift of the transverse centre of gravity by 0.00156m to starboard.

When the model was released within the simulation after 0.5 seconds, both these methods would result in the ship rolling and parametric rolling would commence if the criteria for it to occur were met.

4. PARAMETRIC ROLLING WITH ANGULAR VELOCITY METHOD

4.1 Roll Motion

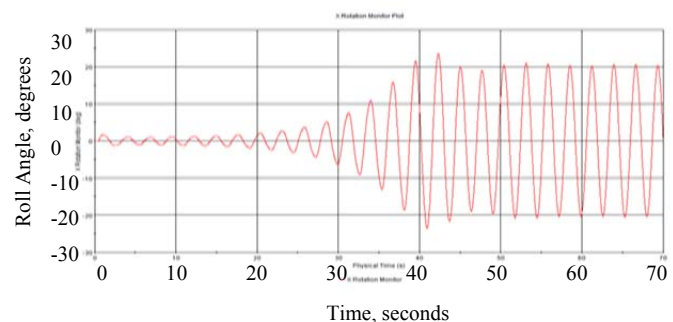


Figure 5. Parametric Rolling Pitch

It was found that the period between oscillations was 2.7s. This is double the wave encounter period of 1.35s, thus demonstrating that the ships motions meets the first criteria of parametric rolling as described in the above literature review (see Figure 5).



The first oscillation reached a peak heel angle of 1.75 degrees due to the initial angular velocity of 0.1 rad/s. The roll motion damped slightly with the following roll amplitude being ± 1 degree. Over the next 20 seconds the roll amplitude for the following 6 oscillations remained relatively steady, increasing gradually over that time to an amplitude of ± 2 degrees. The roll amplitude began to increase substantially with the 9th oscillation plotting a peak roll angle of 2.75 degrees, 10th – 3.5 degrees, 11th – 5.25 degrees, 12th – 7.5 degrees, 13th – 10.8 degrees, 14th – 14.75 degrees, 15th – 21.5 degrees and 16th – 23.5 degrees. For the 17th oscillation onwards, the roll amplitude damped down to an average of 20 degrees where it remained constant for the remainder of the simulation.

This demonstrated that after 45 seconds from the initial angular velocity, the ship encountered steady parametric rolling.

It is noted that with a GM of 1.5m, the vanishing angle of the Tumblehome hull is 64 degrees, therefore these parametric roll motions alone will not result in the loss of the vessel.

4.2 Pitch Motion

The values of pitch are initially large. However this can be explained by the simulation converging and the shock of the model being released as the subsequent pitch angles after 7.5 seconds had an average amplitude of 2.57 degrees (see Figure 6).

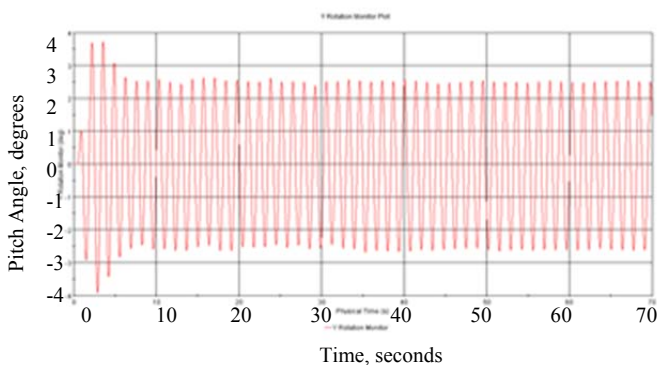


Figure 6. Parametric Rolling - Pitch

It was noted that the average peak pitch was 2.548 degrees while the average trough pitch was -2.587 degrees. Though the difference is 1.5% it does suggest the Tumblehome is following the pattern of diving rather than being lifted over the wave.

The large angles of pitch are coupled with the large angles of roll encountered during the parametric motion.

It is also noted that the pitch period was 1.36s, which is 4.61rad/s or 0.8 rad/s in full scale. This is identical to the encounter period of the wave, suggesting that pitch is dependent on the period of the wave.

4.3 Heave Motion

The heave amplitude of the model was 0.0275m, 0.88m in full scale. The ship heaved around a position of 0 to 0.02m throughout the simulation reaching an average value of 0.02m after 15s before stabilising at 0.01m (see Figure 7).

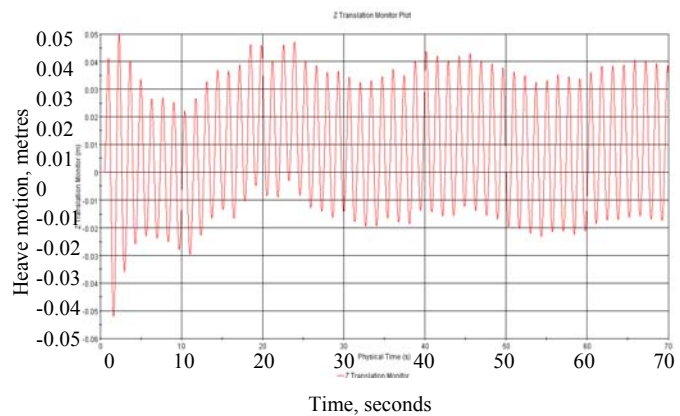


Figure 7. Parametric Rolling - Heave

This motion suggests that the ship is being lifted out the water during the motions of parametric rolling. The heave period was noted to be identical to the pitch and wave encounter period.



5. PARAMETRIC ROLLING WITH DISPLACED TRANSVERSE CENTRE OF GRAVITY

An additional method used to initiate roll in order to promote parametric rolling was moving the centre of gravity off the centreline and to starboard by 0.001486m, 0.0475m in full scale. It would also allow the motions of the ship to be compared with the motions resulted from the previous method.

5.1 Roll

It was again found that the natural roll period of 2.7 seconds was double that of the wave encounter period of 1.35s, confirming that parametric rolling is being detected. (see Figure 8). Parametric rolling became apparent as soon as the ship was released, with the roll amplitude increasing significantly for the first 7 oscillations. After the 8th oscillation, the roll stabilised indicating that the ship had reached its natural roll period with sufficient restoring.

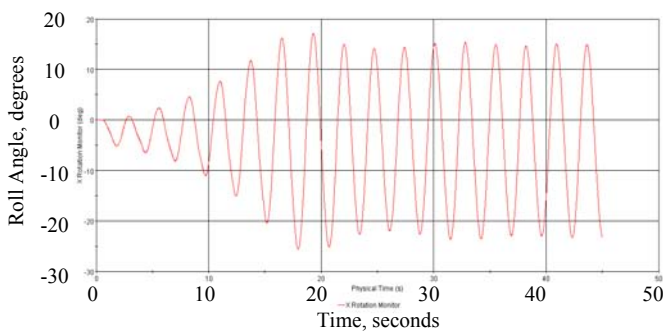


Figure 8. Asymmetric Parametric Motion - Roll

It was noted that steady parametric rolling is detected 20 seconds quicker in this method with the mass off the centreline than compared to the method with the mass on the centreline and angular velocity used to initiate roll.

The first oscillation rolled around the heel angle of -2.5 degrees and had an amplitude of 2.93deg. This amplitude increased to 4.43deg for the 2nd oscillation, 6.73 degrees - 3rd, 9.27 degrees - 4th, 13.36 degrees - 5th, 18.29 degrees - 6th and 21.35 degrees 7th oscillation.

For the 8th oscillation the roll amplitude decreased to 20.06 degrees and then 18.37 degrees where it remained for the continuation of the simulation.

It was noted that the asymmetry of the roll increased from around -2.27 degrees to an average of -4.3 degrees when the rolling became constant.

The Angular Velocity of roll varies between 9 and -7 rads/s. As the roll velocity is at its maximum, the ship is at its upright position. When the velocity is at 0, the ship is at its maximum heeled angles.

5.2 Pitch

The values of pitch are initially large however this could be put down to the simulation converging and the shock of the model being released as the subsequent pitch angles after 7.5 seconds had an average amplitude of 2.57 degrees (see Figure 9).

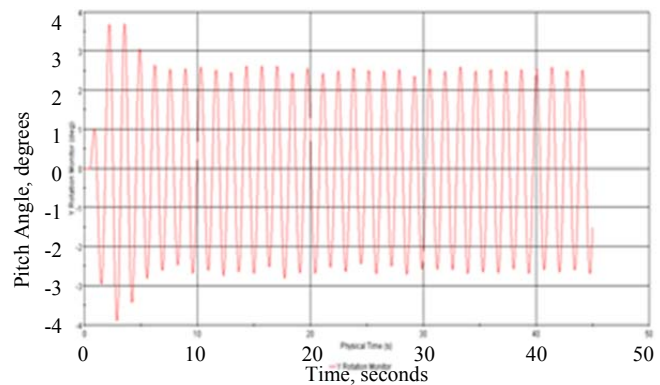


Figure 9. Asymmetric Parametric Motion - Pitch

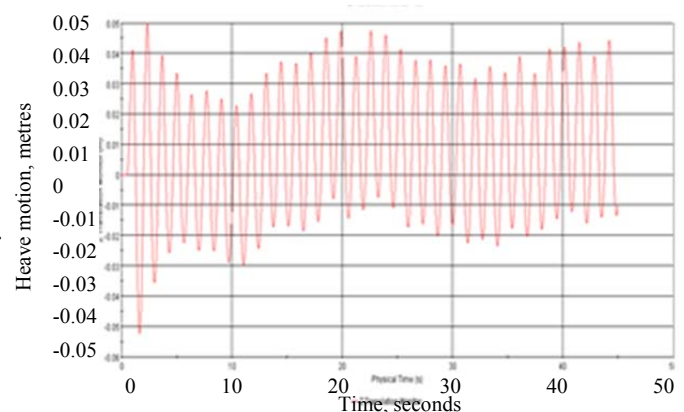


Figure 10. Asymmetric Parametric Motion - Heave



It was noted that the average peak pitch was 2.548 degrees while average trough pitch is -2.587 degrees. Though the difference is 1.5% it does suggest the Tumblehome is again following the pattern of diving rather than being lifted over the wave. The pitch period was noted to be 1.36s, which is 4.61rad/s.

5.3 Heave

The heave amplitude follows the same small values as the previous simulation and is again coupled with pitch. It is also noted that the heave motions are once more oscillating around a moving average that varies between -0.005m and 0.015m again showing that the ship is lifted out of the water (see Figure 10).

5.4 Comparison with Angular Velocity Method

It is noted that the motions of pitch and heave are very similar, regardless to the method used to initiate the roll. It was noted that in the mass off centre method, the parametric rolling was detected 20 seconds sooner, with the amplitude being slightly smaller at 18.37 degrees instead of the 20 degrees. Additionally with the mass off centre, the roll was subsequently asymmetric.

6. INCREASED SHIP SPEED

To investigate the change in parametric rolling and related motions, the ships velocity was increased to a Froude number of 0.145579, 11 knots in full scale. The wave encounter frequency was subsequently increased to 0.87 rad/s in full scale and 4.97 rad/s in model scale. The roll in this simulation was initiated with the mass off centre method.

6.1 Roll

The average period between oscillations was noted through tabulation to be 2.52 seconds,

double the wave encounter period of 1.265s again demonstrating that the ship motion is meeting the criteria of parametric rolling. (see Figure 11)

The first oscillation rolled around the angle of -2.6 degrees and had an amplitude of 2.26 degrees. This amplitude increased to 2.51 degrees for the 2nd oscillation, 2.92 degrees - 3rd, 3.64 degrees - 4th and 4.69 degrees - 5th oscillation. Though the simulation was only run for 15 seconds, it was apparent that the increase in amplitude was significantly smaller with the amplitude only increasing by 107.5% by the 5th oscillation compared to 355.97% when the ship was travelling at a slower speed.

This corresponds with the literature, indicating that the faster the ship speed, the intensity of parametric rolling is reduced. Therefore, a solution to recover from the motion is to increase the speed of the vessel.

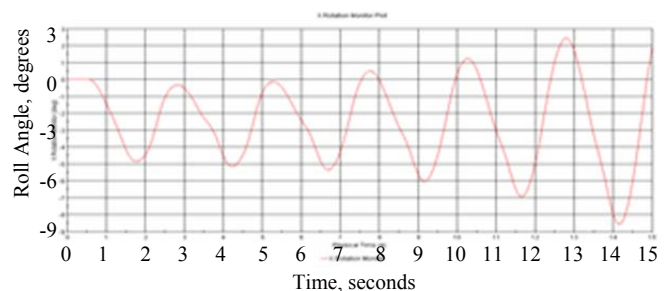


Figure 11. Parametric Motion, Increased Velocity, Roll

It was noted that the asymmetry of the roll for the first oscillation was -2.60 degrees. This increased to -2.65 degrees for the 2nd oscillation, but for the following oscillations, the asymmetry decreased progressively to -2.25 degrees.

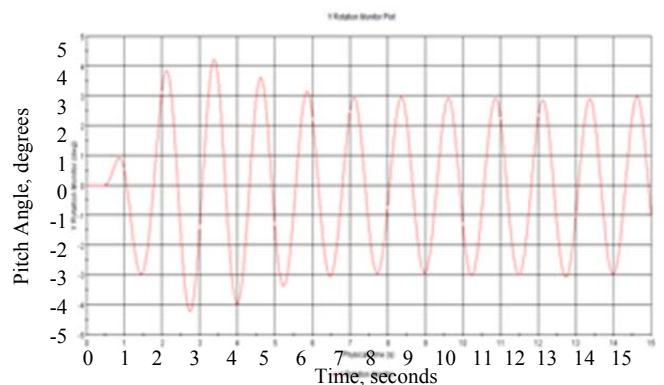


Figure 12. Parametric Motion, Increased Velocity Pitching



6.2 Pitch

It was noted that the pitch amplitude is 15.95% larger than the previous simulation with an amplitude of 2.98 degrees. This suggests that at faster velocities the tumblehome encounters its natural pitch period (see Figure 12).

6.3 Heave

The heave motion amplitude was found to be 0.037m, 1.184m in full scale. This is an increase in amplitude of 48% compared to parametric rolling at a lower speed.

It was noted that the heave motions are oscillating around a moving average that varies between 0.004m and -0.004m for the first 12s before increasing significantly (see Figure 13).

It was noted that though the coupled motion of pitch is larger due to the non-linear motions of roll being reduced, the heave motion is also larger.

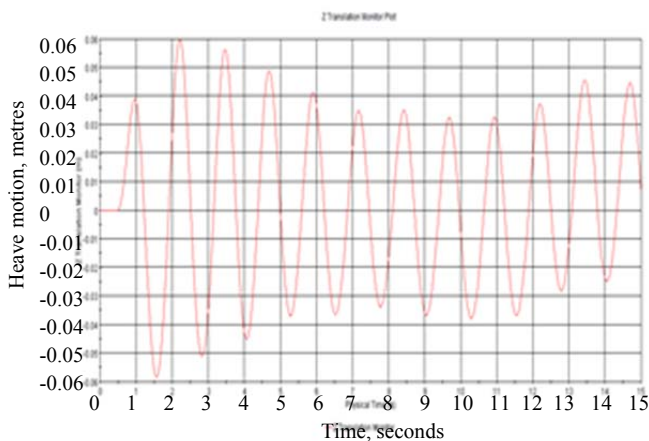


Figure 13. Parametric Motion, Increased Velocity Heaving

7. CONCLUSION

The aims of the study were met whereby using the CFD application Star-CCM+, the non-linear motion of parametric rolling was detected and analysed.

The simulation to find the motion was set-up from scratch using the ONR Tumblehome Model with the bilge keels removed and required an Overset Mesh to allow the essential movements of pitch, heave and roll. The GM for these simulations was set to 1.5m or 0.047m in model scale.

Parametric Rolling was detected at the model scale wave encounter frequency of 4.6 rad/s, Froude number 0.105 and a wave height of 0.234m. It took approximately 45 seconds for steady rolling to occur with an amplitude of 20 degrees. This motion was accompanied with high pitch angles and small heave motions.

It was found that steady parametric rolling occurred 20 seconds quicker when the centre of mass was displaced slightly to starboard than when the mass is above the centreline of the ship, though the roll was asymmetric and the amplitude was smaller at 18.37 degrees.

It was confirmed that when the ship's velocity was increased from 8kn to 11kn, the intensity of parametric rolling decreased substantially with the roll amplitude increasing at a slower rate. This corresponds with other research involving parametric rolling, where a means of avoiding the non-linear phenomenon is to increase speed.

The study has proven that CFD can be a valuable tool for the investigation of this interesting and complex phenomenon and may assist the designers to develop ships "immune" to the risk of parametric rolling.

8. ACKNOWLEDGEMENTS

Results were obtained using the EPSRC funded ARCHIE-WeSt High Performance Computer (www.archie-west.ac.uk). EPSRC grant no. EP/K000586/1.



9. REFERENCES

- ABS, 2004 - "Assessment of Parametric Roll Resonance in the Design of Container Carriers", American Bureau of Shipping September 2004 pp. 2-3.
- ARCHIE-WeSt, 2015, <http://www.archie-west.ac.uk/>.
- Bassler C., Peters A., Belknap W. and McCue L., 2007, "Dynamic Stability of Flared and Tumblehome Hull Forms in Waves", 9th International Ship Stability Workshop, Hamburg, Germany, August 2007, pp. 2-13.
- Bentley, Maxsurf, 2014, <http://www.bentley.com/en-US/>.
- Bishop R.C., Belknap W., Turner C., Simon B. and Joseph H. Kim, 2005, "Parametric Investigation on the Influence of GM, Roll Damping, and Above-Water Form on the Roll Response of Model 5613", Naval Surface Warfare Center NSWCCD-50-TR-2005/027, Hydromechanics Department Report, August 2005.
- CD-Adapco, 2015, Star-CCM+, Website - <http://www.cd-adapco.com/products/star-ccm%C2%AE>
- France W.N., Levadou M., Treacle T.W., Paulling J.R., Michel R.K. and Moore C., 2001, "An Investigation of Head-Sea Parametric Rolling and its Influence on Container Lashing Systems", SNAME Annual Meeting 2001 Presentation, pp. 1-24.
- Hashimoto H., 2009, "Pure loss of Stability of a Tumblehome Hull in Following Seas", Proc. of the 9th Int. Offshore and Polar Engineering Conference (ISOPE 09), 21-26 July, Osaka, Japan, Osaka, Japan, 2009, pp. 626-631.
- Hosseini H.S., Carrica P., Stern F., Umeda N., Hashimoto H., Yamamura S. and Mastuda A., 2011, "CFD, system-based and EFD study of ship dynamic instability events: Surf-riding, periodic motion, and broaching", Ocean Engineering, Volume 38 (1), 2011, pp. 88-110
- IMO Sub-Committee on Ship Design and Construction (SDC), 2014, "Development of Second Generation Intact Stability Criteria - Research on CFD approach application in direct stability assessment criteria of parametric rolling", SDC 2/INF.7, December 2014.
- IMO Sub-Committee on Ship Design and Construction (SDC), 2014, "Draft amendments to Part B of the IS Code with regard to vulnerability criteria of levels 1 and 2 for the parametric rolling failure model", SDC 2/WP.4 Annex 2, December 2014.
- Kruger S., Hatecke H., Billerbeck H., Bruns A. and Kluwe F., 2013, "Investigation of the 2nd Generation of Intact Stability Criteria for Ships Vulnerable to Parametric Rolling in Following Seas" Hamburg University of Technology, Flensburger Schiffbau-Gesellschaft pp. 1-2.
- Liu H., Turan O. and Boulougouris E., 2014, "Sample Calculation on Vulnerability Criteria for Parametric Roll", Monday, 25 August 2014
- McCue L.S., Campbell B.L. and Belknap W.F., 2007, "On the Parametric Resonance of Tumblehome Hullforms in a Longitudinal Seaway", 2007, American Society of Naval Engineers pp. 38-43.

This page is intentionally left blank

Session 8.3 – DYNAMIC STABILITY

Influence of Rudder Emersion on Ship Broaching Prediction

Offshore Inclining Test

Lifecycle Aspects of Stability – Beyond Pure Technical Thinking

**An Experimental Study on the Characteristics of Vertical Acceleration
on Small High Speed Craft in Head Waves**

This page is intentionally left blank



Influence of Rudder Emersion on Ship Broaching Prediction

Liwei Yu, *School of Naval Architecture and Ocean Engineering, Shanghai Jiao Tong University*

(SJTU), liwyu55@sjtu.edu.cn

Ning Ma*, *State Key Laboratory of Ocean Engineering, SJTU*, ningma@sjtu.edu.cn

Xiechong Gu, *State Key Laboratory of Ocean Engineering, SJTU*, xcgu@sjtu.edu.cn

ABSTRACT

Broaching is recognized as one of the major causes of ship capsizing in adverse quartering seas. Loss of rudder effectiveness due to rudder emersion is believed to be very important for broaching. Therefore in the paper, a 6-DOF unified model considering sea-keeping motion at low frequency, manoeuvring motion and rudder propeller hydrodynamics is developed for the numerical analysis of broaching of the ITTC ship A2. A modified model of rudder is proposed to account for the effect of wave orbital velocity and the variation of rudder area and aspect ratio. The modified model of rudder is compared with the original model. Then numerical simulations are conducted in different ship speeds and wave heights, and the influence of rudder emersion on broaching motion is investigated. Results show that rudder immersed depth decreases dramatically and rudder inflow velocity is reduced by wave orbital velocity when surf-riding happens. It is also concluded that rudder emersion is the key factor for the emergence of broaching motion. Moreover the influence of rudder emersion seems to take effect only when Froude number is high.

Keywords: *Broaching, Surf-riding, Unified model, Rudder emersion*

1. INTRODUCTION

Ships have much higher possibility of capsizing when sailing in adverse following and quartering seas comparing to head sea condition. Broaching is one of the major causes of capsizing in following and quartering seas. When sailing in astern seas, ship may encounter large wave induced yaw moment and rudder may lose its course-keeping capability. These will cause ship heading to change suddenly and broaching occurs. Broaching often occurs on small ship and naval vessel with high speed. According to IMO Sub-Committee on Ship Design and Construction (SDC), ship is considered to be vulnerable to broaching if $F_n > 0.3$ or $L_{BP} < 200\text{m}$ (IMO SDC, 2014).

Since the pioneering work of Grim (1951) based on analytical formula, researches on surf-riding and broaching are conducted through theoretical analyses (Umeda, 1999; Makov, 1969; Spyrou, 1996), numerical simulations (Umeda & Hamamoto, 2000; Umeda & Hashimoto, 2002; Yu, Ma, & Gu, 2014) and model experiments (Umeda et al., 1999). As an output of these continuous efforts, the amendments to Part B of the 2008 IS code to assess broaching are proposed recently in IMO (IMO SDC, 2014). However as a strongly nonlinear phenomenon, broaching is influenced by various factors and detailed investigation needs to be conducted.



Loss of rudder effectiveness due to rudder and propeller emersion is believed to be an important factor for the occurrence of broaching. Rudder and propeller emersion is observed in free running model experiment when broaching happens (Araki et al., 2012). Renilson (1982) conducted numerical and experimental study on broaching for ship with standard rudder and rudder with 1/2 depth. Rudder force derivatives in wave were considered in a simplified way. Results showed that loss in rudder effectiveness caused by emersion had an important influence on broaching. Furthermore, Umeda & Kohyama (1990) pointed out that propeller thrust coefficient dropped dramatically when surf-riding happened due to high advance coefficients in wave. This could reduce rudder inflow velocity induced by propeller, in turn weakening rudder force. They also mentioned the possible influence of wave orbital velocity and rudder emersion on surf-riding and broaching. Tigkas & Spyrou (2012) conducted steady-state analysis and bifurcation analysis with a 6 DOF model. In the model, loss of rudder effectiveness was considered by changing rudder area and aspect ratio according to its instantaneous draught. However the influence of rudder on broaching was not further discussed in the paper. Araki et al. (2012) proposed a 6-DOF model with a full consideration of rudder and propeller emersion for the broaching prediction of a tumblehome vessel. In the model the unexpected yaw moment caused by the emersion of twin propellers was also taken into account. Through comparison with experiment and 4-DOF numerical simulation results, it showed that rudder and propeller emersions could be a crucial factor for broaching.

However improvements on the modeling of rudder and propeller are still needed for a better understanding of rudder's influence on broaching. Critical factors such as wave orbital velocity, rudder inflow velocity, propeller and rudder wake near free surface and vortex shedding at rudder edge should be considered in the numerical model. Although very few

data is available for loss of rudder effectiveness caused by rudder and propeller emersion, one can be inspired from researches on reduction of rudder performance in ship ballast condition. Experiments show that rudder force coefficients are reduced due to air bubble and wave making on free surface when rudder is out of water (Lu et al., 1981). Flow straightening coefficient and rudder wake differ significantly with different trims (Liu, Huang, & Deng, 2010) while the hull-rudder interaction coefficients differ slightly for different drafts and trims (Nagarajan et al., 2008).

Therefore in order to investigate rudder's influence on broaching, the 6-DOF weakly nonlinear model proposed by Yu, Ma, & Gu (2012) is adopted for the simulation of broaching motion of the ITTC ship A2 in following and quartering seas. The model couples the manoeuvring and seakeeping motion based on the unified theory. Additionally, modelling of rudder and propeller is modified to account for the effect of wave orbital velocity, change of rudder area and aspect ratio and reduction of rudder inflow velocity. Through the analysis of the numerical results, the reduction of rudder steering capability in adverse following and quartering seas and its influence on broaching motion is investigated.

2. MATHEMATICAL MODEL

In the present numerical model, a combined seakeeping and manoeuvring analysis is carried out based on the unified theory. The modelling of rudder is modified to take the effect of rudder emersion into account.

2.1 6-DOF Weakly Nonlinear Model

In the unified model, the manoeuvring motion is simulated using a 3-DOF surge-sway-yaw MMG model:



$$\begin{bmatrix} m - \bar{X}_U & 0 & 0 \\ 0 & -m + \bar{Y}_V & -m x_G + \bar{Y}_R \\ 0 & -m x_G + \bar{N}_V & -I_z + \bar{N}_R \end{bmatrix} \begin{bmatrix} \dot{u} \\ \dot{v} \\ \dot{R} \end{bmatrix} + \begin{bmatrix} 0 & -mR & 0 \\ 0 & \bar{Y}_V & -mU + \bar{Y}_R \\ 0 & \bar{N}_V & -m x_G U + \bar{N}_R \end{bmatrix} \begin{bmatrix} u \\ v \\ R \end{bmatrix} = \begin{bmatrix} \bar{X}_{HO} \\ \bar{Y}_{HO} \\ \bar{N}_{HO} \end{bmatrix} + \begin{bmatrix} \bar{X}_\delta \\ \bar{Y}_\delta \\ \bar{N}_\delta \end{bmatrix} + \begin{bmatrix} -R(U) \\ +(1-t)T(U) \\ 0 \\ 0 \end{bmatrix} \quad (1)$$

where m and I represent the ship mass and moment of inertia. u , v , R denote surge, sway and yaw velocity. $(X_\delta, Y_\delta, N_\delta)$, $R(U)$ and $T(U)$ are defined as rudder force, ship resistance and propeller thrust respectively. t is the propeller thrust deduction factor. (X_{HO}, Y_{HO}, N_{HO}) is higher order hull hydrodynamic force:

$$\begin{aligned} \bar{X}_{HO} &= X_{vv}v^2 + X_{vr}vr + X_{rr}r^2 \\ \bar{Y}_{HO} &= Y_{vvr}v^2r + Y_{vrr}vr^2 + Y_{vvv}v^3 + Y_{rrr}r^3 \\ \bar{N}_{HO} &= N_{vvr}v^2r + N_{vrr}vr^2 + N_{vvv}v^3 + N_{rrr}r^3 \end{aligned} \quad (2)$$

The sea-keeping motion is simulated by a 6-DOF model based on the IRF approach. The equation of motion can be written as:

$$\begin{aligned} \sum_{j=1}^6 \left[(m_{ij} + a_{ij}(\infty)) \dot{v}_j(t) + \int_0^t R_{ij}(t-\tau) v_j(\tau) d\tau + F_i^{res}(t) \right] \\ = F_i^{FK}(t) + F_i^{dif}(t) + (\bar{K}_\delta, \text{when } i=4) \quad (i=1, \dots, 6) \end{aligned} \quad (3)$$

where m_{ij} and $a_{ij}(\infty)$ stand for the ship mass and the infinite-frequency added mass. The nonlinear restoring forces, F-K forces and diffraction forces are denoted as $F_i^{res}(t)$, $F_i^{FK}(t)$, $F_i^{dif}(t)$ respectively.

According to the IRF approach, the radiation and diffraction forces are calculated in frequency domain by the strip theory and transferred into time domain using the retardation function $R_{ij}(\tau)$. The nonlinear restoring and Froude-Kriloff forces are calculated through pressure integration on instantaneous wetted surfaces. The hull and upper deck consist of several NURBS surfaces are demonstrated in Figure 1.

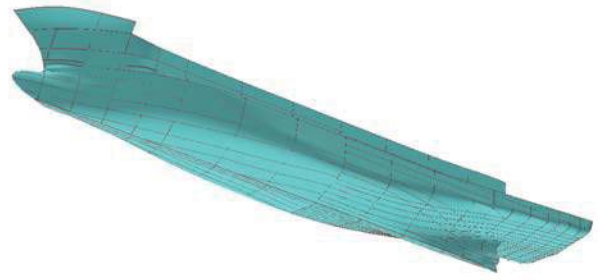


Figure 1 Hull NURBS surface of ITTC ship A2

In the unified model, the manoeuvring and seakeeping models described above are solved in different time scale. The total ship motion is calculated by combining the two motions referring to different coordinate system together:

$$\begin{aligned} [X_T, Y_T, Z_T, \Phi_T, \Theta_T, \Psi_T] = [x^0, y^0, z^0, \phi^0, \theta^0, \psi^0] \\ + \left[\int_0^t U_T dt, \int_0^t V_T dt, \int_0^t W_T dt, \int_0^t P_T dt, \int_0^t Q_T dt, \int_0^t R_T dt \right] \end{aligned} \quad (4)$$

where the subscript T indicates the total motion, and superscript 0 means the initial value for the time $t=0$.

2.2 Modelling of Rudder and Propeller

The rudder forces and propeller thrust are calculated as follows:

$$\begin{cases} \bar{X}_\delta = -0.5(1-t_r)\rho A_R U_R^2 C_N \sin \alpha_R \sin \delta \\ \bar{Y}_\delta = -0.5(1+a_H)\rho A_R U_R^2 C_N \sin \alpha_R \cos \delta \\ \bar{N}_\delta = -0.5(GR_L + a_H x_H)\rho A_R U_R^2 C_N \sin \alpha_R \cos \delta \\ \bar{K}_\delta = -GR\bar{Y}_\delta \end{cases} \quad (5)$$

$$T(U) = \rho K_T D_p^4 n^2$$

where K_δ denotes rudder roll moment. A_R , U_R , GR , GR_L indicate the rudder area, the inflow velocity, the vertical and longitudinal distance between center of gravity and point of rudder force. n , D_p , K_T represent the propeller rotation rate, diameter and thrust coefficient.

In order to account for the effect of rudder emersion, the model for rudder forces and moments need to be modified. Firstly rudder



inflow velocity and propeller advance coefficient are modified to incorporate wave orbital velocity:

$$U_R = \sqrt{(u_r + \bar{u}_w)^2 + v_r^2}$$

$$J_w = \frac{(1 - \omega_p)U \cos \beta + \bar{u}_w}{nD_p} \quad (6)$$

$$K_{T_w} = a_0 + a_1 J_w + a_2 J_w^2$$

where u_r , v_r denote the longitudinal and transversal rudder inflow velocity. ω_p , β denote the propeller wake fraction, and ship drift angle. \bar{u}_w is the longitudinal component of mean value wave orbital velocity around rudder as shown in Figure 2:

$$u_w = C_w k A_w e^{kz} \cos(kx - \omega t) \quad (7)$$

where C_w , A_w , k , ω stand for the wave celerity, wave amplitude, wave number and frequency.

Furthermore, the variation of rudder area A_{Rw} , and aspect ratio λ_w due to rudder emersion are obtained from instantaneous wetted surfaces. The rudder force coefficient C_N is still determined by Fujii's prediction formula (Ogawa & Kasai, 1978):

$$\lambda_w = h_w / b$$

$$C_N = 6.13 \lambda_w / (2.25 + \lambda_w) \quad (8)$$

where b denotes rudder width. h_w is rudder immersed depth which is calculated from the distance between free surface and rudder bottom considering 6-DOF ship motion as shown in Figure 2.

Due to the limitation of present model, the variation of other factors including hull-rudder interaction coefficients, flow straightening coefficient and rudder wake are not yet taken into account.

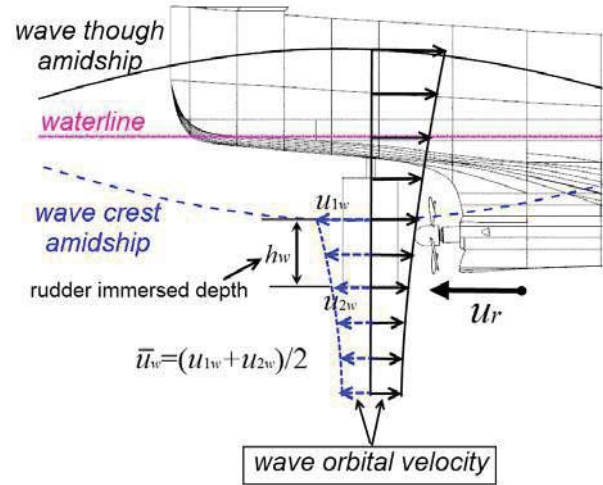


Figure 2 Wave orbital velocity around rudder

3. MODEL VERIFICATION

3.1 Ship Model

The subject ship used for the verification of the weakly nonlinear numerical model accounting for rudder emersion is the ITTC ship A2 fishing vessel (NAOE Osaka University, 2015). Main particulars of the ship and its model are shown in Table 1.

The autopilot system are modeled as follows:

$$T_E \dot{\delta} + \delta = -K_p (\chi - \chi_c) \quad (9)$$

Where the time constant T_E is 0.63s, δ is the rudder angle, $\dot{\delta}$ is rudder rate, χ is the yaw angle, and χ_c is the desired course.

All other data needed for the numerical simulation including hull geometry, hydrodynamic derivatives, rudder and propeller characteristics, roll viscous damping can be found in NAOE Osaka University (2015).



Table 1 Main particulars of ITTC ship A2

Ship		1/15 model
Length between perpendiculars, L_{pp} (m)	34.5	2.3
Breadth, B (m)	7.60	0.507
Depth, D (m)	3.07	0.205
Fore draught, d_f (m)	2.5	0.166
Aft draught, d_a (m)	2.8	0.176
Mean draught, d (m)	2.65	0.186
Block coefficient, C_B	0.597	0.597
Radius of gyration, roll, k_{xx}/L_{pp}	0.108	0.108
Radius of gyration, pitch yaw, k_{yy}/L_{pp} , k_{zz}/L_{pp}	0.302	0.302
Longitudinal position of Buoyancy, L_{CB} (m)	1.31m aft	0.087m aft
Longitudinal position of Floatation, L_{CF} (m)	3.94m aft	0.263m aft
Metacentric height, GM (m)	1.00	0.0667
Natural roll period, T_R (s)	7.4	1.9
Rudder		
Area, A_R (m ²)	3.49	0.0155
Rudder aspect ratio, A	1.84	1.84
Rudder height, h (m)	2.57	0.171

3.2 Validation of rudder modelling

The 6-DOF weakly nonlinear model for the simulation of surf-riding and broaching in astern seas are validated qualitatively based on experiment results of ITTC ship A2 in Yu, Ma, & Gu, (2014). In this paper, the model is further modified based on the method in section 2.2 to account for the effect of rudder emersion. However there is no experimental data for rudder emersion such as rudder immersed depth, wave orbital velocity around rudder and rudder forces and moments. Thus in this paper, the modified model accounting for rudder emersion is only validated through comparison with the original model without rudder emersion. The results of comparison are demonstrated in Figure 3

In Figure 3, (a), (b), (c) and (d) are time history of ship yaw, roll, pitch and heave

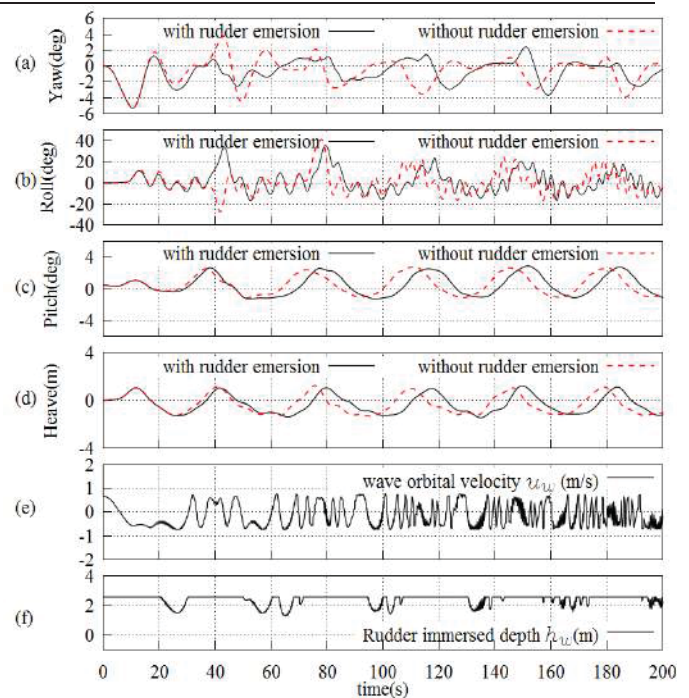


Figure 3 Comparison of ship motions between with and without rudder emersion ($H_w=4m$, $\lambda/L_{pp}=1.637$, $Fn=0.40$ and $\chi=-10$ deg)

motion. (e) and (f) are the time history of wave orbital velocity u_w and rudder immersed depth h_w . The dashed line is results for the original model without rudder emersion, while the solid line is results for the modified model with rudder emersion.

From Figure 3, it can be identified that ship is doing periodic motion in astern sea with and without rudder emersion. However the differences on ship motion between with and without rudder emersion can be easily found. This can be explained by the rudder emersion in astern sea. As shown in Figure 3(a)(b)(c), yaw, roll and pitch motion of the two model are almost the same before 20s. While the time is around 20-30s, rudder emersion starts, rudder immersed depth decreases and rudder inflow velocity is reduced by wave orbital velocity as shown in Figure 3(e)(f). At the same time, there is an overshoot on yaw angle for the modified model (solid line) compared to the original model (dashed line) as shown in Figure 3(a). This overshoot proves that rudder emersion can cause loss of rudder effectiveness and steering capability in astern sea.



Therefore through comparison between results of the original model without rudder emersion and the modified model with rudder emersion, the modified model is verified to be able to account for the effect of rudder emersion. Its influence on broaching motion will be investigated in the next chapter.

4. SIMULATION RESULTS

4.1 Calculation Cases

Numerical simulations using the modified 6-DOF weakly nonlinear model accounting for rudder emersion are conducted to investigate the influence of rudder behaviour on broaching motion. The subject ship is ITTC ship A2, and calculation cases including 5 ship speeds and 11 wave heights are shown in Table 2.

Table 2 Cases for numerical simulation

No.	Fn	$V(\text{m/s})$	$H_w(\text{m})$	λ/L_{pp}	χ	$C_{wx}(\text{m/s})$	ω_e
1-#	0.3	5.52	3.6~6	1.637	-30	8.13	0.563
2-#	0.33	6.07	3.6~6	1.637	-30	8.13	0.516
3-#	0.36	6.62	3.6~6	1.637	-10	9.25	0.453
4-#	0.40	7.36	3.6~6	1.637	-10	9.25	0.295
5-#	0.43	7.91	3.6~6	1.637	-10	9.25	0.228

Where “#” denotes numbers for different wave height H_w . Fn stands for Froude number. H_w , λ , χ are wave height, length and angle, ω_e is encounter frequency taking into account the nonlinearity caused by high wave amplitudes (see Eqn.(10), Umeda et al., 1999). V , C_{wx} denotes ship nominal speed and wave celerity in x direction. They satisfy the followings:

$$\begin{aligned} \omega^2 &= gk(1 + k^2 H_w^2 / 4) \\ \lambda &= 2\pi/k, \omega_e = \omega - kU \cos(\chi), U = Fn \sqrt{gL_{pp}}, \\ C_w &= \lambda \sqrt{gk} / 2\pi, C_{wx} = C_w \cos(\chi) \end{aligned} \quad (10)$$

In order to evaluate the influence of rudder emersion, simulations using the original model without rudder emersion with the same cases are also conducted for comparison.

4.2 Result Analysis

The simulation results obtained from the modified model and the original model are demonstrated in Figure 4, 5 and 6. In Figure 4 and 5, results of the case No. 4-5 and 5-4 are shown. The left figure shows the result of the original model, while the right one shows result of the modified model. (a)-(g) represents the time history of yaw & rudder angle, roll angle, pitch & heave, ship velocity, ship relative position in wave, wave orbital velocity around rudder u_w and rudder immersed depth h_w . Ship relative position in wave is the distance of ship centre of buoyancy to wave trough multiplied with wave number k leading to a value within $[0, 2\pi]$.

From Figure 4, it can be found that ship relative position in wave keeps almost constant within the time range 45-85s for the original and modified model. Meanwhile, the pitch angle stays almost unchanged and the ship is accelerated to wave celerity as shown in Figure 4(c) and (d). This indicates that surf-riding occurs for both models. Because ship relative position in wave is constant when surf-riding happens, wave orbital velocity also keeps constant as presented in Figure 4 right (f). Moreover as shown in Figure 4 right (f)(g), for the modified model rudder immersed depth decreases dramatically even to zero and rudder inflow velocity is reduced by wave orbital velocity when surf-riding happens. Thus the rudder effectiveness is significantly reduced and loss its course keeping capability, which are confirmed by the sudden increase of ship yaw angle despite hard turning of rudder to the opposite side as shown in Figure 4 right (a) within the time range 45-85s. Broaching almost happens. However after 85s, ship escapes from surf-riding, rudder retain its steering capability and ship turns back to original course. That is to say, ship motion by the modified model is further categorized as surf-riding and nearly broaching due to the influence of rudder emersion, while ship motion by the original model can only be categorized as surf-riding.

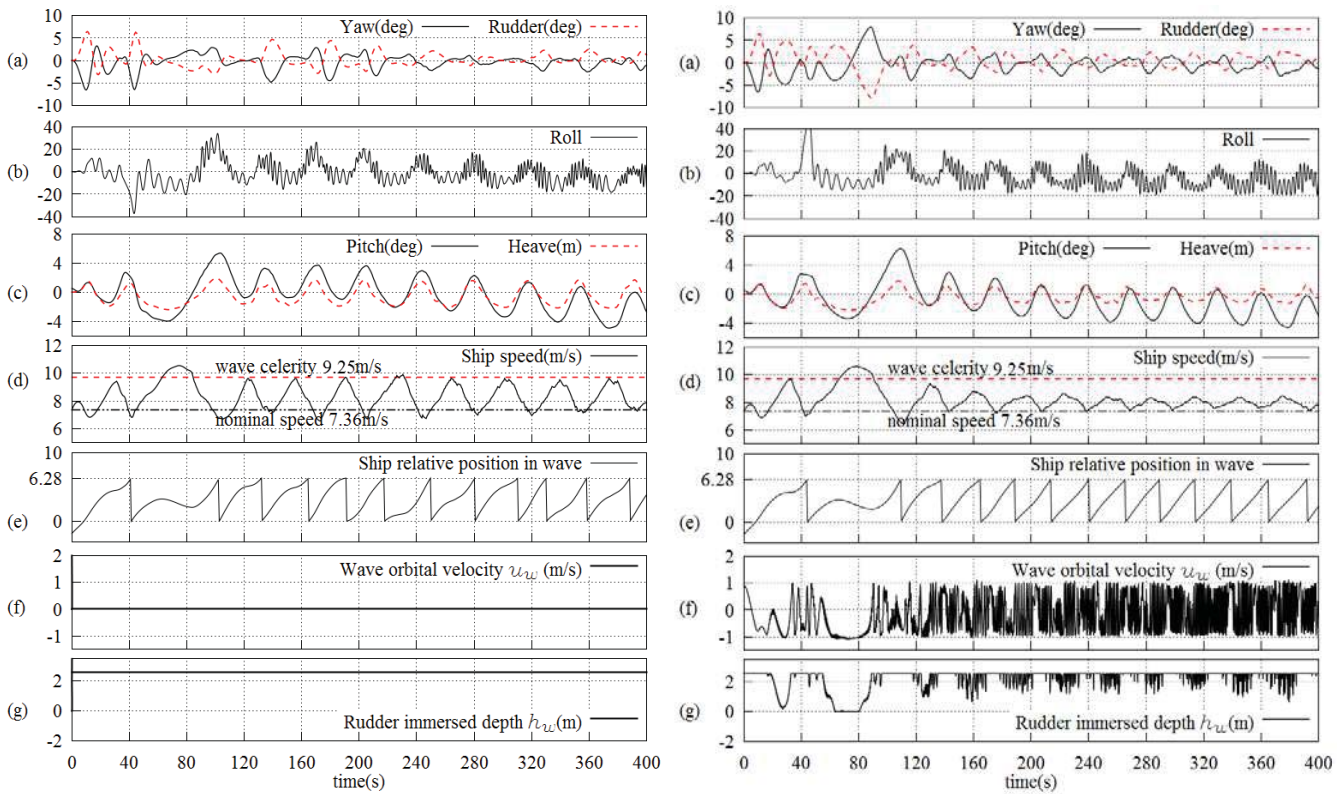


Figure 4 Simulation results of case 4-5 ($H_w=4.6\text{m}$, $\lambda/L_{pp}=1.637$, $Fn=0.40$ and $\chi=-10$ deg)

Left: the original model; Right: the modified model

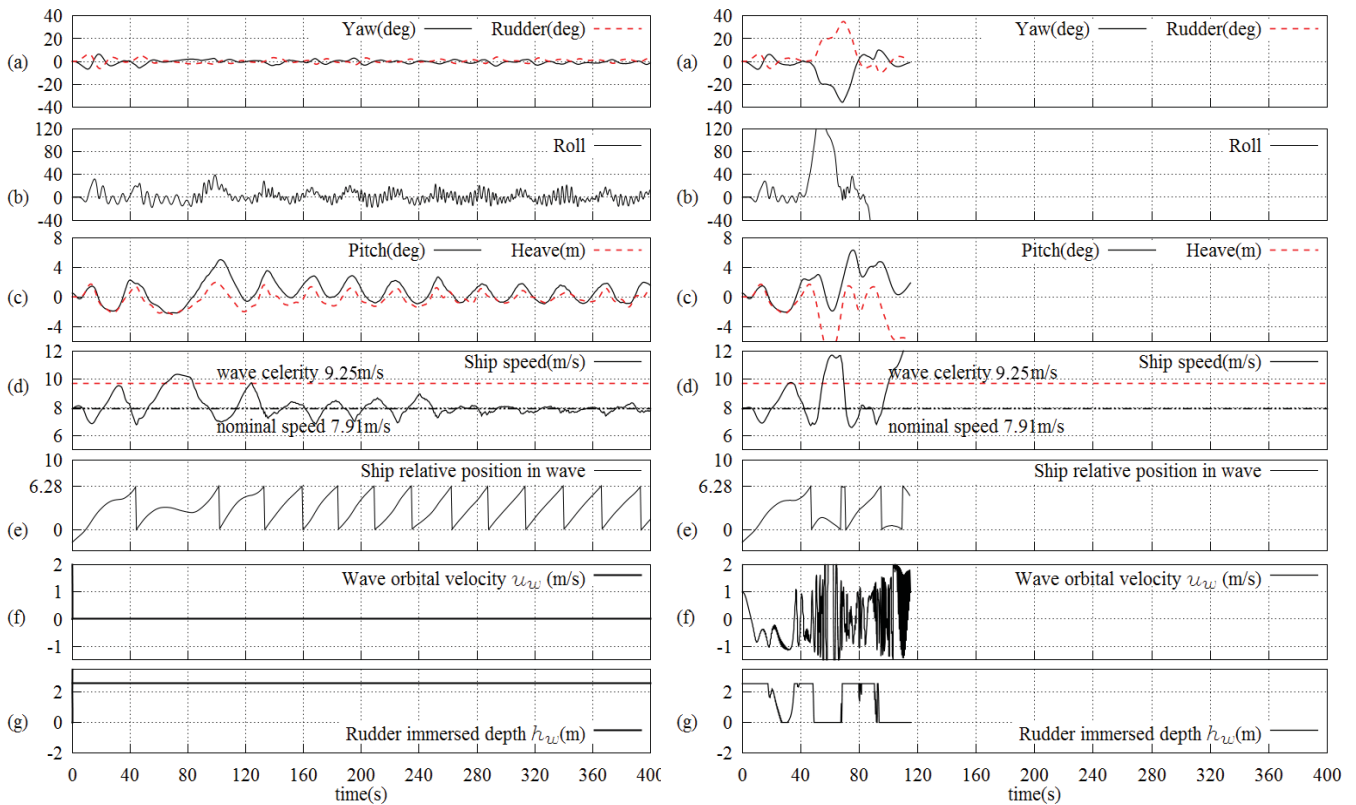


Figure 5 Simulation results of case 5-4 ($H_w=4.8\text{m}$, $\lambda/L_{pp}=1.637$, $Fn=0.43$ and $\chi=-10$ deg)

Left: the original model; Right: the modified model

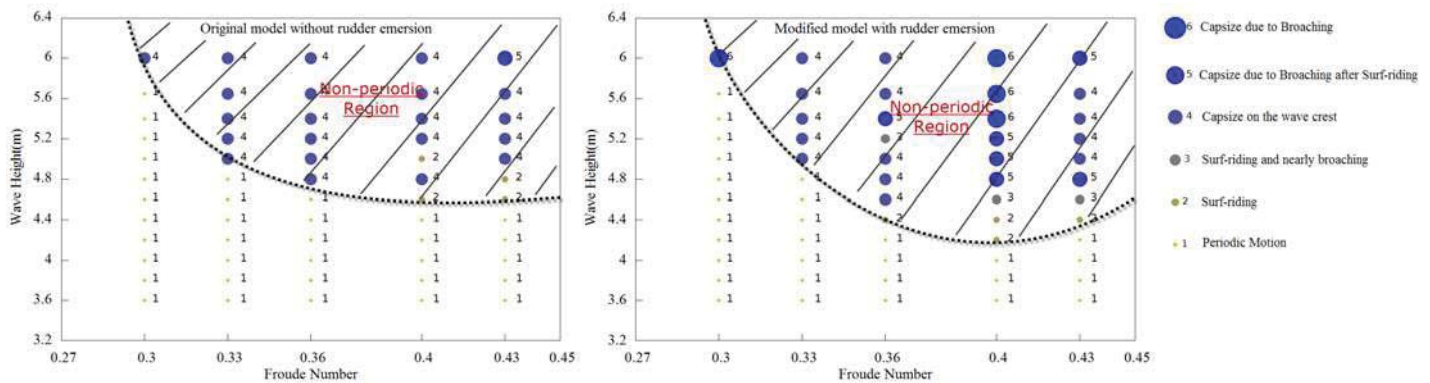


Figure 6 Comparison on simulation results of different cases (Left: the original model; Right: the modified model. The heading angle of cases with $F_n=0.30$ and 0.33 is -30 deg, while the heading angle of cases with $F_n=0.36$, 0.40 and 0.43 is -10 deg which are chosen based on the model experiments of Umeda et al., 1999)

Furthermore in Figure 5, the difference between the original and modified model becomes more obvious. The ship motion by the original model is categorized as surf-riding. Meanwhile, the motion by the modified model is categorized as capsizing due to broaching after surf-riding. As shown in Figure 5 right, ship velocity is accelerated to wave celerity after 50s and rudder lose its steering capability due to emersion. Yaw angle increases suddenly despite max rudder control is applied. Roll angle also starts to raise and eventually causes ship to capsize. Thus capsizing due to broaching after surf-riding has been demonstrated by the modified model. However in Figure 5 left, only surf-riding occurs due to the underestimate on the influence of rudder emersion in the original model.

According to the results presented in Figure 4 and 5, rudder emersion occurs and rudder immersed depth and inflow velocity decrease when surf-riding happens. If these effects are considered in the numerical model, loss of rudder effectiveness can cause sudden increase of yaw angle and even broaching. Therefore rudder emersion is the key factor for the emergence of broaching motion. This conclusion is confirmed by the results shown in Figure 6.

In Figure 6, the results of all the calculation cases including 5 ship speeds and 11 wave heights are presented. The ship motions response are categorized into 6 types: 1 Periodic Motion, 2 Surf-riding, 3 Surf-riding and nearly broaching, 4 Capsizing on the wave crest, 5 Capsizing due to Broaching after Surf-riding and 6 Capsizing due to Broaching. From Figure 6, it is found that for the modified model with rudder emersion, non-periodic motion especially broaching is more likely to be aroused than for the original model. Additionally it is found that the difference between the two models exists mainly in $F_n \geq 0.36$. That is to say, the influence of rudder emersion mainly takes effect in $F_n \geq 0.36$.

5. CONCLUSIONS

In this paper, the 6-DOF weakly nonlinear model proposed by Yu, Ma, & Gu (2012) is adopted for the simulation of broaching motion of the ITTC ship A2 in following and quartering seas. Modelling of rudder and propeller is modified to account for change of rudder area and aspect ratio and reduction of rudder inflow velocity due to wave orbital velocity. Then numerical simulations are conducted in different ship speeds and wave heights. Through analysis of the results, the influence of rudder emersion on broaching



motion is investigated. The following conclusions are drawn:

1. During periodic motion, wave orbital velocity is oscillating, which has no effect on rudder inflow velocity. However when surf-riding happens, wave orbital velocity on rudder keeps almost constant, and the reduction on rudder inflow velocity cannot be neglected.

2. When surf-riding happens, rudder immersed depth decreases dramatically and rudder emersion effect is significant.

3. The loss of rudder effectiveness caused by rudder emersion and wave orbital velocity is the key factor for the emergence of broaching motion in quartering seas.

4. The influence of rudder emersion seems to take effect when Froude number is high and surf-riding is expect to occur.

However modelling of rudder still needs to be verified through experiments. Factors like variation of hull-rudder interaction coefficients, flow straightening coefficient and the thrust reduction due to propeller emersion should also be considered in the model.

6. REFERENCE

- Araki, M., Umeda, N., Hashimoto, H., & Matsuda, A. (2012). An Improvement of Broaching Prediction with a Nonlinear 6 Degrees of Freedom Model. Journal of the Japan Society of Naval Architects and Ocean Engineers, 14, 85–96.
- Grim, O. (1951). Das Schiff in von achtern auflaufender. Schiffbau-Versuchsanstalt.
- IMO SDC1/INF.8 ANNEX 15. (2014). Proposed Amendments to Part B of the 2008 IS CODE to Assess the Vulnerability of Ships to the Broaching Stability Failure Mode. London, UK.
- Liu, X., Huang, G., & Deng, D. (2010). Research of interaction force coefficients based on model test in loading condition. Journal of Shanghai Jiaotong University (Science), 15(2), 168–171. doi:10.1007/s12204-010-8033-x
- Lu, N., Zhu, H., Fei, W., & Wang, W. (1981). Experimental Study on Open Rudders. Journal of Shanghai Jiaotong University, 2, 1.
- Makov, Y. (1969). Some results of theoretical analysis of surf-riding in following seas. T Krylov Soc, (126), 4.
- Nagarajan, V., Kang, D. H., Hasegawa, K., & Nabeshima, K. (2008). Comparison of the mariner Schilling rudder and the mariner rudder for VLCCs in strong winds. Journal of Marine Science and Technology, 13(1), 24–39.
- NAOE Osaka University. (2015). Sample ship data sheet: ITTC A2 fishing vessel. Retrieved from <http://www.naoe.eng.osaka-u.ac.jp/imo/a2>
- Ogawa, A., & Kasai, H. (1978). On the mathematical model of manoeuvring motion of ships. International Shipbuilding Progress, 25(292).
- Renilson, M. R. (1982). An investigation into the factors affecting the likelihood of broaching-to in following seas. In Proceedings of the 2nd International Conference on Stability of Ships and Ocean Vehicles.
- Spyrou, K. J. (1996). Dynamic instability in quartering seas: The behavior of a ship during broaching. Journal of Ship Research, 40(1).



- Tigkas, I., & Spyrou, K. J. (2012). Continuation Analysis of Surf-riding and Periodic Responses of a Ship in Steep Quartering Seas. In Proceedings of the 11th International Conference on the Stability of Ships and Ocean Vehicles (pp. 337–349).
- Umeda, N. (1999). Nonlinear dynamics of ship capsizing due to broaching in following and quartering seas. Journal of Marine Science and Technology, 4(1), 16–26. doi:10.1007/s007730050003
- Umeda, N., & Hamamoto, M. (2000). Capsize of ship models in following/quartering waves: physical experiments and nonlinear dynamics. Philosophical Transactions of the Royal Society of London. Series A: Mathematical, Physical and Engineering Sciences, 358(1771), 1883–1904. doi:10.1098/rsta.2000.0619
- Umeda, N., & Hashimoto, H. (2002). Qualitative aspects of nonlinear ship motions in following and quartering seas with high forward velocity. Journal of Marine Science and Technology, 6(3), 111–121. doi:10.1007/s007730200000
- Umeda, N., & Kohyama, T. (1990). Surf-riding of a ship in regular seas. Journal of Kansai Society of Naval Architects, 11.
- Umeda, N., Matsuda, A., Hamamoto, M., & Suzuki, S. (1999). Stability assessment for intact ships in the light of model experiments. Journal of Marine Science and Technology, 4(2), 45–57. doi:10.1007/s007730050006
- Yu, L., Ma, N., & Gu, X. (2012). Study on Parametric Roll and Its Rudder Stabilization Based on Unified Seakeeping and Maneuvering Model. In 11th Internationalconference on the Stability of Ships and Ocean Vehicles. Greece.
- Yu, L., Ma, N., & Gu, X. (2014). Numerical Investigation into Ship Stability Failure Events in Quartering Seas Based on Time Domain Weakly Nonlinear Unified Model. In Proceedings of the 14th International Ship Stability Workshop (pp. 229–235). Kuala Lumpur, Malaysia.



Offshore Inclining Test

Mauro Costa de Oliveira, *Petrobras* mauro@petrobras.com.br

Rodrigo Augusto Barreira, *Petrobras* barreira@petrobras.com.br

Ivan Neves Porciúncula *Petrobras* ivann@petrobras.com.br

ABSTRACT

The stability test that includes the Lightweight Survey and the Inclining Experiment is the traditional way to determine the light ship and the centre of gravity of a vessel. It is normally conducted in sheltered waters in calm weather conditions and usually requires the vessel to be taken out of service to prepare for and to conduct the test. The motivation to this work began with the application of semisubmersible units (SS) in the oil and gas production activity. These units are planned and installed for long term operation, typically 25 years. Throughout their operational life a SS unit usually requires modifications, basically due to the natural reservoir changes or due to safety or regulatory issues that lead to changes in lightweight. The option of demobilizing a Floating Production System (FPS) to calm waters to execute the Inclining Experiment is neither economical nor technically feasible, due to the impacts to the mooring system, risers system and reservoir management plus the associated costs to tow the unit close to coastal areas. Bearing in mind this scenario, an alternative method to carry out the test with the unit in operation offshore with wind, waves and current and under the influence of the mooring lines and risers could be applied as previously proposed. This paper addresses the main technical issues to be overcome in order to validate and produce reliable results in these new conditions.

Keywords: *inclining test, IMO MODU Code, Centre of Gravity*

1. INTRODUCTION

The stability test that includes the Lightweight Survey and the Inclining Experiment is the traditional way to determine the light ship and the centre of gravity of a vessel. The stability test is required for most vessels upon their completion and is the worldwide recommended and approved method to determine the light vessel characteristics and the Centre of Gravity coordinates. It is normally conducted in sheltered waters in calm weather conditions and usually requires the vessel to be taken out of service to prepare for and conduct the test [1], [2].

The motivation to this work began with the application of semisubmersible units (SS) in the production activity. These units are planned and installed for long term operation, typically 25 years. Throughout their operational life a SS unit requires modifications, basically due to the natural reservoir changes or due to safety or regulatory issues. These changes lead to adjustments in the process plant, typically with the introduction of new equipment to carry out the new processing activities. Safety and legal requirements can also pose the necessity of additional equipment and its structural support.

Once the weight control procedures may not be effective the regulatory bodies and classification societies impose the execution of a new Inclining Test every time the summation of the weight changes surpasses a certain limit.

The option of demobilizing a FPS to calm waters is neither economical nor technically feasible, due to the impacts to the mooring system, risers system and reservoir management plus the associated costs to tow the unit close to the coast. Therefore, instead of the Inclining Test, the classification societies opt to apply penalties to the units, prescribing VCG values above the ones calculated in the weight control reports. Bearing in mind this scenario, this paper evaluates an alternative method to carry out the Inclining Test with the unit in operation offshore, with wind, waves and current and under the influence of the mooring lines and risers, as described in previous studies addressing the same problem [3], [4], [5], [6] and [7].

In order to validate the method an inclining test of a moored semi-submersible with risers and under the action of waves has been carried out in Laboceano ocean basin. The results were analysed and discussed and the error margins were also determined and compared with the traditional approach. After this stage the procedure was applied to a full scale unit of the Petrobras fleet. Ballast transfer was executed to incline the unit and the wave induced motions recorded through a MRU (Motion Recording Unit) equipment. The mooring and risers were carefully modelled in numerical simulation programs and included in the VCG determination. After these two phases, the paper presents the main conclusions and validation of this alternative procedure using only proven measuring equipment and numerical methods to calculate the Centre of Gravity coordinates.

2. SEMISUBMERSIBLE UNIT



Figure 1 – Typical SS production unit

The hull selected to perform the model test is a typical semi-submersible platform. The main characteristics of this unit are shown below:

Table 1 – Platform Main Dimensions

Particular	Value
Length Over All (m)	116.0
Beam (m)	72.0
Depth Main Deck (m)	41.6
Pontoon Width	13.5
Deck length	77.0
Deck width	63.3
Draft (m)	23.47
Displacement (t)	33562

3. MODEL TESTS

3.1 Description

The model tests were conducted at LABOCEANO's ocean basin from UFRJ in Brazil from August to September 2013 with a typical SS to evaluate the proposed procedures to carry out the inclining tests offshore [8].

The main objective of the tests was to evaluate a procedure to perform inclining tests with a moored SS with risers installed at site in the presence of waves and wind mean load. The results from the inclining tests would then be compared with model dry calibration and with still water conventional tests.



A SS hull was constructed at scale of 1:50 and due to basin dimensions limitations, and in order to keep a simplified test, a truncated and simplified mooring and risers system was designed to mimic the influence of such systems on the platform behaviour. The measurements included platform motions, line tensions, local wave heights and waves run-up at four columns.

The structure was firstly tested free floating and then the mooring and risers system was installed. The moored structure was then tested in still water (different draft of free floating condition), and finally wave tests were performed. A set of regular and irregular waves were simulated, and inclining tests in waves were performed using weights in different positions at the deck. A test matrix was defined in a way that the inclining tests in waves could be compared to static inclining tests so that the mean equilibrium angles could be compared. Also, the main parameter to be measured – the vertical centre of gravity, should be well known for both cases. This last requirement was fulfilled by measuring the KG of the instrumented and ballasted model on dry condition before and after the tests.

The environmental conditions chosen for the tests included both regular and irregular waves, with different heights and periods, and two directions (waves from stern and quarter stern).

For the procedure itself, the model deck was prepared with high precision machining so that the weight used to impose the known inclining moment would be precisely positioned at required distances to minimize uncertainty on the results.

On the instrumentation side, a high accuracy visual tracking system was used to measure the model 6 DOF motions, in order to obtain high quality measurements in waves. As additional measurements, the relative wave heights were also measured at four columns, in order to simulate the measured draft at draft

marks. Mooring lines and risers dynamic tensions were also measured, and so were the wave heights at certain points at the basin. The water depth in full scale is 600 m.

3.2 Model Calibration

Figure 2 illustrates the model used in Laboceano basin:



Figure 2 – SS Model in Laboceano Basin

The results at dry "LEVE" condition obtained are summarized below:

Table 2 – Platform Mass Data

	Model Scale		Prototype scale	
Mass	233.450	kg	30091.329	ton
XG	0	mm	0	
YG	0	mm	0	m
ZG	428	mm	21.4	m
IXX	8.90E+07	kg.mm ²	2.87E+07	ton.m ²
IYY	8.86E+07	kg.mm ²	2.86E+07	ton.m ²
IZZ	1.05E+08	kg.mm ²	3.38E+07	ton.m ²

The mass of the model considers the inclining weight (2.32 kg in model scale), positioned at the center of the deck X=0mm, Y=0mm, Z=871mm. The weight and center of gravity coordinates of "LEVE" or LIGHT condition without inclining test mass are shown below as these values will be used later in the proposed procedures to determine the KG.



Table 3 – Mass measured in Dry Conditions

	Prototype scale (light without inclining test mass)	
Mass	29836.11	ton
XG	0	m
YG	0	m
ZG	21.182	m

WAVEFILE	SPEC	HEIGHT (m)	PERIOD (s)	DIR
W02_10304	JS	2.0	9.0	180
W02_20100	JS	1.5	8.0	225

3.3 Mooring and Riser System Design

A mooring system was designed and constructed using eight (8) lines. Also, six (6) risers representing groups were designed and constructed to simulate the influence of such lines.



Figure 3 – Mooring and Risers Model

3.4 Environmental Conditions

Both regular (4) and irregular (4) waves have been tested using the JONSWAP spectrum.

Table 4 – Model Test Wave Data

WAVEFILE	SPEC	HEIGHT (m)	PERIOD (s)	DIR
W01_10101	-	1.0	8.0	180
W01_102010	-	1.5	8.0	180
W01_10301	REG	2.0	9.0	180
W01_20100	REG	1.5	8.0	225
W02_10102	JS	1.0	8.0	180
W02_10201	JS	1.5	8.0	180

3.5 Test Matrix

All tests were grouped into five (5) batteries. The following groups describe the naming convention.

GROUP PT100 – PRE-TESTS - "LEVE" CONDITION, FREE FLOATING: Model freely floating (no mooring, no risers) was tested for equilibrium and inclining test measurements.

GROUP PT120 – PRE-TESTS - "LEVE" CONDITION, MOORED W RISERS: Model moored with risers installed

GROUP T120 – "LEVE" CONDITION, MOORED W RISERS: Same as Group PT120

In all groups the Inclining Weight was placed in 8 different positions from Starboard to Portside in order to incline the platform.

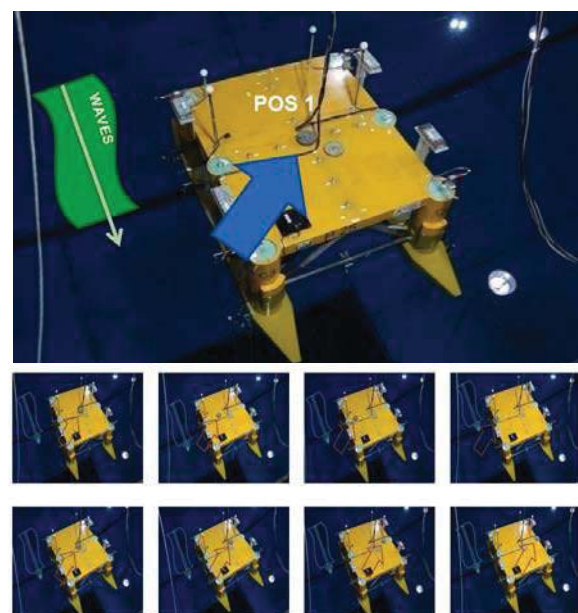


Figure 4 – Test Weight Positions



3.6 Model Test Results

As a sample of the model test results the irregular waves roll motion time trace, mean values and standard deviation for all groups and for the 8 Test Weight positions are shown in Figures 5, 6 and 7:

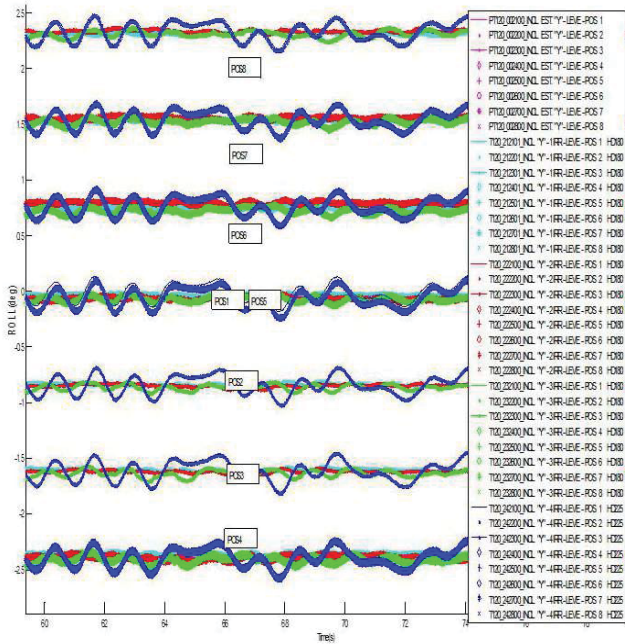


Figure 5 Time traces of roll motion for all irregular waves and test weight positions

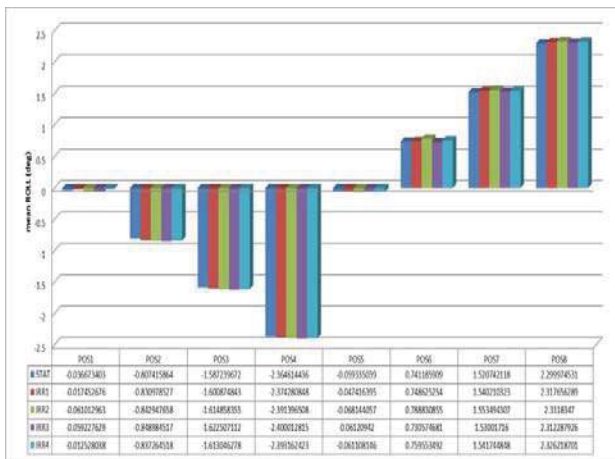


Figure 6 Mean Roll angle for all irregular waves and test weight positions

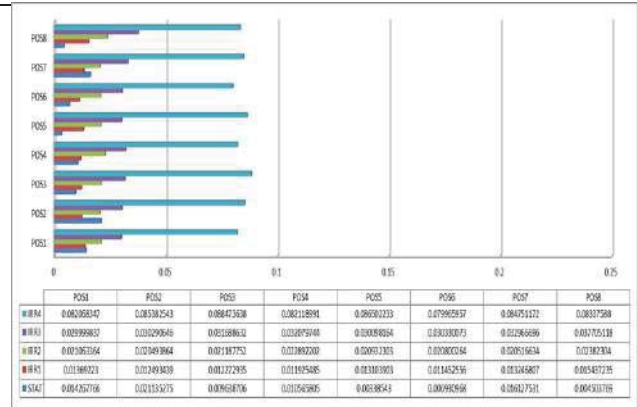


Figure 7 – Standard Deviation of Roll angle for all irregular waves and test weight positions

4. KG CALCULATION PROCEDURE

In order to determine the KG based on the model test results, two approaches were selected:

- 1- Uncoupled Direct Method procedure
- 2- Coupled Iterative Method

Both procedures will use the data generated in the model scale inclining experiment carried out at LabOceano. However to use the model test data it is first necessary to generate numerical models and to calibrated them to obtain the same behaviour as the physical models employed in LabOceano. Two models will be required: the hydrostatic one and the mooring and risers.

4.1 Numerical Hydrostatic Model

The hydrostatic data model was prepared using the in-house hydrostatic and stability program SSTAB, as can be seen below:

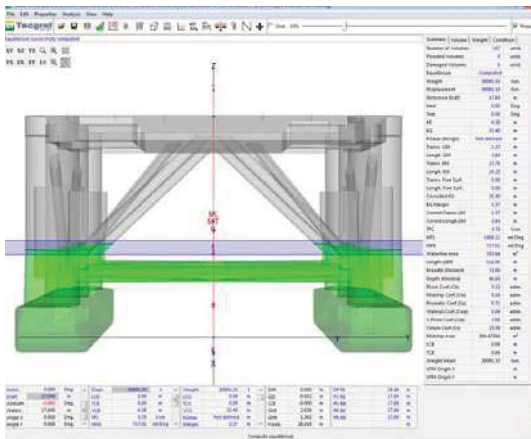


Figure 8 – SSTAB Numerical Model

Table 5 – Test Conditions

#	Cond.	Displac. (t)	Heel (Deg.)	Trim (Deg.)	Draft (m)	KG (m)	KMt (m)	GMt (m)
1	LIGHT	30087.46	0.0	0.0	17.85	21.40	22.76	1.32
2	LIGHT M-R LOADS	34029.00	0.0	0.0	24.87	19.66	22.29	2.63
3	LIGHT M-R CAT	34028.98	0.0	0.0	24.87	19.66	22.29	2.63

LIGHT condition refers to the platform model, plus ballasts, plus the inclining weight, plus the required instrumentation.

LIGHT M-R LOADS: This condition is the same as the LIGHT condition plus the addition of the vertical component of the mooring and risers tensions as point loads.

LIGHT M-R CAT: This condition adds the mooring and risers tensions calculated using a catenary model included in the SSTAB program.

With this model one can calculate the displacement and KM in the mean draft obtained in the model test.

4.2 Mooring and Riser Model

The mooring and risers system was modelled in DYNASIM program using eight (8) mooring lines and six (6) riser

representative groups. The mooring lines in DYNASIM were modelled as close as possible to the LabOceano configuration, using segments of steel wire, steel chains, floaters and stainless steel springs.

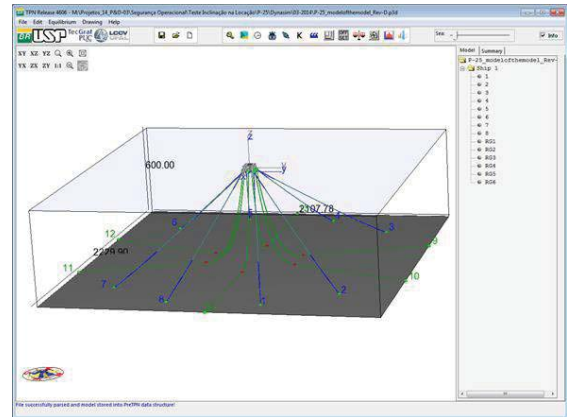


Figure 9 – M&R Numerical Model

As all segments but the springs were highly stiff, all the stiffness was considered to be characterized by the springs. However the main requirement of the numerical model was to match the total stiffness obtained in the pull-out tests PT-120-101000 and PT-120-102000 and the Frame tests with force plate.

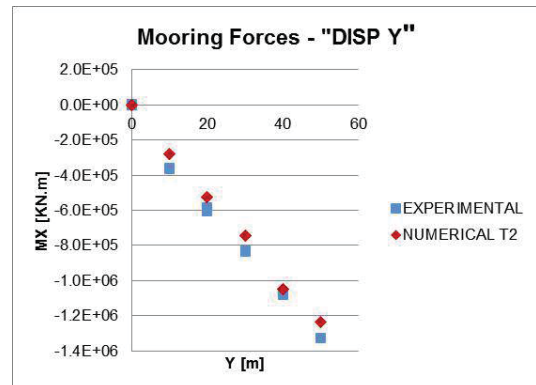


Figure 10 – Restoring Force Calibration

4.3 Uncoupled Direct Method Procedure

A final derivation of GM was performed based on Hydrostatic data and Mooring lines and Risers Moments calculated from Calibrated numerical model. So, for each mean position achieved for the model during wave tests, the Mooring lines and risers moments were



subtracted to allow GM and KG calculations, using the following equation:

$$GM = \frac{w \cdot d \cdot \cos(\theta) - M_{mris}}{Disp \cdot \sin(\theta)} \quad 1$$

where:

w - Inclining weight

d - Inclining distance

θ - Inclining angle

Disp - Displacement

M_{mris} - Total moment for mooring lines and risers calculated for achieved equilibrium position, i.e., mean position for each test. The KG was then calculated by:

$$KG = KM - GM \quad 2$$

The results of KG were then obtained for each test using the conventional expressions [1] and [2]. Implicit in this approach is that it is only valid for small inclination angles due to the change in KM for larger angles.

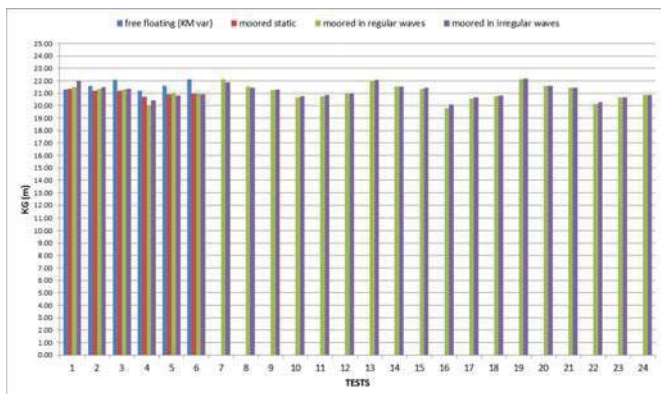


Figure 11 – Uncoupled Procedure Results

KG calculated values are presented in pink lines for free floating test results, brown lines moored static w/o wave results, green lines moored regular waves results (1 REG, 2 REG, 3 REG and 4 REG) and blue lines moored irregular waves results (1 IRR, 2 IRR, 3 IRR and 4 IRR).

4.4 Coupled Iterative Method Procedure

In this item a numerical procedure to determine the KG using the in-house programs SSTAB, for hydrostatic and stability calculations, and DYNASIM for mooring analysis is described. This procedure is based in an iterative search calculation where KG values are input and the equilibrium of the platform is calculated and checked with the model test mean values of heel and trim. When the calculated heel equates the model test heel result the associated KG is the target KG. The procedure is repeated for the 6 positions and the mean KG will be the resultant KG of the platform.

This procedure is fully based in the SSTAB equilibrium algorithm, which does not use any hypothesis of small angle or fixed Metacenter, but determines the coordinate of the Center of Gravity that reproduces the model heel, trim and draft. Therefore the inclining moment is imposed through the change of position of the inclining weight and the platform attains the equilibrium that is dependent of hydrostatic properties and the mooring and risers moments in the inclined position. The forces and moments due to the lines are determined through a catenary model included in the search for equilibrium.

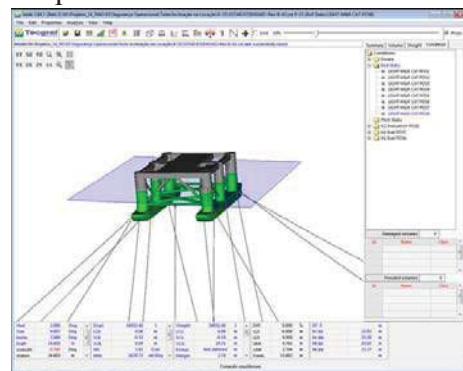


Figure 12 – SSTAB Program

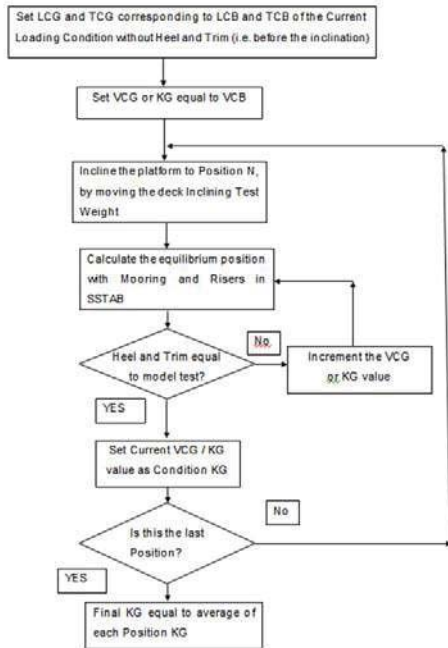


Figure 13 Iterative Coupled procedure

The X and Y displacements can also be considered and input to SSTAB with the objective of including the effect of the offset caused by waves, current and wind in the forces/moments induced by the mooring and risers systems.

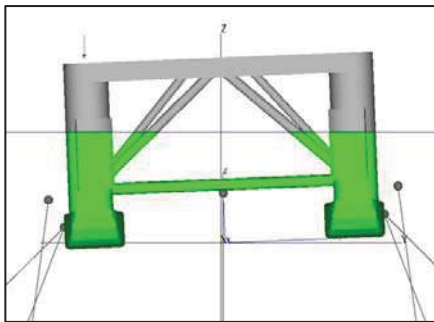


Figure 14 – SSTAB Program mixing hydrostatic and lines static calculations

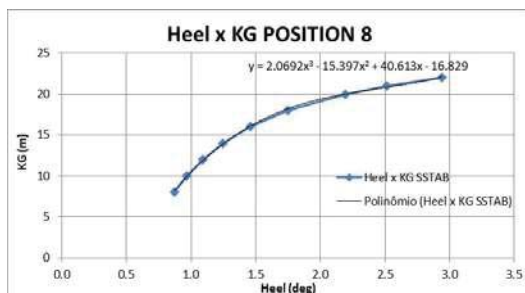


Figure 15 – SSTAB Program based iterative equilibrium calculations mixing hydrostatic and lines static calculations

4.5 Results for Model Test Verification

A KG analysis was performed by using calibrated numerical models leading to the following results:

Table 6 – Test KG results

	KG	Mean	% Diff to ref	% Diff to free floating
		m		
	reference value	21.40	-	-
Conv. Method	free floating small angle	21.01	-	-
	free floating all angles	20.73	-	-
Uncoupled Direct Method	free floating	20.87	-2.48%	-0.67%
	moored static	21.06	-1.61%	0.22%
	moored in regular waves	21.10	-1.42%	0.41%
	moored in irregular waves	21.16	-1.12%	0.72%
Coupled Iterative Method	SSTAB free floating static	21.02	-1.78%	0.05%
	SSTAB moored static	20.70	-3.27%	-1.48%
	SSTAB irregular wave 3	20.73	-3.13%	-1.33%

Comparing the differences to the free floating condition small angles value (KG = 21.01 m), that represents the conventional procedure currently accepted KG determination practice with the other calculation methods, that include different approaches, we can verify an error from -1.96% to 1.65%, that is reasonable considering all the uncertainties involved by the inclining tests.

It can be observed that even the conventional inshore inclining test procedure works with some tolerance ranges, once it is difficult to define precisely some variables, like hull displacement, external weights and variable loads in the platform, draft and angle measurements, etc. Though, the sensitivity analysis performed in this report showed that the error are within an adequate margin of tolerance.

We conclude that this increase in the error is acceptable and within the tolerances of the current practice of inclining tests as performed by the industry and certified by regulatory institutions, therefore we consider that the



inclining test can be performed offshore with the effects of mooring lines and risers and waves consistently taken into account.

5. APPLICATION OF THE OFFSHORE INCLINING TEST PROCEDURE TO AN ACTUAL UNIT

The objective of this item is to apply the procedure to execute the Inclining Experiment offshore in the location as described in the previous items, without removing the unit or stopping the production. This procedure has been approved in principle by ABS.

The proposed procedures have been applied initially in model scale in order to check their feasibility. In this way a model test has been carried out at LabOceano aiming at producing data that has been used to execute all the steps required for the offshore inclining experiment. LabOceano has issued a report [12] and also time series results of all tests in MATLAB format.

As the feasibility of the Model Scale Inclining Experiment has been confirmed and approved in principle, these tests were then performed in a typical semisubmersible unit in order to determine the lightweight and Centre of Gravity with the modifications carried out since the last Stability Experiment, executed in sheltered waters after the construction.

Based on the results of the full test with the SS unit, reported in this document, an official test will be carried out aiming at obtaining the approval of the classification societies and regulatory bodies in order to update the KG of the units in operation after eventual lightweight modifications carried out in the last years. Therefore the penalties imposed could be lifted in a safe and correct way enabling the execution of the required improvements within the safety standards.

The test has been carried out on the 6th of June 2014 from 13:00 to 16:00 (Brasilia Time

Zone) or 16:00 to 19:00 (GMT). The ballast was transferred between tanks S05WBT and S11WBT. There was no admission or discharge of ballast to the sea. In this way only the trim was changed.

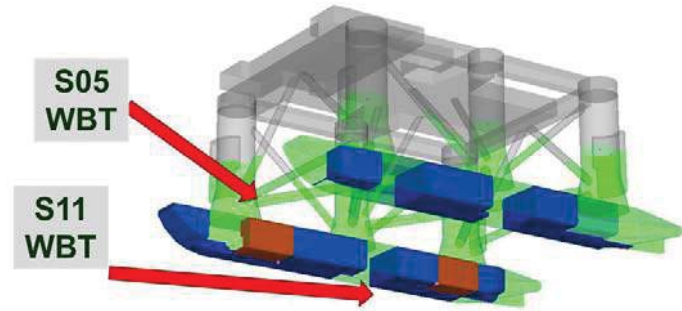


Figure 16 – Tanks used in the experimental test

The following manoeuvres have been executed:

Table 7 Ballast Manoeuvres

	Manoeuvres Time	Ballast transfer	Nominal Trim
POS01	Reference	Parallel Draft	0
	13:00		
POS02	1	11BE==>5BE	2.5
	13:20		
POS03	2	5BE==>11BE	2
	13:49		
POS04	3	5BE==>11BE	1.5
	14:04		
POS05	4	5BE==>11BE	1
	14:24		
POS06	5	5BE==>11BE	0.5
	14:48		
POS07	6	5BE==>11BE	0
	15:07		
POS08	7	5BE==>11BE	-0.5
	15:31		
POS09	8	5BE==>11BE	-1
	15:56		
POS10	9	5BE==>11BE	-1.5
	16:16		
POS11	10	5BE==>11BE	-2
	16:38		
POS12	11	5BE==>11BE	-2.5
	17:02		
POS13	12	11BE==>5BE	0
	17:23		

During the test the consumption of fresh water and of fuel oil was reduced to a



minimum, however it is not possible to eliminate it completely in a producing unit. Therefore the alternative was to carefully register the level of these tanks in order to take this reduction into account.

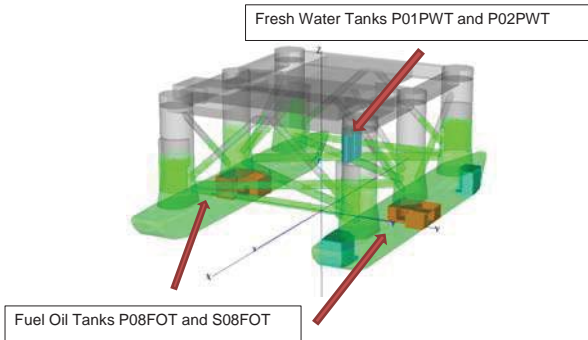


Figure 17 – Tanks with consumption during the test

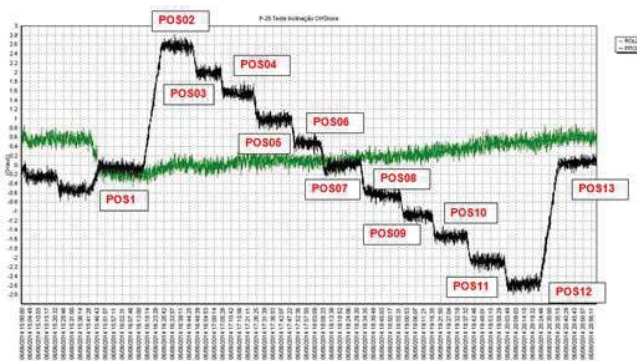


Figure 18 – Heel and Trim Positions

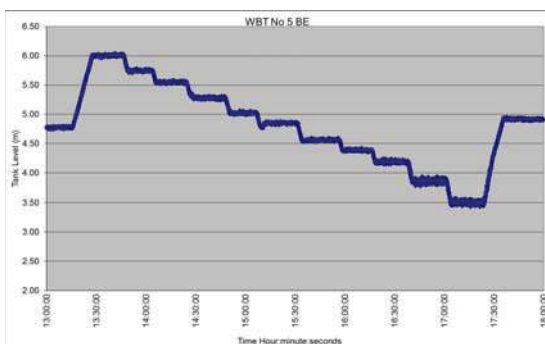


Figure 19 – WBT 5 Tank Ballast Transfers

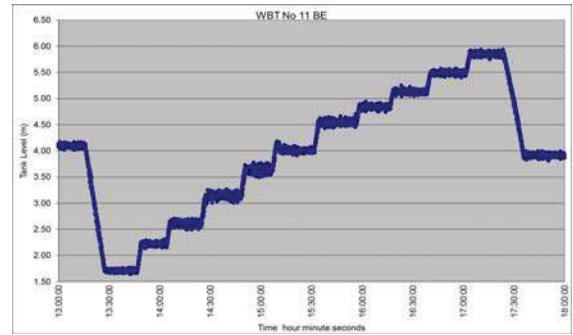


Figure 20 WBT 11 Ballast Transfers

Due to the non-linearities inherent to this method the more general approach of the Coupled Iterative Method has been applied to determine the KG.

5.1 Numerical Hydrostatic Data

The hydrostatic data model was adjusted using the in-house hydrostatic and stability program SSTAB, as can be seen in Figure 21. The SSTAB program has a special feature characterized by the inclusion of a catenary model within the equilibrium calculations taking into account the non-linear behaviour of the mooring and risers system.

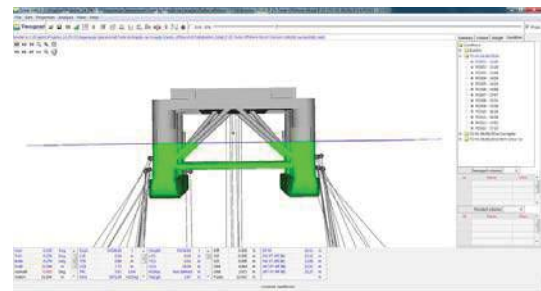


Figure 21 – Initial Position

Table 8 – Initial Position Condition

#	Condition.	Displac. (t)	Heel (Deg.)	Trim (Deg.)	Draft (m)
1	POS01 - 13:00	33350	-0.21	-0.07	23.31



Table 9 – Target Draft, Heel and Trim for All Positions

	Draft Origin (m)	Required Heel Test (deg)	Required Trim Test (deg)
POS01 - 13:00	23.31	-0.21	-0.07
POS02 - 13:20	23.30	-0.02	2.56
POS03 - 13:49	23.30	-0.04	1.99
POS04 - 14:04	23.31	0.05	1.55
POS05 - 14:24	23.30	0.1	0.97
POS06 - 14:48	23.29	0.07	0.48
POS07 - 15:07	23.29	0.06	0
POS08 - 15:31	23.28	0.18	-0.63
POS09 - 15:56	23.28	0.22	-1.09
POS10 - 16:16	23.28	0.32	-1.54
POS11 - 16:38	23.27	0.44	-2.07
POS12 - 17:02	23.25	0.49	-2.58
POS13 - 17:23	23.26	0.61	0.04
Averages	23.29		

	Bottom Chain (m)	Interm. Wire Rope (m)	Chain Connection (m)	Top Chain (m)
1	950	600	10	148
2	1120	600	10	143
3	1135	600	10	202
4	1380	600	10	152
5	1510	600	10	137
6	1410	600	10	130
7	1220	600	10	105
8	1220	600	10	160
9	1130	600	10	160
10	965	600	10	145
11	950	600	10	165
12	840	600	10	173

Table 11 – Mooring Line Properties

	Diam (mm)	MBL (kN)	EA (kN)	Weight in Air (kN/m)	Weight in Water (kN/m)
R3_Stud_Chain	0.084	5550	5.84E+05	1.516	1.315
EIPS_Steel_WireRope	0.096	5740	5.04E+05	0.38	0.315
R4_Stud_Chain	0.078	6295	5.17E+05	1.34	1.17
R4_Stud_Chain	0.078	6295	5.17E+05	1.34	1.17

5.2 Mooring and Riser Model

The mooring and risers systems were modelled in DYNASIM program with 12 mooring lines and 36 risers.

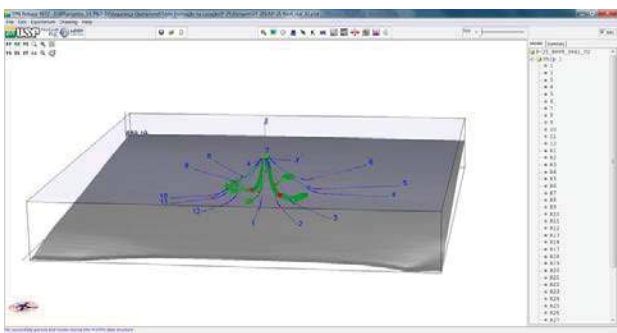


Figure 22 – M&R model as inspected in the field

The mooring lines in DYNASIM were modelled as the AS-LAID configuration [15], using segments of steel wire and steel chains. This model is imported in SSTAB program.

Table 10 – Mooring Line Composition

5.3 KG Calculation – Coupled Iterative Method Procedure

In this item a numerical procedure to determine the KG using the in-house program SSTAB, for hydrostatic and stability calculations, that includes the catenary model imported from DYNASIM program for mooring analysis is described. This procedure is based in an iterative search calculation where KG values are input and the equilibrium of the platform is calculated and checked with the measured offshore test mean values of heel and trim. When the calculated trim equates the measured trim results the current KG is the target KG. The procedure is repeated for the 13 positions and the mean KG will be the resultant KG of the platform.

This procedure is fully based in the SSTAB equilibrium algorithm, which does not use any hypothesis of small angle or fixed Metacentre, but determines the coordinate of the Centre of Gravity that reproduces the model heel, trim



and draft. Therefore the inclining moment is imposed through the change of the ballast level in the test tanks (5SB and 11SB) and the platform attains the equilibrium that is dependent of hydrostatic properties and the mooring and risers moments in the inclined position. The forces and moments due to the lines are determined through a catenary model included in the search for equilibrium. The X and Y displacements can also be considered and input to SSTAB with the objective of including the effect of the offset caused by waves, current and wind in the forces/moments induced by the mooring and risers systems.

In order to determine the overall KG of the condition, all weight items, but liquid cargoes in tanks, have been added to the so called Calibration item. The Calibration item is initially comprised by all items described below based on estimates of the current loading condition.

Table 12 – All Weight Items Summation

Item	Weight (t)	LCG (m)	TCG (m)	VCG (m)
Calibration Item (All weight items Except variable loads)	20093.94	-2.46	1.14	28.41

The Calibration item obtained above is a reference once the actual weight value and X and Y coordinates of the centre of gravity's item has been obtained to attain the equilibrium with the Heel and Trim measured in POSITION01. Four KG calculations have been carried out: One without considering the displacement of the unit in the X and Y directions (offset) due to the environmental actions, other one considering this displacement, another removing the catenary model of the mooring and risers, thus considering them as fixed vertical loads and the last one modelling the tanks cargoes as fixed loads.

5.4 KG Calculation Without Offset Consideration

Table 13 show the weight items considered to assemble the Loading Condition. The Calibration Item comprises, as described above, the Lightweight, consumables, crew, etc. The remaining weight items of the platform are the liquid contained in the tanks, which have been measured through the PI control system and the mooring and risers systems, which are included in the model based on the As-Laid system.

Table 13 – Condition Weight Items

Weight Class	Weight (t)	% of Total	LCG	TCG	VCG
Calibracao	19953.89	59.83	-2.52	1.17	0.00
Mooring Lines	1020.13	3.06	1.03	0.34	16.80
Risers	924.18	2.77	-9.12	2.65	21.06
Ballast_Tanks	8974.40	26.91	3.87	-3.92	3.89
Fresh_Water	1015.32	3.04	17.80	28.08	7.95
Drill Water	323.88	0.97	39.16	-26.22	2.21
Fuel_Oil	1138.21	3.41	-4.35	-7.38	3.10
Total Weight	33350.01	100.00	0.09	0.08	2.51

The procedure described in Figure 13 is applied for the 13 positions beginning with POSITION01. As the trim angle is 0 it is not possible to iterate to determine the KG, this is only possible when the trim is different from 0. The procedure is applied for the remaining 13 positions.

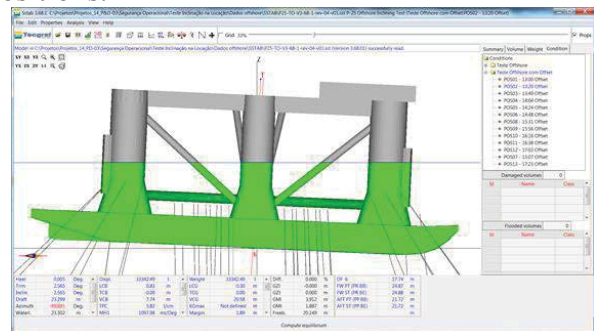


Figure 23 – SSTAB model with lines as catenaries in Position 02 (POS02)

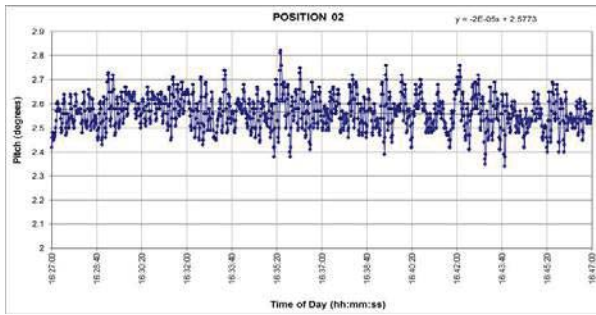


Figure 24 – Trim angle measurement POS02

Table 14 – VCG Coord. Calculated for Inclining Test Positions without Offset

	Displ (t)	Draft Origin (m)	Resultant Heel SSTAB (deg)	Resultant Trim SSTAB (deg)	LCG (m)	TCG (m)	VCG (m)
POS01 - 13:00	33350.01	23.31	-0.21	-0.07	0.056	0.08	
POS02 - 13:20	33343.87	23.3	0	2.57	0.29	0	20.63
POS03 - 13:49	33350.6	23.31	0.13	2	0.24	0	20.7
POS04 - 14:04	33349.96	23.31	0.13	1.56	0.2	0	20.87
POS05 - 14:24	33349.07	23.31	0.15	0.97	0.15	0	21.22
POS06 - 14:48	33350.13	23.31	0.59	0.38	0.1	-0.01	22.44
POS07 - 15:07	33347.34	23.31	0.02	-0.05	0.06	0	
POS08 - 15:31	33344.79	23.3	0.05	-0.65	0	0	18.31
POS09 - 15:56	33349.3	23.31	0.13	-1.12	-0.04	-0.01	19.14
POS10 - 16:16	33347.07	23.31	0.12	-1.54	-0.08	-0.01	19.38
POS11 - 16:38	33343.79	23.3	0.11	-2.1	-0.13	-0.01	19.56
POS12 - 17:02	33342.9	23.3	0.13	-2.61	-0.17	-0.01	19.65
POS13 - 17:23	33342.09	23.3	0.02	-0.04	0.06	-0.01	
Averages	33346.99	23.31			0.06	0.00	20.19

Figure 25 – Balance of ballast between tanks during transfers

5.5 KG Calculation With Offset Consideration

In this chapter the results considering the offset measured through the SMO (Offshore Monitoring System) system are presented. The offsets are calculated based on the GPS data stored in the SMO system from Petrobras.

Table 15 – Offsets X and Y in relation to the Neutral position during the Inclining Test

	Offset X (m)	Offset Y (m)
POS01 - 13:00	3.15	-1.98
POS02 - 13:20	3.49	-1.66
POS03 - 13:49	3.09	-1.71
POS04 - 14:04	2.80	-1.37
POS05 - 14:24	2.80	-1.16
POS06 - 14:48	2.89	-0.70
POS07 - 15:07	2.55	-0.92
POS08 - 15:31	2.64	-0.38
POS09 - 15:56	2.07	-0.43
POS10 - 16:16	1.90	-0.28
POS11 - 16:38	1.69	0.07
POS12 - 17:02	1.53	0.31
POS13 - 17:23	2.17	-0.27

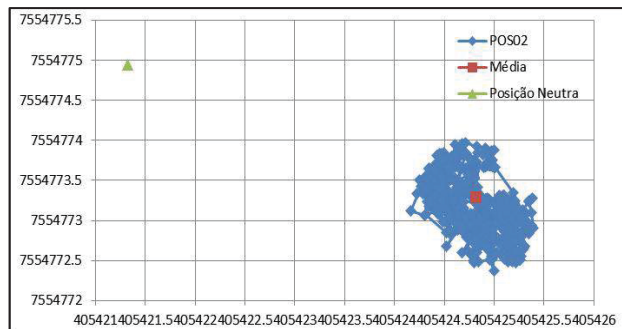
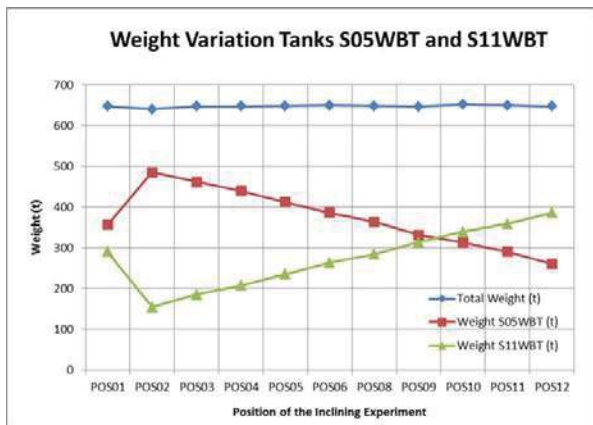


Figure 26 – Planar displacements measured by GPS during Position02 inclination



Table 16 – Calculation of Offsets in relation to the Neutral Position

	Neutral Position without environmental loads	
	East (m)	North (m)
Neutral Position	405421.32	7554774.95
Average of POSITION02	405424.81	7554773.29
Offset	3.49	-1.66

Table 17 – Weight Items for POS02

Summary of Loading Condition for POS02 - 13:20 Offset					
Weight Class	Weight	% of Total	LCG	TCG	VCG
Calibracao	19963.26	59.86	-2.45	1.03	30.04
Mooring Lines	1016.44	3.05	0.03	0.50	16.80
Risers	925.64	2.78	-9.25	2.69	21.12
Ballast_Tanks	8967.29	26.89	4.77	-3.92	3.93
Fresh_Water	1015.56	3.05	17.83	28.08	7.95
Drill Water	323.88	0.97	39.29	-26.25	2.21
Fuel_Oil	1138.21	3.41	-4.24	-7.40	3.10
Total Weight	33350.28	100.00	0.34	0.00	20.51

Table 18 – VCG Coord. Calculated for Inclining Test Positions with Offset

	Displ (t)	Draft Origin (m)	Resultant Heel SSTAB (deg)	Resultant Trim SSTAB (deg)	LCG (m)	TCG (m)	VCG (m)
POS01 - 13:00	33350.51	23.31	-0.21	-0.07	0.01	0.08	
POS02 - 13:20	33350.28	23.31	0	2.57	0.34	0	20.51
POS03 - 13:49	33351.76	23.32	0.17	2	0.3	-0.01	20.41
POS04 - 14:04	33351.1	23.31	0.22	1.55	0.26	-0.01	20.46
POS05 - 14:24	33350.44	23.31	0.09	0.97	0.21	-0.01	20.53
POS06 - 14:48	33351.37	23.32	0.62	0.49	0.16	-0.01	21.3
POS07 - 15:07	33346.55	23.31	-0.17	-0.03	0.06	-0.01	
POS08 - 15:31	33351.23	23.32	0.27	-0.64	0.03	-0.02	19.98
POS09 - 15:56	33349.22	23.31	0.4	-1.1	-0.02	-0.02	20.22
POS10 - 16:16	33346.1	23.31	0.46	-1.55	-0.01	-0.02	20.35
POS11 - 16:38	33344.14	23.3	0.46	-2.08	-0.06	-0.02	20.28
POS12 - 17:02	33347.94	23.31	0.26	-2.59	-0.11	-0.01	19.93
POS13 - 17:23	33343.17	23.3	-0.15	0	0.06	-0.01	
Averages	33348.75	23.31			0.09	-0.01	20.40

5.6 KG Calculation with the Mooring and Risers Modelled as Constant Vertical Weights

This item presents the calculation of the KG for the Calibration Item and for the overall KG of the condition for each Position considering the mooring and riser loads as constant vertical loads applied in the respective fairleads or connection points. It should be noted that this approach is the recommended way by the rules and regulations to take into account the mooring and risers loads. In this type of method the horizontal component (Th) of the mooring loads is not considered and also the variation due to the change in position of the connection points is also not included in the calculations. Only the vertical component (Tv) as a constant load is considered.

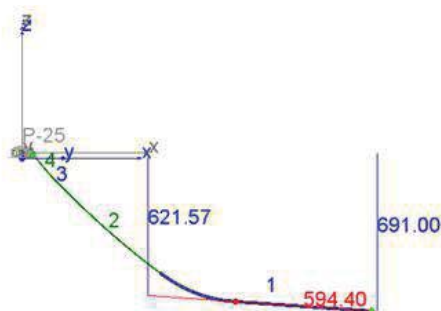


Figure 27 – Mooring Line Catenary

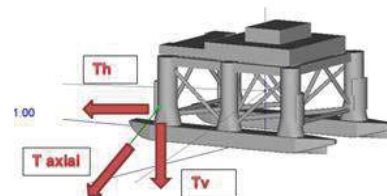


Figure 28 – Mooring line tension components



Table 19 – Vertical Component of Tension

	Vertical Constant Load (t)	X(m)	Y(m)	Z(m)
L1	88.85	39.5	35	16.8
L2	90.07	35.2	36	16.8
L3	86.47	30.6	34.8	16.8
L4	83.69	-30.6	34.8	16.8
L5	83.58	-35.2	36	16.8
L6	82.48	-39.5	35	16.8
L7	81.65	-39.5	-35	16.8
L8	86.83	-35.2	-36	16.8
L9	77.39	-30.6	-34.8	16.8
L10	79.37	30.6	-34.8	16.8
L11	91.55	35.2	-36	16.8
L12	88.20	39.5	-35	16.8

Table 20 – VCG Coord. Calculated for Inclining Test Positions without Offset and with Constant Vertical Tension

	Displ (t)	Draft Origin (m)	Resultant Heel SSTAB (deg)	Resultant Trim SSTAB (deg)	LCG (m)	TCG (m)	VCG (m)
POS01 - 13:00	33350.01	23.31	-0.23	0.01	0.056	0.08	
POS02 - 13:20	33342.52	23.3	-0.02	2.58	0.33	0	18.92
POS03 - 13:49	33349.72	23.31	0.07	2	0.28	0	18.76
POS04 - 14:04	33349.26	23.31	0.06	1.56	0.24	0	18.67
POS05 - 14:24	33348.61	23.31	0.06	0.97	0.19	0	18.34
POS06 - 14:48	33349.9	23.31	0.08	0.49	0.14	-0.01	18.37
POS07 - 15:07	33347.32	23.31	0.01	0.03			
POS08 - 15:31	33345	23.3	0.07	-0.63	0.03	0	19.92
POS09 - 15:56	33349.71	23.31	0.17	-1.09	-0.01	-0.01	19.62
POS10 - 16:16	33347.66	23.31	0.14	-1.56	-0.05	-0.01	19.56
POS11 - 16:38	33344.59	23.3	0.1	-2.08	-0.1	-0.01	19.34
POS12 - 17:02	33343.91	23.3	0.13	-2.58	-0.15	-0.01	19.27
POS13 - 17:23	33342.09	23.3	0.02	0.04			
Averages	33346.95	23.31			0.09	0.00	19.08

5.7 KG Calculation with the Mooring and Risers Modelled as Constant Vertical Weights and with Liquid Cargoes as Solid Weights

In this item the objective is to consider the liquid cargo as a fixed item, without variation due to the inclination of the platform. This is the usual way to perform the hydrostatic calculations, without including the effect of the change in the coordinates of the center of gravity of the liquid cargo inside the tank. The SSTAB program automatically calculates the change in the liquid form of the cargo due to the inclination and the consequent moment that is produced by this change. Usually this effect is taken into account by the correction of the free surface effect by the elevation of the vertical coordinate of the tank center of gravity. The purpose of this item is to investigate the free surface correction in tanks with shapes different from the parallel walls assumption used to determine the increase in the vertical coordinate of the overall KG of the condition. In this way the liquid cargo was considered as fixed and the free surface correction would have to be applied and a comparison with the option with the liquid cargo equilibrium within the tank is performed.

The tanks used to incline the platform, as already mentioned are the tanks S05WBT and S11WBT. The shape of the tanks are the same and as the inclinations are around the Y axis (trim), the resultant shapes of the water line can be seen below.

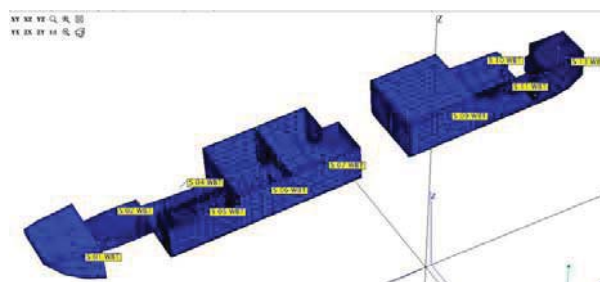


Figure 29 – Pontoon Ballast Tanks Level

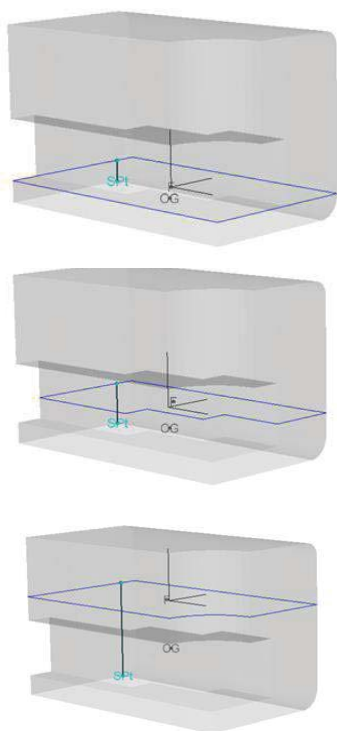


Figure 30 – Three ballast levels of Tank S05WBT showing the complex shape (Level 1, 2 and 5 m)

Table 21 – VCG Coord. Calculated for Inclining Test Positions without Offset with Constant Vertical Tension and with Ballast Tanks as Solid Weights

	Displ (t)	Draft Origin (m)	Resultant Heel SSTAB (deg)	Resultant Trim SSTAB (deg)	LCG (m)	TCG (m)	VCG (m)
POS01 - 13:00	33350.01	23.31	-0.23	0.01	0.056	0.08	
POS02 - 13:20	33343.14	23.3	-0.06	2.57	0.31	0	19.33
POS03 - 13:49	33350.48	23.31	-0.01	1.99	0.27	0	19.24
POS04 - 14:04	33350.54	23.31	-0.01	1.55	0.23	0	19.14
POS05 - 14:24	33350.61	23.31	-0.01	0.97	0.18	0	18.76
POS06 - 14:48	33352.64	23.32	0.01	0.48	0.13	0	18.44
POS07 - 15:07							
POS08 - 15:31	33344.69	23.3	0.05	-0.63	0.04	0	20.48
POS09 - 15:56	33349.27	23.31	0.15	-1.09	0	-0.01	20.19
POS10 - 16:16	33346.99	23.31	0.12	-1.54	-0.03	0	20.06
POS11 - 16:38	33343.63	23.3	0.08	-2.07	-0.08	0	19.85
POS12 - 17:02	33342.66	23.3	0.08	-2.58	-0.13	0	19.76
POS13 - 17:23							
Averages	33347.70	23.31			0.09	0.01	19.53

5.8 Preliminary Verification of Results of the Experimental Offshore Inclining Test

Based on the results obtained above one can verify on Table 22 the estimated KG of the Calibration Item (including all items except the tanks and lines) and the overall condition KG of the typical SS Unit following the 4 different approaches:

Table 22 – Final KG

Option	Liquids Cargoes	Mooring & Riser	Offset	KG Calibrated Item(m)	KG Solid All Items(m)	GMT (m)
1	Fluid	Catenary	Yes	29.89	20.4	2.05
2	Fluid	Catenary	No	29.54	20.19	2.26
3	Fluid	Constant	No	27.68	19.08	3.37
4	Solid	Constant	No	28.43	19.53	2.92

In Table 22 one can see clearly the effect of the Mooring and Risers in the calculation of the KG and hence in the stability. In Option 2 the KG was calculated considering the exact effect of the mooring and risers calculated with the catenary formulation, therefore increasing the Condition KG, whereas in Option 3 this effect was not considered resulting in a smaller KG (19.08 m). In this way the current approach of not considering the mooring and riser contribution results in a difference of 1.11 m in the Condition KG, i.e. with the mooring and riser contribution considered correctly the platform would have a KG of 20.19 m. The conclusion is that the effect of mooring and risers is beneficial for the stability introducing a restoring moment that is not considered in the conventional analysis including the effect of tension as constant weights.

Another aspect that should be considered is the influence of the moment induced by the liquids inside the tanks. In this particular case the comparison of Option 3 and Option 4 leads to a KG increase of 0.45 m. The use of the conventional free surface correction (calculated as Transversal FS = 0.24 m and Longitudinal Free Surface = 0.335) is smaller than 0.45, showing an inadequate correction of the effect



of the inclination of the liquids due to the complex shape of the tanks.

The final KG of the test condition considering the effect of the mooring and risers and the offset is 20.4 m and the KG of all items except the mooring and risers and liquid cargoes is 29.89 m. That leads to a GMT of 2.05 m and a GML of 4.04 m. Without considering the exact catenary effects and the correct effect of the liquids inclination inside complex tanks the Condition KG would be 19.53 m and the Calibration Item KG would be 28.43 m. The latter values are the ones that are used to verify the IMO and Classification Societies rules.

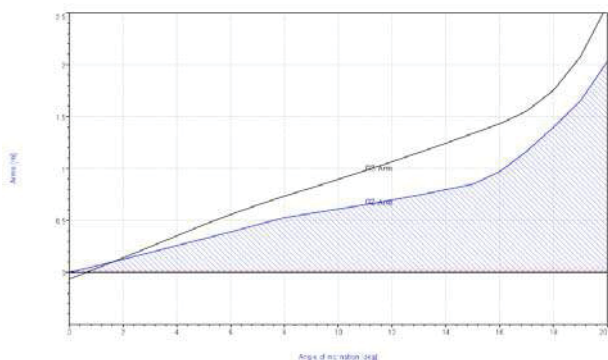


Figure 31 – GZ Curve with Mooring Lines defined as Catenary Model (black) and with Fixed Weights (blue)

Figure 31 shows the GZ curve for inclination around the Y axis (trim) for the SS with the same KG for the Calibration Item (29.89 m) and the Condition of POS01, showing the influence of the Mooring and Risers modelled as catenaries increasing the GZ.

6. CONCLUSIONS

It has been shown, firstly in model test scale and secondly in full scale, that an offshore inclining test is a feasible procedure.

The IMO Rules and Regulations were developed aiming at ships and mobile offshore units, without taking into account permanent

offshore moored units that remain in the field for 25 to 30 years. In this way alternative procedures and regulations shall be implemented in order to consider the special nature of this type of unit.

The offshore test is a sound and robust way to assess and to guarantee the safety of offshore units throughout their operational lives. All procedures are based on proven measurement devices and engineering methodologies.

The mooring and risers effect is beneficial for the stability, introducing an additional restoring moment that is not considered in the current calculations of stability.

7. ACKNOWLEDGMENTS

We acknowledge the great contribution of the TECGRAF Institute from PUC-Rio Pontifical Catholic University of Rio de Janeiro) in the development of the programs MG, SSTAB and DYNASIM.

8. REFERENCES

- ASTM International, 2004, “Standard Guide for Conducting a Stability Test (Lightweight Survey and Inclining Experiment) to Determine the Light Ship Displacement and Centers of Gravity of a Vessel”
- International Maritime Organization IMO, 1989, “Code for The Construction And Equipment Of Mobile Offshore Drilling Units 1989 (Modu Code - 89)”.
- Bradley, M.S. and MacFarlane C.J. Inclining Tests in Service, 1986, “Advances in Underwater Technology”
- MOSIS System MacFarlane C.J. Internet Description
- Brown D.T. and Witz J.A. RINA, 1996,



“Estimation of Vessel Stability at Sea Using
Roll Motion Records”

Nogueira, S., 2009, “Development of a
Inclining Test Procedure Applicable to Semi
Floating Production Units Moored on
Location”, OMAE2009-79184, Honolulu,
Hawaii, USA, 31 may – 5 June.

Nogueira, S., 2010, “Sistemática para Executar
Teste de Inclinação em Unidades
Semissubmersíveis de Produção Operando
na Locação” in Portuguese, Dissertação de
Mestrado (MSc Dissertation),
COPPE/UFRJ

LABOCEANO COPPE/UFRJ, 2013, “Model
Tests for Verification of Inclining Tests
Offshore Procedure” Draft Report -
006_12_RELPRJ03_01A 2013



Lifecycle Properties of Stability – beyond Pure Technical Thinking

Henrique M. Gaspar, *Aalesund University College, Norway* - hega@hials.no

Per Olaf Brett, *Ulstein International AS, Norway* - per.olaf.brett@ulstein.com

Ali Ebrahimi, *Ulstein International AS, Norway* - ali.ebrahimi@ulstein.com

Andre Keane, *Ulstein International AS, Norway* - andre.keane@ulstein.com

ABSTRACT

This paper addresses the importance of understanding a stable ship through its lifecycle, which goes beyond purely technical thinking. Not only is it sufficient to address under what circumstances the vessel is operating during its life cycle, but the vessel needs to be stability wise, prepared to handle safely any likely operational condition. Binary decision-making, such as a Ship A complies with the norm, therefore Ship A is stable throughout its life cycle, is only valid for a specific set of scenarios and pre-defined operational conditions, usually involving most advanced and precise engineering methods on the technical aspect, but not necessarily taking into account accurately other important ship-as-a-complex-system aspects being used for different operational scenarios over its life cycle. Our proposition is that stability is, after all, a system lifecycle property, and should be treated as such. How this proposition is observed by a systems engineering classification, both technically and operationally, is discussed in the paper. Stability as a system lifecycle property is observed via change enabled paths, with its agents, effects and mechanisms. The implications for design of five change related lifecycle properties (ilities) are discussed, namely flexibility, adaptability, robustness, scalability and modifiability. We also reflect upon the use of a complex system engineering five-aspect taxonomy. Structural and behavioural aspects are briefly commented based on classical stability formulation, on how internal (e.g. cargo) and external (e.g. environment) stimulus influence the stability. External factors that influence the concept of stability in a certain scenario, such as mission type, location of the mission and market behaviour, are also considered on the contextual aspect. Uncertainties over time, and how it affects the ship stability, are considered from a temporal perspective. The perceptual aspect presents the understanding of stability as a valuable lifecycle property after the ship is put into initial use. A prescriptive semantic basis for stability is proposed as an extension of this work, applying a general change-related ility pattern introduced by recent systems engineering research.

Keywords: *Lifecycle Properties, Stability and Systems Engineering, Ship as a Complex System.*

1. INTRODUCTION – ON THE VALUE OF STABILITY

Stability is such a fundamental property of the vessel that it is inherently connected to every kind of its operation and design approach. Design for safety, for instance,

would treat stability as the most uncertain aspect of the vessel design solution to be always feared, with designers being asked right on the first meeting: *What is the worst case scenario that this vessel can operate and yet be considered stable, sound safe?* Design



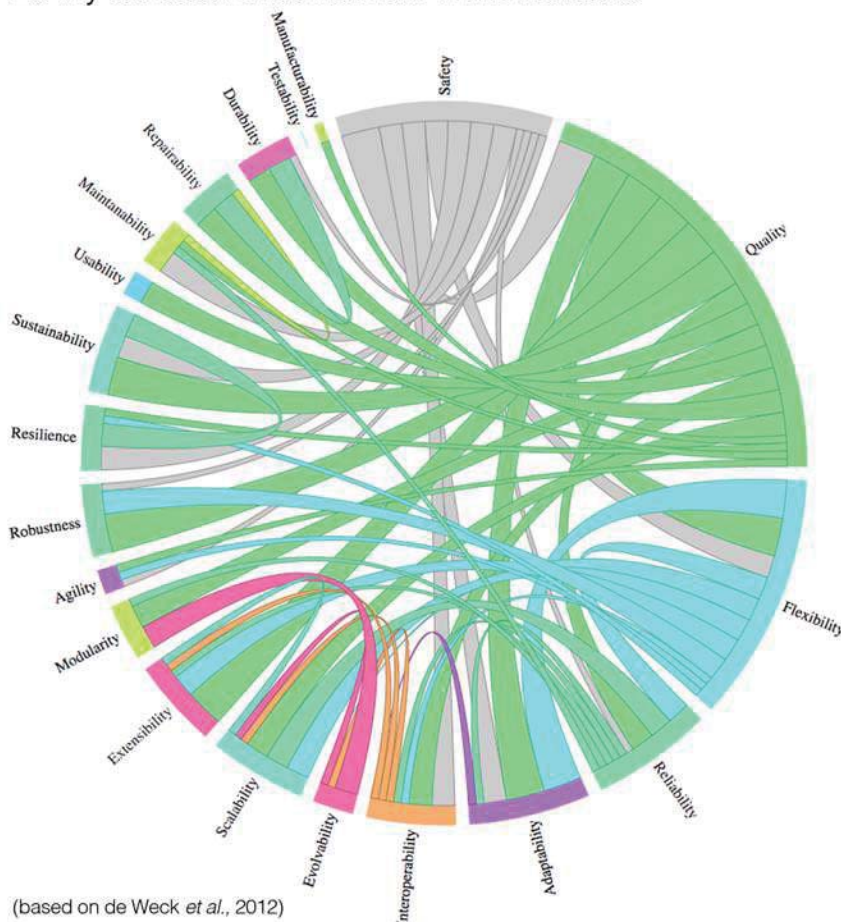
for maximum vessel performance would observe stability as a key constraint for modifications in a current design process, *We could have a bigger crane if the stability criteria did not played such a strong role*, one may say, when designing a new offshore construction vessel. The extension of such an exercise would find stability mentioning in pretty much every X at the Design for X studies (Andrews, 2009; IMDC 2012).

On the other side of the spectre we find new trends on observing qualities of a complex system, such as operability, modularity, maintainability, sustainability and robustness. These new trends and drivers are influencing shipowners' businesses a great deal, shifting perception from the delivery of goods by a ship with a size X and power Y to providing service A and B within safety, economic, and

environmental constraints. As Bodénes describes (2013), a decade ago, a shipowner would sit with the designer and discuss hull and propulsion; Today, the meetings are steered by factors such as safety, fuel consumption, capability, and reliability, necessitating documenting this kind of information as precisely as possible. There is, however, no consensus on how this precision can be achieved, especially since this required knowledge is not easy to access due to the abstract (one may say humanistic or non-metric) nature of these factors. Given that there is a clear shift from purely technical to knowledge-oriented factors, we can ask how then the traditional idea of stability fits on it? How is stability connected to a conception of value that includes not only immediate economic return, but also robustness toward uncertain lifecycle scenarios?

ilities dependency wheel

20 ility-co-occurrence network in the literature



(based on de Weck et al., 2012)

filtering by the three most cited ilities:

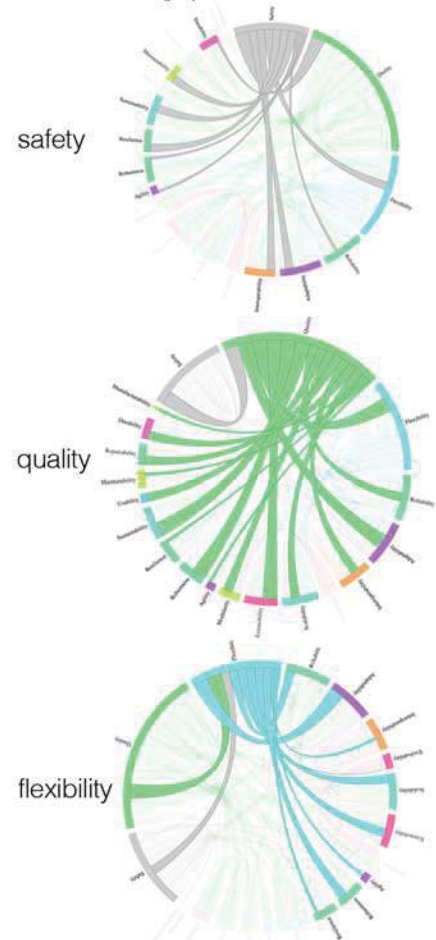


Figure 1 - ilities co-occurrence in engineering literature (based on de Weck et al., 2012)



This paper observes and discusses the stability as a system lifecycle property (ilities), connecting it to other ilities and its implications for vessel design. Section 2 proposes key ship design ilities categorized in top requirements, constraints and change related properties. Stability as a lifecycle property is investigated in Section 3, with its agents, effects and mechanisms, as well as implication for design. A five-aspect taxonomy is used to understand the factors that influence value (Section 4).

Extension of this work using system engineering prescriptive semantic basis is briefly investigated in Section 5. A discussion on the desire for proper stability and its value during the vessel lifecycle appears in the conclusion (Section 6).

2. KEY SHIP DESIGN ILITIES

The traditional understanding of lifecycle properties relates to the satisfactory performance from a quality perspective, over the full lifespan of the vessel system. They describe some essential property of the system connected (or resulted from) the form and function mapping of the system. Iilities typically relates to qualities above and beyond cost/schedule and performance expectations for the system development and operation. In other words, requirements that are not necessarily part of the fundamental set of requirements or constraints, but that act as a response to uncertain factors, such as threats (perturbations) and constraints (limitations) (Ross, 2008, 2014).

Many systems engineering authors are giving emphasis to the study of system lifecycle properties in complex systems during the last decade (Hastings *et al.* 2012). *Croud source* approaches, for instance, gathered in 2012 identified more than 80 ilities that can be used to evaluate the performance of a system (Ross and Rhodes, 2015). Descriptive surveys based on occurrence of ilities in written media attempted to illustrate the occurrence and

dependence of these properties in journal Articles (Figure 1, based on de Weck *et al.*, 2012).

Expressing wishes or expectations for a proper clarification of a property seems essential but, as noted by Rhodes and Ross (2015), tracing and mapping these wishes/expectations remains an ambiguous task. Therefore, selecting and filtering such ilities to the most relevant ones within a specific field is then a necessary challenge.

Table 1 – Key Ship Design Iilities

property	definition	category
QUALITY	The ship is well made to achieve its desired functions (missions) throughout its lifecycle	Top
RELIABILITY	The ship operates throughout its lifecycle without need of unplanned repair or intensive maintenance	Top
SAFETY	The ship operates in a state of acceptable risk, minimizing danger, injury or loss	Top
RESILIENCY	The ship can continue to provide required capabilities in the face of critical failures, such as subsystems malfunctions and environmental challenges	Constraint
AFFORDABILITY	The ship remains delivering value to the stakeholders (e.g. owner, operator, customer) in face of context shifts throughout its lifecycle	Constraint
SURVIVABILITY	The ship minimizes the impact of a finite duration disturbance on overall performance	Constraint
FLEXIBILITY	The ship's dynamic ability to take advantage of external opportunity, mitigating risk by enabling the ship to respond to context shifts in order to retain or increase performance	Change
ADAPTABILITY	The ship's dynamic ability to take advantage of internal opportunity, mitigating risk by enabling the ship to respond to context shifts in order to retain or increase performance	Change
SCALABILITY	A ship parameter can be scaled (e.g. increased/decreased) in order to retain or increase performance	Change
MODIFIABILITY	A ship can modify its form/ essence/ configuration in order to retain or increase performance	Change
ROBUSTNESS	The ship maintains an acceptable level of performance through context shifts with no change in its parameters	Change

(based on Hastings *et al.*, 2012; Ross, 2008; de Weck *et al.*, 2012; Jasionowski and Vassalos, 2010).

Approaching ship design as a complex system problem (Gaspar *et al.*, 2012), we

propose in Table 1 eleven key ilities connected to ship design. A general definition is presented, withihn three main categories. *Quality*, *Reliability* and *Safety* are considered top requirements the “Design for X” concept, meaning that every stakeholder desires a high quality ship (for instance better among peers), with safety (lower risk) and reliable (higher trust). *Resiliency*, *Affordability* and *Survivability* are considered constraints requirements, defined by price (afford) and how much it can survive disturbances (survivability) and critical failures (resiliency), in which the vessels stops to deliver value if not considered resilient, affordable and survivable at any point of its lifespan.

Change related ilities are connected to the changeability concept presented by Ross (2008), where changes can be considered as the transition over time of a parameter of the ship to an altered state (e.g. of stability). For the rest of this work we will use the terms of this last category to situate and compare stability among other lifecycle properties, pointing out how it influences the perception of an “-able” vessel during its lifecycle (e.g. stable, flexible, affordable, adaptable).

3. STABILITY AS A SYSTEM LIFECYCLE PROPERTY

3.1 Changes in Stability as Enabled Paths

Many lifecycle properties can be understood as how *good* the system reacts to changes in its form and function. Our assumption is thus that stability is a change-related ility (Ross and Rhodes, 2015), and should be treated as such, since stability crosses between technical and operational system’s metrics. On the initial phases of the value chain, such as concept and basic design, stability is strongly technical, connected to the system form and architecture. It is measured using a structural/behavioural metric, such as criteria

for GM, GZ curves and classification society rules.

Later, during operation, changes in the form are not an immediate option, and operational metrics gain in relevance. The performance is then measured based on the mission and environment factors that the ship is subjected to. Operational metrics thus are connected to the relation between stability and other attributes of the ship, such as rolling, pitch and heave acceleration, as well as survivability when perturbed/damaged (Neves *et al.*, 2010).

In this context, it is possible to consider changes in the events of a vessel as paths between different situations/states (Ross, 2014), for instance from *stable* to *unstable* as well as to *more operable due to moderate rolling* to *less operable due to heavy rolling*. This path is affected by external and internal agents, as well as mechanisms to balance/infer the effects of these agents.

To exemplify, consider stability having two essential binary states: stable and unstable. A change event in these conditions can be characterized with three elements: i) the agents of change; ii) the mechanism of change; and iii) the effect of change (Figure 2).

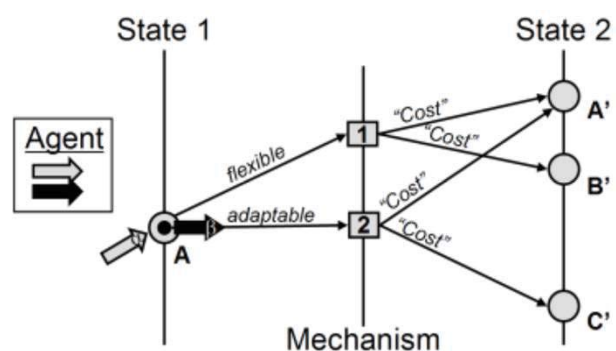


Figure 2 - Changes in stability as paths between states (Ross, 2008)

Consider A the actual state of a ship (for instance stable). An external active change agent α , such as a wave, wind, cargo displacement or damage, acts on the system (ship), affecting its stability. These disturbances accept two paths. First, without



any other agent, the system incorporates a certain mechanism (1), such as listing and/or righting arm, leading to a new state, such as more stable, less stable or unstable (A' , B' , C'). Another external change agent (responsive, β) can be incorporated on the system after the initial change occurs, such as intervention from the bridge to reconfigure anti-heeling tanks, leading to the system to adapt to the new situation with another change mechanism (e.g. movement of liquid cargo to counterbalancing heeling, or roll damping tanks). The cost in this model is not necessary connected to a monetary value, but to any value that represents time and/or resources use, such as energy, fuel, reaction and operation time. A summary of the model is listed in Table 2.

3.2 Agents, effects and mechanisms

During vessel design one must consider which technical (hull size, bow shape, tanks division) and operational (accelerations, risk level) metrics should be considered when analysing the vessel's stability. These choices interfere directly on how the ship will react given a perturbation in its stability state. Our assumption is that change related ilities (Table 1) can be used to define which agents, effects and mechanisms will be used to counteract perturbations in the ship stability (Ross, 2008).

Table 2 – Stability's elements of change

<i>Element</i>	<i>Description</i>	<i>Term</i>
Change agent	Element external to the ship, which affects the stability state, such as humans, software or natural phenomena. It can be considered active agents, such as an external force, environmental conditions (wave, current, wind), cargo handling, accidental forces (e.g. winch break, crane failure); as well as responsive agents (external counteractions), such as human decision to manoeuvring, to fill a ballast tank or to retrofit the ship.	α, β
Change Mechanism	The particular path the ship must take during transition to one prior state (stable) to another post state (more stable, less stable, unstable), such as new heading, tank filling, anchor handling drop, retrofit.	1, 2
Change Effects	Effect on the ship after action from agents - more stable, less stable or unstable.	$A' - A, B' - A, C' - A$

Potential Paths

Possible paths when the ship change from one state to another	$\alpha:A-1-A'$ $\alpha:A-1-B'$ $\alpha,\beta:A-2-A'$ $\alpha,\beta:A-2-C'$
---	--

Stability change agents are divided according to its location. External change agents are considered a flexible-type (e.g. wind heeling the ship, human action to change heading or cargo placement), while internal change agents are considered adaptable-type (e.g. bilge keel or antiroll tanks).

According to this taxonomy, designing for flexibility means facing changes in stability with an external agent, such as the operator at the bridge changing a current parameter of the ship. Designing for adaptability, on the other hand, would tackle changes in the stability state using only internal configurations of the ship-system, such as hull design, automatic antiroll tanks or passive bilge keels.

Effects in stability are considered the difference in states before and after an agent affects the system, indicating that a change in the attribute (e.g. GM value / heeling angle / roll period) has occurred.

A robust effect is the ability of the system to remain relatively constant in parameters in spite of system internal and external disturbances (therefore operable). Design for robustness in stability means that the ship will handle the active change agents by itself, maintain itself operable/survivable under an acceptable level of external forces aging upon it.

When parameters need to be changed we are talking about scalability. It means that, for the system to remain stable within the operational range over time, we need to change the scale of one its parameters, such as fill a ballast tank, modify heading or lower the load of a crane.

Modifiability is when the ship requires a modification in its main form/arrangement to remain stable under a certain operation. This



requires usually a redesign or retrofit of the vessel to incorporate new structural aspects, such as new antiroll tanks and/or structural reinforcement.

Mechanisms can be understood as the paths that the ship must take to transit between states. It includes elements inherent to the ship design process, such as necessary subsystems, components, resources, conditions and constraints that allows a path between two situations, such as *less stable to more stable*, *higher roll acceleration to lower roll accelerations*.

For the sake of exemplification, lets consider a crane operation with heavy cargo. The change agent is the crane, and the change effect is the GM value and heeling angle of the ship. Many possible paths (mechanisms) can be taken to minimize heeling angle and keeping safe GM values. The active agent (crane) can modify its arm length and height or even drop the cargo. The ship operator (responsive agent) can turn on dynamic positioning (DP) or roll compensation mechanism. Each action, thus, is connected to a *cost* in terms of time and resources to correct the effect caused by the crane.

When taking these definitions in the initial design process, design for many potential change mechanisms means design for different costs, with potential costs for a given path in a given condition. Over time, not only the cost of a mechanism may change, but also more paths can be added to the ship via new capabilities on board or retrofit of the ship. Table 3 summarizes the Stability's implications for design in terms of flexibility, adaptability robustness, scalability and modularity

Table 3 – Change related properties in Stability

<i>Design for</i>	<i>Description</i>
Flexibility	The stability change agent is external to the ship-system. Change mechanisms are possible under external (human, computer) actions
Adaptability	The stability change agent is internal to the ship-system.
Robustness	Design a vessel that keeps stable under conditions' change. Change mechanisms are inherent to the design
Scalability	Design a vessel able to be stable under a set of conditions when its parameters are scalable. For instance activate anti-heeling tanks or move deck cargo.
Modifiability	Vessel is only able to be stable after modifications are incorporated in its form, via re-design or retrofit. It may be the case for a low initial capital cost, with option for a retrofit and more stability in the long-term, if future contracts require it.

3.3 Lifecycle implications for ilities in stability during initial design

Our assumption is that designers should no longer only consider stability properties that meet today's regulations and requirements, but rather consider the implications and consequences of the lifecycle technical, operational and commercial context changes early in the design process (Ulstein and Brett, 2012; 2015), including change related mechanisms into the ship, which allow cost-effective reactions on how it behaves to disturbances in its stability related attributes. In order to explicit address the desire of a shipowner to have flexibility, it is necessary to gather more information about the desired responsive change agent, change effect and mechanisms, as *desiring flexibility alone is an imprecise request*. In this sense, we build on Ross (2008) proposition of analysing and evaluating stability related in five basic steps:

i) Specify the origin of the active change agents (perturbances, disturbances), and in which operational conditions they occur. For instance, finite duration active agents such as wave, wind, short operation loads (hanging, moving) or even chaotic motions; as well as long term shifts (likely to last), such as cargo placement/shift, long operation (towing, crane),



damage, free-surface, flooding, collision, grounding should be specified.

ii) Determine the acceptable *cost* threshold, that is, response time and resource uses when disturbed, as well as determining the shipowner willingness to pay for a more stable vessel, such as wider breadth, faster antiroll system, stronger hull or higher dynamic position capability.

iii) Specify if the origin of responsive agent, that is, internal (adaptable and incorporate in the ship as a system) or external (acting on the ship but external to its boundaries).

iv) Consider which effect is expected for each of the responsive agents selected in iii). Robust effects will change no parameter, being inherent to the form/arrangement of the ship. Changes in the level of a vessel parameter creates scalable effects, such as modification of the tension in a towing line, as well as filling up the antiroll tank or activating the DP system. Modifiable effects require changes in the nature of a certain parameter of the ship, such as the installation of a more powerful anti-heeling pump, a new crane or rearrangement of the ship load distribution.

v) Analysis and evaluation of the vessel design space is done in the last phase, considering, which capabilities should be inherent or installed on board the ship, in terms of disturbances (active agents), reactions (responsive agents), and effects on stability related attributes. For example, if the shipowner requires the ship to be adaptable and robust regarding supply operation in North Sea high wave conditions, while flexible when performing anchor-handling operation in more extreme conditions, then response mechanisms that are able to be flexible and adaptable must be considered when evaluating the design space. In this way, the specific *adaptability* (in terms of low accelerations while supplying) and *flexibility* (in terms of controlling safe GM and low acceleration while anchor-handling in extreme conditions) can be weighed against

cost (time/resource) requirements and rules constraints. At the end, we should converge towards a set of quantified lifecycle properties, that is, a value gain versus cost when talking about *robustness* or *scalability*.

4. HANDLING VESSEL STABILITY COMPLEXITY IN A LIFECYCLE CONTEXT VIA A FIVE-ASPECTS TAXONOMY

A systemic approach for defining complexity in ship design is presented by Gaspar *et al.* (2012a, 2012b), where the complexity of a system is captured through five main aspects, namely: Structural (structure and relationships), Behavioural (performance), Contextual (circumstances), Temporal (changes in context and uncertainties) and Perceptual (stakeholders' viewpoint). Here we use these taxonomy to clarify, organize and handle the information necessary to properly identify and build up the elements necessary to understand stability as a lifecycle property.

Structural and behavioural aspects connect to the traditional technical understanding that stability depends on the ship main dimensions, the shape of the submerged hull and tanks/cargo arrangement, as well as location of unprotected openings such as engine room air intakes and the actual location of centre of gravity KG. Well-known trade-offs analysis, when determining the main dimensions and hull form, should be conducted among some major design disciplines, such as sea keeping, stability, manoeuvrability, sufficient cargo hold volume and payload capacity. Considering a ship with large GM, for instance, where the righting arm developed at small angles of heel is also large. Such a ship is usually considered *stiff* and will resist roll. However, if the metacentric height of this ship is small, with smaller righting arm, the vessel may be considered tender, rolling slowly. Practical offshore support vessel (OSV) design experience shows the necessity of balance between generating stiff or tender design, since



they have opposite influences on stability of vessel and convenience of crew during site operation. A *design for safety* thus will be contradictory to a *design for operability*. Therefore, if a shipowner invests in robustness for the reason that his or her vessel may be considered safe for a wide range of conditions, the same investment may lead to a loss in contracts due to limited cargo capacity or smaller crew comfort. What the designer should consider then is the nature of the reaction of the vessel, for instance, by changing one of its change effects, for instance a tank installed in a higher deck (modifiability) that can be filled during site operation (scalability). The initial robust solution is unable to properly consider the extension of the stability complexity, while the modifiable / scalable solution is.

The contextual aspect pertains to the external circumstances to which the vessel is subject to during operation and how its behaviour is affected accordingly. The applied contextual factors in traditional ship design are often dominated by various technical and economic factors during exploration of the technical design space such as meteorological conditions, rules and regulations, supply and demand, breakeven rates and so forth. Such factors will impose a range of requirements and restrictions, the resulting solution space will be significantly delimited, inherently affecting the shape of the vessel and consequently narrowing the diversification of potential stability characteristics. In order to move beyond pure technical thinking, stability as a lifecycle property, which must also be included as input when considering the boundaries of the design space. In other words, stability must be perceived as something more than just metacentric height, a GZ-curve and a characteristic of operational performance. It should also be considered an attribute of value creation across contextual factors, i.e. diversifying the categories of which stability value is commonly quantified by. Exemplifying, a remarkably stable vessel could be considered technically superior, but at the

same time, it may also require compensatory investments leading to an increased capital cost. Viewing this in a contextual lifecycle perspective the value of this increased robustness should also be considered in terms of factors such as flexibility, adaptability, and current and presumed market developments.

When considering a vessel from a temporal perspective, changes in the system's lifespan occurring at disparate points in time, in conjunction with a highly scattered degree of uncertainty, together constitute the fourth taxonomy aspect. When viewing stability as a lifecycle property, a method of quantifying contextual shifts is necessary. The technical perspective would take into account the probable spectre of applicable mission types and operational modes by utilizing a traditional set of analyses, and conclude based on input parameters such as wave height and direction, currents, mass distribution, and hull shape. These types of analyses unquestionably provide excellent sources of information regarding a vessel's stability characteristics; however, they do not take into account contextual variations in an uncertain temporal perspective. One possible method of quantifying such complex information is Epoch Era Analysis (EEA) (Ross and Rhodes, 2008, Gaspar *et al.*, 2012b, Keane *et al.*, 2015), which captures future expectations by encapsulating each factor-variant in a fixed (epoch) and dynamic (era) time-constrained context setting that should be further analysed in terms of probability, optimality, performance, value, and utility, to name a few. This enables the incorporation of multi-values, attributes and assumptions that previously may have been side-lined, generating data for the perceptual aspect.

The overall lifecycle property connected to the perceptual aspect is value robustness, which is used, including but not limited to aspects presented above, to define in multi-perspective a better vessel among a design set. Value robustness is the ability of a system to continue to deliver stakeholder value in face of shifts in



context and needs (Ross and Rhodes, 2008). In ship design, this means a ship perceived successful by stakeholders throughout the lifetime of the vessel. Rather than maximizing value delivered by a ship in one situation, we need to maximize it over a range of situations and preferences of the owner (or other constituents). This might reduce the maximum possible reward but also minimize the maximum possible loss, with relevance increasing as uncertainty grows and investors become more risk aware (Gaspar *et al.*, 2015).

In this context, how to perceive stability as a lifecycle property, and make benefit of it to bring more value to the vessel? How to really decompose the multi-perspective perception of what a stakeholder would understand as a valuable property? Ebrahimi *et al.* (2015) notes that the perception of a better (therefore stable) vessel relies in *a middle term perspective, between the pure satisficing and maximizing the goodness of fit of all stakeholders' expectations*. On one hand, we would like to select the best solution, by creating and analysing all possible risk situations and alternatives, and choose the best. Our limitation as human beings, however, allow us to only compare and contrast a very limited set of variables and alternatives when trying to find the good enough stability. Ulstein and Brett (2015) propose the application of different perspectives to overcome these limitations. *Technical, Operational and Commercial* perspective for instance, links to the vessel skills and level of efficiency needed for a particular operation, while *Smarter, Safer and Greener* perspective connects to a more fashionable idea of effectiveness, increasing the overall effect of the combined technical, operational and commercial performance. The change related properties are tackled in their approach for *design for efficiency*, where flexibility, agility and robustness are observed in terms of the ability of the vessel to perform different operation, move and upgrading itself quickly and not likely to fail.

5. TOWARDS A PRESCRIPTIVE SEMANTIC BASIS FOR STABILITY

We are aware of the challenges when extending the concept of stability, connecting it to less technical lifecycle properties. While stability is traditionally a well-defined and quantified term in ship design, the informal meaning, ambiguity, synonymy and lack of scientific precision (and therefore standard) for the pre-mentioned properties raise a yellow flag. This concern does not relate solely to the stability issue, but to the assessment and quantification of all properties in general. *Flexibility*, for instance, may be connected to the ability *to change* as well as to the ability to *satisfy multiple needs*.

Therefore, to assume that stability can be defined and measured in terms of properties such as flexibility, adaptability, modifiability, scalability and robustness, we need to have a more precise understanding of these terms. Ross and Rhodes (2015) address this issue by proposing a generalization of the change related properties, via a prescriptive semantic basis for these properties. Starting from the same principle of change agent, effect and mechanism, the authors propose a larger set of twenty categories (elements) for defining a larger set of possible changes in a system. This semantic basis aims to capture the essential difference among change-related properties, in the following proposed general statement (categories emphasized): “in response to perturbation in context during phase, desire agent to make some nature impetus to the system parameter from origin(s) to destination(s) in the aspect using mechanism in order to have an effect to the outcome parameter from origin(s) to destination(s) in the aspect of the abstraction that are valuable with respect to the thresholds in reaction, span, cost and benefit”.

For the illustrative purposes, we can use the aforementioned general pattern to create a statement that intends to capture a more precise meaning to which kind of lifecycle property in



stability are we talking about. When talking to *scalability*, for instance, one could state: “In response to a crane failure (*perturbation*) during heavy lift operation (*phase*) in the North Sea (*context*), desire operator (*agent*) to be able to decrease (*nature*) the heeling angle of the ship (*parameter*) from a less stable (*origin*) to more stable (*destination*) position (*aspect*) through turning on the pumps that feeds the anti-heeling tanks (*mechanism*) in less than ten seconds (*reaction*) that results in the increasing of the volume of the tanks (*effect*), decreasing the heeling angle (*aspect*) to an acceptable value (*destination*) in the ship (*abstraction*) taking less than 30 seconds (*span*), with a energy use (*cost*) inferior than the actual installed system (*benefit*)”.

The basis allow then the parsing and decomposition of what one may understand as lifecycle property. When applied to stability, however, this basis can be a bit overwhelming, and simplifications can be done according to phase of the lifecycle studied. When evaluating different mechanisms to overcome unstable conditions, for instance, we may fix the other elements, while leaving the *mechanism* option open, allowing designer to propose and evaluate different alternative paths for meeting the criteria. In this case, considering the example from the last paragraph, rather than proposing the use of anti-heeling tank, one could suggest a second crane to compensate, or adaptations at hull form or at the anti-roll system. In other case, we case vary the causes of failure, investigating which cases of perturbation require robust, scalable and modifiable solutions.

Note also that the concept of *cost* introduced in Section 3.1 is also extended, incorporating common trade-offs that can be used to judge the goodness of a stability performance of a ship, such as *reaction* (timing), *span* (duration), *cost* (resources) and *benefit* (utility).

6. CONCLUDING REMARKS

Much research is currently being developed on the topic of less technical lifecycle properties, and yet many open questions require a more deep study until some consensus is reached as to what this set of agreed upon properties should be like. As for the case described in this paper, our intention was to show that a ship-owner may require a robust vessel system, but in real life situations he or she wants a ship system that can be changed in the future. Market conditions are changing over time and therefore, vessels have to change their capacity and capabilities (internalities) with such externalities. Thus, the way we normally handle the stability of ships from a naval architectural standpoint is not having the process quality of being able to deal with all internalities and externalities to the extent necessary for future flexible/adaptable ship design. Why do people desire higher stability for common initial load cases, while at the same time they know that the vessel over time will be subject to new operational situations not really catered for in the initial design solution space? Stability, may not have a value in and of itself, but rather may represent a significant boundary condition limitation for future adaptability and changeability of the ship at hand. Better prepared for and thought through, in the context of an epoch-era concept framework, stability can be allocated higher value in the future of ship design, than a strict boundary condition, normally,

For the sake of example, let us analyse the main stakeholder and needs of an OSV. It is assumed that the concept of safety considers the protection of human life and environment, and efficiency connects primarily to fuel and the cost (or savings) connected to it. Considering increasingly harsher operating conditions is a necessary precaution in order to reveal adequate stability characteristics when quantifying from a value robustness perspective. The increase of significant wave height, wind speed, and current, all contribute



towards a heightened range of loads and motions, consequentially increasing the risk of destabilizing the vessel, minimizing operational windows, and, inherently, depreciating value from a lifecycle perspective. Creating a vessel with sufficient capabilities to counter these effects increases the operational window, but traditionally will also widen the vessel resulting in increased hull resistance and a need for more power to uphold the same speed during transit and on site DP operations. It will also facilitate a higher payload capacity as well as a larger crane capability, again, enabling a wider range of mission profiles. On the extreme case, even if technically and theoretically science and technology are able to design and construct a vessel that does not capsize, such vessel would end up being unfit to operation or, most commonly, unaffordable. Thus, depending on the viewer's perspective regarding the value of stability, certain trade-offs will be virtually inescapable, e.g. payload capacity versus fuel consumption, or level of acceleration (crew comfort) versus operational utilization (up to allowed level of excitation). Using the concept of ilities can then facilitate the understanding and quantification of these stability trade-offs in future vessel design. In other words, a design can be better perceived as more valuable if stability is observed as a lifecycle system property.

7. REFERENCES

- Andrews, D. IMDC 2009 "State of the Art Report on Design Methodology" in 10th International Marine Design Conference 2009 Proceedings Vol 2, Tapir Academic Press, Trondheim, Norway, 2009.
- Bodénes, G. "Bourbon into the future. Norwegian Maritime Centre of Expertise", NCE Annual Conference, Alesund, 2013
- de Weck, O.L., Ross, A.M., and Rhodes, D.H., "Investigating Relationships and Semantic Sets amongst System Lifecycle Properties (Iilities)," 3rd International Conference on Engineering Systems, TU Delft, the Netherlands, June 2012.
- Gaspar, H., Erikstad, S.O., and Ross, A.M., "Handling Temporal Complexity in the Design of Non-Transport Ships Using Epoch-Era Analysis," *Transactions RINA, Vol. 154, Part A3, International Journal of Maritime Engineering*, Jul-Sep, pp. A109-A120, 2012a
- Gaspar, H., Rhodes, D.H., Ross, A.M., and Erikstad, S.O., "Handling Complexity Aspects in Conceptual Ship Design: A Systems Engineering Approach," *Journal of Ship Production and Design*, Vol. 28, No. 4, November, pp. 145-159, 2012b
- Gaspar, H. M.; P. O. Brett; S. O. Erikstad and A. M. Ross. 2015. "Quantifying value robustness of OSV designs taking into consideration medium to long term stakeholders' expectations". In Proceedings 12th IMDC, Tokyo, 2015.
- Hastings, D.E., La Tour, P., and Putbrese, B., "Value-Driven Analysis of New Paradigms in Space Architectures: An Iilities-Based Approach," AIAA Space 2014, San Diego, CA, August 2014
- IMDC Secretariat. 11th International Marine Design Conference, Proceedings Vol 1&2-IMDC Glasgow, UK, 2012.
- Jasionowski, A., Vassalos, D. "Conceptualizing Risk", University of Strathclyde, in "Contemporary Ideas on Ship Stability and Capsizing Waves", Springer, 2010.
- Keane, A., Brett, P. O., Gaspar, H. M., "Epoch-Era Analysis in the Design of the Next Generation Offshore Subsea Construction Vessels", in 10th International Conference on System of Systems Engineering (SoSE), San Antonio, USA, 2015.
- Neves, M. A. S., Belenky, V. L., de Kat, J. O., Spyrou, K., Umeda, N. "Contemporary Ideas on Ship Stability and Capsizing Waves", Springer, 2010.
- Ross, A. M. "Contributing toward a prescriptive 'Theory of Iilities', SEAr-MIT, Missouri University of Science and Tech. April 2014
- Ross, A. M. "Defining and Using new 'ilities'", SEAr Working Paper Series, MIT, 2008



Ross, A. M., and Rhodes, D. H. “Architecting systems for value robustness: Research motivations and progress”. SysCon 2008 – IEEE International Systems Conference 2008.

Ross, A.M., and Rhodes, D.H., “Towards a Prescriptive Semantic Basis for Change-type Ilities,” 13th Conf. on Systems Engin. Research, Hoboken, NJ, March 2015.

Ulstein, T., and Brett, P. O. “Critical systems thinking in ship design approaches” 11th IMDC, Glasgow, UK, 2012.

Ulstein, T., and Brett, P. O. “What is a better ship? – It all depends...” (accepted) keynote speaker, 12th International Maritime Design Conference – Tokyo, 2015



An Experimental Study on the Characteristics of Vertical Acceleration on Small High Speed Craft in Head Waves

Toru, Katayama, *Graduate School of Engineering, Osaka Prefecture University*

katayama@marine.osakafu-u.ac.jp

Ryosuke, Amano, *Graduate Student, Graduate School of Engineering, Osaka Prefecture University*

sv103001@edu.osakafu-u.ac.jp

ABSTRACT

In this study, the characteristics of vertical acceleration on small high speed passenger craft in head waves are investigated experimentally, an empirical method to estimate it is proposed. First, how to decide the sampling frequency and the test duration (total number of waves encounters) is discussed to measure acceleration accurately. Next, the vertical acceleration on a hull is measured in regular and irregular waves, and the characteristics of the vertical acceleration for wave height, wave period and forward speed are investigated. And its probability density function is also investigated for the results in irregular waves. Moreover, the same measurements for two different hulls are carried out, and the effects of hull form is investigated.

Keywords: *vertical acceleration, small high craft, irregular waves*

1. INTRODUCTION

Recently, the maximum forward speed of small passenger craft is increasing. In case of the craft, the encounter wave period becomes shorter with increase of forward speed, and very large upward vertical acceleration is caused when its bow goes into the water surface. It is known that it cause not only bad ride comfort but also failure of hull or injury of passengers in some cases.

For development hull form, it is necessary to estimate the response of acceleration for its forward speeds and sea conditions. And for safety navigation management, it is important to estimate statistical short-term prediction of

occurrence of un-desired large vertical acceleration.

The purpose of this study is to investigate the above-mentioned characteristics of vertical acceleration of small high speed passenger craft. First, in order to measure accurate vertical acceleration by a partly captive model test, data sampling and data analysis methods are discussed. Next, the vertical acceleration on a hull is measured in regular and irregular waves, and the characteristics of the vertical acceleration for wave height, wave period and forward speed are investigated. And its probability density function is also investigated for the results in irregular waves. Moreover, the same measurements for two additional



different hulls are carried out, and the effects of hull form is investigated.

2. OBJECT SHIP

Table 1 and Fig.1 show the principle particulars of models and their photographs. Fig.2 shows the body plan of Ship A. Their loading condition is full load. They are fast semi-planing craft with warped V and their draft is shallower and L_{pp}/B is larger than typical planing hulls. In the comparisons among the models, L_{pp}/B of Ship B is smaller than others and dead rise angle of Ship B is larger than others.

Table 1 Principal particulars of the models in real scale.

	Ship A	Ship B	Ship C
Scale: 1/S	1/23.4	1/21.0	1/21.0
Length between perpendiculars: L_{pp} [m]	23.4	14.95	18.1
Breadth: B [m]	4.5	4.5	4.4
Deadrise angle at s.s.=5.0: β [deg]	18	18	24
Displacement: W [tonf]	36.76	25.91	31.51
Draft: d [m]	0.760	0.751	0.953



Fig.1 Photographs of the models (Ship A, B and C)

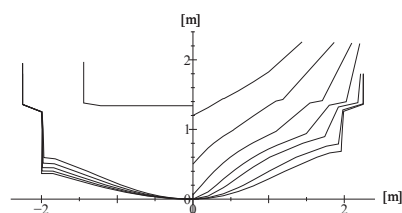


Fig.2 Body plan of the model (ship A).

3. MEASUREMENT AND ANALYSIS

3.1 Measuring device and coordinate system

Fig.2 show a schematic view of experiment and its coordinate system. Fig.3 shows its picture. A model is towed at constant speed with heaving and pitching free condition. And heaving (up: +), pitching (bow up: +) and normal acceleration on the base line of the hull (upward: +) are measured. Three acceleration sensors are installed on bow, midship and stern. Wave height is also measured with a servo type wave height meter attached to the towing carriage.

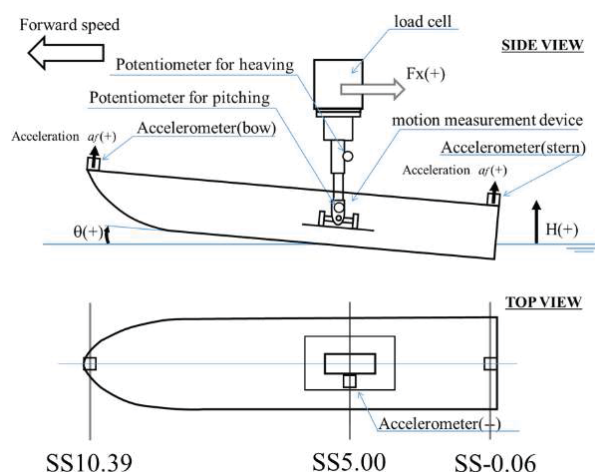


Fig.2 Schematic view of the experiment to measure vertical acceleration on hull

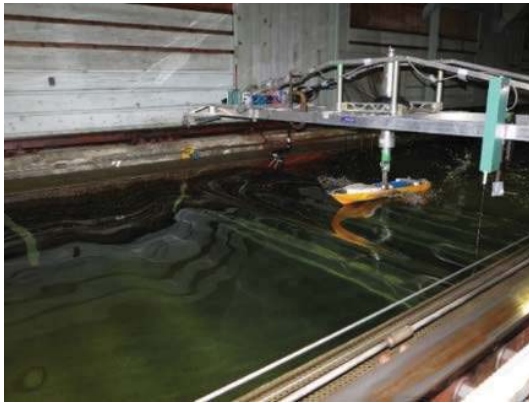


Fig.3 Photograph of the experiment.

3.2 Sampling frequencies

The sampling frequencies f_s [Hz] in the measurement is decided by eq.(1).

$$f_s \geq \frac{n_s}{\Delta t} \sqrt{s} \quad (1)$$

where s is the denominator of scale of model, Δt [sec] is the shortest duration of impact accelerations acting on hull in irregular waves in real scale, n_s is the number of sampling data in the impact acceleration. According to the reference (National Maritime Research Institute, 2007 and Takemoto et al., 1981), Δt is about 120msec in real scale. To express the peak of the impact acceleration, if $n_s = 4$ or 5 (Seakeeping Committee of ITTC, 2011) is assumed, an adequate $f_s = 200\text{Hz}$ is obtained. Fig.4 shows the convergency of average amplitude of vertical acceleration measured for different sampling frequencies (100, 200, 500, 1000Hz). The number of encounter waves is more than 400.

The upper figure shows the average of upward peak value of the acceleration and the under one shows the average of downward peak value of the acceleration, and the horizontal axis is sampling frequency. As a result, it is noted that the margin of error is smaller than 5% when the number of sampling frequencies is more than 200Hz. Therefore, the number of sampling frequencies in the measurement is decided for 200Hz.

Fig.5 shows a time history of measured acceleration at FP. In the measurement, the impact acceleration shown at $t = 0.7\text{seconds}$ in Fig.5 is observed commonly in each measured data. The acceleration occurs when its bow goes down into the water surface. In order to obtain the peak to peak values of the acceleration, zero-down crossing method is used in the analysis. As seen in Fig.5, time history of measured acceleration has noise. To take zero cross points, the data filtered with a central moving average method of 10 datum is used. On the other hand, to take accurate peak value of the acceleration, the data filtered with a central moving average method of 2 datum is used.

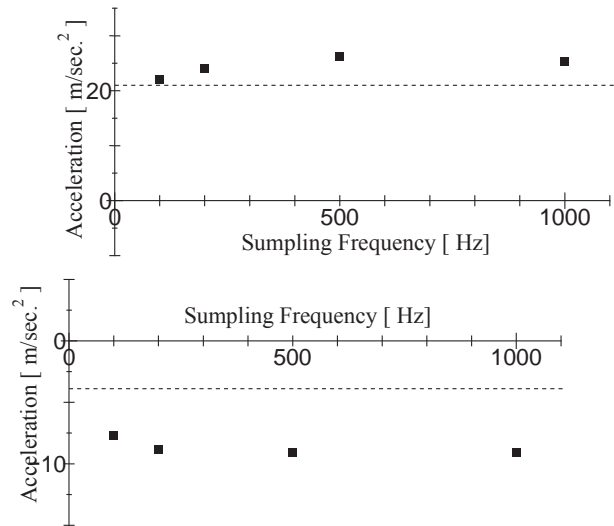


Fig.4 Variation of average of amplitude of vertical acceleration measured for different sampling frequencies. (upper figure: upward acceleration, lower figure: downward acceleration)

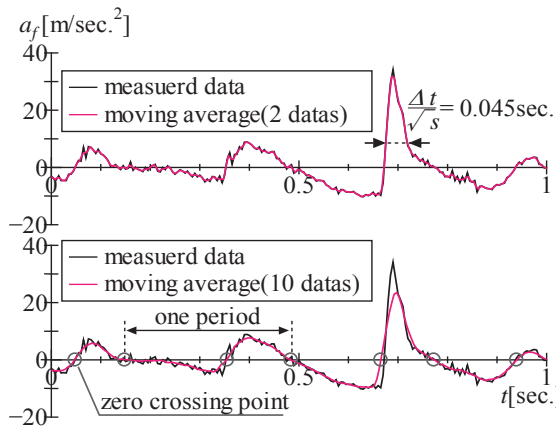


Fig.5 Time histories of measured data in irregular waves. (upper figure: a central moving average method of 2 datum, lower figure: a central moving average method of 10 datum)

3.3 Sampling number of encounter waves

Fig.6 shows the convergency of average amplitude of vertical acceleration measured for different sampling number of encounter waves. The upper figure shows the average of upward peak value of the acceleration and the under one shows the average of downward peak value of the acceleration, and the horizontal axis is sampling number of encounter waves. As a result, it is noted that the margin of error is smaller than $\pm 4\%$ when the sampling number of encounter waves is more than 200. Therefore, measurement in irregular waves is carried out with more than 200 encounter waves.

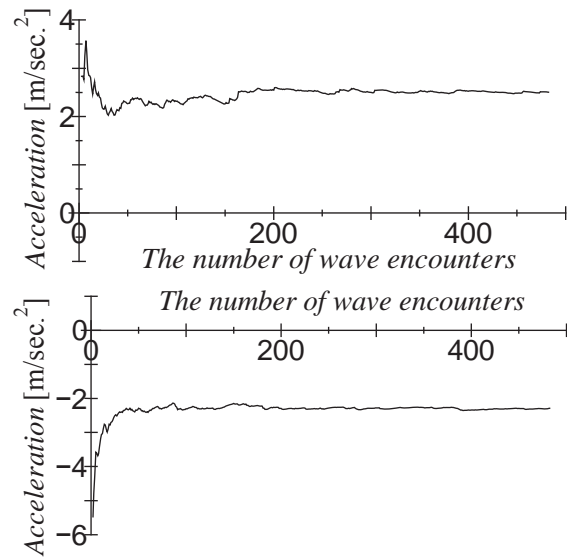


Fig.6 Variation of average of amplitude of measured vertical acceleration for numbers of amplitude data.(upper figure: upward peak value, lower figure: downward peak value)

3.4 Longitudinal distribution of vertical acceleration

The instantaneous acceleration a_x on longitudinal position X on hull is expressed as Eq.(2) with heaving and pitching of an arbitrary position.

$$a_x = \ddot{z} \cos \theta + l_x \ddot{\theta} + (1 - \cos \theta)g \quad (2)$$

Where z is heave displacement (upward: +), θ is pitch angle (bow up: +), l_x is distance (forward:+) from the position of motion measuring and g is the gravitational acceleration (downward: +). Furthermore the heave and pitch accelerations are calculated with numerical differentiation of their data of displacement.

The accelerations measured on two different position on hull (a_A and a_F) are expressed as eq.(3) and eq.(4) by using eq.(2).

$$a_A = \ddot{z} \cos \theta + l_A \ddot{\theta} + (1 - \cos \theta)g \quad (3)$$



$$a_F = \ddot{z} \cos \theta + l_F \ddot{\theta} + (1 - \cos \theta)g \quad (4)$$

$$T_1 = 3.86\sqrt{H_{1/3}} \quad (7)$$

By using eq.(3) and eq.(4), heave and pitch terms in eq.(2) can be erased. Then eq.(5) is obtained.

$$a_X = a_F + (l_X - l_F) \frac{a_F - a_A}{l_F - l_A} \quad (5)$$

where $l_X - l_F$ is the distance from F to X , $l_F - l_A$ is the distance from A to F . Eq.(5) indicated that the instantaneous acceleration a_X is calculated by Eq.(5) with the measured instantaneous accelerations a_A and a_F .

Fig.7 shows the comparison between the calculated acceleration on midship by Eq.(5) using accelerations measured on the stem and stern and the acceleration measured on the midship position. From the results, it is confirmed that the calculated result is good agreement with the measured results.

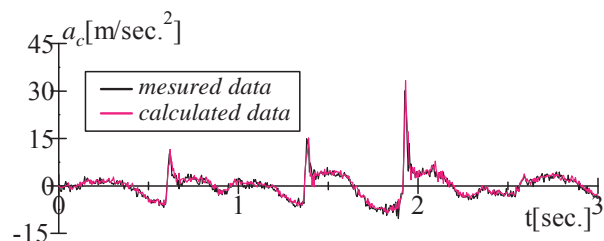


Fig.7 Time histories of measured and calculated results at s.s.5.0 in irregular wave. (sea state 4, $Fn=0.51$, Ship A)

3.5 Making irregular waves

Eq.(6) is ISSC spectrum, and Eq.(7) is the relations between significant wave height $H_{1/3}$ [m] and average wave period T_1 [sec].

$$\frac{S(\omega)}{H_{1/3}^2 T_1} = \frac{0.11}{2\pi} \left(\frac{\omega T_1}{2\pi} \right)^{-5} \exp \left\{ -0.44 \left(\frac{\omega T_1}{2\pi} \right)^4 \right\} \quad (6)$$

where ω [rad/sec] is circular frequency of wave, $S(\omega)$ [$m^2 \text{ sec}$] is energy density function of wave. To make irregular waves, the spectrum is divided into 100 equally in 0.2~2.5Hz, and a sine wave of each frequency component is superposed. In addition, the phase difference of each frequency component is given as random numbers for each measurement. Table 2 shows the range of wave height for sea state in real scale, and the wave height in this study. The towing speeds in the measurement are 0, 10, 15, 20, 25, 40kts in real scale.

Table 2 Wave conditions of the experiment.

sea state	wave height for seastate [m]	typical wave height for a sea state	average wave period : T_1 [sec.]
3	0.50~1.25	0.70	3.2
		1.00	3.9
4	1.25~2.50	2.00	5.5
5	2.50~4.00	3.00	6.7

4. CHARACTERISTICS OF ACCELERATION

4.1 Effects of Type of Ship

As an estimation method of vertical acceleration on hull, Osumi's chart (Osumi, 1992) and Savitsky's empirical formula (Savitsky et al., 1976) are known. Fig.8 shows the comparisons between the measured results (Ship A) and Osumi's results. The measured results are larger than Osumi's results. It is supposed that Osumi's results does not include the impact acceleration shown in Fig.5, because the object ship is the high speed patrol boat. Fig.9 shows the comparisons between the measured results and Savitsky's results. The measured results are smaller than Savitsky's results. It is supposed that Savitsky's results include large impact acceleration, because the object ships is typical planing hulls which is hard chine straight deep V monohedron without bow flare.

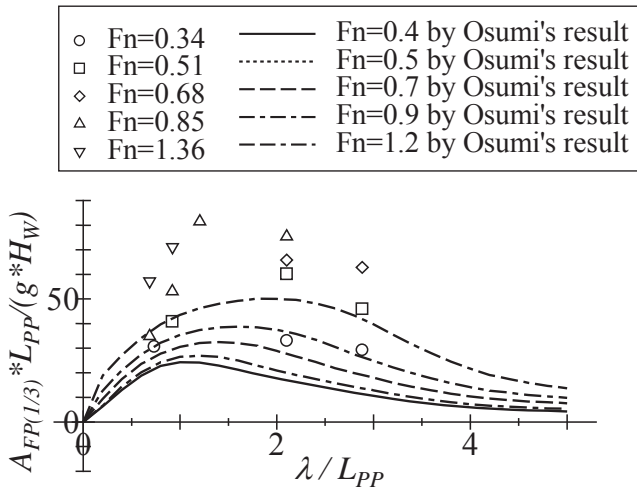


Fig.8 Comparison of non-dimensional significant peak to peak amplitude of acceleration between the measured results and Osumi's results.

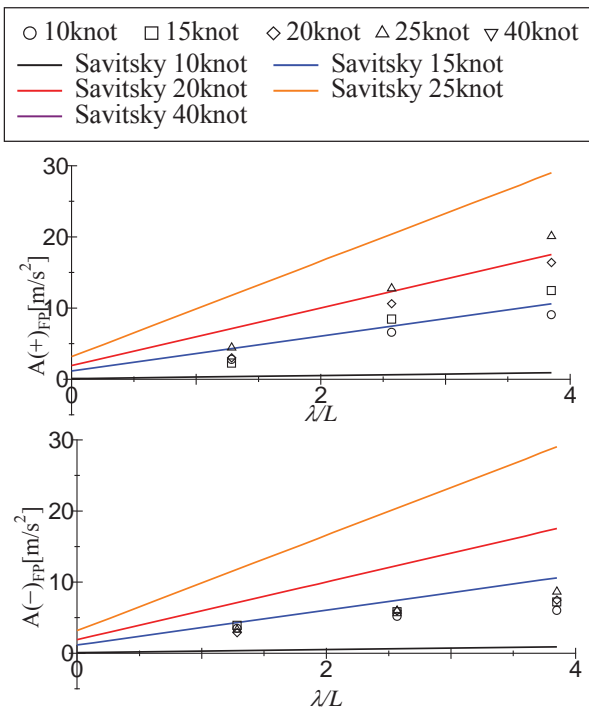


Fig.9 Comparison of average peak value of vertical acceleration between the measured results and Savitsky's results. (upper figure: upward peak value, lower figure: downward peak value)

4.2 Effects of wave length and height

Fig.10 shows non-dimensional average upward or downward peak value of measured

vertical acceleration on hull. In the figure, the horizontal axis is the ratio of wavelength to ship length λ/L_{PP} . The wavelength is calculated from $\lambda = g/(2\pi) \times T_1$. Eq.(8) is proposed to fit to the measured results, and the fitted curves are shown the figure.

$$y = B \times x \times e^{-Cx} \quad (8)$$

To investigate the effect of wave height on the vertical acceleration, the measurement with different wave height, constant forward speed and constant average wave period for Ship A is carried out. Fig.11 shows average upward and downward peak values of vertical acceleration at FP. The horizontal axis is $H_{1/3}/L_{PP}$. From the figure, it is noted that the non-dimensional values of upward and downward acceleration are linearly increased with increase of wave height. The same tendency can be seen in the upward acceleration in the regular wave shown in Fig.12 in the condition where the impact acceleration shown in Fig.5 occurs because of increase of wave height or/and forward speed.

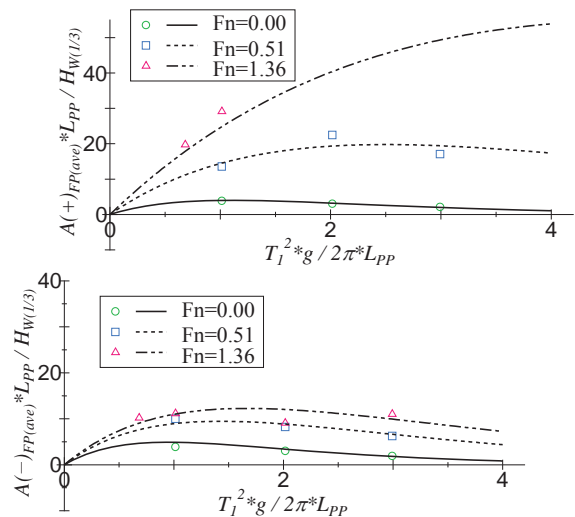


Fig.10 Non-dimensional average peak value of measured vertical acceleration obtained by Eq.(8) for Ship A. (upper figure: upward peak value, lower figure: downward peak value)

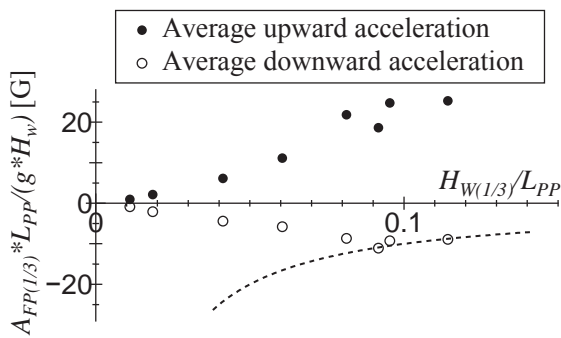


Fig.11 Average upward and downward peak values of vertical acceleration at FP measured for several wave height. (Ship A) In this figure, the black solid line shows the free fall whose acceleration is 1.0 G.

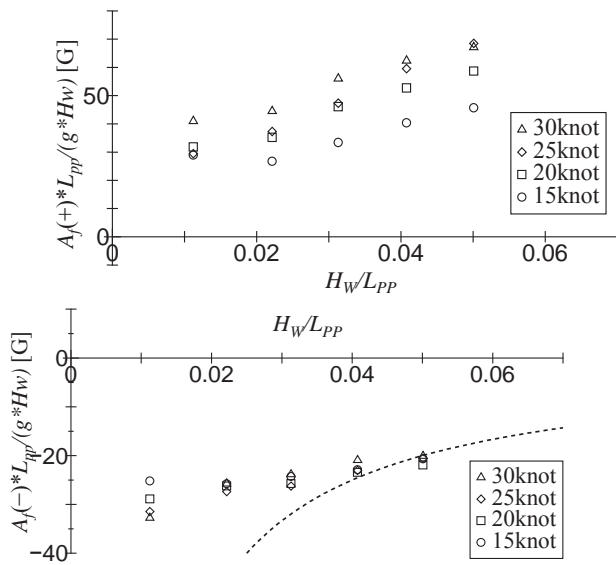


Fig.12 Measured upward and downward peak value of vertical acceleration for wave heights at *s.s.* 10.39 ($T_w=1.0$ sec) (Ship A). (upper figure: upward peak value, lower figure: downward peak value)

4.3 Longitudinal Distribution

Fig.13 shows longitudinal distribution of peak to peak amplitude and peak values of vertical acceleration which is calculated by Eq.(5) with vertical acceleration measured at FP and at AP. The horizontal axis is the square station number (AP=0 and FP=10). The vertical acceleration increases with increase of forward speed, and it linearly increase with

moving forward of longitudinal position from about *s.s.*=4.0. From the lower figure, it is found that upward peak value is larger than downward peak value, because upward acceleration occurs when bow of ship goes into the water surface. Fig.14 shows the longitudinal position of minimum vertical acceleration. The position is different according to forward speeds or wave periods and moves backward with increase of forward speed or/and wave period.

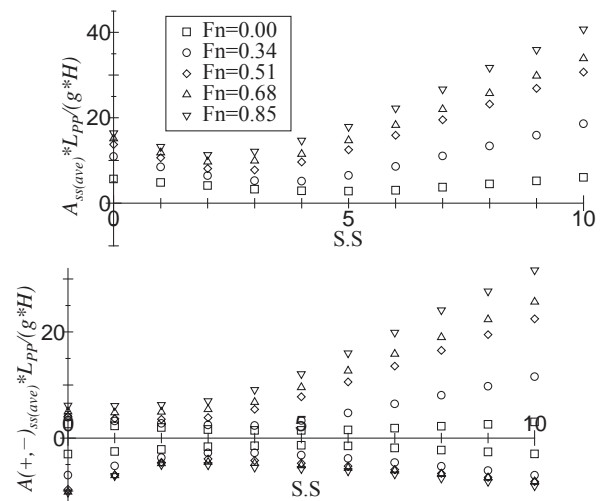


Fig.13 Longitudinal distribution of significant peak to peak value and upward and downward of vertical acceleration on hull. (upper figure: peak to peak value, lower figure, upward and downward of acceleration)

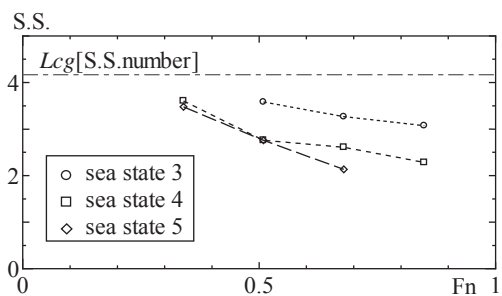


Fig.14 Longitudinal position where amplitude of vertical acceleration is minimum. (Ship A)

Fig.15 shows the non-dimensional value of acceleration shown in Fig.13. Value at arbitrary longitudinal position is divided by the value at FP. To estimate longitudinal



distribution of the acceleration except at $Fn=0$, Eq.(9), (10) and (11) are proposed as empirical formula.

$$\frac{A_{ss(ave)}}{A_{FP(ave)}} = \begin{cases} \frac{s.s.}{10} & (3.0 \leq s.s.) \\ \frac{(6-s.s.)}{10} & (s.s. < 3.0) \end{cases} \quad (9)$$

$$\frac{A_{ss(+)(ave)}}{A_{FP(+)(ave)}} = \begin{cases} \frac{(3 \times s.s. - 2)}{28} & (3.0 \leq s.s.) \\ \frac{(10 - s.s.)}{28} & (s.s. < 3.0) \end{cases} \quad (10)$$

)

$$\frac{A_{ss(-)(ave)}}{A_{FP(-)(ave)}} = \begin{cases} \frac{(2 + s.s.)}{12} & (3.0 \leq s.s.) \\ \frac{(14 - 3 \times s.s.)}{12} & (s.s. < 3.0) \end{cases} \quad (11)$$

11)

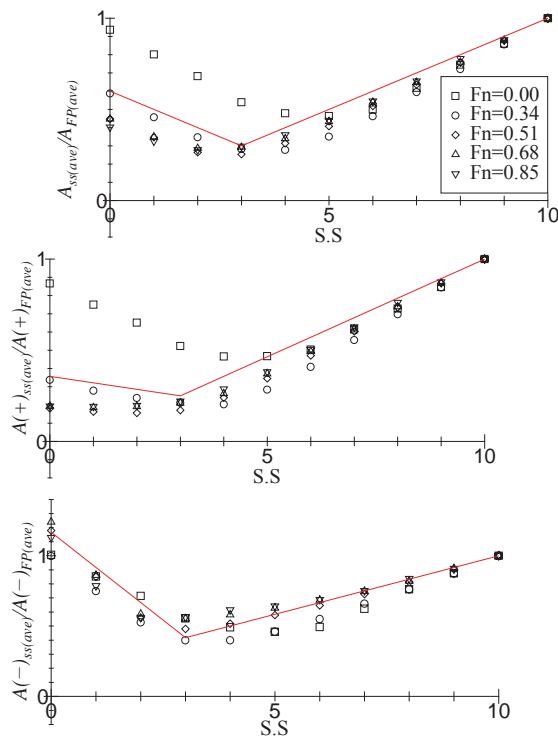


Fig.15 Form of longitudinal distribution of peak to peak value, upward peak value and downward peak value of vertical acceleration on hull in irregular waves. (upper figure: peak to peak value, middle figure: upward peak value, lower figure: downward peak value)

4.4 Effects of Hull Form

Fig.16 shows significant peak to peak value of upward and downward of vertical acceleration on hull with Ship A, B and C. Its horizontal axis is L_{PP} . The extent is different from hull form and vertical acceleration becomes small when deadrise angle becomes large or L_{PP}/B becomes small.

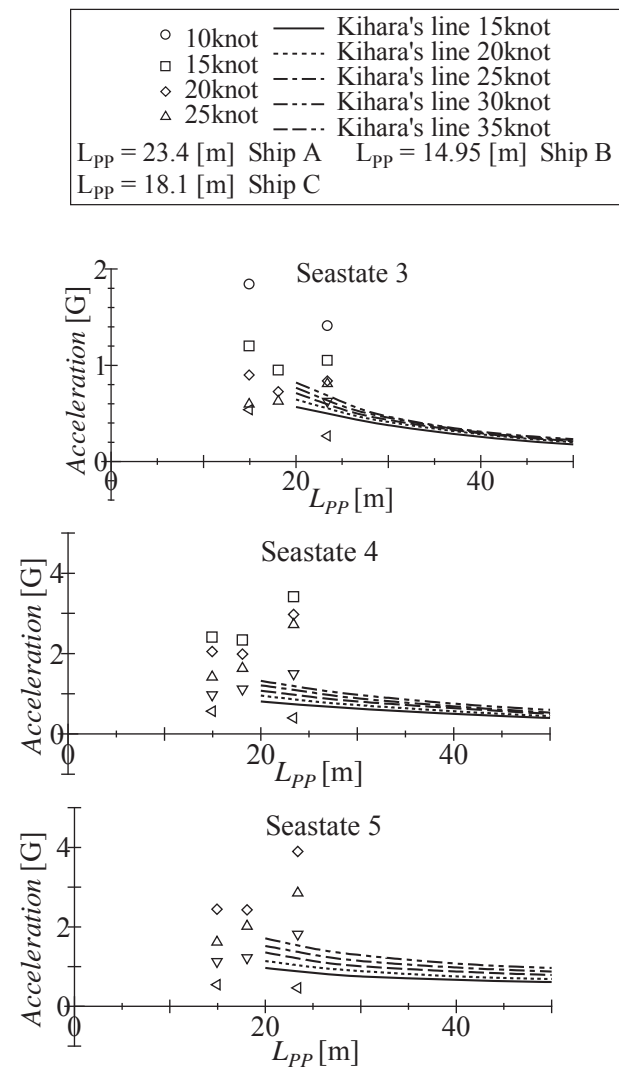


Fig.16 Measured significant amplitude of vertical acceleration on hull at FP vs ship length speed in real scale. (Ship A, B and C) (upper figure: Seastate 3, middle figure: Seastate 4, lower figure: Seastate 5)



4.5 Statistic property

It is well known that the probability density function of amplitudes of acceleration of a displacement type ship in irregular waves can be expressed with Rayleigh distribution of Eq.(12). Rayleigh law describes distribution of the envelope of normal process. In the case of narrow band spectrum, the envelope can be used as a reasonable approximation of the amplitudes. The maximum likelihood estimate of parameter σ is expressed as Eq.(13).

$$p(x) = \frac{x}{\sigma^2} \exp\left(-\frac{x^2}{2\sigma^2}\right) \quad (12)$$

$$\hat{\sigma} = \sqrt{\frac{1}{2n} \sum_{i=1}^n X_i^2} \quad (13)$$

where X_i is measured datum in time step and n is the number of total datum. The relation among parameter σ , average value, significant value and average 1/10 maximum value of Rayleigh distribution is expressed as Eq.(14).

$$\bar{X} = \sigma \sqrt{\frac{\pi}{2}} = \frac{1}{1.6} X_{1/3} = \frac{1}{2.04} X_{1/10} \quad (14)$$

Fig.17 shows the comparison of parameter σ , significant value, average 1/10 maximum value obtained from measured results and estimated results by Eq.(14) with the average amplitude of measured data. From upward acceleration in the upper side Fig.17, measured results are larger than estimated results when the average amplitude is larger than 1.0G. On the other hand, downward acceleration in the lower side Fig.17, measured results smaller than estimated results when the average amplitude larger than 0.5G.

Savitsky proposes a probability density function $p(x)$ (Savitsky et al., 1976) as Eq.(15) with exponential distribution.

$$p(X) = \frac{1}{\bar{X}} \exp\left(-\frac{X}{\bar{X}}\right) \quad (15)$$

where \bar{X} is average amplitude of acceleration. The average 1/N maximum amplitude of acceleration is proposed as Eq.(16).

$$X_{1/N} = \bar{X}(1 + \log_e N) \quad (16)$$

Fig.18 shows comparisons of probability distributions of amplitude of acceleration. The results of Eq.(15) is good agreement with measured results. Fig.19 shows the results of Eq.(16) drowned on the left side Fig.17, and the results is good agreement with the measured results when the average amplitude is larger than 1.0G.

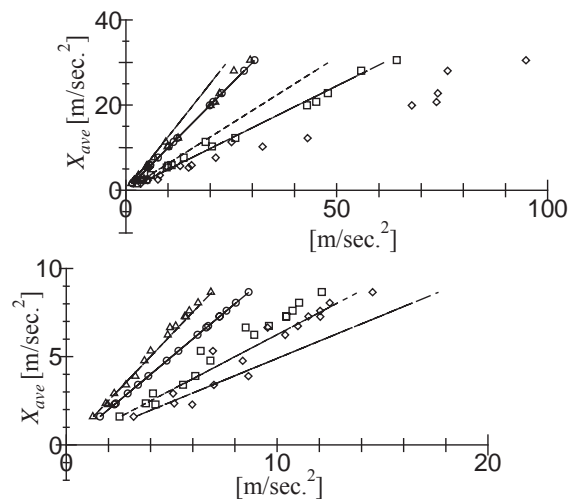
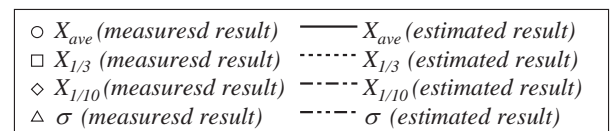


Fig.17 Comparison between measured results and estimated results based on Rayleigh distribution with average value of measured data. (Ship A) (upper figure: upward acceleration, lower figure: downward acceleration)

Fig.20 shows probability distribution of downward peak value of vertical acceleration at FP. The upper figure shows the results when



the average amplitude smaller than 0.5G, and the lower figure shows the results when the average amplitude larger than 0.5G. If average amplitude becomes larger, the mode of amplitude is close to about 1.0G. However when the average is over 0.5G, the mode of amplitude does not becomes much larger than 1.0G and the average amplitude does no becomes larger. Because downward acceleration occurs when ship bow turns rising into falling, bow moves close to free fall when the average is over 0.5G.

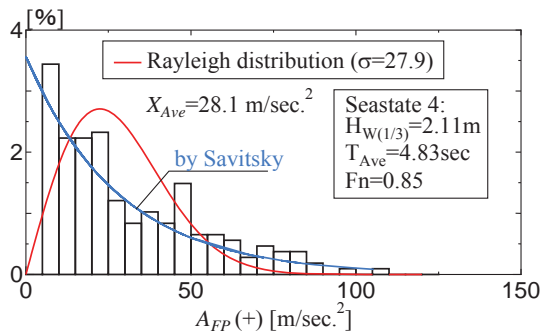


Fig.18 Measured probability distribution of upward peak value of vertical acceleration at FP in irregular wave.

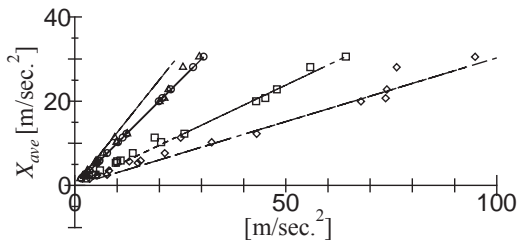


Fig.19 Comparison between measured result and exponential distribution proposed by Savitsky.

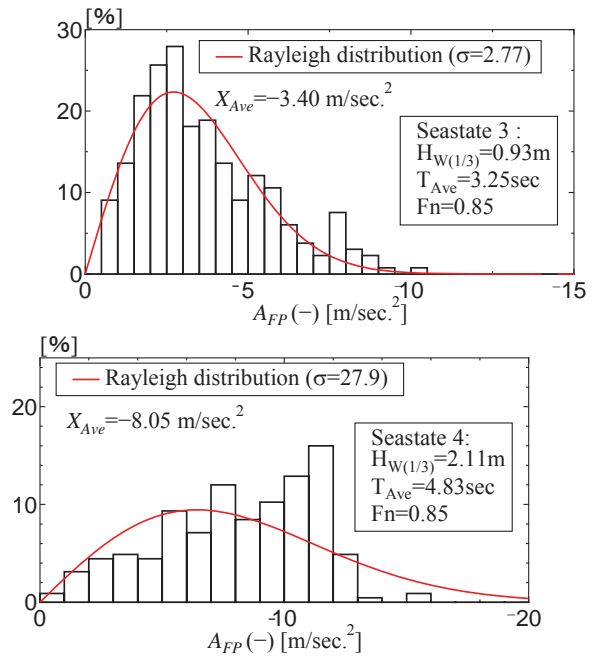


Fig.20 Probability distributions of downward peak value of vertical acceleration at FP in irregular wave. (Ship A)

5. CONCLUSIONS

In this study, the characteristics of vertical acceleration in irregular waves for high speed semi-planing hull is investigated experimentally. The following conclusions are obtained.

1. To measure peak value of impact acceleration accurately, a measurement and analysis procedure is proposed.
2. Based on the measured results, the effects of wave length, wave height and forward speed are indicated and a fitting curve to explain the characteristics of RAO of the acceleration is proposed.
3. Form of longitudinal distribution of the acceleration is discuss, and an empirical equation to express the form expecting at $Fn = 0$ is propose.
4. The vertical acceleration on hull in irregular waves is different with that of



upward and downward acceleration. When impact acceleration doesn't occur, upward acceleration follows Rayleigh distribution and upward acceleration follows that Savitsky's empirical formula. On the other hand, when the average is not over about 0.5G, downward acceleration follows Rayleigh distribution, when over 0.5G, its mode is larger than that of Rayleigh distribution.

Based on the above-mentioned results, the characteristics of the vertical acceleration of a hull can be formulated. It can be possible to estimate vertical on a hull if database of the vertical acceleration for typical hulls are prepared.

6. ACKNOWLEDGEMENT

This work, which was sponsored by JCI (; Japan Craft Inspection Organization), was carried out by Osaka Prefecture University, who is a member of the "Research Committee about the safety of the small high-speed passenger craft of Japan Craft Inspection Organization" which was initiated by JCI.

7. REFERENCES

National Maritime Research Institute, 2007, "Report of research committee of the safety of seat and it equipment for high speed passenger ship".

Osumi, M., 1992, "A design method of a medium-speed boat (continued) (1)", Ship Technology, Vol.45, (in Japanese).

Savitsky, D. and Brown. P. W., 1976, "Procedures for Hydrodynamic Evaluation of Planing Hulls in Smooth and Rough Water", Marine Technology, pp.381-400.

Seakeeping Committee of ITTC, 2011, "Seakeeping Experiments", ITTC

Recommended Procedures and Guidelines
7.5-02-07-02.1, p. 6.

Takemoto, H., Naoi, T., Hashizume, Y., Watanabe, I., Nose, Y. and Osumi, M., 1981, "On the Full Scale Measurement of Motions and Impact Loads of a High Speed Patrol Boat in Waves", Transaction of the west-japan society of naval architects, No.61, (in Japanese).

This page is intentionally left blank

12th INTERNATIONAL CONFERENCE ON THE STABILITY
OF SHIPS AND OCEAN VEHICLES



STAB2015

UNIVERSITY OF STRATHCLYDE,
GLASGOW, 19-24 JUNE 2015

PROCEEDINGS

Volume 2



Session 9.1 – 2nd GENERATION INTACT STABILITY

**An Approach to Assess the Excessive Acceleration based on Defining
Roll Amplitude by Weather Criterion Formula with Modified
Applicability Range**

A Simplified Simulation Model for a Ship Steering in Regular Waves

**Prediction of Wave-Induced Surge Force Using Overset Grid RANS
Solver**

This page is intentionally left blank



An Approach to Assess the Excessive Acceleration Based on Defining Roll Amplitude by Weather Criterion Formula with Modified Applicability Range

Prof. Rudolf Borisov, State Marine Technical University of St. Petersburg, rvborisov@mail.ru

Ph. D. Alexander Luzyanin State Marine Technical University of St. Petersburg,
aaluzyanin@rambler.ru

Dr. Michael Kuteynikov, Russian Maritime Register of Shipping, kuteynikov.ma@rs-class.org

Vladimir Samoylov, Russian Maritime Register of Shipping, samoylov.vr@rs-class.org

ABSTRACT

Development of the second-generation intact stability criteria is focused on five dynamical stability failure modes and three-level approach which indicates susceptibility and degree of susceptibility of a ship to a specific failure mode. The criteria of levels 1 and 2 are based on significant simplifications and have been developed considering substantial safety margins. Until now, the work has been concentrated on the development of levels 1 and 2 criteria and standards. The agreed proposal for excessive acceleration vulnerability criteria was generally made, but some undecided items regarding formulae of roll amplitude and period, formulae for effective wave slope and their applicability still exist. Besides, nonlinear components were not taken into account in the proposed level 1 vulnerability criteria for excessive accelerations, which could decrease the safety margin.

The purpose of the paper is to provide some additional information that can be used during finalization of the development of vulnerability criteria for excessive acceleration.

The possibility of application of a current IMO Weather Criterion to ships with ratio $B/d > 3.5$ and having restricted navigation area is considered. Some drawbacks of formulae for calculation of coefficient c that is necessary for calculation of roll period in the current IMO Weather Criterion are pointed out and the proposal for its correction is made. Criterion for excessive linear acceleration based on the assumptions of IMO Weather Criterion with modified applicability for several types of ships is presented and justification of the value $0.3g$ as a standard is made. The paper also includes information about the influence of nonlinear components on the value of acceleration and contribution of roll to the balance of horizontal accelerations.

Keywords: acceleration, weather, stability

1. INTRODUCTION

This paper contains some information about acceleration criterion, based on the assumptions of IMO Weather Criterion with

modified applicability for ships with different navigation restrictions and ratios $B/d > 3,5$. Presumably it can be used during finalization of the development of vulnerability criterion for excessive acceleration in scope of the



development of second generation intact stability criteria. The proposed criterion is mostly suitable for the 1 level of the vulnerability criteria for excessive acceleration.

2. JUSTIFICATION OF ACCEPTABLE VERTICAL ACCELERATION VALUE 0,3g

There are several types of vessels which have acceleration limitations during roll on heavy sea. This limitations are connected with cargo type, vessel's purpose, or necessity of meeting certain conditions of operation safety.

Vertical accelerations due to roll are usually considered, but sometimes total vertical accelerations are normalized in different combinations of ship motions: roll + heave (on the upper decks and the bridge), pitch + heave (at fore perpendicular) [5]. Here are the main factors, which make normalizing of accelerations necessary.

Biological factors. Roll causes seasickness among crew and passengers. The main reason of seasickness is physiological influence of angular and linear roll accelerations on human body.

Operational factors. These include shifting of containers, bulk and timber cargo, swing of cargo suspended on crane hook, deterioration, and sometimes inoperability of main and auxiliary machinery.

Strength factors. Overall hull strength and strength of particular structures (stern and stem, constructions of cranes and cargo booms and etc.).

Operational and strength factors for transport vessels are basically considered in the appropriate sections of national and international rules [10], [4] for ensuring safe transport technology and marine operations. Stability standards envisage the assessment of

bulk cargo safety conditions and indirectly take inertial forces during roll into account.

Developers of limitations for sea-river vessels [17] considered "... bulk cargo shift, loose cargo shift, especially deck cargo, deterioration of machinery operation conditions, seasickness of the crew, ... dangerous stresses in ship's hull connections", i. e. it seems they created universal mean, that took into account all three groups of factors mentioned above.

Standards which take into account operational and strength factors is often less severe than standards which take into account biological factors. Therefore acceptable accelerations are usually chosen on the basis of biological factors.

Let's look at the factors in more detail. The threshold of human sensitivity to angular accelerations is within $2 - 3 \text{ deg./s}^2$, and to vertical accelerations – within $0,4 - 0,12 \text{ m/s}^2$. Seasickness is significantly increased when the vertical accelerations reach nearly $0,1g \approx 1 \text{ m/s}^2$. Vertical accelerations in the specific point of vessel arises not only from linear but from angular ship motions. Therefore the greatest vertical accelerations occur near vessel's ends.

The majority of the medical scientists tend to think that seasickness is a result of vestibular apparatus malfunction caused by vertical accelerations [11].

The degree of ship motions influence on human body can be seen from the graph, shown in Fig. 1.

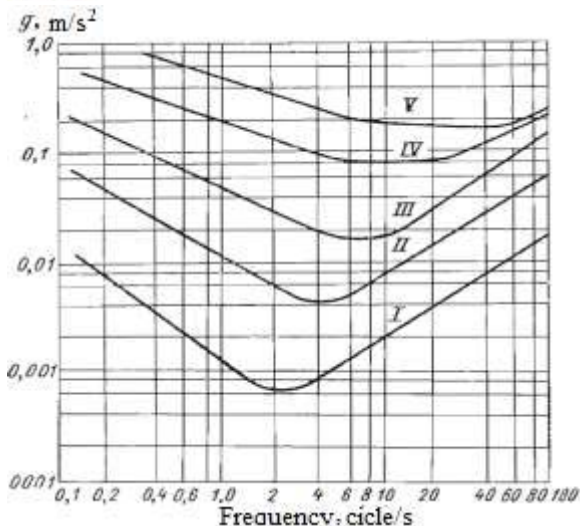


Fig. 1

Curve I marks the boundary of inceptive influence, curve II – boundary of sensible influence, curve III – strong influence, i. e. the beginning of seasickness and discomfort, curve IV – sensible discomfort and curve V – unbearable vibration. The diagram was obtained by Nieuwenhuysen [8]. The graph in Fig. 2 shows that the percentage of diseased passengers increases from 20% to 85% while accelerations increase from 0,1g to 0,4g.

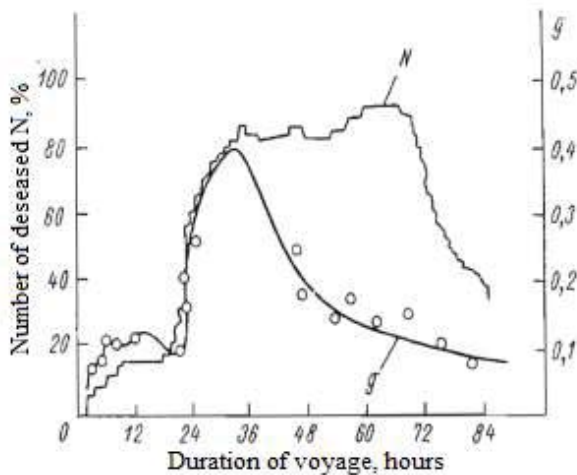


Fig. 2

Professional sailors adapt to seasickness, but this adaptation is not significant, as shown in Fig. 3. Therefore reduction of ship motions is necessary not only for passenger ships.

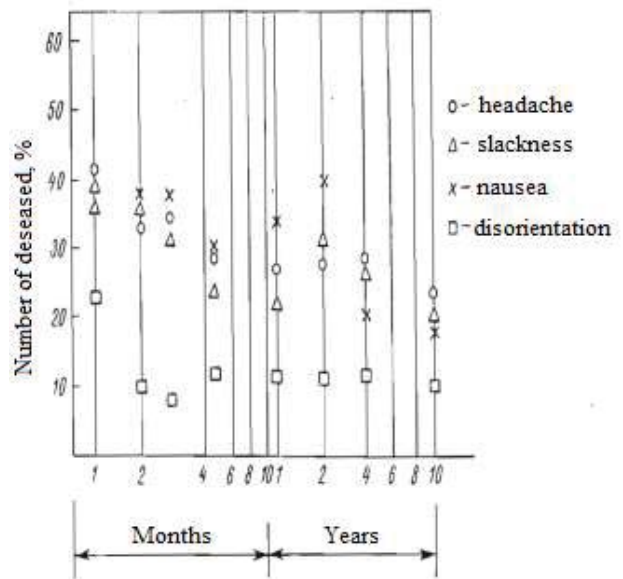


Fig. 3

Proceeding from the graph in Fig. 1 and collected data about the number of diseased people, shown in Figs. 2 and 3, the standard for vertical acceleration 0,3g was selected.

2. PROPOSAL FOR ACCELERATION CRITERION

Acceleration criterion is proposed taking into account the acceptable value of vertical accelerations mentioned above. It allows to input the operational limitations for acceptable

wave height for ships with parameters $\frac{\sqrt{h_0}}{B}$

0,08 and $B/d \geq 2,5$ (where h_0 is initial transverse metacentric height without free surface correction; B is breadth of the vessel; d is draught).

Main proposals in the form of acceleration criterion were included in Rules for Classification and Construction of Sea-Going Ships of Russian Register in 1974 year. These ideas survived to the present day with slight changes in calculation procedure. Their point is as follows.

The stability is judged as satisfactory according to the acceleration criterion if



acceleration (in fractions of g) is not more than the permissible value, i. e. the following condition is fulfilled

$$K^* = 0,3/a_{cal} \geq 1, \quad (1)$$

Where K^* – is the acceleration criterion;
 a_{cal} – is the calculated acceleration (in fractions of g) determined by the formula

$$a_{cal} = 0,0105 \frac{h_0}{c^2 B} k_\theta \theta_r \quad (2)$$

Here, θ_r is the calculated amplitude of roll determined in accordance with [4]

$\theta_r = 109 X_1 X_2 \sqrt{rS}$ as well as in case of weather criterion;

c – is the inertia coefficient determined during calculation of the weather criterion according to the formula

$$c = 0,373 + 0,023B/d - 0,043L_{wl}/100; \quad (3)$$

k_θ – coefficient that takes into account the peculiarities of roll for ships of river-sea navigation determined from Table 1.

Table 1

B/d	$\leq 2,5$	3	3,5	4	4,5	5	5,5	6	6,5
k_θ	1	1,08	1,11	1,11	1,2	1,3	1,45	1,56	1,61

In certain cases, it may be allowed the operation of the ship with the criterion $K^* < 1$. In this case, an additional wave height restriction shall be introduced. The permissible wave height with 3 per cent probability of exceeding level is estimated proceeding from the value of the criterion K^* as given in Table 2. The specific loading conditions with $K^* < 1$ shall be stated in the Stability Booklet.

Table 2

K^*	1,0 and higher	1,0 – 0,75	0,75 and less
Permissible wave height with 3 per cent probability of exceeding level, m	6,0	5,0	4,0

The vessel is assumed to be in beam sea and undergoes rolling and heaving. Vertical accelerations are assessed on amidships at side and actual waterline intersection point.

The acceleration criteria mentioned above can be utilized as the basis for the revision of excessive acceleration vulnerability criterion of 1 level that is being created while developing the second generation intact stability criteria. The formula for calculation of roll amplitude can be used for the vessels with ratio $B/d > 3,5$, as shown below.

3. POSSIBILITY OF APPLICATION OF WEATHER CRITERION TO SHIPS WITH RATIO $B/d > 3,5$

It is well known, the formula for roll amplitude θ_r represents the formula of nonlinear roll theory that is reduced to handy calculation form and was used by authors of Japanese “Stability standards for passenger ships” and then corrected by SLF Subcommittee specialists in order to take into account the influence of B/d , C_B and bilge keels on roll damping in more detail. At the same time multipliers r and s in formula for θ_r are taken right from Japanese “Standards” and multipliers $X_1(B/d)$, $X_2(C_B)$ and k – from “Stability standards” of Russian Maritime Register of Shipping (in the editions published between 1970 and 1995) as noted in MSC.1/Circ. 1281 dated 9 December 2008.

The consideration of the value of r showed it to be a reduction coefficient, averaged on the



basis of the results of many calculations to the main part (Krilov's part) of disturbing moment. It is well known from the roll theory, this coefficient can't be more than one. This is how effective coefficient of wave slope changes (according to the terminology of Japanese "Standards"). It is calculated in compliance with Watanabe method for 60 passenger vessels of Japan and underlies linear statistical dependence of IMO IS Code: $r = 0,73 \pm 0,6 OG / d$, where OG is the distance between center of gravity and waterline (+ if center of gravity is higher than the waterline).

Calculations for other types of ships with high center of gravity mainly cargo ships and industrial ships (for the purpose of this paper it means crane ships, drilling ships and dredgers) shows that in a number of cases the value of r becomes more than one, which is not in compliance with its physical meaning and leads to unreasonable overstating of roll amplitude θ_r . So, $r = 1,06$ for cargo ship ($L = 65,0$ m, $B = 10,0$ m, $C_B = 0,66$) with loading case "without cargo 10% consumables" ($d = 2,42$ m, $OG = 1,34$ m, $GM = 0,88$ m), and $r = 1,29$ for crane ship ($L = 80,4$ m, $B = 25,4$ m, $C_B = 0,60$) during voyage ($d = 3,91$ m, $OG = 3,65$ m, $GM = 10,7$ m) that leads to amplitude $\theta_r = 29^\circ$ which was not observed during operation of this ship in practice. Therefore it is proposed to take $r = 1$ during calculation of θ_r where r turns out to be more than one.

Analysis of dependence $X_I(B/d)$ showed that using scheme of roll calculation θ_r this dependence considers only increasing damping coefficient of rolling with growth of B/d . It is confirmed by results of numerous model tests carried out in different countries. Meanwhile the value of factor X_I in Table 3 at any $B/d \geq 3,5$ is limited by its marginal value $X_I = 0,8$. Such limitation is not appropriate to calculation scheme for roll amplitude θ_r of IMO IS Code. Using of experimental data on damping coefficients of rolling gained in model basin of Saint-Petersburg State Marine Technical

University (SPbSMTU) for different types of ships with wide range of B/d provided the justified prolongation of the dependence $X_I(B/d)$ in region of $B/d > 3,5$ till $B/d = 7,0$. It practically exhausts the real values of dependence B/d for wide range of classes of ships including cargo and industrial ships. Such dependence is presented in Table 3. It is gained by averaging of calculation results of factor X_I for 15 types of cargo, fishing and industrial ships.

Table 3. The values of factor X_I .

B/d	X_I
$\leq 2,4$	1,0
2,5	0,98
2,6	0,96
2,7	0,95
2,8	0,93
2,9	0,91
3,0	0,90
3,1	0,88
3,2	0,86
3,3	0,84
3,4	0,82
3,5	0,80
3,6	0,79
4,0	0,78
4,5	0,76
5,0	0,72
5,5	0,68
6,0	0,64
$\geq 6,5$	0,62

It can be seen that using Table 3 for factor X_I in roll amplitude formulae always leads to decreasing of value θ_r while B/d increases in accordance with physical nature of phenomenon. This decreasing becomes practically sensible starting from $B/d > 4,0$. Such ratios between breadth and draught as shown by statistical analysis of main dimensions of ships are typical for cargo ships with standard loading conditions "without cargo with ballast 10% consumables" (dry cargo, tankers), large fishing vessels (fish cannery ship, whale factory ship) with low production in holds and low consumables and for industrial ships during voyage, when B/d



often more than 5,0 – 6,0. The correction of Table 3 for them has the largest value and may reduce calculated roll amplitudes for 15 – 20%.

So, the formulae for roll amplitude from Weather Criterion can be applied for the vessels with ratio $B/d > 3,5$ which typically has excessive accelerations. Gained value of amplitude may be used in calculation of the acceleration.

4. SOME DRAWBACKS OF FORMULAE FOR CALCULATION OF COEFFICIENT c IN FORMULAE FOR CALCULATION OF ROLL AMPLITUDE

The following formulae is utilized in calculation of roll amplitude according to IMO method [4]:

$$c = 0,373 + 0,023B/d - 0,043L/100 \quad (4)$$

It was obtained for ships of unrestricted service which usually have the ratio of breadth to draught $B/d < 3,5$ and relative metacentric

height is $\frac{\sqrt{h_0}}{B} < 0,08$. Application of this

dependence for sea-river ships, which typically have larger ratios B/d and metacentric heights leads to significant error.

The formulae (4) gives significantly discrepant values of coefficient c and consequently roll period for vessels with different length but with same B/d . So for the

ship with length $L = 100$ m, $B/d = 2,5$, $\frac{\sqrt{h_0}}{B}$

0,06 we will obtain: $c = 0,399$, $T = 12,9$ s, and for ship with length $L = 200$ m, with the same

$B/d = 2,5$, $\frac{\sqrt{h_0}}{B} = 0,06$: $c = 0,345$, $T = 11,5$ s.

The difference is about 10%. It is obvious that with growth of length the error increases.

Taking into account the drawbacks mentioned above, the formulae for calculation of coefficient c also should be revised in order to avoid the above mentioned errors. Besides this, formulae for calculation of c does not take into account the influence of z-coordinate of center of gravity at natural roll period.

Natural roll period is defined by known formulae:

$$T = 2\pi \sqrt{\frac{I_{xx} + \lambda_{44}}{Dh}} \quad (5)$$

Here I_{xx} – moment of inertia of ship's weight about central longitudinal axis;

λ_{44} – associated moment of inertia;

D – displacement.

Coefficient c can be defined from equality

$T = \frac{2cB}{\sqrt{h}}$ taking into account (5) as follows

$$c = \frac{\pi}{B} \sqrt{\frac{I_{xx} + \lambda_{44}}{D}} \quad (6)$$

Moment of inertia of ship's weight about central longitudinal axis and associated moment of inertia are necessary to define coefficient c .

Moment of inertia of ship's weight I_{xx} about central longitudinal axis OX can be determined most accurately by calculation of moments of inertia of the components of weight (shell plating, deck framing, superstructure, cargo, fuel, stores and etc.). The known formulae of theoretical mechanics is used for this purpose:

$$I_{xx} = \sum_i m_i [y_i^2 + (z_i - z_g)^2] + \sum_i I_{xi}^c \quad (7)$$

where m_i – weight of each i component from the whole weight;

y_i – ordinate of center of gravity of each m_i about centerline;

z_i – z-coordinate of its center of gravity about centerline;

I_{xi}^c – natural moment of inertia of each i component of weight.



Calculation according to the formulae (7) is rather laborious. So, approximate formulas are often used in practice. They are based on some facilitating assumptions about the hull form and its load distribution. The most appropriate formulae for many known authors is Duayer formulae [13]:

$$I_{xx} = \frac{D}{12g} (B^2 + 4z_g^2), \quad (8)$$

and also formulae of Y. A. Shimanskiy, [13]:

$$I_{xx} = \frac{D}{g} \left(B^2 \frac{C_w^2}{11,4C_B} + \frac{H^2}{12} \right), \quad (9)$$

where H – depth;

C_w – water plane area coefficient;

C_B – block coefficient.

Duayer formulae is more preferable because it gives the results close to calculation data according to (7) and describes the dependence from z-coordinate of ship's center of gravity.

Roll period of displacement ships which have large ratios L/B and small block coefficients can be calculated using data of V. A. Morenschildt which are obtained as a result of tests of systematic series of ship models [14]. Associated moment of inertia in dependence of B/d , L/B , C_w and C_B can be easily defined by nomograms for fishing vessels and transport ships proposed by V. V. Lugovskiy on the basis of tests of two systematic series (20 models in total), that were carried out in test basin of SPbSMTU [13, 6]. Later S. M. Panenko carried out model tests with larger block coefficients and ratios of B/d that are typical for industrial ships and proposed the nomogram for defining of λ_{44} [13, 9]. According to this data the associated moment of inertia is defined by the following expression:

$$\lambda_{44} = \frac{0,314}{C_B} I_{xx} \frac{\lambda_{44}}{I_{xe}}, \quad (10)$$

where I_{xe} – moment of inertia of underwater part of the ellipsoid, which has the same main dimensions, as the vessel under consideration (model).

The magnitude of λ_{44}/I_{xe} is defined by nomograms depending on B/d , L/B , C_w and C_B . The limits of changing of ships' characteristics for which those nomograms are provided in Table 4.

Table 4

No	Type of vessel	L/B	B/d	C_B	C_w
1	Transport ships	$\approx 7,3$	2,4-3,5	0,59-0,74	0,7-0,82
2	Fishing vessels and tugs	3,5-6,5	2,4-3,5	0,44-0,56	0,7-0,82
3	Industrial ships	4,5-6,5	3-5,6	-	0,75-0,9

The empirical formulae of G. K. Avdeev which is obtained by processing of the same results of model tests of different vessels in test basin of SPbSMTU can be utilized for defining of the associated moment of inertia for wide range of ships and inland-navigation vessels [1, 7].

$$I_{xx} + \lambda_{44} = \frac{I_{xx}}{0,28 + \frac{1,8}{BC_w \left(1 + \frac{1}{6} \frac{B}{d} \right)} \sqrt{\frac{I_{xx} g}{D}}}. \quad (11)$$

It is necessary to know moment of inertia of ship's weight and associated moment of inertia to define natural roll period. Calculation of this moments are preferably to be carried out by approximate empirical methods.

The associated moment of inertia λ_{44} mainly depends on B/d and water plane area coefficient C_w and also moment of inertia of ship's weight I_{xx} . The formulae of G. K. Avdeev (11) and nomograms of V. V. Lugovskiy and S. M. Panenko most fully meets such dependences for wide range of ships and inland-navigation vessels.



Substitution of (11) in expression for coefficient c (6) will give us the following formulae:

$$c = \pi \sqrt{\frac{(1 + 4z_g^2/B^2)}{12g \left[0,28 + \frac{1,8}{C_w(1 + 0,167B/d)} \sqrt{\frac{(1 + 4z_g^2/B^2)}{12}} \right]}} \quad (14)$$

To facilitate calculations it can be reduced with enough for practice degree of accuracy (Fig. 4) to the form:

$$c = 0,114 + 0,012 \frac{B}{d} + 0,26 \frac{z_g}{B} + 0,195C_w \quad (15)$$

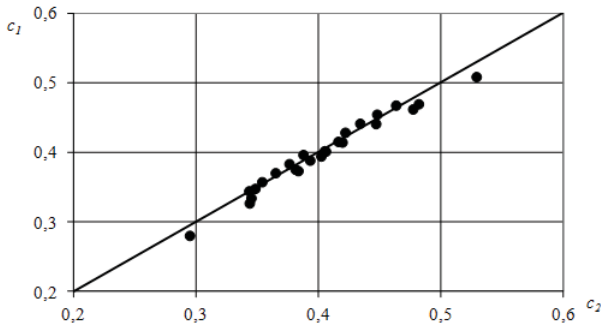


Fig.4 The comparison of the calculation results according to formulas (15) and (14)

Coefficient c can be determined utilizing nomograms of V. V. Lugovskiy and S. M. Panenko (moment of inertia of ship's weight is determined according to Duayer formulae):

$$c = 0,289 \sqrt{\left(1 + 4 \frac{z_g^2}{B^2}\right) \left(1 + \frac{0,314}{C_B} \frac{\lambda_{44}}{I_{x3}}\right)} \quad (16)$$

Here the ratio λ_{44}/I_{xe} is determined by nomograms depending on ship's characteristics B/d , L/B , C_w , C_B . Based on the results of processing of these calculations the approximate dependence is obtained:

$$c = 0,121 + 0,10C_w + 0,025 \frac{B}{d} + 0,35 \frac{z_g}{B} + 0,001 \frac{L}{B} \quad (17)$$

Calculations according to (17) give the results close to data that was obtained directly by nomograms. The error for all values of B/d , L/B , C_w , C_B does not exceed 5 – 7 % excluding

$C_w = 0,9$. The error can reach 15 % for industrial ships where formulae gives understated results.

The results of calculation of coefficient c for determination of natural roll period by different methodologies are provided on Fig. 6:

1. IMO methodology, (2).
2. By formulae (15).
3. By formulae (17).

The calculations are carried out for sea-river vessel with different loading conditions. The ratio B/d is varied from 3.58 to 7,43; ratio z_g/B from 0,19 to 0,38; water plane area coefficient varied slightly ($C_w \approx 0,70 - 0,90$).

Analysis of provided dependences shows that nature of varying coefficient from $\frac{\sqrt{h_0}}{B}$ is practically the same for a number of methods: the value of coefficient c droningly reduces while $\frac{\sqrt{h_0}}{B}$ grows. The exclusion is method (2) (IMO) because coefficient c does not depend from $\frac{\sqrt{h_0}}{B}$.

The dependences of coefficient c which was calculated according to IMO formulae and proposed method (17) with widely varying parameters B/d , z_g/B , C_w are compared on Fig. 7. The range of varying of parameters B/d , z_g/B , C_w practically covers the whole varying range for real vessels: $B/d = 2- 8$; $z_g/B = 0,2 - 0,6$; $C_w = 0,70 - 0,90$. It can be seen from the provided dependences that proposed method of determination of coefficient c is practically in agreement with IMO method with $B/d \geq 4$ but has some advantages because it takes into account the influence of z-coordinate of center of gravity on natural roll period and takes into account more fully the ratio B/d .



Test calculations were carried out for 79 vessels of different types with different loading conditions (289 variants in total).

The difference in natural roll periods between IMO method and proposed method is small and does not exceed 11 % and when $z_g/B \approx 0,33 - 0,35$ they give practically the same results. When $z_g/B < 0,33$ roll period is less according to proposed method and when $z_g/B > 0,35$ it is larger than for IMO method.

Calculation method of natural roll period practically does not affect roll amplitudes for all loading conditions under consideration. It's obvious that Weather Criterion practically does not change when calculating period according to the proposed method.

The revised formulae (17) can be applied for vessels with ratio $B/d > 3,5$ and takes into account z-coordinate of center of gravity, but it practically does not affect roll amplitudes. So the existing formula for calculation of coefficient c can be applied to calculate roll amplitudes that are used for acceleration calculation for vessels with ratio $B/d > 3,5$.

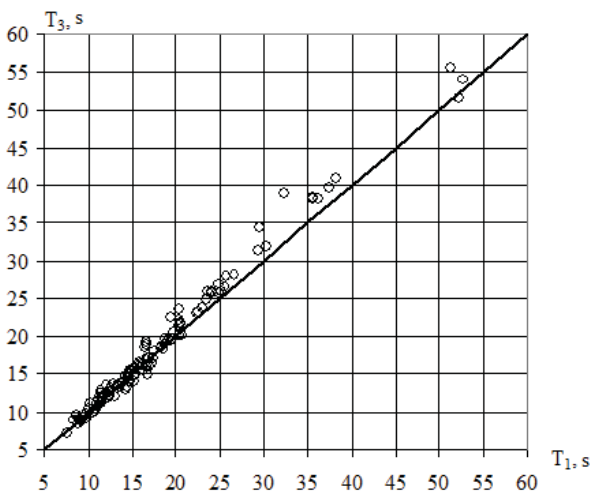


Fig. 5. Roll periods of ships of unrestricted service:
 T_1 – IMO, T_3 – proposed method

5. INFLUENCE OF NONLINEAR COMPONENTS ON THE VALUE OF ACCELERATION, DURING ROLLING

Calculation method for acceleration for other types of ship motions should be considered because of the influence of angular accelerations from roll and horizontal accelerations from sway on people health (“human element” in ship operation and carrying out of different work) [15].

Calculation method for acceleration for all types of roll except surge and yaw in linear and nonlinear formulation on regular waves is proposed in work [2]. This work notes that significant lateral horizontal accelerations are occurred because of the nonlinearity of roll especially at range of low frequencies $\omega < 0,8$. Herewith the acceleration amplitude can be greater on 30 – 50 % of the appropriate amplitudes that are calculated according to the linear theory.

The influence of nonlinear second order factors on the values of accelerations when sway occurs can reach 20 – 40 % at range of frequencies $\omega < 0,5$. The results of acceleration (from sway and roll) calculation in accordance with nonlinear theory at cross point of side and deck is also significantly differs from the same results in accordance with linear theory.

Contribution of roll in common balance of horizontal accelerations for usual loading cases (h_0 below 2 m) constitutes 15 – 20%. Accelerations themselves are 0,15 – 0,20g, but if metacentric height is greater it can reach 60% and summary accelerations significantly exceeds permissible values for horizontal accelerations.

The influence of nonlinear factors on accelerations in different points of vessel first of all depends on value of metacentric height h_0 . Roll amplitudes for vessels with $h_0 < 1$ m which are calculated in accordance with nonlinear theory can exceed 50 – 60 % the



appropriate amplitudes which are calculated according to linear theory at range of main resonance. The influence of nonlinear factors at range of main resonance mode of rolling is practically absent for vessels with $h_0 > 2$ m, but it appears at range of super harmonic resonance.

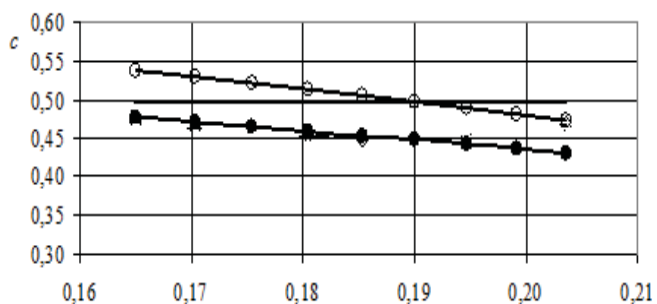
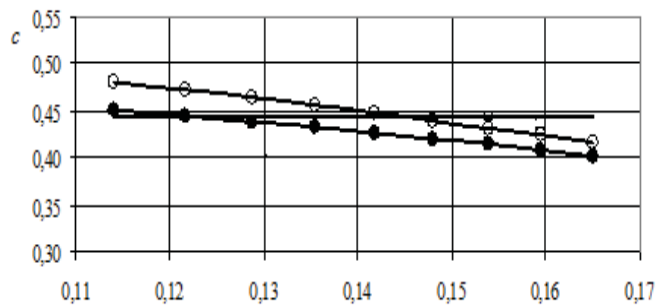
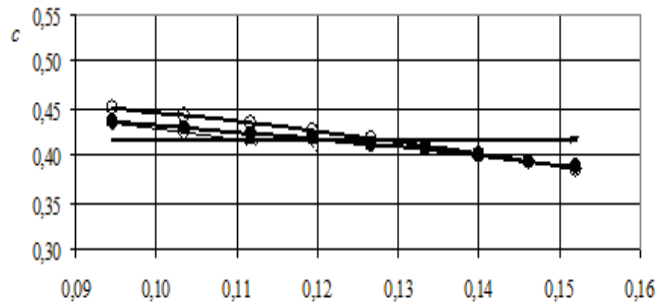
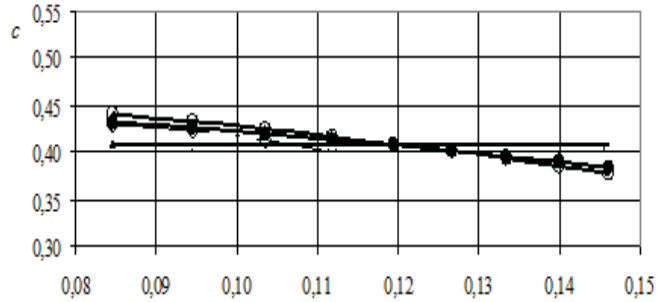


Fig. 6. Coefficient c , calculated according to methodologies:

— 1, ● 2, ⊖ 3,

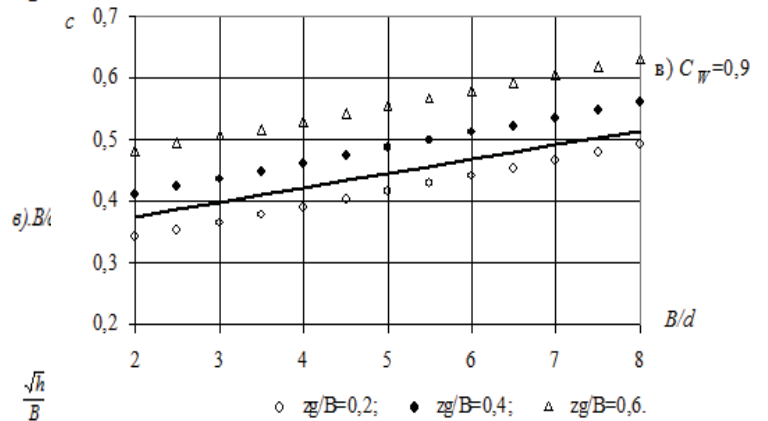
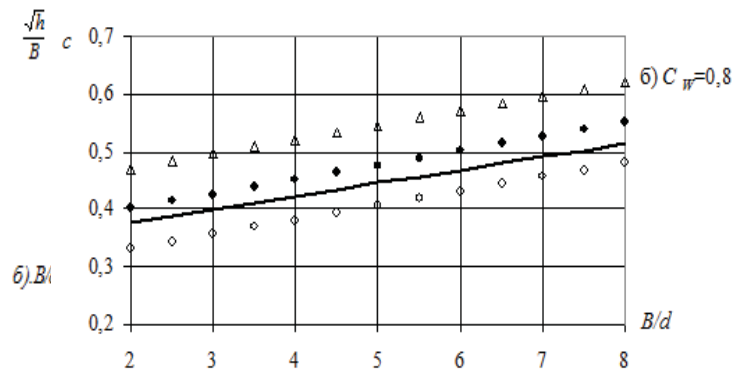
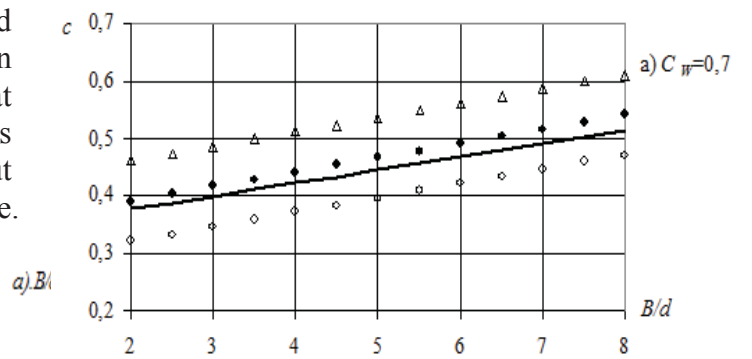


Fig. 7. Coefficient c

○ $z_g/B=0,2$; ● $z_g/B=0,4$; △ $z_g/B=0,6$.



Main contribution to vertical accelerations at fore perpendicular is made by pitching (up to 80%) and contribution that is made by heaving is much less (up to 20%).

Significant influence of speed on acceleration should be noted. Its growth leads to drastic increase of amplitude of vertical accelerations and accelerations from surge at range of main resonance and super harmonic resonance. So the values of acceleration from heaving and surge when $Fr = 0,306$ are higher for 75% and 40% accordingly than when $Fr = 0,2$. The increment of the above mentioned values for 33 – 35 % occurs at range of super harmonic resonance modes.

6. CONCLUSION

Vulnerability criterion for excessive acceleration 1 level is proposed. The possibility of appliance of present formulae for roll calculation from Weather Criterion during acceleration calculation is showed. Data about the influence of nonlinear component on accelerations during rolling are presented. Formulae for calculation of coefficient c is proposed. Information that is contained in this paper can be used for additional work of vulnerability criterion for excessive accelerations 1 level.

7. REFERENCES

- Anfimov V. N., Avdeev G. K. Hydrodynamic characteristics and calculation of roll amplitudes of inland-navigation vessels // Tr. CRI RF. – Ed. XXX. – L., 1955.
- Borisov R. V., Kuteynikov M. A. Semenova V. Y., Luzyanin A. A. About the problem of standardizing of accelerations caused by roll. UDK 629.12.073.243.4 // Scientific and technical compilation No. 27. – SPb.: Russian Maritime Register of Shipping, 2004.
- Borisov R. V., Kuteynikov M. A., Luzyanin A. A. Method of calculation assessment of natural roll period of marine vessels of different types. UDK 629.12.001.11 // Scientific and technical compilation No. 27. – SPb.: Russian Maritime Register of Shipping, 2004.
- Code of Intact Stability for All Types of Ships. IMO Res. MSC.267(85). – 2008.
- Kuteynikov M. A. The development and researching of theoretical basic foundation for setting of operational limitations when standardizing of marine vessels seaworthiness // Abstract for thesis for competition of Ph. D. science degree. – SPb.: SPbSMTU, 2001.
- Lugovskiy V. V. Nonlinear tasks of seaworthiness. – L.: Shipbuilding, 1966.
- Lugovskiy V. V. Roll of the ship. Text-book. – SPb.: Pub. Center SPbSMTU, 1999.
- Nieuwenhuysen J. N. Experimental investigations on seasickness. Diss. Utrecht, 1958.
- Panenko S. M. Hydrodynamic characteristics of roll of hopper dredgers // Scientific and technical compilation of USSR. Book 2. – L.: Transport, 1972.
- Rules for the Classification and Construction of Sea-Going Ships. – SPb.: Russian Maritime Register of Shipping, 2015. – T. 1.
- Semenov-Tyan-Shanskiy V. V., Blagoveshenskiy S. N., Holodilin A. N. Roll of the ship. L.: Shipbuilding, 1971.
- Semenova V. Y. Research and development of programs for calculation of nonlinear hydrodynamic forces which are occurred due to roll of contour of ship form on the free surface of liquid // Thesis for competition of Ph. D. science degree. – SPb.: SPbSMTU, 1999.



Ship theory guide / Ed. Y. I. Voytkunskiy. – L.:
Shipbuilding, 1985. – T.2.

Shmirev. A. N., Morenschildt V. A., Ilyina S. G.
Anti-rolling devices of vessels. – L.:
Transport, 1972.

Skorohodov D. A. Navigation and control of
vessel movement. – SPb.: Almor, 2002.

Borisov R. V., Luzyanin A. A. The
development of theoretical basic foundation
for ships of different types when rolling
//Report on theme. Baltic Engineering
Center. – 2002.

Anfimov V. N., Vasilev A. I., Egorov G. A.,
Mamontov Y. N. The researching of
seaworthiness of marine vessels with
excessive stability and large block
coefficient // Final report on theme 73-632.
– L.: LIWT (Leningrad Institute of Water
Transport), 1974.



A Simplified Simulation Model for a Ship Steering in Regular Waves

Xiechong Gu, *State Key Laboratory of Ocean Engineering, Shanghai Jiao Tong University (SJTU),
Shanghai, China* xcgu@sjtu.edu.cn

Ning Ma, *State Key Laboratory of Ocean Engineering, SJTU, China* ningma@sjtu.edu.cn

Jing Xu, *China Ship Development and Design Centre, Wuhan, China* xujing.sjtu@gmail.com

Dongjian Zhu, *Shanghai Merchant Ship Design and Research Institute* tobya@sjtu.edu.cn

ABSTRACT

A simplified simulation model for a ship steering in regular waves is proposed. It combines the traditional MMG (mathematical manoeuvring group) model with seakeeping model. The former divides hydrodynamic forces into individual ones on the hull, from propeller and due to rudder operation. The latter treats wave forces as the first and second order ones. Impulse response functions, transformed from RAOs, are convoluted with ship motions. Manoeuvring of S175 container ship in regular waves is simulated, and validated by free running tests in regular waves of a S175 model in our ocean engineering basin. Validity and effectiveness of the simulation model are shown.

Keywords: *ship manoeuvring in waves, seakeeping, time domain simulation, impulse response function, second order wave force*

1. INTRODUCTION

Nowadays, manoeuvrability and seakeeping performance has begun to be wholly considered. In the past half a century, manoeuvrability is basically assessed in calm water. A MMG model, out of other theoretical models, was put forward by MMG group in Japan and showed very effective. In MMG model, hydrodynamic forces are split into individual parts, the ones on the ship hull, from the propeller and due to rudder operation, while interactions between them are implicitly, rather than explicitly, shown. Later, Hirano (1981) extended the calm water theory to operation in waves and added second order wave forces into the model. It takes water wave effects into account. Hirano (1981) measured second order wave forces and then calculated turning trajectory in waves. Kijima (1997) further improved the model,

taking first order wave forces and roll response into account, and established a 4DOF MMG model. Kijima (1997) investigated effects of waves on turning trajectories. Yasukawa (2008) extended it to 6DOF motion. Accuracy of the simulated turning trajectory of a container ship in regular waves was apparently improved. On the other hand, Skejec (2008) established a unified manoeuvring and seakeeping model, where first order wave loads are evaluated by STF strip theory by Salvesen (1970). Skejec (2008) systematically investigated estimation methods for various hydrodynamic loads, and only those of suitable ones enter into the model. Turning trajectories simulated are much nice.

This paper presents a 6DOF model, of which manoeuvring and seakeeping are integrated. First order and second order wave loads in frequency domain are calculated in terms of



a code by three dimensional panel method. Impulse response functions are derived from the response amplitude operators (RAOs) by Fourier transformation. Motion equations are solved step by step in time domain. Turning trajectories and history of seakeeping motions are simultaneously obtained. For validation, free running tests of a S175 ship model are performed in our ocean engineering basin.

Below, a mathematical model is described at first, where coordinate systems, estimation method for various hydrodynamic loads, motion equations and solution method are shown. Next, numerical results, model ship specifications, simulated and measured turning trajectories and zigzag motions are given. Finally a brief conclusion is stated.

2. MATHEMATICAL MODEL

2.1 General Equations of Motion

Consider a ship travelling in regular waves. As Fig.1 shows, a global coordinate system, $O_0X_0Y_0Z_0$, is established. O_0X_0 coincides with wave propagation direction. Another coordinate system, $Gx_b y_b z_b$, is fixed on the ship. G denotes the centre of gravity of the ship. Location G , (x_0, y_0, z_0) , in $O_0X_0Y_0Z_0$ and attitude, (ϕ, θ, ψ) , of the ship vary with time t . Heading angle, *i.e.* yaw angle, ψ , is measured from Gx_b to O_0X_0 , pitching angle, θ , is from Gx_b to horizontal plane $O_0X_0Y_0$, and roll angle, ϕ , is from Gz_b to the vertical plane through longitudinal centreline of the ship. We denote (u, v, w) as the velocity at G in $Gx_b y_b z_b$, and $(p,$

$$\begin{bmatrix} \dot{x}_0 \\ \dot{y}_0 \\ \dot{z}_0 \end{bmatrix} = \begin{bmatrix} \cos\psi \cos\theta & -\sin\psi \cos\phi + \cos\psi \sin\theta \sin\phi & \sin\psi \sin\phi + \cos\psi \sin\theta \cos\phi \\ \sin\psi \cos\theta & \cos\psi \cos\phi + \sin\psi \sin\theta \sin\phi & -\cos\psi \sin\phi + \sin\psi \sin\theta \cos\phi \\ -\sin\theta & \cos\theta \sin\phi & \cos\theta \cos\phi \end{bmatrix} \begin{bmatrix} u \\ v \\ w \end{bmatrix} \quad (1)$$

$$\begin{bmatrix} \dot{\phi} \\ \dot{\theta} \\ \dot{\psi} \end{bmatrix} = \begin{bmatrix} 1 & \sin\phi \tan\theta & \cos\phi \tan\theta \\ 0 & \cos\phi & -\sin\phi \\ 0 & \sin\phi / \cos\theta & \cos\phi / \cos\theta \end{bmatrix} \begin{bmatrix} p \\ q \\ r \end{bmatrix} \quad (2)$$

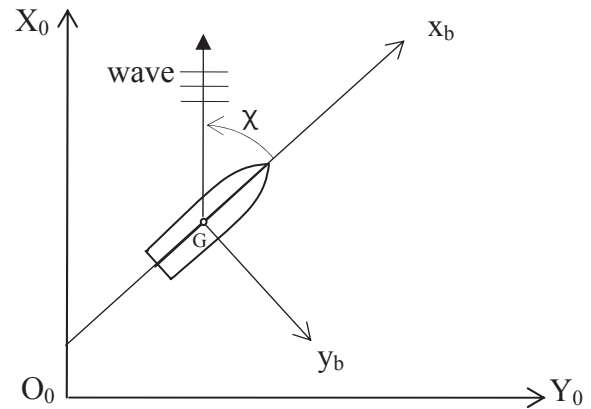


Figure 1 Coordinate Systems

$q, r)$ as angular velocity of the ship. Relations of Eq.1 and Eq.2 can be derived. In these equations, dot over a symbol, say \dot{x}_0 , means time derivative of that symbol, say x_0 .

According to MMG model, forces and moments on a ship are written as the sum of those due to ship hull, propeller, rudder where coupling effect between them is not explicitly shown. In addition, components due to wave, both the first order and the second order wave forces, are also added. This results Eq.3, a general equation of ship motions

$$\begin{cases} m(\dot{u} - vr + wq) = X_H + X_P + X_R + X_{1W} + X_{2W} \\ m(\dot{v} + ur - pw) = Y_H + Y_P + Y_R + Y_{1W} + Y_{2W} \\ m(\dot{w} - uq + vp) = Z_H + Z_{1W} \\ I_{xx}\dot{p} = K_H + K_R + K_{1W} \\ I_{yy}\dot{q} + (I_{xx} - I_{zz})pr = M_H + M_{1W} \\ I_{zz}\dot{r} + (I_{yy} - I_{xx})pq = N_H + N_P + N_R + N_{1W} + N_{2W} \end{cases} \quad (3)$$

where subscripts $H, P, R, 1W$ and $2W$ stand for the forces or moments due to ship hull, propeller, rudder, the first order and the second order wave forces respectively. m is mass of the ship, and I_{xx}, I_{yy}, I_{zz} are moments of inertia of the ship with respect to axes Gx_b, Gy_b, Gz_b respectively, while other cross components are relatively small and ignored. Whenever general forces on the right hand side of Eq.3 are estimated step by step, motions of the ship are accordingly obtained by solving Eq.3. Estimations of these forces will be given below.



2.2 Propeller Forces

For simplicity, propeller is considered only producing either forward or backward forces,

$$X_P = (1 - t_p) \cdot \rho n^2 D_P^4 \cdot K_T(J_P) \quad (4)$$

while Y_P and N_P are reasonably neglected. Here ρ is the water density, D_P diameter of the propeller, n rotational speed. Thrust deduction factor t_p is estimated from empirical formulas. $K_T(J_P)$ is open water propeller thrust coefficient, varies with advance coefficient J_P , where wake coefficient is also estimated from an empirical formula.

2.3 Rudder Forces

Rudder forces are dominantly due to the lift force, F_N , on the rudder. It causes mainly drag and drift forces, yawing and heel moments on the ship.

$$\begin{cases} X_R = (1 - t_R) F_N \sin \delta \\ Y_R = (1 + a_H) F_N \cos \delta \\ N_R = (x_R + a_H x_H) F_N \cos \delta \\ K_R = z_G Y_R \end{cases} \quad (5)$$

where δ is the rudder angle, t_R the rudder drag reduction factor, mainly due to the wake, a_H is drift force modification factor, x_H the distance from rudder centre to G , the centre of gravity of the ship, x_R is the horizontal distance from resultant rudder force to rudder centre, z_G is vertical coordinate of the resultant rudder force.

2.4 Hull Forces

This kind of forces is due to the ship moves advancing in calm water. It can be considered as two parts, one is due to pressures normal to the hull, the other is due to shear stress tangent to the hull.

Eq.6 is the contribution of pressure, which is evaluated by potential flow theory. Eq.7

shows the contribution of shear stress, which could be obtained either from captive model tests or from empirical formulas.

$$\begin{cases} -X_{HI} = A_{11}\dot{u} - A_{22}vr + A_{33}wq \\ -Y_{HI} = A_{22}\dot{v} + A_{11}ur - A_{33}pw \\ -Z_{HI} = A_{33}\dot{w} - A_{11}uq + A_{22}vp \\ -K_{HI} = A_{44}\dot{p} + (A_{66} - A_{55})qr + (A_{33} - A_{22})vw \\ -M_{HI} = A_{55}\dot{q} + (A_{44} - A_{66})pr + (A_{11} - A_{33})uw \\ -N_{HI} = A_{66}\dot{r} + (A_{55} - A_{44})pq + (A_{22} - A_{11})uv \end{cases} \quad (6)$$

$$\begin{cases} X_{HV} = X_{uv}u^2 + X_{vv}v^2 + X_{vr}vr + X_{rr}r^2 \\ Y_{HV} = Y_vv + Y_r r + Y_{|v|} |v|v + Y_{|r|} |r|r + Y_{vr}v^2r + Y_{vr}vr^2 \\ Z_{HV} = -Z_w w - Z_q q - Z_{\dot{q}} \dot{q} - Z_{\theta} \theta \\ K_{HV} = -2K_p p - \rho g \nabla GM \sin \varphi - Y_H \square z_H \\ M_{HV} = -M_w w - M_{\dot{w}} \dot{w} - M_q q - M_{\theta} \theta \\ N_{HV} = N_v v + N_r r + N_{|v|} |v|v + N_{|r|} |r|r + N_{vr}v^2r + N_{vr}vr^2 + Y_H \cdot X_c \end{cases} \quad (7)$$

Subscript I in Eq.6 stands for those due to pressures, and subscript V in Eq.7 for those due to shear stresses, their sum gives the hull forces. For example, $X_{HI} + X_{HV}$ gives out X_H . A_{ij} is the added mass of i -mode motion due to j -mode motion of the ship. ∇ is the volume displaced by the ship, GM the transverse metacentric height of the ship.

2.5 Wave Forces

Wave forces are decomposed into the first order and the second order ones. The former is further separated to the incident wave forces, *i.e.* Froude-Krylov forces, radiation ones and diffraction ones. Panel method is powerful in solution for velocity potential of radiation and diffraction. According to Cummins (1962), the radiation and diffraction forces are expressed as follows.

$$F_{jk}^R = -\mu_{jk} \ddot{\eta}_k(t) - b_{jk} \dot{\eta}_k(t) - c_{jk} \eta_k(t) - \int_0^t K_{jk}(t-\tau) \cdot \eta_k(\tau) d\tau \quad (8)$$

$$F_j(t) = F_j^D + F_j^I = - \int_{-\infty}^t H_j(t-\tau) h(\tau) d\tau \quad (9)$$

where superscript R stands for radiation, I and D are for incident wave and diffraction. $h(\tau)$ is the incident wave elevation at the instant τ . $\eta_k(\tau)$



is the moving displacement of mode k motion at the instant τ . The kernel function $K_{jk}(\tau)$ can be obtained from the damping coefficient $B_{jk}(\omega)$

$$K_{jk}(\tau) = \frac{2}{\pi} \int_0^{\infty} B_{jk}(\omega) \cdot \cos(\omega\tau) d\omega \quad (10)$$

$$\mu_{jk} = A_{jk}^{\infty} \quad (11)$$

$$b_{jk} = B_{jk}^{\infty} \quad (12)$$

that is, μ_{jk} and b_{jk} correspond to the added mass A_{jk} and damping coefficient B_{jk} at extremely high frequency, whereas c_{jk} is restoring forces with nonzero components follows

$$\begin{aligned} c_{33} &= \rho g A_{wp} \\ c_{35} &= c_{53} = -\rho g S_y \\ c_{44} &= \rho g \nabla GM_T \\ c_{55} &= \rho g \nabla GM_L \end{aligned} \quad (13)$$

where A_{wp} is the water plane area, S_y the first order moment of the water plane with respect to Gy_b axis, GM_T and GM_L are the transverse metacentric height and longitudinal metacentric height respectively.

Kernel function $H_j(t)$ is obtained from the wave force $f_{wj}(\omega)$ due to incident wave of unit amplitude and its corresponding diffraction as follows

$$H_j(t) = \frac{1}{2\pi} \int_{-\infty}^{\infty} f_{wj}(\omega) e^{-i\omega t} d\omega \quad (14)$$

As for the second order drift forces, at first we get the response amplitude operator (RAO) from panel method for different frequencies and heading angles, then at any instant the drift force is evaluated by interpolation of the RAO for the specified encounter frequency and heading angle.

2.6 Numerical Algorithm

In simulation, at first by means of the code based on panel method, radiation and diffrac-

tion problems are solved, then added mass and damping coefficient are evaluated, and kernel functions $K_{jk}(\tau)$ and $H_j(t)$ are calculated. At last, the 4th order Runge-Kutta method is applied to solve Eq.3 in time domain step by step.

3. NUMERICAL RESULTS

3.1 Ship for simulation

In simulation, the S175 container ship is used. Table 1 lists principal particulars of S175. Fig.2 shows meshes. In total 1968 quadrilateral meshes are used in calculation.

At first, linear wave force, added mass and damping coefficients, motion response and the second order wave force are calculated by the

Table 1. Principle particulars of S175

symbol	magnitude	unit
L _{OA}	183.0	m
L _{PP}	175.0	m
L _{WL}	178.2	m
B	25.4	m
D	15.0	m
d	9.5	m
▽	24380.6	m ³
C _B	0.5774	
KM	10.5	m
x _B (from AP)	80.64	m
k _{xx}	8.5852	m

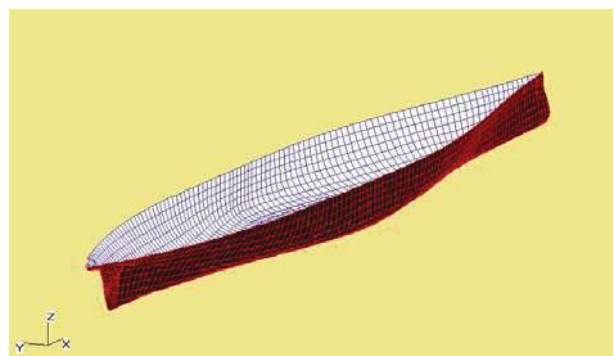


Figure 2 Meshes of S175 for Simulation



using the code based on panel method. In calculation, encounter wave frequency is in between 0.1 and 12 *rad/s*, with increment 0.1 *rad/s*. Heading angle relative to the wave is in between 0 to 360 *deg*, with increment 10 *deg*. It is found that results for 1968 meshes show almost no significant difference with those for more meshes, say 3156 meshes. Service speed corresponds Froude number 0.166. The second order wave force for specified encounter wave frequency and heading angle is evaluated from

the computed results by applying Lagrange interpolation algorithm.

Fig.3 to 8 show response amplitude operators (RAOs) of motions. Fig.9 and 10 are the calculated added mass and damping coefficient. Fig.11 shows the first order wave forces and moments in beam waves. Fig.12 shows the second order wave forces and moments in beam waves.

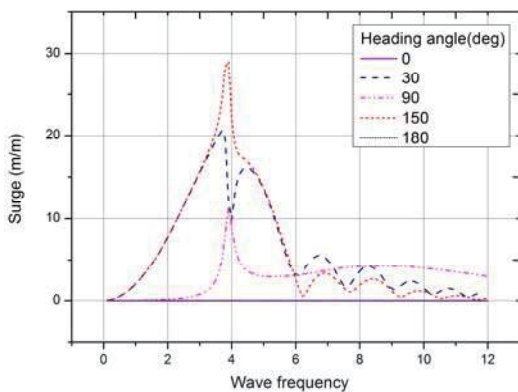


Figure 3 RAO of Surge

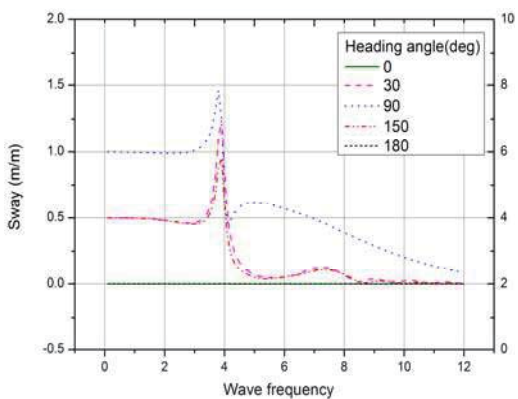


Figure 4 RAO of Sway

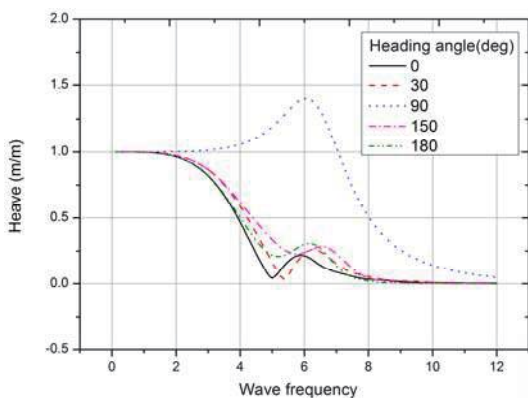


Figure 5 RAO of Heave

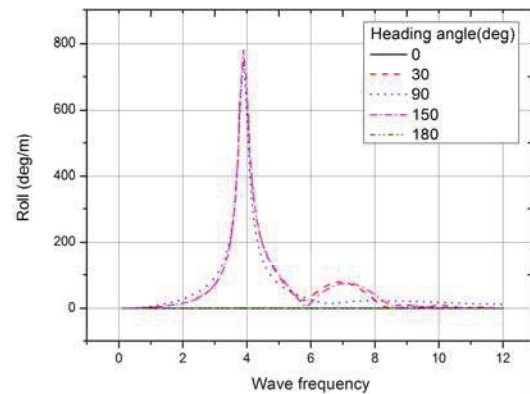


Figure 6 RAO of Roll

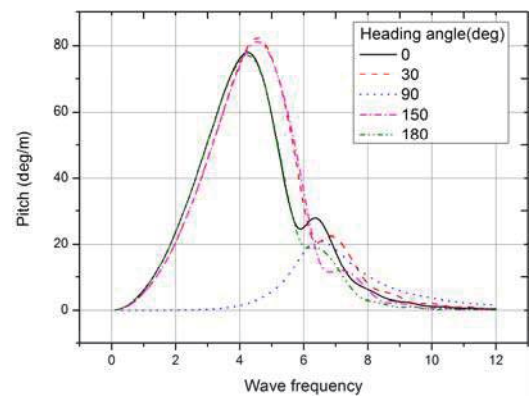


Figure 7 RAO of Pitch

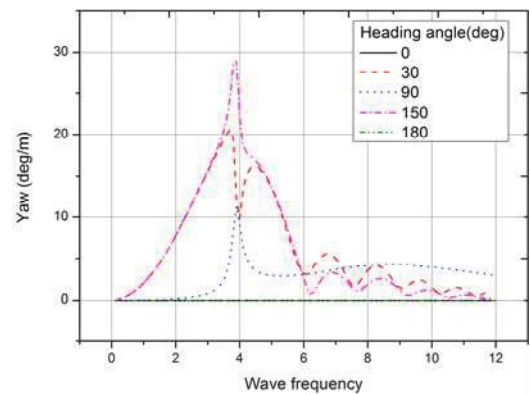


Figure 8 RAO of Yaw

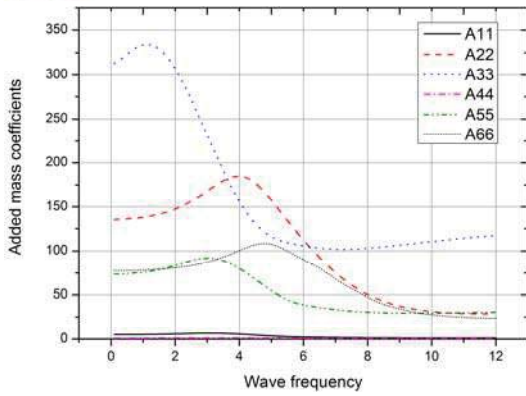


Figure 9 Added Mass

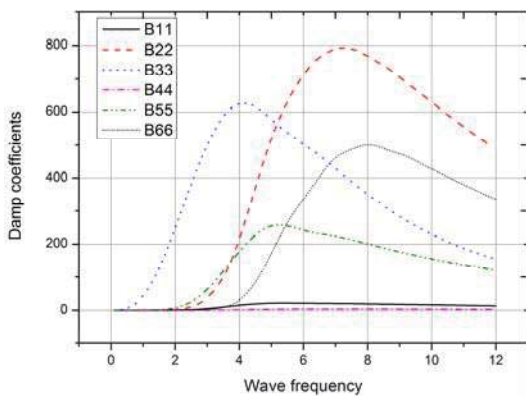


Figure 10 Damping Coefficient

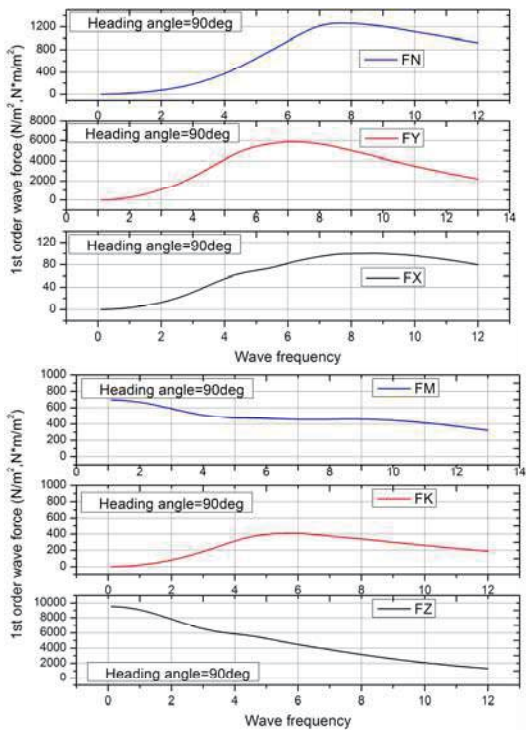


Figure 11 The First Order Wave Forces in Beam Waves

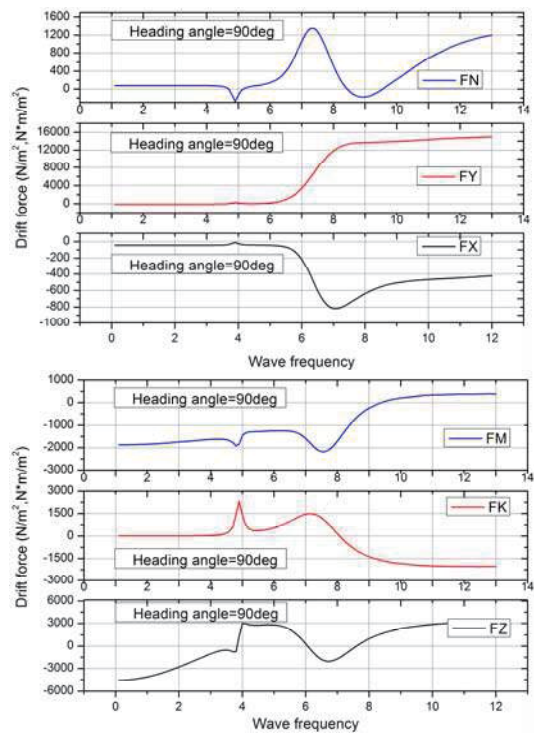


Figure 12 The Second Order Wave Forces in Beam Waves



Figure 13 Ship Model of S175

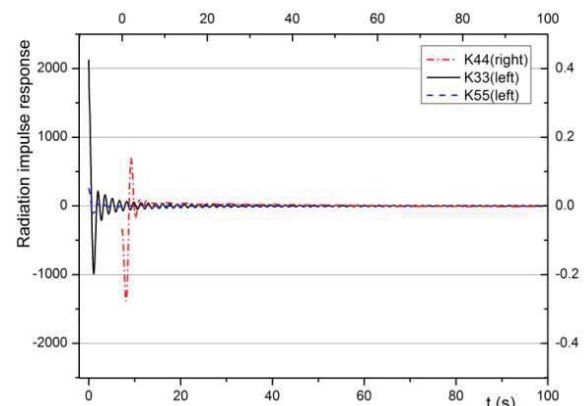


Figure 14 Radiation Impulse Responses



Equations of motion to be solved are summarized in Eq.15. In order to validate simulation method, a free running test for a S175 ship model, see Fig.13, with scale factor 57.69 was performed in the ocean engineering basin of Shanghai Jiao Tong University. Fig.14 shows the calculated radiation impulse responses.

$$\begin{aligned}
 & m(\ddot{u} - v\dot{r} + w\dot{q}) + A_{11}\ddot{u} - A_{22}v\dot{r} + A_{33}w\dot{q} + \int_0^t K_{11}(t-\tau) \cdot u d\tau + \int_0^t H_{11}(t-\tau) \cdot h(\tau) d\tau \\
 & = X_{uv} + X_p + X_R \\
 & m(\ddot{v} + ur - p\dot{w}) + A_{22}\ddot{v} + A_{41}ur - A_{33}p\dot{w} + \int_0^t K_{22}(t-\tau) \cdot v d\tau + \int_0^t K_{23}(t-\tau) \cdot p d\tau \\
 & + \int_0^t K_{26}(t-\tau) \cdot r d\tau + \int_0^t H_{22}(t-\tau) \cdot h(\tau) d\tau = Y_{uv} + Y_p + Y_R \\
 & m(\ddot{w} - uq + vp) + A_{33}\ddot{w} - A_{41}uq + A_{22}vp + C_{33} \cdot \eta_3(t) + C_{35} \cdot \eta_5(t) + B_{33}w + B_{35}q \\
 & + \int_0^t K_{33}(t-\tau) \cdot w d\tau + \int_0^t K_{35}(t-\tau) \cdot q d\tau + \int_0^t H_{33}(t-\tau) \cdot h(\tau) d\tau = Z_{uv} \\
 & I_{xx}\ddot{p} + A_{44}\ddot{p} + (A_{66} - A_{55})qr + (A_{33} - A_{22})vw + B_{44} \cdot p + C_{44} \cdot \eta_4(t) + \int_0^t K_{44}(t-\tau) \cdot p d\tau \\
 & + \int_0^t K_{46}(t-\tau) \cdot v d\tau + \int_0^t K_{48}(t-\tau) \cdot r d\tau + \int_0^t H_{44}(t-\tau) \cdot h(\tau) d\tau = K_{uv} + K_R \\
 & I_{yy}\ddot{q} + (I_{xx} - I_{zz})pr + A_{55}\ddot{q} + (A_{44} - A_{66})pq + (A_1 - A_3)uw + C_{55} \cdot \eta_5(t) + C_{57}\eta_7(t) \\
 & + B_{55} \cdot w + B_{57} \cdot q + \int_0^t K_{55}(t-\tau) \cdot q d\tau + \int_0^t K_{57}(t-\tau) \cdot w d\tau + \int_0^t H_{55}(t-\tau) \cdot h(\tau) d\tau = M_{uv} \\
 & I_{zz}\ddot{r} + (I_{yy} - I_{xx})pq + A_{66}\ddot{r} + (A_{55} - A_{44})pq + (A_{22} - A_{11})uw + \int_0^t K_{66}(t-\tau) \cdot r d\tau \\
 & + \int_0^t K_{68}(t-\tau) \cdot v d\tau + \int_0^t K_{64}(t-\tau) \cdot p d\tau + \int_0^t H_{66}(t-\tau) \cdot h(\tau) d\tau = N_{uv} + N_p + N_R - Y_{uv} \cdot x.
 \end{aligned} \tag{15}$$

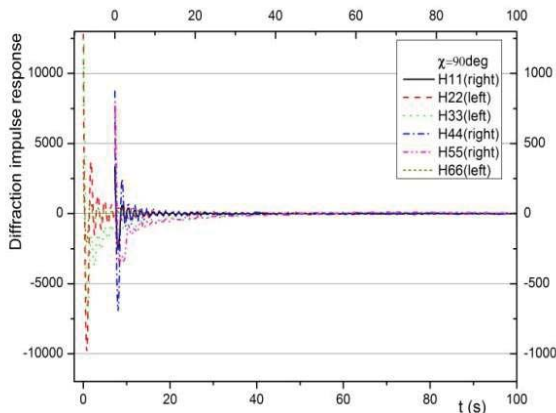


Figure 15 Diffraction Impulse Responses

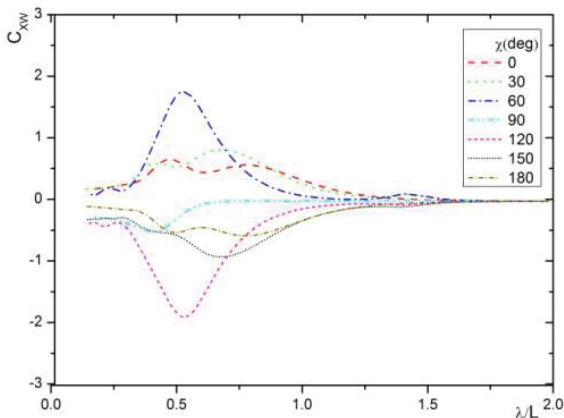


Figure 16 Longitudinal Second Order Wave Force Coefficients

Fig.15 gives out the calculated diffraction impulse responses at beam waves. Fig.16, 17 and 18 show the calculated results of longitudinal, lateral and yawing second order wave forces at various heading angles.

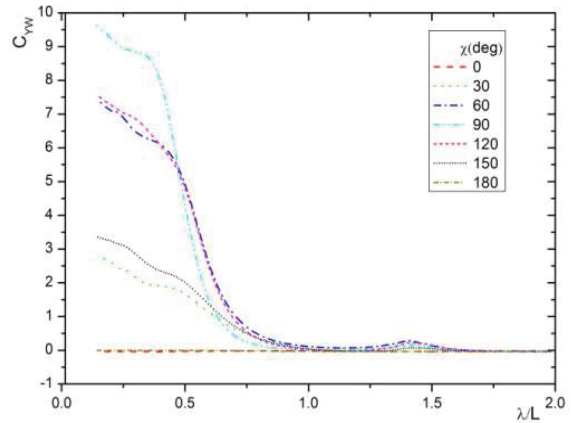


Figure 17 Lateral Second Order Wave Force Coefficients

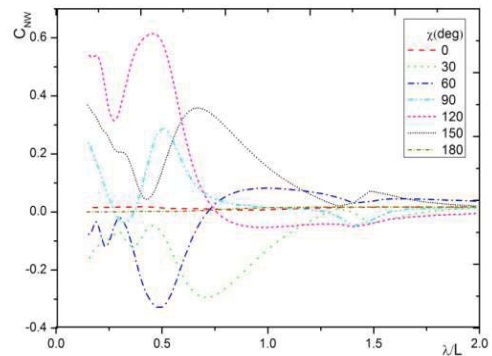


Figure 18 Yawing Second Order Wave Moment Coefficients

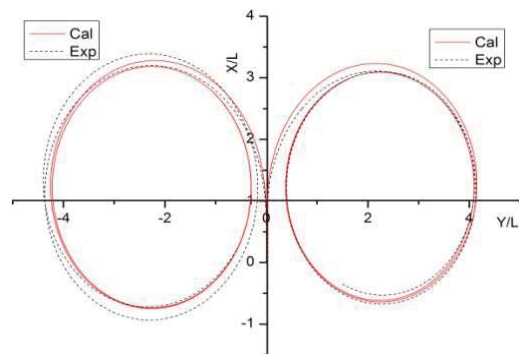


Figure 19 Turning Circle in Still Water with Rudder Angle $\pm 35^\circ$



Based on the above results, turning circle and zigzag test are simulated by solving Eq.15 numerically. Fig.19 shows that in still water the simulated circles agree quite well to measured ones at rudder angles of left and right 35°. Fig.20 and 21 demonstrates that in still water

the simulated zigzag results are very close to the measured records.

Now wave is introduced. As above, initial speed of the ship model is unchanged, also 0.72 m/s. Fig.22 is a comparison of the simulated turning circle in head wave with the test record.

Amplitude of the wave is 13.5 mm, and the ratio of wavelength to ship model length is 1.4. It can be seen that the turning circle drifts along the wave propagating direction downwards. The second order wave drift force seems the main cause of this phenomenon. Agreement of the simulated one with the test result is still quite good.

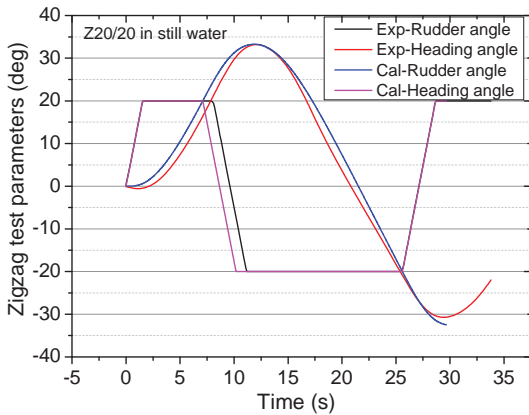


Figure 20 20/20° Zigzag in Still Water

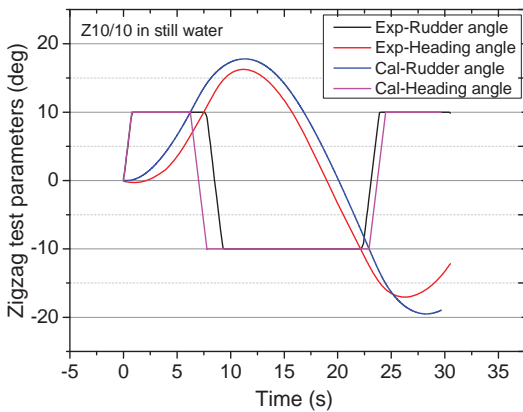


Figure 21 10/10° Zigzag in Still Water

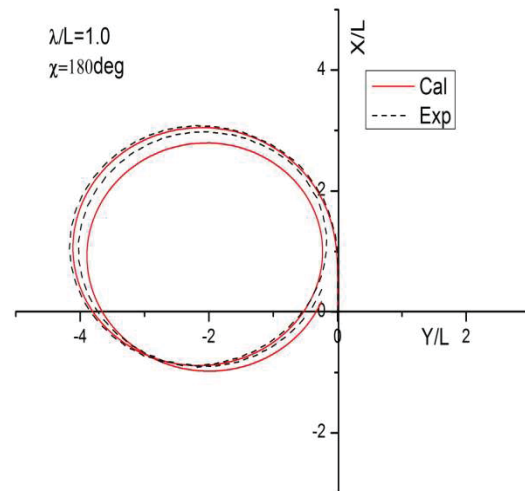
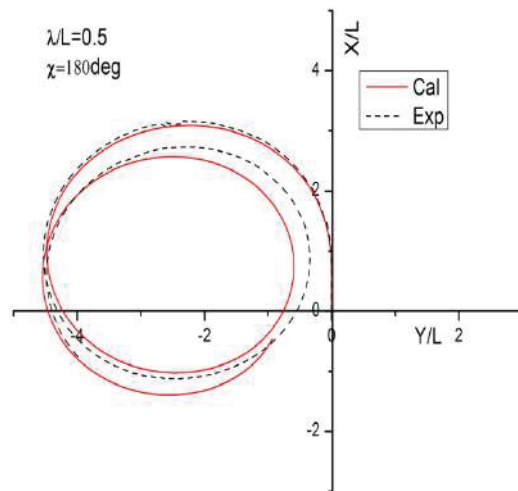


Figure 23 Turning Circle in Head Waves with Different Wave Lengths

Figure 22 Turning Circle in a Head Wave

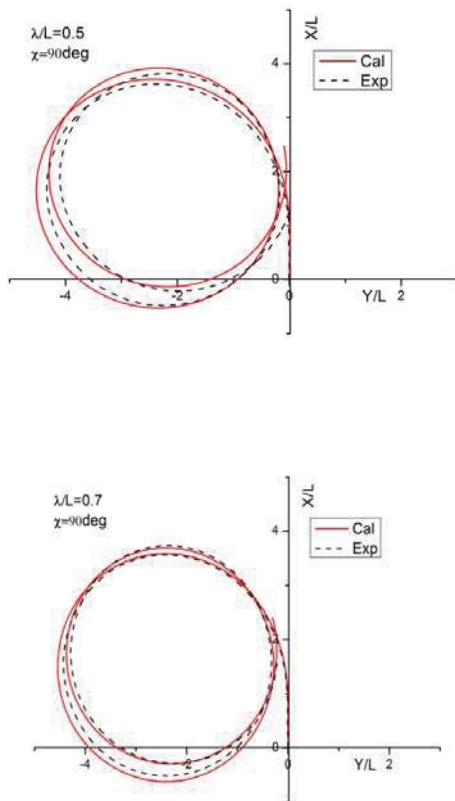


Figure 24 Turning Circle in Beam Waves with Different Wave Lengths

Fig.23 and 24 show turning circles in head and beam waves with different wavelengths. Agreement of the simulated ones with the test results is also quite good.

4. CONCLUSION

A simplified simulation method for a ship steering in regular waves is developed. The traditional MMG (mathematical manoeuvring group) model is combined with the Cummins seakeeping model. The former separates hydrodynamic forces into several individual parts due to different causes, such as the ones on the ship hull, from propeller and due to rudder operation. The latter takes linear and second order wave forces into account.

Based on the investigation for S175 ship, this method seems valid and effective enough. Since a ship steering in waves is affected by a lot of factors, and their mechanisms are quite specific and complicated, further systematic investigations is needed and will be done later, especially for validation, model tests in steeper waves is urgent.

5. ACKNOWLEDGMENTS

This study is a part of Project 51279105 which is financially supported by the National Foundation of China.

6. REFERENCES

- Cummins W.E., 1962, "The Impulse Response Function and Ship Motions", *Schiffstechnik* 9, pp. 101-109
- Hirano, M., Takashima, J., Takeshi, K. and Saruta T., 1981, "Ship turning trajectory in regular waves", *West Japan Society of Naval Architects*, Vol. 60, pp. 17-31
- Kijima, K., Furukawa, Y., 1997, "Ship maneuvering performance in waves", *Proceedings of 3rd International Stability Workshop*
- Salvesen, N., Tuck, E. O. and Faltinsen, O., 1970, "Ship Motions and Ship Loads", *Trans. SNAME*, Vol. 78, pp. 250-287
- Skejec, R. and Faltinsen, O.M., 2008, "A Unified Seakeeping and Maneuvering Analysis of Ships in Regular Waves", *Journal of Marine Science Technology*, Vol. 13, No. 4, pp. 371-394
- Yasukawa, H., 2008, "Simulations of Ship Maneuvering in Waves", *Journal of the Japan Society of Naval Architects and Ocean Engineers*, Vol. 7, pp. 163-170

This page is intentionally left blank



Prediction of Wave-Induced Surge Force Using Overset Grid RANS Solver

Hirotsada Hashimoto, *Kobe University*, hashimoto@port.kobe-u.ac.jp

Shota Yoneda, *Kobe University*, s_yoneda@maritime.kobe-u.ac.jp

Yusuke Tahara, *National Maritime Research Institute*, tahara@nmri.go.jp

Eiichi Kobayashi, *Kobe University*, kobayasi@maritime.kobe-u.ac.jp

ABSTRACT

Prediction of the wave surging force acting on a ship in following seas is a key issue for the accurate prediction of surf-riding phenomenon. It is pointed out that the linear Froude-Krylov component generally overestimates the amplitude of wave-induced surge force. Therefore a simple correction formula for the Froud-Krylov force is proposed in the second-generation intact stability criteria under discussed at IMO. In this study, a RaNS solver with an overset grid system is used to realize more accurate prediction of the wave-induced surge force. Then the current correction formula is evaluated based on the CFD results for a series of hull forms with variety of hull form parameters.

Keywords: *Second-generation intact stability criteria, Broaching/Surf-riding, Wave-induced surge force, Overset grid RaNS Solver, Froude-Krylov force, Correction formula*

1. INTRODUCTION

The second-generation intact stability criteria are under development at International Maritime Organization (IMO). There are five stability failure modes to be discussed, and experimental/numerical prediction of the wave-induced surge force in following and quartering waves became an important issue for relatively high-speed vessels because it has big influence on the threshold of surf-riding and near surf-riding condition, which are triggers for dangerous situations of broaching and pure loss of stability. In a conventional way, the wave-induced surge force is calculated as the Froude-Krylov force. However its accuracy is not satisfactory for a criteria-use purpose because it generally provides the larger amplitude of the wave-induced surge force, and hence the danger of broaching and pure loss of stability could be overestimated. Therefore more

reliable approach is needed for the second-generation intact stability criteria for surf-riding/broaching, i.e. alternative to captive model experiments to measure the wave-induced surge force. In the prediction of the wave-induced surge force for a ship running in following seas, considering the effects of diffraction and ship motion could be candidates to improve the prediction accuracy, and a three-dimensional hydrodynamic effect is also a possible element, which are missing in the linear Froude-Krylov calculation based on the strip theory.

Following these situations, CFD (Computational Fluid Dynamics) simulation to estimate the wave-induced surge force in following waves is executed using an overset grid RaNS Solver (CFDSHIP Iowa ver.4.5). In this study, the ONR tumblehome vessel is used as a sample ship and the CFD results are



compared with an existing experimental result. As a result, it is well confirmed that the CFD provides more accurate prediction than the Froude-Krylov component and the CFD results show fairly good agreement with the experimental results in a sense of practical uses. Then further CFD-based studies are done for a series of ONR-tumblehome hulls with varieties of fineness coefficients to investigate the influence of the hull form on the wave-induced surge force, and then the current correction formula for the Froude-Krylov component in the level 2 vulnerability criterion for broaching, is evaluated.

2. SECOND-GENERATION INTACT STABILITY CRITERIA

In the level 2 vulnerability criterion for broaching, the amplitude of the wave-induced surging force is calculated as the linear Froude-Krylov force by Eq.1 (IMO, 2014) to obtain the critical Froude number corresponding to the threshold of surf-riding for regular waves. However it is pointed out that the Froude-Krylov component has a tendency to overestimate the amplitude of the wave-induced surge force. If a captive model experiment in a towing tank or a numerical test using CFDs is available, more accurate and reliable prediction can be achieved. However they are time- and cost- consuming methods for the ship design in an early stage, so a simple formula for the correction of the Froude-Krylov force is useful. In this reason, one proposal was submitted to IMO, as an alternative to model experiments and CFD simulations in the second-generation intact stability criteria, to introduce an empirical correction coefficient, μ_x , for the linear Froude-Krylov calculation (see Eq.3). This coefficient is aimed to consider the diffraction effect missing in the Froude-Krylov assumption, and is expressed as functions of C_m and C_b as shown in Eq.(4) (Ito et al., 2014) (IMO, 2014).

$$f = \rho g k \frac{H}{2} \mu_x \sqrt{F_C^2 + F_S^2} \quad (1)$$

$$F_C = \int_{AE}^{FE} S(x) e^{-kd(x)/2} \sin kx dx \quad (2)$$

$$F_S = \int_{AE}^{FE} S(x) e^{-kd(x)/2} \cos kx dx$$

ρ : density

g : gravity

k : wave number

H : wave height

AE : ship aft end

FE : ship fore end

$S(x)$: sectional under-water area

$d(x)$: sectional draught

$$f = \rho g k \frac{H}{2} \mu_x \sqrt{F_C^2 + F_S^2} \quad (3)$$

Here μ_x is an empirical correction coefficient derived from several captive model tests using different types of ship.

$$\begin{aligned} \mu_x &= 1.46C_b - 0.05 & C_m < 0.86 \\ &= (5.76 - 5.00C_m)C_b - 0.05 & 0.86 < C_m < 0.94 \\ &= 1.06C_b - 0.05 & C_m \geq 0.94 \end{aligned} \quad (4)$$

\uparrow

C_b : block coefficient

C_m : midship section coefficient \uparrow

3. SUBJECT SHIP

It is important to investigate the accuracy of CFD solvers when trying to discuss a hull form effect on the wave surging force with CFD results. The ONR tumblehome, which is a wave-piercing high-speed mono hull vessel and is prone to suffer surf-riding/broaching because of her small resistance, is selected as the subject ship because a comprehensive experimental data regarding the broaching phenomenon is available. (e.g. Umeda et al. (2008), Hashimoto et al. (2011)) The original hull of the ONR tumblehome is so slender that the midship coefficient, C_m , and the block coefficient, C_b , are small as compared to conventional commercial ships. Principal

particulars of the subject ship are shown in Table 1.

In this study, a naked hull that was not equipped with bilge keels, shaft brackets and rudders is used. The subject ship is designed for a twin screw propulsion system, so a relatively large centre skeg is installed. In order to investigate the effect of ship fineness coefficients (C_m and C_b) used in the correction coefficient, a series of hulls are artificially generated by changing the under-water hull form systematically as shown in Fig.1 and Table 2. In the hull form generation, the original length, breadth and depth of the ship are kept. Since the sonar-dome and transom stern shapes are not simple/smooth, these parts are not modified from the original design.

Table 1 Principal Particulars

Length: L	154.0 m
Breadth: B	18.8 m
Depth: D	14.5 m
Draught: d	5.5 m
Volume: V	8562 m ³
Block coefficient: C_b	0.535
Midship section coefficient: C_m	0.835
Radius of gyration in pitch: κ_{yy}/L	0.25

Table 2 Parameters of the hulls

name	C_m	C_b
H-1 (original hull)	0.835	0.539
H-2	0.880	0.546
H-3	0.950	0.556
H-4	0.950	0.571
H-5	0.950	0.695

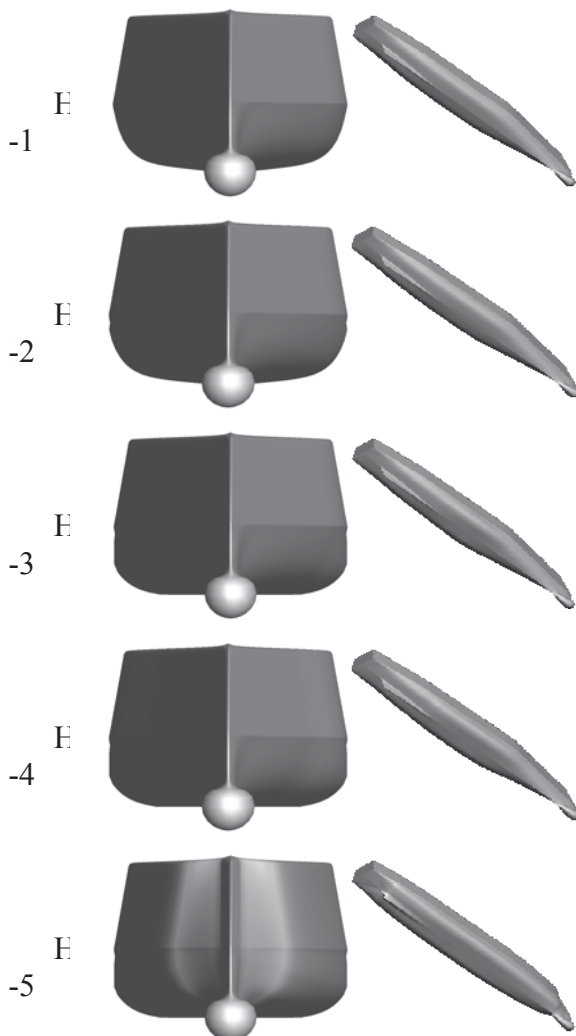


Figure 1 Geometry of the hulls

4. CFD METHOD

4.1 RaNS solver

CFDShip Iowa ver.4.5 (Carrica et al., 2006) (Tahara et al., 2006) is used for numerical computation. CFDShip Iowa solves the RaNS equations using a blended $k-\omega/k-\epsilon$ model for turbulence. The free surface is captured using a single-phase level set approach, in which the air/water interface is the zero level set distance function. The domain is discretized using multi-block structured grids. The capability of the overset is fully dynamic, which enables to simulate large amplitude motions in waves. Numerical methods include a finite difference discretization, with second-order upwind discretization for the convection term and second-order centered scheme for the viscous terms. The temporal terms are discretized using the second-order backwards Euler scheme. Incompressibility is imposed by the strong pressure/velocity coupling by using PISO. Regular waves are implemented through initial and boundary conditions. The fluid flow equations are solved in an earth-fixed inertial reference system, while the rigid body equations are done in the body-fixed system, so

forces and moments are projected to perform the integration of the rigid body equations of motion, which are solved iteratively. The SUGGAR module (Noack, 2007) is used for overset connectivity treatment and the PETSc (<http://www.mcs.anl.gov/petsc/>) is done to solve large simultaneous equations efficiently.

4.2 Grid

The overset grid design consists of 3 grids as shown in Fig.2. Two double-O boundary layer grids model the starboard and port sides of the hull to solve the asymmetric problem due to heeling. Cartesian grid is used as the background for the free surface and the wave propagation. Since the ship motion of heave and pitch is not small in steep waves even the encounter frequency is low, overset grids to accurately capture their effects might be needed to improve the prediction accuracy of the wave-induced surge force. The number of grid points is shown in Table 3. Since the total number is about 1 million, current laptop computers are sufficient enough to obtain CFD solutions. A mobile workstation of Dell Precision M6800 (Intel i7-4800MQ @2.7GHz) is used for this study.

4.3 Numerical condition

Numerical simulation using the overset grid RaNS solver is performed to obtain the wave-induced surge force acting on the subject ship running in pure following waves. Heave and pitch motions are solved in the CFD simulation, but other 4 degrees of surge, sway, roll, and yaw are fixed. Numerical conditions are shown in Table 4. Firstly the wave-induced surge force without heel is demonstrated to discuss the influence of hull form parameters, and then the influence of heel angle, ϕ , is also demonstrated. The wave length to ship length ratio, λ/L , of 1.25 is used in all the simulations because surf-riding and broaching phenomena are frequently observed in a free-running model experiment with this wave length to ship length ratio (Umeda et al., 2008), and the

experimentally confirmed critical Froude number for the surf-riding was about 0.35 for λ/L of 1.25 and wave steepness, H/λ , of 0.05.

Table 3 Number of grid points

Domain	x*y*z direction	Grid points
Ship(S)	72*44*54	171,072
Ship(P)	72*44*54	171,072
Background	95*67*116	738,340
Total		1,080,484

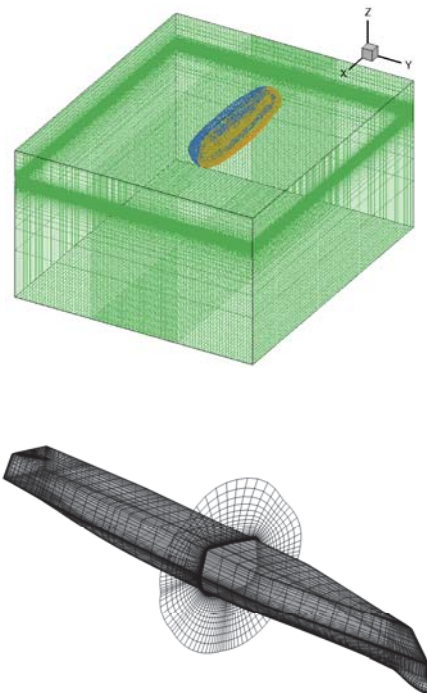


Figure 2 Computational grids

Table 4 Numerical condition

F_n	ϕ [deg]	λ/L	H/λ
0.35	0	1.25	1/40
0.35	0	1.25	1/20
0.35	10	1.25	1/40
0.35	10	1.25	1/20
0.35	20	1.25	1/40
0.35	20	1.25	1/20
0.35	30	1.25	1/40
0.35	30	1.25	1/20

5. RESULTS AND DISCUSSION

Prior to the investigation of the influence of hull form on the wave-induced surge force, the accuracy of the overset grid CFD solver is validated for the original hull (H-1) by comparing with an existing captive model experiment by Hashimoto et al. (2011). In this experiment, a two-meter ship model is used and all the appendages are removed as done in the CFD computation. Comparisons of time histories of wave-induced surge force, heave, and pitch for the wave steepness of 1/40 and 1/20 are shown in Figs.3-4. The non-dimensional time, $t^*=t/T$, of 0 means the moment when the centre of ship gravity passes a wave trough. Here the wave-induced surge force is obtained by subtracting the resistance in calm water at the same Froude number from the measured/calculated surge force in following waves. The wave-induced heave and pitch motions are obtained by the same procedure.

The CFD results show fairly good agreement in the wave-induced surge force and in vertical motions for both wave steepness. Therefore it could be concluded that it is possible to use the same RaNS solver, overset grid treatment, numerical models, and computational grids, to investigate the influence of hull form parameters on the wave-induced surge force in regular following seas.

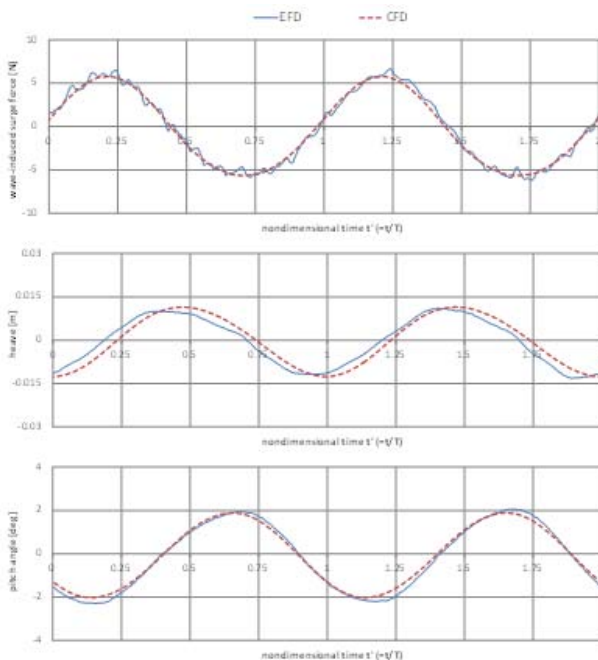


Figure 3 Comparison of wave-induced surge force, heave and pitch motions for the original hull form with $H/\lambda=1/40$

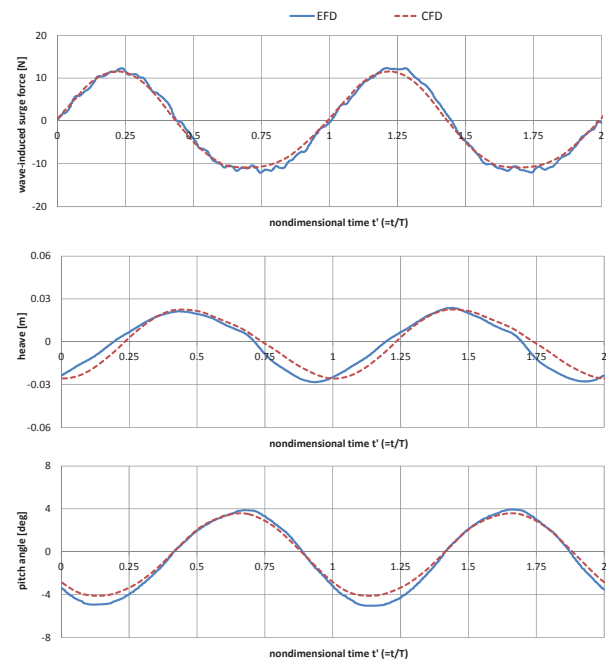


Figure 4 Comparison of wave-induced surge force, heave and pitch motions for the original hull form with $H/\lambda=1/20$

5.1 Influence of C_m and C_b

The CFD simulations are performed for the hull forms derived from the original one, i.e. H-2 to H-5 those have different C_m and C_b values. Because the underwater hull form is modified, the ship volume for the same draught is changed, but we impose the original draught for all hulls in the CFD simulation. Comparisons of CFD results of the wave-induced surge force are shown in Figs.5-6. Here the resistance in calm water of the original hull form in calm water is subtracted from all the calculated data. Therefore the vertical shift of the mean of the wave exciting force is regarded as the increase of the resistance in calm water due to the hull form modification, so the maximum shift can be found in the most-blunt hull (H-5). The amplitude of the wave surging force has a tendency to slightly increase with the fatness of the hull, but it is negligibly small. It is noted that the linearity of the wave-induced surge

force is not confirmed for the H-5 hull. Major difference between wave steepness of 1/40 and 1/20 can be found near wave up-slope position.

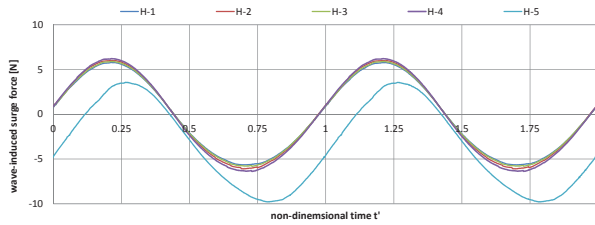


Figure 5 Comparison of wave-induced surge force for five different hull forms with $H/\lambda=1/40$

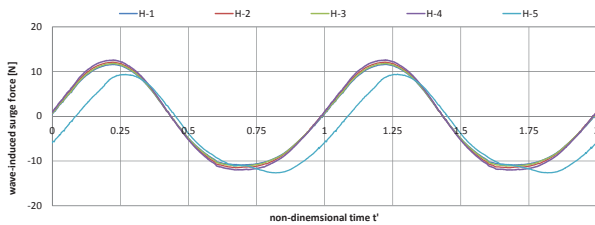


Figure 6 Comparison of wave-induced surge force for five different hull forms with $H/\lambda=1/20$

The CFD result of wave height and pressure on the underwater hull is shown in Fig.7. The ship is located in the wave down-slope portion where the wave presses the ship most strongly. It is difficult to find differences in the wave height distributions among H-1 to H-4. This means that the hull form modification, for H-1 to H-4, has few influences on the wave diffraction, ship-generated waves and their interference. In the result for the H-5 hull bloated over a considerable range, the wave diffraction and bow- and stern-generated waves are much prominent compared to H-1 to H-4 cases. Therefore the wave height distribution is different from the original sinusoidal wave. This might be a possible reason of significant change of the wave-induced surge force for the H-5 hull. The pressure distribution on the underwater hull looks not so different for H-1 to H-3. However, in the H-4 result, high-pressure region appears differently from those of H-1 to H-3, and the appearance of the pressure distribution

becomes much different from others in the H-5 result. Regarding the H-5 hull, the different pattern of the pressure at bow and stern areas could be the reason to explain the phase difference of the wave-induced surge force found in Fig.6.

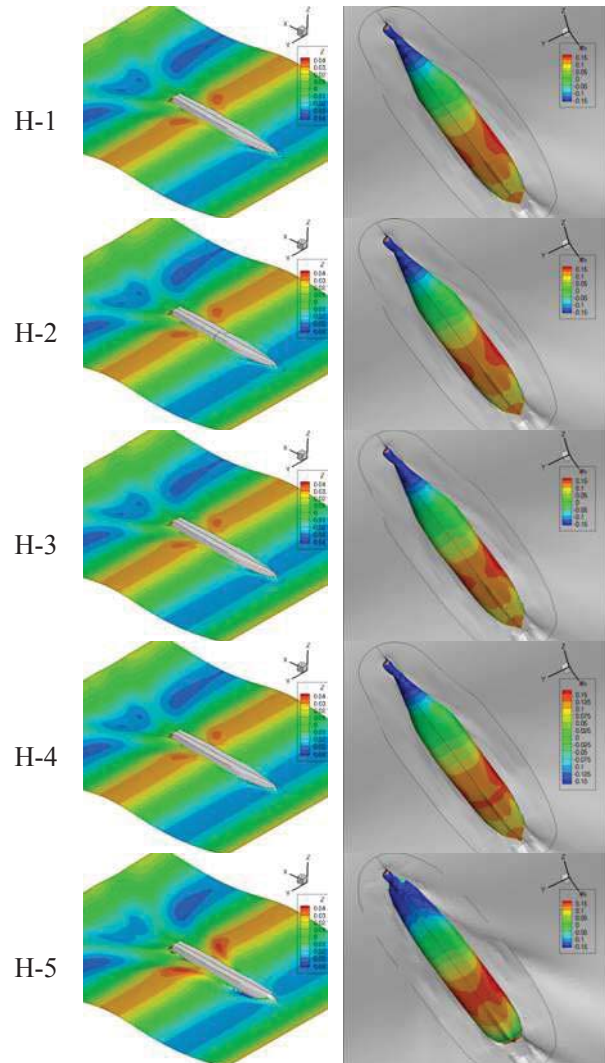


Figure 7 Contour maps of wave height and pressure with $H/\lambda=1/20$

Table 5 shows the non-dimensional amplitude of the wave-induced surge force in following seas, $X'_a = X_a / (\rho g V \times H / \lambda)$, obtained by the CFD and the linear Froude-Krylov calculations. Here the individual volume is used for each hull. The CFD simulation, which shows good agreement with the experimental result, provides much smaller values than the Froude-Krylov force in all



conditions. This means that the linear Froude-Krylov calculation would significantly overestimate the amplitude of the wave exciting force in following waves and hence the danger of surf-riding could be overestimated. Table 6 shows the correction coefficient for the linear Froude-Krylov calculation, which is calculated by the existing correction formula of Eq.4. It would be reasonable to assume the present CFD result is accurate enough, if so the correction coefficient μ_x should coincide with the value of CFD/FK. From the results of H-1 to H-3, in which C_m value is mainly changed, CFD/FK value does not always decrease with the increase of C_m while μ_x decreases monotonically. From the results of H-3 to H-5, with the same C_m but different C_b , the CFD/FK value decreases with the increase of C_b while μ_x increases oppositely.

Table 5 Estimated amplitude of the wave-induced surge force

hull	H/ λ	X'a (CFD)	X'a (FK)	EFD/CFD	EFD/FK
H-1	0.025	1.246	1.546	1.024	0.826
H-2	0.025	1.231	1.557		
H-3	0.025	1.299	1.574		
H-4	0.025	1.291	1.585		
H-5	0.025	1.093	1.412		
H-1	0.05	1.234	1.546	1.055	0.842
H-2	0.05	1.211	1.557		
H-3	0.05	1.268	1.574		
H-4	0.05	1.258	1.585		
H-5	0.05	0.903	1.412		

Table 6 Evaluation of the correction coefficient

hull	H/ λ	C_m	C_b	CFD/FK	μ_x
H-1	0.025	0.837	0.539	0.806	0.737
H-2	0.025	0.88	0.546	0.790	0.693
H-3	0.025	0.95	0.556	0.825	0.539
H-4	0.025	0.95	0.571	0.815	0.555
H-5	0.025	0.95	0.695	0.774	0.687
H-1	0.05	0.837	0.539	0.798	0.737
H-2	0.05	0.88	0.546	0.777	0.693
H-3	0.05	0.95	0.556	0.806	0.539
H-4	0.05	0.95	0.571	0.794	0.555
H-5	0.05	0.95	0.695	0.639	0.687

These results indicate that the existing correction formula, using C_m and C_b as

variables, cannot reasonably explain the influence of the hull form on the wave-induced surge force. Although the current correction formula is based on several captive model tests, the correction coefficient would be only acceptable for the original hull (H-1) and the bluntest hull (H-5). This might be because there is a certain correlation between C_m and C_b values for well-designed ships while such correlation is neglected in the ship hull generation in the present study. However the comparison results show that the current correction formula would be only applicable for limited hull design and does not fully explain the influence of hull form on the wave-induced surge force. Therefore further efforts, to improve/reconstruct the formula using other hull form parameters or additional elements, are expected to realize more rational correction for the regulatory use in the second-generation intact stability criteria.

5.2 Influence of L/B

In order to find more appropriate hull form parameters and/or other elements missing in the current correction formula, the influence of L/B ratio is investigated because the diffraction force would be an important element to improve the prediction accuracy. For this purpose three fattening hulls are additionally generated by stretching the original hull in y-direction uniformly, and the stretched breadths are 1.1, 1.2 and 1.3 times of the original breadth as shown in Table 7 and Fig.8. The projected area to the y-z plane and the entrance angle of the bow becomes larger, so the diffraction effect becomes more significant. The CFD and Froude-Krylov calculations as well as the correction coefficient are shown in Table 8. The correction coefficient is constant because the C_m and C_b values are the same, and the ratio of CFD and the Froude-Krylov force shows the same tendency. Therefore it is confirmed that the diffraction effect is not a dominant, so L/B or bow entrance angle is not a candidate for the improvement of the correction formula. Further investigation is

desired to develop a reasonable correction formula to be applicable for any hull forms.

Table 7 Parameters of the hulls

Hull	B	L/B	Entrance angle [deg]
H-1 (original hull)	18.8	8.19	19.0
H-6	20.7	7.45	20.8
H-7	22.6	6.83	22.7
H-8	24.4	6.30	24.5

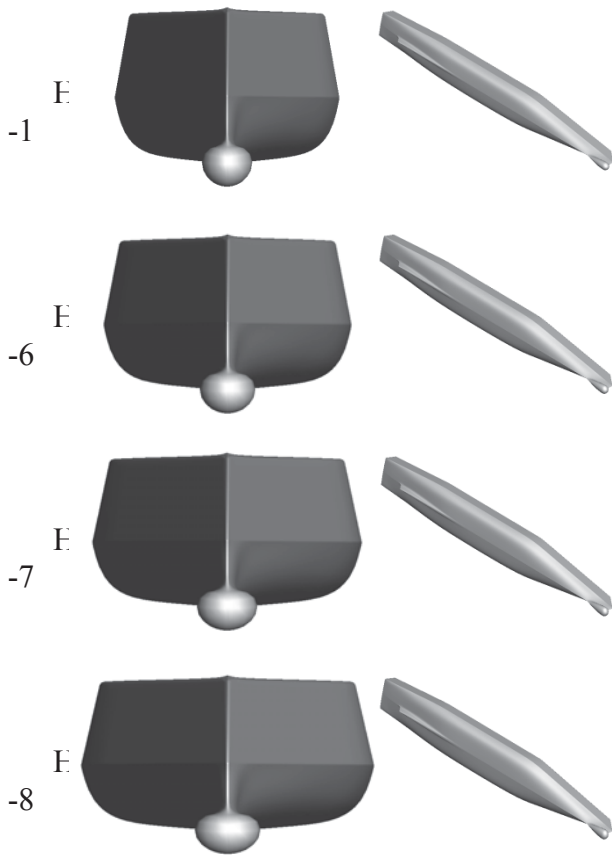


Figure 8 Geometry of the hulls

Table 8 Influence of L/B

hull No.	H/λ	$X'a$ (CFD)	$X'a$ (FK)	CFD/FK	μ_x
H-1	0.025	1.246	1.546	0.806	0.737
H-6	0.025	1.235	1.545	0.799	0.737
H-7	0.025	1.234	1.544	0.799	0.737
H-8	0.025	1.231	1.542	0.798	0.737
H-1	0.050	1.234	1.546	0.798	0.737
H-6	0.050	1.214	1.545	0.786	0.737
H-7	0.050	1.203	1.544	0.779	0.737
H-8	0.050	1.202	1.542	0.780	0.737

5.3 Influence of ship motion

In order to find out the major element to improve the prediction accuracy of wave-induced surge force, the influence of ship motion is examined. The CFD simulation is executed without solving the heave and pitch motions. Time histories of the calculated wave-induced surge force for the original hull is shown in Figs.9-10. Here the steady sinkage and trim in calm water at the same Froude number is neglected, but it is confirmed that their effect is negligibly small at least in the tested condition. These graphs clearly show the neglect of the ship vertical motion significantly affects both the amplitude and the phase of the wave-induced surge force. Therefore the heave and pitch motions should be included for the accurate prediction. However majority of the ship motion here is a component due to hydrostatic balancing in heave and pitch because the encounter frequency is very low and the ship length is comparable to the ship length. Therefore CFD simulation should be performed for the prescribed ship attitude obtained as hydrostatically balanced position in waves, to extract the dynamic effect of ship motion which is neglected in the Froude-Krylov calculation.

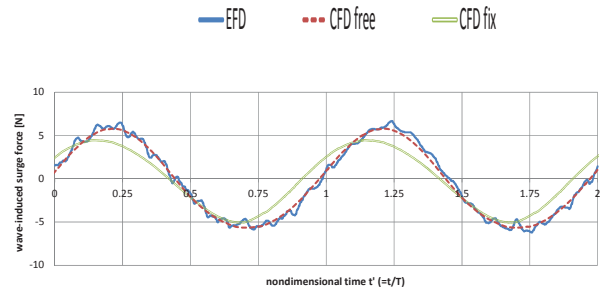


Figure 9 Influence of heave and pitch motions with $H/\lambda=1/40$

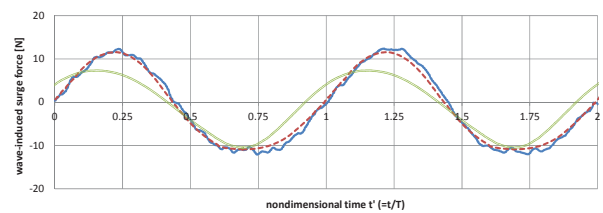


Figure 10 Influence of heave and pitch motions with $H/\lambda=1/20$



5.4 Influence of heel angle

All the discussions until here are done for the ship in upright condition. Once broaching happens, violent yaw motion is induced so that a ship could largely heel due to the centrifugal force. For direct stability assessment of broaching, numerical prediction of the wave-induced surge force in largely heeled condition is also important to quantitatively assess the danger of broaching. Therefore the CFD simulation is executed for the original hull with 10, 20, and 30 degrees of heel angle. The estimated amplitudes of the wave-induced surge force are compared with an existing model experiment by Hashimoto et al. (2011) and their results are shown in Table 9. The experimental result of the amplitude of the wave-induced surge force does not change so much with the increase of heel angle up to 30 degrees. The CFD result can capture this trend and the maximum error is 8.2% and the mean error is 5.2%. The error does not increase with the heel angle, so the overset grid RaNS solver used in this study has possibility to be applicable for the direct stability assessment of surf-riding/broaching phenomenon as the third level of the direct stability assessment.

Table 9 Influence of heel angle

hull No.	H/λ	φ	X'a (CFD)	X'a (EFD)	EFD/CFD
H-1	0.025	0	1.246	1.277	1.024
H-1	0.05	0	1.234	1.302	1.055
H-1	0.025	10	1.248	1.328	1.064
H-1	0.05	10	1.228	1.329	1.082
H-1	0.025	20	1.187	1.262	1.062
H-1	0.05	20	1.222	1.261	1.032
H-1	0.025	30	1.181	1.237	1.047
H-1	0.05	30	1.228	1.197	0.975

6. CONCLUSIONS

The influence of hull parameters on the wave-induced surge force in following seas is investigated using an overset grid RaNS solver. The importance of C_m and C_b is investigated with a series of derived hull forms from the ONR-tumblehome vessel. It is recognized that increasing of C_b affects the amplitude of wave-

induced surge force while C_m does not so. Since it is reconfirmed that the linear Froude-Krylov force significantly overestimates the amplitude of wave-induced surge force, reasonable correction formulae are highly desired to be used in the level two vulnerability criteria for broaching. Therefore current proposal of a correction formula is evaluated by CFD-based numerical tests. As a result, it is demonstrated that the current correction formula has limitation and cannot reasonably explain the influence of the hull form on the wave-induced surge force. Further investigation on the influence of L/B , heave and pitch motions, and heel angle is also performed. The L/B ratio and the heel angle are not influential but the consideration of ship motion is an important element for the accurate prediction of the wave-induced surge force at least for the subject ship. Further comprehensive research is necessary to develop and propose more valid and reliable correction formula to be applicable to any types of ship for the second-generation intact stability criteria for broaching.

7. ACKNOWLEDGMENTS

This work was supported by JSPS KAKENHI Grant Number 25249128 and 24360355, and was also carried out as a research activity of Goal-Based Stability Criterion Project of Japan Ship Technology Research Association in the fiscal year of 2014, funded by the Nippon Foundation. The authors thank Prof. Naoya Umeda from Osaka University for his useful discussion.

8. REFERENCES

Carrica, P. M., Wilson, R.V., Noack, R., Xing, T., Kandasamy, M., Shao, J., Sakamoto, N., and Stern, F. 2006, "A Dynamic Overset, Single-Phase Level Set Approach for Viscous Ship Flows and Large Amplitude Motions and Maneuvering", Proceedings of 26th Symposium on Naval Hydrodynamics,



Rome.

Hashimoto, H., Umeda, N., Matsuda, A. 2011, “Broaching prediction of a wave-piercing tumblehome vessel with twin screws and twin rudders”, Journal of Marine Science and Technology, 16, pp.448-461.

IMO, “Proposed Amendments to Part B of the 2008 IS Code to Assess the Vulnerability of Ships to the Broaching Stability Failure Mode”, SDC1 INF.8 ANNEX15.

IMO, “Proposal of working version of explanatory notes on the vulnerability of ships to the broaching stability failure mode”, SDC1/5/4.

Ito, Y., Umeda, N. and Kubo, H., 2014, “Hydrodynamic Aspects on Vulnerability Criteria for Surf-Riding of Ships”, Jurnal Teknologi, Vol. 66, No. 2, pp. 127-132.

Noack, R., 2007, “Enabling Large Amplitude and Relative Motions Through Overlapping Grids”, Proceedings of 9th International Conference on Numerical Ship Hydrodynamics, Michigan.

Tahara, Y., Wilson, R.V., Carrica, P.M. and Stern, F. 2006, “RANS Simulation of a Container Ship Using a Single-Phase Level Set Method with Overset Grids and Prognosis for Extension to Self-Propulsion Simulator”, Journal Marine Science and Technology, 11, pp. 209-228.

Umeda, N., Yamamura, S., Matsuda, A., Maki, A., Hashimoto, H., 2008, “Model Experiments on Extreme Motions of a Wave-Piercing Tumblehome Vessel in Following and Quartering Waves”, Journal of the Japan Society of Naval Architects and Ocean Engineers, 8, pp.123-129.

Session 9.2 – DAMAGE STABILITY

Life-Cycle Risk (Damage Stability) Management of Passenger Ships

Free- Running Model Tests of a Damaged Ship in Head and Following Seas

Main Contributing Factors to the Stability Accidents in the Spanish Fishing Fleet

This page is intentionally left blank



Life-cycle Risk (Damage Stability) Management of Passenger Ships

Dracos, Vassalos, *Department of Naval Architecture, Ocean and Marine Engineering, University of*

Strathclyde, d.vassalos@strath.ac.uk

Yu, Bi, *Department of Naval Architecture, Ocean and Marine Engineering, University of*

Strathclyde, y.bi@strath.ac.uk

ABSTRACT

Inadequate damage stability, the Achilles heel of passenger ships, has been a critical research objective that industry and academia delved to improve every time following accidents with passenger ships. Most achievements focused on design phase, either for the new-made regulations or rather novel pro-active methodology of risk-based design, which ignored thousands of existing ships and wasted state-of-art knowledge on damage stability. Considering this situation, a framework of life-cycle risk (damage stability) management of passenger ship and its related damage stability verification framework were introduced and established in this paper.

Keywords: damage stability, risk management, damage control

1. INTRODUCTION

Accidents of passenger ships, involving thousands of lives on board, are a matter of grave concern, consequences of which from time to time irritate and astonish the public. As a result, industry and academia's endeavour to improve safety of passenger ships never stops and much of it targets the inadequate damage stability, the Achilles heel of passenger ships. For centuries, traditional passive way of establishment and modification of safety regulations and rules in the aftermath of tragic accidents stays as the dominant method to help control the risk but nowadays it becomes difficult to catch up with the unrelenting pace of ship technology. In contrast, pro-active risk reduction ideas were put forward and various related methods are under development and

tentatively expanding into the ship industry. The typical representative, risk-based ship design method, integrating safety assessment procedure into the ship design process, widens the design envelope and inspires innovations on the new specifications while proactively controlling the risk. Moreover, along with traditional regulations, it focuses on the improvement of damage stability in the design phase, which serves only for the newbuildings, leaving thousands of existing ships still confronted with uncontrollable risk and with state-of-art knowledge on damage stability wasted.

Given the background introduced above, it is not sensible to limit the research of damage stability improvement in ship design phase. Besides the risk control options (RCOs) in



design phase, throughout a ship's life, effective operational (active) measures and measures conducted during emergencies could also serve to improve damage stability and efficiently reduce the loss of lives. This gives birth to the idea of establishment of a complete framework for life-cycle risk (damage stability) management. Built on the life-cycle perspective, this framework is a holistic approach to improve damage stability cost-effectively through risk control measures in design, operation and emergency stages. As the building block of the framework, the risk reduction potential of risk control measures should be known. This could be accomplished by a damage stability verification framework which aims at the verification and measurement of the risk reduction measures in ship's whole life cycle via auditable and measurable means. And this paper would introduce the establishment of these two frameworks respectively.

2. SAFETY MANAGEMENT SYSTEM

The safety management system introduced by HSE (Health and Safety Executive) in its guide -- *successful health and safety management* has served as a mainstream methodology for risk management and has been employed in various different industry fields managing risks and solving safety problem in a holistic view. The system comprises five steps, namely, policy, organizing, planning and implementing, measuring performance, reviewing and auditing (shown in figure 1). 'Policy' describes the corporate approach to safety; 'Organizing' describes the management hierarchy relating to safety with responsibilities defined at each level; 'Planning' shows the safety tasks to be targeted at each stage and 'Implementing' is to conducting measures to reduce or mitigate risks; 'Measuring performance' refers as measurement and verification of the effectiveness the implemented measures; 'Reviewing and Auditing' belongs to the system of continuous improvement, ensuring

new hazards identified, near miss incidents considered and the SMS kept up to date. The importance of this safety management system lies on the classification of a rather complicated situation which includes huge numbers of different aspects into systematic and reasonable five steps.

Based on the HSE's Safety Management System (SMS) guideline, the damage stability risk management framework in this paper also followed the holistic idea of HSE's SMS and utilized the steps in the guideline. Given the particular situation of damage stability problems discussed in the paper, the main concerns of the framework focus on the last three steps which specifically are planning and implementation of risk control measures, measurement of the performance and effectiveness of implemented risk control measures, and acquisition of reviews and suggestions from the former two processes.

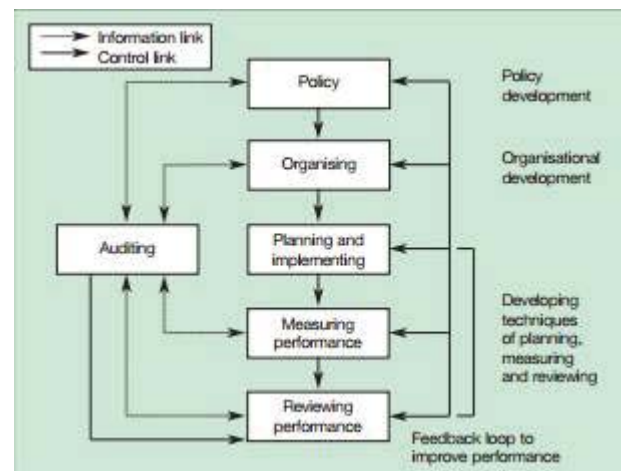


Figure 1: Key Elements of Successful safety management

3. LIFE-CYCLE RISK (DAMAGE STABILITY) MANAGEMENT FRAMEWORK

A literature review on life-cycle risk management (LCRM) for ships would tell us that LCRM is still a developing and immature



subject. Plenty of ideas merged and attempts of managing the overall risk from a life-cycle view have been made. The main target and challenging part of a primary thinking pattern is establishment of linkages among different life periods and among different risk control processes to order to integrate different life periods, safety essentials and risk-based methodologies together in a whole risk management system. A review and feedback system is prone to be established based on this kind of risk management system. However, it seems that this research direction builds on the hypothesis that appropriate measures would be conducted to reduce or mitigate risks and threats to tolerable level during operation and emergency stages, which is not often the case. Complementarily, the objective of the life-cycle risk management framework presented in this paper is assurance of risk being under control in every period of ship's life by managing the risk in ship's different life periods. Disassembly of this holistic goal indicates that target for each life period is the verification of risk reduction or mitigation in this period.

Establishing on a life-cycle perspective, the framework comprises three dominate phases in the life of a ship, namely design, operation, and emergency. The operation stage defined here is from an incident happened to the moment before the ship is going to be abandoned. And emergency stage starts from the moment ship is decided to be abandoned. Correspondingly, risks are divides in terms of life periods into three parts, risk in design, residual risk in operation and residual risk in emergency situation. In each life-cycle phase, three essential safety management steps mentioned in the first section are conducted respectively, reducing and mitigating the risk in every stage and ensuring an overall safety environment.

Verification of the risk control options in each life phase is most direct way to ensure risk reduction or mitigation in every life period. Risk control options in each stage are distinctive from each other. In design phase, traditionally rules always focus on design

solutions, serving as passive risk control measures for damage stability improvement. Operational measures, referred as active risk control measures, are abundant in SOLAS Ch. II-2 (e.g. damage control). In emergency stage, effective risk control measures are mainly systems and measures focusing on emergency response, such as Decision Support Systems for Crisis Management, Evacuation, LSA (Life Saving Appliances), Escape and Rescue.

Whilst a substantial amount of options for planning and implementation of risk control measures exist, measurement of the performance and effectiveness of these risk control measures still remains as a big gap in this approach. Contrary to passive design solutions which has stayed as a primary research target for centuries, operational measures have not been rigorously validated yet. Moreover, the cost-effectiveness of emergency risk reduction potential was never measured nor verified before, since risk reduction of 'residual' risk in this stage falsely perceived to be small by definition. These problems need to be overcome before the overall risk management process can be formalized and adopted. This issue was considered in the next section.

4. DAMAGE STABILITY VERIFICATION FRAMEWORK

In addition to traditional design modifications, identification of alternative means and arrangements such as operational measures and emergency response measures gives credit to their benefit based on their verifiable contribution in improving stability levels. Damage stability verification framework is established, targeting on identification, quantification and validation of the risk-reduction potential of all such measures.

Damage stability verification framework encompasses one proposal for each life stage. The goal for design and operation stage is to assess the ship vulnerability to flooding, while



assessing effectiveness of emergency response is the target for emergency phase. To achieve the goal, objective of the proposal for design stage (Item 1) is establishment of baseline vulnerability and assessment of impact of design measures. Quantitative analysis, including damage stability statutory assessment and damage stability alternative method, are planned to conduct to acquire the effectiveness of various risk control options in design. Correspondingly, assessment of impact of active damage control measures by crew is the objective for operation proposal. Quantitative analysis to fulfill this objective includes damage stability alternative method and ship systems operability assessment, while qualitative analysis, namely assessment of crew performance, could serve as supplementary. Similarly, proposal objective for emergency stage is assessing impact of emergency responses measures. Escape and evacuation analysis and assessment of crew performance are the quantitative and qualitative analysis respectively.

4.1 Proposal for the design phase

The work in design phase comprises the following activities:

Statutory (SOLAS2009) damage stability assessment: The following actions describe in-house developments targeting design vulnerabilities and cost-effective design measures to reduce these.

1. Statutory A-value index calculation (basis calculations) in accordance with SOLAS Ch.II-1 (SOLAS 2009).
2. Vulnerability screening and identification of design modifications aimed at increasing the level of index A as high as it is practicably attainable.
3. The results of the vulnerability screening will be used to define appropriate design modifications on the basis of risk-reduction

potential and cost effectiveness.

4. Taking into account the results of the vulnerability screening, simple solutions (such as closing openings) as well as a number of alternative ship watertight arrangements will be used for further analysis for each ship.

Operational data: The following actions target to identify ship specific data and conditions for use in the stability assessment (rather than the generalised average values used in the probabilistic rules)

5. Collection and analysis of real life on-board data for an agreed period of operation. The data relate to loading conditions, stability parameters, quantity and distribution of loads, etc. Use will be made of any data that already exists.
6. Readily available stability improvements can be specified by reviewing the quantity and distribution of fluid loads (fuel, ballast water, heeling water, fresh water, grey water).
7. Realistic operational data need to be used as a basis for numerical flooding simulations.

Alternative assessment of damage stability: The following actions describe the use of first-principles tools as a supplementary means to assessing damage stability.

8. Alternative assessment based on Monte Carlo (MC) sampling in conjunction with numerical flooding simulations (referred to subsequently as MC simulation). This approach reflects explicitly the damage statistics and accounts realistically for the physics of stability deterioration following a collision event. The MC simulation is a viable technique for stability assessment in accordance with SOLAS Chapter II Part B Regulation 4.2 (alternative method).
9. For the purposes of comparison, the



alternative assessment will be carried out for the same basis design and alternative watertight arrangements developed as part of the statutory damage stability assessment.

10. The MC simulations will allow identification of weak “spots” (e.g. local architecture) contributing to stability deterioration when subject to flooding as a result of water ingress following a large number of collision events.
11. The study will be performed for (a) three watertight arrangements per ship, and (b) two loading conditions, comprising one regulatory condition, and one real life loading condition. In total six cases per ship will be analysed.

for this, a one-day meeting with active crew members (Master, chief engineers, deck hands, etc.) involved in damage control duties on-board the vessels under evaluation will be conducted.

2. Definition of human and organizational (procedural) factors affecting the effectiveness of damage control actions.
3. Effectiveness of crew actions for flooding control will highly depend on the level of crew preparedness and competence necessary to carry out the actions safely, timely and effectively.
4. A qualitative measure reflecting the objective evidence in terms of crew competence and preparedness will be developed

4.2 Proposal for operation stage

The work comprises the following activities, carried out for the same sample ships referred to in Item 1. Measures related to damage stability assessment encompass active damage control which is STAGE 2 activity in a typical muster list.

STAGE 1	STAGE 2	STAGE 3
INCIDENT happens (1) Detection & Alarm	(2) Damage control	(5) Abandon Ship (6) Rescue
	(3) Muster of Pax	
	(4) Preparation of LSA	

Table 1 Generic sequence of events that may occur after a flooding event (typical muster list)

Qualitative analysis includes:

1. Definition of active damage control options by the crew. It is envisaged that

Quantitative analysis includes:

1. One of the watertight arrangements defined in Item 2 will be used as platform to quantitatively assess the impact of possible active flooding control measures by crew when a flooding incident moves to damage control stage (see Table above).
2. The quantitative analysis will be based on the alternative MC simulation method described in Item 1. This entails identification of flooding scenarios where counter-ballasting is effective and feasible, the latter implying availability of ship systems to enable this action.
3. Crew actions to be analysed will comprise counter-ballasting operations. This is based on the premises that available options will be computed, defined and executed in a timely manner.
4. Effectiveness of crew actions for flooding control will depend, in addition



to the necessary ship systems being available, on the possibility of active reconfiguration for that purpose if the systems are impaired by the flooding.

5. The availability of relevant ship systems will be verified by using a design verification tool that allows modeling ship systems architecture, in topological and functional form. The tool is used for verification and analysis of essential ship systems redundancy when applying Safe Return to Port requirements of SOLAS Ch.II-2.

4.3 Proposal for emergency phase

The research comprises the following activities, carried out for the same sample ships referred to in Item 1. Measures related to evacuation include: muster of passengers, preparation of LSA, abandon ship and rescue operations, namely STAGE 2 and 3 activities in a typical muster list.

Qualitative analysis includes:

1. Definition of evacuation-related duties and activities by the crew. It is envisaged that for this, evacuation activities on-board the vessels under consideration will be conducted.
2. A hazard identification type of exercise needs to be conducted with a view to defining human and organisational (procedural) factors affecting the effectiveness of the evacuation process.
3. Effectiveness of crew actions for evacuation purposes will highly depend on the level of crew preparedness and competence necessary to carry out the actions safely, timely and effectively.
4. A qualitative measure reflecting the objective evidence in terms of crew competence and preparedness will be

developed

Quantitative analysis (Evacuation analysis) includes:

5. Evacuation analyses of the ships in question will be conducted with an advanced evacuation analysis tool (as defined in MSC\Circ.1238)
6. The evacuation analysis will cover the mustering and ship abandonment process;
7. Human and LSA systems performance data for the analysis will be collected and validated prior to use on the basis of existing IMO instruments and operators experience
8. The evacuation time will be assessed in the context of the survival time (time to capsize) derived from the damage stability assessment (Items 1 and 2) for all critical emergency scenarios (where damage stability may be compromised)
9. Effectiveness of crew actions for evacuation will depend on the availability of necessary emergency ship systems or the possibility of active reconfiguration for that purpose if the systems are impaired by the flooding.
10. The availability of relevant ship systems will be verified as described in Item 2(9) above.

5. CASE STUDY

Here presented a simplified case study of the damage stability assessment for damage control process. The objective of the study is to identify and qualify the impact of damage control measures. The overall procedures are shown in Figure 2.

Firstly, the original geometry data and loading conditions of representative ship are given and recorded. Monte Carlo simulation



method is employed to generate different damage extents and sea states which would later be applied on the representative ship resulting piles of damage scenarios. By calculating the probabilities of survival under random sea states for each damage extent, critical scenarios that the probability of survival indicates an intolerable chance of capsizing could be elected as research objects in the next step. For each critical scenario, corresponding risk control options are generated, with an alternative loading condition and geometry data comparing to the original one. Then Monte Carlo simulation needs to be employed again to generate random sea states, and with the help of PROTEUS program the motion responses of the damage ship under current circumstances could be obtained. Finally, the probabilities of survival under random sea states for three hours are calculated again, and the differences between the original and new survival probabilities could be counted as the impact of the related risk control options for a certain damage case.

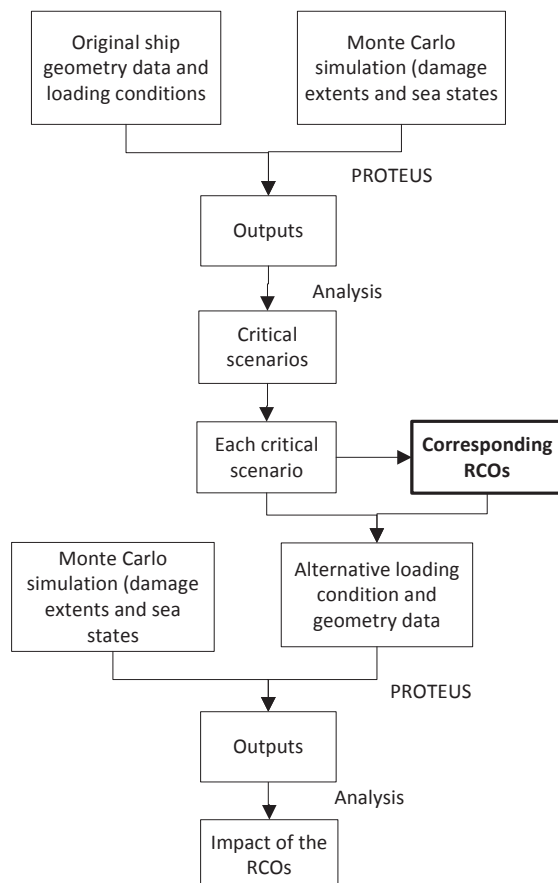


Figure 2 Overall procedures of damage control verification process

The damage control measures considered in this case study mainly include counter-ballasting plans. It is multi-objective optimisation process, and various algorithms could be proposed to determine the most effective risk control option based on both a list of performance and safety criteria.

6. CONCLUSIONS

This paper presented a hostile framework for life-cycle risk (damage stability) management of passenger ships which particularly emphasizes on the benefits and importance of identification and verification of the risk control measures in operation and emergency phases. Correspondingly, as the building block, a damage stability verification framework was established and specific proposals for each life stage were raised. And the last section of the paper outlined a related case study aiming at qualifying and verifying the impact of damage control measures. Further study might include development of the algorithms of generation of damage control measures under various performance and safety criteria at the same time.

7. REFERENCES

- Vassalos, D., Konovessis, D., Jasionowski, A. (2013), "Life-cycle risk management: a safety case approach", Proceedings of the IDFS 2013, pp. 37~42, 25-27 November, Shanghai, China
- Martins, P.T. (2011), "Real-Time Decision Support system for managing ship stability under damage", OCEANS, 2011 IEEE – Spain, ISBN: 978-1-4577-0086-6
- Qi Chen (2012), "Uncertainty Quantification in Assessment of Damage Ship Survivability",



University of Strathclyde, Glasgow, May
2013

Papanikolaou, Apostolos (Ed.) (2009),
“Risk-based ship design – Methods, Tools
and Applications”, ISBN:
978-3-540-89041-6

Health and Safety Executive (1997),
“Successful health and safety management”,
ISBN 978 07176 1276 5



Free-running Model Tests of a Damaged Ship in Head and Following Seas

Taegu, Lim, *Korea Research Institute of Ships and Ocean Engineering* ltg88@kriso.re.kr

Jeonghwa, Seo, *Seoul National University* thamjang@snu.ac.kr

Sung Taek, Park, *Seoul National University* probpst@snu.ac.kr

Shin Hyung, Rhee, *Seoul National University* shr@snu.ac.kr

ABSTRACT

A series of tests using a course-keeping model ship in a towing tank were carried out for research on Safe Return to Port (SRtP). A passenger ship model with a damaged compartment was modified to be equipped with propellers and rudders for a course-keeping maneuver by an onboard autopilot system. The 6DoF motion of the test model was measured by a wireless inertial measurement unit (IMU) and gyro sensors to achieve fully wireless model tests. Advance speed and motion response in various wave conditions were measured and analyzed to investigate the propulsion and maneuvering performances of the damaged ship model in head and following seas.

Keywords: *Free-running test, Safe Return to Port, Damaged ship stability*

1. INTRODUCTION

Recently the scale of damages in maritime accidents has grown with the increasing sizes of vessels. In the case of passenger ship accidents especially, a great number of casualties often results; thus, efforts to improve regulations and vessel designs to prevent casualties are required. The International Maritime Organization (IMO) effected a regulation on the Safe Return to Port (SRtP) of a passenger ship with a length over 120 m in July 2010 (Spanos and Papanikolaou, 2012).

SRtP regulations require the survivability of vessels after fire or flooding under a casualty threshold. After an accident occurs, the vessel must be able to return to a port nearby without external help. It also refers to the minimum requirements of the propulsion performance and maneuverability of the vessel in certain weather conditions; thus, assessing the stability and maneuverability of the vessel under

various weather conditions is needed during the stage of designing the ship to judge whether the vessel follows SRtP regulations.

Traditionally ship stability was analyzed by model tests and analytic methods based on the potential flow theory. Analytic methods have been widely used, as they have the merits of high reliability and low computational resource requirements. For cases of unconventional hull geometry and nonlinear phenomena, however, applying analytic methods with the potential flow theory has limitations, and modifications to the methods are necessary.

Parametric roll and broaching are well-known nonlinear physical phenomena in ship stability. Model tests on those nonlinear vessel motions have been performed, and analytic methods are suggested (Bulian, 2005; Lee et al., 2007; Neves and Rodriguez, 2007).



To achieve an analysis of the nonlinear phenomena, an analysis of the fluid dynamics should precede, i.e., eddy-making, turbulent boundary layer, and viscous roll damping. These features are caused by the viscous nature of fluids; thus, approaching the analysis in consideration of the viscosity of fluid is in high demand and computational fluid dynamics (CFD) is the only viable method to treat the viscous flow field. In these days, CFD techniques have been applied to various fields of naval hydrodynamics: the self-propulsion performance of vessel (Seo et al., 2010; Carrica et al., 2011), the motions in waves (Carrica et al., 2007; Simonsen et al., 2013), and the prediction of maneuverability (Araki et al., 2012; Carrica et al., 2013). Approaches with CFD have produced good results, especially on the roll motion of vessels highly affected by the viscosity of fluid (Wilson et al., 2006). As roll motion is the most important criteria for judging the stability of a ship, it is obvious the CFD analysis will substitute traditional analytic methods based on the potential flow theory.

A CFD analysis also has been introduced to assess the issue of damaged ship stability. In the case of damaged ship stability, the interaction between flooded water and ship motion causes highly nonlinear phenomena (Gao et al., 2011). As damaged ship stability is one of the most important elements of SRtP conditions, approaches with CFD are expected to be essential during the design stage of passenger ships under SRtP regulation.

Before applying the CFD method to practical cases, it should be validated through existing experimental results. In the design of experiments for a validation database for CFD, the existence of nonlinear phenomena should be considered, as CFD approaches aim to predict the nonlinear motion of a vessel.

For experimental study on nonlinear motion of vessel, the motion response of a moored model in various waves was measured, and the parametric roll behavior was identified through a series of model tests (Begovic et al., 2013;

Lee et al., 2012). Also, a gradual increase in the roll motion of a moored model in head seas has been reported and provided for the CFD validation database (Lim et al., 2014). In these tests, however, the restrained motion of the test model was measured, as the model was in a stationary condition with a mooring system.

To predict the stability of practical vessels with high fidelity, tests with a free-running model are required, as it does not require an external towing force. The free-running model has been used to test the seakeeping ability and maneuverability of vessels, but an intact model was used for most tests (Yoon et al., 2007; Sadat-Hosseini et al., 2010; Sadat-Hosseini et al., 2011). For the provision of a CFD validation database, free-running tests in waves must be achieved in damaged condition, and the results should be compared with those achieved in intact condition. Finally, the validated CFD methods can be applied to examine damaged ship stability problems.

In the present study, a free-running model of a passenger ship was used to carry out motion measurements in waves. Tests were designed by SRtP regulations, and the effects of wave conditions and flooded water behaviors on the motion of the test model were investigated.

2. EXPERIMENTAL METHODS

2.1 Test facility

Tests were carried out in the Seoul National University towing tank, the length, width, and depth of which are 110 m, 8 m, and 3.5 m, respectively. Figure 1 shows a schematic diagram of the towing tank, including the eight plunger-type wave makers located at the end of the towing tank. The initial locations of the test model in head seas and following seas were at 50 m and 20 m from the wave maker, respectively.

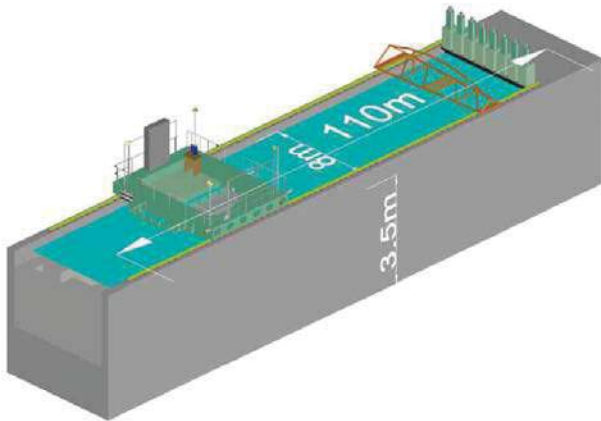


Figure 1 Schematic diagram of the Seoul National University towing tank.

2.2 Test model

A passenger ship hull designed by the Ship Stability Research Centre (SSRC) was used for the test model. It has a bulbous bow and a skeg on the stern. This hull was used for the study on damaged ship stability with a mooring system. Figure 2 shows the design of the test model.

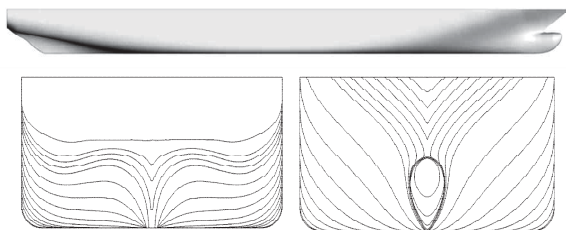


Figure 2 Lines and profile of the test model.

Following the test procedures and recommendations of the seakeeping tests presented by the International Towing Tank Conference (ITTC), the size of the towing tank limited the size of the model ship. The scale ratio of the model was 1/82.57, and the length of the model was 3 m. The principal particulars of the SSRC passenger ship are presented in Table 1. Arrays of studs were attached at station 19 and the bulbous bow to stimulate turbulent flow. Figure 3 shows the constructed test model.

Table 1 Principal particulars of the SSRC passenger ship and test model.

Item	Full Scale	Model Ship
Scale Ratio	1	1/82.57
Length between Perpendiculars (m)	247.7	3
Beam (m)	35.5	0.43
Draft (m)	8.3	0.1
Displacement (m ³)	56514.5	0.312
Propeller Diameter (m)	6	0.073
LCG from amidships (m)	-6.329	-0.077
KB (m)	4.085	0.049
KM (m)	18.781	0.227
KG (m)	16.393	0.199
GM (m)	2.388	0.029
k_{xx}	14.814	0.179
k_{yy}	61.925	0.750



Figure 3 Test model.

A damaged compartment was installed amidships to represent the damaged condition. The location and design of the damaged compartment was identical to the experiments of Lee et al. (2012). Figure 4 shows the design and dimensions of the damaged compartment.

It consisted of two compartments: a damaged compartment located astern (Compartment 1) had an opening to the outside, and a damaged compartment located fore (Compartment 2) had only a connection with Compartment 1. The connection was on the free surface; thus, flooding to Compartment 2 was not expected in a static condition without severe motion. Every compartment had a ventilation hole to minimize the effects of air compression on the flooding behavior. If flooding to Compartment

1 occurred, the model ship gained 5.82 kg of flooded water and an initial heel angle of 2.83°.

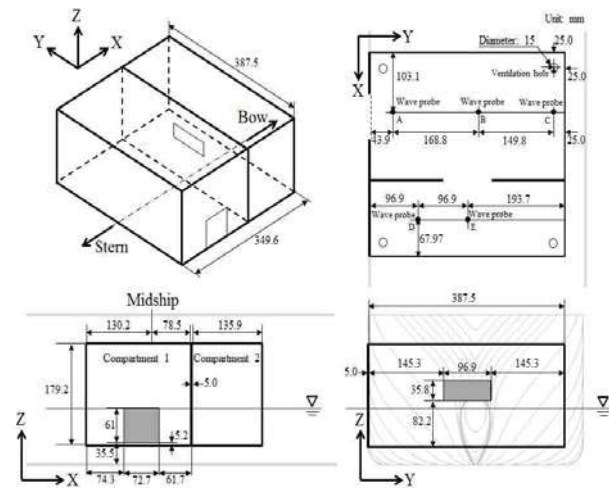
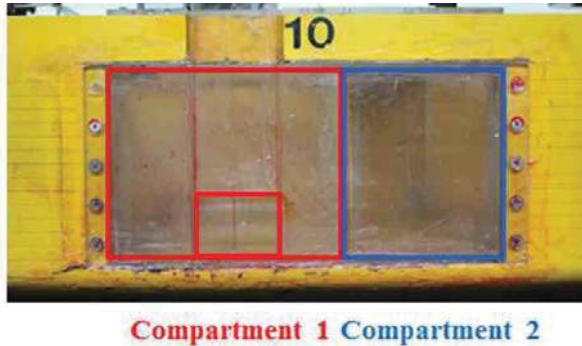


Figure 4 Geometry of the damaged compartment.

2.3 Autopilot system

Two propellers and rudders were appended on the test model to enable maneuverability. The design of a six-blade propeller in the present study was a modified design of the KP505 propeller, of which the design has been open (Paik et al., 2004; Seo et al., 2010). Its pitch ratio at 0.7 R was 0.997. Propeller shafts were supported by L-type struts, which were connected to the center skeg and stern. The profile of the rudder was NACA0012 hydrofoil. Figure 5 shows the fully appended stern of the test model.



Figure 5 Fully appended stern of the test model.

The autopilot system controlled the rudder angle and propeller revolution rate. The heading angle of the test model was measured by a gyro sensor, and the rudder angle was varied by a P controller, the parameter of which was 1.5. The propeller revolution rate was controlled by a PD controller, and the parameters of the P and D controllers were 20 and 8, respectively.

The motion of the model was measured by gyro sensors on the autopilot system and a wireless inertial measurement unit (IMU). Two measurement systems worked independently. The repetition rate of the wireless IMU was 100 Hz. The autopilot system transmitted motion and control signals to a laptop with a repetition rate of 16 Hz.

2.4 Test conditions

Based on the SRtP regulation suggested by Germanischer Lloyd (GL, 2009), the wave and propeller conditions were chosen. In the SRtP regulation, a vessel should achieve an advance speed of 7 knots or half of the design speed in normal weather conditions. In addition, the vessel should preserve maneuverability in unfavorable weather conditions. Normal and unfavorable weather conditions correspond to Sea states 5 and 6, respectively. Table 2 describes the wave conditions for the present SRtP tests.

Table 2 Wave conditions for SRtP tests.

		Normal weather conditions		Unfavorable weather conditions	
		Full scale	Model scale	Full scale	Model scale
Period (s)	T	6.7	0.737	8.3	0.913
Wave number (rad/m)	k	0.090	7.415	0.059	4.832
Wave length (m)	λ	69.9	0.847	107	1.300
Wave Amplitude (m)	A	2.8	0.034	5.4	0.066

To determine the minimum propulsion power, the propeller revolution rate at an advance speed that corresponds to 7 knots in the full scale (0.396 m/s) was investigated in calm water tests. It was 595 rpm, and the propeller revolution rate for tests was fixed at 615 rpm, considering the powering margin in the waves.

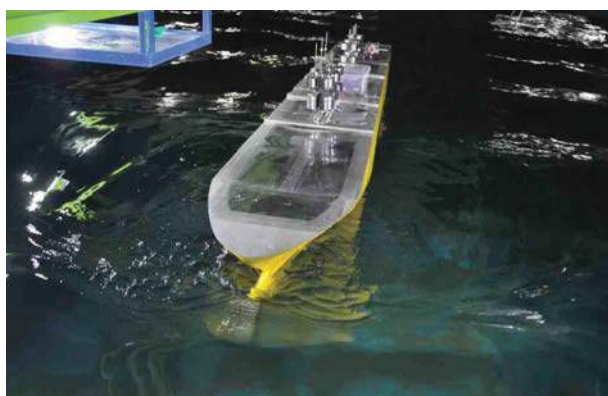


Figure 6 Snapshot of the free-running test.

Tests were performed in head and following seas conditions. The model was released in a stationary condition, and the motion in the time range with a converged speed was sampled and analyzed. Figure 6 shows the snapshot of the model test in head seas.

3. RESULTS AND DISCUSSIONS

3.1 Pitching motion

Figures 7 and 8 show the time history of the pitching motion of the test model. In normal weather conditions, the motion response in following seas was greater than that in head seas, while the pitching motion in head seas increased in unfavorable weather conditions.

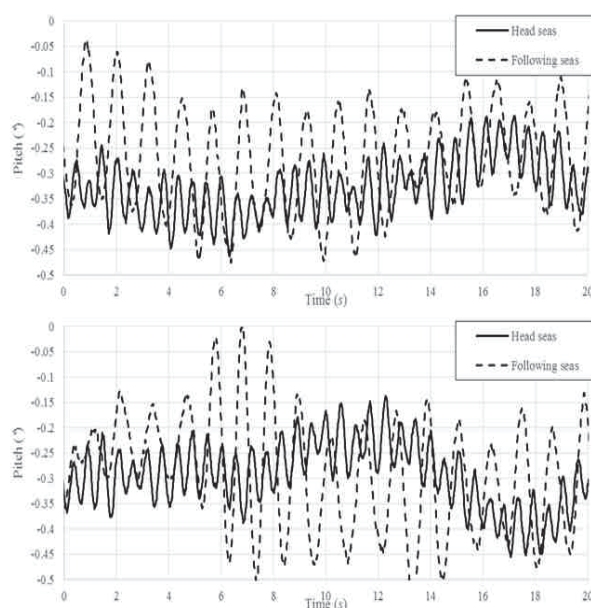


Figure 7 Time history of the pitching motion in normal weather conditions (top: intact condition; bottom: damaged condition).

When the pitching motion of a ship in waves occurs, the bow and stern of the ship move vertically in the water, resulting in slamming. Tendency of slamming, however, showed difference in cases of the bow and stern. As the bulbous bow and the bow flare was immersed, slamming occurred in all wave conditions. Slamming on the stern with flat transom, in contrast to the bow slamming, made high impact over certain wave height condition; thus, slamming on the stern restrained pitching motion in unfavorable weather condition only. In normal weather condition, slamming on the bow was dominant and pitching motion in head seas was smaller than that in following seas.

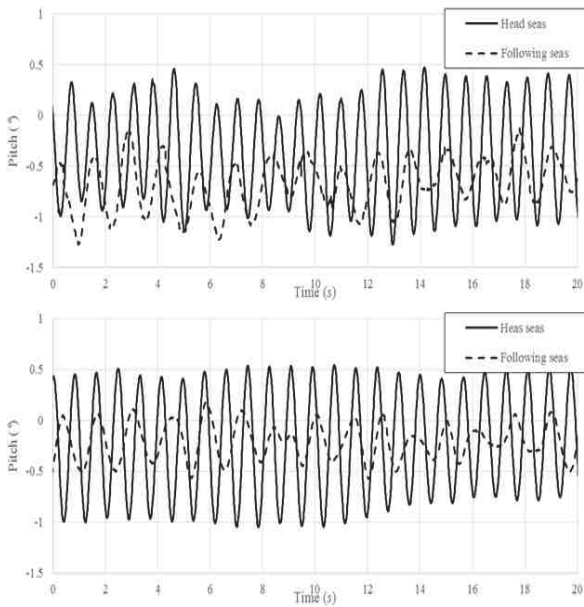


Figure 8 Time history of the pitching motion in unfavorable weather conditions (top: intact condition; bottom: damaged condition).

In all cases, the magnitude and period of the pitching motion in following seas was less regular than in head seas. In following seas, the incoming wave was disturbed by the Kelvin wave and propeller wake and could not maintain its waveform strictly.

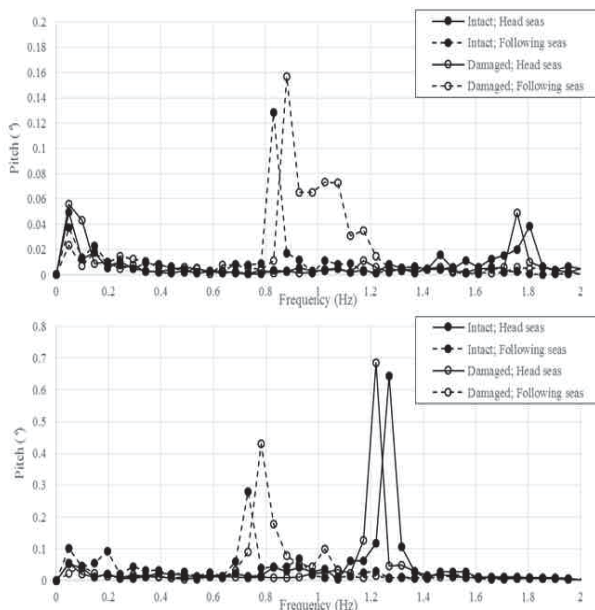


Figure 9 FFT analysis results of the pitching motion (top: normal weather conditions; bottom: unfavorable weather conditions).

Figure 9 shows the results of a fast Fourier transform (FFT) analysis of the pitching motion. The dominant frequency and magnitude of the pitching motion were identified. As stated above, the dominant frequency was clearer in head seas than in following seas due to clear waveform of incoming wave. Also, the magnitude of the pitching motion in damaged condition was greater, as the flooded water led to a loss of stability.

3.2 Speed measurement

The dominant frequency from the FFT analysis was identical to the wave encounter frequency, as the pitching motion was directly induced by waves. Using the incoming and encounter wave frequencies, the advance speed of the model could be derived by the Doppler effect. The derived advance speed of the intact free-running model is presented in Table 3.

Table 3 Advance speed of the intact model ship.

Wave condition		Wave encounter frequency (rad/s)	Advance speed (m/s)
Calm water		-	0.419
Normal weather condition ($\omega_0 = 8.52$ rad/s)	Head seas	11.29	0.382
	Following seas	5.219	0.446
Unfavorable weather condition ($\omega_0 = 6.88$ rad/s)	Head seas	7.933	0.227
	Following seas	4.699	0.471

Advance speed decreased significantly in head seas, while a small increase was observed in following seas because of the difference in the relative velocity of the waves. In head seas condition, the ship and waves were in the opposite direction; thus, the relative velocity of the incoming wave and test model increased,



resulting in large added resistance. As the group velocity of the wave was greater than the advance speed in following seas condition, the ship gained an additional propulsive force from the waves and the advance speed in following seas exceeds that in calm water.

Advance speed results in damaged condition are presented in Table 4. The flooding behavior that caused eddy-making and violent free surface in the damaged compartment was expected to create additional resistance, and a decrease in advance speed was observed in every wave condition. Retardation of the advance speed was more significant in unfavorable weather conditions, as strong flooding behavior occurred through the damaged hole.

Table 4 Advance speed of the damaged model ship.

Wave condition		Wave encounter frequency (rad/s)	Advance speed (m/s)
Calm water		-	0.410
Normal weather condition ($\omega_0 = 8.52$ rad/s)	Head seas	11.12	0.340
	Following seas	5.322	0.404
Unfavorable weather condition ($\omega_0 = 6.88$ rad/s)	Head seas	7.634	0.163
	Following seas	4.865	0.408

3.3 Roll motion

The flooding behavior in the damaged compartment induced roll motion, as well as the retardation of advance speed. Figures 10 and 11 shows the time history of the roll motion in normal weather conditions.

Roll motion was not expected in the ideal case when heading angle was perfectly aligned with wave direction. In the experiments, however, asymmetric flow field developed as the flow around the test model was not exactly symmetric, due to the slight yaw motion during autopilot course-keeping maneuver. Even small asymmetry caused coupled roll and pitching motion in head and following seas condition, and the roll motion period was expected to be identical to the wave encounter period.

In following seas condition, roll motion was regular and its period was identical to the wave encounter period. In normal weather condition, however, the roll motion period was identical to the natural roll period of the test model, although pitching motion period was identical to the wave encounter period. That implied existence of resonance of roll motion only. In the damaged condition, the resonance motion was interfered with by the flooded water; thus, the roll motion was not fully developed and irregular motion was observed.

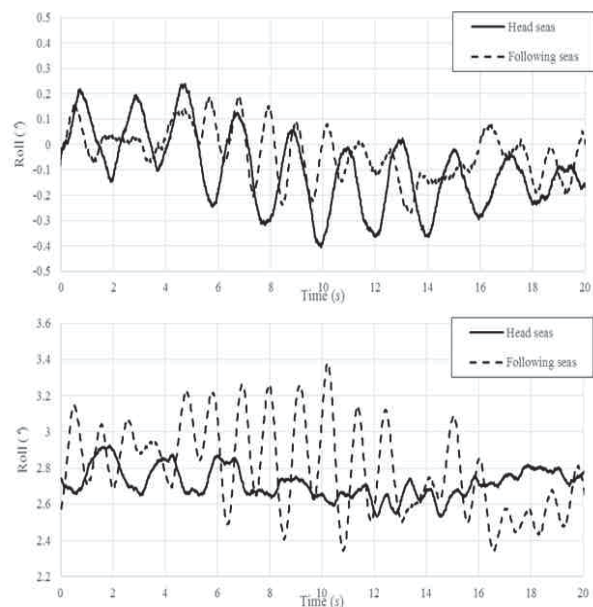


Figure 10 Time history of the roll motion in normal weather conditions (top: intact condition; bottom: damaged condition).

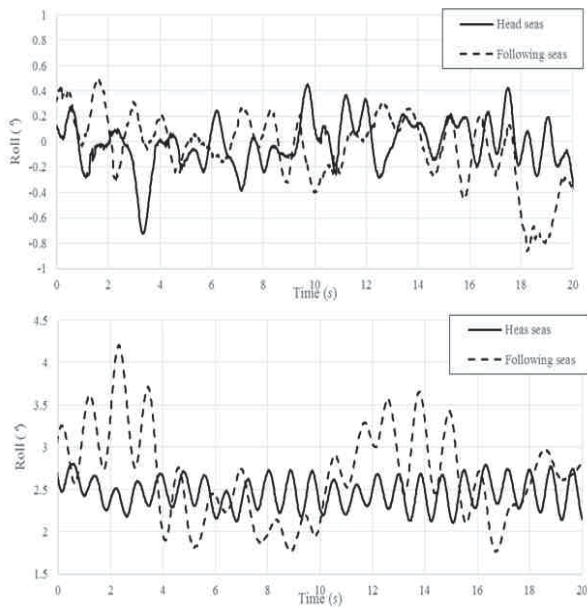


Figure 11 Time history of roll motion in unfavorable weather conditions (top: intact condition; bottom: damaged condition).

Figure 11 shows the time history of roll motion in unfavorable weather conditions. Strong flooding behaviors appear in unfavorable weather conditions; thus, roll motion was induced in damaged condition and its period was identical to the wave encounter period. In intact case, however, roll motion in head seas was irregular and the resonance motion in the natural roll period of the model was not observed, as there was no excitation force of the roll motion.

4. CONCLUSIONS

In the present study, a free-running model ship was constructed to perform experimental research on the SRtP of a damaged ship. Motion responses of the damaged ship model in head and following seas were measured, and the influences of the damaged compartment and wave conditions on the motion responses of the model were identified.

In the course-keeping tests in head and following seas, the characteristics of pitching motion were analyzed first. Slamming on the

stern suppressed the pitching motion of the test model in unfavorable weather conditions; therefore, the pitching motion responses in following seas was less than those in head seas in unfavorable weather conditions.

The advance speed of the model was derived from the wave encounter frequency. In head seas, incoming waves generated additional resistance on the hull and caused the advance speed to decrease severely. In following seas, the phase velocity of the waves was faster than the advance speed of the free-running model; thus, the wave increased the advance speed slightly.

In damaged condition, the flooding behavior in the damaged compartment augmented resistance of the ship, resulting in a lower advance speed than in intact condition. In unfavorable weather conditions, retardation of the advance speed was 13% in following seas and 28% in head seas.

The roll motion responses of the ship in waves were also analyzed. The resonance of the roll motion in the natural roll period of the model was observed in intact and normal weather conditions. In damaged condition, however, the periodic flooding behavior stimulated roll motion, and the distinguishable roll period was identical to the wave encounter period.

Through free-running tests, the characteristics of the motion responses of a damaged ship model under SRtP regulations were identified. As future studies, a wireless measurement system for propulsion performance and wave heights in the damaged compartment will be installed on the free-running system to achieve the provision of a reliable validation database for CFD.

5. ACKNOWLEDGMENTS

The present study is supported by the Office of Naval Research (ONR) under the supervision of Dr. Ki-Han Kim, the National Research



Foundation of Korea (Grant No. 2013R1A1A2012597), and the Multi-Phenomena CFD Research Center (Grant No. 20090093103), funded by the Ministry of Education, Science and Technology of the Korea Government.

6. REFERENCES

- Araki, M., Sadat-Hosseini, H., Sanada, Y., Tanimoto, K., Umeda, N., and Stern, F., 2012, "Estimating Maneuvering Coefficients Using System Identification Methods with Experimental, System-based, and CFD Free-running Trial Data", Ocean Engineering, Vol. 51, pp. 63-84.
- Ayaz, Z., Vassalos, D., and Spyrou, K. J., 2006, "Manoeuvring Behaviour of Ships in Extreme Astern Seas", Ocean Engineering, Vol. 33, pp. 2381-2434.
- Begovic, E., Mortola, G., Incecik, A., and Day, A. H., 2013, "Experimental Assessment of Intact and Damaged Ship Motions in Head, Beam and Quartering Seas", Ocean Engineering, Vol. 72, pp. 209-226.
- Bulian, G., 2005, "Nonlinear Parametric Rolling in Regular Waves-a General Procedure for the Analytical Approximation of the GZ Curve and Its Use in Time Domain Simulations", Ocean Engineering, Vol. 32, pp. 309-330.
- Carrica, P. M., Wilson, R. V., Noack, R. W., and Stern, F., 2007, "Ship Motions Using Single-phase Level Set with Dynamic Overset Grids", Computers & Fluids, Vol. 36, pp. 1415-1433.
- Carrica, P. M., Huiping, F., and Stern, F., 2011, "Computations of Self-propulsion Free to Sink and Trim and of Motions in Head Waves of the KRISO Container Ship (KCS) Model", Applied Ocean Research, Vol. 33, pp. 309-320.
- Carrica, P. M., Ismail, F., Hyman, M., Bhushan, S., and Stern, F., 2013, "Turn and Zigzag maneuvers of a Surface Combatant Using a URANS Approach with Dynamic Overset Grids", Journal of Marine Science and Technology, Vol. 18, pp. 166-181.
- Choi, J.E., Min, K.-S., Kim, J. H., Lee, S.B., and Seo, H. W., 2010, "Resistance and Propulsion Characteristics of Various Commercial Ships Based on CFD Results", Ocean Engineering, Vol. 37, pp. 549-566.
- Gao, Z., Gao, Q., and Vassalos, D., 2011, "Numerical Simulation of Flooding of a Damaged Ship", Ocean Engineering, Vol. 38, pp. 1649-1662.
- Germanischer Lloyd (GL), 2009, "Preliminary Guidelines of Safe Return to Port Capability of Passenger Ships", GL Rules for Classification and Construction, VI-11-02.
- International Towing Tank Conference (ITTC), 2011, "Seakeeping Experiments", ITTC-Recommended Procedures and Guidelines, 7.5-02-07-02.1.
- Lee, D., Hong, S. Y., and Lee, G.-J., 2007, "Theoretical and Experimental Study on Dynamic Behavior of a Damaged Ship in Waves", Ocean Engineering, Vol. 34, pp. 21-31.
- Lee, S., You, J.-M., Lee, H.-H., Lim, T., Rhee, S. H., and Rhee, K.-P., 2012, "Preliminary Tests of a Damaged Ship for CFD Validation", International Journal of Naval Architecture and Ocean Engineering, Vol. 4, pp. 172-181.
- Lim, T., Seo, J., Park, S. T., Rhee, S. H., 2014, "Experimental Study on the Safe-Return-to-Port of a Damaged Ship in Head Seas", Proceedings of 30th Symposium on Naval Hydrodynamics, Hobart, Australia.
- Neves, M. A. S. and Rodriguez, C. A., 2007,



“Influence of Non-linearities on the Limits of Stability of Ships Rolling in Head Seas”, Ocean Engineering, Vol. 34, pp. 1618-1630.

“Estimation of the Roll Hydrodynamic Moment Model of a Ship by Using the System Identification Method and the Free Running Model Test”, IEEE Journal of Oceanic Engineering, Vol. 32, pp. 798-806.

Paik, B. G., Lee, C. M., and Lee, S. J., 2004, “PIV Analysis of Flow around a Container Ship Model with a Rotating Propeller”, Experiments in Fluids, Vol. 36, pp. 833-846.

Sadat-Hosseini, H., Stern, F., Olivieri, A., Campana, E., Hashimoto, H., Umeda, N., Bulian, G., and Francescutto, A., 2010, “Head-wave Parametric Rolling of a Surface Combatant”, Ocean Engineering, Vol. 37, pp. 859-878.

Sadat-Hosseini, H., Carrica, P., Stern, F., Umeda, N., Hashimoto, H., Yamamura, S., and Mastuda, A., 2011, “CFD, System-based and EFD Study of Ship Dynamic Instability Events: Surf-riding, Periodic Motion, and Broaching”, Ocean Engineering, Vol. 38, pp. 88-110.

Seo, J. H., Seol, D. M., Lee, J. H., and Rhee, S. H., 2010, “Flexible CFD Meshing Strategy for Prediction of Ship Resistance and Propulsion Performance”, International Journal of Naval Architecture and Ocean Engineering, Vol. 2, pp. 139-145.

Simonsen, C. D., Otzen, J. F., Joncquez, S., and Stern, F., 2013, “EFD and CFD for KCS Heaving and Pitching In Regular Head Waves”, Journal of Marine Science and Technology, Vol.18, pp. 435-459.

Spanos, D. A. and Papanikolaou, A. D., 2012, “On the Time Dependence of Survivability of ROPAX Ships”, Journal of Marine Science and Technology, Vol. 17, pp. 40-46.

Wilson, R. V., Carrica, P. M., and Stern, F., 2006, “Unsteady RANS Method for Ship Motions with Application to Roll for a Surface Combatant”, Computers & Fluids, Vol. 35, pp. 501-524.

Yoon, H. K., Son, N. S., and Lee, G. J., 2007,



Main Contributing Factors to the Stability Accidents in the Spanish Fishing Fleet

Francisco Mata-Álvarez-Santullano, *Maritime Accident and Incident Investigations Standing*

Commission, Government of Spain, fmata@fomento.es

ABSTRACT

Between November 2008 and November 2014 a total of 28 stability accidents affecting to Spanish fishing vessels were investigated by the Spanish Marine Accident and Incident Investigation Standing Commission. A comprehensive review of these accidents allows determining the nature of the main contributing factors behind the high accident rates in the Spanish fishing sector.

Keywords: *fishing vessel, accident investigation, safety policies, training, complacency*

1. INTRODUCTION

The fishing sector ranks high in the list of mortality rates labor sectors. In Spain, figures published by INE (National Statistics Institute, *Instituto Nacional de Estadística*, <http://www.ine.es/inebmenu/indice.htm>) and various of its bodies (INSHT, 2011) shows the global rate of mortal accidents in 2011 to be 3 deaths for each 100000 workers in Spain (global rate: for all labour sectors). The global rate of severe accidents in Spain in the same year was 25 per 100000 workers. In the fishing sector only, the rate of mortal accidents in that year was of 33 deaths, that is to say, more than ten times the global rate. Similarly, the ratio of severe accidents in the fishing sector rose to 159 per 100000 workers (six times the global rate). According to these data, the fishing and aquiculture labour sector was the third with highest mortality rates in Spain, only behind silviculture¹ (51 deaths per 100000 workers) and extractive industries² (42 deaths per 100000 workers).

Several studies have been conducted studying the relation among fishing safety, research and public policies. Jin and Thunberg

(Jin and Thunberg, 2005) established the importance of probability models in development and quantitative assessment of management mechanisms related to safety in the commercial fishing industry. Pérez-Labajos states (Pérez-Labajos, 2008) that the research work on the safety and accidents of commercial fishing vessels can be broken down into three clearly distinct frameworks of analysis: type of damage (personal and material), types of accidents, and accident inequalities applied to the fishing sector.

The present work belongs to the second type of analysis, but a new approach is proposed: instead of focusing in the type of accident of its consequences, proposes to research into the underlying causes which lead to the accidents.

In the fishing sector in Spain, the relation between type of accident and number of casualties (dead or missing person) shows clearly that the stability related accidents are, by far, the most dangerous.

Being clear that the loss of stability is one of the major risks a vessel may face, it is not so



obvious what can be done to prevent accidents due to loss of stability. For policy makers to develop effective policies to reduce the number of accidents is necessary the causes leading to these accidents be known. It is paradigmatic that accidents are due to multiple factors; not being common accidents which respond to a single cause. In any marine casualty is common to find personal factors (lack of training, fatigue ...), social factors (lack of safety culture, economic conditions ...), technical factors (design faults ...), regulatory factors (inadequate regulations ...), etc.

Consequently the best policy to prevent stability accidents in the fishing fleet should be based on the incidence that each of the contributing factors has over the accidents rates. A possible way to approach such study is by establishing a maritime accident investigation policy with the following characteristics:

- Comprehensive, in the sense of examining accidents from multiple facets,
- Independent from other investigations. Not intended to establish blame or apportion liability.
- Providing a taxonomy which allows contributing factors to be classified for statistical analysis.

At European level, since 2011 there exists a regulation that harmonizes the investigation procedures and fulfils, in principle, those requirements. Directive 2009/18/EC of the European Parliament and of the Council (http://eur-lex.europa.eu/legal-content/EN/TXT/?uri=uriserv:OJ.L_.2009.131.01.0114.01.ENG), which entered into force in June 2011, establishes for European countries the obligation to investigate marine accidents and to notify the Commission on marine accidents and the data resulting from safety investigations in the European Marine Casualty Information Platform (EMCIP).

2. EMCIP ACCIDENT ANALYSIS MODEL

The EMCIP is built over a determined investigation analysis method. The accident analysis method lying below EMCIP is the ECFA (Events and Casual Factors Analysis) method, which is extensively described in the scientific literature of accident investigation.

The ECFA method in EMCIP depicts the necessary and sufficient events and causal factors for accident occurrence in a logical sequence (Buys and Clark, 1995). Under the ECFA scheme, behind the accidental events identified leading to the casualty there are contributing factors which must be identified and corrected to prevent the occurrence of similar accidents.

EMCIP provides taxonomy to classify contributing factors identified during an accident. However the EMCIP system has still to prove its value for accident analysis in the fishing sector, due to the following reasons:

- It is relatively recent; therefore it still does not store a significant amount of safety investigations.
- Fishing vessels with length below 15m are not included in the scope of Directive 2009/18/EC; therefore most countries are not notifying EMCIP with accidents in those vessels.
- EMCIP's taxonomy is adapted from existing models used in other transport modes and is oriented towards merchant marine traffic, but its use in the fishing sector is not always straightforward.

3. MARINE ACCIDENTS INVESTIGATED IN SPAIN

3.1 CIAIM

In Spain the Maritime Accident and Incident Investigations Standing Commission (*Comisión Permanente de Investigación de*



Accidentes e Incidentes Marítimos, CIAIM) is an independent governmental body entrusted with the safety investigation of marine accidents. It acts pursuant to the provisions of Directive 2009/18/EC and the International Maritime Organization (IMO) Casualty Investigation Code. CIAIM was created in September 2008 and since then has received nearly 600 notifications of marine casualties, half of which affect fishing vessels (CIAIM, 2014, 2013, 2012, 2011, 2010, 2009).

3. 2 Stability related accidents of fishing vessels

The author has conducted a study of the stability related accidents of fishing vessels in Spain between September 2008 and December 2014. In this period CIAIM received 305 notifications of fishing vessels casualties, whose distribution according to type of accident and consequences is shown in Table 1.

Type of accident	Number of accidents	Number of dead / missing persons	Number of vessels lost
Capsizing / Listing	32	30	28
Collision	50	8	9
Contact	12	0	5
Damage to equipment	7	0	0
Grounding / Stranding	53	9	22
Fire / explosion	26	3	12
Flooding / foundering	74	8	53
Loss of control	10	1	3
Hull failure	4	0	2
Missing	1	3	1
Non accidental event	3	3	1
Occupational accident	33	27	0
Total	305	92	136

Table 1. Fishing vessel accidents between Sept'08 and Dec'14 in Spain

Definition for types of accidents listed in Table 1 is provided by the European Maritime Safety Agency in the EMCIP taxonomy:

Capsizing/listing: is a casualty where the ship no longer floats in the right-side-up mode due to: negative initial stability (negative

metacentric height), or transversal shift of the centre of gravity, or the impact of external forces. When the ship is tipped over until disabled is called capsizing; when the ship has a permanent heel or angle of loll is called listing.

Collision: a casualty caused by ships striking or being struck by another ship, regardless of whether the ships are underway, anchored or moored. This type of casualty event does not include ships striking underwater wrecks. The collision can be with other ship or with multiple ships or ship not underway.

Contact: a casualty caused by ships striking or being struck by an external object. The objects can be: floating object (cargo, ice, other or unknown); fixed object, but not the sea bottom; or flying object.

Damage to equipment: damage to equipment, system or the ship not covered by any of the other casualty type.

Grounding / stranding: a moving navigating ship, either under command, under power, or not under command, drifting, striking the sea bottom, shore or underwater wrecks.

Fire / explosion: an uncontrolled ignition of flammable chemicals and other materials on board of a ship. Fire is the uncontrolled process of combustion characterized by heat or smoke or flame or any combination of these. Explosion is an uncontrolled release of energy which causes a pressure discontinuity or blast wave.

Flooding / foundering: is a casualty event when the ship is taking water on board. Foundering will be considered when the vessel has sunk. Foundering should only be regarded as the first casualty event if the details of the flooding which caused the vessel to founder are not known. Flooding refers to a casualty when a vessel takes water on board and can be: Progressive if the water flow is gradually; or Massive if the water flow is considerable.

Loss of control: a total or temporary loss of



the ability to operate or maneuver the ship, failure of electric power, or to contain on board cargo or other substances. Loss of electrical power is the loss of the electrical supply to the ship or facility. Loss of propulsion power is the loss of propulsion because of machinery failure. Loss of directional control is the loss of the ability to steer the ship. Loss of containment is an accidental spill or damage or loss of cargo or other substances carried on board a ship.

Hull failure: a failure affecting the general structural strength of the ship.

Missing: a casualty to a ship whose fate is undetermined with no information having been received on the loss and whereabouts after a reasonable period of time.

Non-accidental events: intentional events as a result of illegal or hostile acts. They are: Acts of war, criminal acts, illegal discharge, and others.

Occupational accident: Occupational accident type means the mode in which a person (crewmember, passenger or other person) was injured or killed, not involving in a ship casualty, which can be: accident, illness, suicide/homicide, or unknown.

It is to be noted the high risk of personal loss and vessel loss in stability related accidents in comparison with other types of accident. Focusing on stability related accidents, 28 out of the 32 accidents were investigated or are currently under investigation. These 28 accidents are listed in Table 2, in the appendix, including the following data:

Internal CIAIM accident code.

Vessel total length (Lt, m).

Indicator of the accident having occurred inside or outside territorial waters -12 miles off the coast (High seas, coast).

Mean wind speed (Vw, knots)

Significant wave height, wind and swell waves (Hs, m).

Primary cause of the accident. In the case of accidents still under investigation, the

guessed cause is included.

Number of report published in CIAIM's website www.ciaim.es, in the case the report is published.

3. 3 Underlying causes

Behind the primary causes summarized in the previous table there are several underlying causes. When analysing deeply these 28 accidents the following list of underlying causes has been found.

These underlying causes are listed in Table 3 in the appendix.

3. 4 Contributing factors in the fishing sector

The listed underlying causes may be linked to one or several contributing factors in the EMCIP taxonomy. The individual study of the underlying cause and the specific circumstances of the accident allows for this distribution.

It is not in the scope of the present work to enter in details of the analysis performed in each of the accidents investigated. For the purposes of this study, the results are summarized below.

The results show that most underlying causes are linked to the same type of contributing factors that can be grouped in just six categories according to EMCIP taxonomy:

Type of contributing factor (CF)	Number of CF in CIAIM stability accidents
Lack of training	30
Economic conditions	14
Design error	4
Inadequate regulation	8
Lack of safety awareness	33
Lack of safety culture	20



Table 4. Type of contributing factor in 28 stability related accidents.

Graphically the previous results are presented in Figure 1.

4. ANALYSIS

Most of the contributing factors in the fishing vessel accidents are related to personal economic and social factors: lack of training of crewmembers, economic conditions putting press on the masters to navigate in dangerous areas looking for more abundant catches. Of special relevance is the lack of safety awareness among crew of fishing vessels and the lack of safety culture in fishing companies.



Figure 1 Type of contributing factor (percentage)

It is worth to mention the similarity of these results with those obtained in previous studies by Loughran et al. (Loughran et al, 2002) in their study of fishing vessel safety in the UK: they conclude that fishing industry lacks a safety culture and that more failure data needs to be collected in order to control risks.

Only in four accidents a design error was found to have contributed to the accident.

It is also significant that in 8 accidents the stability regulation has been found inadequate. While the ship fulfilled the stability criteria in force, these were found to be inadequate for correctly managing the stability on board: regulations which did not include any stability, loading or operating information for the master, therefore making impossible to adequately manage stability on board fishing vessels. This was especially true in small fishing vessels, with length below 15 m.

These data may be interpreted in different ways. First, they may indicate the need to design policies which address the basic problems detected: lack of safety awareness and training.

Being this true, the data also show that fishing vessels built and designed according to the approved standards (including safety and stability standards) could be prone to suffer accidents when personal and socio-economic factors are present. For instance, fishing in breaking waves and shoals could be forbidden, or training campaigns to inform about the risks associated to navigating in these areas could be established. Nevertheless it is a fact that fishing vessels will operate where catches can be captured.

This would support the idea of setting more exigent technical standards to fishing vessels, so they are capable to cope with inadequate operation from the crews and fishing companies.

5. CONCLUSIONS

Stability related accidents in Spain in the period September 2008 to December 2014 happened mainly for a combination of personal, social, economic and regulatory factors, being specially relevant the lack of training and lack of safety awareness (complacency) of crews. Marine safety policies in the fishing sector to prevent stability accidents must therefore address these problems.



In addition, the stability standards applicable to fishing vessels, in particular to small fishing vessels, are not capable to deal with the reality of the fishing sector. The maritime authorities should promote the revision of the stability standards applicable to those vessels, so they can bear inadequate operation derived from personal and socio-economic contributing factors present the fishing sector.

6. REFERENCES

- INSHT, 2011. Análisis de mortalidad por accidente de trabajo en España, 2008-2009-2010. Instituto Nacional de Seguridad e Higiene en el Trabajo.
- Loughran C. G., Pillay A., Wang J., Wall A. & Ruxton T., (2002) "A preliminary study of fishing vessel safety", *Journal of Risk Research*, 5:1, 3-21
- Pérez-Labajos, Carlos, 2008, "Fishing safety policy and research", *Marine Policy*, Vol 32, pp. 40-45
- Buyts, J.R., Clark, J.L., 1995, "Events and Causal Factors Analysis (No. SCIE-DOE-01-TRAC-14-95)", Technical Research and Analysis Center.
- CIAIM, 2009. Informe anual. Comisión permanente de investigación de accidentes e incidentes marítimos.
- CIAIM, 2010. Informe anual. Comisión permanente de investigación de accidentes e incidentes marítimos.
- CIAIM, 2011. Informe anual. Comisión permanente de investigación de accidentes e incidentes marítimos.
- CIAIM, 2012. Informe anual. Comisión permanente de investigación de accidentes e incidentes marítimos.
- CIAIM, 2013. Informe anual. Comisión permanente de investigación de accidentes e incidentes marítimos.
- CIAIM, 2014. Informe anual. Comisión permanente de investigación de accidentes e incidentes marítimos.
- Jin, Di and Thunberg, Eric, 2005, "An analysis of fishing vessel accidents in fishing areas off the northeastern United States", *Safety Science*, Vol. 43, pp. 523-540.



APPENDIX

CIAIM accident code	Lt (m)		Vw (kt)	Hs (m)	Primary cause (summarized)	Report number
014/2008	27,85	High sea	25	2,7	Water ingress on main deck	A-05/2010
020/2008	34,5	High sea	25	6,5	Fishing gear stuck	A-15/2010
031/2009	39,3	High sea	20	3	Water ingress on main deck	S-28/2011
033/2009	9,6	Coast	30	1,5	Excessive weather conditions	S-41/2011
035/2009	17,7	High sea	5	1	Water ingress on main deck	A-06/2009
044/2009	10,53	Coast	12	0,25	Cargo shifting	S-20/2011
002/2010	27	High sea	35	3,5	Water ingress on main deck	A-10/2011
007/2010	37,35	High sea	17	4	Water ingress on main deck	S-27/2011
056/2010	7,18	Coast	12	0,25	Fishing gear stuck	S-14/2012
062/2010	24	High sea	20	1,25	Water ingress on main deck	A-01/2013
067/2010	28	High sea	30	4	Water ingress on main deck	A-10/2012
055/2011	14,83	High sea	22	3,5	Excessive weather conditions	A-08/2012
074/2011	5,76	Coast	19	1,4	Excessive weather conditions	S-26/2012
056/2012	15,5	High sea	11	1	Cargo shifting	S-23/2013
003/2013	7,2	Coast	5	1	Green seas	R-27/2013
008/2013	6,37	Coast	23	4,6	Excessive weather conditions	S-24/2013
039/2013	12,5	Coast	27	4,25	Excessive weather conditions	11/2014
047/2013	9,5	Coast	10	2	Green seas	S-42/2013
056/2013	8,45	Coast	11	2	Green seas	R-39/2013
016/2014	9,45	Coast	13	2	Fishing gear stuck	Investigation ongoing
028/2014	32	High sea	5	0,75	Cargo shifting	Investigation ongoing
056/2014	8,64	High sea	22	2	Water ingress on main deck	Investigation ongoing
057/2014	14,48	High sea	17	2	Water ingress on main deck	Investigation ongoing
079/2014	8,7	Coast	20	1	Green seas	Investigation ongoing
072/2014	11,85	Coast	n/a	2	Green seas	Investigation ongoing
088/2014	17,5	High sea	20	2	Water ingress on main deck	Investigation ongoing
089/2014	8,5	Coast	n/a	n/a	Green seas	Investigation ongoing
095/2014	18,6	Coast	20	1,25	Excessive weather conditions	Investigation ongoing

Table 2. Stability related accidents



CIAIM accident code	Contributing factor	CIAIM accident code	Contributing factor
035/2009	Freeing ports sealed	008/2013	Crew inexperienced
035/2009	Overloading: excess of fishing gear	008/2013	Inadequate stability regulation
035/2009	Non authorised modifications to vessel structure	008/2013	Excessive weather conditions
035/2009	Inadequate stability management on-board	003/2013	Loss of propulsion (dead ship)
014/2008	Overloading	003/2013	Fishing close to wave surf or shoal
014/2008	Watertight openings not closed	056/2013	Excessive weather conditions
020/2008	Watertight openings not closed	056/2013	Fishing close to wave surf or shoal
020/2008	Inadequate fishing winch operation	047/2013	Vessel undermanned
020/2008	Inaccessible fishing winch operation post	047/2013	Fishing close to wave surf or shoal
002/2010	Inadequate watertight opening design	047/2013	Excessive weather conditions
002/2010	Watertight openings not closed	039/2013	Excessive weather conditions
044/2009	Inadequate cargo lashing to deck and cargo shifting	039/2013	Fishing gear and catches shifting
044/2009	Overloading	039/2013	Freeing ports sealed
007/2010	Overloading	039/2013	Overloading
007/2010	Watertight openings not closed	016/2014	Excessive weather conditions
031/2009	Overloading	028/2014	Inadequate stability management on-board
031/2009	Watertight openings not closed	028/2014	Overloading
033/2009	Non authorised modifications to vessel structure	056/2014	Inadequate stability management on-board
033/2009	Overloading	056/2014	Inadequate stability regulation
033/2009	Inadequate stability regulation	056/2014	Navigating out of authorised area
055/2011	Inadequate stability regulation	057/2014	Excessive weather conditions
067/2010	Watertight openings not closed	057/2014	Inadequate stability regulation
067/2010	Gear hauling with stern seas	079/2014	Excessive weather conditions
067/2010	Bad watertight opening design	079/2014	Inadequate stability regulation
056/2010	Vessel undermanned	079/2014	Fishing close to wave surf or shoal
056/2010	Fishing winch lack of safety stop system	072/2014	Fishing close to wave surf or shoal
074/2011	Inadequate cargo lashing to deck	072/2014	Inadequate stability regulation
074/2011	Inadequate stability regulation	088/2014	Overloading
062/2010	Watertight openings not closed	088/2014	Bad watertight openings maintenance
062/2010	Navigating in quarter or stern waves	095/2014	Navigating out of authorised area
062/2010	Inadequate stability management on-board: excessive trim	095/2014	Inadequate cargo lashing to deck and cargo shifting
056/2012	Inadequate stowing and cargo shifting	089/2014	Fishing close to wave surf or shoal
056/2012	Inadequate stability management on-board		

Table 3. Underlying causes to 28 stability related accidents.

Session 9.3 – EXTREME BEHAVIOUR

A Time-Efficient Approach for Nonlinear Hydrostatic and Froude-Krylov Forces for Parametric Roll Assessment in Irregular Seas

Non-Stationary Ship Motion Analysis Using Discrete Wavelet Transform

A Study on the Effect of Parametric Rolling on Added Resistance in Regular Head Seas

This page is intentionally left blank



A Time-Efficient Approach for Nonlinear Hydrostatic and Froude-Krylov Forces for Parametric Roll Assessment in Irregular Seas

Claudio A. Rodríguez, *LabOceano, COPPE - Universidade Federal do Rio de Janeiro, Brazil*

claudiorc@laboceano.coppe.ufrj.br

Marcelo A. S. Neves, *LabOceano, COPPE - Universidade Federal do Rio de Janeiro, Brazil*

masn@laboceano.coppe.ufrj.br

Julio César F. Polo, *COPPE - Universidade Federal do Rio de Janeiro, Brazil*

jcfpolo@gmail.com

ABSTRACT

In the context of second generation stability criteria assessments, the present paper introduces a fast time domain algorithm for parametric roll assessment in irregular seas. Two features can be distinguished in the present proposal: a) it involves the essential heave-roll-pitch nonlinear coupling and b) it is a pre-calculated *derivative* model, convenient for the required systematic Monte Carlo simulations.

The main features of the model are described. The proposed methodology is based on a 3D panel method in which hydrostatic and wave-induced forces are computed on the actual body surface considering a set of systematic pre-defined hull positions. This set of data is preprocessed through polynomial fitting and the coefficients of the derivative model, corresponding to a Taylor series expansion defined up to the third order, are obtained. The methodology is applied to a container ship in head seas. The model is capable of reflecting the non-ergodicity of the head seas parametric rolling. At the same time, the heave and pitch motions display "weakly ergodic" responses.

KEYWORDS: *Head seas; Derivative model; Second generation stability criteria; Parametric rolling; Irregular seas.*

1. INTRODUCTION

Nowadays, several numerical methodologies exist for predicting the nonlinear behavior of parametric rolling of ships in waves in time domain. These procedures are usually categorized into fully nonlinear and weakly nonlinear codes. The first type considers nonlinearities in all the involved forces, whereas the second one introduces

nonlinearities basically in the restoring and incident wave forces in a time domain integration scheme. Both approaches demand high computational effort and, as a consequence, appear prohibitive in terms of simulation time when assessing parametric roll motions in stochastic seas.

The first two authors have proposed an analytical derivative model which was



validated in regular waves, Neves and Rodríguez (2006). In order to enhance the capabilities of the *derivative* model, i.e., by considering more general body geometries, the present paper uses an improved approach for the computation of the nonlinear restoring and Froude-Krylov coefficients. The proposed methodology is based on a 3D panel method in which hydrostatic and wave-induced forces are computed on the actual body surface considering a set of systematic pre-defined hull positions. This set of data is preprocessed through polynomial fitting and the coefficients of the derivative model, corresponding to a Taylor series expansion defined up to the third order are obtained. Such strategy does lead to an adequate hydrodynamic modeling capable of taking into consideration the essential nonlinear coupling effects between heave, roll and pitch, see Rodríguez et al. (2007).

In recent years, other authors have proposed mathematically similar approaches to achieve fast time domain algorithm in the context of second generation stability criteria assessments. Song and Kim (2011) used Fourier series decomposition applied to a one-degree-of-freedom roll model. Alternatively, Weems and Wundrow (2013) used a volume-based heave-roll-pitch hybrid model. Finally, Somayajula and Falzarano (2014) used a Volterra series model, again applied in a one degree of freedom model.

The present derivative model, derived in the context of Taylor series expansion is a very fast and reliable time domain algorithm which may be useful in the context of second generation stability criteria assessment. In the present paper the polynomial approach is described and applied in the context of irregular seas. The potentialities of the model are highlighted and some numerical results are presented. It is anticipated that one of the main advantages of the proposed methodology is that after all the derivatives are pre-computed, the equations of motion may be integrated in a very effective and fast way.

2. MATHEMATICAL MODEL

In order to simulate parametric rolling in irregular waves it is necessary to express forces and moments acting on the ship as time series. As these forces and moments depend on the submerged geometry which is governed by a random wave profile and irregular motions of the ship, the problem becomes very complex and costly in computer time. The “exact” approach of the problem implies in not only solving the ship hydrodynamic problem for the random submerged geometry but also the nonlinear hydrostatics in time domain, and additionally, to solve implicitly and iteratively the equations of motion.

To overcome these difficulties and make the solution of the parametric roll problem more practical, the paper proposes a hybrid method which combines some hypothesis from classical seakeeping with the solution of the nonlinear equations in time domain. The equations to be integrated are (Neves and Rodríguez, 2006):

$$\begin{aligned}
 & (m + Z_{\dot{z}})\ddot{z} + Z_{\dot{\theta}}\ddot{\theta} + Z_{\dot{z}}\dot{z} + Z_{\dot{\theta}}\dot{\theta} + \\
 & Z_z z + Z_{\theta}\theta + \frac{1}{2}Z_{zz}z^2 + \frac{1}{2}Z_{\phi\phi}\phi^2 + \frac{1}{2}Z_{\theta\theta}\theta^2 + \\
 & Z_{z\theta}z\theta + \frac{1}{6}Z_{zzz}z^3 + \frac{1}{2}Z_{zz\theta}z^2\theta + \frac{1}{2}Z_{\phi\phi z}\phi^2z + \\
 & \frac{1}{2}Z_{\phi\phi\theta}\phi^2\theta + \frac{1}{2}Z_{\theta\theta z}\theta^2z + \frac{1}{6}Z_{\theta\theta\theta}\theta^3 + Z_{\zeta z}(t)z + \\
 & Z_{\zeta\theta}(t)\theta + Z_{\zeta z\zeta}(t)z + Z_{\zeta z\zeta}(t)z^2 + Z_{\zeta z\theta}(t)z\theta + \\
 & Z_{\zeta\phi\phi}(t)\phi^2 + Z_{\zeta\zeta\theta}(t)\theta + Z_{\zeta\theta\theta}(t)\theta^2 \\
 & = Z_w(t)
 \end{aligned} \tag{1}$$

$$\begin{aligned}
 & (J_{xx} + K_{\ddot{\phi}})\ddot{\phi} + K_{\dot{\phi}}\dot{\phi} + K_{\phi|\phi}|\dot{\phi}| + K_{\phi}\phi + K_{z\phi}z\phi + \\
 & K_{\phi\theta}\phi\theta + \frac{1}{2}K_{zz\phi}z^2\phi + \frac{1}{6}K_{\phi\phi\phi}\phi^3 + \frac{1}{2}K_{\theta\theta\phi}\theta^2\phi + \\
 & K_{z\phi\theta}z\phi\theta + K_{\zeta\phi}(t)\phi + K_{\zeta\zeta\phi}(t)\phi + K_{\zeta z\phi}(t)z\phi + \\
 & K_{\zeta\phi\theta}(t)\phi\theta = K_w(t)
 \end{aligned} \tag{2}$$



$$\begin{aligned}
 & (J_{yy} + M_{\dot{\theta}})\ddot{\theta} + M_{\dot{z}}\ddot{z} + M_{\dot{\phi}}\dot{\phi} + \\
 & M_{\theta}\dot{\theta} + M_{z}z + M_{\theta}\theta + \frac{1}{2}M_{zz}z^2 + \\
 & \frac{1}{2}M_{\phi\phi}\phi^2 + \frac{1}{2}M_{\theta\theta}\theta^2 + M_{z\theta}z\theta + \frac{1}{6}M_{zzz}z^3 + \\
 & \frac{1}{2}M_{zz\theta}z^2\theta + \frac{1}{2}M_{\phi\phi z}\phi^2z + \frac{1}{2}M_{\phi\phi\theta}\phi^2\theta + \\
 & \frac{1}{2}M_{\theta\theta z}\theta^2z + \frac{1}{6}M_{\theta\theta\theta}\theta^3 + M_{\zeta z}(t)z + M_{\zeta\theta}(t)\theta + \\
 & M_{\zeta z z}(t)z + M_{\zeta z z}(t)z^2 + M_{\zeta z\theta}(t)z\theta + M_{\zeta\phi\phi}(t)\phi^2 + \\
 & M_{\zeta\zeta\theta}(t)\theta + M_{\zeta\theta\theta}(t)\theta^2 = M_w(t) \quad (3)
 \end{aligned}$$

Definition of coefficients appearing in the set of equations (1-3) and how to obtain them have been described in Neves and Rodríguez (2007). The same paper demonstrates the good accuracy of the model in regular waves when compared to experimental results for a modern container ship.

3. METHODOLOGY FOR IRREGULAR SEAS

In irregular seas, functions that govern wave excitations lose their harmonic character, becoming random functions in time domain. One way of expressing these direct excitation forces and moments, as well as wave restoring actions associated to a given sea spectrum is through the transfer functions amplitude of excitations (or restoring) in regular waves in frequency domain. Therefore, for example, for the heave excitation force we have:

$$S_{Z_w}(\omega_e) = [RAO_{Z_w}(\omega_e)]^2 S_{\zeta}(\omega_e) \quad (4)$$

and for the roll wave restoring coefficient $K_{\zeta\phi}(t)$:

$$S_{K_{\zeta\phi}}(\omega_e) = [RAO_{K_{\zeta\phi}}(\omega_e)]^2 S_{\zeta}(\omega_e) \quad (5)$$

For the exciting forces and moments in the other degrees of freedom and for the other wave restoring coefficients the same logic as

given in equations (4) and (5) follows. As observed in the structure of eqs. (1-3) the hydrodynamic coupling between the three modes is described by eight time-dependent contributions in the heave equation ($Z_{\zeta z}(t), Z_{\zeta\theta}(t), Z_{\zeta z z}(t), Z_{\zeta z z}(t), Z_{\zeta z\theta}(t), Z_{\zeta\phi\phi}(t), Z_{\zeta z\phi}(t), Z_{\zeta\theta\phi}(t)$), four contributions in the roll mode ($K_{\zeta\phi}(t), K_{\zeta z\phi}(t), K_{\zeta z\phi}(t), K_{\zeta\phi\theta}(t)$) and eight contributions in the pitch mode ($M_{\zeta z}(t), M_{\zeta\theta}(t), M_{\zeta z z}(t), M_{\zeta z z}(t), M_{\zeta z\theta}(t), M_{\zeta\phi\phi}(t), M_{\zeta z\phi}(t), M_{\zeta\theta\phi}(t)$). So, in total there are twenty functions to be pre-computed.

Added mass and damping in the directly excited modes (heave and pitch) may be computed using convolution (Cummins, 1962). However, based on Celis (2008) – which reports small influence of memory effects on the development of parametric rolling in regular waves – and given the aim of simplifying the proposed methodology, added mass and damping are computed at the frequency value corresponding to the peak value, as done by many authors. For roll mode these hydrodynamic coefficients are computed at the roll natural frequency, introducing also nonlinearities in roll damping (adopting the same approach proposed by the Authors in previous articles (Neves and Rodríguez, 2007) for parametric roll in regular waves. Hydrostatic restoring is introduced directly into the equations, as the respective coefficients are independent of time. These are pre-calculated for different hull positions defined around the hull mean position.

In summary, the proposed procedure for parametric roll simulation in irregular waves consists in:

a) Define a sea state, i.e. specify a sea spectrum $S_{\zeta}(\omega)$ for given basic parameters like significant wave height (H_s) and peak period (T_p).

b) Transform sea spectrum defined for wave frequency ω and heading χ into encounter frequency domain ω_e (see Bhattacharyya, 1978):



$$S_{\zeta}(\omega_e) = \frac{S_{\zeta}(\omega)}{1 - \frac{2\omega U}{g} \cos \chi} \quad (6)$$

c) Compute amplitude operators of wave exciting forces and all wave restoring coefficients in frequency domain. The amplitude operators of wave exciting forces may be computed using well known softwares like WAMIT[®] or HANSEL. In the present paper, all twenty wave restoring coefficients are computed using DSSTAB (based on numeric calculation of numerical restoring coefficients based on polynomial fitting, as described in Rodríguez et al., 2007). These operators are computed for unit wave amplitude, analogous to ship RAOs.

d) Transform domains of amplitude operators defined in step (c) from wave frequency to encounter frequency:

$$\omega_e = \omega - \frac{\omega^2 U}{g} \cos \chi$$

e) Calculate spectra of exciting forces and all twenty restoring coefficients, as indicated in equations (4) and (5).

f) Use Fourier analysis to generate time series of all spectra defined in step (e). In the Fourier analysis, a general time series $\gamma(t)$ may be obtained from a given spectrum $S_{\gamma}(\omega)$ using the following well known expressions:

$$\gamma(t) = \sum_{n=1}^N \gamma_{a_n} \cos(k_n x - \omega_n t + \varepsilon_n) \quad (7)$$

$$\text{where: } \gamma_{a_n} = \sqrt{2S_{\gamma}(\omega_n)} \cdot \delta\omega$$

g) Solve nonlinear equations of motion in time domain using, for example, the classical 4th order Runge-Kutta routine.

4. NUMERICAL SIMULATIONS

Now the above presented methodology is applied. A container ship is considered, here denominated SAFEDOR (ITTC A1), described

in Spanos and Papanikolaou (2009). 3D lines of ship hull are shown in Figure 1.



Figure 1 SAFEDOR ship hull.

SAFEDOR hull was tested for a JONSWAP spectrum with significant height $H_s = 5.00$ m, peak period $T_p = 10.63$ s, $\gamma = 3.3$, wave incidence is 180° (head seas). Ship speed corresponds to $Fn = 0.12$. Sea spectrum and transformed spectrum to $Fn = 0.12$ are shown in Figure 2.

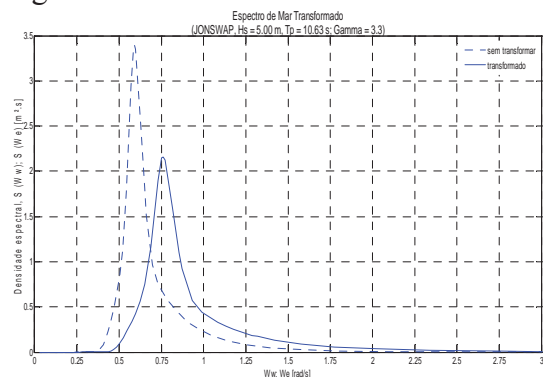


Figure 2 Sea spectrum, wave and encounter frequency domains

Transfer functions of external wave exciting force in heave and moment in pitch are given in Figures 3 e 4, respectively.

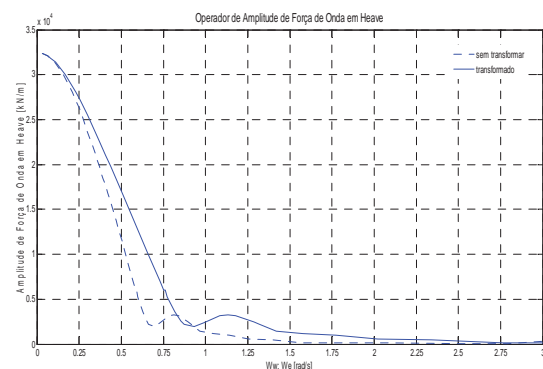




Figure 3 Transfer function, heave wave exciting force, $F_n = 0.12$

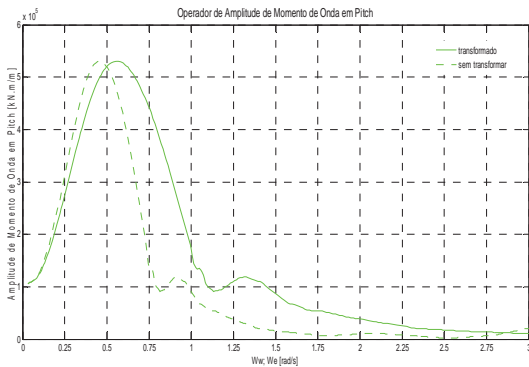


Figure 4 Transfer function, pitch wave exciting moment, $F_n = 0.12$

Transfer functions corresponding to roll wave restoring coefficients $K_{\zeta\phi}$, $K_{\zeta\psi}$ and $K_{\zeta\phi\theta}$ are shown in Figures 5 to 7.

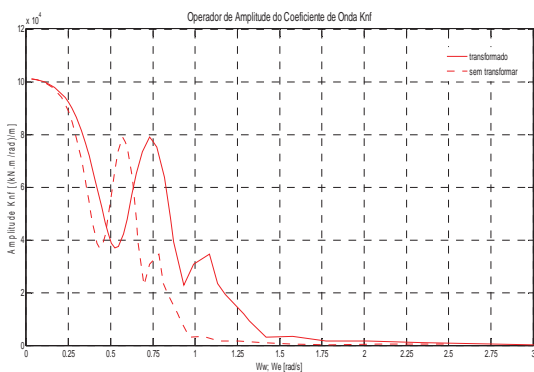


Figure 5 Transfer function, coefficient $K_{\zeta\phi}$

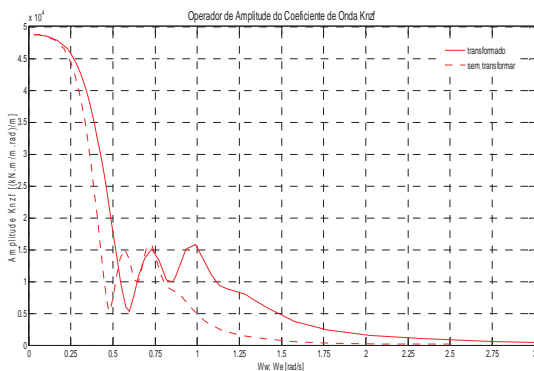


Figure 6 Transfer function, coefficient $K_{\zeta\phi}$

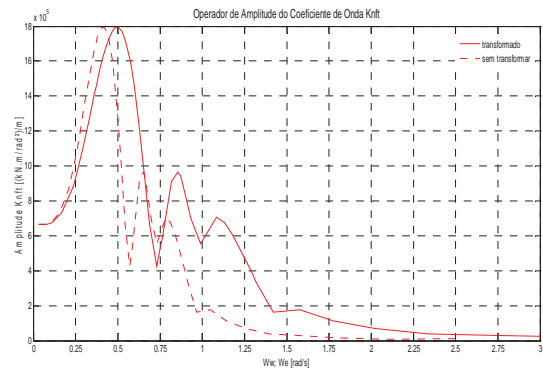


Figure 7 Transfer function, coefficient $K_{\zeta\phi\theta}$

With sea spectrum given in Figure 2 and the transfer functions the corresponding spectra for the specified sea condition are computed, as exemplified in equations (4) and (5). Some of these spectra are shown in Figures 8 to 10. Fourier analysis applied to the various spectra, corresponding time series are generated. Samples are given in Figures 11 to 13.

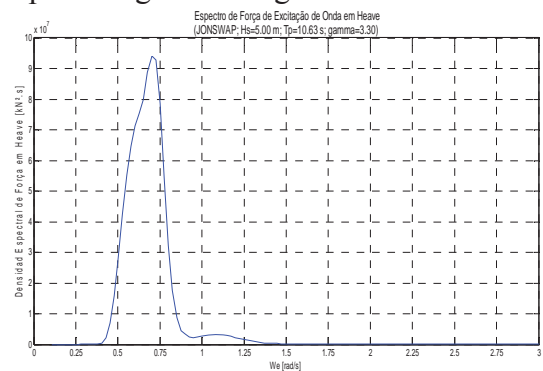


Figure 8 Heave exciting force spectrum

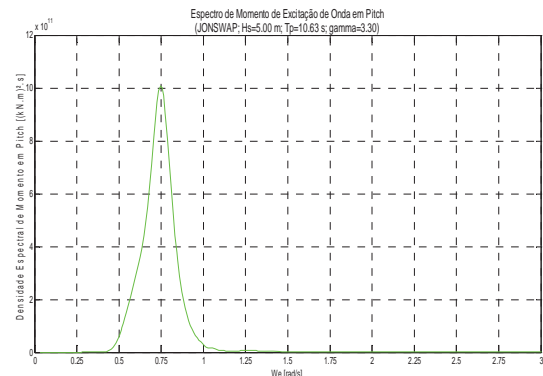


Figure 9 Pitch exciting moment spectrum

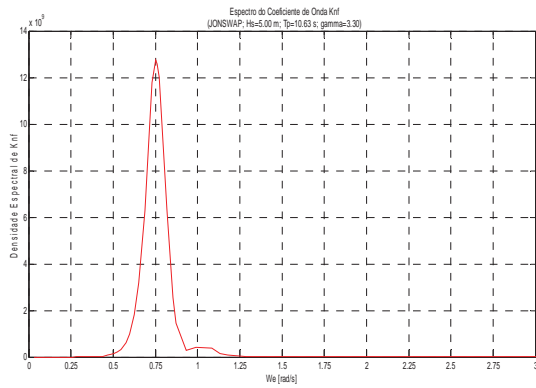


Figure 10 Roll restoring spectrum of K_{ϕ}

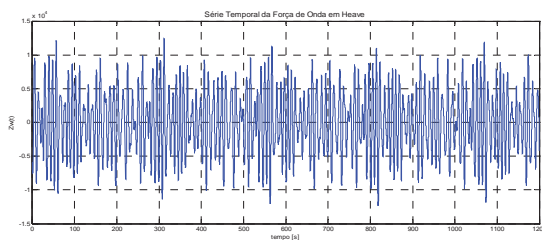


Figure 11 Heave force time series

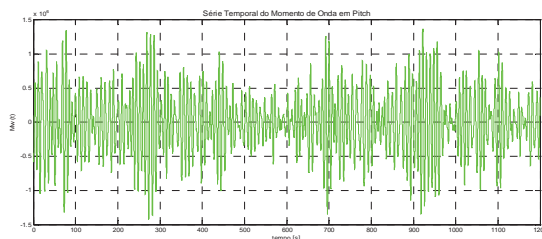


Figure 12 Pitch moment time series

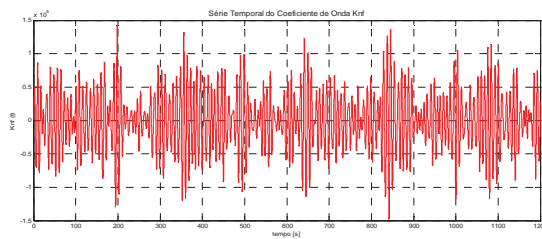


Figure 13 Wave coefficient K_{ϕ} time series

Time series obtained for the excitation forces and moments and all wave restoring coefficients are incorporated into the non linear equations of motion, eqs. (1-3), from which the time series of the heave-roll-pitch ship responses to the specified sea conditions result after integration.

To assess the ergodicity of responses in heave-roll-pitch modes, three realizations have been simulated (obtained from three different

time series of wave excitations) for the specified sea conditions. These are shown in Figures 14 to 16.

Wave elevation is typically an ergodic process; additionally, transfer functions are linear. Therefore, even considering different time series (realizations) sufficiently long, wave excitation is statistically equivalent for the different realizations. In all cases the analyzed time series had a duration of 20', which in practice may be considered representative enough to describe the effects resulting from a given stochastic sea state.

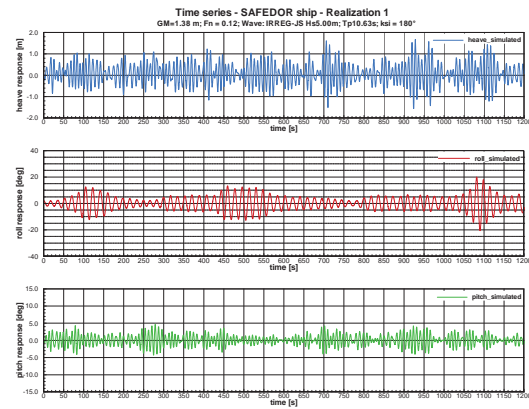


Figure 14 Heave, roll and pitch time series, realization #1

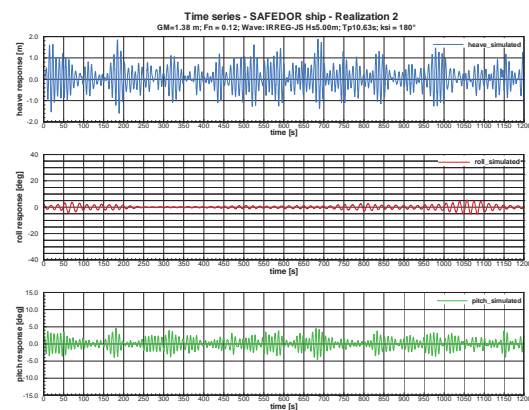


Figure 15 Heave, roll and pitch time series, realization #2

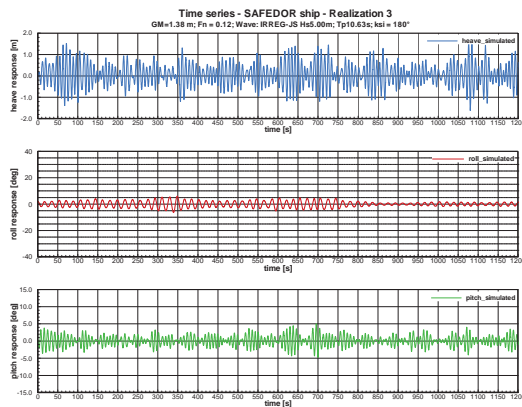


Figure 16 Heave, roll and pitch time series, realization #3

5. DISCUSSION OF NUMERICAL RESULTS

Despite the large frequency band with wave energy content, mainly the range of encounter frequency from 0.50 rad/s to 1.25 rad/s, wave excitation and restoring coefficients spectra are concentrated in a smaller band (0.50 to 0.85 rad/s) around the peak frequency of sea spectrum (0.76 rad/s) and outside the region of natural periods in heave ($\omega_{n3} = 0.82$ rad/s), pitch ($\omega_{n5} = 0.85$ rad/s) and roll ($\omega_{n4} = 0.33$ rad/s).

Roll time series are distinct for the same tested condition. The first realization has moderate development of roll amplification, whereas the second and third realizations present quite small roll amplifications.

Roll responses have a larger period, corresponding typically to the characteristic 2:1 tuning, whereas both heave and pitch respond near encounter period.

Heave, roll and pitch spectra for the three realizations considered (see Figures 17 to 19) show the prevailing frequencies in each degree of freedom: heave and pitch present responses in the region of frequencies between 0.50 and 0.85 rad/s, which coincides with the main band of sea spectrum considered. On the other hand, roll responses are concentrated in a quite narrow band around the roll natural frequency,

thus evidencing the occurrence of parametric rolling.

Roll spectra confirm the distinct character between the three realizations (see Figure 18). So, it is concluded that corresponding to the tested condition there two types of dynamic responses involved in roll: occurrence of parametric roll (realization #1) and non-occurrence of parametric roll (realizations #2 and #3). Thus, evidencing the influence of nonlinearities and the non-ergodicity in the responses.

Nonlinearities discussed in the above paragraph are also visible, but less intense in the heave and pitch spectra. It may be observed that spectral densities are smaller when there is parametric rolling (realization #1), whereas spectral densities are slightly larger in cases where parametric roll is very small (realizations #2 and #3). These results evidence the "weakly ergodic" character of heave and pitch motions, as has been pointed out by distinct authors (Belenky et al., 2003, Ogawa, 2007, Bulian et al., 2008).

It is important to notice here the great advantage in computing time when the derivative model is employed: running 50 time simulations of 10800 seconds with the corresponding 3100 frequency components (in order to avoid the *Self-Repeating Effect*) would take about 4 hours, whereas using full state-of-the-art advanced hydrodynamic code DSSTAB in the same conditions would require about 3 days just to obtain a single realization of the random process on a normal desktop computer. On the other hand, running 20 simulations of 30 minutes with 220 frequency components, after pre-processing the derivative model will take nothing more than 12 seconds.

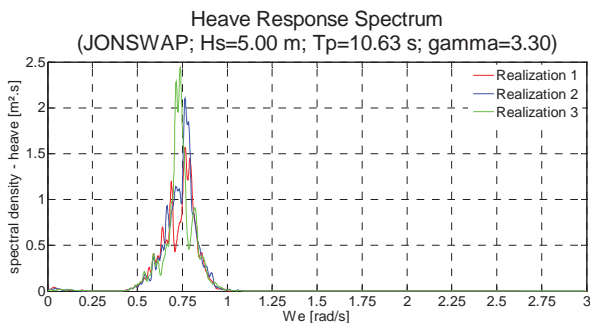


Figure 17 Heave motion spectra

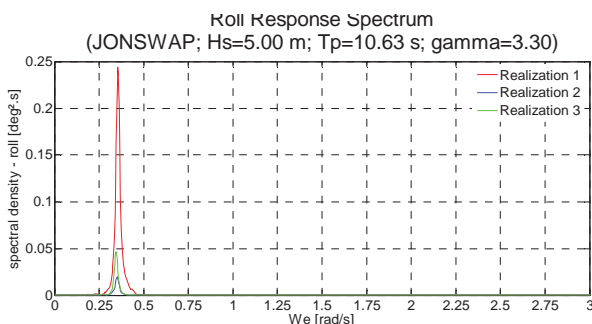


Figure 18 Roll motion spectra.

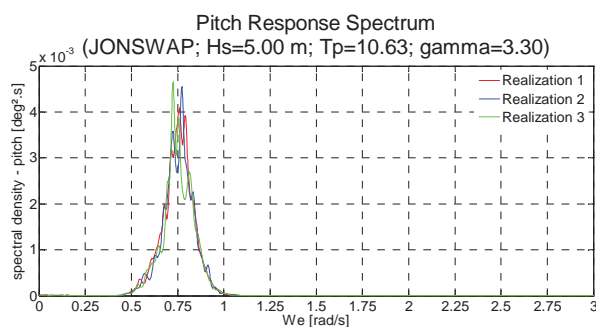


Figure 19 Pitch motion spectra

6. CONCLUSIONS

As previously mentioned, large series of time-domain simulations are required for realistic assessment of coupled heave, roll and pitch motions leading to extreme roll motion in irregular seas.

Some conclusions may be extracted based on the numerical results for the tested condition of SAFEDOR hull in head seas irregular seas.

It is shown that parametric roll affects the irregular responses in heave and pitch – as evidenced by the respective response spectra. In roll, the peak of responses is in the natural frequency, whereas in heave and pitch three

peaks (or contributions) are observed, the larger at the encounter frequency and other two (much smaller) at the wave frequency and at the roll natural frequency.

Distinct realizations corresponding to a given test condition of SAFEDOR have produced qualitatively different responses with regard to occurrence of parametric rolling. This aspect confirms the capability of the proposed methodology to deal with strong nonlinearities, thus evidencing the non-ergodic character of roll responses when parametric rolling takes place.

For the heave and pitch modes the responses are "weakly ergodic".

The derivative model requires much less simulation time than full state-of-the art advanced hydrodynamic codes such as the DSSTAB code. This fact allows systematic Monte Carlo simulations in order to perform a realistic probabilistic assessment of parametric rolling of vessels.

7. ACKNOWLEDGMENTS

The present investigation has been supported by CNPq, CAPES and ANP. Authors greatly acknowledge this crucial support.

8. REFERENCES

- Belenky, V.L., Weems, K.M., Lin, W. and Paulling, J.R., 2003, "Probabilistic Analysis of Roll Parametric Resonance in Head Seas". In: Proceedings of the 8th International Conference on Stability of Ships and Ocean Vehicles (STAB'2003), Madrid, Spain, pp. 325-340, Sep.
- Bhattacharyya, R., 1978, *Dynamics of Marine Vehicles*. John Wiley & Sons, Inc., New York, United States of America.



- Bulian, G., Francescutto, A., Umeda, N. and Hashimoto, H., 2008, "Experimental Investigation on Stochastic Parametric Rolling for a Post-Panamax Containership". In: Proceedings of the 6th Osaka Colloquium on Seakeeping and Stability of Ships (OC'2008), pp. 371-382, Osaka, Japan, Mar.
- Celis, M.A.C., 2008, "Dynamic Stability of Ships: Influence of Memory Effects on Parametric Rolling" M.Sc. Dissertation, COPPE – Ocean Eng., Federal University of Rio de Janeiro, Brazil. (in Portuguese).
- Cummins, W.E., 1962, "The Impulse Response Function and Ship Motions". In: International Symposium on Ship Theory, no. 8, Hamburg, Germany, pp. 101-109, Jun.
- Neves, M.A.S. and Rodriguez, C.A., 2006, "An Investigation of Roll Parametric Resonance in Regular Waves". In: Proceedings of the 9th International Conference on Stability of Ships and Ocean Vehicles (STAB'2006), vol.1, Rio de Janeiro, Brazil, pp. 99-108, Sep.
- Ogawa, Y. (2007): "An Examination for the Numerical Simulation of Parametric Roll in Head and Bow Seas", In: Proceedings of the 9th International Ship Stability Workshop (ISSW'2007), Hamburg, Germany, Aug.
- Rodriguez, C.A., 2010, On the Nonlinear Dynamics of Parametric Rolling. D.Sc. Thesis, COPPE - Ocean Eng., Federal University of Rio de Janeiro, Brazil. (in Portuguese).
- Rodríguez, C.A., Holden, C., Perez, T., Drummen, I., Neves, M.A.S. and Fossen, T.I., 2007, "Validation of a Container Ship Model for Parametric Rolling", In: Proceedings of the 9th International Ship Stability Workshop (ISSW'2007), Hamburg, Germany, Aug.
- Somayajula, A.S. and Falzarano, J.M. 2014, "Non-linear Dynamics of Parametric Roll of Container Ship in Irregular Seas". OMAE2014-24186, San Francisco.
- Song, K.H. and Kim, Y. 2011, "Quantitative Analysis of Parametric Roll and Operational Guidance", In: Proceedings of the 12th International Ship Stability Workshop (ISSW 2011), Washington DC.
- Spanos, D., Papanikolaou, A., 2009, SAFEDOR International Benchmark Study on Numerical Simulation Methods for the Prediction of Parametric Rolling of Ships in Waves, NTUA-SDL Report, rev 1.
- Weems, K.M. and Wundrow, D. 2013, "Hybrid Models for Fast Time Domain Simulation of Stability Failures in Irregular Waves With Volume-Based Calculations for Froude-Krilov and Hydrostatic Forces". In: Proceedings of the 13th International Ship Stability Workshop (ISSW 2013), Brest, France.

This page is intentionally left blank



Non-stationary Ship Motion Analysis Using Discrete Wavelet Transform

Toshio, ISEKI, *Tokyo University of Marine Science and Technology* iseki@kaiyodai.ac.jp

ABSTRACT

The discrete wavelet transform is applied to non-stationary ship motion data. The data was obtained by on-board measurements that were carried out under relatively severe sea conditions. In the full scale measurements, the ship travelled on several courses to investigate the change of frequency response relative to the encounter wave angle. Comparing to the results of Fourier analysis and time-varying autoregressive coefficient modelling, it is shown that the discrete wavelet transform can analyse non-stationary ship motions in the frequency and the time domain.

Keywords: *seakeeping, discrete wavelet transform, full-scale ship measurements, non-stationary time series*

1. INTRODUCTION

The author has been trying to develop a guidance system for heavy weather operation and investigating suitable signal processing methods under the necessity of analysing non-stationary stochastic process. Generally, the assumption of stationary stochastic processes is applied to the seaway, but not to ship response because it also depends on ship manoeuvres. Ship response is strongly affected by changes in the encounter angle and frequency of waves. Therefore, the method is needed to be a real-time algorithm that can deal with non-stationary stochastic processes. In the previous study (Iseki & Terada, 2002, Iseki, 2006), the instantaneous spectral analysis with the Time-Varying coefficient Vector Auto Regressive (TVVAR) model was introduced to deal with non-stationary ship motions. Some problems, however, were pointed out because the maximum likelihood method for determination of the trade-off parameter, which is the ratio of the observation noise and the system noise of Kalman filter, cannot be applied to the real-time algorithm.

On the other hand, the Discrete Wavelet Transform (DWT) is widely used recently in the field of signal processing (Percival and Walden 2000), image compression and analyses of non-stationary time series. In comparison with the Continuous Wavelet Transform (CWT), the process of DWT can be recognized as decomposition of a time series with use of digital filters while the CWT is defined by a convolution integral over entire time axis. In this sense, the DWT is suitable for digital computing and real-time analyses of non-stationary time series.

The author was also applied the Discrete Wavelet Packet Transform (DWPT) to non-stationary ship motion data (Kang and Iseki 2013). Comparing to the results of Discrete Fourier Transform (DFT) and the TVVAR modelling, it was confirmed that the locations of peaks of the DWPT coefficients agree well with the peak frequencies of the spectra estimated by DFT. However, the obvious advantage of DWPT was not observed in comparison with TVVAR modelling.



In this paper, both of DWT and DWPT are applied to analyses of non-stationary ship motion data which was measured during a large course alteration. Comparing to the results of DFT and TVVAR modelling, the validity of the DWT and DWPT is discussed in detail.

2. DISCRETE WAVELET TRANSFORM

2.1 Basic Properties

The DWT of a measured time series $\mathbf{X} = \{x_n : n = 0, 1, 2, \dots, N-1\}$ is defined as follows:

$$\mathbf{W} = \mathbf{w}\mathbf{X} \quad (1)$$

where \mathbf{W} denotes an N dimensional column vector of DWT coefficients, \mathbf{w} an $N \times N$ real-valued matrix defining the DWT.

For the convenience, we assume that the sample size $N = 2^{J_0}$ for an integer J_0 . The DWT coefficient \mathbf{W} and matrix \mathbf{w} could be separated as;

$$\mathbf{W} = [\mathbf{W}_1, \mathbf{W}_2, \dots, \mathbf{W}_{J_0}, \mathbf{V}_{J_0}]^T \quad (2)$$

$$\mathbf{w} = [\mathbf{w}_1, \mathbf{w}_2, \dots, \mathbf{w}_{J_0}, \mathbf{v}_{J_0}]^T \quad (3)$$

where

$$\mathbf{W}_j = \mathbf{w}_j \mathbf{X}^T, \quad \mathbf{V}_{J_0} = \mathbf{v}_{J_0} \mathbf{X}^T \quad (4)$$

The \mathbf{W}_j and \mathbf{V}_j are the wavelet coefficient sub-vector and the scaling coefficient sub-vector for the level j .

$$\mathbf{W}_j = [W_{i,1}, W_{i,2}, \dots, W_{i,N_i}]^T \quad (5)$$

$$\mathbf{V}_j = [V_{i,1}, V_{i,2}, \dots, V_{i,N_i}]^T \quad (6)$$

where $N_j \equiv N/2^j$ denotes the number of components at the level j . Therefore, \mathbf{V}_{J_0} contains only a scaling coefficient.

The “level j ” is closely related to the scale $\tau_j \equiv 2^{j-1}$ ($j = 1, 2, \dots, J_0$) which is the sampling interval of the time series and denotes the number of times of “down-sampling by two”. If the actual sampling time is denoted by Δt (sec), the physical scale can be expressed by $\tau_j \Delta t$.

By orthonormality of the DWT, we can synthesize the vector \mathbf{X} from \mathbf{W} by,

$$\begin{aligned} \mathbf{X} &= \mathbf{w}^T \mathbf{W} = \sum_{j=1}^{J_0} \mathbf{w}_j^T \mathbf{W}_j + \mathbf{v}_{J_0}^T \mathbf{V}_{J_0} \\ &= \sum_{j=1}^{J_0} \mathbf{D}_j + \mathbf{S}_{J_0} \end{aligned} \quad (7)$$

which is also a definition of Multi-Resolution Analysis (MRA) of \mathbf{X} . Here \mathbf{D}_j and \mathbf{S}_{J_0} are called as “details” for level j and “smooth” for level J_0 , respectively. In the actual calculations, the DWT matrix \mathbf{w} is not formed explicitly but rather \mathbf{W} is computed using the “pyramid algorithm” which is effective and fast from the viewpoint of the computational process (Mallat 1989).

If we represent the actual wavelet filter by $\{h_l : l = 0, 1, 2, \dots, L-1\}$, we can also derive the scaling filter by using “quadrature mirror” relationship,

$$g_l \equiv (-1)^{l+1} h_{L-1-l} \quad (8)$$

where L denotes the width of the wavelet filter.

In practice, the wavelet filter $\{h_l\}$ is a high-pass filter, while the scaling filter $\{g_l\}$ is a low-pass filter. Assuming $\mathbf{V}_0 = \mathbf{X}$ with defined $\{h_l\}$, $\{g_l\}$, general j th stage of the pyramid



algorithm yields the n th components of the sub-vector \mathbf{W}_j and \mathbf{V}_j as follows;

$$W_{j,n} \equiv \sum_{l=0}^{L-1} h_l V_{j-1,2n+1-l} \quad (9)$$

$$V_{j,n} \equiv \sum_{l=0}^{L-1} g_l V_{j-1,2n+1-l} \quad (10)$$

$(n = 0, 1, 2, \dots, N_j - 1)$

Therefore, the DWT can be recognized as a decomposition of a time series \mathbf{X} into coefficients that can be associated with different scales and times.

2.2 DWT spectrum

According to the decomposition described in the previous section, the power spectrum of DWT can be defined as follows;

$$P_w(\tau_j) \equiv \frac{1}{N} \|\mathbf{W}_j\|^2 \quad (11)$$

$$\sum_{j=1}^J P_w(\tau_j) = \frac{1}{N} \|\mathbf{W}_j\|^2 = \frac{1}{N} \|\mathbf{X}\|^2 - \bar{\mathbf{X}} = \sigma_x^2 \quad (12)$$

where σ_x^2 denotes the sample variance.

2.3 Wavelet Filters

The filter $\{h_{j,l}\}$ and $\{g_{j,l}\}$ are the band pass filters with pass band given by $1/\Delta t 2^{j+1} \leq f \leq 1/\Delta t 2^j$ and $0 \leq f \leq 1/\Delta t 2^{j+1}$ (Hz), respectively. Meanwhile, scaling filters as well as wavelet filters must satisfy the three basic properties, which are

$$\sum_{l=0}^{L-1} g_l = \sqrt{2}, \quad \sum_{l=0}^{L-1} g_l^2 = 1 \quad (13)$$

$$\sum_{l=0}^{L-1} g_l g_{l+2n} \equiv \sum_{l=-\infty}^{\infty} g_l g_{l+2n} = 0 \quad (14)$$

Additional to the above conditions, Daubechies (1988) specified vanishing moment conditions on the wavelet function and led to obtain the scaling filters which have minimum delay. In this study Daubechies filter of width 8 is used for the DWT. Actual value and the shape are expressed on Figure 1 and Table 1.

Table 1 Daubechies wavelet and scaling filters of width 8.

l	Wavelet filter (h_l)	Scaling filter (g_l)
0	-0.010597401785	0.230377813309
1	-0.032883011667	0.714846570553
2	0.030841381836	0.630880767930
3	0.187034811719	-0.027983769417
4	-0.027983769417	-0.187034811719
5	-0.630880767930	0.030841381836
6	0.714846570553	0.032883011667
7	-0.230377813309	-0.010597401785

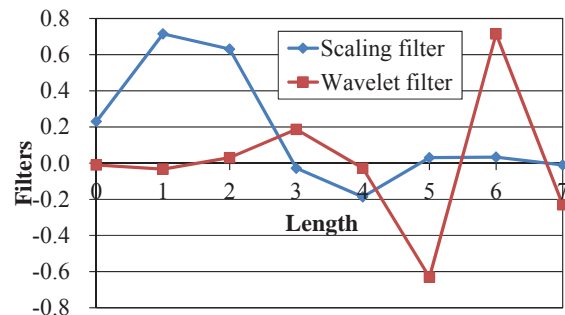


Figure 1 Daubechies wavelet and scaling filters of width 8.

3. DISCRETE WAVELET PACKET TRANSFORM

As shown in the previous section, the DWT decomposes the frequency interval $0 \leq f \leq 1/2\Delta t$ into adjacent individual intervals. The DWPT can be regarded as one of the extension of orthonormal transformation and decomposes the frequency into 2^j equal and individual intervals at the level j . The actual procedure of the calculation is readily



expressed using very simple modification of the pyramid algorithm (Percival and Walden 2000).

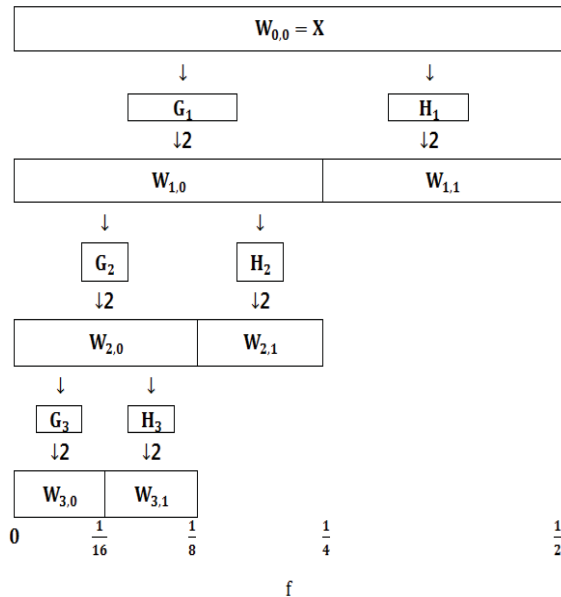


Figure 2 Flow diagram illustrating the analysis of \mathbf{X} into $\mathbf{W}_{3,0}$, $\mathbf{W}_{3,1}$, $\mathbf{W}_{2,1}$ and $\mathbf{W}_{1,1}$ which is identical to partial DWT of level 3.

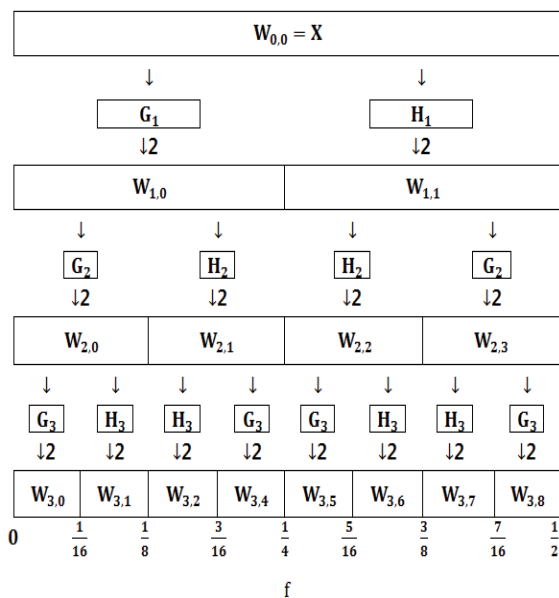


Figure 3 Flow diagram illustrating the analysis of \mathbf{X} into $\mathbf{W}_{3,0}$, $\mathbf{W}_{3,1}$, ..., $\mathbf{W}_{3,8}$ using DWPT of level 3.

Figure 2 shows the flow diagram of the DWT pyramid algorithm described in the previous section, where the level $J_0=3$. The

starting point is defined as $\mathbf{W}_{0,0} = \mathbf{V}_0 = \mathbf{X}$ and other nodes represent $\mathbf{W}_{1,1} = \mathbf{W}_1$, $\mathbf{W}_{2,1} = \mathbf{W}_2$, $\mathbf{W}_{3,1} = \mathbf{W}_3$ and $\mathbf{W}_{3,0} = \mathbf{V}_3$. G_j and H_j represent filtering with use of the wavelet filter $\{h_l\}$ and the scaling filter $\{g_l\}$ at the level j . The ‘ $\downarrow 2$ ’ denotes the “down-sampling by two”. The fractions at the lowest level denote the corresponding frequencies with $\Delta t=1$.

By using the low-pass and high-pass filters, the process of the decomposition of time series \mathbf{X} is simply illustrated in the figure. It should be noted, however, that the nominal frequency intervals for these four nodes are not constant.

Figure 3 shows the flow diagram of the DWPT. It can be seen that the frequency intervals are constant and the resolution is improved by the iterative use of the low-pass and high-pass filters. This is the reason for the introduction of the DWPT.

4. FULL SCALE EXPERIMENT

The full scale ship experiment was carried out on January 25th 2012 using the training ship Shioji-maru of Tokyo University of Marine Science and Technology. A photo and principal particulars of the ship are shown in Figure 4 and Table 2. The location of the experimental area was off Sunosaki cape in Chiba Prefecture, Japan.



Figure 4 The training ship Shioji-maru.

Table 2 Principal particulars of the ship.

Length (P.P.)	46.00(m)
Breadth (M_{LD})	10.00(m)



Depth (M_{LD})	6.10(m)
Draught (M_{LD})	2.65(m)
Displacement	659.4(t)

Figure 5 shows the trajectory of the T.S. Shioji-maru during the experiment. The blue arrow denotes the main direction of waves. In order to measure changes in ship motions with respect to the encounter angle of waves, the angle of CPP was set to 10.5 degrees during 90 minute manoeuvres involving straight sections and changes in course.

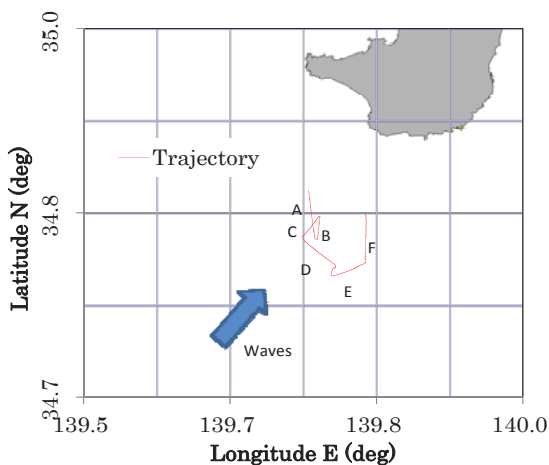


Figure 5 The experimental area at the south of Sunosaki cape and the ship trajectory.

Table 3 Ship course and the sea conditions.

Run	Ship course (deg)	Ship speed (knot)	Wind direction (deg)	Wind speed (m/s)
A	180	8.3	257	10.4
B	0	10.4	260	11.5
C	240	7.3	265	11.5
D	120	9.9	258	11.8
E	60	10.7	267	11.5
F	0	10.5	267	11.4

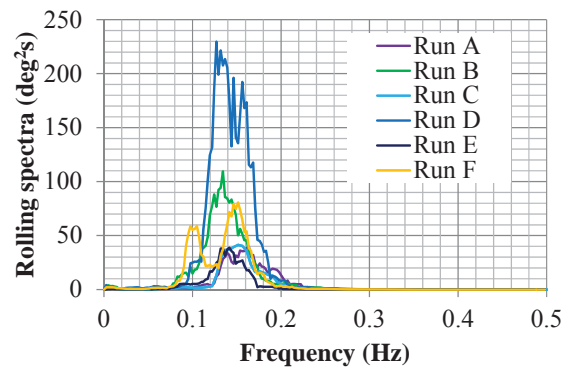


Figure 6 Power spectra of rolling motions.

Table 3 shows the courses and the mean speed-through-water of the ship, and true wind directions and the speeds are also summarized. During the experiment, observed wind waves were: height 1.0-1.5m, period 6-7 sec, direction 200-240 degrees, and swells were: height 2-3m, period 8-10 sec, direction 200 degrees. Note that the wave conditions listed in Table 3 can be recognized rather severe, since the ship is not a large ship (Table 2).

Figure 6 shows power spectra of the rolling motion calculated by FFT. It should be noted that the spectra “D” and “E” show the large difference in spite of adjacent run, because there is a large course alteration between them.

In this paper, the rolling time series between “D” and “E” are analysed in order to concentrate our attention on the non-stationarity. The trajectory is indicated in Figure 7 and seems to be a zigzag line because of beam seas. The analysed time span is 102.4s.

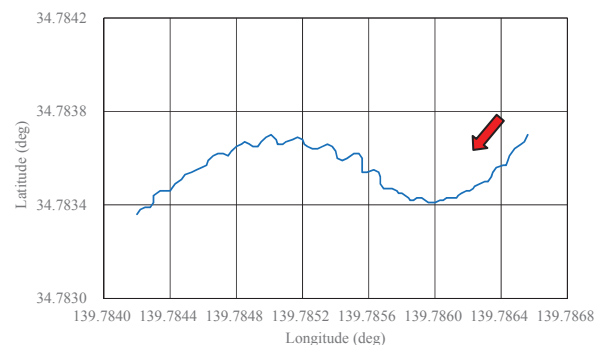


Figure 7 Time series of rolling motion. The red arrow denotes the starting side.

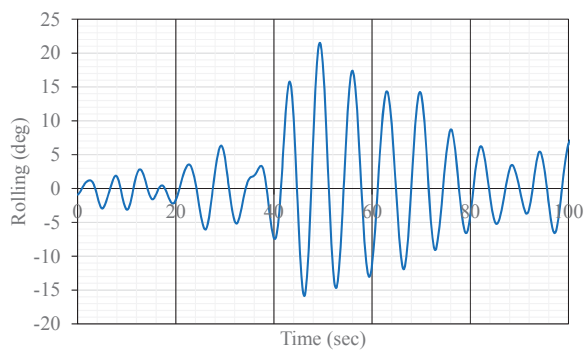


Figure 8 Time series of rolling motion.

Figure 8 shows the time history of the rolling motion that was analysed. The sampling time is 0.1s and 1024 observations are included. It can be seen that the ship was experienced rather large amplitude rolling during the beam seas condition (40 to 70 sec).

Figure 9 shows the power spectrum analysed by DFT ignoring the fact that the data is non-stationary. The peak frequency is 0.152Hz and coincides with the rolling natural frequency of the ship.

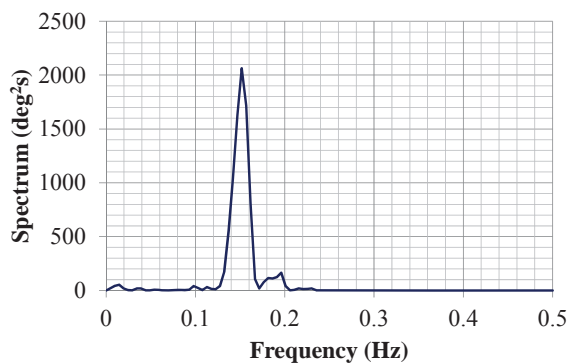


Figure 9 Power spectrum of rolling motion.

5. TVVAR MODEL ANALYSIS

TVVAR modelling was originally applied to analysis of the earthquake data (Kitagawa & Gersch, 1985, Jiang & Kitagawa, 1993). Generally, TVVAR models are transformed into state-space models, and the time varying coefficients can be evaluated by using the Kalman filter algorithm. Using the estimated

time varying coefficients, the instantaneous power spectra of ship motions can be estimated at every moment.

Figure 10 shows the time evolution of the estimated auto spectra of roll angle from 0s to 100s. In this figure, the curves denote estimated instantaneous auto spectra and are superimposed on time axis with time increasing. In this estimation, the model order was set to 9. Comparing with the ship trajectory illustrated in Figure 8, it is found that the rolling motion becomes larger during the beam seas and the peak frequency coincides well with figure 9. On the other hand, it can be seen the “development period” at the beginning of analysis (from 0s to 30s). This comes from the initial conditions of the Kalman filter and means that the TVVAR modelling analysis requires a certain length of time series. In addition to this, some problems were pointed out in the TVVAR modelling. The maximum likelihood method for determination of the trade-off parameter, which is the ratio of the observation noise and the system noise of Kalman filter, cannot be applied to the real-time algorithm.

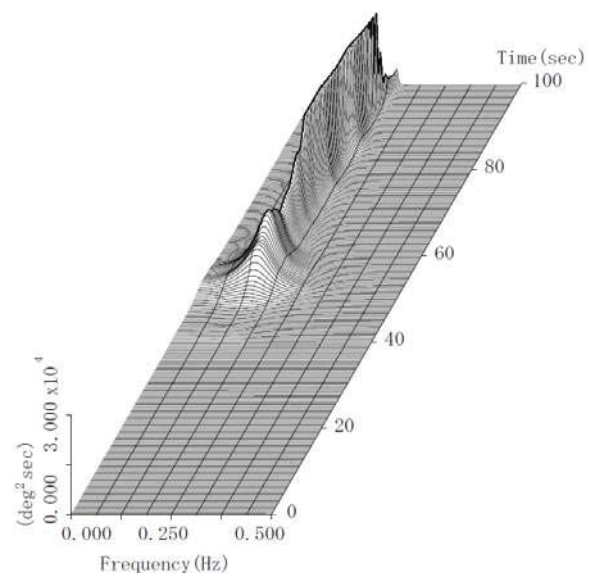


Figure 10 Instantaneous auto spectrum of rolling motions estimated by TVVAR modelling.

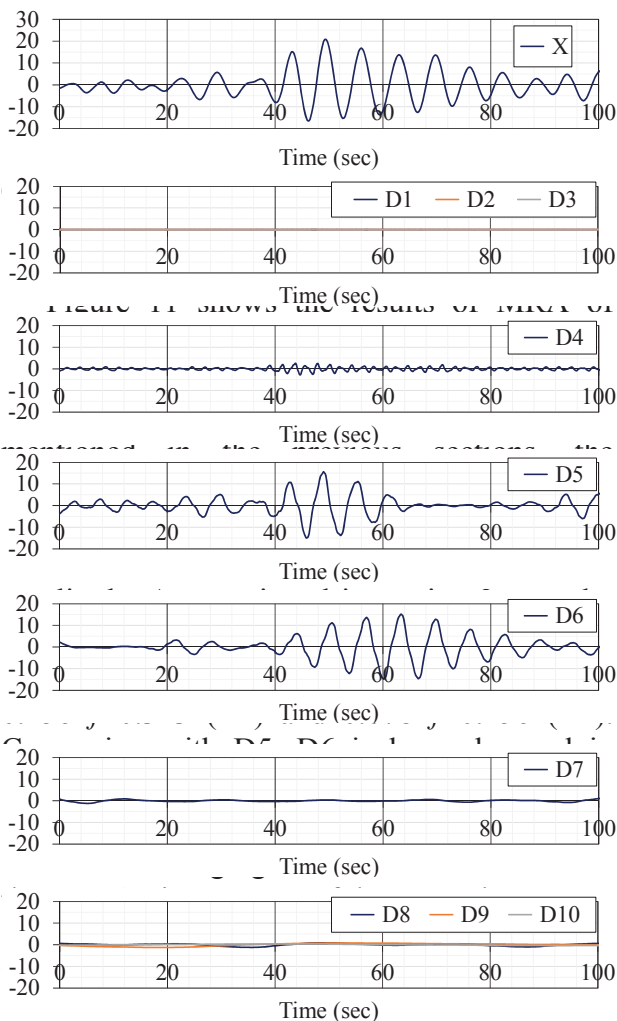


Figure 11 Results of multi-resolution analysis of rolling motion time series.

Figure 12 shows the time evolution of the estimated DWT spectrum from 0s to 100s. The DWT spectrum is expressed by discrete value, therefore, the graph is indicated in a stepwise shape. In this figure, levels of the DWT can be seen from 4 to 10 because frequencies of the smaller level are higher than 0.5Hz. The wide band on the centre (around 0.25Hz) denotes the power of D5 and the neighbouring left band denotes the power of D6. Similar to Figure 11, it can be observed that D6 is less advanced in development and has long duration, comparing

with D5. This concludes that the DWT analysis is very useful for frequency/time analysis.

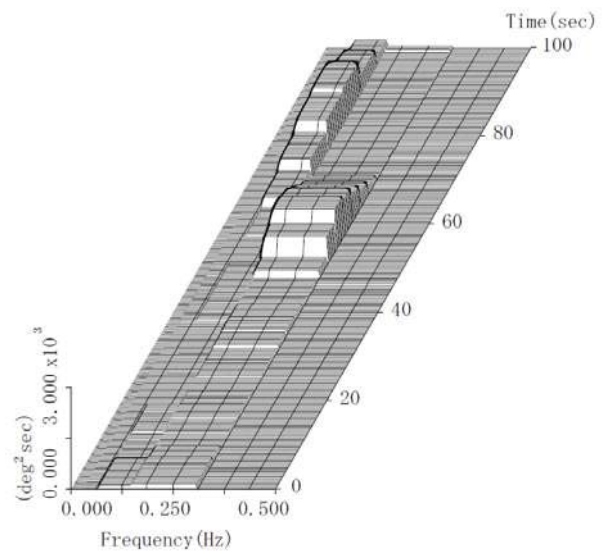


Figure 12 Results of DWT analysis of rolling motion.

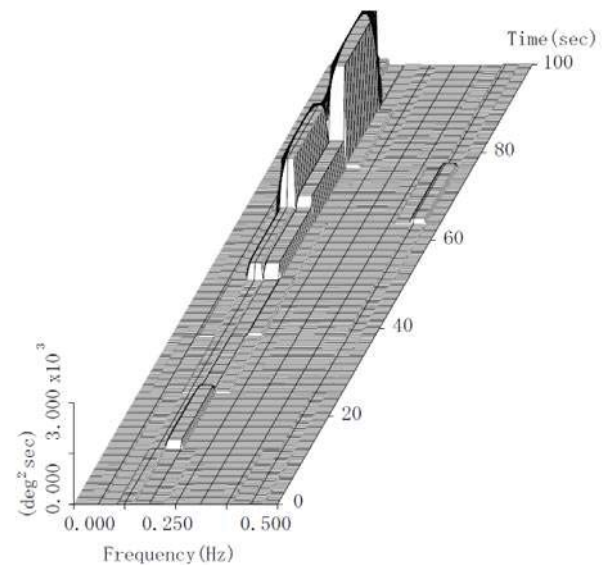


Figure 13 Results of DWPT analysis of level 7 of rolling motion.

Figure 13 shows the time evolution of the estimated DWPT spectrum of level 7. As described in the section 3, the frequency intervals are unified and the resolution is improved than DWT analysis. The peaks of the spectra were sharpened in the frequency-wise. Furthermore, the shape of spectra agree well



with the results of DFT and TVVAR modelling. However, it can be also seen that the resolution in time is worsened in comparison with Figure 12. Therefore, selection of the suitable level is very important for the effective DWPT analysis.

7. CONCLUSIONS

The DWT and DWPT were applied to non-stationary ship motion data. Comparing to the spectra of DFT and the TVVAR modelling, the results obtained in this report can be summarized below:

(1) The MRA can be applied to analyses of non-stationary time series. It is very useful to extract the motion that has a certain frequency band.

(2) The locations of peaks of DWT spectra represent the time evolution of the rolling motion and agree well with the peaks of the spectra estimated by TVVAR modelling.

(3) Selecting a suitable level, the spectra estimated by the DWPT analysis agree well with the results of DFT and TVVAR modelling.

This concludes that the DWT and DWPT are powerful tools for analysing non-stationary ship motion data.

8. ACKNOWLEDGMENTS

This work is partly supported by Grant-in-Aid for Scientific Research of the Japan Society for Promotion of Science (No. 26420822). The author expresses sincere gratitude to the above organizations and thanks the captain and crew of the training ship Shiojimaruru.

9. REFERENCES

Daubechies, I., 1988, "Orthonormal Bases of Compactly Supported Wavelets",

Communications on Pure and Applied Mathematics, 41, pp.909-996.

Iseki, T., Terada, D, 2002, "Study on Real-time Estimation of the Ship Motion Cross Spectra," Journal of Marine Science and Technology, Vol.7, pp.157-163.

Iseki, T., 2006, "Instantaneous Spectral Analysis of Non-stationary Ship Motion Data", Proceedings of the 25th International Conference on Offshore Mechanics and Arctic Engineering, OMAE2006-92197.

Jiang, X. Q., Kitagawa, G., 1993, "A Time Varying Coefficient Vector AR Modeling of Non-stationary Covariance Time Series," Signal Processing, 33, No.3, p.315-331.

Kang, B. and Iseki, T., 2013, "Application of Discrete Wavelet Transform to Ship Motion Analysis", Proceedings of Asia Navigation Conference 2013(ANC2013), pp.20-26.

Kitagawa, G., Gersch, W., 1985, "A Smoothness Priors Time-Varying AR Coefficient Modeling of Nonstationary Covariance Time Series," IEEE Trans. Automatic Control, AC-30, No.1, January, pp.48-56.

Mallat, S.G., 1989, "A Theory for Multiresolution Signal Decomposition", The Wavelet Representation, IEEE Trans. Pattern Analysis and Machine Intelligence, 11, p.674-93.

Percival, D.B. and Walden, A.T., 2000, "Wavelet Methods for Time Series Analysis", Cambridge Series in Statistical and Probabilistic Mathematics, Cambridge University press.



A Study on the Effect of Parametric Rolling on Added Resistance in Regular Head Seas

Jiang Lu, *China Ship Scientific Research Center, Wuxi, China* lujiang1980@aliyun.com

Min Gu, *China Ship Scientific Research Center, Wuxi, China* gumin702@163.com

Naoya Umeda, *Osaka University, Osaka, Japan*, umeda@naoe.eng.osaka-u.ac.jp

ABSTRACT

Both parametric rolling and added resistance in head seas are hot topics in ship hydrodynamics. Parametric rolling with half the encounter frequency is not taken into account in the calculation of added resistance in regular head seas. In order to study the correlation between parametric rolling and added resistance, firstly, a formula of added resistance in regular head seas with parametric rolling taken into account based on Maruo theory is developed to investigate the effect of parametric rolling on added resistance in regular head seas. Secondly, partially restrained free running experiments with and without roll motions are carried out respectively to investigate the effects of parametric rolling on added resistance in regular head seas. The results of experiments and simulations using the C11 containership show that added resistance is affected by parametric rolling, and the results of experiments also show that heave and pitch motions are distinctly affected by parametric rolling.

Keywords: *Parametric rolling, added resistance, heave, pitch, Maruo theory*

1. INTRODUCTION

The second generation intact stability criteria are under development at the International Maritime Organization (IMO) which covers five stability failure modes including parametric rolling as one of roll restoring variation problems, as a supplement to the existing prescriptive criteria (IMO SDC1, 2014).

In case of following waves, the encounter frequency is much lower than the natural frequencies of heave and pitch so that the coupling with dynamic heave and pitch is not important. In addition, added resistance due to waves is generally small in following waves. Thus several successful predictions of parametric rolling in following waves were reported (e.g. Munif and Umeda, 2000). In

particular, clear experimental records of capsize due to parametric rolling in following waves were published by one of the present authors (Umeda et al., 1995).

In case of head seas, however, prediction of parametric rolling is not so easy because coupling with dynamic heave and pitch is significant. In addition, the added resistance and the resulting speed loss cannot be simply ignored. So far, the effect of dynamic heave and pitch motions on parametric rolling was investigated by many researchers and it was well established. The existing research revealed that restoring arm variation depending on dynamic heave and pitch motions is essential for accurately predicting parametric roll in head waves (Taguchi et al., 2006). However, these theoretical works do not deal with the effect of added resistance on parametric rolling.



Umeda et al (2008) and Umeda&Francescutto (2008) executed numerical simulations of parametric rolling in regular and irregular head seas with added resistance taken into account, but their hydrodynamic prediction method for added resistance is different from that for restoring variation. Two of the present authors (Lu et al., 2011a) executed numerical simulation of parametric rolling in head seas with added resistance taken into account, in which both the restoring variation and the Kochin function for added resistance are calculated by a strip theory.

Added resistance in waves is mainly caused by energy dissipation when a ship generates radiation waves and diffraction waves on the ship hull (Kashiwagi et al., 2010). Maruo obtained an well-established formula for added resistance in waves, within linear potential theory, based on the principle of momentum and energy conservation (Maruo, 1963). In linear ship dynamics, the frequency of ship oscillations is equal to encounter frequency, without the consideration of roll, sway and yaw motions in longitudinal waves. Hosoda (1973) and Maruo&Iwase (1980) extended these methods to oblique waves with roll, sway and yaw taken into account. Parametric rolling could occur in head seas with half the encounter frequency, and occasionally the amplitude of parametric rolling is more than 40 degrees. All calculation methods of added resistance mentioned above seem not to include wave radiations due to parametric rolling in head seas, and the effect of parametric rolling on added resistance cannot be discussed. Two of the present authors (Lu et al., 2011b) extended Maruo's theory to study the effect of parametric rolling on added resistance in regular head seas, while the effect of parametric rolling on heave and pitch motions was ignored and the experimental studies with and without parametric rolling were not conducted.

Therefore, the authors attempted to use the extended formula based on Maruo's theory for added resistance with parametric rolling taken

into account to study the effect of parametric rolling on added resistance in regular head seas. Further, the model experiments were conducted to measure roll, heave, pitch motions and wave force in longitudinal direction with and without parametric rolling in regular head seas by a new experimental device.

2. THEORETICAL METHOD

The following formula based on Maruo's theory (Lu et al, 2011b) is used to calculate added resistance in regular head seas with parametric rolling taken into account.

$$\begin{aligned} \bar{R} = & \frac{\rho}{8\pi} \left[\int_{-\pi/2}^{\alpha_0} + \int_{\pi/2}^{\alpha_0} \right] |H(k_1, \alpha)|^2 \frac{k_1^2 (k_1 \cos \alpha - K \cos \chi)}{\sqrt{1-4\Omega \cos \alpha}} d\theta \\ & + \frac{\rho}{8\pi} \left[\int_{-\alpha_0}^{2\pi-\alpha_0} \right] |H(k_2, \alpha)|^2 \frac{k_2^2 (k_2 \cos \alpha - K \cos \chi)}{\sqrt{1-4\Omega \cos \alpha}} d\alpha \\ & + \frac{\rho}{8\pi} \left[\int_{-\pi/2}^{\alpha_0'} + \int_{\pi/2}^{\alpha_0'} \right] |H(k_1', \alpha')|^2 \frac{k_1' (k_1' \cos \alpha' - \frac{1}{2} K \cos \chi)}{\sqrt{1-4\Omega \cos \alpha'}} d\theta \\ & + \frac{\rho}{8\pi} \left[\int_{-\alpha_0'}^{2\pi-\alpha_0'} \right] |H(k_2', \alpha')|^2 \frac{k_2' (k_2' \cos \alpha' - \frac{1}{2} K \cos \chi)}{\sqrt{1-4\Omega \cos \alpha'}} d\alpha' \\ & - \frac{E_1}{\left(\frac{\omega_e}{K}\right)} \cos \chi - \frac{E_2}{\left(\frac{\omega_e}{K}\right)} \cos \chi - \frac{E_3}{\left(\frac{\omega_e}{K}\right)} \cos \chi \end{aligned} \quad (1)$$

where:

$$\alpha_0 = \begin{cases} 0 & (\Omega \leq 1/4) \\ \cos^{-1}\left(\frac{1}{4\Omega}\right) & (\Omega > 1/4) \end{cases}; \quad \alpha_0' = \begin{cases} 0 & (\Omega \leq 1/4) \\ \cos^{-1}\left(\frac{1}{4\Omega}\right) & (\Omega > 1/4) \end{cases} \quad (2)$$

U is ship's forward velocity, ω_0 is wave circular frequency, K is wave number, χ is the angle of wave incidence, ρ is the water density and $\chi = \pi$ corresponds to the heading sea. Here we define that the encounter frequency is $\omega_e = \omega_0 - kU \cos \chi$, the encounter period is T_e , the wavelength is λ for incident wave, diffraction wave and radiation waves due to heave, pitch and surge motions. At the same time, we also define that the frequency is $\omega_{e2} = 1/2\omega_e$, the period is T_{e2} , the wavelength is λ_2 for radiation waves due to parametric roll, sway and yaw motions.



The added resistance can be obtained by averaging forces within the duration that is double the encounter period. According to energy dissipation by viscous roll damping force, the follow equations can be obtained:

$$\begin{aligned} E_1 &= 0 \\ E_2 &= 0 \\ E_3 &= \int_0^{2T_e} (B_{44\phi_a} \dot{\phi}_{roll}) \dot{\phi}_{roll} dt \end{aligned} \quad (3)$$

where ϕ_a is the amplitude of parametric rolling, $B_{44\phi}$ is the viscous roll damping force, $\dot{\phi}_{roll}$ is the angular velocity of parametric rolling. E_3 can be obtained by following formula (Katayama et al.,2010):

$$E_3 = \pi B_{44\phi_a} \phi_a^2 \left(\frac{1}{2} \omega_e\right) \quad (4)$$

Both k_1 wave and k_2 wave are used for incident wave, diffraction wave and radiation waves due to heave, pitch and surge motions.

$$\begin{aligned} k_j &= \frac{K_0 \cdot (1 - 2\Omega \cos \alpha \pm \sqrt{1 - 4\Omega \cos \alpha})}{2 \cos^2 \alpha} \\ (+ \text{for } j=1, - \text{for } j=2, \Omega &= \frac{\omega_e U}{g}, K = \frac{\omega_0^2}{g}, K_0 = \frac{g}{U^2}) \end{aligned} \quad (5)$$

Both k_1 wave and k_2 waves are used for radiation waves due to parametric roll, sway and yaw motions.

$$\begin{aligned} k_j &= \frac{K_0 \cdot (1 - 2\Omega \cos \alpha \pm \sqrt{1 - 4\Omega \cos \alpha})}{2 \cos^2 \alpha} \\ (+ \text{for } j=1, - \text{for } j=2, \Omega &= \frac{\omega_e U}{g} = \frac{1}{2} \Omega, K_0 = \frac{g}{U^2}) \end{aligned} \quad (6)$$

The Kochin function can be calculated by formula (7), if singularity distributions ($\mu(x)$ and $\sigma(x)$) along the centre line of ship submerged with the depth of $z(x)$ are properly provided.

$$\begin{aligned} H(k_i, \alpha) &= \int_L \sigma(x) e^{-k_i z(x)} e^{i k_i x \cos \alpha} dx \\ &+ \int_L i \mu(x) e^{-k_i z(x)} k_i' \sin \alpha e^{i k_i' x \cos \alpha} dx \end{aligned} \quad (7)$$

Based on the comparisons of calculated added resistance by different methods of source distribution $\sigma(x)$ for the modified Wigley model (Lu et al., 2011b), it can be concluded that Maruo and Ishii's method (Maruo and Ishii, 1976) is the most appropriate for the region where parametric rolling could appear. Maruo and Ishii's formula can be described with the two-dimensional Kochin function of heave as follows:

$$\sigma(x) = -H_2^+(x) \times (i \omega_e U \frac{\partial}{\partial x}) (Z_G - x \Theta - \zeta_w) + H_2^+(x) \times U \frac{\dot{B}(x)}{B(x)} (Z_G - x \Theta - \zeta_w), \quad z=0 \quad (8)$$

where $\sigma(x)$ is the source distribution, $Z_G e^{i \omega_e t}$ is the heaving, $\Theta e^{i \omega_e t}$ is the pitching, $\zeta_w e^{i \omega_e t}$ is the wave elevation, $H_2^+(x)$ is the two-dimensional Kochin function in heave, $B(x)$ is the ship breadth at x section and $\dot{B}(x) = \partial B(x) / \partial x$.

For calculating doublet distribution $\mu(x)$, Maruo and Iwase's method (Maruo and Iwase, 1980) is used, which can be described with the two-dimensional Kochin function of sway ($H_1^+(x)$) as follows:

$$\mu(x) = \frac{-1}{2k_e} H_1^+(x) \times \left\{ \frac{1}{B(x)} \left(\frac{\partial}{\partial t} - U \frac{\partial}{\partial x} \right) [B(x) (Y_G - x \psi + |l_w| \phi)] - V_w \right\} \quad (9)$$

where $Y_G e^{i \frac{1}{2} \omega_e t}$ is the swaying, $\psi e^{i \frac{1}{2} \omega_e t}$ is the yawing, $\phi e^{i \frac{1}{2} \omega_e t}$ is the rolling and V_w is the wave particle velocity in y direction.

In this paper, however, the effect of only parametric rolling in head seas is investigated during numerical calculation. The doublet distribution $\mu(x)$ can be rewritten as follow:

$$\mu(x) = \frac{-1}{2k_e} H_1^+(x) \times \left[i \left(\frac{1}{2} \omega_e \right) |l_w| \phi_0 - U \frac{\dot{B}(x)}{B(x)} |l_w| \phi_0 \right] \quad (10)$$

3. EXPERIMENTS

The partially restrained experiment with a 1/65.5 scaled model of the post Panamax C11



class containership were conducted in the seakeeping basin (length: 69m, breadth: 46m, depth: 4m) of China Ship Scientific Research Center, which is equipped with flap wave makers at the two adjacent sides of the basin.

The partially restrained ship model was towed by the towing carriage in regular head seas and a newly designed equipment was used to measure ship motions including roll, pitch and heave motions and exciting wave moment/force including roll moment, yaw moment, sway force and surge force. Roll and pitch motions were measured by potentiometer sensor. Heave motion was measured by displacement sensor. Roll moment, yaw moment, sway force and surge force were measured by four sensors based on electromotive strain gauge.

The principal particulars and body plan of the C11 class containership are shown in Table1 and Fig.1, respectively. The ship model in partially restrained experiment is shown in Fig.2.

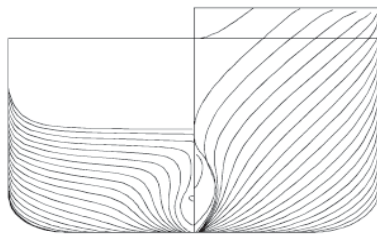


Figure 1 Lines of C11 containership

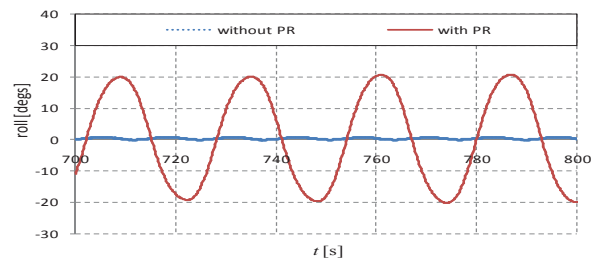
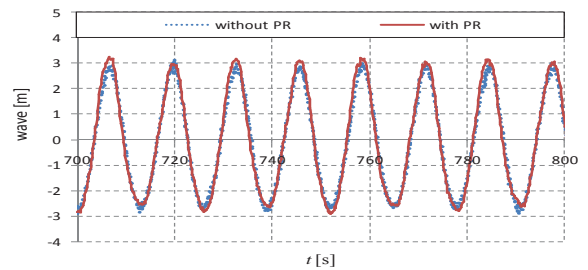


Figure 2 The ship model in partially restrained experiment

Table 1 Principal particulars of the C11 containership

Items	Ship	Model
Length:L	262.0m	4.000m
Draft:T	11.5m	0.176m
Breadth:B	40.0m	0.611m
Depth:D	24.45m	0.373m
Displ.:W	67508ton	240.2kg
C_B	0.560	0.560
GM	1.928m	0.029m
T_ϕ	24.68s	3.05s
K_{YY}	0.24L	0.24L

4. RESULTS AND DISCUSSION



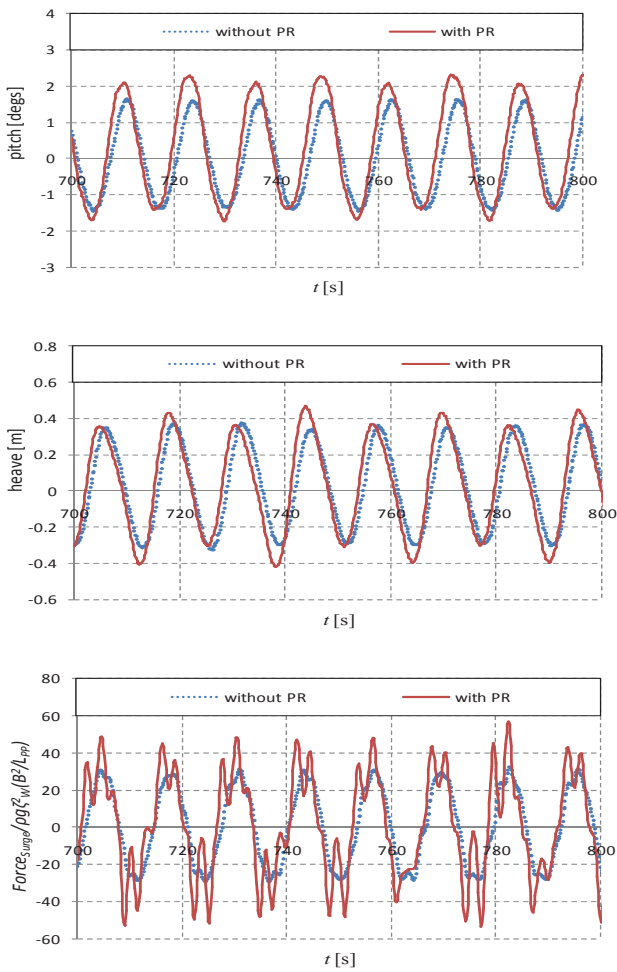


Figure 3 Comparisons of wave, roll, pitch, heave and surge force in time series between with and without parametric rolling in experiments, with $F_n=0.0$, $H/\lambda=0.02$, $\lambda/L_{pp}=1.0$ and $\chi=180$ degs.

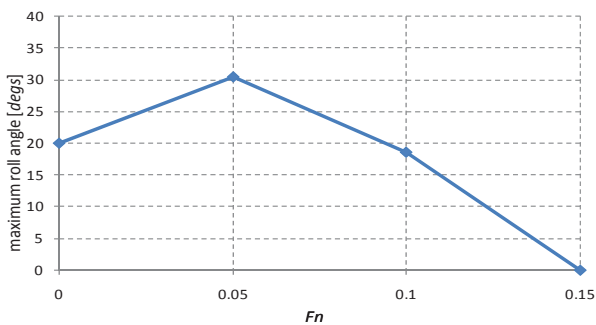


Figure 4 Parametric rolling in experiment as the function of Froude number with $\lambda/L_{pp}=1.0$, $H/\lambda=0.02$ and $\chi=180$ degs.

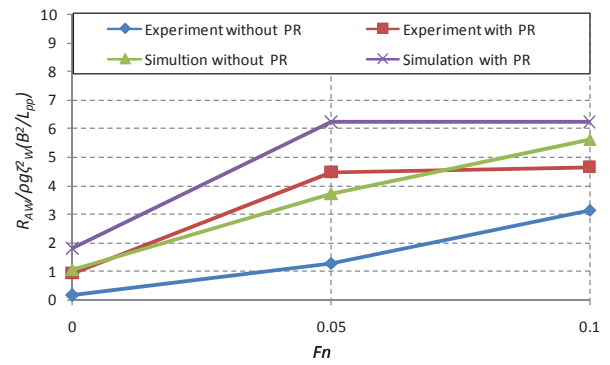


Figure 5 Added resistance with and without parametric rolling in experiments and simulations as the function of the Froude number with $\lambda/L_{pp}=1.0$, $H/\lambda=0.02$ and $\chi=180$ degs.

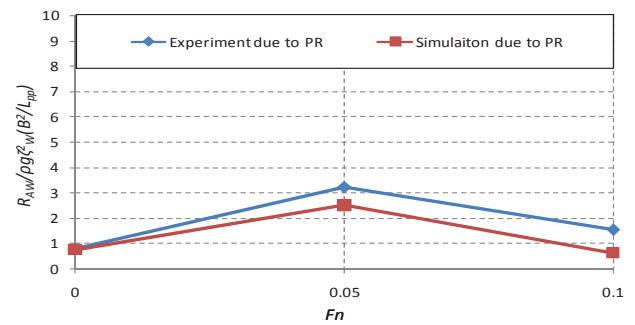


Figure 6 The component of added resistance resulted from parametric rolling in experiments and simulations as the function of the Froude number with $\lambda/L_{pp}=1.0$, $H/\lambda=0.02$ and $\chi=180$ degs.

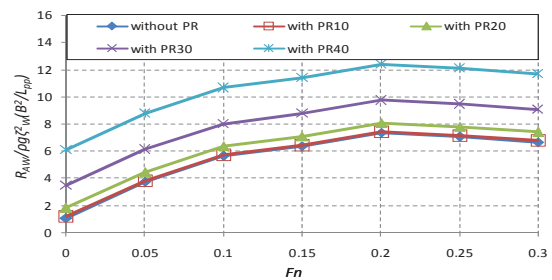
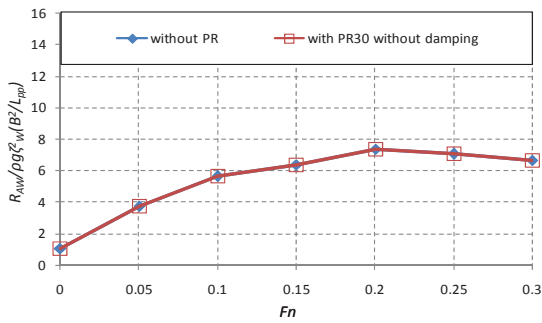


Figure 7 Calculated added resistance with different amplitudes of parametric rolling as the function of the Froude number with $\lambda/L_{pp}=1.0$, $H/\lambda=0.02$ and $\chi=180$ degs.



- Figure 8 Calculated added resistance with parametric rolling and without roll damping force, as the function of the Froude number with $\lambda/L_{pp}=1.0, H/\lambda=0.02$ and $\chi=180$ degs.

We compare heave, pitch, roll motions and surge force containing resistance with and without roll motion in experiment. An example of time series is shown in Fig. 3. When parametric rolling occurs with amplitudes of 20 degrees, heave and pitch motions are affected by parametric rolling and their large and small amplitudes alternatively appear. This phenomenon seems like “subharmonic pitch” and “subharmonic heave” (Neves et al., 2009; Lu et al., 2013, 2014). The phase difference of heave and pitch motion are also small changed as shown in Fig.3. This indicates that both the amplitude and phase difference of heave and pitch motions are distinctly affected by parametric rolling. The surge force is also affected when parametric rolling occurs with amplitudes of 20 degrees as shown in Fig.3. Heave and pitch motions are main cause of added resistance in waves. Therefore added resistance in waves could be affected by parametric rolling. Here we only show the experimental results of time series at zero speed, because the towing carriage has mechanical vibrations with forward speed.

Parametric rolling in regular head seas, as a function of the Froude number, was measured by the partially restrained experiment of C11 containership as shown in Fig.4, and the values of parametric rolling in experiments are used during the numerical simulations of added resistance in waves. The added resistance in

experiments is obtained by subtracting the resistance in calm water from the averaged surge force. Both the experiment and numerical simulation show that the difference of added resistance with and without parametric rolling is not negligible, as shown in Fig.5. The component of added resistance resulted from parametric rolling in experiments and simulations is shown in Fig. 6. Although the calculated results are general larger than experimental results, the tendency of the effect of parametric rolling on added resistance in waves is the same. Here the viscous roll damping coefficient was estimated by roll decay test of the ship model.

In order to investigate the reason, the added resistance was calculated without parametric rolling and with different amplitudes of parametric rolling, as the function of the Froude number. The results shown in Fig.7 indicate that the effect of parametric rolling on added resistance in regular head seas becomes larger as the amplitude of parametric rolling becomes larger. The calculated added resistance with parametric rolling and without viscous roll damping force, as a function of the Froude number, is shown in Fig.8. The effect of parametric rolling on added resistance in regular head seas within a potential flow theory is very small, and it supports Maruo and Iwase's(1980) conclusion in oblique waves, that is to say, the effect of rolling on added resistance is generally small. This means that the major effect of parametric rolling is viscous roll damping. It is noted here the effect of large parametric rolling on heave and pitch motions in simulations is ignored. Heave and pitch motion are main cause of added resistance in waves. Both the amplitude and phase difference of heave and pitch motions are distinctly affected by parametric rolling as show in Fig.3, which could be one of reasons why the added resistance in experiments is smaller than that in simulations as shown in Fig 6.



5. CONCLUSIONS

As a result of experimental and numerical study on the effect of parametric rolling on added resistance in regular head seas for a containership, the following remarks are noted:

1) An extended formula based on Maruo theory for added resistance in head seas with parametric rolling taken into account can be used to study the effect of parametric rolling on added resistance in regular head seas.

2) The effect of parametric rolling on added resistance in regular head seas mainly is due to viscous roll damping and it becomes larger as the amplitude of parametric rolling becomes larger.

Future research is desirable to validate the effect of heave and pitch motion on added resistance while parametric rolling occurs.

6. ACKNOWLEDGEMENTS

Part of this research was once supported by China Scholarship Council [No.2008606031] for the first author's visit to Osaka University. Prof. M. Kashiwagi from Osaka University provided the authors with his useful advice on the theoretical calculation of added resistance in waves. The research is supported by Ministry of Industry and Information Technology of China (No. [2012] 533). The authors sincerely thank the above organizations.

7. REFERENCES

Hosoda, R., 1973, "The Added Resistance in Oblique Waves", Journal of the Society of Naval Architects of Japan, Vol.133,pp.7-22.

Kashiwagi, M., Ikeda, T. and Sasagawa, T., 2010, "Effect of Forward Speed of a ship on Added Resistance in waves", International Journal of Offshore and Polar Engineering, Vol.20(2),pp.1-8.

Katayama, T., Taniguchi, T., and Umeda, N., 2010, "An Experiment Study on Parametric Rolling of a High Speed Trimaran in Head Seas", Journal of the Society of Naval Architects of Japan, Vol. 10, pp.57-63.

Lu, J., Umeda, N. and Ma, K., 2011a. "Predicting parametric rolling in irregular head seas with added resistance taken into account", Journal of Marine Science and Technology, Vol.16, pp.462-471.

Lu, J., Umeda, N. and Ma, K., 2011b. "Theoretical Study on the Effect of Parametric Rolling on Added Resistance in Regular Head Seas", Journal of Marine Science and Technology, Vol.16,pp.283-293.

Lu, J., Min, G. and Umeda, N., 2013, "A Study on the Effect of Parametric Rolling on Heave and Pitch Motions in Head Seas", Proceedings 13th International Ship Stability Workshop, pp.185-191.

Lu, J., Min, G. and Umeda, N., 2014, "Experimental and Numerical Study on Predicting Method of Parametric Rolling in Regular Head Seas", Proceedings 14th International Ship Stability Workshop, pp.117-125.

Maruo, H., 1963. "Resistance in Waves", Chap.5 in Researches on Seakeeping Qualities of Ships in Japan, Soc. Nav. Arch. Japan 60th Anniv. Ser., No. 8, pp.67-102.

Maruo, H. and Ishii, T.,1976, "Calculation of Added Resistance in Head Sea Waves by Means of a Simplified Formula", Journal of the Society of Naval Architects of Japan, Vol.140,pp.136-141.

Maruo. H. and Iwase,K., 1980, "Calculation of Added Resistance in oblique Waves", Journal of the Society of Naval Architects of Japan, Vol.147,pp.79-84(in Japanese).

Munif, A. and Umeda, N. 2000, "Modeling Extreme Roll Motions and Capsizing of a



Moderate-Speed Ship in Astern Waves”,
Journal of the Society of Naval Architects
of Japan, Vol. 187, pp. 405-408.

Neves, Ma.A.S., Vivanco, J.E.M. and
Rodriguez, C.A., 2009, “Nonlinear
Dynamics on Parametric Rolling of Ship in
Head Seas”, Proceedings 10th STAB,
pp.509-520

Taguchi, H., Ishida, S., Sawada, H. and Minami,
M., 2006, “Model Experiment on
Parametric Rolling of a Post-Panamax
Containership in Head Waves”,Proceedings
9th STAB, pp.147-156.

Umeda, N., Hamamoto M., Takaishi, Y., Chiba,
Y., Matsuda, A., Sera W. , Suzuki S. ,
Spyrou K. and Watanabe, K., 1995,
“ Model Experiments of Ship Capsize in
Astern Seas”, Journal of the Society of
Naval Architects of Japan, Vol.177,pp.207-
217.

Umeda, N., Hashimoto, H., Frederick, S.,
Nakamura, S., Seyed, H.S.H., Matsuda, A.
and Pablo, C. 2008, “Comparison Study on
Numerical Prediction Techniques for
Parametric Roll”, Proceedings of the 27th
Symposium on Naval Hydrodynamics,
Seoul,pp.5-10.

Umeda, N. and Francescutto, A., 2008,
“Performance-Based Ship Operation”,Proc
2nd International Workshop on Risk-Based
Approaches in Maritime Industry,2.2.1-
2.2.9.

Session 10.1 – 2nd GENERATION INTACT STABILITY

A Study on Roll Damping Time Domain Estimation for Non Periodic Motion

Investigation of the 2nd Generation of Intact Stability Criteria in Parametric Rolling and Pure Loss of Stability

Requirements for Computational Methods to be Used for the IMO Second Generation Intact Stability Criteria

This page is intentionally left blank



A Study on Roll Damping Time Domain Estimation for Non Periodic Motion

Toru Katayama, *Graduate school of Engineering, Osaka Prefecture University*

katayama@marine.osakafu-u.ac.jp

Jun Umeda, *National Maritime Research Institute, Japan*

umeda@nmri.go.jp

ABSTRACT

In this study, the memory effects of bilge keel component of roll damping in irregular rolling are investigated by numerically. First, in order to validate the results of numerical simulation, a forced irregular roll motion test is carried out, and the characteristics of the memory effects are also confirmed. Second, the mechanism of the memory effects is made clear by the numerical simulation. Finally, based on the simulation results, the roll damping time domain estimation, which is proposed by Katayama et al. (2013) based on the prediction method proposed by Ikeda et al. (1978), is improved.

Keywords: *Roll damping, Memory effects, Transient Effects, Previous Amplitude Effects, Time domain estimation, Non periodic motion*

1. INTRODUCTION

In order to guarantee the safety of vessels, it is important to estimate roll damping accurately. It is well known that there is a prediction method of the roll damping proposed by Ikeda et al. (1978). However, it is indicated by the previous studies that there are some problems in Ikeda's method. Ikeda's method is developed with theoretical and experimental backgrounds for periodical roll motion. Therefore, it is difficult to apply it to a time domain simulation of transitional and irregular roll motions.

In the previous studies (Ikeda et al., 1988, Katayama et al., 2010), it is pointed out that the memory effects of roll damping are necessary to consider for time domain simulations of non-periodical roll motions. Ikeda et al. (1988) show through experiments that the drag coefficient on flat plate increased in the first

few oscillations when the flat plate is started rest (it is called the transient effects in this paper). An additional valuable observation reports from the experiments by Ikeda et al. (1988) is that the memory effects remain important in irregular motion. When an oscillation has a larger amplitude than the oscillation after it, then the drag coefficient is larger than at a steady oscillation amplitude (it is called the memory effects in this paper). Katayama et al. (2010) investigate the effects of transient motion on the drag force of a flat plate. In the region of $KC < 250$, the drag coefficient for acceleration in one direction is larger than the drag coefficient for acceleration in a uniform flow and smaller than that in a steady oscillatory flow. Moreover, in a transient condition under forced oscillation, the drag coefficients from the first to the third oscillation are smaller than that in a steady oscillatory flow. Katayama et al. (2013) propose a time domain estimation method

which is an improved Ikeda's method of bilge-keel component of roll damping based on the results of Katayama et al. (2010). However the improved method include only the transient effects and it is required to include the memory effects.

In this study, the bilge-keel component of roll damping for non-periodic motion is focused. The memory effects is investigated by numerically. First, a forced roll motion test with irregular motion is carried out, and the characteristics of the memory effects are confirmed and the numerical simulation is validated. Second, the mechanism of the memory effects is made clear by the numerical simulation. Finally, based on the CFD results, the roll damping time domain prediction method, which is proposed by Katayama et al. (2013) including the transient effects based on Ikeda's method (1978), is improved.

2. FORCED IRREGULAR ROLL MOTION TEST

2.1 Model and Measurement

In order to investigate the memory effects and take some validation data for the numerical simulation, forced roll motion measurements are carried out at the towing tank of Osaka Prefecture University (length 70m, breadth 3m, depth 1.5m).

Table 1 and Figure 1 show a body plan and principal particulars of a two dimensional model. The model is attached to end plate in order to remove three dimensional effects.

The model is given forced roll moment by the forced irregular roll motion device shown as figure 2, and it is putted on the centre line of the model. The device has three axis of rotation and three rods attached weights are rotated in the horizontal plane at different periods. In the measurement, roll motion and

rotating positions of rods are measured in sampling frequency 100Hz.

Table 2 shows the conditions in the measurement. The measurements at systematically changed forced roll periods and drafts are carried out. In order to reduce wave making component, forced roll period is more than 1.2sec.

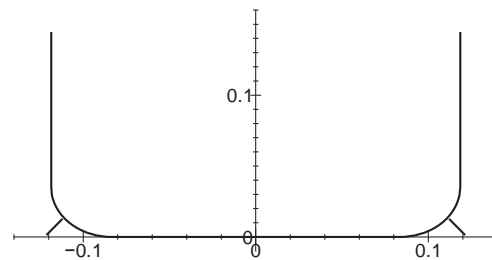


Figure 1 Section of the two dimensional model.

Table 1 Principal particulars of the two dimensional model.

L_{PP} [m]	0.80
B [m]	0.235
D [m]	0.145
Bilge radius [deg]	0.035
Bilge keel [m × m]	0.01 × 0.80



Figure 2 Forced irregular roll motion device.

Table 2 Conditions in the measurement.

height of roll axis [mm]	96
draft [mm]	96, 80, 72, 57
forced roll period [sec]	1.60-1.28, 1.80-1.44
device from roll axis [mm]	119
A mass of weight [g]	150
attached position of weight from centre of rotation [mm]	50

2.2 CFD Calculation

In the tank test, it is difficult to visualize flow around hull and divide the measured hydrodynamic forces into the each component, which are the normal component and the hull surface pressure component of the bilge keel component. In this study, bilge keel component calculated by CFD (Fluent) is divide into the each component and the memory effects on the each component is investigated.

In the calculation, the two dimensional model is given the roll motion expressed by Eq. (1), and roll moment acting on hull is calculated.

$$\phi(t) = \phi_{a1} f_1(t) \sin \omega_1 t + \phi_{a2} f_2(t) \sin \omega_2 t$$

$$f_i(t) = \begin{cases} \frac{1}{2} \sin\left(\frac{1}{4} \frac{\pi}{T_i} t - \frac{1}{2} \pi\right) + \frac{1}{2} & (\text{for } t \leq 4T_i) \\ 1 & (\text{for } t > 4T_i) \end{cases} \quad (1)$$

Eq.(1) can almost express the measured roll motion in the forced irregular roll motion test in the limited cases, which is small amplitude irregular motion caused by two rods. Table 3 shows the calculation conditions and settings.

Table3 Calculation conditions.

Numerical solver	implicit unsteady first order
Viscous model	$k-\varepsilon$ model
Solution algorithm	SIMPLE
Multiphase model	VOF, Geo-reconstructed
Gradient	Least Squares Cell Based
Discretization scheme	Second order Upwind
Interpolation scheme	PRESTO!
Draft[mm]	96
Forced roll period[sec] and amplitude[deg]	2.00-1.2sec and 8.0-5.0deg 1.20-0.67sec and 5.0-5.0deg 1.80-2.00sec and 10.0-8.0deg 1.60-2.00sec and 8.0-6.0deg 1.40-1.8sec and 8.0-6.0deg 1.60-1.28sec (measured) 1.80-1.44sec (measured)

2.3 Analysis of Roll Damping

The roll motion in the measurement and the calculation is expressed as Eq. (2).

$$A_{44} \ddot{\phi}(t) + B_{44} \dot{\phi}(t) + C_{44} \phi(t) = M_E \quad (2)$$

Where the first term of left side of the equation is moment of inertia including added moment of inertia, the second term is the roll damping moment, the third term is the restoring moment and M_E is forced roll moment. It should be noted that A_{44} , B_{44} and C_{44} are not constant value for each time step.

In the measurement, the forced roll moment is given by the forced irregular roll motion device. The given moment can be calculated as follow. Figure 3 shows schematic view and coordinate system.

$$\begin{aligned} x &= r \cos \omega t \\ y &= r \sin \omega t \cos \phi + h \sin \phi \\ z &= h \cos \phi - r \sin \omega t \sin \phi \end{aligned} \quad (3)$$

Kinetic energy and potential energy of weights caused by rotation of weights and roll motion of hull are expressed as Eq. (4) and (5).

$$T = \frac{1}{2} m \{ r^2 \omega^2 + (h^2 + r^2 \sin^2 \omega t) \dot{\phi}^2 + 2hr\omega\dot{\phi} \cos \omega t \} \quad (4)$$

$$U = mg(h \cos \phi - r \sin \omega t \sin \phi) \quad (5)$$

The forced roll moment caused by weights can be obtained from applying Lagrange equation of motion to these energy.

$$\begin{aligned} m_{Ei} &= -mr^2 \sin^2 \omega t \ddot{\phi} \\ &\quad - 2mr^2 \omega_i \dot{\phi} \sin \omega_i t \cos \omega_i t \\ &\quad + mg(h \sin \phi + r \sin \omega_i t \cos \phi) \\ &\quad + mr\omega_i^2 h \sin \omega_i t \end{aligned} \quad (6)$$

C_{44} in Eq.(2) is obtained by the calculated G_z curve corresponding to the roll angle. The

roll angle removed noises by low-pass filter (10Hz) from the measured ones is used in Eq.(2). And roll angular velocity and acceleration obtained from differentiating numerically the filtered roll angle are used in Eq.(2). A_{44} and B_{44} in Eq. (2) are obtained to satisfy the Eq. (2). In concrete terms, the coefficients (A_{44} and B_{44}) at certain time t are decided by using least square method to time history data (data number n) from the starting position where angular velocity of roll is zero to a certain time. Roll damping is obtained in time domain due to decide the coefficients (A_{44} and B_{44}) changed in time step while increasing data number n .

On the other hand, in the calculation, the roll motion expressed by Eq. (1) is given, and the roll moment acting on hull M_E is calculated. The roll damping is obtained from the same way as the above-mentioned method.

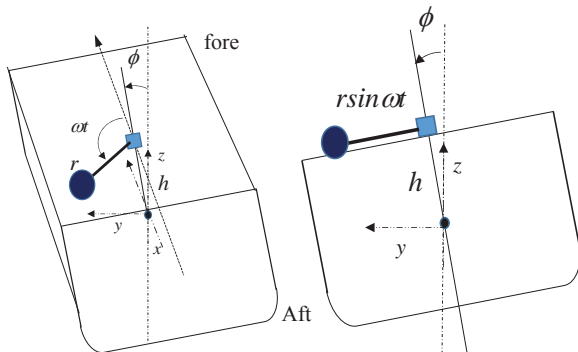


Figure 3 Schematic view of forced irregular motion test.

3. MEMORY EFFECTS

3.1 Comparison of Measured and Calculated results

An example of the comparison between measured and calculated roll damping is shown in Figure 4. The upper and bottom figures of Figure 4 show the time histories of roll angle and roll damping, respectively. The calculated result is good agreement with that of the measured result. It is confirm that roll

damping under irregular motion can be calculated accurately by CFD.

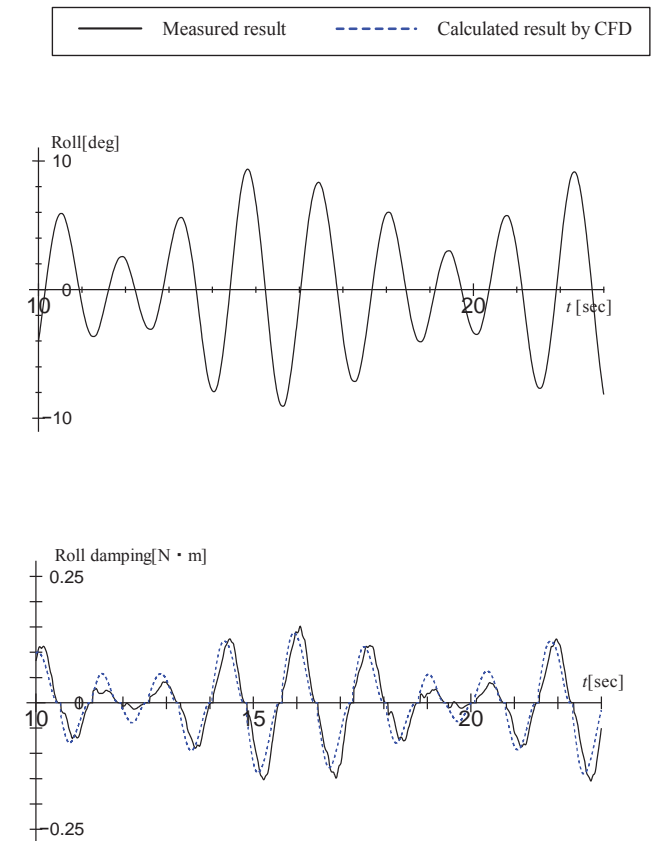


Figure 4 Comparison of measured and calculated roll damping.

3.2 Memory Effects on Normal Force Component

It is confirm that the vortex created by previous swing affects drag force acting on flat plate in present swing by Katayama et al. (2010) and it is assumed that bilge keel component may be affected by the memory effects.

In this section, bilge keel component calculated by CFD is divide into normal force component and hull surface pressure component and the memory effects on normal force component is investigated. Normal force component is the moment due to drag force acting on bilge keel. And the result by CFD is compared with the result estimated by the time

domain estimation proposed by Katayama (2013).

An example of the comparison between calculated and estimated roll damping is shown in Figure 5. The upper, middle and bottom figure of Figure 5 show time history of roll damping, time history of roll damping coefficient and Kc number for half cycle, respectively. When Kc number of the previous swing is larger than Kc number of the present swing, the calculated damping coefficient is larger than the estimated result. On the other hand, when Kc number of the previous swing is smaller than Kc number of the present swing, the calculated damping coefficient is good agreement with the estimated result. Therefore, when Kc number of the previous swing is larger than Kc number of the present swing, the memory effects must be considered in estimation method of normal force component.

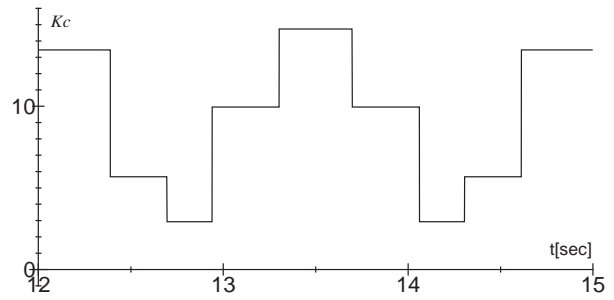
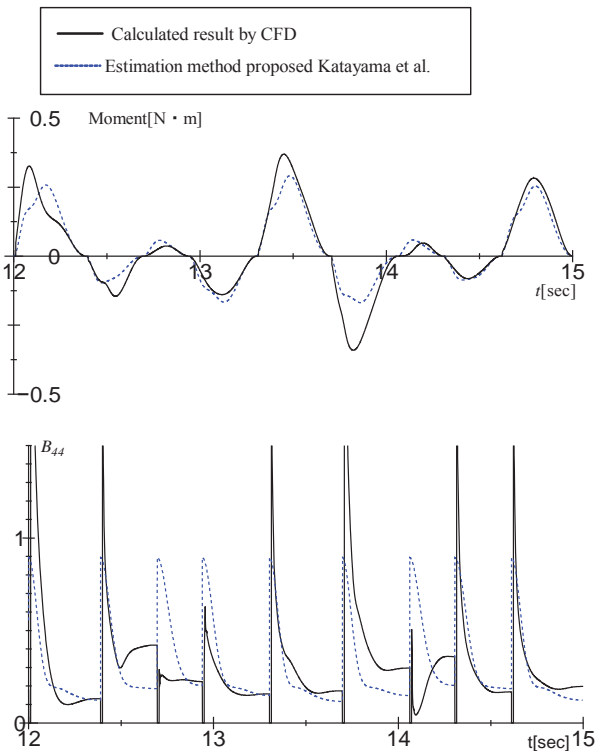


Figure 5 Previous amplitude effects on normal force component shown by comparison between the calculated result of CFD and the estimated result by the estimation method proposed by Katayama et al., (2014).

3.3 Memory Effects on Hull Surface Pressure Component

An example of roll damping coefficients of hull surface pressure component in time domain is shown in Figure 6. It is confirmed that the values are different even if Kc number of the present swing is the same. When Kc number of the previous swing is larger than Kc number of the present swing, the damping coefficient is larger. Therefore, it is also need to consider the memory effects on hull surface pressure component.



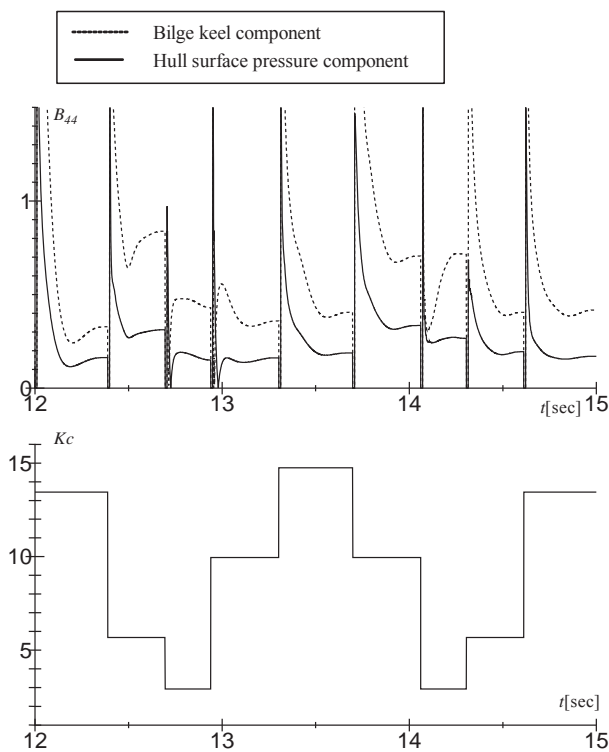
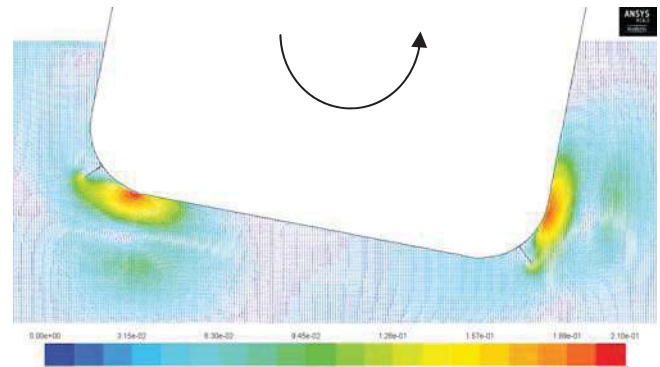


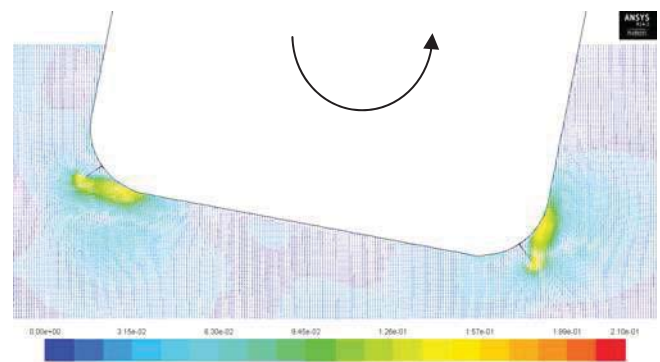
Figure 6 Memory effect for hull surface pressure component calculated by CFD.

3.4 Visualization of Flow around Hull

Flow field around hull is visualized in order to understand the mechanism of the memory effects. Figure 7 shows the velocity vectors around hull at the starting position of swing, and the direction of motion velocity of hull. The scales of these colour contour and arrow figures are the same and these show velocity magnitude. From figure 7(a) and (b), it is found that the fluid in front of bilge keels is given velocity due to the vortexes developed by the previous swing. The fluid velocity in front of bilge keel in the Figure 7 (a) is faster than that in the Figure 7 (b), because Kc number of previous swing of (a) is larger than Kc number of previous swing of (b) and the vortexes developed by previous swing of (a) are larger than that developed by the previous swing of (b). The moment due to the bilge keel is increased by increase of the relative velocity of the fluid in front of bilge keel. Therefore, the memory effects depends on Kc number in previous swing and in present swing.



(a) Kc number of previous swing is 19.61



(b) Kc number of previous swing is 9.35

Figure 7 Calculated velocity vectors around hull starting position of swing for various Kc numbers of previous swing.

4. ROLL DAMPING TIME DOMAIN ESTIMATION

4.1 Time domain Estimation Considering Memory effects

It is confirmed that the memory effects must be considered in time domain estimation of bilge keel component and the memory effects depends on Kc number in previous swing and in present swing. Therefore, the estimation method considering Kc number in previous swing and in present swing is proposed.

The normal force component is calculated by Eq.(7) using a drag coefficient of flat plate under one direction accelerating expressed by Eq.(11) (Katayama et al. (2010)). The hull surface pressure component is calculated by Eq.(8). The coefficient C_P in Eq.(8) is divided into the pressure coefficient C_P^+ on front face of bilge-keels and the pressure coefficient C_P^- on back face of bilge-keels. And the pressure coefficient C_P^- is calculated by Eq.(9) using C_D expressed by Eq.(2). The hull surface pressure component can be obtained from the integration which is shown in Figure 8. Length of negative pressure region S_0 , depends on the Kc number, and it is defined by Eq.(12).

$$M_{BKN} = \frac{1}{2} \rho l_{BK} b_{BK} m C_D l^2 \dot{\phi} |\dot{\phi}| l f^2 \quad (7)$$

$$M_{BKH} = \frac{1}{2} \rho l^2 f^2 \dot{\phi} |\dot{\phi}| \int_G C_P \cdot l_p dG \quad (8)$$

$$C_P^- = C_P^+ - m C_D = 1.2 - m C_D \quad (9)$$

$$S_0 / b_{BK} = 0.3 \left(\frac{\pi l \phi}{b_{BK}} \right) f + 1.95 \quad (10)$$

$$C_D = \left(\begin{array}{l} 14.3e^{-1.80Kc_d} + 4.41e^{-0.37Kc_d} + \\ -10.4e^{-1.03Kc_d} - 0.30e^{-0.17Kc_d} + 1.0 \end{array} \right) \times \left(0.908 + \frac{1.2}{1+1.01^{Kc_d}} \right) \times 2.1 \quad (11)$$

$$(0 < Kc_d \leq 250)$$

$$Kc = Kc_d = \frac{\pi l \phi}{b_{BK}} \quad (12)$$

Where l_{BK} and b_{BK} is the length and breadth of the bilge-keel and l is the distance from the roll axis to the tip of the bilge-keel. f is a correction factor to take account of the increment of flow velocity at the bilge. m is a memory effect factor. The memory effects on normal force component is considered by the memory effect factor in Eq.(7) and the memory effects on hull surface pressure component is considered by the coefficient C_P^- in Eq.(9).

In order to investigate the memory effects factor, the ratio of roll damping coefficients estimated by using Eq. (11) to the coefficients

of normal force component at the velocity is maximum are obtained. When Kc number of the previous swing is smaller than Kc number of the present swing, it is assumed that the memory effects factor equal 1.0.

Figure 9 shows the memory effects factor vs. difference of Kc number between previous swing and in present swing. In order to decide the memory effects factor, a fitting curve is obtained from the results. The memory effects factor is expressed as the following equation.

$$m = 0.0129(Kc_{previous} - Kc_{present})^2 + 0.0647(Kc_{previous} - Kc_{present}) + 1 \quad (12)$$

$$Kc_{previ} - Kc_{present} > 0$$

Where $Kc_{prev.}$ is Kc number in previous swing and Kc_a is Kc number in present swing.

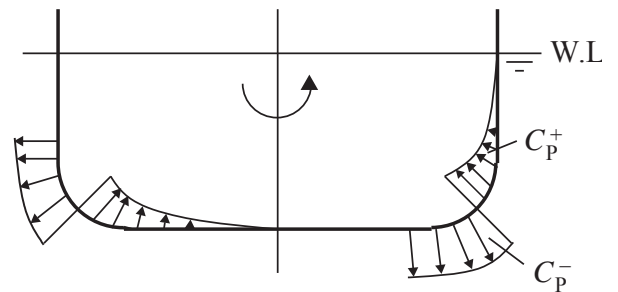


Figure 8 Assumed pressure distribution on the hull surface created by bilge-keels.

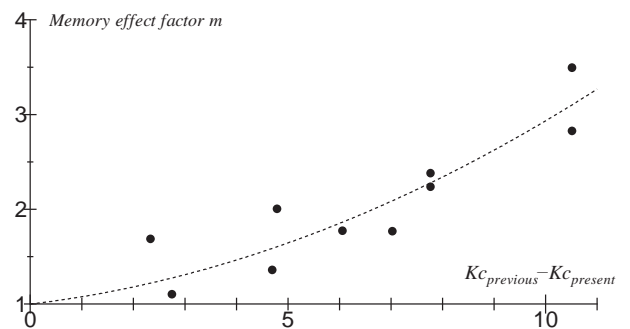


Figure 9 The memory effects factor vs. difference of Kc number between previous swing and in present swing.

4.2 Comparison with Measured Result

Figure 10 shows the result estimated by the proposed method and the result calculated by CFD and the measured result. In the case, the results show that the estimated result is good agreement with the measured and the calculated results. It is confirmed that roll damping can be estimated in time domain by using the method considering the memory effects.

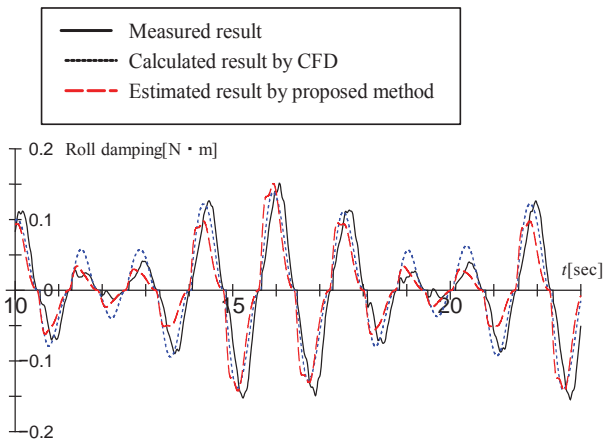


Figure 10 Comparison of estimated and calculated and measured result

5. NUMERICAL SIMULATION USING PROPOSED METHOD

5.1 The Subject Ship and Calculation method

By utilizing the numerical simulation model (H. Hashimoto et al., 2010), the effects of rolling in irregular waves is calculated to investigate the effects of the proposed method.

Fig.11 and Table 4 shows body plan and principal particulars of the subject ship.

In order to investigate effects of different roll damping estimation methods, in the simulation, roll damping component is estimated by two methods. The first one is a simplified method using Ikeda's original method which is used originally (the following section it is called the

previous method) in the numerical simulation, and the other one is the proposed method in this study, which includes the estimation method for bilge-keel component by using the roll damping coefficient considering the memory effects in time-domain.

In the previous method, roll damping is estimated at changed roll amplitudes systematically in roll natural period by Ikeda's original method. And roll damping in the simulation is calculated by interpolation of the results. The roll amplitude is calculated by Eq.(13) with the roll angle and the roll angular velocity in each time step.

$$\phi_a = \sqrt{\phi^2 + \left(\frac{2\dot{\phi}}{\omega_e}\right)^2} \quad (13)$$

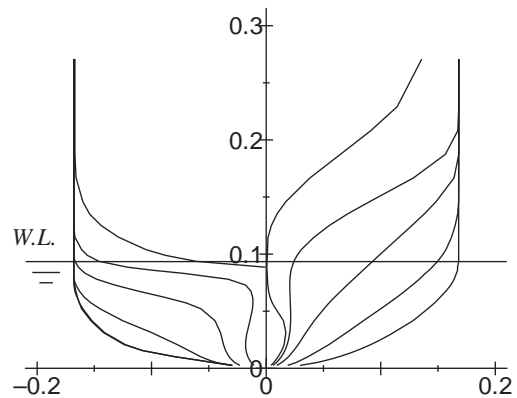


Figure 11 Body plan of the subject ship.

Table 4 Principal particulars of the subject ship.

L_{PP}	192.0 m
B	32.26 m
d	9.0 m
Speed	7knot
Height of gravity: KG	17.0 m
Metacentric height: GM	1.89 m
Natural roll period: T_ϕ	18.42 sec
Displacement: W	27205 ton
Breadth of bilge-keels	0.7 m
Position of bilge-keels	s.s. 3.34-s.s. 5.59

The simulation is carried out at $F_n = 0.083$ in irregular head waves whose significant wave height is 6.0m for 120 minutes (real time scale). The spectrum of irregular wave is the ITTC spectrum expressed by Eq.(14).

$$S(\omega) = 0.0081 \times \frac{g^2}{\omega^5} \exp\left(\frac{-3.11}{H_{1/3}^2 \times \omega^4}\right) \quad (14)$$

The making irregular waves is same and roll motions in time histories are compared between two methods and the effect of the difference of estimation methods on prediction of the parametric rolling.

5.2 Results of Simulations

Figure 12 shows an example of the comparison between the two calculated roll motions in time. The bottom of figure 10 shows the wave elevation at the midship. In this figure, the ratios of mean encounter wave period to the roll natural period (\bar{T}_e / T_ϕ) at T_1 , T_2 and T_3 are also shown. From this figure, it is found that periodic rolling does not occur at T_2 . In the result calculated by simplified method using Ikeda's original method, periodic rolling occurs at T_1 . On the other hand, in the result calculated by proposed method, periodic rolling does not occur at T_1 . In the two results, it is found that periodic rolling occurs at T_3 . However, in the result calculated by the simplified method, roll amplitudes become large rapidly.

Therefore, it is confirmed that parametric rolling occurs more easily in simplified method than in the proposed method.

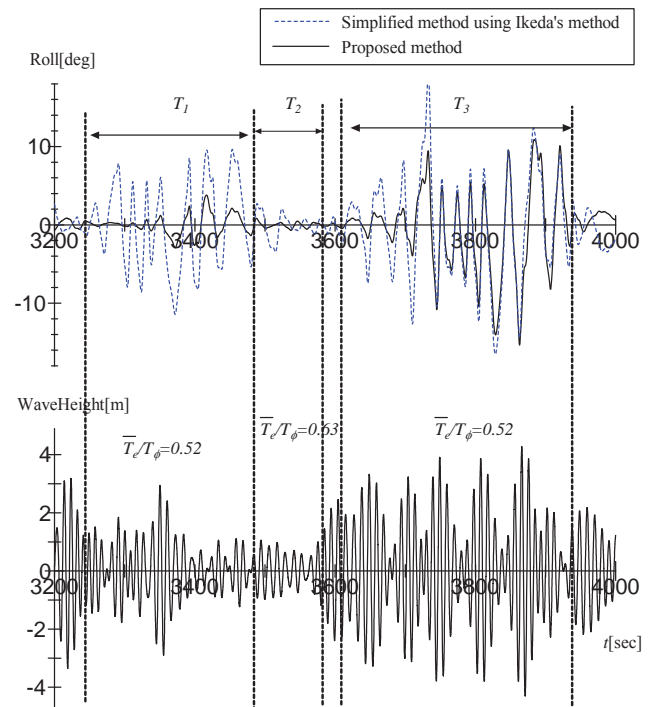


Figure 12 Calculation time history of roll angle and wave height in long crested head irregular waves.

6. CONCLUSIONS

In this study, the memory effects on roll damping is investigated by numerically. The following conclusions are obtained.

In order to take validation data for CFD, forced roll motion test with irregular motion is carried out and the analysis for the test. It is confirmed that the proposed analysis can be applied roll damping under irregular motion and roll damping can be calculated accurately by CFD.

Bilge keel component is divided into normal force component and hull surface pressure component by using CFD and the memory effects are investigated. The memory effects depend on Kc number in previous swing and in present swing. Moreover, in order to clarify the mechanism of the memory effects, the flow field around hull is investigated numerically. The relative fluid velocity in front of bilge keels is increased by the vortices developed by



the previous swing. If K_c number of previous swing is larger, the vortexes developed by previous swing are larger. The moment due to the bilge keel is increased by increase of the relative velocity of the fluid in front of bilge keel.

The estimation method considering the memory effects is proposed. The result estimated by the proposed method is compared with the result calculated by CFD and measured in forced irregular motion test and roll damping can be estimated in time domain by using the method considering the memory effects.

The proposed estimation method is applied for a time domain simulation of parametric rolling in irregular head waves. It is confirmed that parametric rolling occurs more easily in previous method than in the proposed method.

7. REFERENCES

- Ikeda Y., Himeno Y., Tanaka N., (1978). Components of Roll Damping of ship at Forward Speed, Report of Department of Naval Architecture University of Osaka Prefecture, 1978
- Ikeda, Y., Osa, K., Tanaka, N. (1988). Viscous Forces Acting on Irregular Oscillating Circular Cylinders and Flat Plates, Trans. of the ASME, No. 140, Vol. 110, pp.140-147.
- Katayama T., Yoshioka Y., Kakinoki T. and Ikeda Y., "Some Topics for Estimation of Bilge-keel Component of Roll Damping", Proceedings of the 11th International Ship Stability Workshop, 2010, pp.225-230.
- Katayama, T., J. Umeda, H. Hashimoto & B.Yildiz (2013) "A study on roll damping estimation for non-periodic motion." Proc. 13rd Int'l. Ship Stability Workshop, Brest, France, pp. 44-49.
- Hashimoto, H. and Umeda, N., 2010, "A Study

on Quantitative Prediction of Parametric Roll in Regular Waves", Proceedings of the 11th International Ship Stability Workshop, Stability Workshop pp.295-301



Investigation of the 2nd Generation of Intact Stability Criteria in Parametric Rolling and Pure loss of Stability

Haipeng Liu, *University of Strathclyde*, h.liu@strath.ac.uk

Osman Turan, *University of Strathclyde*, o.turan@strath.ac.uk

Evangelos Boulougouris, *University of Strathclyde*, evangelos.boulougouris@strath.ac.uk

ABSTRACT

The International Maritime Organisation is developing the second generation intact stability criteria which include parametric rolling, pure loss of stability and the other three failure modes. This paper will focus on the application of the draft parametric rolling and pure loss of stability criteria on the well-known post-Panamax C11 class containership and a high speed containership developed in the FASTPOD project. The roll amplitude calculated from the proposed analytical method in level 2 parametric rolling criteria is compared to experiment results. The influence of the main particulars on the check by the criteria is investigated.

Keywords: *parametric rolling, pure loss of stability, new generation intact stability criteria*

1. INTRODUCTION

The phenomenon of parametric rolling has been known to naval architects for more than 50 years (Paulling & Rosenberg, 1959). The continued study from Paulling demonstrated parametric roll from a model test in following waves in San-Francisco Bay (Paulling, et al. 1972, 1975). In October 1998, a post-Panamax, C11 class containership experienced severe parametric rolling in the North Pacific Ocean and it confronted the largest container casualty in history (France, et al., 2003). After this accident, parametric rolling attracted increased attention from researchers, and since then, many more studies in parametric rolling prediction have been carried out.

Since the 1800s, the stability changes in waves compared with calm water is known to naval architects (Pollard & Dubeout, 1892; Krylov, 1958). Until the 1960s, a series of model tests were carried out in order to calculate the change of stability in waves. During the model experiments in San-Francisco Bay, pure loss of stability was identified (Paulling, et al., 1972, 1975).

Due to some similar accidents which occurred in the Pacific Ocean and the Atlantic Ocean, it was realised that the existing Intact Stability Code (IS Code) couldn't provide enough safety. Therefore, the International Maritime Organisation (IMO) initiated the revision of the existing regulatory framework with the development of the second generation intact stability criteria which will hopefully fill this safety gap. The new intact stability criteria include five stability failure modes as listed below (SLF, 2012)

- Dead ship condition in beam seas
- Surf riding and broaching-to
- Parametric rolling
- Pure loss of stability
- Excessive acceleration

After the new criteria were generated, the process of stability check is suggested in figure 1. In each stability failure mode, it is divided

into vulnerability layer of level 1 and level 2 and performance-based layer of level 3. With the level increasing, the procedure is more detailed and accurate. The lower the level it is, the more conservative it is. Currently, the IMO finished the simplest level 1 criterion and is developing level 2 criteria. In the following paragraphs a short description of the background and the procedure of vulnerability layer of the criteria will be presented.

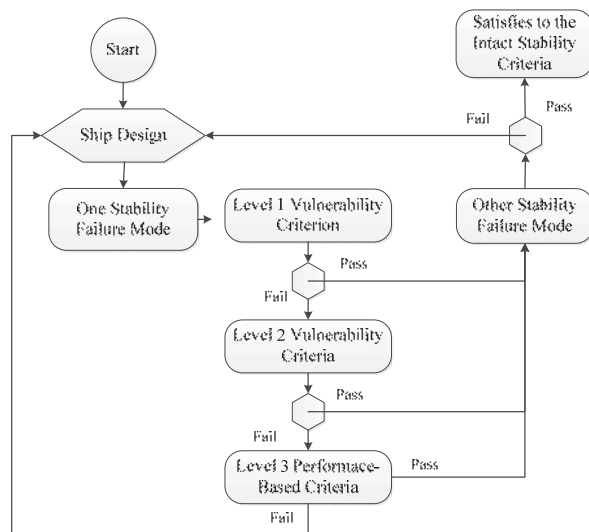


Figure 1 The proposed assessment process for next generation intact stability criteria

- Parametric Rolling

Parametric rolling is the roll amplification which is caused by the periodic change of metacentric height in longitudinal waves under specific conditions (ABS, 2004). The new parametric rolling vulnerability criteria with two levels included are described below.

Level 1 Vulnerability Criterion

As defined by current draft criteria (SDC, 2014), if the ratio of GM variation in reference wave ($\Delta GM/GM$) is larger than the standard R_{PR} , the ship is temporary judged as vulnerable to parametric rolling; otherwise it means the vessel doesn't have any potential danger of parametric rolling. Here GM is the metacentric height of the loading condition in calm water including free surface correction and ΔGM is

the change of metacentric height which can be estimated using two different methods. In the first method (Option A), two different drafts are used and Simpson's rule is applied to calculate the moment of inertia and the average GM variation is achieved. This method is not suitable for a tumblehome hullform but it is applicable to a ship without even keel design (SDC, 2014). In the second method (Option B), ΔGM may be determined as one-half difference between the maximum and minimum GM calculated in sinkage and trim on a series of waves with wave length equals to ship length and the wave height equals to 1/60 of wave length. Both of these two methods are utilised herein.

Level 2 Vulnerability Criteria

Level 2 criteria (SDC, 2014) will check the vessel in the aspects of ship speed, metacentric variation and roll amplitude. If either C_1 or C_2 is larger than safety standard R_{PR0} 0.06, the ship is judged to be in danger of parametric rolling (PR) and needs to be checked in performance-based layer, otherwise it passes the criteria. The aspects of speed and metacentric height variation constitute the first check and the aspect of roll angle computation constitutes the second check.

- First Check

The first check aims to test whether the vessel's speed is within the vulnerable region for PR and GM variation and satisfies the PR safety requirement. The probability of C_1 in the first check is a sum of the product of C_{1i} and the wave weighting factor W_i . The 16 wave series applied in this check are discretisation of the applied wave spectrum (SDC, 2014). The weighting factor is the occurrence probability among the wave series for each wave case. The wave lengths vary from 22.57m to 63.68m and the wave heights vary from 0.35m to 5.95m. The value for criterion 1 in each case, C_{1i} is 0 if both speed check and GM relevant check satisfy with the specific condition as the vessel is considered not vulnerable to PR; otherwise C_{1i} is 1.

Parametric rolling occurs when the encounter frequency is equal to double the natural roll frequency. The speed corresponds to the resonance speed V_{PRi} which is given by the following Equation 1.

$$V_{PRi} = \left| \frac{2\lambda_i}{T_\phi} \cdot \sqrt{\frac{GM(H_i, \lambda_i)}{GM}} - \sqrt{g \frac{\lambda_i}{2\pi}} \right| \quad [1]$$

For GM relevant conditions for avoiding the PR risk region are that $\Delta GM(H_i, \lambda_i)/GM(H_i, \lambda_i) < R_{PR}$ and $GM(H_i, \lambda_i) > 0$. Here, the average metacentric height corresponding to the loading condition under consideration, $GM(H_i, \lambda_i)$; and the one-half of the difference between the maximum and minimum values of the metacentric height GM in wave, $\Delta GM(H_i, \lambda_i)$; are calculated considering the ship balanced in sinkage and trim in the series of waves characteristic by H_i and λ_i .

If total probability of C_1 is greater or equal to the standard value R_{PR0} of 0.06 the ship is judged as potentially vulnerable and it needs to be checked by the second check; otherwise the vessel is not vulnerable and it passes the evaluation of parametric rolling problem.

- Second Check

When C_1 is not smaller than R_{PR0} , the designer should apply the second check. The ship performance is simulated under NO.34 standard wave cases (IACS, 2001). Each wave case has the corresponding weighting factor W_i , which represents the sample wave's occurrence probability among all the 306 wave cases. According to the criteria, if the vessel in each wave case experiences the roll angle which is larger than 25 degrees, the vessel is judged as vulnerable to parametric rolling and C_{2i} is 1, otherwise is 0. An analytical method based on the simplification of Mathieu's equation is used to predict the roll amplitude as given in equation [2] (CGIS, 2014). GM variation in waves is calculated quasi-statically. Ikeda's simplified method, based on an empirical formula, is used for the damping prediction (Kawahara et.al., 2009). It divides the roll

damping into the frictional, the wave, the eddy, the bilge keel and the lift damping components.

$$(I_{xx} + J_{xx}) \cdot \ddot{\phi} + R \cdot (\dot{\phi}) + W \cdot GM \cdot \phi = 0 \quad [2]$$

Where $I_{xx}+J_{xx}$: virtual moment of inertia in roll;

R: nonlinear roll damping;

W: ship weight;

GM: metacentric height

For the second check, if the total probability sum C_2 which is the product of C_{2i} and wave weighting factor W_i , is greater than standard R_{PR0} 0.06, the ship is judged to be vulnerable to parametric rolling and the ship should be checked by level 3; if not, the ship passes the parametric rolling failure mode and it should be checked for the other stability failure modes.

- Pure Loss of Stability

If the stability is reduced for a sufficiently long time, a ship may experience a large roll angle or even capsize, as shown in figure 2 (Belenky, 2008). In the new generated pure loss of stability criteria (SDC, 2014), it mainly concerns the minimum GM value, the vanishing stability and the heel angle under action of specific heeling level. The criteria is proposed to apply to all ships with service speed larger than 0.24.

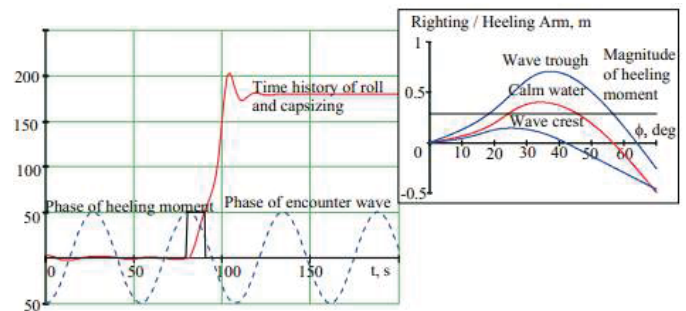


Figure 2: Capsizing due to Pure Loss of Stability (Belenky et.al., 2008)

Level 1 Vulnerability Criteria for Pure Loss of Stability

As proposed, if GM_{\min} is greater than R_{PLA} 0.05, the ship is considered not vulnerable; otherwise it has to be checked by the next level (SDC, 2014).

Similar to the method of GM variation prediction in waves in parametric rolling criteria, the minimum value of metacentric height GM_{\min} can be calculated either from the simplified method (Option A), or from considering the ship is balanced in sinkage and trim quasi-statically (Option B). In this case, the wave length is equal to the ship length and wave steepness is 0.0334 which is twice of that for parametric rolling.

Level 2 Vulnerability Criteria for Pure Loss of Stability

The procedure is quite similar to level 2 criteria for parametric rolling. It requires the stability calculations in a series of longitudinal sinusoidal waves. Here, the criteria totally include 2 checks which evaluate the ship in vanishing stability and the heel angle under action of specific heeling level. The target is for the angle of vanishing stability to be greater than 30 degrees (referred to C_{R1}), and the angle of heel under action of heeling level specified by $R_{PL3} \ 8(H_i/\lambda)dF_n^2$ (referred to C_{R2}) to be larger than 15 degrees for passenger ship or 25 degrees for other ships. The total sum of probability according to corresponding wave probability in each criterion is C_{R1} and C_{R2} . The ship at its service speed is considered not to be vulnerable to pure loss of stability if the largest value among the two criteria, C_{R1} or C_{R2} is less than R_{PLO} ; otherwise, performance-based layer should be applied for further check.

2. SAMPLE VESSELS

2.1 Reference Ship Data

The reference vessels applied with the draft criteria are C11 containership, ITTC ship A-1

and a high speed containership developed in Fastpod project (Turan et. al., 2008). The main particulars of these vessels and geometry are separately listed in table 1-3 and figure 3-5.

Table 1:
Main Parameters of C11 Containership

Item	Value	Unit
Length btw. waterline (L_{pp})	262.00	m
Breadth (B_{DWL})	40.00	m
Depth (D)	24.45	m
Draught (T)	11.50	m
Displacement (Δ)	69,034.40	tons
Block coefficient (C_B)	0.573	/
Transverse metacentric height (GM_T)	1.928	m
Vertical Centre of Gravity (VCG)	18.418	m
Service Speed (V_s)	12.86	m/s
Natural Roll period (T_ϕ)	24.49	s

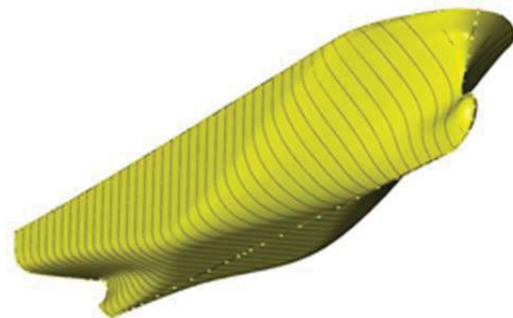


Figure 3: Geometry of C11 Containership

Table 2:
Main Parameters of Ship A-1

Item	Value	Unit
Length btw. Waterline (L_{pp})	150.00	m
Breadth (B_{DWL})	27.20	m
Depth (D)	13.50	m
Draught (T)	8.5	m
Displacement (Δ)	23,751.21	tons
Block coefficient (C_B)	0.668	/
Transverse metacentric height (GM_T)	0.15	m
Vertical Centre of Gravity (VCG)	11.475	m
Service Speed (V_s)	11.50	m/s
Natural Roll period (T_ϕ)	43.30	s

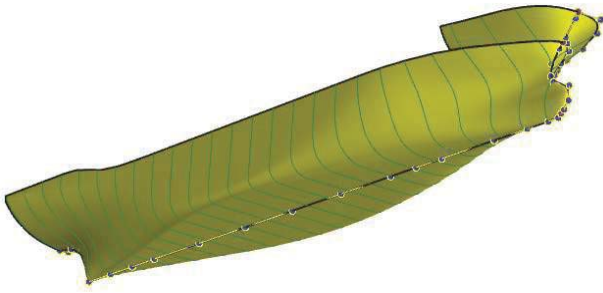


Figure 4: Geometry of ship A1

Table 3:
Main parameters of Fastpod Containership

Item	Value	Unit
Length btw. Waterline (L_{pp})	275.00	m
Breadth (B_{DWL})	30.00	m
Depth (D)	21.65	m
Draught (T)	10.30	m
Displacement (Δ)	49,580.28	tons
Block coefficient (C_B)	0.569	/
Transverse metacentric height (GM_T)	1.926	m
Vertical Centre of Gravity (VCG)	13.678	m
Service Speed (V_s)	18.00	m/s
Natural Roll period (T_ϕ)	19.05	s

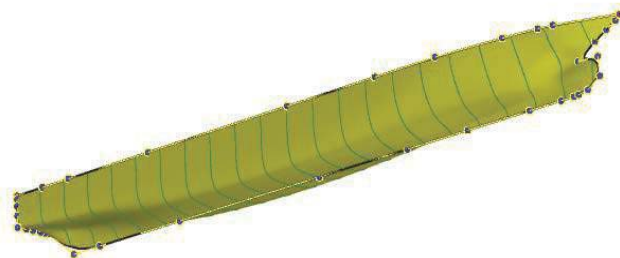


Figure 5: Geometry of Fastpod Containership

3. SECOND GENERATION INTACT STABILITY CRITERIA

The IMO is developing the second generation intact stability criteria of five failure stability modes. In this paper, the application of parametric rolling and pure loss of stability criteria will be introduced in section 3.1 and section 3.2 separately.

3.1 Parametric Rolling

The three sample vessels were tested according to the draft criteria. Roll amplitude results of C11 containership and Fastpod containership were calculated using the analytical methods proposed by the IMO working group and they were compared to model test results. The application of current parametric rolling criteria on the sample vessels is concluded. As C11 containership was tested in danger of parametric rolling, it is useful to investigate the influence of ship parameters on this issue.

- Analytical Method Vs. Experiment

In parametric rolling, the main part is to predict parametric roll amplitude. In level 2 vulnerability criteria, an analytical method is proposed to calculate roll angle (CGIS, 2014). As mentioned, level 2 is more conservative than level 3. If the vessel passes level 2, the vessel won't have any potential danger of parametric rolling. In other words, the roll amplitude calculated from the proposed method in level 2 should be larger than that of the vessel experiencing in practice.

Firstly, the well-known C11 containership is used to carry on the benchmark study. In wave length equals to ship length, wave steepness varies from 0.01 to 0.04 and Froude number changing from 0 to 0.15 in head sea, roll amplitude calculated from analytical method is compared to the experiment result shown in figures 6-9. All these results demonstrate that the analytical method provides a conservative estimate on roll amplitude which matches the purpose of level 2 criteria.

Secondly, the study is also applied to a high speed containership used in the Fastpod project (Turan, 2008). The model was tested for different wave heights for wave frequency 0.525 and vessel speed in 17 knots in head sea (Turan, 2008). The result comparison between analytical method and model test is plotted in figure 10. X axis represents the wave heights of regular wave while Y axis represents the roll amplitude. The data meet the conservative

purpose as well and the analytical method can achieve larger roll angle and provide a reasonable agreement to model test to some extent.

- Parametric Rolling Criteria Application

After validation of the analytical method, parametric rolling vulnerability criteria were applied to the three sample vessels. The results of level 1 and level 2 compared to the safety standard are shown in table 4. C11 is judged to be in potential danger of parametric rolling, while ship A-1 and Fastpod containership passes the criteria. The calculated result of C11 containership has a relative good agreement with IMO published result. Besides, The roll amplitude of most model tests of C11 containership are larger than the safety limit 25 degree while the largest roll amplitude of Fastpod containership reaches to 24.41 degree which is still smaller than the limit 25 degree. It therefore demonstrates that the parametric vulnerability criteria have good accuracy of parametric rolling occurrence prediction.

- Sensitivity Study

C11 containership was judged as being vulnerable to parametric rolling. It is important to investigate the influence of the main parameters on parametric rolling. To achieve the study, parametric transform method, based on Lackenby hull variation method (Lackenby, 1950) is used to generate new hullform. In this study, only one parameter was changed slightly (e.g. $\Delta L \pm 2m$; $\Delta B \pm 0.4m$; $\Delta T \pm 0.4m$; $\Delta C_b \pm 0.01$; $\Delta C_m \pm 0.005$; $T_\phi \pm 0.5s$), keeping the other main parameters constant and leaving the displacement free to vary. Among ship length L_{wl} , breadth B , draft T , block coefficient C_b , midship coefficient C_m and natural roll period T_ϕ , the small change to all the main parameters doesn't have any influence on C_1 of parametric rolling. In figure 11, it is clear that the small change of ship length doesn't have any influence on C_2 while in figure 12, the increase of breadth and block coefficient could slightly

decrease the C_2 value. Compared to these three coefficients, C_m and T_ϕ have a relative larger influence on C_2 value. Overall, increasing draft could decrease the C_2 value but the vessel within this small change still in danger of parametric rolling, as shown in figure 13. From figure 14-15, it demonstrates that decreasing midship coefficient or natural roll period, could reduce the C_2 value and even avoid the vessel from parametric rolling occurrence

3.2 Pure Loss of Stability

In this part, the application of pure loss of stability to the three vessels is applied. The results are listed in table 5. In level 1, the simplified method (option A) seems more conservative. Although most results judged the ship as having a potential danger of pure loss of stability in level 1, all sample vessels still pass the level 2 criteria.

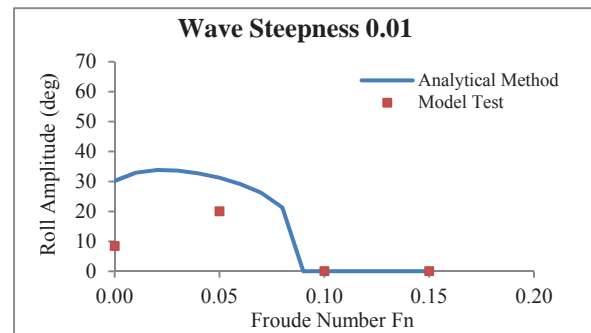


Figure 6 Comparison between Analytical Method and Experiment Result under Wave Steepness 0.01

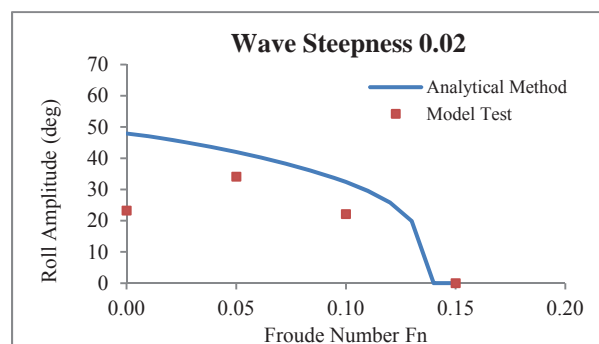


Figure 7 Comparison between Analytical Method and Experiment Result under Wave Steepness 0.02

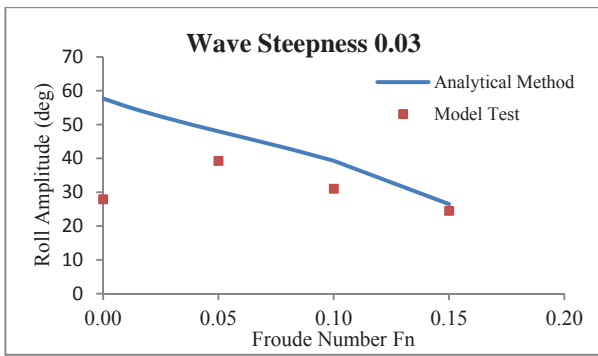


Figure 8 Comparison between Analytical Method and Experiment Result under Wave Steepness 0.03

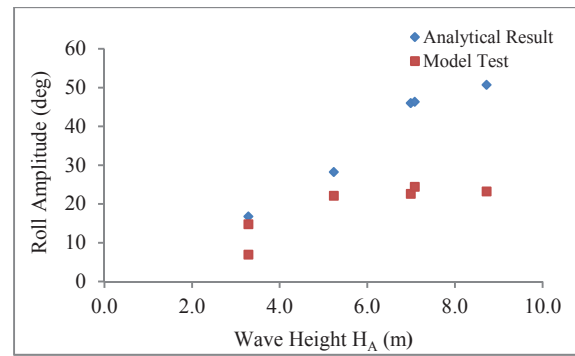


Figure 10 Roll Angle Comparison between the Analytical Method and Experiment Result with Different Wave Height

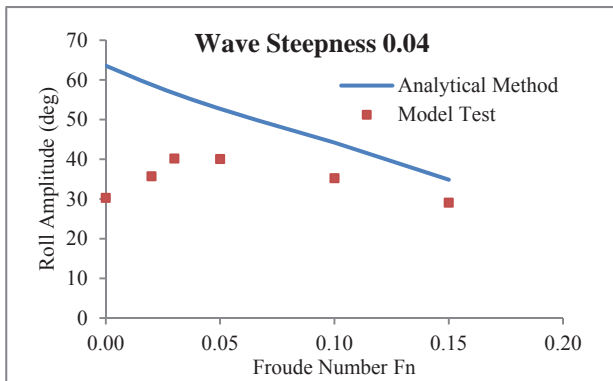


Figure 9 Comparison between Analytical Method and Experiment Result under Wave Steepness 0.04

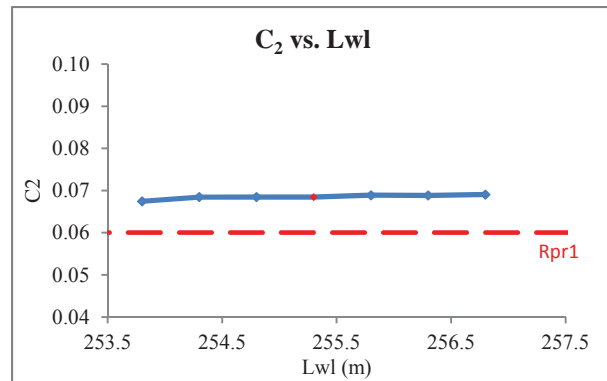


Figure 11 Relationship between ship length and C_2 of Parametric Rolling

Table 4: Application of Parametric Rolling on Sample Vessels (Non-vulnerable; **Vulnerable**)

Ship Type	L_{pp} (m)	$\Delta GM/GM$		R_{PR}	C_1	C_2
		Option A	Option B			
C11 from IMO	262	1.056	/	0.356	0.437	0.073
C11	262	1.067	0.852	0.400	0.436	0.068
Ship A-1	150	3.095	2.477	0.627	0.885	0.002
Containership 1	275	0.837	0.399	0.313	0.225	0.001

Table 5: Application of Pure Loss of Stability on Sample Vessels (Non-vulnerable; **Vulnerable**)

Ship Type	L_{pp} (m)	F_n	Level 1		Level 2	
			Option 1-A	Option 1-B	C_{R1}	C_{R2}
			GMmin-0.05(m)			
C11	262	0.257	-1.969	-0.046	0.000	0.000
Ship A-1	150	0.3	-0.664	-0.201	0.000	0.000
Containership 1	275	0.345	-1.777	0.383	0.000	0.000

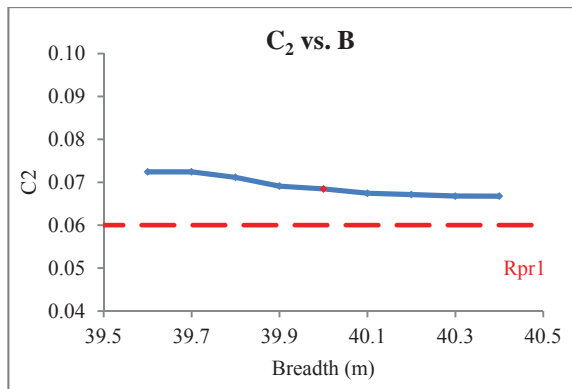


Figure 12 Relationship between Ship Breadth and C_2 of Parametric Rolling

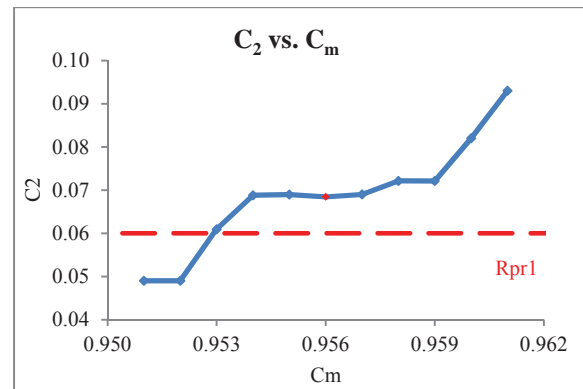


Figure 15 Relationship between Ship Midship Coefficient and C_2 of Parametric Rolling

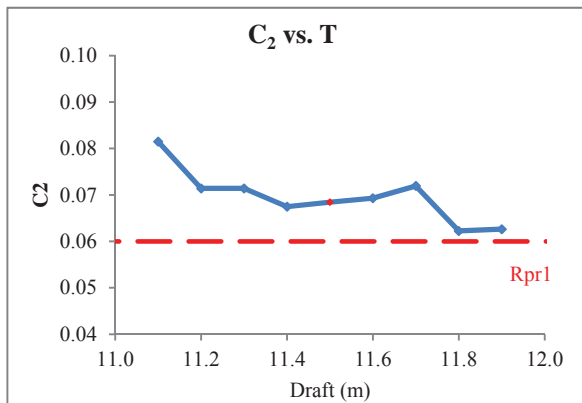


Figure 13 Relationship between Ship Draft and C_2 of Parametric Rolling

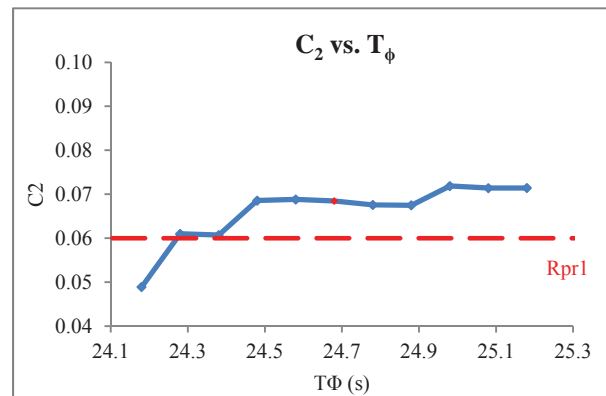


Figure 16 Relationship between Ship Natural Roll Period Coefficient and C_2 of Parametric Rolling

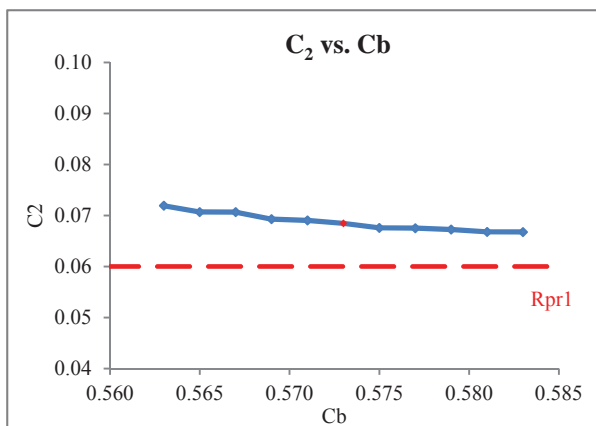


Figure 14 Relationship between Ship Block Coefficient and C_2 of Parametric Rolling

4. CONCLUSIONS

In this paper, the current parametric rolling and pure loss of stability criteria are applied to three sample vessels. C11 containership is judged as vulnerable to parametric rolling while ITTC ship A-1 and Fastpod containership are judged as non-vulnerable to parametric rolling. All the vessels passed the pure loss of stability criteria. Meanwhile, the analytical method from Mathieu equation provides a conservative estimate on the roll angle in comparison to experiments and to some extent; it has a relatively good prediction on the trend. Besides, the sensitivity study demonstrates that among ship length, breadth, draft, block coefficient, midship coefficient, natural roll period, when only one parameter is



changed and the other main parameters are left constant, C_1 is not sensitive but C_2 of parametric rolling is much influenced by draft, midship coefficient and natural period.

5. ACKNOWLEDGMENTS

This project was funded by Lloyd's Register. All internal information relevant to second generation of intact stability was kindly provided by the Royal Institution of Naval Architects. The support from Lloyd's Register and the Royal Institution of Naval Architects is gratefully acknowledged.

The experiment of high speed containership was carried out under the European Commission Research Project FASTPOD (GRD2-2001-50063). The efforts from Dr Zafer Ayaz are very much appreciated.

6. REFERENCES

- American Bureau of Shipping (ABS), 2004, "Guide for the Assessment of Parametric Roll Resonance in the Design of Container Carriers", Houston, Texas.
- Belenky, V., Kat, H.O.D., and Umeda, N., 2008, "Toward Performance-Based Criteria for Intact Stability", Marine Technology, Vol.45, No.2, pp. 101-123.
- Correspondence Group on Intact Stability (CGIS), 2014 "Working Version of Draft Explanatory Notes on the Vulnerability of Ships to the Parametric Rolling Stability Failure Mode", Sub-Committee on Ship Design and Construction, SDC 2/INF.10 Annex 17, pp. 59-74.
- France, W.N., Levadou, M., Treacle, T.W., Paulling, J.R., Michel, R.K. and Moore, C., 2003, "An investigation of head-sea parametric rolling and its influence on container lashing systems", Marine Technology, Vol.40, Number 1, pp.1-19.
- International Association of Classification Societies (IACS), 2001, "No.34 Standard Wave Data".
- Lackenby, H., 1950, "On the Systematic Geometrical Variation of Ship Forms", RINA-Transaction, Vol 92, pp. 289-315.
- Kawahara, Y., Maekawa, K., and Ikeda, Y., 2009, "A Simple Prediction Formula of Roll Damping of Conventional Cargo Ships on the Basis of Ikeda's Method and Its Limitation", The 10th International Conference on Stability of Ships and Ocean Vehicles, St. Petersburg, Russia.
- Krylov, A.N., 1958, Selected Papers, USSR Academy of Sciences, Moscow.
- Paulling, J.R., Kastner, S., and Schaffran, S., 1972, "Experimental Studies of Capsizing of Intact Ships in Heavy Seas", U.S. Coast Guard Technical Report
- Paulling, J.R., Oakely, O.H., and Wood, P.D., 1975, "Ship Capsizing in Heavy Seas: The Correction of Theory and Experiments", Proceedings of 1st International Conference on Stability of Ships and Ocean Vehicles, Glasgow.
- Paulling, J.R. and Rosenberg, R.M., 1959, "On Unstable Ship Motions Resulting from Nonlinear Coupling", Journal of Ship Research, Vol. 3, pp.36-46.
- Pollard, J. and Dudebout, A., 1892, "Theorie Du Navire", Paris.
- Sub-Committee on Stability and Load Lines and on Fishing Vessels Safety (SLF), 2012, "Summary of the Methodologies for the Second Generation Stability Criteria Available for SLF 54", SLF 54-WP, Annex 3.
- Sub-Committee on Ship Design and Construction (SDC), 2014, "Draft Amendments to Part B of the IS Code with



Regard to Vulnerability Criteria of Levels 1 and 2 for the Parametric Rolling Failure Mode”, Development of Second Generation Intact Stability Criteria – Development of Amendments to Part B of the 2008 IS Code on Towing and Anchor Handling Operations: Report of Working Group (Part 1), SDC 2/WP.4, Annex 2.

Turan, O., Ayaz, Z., Aksu, S., Kanar, J. and Bednarek, A., 2008, “Parametric Rolling Behaviour of Azimuthing Propulsion-driven Ships”, Ocean Engineering, 35(13), pp. 1339-1356.



Requirements for Computational Methods to be Used for the IMO Second Generation Intact Stability Criteria

William Peters, *USCG Office of Design and Engineering Standards* william.s.peters@uscg.mil

Vadim Belenky, *Naval Surface Warfare Center Carderock Division*, vadim.belenky@navy.mil

Sotirios Chouliaras, *National Technical University of Athens*, sotchouliaras@gmail.com

Kostas Spyrou, *National Technical University of Athens*, k.spyrou@central.ntua.gr

ABSTRACT

Practical implementation of the second generation of IMO intact stability criteria is not possible without formulation of clear requirements for numerical or other computational methods. Probably, the highest priority should be given to the second-level vulnerability criteria. The first-level is simple enough and, as such, requirements may not be needed or will be obvious based on standard naval architectural practices. While scientifically mature, the application of numerical methods in the second-level may be more difficult as not all of these methods are familiar to practicing naval architects including those employed with administrations and classification societies. This paper focuses on requirements for use of the numerical method for the second-level vulnerability criteria for the parametric roll stability failure mode. Criteria for other modes of stability failure may have similar concerns. Use of a numerical solution of differential equations may be a good way to compute nonlinear ship motions. However, to ensure consistency of its application (i.e. results are reliably repeatable for the same ship in the same condition), all necessary parameters (such as the time increment, the number of steps, the initial conditions, etc.) must be explicitly defined. Further, special attention needs to be given to a ship response on very large waves, for which special procedures may be needed. Since the differential equation is nonlinear, the response to a very large excitation may be chaotic. Also, if capsized equilibrium is not modeled, special measures must be taken to prevent run-time related to a very large, unrealistic roll response.

Key Words: *IMO Second Generation Intact Stability Criteria, Parametric Roll*

1. INTRODUCTION

The development of the second generation IMO intact stability criteria has been an intense multi-year effort. Recognizing the fact that stability failure may be caused by different physical mechanisms, different modes of stability failure are explicitly considered in the new criteria:

- Restoring arm variation problems, such as parametric excitation and pure loss of stability;
- Stability under dead ship condition, as defined by SOLAS regulation II-1/3-8; and
- Maneuvering related problems in waves, such as broaching-to;
- Excessive accelerations (SLF 53/19, paragraph 3.28).

This development was partially motivated by the appearance of novel hull forms that renewed interest in dynamic stability, (see e.g. France, *et al.* 2003). As a result, the emphasis was made on adequate reflection of physics,



making new criteria based on performance (Belenky, *et al* 2008). This means that the assessment is based on hull geometry and physics of stability failure rather than past experience with similar ships.

The multi-tiered structure of new criteria addresses the potential complexity of the application of the new criteria. The first-level vulnerability check is very simple and quick, but conservative. If vulnerability to a particular stability failure mode is determined not to occur, no further assessments are needed. If not, then a more detailed, but less conservative analysis follows, which is the second-level vulnerability assessment.

The IMO Sub-committee on Ship Design and Construction, at its 2nd Session, finalized the first three elements of the criteria:

- Draft Amendments to Part B of The 2008 IS Code with Regard to Vulnerability Criteria of Levels 1 And 2 for the Pure Loss of Stability Failure Mode (Annex 1 of SDC 2/WP.4);
- Draft Amendments to Part B of The 2008 IS Code with Regard to Vulnerability Criteria of Levels 1 And 2 for the Parametric Rolling Failure Mode (Annex 2 of SDC 2/WP.4);
- Draft Amendments to Part B of The 2008 IS Code with Regard to Vulnerability Criteria of Levels 1 And 2 for the Surf-Riding / Broaching Failure Mode (Annex 3 of SDC 2/WP.4).

These documents describe the criteria, standards and contain general requirements for the calculation methods. The explanatory notes are expected to be developed to ensure uniform interpretations and application of the new criteria. The technical background of these criteria is described in Peters, *et al.* (2011). A significant amount of information is being prepared for the explanatory notes, see SLF 53/3/3, Annexes 17, 19, 33, 34 of SDC 2/INF.10, Sections 2.1, 3.1 and 4.1 of Belenky, *et al.* (2011) and Peters, *et al.* (2014). The

particular objective of this paper is to contribute towards the explanatory notes for second-level vulnerability assessment of the parametric roll stability failure mode.

2. MAXIMUM ROLL ANGLE

The second check for the second-level vulnerability criteria requires calculation of the maximum roll angle resulting from parametric roll. This calculation, while not too complex, is beyond the scope of traditional naval architectural calculations; why?

The conventional way to evaluate ship motions is with the use of Response Amplitude Operators (RAO). The RAO expresses dynamic properties of a ship. Its values are the characteristics of motions, multiplied by the values of sea spectrum and summed up to yield the characteristics of motion. RAO is an element or a form of a solution to the linear ship motion equation in waves.

The term “linear ship motion equation” means that the equation assumes that the motions are small and that non-linear parts of the full ship motion equation can be ignored because their effects are negligible (often because the waves are significantly longer than the ship). In particular, GM , which characterizes transverse stability, is used to represent roll stiffness. Indeed, stability at large roll angles cannot be characterized with GM alone.

The maximum angle of parametric roll also cannot be found just with GM even if its variation in waves is known. However, the responsibility for progressively growing roll angles, i.e. parametric roll, is associated with these GM variations together with a frequency ratio in which the encounter frequency is close to twice that of natural frequency (see e.g. SLF 54/3/3).

Once parametric roll motion starts, it grows to a certain maximum angle and the motion



repeats (i.e., it remains stable). This occurs because the GZ curve is not a straight line over the range of roll motion. As a result, the natural roll frequency changes with the increase of the roll angle (the instantaneous GM value also changes). Changing the roll frequency sooner or later will break the parametric roll condition because the supply of energy into roll motion will be stopped. The maximum roll angle is achieved during steady state parametric roll.

Thus, a large portion of the GZ curve is needed to find the maximum roll angle. While the GZ curve is known, the motion equation is no longer linear if GZ is included and a RAO-type of solution is no longer possible.

3. EQUATION OF MOTION

3.1 Overview of Forces Acting on a Ship

The equation of motion takes into account forces acting on the ship. The simplest mathematical model that is capable of evaluating the maximum roll angle includes four moments:

- Inertia, including added inertia (or added mass) as a part of hydrodynamic forces;
- Roll damping, which expresses energy loss from roll motions in creating waves, vortices and skin friction;
- Roll restoring (stiffness) is modeled with the calm water GZ curve; the variation of stability in waves is included by GM represented with a sine function.
- Transverse wave forces are absent for a ship in exact following or head long-crested seas

3.2 Roll Inertia

The roll inertia of a ship as a solid body is measured by the transversal moment of inertia. In absence of ship specific data, it is recommended to assume the radius of gyration r_x as 40% of the molded breadth, B :

$$r_x = 0.4B \quad (1)$$

Then, the moment of inertia, I_x , is calculated as:

$$I_x = \rho \nabla r_x^2 \quad (2)$$

where ρ is the mass density of salt water; ∇ is the volume of displacement. Use of other approximation formulae may be helpful but only if the limits of their applicability are well known.

Inertial forces are proportional to accelerations. There are also hydrodynamic forces acting on a ship subject to accelerated motion that are also proportional to the accelerations. These hydrodynamic forces are usually expressed as an additional mass or a moment of inertia and referred as “added mass”. Again, in the absence of ship specific data, one can assume that the added mass in roll, A_{44} , as:

$$A_{44} = 0.25I_x \quad (4)$$

Finally, the roll inertia is expressed as:

$$M_{IN} = (I_x + A_{44}) \cdot W_\phi \quad (5)$$

where W_ϕ is the angular acceleration in roll.

3.3 Roll Damping

Damping of roll motions is essentially a transfer of kinetic energy of a moving ship to the environment. It is a complex process, because this energy transfer occurs through different physical phenomena. Skin friction causes the layers of water nearest to the hull to move. The moving surface of the hull leads to formation of vortices; the kinetic energy of the water moving in those vortices is taken from the ship. Due to its motion, the ship also makes waves on the surface that also dissipate energy. The complexity of these physical phenomena is the reason why a model test is the most reliable source of information on roll damping. However, recent developments in computational fluid dynamics (CFD) holds

good promise for the availability of this computational method in the future.

In the absence of ship-specific or prototype data, the simplified Ikeda method can be recommended (Annex 3, SDC 1/INF.8). A moment of roll damping is presented in the following form:

$$M_D = (I_X + A_{44}) \cdot (\delta_1 V_\phi + \delta_3 V_\phi^3) \quad (6)$$

where δ_1 and δ_3 are coefficients computed with simplified Ikeda method and V_ϕ is the angular velocity of roll motions.

The simplified Ikeda method contains some empirical elements and, for this reason, the range of its applicability should be observed.

3.4 Roll Restoring

A proper representation of roll restoring is very important for the correct representation of parametric roll. The variation of stability in waves is a primary mechanism of development of parametric roll (an explanation is provide in SLF 54/3/3). The calculation of the instantaneous roll restoring, while straight forward, may be too complex for the level-two vulnerability check. (See the description of one of the simplest algorithms of direct calculation in Weems and Belenky, 2015). Hence, a quasi-static approach can be used instead.

The quasi-static approach means that the GZ curve for the ship on a wave is calculated using the “conventional” static algorithm (in which forces and moments are balanced in heave and pitch as required in Annex 2 of SDC 2/ WP.2), but the waterplane is not flat – it is determined from the intersection of a wave and the hull surface. Known also as “wave-pass” calculations, the capability for this calculation is provided by a number of commercially available hydrostatic software packages (see Figures 1 and 2). For the assessment of parametric roll, calculation of the GZ curve up to 180 degrees is recommended; it sets a natural maximum and prevents the numerical

solution from growing too large and cause a numerical error.

Figures 1 shows the GZ variation in waves as a series of curves. Each curve is calculated for a particular position of the wave crest relative to the midship which results in a surface shown in Figure 2. For the intermediate values of heel angle and of the wave crest position, a bilinear or bi-cubic spline interpolation can be used. The definition of wave crest position is illustrated in Figure 3.

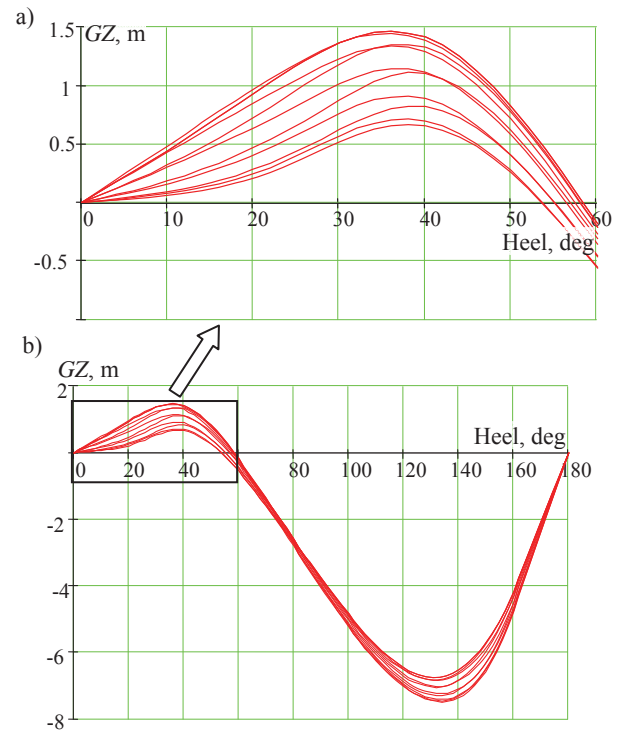


Figure 1: The GZ curve in waves (steepness 0.02, C11 class containership, full load) (a) positive range, (b) full range

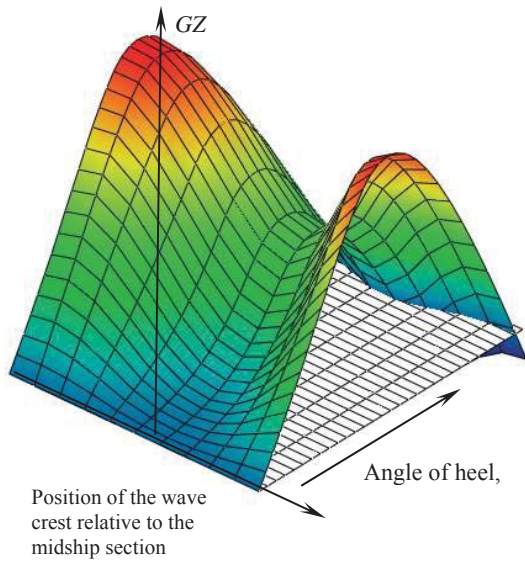


Figure 2: The GZ curve in waves as a surface (steepness 0.02, C11 class containership, full load)

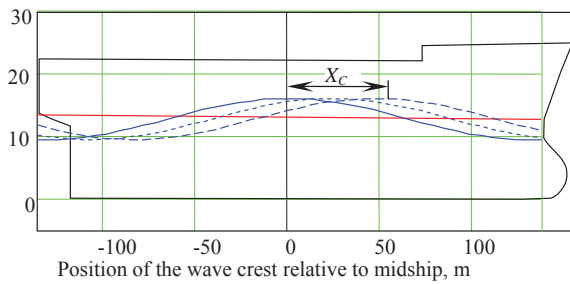


Figure 3: Definition of the position of the wave crest relative to the midship section

The position of the wave crest is a function of time:

$$X_c(t) = 0.5\lambda \sin(\omega_e t) \quad (7)$$

where λ is the length of the wave and ω_e is the wave frequency of encounter:

$$\omega_e = \omega - \frac{\omega^2}{g} V_s \cos \beta \quad (8)$$

where g is the gravity acceleration, β is the relative wave heading (0 degrees – following waves, 180 deg – head waves), and V_s is the forward speed in m/s. Thus, the value of the GZ curve in waves can be presented as a function of time and angle of heel, ϕ :

$$GZ = GZ(t, \phi) \quad (9)$$

If, for some reason, the calculation software is not available, the GZ curve in a wave can be approximated using only the GM value that may be already available from the Level 1 vulnerability check. Indeed, as required by Annex 2 SDC 2/WP.2, the calculation of GM must be done with forces and moments balanced in heave and pitch. An example of the GM variation is shown in Figure 4:

Then, the GZ in waves may be approximated by the calm-water GZ “modulated” by the GM in waves

$$GZ(t, \phi) = \frac{GM(t)}{GM_0} GZ_0(\phi) \quad (10)$$

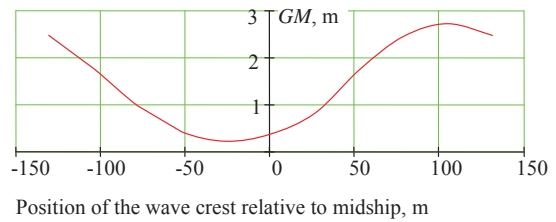


Figure 4: The GM value in waves as a function of wave crest position relative to midship (wave steepness 0.02, C11 class containership, full load)

Assuming that the GZ curve is symmetric, the total restoring moment is expressed as:

$$M_R = \text{sign}(\phi) \cdot \rho \nabla g \cdot GZ(t, |\phi|) \quad (11)$$

$$\text{sign}(\phi) = \begin{cases} 1 & \phi \geq 0 \\ -1 & \phi < 0 \end{cases}$$

3.5 Equation of Motion and Its Solution

Following Newton’s second law, the equation of roll motion is expressed as the inertial force equal to the sum of all other forces. Since the ship is in longitudinal waves, there is negligible or no direct forcing that comes from the waves:

$$M_{IN} = -M_D - M_R \quad (12)$$

In equation (12), the negative sign is inserted because both damping and restoring forces are directed against the roll motion or the rate of motion. The equation of roll motion can be re-written with each force as a function of motion parameters or time:

$$M_{IN}(W_\phi) + M_D(V_\phi) + M_R(t, \phi) = 0 \quad (13)$$

Equation (13) relates the roll motion with the roll rate and the angular roll acceleration. These quantities are related through differentiation: the angular velocity is a derivative of roll and the angular acceleration is a derivative of angular velocity. Thus, equation (13) is a differential equation.

The solution of a differential equation (13) is a time history of roll motions, similar to that shown in Figure 5.

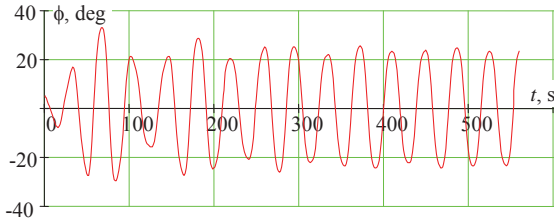


Figure 5 Time history of parametric roll

Figure 5, indeed, shows parametric roll. As the ship is sailing in longitudinal waves, there is no forcing in the transversal plane, so the observed rolling motion is a result of parametric resonance.

The equation (13) is solved by a standard program available from most numerical or engineering software packages. Numerical solvers of differential equation also are available in MS Excel in Visual Basic. To use the solver, the equation (13) must be presented in a form of a vector-valued function:

$$F\left(\begin{pmatrix} \phi \\ V_\phi \end{pmatrix}, t\right) = \frac{1}{I_X + A_{44}} \begin{pmatrix} V_\phi \\ -M_D(V_\phi) - M_R(t, \phi) \end{pmatrix} \quad (14)$$

Besides the vector-valued function (14), the solver requires initial conditions, *i.e.* values of roll angle and roll rate at the beginning (or at time step $t = 0$) of the calculations. The solution, as illustrated in Figure 5, was computed with assumed initial conditions ($\phi = 5$ deg and $V_\phi = 0$ deg/s). While the calculation can assume zero for both ϕ and V_ϕ , the development of parametric roll may not occur until a much longer duration is calculated.

To complete the inputs necessary for the calculation, two more parameters are needed: the time increment Δt and the total number of points N . These parameters can be related to the natural frequency of roll, ω_0 , in calm water because a steady state parametric roll motion in longitudinal waves occurs with this frequency:

$$\omega_0 = \sqrt{\frac{\rho \nabla g \cdot GM_0}{I_X + A_{44}}} \quad (15)$$

Then, the period of the roll motion in calm water is expressed as:

$$T_0 = \frac{2\pi}{\omega_0} \quad (16)$$

The time increment Δt can be expressed in terms of the number of points per period N_{ppp} :

$$\Delta t = \frac{T_0}{N_{ppp}} \quad (17)$$

Thus, the number of points depends on the number of periods N_{per} to be reproduced:

$$N = N_{ppp} N_{per} \quad (18)$$

Practical experience recommends use of the following values:

$$N_{ppp} = 30; \quad N_{per} = 15$$

3.6 Calculation of Maximum Roll Angle

The parametric roll response has a transition from the state where the initial conditions still have an influence to the steady state where the amplitudes are similar or close to each other.

Different criteria for "closeness" can be used: relative (the difference is less than 3 - 5%) or absolute (say, less than one degree). Following this criteria, the steady state portion of the response can be extracted (see Figure 6) and the resultant maximum roll angle can be found as an average of steady state roll amplitudes.

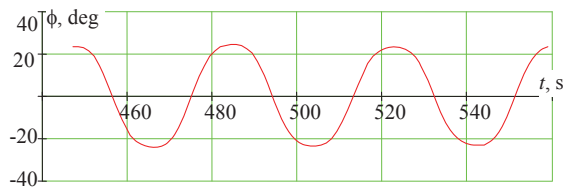


Figure 6 Steady-state portion of the roll motion in parametric resonance conditions

The steady state parametric roll is not the only possible type. If parametric roll is not possible for the given wave conditions, the response is represented by decaying roll oscillations – as shown in Figure 7. Indeed, the maximum roll angle here is the initial roll angle of 5 degrees. The response is not expected to look like a decaying sine function because of both the parametric excitation and nonlinearity of the equation (13).

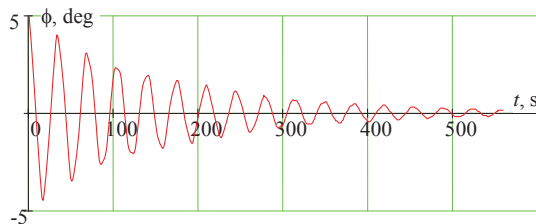


Figure 7 Roll response in absence of parametric roll

Another possible response may include "capsizing" (see Figure 8) if the *GZ* curve was computed for the entire range of 180 degrees (like in Figure 1). If the *GZ* curve is computed only for the positive stability range ($GZ > 0$), the calculation must be explicitly stopped once the roll angle exceeds the angle of vanishing stability.

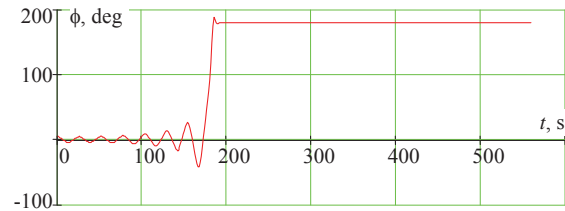


Figure 8 Roll response with parametric roll and capsizing

The mathematical model (13) is, probably, too simple to model actual capsizing, but the response, similar to that shown in Figure 8, indeed indicates a condition of strong parametric roll in which the maximum roll angle exceeds the standard level of 25 degrees as stipulated in Annex 2 of SDC 2/WP.4.

In rare cases, the user may observe response that does not stabilize. The roll amplitude may grow steadily or look like roll in irregular waves. These responses are not the result of an error, but of a known type of nonlinear behavior. In this case, the maximum achieved roll angle during N_{per} periods is used.

4. CALCULATION OF PARAMETRIC ROLL AMPLITUDE FOR A POST-PANAMAX CONTAINER SHIP

An example of a calculation of parametric roll amplitude, in compliance with the Level 2 criteria, is presented below. The investigated ship is a baby post-Panamax container ship with the characteristics as shown in Table 1:

Table 1: Main ship characteristics

Length L_{BP} (m)	238.35
---------------------	--------



Beam (m)	37.3
Depth (m)	19.6
Mean Draught (m)	11.5
Block Coefficient	0.657
GM (m)	0.84

$$I_x \ddot{\phi} + B_{44} \dot{\phi} + mgGZ = 0 \quad (19)$$

$$GZ = GM_0 \phi + l_3 \phi^3 + l_5 \phi^5 + GZ_w \quad (20)$$

The steady amplitude of parametric roll is calculated by using the following four methods:

- a direct numerical solution of the non-linear differential equation of roll that is included in SDC 2/INF.10, Annex 17;
- a numerical solution of the algebraic equation derived after applying the analytical method of averaging on the previous non-linear differential equation. (This algebraic equation is proposed in SDC 2/INF.10, Annex 17 to be used for obtaining the steady amplitude of parametric roll.)
- a numerical solution of the non-linear roll equation used by Spyrou (2005); and
- an analytical, closed-form, formula obtained by the method of harmonic balance, predicting the steady amplitude of parametric roll at principal resonance condition (Spyrou 2005).

The moment of inertia, I_x , and natural roll period T_0 are calculated through the roll radius of gyration by using Kato's formula, as proposed in SDC 2/INF.10-Annex 11. For the loading condition under investigation, $T_0 = 39.3$ s is assumed.

The linear damping coefficient is calculated by using Ikeda's method as proposed in the above IMO document, including the bilge keel component. While acknowledging that the criterion requires both linear and non-linear damping, at this stage, the comparison involves only linear damping.

The four methods use the same inertia and damping terms. Their main differences lie in the representation of the restoring terms. The SDC model (methods a and b above) is in the following form:

$$GZ_w = GM_{mean} \phi + GM_{amp} \cos \omega_e t \left\{ 1 - \left(\frac{\phi}{\pi} \right)^2 \right\} \phi$$

where I_x is roll moment of inertia including added moment of inertia; B_{44} is linear damping coefficient; m is the ship's displacement; g is gravitational acceleration; l_3 , l_5 are third and fifth order coefficients of GZ curve fit; ω_e is the encounter frequency; GM_{amp} is half the difference between the maximum and minimum value of GM on the span of a wave; GM_0 is the initial metacentric height in calm water. GM_{mean} is the mean of metacentric height variation on the span of the wave which, given the expressions in equation (20), and is interpreted to be the difference between the mean value of the GM in waves and the GM in calm water.

On the other hand, methods c) and d) (above) from Spyrou (2005) model parametric roll as follows:

$$\ddot{\phi} + 2\zeta\omega_0\dot{\phi} + \omega_0^2[1 - h\cos(\omega_e t)]\phi - c_3\omega_0^2\phi^3 - c_5\omega_0^2\phi^5 = 0 \quad (21)$$

where ζ is the damping ratio, ω_0 is roll natural frequency, c_3 , c_5 are third and fifth order restoring coefficients and $h = GM_{amp}/GM_{mean}$.

The two differential equations for parametric roll, equations (19) and (21), are not identical and, therefore, the solutions are not expected to replicate on each other completely.

Roll amplitude is calculated for ten different cases where the ship is under the effect of following waves with $\lambda = L_{BP}$ and ten different heights with $H_j = 0.01jL$, where $j = 1, 2, \dots, 10$, as requested in SDC 2/INF.10, Annex 17. This leads to waves some of which are extremely steep and with extremely low probabilities of encounter. For each wave

height, hydrostatic calculations of GM_{mean} and GM_{amp} are carried out by using the well-known commercial software MAXSURF. The ratio of the calculated GM_{amp} to GM_{mean} , together with the corresponding wave heights, are shown in Table 2.

The encounter frequency for the ship when sailing in following waves of length equal to the ship length and with the design speed of 21 knots is 0.224 rad/s. This leads to a frequency index $a = 4\omega_0^2/\omega_e^2 = 2.04$, which is far to the right of the principal resonance value $a=1$. The analytical manipulations that have been applied in the context of SDC and related literature on the parametric roll differential equation assume a condition very near to exact principal resonance. This may lead sometimes to questionable results if the detuning is large. Because the wave length is fixed to ship length, this discrepancy (i.e., a large difference between the frequency index and the principal resonance value) is quite likely to be present whenever a large ship is tested.

Table 2: Wave Height, Probability of Occurrence, and Ratio of GM_{amp} to GM_{mean}

Wave Length $\lambda=238.35\text{m}$			
N	Wave Height $H(\text{m})$	$\frac{GM_{amp}}{GM_{mean}}$	Probability W
1	2.384	0.703	0.2367
2	4.767	1.155	0.1196
3	7.151	1.422	0.0336
4	9.534	1.571	0.006146
5	11.918	1.624	0.0009333
6	14.3	1.632	0.0001025
7	16.685	1.656	0
8	19.068	1.673	0
9	21.452	1.737	0
10	23.835	1.815	0

As said in SDC 2/INF.10, Annex 11, the roll amplitude is calculated by a numerical solution of an algebraic equation deduced through the averaging method. This equation is repeated below for linear damping only:

$$\left(\frac{8\pi^2\omega_e\alpha}{(2\pi^2-A^2)\omega_0^2}\right)^2 + \left(\frac{6A^2-8\pi^2}{4(\pi^2-A^2)}\frac{GM_{mean}}{GM_0}\right) + \frac{8\pi^2-5\pi^2A^4l_5-6\pi^2A^2l_3}{4(\pi^2-A^2)} + \frac{8\pi^2\omega_e^2}{4(\pi^2-A^2)\omega_0^2} = \left(\frac{GM_{amp}}{GM_0}\right)^2 \quad (22)$$

where A is the roll amplitude and α is the linear damping term. Because the analytical solution of equation (22) is not provided in SDC 2/INF.10, Annex 17, the implementation of a numerical scheme to determine the solution cannot be avoided. However, since (22) is nonlinear with respect to amplitude A , more than one solution can exist. Therefore, guidance is required on the process of how to ensure that a solution identified is the correct one for use in the criterion. In general, a numerical calculation performed directly on the differential equation (19), which produces automatically a stable solution, is in many respects preferable to a calculation performed on the averaged form of equation (22), which produces also unstable solutions.

For completeness, the steady roll amplitude of the analytical solution of Spyrou (2005) is given in equation (23) also:

$$A^2 = -\frac{3c_3}{5c_5} \pm \left(\left(\frac{3c_3}{5c_5} \right)^2 - \frac{8}{5c_5} \left(\frac{1}{\alpha} - 1 \pm \sqrt{\frac{h^2}{4} - \frac{4k^2}{\omega_0^2\alpha}} \right) \right)^{0.5} \quad (23)$$

where k is a linear damping coefficient and $\alpha = 4\omega_0^2/\omega_e^2$

In Figure 9, the results obtained by each method, for the ten different wave heights discussed earlier, are shown. As each wave height corresponds to a specific value of GM_{amp}/GM_{mean} , this ratio is selected for the horizontal axis. The numerical simulations are initiated from an assumed roll angle of 0.01 rad (0.57 degrees).

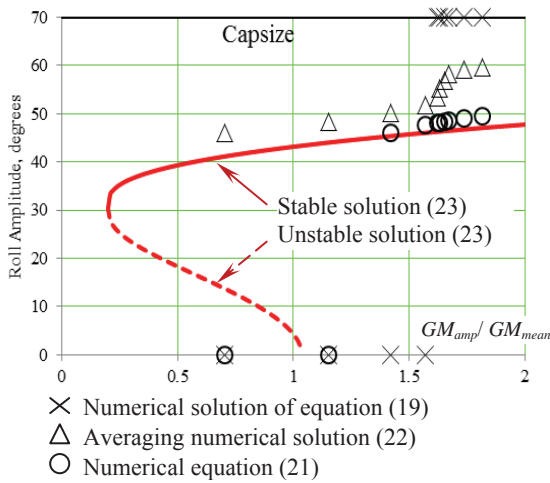


Figure 9: Parametric Rolling Amplitude for ten different wave heights

According to the analytical solution curve appearing in Figure 9, there are two possible responses by the ship: either a stable parametric resonance (continuous curve), similar to what was shown in Figure 6; or a decaying rolling that eventually leads to the upright position (as shown in Figure 7). Unstable solutions represented by the dashed curve cannot be physically realized. Nevertheless, they play the role of establishing a boundary between the coexisting solutions of zero and finite amplitude.

Figure 9 shows that all methods calculate a roll amplitude either close to the curve of parametric resonance or to the x-axis of decaying rolling. The numerical solutions of equation (19) for roll amplitude grow to infinity for the greater values of wave height which can be interpreted as a capsize event in mathematical terms.

When the solutions of parametric resonance and decaying roll coexist, the SDC method that uses equation (19) gives conflicting results. Also, the value of the parameter GM_{amp}/GM_{mean} , after which only parametric resonance occurs, is different for each method. These inconsistencies may lead to important differences between the index values of the

second-level vulnerability check for parametric roll.

For greater values of wave height (and subsequently of the parameter GM_{amp}/GM_{mean}), the response becomes highly non-linear. One such example is shown in Figure 10 which corresponds to the numerical solution of equation (21) for $H = 21.45\text{m}$.

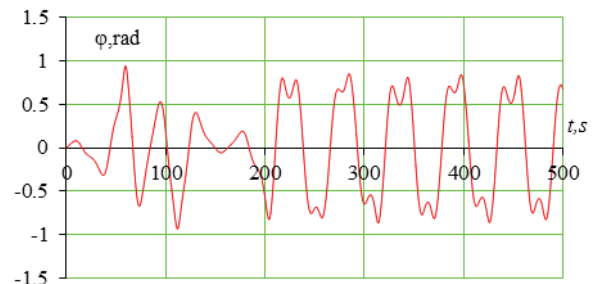


Figure 10: Highly non-linear parametric roll response

According to Figure 10, steady parametric rolling with very large amplitude (about 50 degrees) occurs. This essentially means that capsize is highly likely although the solution remains theoretically bounded. On the other hand, equation (19) for the same wave height detects capsizing, as can be seen from Figure 11. While the standard level of 25 degrees as stipulated in Annex 2 of SDC 2/WP.4 is exceeded in both cases, same order roll equations with similar terms show different dynamic characteristics for large waves.

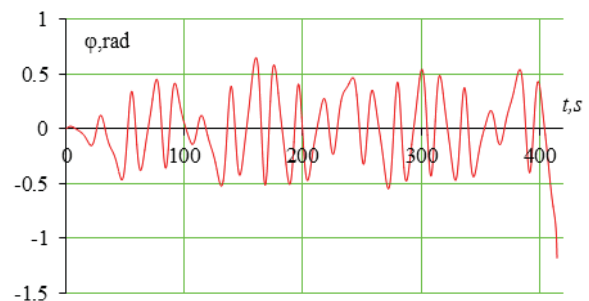


Figure 11: Non-linear parametric rolling that leads to capsize (19)



5. CONCLUSIONS

The second generation intact stability criteria presents new approaches for the assessment of ship stability failure. To perform these assessments, calculation methods are used that are not commonly used by practicing naval architects.

The equation of roll motion for the second check in the second-level of vulnerability criteria for parametric rolling is a differential equation. While the form of this equation may not be the same (see equations (19) and (21) above), a reliable solution of each requires a process to be followed if the solutions are to be replicated. The results show that such reliable solutions can be determined provided that the boundaries of application are respected.

6. REFERENCES

- Belenky, V., J. O. de Kat and Umeda, N., 2008, "Towards Performance-Based Criteria for Intact Stability". Marine Tech., Vol. 45 No 2, pp:101–123.
- Belenky, V., Bassler, C.C. and Spyrou K.J., 2011, Development of Second Generation Intact Stability Criteria, Naval Surface Warfare Center Carderock Division Report NSWCCD-50-TR-2011/065.
- France, W. M, Levadou, M., Treakle, T. W., Paulling, J. R., Michel, K. and Moore, C., 2003, "An Investigation of Head-Sea Parametric Rolling and its Influence on Container Lashing Systems". Marine Tech., Vol 40, No 1, pp:1–19.
- IMO SDC 2/INF.10, 2014, Second Generation Intact Stability Criteria. Information Collected by Correspondence Group on Intact Stability, Submitted by Japan, London, UK
- IMO SDC 2/WP.2, 2015, Development of Second Generation Intact Stability Criteria. Report of the Working Group, London, UK.
- IMO SDC 1/INF.8, 2013, Second Generation Intact Stability Criteria. Information Collected by Correspondence Group on Intact Stability, Submitted by Japan, London, UK
- IMO SLF 54/3/3 2011, Summary of Research into Stability Failures Modes and associated Criteria Development, London, UK
- IMO SLF 53/19, 2011, Report to Maritime Safety Committee, London, UK.
- Peters, W., Belenky, V., Bassler C., Spyrou, K., Umeda, N., Bulian, G. and Altmayer, B., 2011, "The Second Generation of Intact Stability Criteria An Overview of Development", SNAME Trans. Vol. 119.
- Peters, W., Belenky, V. and Spyrou, K., 2014 "Regulatory Use of Nonlinear Dynamics: An Overview" Proc. 14th Intl. Ship Stability Workshop, Kuala Lumpur, Malaysia, pp. 28-37
- Spyrou, K., 2005, "Design Criteria for Parametric Rolling", Oceanic Engineering International, Vol. 9, No 1, pp. 11-27
- Weems, K. and Belenky, V., 2015, "Rapid Ship Motion Simulations for Investigating Rare Stability Failures in Irregular Seas" Proc. 12th Intl. Conf. on Stability of Ships and Ocean Vehicles (STAB 2015), Glasgow, UK.

This page is intentionally left blank

Session 10.2 – NAVAL SHIP STABILITY

Analytical Study of the Capsize Probability of a Frigate

Aerodynamics Loads on a Heeled Ship

**Validation of Time Domain Panel Codes for Prediction of Large
Amplitude Motions of Ships**

This page is intentionally left blank



Analytical Study of the Capsize Probability of a Frigate

Frédéric Le Pivert, *Research Institute of the French Naval Academy, Brest, France*
frederic.le_pivert@ecole-navale.fr

Abdelkader Tizaoui, *Institut Polytechnique des Sciences avancées, DRI, Paris, France*

Radjesvarane Alexandre, *ENSAM, Paristech, Paris, France*

ean-Yves Billard, *Research Institute of the French Naval Academy, Brest, France*

ABSTRACT

The roll motion for a ship in a transverse sea can be represented by a one degree of freedom model. Equations are derived to write analytically the probability density function of roll angle, roll speed and roll excitation moment. Also a capsizing criterion is shown to have a whole process for a capsizing probability calculation.

Keywords: roll motion, capsizing, Fokker-Planck-Kolmogorov equation, characteristic method.

1 INTRODUCTION

Ship stability is one of nowadays worries. The old criteria that were defined in the first part of the 20th century are based on static stability. The new generation of criteria should be based on dynamical stability. These criteria are not simple evaluation but should be also quantification of the risks for a ship on any sea.

All ships are different but their behaviours on sea could be modelled with the same type of equations. Here the problem is limited to a ship sailing in transverse sea. It is assumed that in this case, roll motion could be represented by a one degree of freedom (1-DOF) model. So the goal of the paper is to solve the Fokker-Planck-

Kolmogorov equation (FPK) associated to the dynamical problem and to obtain the probability density function of the three following variables: roll angle, roll speed and roll excitation. The solution obtained has been tested on realistic situation. A capsizing criterion is also added to have a full way to obtain a capsizing probability.

Several methods have already been suggested to estimate large roll angles and stability failures. The Peak Over Threshold Method (McTaggart 2000) and Envelope Peak Over Threshold Method (Belenky & Campbell 2011) use statistical extrapolation on relatively small amplitudes to find the largest motions probability (Campbell 2014). The extrapolation technique is also a real issue for roll motion probability. One way is the split-time method. The split-time method divides the problem in two



parts considering the ship behavior is different whether the roll angle is below or above a given threshold. The idea is to fit only the largest angles distribution (Belenky, 2014) and could be applied for both Peak Over Threshold and Envelope Peak Over Threshold methods.

Melnikov methods have also been largely discussed in the 1990s and in the 2000s (Hsieh et al. 1994, Scolan, 1997, Jiang et al. 2000, McCue & Troesch 2005). Melnikov methods can determine properly whether a sea state is dangerous or not. Markov methods use the dynamics of the system to find the complete expression of the roll motion probability by solving an FPK. The present paper uses one of these methods.

2 MATHEMATICAL ANALYSIS

2.1 Markov Methods

The aim of this group of methods is to consider roll motion as a Markovian process. In their paper Roberts and Vasta (Roberts & Vasta 2000) describe the time evolution of the energy of roll motion with a white noise as system perturbation.

More recent methods preserve the roll motion equation and consider the perturbation as a filtered Gaussian white noise according to Spanos ARMA filters theory (Spanos 1983). This method was applied to uncoupled roll motion by Francescutto and Naito (Francescutto & Naito 2004) and the method was fully developed by Su and Falzarano (Su & Falzarano 2011). This method overcomes the difficulty to deal with a noise which does not have any remarkable property. On the other hand the system becomes larger and new variables appear without any physical sense. By using this method,

the FPK of the complete system for both old and new variables can be obtained. These previous authors derive numerically the equation.

In the present paper the FPK is derived analytically. This derivation needs in return some simplification of dynamics.

2.2 Derivation of the Methods

Consider the following adimensioned roll motion equation:

$$\ddot{\phi} + \lambda_1 \dot{\phi} + \lambda_2 \phi |\dot{\phi}| + c(\phi) = f(t), \quad (1)$$

where:

- ϕ is the roll angle,
- t is the time,
- \dot{y} means the time derivative of the quantity y ,
- λ_1 is the linear damping coefficient,
- λ_2 is the quadratic damping coefficient,
- c is the restoring moment,
- f is the external random moment.

The equation (1) is the expression of the principle of dynamics applied to roll motion. To obtain (1), all the moments were divided by $I_{xx}\omega_0^2$, where I_{xx} is the total inertia in roll of the ship and ω_0 is the natural roll frequency of the ship.



The term f is supposed to be a filtered white noise. The considered filter is defined by the following equation:

$$\ddot{Z} + V_1 \dot{Z} + V_0 Z = \gamma W, \quad (2)$$

where V_1 , V_0 , γ are constant. W is a Gaussian white noise. so it leads to the following system:

$$\begin{cases} \dot{x}_1 = x_2, \\ \dot{x}_2 = -\lambda_1 x_2 - \lambda_2 x_2 |x_2| - c(x_1) + x_3, \\ \dot{x}_3 = x_4, \\ \dot{x}_4 = -V_1 x_4 - V_0 x_3 + \gamma W. \end{cases} \quad (3)$$

In (3), we have:

- $\varphi = x_1$,
- $\dot{\phi} = x_2$,
- $f = x_3$.

The system (3) is rewritten with vectors:

$$\dot{X} = F(X) + GW. \quad (4)$$

This can lead to the Fokker-Planck-Kolmogorov equation:

$$\partial_t P = -\nabla \cdot (P F) + \frac{\gamma^2}{2} \partial_{x_4}^2 P, \quad (5)$$

where P is the probability density function of the random variable X .

Remark: According to (Francescutto & Naito 2004), a 4th order-filter at least should be applied. The present filter has a smaller order filter only to write an analytical formula for P . Here is one simplification to get the formula.

To integrate (5), it was chosen to take the space Fourier transform of this equation. Be-cause F_2 ($F_2 = -\lambda_1 x_2 - \lambda_2 x_2 |x_2| - c(x_1) + x_3$) Fourier transform has no analytical expression, new hypotheses should be made:

- linearization around equilibrium $c(x_1) = c_i(x_1 - x_{eq})$,
- damping linearization, $\lambda_2 = 0$,

where c_i is the restoring coefficient around a considered point of equilibrium x_{eq} , x_{eq} is defined by $c(x_{eq}) = 0$. Here it is chosen to derive (5) assuming the hypotheses. It is assumed a boat has three heel angles of equilibrium on each side: $\varphi = 0$, $\varphi = \pm\varphi_V$, $\varphi = \pm\pi$. Choosing a linearization around these points is considering $c(x_1)$ as a 5th order polynomial. The form of c is given by (6):

$$c(x_1) = C x_1 (x_1^2 - \varphi_V^2) (x_1^2 - \pi^2). \quad (6)$$

This method is equivalent to the piece-wise linearization method (Belenky 1993). The difference is: in the present method the roll motion is supposed to be fully forced by the external moment, whereas in (Belenky 1993) the roll angle is considered as a solution of (1). Using that method, a transition solution calculated by considering $f = 0$ should be taken into account.

The Fourier transform of (5) is:

$$\begin{aligned} \partial_t \hat{P} = & \left(c_i \xi_2 \partial_{\xi_1} + (\xi_1 - \lambda_1 \xi_2) \partial_{\xi_2} \right. \\ & + (\xi_2 - V_0 \xi_4) \partial_{\xi_3} \\ & \left. + (\xi_3 - V_1 \xi_4) \partial_{\xi_4} \right) \hat{P} + \frac{\gamma^2}{2} \xi_4^2 \hat{P} \quad (7) \end{aligned}$$

The equation (7) is a transport equation. So if we know an integrable solution $\hat{P}_0(\xi_1, \xi_2, \xi_3, \xi_4)$ at $t = 0$, there exists an integrable solution $\hat{P}(t, \xi_1, \xi_2, \xi_3, \xi_4) = \hat{P}_t(\xi_1, \xi_2, \xi_3, \xi_4)$ with the same measure at every $t > 0$. Fourier transform make this property true for P solution of (5). Here to obtain (7) \hat{P} has been supposed square-integrable. So P is square-integrable.

A method of characteristics is applied: characteristic curves are curves



$s \rightarrow (t(s), \xi_1(s), \xi_2(s), \xi_3(s), \xi_4(s))$ who check the following condition:

$$\begin{cases} \frac{dt}{ds} = 1, \\ \frac{d\xi_1}{ds} = c_i \xi_2, \\ \frac{d\xi_2}{ds} = \lambda_1 \xi_2 - \xi_1, \\ \frac{d\xi_3}{ds} = V_0 \xi_4 - \xi_2, \\ \frac{d\xi_4}{ds} = V_1 \xi_4 - \xi_3. \end{cases} \quad (8)$$

So $t = s$ and

$$\begin{pmatrix} \xi_1 \\ \xi_2 \\ \xi_3 \\ \xi_4 \end{pmatrix} = \underbrace{\begin{pmatrix} 0 & c_i & 0 & 0 \\ -1 & \lambda_1 & 0 & 0 \\ 0 & 1 & 0 & V_0 \\ 0 & 0 & -1 & V_1 \end{pmatrix}}_A \begin{pmatrix} \xi_1 \\ \xi_2 \\ \xi_3 \\ \xi_4 \end{pmatrix} \quad (9)$$

The solution of (9) is written this way:

$$\begin{pmatrix} \xi_1 \\ \xi_2 \\ \xi_3 \\ \xi_4 \end{pmatrix} = \sum_{k=1}^4 \kappa_k W_k e^{w_k s}, \quad (10)$$

where w_k are the eigenvalues of A , W_k are the eigenvectors of A and κ_k are determined by initial conditions.

Remark: Now the choice for a second order filter can be justified. If a larger order filter had been chosen, this would have lead to a larger ma-trix A . Then it becomes impossible to calculate analytically the eigenvalues and the eigenvectors of A .

$$\begin{aligned} w_1 &= \frac{\lambda_1 + \sqrt{\lambda_1^2 - 4c_i}}{2}, \\ w_2 &= \frac{\lambda_1 - \sqrt{\lambda_1^2 - 4c_i}}{2}, \\ w_3 &= \frac{V_1 + \sqrt{V_1^2 - 4V_0}}{2}, \\ w_4 &= \frac{V_1 - \sqrt{V_1^2 - 4V_0}}{2}, \end{aligned} \quad (11)$$

and

$$W_1 = \begin{pmatrix} -w_2(w_1(\lambda_1 - V_1) - c_i + V_0) \\ w_1(\lambda_1 - V_1) - c_i + V_0 \\ V_1 - w_1 \\ 1 \end{pmatrix} \quad (12)$$

$$W_2 = \begin{pmatrix} -w_1(w_2(\lambda_1 - V_1) - c_i + V_0) \\ w_2(\lambda_1 - V_1) - c_i + V_0 \\ V_1 - w_2 \\ 1 \end{pmatrix}$$

$$W_3 = \begin{pmatrix} 0 \\ 0 \\ w_3 \\ 1 \end{pmatrix}, W_4 = \begin{pmatrix} 0 \\ 0 \\ w_4 \\ 1 \end{pmatrix} \quad (13)$$

After calculation, a formula-tion of $\xi_1(s), \xi_2(s), \xi_3(s), \xi_4(s)$ using $\xi_1(0), \xi_2(0), \xi_3(0), \xi_4(0)$ is obtained. Along the characteristic curves, it can be written:

$$\begin{aligned} \frac{d\hat{P}}{ds} &= \frac{\partial \hat{P}}{\partial t} \frac{dt}{ds} + \frac{\partial \hat{P}}{\partial \xi_1} \frac{d\xi_1}{ds} + \frac{\partial \hat{P}}{\partial \xi_2} \frac{d\xi_2}{ds} \\ &+ \frac{\partial \hat{P}}{\partial \xi_3} \frac{d\xi_3}{ds} + \frac{\partial \hat{P}}{\partial \xi_4} \frac{d\xi_4}{ds} = -\frac{\gamma^2}{2} \xi_4^2 \hat{P} \end{aligned} \quad (14)$$

The only solution is:

$$\hat{P}(s) = \hat{P}(0) \exp \left(-\frac{\gamma^2}{2} \int_0^s \xi_4^2(u) du \right) \quad (15)$$

As the expression $\int_0^s \xi_4^2(u) du$ is difficult to understand written in this way, ξ_i are replaced by $\zeta_i = \kappa_i e^{w_i s}$.



So it leads to:

$$\xi_4 = \zeta_1 + \zeta_2 + \zeta_3 + \zeta_4. \quad (16)$$

Let express the solution as a function of t:

$$\hat{P}_t \begin{pmatrix} \xi_1 \\ \xi_2 \\ \xi_3 \\ \xi_4 \end{pmatrix} = \hat{P}_0 \begin{pmatrix} \xi_1(0) \\ \xi_2(0) \\ \xi_3(0) \\ \xi_4(0) \end{pmatrix} \cdot e^\Psi \quad (17)$$

where $\xi_1(0)$, $\xi_2(0)$, $\xi_3(0)$, $\xi_4(0)$ could be expressed with ζ_1 , ζ_2 , ζ_3 , ζ_4 and t.

$$\Psi = -\frac{\gamma^2}{2} \begin{pmatrix} \frac{\zeta_1^2}{2w_1} + \frac{\zeta_2^2}{2w_2} + \frac{\zeta_3^2}{2w_3} + \frac{\zeta_4^2}{2w_4} \\ + \frac{2\zeta_1\zeta_2}{w_1 + w_2} + \frac{2\zeta_1\zeta_3}{w_1 + w_3} + \frac{2\zeta_1\zeta_4}{w_1 + w_4} \\ + \frac{2\zeta_2\zeta_3}{w_2 + w_3} + \frac{2\zeta_2\zeta_4}{w_2 + w_4} + \frac{2\zeta_3\zeta_4}{w_3 + w_4} \end{pmatrix} \quad (18)$$

With (17) a complete formula for the time depending probability density function of the random variables ξ_1 , ξ_2 , ξ_3 , ξ_4 is given at every time t. The function Ψ depends on the random variables (18) and describes an ellipse. The term \hat{P}_0 is a displacement of the properties at $t = 0$ along the characteristic curves.

So the solution of (5) is:

$$P_t \begin{pmatrix} x_1 \\ x_2 \\ x_3 \\ x_4 \end{pmatrix} = P_0 \begin{pmatrix} x_1(0) \\ x_2(0) \\ x_3(0) \\ x_4(0) \end{pmatrix} * \chi \begin{pmatrix} x_1 \\ x_2 \\ x_3 \\ x_4 \end{pmatrix}, \quad (19)$$

where $x_1(0)$, $x_2(0)$, $x_3(0)$, $x_4(0)$ can be expressed with x_1 , x_2 , x_3 , x_4 and t and * means the convolution product. The function χ is the in-verse Fourier transform e^Ψ and is a gaussian probability law for random variables y_1 , y_2 , y_3 , y_4 which are derived from x_1 , x_2 , x_3 , x_4 with an au-tomorphism. The following initial condition are

applied:

$$P_0 \begin{pmatrix} x_1(0) \\ x_2(0) \\ x_3(0) \\ x_4(0) \end{pmatrix} = \delta \begin{pmatrix} x_1 \\ x_2 \\ x_3 \\ x_4 \end{pmatrix}, \quad (20)$$

where δ is the standard Dirac distributon.

So the final solution of (5) is:

$$P_t \begin{pmatrix} x_1 \\ x_2 \\ x_3 \\ x_4 \end{pmatrix} = \chi \begin{pmatrix} x_1 - x_1(0) \\ x_2 - x_2(0) \\ x_3 - x_3(0) \\ x_4 - x_4(0) \end{pmatrix} \quad (21)$$

In this way, the solution does not depend on time.

The solution has a gaussian form for the 4 variables. This result is in accordance with (Benlenky 1993) considering only forced oscillations.

3 RESULTS

3.1 Method

All results were obtained by generating a large number of simulations in which the sea state remain the same. The software used for the simulation is FREDYN. FREDYN calculate the 6-DOF dynamics of a given boat with the potential flow assumption. Here the boat used for simulation is the F70-frigate of the French Navy. The case tested is the frigate in trans-verse sea with 0 or 6 knots forward speed.

3.2 Time-independance Verification

The time-independance of the probability is tested with long simulations. The hypotheses of calculation used in the first part are not taken into account.



For a series of 50 simulations lasting 5 hours in a sea state defined by a Pierson-Moskowitz spectrum with a significant wave height $H_S = 12.4\text{m}$ and a mean wave period $T_P = 12.7\text{s}$, the maximum of the roll angle for each simulation have been situated in time during the simulation. The number of maxima occurring before a certain time is counted and represented in Figure 1. The frigate's forward speed is 6 knots.

time of the maximum	number of maxima
< 2000s	8
< 4000s	11
< 6000s	23
< 8000s	27
< 10000s	31
< 12000s	33
< 14000s	37
< 16000s	46
< 18000s	50

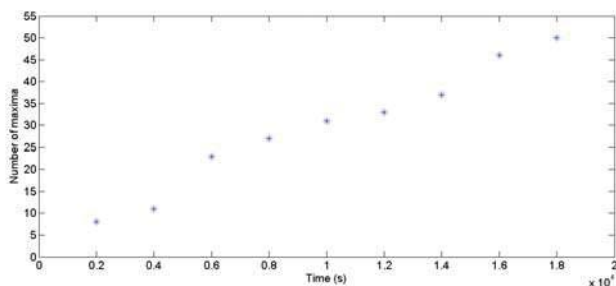


Figure 1: Number of maxima versus time

The number of maxima is linearly growing, so the probability associated to roll motion is time-independent.

3.3 Probability Density Function Estimation

A direct estimation of the probability density function has been calculated for 0 forward speed frigate in 5 sea states. The estimation is made according that over a long time the probability is

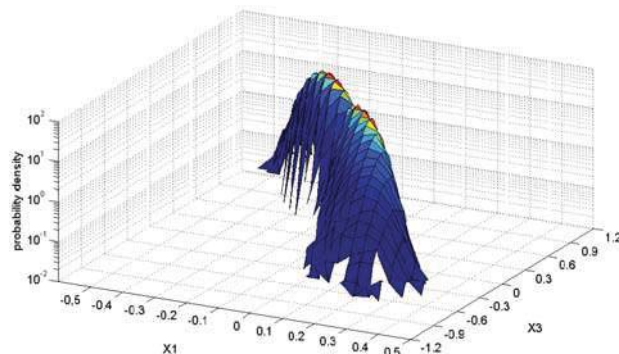


Figure 2: Conditional probability density function $P(x_1, x_2 = 0|x_3)$

stable. The first results showed a similar shape for the probability density function between sea states. To compare the sea states, Bayes' formula was used so:

$$P(x_1, x_2, x_3) = P(x_1, x_2|x_3) \cdot P(x_3), \quad (22)$$

where | means knowing. The conditional probability is supposed to be normal. For representation, the results are taken at $x_2 = 0$. Figure 2 shows a preferred axis of the (x_1, x_3) -plan. A formula is given with variable change: $Y_1 = kx_1 + x_3$ and $Y_2 = kx_3 - x_1$. The variable Y_2 is describing the evolution along the axis and Y_1 describes the evolution perpendicularly to the axis. The formula for $P(x_1, x_2 = 0|x_3)$ is of the following form:

$$P(x_1, x_2 = 0|x_3) = \exp \left(- \left(\begin{array}{c} h_0 + h_1 Y_1 + h_2 Y_1^2 \\ + g_1 Y_2 + g_2 Y_2^2 \\ + g_3 Y_2^3 + g_4 Y_2^4 \end{array} \right) \right). \quad (23)$$

The parameters $k, h_0, h_1, h_2, g_1, g_2, g_3, g_4$ are calculated for 5 different sea states and the results are written in the following table.



H_S	T_P	h_0	h_1	h_2	k
9.270m	12.36s	-4.595	16.26	418.0	-0.4058
9.465m	12.57s	-5.981	15.96	422.6	-0.4141
9.660m	12.79s	-3.557	17.08	395.7	-0.4238
9.758m	12.90s	-3.963	15.68	418.6	-0.4256
10.448m	12.40s	2.994	16.96	401.5	-0.4140

H_S	T_P	g_1	g_2	g_3	g_4
9.270m	12.36s	0.8710	-10.680	-6.489	41.45
9.465m	12.57s	0.6514	-9.714	-4.792	34.70
9.660m	12.79s	0.5147	-9.380	-3.882	31.26
9.758m	12.90s	0.5350	-9.441	-3.870	31.63
10.448m	12.40s	0.1893	-2.475	-1.229	7.584

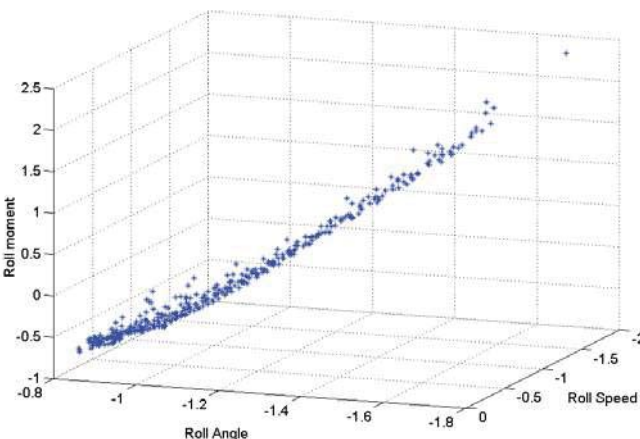


Figure 3: points of the angle-speed-moment-space with $\varphi > 48^\circ$, $\dot{\varphi} > 0$

The parameters h_1 , h_2 , k have really similar values for all the sea state. For the other parameters, the last sea state ($H_S = 10.448\text{m}$, $T_P = 12.40\text{s}$) gives values contrastive in the other sea states. The significative wave height of the last sea state is significantly higher than the others and, in the same time, the mean wave period remains the same. This leads to a much more dangerous sea state and explains why this sea state is associated to contrastive values for h_0 , g_1 , g_2 , g_3 , g_4 . Nonetheless the value of h_0 , g_1 , g_2 , g_3 , g_4 are of close order. This could indicate a slight evolution of these parameters with the sea state. The similar values for h_1 , h_2 , k indicate these parameters are almost constant. The parameter k gives the direction of the preferred axis at $x_2 = 0$ and h_1 , h_2 the decrease of the probability for points of the (x_1, x_3) -plan which are not on the axis.

The form of the results obtained by numerical simulation is in accordance with the analytical development such as the gaussian probability law for the random variable Y_1 .

3.4 Capsizing Criteria

The goal of the probability density estimation is to obtain a capsizing probability. This leads to a

search for criteria of capsizing.

Here are compared simulations in which the roll angle has been really large and simulations leading to capsize. The sea state is still defined by a Pierson-Moskowitz spectrum, $H_S = 12.5\text{m}$ and $T_P = 12.6\text{s}$. In the space defined by angle, speed and moment (x_1, x_2, x_3) , points corresponding to angle over 50° and speed of the same sign like angle (situations getting closer to capsize) are extracted Figure 3.

The points seem to get aligned in a same plan. Figure 4 show the points in this plan defined by two arbitrary variables V_1, V_2 . Red points correspond to simulations getting to capsize and blue points correspond to simulations without capsizing.

A stable area can be defined with the trajectories which do not lead to capsize. So even for a large angle, the boat could escape such dangerous situation. Then the probability of capsizing is the probability for the trajectory in the angle-speed-moment space to come out of the stable domain.

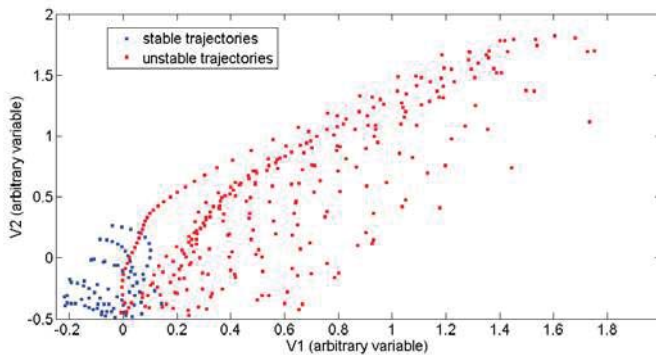


Figure 4: comparison of trajectories either stable or leading to capsize

4 CONCLUSION

In the paper an analytical formula of the probability density function of the linear roll motion has been obtained. The properties have been tested for simulations with realistic sea state. The results are partially in accordance, but the time independence remains exact both for linear and non-linear roll motion. In some case, the gaussian law proved for the linear motion remains exact for the non-linear motion. On top of that capsize criterium has been found for the calculation of a capsize probability with the probability density function of the roll angle, speed and moment.

5 REFERENCE

McTaggart, K.A., 2000, Ship Capsize risk in a Seaway Using Fitted Distributions to Roll Maxima, ASME Journal of Offshore Mechanics and Arctic Engineering, Vol. 122, No. 2, pp.141-146.

Belenky, V. and Campbell, B.L., 2011, Evaluation of the Exceedance Rate of a Stationary Stochastic Process by Statistical Extrapolation Using the Envelope Peaks over Threshold (EPOT) Method, Hydrodynamics Department Report, NSWCCD-50-TR-2011/032, Naval Sur-

face Warfare Center Carderock Division, MD.

Hsieh, S.-R., et al., 1994, A Nonlinear Probabilistic Method for Predicting Vessel Capsizing in Random Beam Seas, Proceedings: Mathematical and Physical Sciences, Vol. 446, No. 1926, pp.195-211.

Scolan, Y.-M., 1997, Technical Note on ship rolling associated to high degree polynomial moment using Melnikov methods, Applied Ocean Research, Vol. 19, pp 225-234.

Jiang, C., et al., 2000, Capsize Criteria for Ship Models with Memory-Dependent Hydrodynamics and Random Excitation, Philosophical Transactions: Mathematical, Physical and Engineering Sciences, Vol. 358, No. 1771 The Nonlinear Dynamics of Ships, pp.1761-1791.

McCue, L. and Troesch, A., Probabilistic determination of critical wave height for a multi-degree of freedom capsize model, Ocean Engineering, Vol. 32, pp. 1608-1622.

Roberts, J.B., Vasta, M., 2000, Markov Modelling and Stochastic Identification for Nonlinear Ship Rolling in Random Waves, Philosophical Transactions: Mathematical, Physical and Engineering Sciences, Vol. 358, No. 1771 The Nonlinear Dynamics of Ships, pp. 1917-1941.

Spanos, P.-T.D., 1983, ARMA Algorithms for Ocean Wave Modelling, ASME Journal of Energy Resources Technology, Vol. 105, pp. 300-309.

Francescutto, A. and Naito, S., 2004, Large amplitude roll motion in a realistic seaway, International Shipbuilding Progress, Vol. 51, No. 2, pp. 221-235.

Su, Z. and Falzarano, J.M., 2011, Gaussian and non-Gaussian cumulant neglect application to



large amplitude rolling in random waves, International Shipbuilding Progress, Vol. 58, No. 2, pp. 97-113.

Campbell, B., et al., 2014, On the Application of Generalized Pareto Distribution for Statistical Extrapolation in the Assessment of Dynamic Stability in Irregular Waves, 14th International Ship Stability Workshop, Kuala Lumpur, Malaysia.

Belenky, V., et al., 2014, Extrapolation and Validation Aspects of the Split-Time Method, 30th Symposium on Naval Hydrodynamics, Hobart, Tasmania, Australia.

Belenky, V., 1993, A Capsizing Probability Computation Method, Journal of Ship Research, Vol. 37, No. 3

This page is intentionally left blank



Aerodynamics Loads on a Heeled Ship

Romain Luquet, *DGA Hydrodynamics, FRANCE*, romain.luquet@intradef.gouv.fr

Pierre Vonier *DGA Hydrodynamics, FRANCE*, pierre.vonier@intradef.gouv.fr

Andrew Prior, *Royal Canadian Navy, DGMEPM, DNPS 2-3*, andrew.prior@forces.gc.ca

Jean-François Leguen, *DGA Hydrodynamics, FRANCE*, jean-francois.leguen@intradef.gouv.fr

ABSTRACT

Verification of ship stability is based on rules which account for the effects of wind. Restrictive hypothesis are employed to define those rules and especially the influence of ship heeling. This study reviews some stability rules and applies them to the case of the F70 frigate. Then, two alternate approaches are considered: (i) accounting for the actual lateral areas and respective centroids of the heeled ship, and (ii) CFD calculations to determine aero and hydro dynamic coefficients at each heel angle. Finally, comparison is made between the results of these alternate approaches and the stability rules.

Keywords: *wind, CFD, rules, naval ships*

1. INTRODUCTION

Strong winds can increase the risk of capsizing, thus, stability assessment must account for wind effects. This study reviews some of the assumptions commonly embedded in stability rules and investigates two alternate approaches.

1.1 Stability Rules

The first phase of this study was a review of some stability rules (i.e. French Navy, Dutch Navy, IMO, Brown & Dreybach). The formulations defined in these rules were employed to calculate wind heeling moments for the French Navy F70 class frigate.

Whether it is because they are very old (sometimes established more than 50 years ago) or to facilitate the calculations, some of the assumptions common to stability rules are simplistic and do not reproduce faithfully the physics of the studied phenomenon. Examples

of such assumptions include:

Fixed value for aerodynamic drag coefficient regardless of ship geometry or heel angle (e.g. $C_D = 1.12$).

Fixed locations (centroid of projected lateral areas) of application of aero and hydro dynamic forces.

Dead ship condition (zero forward speed with a beam wind) considered the worst case. Blendermann (1996) has shown that beam wind is not the worst case.

Constant wind speed. Gusting is accounted for as either an increase in wind lever arm (IMO) or by defining requirements for righting arm area ratios (naval stability rules).

No variation in amplitude of wind against altitude (IMO) or simple wind profile (naval stability rules). No variation in direction.

Simplified windage area.



1.2 Alternate Approaches

The second phase of this study was to address the first two assumptions of the previous section and investigate two alternate approaches:

AERODYNAMIC APPROACH: Uses the same basic wind moment formulation found in the stability rules. Except, the fixed distance between the upright centroid of windage area and half draft (along with cosine function) are replaced with calculated centroids for above waterline windage area and below waterline hull area (Zaero, Zhydro).

CFD APPROACH: Uses a CFD model to generate aerodynamic and hydrodynamic coefficients (C_Y , C_Z , C_k) for the ship at each heel angle.

1.3 Comparison

The last phase of this study was to compare wind heeling moment results to assess their consistency. The study focused only on the determination of the heeling moment on a ship exposed to a given constant wind speed. The relevance of the choice of speed and associated regulatory criteria is not discussed.

2. STABILITY RULES

1.1 French Naval Rules

The wind heeling moment formula in the French military regulations, IG 6018, (1999) is derived from the work of Sarchin and Goldberg (1962). It requires a reference wind speed (at 10 m height above waterline), assumes a wind speed profile ($\sim h^{1/7}$) and integrates over the projected surface area exposed to wind. Integration is simplified by dividing this surface area into horizontal strips, each being subjected to a constant wind speed depending on the average height of the considered strip.

The inclining lever arm in meters or BLI, due to wind (wind heeling moment divided by $\Delta \cdot g$) is then obtained by summing the influence of each strip as follows:

$$B.L.I. = \sum_i \frac{0.0195 \cdot A_i \cdot h_i \cdot V_i^2}{1000 \cdot \Delta} \cos^2 \varphi \quad (1)$$

Where:

- $V_i =$ Wind speed at strip center [knots]
- $A_i =$ Projected area of each strip [m^2]
- $h_i =$ vertical distance between the center of the strip and the drift center (assumed immersed at $T/2$) [m]
- $\varphi =$ Heel Angle [deg]
- $\Delta =$ Vessel displacement [t]

The coefficient 0.0195 is derived from the combination of physical constants and the units used for wind speed:

$$\frac{1}{2} \frac{\rho C_Y}{g} \left(\frac{1.852}{3.6} \right)^2 = 0.0195 \text{ [kg} \cdot \text{m}^{-2} \cdot \text{kts}^{-2}] \quad (2)$$

Where:

- $C_Y = 1.12$,
- $\rho = 1.29 \text{ kg/m}^3$ and
- $g = 9.81 \text{ m}^2/\text{s}$

The \cos^2 term, which is used in many other regulations, comes from historical studies of sail ships (Middendorf, 1903). Sail ships have a large windage area (upright) that decreases drastically with heel (Middendorf, 1903). The formulation is obviously flawed as at 90° heel a ship will still have a windage area.

1.2 Dutch Naval Rules

The formula used in naval regulations of the Netherlands is similar to the French regulations except that it utilizes a \cos^3 term and does not take into account the wind speed profile. These regulations are derived from Germany naval rules (Arndt 1982). The wind heeling arm formula is as follows:



$$B.L.I. = \frac{P.A.I}{1000.\Delta} \cdot \frac{1 + 3\cos^3(\varphi)}{4}$$

$$P = \frac{C_W \cdot \rho_l \cdot V^2}{2} \quad (3)$$

Where:

P = Wind pressure [Pa]

A = Windage surface area [m²]

I = Distance between the half-draft and the windage area center

$C_W = 1.2$

$\rho_l = 0.125 \text{ kg.s}^2.\text{m}^{-4}$

The advantage of this formulation lies in its ability to model the decay of the heeling moment while maintaining a non-zero value at $\varphi = 90^\circ$. The choice to keep one quarter of the zero heel value seems somewhat arbitrary.

2.3 IMO

In the regulations established by the IMO, and therefore applicable to civilian vessels, the pressure applied on the windage surface is specified instead of the wind speed. In addition, the heeling moment is considered invariant with heel angle. The B.L.I. is calculated as follows:

$$B.L.I. = \frac{P.A.Z}{1000.\Delta.g} \quad (4)$$

Where:

P = Pressure applied to windage surface [Pa]

Z = Distance between the center of the windage area and the center of the underwater lateral area (assumed by default located at T/2) [m]

This formulation is acceptable as it applies mainly to large commercial vessels like container ships or tankers, which by their shape, have a windage surface almost independent of the heel angle.

It is possible to compute an equivalent wind speed by comparing the IMO and naval formula at zero heel. Comparing with the French regulations, the relation obtained is:

$$V = \sqrt{\frac{P}{0.0195.g}} \quad (5)$$

With the usual value of $P = 504 \text{ Pa}$ (IMO without gust) and assuming $C_Y = 1.12$, then $V = 51 \text{ knots}$ or 63 knots (IMO with gust) instead of 100 knots generally used in naval stability rules for combatants.

2.4 Brown & Deybach

Brown & Deybach (1998) proposed a formula that considered the principal dimensions of the ship. Their wind heeling arm formula was as follows:

$$B.L.I. = \frac{\frac{1}{2}C_D\rho V^2 \cdot \left[C_W \frac{L_{PP} \cdot B}{2} + \left(A - C_W \frac{L_{PP} \cdot B}{2} \right) \cos(\varphi) \right]}{1000.g.\Delta} \cdot \left[\frac{B}{2} + \left(L - \frac{B}{2} \right) \cos(\varphi) \right] \quad (6)$$

Where:

C_D = Drag coefficient = 1.12

B = Ship beam

L_{pp} = Ship length

C_W = Water plane area coefficient

3. CASE STUDY

The ship chosen for this study is the French Navy F70 type anti-aircraft frigate shown in Figure 1. The CAD model of the ship used for this study has a simplified superstructure (masts and antennae are not considered) as shown in Figure 2. Blendermann (1999) provides guidance on the influence of the details of the superstructure on the



aerodynamic coefficients and its recommendations have been followed. The hydrostatic characteristics of the hull are presented in Table 1.



Figure 1: French frigate “Jean Bart”

Figure 2: CAD model of “Jean Bart”

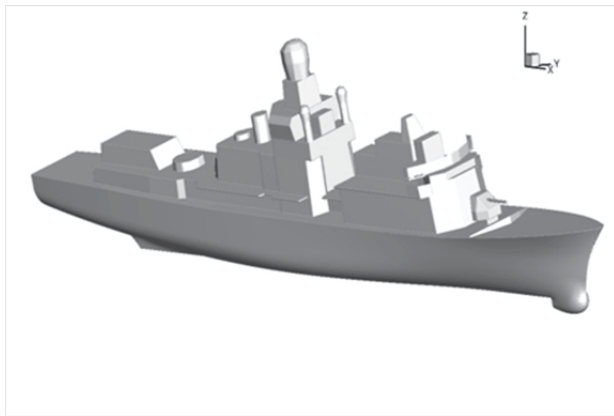


Table 1. Main characteristics

L_{pp}	m	129.00
BWL	m	14.00
T	m	4.82
Δ	t	4873
LCG	m	58.92
YG	m	0.00
VCG	m	5.96

Windage Area	m ²	1346
Z_{aero}	m	6.24
Drift Area	m ²	592
Z_{hydro} / calm water plane	m	-2.37

4. AERODYNAMIC APPROACH (I)

The formulae for wind heeling in the stability rules (other than IMO) use the aerodynamic drag at zero heel angle (or at best taking into account variation using \cos^2 or \cos^3 functions). In addition, they assume that the drift center is located at half draft.

One way to improve upon these formulae is to remove the assumption of an a priori law of decrease (\cos^2 or \cos^3) by calculating the actual projected windage area and centroid height (Z_{aero}) and immersed lateral area and centroid depth (Z_{hydro}) at each heel angle. The wind heel lever formula is thus:

$$B.L.I. = \frac{1}{2} \frac{C_Y \cdot A \cdot (Z_{aero} - Z_{hydro}) \cdot V^2}{1000 \cdot \Delta \cdot g} \quad (6)$$

Where:

V = Wind speed [m/s] (at height Z_{aero})

C_Y = 1.12

ρ = 1.29kg/m³

A , Z_{aero} , Z_{hydro} are calculated at each heel angle. This done by using FASTABI (DGA hydrodynamics code) to establish the hull equilibrium position (waterline position relative to hull) at each heel angle and then using the CAD model to calculate projected areas and centroids. Figure 3 illustrates this procedure.

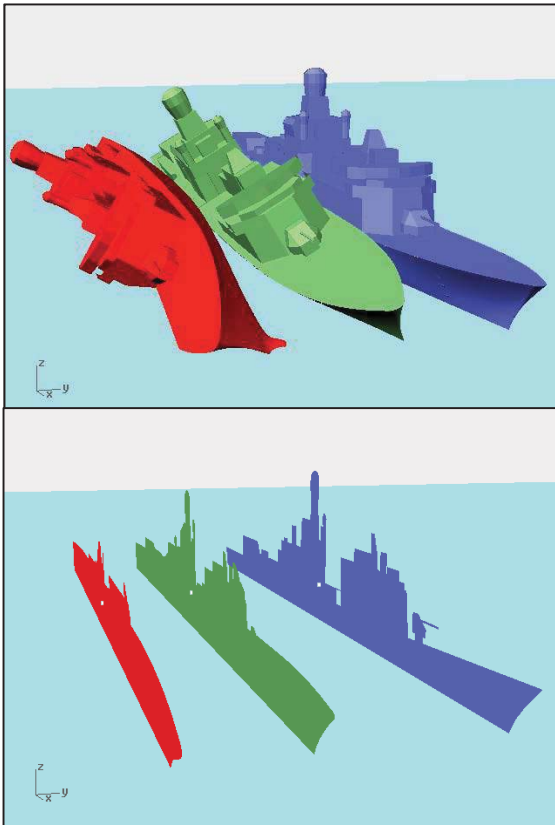


Figure 3: equilibrium and projected wind areas

Figure 4 plots wind lever results for this alternate approach along with the results obtained using the stability rule formula noted in Section 2. To ensure likewise comparison, a wind speed of 100 knots at 10m has been used in all cases, Equation (5) was used to calculate the corresponding pressure for the IMO formula.

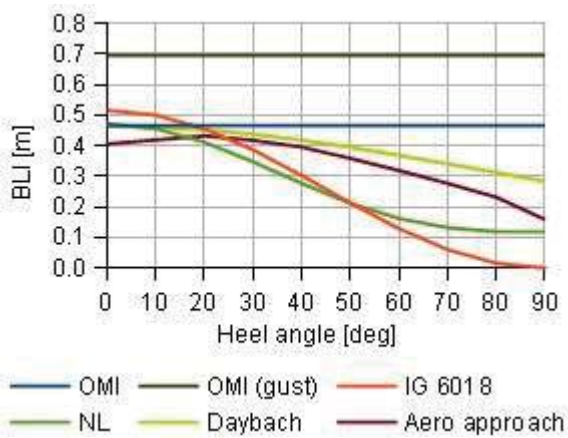


Figure 4: comparisons of BLI

At zero heel, BLI values are all quite similar. However, the shape of the lever arm curves (variance with heel) is very different. This alternative approach shows a maximum around 20° heel angle.

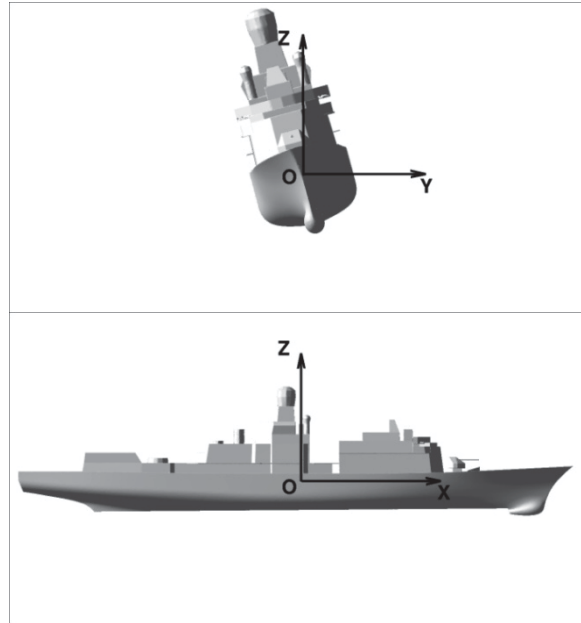


Figure 5: coordinate systems

5. CFD APPROACH (II)

CFD simulations were performed in a dead-ship condition to determine the aero and hydro dynamic forces acting on the ship.

5.1 Coordinate System & Coefficients

CFD work was conducted using the fixed coordinate system shown in Figure 5. The axes are independent of the heel angle, only the position of the origin is linked to the ship. The origin is located as follows:

- Ox : At ship LCG (+ fwd, - aft)
- Oy : At ship Centreline (+port, -starboard)
- Oz : At the waterline (+above, -below)

The coefficients C_Y , C_Z and C_K are defined as:



$$\begin{aligned}
 C_Y &= \frac{F_Y}{\frac{1}{2} \rho U_{ref}^2 S_{ref}} \\
 C_Z &= \frac{F_Z}{\frac{1}{2} \rho U_{ref}^2 S_{ref}} \\
 C_K &= \frac{M_X}{\frac{1}{2} \rho U_{ref}^2 S_{ref}^2 / L_{ref}} \quad (7)
 \end{aligned}$$

Where:

F_Y, F_Z = Force experienced by the ship in the y-axis and z-axis respectively.

M_X = Is the heeling moment acting on the ship (rotation about the x-axis).

L_{ref} = Ship length between perpendiculars.

Depending on whether aero or hydrodynamic forces are being considered:

S_{ref} = Either projected windage area or submersed hull area at zero heel angle.

U_{ref} = Wind speed or drift velocity.

ρ = Air or water density.

5.2 Computational domain and mesh

The computational domain is a parallelepiped as illustrated in Figure 6. A velocity-inlet condition (red) is applied on the upstream boundary and a pressure-outlet condition (blue) is applied at the downstream boundary. A no-slip condition (green) is imposed on the ship and a symmetry condition (gray) on the other boundaries. The computational domain covers $3 L_{pp}$ on each side and $1.5 L_{pp}$ above and below the ship.

The mesh consists of 17 million calculation points constituting 5 million polyhedral cells. The mesh near the walls is made of prisms to ensure proper computation of the boundary layer. The non-dimensional distance from the wall y^+ is fixed at 50 on the hull. The mesh is also made of prisms at the free surface to allow an accurate resolution in this crucial area. The rest of the mesh is covered by polyhedra.

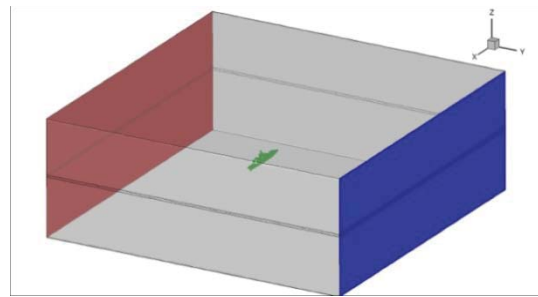


Figure 6: computational domain

5.3 Numerical Method

The calculations were performed using the commercial software FLUENT from ANSYS. It solves RANS equations (Reynolds Averaged Navier-Stokes equations). For these calculations, the Volume Of Fluid (VOF) model was used to simulate the coexistence of the two fluids (air and sea water). A $k\omega$ -SST model was used to model the turbulence of the two fluids.

The simulations are unsteady using an adaptive time step beginning at 0.1s to reach 1s at the end of the calculation. High order discretization schemes have been applied to the momentum equations (MUSCL) and volume fraction (HRIC) to allow an accurate resolution of the air-water interface. The hull was considered to be hydraulically smooth (roughness was not taken into account).

5.4 Calculation Conditions

The simulations were performed on flat sea for a ship at zero forward speed in a fixed position according to the hydrostatic equilibrium at the selected heel angle (the equilibrium is only satisfied on the heave). The characteristics of the two fluids simulated are shown in Table 2. The fluid properties were constant over the computation domain and the effects of temperature, pressure and air hygrometry were neglected.

Table 2. Main characteristics of fluid



Salt water (15°C)			
Dynamic viscosity	μ	(Pa.s)	$1.2200 \cdot 10^{-03}$
Density	ρ	(kg/m ³)	1026
Speed	V_{hydro}	(m/s)	Such that $F_y=0$
Air (15°C, 1% RH, 1013 mbar)			
Dynamic viscosity	μ	(Pa.s)	$1.7894 \cdot 10^{-05}$
Density	ρ	(kg/m ³)	1.225
Wind speed at 10m	V_{aero}	(knots)	100

A uniform lateral current was applied to the flow (water) to model the consecutive drift of the ship due to the efforts of the crosswind. The current speed was determined by balancing the drift forces sustained by the ship (aerodynamic and hydrodynamic loadings). The heeling moments balance is not verified.

Inlet condition imposed on the airflow was determined to correspond to a fully developed turbulent boundary layer profile. For a 100knot wind (at 10m reference height), the turbulent intensity at 10m is of the order of 10%. Theoretical profile, up- and down- stream computed profiles are shown in Figure 7.

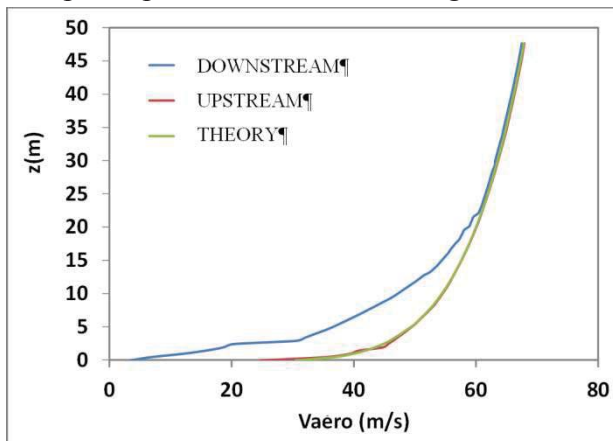


Figure 7: wind profile

5.5 Sensitivity and Convergence

A limited sensitivity analysis was performed. Firstly a higher density of mesh (10 million polyhedra) was tested to quantify the

influence of the discretization of the computational domain. A maximum variation of about 3% was observed on the force coefficients. Then the upstream turbulence flow rate was multiplied and divided by two without observing any significant influence on the results. An evaluation of the influence of Reynolds number was also performed. Computations were performed for different wind speeds at zero heel angle, the results are shown in Table 3. There were no significant changes in the aerodynamic force coefficients; as expected since the Reynolds number remains greater than 10^7 .

Table 3. Main characteristics of fluid

V knots	Re	C_Y	C_Z	C_K
25	$1.23 \cdot 10^{+07}$	0.86	0.65	0.44
50	$2.47 \cdot 10^{+07}$	0.84	0.64	0.45
100	$4.93 \cdot 10^{+07}$	0.83	0.62	0.47

The simulation duration was a period of 500 s which allowed good convergence of the force and moment coefficients as shown in Figure 8. Coefficient values reported in this study are the average over the last hundred seconds of simulation.

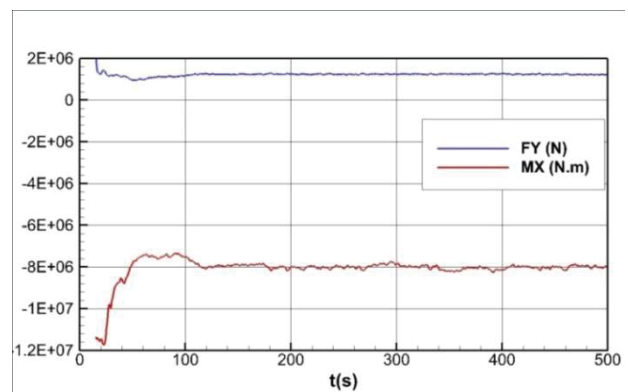


Figure 8: force and moment time trace

The CFD calculation methodology used for this study has not been validated using a



verification procedure. However, some confidence may be taken from comparison of the results obtained to data from wind tunnel tests. Blendermann (1996, 1999) conducted zero heel angle tests for two ships with silhouettes similar to that of the F70 frigate (see Figure 9). Table 4 presents the C_Y and C_K coefficients from CFD and the Blendermann tests.

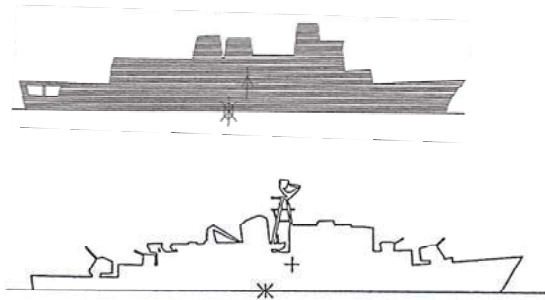


Figure 9: From Blendermann (1996 and 1999)

Table 4. Comparison with Blendermann

	F70 Present CFD	Blendermann Tests	
		1996	1999
C_Y	0.83	0.81	0.85
C_K	0.47	0.48	0.49

Finally, a procedure for CFD simulation has been developed to evaluate the hydrodynamic and aerodynamic loads for vessel in the deadship condition (zero forward speed and drifting in a beam wind); see Figure 10 & 11.”

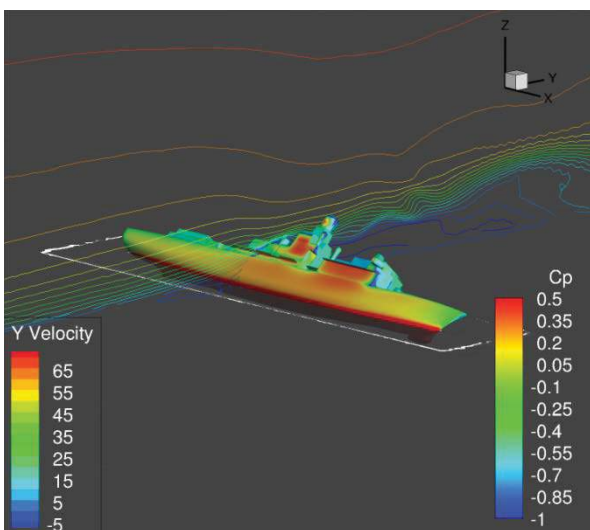


Figure 10: Iso-contours of C_p and iso-lines of transverse speed (m/s) around frigate F70 at +45° heel angle

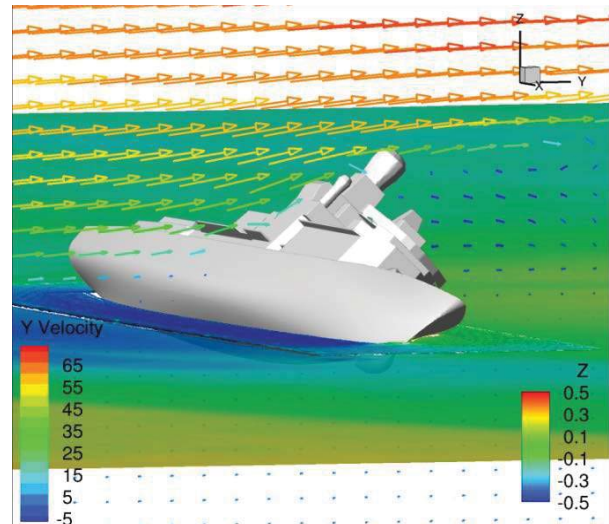


Figure 11: Iso-contours of $Z(m)$ and transverse speed (m/s) around frigate F70 at +45° heel angle

5.6 Results

A series of simulations were performed for a wind speed of 100 knots and heel angles ranging from -60 ° to + 60 °; the positive heel angles correspond to the realistic situation where the ship leans towards leeward. The resulting force and moment coefficients are shown in Figure 12. There is a decrease in C_{Zaero} , C_{Yaero} and C_{Yhydro} with increasing heel angle. Note also that C_{Zaero} and C_{Yhydro} are of the same order of magnitude. C_{Zaero} will influence roll moment because the pressure field on the deck and superstructures of the ship is not symmetrical; this influence is not accounted for in the stability rules reviewed.

Figure 13 shows the vertical location of the point of application of the aerodynamic and hydrodynamic forces. As expected, the point of application of aerodynamic force is located near the centroid of the projected windage area and its height decreases with increasing heel angle. The position of the point of application



of hydrodynamic forces is above the free surface at zero heel but moves below with increasing heel angle to approach the mid-draft position. The heeling moment lever arm, $z(\text{aero}) - z(\text{hydro})$, does not change greatly with heel angle.

Table 5 presents drift velocity (V_{hydro}) and the lateral force coefficients $C_{Y\text{hydro}}$ and $C_{Y\text{aero}}$ for each heel angle. There are little variations in $C_{Y\text{hydro}}$ and $C_{Y\text{aero}}$ and thus V_{hydro} over the range of heel angles.

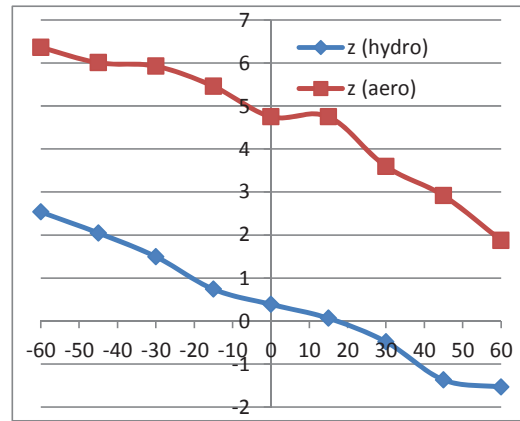


Figure 13: vertical location of hydro and aero forces

Table 5. Drifting speeds for 100 knots of wind

Heel (°)	CY hydro (-)	CY aero (-)	V hydro (knots)
-60	0.65	0.78	5.7
-45	0.69	0.78	5.6
-30	0.85	0.77	5.0
-15	0.73	0.75	5.3
0	0.72	0.83	5.6
15	0.72	0.83	5.6
30	0.69	0.85	5.8
45	0.68	0.78	5.6
60	0.65	0.72	5.5

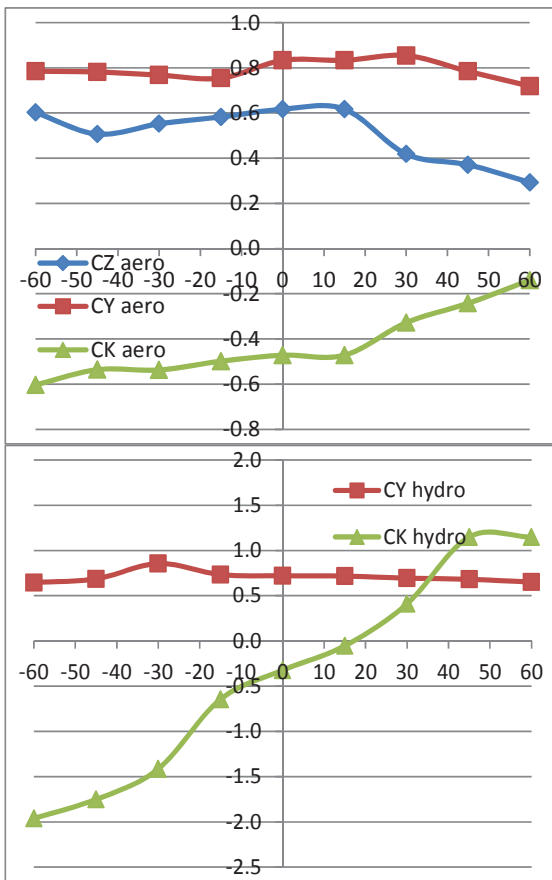


Figure 12: force and moment coefficients for different heel angles

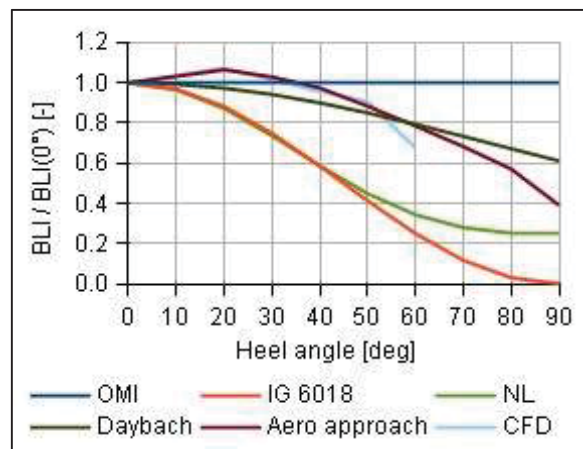


Figure 14: BLI comparisons



6. COMPARISON

Figure 14 presents comparison of the aerodynamic approach and the CFD approach to the stability rules reviewed. Since wind speed and formulation in the rules vary, the curves have been made non-dimensional using values for zero heel. The shape of the aerodynamic and CFD approach curves match well and show a maximums at 20° and 15° respectively. The decrease in BLI is much less pronounced than that obtained by the \cos^2 and \cos^3 function formulae found in the stability rules.

7. CONCLUSIONS

A review was made of different stability rule formulae to account for the effects of wind heeling. These formulae have been applied to the case of F70 frigate. The results obtained were compared to those derived from two alternate approaches. The first approach adopted the same basic formula of the stability rules but replaced the fixed upright windage area, centroids and \cos^2 terms with actual areas and centroids determined for each heel angle. The second approach employed CFD analysis to determine force and moment coefficients at each heel angle. A procedure for CFD simulation has been developed to evaluate the hydrodynamic and aerodynamic loads for vessel in the deadship condition (zero forward speed and drifting in a beam wind).

For the F70 frigate, the two alternate approaches produced similar BLI results. The BLI versus heel angle curves for both have a significantly different shape than that derived from stability rule formula based on a \cos^2 law. Of particular note is that both approaches show a peak in BLI (maximum destabilizing moment) in the 15° to 20° range of heel.

The alternate approaches presented here are interesting and deserves further study. In particular, further work can be done to improve the accuracy of the CFD simulations and

validate the results obtained. This would provide the tool necessary for more comprehensive analysis leading to improved stability rule formulae.

ACKNOWLEDGMENTS

This study was based on CRNAV (Cooperative Research Navies) discussions. Thanks also to H el ene Eudier who started the work in Val de Reuil during a training course. For the French part, the study is funded by the French Ministry of Defence to support DGA Hydrodynamics in its research activities.

REFERENCES

- Arndt B., H. Brandl and K. Vogt, 1982, 20 years of experience – Stability regulations of the West-German Navy, STAB'82, Tokyo pp. 111-121.
- Blendermann W., 1999, Influence of model details on the wind loads demonstrated on a frigate, in Schiff & Hafen.
- Blendermann W., 1996, Wind loadings of ships, - collected data from wind tunnel tests in uniform flow, Institute of Naval Architecture.
- Brown A.J. and Deybach F., 1998, Towards a rational intact stability criteria for naval ships, Naval Engineers Journal.
- DGA/DSA/SPN IG 6018 indice A, 1999, Stabilit e des b atiments de la Marine.
- Middendorf, 1903, Bemastung und takelung des schiffe.
- MSC.267(85).
- Sarchin & Goldberg, 1962, Stability and buoyancy criteria for US naval surface ship, SNAME transactions, vol 70 pp418-434.



Validation of Time Domain Panel Codes for Prediction of Large Amplitude Motions of Ships

Erik Verboom, *Delft University of Technology*, emdverboom@gmail.com

Frans van Walree, *Maritime Research Institute Netherlands*, f.v.walree@marin.nl

ABSTRACT

The paper describes the validation of two time domain methods to simulate the behaviour of a frigate operating in stern quartering seas. The simulation methods differ in the way the seakeeping problem is linearized. The first method is partially body exact while the second method is fully body exact. The validation is based on a statistical analysis as well as a deterministic comparison of simulated and experimental motion time traces.

Keywords: *time domain panel method, statistics, deterministic validation*

1. INTRODUCTION

The operability and safety of a ship depends amongst others on its behaviour in waves. At higher speed in steep waves from aft ward directions dynamic stability risks may exist. These risks can be investigated by means of model tests. Provided these tests are properly executed, they offer the most reliable information on dynamic stability.

Issues in the use of model testing are the costs, the limited statistical reliability of the required tests in irregular waves, the limited flexibility, some limitations in representation of the physics of ship behaviour in waves from the stern quarter and the fact that the test results are not always easy to understand. The limitations in the physical representation relate to viscous effects in the components of the hull resistance with an effect on the propeller loading, in some of the smaller components of the roll damping, in components of the manoeuvring reaction forces and in the (dynamic) stall of the rudders. The neglect of wind on the roll damping and excitation, the wind heel and the propeller loading and related steering has an effect. Issues that are modelled

implicitly correctly are the natural peak-trough asymmetry in steep waves, the presence of breaking waves, the wave induced forces on the propeller and rudder, rudder and propeller ventilation and down-stream effects of vortices from the bilges and bilge keels on the rudder.

In order to understand the physics of dynamic stability, numerical modelling has been pursued for some time. Although the latest CFD techniques have undoubtedly the largest potential, they have not met the expectations yet. This is partly due to the problems of modelling the generation, propagation and absorption of steep waves in a limited computational domain and partly to the local physical character of issues like spilling wave crests on deck, roll damping from bilge keels and rudder stall and ventilation and the role of the propeller herein. In combination with the required domain size, this yields an extreme computational effort.

In between the above two techniques are hybrid calculation methods, which combine the efficiency of potential flow theory with empirical modules covering the non-linear aspects of manoeuvring and roll damping.



After validation, these models are particularly used in assessing capsizing risk.

The present paper deals with validation and comparison of two such simulation methods for a frigate hull form operating in stern quartering seas. A brief description of the simulation methods is given first. Next, the experimental arrangement is described followed by a discussion on the effect of non-linear body boundary conditions on the simulation results.

The simulation methods have been partially developed in a joint industry project on high speed craft called FAST3. Participants are Damen Shipyards (NL), Delft University of Technology (NL), Defence Science Technology Organisation (AUS), MARIN (NL) and the Royal Netherlands Navy (NL).

2. SIMULATION METHODS

Predicting the motion performance of ships operating in stern quartering sea states is more complicated than that for beam or head seas. In stern quartering seas motion amplitudes may be large and both vertical and horizontal plane motions (course keeping) are important. Ideally, prediction methods should be capable of accounting for:

- Six degrees of freedom motions, especially the coupling between sway, yaw and roll,
- Large motion amplitudes,
- Non-linear waves: dynamic stability problems are generally most severe in steep waves for which non-linear effects are of importance,
- Time-varying wetted hull geometry and its effects on restoring forces, wave excitation, wave diffraction and wave radiation forces,
- Forward speed and the effects of friction and flow separation on hydrodynamic properties: in stern quartering seas the wave encounter frequency is low so that potential flow damping is relatively low,
- Propulsion and steering: the speed variations in the horizontal plane should be

predicted adequately, and course keeping is important with respect to broaching,

- The contribution of the wind to the roll damping and the roll excitation.

Prediction methods that are capable of handling the above are in principle capable to simulate phenomena like capsizing due to loss of stability in waves, surf riding and broaching. However, fully non-linear simulation methods are scarce and rather computationally intensive. When a large number of conditions needs to be investigated the required simulation times are impractical. Therefore, there is a need for fast(er) time simulation methods.

One approach that has been proven to lead to reasonable simulation results within a practical time frame is a time domain potential flow simulation. By inserting empirical and semi-empirical components, the errors due to neglecting viscosity, rotation and compressibility, can be minimized. However, also among the time domain potential flow simulations, choices have to be made between simulation time and accuracy. One of these choices is the handling of boundary conditions on the boundaries of the fluid domain.

In an attempt to quantify the effects of linearising boundary conditions, two simulation methods are compared that are identical except for the handling of body boundary conditions. Both simulations are implemented in Panship (Van Walree 2002, De Jong 2011, Van Walree and Turner 2013), a time domain panel method characterised by:

- 3D transient Green function to account for linearized free surface effects, exact forward speed effects, wetted surface, radiated and diffracted wave components along the hull and a Kutta condition for ventilated transoms,
- 3D panel method to account for Froude-Krylov forces on the instantaneous submerged body,
- Cross flow drag method for viscosity effects,



- Resistance (calm water and in waves) is obtained from pressure integration each time step,
- Propulsion and steering using propeller open water characteristics, semi-empirical lifting surface characteristics and propeller-rudder interaction coefficients,
- FDS (Blok and Aalbers 1991) viscous roll damping,
- Autopilot steering,
- Unsteady wind loading based on wind tunnel derived wind load coefficients.

It should be noted that apart from the cross flow drag method there are no “manoeuvring” terms present in PanShip. For instance the sway force and yawing moment due to a drift angle or yaw rate are obtained from the potential flow panel method.

PanShip is used at MARIN for seakeeping predictions for fast and unconventional ships. In the semi non-linear version, the transient Green function is solved for linearized free surface and body boundary conditions. Radiation and diffraction forces are then based on the mean wetted surface and the mean forward speed of the vessel. Since these are both known prior to the start of the time domain simulation, the Green function terms for all time steps can be calculated before the actual simulation starts, resulting in a significant reduction of the computational effort. Froude-Krylov forces are based on the exact wetted surface geometry including ship motions, incident and diffracted waves.

The purpose of the non-linear PanShip version development is to determine wave impact loads on high speed ships. In the non-linear version of PanShip, the Green functions are evaluated at each time step for the instantaneous position of the vessel in the incident and disturbed wave. Since the transient Green function relies on linear free surface boundary conditions, the wetted hull surface

relative to the disturbed water surface ζ is used, i.e. the vertical coordinate z is replaced by $z-\zeta$. For more detailed information on PanShip see Van Walree and Turner (2013).

The present purpose is to investigate the merits of both PanShip versions for a frigate operating in stern quartering seas. This is achieved by comparing simulation results of both methods with experimental results.

3. MODEL TESTS

Model tests were carried out on the parent hull of the FDS systematic hull form series; see Blok and Beukelman (1984). The tests have been performed in MARIN's Seakeeping and Manoeuvring Basin which measures 170x40x5 m in length, width and depth respectively. Table 1 shows the main particulars of the full scale vessel; Figure 1 shows the experimental setup. The model scale used was 15, resulting in a relatively large model.

L _{PP}	100.00	m
L _{WL}	99.982	m
B	12.502	m
T _F	3.125	m
T _A	3.125	m
C _b	0.401	-
Δ	1568.40	m ³
S	1212.30	m ²
GM	2.50	m

Table 1 Main particulars of frigate



Figure 1 Experimental setup

During the tests the model was free sailing in six degrees of freedom and self propelled. Course keeping was realized by an autopilot actuating twin rudders. In order to ensure a negligible effect of the cables connecting vessel and towing carriage, the carriage was able to follow the vessel in its surge, sway and yaw motions.

4. VALIDATION

When validating simulation methods for (irregular) stern quartering waves, a number of aspects have to be taken into account. First, compared to head waves, accelerations, impact pressures and structural loads due to slamming are less relevant. Instead, course keeping and stability are the phenomena that are of interest. However, the low wave encounter frequencies combined with a large, strongly non-linear dependency of the vessels response on the initial speed and position in the wave make the acquisition of reliable statistical data time consuming and expensive.

In this paper two types of validation will be performed. First, a statistical comparison of simulations and model tests is shown. Next, individual model test runs will be used for a deterministic comparison of the vessels motions in stern quartering seas.

4.1 Statistical Validation

The main issue when it comes to validating statistical data for a vessel operating in stern-quartering waves is the acquisition of sufficient data. Due to the low encounter frequency, obtaining a reasonable number of wave encounters can be very time consuming. The model tests discussed here had a duration of 850 seconds (prototype value), obtained by performing 5 to 7 runs (depending on the operational speed) for every condition.

For the statistical validation of the simulation results, two conditions have been selected as shown in Table 2. In both conditions a JONSWAP spectrum has been used with a different wave train realization in each run. A 360 deg wave direction means following seas.

Test case	Speed [kt]	Wave direction [deg]	Wave height [m]	No. of wave encounters [-]
707	17	315	3.8	79
709	23	300	3.8	37

Table 2 Test conditions

As indicated in Table 2, the number of wave encounters during the model tests varied roughly between 40 and 80. In order to get an idea of the statistical significance of the data obtained, 10 simulations in identical conditions with different wave train realizations have been performed with the semi non-linear version of Panship. Each run had a duration of 850 seconds. Mean values and standard deviations of all six degrees of freedom have been determined for each run. An indication of the scatter in results can be obtained from Figures 2 through 5. Figures 2 and 3 show the mean values for all six degrees of freedom, Figures 4 and 5 the standard deviations. Note that for the x-direction the speed is shown instead of the surge motion. In the bar graphs, the left most (darkest) bar describes the values obtained during the model test, the next ten bars are values obtained from simulations for different



wave train realisations (seeds)

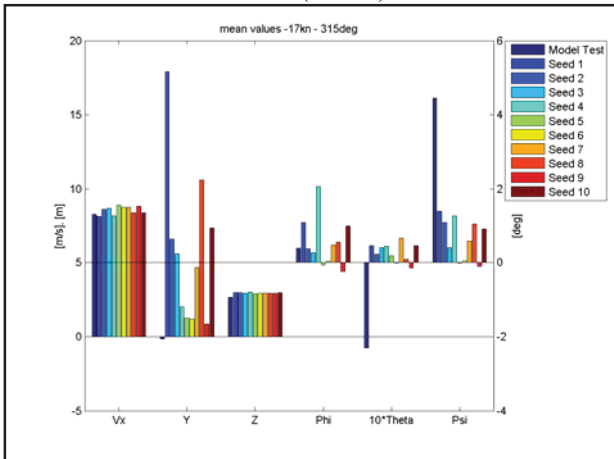


Figure 2 Mean values case 707

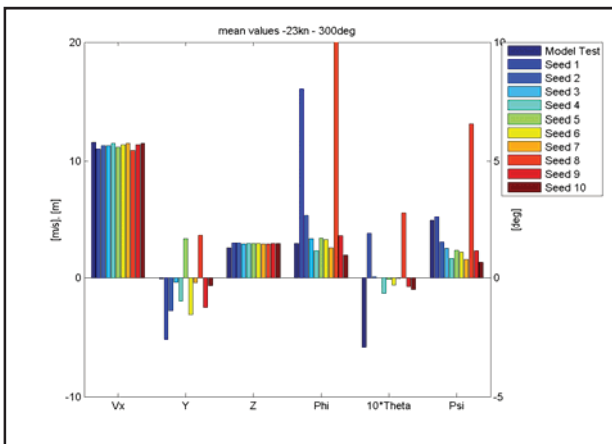


Figure 3 Mean values case 709

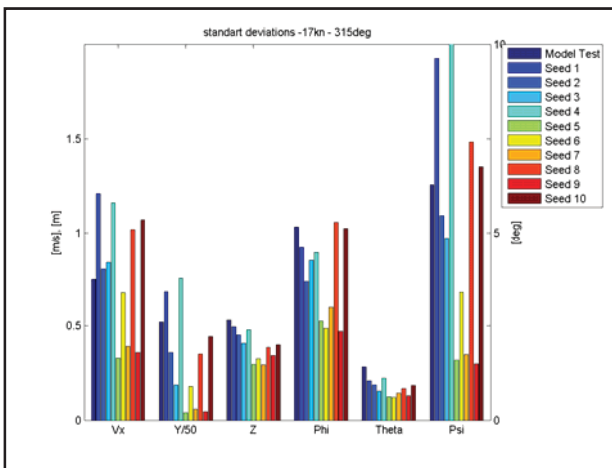


Figure 4 Standard deviations case 707

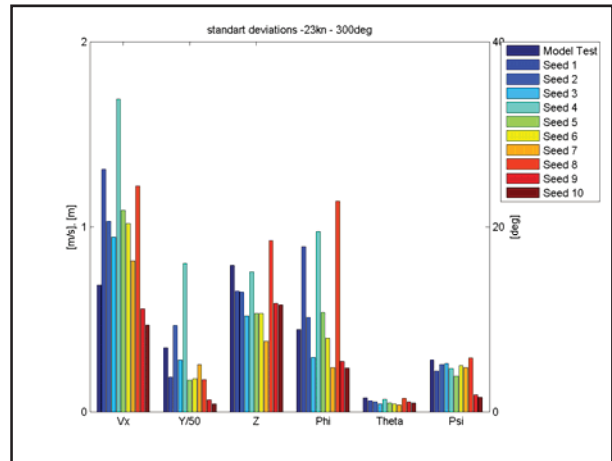


Figure 5 Standard deviations case 709

Individual runs show a significant variation in standard deviation for speed, heave and pitch. This is to be expected when between 40 and 80 waves are met per simulation run. The variation in mean value and standard deviation for sway, roll and yaw is quite large. The plots show that in almost all cases the model test results lie within the scatter of the simulations. The only conclusion that can be made about the validity of the simulation results on basis of these plots is that they are in the right order of magnitude.

In more detailed approach the 95% confidence bounds have been determined on basis of the variance of the variance of individual runs, following methods provided by Belenky et al (2007). Figures 6 through 11 show the mean standard deviation and 95% confidence intervals for sway, roll and yaw for the model tests and the simulations.

It can be seen that for all cases the mean standard deviation of the Panship simulations (indicated by the square symbol) is within the confidence bounds of the model test result. This suggests that Panship simulations are accurate in a statistical sense. The uncertainty in the model test results is expected to be much larger than that of the simulations since its duration is about 10 times lower. Apparently this is only so for case 709 for roll and yaw.

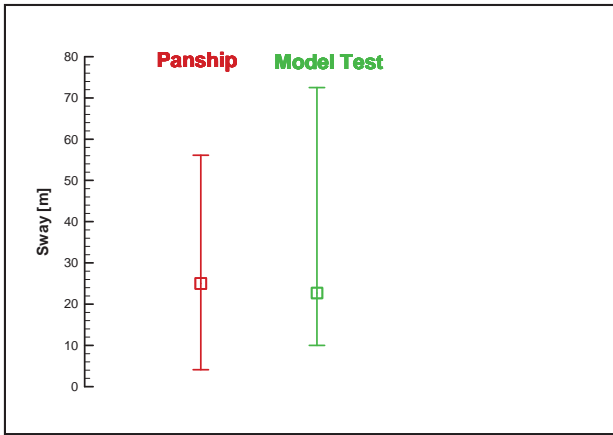


Figure 6 Confidence bounds for sway standard deviation, case 707

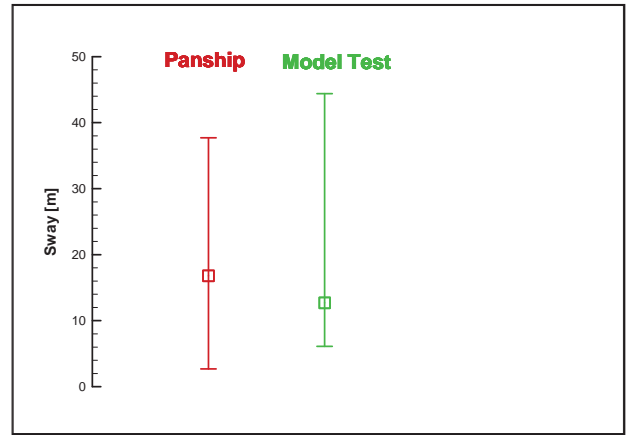


Figure 9 Confidence bounds for sway standard deviation, case 709

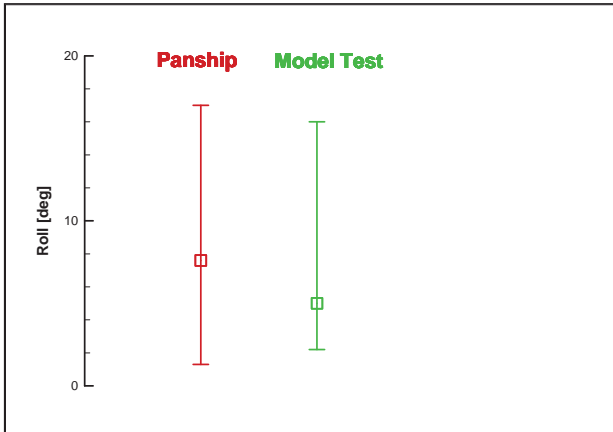


Figure 7 Confidence bounds for roll standard deviation, case 707

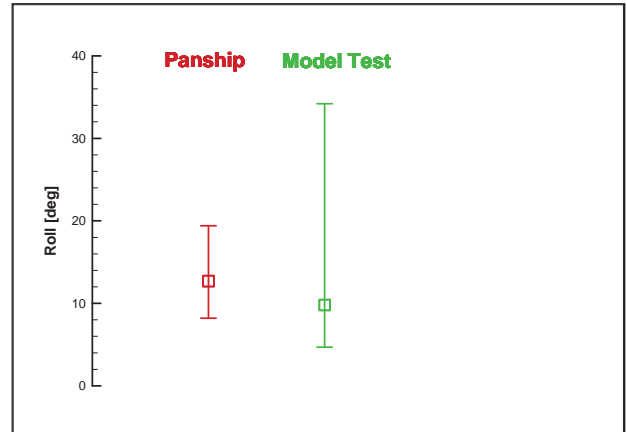


Figure 10 Confidence bounds for roll standard deviation, case 709

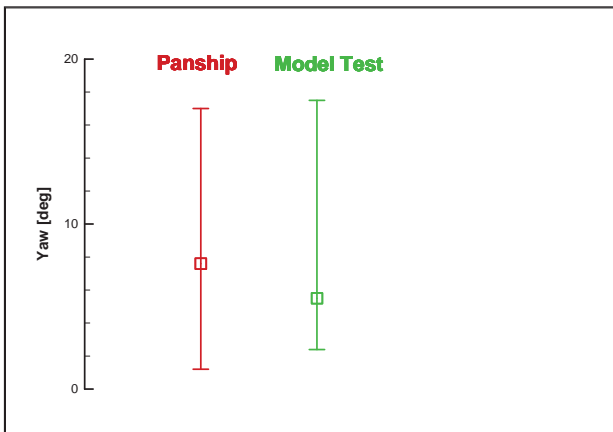


Figure 8 Confidence bounds for yaw standard deviation, case 707

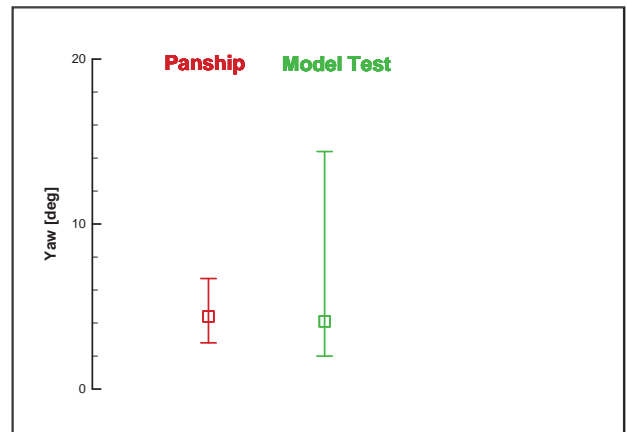


Figure 11 Confidence bounds for yaw standard deviation, case 709

4.2 Deterministic Validation

Next to the statistical method, a deterministic approach has been taken to validate the simulated responses of the vessel. First the experimental wave train needs to be reproduced in the simulations, so that time traces of motions can be compared. For this deterministic validation, single model test runs of about 175 seconds duration have been selected from the model tests runs for cases 707 and 709. For deterministic validation a number of aspects have to be taken into account.

The first point that has to be taken into account is the accumulation of errors over time. In stern quartering waves, the response of a vessel to a wave train is strongly dependent on its initial position, orientation and speed in that particular wave. Hence, in identical wave trains small errors in the simulated position would quickly accumulate, rendering the rest of the validation useless. In order to overcome this problem, during the simulation the vessel's X-Y position required to evaluate the wave kinematics is taken identical to that measured during the model test. In this way, for each time step the wave trains at the centre of gravity for model test and simulation are identical, provided the wave train reconstruction is perfect.

Secondly, attention should be paid to the initial conditions when the simulation is started. During the model tests, when the measurements are started the vessel has already sailed a number of ship lengths in the given conditions. During this period, any forward speed effects and the wave system are fully developed. However, when a simulation is started, there are no memory terms in the Green's function, creating the equivalent of the vessel being instantly accelerated from zero to operational speed the moment the simulation starts. For the deterministic simulations, this has been overcome by forcing the vessel to

attain the velocity of the model test during the first 30 seconds of each run.

The process to reconstruct the experimental wave train in the simulation method is detailed by Van Walree and Carette (2011). Figure 12 shows a typical comparison between the measured and reconstructed wave trains. The reconstruction is reasonably good but not perfect, which will cause some differences between the measured and simulated motions.

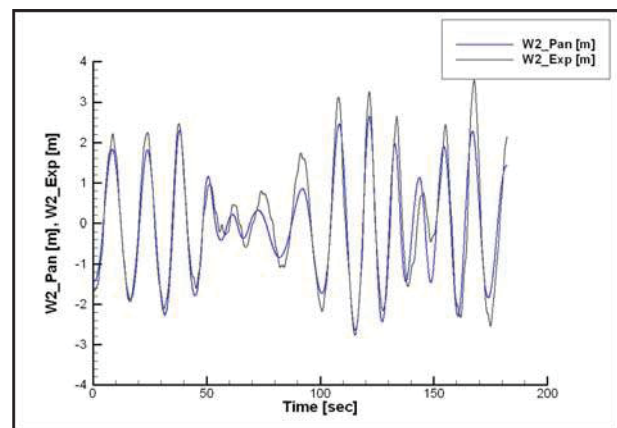


Figure 12 Comparison between reconstructed (blue) and experimental (black) wave trains

Figures 13 through 24 show a comparison between the measured and the simulated ship motions. The red signals denote the non-linear PanshipNL results, the green signals denote the semi-linear Panship results and the blue signal represents the experimental data.

Heave, roll and pitch are adequately predicted by both the semi non-linear and non-linear Panship methods for run 707005. For both methods the sway motion is off mainly due to a persisting difference in the yaw motion. The variations in forward speed are better predicted by the non-linear method.

For run 709003 differences between the semi non-linear and non-linear Panship versions are not large, except near the end of case 709 where relatively large roll and yaw motions occur which are better captured by the non-linear method. Again the speed loss is better predicted by the non-linear method.

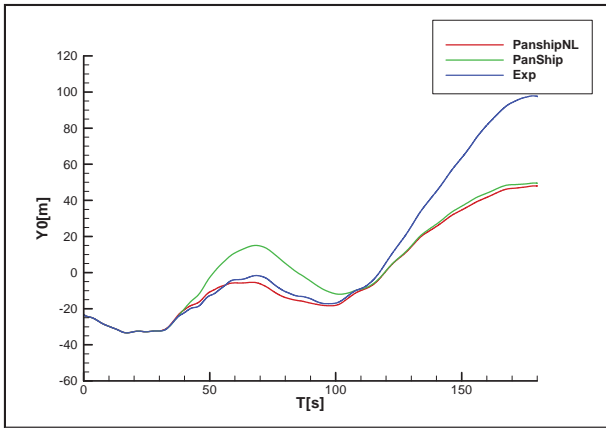


Figure 13 Comparison of sway for run 707005

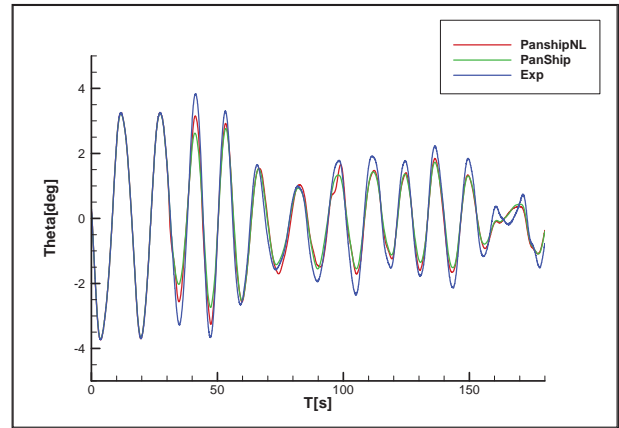


Figure 16 Comparison of pitch for run 707005

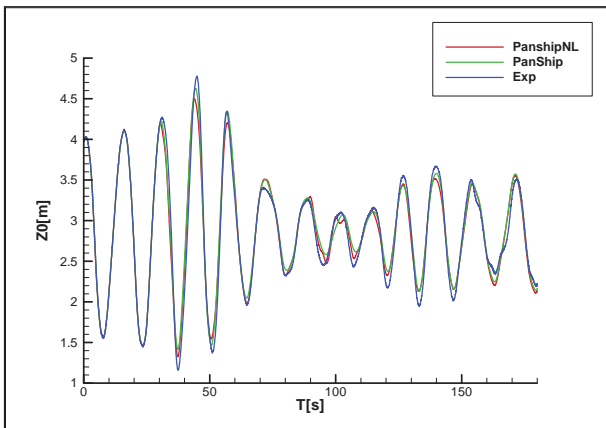


Figure 14 Comparison of heave for run 707005

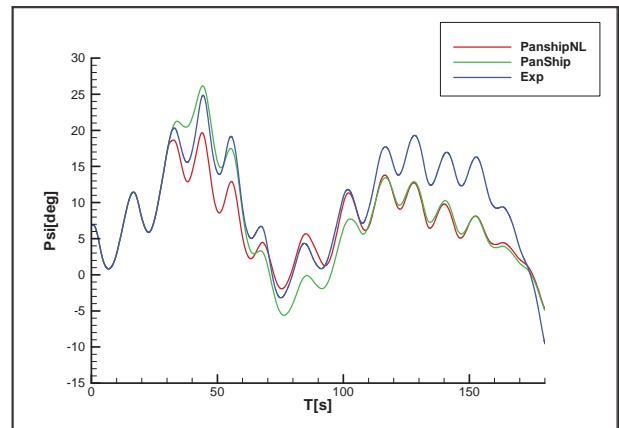


Figure 17 Comparison of yaw for run 707005

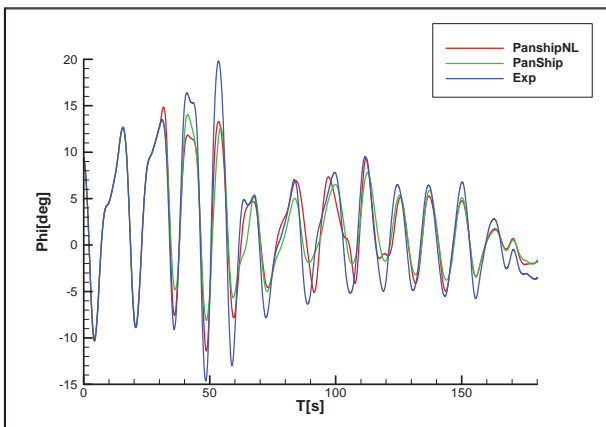


Figure 15 Comparison of roll for run 707005

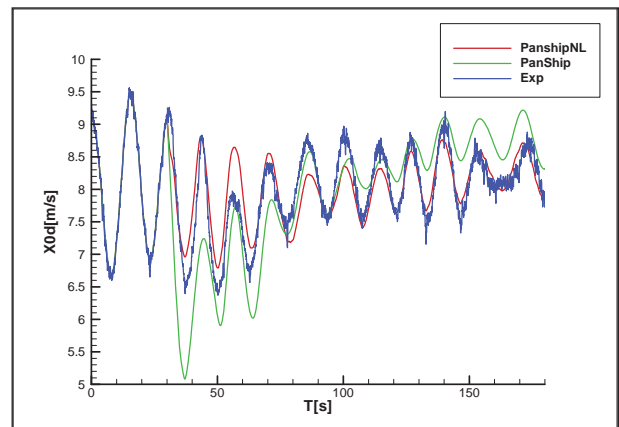


Figure 18 Comparison of speed for run 707005

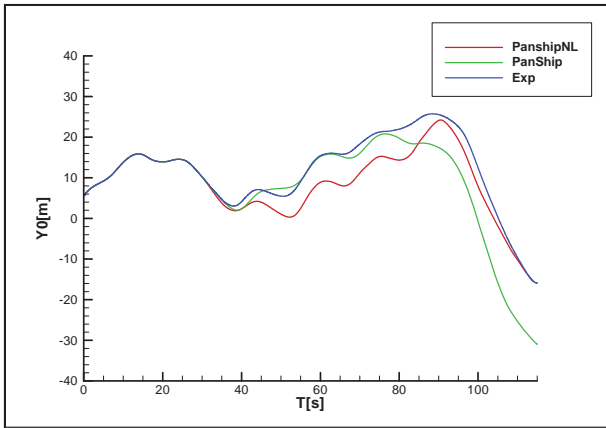


Figure 19 Comparison of sway for run 709003

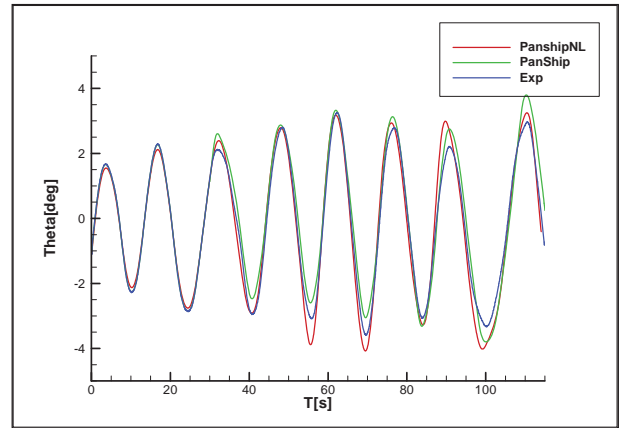


Figure 22 Comparison of pitch for run 709003

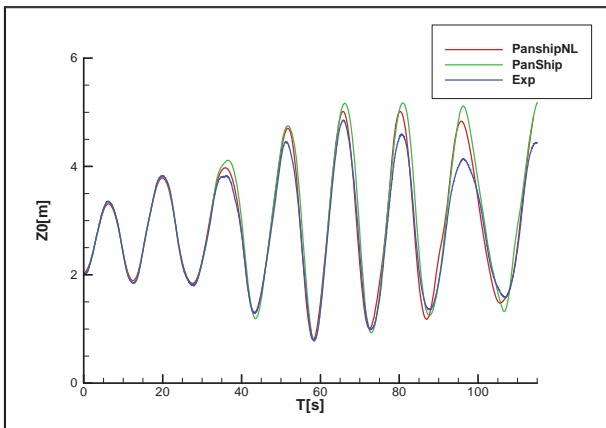


Figure 20 Comparison of heave for run 709003

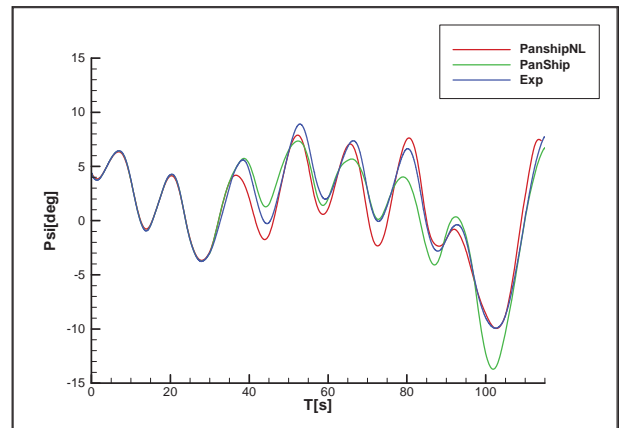


Figure 23 Comparison of yaw for run 709003

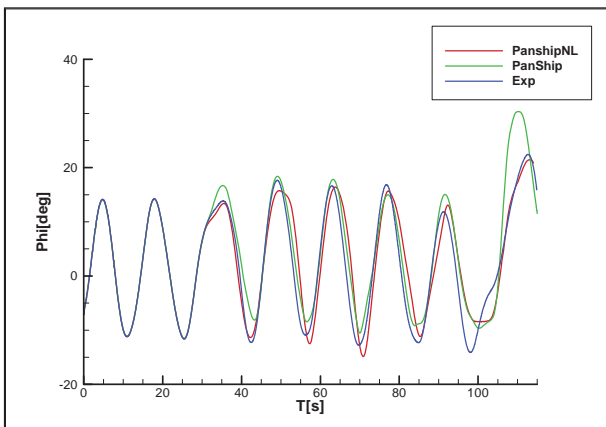


Figure 21 Comparison of roll for run 709003

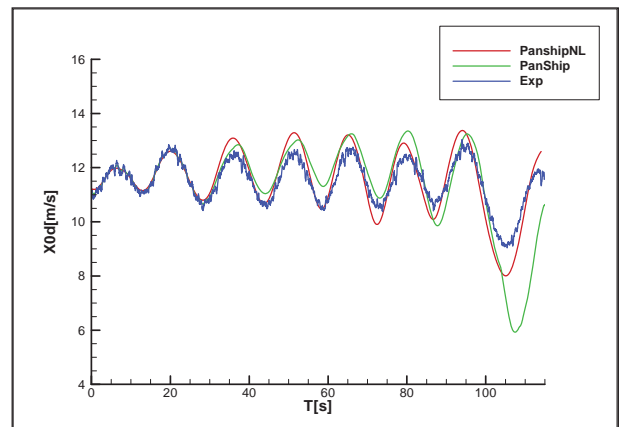


Figure 24 Comparison of speed for run 709003



7. CONCLUSIONS

As is well known for ships operating in stern quartering seas the horizontal plane motions show significant variation in mean value and standard deviation. The mean standard deviation of sway, roll and yaw motions of simulation results are found to be within the experimental confidence range for the standard deviation. Although the duration of the simulations is much greater than that of the model tests for most cases the confidence limits for simulations and model tests are quite similar.

Deterministic validation shows that both the semi non-linear and the non-linear simulation methods yield a fair prediction of motions and speed variations in stern quartering seas. This is not true for case 707 where the sway motion is offset due to a persistent difference in yaw motion. The non-linear simulation methods yield better predictions for the forward speed variations and the large amplitude roll and yaw motions, otherwise differences between the semi non-linear and non-linear simulation methods are small.

8. ACKNOWLEDGMENTS

The authors acknowledge the permission of the FAST3 participants to use the experimental data.

9. REFERENCES

- Belenky, V., Weems, K.M. and Lin, W-M., 2007, "A Probabilistic Procedure for Evaluating the Dynamic Stability and Capsizing of Naval Vessels, Phase 1: Technology Demonstration." SAIC Report ASTD 08-017.
- Blok J.J. and Aalbers A.B., 1991, "Roll damping due to lift effects on high speed monohulls", Proceedings of 1st International Conference of High Speed Sea Transportation, FAST'91, Trondheim, Norway.
- Blok J.J. and Beukelman W., 1984, "The High-Speed Displacement Ship Systematic Series Hull Forms – Seakeeping Characteristics", Transactions SNAME, USA.
- De Jong P. , 2011, "Seakeeping Behaviour of High Speed Ships", Ph.D. Thesis, Delft University of Technology, Netherlands.
- Walree F. van, 2002, "Development, validation and application of a time domain seakeeping method for high-speed craft with a ride control system", Proceedings of 24th Symposium on Naval Hydrodynamics, Fukuoka, Japan.
- Walree F. van and Carette N.F.A.J., 2011, "Validation of Time Domain Seakeeping Codes for a Destroyer Hull Form Operating in Steep Stern-quartering Seas", International Journal Naval Architecture and Ocean Engineering, JNAOE, Vol. 1, pp 1-12.
- Walree F. van and Turner T.G., 2013, "Development and Validation of a Time Domain panel Code for Prediction of Hydrodynamic Loads on High Speed Craft", Proceedings of 12th International Conference of High Speed Sea Transportation, FAST'2013, Amsterdam, Netherlands.

Session 10.3 – EXTREME BEHAVIOUR

Surf-Riding in Multi-Chromatic Seas: “High-Runs” and the Role of Instantaneous Celerity

Stability and Roll Motion of a Ship with an Air Circulating Tank in Its Bottom

A Study on the Effects of Bilge Keels on Roll Damping Coefficient

This page is intentionally left blank



Surf-Riding in Multi-Chromatic Seas: “High-Runs” and the Role of Instantaneous Celerity

Nikos Themelis, *School of Naval Architecture and Marine Engineering, National Technical University of Athens*, nthemelis@naval.ntua.gr

Kostas J. Spyrou, *School of Naval Architecture and Marine Engineering, National Technical University of Athens*, k.spyrou@central.ntua.gr

Vadim Belenky, *David Taylor Model Basin / NSWCCD, Maryland, USA*,
vadim.belenky@navy.mil

ABSTRACT

We investigate “high-run” events of ships in following seas. These are cases of ship motion when, due to waves’ effect, a ship attains abnormally high speed. Investigations are carried out in three directions: firstly, the statistics of high-runs are calculated, exploring in particular their dependence on the wave spectrum and the sea state. Secondly, a rather neglected up to now method, proposed by Grim, for the quantification of the probability of high-run occurrence is implemented. Lastly, the focus is set on the connection of the instantaneous wave celerity with the mean surge velocity during high-run. For its evaluation, two different error metrics are implemented.

Keywords: *ship surging, surf-riding, high-run*

1. INTRODUCTION

A direct approach for calculating the probability of surf-riding of a ship operating in extreme irregular waves could be based on the identification of time intervals in which her speed is maintained at a level that is consistently above the normally expected range. Any individual realisation of such behaviour will be called hereafter “a high run” and it could be considered as generalisation of surf-riding for a multi-frequency wave environment. Whilst its inception requires careful consideration of system’s phase-space, empirically it could be recognised by the up-crossing of an appropriate surge velocity threshold such as the instantaneous wave

celerity. It is noted however that, for irregular seas, the role of wave celerity for surf-riding capture is still inferred from phenomenology rather than from proof (for some insights see Spyrou et al 2014a). A high-run’s end could be similarly defined by the down-crossing of a suitable threshold, which however it is not easy to be uniquely defined through experience.

The literature in the topic is scarce. However, in a pioneering (but rather oversighted) work, Grim had attempted to determine how a ship could be accelerated by waves and then maintain a speed higher than her mean speed, for extended time intervals in irregular seas (Grim 1963). He had called such phenomena “long-runs”. By a string of

eloquent and yet quite severe analytical approximations, he had produced statistical estimates of their existence (based on up-crossing of a speed level that he had considered as critical) and their duration.

In the current study the aim was the systematic examination of the probabilistic properties of the high-runs. It is well-known that, the longer a ship maintains a speed higher than normal, the more likely it is to experience the broaching-to instability (Spyrou 1995). The importance of the topic is thus prevalent. Firstly, a campaign of numerical simulations with direct counting of high-run durations was performed. Targeted quantities were: the mean duration of high-run; and the mean time between successive high-runs. Then, the key elements of Grim's approach were implemented, taking advantage however of current numerical calculation capability. Thus, alternative probability figures were derived which could be contrasted against those obtained by direct counting. Our final goal was to examine the correlation of instantaneous wave celerity with surge velocity during high-run incidents.

2. HIGH-RUN STATISTICS

2.1 Mathematical model

The mathematical model of surge motion in following seas was written for an earth-fixed observer, as follows:

$$(m - X_{\ddot{u}})\ddot{\xi} - (\tilde{\tau}_2\dot{\xi}^2 + \tilde{\tau}_1n\dot{\xi} + \tilde{\tau}_0n^2) + (r_1\dot{\xi} + r_2\dot{\xi}^2 + r_3\dot{\xi}^3) - \sum_{i=1}^N Fx_i \sin(k_i\xi - \omega_i t + \varepsilon_i + \varepsilon_{fi}) = 0 \quad (1)$$

where ξ is the longitudinal position of the ship and m , $X_{\ddot{u}}$ are her mass and "surge added mass" respectively. In the summation term denoting wave force, k_i , ω_i and ε_i stand respectively for the i harmonic's wave number,

frequency and random phase. Fx_i denotes the amplitude and ε_{fi} the phase of the harmonic wave force component. Also, n is the propeller rate and r_i , $\tilde{\tau}_i$ are polynomial coefficients appearing in the resistance and thrust force expressions, respectively.

2.2 "High-run" definition

An apparent choice of a velocity threshold whose upcrossing would signal a high-run is the instantaneous wave celerity. Yet, it is known that attraction towards surf-riding is very likely to have started from a slightly earlier time (and thus from a lower velocity). If this early stage is neglected, a small underestimation of the probability should be expected. As down-crossing threshold was set, at first step, the nominal speed. This threshold should not be crossed by speed fluctuations occurring during surf-riding. The nominal speed is a safe choice from this point of view, although a conservative one, possibly contributing to a slight overestimation of probability. This may be statistically cancelled out, at least partly, with the underestimation linked with the beginning of the high-run. As an extra condition we request the surge velocity to be always higher than the nominal speed in order to exclude, in relatively short wave lengths and mild wave height conditions, cases that qualitatively, should not be counted as high runs. In Figure 1 are shown time segments of high-run in accordance to the presented definition. It is desired to obtain the statistics of the high-run's duration as well as of the time interval between successive events of this kind. The mean duration is obtained by summing up all individual durations and then dividing by the number of events:

$$\bar{t}_{\text{high run}} = \frac{\sum_{i=1}^N t_{\text{high-run}}^{(i)}}{\sum_{i=1}^N i} \quad (2)$$

A similar formula is applied for the mean time between high-runs.

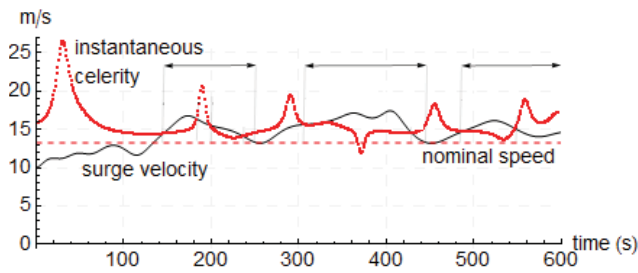


Figure 1 Schematic definition of high-run.

2.3 Simulation settings

The ship selected for applying the calculation schemes is the ONR “tumblehome topside”, well-known from several previous studies (for example, Spyrou et al 2014a). A JONSWAP spectrum is considered, discretized by applying a fixed frequency increment $\delta\omega = 2\pi/t_{sim}$ where $t_{sim} = 300$ s is the so-called “basis simulation time”. The total simulation time was a multiple of it (up to $40 \times t_{sim}$). Four ranges around spectrum’s peak were separately examined, assumed containing the wave frequencies participated in the simulations. In Figure 2 are shown the wave amplitudes obtained from the spectrum, considering frequency ranges $0.2\omega_p$ and $0.4\omega_p$. A different choice would have been to modify the wave amplitude so that the variance remains constant. In that case the wave amplitudes obtained would be considerably higher (see again Figure 2). In the current study wave realizations were produced according to the first method, meaning that, the increase of the frequency range increased also the energy.

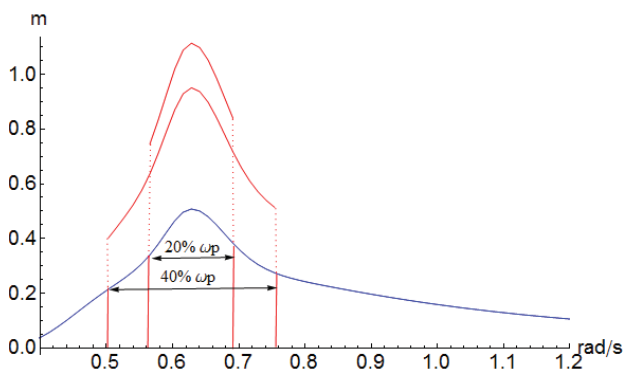


Figure 2 Wave amplitudes for 2 frequency ranges and their modified values when the variance is kept constant. $H_S=6$ m and $T_P=10$ s.

Lastly, in Table 1 appear the values of the remaining simulation parameters. Sensitivity studies in relation to the sea state, narrowness of the spectrum and the simulation time were carried out. We run 100 wave realizations per parameters’ setting. The nominal and the initial speed of the ship, in each scenario, were not changed (for extra explanations see Spyrou et al 2014b).

2.4 Results

In Figure 3 appear characteristic high-run durations, obtained by simulation. Vast differences are noticed, some high-runs lasting just a few seconds and others reaching 1000 seconds! The probability density function (*pdf*) of the mean duration, based on 100 simulations, is shown in Figure 4. The effect of the sea condition on the mean, and also on certain percentiles, appear in Figures 5 and 6. Convergence with respect to the simulation time is confirmed from Figure 7.

Effect of wave frequency range on mean duration of high-run

When the frequency range is narrow, mean times are higher and they are concentrated around the lower peak periods (Figure 9).



Table 1 Range of the parameters of simulation

Parameter	Value
V_{nom} (m/s) - F_n	12 – 0.308
$V(0)$ (m/s)	10
wave realizations per scenario	100
H_S (m)	(3-6)
T_P (s)	(8.5-13)
(% ω_p one side)	(5-30)
Total simulation time (s)	($t_{sim} - 40xt_{sim}$)

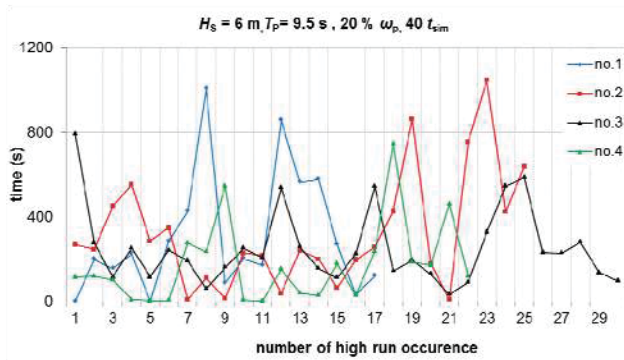


Figure 3 Recorded durations of high-run incidents in different simulations.

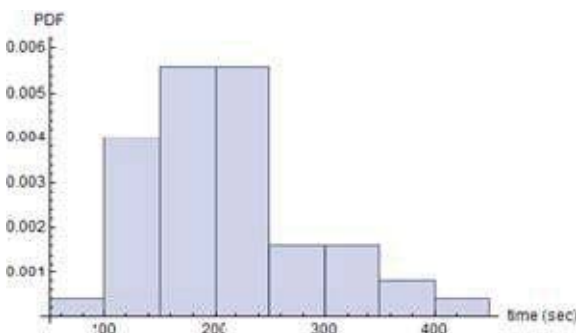


Figure 4 pdf of mean high-run duration [$H_S=6$ m, $T_P=9.5$ s, $40 t_{sim}$, frequencies in 10% ω_p (one side)].

When the range is broadened, so do the peak values of the mean. The trend depends on the assumed significant wave height and it is more pronounced at higher significant wave heights.

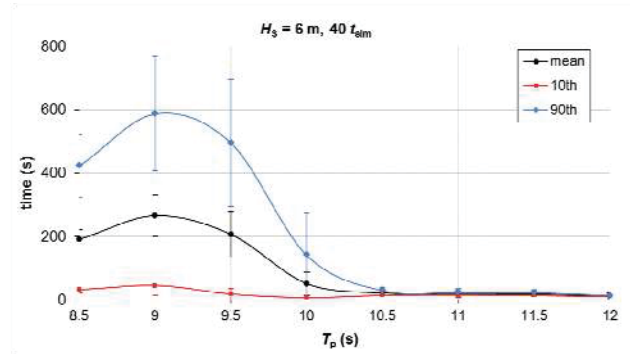


Figure 5 Mean value and percentile means (10th and 90th), as T_P is varied ($H_S=6$ m and simulation time $40 t_{sim}$). Standard deviations are included.

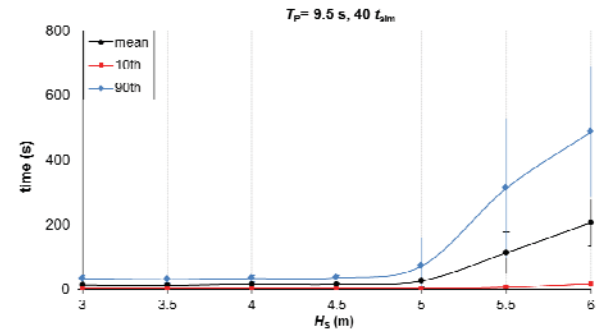


Figure 6 As in Figure 5, with varied significant wave height and fixed peak period.

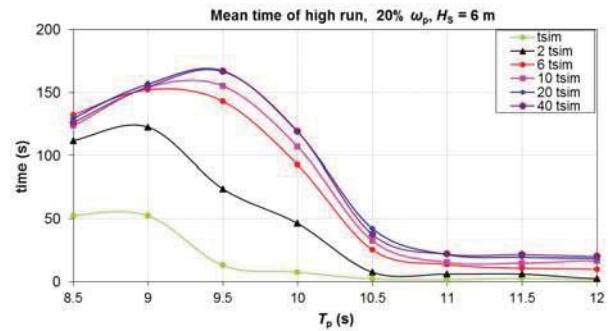


Figure 7 Convergence of statistics.

Effect of wave frequency range on mean time between high-runs

The mean time between successive high-runs is increased with the peak period (Figure 9). The effect of varying the significant wave height can be similarly assessed from Figure 10. The broader the frequency range, the more frequent the high-run occurrence. There seems to be a sharp increase of the mean time beyond a certain value of peak period. On the other

hand, the significant wave height seems more influential when the frequency range is narrow.

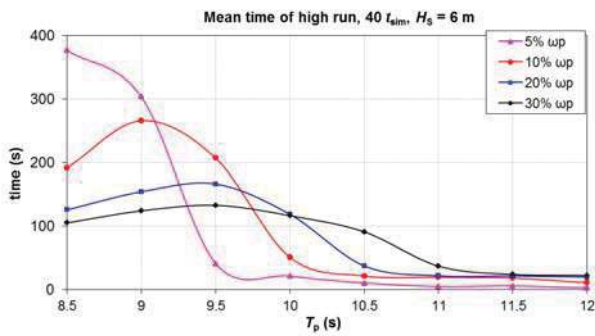


Figure 8 Mean duration of high-run for a gradually broader frequency range, as peak period is varied.

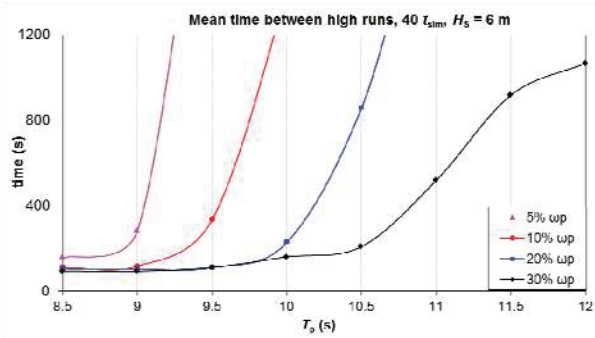


Figure 9 Mean time between successive high-runs as the peak period is varied.

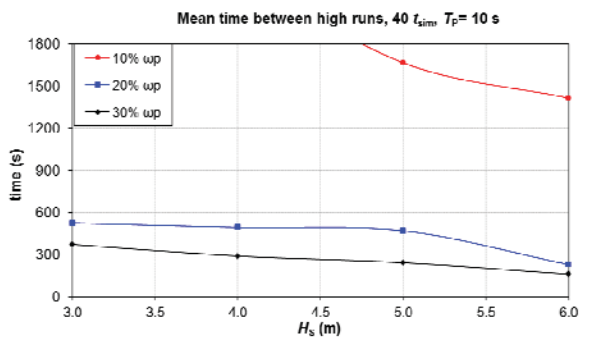


Figure 10 Mean time between high-runs as significant wave height is varied.

3. THE APPROACH OF GRIM

3.1 Key points

The main issue addressed by Grim was the probabilistic quantification of the occurrence and duration of high-run (“long run”), taking

into account the strongly nonlinear character of surge motion when the phenomenon occurs, in a following irregular sea (Grim 1963). However, the lack of computer power for the demanding numerical calculations, together with the lack of a theory explaining surf-riding, at that time, had led him to incorporate several simplifying assumptions whose influence was unknown. Grim had focused on the condition generating unusually high surge acceleration and on the duration of the ensuing high speed run, which he assumed represented by a velocity plateau. Thus a simple, trapezoidal structure of ship speed was considered during such incidents. Next is presented a summary of Grim’s method.

3.2 Mathematical model set-up

The surge equation is written with respect to an inertial system that moves with the ship’s constant nominal speed V . The method assumes that the time is paused at the instant t when high-run’s acceleration begins. Later time is measured through a new time variable τ :

$$\ddot{x}_0 + N(\dot{x}_0, x_0^2, x_0^3) / (m - X_{\dot{u}}) = \int_0^{\infty} \cos \left[\frac{\omega^2}{g} x_0 - \omega \left(1 - \frac{\omega \cdot V}{g} \right) (t + \tau) + \varepsilon \right] \sqrt{f_x^2(\omega) S(\omega)} d\omega \quad (3)$$

The distance variable x_0 determines ship’s position. Function $N(\dot{x}_0, x_0^2, x_0^3)$ refers to the resistance and thrust forces, f_x is the RAO of the Froude-Krylov surge wave force [divided by the mass (including added mass) of the ship] and S is the wave spectrum. Consistently with the model of section 2, the term $N(\dot{x}_0, x_0^2, x_0^3)$ should take the following form:

$$N(\dot{x}_0, x_0^2, x_0^3) = [3r_3 V^2 + 2(r_2 - \tilde{r}_2)V + r_1 - \tilde{r}_1 n] \dot{x}_0 + (4) + (3r_3 V + r_2 - \tilde{r}_2) \dot{x}_0^2 + r_3 x_0^3 + R(V) - T(V; n)$$

where resistance and thrust, at the nominal speed are, respectively:



$$\begin{aligned} R(V) &= r_1 V + r_2 V^2 + r_3 V^3 \\ T(V; n) &= \tilde{\tau}_2 V^2 + \tilde{\tau}_1 V n + \tilde{\tau}_0 n^2 \end{aligned} \quad (5)$$

At the critical stage, the ship is assumed under a constant acceleration for a time duration τ_1 . When the critical velocity V_{crit} is reached the ship maintains this velocity for time $\tau_2 - \tau_1$ (see eq. 6). Thus, the required acceleration to realise the high run should be: $b = (V_{crit} - V) / \tau_1$.

$$\dot{x}_0 = \begin{cases} b \cdot \tau, & 0 \leq \tau \leq \tau_1 \\ b \cdot \tau_1, & \tau_1 \leq \tau \leq \tau_2 \end{cases} \quad (6)$$

We note that, whilst for the regular sea he identified celerity as the critical speed, he gave no similar indication for the choice of critical speed in an irregular sea.

The wave force in (3) is considered through its integral for a finite duration τ_1 (impulse function) – this leads to the key idea of producing an impulse spectrum. Integration of (3) in time leads to an equation based on momentum:

$$\begin{aligned} \int_0^{\tau_1} \left[\ddot{x}_0 + \frac{N(\dot{x}_0, x_0^2, x_0^3)}{(m - X_{\ddot{u}})} \right] d\tau &= \\ = \int_0^{\tau_1} \int_0^{\infty} \cos \left[\frac{\omega^2}{g} x_0 - \omega \left(1 - \frac{\omega \cdot V}{g} \right) (t + \tau) + \varepsilon \right] \sqrt{f_x^2(\omega) S(\omega)} d\omega d\tau \end{aligned} \quad (7)$$

Calculating partly the force integral leads to the following expression of the impulse (for details see Grim 1963):

$$\int_0^{\infty} \cos \left[\omega \left(1 - \frac{\omega V}{g} \right) t + \varepsilon' \right] \sqrt{f_x^2(\omega) T^2 (I^2 + Y^2) S(\omega)} d\omega \quad (8)$$

where:

$$T^2 (I^2 + U^2) = \left\| \int_0^{\tau_1} e^{i \left[-\omega \left(1 - \frac{\omega V}{g} \right) \tau + \frac{\omega^2 b}{g} \tau^2 \right]} d\tau \right\|^2 \quad (8')$$

The term $f_x^2(\omega) T^2 (I^2 + Y^2) S(\omega)$ is the sought impulse spectrum, while ε' is another, but still random, phase. Since the maximum value of the impulse is of interest, the cosine term is set to 1. The impulse is a random

function and Grim assumed that its amplitude follows the Rayleigh distribution. In analogy to the mean wave amplitude, the mean impulse amplitude (or some other percentile average of it) is obtained from the square root of the area under the impulse spectrum, for ω from 0 to ∞ .

$$\bar{I}^{(1/n)} = \alpha_{1/n} \sqrt{\int_0^{\infty} f_x^2(\omega) T^2 (I^2 + Y^2) S(\omega) d\omega} \quad (9)$$

where the coefficient $\alpha_{1/n}$ obtains specific values depending on the average of the impulse highest $1/n$ amplitudes. For example, $\alpha_{1/10} = 1.8$ corresponds to the average of the 1/10 highest amplitudes. Additionally, the probability to exceed this average value can be obtained from the Rayleigh density function (3.92%). So, eq. 7 is transformed to the next equation where one can solve for $\alpha_{1/n}$ in order to obtain the probability to reach a critical velocity within time τ_1 :

$$b \cdot \tau_1 + \int_0^{\tau_1} \left[N(\dot{x}_0, x_0^2, x_0^3) / (m - X_{\ddot{u}}) \right] d\tau = \bar{I}^{(1/n)} \quad (10)$$

By integrating eq. 3 up to $\tau = \tau_2$ and repeating the above procedure, a statistical estimate of the time duration of high-run can be obtained.

3.3 Application and results

The above methodology has been applied through the next steps:

- The critical velocity is set equal to the celerity of spectrum's peak frequency.
- The probability to exceed the targeted velocity in a given time τ_1 is calculated.
- Assuming that the critical velocity has been reached in τ_1 , we calculate the probability to exceed certain durations $\tau_2 - \tau_1$ of high runs.
- The procedure is repeated by selecting various critical velocity levels, deriving from the nominal speed.



The nominal speed is 12 m/s and the spectrum is JONSWAP with its full frequency range.

Accelerated motion

In Figures 11 and 12 are shown plots of the calculated probability the ship speed to exceed the defined wave celerity. One could regard the time τ_1 as a fraction of the apparent wave period, i.e. it is comparable to the time, during an encounter wave cycle, when the ship is pushed by the wave. For the selected speed and peak periods, the τ_1 value should be somewhere in the range 18-26s. In Figure 13 several velocity thresholds have been tried. To be noted that the threshold $1.3V_{nom}$ corresponds to the wave celerity of $T_p = 10$ s.

Duration of high-run

The statistics of high-run duration depends on the time τ_1 (see Figure 14). It appears that, the sooner the threshold is reached the longer the high-run will last. However, according to Figure 11, the probability of a velocity threshold crossing becomes significant for $\tau_1 > 20$ s. Given that the threshold has been reached, we examine the effect of peak period and significant wave height on high-run's duration. Thus, Figures 15 and 16, showing the effect of peak period and significant wave height on high-run duration, were drawn for $\tau_1 = 20$ s.

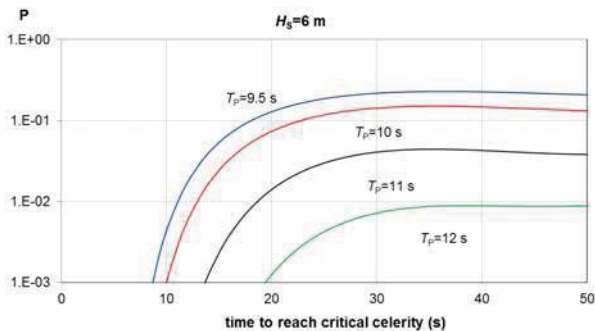


Figure 11 Probability to exceed the celerity value corresponding to the peak frequency, within a certain time, for $H_s=6$ m.

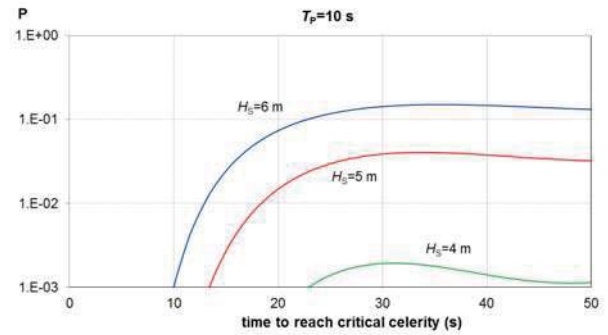


Figure 12 Probability to exceed the celerity value corresponding to the peak frequency, within a certain time, for $T_p=10$ s.

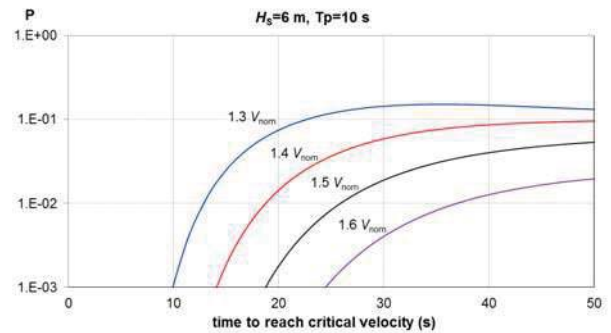


Figure 13 Probability to exceed various values of critical velocity (defined by a constant times the nominal speed) as a function of τ_1 ($H_s=6$ m and $T_p=10$ s).

By increasing the peak period, the high-run occur less frequently. One notes in Figure 16 the substantial decrease of the duration for lower significant wave heights. Also, from Figure 17 it is recovered that, setting a higher velocity threshold induces a significant reduction of probability.

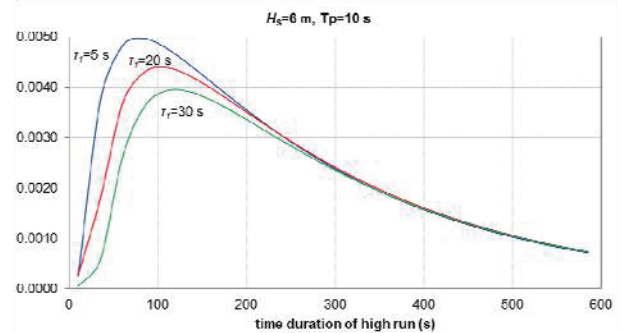


Figure 14 pdf of high-run duration for certain wave parameters (3 cases of τ_1).

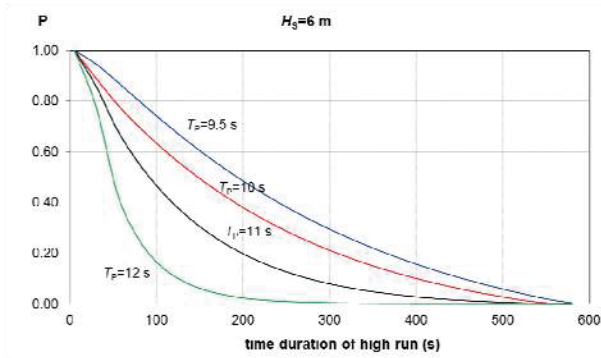


Figure 15 Probability of exceeding a duration value, for several peak periods ($\tau_1 = 20$ s).

3.4 Comparison with direct counting

We contrasted the statistics of high-run duration obtained with the method described in section 2, against the respective result based on Grim's approach (Figure 18). As observed, Grim's method suggests that the longer high-run are more probable (when compared with the mean durations obtained from simulation). This could be also verified by the fact that the mean duration derived from Grim's method (150 s) is approximately equal with the mean obtained for the 80th percentile. A qualitatively similar tendency was noticed also in other sea states.

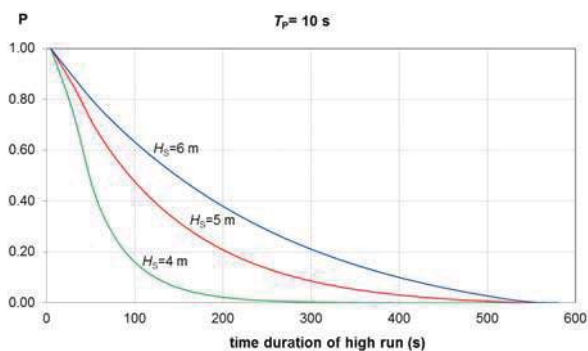


Figure 16 Probability to exceed a duration value. The threshold speed is the celerity corresponding to the peak frequency of the spectrum ($\tau_1 = 20$ s).

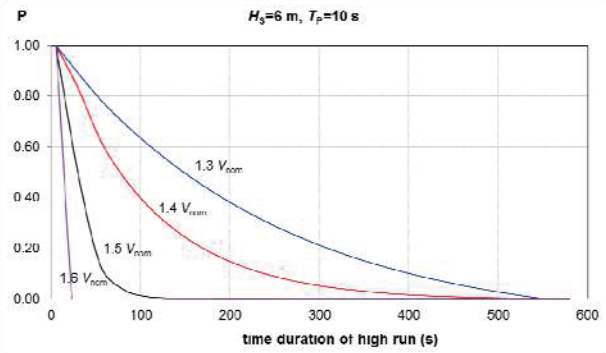


Figure 17 Probability of high-run duration for various velocity thresholds ($\tau_1 = 20$ s).

In interpreting any discrepancies between the results of the two methods, one should take into account their main differences: firstly, Grim's method assumes a constant (and equal to the targeted threshold) surge velocity during the high-run (possibly inspired by the regular wave case when surf-riding occurs). Nonetheless, we have observed fluctuations (sometimes strong) in high-runs. Furthermore, the velocity thresholds that bound the high-run in the two methods are different. In the direct counting, it is specified by the instantaneous wave celerity and the nominal speed while on Grim's approach the limit threshold is constant and equal to the celerity of peak frequency.

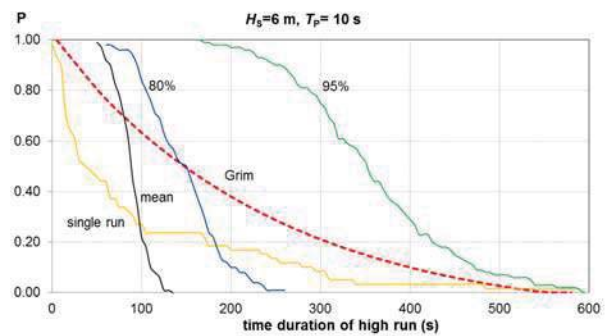


Figure 18 Comparison of probabilities of high-run duration between simulation statistics and Grim's method ($H_s = 6$ m, $T_p = 10$ s).

4. CORRELATION OF CELERITY AND MEAN SPEED IN HIGH-RUNS

4.1 Objectives of the study and error metrics

The aim of this final study is to examine whether could be objectively established that the instantaneous wave celerity truly dictates the mean surge velocity during high-run events. The frequency range is systematically varied in order to study the effect of a transition from a “narrow” to a “broad-band” spectrum. Methods of calculation of the instantaneous wave celerity $c(t)$ in irregular waves were discussed earlier (see Spyrou et al. 2014c). The one used here is derived from the concept of instantaneous frequency.

The mean speed $\bar{U}(t)$ is based on several speed values sampled between successive speed maxima and minima. Details of the calculation procedure are found in Spyrou and Themelis (2013). To quantify the difference between the two time-varying processes of interest (the instantaneous celerity and the mean speed), two error metrics commonly employed in studies addressing discrepancies of time histories will be used (Sarin et. al. 2010). The first metric is the well-known Euclidean vector norm:

$$L_2 = \|\mathbf{c} - \bar{\mathbf{U}}\| = \left(\sum_{i=1}^N |c_i - \bar{U}_i|^2 \right)^{1/2} \quad (11)$$

where $\mathbf{c}, \bar{\mathbf{U}}$ are the discretised time histories (vectors of equal dimension N) of instantaneous celerity and mean speed, respectively. It should be noted that vector norms cannot distinguish an error due to phase difference from an error due to magnitude.

The second error metric has been proposed by Sprague and Geers (2004). It combines the error M due to magnitude differences (eq. 12) and the error P due to those of phase (eq.13):

$$M = \sqrt{\frac{\psi_{AA}}{\psi_{BB}}} - 1 \quad (12)$$

$$P = \frac{1}{\pi} \cos^{-1} \left(\frac{\psi_{AB}}{\sqrt{\psi_{AA} \cdot \psi_{BB}}} \right) \quad (13)$$

where

$$\psi_{AA} = \frac{\sum_{i=1}^N c_i^2}{N}, \quad \psi_{BB} = \frac{\sum_{i=1}^N \bar{U}_i^2}{N}, \quad \psi_{AB} = \frac{\sum_{i=1}^N c_i \bar{U}_i}{N} \quad (14)$$

The combined error is:

$$C_{er} = \sqrt{M^2 + P^2} \quad (15)$$

These two error metrics will be applied not only to the instantaneous celerity versus the mean speed, but also to the celerity corresponding to the peak frequency versus the mean speed, because the latter is also a strong candidate for the critical speed of surf-riding.

4.2 Simulation settings

The “tumblehome” vessel is assumed operating at nominal speed 14 m/s. Ranges of wave frequency with gradually increasing width are tested (JONSWAP spectrum). Per frequency range, 10 realisations are generated. The significant wave height and the peak period are 6 m and 10 s, respectively. The total simulation time is 5000 s; however the first 2000 s of each run are excluded from further processing. The time step is 1 s.

4.3 Results

Error mean values according to the two applied metrics were obtained. To ensure that the comparison is carried out only during time segments of high run occurrence, we introduced a velocity condition requiring, the mean surge velocity to be greater than the nominal speed ($\bar{U}(t) > U_{nom}$) (“1st velocity condition”). We tested also a slightly modified version of it: $\bar{U}(t) > 1.1 \cdot U_{nom}$ (“2nd velocity condition”). Finally, we calculate the error values between the mean of the surge velocity and the mean of the instantaneous celerity. For

the latter, we follow the same calculation procedure as for the mean surge velocity.

Typical time histories on which the two metrics are applied are shown in Figure 19. Errors according to the Euclidean metric are seen in Figure 21 and 22, for the first and the second velocity condition, respectively. In contrast, Figures 23 and 24 show the errors according to the Sprague and Speers metric. The results based on the Euclidean metric suggest that, the discrepancy of mean speed from the celerity of peak frequency is consistently less than that of mean speed from instantaneous celerity. This trend appears too if the 2nd velocity condition ($\bar{U}(t) > 1.1 \cdot U_{nom}$) is imposed. The same conclusion is drawn when the Sprague-Geers metric is used, if the first velocity condition is applied.

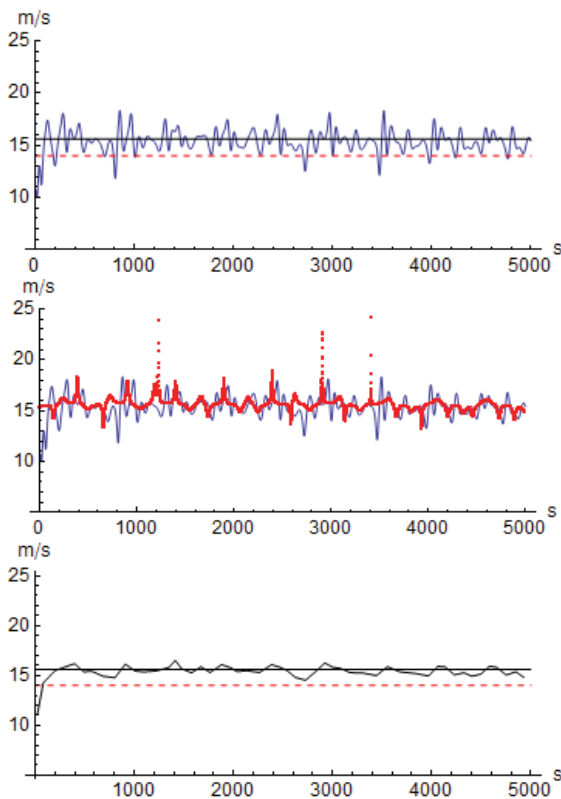


Figure 19 Time histories of surge velocity (upper diagram), instantaneous wave celerity (middle) and mean surge velocity (low). Continuous and dashed straight lines show the wave celerity of the peak frequency and the nominal speed, respectively. The simulations

were based on a frequency range $20\% \omega_p$ (both sides).

However, for the second velocity condition the situation is reversed and the correlation of instantaneous celerity with mean speed is superior, for frequency ranges up to $45\% \omega_p$. Even better correlation is achieved when the mean of the instantaneous celerity is taken, in place of the instantaneous celerity itself. In general, the error increases as the frequency range of the spectrum is broadened.

5. CONCLUDING REMARKS

The statistics of high-run occurrences in irregular seas were investigated by simulation-based direct counting and by an approximate semi-analytical method. The topic remains open since the dynamics behind these events is not completely understood yet. The velocity of the high-run shows good correlation with the mean instantaneous celerity when an error metric combining errors of amplitude and phase is applied.

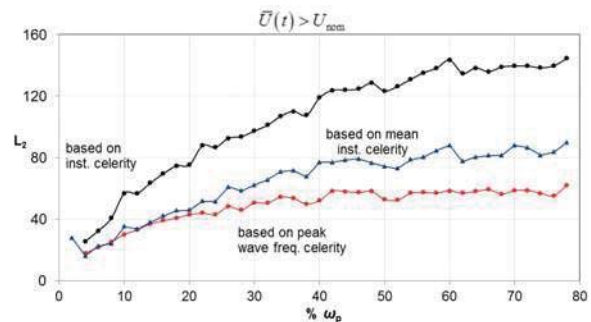


Figure 20 Calculated error according to Euclidean metric (1st velocity condition)

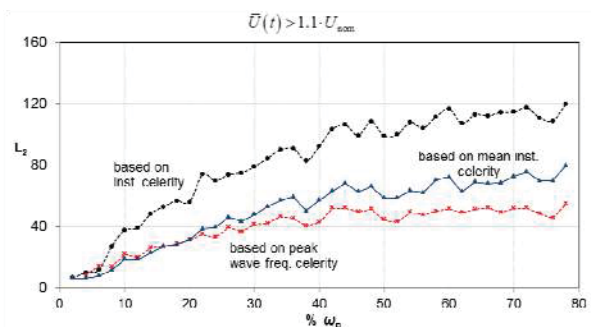


Figure 21 Calculated error according to Euclidean metric (1st velocity condition).

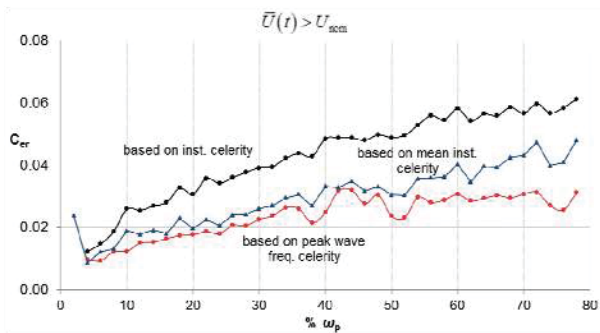


Figure 22 Error according to the Sprague and Geers metric, when satisfying the 1st velocity condition.

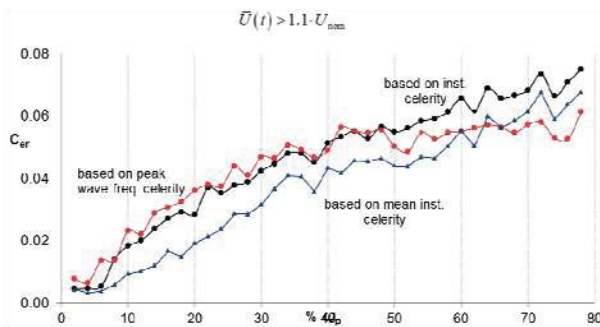


Figure 23 Error according to the Sprague and Geers metric when satisfying the 2nd velocity condition.

6. ACKNOWLEDGEMENTS

Parts of the work described in this paper (sections 2 and 3) have been funded by the Office of Naval Research under Dr. Ki-Han Kim and Dr. Woei-Min Lin. Section 4 has been supported by the Greek General Secretariat of Research and Technology under the General Program ARISTEIA I (contract reference number GSRT-252).

7. REFERENCES

Grim, O., 1963, "Surging motion and broaching tendencies in a severe irregular sea", *Ocean Dynamics*, Vol. 16, No 5, Springer Berlin/Heidelberg, pp. 201-231

Spyrou, K., 1995, Surf-riding, yaw instability and large heeling of ships in following/quarterming waves, *Ship Technology Research/Schiffstechnik*, 42 (2), 103-112

Spyrou, K., Themelis, N., 2013, "Wave celerity in a multi-chromatic sea: a comparative study", *Proceedings, 13th International Ship Stability Workshop*, Brest, France.

Spyrou, K., Belenky, V., Themelis, N., Weems, K., 2014a, "Detection of surf-riding behavior of ships in irregular seas", *Nonlinear Dynamics*, Vol. 78 (1), 649-667, Springer.

Spyrou, K., Themelis, N., Kontolefas, I., 2014b, "What is surf-riding in irregular seas?", *Proceedings, 14th International Ship Stability Workshop*, Kuala Lumpur, Malaysia, 29th September- 1st October 2014.

Spyrou, K., Belenky, V., Reed, A., Weems, K., Themelis, N., Kontolefas, I., 2014c, "Split-Time Method for Pure Loss of Stability and Broaching-To", *Proceedings, 30th Symposium on Naval Hydrodynamics*, Hobart, Tasmania, Australia, 2-7 November 2014.

Sarin, H., Kokkolaras, M., Hulbert, G., Papalambros, P., Barbat, S., Yang, R., 2010, "Comparing time histories for validation of simulation models: error measures and metrics", *Journal of Dynamic Systems, Measurement, and Control*, vol.132.

Sprague, M. A., and Geers, T. L., 2004, "A Spectral-Element Method for Modelling Cavitation in Transient Fluid-Structure Interaction," *Int. J. of Numerical Methods Eng.*, vol. 60, pp. 2467-2499.

This page is intentionally left blank



Stability and Roll Motion of a Ship with an Air Circulating Tank in Its Bottom

Ikko Watanabe, *Osaka Prefecture University* sv103027@edu.osakafu-u.ac.jp

Satowa Ibata, *Osaka Prefecture University* ibata@marine.osakafu-u.ac.jp

Seijiro Miyake, *Osaka Prefecture University* miyake@marine.osakafu-u.ac.jp

Yoshiho Ikeda, *Osaka Prefecture University* ikeda@marine.osakafu-u.ac.jp

ABSTRACT

A ship with an air circulating tank in its bottom has been developed in Osaka Prefecture University with several Japanese shipyards to reduce the frictional resistance drastically and to save fuel consumption of the ship. It was pointed out that the moving air in the tank due to heel and roll motions may reduce the stability, and changes the roll motion characteristics of the ship.

In the present paper, at first, the effects of the moving air on the stability of a ship with an air circulating tank which has a single compartment are theoretically and experimentally investigated to confirm the loss of stability. To resolve the stability loss, the air circulating tank is divided into some transverse compartments. The stability calculation suggests that four compartments can keep enough stability in small roll angle. For the new tank, the stability, roll damping and roll motions are experimentally investigated.

Keywords: *air circulating tank, frictional resistance, stability, roll motions, roll damping*

1. INTRODUCTION

Reduction of the frictional resistance acting on a ship by using air has been studied in more than hundred years. In Russia (Soviet Union), Europe and Japan, research and development of ship drag reduction by using air were carried out from 1960's to 2000's. Comprehensive reviews were published (Gorbachev, Y, 2012 and Makiharju, S, 2012). For a large ship which runs in lower Froude number, drag reduction devices by using air-micro-bubbles were successively installed to module carriers, bulk carriers and a Ro-Ro ferry in Japan, and revealed that the devices gave a 3-12% reduction of fuel consumptions.

To get more effective drag reduction tools, the authors have been developing an air circulating tank (ACT) which is installed in

the bottom of a ship and in which air is kept and circulates. Reduction of the frictional resistance can be more than the air micro-bubble method mentioned above. The experiments carried out by the authors showed that a 25-30% reduction of frictional resistance can be achieved in lower Froude numbers (Furuo, A, 2015). There are some problems to keep the drag reduction, for examples, how to keep the air in trim, heel and ship motions, how to reduce generated waves on the free surface between inside air and outside bottom water flow, how to keep the stability of the ship with the air circulating tank.

In the present study, fundamental characteristics of the stability of a ship with ACT are theoretically and experimentally studied, and an ACT to avoid the stability

reduction due to the bottom air is developed. Roll damping and roll motions in beam waves are also experimentally investigated.

2. STABILITY OF A SINGLE-COMPARTMENT ACT

Stability characteristics of a box shape model with a single-compartment ACT in the bottom are investigated. The cross section of the model are shown in Fig. 1. Air is accumulated in the ACT or the well.

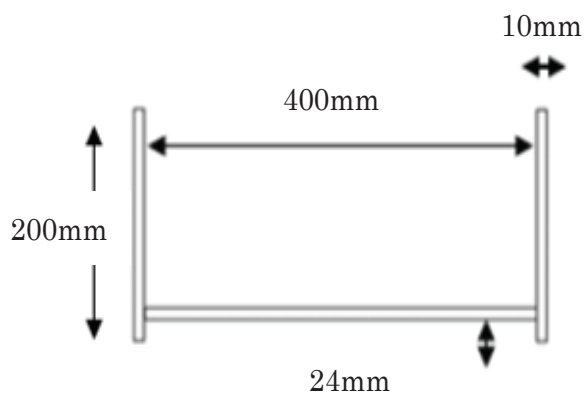


Figure 1 Cross section of the box shape model with a single-compartment ACT .

With increasing heel angle, the inside air shifts and generates a negative restoring moment as shown in Fig. 2. The inside air escapes from the tank in larger heel angle and the draft increases due to reduction of buoyancy as shown in the fourth figure in Fig. 2.

The stability reduction due to the air shift and escape in the ACT can be easily calculated. The results are shown in Fig. 3 with experimental results obtained by the authors. We can see that the air in ACT significantly reduces the stability of the model. It should be noted that the stability in small heel angle becomes very small as shown in Fig. 3. This means that the ship may be unstable in some degree, and needs appropriate GM to compensate the reduction of the stability due to the air. In larger heel angle, however, the inside

air escapes from the ACT, and the stability may recover to the safety side.

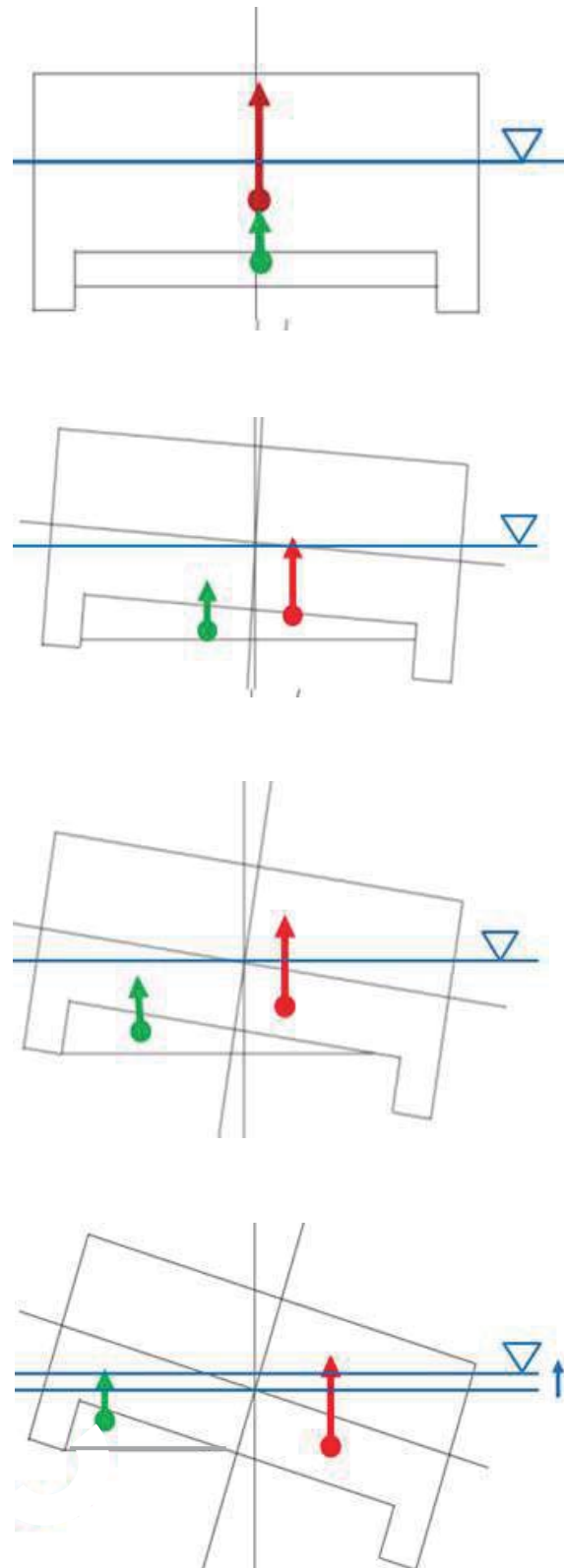


Figure 2 Inclining of a ship and air in ACT (red arrow: buoyancy acting on the body, green arrow: buoyancy by trapped air).

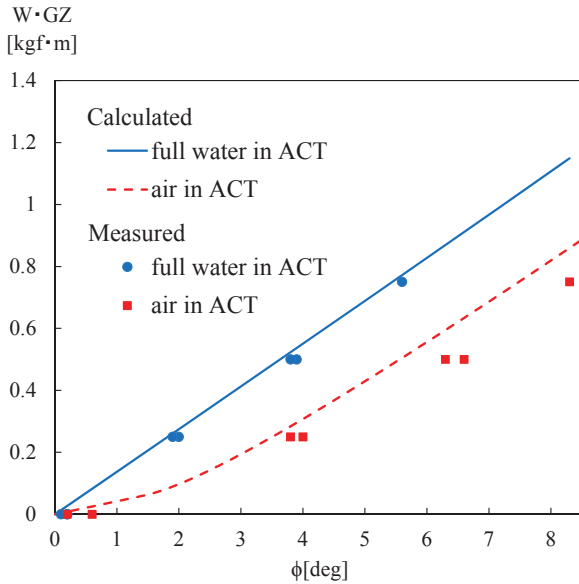


Figure 3 Reduction of stability of a box model due to air in a single-compartment ACT (lines: calculated, marks: measured)

3. IMPROVED ACT

The easiest way to resolve the reduction of the stability of a ship with ACT may be to transversely divide the tank into some compartments. Fig. 4 shows air shift in each compartments of the box model with a four-compartment ACT. Stability calculations for various numbers of the compartments are carried out, and the results are shown in Fig. 5. The results demonstrate that the transverse compartments drastically improve the stability, and the stability of a model with four compartments are almost same as that of the case of no air in the ACT. We can safely said that the four compartments can resolve the stability problem of a ship with an air circulating tank.

4. STABILITY AND ROLL MOTIONS OF ULCC

The authors developed a 20,000TEU ultra-large container carrier with shallow draft and wide beam. To reduce the frictional resistance of the ship, an ACT was developed for the ship as shown in Fig. 6.

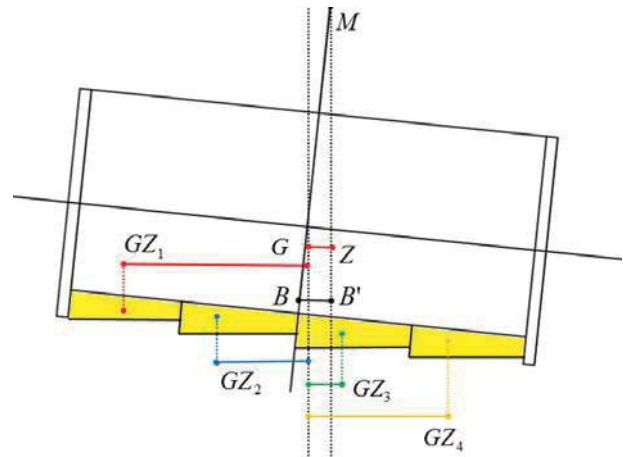


Figure 4 Schematic view of an inclining box model with an ACT with four-compartment.

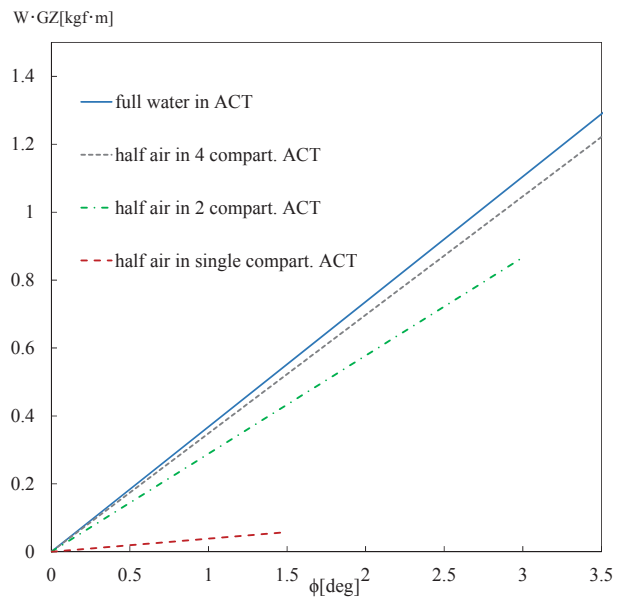


Figure 5 Calculated stability reduction of ACTs with single, two and four compartments.

Model experiments to measure the resistance acting on the model were carried out in a circulating water channel and a towing tank to find a 26% reduction of the frictional



resistance in low Froude number (Furuo, A, 2015).

In the present study, roll motions in beam waves are experimentally investigated. The body plan and the principal particulars of the model are shown in Fig. 7 and Table 1. The experimental results are shown in Figs. 8 and 9. The roll damping shown in Fig. 8 demonstrates that the air decreases the damping drastically. It can be seen that the damping for the case of no air in the ACT is much larger than those for the cases of air in the ACT and normal bottom. The increase of the roll damping may be because that the longitudinal walls which divide compartments in ACT works as the same as bilge keels of a ship. Roll amplitudes of the ship in beam waves shown in Fig. 9, however, suggest that the air in the ACT has only slight effects on the roll motions. The peak value at resonance of the case of air in the ACT is slightly larger than that full water in the ACT.

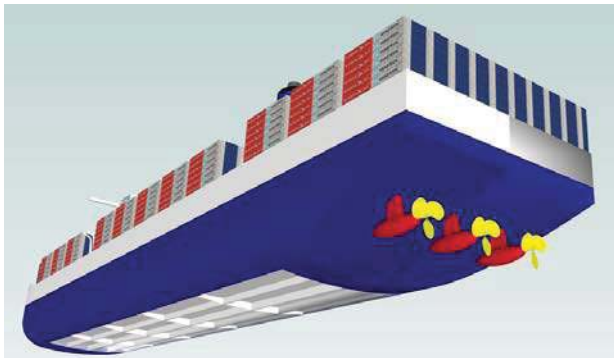


Figure 6 Artist impression of a 20,000TEU container ship with ACT.

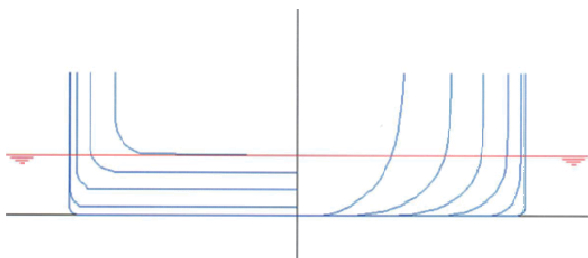


Figure 7 Body plan of the model without ACT

Table 1 Principal particulars of the model of ULCC

Model ship	Loa(m)	2.770
	Lwl(m)	2.670
	B(m)	0.500
	D(m)	0.150
	d(full load)(m)	0.063
	Wetted Surface Area (full load)(m ²)	1.549
	Cb	0.955
Air Circulating Tank	L(m)	2.000
	B'(m)	0.476
	H(m)	0.0125
	Surface Area (m ²)	0.952

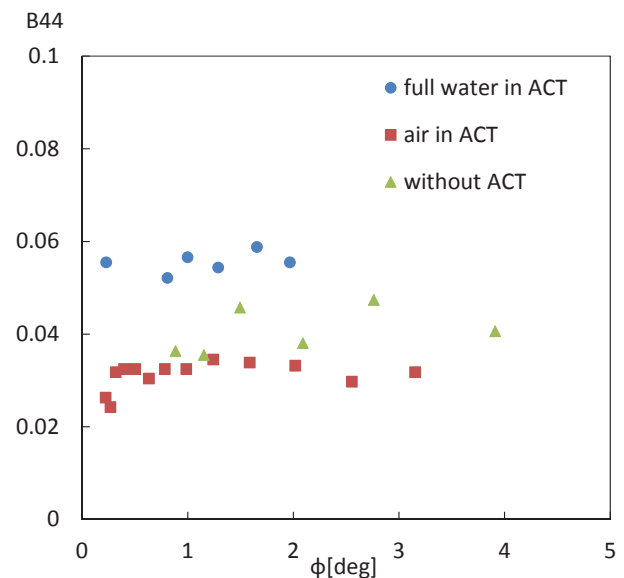


Figure 8 Measured roll damping coefficients by free decay tests

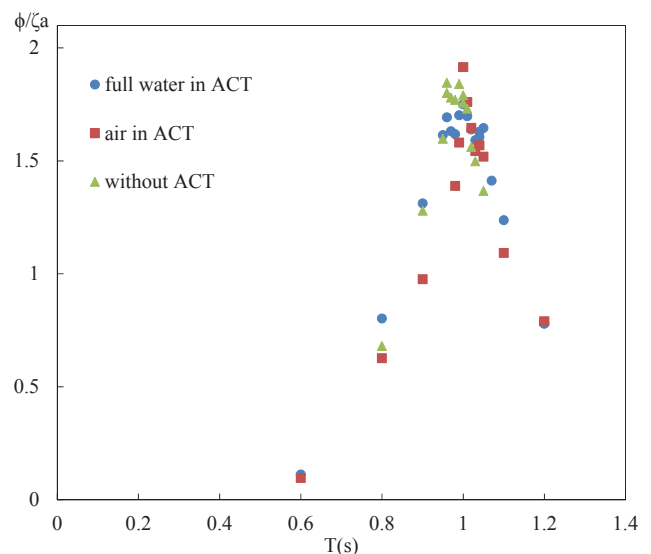




Figure 9 Measured roll amplitudes in beam waves of ULCC model with and without ACT

5. CONCLUSIONS

Effects of air in an air circulating tank (ACT) on the stability and the roll characteristics of a ship are theoretically and experimentally investigated, and following conclusions have been obtained.

- 1) Air in an air circulating tank of a single compartment reduces the transvers stability, particularly in small heel angle.
- 2) By dividing the ACT into some transverse compartments, the reduction of the stability decreases. The reduction disappears for four compartments.
- 3) Effects of the air in ACT on roll motions in beam waves are slight.

6. REFERENCES

- Furuo, A, 2015, "A study on an air circulating tank to reduce the frictional resistance of a ship", Master thesis, Osaka Prefecture University, Japan (in Japanese).
- Furuo, A, 2015, "Development of an Air Circulating Tank to Reduce the Frictional Resistance of a Ship", the 25th ISOPE Conference.
- Gorbachev, Y, Amromin, E, 2012, "Ship Drag Reduction by Hull Ventilation from Level to Near Future", Proc. of ATMA,
- Makiharju. S, Ceccio. S. L, 2012, "Air Lubrication Drag Reduction on Great Lakes Ships", Presentaion material at University of Michigan.

This page is intentionally left blank



A Study on the Effects of Bilge Keels on Roll Damping Coefficient

Yue Gu, *Department of Naval Architecture, Ocean and Marine Engineering, University of Strathclyde, Glasgow, UK.* yue.gu.2013@uni.strath.ac.uk

Prof. Sandy Day, *Department of Naval Architecture, Ocean and Marine Engineering, University of Strathclyde, Glasgow, UK.* sandy.day@strath.ac.uk

Dr. Evangelos Boulougouris, *Department of Naval Architecture, Ocean and Marine Engineering, University of Strathclyde, Glasgow, UK.* evangelos.boulougouris@strath.ac.uk

ABSTRACT

A study of the roll damping of a two-dimensional FPSO model produced by bilge keels using CFD method is presented in this paper. The tool to be utilized is the well-known code Star-CCM+, which uses the Volume of Fluid (VOF) approach to capture the free surface. The results are validated by comparison with experiments. Using the results from a number of simulations, the roll damping coefficient resulting from locating the bilge keels at different positions will be calculated. The analysis of the rolling damping coefficients for the different locations will provide a useful design tool for optimising the roll damping of vessels with bilge keels.

Keywords: roll damping coefficient, bilge keels, FPSO, 2-D, Star CCM+

1. INTRODUCTION

Roll motion although it is a significant parameter in the prediction of a ship's seakeeping performance, is one of the most difficult to calculate for seagoing vessels. This is due to fact that roll damping has a large influence on the roll motion up to the point that it may even cause the vessel's capsize (Haddara, 1989). It plays a dominant role on reducing the roll amplitude and that is why many researchers pay attention to the improvement of its prediction (Pesman at al, 2007). Since 1970s, many investigations have been carried out on the effects of bilge keels, which are used for many years on ships to enhance roll damping (Ikeda, 1977, Ikeda, 1978, Ikeda, 2004). However, due to the complicated nature of roll motion, mainly due to the influence of the viscosity, as well as other factors such as wind, waves and the interaction between the ship and the free

surface, it is difficult to make accurate predictions using the potential theory or analytical solutions, which result in many cases in an over-estimation of the roll amplitude (ITTC, 2011). The most well-known and accepted empirical formula is Ikeda's method, but its limitations and inaccuracies have been revealed over time (Yuki, 2003a, Yuki, 2003b, Bassler, 2011). The most accurate way of predicting roll damping remains until today model testing. An efficient and low-cost method to minimise the number of model tests and improve the accuracy of the predictions is the roll damping simulation using CFD (Yang, 2012). Using such method the impact of bilge keels can be simulated and their roll damping coefficient can be predicted quite accurately.

2. BACKGROUND



A study on roll damping on a non-conventional 2-D cross-section was proposed by Yuck (2003a) to investigate the operational efficiency and stability of FPSO. Three kinds of models, namely bilge model, box model and step model, were established in the roll damping coefficient analysis under small roll angle. The results revealed a fact on midships cross-section that affects damping coefficient without bilge keels. Additional work was performed by Van't (2011) to predict the roll damping motion of a FPSO with bilge keels comparing experiment results with CFD simulations using Star CCM+, however, the entire work was limited on two bilge-keels positions.

Comparisons between experimental data and numerical results of roll damping decay for a FPSO with bilge keels was carried out by Avalos (2012, 2013, 2014) to validate accuracy of numerical methods.

Due to the limitation of Ikeda's method for large amplitude roll motions, a DTMB model with bilge keels has been developed by Bassler (2010a, 2010b, 2011) to increase the prediction accuracy of the ship's motions for design assessments.

A numerical model using RANS (Reynolds Averaged Navier Stokes) flow solver compared with experiments has been developed to improved predictions of the bilge keels effect on viscous roll damping coefficients (Querard, 2010). The results revealed that due to friction and eddy making, bilge keels have a dominant impact on the viscous roll damping coefficient.

Considering the effect of bilge keels on the roll damping, Chakrabarti (2001) investigated the features of roll damping with various ship hullform with experiments. Based on Ikeda's method, it was concluded that the impact of bilge keels on the roll damping depends on the locations of the bilge keels.

The effects of putting bilge keels at different positions on the a new non-ballast ship with rounder cross section was investigated by Miyake (2013), and results revealed that the effect of bilge keels on damping motion for a rounder cross-section are much smaller compared with a conventional square cross-section.

In this work, the effect of bilge keels at different locations for roll damping coefficients is investigated in a 2-dimensional FPSO model. Star CCM+ solver is used to simulate roll motion of the rectangular model and FPSO model. Initially, CFD simulations results are compared with previous work for validating the accuracy and feasibility of the scheme. Results obtained by Jung (2006) from roll decay tests on a rectangular structure in calm water and waves are used to be compared. Utilizing the FPSO model provided by Avalos (2012, 2013, 2014), an investigation is performed on the effects of bilge keels at different location on roll damping coefficients.

3. NUMERICAL FORMULAE

3.1 Rolling Motion

A simple equation for ship roll motion including single degree of freedom can be given by

$$A\ddot{\phi} + B(\dot{\phi}) + C\phi = M(\omega t) \quad (1)$$

However, the damping term $B(\dot{\phi})$ includes linear and nonlinear components

$$B(\dot{\phi}) = B_1\dot{\phi} + B_2\dot{\phi}|\dot{\phi}| + B_3\dot{\phi}^3 + \dots \quad (2)$$

It can be assumed that the nonlinear component can be approximated by being linearized so that the damping term can become (Bassler, 2009)

$$B(\dot{\phi}) = B_{44}\dot{\phi} \quad (3)$$

3.2 Rolling in Calm Water

According to Bhattacharyya (1978), the equation of rolling motion in calm water can be expressed in a differential form given by

$$a \frac{d^2 \phi}{dt^2} + b \frac{d\phi}{dt} + c\phi = 0 \quad (4)$$

where,

a is the virtual mass moment of inertia

$d^2\phi/dt^2$ is the acceleration of rolling

$a(d^2\phi/dt^2)$ is the inertial moment

b is damping moment coefficient

$d\phi/dt$ is angular velocity

$b(d\phi/dt)$ is the damping moment

$c\phi$ is the restoring moment

c is the restoring moment coefficient

ϕ is the angular displacement of rolling.

Parameters of ship roll motion are substituted into a , b and c , and the expression of roll motion in calm water can be given as

$$I' \frac{d^2 \phi}{dt^2} + b \frac{d\phi}{dt} + \Delta GM \phi = 0 \quad (5)$$

where I' is the virtual mass moment of inertia, which is the sum of the actual mass moment of inertia I and the added mass moment of inertia δI

$$I' = I + \delta I \quad (6)$$

Equation (5) is divided by I' , then the equation becomes

$$\frac{d^2 \phi}{dt^2} + 2\zeta\omega_N \frac{d\phi}{dt} + \omega_N^2 \phi = 0 \quad (7)$$

where ζ is the damping factor, ω_N is the natural frequency given by

$$2\zeta\omega_N = \frac{b}{I'} \quad (8)$$

$$\omega_N^2 = \frac{\Delta GM}{I'} \quad (9)$$

4. METHODOLOGY VALIDATION AND ANALYSIS

The present work uses the experimental data provided by Jung (2006) for its validation. Roll decay simulations in calm water and waves use the same setup as the experiment.

4.1 Geometric Characteristics of Model

The model is a rectangular structure, which is 0.3m wide and 0.1m high with 0.05m draft shown as below

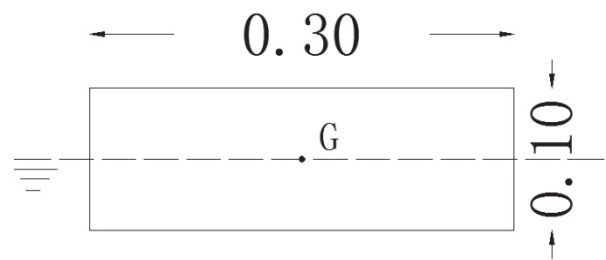


Figure 1 - Definition of geometric feature of model

4.2 Flow Domain in Free Decay Test

The roll decrement simulation is performed in a 2-D domain with the dimension of 5.7m long and 1.8m high with 0.9m water depth, shown as

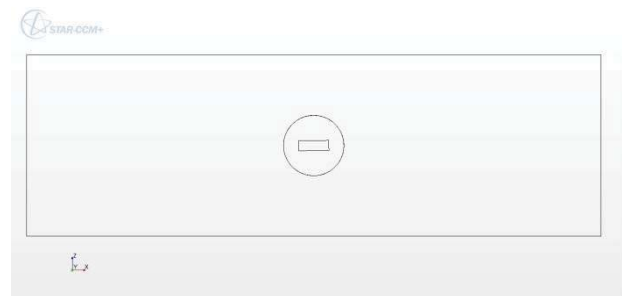


Figure 2 - Flow domain of free decay simulation

4.3 Generation of the Grid

As the body rolls in the domain, not all the mesh would be fixed. A mesh scheme is established by Manzke (2012) including deforming mesh, which changes shapes of grid

as the body rolls. However, deforming mesh is decreasing the quality of the calculations. In this work, a finer mesh scheme is utilized so that the mesh around the body can move rigidly with body without deformation. The trimmed mesh and prism layer mesher are used in the entire flow domain except the body itself. Fig.3 shows the distribution of grid through the whole domain, and Fig.4 gives the concentration of refined mesh around the free surface. Fig.5 demonstrates a refined mesh and prism layer mesh distribution around the body.

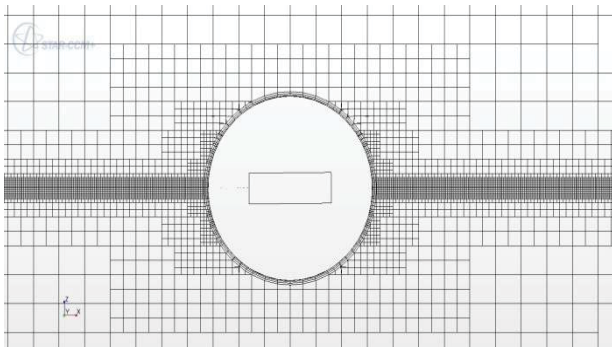


Figure 3 - Mesh scheme through the whole domain

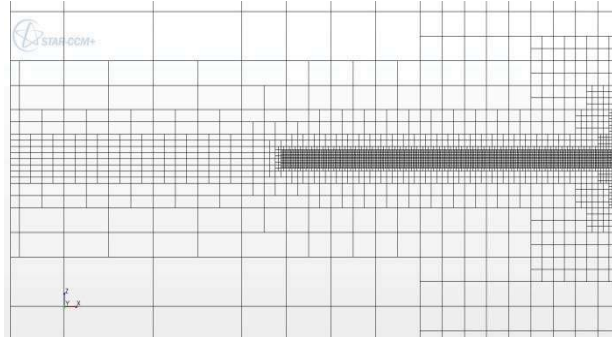


Figure 4 - Mesh distribution around free surface

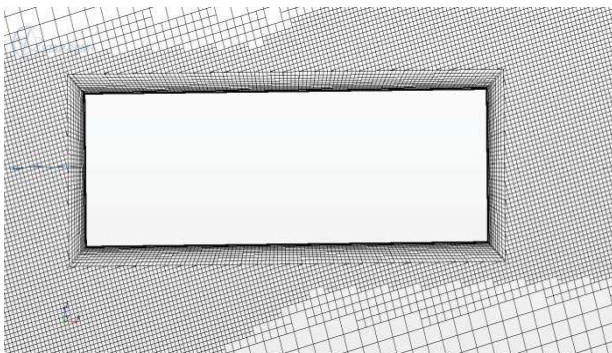


Figure 5 - Refined mesh around the body

4.4 Analysis of Free Decay Simulation

Fig.6 shows the time history of angle of inclination in the simulation of free decay. The body is initialized and released at 15 degree, inclination angle decreases after each time of roll.

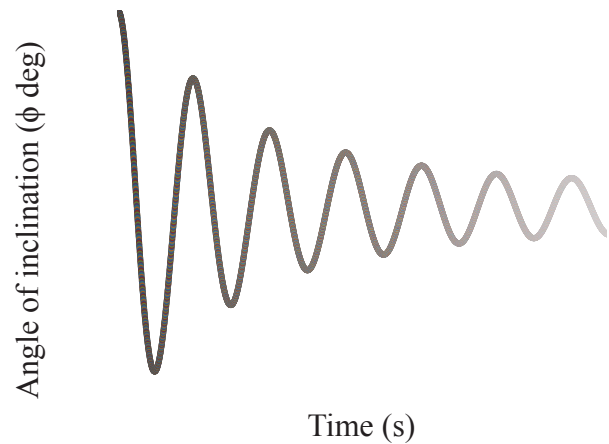


Figure 6 - Time history of angle of inclination

From Fig.6 the natural period of the structure can be obtained $T_N = 0.931s$, so that the natural frequency is $\omega_N = 6.746rad/s$, the virtual mass moment of inertia $I' = 0.364 kgm^2$ and the added mass moment of inertia $\delta I = 0.128 kgm^2$, which gives a good agreement with experiment data provided ($T_N = 0.93s$, $\omega_N = 6.78rad/s$ and $\delta I = 0.124 kgm^2$). Fig.7 shows curve of the decrease of angles.

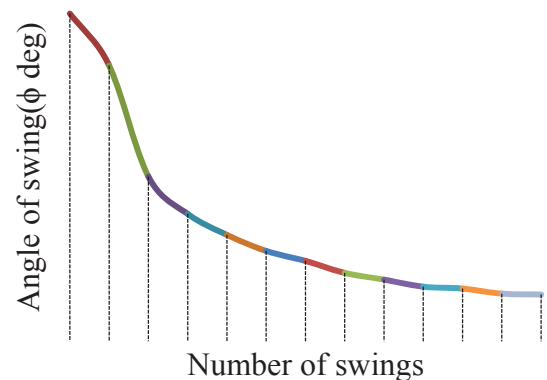


Figure 7- Curve of declining angles

According to the approach suggested by Bhattacharyya (1978), the coefficient K can be

found from the trendline of the curve of extinction that can be represented as

$$\delta\phi \text{ per swing} = K \phi_m \quad (10)$$

Analysis of the calculated data gives $K=0.3214$. With the coefficient K obtained, the damping coefficient b can be obtained by the equation given below

$$b = \frac{KT_N \Delta GM}{\pi^2} \quad (11)$$

So the damping coefficient b is 0.503kg-m-s . Compared with $b=0.519\text{kg-m-s}$ from experiment data, the different percentage is 3.16% . And the damping factor $\zeta=0.103$.

Since the simulation results demonstrate a good agreement with experiment data, the methodology can be considered valid for predicting the effect of bilge keels on the damping coefficients of FPSO model.

5. ROLL DECAY SIMULATIONS WITH BILGE KEELS

A FPSO model given by Avalos (2012, 2013, 2014) is used to investigate the damping effects of bilge keels at different locations through a series of roll decay simulations. The results demonstrate the correlation between bilge keels' locations and damping coefficients.

5.1 Characteristics of Models

Table 1 demonstrates the model features of FPSO in the present study, and bilge keels are distributed around the midship frame of FPSO at 10 positions (from position A to position J). Fig. 8 shows the distribution of bilge keels' positions at the cross-section of midships which can be given by

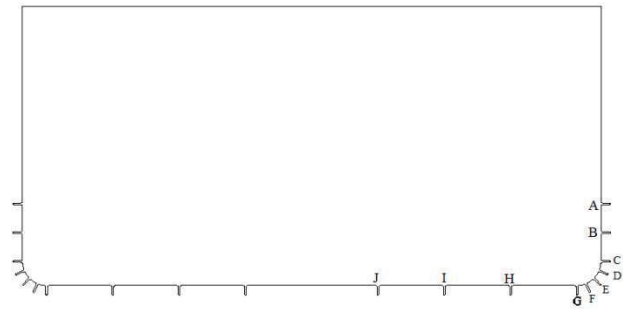


Figure 8 - Bilge keels distributions at midships cross-section

Characteristics of FPSO	Magnitude
Breath	0.725m
Draft	0.196m
Length	0.90m
Centre of gravity (KG)	0.175m
Radius of gyration (R _{xx})	0.264m
Mass per unit length	169.76Kg/m
Transverse moment of inertia per unit length	13.269Kg/m
Bilge radius	0.03m
Bilge keel	0.016m

Table 1- Model characteristics of FPSO

5.2 Mesh Generation

Fig. 9 gives a view at the mesh generated based on the present scheme when the bilge keels are located at position E and refined mesh at bilge keels are illustrated by Fig.10.

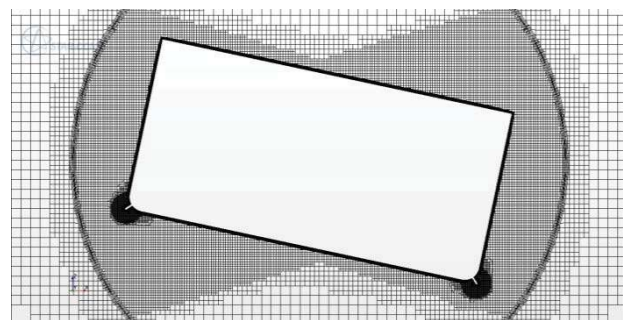


Figure 8 - Generated mesh at position E

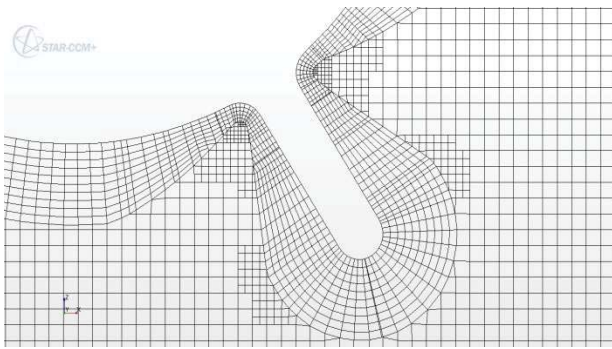


Figure 10 - Refined mesh at bilge keels

5.3 Results

Free decay simulations are carried out with each bilge keel's location (A to J). The results are compared with that of free decay without bilge keels. The initial rolling angle is 12 degree. All results are analysed to obtain the natural period T_N (s), natural frequency ω_N (rad/s), the coefficient Kn ($n=1, 2, \dots, 10$ corresponding to position A to J) based on Equ.(10) and the calculated damping coefficient b (kg-m-s) based on Equ.(11). The results can be given as Table 2. Comparison of rolling period between free decay with bilge keels and without bilge keels is shown in Fig.11. It should be noted that with bilge keels, rolling period increases obviously compared with that of the model without bilge keels (from 1.68s to approximately 1.87s).

The same effectiveness can be also seen from Fig.12 (a), which shows the time history of roll decay simulation without bilge keels and with bilge keels, which are located at position E (45° to the bilge). Fig.12 (b) is the result of roll decay test obtained by Avalos at the same position with the same magnitude of bilge keels. The comparison between Fig.12 (a) and Fig.12 (b) shows a good agreement. However, it should be noted that the decay rate is underestimated in both Fig. 12(a) and Fig. 12(b) for the smaller angles of roll oscillation. The phenomenon of under-estimated damping for smaller angle is recommended to be investigated further.

Fig.13 demonstrates the correlation between locations of bilge keels and damping coefficients based on Table 2.

Fig.14 (a) to Fig.14 (d) are the velocity distribution around the FPSO, and it can be clearly seen that the vortices at the bilge corners.

Positions	T_N	ω_N	Kn	b (kgms)
A (1)	1.8546	3.3861	0.0464	0.1818
B (2)	1.8661	3.3653	0.0617	0.2433
C (3)	1.8810	3.3386	0.1530	0.6080
D (4)	1.8748	3.3497	0.2225	0.8813
E (5)	1.8787	3.3428	0.2610	1.0360
F (6)	1.8737	3.3516	0.1850	0.7324
G (7)	1.8723	3.3541	0.1697	0.2790
H (8)	1.8375	3.4176	0.0024	0.0093
I (9)	1.8285	3.4345	0	0
J (10)	1.8276	3.4362	0	0
NO BK	1.6816	3.7345	0.0618	0.2196

Table 2 - Results of free decay simulations

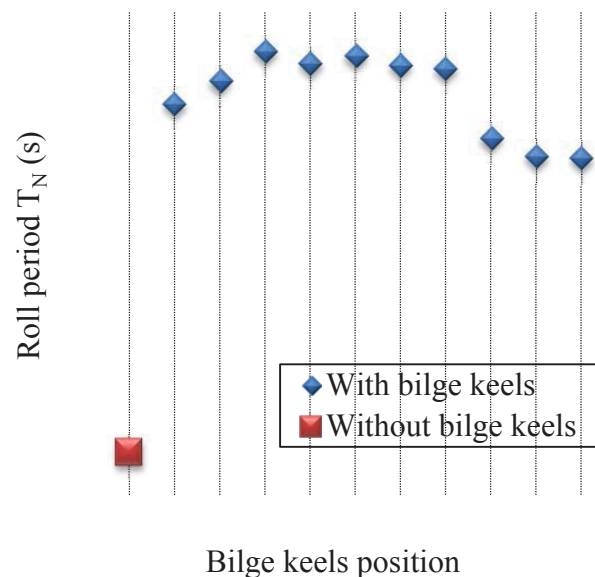


Figure 9 - Rolling period of free decay

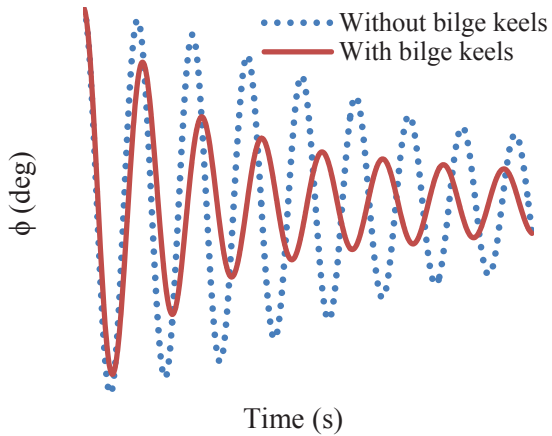


Figure 10 (a) – Results of angle of inclination at present study

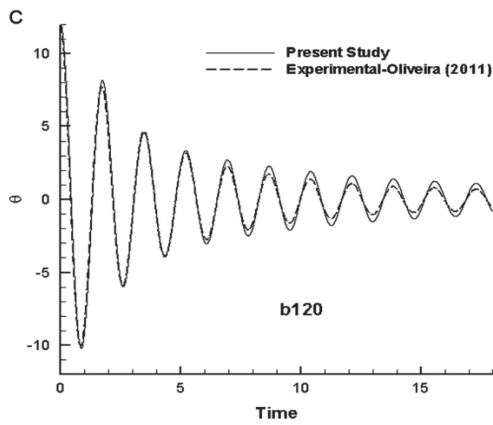


Figure 12 (b) - Result of roll decay test obtained by Avalos

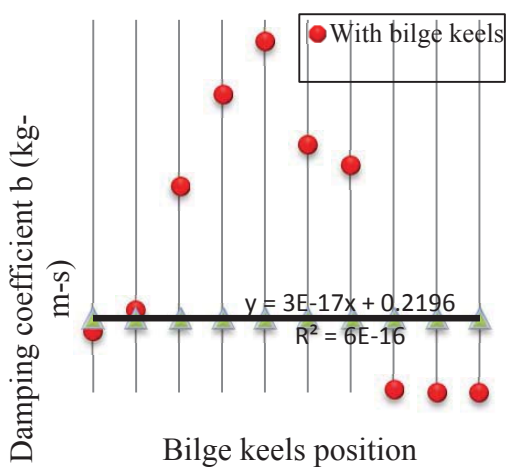
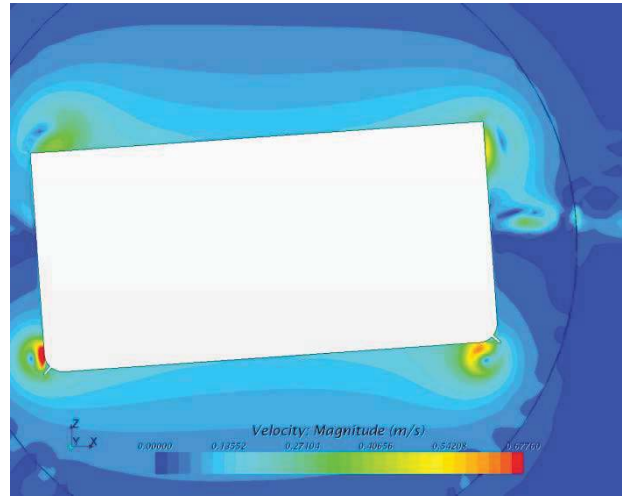
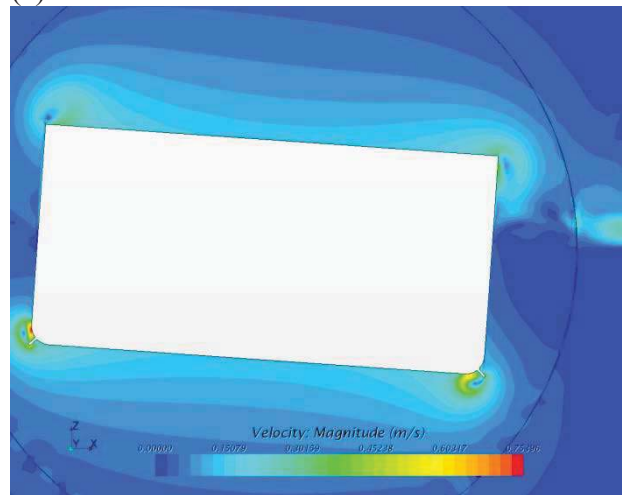


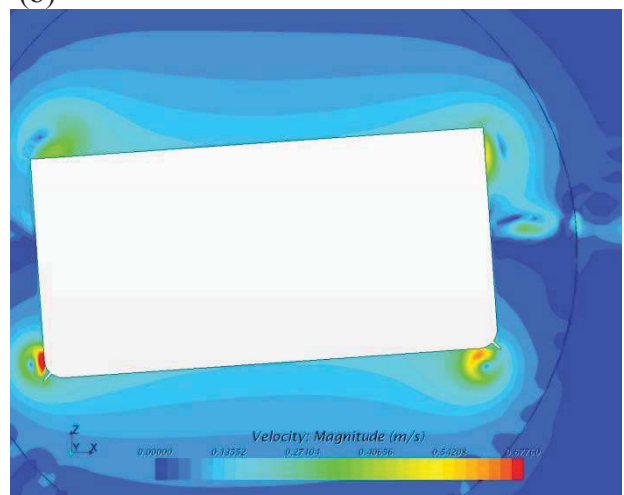
Figure 11 - Damping coefficient of FPSO model with bilge keels at each position (A to J) of bilge keels and without bilge keels



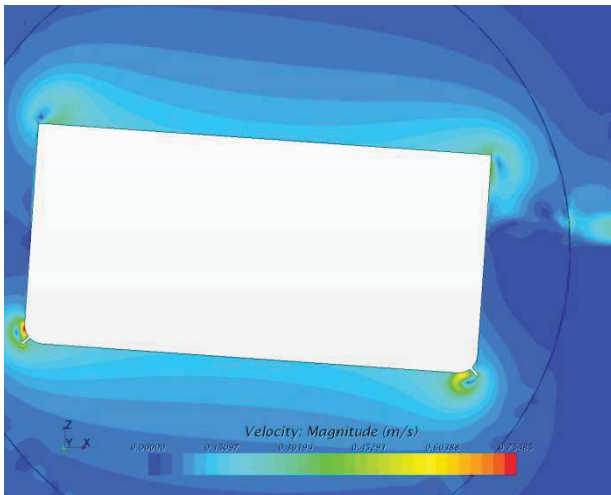
(a)



(b)



(c)



(d)

Figure 14 (a to d) – Velocity and vortex distributions

6. CONCLUSIONS

Table 2 and Fig.11 reveal that bilge keels, which located at ship side and bilge, do have an impact on damping the ship's roll motion. However, the effect can be negligible when bilge keels are positioned at ship bottom.

From Fig.13 it can be seen that bilge keels yield a larger damping coefficient when they are located at the bilge compared with other positions, which means when at the bilge, bilge keels can have a greater impact on the roll motion. Bilge keels at ship side and bottom also affect the damping, and the more they are close to the bilge the larger impact they have on the damping effectiveness.

Comparing results between side locations and bottom locations, bilge keels at the side have greater influence on the roll damping. Additionally, it can be seen from Table 2 that the coefficient K of position H, I and J are close to zero, so that bilge keels that are close to the ship keel are not effective in damping the motion.

Further work will be concentrated on investigating the effect of bilge keels on roll damping when the FPSO is rolling in waves.

7. REFERENCE

- Avalos, G. O. G. & Wanderley, J. B., 2012, "A Two-Dimensional Numerical Simulation of Roll Damping Decay of a FPSO Using the Upwind TVD Scheme of Roe-Sweby", The 31st International Conference on Ocean, Offshore and Arctic Engineering, pp. 395-402.
- Avalos, G. O. G., Wanderley, J. B. V. & Fernandes, A. C., 2013, "Roll Damping Decay of a FPSO With Bilge Keel", Proceedings of the ASME 2013 32nd International Conference on Ocean, Offshore and Arctic Engineering.
- Avalos, G. O., Wanderley, J. B., Fernandes, A. C. & Oliveira, A. C., 2014, "Roll Damping Decay of a FPSO with Bilge Keel", Ocean Engineering, vol. 87(2014), pp. 111-120.
- Bassler, C. C. & Reed, A. M., 2009, "An Analysis of the Bilge Keel Roll Damping Component Model", The 10th International Conference on Stability of Ships and Ocean Vehicles, pp. 369-386.
- Bassler, C., Reed, A., & Brown, A., 2010, "Characterization of Physical Phenomena for Large Amplitude Ship Roll Motion", Proceedings of 29th American Towing Tank Conference.
- Bassler, C. C., Reed, A. M., & Brown, A. J., 2010, "A Method to Model Large Amplitude Ship Roll Damping", Proceedings of the 11th International Ship Stability Workshop.
- Bassler, C., Miller, R., Reed, A., Brown, A., 2011, "Considerations for Bilge Keel Force Models in Potential Flow Simulations of Ship Maneuvering in Waves", Proceedings of 12th International Ship Stability Workshop.
- Bhattacharyya, R., 1978, "Dynamics of Marine Vehicles", John Wiley & Sons Inc., pp.75-95.



- Chakrabarti, S., 2001, "Empirical Calculation of Roll Damping for Ships and Barges", Ocean Engineering, vol. 28(7), pp. 915-932.
- Chan, H. S. Y., Xu, Z., & Huang, W. L., 1995, "Estimation of Nonlinear Damping Coefficients from Large-Amplitude Ship Rolling Motions", Applied Ocean Research, vol. 17(4), pp. 217-224.
- Haddara, M. R., & Bennett, P., 1989, "A Study of the Angle Dependence of Roll Damping Moment", Ocean Engineering, vol. 16(4), pp. 411-427.
- ITTC, 2011, "ITTC-Recommended Procedures: Numerical Estimation of Roll Damping", vol. 7.5-02-07-04.5, pp.1-33.
- Ikeda, Y., 2004, "Prediction Methods of Roll Damping of Ships and Their Application to Determine Optimum Stabilization Devices". Marine Technology, vol. 41(2), pp. 89-93.
- Ikeda, Y., Himeno, Y., & Tanaka, N., 1978, "A Prediction Method for Ship Roll Damping", Report of the Department of Naval Architecture, University of Osaka Prefecture.
- Ikeda, Y., Komatsu, K., Himeno, Y., & Tanaka, N., 1977, "On Roll Damping Force of Ship, Effects of Hull Surface Pressure Created by Bilge Keels", Journal of Kansai Society of Naval Architects, vol. 165, pp. 31-40.
- Jung, K. H., Chang, K.-A. & JO, H. J., 2006, "Viscous Effect on the Roll Motion of a Rectangular Structure", Journal of Engineering Mechanics, vol. 132, pp. 190-200.
- Kawahara, Y., & Maekawa, K., 2012, "A Simple Prediction Formula of Roll Damping of Conventional Cargo Ships on the Basis of Ikeda's Method and its Limitation", Journal of Shipping and Ocean Engineering, vol. 2, pp. 201-210.
- Miyake, T. & Ikeda, Y., 2013, "A Study on Roll Damping of Bilge Keels for New Non-Ballast Ship with Rounder Cross Section". Proceedings of the 13th International Ship Stability Workshop.
- Manzke, M. & Rung, T., 2012, "Prediction of Roll Damping Using Viscous Flow Solvers", The 31st International Conference on Ocean, Offshore and Arctic Engineering, pp. 695-704.
- Pesman, E., Bayraktar, D., & Taylan, M., 2007, "Influence of Damping on the Roll Motion of Ships", The 2nd International Conference on Marine Research and Transportation (ICMRT'07), pp. 28-30.
- Querard, A. B. G., Temarel, P., & Turnock, S. R., 2010, "Application of RANS to Hydrodynamics of Bilge Keels and Baffles", William Froude Conference on Advances in theoretical and applied hydrodynamics – Past and Future.
- Van't Veer, R., Fathi, F., & Kherian, J., 2011, "On Roll Hydrodynamics of FPSO's Fitted with Bilge Keels and Riser Balcony", ASME 30th International Conference on Ocean, Offshore and Arctic Engineering.
- Yang, B., Wang, Z.-c., & Wu, M., 2012, "Numerical Simulation of Naval Ship's Roll Damping Based on CFD", Procedia Engineering, vol. 37, pp. 287-293.
- Yuck, R. H., Lee, D. H., & Choi, H. S., 2003, "Estimation of Roll Damping Coefficients for Non-conventional Mid-ship Sections", The Thirteenth (2003) International Offshore and Polar Engineering Conference, pp. 540-543.
- Yuck, R. H., Lee, D. H., Choi, H. S., Jin, Y. M., & Bang, C. S., 2003, "A Study on Roll Damping of 2-D Cylinders", International Journal of Offshore and Polar Engineering, vol. 13(03), pp. 205-208.

This page is intentionally left blank

Session 11.1 – RISK-BASED STABILITY

Influence of Linear Filters and Nonlinear Damping Models on the Stochastic Roll Response of a Ship in Random Seas

Risk Analysis of a Stability Failure for the Dead Ship Condition

Application of the Envelope Peaks over Threshold (EPOT) Method for Probabilistic Assessment of Dynamic Stability

Split-Time Method for Estimation of Probability of Capsizing Caused by Pure Loss of Stability

This page is intentionally left blank



Influence of Linear Filters and Nonlinear Damping Models on the Stochastic Roll Response of a Ship in Random Seas

Wei Chai, *Department of Marine Technology,*

Norwegian University of Science and Technology chai.wei@ntnu.no

Arvid Naess, *Centre for Ships and Ocean Structures & Department of Mathematical Sciences,*

Norwegian University of Science and Technology arvid.naess@ntnu.no

Bernt J. Leira, *Department of Marine Technology,*

Norwegian University of Science and Technology bernt.leira@ntnu.no

ABSTRACT

Roll motion is the most critical ship motion leading to capsizing. The single-degree-of-freedom (SDOF) model is applied in order to simulate the roll motion in random beam seas. The random wave excitation term in the SDOF model is approximated by a second-order linear filter or more accurately, by a fourth-order linear filter as a filtered white noise process. Then the original SDOF model would be extended into a four-dimensional (4D) or a six-dimensional (6D) dynamic system, respectively. For the 4D coupled system, it can be viewed as a Markov system whose probability properties are governed by the corresponding Fokker-Planck equation. With the advantage of Markov property, the stochastic roll response can be obtained by the efficient 4D path integration (PI) method. The effect of different damping models, i.e. the linear-plus-quadratic damping (LPQD) model and linear-plus-cubic damping (LPCD) model, on the stochastic roll response is investigated. Furthermore, Monte Carlo simulation is introduced in order to validate the stochastic roll responses calculated by the 4D PI method as well as to study the influence of two different linear filter models on the response statistics.

KEYWORDS: *stochastic roll response; path integration method; filtering technique; nonlinear damping; Monte Carlo simulation.*

1. INTRODUCTION

For large amplitude roll motion in random seas, ship motion is strongly nonlinear and the dynamic behaviour of the vessel as well as the stochastic nature of random wave excitation should be taken into consideration in ship stability analysis. Moreover, the problem of estimating the stochastic response of nonlinear dynamic system excited by random external loads has been a demanding challenge for several decades (Naess & Johnsen, 1993).

Markov models have been widely applied in the area of stochastic dynamic analysis of roll motion in random seas. The shaping filter technique is introduced in order to approximate the wave excitation as a filtered white noise process. Subsequently, an augmented dynamic system is created when the original dynamic system is coupled with the filter model. Under the Markov theory, the joint probability density function (PDF) of the roll response can be obtained by solving the governing equation, i.e.

the Fokker-Planck (FP) equation. However, extended dynamic system usually corresponds to a high-dimensional FP equation and analytical solutions to high-dimensional FP equations are only available for some linear systems and a very restricted class of nonlinear systems.

The path integration (PI) method is an efficient approximation for solving the high-dimensional FP equations with reliable accuracy. This method is based on the Markov property of the dynamic system and the global solution of the FP equation can be constructed by linking the explicitly known local solutions. Recently, this algorithm was successfully extended to 4D for studying the stochastic roll response of a ship in random beam seas (Chai et al. 2014).

Besides the efficient PI method, Monte Carlo simulation is another methodology to determine the response statistics of the nonlinear dynamic systems subjected to random external forcing. The nonlinear and time-dependent terms can be easily and directly dealt with. However, the main drawback of Monte Carlo simulation is the associated computational efficiency will be sacrificed for estimation of the extreme responses with low probability levels.

The nonlinearity of the roll damping has been recognized to be crucial for evaluating the ship stability since Froude's time (Bikdash et al., 1994). Since the quantitative evaluation of roll damping is difficult, empirical models are used to describe the roll damping term. The linear-plus-quadratic damping (LPQD) model has been verified by numerous studies of experimental data (Roberts & Vasta, 2000). On the other hand, the linear-plus-cubic damping (LPCD) model is infinitely differentiable, and mathematically preferable to the LPQD model. Bikdash et al (1994) derived a condition under which the LPCD model approximates well with the LPQD model in a least-squares sense.

In this paper, the wave excitation spectrum is modelled by a second-order linear filter and a more precise fourth-order linear filter. The effect of different linear filters on the stochastic roll response is investigated by comparison with the Monte Carlo data. The LPQD model is transformed into a LPCD model by the least square method. Then, the influence of two different damping models on the stochastic roll response, especially on the extreme response are evaluated. The accuracy of the 4D PI method is verified by means of the versatile Monte Carlo simulation technique.

2. THEORETICAL BACKGROUND

2.1 Mathematical model of roll motion

When the ship is excited by beam wave loads, the rolling behaviour can be represented by the following single-degree-of-freedom (SDOF) equation:

$$(I_{44} + A_{44})\ddot{\theta}(t) + B_{44}\dot{\theta}(t) + B_{44q}\dot{\theta}(t)|\dot{\theta}(t)| + \Delta(C_1\theta(t) - C_3\theta^3(t)) = M(t) \quad (1)$$

where $\theta(t)$ and $\dot{\theta}(t)$ are the roll angle and the roll velocity, respectively. I_{44} is the moment of inertia with respect to an axis through an assumed roll center, A_{44} denotes the added mass coefficient. B_{44} and B_{44q} are the linear and quadratic damping coefficients. Δ is the displacement of the vessel, C_1 and C_3 are the linear and nonlinear roll restoring coefficients of the restoring arm. $M(t)$ represents the random wave excitation moment.

The wave elevation and wave excitation moment are assumed to be stationary Gaussian stochastic processes. The wave excitation moment spectrum, $S_{MM}(\omega)$, can be determined as follows (Jiang et al., 1996):

$$S_{MM}(\omega) = |F_{roll}(\omega)|^2 S_{\zeta\zeta}(\omega) \quad (2)$$



in which $S_{\zeta\zeta}(\omega)$ is the wave energy spectrum, $|F_{roll}(\omega)|$ represents the roll excitation moment amplitude per unit wave height.

Dividing equation (1) by $(I_{44} + A_{44})$, the final form of the differential equation is obtained as:

$$\ddot{\theta}(t) + b_{44}\dot{\theta}(t) + b_{44q}\dot{\theta}(t)|\dot{\theta}(t)| + c_1\theta(t) - c_3\theta^3(t) = m(t) \quad (3)$$

where b_{44} , b_{44q} , c_1 and c_3 are relative roll parameters. The spectrum of the relative roll excitation moment, $S_{mm}(\omega)$, is expressed as:

$$S_{mm}(\omega) = |F_{roll}(\omega)|^2 S_{\zeta\zeta}(\omega) / (I_{44} + A_{44})^2 \quad (4)$$

Furthermore, the SDOF model (3) can be transformed into the following state-space equation:

$$\begin{cases} dx_1 = x_2 dt \\ dx_2 = (-b_{44}x_2 - b_{44q}x_2|x_2| - c_1x_1 + c_3x_1^3 + x_3) dt \end{cases} \quad (5)$$

where $x_1 = \theta(t)$, $x_2 = \dot{\theta}(t)$, $x_3 = m(t)$.

2.2 Shaping filter technique

Dostal and Kreuzer (2011) proposed a second-order and a fourth-order linear filter to fit the desired narrow-banded spectrum. In this work, both of the linear filters can be applied in order to model the target spectrum, i.e. the relative wave excitation moment spectrum $S_{mm}(\omega)$. The second-order linear filter is given by the following differential equation

$$\begin{cases} dx_3 = (x_4 - \beta x_3) dt + \gamma dW \\ dx_4 = -\alpha x_3 dt \end{cases} \quad (6)$$

where x_3 and x_4 are the state variables in the filter equation with x_3 representing the output $m(t)$. $dW(t) = W(t+dt) - W(t)$ is the increment of a Wiener process with $E\{dW(t)\} = 0$ and $E\{dW(t)dW(t+dt)\} = \delta(dt)$, where $\delta(\cdot)$ represents the Dirac function. The spectrum generated by equation (6) is given by

$$S_{2nd}(\omega) = \frac{1}{2\pi} \frac{\gamma^2 \omega^2}{(\alpha - \omega^2)^2 + (\beta\omega)^2} \quad (7)$$

The fourth-order linear filter which represents a more accurate approximation is given by the following expression:

$$\begin{cases} dx_5 = (x_6 - \lambda_1 x_5) dt \\ dx_6 = (x_7 - \lambda_2 x_5) dt + \gamma_1 dW \\ dx_7 = (x_8 - \lambda_3 x_5) dt \\ dx_8 = -\lambda_4 x_5 dt \end{cases} \quad (8)$$

where x_5, x_6, x_7, x_8 are variables introduced for the state-space representation and x_5 represents the filter output $m(t)$. The spectrum generated by equation (11) will have the following form:

$$S_{4th}(\omega) = \frac{1}{2\pi} \frac{\gamma_1^2 \omega^4}{[(\beta_1 - \omega^2)^2 + (\alpha_1 \omega)^2][(\beta_2 - \omega^2)^2 + (\alpha_2 \omega)^2]} \quad (9)$$

where the parameters $\lambda_1, \lambda_2, \lambda_3, \lambda_4$ in equation (9) can be determined by the following relationship: $\lambda_1 = \alpha_1 + \alpha_2$, $\lambda_2 = \beta_1 + \beta_2 + \alpha_1 \alpha_2$, $\lambda_3 = \alpha_1 \beta_2 + \alpha_2 \beta_1$, $\lambda_4 = \beta_1 \beta_2$. The parameters α, β, γ in the second-order linear filter and the parameters $\alpha_1, \alpha_2, \beta_1, \beta_2, \gamma_1$ in the fourth-order filter are determined by a least-square algorithm which is utilized for fitting of the target spectrum, $S_{mm}(\omega)$. The bandwidth and the peak frequency of the filtered spectrum can easily be adjusted by changing the values of these parameters.

By combining the governing equation of the roll motion (5) with the linear filter equation (6) or (8), ship roll motion in random beam seas can be described by a 4D or a 6D state space equation, respectively.

2.3 Path integration method

The 4D state space equation can be expressed as follows:

$$\begin{cases} dx_1 = x_2 dt \\ dx_2 = (-b_{44}x_2 - b_{44q}x_2|x_2| - c_1x_1 + c_3x_1^3 + x_3) dt \\ dx_3 = (x_4 - \beta x_3) dt + \gamma dW \\ dx_4 = -\alpha x_3 dt \end{cases} \quad (10)$$



Equation (10) represents a Markov dynamic system driven by Gaussian white noise. It can be expressed as an Itô stochastic differential equation (SDE):

$$d\mathbf{x} = a(\mathbf{x}, t)dt + b(t)d\mathbf{W}(t) \quad (11)$$

where $x(t)=(x_1(t), \dots, x_4(t))^T$ is a 4D state space vector process, the vector $a(\mathbf{x}, t)$ represents the drift term and $b(t)d\mathbf{W}(t)$ is the diffusive term. The vector $d\mathbf{W}(t)=\mathbf{W}(t+dt)-\mathbf{W}(t)$ denotes independent increments of a standard Wiener process.

The solution $\mathbf{x}(t)$ to equation (11) is a Markov process and its transition probability density (TPD), also known as the conditional PDF, $p(\mathbf{x}, t | \mathbf{x}', t')$ satisfies the FP equation which is casted in the following form:

$$\begin{aligned} \frac{\partial}{\partial t} p(\mathbf{x}, t | \mathbf{x}', t') &= - \sum_{i=1}^4 \frac{\partial}{\partial x_i} a_i(\mathbf{x}, t) p(\mathbf{x}, t | \mathbf{x}', t') \\ &+ \frac{1}{2} \sum_{i=1}^4 \sum_{j=1}^4 \frac{\partial^2}{\partial x_i \partial x_j} (b(t) \cdot b^T(t))_{ij} p(\mathbf{x}, t | \mathbf{x}', t') \end{aligned} \quad (12)$$

Unlike direct numerical techniques, such as the finite-element method and the finite difference method, aiming to solve the FP equation (12) and obtain the TPD directly, the PI method captures the probabilistic evolution of the process $\mathbf{x}(t)$ by taking advantage of the Markov property of the dynamics system (11). In principle, the PI method is an approximation approach and the PDF of the process $\mathbf{x}(t)$ can be determined by the following basic equation:

$$p(\mathbf{x}, t) = \int_{R^4} p(\mathbf{x}, t | \mathbf{x}', t') p(\mathbf{x}', t') d\mathbf{x}' \quad (13)$$

where $d\mathbf{x}' = \prod_{i=1}^4 dx'_i$.

Specifically, the value of the PDF at time t , $p(\mathbf{x}, t)$, can be calculated by equation (13) with the value of previous PDF at time t' as well as the value of conditional PDF, $p(\mathbf{x}, t | \mathbf{x}', t')$. For a numerical solution of the SDE (11), a time discrete approximation should be introduced. Naess and Moe (2000) proposed a fourth-order

Runge-Kutta-Maruyama (RKM) discretization approximation:

$$\mathbf{x}(t) = \mathbf{x}(t') + r(\mathbf{x}(t'), t')\Delta t + b(t')\Delta\mathbf{W}(t') \quad (14)$$

where the vector $r(\mathbf{x}(t'), t')$ is the explicit fourth-order Runge-Kutta approximation or the Runge-Kutta increment. Since $\mathbf{W}(t)$ is a Wiener process, the independent increment $\Delta\mathbf{W}(t') = \mathbf{W}(t) - \mathbf{W}(t')$ is a Gaussian variable for every t' .

If we consider only the deterministic part of equation (11), the approximation (14) reduces to the fourth-order Runge-Kutta approximation $\mathbf{x}(t) = \mathbf{x}(t') + r(\mathbf{x}(t'), t')\Delta t$. Experiments have shown that, for the Markov systems, the accuracy associated with approximating the deterministic terms is the most important (Mo, 2008). In this regard, the accuracy of the fourth-order RKM approximation is satisfactory since the fourth-order Runge-Kutta approximation follows the time evolution of the deterministic part of equation (11) with an accuracy to the order of $O(\Delta t^5)$.

The time sequence $\{\mathbf{x}(i \cdot \Delta t)\}_{i=0}^{\infty}$ is a Markov chain and it can approximate the time-continuous Markov process solution of the SDE (11) when the time increment $\Delta t = t - t'$ is sufficiently small. Moreover, the conditional PDF of the process $\mathbf{x}(t)$, $p(\mathbf{x}, t | \mathbf{x}', t')$, follows a (degenerate) Gaussian distribution and it can be written as (Naess & Johnsen, 1993):

$$\begin{aligned} p(\mathbf{x}, t | \mathbf{x}', t') &= \delta(x_1 - x'_1 - r_1(\mathbf{x}', \Delta t)) \\ &\cdot \delta(x_2 - x'_2 - r_2(\mathbf{x}', \Delta t)) \cdot \tilde{p}(x_3, t | x'_3, t') \\ &\cdot \delta(x_4 - x'_4 - r_4(\mathbf{x}', \Delta t)) \end{aligned} \quad (15)$$

where $\tilde{p}(x_3, t | x'_3, t')$ is given by the relation:

$$\begin{aligned} \tilde{p}(x_3, t | x'_3, t') &= \frac{1}{\sqrt{2\pi\gamma^2\Delta t}} \\ &\cdot \exp\left\{-\frac{(x_3 - x'_3 - r_3(\mathbf{x}', \Delta t))^2}{2\gamma^2\Delta t}\right\} \end{aligned} \quad (16)$$

in which $r_i(\mathbf{x}', \Delta t)$, $i=1,2,3,4$, are the Runge-Kutta increments for the state space variables.

Since the expression for the conditional PDF is known, the time evolution of the PDF of $\mathbf{x}(t)$ can be determined by the iterative algorithm (17) if an initial PDF $p(\mathbf{x}^{(0)}, t_0)$ is given

$$p(\mathbf{x}, t) = \int_{R^4} \cdots \int_{R^4} \prod_{i=1}^n p(\mathbf{x}^{(i)}, t_i | \mathbf{x}^{(i-1)}, t_{i-1}) \cdot p(\mathbf{x}^{(0)}, t_0) d\mathbf{x}^{(0)} \dots d\mathbf{x}^{(n-1)} \quad (17)$$

where $\mathbf{x} = \mathbf{x}^{(n)}$, $t = t_n = t_0 + n \Delta t$.

Equation (17) describes the mathematical principle of the PI approach. In this work, the initial PDF $p(\mathbf{x}^{(0)}, t_0)$ is chosen as a 4D Gaussian PDF with zero mean and variances evaluated by a simple Monte Carlo simulation. The straightforward Monte Carlo simulation ensures that the initial 4D Gaussian PDF includes all the information corresponding to the selected parameters of the dynamic system, and it also provides a rational computational domain for the subsequent simulation. For the numerical implementation of the iterative algorithm (17), it represents the PDF at the previous time t' as an interpolating spline surface via parabolic B-spline and then it evaluates the PDF at time t by several specific steps. The numerical iterative algorithm and the associated specific computational steps have been systematically described by Iourtchenko et al (2006) and Yurchenko et al (2013). Moreover, the capability of the PI method in producing accurate and reliable solutions for the stochastic dynamic systems has been demonstrated by numerous examples (Mo, 2008).

3. MEAN UPCROSSING RATE

The mean upcrossing rate is a key parameter for estimating the stochastic responses, especially the large and extreme responses. A nice aspect of the PI method is that the joint PDF of the roll angle and the roll velocity can be calculated directly. Then the mean upcrossing rate can be given by the Rice formula

$$v^+(\zeta; t) = \int_0^\infty \dot{\theta} f_{\theta\dot{\theta}}(\zeta, \dot{\theta}; t) d\dot{\theta} \quad (18)$$

where $v^+(\zeta; t)$ denotes the expected number of upcrossing for the ζ -level per unit time at time t by the roll angle $\theta(t)$, $f_{\theta\dot{\theta}}(\theta, \dot{\theta}; t)$ is the joint PDF of the roll angle and the roll velocity at the time instant t .

For nonlinear ship rolling in beam seas, due to the presence of negative nonlinear stiffness term in the SDOF model (1), ship capsizing may happen when the predetermined simulation time T is long enough or the intensity of the external excitation is strong enough. If the mean time to capsize is long enough, the dynamic system can be regarded as a highly reliable system and the corresponding roll response reaches stationarity in an approximate sense (Roberts & Vasta, 2000).

As for the four-dimensional dynamic system (10) or the six-dimensional dynamic system obtained by combining the equations (5) and (8), the fourth-order RKM method is adopted to solve the corresponding SDE. The mean upcrossing rates can be estimated from the time series of responses. Let $n_i^+(\zeta; T_i)$ denote the counted number of upcrossing for the level ζ during the time interval $(0, T_i)$ for simulated time history No. i . The appropriate sample mean value of averaged mean upcrossing rate, $\hat{v}^+(\zeta)$ is then obtained as:

$$\hat{v}^+(\zeta) = \frac{\sum_{i=1}^k n_i^+(\zeta; T_i)}{\sum_{i=1}^k T_i} \quad (19)$$

A fair approximation of the 95% confidence interval, $CI_{0.95}$, for the value of $\hat{v}^+(\zeta)$ can be obtained as (Naess et al, 2007):

$$CI_{0.95}(\zeta) = \left(\hat{v}^+(\zeta) - 1.96 \frac{\hat{s}(\zeta)}{\sqrt{k}}, \hat{v}^+(\zeta) + 1.96 \frac{\hat{s}(\zeta)}{\sqrt{k}} \right) \quad (20)$$

Where the empirical standard deviation $\hat{s}(\zeta)$ is given as



$$\hat{s}(\zeta)^2 = \frac{1}{k-1} \sum_{i=1}^k \left(\frac{n_i^+(\zeta; T_i)}{T_i} - \hat{v}^+(\zeta) \right)^2 \quad (21)$$

Moreover, the selection of the number of simulation, k , for the Monte Carlo simulation is selected according to the upcrossing rates in the tail region and the length of the predetermined simulation time T . Usually, low upcrossing rates and short time periods T corresponds to a large simulation number k .

Ship stability failure occurs when the roll angle exceeds some certain values, such as the angle of vanishing stability or some large roll angle leading to damage. Assume that the upcrossing events in the high level response region are statistically independent and the random process $\theta(t)$ is not extremely narrow-banded, the exceedance probability for a duration of exposure time T , $P_\theta(T)$, can be approximated by a widely used Poisson estimate, which is given as follows:

$$P_\theta(T) = 1 - \exp\left(-\int_0^T v^+(\zeta; t) dt\right) \quad (22)$$

$$\approx 1 - \exp(-v^+(\zeta) \cdot T)$$

where $v^+(\zeta)$ represents the mean upcrossing rate of the level ζ at a suitable reference point in time, which can be determined directly by the 4D PI approach and the Rice formula (18).

4. SIMULATION RESULTS

4.1 Ship parameters and excitation spectrum

In this section, an ocean surveillance ship (Su, 2012), is selected for studying the stochastic responses of ship rolling. The parameters of the vessel and the natural roll frequency, ω_0 , are given in Table 1.

The modified P-M spectrum, widely used for the fully developed ocean waves, is adopted in this analysis.

$$S_{\xi\xi}(\omega) = \frac{5.058 g^2 H_s^2}{T_p^4 \omega^5} \exp\left(-1.25 \frac{\omega_p^4}{\omega^4}\right) \quad (23)$$

in which H_s denotes the significant wave height, ω_p is the peak frequency at which the wave spectrum $S_{\xi\xi}(\omega)$ has its maximum, and T_p is the corresponding peak period.

Table 1 List of parameters for the vessel

Parameters	Dimensional value
$I_{44}+A_{44}$	$5.540 \times 10^7 \text{ kg}\cdot\text{m}^2$
B_{44}	$5.266 \times 10^6 \text{ kg}\cdot\text{m}^2\cdot\text{s}^{-1}$
B_{44q}	$2.877 \times 10^6 \text{ kg}\cdot\text{m}^2$
Δ	$2.017 \times 10^7 \text{ N}$
C_1	3.168 m
C_3	2.513 m
ω_0	1.074 rad/s

Three different sea states, i.e. different external excitations, are selected for analyzing the stochastic roll responses. The wave spectra and rolling excitation moment amplitude per unit wave height of the vessel are plotted in Figure 1.

The parameters α, β, γ in the second-order filter (6) and parameters $\lambda_1, \lambda_2, \lambda_3, \lambda_4$ in the fourth-order filter (8) can be determined by the least square scheme which is available in the curve fitting algorithms of MATLAB. The parameters in these two linear filters for different sea states are presented in Tables 2 and 3. Moreover, the fitting results of the relative wave excitation spectrum for sea state 1 are shown in Figure 2.

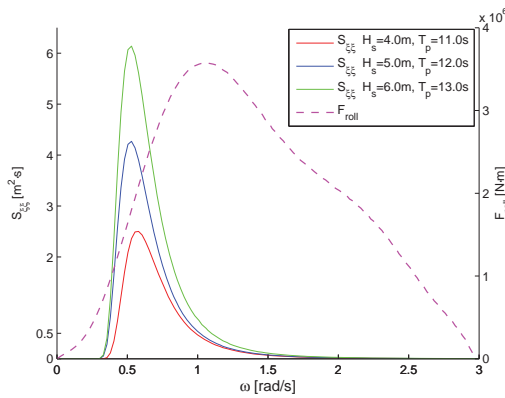


Figure 1 Wave spectra for different sea states and rolling excitation moment amplitude per unit wave height

Table 2 Parameters of the second-order linear filter for different sea states

Sea States	H_s (m)	T_p (s)	α	β	γ
Sea state 1	4.0	11.0	0.495	0.366	0.0432
Sea state 2	5.0	12.0	0.441	0.364	0.0498
Sea state 3	6.0	13.0	0.390	0.365	0.0555

Table 3 Parameters of the fourth-order linear filter for different sea states

H_s (m)	T_p (s)	λ_1	λ_2	λ_3	λ_4	γ_1
4.0	11.0	0.934	1.431	0.486	0.310	0.0363
5.0	12.0	0.924	1.309	0.429	0.249	0.0414
6.0	13.0	0.931	1.212	0.390	0.202	0.0461

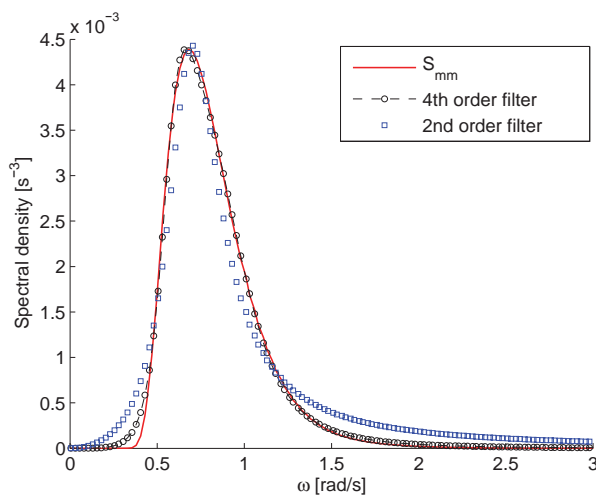


Figure 2 Relative wave excitation spectrum in equation (4) and filtered spectra for sea state 1

4.2 Influence of linear filter

The transfer function between wave excitation and roll response in the SDOF model (1) is narrow-banded due to the light roll damping. Thus, the fitting accuracy near the natural roll frequency, ω_0 , has a significant effect on the subsequent rolling responses. However, there is a slight discrepancy between the spectral density generated by the second-order filter and the target spectral density in Figure 2. Therefore, a constant, c , should be introduced as a correction factor for the filtered spectral density to decrease the discrepancy in the critical region near roll frequency ω_0 . The filtered spectrum (12) can be changed to:

$$S_{2nd}(\omega) = \frac{1}{2\pi} \frac{(c \cdot \gamma)^2 \omega^2}{(\beta - \omega^2)^2 + (\alpha\omega)^2} \quad (24)$$

The correction factor c is taken to be 1.07 by considering the mean difference of the two spectral densities in the critical frequency region. As mentioned in section 3, the joint probability density function (PDF) of the roll angle and the roll velocity can be obtained directly by the 4D PI method. The joint PDF of the roll response for sea state 1 is presented in Figure 3, while Figure 4 displays the contour lines of the joint PDF.

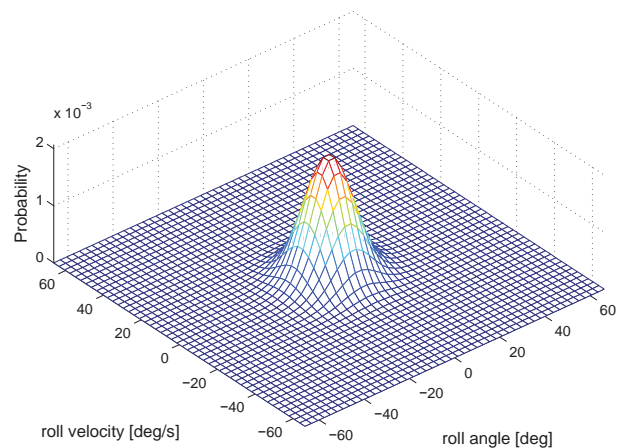


Figure 3 Joint PDF of the roll response for sea state 1 with $H_s=4.0m$, $T_p=11.0s$

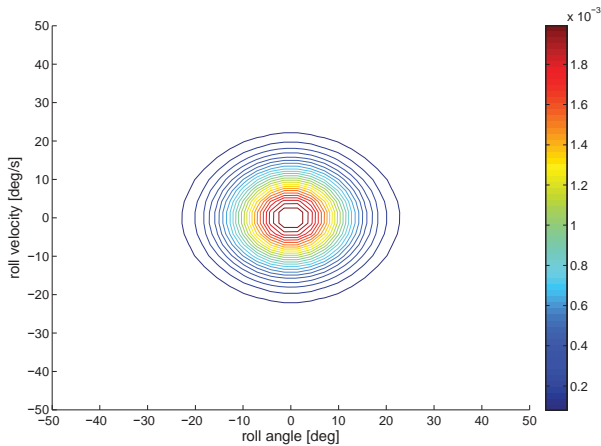


Figure 4 Contour lines of the joint PDF of the roll response for sea state 1

It can be observed in Figures 3 and 4 that the PDF of the roll response is symmetric. This is reasonable since the distribution of the random wave excitation, i.e. the filtered white noise process, and the vessel properties are symmetric with respect to the origin. Moreover, the marginal PDF of the roll angle process and the marginal PDF of the roll velocity process obtained by the 4D PI method and the 4D Monte Carlo simulation are plotted in Figure 5 and 6, respectively.

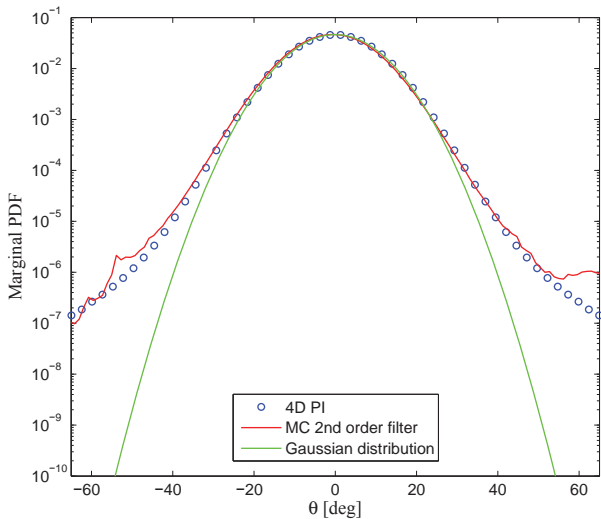


Figure 5 Marginal PDF of the roll angle process for sea state 1

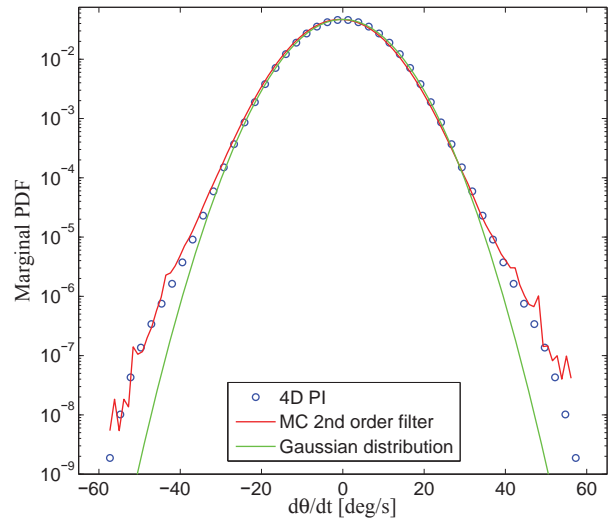


Figure 6 Marginal PDF of the roll velocity process for sea state 1

It is shown in Figures 5 and 6 that the Gaussian distribution gives a reasonable approximation of the statistics of small-amplitude roll motions. However, for the high-level responses, Gaussian distribution underestimates the corresponding low probability levels in this region. Moreover, the 4D PI method provides nice results for the low probabilities, where the distributions obtained by the versatile Monte Carlo simulation are suffering from uncertainties.

The importance of the correction factor c for the stochastic roll response is illustrated in Figure 7. It can be observed that, the slight discrepancy between the second-order filtered spectrum and the target spectrum in the critical region, which is shown in Figure 2, results in noticeable influence on the subsequent roll response. If there is no correction factor for the second order linear filter, the stochastic roll response, will be significantly underestimated. In addition, the good agreement of the upcrossing rates obtained by 4D PI method and 6D Monte Carlo simulation (MCS) verify the rationality of the correction factor.

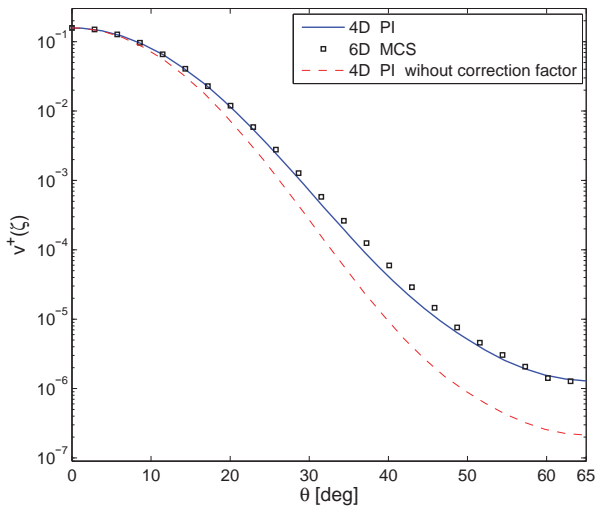


Figure 7 Influence of the correction factor, c , on the upcrossing rate for sea state 1 with $H_s=4.0m$, $T_p=11.0s$

The comparisons between the upcrossing rates calculated by the 4D PI method and the empirical estimation of the upcrossing rates as well as the 95% confidence intervals obtained by 4D Monte Carlo simulations for different sea states can be viewed in Figures 8, 9 and 10. It can be readily seen that the 4D PI approach yields accurate and reliable results for various external excitation cases. Next, the empirical estimation of the upcrossing rates computed by 6D Monte Carlo simulations are plotted in these Figures. The good agreement of the 4D results and 6D results extracted from Monte Carlo simulation verify the rationality of introducing the correction factor for all of the cases.

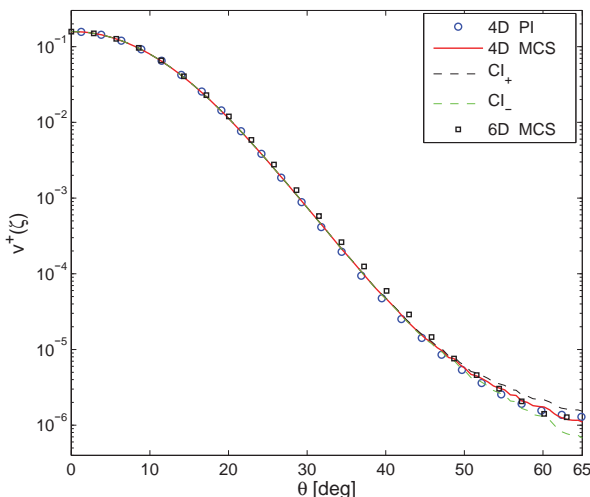


Figure 8 Upcrossing rate for sea state 1 with $H_s=4.0m$, $T_p=11.0s$

$H_s=4.0m$, $T_p=11.0s$ (simulation number $k=3000$)

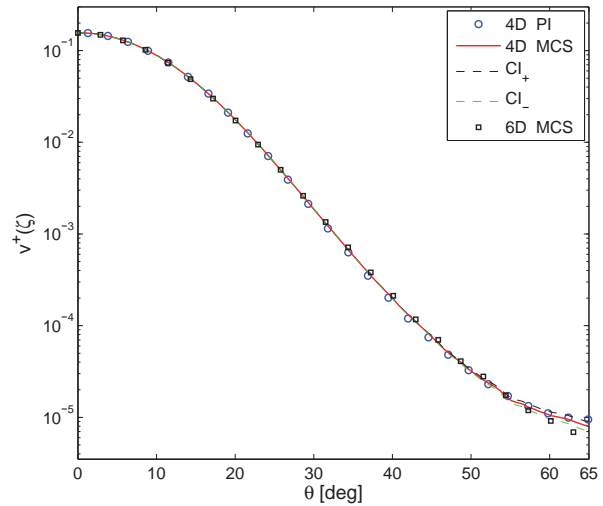


Figure 9 Upcrossing rate for sea state 2 with $H_s=5.0m$, $T_p=12.0s$ (simulation number $k=1500$)

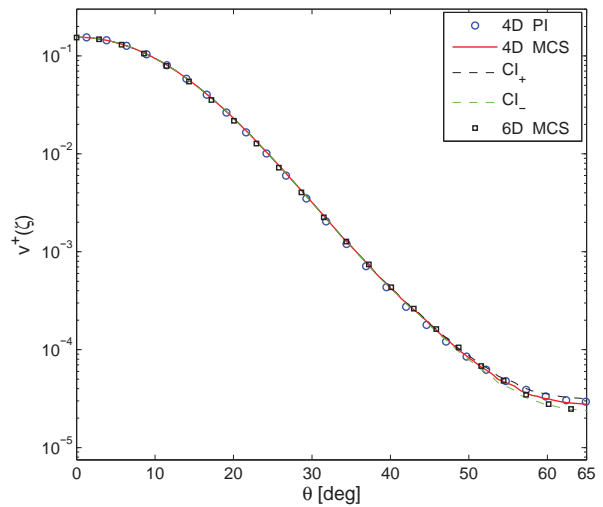


Figure 10 Upcrossing rate for sea state 3 with $H_s=6.0m$, $T_p=13.0s$ (simulation number $k=1000$)

4.3 Influence of nonlinear damping models

The roll damping is mainly due to three different sources: the free surface radiated wave damping, the damping caused by vortex shedding and flow separation and finally the

viscous friction damping. In general, these damping terms are coupled with each other. The linear-plus-quadratic damping (LPQD) model is one of the most common expressions used in the SDOF equation (1). This model is given as:

$$b_{44} \dot{\theta}(t) + b_{44q} \dot{\theta}(t) |\dot{\theta}(t)| \quad (25)$$

However, the LPQD model is only once continuously differentiable and mathematically inferior to the infinitely differentiable linear-plus-cubic damping (LPCD) model. The LPCD model is written as:

$$b'_{44} \dot{\theta}(t) + b_{44c} \dot{\theta}^3(t) \quad (26)$$

The least square method is a typical approach used to transform the LPQD model into the LPCD model. The result of fitting the two damping models is shown in Figure 11. Moreover, the roll response spectra for the dynamic systems with different damping models for sea state 1 are plotted in Figure 12.

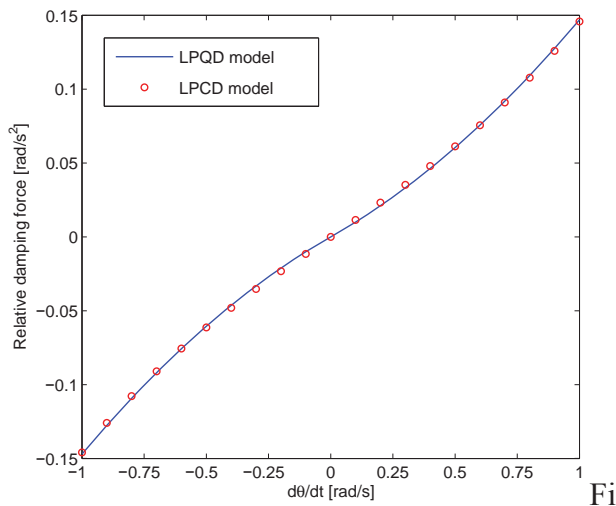


Figure 11 Fitting result for the LPQD and LPCD models

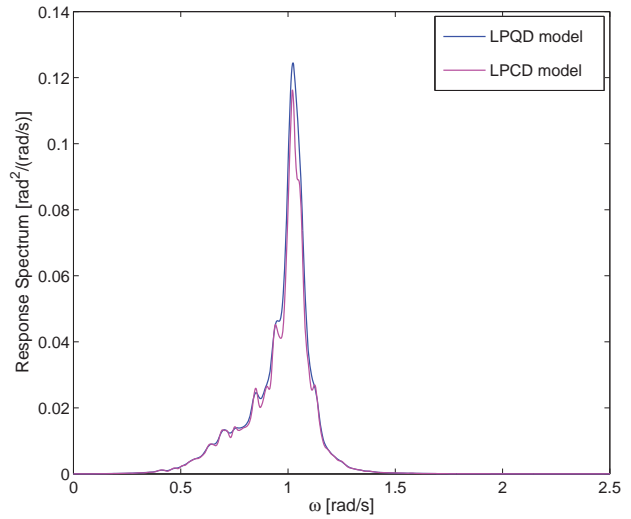


Figure 12 Roll response spectra for the LPQD and LPCD models for sea state 1

It is illustrated in Figure 11 that the two damping models have a good agreement in the least-square sense. Nevertheless, in Figure 12, there is still a slight discrepancy between the response spectra in the peak region, i.e. the critical frequency region near natural roll frequency ω_0 . The upcrossing rates, obtained by the 4D PI method and the 4D Monte Carlo simulation, for the LPQD model versus the LPCD model for different sea states are plotted in Figures 13, 14 and 15, respectively.

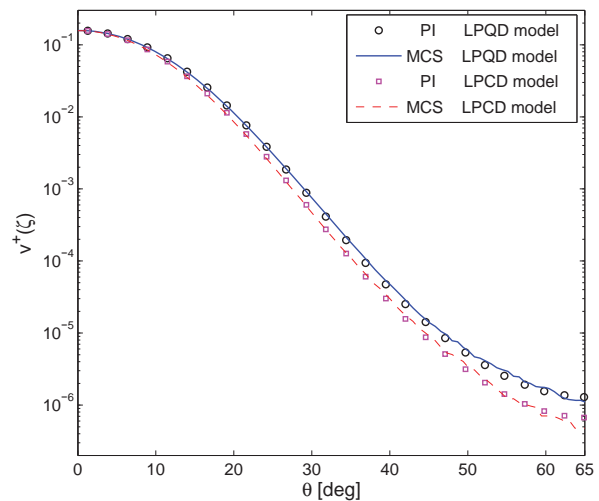


Figure 13 Upcrossing rate for different damping models for sea state 1

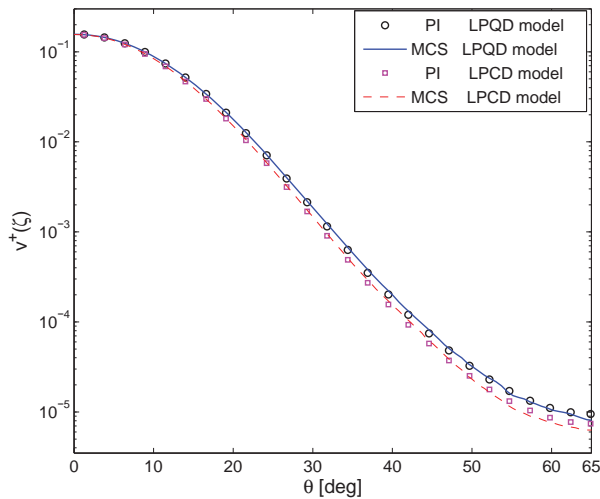


Figure 14 Upcrossing rate for different damping models for sea state 2

The 4D PI approach is available to provide high-accuracy results for both models when compared with the corresponding empirical estimations obtained by 4D Monte Carlo simulations. However, the corresponding upcrossing rates under the same sea state are quite different, even though the two damping models match well in the least-square sense. The discrepancies between the upcrossing rates in the tail regions, suggest that the LPCD model might underestimate the extreme response of the dynamic system. Therefore, the traditional least square method, applied to transform the LPQD model into the LPCD model, cannot guarantee the accuracy of the subsequent stochastic roll response. Furthermore, from the observations in Figures 13-15, it can be predicted that when the stochastic linearization technique is applied in order to linearize the nonlinear damping term (25), even more significant discrepancy of the upcrossing rate would be observed in the tail region.

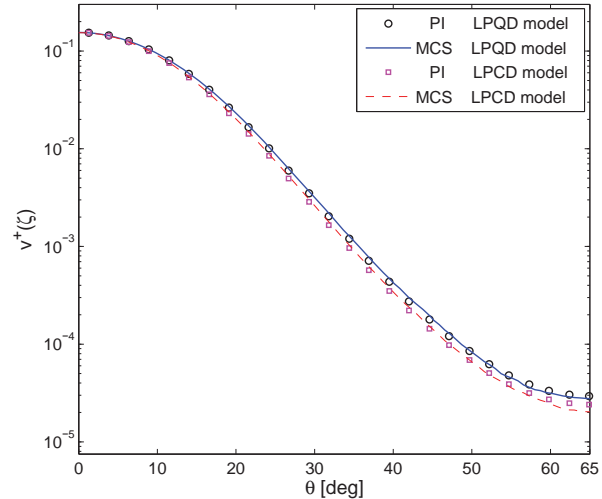


Figure 15 Upcrossing rate for different damping models for sea state 3

5. CONCLUSIONS

In this paper, the 4D path integration technique and Monte Carlo simulation were applied in order to investigate the influences of linear filter models and nonlinear damping models on the stochastic roll response of a vessel in random beam seas. From the numerical results and discussions above, some of the results can be summarized:

The correction factor, c , is important and reasonable to be introduced into the second-order linear filter. Moreover, the accuracy of the filtered spectrum in the critical frequency region is crucial for prediction of the response statistical. The 6D dynamic system can be simplified as a corresponding 4D dynamic system with a modified second-order linear filter due to the high-accuracy agreements for the upcrossing rates.

The typical least square method results in an underestimation of the upcrossing rate when it is used to transform a LPQD model into a LPCD model. The discrepancies between the upcrossing rates generated by different damping models should not be ignored.

It has been shown that the 4D PI approach yields reliable results for different damping



models and various excitation cases, even in the tail regions with low probability levels. Therefore, the 4D PI technique can be applied for the stochastic analysis of nonlinear ship rolling in random beam seas.

6. ACKNOWLEDGMENTS

The first author would like to thank the financial support from the China Scholarship Council (CSC) (Grant No. 201306230077), affiliated with the Ministry of Education of the P.R. China. The funds from the Department of Marine Technology's budget for scientific travels and the "Norwegian ship-owners' association fund" at NTNU to scientific travels are gratefully acknowledged.

7. REFERENCES

- Bikdash, M., Balachandran, B., Navfeh, A., 1994, "Melnikov analysis for a ship with a general roll-damping model", Nonlinear Dynamics, Vol. 6, pp. 101-124.
- Chai, W., Naess, A., Leira, B. J., 2014, "Stochastic dynamic analysis of nonlinear ship rolling in random beam seas", Proceeding of the 7th International Conference on Computational Stochastic Mechanics, in press.
- Dostal, L., Kreuzer, E., 2011, "Probabilistic approach to large amplitude ship rolling in random seas", Proceedings of the Institution of Mechanical Engineers, Part C: Journal of Mechanical Engineering Science, Vol. 225, pp. 2464-2476.
- Iourtchenko, D.V., Mo, E., Naess, A., 2006, "Response probability density functions of strongly non-linear systems by the path integration method", International Journal of Non-Linear Mechanics, Vol. 41, pp. 693-705.
- Jiang, C., Troesch, A.W., Shaw, S., 1996, "Highly nonlinear rolling motion of biased ships in random beam seas", Journal of ship research, Vol. 40, pp. 125-135.
- Mo, E., 2008, "Nonlinear stochastic dynamics and chaos by numerical path integration", Ph.D. Thesis, Norwegian University of Science and Technology, Trondheim, Norway.
- Naess, A., J. Johnsen, 1993, "Response statistics of nonlinear, compliant offshore structures by the path integral solution method", Probabilistic Engineering Mechanics, Vol. 8, pp. 91-106.
- Naess, A., Gaidai, O., Teigen, P.S., 2007, "Extreme response prediction for nonlinear floating offshore structures by Monte Carlo simulation", Applied Ocean Research, Vol. 29, pp. 221-230.
- Naess, A., Moe, V., 2000, "Efficient path integration methods for nonlinear dynamic systems", Probabilistic Engineering Mechanics, Vol. 15, pp. 221-231.
- Roberts, J. and Vasta, M., 2000, "Markov modelling and stochastic identification for nonlinear ship rolling in random waves", Philosophical Transactions of the Royal Society of London. Series A: Mathematical, Physical and Engineering Sciences, Vol. 358, pp. 1917-1941.
- Su, Z., 2012, "Nonlinear response and stability analysis of vessel rolling motion in random waves using stochastic dynamical systems", Ph.D. Thesis, Texas A & M University, Texas.
- Yurchenko, D., Naess, A., Alevras P., 2013, "Pendulum's rotational motion governed by a stochastic Mathieu equation", Probabilistic Engineering Mechanics, Vol. 31, pp. 12-18.



Risk Analysis of a Stability Failure for the Dead Ship Condition

Tomasz Hinz, *Deltamarin LTD*, Tomasz.Hinz@deltamarin.com

ABSTRACT

In this article, the application of the risk analysis of a stability failure for the dead ship condition is presented. The analysis combines deterministic and probabilistic approach. First, the number of simulation runs is carried out for a specific RoPax ship with the use of LaiDyn model. Second, the obtained results were organized in a probabilistic meta model with the use of Bayesian Belief Network. Finally, the BBN-based model was used as a platform for risk assessment. The adopted measure of risk is a number of fatalities that results from an accident, when a ship is in Dead Ship Condition (DSC) capsizes. The results are presented in a form of F-N. Finally the sensitivity of the model is evaluated along with the assessment of associated uncertainties.

Keywords: *stability, Dead Ship Condition, risk, Bayesian Belief Network*

1. INTRODUCTION

Discussions on the improvement of the IS Code (Francescutto, 2007), which were conducted at IMO forum, resulted in the identification of several major stability accident scenarios (Umeda, 2013):

- events related to the changes of righting arm – the parametric resonance and the pure loss of stability
- Dead Ship Condition - ship losing propulsion and manoeuvring characteristics (DSC)
- Problems with manoeuvrability on the wave - broaching, surf-riding,
- Problems with excessive accelerations.

Because the scenarios proposed by the IMO, still do not provide all possible causes of the loss of stability, it is necessary to approach the problem in another way. Consequently, the new rules are losing their passive and retroactive approach and shift towards active feature. Which are not the result of the study of the stability accidents, but are based on the previous in-depth analysis of the phenomena associated with the behaviour of a ship on a

wave. Such an approach allows the extension of regulations of further scenarios more easily.

This means that when creating the next generation of rules, it is advisable to develop methods for assessing the safety of the ship, where they not only physical, but also the operational characteristics of vessels will be taken into account.

Well known methods, which take into account the above mentioned elements are methods based on analysis and risk assessment, such as the one based on Safety Cases (Wang, 2002), widely used in the offshore industry - or another one called Formal Safety Assessment (Psaraftis, 2012) (Montewka, Goerlandt, & Kujala, 2014), which is used in the shipbuilding industry to create new rules (IMO, 2002). There is also a Risk-Based Design methodology (Papanikolaou et al., 2009), which is more and more widely used in the design of ships in the damaged condition.

Risk-based methods allow taking into account even the most unlikely accident scenario, and also the interactions between the

scenarios, or some of their components. The probabilistic causal models (Bayesian networks (BN), Fault Tree (FT) and Event Tree (ET))(Goerlandt & Montewka, 2015; Montewka, Ehlers, et al., 2014; Pillay & Wang, 2003) are more and more frequently used as a tool in the risk assessment process.

The main objective of this project was to create a probabilistic risk model of the ship stability accident, which might be applied to the assessment of the intact stability safety with the usage of the probabilistic casual model. One of previously presented scenario, i.e. Dead Ship Conditions, was chosen for the further analysis. The following sections will present the risk model built with the usage of the Bayesian Network and its application in RoPax ship. They allow exploring easily the influence of particular elements on the other ones, and in both directions. Having BN at disposal, it is possible to conduct the casual analysis, examine the strength of the impact of some elements on the other ones and make decisions under conditions of uncertainty.

2. RISK MODEL OF DEAD SHIP CONDITION ACCIDENTS

The aim of the proposed method is to estimate the risk of the stability accidents in the intact condition for the loss of the propulsion and manoeuvrability scenario. Such scenario might results in ship drifting, increased rolling, which in turn may lead to the capsizing and the ensuing loss of life by passengers. For the given meteorological conditions, the probability of exceeding the limits of ship motions is determined with the usage of 'LaiDyn' model. The following factors are taken into account concerning: meteorological conditions, ship dynamic and ship loading conditions. The total number of fatalities (N) resulting from an accident is modelled using the concept of death rates. This factor is determined with the participation of evacuation time and time of capsizing. The number of passengers on board is modelled based on data

from the operators of RoPax form the Gulf of Finland. All these elements together, also with the associated probabilities (P) of the number of victims, is shown in the graph FN. The risk is measured adopting societal measure pressed as the probability of a given number of fatalities.

3. DEFINING THE RISK MODEL

The risk model of the DSC accident for RoPax ship was built with the support of the probabilistic casual model, which is the Bayesian network (BBN). The BBN structure was built with the participation of experts. The parameters were developed with the participation of the PC classifier based on the training data. It was created using the GeNie software developed at the University of Pittsburgh(Druzdzel, 1999).

Due to the limited statistic data, it was primarily the knowledge of experts that was used to create the structure of the model.

The analysed system is quite wide and multidisciplinary, therefore the model is divided into sections associated with (i) stability, (ii) propulsion and manoeuvring system, and (iii) finally with the consequences of an accident.

Experts' knowledge about the domain was used during a brainstorming session and individual meetings. During the session, they were presented with a preliminary version of the structure. Then, based on their advice, the structure under went the further modifications. Once the final structure of the model was established, it was necessary to define the qualitative part of the model.

The structure of the risk model is shown in **Figure 1**.

Table 1 contains all the variables included in the model. If the variable is determined by means of literature, it is marked by reference.

Variables marked as E are determined with the support of experts' knowledge. Simulations were used for variables marked with the letter S. The letter N in the description of a variable indicates that it was obtained by numerical analysis.

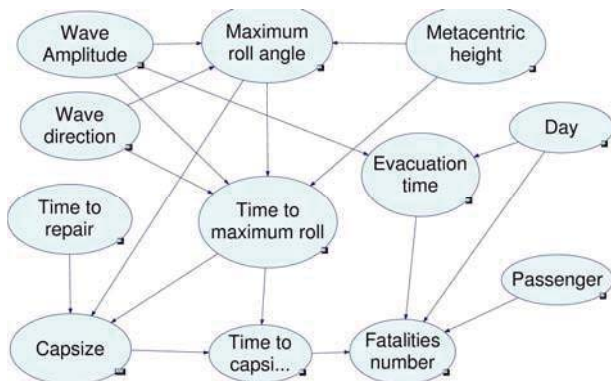


Figure 1 Structure of risk model

Table 1 Parameters of risk model

Name	Symbols	Source
Wave amplitude	Ampl	(IMO, 2013)
Wave direction	Beta	E
Maximum roll angle	Roll _{max}	S
Metacentric height	GM	E
Day	DAY	E
Time to repair	TTRep	(Ravn, 2006)
Evacuation time	TTE	(Montewka, Ehlers, et al., 2014)
Time to maximum roll angle	TTR	S
Capsize	Capsize	N
Time to capsiz	TTC	S,N
Passenger	N _{PASS}	(Montewka et al., 2011), E
Fatalities number	N _{LOSA}	N

The simulation was conducted with the usage of the numerical model of the ship's movement on the wave. 17388 simulations of ship motions on the wave were performed. The simulation results were used to estimate the

probability of exceeding the angle, which is considered to be the angle of capsizing. The results of simulations provided also data about the time at which the ship reaches the capsizing angle ('Maximum roll angle').

4. PARAMETERS OF THE RISK MODEL

This section describes the methods adopted to determine the parameters of the risk model.

The analysed accident scenario involves RoPax ship, which due to various reasons loses its propulsion and manoeuvring characteristics and enters a dead ship condition. This transition may be caused by a spontaneous failure of systems as well as the environment (large motions).

The basic elements of the model are:

- the probability of staying in a blackout state and time needed to exit this state,
- wave parameters,
- hydrostatic properties and ship loading conditions,
- ship's response to waves,
- the probability of capsizing of the ship in the DSC,
- elements related to the rescue of passengers, cargo and the ship,
- the number of victims of the stability accident.

Elements of the model presented in this paper relate to the ship RoPax, for unrestricted service area. However, the manner of use and modularity of the methodology allow its (this model) use for other types of ships, as well as for limited service areas.

The behaviour of the ship on waves was studied using a mathematical model developed by prof. Jerzy Matusiak(2007)(Acanfora & Matusiak, 2014). "LaiDyn" method is based on the assumption that the complete answer of a ship equals the sum of linear and non-linear parts. Such division results from the fact that



the linear computation methods are well-known. It causes the situation where the radiation and diffractive forces are presented by linear equations quite well (Kukkanen, 1995) (Journee & Adegeest, 2003). In this method, the main part of the first order load is calculated with the linear approximation, based on the current heading and location in relation to a wave. Defining the non-linear part, such elements as non-linearity as a result of ship shape, hydrostatics, wave force were taken into consideration. (Matusiak, 2011).

The LaiDyn program conducted over 17.000 simulations. The simulations conducted for four loading conditions. The wave statistics were taken from IACS documents (IACS, 2001). The information about the maximum roll angle and the time of reaching it, which were obtained as a result of conducted calculations, were applied to construct a risk model. When the time of reaching the critical angle was smaller than the time of repair, it was stated that the ship will capsize. The probability distributions of the variables, marked with references in **Table 1**, were prepared with the usage of the information included in various publications. The 'Fatalities number' variable includes information about the life lost probabilities of the N-passengers. BBN was created using the GeNie software developed at the University of Pittsburgh (Druzdzal, 1999).

5. RISK FRAMEWORK VALIDATION – SENSITIVITY ANALYSIS

The sensitivity analysis allows to investigate how sensitive the results obtained from the risk model are to changes of individual variables (Montewka et al., 2011). To do this, it is necessary to determine the function of the sensitivity for each individual node in the network (Chan & Darwiche, 2002):

$$f(t) = \frac{(c_1 t + c_2)}{(c_3 t + c_4)} \quad (1)$$

where f is the output probability of interest given observations, c_1 , c_2 , c_3 and c_4 which are identified based on the risk model (Goerlandt & Montewka, 2015). The effect of small changes in the input parameters on the result is called sensitivity. The sensitivity is determined from the first derivative of the sensitivity function (see eq. (1)).

Figure 2 provides a graphical result of the sensitivity model analysis, on the assumption that the resulting variable is the 'Fatalities number' of the accident.

The presented graph shows that these variables - 'Capsize', 'Time to capsize', and 'Evacuation time' - have the most crucial impact on the results from the risk model. The 'Capsize' and 'Time to capsize' variables are considered as ones of the most important in the model constructed with the usage of the simulations and additional transformations. The 'Evacuation time' variable was created using data from the literature. So, if the Bayes network were to be applied in practice, it would be required to prepare a better model of the evacuation.

A similar analysis was performed for the 'Capsize' variable, as it is shown in **Figure 3**.

In the case where the 'Capsize' variable is analysed, it is impossible to observe any strong dominant variable. Concerning their dominant character, the average variables are the following ones: the 'Wave amplitude', 'Maximum roll angle', and 'Metacentric height'.

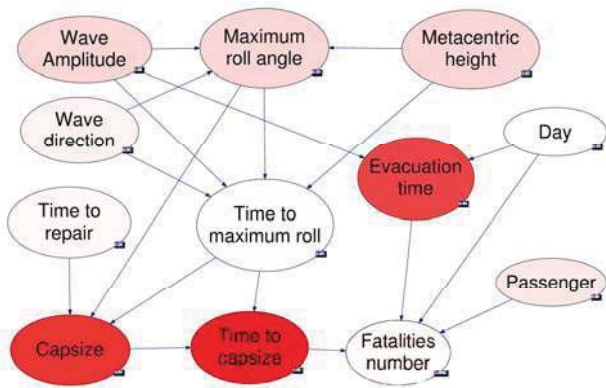


Figure 2 Sensitivity analysis – ‘Fatalities number’ variable

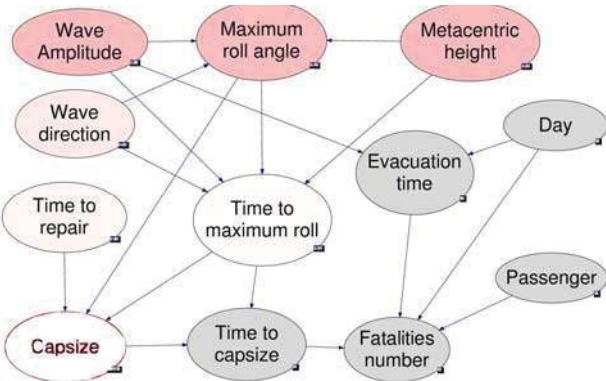


Figure 3 Sensitivity analysis - 'Capsize' variable

6. EXAMPLES

In this section, the methods currently applied to the assessment of stability safety are compared with the results obtained with the method based on risk analysis.

The comparison of two methods is used to show the applicability of the risk to the assessment of the ship stability safety. Such a comparison can also show the level of safety of ships built in accordance with modern requirements.

In the comparison, we used a RoPax type of ship, described below.

Table 2 contains the basic dimensions and hydrostatic characteristics of a hull that was used in the risk analysis (Mattila, 1999). **Figure 4** presents the hull profile.

Table 2 Main dimension

Name	Symbol		
Length	Lpp	[m]	158
Breadth	B	[m]	25
Draft	T	[m]	6.1
Depth	H	[m]	15
Block Coefficient	C _b	[-]	0.571
Displacement		[ton]	13766
Wetted surface	S	[m ²]	4356

Four different loading conditions for the draught of T=6.1 [m] were taken for the calculations.

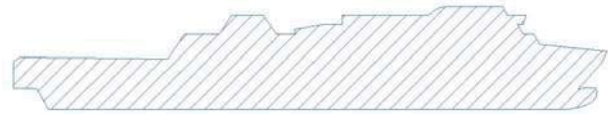


Figure 4 RoPax profile

The standard stability document created in the process of ship design takes a shape of a curve of minimum metacentric heights and maximal centres of gravity. It shows the loading conditions for which the ship complies with the criteria contained in the Code and for which the criteria are not met. The curve of the minimum GM is presented in the **Figure 5**. **Figure 6** shows the curve of the maximum centres of gravity. Both **Figure 5** and **Figure 6** also present the loading conditions used in the simulation.

The analysis of that graphs shows that LC1 condition does not meet the regulations, which are currently in force. Other loading conditions do meet the criteria defined by the rules, wherein LC2 condition is exactly on the limiting curve. According to the approach, that is used nowadays, LC1 condition cannot be considered as a safe one, whereas the remaining conditions are seen as safe ones.

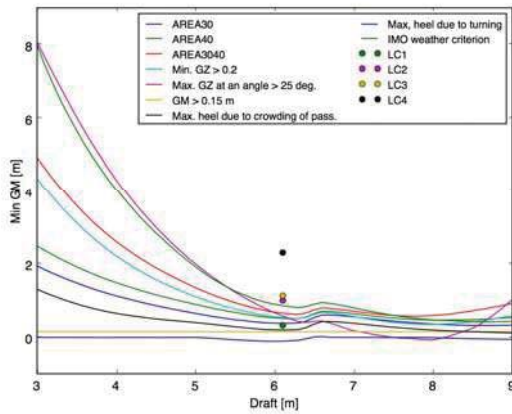


Figure 5 Minimum GM curve

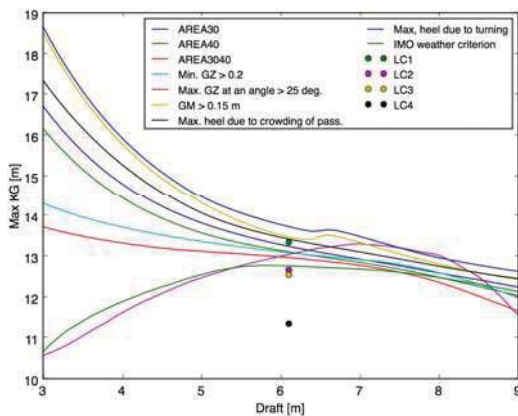


Figure 6 Maximum KG curve

Each FN curve in **Figure 7** corresponds to one load conditions (LC1-LC4). The horizontal position of each curve shows that the higher the GM is the fewer victims of the accident.

Loading condition coded LC4 has the highest GM. This condition meets current stability requirements with a large margin. Also the FN chart confirms this.

7. CONCLUSIONS

The assessment of the safety level has not been performed for the current legislation. So it is unknown how safe ships built with its use are.

Only by using the risk analysis it is possible to decide how safe a ship might be. The measure of safety is presented by the FN curve.

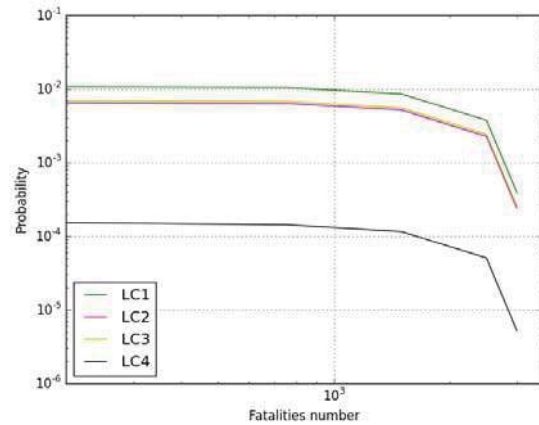


Figure 7 FN curves

Figure 8 is an extension of the graph in **Figure 7** and covers additional ALARP region (Pillay & Wang, 2003). According to the analysis of FN chart include the ALARP area, only LC4 loading condition is entirely included in the area or is located below it. Remaining loading conditions fall outside the area. One should assume that these conditions are not safe. In case of a real project, the group of experts should perform the third stage of

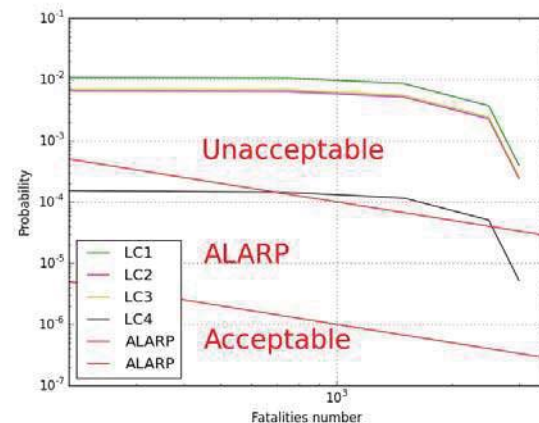


Figure 8 FN curve with ALARP region

According to the designers' experience it should be necessary to check the loading



conditions i.e. to verify whether these conditions are realistic. In the case of the situation where there are no results of the inclining experiment, at least not yet, one could verify the weight estimation. If the previous steps did not provide any appropriate outcome, it would be necessary to modify the shape of the hull. One could also develop an operation manual with the basic information about the limitations of loading conditions and the operating areas.

There are advantages and disadvantages of the risk analysis when used as a tool to assess the stability safety of the ship in the intact condition.

The great advantage of the methods based on the risk analysis is the fact that it might be applied in the new projects or even innovative ones, which cannot be compared to data taken from previous projects. In the process of designing modern vessels or offshore structures, it is possible to use model tests or computer simulations. Such an approach enables the prediction of certain properties in a much more accurate way than using a simple empirical formulas based on experience.

It is possible to use the risk analysis in the evaluation of only one of the scenarios; however such narrowing is not practical. Much better results are obtained by the application of a holistic approach using a variety of scenarios. The risk analysis can give an overall view of the causes and consequences of the accident, as well as examine the impact of the Risk Control Options (RCO) at risk.

The disadvantages of the risk analysis may include primarily large costs associated with the time-consuming experiment; regarding not only its financial side but also the issue of time and personnel. To perform a detail risk analysis, it is necessary to collect a group of experts what might be difficult to achieve in a small design office.

The lack of good probability models of the ship capsizing makes it more difficult to accurately estimate the risk. In many areas of technology, a rich statistic material replaces this lack of probability models of accidents. Concerning the stability accidents, such an approach cannot be applied because the statistical material is rather poor and the analysed accidents do not have any characteristics of repeatability.

8. ABBREVIATIONS

ALARP – As Low As Reasonably Practicable

BBN - Bayesian (Belief) Network

FN – Fatalities number

LC – Loading Condition

RCO – Risk Control Option

9. REFERENCES

- Acanfora, M., & Matusiak, J. (2014). Quantitative Assessment of Ship Behaviour in Critical Stern Quartering Seas. In 14th International Ship Stability Workshop (pp. 19–27).
- Chan, H., & Darwiche, A. (2002). When do numbers really matter? Journal of Artificial Intelligence Research, 17, 265–287.
- Druzdzel, M. (1999). Genie: A development environment for graphical decision-analytic models. In Annual Symposium of the American Medical Informatics Association (p. 1206). Washington, D.C., USA.
- Francescutto, A. (2007). THE INTACT SHIP STABILITY CODE : PRESENT STATUS AND FUTURE. In 2nd



- INTERNATIONAL CONFERENCE ON MARINE RESEARCH AND TRANSPORTATION (pp. 199–208). Ischia, Naples, Italy.
- Goerlandt, F., & Montewka, J. (2015). An extended risk analysis approach for oil spill from tankers in a ship-ship collision. *Safety Science*, Submitted, 42–66. doi:10.1016/j.ssci.2015.02.009
- IACS. (2001). Standard Wave Data. IACS (Vol. 34). IACS.
- IMO. (2002). MSC/Circ.1023, MEPC/Circ.392 - GUIDELINES FOR FORMAL SAFETY ASSESSMENT (FSA) FOR USE IN THE IMO RULE-MAKING PROCESS. International Maritime Organization.
- IMO. (2013). SDC 1/INF.6 - DEVELOPMENT OF SECOND-GENERATION INTACT STABILITY CRITERIA Vulnerability assessment for dead-ship stability failure mode Submitted by Italy and Japan. International Maritime Organization (Vol. SDC 1/INF.). London, UK.
- Journee, J. M. J., & Adegeest, L. J. M. (2003). Theoretical Manual of Strip Theory Program “SEAWAY for Windows.” Technische Universiteit Delft. Delft, Netherlands.
- Kukkanen, T. (1995). Sealoads version 6.0 - software manual. VTT Technical Research Centre of Finland. Espoo, Finland.
- Mattila, M. (1999). Experimental study on transverse stability of fast Ropax vessels on waves. Helsinki University of Technology. Helsinki University of Technology.
- Matusiak, J. (2007). On certain types of ship responses disclosed by the two-stage approach to ship dynamics. Archives of Civil and Mechanical Engineering, 7(4), 151–166. doi:10.1016/S1644-9665(12)60233-7
- Matusiak, J. (2011). On the non-linearities of ship’s restoring and the Froude-Krylov wave load part. International Journal of Naval Architecture and Ocean Engineering, 3(1), 111–115. doi:10.3744/JNAOE.2011.3.1.111
- Montewka, J., Ehlers, S., Goerlandt, F., Hinz, T., Tabri, K., & Kujala, P. (2014). A framework for risk assessment for maritime transportation systems—A case study for open sea collisions involving RoPax vessels. Reliability Engineering & System Safety, 124, 142–157. doi:10.1016/j.ress.2013.11.014
- Montewka, J., Goerlandt, F., Ehlers, S., Kujala, P., Erceg, S., Polic, D., ... Tabri, K. (2011). A model for consequence evaluation of ship-ship collision based on Bayesian Belief Network. In E. Rizzuto & C. Guedes Soares (Eds.), Sustainable Maritime Transportation and Exploitation of Sea Resources (pp. 721–728). LONDON, UK: Taylor & Francis Group.
- Montewka, J., Goerlandt, F., & Kujala, P. (2014). On a systematic perspective on risk for formal safety assessment (FSA). *Reliability Engineering & System Safety*, 127, 77–85. doi:10.1016/j.ress.2014.03.009
- Papanikolaou, A. D., Guedes Soares, C., Andrzej Jasionowski, Jensen, J. J., McGeorge, D., Poylio, E., ... Vassalos, D. (2009). Risk-Based Ship Design. (A. D. Papanikolaou, Ed.)Springer. Springer. doi:10.1007/978-3-540-89042-3
- Pillay, A., & Wang, J. (2003). Technology and Safety of Marine Systems. (R. Bhattacharyya & M. E. McCormick, Eds.)Elsevier Ocean Engineering Series (Vol. 7). Elsevier.



- Psaraftis, H. N. (2012). Formal Safety Assessment: an updated review. Journal of Marine Science and Technology, 17(3), 390–402. doi:10.1007/s00773-012-0175-0
- Ravn, E. (2006). Risk based model for failure of propulsion and steering gear system. *Safedor* (Vol. 2.4.7).
- Umeda, N. (2013). Current Status of Second Generation Intact Stability Criteria Development and Some Recent Efforts. In 13th International Ship Stability Workshop (pp. 138–157). Brest, Brittany, France.
- Wang, J. (2002). Offshore safety case approach and formal safety assessment of ships. Journal of Safety Research, 33(1), 81–115.

This page is intentionally left blank



Application of the Envelope Peaks over Threshold (EPOT) Method for Probabilistic Assessment of Dynamic Stability

Bradley Campbell *NSWCCD (Naval Surface Warfare Center Carderock Division)*,

bradley.campbell@navy.mil

Vadim Belenky, *NSWCCD (Naval Surface Warfare Center Carderock Division)*,

vadim.belenky@navy.mil

Vladas Pipiras, *University of North Carolina at Chapel Hill*, pipiras@email.unc.edu

ABSTRACT

This paper reviews the research and development of the Envelope Peaks over Threshold (EPOT) method that has taken place since the previous STAB conference. The EPOT method is intended for the statistical extrapolation of ship motions and accelerations from time-domain numerical simulations, or possibly, from a model test. To model the relationship between probability and time, the large roll angle events must be independent, so Poisson flow can be used. The method uses the envelope of the signal to ensure the independence of large exceedances. The most significant development was application of the Generalized Pareto Distribution (GPD) for approximation of the tail, replacing the previously used Weibull distribution. This paper reviews the main aspects of modeling the GPD, including its mathematical justification, fitting the parameters of the distribution, and evaluating of the probability of exceedance and its confidence interval.

Keywords: *Large roll, Statistical extrapolation, Generalized Pareto Distribution, EPOT*

1. INTRODUCTION

The rarity of dynamic stability failures in realistic sea condition makes the problem of extrapolation inevitable. This can be illustrated in the following example. If we assume an hourly stability failure rate of 10^{-6} hr^{-1} (Kobylinski and Kastner, 2003), then we can expect to see (on average) one failure every 1,000,000 hours. If we require 10 observations for a reliable statistical estimate; then we need to simulate 10,000,000 hours. Even if an advanced hydrodynamic code could run in a real time and a cluster with 1,000 processors is dedicated to the task, it would take 10,000 hours per condition (combination of seaway,

speed and heading) to perform the assessment. The cost of the calculations prohibits direct simulation in this manner.

Additionally stability failure is associated with large-amplitude motions and is expected to be nonlinear. Indeed, capsize is related to the ultimate nonlinearity – transition to another equilibrium. In order to have enough fidelity to model this problem, the hydrodynamic code must be quite sophisticated (see a review by Reed, *et al.*, 2014). The probability of capsizing the topic of a multi-year ONR research project titled “A Probabilistic Procedure for Evaluating the Dynamic Stability



and Capsizing of Naval Vessels” (Belenky, *et al.*, 2015).

IMO document SLF 54/3/1 (Annex 1) defines intact stability failure as a state of inability of a ship to remain within design limits of roll (heel, list) angle combined with high rigid body accelerations. This includes also partial stability failure when a ship is subjected to a large roll angle or excessive accelerations, but does not capsizes. Following the same logic one could also include an excessive pitch angle. As this study focuses on partial stability failure, peak over threshold method (POT) was chosen (Pickands, 1975). Introducing a threshold allows considering the data that are more influenced by nonlinearity; this incorporates changing physics into the statistical estimates.

To satisfy the requirement of independent peaks over threshold, the peaks of envelope were used instead of the peaks of the process itself (Campbell and Belenky, 2010). The review of this research effort is available from Belenky and Campbell (2012). That work included consideration of the relationship between probability and time, the probabilistic properties of peaks, application of envelope theory and the extreme value distribution.

The relationship between time and probability is key to the proper treatment of the partial stability failures. It is modeled with Poisson flow and requires independence of the failures. In the case of capsizing, the enforcement of Poisson Flow is not required, since capsizing can only occur once per record (the possibility of several capsizings within one record can be safely ignored for practical cases). Belenky and Campbell (2012) also review different ways of statistical characterization of the rate of events, the only parameter of the Poisson flow.

Classical POT methods use the Generalized Pareto Distribution (GPD) to approximate the tail of the distribution above a threshold. However, under certain conditions the GPD

may be right bounded, that is, there is some value above which the probability of exceedances is zero. This is not a problem for conventional statistical consideration, when we are interested in the quantiles of the (i.e. the probability is given and the level needs to be found). In ship stability generally the failure level is known and related to down flooding or cargo shifting angles and probability is to be found. The physical meaning of the right bound was not clear at that time (and still is not completely clear). As a result, the Weibull distribution was used for modeling the tail.

Normally distributed wave elevation was the subject of study in Belenky and Campbell (2012). This was a logical first test for these techniques. The study concluded that the distribution of large absolute values of peaks can be approximated by Rayleigh law. The Rayleigh distribution is a particular case of Weibull distribution when the shape parameter equals two. Thus, deviation of this parameter from two may be suitable for representing nonlinearity in a dynamical system.

To investigate the performance of a POT scheme based on the Weibull distribution, a model representing ship motions with realistic stability variation was used (Weems and Wundrow, 2013; Weems and Belenky, 2015). It was found that Weibull distribution does not have enough flexibility to approximate the tail of large-amplitude ship motions and the consideration of the GPD was started again.

Application of the GPD with EPOT produced very reasonable results (Smith and Zuzick, 2015). The techniques used to fit GPD, estimate the probability of exceedance of a given level and evaluate its uncertainty are described in Campbell, *et al.* (2014, 2014a) and Pipiras, *et al.* (2015) and briefly reviewed in the rest of this paper.

2. MATHEMATICAL BACKGROUND

2.1 Distribution of Order Statistics

In order to understand why statistical extrapolation is possible when the underlying distribution is unknown, we begin with order statistics.

Consider a set of n independent realizations of random variable z . Assume that the distribution is given in a form of a cumulative distribution function (CDF) and probability density function (PDF). Sorting the observed values from the largest to smallest we have:

$$y_i = \text{sort}(z_i) \quad i = 1, \dots, n \quad (1)$$

Indeed, for a randomly selected values y and z :

$$pdf(y) = pdf(z); \quad CDF(y) = CDF(z) \quad (2)$$

Consider a value that happens to be k -th in the list ($1 \leq k \leq n$). It is a random number, because, if one generates another set of realizations of variable z , and sorts them, another value will be the k -th. This random number is referred as k -th order statistic. Like any other random variable, y_k has its own distribution. This distribution is (see, e.g. David and Nagaraja, 2003):

$$pdf(y|k) = pdf(y) \frac{n!}{(k-1)!(n-k)!} \cdot (CDF(y))^{k-1} (1-CDF(y))^{n-k} \quad (3)$$

2.2 Generalized Extreme Value (GEV) Distribution

Consideration of distribution of the largest value ($k=1$) when the number of observations n grows, leads to a limit, known as Generalized Extreme Value (GEV) distribution (see e.g. Coles, 2001):

$$pdf(x) = \frac{1}{\sigma} \left(1 + \xi \frac{x-\mu}{\sigma} \right)^{-\left(1+\frac{1}{\xi}\right)} \cdot \exp \left[- \left(1 + \xi \frac{x-\mu}{\sigma} \right)^{\frac{1}{\xi}} \right] \quad (4)$$

ξ is a shape parameter, σ is scale parameter ($\sigma > 0$); μ is a shift parameter, Equation (4) is non-zero for:

$$x > \mu - \frac{\sigma}{\xi} \quad \text{for } \xi > 0 \quad (5)$$

$$x < \mu - \frac{\sigma}{\xi} \quad \text{for } \xi < 0$$

and is zero otherwise. If the shape parameter $\xi=0$:

$$pdf(x) = \frac{1}{\sigma} \exp \left(\frac{x-\mu}{\sigma} \right) \cdot \exp \left(- \exp \left(\frac{x-\mu}{\sigma} \right) \right) \quad (6)$$

for any values of x .

It is important that the limit (4-6) does not depend on the distribution z . That means that all the extreme values have the same distribution if one considers a sample of sufficient volume. This is the essence of the extreme value theorem, sometimes referred to as the Fisher-Tippet-Gnedenko theorem (see, e.g. Coles, 2001).

Direct application of the extreme value theorem for probabilistic assessment of dynamic stability can be found in MacTaggart, (2000), MacTaggart and deKat (2000). However, several issues remained unresolved; including the question how large the sample should be (in terms of record length and number of records) to claim limiting properties of GEV.

2.3 Generalized Pareto Distribution (GPD)

The large sample volume needed for direct application of the GEV is partially driven by the fact that only a single value (the largest one

from the time window) is used to find the parameters of distribution. The desire to use more data leads to the idea of peaks over threshold methods.

Take μ as a threshold and find the distribution of the data exceeding this threshold, i.e. consider conditional probability. The Generalized Pareto distribution is derived from the GEV with the threshold condition applied. The basic logic of this derivation is available in Coles (2001). The GPD is expressed as

$$f(x) = \begin{cases} \frac{1}{\sigma} \left(1 + \xi \frac{x - \mu}{\sigma} \right)^{-\left(1 + \frac{1}{\xi}\right)} ; \\ \quad \text{if } \mu < x, \quad \xi > 0, \quad \text{or} \\ \quad \mu < x < \mu - \frac{\sigma}{\xi}, \quad \xi < 0 \\ \frac{1}{\sigma} \exp\left(-\frac{x - \mu}{\sigma}\right) ; \\ \quad \text{if } \mu < x, \quad \xi = 0 \end{cases} \quad (7)$$

where ξ is the shape parameter, σ is the scale parameter ($\sigma > 0$) and μ is the threshold, above which, the GPD is believed to be applicable.

Equation (7) expresses the second extreme value theorem, referred as Pickands-Balkema-de Haan theorem. It states that the tail of independent random variables can be approximated with the GPD.

3. FITTING THE GPD

3.1 Preparing Independent Data

Ship motions are characterized by strong dependence of the data points on each other, especially in following and stern quartering seas when a spectrum is narrow and autocorrelation function takes a long time to decay. However, the peaks of the piecewise linear envelope (see Figure 1) represent independent data points. The difference between piecewise linear and theoretical

envelope is considered by Belenky and Campbell (2012). However, this technique may not work for the cases of parametric roll, where mutual dependence is much stronger. The method of collecting independent data for the case of parametric roll is described in Kim, *et al.* (2014).

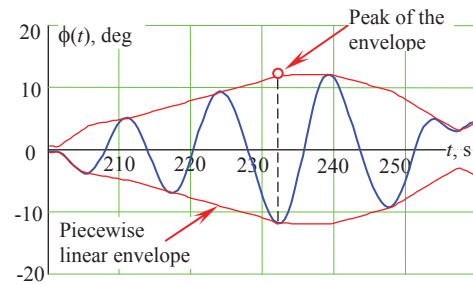


Figure 1: Piecewise linear envelope and its peak

3.2 Estimating Shape and Scale Parameters

To facilitate the choice of the threshold at a later step, fitting the shape and scale parameters are carried out for a series of prescribed thresholds. The maximum likelihood estimator (MLE) method is a standard way of estimating the parameters for the GPD. The idea of MLE method is quite intuitive: to find such values of parameters that are “most likely” to fit the data.

What is “most likely”? The data points that have been observed are the facts. At the same time they are instances of a random variable. Because these particular values were observed, they are more likely to occur than others. That means that the probability of observing these particular values reaches maximum when the correct parameters are used for distribution. The parameters are found by maximizing the value of the likelihood function. In practice this is made easier by taking the natural logarithm of the likelihood function (Equation 8 below).

$$l(\xi, \sigma) = -n \cdot \ln(\sigma) - \left(1 + \frac{1}{\xi}\right) \cdot \sum_{i=1}^n \ln\left(1 + \xi \cdot \frac{z_i}{\sigma}\right) \quad (8)$$

$$z_i = x_i - \mu$$

Where n is the number of data points above a threshold μ , z_i are the sample data points above a threshold μ (sometimes referred to as *excesses*).

3.3 Distribution the GPD Parameters

Since the shape and scale parameters are estimated from the envelope peak data (which are random numbers), the estimated parameters are also random numbers. Their distribution can be approximated with a bivariate normal distribution (Smith, 1987).

$$f_N(\hat{\xi}, \hat{\sigma}) = \frac{1}{2\pi V_\xi V_\sigma \sqrt{1 - \rho_{\xi\sigma}^2}} \cdot \exp\left(-\frac{1}{2(1 - \rho_{\xi\sigma}^2)} \left(\frac{(\hat{\xi} - E_\xi)^2}{V_\xi} + \frac{(\hat{\sigma} - E_\sigma)^2}{V_\sigma} - \frac{2\rho_{\xi\sigma}(\hat{\xi} - E_\xi)(\hat{\sigma} - E_\sigma)}{\sqrt{V_\xi V_\sigma}} \right)\right) \quad (9)$$

Here $\hat{\xi}$ and $\hat{\sigma}$ are estimates of ξ and σ , E is used for expected (or mean) value, V is the variance and ρ is the correlation coefficient between ξ and σ . The parameter estimates produced by maximizing equation (8) are the mean values, while the covariance matrix M_C is found using the method outlined below.

$$M_C = \begin{pmatrix} V_\xi & \rho_{\xi\sigma} \sqrt{V_\xi V_\sigma} \\ \rho_{\xi\sigma} \sqrt{V_\xi V_\sigma} & V_\sigma \end{pmatrix} \quad (10)$$

The delta method allows one to find the estimates of mean and variance of the output, if estimates of the input are known and the function that turns input into output can be linearized, such as by a Taylor series. Because of this the delta method is an approximation.

Applying the delta method to maximization of equation (8) yields the Fisher information matrix M_F that is an inverse of the covariance matrix (10) (Boos and Stefanski, 2013):

$$M_F = \begin{pmatrix} -\frac{\partial^2 l(\xi, \sigma)}{\partial \xi^2} & -\frac{\partial^2 l(\xi, \sigma)}{\partial \xi \partial \sigma} \\ -\frac{\partial^2 l(\xi, \sigma)}{\partial \xi \partial \sigma} & -\frac{\partial^2 l(\xi, \sigma)}{\partial \sigma^2} \end{pmatrix} \quad (11)$$

The derivatives in (11) are expressed as follows:

$$\frac{\partial^2 l(\xi, \sigma)}{\partial \xi^2} = \frac{2}{\xi^3} \sum_{i=1}^n \ln\left(1 + \xi \cdot \frac{z_i}{\sigma}\right) - \frac{2}{\xi^2} \sum_{i=1}^n \frac{z_i}{\sigma + \xi \cdot z_i} - \left(1 + \frac{1}{\xi}\right) \cdot \sum_{i=1}^n \frac{z_i^2}{(\sigma + \xi \cdot z_i)^2} \quad (12)$$

$$\frac{\partial^2 l(\xi, \sigma)}{\partial \sigma^2} = \frac{n}{\xi \cdot \sigma^2} - \left(1 + \frac{1}{\xi}\right) \cdot \sum_{i=1}^n \frac{1}{(\sigma + \xi \cdot z_i)^2} \quad (13)$$

$$\frac{\partial^2 l(\xi, \sigma)}{\partial \xi \partial \sigma} = \frac{n}{\xi^2 \cdot \sigma} - \frac{1}{\xi^2} \sum_{i=1}^n \frac{1}{\sigma + \xi \cdot z_i} - \left(1 + \frac{1}{\xi}\right) \cdot \sum_{i=1}^n \frac{z_i}{(\sigma + \xi \cdot z_i)^2} \quad (14)$$

The covariance matrix is finally found as:

$$M_C = M_F^{-1} \quad (15)$$

Equations (10) through (14) completely define the bivariate normal distribution (9), as shown in Figure 2.

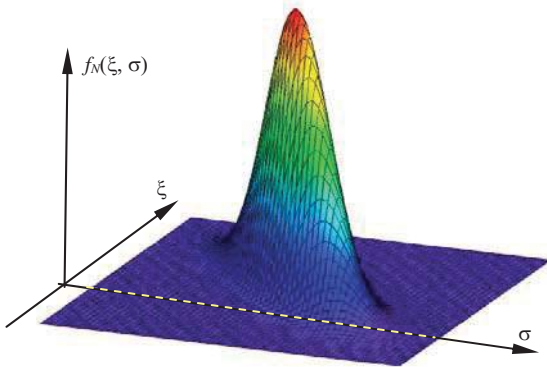


Figure 2: Joint distribution of GPD parameters

It is important to note that the scale parameter is by definition a positive quantity, while the bivariate normal distribution formally supports negative values for the scale parameter. To avoid negativity of σ as an artifact of approximation (9), Pipiras, et al. (2015) proposed using the $\hat{l}_\sigma = \ln \hat{\sigma}$ instead of σ . This leads to a new distribution:

$$f_{LN}(\hat{\xi}, \hat{l}_\sigma) = \frac{1}{2\pi V_\xi V_{l_\sigma} \sqrt{1 - \rho_{\xi/l_\sigma}^2}} \cdot \exp\left(-\frac{1}{2(1 - \rho_{\xi/l_\sigma}^2)} \left(\frac{(\hat{\xi} - E_\xi)^2}{V_\xi} + \frac{(\hat{l}_\sigma - E_{l_\sigma})^2}{V_{l_\sigma}} - \frac{2\rho_{\xi/l_\sigma}(\hat{\xi} - E_\xi)(\hat{l}_\sigma - E_{l_\sigma})}{\sqrt{V_\xi V_{l_\sigma}}} \right)\right) \quad (16)$$

$$E_{l_\sigma} = \ln(E_\sigma); \quad V_{l_\sigma} = \frac{V_\sigma}{E_\sigma^2}; \quad \rho_{\xi/l_\sigma} = \frac{\rho_{\xi\sigma}}{E_\sigma} \quad (17)$$

Difference between distribution (16) and bivariate normal (9) is not very large (Pipiras, et al., 2015).

3.4 Choice of the Threshold

Choosing a correct threshold is a critical to ensuring the applicability of the GPD. If the threshold is too low, the fitted GPD is not an approximation of the tail, because the conditions of the second extreme value

theorem have not been met. If the threshold is too high, “eligible” data have been wasted and the result will more scatter or uncertainty than necessary.

The second extreme value theorem states that the GPD can be used for approximation of the tail of any distribution if the threshold is high enough. That means that above certain threshold the GPD approximation must be invariant to the threshold (Coles, 2001). The simplest way is to observe stabilization of the shape parameter, see Figure 3.

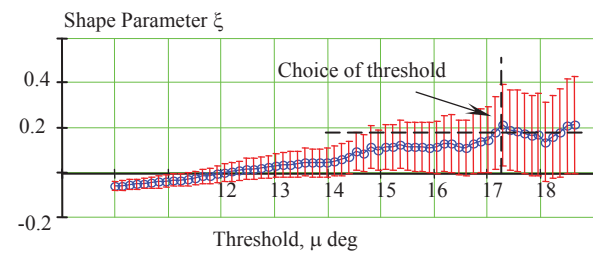


Figure 3 Choice of threshold by stabilization of the shape parameter

Campbell, et al. (2014) describes study of five different methods of setting the threshold:

1. Stabilization of shape parameter
2. Stabilization of modified scale parameter
3. Stabilization of mean residual life estimate
4. Ad-hoc method based on minimum absolute difference between the shape parameter and its median above the threshold
5. Ad-hoc method based on minimum squared difference in the shape from its mean above the threshold

The first three methods are taken from Coles (2001) and they were mostly intended for “manual” calculation with “a human in a loop”. The methods 4 and 5 are similar to the methods proposed in Reiss and Thomas (2007) for automatic choice of the threshold. The referred study (Campbell, et al., 2014) has shown that automation of the method 1 through 3 makes the threshold lower than the visual choice. For the example shown in Figure 3, these methods put the threshold somewhere

around 13~14 degrees, while the visual choice is somewhere above 17 degrees.

At the same time methods 4 and 5 have returned the threshold that is more close to the “visual” choice. The method 4 is quickly reviewed below. It is based on minimizing the following function:

$$f(\mu_k) = \frac{1}{N_{Tr} - 1 - k} \sum_{i=k}^{N_{Tr}-1} (N_{Tr} - i)^b \left| \hat{\xi}_i - \text{median}(\hat{\xi}_k, \dots, \hat{\xi}_{N_{Tr}}) \right| \quad (18)$$

The value of b was taken as 0.5; N_{Tr} is the number of the thresholds considered. A plot of (16) is shown in Figure 4. A global minimum (ignoring that the function goes to zero at the right) occurs just below $\mu=17.4$ deg, which is close to one of the visual choices made at Figure 3.

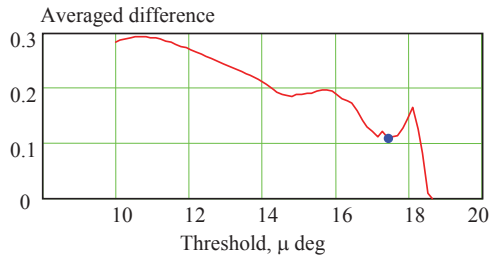


Figure 4 Choice of the Threshold based on the Global Minimum of the Equation (16)

4. EXTRAPOLATION AND UNCERTAINTY OF THE PROBABILITY OF EXCEEDANCE

4.1 Extrapolated Estimate

Using the GPD to extrapolate the probability of exceedance yields the conditional probability that the level of interest c has been exceeded if the threshold μ has been exceeded:

$$\hat{P} = \begin{cases} \left(1 + \hat{\xi} \cdot \frac{c - \mu}{\hat{\sigma}} \right)^{-\frac{1}{\hat{\xi}}} & \text{if } \hat{\xi} > -\frac{\hat{\sigma}}{c - \mu} \\ 0 & \text{if } \hat{\xi} \leq -\frac{\hat{\sigma}}{c - \mu} \end{cases} \quad (19)$$

c is the limit that constitutes the stability failure. The probability that μ has been exceeded can be estimated statistically, since it has been exceeded often enough so that we have enough data to build the distribution of peaks above it.

Now let's consider the problem of the right bound. As can be seen from equation (19), the probability of exceedance is equal zero for negative shape parameters and $c \geq \mu - \hat{\sigma} / \hat{\xi}$. This has several implications.

First, the extrapolated estimate is a random number. The joint distribution of the shape and scale parameters is approximated using distribution (16). That also means that the mean values of the shape and scale parameters are the most probable values at the same time (because normal distribution has a maximum at its mean value). Thus, one could expect that the most probable values used for formulae (19) returns the most probable value of extrapolated estimate.

So if the formula (19) returns zero, it is the most probable answer, but not the only one possible. In fact, the formula (19) must be accompanied with confidence interval that may be seen as a “range of answers”.

4.2 Mean and Distribution of the Extrapolated Estimate

In contrast to the most probable value of the extrapolated estimate, the mean value is never zero for a finite volume of data. Consider formula (19) as a deterministic function of random arguments:

$$\hat{P} = g(\hat{\xi}, \hat{\sigma}) \quad (20)$$

Its mean value can be found as using well known formula for the mean value of deterministic function of random arguments:

$$E(\hat{P}) = \int_0^{\infty} \int_{-\infty}^{\infty} g(\xi, \sigma) f_{LN}(\xi, \sigma) d\xi d\sigma \quad (21)$$

Using (21) the PDF of the extrapolated estimate is derived as:

$$f_p(x) = \int_{-\infty}^{\infty} f_{LN}\left(\xi, \frac{\xi(c-\mu)}{x^{-\xi}-1}\right) \cdot \frac{\xi^2 x^{-\xi-1}}{(x^{-\xi}-1)^2} (c-\mu) d\xi \quad (22)$$

Figure 5 depicts the PDF of the extrapolated estimate

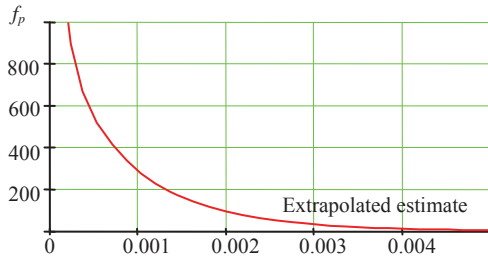


Figure 5: PDF of the Extrapolate Estimate (Campbell, *et al.*, 2014).

More details are available from Campbell *et al.* (2014). The formula (22) also can be written using the bivariate normal distribution (9).

4.3 Confidence Interval of the Extrapolated Estimate

Quantiles of distribution (22) can be used to evaluate the confidence interval of the extrapolated estimate. The profile log likelihood PLL method (Coles, 2001) adapted for the extrapolated estimate is another way to find the confidence interval (Campbell, *et al.*, 2014). The log likelihood estimator (8) is expressed in terms of the extrapolated estimate \hat{P} (19):

$$l_p(\hat{\xi}, \hat{P}) = -n \ln \left(\frac{\hat{\xi} \cdot c}{\hat{P}^{-\hat{\xi}} - 1} \right) - \left(1 + \frac{1}{\hat{\xi}} \right) \sum_{i=1}^n \ln \left(1 + \frac{z_i (\hat{P}^{-\hat{\xi}} - 1)}{c} \right) \quad (23)$$

and maximized by the shape parameter:

$$l_m(\hat{P}_x) = \arg \max_{\hat{\xi}} l_p(\hat{\xi}, \hat{P}_x) \quad (24)$$

and the extrapolated estimate:

$$\hat{P} = \arg \max_{\hat{P}_x} l_m(\hat{P}_x) \quad (25)$$

The difference between them, referred as deviance statistic D and is assumed to have χ^2 distribution:

$$D(\hat{P}_x) = l_m(\hat{P}) - l_m(\hat{P}_x) \quad (26)$$

The confidence interval includes the space where:

$$D(p) < 0.5 Q_{\chi^2}(P_\beta, dof=1) \quad (27)$$

P_β is the confidence probability and Q_{χ^2} is the quantile function of the χ^2 distribution. The boundaries are found as the limits of P_x that satisfy the condition (27), see Figure 6.

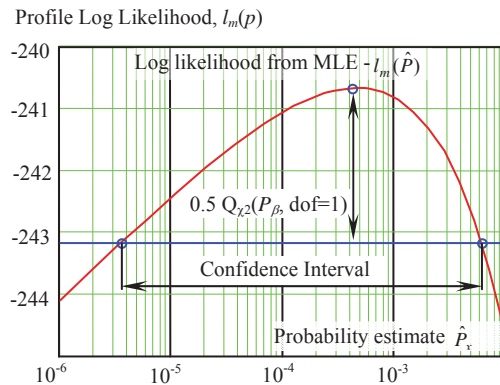


Figure 6. Profile Log Likelihood Method for Confidence Interval (Campbell, *et al.* 2014)

Pipiras, *et al.* (2015) systematically studied and compared different methods of calculating the confidence interval for the extrapolated

estimate. The following methods were considered:

1. Delta method
2. "Normal" method (distribution 9)
3. "Lognormal" method (distribution 22)
4. "Boundary" method
5. Standard bootstrap method
6. Profile likelihood method (as briefly described above)

In addition to those six methods, three more techniques, termed indirect techniques, investigated were based on quantiles rather than extrapolated estimate for exceedance probability. Any of the methods mentioned above can be used to construct a confidence interval for the return level (the level to be exceeded with given probability p):

$$x_p = \frac{\sigma}{\xi} (p^{-\xi} - 1) \quad (28)$$

The general scheme of calculations of the confidence interval through quantiles / return level is shown in Figure 7. The three methods adapted to the indirect approach using quantiles were:

7. Indirect "Lognormal" method
8. Indirect "Boundary" method
9. Indirect Profile likelihood method

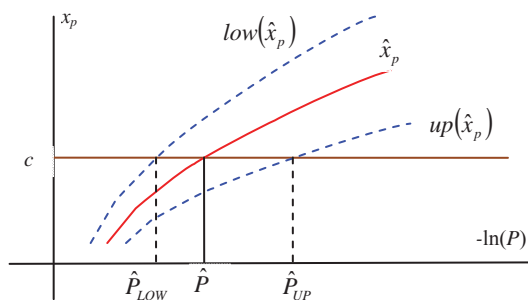


Figure 7 On Calculation of Confidence Interval using quantiles (Pipiras, *et al.*, 2015)

A comparison study was performed on simulated data sampled from a GPD distribution. The performance was judged based on the percentage of cases where the confidence interval contained the true value

(coverage). An accurate method should have the coverage close to the given confidence probability ($P_\beta=0.95$). There were two series of calculations with 100 and 50 samples each.

The indirect profile likelihood method was shown to have the best performance, see Pipiras, *et al.* (2015). The delta method does not perform well for probability estimates and should not be used. The "normal", "log-normal", and indirect "log-normal" methods are slightly anticonservative (coverage < 95%) with the log-normal method preferred among the three. The boundary method and indirect boundary methods are slightly conservative (coverage > 95%). The bootstrap and profile likelihood methods performed poorly for negative and near-zero shape parameters.

4.4 Convergence Study

Campbell, *et al.* (2014) describes convergence study for the EPOT method, using of the datasets from Smith *et al.* (2014) and Smith and Zuzick (2015). The results are shown in Figure 8.

The convergence test uses a moving average for 100 extrapolation data sets; the moving average is performed for the most probable value, mean value, and the upper boundary of the confidence interval calculated with the "log-normal" method. The most probable value is a better estimator when the sample volume is large, while the mean shows better (and more conservative) performance for smaller sample volumes. More details are available from Campbell, *et al.*, (2014).

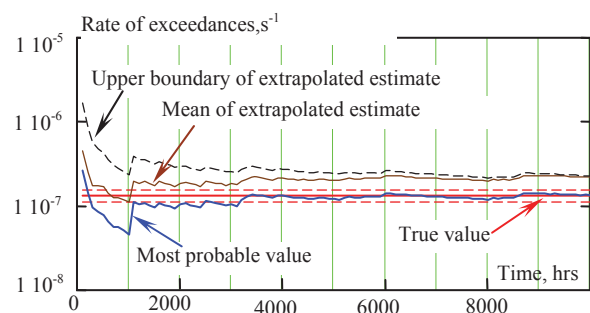


Figure 8 Convergence Test Using Moving



Averages to Approximate Extrapolated Estimates (Campbell, *et al.*, 2014)

4.5 On the Validation of EPOT

A comprehensive validation study of the EPOT method is reported by Smith and Zuzick (2015). Motions of the ONR Tumblehome topsides (Bishop *et al.*, 2005) configuration were simulated with a 3-DOF volume-based simulation (Weems and Wundrow, 2013; Weems and Belenky, 2015) for hundreds of thousands of hours to produce “true” values on rare exceedances. Then small subsets (100 hrs each) was used by EPOT extrapolation. Smith and Zuzick (2015) used log-normal and boundary methods in carrying out their validation procedure for six relative wave headings considering roll, pitch, lateral and vertical accelerations. Using the same data set, Pipiras, *et al.* (2015) reported results for heave and pitch only for 30 and 45 degrees of heading, but used methods 2 through 9 for the confidence interval.

Total number of conditions reported by Smith and Zuzick (2015) was 23. The minimal acceptable coverage was set to 90%. With log-normal confidence interval six conditions failed, while all the conditions are passed using the boundary method. These results could be expected as the log-normal method is slightly anti-conservative and the boundary method is slightly conservative, as mentioned above. Smith and Zuzick (2015) noted that all the conditions show acceptable results for restricted range of headings – aft of the beam seas. Similar conclusions were reached by Pipiras, *et al.* (2015).

5. CURRENT STATUS AND FUTURE WORK

The EPOT method has evolved significantly in the three years since the previous STAB conference. The main idea remains the same, however: extrapolate peaks

over a threshold and use the envelope to ensure independence. The idea of threshold was originally aimed to emphasize influence of nonlinearity. Now it is also has a mathematical interpretation – it ensures the applicability of the second extreme value theorem.

Use of the second extreme value theorem leads to use of the Generalized Pareto distribution (GPD) to approximate the distribution above a certain large threshold. The selection of the threshold is done based on applicability of GPD approximation above the chosen threshold. Five different techniques for selecting the threshold have been considered.

Fitting the GPD is performed with the maximum likelihood estimation (MLE) method. These parameter estimates from the MLE fit are assumed to follow a normal distribution. Several methods were considered for estimating the confidence interval of the extrapolated probability of exceedance. Some of them were anti-conservative and some were conservative. A definitive recommendation on which to use is still outstanding.

Significant progress has been achieved in the validation techniques of EPOT and the problems of extreme rarity in general. A very fast simulation code has been developed that is capable of producing statistics for events that occur only a few times during millions of hours. The simulation was shown to be qualitatively similar to higher fidelity codes like LAMP (Weems and Belenky, 2015). A procedure for the validation of statistical extrapolation techniques has been developed and applied to EPOT (Smith and Zuzick, 2015). While not all the tested environmental conditions satisfied the currently proposed requirements, the EPOT method shows promise and potential to be acceptable.

In addition to finalizing the confidence interval formulation, attention needs to be paid to reducing the uncertainty in the extrapolated probability of exceedance estimates. It may be possible to reduce the uncertainty if a



relationship between the GPD parameters and physical considerations can be established. Pipiras, *et al.* (2015) investigated fixing the ratio between the GPD parameters for the case of pitch based on shape of the longitudinal GZ curve. This resulted in decreasing of width of the confidence interval and spread of the estimates around the “true” value. Such a decrease of uncertainty was the result of introducing additional physical information into the problem. The idea of a limiting roll angle is discussed by Campbell, *et al* (2015) and may lead to a similar result for roll. It is anticipated that further study into the nature of the tail of the distribution of large ship motions will lead to an application-ready EPOT method.

6. ACKNOWLEDGEMENTS

The work described in this paper has been funded by the Office of Naval Research, under Dr. Patrick Purtell, Dr. Ki-Han Kim and Dr. Thomas Fu. The authors greatly appreciate their support. The participation of Prof. Pipiras was facilitated by the Summer Faculty Program supported by ONR and NSWCCD under Dr. Jack Price (David Taylor Model Basin, NSWCCD). The authors would like to acknowledge fruitful discussions with Prof. Pol Spanos (Rice University), Dr. Art Reed, Mr. Tim Smith (David Taylor Model Basin, NSWCCD), and Prof. Ross Leadbetter (University of North Carolina, Chapel Hill).

7. REFERENCES

- Belenky, V. and Campbell, B.L., 2012 “Statistical Extrapolation for Direct Stability Assessment”, Proc. 11th Intl. Conf. on Stability of Ships and Ocean Vehicles STAB 2012, 243-256, Athens, Greece.
- Belenky, V., Weems, K. and Lin, W.M., 2015 “Split-time Method for Estimation of Probability of Capsizing Caused by Pure Loss of Stability” in Proc. 12th Intl. Conf. on Stability of Ships and Ocean Vehicles STAB 2015, Glasgow, UK.
- Bishop, R. C., W. Belknap, C. Turner, B. Simon, and Kim J. H., 2005 “Parametric Investigation on the Influence of GM, Roll damping, and Above-Water Form on the Roll Response of Model 5613.” Report NSWCCD-50-TR-2005/027.
- Boos, D. D. and Stefanski, L. D., 2013 *Essential Statistical Inference: Theory and Method*. Springer.
- Campbell, B. and Belenky, V., 2010 “Assessment of Short-Term Risk with Monte-Carlo Method” Proc. 11th Int. Ship Stability Workshop, Wageningen, the Netherlands.
- Campbell, B., Belenky, V. and Pipiras, V., 2014 “Properties of the Tail of Envelope Peaks and their Use for the Prediction of the Probability of Exceedance for Ship Motions in Irregular Waves” CSM7 Computational Stochastic Mechanics, Deodatis, G. and P. D. Spanos, eds. (accepted).
- Campbell, B., Belenky, V. and Pipiras V., 2014a “On the Application of the Generalized Pareto Distribution for Statistical Extrapolation in the Assessment of Dynamic Stability in Irregular Waves” Proc. 14th Intl. Ship Stability Workshop, Kuala Lumpur, Malaysia, pp. 144-148.
- Coles, S., 2001 *An Introduction to Statistical Modeling of Extreme Values*. Springer, London.
- David, H. A. and Nagaraja, H. N., 2003. *Order Statistics*. Wiley Series in Probability and Statistics
- IMO SLF 54/3/1 Development of Second Generation Intact Stability Criteria. Report of the Working Group at SLF 53 (part 2). Submitted by the Chairman of the Working Group, 2011, London, UK.



- Kim, D.H., Belenky, V., Campbell, B. L. and Troesch, A. W., 2014 “Statistical Estimation of Extreme Roll in Head Seas” in Proc. of 33rd Intl. Conf. on Ocean, Offshore and Arctic Engineering OMAE 2014, San-Francisco, USA.
- Kobylnski, L. and Kastner, S. 2003 *Stability and Safety of Ships. Regulation and Operation*, Elsevier.
- McTaggart, K. A., 2000 “Ongoing Work Examining Capsize Risk of Intact Frigates Using Time Domain Simulation”. In *Contemporary Ideas of Ship Stability*, D. Vassalos, et al. (eds), Elsevier Science, pp. 587–595.
- McTaggart, K. A., de Kat J.O., 2000 “Capsize Risk of Intact Frigates in Irregular Seas”. Trans. SNAME, Vol. 108, pp 147–177.
- Pickands, J., 1975 “Statistical Inference Using Extreme Order Statistics”. The Annals of Statistics Vol. 3, No 1, pp. 119-131.
- Pipiras, V., Glotzer, D., Belenky, V., Campbell, B., Smith, T., 2015 "Confidence Interval for Exceedance Probabilities with Application to Extreme Ship Motions", J. of Statistical Planning and Inference (Submitted)
- Reed, A., Beck, R. and Belknap, W., 2014 “Advances in Predictive Capability of Ship Dynamics in Waves”, Invited Lecture at 30th Symposium of Naval Hydrodynamics, Hobart, Australia.
- Reiss, R.-D. and Thomas, M., 2007 *Statistical Analysis of Extreme Values with Application to Insurance, Finance, Hydrology and Other Fields*. 3rd Edition, Basel: Birkhäuser Verlag.
- Smith, R. L., 1987 “Estimating tails of probability distributions.” The Annals of Statistics Vol 15, pp.1174–1207.
- Smith, T. C., 2014 “Example of Validation of Statistical Extrapolation Example of Validation of Statistical Extrapolation,” Proc. of the 14th Intl. Ship Stability Workshop, Kuala Lumpur, Malaysia.
- Smith, T. C., and Zuzick, A., 2015 “Validation of Statistical Extrapolation Methods for Large Motion Prediction” in Proc. 12th Intl. Conf. on Stability of Ships and Ocean Vehicles (STAB 2015), Glasgow, UK.
- Weems, K., and Wundrow, D., 2013 “Hybrid Models for Fast Time-Domain Simulation of Stability Failures in Irregular Waves with Volume-Based Calculations for Froude-Krylov and Hydrostatic Forces”, Proc. 13th Intl. Ship Stability Workshop, Brest, France.
- Weems, K. and Belenky, V., 2015 “Fast Time-Domain Simulation in Irregular Waves With Volume-Based Calculations for Froude-Krylov and Hydrostatic Force” in Proc. 12th Intl. Conf. on Stability of Ships and Ocean Vehicles (STAB 2015), Glasgow, UK.



Split-time Method for Estimation of Probability of Capsizing Caused by Pure Loss of Stability

Vadim Belenky, *NSWCCD (David Taylor Model Basin)*, vadim.belenky@navy.mil

Kenneth Weems, *NSWCCD (David Taylor Model Basin)*, kenneth.weems@navy.mil

Woei-Min Lin, *Office of Naval Research – Global*, woei-min.lin.civ@mail.mil

ABSTRACT

The paper reviews a multi-year research effort for using the split-time method to calculate the probability of ship capsizing due to pure loss of stability in irregular waves. The idea of the split-time method is to separate the complex problem of the probability of capsizing into two less complex problems: a non-rare problem that involves the upcrossing of an intermediate level of roll and a rare problem that focuses on capsizing after an upcrossing. An initial implementation using a dynamic model with piecewise linear stiffness, which can be considered to be the simplest model of capsizing in beam seas, led to the concept of critical roll rate as the smallest roll rate at the instant of upcrossing that inevitably leads to capsizing. The piecewise linear system allows a closed-form solution for the critical roll rate, but a more general approach using perturbations can be used for numerical models including advanced hydrodynamic simulation codes. The extension of the split-time method to pure loss of stability required the consideration of the change of roll stiffness in waves and led to calculating the critical roll rate at each upcrossing. A metric of the likelihood of capsizing has been defined as the difference between the observed and critical roll rate at the instances of upcrossing. The probability of capsizing after upcrossing becomes an extrapolation problem for the value of the metric, which can be performed by approximating the tail of the metric's distribution with the Generalized Pareto Distribution. This probability is combined with the observed rate of upcrossings to estimate the rate of capsizing in irregular seas.

Keywords: *Capsizing, Probability, Pure Loss of Stability, Split-Time Method*

1. INTRODUCTION

The dynamic capsizing of a ship is a complex phenomenon dominated by the nonlinearity of the large amplitude roll response, so that linearized mathematical models cannot retain the phenomenon's essential properties. Capsizing of an intact ship in realistic irregular waves represents an even bigger challenge, as this extreme nonlinearity is combined with extreme rarity, leaving no chance for using brute-force Monte-Carlo simulation with hydrodynamic codes of sufficient fidelity.

This challenge has been taken up by the US Office of Naval Research (ONR) project "A Probabilistic Procedure for Evaluating the Dynamic Stability and Capsizing of Naval Vessels". The objective of the project is to create a robust theory of probabilistic capsizing in irregular waves and a numerical procedure based on this theory.

As is well known, an intact ship in realistic ocean waves can capsize in a number of different scenarios or modes. The physical mechanism is different for each scenario, so the

theory must be mode-specific. The pure loss of stability is, in a sense, a simplest scenario. It can be modeled in a basin just with waves, assuming that roll damping is high enough to prevent parametric roll resonance and the forward speed is too low for surf-riding and broaching-to.

The split-time method has been developed to simultaneously address the phenomenon's extreme nonlinearity and rarity by providing an evaluation of the probability of capsizing from a relatively small volume of irregular sea response data, perhaps hundreds of hours of simulation rather than the millions of hours required for a Monte-Carlo approach. Numerical implementation has largely been carried out using the Large Amplitude Motion Program (LAMP), although the procedure is fundamentally code-independent.

The split-time method is being developed in phases. The initial phase considered a ship with time-invariant stiffness. While this can be considered to be a model of capsizing at zero speed in beam seas, the primary objective was to develop a basic theory of the method for both a simplified mathematical model and numerical simulation codes. The second phase of the development has extended the theories to the problem of pure loss of stability by considering the ship's change of stiffness as it moves in waves. This paper discusses the development of the theory for these initial two phases.

2. BASIC THEORY OF RARE RANDOM TRANSITIONS

2.1 Piecewise Linear System

Capsizing can be considered as a transition of a ship moving about its stable upright equilibrium to motions about its stable "mast down" equilibrium. A dynamical system with a piecewise linear stiffness is, possibly, the

simplest way to describe a transition between two stable equilibria:

$$\ddot{\phi} + \omega_{\phi}^2 f_L^*(\phi) = 0 \quad (1)$$

ω_{ϕ} is a natural frequency of roll and f_L^* is a piecewise linear stiffness function. As illustrated in Figure 1, equation (1) models the phase plane topology of a ship in calm water, and has a closed-form solution for each range.

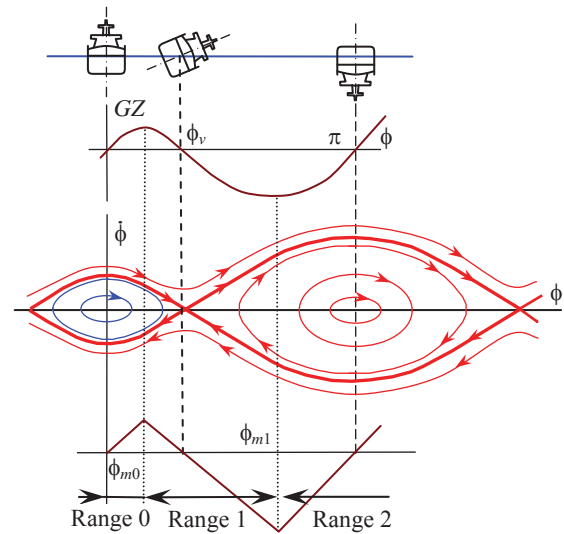


Figure 1: Phase plane topology of capsizing and piecewise linear stiffness (Belenky, 1993)

Adding linear damping and random excitation to the dynamical system (1) makes it a model of random transition between stable equilibria:

$$\ddot{\phi} + 2\delta\dot{\phi} + \omega_{\phi}^2 f_L^*(\phi) = f_{E\phi}(t) \quad (2)$$

δ is a linear damping coefficient and $f_{E\phi}$ is a stochastic process of roll excitation, modeled as:

$$f_{E\phi}(t) = \sum_{i=1}^{N_{\omega}} \alpha_{Ei} \sin(\omega_i t + \phi_{0i}) \quad (3)$$

α_{Ei} are amplitudes, ω_i are frequencies and ϕ_{0i} are initial phases of the i^{th} component of an excitation process presented as a Fourier series with N_{ω} frequencies. Equation (2) has a known closed-form solution in each range:

$$\phi = \begin{cases} \phi_a e^{-\delta t} \sin(\omega_{d0} t + \varepsilon) + p_0(t) & \text{if } -\phi_{m0} \leq \phi \leq \phi_{m0} \\ Ae^{\lambda_1 t} + Be^{\lambda_2 t} + p_1(t) & \text{if } \phi_{m0} < \phi \leq \phi_{m1} \\ \phi_{a2} e^{-\delta t} \sin(\omega_{d2} t + \varepsilon_2) + p_2(t) & \text{if } \phi > \phi_{m0} \end{cases} \quad (4)$$

ϕ_a , ε , A , B , ϕ_{a2} and ε_2 are arbitrary constants that are dependent on the initial conditions at the “switching” of the ranges; ω_{d0} and ω_{d2} are frequencies of the damped oscillation in ranges 0 and 2, respectively; λ_1 and λ_2 are eigenvalues for the solution in Range 1. The particular solutions for each range are expressed as:

$$p_j(t) = \sum_{i=1}^{N_{\omega}} p_{ij} \sin(\omega_i t + \beta_{ij} + \varphi_{0i}) + E_j \quad (5)$$

$j=0, 1, 2$ is a range number, p_{ij} is an amplitude and β_{ij} is a phase shift of the i^{th} component of the response. E_j is a position of equilibria for each range:

$$E_0 = 0; \quad E_1 = \phi_v; \quad E_2 = \pi \quad (6)$$

ϕ_v is the angle of vanishing stability. One of the eigenvalues for the Range 1 is positive while another is negative:

$$\begin{aligned} \lambda_1 &= -\delta + \sqrt{\omega_{\phi}^2 k_{f1} + \delta^2} > 0 \\ \lambda_2 &= -\delta - \sqrt{\omega_{\phi}^2 k_{f1} + \delta^2} < 0 \end{aligned} \quad (7)$$

k_{f1} is the slope coefficient for Range 1 taken with opposite sign.

2.2 Condition of the Transition

Whether the transition to the “mast down” equilibrium (*i.e.* capsizes) occurs is determined by the sign of the arbitrary constant A , as the first term in Range 1 in solution (4) is unlimited (for non-zero A):

$$A = \frac{(\dot{\phi}_1 - \dot{p}_{01}) - \lambda_2(\phi_{m0} - p_{01} - \phi_v)}{\lambda_1 - \lambda_2} \quad (8)$$

$\dot{\phi}_1$ and ϕ_{m0} are initial conditions, and \dot{p}_{01} and p_{01} are values of particular solution (5) at the instant of crossing from Range 0 into Range 1. If $A > 0$, the transition occurs immediately, as illustrated in Figure 2. One can express the condition of transition in terms of the roll rate at the instant of upcrossing ϕ_{m0} :

$$\dot{\phi}_{cr} = \lambda_2(\phi_{m0} - p_{01} - \phi_v) + \dot{p}_{01} \approx -\lambda_2 \phi_v \quad (9)$$

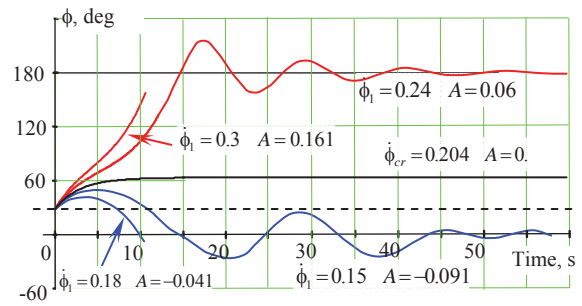


Figure 2: General solution of homogenous equation (2), the derivative values are expressed in rad/s

Values of a particular solution and its derivative at the instant of upcrossing are small and can be neglected. The dynamical system (4) is a repeller in Range 1, so resonance is impossible and the particular solution is small; see Figure 3. The same argument can be applied to the value of the derivative of the particular solution in Range 1 (Belenky, 1993).

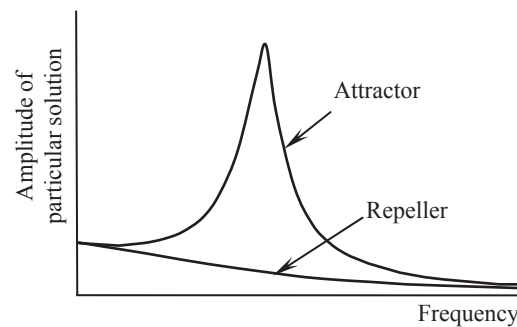


Figure 3: Amplitudes of frequency-domain response of attractor and repeller (Belenky *et al.*, 2008)

Thus, the random transition occurs whenever the process upcrosses the threshold ϕ_{m0} and its derivative exceeds the critical value (9) at the instant of upcrossing. Some upcrossings will result in the transition, while other will not. The transition can be seen as an upcrossing, with its rate reduced by the probability of the derivative's exceeding the critical value (9):

$$\xi_C = \xi_U(\phi_{m0}) \cdot P(\dot{\phi}_1 > \dot{\phi}_{Cr}) \quad (10)$$

where $\xi_U(\phi_{m0})$ is the upcrossing rate through the threshold ϕ_{m0} .

Formula (10) expresses the main idea of the split-time method. The complex problem of transition has been divided into two less complex problems: characterizing the upcrossing of the intermediate level (non-rare problem) and finding the probability of transition if the upcrossing has occurred (rare problem).

2.3 The Non-Rare Problem

The random transitions (capsizings) are expected to be rare. If one assumes that upcrossings of the threshold ϕ_{m0} are also rare, then influence from the general solution of the homogenous equation on Range 1 can be neglected. For this model, the process of the particular solution is normal and the rate of upcrossing can be expressed as:

$$\xi_U(\phi_{m0}) = \frac{1}{2\pi} \sqrt{\frac{V_{\dot{\phi}}}{V_{\phi}}} \exp\left(-\frac{\phi_{m0}^2}{2V_{\phi}}\right) \quad (11)$$

$V_{\phi} = V_{p0}$ and $V_{\dot{\phi}} = V_{\dot{p}0}$ are the variances of the particular solution and its derivative in Range 0, and can be found from formula (5):

$$V_{p0} = \sum_{i=1}^{N_{\omega}} p_{0i}^2 \quad ; \quad V_{\dot{p}0} = \sum_{i=1}^{N_{\omega}} \omega_i p_{0i}^2 \quad (12)$$

The calculation of these variances does not present a problem.

2.4 The Rare Problem

The difference between the observed and critical values of the derivative is the metric of the transition's likelihood. Since the critical value for the derivative is constant, it is only necessary to find the distribution of the value of the derivative at upcrossing. The original derivation was published in Appendix 3 of Belenky *et al.* (2008), while the abridged and updated version is given below.

The upcrossing event is defined as follows (Kramer and Leadbetter, 1967):

$$U = \begin{cases} \phi(t) < \phi_{m0} \\ \phi(t+dt) > \phi_{m0} \end{cases} = \begin{cases} \phi(t) < \phi_{m0} \\ \phi(t) > \phi_{m0} - \dot{\phi}(t)dt \end{cases} \quad (13)$$

The probability that U occurs at time t is

$$P(U) = \int_0^{\infty} \int_{\phi_{m0} - \dot{\phi}dt}^{\phi_{m0}} pdf(\phi, \dot{\phi}) d\phi d\dot{\phi} = dt \int_0^{\infty} \dot{\phi} \cdot pdf(\phi = \phi_{m0}, \dot{\phi}) d\phi d\dot{\phi} \quad (13)$$

$pdf(\phi, \dot{\phi})$ is the joint probability distribution function of the process and its derivative.

Consider a random event V such that:

$$V = \begin{cases} \dot{\phi}(t) \leq \dot{\phi}_1 \\ \dot{\phi}(t) > 0 \end{cases} \quad (15)$$

A random event that the events U and V occur simultaneously:

$$U \cap V = \begin{cases} \phi(t) < \phi_{m0} \\ \phi(t) > \phi_{m0} - \dot{\phi}(t)dt \\ \dot{\phi}(t) \leq \dot{\phi}_1 \\ \dot{\phi}(t) > 0 \end{cases} \quad (16)$$

The probability that U and V occur simultaneously at time t is:

$$\begin{aligned}
 P(U \cap V) &= \int_0^{\dot{\phi}_1} \int_{\phi_{m0}-\dot{\phi}t}^{\phi_{m0}} pdf(\phi, \dot{\phi}) d\phi d\dot{\phi} \\
 &= dt \int_0^{\dot{\phi}_1} \dot{\phi} \cdot pdf(\phi = \phi_{m0}, \dot{\phi}) d\dot{\phi}
 \end{aligned} \quad (17)$$

By definition, the Cumulative Distribution Function (CDF) is:

$$\begin{aligned}
 CDF(\dot{\phi}_1 | \phi_{m0}) &= P(\dot{\phi}(t) < \dot{\phi}_1 | \phi_{m0}) = \\
 \frac{P(V \cap U)}{P(U)} &= \frac{\int_0^{\dot{\phi}_1} \dot{\phi} \cdot pdf(\phi = \phi_{m0}, \dot{\phi}) d\dot{\phi}}{\int_0^{\infty} \dot{\phi} \cdot pdf(\phi = \phi_{m0}, \dot{\phi}) d\dot{\phi}}
 \end{aligned} \quad (18)$$

Differentiation of (18) yields the *pdf* of the derivative value at the instant of upcrossing:

$$pdf(\dot{\phi}_1 | \phi_{m0}) = \frac{\dot{\phi}_1 \cdot pdf(\phi = \phi_{m0}, \dot{\phi}_1)}{\int_0^{\infty} \dot{\phi} \cdot pdf(\phi = \phi_{m0}, \dot{\phi}) d\dot{\phi}} \quad (19)$$

If upcrossings are rare, the response process and its derivative can be assumed to be normal. This also means that they are independent, as the stationary process is not correlated with its first derivative and two uncorrelated normal processes are independent. Substitution of the normal distribution into (19) yields:

$$pdf(\dot{\phi}_1) = \frac{\dot{\phi}_1}{V_{\dot{\phi}}} \exp\left(-\frac{\dot{\phi}_1^2}{2V_{\dot{\phi}}}\right) \quad (20)$$

Formula (20) is the Raleigh distribution.

The distribution of the derivative at the instant of upcrossing is different from the distribution of the derivative in general. The distribution “in general” is obtained if the sampling is done in “any” (or random) instant. The instant of upcrossing of the primitive is not a random instant. A condition when the upcrossing is occurred is expressed by equation (13). Thus, the distribution of the derivative at

upcrossing is not equivalent to the distribution of the derivative “in general”.

Finally, the conditional probability of the transition after upcrossing has occurred is derived using equations (9) and (20):

$$P(\dot{\phi}_1 > \dot{\phi}_{Cr}) = \exp\left(-\frac{(\lambda_2 \phi_V)^2}{2V_{\dot{\phi}}}\right) \quad (21)$$

Equation (20) is the solution of the rare problem.

2.5 Probability of Rare Transitions

The combination of equations (10) and (20) yields the solution for the rate of rare random transitions:

$$\xi_c = \frac{1}{2\pi} \sqrt{\frac{V_{\dot{\phi}}}{V_{\phi}}} \exp\left(-\frac{1}{2} \left(\frac{\phi_{m0}^2}{V_{\phi}} + \frac{(\lambda_2 \phi_V)^2}{V_{\dot{\phi}}} \right)\right) \quad (21)$$

For the ship-like dynamical system with piecewise linear stiffness (Figure 1), the domain of attraction to the capsized equilibrium is larger than for the one with “mast up”. Thus, while the transition to capsized equilibrium is rare, the probability of transition in the opposite direction can be neglected. It is safe to assume that once transition has occurred, the dynamical system will stay capsized. That means that any two transitions are independent, as they must occur in two independent records. This means the transition meets the requirement of Poisson flow (Sevastianov, 1963, 1994), which leads to the following formula for the probability of transition (capsizing) during a given time T :

$$P(T) = 1 - \exp(-\xi_c T) \quad (22)$$

2.6 Summary of the Basic Theory

The original solution for random rare transitions in a dynamical system with



piecewise linear stiffness was found in the late 1980s (Belenky, 1993). It has been applied to the probability of capsizing of a ship in beam wind and seas (Paroka and Umeda, 2006; Paroka *et al.*, 2006). Some verification of self-consistency was carried out within the framework of the ONR project, which resulted in the refinement of the solution; the distribution of the derivative value at the instant of upcrossing was found to be Rayleigh (Belenky *et al.*, 2008).

The dynamical system with the piecewise linear stiffness likely represents the simplest model of a rare random transition between two stable equilibria. Nevertheless, considering this simple model, the following conclusions can be reached:

- A “critical derivative” (“critical roll rate”) can be defined as the value of the derivative which, if exceeded at upcrossing, inevitably leads to transition (capsizing)
- The difference between the observed and critical derivatives (roll rates) can be used as a metric of the likelihood of transition (capsizing)
- The rate of transitions (capsizings) can be defined as the rate of upcrossings of a maximum stiffness level in which the observed derivative (roll rate) exceeds the critical derivative (roll rate)
- The calculations of upcrossings and critical roll rate can be considered separately as non-rare and rare problems, respectively.

3. NUMERICAL EXTENSION OF THE BASIC THEORY OF RARE RANDOM TRANSITIONS

3.1 Toward a Time-Domain Solution

The dynamical system with piecewise linear restoring (2) yields a closed-form solution for the probability of random rare transition (21), which is the simplest mathematical model of a ship capsizing in

waves. Is it possible to apply the split-time method if a dynamical system is represented by a time-domain hydrodynamic simulation code?

The non-rare problem can be readily solved in the time domain, as long as the code can provide a sufficient statistical sample. If the intermediate threshold is set appropriately, one can count the upcrossings and estimate the upcrossing rate and an average number of events per unit of time.

The rare problem can also be recast in the time domain. If one assumes that roll stiffness of the dynamical system does not change in time and can be represented by the calm water GZ curve, then the critical roll rate can be found by an iterative set of numerical simulations. The calculations start at the intermediate level and the initial roll rate is perturbed for each run until capsizing is observed. The iteration scheme will create a picture similar to the one in Figure 2.

The distribution of the roll rate at upcrossing can be estimated statistically. Because capsizing is a rare event, the observed roll rates are expected to be smaller than the critical roll rate. The solution of the rare problem in the numerical case therefore involves statistical extrapolation, so only the tail of the distribution needs to be modeled. Generalized Pareto Distribution can be used for this purpose.

3.2 Numerical Non-Rare Problem

The non-rare problem will be solved using a set of time-domain simulations in “random” realizations of stationary irregular waves, which will typically be derived by discretizing an ocean wave spectrum into a set of component wave frequencies with pseudo-random phases. For the upcrossing rate to be estimated correctly, this model of wave excitation should be statistically representative for the duration of each record. To ensure this, the frequency set must be selected so as to

avoid a possible self-repeating effect (Belenky, 2011). Since long records require a very large number of incident wave frequencies to avoid this effect, it is generally more efficient to use a number of relatively short records – about 30 minutes each – than a smaller number of long records.

Following the approach developed for the model with piecewise linear stiffness, the level of the intermediate threshold is set to the maximum of the roll restoring (GZ) curve, where the slope of the curve becomes small enough that the corresponding instantaneous frequency does not support resonance under realistic wave excitation. Wave excitation will then add little energy to the dynamical system after this threshold is exceeded, which justifies the solution of the rare problem for the critical roll rate value without excitation, *i.e.* in clam water.

Once the non-rare simulations are completed, the upcrossing rate is estimated as:

$$\hat{\xi} = \frac{N_U}{N_T \Delta t} \quad (23)$$

N_U is the observed number of upcrossings, N_T is total number of data points in all records, and Δt is the time increment (data sampling rate), which is assumed to be the same for all records.

This estimate is a random number and requires an evaluation of statistical uncertainty. Assuming independence of upcrossings (for the purposes of statistical uncertainty assessment only), the occurrence of an upcrossing at a particular time step can be seen as a Bernoulli trial. The number of observed upcrossings then has a binomial distribution:

$$pmf(N_U) = \binom{N_T}{N_U} p^{N_U} (1-p)^{N_T-N_U} \quad (24)$$

p is a parameter of binomial distribution that has the meaning of the probability of a “success” (*i.e.* upcrossing) at a particular time increment. It can be estimated as:

$$\hat{p} = \frac{N_U}{N_T} \quad (25)$$

The boundary of the confidence interval corresponding to a confidence probability P_β can be computed as:

$$\hat{\xi}(low, up) = \frac{Q_{Bin}(0.5(1 \mp P_\beta) | \hat{p})}{N_T \Delta t} \quad (26)$$

Q_{Bin} is the quantile of the binomial distribution. Its calculation, however, may encounter numerical difficulties as the total number of points N_T may be large. If this is the case, a normal approximation of the binomial distribution can be used with the following variance estimate:

$$Var(\hat{\xi}) = \frac{\hat{\xi} \cdot (1 - \hat{\xi})}{N_T \Delta t} \quad (27)$$

The boundaries of the confidence interval are then expressed as:

$$\hat{\xi}(low, up) = \hat{\xi} \pm K_\beta \sqrt{Var(\hat{\xi})} \quad (28)$$

K_β is $0.5(1 + P_\beta)$ quantile of a standard normal distribution. Further details may be found in Belenky *et al.* (2008) and Campbell and Belenky (2010).

3.3 Numerical Rare Problem

As described above, the numerical solution of the rare problem starts with an iterative set of simulations with different initial conditions to compute the critical roll rate at upcrossing that leads to capsizing. These simulations must include an accurate calculation of the restoring at large roll angles.

The numerical solution of the rare problem was implemented using the Large Amplitude Motion Program (LAMP). LAMP is a mature hybrid time-domain code (Lin and Yu, 1990) incorporating a number of hydrodynamic modeling options of different fidelity.

Figure 4 shows a sample rare solution using a simplest option based on hydrostatics only solution (LAMP-0) with the following features:

- 3-D hydrostatics up to the instantaneous waterline
- Does *not* solve the wave-body disturbance problem
- “Tunable” terms for viscous damping and wave interaction effects (*e.g.* added mass)
- CPU time per 2.5-minute simulation: ~3 seconds.

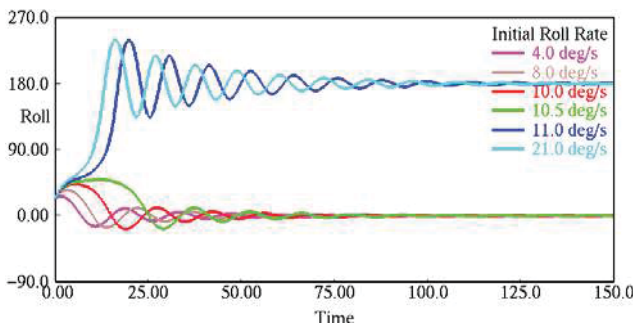


Figure 4: Calculation of critical roll rate via iterative numerical simulation (LAMP-0)

Figure 5 shows the next level of complexity: the approximate body-nonlinear solution (LAMP-2). LAMP-2 is characterized by the following features:

- 3-D hydrostatics up to the instantaneous waterline
- Solves the wave-body disturbance potential over the mean wetted hull surface
- “Tunable” damping terms for viscous effects
- CPU time per 2.5-minute simulation: ~2 minutes (Direct) or ~8 seconds (pre-computed impulse response functions for disturbance potential).

Figure 6 shows the complete body-nonlinear solution (LAMP-4), which is characterized by the following features:

- 3-D hydrostatics up to the instantaneous waterline

- Solves the wave-body disturbance potential over the instantaneous wetted hull surface
- “Tunable” damping terms for viscous effects
- CPU time per 2.5 minute simulation: ~3 hours.

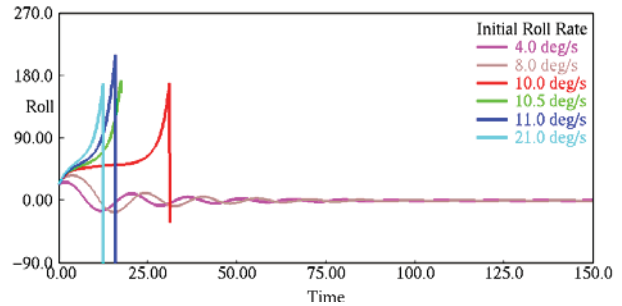


Figure 5: Calculation of critical roll rate via iterative numerical simulation (LAMP-2)

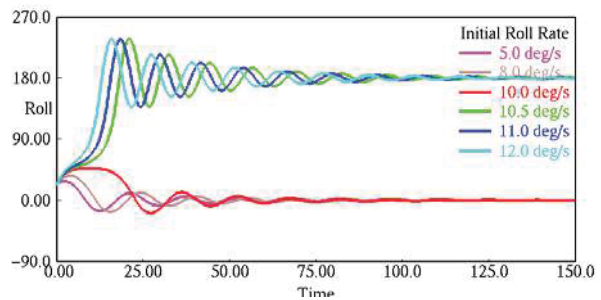


Figure 6: Calculation of critical roll rate via iterative numerical simulation (LAMP-4)

The next step in solving the rare problem is estimating the probability of capsizing after upcrossing. It is associated with exceedance of the critical value by the roll rate at the instant of upcrossing. Its distribution is not known, however, and must be modeled based on the time-domain results. If a good model were available for the joint distribution of roll and roll rate, formula (19) could be used to derive the distribution of the roll rate at the instant of upcrossing; however, no such model is available. Instead, one can attempt to directly model this distribution using the upcrossing data. As the critical roll rate is relatively large, only the tail of the distribution needs to be modeled. Since direct observation of capsizing is not expected, modeling the tail of the

distribution is, in fact, a statistical extrapolation problem.

The mathematical background of statistical extrapolation is based on two extreme value theorems (Coles, 2001):

- Fisher-Tippet-Gnedenko theorem states that the largest value of independent identically distributed (IID) random variables asymptotically tends to the Generalized Extreme Value (GEV) distribution
- Pickands-Balkema-de Haan theorem states that the tail of IID random variables can be approximated with the Generalized Pareto Distribution (GPD).

The *pdf* of the GPD is expressed as:

$$pdf(\dot{\phi}_1) = \begin{cases} \frac{1}{\sigma} \left(1 + k \frac{\dot{\phi}_1 - \mu}{\sigma} \right)^{-\left(1 + \frac{1}{k}\right)} ; \\ \text{if } \mu < \dot{\phi}_1, \quad k > 0, \quad \text{or} \\ \mu < \dot{\phi}_1 < \mu - \frac{\sigma}{k}, \quad k < 0 \\ \frac{1}{\sigma} \exp\left(-\frac{\dot{\phi}_1 - \mu}{\sigma}\right) ; \\ \text{if } \mu < \dot{\phi}_1, \quad k = 0 \end{cases} \quad (29)$$

k is the shape parameter, σ is the scale parameter, and μ is the threshold above which GPD is applicable.

These three parameters must be estimated in order to approximate the tail. Belenky *et al.* (2014) describes the technique for fitting the GPD for the more complex case that accounts for stability variation, which will be reviewed later in this paper. One can see that the constant stiffness is the particular case where the critical roll rate remains the same for each upcrossing. There seems to be no reason to believe that the fitting technique will not work for this particular case, as it worked for more general case.

The fitting procedure consists of the following steps (see Belenky *et al.* (2014) for details):

- Set a series of thresholds μ for the observed roll rates at upcrossing – this threshold is the value of the roll rate at which the GPD becomes valid (*i.e.* the start of the tail) and is not to be confused with the intermediate threshold for roll angle
- Use the log-likelihood method (Grimshaw, 1991) to find the estimate of shape and scale parameter for each threshold μ
- Using the Delta method, find variances and covariances of the shape and scale parameter for each threshold μ (Boos and Stefanski, 2013)
- Find the minimum threshold μ providing applicability of GPD, using techniques described in Coles (2001) and based on Reiss and Thomas (2007).

The probability of capsizing if the threshold μ is exceeded is then expressed as:

$$\hat{P}_1 = \begin{cases} \left(1 + \hat{k} \cdot \hat{\sigma}^{-1} \cdot (\dot{\phi}_{cr} - \mu) \right)^{-\hat{k}^{-1}} \\ \text{if } \hat{k} > -\frac{\hat{\sigma}}{\dot{\phi}_{cr} - \mu} \\ 0 \quad \text{otherwise} \end{cases} \quad (30)$$

The probability (30) is computed using estimates, which are random numbers, so the result of (30) is also an estimate and a random number. It can also be considered as the most probable value, because the scale and shape parameters were estimated with the log likelihood method, *i.e.* they are the most probable values for the parameters.

The next step is evaluating the confidence interval for the probability estimate (30). This is done by considering it as a deterministic function of random arguments. Assuming a normal distribution for the estimates of shape parameter and the logarithm of scale parameter (scale parameter is always positive), the

following formula was derived for the distribution of the estimate of probability of capsizing after upcrossing:

$$pdf_{P_1}(P_1) = \int_{-\infty}^{\infty} f_N \left(k, \frac{k(\dot{\phi}_{cr} - \mu)}{P_1^{-k} - 1} \right) \cdot \frac{k^2 P_1^{-k-1}}{(P_1^{-k} - 1)^2} (\dot{\phi}_{cr} - \mu) dk \quad (31)$$

where $f_N(k, \ln(\sigma))$ is a normal joint distribution of the shape parameter and the logarithm of the scale parameter. The boundaries of the confidence interval are computed with the quantiles of the distribution (31). The most probable value of P_1 may be zero; however, this does not necessarily mean that the upper boundary of the confidence interval is zero.

The GPD distribution approximates a tail of the distribution when it exceeds the threshold μ . Equation (31) therefore estimates a conditional probability under the condition that the threshold was exceeded, so the solution of the rare problem is expressed as:

$$\hat{P}(\dot{\phi}_1 > \dot{\phi}_{cr}) = \frac{N_{\mu}}{N_U} \hat{P}_1 \quad (32)$$

N_{μ} is the number of upcrossings when the roll rate has exceeded the threshold μ . The complete estimate of the capsizing rate is:

$$\hat{\xi}_C = \frac{N_U}{N_T \Delta t} \cdot \frac{N_{\mu}}{N_U} \hat{P}_1 = \frac{N_{\mu}}{N_T \Delta t} \cdot \hat{P}_1 \quad (33)$$

The number of upcrossings of the intermediate threshold has disappeared from equation (33). Thus, the choice of the intermediate threshold μ can only affect the independence of the upcrossings as a condition of the GPD's applicability.

The fraction in equation (33) is the estimate of the rate of events: upcrossings of the intermediate level when the roll rate has exceeded μ . The confidence interval of this estimate can be computed using formula (26), but N_U must be substituted N_{μ} :

$$\hat{\xi}_{\mu}(low, up) = \frac{Q_{Bin}(0.5(1 \mp P_{\beta 1}) | \hat{P}_{\mu})}{N_T \Delta t} \quad (34)$$

$$\hat{P}_{\mu} = \frac{N_{\mu}}{N_T}$$

$P_{\beta 1}$ is the “new” confidence probability; it reflects the fact that the estimate of capsizing rate is a product of two random numbers, each of which has its own confidence interval. As these numbers are independent,

$$P_{\beta 1} = \sqrt{P_{\beta}} \quad (35)$$

The confidence interval of the estimate P_1 must therefore use $P_{\beta 1}$ as a confidence probability:

$$\hat{P}_1(low, up) = Q_{P_1}(0.5(1 \mp P_{\beta 1})) \quad (36)$$

Q_{P_1} is the quantile of the distribution (29). Finally, the boundaries of the confidence interval for the capsizing rate estimate (33) are:

$$\begin{aligned} low(\hat{\xi}_C) &= low(\hat{\xi}_{\mu}) \cdot low(\hat{P}_1) \\ high(\hat{\xi}_C) &= high(\hat{\xi}_{\mu}) \cdot high(\hat{P}_1) \end{aligned} \quad (37)$$

3.4 Summary for the Numerical Extension of the Basic Theory

The numerical extension of the basic probabilistic theory of capsizing was published in Belenky *et al.* (2008), where most of the numerical problem's specifics were formulated. However, the problem of modeling the distribution of the roll rate remained without practical solution until the applicability of the GPD was fully appreciated (Belenky *et al.*, 2014).

The extension demonstrated that the split-time method is applicable for a dynamical system presented by an advanced hydrodynamic simulation code instead of an ordinary differential equation (ODE). The simplest numerical extension involves:

- Assuming that the roll stiffness of the dynamical system can be modeled by the GZ curve in calm water
- Finding the critical roll rate by a series of iterative simulations starting from an intermediate threshold with different rates; the critical roll rate is defined as the largest roll rate not leading to capsizing
- Modeling the tail of the distribution of roll rate at upcrossing with GPD
- Evaluating the statistical uncertainty for the estimates of upcrossing rate and probability of capsizing after upcrossing.

The transition to the numerical solution involves working with time-domain data and requires statistical methods to handle the results of numerical simulation, including the modeling of distributions and the assessment of statistical uncertainty.

4. BASIC THEORY OF RARE RANDOM TRANSITIONS WITH RANDOM STIFFNESS

4.1 Piecewise Linear System

The next step is to find out if the assumption of time-invariant stiffness may be abolished and if a solution can still be obtained in the simplest case with random stiffness. Consider the dynamical system (2), but with the stiffness in Range 1 now time dependent; its intercept is random, but the slope remains the same, as shown in Figure 7.

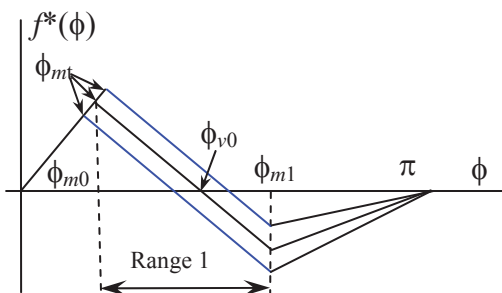


Figure 7: Time-variant piecewise linear stiffness

The variation of the stiffness in waves can be caused by the wave pass effect and ship motions. Both phenomena have certain inertia, so the parameters of time-varying stability are described by stochastic processes rather than random variables. Belenky *et al.* (2011) describes a simple mathematical model where the intercept in Range 1 is a linear function of heave:

$$\ddot{\phi} + 2\delta_{\phi}\dot{\phi} + \omega_{\phi}^2 f^*(\phi, \zeta_G) = f_{E\phi}(t) \quad (38)$$

ζ_G is the heave displacement modeled with a linear ODE. The boundary ϕ_m between Ranges 0 and 1 in equation (38) now depends on time. However, within Range 0 equation (38) is identical to equation (2). The difference caused by the stiffness variation in Range 1 makes equation (38) appear as follows:

$$\begin{aligned} \ddot{\phi} + 2\delta_{\phi}\dot{\phi} + \omega_{\phi}^2 k_{f1}\phi \\ = \omega_{\phi}^2 k_b \zeta_G(t) + \omega_{\phi}^2 k_{f1}\phi_{v0} + f_{E\phi}(t) \end{aligned} \quad (39)$$

- Coefficient k_b reflects the dependence of the intercept on the heave displacement ζ_G . The term containing ζ_G is the only difference between (39) and (2).

Taking into account that the slope coefficient k_{f1} has been taken with the opposite sign, equation (39) describes a repeller and its general solution is:

$$\begin{aligned} \phi(t) = A \exp(\lambda_1 t) + B \exp(\lambda_2 t) \\ + p_1(t) + \phi_{v0} \end{aligned} \quad (40)$$

The difference between solutions (40) and (4) in Range 1 is the particular solution that now includes the influence of the random variation of stiffness.

4.2 Condition of Transition

The homogenous part of equation (39) does differ from the homogenous part of equation (2) in Range 1, but the condition of transition at the instant of upcrossing t_1 is still the same:

$$A(t_1) > 0 \Rightarrow \dot{\phi}(t_1) > \dot{\phi}_{cr}(t_1) \quad (41)$$

The critical roll rate is still defined by the same formula (9), but the particular solution can no longer be neglected. As a result, the critical roll rate becomes a function of time, *i.e.* it is a stochastic process:

$$\dot{\phi}_{cr}(t) = \lambda_2(\phi_m(t) - p_1(t) - \phi_{v0}) + \dot{p}_1(t) \quad (42)$$

4.3 Non-Rare Problem

The boundary between Ranges 0 and 1 is now time-dependent, so it makes sense to formulate the non-rare problem for a difference between the boundary and the roll motion, introducing a new stochastic process:

$$x(t) = \phi(t) - \phi_m(t) + \phi_{m0} \quad (43)$$

Upcrossing of the process $x(t)$ through the threshold ϕ_{m0} makes the switch from Range 0 to Range 1.

The time-dependent boundary $\phi_m(t)$ is a linear function of the heave motion, which is also linear. A Fourier series presentation for $x(t)$ is available from Belenky *et al.* (2011), which allows the upcrossing rate to be expressed using formula (11):

$$\xi_U(\phi_{m0}) = \frac{1}{2\pi} \sqrt{\frac{V_{\dot{x}}}{V_x}} \exp\left(-\frac{\phi_{m0}^2}{2V_x}\right) \quad (44)$$

V_x and $V_{\dot{x}}$ are variances of the process $x(t)$ and its derivative.

4.4 Rare Problem

To formulate the rare problem, consider a difference between the critical roll rate and the instantaneous roll rate $y(t)$:

$$y(t) = \dot{\phi}_{cr}(t) - \dot{\phi}(t) \quad (45)$$

The process $y(t)$ is a linear combination of normal processes and can be presented with a Fourier series (Belenky *et al.*, 2011). The capsizing event is associated with a negative value of y at the instant of upcrossing. One therefore needs to find the distribution of the process $y(t)$ at the instant when the dependent process $x(t)$ has an upcrossing. The problem is similar to the one considered in Section 2.4, but instead of a derivative, a dependent process is considered.

To derive the distribution of the process $y(t)$ at the instant of upcrossing, consider a random event W :

$$W = (y(t) \leq y_c) \quad (46)$$

The events of U (defined by equation (13), but re-formulated for the process $x(t)$) and W occur simultaneously:

$$U \cap W = \begin{cases} x(t) < \phi_{m0} \\ x(t) > \phi_{m0} - \dot{x}(t)dt \\ \dot{x}(t) > 0 \\ y(t) \leq y_c \end{cases} \quad (47)$$

The probability that U and W occur simultaneously at time t is:

$$\begin{aligned} P(U \cap W) &= \int_{-\infty}^{\phi_{m0}} \int_{a-\dot{x}dt}^{\phi_{m0}} p df(x, \dot{x}, y) dx d\dot{x} dy \\ &= dt \int_{-\infty}^{\phi_{m0}} \int_0^{\infty} \dot{x} \cdot p df(x = \phi_{m0}, \dot{x}, y) d\dot{x} dy \end{aligned} \quad (48)$$

By definition, the CDF is:

$$\begin{aligned} CDF(y_c | \phi_{m0}) &= \frac{P(W \cap U)}{P(U)} \\ &= \frac{\int_{-\infty}^{\phi_{m0}} \int_0^{\infty} \dot{x} \cdot p df(x = \phi_{m0}, \dot{x}, y) d\dot{x} dy}{\int_0^{\infty} \dot{x} \cdot p df(x = \phi_{m0}, \dot{x}) d\dot{x}} \end{aligned} \quad (49)$$

Differentiation of (49) yields a *pdf* of the value of the dependent process at the instant of upcrossing:

$$pdf(y_c) = \frac{\int_0^{\infty} \dot{x} \cdot pdf(x = \phi_{m_0}, \dot{x}, y_c) d\dot{x}}{\int_0^{\infty} \dot{x} \cdot pdf(x = \phi_{m_0}, \dot{x}) d\dot{x}} \quad (50)$$

For the considered case of a dynamical system with piecewise linear term, all of the processes are normal and their mutual dependence is completely described by the appropriate covariance moments. This information is available as all of these processes are presented by Fourier series. The integrals in equation (50) can be evaluated symbolically:

$$pdf(y_c) = \frac{\sigma_{\dot{x}|y_c}}{\sqrt{2\pi}} \exp\left(-\frac{(m_{\dot{x}|y_c}(y_c))^2}{2\sigma_{\dot{x}|y_c}^2}\right) + \frac{m_{\dot{x}|y_c}(y_c)}{2} \left(1 - \operatorname{erf}\left(-\frac{m_{\dot{x}|y_c}(y_c)}{\sqrt{2}\sigma_{\dot{x}|y_c}}\right)\right) \quad (51)$$

- $m_{\dot{x}|y_c}$ and $\sigma_{\dot{x}|y_c}$ are the conditional mean and the conditional standard deviation of the derivative of the process $x(t)$ if the processes $x(t)$ and $y(t)$ took particular values. Note that the conditional mean is a function of the value of the process y at upcrossing, while the standard deviation is a constant; erf is the standard error function (see Belenky *et al.* (2013) for details).

The probability of capsizing after an upcrossing event is expressed as:

$$P(y_c < 0) = \int_{-\infty}^0 pdf(y_c) dy_c \quad (52)$$

Equation (52) completes the solution of the rare problem.

4.5 Probability of Rare Transitions

The final result of the rate of transitions (capsizes) can only be resolved using quadratures:

$$\xi_c = \frac{1}{2\pi} \frac{\sigma_{\dot{x}}}{\sigma_x} \exp\left(-\frac{\phi_{m_0}^2}{2\sigma_x^2}\right) \int_{-\infty}^0 f_c(y_c) dy_c \quad (53)$$

- σ_x and $\sigma_{\dot{x}}$ are the standard deviation of process x and its derivative.

Most of the basic theory of rare transitions with random stiffness was published in Belenky *et al.* (2010, 2011). The assumption of the independence of the process x and its derivative, which appeared in those publications, was abolished in order to obtain a more general solution (Belenky *et al.*, 2013, 2013a). The latter works also contain a closed-form solution to (51), which was not available in the earlier publications.

The main outcome of the basic study of rare transitions in dynamical system with random stiffness is that the critical roll rate becomes time variant and random as well. As part of this study, the distribution of the value of dependent process at the instant of upcrossing was derived.

5. NUMERICAL EXTENSION OF BASIC THEORY OF RARE RANDOM TRANSITIONS WITH RANDOM STIFFNESS

5.1 Towards a Time-Domain Solution

A comparison of a basic theory of random transition (Section 2) with its numerical extension (Section 3) shows a commonality in their approaches but some significant differences in technique. The understanding that numerical techniques may be quite different from the solution for the simpler piecewise linear system came from a number of

studies, where “theoretical” methods were attempted in a more direct way.

The calculation of instantaneous GZ curve in waves was described in Belenky and Weems (2008). Belenky *et al.* (2010) describe a method of tracking the maximum of the GZ curve in waves. However, an attempt to use the theoretical formula for upcrossing rate, as proposed in Belenky *et al.* (2008), showed a significant discrepancy from statistical estimates for stern quartering seas. This discrepancy was not observed in beam seas.

The reason for this discrepancy is the dependence between roll angles and roll rate in stern quartering seas (Belenky and Weems, 2012; Belenky *et al.*, 2013). The roll angles and rates are not correlated (see, for example, Bendat and Piersol, 1986). However, the absence of correlation means independence only for a normal process. Since large-amplitude roll motions may be not normal, independence cannot be assumed based on an absence of correlation. In this case, dependence can be characterized through the joint moments of higher order, say the fourth joint moment (covariance is the second joint moment). It is possible that the dependence is somehow related with stability variation in stern quartering seas, as it was not observed in beam seas.

The probabilistic properties of the elements of GZ curve in waves was found to be quite complex (Belenky and Weems, 2008). As a result, the modeling of a threshold distribution is difficult. Difficulty is further increased by the necessity to include all dependencies in order to get the joint distribution required in formula (50). Even if such a distribution fit is proposed, it may be reasonable only near the mean value, while the distribution needs to be evaluated on the tail. It was concluded that this approach did not offer a practical solution.

The difficulties fundamentally originated from the necessity to model tails of multi-dimensional distributions. These distributions

are needed for characterizing the values at the instant of upcrossing. Why not get this information directly from the simulated data?

This simple question has led to understanding that numerical methods may be quite specific and should be based on direct data analysis, *i.e.* statistics. This motivated a revision of the original work on the evaluation of probability of capsizing in beam seas. The description in Section 3 reflects the authors’ current understanding of how the problem should be handled, which has evolved significantly since its first publication in Belenky *et al.* (2008).

5.2 Numerical Non-Rare Problem

The formulation of the non-rare problem for the case of time-dependent stiffness is almost identical to the case of constant stiffness. However, the requirement of the independence of upcrossings can be removed. Dependent crossing events will be addressed as a part of rare problem as will be described in the next subsection. As a result, the choice of the intermediate threshold becomes a matter of computational efficiency only.

5.3 Numerical Rare Problem

The solution for a dynamical system with random piecewise stiffness has shown that the critical roll rate depends on time. To account for the stability changes in wave in the numerical case, the critical roll rate is calculated at each upcrossing, and the effect of the wave is included in the rare simulations. The calculations start from the instant of upcrossing; and roll rate is perturbed until capsizing is reached; see Figure 8.

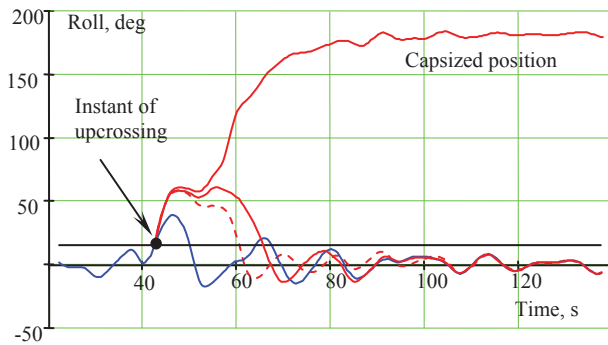


Figure 8: Calculation of critical roll rate

A detailed discussion of this algorithm, further referred as the Motion Perturbation Method (MPM), can be found in Spyrou *et al.* (2014). A particularly important point is how MPM is related to the definition of motion stability and the classic definition of ship stability given by Euler (1749). The result of the MPM calculation is a value of the metric of likelihood of capsizing (Belenky *et al.*, 2014):

$$y_i = 1 - \dot{\phi}_{Ui} + \dot{\phi}_{Cri}; \quad i = 1, \dots, N_U \quad (54)$$

- $\dot{\phi}_{Cri}$ is the critical roll rate calculated for the i^{th} upcrossing, and $\dot{\phi}_{Ui}$ is the roll rate observed at the i^{th} upcrossing.

The next step should be the GPD extrapolation of the metric y to find the probability of exceeding 1, which is the value associated with capsizing per equation (54). However, GPD requires independent data and the independence of upcrossings is no longer required when choosing the intermediate threshold. To resolve this, the dependence or independence of successive upcrossings must be determined.

If capsizing does not occur, the perturbed time history returns to the unperturbed state after some time (“time of convergence”); see Figures 9. If the next upcrossing occurs within this time of convergence, it is considered to be dependent. If the effect of perturbation has no further influence, the next upcrossing is considered to be independent; see Figure 9. The critical roll rate is calculated for all upcrossings, but only the largest value in each

set of dependent upcrossings is retained for further processing; see Spyrou *et al.* (2014) for further details.

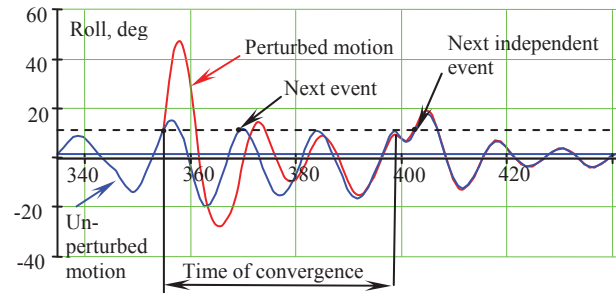


Figure 9: Dependent and independent upcrossings

The procedure for GPD extrapolation is similar to the constant stiffness case that was reviewed in Section 3.3. The only difference is that metric y is extrapolated and the target value associated with capsizing equals 1.

5.4 Initial Validation

As with any analytical method, validation is required if the method is to be put to practical use. But what would constitute validation of the split-time method of probability of capsizing? The split-time method is essentially the method of extrapolation; it is intended to evaluate the probability of capsizing based on a limited simulation data set. Thus, the validation of extrapolation is the more general question.

A statistical extrapolation method can be considered valid if its prediction is identical to value directly estimated from a sample. To do this, the sample must be large enough to support the estimation of the predicted event. To estimate the probability of capsizing, a sample must contain a number of capsizes so that the rate of capsizing can be estimated by direct counting. The extrapolation can then be applied to one or more small sub-samples of the data, each of which may or may not contain any capsizing events. If the estimates from the extrapolations and direct counting match, then the extrapolation method is valid.

While this idea seems straightforward, many issues need to be resolved to create a procedure of extrapolation. The development of this procedure is described by Smith and Campbell (2013), Smith (2014), and Smith *et al.* (2014) and summarized in Smith and Zuzick (2015). A key idea of the procedure is that the validation must be repeated systematically for the same condition in order to verify the confidence interval as well as for different speed, heading and wave environment in order to verify the robustness of the method.

Another question is how to get a sample that is large enough to capture such a rare event while retaining the essential nonlinear physics? For realistic wave conditions, millions of hours of simulation may be required to see capsizing. A particular problem is how to model stability variations in waves that play the central role in capsizing caused by pure loss of stability. ODE solvers may be fast enough to provide required simulation time, but ODE models may be quite questionable in terms of reproducing the stability variation.

For the present study, simulations were made with a 3 degree-of-freedom (heave, roll, pitch) time-domain simulation code which incorporates a novel volume-based calculation of the body-nonlinear Froude-Krylov and hydrostatic pressure forces. The algorithm is almost as fast as an ODE solver, but it captures the key features of the nonlinear wave forcing and restoring, allowing large, realistic irregular sea motion data sets to be generated. Description of the algorithm, implementation and verification is available from Weems and Wundrow (2013) and Weems and Belenky (2015).

The code was used to generate 1,000,000 hours of motion data for the ONR Topsides Tumblehome hull in random realizations of large, irregular stern quartering seas. 157 capsizes were observed, which allows a “true” value to be estimated. The split-time method was applied to 50 different sub-sets of the data, each of which consisted of 100 hours of data.

The observed and extrapolated capsizing rates, with confidence intervals, are plotted in Figure 10. The percentage of successful extrapolations is 96%, which is very close to 95% of confidence probability. Details of the validation can be found in Belenky *et al.* (2014).

5.5 Summary on the Numerical Extension of the Basic Theory for Random Stiffness

Numerical extension of the basic theory of random transition in a dynamical system with random stiffness was initially published in Belenky *et al.* (2013), with an exponential distribution as a model for the tail of the metric. Subsequent publications (Belenky *et al.*, 2014; Spyrou *et al.*, 2014) include the switch to GPD, which has led to a successful initial validation.

The development of this numerical extension can be summarized as follows:

- It is possible to estimate the probability of capsizing numerically without any assumption on roll stiffness
- The problem can be solved by GPD extrapolation of the metric of likelihood of capsizing (equation 54)
- The metric fully accounts for the nonlinearity of dynamical system; it contains a critical roll rate computed by perturbations
- The metric can be seen as an implementation of both the classical definition of ship stability and the general definition of motion stability
- Roll rate and angles may be dependent in stern quartering seas, while remaining uncorrelated.

The method has been successfully tested using a large volume of ship motion generated with a volume-based 3-DOF simulation code. This test provides a very promising but limited validation of the method, as the results of the 3-DOF simulation should be considered to be a

qualitatively rather than a quantitatively correct representation of ship capsizing. The numerical extension cannot be considered complete until

it has been fully implemented and validated with a more complete time-domain simulation code such as LAMP.

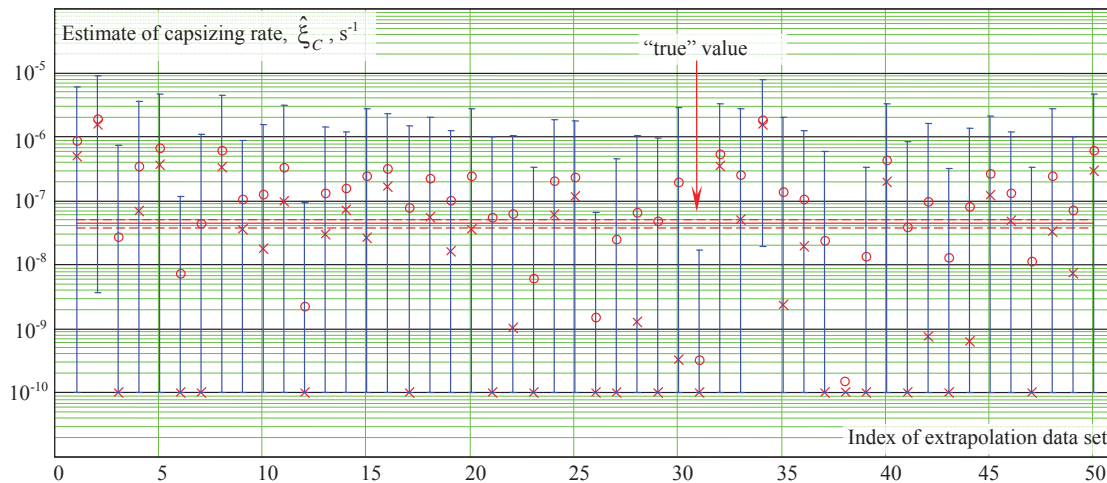


Figure 10: Results of initial validation performed for 50 validation data sets for ONR tumblehome

6. CONCLUSIONS AND FUTURE WORK

This paper has reviewed work under the ONR project “A Probabilistic Procedure for Evaluating the Dynamic Stability and Capsizing of Naval Vessels”. The review was limited to the results related to pure loss of stability, without consideration of effects from wind, surge, sway, or yaw. The main focus of the study was on the effect of random stability variations in waves. The research was reviewed in four following steps:

- Basic theory of rare random transitions
- Numerical extension of the basic theory of rare random transition
- Basic theory of rare random transition in a dynamical system with random stiffness
- Numerical extension of the theory of rare random transition in a dynamical system with random stiffness.

The result of the study is a procedure of physics-based statistical extrapolation using a limited data set from nonlinear time-domain numerical simulation. The procedure consists of the following steps:

- Prepare an extrapolation data set of simulation data; typically about 100 hours of total duration and consisting of a number of records approximately 30 minutes each
- Set an intermediate threshold providing a reasonable number (thousands) of upcrossings to be observed
- For each upcrossing, use perturbation simulations to find the critical roll rate leading to capsize, and then use the difference between the observed and critical roll rate to calculate the value of the metric of the likelihood of capsizing; then remove dependent data from the dataset
- Fit GPD with the metric data; evaluate the estimate of the capsizing rate and its confidence interval.

So far, this procedure has had a very limited validation for one condition and has not been fully implemented with LAMP or other advanced hydrodynamic code. The following are the next steps in the development of the method:



- Bring the validation to reasonable completion by considering more conditions
- Address implementation issues related with the consideration of 6 DOF in the solution of the non-rare and rare problems
- Consider the inclusion of hydrodynamic diffraction and radiation forces in the solution of the rare problem.

7. ACKNOWLEDGEMENTS

The work described in this paper has been funded by the Office of Naval Research, under Dr. Patrick Purtell, Dr. Ki-Han Kim, and Dr. Thomas Fu. The authors greatly appreciate their support.

Over the years of the development, many colleagues have influenced and contributed to our work. The authors would like acknowledge Prof. Pol Spanos (Rice University), Dr. Art Reed, Mr. Tim Smith, Mr. Brad Campbell (NSWCCD, David Taylor Model Basin), Prof. Kostas Spyrou (National Technical University of Athens), and Profs. Ross Leadbetter and Vlas Pipiras (University of North Carolina Chapel Hill).

The participation of Prof. Pipiras was facilitated by the Summer Faculty Program supported by ONR and managed by Dr. Jack Price (NSWCCD, David Taylor Model Basin).

8. REFERENCES

- Belenky, V. L. 1993, "A Capsizing Probability Computation Method", J. Ship Research, Vol. 37, pp. 200- 207.
- Belenky, V. and Weems K. M. 2008, "Probabilistic Qualities of Stability Change in Waves", Proc. 10th Intl. Ship Stability Workshop, Daejon, Korea, pp. 95-108.
- Belenky, V. L., Weems, K. M., and Lin, W.-M. 2008, "Numerical Procedure for Evaluation of Capsizing Probability with Split Time Method", Proc. 27th Symp. Naval Hydrodynamics, Seoul, Korea.
- Belenky, V. L., Weems, K. M., Lin, W.-M., and Spyrou, K. J. 2010, "Numerical Evaluation of Capsizing Probability in Quartering Seas with Split Time Method", Proc. 28th Symp. Naval Hydrodynamics, Pasadena, California, USA.
- Belenky, V., Reed, A.M., and Weems K. M. 2011, "Probability of Capsizing in Beam Seas with Piecewise Linear Stochastic GZ Curve", Chapter 30 of "Contemporary Ideas on Ship Stability", edited by M.A.S. Neves, V. L. Belenky, J. O. de Kat, K. Spyrou, and N. Umeda, Springer, pp. 531-554.
- Belenky, V. L. 2011, "On Self-Repeating Effect in Reconstruction of Irregular Waves", Chapter 33 of "*Contemporary Ideas on Ship Stability*", edited by M.A.S. Neves, Belenky, J. O. de Kat, K. Spyrou, and N. Umeda, Springer, pp. 589-598.
- Belenky, V., and Weems, K. 2012, "Dependence of Roll and Roll Rate in Nonlinear Ship Motions in Following and Stern Quartering Seas", Proc. 11th Intl. Conf. on Stability of Ships and Ocean Vehicles (STAB 2012), Athens, Greece, pp. 59-66.
- Belenky, V., Weems, K. M., and Pipiras, V. 2013, "Split-time Method for Calculation of Probability of Capsizing Due to Pure Loss of Stability", Proc. 13th Intl. Ship Stability Workshop, Brest, France, pp. 70-78.
- Belenky, V., Spyrou, J., Weems, K. M., and Lin W.-M. 2013a, "Split-time Method for the Probabilistic Characterization of Stability Failures in Quartering Waves", Intl. Shipbuilding Progress, Vol. 60, No. 1-4, pp. 579-612.
- Belenky, V., Weems, K., Campbell, B., and



- Pipiras, V. 2014, "Extrapolation and Validation Aspects of the Split-Time Method", Proc. 30th Symp. Naval Hydrodynamics, Hobart, Tasmania, Australia.
- Bendat, J. S., and Piersol, A.G., 1986, *Random Data: Analysis and Measurement Procedures*, 2nd edition, New York: John Wiley & Sons.
- Boos, D. D. and Stefanski L. D. 2013, *Essential Statistical Inference: Theory and Method*, Springer.
- Campbell, B. and Belenky, V. 2010, "Assessment of Short-Term Risk with Monte-Carlo Method", Proc. 11th Intl. Ship Stability Workshop, Wageningen, Netherlands, pp. 85-92.
- Coles, S. 2001, *An Introduction to Statistical Modeling of Extreme Values*. London: Springer-Verlag.
- Euler, L. 1749, *Scientea Navalis*, St.Petersburg, Russia.
- Grimshaw, S. D. 1991, "Calculating Maximum Likelihood Estimates for the Generalized Pareto Distribution", Proc. 23rd Symp. Interface of Computing Science and Statistics, Seattle, Washington, USA, pp 616-619.
- Kramer, H., and Leadbetter, M. R. 1967, *Stationary and Related Stochastic Processes*, New York: John Wiley.
- Lin, W.-M., and Yue, D.K.P. 1990, "Numerical Solutions for Large Amplitude Ship Motions in the Time-Domain" Proc. 18th Symp. on Naval Hydrodynamics, Ann Arbor, Michigan, USA, pp. 41-66.
- Paroka, D., Okura, Y., and Umeda, N. 2006, "Analytical prediction of capsizing probability of a ship in beam wind and waves", J. Ship Research, Vol. 50, No. 2, pp. 187-195.
- Paroka, D. and Umeda, N. 2006, "Capsizing probability prediction of the large passenger ship in irregular beam wind and waves: comparison of analytical and numerical methods" J. Ship Research, Vol. 50, No. 4, pp. 371-377.
- Reiss, R.-D., and Thomas, M. 2007, *Statistical Analysis of Extreme Values with Application to Insurance, Finance, Hydrology and Other Fields*, 3rd Edition, Basel: Birkhäuser Verlag.
- Sevastianov, N. B. 1963, "On Probabilistic Approach to Setting Stability Standards". Trans. of Kaliningrad Institute of Technology, Vol. 18 (in Russian).
- Sevastianov, N. B. 1994, "An Algorithm of Probabilistic Stability Assessment and Standards", Proc. 5th Intl. Conf. on Stability of Ships and Ocean Vehicles (STAB 1994), Melbourne, Florida, USA, Vol. 5.
- Smith, T. C. and Campbell, B. L. 2013, "On the Validation of Statistical Extrapolation for Stability Failure Rate" in Proc. of 13th Intl. Ship Stability Workshop, Brest, France, pp. 79-87.
- Smith, T. C., Campbell, B. L., Zuzick, A. V., Belknap, W. F., and Reed, A. M. 2014, "Approaches to Validation of Ship Motion Predictions Tools and Extrapolation Procedures for Large Excursions of Ship Motions in Irregular Seas" in Computational Stochastic Mechanics – Proc. of the 7th Intl. Conference (CSM-7), edited by G. Deodatis and P. Spanos, Santorini, Greece.
- Smith, T. C. 2014, "Example of Validation of Statistical Extrapolation," in Proceedings of the 14th Intl. Ship Stability Workshop, Kuala Lumpur, Malaysia.
- Smith, T. C., and Zuzick, A. 2015, "Validation of Statistical Extrapolation Methods for Large Motion Prediction" in Proc. 12th Intl. Conf. on Stability of Ships and Ocean Vehicles (STAB 2015), Glasgow, UK.



Spyrou, K. J., Belenky, V., Reed, A., Weems, K., Themelis, N., and Kontolefas, I. 2014, “Split-Time Method for Pure Loss of Stability and Broaching-To”, Proc. 30th Symp. Naval Hydrodynamics, Hobart, Tasmania, Australia.

Weems, K., and Wundrow, D., 2013, “Hybrid Models for Fast Time-Domain Simulation of Stability Failures in Irregular Waves with Volume-Based Calculations for Froude-Krylov and Hydrostatic Forces”, Proc. 13th Intl. Ship Stability Workshop, Brest, France.

Weems, K. and Belenky, V. 2015, “Fast Time-Domain Simulation in Irregular Waves With Volume-Based Calculations for Froude-Krylov and Hydrostatic Force” in Proc. 12th Intl. Conf. on Stability of Ships and Ocean Vehicles (STAB 2015), Glasgow, UK.

Session 11.2 – NAVAL SHIP STABILITY

Beyond the Wall

Exploration of the Probabilities of Extreme Roll of Naval Vessels

**Comparative Stability Analysis of a Frigate According to the Different
Navy Rules in Waves**

**Towing Test and Motion Analysis of a Motion-Controlled Ship - Based
on an Application of Skyhook Theory**

This page is intentionally left blank



Beyond the Wall

Richard Dunworth, *Department of Defence, Australia* richard.dunworth@defence.gov.au

ABSTRACT

Inaccuracy in evaluation of inclining experiments by the application of the wall-sided concept was discussed by Dunworth (2014). KG can be significantly underestimated for V-bottomed hull forms when relying on GM to evaluate inclining experiments. A solution was proposed which derived KG and TCG to align heeling and righting moments without reference to the metacentre.

Looking beyond the theory, this paper describes practical model testing to explore the accuracy of the new method, reviews experiences in its use by the Australian Department of Defence and offers guidance in its application.

Keywords: *Stability; Inclining; Metacentre; Wall-sided*

NOMENCLATURE

Δ	Displacement of the system (ship plus inclining masses) (t)	KN	Righting arm about the origin (m)
d	Distance of inclining mass shift (m)	KN_0	Righting arm about the origin when upright (m)
φ	Angle of heel (degrees)	TCB_0	Transverse centre of buoyancy when upright (m)
GG'	Shift of centre of gravity (m)	TCG	Transverse centre of gravity (m)
GM_0	Transverse metacentric height when upright (m)	TCG_0	Estimated transverse centre of gravity when in upright equilibrium (m)
GZ	Righting arm (m)	TCG_1	Estimated transverse centre of gravity of the system with inclining masses in their initial position (m)
GZ'	Righting arm corrected for TCG_1 (m)	w	Inclining mass (t)
HZ	Heeling arm (m)		
HZ_0	Heeling arm when upright (m)		
KG	Height of vertical centre of gravity above baseline (m)		
KG_1	Estimated height of vertical centre of gravity above the origin, in global coordinates, with inclining masses in their initial position (m)		
KG_L	Estimated height of vertical centre of gravity above baseline, in local (ship) coordinates, with inclining masses in their initial position (m)		
KM_0	Height of transverse metacentre above baseline (m)		

1. INTRODUCTION

The concept of an inclining experiment was first proposed by Hoste (1697), a professor of mathematics at the Royal Naval College in Toulon, France. However it was nearly fifty years before a practical method of conducting an inclining experiment was described by Bouguer (1746).

The traditional calculation associated with an inclining experiment led directly to a value of GM_0 and, as this was the primary measure of



stability, it was not necessary to know KG itself until the development of the concept of GZ . By that time, Bouguer's calculation method was well established and continues to be used to this day.

Growth in displacement and KG is common on naval ships. Communication, navigation and armament equipment increase with time and tend to be placed high up. Conversely, when heavy machinery low down in the ship is upgraded, it is often replaced with more efficient, lighter equipment. Without compensation, these effects almost guarantee that KG will rise over time. Growth must be captured and updated regularly in the stability information provided to ships.

For RAN ships, stability is managed by comparison of a load condition's KG with a curve of limiting KG . If KG has been over-estimated, then unnecessary operational restrictions may result but, if KG has been under-estimated, then the vessel may be at risk if it encounters the environment and/or damage which underlie the curve of limiting KG .

The lightship characteristics of RAN ships are regularly checked by inclining experiments with the interval determined by the expected time before any standard load condition will exceed the limiting KG , due to growth. Over the whole fleet, there is about one ship checked every three or four months.

Although there is ample guidance available on the conduct of an inclining, Administrations rarely, if ever, prescribe the method of deriving KG from the recorded data.

2. THE CLASSIC METHOD

2.1 Relying on the Metacentre

It has previously been assumed that the metacentre does not move significantly at small angles of heel. On this premise, the wall-sided

concept has been used to derive GM from inclining experiment results using the relationship:

$$GM = \frac{w d}{\Delta \tan \varphi} \quad (1)$$

and KG is then calculated as:

$$KG = KM - GM \quad (2)$$

The derivation of GM is most commonly performed by fitting a line of best fit (trendline) through the plot of $w d$ against $\Delta \tan \varphi$. GM is then equal to the slope of that trendline.

2.2 The Moving Metacentre

Even for a wall-sided ship, the metacentre moves at small angles of heel and, for some hull forms, the movement is significant. Where a hull has a relatively shallow V-bottom over a significant proportion of its length, reliance on GM for determining KG is unsafe.

3. THE NEW METHOD

3.1 Balancing Heeling and Righting Arms

The new method recognises that, after each weight move, the vessel is in equilibrium and that there must be a righting arm, GZ , equal and opposite to the heeling arm HZ developed by the shift of inclining weights. With the vessel's trim and displacement known from draught readings, it is possible to calculate the corresponding value of KN for each weight move. GZ is derived from KN by the relationship:

$$GZ = KN - KG \sin \varphi - TCG \cos \varphi \quad (3)$$

In the absence of experimental error, there is a pair of unique values for TCG and VCG which will result in values of GZ for each heel which exactly match the corresponding HZ

values. Similarly, even when there are experimental errors present, there will be a pair of unique values for TCG and KG which will result in the trendlines through HZ and GZ against heel being coincident. When close to upright, TCG can be considered to raise or lower the trendline, while VCG skews the trendline about zero heel.

A method for deriving TCG and KG has been proposed (Dunworth, 2014) and is briefly described below.

3.2 The Solution for TCG_I

When $\varphi = 0$, $\sin\varphi = 0$ and $\cos\varphi = 1.0$, so Equation 3 reduces to:

$$HZ_0 = KN_0 - TCG_I \quad (4)$$

Equation 4 can be re-arranged to give a solution for TCG_I :

$$TCG_I = KN_0 - HZ_0 \quad (5)$$

KN_0 is identical to TCB_0 and could therefore be found from upright hydrostatics. However, it is more convenient to calculate KN_0 with the other KN values which will be required. KN_0 can be expected to be close to zero, but will only be exactly so if both hull and appendages are truly symmetric about the centreline. The actual value should generally be calculated.

HZ_0 can be found from the trendline through the HZ points when plotted against heel angle and is the value of HZ when heel = 0, i.e. the intercept of the trendline.

A third-order polynomial trendline should be used because it can closely match non-linear data sets which include a point of inflection - which generally occur near equilibrium in GZ plots.

When there is known to be a discontinuity in GZ within the range of heels at the inclining

experiment, the points should be divided into two sets, either side of the discontinuity, and only the set which spans upright used to determine HZ_0 . If the discontinuity is exactly at upright, both sets may be used and HZ_0 taken to be the mean of the two intersections.

3.3 The Solution for KG_I

Equation 3 can be re-arranged as:

$$KG_I \sin\varphi = KN - HZ - TCG_I \cos\varphi \quad (6)$$

and the solution for KG_I is therefore:

$$KG_I = \frac{KN - HZ - TCG_I \cos\varphi}{\sin\varphi} \quad (7)$$

For each mass move, $KG_I \sin\varphi$ (from Equation 6) is plotted against $\sin\varphi$. All points should lie on a straight line and the value of KG_I is then equal to the slope of the linear line of best fit through the points.

KG_I is a vertical measure and, to account for trim, G_I will need to be rotated about the ship's origin to give VCG in ship coordinates.

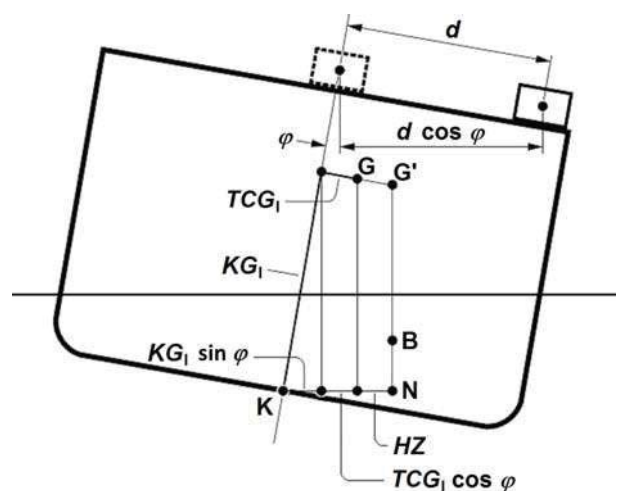


Figure 1 Illustration of Equation 6

4. VALIDATING THE NEW METHOD BY MODEL TESTING

4.1 Selection of the Hull Form

As part of the validation process for the new method, a scale model of a hull section was built and tested. The model was sized to fit into an existing trough used for teaching inclining experiments and was a practical size and weight to handle. As will be shown, there was sufficient difference between KG s calculated by the two methods for the result to be conclusive and not lost within variations caused by experimental error.

Being representative of a hull section only, the model is considerably wider than it is long with a beam of 1.2 m and length of only 0.3 m. Details are shown in Table 1 and Figure 2.

Table 1 Model particulars

Length	0.3 m
Beam	1.2 m
Displacement	17.560 kg
Inclining weight	3.098 kg
KM_0	1.073 m
Forward pendulum length	1086.35 mm
Aft pendulum length	1085.25 mm

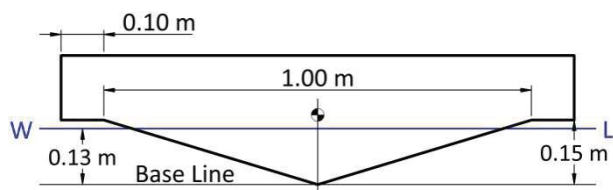


Figure 2 Model section

The model is not intended to accurately reflect any particular vessel, with the shape having been chosen specifically to demonstrate the difference in results between the classic and new methods. It is, however, geometrically similar to a section through the aft portion of the small aluminium survey boats operated by RAN.

On one occasion, one of these craft was presented for inclining with a list of just under three degrees. This would not normally be acceptable, in part because of the unreliability of tank dips at that angle, but it was decided to proceed with the experiment so that the results could be used in planning appropriate remedial measures. A heel of over two degrees each way was developed, but the vessel never came upright during the experiment. This inclining is of interest and will be referred to later at 5.5.

4.2 Model Construction

The model was of plywood construction and subsequent measurements showed it to be generally quite accurate.

Aluminium angle rails, forward and aft, were pre-drilled at 50 mm centres out to 550 mm either side of the centreline. This allowed quick and accurate movement of the inclining weight without having to measure the shift at each weight move and also provided a secure mounting for a pair of ballast weights.



Figure 3 Model Arrangement

The ballast weights were suspended on threaded rods and could be wound up and



down to vary *KG*. A disadvantage of this arrangement is that two pairs of the pre-drilled holes were occupied by the ballast and were therefore not available for inclining weight shifts. Ballast was chocked to prevent any movement.

To date, only one set of readings has been taken: at a single displacement and with ballast in its lowest position.

As ballasted, the model floated close to level trim (0.07°) and heel (0.05°) with the chine flat about 19 mm clear above the waterplane. The chine outer edge touched the waterplane at a heel of 1.9 degrees and the chine flat was completely immersed beyond 2.2 degrees. The significance of the small trim was not realised until the inclining results were analysed and is discussed later at 5.1.

4.3 Determining the Model Weight

An unexpected difficulty came with the determination of the model weight.

For the first measurement, a pair of scales, each with an upper limit of 5 kg, was used to weigh the bare hull and individual components. It was immediately apparent that the two scales gave different readings, but there was no way of determining which, if either, was correct.

A second measurement was taken by measuring the rise of water in the trough; from the trough dimensions and water density (0.9985 kg/l), the weight of the model could be calculated. Once the model was in the trough, the depth of water and height to gunwale were used to determine the freeboard at each corner. Both methods required measurement of water depths, but the height of the meniscus where the water surface met the measuring scale was difficult to determine. This was a concern as the effect of change of draught for the model is about 0.265 kg/mm.

A set of as-built offsets was lifted so that a new numerical model could be generated and the results re-worked.

Finally, a larger set of scales was used to weigh the entire model. Although the scales were not calibrated, this was thought likely to be the most accurate measurement and differs by less than 0.5 percent from the mean value of 17.560 kg which was taken to be the model weight for calculation purposes. Results are shown in Table 2.

Table 2 Results of the methods used to determine model weight

Method	Weight
Weigh parts	17.473 kg
Weigh whole	17.575 kg
Freeboards	17.928 kg
Draughts	17.223 kg
Displaced volume	17.698 kg
Mean weight	17.560 kg

4.4 Establishing *KG*

Six strong points were incorporated in the model to allow it to be freely suspended from a spreader bar, via solid wire strops, onto large washers; pendulums were hung from the same points – see Figures 4 and 5. On one face, all three pendulum lines intersected at a single point: on the other, they formed a very small triangle or ‘cocked hat’.

Values forward and aft of 162.0 mm and 161.5 mm respectively were found and the mean value of 161.75 mm was taken to be the model *KG*.

4.5 Inclining the Model

By sighting across the two pendulums, both during the measurement of *KG* and during the inclining at each weight move, parallax errors in the readings were minimised. All readings were photographed for later analysis. A short video of each would have been useful as it



Figure 4 Establishing KG by suspension

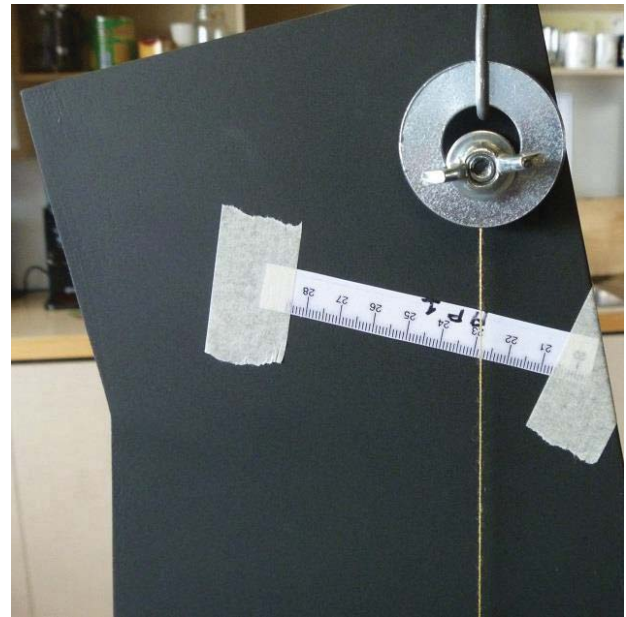


Figure 5 Suspension point detail

would have shown the extent of any movement at pendulum readings.

The inclining weight was then moved progressively along the rails with pendulum readings taken at each move. In addition to the pre-determined positions, the weight was also placed as close as practicable to either side of each ballast weight (moves 11, 12, 14 & 15), and the positions measured, to give additional readings close to upright.

In analysing the results, deflections were normalised to the respective mean zero readings. The full set of inclining readings is shown in Table A-1.

For the classic workup, $w d$ and $\tan\phi$ are calculated and the derived data over all weight moves is included in Table A-1.

Table A-2 shows the derived data for the new method over all weight moves. There was a small initial list of 0.054 degrees measured by freeboards. This was added to each heel determined by pendulum deflection to give actual heels. KN s were then calculated from the numerical hull mesh model.

5. INTERPRETING THE MODEL TEST RESULTS

5.1 Balancing Heeling and Righting Arms

The concept of the new method is based on heeling and righting arms being equal after each weight shift. Knowing KG_1 , upright TCG_1 can be calculated and a set of righting arms developed from the KN values. These righting arms are, in effect, GZ values shifted to take account of TCG_1 . The comparison between experimental heeling arms and calculated righting arms is included in Table A-2.

It can be seen that the greatest differences occur at weight moves 9 and 17. These are symmetrical port and starboard and it is possible that they resulted from the small initial trim. This would have caused the low corners of the chine flats to touch the water surface early, generating small additional righting moments at those weight moves.

The use of readings with large differences between heeling and righting arms should be avoided in further calculations if practicable.

5.2 Simulating Actual Inclining Experiments

The full data set was analysed, together with four combinations of weight moves to represent inclining experiment scenarios. Not all sets use the same number of weight moves.

5.3 Case 1: Full Data Set

Using the full set of results the new method gives an accurate KG of 0.162 m. Despite a high coefficient of determination of 0.998, the classic method is significantly in error with KG of 0.010 m. See Figure 6 and Table 3.

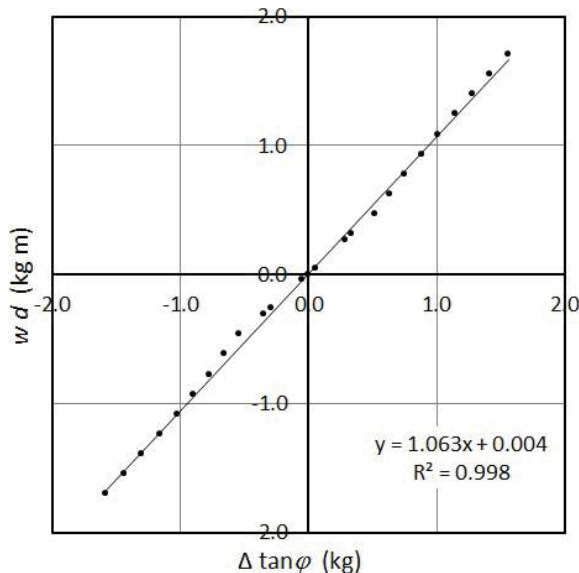


Figure 6 Plot of full data set $w d$ vs. $\Delta \tan \phi$

Table 3 Results using the full data set

Classic – Full Set		New – Full Set	
GM_0 (m)	1.063	TCG_1 (m)	0.001
KG_1 (m)	0.010	KG_1 (m)	0.162

5.4 Case 2: Typical

A typical set of inclining results can be selected with a heel range a little over two degrees each way. Results are shown in Table A-3. KG by the new method is 2 mm low, but significantly better than by the classic method.

5.5 Case 3: Large Initial List to Port

A set can be selected which is similar to the inclining experiment on the survey boat described previously at 4.1. TCG is known to be -0.053 m from the inclining weight shift at the initial state (move 20) and values for the classic method have been adjusted to reflect this.

The resulting KG is 0.163 m by the new method (1 mm error) with TCG slightly in error at -0.050 m. The small error in TCG may be caused by extrapolation of the trendline through HZ vs. Heel to obtain the intersection at upright. KG is -0.063 m by the classic method – placing the centre of gravity below the baseline. Results are shown in Table A-4.

The fact that the classic method can give a negative KG , well below the underside of keel, is alarming – though hopefully would not go unnoticed.

5.6 Case 4: Restricted Heel

It has been pointed out that, since the new method relies on division by $\sin \phi$, the results can be erratic when measurement of heels close to upright is not completely accurate. When calculating individual results, division by zero would occur at upright.

This is not an issue with a reasonable range of heels to either side of upright. By using the slope of a trendline, values close to the mean have little effect as they tend to shift, rather than skew, the line of best fit. However a set of inclining values over a small range near upright may cause a problem. In fact, the model test shows a good result by the new method, even with less than one degree heel to either side of upright.

Though still a little low, the result for the classic method is almost correct – as would be expected with such a small range of heel. Results are shown in Table A-5.

5.7 Case 5: One Extreme Heel Close to Upright

Division by $\sin\phi$ may also result in error if one of the extreme heels is close to upright.

The current set of model results cannot be used to reliably illustrate the problem. Upright was the starting point for model readings and the mean of three readings (0, 13 & 26) gives better accuracy than would be expected in practice. Results in Table A-6 show that the new method has an error of 2 mm but, as in Case 3, the classic method gives a nonsensical result with KG below the baseline!

5.8 Summary of the Simulation Cases

Figure 7 shows the KG s for the five cases by each method. The horizontal line is at the KG found by suspending the model. Clearly the new method is the more reliable for this model.

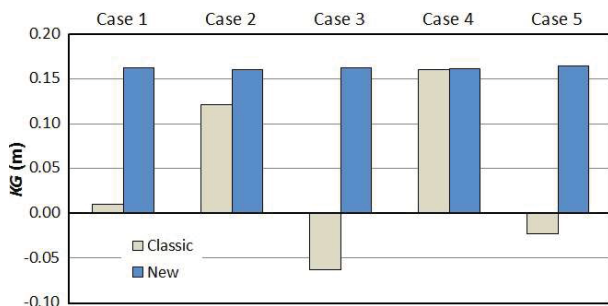


Figure 7 Comparison of inclining simulations

6. GENERAL OBSERVATIONS

6.1 Discarding Readings Near Upright

The new workup method benefits from values near upright for calculating TCG but, in the subsequent calculation of KG , there may be justification for discarding any readings with the vessel close to upright unless good accuracy in the measurements of those heel angles can be assured.

6.2 Measuring Pendulum Deflections

The problem of measuring small pendulum deflections can be overcome to some extent by the use of longer pendulums. However, these can often fail to settle at a measurable point and are influenced by ship movement transmitted through the pivot point. The practice of hanging pendulums high in the ship is not helpful and, wherever practicable, they should be low down with the pivot point close to the waterline for best results.

Damping of the pendulum bob in a trough of viscous fluid will assist. In the past, DNPS has recommended the use of spent oil as a damping medium, but now advocates the use of a thin wallpaper paste – about 5 g/l. This has several advantages: it is readily available, light (it can be taken in powder form to the inclining) and, being basically starch, is more environmentally friendly. There are no special precautions or equipment required for disposal.

7. EXPERIENCES WITH THE NEW METHOD

7.1 Applying the New Method

RAN generally employs contractors to conduct inclining experiments and to produce the associated reports. Since the use of the new workup method was introduced in 2013, a number of inclining experiments have been conducted on RAN ships and the new method used with varying degrees of success.

Some contractors have chosen to use the resources of DNPS to provide the as-inclined characteristics, but several have used the new method for themselves. DNPS offers an Excel spreadsheet which will perform the necessary calculations.

Apart from KN s, the data input required is the same as for the classic method.



7.2 Generating *KN* Values

The calculation of *KN* values is clearly an issue. Few contractors hold good numerical models of our ships and even those who do so are not necessarily able to produce *KNs* at the specific heel angles, and to sufficient accuracy, to be of use.

One solution has been to provide *KN* data tabulated at fine intervals of heel, trim and volume which can be interrogated by linear interpolation. Volume is used rather than displacement as it is independent of the water density at the time of the inclining experiment. Considerable effort has gone into determining how fine the intervals need to be and experience has shown that the requirements are specific to each hull form. To date, no general rules have been found which will enable the intervals to be determined by simple inspection of the hull characteristics.

8. CONCLUSIONS

Although some issues, particularly the generation of accurate *KN* values, need to be resolved before the new method can be readily and universally applied, the practical model inclining has shown how robust and versatile it is. By comparison, on only one occasion did the classic method come closer than 0.04 m (25%) to the correct *KG* in the scenarios which were simulated for this particular model.

It has been clearly demonstrated that this is a superior method for application to non-wall-sided hull forms, even when they are inclined to extreme angles, and its adoption is strongly recommended.

9. ACKNOWLEDGMENTS

The author is grateful for the assistance given by members of the Stability and Hydrodynamics Sections of DNPS in the conduct of the model testing described above.

10. FUTURE WORK

10.1 Extending the Experimental Data Set

To date, only a single set of readings has been taken on this model at one displacement and *KG*. The work should be extended to cover a range of hull forms, displacements and *KGs*. This should include a true wall-sided model.

10.2 Investigating Sensitivity

The sensitivity of the new method to both hull type, and to inaccuracies in measurements taken at the inclining experiment, needs to be investigated.

10.3 Deviations in Hull Form

Deviations of the hull from the original design and errors in numerical modelling may be significant. Work is needed to establish the extent of this problem in practice and the influence it has on inclining experiment results.

11. REFERENCES

- Bouguer, P., 1746, *Traité du Navire, de sa Construction et de ses Mouvements* (Treatise of the Ship, its Construction and its Movements), Jombert, Paris.
- Dunworth, R.J., 2014, "Back Against the Wall", *The Transactions of The Royal Institution of Naval Architects*, vol. 156, part B2 (International Journal of Small Craft Technology), pp. 99-106.
- Hoste, P., 1697, *Théorie de la Construction des Vaisseaux* (Theory of the Construction of Vessels), Arisson & Posule, Lyon.



Appendix A – Tables of Data and Results

Table A-1 Pendulum deflections and classic workup

Move No.	Weight Shift mm	Forward Pendulum			Aft Pendulum			Mean Heel (ϕ) deg.	$w d$ kg m	$\Delta \tan \phi$ kg
		Reading mm	Deflection mm	Heel (ϕ) deg.	Reading mm	Deflection mm	Heel (ϕ) deg.			
0	0	151.5	0.00	0.000	153.2	0.00	0.000	0.000	0.0000	0.0000
1	550	54.4	96.90	5.097	249.9	96.73	5.094	5.095	1.7039	1.5658
2	500	63.7	87.60	4.610	241.0	87.83	4.627	4.619	1.5490	1.4186
3	450	72.0	79.30	4.175	232.2	79.03	4.165	4.170	1.3941	1.2803
4	400	80.5	70.80	3.729	223.8	70.63	3.724	3.726	1.2392	1.1437
5	350	88.6	62.70	3.303	215.5	62.33	3.287	3.295	1.0843	1.0110
6	300	96.6	54.70	2.883	207.8	54.63	2.882	2.882	0.9294	0.8841
7	250	104.5	46.80	2.467	200.0	46.83	2.471	2.469	0.7745	0.7571
8	200	111.8	39.50	2.082	192.5	39.33	2.076	2.079	0.6196	0.6375
9	150	119.0	32.30	1.703	185.2	32.03	1.691	1.697	0.4647	0.5202
10	100	130.2	21.10	1.113	174.1	20.93	1.105	1.109	0.3098	0.3399
11	84.50	133.5	17.80	0.939	171.0	17.83	0.941	0.940	0.2618	0.2881
12	16.00	147.8	3.50	0.185	156.5	3.33	0.176	0.180	0.0496	0.0553
13	0	151.2	0.00	0.000	153.2	0.00	0.000	0.000	0.0000	0.0000
14	-14.00	154.2	-2.90	-0.153	150.3	-2.87	-0.151	-0.152	-0.0434	-0.0466
15	-84.25	168.9	-17.60	-0.928	135.5	-17.67	-0.933	-0.930	-0.2610	-0.2852
16	-100	172.3	-21.00	-1.107	132.0	-21.17	-1.117	-1.112	-0.3098	-0.3410
17	-150	184.5	-33.20	-1.750	120.3	-32.87	-1.735	-1.743	-0.4647	-0.5342
18	-200	191.5	-40.20	-2.119	113.2	-39.97	-2.109	-2.114	-0.6196	-0.6482
19	-250	198.8	-47.50	-2.504	105.8	-47.37	-2.499	-2.501	-0.7745	-0.7671
20	-300	206.5	-55.20	-2.909	98.2	-54.97	-2.899	-2.904	-0.9294	-0.8908
21	-350	214.5	-63.20	-3.330	90.4	-62.77	-3.310	-3.320	-1.0843	-1.0186
22	-400	222.4	-71.10	-3.745	82.0	-71.17	-3.752	-3.748	-1.2392	-1.1504
23	-450	231.2	-79.90	-4.206	73.1	-80.07	-4.219	-4.213	-1.3941	-1.2935
24	-500	239.8	-88.50	-4.657	64.8	-88.37	-4.655	-4.656	-1.5490	-1.4302
25	-550	248.9	-97.60	-5.134	55.8	-97.37	-5.127	-5.130	-1.7039	-1.5765
26	0	151.2	0.00	0.000	153.1	0.00	0.000	0.000	0.0000	0.0000
Mean Zero		151.30			153.17					



Table A-2 New workup and heeling / righting arm comparison

Move No.	Actual Heel (ϕ) deg.	KN m	$\sin \phi$	$\cos \phi$	HZ m	KG $\sin \phi$ m	HZ mm	GZ' mm	Delta mm
0	0.054	0.0013	0.0009	1.0000	0.0000	0.0002	0.00	0.00	0.00
1	5.149	0.1123	0.0898	0.9960	0.0966	0.0146	96.64	96.65	0.01
2	4.673	0.1022	0.0815	0.9967	0.0879	0.0131	87.92	87.85	-0.07
3	4.224	0.0924	0.0737	0.9973	0.0792	0.0121	79.18	79.30	0.12
4	3.780	0.0824	0.0659	0.9978	0.0704	0.0108	70.42	70.55	0.14
5	3.349	0.0724	0.0584	0.9983	0.0616	0.0096	61.64	61.78	0.14
6	2.936	0.0625	0.0512	0.9987	0.0529	0.0085	52.86	53.11	0.25
7	2.523	0.0524	0.0440	0.9990	0.0441	0.0072	44.06	44.14	0.08
8	2.133	0.0426	0.0372	0.9993	0.0353	0.0062	35.26	35.41	0.15
9	1.751	0.0334	0.0306	0.9995	0.0265	0.0058	26.45	27.27	0.82
10	1.163	0.0221	0.0203	0.9998	0.0176	0.0033	17.64	17.69	0.05
11	0.994	0.0189	0.0173	0.9998	0.0149	0.0029	14.91	14.99	0.08
12	0.234	0.0047	0.0041	1.0000	0.0028	0.0007	2.82	2.87	0.04
13	0.054	0.0013	0.0009	1.0000	0.0000	0.0002	0.00	0.00	0.00
14	-0.098	-0.0016	-0.0017	1.0000	-0.0025	-0.0002	-2.47	-2.42	0.05
15	-0.876	-0.0162	-0.0153	0.9999	-0.0149	-0.0024	-14.51	-14.81	-0.30
16	-1.058	-0.0196	-0.0185	0.9998	-0.0176	-0.0031	-17.64	-17.72	-0.08
17	-1.689	-0.0315	-0.0295	0.9996	-0.0265	-0.0062	-26.45	-27.84	-1.39
18	-2.060	-0.0396	-0.0359	0.9994	-0.0353	-0.0055	-35.26	-34.89	0.37
19	-2.447	-0.0494	-0.0427	0.9991	-0.0441	-0.0064	-44.07	-43.59	0.48
20	-2.850	-0.0593	-0.0497	0.9988	-0.0529	-0.0076	-52.86	-52.41	0.46
21	-3.266	-0.0693	-0.0570	0.9984	-0.0616	-0.0088	-61.65	-61.22	0.42
22	-3.694	-0.0793	-0.0644	0.9979	-0.0704	-0.0100	-70.42	-70.02	0.40
23	-4.159	-0.0899	-0.0725	0.9974	-0.0792	-0.0118	-79.18	-79.26	-0.08
24	-4.602	-0.0996	-0.0802	0.9968	-0.0879	-0.0129	-87.93	-87.78	0.15
25	-5.076	-0.1098	-0.0885	0.9961	-0.0967	-0.0143	-96.65	-96.60	0.05
26	0.054	0.0013	0.0009	1.0000	0.0000	0.0002	0.00	0.00	0.00

Table A-3 Case 2: Data set representing a typical inclining experiment

Move No.	Shift m	$w d$ kg m	$\Delta \tan \phi$ kg	Heel (ϕ) deg.	KN m	$\sin \phi$	$\cos \phi$	HZ m	KG $\sin \phi$ m
13	0.000	0.0000	0.0000	0.0540	0.0013	0.0009	1.0000	0.0000	0.0004
10	0.100	0.3098	0.3399	1.1629	0.0221	0.0203	0.9998	0.0176	0.0036
8	0.200	0.6196	0.6375	2.1330	0.0426	0.0372	0.9993	0.0353	0.0065
13	0.000	0.0000	0.0000	0.0540	0.0013	0.0009	1.0000	0.0000	0.0004
16	-0.100	-0.3098	-0.3410	-1.0584	-0.0196	-0.0185	0.9998	-0.0176	-0.0028
18	-0.200	-0.6196	-0.6482	-2.0602	-0.0396	-0.0359	0.9994	-0.0353	-0.0052
13	0.000	0.0000	0.0000	0.0540	0.0013	0.0009	1.0000	0.0000	0.0004
		GM_0	0.952		TCG_1	0.001			
		KG_1	0.121		KG_1	0.160			



Table A-4 Case 3: Data set representing an inclining experiment with large initial list

Move No.	Shift m	$w d$ kg m	$\Delta \tan \phi$ kg	Heel (ϕ) deg.	KN m	$\sin \phi$	$\cos \phi$	HZ m	$KG \sin \phi$ m
20	0.000	0.0000	0.0000	-2.8502	-0.0593	-0.0497	0.9988	0.0000	-0.0094
22	-0.100	-0.3098	-0.2587	-3.6942	-0.0793	-0.0644	0.9979	-0.0176	-0.0118
25	-0.250	-0.7745	-0.6826	-5.0763	-0.1098	-0.0885	0.9961	-0.0439	-0.0161
20	0.000	0.0000	0.0000	-2.8502	-0.0593	-0.0497	0.9988	0.0000	-0.0094
18	0.100	0.3098	0.2421	-2.0602	-0.0396	-0.0359	0.9994	0.0176	-0.0072
15	0.216	0.6676	0.6052	-0.8764	-0.0162	-0.0153	0.9999	0.0380	-0.0042
20	0.000	0.0000	0.0000	-2.8502	-0.0593	-0.0497	0.9988	0.0000	-0.0094
		GM_0	1.136		TCG_1	-0.050			
		KG_1	-0.063		KG_1	0.163			

Table A-5 Case 4: Data set representing an inclining experiment with restricted heel

Move No.	Shift m	$w d$ kg m	$\Delta \tan \phi$ kg	Heel (ϕ) deg.	KN m	$\sin \phi$	$\cos \phi$	HZ m	$KG \sin \phi$ m
13	0.000	0.0000	0.0000	0.0540	0.0013	0.0009	1.0000	0.0000	0.0002
11	0.085	0.2618	0.2881	0.9941	0.0189	0.0173	0.9998	0.0149	0.0029
13	0.000	0.0000	0.0000	0.0540	0.0013	0.0009	1.0000	0.0000	0.0002
15	-0.084	-0.2610	-0.2852	-0.8764	-0.0162	-0.0153	0.9999	-0.0149	-0.0024
11	0.000	0.0000	0.0000	0.0540	0.0013	0.0009	1.0000	0.0000	0.0002
		GM_0	0.912		TCG_1	0.001			
		KG_1	0.161		KG_1	0.163			

Table A-6 Case 5: Data set representing an inclining experiment with an extreme heel close to upright

Move No.	Shift m	$w d$ kg m	$\Delta \tan \phi$ kg	Heel (ϕ) deg.	KN m	$\sin \phi$	$\cos \phi$	HZ m	$KG \sin \phi$ m
8	0.000	0.0000	0.0000	2.1330	0.0426	0.0372	0.9993	0.0000	0.0142
6	0.100	0.3098	0.2462	2.9362	0.0625	0.0512	0.9987	0.0176	0.0166
3	0.250	0.7745	0.6412	4.2241	0.0924	0.0737	0.9973	0.0440	0.0201
8	0.000	0.0000	0.0000	2.1330	0.0426	0.0372	0.9993	0.0000	0.0142
11	-0.116	-0.3578	-0.3491	0.9941	0.0189	0.0173	0.9998	-0.0204	0.0110
13	-0.200	-0.6196	-0.6375	0.0540	0.0013	0.0009	1.0000	-0.0353	0.0082
8	0.000	0.0000	0.0000	2.1330	0.0426	0.0372	0.9993	0.0000	0.0142
		GM_0	1.096		TCG_1	0.028			
		KG_1	-0.023		KG_1	0.164			



Exploration of the Probabilities of Extreme Roll of Naval Vessels

Douglas Perrault, *Defence Research and Development Canada – Atlantic Research*

Centre Doug.Perrault@DRDC-RDDC.GC.Ca

ABSTRACT

Dynamic stability simulation tools developed by the Cooperative Research Navies have been used to investigate the relationship between a number of stability criteria and the probability of exceeding a critical roll angle. Multiple roll response time series for several ships in various seaway conditions are generated to provide the probabilities. This paper describes the investigation into the probability results themselves, as a precursor to regression against GZ curve parameters. Specifically, it examines the effects of modelling choices and of variation and range in the input control variables.

Keywords: *Dynamic Stability, Probability of Capsize, Simulation*

1. INTRODUCTION

Tools for assessing dynamic stability of intact ships have been developed within the Cooperative Research Navies (CRNav) Dynamic Stability Project. Under tasking from the Naval Stability Standards Working Group (NSSWG), the tools were employed to investigate the relationship between risk of capsizing and various geometry and stability parameters. The risk of capsizing is characterized by the probability of exceeding a critical roll angle (PECRA), and although in the present case it is related to capsizing, the critical roll angle may also take on a number of other important connotations, such as machinery or weapon limits.

The probability of exceeding a critical roll angle (PECRA) is determined by running multiple, time-domain simulations of a ship in a specific loading condition at a mean speed and heading (the operating point of the vessel) in waves of a given significant height and modal period (the environmental condition). The time series of roll responses are used to

determine the PECRA. The probability outcomes are later used as the regressands (response variables) in regression analysis investigating relationships with parameters associated with ship stability.

This paper records the study into how the PECRA vary with the input control variables of ship speed (V), ship heading relative to the wave system (β), significant wave height (H), and modal wave period (τ). It also looks into the differences between ships and between loading conditions. It further seeks to address the issue of the range and resolution of the sets of input control variables that will fully characterize the total probability of exceeding a critical roll angle (TPECRA) across all input variables for each load condition of each ship.

The next section will discuss the scope of work to date, looking at the similarities and differences between three phases of work, each with slightly different goals. Following that will be a look at the different geometries of the ships used in Phase 2. The next section will briefly examine the effects of load conditions,



operating points, and environmental conditions. After that will be a study into the consequences of choices relating to range and resolution of the input control variables (V , β , H , τ). This will be followed by a discussion on the use of Operational Overlays. Finally conclusions will be presented.

2. SCOPE OF WORK – 3 PHASES

2.1 Determination of Probabilities

FREDYN is a non-linear, semi-empirical, time-domain software for simulating ship motions in environmental conditions from calm water to severe wind and waves. It allows for studies in stability, seakeeping and manoeuvring. FREDYN is appropriate for any type of a relatively slender mono-hull with a Froude number less than 0.5. Specific to the current study, FREDYN is capable of predicting a range of capsize modes in regular and irregular waves.

Since 1999, the objectives of the NSSWG have been pursued through three phases of study for intact ships. Phase 1 (FREDYN version 8.2) used a strip theory approach to look at relationships between the risk of capsize and various stability-related and ship-form parameters. Phase 2 (FREDYN version 9.9) used panel methods and the emphasis of the study shifted to looking for the level of safety inherent in the current naval stability standards. In addition to using a panel method for the Froude-Krylov forces, the Frank Close Fit Method was implemented to replace a conformal mapping method, the roll damping method was improved, and the ship motion algorithm was upgraded. Phase 3 (FREDYN version 10.2) was conducted after a complete rewrite of the software to modularize the code. The Phase 3 study still used panel methods, but included a more accurate modelling of the effects of deck-edge immersion, as well as an automatic determination of the retardation function time interval and time step. The focus

in Phase 3 was narrowed to finding criteria that would be suitable for stability standards, in particular the Naval Ship Code (ANEP 77, 2012).

The set of ships investigated was largely the same for all three phases, and included slender hulls with twin propellers and one or two rudders. Several different load conditions are explored for each ship, with each load condition delineated by draft (T) and vertical position of the centre of gravity (KG). The radii of gyration were held constant for a given ship for all load conditions (TKG). Some of the load conditions were common in two or more phases, but most were not.

What is common to all three phases is the general approach to determining the probability of exceeding the critical roll angle (PECRA). Simulations were run for each ship in specific load conditions, at standard operating points and environmental conditions.

The standard operating points are three speeds chosen by the NSSWG as typical for frigates, and 7 headings covering 0° to 180° , following the standard assumption that the symmetry of the ship will make the results from 180° to 360° a mirror image of those from 0° to 180° . In fact the 0° and 180° headings were changed to 1° and 179° to mimic the asymmetry of real vessels. The standard environmental conditions were taken as those defined by the Bales North Atlantic scattergram (see Bales, Lee, and Voelker, 1981) as modified by McTaggart and De Kat (2000).

The same set of operating points and environmental conditions was used in Phase 2 as in Phase 1, but in Phase 3 there were fewer wave heights and periods and only one ship speed.

To be conservative, a single sea direction was assumed and wave spreading was not used, so that all the energy associated with the sea spectrum would be concentrated in the



unidirectional wave train. This is expected to result in a more pessimistic estimate of risk.

Wind was modelled as a function of wave height and was set to be collinear with the wave, again to be conservative. No currents were included in the simulations.

Each environmental condition was modelled as a Bretschneider spectrum defined by the significant wave height and modal wave period. The spectrum is built by summing regular waves of different amplitudes, wavelengths and phase angles, and there are an infinite number of ways to realize (achieve) the spectrum, with each realization accomplished by a different choice of the pseudo-random seed number used to generate the component wave phase angles. Each realization is capable of producing a unique time series of wave conditions, and thus ship responses. This is the key to generating probabilistic results: under the assumption that any one of the unique realizations is equally likely to occur, performing multiple simulation runs (where each run is a unique realization) generates a statistical sample leading to the probability of exceeding the critical roll angle (PECRA).

The same operating points and environmental conditions were used in all cases within a given phase, but the number of seaway realizations was not necessarily the same for each ship, or even for each load condition for the same ship. The number of realizations depended on the quality of the probability result; (small) batches of simulations were added when the uncertainty in the probability result was higher than acceptable.

2.2 Post-Analysis

For Phases 1 and 2 a block maxima method called PCAPSIZE (see McTaggart and De Kat, 2000) was used to determine the probability of exceeding the critical roll angle (which for Phases 1 and 2 was 90°) within one hour.

For Phase 3 an envelope-peaks-over-threshold (EPOT) method called LORELEI (see Ypma and Harmsen, 2012) was developed to obtain the probability of exceeding the critical roll angle (which for Phase 3 was 70°) within an hour. This method makes fuller use of the time-series data and thus theoretically provides a more accurate value.

2.3 Current Investigation

For each load condition, the simulation results can be stored as a 4-dimensional hypercube with each dimension representing a single input control variable. While this makes it easy to index into the data, as well as to partition the data along any subset of variable ranges, for visually examining the data, it is necessary to “flatten” the data into at most 2 dimensions. It is intuitive to group the speed and heading together, and the wave height and period together. For each ship loading condition there can be up to 148 speed-heading tables or plots and up to 21 height-period tables or plots. Each phase has at least 37 loading conditions to consider, and over all 3 phases there are a total of 152 distinct loading conditions (i.e., not including repeated loading conditions) over 14 ships. The number of tables and/or plots to examine is large, so generalizations will be made by looking at single speed-heading plots that represents a sum of PECRA over all wave heights and periods for a given ship loading condition, and single height-period plot that represents a sum of PECRA over all ship speeds and headings for a given ship loading condition. These summations are known as marginal sums and can be denoted as MPECRA-HT and MPECRA-VB respectively. Each of these marginal summations can be further summed to a common number representing the total probability of exceeding the critical roll angle (TPECRA) for the load condition.

The marginal sums and the total sum are only possible by applying suitable probability distributions for the wave conditions, and/or



ship's speed and heading. The choice of probability distributions for the input control variables will be discussed more fully under Operator Overlays. For this paper, uniform distributions were used to make it easy to investigate the relationships without any weighting issues.

The probability results vary across several orders of magnitude. It is arguably more intuitive to talk about these probabilities in terms of their order of magnitude than about the values themselves. Therefore the remainder of this paper concerns itself with the data in terms of the base-10 logarithm of the probabilities; i.e., O(PECRA), O(MPECRA-HT), O(MPECRA-VB), O(TPECRA).

2.4 Data Presentation

Typically, the data with respect to the operating point (ship speed and heading) would be plotted on a polar plot, or a half-polar plot given an assumption of symmetry of the ship leading to similar results for relative headings from 180° to 360° as for 0° to 180°. In this paper, a contour plot of the order of magnitude of TPECRA with respect to speed and heading will be given in the form of a rectangular contour plot.

Figure 1 shows the more complicated contour plot in terms of environmental conditions (wave height and period), in this case for the order of magnitude of the probability of observing the wave height-period combination according to Bales as modified by McTaggart and De Kat (2000). The plot is more complicated because of several features. Wave steepness (significant wave height divided by wavelength) is taken into account so that waves that are too steep to exist are not included. This results in the lower left corner being empty; other empty areas are the result of not having data for the height-period combination. Overlaid on the plot are wave steepness contours (lines sweeping down from the top left corner). Stokes wave theory

predicts a limit of steepness of 1/7, while Buckley (see McTaggart and De Kat, 2000) gives an observed limit of about 0.049, based on significant wave height and peak wave period. Note that the Bales data only has valid elements below both limits (i.e. above those contours in the figure). The lines crossing the steepness contours are contours of constant (normalized) energy due to the incident wave.

The average energy per unit meter along the wave¹ (perpendicular to the direction of wave travel) is given by:

$$E = (1/16\pi)\rho g^2 H^2 \tau^2 \quad (1)$$

This is clearly a function of the wave height and period only (for a given density of water). The energy is normalized by the highest value, which would be at the largest values of height and period; hence the contours show an increase towards the lower right corner.

The dashed boxes added to this particular figure indicate the NATO STANAG 4194 (1994) Sea State definitions for reference (see also Bales, Lee, and Voelker, 1981).

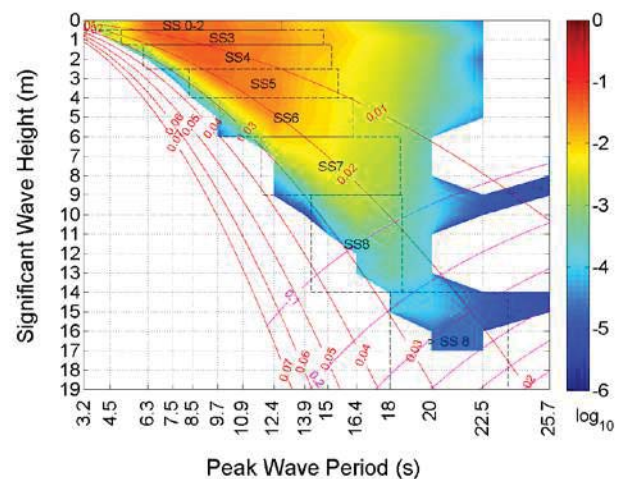


Figure 1. Order of Magnitude of Probabilities of Occurrence in Bales (modified) North Atlantic Wave Table.

¹ An estimate of the total energy imparted to the ship by the incident wave can be calculated by multiplying E by the waterline length of the ship times the sin of the relative heading to the wave. This estimate does not take into account radiation, diffraction, or other physical phenomena – only the energy in the incident wave.



2.5 Effects of Modelling and Analysis Choices

An attempt was made to track the changes between the phases of the intact stability study, in order to establish the effects of specific modelling choices, like the difference between strip theory and panel methods.

Across the set of ships and loading conditions in the three phases, there were 9 common loading conditions, representing 5 different ships. Some ships have one common condition and others have more. The loading conditions are numbered from 1 to 9 without regard to which ship they are associated with. Figures 2 through 4 show an example of the same loading condition in each phase. They show the maximum order of magnitude of PECRA over all speeds and headings, and do not, therefore, represent any particular operating point, nor are they marginal sums.

Because the ranges of wave heights and periods in phase 3 were reduced, Figures 2 and 3 have been cropped to show the Phase 3 Equivalent (P3E) ranges.

It is clear that each phase shows different orders of magnitude of the probabilities for the same conditions. Unfortunately, there were too many changes to the software in between phases to definitively assign changes in the probability results to specific modelling choices. Phase 2 data was chosen for this analysis because, as will be seen later, the ranges of input control variables provide for a more accurate characterization of the TPECRA.

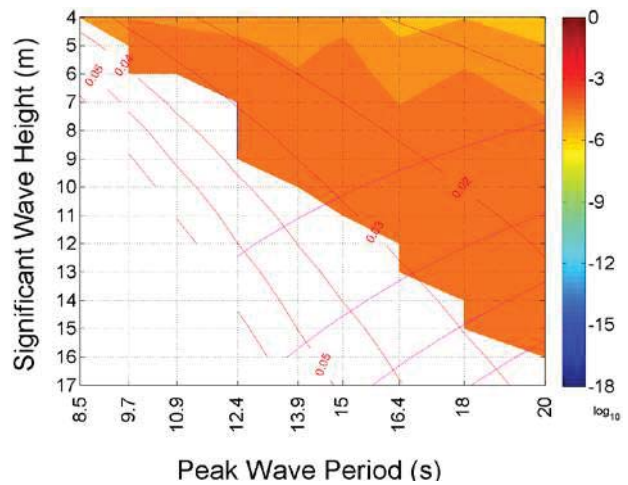


Figure 2. Maximum O(PECRA-VB) by Wave Height and Period – Phase 1 Load Condition 6.

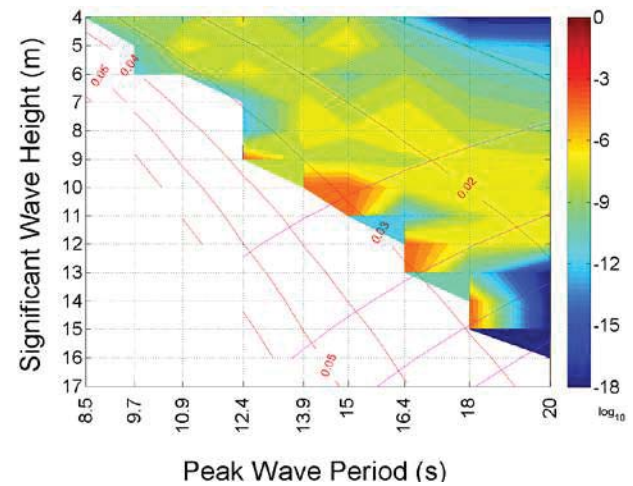


Figure 3. Maximum O(PECRA-VB) by Wave Height and Period – Phase 2 Load Condition 6.

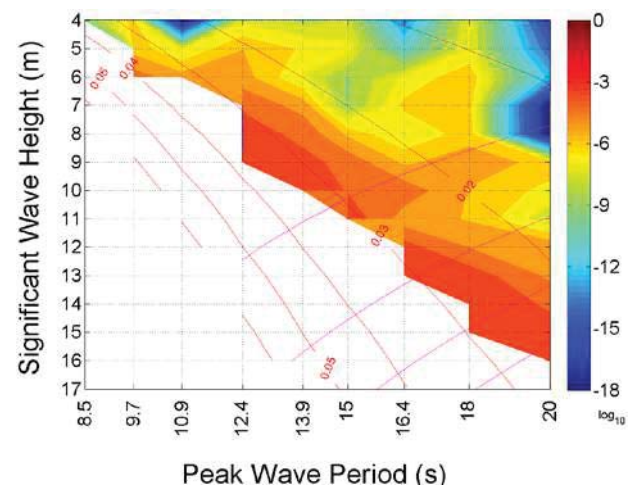


Figure 4. Maximum O(PECRA-VB) by Wave Height and Period – Phase 3 Load Condition 6.



3. SHIP GEOMETRY

The study looked at three forms of geometry:

1. A binary factor defining appendages
 - a. Single vs double rudders
 - b. Presence vs absence of skeg
 - c. Presence vs absence of stabilizing fins
2. Dimensional geometry
3. Non-dimensional geometry

Scatter plots of TPECRA are used to investigate the effects of ship geometry.

3.1 Appendages

Within the set of ships simulated there are vessels with a skeg and/or fins, and some ships have a single rudder rather than twin rudders. The set of ships can be partitioned into groups having the various features:

Skeg Exclusively: ship(s) with skegs and double rudders, but no fins vs. all ships with a single rudder and/or fins and/or no skeg.

Fins Exclusively: ship(s) with fins and double rudders, but no skeg vs. all ships with a single rudder and/or a skeg and/or no fins.

Single Rudder Exclusively: ship(s) with a single rudder, but no skeg or fins vs all ships with a skeg and/or fins and/or double rudders.

Skeg Inclusive: ship(s) with skegs, with or without double rudders and/or fins vs. all ships without a skeg.

Fins Inclusive: ship(s) with fins, with or without double rudders and/or a skeg vs. all ships without fins.

Single Rudder Inclusive: ship(s) with a single rudder, with or without a skeg and/or fins vs. all ships with double rudders.

Skeg and Fins and Single Rudder: ship(s) with a skeg, fins, and double rudders vs. all ships not having all three features.

Other partitions are possible, but either the ship subsets already exist in the partitions above, or the ships used do not support them; i.e., one of the partitions is a null set and the other is the set of all ships.

Figure 5 shows a typical result. The filled markers in this figure indicate the load conditions of those ships with a single rudder only, but no fins, and no skeg, while the unfilled markers represent load conditions of all other ships. Although all the load conditions for the single-rudder ships are in one corner of the grouping, there is no definitive distinction between the filled and unfilled markers, at least in terms of the KG and O(TPECRA). Figure 6 shows that when ships with single rudders and fins or skegs are included, there is even less distinction. Figures 7 and 8 show the same thing when O(TPECRA) is plotted against the draft of the ship.

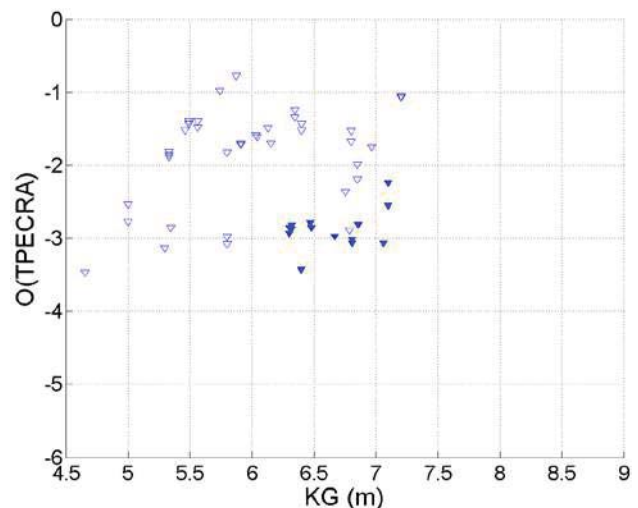


Figure 5. O(TPECRA) for each KG grouped by Single Rudder Exclusively (Phase 2).

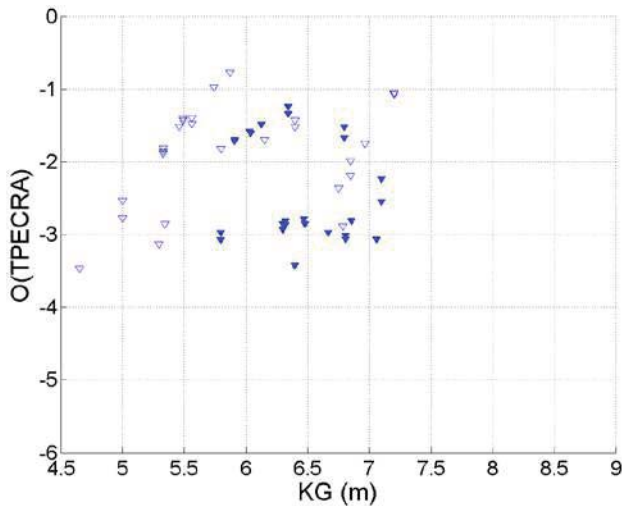


Figure 6. O(TPECRA) for each KG grouped by Single Rudder Inclusively (Phase 2).

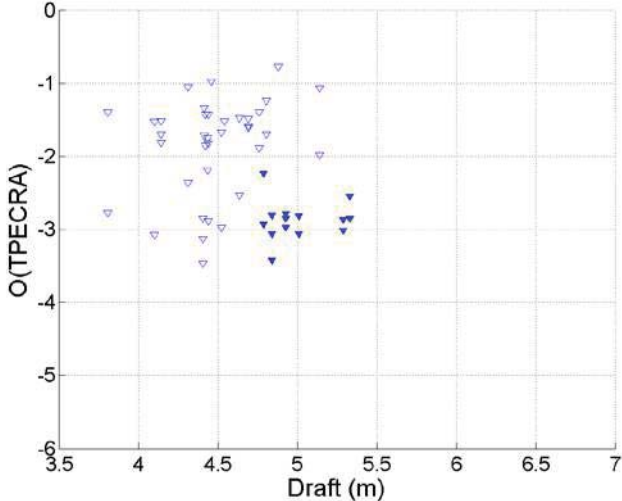


Figure 7. O(TPECRA) for each Draft grouped by Single Rudder Exclusively (Phase 2).

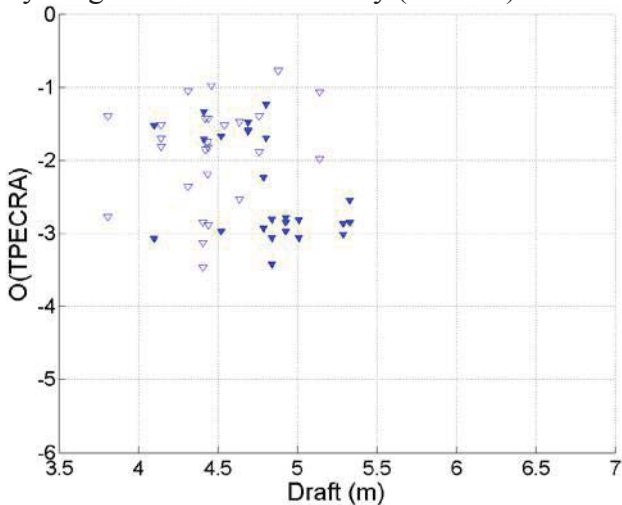


Figure 8. O(TPECRA) for each Draft grouped by Single Rudder Inclusively (Phase 2).

3.2 Dimensional Geometry

Dimensional measures of lengths, areas, and volumes were also examined to find any trends in the probability data. For some typical measures it is possible to look at the fore-aft differences as well.

LWL: Length along waterline², L_{WL} .

BMSWL: Beam at midships on the waterline.

BmaxWL: Maximum beam on the waterline³

TMS: Draft at midships.

AMS: Area of the (immersed) midship section.

AWP: Area of the waterplane.

VDisp: Volume of displacement, ∇ .

The length (LWL), waterplane area (AWP) and volume of displacement (VDisp) can be examined for fore-aft variations. The following postscripts are added to distinguish each case:

FWDMS/AFTMS: Forward/aft of midships.

FWDLCF/AFTLCF: Forward/aft of the center of flotation.

FWDLCB/AFTLCB: Forward/aft of the center of buoyancy.

Midships (MS) represents a division in two based on ship length; the longitudinal center of flotation (LCF) represents division on the basis of waterplane area; and the longitudinal center of buoyancy (LCB) represents a division in two on the basis of volume.

The relationships between dimensional geometry (lengths, areas, volumes) are very similar to those for non-dimensional geometry, with lengths behaving like the ratios and

² The waterline is at the draft associated with the specific load condition, which is not necessarily the design draft.

³ Because the maximum beam typically exists for some distance along the length of a ship, rather than only at a single, specific point, it is not suitable for dividing the ship into clear fore and aft parts.



coefficients in Figures 9 through 12, and areas and volumes more like Figure 13.

3.3 Non-Dimensional Geometry

Non-dimensional measures are ratios of dimensional measures, including classical form coefficients.

- LWLowerTMS: Length to draft ratio.
- LWLowerBMS Length to beam ratio.
- WL:
- BMSWLowerT Beam to draft ratio.
- MS:
- CM: Midship coefficient
 $AMS/(BMSWL*TMS)$.
- CW: Waterplane coefficient
 $AWP/(LWL*BMSWL)$.
- CB: Block coefficient
 $Vdisp/(LWL*BMSWL*TMS)$.
- CLP: (Longitudinal) prismatic
coefficient
 $Vdisp/(AMS*LWL) = CB/CM$.
- CVP: Vertical prismatic coefficient
 $Vdisp/(AWP*TMS) = CB/CW$.

Length over beam, length over draft, the waterplane area coefficient, the block coefficient, and both prismatic coefficients allow for fore-aft versions, which are delineated by the same suffixes as the dimensional measures.

The O(TPECRA) was plotted against each of the geometry parameters to look for obvious trends. Figure 9 shows both forms of the typical results. On the left, the L/B ratios are tight-banded, while the more wide-banded data are like those of the B/T data on the right. None of the geometry parameters show a trend with the O(TPECRA); they were all vertical bands like those in Figure 9.

Figure 10 shows that the most common form coefficients do not have a meaningful relationship with O(TPECRA) either.

Figure 11 and Figure 12 show the situation is not changed by splitting the coefficients into fore and aft measures at midships (equal length halves). The results for division at the LCF (equal area halves) and the LCB (equal volume halves) show the same (lack of) trend.

Finally the freeboard is examined via the volume of reserve of buoyancy in Figure 13. It does not show any clear trend with O(TPECRA) either.

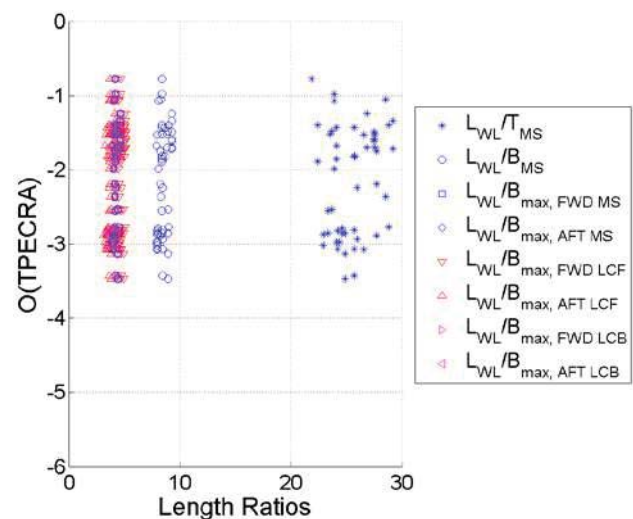


Figure 9. O(TPECRA) vs. Non-Dimensional Length (Beam) Ratios

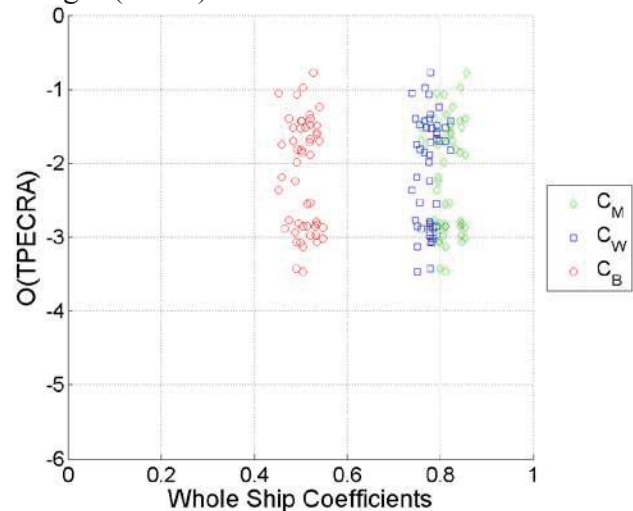


Figure 10. O(TPECRA) vs. Coefficients of Form for the Ship as a Whole.

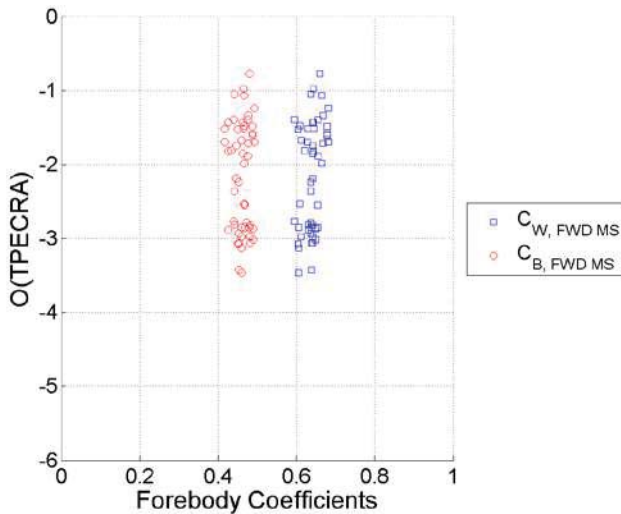


Figure 11. O(TPECRA) vs. Coefficients of Form for the Fore Body.

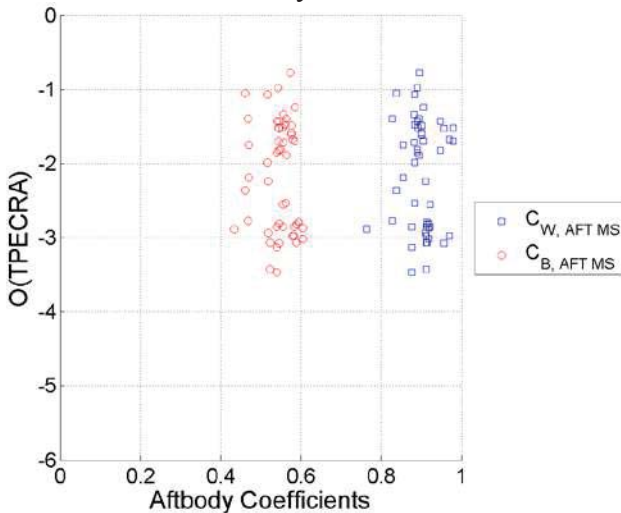


Figure 12. O(TPECRA) vs. Coefficients of Form for the Aft Body.

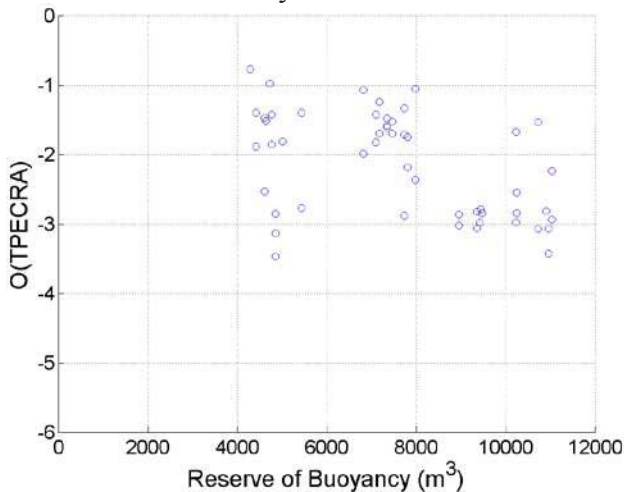


Figure 13. O(TPECRA) vs. Volume Reserve of Buoyancy

4. LOADING CONDITIONS, OPERATING POINTS, AND ENVIRONMENTAL CONDITIONS

In Phases 1 and 2, the loading conditions were picked such that for each ship at least four T-KG combinations constituted a matrix where two KG were simulated at two (or more) values of draft. This was not the case in Phase 3.

Contour plots over environmental conditions have been generated where the order of magnitude of the highest PECRA for all speeds and headings are shown for each height-period combination. For example, see Figure 14. Note that these plots show maxima results rather than marginal summations. Examination of contour plots for each loading condition of a ship will show that there can be a wide variation in the TPECRA for different loading conditions. Typically the effect of change in KG is more pronounced than that of a change in draft; however, this is not always true. Arguably, the expected outcome within each matrix is that the combination of the highest T and lowest KG would have the least O(PECRA), while the lowest T and the highest KG would have the greatest O(PECRA), with the other two combinations between the two extremes. Out of 8 ships, only 2 showed the expected outcome.

Contour plots over operating points were also generated where the order of magnitude of the highest PECRA for all heights and periods are shown for each speed-heading combination. Out of 8 ships, only 1 ship shows the expected outcome described above. These results indicate that the relationship between O(PECRA) and the draft and KG is complex and likely is affected by other factors, including the environmental conditions and the ship operating point.

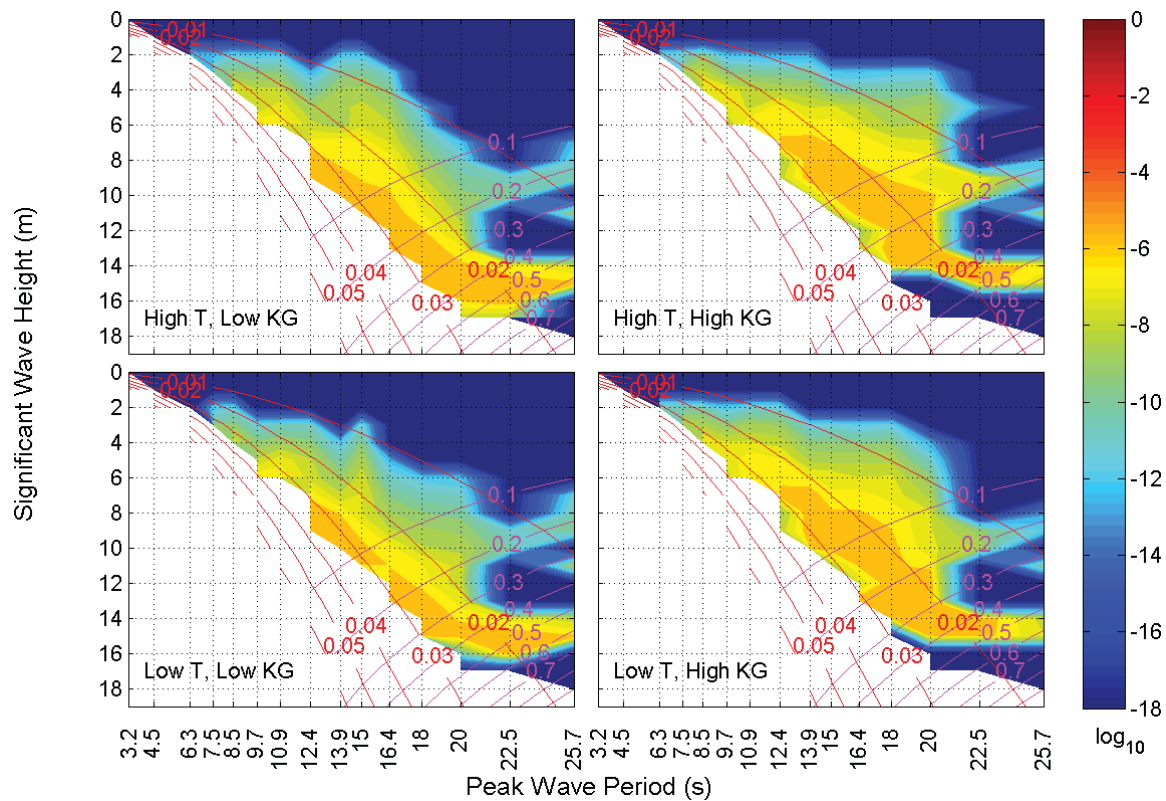


Figure 14. Typical Set of Environmental Relationships for Matrix of Load Conditions.

5. RANGE AND RESOLUTION OF INPUT CONTROL VARIABLES

The amount of data generated for each ship loading condition is sizeable, such that it is an onerous task to examine it all. It would be useful to reduce the number of conditions/points that need to be simulated. On the other hand, it is necessary to ensure that a sufficient number of conditions/points are simulated that an accurate characterization of the ship's behaviour is captured.

The idea of reduced data sets suggests that fewer simulations can be run to obtain the needed results. This was in fact practiced for the Phase 3 study, based on an educated guess of the new ranges of ship speed, and wave height and period. The question naturally arises as to whether or not the guess is reasonable, and further, how far the variable ranges can be reduced before the characterization of extreme roll probability is significantly affected.

Before either of these questions can be answered “significant” must be quantified. As stated above, when dealing with probabilities it is reasonable to speak in terms of orders of magnitude, and “significantly affected” can be thought of in terms of the difference between the order of magnitude of the sum of probabilities (TPECRA) for the reduced range and that for the full range. Five levels of significance have been examined in this study: 0.01, 0.05, 0.1, 0.5, and 1.0. These values represent approximately 2%, 12%, 26%, 300%, and 1000% changes respectively. The first level is very demanding, while the last level allows a 10x difference, and should be considered to be at or near the limit of acceptable difference, and in some cases may be too much of a difference.

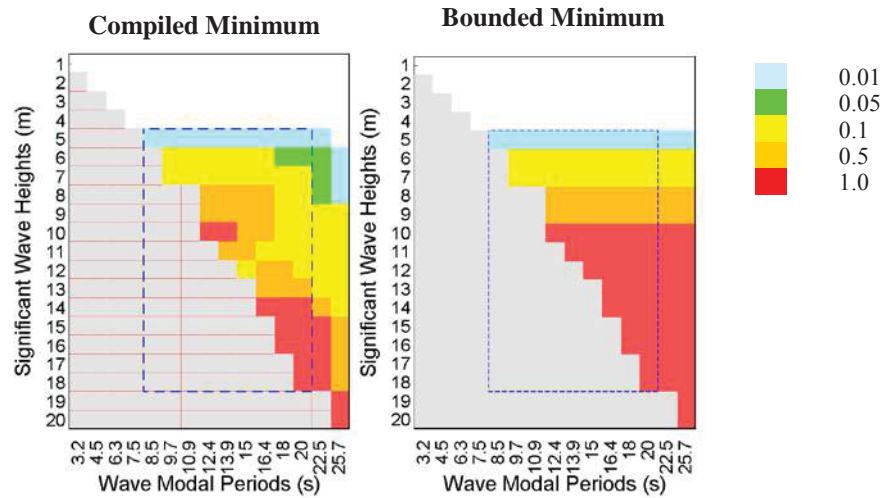


Figure 15. Minimum ranges of Wave Height and Period.

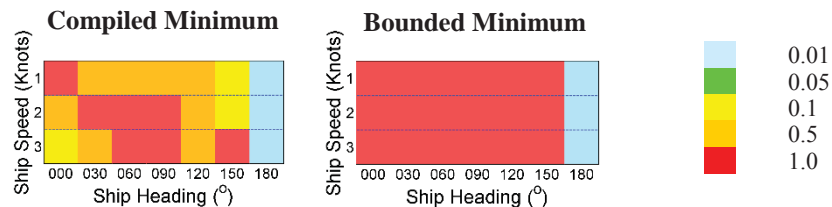


Figure 16. Minimum ranges of Ship Speeds and Headings.

The effect of reducing the range of the variables was investigated via a set of systematic reductions of the marginal sums over every possible range of the input control variables, leading to range-specific PECRA (RPECRA).

Figure 15 shows a compilation of results of the minimum-height-period-range search for all ship load conditions in Phase 2. The figure shows two wave height-period tables, each with all the possible wave conditions as non-greyed-out cells. The left-hand table shows the actual compilation of ranges; i.e., the minimum required range of environmental conditions for each load condition of all ships is included in the same figure, with the ranges corresponding to the less demanding levels of significance overlaid on the more demanding levels. Each level of significance is depicted in a different colour, with blue as the most demanding level and red as the least demanding level; the blue

cells show the ranges of conditions required to provide a probability of exceeding the critical roll angle with an order of magnitude within 0.01, while the green cells represent a difference in the order of magnitudes of 0.05, the yellow cells a difference of 0.1 order of magnitude, the orange cells represent a difference in the order of magnitudes of 0.5, and the red cells a difference of 1 order of magnitude. The right-hand side shows the single contiguous range for each level needed to capture all the individual load condition ranges indicated in the left-hand side. These contiguous ranges represent the number of simulations that would be required if there was no prior knowledge of the individual constituent ranges. The blue dashed lines indicate the range of speeds and headings in the P3E (reduced) set.

Figure 15 shows that as the margin of difference is reduced, the ranges of conditions



must increase. It also indicates that, based on the compilation of results from all ship load conditions, the range of wave heights go from 4 to 20 m and the range of wave periods is from 8.5 to 25.7 s to ensure that extreme roll probability is within 0.01 order of magnitude of the full-table value. The range of wave heights go from 10 to 20 m and the range of wave periods is from 12.4 to 25.7 s to ensure that extreme roll probability is within 1 order of magnitude of the full-table value.

Figure 16 shows a compilation of results of the minimum-speed-heading-range search. At the 0.01 level of significance, the whole range of speeds and headings are necessary, while at levels of significance of 0.05 and greater all speeds and most headings are still required. Note that a heading of 0° represents the ship in following seas.

Figures 15 and 16 indicate that the Phase 3 range reductions are somewhat reasonable in terms of wave height and period, but are not appropriate for ship speed. The results in Figures 15 and 16 do not necessarily reflect the characteristics of the individual ships used in the compilation.

Table 1 summarizes the check on the validity of reducing the ranges of ship speeds and wave heights and periods as done in Phase 3. The table shows that the reduction in wave conditions will still give results within half an order of magnitude of the full table, for most ships. However, reducing the range of speeds will lead to a difference in extreme roll probability of up to an order of magnitude for most ships, and greater for some ships.

Table 1. Adequacy of Phase 2 data when ranges reduced to those of Phase 3.

	Reduced Environmental Profile			Reduced Operational Profile		
	0.1	0.5	1.0	0.1	0.5	1.0
Ship A	✗	✓	✓	✗	✗	✓
Ship B	✗	✓	✓	✗	✗	✓
Ship C	✗	✓	✓	✗	✗	✓

Ship D	✓	✓	✓	✗	✗	✓
Ship E	✗	✓	✓	✗	✗	✓
Ship F	✗	✓	✓	✗	✗	✓
Ship G	✗	✗	✗	✗	✗	✗
Ship H	✗	✓	✓	✗	✗	✓

The ranges of environmental conditions and operating points are not the only determining factors for ensuring coverage of the phenomena that accurately characterizes the ship behaviour. The number of simulations required is also dependent on the resolution of the environmental condition and operating point sets. The resolution for the operating points was arbitrarily assigned by the NSSWG. The resolution of the environmental conditions is that of the Bales scattergram.

Figure 17 is an example of a Phase 2 contour plot over environmental conditions. Figure 18 shows the data cropped to the Phase-3-Equivalent range of wave headings and periods; that is, all the data is available but the axes scales are reduced to show only the ranges similar to the Phase 3 plots. Figure 19 shows the same data set when only the data from the heights and periods that are common to Phase 3 are kept. Figure 19 is different from Figure 18, indicating that the range and resolution of the data affects the plot. If the resolution were sufficient, the plots would be similar. Essentially, the contours are being affected by “far field” values. Better resolution would make it more difficult for the “far field” to affect the results.

6. OPERATIONAL OVERLAYS

Advice to the designer or operator would have to take into account the probabilities of being at each loading condition, operating point, and in each environment.

For the sake of the current work however, because summation across input variables required the use of probability distributions, the probabilities for the operating points and environmental conditions were taken as



uniformly distributed over the ranges employed, while the probability of the load condition has not been considered. This was done to avoid obscuring relationships between the conditional probabilities and the conditions.

Naval Administrations can replace the uniform distributions with distributions more representative of their own particular pattern of use for the vessel. The replacement may require some interpolation. Any extrapolation must be limited to values very near the original data.

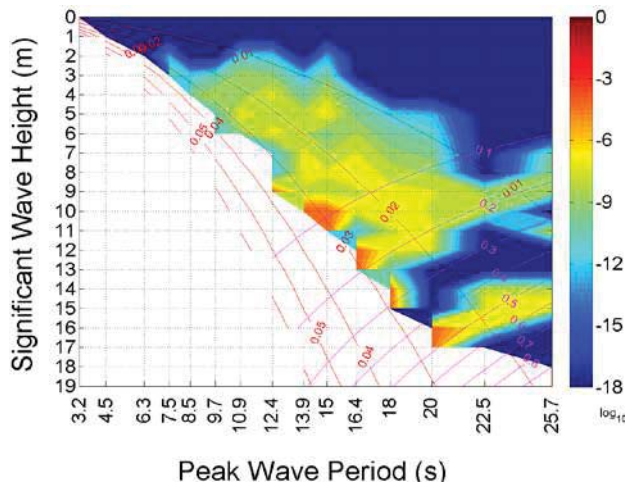


Figure 17. O(MPECRA-VB) by Wave Height and Period in Phase 2 Load Condition 6 (Full Range of Height and Period).

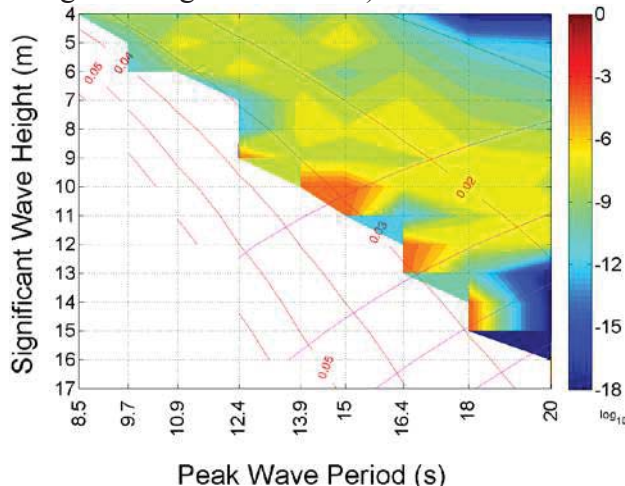


Figure 18. O(MPECRA-VB) by Wave Height and Period in Phase 2 Load Condition 6 (Full Range of Height and Period Cropped).

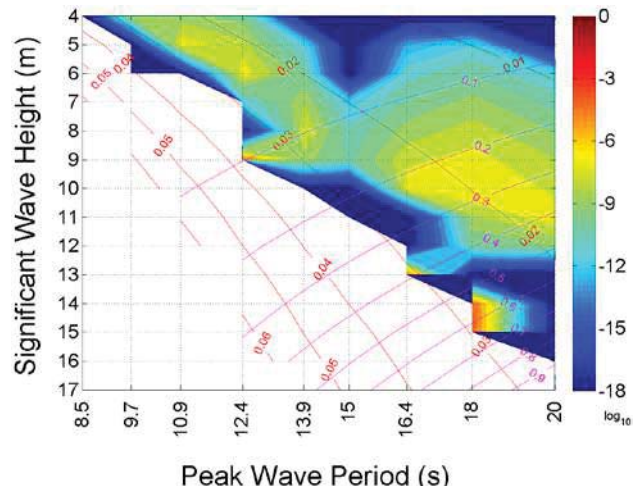


Figure 19. O(MPECRA-VB) by Wave Height and Period in Phase 2 Load Condition 6 (Phase 3 Equivalent Range of Height and Period).

For the main work of regression against stability parameters, the ships were assumed to be equally likely to take on any heading relative to the waves, but a generic 3-speed profile based on experience was agreed on and used (Phases 1 and 2; reduced to the most common speed for Phase 3). Further, the Bales' scattergram for the North Atlantic (see Bales, Lee, and Voelker [1981]) as modified by McTaggart and De Kat [2000] was used as the joint probability distribution of wave heights and periods.

Other options for operational overlays include the capability to use different wave height-and/or wave period distributions (e.g., the North Pacific scattergram) with the same underlying PECRA (via interpolation), and the ability to rule out certain environmental conditions based on restrictions due to design or change of vessel state. Operational overlays may also be used to account for operator influence, such as voluntary speed reductions and course changes in more severe seas.

7. CONCLUSIONS

This study has looked at probability data generated to investigate relationship between the probability of exceeding a critical roll angle (PECRA) and ship form and stability



parameters. The probabilities were produced for several ships at a number of loading conditions, and for a standard set of operating points (speeds and headings) and environmental conditions (wave heights and periods).

Similar simulations were run for each of 3 phases which each had a different goal. There are notable differences in the results between the 3 phases of the intact stability project. Unfortunately, because of the number of changes in modelling capabilities and choices between the phases, it is not possible to attribute the changes to specific choices.

Within each phase, a careful examination of the probabilities for each ship did not provide any clear patterns related to the typical appendages, or due to geometric parameters, whether expressed in dimensional or non-dimensional form. However, the set of ships used represents a relatively small sample of closely related hull forms with similar features, and it is possible that a larger sample, using more divergent ship types may identify relationships between PECRA and geometry.

When differences between loading conditions for each ship were studied, there was clear evidence of the expected variation due to draft and, more strongly, vertical center of gravity, but these expected variations were not observed in all cases. This suggests greater complexity, and perhaps the influence of other factors. More investigation is warranted.

The study did not investigate the data at the level of each combination of control input variables, because the number of combinations is essentially too large to manually observe. Instead, marginal sums and maxima over operating points and/or environmental conditions provided the basis of analysis. It is possible that there may be some method to examine the large data set, but it is thought that such an investigation would be more suitable when a specific behaviour or anomaly is in view. It was noted that the O(PECRA) contours

tended to align with wave steepness, indicating that future work with wave steepness and energy is needed.

The question of how to efficiently and accurately characterize PECRA was addressed by looking at the range and resolution of the input control variables. It was found that the environmental conditions might be reduced in range, but probably need to be increased in resolution. It was also found that both the range and resolution of the operating points may need to be increased, particularly in terms of the range of speeds. Further investigation is required.

Finally, the utility of Operational Overlays was introduced as a means of extending usefulness of underlying probability data for all users, from the designer to the operator.

8. REFERENCES

- ANEP-77, Naval Ship Code, NATO, Ed. 4, December 2012
- Bales, S.L., Lee, W.T., and Voelker, J.M. 'Standardized Wave and Wind Environments for NATO Operational Areas'. DTNSRDC, (Report DTNSRDC/SPD-0919-01), 1981.
- McTaggart, K.A., De Kat, J. O., 'Capsize Risk of Intact Frigates in Irregular Seas', SNAME Transactions, 2000.
- STANAG 4194, Standardized Wave and Wind Environments and Shipboard Reporting of Sea Conditions, Ed. 2, 1994.
- Ypma, E., Harmsen, E., Development of a new methodology to predict the capsize risk of ships, 11th International Conference on the Stability of Ships and Ocean Vehicles, Athens, Greece, 2012.



Comparative Stability Analysis of a Frigate According to the Different Navy Rules in Waves

Emre Kahramanoğlu, *Yıldız Technical University*, emrek@yildiz.edu.tr

Hüseyin Yılmaz, *Yıldız Technical University*, hyilmaz@yildiz.edu.tr

Burak Yıldız, *Yıldız Technical University*, buraky@yildiz.edu.tr

ABSTRACT

As it is known, the naval ships are vulnerable to be damaged because of their mission. Therefore the most important parameter is survivability for them. This parameter is directly related to damaged stability analysis. In this study, the intact and damaged stability analysis of a frigate which is partially modernized have been carried out in waves according to three different navy rules. In addition to its conformity with these three different groups of rules, it has been examined that whether there are conflicting and varying points of different group of rules with each other and it has been tried to determine which one is more realistic.

Keywords: *damage stability, frigate, naval ship stability*

1. INTRODUCTION

Probability of damaging is very high for naval ships and it is related to their vocation. Therefore survivability is one of the most important parameter for them. Thereby intact and damaged stability analyses are so important for these ships in every circumstance.

Up to today there are many the studies which include the ships' intact and damaged stability analysis in waves. Some of them are mentioned.

A ship's intact and damaged stability analyses were made by Lee et al. (2012) via 2D linear method to determine the response of the ship in waves. On another study the waves were sent to model in different directions by Begovic et al. (2013). In that study the different scale of models' results were compared by the investigators. The global wave loads on ship which has zero speed was tried to determine by Chan et al. (2003). The analyses were made

intact and damaged situations. An algorithm was developed by Hu et al (2013) to determine the optimum response when a naval ship has damage. A study about second generation intact stability criteria was done by Belenky et al (2011). It also included the effect of wave crest or through which were on the amidships on stability. A study about parametric roll motion of ships which come across a longitudinal wave was carried out by Taylan et al (2012).

In this study, the intact and damaged stability analyses of a frigate which is designed conceptually are implemented in waves according to three different navy rules. Also the results are compared with each other.

2. NAVY RULES

Basically, the stability analyses are made depend on two curves with regard to navy rules. One of them is the righting arm and the other is heeling arm. The heeling arm curve can



be made by beam winds, icing, lifting of heavy weights over the side, crowding passengers on one side or high speed turning.

2.1 American Navy Rules (DDS079)

Basically, in reference to DDS079 stability criteria depend on the areas under the righting and the heeling arm curves, the ratio of these areas, the equilibrium angle of the two curves and the ratio of arm's value at the equilibrium angle and the maximum righting arm (GZmax) (DDS079,2002). On the Figure 1 classically, the areas and the curves are shown.

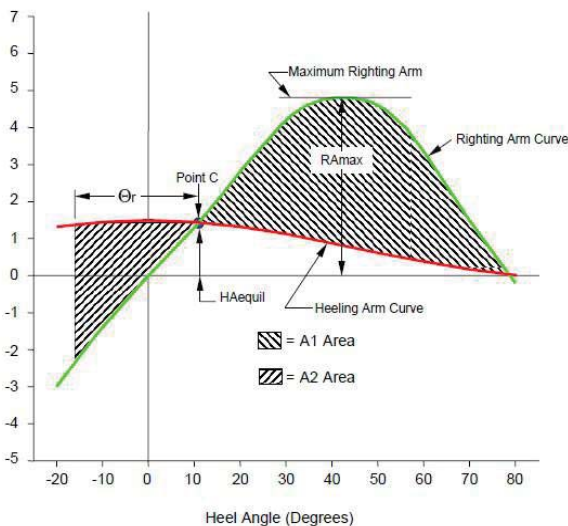


Figure 1. The areas and the curves with reference to DDS079 (2002)

With respect to the DDS079 the heeling arms are calculated by using these formulas:

Caused by beam winds:

$$HA = \frac{0.0195 * V_w^2 * A * z * \cos^2 \varphi}{1000 * \Delta} \quad (1)$$

Caused by lifting of heavy weights or crowding passengers over the side:

$$HA = \frac{w * a * \cos \varphi}{\Delta} \quad (2)$$

Caused by high speed turning:

$$HA = \frac{V^2 * a_1 * \cos \varphi}{g * R} \quad (3)$$

In here,

A: projected sail area

V_w : wind speed

z: lever arm from half draft to centroid of sail area

a: transverse distance from centreline to end of boom

a_1 : distance between ship's centre of gravity (KG) and centre of lateral resistance with ship upright

g: acceleration due to gravity

R: radius of turning circle

φ : angle of inclination

Δ : displacement

2.2 German Navy Rules (BV1030)

10. Basically, with reference BV1030 stability criteria depend on the equilibrium angle of the two curves. By using this angle a reference angle is determined. At the reference angle the residual arm must be greater than the minimum value (BV1030, 2001). In the Figure 2, the residual arm and the equilibrium angle are shown.

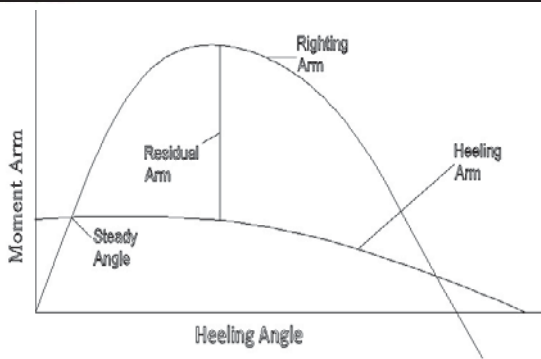


Figure 2. In regard to BV1030 (2001) the arm curves

With respect to the BV1030 (2001) some of the heeling arms can be calculated by using these formulas:

Caused by beam winds:

$$HA = \frac{A_w * (A_{WOH} - 0.5 * T)}{\Delta * g} * P_w * (0.25 + 0.75 * \cos^3 \varphi) \quad (4)$$

Caused by free surface effect:

$$HA = \frac{\sum (\rho * i)}{\Delta} * \sin \varphi \quad (5)$$

Caused by high speed turning

$$HA = \frac{C_D * V^2 * (KG - 0.5 * T)}{g * LWL} * \cos \varphi \quad (6)$$

Caused by crowding passenger over the side:

$$HA = \frac{P * Y}{\Delta * g} * \cos \varphi \quad (7)$$

In here,

A_w : projected sail area

A_{WOH} : centroid of sail area

P_w : wind pressure

ρ : density of liquids in the tanks

Y : transverse distance from centreline to centroid of passengers

i : moment of inertia of liquids in tanks

g : acceleration due to gravity

C_D : coefficient for turning

V : vessel speed

KG : centre of gravity

T : draft of vessel

φ : angle of inclination

Δ : displacement

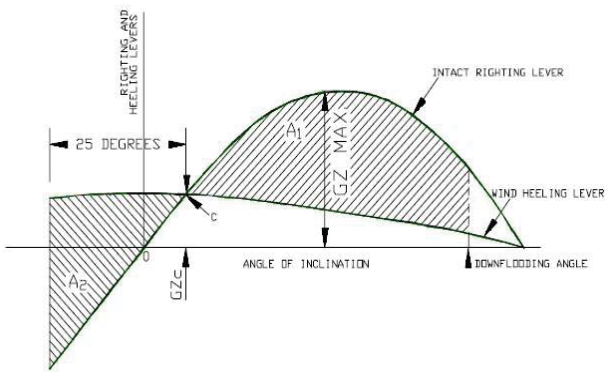
LWL : length of waterline

P : weight of passenger

2.3 English Navy Rules (NES109)

Basically, in accordance with NES109 stability criteria depend on the areas under righting and heeling arm curves, the ratio of these areas, the equilibrium angle of the two curves and the ratio of arm's value at the equilibrium angle and the maximum righting arm (GZ_{max}). In addition of these criteria it has some other requirements. For example the value of GM , GZ_{MAX} , and the area of from 30° to 40° etc. (NES109, 2000)

Formulas in order to calculate heeling arms are same as the DDS079. But it has different notations and different limitations. In the Figure 3 classically; the areas and the curves are shown.



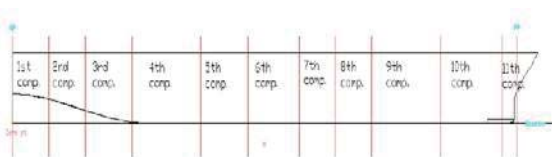
11. Figure 3. In regard to NES109 (2000) the areas and the arm curves

3. SPECIFICATIONS OF THE SHIP

12. Form used in analyses was designed by Sener (2012). This form has been designed conceptually in this study. During the design, from steel weight to weapon and electronic systems lots of parameters have been chosen, calculated and placed originally. In Table 1 the main values of the frigate are shown.

13. Table 1. Main values of the vessel

LOA	145	<i>m</i>
LPP	139	<i>m</i>
B _{MAX}	18,2	<i>m</i>
D	11,2	<i>m</i>
T	5,05	<i>m</i>
C _B	0,49	-
V	18	<i>knot</i>
V _{MAX}	30	<i>knot</i>



14. Figure 4 Subdivision of the frigate (Kahramanoglu, 2015)

15. In the Figure 3 the watertight bulkheads are shown on the vessel. The location of them has been settled by originally via taking into consideration experiments and other frigates (Kahramanoglu, 2015). But the damaged stability criteria are not considered when the locations are specified. Just the effect of this

localization has been tried to observe on the different navy rules.

4. COMPARATIVE STABILITY ANALYSES IN WAVES

Calculations are made considering each navy rules. On the intact stability analysis, initially, all calculations are made for the calm water. Then a sinus wave which has the same length and direction with the vessel is sent to the vessel. The wave crest is moved from fore to aft step by step. The same methodology is also used for the damaged stability analyses. On the damaged stability analyses, the wave crest is also considered.

4.1 Basic Differences Between Navy Rules

There are some differences between the navy rules. The calculation method of heeling arms and the assumptions are different. Therefore the results of the same analyses differentiate for each navy. The effects of the basic differences on the results are the main aim of this study.

Table 2. Basic differences among navy rules

Parameter	DDS079	NES109	BV1030
Wind speed (intact) (knot)	100	90	90
Wind speed (damaged) (knot)	35	34	40
Roll back (intact)(deg.)	25	25	-
Roll back (damaged) (deg.)	10,5	15	-
Damage length (m)	20,58	25	18
Wave height (m)	7,126	7,126	8,2
Limit of Initial heeling angle (damaged) (deg.)	15	20	25



In the Table 2, the values are demonstrated. Some of them are calculated and some of them are assumed such as wave height with regard to navy rules. Wave height has been assumed equal to DDS079 because of their methodology's similarity.

Damage cases are directly related to damage extents. The damage length values can be seen Table 2. So, as it is seen in Table 3, the damage compartments are different for each navy rules for some damage cases. Thereby the damage cases differentiate. It is assumed that the longitudinal extent of damage starts the near of the bulkhead shown in Figure 2 and moved towards to fore of the vessel. The transverse extent of damage is limited by centre line. The vertical extent of damage is limited by main decks. These limitations are chosen with regard to all navy rules.

Table 3. Damage scenarios

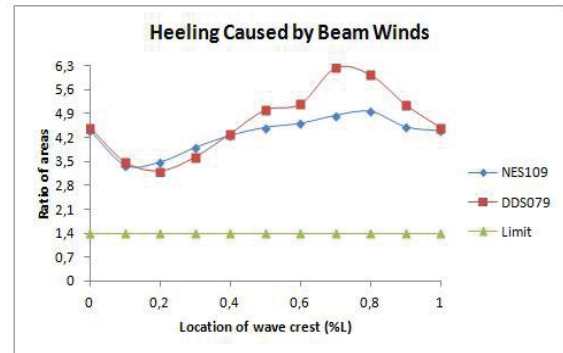
Damage Scenario	Damaged Compartments		
	BV1030	NES109	DDS079
D1	1-2	1-2-3	1-2-3
D2	2-3	2-3-4	2-3
D3	3-4	3-4	3-4
D4	4-5	4-5	4-5
D5	5-6	5-6	5-6
D6	6-7	6-7-8	6-7
D7	7-8	7-8-9	7-8-9
D8	8-9	8-9	8-9
D9	9-10	9-10	9-10
D10	10-11	10-11	10-11

4.2 Intact Stability Analysis

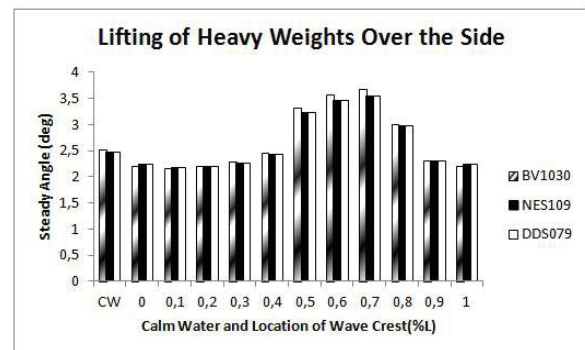
All analyses are made for full load case. Firstly, analyses are carried out for calm water. Then they are repeated in waves. From fore to aft wave crest is moved $0.1 \cdot L$ step by step (Kahramanoglu, 2015).

16. In this section, effects of the beam winds, lifting of heavy weights and crowding passenger over the side, high speed turning and

icing are investigated. In the figures some of the most critical results are shown. In Figure 5 effects of beam winds are shown. With respect to NES109 and DDS079 the ratios of areas are compared for different location of the wave crest.



17. Figure 5. Ratio of areas when beam winds cause heeling



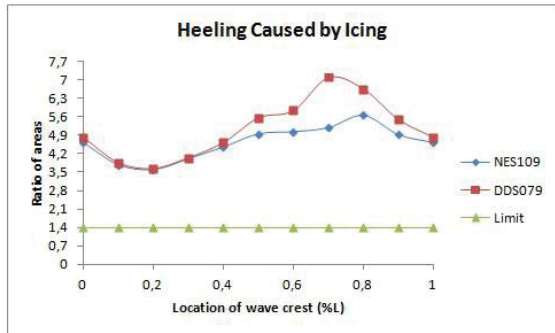
18. Figure 6. Effects of lifting of heavy weights over the side on the steady angle

In figure 6 the effects of lifting of heavy weights on steady angle are shown. In this figure the results of DDS079 and NES109 are the same because their calculation methods of heeling arm caused by lifting of heavy weights are the same. However, there are some differences for BV1030. The reason is that, the calculation method is different for BV1030. (2) and (7)

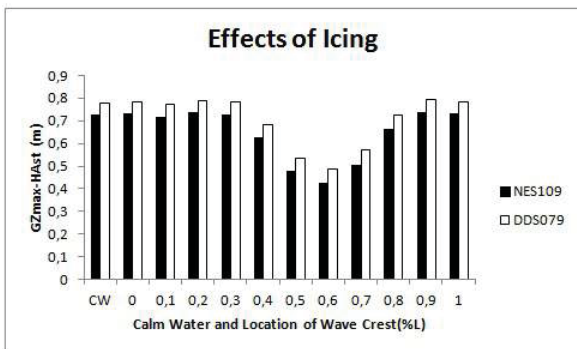
19. Effect of icing has similarities. For this section the calculation method and assumptions are different between NES109 and DDS079.



Therefore, the results differentiate. There are no extra criteria for BV1030 for icing. In Figure 7 and Figure 8 the differences of effects of icing are shown.



20. Figure 7. Ratio of areas when icing causes heeling



21. Figure 8. The differences about the arms when icing causes heeling

4.3 Damaged Stability Analyses

For damaged stability analysis the scenarios in Table 3 are used. The analyses are carried out for each navy rules. At first, all calculations are performed for calm water alike intact stability analyses. Then they are repeated for different location of the wave crest (Kahramanoglu, 2015).

In both intact and damaged stability analyses, it is considered that ship is operating in head wave condition in addition to calm water. With respect to all of three navies the damaged stability analyses are performed for

damaged conditions. Wind is coming to the ship from beam direction in all cases while the wind velocity differs in regard to the navy rules. However, wind velocities are different from intact ones (Table 2). The criteria are about the angles, areas and the ratio of GZ_{MAX} and GZ_{ST} ($=HA_{ST}$) for NES109 and DDS079. However, for BV1030 the criteria of damaged stability are about the angles and residual arm alike intact one.

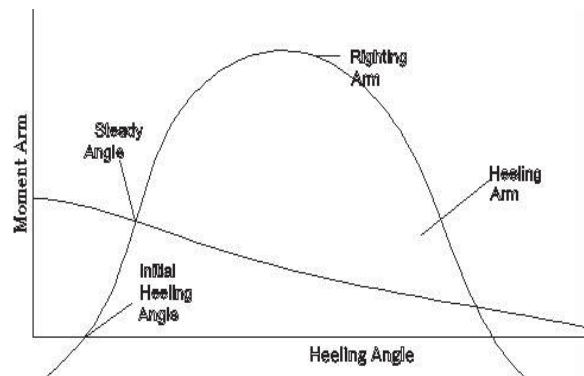
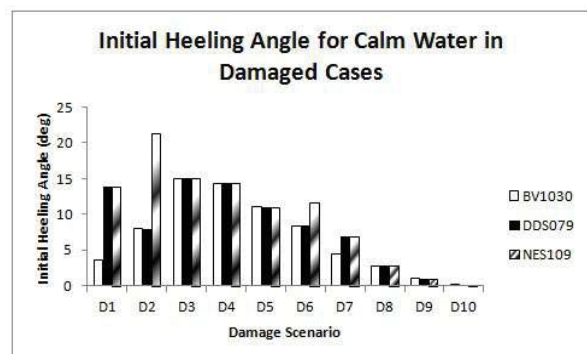


Figure 9. Initial heeling angle and steady angle in damaged stability analysis

In Figure 9 steady angle and the initial heeling angle are shown. These two parameters are crucial for each navy rules.

In Figure 10 and Figure 11, the steady angles and the initial heeling angles are shown for each navy rules and each damaged



scenarios in calm water.

Figure 10. Initial heeling angle for calm water in damaged cases

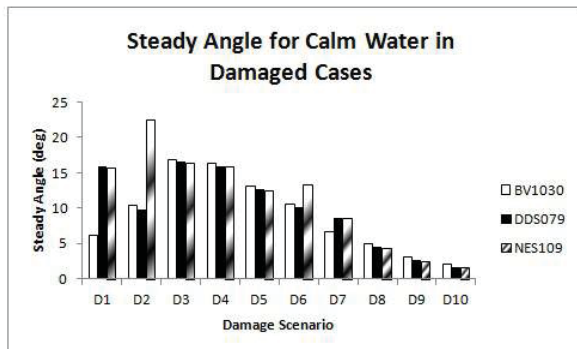


Figure 11. Steady angle for calm water in damaged cases

22. As can be seen from Figure 10 when number of damaged compartments is also same, the initial heeling angles are the same because this is related to vessel's hull form and distribution of weights. Figure 11 shows some differences for steady angles. This is related to the calculation of heeling arm in addition to vessel's hull form and distribution of weights.

Results of D1, D2, D6 and D7 scenarios are shown with more detail. Because these scenarios have differences in terms of initial heeling angle and steady angle and also they are more critic than the others (Kahramanoglu, 2015).

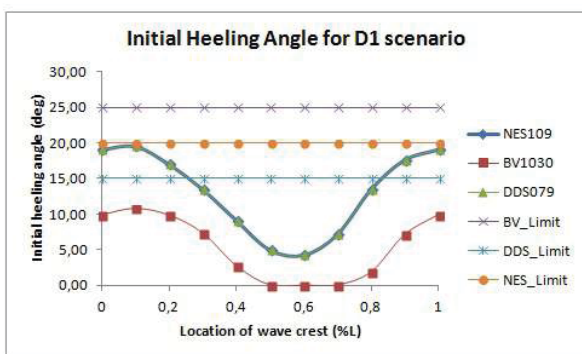


Figure 12. Initial heeling angle for D1 scenario

In Figure 12, initial heeling angles are shown for D1 scenario. It is observed that, the results of NES109 and DDS079 are the same. However, results of BV1030 are different and it can be also realised that the results of

BV1030 are less than the others. All these results are just related to number of damaged compartments. For D1 scenario, NES109 and DDS079 have same number of damaged compartments which is more than BV1030 (Table 3).

In Figure 13, initial heeling angles are shown for D2 scenario. For this scenario, because NES109 has more damaged compartments than BV1030 and DDS079, its results are higher. Moreover when the location of the wave crest is between $0,6 \cdot L$ and $0,8 \cdot L$, the criteria of damaged stability for NES109 is not adequate. The reason of differences between DDS079 and BV1030 is the wave height for this scenario (Table 2).

There are similarities between Figure 13 and Figure 14. As before the number of damaged compartments is higher for NES109. Because of this reason, the initial heeling angle values are higher. In addition to NES109, the criteria of damaged stability for DDS079 for D6 scenario are not adequate for some location of wave crest, too.

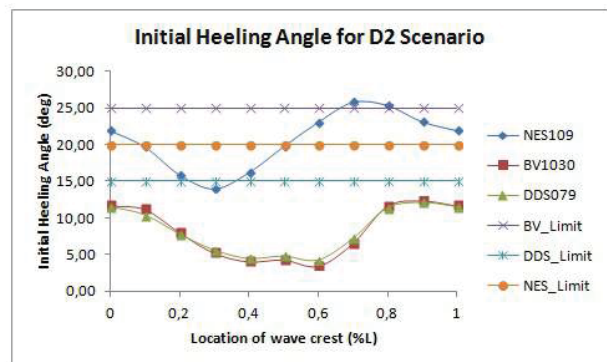


Figure 13. Initial heeling angle for D2 scenario

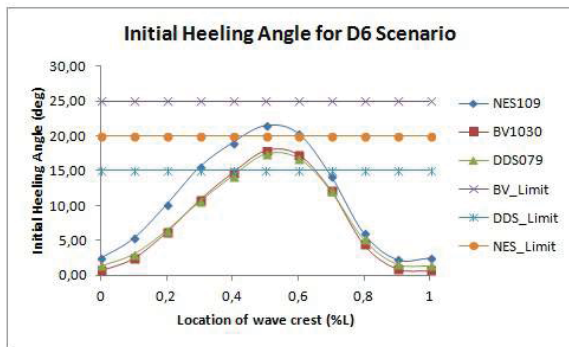


Figure 14. Initial heeling angle for D6 scenario

The results of other scenarios for initial heeling angle do not have significant differences between each other. The little differences' reason is the wave height (Kahramanoglu, 2015).

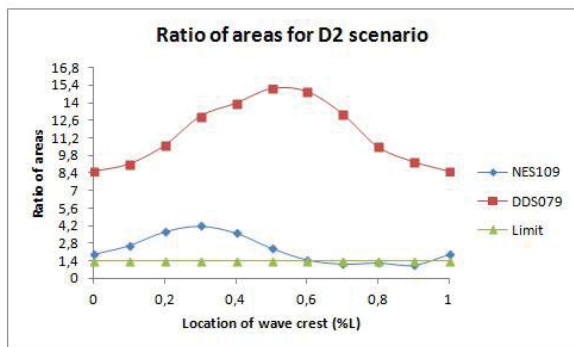


Figure 15. Ratio of areas for D2 scenario

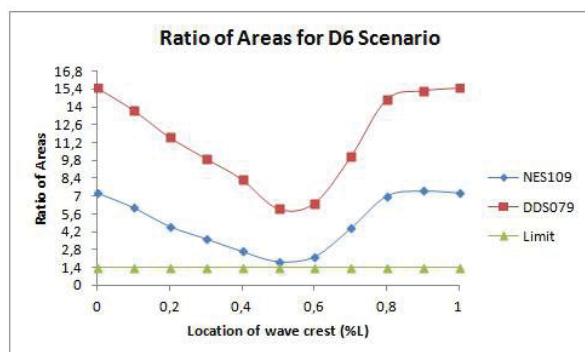


Figure 16. Ratio of areas for D6 scenario

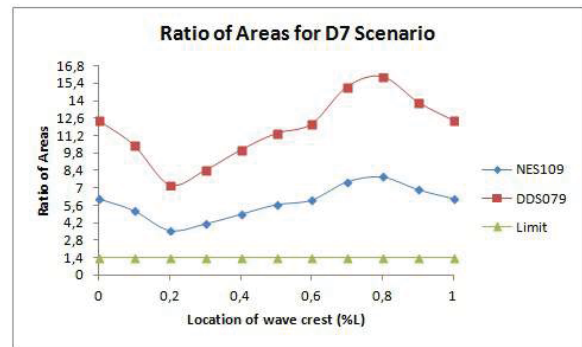


Figure 17. Ratio of areas for D7 scenario

When Figure 15 is examined, it can be realised that when the location of crest is between $0,6*L$ and $0,7*L$ the ratios of areas are lower than minimum value for NES109. It means that the stability requirements are not satisfied for NES109 when the location of crest is between $0,6*L$ and $0,7*L$. However, according to DDS079 all the points satisfy the criteria. The reason of these differences is same as before ones. The calculation method of areas and the number of damaged compartment are different so the results differ.

In Figure 16, the reasons of differences are same with Figure 15. Moreover, the ratios are lower for NES109 for both figures.

In Figure 17, one of the reasons mentioned just before is disappeared. The number of compartments is the same for NES109 and DDS079 for D7 scenario. However, the values of NES109 are again lower. At this point, while it is known that the only difference is the calculation method of areas. The effects of the method can be picked out easily. The other scenarios' results for ratios are just same with D7 scenario.

5. CONCLUSIONS

For each navy rules, effects of beam winds are more important than the others for intact stability analysis. NES109 and DDS079 have more strict rules than BV1030 for intact stability.



For damaged stability analysis the most important parameter was length of damage. In this respect, NES109 had the maximum value and BV1030 is the minimum. Therefore, sometimes NES109 had more damaged compartments than BV1030 and sometimes it had more damaged compartments than BV1030 and DDS079. This has made it difficult to meet adequate stability criteria.

When present form and load case are taken into consideration;

- Satisfying criteria of initial heeling angle was more difficult than criteria of ratio of areas.
- Among three navy rules, BV1030 was the simplest to meet criteria.
- Because considering areas and being limit values higher, NES109 was the most suitable one (just for this form and loadcase)
- Location of wave crest was very important for stability analyses and the most critical points of it were a little bit forward from amidships and it is thought that it could be related to vessel's form.
- When damage was near amidships, it could be more critical for each navy rules.

6. REFERENCES

- Lee, Y., Chan, H.S., Pu, Y., Incecik, A. and Dow, R.S., (2012). "Global Wave Loads on a Damaged Ship", Ship and Offshore Structures, 7:237-268.
- Begovic, E., Mortola, G., Incecik, A. and Day, A.H.,(2013). "Experimental Assessment of Intact and Damaged Ship Motions in Head, Beam and Quartering Seas", Ocean Engineering, 72:229-236.
- Chan, H.S., Atlar, M. and Incecik, A., (2003). "Global Wave Loads on Intact and Damaged Ro-Ro Ships in Regular Oblique Waves", Marine Structures, 16:323-344.
- Hu, L.F., Ma, K. and Ji, Z., (2013). "A M-H Method-Based Decision Support System for Flooding Emergencies Onboard Warship", Ocean Engineering, 58:192-200.
- Belenky, V., Bassler, C.C. and Spyrou, K.J., (2011). "Development of Second Generation Intact Stability Criteria", NSWCCD, 3-24.
- Peşman, E. and Taylan, M., (2012). "Influence of Varying Restoring Moment Curve on Parametric Roll Motion of Ships in Regular Longitudinal Waves", Marine Science and Technology, 17:511-522
- DDS 079-1, (2002). Stability and Buoyancy of U.S. Naval Surface Ships, Department of The Navy, Version 1.2.
- NES 109, (2000). Stability Standards for Surface Ships, Ministry of Defence, Bristol.
- BV1030, (2001). Construction Regulations for German Vessels 1030-1 Stability of Surface Combatants, Koblenz.
- Sener, B., (2012). Developing of frigate type hull form series and hydrodynamic form optimization, PhD Thesis, YTU Institute of Science, Istanbul (in Turkish).
- Kahramanoglu, E. (2015). Naval ships' intact and damaged stability analysis in waves, MSc. Thesis, YTU Institute of Science, Istanbul (in Turkish).

This page is intentionally left blank



Towing Test and Motion Analysis of a Motion- Controlled Ship - Based on an Application of Skyhook Theory

Jialin Han, *Doctoral Student, Department of Systems Innovation, School of Engineering, the
University of Tokyo, Japan* kankarin@iis.u-tokyo.ac.jp

Teruo Maeda, *OPD Research Center* t-maeda@theia.ocn.ne.jp

Takeshi Kinoshita, *Adjunct Professor, Department of Oceanic Architecture and Engineering,
College of Science and Technology, Nihon University, Japan* kinoshit@iis.u-tokyo.ac.jp

Daisuke Kitazawa, *Associate Professor, Institute of Industrial Science, the University of Tokyo,
Japan* dkita@iis.u-tokyo.ac.jp

ABSTRACT

A novel-concept catamaran called the Motion-Controlled Ship (MCS) Type-6 is proposed. It consists of a cabin, two hulls, four suspension setting units as well as four relative dependence control system units. The cabin and hulls are separated by suspensions. By implementing adaptive control algorithms, the motion modulation of the cabin is realized. A hull-excited bench test is conducted to validate the function of the control systems, following which a model ship towing test is performed in regular wave conditions. The motion responses of the MCS in terms of heave, pitch and roll are analysed under five control algorithms at two different towing speeds. Compared to a rigid body catamaran (in which suspension systems are invalid), pitch is eliminated by a maximum of 93% and an average of 74.8% under certain test conditions.

Key Words: *Catamaran, Motion Control, Stability, Skyhook, Suspension System*

1. INTRODUCTION

Ride comfort plays an important role in ground vehicle evaluation. Numerous researchers have dedicated themselves to the investigation and improvement of devices for shock absorption or vibration elimination. Currently, suspension setting, which comprises springs and dampers, is commonly applied in such motion control systems.

Comparing road profiles to the ocean surface, one finds that the latter is much

rougher and can easily lead to violent shaking; however, suspension settings have seldom been used in ocean vehicles to improve ride comfort and stability.

The development of a Motion-Controlled Ship (MCS) has been ongoing since 2008. The MCS Type-1, shaped similar to a tricycle, had

three small hulls and one big submerged float (Figure 1). One suspension setting, which consisted of a spring and an oil damper, was equipped between the cabin and one of the hulls. It was found that strong dampers had a relatively high efficiency in reducing the motion of the small hulls but had less effect on the cabin (Lu. 2010).

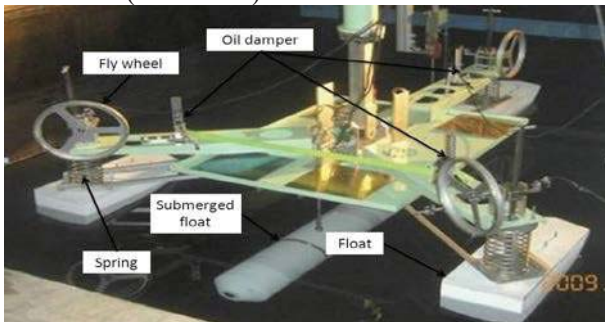


Figure 1 Structure of the MCS Type-1

The MSC Type-2 was a catamaran. It had two suspension setting units on each hull, located at the front and rear (Figure 2). The test results indicated that the reduction of the heave and pitch motions of the cabin was improved along with the increase of the damping coefficient when the towing speed was 1.5 m/s . The results also suggested that the relative displacement between the cabin and hulls could produce sufficient kinetic energy to be reused (Tsukamoto. 2012).



Figure 2 Structure of the MCS Type-2

Instead of oil dampers, the so-called electronic damper was formed and applied to the MCS Type-3 (Figure 3). A stepping motor was connected to a load resistor in series to construct an electrical circuit; by tuning the value of the resistance, the current in the circuit was made to vary and therefore the rotations of the motor shafts were adjusted. This affected

the angular velocity of a pinion that meshed with a rack, leading to a change in the relative velocity between the cabin and hulls. This can be seen as an equivalent result of that obtained by damper tuning. A towing test was performed; it was shown that the ability of motion elimination increased along with the reduction of load resistance, which meant an increase in the damper coefficient. It also implied that a strategy of simultaneously enhancing motion control and energy harvesting is possible. A compromise between those aims is necessary and should be made according to the use of the ship (Han. 2013a).

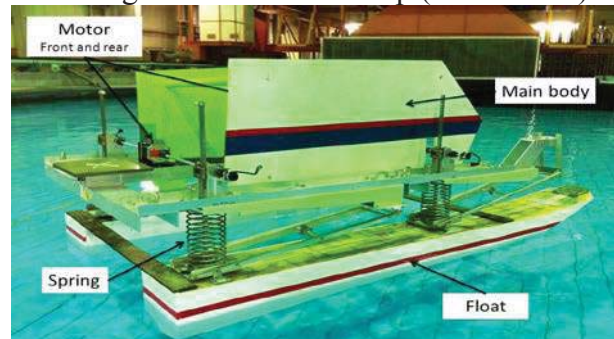


Figure 3 Structure of the MCS Type-3

A semi-active motion control system was developed for the MCS Type-4. The ship structure was similar to the Type-3, except the number of motors in one control system was increased from one to two. The control system analysed the feedback signals of the acceleration of the cabin as well as the relative velocity between the cabin and hulls, then determined whether or not to trigger the motion-control system. Through the inductive force generated by the motors, the heave and pitch of the cabin could be reduced. This was proved by a towing test. In the wave energy harvesting phase, the motors acted as generators, and a wave energy harvesting potential (defined as the ratio of the harvested energy to the wave energy contained by the crest over the width of the hulls) of 110% was achieved (Han. 2013b).

Between Type-2 and Type-4, the MCS can be seen as a high speed ship with hulls that planed on the sea surface. Type-5 adopted displacement type hulls.



an inspiration for the design concept of the proposed motion control system.

In the model ship, the hulls are excited by waves. The wave force can be illustrated as a combination of a spring force (K_w) and a damping force (C_w). Meanwhile, the suspension system, set between the cabin and hulls, provides another spring force (K), while the motor fit on the cabin produces a reaction force meant to counteract the force that acts on the cabin. This skyhook-like dynamic configuration is shown in Figure 6.

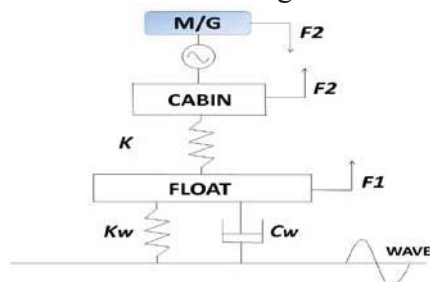


Figure 6 Configuration of the model ship dynamic

Specifically, when a spring starts to expand or contract from its neutral length, the motor applies power to restrain it (motor mode); when the spring expands or contracts to the normal length, the generator absorbs the spring power and converts it into electricity (generator mode); hence, the external force acting on the cabin is supposed to be zero.

3.2. DC Motor and Sensor

Considering the affordability of the control system, a brushed DC motor Maxon-353300, made by Maxon Japan Co. Ltd, is selected and tested. The stall torque of the motor is $1.41Nm$, the terminal resistance is 1.06Ω . The sensitivity of the G-sensor is $1.2V$ per gravitational acceleration.

3.3. PI Control System

Our control contains both proportional and integral elements and is therefore known as PI control. In P control the system acts in such a

manner that the control effort is proportional to the error, while which of I control is proportional to the integral of the error.

In the current study, only I control is activated. The acceleration of the cabin is detected by a G-sensor and transferred to an integral operator to calculate the cabin's absolute velocity. The difference between the reference velocity (set to zero) and the cabin absolute velocity is analysed. By tuning the gain of the I control, the instruction signal measured in voltage (V_{out}) is varied. This signal is fed to the motor and determines the value of the torque force it generates. Such torque force acts on the hull through a rack-pinion unit that eventually restrains the motion of the cabin. Therefore a new acceleration is generated, and causes the control circle to repeat until the current velocity of the cabin reaches $0m/s$, this procedure is shown in Figure 7.

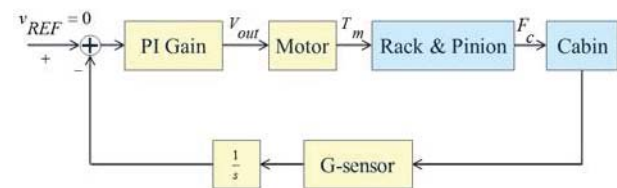


Figure 7 PI control procedure

4. HULL-EXCITED BENCH TEST AND SIMULATION

A hull-excited bench test is performed to validate the proposed skyhook control system, simplified to one degree of freedom.

4.1 Experiment Setting

An oscillation machine is settled on a heavy steel framework (Figure 8). The oscillation operator is connected to a metal support on which the model ship rides. The hulls are tightly tied to the bottom of the metal support, when the oscillation machine exerts a force at the centre of gravity of the frame-ship structure, the hulls move along with the metal support,

therefore yielding heave motion in the cabin.

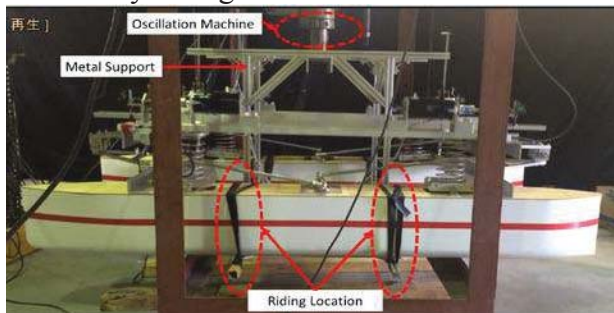


Figure 8 Experimental set-up of the bench test

4.2 Experiment Conditions

A simulation model with one degree of freedom is built in LTspice[®], which is an open source analogue electronic circuit simulator produced by the semiconductor manufacturer Linear Technology (LTC).

The value of the mechanical friction is estimated in two steps. First, the skyhook control system is eliminated; therefore a simple mass-spring-mass structure is constructed. Under this condition a bench test is implemented and the heave response of the cabin is recorded. Second, tuning the value of the friction in the simulation program until the similar motion response of the cabin is obtained. The value of friction is determined at this point.

The I-gain (G_I) based on the design of our PI control system is expressed as a multiplication of several components, shown in Equation (1):

$$G_I = G_G \times G_{IC} \times G_{PA} \times G_A \quad (1)$$

where G_G is the gain of the G-sensor, equal to $0.122V/(m/s^2)$; G_{IC} is the gain of the integrator circuit, expressed as $25s^{-1}$ (s is the Laplace Operator); G_{PA} is the gain of a power amplifier, equal to 4; G_A is the gain of an adjusting unit, which is a ratio of a reference resistance ($47k\Omega$) to R_{sky} . Note that R_{sky} is an adjustable resistance, so G_I therefore can be described as

$$G_I = 573.4 / (s \cdot R_{sky}) \quad (2)$$

Here, R_{sky} can be seen as a medium for modulating the magnitude of the PI control system. According to the test results, we find that if R_{sky} is smaller than $4k\Omega$, an unstable motion is observed for the cabin. Therefore, we consider that $4k\Omega$ is the threshold value of R_{sky} . In order to make a comparison between the performance of several skyhook control conditions, another two R_{sky} are decided: $10k\Omega$ and $20k\Omega$. The equivalent I-gains of these cases are 143.35, 57.34 and 28.67, respectively.

The stroke amplitude of the hulls is set as $3cm$, while frequency is $0.8Hz$, $1.0Hz$, $1.2Hz$ and $1.4Hz$.

4.1 Experimental Results

The results of the bench test and the simulation for the dimensionless heave and power consumption are shown in Figure 9 to Figure 12. The x-axis represents stroke frequency, while y-axis is either dimensionless heave or power consumption.

In Figure 9, it is found that among the three resistances, $R_{sky} = 4k\Omega$ shows the strongest motion-elimination ability, reducing the heave by more than 50%. When R_{sky} gets bigger, such elimination ability gets weaker. Moreover, in the same control algorithm, a higher stroke frequency achieves better motion elimination. The heave motion is mitigated to 20.5% when $R_{sky} = 4k\Omega$ and $f = 1.4Hz$.

In Figure 10, the simulation results show the same trend, along with the variety of R_{sky} and f . However, compared to Figure 9, a significant deviation of the magnitude of heave is observed, which might be caused by the rough estimation of the friction or other unconsidered factors.

In Figures 11 and 12, it is easy to determine



that when $R_{sky} = 4k\Omega$, the power consumption maintains its highest level, which decays if R_{sky} grows bigger. This proves that in order to achieve better motion control, more power consumption is necessary. The power can be seen as partially used to maintain the stability of the cabin and partially devoted to overcoming friction. Note that the stability in the bench test is worse than that in the simulation, which implies that the power consumption should be smaller. However, the overall power consumption in the bench test is higher than that in the simulation, suggesting that more power is consumed in overcoming friction during the test than the simulation. This conclusion agrees with the inference in the above motion analysis.

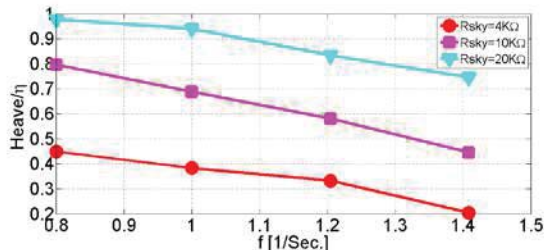


Figure 9 Dimensionless heave in bench test

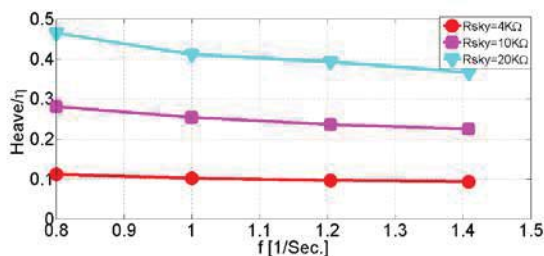


Figure 10 Dimensionless heave in simulation

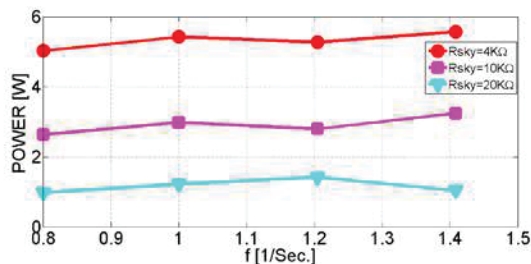


Figure 11 Power consumption of bench test

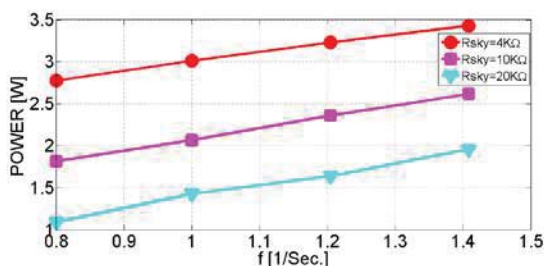


Figure 12 Power consumption of simulation

4.3 Conclusions

Through the comparison between the simulation and the bench test, the one-degree-of-freedom control system was evaluated. Conclusions can be summarized as:

- The control circuit and control panel are well-designed and the brushed DC motor is well functioned. Four one-degree-of-freedom control system sets perform reasonably.
- Higher I-gain produces better heave motion reduction. $R_{sky} = 4k\Omega$ is currently the optimal skyhook control condition and could be adopted as a test condition in the towing tank test.
- A better motion control strategy consumes more power.
- The friction of the ship structure should be discussed further so as to improve the accuracy of the simulation program.

5. TOWING TEST AND RESULTS

5.1 Model Ship Specifications

The components and the structure of MCS Type-6 are given in Figure 13. The model ship is 1.6m in length and 0.83m in width. The weight of the cabin session is 34.71kg, which of the hulls session is 13.14kg. The mass of the suspension parts is equally distributed into those two sessions. The spring constant is 615N/m and water surface is 0.498m². The locations of the four control spots are arranged symmetrically 0.445m from the centre of gravity of the hulls from bow to stern.

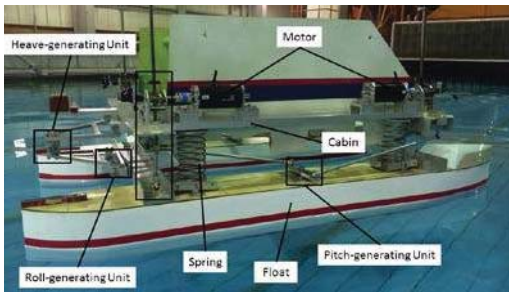


Figure 13 Structure of the MCS Type-6

1.11	0.9	3.06	0.050
1.25	0.8	1.94	
1.43	0.7	2.54	
2.00	0.5	4.97	

Table 2 Regular wave conditions $\beta = 90^\circ$

Wave Period [sec]	Frequency [Hz]	Wave Amplitude [cm]	Wave slope
0.67	1.5	1.12	0.100
0.77	1.3	1.47	
0.83	1.2	1.71	
0.91	1.1	2.06	
1.00	1.0	2.48	
1.11	0.9	3.06	
1.25	0.8	3.88	0.050
1.43	0.7	5.08	
2.00	0.5	4.97	

5.2 Experiment Descriptions

A towing test was performed in December 2014, at Ocean Engineering Basin in the Chiba Campus of the University of Tokyo.

In order to evaluate the efficiency of the skyhook control system, a rigid body catamaran is used as a reference model. By connecting the cabin and the hulls with four metal plates, the suspension system was invalid, therefore an equivalent model of rigid body catamaran is formed, called Rigid Body mode.

Control OFF mode, is a test condition when the skyhook control system is turned off, by only letting springs be functioned.

Skyhook control algorithms are $R_{sky} = 4k\Omega$, $10k\Omega$ and $20k\Omega$, which are the same as the bench test.

The towing test is performed in regular wave conditions which are listed in Table 1 and Table 2. The direction of wave propagation β is 180° and 90° . Due to the limitation of the towing tank, the towing speed is chosen as 0.0m/s and 1.5m/s.

Table 1 Regular wave conditions $\beta = 180^\circ$

Wave Period [sec]	Frequency [Hz]	Wave Amplitude [cm]	Wave slope
0.67	1.5	1.12	0.100
0.77	1.3	1.47	
0.83	1.2	1.71	
0.91	1.1	2.06	
1.00	1.0	2.48	

5.3 Motion Responses

The results of the heave, pitch and roll of the cabin are given from Figure 14 to Figure 19. The x-axis represents the encounter wave frequency, while the y-axis represents dimensionless value.

When $\beta = 180^\circ$, Control OFF mode shows the biggest motion response and significant resonances are observed. Compared to the rigid body mode, control modes show several levels of reduction in heave and pitch motion, the potential of which increases along with the decrease of R_{sky} . In other words, $R_{sky} = 4k\Omega$ shows the best motion elimination. It agrees with the conclusion in the bench test.

When $\beta = 90^\circ$, only the control mode in $R_{sky} = 4k\Omega$ is tested. Comparing the control mode to the rigid body mode, heave motion is greatly reduced, especially around the resonance frequency. However, in roll motion such reduction only appears around the resonance frequency. In other wave frequencies, rigid body shows relatively smaller motion response. In general, Control OFF mode



generates the largest motion magnitude.

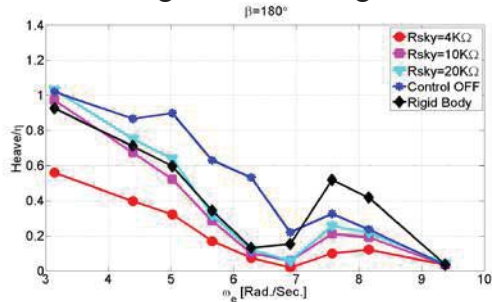


Figure 14 Dimensionless heave when $V = 0.0\text{m/s}$ at $\beta = 180^\circ$

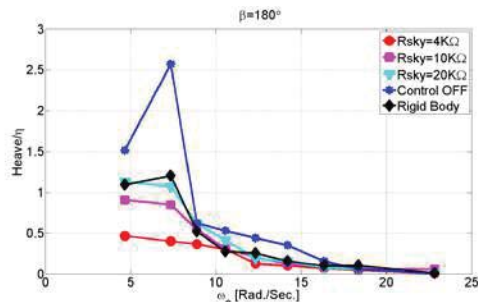


Figure 15 Dimensionless heave when $V = 1.5\text{m/s}$ at $\beta = 180^\circ$

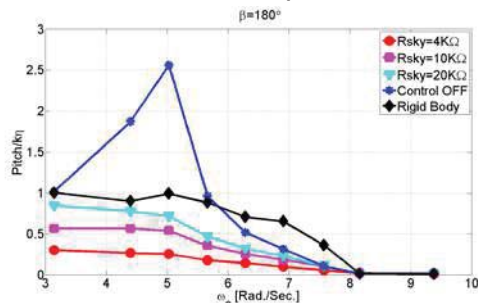


Figure 16 Dimensionless pitch when $V = 0.0\text{m/s}$ at $\beta = 180^\circ$

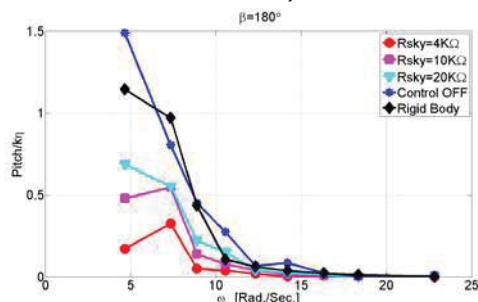


Figure 17 Dimensionless pitch when $V = 1.5\text{m/s}$ at $\beta = 180^\circ$

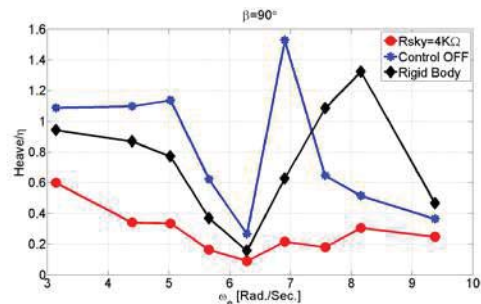


Figure 18 Dimensionless heave when $V = 0.0\text{m/s}$ at $\beta = 90^\circ$

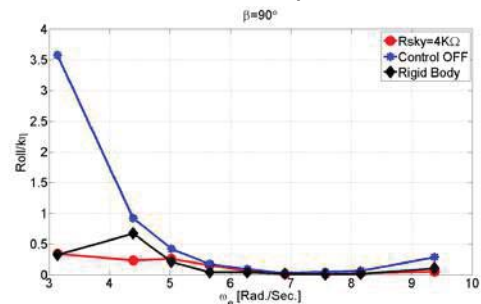


Figure 19 Dimensionless roll when $V = 0.0\text{m/s}$ at $\beta = 90^\circ$

5.4 Stability Evaluation of the Cabin

A ratio of motion response in Control Mode against Rigid Body mode is applied as an index of stability evaluation, which is expressed as

$$Ratio = \frac{ControlMode}{RigidBodyMode} \times 100 \quad (3)$$

The lower the ratio is, the better the stability represents. Assuming the benefit of a control mode is expressed in Equation (4). When the value is positive, a certain benefit is gained, otherwise a certain loss is obtained.

$$B = 100 - Ratio \quad (4)$$

The results of the ratio are shown from Figure 20 to Figure 24. When $\beta = 180^\circ$, in most of cases benefits are obtained. The highest benefit reaches up to 93% in pitch when $R_{sky} = 4k\Omega$, $V = 1.5\text{m/s}$, $\omega_e = 14.19\text{Rad/Sec}$.

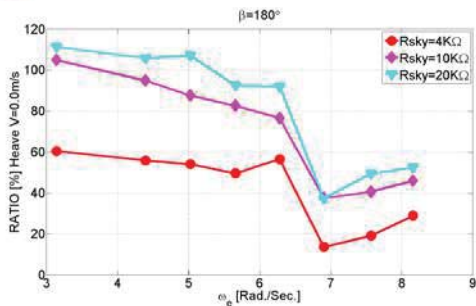


Figure 20 Stability of heave when $V = 0.0\text{m/s}$ at $\beta = 180^\circ$

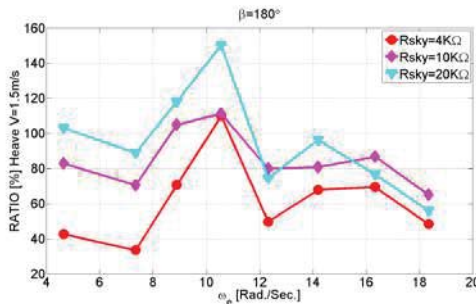


Figure 21 Stability of heave when $V = 1.5\text{m/s}$ at $\beta = 180^\circ$

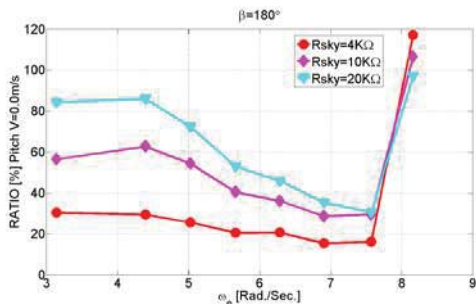


Figure 22 Stability of pitch when $V = 0.0\text{m/s}$ at $\beta = 180^\circ$

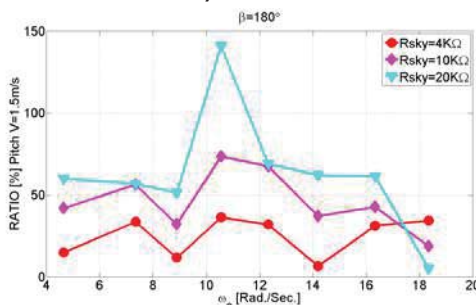


Figure 23 Stability of pitch when $V = 1.5\text{m/s}$ at $\beta = 180^\circ$

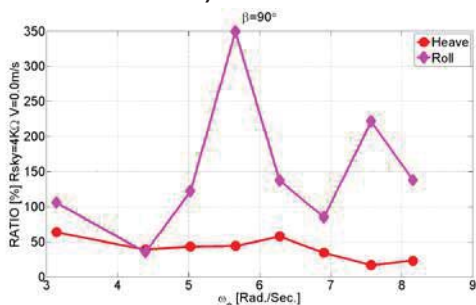


Figure 24 Stability of the cabin when $V = 0.0\text{m/s}$ at $\beta = 90^\circ$

If the average benefit is given by

$$B_{avg} = \sum_{n=1}^{n=8} (100 - Ratio_n) \quad (5)$$

Then the B_{avg} at $R_{sky} = 4k\Omega$ can be summarized and shown in Table 3. An average benefit in pitch reaches up to 74.8%, when the towing speed $V = 1.5\text{m/s}$ and $\beta = 180^\circ$. However, an average loss of 49.35% in roll is obtained when $V = 0.0\text{m/s}$ and $\beta = 90^\circ$.

Table 3 Average benefit level at $R_{sky} = 4k\Omega$

	$\beta = 180^\circ$		$\beta = 90^\circ$	
	0.0m/s	1.5m/s	0.0m/s	0.0m/s
heave	57.7	38.5	heave	59.7
pitch	65.5	74.8	roll	-49.35

6. CONCLUSIONS

In the current study, a 1/5-scale model ship that contains suspension systems and brushed DC motors was tested and evaluated. A hull-excited bench test and a tank towing test were performed. The motion reduction of the heave, pitch and roll of the cabin under several control modes were validated.

The bench test showed that a reasonable heave motion reduction was obtained and the highest level reached up to 79.5% of reduction. A higher I gain in PI control algorithm, generated stronger motion elimination ability. However, because of the friction of the structure, extra power consumption was unavoidable. Further work will be required to understand friction control.

In the towing test, the optimal control algorithm agreed with the bench test, with an average benefit level of 74.8% in pitch when towing velocity is 1.5m/s. The peak reduction of pitch reached to 93% at a certain wave and control condition. However, this reduction was



not reproduced in roll motion.

In next step, the research might focus on improving the motion control system by developing an absolute position control model, and evaluating the motion responses in irregular wave conditions.

7. ACKNOWLEDGEMENT

I am sincerely grateful, to Mr. Yukitsugu Hirota who is a responsible, sophisticated and enthusiastic electro-dynamics expert and taught me a lot of principles about system controls and motors and to Mr. Hiroshi Itakura, an excellent technical staff member, who gave me sufficient support about parts manufacture and ship building.

The major part of this paper is based on results obtained from a project commissioned by the New Energy and Industrial Technology Development Organization (NEDO). A part of the paper was supported by Japan Society for the Promotion of Science (JSPS), Grant-in-Aid for Challenging Exploratory Research, 25630399.

8. REFERENCE

Jialin Han, Teruo Maeda, Takeshi Kinoshita, Daisuke Kitazawa, 2013a, "Towing Test and Analysis of an Oscillation Controlled Small Ship with Wave Energy Converters", World NAOE Forum 2013 & International Symposium on Marine and Offshore Renewable Energy, Tokyo, Japan.

Jialin Han, Teruo Maeda, Takeshi Kinoshita, Daisuke Kitazawa, 2013b, "Research on a Motion-Controlled Ship by Harvesting Wave Energy-Based on a Semi-Active Control System", The 6th East Asia Workshop for Marine Environment and Energy, Qingdao, China.

Chenliang Lu, 2010, "A Comfortable Boat with

Suspensions Absorbing Wave Power", Master Thesis, Department of Systems Innovation, School of Engineering, the University of Tokyo.

Daisuke Tsukamoto, 2012, "Basic research on a wave energy absorbing and motion-controlled ship", Master Thesis, Department of Systems Innovation, School of Engineering, the University of Tokyo. (In Japanese)

Session 11.3 – EXTREME BEHAVIOUR

Statistical Uncertainty of Ship Motion Data

An Investigation into the Capsizing Accident of a Pusher Tug Boat

**Rapid Ship Motion Simulations for Investigating Rare Stability
Failures in Irregular Seas**

**Dynamic Instability of Taut Mooring Lines Subjected to Parametric
Excitation**

This page is intentionally left blank



Statistical Uncertainty of Ship Motion Data

Vadim Belenky, *NSWCCD (David Taylor Model Basin)*, vadim.belenky@navy.mil

Vladas Pipiras, *University of North Carolina at Chapel Hill*, pipiras@email.unc.edu

Kenneth Weems, *NSWCCD (David Taylor Model Basin)*, kenneth.weems@navy.mil

ABSTRACT

Records of nonlinear ship motion data, which are the basis for a probabilistic assessment of dynamic stability of a ship in irregular waves, are produced by time-domain numerical simulations or model tests in a basin. The volume of such samples is finite, so any statistical estimates calculated from a sample are random numbers and need to have a confidence interval, which quantifies the statistical uncertainty of the estimate. Ship motion data samples generally come in the form of an ensemble of records for a given condition, in which dependence may be very strong within the record, while the records themselves are independent of one another.

Since multiple data points describe the same feature of the process, statistically dependent data usually contains less information in comparison to independent data, so the confidence interval is wider for a set of dependent data than for the same amount of independent data. The paper revisits known mathematical methods to account for data dependency in computing the variance of the mean estimate and the variance of the variance estimate, which are the basis for computing a confidence interval of these estimates. The paper also addresses the calculation of the variance of the mean and variance of the variance for an ensemble of independent records of different length. The issue of minimum record length is considered and it is shown that a record of any length can contribute to the ensemble estimates of mean and variance.

Keywords: *Confidence interval, Statistical estimate*

1. INTRODUCTION

The development of probabilistic models for the assessment of the dynamic stability of a ship requires a characterization of the nonlinear response of the ship to severe sea conditions. This characterization is generally based on time-domain numerical simulations or model-scale experiments in large, “random” waves derived from theoretical or experimental representations of severe ocean waves. The direct results of such model test or numerical simulation campaigns are presented as a set of time histories of ship motion in large amplitude, irregular waves.

As the waves are irregular, the time histories are records of a stochastic process of ship motions. The most basic statistical processing includes the estimation of the mean value and variance or standard deviation. These estimates are essentially random numbers, which tend to the true value as the volume of data increases. A confidence interval is a measure of how close the estimate is likely to be to the true value, and is presented as a range of values and a probability, P_β , that the true value is within that range. For example, an estimate of standard deviation with its confidence interval can be presented as:

$$\hat{\sigma} = [\sigma_{low}; \sigma_{up} | P_\beta] \quad (1)$$



It means that there is a P_β chance that the true value of the standard deviation is between the lower boundary σ_{low} and upper boundary σ_{up} . The confidence probability P_β is an *a priori* given or agreed value; $P_\beta=0.95$ is widely used for engineering purposes. The “hat” above a symbol indicates an “estimate”, which is a random value. The absence of a “hat” indicates that the value is deterministic.

Engineering calculations will typically use the upper and/or lower values of the confidence interval as a bound of the actual expected value. For example, if a measure of the intensity of ship motion is needed for further assessment or calculation, the upper boundary of confidence interval can be used as a conservative value. A change to the confidence probability P_β allows the conservatism of the assessment to be “tuned” to a level appropriate for the task in hand. A larger P_β will result in a wider confidence interval for an estimate and a wider range of values for assessments based on that estimate, but reduce the likelihood that the true value of the assessment is outside of the computed range.

Confidence intervals are heavily used in validation as they enable the comparison of two estimates; this application aspect (among others) is considered in Smith and Zuzick (2015) and is outside of the scope of this paper. Another use for the confidence interval is in the planning of model tests and numerical simulations, as it can help to determine the number and length of model tests or simulation runs that are needed to achieve required accuracy; this type of application is also outside the scope of this paper.

The uncertainty of statistical estimates is of particular concern for assessments, which involve the prediction of extreme responses or low-probability events from non-linear time domain data. Since these assessments are fundamentally extrapolations, the uncertainty in the results will tend to be very sensitive to the uncertainty in the statistical characterization of the data. For this reason,

the consideration of the statistical uncertainty of ship motions is an important part of the ONR project “A Probabilistic Procedure for Evaluating the Dynamic Stability and Capsizing of Naval Vessels” (Belenky, *et al.*, 2015).

2. CONCEPT OF ENSEMBLE

The ensemble is a set of ship motion data records which represent a single or narrow range of sea and operating conditions. By its definition, it presumes that more than one record may be needed. Why is this so?

- Limitations on record length; for model tests in a seakeeping basin, the limited size of the facility will limit the duration of any test run with forward speed. As a result, a single record may have too few wave encounters to assess motions. This will particularly be true for cases with high speed and/or following or quartering seas.
- Practical non-ergodicity; the nonlinearity of ship behavior may cause one run to be insufficient for a complete assessment, even if it is relatively long. A typical example is parametric roll in head seas (Reed 2011), for which a typical run in a linear basin did not provide the necessary variation in initial conditions for proper statistical characterization of parametric roll.
- Valid modeling of irregular waves for numerical simulation. The elevation, pressure and velocity field of the incident wave is generally modeled using Fourier series, where amplitudes are defined by spectra and phases are random. The duration for which such a model will produce statistically independent waves will depend on the number of frequencies used for the discretization of a spectrum (Belenky, 2011). Increasing the number of frequencies in the wave model incurs a significant computational cost, so a set of

relatively short records, each of which requires fewer wave frequencies, is computationally more efficient than one long record requiring many frequencies.

The records in ensemble are not necessarily of the same length. It is both difficult and unnecessary to ensure that experimental runs have exactly the same duration.

In the analysis of irregular wave motion data, the processes of waves and ship motions are assumed to be stationary. If the ship capsizes, the response of the “mast-down” ship will be fundamentally different for its upright response, which has to be considered as a violation of the stationarity of the motion process. Attempting to include pre-capsize, capsize and post-capsize motion as part of a single stationary process will make the required volume of the data impractical. As a result, the record has to be cut immediately prior to capsizing. Similarly, it may be necessary to truncate a model test run if variations in the speed or relative heading of the ship become too large. Both of these scenarios may result in records of different lengths.

Thus, the ensemble for a particular wave environment, speed and heading is an irregular data structure that can be described by a “nested array” defined as an array that contains other arrays as elements. To avoid confusion with typical matrix notation, the following nomenclature will be used:

$$X = [x_i]_j ; \quad i = 1, \dots, Np_j ; \quad j = 1, \dots, Nr \quad (2)$$

The index within the square bracket refers to a data point within a record while the index outside of the square brackets relates to the record number. An example data structure is illustrated in Figure 1.

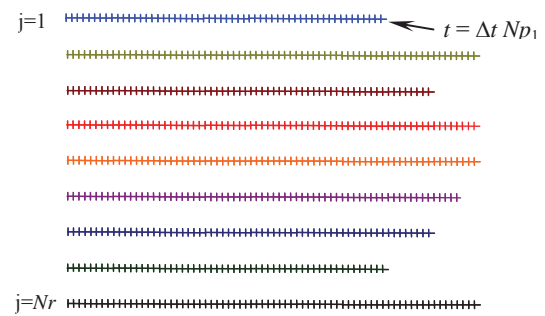


Figure 1: Illustration of a nested array

The data points within each record are dependent, while no dependence is expected between the records. Dependence between the data points is a result of inertia of ship motions, hydrodynamic memory and inertia of water particles in wave. Independence between simulation records is ensured by using different pseudo-random sets of initial phases in the model of the irregular waves. Independence between model test records is supported by the pseudo-random actuation of the wave maker and by the time lag between runs; this time usually is sufficient for the waves to be radiated and decay on the damping beach of a basin.

The combination of dependent and independent data within a single sample is specific to ship motion data.

3. ESTIMATES FOR A SINGLE RECORD

The consideration starts with examining mean value and variance estimates and their confidence interval for a single record. To simplify the notation, the square brackets and record index are not used in this section.

3.1 Dependence and Uncertainty

Consider the mean value and variance estimates.

$$\hat{E} = \frac{1}{Np} \sum_{i=1}^{Np} x_i \quad (3)$$

$$\hat{V} = \frac{1}{Np-1} \sum_{i=1}^{Np} (x_i - \hat{E})^2 \quad (4)$$

The dependency within a record does not matter for these estimates. Changing the sampling rate or time increment will change the number of data points, but it will be reflected in the number Np . As long as the time increment remains within the reasonable range, *e.g.* it does not become large compared to the response period of the ship, the estimates (3) and (4) are affected very little.

This is not true for the confidence interval. The confidence interval is a metric of statistical uncertainty, which generally decreases with an increased volume of the sample. Theoretically, the width of the confidence interval goes to zero when the volume of the sample becomes infinite, because the estimate becomes a true value. Increasing the sampling rate does not increase the amount of information available in the sample; however the number of data points becomes larger. The data points become closer to each other. Since the same information is carried by more points, the dependence between data points becomes stronger, and the contribution of each of them is decreased.

Conversely, if the increment between the data points is increased, their dependence is decreased and the contribution of each individual data point becomes larger. Further increase of the increment (decrease of the sampling rate) should lead to independence. Once the independence is achieved, the contribution of each data point can no longer be affected by other points. This means that the number of independent points will define the amount of information available in the sample. The dependence between the data points may therefore have a serious effect on uncertainty and the width of the confidence interval. The mathematical treatment of this influence is considered further.

3.2 Variance of the Mean Value

Estimates of the mean value and variance of the process X are random numbers and, as any other random numbers, may have a variance. Priestley (1981) gives a general direction for the derivation of the formulae for the variance of mean value and variance estimates. That derivation was reproduced in Belenky *et al.* (2013) in order to examine the role of the assumption of normal distribution for X . An abridged version of this derivation is included below for the sake of completeness.

Apply a variance operator to both sides of equation (3) and treat the sum as if the values are dependent, so the variance of the sum is a sum of all of the terms of the covariance matrix:

$$\begin{aligned} \text{var}(\hat{E}) &= \text{var}\left(\frac{1}{Np} \sum_{i=1}^{Np} x_i\right) = \\ &= \frac{1}{Np^2} \sum_{i=1}^{Np} \sum_{j=1}^{Np} \text{Cov}(x_i, x_j) \end{aligned} \quad (5)$$

$\text{Var}(\cdot)$ is the variance operator and $\text{Cov}(\cdot)$ is the covariance operator. Since the process X is assumed to be stationary, its auto-covariance function depends only on the difference in time (time lag) between the two points and does not depend on particular time instances:

$$\begin{aligned} \text{Cov}(x_i, x_j) &= R(t_{i-j}) = R(\tau_k) \\ k &= 0, 1, \dots, Np-1 \end{aligned} \quad (6)$$

Consider a sum of all the elements of the covariance matrix in Equation (5):

$$\sum_{i=1}^{Np} \sum_{j=1}^{Np} \text{Cov}(x_i, x_j) = \sum \begin{pmatrix} R(\tau_0) & R(\tau_1) & \dots & R(\tau_{N-2}) & R(\tau_{N-1}) \\ R(\tau_1) & R(\tau_0) & \dots & R(\tau_{N-3}) & R(\tau_{N-2}) \\ \dots & \dots & \dots & \dots & \dots \\ R(\tau_{N-2}) & R(\tau_{N-3}) & \dots & R(\tau_0) & R(\tau_1) \\ R(\tau_{N-1}) & R(\tau_{N-2}) & \dots & R(\tau_1) & R(\tau_0) \end{pmatrix} \quad (7)$$

The elements of the main diagonal are variances:

$$R(\tau_0) = R(0) = V \quad (8)$$

The other elements on the line parallel to the main diagonal are also the same; the next element to the term $R(\tau_0)=V$ is always $R(\tau_1)$, then $R(\tau_2)$ and so forth. The main diagonal of a $Np \times Np$ square matrix contains Np elements. The lines of elements parallel to the main diagonal and located next to it contain only $Np-1$ elements. Each subsequent line will have one fewer element, until diagonals at the low-left or upper-right corner have only one element. Having in mind that the covariance matrix is symmetric relative to its main diagonal and all the “lines of elements” except the main diagonal are encountered twice:

$$\begin{aligned} \sum_{i=1}^{Np} \sum_{j=1}^{Np} Cov(x_i, x_j) &= Np \cdot V + \\ 2((Np-1)R(\tau_1) + (N-2)R(\tau_2) + \dots + R(\tau_{N-1})) &= \\ Np \cdot V + 2 \cdot \sum_{i=1}^{Np-1} (N-i)R(\tau_i) \end{aligned} \quad (9)$$

Substitution of Equation (9) into Equation (5) leads to the standard formula for the variance of the mean value estimate (see *e.g.* Priestley 1981):

$$\text{var}(\hat{E}) = \frac{V}{Np} + \frac{2}{Np} \cdot \sum_{i=1}^{Np-1} \left(1 - \frac{i}{Np}\right) \cdot R(\tau_i) \quad (10)$$

The first term in Equation (10) is actually the variance of the mean estimate of a random variable, while the second term accounts for the dependence between the data points of a stochastic process. As expected, if the process X is uncorrelated white noise (Wiener process), the result is identical to the one for a random variable, because the auto-covariance function of the white noise equals zero for all non-zero time lags.

3.3 Variance of the Variance

Variance is, by definition, the average of centered squares, so a process Y is introduced as:

$$y_i = (x_i - E)^2 \approx (x_i - \hat{E})^2 \quad (11)$$

The estimate of the mean value of the process Y is the estimate of the variance of the original process x :

$$\hat{E}_y = \hat{V} \quad (12)$$

The variance of the mean estimate of the process Y is then the variance of the variance estimate of the process X :

$$\text{var}(\hat{V}) = \frac{V_y}{Np} + \frac{2}{Np} \cdot \sum_{i=1}^{Np-1} \left(1 - \frac{i}{Np}\right) \cdot R_y(\tau_i) \quad (13)$$

V_y and R_y are, respectively, the variance and the auto-covariance function of the process of centered squares Y .

The standard formula for the variance of the variance (*e.g.* Priestley 1981) uses the assumption that the process X is normal, which leads to

$$\text{var}(\hat{V}) = \frac{2V^2}{Np} + \frac{4}{Np} \sum_{i=1}^{Np-1} \left(1 - \frac{i}{Np}\right) (R(\tau_i))^2 \quad (14)$$

Because for the normal process

$$V_y = 2 \cdot V^2; \quad R_y(\tau) = 2 \cdot (R(\tau))^2 \quad (15)$$

Reed (2011) uses an alternative form of (14):

$$\text{var}(\hat{V}) = \frac{2}{Np} \sum_{i=-(Np-1)}^{Np-1} \left(1 - \frac{|i|}{Np}\right) (R(\tau_{|i|}))^2 \quad (16)$$

As noted in Belenky, *et al.* (2013), there is no apparent reason to use the normal assumption for the process X . The calculation of the auto-covariance function of the centered squares requires little additional computation effort in comparison with the straight auto-covariance function.

3.4 Estimate of Auto-Covariance

To use Equations (10) and (13), it is necessary to estimate the auto-covariance functions of the processes X and Y . The estimate is expressed as:

$$\hat{R}'(\tau_i) = \frac{1}{Np-i} \sum_{j=1}^{Np-i} (x_j - \hat{E})(x_{j+i} - \hat{E}) \quad (17)$$

Accuracy of the estimate (17) deteriorates very quickly for larger time lags due to insufficient data – as the time lag gets larger there are fewer pairs of data points with that time lag. This leads to statistical “noise” as shown Figure 2. This is obviously noise as there is no reason why the dependence could that strong after 500 seconds.

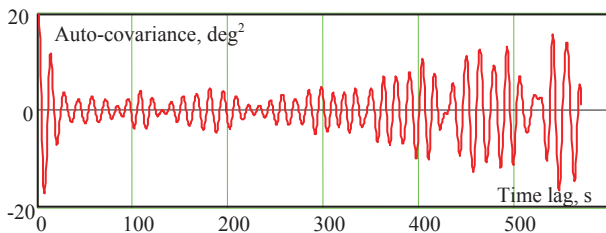


Figure 2 Estimate of auto-covariance function

This loss of accuracy can be alleviated by a simple weighting factor: $(Np-i)/Np$. Such weighting results in little change to the auto-covariance function for small time lags as the difference between Np and $Np-i$ is not significant for small i . When the index i becomes large, the amount of available data decreases and therefore the influence of its contribution also decreases. The weighted estimate is expressed as:

$$\hat{R}(\tau_i) = \frac{1}{Np} \sum_{j=1}^{Np-i} (x_j - \hat{E})(x_{j+i} - \hat{E}) \quad (18)$$

The result of weighting the estimate of the auto-covariance function is shown in Figure 3. It is apparent that the amount of “noise” has subsided, while the initial part (first 100 seconds) has not changed very much. Details on the numerical example can be found in Belenky *et al.* (2013).

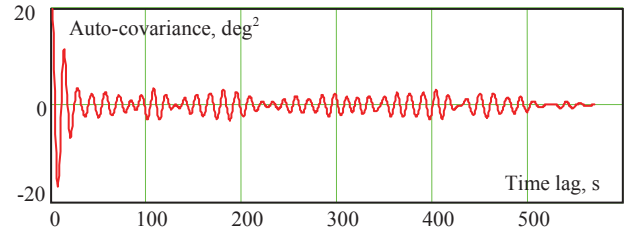


Figure 3 Weighted estimate of auto-covariance function

However, weighting the estimate may not be sufficient to get rid of all of the “noise”. Cases are still possible when the “noise” makes the calculations completely senseless (*e.g.* producing negative value of the variance of the mean) if one uses the estimate (18) in formulae (10) or (13). Since the auto-covariance estimates at large lags are still not very reliable, they can be cut off, at a point designated M . Equations (10) and (13) are re-written as:

$$\hat{\text{var}}(\hat{E}) = \frac{V}{Np} + \frac{2}{Np} \cdot \sum_{i=1}^{M-1} \left(1 - \frac{i}{M}\right) \cdot \hat{R}(\tau_i) \quad (19)$$

$$\hat{\text{var}}(\hat{V}) = \frac{V_y}{Np} + \frac{2}{Np} \cdot \sum_{i=1}^{M-1} \left(1 - \frac{i}{M}\right) \cdot \hat{R}_y(\tau_i) \quad (20)$$

Belenky, *et al.* (2013) considered $M=Np/2$, which works well if the estimate of the auto-covariance is fairly accurate. Further review of the literature has led to (Priestly, 1981; Brockwell and Davis, 2008):

$$M = \sqrt{Np} \quad (21)$$

Some sources also suggest $2\sqrt{Np}$ or $\sqrt{Np}/2$. The origin of this formula is optimality of spectral smoothing. The range $[0.5Np^{0.5}; 2Np^{0.5}]$ appears to represent an area where the result is not very sensitive to the specific value of M . The operation of cutting off the autocorrelation function is essentially the same as smoothing the spectral estimate. Spectral representations are a traditional way of processing ship motion information and can also be used for the estimate of the auto-covariance. However, the discussion of estimation of spectra is outside of the scope of this paper.

4. ESTIMATES OF AN ENSEMBLE

4.1 Estimate of Mean and Variance

Consider an ensemble of Nr records, each of which has Np_j data points. The time increment Δt is assumed to be the same for all the records, which is the usual practice for both numerical simulations and model tests. The statistical weight for each record is expressed as follows:

$$W_j = \frac{Np_j}{Nt} \quad (22)$$

Nt is the total number of points in the ensemble:

$$Nt = \sum_{j=1}^{Nr} Np_j \quad (23)$$

The ensemble estimate for the mean value is calculated for all of the points:

$$\hat{E}_a = \frac{1}{Nt} \sum_{j=1}^{Nr} \sum_{i=1}^{Np_j} [x_i]_j = \frac{1}{Nt} \sum_{j=1}^{Nr} \frac{Np_j}{Np_j} \sum_{i=1}^{Np_j} [x_i]_j = \sum_{i=1}^{Nr} W_i \left(\frac{1}{Np_j} \sum_{i=1}^{Np_j} [x_i]_j \right) = \sum_{i=1}^{Nr} W_i \hat{E}_i \quad (24)$$

\hat{E}_j is the mean value estimate for a record j . The ensemble estimate of the variance is:

$$\hat{V}_a = \frac{1}{Nt-1} \sum_{j=1}^{Nr} \sum_{i=1}^{Np_j} ([x_i]_j - \hat{E}_a)^2 = \sum_{i=1}^{Nr} W_j' \hat{V}_j' \quad (25)$$

$$\hat{V}_j' = \frac{1}{Np_j-1} \sum_{i=1}^{Np_j} ([x_i]_j - \hat{E}_a)^2 \quad (26)$$

$$W_j' = \frac{Np_j-1}{Nt-1} \quad (27)$$

The weights (27) are slightly different from (22). However, as the number of points is quite large (thousands and tens of thousands), one can state that

$$W_j \approx W_j' \quad (28)$$

Note that the variance estimate in (26) is not exactly the same as the record variance estimate from (4), as it uses the ensemble mean estimate instead of record mean estimate.

4.2 Estimate of Auto-Covariance Function

As the records may have different length, the estimate of the auto-covariance function (18) is padded with zeros to facilitate averaging across the record:

$$[\hat{R}_m]_j = \frac{1}{Np_j} \begin{cases} \sum_{i=1}^{Np_j-m} ([x_i]_j - \hat{E}_a)([x_{i+m}]_j - \hat{E}_a) & i+m < Np_j \\ 0 & i+m \geq Np_j \end{cases} \quad (29)$$

$m = 1, \dots, \max(Np_j)$

Like the data, the record estimate of the auto-covariance is presented in a form of nested array, with j being the index of record, while m is the index of the time lag. Since they have been padded by zeros, all of the record estimates of the auto-covariance function have the same length.

The ensemble estimate of the auto-covariance function is obtained by averaging across the records (assuming that if very short records are present in the ensemble, their statistical weight is small):

$$\hat{R}_a(\tau_m) = \sum_{j=1}^{Nr} W_j [\hat{R}_m]_j = \frac{1}{Nt} \sum_{j=1}^{Nr} \sum_{i=1}^{Np_j-m} \begin{cases} ([x_i]_j - \hat{E}_a)([x_{i+m}]_j - \hat{E}_a) & i+m < Np_j \\ 0 & i+m \geq Np_j \end{cases} \quad (30)$$

Note that for $m=0$, equation (30) yields an expression identical to the formula for ensemble averaged variance. The averaging procedure significantly decreases the amount of “noise”, as illustrated in Figure 4.

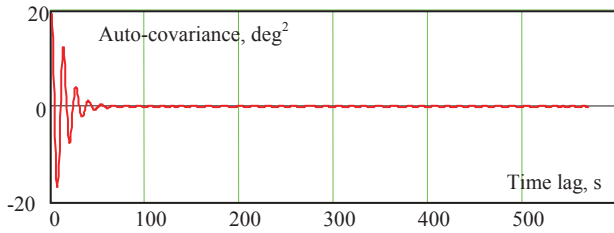


Figure 4 Ensemble-averaged estimate of auto-covariance function (Belenky *et al.*, 2013)

The formula for the ensemble averaged estimate for the process Y (the process of the centered squares) is similar to equation (30):

$$\hat{R}_{Ya}(\tau_m) = \frac{1}{Nt} \sum_{j=1}^{Nr} \sum_{i=1}^{Np_j-m} \begin{cases} ([y_i]_j - \hat{V}_a)([y_{i+m}]_j - \hat{V}_a) & i+m < Np_j \\ 0 & i+m \geq Np_j \end{cases} \quad (31)$$

The ensemble-averaged estimate of auto-covariance function of centered squared for an example set of roll data is plotted in Figure 5.

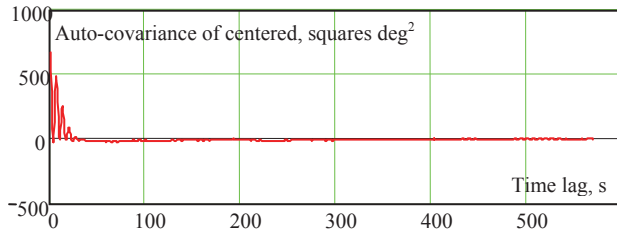


Figure 5: Ensemble-averaged estimate of auto-covariance function of centered squares (Belenky *et al.*, 2013)

4.3 Variances of Mean and Variance

In order to get the variance of the ensemble-averaged mean estimate, the variance operator is applied to both sides of equation (24):

$$\text{var}(\hat{E}_a) = \text{var}\left(\sum_{j=1}^{Nr} W_j \hat{E}_j\right) = \sum_{j=1}^{Nr} W_j^2 \text{var}(\hat{E}_j) \quad (32)$$

$\text{var}(\hat{E}_j)$ is the variance of the record mean value estimate, expressed with equation (19) where the auto-covariance function is estimated by equation (29). The cut-off point M can be taken for the ensemble:

$$M = \sqrt{\max(Np_j)} \quad (33)$$

Substitution of equations (19), (22) and (29) into (32) leads to:

$$\text{var}(\hat{E}_a) = \frac{1}{Nt} \sum_{j=1}^{Nr} W_j \hat{V}_j + \frac{2}{Nt} \sum_{m=1}^M \left(1 - \frac{m}{M}\right) \cdot \sum_{j=1}^{Nr} W_j [\hat{R}_m]_j \quad (34)$$

Here, the variance estimate (26) is used instead of the record estimate (4) for consistency with the auto-covariance estimate (29), so the ensemble mean estimate is used instead of record mean estimate.

Equations (25), (28) and (30) can be used to re-write equation (34) in terms of ensemble-averaged estimates:

$$\text{var}(\hat{E}_a) = \frac{\hat{V}_a}{Nt} + \frac{2}{Nt} \sum_{m=1}^M \left(1 - \frac{m}{M}\right) \cdot \hat{R}_a(\tau_m) \quad (35)$$

A similar argument can be made for the ensemble-averaged variance of the variance estimate:

$$\text{var}(\hat{V}_a) = \sum_{i=1}^{Nr} (W_j')^2 \text{var}(V_j) \quad (36)$$

$$\text{var}(\hat{V}_a) = \frac{\hat{V}_{Ya}}{Nt} + \frac{2}{Nt} \sum_{m=1}^M \left(1 - \frac{m}{M}\right) \cdot \hat{R}_{Ya}(\tau_m) \quad (37)$$

\hat{V}_{Ya} is the ensemble-averaged estimate of the variance estimate of the process Y (centered squares) based on the ensemble-averaged mean value estimate:

$$\hat{V}_{Ya} = \hat{R}_{Ya}(0) = \frac{1}{Nt} \sum_{j=1}^{Nr} \sum_{i=1}^{Np_j} ([y_i]_j - \hat{V}_a)^2 \quad (38)$$

4.4 Alternative Method for Variances of Mean and Variance

If the number of records is large enough, the variances of the mean and variance estimates can be computed without an auto-covariance estimate. Consider equation (32) for the special case where all of the records have the same length, so all the weights are the same and equal to $1/Nr$. The theoretical values of the variances of the mean estimates $\text{var}(\hat{E}_j)$ are the same for all the records. The variance of ensemble-averaged mean estimate for the records of the same length is expressed as:

$$\text{var}(\hat{E}_a) = \frac{\text{var}(\hat{E}_j)}{Nr} \quad (39)$$

If the bias is assumed to be small, the estimate can be used instead of theoretical value:

$$\hat{\text{var}}(\hat{E}_a) = \frac{1}{Nr^2} \sum_{j=1}^{Nr} (\hat{E}_i - \hat{E}_a)^2 \quad (40)$$

Equation (40) can then be presented as:

$$\hat{\text{var}}(\hat{E}_a) = \sum_{j=1}^{Nr} W^2 (\hat{E}_i - \hat{E}_a)^2 \quad (41)$$

$$W = \frac{1}{Nr}$$

The weight lacks a record index as all of the records are of the same length. However, this requirement is no longer necessary as the weight is inside the summation sign, so the record index j can be brought back:

$$\hat{\text{var}}(\hat{E}_a) = \sum_{j=1}^{Nr} W_j^2 (\hat{E}_i - \hat{E}_a)^2 \quad (42)$$

Formula (42) is equivalent to formula (35). To prove this, start by substituting (3) into (39):

$$\hat{\text{var}}(\hat{E}_a) = \sum_{j=1}^{Nr} W_j^2 \left(\frac{1}{Np_j} \sum_{i=1}^{Np_j} [x_i]_j - \hat{E}_a \right)^2 =$$

$$\sum_{j=1}^{Nr} W_j^2 \left(\frac{1}{Np_j} \sum_{i=1}^{Np_j} [x_i]_j - \frac{1}{Np_j} \sum_{i=1}^{Np_j} \hat{E}_a \right)^2 \quad (43)$$

$$\sum_{j=1}^{Nr} \frac{W_j^2}{Np_j^2} \left(\sum_{i=1}^{Np_j} ([x_i]_j - \hat{E}_a) \right)^2$$

Using the well-known formula for the square of a sum:

$$\left(\sum_{i=1}^N a_i \right)^2 = \sum_{i=1}^N \sum_{j=1}^N a_i a_j =$$

$$\sum_{i=1}^N a_i^2 + \sum_{i=1}^N \sum_{j=1, j \neq i}^N a_i a_j \quad (44)$$

$$\sum_{i=1}^N a_i^2 + 2 \sum_{i=1}^N \sum_{j=1}^{N-i} a_i a_{i+j}$$

Note the algebraic equivalence of the structure of equations (44) and (7). Applying the expansion (44) to equation (43) leads to:

$$\hat{\text{var}}(\hat{E}_a) = \sum_{j=1}^{Nr} \frac{W_j^2}{Np_j^2} \left(\sum_{i=1}^{Np_j} ([x_i]_j - \hat{E}_a) \right)^2 +$$

$$2 \sum_{m=1}^{Np_j} \sum_{i=1}^{Np_j-m} \left([x_i]_j - \hat{E}_a \right) \left([x_{i+m}]_j - \hat{E}_a \right) \quad (45)$$

The first term of (45) can be converted into a biased estimate of the record estimate and the second term can be converted into a non-weighted estimate of the auto-covariance function (17):

$$\hat{\text{var}}(\hat{E}_a) = \sum_{j=1}^{Nr} \frac{W_j^2}{Np_j} (V_j'' +$$

$$2 \sum_{i=1}^{Np_j} \frac{Np_j - i}{Np_j} \cdot \frac{1}{Np_j - i} \sum_{k=1}^{Np_j-i} ([x_i]_j - \hat{E}_a) \times$$

$$([x_{i+k}]_j - \hat{E}_a)) =$$

$$\sum_{j=1}^{Nr} W_j^2 \left(\frac{\hat{V}_j''}{Np_j} + \frac{1}{Np_j} \sum_{m=1}^{Np_j} \left(1 - \frac{m}{Np_j} \right) \cdot [\hat{R}_m']_j \right)$$

$$(46)$$

\hat{V}_j'' is the biased estimate of record variance.

$$\hat{V}_j'' = \frac{Np_j - 1}{Np_j} \hat{V}_j' \approx \hat{V}_j' \quad (47)$$

$$[\hat{R}_m']_j = \frac{1}{Np_j - m} \begin{cases} \sum_{i=1}^{Np_j - m} ([x_i]_j - \hat{E}_a)([x_{i+m}]_j - \hat{E}_a) & i + m < Np_j \\ 0 & i + m \geq Np_j \end{cases} \quad (48)$$

$m = 1, \dots, \max(Np_j)$

Substitution of equation (22) into (46) yields

$$\begin{aligned} \text{var}(\hat{E}_a) &= \frac{1}{Nt} \sum_{j=1}^{Nr} W_j \hat{V}_j'' + \\ &\frac{1}{Nt} \sum_{j=1}^{Nr} W_j \sum_{m=1}^{Np_j} \left(1 - \frac{m}{Np_j}\right) \cdot [\hat{R}_m']_j \end{aligned} \quad (49)$$

Introducing the cut-off point M defined by equation (33) completes the derivation

$$\text{var}(\hat{E}_a) = \frac{\hat{V}_a''}{Nt} + \frac{1}{Nt} \sum_{m=1}^M \left(1 - \frac{m}{M}\right) \cdot \hat{R}_a'(\tau_m) \quad (50)$$

Equation (50) is identical to equation (35), taking into account that the large number of points and insignificant bias:

$$\hat{V}_a'' = \sum_{j=1}^{Nr} W_j \hat{V}_j'' \approx \hat{V}_a \quad (51)$$

Estimates of auto-covariance (29) and (48) differ by weighting. However, they can still be considered to be approximately equal because the cut-off limits the influence of weighting, so

$$\hat{R}_a'(\tau_m) = \sum_{j=1}^{Nr} W_j [\hat{R}_m']_j \approx \hat{R}_a(\tau_m) \quad (52)$$

A similar argument can be made for the variance of the variance, allowing the following formula to be used for the

calculation of the variance of the ensemble-averaged variance estimate:

$$\text{var}(\hat{V}_a) = \sum_{j=1}^{Nr} W_j^2 (\hat{V}_j' - \hat{V}_a)^2 \quad (53)$$

Further consideration of equation (53) can be found in Belenky *et al.*, (2013).

4.5 Confidence Interval for Mean and Variance Estimates

The calculation of the boundaries of the confidence interval requires knowledge of the distribution of the estimates. This information is rarely available as distribution of the estimate is related with the distribution of the process itself. For example, if a sample of independent random variables is known to have normal distribution, the estimate of the mean will have student-t distribution and the distribution of variance estimate is related to 2 distribution.

The distributions of the processes of ship motion are not known. Even if the central part of the distribution can be approximated with normal for some motions and some ships, the mutual dependence of data points creates difficulties with using Student-t and 2 distribution. On the other hand, the sample, i.e. ensemble of records, is presented with large number of points. The calculations of the estimates involve mostly summation, so it seems appropriate to invoke the Central Limit Theorem, which allows the distribution of the estimates to be assumed to be normal.

This assumption presents no difficulties for the mean value, but may be a problem with variance estimate. The normal distribution supports negative values, while the variance and its estimate cannot be negative. Practical experience, however, shows that the confidence interval of variance is usually small enough to keep the low boundary of the variance far from zero. Nevertheless, the

possibility of numerical difficulties does exist, especially for smaller ensemble data volume.

Once the assumption of normality of distribution of the estimate is accepted, the calculation of the boundaries of confidence interval is trivial:

$$\begin{aligned} E_{low} &= \hat{E}_a - K_\beta \sqrt{\text{Var}(\hat{E}_a)} \\ E_{up} &= \hat{E}_a + K_\beta \sqrt{\text{Var}(\hat{E}_a)} \end{aligned} \quad (50)$$

$$\begin{aligned} V_{low} &= \hat{V}_a - K_\beta \sqrt{\text{Var}(\hat{V}_a)} \\ V_{up} &= \hat{V}_a + K_\beta \sqrt{\text{Var}(\hat{V}_a)} \end{aligned} \quad (51)$$

K_β is the $0.5(1+P_\beta)$ quantile of a standard normal distribution (with zero mean and unity variance):

$$\begin{aligned} K_\beta(P_\beta) &= Q_N\left(\frac{1+P_\beta}{2}\right) \\ K_\beta(0.95) &= 1.959964.. \approx 1.96 \end{aligned} \quad (52)$$

The confidence interval for standard deviation can be calculated using the “boundary” method (Bickel and Doksum, 2001):

$$\sigma_{low} = \sqrt{V_{low}} \quad ; \quad \sigma_{up} = \sqrt{V_{up}} \quad (53)$$

5. CONCLUSIONS AND FUTURE WORK

The analysis of dynamic stability in ocean waves is based primarily on irregular sea ship motion data obtained from model tests in the basin or time-domain nonlinear numerical simulations. As the volume of data from these sources is, by necessity, limited, such analyses must account for uncertainties that result from the finite volume of data. The present paper presents robust and easy-to-use formulae for the calculation of estimates of the mean value and variance, with confidence intervals, from such data.

Ship motions in irregular waves are generally presented as an “ensemble” of records of time-domain data which has been computed or measured for the same environmental conditions, loading conditions, speed and heading. The records are independent of each other, but there is a strong dependence between data points within each record. Different records may have different length, so the natural data structure for an ensemble is a nested array (*i.e.* an array containing other arrays).

The structure of the dependence (strong dependence within each record and independence of records to each other) does not affect the ensemble-averaged estimates of mean value and variance, but must be accounted for when evaluating the statistical uncertainty of those estimates. The dependence within each record is accounted for through estimates of the auto-covariance function of the value of ship motion processes and their centered squares. As these quantities are estimated from a finite-length time series, a cut-off point is introduced to limit the possible influence of statistical “noise” caused by a deterioration of accuracy for large time lags. The estimation of the auto-covariance functions may be avoided if an ensemble contains a sufficient number of independent records.

Future development may be expected in the relation of the statistical uncertainty with spectral characteristics. In particular, the smoothed spectral estimate can be seen as a natural source for the estimate of auto-covariance function. Further test calculations are desirable in order to determine how many independent records are “sufficient” to use formulae (39) and (48) instead of (32) and (37).

Future work may also include further testing of the formulae. This would include creating or collecting a large set of ensembles from different experimental and numerical sources in order to see how well the computed confidence interval captures the expected



values of the ensemble estimates. The fraction of estimates falling within the confidence interval should be close to the given confidence probability.

6. ACKNOWLEDGEMENTS

The work described in this paper has been funded by the Office of Naval Research, under Dr. Patrick Purtell, Dr. Ki-Han Kim and Dr. Thomas Fu. The authors greatly appreciate their support. The participation of Prof. Pipiras was facilitated by the Summer Faculty Program supported by ONR and managed by Dr. Jack Price (David Taylor Model Basin, NSWCCD). The authors are grateful to Dr. Mike Levine for internal support of this work.

Over the years of the development, many colleagues have influenced and contributed to our work. The authors would like acknowledge Prof. Pol Spanos (Rice University), Dr. Art Reed, Mr. Tim Smith, Mr. Brad Campbell, Dr. Mike Hughes (David Taylor Model Basin, NSWCCD), and Prof. Ross Leadbetter (University of North Carolina Chapel Hill).

7. REFERENCES

Belenky, V.L. 2011, "On Self-Repeating Effect in Reconstruction of Irregular Waves", Chapter 33 of "Contemporary Ideas on Ship Stability", Neves, M.A.S., *et al.* eds., Springer, pp. 589-598.

Belenky, V., Pipiras, V., Kent, C., Hughes, M., Campbell, B. and Smith, T. 2013, "On the Statistical Uncertainties of Time-domain-based Assessment of Stability Failures: Confidence Interval for the Mean and Variance of a Time Series", Proc. 13th Intl. Ship Stability Workshop, Brest, France, pp. 251-258.

Belenky, V., Weems, K. and Lin, W.M., 2015 "Split-time Method for Estimation of

Probability of Capsizing Caused by Pure Loss of Stability" in Proc. 12th Intl. Conf. on Stability of Ships and Ocean Vehicles STAB 2015, Glasgow, UK

Bickel, J. P. and Doksum, K. A., 2001 Mathematical Statistics: Basic Ideas and Selected Topics. Vol. 1, Prentice-Hall, Upper Saddle River, NJ.

Brockwell, P. J. and Davis, R. A., 2006, Time Series: Theory and Methods, Springer, 2nd edition.

Priestley, M. B., 1981, Spectral Analysis and Time Series, Vol. 1, Academic Press, New York.

Reed, A., 2011, "26th ITTC Parametric Roll Benchmark Study", Proc. 12th Intl. Ship Stability Workshop, Washington DC, USA pp 195-204.

Smith, T. C. and Zuzick A. 2015, "Validation of Statistical Extrapolation Methods for Large Motion Prediction" in Proc. 12th Intl. Conf. on Stability of Ships and Ocean Vehicles STAB 2015, Glasgow, UK.



An Investigation into the Capsizing Accident of a Pusher Tug Boat

Harukuni Taguchi, *National Maritime Research Institute (NMRI)* taguchi@nmri.go.jp

Tomihiko Haraguchi, *National Maritime Research Institute (NMRI)* haraguch@nmri.go.jp

Makiko Minami, *Japan Transport Safety Board (JTSB)* mminami@nmri.go.jp

Hidetaka Houtani, *National Maritime Research Institute (NMRI)* houtani@nmri.go.jp

ABSTRACT

This paper outlines a technical investigation into an accident of a pusher tug boat, which capsized whilst navigating near the outer boundary of Seto Inland Sea, Japan on 27 May 2013. In order to clarify the relation between rudder angle and heel angle in the manoeuvring motion of the capsized boat, an experiment using an actual similar boat was carried out. Utilising the experimental results and a stability calculation of the boat at the accident along with a statistically estimated roll angle in the waves at that time, a mechanism of capsizing was identified from energy balance like the IMO weather criterion concept.

Keywords: *accident investigation, pusher tug boat, capsizing, experiment with an actual boat, heel due to manoeuvring*

1. INTRODUCTION

A typical Japanese pusher tug boat “No. 38 Sankyo Maru” capsized off Awaji Island in Seto Inland Sea on 27 May 2013. The accident claimed two lives of crew on board. The Japan Transport Safety Board (JTSB) had investigated this accident and identified probable causes of the accident. The results of the investigations were compiled into an investigation report and submitted to the Minister of Land, Infrastructure, Transport and Tourism and publicized (JTSB, 2014).

As a technical part of the investigation, the National Maritime Research Institute (NMRI) carried out a manoeuvring experiment using an actual similar boat and utilising the experimental results a mechanism of capsizing was examined along with a stability calculation. Based on the technical investigation the JTSB concluded the probable causes of the accident

and issued recommendations in order to prevent similar accidents.

In this paper the main points of technical investigation are presented.

2. OUTLINE OF THE ACCIDENT

2.1 Summary of the Accident

“No. 38 Sankyo Maru” whilst returning to Osaka from Tokushima without a box barge capsized off Awaji Island around 15 o'clock on 27 May 2013. Two members of the crew in the bridge died and a skipper in the cabin inside the hull was rescued from the capsized boat. A high sea warning was issued at that time. The estimated wind and sea conditions at the time of the accident are summarised in Table 1.

According to the skipper, who took a nap at the accident, the boat suddenly heeled to the port side largely then capsized in a short time. But sequence and mechanism of the accident were not clear.

Table 1. Wind and Sea Conditions at the Accident.

Average wind speed	about 7 m/s ~ 8 m/s
Wind direction	SSW
Significant wave height	about 2 m ~ 3 m
Average wave period	about 5 s
Wave direction	S

2.2 Capsized Pusher Tug Boat “No. 38 Sankyo Maru”

“No. 38 Sankyo Maru” (Lr = 16.00 m, B = 5.50 m and D = 2.00 m) constructed in 2007 was a twin-propeller and twin-rudder pusher tug boat of 19 gross tons. The general arrangement of the boat is shown in Figure 1.

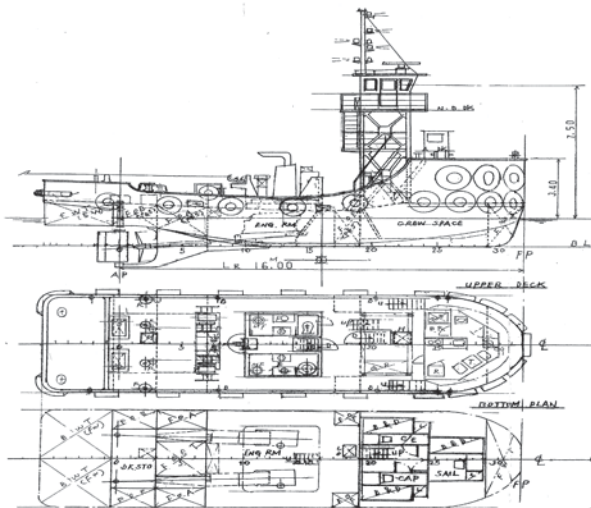


Figure 1 General Arrangement of “No. 38 Sankyo Maru”.

In order to secure enough manoeuvrability during linking with a box barge the rudder area ratio of the boat was relatively large and even with small rudder angle its steering quality was good. However, relatively large rudder area also led to inducing large heeling moment in

manoeuvring motion. Therefore, during navigating without a box barge in order to prevent large heel in changing course the skipper used to limit the rudder angle to about 5 degrees and ease the wheel immediately. And he instructed the crew to follow his way of steering the boat.

3. AT-SEA EXPERIMENT

Due to the above mentioned feature of the capsized boat it was presumed that heel angle in manoeuvring motion might be related to the occurrence of the accident but its characteristic was unknown. Therefore, in order to clarify the relation between rudder angle and heel angle in manoeuvring motion of the capsized boat, an experiment using an actual similar boat was carried out. From the experimental results an estimation method for heel angle of the capsized boat in manoeuvring motion was derived.

3.1 Outline of the Experiment

A twin-propeller and twin-rudder pusher tug boat “No. 58 Sankyo Maru” whose principal particulars, rudder area and output of main engines were the same as for the capsized boat was used in the experiment. At the experiment the boat was almost full loaded with fuel oil and fresh water.

Table 2. Hull Condition at the Experiment.

Displacement: W	141.31 t
Mean draft: d	1.69 m
Trim by stern: τ	1.11 m
Vertical C.G.: KG	1.99 m
Metacentric height: GM	0.76 m

An inclining test was carried out first to clarify the condition of the boat at the experiment and the result (Table 2) was used to estimate the condition of the capsized boat at the accident. Then, a manoeuvring experiment

was carried out and the boat motion (roll angle, yaw angle, yaw rate and so on) and the boat speed were measured. In the experiment not only rudder angle but also way of steering was changed (Table 3).

Table 3. Summary of the experiment

Kind of test	Turning test, weave manoeuvre test.
Approach speed	9 kn, the same as the presumed speed of the capsized boat at the accident.
Rudder angle (degrees)	(1)Turning test 5, 8, 10 (port), 10 (stbd.).
	(2) Weave manoeuvre test 7(port)-7(stbd.)-8(port)-6(stbd.), 9(stbd.)-8(port)-9(stbd.)-9(port), 10(port)-9(stbd.)-12(port)-12(stbd.), 13(port)-10(stbd.)-10(port)-13(stbd.), 22(stbd.)-17(port)-23(stbd.)-7(port).

3.2 Experimental Results

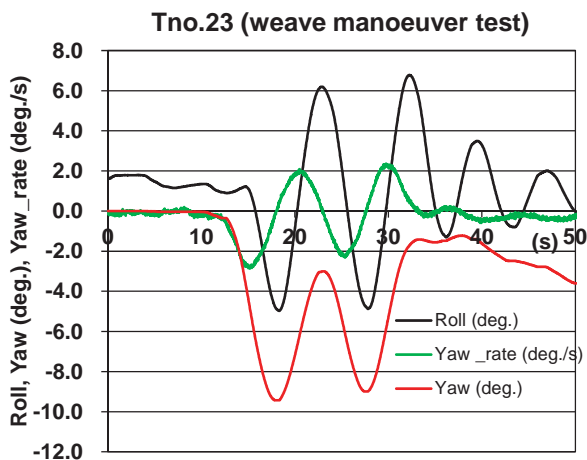


Figure 2 Measured roll angle, yaw angle and yaw rate in a weave manoeuvre test with a series of rudder angles of 13(port)-10(stbd.)-10(port)-13(stbd.) degrees.

Figure 2 shows an example of measured time histories of roll angle, yaw angle and yaw rate in a weave manoeuvre. Roll angle is positive for the port side down and yaw angle and yaw rate are positive for a starboard turn. From the measured boat motion and observation during the experiment the characteristic of heel angle in manoeuvring

motion of the similar boat could be summarised as follows (refer to Figure 2).

- (1) No clear inward heel occurs in the initial stage of manoeuvring motion.
- (2) Corresponding to the magnitude of rudder angle relatively large outward heel occurs during manoeuvring motion.
- (3) Response speed of heel to steering is relatively fast and outward heel develops quickly.

Heel Angle. Figure 3 shows relation between heel angles and rudder angles measured in the experiment. The horizontal axis is rudder angle δ , positive for the starboard side, and the vertical axis is outward heel angle ϕ_2 , positive for the port side down. From Figure 3 it is noticed that within the measured extent the relation between heel angles and rudder angles is approximated by a linear function (showed in the dotted line) and in manoeuvring motion of the similar boat outward heel of almost half as large as rudder angle is induced.

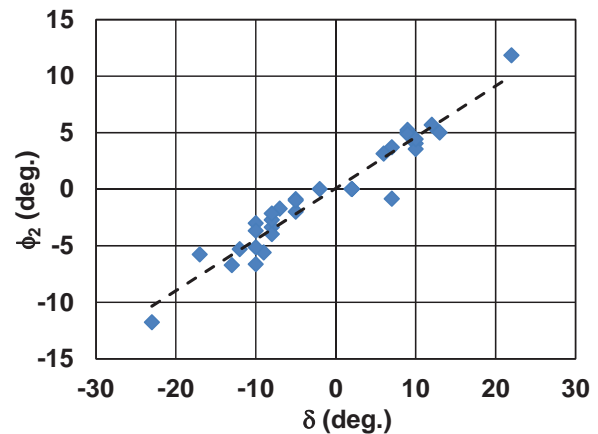


Figure 3 Measured heel angles and rudder angles in the experiment.

Turning Rate. Figure 4 shows the relation between turning rates (yaw rates) and rudder angles measured in the experiment. The vertical axis is normalised turning rate r' , which is positive for a starboard turn. The normalised turning rate r' was calculated with equation (1).

$$r' = \frac{L_{pp}}{r} = \frac{\omega \cdot L_{pp}}{V} \quad (1)$$

where ω is the measured turning rate, V is the measured boat speed, r is the local radius of trajectory and L_{pp} is the length between perpendiculars of the boat.

From Figure 4 it is noticed that within the measured extent the relation between normalised turning rates and rudder angles is approximated by a linear function as equation (2) (the dotted line in Figure 4).

$$r' = 0.0122 \times \delta - 0.0078 \quad (2)$$

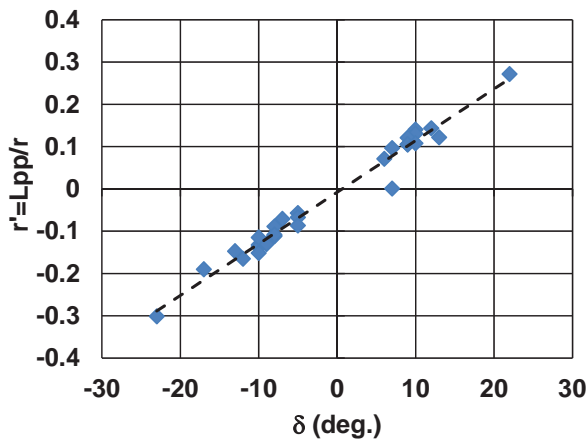


Figure 4 Measured turning rates and rudder angles in the experiment.

3.3 Estimation of Outward Heel Angle of the Capsized Boat

Outward heel in manoeuvring motion is induced by a couple consisting of a centrifugal force acting on the centre of gravity and a fluid reaction force acting on the side of hull. If the fluid reaction force is assumed to act at half the mean draft ($d/2$), outward heeling moment M is estimated with equation (3) (Morita, 1985).

$$M = \frac{W}{g} \frac{V^2}{r} \left(\overline{KG} - \frac{d}{2} \right) \quad (3)$$

where W is the displacement of the boat, g is the gravitational acceleration, \overline{KG} is the vertical centre of gravity of the boat.

Figure 5 shows a comparison between the outward heeling moments estimated by substituting experimental data in equation (3) and the righting moments corresponding to the measured heel angle, $W \cdot \overline{GM} \cdot \sin \phi_2$. From Figure 5 it is noticed that the righting moment is almost 2.77 times (the dotted line in Figure 5) larger than the outward heeling moment estimated with equation (3). This indicates that for the similar boat the fluid reaction force acts at a position, which differs largely from half draft ($d/2$). And in addition to this due to inertia of the boat and change in rudder force at reversing rudder angle in weave manoeuvre might increase the outward heel angle.

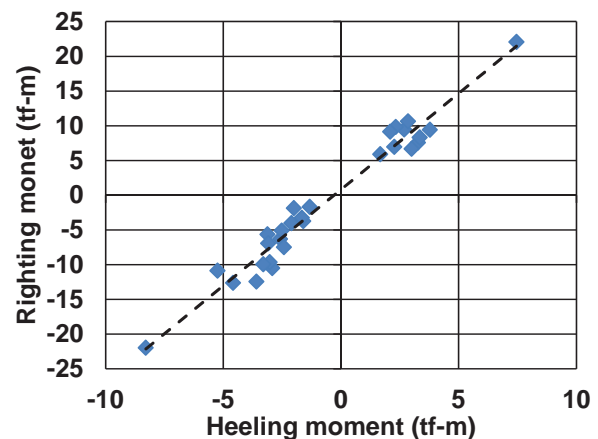


Figure 5 Outward heeling moments estimated with equation (3) and righting moments corresponding to measured heel angles.

If the following are supposed, outward heel angle ϕ_2 of the capsized boat in manoeuvring motion for given rudder angle δ can be estimated with equations (2), (4) and (5).

- (1) Turning characteristics, the relation between rudder angle and turning rate, of the capsized boat at the accident is the same as the similar boat at the experiment (Figure 4).
- (2) Speed reduction in manoeuvring motion is negligible.
- (3) Feature of outward heeling moment of the similar boat at the experiment (Figure 5) is

applicable to the capsized boat at the accident.

$$r = \frac{L_{pp}}{r'} \quad (4)$$

$$\sin \phi_2 = 2.77 \times \frac{V^2}{g \cdot r \cdot \overline{GM}} \left(\overline{KG} - \frac{d}{2} \right) \quad (5)$$

4. CONSIDERATION ON CAPSIZING MECHANISM

As the high sea warning was issued at the time of the accident and for the capsized boat quite careful steering was necessary to prevent large heel in changing course during navigating without a box barge, it is presumed that the following factors, wind and waves at the accident and careless steering of the boat, were related to the accident. As the skipper explained that the boat suddenly heeled to the port side largely then capsized in a short time, the situation of occurrence of the capsizing was supposed to be similar to that of the IMO weather criterion. Therefore, with calculating maximum heel angle based on an energy balance concept like the weather criterion, the capsizing mechanism was examined.

4.1 Stability at the Accident

Table 4 shows the estimated loading condition of the boat at the time of the accident, which is based on the inclining test result of the similar boat and the fuel oil and fresh water, supposed to be loaded into the capsized boat at the accident. Stability calculation was carried out with trim free condition. Figure 6 shows the stability curve at the time of the accident and Table 5 shows the estimated draft, trim, metacentric height and angle of bulwark top immersion. In Figure 6 the stability curve of the similar boat at the experiment is also shown.

From Figure 6 and Tables 2, 4 and 5 it is noticed that as the full loaded fuel oil and fresh

water increase the draft and trim of the boat, for large heel angle the stability of the similar boat at the experiment is smaller than that of the capsized boat at the accident. Therefore, for pusher tug boats of similar type to the capsized one, in order to maintain sufficient stability special attention is needed in loading fuel oil and fresh water.

Table 4. Loading condition at the accident.

Displacement: W	129.21 t
Vertical C.G.: KG	2.03 m
Longitudinal C.G.: mid-G	-1.19 m
Free surface effect: GG ₀	0.11 m

Table 5. Draft, trim, metacentric height and angle of bulwark top immersion at the accident.

Mean draft: d	1.66 m
Trim by stern: τ	0.37 m
Metacentric height: G ₀ M	0.70 m
Angle of bulwark top immersion: φ _b	20.7 deg.

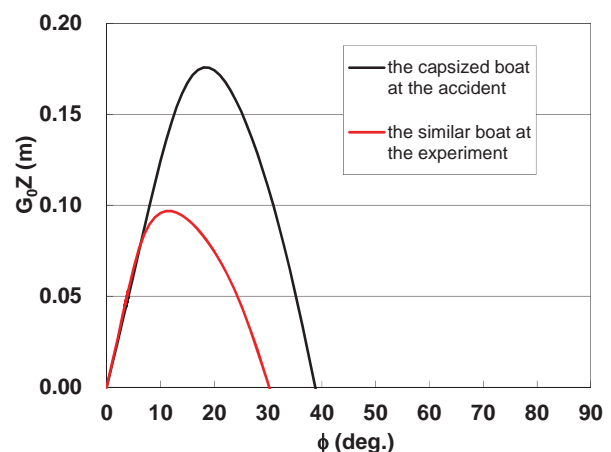


Figure 6 Stability curves at the accident and at the experiment.

4.2 Influence of Wind and Waves

Heel due to the Wind at the Accident.
Assuming beam wind condition, heel angle under action of steady wind and gust wind at

the accident were estimated with the same method as the weather criterion except wind pressure at 8 m/s. Table 6 shows the estimated heel angles due to the wind at the accident. Even gustiness considered, the heel angle due to the wind at the accident is estimated to be less than 1 degree. Taking the stability curve at the accident, Figure 6, into account, influence of the heel due to the wind at that time on the capsizing of the boat would be quite small. Therefore, the influence of the wind was excluded from consideration on capsizing mechanism.

Table 6. Heel angle due to the wind at accident (steady wind speed of 8 m/s).

Lateral windage area: A	49.06 m ²
Vertical distance from centre of "A" to a point at half the mean draft: Z	2.82 m
Wind pressure at 8 m/s: P	47.7
Heeling lever due to steady wind: $l_{w1} = PAZ/1000gW$	0.005 m
Heeling lever due to gust wind: $l_{w2} = 1.5l_{w1}$	0.008 m
Heel angle due to steady wind: ϕ_0	0.44 deg.
Heel angle due to gust wind: $1.5\phi_0$	0.65 deg.

Roll due to the Waves at the Accident. It was presumed that the speed of the boat was 9 knots and its heading angle was about 60 degrees at the time of the accident. Based on this information and the estimated sea condition at the time of the accident, Table 1, roll response of the capsized boat in a short crested sea was statistically estimated with the condition that the significant wave height was 2 m, the average wave period was 4.8 s and the mean encounter angle was 60 degrees. As a result, the expected largest in 200 successive roll amplitudes, ϕ_1 of the capsized boat is estimated to be 15.6 degrees (Table 7). Considering the stability at the accident, the estimated roll in the waves at the accident should be one of main factors related the capsizing of the boat.

As shown in Table 7, the expected largest in 200 successive roll amplitudes of the similar boat in the wave at the accident is 6.2 degrees, which is less than half that of the capsized boat. However, considering the stability of the similar boat at the experiment, the estimated roll angle in the waves at the accident might impair its safety.

Table 7. Roll angle of 1/200 maximum expectation in waves at the accident.

The capsized boat at the accident	15.6 deg.
The similar boat at the experiment	6.2 deg.

4.3 Influence of Steering

No information on the way of steering the capsized boat at the accident was provided. Therefore, outward heel angle ϕ_2 of the capsized boat at speed of 9 knots in manoeuvring motion with rudder angle of 5 to 15 degrees was estimated with equations (2), (4) and (5). Figure 7 shows the estimated outward heel angle due to steering of the capsized boat along with that of the similar boat at the experiment.

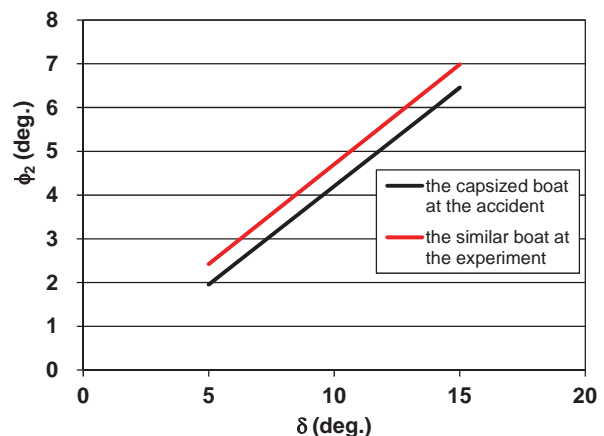


Figure 7 Outward heel angle due to steering.

The outward heel angle of the capsized boat at the accident is smaller than that of the similar boat at the experiment. At the condition of the accident the outward heel angle of the capsized boat with rudder angle of 10 degrees is estimated to be 4.2 degrees, which is much



smaller than the estimated roll angle in the waves at the accident. However, during steering the capsized boat outward heeling moment was supposed to keep working at the accident. In that case the outward heeling moment should reduce the residual dynamical stability of the capsized boat significantly.

4.4 Consideration on Capsizing Mechanism

As mentioned above it was presumed that rolling in waves at the accident and outward heel due to steering played a key role to the capsizing of the boat. Therefore, assuming that the capsized boat rolling in waves was carelessly steered at the accident, the mechanism of the capsizing was examined by calculating maximum heel angle with an energy balance concept like the weather criterion. In the examination as the worst case, the capsized boat was assumed to suffer outward heeling moment induced by starboard steering when it rolled to starboard side at an angle corresponding to the 1/200 maximum expectation in the waves at the accident and energy balance between rolling energy and dynamical stability was calculated. As no information on the steering of the capsized boat at the accident was available, the energy balance calculation was carried out at various rudder angles. The rudder angles, which induced the bulwark top immersion and the capsizing, were estimated and their feasibility was considered.

Table 8. Calculation results

δ (deg.)	ϕ_2 (deg.)	$b(\phi_b)/a$	b/a	ϕ_1 (deg.)
4.7	1.8	1.00	1.77	20.7
5.0	2.0	0.97	1.70	21.1
9.7	4.1	0.58	1.00	34.9

Calculation results are shown in Table 8 and graphs used for calculation are shown in Figure 8. In Table 8, ϕ_2 is the outward heel angle due to starboard steering with rudder

angle of δ , “a” and “b” are the rolling energy to the port side (the capsizing direction) and the residual dynamical stability respectively (refer to Figure 8), “b (ϕ_b)” is the residual dynamical stability up to the angle of bulwark top immersion (refer to Figure 8) and ϕ_1 is the maximum heel angle to the port side.

From Table 8 it is noticed that if the outward heeling moment induced by the steering with rudder angle of 4.7 degrees is assumed to act on the boat when it rolls to the starboard side at the maximum, the resultant port side heel reaches the angle of bulwark top immersion (ϕ_b), 20.7 degrees. If the assumed rudder angle is larger than 4.7 degrees, the maximum heel angle to the port side exceeds the angle of bulwark top immersion. For example with the assumed rudder angle of 5.0 degrees the maximum heel angle to the port side is 21.1 degrees, and the bulwark top is considered to be immersed. After the top of bulwark is immersed, it should induce a resistance force against up-righting the boat. Therefore, if the bulwark top is immersed the boat would not upright readily and the successive waves might capsize it. Table 8 also shows that if the assumed rudder angle of starboard steering at the accident is larger than 10 degrees, the boat is considered to capsize immediately to port.

Although during navigating without a box barge in order to prevent large heel in changing course steering with small rudder angle used to be carried out for the capsized boat, it seems not unrealistic to assume that steering with rudder angle of about 5 degrees was carried out at the accident. In any case the calculation results indicate that if the worst case that when the boat rolls to one side at the maximum heeling moment due to steering to the same side is assume to act on the boat, steering with rudder angle of less than 10 degrees could lead the boat to capsize. Therefore it seems that for pusher tug boats of similar type to the capsized one, careful steering with small rudder angle is indispensable to ensure safety during navigating without a box barge.

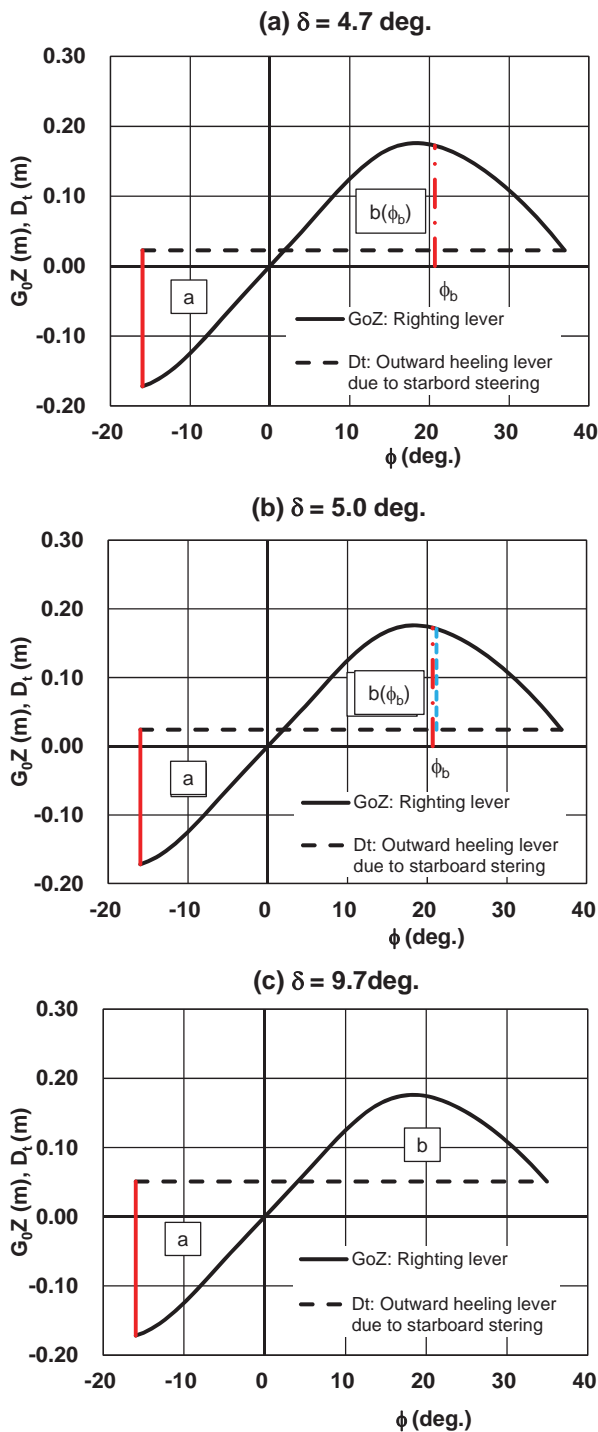


Figure 8 Comparison between dynamical stability and heeling energy with various rudder angles.

5. CONCLUSIONS

With the above mentioned technical investigation and so on the JTSC compiled the

investigation report on the capsizing accident of “No. 38 Sankyo Maru” and publicised it (JTSC, 2014). In the report, the probable cause of the accident is summarised as follows. Due to the steering with rudder angle of larger than 4.7 degrees the capsized boat navigating without a box barge at speed of about 9 knots with suffering starboard waves of about 2 ~ 3 meters in significant wave height and about 5 seconds in average wave period was forced to heel beyond the angle of bulwark top immersion to the port side and fell into a difficult situation for up-righting. Then with successive waves action the boat might have capsized.

In the report the following feature of pusher tug boats of similar type to the capsized one are pointed out too.

- (1) Depending on the loading condition of fuel oil and so on, the stability of these boats tends to reduce considerably.
- (2) In rough weather large rolling due to waves may occur easily in these boats.
- (3) As the rudders of these boats are designed to secure enough manoeuvrability during linking with a box barge, in case of navigating solely these boats are liable to heel largely by the action of rudders.

In order to prevent similar accident, the operating company is instructed to prepare a manual, which explains precautions for pusher tug boats in navigating solely, limitation on loading fuel oil and so on, wind and sea conditions where planned navigation should be abandoned, appropriate way of steering etc. and advise skippers to follow it.

6. REFERENCES

Japan Transport Safety Board, 2014, "Push boat SANKYO MARU No. 38 Capsizing", Marine Accident Investigation Report, MA2014-3 (in Japanese).

Morita, T., 1985, "Theory of Ship Stability - Basis and Application -", Kaibun-do, pp. 134-136 (in Japanese).



Rapid Ship Motion Simulations for Investigating Rare Stability Failures in Irregular Seas

Kenneth Weems, *NSWCCD (Naval Surface Warfare Centre Carderock Division)*,

kenneth.weems@navy.mil

Vadim Belenky, *NSWCCD (Naval Surface Warfare Centre Carderock Division)*,

vadim.belenky@navy.mil

ABSTRACT

The use of time-domain numerical simulations for the investigation of stability failures and other rare events in random, irregular seas requires a challenging combination of speed and accuracy. Simulations must be fast enough to observe a statistically significant number of failure or near failure events in order to build a reliable stochastic model of the event or conditions leading up to the event, while also being accurate and complete enough to capture the physical behavior that drives the event. Of particular importance are the body-nonlinear hydrostatic and Froude-Krylov forces, which are critical for large-amplitude roll motion and may also play a significant role in the surge and sway forces involved in surf-riding and broaching.

This paper presents a volume-based evaluation of the body-linear Froude-Krylov and hydrostatic pressure forces, which retains the inseparability of hydrostatic and Froude-Krylov forces and the effects of large-amplitude relative motion along the length of a ship. Implementation of the method requires a minimum number of evaluations of the incident wave, so it can run at a fraction of the computational cost for traditional surface pressure integration schemes. The calculation has been implemented in a hybrid numerical method that incorporates ordinary differential equation (ODE) like models for wave-body perturbation forces. The hybrid method has been used to produce a very large number of realizations of irregular sea responses, including a statistically significant number of stability failures, for validating schemes for the extrapolation of extreme motion responses.

Keywords: *Seakeeping, Nonlinear Restoring, Froude-Krylov Forces*

1. INTRODUCTION

The use of time-domain numerical simulations for the investigation of stability failures and other rare events in random, irregular seas requires a challenging combination of speed and accuracy. The rarity of such events requires an extremely long set of simulations in order to observe a statistically significant number of events, while the complexity of the physics precludes the use of excessively simple models.

Of particular importance are the body-nonlinear restoring (hydrostatic) and incident wave (Froude-Krylov) forces, which are critical for large-amplitude roll motions and may also play a significant role in the surge and sway forces involved in surf-riding and broaching. France *et al.* (2003) described how these forces were key to describing parametric roll, while Spyrou *et al.* (2014) and others have linked the change of roll stability in waves to



large roll events and capsizing in pure loss-of-stability events.

Hybrid time-domain simulation codes, which generally combine a body-nonlinear calculation of the hydrostatic and Froude-Krylov forces with a potential-flow solution of the wave-body hydrodynamic disturbance forces (radiation, diffraction, etc.) and theoretical or semi-empirical models of viscous and lift forces, have become the principal tool for simulating non-linear ship motion in irregular waves. These tools provide a reasonable compromise between accuracy and speed, and they can readily generate hundreds or thousands of hours of motion data for different realizations of ocean waves.

This, of course, is not nearly enough simulation time to observe a statistically significant number of failure or near failure events; building a reliable stochastic model of the event or conditions leading up to the event may require millions of hours of simulation for a single wave and operating condition. This has led to the development of extrapolation methods that attempt to characterize the probability of rare events from limited motion data (see, for example, Belenky et al. 2015 and Campbell et al. 2015). However, the development, testing, and validation of such methods still require extremely large simulation data sets of motions in extreme conditions.

Faster methods, therefore, are needed. For the development and validation (or at least testing) of extrapolation methods, they need not be quantitatively accurate to a high degree, but they do need to be qualitatively accurate in that they capture the key physics of the large-amplitude roll motion (Smith and Zuzick 2015). As mentioned above, a key part of such a calculation is the body-nonlinear hydrostatic and Froude-Kyrlov forces. While it is relatively straightforward to calculate these forces via direct pressure integration, they can be computationally expensive: they require a very

large number of evaluations of the incident wave, and a very large number of component frequencies are required for a statistically valid representation of the irregular wave field for long simulations (Belenky 2011).

To provide a fast but complete calculation of the body-nonlinear Froude-Krylov and hydrostatic pressure forces, a sectional, volume-based evaluation has been developed that retains the inseparability of hydrostatic and Froude-Krylov forces and the effects of large-amplitude relative motion along a ship's length. Implementing the method requires a minimum number of evaluations of the incident wave, so it can run at a fraction of the computational cost of traditional surface pressure integration schemes. The calculation has been implemented in a hybrid numerical method that incorporates ordinary differential equation (ODE) like models for wave-body perturbation forces. The hybrid method has been used to produce a very large number of realizations of irregular sea responses, including a statistically significant number of stability failures, for validating schemes to extrapolate extreme motion responses (Weems and Wundrow 2013).

In this initial implementation, the simplified model of wave-body hydrodynamics prevents this simulation from being considered as quantitatively accurate. In the future, however, rapid, quantitatively accurate simulations may be possible by combining volume-based restoring and wave forces with a more complex but still fast model of the wave-body hydrodynamics, perhaps based on impulse response potentials or a more sophisticated coefficient representation.

2. FORMULATION OF VOLUME-BASED CALCULATIONS

The non-linear wave forcing and restoring forces can generally be computed by integrating the incident wave and hydrostatic pressure over the instantaneous wetted hull surface (in the Earth-fixed frame):



$$\mathbf{F}_{FK+HS}(t) = -\rho \iint_{S_B(t)} \left(\frac{\partial \phi_0(x, y, z, t)}{\partial t} + gz \right) \hat{\mathbf{n}} ds \quad (1)$$

$\partial \phi_0(x, y, z, t) / \partial t$ is the pressure of the undisturbed incident wave field (Froude-Krylov pressure) and $S_B(t)$ is the instantaneous wetted portion of the hull surface up to the incident wave waterline $\eta(x, y, t)$. The key element of this expression is that it captures the geometric non-linearity due to large vertical motion relative to the wave surface, ranging from the effect of bow flare to full emergence or submergence of the bow and stern.

It should be noted that this expression can be used with linear or nonlinear incident wave models as long as the incident wave model expresses a pressure and velocity field in the body-nonlinear domain, that is up to $z = \eta(x, y, t)$. For the typical linear wave model – in which the wave is represented by a superposition of sinusoidal components – this can be accomplished by applying the Wheeler stretching technique, in which the exponential decay term in the expressions for pressure, velocity, and their derivatives is expressed as $e^{k(\eta-z)}$.

As noted above, this expression is relatively straightforward to evaluate but can be expensive to generate, as it generally involves a large number of evaluations of the incident wave. To provide a much faster calculation, a volume-based calculation scheme is considered, using the submerged volume at each instant in time, which can be calculated with a minimal number of incident wave evaluations. It is, however, imperative that the scheme capture the effect of the longitudinal variation of the relative motion, as this is a principle driver in dynamic stability phenomena such as parametric roll and pure loss of stability in waves. To do so, Equation (1) is expressed as the sum of incremental forces calculated on a set of incremental sections distributed along the ship's length:

$$\mathbf{F}_{FK+HS}(t) = \sum \delta \mathbf{F}_{FK+HS}(x_i, t) \quad (2)$$

$\delta \mathbf{F}_{FK+HS}(x_i, t)$ is the force *computed* over the incremental submerged portion of the hull's surface running from $x_i - \Delta x / 2$ to $x_i + \Delta x / 2$, which is designated $\delta S_B(x_i, t)$:

$$\delta \mathbf{F}_{FK+HS}(x_i, t) = -\rho \iint_{\delta S_B(x_i, t)} \left(\frac{\partial \phi_0(x, y, z, t)}{\partial t} + gz \right) \hat{\mathbf{n}} ds \quad (3)$$

Note that the incremental hull surface $\delta S_B(x_i, t)$ is *considered* to include the wetted portion of the hull for that section as well as the wetted (below the incident wave) portions of the planes (cross-sections) separating this section from adjacent sections.

Within each section, a Taylor series expansion (neglecting higher-order derivatives) can be used to approximate the distribution of the incident wave pressure over an incremental hull section in terms of the value and derivatives of the pressure at a nominal point (x_0, y_0, z_0) on the section:

$$\begin{aligned} \frac{\partial \phi_0(x, y, z, t)}{\partial t} \cong & \frac{\partial \phi_0(x_0, y_0, z_0, t)}{\partial t} + \\ & \frac{\partial^2 \phi_0(x_0, y_0, z_0, t)}{\partial t \partial x} (x - x_0) + \\ & \frac{\partial^2 \phi_0(x_0, y_0, z_0, t)}{\partial t \partial y} (y - y_0) + \\ & \frac{\partial^2 \phi_0(x_0, y_0, z_0, t)}{\partial t \partial z} (z - z_0) \end{aligned} \quad (4)$$

The dynamic free surface *boundary* condition can be used to relate the Froude-Krylov pressure at the free surface to the incident wave elevation:

$$\frac{\partial \phi_0(x, y, \eta, t)}{\partial t} = -g\eta(x, y, t) \quad (5)$$

If the *evaluation* point is chosen to be on the incident wave surface, $z_0 = \eta$, Equation (4) can be written as:



$$\begin{aligned} \frac{\partial \phi_0(x, y, z, t)}{\partial t} &\cong -g\eta(x_0, y_0, t) \\ &- g \frac{\partial \eta(x_0, y_0, t)}{\partial x} (x - x_0) \\ &- g \frac{\partial \eta(x_0, y_0, t)}{\partial y} (y - y_0) \\ &+ \frac{\partial^2 \phi_0(x_0, y_0, \eta, t)}{\partial t \partial z} (z - \eta) \end{aligned} \quad (6)$$

Using an overbar to designate the mean or nominal value of the elevation, etc. for a section, the sectional force can be written as:

$$\begin{aligned} \delta \mathbf{F}_{FK+HS}(x_i, t) &\cong \rho \iint_{\delta S_B(t)} (g\bar{\eta} - gz \\ &+ g \frac{\partial \bar{\eta}}{\partial x} (x - x_0) + g \frac{\partial \bar{\eta}}{\partial y} (y - y_0) \\ &+ \frac{\partial^2 \bar{\phi}_0}{\partial z \partial t} (z - z_0)) \hat{\mathbf{n}} ds \end{aligned} \quad (7)$$

Since the incremental surface $\delta S_B(x_i, t)$ includes x =constant plane separating adjacent sections and the pressure over the free surface above the section will be zero, the RHS of (7) complete encompasses the submerged portion of the section. Gauss's theorem can then be applied in order to define the sectional force in terms of the integral of the gradient of the approximated pressure field over the incremental volume:

$$\delta \mathbf{F}(t) = \iint_{\delta S_B(t)} P \hat{\mathbf{n}} ds = - \iiint_{\delta V(t)} \nabla P dv \quad (8)$$

This results in a volume-based formula for the sectional incident wave and restoring force:

$$\begin{aligned} \delta \mathbf{F}_{FK+HS}(x_i, t) &\cong \rho g \delta V(x_i, t) \hat{\mathbf{k}} \\ &- \rho g \delta V(x_i, t) \frac{\partial \bar{\eta}}{\partial x} \hat{\mathbf{i}} \\ &- \rho g \delta V(x_i, t) \frac{\partial \bar{\eta}}{\partial y} \hat{\mathbf{j}} \\ &+ \rho g \delta V(x_i, t) \frac{\partial^2 \bar{\phi}_0}{\partial z \partial t} \hat{\mathbf{k}} \end{aligned} \quad (9)$$

$\delta V(x_i, t)$ is the instantaneous volume of the submerged portion of the i^{th} section up to the

incident wave surface. The first term in Equation (9) is the familiar buoyancy term, but with the volume integrated up to the incident wave surface. The second and third terms are longitudinal and side forces from the gradient of the incident wave pressure field, evaluated in terms of the incident wave slope. The final term can be considered to be a "correction" to the vertical incident wave force, using a linear approximation of the exponential decay of the incident wave pressure field with depth.

Similarly, expressions for the moments can be derived by applying the relation:

$$- \iint_S (\hat{\mathbf{n}} \times \mathbf{Pr}) ds = \iiint_V \nabla \times \mathbf{Pr} dv \quad (10)$$

This gives the following formula for the roll and pitch moments:

$$\begin{aligned} \delta Mx_{FK+HS}(x_i, t) &\cong \rho g \delta V(x_i, t) y_{CV}(x_i, t) \\ &- \rho g \delta V(x_i, t) \frac{\partial \bar{\eta}}{\partial y} z_{CV}(x_i, t) \\ &+ \rho g \delta V(x_i, t) \frac{\partial^2 \bar{\phi}_0}{\partial z \partial t} y_{CV}(x_i, t) \end{aligned} \quad (11)$$

$$\begin{aligned} \delta My_{FK+HS}(x_i, t) &\cong -\rho g \delta V(x_i, t) x_{CV}(x_i, t) \\ &+ \rho g \delta V(x_i, t) \frac{\partial \bar{\eta}}{\partial x} z_{CV}(x_i, t) \\ &- \rho g \delta V(x_i, t) \frac{\partial^2 \bar{\phi}_0}{\partial z \partial t} x_{CV}(x_i, t) \end{aligned} \quad (12)$$

$x_{cv}(x_i, t)$, $y_{cv}(x_i, t)$ and $z_{cv}(x_i, t)$ are coordinates for the center of the instantaneous submerged volume for the i^{th} section up to the incident wave waterline. The sectional roll and pitch moments can be summed to get the total moments on the ship:

$$Mx_{FK+HS}(t) = \sum \delta Mx_{FK+HS}(x_i, t) \quad (13)$$

$$My_{FK+HS}(t) = \sum \delta My_{FK+HS}(x_i, t) \quad (14)$$

The yaw moment can be computed from the sectional lateral forces as:



$$M_{z_{FK+HS}}(t) = \sum -\rho g \delta V(x_i, t) \frac{\partial \eta}{\partial y}(x_i - x_{cg}) \quad (15)$$

With these formulae, the body-nonlinear Froude-Krylov and hydrostatic restoring forces can be computed with a single evaluation of the incident wave per section. The only major assumption in the derivation of these formulae is the Taylor series expansion of the incident wave pressure in Equation (4). This expansion assumes that the wave slope is constant over the beam and the incremental length of each section Δx , and can be considered a long-wavelength assumption in which the wave length is assumed to be long with respect to the beam and increment section length. This assumption should be quite reasonable for waves, or wave components in an irregular sea model, that are longer than two or three times the beam, but the linear approximation of the sinusoidal wave profile will become inaccurate for shorter waves. However, the section-based derivation retains the variation of elevation and slopes from section to section, so the waves are not assumed to be long relative to the ship length and the variation of relative motion along the ship's length, which the primary driver of the change of stability in waves, is considered.

The expansion considers the vertical pressure gradient to be, at most, linear with depth, so the wave is also assumed to be long compared to the draft of the ship. The linear approximation of the exponential pressure decay will become quite inaccurate for shorter waves, so any implementation of the $\partial^2 \phi_0 / \partial z \partial t$ term will need to treat of short waves or wave components carefully.

3. IMPLEMENTATION OF VOLUME-BASED CALCULATIONS

The implementation of these volume-based formulae in a time-domain numerical code requires the calculation of the submerged

volume, up to the incident wave, and volume center for a set of ship hull sections at each time step. In order to accommodate extreme motion problems, these sectional volume calculations should accommodate large amplitude heave and pitch including fully submerged and emerged sections, and large amplitude roll motions including a fully inverted ship.

In the initial implementation, the sectional volume calculations were implemented using an approach similar to the Bonjean curves used for classic stability analysis. Prior to starting the simulation, a set of x =constant stations are cut through the hull and the volume and volume moments for the $y > 0$ half of the hull section are pre-computed for 0 heel up to each station offset point.

At each time of a simulation (or heel angle of a restoring curve calculation), the Froude-Krylov and hydrostatic restoring force for each section is computed as follows:

1. Evaluate the incident wave elevation and slope at the centerline of each station
2. Find the intersection of the incident wave surface and the section centerline considering the wave elevation and vertical motion of the station due to the ship's heave and pitch
3. Find the port and starboard waterline points from the incident wave/center intersection and an effective heel angle, which is the sum of the ship's roll angle and the lateral wave slope at the centerline
4. Interpolate the volume and volume moments up to the waterline point for each side of the hull (dark blue in Figure 1)
5. Correct the volume and volume moments for the effective heel angle by adding or subtracting the contribution of the light blue triangular regions in Figure 1
6. Combine the volume and volume moments for the two sides to determine the volume and volume center for the section

7. Compute sectional forces and moments via Equations (9), (11), and (12).

The sectional forces and moments are then integrated along the length of the ship to get the total forces and moments.

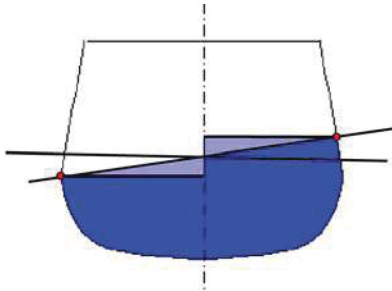


Figure 1: Sample sectional volume calculation for a midships section of the ONR Topsides Series Tumblehome hull

Figure 2 shows the station offsets and the waterline intersection points of each station for a time instant from a simulation in stern oblique irregular waves.

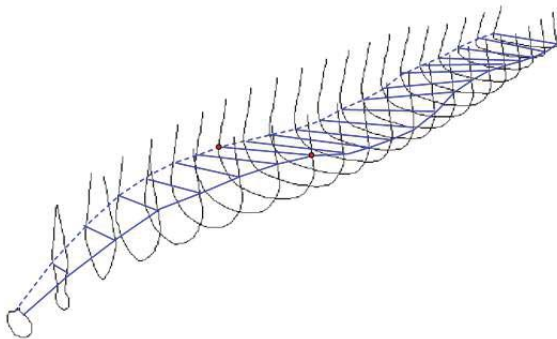


Figure 2: Station/incident wave intersection points for the ONR Tumblehome hull in stern oblique seas

In the initial implementation of the volume-based calculation, the $\partial^2\phi_0/\partial z\partial t$ term has *not* been included. Further work may be required to explore the $\partial^2\phi_0/\partial z\partial t$ term and to develop a robust and accurate handling for shorter waves and irregular wave representation, including short wave components.

The procedure is very fast, since it requires only a single evaluation of the incident wave elevation and its derivatives for each station at each time step. Even this effort can be mitigated by interpolating the wave in space and/or time. For a 3-DOF (heave, roll, pitch) simulation in which surge, sway, and yaw are prescribed based on constant forward speed, the global position of the sections is known *a priori*, so the incident wave values can be pre-computed at a larger time increment and interpolated to the simulation time step.

4. RESTORING CURVE CHECK

In order to verify the formulation and implementation of the sectional volume-based calculation, the roll restoring arm (GZ) curve was computed in both calm water and for the quasi-static wave-pass problem, and the results were compared to results from 3-D surface pressure integration in the Large Amplitude Motions Program (LAMP) and to results from a standard statics code. Figure 3 compares the calm water restoring arm of the different calculations for a 100m x 20m x 6m rectangular barge, while Figure 4 presents a similar comparison for the ONR Topsides Series Tumblehome hull.

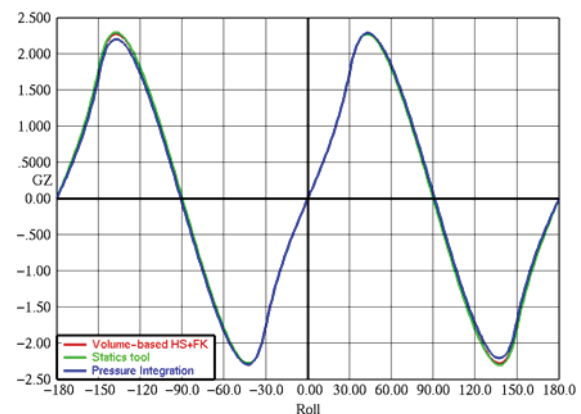


Figure 3: Calm water restoring curve for rectangular barge

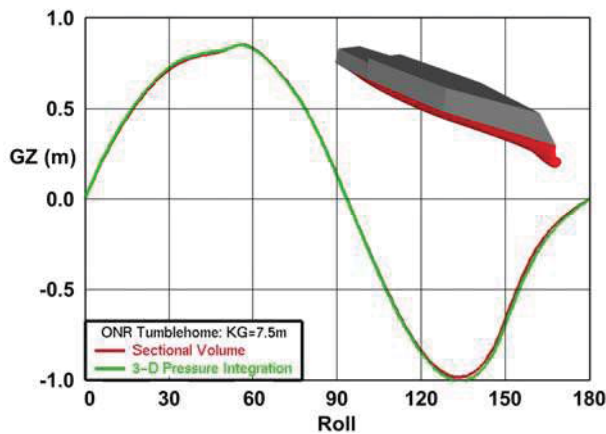


Figure 4: Calm water roll restoring arm (GZ) curve for ONR Tumblehome hull

As expected, the curves are nearly identical. As the calculation of the restoring moment is based on a volume calculation that is nearly exact, the incremental restoring moment about its static or instantaneous dynamic position, which is to say its restoring curve in calm water or in waves, will be nearly exact as well.

5. MOTIONS IN REGULAR WAVES

The volume-based Froude-Krylov and hydrostatic force calculation has been implemented in a 3-DOF (heave, pitch, roll) hybrid numerical simulation tool that incorporates ODE-like models for wave-body perturbation forces and viscous roll damping. In order to test the tool, the predicted response in regular waves was compared to LAMP simulations. LAMP is a general hybrid time-domain ship motions prediction tool that incorporates a conventional surface pressure integration of the hydrostatic and Froude-Krylov pressures with several different options for the wave-body hydrodynamic force (Shin *et al.*, 2003). Most LAMP simulations use its 3-D potential flow solution of the wave-body hydrodynamics, but LAMP also has the option, sometimes referred to as LAMP-0, of substituting coefficient-based added mass and damping terms for the potential flow solution. LAMP's Froude-Krylov pressure terms can

also be evaluated without the pressure decay term (e^{kz}).

Figures 5 and 6 show the roll and heave response for a 3-DOF (heave, roll, pitch) simulation of a 100m x 20m x 6m rectangular barge in regular quartering waves with wave length equal to ship length and wave height equal to 1/3rd of the draft. The roll and pitch responses are nearly identical, as was heave (not plotted).

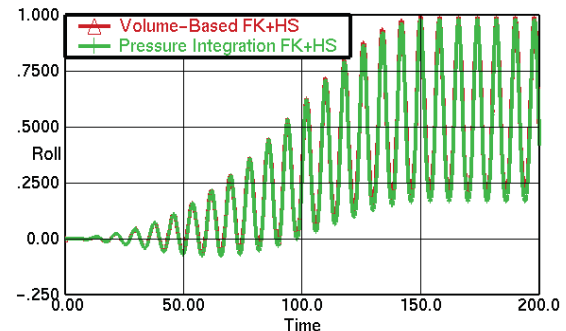


Figure 5: Roll motion for rectangular barge in quartering regular waves, $\lambda=L$ $h=d/3$

The “Pressure Integration” results in Figures 5 and 6 are LAMP-0 results in which the incident wave decay (e^{kz}) has been turned off. As such, the incident wave and hydrostatic forces will differ only by the calculation method: volume vs. pressure integration. The viscous damping models and implementation of the hydrodynamic coefficient are similar but not identical. The results indicate that for a wave that is equal to the ship length and long relative to the beam, the magnitude and phase of the wave forcing and restoring, including the coupling that results in the asymmetric roll response, is well represented in the volume-based calculation.

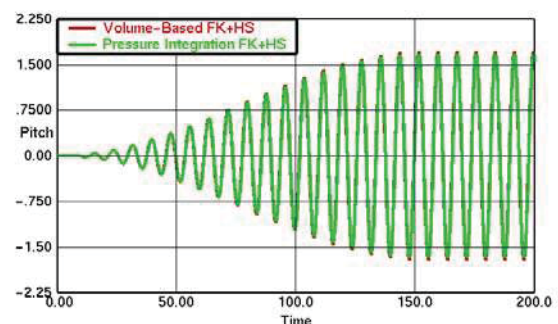


Figure 6: Pitch motion for rectangular barge in quartering regular waves, $\lambda=L$ $h=d/3$

In order to evaluate the effects of wave length and calculation options, a series of regular wave response calculations were made for the ONR Topsides Series Tumblehome hull in regular, quartering seas at zero speed. Figures 7 through 9 plot the normalized response amplitude vs. the ratio of ship length to wave length for a wave slope of $H/\lambda=50$. The heave response is normalized by wave amplitude while the roll and pitch response are normalized by wave slope (ka).

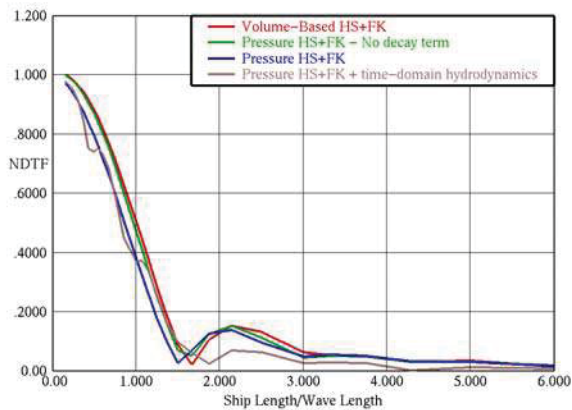


Figure 7: Heave response of ONR Tumblehome in regular, stern quartering waves, 0 knots

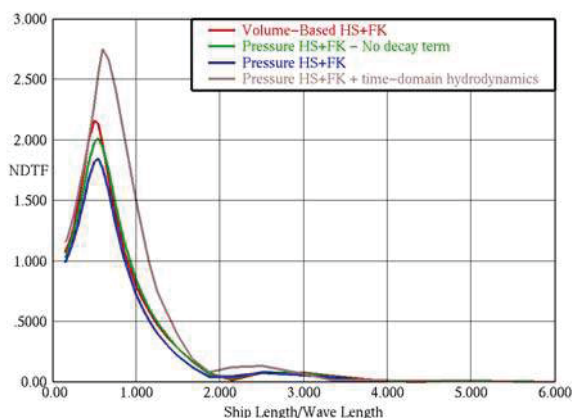


Figure 8: Roll response of ONR Tumblehome in regular, stern quartering waves, 0 knots

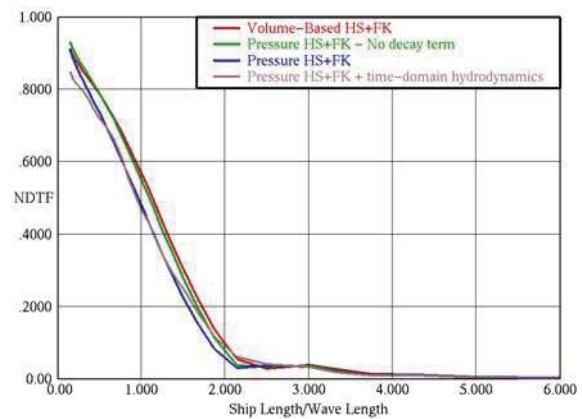


Figure 9: Pitch response of ONR Tumblehome in regular, stern quartering waves, 0 knots

These calculations were made with four different methods, labeled as:

- **Volume-Based HS+FK** is the simulation tool incorporating the new, volume-based calculation (red line)
- **Pressure HS+FK – No decay term** is a LAMP-0 simulation with surface pressure integration of HS+FK pressure neglecting the decay (e^{kz}) term (green line)
- **Pressure HS+FK** is a LAMP-0 simulation with surface pressure integration of HS+FK pressure including the decay (e^{kz}) term (blue line)
- **Pressure HS+FK + time-domain hydrodynamics** is a regular LAMP simulation with 3-D potential flow solution of the wave-body interaction. (brown line)

The difference between the red and green curves is primarily the difference between the new, volume-based calculation of the HS+FK forces vs. the traditional, pressure integration calculation, but with the effect of the pressure decay removed. There is also some difference in the coefficient-based hydrodynamics and damping models, which is most likely responsible for the difference in the roll response peak. The largest difference between the two calculations is expected to be for the

shorter waves, but the response there is equally small for both.

The difference between the green and blue curves is entirely the effect of the decay (e^{kz}) term in the Froude-Krylov pressure integration. The effect is evident, especially in heave and pitch, but does not dominant the results. It is probably worth investigating the $\partial^2\phi_0/\partial z\partial t$ term in Equations (9), (11), and (12), which has been neglected in the initial implementation over the method, to correct for this difference.

The difference between blue and the brown curves is the effect of the more accurate hydrodynamics in the regular LAMP calculation. The effect is large enough that volume-based method must be coupled with a more complete model of hydrodynamics in order to create a quantitative tool for ship motions.

6. MOTIONS IN IRREGULAR SEAS

As described above, the primary purpose for developing the volume-based calculation of the hydrostatic restoring and incident wave forcing was to produce a tool capable of creating very large data sets of ship motions in severe, irregular seas that are at least qualitatively representative of actual, nonlinear data. These data would be used in developing and testing of extrapolation methods for severe roll motion including capsizing.

Figure 10 shows 20 records of the roll response for the ONR Tumblehome ship at a low GM condition ($GM=1.5m$) in large (Sea State 8) steep stern quartering waves. The seaway is modeled by 220 wave components to provide a statistically independent wave representation over each 30-minute realization. The total calculation time for these 20 realizations was about 7 seconds on a single processor laptop computer. 2,000,000 realizations comprising 1,000,000 hours of data can be generated in a day or so on a modest sized cluster.

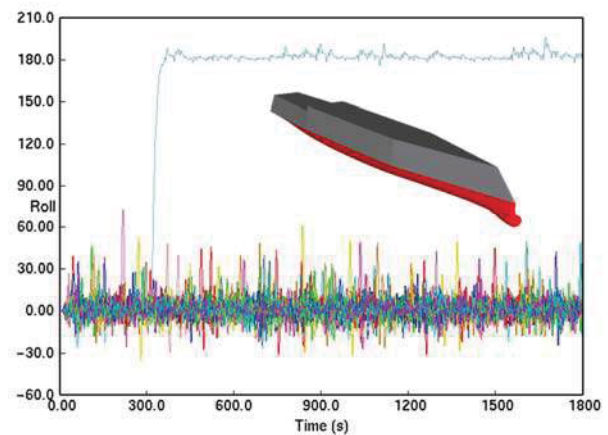


Figure 10: Roll motion for 20 realizations of ONR Tumblehome hull in steep Sea State 8

This example shows that the code is fast enough, but does it reproduce the significant nonlinearities of realistic severe ship motion, especially roll? Since the method captures the key features of the change of stability in waves, it should, at least to some extent. But how does one demonstrate, let alone prove, that it does?

For the present, we look at the distribution of predicted roll motion for the ONR Tumblehome hull at 6 knots in long-crested quartering seas with a significant wave height ($H^{1/3}$) of 9.5m, which is one of the cases used to test the extrapolation methods described in Belenky *et al.* (2015). Figures 11 through 13 compare a histogram of the roll angle from 15 hours of regular (with potential flow hydrodynamics) LAMP simulations (30 30-minute realizations) to a curve derived from 500 hours of simulations using the volume-based HS+FK calculation with simplified hydrodynamics. The horizontal axis is the roll angle divided by its standard deviation (σ). A normal distribution is overlaid for reference.

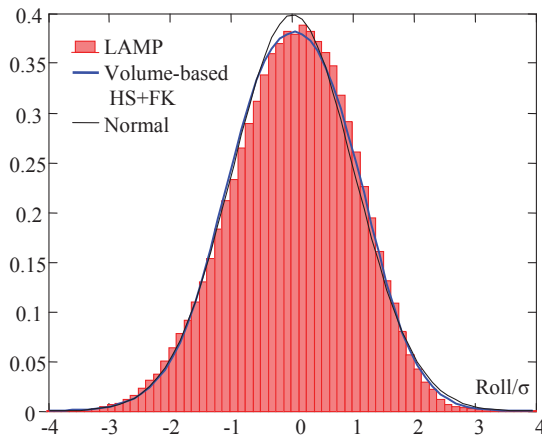


Figure 11: Distribution of Roll Angle for ONR Tumblehome at 6 knots in quartering seas, $H^{1/3}=9.5\text{m}$

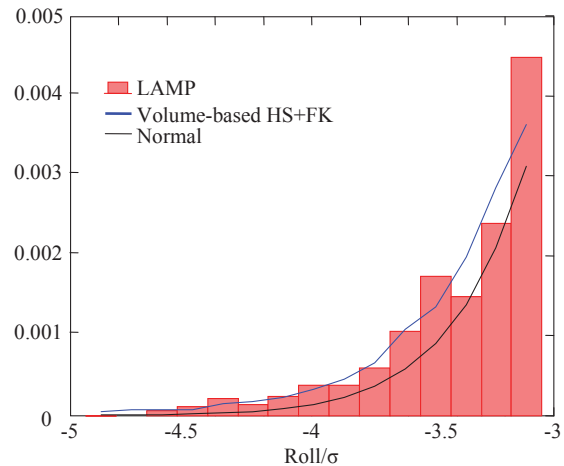


Figure 13: Distribution of Roll Angle – negative tail

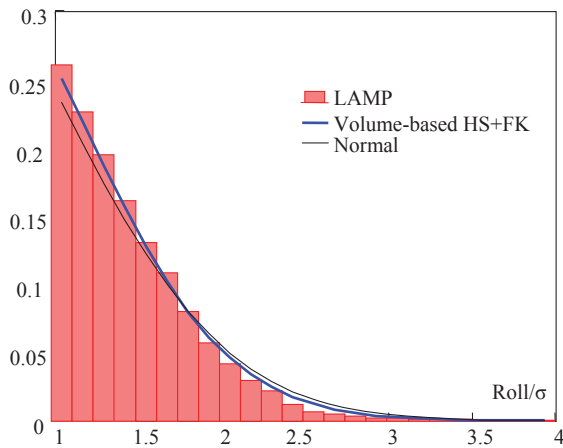


Figure 12: Distribution of Roll Angle – positive tail

The difference between the normal distribution and the LAMP results is not huge, but it has been shown that this difference is important, especially at the tail. Most important is the relative thinness of the positive tail (Figure 12) thickness of the negative tail (Figure 13). The trending of the volume-based result follows the LAMP results rather well. This result is not conclusive by any means, but it is encouraging and provides justification for using the results of the volume-based simulations for the testing of the extrapolation techniques.

7. CONCLUSIONS AND FUTURE WORK

The analysis of rare dynamic stability failures, including extreme roll events and capsizing, can gain considerable benefit from very rapid numerical simulations in irregular waves, as long as the simulations capture the principal physical phenomenon of the events. The very large data sets of irregular sea ship motion generated by such methods would allow the direct observation of rare events or near events and provide a basis for building and testing probabilistic models. Simulations that are even qualitatively correct have potential application for testing such models, especially those which are based on the extrapolation of smaller data sets.

In order to enable the development of such a numerical simulation tool, a very fast calculation method has been developed for the body-nonlinear hydrostatic restoring and incident wave (Froude-Krylov) forcing, which has been identified as a principal contributor to parametric roll and pure-loss-of-stability events. The calculation method uses volume-based formulae for the forces and moments on a series of hull stations as a function of the local relative motion and effective heel angle. The method is very accurate in the assessment of roll restoring and its changes due to relative motions in waves, but is approximate in the



evaluation of the incident wave forcing. By requiring only one evaluation of the incident wave per section, it is far faster than traditional methods based on the integration of pressure over the hull surface.

The method has been implemented in a 3-DOF (heave, roll, pitch) hybrid simulation tool which incorporates simple, coefficient-based models for wave-body hydrodynamics and viscous damping. The tool is capable of practically generating very large data sets, *e.g.* millions of hours, but can be considered only qualitatively accurate with its simplified hydrodynamic model. Future work will include an investigation of the vertical derivative term in the formulae, a more complete verification that the method provides a qualitatively accurate representation of ship motion in large waves and the integration of the volume-based calculation with more complete models for the wave-body hydrodynamics, maneuvering forces such as propulsion and hull lift, and other effects.

8. ACKNOWLEDGEMENTS

The work described in this paper has been funded by the Office of Naval Research, under Dr. Patrick Purtell and Dr. Ki-Han Kim. The authors greatly appreciate their support.

The authors would like to recognize the contributions of Dr. A. Reed, B. Campbell, Dr. D. Wundrow and T. Smith of NSWCCD during the development and testing of this method.

9. REFERENCES

Belenky, V. L., 2011, "On Self-Repeating Effect in Reconstruction of Irregular Waves", Chapter 33 of Contemporary Ideas on Ship Stability" edited by M.A.S. Neves, V. L. Belenky, J. O. de Kat, K. Spyrou, and N. Umeda, Springer, pp. 589-598.

Belenky, V., Weems, K. and Lin, W.M., 2015, "Split-time Method for Estimation of Probability of Capsizing Caused by Pure Loss of Stability," Proc. 12th Intl. Conf. on Stability of Ships and Ocean Vehicles (STAB 2015), Glasgow, UK.

Campbell, B., Belenky, V. and Pipiras, V. 2015 "Statistical Extrapolation in the Assessment of Dynamic Stability in Irregular Waves" Proc. 12th Intl. Conf. on Stability of Ships and Ocean Vehicles (STAB 2015), Glasgow, UK

France, W.M, Levadou, M, Treacle, T.W., Paulling, J. R., Michel, K. and Moore, C. (2003). "An Investigation of Head-Sea Parametric Rolling and its Influence on Container Lashing Systems," Marine Technology, Vol. 40, No. 1, pp. 1-19.

Shin, Y.S., Belenky, V., Lin, W.M., Weems, K. and Engle, A. (2003), "Nonlinear Time Domain Simulation Technology for Seakeeping and Wave-Load Analysis for Modern Ship Design," SNAME Transactions, Vol. 111.

Smith, T., and Zuzick, A., 2015, "Validation of Statistical Extrapolation Methods for Large Motion Prediction," Proc. 12th Intl. Conf. on Stability of Ships and Ocean Vehicles (STAB 2015), Glasgow, UK.

Spyrou, K. J., Belenky, V., Reed, A., Weems, K., Themelis, N., and Kontolefas, I., 2014, "Split-Time Method for Pure Loss of Stability and Broaching-To," Proc. 30th Symp. Naval Hydrodynamics, Hobart, Tasmania, Australia.

Weems, K. and Wundrow, D. 2013, "Hybrid Models for Fast Time-Domain Simulation of Stability Failures in Irregular Waves with Volume-Based Calculations for Froude-Krylov and Hydrostatic Force", Proc. 13th Intl. Ship Stability Workshop, Brest, France.

This page is intentionally left blank



Dynamic Instability of Taut Mooring Lines Subjected to Bi-frequency Parametric Excitation

Aijun Wang, *University of Strathclyde*

Hezhen Yang, *State Key Laboratory of Ocean Engineering, Shanghai Jiao Tong University*

Nigel Barltrop, *University of Strathclyde*

Shan Huang, *University of Strathclyde*

ABSTRACT

Parametric excitation or parametric resonance occurs when the offshore structure system parameter varies with time and meets a certain condition. Moored structure during the swell sea states causes the taut mooring line tension fluctuation which may induce very large dynamic motion of mooring lines. In this work, the taut mooring lines subjected to bi-frequency parametric excitation are studied. The parametric excitation equation of mooring lines is derived. The Bubnov-Galerkin approach is employed to obtain stability chart when consider the bi-frequency excitation. The responses of the mooring lines subjected to single- and bi-frequency excitation are discussed.

Keywords: *dynamic instability; mooring line; parametric excitation; Mathieu; bi-frequency*

1. INTRODUCTION

The dynamic instability is the oscillatory motion of dynamic system due to time-dependent variation of structure parameters e.g. inertia or stiffness due to the influence of externally applied force. Different the forced excitation, the parametric excitation is nonautonomous system. It can have catastrophic effects on the structures. The study indicated parametric excitation would cause very large increase in lateral dynamic motion of mooring lines due to the variation of axial tension. (Rönnquist et al., 2010). It is beneficial to avoid the mooring line design to locate in the unstable zone. Recently, some researchers have studied the dynamic instability due to parametric excitation such as parametric rolling of ships, spar and risers (Falzarano et. al 2003, Yang et al. 2015, and Zhang et. al 2010). However, previous work all focused on the single frequency excitation. Actually, the offshore structure is exposed to random waves

which are multi-frequency excitation. So, it is necessary and beneficial to study the taut mooring lines subjected to bi-frequency parametric excitation.

2. THEORY AND MATHEMATICAL MODEL

The general dynamic equation of Bernoulli-Euler beam can be expressed as follow.

$$EI \frac{\partial^4 y}{\partial x^4} - T \frac{\partial^2 y}{\partial x^2} + m \frac{\partial^2 y}{\partial t^2} = f(x, t) \quad (1)$$

Where EI is the bending stiffness, T is the axial tension, m is mass per unit length, $f(x, t)$ is external force on the beam.

For the mooring lines, the bending stiffness often can be neglected and the axial tension can be expressed by

$$T = T_0 + T_A \phi(t) \quad (2)$$



Where $\phi(t) = \sum_{n=0}^{\infty} A_n \cos(\omega_n t + \theta_n)$.

T_0 is the mean tension of the line.

T_A is the amplitude of lines dynamic tension.

ω_n is the tension variation frequency of the line.

θ_n is the random phase.

The hydrodynamic on the lines are calculated by Morison equation. It is nonlinear and can be linearized as the follows.

$$f(x,t) = -\frac{1}{2} \rho D C_D \left| \frac{\partial y}{\partial t} \right| \frac{\partial y}{\partial t} = -\sqrt{\frac{2}{\pi}} C_D \rho D \sigma \frac{\partial y}{\partial t} \quad (3)$$

Combing equations (1)-(3) leads to

$$m \frac{\partial^2 y}{\partial t^2} + \sqrt{\frac{2}{\pi}} C_D \rho D \sigma \frac{\partial y}{\partial t} - \left(T_0 + T_A \sum_{n=0}^{\infty} A_n \cos(\omega_n t + \theta_n) \right) \frac{\partial^2 y}{\partial x^2} = 0 \quad (4)$$

Assumed that the ends are pinned, the lateral motion of lines can be written as

$$y(x,t) = \sum_{n=1}^{\infty} y_n(t) \sin \frac{n\pi x}{l} \quad (5)$$

Submit Eq. (2) into Eq. (1), it follows that

$$\sum_{n=1}^{\infty} \left[m \frac{d^2 y_n(t)}{dt^2} + \sqrt{\frac{2}{\pi}} C_D \rho D \sigma \frac{dy_n(t)}{dt} + \left(T_0 + T_A \sum_{n=0}^{\infty} A_n \cos(\omega_n t + \theta_n) \right) \left(\frac{n\pi}{l} \right)^2 y_n(t) \right] \sin \frac{n\pi x}{l} = 0 \quad (6)$$

The above equation can be rewritten into the general form,

$$\frac{d^2 y_n(\tau)}{d\tau^2} + 2c_n \frac{dy_n(\tau)}{d\tau} + \left(a_n + 2q_n \sum_{n=0}^{\infty} A_n \cos(k\tau + \theta_n) \right) y_n(\tau) = 0 \quad (7)$$

where $\tau = \omega_0 t$, ω_0 is the basic frequency.

$$k = \frac{\omega_n}{\omega_0}, \quad a_n = \left(\frac{\bar{\omega}_n}{\omega_0} \right)^2, \quad q_n = \frac{1}{2} \frac{T_A}{T_0} \left(\frac{\bar{\omega}_n}{\omega_0} \right)^2,$$

$$c_n = \sqrt{\frac{1}{2\pi}} \frac{C_D \rho D \sigma}{m \omega_0}.$$

$$\bar{\omega}_n = \frac{n\pi}{l} \sqrt{\frac{T_0}{m}} \quad n=1, 2, \dots$$

$\bar{\omega}_n$ is the natural frequency of the line.

This is the second order homogenous equation which named Hill equation.

3. SINGLE-FREQUENCY EXCITATION CASE

In this section, only single-frequency excitation is taken into account, and then the Eq. (7) can be expressed as follow. It is the well-known Mathieu equation.

$$\ddot{y} + 2c\dot{y} + (a + 2q \cos(2\tau)) y = 0 \quad (8)$$

For the single-frequency excitation, the top end motion of mooring lines corresponds to the floating structure during the regular sea.

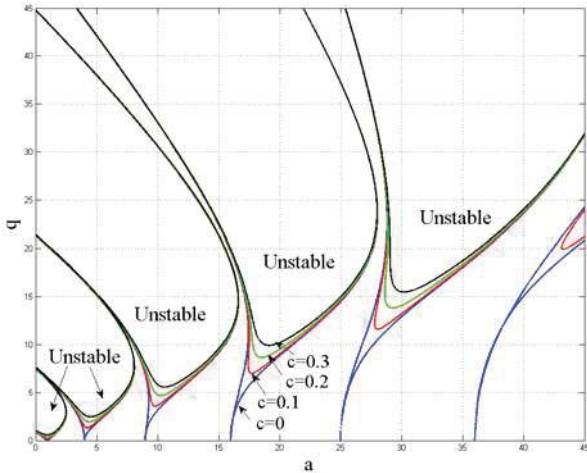
3.1 Stability chart of single-frequency excitation

The stability chart is often used to identify the unstable and stable zones of dynamic instability due to parametric excitation. The stability chart can show the change instability as the parameters are varied and are very useful for the design guidance. It can be solved by Floquet theory or perturbation method. The stability chart of single-frequency excitation for



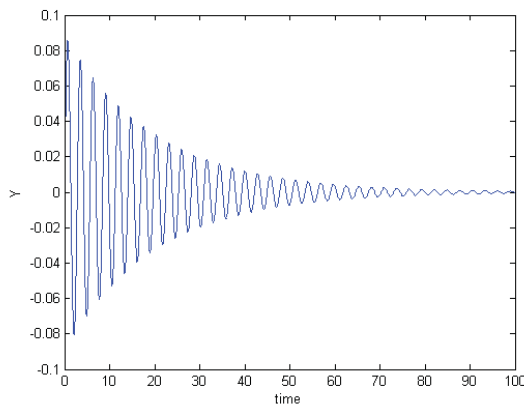
the taut mooring lines is shown in the Fig.1. It can be seen that the unstable zone will shrink as the damping increases. The resonance will occur when excitation is integral or sub multiple of fundamental frequency.

Fig.1 Stability chart of single-frequency excitation
(Blue line-- $c=0$; red line-- $c=0.1$; green line-- $c=0.2$; black line-- $c=0.3$)



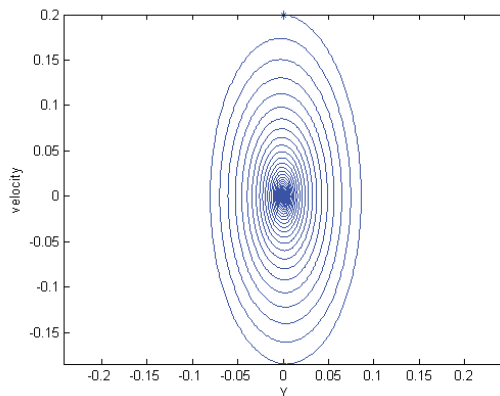
3.2 Dynamic response due to single-frequency excitation in time domain

Fig.2 present two case for the lateral dynamic response at the midpoint of the mooring line (Case I locate at stable zone and case II locate at unstable zone). The direction of response is orthogonal to the direction of the excitation. For the case II, It can be seen that the response will increase exponentially. This case should be removed for the design.

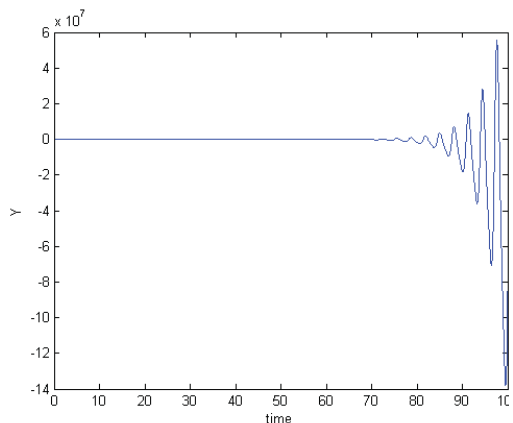


Response

(Case I)

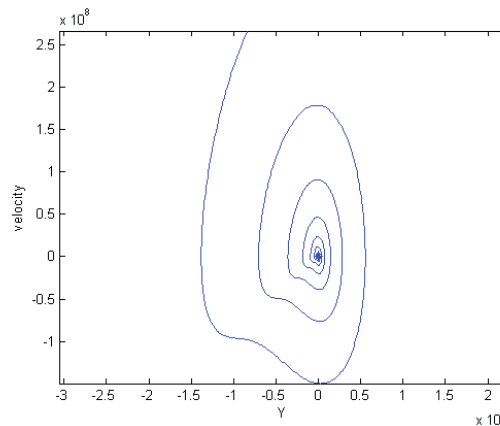


Phase plane trajectory



Response

(Case II)



Phase plane trajectory

Fig.2 Dynamic response due to single-frequency excitation in time domain
(Case I: $a=5$; $q=0.04$; $c=0.1$; Case II: $a=5$; $q=2.5$; $c=0.1$)

4. BI-FREQUENCY EXCITATION CASE

For real sea conditions, the top end of mooring line is subjected to multi-frequency excitation from floating motions in the random waves. The parametric instability property of mooring line has great effects on the safety of the design case and it can cause the lateral motion exponential increase in the oscillation. Here, the parametric instability due to bi-frequency excitation is studied which is conducive to understand the mechanism of the dynamic instability.

$$\ddot{y} + 2c\dot{y} + (a + 2q(\cos(2\tau) + d\cos(4\tau)))y = 0 \quad (9)$$

The dynamic instability for the bi-frequency excitation is obtained by the Bubnov-Galerkin approach (Perdesen, 1980). Fig.3 shows the stability chart for the bi-frequency excitation. It can be seen that the unstable zone for the bi-frequency excitation is obviously different from the single-frequency excitation.

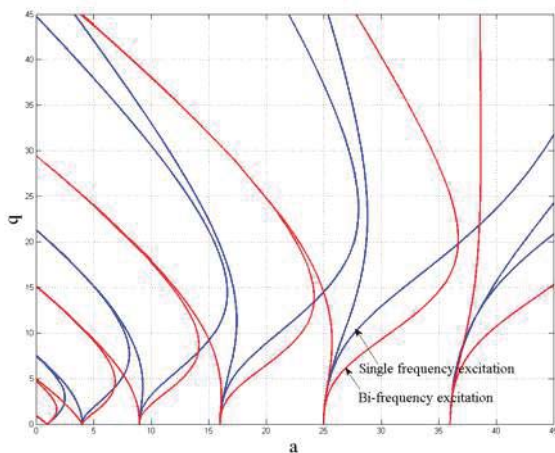


Fig.3 Stability chart for single- and bi-frequency excitation ($d=-0.5$) (Blue line- single-frequency excitation; red line- bi-frequency excitation)

4.1 Effects of different d

Fig.4 and 5 give the stability charts for different $d=0.5$ and -0.5 respectively. The sign of d mean the different phase between the two excitations. The unstable zone changes when d turns into negative and the shape is also different. It is interesting to find that the closed zone exists.

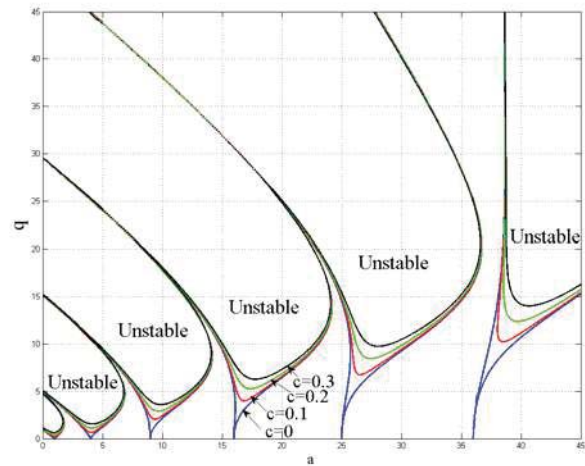


Fig.4 Stability chart for bi-frequency excitation for different damping ($d=-0.5$) (Blue line-- $c=0$; red line-- $c=0.1$; green line-- $c=0.2$; black line-- $c=0.3$)

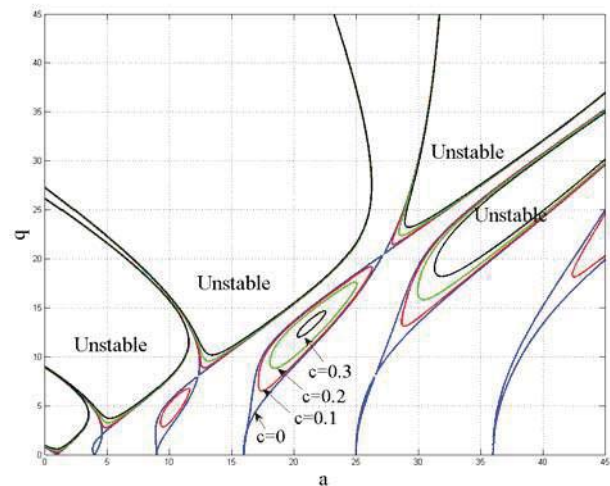


Fig.5 Stability chart for bi-frequency excitation for different damping ($d=0.5$) (Blue line-- $c=0$; red line-- $c=0.1$; green line-- $c=0.2$; black line-- $c=0.3$)



4.2 Effects of different damping for positive d

The effects of different damping for positive d are compared in the Fig.6-8. The damping varies from 0 to 0.3. It can be seen that the unstable zone of bi-frequency excitation is more sensitive than the single-frequency excitation. The unstable zone changes more as the damping varies.

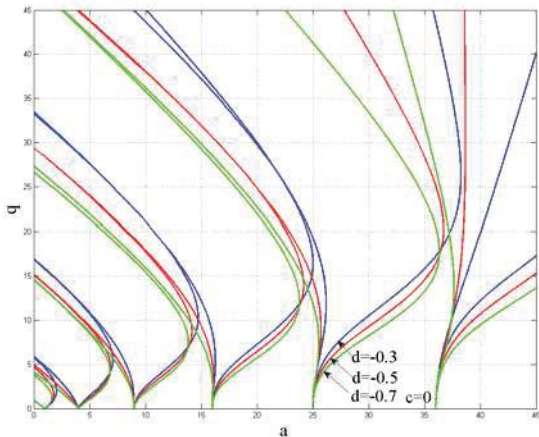


Fig.6 Stability chart for bi-frequency excitation for different damping ($c=0.0$) (Blue line-- $d=-0.3$; red line-- $d=-0.5$; green line-- $d=-0.7$)

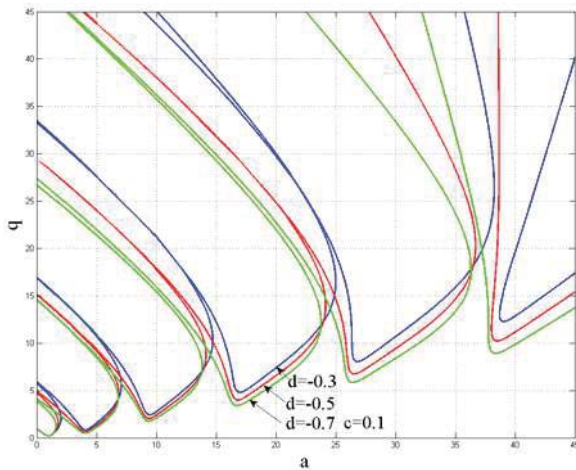


Fig.7 Stability chart for bi-frequency excitation for different d ($c=0.1$) (Blue line-- $d=-0.3$; red line-- $d=-0.5$; green line-- $d=-0.7$)

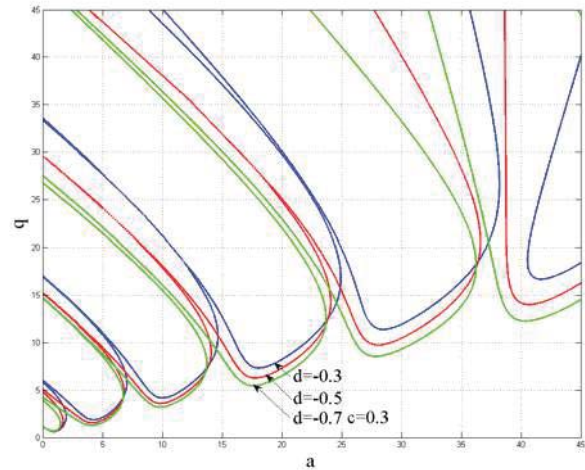


Fig.8 Stability chart for bi-frequency excitation for different d ($c=0.3$) (Blue line-- $d=-0.3$; red line-- $d=-0.5$; green line-- $d=-0.7$)

4.3 Effects of different damping for negative d

Fig.9-11 present the effects of different damping for negative d on the dynamic instability zone. The damping varies from 0 to 0.3. It can be seen that the unstable zone of bi-frequency excitation is completely different from the single-frequency excitation. The unstable zone changes more as the damping varies. The safety case will turn into unsafely when damping varies or the sign of d changes.

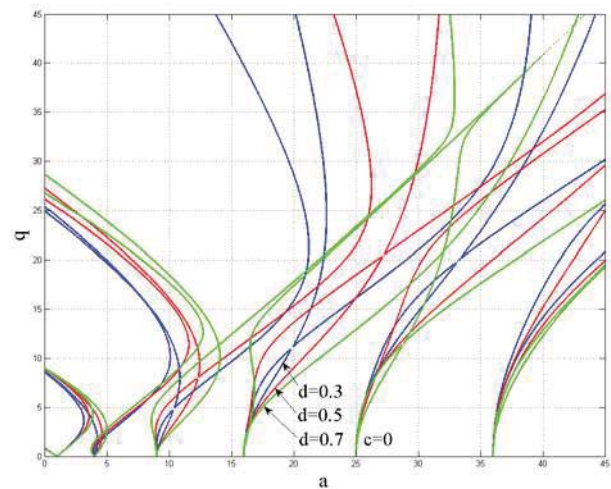


Fig.9 Stability chart for bi-frequency excitation for different d ($c=0.0$)

(Blue line-- $d=0.3$; red line-- $d=0.5$; green line-- $d=0.7$)

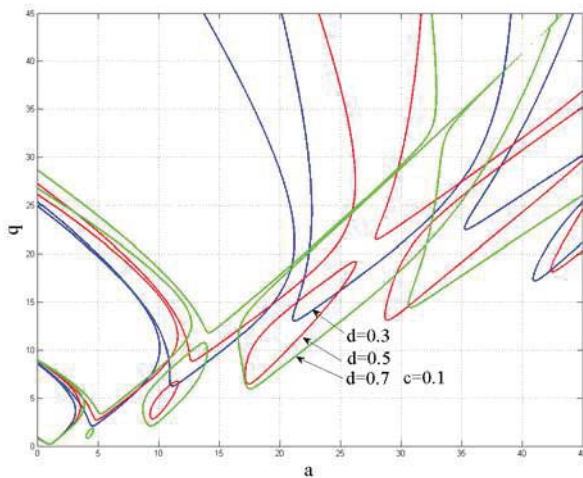


Fig.10 Stability chart for bi-frequency excitation for different d ($c=0.1$)

(Blue line-- $d=0.3$; red line-- $d=0.5$; green line-- $d=0.7$)

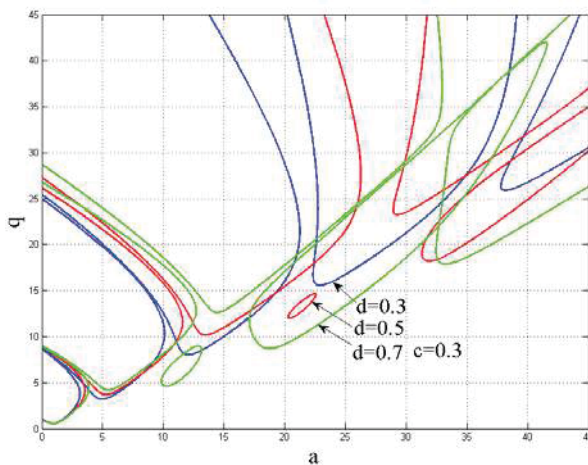


Fig.11 Stability chart for bi-frequency excitation for different d ($c=0.3$)

(Blue line-- $d=0.3$; red line-- $d=0.5$; green line-- $d=0.7$)

5. CONCLUSIONS

In this work, the taut mooring lines subjected to single and bi-frequency parametric excitation were studied. The responses of the mooring lines subjected to single- and bi-frequency excitation were discussed. The unstable zone of bi-frequency excitation is obviously different from the single-frequency

excitation. The safety case in the single-frequency excitation may become unsafely in the bi-frequency excitation. The effects of different parameters on the stability chart were discussed. The results indicate that multi-frequency should be given consideration in a more accurate prediction of parametric excitation.

ACKNOWLEDGEMENTS

This work was financially supported by the National Natural Science Foundation of China (Grant No. 51379005).

6. REFERENCES

- Rönquist, A. Remseth, S. and Udahl, G. 2010. Unstable Non-Linear Dynamic Response Investigation of Submerged Tunnel Taut Mooring Elements Due to Parametric Excitation. 23rd Nordic Seminar on Computational Mechanics.
- Jeffrey Falzarano, Jun Cheng, and Samrat Das. 2003. Parametric excitation of floating offshore platforms. 8th International Conference on the Stability of Ships and Ocean Vehicles.
- Yang H.Z., Xu P. , 2015. Effect of hull geometry on parametric resonances of spar in irregular waves. Ocean Engineering. 99:14-22.
- Libang Zhang, Ayman Eltaher, Paul Jukes. 2010. Mathieu instability of TTR due to VIV. Proceedings of the 5th International Offshore Pipeline Forum.
- Pedersen, P. 1980. Stability of the solutions to Mathieu-Hill equations with damping. Ingenieur-Archiv, 149 (1),15-29.

Session 12.1 – DAMAGE STABILITY

Flow Model for Flooding Simulation of a Damaged Ship

An Overview of Warships Damage Data from 1967 to 2013

Advanced Damaged Stability Assessment for Surface Combatants

Dynamic Stability Assessment of Naval Ships in Early-Stage Design

This page is intentionally left blank



Flow Model for Flooding Simulation of a Damaged Ship

Gyeong Joong Lee, *KRISO*, gjlee@kriso.re.kr

ABSTRACT

In this paper, new models for vented compartments and an accumulator model were proposed, which can adjust the inner pressure automatically, even for systems with many compartments and openings. The dynamic-orifice equation was investigated for use in the case of large openings, so that the ripples in the air pressure that had been caused by the square-root singularity of the existing orifice equation could be eliminated. In addition, some models of flow between compartments were investigated, so that the simulation could reflect more realistic situations. Application to a recent real accident validated the effectiveness of the proposed models.

Keywords: *orifice equation, flooding, air compressibility, damaged ship*

1. INTRODUCTION

While the number of flooding and sinking accidents is relatively small, they often lead to the tragic loss of personnel. Therefore, better knowledge about the processes that occur during flooding and sinking is required, and optimal response measures should be prepared according to the results of the study. For this purpose, a great deal of research about flooding has been conducted for specific real accidents, and safety assessments have been conducted during ship design, in anticipation of possible damage in the field.

The flooding simulation of a damaged ship seems to have been started by Spouge (1986), when he investigated the Ro-Ro Ferry sinking. He used a hydraulic-flow model to calculate the flood rate, and used an empirical formula to determine the center-of-gravity of the floodwater and its movement. Sen and Konstantinidis (1987) developed his method further, and they obtained the position of the center-of-gravity by assuming the free surface always remains horizontal. Later, to take into account the dynamic effect of the floodwater, Papanikolaou et al. (2000) developed the method of lumped mass. A flow equation for

shallow water and the movement of point mass followed (Chang and Blume, 1998; Chang, 1999). These two papers were cited in Ruponen (2007). Computational fluid dynamics followed (van't Veer and de Kat, 2000; Woodburn et al., 2002; Cho et al., 2005); then the depth-averaged Euler equation was introduced (Lee, 2010a).

Until now, the hydraulic orifice equation has been used to obtain the flow between compartments. For the application of this equation, the following assumptions are required: incompressible fluid, inviscid fluid, steady conditions, and small openings (area). The most troublesome assumption is that steady state: the flow velocity can change instantly as the pressure changes. Lee (2014) newly derived the dynamic-orifice equation from the basic equations of fluid mechanics. In this study, the property of this dynamic-orifice equation was investigated, and the sample calculations with analysis were given.

Another problem that occurs in the simulation of ship flooding, involves the calculation of the pressure in each compartment, when many compartments are connected to each other in complicated ways. This problem has been addressed previously (van't Veer et al., 2002, 2004; Ikeda et al.,

2004; Vassalos et al., 2005). The most important thing is the determining a reference pressure for use in each compartment. Ruponen (2007) made a comprehensive study of this problem and proposed a pressure-correction method that satisfied the mass-conservation law. In this study, a new compartment model was proposed that adjusts the reference pressure simply, even for systems with many compartments and openings. And a method that takes into consideration the dynamic effect for quasi-static analysis was investigated.

2. RE-ANALYSIS OF THE ORIFICE EQUATION

In many studies, the following ‘orifice equation’ has been used in calculating the flow through an opening.

$$q = \rho C_D A v = \rho C_D A \sqrt{\frac{2\Delta p}{\rho}} \quad (1)$$

where, q and ρ are the mass flux and density of the flow through the opening, A is the area of the opening, Δp the pressure difference, and C_D the discharge coefficient. The above orifice equation was derived from the steady Bernoulli’s equation.

2.1 Hydraulic Orifice Equation

Let us derive the hydraulic orifice equation. Bernoulli’s equation can be applied to the flow of an incompressible, inviscid fluid in steady state along a stream line. Bernoulli’s equation and the continuity equation used for Fig. 1 are Equations 2 and 3, respectively.

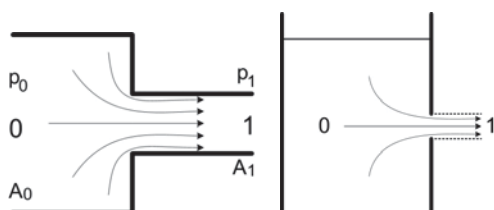


Fig. 1 Orifice and stream lines

$$\frac{p_0}{\rho} + \frac{1}{2}V_0^2 + gz_0 = \frac{p_1}{\rho} + \frac{1}{2}V_1^2 + gz_1 \quad (2)$$

$$A_0V_0 = A_1V_1 \quad (3)$$

where, g is the gravitational acceleration, z the height of the position, the subscripts ‘0’ and ‘1’ indicate the orientation (position), the fluid flows from side ‘0’ to side ‘1’. The total speed of the flow is the square root of the component velocity squared, $V = \sqrt{u^2 + v^2 + w^2}$. From Equations 2 and 3, the flow velocity through the orifice can be expressed as in Equation 4.

$$V_1 = \sqrt{\frac{2}{\rho} \frac{(\Delta P + \rho g \Delta z)}{1 - (A_1/A_0)^2}} \quad (4)$$

If the area of side ‘0’ is large, and the height difference vanishes, then Equation 4 can be reduced to the simpler form below.

$$V_1 = \sqrt{\frac{2}{\rho} \Delta p} \quad (5)$$

The flux can then be obtained by multiplying the area of orifice and fluid density.

$$q = C_D \rho A V_1 = C_D \rho A \sqrt{\frac{2\Delta p}{\rho}} \quad (6)$$

where, the discharge coefficient C_D is related to the inlet/outlet shape, and the Reynolds number. Usually for an orifice with right-angled edges, a discharge coefficient of 0.6–0.7 is used.

Equation 6 has a singular behavior of the square root function for small pressure differences. The rate of change with respect to the pressure difference, goes to infinity as the pressure difference goes to zero. Because of this, an unrealistic oscillation takes place when the pressure difference is small (as for an opening between two compartments with no

other openings), while there is no problem when the pressure difference is large. This phenomenon of square root instability is explained in detail in Appendix A. Thus, the hydraulic orifice equation (6) is for a large pressure difference, subject to the assumptions stated previously.

2.2 Dynamic Orifice Equation

There are two problems with the hydraulic orifice equation. One is that it applies to steady state conditions. The second is that it applied orifices of small cross-section (area). In order to conduct a time-domain flooding simulation, it is required to include the dynamic effect, and to expand the applicability to include orifices of large area. Let us shortly introduce the work of Lee (2014), derivation of a new dynamic orifice equation. The momentum conservation law can be represented by the Euler equation for an incompressible, inviscid fluid (Equations 7 and 7').

$$\frac{\partial \vec{v}}{\partial t} + (\vec{v} \cdot \nabla) \vec{v} = \vec{F} - \frac{1}{\rho} \nabla p \quad (7)$$

$$\frac{\partial \vec{v}}{\partial t} + \frac{1}{2} \nabla(\vec{v} \cdot \vec{v}) = \vec{F} - \frac{1}{\rho} \nabla p \quad (7')$$

where, \vec{v} is a velocity vector, p the pressure, ρ the density of fluid, and \vec{F} is the body force, including gravity. The above two equations are the same for incompressible and inviscid fluid. In this study, the integral version of the Euler equation will be used, so the momentum conservation law can be represented as in Equations 8 and 8' for a specific control volume.

$$\int_{\Omega} \frac{\partial}{\partial t} (\rho \vec{v}) dV + \int_{\partial\Omega} \rho \vec{v} (\vec{v} \cdot \vec{n}) dS = \int_{\Omega} \rho \vec{F} dV - \int_{\partial\Omega} p \vec{n} dS \quad (8)$$

$$\int_{\Omega} \frac{\partial}{\partial t} (\rho \vec{v}) dV + \frac{1}{2} \int_{\partial\Omega} \rho (\vec{v} \cdot \vec{v}) \vec{n} dS \quad (8')$$

$$= \int_{\Omega} \rho \vec{F} dV - \int_{\partial\Omega} p \vec{n} dS$$

where, Ω is the control volume of concern, and $\partial\Omega$ is the boundary of the control volume. The orientation of the normal vector is outward normal.

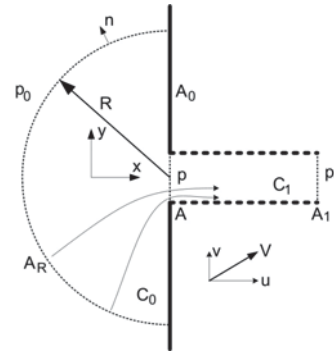


Fig. 2 Orifice, control volumes and related parameters

Fig. 2 shows the orifice and the overall shape of the control volume, where R is the distance from the center of orifice and is chosen to be large so that the flow velocity at that distance will be small enough. On the boundary, A_R , the pressure is constant as p_0 , and the flow velocity is parallel to the normal vector. Let us represent the velocity vector as \vec{v} , the velocity normal to orifice as u , and the total velocity as $V = \sqrt{u^2 + v^2 + w^2}$, here and after. At the right side of the orifice, the velocity and pressure are assumed to be constantly distributed. The area of the orifice is $A = A_1$, the area of the wall in which the orifice exists is A_0 . The control volumes on the left and right are C_0 and C_1 , respectively. The velocity components, excluding u , are asymmetric about the centerline of the orifice.

Applying the mass and momentum conservation law to the control volume C_0 and C_1 , we can obtain the resulting equation (9) which relates the velocity at the orifice and the pressure difference. (Lee (2014) finally got Equation 9 for the dynamic-orifice equation.)

$$\frac{\sqrt{A} \partial \bar{u}}{2 \partial t} + \frac{7}{8} (\bar{u})^2 = \frac{(p_0 - p_1)}{\rho} \quad (9)$$

where, \bar{u} is the average normal velocity at the orifice. The final velocity for a steady state of the above equation is:

$$\bar{u}_f = \sqrt{\frac{8(p_0 - p_1)}{7\rho}} \quad (10)$$

This final steady state value is less than that provided by Equation 5. As briefly explained previously, the velocity from Equation 5 is the total velocity, and that of Equation 10 is the normal velocity at the orifice. It is reasonable to use the normal velocity for the calculation of flux through an orifice. Comparing Equations 5 and 10, it can be seen that the theoretical value of the contraction coefficient of a circular orifice with right-angle edge, is $\sqrt{4/7} \cong 0.756$ for an inviscid fluid. We can obtain the initial rate of velocity (i.e., initial acceleration) from rest using Equation 9.

$$\left. \frac{\partial \bar{u}}{\partial t} \right|_{t=0} = \frac{1}{\sqrt{A}} \frac{2(p_0 - p_1)}{\rho} \quad (11)$$

The time to reach final velocity using the initial rate of change would be:

$$T = \frac{\bar{u}_f}{d\bar{u}/dt|_{t=0}} = 2 \sqrt{\frac{A}{7}} \sqrt{\frac{\rho}{2(p_0 - p_1)}} \quad (12)$$

Fig. 3 shows the velocity rise with respect to time, when the pressure difference is a step-function.

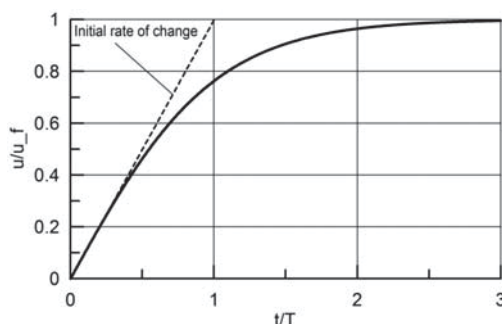


Fig. 3 Orifice velocity behavior when the pressure difference is a step function

The velocity reaches 0.765 of the final velocity at $t = T$, 0.965 at $t = 2T$, and 0.99 at $t = 3T$. From Fig. 3, the numerical time integration using Equation 9 seems not to be desirable if the size of time step of the simulation is less than T . For that case, one can use Equation 10 rather than 9. Here, T (from Equation 12) becomes larger as the pressure difference becomes smaller. This means that the dynamic model works for the case of small pressure differences, even if we use a fixed size of time step.

For the discharge coefficient, the use of $C_D/\sqrt{4/7}$ is desirable because of the difference between the normal velocity and total velocity in Equations 10 and 5. The density in Equation 10 should be determined according to the sign of the velocity, not the sign of the pressure difference. Equation 9 stands for positive velocity only, and we can modify the equation a little bit for both directions.

$$\frac{\sqrt{A} \partial \bar{u}}{2 \partial t} + \frac{7}{8} \bar{u} |\bar{u}| = \frac{(p_0 - p_1)}{\rho} \quad (13)$$

if $\bar{u} \geq 0$, $\rho = \rho_0$
if $\bar{u} < 0$, $\rho = \rho_1$

2.3 Large Opening

The pressure difference can vary across the orifice when it is large. If the pressure difference is constant over the orifice area, Equations 5 and 14 can give the flow velocity, but if it varies; it is possible to obtain the flow by solving the Euler equation or the Navier-Stokes equation. However, this is impractical for a system with many compartments and orifices. A more practical way is to integrate the expression over the orifice area in order to obtain the flux through the orifice. The hydraulic orifice equations (5 and 6) do not include the concept of average velocity, but for practical calculation, one can use the average concept of velocity by integrating them over

the orifice area. Meanwhile, the dynamic orifice equation (13) uses the average velocity, so it creates no logical problem to integrate the pressure difference in order to get the forces acting on the surrounding fluid. Therefore, the average velocities could be obtained using the following equations, and multiplying the orifice area gives the flux.

$$V = \frac{1}{A} \int_A \sqrt{\frac{2}{\rho} \Delta p} dA = \frac{1}{A} \sqrt{\frac{2}{\rho}} \int_A \sqrt{\Delta p} dA \quad (14)$$

$$\frac{\sqrt{A}}{2} \frac{\partial \bar{u}}{\partial t} + \frac{7}{8} \bar{u} |\bar{u}| = \frac{1}{\rho A} \int_A \Delta p dA \quad (15)$$

where, $\Delta p = p_0 - p_1$ is the pressure difference across the orifice. The mass flux can be obtained by the following equations. (The subscripts 'h' and 'd' mean the flux from the hydraulic orifice equation and dynamic orifice equation, respectively.)

$$q_h = \rho C_D A V \quad (16)$$

$$q_d = \rho C_D' A \bar{u} \quad (17)$$

where the value of C_D is from the hydraulic experiment, so use C_D' as $C_D / \sqrt{4/7}$.

Another big problem with larger openings is the fact that the free surface may lie upon cross section of the orifice. Followings are a number of cases (Fig. 4) that could occur, depending on the height of the free surface, and the substances on both sides of the orifice.

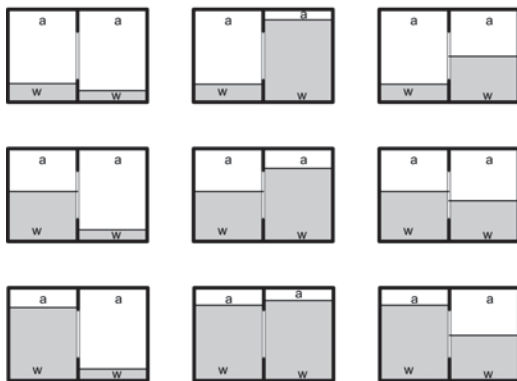


Fig. 4 Orifice and adjacent substances ('a' is air, 'w' is water)

These cases can be classified into four boundary types (within the orifice) according to the substances in contact: Air-Air, Air-Water, Water-Air, and Water-Water. The integration of Equations 14 and 15 can be obtained by dividing the orifice area into sub-regions so that each sub-region has one type of material boundary, then integrating the equations (14, 15) over each sub-region, and adding the results.

Regarding the shape of the openings, many have long, narrow shapes (e.g., doors and gaps). In these cases, one-dimensional (1-D) integration may be helpful, but for other cases the integration should be done in 2-D.

In order to calculate the flow through an opening, there is a need for several definitions. First, the identification of the compartment of interest is needed because the opening connects two compartments; thus, we have Compartment 0 and Compartment 1. This identification may be provided by adding the subscript '0' or '1'. The velocity is defined as positive when the flow is from Compartment 0 to Compartment 1; whereas, negative velocity means flow in the opposite direction. Compartment 0 is called the 'donor'; Compartment 1 is the 'acceptor'. The subscripts 'w' and 'a' refer to the substances water and air, respectively.

The two substances can flow through the opening simultaneously, so the flux may be identified by adding subscript as follows,

q_{ha} : mass flux of air using hydraulic orifice equation

q_{hw} : mass flux of water using hydraulic orifice equation

q_{da} : mass flux of air using dynamic orifice equation

q_{dw} : mass flux of water using dynamic orifice equation

First, let us divide the opening area into sub-regions with one of the four types of boundary (i.e., 'air-air', 'air-water', 'water-air', and 'water-water'). If the sign of the pressure difference changes in any sub-region, this sub-region is divided into two sub-regions so that each sub-region has a distinct sign of pressure

difference, and one boundary type. For each sub-region, calculate the following integrals,

$$I_i = \int_{A_i} \text{sgn}(\Delta p) \sqrt{|\Delta p|} dA \quad (18)$$

$$J_i = \int_{A_i} \Delta p dA \quad (19)$$

$$A_i = \int_{A_i} dA \quad (20)$$

where, $\text{sgn}(\Delta p)$ is the sign of Δp . Because the integrand has one sign, the sign of the integral is the same as the sign of the pressure difference.

The mass flux can be calculated using the above integrals, if we use the hydraulic orifice equation (21 and 22).

$$q_{ha} = \sum_i \begin{cases} \rho_{a0} C_D \sqrt{2/\rho_{a0}} I_i & \text{for } I_i \geq 0, \text{ and donor is air} \\ \rho_{a1} C_D \sqrt{2/\rho_{a1}} I_i & \text{for } I_i < 0, \text{ and acceptor is air} \end{cases} \quad (21)$$

$$q_{hw} = \sum_i \begin{cases} \rho_{w0} C_D \sqrt{2/\rho_{w0}} I_i & \text{for } I_i \geq 0, \text{ and donor is water} \\ \rho_{w1} C_D \sqrt{2/\rho_{w1}} I_i & \text{for } I_i < 0, \text{ and acceptor is water} \end{cases} \quad (22)$$

To use the dynamic orifice equation (15), the calculation should be done according to the sign of the velocity not the sign of the pressure difference. Because the velocity is the unknown, two cases (positive and negative) should be prepared. Thus,

$$\text{For air-air, } J_{Pa} = \sum_i J_i, A_{Pa} = \sum_i A_i$$

$$J_{Ma} = \sum_i J_i, A_{Ma} = \sum_i A_i$$

$$\text{For water-water, } J_{Pw} = \sum_i J_i, A_{Pw} = \sum_i A_i$$

$$J_{Mw} = \sum_i J_i, A_{Mw} = \sum_i A_i$$

$$\text{For air-water, } J_{Pa} = \sum_i J_i, A_{Pa} = \sum_i A_i \text{ if } J_i \geq 0$$

$$J_{Mw} = \sum_i J_i, A_{Mw} = \sum_i A_i \text{ if } J_i < 0$$

$$\text{For water-air, } J_{Pw} = \sum_i J_i, A_{Pw} = \sum_i A_i \text{ if } J_i \geq 0$$

$$J_{Ma} = \sum_i J_i, A_{Ma} = \sum_i A_i \text{ if } J_i < 0$$

According to the sign of the velocity, the following equations give the averaged water and air velocities.

$$\frac{\sqrt{A_{Xa}}}{2} \frac{\partial(\bar{u})_a}{\partial t} + \frac{7}{8} \bar{u} |\bar{u}|_a = \frac{1}{\rho A_{Xa}} J_{Xa} \quad (23)$$

$$\frac{\sqrt{A_{Xw}}}{2} \frac{\partial(\bar{u})_w}{\partial t} + \frac{7}{8} \bar{u} |\bar{u}|_w = \frac{1}{\rho A_{Xw}} J_{Xw} \quad (23')$$

Equation 23 is for the air flow, and 23' is for the water flow. In the above equation 'X' is 'P' if the velocity is positive; while 'M' is negative. The mass flux can be obtained by the following equations.

$$q_{da} = \rho_a C'_D A_a (\bar{u})_a \quad (24)$$

$$q_{dw} = \rho_w C'_D A_w (\bar{u})_w \quad (24')$$

In some cases, the force acting on a door is required to determine when the door will collapse; the force can be obtained by simply adding all J_i .

1-D Opening

Sometimes, it is convenient to neglect the variation of the pressure difference along width and to integrate it along the height, for a door or its gap, as shown in Fig. 5.

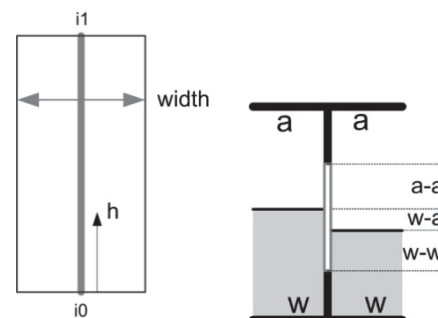


Fig. 5 Shape of 1-D opening and sub-regions of orifice

The integration of Equations (18), (19), (20) can be carried out analytically by assuming the linear variation of pressure difference in each sub-region. For the i -th sub-region, ($h_i \leq h < h_{i+1}$) the pressure difference can be represented as,

$$\Delta p = a_i (h - h_i) + b_i$$

$$b_i = \Delta p_i, \quad a_i = (\Delta p_{i+1} - \Delta p_i) / (h_{i+1} - h_i)$$



Then, substitute the above into Equations 18 and 19, and integrate them analytically. The results of the integrations for $a_i = 0$ are:

$$I_i = \text{sgn}(\Delta p_i) w_0 \int_{h_i}^{h_{i+1}} (|\Delta p|)^{\frac{1}{2}} dh \quad (25)$$

$$= \text{sgn}(\Delta p_i) w_0 (|\Delta p|)^{\frac{1}{2}} (h_{i+1} - h_i)$$

$$J_i = w_0 \int_{h_i}^{h_{i+1}} \Delta p dh = w_0 \Delta p (h_{i+1} - h_i) \quad (26)$$

$$A_i = w_0 \int_{h_i}^{h_{i+1}} dh = w_0 (h_{i+1} - h_i) \quad (27)$$

and for $a_i \neq 0$,

$$I_i = \text{sgn}(\Delta p_i) w_0 \int_{h_i}^{h_{i+1}} (|\Delta p|)^{\frac{1}{2}} dh \quad (28)$$

$$= \text{sgn}(\Delta p_i) w_0 \frac{2}{3a_i} \left[\Delta p (|\Delta p|)^{\frac{1}{2}} \right]_i^{i+1}$$

$$J_i = w_0 \int_{h_i}^{h_{i+1}} \Delta p dh = w_0 \frac{1}{2a_i} [(\Delta p)^2]_i^{i+1} \quad (29)$$

$$A_i = w_0 \int_{h_i}^{h_{i+1}} dh = w_0 (h_{i+1} - h_i) \quad (30)$$

where, $[]_i^{i+1}$ means the subtraction of i indexed value from $i+1$ indexed value. The above expression was drawn to be independent of the sign of the pressure difference.

2-D Opening

For the general shape of an opening, the integration would be carried out in 2-D. Let us divide the opening area into sub-regions as explained previously, which can be represented as a closed polynomial. Next, integrate them over each sub-region using the Stokes theorem. Let us fit the pressure difference by bi-linear interpolation as in Equation 31.

$$\Delta p = ax + by + c \quad (31)$$

Three constants a, b , and c can be found from three conditions at three vertices of that polynomial.

Let us change the area integral to the contour integral, along the contour C_i using Stokes theorem.

$$I_i = \text{sgn}(\Delta p) \iint_{R_i} \sqrt{|\Delta p|} dx dy \quad (32)$$

$$= \frac{2}{3a} \oint_{C_i} |\Delta p|^{2/3} dy$$

$$J_i = \iint_{R_i} \Delta p dx dy = \frac{1}{2a} \oint_{C_i} (\Delta p)^2 dy \quad (33)$$

$$A_i = \iint_{R_i} dx dy = \oint_{C_i} x dy \quad (34)$$

On the j -th line segment of the i -th sub-region, the following geometric relation exists.

$$x = b_{xj}y + c_{xj}, \quad b_{xj} = \frac{x_{j+1} - x_j}{y_{j+1} - y_j},$$

$$c_{xj} = x_j - \frac{x_{j+1} - x_j}{y_{j+1} - y_j} y_j$$

Therefore, the pressure difference (31) can be expressed as follows on the j -th line segment.

$$\Delta p = ax + by + c = b'_j y + c'_j$$

$$b'_j = b + ab_{xj}, \quad c'_j = c + ac_{xj}$$

If we integrate Equation 32, the results are (for $a \neq 0$),

$$I_i = \text{sgn}(\Delta p) \frac{2}{3a} \times \sum_j \begin{cases} \frac{2}{5b'_j} [(\Delta p)^2 (|\Delta p|)^{\frac{1}{2}}]_j^{j+1} & \text{for } b'_j \neq 0 \\ (\Delta p) (|\Delta p|)^{\frac{1}{2}} (y_{j+1} - y_j) & \text{for } b'_j = 0 \end{cases} \quad (35)$$

and for $a = 0$, ($b'_j = b, c'_j = c$)

$$I_i = \text{sgn}(\Delta p) \times \sum_j \begin{cases} \frac{2}{15b^2} [(5bx - 2b_{xj}\Delta p)(\Delta p)(|\Delta p|)^{\frac{1}{2}}]_j^{j+1} & \text{for } b \neq 0 \\ \frac{1}{2} (|\Delta p|)^{\frac{1}{2}} (x_{j+1} + x_j)(y_{j+1} - y_j) & \text{for } b = 0 \end{cases} \quad (36)$$

The results of equation (33) are (for $a \neq 0$),

$$J_i = \frac{1}{2a} \sum_j \begin{cases} \frac{1}{3b_j'} [(\Delta p)^3]_j^{j+1} & \text{for } b_j' \neq 0 \\ (\Delta p)^2 (y_{j+1} - y_j) & \text{for } b_j' = 0 \end{cases} \quad (37)$$

and for $a = 0$, ($b_j' = b$, $c_j' = c$)

$$J_i = \sum_j \begin{cases} \frac{1}{6b^2} [(3bx - b_x \Delta p)(\Delta p)^2]_j^{j+1} & \text{for } b \neq 0 \\ \frac{1}{2} (\Delta p)(x_{j+1} + x_j)(y_{j+1} - y_j) & \text{for } b = 0 \end{cases} \quad (38)$$

The area, from Equation 34, can be rewritten as follows.

$$A_i = \sum_j \frac{1}{2} (x_{j+1} + x_j)(y_{j+1} - y_j) \quad (39)$$

2.4 Sample Applications

Let us consider the case in which two compartments are adjacent, and an opening is located in the wall between them. The size of the compartment is 5 m (L) x 5 m (W) x 5 m (H), and there is no vent. The sample calculations were carried out for a point and a

1-D opening, the compressibility of air was included, and an iso-thermal process was assumed. The result from the dynamic orifice equation was compared with that from the hydraulic orifice equation.

For a point opening, the area of the opening is 1 m² and the location of the orifice 1 m from the bottom. A 1-D calculation was also made for the comparison. The calculation cases are shown in Fig.6. The results are shown in Fig. 7 in comparison with 1-D calculation.

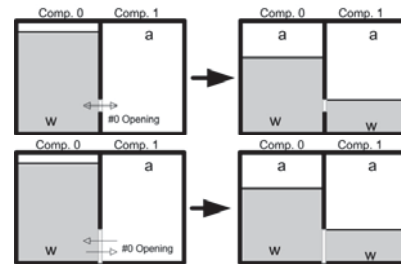


Fig. 6 Sample model for point opening (upper two) and equivalent 1-D opening (below two) (In each pair of figures, the left figure shows the initial state, and the right figure shows the expected final state.)

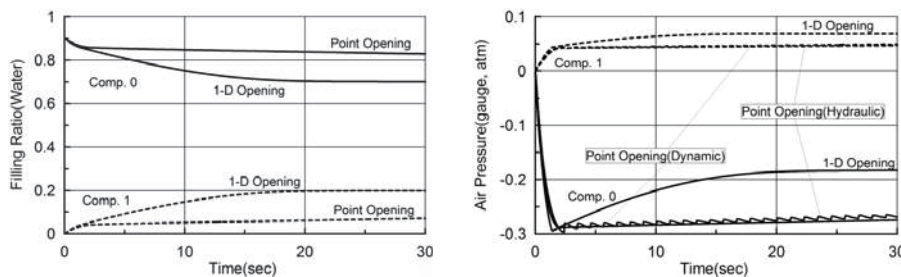


Fig. 7 Filling ratio (left) and the air pressure (right) in compartments with a point-opening

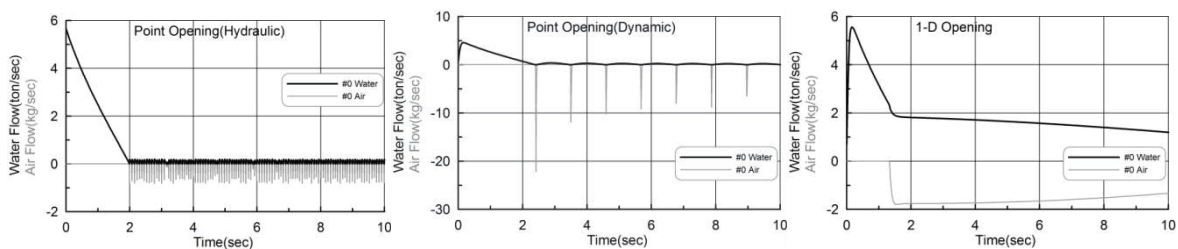


Fig. 8 Flow rates of water and air for point (left and center) and 1-D openings (right)

The filling ratio of Compartment 0 decreases with time, and the filling ratio of Compartment 1 increases. However, the results for the point-opening vary slowly, except in the initial stage, and the pressure in Compartment 0 oscillates. The flows of water and air are shown in Fig. 8.

The flow of air exhibits many rapid small oscillations with the hydraulic orifice equation, while it exhibits intermittent large oscillations with the dynamic orifice equation. This affects the pressure fluctuation in Fig. 7. This is because a point opening can only allow the flow of one substance at a time. For 1-D openings, the water and air can flow simultaneously in opposite directions, the flow is smoother, and the filling ratio reaches the value we anticipated. From these results, we now know that point-openings should not be used when there is only one opening in a compartment.

1-D opening

The next sample calculations were made with 1-D openings. The sample cases were for situations with a low opening (Case 1), a centered opening (Case 2), and two openings, one upper and one lower (Case 3). The results with a 2-D opening would be the same as the results with a 1-D opening of the same shape, if the compartments were not inclined. Here, the focus is on the comparison of the results of the hydraulic and dynamic orifice equations.

For Case 1, the model was set as in Fig. 9; the opening was located in the lower part of the wall, the height of opening was 1m and the area was 1m².

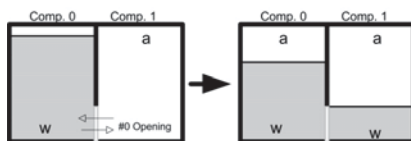


Fig. 9 Sample Case 1: low 1-D opening (The left figure shows the initial state, and the right figure shows the expected final state.)

As can be seen in Fig. 10, the calculation results for the hydraulic-orifice and dynamic-orifice equations are similar. There was no oscillation phenomenon in the results. This might be because the water totally covers the opening in the final steady stage.

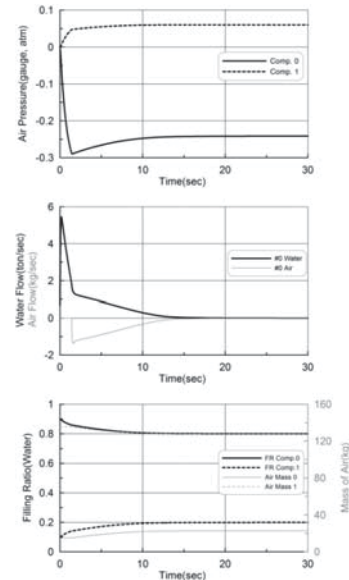


Fig. 10 Time simulation results for Sample Case 1 (low 1-D opening)

Next was Case 2, involving a 1-D opening in the middle of the wall (Fig. 11).

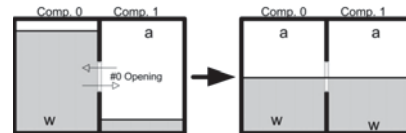


Fig. 11 Sample Case 2: centered 1-D opening (The left figure shows the initial state, and the right figure shows the expected final state.)

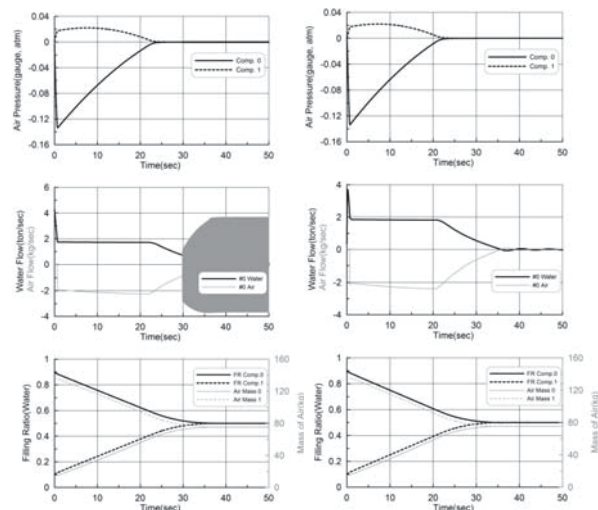




Fig. 12 Time simulation results for Sample Case 2 (centered 1-D opening), left—results from the hydraulic orifice equation, right—results from the dynamic one

The Case 2 results are shown in Fig. 12. The filling ratios are similar, but the air flows after 30 seconds are quite different from each other. The result from the hydraulic orifice equation starts to oscillate highly around 30 seconds; an enlarged view of this oscillation was drawn in Fig. 13. This oscillation is due to the numerical stability of the square root. However, the results from the dynamic orifice equation oscillated smoothly. This might be from an inertia effect.

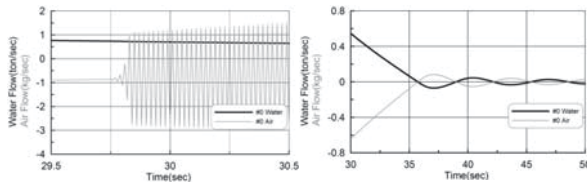


Fig. 13 Enlarged view of the flow rates of water and air: left—for hydraulic orifice equation, right—for the dynamic one)

The third sample, Case 3, involves two openings, one upper and one lower. The height of both openings is 1 m, and both openings are 1 m², the model was set in Fig. 14.

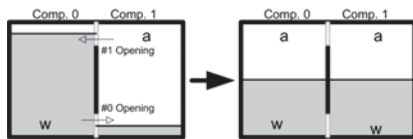


Fig. 14 Sample Case 3: two 1-D openings, one upper and one lower (The left figure shows the initial state, and the right figure shows the expected final state.)

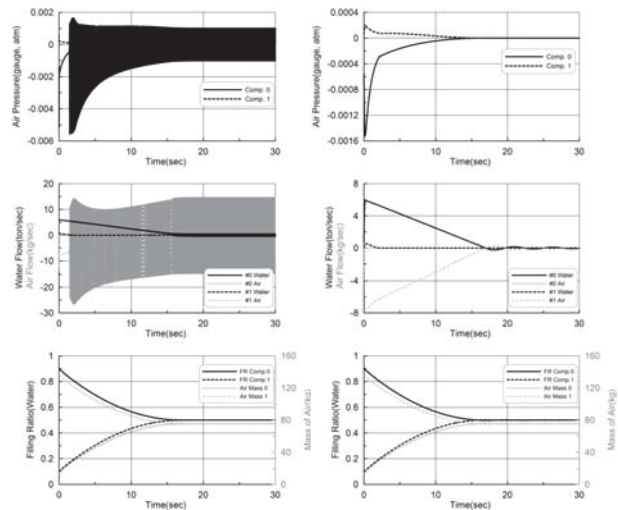


Fig. 15 Time simulation results for Sample Case 3 (two 1-D openings, one upper and one lower), left—for hydraulic orifice equation, right—for dynamic one

In this case also, the filling ratios were similar. However, the air pressure and air flow through the upper opening started to oscillate from an early stage, as in Fig. 15. Fig. 16 shows the enlarged view of the air flow and air pressure around the start of oscillation.

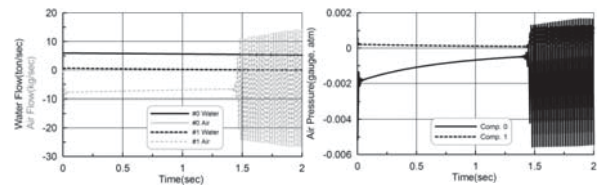


Fig. 16 Enlarged view of flow rates of water and air, and air pressure (around the starting point of the oscillation)

The results from the three sample calculations above show that the point opening should not be used for the cases with one opening in a compartment, and that the numerical instability takes place when the air in both compartments is connected through an opening. Surely, for the case of many compartments, the numerical instability due to the square-root function can ruin the flooding simulation. The dynamic orifice equation can solve this problem as it did in the above calculations.



3. COMPARTMENT MODEL

If damage occurs in a ship with many rooms, like a passenger ship, the flows of floodwater and air through the inside passages is quite complicated. The air could block the flow of water into some compartments, and retard the flooding rate. Thus, the compressibility of air plays a crucial role in the transient stage of flooding. Moreover, it is necessary to provide a reference pressure for every compartment. If a compartment is partially filled with water, the reference pressure is the one on the free surface, i.e. the air pressure. In fully water-filled compartment, there exist no free surface; so no air pressure. In such cases, selection of the reference pressure is a problem.

For a fully water-filled compartment, there is no reference pressure, while the reference pressure in a partially filled compartment is the air pressure. Ruponen (2007) introduced the idea of water height at each compartment to play the role of reference pressure in fully filled compartments. He used a method in which the pressure should be determined to satisfy the mass conservation law for each compartment, by pressure-correction. However, this method is complex and he had no choice but to use iteration to solve the pressure-correction equation

However, there is no need to focus on mass conservation. It can be satisfied automatically if we calculate the mass flux in the right way. For steady state, there is no choice but to use the iteration method to solve the non-linear pressure-correction equation. On the other hand, for unsteady problems, dynamics gives the relation between mass flow and pressure, so that the mass flow and pressure vary continuously with time, in order to maintain mass and momentum balance (i.e., via the law of conservation of mass and momentum). Therefore, if we solve the dynamic equation derived from the conservation law, the conservation will be satisfied intrinsically. The compartment that can be fully flooded is

usually one with a vent. For this compartment, the mass conservation law will be satisfied if we count on the mass flowing through the air vent, that is, mass conservation for the compartment and vent, not the compartment only.

In this section, the compartment model was adapted. Then the mass of water and air, the calculation of flow in and out, and the reference pressure of the compartment, were analyzed for vented and unvented compartments.

3.1 Basic Compartment Model

Consider a compartment in which all the openings, including vents, are well defined. The mass of water and air can be calculated as,

$$\begin{aligned} \dot{m}_w &= q_w \\ \dot{m}_a &= q_a \quad (\text{for } m_a \geq 0) \end{aligned} \quad (40)$$

where, m_w , m_a are the mass of water and air; q_w , q_a are the mass flux of each substance into the compartment through all openings. The volume charged by water V_w is calculated by m_w/ρ_w , then the remaining volume of the compartment is the volume charged by air.

$$\begin{aligned} V_w &= m_w/\rho_w \\ V_a &= V_{max} - V_w \end{aligned} \quad (41)$$

The above equation (41) can be applied for ($V_w \leq V_{max}$) only. The state equation of ideal gas gives the pressure of the air. The state equation using pressure and density is

$$pV^\gamma = const. \rightarrow p/\rho^\gamma = const. \quad (42)$$

where, γ is the ratio of specific heat of ideal air, for the iso-thermal process its value is '1', and for the iso-entropic process its value is 7/5. The pressure of the air can be calculated as

$$p_a = k_{atm} \rho_a^\gamma - p_{atm} \quad (43)$$

where, the density of air $\rho_a = m_a/V_a$, and the constant coefficient of the atmospheric condition $k_{atm} = p_{atm}/\rho_a^\gamma$. The pressure p_a is the gauge pressure, and p_{atm} is the atmospheric pressure. About the ratio of specific heat γ , the value '1' is adequate for the case that the flooding is proceeded slowly (i.e., the slow compression), and 7/5 for the case of rapid compression.

3.2 Vented Compartment Model

A vented compartment is one from which the air can flow out, if the water flows into it, without actually describing the vent duct. If the vent area (cross-section) is large enough, the pressure will remain at atmospheric. However, for a small vent area, the air would become compressed, so that the pressure of the air inside is greater than atmospheric pressure. There is no problem in calculating the flows of water and air, and the pressure, if air remains in the compartment, as in Fig. 17 (left). If, however, all the air flows out (Fig. 17, right) there is no means to calculate the pressure in it without comparing the surrounding pressure (i.e., there is no reference pressure). In this case, water can enter the compartment; the mass conservation law seems to be violated without considering the flow through the vent. If the same amount of water is understood to flow out through the vent, the mass conservation law is satisfied. We found a way to designate a reference pressure, considering the pressure at the position of the vent. For this purpose, we propose the following compartment model (Fig. 18).

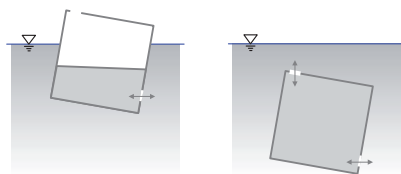


Fig. 17 Previous vented-compartment concept: floating (left) and submerged (right)

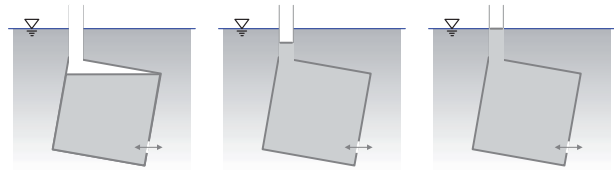


Fig. 18 Alternative air-water column concept for vented compartments

For the real vent duct (or ducts) substitute a simple vertical (virtual) vent (i.e., introduce a vertical air-water column at the top of the compartment). For the case of partial filling, there is no problem, and the reference pressure is the air pressure. Even for the case of full filling, the water can flow into the compartment; the surplus water flows up through the vertical vent. The surplus water fills the vertical vent and the top surface goes up to the free surface, and the reference pressure will be set to the pressure corresponding to the height of the water column in the vertical vent. If more water flows into it, the height of water column will be higher than the free surface, and the reference pressure will be higher than the surrounding compartment. If so, the water in that compartment could flow out to another compartment, and the water column could be reduced (that is, the reference pressure will be set to the correct value automatically as the event progresses). The above assumptions explain real situations well, and the conservation of mass is satisfied.

To continue, the compartments can then be categorized into partially vented and fully vented compartments. If the vent area is large, the air is easily vented if the water flows in, so the air pressure is almost the same as atmospheric pressure. If the vent area is small, the air will be compressed. From these, the criterion for a fully vented compartment can be drawn. It seems reasonable that a fully vented compartment has a virtual vent area greater than 1/100 of the top area. A compartment with a vent area less than 1/100 of the top area would be classified as a partially vented compartment.



Fully Vented Compartment

Let us assume the vent area $A_v = 0.01 \times (V_{max})^{2/3}$ or the area of water flow in. Then air compressibility is nearly absent. For fully vented compartments, the flow model can be described for $V_w/V_{max} < 1$, i.e., the case in which air remains,

$$\begin{aligned} \dot{m}_w &= q_w \\ V_w &= m_w / \rho_w \\ p_a &= 0 \end{aligned} \quad (44)$$

for $V_w/V_{max} \geq 1$, i.e. fully water-filled, ($V_v \geq 0$)

$$\begin{aligned} V_w &= V_{max} \\ \dot{V}_v &= q_w / \rho_w \\ h_v &= V_v / A_v \\ p_a &= \rho_w g h_v \end{aligned} \quad (45)$$

where, h_v , V_v are the height and volume of the water column in the vertical vent, respectively.

Partially Vented Compartment

In this model, the air pressure is sought. Suppose that A_v is given.

For $V_w/V_{max} < 1$,

$$\begin{aligned} q_{av} &= \begin{cases} C_D \rho_a A_v \sqrt{2p_a / \rho_a} & \text{for } p_a \geq 0 \\ -C_D \rho_{atm} A_v \sqrt{-2p_a / \rho_{atm}} & \text{for } p_a < 0 \end{cases} \\ \dot{m}_w &= q_w \\ \dot{m}_a &= q_a + q_{av} \\ V_w &= m_w / \rho_w \\ V_a &= V_{max} - V_w \\ \rho_a &= m_a / V_a \\ p_a &= k_{atm} \rho_a - p_{atm} \end{aligned} \quad (46)$$

For $V_w/V_{max} \geq 1$, i.e. fully filled, ($V_v \geq 0$)

$$\begin{aligned} V_w &= V_{max} \\ \dot{V}_v &= q_w / \rho_w \\ h_v &= V_v / A_v \end{aligned} \quad (47)$$

$$p_a = \rho_w g h_v + p_{vent}$$

where, in the last equation p_{vent} is the pressure loss due to the flow through the vent. It can be represented by the equation $p_{vent} = 1/2 \rho v^2$, in which the velocity and density is assumed to be those of the air flowing through the vent.

When the filling ratio (V_w/V_{max}) reaches '1' (i.e., the substance that flows through the inlet of the vent changes from air the water), the volume of the air (V_a) vanishes. So, we have trouble in calculating the density of air. To remedy this, it is required to add the volume of the vent to V_a , and the mass of air in the vent to the air mass of the compartment. At the moment when the compartment is just fully filled, the pressure of air (i.e., the reference pressure) has a jump to p_{vent} . If we use the density and velocity of the water, this gives very large value at that moment, whereas it will soon be balanced with the adjacent compartment. So it is recommended to use the density and velocity of the air through the vent, and add some damping to it.

3.3 Accumulator Model

If a compartment is not vented, usually all the air does not flow out. Of course, all the air could flow out if there were any openings at the top of the compartment. If air remains in the compartment, the air pressure can be calculated using the state equation of air (Equation 43). On the other hand, if the amount of air is very small, the air pressure is so largely affected by the amount of water inflow, that it is difficult to calculate the air pressure. Furthermore, if all the air flows through an opening, there is no means to calculate the air density, thus a problem arises in calculating the reference pressure. In fact, a compartment in a ship might have machinery, freight, and many other things in it, so that there might be many small spaces that could contain air. This means that all the air in a compartment seldom flows out. Let us

introduce a virtual accumulator that could solve this problem.

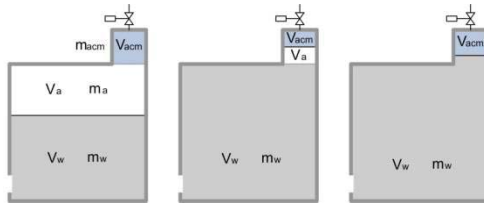


Fig. 19 Virtual Accumulator Model

Fig. 19 shows the concept of a virtual accumulator for several cases: a case with remaining air, a case with a very small amount of remaining air, and a case without air. Air fills the accumulator, and its maximum volume is represented as V_{acmmax} , the operating volume is V_{acm} , and the air mass in the accumulator is m_{acm} .

A simple way to apply the accumulator is by adding the extra air volume without pre-charged pressure to the compartment volume, which cannot flow out. This is a passive accumulator, and its mathematical model is Equation 48.

$$\begin{aligned}
 \dot{m}_w &= q_w \\
 \dot{m}_a &= q_a \text{ (for } m_a \geq 0) \\
 V_w &= m_w / \rho_w \\
 V_a + V_{acm} &= V_{max} + V_{acmmax} - V_w \\
 \rho_a &= \frac{m_a + m_{acm}}{V_a + V_{acm}} \\
 p_a &= k_{atm} \rho_a - p_{atm} \\
 V_a &= m_a / \rho_a \\
 V_{acm} &= m_{acm} / \rho_a
 \end{aligned} \tag{48}$$

The virtual accumulator has the effect of enlargement of the volume. Even when there is no air the accumulator can provide a reference pressure and stabilize pressure fluctuation. If a passive accumulator is used, the mass conservation law is violated a little. However, if we want to conserve mass strictly, the active accumulator ensures it. An active accumulator makes the accumulator volume constant by controlling the amount of air. If the water flows in, the air in the accumulator is compressed so that the reference pressure rises and blocks the

inflow of water. In this way, the active accumulator can give the reference pressure and ensures the mass conservation law in that compartment. A sudden inflow violates the mass conservation law, but in a short time, the appropriate amount of water flows out, so that the inner mass of compartment remains constant in reference to the concept of time average. The active accumulator model simply adds a feedback control law to regulate the volume of the accumulator. This allows the accumulator to maintain a nearly constant volume, and this feedback control changes the mass of the accumulator as in Equation 49.

$$\begin{aligned}
 V_{in} &= V_{acmmax} - V_{acm} \\
 \dot{m}_{acm} &= k_p V_{in} + k_D \dot{V}_{in}
 \end{aligned} \tag{49}$$

where, k_p , k_D are the proportional and differential gains respectively, V_{in} means the change of the accumulator volume from its initial one (i.e., the volume that enters the accumulator). Through many calculations, we found that 5% of the compartment volume is reasonable for a maximum accumulator volume, and $k_p = 1$, $k_D = 10$ are adequate for almost all the cases with $\Delta t = 0.01s$. For other values of Δt , the adequate values of control gains may differ, of course.

3.4 Floodwater Dynamics

In this study, the movement of the center-of-gravity was analyzed using quasi-static analysis. This analysis has no dynamics, so that the center-of-gravity moves instantly to a new position if a compartment inclines. However, in real situations, time is required for the floodwater to accumulate in new locations, and some complicated flow motions arise, typically waves. Quasi-static analysis has no dynamics effect, so it cannot reflect this reality. In flooding simulation, this effect is large for a ship like a Ro-Ro ferry, which has a large car deck. Suppose that a ship contains floodwater, even if it is inclined only a little bit, the shift in the floodwater center-of-gravity is largely



instantaneous (by previous methods). Therefore, the calculated motions of the ship include unrealistic motions because of the instant large shifts in the center-of-gravity. In this study, a simple method is proposed that considers the dynamics of the floodwater.

The center-of-gravity moves toward the geometric center as time goes, so we want a method that provides a force toward the static center-of-gravity, and that also provides adequate damping. The appropriate mathematical model for the movement of floodwater might be a second-order differential equation in the form of Equation 50.

$$m\dot{v} + bv = f \times (x_s - x) \quad (50)$$

where, x is the center-of-gravity of floodwater, while x_s is the static one; m is the mass of floodwater, and v the moving velocity of the center-of-gravity. If the static center-of-gravity does not move, the center-of-gravity moves toward the static one.

The forcing factor f seems to be proportional to the mass and gravity, and be a function of the filling ratio f_r . So, we propose the equation of motion of the center-of-gravity as follows,

$$m\dot{v} + bv = mg \frac{1 + 2f_r}{l/2} (x_s - x) \quad (51)$$

where, l is a characteristic length of the compartment. Dividing the above equation by the mass, the equation can be represented as a typical second-order differential equation.

$$\begin{aligned} \ddot{x} + b'\dot{x} + \omega_n^2 x &= \omega_n^2 x_s \\ \omega_n^2 &= \frac{2(1 + 2f_r)g}{l} \\ b' &= \omega_n \end{aligned} \quad (52)$$

Let us also consider the damping coefficient b' . If the damping is critical, it is $b'_c = 2\omega_n$. In order to reflect more realistic situations, it is

better to have an overshoot, so let us take 1/2 of the critical value. If we take this value, the amplitude of RAO at resonance is '1'. The above equation shows that the center-of-gravity moves slowly if the characteristic length is long, and moves quickly if the length is short. This reflects reality. Consider the natural frequency of Equation 52. The natural frequency of the first resonance mode of a standing wave in a tank whose length is l can be found in Equation 53.

$$\begin{aligned} \omega_n^2 &= \frac{\pi g}{l} \\ \text{from } \left(\frac{1}{2}\lambda = l, k = \right) & \quad (53) \\ \frac{2\pi}{\lambda} &= \frac{\pi}{l} \end{aligned}$$

Comparing the two resonance frequencies (52, 53), if the filling ratio is about 0.3, the two frequencies are similar. As the filling ratio decreases, the effect of shallow water makes the natural frequency lower, and as the filling ratio increases, the natural frequency becomes higher. This characteristic is already included, approximately, in Equation 52.

The advantage of this equation is the fact that we can consider the effect of the filling ratio in a simple manner. If we can determine the static center-of-gravity, Equation 52 gives the motion of the center-of-gravity without involving complex fluid dynamics.

4. VALIDATION

Recently, there was a sinking accident with the loss of many people in Korea. The ship, MV Sewol, was a Ro-Ro ferry of 132m length, 22m breath, and 9,610ton displacement. It has two car decks and a freight deck in it. The simulation team in KRISO was launched in order to make data to reasonably explain the cause and effect of the accident (KRISO, 2014). The main reason of the accident turned out to be the lack of restoring and the movement of freight during its turn. The ship was modeled



with 27 internal compartments and 81 openings for flooding simulation. Figure 20 shows the shape of the ship and compartments in it. The flooding simulation team had tried to tune up the parameters (especially related with openings, the gap of doors and ramps) so that the simulation results resemble the official data from the cooperative investigation headquarter for MV Sewol. Then, the team provided explanations about the process of the flooding and sinking.

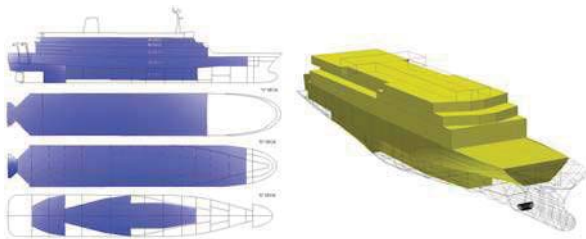


Fig. 20 Shape and the internal compartments of MV Sewol

It was presumed that the ship tumbled down due to an excessive steering and the resulting movement of freight in it. It was reported the initial angle of heel was 30 degrees port after its tumble and there was no collision accident. The flooding simulation started from the condition in which the roll angle was negative 30 degree (i.e., the left side of the ship went down). Fig. 21 shows the roll angle (inclination) compared with the official data provided by the cooperative investigation headquarter for MV Sewol. Fig. 22 shows the pitch and heave motion during flooding and sinking.

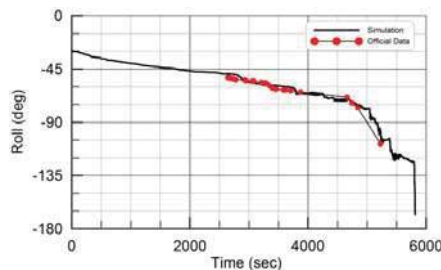


Fig. 21 Inclination angle(roll) compared with the official data

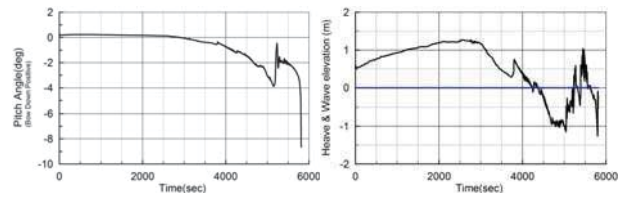


Fig. 22 Pitch(left) and heave(right)

Fig. 23 shows the flow rate through some important openings from outside. And Fig. 24 shows the filling ratios in compartments below the main deck. At the start, the flow-in took place only through the side door located at D deck. As the inclination went larger, the flow-in through the stern ramps began to grow. There were only 3 openings through which the sea water flows in before 2,700 seconds. The resulting floodwater was piled up in D deck and E deck (these decks is located under the main deck). After 2,700 seconds, the sea water flowed in through the vent of the left stabilizer room. And after, many other compartments flooded.

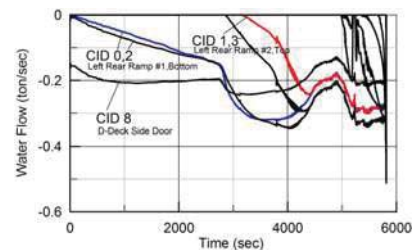


Fig. 23 Flow rate of water through important openings

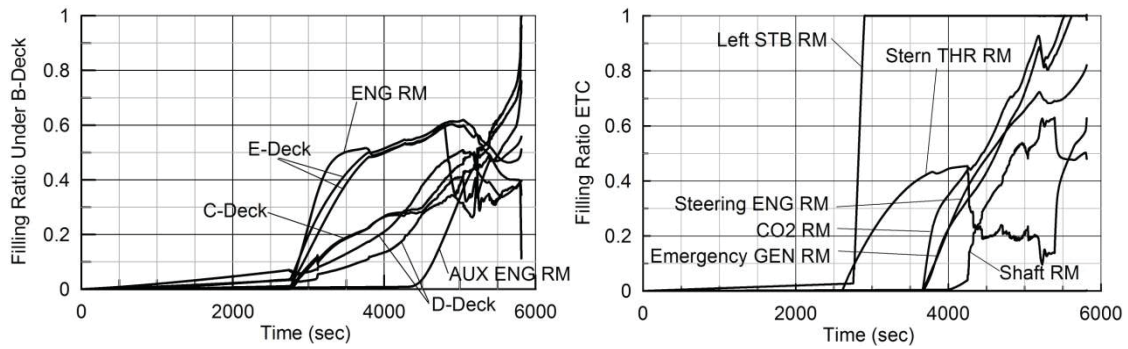


Fig. 24 Filling ratios of the lower compartments (below main deck)

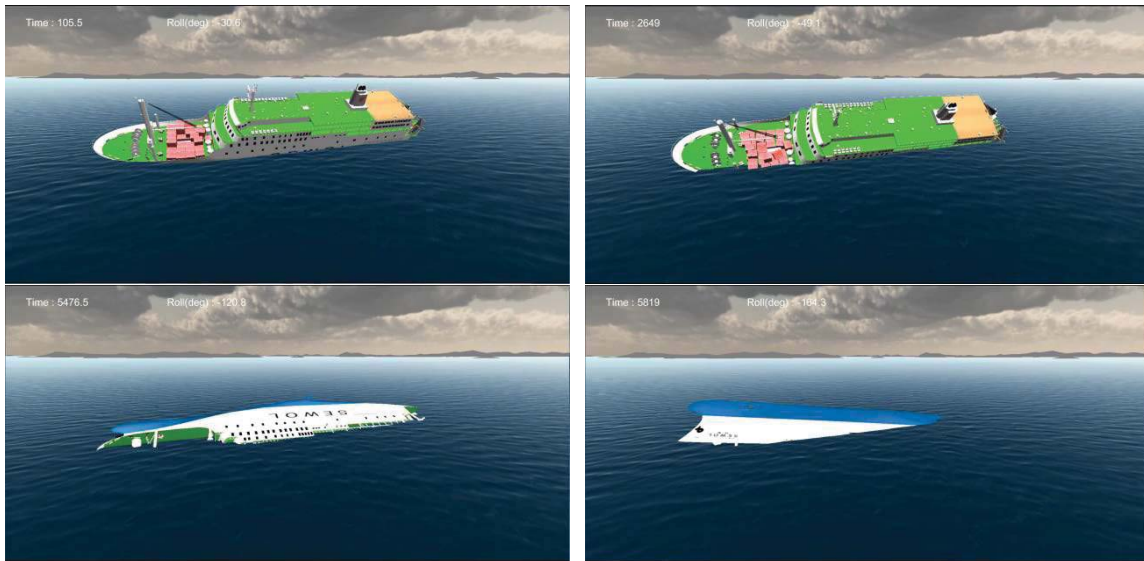


Fig. 25 Visualizations of the simulation results (upper left: initial state, upper right: when the coast guard arrived, lower left: when the last rescue action, lower right: final state)

The side door located at D deck and the rear ramps are assumed to be closed. The simulation team assumed gap of 0.01m along the edge of the door and ramps. It could be said that the only 0.01m of gap size of a side door and rear car ramp are sufficient to flooding and sinking of Ro-Ro ferry.

Fig. 25 shows the important situations to be noticed: initial condition of flooding simulation, the ship when coast guard arrived, when the last rescue action played, finally capsized. The results reflect the actual situations well, in comparison with the pictures that have shown in many mass medias.

5. CONCLUSIONS

In this study, flow models for simulation of ship flooding were investigated. The most important matters were the orifice equations and the compartment models. For the orifice equation, it was shown that numerical instability could occur involving the air flow, if the hydraulic orifice equation is used to calculate the flow through an opening. A newly derived dynamic orifice equation by Lee (2014) was investigated that could resolve the numerical instability that comes from the square root of the pressure difference. A new compartment model that can provide pressure balance automatically was proposed. It reduces the computational burden and difficulty in applying the pressure-correction method.



Furthermore, practical models indispensable for application to realistic situations were investigated. These included down flooding and a simple method for giving the dynamic effect of floodwater in quasi-static analysis.

Using these models, the flooding simulation of a recent actual accident was carried out. When the results were compared with official data, the process of the flooding and sinking could be explained approximately, but reasonably.

6. ACKNOWLEDGMENTS

In the accident mentioned in this study, the ship sank with the loss of many people, dead or missing. The data included in section 5 are parts of the report of the simulation team for the accident of Ro-Ro ferry. The writer feels sorry for not adding the details of the report of the simulation team of this accident in this paper. The writer hopes that this study helps to make ships safer. This study was partially supported through a basic project of KRISO(PES1990).

7. REFERENCES

- Chang, B.-C., Blume, P., 1998. "Survivability of Damaged Ro-Ro Passenger Vessels", Schiffstechnik – Ship Technology Research, Vol. 45, pp. 105-112.
- Chang, B.-C., 1999. "On the Damage Survivability of Ro-Ro Ships Investigated by Motion Simulation in a Seaway", Schiffstechnik – Ship Technology Research, Vol. 46, pp. 192-207.
- Cho, S. K., Hong, S. Y., Kim, Y. H., and Lee, K. J., 2005. "Investigation of dynamic characteristics of the flooding water of the damaged compartment of an ITTC RORO Passenger Ship", Proceedings of the 8th International Ship Stability Workshop, Istanbul, Turkey, 6-7 October 2005.
- Clift, R., Grace, J.R., and Weber, M.E., 1978. Bubbles, Drops, and Particles, Academic Press Inc., New York, p.205.
- FLOODSTAND Project Consortium, 2011. WP2 - Flooding Progression Modelling, Deliverable No. D2.3, D2.4a, D2.4b, FLOODSTAND Project Consortium, EU.
- Ikeda, Y., Ishida, S., Katayama, T., and Takeuchi, Y., 2004. "Experimental and Numerical Studies on Roll Motion of a Damaged Large Passenger Ship in Intermediate Stages of Flooding", Proceedings of the 7th International Ship Stability Workshop, Shanghai, China, 1-3 November 2004, pp. 42-46.
- ITTC, 2011. "Final Report and Recommendations to the 26th ITTC, The Specialist Committee on Stability in Waves", Proceedings of 26th ITTC, Rio de Janeiro, Brazil, 28 August - 3 September 2011, pp.523-560.
- KRISO, 2014. Analysis of the cause of a sinking accident of MV Sewol (Simulation of Maneuvering, Flooding, and Sinking), Report No. UCPGS2750-10546-6. KRISO, Korea, pp.114-129. (in Korean)
- Lamb, H., 1945. Hydrodynamics, Dover Publications, Inc., New York. (republication of the 6th(1932) edition by Cambridge University Press), p.164.
- Lee, G. J., 2010a. "Simplified Modelling of Floodwater Dynamics", Proceedings of the Annual Autumn Meeting, SNAK, Changwon, 21-22 October 2010, pp.969-974. (in Korean)
- Lee, G. J., 2010b. "Flow through Openings for Flooding Calculation", Proceedings of the Annual Autumn Meeting, SNAK, Changwon, 21-22 October 2010, pp.979-990. (in Korean)
- Lee, G. J., 2014. "A Study on the Dynamic Orifice Equation for the Flooding Simulation of a Ship", Journal of Ships & Ocean Engineering, vol. 55., pp.17-27. (in Korean)
- Lee, G. J., 2015. "Dynamic orifice flow model and compartment models for flooding simulation of a damaged ship", Ocean Engineering (submitted).
- Papanikolaou, A., Zaraphonitis, G., Spanos, D., Boulougouris, E., and Eliopoulou, E., 2000. "Investigation into the Capsizing of Damaged Ro-Ro Passenger Ships in Waves", Proceedings of the 7th International Conference on Stability of Ships and Ocean Vehicles, Launceston, Tasmania, Australia, 7-11. February 2000, pp. 351-362.
- Ruponen, P., 2007. Progressive Flooding of a

Damaged Passenger Ship, Doctoral Dissertation, Helsinki University of Technology, Finland.

Spouge, J. R., 1986. "The Technical Investigation of the Sinking of the Ro-Ro Ferry European Gateway", Transactions of Royal Institute of Naval Architects, RINA, Vol. 128, pp. 49-72.

Sen, P. and Konstantinidis, C., 1987. "A Time Simulation Approach to the Assessment of Damage Survivability of Ro/Ro Cargo Ships", Transactions of Society of Naval Architects and Marine Engineers, SNAME, Vol. 95, pp. 337-355

van't Veer, R. and de Kat, O., 2000. "Experimental and Numerical Investigation on Progressive Flooding in Complex Compartment Geometries", Proceedings of the 7th International Conference on Stability of Ships and Ocean Vehicles, Launceston, Tasmania, Australia, 7-11 February 2000, pp. 305-321.

van't Veer, R., de Kat, O., and Cojeen, P., 2002. "Large Passenger Ship Safety: Time to Sink", Proceedings of the 6th International Ship Stability Workshop, New York, U.S.A, 13-16 October, 2002.

van't Veer, R., Peters, W., Rimpelä, A-L., and de Kat, J., 2004. "Exploring the Influence of Different Arrangements of Semi-Watertight Spaces on Survivability of a Damaged Large Passenger Ship", Proceedings of the 7th International Ship Stability Workshop, Shanghai, China, 1-3 November 2004.

Vassalos, D., Jasionowski, A., and Guerin, L., 2005. "Passenger Ship Safety – Science Paving the Way", Proceedings of the 8th International Ship Stability Workshop, Istanbul, Turkey, 6-7 October 2005.

White, F. M., 1979. Fluid Mechanics, McGraw-Hill, New York, pp. 159-163, Chapter 6,10.

Woodburn, P., Gallagher, P., and Letizia, L., 2002. "Fundamentals of Damage Ship Survivability", Transactions of Royal Institute of Naval Architects, RINA, Vol. 144, pp.143-163.

APPENDIX A. Square Root Instability

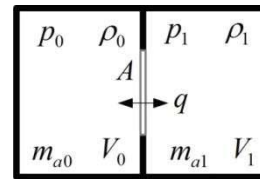


Fig. A-1 Arrangement of the sample problem

The hydraulic orifice equation was originally for steady state, let us see what happens if we apply it for an unsteady case. Here, the point of focus is the fact that the flow velocity is represented using the square root of the pressure difference. Consider the situation in Fig. A-1, in which both sides are filled with air, and there is an opening between them. The final state is the one in which the pressures on both sides are the same, so the pressure difference is zero.

Let us formulate the above situation. The flow could be represented as

$$q = \text{sgn}(\Delta p) \rho A \sqrt{\frac{2|\Delta p|}{\rho}} \quad (\text{A-1})$$

$$= \text{sgn}(\Delta p) A \sqrt{2\rho} \sqrt{|\Delta p|}$$

The mass would change to

$$\begin{aligned} \dot{m}_{a0} &= -q \\ \dot{m}_{a1} &= q \end{aligned} \quad (\text{A-2})$$

The density at each compartment could be represented by

$$\begin{aligned} \rho_0 &= m_{a0}/V_0 \\ \rho_1 &= m_{a1}/V_1 \end{aligned} \quad (\text{A-3})$$

The pressure in each compartment can be determined under the assumption of iso-entropic process of air. (γ is the specific heat, 7/5 for an iso-entropic process, and 1 for an iso-thermal process)



$$\begin{aligned}
 p_0 &= k_a \rho_0^\gamma - p_{atm} = k_a \left(\frac{m_{a0}}{V_0} \right)^\gamma - p_{atm} \\
 p_1 &= k_a \rho_1^\gamma - p_{atm} = k_a \left(\frac{m_{a1}}{V_1} \right)^\gamma - p_{atm} \\
 \text{where } k_a &= p_{atm} / \rho_{atm}^\gamma.
 \end{aligned} \tag{A-4}$$

Take the time differentiation of the above equations,

$$\begin{aligned}
 \dot{p}_0 &= \gamma \frac{k_a}{V_0} (m_{a0})^{\gamma-1} \dot{m}_{a0} = -\gamma \frac{k_a}{V_0} (m_{a0})^{\gamma-1} q \\
 \dot{p}_1 &= \gamma \frac{k_a}{V_1} (m_{a1})^{\gamma-1} \dot{m}_{a1} = \gamma \frac{k_a}{V_1} (m_{a1})^{\gamma-1} q
 \end{aligned} \tag{A-5}$$

Here, we assume the same volume of compartments (i.e., $V_0 = V_1$). If the pressures are the same initially, then air masses in both compartments are the same initially. Assume the change of air masses is small, and the mass could be assumed as constant m_a for the last expression of Equation A-5. If the flow through an opening increases the pressure of one compartment, the pressure of the other compartment goes down, so that $p_1 = -p_0$.

$$\dot{p}_0 = -\gamma \frac{k_a}{V} (m_a)^{\gamma-1} \text{sgn}(p_0) A \sqrt{2\rho} \sqrt{2|p_0|} \tag{A-6}$$

The atmospheric pressure is large enough so that the density is nearly constant, so Equation A-6 can be rewritten as

$$\begin{aligned}
 \dot{p}_0 &= -\gamma \frac{k_a}{V} (m_a)^{\gamma-1} \text{sgn}(p_0) 2A \sqrt{\rho_{atm}} \sqrt{|p_0|} \\
 &= -2\gamma \frac{A}{V^{2-\gamma}} \frac{p_{atm}}{\sqrt{\rho_{atm}}} \text{sgn}(p_0) \sqrt{|p_0|}
 \end{aligned} \tag{A-7}$$

Let us rewrite this into a simpler form.

$$\begin{aligned}
 \dot{p} &= -K \text{sgn}(p_0) \sqrt{|p_0|} \\
 \text{where } K &= 2\gamma \frac{A}{V^{2-\gamma}} \frac{p_{atm}}{\sqrt{\rho_{atm}}}
 \end{aligned} \tag{A-8}$$

The value of K is very large. One solution of the above equation is $p = 0$, which is what we want. Let us examine the numerical solution, using the Euler method,

$$p^{n+1} = p^n - K \text{sgn}(p) \sqrt{|p^n|} \Delta t \tag{A-9}$$

We know the pressure would bounce around zero, because of the large value of K . Let us seek the amplitude of oscillation p^* .

$$\begin{aligned}
 -p^* &= p^* - K \sqrt{p^*} \Delta t \rightarrow 2p^* = K \sqrt{p^*} \Delta t \\
 \therefore p^* &= 0 \text{ or } p^* = \frac{(K \Delta t)^2}{4}
 \end{aligned} \tag{A-10}$$

The oscillating solution is as follows.

$$p^n = (-1)^n (K \Delta t)^2 / 4 \tag{A-11}$$

No matter what the absolute value of the pressure was initially, the amplitude of pressure oscillation converges to p^* . That is a type of self-sustained oscillation (or self-excited). Even though we use the predictor-corrector, or Runge-Kutta method, the pressure will not go to zero, and does not oscillate as in Fig. A-2.

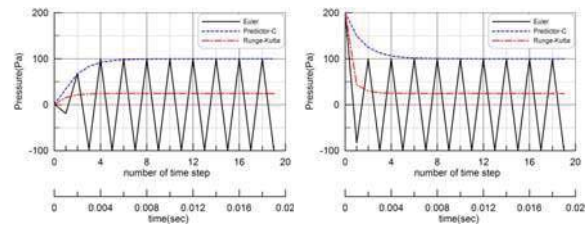


Fig. A-2 Numerical solution of the air pressure revealing the square root instability.
($K=20000$, $\Delta t=0.001$, $p^*=100$)

The above figure shows that even if the initial value is infinitesimally small (not zero) or larger than p^* , the result of the Euler method oscillates back and forth around zero and the amplitude grows to p^* . However, the results of the predictor-corrector do not oscillate and go to the value of p^* . Even for the Runge-Kutta method, it goes to about $1/4 p^*$, not zero. This is numerically unstable. Because the predictor-corrector and Runge-Kutta methods give non-zero solutions, they are dangerous compared with the Euler method. The result of the Euler method gives values whose average is zero. We expected the solution to go to zero, but it does not, so this phenomenon can be called numerical instability.

Let us investigate the value of K ,



$$K = 2\gamma \frac{A}{V^{2-\gamma}} \frac{p_{atm}}{\sqrt{\rho_{atm}}}$$

Substitute the real values except A and V ($\rho_{atm}=1.26$, $p_{atm} \cong 100,000$)

$$K = 178,174 \times \gamma \frac{A}{V^{2-\gamma}} = 356,348 \times \frac{A}{V^{0.6}} \quad (\text{A-12})$$

In order to maintain p^* as less than 100 Pa (i.e., 1/1000 of atmospheric pressure; this would be accepted as a negligible amount in the engineering sense) the time interval of simulation should be the following value.

$$\Delta t^* = 20/K = 5.6 \times 10^{-6} \frac{V^{0.6}}{A}$$

For example, a passenger ship has many rooms in which the dimensions are about 4m(depth), 3m(width), and 2.5m(height), for which the area of door is 2m^2 , and for that room $\Delta t=0.00022$. This is not practical. For a larger compartment of 10m x 10m x 5m, with a 2m^2 door, the time interval should be $\Delta t=0.001$. Therefore, this is impractical because of the numerical instability of the square root.

This page is intentionally left blank



An Overview of Warships Damage Data from 1967 to 2013

Andrea Ungaro, *CETENA spa, Genoa, ITALY* andrea.ungaro@cetena.it

Paola Gualeni, *DITEN University of Genoa, ITALY* paola.gualeni@unige.it

ABSTRACT

In the last decade, in the field of merchant ships, a long harmonization process has taken place at IMO, resulting in the enforcement of the so called probabilistic SOLAS2009 for the residual buoyancy and stability assessment of a ship in a damaged condition.

In the warships design process, the probabilistic methodology might represent a consistent approach to complement the fundamental overall ship survivability assessment. Nevertheless among the most critical issues, while discussing the possible implementation of this innovative approach, are the lack of a damage database and the significantly different threat typology.

In this perspective, significant damage cases in the field of warships are investigated and critically analyzed. The observed time period will regard the period from 1967 (sinking of the Eilat) to 2013.

Keywords: *warships, damage, survivability assessment*

1. INTRODUCTION

In the field of merchant ships, the rules for stability assessment of a damaged ship have been renewed a few years ago by the International Maritime Organization (IMO).

The new requirements are based on the probabilistic approach and represent a significant change in one of the most long-established safety issues i.e. the ship subdivision criteria.

They are the result of a prolonged process having its roots in the sixties (IMO, 1960) and passing by the adoption of the mandatory probabilistic regulation for cargo ships (IMO, 1990). An harmonization process has subsequently originated, leading to a comprehensive SOLAS Convention text for

both passenger and cargo ships that has been enforced from January 1st 2009 (IMO, 2007), the reason why in the following it is going to be mentioned as SOLAS2009.

This paper is developed in the perspective that the probabilistic approach might represent an interesting hint also within the warship design context (Harmsen & Krikke, 2000; Papanikolaou & Boulougouris, 2000). In fact, in principle, it is particularly suitable to address the vulnerability characteristics of the ship in terms of survivability after damage and it can be exploited also in terms of risk assessment, for the discussion of ship survival attitude after damage due to a weapon hit (Boulougouris & Papanikolaou, 2012).

At the same time, some critical points can be raised, for example in relation with the totally different context in terms of threat and operational situations.



Moreover the lack of a rational and comprehensive damage database is another fundamental issue in order to define the statistical characteristics of hull damages.

2. PRESENT CRITERIA FOR THE DAMAGED SHIP: NAVAL AND MERCHANT FIELD

At present, major Navies in the world apply the so called “deterministic” approach for the design and assessment of the appropriate ship subdivision, derived from the World War II experience and from the Sarchin and Goldberg studies (1962).

Damaged stability criteria are based on standard extents of damage, margin line and V-line concepts for buoyancy assessment and progressive flooding prevention; for the residual stability assessment, criteria are developed processing the righting arm characteristics in comparison with standard.

A remarkable overview about the current warship damaged stability criteria is given in Surko (1994), where a compared analysis is carried out among the deterministic criteria applied by Canada, France, Germany, Israel, Italy, United Kingdom, United States, Australia. In the same paper many interesting hints for improvement are suggested for example the need to treat the survivability and the damage control as a single issue in the 21st century. The same author raise the attention toward the residual strength after damage, in a comprehensive performance assessment perspective (Surko, 1988).

In the field of merchant ships, before the SOLAS2009 enforcement the “deterministic” approach was the general SOLAS damage stability paradigm. At present, the traditional set of rules has been replaced by the probabilistic approach that in principle can be described as a rational, comprehensive and able to deliver a synthetic final score parameter,

representative of the damaged ship survivability global attitude. Furthermore it has the characteristic of being a versatile instrument, able to deal with innovative and peculiar ship typologies.

Notwithstanding many positive conceptual features, its implementation in actual design poses a number of problems. In general, among the less encouraging features, is the extremely long, elaborate and intricate procedure it requires (only the significant increase and availability of cheap calculation power have practically allowed the introduction of this new methodology). At the same time, a critical aspect is represented by the feeble chance to appreciate intuitively the effects of even a light modification in the ship general layout in terms of damage stability compliance. This in turn could mean that in case the investigated ship doesn't satisfy the requirements, the designer's options to improve the situation are not so clear and straightforward.

3. CRITICAL ISSUES FOR PROBABILISTIC APPROACH TRANSFERABILITY FROM MERCHANT TO WARSHIP DESIGN

A very short and not exhaustive description of the SOLAS 2009 probabilistic methodology is given in the following. The methodology is based on a calculation of the attained subdivision index A and the required subdivision index R . The ship is sufficiently subdivided when

$$A > R, \quad R = R(L_S, N_1, N_2) \quad (1)$$

In particular coefficient R , besides its dependence on the ship length (L_S), is defined as a function of the number of people for whom lifeboats are provided (N_I) and of the number of people (including officers and crew) the ship is permitted to carry in excess of N_I .



The formulation of the attained coefficient A is more complex, it is obtained after relevant calculations for three different draughts: the deepest subdivision draught (ds , the waterline which corresponds to the summer load line), the light service draught (dl , related with the lightest loading condition of the vessel) and the partial subdivision draught (dp , the light service draught plus 60% of the difference between the light service draught and the deepest subdivision draught). For each of the aforementioned calculation draughts ds , dp and dl , partial indices respectively A_s , A_p , A_l , are to be found. The global attained coefficient A is calculated as the linear combination of the partial subdivision indices at each defined draught:

$$A = 0.4A_s + 0.4A_p + 0.2A_l \quad (2)$$

Every partial index A_s , A_p , A_l is the summation of the products of two parameters (p_i and s_i) representing respectively, the probability that only the compartment or group of compartments under consideration may be flooded p_i , (disregarding any horizontal subdivision) and the probability of survival s_i after flooding of the compartment or group of compartments under consideration, (including the effect of any horizontal subdivision). Each partial index A_j is therefore calculated as follows:

$$A_j = \left[\sum_i p_i \quad s_i \right]_j \quad (3)$$

The formulation of the p_i coefficients is based on the damage length and on its longitudinal position along the ship. As a matter of fact when dealing with a certain zone within two transversal bulkheads it is possible to take into account different transversal damage penetrations, correcting p_i by the r_i coefficient, that accounts for the probability not to damage the longitudinal bulkhead.

The s_i , parameter the survivability index, is calculated with reference to the residual buoyancy and stability characteristics of the ship after damage and accounts also for

intermediate stages of flooding and external heeling moments such as wind, movement of passengers and launch of a survival craft. Moreover the survivability index coefficient can be corrected by the factor v_i in case the horizontal watertight boundaries are fitted above the waterline under consideration and they are limiting superiorly the damage: the v_i factor in fact, represents the probability that the spaces above the horizontal subdivision will not be flooded. The attended index A takes therefore the following form,

$$A_j = \left[\sum_i (p_i \quad r_i) \quad (v_i \quad s_i) \right]_j \quad (4)$$

In order to avoid that global index A is attained also in case of extremely unbalanced situations some corollary requirements have been introduced: for passenger ships, prescriptions on the s_i values are imposed regarding some specific damage scenarios defined in terms of position and extensions, depending on the number of passengers onboard. Moreover a minimum value of for partial A_s , A_p , A_l indices is imposed (at least $0.5 \cdot R$ for cargo ships and $0.9 \cdot R$ for passengers ships).

To discuss the opportunity of the probabilistic approach application in the field of warship design it is worth mentioning that "survivability" in such cases is a very wide concept and also includes the concepts of vulnerability and susceptibility (Ball & Calvano, 1994).

The possible application, moreover, would imply an extensive work of re-formulation of the probabilistic parameters characterizing the damage scenario probability and of the survivability index.

In fact, one of the biggest issues for the probabilistic approach application in the warship field is the redefinition of coefficients exploited in the methodology. In this process it would be necessary to take into account the different environmental, operational scenarios



and the boundary conditions the naval ship has to operate in.

Two points should be properly considered: the first one is the different performances required after damage and the second is the origin and nature of the damage.

The ship performances after damage should be tackled through the definition of a new *si* survivability factor within the probabilistic methodology.

The nature of the damage should be introduced with the definition of damage probability factors i.e. *pi*, *ri*, *vi*, respectively representing the longitudinal transverse and vertical extents of damage.

The occurrence of a damage has different features in case of a merchant ship or a naval ship: in general the first suffers damage due to collision and grounding while the second suffers damage due to offensive /aggressive threats (weapons) put in act to destroy the ship herself and characterized by more devastating effects.

Moreover a new definition of the required index *R* is necessary, since in the SOLAS 2009 it has a statistical origin too; the harmonized SOLAS has been applied to several ships which complied with the old deterministic rules and their attained indexes *A* have been calculated. The index *R* has been defined by means of a regression of such set of values with the aim to keep an equivalent level of safety. A similar approach should be followed with a proper set of naval ships to define its naval formulation.

From what above, the critical points for probabilistic approach transferability to navy ships are summarized below:

- Definition of suitable probabilistic terms to evaluate damage extensions statistics and damage effects
- Definition of survivability index
- Definition of a new *R* factor, i.e. the level

of sufficient subdivision

Unfortunately a database of damage cases for ships in the military context with all the necessary data for a statistical analysis is not available.

In the following paragraph an overview about the damage scenario of warships in the latest decades is carried out; the aim is to investigate what kind of framework and information would be useful in the perspective of a possible probabilistic approach for damage stability assessment for warship design. A special attention is given also to the threat typology as a fundamental parameter to class the damage size and typology.

4. A TAXONOMY FOR A WARSHIP DAMAGE DATA OVERVIEW

Year 1967 marks a breakthrough in naval warfare, specifically the sinking of INS Eilat by means of guided ship-launched anti-ship missiles (ASMs) a few months after the Six-Day War.

Guided weapons had already been used during the Second World War: the German Luftwaffe used several kinds of remotely-controlled glide bombs, such as the Henschel Hs293 and the so-called "Fritz-X"; two hits from the latter in fact sunk the RN Roma in 1944. All of these weapons were however dropped by a bomber and usually controlled via radio signals by an operator within visual range, following the smoke trail left by the bomb to help steering.

When INS Eilat was sunk in October 21st, 1967, the three hits were by P-15 Termit (NATO name: SS-N-2 Styx) missiles, fired from two Komar-class missile boats, carrying their own radar sensors, and attacking well outside visual range (17 nm as reported).



From 1967 to 2013, 45 hits by guided anti-ship missiles, both surface- and aircraft-launched, have been suffered by naval ships. Of these hits, 16 concerned 9 different naval ships with a displacement larger than 1000 t (corvette-sized or bigger) and are therefore interesting for our study; hits on smaller ships are less interesting because smaller platforms can hardly survive missile impacts. In those cases, specific details are also hard to come by (the ship, typically a missile boat, is usually listed as “sunk”, without other information).

Of these 16 hits, 6 were by P-15 Termit (3 of those during the Eilat attack and 3 during Operation Trident), 4 by some versions of the Exocet, 3 by Harpoon missiles, 2 by Sea Sparrow missiles (a “blue-on-blue” incident) and 1 by a YJ-82. 4 out of 9 of the hit ships were sunk. In 7 cases out of 9, the ships were clearly mission-killed, i.e. lost the capability to carry out their operational tasking.

In 6 out of 9 ships, and in 3 out of 4 ships being sunk, fire is mentioned as a significant damage mechanism; specifically, HMS Sheffield and IRS Sahand were lost due to uncontrollable fires, even though the first one eventually sunk due to flooding and the second due to secondary ammunition explosions. INS Eilat on the other hand suffered a complete loss of integrity of the hull girder (i.e. “broke in two”) after the third hit whereas the fate of PNS Khaibar was probably caused by extensive flooding.

Note that this statistic doesn’t include non-naval ships (several oil carriers were hit by ASMs during the so-called Tanker War, for example) and doesn’t include merchant ships in military use such as the Atlantic Conveyor, which despite being a container ship was in military use during the 1982 Falklands War, and the Venus Challenger, which was reportedly carrying ammunition (this is contested) when sunk during the 1971 Operation Trident.

In the same historical period, 15 ships larger than 1000 t sustained hits from weapons other than guided missiles: 3 were torpedoed, 8 were hit by bombs, 3 struck a mine and 1 was struck by a suicide boat. One of the ships hit by bombs (IIS Sahand) was also hit by missiles, and therefore our list below is composed of 23 entries rather than 24.

The three ships that were hit by torpedoes all sunk, in a quite short time frame and with large loss of life.

The three ships that were hit by mines received severe damage and were mission-killed in two cases, whereas USS Tripoli, undoubtedly also due to her large displacement, remained mission-capable. Casualties were low.

USS Cole, struck by a suicide boat, was certainly unable to continue her mission, and was ultimately drydocked and brought back to the US for repairs.

Finally, the 8 ships that were struck by bombs: 3 were hit by multiple bombs and sunk (HMS Ardent during defusing operations); 3 were struck by unexploding bombs only and survived (HMS Argonaut suffered a partial missile magazine explosion and fire and had to be towed away); 1 was struck by a single bomb and lost propulsion but survived (IIS Sabalan) and 1 was struck by multiple bombs and missiles and sunk (IIS Sahand).

In 4 out of 5 cases of ships struck by bombs which exploded successfully, and in 1 case out of 3 of unexploded bomb hits only, fire is mentioned as a significant factor. Only HMS Coventry was lost mainly due to loss of stability.

The following review goes into some detail, as available from unclassified or de-classified sources, about the damage sustained by the ships as listed in table 1.



It appears evident that the definition of damage as described in the SOLAS2009 (i.e. in terms of longitudinal, transverse and vertical extension) is not commonly available, and that the damage is usually described in terms of source (i.e. kind of weapon) and effects (i.e. residual buoyancy, total loss, fire, fatalities).

INS Eilat (1967)

INS Eilat (ex HMS Zealous) was a WWII Z-class destroyer with a displacement of about 1700 t. She received three hits (sources report anything from 2 to 4 hits), all by P-15 Termit missiles (carrying 454 kg warheads), which sunk her.

Reports are unclear on the location of the hits but it's clear that after the two first hits the ship was dead in the water (boiler rooms out of order) and with severe structural damage; some sources report one hit very close to the waterline (and therefore flooding) and fire is reported as well.

The ship was still floating when two hours later the third hit finished her by splitting the already damaged hull into two parts. Further underwater damage from a near-miss by a 4th

missile was reported (the ship was attacked by two Osa missile boats carrying two missiles each).

PNS Khaibar (1971)

PNS Khaibar (ex HMS Cadiz) was a WWII Battle class destroyer with a displacement of about 2300 t standard (3300 full load). She received two hits by P-15 Termit missiles which sunk her (Harry, 2002).

The first hit was on the starboard side, low on the water; propulsion and electrical power were lost (possibly due to shock?) Boiler room 1 was lost and the ship was engulfed in thick black smoke, with spreading fires reported. The second subsequent hit was on the same side and destroyed boiler room 2 as well as some boats, causing a heavy list. The ship sunk shortly thereafter.

Name	Year	Country	Weapons	Final status
INS Eilat	1967	Israel	3 x P-15 Termit	Sunk
PNS Khaibar	1971	Pakistan	2 x P-15 Termit	Sunk
PNS Shah Jahan	1971	Pakistan	1 x P-15 Termit	Unknown, did not sink
INS Khukri	1971	India	1 x 550-mm torpedo	Sunk
ARA General Belgrano	1982	Argentina	2 x Mk 8 torpedo	Sunk
HMS Sheffield	1982	UK	1 x Exocet (did not explode)	Sunk
HMS Ardent	1982	UK	Multiple aircraft bombs	Sunk
HMS Antelope	1982	UK	2 aircraft bombs	Sunk during defusing operations
HMS Coventry	1982	UK	Multiple aircraft bombs	Sunk
HMS Broadsword	1982	UK	1 unexploded bomb	Mission capable
HMS Argonaut	1982	UK	2 unexploded bombs	Towed away
HMS Antrim	1982	UK	1 unexploded bomb	Unknown



HMS Glamorgan	1982	UK	1 x Exocet	Mission capable after damage recovery
USS Stark	1987	USA	2 x Exocet (1 did not explode)	Severe damage, maintained propulsion
USS Samuel B. Roberts	1988	USA	1 x M-08 contact mine	Severe damage, reduced propulsion
IIS Sahand	1988	Iran	3 x Harpoon, 2 x CBU, 2 x LGB	Sunk
IIS Sabalan	1988	Iran	1 x LGB	Severe damage, towed away
USS Tripoli	1991	USA	1 x LUGM-145 contact mine	Mission capable after damage recovery
USS Princeton	1991	USA	1 x MN-103 influence mine	Severe damage, towed away
TCG Muavenet	1992	Turkey	2 x Sea Sparrow	Crippled by loss of staff
USS Cole	1999	USA	1 x suicide boat	Severe damage, drydocked
INS Hanit	2006	Israel	1 x YJ-82 missile	Moved away from the area
ROKS Cheonan	2010	South Korea	1 x unknown torpedo	Sunk

Table 1: List of the analyzed ships with some summarized details

PNS Shah Jahan (1971)

PNS Shah Jahan (ex HMS Charity) was a C-class destroyer with a displacement of about 2500 t. She received one hit by a P-15 Termit missile.

Not much is known about this attack, except that the ship did not sink but was eventually scrapped due to the extensive damage.

INS Khukri (1971)

INS Khukri was a Type 14 (Blackwood-class) frigate with a displacement of about 1450 t (full load). She received one hit by a 550-mm torpedo which sank her.

According to open literature accounts, the torpedo hit “exploded under the oil tanks”. This apparent fact, taken together with the small displacement of the ship, explains the reportedly quick sinking of the ship and proportionally large loss of life.

ARA General Belgrano (1982)

ARA General Belgrano was a WWII Brooklyn-class light cruiser with a displacement of about 12200 t at full load. She was hit by two Mk 8 torpedoes which sank her, earning her the dubious distinction of being the first and only ship to be killed by a nuclear submarine in history.

The torpedoes hitting the Belgrano had a 363 kg warhead. The first hit came very close to the bow, outside both the armored belt and the anti-torpedo bulge, and blew it up; the damage was however ultimately very small as the ship water integrity was preserved.

The second hit was sustained aft, again outside the armored area, and proved catastrophic: the aft machinery room and two mess rooms were immolated causing about 275 casualties, and subsequently the explosion vented through the main deck.

The ship very quickly filled with smoke. Electrical power was lost due to the explosion



and the list that the ship soon developed could not be countered by pumping. Twenty minutes later the order to abandon ship was given and she eventually slipped beneath the waves.

HMS Sheffield (1982)

HMS Sheffield was a Type 42 destroyer with a displacement of about 4800 t. She received one hit by an Exocet which sunk her.

This is probably the missile attack that has been discussed most in the brief history of naval missile combat. According to the official RN account (UK-MOD 1982a) Sheffield sustained the hit on her second deck, 2.4 meters above the waterline. Immediate damage included the control room, fire main, forward auxiliary and machinery room being lost. Fire spread and could not be fought due to heavy smoke and no fire main, so eventually the ship was abandoned. Sheffield then sunk during towing due to flooding through the side hole, but fire (and smoke) was definitely the primary damage mechanism in this attack.

It is significant that the missile with its 165 kg warhead did not detonate, according to official statements, though this is contested by some.

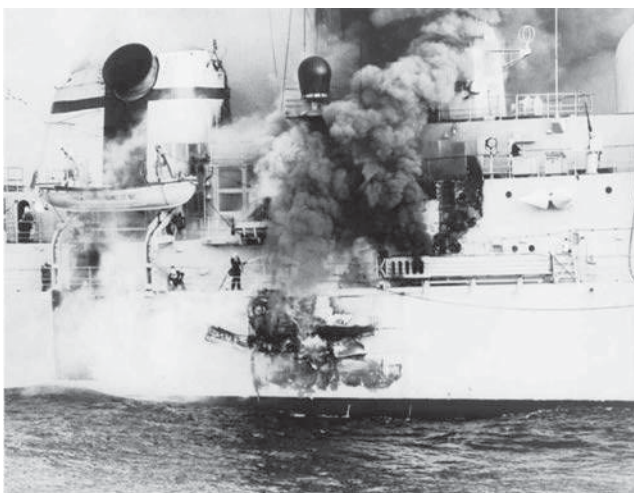


Figure 1: HMS Sheffield on fire after the Exocet hit
(photo credit: UK MoD - believed to be in the public domain)

HMS Ardent (1982)

HMS Ardent was a Type 21 frigate with a displacement of about 3200 t. She received several bomb hits which sunk her (UK-MOD 1983).

Ardent was hit by several waves of air attacks.

The first three hits were sustained in the hangar (two weapons) and aft auxiliary machinery room (one weapon, which failed to explode but caused significant damage nonetheless by destroying a switchboard which left, among other things, the main gun inoperative). The hangar hits destroyed the helicopter and a missile launcher, as well as started a large fire and caused significant crew casualties.

A subsequent wave of attackers hit the ship in the aft area with an unknown number of weapons, estimates range from two to four bombs. There are reports of more weapon hitting the ship at the same time but failing to explode, which was fairly common due to the low altitude the attacks were performed at. These attacks caused many casualties and the ship lost steering as well. Fires aft grew out of control and a list was developed from flooding due to underwater explosions of near misses. The ship was abandoned and sunk about 12 hours later.

According to Argentine sources both Mk 83 (450 kg) and Mk 82 (230 kg) bombs were used, in the normal and retarded type.

HMS Antelope (1982)

HMS Antelope was a Type 21 frigate with a displacement of about 3200 t. She was sunk when the defusing attempts on two bombs that she had received failed (UK-MOD, 1982b).

Antelope sustained two bomb hits, the first in the starboard side, the second close to the



main mast, from an aircraft that crashed through it. No one of the bombs exploded.

Defusing attempts on the aft bomb failed and the ship was torn open from waterline to funnel. Major fires were started in both engine rooms. Electrical power was lost and the starboard fire main was fractured as well, making fire fighting all but impossible.

The ship was abandoned and shortly thereafter missile magazines began exploding. The ship was still afloat, her keel broken and her substructure all but melted, the following day, but eventually sunk after breaking in half.

HMS Coventry (1982)

HMS Coventry was a Type 42 destroyer with a displacement of about 4800 t. She received four hits by bombs, two of which exploded, and eventually sunk.

Coventry was hit a first time on her flight deck by a 450-kg bomb which destroyed her helicopter but did not explode. Then, she was hit by three 225-kg bombs on her port side, just above the waterline: two of the bombs exploded, one putting the computer room and most of the senior staff out of commission; the second in the forward engine room. The latter hit destroyed the bulkhead separating the two engine rooms, causing an uncontrollable flooding (the ship could survive two compartments being flooded but not the two engine rooms as they were too large).

The ship capsized in about twenty minutes and sunk shortly thereafter.

HMS Broadsword (1982)

HMS Broadsword was a Type 22 frigate with a displacement of about 4400 t. She received one hit by a bomb which did not explode.

During the same action in which Coventry was sunk, Broadsword was hit by a bomb of

unknown weight, which bounced on her flight deck, destroying her helicopter (similarly to Coventry) and then exploded harmlessly in the water.

The ship remained mission capable (but for the loss of her helicopter of course) and in fact was instrumental in rescuing most of the crew of Coventry.

HMS Argonaut (1982)

HMS Argonaut was a Leander-class frigate with a displacement of about 3250 t at full load. She received two hits by bombs which did not explode.

HMS Argonaut was hit by two bombs which did not explode; however, one of them entered a missile magazine, detonating two missiles and causing some casualties and a fire.

The ship moved away from the area under tow, which suggests some internal damage for which however documentation is lacking.

HMS Antrim (1982)

HMS Antrim was a County-class destroyer with a displacement of about 6850 t at full load. She received one hit by a bomb which did not explode.

HMS Antrim was hit by one 450-kg bomb which did not explode.

Information is lacking about what damage, if any, was caused by the impact.

HMS Glamorgan (1982)

HMS Glamorgan was a County class destroyer with a displacement of about 5400 t (6200 full load). She received one hit by an Exocet which she survived despite some extensive fire damage.

The hit was sustained on the port side of the hangar deck, close to the Sea Cat launcher, and



deflected upwards (the ship was violently maneuvering to present the stern to the missile). The hangar deck was holed by the explosion, fire spread in the galley below; the missile body kept going and penetrated the hangar, destroying the ship helicopter. Eventually the crew managed to contain the spread of fire but there was extensive damage in the hangar area (Inskip, 2012). The ship was definitely able to float, though there was some list caused by the extensive quantity of water used in firefighting, and moved away at high speed soon after the attack; her fighting capabilities are unclear, but her main sensors were probably still active. The following day however saw the ship in sheltered waters for repairs. After the end of the war the ship traveled back to the UK under her own power.

USS Stark (1987)

USS Stark was a Perry class frigate with a displacement of about 4200 t (full load). She received two hits by Exocet missiles which she survived despite significant, fire, flooding and crew losses.

The ship received two hits in the same location, on the port side close to the waterline (more or less below the bridge); the first missile did not detonate but started a fire, the second exploded in crew quarters causing large losses among the crew.

Official statements (USN, 1987) indicate that the first hit was more damaging as a large quantity of propellant was injected further inside the ship, whereas the second hit is estimated to have occurred about 1 m inside the ship and vented some of its energy outside her.

Energetic damage control carried out for several hours with the help of nearby ships managed to contain the spreading of fires and saved the ship, which at a point had an extensive list, reported as 15° (USN, 1987). The ship eventually made it to Bahrain where she sustained temporary repairs before returning home.

While propulsion was maintained, it took a while before the ship was able to move safely; also, the Standard launcher was reportedly down and the ship could not retaliate nor defend herself (except with the CIWS) from further attacks.

USS Samuel B. Roberts (1988)

USS Samuel B. Roberts was a Perry class frigate with a displacement of about 4200 t (full load). She sustained one hit by a contact mine which caused extreme damage but did not sink her.

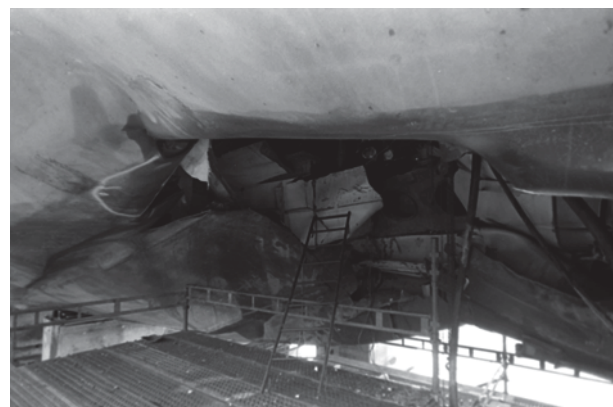


Figure 2: The damaged hull of USS Samuel B. Roberts

(photo credit: PH2 Rudy D. Pahoyo - USN - public domain)

Samuel B. Roberts struck an M-08 contact mine with a nominal charge of about 115 kg (Watts, 1991). Literature suggests however that some of the mines encountered in the Persian Gulf had a higher than normal charge in exchange for flimsier chains, which could explain the fact that the mine was encountered in a commercial shipping lane.

The hit broke the keel of the ship and blew a 5 m hole in the hull, flooding the engine room and knocking the two gas turbines from their mounts; a large fire was also initiated. Heroic damage control managed to contain the damage and save the ship, which then moved away under the power of her auxiliary thruster and reportedly maintained (or quickly



regained) radar coverage and weapon readiness; however her extreme structural damage as well as her much reduced mobility still qualifies this hit as a mission-kill.

IIS Sahand (1988)

IIS Sahand was a British-made Alvand-class 1500 t full load frigate that was sunk after sustaining 3 Harpoon hits plus further hits by 2 cluster bombs and at least 2 laser guided bombs.

It is reported that either of the first two Harpoon shots (with a 220 kg warhead) hit the superstructure in the command area, effectively disabling the fighting capabilities of the ship; further hits had the ship ablaze from bow to stern, dead in the water and listing; eventually the ship blew up when the flames reached her ammunition magazines.

IIS Sabalan (1988)

IIS Sabalan was a British-made Alvand-class 1500 t full load frigate that was hit by 1 225-kg laser-guided bomb.

Sabalan sustained a hit by a Mark 82 bomb, reportedly close to her exhaust stack, which caused the ship to lose propulsion and set her on fire. It was eventually towed back to port and repaired. Not much more is known about this event.

USS Tripoli (1991)

USS Tripoli was a Iwo Jima-class amphibious assault ship with a displacement of 19300 t that was hit by a contact mine (USN 1992, Atkinson 1994).

Tripoli was hit on her starboard bow by an LUGM-145 mine carrying about 145 kg of explosives, the effect of the hit being magnified

by the close bottom. The explosion ripped a 5 by 7 m hole in the hull and caused damage throughout the bow, including an artillery magazine being flooded with JP5 kerosene and water and a mixture of paint and thinner being vaporized and filling part of the hull with its toxic vapors.

Damage control managed to contain the effects of the damage; the ship resumed operations after 20 hours, remaining in the combat area for several days until relieved, though she was unable to deploy her mine-hunting helicopter due to the relevant fuel tanks having been damaged by the hit.

USS Princeton (1991)

USS Princeton is a Ticonderoga-class cruiser with a displacement of 9800 t at full load. She was hit by two influence mines (USN 1992, Atkinson 1994).

Princeton was hit by the blast of an Italian-made MN-103 Manta, a bottom-mounted influence mine, which exploded under the port rudder; immediately thereafter a second mine of the same type (probably in a sympathetic detonation) exploded forward of the starboard bow. The whipping induced by the detonations caused the ship to suffer severe structural damage.

The fantail nearly separated from the rest of the ship. Cracks developed in the hull and in the superstructure which was nearly divided in two parts by a crack going completely through its sides. The port rudder was jammed and the starboard propeller shaft was damaged. A fire main was damaged, flooding part of the ship and shorting one of the main switchboards.

The AEGIS system was brought back online in a short while and the forward weapons were still operational, but the ship could not be safely moved due to the severe structural damage and eventually had to be towed away, so as in the case of Samuel B.



Roberts this must be considered a mission-kill as well.

TCG Muavenet (1992)

TCG Muavenet (ex USS Gwin) was a mine layer destroyer that was hit by two Sea Sparrow missiles fired inadvertently by USS Saratoga.

The missiles were meant for AA use and therefore had smaller 40-kg warheads; however the first hit destroyed the bridge and the CIC, whereas the second struck the aft magazine but did not detonate.

Damage control operations saved the ship which was still capable of floating and moving, but she had been effectively crippled due to the loss of most of her bridge crew and command rooms.

USS Cole (1999)

USS Cole is an Arleigh Burke-class destroyer with a displacement of 9000 t at full load. She was hit by a suicide small boat on her port side. It is estimated that 200-300 kg of explosives, possibly formed in a shaped charge, were used. The attack was probably the most successful attempt at asymmetric warfare in the post Cold War era and has influenced naval thinking and design in recent times.

The hit opened an 18 by 12 m gash in the ship at the waterline, driving two lower decks upward toward the main deck and opening the room containing the starboard main engine to the sea. Fuel lines were ruptured and power throughout the vessel went out as well. Damage control took three days until the situation was stabilized enough for the ship to be towed and then dry-docked.

INS Hanit (2006)

INS Hanit is a Sa'ar 5 class corvette with a displacement of 1300 t (full load) which

received a single hit by what has been reported as a YJ-82 missile.

The hit was sustained in the stern area of the ship; the explosion split the helo deck, caused crew casualties and reportedly extensive damage to propulsion. Despite this the ship made it back to a safe port under her own power; her fighting capabilities after the impact remain however unknown.

ROKS Cheonan (2010)

ROKS Cheonan was a Pohang-class corvette with a displacement of 1200 t which, according to the official investigation, received a single torpedo hit which sunk her.

The matter is contested, but what is clear is that a medium-sized explosive charge, estimated as 250 kg of TNT equivalent, detonated just below the hull in the stern area, somewhat off to port; the resulting bubble jet broke the ship in half, separating the stern, and the ship capsized and sunk in a very short time frame.

5. CONCLUSIONS

At the base of this paper there is the opinion that the SOLAS2009 probabilistic approach might represent an interesting methodology to be implemented in the warship survivability assessment. After the indication of the main critical points for the approach transferability to the warship design process, attention is given to the need of a consistent and comprehensive investigation, about the different damage scenario characteristics..

As an initial approach to the problem an overview is carried out evidencing the importance to discuss about the ship characteristics, the kind of threat, the primary effects (hull damage and flooding), the secondary effects (for example fire or systems failures) and the final evolution of the situation.



It appears evident that the damage size description in terms of length, penetration and height is not a straightforward activity and that some further studies are necessary in the perspective of a probabilistic approach, SOLAS2009 like, the field of naval ship assessment. Actually some analytical probability density function derived from literature (Przemieniecki, 2000) able to describe the ship damage statistics, might represent a more suitable way to move forward, as already proposed by some authors.

The efficiency that the watertight subdivision can express is of course in close relation with the weapon overall power intensity that in some occasions is really devastating. To this regard, it might be more interesting to focus on a possible optimization of the ship subdivision considering the effect of an asymmetric threat, characterized by a lower power, but usually oriented to possibly offend a sensitive part of the ship. However there is growing attention to the assessment of a warship performance not only to survive a hostile damage, but also in relation with typical merchant fleet accidents like collision and grounding (Smith & Heywood, 2009) and in this sense the possible application of the probabilistic approach for the warship design might find its exploitation.

6. REFERENCES

- Atkinson, R. 1994 "Crusade: The Untold Story of the Persian Gulf War" Mariner Books
- Ball, R.E.; Calvano, C.N. (1994), "Establishing the fundamentals of a surface ship Survivability Design Discipline", Naval Engineers Journal, Vol. 106, No. 1, pp. 71-74
- Boulougouris E., Papanikolaou A., 2012, "Risk-based Design of Naval Combatants" 11th International Marine Design Conference IMDC 2012 Glasgow UK
- Harmsen, E., Krikke, M., 2000, "A probabilistic damage stability calculation method for naval vessels", 7th International Conference on Stability of Ships and Ocean Vehicles (STAB '00), Tasmania, Australia.
- Harry, B. 2002 "Trident, Grandslam and Python: Attacks on Karachi". Pages from History. Bharat Rakshak Monitor - Volume 4 (4) IMO, 1960, "Resolution A.265 (VIII) - Regulations on Subdivision and Stability of Passenger Ships as an Equivalent to Part B of Chapter II of the International Convention for Safety of Life at Sea", London, UK.
- IMO, 1990, "Resolution MSC 19 (58) on the Adoption of Amendments to the SOLAS 1974 Convention, regarding the Subdivision and Damage Stability of Dry Cargo – MSC 58/25 Annex 2" London, UK.
- IMO, 2007, "MSC 82/24/Add.1 Report of the Maritime Safety Committee on its eighty-second Session - ANNEX 2 MSC.Res.216(82)" London UK.
- Inskip, I., 2012 "Ordeal by Exocet: HMS Glamorgan and the Falklands War 1982" Frontline Books
- Papanikolaou, A.; Boulougouris, E., 2000, "On a rational approach to the assessment of survivability of surface naval and merchant ships", Proc. 9th congress of the Int. Maritime Association of Mediterranean, IMAM 2000, Ischia, April 2000
- Przemieniecki, J.S. (2000), "Mathematical Methods in Defense Analyses", Third Edition, American Institute of Aeronautics and Astronautics, Reston VA, USA.
- Sarchin T.H., Goldberg, L.L., 1962 "Stability and Buoyancy Criteria for U. S. Naval Surface Ships" Transactions SNAME Vol. 70.
- Smith, D., Heywood, M., 2009 "Accidental



Damage Templates (ADTs) A basis for the future of Naval Ship Safety Certification?"
Proceedings of the 10th International Conference on Stability of Ships and Ocean Vehicles, STAB 2009 St. Petersburg Russia

Surko, S.W., 1994, "An Assessment of Current Warship Damaged Stability Criteria", Naval Engineers Journal, Vol. 106, No. 3, pp. 120-131.

Surko, S.W., 1988, "The residual strength of a ship after an internal explosion" Thesis (M.S.)--Massachusetts Institute of Technology, Dept. of Ocean Engineering, 1988, and (M.S.)--Massachusetts Institute of Technology, Dept. of Mechanical Engineering.

UK MOD, 1982a "Loss of HMS Sheffield – Board of Enquiry" reference 520/237.L

UK MOD, 1982b "Loss of HMS Antelope – Board of Enquiry" reference 520/4.X

UK MOD, 1983 "Loss of HMS Ardent – Board of Enquiry" reference 520/241L

USN, 1987 "Formal investigation into the circumstances surrounding the attack on the USS Stark (FFG 31)"

USN 1992 "Salvage Report Operations Desert Shield / Desert Storm" Volume I. Naval Sea System Command.

Watts A.J., 1991 "Jane's Underwater Warfare Systems 1991-1992" Jane's Information Group



Advanced Damaged Stability Assessment for Surface Combatants

Evangelos Boulougouris, *University of Strathclyde*, evangelos.boulougouris@strath.ac.uk

Stuart Winnie, *University of Strathclyde*

Apostolos Papanikolaou, *National Technical University of Athens*

ABSTRACT

One of the major contributors to survivability of a surface combatant is her vulnerability to weapon effects and as such the damage stability characteristics have a direct influence on vulnerability. There are serious concerns about the limitations of the current semi-empirical deterministic criteria in which a combatant's damage stability is assessed upon. This paper details a comparison between the current approach and a newly presented probabilistic approach with the aim of determining which will result in a more accurate way of estimating the level of survivability of a particular design. A study is also presented in which the damage length used is increased to merchant standards of $0.24L_{bp}$.

Keywords: *naval ships, damage stability, probabilistic, survivability*

1. INTRODUCTION

Surface warships differ from other categories of ships in that they are designed to operate in a man-made hostile environment. In addition to being able to withstand damage from collision and grounding a surface combatant must be able to avoid and withstand the effects of modern anti-ship weapons. As warships are designed and built to support high-end combat operations, survivability and the ability to 'fight hurt' is a vital design objective.

One of the main contributors to a surface combatants survivability is her vulnerability to weapon effects and as such the damage stability and floatation characteristics of the vessel determine the vulnerability of the vessel. Therefore it is critical for the designer to minimise the vulnerability of the vessel from the early design stages in order to maximise its survivability. This can be achieved through the use of optimal subdivision and by considering

a large number of damage scenarios and operational /environmental conditions.

The majority of modern warship stability criteria used is based on a set of empirically defined stability criteria proposed by Sarchin and Goldberg (1962). The survivable damage lengths and criteria are based largely on WWII battle damage experience. The criteria used by major navies such as the U.S Navy (USN) and Royal Navy (RN) have been reviewed over the years however, there have been no significant changes. Although the criteria have served their purpose for many years, they now appear to be outdated and there are serious concerns about their limitations and applicability to modern naval ship designs. Some of the shortfalls of the criteria include (Surko, 1994);

- Capability of modern warships to survive damage from current threats, in demanding environmental conditions, is not known
- Modern hull forms and construction techniques differ greatly from the ships



used to determine the criteria

- Assumption of moderate wind and sea conditions at the time of damage

This suggests that even though a vessel may comply with the standards outlined, the designer and operator may not have a clear understanding of the survivability performance and operational limits of their vessel.

In contrast the International Maritime Organisation (IMO) have made significant advances in terms of upgrading safety standards of merchant vessels. The acceptance of the new harmonized probabilistic damage stability framework of SOLAS 2009 for the damage stability assessment of passenger and dry cargo vessels shows that the maritime industry and regulatory bodies are convinced this is the only way forward. Boulougouris and Papanikolaou (2004) previously presented a methodology for the probabilistic damaged stability assessment of naval combatants and its application to design optimisation. The methodology allows the risk that the vessel will be lost as a result of damage to be quantified. Therefore minimal risk can become a design objective and the surface ship can be optimised for minimum risk while still being efficient and economical.

This paper details a comparative study of the currently used semi-empirical deterministic approach and the proposed quasi-static probabilistic approach to assessing the damage stability of a surface combatant. Each approach is applied to a generic frigate and the merits and shortcomings of each method along with the results are presented. In addition, a study was carried out to observe the effects of increasing the damage length on a frigate which meets the current deterministic criteria.

2. SURVIVABILITY

The survivability of a naval combatant can be defined as “*the capability of a (naval) ship and its shipboard systems to avoid and*

withstand a weapons effects environment without sustaining impairment of their ability to accomplish designated missions” (Said, 1995). Survivability consists of two main aspects;

- Susceptibility – Inability of the ship to avoid being damaged in operation and is also referred to as the probability of being hit (P_H)
- Vulnerability – Inability of the ship to withstand the effects of a threat weapon and is also referred to as the probability of serious damage or loss when hit ($P_{K/H}$)

Survivability is the opposite of killability which is the probability that the ship will be lost due to enemy action. Killability can be described mathematically as the product of susceptibility and vulnerability. A ship kill can be expressed in many different ways, in this case the definition given by Ball & Calvano (1994) is referred to;

- System Kill – damage of one or more compartments which leads to the failure of a ship system.
- Mission Area Kill – damage which leads to the loss of a mission critical area such as AAW
- Mobility Kill – damage which leads to the ship being immobilised through the loss of propulsion or steering.
- Total Ship Kill – damage which leads to the loss of the ship through insufficient buoyancy, loss of transverse stability or abandonment due to fire.

The mathematical relationship between survivability (P_s), susceptibility and vulnerability is as follows (Ball & Calvano, 1994);

$$P_s = 1 - (P_H \times P_{K/H}) \quad (1)$$

The relationship highlights that both susceptibility and vulnerability are of equal importance to the survivability of the vessel.



Some naval design philosophies have included to ‘design for peace’ as the probability of being damaged in operation is very low. They will therefore accept that in the event of a hit that the vessel will be out of action or have limited participation in the operation. Thus their focus has been to minimise the susceptibility of the vessel. Most of the scenario simulations ran would assume a single hit has a kill probability equal to one for smaller vessels and two hits would be sufficient to sink a larger vessel. Although modern surface ships are powerful military assets on the open ocean, they lose their advantage near shore. Even the stealthiest vessel is susceptible to asymmetrical threats. By treating the vulnerability as a property with a deterministic outcome, pass or fail, it is not possible to truly quantify the survivability of the vessel.

3. DETERMINISTIC

Currently both the USN and RN use deterministic criteria to assess the stability of naval ships after damage. The stability standards previously used by the UK MOD, NES 109, was recently reissued in DEFSTAN 02-900 part 1: Ship safety & Environmental Protection (UK MOD, 2013). However the criteria used in the assessment of stability and reserve buoyancy after damage remain unchanged. Table 1 shows the semi-empirical damage stability criteria currently used by the USN and RN for surface combatants. Both use a damage length of 15% L_{wl} for larger vessels however the UK also implements a minimum damage length of 21m. Although the survivability requirements between naval ships and merchant vessels differ significantly it is of

interest to note that the current IMO probabilistic damage approach considers damage extents up to 24%.

Although both criteria are very similar the UK criteria is slightly more demanding, the use of a 15 degree roll back angle requires that UK warships have a greater righting energy to achieve the same reserve dynamic stability criteria. In addition the use of a minimum length of damage shows progress towards a threat based standard for damage length.

4. PROBABILISTIC ASSESSMENT

Boulougouris and Papanikolaou (2004, 2013) previously presented a methodology for the probabilistic damaged stability assessment and its application to design optimisation. It is based on the fundamentals of the probabilistic damage stability concept for passenger vessels introduced by Wendel (1960) and its derivatives (IMO Resolution A.265; IMO MSC.19 (58); IMO MSC.216 (82)) which are used to assess the ships level of safety after damage. The probabilistic approach uses the probability of survival after damage as a measure of the ships safety when damaged. The approach considers the following probabilities of events as being relevant to the ships damage stability;

- The probability that a compartment or group of compartments i may be flooded (damaged), p_i .
- The probability that the ship will survive after flooding of the compartment or group of compartments i under consideration, s_i .

Table 1
Current UK and US damage stability criteria for surface combatants

Criteria	UK Defstan 02-900		U.S.N DDS 079-1	
Damage Length	LWL < 30m	1 Compartment	LWL < 100ft	1 Compartment
	30m < LWL < 92m	2 comp of at least 6m	100ft < LWL < 300ft	2 comp of at least 6m
	LWL > 92m	max{15%LWL or 21m}	300ft < LWL	15% LWL
Permeability	Watertight void	97%	Watertight void	95%
	Accommodation	95%	Accommodation	95%
	Machinery	85%	Machinery	85-95%
	Stores etc.	80-95%	Stores etc.	60-95%
Angle of list or lol	< 20°		List < 15°	
GZ at C	60% of Gzmax		-	
Area A1	> 1.4 A2		> 1.4 A2	
Longitudinal GM	> 0		0.69	
Buoyancy	longitudinal trim less than required to cause down-flooding		3 in margin line	



The total probability of survival is expressed by the attained subdivision index, A , and is given by the sum of the product of p_i and s_i for each compartment and compartment group, i along the ship's length.

$$A = \sum_i p_i \cdot s_i \quad (2)$$

In order for a vessel to comply with the IMO probabilistic method for passenger and cargo ships (IMO MSC.216 (82)) the attained subdivision index must be greater than or equal to the required index. This ensures that the vessel is designed with an acceptable level of risk. The required attained index is based on the number of passengers carried, safety equipment on-board and the length of subdivision. The calculated required index (R) of the ship is consistent with the mean value of the attained index (A) from a sample of ships which in theory face a similar level of risk. This consists of ships of a similar size and number of passengers which have acceptable damage stability/ survival characteristics. Similarly for warships an acceptable level of risk should be specified by either the owner (navy) or approval authority (NATO/ classification society).

For naval vessels there is a probability that the ship will be targeted and engaged leading to the flooding of one or more compartments. The damage can occur at any point along the ship's hull and can vary extensively in magnitude. The extent of damage is dependent on both the characteristics of the target (ship) and the threat weapon. As the survivability of the vessel is determined by the vulnerability and susceptibility, the probability distribution for damage of a naval ship relates these characteristics.

The probability of survival of a particular function of the ship can be extracted from the total attained index, which represents ship's floatability and stability after damage. If $j^* = \{j_1, j_2, j_3, \dots, j_n\}$ is the set of compartments

that host all systems of the particular function F , then the damage of any set j that includes j^* will impair the ship from function F . Therefore the probability of survival of the particular function is calculated using the following formula:

$$S_f = \sum_i p_i \cdot s_i - \sum_j p_j \cdot s_j \quad (3)$$

where j are all damage cases, which include the compartment set j^* .

4.1 Determining p_i

During the initial stages of a naval ship's design, when there is a lack of refined information for the threat's signature distribution along the ship it can be assumed that the probability of weapon impact along the hull follows a basic mathematical distribution, such as the piecewise linear distribution. Boulougouris and Papanikolaou (2004) propose that for air-to-surface missile (ASM) threats, a piecewise linear distribution with maximum probability amidships can be used. As both the ship's radar profile and heat emissions due to machinery and exhaust are highest at amidships this is the most likely aim point of the weapon. For contact mines a linear distribution can be assumed (Harmsen & Krikke, 2000). Thus the impact point probability density function in the missile's case with a piecewise linear distribution is;

$$imp(x) = \begin{cases} 4x & x \leq 0.5 \\ -4x + 4 & x \geq 0.5 \end{cases} \quad (4)$$

The damage length probability density distribution is based on the concept of the Damage Function used in the theory of Defence Analysis (Przemieniecki, 1994). The well-known log-normal distribution considered the most appropriate for this case. Therefore the damage length probability density distribution is given by the following formula;



$$Dam(y) = \frac{1}{\sqrt{2\pi}\beta y} \cdot \exp\left[-\frac{\ln^2(y-\alpha)}{2\beta^2}\right] \quad (5)$$

Where;

$$\alpha = \sqrt{L_{SS}L_{SK}}, \beta = \frac{1}{2\sqrt{2}z_{SS}} \ln\left(\frac{L_{SS}}{L_{SK}}\right) \quad (6)$$

Where L_{SK} is the sure kill length which means that $d(L_{SK})=0.98$, L_{SS} is the sure save length which means $d(L_{SS})=0.02$ and z_{SS} is a constant equal to 1.45222.

For defining the damage extent range, it is a common approach in naval ship design to consider 2 or 3 damaged compartments around the detonation compartment especially in case of absence of blast resistant bulkheads (Erkel & Galle, 2003). More detailed estimates may result from a careful risk assessment based on live firing tests analysis, the analysis of data from actual engagements, empirical formulas linking the damage range with the type and weight of the warhead or from the use of damage lengths/extents defined in current deterministic damage stability regulations for naval ships. In the latter case, which is the one proposed by Boulougouris and Papanikolaou (2004), a first approximation of the L_{SS} can be taken according to naval codes DefStan 02-900 and DDS-079 and it would be 0.15L (see Table 1). The author's state that the L_{SK} has can be assumed equal to 0.02L.

By combining the impact point and damage length density functions the probability of damage lying between the boundaries x_1 and x_2 or a naval ships compartments is;

$$p_i = \int_0^y Dam(y) \int_{x_1 + \frac{y}{2}}^{x_2 - \frac{y}{2}} imp(x) dx dy \quad (7)$$

The equations resulting from substituting $Dam(y)$ and $Imp(x)$ into equation (7) were presented in Boulougouris and Papanikolaou (2004).

Similar to collision damage the extent from a threat weapon will vary in magnitude transversely and vertically. The transverse damage penetration especially from ASM threats can vary extensively and in cases can extend across the full hull. Weapons fitted with time-delay fuses will penetrate the hull to an optimum position before detonating. However the damage penetration distribution is not an 'issue' for surface combatants as longitudinal subdivision which would lead to asymmetrical flooding is avoided by design.

For the assessment carried out a piecewise linear distribution with maximum probability at the centreline was utilised for the damage penetration distribution in order to calculate reduction factors for various damage cases. The vertical extent of damage may also vary depending on the weapon's characteristics. In a surface combatant such as a frigate or a destroyer there are 3 vertical watertight boundaries, namely the tanktop, the damage control deck and the main deck. Excessive vertical watertight boundaries are avoided by design as high flooding can lead to poor stability thus it can be favourable to allow lower decks to flood. In the case of an air delivered weapon (e.g. Anti-Ship Cruise Missile) it will generally detonate close to the waterline causing greater damage above the waterline and the tank top will most likely remain intact. However in the case of an underwater weapon (e.g. contact mine or torpedo) which detonates close to the keel, the damage control deck will likely remain intact. The problem with an underwater explosion is that modern under-keel torpedoes are capable of causing extensive damage to the keel girder of even a cruiser sized ship, often this is sufficient to cause breaking and sinking of the ship. Such cases are not covered in the proposed methodology as the maintenance of structural integrity is a prerequisite for the assessment of the ships damage stability.

For a hit by an air-delivered weapon, a linear distribution for the probability density function of the vertical extent of damage can be

used. Its maximum is at the main deck and the minimum at the keel, the opposite is valid for an underwater weapon (see Figure 1) (Boulougouris & Papanikolaou, 2013). By considering the vertical extent of damage the effect of the position of vertical watertight boundaries on the overall survivability of the vessel can be observed. In order to take into account both threats a weighting factor can be applied according to an operational analysis of the potential threats.

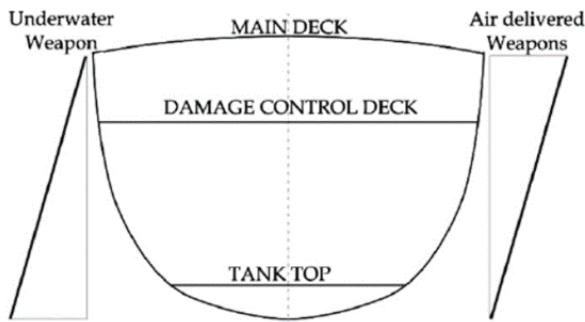


Figure 1 Naval Ship Vertical Watertight Boundaries

4.2 Survival index S_i

The approach used to assess the probability of survival after damage is a probabilistic quasi-static approach adjusted for the currently valid, semi-empirical deterministic criteria for naval ships (Boulougouris & Papanikolaou, 2013). The approach considers the probability of survival after damage and is based on quasi-static survival criteria such as those used by the Royal Navy and US Navy. The criteria were developed from real life damage incidences of

WWII and although the current criteria have been under criticism as being outdated they have proved reliable over the years and thus there have been no significant changes. One of the main criticisms of the current criteria is the fundamental assumption that the sea conditions at the time of damage are “moderate.” This constraint was lifted in the proposed methodology with the requirement for a specific survival sea state in case of damage.

This allows the correction of these requirements by consideration of the probability of exceedance of the wave height considered as basis for the current deterministic RN and USN criteria, namely a significant wave height H_s of merely 8 ft. The wave height is used in the criteria in order to define ϕ_{roll} , the roll amplitude due to wave action. It was also the underlying assumption behind the guidelines for establishing the watertight features/closures to prevent progressive flooding. Thus, any attempt to change the wave amplitude must take into account changes in both ϕ_{roll} as well as the margin line or equivalent.

The wind speed is another important parameter which needs to be considered, however given the small probability of exceeding the values given by RN and U.S Navy standards, the values were left unchanged (approximately 33 knots for a 3500t frigate). Table 2 shows the criteria which were applied in the frame of a probabilistic approach to assess the survivability of a generic frigate.

Table 2
Probabilistic damage stability criteria for naval combatants

$s_i = 1$	$\Theta_{roll} = 25 \text{ deg}$	Wind Speed = According to Defstan 02-900
	$A_1 \geq 1.4 A_2$	Min Freeboard $\geq 3in + 0.5(H_s(0.99) - 8ft)$
$s_i = P(H_s \leq 8ft)$	Ship meets Defstan 02-900 damage Stability Criteria	
$s_i = 0$	$\Theta_{roll} = 15 \text{ deg}$	Wind Speed = According to Defstan 02-900
	$A_1 \leq 1.05 A_2$	Longitudinal trim < required to cause downflooding



For intermediate stages, interpolant values can be used. Figure 2 shows the meaning of various notions of the righting arm curve.

Implementing the above criteria for ships operating in North Atlantic ($P(H_S \leq 8 \text{ ft})$) would be 0.56 and for East Mediterranean Sea 0.90 (Athanassoulis & Skarsoulis, 1992). For the North Pacific $P(H_S \leq 8 \text{ ft})$ would be 0.42 (Lee, 1995) and for the South China Sea 0.71 (Haveman et al, 2006).

Therefore, a combatant, meeting the U.S. Navy criteria for warships, should have according to the proposed criteria a 56% probability of survival in the North Atlantic for a damage length not exceeding the current regulations (Ochi, 1978). This probability will increase to 90% probability of survival in the Mediterranean Sea and to 71% in the South China Sea. However in the case of the North Pacific the probability of survival will decrease to 42%. Obviously a similar methodology can be introduced for auxiliary naval vessels. The minimum required values for compliance could be estimated after application of the above procedure to sample/existing ships.

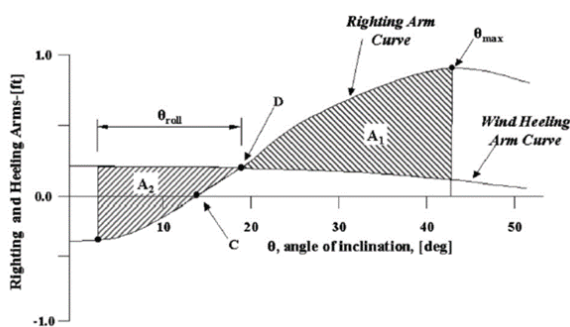


Figure 2 Damaged ship GZ criteria

5. CASE STUDY

Both the current deterministic approach and proposed probabilistic approach were applied to a generic frigate model which was defined in the Maxsurf package (Bentley Systems, 2013). The stability of the vessel was assessed using Maxsurf stability advanced. The

ships main particulars are given in Table 3 and the 3D hull model is shown in Figure 3.

Table 3

Main Particulars	
Loa (m)	148.1
Lwl (m)	137
Twl (m)	4.31
Depth (m)	9.3
Displacement (tons)	4528



Figure 3 Frigate 3D hull model

The arrangement is typical for a frigate of this size with a centreline passageway providing an un-flooded route across the full length of the damage control deck. The ship has two main engine rooms, one for two cruise gas turbines and the other for two boost gas turbines. In addition there are two auxiliary machinery rooms forward and aft of the GT rooms.

The internal layout of the frigate consisted of 13 watertight transverse bulkheads which subdivide the hull into 14 main compartments. Three decks form the horizontal watertight boundaries, namely the main deck (1st deck), damage control deck (2nd deck) and the tank top (4th deck).

The ship has a 4528t displacement at full load condition without a growth margin and has a VCG of 5.53m resulting in a GMcorr of 1.097m. At this condition the ship fulfils the intact stability criteria outlined in DefStan 02-900.



Initially the deterministic assessment was carried out in which all damage cases had to meet the criteria outlined in DefStan 02-900. The damage length specified (15%Lwl) resulted in a damaged length of 20.55m, thus the minimum length of 21m was used to define the damage cases. This resulted in mainly 3 compartment damage cases. Several different transverse extents were taken for each damage case including B/5, B/2 and penetration across the full beam to ensure to worst possible cases were considered. As the frigate model was designed to this standard all damage cases fulfilled the criteria.

For the quasi-static probabilistic approach damage cases up to 6 adjacent zones were initially considered, however the probability of occurrence of both 5 and 6 compartment damage extents was found to be insignificant.

A total of 226 damage cases extending up to 4 adjacent damage zone were defined in Maxsurf stability. The formulas for the calculation of the probability of damage occurring, p_i , from equation (7), were applied to the basis ship and results for single compartment damage are given in Table 4.

Table 4 p_i for frigate 1-comp damages

Room	NZ	x_1	x_2	x_{1u}	x_{2u}	y	P_i
1	1	0	13.06	0.000	0.095	0.095	0.0071
2	1	13.06	23.53	0.095	0.172	0.076	0.0117
3	1	23.53	29.32	0.172	0.214	0.042	0.0024
4	1	29.32	41.19	0.214	0.301	0.087	0.0309
5	1	41.19	51.61	0.301	0.377	0.076	0.0293
6	1	51.61	62.06	0.377	0.453	0.076	0.0362
7	1	62.06	72.5	0.453	0.529	0.076	0.0421
8	1	72.5	79.58	0.529	0.581	0.052	0.0118
9	1	79.58	89.11	0.581	0.650	0.070	0.0261
10	1	89.11	102.37	0.650	0.747	0.097	0.0466
11	1	102.37	109.01	0.747	0.796	0.048	0.0048
12	1	109.01	117.64	0.796	0.859	0.063	0.0088
13	1	117.64	128.06	0.859	0.935	0.076	0.0089
14	1	128.06	137	0.935	1.000	0.065	0.0018

For the given subdivision arrangement, damage length and longitudinal distribution, 1 compartment damage cases contribute approximately 0.27 whereas 2, 3 and 4

compartment cases contribute 0.6, 0.11 and 0.01 respectively.

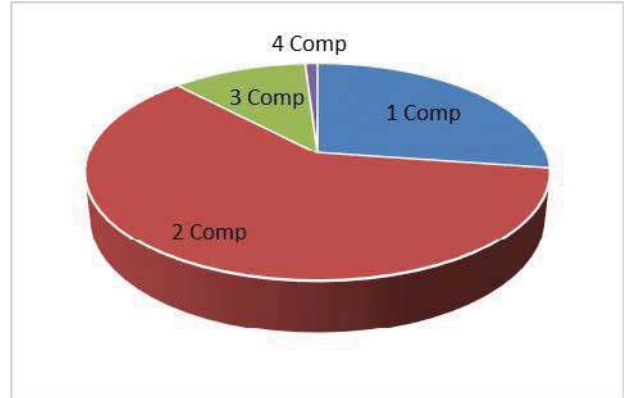


Figure 4 Contribution of various damage cases to attained index

Two different operational areas were considered in order to determine the influence of sea state on survivability, considering the criteria given in Table 2. For the North Atlantic Scenario, we assume $P(H_s \leq 8ft) = 0.56$ and $H_s(0.99) = 10m$, for the North Pacific $P(H_s \leq 8ft) = 0.42$ and $H_s(0.99) = 11.2m$.

For the frigate under consideration at full load condition the attained index was found to be $A=0.98$ for the North Atlantic and $A=0.95$ for the North Pacific Scenario. The survivability of the mobility function was calculated using equation (3) where j are all the main engine room compartments; in this case 5, 6 and 7. This resulted in a mobility survivability index of 0.87.

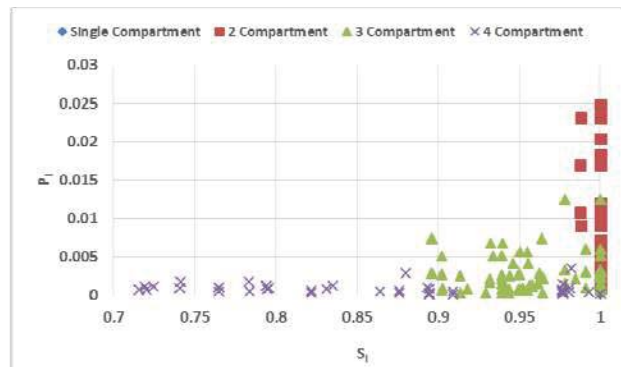


Figure 5 North Pacific p_i against s_i



Figure 5 shows that for the given damage length and longitudinal distribution, the damage cases which are most likely to occur and their corresponding probability of survival. The results illustrate that the vessel has a low risk of being lost due to damage up to two compartments. Due to the length of damage utilised, up to two adjacent compartments contributes approximately 0.87 to the attained index. The risk increases significantly for four or more adjacent compartments however the probability of occurrence of this extent of damage is too low to affect the overall attained index.

It was readily observed that the probabilistic approach can result in minimising the vulnerability of the vessel in the early stages of the design. The results from this approach can be easily visualised making the comparison of many different designs more concise for the designer. As the result of a deterministic assessment is simply a 'pass or fail' for each of the damage cases, it is difficult to quantify the effect of any major design changes on the overall survivability of the vessel. The use of the attained survivability index in the probabilistic approach enables the designer to adopt a holistic approach to naval ship survivability and allows him to easily monitor the influence of his decisions on the survivability.

The defined deterministic length of damage criteria directly influences the position of transverse watertight bulkheads; the specified length of damage implies that the length of either two or three compartments should be slightly larger than the damage length. This results in larger ships being designed with longer compartments to limit the extent of flooding in fewer compartments. Therefore the subdivision methodology simply following the concept of compliance with a set of deterministic criteria, as opposed to an optimisation for maximum survivability. The use of the probabilistic approach in a formal, multi-objective optimisation procedure allows the designer to achieve the optimum level of

survivability, while keeping ship's weight and shaft length to a minimum (Boulougouris & Papanikolaou, 2013).

Relaxing the assumption for a moderate sea state ($H_s=2.4\text{m}$ or 8ft) at the time of damage, it gives a more demanding and realistic set of criteria, which can ultimately result in a higher level of survivability. The currently used significant wave height in the deterministic approach has a 58% chance of exceedance in the North Pacific and a 44% chance of exceedance in the North Atlantic. Thus, it does not properly reflect the harsh environments, which modern surface combatants are expected to operate in.

5.1 Damage Length

The current IMO regulations for dry cargo and passenger ships (IMO MSC.216 (82)) consider collision damage lengths of up to 24% L_{bp} , thus any length of damage over 24% L_{bp} is considered as statistically insignificant. This means that collision damage extents of less than 24% L_{bp} (but still greater than 15% weapon damage length) are statistically significant.

In order to develop a proper set of probabilistic criteria for naval ships extensive calculations must be carried out on a sample of ships, which comply with the current damage stability regulations. A study was carried out in order to explore the effects of the damage length in which the ship is expected to survive on the overall survivability. This will provide insight regarding the extent of damage modern naval ships are capable of surviving. This can therefore lead to a more rational approach of basing the damage extent on an assessment of threat while still having a set of criteria which can be reasonably met resulting in a higher level of survivability.

Initially the maximum length of damage was increased from 15% L_{wl} (or 21m) to 20% L_{bp} for the deterministic assessment. This led to a damage length of 27m resulting in a majority of four compartment damage cases. The new length of damage fulfilled the deterministic criteria for all cases; however, the criteria were met with a much lower margin for the 4 compartment cases. A single 5 compartment case at the bow of the vessel was also assessed in which it passed the reserve buoyancy criteria by 0.17m.

Similarly for the quasi-static probabilistic assessment the maximum length of damage in the distribution was increased from 15% L_{wl} . The value of L_{ss} was set to 20% L_{bp} which altered the damage length distribution. For the new damage length, 1 compartment cases now contribute 0.22 and 2, 3 and 4 compartment damage cases contribute 0.57, 0.17 and 0.03 respectively. For a 15% damage length, 1 and 2 compartment cases contributed 0.87 to the attained index; however that has fallen to 0.79 for a 0.2L damage. An attained index of $A=0.96$ was obtained for the North Atlantic scenario and $A=0.93$ for the North Pacific scenario. Finally the damage length was increased to 0.24L. As collision damage extents over 0.24L are considered to be statistically insignificant this was taken as the maximum value for the study. At approximately $\frac{1}{4}$ of the ships lengths this resulted in a large number of 5 compartment damages for the deterministic assessment. At this point the basis frigate failed the assessment in several cases due to both insufficient transverse stability and reserve buoyancy.

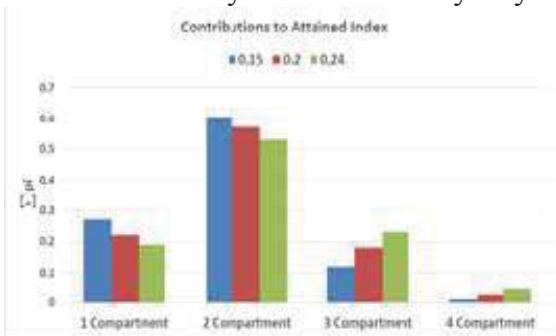


Figure 6 Contributions to attained index

For the probabilistic assessment the 0.24L damage length led to an attained index of $A=0.94$ for the North Atlantic and $A=0.90$ for the North Pacific Scenario. The 4 and 5 compartment cases now contribute a maximum of 0.05 to the attained index as opposed to approximately 0.01 for the 0.15L case.

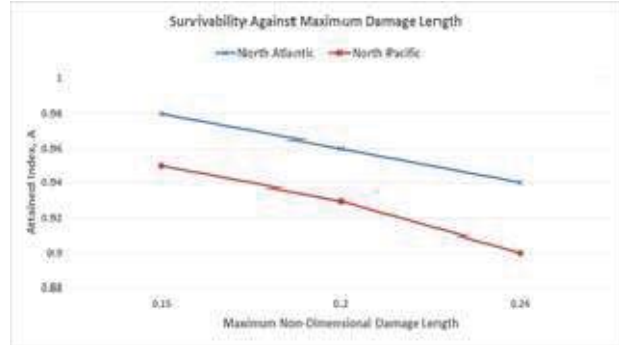


Figure 7 Survivability against max damage length

Figure 6 and 7 show the difference in contribution to the attained index for various damage cases and the effect on the attained index for each of the maximum damage lengths investigated.

Figure 8 illustrates the different contributions to the attained index for the frigate under consideration in the outlined probabilistic approach and also when considering IMO MSC.216 (82); both assessments are for a damage length of 0.24L.

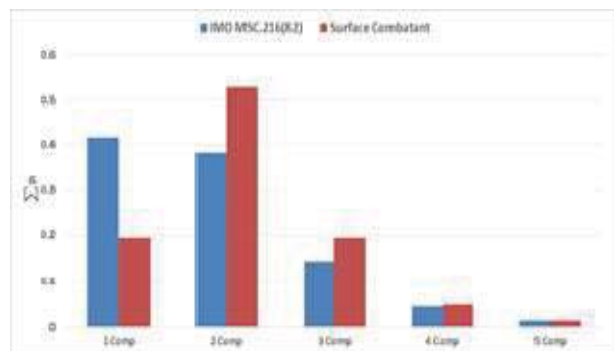


Figure 8 Comparison of damage length distributions

As a damage from a threat weapon will result in greater damage extent than from collision, there is a peak at two compartment damage as opposed to one compartment damage in the case of the linear distribution of SOLAS.



Although SOLAS considers damage lengths up to $0.24L_{bp}$, the use of the linear damage length distribution results in a more conservative estimate of the level of survivability. The linear distribution from SOLAS 2009 was applied and an attained index of $A=0.97$ was obtained for the North Atlantic and $A=0.94$ for the North Pacific. Using the log-normal distribution with the same maximum length of damage ($0.24L$) the values obtained were $A=0.94$ for the North Atlantic and $A=0.90$ for the North Pacific.

It is observed that the log-normal distribution is more practical for naval ships as it can accurately represent the extent of damage associated with weapon effects. The use of the log-normal distribution will increase the likelihood of occurrence of damage cases involving multiple adjacent zones, therefore resulting in a more accurate estimate of survivability.

6. CONCLUSION

The use of a probabilistic approach to assess the damage stability of a naval combatant can lead to a higher level of survivability. The use of the probabilistic assessment through the attained subdivision index allows a holistic approach to be taken to surface ship survivability. This allows ship's subdivision to be optimised for *minimum risk* (or *maximum Attained Index*) making survivability a distinct feature of the naval ship design and no longer a requirement. In addition, the use of more realistic operating conditions such as sea state at the time of damage will give the designer a better understanding of the damaged ship's performance and limitations.

The conducted study on the damage length margin for a naval ship shows that the length can be readily increased to more accurately represent damages reflecting possible weapon threats and without compromising the position of bulkheads. It illustrates that current naval

vessels are capable of surviving greater damage lengths than previously specified. Thus, altering the damage length distribution for naval ships appears to be fully justified, whereas the impact on design is not anticipated to be drastic. In any case, the length of damage can be more rationally refined, namely based on current weapon threats which a combatant may face in its life cycle, resulting in a more realistic representation of the ship's survivability.

7. REFERENCES

- Athanassoulis, G., & Skarsoulis, M. (1992). Wind and wave atlas of the North-Eastern Mediterranean Sea. NTUA-SMHL.
- Ball, R. E., & Calvano, C. N. (1994). Establishing the fundamentals of a surface ship Survivability Design Discipline. Naval Engineers Journal 106, 71-74.
- Bentley Systems. (2013). Maxsurf Marine Vessel Analysis and Design Software. Retrieved from <http://www.bentley.com/en-US/Products/Maxsurf/Marine+Vessel+Analysis+and+Design.htm>
- Boulougouris, E. K., & Papanikolaou, A. D. (2004). Optimisation of the Survivability of Naval Ships by Genetic Algorithms. 3rd Int. EuroConference of Computer Applications and Information technologies in the Maritime Industries.
- Boulougouris, E., & Papanikolaou, A. (2013). Risk-based design of naval combatants. Ocean Engineering 65, 49-61.
- Department of US Navy. (2002). DDS 079-1 Stability and Buoyancy of U.S Naval Surface Ships. Department of US Navy.
- Erkel, A. v., & Galle, L. F. (2003). TNO-PML Developments of Blast Resistant Doors and Walls. 8th International Marine Design Conference, (pp. 753-764). Athens.



- Ferreiro, L. D., & Stonehouse, M. H. (1991). A Comparative Study of US and UK Frigate Design. SNAME Transactions Vol. 99, 147-175.
- Harmsen, E., & Krikke, M. (2000). A probabilistic damage stability calculation method for naval vessels. 7th International Conference on Stability of Ships and Ocean Vehicles (STAB'00). Tasmania.
- Haveman, C., Parliament, J., Sokol, J., Swenson, J., & Wagner, T. (2006). Design of a Floating, Production, Storage, and Offloading Vessel for Operation in the South China Sea. Texas: Texas A&M University.
- IMO. (2007). MSC.1/Circ.1226 Interim Explanatory Notes to the Solas Chapter II-1 Subdivision and Damage Stability Regulations. IMO.
- Lee, W. T. (1995). Global Wave Statistics for Structural Design. Maryland: Naval Surface Warfare Center.
- MOD. (2010). MAP 01-024 Stability of Surface Ships part 1.
- NATO/PfP. (2004). NATO/PfP Working Paper on Small Ship Design (Unclassified). NATO.
- Perrault, D. E., Hughes, T., & Marshall, S. (2010). Naval ship stability guidelines: developing a shared vision for naval stability assessment. Trans. RINA. Inr. J Marit. Eng., 99-118.
- Przemieniecki, J. S. (1994). Mathematical Methods in Defence Analysis. American Institute of Aeronautics and Astronautics.
- Rawson, K. J., & Tupper, E. C. (2001). Basic Ship Theory Vol 2.
- Said, M. O. (1995). Theory and Practice of Total Ship Survivability for Ship Design. pp 191-203.
- Sarchin, T. H., & Goldberg, L. L. (1962). Stability and buoyancy Criteria for U.S. Naval Surface Ships.
- Surko, S. W. (1994). An Assessment of Current Warship Damaged Stability Criteria. Naval Engineers Journal, 120-131.
- UK MOD. (2013). DEFSTAN 02-900 Part 1.
- Walree, F. v., & Carette, N. (2011). Validation of time domain seakeeping codes for a destroyer hull form operating in steep stern-quartering seas. JNAOE, 9-19.
- Wendel, K. (1960). Die Wahrscheinlichkeit des Überstehens von Verletzungen. Journal of Ship Technology Research, 47-61.



Dynamic Stability Assessment of Naval Ships in Early-Stage Design

Heather A. Tomaszek, *Naval Surface Warfare Center Carderock Division*

heather.tomaszek@navy.mil

Christopher C. Bassler, *Naval Surface Warfare Center Carderock Division*

christopher.bassler@navy.mil

ABSTRACT

A method is currently under development at the International Maritime Organization (IMO) to assess dynamic stability susceptibility during early-stage ship design. The method is intended to provide a physics-based, preliminary analysis of relative risk for ship designs to dynamic stability phenomena, including parametric roll and surf-riding and broaching, with only minimal information about the ship design of interest for evaluation. The method uses a two-stage approach to determine the susceptibility to dynamic intact stability failure modes. This approach can be used to identify designs with increased susceptibility to dynamic stability behavior, which will then require a more detailed analysis and possibly the development of ship-specific operator guidance. Using the mature method developed specifically to assess parametric roll and surf-riding, and to demonstrate the robustness of the method, results for eight naval ship types are presented and discussed. These results were also used to establish an estimate of the criteria corresponding to the second threshold for a sample population of eight notional naval vessels.

Keywords: *Early-stage design, Dynamic Stability, Parametric Roll, Surf-riding / Broaching-to*

1. INTRODUCTION

The International Maritime Organization (IMO) is currently developing the second generation intact stability criteria - SGISC (IMO SDC 2/WP.4). The new criteria are focused on dynamic stability and have a multi-tiered structure. The first two tiers are susceptibility checks that are suitable for early stage ship design (Peters, et al. 2011). In early stage ship design many detailed parameters of a ship design are unknown. The method to evaluate these criteria relies on basic hull geometry defined by a table of offsets, design speed, and basic dimensions such as length, beam, and draft. The results of dynamic stability assessment provide additional information to the ship designer to aid in decision making for either down selection or design modification.

The criteria are being developed for ships covered by IMO instruments. The complex designs typically associated with naval ships differ from typical commercial vessels. To demonstrate the robustness of the criteria and the applicability to naval vessels, a notional naval fleet of eight ships was assessed using the susceptibility criteria from IMO SGISC. The benefits of early identification of dynamic stability failure susceptibilities in naval ship design are discussed. Further discussion of the mathematical models and criteria can be found in the references, and are discussed only briefly here.

Other IMO efforts on dynamic stability criteria include failures related to pure loss of stability, dead ship conditions and excessive accelerations. A study of methods for early-stage design evaluation of pure loss of stability of notional navy ships has been performed earlier by Belenky and Bassler (2010). This



paper can be seen as a continuation of those efforts.

2. PARAMETRIC ROLL

2.1 Physical Description

Periodic stability changes at certain frequencies resulting from the changing hull submergence while operating in waves causes the development of parametric roll. Increased stability from roll on the wave trough increases the restoring moment causing greater angles and increased roll rate. With stability decreasing as the ship is restored to upright, the ship rolls further to the opposite side due to the increased roll rate, see Figure 1 (SLF 54/3/3). The roll period during this phenomenon is generally about two times the wave period.

2.2 Sample Notional Naval Ship Calculations

The level 1 susceptibility check uses the Mathieu equation to check if both the frequency is within the necessary range and the magnitude of the stability change is above the threshold (Belenky, et al. 2011). The level 1 assessment accounts for bilge keels. The calculations were done following the requirement identified in Annex 2 of SDC 2.WP.4.

The level 2 susceptibility check increases the fidelity by accounting for certain aspects of irregular waves. The first check accounts for the possibility of encountering waves of different lengths. The second check accounts for roll damping and maximum roll angle during parametric roll. The standard for the criterion used in the level 2 calculations was 0.06 (Annex 2 of SDC 2/WP.4).

Calculations generally follow Annex 3 of SDC 1/INF.8. A wave scatter diagram from IACS Recommendation 34 was used as a data source for wave cases. Representative wave

characteristics were calculated using Grimm Effective Wave as described in the document referred to above. As a result, the length of the representative wave equals to ship length. The height of the representative wave depends on spectral characteristics and roughly reflects the likelihood of encountering a wave of that length in a given sea conditions. Roll damping was calculated with a simplified Ikeda method as described in Annex 3 SDC 1/INF.8.

Three options to apply the second check of the level 2 criteria are considered in the calculations:

- Option 1. Numerical solution of a 1 degree of freedom (DOF) for the equation of roll motion, using the interpolated GZ curve defined by the user (as in Annex 22 of SDC-2/INF.10)
- Option 2. The GZ curve is fitted with a 5th order polynomial, then the maximum roll angle is evaluated by the averaging method as described in paragraph 2.6 of Annex 3 of SDC 1/INF.8.
- Option 3. The GZ curve is fitted with a 5th order polynomial, but the maximum roll angle is found by numerical solution of 1 DOF for the equation of roll motion (the result is expected to be close to the result in option 2)

Results are shown in Table 1. All calculations assume the ship is at the storm draft loading condition.

2.3 Discussion of Results

Several of the results are consistent with expected results. Where the second level shows susceptibility, the first level does as well. The level 1 criterion indicates susceptibility for more ships. This provides a conservative filtering method to identify ships with potential susceptibility to this dynamic stability failure mode. Some inconsistencies among the methods are discussed below.

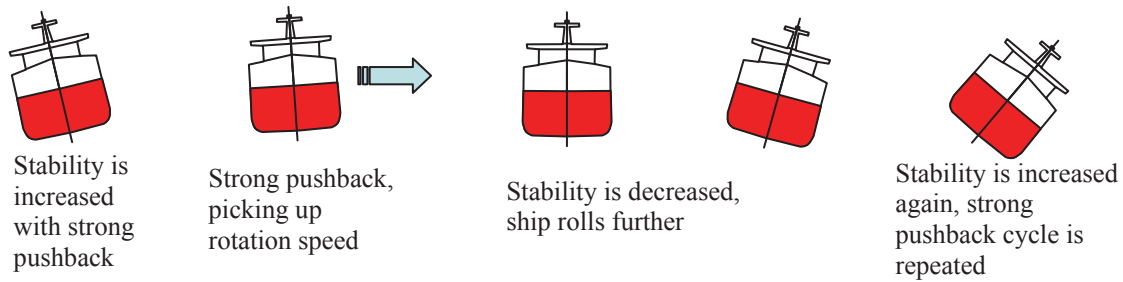


Figure 1. Development of Parametric Roll Resonance (Parametric Roll)

Table 1 Results of Susceptibility Check on Notional Navy Ships for Parametric Roll

Notional Ship	L, m	GM	Vs, kts	Level 1			Level 2				
				Criterion	Standard	Y/N	Criterion Check 1	Criterion Check 2 Option 1	Criterion Check 2 Option 2	Criterion Check 2 Option 3	Y/N
Amphib	200	4.6	20	0.390	0.297	Y	0	0	0.1385	0	N
Carrier	317	3.0	30	0.287	0.334	N	0	0.0224	0.1031	0	N
Cruiser	161	0.8	30	0.401	0.386	Y	0	0.0015	0.0008	0.0011	N
Destroyer	142	1.4	30	0.599	0.378	Y	0	0.0007	0.0003	0.0004	N
Frigate	127	1.1	30	0.459	0.378	Y	0	0.0003	0.0003	0.0003	N
Minehunter	53	4.9	20	0.125	0.474	N	0	0	0	0	N
Patrol Craft	48	1.2	20	0.312	0.578	N	0	0	0	0	N
Small Combatant	98	1.5	30	0.696	0.170	Y	0.5634	0	0	0	Y

Two of the options to check parametric roll susceptibility rely on an approximated GZ curve, so the approximation method should match well with the calculated curve. Two examples are shown below where the approximated curve closely mimics the calculated curve past the useful range to 25~30 degrees of heel before deviating substantially (see Figures 2, 3). Because the offsets of the ship must be known for the calculation the preferred method for naval ship designs is to use actual GZ curve, due to the sensitivity of the hull forms the fitted curve may not always be accurate.

Additionally for the amphibious ship and the carrier, ship specific data indicates that the two ships would not be susceptible to parametric roll. The geometry of these ships indicates that the change in stability would not be significant enough along the length of the ship to produce parametric roll. The simplified Ikeda method for predicting roll

damping may be under-predicting the damping. Similarly, the small combatant indicates a very low standard on the level 1 check. Hard chines on the small combatant may provide greater damping than estimated. The under-predicted damping indicates a susceptibility that isn't supported by the specific information of the ships. Consideration to the applicability of the Ikeda method for roll damping should be made by the designer. Additional research for a more accurate prediction of damping in naval ships is still needed.

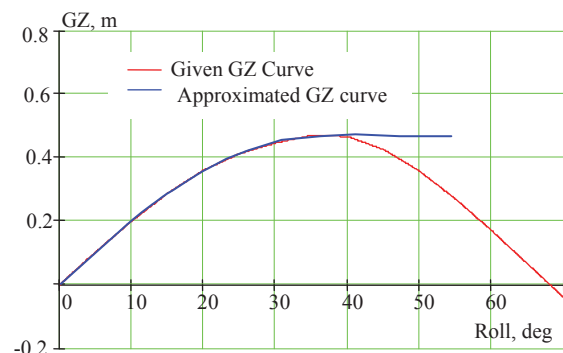


Figure 2. GZ Curve of a Notional Cruiser

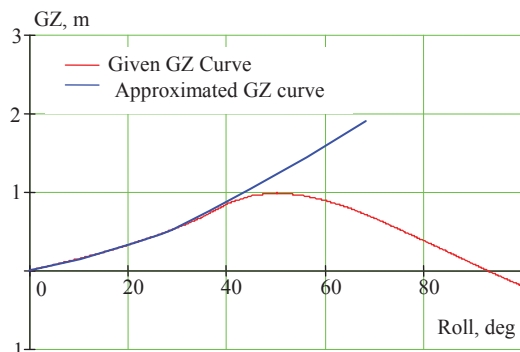


Figure 3. GZ Curve of a Notional Patrol Craft

3. SURF-RIDING AND BROACHING-TO

3.1 Physical Description of Broaching-to

Broaching-to is an operational phenomenon, which results in an uncontrolled turn, which is associated with unsuccessful efforts to reverse direction with maximum steering to the opposite direction. The result of a broaching-to event is often an excessive heel angle resulting from the sharp turn. This excessive heeling of the ship may cause a ship to sustain damage or even capsize. Surf-riding precedes the most common case of broaching-to. As the calculation of likelihood of surf-riding in early stages of design is easier than broaching-to, the susceptibility criteria use probability of surf-riding (Belenky, et al. 2011).

3.2 Sample Naval Ship Calculations

The level 1 susceptibility check assumes the possibility of surf-riding occurs when Froude number is greater than or equal to 0.3, while ship length is less than 200 m. If the length of the ship more than 200 m, then the ship is not considered susceptible even if Froude number exceeds 0.3 (Annex 3 of SDC 2/WP.4). Length is considered due to surf-riding being caused by steep waves with

the length equal to about ship length. Encountering a long and steep wave is not very likely.

The level 2 criterion is based on the critical Froude number. If the critical Froude number is exceeded, surf-riding occurs from any location on the wave and with any initial speed. Melnikov's method is applied to calculate the critical Froude number as described in Annex 35 of SDC 2/INF.10; theoretical background can be found in (Spyrou, 2006). Melnikov's analysis is applied to a single wave; the probability of encounter of the wave where the critical Froude number is exceeded by the service Froude number is associated with the probability of the ship surf-riding. The standard criterion used in the level 2 calculations was 0.005 (Annex 3 of SDC 2/WP.4).

Two options for the method of calculation were used in determining the probability surf-riding. Option 1 uses a cubic polynomial fit for resistance in calm water, while option 2 uses a 5th degree polynomial fit.

Results are shown in Table 2. All calculations assume the ship is at the storm draft loading condition.

3.3 Discussion of Results

There was consistency among the criterion. Additionally, the calculations were consistent with what a designer would expect. Relatively short, fast ships are most susceptible to surf-riding and broaching-to. Short steep waves are more likely to occur naturally than long steep waves. Because surf-riding and broaching-to is most likely to occur on steep waves where the ship is similar in speed and length to the wave, shorter ships with significant speed are intuitively more susceptible to surf-riding.



Table 2 Results of Susceptibility Check on Notional Navy Ships on Surf-riding /Broaching-to

Notional Ship	L, m	Vs, kts	Fn	Criterion, option 1	Criterion, option 2	Y/N
Amphib	200	20	0.23	0	0	N
Carrier	317	30	0.28	0.0005	0	N
Cruiser	161	30	0.39	0.0186	0.0183	Y
Destroyer	142	30	0.41	0.0278	0.0276	Y
Frigate	127	30	0.44	0.0386	0.0386	Y
Minehunter	53	20	0.45	0.1094	0.1094	Y
Patrol Craft	48	20	0.47	0.1090	0.1090	Y
Small Combatant	98	30	0.50	0.0640	0.0640	Y

4. DESIGN CHANGES OR OPERATIONAL GUIDANCE

As with all early stage design calculations, the accuracy of the susceptibility assessments here are not significantly high, because of the minimal information available to make the assessment. The ship designer must take into account the limited accuracy of the calculation when making decisions to modify hull geometry or make recommendations for operational limitations guidance.

The information gained from the above calculations in early stage design can lead the ship designer to either modify the hull geometry design to reduce the susceptibility to parametric roll or broaching, or develop operational guidance to avoid parametric roll or broaching events. In some cases other ship design requirements may outweigh the risk of stability failure events and the hull geometry is not able to be changed. Other considerations for hull geometry can be signature, hydrodynamic, or weapons systems related. In the case that signature reduction or speed will be compromised to reduce the risk of dynamic stability failure, often the ship designer will assume the risk in favor of a more capable warship in the safe operating environment. If the risk of dynamic stability is identified but the hull geometry is unable to be modified the early stage design calculations still provide significant value to the ship designer.

The ship designer is able to identify early on an operational limitation of the ship in certain seaways. From a naval fleet perspective, the early identification of operational limitation offers a gap which may be filled by several other ships in the fleet already.

If greater operational area is a higher priority for a certain class of naval ship than speed or signature reduction, the susceptibility assessment allows the designer to modify geometry early in the design when modifications are most cost effective. In cases where these susceptibilities may not be identified until much later in the design process through computational fluid dynamics modelling or model testing, the design may be too mature to allow for significant modifications. Later designs changes in hull geometry can lead to changes in other aspects of the design leading to schedule delays.

5. CONCLUSIONS

Not all methods used in commercial ship designs are viable for assessing naval ship designs. Use of actual GZ curve is preferable over the fitted GZ curve, unless, there are some substantial benefits like use of closed-form solutions. The simplified Ikeda method for roll damping is also may be not applicable to all types of Naval ships.



While there are some limitations, the sample calculations shown indicate that provide a realistic susceptibility checks for naval ship designs. The accuracy of the assessment should be considered in relation to the accuracy and fidelity of the available information to be input to the models. The assessments discussed provide an advantage of additional decision making information to early stage naval ship designers.

6. ACKNOWLEDGMENTS

Portions of the dynamic stability criteria research was sponsored by the Office of Naval Research under Dr. Ki-Han Kim.

The authors of this paper would like to acknowledge all those involved in the development of the criteria used in this assessment, especially Dr. Vadim Belenky (NSWCCD). The second author would like to express his gratitude to Prof. Kostas Spyrou (National Technical University of Athens, Greece) for many fruitful discussions on dynamic stability.

7. REFERENCES

- Belenky, V. and Bassler, C. 2010, "Procedures for Early-Stage Naval Ship Design Evaluation of Dynamic Stability: Influence of the Wave Crest," Naval Engineers Journal, 122(2), pp.93-106
- Belenky, V., Bassler, C. C. and Spyrou, K. J. (2011), "Development of Second Generation Intact Stability Criteria," Hydromechanics Dept. Report, NSWCCD-50-TR-2011/065, December
- IMO SDC 2/INF.10, 2014 Second Generation Intact Stability Criteria. Information Collected by Correspondence Group on Intact Stability, Submitted by Japan, London, UK
- IMO SDC 2/WP.4, 2015, Development of
- Second Generation Intact Stability Criteria. Report of the Working Group, London, UK.
- IMO SDC 1/INF.8, 2013 Second Generation Intact Stability Criteria. Information Collected by Correspondence Group on Intact Stability, Submitted by Japan, London, UK
- IMO SLF 54/3/3 2011 Summary of Research into Stability Failures Modes and associated Criteria Development, London, UK.
- Peters, W., Belenky, V., Bassler C., Spyrou, K., Umeda, N., Bulian, G. and B. Altmayer, 2011 "The Second Generation of Intact Stability Criteria An Overview of Development", SNAME Trans. Vol. 119.
- Spyrou, K. J., 2006 Asymmetric Surging of Ships in Following Seas and its Repercussion for Safety. Nonlinear Dynamics, Vol 43, pp. 149–172.

Session 12.2 – DECISION SUPPORT

**Prediction of Survivability for Decision Support in Ship Flooding
Emergency**

**Crew Comfort Investigation for Vertical and Lateral Responses of a
Container Ship**

**Novel Statistical Prediction on Parametric Roll Resonance by Using
Onboard Monitoring Data for Officers**

**Target Ship Design and Features of Navigation for Motion
Stabilization and High Propulsion in Strong Storms and Icing**

This page is intentionally left blank



Prediction of Survivability for Decision Support in Ship Flooding Emergency

Pekka Ruponen *NAPA Ltd* pekka.ruponen@napa.fi

Daniel Lindroth, *NAPA Ltd* daniel.lindroth@napa.fi

Petri Pennanen, *NAPA Ltd* petri.pennanen@napa.fi

ABSTRACT

Several recent flooding emergencies on passenger ships have pointed out the need to quickly get a better assessment of the survivability onboard a damaged ship. The development of time-domain flooding prediction methods has enabled advanced decision support tools. In this paper a method for assessment of the survivability of the people onboard a damaged ship is presented. The level sensor data is used to detect the breach and calculate progressive flooding in time-domain. The predictions are constantly updated to increase the reliability of the results. The method is tested with two realistic damage scenarios for a large cruise ship.

Keywords: *damage stability, flooding simulation, decision support*

1. INTRODUCTION

Several recent flooding emergencies concerning passenger ships, such as the Costa Concordia incident, have clearly pointed out the need to quickly get an accurate assessment of the survivability onboard a damaged ship. It is essential for the crew of the ship to know the extent of the damage and how the situation will develop. If the ship will survive the damage with sufficient reserve stability, the ship is likely the safest place for the passengers and the crew. On the other hand, if the ship is expected to capsize or sink, evacuation and abandonment of the ship should be started as soon as possible. Every minute counts when a large number of persons needs to be evacuated in a safe manner. In this context the term survivability is associated with the survivability of the people onboard the damaged ship, not the survivability of the ship itself, as it is in the damage stability calculations in ship design.

Several different methods have been presented for decision support for flooding

emergencies onboard a damaged ship. *Ölcer and Majumder (2006)* presented a method based on pre-calculated damage cases. *Jasionowski (2011)* presented a method for assessing the safety level of an intact ship, based on increased vulnerability due to open watertight doors. A fast time-domain flooding prediction method was introduced by *Ruponen et al. (2012)*, and more recently, also *Varela et al. (2014)* have described a tool for decision support for damaged ships.

Recent developments in the time-domain prediction of progressive flooding now enable a new kind of decision support system that produces more detailed information on the damage case. The actual loading condition and flood level sensors can provide input data for predicting the progress of flooding. Yet the interpretation of the results is a challenge. One major question that remains is how to assess the survivability of the people onboard a damaged ship, even when the actual damage case is known with a fairly good accuracy.

Spanos and Papanikolaou (2014) have concluded that for actual damage incidents a reliable assessment onboard is still a technical



challenge as the identification of the damage extent and related survivability suffers from uncertainty. This paper describes a new approach, where information from systems already available is utilized for fast time-domain flooding predictions. The results are continuously updated in an attempt to improve the accuracy. As the flooding progresses, more information is collected by the level sensors that can be used to update the breach definitions for the calculations. This approach will decrease the uncertainty in the results.

The key factors that affect the survivability are reviewed. These include the extent of flooding, stability and possibility for an orderly evacuation and abandonment. Based on these, a method for assessing the survivability on the basis of a time-domain flooding prediction is presented. Finally, the developed method is tested with a large passenger ship design and two realistic damage scenarios.

2. FLOODING PREDICTION

2.1 Progressive Flooding

Over the past two decades, several time-domain flooding simulation tools have been developed and successfully validated. Most of these are based on an application of Bernoulli's equation. However, for use onboard a damaged ship, the computational performance is of utmost importance. This combined with the fact that the available input data is never fully accurate, justifies the use of a more approximate and robust method with good computational performance.

In this study a time-domain simulation method, *Ruponen (2007)*, is used with a long time step of 30 s. The implicit time integration of the pressure-correction method ensures numerical stability, even with such a long time step. However, this means that the results are not as time-accurate, as they would be with a shorter time step. Consequently, the word

“prediction” is used instead of “simulation”. The applied method has been validated also against full-scale measurements, *Ruponen et al. (2010)*. Updating the flooding predictions at certain intervals will provide better information of the situation at hand. The actual measured floodwater is added to the initial condition. For rooms without level sensors, the volumes obtained from the previous prediction can be used as input for the updated prediction.

2.2 Ship Motions

Ship motions are considered to be quasi-static, so that at each time step a static floating position of the ship is calculated based on the distribution of floodwater inside the ship. It is also assumed that the sea is calm. This simplification allows for purely deterministic approach, based on the real flooding scenario. On the other hand, the increased flooding due to waves is disregarded. However, the HARDER statistics indicate that over 90% of the collision damages occur in a sea state, where the significant wave height is less than 2.0 m, *Tagg and Tuzcu (2003)*. For a large passenger ship with a dense internal subdivision, the effect of waves on the flooding process can be considered as minimal.

2.3 Ship Model

The flooding prediction requires a detailed 3D model of the rooms and openings. For non-watertight doors, additional parameters are needed for modelling leakage or collapsing due to floodwater pressure. Results from the FLOODSTAND, *IMO SLF54/INF.8/Rev.1*, can here be used as the best available approximation for this data.

The status of the watertight (WT) doors (open/closed) is obtained from the automation system. For most of the non-watertight doors this information may not be available. The cold room doors can be assumed as closed, while fire doors to staircases and along the service

corridor may be open. In order to achieve some level of conservativeness, all fire doors are assumed to be open, unless the status is available from the automation system.

3. BREACH DETECTION

A breach in the hull of the ship is detected by the floodwater level sensors. Both the size and the location of the breach need to be estimated based on this sensor data. Thus every WT compartment should have sensors on all deck levels on both sides of the ship, *IMO SDC2 INF.6*. Problems related to breach detection has previously been studied by *Penttilä and Ruponen (2010)*.

The rooms, where floodwater is initially detected within the first 30...60 s, are considered to be breached. Based on the measured water level rate and the floating position of the ship, a rough approximation of the breach size is done. If the room is limited to the hull surface the breach is modelled on the side, Fig. 1. Otherwise the breach is placed on the bottom of the room.

The ship is assumed to heel towards the breached side, and the area of the breach is approximated based on Bernoulli's equation:

$$A \approx \frac{\mu S \frac{dH}{dt}}{C_d \sqrt{2g(T-H)}} \quad (1)$$

where H is floodwater level, S is the surface area of the room corresponding the level, μ is the permeability, g is gravitational acceleration, T is the draft of the ship and t is time. A constant discharge coefficient $C_d = 0.6$ can be used.

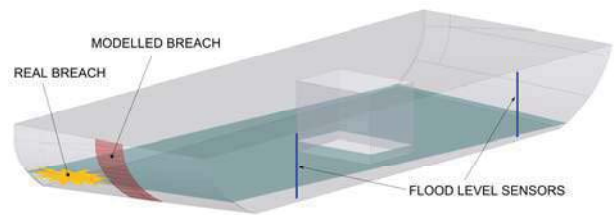


Figure 1: Approximated breach based on level sensor data

For an updated flooding prediction, the original breach is by default unchanged. Other flooded rooms are checked against the result of the previous prediction. If the room is not predicted to be flooded, the water may come from a previously undetected breach or through unknown progressive flooding (e.g. broken pipelines). For the updated prediction, these rooms are also modelled as breached in addition to the original breaches, Fig. 2.

The detected breaches and the door statuses from the automation system form the basis for the time-domain flooding prediction. The main challenge is to separate progressive flooding through the modelled openings from the flooding through breaches in the hull. This is essential since too many breaches will result in too fast flooding.

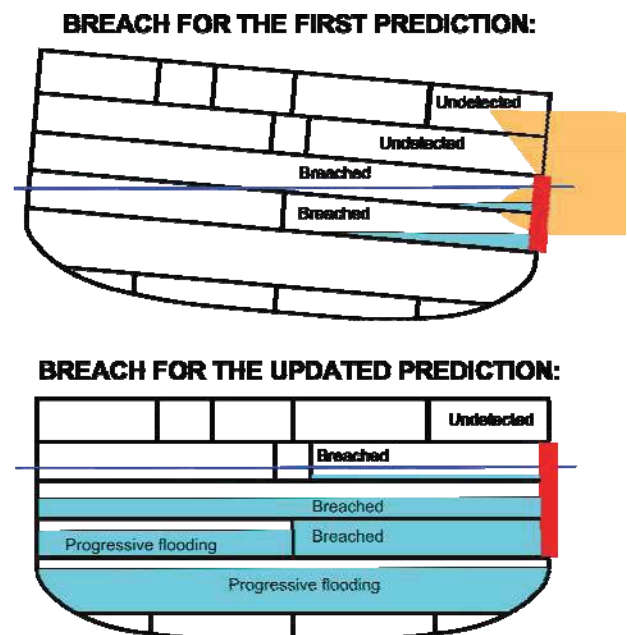


Figure 2: Update of breach for a new prediction

4. ASSESSMENT OF SURVIVABILITY

4.1 Methodology

In this study the survivability level is evaluated with the following equation:

$$F_{tot} = \min(F_{ext}, F_{stab}, F_{evac}) \quad (2)$$

The sub factors for flooding extent, stability and evacuation (F_{ext} , F_{stab} and F_{evac}) are presented in detail in the following sections. Each of them is a function of time, and the applied value is the minimum during a time window extending from the current time to the approximate maximum required evacuation time, see Fig. 3.

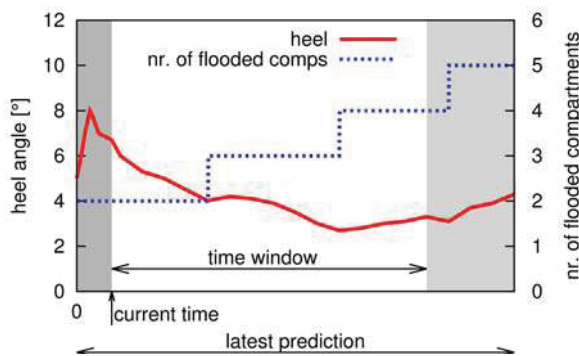


Figure 3: Time window for evaluation of the survivability level from the prediction results

4.2 Floating Position

Heel angle is considered to be the most important factor that affects the survivability level. At large heel angles launching of the lifeboats becomes impossible. Moreover, large heeling also increases the required evacuation time. Consequently, the predicted development of the heel is a primary information to the master for decision making. However, in the presented approach heel angle is only considered indirectly through its effects on stability and evacuation.

4.3 Damage Extent

The new probabilistic damage stability regulations do not set any specific requirements on how many watertight compartments can be flooded without a risk of sinking or capsizing. Despite of this, it is considered to be of the utmost importance to clearly identify how many WT compartments are flooded, since this is vital information for the decision making. If water is detected on the bulkhead deck, or at the time when floodwater is predicted to reach the bulkhead deck, the survivability level is significantly decreased. The reason for this is the increased risk of progressive flooding to undamaged WT compartments. In this study, the following approach is used:

$$F_{ext} = 1.0 \quad \text{when } N_f \leq N_1$$

$$F_{ext} = C \cdot \frac{N_0 - N_f}{N_0 - N_1} \quad \text{when } N_1 < N_f < N_0 \quad (3)$$

$$F_{ext} = 0.0 \quad \text{when } N_f \geq N_0$$

where N_f is the number of flooded WT compartments during the time window (see Fig. 3), i.e. the flooding extent at the end of prediction. N_1 is the number of compartments that can be flooded without significant risk and N_0 is the number of flooded compartments when the survivability level is set to zero. The additional coefficient C is 0.5 if the bulkhead deck is flooded, otherwise 1.0. The function is illustrated in Fig. 4.

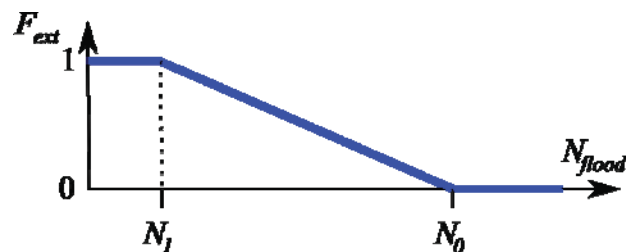


Figure 4: Flooding extent factor

In the present study $N_1 = 1$ and $N_0 = 6$ are used. However, N_0 should also be considered to depend on the size of the ship, i.e. the total number of WT compartments or the length of the ship. With $N_1 = 1$ it is ensured that $F_{tot} = 1.0$ only for one compartment flooding cases.

4.4 Stability

Even with a small heel angle the risk of capsizing can be significant if the stability of the ship is not good enough. The *s*-factor in SOLAS II-1 Part II-1 Regulation 7 is applied:

$$s_{final} = K \cdot \left(\frac{GZ_{max}}{0.12} \cdot \frac{range}{16} \right)^{\frac{1}{4}} \quad (4)$$

where GZ_{max} is limited to 0.12 m and *range* to 16°. The effect of the heel angle ϕ is accounted with the coefficient:

$$K = \sqrt{\frac{15^\circ - \phi}{15^\circ - 7^\circ}} \quad (5)$$

when the heeling angle is between 7° and 15°. If the heeling exceeds 15° the effective *s*-factor is taken as zero.

The *range* is limited to the angle where the first unprotected opening is immersed, Fig. 5. Only real unprotected openings above the bulkhead deck should be considered in order to avoid too conservative approach that limits the reserve buoyancy of the hull. On the other hand, if no limitation of the range is used, the results could be too optimistic. This approach also allows for a simple inclusion of the external heeling moments through the factor:

$$s_{mom} = \min\left(\frac{(GZ_{max} - 0.04) \cdot \Delta}{M_{heel}}, 1.0\right) \quad (6)$$

where Δ is the intact displacement of the loading condition and M_{heel} is the maximum external heeling moment caused either by crowding of passengers, launching of survival craft or wind. In the present study the SOLAS wind pressure is applied.

The stability factor in the survivability assessment is taken as the smallest value during the time window t_{window} (see Fig. 3):

$$F_{stab} = \min(s_{final}(t_i) \cdot s_{mom}(t_i)), t_i \in t_{window} \quad (7)$$

Although in SOLAS there is a separate, less stringent, *s*-factor formula for intermediate flooding stages, it is believed that the application of the *s*-final formula is more suitable for the assessment of damage stability onboard a damaged ship, since the flooding process can be slow.

For better computational performance, the *s*-factor does not need to be evaluated at every time step, but frequently enough, e.g. every 5 min. Still, for each intermediate time step without the stability curve calculated, the effect of the heeling angle can still be taken into account through the *K*-factor, eq. (5).

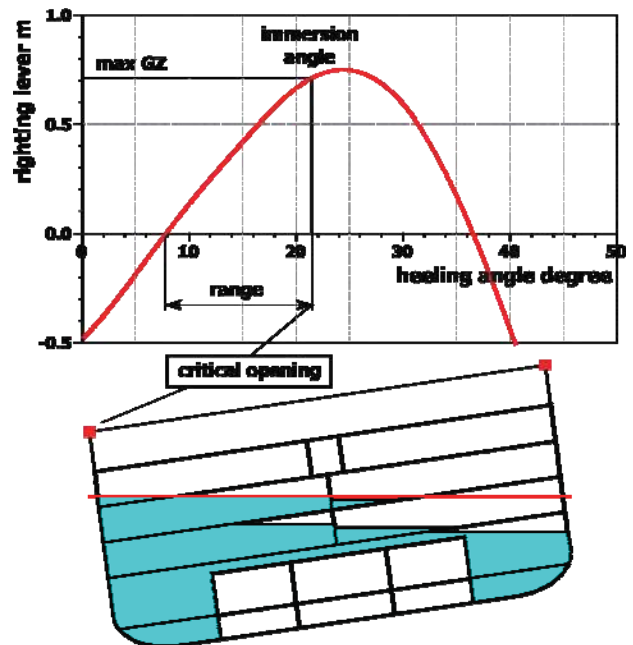


Figure 5: Effect of unprotected openings above the bulkhead deck on the GZ curve

For the survivability assessment onboard a damaged ship, the calculation of stability is somewhat different since the flooding process still continues. The traditional approach with the lost buoyancy method cannot be applied. Instead, the volumes of floodwater in the flooded rooms are kept constant for the calculation of the GZ curve. However, contrary to the added weight method, a constant displacement is used. With this approach also the so-called multiple free surface effect, see Fig. 5, is properly taken into account in the intermediate phases of flooding.

4.5 Evacuation Time

A key factor for evaluation of the survivability is the relation between the required evacuation time T_R and available evacuation time T_A . The following simple formula, providing some safety margin, is applied:

$$F_{evac} = 1.0 \quad \text{when } T_R/T_A \leq R_{evac}$$

$$F_{evac} = \frac{\left(1 - \frac{T_R}{T_A}\right)}{1 - R_{evac}} \quad \text{when } R_{evac} < T_R/T_A < 1.0 \quad (8)$$

$$F_{evac} = 0.0 \quad \text{when } T_R/T_A \geq 1.0$$

This function is illustrated in Fig 6. The applied critical ratio of evacuation times was $R_{evac} = 0.75$. The available time is limited by maximum allowed heel of 15° .

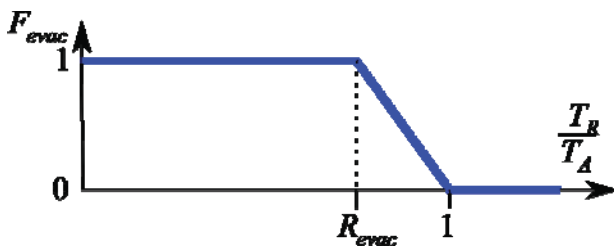


Figure 6: Evacuation time factor

The *IMO MSC.1/Circ.1238* gives the required evacuation time as 80 min for a passenger ship with more than three vertical fire zones. In the absence of more accurate data this value can be used as the best approximation.

Adverse conditions, such as extensive heel, will increase the required evacuation time. The simplest approach is to integrate over the predicted development of heel angle:

$$\int_0^{T_R} r(\phi(\tau)) d\tau = T_0 \quad (9)$$

where $r(\phi)$ is the reduction factor due to the heel/trim angle and T_0 is the required evacuation time at zero heel and trim. The latter can also include the time of the day and other factors such as the number of passengers

onboard. *Bles et al. (2002)* have concluded that the walking speed is linearly decreased with an increasing heel angle. In the presented calculations, it is assumed that the reduction factor is 0.5 at a heel angle of 20° . This is somewhat more conservative than in previous studies, *Meyer-König et al. (2005)*, but even more radical decrease was initially presented by *Vassalos et al. (2002)*, Fig. 7.

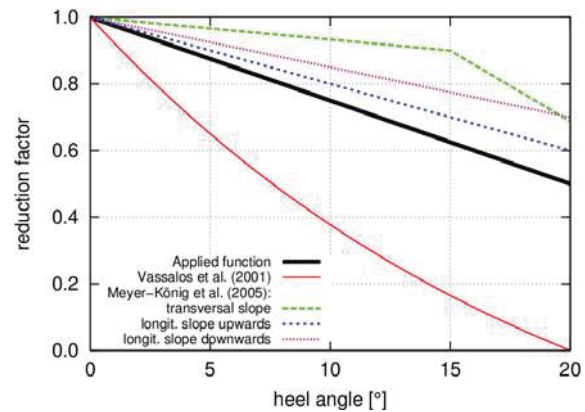


Figure 7: Reduction factor due to heel angle

4.6 Survivability Level

The vessel TRIAGE categorization¹ can be used to present the survivability level with color codes. This is very important in communication with the MRCC (Maritime Rescue Coordination Centre). A similar three-level categorization for stability of a damaged ship was presented by *Lee et al. (2005)*. The present approach is shown in Table 1. The limit between yellow and red was set on the basis of equation (5), corresponding to a heel angle of 10° . Also eq. (3) results in $F_{ext} = 0.8$ when flooding is limited to two compartments.

¹ <http://www.raja.fi/vesseltrriage>

Table 1: Color coding for survivability level

Color	Description	<i>F</i>
green	<ul style="list-style-type: none"> • flooding is limited • ship is stable enough • orderly evacuation can be done 	1.0
yellow	<ul style="list-style-type: none"> • ship is still safe but flooding is extensive • notable heeling can occur • orderly evacuation can be done 	≥ 0.8 & < 1.0
red	<ul style="list-style-type: none"> • very extensive flooding • progressive flooding to undamaged WT compartments • very large heel angles • orderly evacuation may not be possible 	< 0.8
black	<ul style="list-style-type: none"> • ship has capsized or sunk 	-

5. TEST CASES

5.1 Testing Methodology

The 125 000 GT large cruise ship design, *Kujanpää and Routi (2009)*, developed in the FLOODSTAND project, is used. The actual breach geometry was first modelled, and the damage scenarios were calculated using an accurate time-domain flooding simulation, *Ruponen (2007)*, with a short time step of 2.0 s. The simulation results were then used to generate the level sensor data in the flooded rooms.

Total of 292 rooms, including the tanks, were modelled, as well as 313 internal openings, Fig. 8. A typical loading condition with GM_0 of 2.72 m, draft of 8.45 m and small bow trim of 0.05 m was used as an initial intact condition.

All cold room doors and WT doors were closed. 169 of the 227 fire doors were open. These open doors were located either in the passenger areas on Deck 5 or in locations where the crew frequently passes the door. Random variation, based on the Raleigh distribution, was applied to the leaking and collapsing parameters of the non-watertight

doors in the accurate simulations of the reference data. In the flooding predictions the standard values were used.

The ship was considered to be equipped with 123 level sensors in the dry spaces, following the guidelines provided in *IMO SDC2/INF.6*. This represents 66 % of the rooms below the bulkhead deck and 50 % of the rooms on the bulkhead deck.

The first flooding prediction and analysis of the survivability level is done by using the sensor data from the first 60 s after the damage. The results are then updated by performing new predictions with a measured floodwater volumes as input for rooms with a level sensor. For the rooms without a sensor, the volumes of floodwater from the previous prediction were used as an initial condition. The predictions were repeated at the interval of 5...10 min. Calculation time for each prediction was about 2 min.

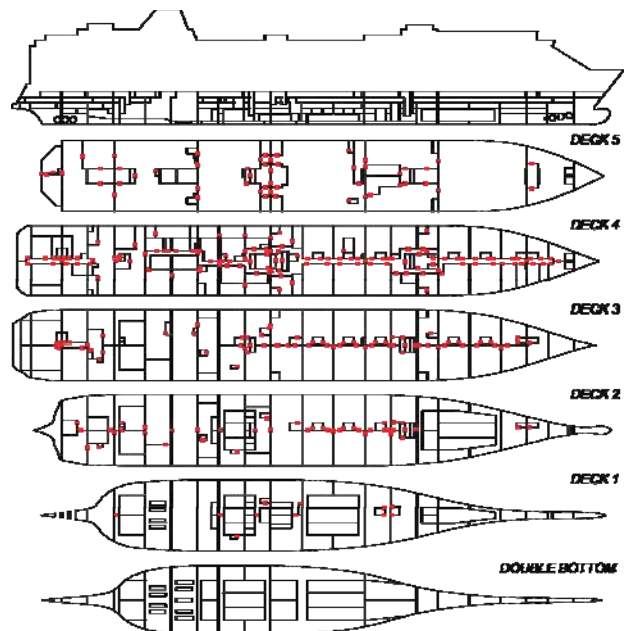


Figure 8: Modelled room arrangement and openings for the studied large passenger ship

5.2 Extensive Side Grounding Damage

This damage scenario is similar to the Costa Concordia accident. The grounding causes a 61

m long very narrow breach on the starboard side of the ship about 6 m below the sea level, Fig. 9. The damage extends over six WT compartments, including both engine rooms. Also part of the double bottom is breached.

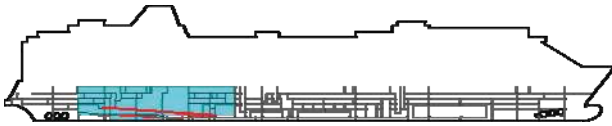


Figure 9: Damage case for extensive side grounding

The damage is so extensive that the bulkhead deck is flooded within 32 min, and water progresses also to undamaged WT compartments. In the reference simulation the ship capsizes after 3 h. The predictions indicate somewhat faster flooding, where the critical heel angle of 15° is achieved in about 2 h after the damage, Fig. 10. By this time there is already floodwater in nine WT compartments. The predictions assume that all A-class fire doors are open, whereas in reality the closed doors slow down the progress of floodwater, especially on the bulkhead deck. Thus also in the updated predictions the flooding rates are immediately somewhat faster than measured, Fig. 11. Consequently, the updated predictions indicate slightly faster time-to-capsize.

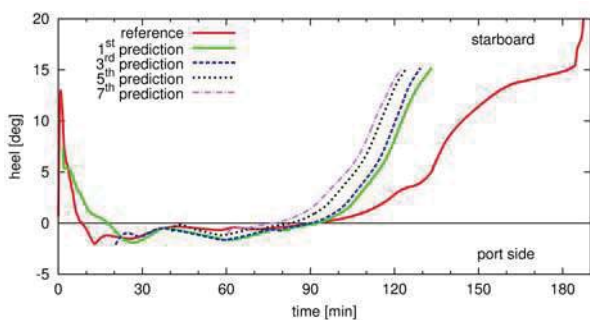


Figure 10: Comparison of heel angle for the initial and updated predictions against the simulated reference result

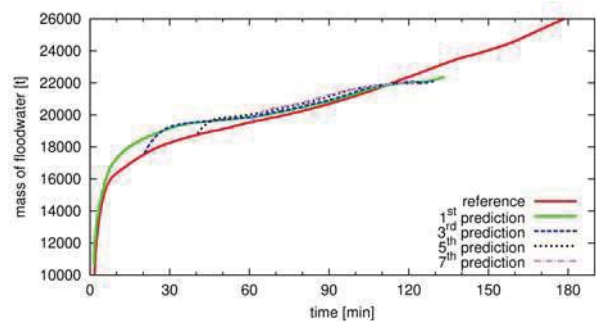


Figure 11: Comparison of the total mass of floodwater

Due to the very extensive damage, the survivability level is very poor. The color code is red (see Table 1) instantly since $F_{ext} = 0$. From the start, the prediction results provide important information to the crew that evacuation needs to be started immediately after the initial transient heeling has equalized. For a time frame of about 90 min the heeling is predicted to be less than 5°. And since the required evacuation time is about 85 min, there should be just enough time for orderly evacuation and abandonment before the ship is predicted to capsize.

5.3 Collision Damage

The second scenario is a typical collision damage, breaking two WT compartments. The breach extends above the waterline, but it is vertically limited so that the double bottom remains intact. Here however, one transverse bulkhead is not fully watertight, and also a third compartment is eventually flooded. This is accounted for in the reference simulation results by modelling a small additional internal opening in the bulkhead, Fig. 12.

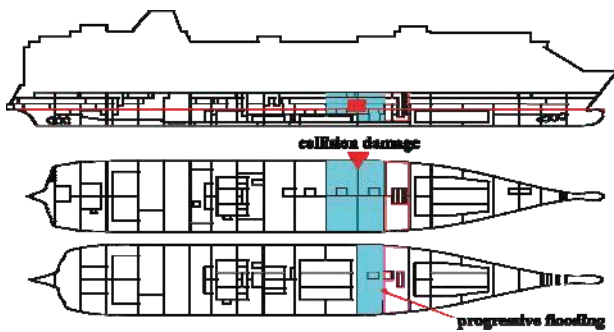


Figure 12: Collision damage case with progressive flooding

The first prediction that is started 60 s after the damage properly estimates the equalization of the initial heel towards the damaged side, Fig. 13. The predicted survivability level is fairly good with only the two damaged compartments rapidly filled up with water. The flooding extent factor is $F_{ext} = 0.8$, corresponding to a yellow color code, Table 1. Thus the initial result is too optimistic when compared to the reference simulation results for total amount of floodwater, Fig. 14.

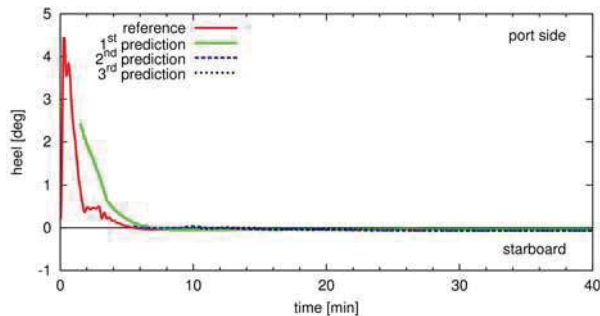


Figure 13: Comparison of initial and updated prediction against the simulated reference result

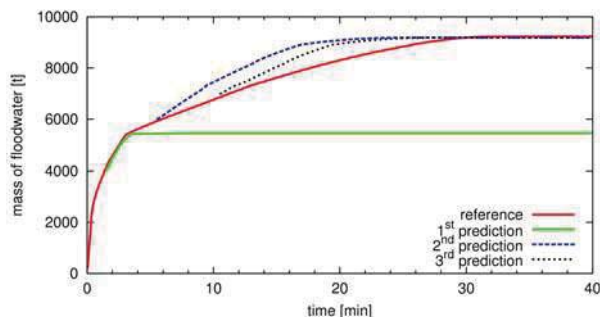


Figure 14: Comparison of the total mass of floodwater for collision damage

The updated prediction, starting 5 min later, accounts for the progressive flooding through

the WT bulkhead and results in the same equilibrium as the reference result, Figs. 13 and 14. Now only the time-to-flood is somewhat shorter. The origin of the floodwater in the third compartment remains unknown, but an additional breach to one room is modelled, see Fig. 15.

The increased flooding extent results in $F_{ext} = 0.6$, and the color code changes to red. The ship is still very stable ($F_{stab} = 1.0$) and there is plenty of time for an orderly evacuation. Still, the fact that there is progressive flooding to a new undamaged WT compartment means that the situation could become more severe.

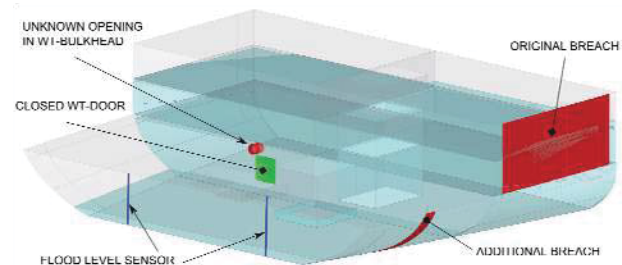


Figure 15: Additional breach in the hull to model detected flooding from an unknown source

6. CONCLUSIONS

A new approach has been developed for assessing the survivability of people onboard a damaged ship. Critical factors, such as stability of the ship and the evacuation time are accounted for. Data from level sensors is utilized and a fast time-domain flooding prediction method is used to assess the progressive flooding and the development of heel. Following the suggested principles for vessel TRIAGE, a color code representation for the severity of the situation can be determined based on the calculated factors for flooding extent, stability and available evacuation time.

The developed method has been tested with two realistic damage cases. The predicted time-to-capsize or time-to-flood is in general shorter than in the reference simulation due to the assumption that all A-class fire doors are open.



Thus the prediction results are normally somewhat more conservative. Fine-tuning of the presented criteria for the survivability level may still be needed, but the present approach forms a solid basis for further work.

It must be noted that a sufficient number of properly located flood level sensors is a prerequisite for a reliable assessment of the survivability. The combination of available measurement data from the sensors and the results from the previous prediction is a challenge. Based on the presented case studies the applied method seems to work well, but some improvements may still be needed.

Further studies are needed to ensure that the developed method works also in other damage scenarios. These cases could include also real accidents. In addition, the impact of inaccuracies in flood level sensor data needs to be further investigated.

The developed method for a fast analysis of the survivability onboard a damaged ship seems to work well in both tested scenarios. The results provide essential information on how the flooding will progress and how serious the situation is. The updated predictions can also account for additional breaches or unknown sources of flooding. This information is very useful and support the master in the decision making.

7. REFERENCES

- Bles, W., Nooy, S., Boer, L.C. 2002 Influence of Ship Listing and Ship Motions on Walking Speed, Pedestrian and Evacuation Dynamics, Springer Verlag, pp. 437-452.
- IMO MSC.1/Circ.1238 Guidelines for Evacuation Analysis for New and Existing Passenger Ships, 30 October 2007.
- IMO SDC2/INF.6 Guidelines for Flood Sensor Placement and Technical Requirements, submitted by Finland, 2014.
- IMO SLF/54/INF.8/Rev.1 Modelling of leaking and collapsing of closed non-watertight doors, submitted by Finland, 28 Oct. 2011.
- Jasionowski, A. 2011. Decision Support for Ship Flooding Crisis Management, Ocean Engineering, Vol. 38, pp. 1568-1581.
- Kujanpää, J. Routi, A-L. 2009. Concept Ship Design A, FLOODSTAND Deliverable D1.1a.
- Lee, D., Lee, S-S., Park, B-J., Kim, S-Y. 2005. A Study on the Framework for Survivability Assessment System of Damaged Ships, Ocean Engineering, Vol. 32, pp. 1122-1132.
- Meyer-König, T., Valanto, P., Povel, D. 2005. Implementing Ship Motion in AENEAS – Model Development and First Results, Pedestrian and Evacuation Dynamics 2005, pp. 429-441.
- Ölcer, A. I., Majumder, J. 2006. A Case-Based Decision Support System for Flooding Crises Onboard Ships, Quality and Reliability Engineering International, Vol. 22, pp. 59-78.
- Penttilä, P., Ruponen, P. 2010. Use of Level Sensors in Breach Estimation for Damaged Ship, Proceedings of the 5th International Conference on Collision and Grounding of Ships ICCGS 2010, Finland, pp. 80-87.



Ruponen, P. 2007. Progressive Flooding of a Damaged Passenger Ship, TKK Dissertations 94.

Ruponen, P., Kurvinen, P., Saisto, I., Harras, J. 2010. Experimental and numerical study on progressive flooding in full-scale, Transactions of the Royal Institute of Naval Architects, Vol. 152. pp., A197–A207.

Ruponen, P., Larmela, M., Pennanen, P. 2012. Flooding Prediction Onboard a Damaged Ship, Proceedings of the 11th International Conference on Stability of Ships and Ocean Vehicles STAB2012, Athens, Greece, pp. 391-400.

Spanos, D., Papanikolaou, A. 2014. On the time for the abandonment of flooded passenger ships due to collision damages, Journal of Marine Science and Technology, Vol. 19, pp. 327-337.

Tagg, R., Tuzcu, C. 2003. A Performance-Based Assessment of the Survival of Damaged Ships: Final Outcome of the EU Research Project HARDER, Marine Technology, Vol. 40, No. 4, pp.288-295.

Varela, J.M., Rodrigues, J.M., Guedes Soares, C. 2014. On-board Decision Support System for Ship Flooding Emergency Response, Procedia Computer Science, Vol. 29, pp. 1688-1700.

Vassalos, D., Kim, H., Christiansen, G., Majumder, J. 2002. A Mesoscopic Model for Passenger Evacuation in a Virtual Ship-Sea Environment and Performance-Based Evaluation, Pedestrian and Evacuation Dynamics, Springer Verlag, pp. 437-452.

Vessel TRIAGE project:

<http://www.raja.fi/vesseltriage>

This page is intentionally left blank



Crew Comfort Investigation for Vertical and Lateral Responses of a Container Ship

Ferdi Çakıcı, *Yildiz Technical University*, fcakici@yildiz.edu.tr

Burak Yıldız, *Yildiz Technical University*, buraky@yildiz.edu.tr

Ahmet Dursun Alkan, *Yildiz Technical University*, alkanad@yildiz.edu.tr

ABSTRACT

This study deals with the crew comfort on board analyses based on vertical and lateral responses of a container ship in sea states 4, 5 and 6. Crew on board might be affected by excessive motions of the ship where fatigue and lack of morale might began gradually and it leads to low concentration for deck operations. This is all called as seasickness phenomena and it should be investigated/evaluated influence on conceptual design decisions. Vertical and lateral responses calculations of the ship are carried out by using strip theory and short statistical method. The total roll damping coefficient is defined using Ikeda's estimation method. The obtained results are combined with the published seakeeping criteria in terms of human factor. In the end of study, operability indices of the container ship are shown with respect to sea states and selected criteria in polar diagrams and tables.

Key Words: *Operability, Ikeda's Method, Potential Theory, Human Factor*

1. INTRODUCTION

It always has been a significant issue to have seakeeping characteristics of ships in waves during design stage. It is very important to obtain the responses in waves due to the effects of the ship motions on human. Minimization for responses can definitely advance the operability and safety of the crew on deck. Reducing motions and accelerations in several sea states is necessary for the sake of crew on ship. Operability index (OI) for the bridge and bow operations should be increased. Intensive operability calculations on board for the commercial ships have to be evaluated during design stage.

It is very common to evaluate container ships as regard to their mobility in terms of seakeeping. However seakeeping performance of commercial ship in terms of crew morale has an important impact on overall performance and it is a measure of being under the specified seakeeping criterion. Absolute vertical and lateral accelerations are significant responses for the safety of crew. People who are not familiar with the excessive responses easily may get seasick.

Seakeeping analysis has been widely used after the development of the first practical strip theory. It is mainly based on the evaluation of the hydrodynamic characteristics of hull sections by using Lewis conformal mapping technique or Frank Close-

Fit approach (Frank, 1967). Although the strip theory is the quickest and relatively most accurate one it has main restrictions due to its theoretical assumptions. It has been most preferred tool during conceptual design stage for calculation of motions. Due to its theory is linear; solutions are more realistic for slender hulls and low Froude numbers. However, strip theory has been widely accepted and a large number of computer codes are developed.

A large number of researches could be found in the seakeeping literature. In the study of Sariöz and Narlı (2005), they showed that the chosen criterion directly affects seakeeping performance of a ship and they calculated operability index values for selected criteria for sea state 5 and 6. In another study, they tabulated the operability performance indices for a passenger ship by using wave distribution scatter (Sariöz and Sariöz, 2005). In both studies, they deal with the vertical accelerations and obtain the limiting values by the help of ISO 2631 standards. In addition to what is mentioned above, seakeeping computations and comfort analyses for three different mono hull yachts are investigated by Nabergoj (2006). On the other hand, Scamardella and Piscopo obtained the overall motion sickness incidence for passenger ships (Scamardella and Piscopo, 2014). Cakici and Aydin discovered the overall seakeeping properties up to several sea states for the gulet type pleasure boats (2014). In another study, Cakici et al. presented the MSI and HI percentages of mega yacht and catamaran hulls for their general arrangements (2014).

In this study, a container ship model is taken as a sample for seakeeping calculations with 2-D strip method. It is shown the OI values of the ship model via polar diagrams according to specified sea conditions and suggested criteria. Selected responses are vertical-lateral accelerations and roll motion. For this responses, criteria are selected as

regards to NORDFORSK project (1987) and Ferdinande V. (1969).

2. SEAKEEPING PERFORMANCE PREDICTION

The seakeeping performance of a ship in a particular sea environment depends on 4 main factors. These are:

- Response in regular waves (RAO)
- Sea state (SS)
- Vessel's speed and heading
- Standardized seakeeping criteria.

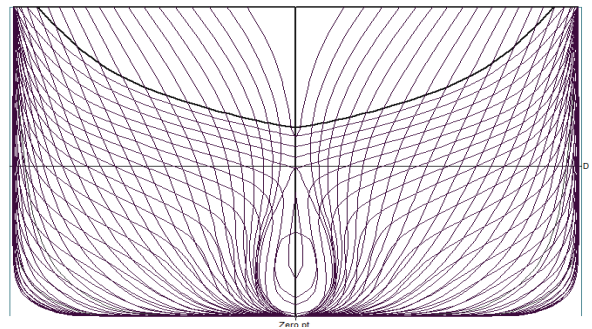


Figure 1 Body plan of the vessel

Body plan and geometric features of the chosen container ship is shown in Fig.1 and Table 1 respectively.

Table 1 Geometric properties of the vessel

Ship	Figures
Displacement, Δ (kN)	48562.16
Draft, T (m)	5.250
Waterline length, L_{OA} (m)	104.321
Waterline length, L_{WL} (m)	100.453
Waterline beam, B_{WL} (m)	16.495
Prismatic coefficient, C_P	0.582
Block coefficient, C_B	0.570
Waterplane area coefficient, C_{WP}	0.698
LCB from FP, LCB, %LWL	-53.871 (+fwd)
Vertical center of buoyancy, KB (m)	2.852
Vertical center of gravity, KG (m)	6.562
Cruise Speed (kts)	18.26
GM_T (m)	0.824

While the behaviour of a ship in regular waves depends on its weight, main dimensions, hull form parameters and weight distribution, the sea state information is based on annual measurements and it may differ for each sea states. Vertical and lateral plane accelerations in regular waves can be



calculated by using 2D strip methods in conceptual design phase. Typical RAO, wave spectrum and response spectrum curve is shown in Fig.2, 3 and 4, respectively, for seakeeping calculations.

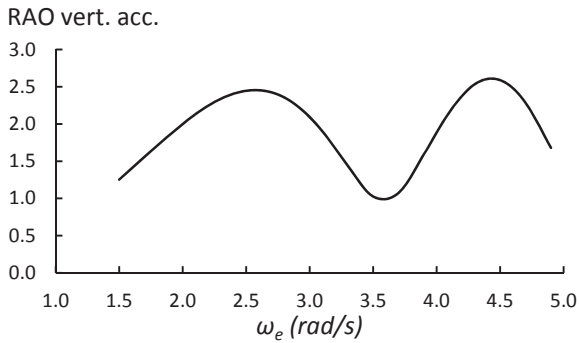


Figure 2 Typical RAO curve

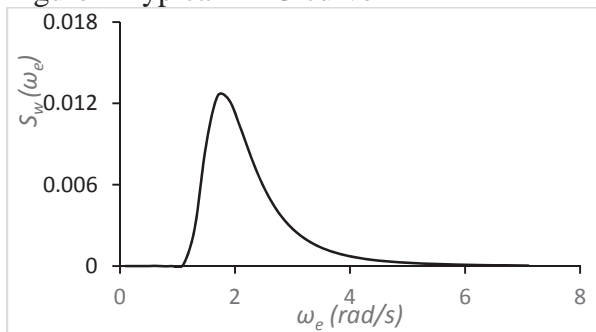


Figure 3 Typical wave spectrum curve

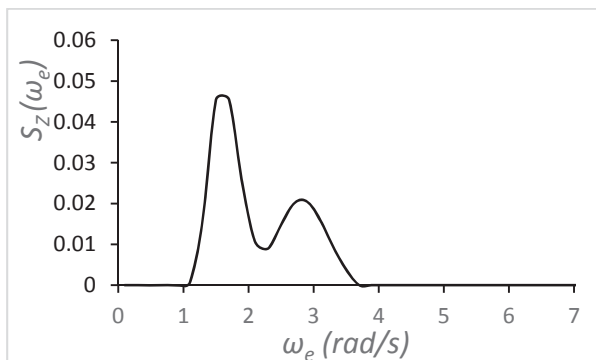


Figure 4 Response spectrum curve

Roll motion is the most critical response of a ship in waves among ship motions and it is important to calculate the roll motion during design stage. Roll motion affects the crew performance, ship habitability, limits the operability, causes the cargo shift, loss of deck cargo and even leads to ship capsizing.

Accurate prediction of roll motion is necessary for operational and safety considerations, especially for container ships. Roll damping coefficient has to be determined correctly for an exact prediction of the roll motion. One of the most used methods to determine roll damping is Ikeda's estimation method. According to Ikeda (1978), see also Himeno (1981), the total equivalent linear roll damping coefficient can be divided into five components. These components are composed of skin friction damping, eddy damping, wave damping, lift damping and bilge keel damping. These are indicated in equation 1.

$$B_e = B_F + B_E + B_W + B_L + B_{BK} \quad (1)$$

In this study, Ikeda's method is used for the prediction of roll damping coefficient.

2.1 Definition of environmental conditions

Motion responses in irregular waves are significant since there are almost no regular waves in nature. Irregular sea surfaces can be defined by the help of wave spectra that is composed through a probabilistic distribution model. This function must be adoptable with the characteristics of the seaway. In this study, the seaway is taken on one parameter Pierson – Moskowitz formulation. The analyses are performed at sea states 4, 5 and 6 and the corresponding characteristic wave heights and modal periods of North Atlantic are shown in Table 2.

Table 2 Wave heights of North Atlantic

Sea State	Significant wave height (m)
4	1.88
5	3.25
6	5.00

2.2 Operability Index Based on Ship Motions

A typical seakeeping polar diagram involves wave heading and sea state for a



given seakeeping limit by using the results of ship motion analyses in irregular seas. Thus polar diagram shows an area where human tolerance is valid and the rest of area refers at least one seakeeping limit criterion is violated. The percentage rate between human tolerant or safer area to violating area of any seakeeping limiting criterion of a seakeeping polar diagram is so-called as Operability Index (OI). This one is defined by both mechanical vibrations from various sources and vibrations resulting from ship motions in waves. In this study OI values are computed by integrating the limiting speeds from stationary speed to cruise speed for all headings, specified sea conditions and seakeeping criterion by employing

$$OI = \frac{1}{2\pi V_0} \int_0^{2\pi} V_{lim}(H_{1/3}, \mu) d\mu \quad (2)$$

Where:

OI: Operability Index based on ship motions (-)

V_0 : Ship Speed (m/s)

V_{lim} : Limiting Criterion Speed (m/s)

μ : Heading (rad)

$H_{1/3}$: Characteristic Wave Height (m)

Operability indices of the container ship are computed for sea state four to six at speeds from zero to cruise speed. OI gives a robust idea according to limit vertical and lateral accelerations defined by existing studies. Safety of crew is closely related to vertical and lateral accelerations. In Figure 5-8, one can easily have an idea for safer places at bridge and bow of the container ship and as well as roll motion in terms of speed and route. The coloured zones show safer regions. Selected criteria are shown with Table 3.

Table 3 Selected Criteria

RMS Lat. Acc. (m/s^2)	RMS Vert. Acc. (m/s^2)	RMS roll motion (deg)
0.12g (bridge)	0.15g (bridge)	6°
	0.20g (bow)	

2.3 Limiting Wave Height for all heading and speed range

The limiting significant wave heights are computed based on each criterion. The results are displayed in Fig. 10. This figure clearly illustrates the influence of the selected response on the maximum allowed significant wave heights.

Necessary computation method is presented in Eq.3.

$$LSWH = Max H_{1/3} \{R_i(V_j \mu_k) \leq R_i^{cr}\} \quad (3)$$

Where:

LSWH: Limiting Significant Wave Heights (m)

μ_k : Heading $0:\pi^\circ$ (rad)

$H_{1/3}$: Characteristic Wave Height (m)

R_i : Computed Response

R_i^{cr} : Criterion Defined Response

V_j : Ship speed $0: V_{cruise}$ (m/s)

3. SEAKEEPING CALCULATIONS AND RESULTS

In this part of the study calculated polar diagrams for lateral and vertical responses are presented with figures.

For sea state four and five, polar diagrams are all safe due to there is no exceed values of specified responses in accordance with selected criteria. Therefore, this sea conditions are not dangerous for crew on deck. However, in sea state six, polar diagrams give two different regions. While coloured zone is safe for the operation; the non-coloured zone is critical. Figure 5-8 show the polar diagrams for selected responses.

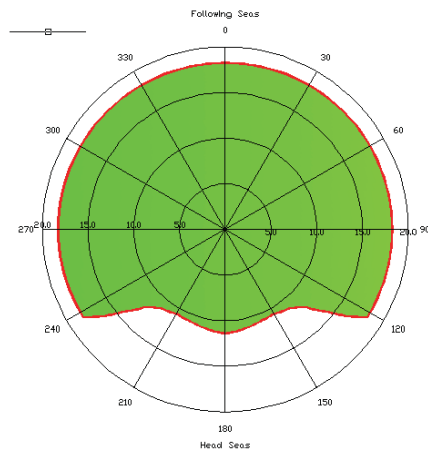


Fig.5 Bow Vert. Acc. Operability Diagram for SS6

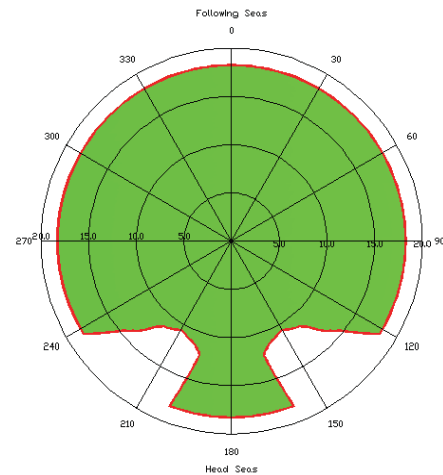


Fig.6 Bridge Vert. Acc. Operability Diagram for SS6

Table 4 Exceeding routes and limiting speeds (knots) for Bow Vert. Acc.

μ	V_{lim} @150°	V_{lim} @180°
122°-180°	11.1 knot	11.3 knot

Table 5 Exceeding routes and limiting cruise speed for Bridge Vert. Acc.

μ	V_{lim} @150°	V_{lim} @160°
123°-160°	11.2 knot	11.9 knot

While figure 5 shows the bow vertical acceleration polar diagram, figure 6 shows the bridge vertical acceleration polar diagram for SS6. Exceeding routes and limiting cruise speed for specified responses are shown in Table 4-6.

Table 6 Exceeding routes and limiting cruise speed for Roll Motion

μ	V_{lim} @60°	V_{lim} @70°
55°-70°	6.9 knot	6.9 knot

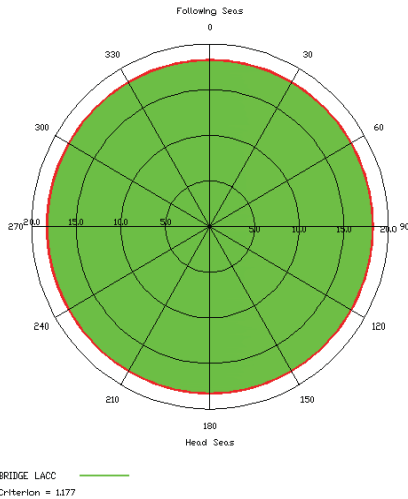


Fig.7 Bridge Lat. Acc. Operability Diagram for SS6

Bridge lateral acceleration polar diagram in Fig. 7 gives an idea that calculated lateral acceleration values are under the selected criterion. There is no exceeding route and limiting cruise speed value for this response.

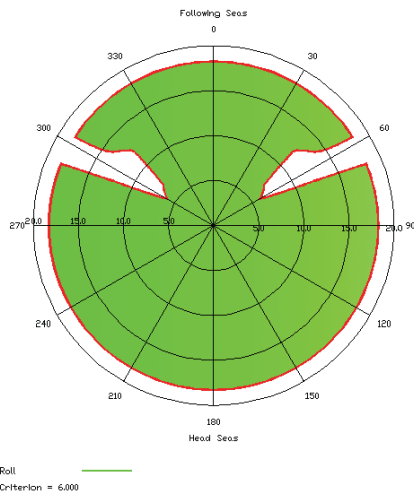


Fig.8 Roll Motion Operability Diagram for SS6

Roll motions of chosen container ship are calculated in irregular waves for sea states 4, 5 and 6. Safe regions are shown in polar diagram as seen in Fig. 8.

Fig. 9 can be obtained by the help of figures 5 -8. OI values are shown between 0-1 for the three sea states.

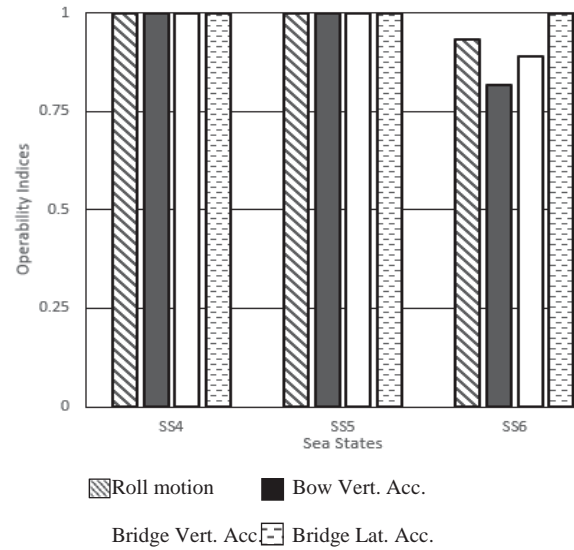


Fig.9 Comparison of Operability Indices

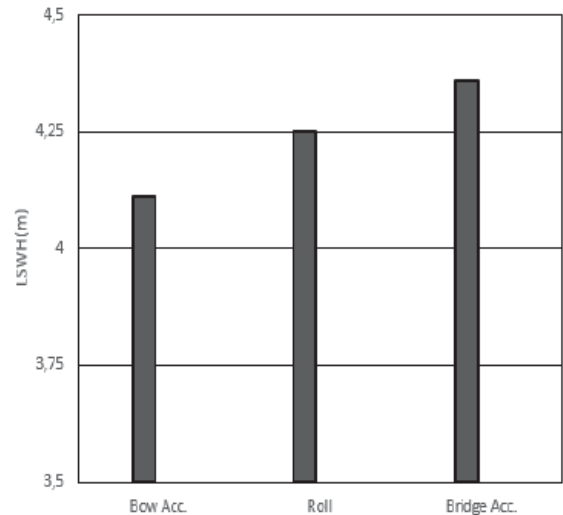


Fig.10 Limiting Significant Wave Heights for Selected Responses

4. CONCLUSIONS

Operability indices regarding crew comfort on board for a container ship are investigated with respect to different sea states, seakeeping phenomena and criteria. The study underlines the crew comfort operability percentages under the lateral and vertical responses for a given seaway and sea state. The limiting wave heights are calculated for each response.

The authors suggest that seakeeping analyses on crew comfort on board as well as



on vessel behavior are remarkably important that must be considered during concept design level. Such analyses will gain useful information on optimal positioning of bridge and accommodation locations as well as defining seakeeping ship.

5. REFERENCES

- K. Sarioz, E. Narli, "Effect of Criterion on Seakeeping Performance Assessment", Ocean Engineering 32, (2005) 1161–1173.
- K. Sarioz, E. Narli, "Effect of Criterion on Seakeeping Performance Assessment", Ocean Engineering 32, (2005) 1161–1173.
- Nabergoj, R. (2006). "Passenger comfort and seakeeping: A new challenge for high-tech ship design", Proceedings of SMALL CRAFT: An International Conference on Small Craft Related Sciences and Technology, Bodrum, Muğla.
- Scamardella, A. and Piscopo, V. (2014), "Passenger ship seakeeping optimization by the Overall Motion Sickness Incidence", Ocean Engineering, Vol:76, pp: 86-97.
- Çakici F. and Aydın M., (2014) "Investigation of Habitability Indices of YTU Gulet Series in Various Sea States", Brodogradnja/Shipbuilding.
- Çakici, F., Sukas, O. F. and Alkan, A. D., (2014) "An Investigation of Comfort on Board Calculations for a Passenger Catamaran and Mega Yacht Hulls", 2nd International Symposium on Naval Architecture and Maritime. INT-NAM 2014, (pp. 589-594).
- NORDFORSK 1987, "The Nordic Cooperative Project, Seakeeping Performance of Ships Assessment of a Ship's Performance in a Seaway", Marintek, Trondheim.
- Ferdinande V. 1969, "Analysis of Slamming Phenomena on a Model of a Cargo Ship in Irregular Waves", International Shipbuilding Progress, November
- Ikeda, Y., Y. Himeno, and N. Tanaka, "A Prediction Method for Ship Roll Damping", Report of the Department of Naval Architecture, University of Osaka Prefecture, 1978e, No. 00405.
- Himeno, Y., "Prediction of Ship Roll Damping-State of the Art", U. Michigan Dept. of Naval Arch. and Marine Engineering, 1981, Report 239

This page is intentionally left blank



Novel Statistical Prediction on Parametric Roll Resonance by Using Onboard Monitoring Data for Officers

Daisuke Terada, *Fisheries Research Agency* dterada@affrc.go.jp
Hirotada Hashimoto, *Kobe University* hashimoto@maritime.kobe.ac.jp
Akihiko Matsuda, *Fisheries Research Agency* amatsuda@affrc.go.jp

ABSTRACT

A novel statistical prediction method on occurrence of roll with large amplitude is proposed based on a methodology applied exponential autoregressive (ExpAR) modeling procedure, which is a kind of nonlinear time series analysis. The verification of the proposed method is implemented by using results of model experiments concerning the parametric roll resonance. It can be confirmed that the large amplitude roll motion can be predicted based on the predictive probability distribution calculated by using the statistically optimum ExpAR model determined by Akaike Information Criterion (AIC).

Keywords: *Parametric roll resonance, ExpAR model, AIC, Predictive probability distribution*

1 INTRODUCTION

There are many studies concerning a parametric roll resonance that have been published in the past Stability of Ships and Ocean Vehicles (STAB) conference and the International Ship Stability Workshop (ISSW) (e.g. Belenky & Campbell 2012; Bulian & Francescutto 2012; Cooper & McCue 2012; Katayama *et al.* 2012; Miguez-Gonzalez *et al.* 2012; Hashimoto & Umeda 2012; Ovegard *et al.* 2012; and so on) from the viewpoint of naval architecture. And excellent knowledges concerning this issue has been showed. However, they are not enough from the viewpoint of ship officers, since ship motions under navigation are big different due to lording conditions of cargoes and external forces such as waves, wind, current and so on. Therefore, it is very important for officers to understand the state of roll motion in which it is the steady or the unstable.

From this background, one of authors (Terada, 2014) suggested that during navigation, of-

icers should keep monitoring the roll motion. In that study, the dynamical system on roll motion can be approximated by an exponential autoregressive (ExpAR) model that is a kind of a nonlinear time series model, and it showed that roots of a characteristic equation on the ExpAR model are an evaluation index useful as the method to confirm the state of roll motion. In short, if all characteristic roots lie inside of the unit circle, then the system is stationary and stable. Moreover, when the real part of the characteristic root changes from positive/negative to negative/positive, the dynamical system for the roll motion can be evaluated as nonlinear for the damping force. Moreover, when the imaginary part of the characteristic root changes from positive/negative to negative/positive, the dynamical system for the roll motion can be evaluated as nonlinear for the restoring force. Therefore, since officers can understand the detailed dynamics of the roll motion under navigation, it is considered that the proposed method is useful for promoting safer



navigation. However, we has been pointed out that it is very difficult for officers to understand the result, and we need to solve this issue.

On the other hand, it is possible to consider that the ExpAR model is one class of the radial basis function (RBF) approximation model in the neural network approach. Ueno & Han (2013) attempted to predict the time series of the roll motion, they showed it's effectiveness. Note that this kind of approach cannot use in actual navigation, since officers do not steer confirming the time series of the roll motion and serious accidents occur with the failure of the prediction.

In this study, we attempt to establish a novel statistical prediction method, which uses an upper and lower endpoint of a predictive probability distribution calculated from a stochastic simulation based on the ExpAR model, in order to give the significant information concerning the roll motion to officers. To confirm the effectiveness of the proposed method, we analyzed the data of the parametric roll resonance. The obtained findings are reported.

2 RELATIONSHIP BETWEEN NONLINEAR STOCHASTIC DYNAMICAL SYSTEM AND TIME SERIES MODEL

Firstly, we mention a relationship between nonlinear stochastic dynamical system and time series model according to Terada& Matsuda (2011) and Terada (2014).

Consider the following nonlinear stochastic dynamical system concerning the roll motion:

$$\ddot{x}(t) + f(\dot{x}(t)) + g(x(t)) = u(t) \quad (1)$$

where $x(t)$ indicates a roll angle, the notation (\cdot) and $(\ddot{\cdot})$ indicate the 1st and the 2nd order differential operator with time, $f(*)$ indicates the nonlinear mapping function concerning the damping force, $g(*)$ indicates the non-

linear mapping function concerning the restoring force and $u(t)$ indicates an external disturbance that is treated with the random variable, respectively. Note that $u(t)$ has the finite variance, but is not white noise sequence. And Equation 1 can be written in the following vector form:

$$\dot{\mathbf{x}}_t = \mathcal{F}(\mathbf{x}_t) + \mathbf{u}_t \quad (2)$$

where, as the notation (T) means the transpose,

$$\begin{aligned} \mathbf{x}_t &= [\dot{x}(t), x(t)]^T, \\ \mathcal{F}(\mathbf{x}_t) &= \left(-f(\dot{x}(t)) - g(x(t)), \dot{x}(t) \right)^T, \\ \mathbf{u}_t &= [u(t), 0]^T. \end{aligned}$$

According to the locally linearization method (Ozaki, 1986), Equation 2 can be discretized as follows:

$$\mathbf{x}_n = \text{EXP}[\mathbf{K}_{n-1}\Delta t] \cdot \mathbf{x}_{n-1} + \mathbf{B}_{n-1}\mathbf{u}_n \quad (3)$$

where,

$$\begin{aligned} \mathbf{x}_n &= [\dot{x}_n, x_n]^T, \\ \mathbf{K}_n &= \frac{1}{\Delta t} \text{LOG}(\mathbf{A}_n), \\ \mathbf{A}_n &= \mathbf{I} + \mathbf{J}_n^{-1} \left\{ \text{EXP}[\mathbf{J}_n \Delta t] \right\} \mathbf{F}_n, \\ \text{LOG}(\mathbf{A}_n) &= \sum_{k=1}^{\infty} \frac{(-1)^k}{k} (\mathbf{A}_n - \mathbf{I})^k, \\ \mathbf{J}_n &= \frac{\partial \mathcal{F}(\mathbf{x}_n)}{\partial \mathbf{x}_n}, \\ \mathbf{F}_n \mathbf{x}_n &= \begin{pmatrix} -f(\dot{x}_n) & -g(x_n) \\ \dot{x}_n & 0 \end{pmatrix}, \end{aligned}$$

and, Δt indicates a discrete interval and $\mathbf{B}_{n-1}\mathbf{u}_n$ is a two-dimensional colored noise sequence, which is obtained by the stochastic integral.

In Equation 3, since the term of the noise is not the white noise sequence, it is necessary to transform the colored noise sequence into a white noise sequence in order to deal with the problem stochastically. To do the whitening,



Yamanouchi (1956) showed how to use the discrete autoregressive process: in Equation 3, let

$$\boldsymbol{\varepsilon}_n \equiv \mathbf{B}_{n-1} \mathbf{u}_n. \quad (4)$$

Then this can be approximated by the following m -th order discrete autoregressive process.

$$\boldsymbol{\varepsilon}_n = \sum_{i=1}^m \mathbf{D}_i \boldsymbol{\varepsilon}_{n-i} + \mathbf{w}_n, \quad (\boldsymbol{\varepsilon}_n = \mathbf{w}_n \text{ for } i = 0), \quad (5)$$

where w_n is a 2×2 Gaussian white noise sequence with $N(0, \text{diag}(\sigma_1^2, \sigma_2^2))$ and D_n indicates a 2×2 autoregressive coefficient matrix. On the other hand, the following relation is evident.

$$\begin{aligned} \boldsymbol{\varepsilon}_n &= \mathbf{x}_n - \mathbf{A}_{n-1} \mathbf{x}_{n-1} \\ \boldsymbol{\varepsilon}_{n-1} &= \mathbf{x}_{n-1} - \mathbf{A}_{n-2} \mathbf{x}_{n-2} \\ &\vdots \\ \boldsymbol{\varepsilon}_{n-m} &= \mathbf{x}_{n-m} - \mathbf{A}_{n-m-1} \mathbf{x}_{n-m-1}. \end{aligned} \quad (6)$$

Therefore, by substituting Equations 6 into Equation 5, we can obtain the following two dimensional $(m + 1)$ -th order time-varying autoregressive model.

$$\mathbf{x}_n = \sum_{i=1}^{m+1} \mathbf{C}_i \mathbf{x}_{n-i} + \mathbf{w}_n. \quad (7)$$

Here C_i ($i = 1, \dots, m + 1$) is the time-varying autoregressive coefficient matrix, which is expressed as follows:

$$\begin{aligned} \mathbf{C}_1 &= \mathbf{D}_1 + \mathbf{A}_{n-1}, \\ \mathbf{C}_2 &= \mathbf{D}_2 - \mathbf{D}_1 \mathbf{A}_{n-2}, \\ &\vdots \\ \mathbf{C}_m &= \mathbf{D}_m - \mathbf{D}_{m-1} \mathbf{A}_{n-m}, \\ \mathbf{C}_{m+1} &= -\mathbf{D}_m \mathbf{A}_{n-m-1}. \end{aligned}$$

Moreover, by using the following relation

$$\dot{x}_n \cong \frac{1}{\Delta t} (x_n - x_{n-1}), \quad (8)$$

Equation 7 can be approximated by the following the $M(= m + 2)$ -th order scalar time-varying autoregressive model

$$x_n = \sum_{i=1}^M a_{n,i} x_{n-i} + w_n. \quad (9)$$

where $a_{n,i}$ indicates time-varying autoregressive coefficients, w_n is the Gaussian white noise sequence with $N(0, \sigma_2^2)$. Now, since $a_{n,i}$ is time-varying autoregressive coefficients, suppose that the following relation

$$\sum_{i=1}^M a_{n,i} \cong \sum_{i=1}^M \{ \phi_i + \pi_i \exp[-\gamma x_{n-1}^2] \} \quad (10)$$

where ϕ_i is a linear term of autoregressive coefficients, π_i is a time-varying term of autoregressive coefficients and γ is a scaling parameter. Thus, Equation 9 can be written as follows:

$$x_n = \sum_{i=1}^M \{ \phi_i + \pi_i \exp[-\gamma x_{n-1}^2] \} x_{n-i} + w_n \quad (11)$$

This time series model, which is called an exponential autoregressive (ExpAR) model, was first introduced by Ozaki & Oda (1978). And then characteristics are investigated by Haggan & Ozaki (1981). According to Haggan & Ozaki (1981), consider the following characteristic equations of Equation 11:

$$\lambda^M - \phi_1 \lambda^{M-1} - \dots - \phi_{M-1} \lambda - \phi_M = 0 \quad (12)$$

$$\begin{aligned} \lambda^M - (\phi_1 + \pi_1) \lambda^{M-1} - \dots - \\ (\phi_{M-1} + \pi_{M-1}) \lambda - (\phi_M + \pi_M) = 0 \end{aligned} \quad (13)$$



If all roots of these equations lie inside of the unit circle, then the nonlinear stochastic dynamical system is stationary and stable. Moreover, when the real part of the characteristic root changes from positive/negative to negative/positive, the dynamical system for the roll motion can be evaluated as nonlinear for the damping force. And also, when the imaginary part of the characteristic root changes from positive/negative to negative/positive, the dynamical system for the roll motion can be evaluated as nonlinear for the restoring force.

3 FITTING OF THE ExpAR MODEL AND PARAMETER ESTIMATION

As to the estimation of the model order M and the coefficients γ , $(\phi_i, \pi_i, i = 1, \dots, M)$ in the ExpAR model, for simplicity, by fixing the parameter γ at one of a grid of values, we estimated the model order M and the corresponding ϕ_i, π_i parameters as well as Haggan & Ozaki (1981). As N is the total number of observations, after fixing $\gamma = \gamma_0$, the ExpAR model for $n = M + 1, \dots, N; i = 1, \dots, M$ can be written as follows:

$$x_n = \sum_{i=1}^M \{ \phi_i + \pi_i \exp[-\gamma_0 x_{n-1}^2] \} x_{n-i} + w_n. \quad (14)$$

So the matrix form of Equation 14 can be written as

$$\mathbf{X}^{(n)} = \mathbf{H}\boldsymbol{\beta} + \mathbf{w}. \quad (15)$$

where, $n = N - M, \dots, N$ and

$$\begin{aligned} \mathbf{X}^{(n)} &= (x_n, x_{n-1}, \dots, x_{n-(N-M-1)})^T, \\ \mathbf{Y}^{(n)} &= (\exp[-\gamma_0 x_n^2] x_n, \exp[-\gamma_0 x_{n-1}^2] x_{n-1}, \dots, \\ &\quad \exp[-\gamma_0 x_{n-(N-M-1)}^2] x_{n-(N-M-1)})^T, \end{aligned}$$

$$\mathbf{H} = (\mathbf{X}^{(n-1)}, \mathbf{Y}^{(n-1)}, \mathbf{X}^{(n-2)}, \mathbf{Y}^{(n-2)}, \dots, \mathbf{X}^{(n-i)}, \mathbf{Y}^{(n-i)}),$$

$$\boldsymbol{\beta} = (\phi_1, \pi_1, \phi_2, \pi_2, \dots, \phi_i, \pi_i)^T,$$

$$\mathbf{w} = (w_n, w_{n-1}, \dots, w_{M+1})^T,$$

so that the normal equations for $\boldsymbol{\beta}$ become $\mathbf{X}^{(n)} = \mathbf{H}\boldsymbol{\beta}$, hence $\boldsymbol{\beta}$ can be found from

$$\hat{\boldsymbol{\beta}} = (\mathbf{H}^T \mathbf{H})^{-1} \mathbf{H} \mathbf{X}^{(n)}. \quad (16)$$

The model order M of the fitted model is selected by using the Akaike Information Criterion (AIC) for nonlinear time series (Ozaki & Oda, 1978)

$$\text{AIC}(M) = (N - M) \log \hat{\sigma}_{2,M}^2 + 2(2M + 1), \quad (17)$$

where,

$$\hat{\sigma}_{2,M}^2 = \frac{(\hat{w}_N^2 + \hat{w}_{N-1}^2 + \dots + \hat{w}_M^2)}{N - M} \quad (18)$$

is the least squares estimate of the residual variance of the model.

4 STATISTICAL PREDICTION OF ROLL WITH LARGE AMPLITUDE

As mentioned before, we can evaluate the stability of the dynamical system by using the characteristic roots calculated from Equation 12 and 13. However, it is impossible to understand the absolute amount of roll amplitude based on this method, and we cannot give the accurate information concerning the future roll motion to officers. Therefore, we propose a novel procedure to solve this problem. In this procedure, We firstly consider a predictive probability distribution calculated from a stochastic simulation based on the optimum ExpAR model determined by Equation 17. Then, as the results we can estimate the



upper and lower endpoint of the probability distribution, and can use them as evaluation index concerning the absolute amount of roll amplitude.

The concrete procedure is as follows:

Step 1:

Fit the ExpAR model to the data of N samples, and the model order, and estimate parameters such as the model order, the scaling factor and so on based on Equation 16 to 18.

Step 2:

Reduce the model order M from the data of N samples.

Step 3:

Prepare the $N - M$ sequence, and give the data of $N - M$ samples as the initial values of their sequence. After that, perform the stochastic simulation of roll motion based on the ExpAR model determined by the AIC.

Step 4:

Calculate the histogram by using the obtained realizations at [Step 1]. Estimate the predictive probability distribution of roll motion by normalization of the histogram. In this case, the the upper and lower endpoint of the probability distribution are simultaneously obtained.

Step 5:

Evaluate the safety level of the roll amplitude based on the upper and lower endpoint of the probability distribution. If values exist within the safety level of the roll amplitude then return to [Step 1] to consider next data set. Otherwise, inform officers the information in which the present state is danger.

Step 6:

Return to [Step 1] to consider next data set.

5 VERIFICATION

To verify the proposed procedure, we analyzed the two kinds of data of the parametric roll resonance concerning a container model ship obtained by Hashimoto *et. al.* (2005). First one is regular waves, and other one is irregular waves. They were measured at sampling interval 0.1[sec] when the ship was running in head seas.

Figure 1 shows a time series of roll motion in regular waves. We analyzed 1,200 samples every 300 samples, namely every 30[sec], concerning this data. In this figure, we defined them as form "Data set 1" to "Data set 4". As shown this figure, the amplitude of roll motion is small in "Data set 1", and becomes gradually large after "Data set 1".

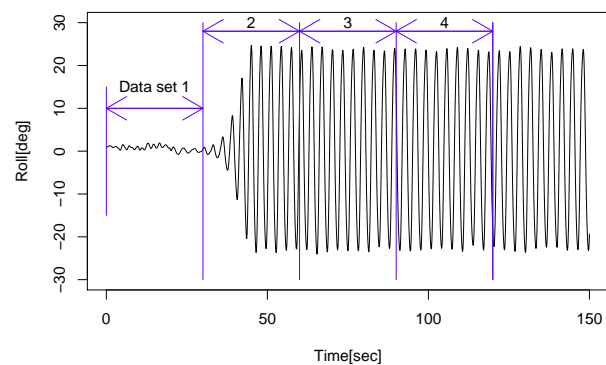


Figure 1 Time series in the case of regular waves

Results of the ExpAR modeling are summarized in Table 1. The probability distribution are calculated based on values shown in this table.

As to the regular waves shown in Figure 1, the predictive probability distribution of next data set calculated from optimum ExpAR model determined by AIC concerning present data set is shown in from Figure 2 to Figure 5.



Table 1 Results of the ExpAR modeling concerning the data of Fig.1

Data	1	2	3	4
Order	3	6	2	2
AIC	-4462.8	-3309.4	-2555.1	-2507.9
γ	8321.8	49.6	51.1	51.7
$\hat{\sigma}^2$	1.04×10^{-7}	4.32×10^{-6}	6.68×10^{-5}	7.82×10^{-5}
ϕ_1	2.79	2.31	1.88	1.86
π_1	0.0419	-0.0545	-0.0344	-0.0358
ϕ_2	-2.70	-1.15	-0.935	-0.933
π_2	-0.0827	0.177	0.0322	0.0332
ϕ_3	0.910	-0.809	-	-
π_3	0.0428	-0.164	-	-
ϕ_4	-	0.373	-	-
π_4	-	0.00175	-	-
ϕ_5	-	0.653	-	-
π_5	-	0.0519	-	-
ϕ_6	-	-0.395	-	-
π_6	-	-0.0110	-	-

In these figures, the horizontal axis indicates the roll angle and the vertical axis indicates the density of the probability, respectively. As you can see from Figure 2, the predictive probability distribution of "Data set 2" calculated from optimum ExpAR model of "Data set 1" shows that the amplitude of roll motion has danger of growing in the future, since the density of the probability exists in the range of from -30[deg] to 30[deg]. In actual, the amplitude of roll motion is growing in "Data set 2". Therefore, it is considered that it is possible to predict the absolute amount of roll amplitude based on this method. As to the results of from Figure 3 to Figure 5, the predictive probability distribution is nearly normal distribution, since time series is stationary, although their amplitude are large.

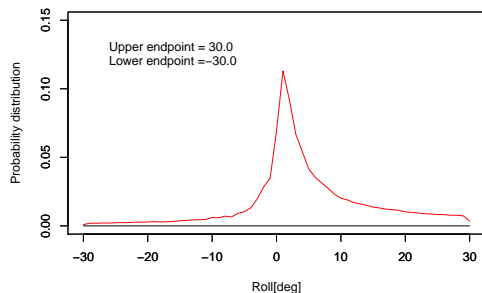


Figure 2 Probability distribution in Data 2 predicted by using "Data set 1" of Fig.1

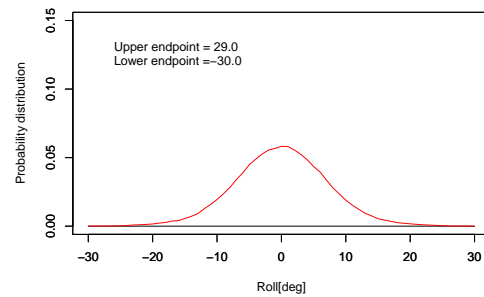


Figure 3 Probability distribution in Data 3 predicted by using "Data set 2" of Fig.1

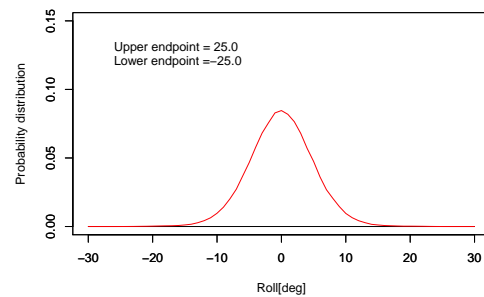


Figure 4 Probability distribution in Data 4 predicted by using "Data set 3" of Fig.1

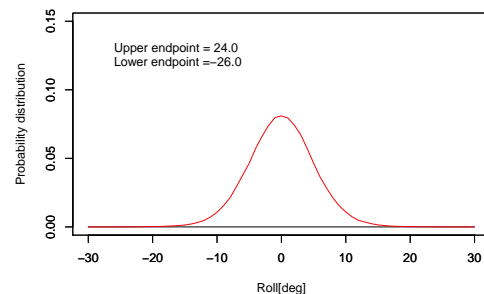


Figure 5 Probability distribution in after Data 5 predicted by using "Data set 4" of Fig.1

Figure 6 shows a time series of roll motion in irregular waves. We analyzed 1,500 samples every 300 samples, namely every 30[sec], concerning this data. In this figure, we defined them as form "Data set 1" to "Data set 5". As shown this figure, the amplitude of roll motion becomes large in after "Data set 5".

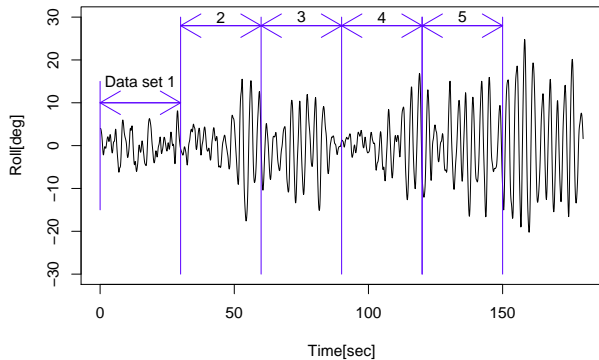


Figure 6 Time series in the case of irregular waves

Results of the ExpAR modeling are summarized in Table 2. The probability distribution are calculated based on values shown in this table.

Table 2 Results of the ExpAR modeling concerning the data of Fig.6

Data	1	2	3	4	5
Order	4	4	6	4	5
AIC	-3306.1	-3389.7	-3335.4	-3255.9	-3172.385
γ	458.7	97.7	132.1	106.4	109.5
$\hat{\sigma}^2$	4.85×10^{-6}	3.66×10^{-6}	3.96×10^{-6}	5.75×10^{-6}	7.25×10^{-6}
ϕ_1	3.02	3.21	2.97	3.06	2.69
π_1	0.0162	-0.0361	-0.00426	0.0373	-0.0273
ϕ_2	-3.61	-4.09	-3.14	-3.66	-2.16
π_2	-0.00978	0.126	-0.0263	-0.0749	0.125
ϕ_3	2.06	2.48	0.824	2.05	-0.391
π_3	-0.0184	-0.150	0.128	0.0258	-0.219
ϕ_4	-0.487	-0.617	1.02	-0.468	1.41
π_4	0.0125	0.0607	-0.181	0.0148	0.178
ϕ_5	-	-	-0.918	-	-0.574
π_5	-	-	0.105	-	-0.0567
ϕ_6	-	-	0.222	-	-
π_6	-	-	-0.0207	-	-

As to the irregular waves shown in Figure 6, the predictive probability distribution of next data set calculated from optimum ExpAR model determined by AIC concerning present data set is shown in from Figure 7 to Figure 11. In these figures, as well as the case of regular waves, the horizontal axis indicates the roll angle and the vertical axis indicates the density of the probability, respectively. As you can see from Figure 11, the predictive probability distribution in after "Data set 5" calculated from

optimum ExpAR model of "Data set 5" shows that the amplitude of roll motion has danger of growing in the future, since the density of the probability exists in the range of from -30[deg] to 30[deg]. It means that it is possible to predict the absolute amount of roll amplitude based on this method even the case of irregular waves. As to the results of from Figure 7 to Figure 10, the upper and lower endpoint of the probability distribution is from about -20[deg] to about 20[deg]. Thus, we can judge that this experimental condition is overall dangerous. For officers, this information is very important from the view point to remain safe navigation.

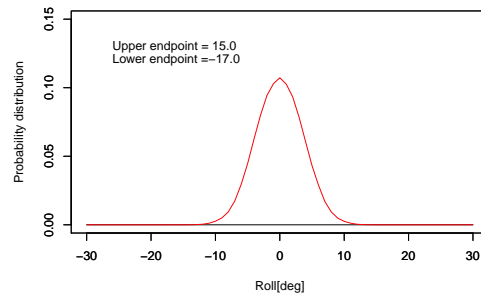


Figure 7 Probability distribution in Data 2 predicted by using "Data set 1" of Fig.6

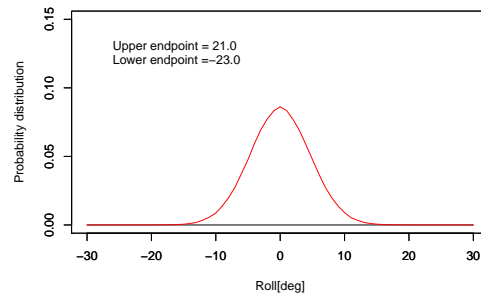


Figure 8 Probability distribution in Data 3 predicted by using "Data set 2" of Fig.6

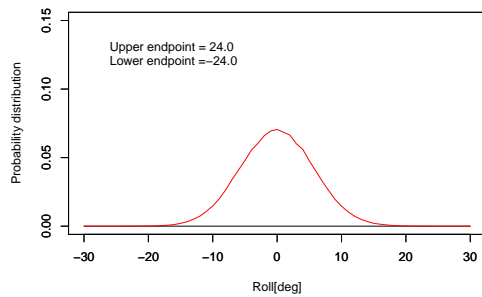


Figure 9 Probability distribution in Data 4 predicted by using "Data set 3" of Fig.6

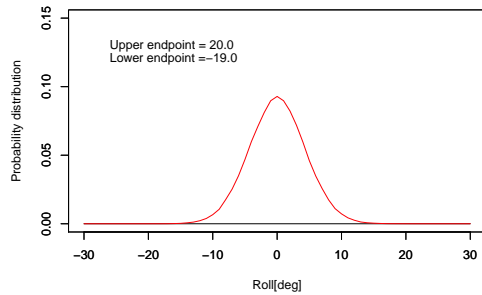


Figure 10 Probability distribution in Data 5 predicted by using "Data set 4" of Fig.6

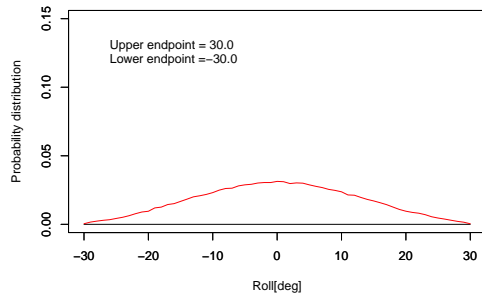


Figure 11 Probability distribution in after Data 5 predicted by using "Data set 5" of Fig.6

6 CONCLUSIONS

In this study, we attempt to establish a novel statistical prediction method, which uses an upper and lower endpoint of a predictive probability distribution calculated from a stochastic simulation based on the exponential autoregressive (ExpAR) model, in order to give

the significant information concerning the roll motion to officers. To confirm the effectiveness of the proposed method, we analyzed the data of the parametric roll resonance. Main conclusions are summarized as follows:

1. As to the regular waves, it is roughly possible to predict the absolute amount of roll amplitude based on this method.
2. It is roughly possible to predict the absolute amount of roll amplitude based on this method even the case of irregular waves.

As mentioned before, it is very important for officer to obtain the predictive information concerning the parametric roll resonance from the view point to remain safe navigation, and we confirmed that the proposed procedure is possible to realize it. Therefore, we consider that the proposed procedure is practical usefulness, and can be used as a powerful tool to remain safe navigation.

Note that we need to verify the proposed procedure more concerning many kind of ships as future task.

7 ACKNOWLEDGMENTS

This work was supported by JSPS KAKENHI Grant Number 25289328. Authors would like to thank President Genshiro KITAGAWA (Research Organization of Information and System) and Prof. Kohei OHTSU (Tokyo University of Marine Science and Technology) for helpful suggestions.

8 REFERENCES

- Belenky, V. and Campbell, B. (2012): Statistical extrapolation for direct stability assessment, Proc. of 11th International conference on STAB, pp.243–256.



- Bulian, G. and Francescutto, A. (2012): Roll motion of a ship with low metacentric height in bi-chromatic beam waves, Proc. of 11th International conference on STAB, pp.187–200.
- Cooper, M D, and McCue, L S. (2012): Effectiveness of chaotic system measures for the validation of ship dynamics simulation, Proc. of 11th International conference on STAB, pp.363–372.
- Katayama, T., Miyamoto, S., Hashimoto, H. and Tai, Y. (2012): An experimental study on characteristics of rolling in head waves for a vessel with non-linear GZ-curve, Proc. of 11th International conference on STAB, pp.281–290.
- Miguez-Gonzalez, M., Diaz-Casas, V., Lopez-Pena, F. and Perez-Rojas, L. (2012): Experimental parametric roll resonance characterization of a stern trawler in head seas, Proc. of 11th International conference on STAB, pp.625–634.
- Haggan, V. and Ozaki, T. (1981): Modelling nonlinear random vibrations using an amplitude-dependent autoregressive time series model, Biometrika, 68, 1, pp.189–196.
- Hashimoto, H., Matsuda, A. and Umeda, N. (2005): Model Experiment on Parametric Roll of a Post-Panamax Container Ship in Short-Crested Irregular Seas, Conference Proc. of the Japan society of naval architects and Ocean Engineers, vol.1, pp.71–74.
- Hashimoto, H. and Umeda, N. (2012): Validation of a numerical simulation model for parametric rolling prediction using a PCTC, Proc. of 11th International conference on STAB, pp.141–150.
- Ovegard, E., Rosen, A., Palmquist, M. and Huss, M. (2012): Operational guidance with pure loss of stability and parametric rolling, Proc. of 11th International conference on STAB, pp.363–372.
- Ozaki, T. and Oda, H. (1978): Nonlinear time series model identification by Akaike's information criterion, Information and Systems, Dubuisson (eds) (1978), Pergamon Press, pp.83–91.
- Ozaki, T. (1986): Local Gaussian modelling of stochastic dynamical systems in the analysis of nonlinear random vibrations, Essays in Time Series and Allied Processes, Festschrift in honour of Prof.E.J.Hannan (1986), Probability Trust, pp.241–255.
- Terada, D. and Matsuda, A. (2011): Study on a relationship between nonlinear dynamical system and stochastic model - Application to stability judgment system of ships - (in Japanese), Journal of the Japan Society of Naval Architects and Ocean Engineers, 14, pp.75–84.
- Ueno, K. and Fan, C. (2013): Quasi-chaotic behaviors of narrow-band response of a non-deterministic resonant System -Application to analysis of ship motion in irregular seas, Japan Journal of Industrial and Applied Mathematic, Vol.30, No.1, pp.203–225.
- Yamanouchi, Y. (1956): On the Analysis of ships, Oscillations as a Time Series, Journal of zosen kyokai, Vol. 99, pp.47–64.

This page is intentionally left blank



Target Ship Design and Features of Navigation for Motion Stabilization and High Propulsion in Strong Storms and Icing

Vasily N. Khramushin,

*Applied mathematics and control processes faculty, St. Petersburg State University,
Russian science-engineering society of shipbuilders of Alexey Krylov, Yuzhno-Sakhalinsk,
V.Khram@Gmail.com*

ABSTRACT

Statement of the design problem for ocean vessel of unlimited sailing can be based on the active use of the historical experience of designing of the good-quality ships. Such experience includes good sea practice of the most authoritative seafarers. It is reflected in the navigational instructions on achievement of efficient operation of ships, in pilot recommendations of practical navigation and unwritten rules of carrying out dangerous and hard sea work in the complicated, storm and ice conditions. Particular specialization of the ship for a concrete type of sea activity in the originally specified geographical and navigational conditions allows the use of achievements of noncontradictory design. It is formally reduced to global optimization (as well as in mathematician) under the terms of minimum external impact on a ship hull. Such approach certainly requires special navigator skills or adaptation of the automated navigation complexes in a variety of special or emergency situations, unpredictable in long ocean voyages. Each new design solution of the vessel of the improved seaworthiness should be complemented by the corresponding techniques on efficient carry out of sea works in storm conditions. In this paper, various examples show how to implement this concept in order to address the engineering problem of the highest efficiency of maritime activities of specialized ships. As target parameters are considered safety of navigation (including in extreme situations), achievement of optimum propulsion in strong storms and severe icing.

Keywords: *seafaring, shipbuilding, sensible target design, trochoidal wave, ninth wave, propulsive and pitching quality of the ship*

1. INTRODUCTION

Seamanship and maritime infrastructure development is an important indicator of efficiency of use of high technologies, general geographic knowledge and creative art marine engineers and navigators authoritative, in general, forming the foundation of "good seamanship" and exclude the possibility "of vainly invention not for mariners".

The concept of a consistent target of ship design is aimed at full harmonization of engineering solutions to well-defined geographical, navigational and meteorological conditions of navigation; for a given level arrangement of regional marine infrastructure and adequate competence shore-based and ship crews. Priority in the selection of design decisions and responsible for the formation of sailors ship's architecture; for the layout of ship equipment and mechanisms, as a consequence, lead to a mismatch of formal methods model shipbuilding and claim new research to test the special in-



structions on the efficacy and safety of navigation and marine operations for the intended purpose of the vessel.

A sensible design of the ship means the execution of the whole complex of marine research to optimize engineering solutions in shipbuilding for extremely accurate and complete realization of the real operating experience and good seamanship all-weather control of the ship in specific geographical areas of the ocean, that the Russian Far East is the need of understanding all aspects of navigation in complex, ice and storm conditions navigation ensuring with all-season and all-weather works maintenance of ship for its original purpose, and without the possibility of reliable shelter while waiting for the sea "fair weather".

2. THE EVOLUTIONARY GENESIS OF THE SHIP'S AFFAIRS AND GOOD SEAMANSHIP

Appearance, contours and architecture of the historic ship uniquely determine the possibility of its maneuvering in a storm winds and waves (Khrumushin, 2011). Historically, as well as in real engineering and seamanship, seaworthiness of ships predetermined by relative strength of the shiphull and reserves its weighting to achieve the best propulsion in rough weather, or to keep the storm safe course in any one of the three historically verified modes storming, relying only on the ability of the crew to provide maneuvering in complex and storm sailing conditions:

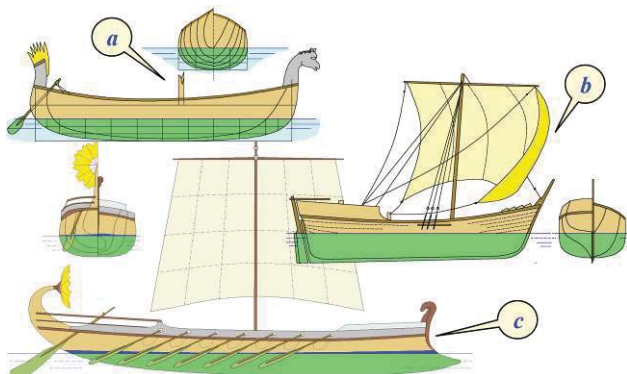


Figure 1 Design solutions ancient shipbuilding

techniques associated storm navigation:

- a) - with a course along to a wave;
- b) - active move in the wind and wave;
- c) - passive storming bow on a wave.

a) – course of along to a wave (Figure 1-a) so far implemented on a wooden boat on the Volga river; previously used by the ancient Egyptian ships on the Nile river; as well as the broad Norwegian boats for shallow water areas, including long-range maritime and ocean navigation. Such vessels have excessive initial stability, why are experiencing intense rolling and pitching in the tempo of fast surface slope of storm waves, and, of course, need to be active course correction to keep the shiphull along the ridge for largest and most dangerous storm waves that ancient vessels was performed with a feed fin oars. This mode of stormy navigation fundamentally unacceptable to consider as the base for the vessels with a large displacement;

b) – active storm course on a wave fronts (Figure 1-b) is sometimes used by modern sailing yachts with a broad stern, as well as quite large rescue tugs with advanced bow superstructure; previously been used extensively the sloops Russian Pomors on a northern latitudes of the Arctic Ocean. The vessel medium displacement on the course with the wind must feels smooth pitching with a significant reduction in power loads on the shiphull by large ridges for passing storm waves, that provided the maintenance of sustainability and maneuverability via hinged aft rudder, effectively operating at a relatively high speed movement under the bow square sail;

c) – storming the course bow on a wave (Figure 1-c), unfortunately, has now become is practically the sole means of aimless containment of forward propulsion to provide its safety in heavy weather at extreme external loads on the host machine and the steering gear. This method has historically inherited from the ancient Phoenician warships with bulbous bowram; in the Middle Ages storming by a bow wave created conditions for safety far ocean sailing expeditions of the Geographical Dis-

covery Age. Asymmetry forms of fore and aft ends shiphull gives the ship weathervanes properties in relation to the wind and the waves, which is achieved by the creation of special contours and perfecting form a surface part shiphull to minimize power influence on the intensity of the storm loads on the hull of the vessel by the oncoming wave fronts, and this asymmetry is quite enough to safely the sea waiting for good weather with no active of the crew.

Last method of a stormy timelessness on course "bow on a wave" is a special captain's ability to save the ship in a stormy sea, which often require a hazard to pull by the main engines, with extremely high overloading mechanisms of steering device, that ship changes a favorable course before impact with each storm wave ridges – with the dangerous ninth wave. This ability does not correct the disastrous mistakes shipbuilders, and the use of such "skills" in a large vessel is limited by the fact that the crew and passengers survive unbearable conditions of habitability; until main deck sheer strake belt of shiphull is not broken under the blows of the ship's cargo in the cycles of rise in weightlessness - to fold multiplication of forces under the influence of the weight onboard and heaving; and immense overload onboard mechanisms do not overpower the technical capabilities and resources efficiency of main machine and control systems.

3. TARGET SHIP DESIGN AND EFFECTIVENESS OF STORM NAVIGATION

Modern fleet with the current power availability by each ocean ships can be used in combination regimens of maneuvering in heavy weather, and steady maintenance of propulsion by arbitrary course throw hurricane winds on stormy waves, if the original design of the ship provides a thorough engineering study of ship contours, the hull shape and the ship's architecture for specific geographic conditions, with the obligatory agreement of all the navigator's

requirements and practical methods of seafaring and exploitations of perspective fleet in a predetermined maritime area. Search and optimization of technical solutions determines are "sensible target ship design", is the key results of which are discussed in this paper.

At the time the Great Geographical Discoveries ocean fleet (Figure 2-*a*) has gained universal understanding of good seamanship for a far transoceanic expeditions, which was supported by a universal ship's architecture for reducing impacts to ship from stormy waves, and provides passive storming on the course bow on a wave. Draught becomes comparable with half the width of the shiphull and freeboard tumblehome inwardly to compensate for the hydrodynamic force action of storm waves. The external appearance of ocean ship has a high aft superstructure – as storm weather vane, and very low deck of bow under privy head and vessel there (knee of the head), dived under the ridges of counterpropagating waves for a hydrodynamic compensation of pitching, and as a result, prevent the wave impact loads on a wooden shiphull and deck superstructures, which has a relatively lower strength.

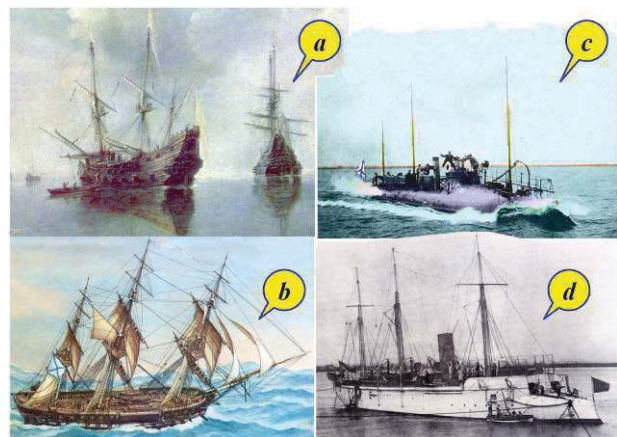


Figure 2 The optimal design for a ocean sailing ships: left side – *a*) and *b*); and their evolutionary improvement to a ships with enhanced stormy seaworthiness by using the power-driven propulsion: right side – *c*) and *d*).

By the beginning of the XIX century a structure and governance by sailing equipments

was up to the highest technical perfection, and, as evidence of optimal engineering solutions – there is a universal uniformity of sailing fleets all over the world. In the latest projects of sailing ships begins traceable target concept of designing to achieve the highest efficiency seafaring in a fresh ocean winds and intense stormy waving for specific geographical conditions maritime communications. On the example of the cruiser-frigate “Pallada” (Figure 2-*b*) there is a decrease of height and alignment of the continuous upper deck, which indicates assurance of the crew in the adequacy of sailing equipments for all-weather control and manoeuvrable of yours best ship. Noncontradictory design concept, however, keep it up in using the old method of passive support storming course by the “bow on a wave”, that enables the use of storm the aft mizzen instead of high aft superstructure, and in the event of the hazard of hurricane force winds, and still foremast can go overboard as a drogue anchor, which also weighting and stabilizing the ship bow on a stormy waves.

Evolutionary perfection design of contours, hull shapes and ship's architecture in general for new fleet is achieved by implementation of steam engines, propeller screws and highly durable steel hulls of ships and vessels at the end of XIX – beginning of XX centuries (Figure 2-*c*, *d*). In the external appearance the newest ships disappear multitude bulky devices except the mizzen mast gaff on, indicates the possibility of quickly setting the mizzen storm sail to bring the ship on course bow on a wave during storm strong wind. Draught of ship hull was remains relatively deep, and the freeboard has a tumblehome form to compensation force action of the waves and reduce roll. The bow deck is very low, the stem to the stern tumble-

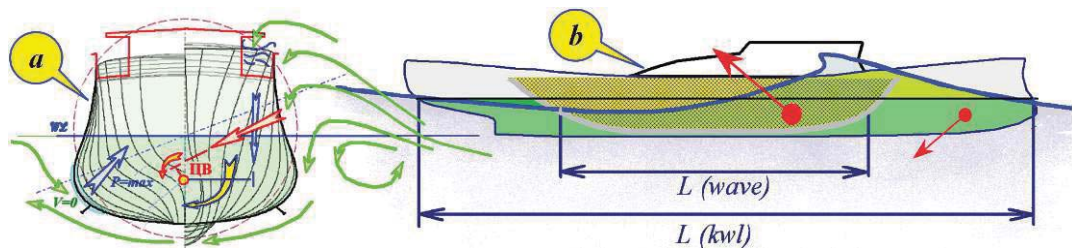


Figure 3 The hull form must given the hydrodynamic compensation: *a*) – a rolling using by minimizing height of tumblehome board in the middle, and: *b*) – pitching of ship through the redistribution of pressures in trochoidal wave on board.

home, or is almost vertical stem, it is necessary to sharpen the waterlines and reduce the risk of intense pitching.

4. KEY TECHNICAL SOLUTIONS TO ACHIEVE THE BEST STORM SEAWORTHINESS

The main engineering solutions to achieve efficiency of navigation in heavy weather, and especially their involvement in good seamanship outlining maritime forum STAB-2009 in St-Petersburg in the report “Key design solutions and specifics of operation in heavy weather, fluid mechanics approach to stabilization of ship in heavy seas” (Khramushin). And we restrict ourselves the illustrations and brief explanations necessary in subsequent submissions by the refined of geometric constructions ship contours and shape of the hull of ships and vessels enhanced storm seaworthiness and ice passability, which is very important for navigation on the Russian Far East seas.

In real navigating practice are preserving the tradition visual interpretation the force distribution and hydrostatic pressure changes of flow field (by Bernoulli's law) in the hydrodynamics ascent by account of water flows near the hull and outboard stabilizers, also under the influence of sea waves, which performed by analogy of engineering decision-making for maneuvering using of spatial images and laws ship fluid mechanics, generally accepted in the international language of navigator communication on duty watches, with pilots, marine res-

cuers and captain's mentors from a coastal services. The scheme of hydrodynamic effects of storm waves impact to the shipboard, was built on navigator's principles, mentioned (Figure 3) in the design and optimization of contours and shape of the hull to minimize rolling (Patent of invention № 2360827, 2009) (Figure 3-a) and pitching (Order of invention 2007133625, 2007) (Figure 3-b), found experimentally confirmed for almost complete compensation rolling under the influence of extremely high ridges storm waves (Figure 3-a), which free passing under the tumblehome shiphull, and emerging from the other board with little or no shape distortion and intensity collapsing wave's ridges, as well as visually complete transformation pitching hull in the heaving (Figure 3-b), which helps to maintain the best propulsion and better habitability conditions in the active movement of the ship relatively an arbitrary course of progressive wave ridges and ninth wave, resulting in packages trochoidal wave structures.

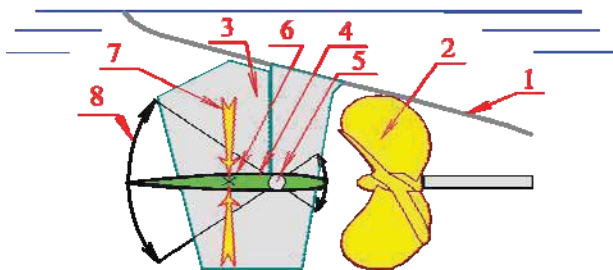


Figure 4 Screw steering system (2, 3) with stabilizing wings (4) - storm emergency propulsion. 1 – the ship's hull; 5 – axis of blow in the stream behind the propeller-driven and allows the elastic rotation of the wings; 6 – the abscissa of summary forces (7) of the heaving motion of a stern extremity; 8 – the turn angles for the plane of stabilizing – propulsion wing.

Hydrodynamic compensation effects on the hull by storm trochoidal waves in deep water is formally responsible solution of the inverse problem of the project is minimal body reaction to external force is well-defined wave nature. If the ship would be under the influence of any other roll and different forces, such as in the circulation; mode porpoise on a wave; or in the zone of cnoidal wave ridges in shallow wa-

ter; et al., the ship may be subject to unacceptably large angles of roll or different of uncontrollably increasing, with a sweeping flow of water on upper decks on the bow and aft decks; and the like. Assuming that the external forces of nature nonwave have significantly lower intensity may direct opposition to their negative impact with active wing devices to compensate for residual pitch and roll (Patent 2384457, at 2010).

In stormy conditions stabilized in the direction of flow of the water near the ship's hull, going full speed ahead, there is only a flow of working propellers (Figure 4-4). There is also is possible to obtain the greatest moments of forces for active roll stabilization and pitch of the ship in stormy weather on the fast circulation et al.

In case of loss of ship way ahead, the influence of storm waves may there are heave for aft in a large amplitude, which will lead to the wing unit with elastic axis shaft to mode flapping fin propulsion, which auto activating in a dangerous conditions on stormy sailing of the ship with the machine stopped. Passive fin propulsion requires no additional power or control actions on the wing device, and elastic rotation (backlash) on the rudder angle of $\pm 30^\circ$ to protect the ship from hitting the surface of the water that is no less important and active stabilization mode on the fly pitching ship.

5. GEOMETRIC CREATION OF LINE CONTOURS AND FORM OF THE HULL FOR A NEW SEAFARING VESSEL

The result of research into the historical evolution of shipbuilding, it is possible to formulate the main design features of construction contours and form of the hull of the typical ship and a low-speed vessel, which considering the need to achieve effective navigation in ice and storm on the Far Eastern seas.

Stem and bilge contours of the high-speed surface ship (Figure 5) or relatively low-speed commercial vessel (Figure 6) determine the conditions of preservation of the storm propulsion at arbitrary courses; lessening all kinds of stormy hull motions; prevent dangerous icing upper decks; and to enable autonomous navigation in ice conditions. A large series of computational and towing experiments with models of ships and vessels of different classes, has identified the most important geometric elements and design features of the stem and hull lines in the bow:

- slope to aft (*tumblehome*) or vertical (*plumb*) and arrow-headed stem (Figures 5, 6–3) in the range of variables waterlines when sailing at a moderate sea state (about one-third or one-half of the draught) for non-impact cutting of a stormy waves ridges and rising the edge of breaking ice by ship under way, from the ice fields diving under the bilge or the bottom of the hull;

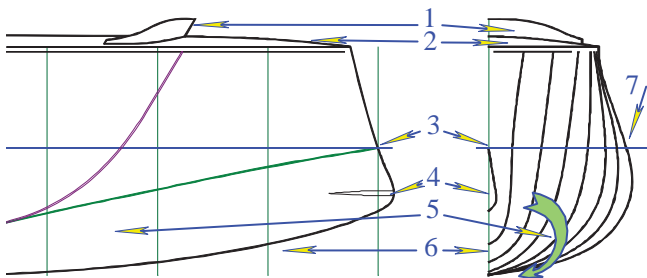


Figure 5 The bow with tumblehome stem of fast ship hull, capable to actively maneuvering in a gale-force winds, stormy waves, and also for autonomous navigation in the ice conditions with average continuity.

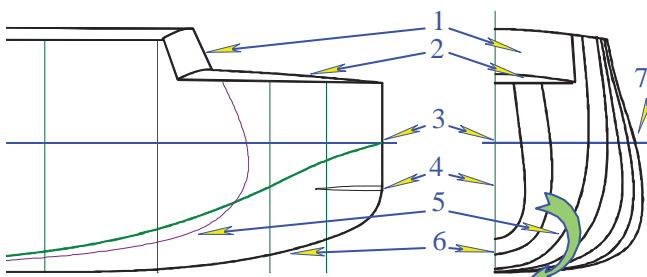


Figure 6 The bow with plumb stem of slow-speed vessel hull, capable to keep a given course with relative slowly way under hurri-

cane-force winds and waves, and for autonomous sailing through average continuity ice fields.

- stormy undercut at bottom to stem (Figure 5, 6–6) with an average slope of 20° – 30° from the keel line, which need to allow free yaw under heavy rolling and pitching with the active movement of the ship on a stormy sea-way;

- with a special strengthening of the collision part of stem (Figure 5, 6–4) to an impact load for splitting of medium ice fields on the speed way up to 6 knots, or with immediately stop the ship at speeds up to 3 – 4 knots, with the ability to create maximum force thrust to lower part of large ice floes and ridges, where the ice is warmed up to a temperature of the water, with the vector force on a small rise of the ice edge to prevent of diving an ice fragments to a bilge and under bottom of the ship;

- branches of a bow freeboard frames may have little rake for hydrodynamic compensate of possible burrowing the bow deck under oncoming storm waves ridges for speed movement ship at high speed ahead (Figure 5), or have a tumblehome upper part of the all frame's height contours with descent of connection point with sheerstrake belt under forecastle deck of slow-speed vessels (Figure 6), that is required to compensate for pitching and heaving due to admission to bow deck big flows of water from storm waves ridges;

- wave screen of fast ship (Figure 5-1) and the shelterdeck's superstructure bulkhead of a slow-speed vessel (Figure 6-1) to protect crew on the upper deck of the direct impacts of waves in rough weather;

- at the expense of the bulb-board shell in the range of variables waterplanes (Figure 5, 6–3) creates screw surface on the length of the stem to the area of divergent ship waves break-away, including comparable in length with external storm waves to tighten the counter-flow

and wave ridges under the bow and bilge bottom of the hull;

– just behind the plot waterlines at diverging ship-waves in break-away zone, can begin a convex bend in the frame's loops to form a boules and tumblehome boards in the middle part of the shiphull (Figure 5, 6–7), that it is necessary for the hydrodynamics compensation of rolling when sailing an arbitrary course relative on storm waves, and also creates the conditions for the repulsion of large ice floes floating under the large around ice fields, and, as a consequence, prevent tightening of ice fragments to the zone with propeller-rudder system at the astern part of the shiphull.

Stern-post, bottom bilge, aft quarter and valance above propeller-rudder system, are arranged in a single or twin-screw in the propulsion options, including the ability to install stabilizers residual pitching and rolling in a stabilized flow directly behind the propeller propellers (Figure 7), and optimized under the terms of the hydrodynamic stabilization running trim at movement in calm water and in heavy storm waves, for which:

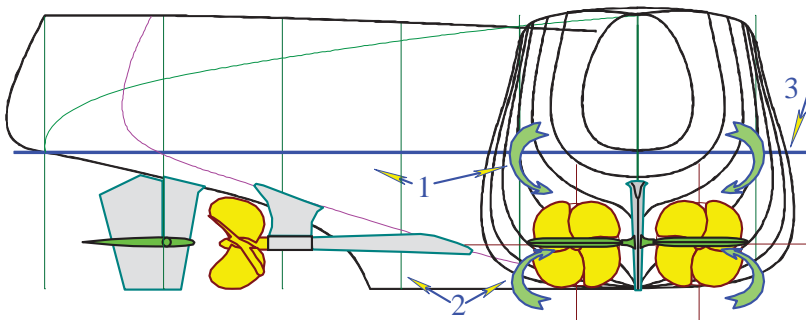


Figure 7 Aft valance, quarter, bottom bilge and stern-post of twin-screw ship, optimized to minimal trim on calm water way

– at the level of a heaving variables waterplanes must created helical surface along from boules on middle board (Figure 7–3) to the astern overhangs (Figure 7–1) for tightening and partial redirection of water flow near the side plating up, thereby compensating cocurrent (hydrostatic) slipstream and break away prevent of the high-frequency component of the ship's wave, followed by the dispersion

concentration of wave energy in long-end of the spectrum, with phase shift for damping of interference with the main component of wave – a wave of cross-ship;

– helical surface in variable waterplanes will reduce the volume of the aft freeboard, and natural sharpening shell for cruising ship over astern overhangs, thereby reducing external force by storm waves and corresponding of slowing to heaving and pitching; not least to prevent shock and danger of capture the stern of the ship (*broaching*) by the ridges of ninth waves and especially on dangerous courses to wave moves by slow speed way, and in the case of an emergency loss of moving;

– a pointed cruising stern does not deform hydrodynamic field in storm waves water flows under the aft shell and astern overhangs hull, when stopping the main machinery, which automatically switches from regime of active wing stabilizers for pitching and rolling, to new mode of the passive storm emergency, which thrusters to bring the ship to a safe course of the storm, bringing the total for the device and the shape of the aft end must be optimized in order to maintain control, even at the minimum power, which arises as a result of the elastic reaction on the rudder passive wing propellers;

– on extended from bottom bilge shell to pairing with stern contour must created a second helical surface (Figure 7-2) to the on-coming flow rotation with over waterplanes (supporting) depth, thus allowing for the mutual compensation of the lower and upper flow vorticity in the area aft overhangs and in the scope of the rudder and horizontal stabilizers of residual (non-linear) pitching and rolling of the ship, as well as through the creation of a total vertical component of flow at small distance from the side shell plating is prevented delays in broken ice from the area of on-board bulls in the area aft propeller-steering and stabilizing the complex, including the possibility of creat-



ing a sustainable ice channel at the astern of the ship;

– tumblehome board in the middle of the hull at the level of current waterplane (Figure 7-3) promotes hydrodynamic compensation of the ship rolling, as well as the raised ridge intercepts ship waves ice fields and does not allow them to flooding and diving the area of propeller-rudder system and wing stabilizers under stern overhand.

6. CONCLUSIONS

The paper presents some special engineering solutions for ships and vessels average displacement, showing features of "design target" for storm conditions in the cold polar seas, with options "consistent design" based on matching the experience of good seamanship, navigation practices to achieve efficient and all-weather safe navigation in the precarious waters of the Russian Far East - in the polar latitudes storm the North and South Pacific Ocean, historically successfully develop Sakhalin sailors, fishermen.

Usage target consistent design is characterized by the search for geometric shapes in order to reduce the external power load on the ship from the storm waves, high winds and ice hazards, followed by naturally developing are ship mechanisms, devices, and the appearance of the ship as a whole as it appears in the light engineering the evolution of the best shipbuilding solutions for ocean and coastal fleet – for the effective conduct of offshore operations in specific geographic conditions.

Due to the involvement of competent seafarers to design and build a new and prospective fleet, what allowed to return to seafarers practice a natural concern for the safety of navigation in difficult, storm and emergency conditions using proven captain and boatswain's methods, such as: installation of storm mizzen or staging sea anchor and all other useful nautical fittings to achieve sustainable and safe nav-

igation in all seasons in all meteorological and weather conditions.

7. ACKNOWLEDGMENTS

This study summarizes the results of many years of discussion on the creation of contours and ship's architecture and historical perspective ships, covering the time period from the 60s to the ship-modeling studios mentors students in the city of Syzran on the Volga (*Vladimir and Alexander Lagutin, Arkady Aksenov*). followed by the formulation of principles of good seamanship on the authority of mariners and confirmation of the advantages of ships late XIX – early XX centuries from older teachers and navy officers of the Kaliningrad Marine College, insisted on the experimental verification of the historical merits of the steam fleet in the 70s (*Alexander Kamyshev, Gregory Malenko, Dalen Bronstein*). Special gratitude for chair teachers of fluid mechanics and the theory of the ship of the Leningrad Shipbuilding Institute, delivered the first professional seaworthiness experiments for historical views on good-quality design of the ship in the 80s (*Alexander Kholodilin, Walter Amphilokhiev*), and put on the path of the present study thirty years approbation with the sailors and shipbuilders of the Far East of Russia (*Sergey Antonenko, Igor Tikhonov, Nikolai Mytnyk, Sergey Chizhiumov and Nikolay Taranukha et al.*), and then - St. Petersburg (*Sergey Krolenko, Alexander Promyslov and Alexander Degtyarev*).



8. REFERENCES

Khramushin V. N. Exploratory studies of storm seaworthiness of the ship (History of evolutionary engineering solutions and architecture of the contours of the ship, of the unity of marine science and good seamanship). Lambert Academic Publishing, Germany. (2011-01-20). 288 c, in Russian: ShipDesign.ru/Khram/History-II.pdf

Khramushin V. Key Design Solutions and Specifics of Operation in Heavy Weather (Fluid Mechanics Approach to Stabilization of Ship in Heavy Seas) // Proceedings. 10th International Conference on Stability of Ships and Ocean Vehicles. STAB-2009, June 22-26, 2009. S-Petersburg, Russia. P. 473-482. ShipDesign.ru/Khram/Art/STAB2009-eng.html

Khramushin V. N. Ship without rolling in rough seas. Patent 2360827 on July-10, 2009. ShipDesign.ru/Invent/01.html

Khramushin V. N. Ship without pitching under way on seaway. Order for invention № 2007133625, 2007.09.07, Bull.N 8 on 2009.03.20. Shipdesign.ru/Invent/02.html

Khramushin V. N. Active stabilizer pitching and rolling of the ship - a storm emergency propulsion. Patent number 2384457 to 2010.03.20. Shipdesign.ru/Invent/04.html

This page is intentionally left blank

Session 12.3 – INSTABILITY OTHER THAN ROLL MOTION

**Prediction of Parametric Rolling of Ships in Single Frequency Regular
and Group Waves**

**Probabilistic Response of Mathieu Equation Excited by Correlated
Parametric Excitation**

Coupled Simulation of Nonlinear Ship Motions and Free Surface Tanks

**Modelling Sailing Yachts Course Instabilities Considering Sail Shape
Deformations**

This page is intentionally left blank



Prediction of Parametric Rolling of Ships in Single Frequency Regular and Group Waves

Shukui Liu, *National Technical University of Athens*, liushukui@deslab.ntua.gr

Apostolos Papanikolaou, *National Technical University of Athens*, papa@deslab.ntua.gr

ABSTRACT

In this paper, a 3D nonlinear time domain numerical simulation method, which is based on the impulse response function concept, is applied to the investigation of parametric rolling of the ITTC-A1 ship. During the simulation, the hydrodynamic coefficients are determined by 3D panel code on the basis of linear potential theory, whereas several nonlinear terms are considered in the equations of motion, such as the excitation by large amplitude waves, the exact restoring forces and moments resulting from the actual wetting of the ship hull geometry and the semi-empirical nonlinear viscous damping. In addition, nonlinear inertia terms are retained when considering motions of large angles. The parametric rolling of the ship is predicted by simulating 6 degree of freedom (DoF) nonlinear motions in response to single frequency regular waves and triple frequency group waves. The obtained numerical results are compared with corresponding experimental measurements and good agreement has been observed.

Keywords: *numerical simulation, parametric resonance, roll motion, non-linear dynamics, ship safety*

1. INTRODUCTION

Parametric rolling is the induced roll motion of a ship due to the periodic change of the restoring characteristics as the ship advances in waves. This phenomenon is often observed on ships with excessive bow flares and very flat sterns, such as modern containerhips, car carriers etc. Typically it takes place when the wave frequency of encounter is close to twice of the natural roll frequency of the ship and near the heave/pitch resonance frequency. Under such condition, the occurrence of the parametric roll phenomenon, which is a strongly nonlinear oscillatory motion phenomenon, is actually subject to the incident wave amplitude, the ship's loading condition, ship's speed and roll damping feature.

The prediction of parametric rolling has high practical value, as it can lead to not only the loss of cargo, but also to the loss of the ship, thus it is an important safety issue already considered in IMO regulations (Peters et al, 2011). It is, also, a popular research subject, because of the complexity of the associated nonlinear ship dynamics and hydrodynamic phenomena; thus the correct prediction of parametric rolling, in terms of likelihood of *occurrence and resulting roll amplitude*, in regular waves and irregular seas remains a challenge to state-of-the-art numerical simulation methods and software tools.

The investigation of parametric rolling by numerical and experimental methods has a long history, dating back to the 1930s (see Paulling, 2006 for historical review). The phenomenon attracted special interest only in the last few decades with the serious accidents on large



ships, for instance, the containership APL CHINA casualty in 1998 (France et al, 2003).

Several approaches are being employed to analyze and understand the parametric roll phenomenon, ranging from the uncoupled, one degree of freedom non-linear roll equation, adjusted with appropriate parameters, for instance, Paulling (1961), Francescutto (2002), Umeda et al. (2003), to models of multi degrees of freedom, where the roll motion and ship hydrodynamics are appropriately coupled with the other degrees of freedom, Ribeiro et al. (2005), Neves, (2005), Krueger (2006), Spanos and Papanikolaou (2006). Parametric rolling has been investigated for both regular and irregular seaways (Belenky, 2003), as well as for following and head seas conditions. A thorough review of the related literature has been carried out by ITTC (2005).

In this paper, a nonlinear time domain method based on the impulse response function concept (Liu et al., 2014), is applied to the simulation of parametric rolling. This method has been developed (independently of earlier work by Spanos and Papanikolaou, 2006) at the Ship Design Laboratory of National Technical University of Athens in the frame of NTUA-SDL's HYBRID software system, aiming to facilitate the analysis of the seakeeping performance and safety of ships in complex environmental and/or adverse sea conditions. In the framework of potential theory, the wave excitation is decomposed into Froude-Krylov, radiation and diffraction forces. Incident wave forces (both hydrodynamic and hydrostatic parts) are calculated through direct integration of the corresponding pressures over the instantaneous wetted surface, which is defined by the undisturbed incident wave and the instant position of the ship. The radiation forces are calculated using the added mass and damping coefficients calculated by a 3D frequency domain code NEWDRIFT (Papanikolaou et al. 1985, 1990) and transformed in the time domain by application of the impulse response function concept.

Diffraction forces are obtained in a similar manner, using corresponding results obtained by NEWDRIFT. Solving the six coupled nonlinear integro-differential equations of motion by a time integration method, the six DOF motions of the ship are obtained in the time domain.

2. MATHEMATICAL MODEL

In order to study the nonlinear ship motion problem, three coordinate systems are defined: the earth-fixed $OXYZ$ system, a system $O'X'Y'Z'$ travelling with the mean ship speed, always parallel to $OXYZ$ and a body-fixed $Gxyz$ system, with its origin G at the center of gravity. It is assumed that at $t=0$ both O and O' coincide with G . The two coordinate systems, $O'X'Y'Z'$ and $Gxyz$ are connected by the three Euler angles: θ (roll), ψ (pitch), and ϕ (yaw). If $O'X'Y'Z'$ is rotated by the three Euler angles, it becomes parallel with $Gxyz$. The order of rotation is θ , ψ , and ϕ . A vector \bar{x} in the $Gxyz$ system may be expressed as \bar{x}' in $O'X'Y'Z'$ system as follows:

$$\bar{x}' = \mathbf{T}\bar{x} \quad (1)$$

where \mathbf{T} is the transformation matrix:

$$\mathbf{T} = \begin{bmatrix} \cos\psi \cos\phi & \sin\theta \sin\psi \cos\phi - & \cos\theta \sin\psi \cos\phi + \\ & -\cos\theta \sin\phi & +\sin\theta \sin\phi \\ \cos\psi \sin\phi & \sin\theta \sin\psi \sin\phi + & \cos\theta \sin\psi \sin\phi - \\ & +\cos\theta \cos\phi & -\sin\theta \sin\phi \\ -\sin\psi & \sin\theta \cos\psi & \cos\theta \cos\psi \end{bmatrix} \quad (2)$$

The ship is assumed travelling on the free-surface with a mean speed $\vec{V}_{O'} = [U, 0, 0]^T$ parallel to the OX axis, subject to incident regular waves. The location of the ship in the $OXYZ$ system is expressed by the location of the center of gravity (G) and the three Euler angles. The location of the center of gravity is defined by $\vec{X}_G(t) = [X_G(t), Y_G(t), Z_G(t)]^T$ and it's velocity $\vec{V}_G(t)$ by the time derivative of $\vec{X}_G(t)$. The relationship between the absolute velocity of the ship and the relative velocity (both



expressed in the earth-fixed coordinate system) is:

$$\vec{V}_G^R = \vec{V}_G - \vec{V}_{O'} = \vec{V}_G - [U, 0, 0]^T \quad (3)$$

The angular velocities about the ship-fixed coordinate axes given by $\vec{\omega}$ are related to the time derivatives of the Euler angles as follows:

$$\vec{\omega} = \begin{bmatrix} \omega_1 \\ \omega_2 \\ \omega_3 \end{bmatrix} = \begin{bmatrix} 1 & 0 & -\sin\psi \\ 0 & \cos\theta & \sin\theta\cos\psi \\ 0 & -\sin\theta & \cos\theta\cos\psi \end{bmatrix} \begin{bmatrix} \dot{\theta} \\ \dot{\psi} \\ \dot{\phi} \end{bmatrix} = \mathbf{B} \begin{bmatrix} \dot{\theta} \\ \dot{\psi} \\ \dot{\phi} \end{bmatrix} \quad (4)$$

where:

$$\mathbf{B} = \begin{bmatrix} 1 & 0 & -\sin\psi \\ 0 & \cos\theta & \sin\theta\cos\psi \\ 0 & -\sin\theta & \cos\theta\cos\psi \end{bmatrix} \quad (5)$$

Let \vec{a}_G be the (total) acceleration vector of the center of gravity G , expressed in the body-fixed system; \vec{a}_G may be expressed as follows:

$$\vec{a}_G = \dot{\vec{v}}_G + \vec{\omega} \times \vec{v}_G \quad (6)$$

The first term in the above equation corresponds to the rate of change of the translational velocity of the ship, while the second one takes into account the effect of rotation of the body-fixed coordinate system.

The equations of motion are given by application of Newton's second law:

$$m(\dot{\vec{v}}_G + \vec{\omega} \times \vec{v}_G) = \vec{F} \quad (7)$$

$$\mathbf{I}\dot{\vec{\omega}} + \vec{\omega} \times \mathbf{I}\vec{\omega} = \vec{M} \quad (8)$$

In the above equations, the external forces and moments are expressed in the body-fixed system of coordinates and they consist of the gravitational, radiation, diffraction, incident wave force, restoring forces and possible viscous terms, while \mathbf{I} is the moment of inertial matrix of the ship.

2.1 Diffraction forces

For weakly nonlinear motions, assuming the ship in the upright/mean position when calculating the diffraction forces due to the incoming waves is a reasonable approach. However, as the motions increase and particularly when the dimensions of the ship are small compared to the wave length (e.g. the case of a small boat in large waves), the effect of the oscillatory ship motions on the diffraction forces increases, and their calculation assuming the ship at its instantaneous position may be considered. On the other hand, in this latter case, diffraction effects will tend to zero, due to the small disturbance to the incoming waves, caused by the presence of the ship.

In the current study, diffraction forces and moments are calculated assuming the ship in the upright/mean position using the velocity potential results obtained by NEWDRIFT. This code is based on a 3D panel method for the evaluation of the responses (ship motions, structural loads and drift forces) of arbitrarily shaped marine structures and shiplike bodies subject to the excitation of incident regular waves; it has been widely benchmarked over the last 35 years and applied to a variety of problems and ship types by marine industry professionals and university researchers. NEWDRIFT was initially developed for the zero speed case (Papanikolaou, 1985), based on the distribution of zero-speed pulsating Green sources over the mean wetted body surface to express the radiation and diffraction potentials and was subsequently extended to the case of shiplike bodies advancing with forward speed in waves (Papanikolaou et al. 1990).

2.2 Incident wave forces

The Froude-Krylov and restoring forces/moments are calculated by integrating the pressure over the *instantaneous* wetted surface of the ship. The incident wave pressure



is herein defined by the sum of linear dynamic pressure and hydrostatic pressure:

$$p = -\rho \frac{\partial \Phi_I}{\partial t} - \rho g Z \quad (9)$$

According to the linear wave theory, the dynamic pressure is assumed constant from the mean free surface to the actual free surface, whereas the hydrostatic component increases linearly from zero at the actual water surface and is being added to the dynamic component.

2.3 Radiation forces

Following Cummins (1962), the radiation forces and moments in the body-fixed coordinate system are evaluated by:

$$F_i(t) = -\sum_{j=1}^6 \left[A_{ij} \dot{v}_j + \int_0^t L_{ij}(t-\tau) v_j(\tau) d\tau \right] \quad i = 1 \sim 6 \quad (10)$$

where A_{ij} are the added mass coefficients, v_j stand for the velocities of the ship in 6DOF, while the kernel functions L_{ij} may be calculated from the damping coefficients B_{ij} :

$$L_{ij}(\tau) = \frac{2}{\pi} \int_0^\infty B_{ij}(\omega) \cos \omega \tau d\omega \quad (11)$$

The added mass and damping coefficients appearing in (10) and (11) are calculated by NEWDRIFT.

2.4 Time domain integration

In order to smoothly introduce the incident wave disturbance into the numerical scheme and to mitigate the effect of initial transients on the steady response to an incident regular wave, the velocity potential of the incident wave is defined as following:

$$\Phi_0 = \frac{g\zeta}{\omega} e^{kz} \sin[k(x \cos \beta + y \sin \beta) - \omega t] \quad (12)$$

$$\zeta = \begin{cases} \zeta_a \left[\frac{1}{2} \left(1 - \cos \frac{t\pi}{nT} \right) \right]^2 & t < nT \\ \zeta_a & t \geq nT \end{cases} \quad (13)$$

where ω is the wave frequency, ζ_a the wave amplitude, k the wave number, β the angle of incidence (with 180deg corresponding to head waves) and n is a pre-defined integer parameter.

During the numerical simulation of the motion of the ship, the determination of the instantaneous wetted surface, considering the ship motions as well as the actual wave elevation is required. This is done according to the following procedure:

1. Prepare a panelization for the ship, including the part of the outer shell above the waterline, up to and including the deck;
2. At each time instant, check the position of each panel in relation to the instantaneous wave surface, mark the panels that are fully wetted, partially wetted, or non-wetted;
3. The non-wetted panels are skipped. Regarding the partially wetted panels, if only one node is immersed, a new triangular panel will be formed; if 2 nodes are immersed, a new rectangular panel will be formed; if 3 nodes are immersed, the wetted area will be split into 2 panels.

3. THE EXPERIMENT

In order to investigate the occurrence of roll resonance and its dependence on the basic parameters of the problem, tank tests have been conducted within SAFEDOR project for the validation of numerical simulation methods in an international benchmark study, coordinated by NTUA-SDL (Spanos and Papanikolaou, 2009).

This benchmark study was based on parametric roll investigations of the

standardized containership ITTC-A1. The principal particulars and body plans of these ships are shown in Table 1 and Figure 1. The two ship loading conditions investigated are shown in Table 2, while in Table 3 the matrix of simulated tests which will be described and discussed in the following section is presented.

The ship model has been investigated with a constant forward speed in head waves. The model was free to move in 3 DoF, namely, in heave, roll and pitch. Tests were independent of any course keeping mechanism. The model was tested both in regular and irregular waves. Free decay tests were also performed in order to evaluate the damping properties of the ship model. The motion of the model, the restraining forces and moments and the wave elevation have been measured. This type of semi-captive tests can be considered “ideal” for the benchmarking of numerical simulation methods (even deviating from the actual, free to move ship performance), as the uncertainties related to the speed and course keeping are suppressed. The experimental results as well as the numerical results of the benchmark study have been extensively reported by Spanos D. (2009) within SAFEDOR framework.

Table 1 Main Particulars of ITTC-A1 ship

Items	Ship
length : L_{pp}	150.0 m
breadth : B	27.2 m
depth : D	13.5 m
draught at FP : T_f	8.5 m
mean draught : T	8.5 m
draught at AP : T_a	8.5 m
block coefficient : C_b	0.667
prismatic coefficient : C_p	0.678
water plane coefficient : C_w	0.787
wetted surface area : S	5065 m ²

Table 2. Loading conditions tested in benchmark study

Tests 01 ~ 11	GM = 1.38 m
	i_{xx} = 10.33 m
	i_{yy} = 37.5 m
Tests 12 ~ 22	GM = 1.00 m
	i_{xx} = 10.33 m
	i_{yy} = 38.2 m

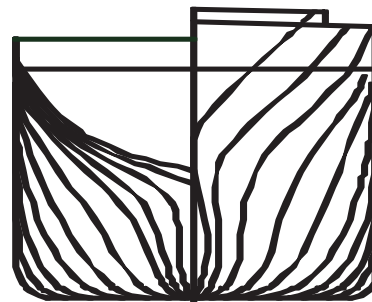


Figure 1. Body plan of ITTC-A1 Ship

Table 3. Matrix of simulated tests from SAFEDOR benchmark study

TEST	GM (m)	Heading (deg)	F_n	H (m)	T (sec)	Comment
T01	1.38	180	0.00	-	-	Roll decay
T02	»	»	0.08	3.6	10.63	Regular
T03	»	»	»	5.7	»	»
T04	»	»	0.12	3.6	»	»
T05	»	»	»	5.7	»	»
T06	»	»	»	2.4 2.4 2.4	10.63 9.66 11.55	Group
T07	»	»	»	4.0 1.0 1.0	10.63 9.66 11.55	»
T09	»	160	»	3.6	»	Regular
T10	»	»	»	5.7	»	»
T11	»	»	»	4.0 1.0 1.0	10.63 9.66 11.55	Group
T20	1.00	180	0.08	5.0	12.12	Regular
T21	»	»	0.12	5.0	»	»
T22	»	»	0.08	4.0 1.0 1.0	12.12 10.77 13.47	Group



4. NUMERICAL RESULTS AND DISCUSSION

In this section we apply the 6 DoF model described, outlined in section 2, to the simulation of parametric rolling phenomenon.

Before proceeding to the parametric rolling simulation, it is necessary to calibrate the roll damping and gyration properties of the model according to the decay test results. Figure 2 shows the tuned decay simulation for Test 01. Using this result, the actual roll viscous damping may be adjusted, as well as the radius of gyration.

For simulating the parametric roll phenomenon in a longitudinal, symmetric wave load condition, we need to introduce a small roll disturbance (by a small initial roll displacement of 1-2 degrees), upon the excitation of which the ship will start rolling with a continuously decreasing roll amplitude, unless the condition for the occurrence of a parametric roll instability is met. This initial disturbance corresponds in practice to the excitation by a sudden side wind or other acting transverse force, while the ship is sailing in exactly head or following sea condition.

When analysing the roll amplitude time records, the mean roll amplitude of the stationary response is used for the quantification of the performance of the numerical method in terms of the predictability of the roll motion magnitude, which is the mean value of successive amplitudes.

Figure 3 shows the overall results for the mean roll amplitude from the present method against the tank tests. In general, numerical predictions of the roll amplitude are consistently higher than experimentally measured amplitudes. Examining the testing conditions, it is noted that going from Test 02 to Test 03, or from Test 04 to Test 05, or from Test 09 to Test 10, the only difference has been the *increase of wave amplitude*, while the wave frequency remained the same. The results for

such an *increase of incident wave amplitude* were the *decrease of resonance amplitude*, both in the experimental and numerical simulation. *This is a clear indication of a rare nonlinear motion phenomenon, for which an increase of the excitation amplitude leads to a decrease of the response amplitude* (or even to zero response, see Spanos D. and Papanikolaou A. 2009b). Commenting on conducted Test 20 and Test 21, the only difference in testing conditions is the increase of speed from $F_n=0.08$ to $F_n=0.12$; this change has induced the disappearance of the roll resonance, as could be also numerically predicted.

Figure 4-11 show the time histories and tank results of several test cases. It is observed that for regular waves, after the initial transient time (depending on the numerical set-up), the ship response is fully developed and a stationary rolling behaviour (constant amplitude) is achieved. Another observation is that the period of roll resonance is twice that of the encounter wave period, which shows the essentially different mechanism of the parametric rolling from a normal (prime resonance) rolling motion excited by incident waves.

At last in Figure 12 the mean roll amplitude results based on the present method are plotted against the simulations of the four best performing methods from the SAFEDOR benchmark study together with the experimental data (full diamond symbols). Interestingly the present method correctly simulated the outcome of Test 21, where no parametric rolling has been observed in tank test, but even the four best performers of SAFEDOR benchmark participants failed to properly simulate it. Comparing the conditions for Test 20 and Test 21, which only differ slightly with respect to ship's speed of advance, but are associated with the initiation of parametric rolling or not, it proves that the sensitivity of prediction methods with respect to the ensuing parameters is very crucial for the reliable prediction if the parametric roll phenomenon.

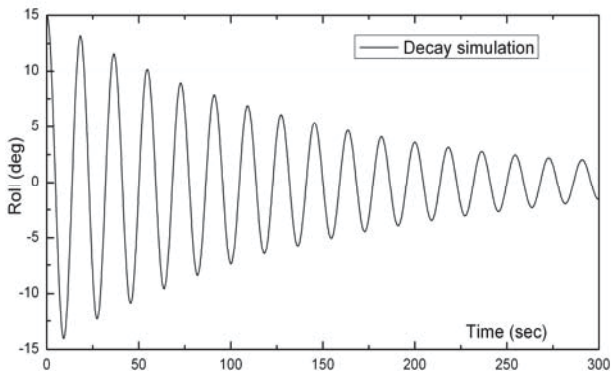


Figure 2. Roll decay simulation GM=1.38m

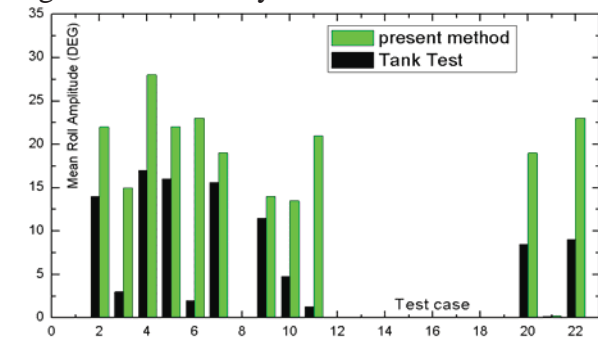


Figure 3. Predicted mean roll amplitude by present method against the experimental results

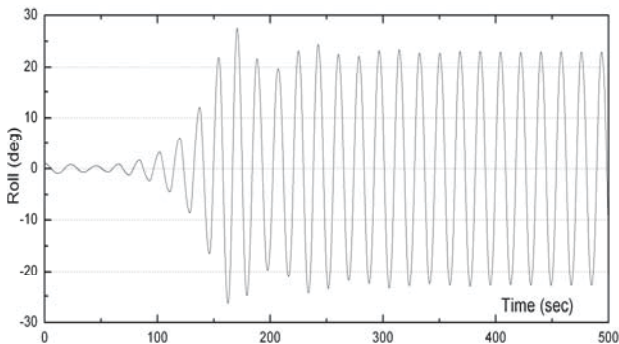


Figure 4. Simulated roll angle history, Test 02

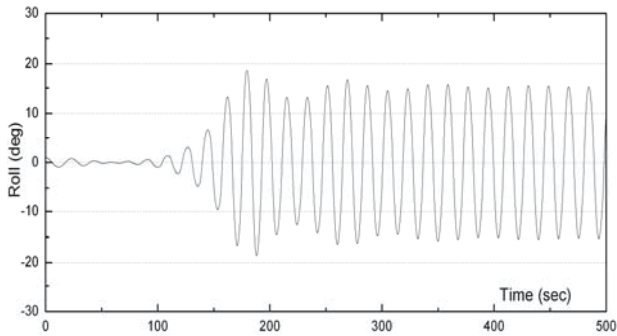


Figure 5. Simulated roll angle history, Test 03

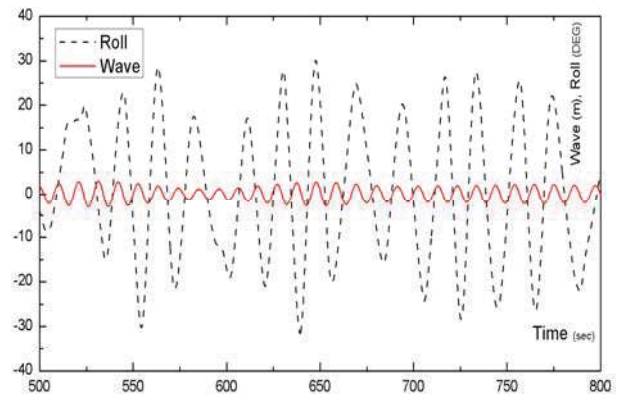


Figure 6. Time history of roll angle simulation in test case T07, head sea, group wave

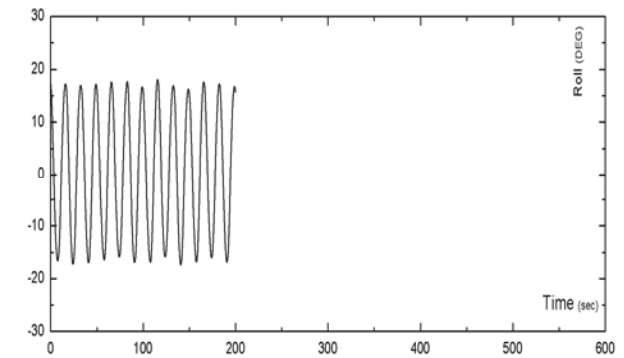
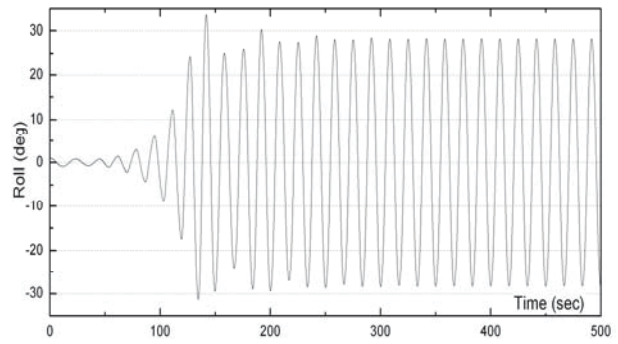
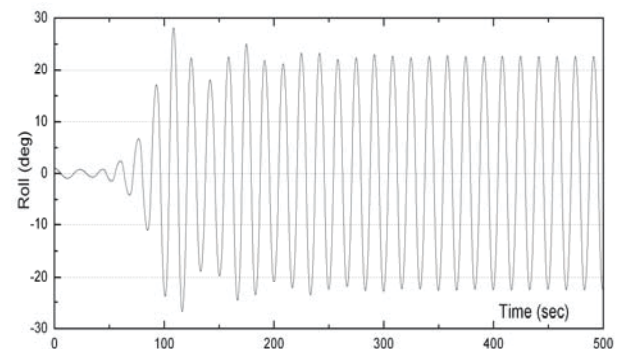


Figure 7. Time history of roll angle of Test 04, simulation (above) vs experiment (below)



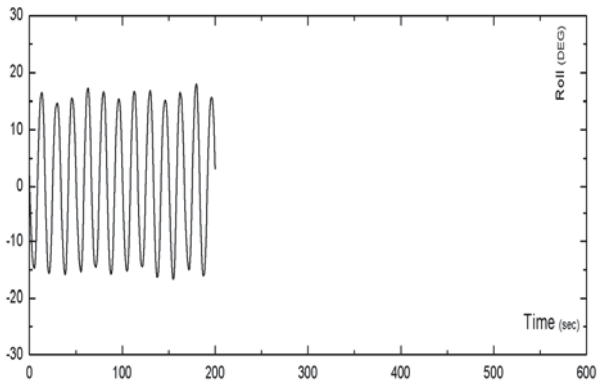


Figure 8. Time history of roll angle of Test 05, simulation (above) vs experiment (below)

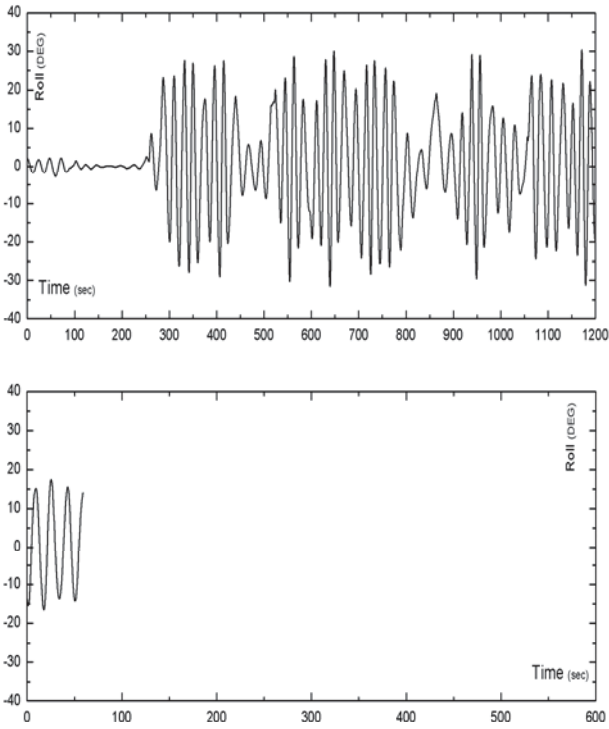


Figure 9. Time history of roll angle of Test 07, simulation (above) vs experiment (below)

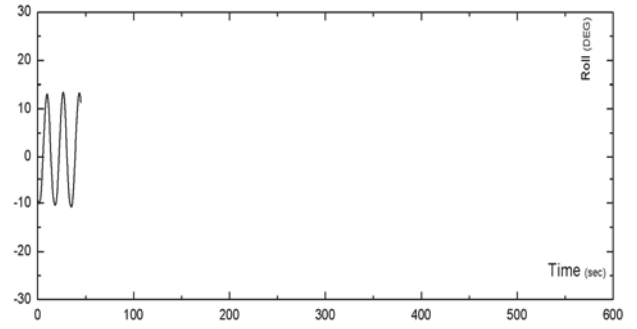
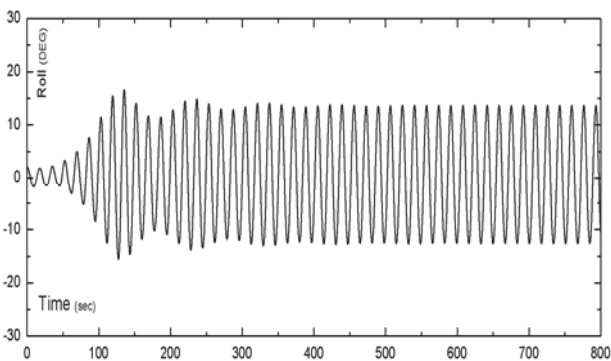


Figure 10. Time history of roll angle of Test 09, simulation (above) vs experiment (below)

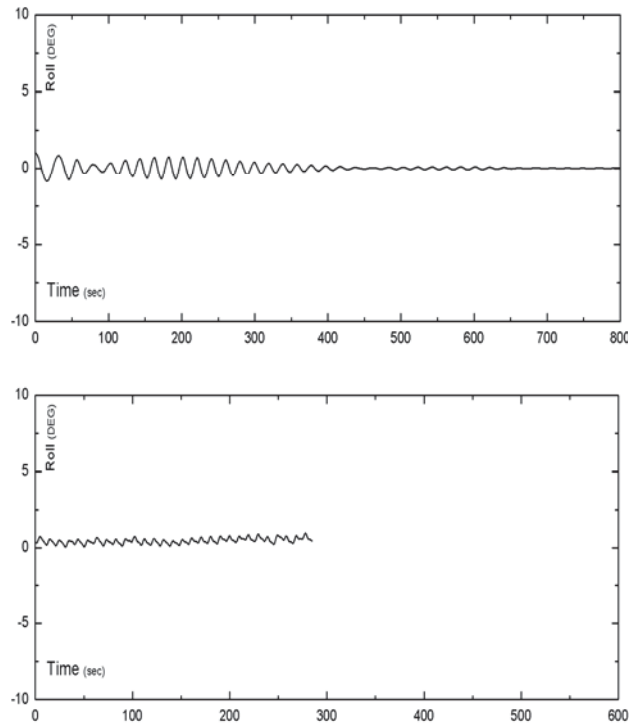


Figure 11. Time history of roll angle of Test 21, simulation (above) vs experiment (below)

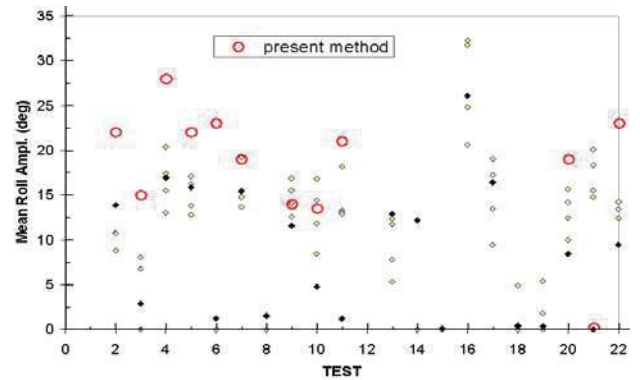


Figure 12 Mean roll amplitude as estimated from current method and the best performing



(four) methods of SAFEDOR benchmark, as well as experimental results

5. CONCLUSIONS

The prediction of parametric roll resonance is inherently a difficult subject, as revealed by the large scattering of numerical results presented in the SAFEDOR benchmark study. Hence it is a good test case for any under development numerical method and software tool to test its performance in such conditions. The quality of the numerical results should be judged by two criteria, as suggested by the SAFEDOR benchmark study:

1. Is the occurrence of resonance correctly captured?
2. Is the amplitude correctly predicted?

Based on these two criteria, we may draw a preliminary conclusion regarding the performance of the herein presented method.

1. The current method has been successfully applied to the prediction of parametric rolling phenomenon of ships in regular waves and triple-frequency group waves. For the 8 tested regular wave cases and 4 tested triple-frequency group wave cases, parametric rolling phenomenon has been correctly predicted in all tested cases (100%).
2. The importance of proper prediction in triple frequency wave group excitation is highlighted, noting that the predictability of parametric roll in natural irregular seas is inherently related to the occurrence of dominating wave groups within the multi-frequency wave ensemble.
3. The amplitude of roll resonance has been in general over-predicted. This is due to the employed linear viscous roll damping model. Despite this, the fact is,

as shown in Test Cases 2 3, Test Case 4 and 5, that the gradient of predicted amplitude change against the incident wave amplitude, has been correctly captured.

3. The correction of the potential theory linear damping by an equivalent viscous damping that may be deduced from roll decay tests, appears to have little effect on the correct prediction of the parametric rolling amplitude. Hence, it is advisable to test higher order roll damping models and to consider in addition the enhanced damping in other modes of motion (heave and pitch), before concluding.

6. ACKNOWLEDGMENTS

The work presented in this paper is supported by the Collaborative Project (Grant Agreement number 605221) SHOPERA (Energy Efficient Safe **SH**ip **OP**eration) co-funded by the Research DG of the European Commission within the RTD activities of the FP7 Thematic Priority Transport / FP7-SST-2013-RTD-1/ Activity 7.2.4 Improving Safety and Security / SST.2013.4-1: Ships in operation. The European Community and the authors shall not in any way be liable or responsible for the use of any knowledge, information or data of the present paper, or of the consequences thereof. The views expressed in this paper are those of the authors and do not necessarily reflect the views and policies of the European Community.

7. REFERENCES

- Cummins, W., 1962, "The impulse response function and ship motions", Journal Schiffstechnik, Vol. 9, no. 47, pp. 101-109.
- France W. N., Levadou M., Treacle T. W., Paulling J. R., Michel R. K., Moore C. (2003), "An investigation of head-sea



- parametric rolling and its influence on container lashing systems”, Marine Technology, 40(1), 1-19.
- Francescutto, A., Bulian G., 2002, Nonlinear and Stochastic Aspects of Parametric Rolling Modeling., Proceedings of International Ship Stability Workshop, Webb Institute, USA.
- ITTC, The specialist committee on Stability in Waves, 2005, Final report and recommendations to the 24th ITTC.
- Krueger S., Kluwe, F., 2006, “Development of Dynamic Stability Criteria from Direct Seakeeping Simulations”, Proc. of the 9th Inter. Marine Design Conference, Ann Arbor, USA.
- Liu S., Papanikolaou A. and Zaraphonitis G., 2014, “Time domain simulation of nonlinear ship motions using an impulse response function method”, Proceeding of ICMT2014, 7th-9th July, Glasgow, UK
- Neves M. A. S. and Rodriguez C.A., 2005, “Stability Analysis of Ship Undergoing Strong Roll Amplifications in Head Seas”, Proceedings of the 8th International Ship Stability Workshop, Istanbul, Turkey.
- Papanikolaou A., 1985, "On Integral-Equation-Methods for the Evaluation of Motions and Loads of Arbitrary Bodies in Waves," Journal Ingenieur - Archiv., 55:17-29.
- Papanikolaou A. and Schellin Th., “A Three Dimensional Panel Method for Motions and Loads of Ships with Forward Speed”, Journal Schiffstechnik - Ship Technology Research, Vol. 39, No. 4, pp.147-156,1992
- Papanikolaou A. and Spanos D., 2008, “SPECIFICATION OF SAFEDOR BENCHMARK SHIP MODEL TESTS”, Rev.00, SAFEDOR technical document.
- Peters W., Belenky V., Bassler C., Spyrou K. J., Umeda N., Bulian G. and Altmayer B., 2011, “The Second Generation Intact Stability Criteria: An Overview of Development”, SNAME Transactions, 121, Houston.
- Paulling J. R., 1961, “The transverse stability of a ship in a longitudinal Seaway”, Journal of Ship Research, V 4:4
- Paulling J. R., 2006, “Parametric resonance in head seas - Then and Now”, Proc. 9th International Conference on Stability of Ships and Ocean Vehicles, Rio de Janeiro-Brazil
- Spanos D., 2009, “SAFEDOR International Benchmark Study on Numerical Simulation Methods for the Prediction of Parametric Rolling of Ships in Wave”, Document Id. SAFEDOR-R-7.3.9-2009-02-13
- Spanos D., Papanikolaou A., 2006a, “Numerical Simulation of a Fishing vessel in Parametric Roll in Head Seas”, Journal of Marine Systems & Ocean Technology, SOBENA, Vol. 2, No. 1-2, pp. 39-44.
- Spanos D. and Papanikolaou A., 2006b, “Numerical Simulation of Parametric Roll in Head Seas”, Proc. 9th International Conference on Stability of Ships and Ocean Vehicles, Rio de Janeiro-Brazil
- Spanos D. and Papanikolaou A., 2009a, “Benchmark Study on Numerical Simulation Methods for the Prediction of Parametric Roll of Ships in Waves”, Proceedings of the 10th International Conference on Stability of Ships and Ocean Vehicles, St. Petersburg, Russia
- Spanos D., Papanikolaou A., 2009b, “On the Decay and Disappearance of Parametric Roll of Ships in Head Steep Waves”, Proc. 10th International Conference on Stability of Ships and Offshore Vehicles, St. Petersburg, Russia,.



Umeda N., 2001, “Final Report on the benchmark tests for intact ships (Ships A-1 & A-2)”, ITTC Specialist Committee on Prediction of Extreme Ship Motions and Capsizing.

Umeda N., Hashimoto H., Vassalos D., Urano S., Okou K., 2003, “Nonlinear Dynamics on Parametric Roll Resonance with Realistic Numerical Modeling”, Proc. of 8th Inter. Conference on the Stability of Ships and Ocean Vehicles STAB03.

This page is intentionally left blank



Probabilistic Response of Mathieu Equation Excited by Correlated Parametric Excitation

Mustafa A. Mohamad, *Massachusetts Institute of Technology*,
Themistoklis P. Sapsis, *Massachusetts Institute of Technology*,

Abstract

We derive analytical approximations for the probability distribution function (pdf) for the response of the Mathieu equation with random parametric excitation at the main resonant frequency. The inclusion of stochastic excitation renders the otherwise straightforward response into a system exhibiting intermittent resonance. Due to the random amplitude term the system may momentarily cross into the instability region, triggering an intermittent system resonance. As a result, the statistics of the response are characterized by heavy-tails. We develop a mathematical approach to study this problem by conditioning the density of the system response on the occurrence of an instability, and analyze separately the stable and the unstable regimes.

Keywords: *Mathieu equation, random excitation, heavy-tails quantification, intermittent instabilities.*

1 INTRODUCTION

In this work we consider a Mathieu type stochastic differential equation of the form

$$\ddot{x}(t) + 2\varepsilon\zeta_0\omega_0\dot{x}(t) + \omega_0^2(1 + \varepsilon\beta(t)\sin\Omega t)x(t) = \sqrt{\varepsilon}\xi(t), \quad (1)$$

where ζ_0 is the damping ratio, ω_0 is the undamped natural frequency of the system, Ω is the frequency of the harmonic excitation term and $\beta(t)$ its (random) amplitude, ε is a small positive parameter, and $\xi(t)$ is a broadband weakly stationary random excitation. It is well known that the Mathieu equation

$$\ddot{x}(t) + 2\zeta_0\omega_0\dot{x}(t) + \omega_0^2(1 + \lambda\sin\Omega t)x = 0, \quad (2)$$

displays instability due to resonance depending upon the parametric excitation frequency and amplitude parameters in the (Ω, λ) plane. Near $\Omega/2\omega_0 = 1/n$ for positive integers n , we have regions of instabilities, with the widest instability region being for $n = 1$. Damping has the effect of raising the instability regions from the $\Omega/2\omega_0$ axis by $2(2\zeta)^{1/n}$. Therefore,

for $\zeta \ll 1$ the instability region near $n = 1$ is of greatest practical importance (Lin & Cai, 1995, Nayfeh & Mook, 1984). In the following we consider (1) tuned to the important resonant frequency $\Omega = 2\omega_0$. The case, where the frequency is slightly detuned can be generalized following exactly the same approach, but for simplicity of the presentation we consider no detuning. In realistic systems the parameter λ in (2) that controls the stability of the system for a fixed Ω and ζ_0 may be a random quantity and not necessarily deterministic. If this is the case, intermittent resonant instabilities may occur due to the randomly varying parameter $\beta(t)$ in (1) crossing momentarily into the instability region which induces a short-lived large amplitude spike in the response after which the system is relaxed back to its stable response (Fig. 1). In other words, we are interested in the case where $\beta(t)$ is on average stable, but can momentarily transition into the instability region due to randomness. From an applications standpoint ignoring randomness in



$\beta(t)$, would severely underestimate the probability for extreme events since the corresponding averaged equation would lead to Gaussian statistics, whereas the original system features heavy-tailed statistics. It is the purpose of this work to quantify the probabilistic response of (1), in other words the probability distribution function (pdf), for the case when $\beta(t)$ is a random quantity. The strategy we employ utilizes a decomposition of the probabilistic system response into stable and unstable regimes, which are then individually analyzed and combined to construct the full distribution of the response.

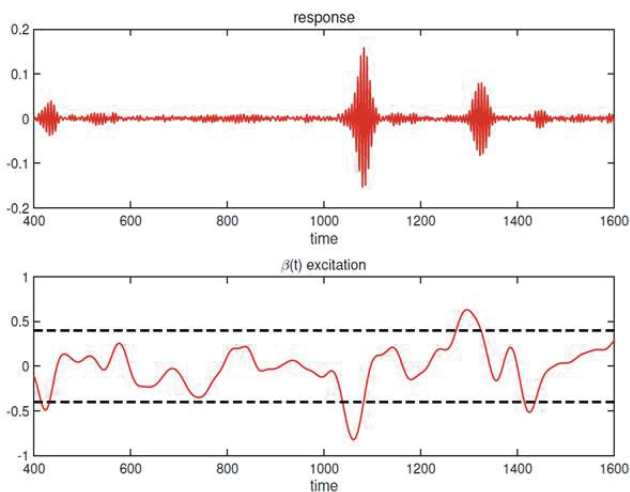


Figure 1 Sample realization of the Mathieu equation (3) (top). The parametric amplitude stochastic excitation term $\beta(t)$ (bottom) triggers intermittent resonance when it crossing above or below the instability threshold (dashed lines).

2 PROBLEM STATEMENT

We consider the following equation

$$\ddot{x}(t) + 2\zeta_0\omega_0\dot{x}(t) + \omega_0^2(1 + \beta(t)\sin 2\omega_0 t)x(t) = \xi(t), \quad (3)$$

where it is understood that the order of the terms are as in (1), $\xi(t)$ is a broadband weakly stationary excitation, and $\beta(t)$ is a correlated weakly stationary Gaussian process. To derive the probability distribution of (3) the standard approach is by a coordinate transformation to a pair of slowly varying variables and then to

apply the stochastic averaging procedure to arrive at a set of Ito stochastic differential equations for the transformed coordinates. The Fokker-Plank equation can then be used to solve for the response pdf (Lin & Cai, 1995, Floris 2012). This standard approach, applied to the problem (3) leads to Gaussian statistics. In reality, randomness in the amplitude $\beta(t)$ leads to intermittent parametric instabilities, and therefore non-Gaussian statistics. To account for the statistics due to intermittent events triggered by $\beta(t)$ we decompose the probabilistic system response into the stable regime and unstable regime according to

$$\mathbf{P}(X) = \mathbf{P}(X | \text{stable regime})\mathbf{P}(\text{stable regime}) + \mathbf{P}(X | \text{unstable regime})\mathbf{P}(\text{unstable regime}), \quad (4)$$

and derive the corresponding distributions for each term in (4). We assume that instabilities are statistically independent so that the decomposition is applicable; in other words that the frequency of $\beta(t)$ crossing into the instability region is sufficiently rare. We remark that for the system to feature intermittent instabilities it is required that the correlation length of the process $\beta(t)$ must be sufficiently large compared the time scale of damping $\approx 1/\zeta_0$ so that instabilities develop. In the following sections our attention will be aimed for the case where the excitation $\beta(t)$ is described by a *Gaussian* process to facilitate the analytic determination of the terms in (4). However, the ideas developed can be generalized to the case when $\beta(t)$ is a non-Gaussian process by carrying out the procedure using numerically generated realization of the excitation process.

To proceed we will average the governing system (3) over the fast frequency ω_0 . We assume that correlation length of the stochastic process $\beta(t)$ varies slowly over the systems natural period $2\pi/\omega_0$ so that $\beta(t)$ can be treated constant over the period, which will be the case in order for (3) to exhibit intermittent instabilities. To apply the method of averaging to (3) we introduce the following transformation



$$\begin{aligned} x(t) &= x_1(t)\cos(\omega_0 t) + x_2(t)\sin(\omega_0 t) \\ \dot{x}(t) &= -\omega_0 x_1(t)\sin(\omega_0 t) + \omega_0 x_2(t)\cos(\omega_0 t) \end{aligned} \quad (5)$$

for the slowly varying variables $x_1(t)$ and $x_2(t)$. Inserting (5) into (3) and using the additional relation $\dot{x}_1 \cos(\omega_0 t) + \dot{x}_2 \sin(\omega_0 t) = 0$ gives the following pair of differential equations

$$\begin{aligned} x_1(t) &= -[2\zeta_0 \omega_0 (x_1 \sin^2(\omega_0 t) - \\ &\frac{1}{2} x_2 \sin(2\omega_0 t)) - \frac{\omega_0 \beta}{2} x_1 \sin^2(2\omega t) - \\ &\omega_0 \beta x_2 \sin^2(\omega_0 t) \sin(2\omega t)] - \frac{1}{\omega_0} \sin(\omega_0 t) \xi(t) \end{aligned} \quad (6)$$

$$\begin{aligned} x_2(t) &= [2\zeta_0 \omega_0 (\frac{1}{2} x_1 \sin(2\omega_0 t) - \\ &x_2 \cos^2(\omega_0 t)) - \frac{\omega_0 \beta}{2} x_2 \sin^2(2\omega t) - \\ &\omega_0 \beta x_1 \cos^2(\omega_0 t) \sin(2\omega t)] + \frac{1}{\omega_0} \cos(\omega_0 t) \xi(t) \end{aligned} \quad (7)$$

Averaging the deterministic terms in brackets in (6) and (7) over the fast frequency $\frac{\omega_0}{2\pi} \int_0^{2\pi/\omega_0} dt$ we have

$$\dot{x}_1 = -\left(\zeta_0 - \frac{\beta}{4}\right) \omega_0 x_1 - \frac{1}{\omega_0} \sin(\omega_0 t) \xi(t) \quad (8)$$

$$\dot{x}_2 = -\left(\zeta_0 + \frac{\beta}{4}\right) \omega_0 x_2 + \frac{1}{\omega_0} \cos(\omega_0 t) \xi(t). \quad (9)$$

The averaged variables x_1 and x_2 provide an excellent statistical and pathwise approximation to the original system. Applying the stochastic averaging procedure to the random forcing gives the following set of Ito stochastic differential equations for the transformed coordinates

$$\dot{x}_1 = -\left(\zeta_0 - \frac{\beta(t)}{4}\right) \omega_0 x_1 + \sqrt{2\pi K} \dot{W}_1(t) \quad (10)$$

$$\dot{x}_2 = -\left(\zeta_0 + \frac{\beta(t)}{4}\right) \omega_0 x_2 + \sqrt{2\pi K} \dot{W}_2(t), \quad (11)$$

with $K = S_{\xi\xi}(\omega_0)/2\omega_0^2$, where $S_{\xi\xi}(\omega_0)$ is the spectral density of the additive excitation $\xi(t)$

at frequency ω_0 , and \dot{W}_1 and \dot{W}_2 are independent white noise of unit intensity (Lin & Cai, 1995). The slowly varying coordinates after averaging transform into two decoupled Ornstein-Uhlenbeck (OU) processes. While averaging the forcing term provides poor pathwise agreement with the original system, it does however provide excellent statistical agreement.

3 PROBABILITY DISTRIBUTION OF THE SLOW VARIABLES

Here we will present the main results on how the heavy-tailed statistics of the averaged slowly varying variables in (10) can be approximated by separating the response into stable and unstable regimes according to (4). If $\beta(t)$ is a zero mean process both x_1 and x_2 will follow the same distribution. Incorporating bias in the amplitude excitation term $\beta(t)$ is straightforward. We will however concentrate on a zero mean process which we write as $\beta(t) = k\tilde{\gamma}(t)$, where $\tilde{\gamma}(t)$ is a Gaussian process with zero mean and unit variance. We consider the following OU process which represents x_1 or x_2

$$\dot{x} = -\left(\zeta_0 - \frac{\beta(t)}{4}\right) \omega_0 x + \sigma \dot{W}(t) \quad (12)$$

We write (12) as

$$\dot{x} = -\gamma(t)x + \sigma \dot{W}(t), \quad (13)$$

so that $\gamma(t) = \tilde{m} - \tilde{k}\tilde{\gamma}(t)$ is a Gaussian process with mean $\tilde{m} = \zeta_0 \omega_0$ and standard deviation $\tilde{k} = k\omega_0/4$. From (13) it is clear that intermittency is triggered when γ has zero downcrossings.

We define the threshold of an instability by $\eta = \tilde{m}/\tilde{k}$. So that the probability of γ being in a regime that does not trigger instabilities is given by $\mathbf{P}(\gamma > 0) = \Phi(\eta)$ and otherwise by $\mathbf{P}(\gamma < 0) = 1 - \Phi(\eta)$ (where $\phi(\cdot)$ denotes the standard normal pdf and $\Phi(\cdot)$ denotes the standard normal cdf). However due to the relaxation phase after an instability the probability $\mathbf{P}(\text{unstable regime})$ is not exactly $1 - \Phi(\eta)$. To determine the typical duration of



the decay phase, we note that during the growth phase the dynamics are approximately given by $x_p = x_0 e^{-\bar{\gamma}|_{\gamma < 0} T_{\gamma < 0}}$, where $T_{\gamma < 0}$ is the duration for which $\gamma < 0$, x_p is the peak value of x during the instability, and $\bar{\gamma}|_{\gamma < 0}$ is the conditional mean of γ given $\gamma < 0$. Similarly, for the decay phase $x_0 = x_p e^{-\bar{\gamma}|_{\gamma > 0} T_{\text{decay}}}$. Combining these two results we have that the typical ratio between the growth and decay phase is given by

$$\frac{T_{\text{decay}}}{T_{\gamma < 0}} = -\frac{\bar{\gamma}|_{\gamma < 0}}{\bar{\gamma}|_{\gamma > 0}} = -\frac{\tilde{m} - \tilde{k} \frac{\phi(\eta)}{1 - \Phi(\eta)}}{\tilde{m} + \tilde{k} \frac{\phi(\eta)}{\Phi(\eta)}} = \nu. \quad (14)$$

The total duration of an unstable event is thus given by the sum of the duration of $T_{\gamma < 0}$ and T_{decay} : $T_{\text{inst}} = (1 + \nu)T_{\alpha < 0}$. Making this modification we have

$$\mathbf{P}(\text{unstable regime}) = (1 + \nu)\mathbf{P}(\gamma < 0), \quad (15)$$

$$\mathbf{P}(\text{stable regime}) = 1 - (1 + \nu)\mathbf{P}(\gamma < 0). \quad (16)$$

3.1 Stable Regime Distribution

In the stable regime we have by definition no intermittent events. The dynamics can therefore be well approximated by replacing $\gamma(t)$ by its conditionally stable average $\bar{\gamma}|_{\gamma > 0} = \tilde{m} + \tilde{k} \frac{\phi(\eta)}{\Phi(\eta)}$ so that

$$\dot{x} = -\bar{\gamma}|_{\gamma > 0} x + \sigma \dot{W}(t). \quad (17)$$

The corresponding stationary pdf of (17) is a Gaussian distribution by the Fokker-Planck equation (Soong & Grigoriu, 1993). This gives us the following distribution for the conditionally stable dynamics

$$\mathbf{P}(X = x | \text{stable regime}) = \sqrt{\frac{\bar{\gamma}|_{\gamma > 0}}{\pi \sigma^2}} e^{-\frac{\bar{\gamma}|_{\gamma > 0} x^2}{\sigma^2}}. \quad (18)$$

3.2 Unstable Regime Distribution

Next we will derive the pdf for the system response for the unstable regime. In the unstable regime there is a growth phase due to

the stochastic process $\gamma(t)$ crossing below the zero level, which triggers the instability. During this stage we assume that the parametric excitation is the primary mechanism driving the instability and ignore the small white noise forcing term which has a negligible minimal impact on the pdf of the response. We characterize the growth phase by the envelope of the response $u \simeq u_0 e^{\Lambda T_{\gamma < 0}}$, where u_0 is a random variable that characterizes the stable envelope pdf, Λ is a random variable that represents the Lyapunov exponent, and $T_{\gamma < 0}$ is the random length of time that the stochastic process γ spends below the zero level.

We first determine the energy growth distribution $Q = \Lambda T_{\gamma < 0}$. By substituting the representation $u \simeq u_0 e^{\Lambda T_{\gamma < 0}}$ into (13) we obtain that the eigenvalue is given by $\Lambda = -\gamma$ so that

$$\begin{aligned} f_{\Lambda}(x) &= \mathbf{P}(-\gamma | \gamma < 0) \\ &= \frac{1}{k(1 - \Phi(\eta))} \phi\left(\frac{x + \tilde{m}}{\tilde{k}}\right). \end{aligned} \quad (19)$$

To determine analytically the distribution of the time that the stochastic process $\tilde{\gamma}$ spends below an arbitrary threshold level η is not in general possible. However an asymptotic expression is available for the case of rare crossings $\eta \rightarrow \infty$ (Rice 1958)

$$f_{T_{\gamma < 0}}(t) = \frac{\pi t}{2\bar{T}} e^{-\frac{\pi t^2}{4\bar{T}}}, \quad (20)$$

which in our case provides a very good approximation since we assume that instabilities are rare so that η is relatively large. In (20) \bar{T} represents the average length of an instability which for a Gaussian process is given by the ratio between the probability of $\gamma < 0$ and the average number of upcrossings of level η per unit time $\bar{N}^+(\eta)$ (Rice 1958)

$$\bar{T}_{\gamma < 0} = \frac{\mathbf{P}(\tilde{\gamma} > \eta)}{\bar{N}^+(\eta)} = \frac{1 - \Phi(\eta)}{\frac{1}{2\pi} \sqrt{-R_{\tilde{\gamma}}''(0)} \exp\left(-\frac{\eta^2}{2}\right)}, \quad (21)$$

where we have used Rice's formula for the expected number of upcrossings (Blake & Lindsey, 1973, Kratz 2006) and where $R_{\tilde{\gamma}}(x)$ represents the correlation of the process $\tilde{\gamma}$. With these results we can determine the



distribution of the energy excitation statistics by the product distribution

$$f_Q(z) = \int_0^\infty f_\Lambda(x) f_{T_{Y<0}}(z/x) \frac{1}{|x|} dx. \quad (22)$$

With the distribution of the energy excitation statistics from (22) we can now derive the pdf for the unstable response. For simplicity let $U = Ye^Q$ and $\Lambda = Q$, so that by a random variable transformation we have

$$\begin{aligned} f_{U\Lambda}(u, \lambda) &= f_{YQ}(y, q) \det|\partial(y, q)/\partial(u, \lambda)| \\ &= \frac{1}{e^Q} f_Y(y) f_Q(q) \\ &= \frac{1}{e^\lambda} f_Y(u/e^\lambda) f_Q(\lambda). \end{aligned} \quad (23)$$

Therefore the general form of the system pdf is given by

$$f_U(u) = \int_0^\infty \frac{1}{e^\lambda} f_Y(u/e^\lambda) f_Q(\lambda) d\lambda. \quad (24)$$

Where the pdf f_Y corresponds to the pdf of the initial point of the instability. We note that the OU process has the property that its interaction with the parametric excitation gives rise to “instabilities” of very small intensity which are indistinguishable from the typical stable state response. To enforce the separation of the unstable response from the stable state requires we introduce the following correction to the initial point of the instability $Y = |x_s| + c$, where $|x_s|$ is the pdf of the envelope of the stable response (Rayleigh) and c is a constant that enforces the separation. We find that choosing c such that it is one standard deviation of the typical stable response is sufficient to enforce this separation and works well in practice. In addition, this choice is associated with very robust performance over different parametric regimes. Therefore we have that the distribution of the initial point of an instability is given by

$$f_Y(x) = \frac{2\bar{v}|_{Y>0}}{\sigma^2} (x - c) \exp\left(-\frac{\bar{v}|_{Y>0}}{\sigma^2} (x - c)^2\right), \quad (25)$$

for $x \geq c$.

Thus after transforming the envelope representation into the full response distribution by a narrowbanded argument we

finally have the conditionally unstable distribution

$$\mathbf{P}(X = x \mid \text{unstable regime}) = \frac{1}{2} f_U(|x|) \quad (26)$$

4 COMPARISON WITH MONTE-CARLO EXPERIMENTS

With the results from Section 3 constructing the full probability distribution for the slow variable is straightforward and requires using the result from the unstable regime (26) and stable regime (18) and combining them with the appropriate weights (15) according to the decomposition (4). Since we considered that the noise term $\beta(t)$ is unbiased with zero mean the corresponding distribution for the response of the Mathieu equation (3) will be given by the distribution of the average of the slow variable x_1 and x_2 (which are equivalent) since the response is a narrowbanded process according to $x(t) = x_1(t)\cos(\omega_0 t) + x_2(t)\sin(\omega_0 t)$. This can be seen by considering the probability distribution for $\cos(\varphi)$, where φ is a uniform random variable between 0 and 2π . The pdf for $z = \cos(\varphi)$ is given by $f_z(x) = 1/(\pi\sqrt{1-x^2})$, $x \in [-1, 1]$, which we approximate by $f_z(x) = \frac{1}{2}(\delta(z+1) + \delta(z-1))$.

For the Monte-Carlo experiments we solve (3) with white noise forcing and non-dimensionalize time by ω_0 so that

$$\ddot{x}(t) + 2\zeta_0 \dot{x}(t) + (1 + \beta(t)\sin 2t)x(t) = \delta W(t), \quad (27)$$

for 2500 realization using forward-Euler integration with a time step $dt = 5 \times 10^{-3}$ from $t = 0$ to $t = 3500$ and discard the first 500 time units to ensure statistical steady states from any initial transients. Moreover we simulate the stochastic process $\beta(t)$ according to the method presented in Percival 1992.

For comparisons we present three cases. Moreover, even in very turbulent regimes with frequent instabilities our results capture the



trend of the tails. We set the damping at $\zeta_0 = 0.1$, $\delta = 0.002$, the correlation length of $\beta(t)$ to be 50 times the time scale of damping $L_{\text{corr}} = 500$, and show three cases with varying frequency of instabilities by changing the variance of β . For the most intermittent regime we set the standard deviation of $\beta(t) = k\tilde{\gamma}(t)$ to $k = 0.229$ so that rare event crossings occur with a 4.0% chance, for the middle regime $k = 0.200$ with a 2.3% chance of rare event crossings, and finally for the least intermittent regime $k = 0.178$ with a 1.2% rare event crossing frequency, see Fig. 2. Overall we have good agreement between the analytic distribution and Monte-Carlo results for these three cases, we stress that the results are robust across a range of parameters that satisfy the assumptions.

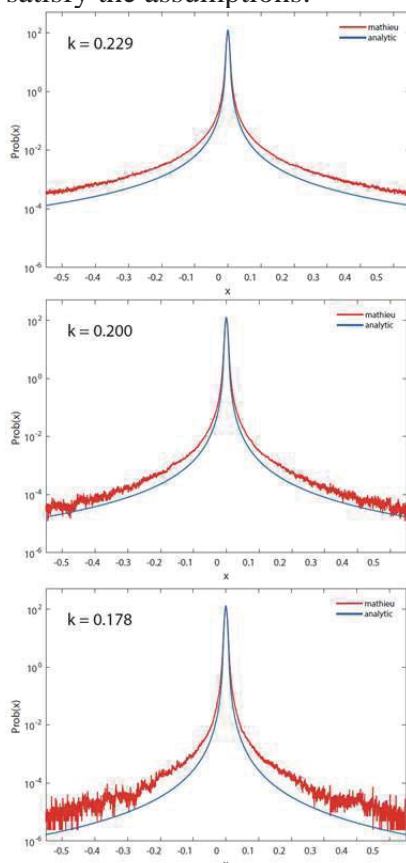


Figure 2 Comparison of Monte-Carlo results of the Mathieu equation (27) (red curve) and analytic probability distribution (blue curve) for various intermittency levels with (left) being most intermittent and (right) least intermittent (semilogarithmic y-axis scale).

5 CONCLUSIONS

In this work we derive an analytic approximation to the pdf for the damped Mathieu equation tuned to the main resonant frequency with random amplitude on the harmonic parametric excitation term. This system features intermittent resonance due the random nature of the amplitude term that triggers intermittent resonance and these intermittent events lead to complex heavy-tailed statistics. To derive the pdf for the response we average the governing equation over the fast frequency to arrive at a set of parametrically excited OU processes. We then decompose the response for the slow variables by conditioning on the stable regime and the unstable (transient) state. In the stable regime we employ classical results to describe the pdf of the statistical steady state. In the unstable regime we capture the response by characterizing the transients bursts by an exponential representation with a random Lyapunov exponent and growth duration. This method allows us to capture the statistics associated with the dynamics that give rise to the heavy-tailed distributions and the resulting analytical approximations compare favorably with direct numerical simulations for a large parameter range.

Acknowledgments

This research has been partially supported by the Naval Engineering Education Center (NEEC) grant 3002883706 and by the Office of Naval Research (ONR) grant ONR N00014-14-1-0520. The authors thank Dr. Craig Merrill (NEEC Technical Point of Contact), Dr. Vadim Belenky, and Prof. Andrew Majda for numerous stimulating discussions.

6. REFERENCES

- Blake, Ian F. and William C. Lindsey (1973). "Level-crossing problems for random processes". In: *IEEE Trans. Information Theory* IT-19, pp. 295–315.



- Floris, Claudio (2012). “Stochastic Stability of Damped Mathieu Oscillator Parametrically Excited by a Gaussian Noise.” In: Mathematical Problems in Engineering 2012, pp. 1–18.
- Kratz, Marie F. (2006). “Level crossings and other level functionals of stationary Gaussian processes”. In: Probab. Surv. 3, pp. 230–288.
- Lin, Y. K. and C. Q. Cai (1995). Probabilistic Structural Dynamics. McGraw-Hill, Inc.
- Nayfeh, A. H. and D. T. Mook (1984). Nonlinear Oscillations. New York: Wiley-Interscience.
- Percival, D. B. (1992). “Simulating Gaussian Random Processes with Specified Spectra”. In: Computing Science and Statistics 24, pp. 534–538.
- Rice, S. O. (1958). “Distribution of the duration of fades in radio transmission: Gaussian noise model”. In: Bell System Tech. J. 37, pp. 581–635.
- Soong, T. and M. Grigoriu (1993). Random Vibration of Mechanical and Structural Systems. PTR Prentice Hall.

This page is intentionally left blank



Coupled Simulation of Nonlinear Ship Motions and Free Surface Tanks

Jose Luis Cercos-Pita, *Technical University of Madrid, Spain*, jl.cercos@upm.es

Gabriele Bulian, *University of Trieste, Italy*, gbulian@units.it

Luis Pérez-Rojas, *Technical University of Madrid, Spain*, luis.perezrojas@upm.es

Alberto Francescutto, *University of Trieste, Italy*, francesc@units.it

ABSTRACT

This paper investigates the coupled nonlinear dynamics of a vessel with a free surface tank onboard. To this end, a 6-DOF ship motions simulation code is coupled with a CFD solver addressing the behaviour of the fluid in the tank. The nonlinear ship motions code is of the blended (hybrid) type, intended for the simulation of free running vessels in waves. The nonlinear CFD solver is a GPU-based 3D Weakly-Compressible Smoothed-Particle Hydrodynamic (WCSPH) solver. Numerical results are presented for the nonlinear roll motion of a vessel with and without a free surface tank in regular beam waves with different steepnesses.

Keywords: *nonlinear ship motions; sloshing; smoothed-particle hydrodynamics (SPH); GPU; anti-rolling tanks; 6-DOF simulations; blended codes; coupling*

1. INTRODUCTION

Tanks characterised by the presence of a free surface are almost invariably present onboard vessels, with different scopes: fuel tanks, ballast tanks, cargo tanks, anti-rolling devices, etc. While taking exactly into account their effect on static restoring is, nowadays, a matter of routine stability calculations, the same cannot be said when ship dynamics and fluid cargo dynamics are to be accounted for in a coupled way. Due to the complexity of the involved phenomena, a coupled dynamic approach is particularly challenging when nonlinear effects are to be considered in both ship motions and fluid dynamics in the free surface tanks.

Different approaches have been used in the past to simulate the behaviour of a vessel in

presence of liquid tanks onboard. Fully linear approaches for ship motions, internal hydrodynamics and external hydrodynamics, have been developed by Malenica et al. (2003) and Kim & Shin (2008). Such approaches are very suitable for design purposes in mild sea conditions. However, when sloshing within the tanks becomes violent and/or ship motions become large, the linearity assumption become too restrictive and the underlying models fail to reproduce the actual fluid and ship dynamics. As a result, nonlinearities need to be introduced, and different authors, recognising this need in certain conditions, have tackled the problem with approaches having different levels of sophistication.

In case ship motions can be considered small enough to be treated linearly, nonlinear effects can be introduced only in the numerical solution of the sloshing problem. Approaches along this line can be found, for instance, in



(Kim et al., 2007, Zhao et al., 2014), where nonlinear time domain potential flow approaches are used under the assumption of a free surface retaining a single-valued behaviour. However, this assumption does not allow taking into account strong nonlinear phenomena such as free surface fragmentation or wave breaking, which characterise violent sloshing. The possibility of handling complex, non-single valued, free surface dynamics was instead introduced in the work of Bunnik & Veldman (2010), where a VOF solver for the internal sloshing flow was coupled in time domain with a linear ship motions model handling the linear potential external fluid-structure interaction and the linearized rigid body dynamics.

However, there are many situations when linear approaches to ship motions are insufficient. This is, for instance the case when the interest is on the assessment of ship behaviour in severe environmental conditions, or when the interest is on typically nonlinear dynamic stability phenomena in waves (e.g. parametric roll, pure loss of stability, surf riding and broaching, large rolling amplitudes in beam waves – see IMO (2009)), or when the interest is on the simulation of the behaviour of a vessel, having free surface tanks onboard, and which is free running in waves. In all such, and other, cases, nonlinear models need to be used for simulating the dynamics of the vessel. Approaches making use of nonlinear ship motions models together with simplified models for the behaviour of the fluid in the tank can be found in Francescutto & Contento (1999) for the beam sea case, and in Neves et al. (2009) for the case of longitudinal sea and, in particular, parametric roll. 6-DOF ship motions models coupled with 1-DOF U-tube tank models have been reported by Youssef et al. (2003) and Holden & Fossen (2012).

More sophisticated models are required when nonlinear effects are to be introduced in both ship motions and in the solution of the fluid flow in the tank. Nonlinear effects in the fluid flow can become particularly relevant in

case of tanks featuring large free surfaces. Along the line of increasing the accuracy of the CFD solver for the internal flow, Hashimoto et al. (2012) coupled a nonlinear 1-DOF roll motion model for the simulation of parametrically excited roll motion, with a fully nonlinear solution of the fluid flow in the tank using the Moving Particle Semi-implicit (MPS) method, which is able to take into account strongly nonlinear free surface flows. In Mitra et al. (2012) a nonlinear potential flow model was solved by FEM for the internal tank, assuming the free surface to be single valued (therefore, also in this case, free surface fragmentation, breaking and strong nonlinearities cannot be accounted for), and the coupling was done with a partially nonlinear 6-DOF ship motions model.

In this study an approach is used where a 6-DOF ship motions simulation code is coupled with a CFD solver addressing the behaviour of the fluid in the tank. The nonlinear ship motions code is of the blended (hybrid) type, intended for the simulation of free running vessels in waves. The nonlinear CFD solver is a 3D Weakly-Compressible Smoothed-Particle Hydrodynamic (WCSPH) solver, allowing the use of graphical processing units (GPUs). In the following, the simulation tool is firstly described. Then, numerical results are presented for the nonlinear roll motion of a vessel with and without a free surface tank in regular beam waves with different steepnesses.

2. SIMULATION TOOL

The tool developed in the present study is intended to be able to simulate the general case of nonlinear motions for a free running ship sailing in regular or irregular waves, with a liquid tank onboard. Since nonlinear motions and nonlinear fluid flow inside the tank are of interest, and since the tool is expected to be able to deal with the general case of a ship free running in waves, linear frequency domain approaches (Malenica et al., 2003, Kim & Shin, 2008) do not represent a relevant option



for the scope of the study. Although research is ongoing (Sadat-Hosseini et al., 2010, Carrica et al., 2012) regarding the use of direct computational fluid dynamics approaches for nonlinear ship motions of, possibly free running, ships in waves, the required computational time and resources are still prohibitive for practical applications.

Considering the situation, herein an intermediate approach has been followed, where the nonlinear rigid body dynamics and the ship-waves interaction is dealt with by means of a blended (hybrid) nonlinear 6-DOF approach, while the internal fluid-structure interaction, i.e. the fluid dynamics within the tank, is handled through a CFD approach based on a fully nonlinear SPH solver. The two tools are then coupled, in order to incorporate the tank effects in the solution of ship motions.

In particular, the ship dynamics is handled by the 6-DOF blended simulation code SHIXDOF ("nonlinear SHIP motion simulation program with six Degrees Of Freedom"), under development at the University of Trieste. The code has been described and applied previously in (Bulian et al., 2012, Bulian & Francescutto, 2013) and herein some main details are reported.

The simulation approach used in SHIXDOF is a typical hybrid approach along the line of de Kat & Paulling (1989). To date, approaches of such type have been considered suitable for practical assessment of nonlinear ship motions in waves, and their suitability for such purpose has been stated also in the framework of IMO "Second Generation Intact stability Criteria" (Bulian & Francescutto, 2013, IMO, 2010, 2013). As described in some more details by Bulian et al. (2012) and Bulian & Francescutto (2013), SHIXDOF solves nonlinear rigid body motions equations with respect to the ship-fixed reference system:

$$\left\{ \begin{array}{l} m \cdot \left[\underline{u}_O' + \underline{\omega} \wedge \underline{u}_O + \right. \\ \left. + \underline{\omega}' \wedge \underline{x}_G + \underline{\omega} \wedge (\underline{\omega} \wedge \underline{x}_G) \right] = \underline{F}_{ext}(t) \\ \underline{I}_O \cdot \underline{\omega}' + \underline{\omega} \wedge (\underline{I}_O \cdot \underline{\omega}) + m \cdot \underline{x}_G \wedge \underline{u}_O' + \\ \left. + m \cdot \underline{x}_G \wedge (\underline{\omega} \wedge \underline{u}_O) \right] = \underline{M}_{ext,O}(t) \end{array} \right. \quad (1)$$

The vessel is then moved and oriented with respect to an earth-fixed reference system. The external force $\underline{F}_{ext}(t)$ and moment $\underline{M}_{ext,O}(t)$ comprise the following main effects: Froude-Krylov pressure, including hydrostatic term, calculated up to the instantaneous wetted surface of the hull (to catch geometrical nonlinearities); linear hydrodynamic radiation terms through convolution of kernel functions and infinite frequency added mass terms obtained from linear potential flow pre-calculations; instantaneous diffraction forces from linear frequency domain pre-calculations; manoeuvring forces, comprising a cross-flow model. Furthermore, it is possible to consider: constant and gusty wind effects; additional empirical damping terms (typically for, but not limited to, roll); linear/nonlinear, mooring-like springs; propulsors; lifting surfaces (rudders, fins).

In addition to the abovementioned effects, in the simulation tool developed herein, $\underline{F}_{ext}(t)$ and $\underline{M}_{ext,O}(t)$ also contain the instantaneous action, on the vessel, of the fluid in the tank. Such actions are calculated by the coupled CFD solver, which is based on the numerical solution of the 3D fluid field through a meshless Smoothed-Particle Hydrodynamics (SPH) approach.

The SPH approach has become very popular in CFD field thanks to the adaptability to complex geometries, and the capability of dealing with heavily fragmented fluids, while keeping a reasonable computational cost. The particular solver used herein is AQUA_gph (Cercos-Pita et al., 2013, Cercos-Pita, 2015), developed at University of Madrid. To address the actually incompressible flow,



AQUA_{gpusph} uses the commonly employed weakly-compressible SPH approach (WCSPH) (Monaghan, 2005, Colagrossi et al., 2009), which is based on the solution of the Navier-Stokes equations, where an artificial weak compressibility is considered through a pressure-density state equation which provides small density variations:

$$\begin{cases} \frac{d\rho_a}{dt} = -\rho_a \nabla \cdot \underline{u}_a \\ \frac{d\underline{u}_a}{dt} = -\frac{\nabla p_a}{\rho_a} + \frac{\mu}{\rho_a} \Delta \underline{u}_a + \underline{g} \\ p_a = p_a(\rho_a) \end{cases} \quad (2)$$

AQUA_{gpusph} solves the discretised version of (2) using the Lagrangian kernel-based SPH formalism. Other formulations can be found in order to perform truly incompressible SPH simulations (e.g. Cummins & Rudman, 1999, Souto-Iglesias et al., 2014), but the WCSPH formulation has the main benefit that a purely explicit scheme can be used to perform the integration, and hence, no linear system of equations needs to be solved in order to compute the pressure field at each time step. In order to speed up the computation, AQUA_{gpusph} can exploit, through OpenCL, the parallel computing capabilities of graphical processing units (GPUs), if such hardware, as in the present application, is available (Cercos-Pita et al., 2013, Cercos-Pita, 2015).

To allow coupled simulations, an explicit coupling strategy has been implemented, where SHIXDOF performs the time stepping by means of an explicit integration scheme, receiving force and moment from AQUA_{gpusph} at the beginning of each step, and passing to AQUA_{gpusph} the updated ship and tank motions at the end of the step. With such information, AQUA_{gpusph} simulates the fluid motion in the tank within the considered time step, while SHIXDOF waits to receive the

force and moment at the beginning of the next time step. The integration in SHIXDOF is carried out by means of a 4th-order Adams-Bashforth integration scheme with fixed time step. On the other hand, AQUA_{gpusph} integrates in time by means of a Leap-Frog method (Souto-Iglesias et al., 2006) with variable time step controlled by a Courant condition.

3. APPLICATION

An application of the developed nonlinear coupled simulation tool has been carried out using a freely available and well-known hull form geometry. This allows present results to serve as possible comparison cases for other researchers developing similar tools. Furthermore, the considered hull has been selected because experimental data regarding nonlinear rolling motion without tank were available from previous studies.

The geometry and positioning of the tank in the simulations was chosen, and constraint, to be compatible with an already existing 1:100 scale model of the hull. As a result of such choice, the positioning of the tank in the simulations is quite high above the waterline and above the centre of gravity.

Simulations have been targeted at assessing nonlinear effects on the roll response curve, coming from external hydrodynamics (ship-wave interaction) and internal hydrodynamics (ship-tank interaction). To this end, numerical experiments have been carried out, for one specific tank geometry, in regular beam waves having different steepnesses (ratio between wave height and wave length).

3.1 Sample hull and free surface tank

The simulation tool has been used for simulating the behaviour of a Series 60 hull form, in bare hull condition, and equipped with a box-shaped free surface tank. The bodyplan

of the hull, together with a transversal view of the tank geometry is shown in Figure 1, while the main characteristics of the hull and the loading condition (with empty tank) are reported in Table 1. Such hull form, without any tank onboard, was used in previous numerical and experimental studies regarding nonlinear roll motion in beam regular, bi-chromatic and irregular waves (Tzamtzis, 2004, Bulian et al., 2012, Bulian & Francescutto, 2013). As a result, a certain amount of reference experimental data was available for the present study.

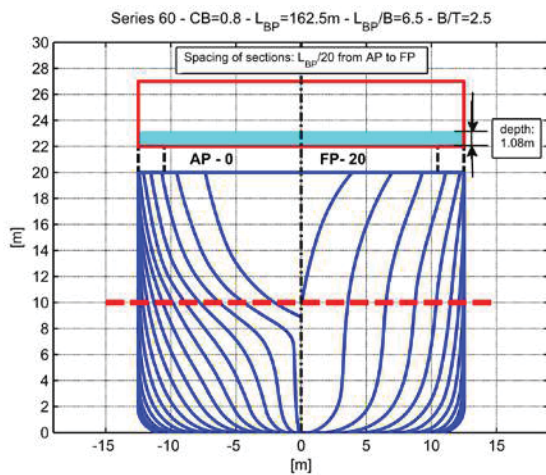


Figure 1: Hull bodyplan and tank geometry.

Table 1: Main data of hull and loading condition (without tank).

L_{BP}	[m]	162.5	Length b.p.
B	[m]	25.0	Beam
T	[m]	10.0	Draught
C_B	[-]	0.8	Block coefficient
\overline{GM}	[m]	1.65	Transversal metacentric height
\overline{KG}	[m]	8.59	Height of CoG above baseline
ω_0	[rad/s]	0.408	Roll natural frequency
$R_{xx,G}$	[m]	9.1	Dry roll radius of inertia (w.r.t. CoG)
$R_{yy,G}$	[m]	40.6	Dry pitch radius of inertia (w.r.t. CoG)
$R_{zz,G}$	[m]	40.6	Dry yaw radius of inertia (w.r.t. CoG)

The tested tank has the main characteristics reported in Table 2. The tank is longitudinally positioned at the mid perpendicular, spanning a total length of 10m in longitudinal direction (5m aft and 5m forward of the mid perpendicular). The transversal width of the tank corresponds to the ship breadth, and the fluid depth is set in such a way to obtain a first transversal linear natural sloshing mode matching the roll natural frequency of the vessel with empty tank. In such configuration, the ratio between the mass of the fluid in the tank and the mass of the vessel with empty tank is 0.83%. The increase of draught due to the additional weight loaded in the tank is 76mm, i.e. 0.76% of the ship draught without fluid in the tank. It is also to be noted that the depth to width ratio for the fluid in the tank is 0.0432, meaning that sloshing occurs in a shallow water regime. Even under purely static inclinations, the bilge corner of the tank becomes dry at a heel angle of just 4.9deg. It is herein assumed that the hull without tank has the same mechanical properties (mass, position of centre of gravity, radii of inertia) of the hull equipped with the empty tank. As a result, the indications “without tank” and “empty tank” are to be assumed, herein, as synonymous.

The righting lever (\overline{GZ}) curve has been calculated for the vessel without tank and with the tank. For sake of comparison, the calculation of the righting lever with the tank was carried out considering the cargo as both solid (frozen) and fluid. Results are shown in Figure 2. Since the liquid cargo is loaded high above the baseline, part of the reduction in the righting lever is due to the increase of \overline{KG} (the variation of \overline{KM} due to the small variation of draught, associated with the loading of the fluid in the tank, is very small). Then, the majority of the reduction in the restoring is due to the free surface effect. As a consequence of the large fluid depth to tank width ratio, free surface effects are practically linear with respect to the heeling angle until the tank bilge corner gets dry (abt. 5deg) then the overall free surface effect reduces as the heeling increases.



Table 2: Main characteristics of the tank.

Tank dimensions $L_{\text{tank}} \times W_{\text{tank}} \times H_{\text{tank}}$	10m x 25m x 5m
Longitudinal position	Centre at mid perpendicular
Height of tank bottom from baseline	22m
Fluid depth - d_{fluid}	1.08m
$d_{\text{fluid}} / W_{\text{tank}}$	0.0432
Filling ratio	0.2160

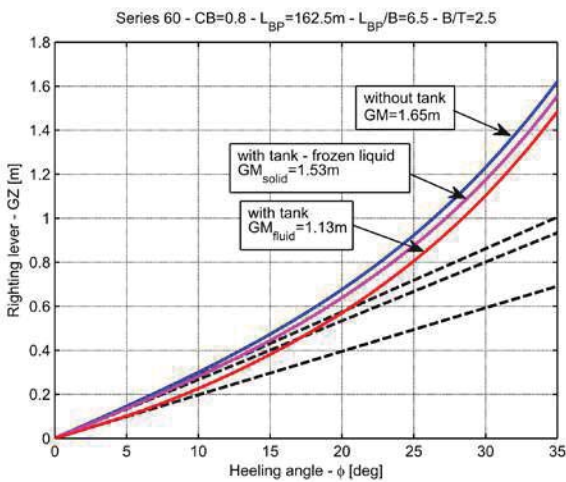


Figure 2: Righting lever curves without tank, with frozen liquid in the tank and with fluid in the tank.

3.2 Roll motion in regular beam waves without free surface tank

Before running a set of coupled simulations, the 6-DOF software tool has been compared and tuned, in terms of additional roll damping coefficients. The tuning has been performed making reference to a set of experimental data without tank for roll motion in regular beam waves at zero speed (Tzamtzis, 2004). A first tuning of the 6-DOF code on roll decay experimental data for the considered loading condition was carried out by Bulian & Francescutto (2013). Herein the tuning has been improved to achieve a better matching between simulations and experimental roll response at large forcing wave steepnesses in beam regular waves, while still keeping a good

matching with roll decay data and experiments in milder regular beam waves.

In the tuning process, the drag coefficient used in the cross flow model has been kept constant to a value equal to 0.8, which is in line with typical lateral drag coefficients for quite full vessels with similar beam to draught ratios (e.g. Kijima, 2003, Faltinsen, 1990). In view of the experimentally observed behaviour of equivalent linear roll damping coefficient as a function of the oscillation amplitude from roll decays, the tuning of damping in roll was carried out through an additional empirical linear-in-velocity term ($-B_{L,add} \cdot \dot{\phi}$) and an additional cubic-in-velocity term ($-B_{C,add} \cdot \dot{\phi}^3$). Such terms have been added to the moment acting on the vessel around the longitudinal axis of the ship-fixed reference system. It is to be noted that, as a result, such additional damping terms are not independent from the considered reference system.

Simulations have then been carried out in regular beam waves, without tank, for different frequencies close to the roll natural one, and considering two wave steepnesses, 1/100 and 1/30, as in the experimental conditions (Tzamtzis, 2004, Bulian & Francescutto, 2013). In both experiments and simulations the vessel was free to drift. In the experiments the beam sea condition was maintained by manual control, while in the simulations a linear, with respect to yaw, restoring moment directed along the earth-fixed vertical axis and with spring constant equal to $5.3 \cdot 10^8 \text{ N} \cdot \text{m} / \text{rad}$ was used in order to keep the heading at about 90deg. The introduction of this artificial spring leads to a yaw natural frequency, as measured from yaw decays, of $0.0673 \text{ rad} / \text{s}$, which is far enough from the roll natural frequency to reduce the risk of spurious couplings. The comparison between experimental results and results from simulations is shown in Figure 3 (at ship scale). Although there is still a small overestimation of the experimental roll amplitude at the larger forcing steepness, the re-tuning of additional roll damping has led to a reduction in the difference between

experimental and numerical maximum roll response at $s_w = 1/30$, from about 15% in Bulian & Francescutto (2013), to about 9% herein. The difference in the peak roll between experiments and simulations for $s_w = 1/100$ is, instead, 2%. It can be noticed that the bending towards high frequencies of the roll response curve, associated with the hardening roll restoring, is well captured by the simulations.

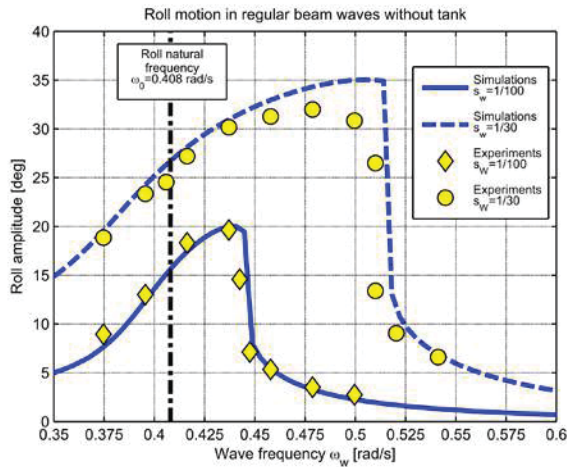


Figure 3: Roll motion in regular beam waves, without tank.

In order to analyse the obtained roll dissipation level in calm water after tuning the ship motions code, a numerical roll decay has been simulated. The resulting roll time history has then been analysed on the basis of the classical 1-DOF nonlinear model:

$$\ddot{\phi} + 2 \cdot \mu \cdot \dot{\phi} + \beta \cdot \dot{\phi} |\dot{\phi}| + \delta \cdot \phi^3 + \omega_0^2 \cdot r(\phi) = 0 \quad (3)$$

with $r(\phi) = \phi + \gamma_3 \cdot \phi^3 + \gamma_5 \cdot \phi^5 + \dots$

Results from the roll decrement analysis according to the methodology described by Bulian et al. (2009), lead to $\omega_0 = 0.408 \text{ rad} / \text{s}$, $\mu = 0.00340 \text{ s}^{-1}$, $\beta = 0.0994 \text{ rad}^{-1}$ and $\delta = 0.554 \text{ s} \cdot \text{rad}^{-2}$.

On the basis of the reported results, it can therefore be concluded that the 6-DOF

nonlinear ship motions code can be considered validated for the intended scope of this study.

3.3 Validation of the SPH solver

The SPH solver has been validated by simulating the SPHERIC validation test 9 (Botia-Vera et al., 2010, Bulian et al., 2010), for which data are available from <https://wiki.manchester.ac.uk/spheric/> under the “Validation Tests” section.

The validation test 9 consists in a simplified 1-DOF mechanical model of a tuned liquid damper (TLD), where a rectangular tank is allowed to rotate around a fixed point under the forcing of a translating mass with prescribed oscillatory motion. The motion of the mass is rectilinear in the tank-fixed reference system. The tank is partially filled with liquid, and the resulting system is, therefore, a 1-DOF mechanical system coupled with the action of the fluid inside the tank. Such system, can also be considered as a simplified model relevant for the dynamics of a vessel equipped with a free surface tank.

The equation of motion of the coupled system, in such condition, and the values for the model parameters can be found in (Pérez-Rojas et al., 2011, Botia-Vera et al., 2010, Bulian et al., 2010) and can also be obtained from the already mentioned SPHERIC website.

Figure 4 shows a comparison between experiments and simulations carried out with a total of about 100000 particles. The very good agreement between predictions and experimental outcomes can be noticed. The SPH solver can therefore be considered suitable for the intended purpose of this study.

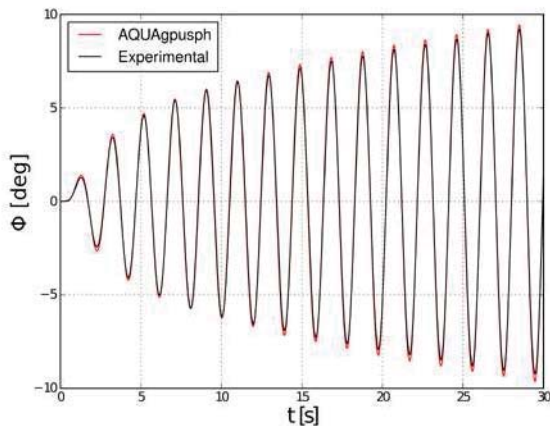


Figure 4: Roll angle of the tuned liquid damper. Comparison between SPH simulation and experiments. Amplitude of the motion for the moving mass: 100 mm . Forcing frequency equal to natural frequency of the dry system.

3.4 Roll motion in regular beam waves with free surface tank

After checking the capability of the 6-DOF nonlinear ship motions code to reproduce experimental data without the effect of the free surface tank, and after checking the capability of the SPH solver to properly reproduce the fluid action in a simplified 1-DOF coupled TLD model, a series of 6-DOF coupled ship-tank simulations have been carried out considering the tank partially filled with fluid as reported in Table 2.

Coupled 6-DOF simulations have been carried out in beam regular waves at zero speed, with the same numerical setup used for simulating the motion of the vessel without tank. The ship was free to drift, but rotations around the earth fixed vertical axis were partially restrained as in the case without tank.

The number of particles used for the fluid discretisation in the SPH solver was set to about 12000.

The primary scope of the simulations described herein was to analyse the behaviour of the coupled system for different levels of the wave forcing. Roll motion is known to behave nonlinearly as the wave forcing increases. Similarly, it can be expected to observe a nonlinear behaviour also for the action on the vessel of the fluid inside the tank as the motion of the tank boundaries, which are forcing the fluid, increases. For the considered tank this is particularly expectable, as a consequence of the small depth to width ratio, and the associated very shallow water regime in which the tank is working. To this end, four wave steepnesses have been tested, namely: $1/80$, $1/67$, $1/57$ and $1/50$. A specific set of wave frequencies was simulated for each steepness in order to have a clear representation of the roll response curve.

To allow an assessment of the effectiveness of the tank as a passive anti-rolling device, simulations have been carried out for the same four steepnesses also for the vessel without tank.

The total length of each simulation was set to 500s, with an initial ramp of 50s on the wave forcing. A 2s pre-stabilization of the SPH solver is performed before starting each simulation. The average roll amplitude was measured considering the final part of each simulation. Herein, the roll amplitude is defined as half of the difference between maximum and minimum roll within each cycle. The roll response curves resulting from the simulations are shown in Figure 5.

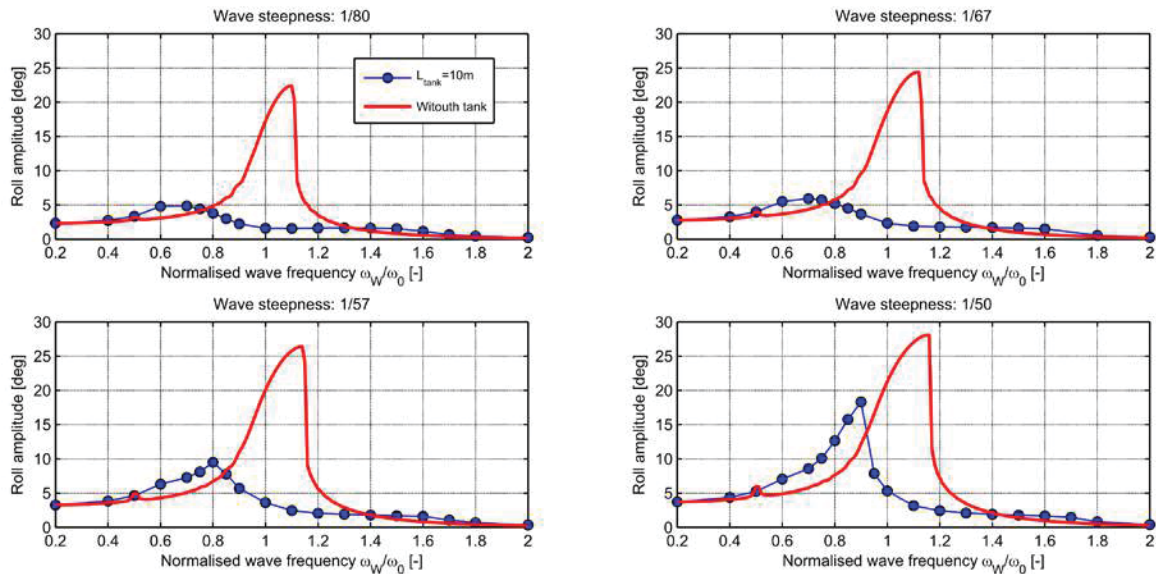


Figure 5: Roll response in regular beam waves with different steepnesses, with and without tank.

From the results reported in Figure 5, it can be noticed that the vessel without the tank follows the classical well-known nonlinear behaviour in regular beam waves, with a peak roll response which increases less-than-linearly as a function of the wave steepness, and a bending of the response curve towards the region of high frequencies, in accordance with the hardening behaviour of the roll righting moment in calm water. A small secondary peak is also visible at $\omega_W \approx 0.5\omega_0$, particularly for the largest steepnesses. Such small peak is associated with the inception of ultra-harmonic roll motions (Cardo et al., 1981), where the roll response, in addition to the harmonic at the encounter frequency, features a significant harmonic at twice the encounter frequency of the forcing.

Looking at the behaviour of the roll response with the tank partially filled with fluid, it can be noticed that the effect of the tank, as an anti-rolling device, is very significant in case of the two lowest forcing steepnesses ($s_W = 1/80$ and $s_W = 1/67$). In such cases the roll response shows the well-known double-peak shape (e.g., Field & Martin, 1976, Lee & Vassalos, 1996, Francescutto & Contento, 1999, Kim et al., 2007, and discussion by Bell in van den Bosch & Vugts, 1966): in the frequency region close to the roll natural frequency the roll motion is

strongly suppressed, while, on the other hand, the roll response with the tank is larger than without the tank in the frequency regions close to the two peaks appearing at low and high frequency.

However, the roll motion has a totally different behaviour for the largest forcing steepness ($s_W = 1/50$). In such case, the maximum roll amplitude with tank is much closer to the maximum roll amplitude without tank, and the effectiveness of the tank, as an anti-rolling device, is very significantly reduced. Looking at the shape of the response curve, although a small high-frequency peak is still present, the roll response with tank approximately resembles the one without tank, with a shifting towards lower frequencies and a reduction in the maximum peak. A small but noticeable hump is still present in the frequency region corresponding to the low frequency peak for at $s_W = 1/80$ and $s_W = 1/67$, as a reminiscence of the behaviour of the roll response curve for small wave forcing. The case of forcing steepness $s_W = 1/57$ seems to represent, instead, a sort of transition case. In this case, the roll response behaves, in part, similarly to the case of small wave forcing. However the inception of the peak which will then become dominant at $s_W = 1/50$, is already noticeable at wave frequencies around $0.8\omega_0$. In the same

frequency region, the transitional character of this forcing condition manifests also in time domain, as long transients before stationarity.

The behaviour described above on the basis of Figure 5 is more evident when plotting the roll response curves with tank for different steepnesses, on the same graph, as shown in Figure 6. From the response curves in Figure 6 it is also interesting to note that, similarly to the case without tank, also in case of vessel equipped with the tank the roll response curve, in the region of the low-frequency peak, tends to bend towards higher frequencies. Furthermore, it is also interesting to report that the observation of the time histories at $\omega_w = 0.5\omega_0$ indicates that, for all forcing steepnesses, the presence of the tank is able to suppress the inception of the small ultra-harmonic response which was instead observed in the simulations without tank.

Finally, Figure 7 shows the simulated fluid behaviour inside the tank for two example cases. The two cases correspond to the frequency ratio $\omega_w / \omega_0 = 0.9$ for the minimum and maximum simulated wave steepness, i.e. $s_w = 1/80$ and $s_w = 1/50$ respectively. The reported snapshots are taken at four representative time instants within the last available roll cycle, corresponding to: minimum roll, up-zero-crossing for roll, maximum roll and down-zero-crossing for roll. It can be noticed that impacts on the tank side take place at the lowest steepness. At the highest steepness, where the rolling amplitude exceeds 18deg, the fluid also impacts the top of the tank.

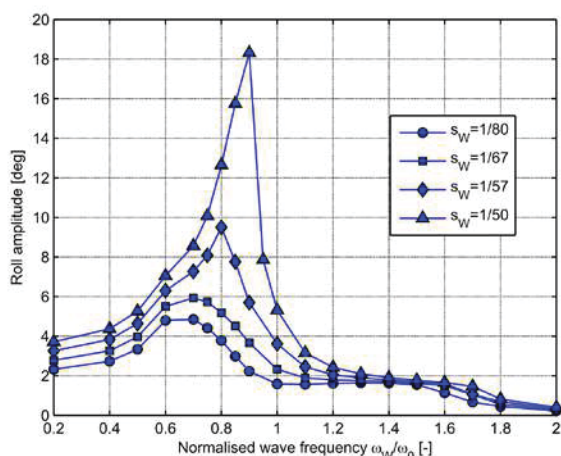


Figure 6: Roll response in regular beam waves with different steepnesses, with tank.

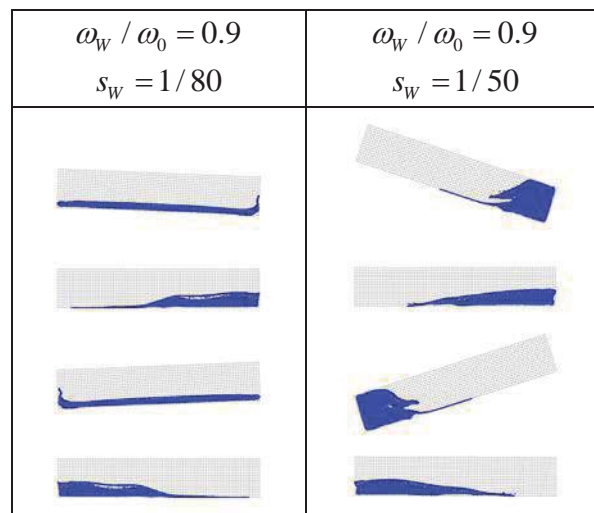


Figure 7: Representative snapshots of fluid inside the tank for two example cases.

4. FINAL REMARKS

Since vessels almost invariably sail with tanks partially filled by liquids, the analysis of ship motions in presence of free surface tanks onboard represents an interesting research topic, having also significant practical implications.

In this paper a time domain simulation approach has been presented where a blended (hybrid) nonlinear 6-DOF ship motions simulation code has been coupled with a nonlinear SPH solver intended to address the flow in the internal tank.

An application of the developed tool has been carried out for a Series-60 hull, with one rectangular tank meant to act as anti-rolling device. The tuning of the tank with the roll natural frequency of the vessel led to a small fluid depth to tank width ratio, and therefore a shallow water fluid regime.

The primary scope of the simulations described in the paper was to analyse the



behaviour of the coupled system for different levels of the wave forcing, in order to highlight the possible occurrence of nonlinear behaviours. To this end, simulations have been carried out in regular beam waves with different steepnesses.

Before carrying out coupled ship-tank simulations, the 6-DOF ship motions code was tuned, in terms of roll dissipation, using available experimental data. Validation comparisons between simulations without tank and available experimental data indicated a good agreement. Similarly, the SPH solver was separately validated on the basis of available experimental data for a 1-DOF coupled mechanical system representing a tuned liquid damper.

Results of coupled ship-tank simulations have been reported in terms of roll response curves, with and without tank, for a range of frequencies. Outcomes from simulations have clearly shown the occurrence of nonlinear phenomena. The most notable behaviour was found to be a reduction of effectiveness of the anti-rolling tank as the wave forcing, and the consequent motions, increase. Also, simulations without tank showed the occurrence of a small ultra-harmonic roll response at wave frequencies close to half the roll natural frequency. Such type of response, instead, did not appear with the tank partially filled by fluid. Also, bending of the response curves, with and without tank, was observed, in line with the hardening restoring of the vessel.

Although the developed approach has been tested herein at zero forward speed in beam regular waves with a box-shaped tank, the software architecture is more flexible. Indeed, the 6-DOF code allows simulating ship motions in case of the vessel manoeuvring in regular/irregular waves, considering the coupling with the tank. Furthermore, the SPH solver allows taking into account more complex tank geometries (e.g. non box-shaped tanks, presence of baffles and obstructions, etc.). As a result, in addition to representing a

valuable tool for research purposes, there are potentialities for this approach to be used for more practical engineering applications. Research is presently ongoing regarding the application of the present approach in different conditions and, in particular, in cases associated with different tank dimensions.

5. REFERENCES

- Bosch, J.J. van den, Vugts, J.H., 1966 "On roll damping by free-surface tanks" Transactions of the Institution of Naval Architects, Vol. 69, pp. 345-361.
- Botia-Vera, E., Souto-Iglesias, A., Bulian, G., Lobovský, L., 2010, "Three SPH novel benchmark test cases for free surface flows", Proc. 5th ERCOFTAC SPHERIC workshop on SPH applications, pp. 146-155
- Bulian, G., Francescutto, A., 2013, "Second Generation Intact Stability Criteria: on the validation of codes for direct stability assessment in the framework of an example application", Polish Maritime Research, Vol.20, Issue 4, pp. 52-61
- Bulian, G., Francescutto, A., Fucile, F., 2009, "Determination of Relevant Parameters for the Alternative Assessment of Intact Stability Weather Criterion on Experimental Basis", Final report HYD-III-CEH-5, University of Trieste
- Bulian, G., Francescutto, A., Sinibaldi, M., 2012, "Roll motion of a ship with low metacentric height in bi-chromatic beam waves", Proc. 11th International Conference on the Stability of Ships and Ocean Vehicles (STAB2012), 23-28 September, Athens, Greece, pp. 187-200
- Bulian, G., Souto-Iglesias, A., Delorme, L., Botia-Vera, E., 2010, "SPH simulation of a tuned liquid damper with angular motion,"



- Journal of Hydraulic Research, Vol. 48, Extra Issue, pp. 28–39
- Bunnik, T., Veldman, A., 2010, “Modelling the effect of sloshing on ship motions”, Proc. 29th International Conference on Ocean, Offshore and Arctic Engineering (OMAE2010), June 6-11, Shanghai, China, paper OMAE2010-20458
- Cardo, A., Francescutto, A., Nabergoj, R., 1981, “Ultraharmonics and Subharmonics in the Rolling Motion of a Ship: Steady-State Solution”, International Shipbuilding Progress, Vol. 28, pp. 234-251
- Carrica, P.M., Sadat-Hosseini, H., Stern, F., 2012, “CFD analysis of broaching for a model surface combatant with explicit simulation of moving rudders and rotating propellers”, Computers & Fluids, Vol. 53, pp. 117–132
- Cercos-Pita, J.L., 2015, "AQUAgpusph, a new free 3D SPH solver accelerated with OpenCL", Accepted for publication in Computer Physics Communications.
- Cercos-Pita, J.L., Souto-Iglesias, A., Gonzalez, L.M., Macià, F., 2013, “AQUAgpusph, a free 3D SPH solver accelerated with OpenCL”, Proc. 8th International SPHERIC Workshop, 4-6 June, Trondheim, Norway
- Colagrossi, A., Antuono, M., Touzé, D.L. 2009, “Theoretical considerations on the free-surface role in the Smoothed-particle-hydrodynamics model”, Physical Review E (Statistical, Nonlinear, and Soft Matter Physics), vol. 79(5), 056701
- Cummins, S., Rudman, M., 1999, “An SPH projection method”, Journal of Computational Physics, Vol. 152 (2), July, pp. 584–607
- de Kat, J.O., Paulling, J.R., 1989, “The Simulation of Ship Motions and Capsizing in Severe Seas”, Trans. SNAME, Vol. 97, pp. 139-168
- Faltinsen, O.M., 1990, "Sea Loads on Ships and Offshore Structures", Cambridge University Press
- Field, S.B., Martin, J.P., 1976, “Comparative effects of U-tube and free surface type passive roll stabilization systems”, Transactions of the Royal Institution of Naval Architects, Vol. 118, pp. 73-92.
- Francescutto, A., Contento, G., 1999, “An Investigation on the Applicability of Simplified Mathematical Models to the Roll-Sloshing Problem”, International Journal of Offshore and Polar Engineering, Vol. 9, pp. 97-104
- Hashimoto, H., Ito, Y., Kawakami, N., Sueyoshi, M., 2012, “Numerical Simulation Method for Coupling of Tank Fluid and Ship Roll Motions”, Proc. 11th International Conference on the Stability of Ships and Ocean Vehicles (STAB2012), 23-28 September, Athens, Greece, pp. 477-485
- Holden, C., Fossen, T.I., 2012, “A nonlinear 7-DOF model for U-tanks of arbitrary shape”, Ocean Engineering, Vol. 45, pp. 22–37
- IMO SDC1/INF.8-Annex 27, 2013, “Draft Guidelines of Direct Stability Assessment Procedures as a Part of the Second Generation Intact Stability Criteria – Submitted by Japan and United States”, in SDC1/INF.8 submitted by Japan, 15 November, London, UK
- IMO SLF52/WP.1-Annex 2, 2010, “Preliminary Specifications for the New Generation Intact Stability Criteria”, 28 January, London, UK
- IMO, 2009, "International Code on Intact Stability, 2008 - 2009 Edition"



- Kijima, K., 2003, "Some studies on the prediction for ship manoeuvrability", Proc. International Conference on Marine Simulation and Ship Maneuverability (MARSIM'03), pp. KN-3-1 – KN-3-10.
- Kim, B., Shin, Y.S., 2008, "Coupled seakeeping with liquid sloshing in ship tanks", Proc. 27th ASME International Conference on Offshore Mechanics and Arctic Engineering, 15-20 June, Vol. 6, pp. 247-257
- Kim, Y., Nam, B.W., Kim, D.W., Kim, Y.S., 2007, "Study on coupling effects of ship motion and sloshing", Ocean Engineering, Vol. 34, pp. 2176–2187
- Lee, B.S., Vassalos, D., 1996, "An investigation into the stabilization effects of anti-roll tanks with flow obstructions", International Shipbuilding Progress, Vol. 43, No. 433, pp. 70-88
- Malenica, Š., Zalar, M., Chen, X.B., 2003, "Dynamic coupling of seakeeping and sloshing", Proc. 13th International Offshore and Polar Engineering Conference, 25-30 May, Honolulu, Vol. III, pp. 486-492
- Mitra, S., Wang, C.Z., Hai, L.V., Reddy, J.N., Khoo, B.C., 2012, "A 3D fully coupled analysis of nonlinear sloshing and ship motion", Ocean Engineering, Vol. 39, pp. 1–13 (see also Corrigendum Ocean Engineering, Vol. 52, 2012, p. 128)
- Monaghan, J.J., 2005, "Smoothed particle hydrodynamics", Reports on Progress in Physics, vol. 68, pp. 1703–1759
- Neves, M.A.S., Merino, J.A., Rodríguez, C.A., 2009, "A nonlinear model of parametric rolling stabilization by anti-roll tanks", Ocean Engineering, Vol. 36, pp. 1048–1059
- Pérez-Rojas, L., Botia-Vera, E., Cercos-Pita, J.L., Souto-Iglesias, A., Bulian, G., Delorme, L., 2011, "A combined Experimental and SPH Approach to Sloshing and Ship Roll Motions", in "Contemporary Ideas on Ship Stability and Capsizing in Waves", Fluid Mechanics and Its Applications, Springer, Volume 96, Part 10, pp. 735-749 (see also Proc. STAB2009, pp. 261-270)
- Sadat-Hosseini, H., Stern, F., Olivieri, A., Campana, E.F., Hashimoto, H., Umeda, N., Bulian, G., Francescutto, A., 2010, "Head-wave parametric rolling of a surface combatant", Ocean Engineering, Vol. 37, pp.859–878
- Souto-Iglesias, A., Delorme, L., Pérez-Rojas, L., Abril-Pérez, S., 2006, "Liquid moment amplitude assessment in sloshing type problems with smooth particle hydrodynamics", Ocean Engineering, vol. 33, , pp. 1462–1484
- Souto-Iglesias, A., Macià, F., González, L.M., Cercos-Pita, J. L., 2014, "Addendum to on the consistency of MPS", Computer Physics Communications, Vol. 185(2), pp. 595 – 598
- Tzamtzis, S., 2004, "Development and testing of a procedure for the alternative assessment of Weather Criterion on experimental basis", Thesis, University of Trieste and National Technical University of Athens.
- Youssef, K.S, Mook, D.T., Nayfeh, A.H., Ragab, S.A., 2003, "Roll Stabilization by Passive Anti-Rolling Tanks Using an Improved Model of the Tank-Liquid Motion", Journal of Vibration and Control, Vol. 9, pp. 839-862
- Zhao, W., Yang, J., Hu, Z., Tao, L., 2014, "Coupled analysis of nonlinear sloshing and ship motions", Applied Ocean Research, Vol. 47, pp.85–97

This page is intentionally left blank



Modeling Sailing Yachts' Course Instabilities Considering Sail Shape Deformations

Emmanouil Angelou, *National Technical University of Athens*, angeloum@mail.ntua.gr

Kostas J. Spyrou, *National Technical University of Athens*, k.spyrou@central.ntua.gr

ABSTRACT

The performance of sailing yachts depends partly on the fluctuating pressure field around the sails which causes continual change of the shape of the sails. The present study focuses on the development of a mathematical model for predicting the behaviour of sailing yachts, with a twofold purpose: to evaluate the variations of forces and moments sustained by the sails due to wind induced sails-shape deformations; and to assess the impact of these variations on the development of course-keeping instability phenomena during downwind sailing conditions. The fluid-structure interaction problem of the sails is handled by coupling, in an iterative way, a Vorticity-Stream Function formulation to a Finite Element Method for flexure elements.

Keywords: *Sailing Yachts, Sail Modeling, Downwind Course*

1. INTRODUCTION

The course stability of sailing yachts is a topic that has not attracted much attention, although, historically, several records exist referring to broaching-to incidents of ships with sails (Spyrou 2010). The present study is a first step towards setting up a systematic study of the course stability of sailing yachts operating in wind and waves. A mathematical model is under development, consisted of two major components: an aerodynamic one, addressing the forces on the sails and the variation of their shape due to wind flow; and a hydrodynamic, handling the hull and its appendages.

Sails produce the aerodynamic forces exploited for propulsion. However, because they are very thin, they have their shape continually adapted according to the locally developing pressures. Thus the flying shape of a sail in real sailing conditions differs from its design shape and it is basically unknown. In terms of physical modelling, one can

distinguish sailing cases as *upwind* (running to the wind) where the flow is characterized as lifting and can be assumed as attached to the sails; and as *downwind* (running away from the wind) where viscous effects cannot be disregarded and drag effects are dominant. Recently, the fluid-structure interaction problem of the sails in the upwind case has been tackled, by coupling a low order Boundary Element Method for the aerodynamic part (Lifting Surface) to a Finite Element Method for the structural part (Shell Elements), in combination with an iterative scheme that provided the converged flying shape of the sail and the sustained forces and moments (Angelou & Spyrou 2013).

In the current paper, the sails model is expanded to a wider operational range of inflow angles, from the outskirts of upwind sailing, to beam and fully downwind cases. The method is a pseudo-3d approach, based on the evaluation of vorticity of the flow field around certain cross sections of the sails in order to obtain the force and moment coefficients, while the deformed shape of each sail is obtained using a finite element formulation for flexure

elements. The hydrodynamic part is not complete yet. However, in order to qualitatively evaluate our aerodynamic model we coupled it with a typical semi-empirical manoeuvring model accounting qualitatively for hull reaction and wave forces.

2. MATHEMATICAL MODEL

2.1 Equations of Motion and Coordinate Systems

Since downwind following seas are the cases of main interest, the model includes 4 degrees of freedom, surge, sway, roll and yaw and it used three different coordinate systems: an earth-fixed non-rotating coordinate system (X_0, Y_0, Z_0) , a wave fixed body system that travels with the wave celerity (x_w, y_w, z_w) and a body fixed system (x, y, z) with its origin fixed on the midship point where the centerplane and waterplane intersect (Fig. 1);

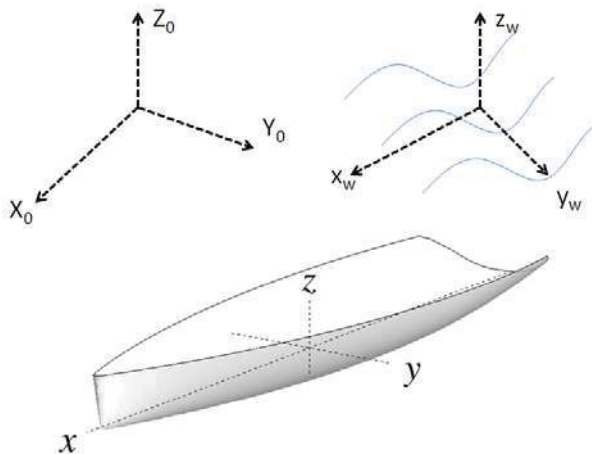


Figure 1: Coordinate Systems.

The systems are in accordance with the right hand rule where 'x' axis points positive forward, having on its left the positive 'y' axis, while positive 'z' axis points upwards.

Assuming the hull as a rigid body, the equations of motions for the 4 degrees of

freedom are as in Masuyama & Fukasawa (2011)

$$(m + m_x) \ddot{x} - (m + m_y \cos^2 \varphi + m_z \sin^2 \varphi) \dot{y} \cdot \dot{\psi} = X_{HR} + X_R + X_W + X_S \quad (1)$$

$$(m + m_y \cos^2 \varphi + m_z \sin^2 \varphi) \ddot{y} + (m + m_x) \dot{x} \cdot \dot{\psi} + 2(m_z - m_y) \sin \varphi \cos \varphi \cdot \dot{y} \cdot \dot{\varphi} = Y_{HR} + Y_R + Y_W + Y_S \quad (2)$$

$$(I_{xx} + J_{xx}) \ddot{\varphi} - [(I_{yy} + J_{yy}) - (I_{zz} + J_{zz})] \sin \varphi \cos \varphi \cdot \dot{\psi}^2 = K_{HR} + K_R + K_W + K_S \quad (3)$$

$$[(I_{yy} + J_{yy}) \sin^2 \varphi + (I_{zz} + J_{zz}) \cos^2 \varphi] \ddot{\psi} + 2[(I_{yy} + J_{yy}) - (I_{zz} + J_{zz})] \sin \varphi \cos \varphi \cdot \dot{\psi} \cdot \dot{\varphi} = N_{HR} + N_R + N_W + N_S \quad (4)$$

The subscripts on the right-hand-side of the equations indicate force contribution from *Hull Reaction, Rudder, Waves* and *Sails*. These terms are grouped into two modules, named *Hull* and *Sails Model* respectively, in accordance with the excitation being of hydrodynamic or aerodynamic origin.

3. SAILS MODEL

3.1 Sails Variation

Sails are surfaces of very small thickness and while this allows a major simplification in the fluid modelling, it simultaneously induces a drawback. This insignificant thickness makes the sail to be a very flexible surface, subjected to deformations due to the pressure forces it sustains under wind flow. Calculating the flow around them then is not enough, as one should



be able to account for the difference between the design shape of the sail and the flying shape it adopts. Moreover, it is important to know the effect this bears to the forces and moments on the sail. Excluding wind tunnel tests and real-time measurements at sea, a common computational approach is to combine a fluid solver for the flow field around the sail with a structural solver for the transition of the initial to the new shape.

Regarding the *upwind* case and in terms of the aforementioned simplification, the small thickness of the sail makes it ideal for being modelled with a potential flow method, such as the one using the Lifting Surface Theory (L.S.T.) (Angelou & Spyrou 2013). This is a formulation for lifting flows that allows the effects of camber and thickness to be decoupled and it is usually applied through a numerical scheme based on the Vortex Lattice Method (V.L.M.). While the lifting surface bears minimal computational cost, it requires that the flow always remains attached to the surface, thus restraining L.S.T.'s applicability to a relatively narrow range of fluid inflow angles.

To examine the behaviour of a sail in a wider operational range, notably *downwind*, as is the scope of this study, the use of viscous flows methods is unavoidable as drag effects become dominant. These methods provide great detail of the flow field, yet they induce a considerable computational cost.

The numerical schemes involving the solution of the Vorticity Transport – Stream Function equations in a computational mesh may appear at first instance outdated compared to modern schemes that handle the primitive variable form of the Navier-Stokes equations. However as the long term objective of this study is directional stability analysis using 6 degrees of freedom while taking into account the instant position and shape of the sail(s), this method was chosen as an intermediate step towards a Lagrangian “free” vorticity formulation, where remeshing of the domain

and the induced computational cost can be avoided.

3.2 Sails Modelling

Considering wind flow velocity V_{TW} and a sailing yacht that moves with boat velocity V_B , then the apparent wind, i.e., the wind that actually excites the sails, is defined as in Fossati (2009):

$$V_{AW}^2 = (V_{TW} \cdot \cos a_{TW} + V_B)^2 + V_{TW}^2 \sin^2 a_{TW} \cos^2 \varphi \quad (5)$$

$$a_{AW} = \text{atan} \left(\frac{V_{TW} \sin a_{TW} \cos \varphi}{V_{TW} \cos a_{TW} + V_B} \right) \quad (6)$$

where a_{TW} is true wind angle and a_{AW} is the apparent wind angle.

The sail forces are obtained in terms of *drag* (C_D) and *lift* (C_L) coefficients, where *drag* (D) is the resulting force on the direction of the free stream flow (apparent wind), while *lift* (L) is normal to it:

$$D = \frac{1}{2} \rho \cdot V_{wind}^2 \cdot S \cdot C_D \quad (7)$$

$$L = \frac{1}{2} \rho \cdot V_{wind}^2 \cdot S \cdot C_L \quad (8)$$

Through transformation to the ship coordinate system the surge and sway forces are obtained:

$$X_S = D \cdot \cos a_{AW} + L \cdot \sin a_{AW} \quad (9)$$

$$Y_S = D \cdot \sin a_{AW} + L \cdot \cos a_{AW} \cdot \cos \varphi \quad (10)$$

Roll and yaw sail induced moments are:

$$K_S = -Y_S \cdot z_{cef} \cdot \cos \varphi \quad (11)$$

$$N_s = (Y_s \cdot x_{cef} + X_s \cdot y_{cef}) \quad (12)$$

In this study, the method of aerodynamic force calculation is pseudo-transient, meaning that calculations are performed on certain sections of the sails, and vertical flow interaction effects are ignored. Every section has a computational flow field constructed around it, in the form of an unstructured meshed domain of triangular elements. A Finite Volume numerical scheme is applied on these elements for the solution of the Vorticity Transport and Stream Function equations.

Once the velocity and pressure fields are computed, pressure loads are transformed to nodal forces and they are used for deriving the deformation of the sail via a Finite Element Formulation for flexure beams. When the sail shape has converged, lift and drag coefficients of the section are used in order to calculate total sail excitation. Each section sail coefficient (red lines Fig. 2) is averaged over a surface that extends bilaterally off the section's vertical position (black lines Fig. 2). Total Drag and Lift forces of the sail are defined as

$$D = \frac{1}{2} \rho \cdot V_{wind}^2 \cdot \sum \{S_i \cdot C_{Di}\} \quad (13)$$

$$L = \frac{1}{2} \rho \cdot V_{wind}^2 \cdot \sum \{S_i \cdot C_{Li}\} \quad (14)$$

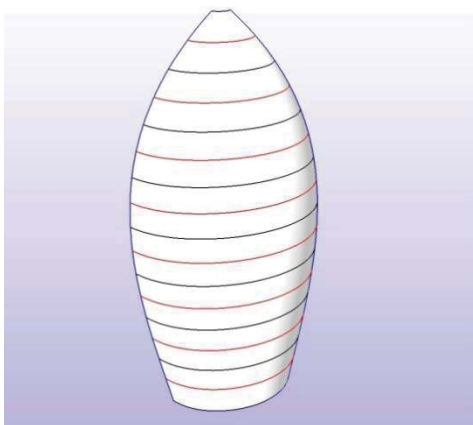


Figure 2: Spinnaker Sail and sections.

3.3 Meshing

The mesh is constructed using the Advancing Front Method – AFV (Peraire et al 1987), which was chosen due to its ability to handle complex geometries whilst its implementation is straightforward. Given the boundary of an outer domain Ω and any internal boundaries Ω_i , this formulation creates an initial front of connected segments, each of which is used as the edge of a candidate triangle element to be added. With every triangle addition, the respective initial segment is replaced by the new edge or edge(s), and the front is reduced until the domain is completely meshed.

However, the obtained mesh may contain triangles with highly acute angles, prone to cause numerical errors during the solution. To overcome this, the smoothing technique of Zhou & Shimada (2000) is applied on the domain. This method treats all triangle edges as springs, either on a compressed or on an elongated state. By iterating through probable nodal positions, this method seeks to find an optimized set, where the torsional energy of every spring is minimized. All non-boundary nodes are moved accordingly and each triangle tends to reach an equilateral shape (Fig. 3).

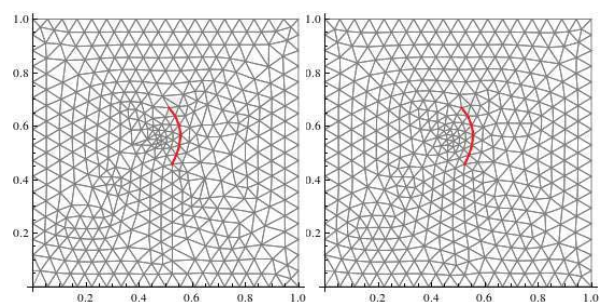


Figure 3: Initial (left) and Smoothed (Right) Mesh around a Sail Section (Bold Red).

While the obtained mesh is smoothed, the size of the triangles in regions away from the given boundaries tends to increase. This is a drawback in accuracy, especially in case the triangles are located in areas where state variables are characterized by large gradients.



A future step is the local refinement in these areas using mesh enrichment techniques.

3.4 Aerodynamic Component

The fluid domain around the sails is obtained by solving the non-conservative Vorticity Transport Equation (15) and the Stream Function Equation (16) using a Finite Volume scheme on an unstructured triangular meshed domain. The triangles are virtually treated as P2 elements, meaning that mid-edge point values of vorticity are included in the calculations, but only in order to update the vorticity on the centres and vertices.

$$\frac{\partial \omega}{\partial t} + u \frac{\partial \omega}{\partial x} + v \frac{\partial \omega}{\partial y} = \nu \left(\frac{\partial^2 \omega}{\partial x^2} + \frac{\partial^2 \omega}{\partial y^2} \right) \quad (15)$$

$$\frac{\partial^2 \psi}{\partial x^2} + \frac{\partial^2 \psi}{\partial y^2} = -\omega \quad (16)$$

The numerical solution of the Vorticity Transport equation is dictated by the viscous split technique where the advection and diffusion terms are treated separately (e.g. see Cottet & Koumoutsakos, 2000) :

$$\frac{\partial \omega}{\partial t} + u \frac{\partial \omega}{\partial x} + v \frac{\partial \omega}{\partial y} = 0 \quad (17)$$

$$\frac{\partial \omega}{\partial t} = \nu \left(\frac{\partial^2 \omega}{\partial x^2} + \frac{\partial^2 \omega}{\partial y^2} \right) \quad (18)$$

The pure advection part (17) of the Vorticity Transport equation is treated using the fluctuation-splitting scheme of Nishikawa & Roe (2005). This method provides a way for the calculation of the fraction of the fluctuation of a variable inside any triangle, as that fluctuation is directed to the triangle's downstream nodes. The nodes are characterized as upwind or downwind, according to the triangle's orientation in relation with the local convection velocity

vector \vec{V} . Thus, in every triangle, transport effects are accounted for, by updating only the downstream nodes.

The pure diffusion equation (18) is treated as in Hoffman & Chiang (2000). Considering any triangle T, by applying Green's theorem on the surface integral of the diffusion equation, the right hand side is transformed to a line integral that can be calculated using the mid-point vorticity values of the triangle edges. These are obtained by interpolation of vorticity value that is assigned on the neighbouring triangles centres, as also on the common nodes they share with triangle T.

The Stream Function, as in Hoffman & Chiang (2000), can be transformed from an elliptic (16) to a pseudo-transient (19) parabolic equation:

$$\frac{\partial \psi}{\partial t} = - \left(\frac{\partial^2 \psi}{\partial x^2} + \frac{\partial^2 \psi}{\partial y^2} + \omega \right) \quad (19)$$

Equation (19) is treated as the diffusion equation (18) with the addition of the calculated vorticity during the current time step as a source term.

The free stream flow is considered to enter a rectangular computational domain from the left side bearing horizontal velocity of constant magnitude u_0 , and exit from the right side far downstream of the sails. The same value of inflow velocity is considered at the top and bottom domain boundaries in order to simulate infinite fluid extent normal to them. The stream function is assigned a constant value across the bottom boundary and gradually increases with increasing height according to $u = \partial \psi / \partial y$ so as to provide a constant velocity u_0 . The stream function value on the top boundary remains constant until the end of the domain. Initial vorticity values have been set to zero all over the domain. When the wind vector has a non-zero angle of attack then inflow conditions for the velocity remain the same and it is the initial geometry of the sail that is rotated accordingly.



3.5 Aeroelastic Component

The structural response of every discrete sail section to wind loads is modelled using a Finite Element Method for *flexures*. A flexure is an enriched beam element, capable of being subjected to both axial and bending loading. Each section is divided to small segments that correspond to all triangle edges that consist of sail nodes explicitly. Considering a linearly elastic, isotropic and homogeneous material, the displacements \mathbf{U} of the nodes are calculated by solving the linear system

$$K_{STIFF} \cdot \mathbf{U} = \bar{\mathbf{F}} \quad (20)$$

The total stiffness matrix K_{STIFF} is composed by superposition of all element stiffness matrices k_E according to their connectivity. The matrix k_E is a joint matrix of a bar and a flexure element, for axial and bending loads respectively without considering any coupling between them. The formation of the bending flexure stiffness matrix for each segment is obtained through the application of the first theorem of Castigliano, with respect to nodal translational and rotational displacements, to the strain energy function U_E of the element (Hutton 2004).

$$U_E = \frac{1}{2} \int \sigma_x \varepsilon_x dV \quad (21)$$

Assuming that each segment can be considered as an elastic bar of constant cross section, the axial stiffness matrix of the element is formulated by analyzing the axial forces using the stress and strain formulae (Hutton 2004). After solving the linear system, nodal positions are adjusted according to the displacements vector of the solution and the domain is re-meshed.

4. HULL MODEL

As the scope of this study is to emphasize on the sail-induced impact on the development

of instabilities, the hull modular parts of the mathematical model have been treated so far using methods that do not necessarily lead to a precise quantification of hull responses. In addition, as the appendages have been approximated by simplified geometries and in the general case flow interaction effects between them have been omitted, hull realistic modelling is underacted. However as this manoeuvring model is still under development and bears a potential for growth of modelling detail regarding the modular parts it consists of, compromising with low level analysis on these components has been tolerated.

4.1 Inertia Terms

The calculation of the moments of inertia is based on the mass distribution of the yacht. For the canoe body, the added masses along y and z axes are calculated by considering sections along the hull and approximating their corresponding added mass coefficients from Korotkin (2008), while for the x axis and added moments of inertia around all axes as in Ridder (2004). The appendages are treated as elongated ellipsoids and their added masses as also their added moments of inertia are approximated as in Korotkin (2008).

4.2 Resistance

The resistance of the yacht can be decomposed to viscous, induced (which is the lift-induced Drag force component that is developing on the body and appendages due to the inflow angle) and wave-making parts. Viscous and induced terms are calculated as in Oossanen (1993) with some modifications regarding the contribution of the canoe body of the hull and the bulbous part of the keel, where a drag coefficient and a form factor have been added respectively, as in Nesteruk & Cartwright (2011) and in Scragg & Nelson (1993). Wherever included in the above formulation, the wetted surface is calculated from the summation of the areas of the hull

panels (Fig. 4) that are immersed at that instant under heel, if any. Lastly, the wave-making resistance of the yacht is calculated as in Pascual (2007).

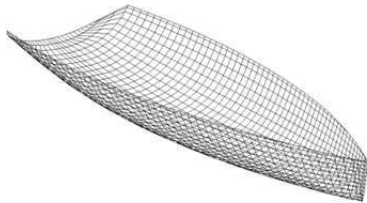


Figure 4: Canoe Body Panels.

4.3 Other Hull Reaction and Rudder

Other hull reaction forces and moments for sway and yaw modes are taken into account using the model of Inoue et al (1979), where the linear hydrodynamic coefficients are as in Clarke (1983) and the nonlinear as in Inoue et al(1979). Heel effects for the same modes have been added as in Hirano & Takashina (1980). Though the aforementioned references provide coefficients suitable for much larger hulls and need treatment regarding appendages effects, they were chosen as a rough indication due to our lack of data regarding the hydrodynamic responses of the studied sailing yacht. Roll terms are limited to damping and restoring moments. Rudder forces and moments in the model are accounted for as in Masuyama&Fukasawa (2011).

4.4 Waves

Considering an undisturbed pressure field around the yacht, the wave excitation is limited to Froude-Krylov forces and moments. These are calculated by integrating the unit potential φ_0 (e.g. Belenky & Sevastianov 2003) on every immersed panel of the hull up to the elevated running waterline, after the panel

coordinates have been transformed suitably for the relative position of the hull on the encountered wave.

5. CASE STUDY– RESULTS

5.1 Principal Dimensions

Problems of course stability in strong wind are well known for motorships (e.g. Spyrou 1995, Spyrou et al 2007), while for sailing yachts the available studies are only a few (e.g. Harris et al 2000). The yacht used as a case study is a one-mast modern cruiser, carrying a main and a jib sail, or a main and a spinnaker sail, for upwind and downwind courses respectively. Principal dimensions of the hull are on table 1.

HULL	
Length Overall	13.90 m
Length Waterline	12.86 m
Beam Waterline	2.79 m
Draught [Canoe Body Total]	0.525 m 3.45 m
Displacement	7830 kg

Table 1.Hull and Sails Dimensions.

The concept of the first two “trial” simulated scenarios is to apprehend the sensitivity of the model. The first scenario handles a case where the yacht is sailing under the influence of constant wind of 10 knots speed and $\alpha_{TW}=0^\circ$ direction off the stern (*true* wind angle) while wave excitation is omitted.

After a small simulated time ($t = 10\text{sec}$) the wind direction is considered to change to $\alpha_{TW} = 10^\circ$ off the stern while the rudder angle is kept fixed to zero position. On both cases counter-rotating vortices develop in front and back of the sail (Fig.5). This vorticity trend was expected, as compared with a bluff canopy body, bearing strong similarity to a sail (Johari & Desabrais 2005). As the wind angle changes, the yacht commences a turn. Trajectory and responses for 30 seconds of simulation are depicted in Figures 6 to 8.

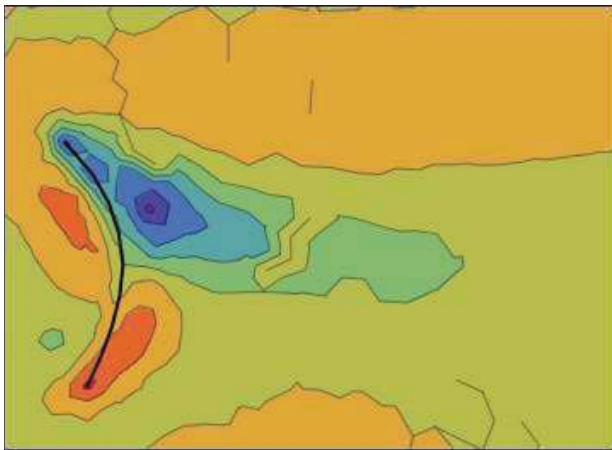


Figure 5a: Vorticity field, V_{wind} : 10kn, a_{TW} : 0°

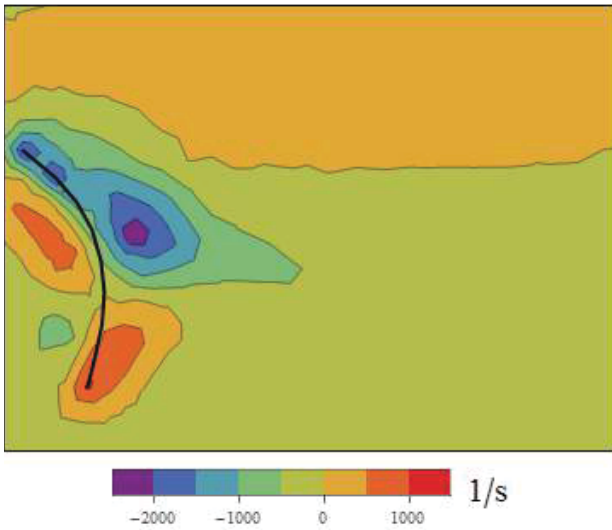


Figure 5b: Vorticity field, V_{wind} : 10kn, a_{TW} : 10°

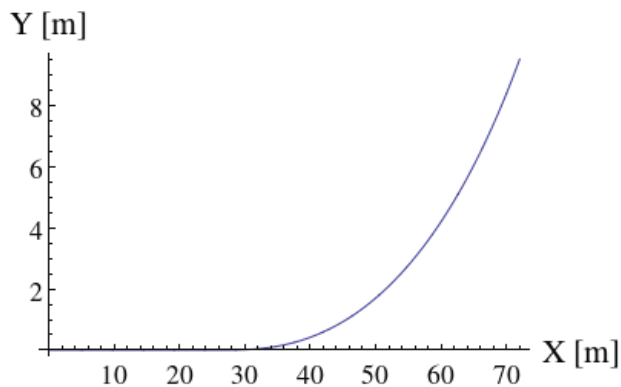


Figure 6: Course trajectory: scenario 1.

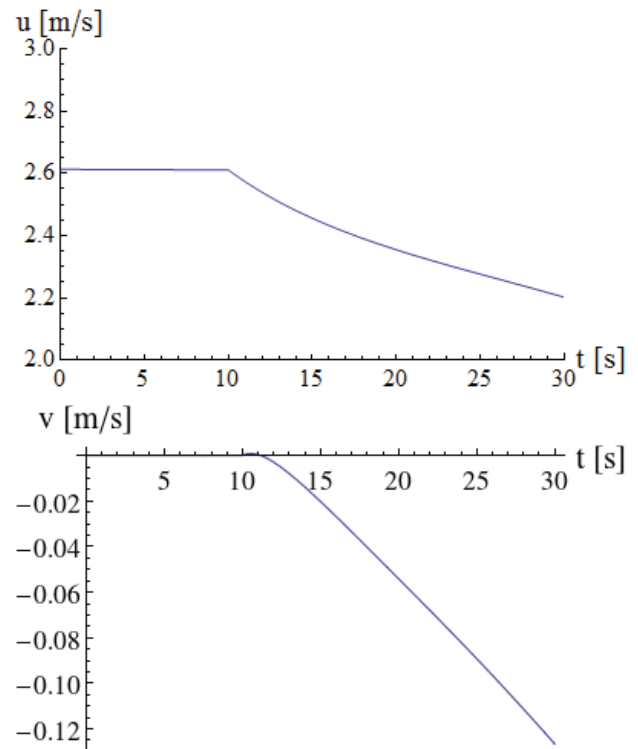


Figure 7: Surge (top) and sway (bottom) velocity.

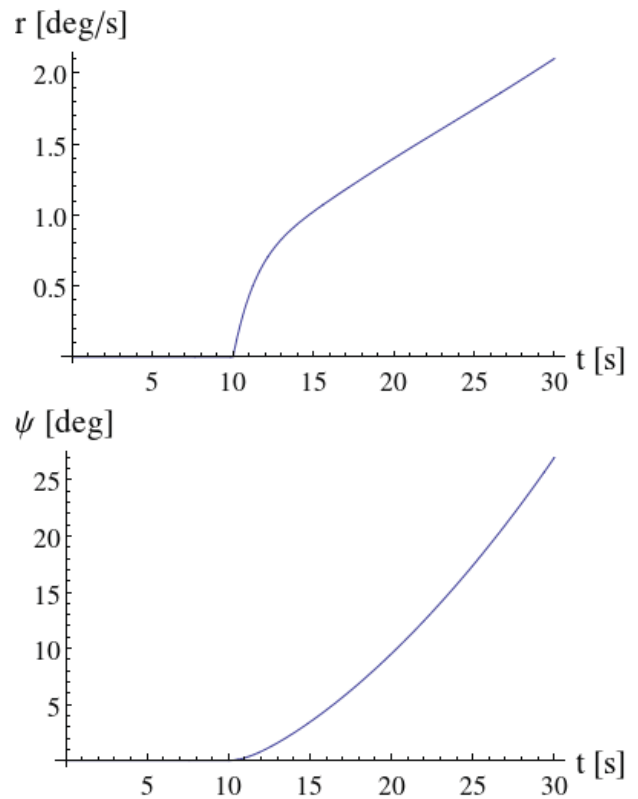


Figure 8: Yaw turning rate (top) and angle (bottom).

In the second scenario the yacht is sailing under the influence of a purely following *true* wind (0° off the stern) of constant speed of 10 knots. Simultaneously it is excited by following harmonic waves of $\lambda = 1.5 L_{wl}$ with steepness $H/\lambda = 0.036$. As shown in Fig. 9, the yacht experiences asymmetric surging. Moreover, for a very steep wave ($H/\lambda = 0.051$) it adopts surf-riding behaviour (Fig. 9).

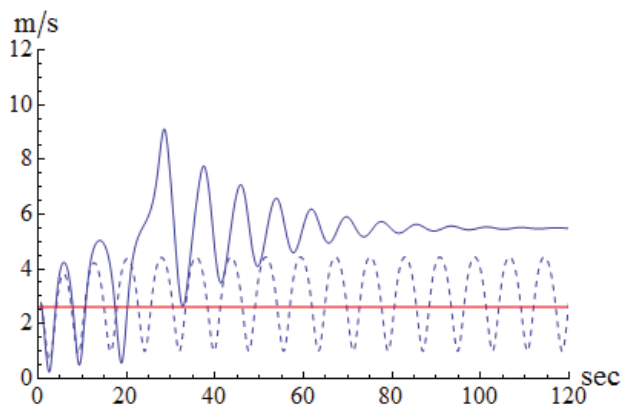


Figure 9: Asymmetric surging and surf-riding.

6. CONCLUSIONS – FUTURE WORK

This study is the first step towards a mathematical model suitable for the analysis of directional instabilities phenomena of sailing yachts. As the authors' intention is to evaluate the impact of sail shape deformations and sail forces variations on the behaviour of yachts, the hull model has been formulated inside the context of low level detail analysis, while the sails have been modelled by coupling two relatively simple models, among the family of the finest advanced methods: a pseudo-3d Vorticity-Stream function formulation and a Finite Element Method for flexure elements.

The performance of the sails model seems realistic, in qualitative terms. Future steps include further development by implementing turbulence effects and by moving towards a full 3d method for both the fluid and structural formulations.

The hull model has proved to be hypersensitive to excitations. This was expected and it is attributed to the choice of handling (in lack of any full scale data or of a more appropriate formulation) the performance of a small sailing yacht using methods intended for hulls of significant greater displacement; doing so, the influence of the appendages was underacted and the damping of the hull underestimated.

The same method used for the fluid part of the sails model can be modified to tackle the problem of finding a realistic pattern of hull reaction forces and moments.

7. ACKNOWLEDGMENTS

Mr. Angelou acknowledges with gratitude his support by NTUA's PhD Research Fund for Doctoral Candidates (EAKE).

8. REFERENCES

- Angelou, E. and Spyrou, K.J., 2013, "Simulations of Sails of a Yacht Using a Fluid-Structure Interaction Model", 10th HSTAM International Congress on Mechanics, Chania, Greece.
- Belenky, V.L. and Sevastianof, N.B., 2003, "Stability and Safety of Ships, Vol. II : Risk of Capsizing", *Elsevier Ocean Engineering Book Series*, Vol.10-II, pp. 83-86.
- Clarke D., Gedling P. and Hine G., 1983, "The Application of Manoeuvring criteria in Hull Design using Linear Theory", *RINA Transactions*, Vol. 125, pp. 45-68.
- Cottet, G.H., Koumoutsakos, P.D., 2000, "Vortex Methods: Theory and Practice", Cambridge University Press, Cambridge, UK.



- Fossati, F., 2009, "Aero-Hydrodynamics and the Performance of Sailing Yachts", Adlard Coles Nautical, London, pp. 265-287.
- Harris, D., Thomas, G., Renilson, M., 2000, "Towards Predicting the Behaviour of Yachts in Following Seas", 7th International Conference on Stability of Ships and Ocean Vehicles, pp. 595-608.
- Hirano, M. and Takashina, J., 1980, "A Calculation of Ship Turning Motion Taking Coupling Effect Due to Heel into Consideration", Journal of the West-Japan Society of Naval Architects and Ocean Engineers, Vol. 59, March 1980, pp. 71-81.
- Hoffmann, K.A. and Chiang, S.T., 2000, "Computational Fluid Dynamics", Vol. II, Engineering Education System, pp. 391-402.
- Hutton, D.V., 2004, "Fundamentals of Finite Element Analysis", Mc-Graw Hill, pp. 91-131.
- Inoue, S., Hirano, M. and Mukai, K., 1979, "The Non-linear Terms of Lateral Force and Moment Acting on Ship Hull in Case of Maneuvering", The Japan Society of Naval Architects and Ocean Engineers, Vol 58, August 1979, pp. 153-160.
- Johari, H. and Desabrais, J.K., 2005, "Vortex Shedding in the Near Wake of a Parachute Canopy", Journal of Fluid Mechanics, vol. 536, pp.185-207.
- Korotkin, A.I., 2008, "Added Masses of Ships Structures", Springer, Series of Fluid Mechanics and its Applications, Vol.88, pp. 82.
- Masuyama, Y. and Fukasawa T., 2011, "Tacking Simulation of Sailing Yachts with New Model of Aerodynamic Force Variation During Tacking Maneuver", SNAME Journal of Sailboat Technology, Article 2011-01.
- Nesteruk, I. and Cartwright, J.H.E., 2011, "Turbulent Skin-Friction Drag on a Slender Body of Revolution and Gray's Paradox", 13th European Turbulence Conference (ETC13), Journal of Physics: Conference Series 318.
- Nishikawa, H. and Roe, L.P., 2005, "Towards High-Order Fluctuation-Splitting Schemes for Navier-Stokes Equations", 17th AIAA CFD Conference, Toronto.
- van Oossanen, P., 1993, "Predicting the Speed of Sailing Yachts", SNAME Transactions, Vol. 101, pp. 337-397.
- Pascual, E., 2007, "Revised Approach to Khaskind's Method to Calculate the Wave-Making Resistance Depending on the Sectional Area Curve of the Ship", Journal of Ship Research, Vol. 51, September 2007, pp. 259-266.
- Peraire, J., Vahdati, M., Morgan, K. and Zienkiewicz, O.J., 1987, "Adaptive Remeshing for Compressible Flow Computations", Journal of Computational Physics, Vol. 72, pp. 449-466.
- Ridder, E.J., Vermeulen, K.J. and Keuning, J.A., 2004, "A Mathematical Model for the Tacking Maneuver of a Sailing Yacht", The International HISWA Symposium on Yacht Design and Yacht Construction, Amsterdam, Netherlands.
- Scragg C.A. and Nelson B.D., 1993, "The Design of an Eight-Oared Rowing Shell", SNAME Marine Technology, Vol. 30, No.2, April 1993, pp. 84-49.
- Spyrou K., 1995, "Yaw Stability of Ships in Stationary Wind", Ship Technology Research/Schiffstechnik, 42, No.1, pp. 21-30.
- Spyrou K., Tigkas, I., Hatzis, A., 2007, "Dynamics of a Ship Steering in Wind



Revisited”, Journal of Ship Research, 51,
pp. 160-173.

Spyrou, K.J., 2010, “Historical Trails of Ship
Broaching-To”, The Transactions of the
Royal Institution of Naval Architects: Part
A - International Journal of Maritime
Engineering, 152, Part A4, pp. 163-173.

Zhou, T. and Shimadi, K., 2000, “An Angle-
Based Approach to Two-Dimensional Mesh
Smoothing”, Proceedings of the Ninth
International Meshing Roundtable, New
Orleans, pp. 373–384.

This page is intentionally left blank

Session 13.1 – STABILITY IN ASTERN SEAS

Coherent Phase-Space Structures Governing Surge Dynamics in Astern Seas

Toward a Split-Time Method for Estimation of Probability of Surf-Riding in Irregular Seas

The Effect of Ship Speed, Heading Angle and Wave Steepness on the Likelihood of Broaching-To in Astern Quartering Seas

This page is intentionally left blank



Coherent Phase-Space Structures Governing Surge Dynamics in Astern Seas

Ioannis Kontolefas, *National Technical University of Athens*, ikon@central.ntua.gr

Kostas J. Spyrou, *National Technical University of Athens*, spyrou@deslab.ntua.gr

ABSTRACT

Consideration of a steep multi-chromatic wave field greatly increases the complexity of ship surge dynamics as it renders the underlying strongly nonlinear system also time-dependent. Consequently, conventional concepts used for the analysis of stationary phase-space flows are no longer sufficient to support an in-depth investigation of ship dynamics. To overcome this hindrance, the concept of hyperbolic Lagrangian Coherent Structures (LCSs) is employed. These phase-space objects can be regarded as finite-time generalizations of the stable and unstable manifolds of hyperbolic trajectories defined in dynamical systems with special (such as periodic or quasiperiodic) time dependencies. LCSs represent, locally, the strongest repelling or attracting material surfaces (curves in the case of 2-dimensional systems) advected with the phase flow. We identify hyperbolic LCSs that are intrinsic to the phase flow associated with the surge motion of a ship in astern seas. To the global approach of LCSs is incorporated a scheme aiming to track in space-time “local features” of the flow. The emerging new toolset can enhance substantially current efforts towards a rigorous assessment of ship dynamic stability in steep following seas.

Keywords: *Surf-riding, Multi-frequency Waves, Lagrangian Coherent Structures*

1. INTRODUCTION

The mechanisms generating surf-riding for a ship in regular seas have been extensively studied in the past (Kan 1990; Spyrou 1996). However, gaining understanding beyond the context of harmonic waves has been considered as a daunting task, till recently. The consideration of a multi-frequency wave field brings in new concepts accruing from the time-dependent nature of the problem.

For the regular sea scenario, it is well known that surf-riding can be identified as an equilibrium solution of the surge equation of

motion. The consideration, though, of more general wave forms introduces profound complications. For an irregular seaway, this key definition needs to be revised, since stationary states are not likely to exist; i.e., one cannot assume that the underlying non-autonomous dynamical system will admit constant solutions. Therefore, a broader definition of surf-riding needs to be sought.

These difficulties have been recognized and a phenomenological approach to surf-riding in irregular seas has been proposed, expanding upon the notion of wave celerity and its role in signaling the capture to surf-riding (Spyrou et al. 2012, 2014a). In particular, definition and methods for the calculation of wave celeri-



ty for an irregular seaway were proposed and their relevance to the problem of surf-riding was examined. The appeal of such an approach is that it can permit the evaluation of the probability of surf-riding in irregular seas, by setting up the latter as a threshold exceedance problem.

Through the identification of “surf-riding equilibria”, i.e. points on the wave where the equilibrium of forces in the longitudinal direction of the ship is instantaneously satisfied, Belenky et al. (2012) endeavoured to gain insight into the dynamics of surge equation in multi-frequency following waves. It is noted that for the calculation of such points, celerity of irregular waves needs to be evaluated.

In another study, Spyrou et al. (2014b) examined the possibility of extracting and tracking “features” related to the surge dynamics in irregular seas (the term is used to characterize objects that are relevant to the problem considered). It was concluded that meaningful features are found among the elements of the zero set of the “acceleration field” i.e., points on the phase space where the acceleration and its time derivative attain, instantly, zero values. Moreover, it was conjectured that certain points satisfying such a condition correlate with surf-riding events.

In the current work, new methods with potential to yield further insights into the dynamics of the surge motion in multi-chromatic astern seas are applied. In particular, the concept of hyperbolic Lagrangian Coherent Structures (LCSs) is tested for unveiling the changing-in-time organization of system’s phase-space. Through their organizing role, these structures can be considered as analogues of the stable and unstable manifolds of hyperbolic fixed points, defined in autonomous dynamical systems. For their identification different methods can be applied. Here, a popular, in the nonlinear dynamics literature, numerical scheme is applied, based on the calculation of the spatial distribution of the

largest finite-time Lyapunov Exponent of system’s trajectories.

2. LAGRANGIAN COHERENT STRUCTURES

2.1 General

The concept of Lagrangian Coherent Structures seems to have emerged as result of the interbreeding of ideas originating from the fields of dynamical systems theory and fluid dynamics. Although the term was first introduced by Haller & Yuan (2000) many people have contributed in the development of computational strategies – for a short review see Shadden (2011). In the context of fluid flows, LCSs can be physically observed as the cores of emergent trajectory patterns and are identified as, locally, the strongest attracting/repelling material surfaces advected with the flow. LCSs have been extensively used during the last years in a wide range of applications concerning physical and biological flows, while the theory, as well as efficient calculation methods, are still developing.

2.2 Identification of LCSs

Although one can choose among different identification schemes (such as the finite size Lyapunov Exponent (FSLE) approach, or the variational theory of hyperbolic LCSs developed recently by Haller (2011) that enables a more rigorous computation) for the needs of the current study we will consider a widely used computational procedure, which involves the calculation of the largest finite-time Lyapunov Exponent (FTLE) field.

Let us consider the following dynamical system that defines a flow on the plane,

$$\dot{x} = f(x, t), \quad x \in D \subset \mathbb{R}^2, \quad t \in [t^-, t^+] \quad (1)$$



A trajectory of system (1) at time t , starting from the initial condition x_0 at t_0 , will be denoted by $x(t; t_0, x_0)$. We can write for the flow map $F_{t_0}^t(x_0)$ of (1),

$$F_{t_0}^t : D \rightarrow D \quad (2)$$

$$x_0 \mapsto x(t; t_0, x_0)$$

Through (2), the phase-particle passing from x_0 at time t_0 , is associated with its position $x(t; t_0, x_0)$ at time t . If we furthermore consider two phase-particles, located at x_0 and $x_0 + \xi_0$ at time t_0 , we can write for their distance $\|\xi_t\|$, in a first order approximation with respect to $\|\xi_0\| \ll 1$,

$$\|\xi_t\| \approx \|\nabla F_{t_0}^t(x_0) \xi_0\| = \|\xi_0\| \sqrt{\hat{\xi}_0^T \left[\nabla F_{t_0}^t(x_0) \right]^T \nabla F_{t_0}^t(x_0) \hat{\xi}_0} \quad (3)$$

In the above $\hat{\xi}_0$ is the unit vector along the direction of ξ_0 , A^T denotes the transpose of A , while $\nabla F_{t_0}^t(x_0)$ is the deformation gradient and $C_{t_0}^t(x_0) = \left[\nabla F_{t_0}^t(x_0) \right]^T \nabla F_{t_0}^t(x_0)$ the right Cauchy-Green deformation tensor, both evaluated at x_0 . $C_{t_0}^t(x_0)$ is a real symmetric, positive definite tensor and as such has real positive eigenvalues,

$$0 < \lambda_1 \leq \lambda_2 \quad (4)$$

Moreover, the corresponding eigenvectors e_i , $i=1,2$ form an orthonormal basis. The Cauchy-Green deformation tensor provides a measure of how line elements in the neighbourhood of x_0 deform under the flow i.e., how the lengths and the angles between line elements change, when considering the configuration in the close vicinity of $x(t; t_0, x_0)$ at times t_0 and t . A circular blob of initial conditions centred at x_0 will evolve into an ellipse, with the major (minor) axis aligned with the direction of the eigenvector e_2 (e_1). The coefficients of expansion along these directions will be given by $\sqrt{\lambda_i}$, $i=1,2$.

The finite-time Lyapunov exponents (FTLEs) are defined as follows,

$$\Lambda_i = \frac{1}{|t-t_0|} \ln \sqrt{\lambda_i}, \quad i=1,2 \quad (5)$$

The largest FTLE, Λ_2 , is usually referred to as ‘‘FTLE’’ without distinction. By virtue of (5) Λ_2 can be regarded as a time-averaged measure of stretching and therefore, as a (rough) measure of a trajectory’s hyperbolicity. Yet, as noted by Shadden (2011) and Haller (2011), this does not hold in general.

Through the calculation of the spatial FTLE distribution, the identification of LCSs can be made possible. The latter will appear as local maximizing curves of the FTLE field. Typically, the calculation of the field is performed on the basis of a structured grid of initial conditions spanning a considered domain at a given time t_0 . The grid is integrated over a specified time interval, $\tau = t - t_0$, using a numerical integration algorithm. Once the final position of each grid point is calculated, the deformation gradient is obtained by implementing a finite difference scheme on the nodes of the initial grid. In the final step of the procedure, the largest eigenvalue of the deformation gradient is computed and the FTLE field is calculated directly from expression (5). The location of repelling/attracting LCSs can be identified as ridges of the FTLE field when forward/backward integration times are considered – contraction can be viewed as expansion in reverse time.

3. MATHEMATICAL MODEL OF SURGE MOTION

Consider the following unidirectional waveform comprised of N propagating, harmonic wave components,

$$\zeta(x;t) = \sum_{i=1}^N A_i \cos \left[k_i x - \omega_i t + \varepsilon_i^{(r)} \right] \quad (6)$$



In the above, x is the distance from an earth-fixed point of reference, while A_i , k_i and ω_i are the amplitude, wave number and frequency, respectively, of the distinct wave component i ; $\varepsilon_i^{(r)}$ denotes the random phase of the latter, uniformly distributed in the range $[0, 2\pi)$.

We, furthermore, consider an elementary mathematical model that can reproduce asymmetric surging and surf-riding occurrences in following waves of the form (6) – Spyrou et al. (2012, 2014a),

$$\underbrace{(m - X_{\dot{u}})}_{\text{inertia}} \ddot{\xi} = \underbrace{(\tau_0 n^2 + \tau_1 n \dot{\xi} + \tau_2 \dot{\xi}^2)}_{\text{thrust}} - \underbrace{(r_1 \dot{\xi} + r_2 \dot{\xi}^2 + r_3 \dot{\xi}^3)}_{\text{resistance}} + \underbrace{\sum_{i=1}^N A_i RAO_i \sin[k_i \xi - \omega_i t + \varepsilon_i^{(r)} + \varepsilon_{fi}]}_{\text{wave force}} \quad (7)$$

In the equation above, ξ is the position of a ship-fixed point of reference with respect to the earth-fixed origin, while RAO_i and ε_{fi} denote the response-amplitude-operator and phase, respectively, of the surging force corresponding to the wave component i ; n corresponds to the propeller revolutions. The overdot denotes differentiation with respect to time t . Setting,

$$x_1 = \xi, \quad x_2 = \dot{\xi} \quad (8)$$

equation (7) can be written in normal form,

$$\begin{aligned} \dot{x}_1 &= x_2 \\ \dot{x}_2 &= \left\{ \tau_0 n^2 + \sum_{i=1}^N f_i \sin[k_i x_1 - \omega_i t + \varepsilon_i^{(r)} + \varepsilon_{fi}] - \right. \\ &\quad \left. - (r_1 - \tau_1 n)x_2 - (r_2 - \tau_2)x_2^2 - r_3 x_2^3 \right\} / (m - X_{\dot{u}}) \end{aligned} \quad (9)$$

where in the above $f_i = A_i RAO_i$.

4. APPLICATION

We select, as a case study, the tumblehome hull from the ONR topside series with $L = 154 \text{ m}$, $B = 18.8 \text{ m}$ and $T = 5.5 \text{ m}$. To test the applicability of the method in the problem considered, we first write system (9) for $N = 1$ (regular waves),

$$\begin{aligned} \dot{x}_1 &= x_2 \\ \dot{x}_2 &= (m - X_{\dot{u}})^{-1} \left[(\tau_1 n - r_1)x_2 + (\tau_2 - r_2)x_2^2 - r_3 x_2^3 + \right. \\ &\quad \left. + f \sin(kx_1 - \omega t + \varepsilon) + \tau_0 n^2 \right] \end{aligned} \quad (10)$$

We set the wave length and steepness values to $\lambda = L$ and $H / \lambda = 0.04$, respectively, where H the wave height. Deep water is assumed. For the calculation of the FTLE field, a grid is considered at $t_0 = 300 \text{ s}$ on a (x_1, x_2) domain. Integration time is set to $\tau = 45 \text{ s}$. The graph of the resulting field can be seen on the left part of figure 1. On the right part of the same figure, we visualize loci of points where the field surpasses a selected threshold of $0.85 \text{Max}(\Lambda_2)$. The emergent curves correspond to repelling LCSs over the interval $[t_0, t_0 + \tau]$.

To further examine the relevance of these structures with the stable and unstable manifolds of hyperbolic fixed points arising in the context of surf-riding in regular waves, we render (10) in autonomous form by considering the following transformations,

$$x_1 = x_1^w + ct, \quad x_2 = x_2^w + c \quad (11)$$

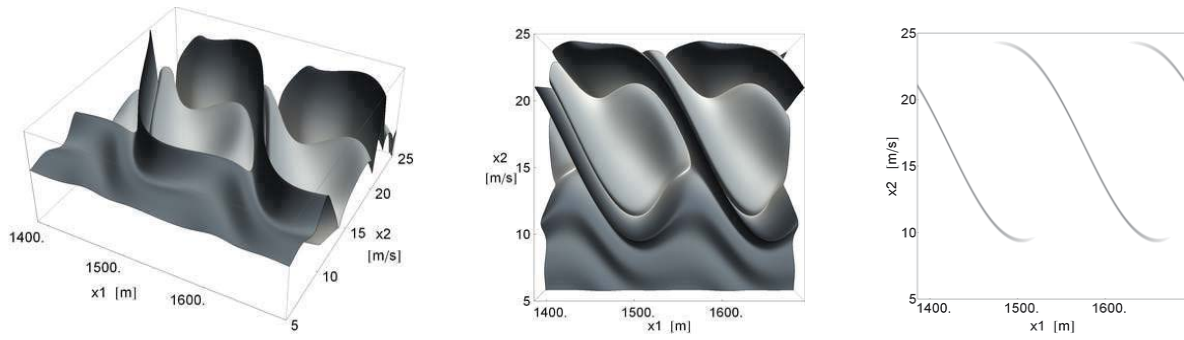


Figure 1 Harmonic excitation: The graph of the forward FTLE field over a (x_1, x_2) domain (left, middle). Loci of points where the field surpasses a selected threshold (right).

In the above, x_1^w and x_2^w is the longitudinal position and velocity, respectively, of the ship with respect to a frame located at a wave crest, translating with the wave celerity c .

Applying expressions (11) to system (10) we obtain, after rearranging, the following set of equations,

$$\begin{aligned} \dot{x}_1^w &= x_2^w \\ \dot{x}_2^w &= (m - X_{ii})^{-1} \\ &\left\{ \left[\tau_1 n - r_1 + 2c(\tau_2 - r_2) - 3r_3 c^2 \right] x_2^w + \right. \\ &\quad \left. + (\tau_2 - r_2 - 3r_3 c)(x_2^w)^2 - r_3 (x_2^w)^3 + \right. \\ &\quad \left. + f \sin(k x_1^w + \varepsilon) + g(c, n) \right\} \end{aligned} \quad (12)$$

where,

$$\begin{aligned} g(c, n) &= \tau_0 n^2 + \\ &\quad + (\tau_1 n - r_1)c + (\tau_2 - r_2)c^2 - r_3 c^3 \end{aligned} \quad (13)$$

It can be seen that system (12) does not depend (explicitly) on time. Stationary solutions can be obtained by setting the right hand side to be equal to zero and solving with respect to x_1^w and x_2^w . In the upper part of figure 2, a number of saddle points are identified and the unstable/stable manifolds are “grown” by integrating perturbed, with respect to the fixed points and along the eigendirections, initial

conditions forward and backward in time. Wave length and nominal speed are set to $\lambda = L$ and $u_{nom} = 12.5 \text{ m/s}$. The figure on the left (right) correspond to a wave steepness of $s = 0.015$ ($s = 0.04$).

We, consequently, consider system (10) and calculate, for the same settings, the forward ($\tau = 420 \text{ s}$) and backward ($\tau = -240 \text{ s}$) FTLE field at $t_0 = 0 \text{ s}$. LCSs are identified as in the case of figure 1. Results are presented in the lower part of figure 2; grey (black) lines correspond to repelling (attracting) LCSs. We note that the arrangement of the structures revealed is, substantially, identical to the arrangement of manifolds integrated from the saddle points. The only difference is that the former are translating with the wave celerity – as system (10) is expressed with respect to an earth-fixed frame.

We now introduce a second wave component i.e., system (9) is considered with $N = 2$. The length and steepness of the reference wave are set to $\lambda_1 = L$ and $s_1 = 0.04$. The parameters of the second wave component are fixed such that $\omega_2/\omega_1 = 0.91$ and $s_2/s_1 = 0.4$. Nominal speed is set to $u_{nom} = 12 \text{ m/s}$. FTLE fields are calculated at 258 s and 282 s (figure 3). As it can be noticed, LCSs seem to persist while their arrangement resembles, in a sense, to that observed in the regular case. This time though, the image is somehow “distorted” – as expected.

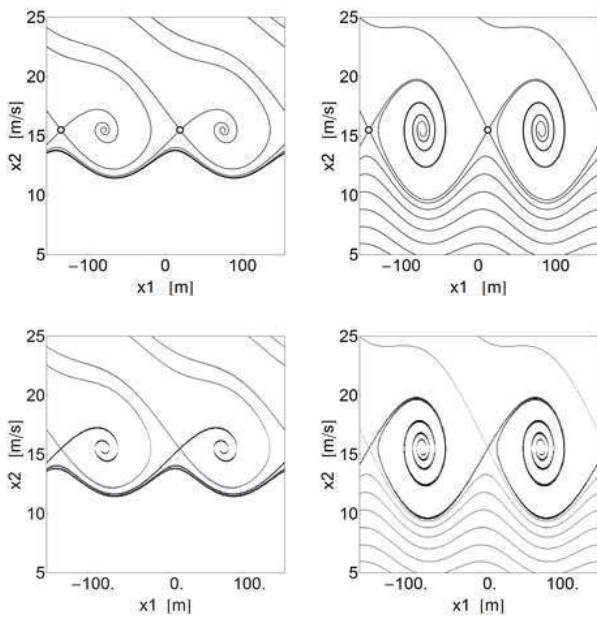


Figure 2 Top: Manifolds of hyperbolic points of (12). Bottom: LCSs of (10) obtained from forward (grey) and backward (black) FTLE fields.

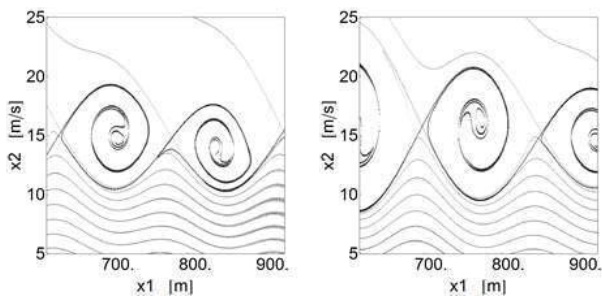


Figure 3 Bi-chromatic excitation: Attracting (black) and repelling (grey) LCSs.

The same procedure is repeated for the case of a JONSWAP spectrum with a peak period and significant height of $T_p = 10$ s and $H_s = 5.5$ m, respectively. A frequency range of $0.5\omega_p$ is considered around the peak value ω_p and a 51-component wave is produced. Nominal speed is set to $u_{nom} = 12$ m/s. Results are displayed in figure 4. As it can be seen, the arrangement of the identified structures appears to be fairly complicated.

Returning to the bi-chromatic scenario, we attempt, this time, to ascertain the organizing

role of LCSs on the time-varying phase-flow. We set $\lambda = L$, $s_1 = 0.025$, $\omega_2/\omega_1 = 0.76$,

$s_2/s_1 = 0.4$ and $u_{nom} = 12$ m/s. In figure 5 a parcel of particles is integrated – these correspond to different initial conditions for the ship. The evolution of the parcel under the flow reveals different “long-term” behaviour of particle trajectories, as the former, after some time, splits in two. Some particles seem to respond in a surging-like manner (figure 5, particles on the left part of the last snapshot), while others seem to be engaged to surf-riding (same snapshot, right part).

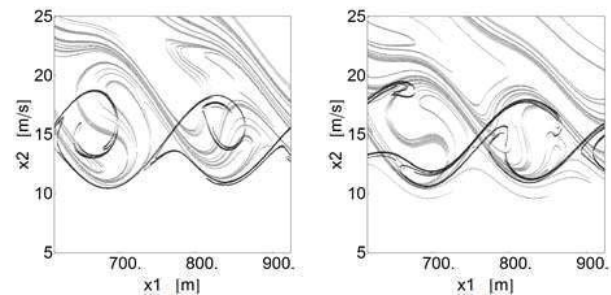


Figure 4 Attracting (black) and repelling (grey) LCSs for the case of a JONSWAP spectrum (51 wave components).

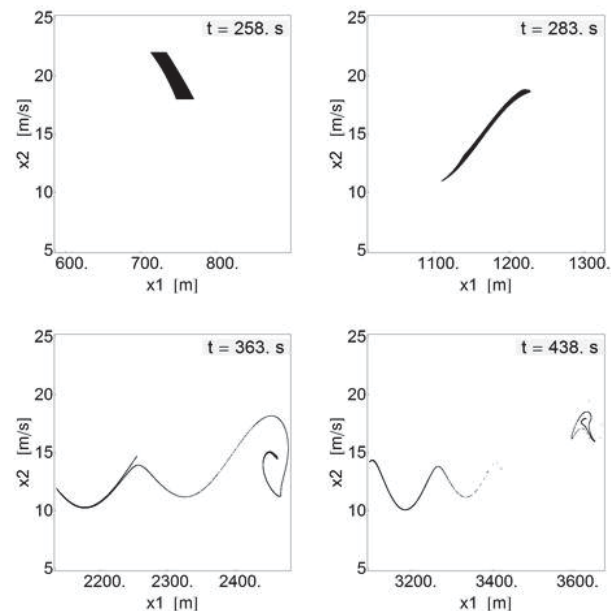


Figure 5 Bi-chromatic excitation: Integration of a dense patch of initial conditions reveals qualitatively different “long-term” behaviour of particle trajectories.

We keep the same setting and calculate the FTLE field on a domain containing the initial conditions ($t = 258$ s). It seems that the “sus-

pect” for the situation depicted above can be identified among the repelling LCSs of the phase flow. Specifically, the repelling LCS associating with the hyperbolic trajectory passing near (790,16) at time $t = 258$ s (figure 6, snapshots on the left), acts as a transport barrier between regions of the flow with distinct dynam-

ics. In fact, particles travel along this repelling structure towards the hyperbolic trajectory, where they are redirected towards different branches of the attracting LCS correlating with the same trajectory (figure 6, last three snapshots, top and bottom row).

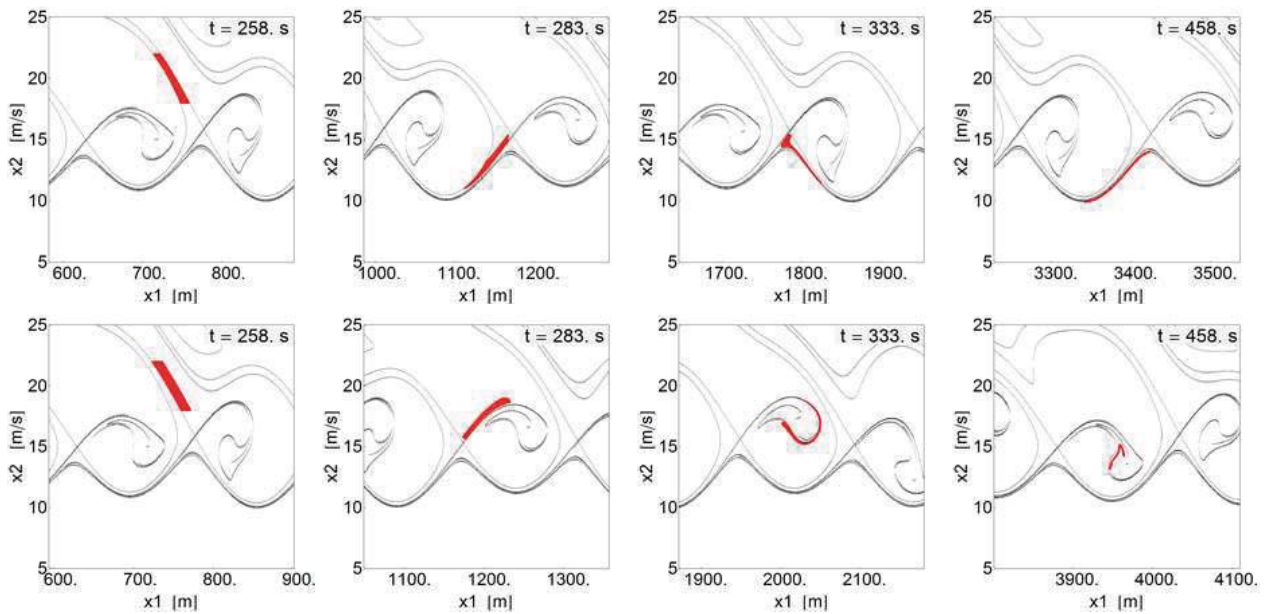


Figure 6 Same setting as in figure 5. Advection of two adjacent phase-particle parcels (red); integration of 91.000 and 118.000 (approx.) initial conditions, top and bottom row respectively.

Lastly, a bi-chromatic scenario is considered, with the frequency and steepness ratio of the two related wave components set to $\omega_2/\omega_1 = 0.93$ and $s_2/s_1 = 0.5$, respectively. The reference wave has been chosen such that $\lambda_1 = L$ and $s_1 = 1/30$, while nominal speed is set to $u_{nom} = 12$ m/s.

We differentiate (9) with respect to time to obtain the acceleration field $a = (\ddot{x}_1, \ddot{x}_2)$ – the use of this term is justified from the fact that one can interpret (9) as a velocity field on the phase plane. Our objective is to track critical points of a i.e., points where the acceleration vector vanishes. In Spyrou et al. (2014b) it has been conjectured that certain critical points of this field correlate with surf-riding events. Furthermore, in Spyrou et al. (2015) it has been argued that critical points of a moving along paths that “resemble” to solutions of (9) seem

to mark regions in the extended phase space where ensembles of trajectories are engaged to surf-riding.

In figure 7, a simulation corresponding to the aforementioned scenario can be seen (red line). Distance is measured from amidships (x -axis) while u -axis refers to velocity as measured by an on-shore observer. Three critical points of the acceleration field have been detected at around $t = 220$ s (these have been selected as they are related to the calculated trajectory; one could find more critical points at different space-time intervals). Their paths (grey and black lines) have been computed using the Feature Flow Field method (Theisel & Seidel 2003). In the same figure, we have included sections depicting LCSs that have been identified on phase-space windows around the ship at selected time instants. There seems to be a strong correspondence between the paths

of two critical points (denoted with grey lines) and hyperbolic trajectories revealed via the FTLE fields. The third critical point, on the other hand, appears near the core of an attracting LCS, in a region of the phase flow where a

surf-riding state can be revealed (Spyrou et al. 2015). It is noted that for the considered arrangement, this would be a periodic trajectory with an attracting character.

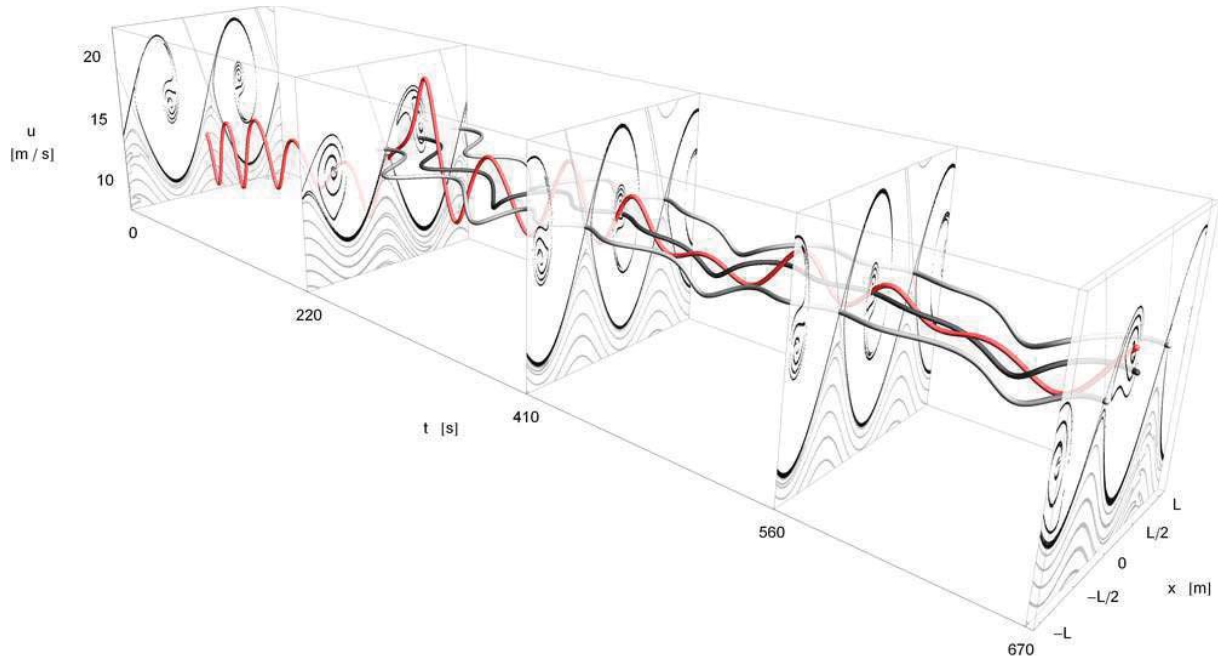


Figure 7 Bi-chromatic excitation: Ship trajectory (red line), LCSs at selected time instants and paths of three critical points of the acceleration field (black and gray lines).

5. CONCLUDING REMARKS

Methods for gaining insight into the dynamics of ship surge motion in astern multi-chromatic seas are introduced. Specifically, an identification method for Lagrangian Coherent Structures (LCSs) is applied on the phase flow defined by the surge equation of motion. It is based on a well-known scheme with a wide range of applications in the literature, which involves the calculation of the spatial distribution of the largest finite-time Lyapunov exponent (FTLE). Through the FTLE field, LCSs i.e., influential material lines shaping the pattern of the time-dependent flow, were obtained. Their role as phase-flow organizing structures was examined. It was found that, for the case of a bi-chromatic scenario, LCSs can help to understand the evolution of ensembles of initial

conditions, by providing the location of transport barriers, as well as the final destinations of particle trajectories.

Furthermore, the Feature Flow Field method was implemented for the tracking of features, corresponding to elements of the zero set of the acceleration field defined by the surge equation of motion. Results obtained from the tracking of such features and the LCSs identification procedure were combined. It has been shown that the paths of certain features correlate to hyperbolic trajectories of the surge equation, while others to trajectories with attracting character that seem to evolve in the core of specific branches of attracting LCSs.



6. ACKNOWLEDGEMENTS

The calculation and testing of LCSs for surging and surf-riding behaviour described in this paper have been funded by the Greek General Secretariat of Research and Technology under the General Program ARISTEIA I (contract reference number GSRT-252). The work regarding the feature tracking method applied in Section 4 has been funded by the Office of Naval Research, ONRG grant number N62909-13-1-7, under Dr. Ki-Han Kim, Dr. Tom Fu and Dr. Woei-Min Lin.

7. REFERENCES

- Belenky, V., Spyrou, K., & Weems, K., 2012, "Evaluation of the probability of surf-riding in irregular waves with the time-split method", Proceedings of 11th International Conference on the Stability of Ships and Ocean Vehicles, Athens, Greece, pp. 29-37.
- Haller, G. and Yuan, G., 2000, "Lagrangian coherent structures and mixing in two-dimensional turbulence", Physica D, 147, pp. 352-370.
- Haller, G., 2011, "A variational theory of hyperbolic Lagrangian Coherent Structures", Physica D, 240, pp. 574-598.
- Kan, M., 1990, "Surging of Large Amplitude and Surf-riding of Ships in Following Seas", Selected Papers in Naval Architecture and Ocean Engineering, The Society of Naval Architects of Japan, 28.
- Shadden, S. C., 2011, "Lagrangian Coherent Structures", Transport and Mixing in Laminar Flows: From Microfluidics to Oceanic Currents, Roman Grigoriev, Ed., Wiley-VCH.
- Spyrou, K., 1996, "Dynamic instability in quartering seas: The behaviour of a ship during broaching", Journal of Ship Research, SNAME, 40, No 1, pp. 46-59.
- Spyrou, K., Belenky, V., Themelis, N., & Weems, K., 2012, "Conditions of surf-riding in an irregular seaway", Proceedings of 11th International Conference on Stability of Ships and Ocean Vehicles, Athens, Greece, pp. 323-336.
- Spyrou, K., Belenky, V., Themelis, N., & Weems, K., 2014a, "Detection of surf-riding behaviour of ships in irregular seas", Nonlinear Dynamics, DOI 10.1007/s11071-014-1466-2.
- Spyrou, K., Belenky, V., Reed, A., Weems, K., Themelis, N., Kontolefas, I., 2014b, "Split-Time Method for Pure Loss of Stability and Broaching-To", Proceedings of 30th Symposium on Naval Hydrodynamics, Hobart, Tasmania, Australia.
- Spyrou, K., Themelis, N., Kontolefas, I., 2015, "Development of Probabilistic Models for Evaluating the Dynamic Stability and Capsize Tendency of Naval Vessels with Respect to Broaching-to", Technical Report to the Office of Naval Research (2015), ONRG grant number: N62909-13-1-7.
- Theisel, H., Seidel, H-P., 2003, "Feature flow fields", Data Visualization 2003, Proc. VisSym 03, 2003, pp. 141-148.

This page is intentionally left blank



Toward a Split-Time Method for Estimation of Probability of Surf-Riding in Irregular Seas

Vadim Belenky, *Naval Surface Warfare Center Carderock Division*, vadim.belenky@navy.mil

Kenneth Weems, *Naval Surface Warfare Center Carderock Division*, kenneth.weems@navy.mil

Kostas Spyrou, *National Technical University of Athens*, k.spyrou@central.ntua.gr

ABSTRACT

The paper reviews the status of a multi-year research effort for using the split-time method to calculate the probability of ship capsizing due to broaching-to in irregular waves. The present work focuses on extending the existing theory of surf-riding and broaching-to from regular waves to irregular waves and applying it to numerical simulation codes. Extending the theory for irregular waves leads to the formulation of a spatial-temporal framework for considering surf-riding where the celerity of irregular waves must be defined. An approximate metric for the likelihood of surf-riding in irregular waves has been proposed as the distance, in the phase plane, between the instantaneous position of a ship and the stable surf-riding equilibrium at that instant. Further work includes studying the properties of the surf-riding phase plane in irregular waves and statistics of surf-riding occurrences.

Keywords: *Probability, Surf-Riding, Celerity, Split-Time Method*

1. INTRODUCTION

Surf-riding and broaching-to are associated, complex phenomena linked through the generation of attraction towards a point of equilibrium located near a wave trough, appearing to be stable in surge but unstable in yaw. This yaw instability leads to a rapid, uncontrollable turn which can induce a large roll angle or capsize. The standing theory of surf-riding and broaching-to was proposed on the basis of the nonlinear dynamics theory (Spyrou 1996, 1997). It used an ordinary differential equations (ODE) model of ship motion in regular following/quarterming waves. The minimal mathematical model for describing these phenomena includes surge-sway-yaw for modeling broaching-to plus a roll motion equation to model capsize. An auto-pilot equation also must be included for the directional control of the ship. The resulting system has a 10-dimensional phase space.

This already complex description becomes even more complex if one considers the fact that large-amplitude ship motions are described

by integro-differential equations, where wave excitation cannot be separated from stiffness and hydrodynamic memory effects, such as radiation and diffraction forces, are present. Furthermore, the irregularity of realistic ocean introduces new physical qualities to the phenomenon.

The challenge to include surf-riding and broaching into a probabilistic assessment of stability based on advanced hydrodynamic codes has been taken up by the US Office of Naval Research (ONR) project "A Probabilistic Procedure for Evaluating the Dynamic Stability and Capsizing of Naval Vessels". The project's main objective is to create a robust theory of probabilistic capsizing in irregular waves and a numerical procedure based on this theory.

The split-time method is the probabilistic framework of this project. The idea of the split-time method is to separate the complex problem of the probability of a rare, extreme event in two problems that may be less complex. The "non-rare" problem is associated with an intermediate random event, statistics of which can be obtained by running an advanced code for sufficient time. This "non-rare"

problem ensures a correct relation between time and probability in irregular waves. The “rare” problem is responsible for modeling the physics of the rare event. Its core is a metric of the danger of the severe event, for example capsizing or large roll angle caused by broaching, that is computed when the intermediate random event occurs. The procedure is repeated for each intermediate random event observed during the non-rare simulations. The sample of metric values is then statistically extrapolated to determine the likelihood of the rare event. Since the metric value is expected to include the physics of the extreme event, actual observations of the event are not required, so the method is expected to work for conditions (sea states, speed, loading) where extreme events are rare.

2. SURF-RIDING AND BROACHING-TO IN LAMP

2.1 Objective and Approach

As the current theory of surf-riding and broaching-to was developed using ODE, application to more general models raises certain questions. Can this theory be extended to the cases when ship motions are presented with integro-differential equations with 6 degrees of freedom and hydrodynamic memory effects? How well will the analysis tools of nonlinear dynamics work with the dynamical system represented by the advanced hydrodynamic code? The results of a study of these issues are presented in Spyrou *et al.* (2009) and Belenky *et al.* (2010).

While the Large-Amplitude Motion program (LAMP) was used as the main hydrodynamic code for this study, the results are meant to be code-independent and applicable to any code capable of reproducing surf-riding, broaching-to, and capsizing. LAMP is based on a boundary value problem for radiation and diffraction (potential flow), a body non-linear evaluation of the hydrostatic

and Froude-Krylov forces, and force models for vortex and viscous effects (Lin and Yue 1990). The use of LAMP for the simulation of ship maneuvering is described in Lin *et al.* (2006) and Yen *et al.* (2010).

The ship configuration used for demonstrating the surf-riding and broaching phenomena is the “tumblehome” form of the ONR Topsides Study (Bishop *et al.* 2005).

2.2 Time-Domain Simulations

The study first looked at the modeling of large heel angle (up to capsize) caused by a sharp turn. Figure 1 shows predicted time histories of roll with two values of the transverse metacentric height (GM) after a 30° rudder application while sailing at 38 knots in calm water. At the higher GM value, the ship attains a large heel angle before recovering. At the lower GM value, the ship capsizes.

The study then looked at surf-riding in combinations of wave frequency and height and ship speed for which the theory predicts a co-existence of surging and surf-riding. Figure 2 shows different responses depending on the initial conditions. Systematic simulations were performed for a nominal Froude number (Fn) from 0.3 to 0.41 and commanded headings relative to the wave direction from 10 to 32 degrees. A summary of the results is presented in Figure 3.

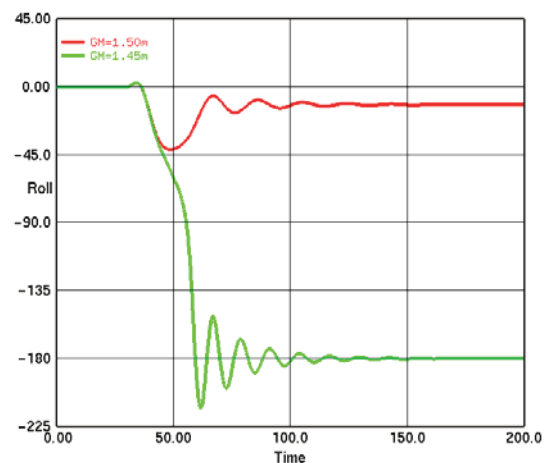


Figure 1: Large heel angle and capsizing due to sharp turn in calm water (Belenky *et al.* 2010)

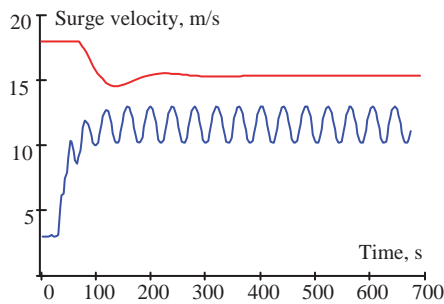


Figure 2: LAMP simulations showing coexistence of surging and surf-riding (Belenky *et al.* 2010)

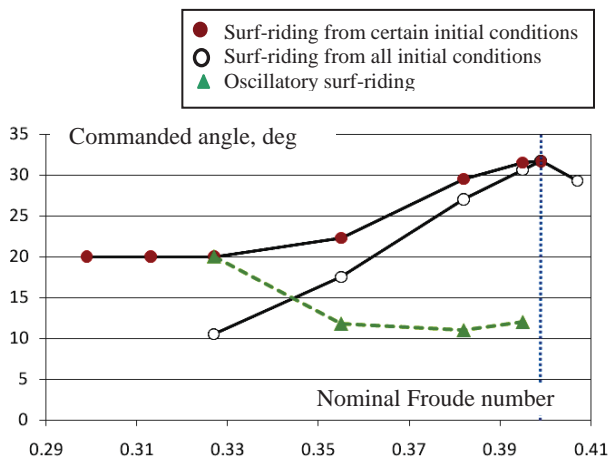


Figure 3: Boundaries of surf-riding in terms of commanded heading as a function of nominal Froude number (Spyrou *et al.* 2009)

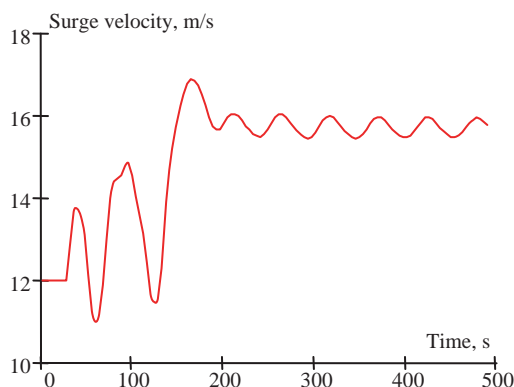


Figure 4: Capture into oscillatory surf-riding for commanded relative heading of 12 deg, $Fn=0.36$; notice the upward jump of mean speed (Spyrou *et al.* 2009)

A remarkable feature that appeared at the higher nominal speeds ($Fn>0.33$) was a stable

oscillatory type of surf-riding, for which the time history of ship speed is shown in Figure 4. As the ship is carried along by a single wave, it is also oscillating up-and-down the wave face. This fascinating occurrence has been observed in the past and has been explained as being due to a Hopf bifurcation (Spyrou 1996).

2.3 The Continuation Method

The continuation method is a powerful approach for studying the behavior of nonlinear systems by mapping and characterizing equilibria. However, continuation techniques were developed for dynamical systems described by ODE, and the application of continuation with advanced hydrodynamic codes presents many challenges, mostly caused by hydrodynamic hysteresis (memory effect). The first use of the continuation method (DERPAR) with a potential flow code (LAMP) was described by Spyrou *et al.* (2009). To avoid excessive complexity associated with the memory effect, the diffraction and radiation forces have been approximated with constant added mass and damping coefficient.

A sample result from LAMP-based continuation analysis is given in Figure 5. The curve shows the positions of surf-riding equilibria in the coordinates as yaw vs. rudder angle, and follows the similar curve from Spyrou (1996). This curve contains both stable and unstable surf-riding equilibria. That is why the continuation method is necessary, as direct time-domain simulations are not capable of capturing unstable equilibria.

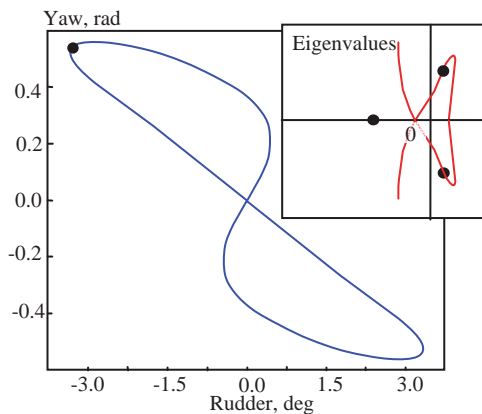


Figure 5: Curve of yaw vs. rudder angle for surf-riding equilibria calculation with DERP and LAMP (Belenky *et al.* 2010)

The stability of regions of the equilibrium curve was analyzed by examining the eigenvalues. The inset plot shows eigenvalues in the complex plane for a point on the curve at which the Hopf bifurcation (Figure 4) can be expected. Further development has led to the inclusion of hydrodynamic memory effects into the continuation analysis (Spyrou and Tigkas 2011).

2.4 The Theory and Code

The analysis carried out by Spyrou *et al.* (2009) demonstrated that the LAMP-simulated behavior is consistent with the current theory of broaching-to and surf-riding. It also confirmed the generic nature of the phenomena that had been identified independently and for a very different configuration in earlier research. In particular, the consideration of all six degrees does not change the qualitative picture of the phenomenon.

LAMP-based continuation analysis produced results that are consistent with direct simulation of the stable equilibria as well as the results of previous continuation research of a more theoretical nature.

These results lead to the conclusion that the current theory can be used to explain the outcomes of time-domain simulation with

advanced hydrodynamic codes and that advanced hydrodynamic codes can describe a nonlinear dynamical system.

3. SPATIAL-TEMPORAL FRAMEWORK FOR SURF-RIDING

In regular waves, a sliding coordinate system with its origin on the wave crest (or any other point fixed to the wave) allows a space-only consideration for surf-riding, as the next or previous wave in space and time is exactly the same. Figure 6 illustrates this approach; the upper part (Figure 6a) shows the balance of thrust and resistance plotted with the spatial representation of the surging wave force. The intersections of these two lines correspond to surf-riding equilibria, which define the topology of the phase plane shown in the lower part (Figure 6b). As the wave is regular, shifting coordinates in space corresponds to shifting coordinates in time, so only one coordinate – usually space – has to be considered.

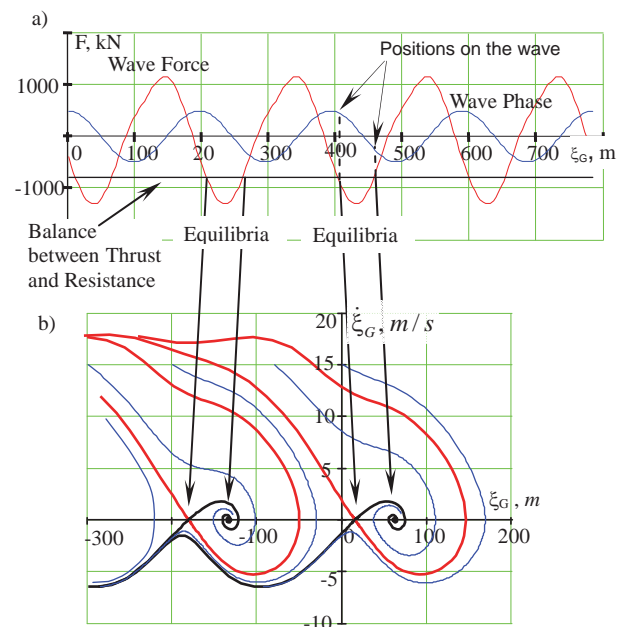


Figure 6: Surf-riding in regular waves – space consideration only: (a) balance of forces and (b) phase plane

In irregular seas, the waves are changing in both space and time. Consider an Earth-fixed coordinate system and imagine Figure 6 slowly changing in space for a fixed instant of time. The picture then changes slightly for the next time instant. As the waves change, surf-riding equilibria (actually quasi-equilibria) appear and disappear at different instances of time and points in space. This qualitative description is illustrated in Figure 7.

This rather qualitative consideration produces two main outcomes:

- Celerity of irregular waves must be defined in order to find the equilibria
- All elements of the mathematical model of surf-riding in irregular waves must be functions of position (x-coordinate) and time.

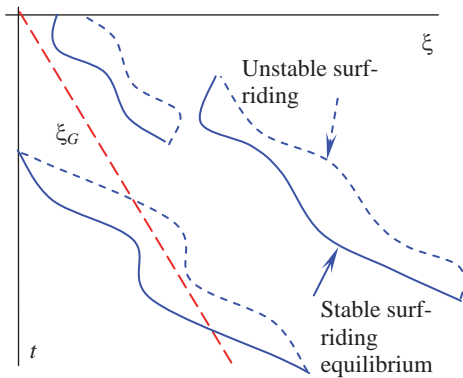


Figure 7: Spatial-temporary framework for surf-riding in irregular seas (Belenky *et al.* 2011)

4. CELERITY OF IRREGULAR WAVES

4.1 Velocity of a Profile

The most evident idea for irregular wave celerity was to find characteristic points in the profile, track them in time, and take their velocity as an approximation of wave celerity at these points. Belenky *et al.* (2012) proposed the tracking of zero-crossing points as illustrated in Figure 8. Each curve in Figure 9 is a spatial wave profile plotted at a time instant. Three zero-crossing points, marked by circles,

are tracked. The celerity calculated by this method is generally reasonable, but at times can become negative or jump to a very large value.

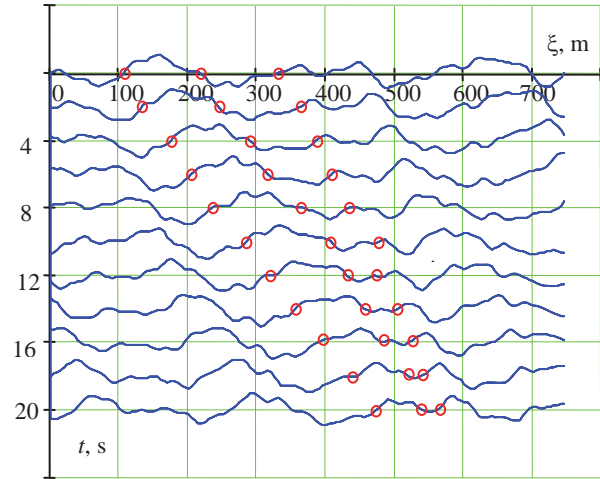


Figure 8: Celerity based on zero-crossing points (Belenky *et al.* 2012)

To gain a better understanding of the nature of this behavior, simplified cases were created with only two and three components (bi- and tri-chromatic waves), as shown in Figures 9 and 10. The tendency for large peaks can be seen even for two frequencies, and is even more dramatic for three frequencies.

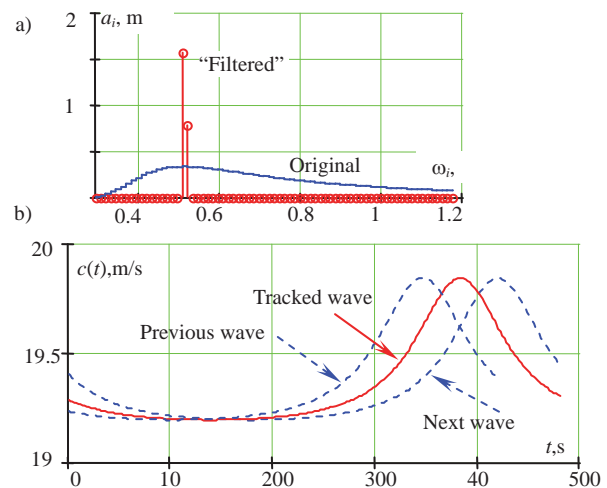


Figure 9: Bi-chromatic waves: (a) spectrum and (b) time history of celerity (Belenky *et al.* 2012)

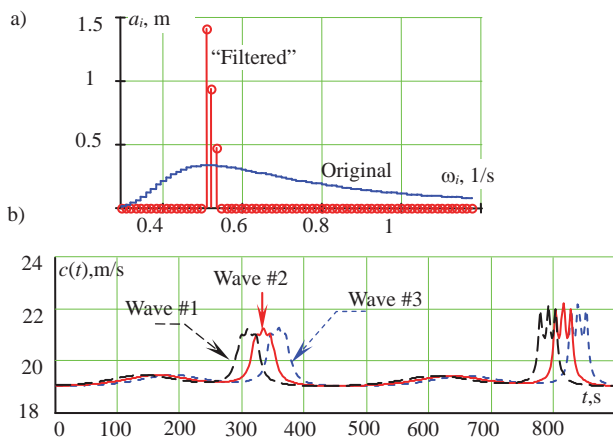


Figure 10: Tri-chromatic waves: (a) spectrum and (b) time history of celerity (Belenky *et al.* 2012)

Spyrou *et al.* (2012) had preferred to track the points of constant wave slope, proposing the concept of instantaneous celerity which can be calculated at the exact ship position at each time step. Figure 11 shows the celerity curves calculated for seaway derived from a JONSWAP spectrum. In a further development, they also proposed calculating a characteristic local celerity value corresponding to the point of maximum wave slope that is found in the vicinity of the ship. All these methods converged to the finding that the peaks in the celerity curve are intrinsic to the problem.

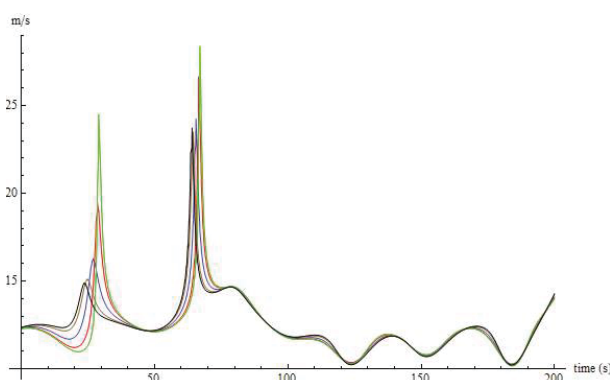


Figure 11: Celerity curves corresponding to wave slopes 1/75, 1/100, 0, -1/100, -1/75 (Spyrou *et al.* 2012)

The peaks appear to be related to changes in the local wave features, as when one wave overtakes another. As this occurs, a local wave

feature may cease to exist and the tracked points disappear and appear in another place, leading to a “spike” in the velocity of those points. Several candidate wave features were considered as points to track, and the smoothest behavior was found for the point of the maximum wave slope on the forward face. As this point can also be associated with the maximum surging force on a ship, it has a physical meaning with regard to surf-riding.

The calculation of wave celerity by tracking the points of maximum wave slope has been implemented in LAMP. In order to consider oblique and short-crested (multi-directional) seas, the algorithm searches for zeros of the derivative of the wave slope in the ship’s direction of travel,

$$\frac{\partial^3 \zeta_W(\xi_{\alpha_{\max}}, t)}{\partial \xi^3} = 0 \quad (1)$$

with the condition that they are on the down-slope:

$$\frac{\partial^2 \zeta(\xi_{\alpha_{\max}}, t)}{\partial \xi^2} < 0 \quad (2)$$

ζ_W is wave elevation, ξ is a coordinate in the mean direction of travel, and $\xi_{\alpha_{\max}}$ is a position of maximum wave slope angle. ξ is related to this Earth-fixed coordinate system as:

$$\begin{aligned} x &= x_G(t) + \xi \cos \psi \\ y &= y_G(t) + \xi \sin \psi \end{aligned} \quad (3)$$

(x_G, y_G) is the current position of the center of gravity of the ship and ψ is the mean heading angle with respect to the global frame.

For efficiency, the algorithm computes the elevation and its derivatives on a line of points within a characteristic wave length of the ship, then iterates within intervals containing a maximum slope point. The local maximum slope points are tracked in time and the propagation speed of the point closest to the ship provides a practical celerity.

Figure 12 shows a snapshot of a LAMP simulation for the ONR tumblehome hull form running in long-crested irregular waves. The plot shows the wave profile at that time instance along the ship's travel direction with marks for the points of maximum down slope and elevation (crest). The wave in this case is derived from a Bretschneider spectrum with $H_s=7\text{m}$ and $T_m=12.0\text{s}$. A portion of the time history of the ship speed and the local wave celerity is shown in Figure 13.

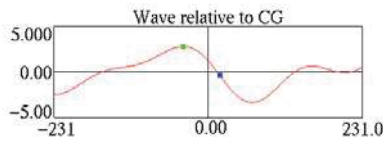


Figure 12: LAMP simulation of ONR Topsides tumblehome hull in irregular following seas (Spyrou *et al.* 2012)

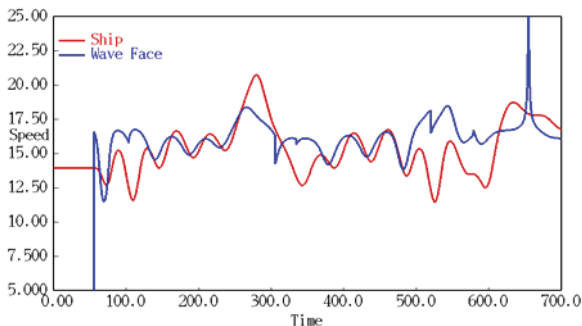


Figure 13: Ship speed and wave celerity for case with significant surf-riding in irregular waves (Spyrou *et al.* 2012)

The comparison of ship speed and local wave celerity clearly shows periods of surf-riding (*e.g.* $t=380\text{-}480$) and periods where the wave is overtaking the ship (*e.g.* $t=480\text{-}600$). While the initial wave celerity jump at 60 seconds is an artifact of ramping-up the wave, the “spike” in wave speed at $t=675$ is a case where the phasing of the wave component produces a very rapid local translation of the point of maximum slope and is related to a “merging” of wave faces. However, other discontinuities in the celerity, such as the one at $t=530$, are simply cases where the closest

point of maximum slope switches from one face to another as the waves overtake the ship.

In general, the problem of celerity in irregular waves and how it can affect ship motion is a very deep problem. Spyrou *et al.* (2014) provided a comprehensive theoretical analysis with an emphasis on the detection of surf-riding.

4.2 Celerity Based on Instantaneous Frequency

Looking for a method capable of producing a smoother celerity curve, Spyrou *et al.* (2014a) proposed an alternate scheme based on the instantaneous frequency derived from an envelope presentation of the wave elevation:

$$\zeta(t, \xi) = A(t, \xi) \cos(\vartheta(t, \xi)) \quad (4)$$

For a case where the wave elevation ζ_W is presented as typical cosine series, the amplitude $A(t, \xi)$ and phase $\vartheta(t, \xi)$ functions are computed from the wave elevations ζ_W and the Hilbert transform of the wave elevations $H(\zeta_W)$:

$$A(t, \xi) = \sqrt{\zeta_W^2 + (H(\zeta_W))^2} \quad (5)$$

$$\vartheta(t, \xi) = \arctan \frac{\zeta_W}{H(\zeta_W)}$$

$$\zeta_W(t, \xi) = \sum_{i=1}^{N_\omega} a_i \cos(k_i \xi - \omega_i t + \varphi_i) \quad (6)$$

$$H(\zeta_W(t, \xi)) = \sum_{i=1}^{N_\omega} a_i \sin(k_i \xi - \omega_i t + \varphi_i)$$

a_i , ω_i , and k_i are the amplitude, frequency, and wave number of the i^{th} component, while φ_i is a random phase shift.

The instantaneous frequency ω_W and the instantaneous wave number k_W are then computed as:

$$\omega_w(t, \xi) = -\frac{\partial \vartheta(t, \xi)}{\partial t} \quad (7)$$

$$k_w(t, \xi) = \frac{\partial \vartheta(t, \xi)}{\partial \xi} \quad (8)$$

This leads to the following definition of the wave celerity:

$$c(t, \xi) = \frac{\omega_w(t, \xi)}{k_w(t, \xi)} \quad (9)$$

For numerical calculations, it is convenient to substitute equations (5, 7, 8) into equation (9) and perform differentiation:

$$c(t, \xi) = -\frac{\frac{\partial H(\zeta_w)}{\partial t} \zeta_w - \frac{\partial \zeta_w}{\partial t} H(\zeta_w)}{\frac{\partial H(\zeta_w)}{\partial \xi} \zeta_w - \frac{\partial \zeta_w}{\partial \xi} H(\zeta_w)} \quad (10)$$

Equation (10) presents the wave celerity as a function of time and space that can be computed everywhere. The result can be compared against the instantaneous celerity calculated through the tracking method. Spyrou *et al.* (2014a) shows a series of comparisons between the “wave profile” and “instantaneous frequency” calculation schemes, an example of which is reproduced in Figure 14. The two calculations are generally very similar and both show “spikes” in celerity, although there is significant difference at the second spike at 440 s. What causes the “spikes” in formula (10)?

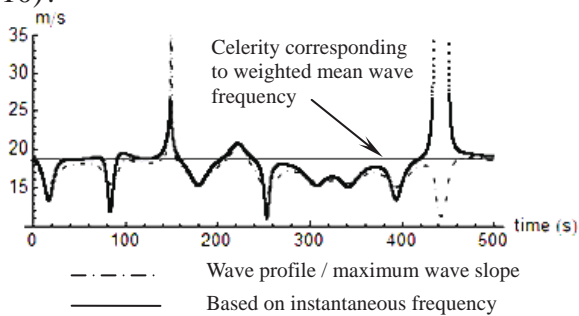


Figure 14: Instantaneous celerity for the bandwidth limited to 20% of the peak period (Spyrou *et al.* 2014a)

Figure 15 shows the spatial profile of the wave celerity calculated for Sea State 7 (Significant wave height 7.5 m, modal period 15 s) using a full-bandwidth Bretschneider spectrum and random phases. At this instant in time, there are four spikes at around 1500 m.

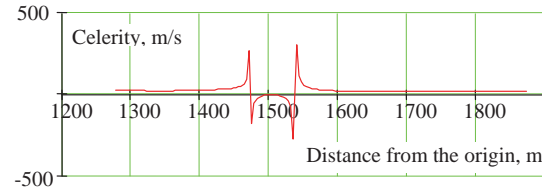


Figure 15: Spatial profile of wave celerity

One of the advantages of the present scheme of celerity calculation is that the origin of a spike can be analyzed. Consider the instantaneous wave number, which is the denominator in formula (9):

$$\begin{aligned} k_w(t, \xi) &= \frac{\partial \vartheta(t, \xi)}{\partial \xi} \\ &= \frac{\frac{\partial H(\zeta_w)}{\partial \xi} \zeta_w - \frac{\partial \zeta_w}{\partial \xi} H(\zeta_w)}{\zeta_w^2 + (H(\zeta_w))^2} \end{aligned} \quad (11)$$

The spatial profile of the instantaneous wave number is shown in Figure 16. It has a minimum around 1500 m and this minimum is negative. The curve of the instantaneous wave number crosses zero twice, which results in spikes in the value of instantaneous wave celerity. Figure 17 plots the spatial profile of wave elevations and shows that the minimum of the wave number and spikes of the celerity occur near the secondary maximum, *i.e.* the local maximum without crossing the line of calm water.

The secondary maxima and minima are related to the origination of new waves. If the local maximum at 1500 m raises and crosses the calm water line, the new wave will appear. Appearance of the new wave will lead to appearance of a new point of maximum of the wave slope and new zero-crossing. At the instance the new wave appears, the tracked points will make a finite “jump” in the infinitely small period of time causing a

theoretically infinite “spike” in celerity. Limiting the smallest value of the instantaneous wave number will limit the value “spike” and will make the celerity equation (10) into a practical formula for calculation.

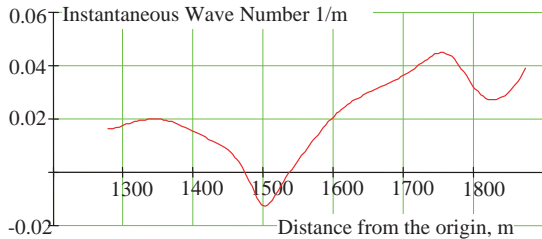


Figure 16: Spatial profile of the instantaneous wave number

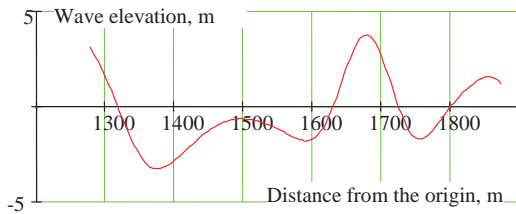


Figure 17: Spatial profile of the wave elevation

5. SURF-RIDING IN IRREGULAR WAVES

5.1 Simple Mathematical Model of Surging and Surf-Riding in Irregular Waves

A simple model for one-degree-of-freedom nonlinear surging was proposed in Belenky *et al.* (2011):

$$(M + A_{11})\ddot{\xi}_G + R(\dot{\xi}_G) - T(\dot{\xi}_G, n) + F_X(t, \xi_G) = 0 \quad (12)$$

M is mass of the ship, A_{11} is the longitudinal added mass, R is resistance in calm water, T is the thrust in calm water, n is the propeller rotation rate, F_X is the surging component of the Froude-Krylov wave force, and ξ_G is longitudinal position of the center of gravity in the Earth-fixed coordinate system. The dot above the symbol indicates temporal

derivative. Following Spyrou (2006), a polynomial approximation for thrust and resistance are used:

$$\begin{aligned} R(U) &= r_1U + r_2U^2 + r_3U^3 \\ T(U, n) &= \tau_1n^2 + \tau_2nU + \tau_3U^2 \end{aligned} \quad (13)$$

As the model is meant at this stage to be qualitative, a linear wave-body formulation seems to be appropriate for the case. Therefore:

$$F_X(t, \xi_G) = \sum_{i=1}^N A_{Xi} \cos(k_i \xi - \omega_i t + \varphi_i + \gamma_i) \quad (14)$$

As a body-linear formulation is adopted, the amplitude A_{Xi} and phase shift γ_i are available via response amplitude and phase operators:

$$A_{Xi} = a_i RAO(k_i) \quad (15)$$

$$\begin{aligned} RAO(k_i) &= \rho g k_i \left(\left(\int_{-0.5L}^{0.5L} C(x, k_i) \cos(k_i x) dx \right)^2 \right. \\ &\quad \left. + \left(\int_{-0.5L}^{0.5L} C(x, k_i) \sin(k_i x) dx \right)^2 \right)^{1/2} \end{aligned} \quad (16)$$

$$C(x, k_i) = 2 \int_{-d}^0 \exp(k_i z) b(x, z + d) dz \quad (17)$$

Here x and z are measured in the ship-fixed coordinate system (positive forwards of amidships and upward from the baseline), $b(x, z)$ is the molded local half-breadth, and d is the draft amidships. The surging phase shift is expressed as:

$$\gamma_i = \arctan \left(\frac{\int_{-0.5L}^{0.5L} C(x, k_i) \sin(k_i x) dx}{\int_{-0.5L}^{0.5L} C(x, k_i) \cos(k_i x) dx} \right) \quad (18)$$

The mathematical model described by equations (12 through 18) is essentially an

extended time domain version of the model presented in Spyrou (2006). It is expected to reproduce nonlinear surging and surf-riding, which is illustrated in Figure 18.

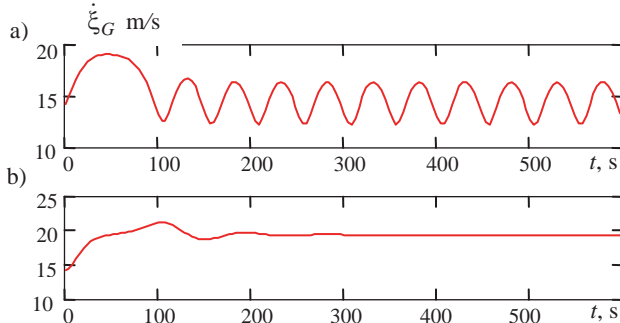


Figure 18: Solution in regular waves: co-existence of (a) surging and (b) surf-riding (Belenky *et al.* 2011)

5.2 Identification of Surf-Riding Instances in Irregular Waves

There are two aspects to the problem of identifying instances of surf-riding. The first is that surf-riding in irregular seas is not visually evident from the ship speed, as was illustrated in Figure 13. Without the wave celerity plotted alongside, an observer sees just a periodic stochastic process. The second aspect is to see how well definition of the wave celerity in irregular seas can explain the observed behavior. In a sense, the identification of surf-riding can be used as qualitative validation of the celerity calculation scheme.

A very basic example of such identification is described by Belenky *et al.* (2012), using tri-chromatic waves and zero-crossing wave celerity (see Figure 10). The time histories of surging speed and celerity are shown in Figure 19. The evolution of the surging speed for the first hundred seconds suggests attraction to a surf-riding equilibrium. But is this really the case?

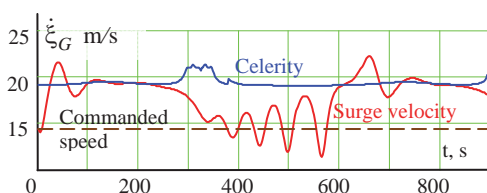


Figure 19: Time histories of surging velocity and celerity for tri-chromatic waves (Belenky *et al.* 2012)

Figure 20 shows a “spatial snapshot” of the forces (surging force vs. balance of thrust and resistance) superimposed with a spatial profile of the wave and its zero-crossing points. The time instant is $t=150$ s. The instantaneous position of the ship is indicated via the x-coordinate of the diamond, while the balance between thrust and resistance is indicated by its y-coordinate. The diamond is located at the intersection of the surging force and the balance of the thrust and resistance at the wave celerity. This means that the ship is in equilibrium and surf-riding is observed.

This simple example shows how wave celerity allows an interpretation of the observed motion and establishes the fact of surf-riding. The example also verifies the physical relevance of the calculated wave celerity. The method of calculating celerity based on maximum wave slope was successfully tested for identification of surf-riding by Spyrou *et al.* (2012, 2014). Spyrou, *et al.* (2014a) used both methods to calculate the celerity; see Figure 21.

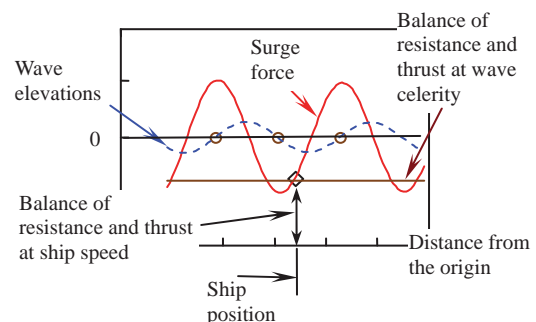


Figure 20: “Spatial snapshot” for $t=150$ s (Belenky *et al.* 2012)

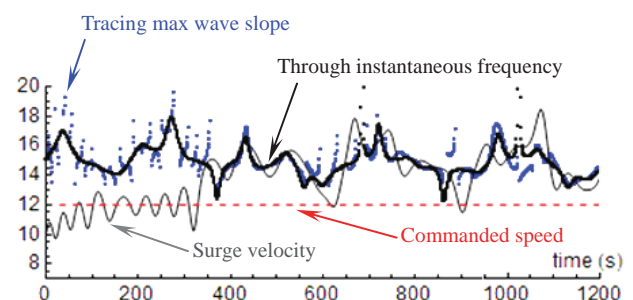


Figure 21: Time histories of surge velocity and celerity calculated with max wave slope and instantaneous frequency (Spyrou *et al.* 2014a)

Both methods of the wave celerity calculation seem to identify surf-riding instance in the same way, which is not surprising considering the similarity in the results of the two methods (Figure 14).

5.3 Phase Space in Irregular Waves

The position and type of the equilibria defines the topology of the phase plane, so the evolution of surf-riding equilibria in space and time is a logical starting point for analyzing surf-riding in irregular waves. Figure 22 shows the calculated loci of equilibria for the trichromatic case described above. The result is remarkably consistent with the notional topology presented in Figure 7.

The accuracy of the evaluation of the equilibrium stability was not always sufficient near the points where the equilibria appeared or disappeared, so the stability status of those point was corrected based on geometric considerations. Correct points are shown as two-color symbols. The inset in Figure 22 shows a close-up where the geometrical correction was applied.

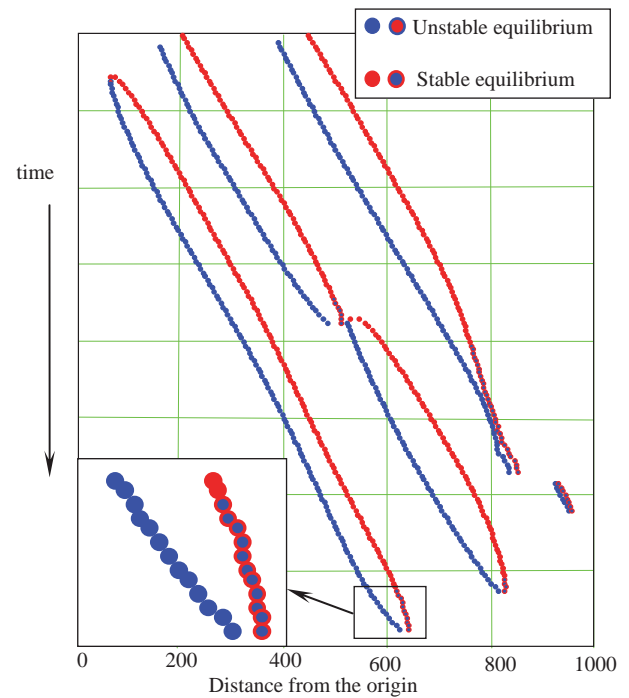


Figure 22: Calculated traces of equilibria

The unsteady motion of the equilibria qualitatively changes the phenomenon. A frame of reference moving with the equilibrium is no longer inertial. Also, the dynamical system cannot stay at the equilibrium position, even if the initial conditions correspond exactly to the equilibrium, because the equilibrium will move away. As an analogy, imagine a small heavy ball in a wine glass that is being moved in a circular motion. The ball will continuously “chase” a quasi-equilibrium point that moves around the inside of the glass.

The phase plane is also changing with time; strictly speaking, the phase plane by itself does not make sense beyond the “spatial snapshot”. The phase trajectory becomes a 3D line in hybrid phase-time coordinates (Kontolefas and Spyrou 2015). Projecting to a plane, the set of trajectories behaves as a non-stationary fluid flow. Spyrou *et al.* (2014a) describe an application of the concept of a Feature Flow Field (Theisel and Seidel 2003), which addresses the problem of feature tracking in non-stationary flow fields. The Feature Flow Field (FFF) method has been proposed for the tracking of a variety of different local features, including critical points of vector fields (such

as, in our case, the surf-riding equilibria). Figure 23 shows an example plot for surf-riding, where “saddle and focus-like” structures are present.

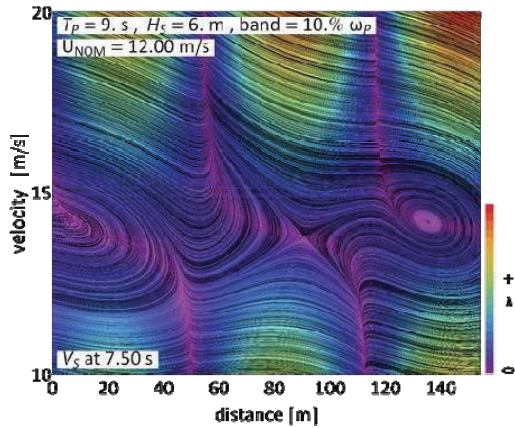


Figure 23: Streamlines and magnitude of forward velocity; JONSWAP Spectrum (Spyrou *et al.* 2014a)

Further developments towards the understanding of this time-dependent phase plane are described in Kontolefas and Spyrou (2015). Here is discussed a combined consideration of the feature flow field concept for tracking surf-riding states with the concept of hyperbolic Lagrangian Coherent Structures which can be seen as the finite-time generalization of the manifolds.

5.4 Statistics of High-Runs

The study of surf-riding in irregular waves requires the capability to characterize observations from simulations or model tests. However, the identification of surf-riding events in irregular waves is not trivial, particularly if the wave celerity cannot be calculated, which will generally be the case in a model test. It therefore makes sense to also look at the statistics of significant exceedances of the nominal speed by the surge velocity, also known as “high-runs”. Themelis *et al.* (2015) studied the statistics of high-runs depending on spectrum and sea state.

The idea of high-runs is not new. As pointed out in that work, Grim (1963) had

looked into the probabilistic quantification of the occurrence and duration of high-runs (“long run”) in a following irregular sea, taking into account the strongly nonlinear character of surge motion when the phenomenon occurs. Themelis *et al.* (2015) also examined the relation between the high-run occurrences and the instantaneous wave celerity (Figure 24).

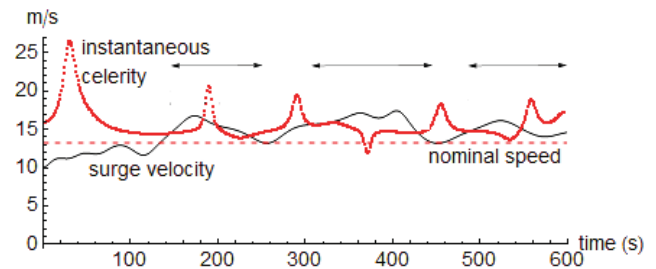


Figure 24: Schematic definition of high-run with the superimposed instantaneous wave celerity (Themelis *et al.* 2015)

The conclusion was that the velocity of the high-run shows good correlation with the mean instantaneous celerity when an error metric combining errors of amplitude and phase is applied.

5.5 Metric for Likelihood of Surf-Riding

As described at the beginning of this paper, a central element in the implementation of the split-time method is developing a metric for the likelihood of a rare event which can be evaluated at the occurrence of an intermediate event of some sort. An initial proposal for a metric of the likelihood of surf-riding can be found in Spyrou *et al.* (2014a) and is illustrated in Figure 25. The idea is to compute a “critical distance” in the phase plane between the ship’s state (position and velocity) at up-crossing and a critical state (point in the phase plane) from which the ship would be captured into surf-riding.

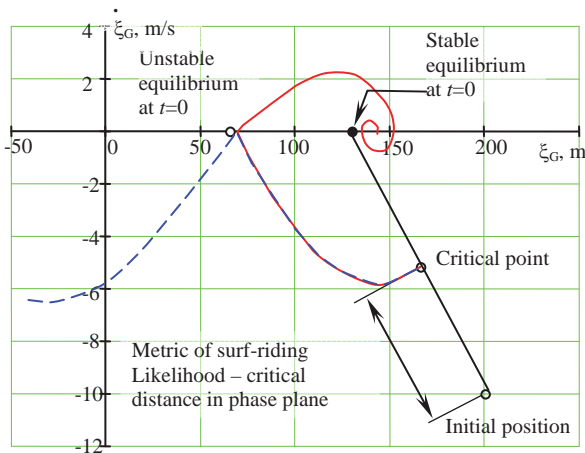


Figure 25: Initial idea for the metric of the likelihood of surf-riding

The critical point would lie on the line between the initial position of a ship (state at upcrossing) and the position of the stable quasi-equilibrium at the initial instant. A series of “rare” simulations would be performed for initial conditions corresponding to points along this line, and these simulations would determine the conditions that led to surf-riding.

This metric was initially tested with a slowly changing regular wave for which it is possible to explicitly consider the motion of the equilibria. The critical distance could be calculated, but the point to which the system was attracted and, once the critical point was reached, captured into surf-riding was different from the stable equilibrium at the initial moment.

A method of calculating wave celerity based on instantaneous frequency allowed the metric to be tried in irregular waves. The observed picture was more complex. The acceleration of the equilibria is not small and, as a result, the actual attraction does not occur. Instead, the dynamical system moves around the equilibrium path, similar to the picture on Figures 13 and 24. Figure 26 shows the phase plane computed for a moving frame of reference. The velocity of this frame of reference is constant and corresponds to a

velocity of the stable equilibrium at the initial moment.

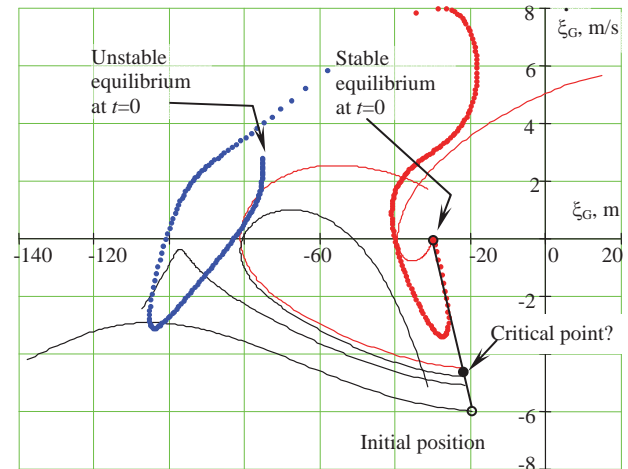


Figure 26: Phase plane trajectories for the critical point determination in calculating a metric for the likelihood of surf-riding in irregular waves

The main difference is that the dynamical system does not follow the stable equilibrium, even if it was placed exactly in the equilibrium position at the initial moment. Furthermore, the equilibria can move toward each other and disappear, releasing the ship from the surf-riding. This means that the criterion for attraction to equilibrium is not as evident as in the case shown in Figure 25. While it is possible to find the critical point visually, the development of a formal criterion of attraction remains for the future work.

6. CONCLUSIONS AND FUTURE WORK

This paper has reviewed work related to surf-riding and broaching-to that has been and continues to be performed under the ONR project entitled “A Probabilistic Procedure for Evaluating the Dynamic Stability and Capsizing of Naval Vessels”. The present work focusses on how irregular waves influence the phenomenon. The review addressed three major areas:



- Simulation of surf-riding and broaching-to by advanced hydrodynamic codes and the applicability of nonlinear dynamics tools
- Celerity of irregular waves
- Properties of time-dependent phase space of surging and surf-riding in irregular seas and their characterization.

The results of the studies may be summarized in the following conclusions:

- Surf-riding and broaching-to responses predicted via hybrid hydrodynamic codes are consistent with theoretical results, and the concepts and tools developed from ODE-based analysis can be applied to simulation tools as well
- The introduction of irregular waves leads to qualitative changes in surf-riding and broaching-to, including:
 - Problem must be considered in space and time
 - Surf-riding equilibria moves in an unsteady (accelerating) manner, and can appear and disappear in time
 - Surf-riding modes exist for a limited period of time
 - The system attracted to an equilibrium cannot stay with the equilibrium, but instead moves around it.

Problems to be addressed in the next stage of the research project include:

- Formulation of convergence criteria for the metric of likelihood of surf-riding
- Inclusion of sway and yaw into the simplest mathematical model, and study of the uncontrolled turn in irregular waves
- Formulation of the metric of likelihood of broaching-to and capsizing caused by broaching-to.

Solution of these problems is aimed at the developing the procedure for a physics-based statistical extrapolation using a limited data set from nonlinear time-domain numerical simulation. It is envisioned that the procedure will consist of the following steps:

- Prepare an extrapolation data set of simulation data
- Set an intermediate threshold providing a reasonable number (thousands) of upcrossings to be observed
- For each upcrossing, compute a metric of the likelihood of surf-riding, broaching-to, or capsizing due to broaching
- Fit a Generalized Pareto Distribution (GPD) to the metric data and evaluate the estimate of the capsizing rate and its confidence interval from the extrapolation of the metric to the level at which capsizing is inevitable.

7. ACKNOWLEDGEMENTS

The work described in this paper has been funded by the Office of Naval Research, under Dr. Patrick Purtell, Dr. Ki-Han Kim, and Dr. Thomas Fu, and by ONR Global under Dr. Richard Vogel song and Dr. Woei-Min Lin. The authors greatly appreciate their support.

Many colleagues have influenced and contributed to our work. The authors would like to acknowledge Prof. Pol Spanos (Rice University); Dr. Art Reed, Mr. Tim Smith, and Mr. Brad Campbell (NSWCCD, David Taylor Model Basin); Dr. Nikos Themelis and Mr. Ioanis Kontolefas (National Technical University of Athens); and Profs. Ross Leadbetter and Vladas Pipiras (University of North Carolina Chapel Hill).

8. REFERENCES

- Belenky, V.L., Weems, K.M., Lin, W.M., and Spyrou, K.J. 2010, "Numerical Evaluation of Capsizing Probability in Quartering Seas with Split Time Method," Proc. 28th Symp. on Naval Hydrodynamics, Pasadena, California, USA.
- Belenky, V., Spyrou, K., and Weems, K.M. 2011, "Split-Time Method for Surf-Riding and Broaching-To," Proc. 12th Intl. Ship



- Stability Workshop, Washington D.C., USA, pp. 163-168.
- Belenky, V., Spyrou, K., and Weems, K. 2012, "Evaluation of the Probability of Surf-Riding in Irregular Waves with the Time-Split Method," Proc. 11th Intl. Conf. on Stability of Ships and Ocean Vehicles STAB 2012, Athens, Greece, pp. 29-37.
- Bishop, B., Belknap, W., Turner, C., Simon, B., and Kim, J. 2005, Parametric Investigation on the Influence of GM, Roll Damping, and Above-Water Form on the Roll Response of Model 5613, Report NSWCCD-50-TR-2005/027, Naval Surface Warfare Center/Carderock Division, West Bethesda, Maryland.
- Grim, O. 1963, "Surging motion and broaching tendencies in a severe irregular sea," Ocean Dynamics, Vol. 16, No 5, Springer Berlin/Heidelberg, pp. 201-231.
- Kontolefas, I, and Spyrou, K.J. 2015, "Coherent Phase-space Structures Governing Surge Dynamics in Astern Seas," Proc. 12th Intl. Conf. on Stability of Ships and Ocean Vehicles (STAB 2015), Glasgow, UK.
- Lin, W.M., and Yue, D.K.P. 1990, "Numerical Solutions for Large Amplitude Ship Motions in the Time-Domain," Proc. 18th Symp. on Naval Hydrodynamics, Ann Arbor, Michigan, USA, pp. 41-66.
- Lin, W.M., Zhang, S., Weems, K., and Luit, D. 2006, "Numerical simulations of Ship Maneuvering in Waves," Proc. of 26th Symp. on Naval Hydrodynamics, Rome, Italy.
- Spyrou, K.J. 1996, "Dynamic instability in quartering seas: The behavior of a ship during broaching," J. of Ship Research, Vol. 40, No 1, pp46-59.
- Spyrou, K.J. 1997, "Dynamic instability in quartering seas-Part III: Nonlinear effects on periodic motion," J. of Ship Research, Vol. 41, No 3, pp210-223.
- Spyrou, K.J. 2006, "Asymmetric Surging of Ships in Following Seas and its Repercussions for Safety," Nonlinear Dynamics, Vol. 43, pp. 149-172.
- Spyrou, K., Weems, K.M., and Belenky V. 2009, "Patterns of Surf-Riding and Broaching-to Captured by Advanced Hydrodynamic Modeling," Proc. 10th Intl. Conf. on Stability of Ships and Ocean Vehicles STAB2009, St. Petersburg, Russia, pp. 331-346.
- Spyrou, K., and Tigkas, I. 2011, "Nonlinear Surge Dynamics of a Ship in Astern Seas: "Continuation Analysis" of Periodic States with Hydrodynamic Memory," J. Ship Research, Vol. 55 No 1, pp 19-28.
- Spyrou, K., Belenky, V., Themelis, N., and Weems, K. 2012, "Conditions for Surf-riding in an Irregular Seaway," Proc. 11th Intl. Conf. on Stability of Ships and Ocean Vehicles STAB 2012, Athens, Greece, pp. 323-336.
- Spyrou, K.J., Belenky, V., Themelis, N., and Weems, K. 2014, "Detection of Surf-riding Behavior of Ships in Irregular Seas," Nonlinear Dynamics, Vol. 78, No. 1, pp 649-667.
- Spyrou, K.J., Belenky, V., Reed, A., Weems, K., Themelis, N., and Kontolefas, I. 2014a, "Split-Time Method for Pure Loss of Stability and Broaching-To," Proc. 30th Symp. Naval Hydrodynamics, Hobart, Tasmania, Australia.
- Theisel, H., and Seidel, H. P. 2003, "Feature Flow Fields," Data Visualization 2003. Proc. VisSym 03, pp. 141-148.
- Themelis, N., Spyrou, K., and Belenky, V. 2015, "Surf-riding in Multi-chromatic Seas: "High-runs" and the Role of Instantaneous Celerity," Proc. 12th Intl. Conf. on Stability of Ships and Ocean Vehicles (STAB 2015), Glasgow, UK.
- Yen, T.-G., Zhang, S., Weems, K., and Lin,



W.M. 2010, "Development and Validation
of Numerical Simulations for Ship
Maneuvering in Calm Water and in Waves,"

Proc. of 28th Symposium on Naval
Hydrodynamics Pasadena, California USA.



The Effect of Ship Speed, Heading Angle and Wave Steepness on the Likelihood of Broaching-To in Astern Quartering Seas

Pepijn de Jong, *Delft University of Technology*, pepijn.dejong@tudelft.nl

Martin. R. Renilson, *Higher Colleges of Technology, UAE*,
and *Australian Maritime College*, martin@renilson-marine.com

Frans van Walree, *Maritime Research Institute Netherlands*, f.v.walree@marin.nl

ABSTRACT

A time domain simulation method that has been developed to investigate the non-linear behaviour of fast ships in waves is applied to following and astern quartering seas. The basis for the simulation method is a panel method employing linearization of some aspects of the hydrodynamics, combined with semi-empirical viscous models to enable faster computations and enabling a range of parameters to be studied in a realistic time frame.

This paper describes the application of the simulation method to the behaviour a fine form displacement hull shape in following and astern quartering seas. The effects of: vessel speed; wave length; heading angle to the waves; and wave steepness are investigated, and the implications on the likelihood of broaching-to in a realistic irregular seaway are inferred.

Keywords: *broaching-to, seakeeping and manoeuvring, time-domain panel method*

NOMENCLATURE

Roman

B	Beam	(m)
c	Wave celerity	(m/s)
Fr	Froude number	(-)
GM	Metacentric height	(m)
H	Wave height	(m)
L	Length	(m)
K, N	Manoeuvring moments	(Nm)
m	Ship mass	(kg)
r	Yaw rate	(rad/s)
R	Resistance	(N)
S	Wetted surface area	(m ²)
T	Draught	(m)
U	Forward speed	(m/s)
x, y, z	Spatial reference coordinates	(m)
X, Y, Z	Manoeuvring forces	(N)

Greek

β	Drift angle	(deg)
δ	Rudder deflection	(deg)
φ	Heel angle	(deg)
λ	Wave length	(m)
ρ	Density of sea water	(kg/m ³)
ξ	Long. position in the wave	(m)
ψ	Yaw (course deviation)	(deg)
ψ_w	Desired heading	(deg)
ζ	Wave elevation	(m)

An over-dot denotes a derivative with respect to time.

Non-dimensional parameters

$$Y' = \frac{Y}{\frac{1}{2} \cdot \rho \cdot U^2 \cdot L^2} \quad N' = \frac{N}{\frac{1}{2} \cdot \rho \cdot U^2 \cdot L^3}$$

$$r' = \frac{r \cdot L}{U} \quad v' = \frac{v}{U} \quad m' = \frac{m}{\frac{1}{2} \cdot \rho \cdot L^3}$$



1. INTRODUCTION

The control of vessels operating in severe following or astern quartering seas can be difficult, and in many cases can lead to broaching-to. Broaching occurs when a vessel is forced to yaw, and turns away from the wave direction, and towards a direction parallel to the waves. Often, the yaw is particularly violent, which, when combined with the rolling moment due to the counter rudder, and the wave induced rolling moment, can result in a sudden capsize (du Cane and Goodrich, 1962 and Renilson, 1980).

A time domain simulation model, termed PANSHIP, has been developed to investigate the broaching of a fast rescue craft (de Jong *et al.*, 2013). The results from this work showed that the method was able to predict the tendency of this vessel to broach in regular waves of varying length and steepness over range of forward speeds.

The current paper describes the application of the simulation model to investigate the broaching of a high speed fine form displacement vessel. In particular the influence of: ship speed; heading angle to the waves; wave length; and wave steepness have been investigated.

2. SIMULATION MODEL

The simulation of broaching in stern to stern-quartering waves is more complex than simulating ship motions in head to beam seas. One of the main difficulties is that in stern to stern-quartering seas a vessel's speed is likely to vary substantially due to the large longitudinal wave force, and the low encounter frequency. As the ship's hydrodynamic characteristics are functions of its longitudinal position in the wave, it is not normally possible to assume an "average" value, as is the usual practice in head seas. Thus, the situation is complicated by a substantial non-linearity, which must be taken into account carefully.

This is unlike the behaviour in head seas, where to a large extent it is enough to consider the average position of the vessel in the wave.

On the other hand, as the encounter frequency is low it is often possible to assume quasi-steadiness, which can considerably simplify the situation. This low encounter frequency has inspired some authors to deal with surf-riding and broaching problems in a quasi-steady fashion, see for instance Renilson and Driscoll (1982). As a result of these low encounter frequencies potential flow damping is only slight and viscous forces due to friction and flow separation are important.

As the steepness of the waves increases, so does the tendency to broach, requiring simulation methods to deal with non-linear effects both in the waves and in the body motions. The resulting large variations in the instantaneous submerged body have an influence on the hydrostatic forces, the wave exciting forces, and the hydrodynamic disturbance forces. In extreme cases the large relative motions may lead to deck immersion, requiring incorporation of the dynamics of water on deck.

To completely deal with the above requires a fully non-linear simulation method, preferably including viscous flow effects. Up to now, these methods require a prohibitive amount of computational time and effort for a full time-domain simulation. Consequently, computational techniques, together with captive model experiments, are mostly used to derive manoeuvring coefficients for use in time domain simulations based on differential equations to simulate manoeuvring performance.

Here a time domain panel method is used, employing a linearization of part of the hydrodynamic problem combined with semi-empirical viscous models to enable faster computations and enabling full time domain simulation. This method, termed PANSHIP, is

described in detail in van Walree (2002) and de Jong (2011), and can be characterized by:

- Three-dimensional transient Green function to account for linearized free surface effects, exact forward speed effects, mean wetted surface, mean radiated and diffracted wave components along the hull and a Kutta condition at the stern;
- Three-dimensional panel method to account for Froude-Krylov forces on the instantaneous submerged body;
- Cross flow drag method for viscosity effects;
- Resistance obtained from pressure integration at each time step combined with empirical viscous drag;
- Propulsion using propeller open water characteristics or a semi-empirical water jet model;
- Motion control and steering using semi-empirical lifting-surface characteristics, water jet steering, and propeller-rudder interaction coefficients;
- Empirical viscous roll damping; and
- Autopilot steering and motion control.

The method has partly been developed and validated in the FAST2 and FAST3 research projects. The participants of these projects are Damen Shipyards (NL), Defence Science Technology Organisation (AUS), Royal Netherlands Navy (NL), Marin (NL) and Delft University of Technology (NL). The method has been validated using a range of physical model experiments, some of which are described in de Jong *et al.* (2013), including:

- Prediction of calm water running attitude and resistance;
- Steering moments from water jet propulsion; and
- Sway, yaw and roll manoeuvring forces/moments due to sway and yaw velocities.

3. APPLICATION

3.1 Fine form displacement vessel

The method was applied to the simulation of the motions of a fine form displacement vessel in following to quartering regular waves. This particular hull shape was used earlier in work published by Renilson and Driscoll (1982). They experimentally determined the manoeuvring coefficients for this hull form in slowly overtaking following and quartering regular waves. This was done by performing forced oscillations with the model mounted under a PMM in a circulating water channel outfitted with a wavedozer. The set of coefficients reported in that paper were used in this work to determine whether the current simulation model reflects a realistic manoeuvring behaviour for this type of vessel.

Figure 1 shows the body plan of the fine form displacement vessel and Table 1 presents the main particulars of the vessel. The hull lines were obtained by digitizing the body plan given in the original paper. For the purpose of this paper the main dimensions were scaled to a length between the perpendiculars of 120 m. The experiments were not performed at the design waterline (DWL) of the vessel, but at a larger draught of 5.28 m, denoted EXPWL in **Figure 1**.

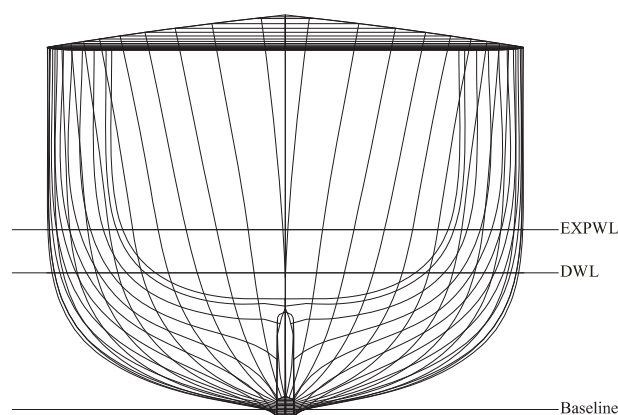


Figure 1 Section plan



Due to the conversion process from a two-dimensional section plan and a lack of longitudinal hull shape information, the displacement and the centre of buoyancy location of the final design differed from the original design. As the intention of the current work was to investigate the behaviour of a generic slender vessel in following waves no further attempt was made to correct the differences in hull parameters.

The propeller and rudder arrangement were not described in the original paper other than the specification of a twin rudder, twin screw arrangement. For this work, a rudder area was chosen of 1% of the lateral area formed by the length between the perpendiculars and the design draught. This is at the lower limit of the usual rudder area for this type of vessel. The propellers were placed at a short distance in front of the rudders, with a diameter of 3.00 meters and a P/D ratio of 1.2.

Table 1 Main particulars

Description	Unit	1982 Value	Current Value
Length between perpendiculars	m	3.660	120.00
Beam	m	0.417	13.67
Draught (EXPWL)	m	0.161	5.28
Draught (DWL)	m	0.122	4.00
Longitudinal centre of buoyancy aft of amidships	m	0.012	6.36 ¹
Displacement at EXPWL	kg	127.65	4499054 ¹
Radius of gyration about vertical axes	m	0.218 L	0.218 L
Stern arrangement	-	Twin rudder, twin screw	Twin rudder, twin screw
Metacentric height	m	Unknown	1.50
Rudder area	%	Unknown	1%

¹ The center of buoyancy and the displacement given in the original paper were not achievable with the lines provided.

3.2 Numerical modelling details

The forces obtained from the rudders, propellers, and the propeller shafts were determined by using semi-empirical formulations. The rudder formulations accounted for the actual disturbed inflow velocity at the rudder based on the potential flow solution taking into account the orbital velocity from the wave. Rudder emergence was taken into account by determining the wetted span and chord of the rudder below the disturbed water surface and adjusting the forces accordingly. The steering angle was controlled by an autopilot. The settings of the autopilot that were used are given in Table 2.

The propulsion force was determined by the constant rpm setting of the propellers, combined with the inflow velocity at the propeller plane. The rpm setting was determined for the corresponding nominal forward speed in calm water and kept constant during the simulation, The centreline skeg was modelled using combined source and doublet elements combined with a wake sheet extending from its trailing edge. To avoid unrealistic large induced velocities at the hull surface above the skeg, the skeg was extended to the waterline inside the vessel using dummy panels.

Table 2 Auto-pilot settings for course keeping

Description	Symbol	Unit	Value
Damping coefficient	$b_{\delta\dot{\nu}}$	deg/(deg/s)	9.00
Proportional coefficient	$c_{\delta\nu}$	deg/deg	3.00
Max deflection angle	δ_{\max}	deg	35
Max deflection speed	$\dot{\delta}_{\max}$	deg/s	6.00

Care was taken to ensure fully converged solutions with respect to panel size, time step, wake sheet length, and memory effect length and resolution. Typically around 1300 panels were used on the submerged part of the geometry. The memory effect contributions were truncated at 150 history time steps, and the wake sheet extending from the centre skeg was truncated at 150 panels as well. Time steps



were chosen equivalent to the time necessary to travel 1/50 of the ship length L and kept constant during each simulation.

3.3 Simulation setup

To study the behaviour in following waves, a series of time domain simulations were performed in regular waves. Table 3 presents an overview of the conditions that were simulated. The three different initial headings were tested at the intermediate wave steepness of 1/20 and the three wave steepness were tested at the intermediate initial heading of 20 degrees. This led to a total of 280 individual regular wave time domain simulations of 200 seconds each, requiring about 28 hours in total on a regular desktop computer.

Table 3 Parameter ranges investigated

Description	Parameter	Range	# Variations
Nominal forward speed	Fr	0.30–0.44	7
Wave length	λ/L	0.5–3.0	8
Wave steepness	H/λ	1/25, 1/20, 1/17	3
Initial heading	λ/L	10°, 20°, 30°	3

At the start of each simulation the vessel was set to sail at the nominal forward speed with the corresponding rpm setting. The vessel was placed with a wave trough amidships. The wave height and consequently the ship motions were ramped up over 100 time steps. Each time trace was analysed and categorized into one of the following:

- Surf-riding;
- Marginal surf-riding;
- Broaching; or
- None of the above.

The definitions of these characterisations are given in Table 4 and **Table 5**, based on the work of Renilson and Tuite (1998). For the

current work no distinction was made between marginal broaching or full broaching, which is the same as the approach taken in an earlier paper (de Jong *et al.*, 2013). The distinction was not found to be very meaningful for this type of simulation and in some cases rather arbitrary.

Table 4 Surf-riding

Description	Surf-riding	Marginal surf-riding
Forward speed	$U = c$	$U \geq 0.9 \cdot c$

Table 5 Broaching (Renilson and Tuite, 1998)

Description	Broach	Marginal broach
Heading deviation	$\psi \geq 20^\circ$	$\psi \geq 20^\circ$
Rudder angle	$\delta = \delta_{\max}$	$\delta = \delta_{\max}$
Yaw rate	$r > 0$	$r > 0$
Yaw acceleration	$\dot{r} > 0$	-

Prior to the full six degrees of freedom time domain simulations, a number of more basic simulations were carried out. First, a series of calm water runs were performed in order to iteratively determine the calm water trim and sinkage (or rise), as well as the rpm setting necessary for each of the nominal forward speeds. The calm water trim and sinkage were used for determining the mean wetted surface geometry to be used for the linearized radiated and diffracted wave solution.

Second, captive time domain simulations were performed in calm water conditions to capture the manoeuvring coefficients and the steering forces of the vessel and to determine the directional stability over the range of forward speeds of the vessel.

The captive manoeuvring and free running broaching results that are presented in the next section are defined using the axis system given in **Figure 2**. The origin of the ship-fixed frame lies at the centre of gravity of the vessel in the calm water plane. The system is similar to that used for calm water manoeuvring studies. The wave definitions relative to the vessel are used in the free running simulations.

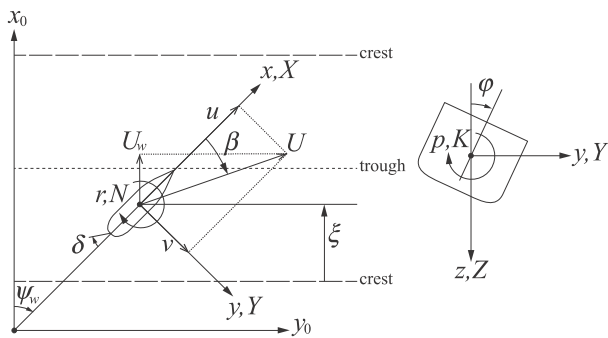


Figure 2 Axis system used for the manoeuvring forces

4. RESULTS

4.1 Manoeuvring

Calm water captive simulations were performed to ensure that the method captured the manoeuvring characteristics of the slender displacement vessel in a realistic manner. The predicted forces and moments in calm water at Froude number 0.40 are compared to those measured by Renilson and Driscoll (1982) at Froude number 0.41 in **Figure 3** to **Figure 6**, and the resulting hydrodynamic coefficients given in **Table 6**.

The dotted blue lines in the figures denote the non-dimensional forces as predicted. The blue solid lines represent the linear component of the fitted polynomial to these forces. The slope of these lines corresponds to the value of the corresponding linear manoeuvring derivative. Deviations between the measured force and the linear fit indicate non-linear contributions to that force component. The slope of green dashed lines represent the value of the calm water manoeuvring coefficients that were reported in the 1982 paper.

The results of the steady drift predictions in **Figure 3** and **Figure 4** show that both the Y_v and N_v coefficients compare well between prediction and measurement. The results of the yaw oscillations also show a good agreement for N_r in **Figure 6**. However, the results for the (Y_r-m) -derivative in **Figure 5** do not match very

well. A possible explanation for this is that this coefficient is the result of the side force distribution over the length of the vessel. For yaw oscillations the contributions to the side force of fore ship and aft ship counteract each other. The difference in their absolute value determines the relatively small magnitude of the resultant side force. The significant mismatch in the longitudinal centre of buoyancy between the original hull and the reconstructed one could cause a relatively large difference, particularly in (Y_r-m) .

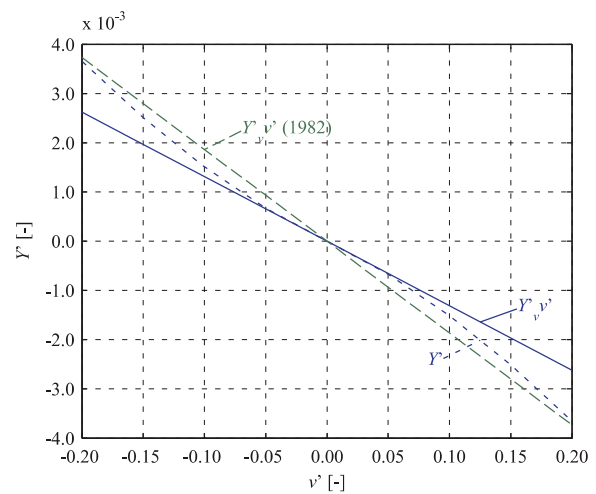


Figure 3 Steady drift: side force computed at three forward speeds and the 1982 measured results

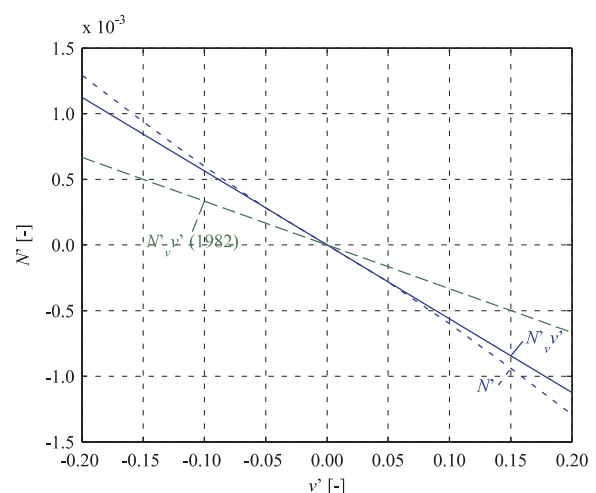


Figure 4 Steady drift: yawing moment computed at three forward speeds and the 1982 measured result

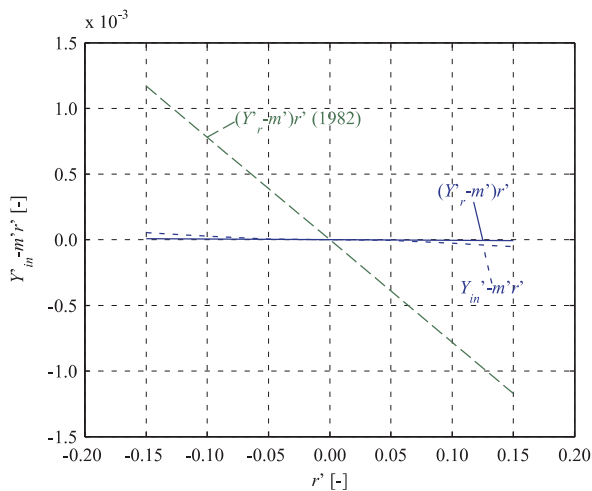


Figure 5 Yaw oscillations: in-phase side force computed at three forward speeds and the 1982 measured results

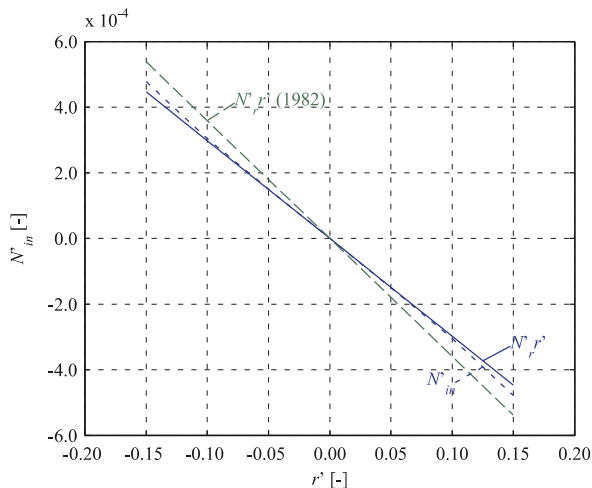


Figure 6 Yaw oscillations: in-phase yawing moment computed at three forward speeds and the 1982 measured results

Table 6 shows the values of the linear manoeuvring coefficients for the 1982 measurement and the current predictions. Also the value of C , given by Eq. (1), is reported.

$$C = Y'_v N'_v - N'_r (Y'_r - m') \quad (1)$$

The quantity C is considered the discriminator for determining whether a ship possesses control-fixed straight-line stability (Lewis, 1989). A positive value for C means, in most cases, that a ship is dynamically stable in the horizontal plane, and will resume on a straight-line path after a disturbance has ended.

Table 6 Results for manoeuvring

	Measured	Computed
Fr	0.412	0.400
Y'_v	-1.87E-02	-1.28E-02
N'_v	-3.33E-03	-5.49E-03
$Y'_r - m'$	-7.81E-03	-5.07E-05
N'_r	-3.59E-03	-2.98E-03
C	+4.09E-05	+3.78E-05

Table 6 indicates that despite the deviation in $Y'_r - m'$, the value of C agrees well between the 1982 measured value and the prediction. The main reason is that the contribution of the first term in Eq. (1) is at least an order of magnitude larger than the contribution of the second term. It can be concluded that both hulls have similar controls-fixed directional stability.

Finally, in **Figure 7** a comparison of the predicted and the 1982 measured steering forces is presented. Although the side force agrees well between computation and measurement, the predicted steering moment was found to be slightly lower than in the 1982 measurements. As the 1982 rudder size could not be recovered, the comparison seems to confirm the chosen relatively small rudder area for the computations. The deviation in steering moment arm can only partly be explained by the deviation in longitudinal centre of buoyancy between original and reconstructed hull.

Although not presented here, turning circle manoeuvres were simulated resulting in predicted turning circles diameters in the order of 4 to 6 times L at full rudder, depending on the nominal forward speed.

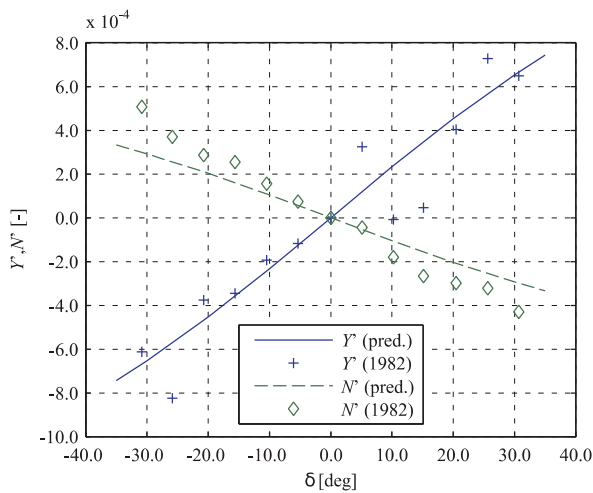


Figure 7 Steering forces: side force and steering moment

4.2 Broaching

The results of the full six degrees of freedom time domain simulations are presented in **Figure 8** to **Figure 13**. First, in **Figure 8** an overview plot is presented for a heading of 20 degrees and wave steepness of 1/20 as an example. Each symbol in the figure represents the outcome of one 200 second time domain simulation. The shape of the symbol indicates categorization of that time trace, using the definitions presented in the previous section.

Furthermore, the figure shows two additional lines. One is marked 'broaching zone' and demarcates the region within which broaches were detected. The other line, marked ' $U = c$ ', indicates the line of zero frequency of encounter, based on the nominal forward speed and wave heading. Below this line, the vessel is initially overtaking the waves, above this line initially the waves are overtaking the vessel.

In both cases the vessel can become entrapped between two wave crests. When the waves are initially overtaking the vessel, this is known as surf-riding. The vessel rides on the front face of the wave, leading to a wave induced moment that tends to force the vessel off course, possibly leading to a broach. The situation where the vessel is initially overtaking the waves has been termed wave-blocking

(Maki *et al.*, 2013). In this case the vessel is travelling on the back face of a wave and there is much less risk of upsetting wave forces being built up.

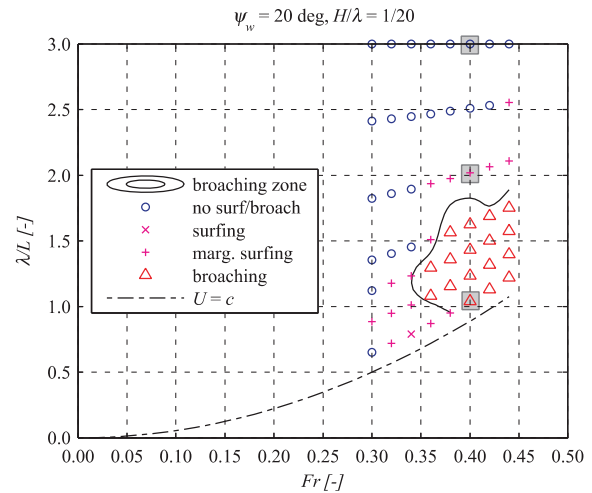


Figure 8 Broaching plot ($\psi_w = 20^\circ$, $H/\lambda = 1/20$)

Figure 9 to **Figure 11** show relevant time traces of three particular individual time domain simulations performed at Froude number 0.40. The top time trace in each of these figures shows the component of the forward speed of the vessel in the direction of the wave, denoted U_w . The two horizontal red dotted lines mark the wave celerity and 90% of the wave celerity (the threshold for marginal surf-riding). The fourth time trace in each of these figures shows the yaw motion, and the red dotted line indicates a course deviation of 20 degrees (the main threshold value for broaching). The red lines in the last time trace indicate the maximum steering angle. The red circles in the first figure mark the broaches that were detected.

Figure 9 shows the time traces of a run in which broaches were detected. The broaching behaviour is cyclic: within the simulation two broaches occurred. **Figure 10** shows marginal surf-riding, characterised by asymmetric surging with the vessel spending relatively more time close to the wave crest.

Figure 11 shows a situation without surfing or broaching. Although there is still significant



asymmetry in the surge motion, the forward speed in the direction of the wave does not exceed 90% of the wave celerity.

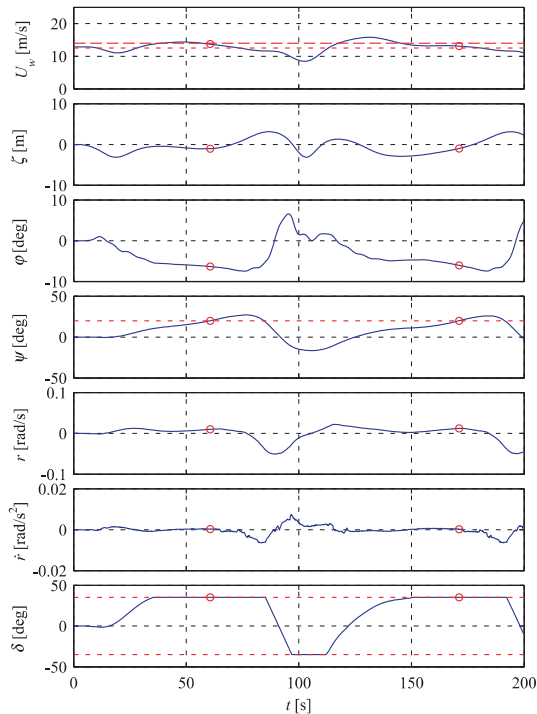


Figure 9 Time traces showing broaching ($Fr = 0.40$, $\psi_w = 20^\circ$, $H/\lambda = 1/20$, $\lambda/L = 1.04$)

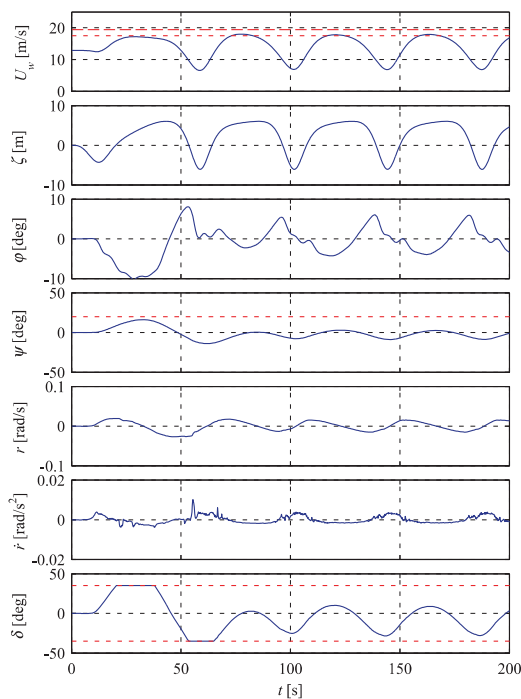


Figure 10 Time traces showing marginal surf-riding ($Fr = 0.40$, $\psi_w = 20^\circ$, $H/\lambda = 1/20$, $\lambda/L = 2.02$)

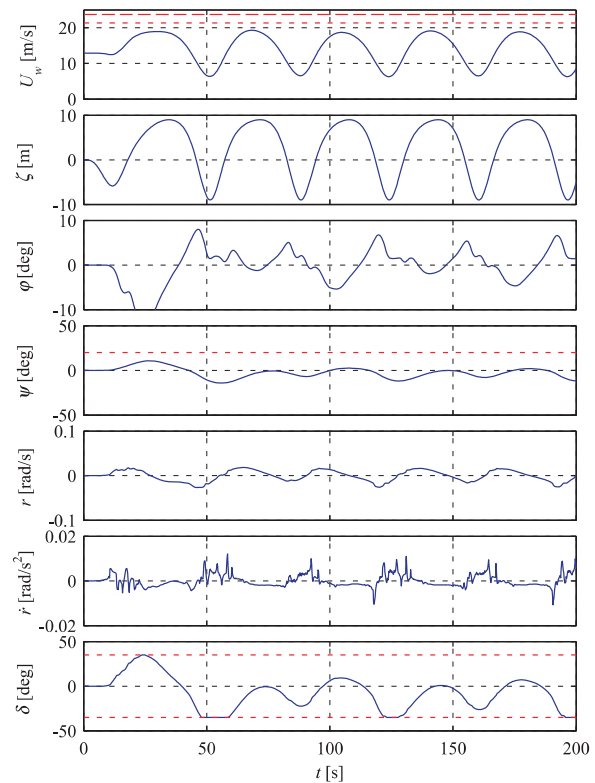


Figure 11 Time traces of no broaching/surf-riding ($Fr = 0.40$, $\psi_w = 20^\circ$, $H/\lambda = 1/20$, $\lambda/L = 3.00$)

The broaching zones for the variations in initial heading angle are presented in **Figure 12** and the broaching zones for the variations in wave steepness in **Figure 13**. Both figures also show the zero frequency of encounter lines for reference. There is no broaching zone for the smallest heading of 10 degrees in **Figure 12**. For this heading, although surf-riding took place over a significant region, no broaches were detected.

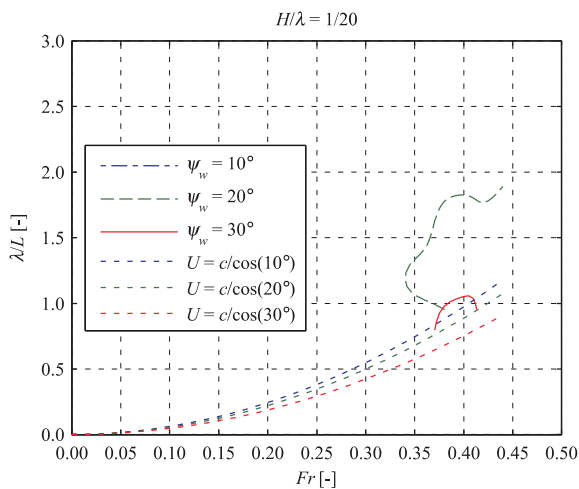


Figure 12 Broaching zones for varying headings

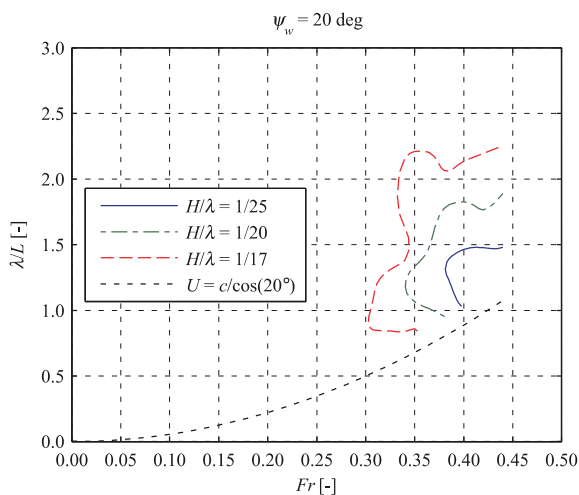


Figure 13 Broaching zones for varying values of the wave steepness

There seems to be a clear progression from no broaching at 10 degrees heading, to a significant broaching region for 20 degrees heading, before diminishing again towards 30 degrees of heading. The fact that the broaching zone is smaller for an initial heading of 30 degrees is counterintuitive, as the wave induced yaw moment at 30 degrees is larger than at 20 degrees. However, this is due to the lower component of the ship velocity in the wave direction when the heading is 30 degrees, resulting in a much lower likelihood of surf-riding.

Figure 13 confirms the expected outcome that the broaching zone expands significantly with increasing wave steepness.

5. DISCUSSION

For a broach to occur there are two conditions to be satisfied: (1) the upsetting wave induced yaw moment should exceed the available restoring steering moment; and (2) this should happen for enough time for the course deviation to build up – hence the link of broaching with surf-riding. The upsetting yaw moment increases with an increasing heading angle, whereas the tendency to surf diminishes with increasing heading angle. This appears to be confirmed by the results presented in this work, showing the largest broaching zone at the intermediate heading.

To compare the results presented in this work with experimental work use was made of results reported by Renilson and Driscoll (1982) and by Nicholson (1974) for similar fine form displacement vessels. Despite differences in hull design and control parameters with these free running experimental investigations, very similar broaching zones were found. The work of Nicholson seems to tend to larger zones at smaller values of the initial heading. Design parameters as metacentric height, rudder size, maximum rudder turning speed and control parameters can have a significant impact on the broaching behaviour and possibly can explain this difference.

De Jong *et al.* (2013) used the same simulation method applied to a water jet powered small rescue craft. Some simulations were carried out at a wave steepness of 1/17 and an initial heading of 20 degrees, allowing a comparison with **Figure 13** in this paper. Although the broaching zones were similar shaped, the rescue craft showed less tendency to broach, with broaching zones starting at slightly larger Froude numbers (0.32 and above) and longer wave lengths (1.1L and above).

Although broaching zones are an useful tool for obtaining a systematic overview of the broaching behaviour of a vessel, and for



comparing the relative performance of alternative designs, the question remains how to use the broaching zone plots for predicting the chance of occurrence and the severity of broaches in realistic irregular seas with directional spreading. Aided by the low frequency of encounter and near quasi-steady behaviour, it might be possible to identify an equivalent regular wave with its own length, height and heading for each passing irregular wave crest and subsequently using the broaching plot to determine the consequences of that wave. The authors are planning to investigate this approach, and compare the results with those obtained in irregular waves, in the future.

6. CONCLUDING REMARKS

Time domain simulations were performed for a fine form displacement vessel with semi-nonlinear panel method with empirical viscous flow corrections. The broaching in regular following to astern quartering waves was simulated to study the effect of: vessel speed; wave length; heading angle to the waves; and wave steepness.

To ensure realistic manoeuvring and course keeping characteristics the results of captive manoeuvring simulations in calm water were compared with earlier experimental data, showing good agreement, despite some differences and unknowns in the design parameters. The deviations found in the side force due to yaw oscillations were shown not to significantly influence the horizontal plane dynamic stability.

The results of time domain simulations were presented as broaching zones, showing the influence of wave heading and wave steepness.

It was found that the broaching zone was larger for a heading of 20 degrees compared to headings of both 10 degrees and 30 degrees. This is due to a greater wave upsetting moment

occurring at the greater heading angle, but a lower component of ship speed in the wave direction, and hence less surf-riding at the higher wave heading.

As expected, the tendency to broach was shown to increase with increasing wave steepness.

The broaching zones were found to be similar to zones based on previous free running experimental work with comparable vessels. The question remains how to use these plots for studying the behaviour in realistic irregular seas, and the authors plan to address this in the future.

REFERENCES

- Cane, P. du and Goodrich G.J., 1962, "The following sea, broaching and surging", Transactions of the Royal Society of Naval Architects, Vol. 104, pp. 221-228.
- Jong, P. de, 2011, "Seakeeping behaviour of high speed ships - An experimental and numerical study", Ph.D. Thesis, Delft University of Technology.
- Jong, P. de, Renilson, M.R. and Walree, F. van, 2013, "The broaching of a fast rescue craft in following seas", Proceedings of the 12th International Conference of Fast Sea Transportation, Amsterdam, The Netherlands.
- Lewis, E.V. (ed.), 1989, "Motions in Waves and Controllability", In Principles of Naval Architecture, Vol. 3, The Society of Naval Architects and Marine Engineers, NJ, USA.
- Maki, A., Umeda, N., Renilson, M.R., and Ueta, T., 2013, "Analytical methods to predict the surf-riding threshold and the wave-blocking threshold in astern seas", Journal of Marine Science and Technology, Vol.19(4), pp. 415-424.
- Nicholson, K., 1974, "Some parametric model experiments to investigate broaching-to", International Symposium on the Dynamics



of Marine Vehicles and Structures in Waves, London, UK, pp. 171-177.

Renilson, M.R., 1980, "Broaching in a heavy following sea", The Motor Ship.

Renilson, M.R. and Driscoll, A., 1982, "Broaching – An investigation into the loss of directional stability in severe following seas", Transactions Royal Institution of Naval Architects, Vol. 124, pp. 253-273.

Renilson, M.R. and Tuite, A.J., 1998, "Broaching-to – A proposed definition and analysis method", Proceedings of the 25th American Towing Tank Conference, Iowa, USA.

Walree, F. van, 2002, "Development, Validation and Application of a Time Domain seakeeping method for High Speed Craft with a Ride Control System", Proceedings of the 24th Symposium on Naval Hydrodynamics, Fukuoka, Japan, pp. 475-490.

Session 13.2 – LIQUEFACTION

Computation of Pressures in Inverse Problem in Hydrodynamics of Potential Flow

Potential Assessment of Cargo Liquefaction Based on an UBC3D-PLM Model

Coupled Granular Material and Vessel Motion in Regular Beam Seas

This page is intentionally left blank



Computation of Pressures in Inverse Problem in Hydrodynamics of Potential Flow

Ivan Gankevich, *Saint Petersburg State University* igankevich@yandex.com

Alexander Degtyarev, *Saint Petersburg State University* deg@csa.ru

ABSTRACT

The inverse problem in hydrodynamics of potential flow consists of finding velocity and wave pressures under assumption that a wavy surface elevation is known beforehand. The solution to this problem in both two and three dimensions is known but is based on theory of small-amplitude waves. Since some hydrodynamic problems involve waves of arbitrary amplitudes a more general solution is needed. In the paper such solution is given for two and three dimensions and it is shown that it is efficient from computational point of view and more accurate than the solution for small-amplitude waves.

Keywords: *inviscid flow, irrotational flow, analytical solution*

1. INTRODUCTION

A potential flow is the flow of inviscid incompressible fluid which is described by the system of equations (Kochin et al, 1966)

$$\begin{aligned} \nabla^2 \varphi &= 0, \\ \varphi_t + \frac{1}{2} |\vec{v}|^2 + g\zeta &= -\frac{p}{\rho}, \quad \mathfrak{D}\diamond = \zeta(x, y, t), \\ D\zeta = \nabla \varphi \cdot \vec{n}, \quad \mathfrak{D}\diamond &= \zeta(x, y, t), \end{aligned} \quad (1)$$

where φ is velocity potential, ζ is wavy surface elevation, p is wave pressure, ρ is water density, $v=(\varphi_x, \varphi_y, \varphi_z)$ is velocity vector, g is gravitational acceleration and D is a substantial derivative. The first two equations are equation of continuity and equation of motion (the so called dynamic boundary condition) and both are derived from Navier-Stokes equations for incompressible inviscid fluid. The last one is kinematic boundary condition for free wavy surface which states that rate of change of wavy surface elevation equals to the change of velocity potential derivative along the wavy surface normal.

In previous paper (Degtyarev & Gankevich, 2012) the solution to inverse problem is given for small-amplitude waves when wave length is much larger than wave height ($\lambda \gg h$). It is shown that the inverse problem is linear and can be reduced to a Laplace equation with a mixed boundary condition with equation of motion being used only to determine wave pressure. The assumption of small amplitudes means the slow decay of wind wave coherence function, i.e. a small change of a local wave number in time and space compared to the wave elevation. This assumption allows the use of special derivative formula $\zeta_z = k\zeta$, where k is the wave number; using this formula the solution is constructed. In two-dimensional case the solution is given by

$$\begin{aligned} \frac{\partial \varphi}{\partial x} \Big|_{x,t} &= -\frac{1}{\sqrt{1+\alpha^2}} e^{-I(x)} \int_0^x \frac{\partial \zeta / \partial z + \alpha \dot{\alpha}}{\sqrt{1+\alpha^2}} e^{I(x)} dx, \\ I(x) &= \int_0^x \frac{\partial \alpha / \partial z}{1+\alpha^2} dx, \end{aligned} \quad (2)$$



where α is the wave slope. In three-dimensional case the solution is given by

$$\begin{aligned} & \frac{\partial^2 \varphi}{\partial x^2} (1 + \alpha_x^2) + \frac{\partial^2 \varphi}{\partial y^2} (1 + \alpha_y^2) + 2\alpha_x \alpha_y \frac{\partial^2 \varphi}{\partial x \partial y} + \\ & \left(\frac{\partial \alpha_x}{\partial z} + \alpha_x \frac{\partial \alpha_x}{\partial x} + \alpha_y \frac{\partial \alpha_x}{\partial y} \right) \frac{\partial \varphi}{\partial x} + \\ & \left(\frac{\partial \alpha_y}{\partial z} + \alpha_x \frac{\partial \alpha_y}{\partial x} + \alpha_y \frac{\partial \alpha_y}{\partial y} \right) \frac{\partial \varphi}{\partial y} + \\ & \frac{\partial \zeta}{\partial z} + \alpha_x \dot{\alpha}_x + \alpha_y \dot{\alpha}_y = 0. \end{aligned}$$

Here the formula is not explicit and represents elliptic equation which is intended to be solved by a variety of known numerical methods.

Although, these methods are efficient and work well for a wide range of wavy surfaces some weather conditions produce waves with wave numbers which change frequently in time and space. These are transitions between normal and storm weather, wind wave and swell heading from multiple directions and some others. These weather conditions and a possibility to obtain a more general solution are the main reasons for solving the potential flow problem for arbitrary amplitude waves case.

2. TWO-DIMENSIONAL CASE

For two-dimensional flow equation (1) can be rewritten as follows.

$$\begin{aligned} \varphi_{xx} + \varphi_{zz} &= 0, \\ \varphi_t + \frac{1}{2}(\varphi_x^2 + \varphi_y^2) + g\zeta &= -\frac{p}{\rho}, \quad \varphi = \varphi(x, y, t), \\ \zeta_t + \zeta_x \varphi_x &= \frac{\zeta_x}{\sqrt{1 + \zeta_x^2}} \varphi_x + \varphi_z, \quad \varphi = \varphi(x, y, t), \end{aligned}$$

The first step is to solve Laplace equation using Fourier method. The solution can be written as integral similar to Fourier transform:

$$\varphi(x, z) = \int_{-\infty}^{\infty} E(\lambda) e^{\lambda(z+ix)} d\lambda \quad (3)$$

Then coefficients E can be determined by plugging this integral into kinematic boundary condition and evaluating derivatives. This step gives equation

$$\frac{\zeta_t \sqrt{1 + \zeta_x^2}}{1 - i\zeta_x (\sqrt{1 + \zeta_x^2} - 1)} = \int_{-\infty}^{\infty} \lambda E(\lambda) e^{\lambda(\zeta+ix)} d\lambda$$

which represents forward bilateral Laplace transform and thus can be inverted to yield formula for coefficients E :

$$E(\lambda) = \frac{1}{2\pi i \lambda} \int_{-\infty}^{\infty} \frac{\zeta_t \sqrt{1 + \zeta_x^2}}{1 - i\zeta_x (\sqrt{1 + \zeta_x^2} - 1)} e^{-\lambda(\zeta+ix)} dx \quad (4)$$

The third step is to plug (4) into (3) which yields the final result:

$$\begin{aligned} \varphi(x, t) &= \frac{1}{2\pi i} \int_{-\infty}^{\infty} \frac{1}{\lambda} e^{\lambda(\zeta+ix)} d\lambda \\ & \int_{-\infty}^{\infty} \frac{\zeta_t \sqrt{1 + \zeta_x^2}}{1 - i\zeta_x (\sqrt{1 + \zeta_x^2} - 1)} e^{-\lambda(\zeta+ix)} dx. \end{aligned} \quad (5)$$

When equation (1) is solved that way, wave pressures can be determined from dynamic boundary condition.

Since velocity potential is the only unknown prerequisite for determining wave pressures it is feasible to use it to validate the solution. A comparison was done to the known small-amplitude wave solution (2) and numerical experiments showed good correspondence rate between resulting velocity potential fields.

In order to obtain velocity potential fields the wavy sea surface was generated by autoregressive model differing only in wave amplitude. In numerical implementation infinite outer and inner integral limits of (5) were replaced by the corresponding wavy surface size (x_0, x_1) and wave number interval (λ_0, λ_1) so that inner integral of (5) converges.

Experiments were conducted for waves of both small and large amplitudes and in case of small-amplitude waves both solutions produced similar results, whereas in case of large-amplitude waves only general solution produced

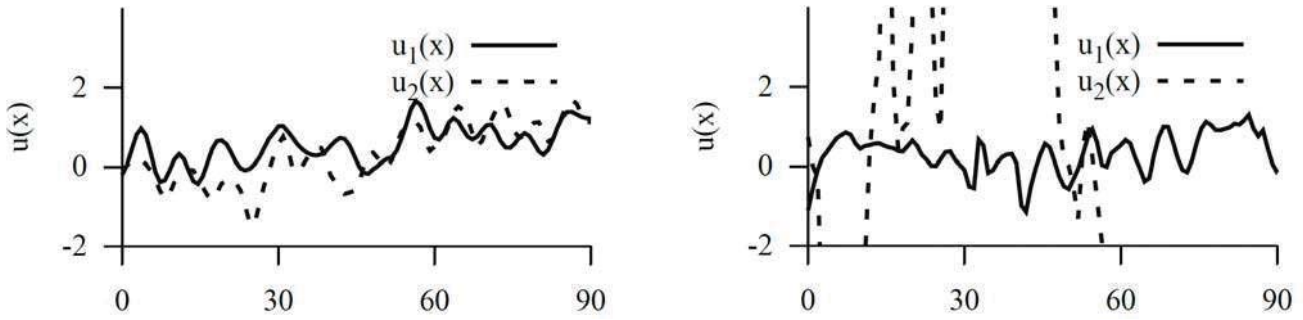


Fig. 1 Comparison of velocity fields produced by general solution (u_1) and solution for small-amplitude waves (u_2).
Velocity fields for small-amplitude (left) and large-amplitude (right) wavy sea surfaces.

stable velocity field (Figure 1). The fact that velocity fields for small-amplitude waves are not equal can be explained by stochastic nature of autoregressive wind wave model (i.e. the amplitude is small in a statistical sense only). Therefore, general solution in two-dimensional case works for different wavy sea surfaces without restriction on wave amplitude.

3. SPECIAL TRANSFORM

Three-dimensional problem can be solved with help of special inversion formula which serves as a modified version of Fourier transform. The transform has the following form:

$$F(x, y) = \iint_{-\infty}^{\infty} f(\lambda, \gamma) e^{i(\lambda x + \gamma y) + \zeta(x, y) \sqrt{\lambda^2 + \gamma^2}} d\lambda d\gamma. \quad (6)$$

In order to derive inversion formula this expression should be reduced to a two-dimensional convolution. By applying transformations

$$\begin{aligned} (\lambda, \gamma) &\rightarrow (r, \theta), \lambda = r \cos \theta, \gamma = r \sin \theta, |J| = r, \\ (x, y) &\rightarrow (\rho, \psi), x = \rho \cos \psi, y = \rho \sin \psi, \end{aligned} \quad (7)$$

the formula is rewritten in polar coordinates for both f and F :

$$F(\rho, \psi) = \int_0^{\infty} \int_0^{2\pi} r f(r, \theta) e^{ir\rho \cos(\psi - \theta) + r\zeta(\rho, \psi)} d\theta dr.$$

Then applying additional transformations

$$\begin{aligned} r &\rightarrow r', r = e^{r'}; \rho = \rho', \rho = e^{-\rho'}; \\ \zeta &\rightarrow \zeta', \zeta = e^{\rho'} \zeta' \end{aligned} \quad (8)$$

to the radius vectors and function ζ a convolution can be obtained:

$$\begin{aligned} F(\rho', \psi) &= f_1 * f_2, \\ f_1(r', \theta) &= e^{2r'} f(r', \theta), \\ f_2(\rho', \psi) &= \exp[ie^{-\rho'} \cos \psi + e^{-\rho'} \zeta'(\rho', \psi)] \end{aligned} \quad (9)$$

Since convolution theorem permits any converging integral transform to be applied to a convolution, here a modified polar version of Fourier transform

$$\begin{aligned} \mathfrak{F}'\{g(r, \theta)\}(r_1, \theta_1) &= \int_0^{\infty} \int_0^{2\pi} -e^{-2r} g(r, \theta) \\ &\exp[-ie^{-r} r_1 \cos(\theta_1 - \theta)] d\theta dr \end{aligned} \quad (10)$$

is used. Applying this transform to the both sides of equation (9) yields the final formula

$$\begin{aligned} \mathfrak{F}'\{F(x, y)\} &= \mathfrak{F}'\left\{\frac{f(x, y)}{x^2 + y^2}\right\} \\ &\mathfrak{F}'\{\exp[ix + \zeta(x, y)]\}, \end{aligned} \quad (11)$$

where \mathfrak{F}' is ordinary forward Fourier transform.

This formula is useful in two cases. First, it allows inversion of initial modified Fourier transform (6) which is needed when solving three-dimensional problem. Second, it can be used to compute F efficiently with use of fast Fourier transform family of algorithms. So, special transform is the tool to solve three-dimensional problem.



4. THREE-DIMENSIONAL CASE

Three-dimensional problem is solved mostly the same way as its two-dimensional counterpart, however, special transform developed in the previous section should be used instead of bilateral Laplace transform and some terms from system of equations (1) should be rewritten in dimensionless form for convolution to be physically feasible.

4.1 Formula derivation

Consider a square region with a side N where the problem is being solved. Then coordinate transform $(x, y) \rightarrow (xN, yN)$ produces system of equations with dimensionless x and y :

$$\frac{1}{N^2} \varphi_{xx} + \frac{1}{N^2} \varphi_{yy} + \varphi_{zz} = 0,$$

$$\varphi_t + \frac{1}{2} \left(\frac{\varphi_x^2}{N^2} + \frac{\varphi_y^2}{N^2} + \varphi_z^2 \right) + g\zeta = -\frac{p}{\rho},$$

$$\mathfrak{D}\diamond = \zeta(x, y, t),$$

$$\zeta_t + \frac{\zeta_x}{N^2} \varphi_x + \frac{\zeta_y}{N^2} \varphi_y = \frac{\zeta_x}{Nd} \varphi_x + \frac{\zeta_y}{Nd} \varphi_y + \varphi_z,$$

$$\mathfrak{D}\diamond = \zeta(x, y, t),$$

$$\text{where } d = \sqrt{N^2 + \zeta_x^2 + \zeta_y^2}.$$

The first step is to solve Laplace equation with Fourier method which yields

$$F(x, y, z) = \int_{-\infty}^{\infty} \int_{-\infty}^{\infty} E(\lambda, \gamma) e^{M(iN(\lambda x + \gamma y) + z(x, y)\sqrt{\lambda^2 + \gamma^2})} d\lambda d\gamma. \quad (12)$$

Here λ and γ represent wave numbers which were made dimensionless with transform $(\lambda, \gamma) \rightarrow (\lambda M, \gamma M)$. Then the expression is plugged into the kinematic boundary condition yielding

$$\zeta_t = \int_{-\infty}^{\infty} \int_{-\infty}^{\infty} d\lambda d\gamma E(\lambda, \gamma) e^{M(iN(\lambda x + \gamma y) + \zeta \sqrt{\lambda^2 + \gamma^2})}$$

$$\frac{M}{Nd} \left[N^3 \sqrt{\lambda^2 + \gamma^2} - i\lambda \zeta_x (d - N) - i\gamma \zeta_y (d - N) \right]$$

In order to obtain convolution formula transformations (7) and (8) from the previous section are applied:

$$\zeta_t = \int_{-\infty}^{\infty} \int_{-\infty}^{\infty} d\theta dr' e^{Me^{r'-\rho'}(iN \cos(\theta-\psi)+\zeta)} \frac{Me^{2r'}}{Nd'} E(r', \theta) \left[\begin{array}{l} N^3 - ie^{\rho'} \cos(\theta-\psi) \zeta_{\rho'} (d'-N) \\ - ie^{\rho'} \sin(\theta-\psi) \zeta_{\psi} (d'-N) \end{array} \right],$$

$$\text{where } d' = \sqrt{N^2 + e^{2\rho'} (\zeta_{\rho'}^2 + \zeta_{\psi}^2)}.$$

Finally, after applying modified Fourier transform (10) to the both sides of this equation the formula for coefficients E can be derived:

$$\mathfrak{F}\{\zeta_t(x, y)\} = \mathfrak{F}\left\{ \frac{E(\lambda, \gamma)}{\lambda^2 + \gamma^2} \right\} \mathfrak{F}\{f(x, y) e^{M(iNx + \zeta)}\},$$

$$f(x, y) = M \frac{N^2 + i\zeta_x \left(\sqrt{N^2 + \zeta_x^2 + \zeta_y^2} - N \right)}{N \sqrt{N^2 + \zeta_x^2 + \zeta_y^2}}.$$

4.2 Numerical implementation

Using formula (11) the integral from (12) can be decomposed into two forward and one inverse Fourier transforms, so the whole solution can be computed efficiently:

$$\varphi(x, y, z) = \mathfrak{F}^{-1} \left\{ \mathfrak{F} \left\{ \frac{E(\lambda, \gamma)}{\lambda^2 + \gamma^2} \right\} \mathfrak{F} \left\{ e^{M(iNx + \zeta)} \right\} \right\}.$$

Forward and inverse Fourier transform of E cancel each other:

$$\varphi(x, y, z) = \mathfrak{F}^{-1} \left\{ \frac{\mathfrak{F}\{\zeta_t(x, y)\} \mathfrak{F}\{e^{M(iNx + \zeta)}\}}{\mathfrak{F}\{f(x, y) e^{M(iNx + \zeta)}\}} \right\}.$$

There is no easy way to derive analogous formula for velocity potential derivatives, however, numerical experiments have shown that there is no need to do it. These derivatives can be obtained numerically via finite difference formulae. Less number of integral transforms means less numerical error and faster computation.

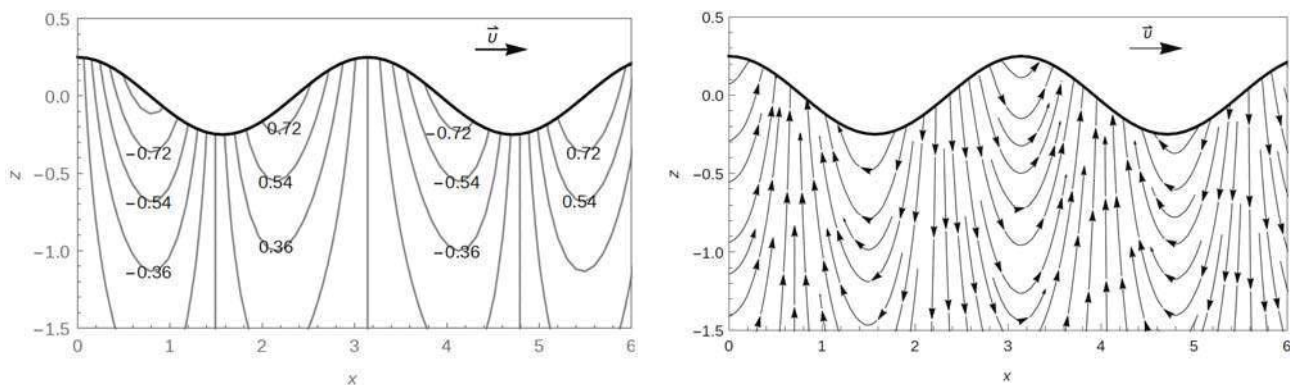


Fig. 2 Slices at $y=3.1$; $t=0$ of propagating waves' velocity potential field (left) and stream lines (right). Here $\zeta(x, y, t) = \frac{1}{4} \cos(4\pi x - 0.25t)$.

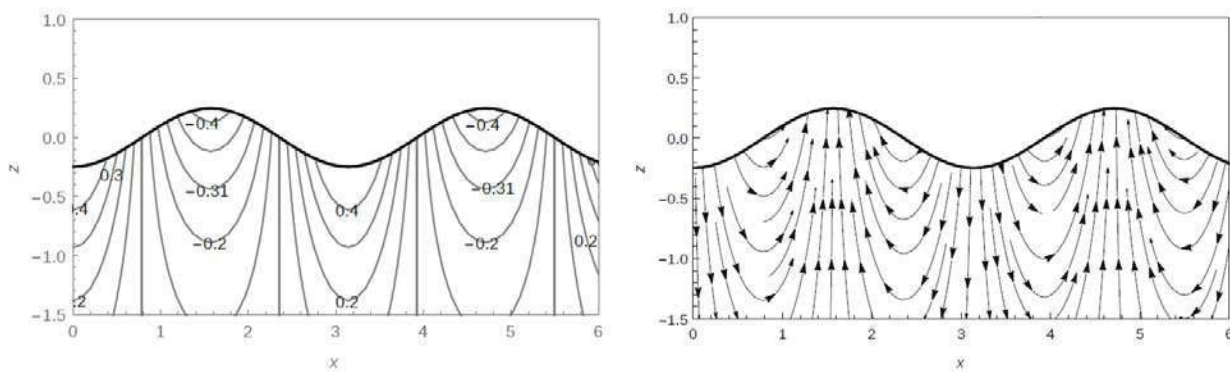


Fig. 3 Slices at $y=3.1$; $t=1$ of standing waves' velocity potential field (left) and stream lines (right). Here $\zeta(x, y, t) = \cos(4\pi x) \sin(-0.25t)$.

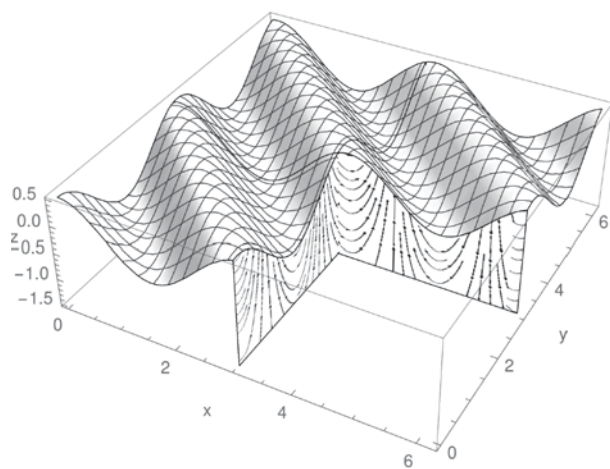


Fig. 4 Slice at $y = 3.1$; $t = 0$ of propagating waves' velocity potential stream lines. Here $\zeta(x, y, t) = \frac{1}{2} \cos(4\pi(x + y) - 0.25t)$.

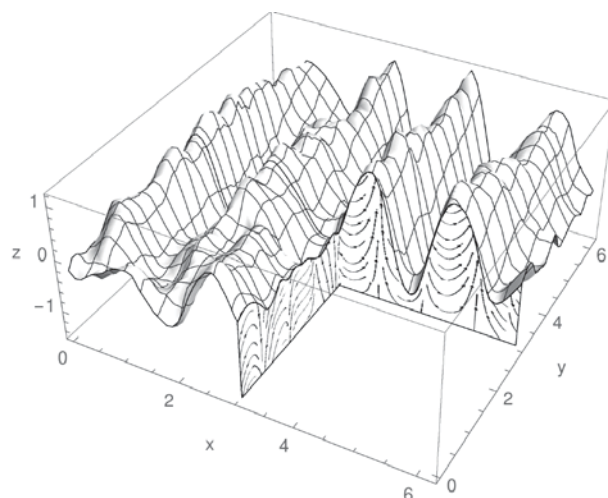


Fig. 5 Slice of a wavy surface with waves of large amplitude generated by autoregressive wind wave model.



So, from computational point of view velocity potential is given by four fast Fourier transforms plus three numerical differentiations (one for each coordinate), in other words its asymptotic complexity is roughly $4n \log_2 n + 3n$, where n is the total number of points in the volume.

4.3 Evaluation

Three-dimensional solution was evaluated on different types of waves: propagating, standing and real ocean waves generated by autoregressive model. For the first two types of waves the shape of velocity potential and velocity field is known and can be found elsewhere (van Dyke, 1982), so they were used to validate the solution. The last type of wave was used to see how the solution behaves in case of large amplitude waves.

Since computation is done with discrete Fourier transforms the resulting data is sometimes perturbed on the edges (Lyons, 2010). In real world those perturbations should be removed from the solution but here they were left for the sake of transparency of results.

Propagating waves are known to have region of negative velocity potential under the front slope and region of positive potential under the back slope while standing waves are known to have region of negative potential under their crests and region of positive potential under their bottoms. Velocity of a water particle is always in the direction of negative potential and it is perpendicular to the contours of velocity potential. This behaviour is fully captured by the solution (Figures 2–4).

For large amplitude waves the solution was tested on the wavy surface generated by autoregressive wind wave model and in this case the shape of stream lines and potential field is asymmetric. As can be seen in Figure 5 stream lines are skewed in the direction which is opposite to the direction of wave propagation.

5. CONCLUSIONS

To sum up, new solution allows determining velocity field for waves of arbitrary amplitudes and is fast from computational point of view. For plain waves the solution gives the same field as previously known solutions and for large-amplitude waves it gives asymmetrical velocity field.

6. ACKNOWLEDGEMENTS

The research was carried out using computational resources of Resource Centre “Computational Centre of Saint Petersburg State University” (T-EDGE96 HPC-0011828-001) within frameworks of grants of Russian Foundation for Basic Research (project no. 13-07-00747) and Saint Petersburg State University (projects no. 9.38.674.2013 and 0.37.155.2014).

7. REFERENCES

- A. Degtyarev and I. Gankevich. Evaluation of hydrodynamic pressures for autoregression model of irregular waves. *In Proceedings of 11th International Conference on Stability of Ships and Ocean Vehicles*, Athens, pages 841–852, 2012.
- N. Kochin, I. Kibel, and N. Roze. *Theoretical hydrodynamics* [in Russian]. FizMatLit, 1966.
- Richard G Lyons. *Understanding digital signal processing*. Pearson Education, 2010.
- Milton Van Dyke. *An album of fluid motion*. 1982.



Potential Assessment of Cargo Fluidization based on an UBC3D-PLM Model

Lei Ju, *Ship Stability Research Centre, University of Strathclyde*, lei.ju@strath.ac.uk

Dracos Vassalos, *Ship Stability Research Centre, University of Strathclyde*, d.vassalos@strath.ac.uk

ABSTRACT

Fluidization of fine particle cargoes, resulting in cargo shift and loss of stability, has caused the loss of many lives in numerous marine casualties over the past decades. Since the dangers of cargo fluidization have long been known to the shipping industry, the question of why the phenomenon is resurfacing now would be a legitimate one. With this in mind, an UBC3D-PLM model based on FEM theory in the commercial software PLAXIS is presented in this paper to consider soil DSS (Direct Simple Shear) test to verify the model. To assess the cargo fluidization potential, an evaluating method is presented in the paper considering cargo fluidization. Shaking table tests with different amplitude, frequency and initial degree of saturation of cargoes were studied to predict time-domain characteristics. This method in the paper could be feasibly used as a reference and possibly support a suitable regulatory framework to the fluidization analysis of ship stability.

Keywords: *Cargo Liquefaction; UBC3D-PLM; Ship Stability*

1. INTRODUCTION

Liquefaction of mineral ores, such as ore fines from India and nickel ore from Indonesia, the Philippines and New Caledonia, resulting in cargo shift and loss of stability, has been a major cause of marine casualties over the past few years. Such a transition during ocean carriage can cause a sudden loss of stability of the carrying vessel. While cargoes are loaded on board a vessel, the material is exposed to mechanical agitation and energy input in the form of engine vibrations, vessel movement and wave impact, resulting in a gradual settling and compaction of the cargo. The gaps between the particles become smaller in the process, while the pore pressure between particles will increase. The water holding ability or matric suction of particles decreases and the water in the cargoes will separate from the cargo. Then cargoes turn into a viscous fluid, i.e. fluidization.

The UBC3D-PLM is a powerful constitutive model, which is a 3-D extension of the UBCSAND model introduced by Beaty & Byrne (1998). The Mohr-Coulomb yield condition in a 3-D principal stress space is used. The bulk modulus of water is depended with the degree of saturation, which is specified via PLAXIS input, enabling the prediction of the pore pressure evolution in unsaturated particles.

2. KEY FEATURES OF UBC3D-PLM

2.1 Yield Surface

Mohr-Coulomb yield function generalized in 3-D principal stress space is used in UBC3D-PLM model (Alexandros & Vahid, 2013) as presented in Figure 1.

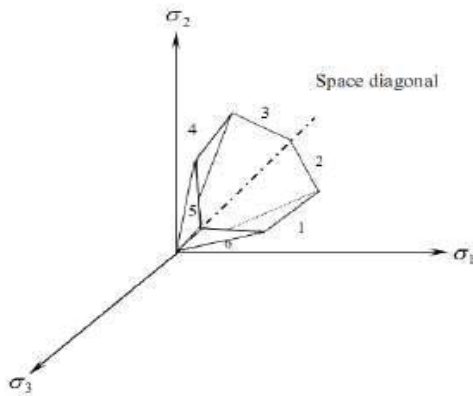


Figure 1 The Mohr-Coulomb yield surface in 3-D principal stress space

The critical yield surface could be defined given by Equation (1):

$$f_m = \frac{\sigma'_{\max} - \sigma'_{\min}}{2} - \left(\frac{\sigma'_{\max} + \sigma'_{\min}}{2} + c' \cot \phi'_p \right) \sin \phi'_{mob} \quad (1)$$

Where, σ'_{\max} and σ'_{\min} are the maximum and minimum principal stresses respectively, c' is the cohesion of the soil, ϕ'_p is the peak friction angle of the soil, ϕ'_{mob} is the mobilized friction angle during hardening.

2.2 Elasto-plastic Behaviour

The elastic behaviour which occurs within the yield surface is controlled by two parameters expressed in terms of the elastic bulk modulus K_B^e and the elastic shear modulus K_G^e as shown below:

$$K_B^e = k_B^e P_A \left(\frac{p'}{P_A} \right)^{me} \quad (2)$$

$$K_G^e = k_G^e P_A \left(\frac{p'}{P_A} \right)^{ne} \quad (3)$$

Where, p' is the mean effective stress, P_A is the reference stress (usually equal to 100kPa), k_B^e and k_G^e are the bulk and shear modulus numbers respectively and, me and ne

are the elastic exponents which define the rate dependency of stiffness.

The hardening rule as reformulated by Tsegaye (2011) in UBC3D-PLM model is given as:

$$d \sin \phi'_{mob} = 1.5 K_G^p \left(\frac{p}{P_A} \right)^{np} \frac{P_A}{P_m} \left(1 - \frac{\sin \phi'_{mob}}{\sin \phi'_{peak}} R_f \right)^2 d\lambda \quad (4)$$

Where, $d\lambda$ is the plastic strain increment multiplier, np is the plastic shear modulus exponent, ϕ'_{mob} is the mobilized friction angle, which is defined by the stress ratio, ϕ'_{peak} is the peak friction angle and R_f is the failure ratio n_f / n_{ult} , ranging from 0.5 to 1.0.

2.3 Plastic Potential Function

The plastic potential function specifies the direction of the plastic strain. A non-associated flow rule based on the Drucker-Prager plastic potential function is used in the UBC3D-PLM (Tsegaye, 2011). The plastic potential function is formulated as:

$$g = q - a(p' + c \cot \phi'_p) \quad (5)$$

$$a = \frac{\sqrt{3} \sin \psi'_{mob}}{\cos \theta + \frac{\sin \theta \sin \psi'}{\sqrt{3}}} \quad (6)$$

Where, θ equals 30° cause the Drucker-Prager surface is fixed in the compression point.

2.4 Post-liquefaction Rule and Cyclic Mobility

From the experimental studies, the stiffness degradation of soil due to the post-liquefaction behaviour of loose non-cohesive soils or due to the cyclic mobility of dense non-cohesive sands is occurred. For modelling this, an



equation is implemented in UBC3D-PLM which gradually decreases the plastic shear modulus as a function of the generated plastic deviatoric strain during dilation of the soil element.

This behaviour is presented in Figure 2 picturing the process of cyclic mobility of dense sand. The stiffness degradation is computed as follows:

$$K_G^P = K_{G, primary}^P * e^{E_{dil}} \quad (7)$$

$$E_{dil} = \min(110 * \varepsilon_{dil}, fac_{post}) \quad (8)$$

Where ε_{dil} is accumulation of the plastic deviatoric strain which is generated during dilation of the soil element, the input parameter fac_{post} is the value of the exponential multiplier term.

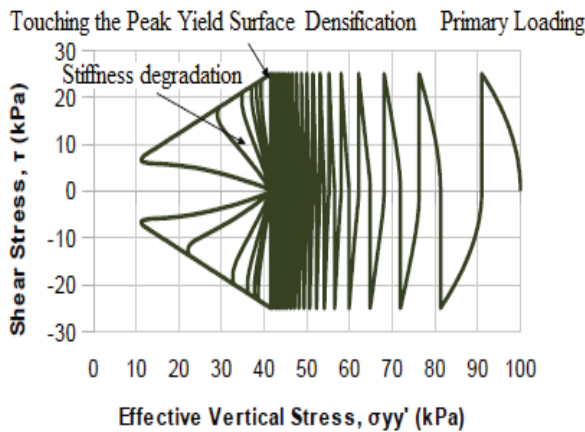


Figure 2 Undrained cyclic shear stress path reproduced with UBC3D-PLM for dense sand. Cyclic mobility, stiffness degradation and soil densification are mentioned on the graph

2.5 Undrained Behaviours

The increment of the pore water pressure is computed by the following equation:

$$dp_w = \frac{K_w}{n} d\varepsilon_v \quad (9)$$

Where K_w is the bulk modulus of the water and n is the soil porosity and $d\varepsilon_v$ is the volumetric strain of the fluid.

The bulk modulus of water is dependent with the degree of saturation of the soil. The bulk modulus of the unsaturated water is defined as follows:

$$K_w^{unsat} = \frac{K_w^{sat} K_{air}}{SK_{air} + (1-S)K_w^{sat}} \quad (10)$$

Where K_w^{sat} is the bulk modulus of the saturated water and K_{air} is the bulk modulus of air which equals 1 kPa in this implementation having the minimum value which enables to avoid the generation of pore pressures during modelling a dry sand. S is the degree of saturation in the soil.

3. VALIDATION OF THE UBC3D-PLM IN ELEMENT TEST

3.1 Validation of the UBC3D-PLM in Monotonic Loading

The validation of the UBC3D-PLM in monotonic loading is presented in this section. The input parameters for modelling the tri-axial compression test (TxC) and the direct simple shear test (DSS) on loose Syncrude sand are given in Table 1. The results of the UBC3D-PLM are in a good agreement with the experimental data (Puebla & Byrne & Philips, 1997) as shown in Figure 3 and Figure 4.

Table 1 UBC3D input parameters for all the validation tests

Parameter	Syncrude S. (TxC, DSS)	Fraser S. (Cyclic DSS)	Cargo (FEM)



$\phi_p(\circ)$	33.7	33.8	31.2
$\phi_{cv}(\circ)$	33	33	34.6
k_B^e	300	607	720
k_G^e	300	867	1031
$K_G^p(TxC)$	310	-	
$K_G^p(DSS)$	98.3	266	700
$me = ne$	0.5	0.5	0.5
np	0.5	0.4	0.4
R_f	0.95	0.81	0.74
$N1(60)$	8	8	13
fac_{hard}	1	1	0.45
fac_{post}	0	0.6	0.01

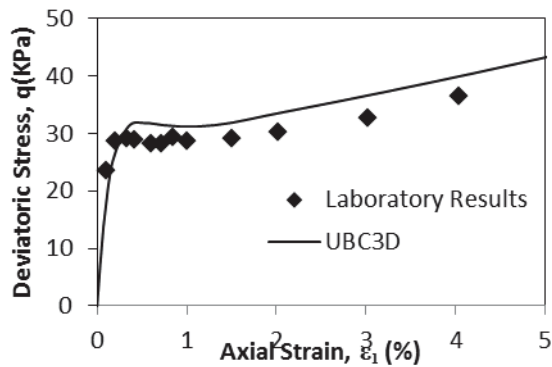


Figure 3 Undrained tri-axial compression

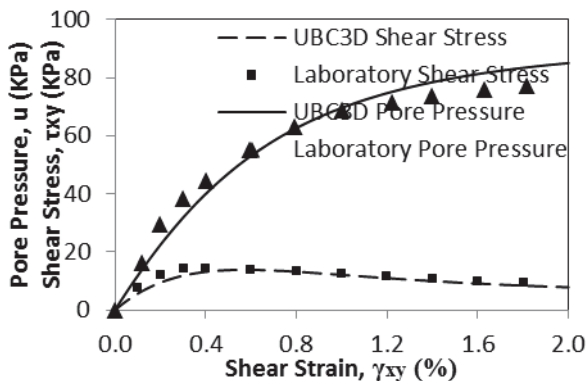


Figure 4 Undrained simple shearing

3.2 Validation of the UBC3D-PLM in Cyclic Loading

The behaviour of loose Fraser sand under cyclic direct simple shear is modelled and the numerical results are compared with experimental data as published by

Sriskandakumar (2004). The relative density (RD) of the tested sand is 40%. In Figures 5, the evolution of stress-strain is presented. The applied CSR equals 0.08. The vertical applied stress is 100 kPa in all cases. The K0 factor is assumed to be 1 for simplification.

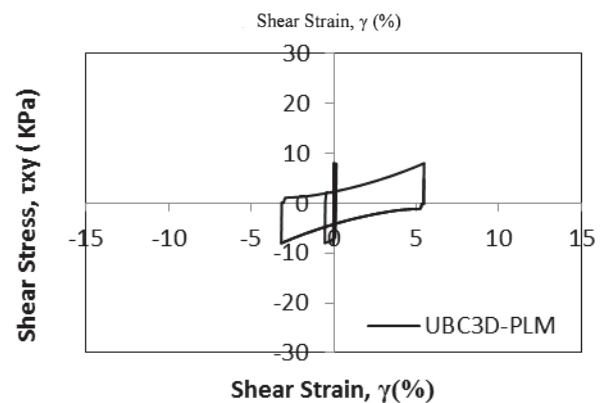
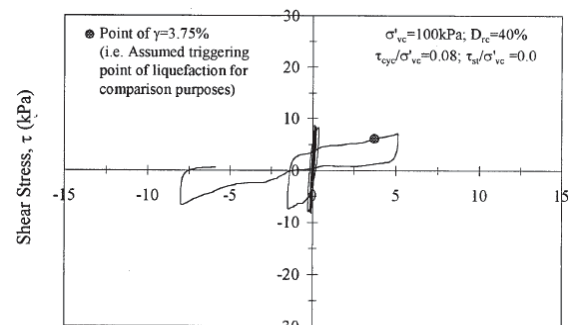
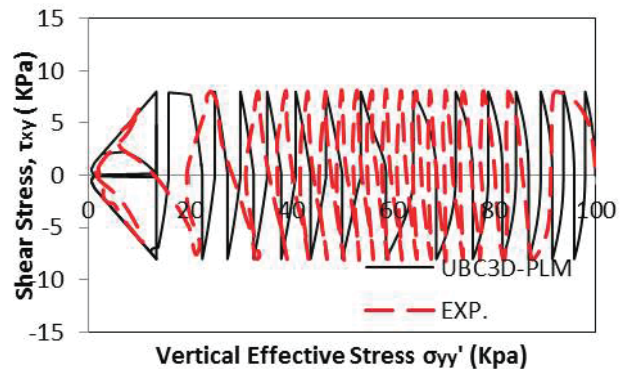


Figure 5 Cyclic DSS stress controlled (RD=0.4 CSR=0.08 $\sigma_v=100kpa$)



4. CARGO FLUIDIZATION IN A FINITE ELEMENT SCHEME

4.1 Evaluating cargo fluidization

The soil-water characteristic curve is the basis for estimating the dynamic analysis of particles. Unsaturated particles are composed of three phases; including particle skeleton (solid), pore water (liquid) and pore air (gas). The air-water interface has a surface tension. In the unsaturated particles, the pore air pressure and pore water pressure are unequal and greater than the latter. The interface is under the part pore air pressure of larger pore water pressure. The pressure difference (i.e., pore air pressure minus pore water pressure) across the interface of air and water is called the matric suction. Matric suction is generally the key parameter describing the mechanical property of unsaturated particles.

In the capillary tube, the surface between pore air and pore water displays curved interface. The fluid pressure of sides interface is discontinuous. If the upside of the interface is connected with atmosphere, the pressure upside interface is larger than the water pressure. The pressure difference is called matric suction. S depends on the curvature of the curved interface and surface tension.

$$S = u_a - u_w \quad (11)$$

The soil-water characteristic curve (SWCCs) relates the water content or degree of saturation to matrix suction of a particle. A representative SWCCs is shown in Fig 6. We can see different iron ore has different water holding ability. When the cargo compaction, the volume decreases resulting in increasing pore water pressure and decreasing matric suction of cargos. Cargos cannot hold any water in case of suction equals zero. Water is progressively displaced in the hold base, which

may result in some portions or all of the cargo developing a flow state.

For earthquake liquefaction, the acceleration is large and soil could be regarded as un-drained soil, where acceleration for cargo fluidization is small and the water could drain from cargos. When the degree of saturation turns 100% and water comes out from the cargos, the cargos have reflected the nature of fluidization. Therefore, take suction=0 as the onset of cargo fluidization in the paper.

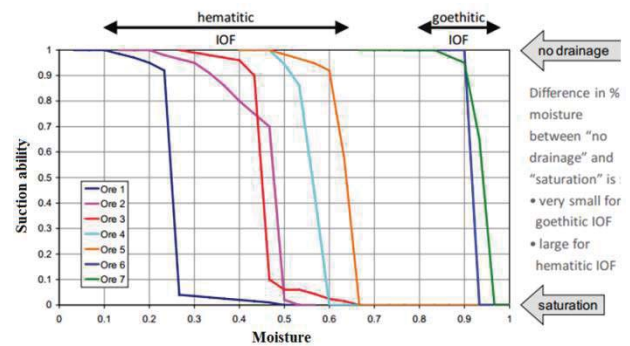


Figure 6 Soil-water characteristic curves

4.2 Centrifuge Test

The influence of degree of saturation on the free field response is investigated. The geometry of layer is shown in Figure 7. Locations L, N, O are monitored through the test. The initial degree of saturation is supposed uniform.

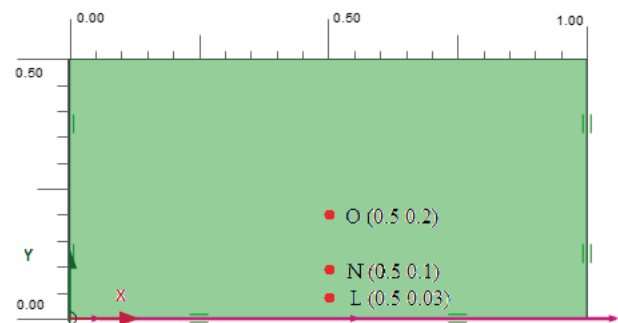
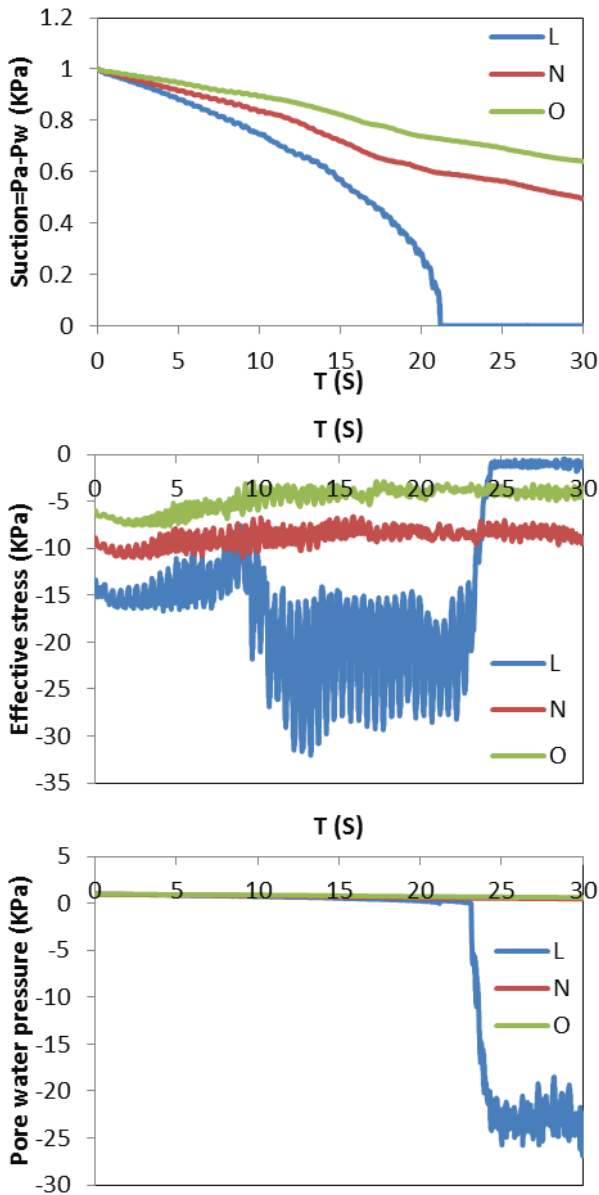


Figure 7 Centrifuge test model

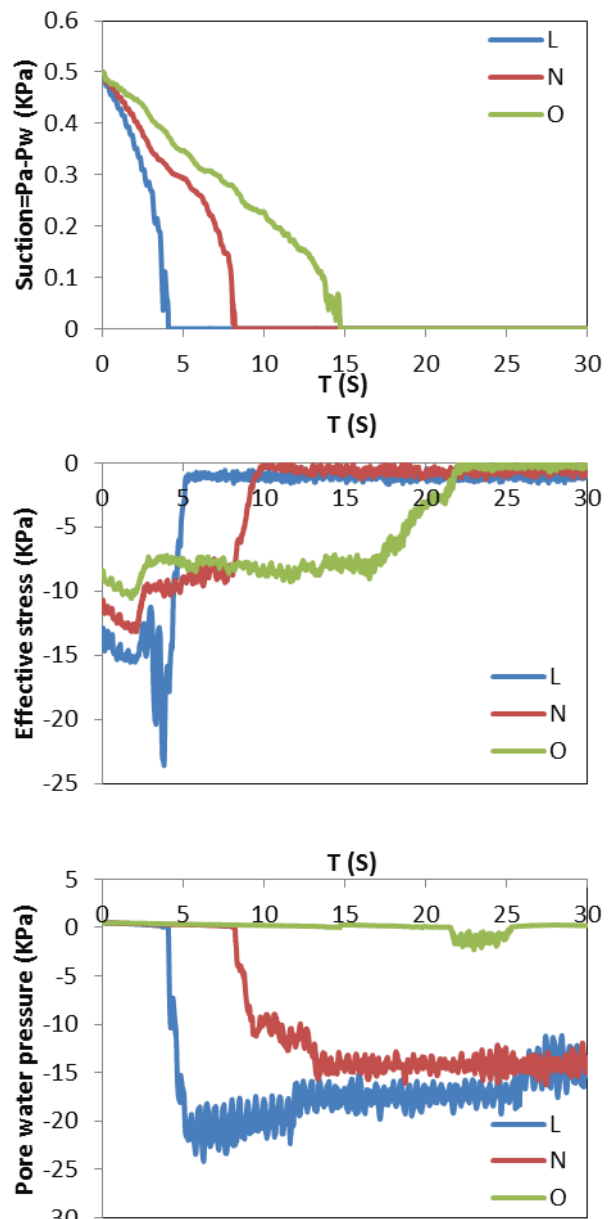
The degree of saturation varies as $S=99.0\%$, 97.0% and 94.0% . The initial stress may have a



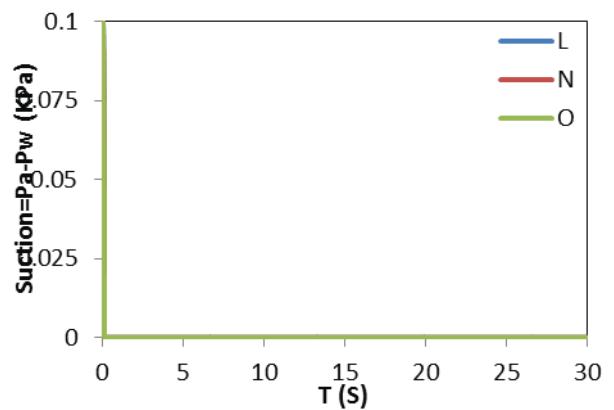
great influence on the results and the initial stress used is due to the gravity action during all the tests. The boundary conditions are defined as: at the base of layer, the vertical displacement is blocked, and the input energy is sinusoidal horizontal acceleration with the amplitude $0.02m/s^2$ and the frequency 2HZ. At the lateral boundaries, the horizontal displacement is blocked. The model parameters are listed in Table 1.

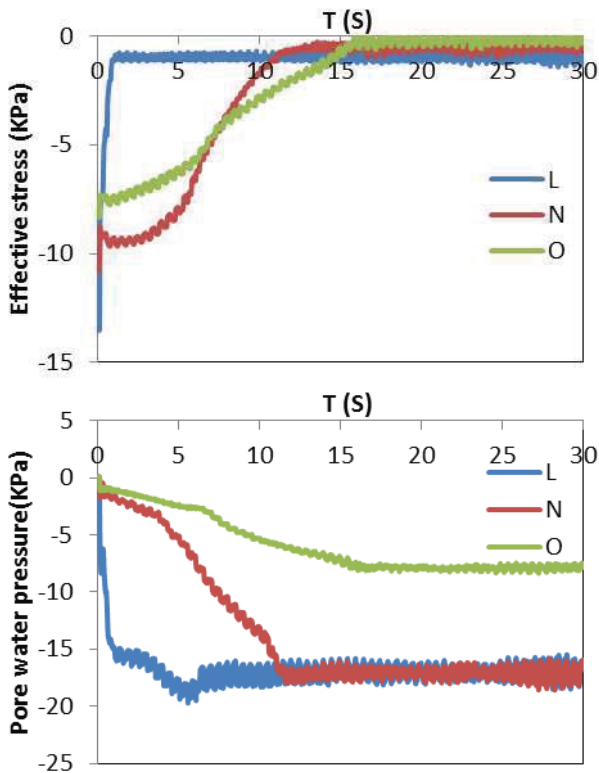


(a) Degree of saturation=94%



(b) Degree of saturation=97.0%





(c) Degree of saturation =99.0%

Figure 8 Evolution of suction, effective stress and pore water pressure of the column during centrifuge test

From Figure 8, we can see that variation of the degree of saturation has a significant influence on matric suction, effective stress and pore water pressure generation. When the matric suction decreases to 0, the degree of saturation turns 100%. From the figure, after full degree of saturation, the pore water pressure increases rapidly and the effective stress decreases to zero and fluidization occurs immediately. when the degree of saturation is less 94%, the onset of fluidization at point L could be delayed to 23s. With the increase in the initial degree of saturation, the onset of fluidization is easier to reach.

4.3 Shaking Table Test

Shaking table tests considering sway motion of ship with different amplitude, frequency and initial degree of saturation of cargos are investigated to predict time-domain

characteristics during liquefaction based on UBC3D-PLM Model in commercial software PLAXIS. The geometry of layer is shown in Figure 9. Locations M, L, K, P, O and N are monitored through the test. The initial degree of saturation is supposed uniform and varies as 99%, 95.16% and 92.38%. The frequency varies as 0.25HZ, 0.35HZ and 0.5HZ. The amplitude varies as 0.02m, 0.04m and 0.06m. The boundary conditions are defined as: rigid box is used in the shaking table test; at the base of layer, the vertical displacement is blocked, and the input energy is sinusoidal horizontal displacement condition. At the lateral boundaries, the horizontal displacement is free and has the same motion with the base of box. The initial stress due to the gravity is shown in Figure 10.

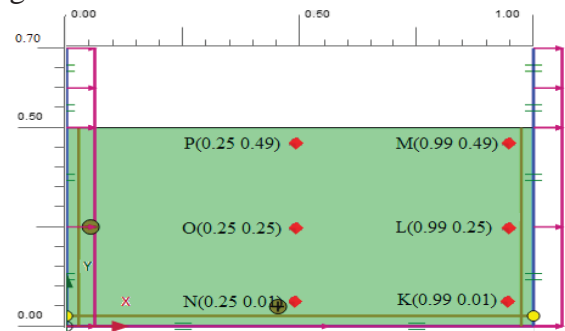


Figure 9 Shaking table test model

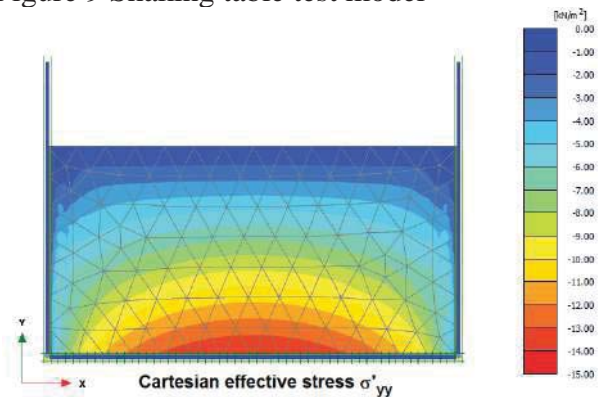


Figure 10 The effective stress contour after gravity action

From Figure 11 in the calculation of amplitude 0.04m, frequency 0.25HZ and degree of saturation 95.16%, we can see the soil near locations L, O and K is at the edge of liquefaction due to severe contraction. Locations M and P occurs dilation and N has a



high effective stress which are difficult to liquefy.

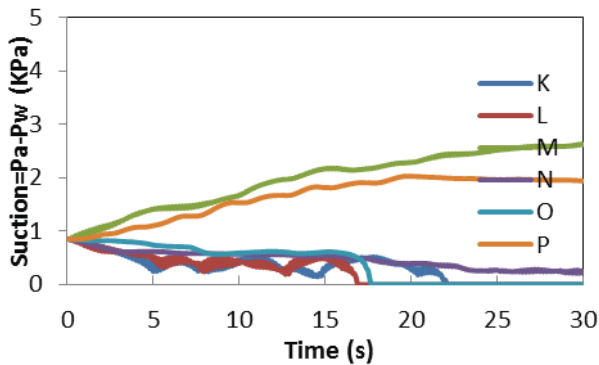
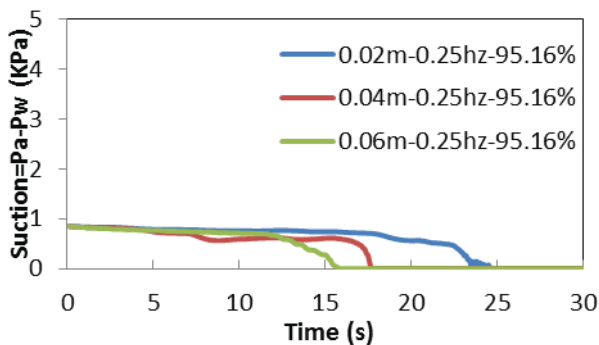
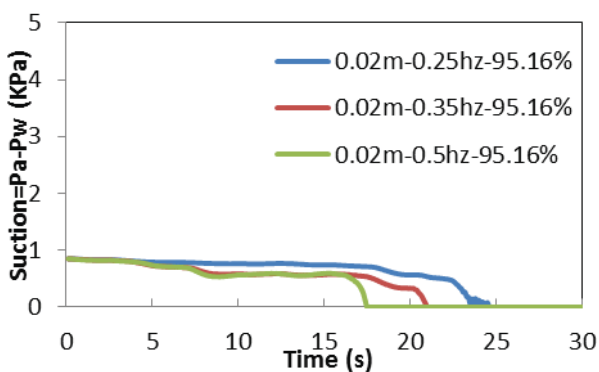


Figure 11 Evolution of suction during shaking table test

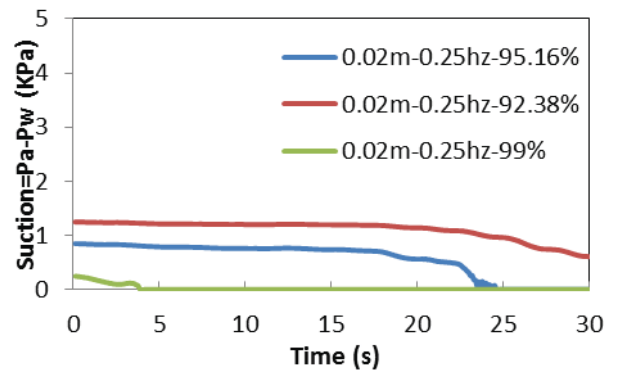
Emphasis could be put on the middle column of location O. From Figure 12, we can see that the higher degree of saturation, frequency and amplitude, the easier the onset of liquefaction. Due to the interaction between soil and rigid box, liquefaction of the soil displays more complicated from the curves of effective stress. From (a) to (c), varies of the amplitude and the frequency have small impact on liquefaction, where degree of saturation is just the reverse.



(a) Variation with amplitude



(b) Variation with frequency



(c) Variation with degree of saturation

Figure 12 Evolution of suction at the middle of the column during shaking table test

5. CONCLUSIONS

Tests for monotonic loading and cyclic loading agree well with experimental data. Finite Element Method combined with UBC3D-PLM model could be used to simulate cargo liquefaction potential assessment. Accurate description for properties of cargos is the key factor to predict cargo liquefaction. In the tests, special properties of soil were used to model the cargo liquefaction.

With the higher degree of saturation, frequency and amplitude, cargo has smaller liquefaction resistance. Among these three factors, the only one we could control is the degree of saturation. Therefore, reducing the degree of saturation of cargos will enormously improve the stability of the cargo ship during transportation. Comparison with centrifuge test of the single vibration source on the base of column, soil liquefaction with shaking table is more complicated due to the interaction between soil and rigid box.

This method in the paper could be feasibly used as a reference and possibly support a suitable regulatory framework based on time domain analysis of cargo liquefaction.



6. REFERENCES

- Beatty, M. and Byrne, P., 1998, "An Effective Stress Model for Predicting Liquefaction Behaviour of Sand", ASCE Geotechnical Earthquake Engineering and Soil Dynamics (geotechnical special publication III), Vol. 75(1), pp. 766-777.
- Petalas, Alexandros. and Galavi, Vahid., 2013, "Plaxis Liquefaction Model UBC3D-PLM", PLAXIS Report.
- Puebla, H., Byrne, M., and P.Philips, P., 1997, "Analysis of canlex liquefaction embankments prototype and centrifuge models", Canadian Geotechnical Journal, Vol. 34, pp. 641-651.
- Sriskandakumar, S., 2004, "Cyclic loading response of fraser sand for validation of numerical models simulating centrifuge tests", Master's Thesis, The University of British Columbia, Department of Civil Engineering.
- Tsegaye, A., 2011, "Plaxis Liquefaction Model", PLAXIS Report.
- G.R. Martin, W.D.L. Finn, and H.B. Seed., 1975, "Fundamentals of liquefaction under cyclic loading", Journal of the Geotechnical Engineering Division, ASCE, 101.

This page is intentionally left blank



Coupled Granular Material and Vessel Motion in Regular Beam Seas

Christos C. Spandonidis & Kostas J. Spyrou

*School of Naval Architecture and Marine Engineering
National Technical University of Athens*

spandonx@mymail.ntua.gr, k.spyrou@central.ntua.gr

ABSTRACT

The behaviour of granular cargos under the effect of ship motions has not been sufficiently studied and international regulations on bulky cargos' loading and stowage, despite their updating and improvement, remain empirical. In the current work we investigate the interplay of granular material flow with a vessel's motion. The method of molecular dynamics is employed for modelling granular material dynamics, combined with a standard model of ship rolling for regular beam seas. Dry granular materials, spherical particle approximation and non-linear frictional forces are the key assumptions in modelling the cargo's movement. Characteristic simulation results including comparisons against cases of rigid cargo are presented.

Keywords: *granular material, molecular dynamics, ship cargo shift, ship motion*

1. INTRODUCTION

The problem of cargo shift is one of the most important ship safety issues. The recent upgrading of international regulations concerning the loading and stowage of ship cargos in bulky form is based, almost entirely, on empirical considerations (IMO, 2012). Approaches with potential to establish a solid scientific basis for this problem, using micro-scale modelling of cargo particles' motion and their interaction with the moving ship under wind/wave excitations, are still lacking. A possible reason is because such modelling is very demanding and it calls for an interdisciplinary approach, overcoming the often fragmented nature of scientific efforts. As type of problem, cargo shift could be classified along with sloshing; with clear methodological analogies prevalent in particular when, for the latter, a smooth particles hydrodynamics (SPH) modelling approach is applied. As well known, coupled ship motions affected by liquid

sloshing have been extensively studied in the past, since high impacting pressures on tank walls constitute a perennial operation hazard. Faltinsen & Timokha (2009) provided an in depth presentation of analytical and numerical models for the coupled fluid motion in a tank. Moreover, in Monaghan (2005) was included a review of commonly applied SPH techniques. When it comes to granular cargos however, the authors could not identify any research effort of similar standing. A category of interesting works have dealt, for example, with the dynamics of sloshing cargos in silo vehicles (e.g. Fleissner et al 2009). But they have not presumed any link to the ship motion problem.

A key element in the coupled roll-granular cargo problem formulation is the feedback from ensemble of discontinuously moving particles to the ship's body. Such abrupt particle movement is a characteristic of container-body motions receiving external excitations predominantly of low frequency, with some higher frequencies appearing in the excitation from time to time. Such sudden



motion of the cargo constitutes the main contributing factor for a ship to acquire large roll bias, a state wherefrom capsizing becomes imminent. In general, in terms of dynamics, the particles behave like oscillating masses interacting with each other and also, in unison, with the hold they are transported wherein. As a matter of fact, significant quantities of energy can be exchanged between the particles and the carrying body in a rather intermittent manner. These effects of interaction take the problem out of the convenient field of rigid body dynamics where ship stability studies are customarily performed.

In a line of research initiated at NTUA since 2011 to fill this gap, we have investigated already the excited motion of granular materials when the hold is subjected to series of prescribed oscillations. It was studied in particular the mechanism of formation of the cargo's angle of repose and associated phenomena (Spandonidis & Spyrou 2012 & 2013). In the current paper we take a step further, to study how the ship and the granular material behave, as a system, under the effect of wave excitation on the hull. Our intention is to understand how the coupling between material and ship works, in order to create a suitable tool for assessing the severity of such coupling effect. Although it is aimed to develop, in the longer run, a full ship motion model, at present we have restricted our study to regular beam sea waves in deep water, applied on a prism with rectangular cross section restrained to move only in roll.

2. ASPECTS OF THE BEHAVIOUR OF VIBRATED GRANULAR MATERIAL

As it is intended to combine a ship roll model with a suitable granular material flow model, in this part are reviewed briefly some aspects of their modelling and behaviour. General interest for the study of granular flows is inspired by their several industrial applications as well as by their complex rheological character. A granular material flow

typically is comprised of a particulate solid in an interstitial fluid (usually air) subjected to a shearing force. In the most common granular material vibration experiments the considered materials are sand, grain or glass spheres (usually 0.5 – 3 mm diameter with standard deviation 5%). They are placed in a rectangular or cylindrical container mounted on a rigid base which is subjected to multi axial, sinusoidal oscillations. Even these simple systems can exhibit surprisingly complex behaviour that has yet to be fully explained. For example, the particle bed can behave as a "cloud" of particles with little or no structure; and in other cases the particle bed moves as a coherent mass. Depending on the frequency and amplitude of acceleration, vibrated granular materials can give rise to various phenomena such as compaction, convective flow, size segregation and "arching". Particle rearrangements induced by vibrations lead to lower shear strength and higher ability to flow. In the full fluidization regime, there are no permanent contacts between particles and the system behaves as a dissipative gas. When particle accelerations remain below the gravitational acceleration, the system keeps its static nature and the vibrational energy propagates through a rather compact network of inter-particle contacts. On the other hand, vibrations at high frequency and low amplitude lead to slow (logarithmic) decay of the pore space as a function of time. Several theories trying to explain this behaviour have been proposed (e.g. Laroche et al. 1989; Gallas et al. 1992; Corwin et al. 2005); yet none seem to be universally accepted. Another phenomenon that is observed for deep beds is the formation of surface waves. The waves travel from the lowest point of the heap up the slope to the peak but do not interfere with the continuous avalanche of particles associated with the convection pattern. The waves increase in length and decrease in height as they travel up the slope and eventually disappear at the peak. The onset of the travelling surface waves depends on the vibration- amplitude-to-particle-diameter ratio. Standing surface waves form at half the excitation frequency for certain

ranges of the excitation amplitude and frequency, following a mechanism similar to the Faraday instability (Douady & Fauve 1988; Miles & Henderson 1990).

3. EQUATION OF MOTION

The analysis is performed in model scale and a small rectangular hold is considered. It is placed inside a box barge that is allowed to be rotated in roll only, around a specific axis (1-DOF approach). That is, the roll centre is considered fixed (point P in Figure 1). Each particle's motion is monitored from another coordinate system, whose origin is placed at the hold's bottom left corner (ZOY). This coordinate system remains always horizontal (i.e. it does not follow vessel's rotation). System yKz is also placed at the bottom left corner; but it follows the motion of the hold in such a manner that its z -axis is always perpendicular to the bottom. The reference system aPb is assumed to be at the centre of rotation of the vessel (which in the current study coincides with the middle point of the ideal flat free surface). This coordinate system follows vessel's rotation.

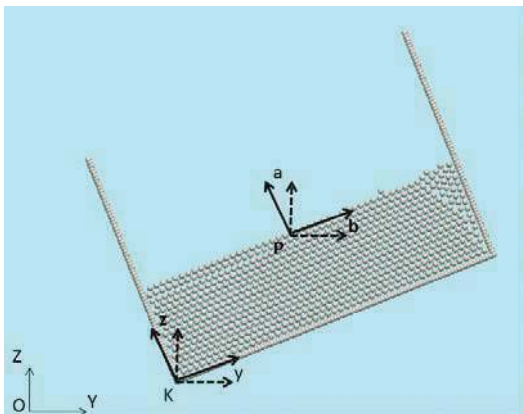


Figure 1 The three different coordinate systems (solid lines) and their irrotational equivalents (dashed lines) are being depicted.

In Figure 1 systems yKz and aPb are depicted with solid lines. In what follows, only the dynamics on the xy plane is under investigation due to the 2D nature of the

developed granular material algorithm. Thus, the barge is assumed to be long enough (2 m) compared to her height (0.3 m) and beam (0.34 m). These dimensions should facilitate direct comparison with the results of experiments in the future.

Two different problems need to be tackled simultaneously: The wave induced ship motion and the motion of the granules inside the hold. On the basis of the so called “molecular dynamics” method we predict the trajectory of each individual particle, assumed to interact with all its neighbouring particles through non-linear elastic and frictional forces. “Molecular dynamics” is the most important among the simulation methods that have been used for granular flows. It involves solution of Newton's equation of motion for every particle. Normally to the line of contact of particle collisions we have considered nonlinear elastic and frictional forces; while transversely we have assumed acting a purely frictional force:

$$F_{nor} = -k_n \xi^{3/2} - \gamma_n \xi^{1/2} \dot{\xi} \quad (1)$$

$$F_{tan} = -\min(|\gamma_s u_s|, |\mu F_n|) \cdot \text{sign}(u_s)$$

γ_n and γ_s are normal and shear damping constants respectively; k_n is non-linear stiffness coefficient, u_s is the shear velocity component and μ stands for the dynamic friction coefficient (see Spandonidis & Spyrou 2012 for details). Collision forces are computed for each couple and at every time step. From them, the forces that act on the side plates of the hold are obtained.

Newton's equation for ship roll motion is also solved at each time step, with loads considered due to added moment of inertia, hydrodynamic damping, restoring, “Froude-Krylov” moment and the impacting moment due to possible particles' impact with hold's side walls. Vessel's roll motion can be described then by Eq. (2) which is solved in time, coupled with the nonlinear molecular dynamics model of the granular material:



$$(I + \delta I)\ddot{\phi} + B_1\dot{\phi} + B_2\phi|\dot{\phi}| + M_R = \\ = mg GM r Ak \cos(\omega t) + M_I \quad (2)$$

ϕ is the roll angle, I and δI are respectively the roll moment of inertia and the added moment of inertia, B_1 and B_2 are the linear and the quadratic roll damping coefficients. δI and B_1 were calculated with a linear BEM code while B_2 was taken as frequency independent. M_R is the restoring moment calculated as the sum of three moments (M_B due to buoyancy, M_S due to ship's weight and M_C due to cargo's weight) calculated around the fixed axis of rotation:

$$M_R = M_B + M_S + M_C \quad (3)$$

Moreover, the impact moment M_I generated by the particles' contact with nonzero relative velocity with hold's walls is calculated.

In order to verify our results we performed reliability tests as proposed by Haile (1997). Different operating systems (Windows 8, Windows XP, Linux RedHat 5.1), hardware configuration and computational software (Microsoft Visual C++, Mathematica, Matlab) were used, in order to calculate the systemic error. Also, several repetitions were performed for each numerical experiment in order to check conservation principles and monitor the statistical error. The algorithm can provide accurate calculations with a statistical and systemic error whose deviation does not exceed 2%. Validation of the coupled motion results could not be done at this stage due to lack of suitable experimental measurements and we relied on separate validation of the two sub-algorithms. For the validation of the molecular dynamics algorithm see Spandonidis & Spyrou (2013). Concerning the ship motion equation, results for "empty hold" and for "hold with solid (frozen) cargo" were compared against similar experimental results obtained by Rogenbake & Faltinsen (2003) and by Murashige & Aihara (1998), indicating that the algorithm performs very well with a standard deviation less than 1%.

4. CASE STUDY

We assumed the hold filled with cellulose acetate particles of diameter 0.3 cm such that the particle parameters (friction, stiffness etc) coincide with these experimentally measured by Forester et al (1994). The draft with the material inside is (in initial position) 0.11 m. The material height-to-width-ratio is 0.36 which corresponds certainly to a "finite" material depth case. The vessel was free to move only in roll, with an external excitation owed to waves that were fixed in amplitude and frequency. Granules were considered as smooth spheres with diameters that could be either fixed or varied in some range and they could be translated (horizontally-vertically) or rotated. At this specific stage we assumed dry granules and the weight of the cargo equalled that of the vessel itself (even though this would not be the real case e.g. for a bulk-carrier). Several tests were performed before beginning the actual numerical experiments, in order to identify the critical parameters. At first step, the material was left to balance in calm water. In this way the draught of the barge and its initial roll angle were calculated for several slightly different initial free surface configurations. The eigenperiod of the barge lies within acceptable, for real case scenario, limits. In addition, following the tilting table method described in the International Maritime Solid Bulk Cargoes code -IMSBC (IMO 2012), we determined the critical angles leading to cargo shift. In Figure 2 is depicted the horizontal displacement of the centre of mass versus the tilting angle, for different tilting rates. As indicated, when relatively slow rates are applied (smaller than 1 rad/s) two angles with values close to 25 and 42 deg are identified.

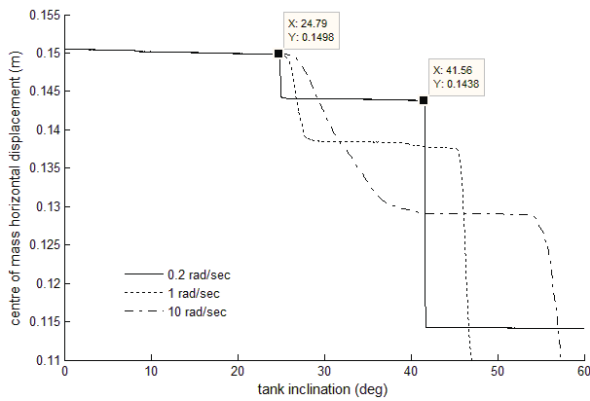


Figure 2 Center of mass displacements versus vessel inclination (the illustration is based on the zKy coordinate system).

The former is the angle where heap formation occurs; while the latter should be considered as the true angle of repose (Spandonidis & Spyrou, 2013). Moreover, it is shown that when a large enough tilting ratio is used, the cargo behaves in a slightly different way. In that case, the flow of the cargo is larger after the first critical value is reached.

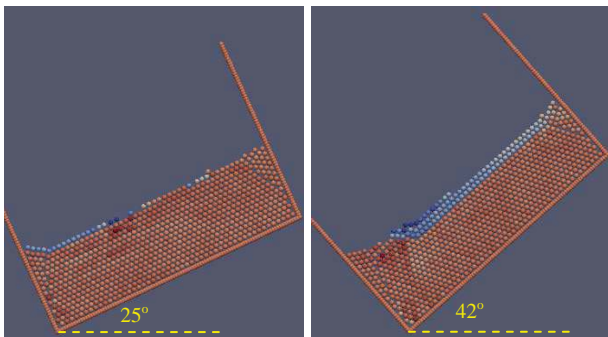
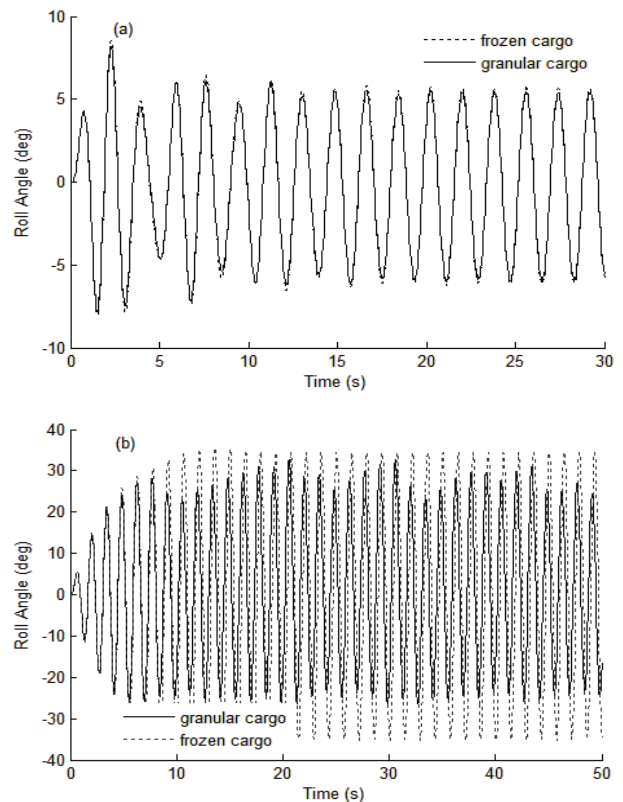


Figure 3 Time shots of inclined vessel when roll angle has a value of 25° (left) and 42° (right).

In Figure 3 is shown cargo's state inside the hold at specific time instants when critical angles are reached. Red colour is used when the particle has kinetic energy close to 0 and blue when it has clearly nonzero kinetic energy. In this way the percentage of material involved in cargo shift can be illustrated. Our main goal was the identification of critical parameters affecting system's dynamic response.

Two kinds of numerical experiments were performed. The first was basically a reference case and the vessel was loaded with *solid cargo*; that is cargo with the same weight and mass centre with the granular but without the ability to move. It was tested in several wave frequencies and amplitudes. Analysis of these results provided a good feeling of the most significant frequency region for further investigation. The second series involved tests with actual granular cargo. The wave frequency and amplitude region of interest were 2.3-6.5 rad/s and 0.005-0.025 m, respectively.

In Figure 4 are shown some examples of comparison of behaviour, for four different frequency values and wave amplitude fixed at 0.01m. The key findings are as follows:



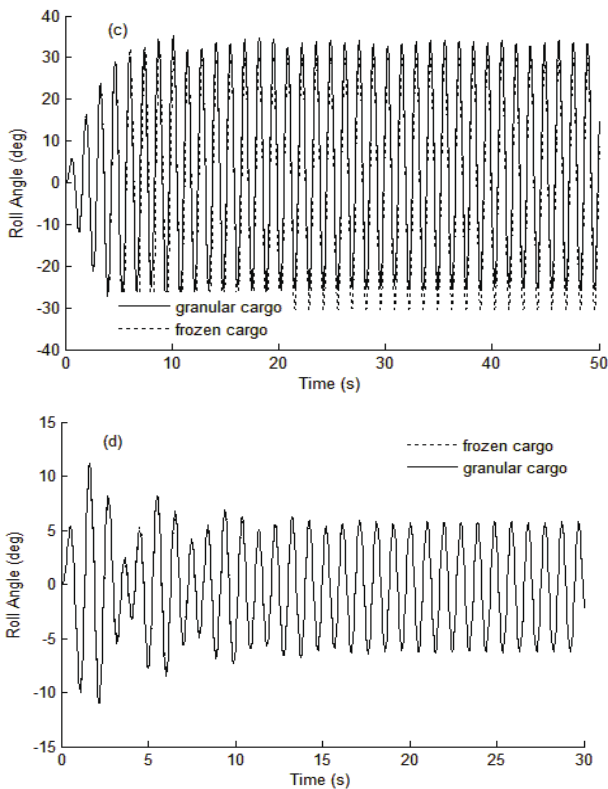
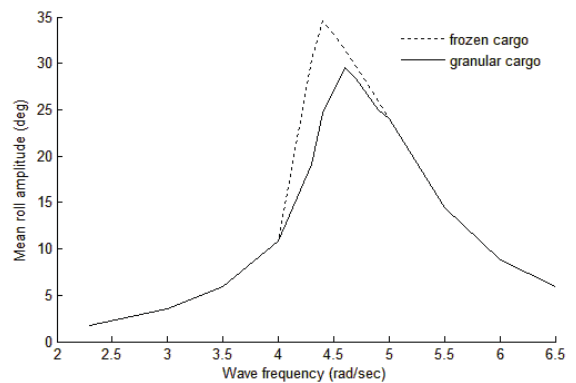


Figure 4 Comparison of response of frozen and granular cargo. The excitation amplitude s fixed at 0.01m and the frequency varies: a) 3.5 rad/s, b) 4.4 rad/s, c) 4.7 rad/s and d) 6.5rad/s.

- a) For wave frequency values below 3.5 or above 6 rad/s, barge's response is limited (Fig. 4 (a) and (d)). After a short transient, she reaches a max roll angle less than 5 deg. The behaviour of the barge does not depend on whether she is frozen or with movable cargo (i.e. the granular material does not perform any substantial motion).
- b) For wave frequency between 3.5 and 6 rad/s, the barge, in either condition, enters a resonant region. As shown in Figure 4b, the peak response amplitude for the case of frozen cargo appears at frequency 4.4 rad/s and a maximum roll angle about 36 deg is reached. The "unfrozen" system shows smaller response, mainly apparent after a frequency about 4 rad/s. The peak roll angle reached is less than 30 deg. The lower response is because the granular material reaches the first critical angle of heap formation which sets it in motion. As the phase of cargo's movement opposes

that of the vessel, the overall motion becomes smaller. Calculation of moments indicates that, the moment due to cargo's mass centre, and not the impact moment, is the primary cause of this effect.

- c) Further observation of Figure 4b produces two more, secondary, findings. Firstly, the motion of the vessel with the granular cargo has become asymmetrical. Local movement of cargo occurring around the one corner of the free surface, leads to lower absolute roll peak when the hold rotates clockwise. Secondly, for certain values of wave frequency, the steady-state is characterized by more than one frequency. As confirmed from Figs. 4b and 4d where the simulation was run for 50 s, this phenomenon is not transient but it is true long-term response.
- d) Inside the resonant region and after a critical value of 4.7 rad/s the two systems present almost identical mean responses. Despite though their similar behaviour, the initial movement of the granular cargo during the transient stage leads to larger absolute roll amplitude. For the case of 4.7 rad/s (Fig. 4c) both systems oscillate with mean roll amplitude of 30 deg. But for the granular cargo, an almost 2 degree dynamic roll bias is incurred, generating a higher absolute roll peak. These findings are summarized in Fig.5.



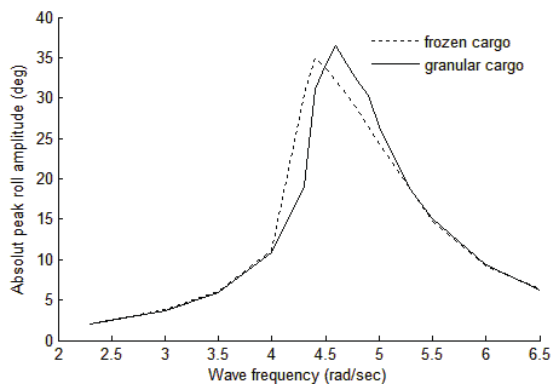


Figure 5 Mean roll amplitude (up) and absolute roll peak (down), for 0.01m excitation.

For wave amplitudes between 0.005 and 0.15 m, our simulations yielded that the behaviour remains qualitatively similar to that obtained for 0.01 m excitation.

In Figure 6 appear comparisons at the two ends of the investigated region of wave amplitude [0.005 m (up) and 0.015 m (down) - wave frequency, respectively, 4.5 and 4.3 rad/s]. Notably, for wave amplitude 0.015 m, the granular cargo case is associated with smaller response but with a “clear” second frequency existing in the steady state due to material’s displacement.

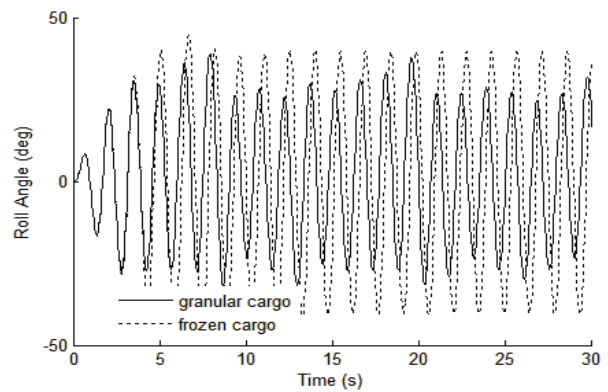


Figure 6 Comparison of response of solid and granular cargo: (up) excitation amplitude 0.005m and frequency 4.5 rad/s; (down) excitation 0.015m and frequency 4.3 rad/s.

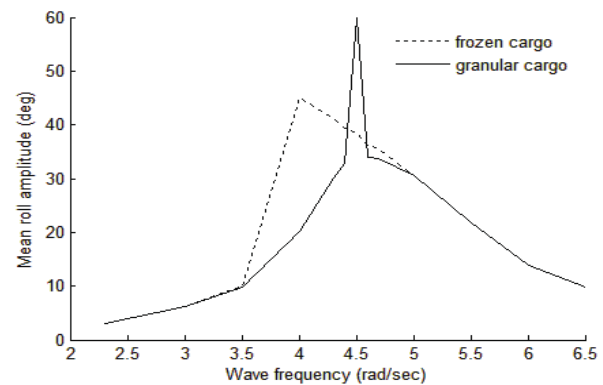


Figure 7 Mean roll amplitude for wave amplitude 0.017 m and frequency 4.3 rad/s

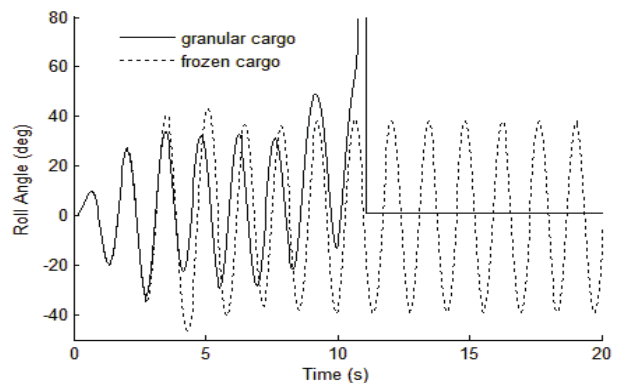
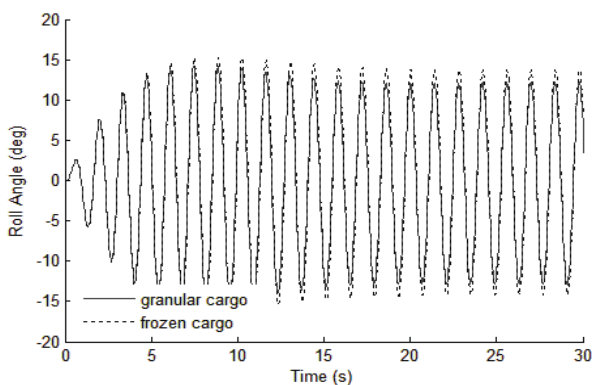


Figure 8 Comparison between frozen and granular cargo for wave amplitude 0.0017m and frequency 4.5 rad/s.

Further increase of the excitation leads however to a substantially different behaviour (Figure 7): for wave amplitude 0.017 m and frequency 4.5 deg/s, the material inside the

hold moves in such a way that the barge cannot return towards the upright position and capsizing is finally realized.

To investigate deeper this behaviour we considered the first seconds of motion. Figure 8 depicts in a comparative manner the 20 first seconds for the two systems. At about the 10th second, the barge with the granular cargo capsized. Whilst she initially behaved in a similar to the 0.01m wave amplitude case (that is, smaller mean roll angle and quasi-steady state response), suddenly a large peak value appeared (almost 45 deg). This is above the material's second critical angle associated with its angle of repose. In the ensuing cycle the roll angle grows further and capsizing finally occurs. Visual inspection of the cargo inside the hold indicates that, due to high acceleration, significant amount of material is displaced during the two roll cycles before capsizing (Figure 9). Wave amplitudes larger than 0.02m generate qualitatively similar results for material's behaviour.

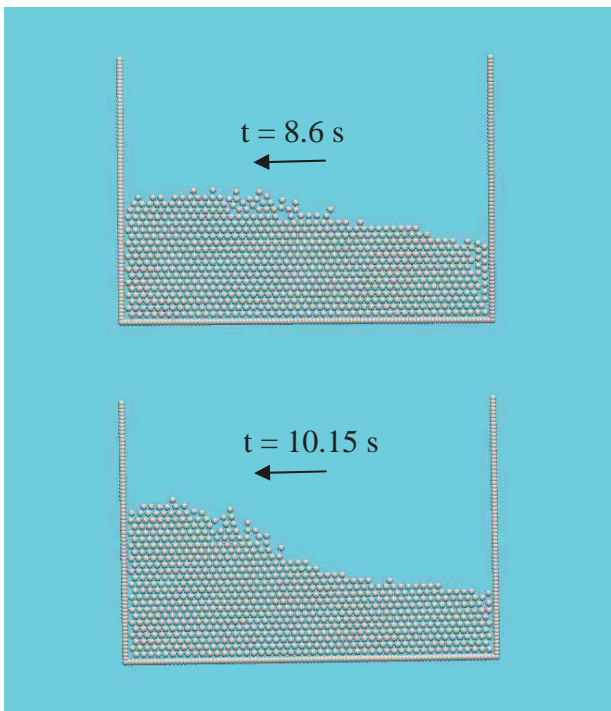


Figure 9 State of cargo inside the hold at two successive passages of the barge from the upright position: (up) seventh roll cycle; (down) 8th roll cycle in which capsizing occurs. The arrow indicates the direction of motion

(anti-clockwise).

5. CONCLUDING REMARKS

A step towards a systematic investigation of the coupled granular material-and-vessel-motion in regular beam seas, based on numerical procedures, was presented. The vessel was allowed to move only in roll direction performing thus a restricted 1 DOF motion. Several values of wave amplitude and frequency were applied on a scaled container containing spherically shaped particles of granular material in order to capture the response of the system. Special attention was given in the comparison of the results against corresponding cases where the cargo was treated as solid ("frozen").

These results indicated that, although the same resonant region occurs for both systems, in the case of granular cargo and for wave amplitudes below a certain limit, the motion of the system is smaller. This leads to a system that is even more stable than its frozen counterpart, even though it appears to have some difficulty in reaching steady state. For higher wave amplitudes a new region appears where the vessel due to her cargo's movement, shows larger response and in some cases it capsizes. An effort to analyse this behaviour revealed that, this is related with a shift of the roll resonance peak value.

A logical next step in our research would be the experimental examination of these results. In the meantime, several different numerical experiments are executed in a systematic way. Specifically, different material-height-to-hold-width ratios, constant wave steepness, more than one frequency wave packets, different material parameters and different vessel shapes are under study. Furthermore, dynamical analysis tools are being considered for capturing more rigorously vessel dynamics as influenced by the granular material's movement. It is remarked that, a further investigation based on a 3 DOF coupled



motion is currently under verification /validation. Early results indicate some significant effects for higher frequencies.

6. ACKNOWLEDGMENTS

The present work was supported by the Greek General Secretariat for Research and Technology under the General Programme ARISTEIA (EXCELENCE) I, with contract reference number GSRT-252.

7. REFERENCES

- Corwin E.I., Jaeger H.M., Nagel S.R., 2005. "Structural signature of jamming in granular media", Nature, 435: 1075-1078.
- Douady S., Fauve S., 1988. "Pattern selection in Faraday instability", Europhysics Letters, 6: 221-226.
- Faltinsen O.M., Timokha A.N., 2009. "Sloshing", New York: Cambridge University Press.
- Fleissner F., Alessandro V., Schiehlen Wand Eberhard P., 2009. "Sloshing cargo in silo vehicles", Journal of Mechanical Science and Technology 23: 968-973.
- Foerster S. F, Louge M.Y, Chang H, Allia K., 1994, "Measurements of the collision properties of small spheres", Phys. Fluids 6: 1108.
- Gallas J. A. C., Herrmann H. J., Sokolowski, S., 1992. "Convection Cells in Vibrating Granular Media", Physics Review Letters, 69:1371-1374.
- International Maritime Organization (IMO), 2012. "Solid Bulk Cargoes Code [IMSB Code 268(85)]", IMO publishing, ISBN: 978-92-801-1535-2.
- Laroche C., Douady S., Fauve S., 1989. "Convective flow of granular masses under vertical vibrations", Journal de Physique France, 50: 699-706.
- Miles J., Henderson D., 1990. "Parametrically forced surface waves", Annual Review of Fluid Mechanics, 22: 143-165.
- Monaghan J.J., 2005. "Smoothed Particle Hydrodynamics", Reports on Progress in Physics, 68: 1703-1759.
- Murashige S., Aihara K., 1998. "Coexistence of periodic roll motion and chaotic one in a forced flooded ship", International Journal of Bifurcation and Chaos 8:619-626
- Rognebakke O.F, Faltinsen O.M., 2003, "Coupling of sloshing and ship motions", Journal of Ship Research 47, no 3, 208-221.
- Spandonidis C., Spyrou K. J., 2013. "Micro-scale modelling of excited granular ship cargos: A numerical approach", Ocean Engineering 74: 22-36.
- Spandonidis C., Spyrou J., 2012. "Use of granular material dynamics simulation for the study of cargo shift of ships", Proceedings of 11th International Conference on the Stability of Ships and Ocean Vehicles, Athens, pp. 497-507.

This page is intentionally left blank

Session 13.3 – EXTREME BEHAVIOUR

Numerical Simulation of Ship Parametric Roll Motion in Regular Waves Using Consistent Strip Theory in Time Domain

Validation of Statistical Extrapolation Methods for Large Motion Prediction

Coupled Hydro – Aero – Elastic Analysis of a Multi – Purpose Floating Structure for Offshore Wind and Wave Energy Sources Exploitation

This page is intentionally left blank



Numerical Simulation of Ship Parametric Roll Motion in Regular Waves Using Consistent Strip Theory in Time Domain

Shan Ma, *College of Shipbuilding Engineering, Harbin Engineering University,*

mashan01@hrbeu.edu.cn

Rui Wang, *College of Shipbuilding Engineering, Harbin Engineering University,*

wangrui10653@163.com

Wenyang Duan, *College of Shipbuilding Engineering, Harbin Engineering University,*

duanwenyang@hrbeu.edu.cn

Jie Zhang, *College of Shipbuilding Engineering, Harbin Engineering University,*

pressme@163.com

ABSTRACT

In this paper, a numerical method is proposed to simulate the parametric rolling of ship in regular head seas. The numerical method aims at solving the coupled 3 degrees of freedom heave, pitch and roll together for better modelling of this nonlinear motions. The method is developed in time domain based on strip theory. The concept of impulse response function method is used to take into account the memory effect of fluid due to ship motion generated wave. Via theoretical analysis, a consistent way of estimating the impulse response function using strip theory is presented.

In order to model the nonlinear time variation of restoring force coefficients in wave, the Froude-Krylov forces (incident wave forces) and hydrostatic force are evaluated on the instantaneously wetted surface of the ship. Based on the developed method, the parametrically excited roll motions of C11 containership is simulated and the numerical results are compared with model tests.

Keywords: *Parametric rolling of ship, numerical model, nonlinear ship motions, impulse response function method*

1. INTRODUCTION

In a seaway the parametrically excited roll motion of a ship unexpectedly generated in either following or head sea conditions is quite a dangerous phenomenon due to its occurrence with large rolling amplitudes. Therefore, the quantitative prediction of the parametric roll

phenomenon are absolutely essential to ensure the safety of life and property on ships. Authoritative organizations of the maritime industry correspondingly published prediction guidelines (ABS, 2004, ITTC, 2005). The vulnerability criteria on parametric rolling are also under development by the International Maritime Organization (IMO) in the second intact stability criteria.



Parametric rolling in head seas as one of transverse stability problems resulting from time-varying changes in the underwater hull geometry is a nonlinear phenomenon with dynamic pitch and heave motions, which make it difficult to accurately predict parametric rolling in head seas. Before several accidents with ships operating in head seas (France et al., 2003, Hua et al., 2006), parametric rolling is largely handled in the cases of following waves (Kerwin, 1955) or beam waves (Blocki, 1980). In case of following waves the encounter frequency is much lower than the natural frequency of heave and pitch, so that coupling with heave and pitch is not important. As for head seas, however, prediction of parametric rolling is not so easy because parametric roll in head seas is more likely influenced by and coupled with heave and pitch motions, which are typically more pronounced in head waves (Shin et al., 2004). Effect of dynamic heave and pitch motions on parametric rolling was investigated so far by many researchers and is well established that restoring arm variation in head waves depends on dynamic heave and pitch (Taguchi et al., 2006). Nevertheless, the effect of coupling from roll into heave and pitch on parametric rolling in regular head seas is not significant in case the wavelength is equal to the ship length (J. Lu et al., 2012). Naoya Umeda et al. (2003) confirmed that a mathematical model with a roll-restoring moment in waves calculated with the Froude-Krylov assumption could considerably overestimated the danger of capsizing associated with parametric rolling. Neves and Rodriguez (2005) used a two-dimensional analysis for a set of coupled heave, pitch and roll equations of motion with 2nd and 3rd order non-linearities describing the restoring actions. Ahmed et al. (2006, 2008) used a system with 3 degrees of freedom, with the coupled heave and pitch motions providing input to the parametric excitation simulated using a one degree of freedom non-linear roll equation of motion. Levadou and van't Veer (2006) used coupled non-linear equations of motion in the time domain with 3 (heave, roll and pitch) and 5 (sway, heave, roll, pitch and yaw) DOF, where

nonlinear excitations are evaluated considering the actual submerged surface whereas diffraction forces are considered linear. Hydrodynamics are calculated in the frequency domain and are incorporated in the time domain by adopting the impulse response functions method. More recently, Ahmed et al. (2010) employed a system with 4 DOF (sway, heave, roll, pitch) to investigate parametric rolling in regular waves. The non-linear incident wave and hydrostatic restoring forces/moments are incorporated considering the instantaneous wetted surface while the hydrodynamic forces and moments, including diffraction, are expressed in terms of convolution integrals based on the mean wetted hull surface. Kim et al. (2010) and Park et al. (2013) also used impulse response function method (IRFM) to predict the parametric roll. Ribeiro e Silva and Guedes Soares (2013) described a time-domain non-linear theory model of ship's motions in 6 DOF, with the time variations of the restoring force calculated over the instantaneous submerged hull and hydrodynamic effects based on a potential flow strip theory using Frank's close fit method.

Analysis of parametric roll of container ships in regular head waves has been studied extensively. However, the ships do not encounter regular waves in the ocean. So, it is necessary to study how important parametric roll is in irregular seas. The work conducted by Ribeiro e Silva et al. (2003, 2005, 2013) and Bulian et al. (2006) are examples of investigations in this field. Nonetheless, numerical simulations and experimental measurements in regular waves are a useful way of observing and understanding the physics of the parametric roll phenomenon as well as validating numerical methods. According to past research, it is necessary for parametric roll to occur that four certain conditions need to be satisfied, namely, an encounter frequency equal or close to twice the natural frequency of roll, a wave length of the same order as the ship length, a wave height exceeding a critical level and finally, roll damping to be below a threshold value (France



et al., 2003). As well known, non-linear damping tends to increase with roll velocity, thus, it will eventually exceed the damping threshold leading to stabilization of the roll motion and reaching a steady roll amplitude. It is worth noting the fact that rationally accounting for non-potential roll damping is of substantial importance for an accurate simulation of parametric rolling.

When the impulse response function method (IRFM) is used, the coefficients and the IRF in Cummins's equation (Cummins, 1962) must be estimated in advance. Liapis et al. (1986) and King (1987) established the complete time domain framework of ship motion with forward speed by 3D time domain potential flow theory in which the coefficients are directly calculated by 3D boundary element method in time domain. While in time domain strip theory using IRFM, the impulse response function is often transformed from frequency domain hydrodynamic coefficients without any extra modification. This transformation seems already being a common practice. Although during the transformation, there are some different methods in the way to estimate the hydrodynamic damping and radiation restoring forces. It looks that people seldom noticed that there is some theoretical inconsistency during the transformation. The hydrodynamic radiation and damping coefficients in Cummins's equation is theoretically derived using the conception of strip theory by us and some of the modification to restoring radiation coefficients is proposed to ensure the consistent transformation.

In this work, the effect of parametric resonance on a containership sailing in head seas is investigated using a partly non-linear numerical model with 3 DOF (heave, roll and pitch). In this model, the incident wave and hydrostatic restoring forces/moments are assumed non-linear and are evaluated at every time step considering the instantaneous submerged surface while hydrodynamic forces and moments are assumed linear. Radiation forces and moments are expressed in terms of

convolution integrals and diffraction forces and moments are calculated in the frequency domain by strip method and then incorporated in the time domain. The requisite impulse response functions are obtained from Fourier transforms performed on hydrodynamic coefficients evaluated from STF method (Salvesen et al., 1970) in frequency domain based on the mean wetted surface. Comparisons between numerical and experimental results demonstrate the usefulness and accuracy as well as some limitations of the method proposed.

2. MATHEMATICAL MODEL OF PARAMETRIC ROLLING SHIP MOTIONS IN WAVES

2.1 Ship Motion Equations

A right-handed inertial coordinate system fixed with respect to the mean position of the ship *oxyz* is established with *z* in the vertical upward direction and passing through the centre of gravity of the ship and *x* directed to the bow. The origin is in the plane of the undisturbed free surface. This coordinate moves with the ship but remains unaffected by its parasitic motions. Parallel with *oxyz*, the inertial coordinate system *cx1y1z1* with origin at center of gravity of the ship can also be formed. In order to express the large amplitude rolling motions, the right-handed body-fixed coordinate system *cxbybzb*, with origin *c* at the center of mass of the ship is also formed.

The unrestrained 3 DOF rigid body motions of a vessel with or without advancing speed are considered. The ship motions in time domain is formed as followed:

$$\begin{aligned} (M + \mu_{33})\ddot{\eta}_3 + b_{33}\dot{\eta}_3 + \int_0^t K_{33}(t-\tau)\dot{\eta}_3(\tau)d\tau + (c_{33} + C_{33})\eta_3 \\ + \mu_{35}\ddot{\eta}_5 + b_{35}\dot{\eta}_5 + \int_0^t K_{35}(t-\tau)\dot{\eta}_5(\tau)d\tau + c_{35}\eta_5 \\ = F_3^I + F_3^S + F_3^D - Mg \end{aligned}$$



$$\begin{aligned}
 (I_{44} + \mu_{44})\ddot{\eta}_4 + b_{44}\dot{\eta}_4 + \int_0^t K_{44}(t-\tau)\dot{\eta}_4(\tau)d\tau + c_{44}\eta_4 \\
 = F_4^I + F_4^S + F_4^D \\
 \mu_{53}\ddot{\eta}_3 + b_{53}\dot{\eta}_3 + \int_0^t K_{53}(t-\tau)\dot{\eta}_3(\tau)d\tau + c_{53}\eta_3 \\
 + (I_{55} + \mu_{55})\ddot{\eta}_5 + b_{55}\dot{\eta}_5 + \int_0^t K_{55}(t-\tau)\dot{\eta}_5(\tau)d\tau \\
 + c_{55}\eta_5 = F_5^I + F_5^S + F_5^D \quad (1)
 \end{aligned}$$

Where η_3 , η_4 , η_5 are heave, roll and pitch motion respectively where η_3 is given along cz_1 , η_4 , η_5 is given along $cx_b y_b z_b$ coordinate system. M , I_{44} , I_{55} are the mass, inertial moment of the ship along the cx_b and cy_b axis. The radiation forces/moments are expressed by convolution integrals, with accounted for the memory effect. Diffraction forces/moments F_3^D , F_4^D , F_5^D are obtained from strip theory. Both radiation and diffraction forces/moments are represented on $cx_1 y_1 z_1$ coordinate system.

The incident wave excitations F_3^I , F_4^I , F_5^I and restoring forces/moments F_3^S , F_4^S , F_5^S are referenced to another right-handed body-fixed coordinate system $cx_b y_b z_b$, with origin c at the center of mass of the ship.

2.2 Radiation Forces and Moments Modelling

According to Cummins's theory, the added mass and damping coefficients is referenced to an equilibrium axis system, Cummins (1962) showed that the linear radiation forces in time domain can be written as followed:

$$\begin{aligned}
 F_{jk}(t) = -\mu_{jk}\ddot{\eta}_k(t) - b_{jk}\dot{\eta}_k - c_{jk}\eta_k(t) \\
 - \int_0^t K_{jk}(t-\tau)\dot{\eta}_k(\tau)d\tau \quad (2)
 \end{aligned}$$

where, $\eta_k(t)$ represents the oscillation motion in k -mode and the overdot represents the derivative with respect to time. K_{jk} is the impulse response function (IRF) representing the memory effect of fluid. μ_{jk} and b_{jk} are the asymptotic values of the radiation coefficients at high frequency, and c_{jk} is the radiation

restoring force coefficient. The IRF K_{jk} can be directly related to the frequency-domain hydrodynamic coefficient:

$$K_{jk}(\tau) = \frac{2}{\pi} \int_0^\infty (B_{jk}(\omega) - b_{jk}) \cos \omega \tau d\omega \quad (3a)$$

$$K_{jk}(\tau) = \frac{2}{\pi} \int_0^\infty \left(\omega \mu_{jk} - \omega A_{jk}(\omega) - \frac{1}{\omega} c_{jk} \right) \sin \omega \tau d\omega \quad (3b)$$

where, ω is the encounter frequency of ship in waves.

By Fourier transformation, Eq. (3) can be written as follows:

$$A_{jk} = \mu_{jk} - \frac{1}{\omega^2} c_{jk} - \frac{1}{\omega} \int_0^\infty K_{jk}(\tau) \sin \omega \tau d\tau \quad (4a)$$

$$B_{jk} = b_{jk} + \int_0^\infty K_{jk}(\tau) \cos \omega \tau d\tau \quad (4b)$$

Eq.3 means that the hydrodynamic impulse response function K_{jk} can be expressed using frequency domain hydrodynamic coefficients without solving the problem directly in time domain. Presently strip theory is used to calculate the hydrodynamic coefficients and estimate IRF. However it's known that this theory is not a fully strict theory to solve the hydrodynamics of ship with forward speed in frequency domain. While Eq. 2 is established using strict 3D hydrodynamic theory in time domain. Because of the discrepant mathematical model described in both domains, the inconsistency may occur if the hydrodynamic coefficients obtained by STF are directly used to calculate the IRF based on Eq. (3a) or Eq. (3b).

With the theoretical analysis followed, the inconsistency can be shown and some modifications are derived.



In the following procedure, the pitch added mass A_{55} and damping B_{55} are taken as example to show the modification. According to STF method, the hydrodynamic coefficients of the ship can be written as follows:

$$A_{55}(\omega) = A_{55}^0(\omega) + \frac{u^2}{\omega^2} A_{33}^0 - \frac{u}{\omega^2} x_A^2 b_{33}^A(\omega) + \frac{u^2}{\omega^2} x_A a_{33}^A(\omega) \quad (5a)$$

$$B_{55}(\omega) = B_{55}^0(\omega) + \frac{u^2}{\omega^2} B_{33}^0 + u x_A^2 a_{33}^A(\omega) + \frac{u^2}{\omega^2} x_A b_{33}^A(\omega) \quad (5b)$$

where, A_{55}^0 and B_{55}^0 represent added mass and damping coefficients at zero speed, a_{33}^A and b_{33}^A are stern sectional added mass and damping coefficient, respectively. x_A is the longitudinal distance between stern section and the gravity center of the ship. According to (3a) and (4a):

$$K_{55}(\tau) = \frac{2}{\pi} \int_0^{\infty} (B_{55}(\omega) - b_{55}) \cos \omega \tau d\omega \quad (6a)$$

$$A_{55} = \mu_{55} - \frac{1}{\omega^2} c_{55} - \frac{1}{\omega} \int_0^{\infty} K_{55}(\tau) \sin \omega \tau d\tau \quad (6b)$$

Substituting (6a) into the third term in the right hand side of (6b) leads to the following equation which is not identical to equation (5a) excluding the additional modification term $c_{55 plus}$.

$$A_{55} = \mu_{55} - \frac{1}{\omega^2} (c_{55} + c_{55 plus}) - \frac{1}{\omega} \int_0^{\infty} K_{55}(\tau) \sin \omega \tau d\tau \quad (7a)$$

$$c_{55 plus} = -u^2 \frac{2}{\pi} \int_0^{\infty} \frac{B_{33}^0 + x_A b_{33}^A}{\omega_1^2} d\omega_1 - u x_A^2 \frac{2}{\pi} \int_0^{\infty} (a_{33}^A(\omega) - \mu_{33}^A) d\omega_1 \quad (7b)$$

From the above, we can see that the direct transformation from strip theory to get IRF will cause the inconsistency between hydrodynamics in time domain and frequency domain. The modification to the hydrodynamic

coefficients like radiation restoring coefficients $c_{55 plus}$ is necessary to assure the transformation consistent. The numerical results to be shown in section 4 will demonstrate the necessity of the modification.

2.3 Diffraction Forces Modelling

Similarly, the diffraction forces/moments contribution can also be represented using convolution integrals (King, 1987, Ahmed et al. 2010), which is what we will study in next step. In the present method, the strip theory in frequency-domain is employed to calculate the diffraction force directly. The diffraction forces/moment can be expressed in time-domain as followed:

$$F_j^D(t) = \zeta_a F_{ja}^D \cos(\omega_e t + \varphi_j) \quad j = 3,4,5 \quad (8)$$

Where ω_e is the encounter frequency of ship in waves. F_{ja}^D , φ_j are amplitude and phase angle of diffraction force transfer function using strip theory, ζ_a is the amplitude of incident regular wave.

2.4 F-K and hydrostatic restoring forces modelling

In order to capture the ship rolling restoring moment variation in wave, the main cause for parametric rolling, the restoring force/moment should be accurately modelled accounting for the exact ship geometry and the position on waves at each time step. In the method presented here, the non-linear incident wave excitation is also incorporated. Together with the corresponding weight contributions, the fluid loads $F_j^I + F_j^S$ from incident wave excitation and hydrostatic restoring force are determined by integration of the incident wave pressure and hydrostatic pressure over the actual submerged part of the hull as shown in Fig. 1.

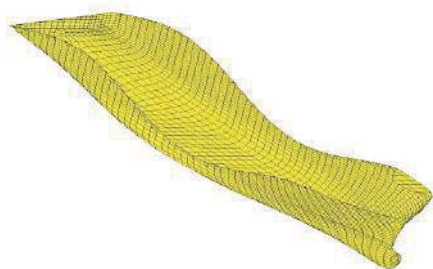


Fig. 1 The instantaneous wetted ship surface under incident wave profile

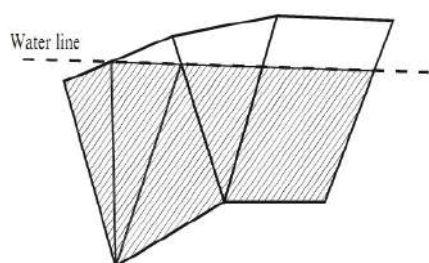


Fig. 2 panels subdivision across the incident wave free surface

The entire surface of the ship hull (up to deck line) is discretised with quadrilateral or triangular panels. At each time step, panels which are above the instantaneous incident wave free surface are directly ignored while panels below the instantaneous free surface are accounted. In particular, panels which are cross the free surface are subdivided and the smaller panels are newly formed, as shown in figure 2. The pressure acting on each panel is assumed uniform and equal to that acting at the centroid of the panel. At each time step, the total ship rolling moment is given by summing up contributions of all the accounted panels.

2.5 Ship roll damping modelling

In general, ships rolling on the free surface of the sea are subjected to the damping of the water where the viscous effect contributes quite large amount and can't be calculated using traditional potential flow theory. The most

accurate way to account for the damping moment is to conduct experiments on models or actual ships. In this study, a series of free-decay experiment with different advancing speed are conducted on a scaled model of C11 class containership.

In order to confine the case to the problem of non-linear roll damping, the following roll equation are considered, where the original damping term is expressed as a series expansion of $\dot{\eta}_4$:

$$(I_{44} + \mu_{44})\ddot{\eta}_4 + b_{44}\dot{\eta}_4 + b_{441}\dot{\eta}_4 + b_{442}\dot{\eta}_4^3 + \int_0^t K_{44}(t-\tau)\dot{\eta}_4(\tau)d\tau + c_{44}\eta_4 = F_4^I + F_4^S + F_4^D \quad (9)$$

where b_{441} is the linear damping term, and b_{442} is the cubic damping term. The terms b_{441} and b_{442} can be determined by analyzing the free-decay rolling experimental data.

3. THE MODEL TEST ABOUT THE PARAMETRIC ROLLING FOR C11 CONTAINERSHIP

The free running experiment with a 1/65.5 scaled model of the post Panamax C11 class containership in regular waves is conducted at the seakeeping basin of China Science Research Center in China, in which the ship model is propelled by one propeller whose revolution is controlled to keep the same mean speed with the tow carriage (J. LU, 2012). The principal particulars and the line plan of the C11 class containership are shown in Table 1 and Fig. 3.

Table 1 Main particulars of C11 class containership

Principal particular	Value
Length between perpendiculars (L_{pp})	262.0 m
Breadth (B)	40.0 m
Mean draught (T)	11.5 m
Block coefficient (C_b)	0.560
Pitch radius of gyration (κ_{yy})	0.24 L_{pp}
Longitudinal position of center of gravity from amidship (x_{CG})	5.483 m aft



Transverse metacentric height, still water (GM)	1.952 m
Natural roll period (T_ϕ)	24.20 s

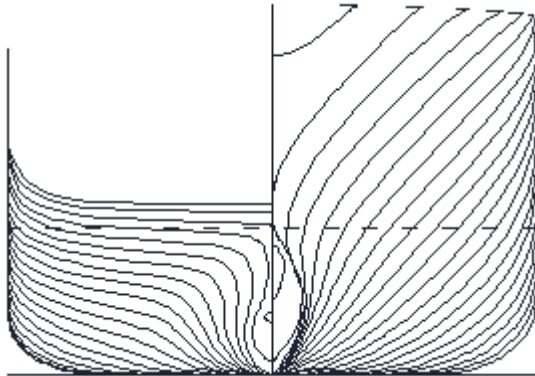


Fig.3. Lines plan for the C11 class containership

The test carried out covering a range of Froude numbers of 0.0, 0.05, 0.1, 0.15 and a range of wave steepness varying from 0.01 to 0.04. And the wavelength is equal to ship length between perpendiculars. Roll damping is determined directly from free roll decay tests at different speed based on extinction curve method. For example, the time history of a free-decay test with Froude number of 0.1 is illustrated in Fig. 4, imposing the largest heeling angle of 19.25° . Then the extinction curve obtained by regressive analysis and demonstrated in Fig. 5 can be calculated as follow:

$$\Delta\eta_4 = a\eta_{4m} + b\eta_{4m}^3 \quad (10)$$

where η_{4m} and $\Delta\eta_4$ are mean roll amplitude and roll amplitude decrement per half cycle, respectively.

After obtaining the coefficients a and b, the roll damping then can be calculated. The method is based on the concept that the rate of change of the total energy in roll motion equals to the rate of energy dissipated by the roll damping.

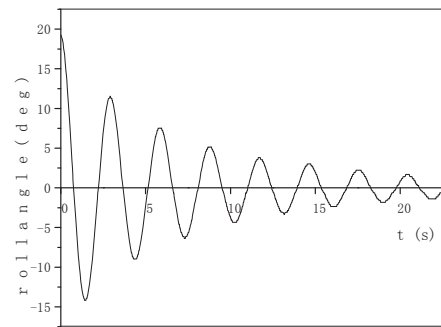


Fig.4. Time history of free roll decay test with Froude number of 0.1

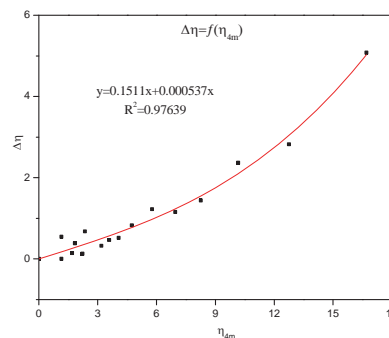


Fig.5. The extinct curve of the corresponding free roll decay test

4. NUMERICAL RESULTS AND DISCUSSIONS

4.1 The numerical results and discussion on the modification of radiation restoring coefficients using IRF method

The comparison of linear hydrodynamics-radiation pitch moment with or without considering the term c_{55plus} -for C11 containership using Eq. 2 and numerical result using strip theory in frequency domain is illustrated in Fig. 6. In the plot, the results are obtained assumed that the ship is performing harmonic pitch motion with unit amplitude. Obviously, the result from “new transformation” considering the term c_{55plus}



keeps highly consistence with that from STF method.

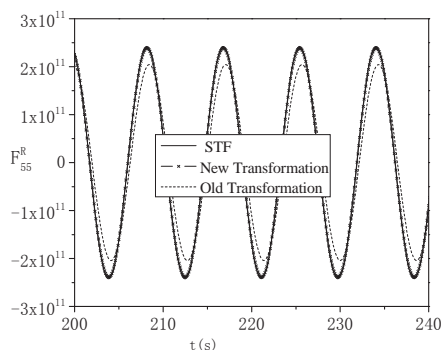


Fig.6 The comparison of radiation pitch moment between strip theory and time domain hydrodynamics using IRF

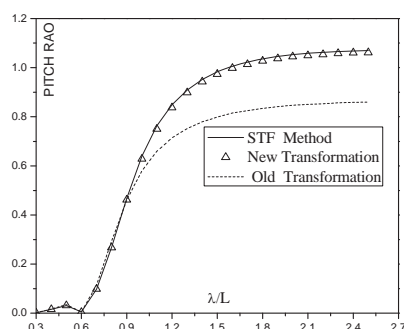


Fig.7 The comparison of pitch motion between strip theory and time domain solution using IRF

To further show the influence of the modification to hydrodynamic coefficients like term c_{55plus} using IRF method, The comparison of linear pitch motion- between time domain calculation and strip theory results in frequency domain are demonstrated in Fig. 7. It is evident that the present method can provide consistent results with those from original strip theory.

4.2 The numerical simulation of parametric rolling and compared with model test using 3 DOF coupled method in time domain

Based on the numerical model for parametric rolling prediction, the time-domain simulation of vessel's motions is carried out using fourth order Runge-Kutta method. As mentioned before, only three degrees of freedoms are considered, i.e., heave, roll, pitch.

In table 2, Experimental and numerical results for C11 class containership are presented. The table provides the final steady roll amplitudes comparisons between numerical predictions and experimental data. From the comparison, it's seen that the numerical code generally presents quite well predictions on the steady amplitude of parametric rolling. While it can also be observed that the numerical code fails to predict properly in four cases where three of them fail to predict its occurrence and one of them overestimated the steady magnitude. From the discussion by Belenky et. al. (2011) about the influence of roll damping on parametric rolling, it is known that the linear damping will make the instability zone narrower and increase the threshold value of minimum GM variation. Therefore the possible reason of numerical code unable to predict the occurrence of parametric roll is related to damping. The numerical damping used in simulation is a little larger and consequently move the system out of the instability region. For the case Test No. 1 where the numerical code overestimate the experiment value, the possible reason is not clearly yet.

Table 2. Experimental and numerical results for the C11 class containership

Test No.	Fr. #	Wave steepness	Experimental Roll Amp.(deg.)	Numeric al Roll Amp.(deg.)
1	0.0	0.01	8.12	30.65
2		0.02	24.77	33.46
3		0.03	28.61	33.91



4		0.04	30.23	34.52
5	0.0	0.01	17.77	0.0
6		0.02	30.6	37.15
7		0.03	34.7	42.87
8		0.04	39.97	44.69
9	0.1	0.01	0.0	0.0
10		0.02	21.16	0.0
11		0.03	31.07	37.1
12		0.04	34.43	48.33
13	0.1	0.01	0.0	0.0
14		0.02	0.0	0.0
15		0.03	21.89	0.0
16		0.04	28.13	36.89

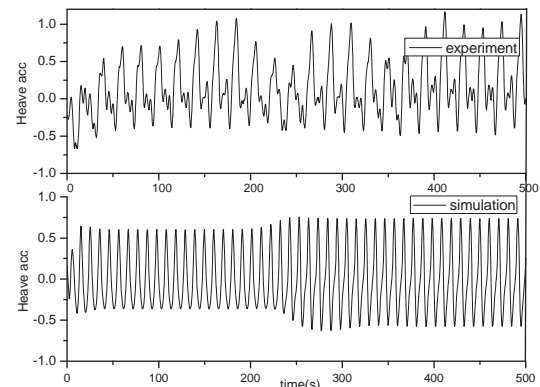


Fig. 8a Time history of heave acceleration

The following Fig. 8 presents the comparison of time history between numerical code and model test. The model test case is referred to Test No.11 in Tab. 2. where the Froude number is 0.1, the wave height is $H_w=7.86$ m and incident wave period is 12.95s.

As we can see, the parametric roll stabilizes at a roll angle of about 37 degrees, which is close to the experimental result of 31.07 degrees. The successful prediction justifies the usefulness and accuracy of the presented method. The associated heave acceleration and pitch motions are also illustrated. In term of numerical predictions for heave and pitch motions itself, it's seen that there is a increase in heave and a very slight decrease in pitch motions accompanied with parametric rolling compared with those when ship roll motions is not excited. These phenomena should be the influence of non-linearity from fluid loads and coupling between heave-roll-pitch.

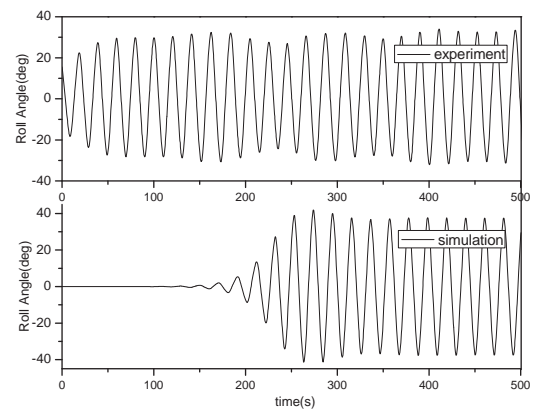


Fig. 8b Time history of roll angle

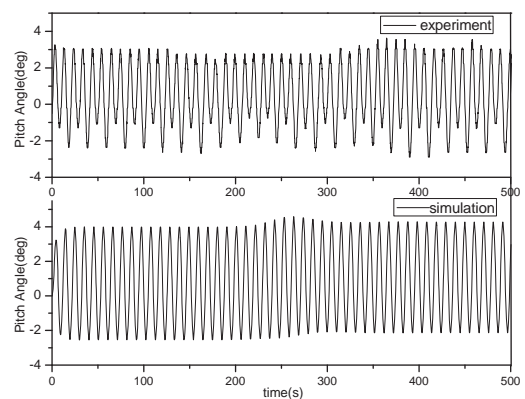


Fig. 8c Time history of pitch angle



Fig. 8. Time history comparison for test No. 11 obtained from numerical simulations and experimental measurements

5. CONCLUSION

In this paper, a partly non-linear time-domain numerical model is presented and utilized to simulate parametric excited rolling resonance in regular head waves. In the present numerical model, the impulse response function method is used to model the time domain radiation forces of ship motions. The impulse response function is obtained from strip theory. Via theoretical analysis, consistent transformation from frequency domain to time domain has been performed. Results obtained for C11 class containership demonstrate that the method succeeds in obtaining steady roll angles of parametric roll that mostly compares reasonably well with experimental data. In addition, it should be noted that the presented model undesirably fails to predict the occurrence of parametric ship rolling under some cases. The possible reason is due to the numerical modelling of rolling damping which will influence the occurrence of parametric rolling. Further developments needed to improve the capability of the presented method will include: considering the hydrodynamic coupling effects from heave and pitch to rolling and vice versa, the numerical modelling of parametric rolling in irregular wave.

6. ACKNOWLEDGEMENT

In this paper, the model test data of parametric rolling for C11 containership is provided by Prof. M. Gu and Dr. J. Lu from CSSRC. The model test data is very useful for validating our numerical code. Their help is gratefully acknowledged.

The present work is supported by the National Natural Science Foundation of China (Grant no. 51079032, 51109040) and Defense Industrial Technology Development Program

(Grant no. B2420132001). Young Faculty Academic Supporting Program of Heilongjiang Province (Grant No.1252G017) is also gratefully acknowledged.

7. REFERENCES

- Ahmed, T.M., Ballard, E.J., Hudson, D.A., and Temarel, P., 2006, "Prediction of parametric roll resonance in longitudinal regular waves using a non-linear method", Proceedings of the Ninth International Conference on Stability of Ships and Ocean Vehicles STAB'06, vol. 1, Rio de Janeiro, Brasil, pp.89–97.
- Ahmed, T.M., Ballard, E.J., Hudson, D.A., and Temarel, P., 2008, "A non-linear numerical method for the simulation of parametric roll resonance in regular waves", Proceedings of the ASME 27th International Conference on Offshore Mechanics and Arctic Engineering OMAE 2008, Estoril, Portugal.
- Ahmed T M, Hudson D A, Temarel P. 2010, "An investigation into parametric roll resonance in regular waves using a partly non-linear numerical model", Ocean Engineering, 37(14): 1307-1320
- Bulian, G. Francescutto, A., 2006, "On the effect of stochastic variations of restoring moment in long-crested irregular longitudinal seas", Proceedings of the Ninth International Conference on Stability of Ships and Ocean Vehicles (STAB'06), vol. 1, pp. 131–146.
- Blocki W., 1980, "Ship Safety in Connection with Parametric Resonance of the Roll", International Shipbuilding Progress, 27:36-53.
- Cummins, W. E., 1962, "The impulse response function and ship motions", DTMB-1661. David Taylor Model Basin Washington DC.



- France, W.N., Levadou, M., Treacle, T.W., Paulling, J.R., Michel, R.K. and Moore, C., 2003, "An investigation of head-sea parametric rolling and its influence on container lashing systems", Marine Technology, Vol. 40, pp. 1-19
- "Guide for the assessment of parametric roll resonance in the design of container carriers", 2004, American Bureau of Shipping, Houston, TX. USA.
- Hua, J., Palmquist, M. and Lindgren, G., 2006, "An analysis of the parametric roll events measured onboard the PCTC Aida", Proc. STAB 2006, pp. 109-118
- Kerwin J.E., 1955, "Note on Rolling in Longitudinal Waves", International Shipbuilding Progress, 2(16): 597-614.
- Kim, T.Y. and Kim, Y., 2010, "multi-level approach of parametric roll analysis", The 7th International Workshop on Ship Hydrodynamics. ITTC Workshop on Seakeeping, Seoul, Korea, Oct. 19-21
- King, B., 1987, "Time-domain analysis of wave exciting forces on ships and bodies.", Ph.D. Thesis, The University of Michigan.
- Liapis, S. J., 1986, "Time-Domain Analysis of Ship Motions", Ph.D. Thesis, University of Michigan.
- Levadou, M. van 't Veer, R., 2006, "Parametric roll and ship design". Proceedings of the Ninth International Conference on Stability of Ships and Ocean Vehicles (STAB'06), vol. 1, pp. 191-206.
- LU J., GU M., Umeda N., 2012, "Numerical Approaches on Parametric Rolling in Head Seas", 10th International Conference on Hydrodynamics, St. Petersburg, Russia. October 1-4, 2012.
- Neves, M., Rodriguez, C., 2005. "A non-linear mathematical model of higher order for strong parametric resonance of the roll motion of ships in waves", Marine Systems & Ocean Technology 1 (2), 69-81 .
- Park, D. M., Kim, Y., Song, K. H., 2013. "Sensitivity in numerical analysis of parametric roll", Ocean Engineering, 67, 1-12.
- Ribeiro e Silva S, Guedes Soares C. 2013, "Prediction of parametric rolling in waves with a time domain non-linear strip theory model", Ocean Engineering, 72: 453-469.
- Ribeiro e Silva, S., Santos, T. Guedes Soares, C. 2003, "Time domain simulation of a fully coupled parametrically excited roll response in regular and irregular head seas", Proceedings of the Eighth International Conference of Ships and Ocean Vehicles (STAB'03), Madrid, Spain, pp. 349-360.
- Ribeiro e Silva, S., Santos, T.A., Guedes Soares, C., 2005, "Parametrically excited roll in regular and irregular head seas", International Shipbuilding Progress 52, 29-56.
- Salvesen, N., Tuck, E. O., Faltinsen, O. M.. "Ship motions and sea loads", SNAME, 1970
- Shin, Y.S., Belenky, V.L., Paulling, J.R., Weems, K.M., Lin, W.M., 2004. "Criteria for parametric roll of large containerships in longitudinal seas". Transactions of SNAME 112, 14-47.
- "Testing and Extrapolation Methods Loads and Responses, Stability Predicting the Occurrence and Magnitude of Parametric Rolling", Revision 00, 2005, ITTC-international towing tank conference 7.5-02-07-04.3,
- Taguchi H., Ishida S., Sawada H. and Minami, M., 2006, "Model Experiment on Parametric Rolling of a Post-Panamax Containership in Head Waves", Proceedings of the 9th



International Conference of Ships and
Ocean Vehicles, COPPE Univ Fed Rio de
Janeiro, 147-156

Umeda N, Hashimoto H, Vassalos D, et
al, 2003, "Nonlinear dynamics on parametric
roll resonance with realistic numerical
modelling", Proceedings of the 8th
International Conference on Stability of
Ships and Ocean Vehicles, Madrid, pp 281–
290.

Belenky V., Bassler C.C., Spyrou K.J., 2011,
"Development of Second Generation Intact
Stability Criteria", NSWCCD-50-TR-
2011/065, Hydromechanics Department
Report, Naval Surface Warfare Center,
Carderock Division.



Validation of Statistical Extrapolation Methods for Large Motion Prediction

Timothy Smith, *NSWCCD (Naval Surface Warfare Center, Carderock Division)*

timothy.c.smith1@navy.mil

Aurore Zuzick, *NSWCCD (Naval Surface Warfare Center, Carderock Division)*

aurore.zuzick@navy.mil

ABSTRACT

Large amplitude ship motion often results from nonlinear aspects of hull geometry and wave excitation. As a result, large amplitude ship motion occurs infrequently, making direct simulation problematic. Statistical extrapolation is a methodology to assess the probability of large amplitude ship motion from shorter duration simulations or model test data that may not contain such large motion. The validation process involves the fitting of an extreme value distribution to data, generation and identification of a “true value,” and formulation of a comparison such that a definitive answer can be made.

This paper presents a worked numerical example of statistical extrapolation considering large amplitude roll, pitch, vertical acceleration, and lateral acceleration. Examining different motions addresses different types and levels of nonlinearity. Data are fit with the Generalized Pareto Distribution to formulate a statistical extrapolation. The generation of a “true value” for comparison is discussed. Lastly, the formulation of three-tier acceptance criteria is demonstrated to fully answer the question of statistical extrapolation accuracy. The paper will stress the desired traits and interactions between the main parts of extrapolation, true value, and acceptance criteria.

Keywords: *statistical extrapolation, validation, non-linear motion*

1. INTRODUCTION

The validation of numerical simulations is addressed by various professional societies and governmental bodies for many engineering disciplines. There are established verification and validation outlines, guides, and processes to follow when performing numerical simulation verification and validation (AIAA, 1998; ASME, 2009; ITTC, 2011). These processes and guides are often generalized with details left to the engineers actually performing the verification and validation. Validation at its core consists of a comparison between the simulation and the “true value,” and becomes the basis for a validation decision. The true value comes from scale model testing or higher fidelity simulations and implies enough

physical understanding to recognize it as the true value.

Focusing on the phenomena of large motion and capsizing, the true value is at once both non-linear and rare. The simulation of these phenomena requires advanced, hydrodynamic blended method prediction tools due to the non-linearity involved (de Kat and Pauling, 1989; Lin and Yue, 1990; Shin *et al.*, 2003). Furthermore, the ITTC parametric roll study (Reed, 2011; ITTC Stability in Waves, 2011) showed the uncertainty can be quite large due to practical non-ergodicity. This further increases the difficulty in understanding the result of the validation effort and achieving a definitive result.

This paper continues Smith (2014) and Smith and Campbell (2013) by providing a complete worked example to demonstrate a



multi-tiered validation approach with large amplitude motions and accelerations including statistical extrapolation of rare events.

2. TEST CASE

This test case considers ship roll and pitch motion and lateral and vertical acceleration for a range of relative wave heading in a high sea state. Extrapolations are made based on a sub-set of time history data and compared to a directly counted true value at a motion level not necessarily seen in the data sub-set.

2.1 Extrapolation Method

Following (Smith, 2014), this paper uses the extrapolation technique based on Generalized Pareto Distribution (GPD) as implemented by Campbell, *et al*, (2014). GPD can be used to approximate the tail of any distribution that makes use of a scale and shape parameter to fit the data. There are various implementation details in terms of selecting a threshold and determining the scale and shape parameter.

The confidence intervals for the extrapolated estimate were calculated using two approaches assuming a normal distribution of the GPD parameters. The first is based on the confidence interval of the GPD parameters and generation of a boundary based on the upper and lower extremes of the possible combinations. The second follows the confidence interval method from Campbell, *et al*, (2014) except the logarithm of the scale parameter was used instead of the scale parameters itself. The use of the logarithm of the scale parameter ensures its positive value. These are referred to as the boundary CI and logarithm CI in this paper.

2.2 True Value

The true value was determined by calculating hundreds of thousands of hours of ship motion simulation using a fully coupled, 3 degree of freedom (DOF) simulation tool based on volume calculation (Weems and Wundrow, 2013, Weems and Belenky, 2015). This model assumes constant radiation and diffraction forces with non-linear hydrostatics on 2D strip hull representation. As such it captures essential hydrostatic non-linearity and maintains very fast computation time. Note that in the case of validation against model test data, the true value is typically characterized by some non-negligible amount of uncertainty related to instrumentation and sampling limitations. By simulating against large amounts of simulated data, this uncertainty can be reduced such that a single true value may be identified.

The appropriateness of the 3DOF simplified simulation tool was checked by comparing various instantaneous roll and pitch parameters to those same parameters as calculated with a higher fidelity, 6 DOF blended simulation tool (Lin and Yue, 1990). The parameters compared dealt with the roll and pitch restoring force such as metacentric height, area under GZ curve, and peak of the GZ curve. The most useful comparison was plotting instantaneous roll angle and GZ value. Due to the difference in degree of freedom, the simulation tools could not be compared time step by time step for the same wave realization. The determination of appropriate and adequate physical representation was based on general agreement between the 3DOF and 6DOF simulations (Weems and Belenky 2015).

The peaks were extracted using an envelope approach (Belenky and Campbell, 2012). This method ensures independent data samples as required to apply GPD. The true value of the exceedance rate is found using a direct counting procedure studied in detail in Belenky and Campbell (2012).



3. VALIDATION APPROACH

This example expands the multi-tier validation approach consisting of a parameter, condition and set criteria to include vertical and lateral acceleration (Smith, 2012). The three tiered structure reflects typical scale model data structures of individual motion channels, a run condition of speed-heading-seaway, and a test consisting of many conditions. Criteria are set to determine an acceptable parameter comparison, and what constitutes an acceptable condition and overall set.

A parameter comparison, Tier I, is the elemental comparison between the simulation and true value. It refers to a single motion or response. Choosing an appropriate parameter-level comparison metric depends largely on the problem under examination. Metric options typically share underlying principles and utilize similar properties of the sample data to draw conclusions. They tend to differ in terms of the specific information they provide about each comparison. Some metrics produce binary outcomes (pass or fail) while others provide quantified measures of correlation. Smith (2012) discusses possible comparisons for motions. Further discussion of comparison methods appears later in this paper.

Tier II is a condition comparison. Typically, a condition is the environment, speed and heading used to define the simulation and the associated motion response. So a set of environmental descriptors (e.g. significant wave height, period, etc.), speed and heading and four motions would be four conditions due to the four motions. Thus, a condition can be defined as a deterministic vector:

$$\vec{S} = (H_S, T_m, V_S, \beta, i_{dx}) \quad (1)$$

where H_S is a significant wave height, T_m modal frequency, V_S , forward speed, β -heading, i_{dx} -motion index (say, $i_{dx}=4$ corresponds to roll). This considers motions or parameters independently and Tier II mirrors Tier I.

Alternatively, motions (parameters) can be considered collectively with all or multiple motions (parameters) being included in the condition definition. Then the number of passing motion (parameter) responses becomes a criterion for a condition passing. This is a more stringent criterion to pass with slightly different bookkeeping. The Tier II criterion defines what constitutes a passing condition in terms of number or combinations of passing Tier I comparisons.

Tier III, the set comparison, defines how many conditions have to pass for the simulation to pass the validation criteria. The condition definition needs to be considered in setting the Tier III validation criteria to avoid an impossible criterion.

There is an inter-relationship between the parameter comparisons, second tier condition definition and third tier acceptance levels. Other parameter comparisons besides confidence interval capture of the true value may be used depending on what is important to the application. For instance, the amount of conservatism or absolute difference may be used as a metric. A change of the parameter comparison could change the condition criteria. The multi-tier validation definition used in this study provides a check on both the extrapolation and the confidence interval formulation as both are included in the parameter comparison.

For this example, the parameter comparison is the comparison of a statistical extrapolation to the true value at a specified critical motion level. The parameter comparison passes the test if the extrapolation confidence interval captures the true value. Multiple extrapolations are made from different data sets all representing the same condition, that is speed-heading-seaway-motion combination. A condition passes if the true value is captured by the confidence interval at a percentage roughly equal to the confidence probability. This is repeated for a number of different conditions.



The extrapolation method is considered valid if a high percentage of conditions pass.

These acceptance criteria assume a valid confidence interval formulation. As two confidence interval calculation methods are assessed, this example also serves as a validation of the confidence interval calculation method.

4. FURTHER PARAMETRIC COMPARISONS

The validation approach described above examines the effectiveness of the method used to calculate the confidence interval on the extrapolated value. If the acceptance criteria are passed, we have demonstrated that the 95% confidence interval for any given population sample set does indeed capture the true population value 95% of the time. Once we have confidence that our methods can accurately calculate the uncertainty associated with an extrapolated value, the extrapolated values and their associated uncertainty can be used to validate the simulation tool's ability to model real ship motions. This section discusses parameter comparisons appropriate for non-rare and rare comparisons between simulation data and model test data as an expansion of Smith (2012, 2014). The comparisons discussed are: confidence interval overlap, hypothesis testing, and quantiles (percentiles).

4.1 Confidence Interval Overlap

Confidence interval overlap is a straightforward comparison metric which provides an unambiguous outcome applicable to both non-rare and rare comparisons. Note that the application of the confidence interval overlap metric described earlier for validation of the confidence interval formulation is distinctly different from its use as validation metric for comparisons between simulation and model test data. When evaluating the confidence interval formulation, a true value is

known and there are many sample sets of the population from which to draw conclusions. For model test comparisons, the "true values" from two populations (model and simulation) are being compared, and only one sample set from each population is available. When validating simulation results against model test data, confidence intervals are calculated at a specified confidence probability for both sets of sample data; if the intervals from both sets overlap one another, the comparison is considered successful. However, the existence of overlapping 95% confidence intervals does not necessarily signify a 95% chance that both samples share the same underlying population characteristics. The combined probability that the true population values of both data sets lie within the overlapped interval range is significantly less than 95% and depends on the lengths and relative position of both confidence intervals.

The interval overlap metric also provides no information about the probability of differences between the populations. For example, significant overlap of relatively long intervals (high uncertainty) suggests that both populations lie on the same interval; but if the interval is large, the populations could be very different. Alternatively, if intervals are very small, this metric can reject comparisons when population differences are very (perhaps acceptably) small. A perhaps undesirable characteristic of the interval overlap metric is that comparisons are inherently less likely to pass the criteria as uncertainty is reduced.

The confidence interval on the difference between parameter populations is an extension of the interval overlap method. The level of significance is associated with the comparison (i.e. a form of combined probability), rather than with each individual data set. The extents of the confidence interval on the difference provide information about how similar and how different the populations are likely to be. A 95% confidence interval on difference provides the range of values for which the following is true: there is a 95% probability



that the true difference between the two populations lies within that range. Setting limits on the allowable difference (including uncertainty) forms a pass/fail application of this comparison metric. Unlike the interval overlap method, this criterion does not become more difficult to pass when the data are more well-known (less uncertainty). In addition, the difference (including uncertainty) can be used to quantify the simulation's overall level of accuracy. For example, basic statistics (minimum, mean, etc.) of the observed lower uncertainty limits across Tier I comparisons quantify the amount of under-prediction and provide information on safety margin for simulation results.

Another metric making use of the confidence interval is the maximum conservative distance (MCD) which is the difference between the extrapolation upper confidence level and the true value. The upper confidence level is often the "not to exceed" limit. Maximum conservative distance then provides a direct measurement of accuracy of the important parameter.

4.2 Hypothesis Testing

Hypothesis testing on the difference between population statistics is another way to associate a level of significance with a quantified measure of correlation agreement based on two sets of sample data. Formulation of an appropriate null hypothesis is integral to applying this metric. When attempting to identify evidence of good correlation that cannot initially be assumed to exist, the null hypothesis should be contrary to the outcome desired. Formulated this way, strong evidence must be present in the sample data to reject the null hypothesis (acceptance of desired outcome).

For example, the following null hypothesis for a one-tailed Student's t-test may be well-suited as parameter-level criteria metric: the difference between the population mean

significant single amplitude (SSA) values is greater than a specified amount. The level of significance used in the test dictates the probability of wrongly rejecting the null hypothesis. For the given null hypothesis, it is possible to quantify (and set to an acceptably low level) the probability of incorrectly identifying good correlation. The probability of failing to correctly identify good correlation is not associated with a specific probability (often known as the Type II or beta error); while this value is of interest, it is typically of less concern than incorrectly identifying poor correlation as good correlation. By defining both a specific limit on the allowable population difference and a level of significance for the test, the Student's t-test can provide a pass/fail outcome for the comparison.

Alternatively, by specifying the level of significance and solving for the critical value of the limit on the difference allowed to pass the test, a quantified measure of correlation agreement is produced. Similarly, by specifying the limit on the difference and solving for the critical level of significance to pass the test, the probability associated with success of the comparison is produced; see Appendix A. Both the quantified measure of agreement and probability of test success are comparison outcomes which can be used to develop measures of correlation across multiple comparisons. The beta error is not explicitly calculated in this process.

Hypothesis tests rely upon measures of the variance in both populations; for comparison of extrapolated values, the confidence intervals on the extrapolated values can be used to calculate the parameters necessary for hypothesis test calculations.

4.3 Percentiles – Rare Comparisons

To make comparisons farther out on the tail of the motion distribution, a cumulative distribution of the measured peaks is useful. The cumulative distributions or quantiles can



be compared at specific percentiles with uncertainty bands. Uncertainty bands at any percentile can be calculated using the normal approximation to the binomial distribution (Belenky and Campbell, 2012).

Percentiles comparisons across the range of available data (shown as a Quantile-Quantile (Q-Q) plot) provide strong visual indications about model and simulation correlation across the distribution of ship response. However, establishing parameter criteria metrics to quantify correlation (including uncertainty) across a range of percentiles is challenging; applying comparison metrics at one or more discrete percentile of peak values is recommended.

One should be cautious when deciding at which percentile to apply parameter criteria comparison metrics. Data at the highest percentiles are prone to large sampling uncertainties; repetition of an ensemble of runs often leads to very different values of the 99th percentile of roll peaks due to the small number of samples associated with extreme motions. The 90th percentile of ship motion peak responses has been observed to be a stable level at which quasi-rare behavior can be observed without being obscured by very large uncertainty. Note that high percentile of peak values are related to threshold exceedance rate. Both high percentiles of peaks and exceedance rates are useful parameters for which non-rare motion channel criteria may be applied, though percentiles tend to lend themselves more easily to the definition of margins and limits. The authors have not yet attempted to apply this to extrapolations.

5. RESULTS

Ten of thousands of hours simulated ship motions were calculated using the 3DOF simplified simulation tool in large sea states for a range of heading. The seaway was a 9.5 m significant wave height and 15 sec modal period with a Bretschneider spectral shape.

The headings ranged from near following (15 deg) to bow seas (135 deg). The headings were 15, 30, 45, 60, 90, and 135 deg. The speed was 12 knots for all cases.

The total exposure time was accumulated by ensembling many half-hour simulations. Each simulation had a unique set of random phases to generate a unique and independent wave realization. Time histories of roll, pitch, vertical acceleration, and lateral acceleration were analyzed to extract peaks. This distribution of peaks is the true value for each heading-motion combination. The length of exposure time varies between headings as a matter of convenience. The difference in exposure time does not affect the validation results beyond potentially limiting the maximum comparison value.

Around 100 extrapolations were made with sub-sets of the total exposure time for each heading-motion combination. The use of multiple extrapolations allows for a direct check on confidence interval formulation and gives understanding of data sub-set dependency. The data sub-set exposure time was either 50 hours or 100 hours depending on the number of peaks extracted, with 50 hours being used for cases with more peaks. This was due to a memory limitation on the analysis software.

The extrapolations were compared to the true value at an evaluation level corresponding to a high motion level in the true data set. The comparison was based on overlap of the 95% confidence interval with the true value. The evaluation level was selected as the highest level in the true data set that had more than 30 data samples. Thirty samples are enough to have meaningful uncertainty. With less than 30 samples, the uncertainty becomes very large and the true value has not stabilized.

Figure 1 shows an example of the roll parameter comparisons for stern seas, 30 deg heading. In this figure, the true value is represented by a solid line (1.1111°). Each extrapolation confidence interval is represented



by a vertical line and represents a single Tier I comparison. The extrapolation captures the true value if the vertical line crosses the horizontal true value line. The estimate of mean value of crossing rate is denoted by a circle and the most probable crossing rate is denoted by a cross. The confidence intervals are asymmetric relative to the mean or most probable crossing rate. This is a property of GPD and different than the symmetric confidence intervals more commonly seen with the normal distribution.

The entirety of Figure 1 represents a Tier II comparison comprised of 100 Tier I comparisons. The expected passing rate percentage is the same as the confidence interval due to use of confidence interval overlap for the parameter comparison. Due to the finite number of data sets, the passing rate can vary from 90 to 100% and still be acceptable; though the mean rate across all the conditions should be close to the confidence level. Table 1 shows the passing rates for all the conditions for the two different confidence formulations. Conditions that pass are bold; failing conditions are italicized. Smith (2014) indicated both CI approaches were acceptable based on roll and pitch. The addition of lateral and vertical acceleration shows a difference between the two CI approaches. The logarithm CI has many instances where the true value capture rate is less than 90% and fail the Tier I comparison (parameter).

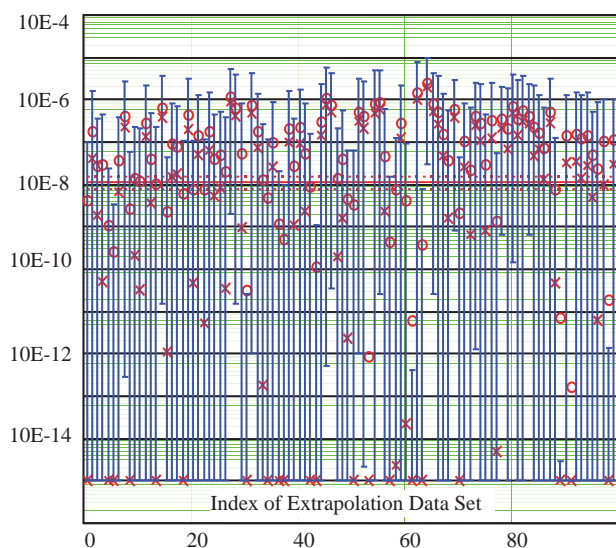


Figure 1 Confidence interval overlap of true value for roll at 30 deg heading at 30 deg comparison level using logarithm CI (91%) (true value 1.111E-08)

As noted in Smith (2014), the GPD can have zero probability which results in asymmetric confidence intervals that have very small lower confidence limits. This can result in automatically capturing the true value if the extrapolation is at all conservative; larger than the true value.

Figure 1 shows roll comparison at 30 deg wave heading for the logarithm boundary CI. The estimates of the mean value are distributed about the true value, while the most probable values are mainly less than the true value. This is a property of the mean value averaging over the entire confidence interval region, whereas the most probable value is selected at a particular point. This difference is discussed in Campbell *et al.* Figure 2 shows the pitch comparison at the same condition where both the mean value estimates and most probable values are greater than the true value. This is indicative of a conservative bias.

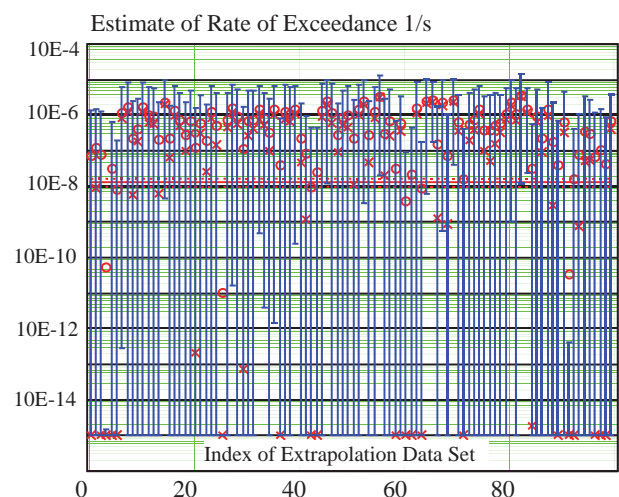


Figure 2 Confidence interval overlap of true value for pitch at 30 deg at 11.5 deg using logarithm CI (97%)

Figures 3 and 4 show the difference in confidence interval method for pitch at 45 deg heading at 11.5 deg comparison level. The



boundary CI method has a higher average upper boundary and a lower boundary always at the lowest value considered (10^{-15}). The logarithm CI method produces smaller confidence intervals.

value for pitch at 45 deg heading at 11.5 deg comparison level using boundary CI (100%)

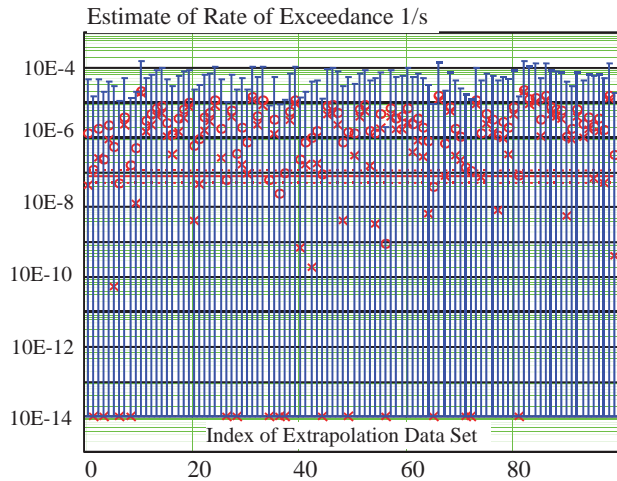


Figure 3 Confidence interval overlap of true
Table 1 Confidence interval overlap results

Heading	Motion	Avg GPD Threshold	Comparison Level	# Points at Threshold	Exposure Hours	Boundary CI		Logarithm CI		Shooting Distance
						pass %	MCD	pass %	MCD	
15	roll	6.947	15	53	230000	96	119.210	84	60.867	1.159
15	pitch	7.359	12	69	230000	99	278.512	94	166.585	0.653
15	lat accel	No data > 0.2g								
15	vert accel	0.125	0.2	468	230000	100	89.878	86	49.892	0.607
30	roll	12.877	30	40	100000	96	178.616	91	101.038	1.330
30	pitch	7.296	11.5	46	100000	99	420.751	97	244.296	0.576
30	lat accel	0.091	0.2	16	100000	100	1061.000	98	591.799	1.186
30	vert accel	0.133	0.25	13	100000	100	955.188	96	484.258	0.877
45	roll	17.094	60	30	230000	99	193.110	94	112.282	2.510
45	pitch	7.012	11.5	28	230000	100	503.342	98	269.962	0.640
45	lat accel	0.135	0.3	37	230000	98	237.340	94	118.744	1.221
45	vert accel	0.158	0.25	518	230000	99	74.673	90	41.558	0.578
60	roll	18.754	50	49	100000	100	276.284	100	169.168	1.666
60	pitch	6.257	9.5	71	100000	100	330.874	91	179.786	0.518
60	lat accel	0.157	0.35	19	100000	98	415.630	97	213.923	1.227
60	vert accel	0.194	0.3	169	100000	100	193.528	86	98.556	0.547
90	roll	16.055	32.5	41	230000	99	329.773	99	192.832	1.024
90	pitch	1.517	2.5	170	230000	100	136.716	94	68.382	0.648
90	lat accel	0.154	0.25	43	230000	94	136.448	86	74.551	0.621
90	vert accel	0.270	0.4	287	230000	100	98.103	96	52.179	0.480
135	roll	12.350	17.5	186	230000	100	92.851	92	60.694	0.417
135	pitch	4.909	7	172	230000	100	134.019	94	70.853	0.426
135	lat accel	0.137	0.25	25	230000	96	424.676	88	232.106	0.827
135	vert accel	0.283	0.4	192	230000	98	150.486	96	85.572	0.416
Average Value						99		93		

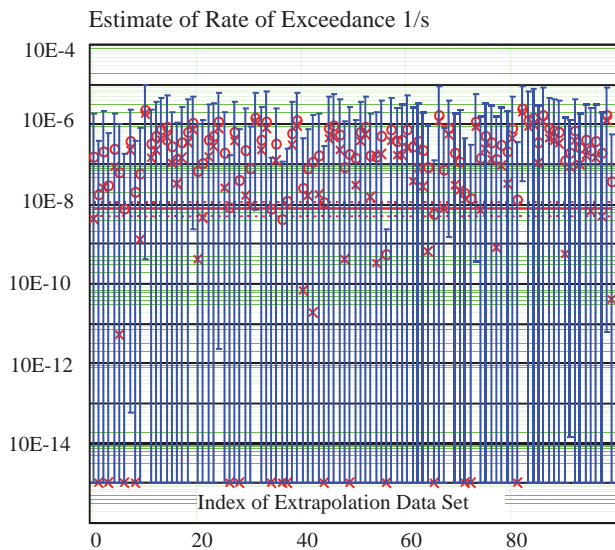


Figure 4 Confidence interval overlap of true value for pitch at 45 deg heading at 11.5 deg comparison level using logarithm CI (98%)

Figure 5 shows asymmetric confidence intervals for the 45 deg heading, lateral acceleration logarithm CI at 0.3 g comparison. At 0.2g comparison level for lateral acceleration at 45 deg heading, Figure 6 shows much smaller confidence intervals and a conservative bias. Although the true value capture rate is very low, the actual difference is small.

Figures 7 and 8 compare the boundary and logarithm CI methods for vertical acceleration at 30 deg heading and 0.2g comparison level. For comparisons at higher levels, both methods have 100% capture rate. The boundary method has larger confidence intervals; both a higher upper bound and many more instances of near zero lower bound. The boundary CI higher upper bound is indicated by the higher MCD; 99.5 vice 54.2. These are similar to the trends seen for pitch in Figures 3 and 4.

Pipiras, *et al.* (2015) compares the boundary and logarithm (lognormal) confidence interval approaches with a preference for lognormal as anti-conservative.

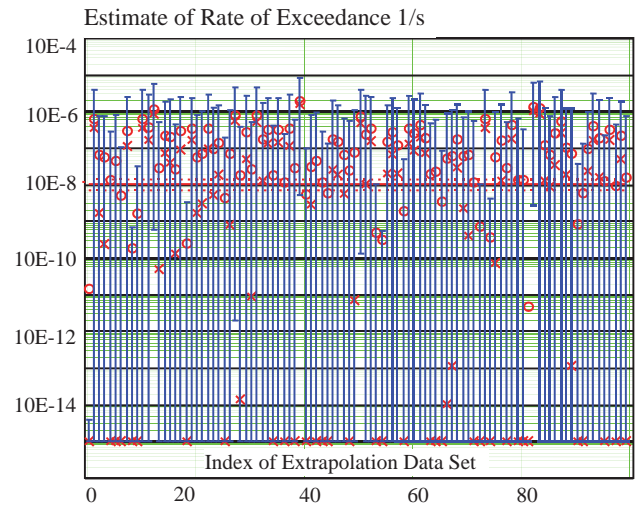


Figure 5 Confidence interval overlap of true value for lateral acceleration at 45 deg heading at 0.3g comparison level using logarithm CI

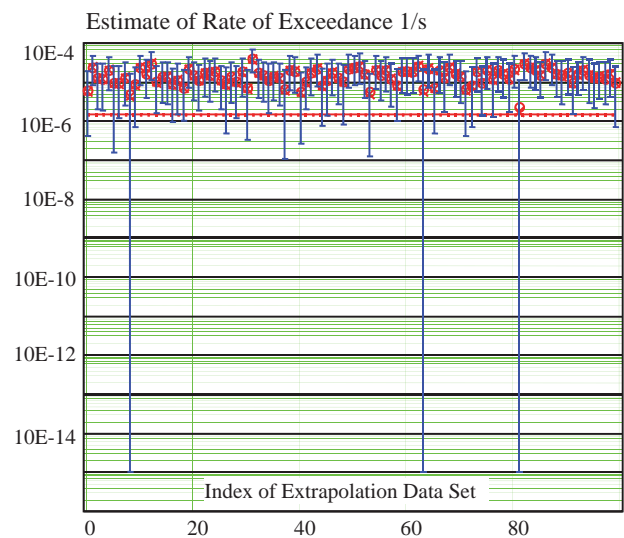


Figure 6 Confidence interval overlap of true value for lateral acceleration at 45 deg heading at 0.2g comparison level using logarithm CI

In terms of acceptance criteria, the boundary CI approach had all the parameter comparisons pass. Therefore, all the Tier II conditions pass and overall acceptance, Tier III, automatically passes if all condition comparisons, Tier II, are acceptable. In this case, even the alternate Tier II definition requiring all the motions to pass for a condition to pass results in overall acceptance.

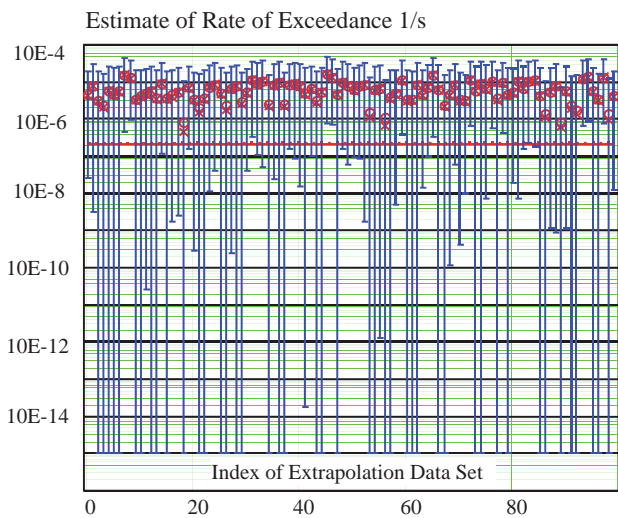


Figure 7 Confidence interval overlap of true value for vertical acceleration at 30 deg heading at 0.2g comparison level using boundary CI

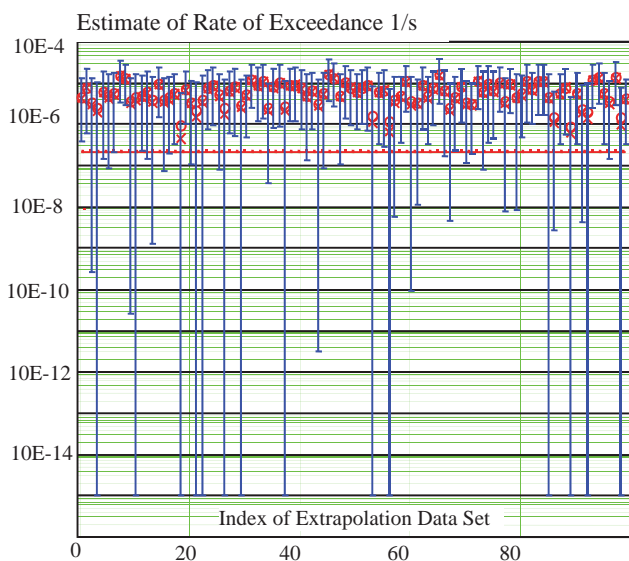


Figure 8 Confidence interval overlap of true value for vertical acceleration at 30 deg heading at 0.2g comparison level using logarithm CI

It is perhaps more instructive to look at the logarithm CI results. Here some of the acceleration parameter comparisons are not acceptable; true value capture rates less than 90%. As a result, some conditions do not pass but the condition pass rate is acceptable for overall acceptance, 18/23 (78%). However, a condition criterion requiring the passing of all motion comparisons is failed for two-thirds the conditions defined by unique speed-heading-

seaway combination. There are six such conditions in this example. Overall acceptance fails as well.

However, this does show there is a heading range that is acceptable; aft of beam seas. There could be a limited acceptance with the restricted range of headings. This may also highlight a difference in performance due to behavior of the distribution tail, that is, heavy or light.

As an alternative, the mean conservative distance is a metric which uses the upper confidence limit on an extrapolated sample value. This metric estimates how much conservatism (or over-prediction) is present in the simulation results. For validation of a simulation tool against model data for ship guidance, this quantity may be more important than overall total confidence interval. The difficulty is agreeing to what is an acceptable value. In this example, only one case was over 3 orders of magnitude and almost all were over 2 orders of magnitude. At first glance, this appears to be completely unacceptable as a 100% difference is usually considered unacceptable. However, for exceedance rates of extreme values the uncertainty is inherently high and 1 in a billion is essentially the same as 10 in a billion. The acceptable MCD can be determined by the level at which the over conservatism produces an undesired operational restriction or life time risk level.

The MCD is calculated from the upper confidence limit; the upper confident limit suggests that 95% of the time, the true value is smaller than the limit value. Re-analysis of the existing data would show how successfully both methodologies estimate this quantity. Because this investigation would be focused on only the upper interval limit, the overall methodology validation conclusions may differ from those related to formulation of the entire confidence interval.



This example demonstrates the many factors influencing the comparison: CI method, comparison level, and comparison metric.

6. CONCLUSIONS

This paper demonstrated the applicability of a multi-tier validation approach to the validation of an extrapolated value confidence interval calculation method based on the Generalized Pareto Distribution. The first tier, parameter comparison, was made by comparing the 95% confidence interval from a GPD extrapolation to the true value. This was done 50 to 100 times to determine a passing rate for the Tier II, condition, comparison. Lastly, most of the conditions passed the second tier criterion, which passes the Tier III, or set, comparison. The extrapolation method would be considered validated. A rigorous validation effort would specify passing percentages at Tiers I and II.

Discussion was extended from parameter comparisons of a confidence interval calculation methodology against a known population to comparisons of extrapolated data between simulation and model data. The confidence interval overlap validation approach for these Tier I comparisons requires a validated confidence interval formulation. Other comparison metrics such as maximum conservative distance, mean difference, hypothesis testing, and percentiles were discussed as alternatives to confidence interval overlap. The boundary CI method proved marginally better than the logarithm CI method due to more acceptable conditions and mean value closer to confidence level. Still the boundary CI has many instances of 100 percent capture. This could be indicative of an overly large CI. The logarithm CI method had many failing conditions. Both approaches showed a conservative bias. Extrapolation of acceleration peaks tended to have lower capture rates than for roll or pitch for both CI methods. In terms of the acceptance criteria, the boundary CI method passed when

accelerations are included and the logarithm CI method did not. It was shown that the acceptance criteria can indicate the presence of different behavior of distribution tail based on which parameters/motions pass.

The ratio of the GPD threshold and the evaluation level provides a metric for practical use. This ratio was less for accelerations than motions. The conditions with low motions can either have more data added, in the hope of increasing the GPD threshold level, or ignoring the condition as having negligible motions.

7. ACKNOWLEDGEMENT

This work was funded by the Office of Naval Research under Dr. Ki-Han Kim. The authors are grateful to Dr. V. Belenky for providing the data and analysis tools for the numerical example and thorough editing of the manuscript.

8. REFERENCES

- AIAA, 1998, Guide for the Verification and Validation of Computational Fluid Dynamics Simulations. American Institute for Aeronautics and Astronautics, Reston, Virginia.
- ASME, 2009, *Standard for Verification and Validation in Computational Fluid Dynamics and Heat Transfer*, American Society of Mechanical Engineers, NY.
- Belenky, V. and Campbell, B. 2012 "Statistical Extrapolation for Direct Stability Assessment", Proc. 11th Intl. Conf. on Stability of Ships and Ocean Vehicles STAB 2012, Athens, Greece, pp. 243-256.
- Belenky, V., Pipiras, V., Kent, C., Hughes, M., Campbell, B. and Smith, T. 2013 "On the Statistical Uncertainties of Time-domain-based Assessment of Stability Failures: Confidence Interval for the Mean and Variance of a Time Series", Proc. 13th Intl.



- Ship Stability Workshop, Brest, France, pp. 251-258.
- Belenky, V., Pipiras, V. and Weems, K. 2015 "Statistical Uncertainty of Ship Motion Data" Proc. of 12th Intl Conference of the Stability of Ships and Ocean Vehicles STAB 2015, Glasgow, UK
- Campbell, B., Belenky, V. and Pipiras, V. 2014, "On the Application of the Generalized Pareto Distribution for Statistical Extrapolation in the Assessment of Dynamic Stability in Irregular Waves," Proc. 14th Intl. Ship Stability Workshop, Kuala Lumpur, Malaysia.
- de Kat, J. O. and Paulling, J. R., 1989, "The Simulation of Ship Motions and Capsizing in Severe Seas," Transactions of The Society of Naval Architects and Marine Engineers, vol. 97.
- ITTC Loads and Responses Seakeeping, 2011, "Verification and Validation of Linear and Weakly Nonlinear Seakeeping Computer Code," Procedure 7.5-02-07-02.4 Rev 1.
- Lin, W.M., & D.K.P. Yue, 1990, "Numerical Solutions for Large Amplitude Ship Motions in the Time-Domain." Proc. 18th Symp. of Naval Hydrodynamics, Ann Arbor, Michigan, pp. 41-66.
- Pipiras, V., Glotzer, D., Belenky, V., Campbell, B., Smith, T. 2015 "Confidence Interval for Exceedance Probabilities with Application to Extreme Ship Motions", Journal of Statistical Planning and Inference (Submitted).
- Reed, A. M., 2011, "26th ITTC Parametric Roll Benchmark Study," Proc. 11th Intl. Ship Stability Workshop, Washington, DC, USA.
- Shin, Y.S., Belenky, V. Lin, W.M. Weems, K.M. and Engle, A.H. 2003, "Nonlinear Time Domain Simulation Technology for Seakeeping and Wave-Load Analysis for Modern Ship Design," SNAME Transactions, Vol. 111.
- Smith, T. C., 2012, "Approaches to Ship Motion Simulation Acceptance Criteria" Proc. of 11th Intl Conference of the Stability of Ships and Ocean Vehicles STAB 2012, Athens, Greece pp 101-114.
- Smith, T. C., 2014, "Example of Validation of Statistical Extrapolation Example of Validation of Statistical Extrapolation," Proc. of the 14th Intl. Ship Stability Workshop, Kuala Lumpur, Malaysia.
- Smith, T. and Campbell, B. 2013, "On the Validation of Statistical Extrapolation for Stability Failure Rate," Proc. 13th Intl. Ship Stability Workshop, Brest, France.
- The Specialist Committee on Stability in Waves, 2011, Final Report and Recommendations to the 26th ITTC, Proc. 26th International Towing Tank Conference, Vol II, Rio de Janeiro, Brazil.
- Weems, K. and Wundrow, D. 2013, "Hybrid Models for Fast Time-Domain Simulation of Stability Failures in Irregular Waves with Volume-Based Calculations for Froude-Krylov and Hydrostatic Force", Proc. 13th Intl. Ship Stability Workshop, Brest, France.
- Weems, K. and Belenky, V. 2015, "Fast Time-Domain Simulation in Irregular Waves With Volume-Based Calculations for Froude-Krylov and Hydrostatic Force" Proc. of 12th Intl Conference of the Stability of Ships and Ocean Vehicles STAB 2015, Glasgow, UK

9. APPENDIX A: DISCUSSION OF HYPOTHESIS TESTING ERROR

Hypothesis testing involves the formulation of a null hypothesis and has two errors that need to be controlled. The Type I error is associated with rejecting a null hypothesis that should be accepted - false negative. It is characterized with probability α (also known as the level of significance). On the probability

density function (PDF), this is the area in the tails of the distribution. The confidence interval is the area between the tails, $1-\alpha$ (probability that null hypothesis is accepted correctly).

Type II error is the error associated with accepting a null hypothesis that should be rejected - false positive. It is characterized with probability β . Indeed, $1-\beta$ is the probability that the null hypothesis is rejected correctly. Type II error is calculated based on the difference in means between the data sets relative to an allowable or desired difference. The Type II error is overlap area of the original PDF and a PDF shifted by the difference in means.

If the mean shift is large, then it is relatively easy to detect false positives as the means being compared are far apart and β is small. Conversely, if the mean shift is small, then it is difficult to detect false positives and they are more likely to occur. For this case, β would be larger and even greater than 50%. A normal distribution is often used to describe the data probability density function for the Type II comparison.

This example deals with motion data sets with equal number of records and the comparison metric is the standard deviation. The null hypothesis is that the two variances are assumed to come from the same data set or the variances are statistically the same. Probability of Type II error is arbitrarily desired to be less than 50% using 90% confidence probability.

It is possible to check if $\beta < 0.5$ without actually calculating β by taking advantage of the fact that once normalized, the mean difference must be greater than 1.645 (90% quintile of a normal distribution with zero mean and unity variance) based on the shift to achieve less than 50% probability with 90% confidence and two-tailed Normal distribution. This critical difference, δ_{cr} , is applicable to all comparisons using the same confidence and β .

Using other values of β results in different mean critical differences.

As the comparison metric is related to standard deviation, the starting point is normalizing the allowable mean difference D_A between the variance estimates of the two data samples:

$$\delta_{cr} = \frac{D_A}{\sqrt{Var(\hat{D})}} \quad (A1)$$

\hat{D} is the difference between variance estimates of the two samples and $Var(\hat{D})$ is the variance of this difference.

$$\hat{D} = \hat{V}_1 - \hat{V}_2 \quad (A2)$$

The samples are independent, thus:

$$Var(\hat{D}) = Var(\hat{V}_1) + Var(\hat{V}_2) \quad (A3)$$

Each sample consists of a number of records obtained from simulation or model experiment. Variance estimates of each sample are the result of averaging the variance estimates of each record. Thus, variance of the variance estimate is expressed as:

$$Var(\hat{V}_1) = \frac{Var(\hat{V}_{R1})}{N_1}; Var(\hat{V}_2) = \frac{Var(\hat{V}_{R2})}{N_2} \quad (A4)$$

$Var(\hat{V}_{R1})$ and $Var(\hat{V}_{R2})$ are the variances of the variance of a single record.

The validity of the code is the hypothesis being tested. Thus, the code is expected to recover the theoretical variance reflected in a model test. It also means that the variance of the variance estimate of a single record is the same between the code and model test:

$$Var(\hat{V}_{R1}) = Var(\hat{V}_{R2}) = Var(\hat{V}_R) \quad (A5)$$

Thus, the theoretical value of the variance of the differences is



$$\begin{aligned} \text{Var}(\hat{D}) &= \frac{\text{Var}(\hat{V}_{R1})}{N_1} + \frac{\text{Var}(\hat{V}_{R2})}{N_2} \\ &= \text{Var}(\hat{V}_R) \left(\frac{1}{N_1} + \frac{1}{N_2} \right) \end{aligned} \quad (\text{A6})$$

The problem is that the theoretical value $\text{Var}(\hat{V}_R)$ is not known. Instead, the estimates \hat{V}_{R1} and \hat{V}_{R2} can be computed using an option for a large number of records, see Belenky, *et al.* (2013, 2015). The best estimate of $\text{Var}(\hat{V}_R)$ can be obtained by pooling together the two available estimates:

$$\begin{aligned} \hat{V}_{R} &= \frac{(N_1 - 1)\hat{V}_{R1} + (N_2 - 1)\hat{V}_{R2}}{N_1 + N_2 - 2} \end{aligned} \quad (\text{A7})$$

Finally:

$$\begin{aligned} \hat{D} &= \frac{(N_1 - 1)\hat{V}_{R1} + (N_2 - 1)\hat{V}_{R2}}{N_1 + N_2 - 2} \\ &\times \left(\frac{1}{N_1} + \frac{1}{N_2} \right) \end{aligned} \quad (\text{A8})$$

Setting δ_{cr} to 1.645 and substituting (A8) into equation (A1)

$$1.645\sqrt{\hat{D}} < D_A \quad (\text{A9})$$

For the case when number of records in each sample is the same: $N_1=N_2=N$:

$$\hat{D} = \frac{\hat{V}_{R1} + \hat{V}_{R2}}{N} \quad (\text{A10})$$

Equal number of records allows producing a simple final formula to assess Type II error:

$$1.645\sqrt{\frac{\hat{V}_{R1} + \hat{V}_{R2}}{N}} < D_A \quad (\text{A11})$$



Coupled Hydro – Aero – Elastic Analysis of a Multi – Purpose Floating Structure for Offshore Wind and Wave Energy Sources Exploitation

Thomas P., Mazarakos, *Laboratory for Floating Structures and Mooring Systems, School of Naval Architecture and Marine Engineering*, tmazarakos@naval.ntua.gr

Dimitrios N., Konispoliatis, *Laboratory for Floating Structures and Mooring Systems, School of Naval Architecture and Marine Engineering*, dkonisp@naval.ntua.gr

Dimitris I., Manolas, *Aerodynamic Laboratory, School of Mechanical Engineering National Technical University of Athens*, manolasd@fluid.mech.ntua.gr

Spyros A., Mavrakos, *Laboratory for Floating Structures and Mooring Systems, School of Naval Architecture and Marine Engineering*, mavrakos@naval.ntua.gr

Spyros G., Voutsinas, *Aerodynamic Laboratory, School of Mechanical Engineering National Technical University of Athens*, spyros@fluid.mech.ntua.gr

ABSTRACT

A coupled hydro–aero–elastic analysis of a multi–purpose floating structure suitable for offshore wind and wave energy sources exploitation is presented. The floating structure encompasses an array of hydrodynamically interacting Oscillating Water Column (OWC) devices consisting of concentric vertical cylinders, which are moored through tensioned tethers as a Tension Leg Platform (TLP) supporting a 5 MW W/T. The solutions of the diffraction and the pressure– and motion– dependent radiation problems around the floating structure and the aerodynamics of the Wind Turbine (W/T) are properly combined in the frequency and time domain. Results are compared at the level of RAOs and consistent results are obtained.

Keywords: *Multi purpose floating structure, Oscillating water column device, Wind turbine*

1. INTRODUCTION

In the last years considerable efforts and advances have been made worldwide in developing renewable energy devices. Among the numerous concepts proposed for wave energy conversion one of the most promising is the multi bodied floating structure based on the oscillating water column principle. Such type

of devices have been reported in connection with the wave energy extraction (Konispoliatis & Mavrakos, 2013a) or in composing semi–submersible platforms for renewable electricity generation from the combined wind and wave action (Aubault et al., 2011; Mavrakos et al., 2011).

In the present contribution we consider a system of three identical OWC devices which

are placed at the corners of a triangular floater and can oscillate about their mean equilibrium position moving as a unit. The geometric configuration of each device consists of an exterior partially immersed toroidal oscillating chamber of finite volume supplemented by a concentric interior piston-like truncated cylinder. The wave action causes the captured water column to oscillate in the annular chamber, compressing and decompressing the air above the inner water surface. As a result, there is an air flow moving forwards and backwards through a turbine coupled to an electric generator. In the centre of the platform a solid cylindrical body is arranged in order to support the W/T (Figure 1).

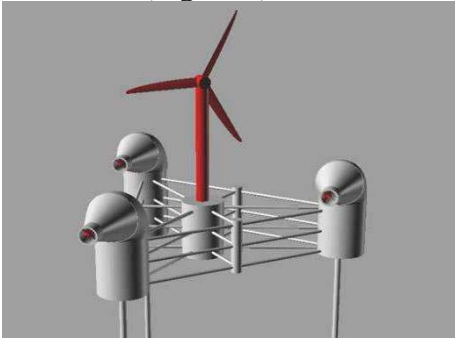


Figure 1: Multi-purpose floating structure with three OWC devices and a W/T

The latter is a typical 5MW horizontal axis turbine which is a variable-speed variable-pitch controlled WT. Detailed data are given in Jonkman et al. 2009. The tower of the WT is cantilevered at an elevation of 10m above the sea water level (SWL) to the top of the main column of the floating platform.

2. FORMULATION OF THE PROBLEM

2.1 Calculation of the velocity potential function

We consider that the group of three OWCs is excited by a plane periodic wave of amplitude $H/2$, frequency ω and wave number k propagating in water of finite water depth d . The distance between each device is L . The outer and inner radii of each device's chamber

$q, q=1, 2, 3$, are denoted by α_q, b_q , respectively, whereas the distance between the bottom of the q device and the sea bed is denoted by h_q . The radius of the interior concentric cylindrical body in each device q , is denoted by $b_{1,q}$ and the distance between its bottom and the sea bed is $h_{1,q}$. The radius of the central cylindrical body that supports the WT is c and the distance between its bottom and the sea bed is h_c (Fig2 & Fig3). Small amplitude waves, inviscid, incompressible and irrotational flow are assumed, so that linear potential theory can be employed. A global Cartesian co-ordinate system O-XYZ with origin on the sea bed and its vertical axis OZ directed positive upwards and coinciding with the vertical axis of symmetry of the central body is used. Moreover, three local cylindrical co-ordinate systems (r_q, θ_q, z_q) , $q = 1, 2, 3$ are defined with origins on the sea bottom and their vertical axes pointing upwards and coinciding with the vertical axis of symmetry of the q device.

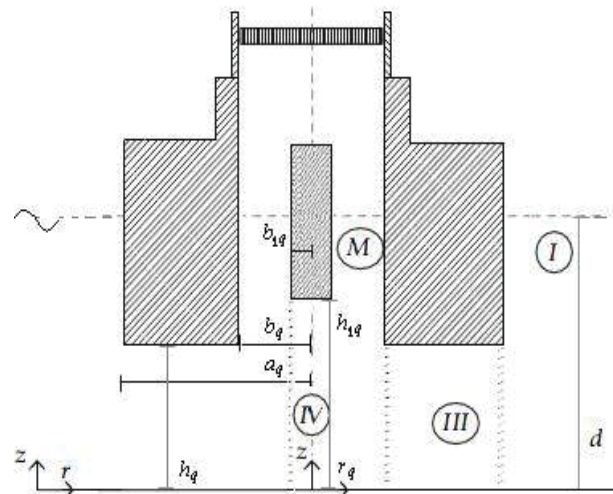
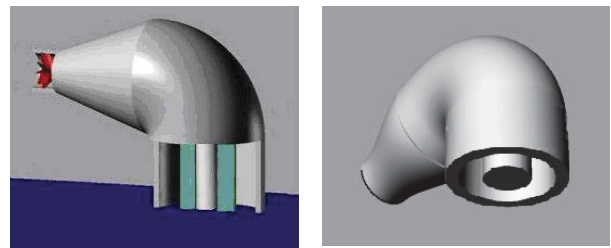


Figure 2: Definition sketch of the q OWC device of the array

The fluid flow around the $q = 1, 2, 3, 4$ device/body (three OWCs & one solid body) can be described by the potential function:

$$\Phi^q(r_q, \theta_q, z; t) = \text{Re} \left\{ \phi^q(r_q, \theta_q, z) \cdot e^{-i\omega t} \right\} \quad (1)$$

Following Falnes (2002) the spatial function ϕ^q can be decomposed, on the basis of linear modelling, as:

$$\varphi^q = \varphi_0^q + \varphi_7^q + \sum_{p=1}^4 \sum_{j=1}^6 \dot{x}_{j0}^p \cdot \varphi_j^{qp} + \sum_{i=1}^3 P_{in0}^i \cdot \varphi_P^{qi} \quad (2)$$

Here, ϕ_0^q is the velocity potential of the undisturbed incident harmonic wave (Mavrakos & Koumoutsakos, 1987); ϕ_7^q is the scattered potential around the q device/body, when it is considered fixed in waves with the duct open to the atmosphere, so that the pressure in the chamber is equal to the atmospheric one (for the OWCs); ϕ_j^{qp} is the motion-dependent radiation potential around the device/body q resulting from the forced oscillation of the p -th device/body, $p=1,2,3,4$, moving with unit velocity amplitude, $\dot{x}_j^p = \text{Re} \left\{ \dot{x}_{j0}^p \cdot e^{-i\omega t} \right\}$; ϕ_P^{qi} is the pressure-dependent radiation potential around the q -th device/body when it is considered fixed in the wave field and open to the atmosphere (for the OWCs), due to unit time harmonic oscillating pressure head, $P_{in}^i = \text{Re} \left\{ P_{in0}^i \cdot e^{-i\omega t} \right\}$, in the chamber of the $i=1,2,3$ device which is considered fixed in otherwise calm water.

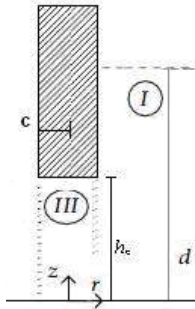


Figure 3: Definition sketch of the central cylindrical body basing the W/T

The diffraction, i.e. $\phi_D^q = \phi_0^q + \phi_7^q$, $q=1,2,3,4$, the motion-dependent radiation potentials around the isolated q device/body and pressure-dependent radiation potential around the

isolated q device, when it is considered alone in the field, are expressed in its own cylindrical co-ordinate system (r_q, θ_q, z) as follows:

$$\phi_D^q(r_q, \theta_q, z) = -i\omega \frac{H}{2} \sum_{m=-\infty}^{\infty} i^m \Psi_{D,m}^q(r_q, z) \cdot e^{im\theta_q} \quad (3)$$

$$\phi_j^{qq}(r_q, \theta_q, z) = -i\omega \sum_{m=-\infty}^{\infty} \Psi_{j,m}^{qq}(r_q, z) \cdot e^{im\theta_q} \quad (4)$$

$$\phi_P^{qq}(r_q, \theta_q, z) = \frac{1}{i\omega\rho} \sum_{m=-\infty}^{\infty} \Psi_{P,m}^{qq}(r_q, z) \cdot e^{im\theta_q} \quad (5)$$

Here ρ is the water density.

The potentials ϕ_j^l ($l \equiv q, qp; j=D, 1, \dots, 6, P; p, q = 1,2,3,4; i=1,2,3$) are solutions of Laplace's equation in the entire fluid domain and satisfy the following boundary conditions:

$$\omega^2 \phi_j^l - g \frac{\partial \phi_j^l}{\partial z} = \begin{cases} 0 & \text{for } r_q \geq a_q; \text{ or } r_q \geq c \\ & l \equiv q, j = D; \text{ or} \\ & l \equiv qp, j = 1,2,\dots,6, P \\ 0 & \text{for } b_{1,q} \leq r_q \leq b_q; \\ & l \equiv q, j = D; \text{ or} \\ & l \equiv qp, j = 1,2,\dots,6 \\ -\delta_{q,i} \frac{i\omega}{\rho} & \text{for } b_{1,q} \leq r_q \leq b_q; \\ & l \equiv qi; j = P \end{cases} \quad (6)$$

on the outer and inner free sea surface ($z=d$), and the zero normal velocity on the sea bed ($z=0$). Moreover, the potentials have to fulfil kinematic conditions on the mean device/body's wetted surface. Finally, a radiation condition must be imposed which states that propagating disturbances must be outgoing.

The unknown potential functions $\Psi_{j,m}^{k,l}$, $k=I, III, M, IV$, see Eq3 – Eq5, can be established in each fluid region surrounding the q -th device/body (see Figs. 2 and 3) using the method of matched axisymmetric eigenfunction expansions.

Next, the potentials, ϕ_j^{qp}, ϕ_P^{qi} , ($j=1, \dots, 6$) around anybody q of the multi-body configuration due to oscillation of body p ,



$p=1,2,3,4$, in otherwise still water (motion – dependent radiation potential) or due to inner time harmonic oscillating pressure head in the air chamber of the device i , $i=1,2,3$, (pressure – dependent radiation potential), can be expressed in the q -th body's cylindrical coordinate system, as:

$$\phi_j^{qp}(r_q, \theta_q, z) = -i\omega \sum_{m=-\infty}^{\infty} \Psi_{j,m}^{qp}(r_q, z) \cdot e^{im\theta_q} \quad (7)$$

$$\phi_p^{qi}(r_q, \theta_q, z) = \frac{1}{i\omega\rho} \sum_{m=-\infty}^{\infty} \Psi_{p,m}^{qi}(r_q, z) \cdot e^{im\theta_q} \quad (8)$$

In order to express the potentials, ϕ_j^{qp} , ϕ_p^{qi} in the form of Eq7 and Eq8, use is made of the multiple scattering approach (Twersky, 1952; Okhusu, 1974). This method has been further elaborated to solve the diffraction and the motion – dependent radiation problems around arbitrarily shaped, floating or / and submerged vertical axisymmetric bodies by Mavrakos & Koumoutsakos (1987) and Mavrakos (1991) and for the diffraction and the pressure–dependent radiation problems for an interacting array of OWC's devices by Konispoliatis & Mavrakos (2013b); thus, it will be no further elaborated here.

2.2 Volume flow

The time dependent volume flow produced by the oscillating internal water surface in q OWC device, $q = 1, 2, 3$, is denoted by $Q^q(r_q, \theta_q, z; t) = \text{Re}[q^q(r_q, \theta_q, z) \cdot e^{-i\omega t}]$, where:

$$q^q = \iint_{S_i^q} u_z dS_i^q = \iint_{S_i^q} \frac{\partial \phi^q}{\partial z} r_q dr_q d\theta_q \quad (9)$$

Here u_z denotes the vertical velocity of the water surface, and S_i^q the inner water surface in the q device, $q=1, 2, 3$.

Assuming that the Wells turbine is placed in a duct between the q device's chamber and

the outer atmosphere and that it is characterized by a pneumatic admittance Λ^q , then the total volume flow is equal to (Evans & Porter; 1996, Falnes; 2002):

$$Q^q(t) = \Lambda^q \cdot P_{in}^q(t) \quad (10)$$

Assuming isentropy so that variations of air density and pressure are proportional to each other with $c_{air}^2 = dp_{in}^q / d\rho_{air}$, c_{air} being the sound velocity in air, the pneumatic complex admittance Λ^q is equal to (Martins–Rivas & Mei, 2010):

$$\Lambda^q = \frac{KD}{\rho_{air}N} + (-i\omega) \frac{V_0^q}{c_{air}^2 \rho_{air}} \quad (11)$$

Where K is constant for a given turbine geometry (independent of turbine size or rotational speed), D is turbine rotor diameter, N is the rotational speed (radians per unit time), ρ_{air} is the atmospheric density and V_0^q the q device's air chamber volume.

Decomposing the total volume flow, q^q , of the q -th device, same as for the velocity potential; see Eq2, into three terms associated with the diffraction, q_D^q , and the motion– and pressure–dependent radiation problems, q_R^q , q_P^q , respectively, we can obtained:

$$q^q = q_D^q + q_R^q + \sum_{i=1}^3 P_{in0}^i \cdot q_P^{qi} \quad (12)$$

Here:

$$q_R^q = \sum_{p=1}^4 \sum_{j=1}^6 \dot{x}_{j0}^p \cdot q_{3,j}^p - \dot{x}_{30}^p \cdot S_i^p \quad (13)$$

Where S_i^p is the inner water surface in the p device, $p=1, 2, 3$.



The pneumatic admittance Λ^q for the OWCs, for the presented results, was considered as a real and positive number equal to the optimum coefficient Λ_{opt} of the same restrained OWC device but in isolation condition as in Evans and Porter (1996) work.

2.3 Hydrodynamic forces

The various forces on the q device/body can be calculated from the pressure distribution given by the linearised Bernoulli's equation:

$$P(r_q, \theta_q, z; t) = -\rho \frac{\partial \Phi^q}{\partial t} = i\omega \rho \phi^q \cdot e^{-i\omega t} \quad (14)$$

Where ϕ^q is the q devices' velocity potential in each fluid domain I , III , M and IV (see Figs. 2 and 3). The horizontal and vertical exciting forces and moments acting on an array of OWC devices have been presented in Konispoliatis & Mavrakos (2013b).

The hydrodynamic reaction forces and moments F_{ij}^{qp} acting on the device/body q , $q=1,2,3,4$, in the i -th direction due to the oscillation of device/body p , $p=1,2,3,4$, in the j -th direction, can be calculated by the Eq14 and the complex form f_{ij}^{qp} may be written in the form (Newman, 1977):

$$f_{ij}^{qp} = \omega^2 (a_{ij}^{qp} + i/\omega b_{ij}^{qp}) x_{j0}^p \quad (15)$$

Here, a_{ij}^{qp} , b_{ij}^{qp} , are the well-known added mass and damping coefficients.

In the same way, the hydrodynamic pressure forces and moments f_i^{ql} acting on the device/body q in the i -th direction due to oscillating pressure head in the $l=1,2,3$ device can be written in the form:

$$f_i^{ql} = (-e_i^{ql} + id_i^{ql}) \cdot p_{in0}^l \quad (16)$$

Here e_i^{ql} , d_i^{ql} are the pressure damping coefficients.

The total hydrodynamic forces on the entire multi-body configuration can be calculated by properly superposing the corresponding forces on each device with respect to the reference point of motion, G , of the entire structure. (for details see Mavrakos, 1991).

2.4 Mooring system

The floating structure is moored with a TLP mooring system of three tendons spread symmetrically about the platform Z-axis. The fairleads are located at the base of the offset columns, at a depth of 20.0m below the sea water level. The anchors (fixed to the inertia frame) are located at a water depth of 200m below the sea water level. Each of the 3 tendons has an unstretched length of 180m, a diameter of 0.130m, an equivalent mass per unit length of 104kg/m and a submerged weight per unit length equal to 888.6N/m. The pretension of each tendon is 10800 kN. The mooring line stiffness k_{xx} and k_{zz} of each tendon is 60KN/m and 14700KN/m, respectively.

2.5 Aerodynamic loading

In the frequency domain formulation, the contribution of the W/T is projected on the degrees of freedom of the floater motion. This is carried out in the context of Hamiltonian dynamics with gravity and aerodynamics being the external forcing. The aerodynamic loading is defined from the Blade Element Momentum theory. After a linearization procedure, additional mass, damping and stiffness matrices are defined which contribute the W/T aerodynamic, inertial-gyroscopic and gravitational loading (Papadakis et al. 2014).

2.6 The time domain problem

The time domain simulations are carried out using the advanced full model hydroGAST developed at NTUA (Riziotis et al., 1997, 2004, Manolas et al. 2012). hydroGAST is a multi-body FEM dynamic model of the complete system. The aerodynamic loading is based on BEM modeling, the hydrodynamic loading is based on linear theory, and the mooring tendons as co-rotating non-linear truss elements. The specific model has been verified within the OC4 IEA project (Popko et al., 2012, Robertson et al., 2014a).

3. RESPONSE AMPLITUDE OPERATORS (RAO'S)

The investigation of the dynamic equilibrium of the forces acting on the freely floating array of OWC devices/body without the W/T leads to the following well – know system of differential equations of motions, in the frequency domain, i.e.:

$$\sum_{j=1}^6 \left[-\omega^2 (M_{i,j} + A_{i,j} + \frac{i}{\omega} B_{i,j}) + C_{i,j} \right] \cdot x_{j0} - F_{P,i} = F_i \quad (17)$$

for $i=1, \dots, 6$.

where $M_{i,j}$ and $C_{i,j}$ are elements of the (6x6) mass and stiffness matrices of the entire configuration; $A_{i,j}, B_{i,j}$, are the hydrodynamic masses and potential damping of the entire configuration; F_i are the exciting forces acting on the multi–body system at the i –th direction; $F_{P,i}$ are the pressure hydrodynamic forces acting on the multi–body system at the i –th direction; x_{j0} is the motion displacement of the entire OWC system at the j –th direction with respect to a global co – ordinate system G .

By inserting the TLP mooring system and the W/T characteristics in the multi – body system, Eq17 can be reduced to the following form (Mazarakos et al. 2014a), describing the couple hydro – aeroelastic problem of the investigated

moored multi-purpose floating structure in the frequency domain:

$$\sum_{j=1}^6 \left[\begin{array}{c} -\omega^2 (M_{i,j} + A_{i,j} + M^{WT}) \\ + \frac{i}{\omega} B_{i,j} + \frac{i}{\omega} B_{i,j}^{WT} \\ + C_{i,j} + C_{i,j}^{WT} + C_{mooring} \end{array} \right] \cdot x_{j0} = \quad (18)$$

$$= F_i + F_{P,i}$$

where M^{WT} , B^{WT} and C^{WT} , are the mass, damping and stiffness which contribute the W/T aerodynamic, inertial-gyroscopic and gravitational loading respectively, while $C_{mooring}$ is the mooring lines stiffness matrix.

The RAO's can be estimated from time series data from the following equation:

$$RAO(\omega) = \frac{|P_{xy}(\omega)|}{P_{xx}(\omega)} \quad (19)$$

where P_{xx} is the auto power spectral density and P_{xy} is the cross spectral density. P_{xx}, P_{xy} are calculated using Welch's method with a sufficient number of data split and 50% overlap between the split data parts. x refers to the input (wave elevation) and y to the output (each motion). The simulations lasted 3600sec - the first 600sec are excluded – assuming a uniform wind speed and white noise waves of 1m significant wave height.

4. NUMERICAL MODELING

4.1 Eigen values

In Table 1 the first 12 eigenvalues of the coupled system are presented, as provided by hydroGAST. In the flexible case, the flexibility of the W/T's members (tower, shaft, blades) is considered, while in the rigid case the members are stiff. The rigid case corresponds to the frequency domain analysis as well, because

only the 6 rigid modes of the floater are considered.

The main differences, between the two cases, are: the reduction of the roll/pitch eigenvalues from 0.3 Hz to 0.25 Hz and the presence of the tower fore-aft and side-to-side frequencies at ~ 0.85 Hz. Flexibility is important in the TLP case due to the strong coupling between the roll/pitch motion and the side-to-side/fore-aft bending moments of the tower. The modes of the blades and the shaft are not coupled with the motions of the floater, so they are not expected to appear in the RAOs.

Table 1: Coupled system eigen values [Hz]

Mode description	flexible	rigid
Platform Surge	0.026	0.026
Platform Sway	0.026	0.026
Platform Yaw	0.028	0.028
Platform Roll	0.244	0.301
Platform Pitch	0.245	0.301
Platform Heave	0.569	0.569
1st Drivetrain Torsion	0.585	-
1st Blade Flapwise Yaw	0.634	-
1st Blade Flapwise Pitch	0.653	-
1st Blade Collective Flap	0.702	-
1st Tower Fore-Aft	0.854	-
1st Tower Side-Side	0.861	-

4.2 RAO's comparison

Frequency and time domain methods consistently predict similar RAOs, in the case of a TLP floating W/T (Mazarakos et al. 2014b). In the present paper, RAOs for the TLP floating W/T with 3 OWC devices predicted by the frequency domain (fd) and the time domain (td) method are compared. Two inflow conditions are modelled; the zero wind speed case where the rotor is still and the 11.4 m/s case

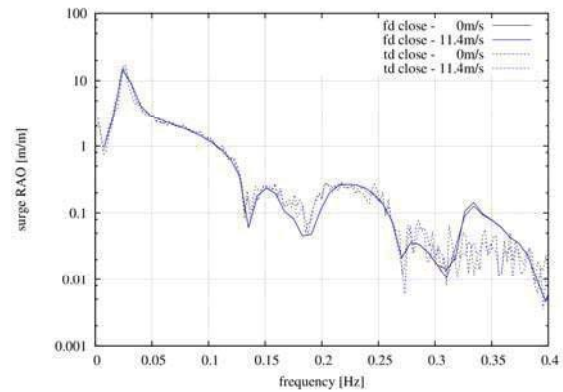


Figure 4: Surge RAO's comparison

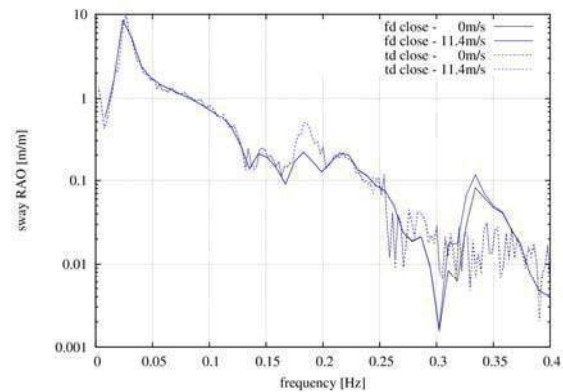


Figure 5: Sway RAO's comparison

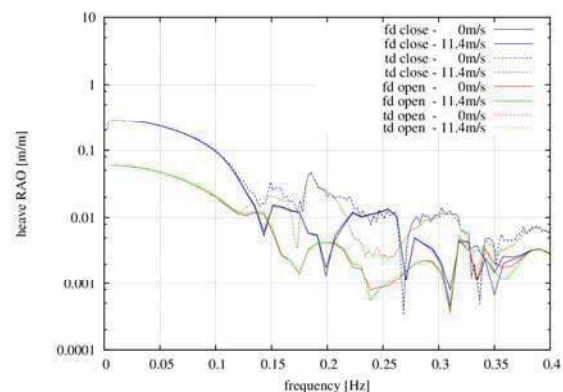


Figure 6: Heave RAO's comparison

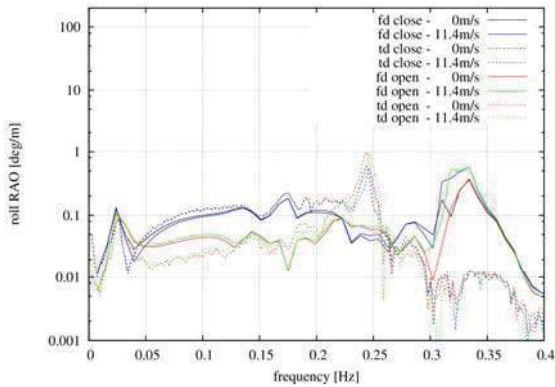


Figure 7: Roll RAO's comparison

which corresponds to the rated wind speed at which the rotational speed is 12 rpm. The wave heading angle is 30 deg.

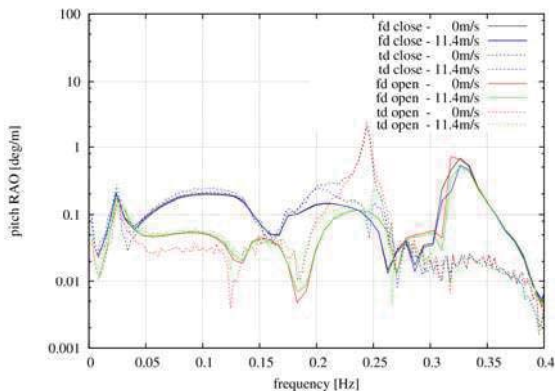


Figure 8: Pitch RAO's comparison

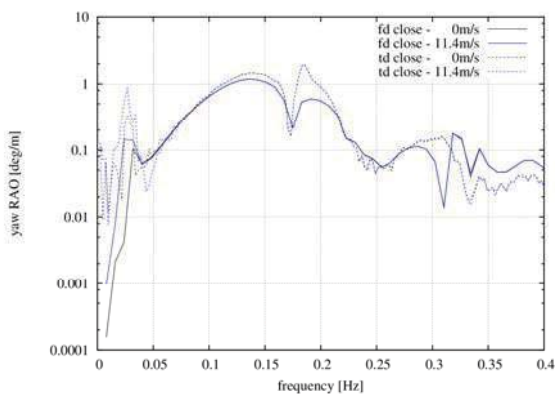


Figure 9: Yaw RAO's comparison

The 'open' case RAOs plots in the heave, roll and pitch motions correspond to the case where the OWC does not contribute additional pressure terms. The surge, sway and yaw RAO's are not affected by the OWC. Time domain simulations consider additional elastic degrees of freedom and nonlinear modeling of the aerodynamics, the complete dynamics, the mooring lines and the viscous term of the Morison's equation. Both methods consider the same linear hydrodynamic theory.

In general both methods predict similar RAOs and the eigen frequencies of table 1 are clearly identified. Focusing on the differences, in the frequency domain results the surge-pitch and the sway-roll coupling at 0.35 Hz are excited, contrary to that shown in the time domain ones (Figures 4, 5). Excellent agreement is observed in the heave motion (Figure 6) up to 0.15 Hz. At higher frequencies the heave exciting force, which is not presented due to space limitation, is almost zero and explains the difference. In the roll and the pitch motions (Figures 7, 8) the reduction of the natural frequency is clearly depicted, as already discussed in section 4.1. Both methods capture the reduction of the roll and pitch amplitudes at the corresponding eigen frequencies due to the aerodynamic damping. The influence of the aerodynamic damping in the time domain predictions is by far more significant due to nonlinear aerodynamics. It is noted that viscous drag could not be the reason, because it is present in the 0 wind case as well, in which the amplitudes are high and comparable to those in the frequency domain results. The OWC also does not seem to influence the peak amplitude, as the roll and pitch eigen frequencies are outside the wave region. In the range of the wave frequencies, the amplitudes of the heave (Figure 6) and the roll/pitch (Figures 7, 8) motions are more excited when the contribution of the OWC is considered. Finally, the time domain method predicts slightly higher yaw amplitude RAOs. Both methods capture the gyroscopic effects at



~0.03 Hz where the rotation of the blade increases the yaw motion.

5. CONCLUSIONS

A TLP floater supporting the NREL 5MW RWT and 3 OWC devices has been analyzed. For this design, RAO's of the complete system have been calculated using frequency as well as time domain simulations.

By comparing the results from the two methods, the following conclusions were drawn:

1 Both methods consistently predict the system RAO's, which gives confidence to the specific frequency domain approach as a preliminary design tool.

2 The frequency domain method does not include structural flexibilities which affect the roll/pitch RAO's. The natural frequency in roll/pitch for the rigid WT is 0.3Hz, while for the flexible WT is 0.25Hz and the tower bending frequencies about 0.85Hz. On the other hand roll and pitch is very small for a TLP - in time domain calculations do not exceed 0.1 deg. - and not within the wave frequency range.

3 As regards the design, it seems difficult to increase the roll/pitch natural frequencies above 0.25 Hz and keep the cost reasonable, due to the strong coupling with the tower that is counteracting.

4 Both methods capture the aerodynamic damping that reduces the amplitude of the roll/pitch motions around resonance and the gyroscope effect affecting the yaw amplitude.

5 The roll and pitch RAO's amplitudes near resonance as predicted by the time domain method are smaller, most probably due to aerodynamic nonlinearities, and not viscous damping as was initially supposed.

6 The action of the OWC devices increase heave, roll and pitch RAO's. In this respect, the IEC load cases should be performed in time domain.

6. ACKNOWLEDGMENTS

This research has been co-financed by the European Union (European Social Fund – ESF) and Greek national funds through the Operational Program "Education and Lifelong Learning" of the National Strategic Reference Framework (NSRF) 2007 – 2013: Research Funding Program: ARISTEIA, Program POSEIDON (2041).

7. REFERENCES

- Aubault, A., Alves, M., Sarmiento, A., Roddier, D., Peiffer, A., 2011. Modeling of an oscillating water column on the floating foundation WINDFLOAT; Proceedings, 30th International Conference on Ocean, Offshore and Arctic Engineering (OMAE2011), Rotterdam, The Netherlands.
- Evans, D.V., Porter, R., 1996. Efficient calculation of hydrodynamic properties of OWC type devices; OMAE–Volume I – Part B; p. 123–132.
- Falnes, J., 2002. Ocean waves and oscillating systems: linear interactions including wave-energy extraction; Cambridge University Press.
- Jonkman, J., Butterfield, S., Musial, W. and Scott G., 2009 Definition of a 5-MW Reference Wind Turbine for Offshore System Development, Technical Report, NREL/TP-500-38060, USA.
- Konispoliatis, D.N., Mavrakos, S.A., 2013 a. Hydrodynamics of multiple vertical axisymmetric OWC's devices restrained in waves; Proceedings, 32nd International



- Conference Ocean, Offshore and Arctic Engineering (OMAE2013), Nantes, France.
- Konispoliatis, D.N., Mavrakos, S.A., 2013 b. Hydrodynamics of arrays of OWC's devices consisting of concentric cylinders restrained in waves; Proceedings, 10th European Wave and Tidal Energy Conference (EWTEC 2013), International Conference Ocean, Aalborg, Denmark.
- Manolas, D., Riziotis, V., Voutsinas, S., 2012. Assessment of 3D aerodynamic effects on the behaviour of floating wind turbines, The science of making torque from Wind, TORQUE 2012, Oldenbourg, Germany.
- Martins-rivas H. & Mei C.C., 2009. Wave power extraction from an oscillating water column along a straight coast. In: Ocean Engineering 36; p. 426–433.
- Mavrakos, S.A. & Koumoutsakos, P., 1987. Hydrodynamic interaction among vertical axisymmetric bodies restrained in waves; Applied Ocean Research, Vol. 9, No. 3.
- Mavrakos, S.A., 1991. Hydrodynamic coefficients for groups of interacting vertical axisymmetric bodies; Ocean Engineering, Vol. 18, No. 5, p. 485–515.
- Mavrakos, S.A., Chatjigeorgiou, I.K., Mazarakos, T., Konispoliatis, D.N, Maron, A., 2011. Hydrodynamic forces and wave run-up on concentric vertical cylinders forming piston-like arrangements; Proceedings, 26th International Workshop on Water Waves and Floating Bodies, Athens, Greece.
- Mazarakos, T.P., Mavrakos, S.A., Konispoliatis, D.N., Voutsinas, S.G., Manolas, D., 2014a. Multi- purpose floating structures for offshore wind and wave energy sources exploitation. COCONET Workshop for Offshore Wind Farms in the Mediterranean and Black Seas, Anavyssos- Greece, 9- 10 June 2014.
- Mazarakos, T.P., Manolas, D.I., Grapsas T., Mavrakos, S.A., Riziotis V.A., Voutsinas S.G., 2014b, Conceptual design and advanced hydro-aero-elastic modeling of a TLP concept for floating wind turbine applications. RENEW 2014, Lisbon, Portugal.
- Newman, J.N., 1977. The motions of a floating slender torus; J. Fluid Mech, Vol. 83, p. 721–735.
- Okhusu, M., 1974. Hydrodynamic forces on multiple cylinders in waves; Int. Symp. on the Dynamics of Marine Vehicles and structures in Waves, University College London, London.
- Papadakis, G., Riziotis, V., Voutsinas, S., Mavrakos, S.A., 2014. W/T's reduced order aeroelastic models (in Greek). Technical Report No. D3.2, Program POSEIDON (2014), Greek General Secretariat for Research and Technology.
- Popko et al., 2012. Offshore Code Comparison Collaboration Continuation (OC4), Phase I – Results of Coupled Simulations of an Offshore Wind Turbine with Jacket Support Structure, ISOPE 2012, Rhodes, Greece.
- Riziotis. V.A., Voutsinas, S.G., 1997. GAST: A general aerodynamic and structural prediction tool for wind turbines. Proceedings of the EWEC' 97, Dublin, Ireland, 1997.
- Riziotis, V., S.G. Voutsinas, E.S. Politis, P.K. Chaviaropoulos 2004. Aeroelastic Stability of Wind Turbines: the problem, the methods, the issues”, Wind Energy, 7, pp 373-392.
- Robertson Amy et al., 2014. Offshore code comparison collaboration, continuation within IEA wind task 30: phase II results regarding a floating semisubmersible wind system, OMAE 2014, San Francisco, USA.



Twersky, V., 1952. Multiple scattering of radiation by an arbitrary configuration of parallel cylinders; J. Acoustical Soc. of America, 24 (1).

This page is intentionally left blank

Session 14 – 40 YEARS OF STABILITY

SOTA on Damage Stability of Cruise Ships – Evidence and Conjecture

SOTA on Dynamic Stability of Ships – Design and Operation

SOTA on Intact Stability Criteria of Ships – Past, Present and Future

This page is intentionally left blank



Damage Survivability of Cruise Ships – Evidence and Conjecture

Dracos Vassalos, *The Ship Stability Research Centre, Department of Naval Architecture, Ocean
and Marine Engineering, University of Strathclyde, Glasgow, Scotland, UK,*

d.vassalos@strath.ac.uk

ABSTRACT

This paper delves into damage stability legislation as it applies to passenger ships. The Concordia accident, like many others before it, has shaken the maritime profession once again with many questions being asked without being able to provide credible answers. Old ships have been designed to lower standards (it is common knowledge that new ships are safer than old ships, with the latter comprising the majority of the population), new standards are holistic and goal-based offering knowledge of the standard these ships are designed to, which is not true for old ships, emergency response is an altogether different science in modern ships and many others. Notwithstanding this state of affairs, there is another more fundamental weakness in the regulations for damage stability, perhaps at the heart of most problems with cruise ships safety, old and new. A critical review into damage stability legislation, as it applies to passenger ships, offers compelling evidence that cruise ship characteristics and behaviour have not been accounted for in the derivation of relevant damage stability rules. As a result, the regulatory instruments for damage stability currently in place do not provide the right measure of damage stability for cruise ships and, even more worryingly, the right guidance for design improvement. This leads to a precarious situation where cruise ships are underrated when it comes to assigning a damage stability standard whilst depriving designers of appropriate legislative instruments to nurture continuous improvement. Documented evidence is being presented and the ensuing results and impact discussed. Recommendations are given for a way forward.

Keywords: *damage stability and survivability, cruise ships*

1. INTRODUCTION

SOLAS regulations is the Bible of safety and like the latter, it is considered “holy” by many and it will take endless debates to change a line, even though the former has been written, in the best of circumstances, by naval architects not yet canonised. A passenger ship is a vessel carrying 12 or more passengers (... and is involved in international trade), irrespective of size, shape, age, construction and condition. This state of affairs has served the maritime industry well for over a century, as it has taken

half as long for all concerned to realise that current rules are becoming progressively less relevant and amendments have run their course. The Secretary General of the International Maritime Organization (IMO) Koji Sekimizu, realising fully this state of affairs has set 2029 (the 100th anniversary of SOLAS) as the date by which a new, more relevant, SOLAS will be introduced. Sadly, he is leaving in less than a year’s time and the chance that another Naval Architect will be filling his shoes is slim. In the interim, we have reached the embarrassing situation of having to conceal knowledge on the fact that treating all IMO-defined passengers ships the same, is alienating the



profession when it comes to developing and setting standards for damage stability. It is certain there are many other “anomalies” in SOLAS concerning all sort of different issues but damage stability is big enough a subject when it comes to passenger ships to consider it in isolation. More specifically, there is documented evidence to demonstrate that passenger ship damage stability rule development to date is based almost 100% on RoRo Passenger vessels and this has led to an unfathomable situation where cruise ship safety is underrated by the rules whilst rendering any attempts to improve damage stability of cruise ships futile, using current IMO cost-effectiveness criteria for decision making. This is a precarious position for the cruise ship industry to be in for both the safety-cultured and the rule-evading owners; the former because the current regulatory framework does not justify improving cruise ship safety, which we know cannot be right, and the latter because newbuildings cruise ships can easily meet the common “passenger ships pool” regulations and are relaxed in this futility. This situation must change. We must change it. As Naval Architects, we owe it to the travelling public, who board these ships by the thousands at a time.

2. PROBABILISTIC CONCEPT OF SHIP SUBDIVISION

2.1 Conceptual Formulation

A direct link between the probabilistic concept of ship subdivision and modern concepts of risk estimation may simplistically be expressed as follows:

$$R_c = P_c \times P_{w/c} \times P_{f/w/c} \times P_{l/f/w/c} \quad (1)$$

Where:

P_c Probability of a collision event, dependent on loading condition, area of

operation, geography, topology, bathymetry, route, traffic density, ship type, human factors, etc.;

$P_{w/c}$ Probability of water ingress, conditional on collision event occurring (accounting for all the above);

$P_{f/w/c}$ Probability of failure (capsize / sinking / collapse), conditional on collision and water ingress events occurring – expressed as a function of e.g., sea state, structural strength and time;

$P_{l/f/w/c}$ Consequences (Probability of Loss) deriving from the collision event, conditional on all the foregoing; this accounts for loss of (or injury to) life, property damage / loss and impact to the environment. The former will depend on time to capsize and time to abandon ship (as determined from evacuation analysis – passenger ships) and the latter of e.g., probabilistic oil outflow using relevant models of oil spill damages and results from known accidents or through analysis using first-principles tools.

Considering the above and on the basis of work by (Lutzen, 2001), the relevant probabilities can be calculated from first-principles. Hence, if a more specific analysis is warranted for a novel ship design concept, the probability of collision damage that leads to hull breaching and flooding can be calculated. Moreover, based on work reported in (Jasionowski and Vassalos, 2006) and (Dogliani, et al., 2004), the various terms in [1] could also be addressed for each pertinent scenario from first principles. This allows for complete risk analysis of any damage case.



2.2 Basic Formulation (SOLAS 2009)

One of the fundamental assumptions of the probabilistic concept of ship subdivision in SOLAS 2009 is that the ship under consideration is damaged, i.e. the hull is assumed to be breached and there is (large scale) flooding. This implies that the cause of the breach, the collision event and the circumstances leading to its occurrence are disregarded; hence the interest focuses on the conditional probability of survival. Other pertinent factors, such as size of ship, number of persons on board, life-saving appliances arrangement, and so on, are directly or indirectly accounted for by the Required Index of Subdivision R. Therefore, the probability of ship surviving collision damage is given by the Attained Index of Subdivision, A, using the following expressions:

$$A = \sum_{j=1}^J \sum_{i=1}^I w_j \cdot p_i \cdot s_i \quad (2)$$

Where,

$j =$ represents the loading conditions (draught) under consideration

$J =$ is the number of loading conditions considered in the calculation of the attained index (normally 3 draughts)

w_j is weighting factor for each draught;

i represents each compartment or group of compartments under consideration for loading condition j

I is the set of all feasible flooding scenarios, comprising single compartments and groups of adjacent compartments for loading condition j ; The sum is taken for all cases of flooding in which one, two, three or more adjacent compartments are involved.

P_i is the probability that, for loading condition j , only the compartment(s) under consideration are flooded weighted by the probability that the space above a horizontal subdivision may not be flooded (note that $\sum p_i = 1$ for each draught considered)

s_i is the (conditional) probability of surviving the flooding of compartment(s) under consideration for loading condition j

The summation in equation (2) covers only flooding scenarios for which both p_i and s_i are positive (i.e., survivable scenarios, which contribute to the summation). In other words, A is the weighted average “s-factor”, with “p-factors” being the weights, i.e.:

$$A = \hat{E}(s) \text{ on } I \quad (3)$$

The Attained Index of Subdivision, A, must be greater than the Required Index, R, as specified by the regulations, i.e.:

$$A > R \quad (4)$$

Deriving from the above, it is further implied that two different ships achieving the same Attained Index of subdivision are equally safe. The philosophy behind the probabilistic concept is that two different ships with the same index of subdivision have equal *overall* capacity to resist flooding following collision, although these ships may have quite different actual capabilities to withstanding individual damage scenarios (*local*) in addition to being subjected to different collision risk altogether. Therefore, it is this summary statistic that is the key.

Having said this, there is a profound knowledge hidden in the basic formulation of the probabilistic rules for damage stability, especially when the targeted population is



cruise ships, carrying thousands of people onboard. In this case, given that capsizing or sinking of any such ship will be catastrophic, the emphasis in the risk model shifts towards damage limitation rather than reducing the probability of such an event taking place. Hence, the emphasis by (Wendel, 1968) on Index-A alone. This is key to understanding Wendel's formulation and to ensuring that no effort will be spared with e.g., large cruise ships to making A as close to 1 as possible.

Considering (1) and (3) and allowing for large time intervals, it is apparent that

$$R_{1/f/w/c} = (1-A) \quad (5)$$

This means that Index A is the marginal probability for time to capsize within certain time, assuming that the time being considered is sufficiently long for capsizing to have occurred in the majority of cases. This is a key observation, as this can be used to derive the flooding risk contribution, as indicated in the following. However, the assumption on time being sufficiently long is critical.

Finally, the Required Index of Subdivision, R represents the "level of safety" associated with collision and flooding events that is deemed to be acceptable by society, in the sense that it is derived using ships that society considers fit for purpose, since they are in daily operation.

3. STATUTORY A-INDEX CALCULATION (SOLAS 2009)

3.1 Capsize band

Capsize band is a concept describing the transition of sea-states from those at which no capsizing is observed (lower boundary) to those at which the probability of capsizing equals unity (upper boundary). In simpler terms, it is a band outside which capsizing is either unlikely to happen or certain. For a finite observation time,

the probability of capsizing can be approximated either as a sigmoid function (Tsakalakis et al, 2010) or alternatively as a Gaussian distribution (Jasionowski et al, 2007). Significantly, it can be observed that as the time of observation increases the capsizing band contracts towards its lower boundary, becoming a unit step function as time approaches infinity (Figure 1). This property is of major importance, particularly when the focus is cruise ships where the time it takes the vessel to capsize is normally much longer than the current SOLAS-based evaluation of 30 minutes. In this respect, $H_{S,Crit}$ is associated with the sea state at which the probability of capsizing (P_f) is equal to 0.5, based on 30-minute tests.

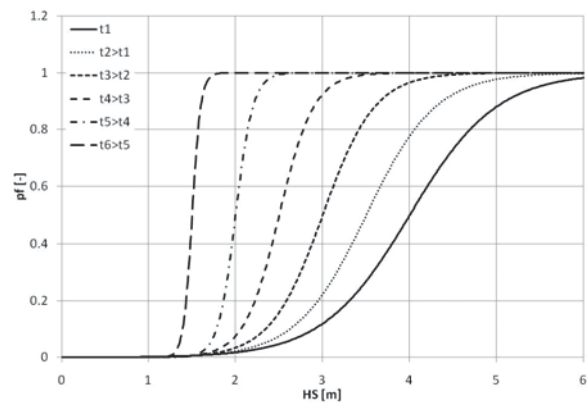


Figure 1: Capsize band as function of the observation time.

3.2 Survival Factor-s (Projects HARDER and GOALDS)

Although it is not explicitly stated in SOLAS, the s-factor is a measure of the probability of survival of a damaged ship in waves, namely:

$$s = \int_0^{\infty} dH_S \cdot f_{H_S|coll}(H_S) \cdot F_{surv}(H_S) \quad (6)$$

Where: $f_{H_S|coll}(H_S)$ is the probability density distribution of sea states expected to be encountered during collision and $F_{surv}(H_S)$ is



the probability of survival in that sea state when exposed to a specific flooding case. More importantly, deriving from the observations made in 3.1 above, the probability of survival is in fact a conditional probability:

$$F_{surv}(H_S) \equiv F_{surv}(t = 30 \text{ min} | H_S) \quad (7)$$

This yield:

$$s(t = 30 \text{ min}) = \int_0^{\infty} dH_S \cdot f_{H_S|coll}(H_S) \cdot F_{surv}(t = 30 \text{ min} | H_S) \quad (8)$$

Furthermore, it has been assumed that the probability of survival, $F_{surv}(H_S)$ can be approximated by a step function centred on the sea state. That is, the $H_{S,crit}$ constitutes the 50th percentile of the significant wave height the vessel, subjected to a particular damage scenario, can survive for 30 minutes (this corresponds to the abscissa of the inflection point of the sigmoid that defines the capsizing band, obtained for $t=30\text{min}$). In Project GOALDS, the capsizing band itself was substituted by a step function, as outlined next:

$$F_{surv}(H_S) = \begin{cases} 1 & \Leftrightarrow H_S \leq H_{S,crit} \\ 0 & \Leftrightarrow H_S > H_{S,crit} \end{cases} \quad (9)$$

On the basis of this, the final formulation becomes:

$$s = \int_0^{H_{S,crit}} dH_S \cdot f_{H_S|coll}(H_S) = \exp(-\exp(0.16 - 1.2 \cdot H_{S,crit})) \quad (10)$$

Where the $H_{S,crit}$ is given as:

$$H_{S,crit} \Big|_{t=30\text{min}} = 4 \left(\frac{\min(GZ_{\max}, 0.12)}{0.12} \frac{\min(Range, 16)}{16} \right) = 4 \cdot s(t = 30 \text{ min})^4 \quad (11)$$

In essence, the approach adopted within the GOALDS Project is similar to that of the HARDER project with the main difference stemming from the assumption of $H_{S,crit}$ corresponding to the lower limit of the capsizing band, thus allowing for a justified assumption of very long (“infinite”) time of survival. Therefore, the limiting assumption of short survival time, implicit in the formulation of HARDER has been addressed properly in GOALDS. This makes the GOALDS s-factor formulation better suited to cruise ships than the current SOLAS formulation.

Moreover, in the analysis of results pertaining to small and large vessels (sample ships in Project GOALDS), it was made apparent that there is a significant effect deriving from scale. Indeed, one of the major concerns related to SOLAS 2009 formulation for the s-factor was that it does not account for the ship size and that it might be inaccurate when applied to vessels deviating significantly from the size of the test vessels used in HARDER as basis for its derivation. In addition, the fact that the SOLAS 2009 s-factor formulation (residual GZ curve characteristics) is limited to relatively small range and maximum GZ values fails to account for the contribution of watertight volume distributed high enough not to be “seen” by the formulation. This, in essence deviates from normal Naval Architecture practice, previously expressed through the explicit demand for and provision of residual/effective freeboard.

Accounting for the above and using a systematic approach based on applying Design of Experiments (DoE), the formulation finally proposed is given by the following expression (Cichowicz, et al. 2011):

$$H_{S,crit} = \frac{A_{GZE}}{\frac{1}{2} GM_f \cdot Range} V_R^{1/3} \quad (12)$$

And,



$$s(H_s) = \begin{cases} e^{-e^{(0.16-1.2H_s \text{ crit})}}, & \forall (A_{GZ}, V_R, Range, k > 0) \\ 0, & \text{otherwise} \end{cases} \quad (13)$$

Where $A_{GZ E}$ is an effective area under the GZ curve taken up to the heel angle corresponding to the submersion of the opening in question and V_R is the residual volume mentioned above; GM_f is residual metacentric height. This formulation, by incorporating residual volume accounts for the effect of scale on one hand whilst on the other incorporates a key feature of the cruise vessels, namely residual volume high up in the vessel, which is a key characteristic of modern cruise vessel design.

The overall improvement between Projects HARDER (SOLAS 2009) and GOALDS, pertaining to cruise ships, is best visualised (hard evidence) in Figure 2 next.

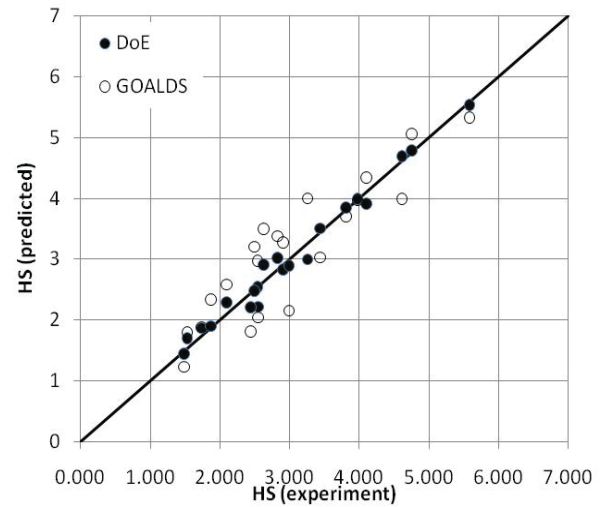
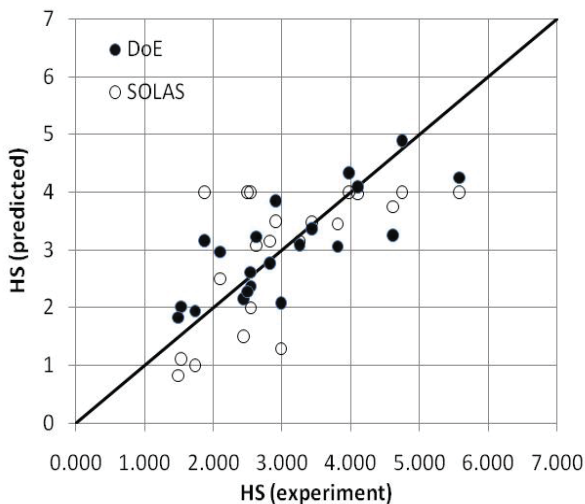


Figure 2: Comparison between predicted and experimental survivability results, using SOLAS 2009 (HARDER - Top) and (GOALDS - bottom) s-factor formulations.

As indicated in the introduction, the formulation for the s-factor in current SOLAS is based almost exclusively on results of either RoPax or cargo ships. The one cruise ship used in GOALDS provides evidence that the SOLAS formulation for s-factors

- (a) Does not relate to cruise ships and, this fact leads to another truth, namely that
- (b) Current SOLAS does not account for the known survival resilience of cruise ships

Figures 3 and 4 next provide rare evidence.

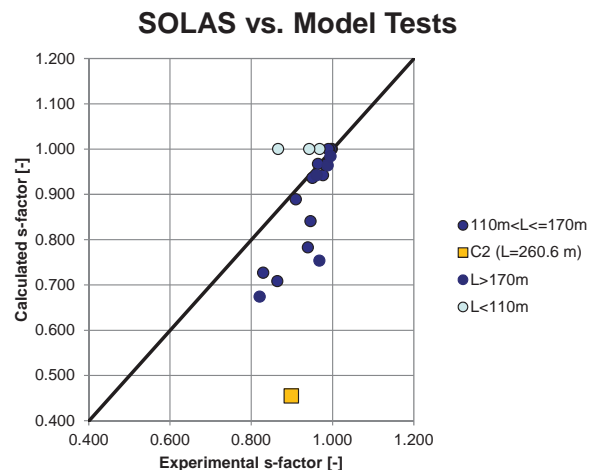


Figure 3: Comparison between predicted and experimental survivability results, using SOLAS 2009 (HARDER) s-factor formulation

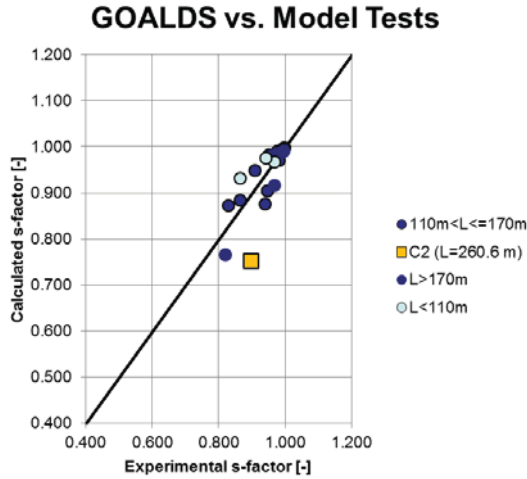


Figure 4: Comparison between predicted and experimental survivability results, using Project GOALDS s-factor formulation

In this light, it is important mentioning here that similar to Project GOALDS, the formulation of the s-factors for the current SOLAS formulation (Project HARDER) contains only one survivability experiment of a cruise ship, which again illustrates higher capsizes resilience (Figure 5). The graph also illustrates that the s-factor in current SOLAS is, in fact, based on cargo ships results!

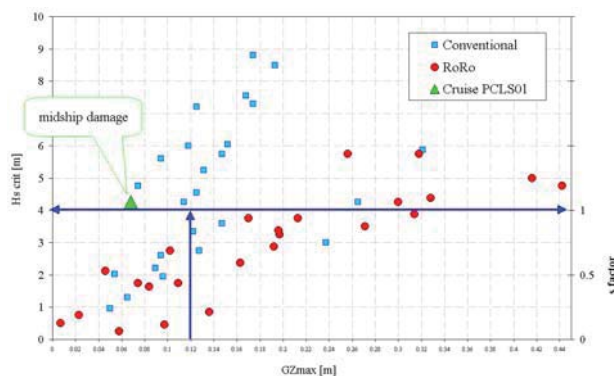


Figure 5: Experimental damage survivability results used to support SOLAS 2009 (HARDER) s-factor formulation

4. DIRECT APPROACH A-INDEX DERIVATION

4.1 Approval of Alternative and Equivalents

With direct influence from regulations, and because of the level of effort that is still needed to implement Risk-Based Design (RBD) in full, the real innovation attributable to RBD is currently witnessed mainly at local level. Known as “Approval of Alternatives and Equivalents” (MSC.1/Circ. 1455, 24 June 2013), it is using the principle of equivalent safety to consider alternative design and arrangements other than those supported by SOLAS legislation. This has taken a more generalised character than initially envisaged, with legislative instruments currently in place to address Fire Safety (SOLAS II-2, Reg. 17, MSC/Circ.1002); Life Saving Appliances (SOLAS III/Reg. 38, MSC/Circ. 1238), Damage Stability (Ch. II-1, Re, 4) and general Approval of Equivalents (MSC/Circ. 1455).

This opens the door to using an equivalent approach to A-Index derivation, as reported in (Vassalos et al, 2008) and highlighted in the following.

4.2 Impact of Time to Capsize

As discussed earlier, the survival factor “s” is estimated based on the assumption that the ship capsizes within half an hour, deriving mainly from work on RoPax. This, however, is not the case with cruise ships and it will be of interest to have another introspective look into this with the view to ascertaining the impact of a more prolonged time to capsize. The time to capsize (t_c), is a random variable, hence only known as a distribution determined through probability methods. Moreover, it is dependent upon a number of parameters (e.g. flooding condition, sea state, damage extent) all of which are also random in nature. In this respect, accounting only for the damage case scenarios implicit in SOLAS 2009 (normally



over 1,000 for a typical passenger ship) and considering the 3 loading conditions, also implicit in the rules, and some 10 sea states per damage case, it becomes readily obvious that some form of simplification and reduction will be meritorious. In view of this, two lines of action have been pursued and two methods are currently available. The first relates to the development of a simple (inference) model for estimating the time to capsize, for any given collision damage scenario; the second entails automation of the process using Monte Carlo sampling of the random variables and time domain simulation, as outlined next.

Method 1: Univariate Geometric Distribution

Considerable effort has been expended over many years to develop an analytical expression, which could provide an overall description of the character of the stochastic process of ship capsize when subjected to collision damage in a seaway, (Jasionowski, et. al, 2004, 2006, 2008). The inference model used is based on a Univariate Geometric Probability (UGD) density distribution for time to capsize for each flooding scenario, where the only random variable being considered is the survival factor “s” as defined in SOLAS. Hence, the result will be subjected to the same limiting assumptions, inherent in the rules, e.g., applicable to scenarios where the time to capsize is short. Figure 6 presents a result for a typical ship at scenario level where using this simple inference model, it is possible to predict instantly the likelihood of a vessel to capsize within a given time in any given flooding scenario.

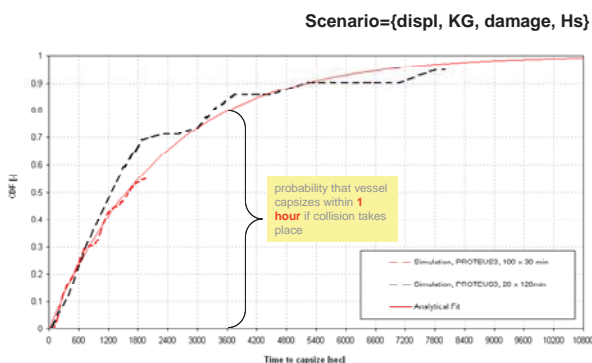


Figure 6: Cumulative probability function for time to capsize (scenario level) - Comparison between analytical model and numerical simulation results

Considering the ease of this operation, tens of thousands of scenarios may be considered to develop pertinent distributions at ship level, see Figure 7. Considering all flooding scenarios of interest for a typical ship, the outcome is the marginal cumulative probability distribution for time to capsize, shown in Figure 7.

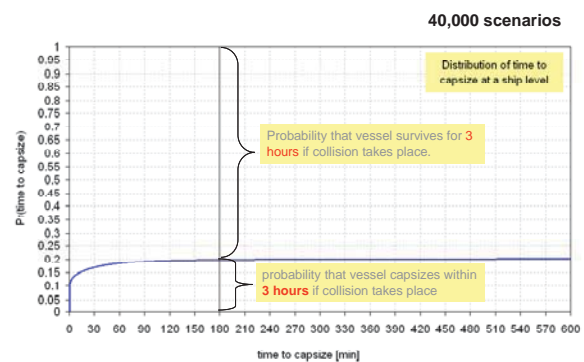


Figure 7: Cumulative marginal probability distribution for time to capsize within a given time

A close examination of Figure 7 reveals the following noteworthy points:

- If a vessel did not capsize within the first hour post-accident, capsize is unlikely, on average.
- The marginal probability distributions for time to capsize tends asymptotically (i.e., after infinite time, in principle) to values defined by (1-A), as indicated earlier.

Method 2 – Monte Carlo Simulation

To overcome problems associated with “averaging” the following approach may be adopted instead:

- Use of actual statistics (e.g., loading, sea state, damage size, survival time);
- Account properly for physical phenomena of ship motion and floodwater dispersion;

- Disclose ship attitude and behaviour as a function of time (including time to capsize);
- Aiming to avoid any “unnecessary” conservatism and other approximations and potential weaknesses embedded in the formulation of the probabilistic rules (e.g., heel limitations, down flooding points, etc.), the random variables distributions comprising loading conditions, sea states and damage characteristics are sampled using Monte Carlo Sampling and each ensuing damage scenario is simulated using explicit dynamic flooding simulation by PROTEUS3, (Jasionowski, 2005);
- Random variables to be considered would involve for collision: location, length, height, penetration according to the damage statistics adopted in the probabilistic rules and sea state. The resolution could be as high as necessary (every second of each scenario) accounting for transient- cross- and progressive-flooding, impact of multi-free surfaces, watertight and semi-watertight doors (relevant to cruise ships).

Applications of this method indicate that 500 scenarios would result in an absolute sampling error for the cumulative probability of time to capsize in the order of 4%-5%. Examples of Monte Carlo simulations setup are shown in Figures 8-9 for collision.

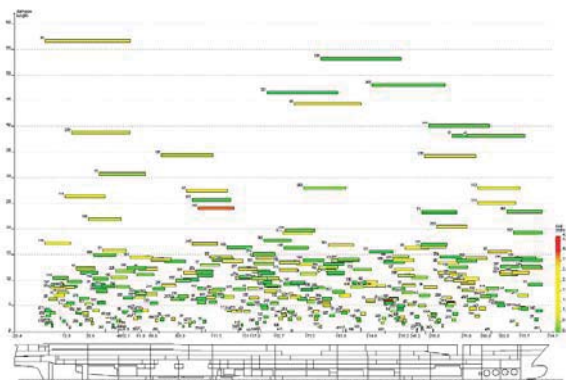


Figure 8: Monte Carlo Simulation Set up – Collision (342 scenarios) – Large Cruise Ship

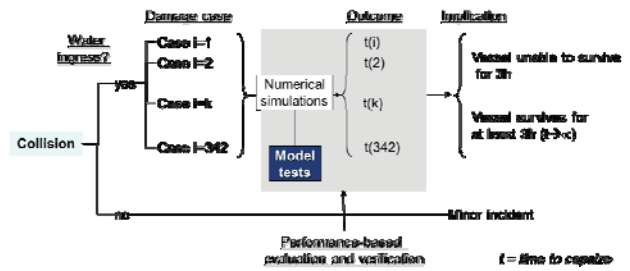


Figure 9: Monte Carlo Simulation and post-processing set up – Collision (342 scenarios) – Large Cruise Ship

Typical results are shown in Figures 10 and 11 for a RoPax and a Cruise Ship respectively as cumulative distribution functions of time to capsize. From the latter it will be seen that differences between the two methods of nearly an order of magnitude have been encountered and this led to renewed scrutiny of the probabilistic rules, as reported in (Vassalos and Jasionowski, 2007) that led to the EC-funded Project GOALDS.

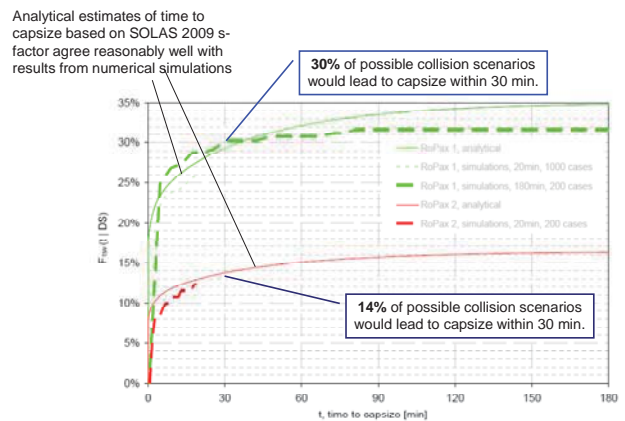


Figure 10: Probability Distributions of Time to Capsize (RoPax) – SOLAS 2009 Vs Direct Approach

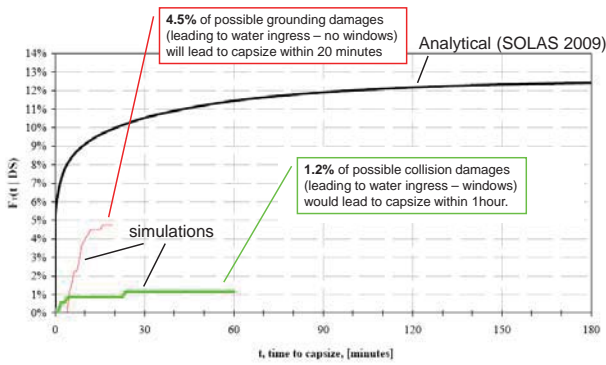


Figure 11: Probability Distributions of Time to Capsize (Cruise Ship) – SOLAS 2009 Vs Direct Approach

The results shown in the above figures offer another piece of evidence that the s-factor in current SOLAS does not represent the survivability of cruise ships by far. The fact that time to capsize for cruise ships is considerably longer than RoPax or indeed cargo ships on which the current SOLAS is based (i.e., half an hour) appears to have much larger impact on the ability to predict survivability of cruise ships than initially envisaged. Efforts to rectify this in Project GOALDS by encompassing cruise ship characteristics in the final formulation appear to have improved this situation as shown in Figure 12. However, the fact that only one data point related to a cruise ship was used in such derivation has not had as full an impact on the final formulation of the s-factor as focusing on cruise ships alone would bring.

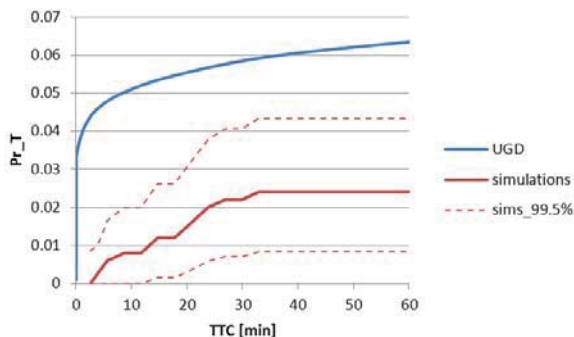


Figure 12: Probability Distributions of Time to Capsize (Cruise Ship) – GOALDS Project s-factor Vs Direct Approach

5. RECOMMENDATIONS FOR A WAY FORWARD

All the evidence available to date strongly suggests that the current SOLAS misrepresents the survivability of cruise ships. Continuing to group these with RoPax is no longer workable and more importantly largely unjustifiable. It is time to address survivability of cruise ships as a separate group of ships from RoPax. This will incentivise research to focus on these ships for the first time ever with the view to understanding the underlying characteristics that define survivability of cruise ships and to attempt to capture these in formulating and proposing a new s-factor for cruise ships. Following verification, application and calibration by the industry, this will lead to a legislative instrument, specifically for cruise ships, that will incentivise industry to seek continuous improvement and to facilitate designers in this quest. This time, it has to be the industry that takes initiative and leadership to put together a Joint Industry Project to target and accomplish this in a relatively short time. This is the only way forward!

6. CONCLUDING REMARKS

- The general formulation of the s-factor for cargo ships was adopted as the harmonised solution for both cargo and passenger ships. This is irrational considering that cruise ships are vastly different to both types of ships on which the formulation is based.
- SOLAS 2009 formulation considerably underestimates cruise ship survivability. This implies that due credit is not given to the damage resilience of cruise ships, which, in turn, affects industry image (ships being seen less safe than they actually are).
- SOLAS 2009 formulation does not support best-practice design, meaning that potential solutions for improving cruise



ship survivability will not be properly rated and hence dismissed. Adding to this is the risk of alienating the designers in that what they know to improve survivability in their designs does not appear to be justifiable.

- Emphasis on continuous safety improvement is, as a result, being hindered and safety culture undermined.
- The general formulation of the s-factor for cargo ships was adopted as the harmonised solution for both cargo and passenger ships. This is irrational considering that cruise ships are vastly different to both types of ships on which the formulation is based.
- SOLAS 2009 formulation considerably underestimates cruise ship survivability. This implies that due credit is not given to the damage resilience of cruise ships, which, in turn, affects industry image (ships being seen less safe than they actually are).
- SOLAS 2009 formulation does not support best-practice design, meaning that potential solutions for improving cruise ship survivability will not be properly rated and hence dismissed. Adding to this is the risk of alienating the designers in that what they know to improve survivability in their designs does not appear to be justifiable.
- Emphasis on continuous safety improvement is, as a result, being hindered and safety culture undermined.

7. REFERENCES

- Lutzen, M, 2006, "Damage Distributions, Report No.: 2-22-D-2001-01-1, Task 2.2, EU Project No: GRD1- Harder", November 2001, 66 pp.; also in: Ship collision damage, PhD thesis, Department of Mechanical Engineering, Technical University of Denmark, Lyngby.
- Jasionowski, A. and Vassalos, D., 2006, "Conceptualising Risk", STAB 2006, Rio de Janeiro, Brazil
- Dogliani, M, Vassalos, D and Strang, T, 2004, "Evacuation Notation – A New Concept to Boost Passenger Evacuation Effectiveness in the Cruise Industry", COMPIT 2004, 3rd Int. Euro-Conference on Computer Applications and Information Technology in the Marine Industries, Parador Sigüenza, Spain
- Wendel, K, 1968, "Subdivision of Ships", Diamond Jubilee International Meeting, New York, June 1968, pp 12-1 to 12-21.
- Tsakalakis, N., Cichowicz, J., Vassalos, D., 2010, "The concept of the capsized band revisited", 11th International Workshop on Stability of Ships and Ocean Vehicles, Wageningen
- Jasionowski, A, Dodworth, K, Vassalos, D, 1999, "Proposal for Passenger Survival-Based Criteria for Ro-Ro Vessels", International Shipbuilding Progress, Vol. 46, No 448
- Cichowicz, J, Tsakalakis, N, Vassalos, D and Jasionowski, A, 2011, "Survivability of Passenger Vessels - Re-engineering of the s-Factor", Proceeding of the 12th International Ship Stability Workshop, Washington D.C., USA.
- Vassalos, D, Jasionowski, A and Guarin, L, 2008, "Risk-Based Design: A Bridge too far?", OC 2008 Seakeeping and Stability, Osaka, Japan.
- Jasionowski A, Vassalos D, Guarin L, 2004, "Theoretical Developments on Survival Time Post-Damage", Proc. The 7th Int Ship Stability Workshop, Shanghai.



Jasionowski A, Bulian G, Vassalos D,
Francescutto A, Pawlowski, M, Maccari A,
2007, “Modelling survivability”,
SAFEDOR, D2.1.3, www.safedor.org.

Jasionowski, A, 2005: “An integrated approach
to damage ship survivability assessment”,
PhD, University of Strathclyde.

Vassalos, D and Jasionowski, A, 2007,
“SOLAS 2009 – Raising the Alarm”, 9th
International Stability Workshop, Hamburg,
Germany

SOTA on Dynamic Stability of Ships – Design and Operation

Jan Otto de Kat

This page is intentionally left blank



Intact Stability Criteria of Ships – Past, Present and Future

Alberto Francescutto, *University of Trieste, Italy*, francesc@units.it

ABSTRACT

This paper contains a brief excursus of the developments of intact stability of ships through the time from stone age, through historical period, modern age, renaissance, completion of the first intact stability code, beginning of development of 2nd generation intact stability criteria, present status and the foreseeable future developments.

Keywords: *Ship stability, 2nd generation stability criteria, ship safety*

1. INTRODUCTION

Sinking due to insufficient buoyancy and capsizing because of insufficient stability are two of the major threats to ship survivability at sea. The safety from sinking and capsizing is thus an important part of the safety of navigation with the entailed safety of life and protection of the environment in waterborne transportation. The two aspects had an extremely different development through history. As we will see, this is substantially due to the different perception of the immediacy of danger and to the very different entailment of physical and mathematical aspects in the two aspects. An important change in the perception was given by the change in propulsion, in particular the passage from sail ships to mechanical propulsion.

Due to the short time available, the paper is just a working scheme for presentation, mostly composed of quotations from relevant literature. The adopted nomenclature for historical periods doesn't conform to the standard use. It has been adapted by the author (Francescutto 1993, Francescutto 2004, Francescutto 2007) to the slow development of ship stability as a science.

2. FROM THE STONE AGE TO THE BEGINNING OF HISTORY

Man has travelled for thousands of years throughout the oceans without knowing how and why this was possible. Although the basic concepts of floatability and stability will have been known before, the basic laws of hydrostatics of floating bodies were introduced by the great Archimedes in 300 BC. It is well established that he was the first to formulate the basic law of buoyancy and eventually floatability. It was, however, only quite recently that it was found that he had also set the foundations of stability of floating bodies, namely by introducing the concept of the balance of couples of forces or moments.

The part of naval architecture known as buoyancy and stability is directly founded on the roots of Archimedes' principle, but it is not clear whether his early findings about the stability of floating paraboloids were generalized by himself to actual ship forms or not. What is certain, is the fact that, after some great scientific achievements in the Hellenistic era, there was a long silence (Russo, 2004). Gained knowledge remained unexploited for centuries (or was simply ignored and not



referenced) and it is not known what its impact on later developments in ship stability actually was. The development of ship stability as a science, indeed, occurred very late in the 18th century with two different approaches based on the introduction of the metacentre and the righting moment notions respectively. These approaches were developed respectively by Bouguer and Eulero.

3. THE BEGINNING OF HISTORY

Additional details on the similarities and differences between Bouguer and Eulero are contained in references [Nowacki 2001, Nowacki and Ferreiro 2003 and Francescutto and Papanikolaou 2011]. What is important to remark here is that, after the bright but isolated spot of Archimedes, the decisive progress of ship stability, as we know it now, came from the (mostly) geographer Bouguer while he was strolling up-and-down the Andes in search of a proof that Earth shape was following Descartes theories against Newton's theories. The result was the notion of metacentre, i.e. the upper limitation of the position of centre of gravity that guarantees the stability-in-the-small or initial stability.

It is important to note the observation made by Bouguer in the Preface to his book (Bouguer 1746): "Il n'était guère possible que l'Architecture navale, compliquée comme l'est par la multitude des diverses connoissances qu'elle suppose, fit des progrès aussi rapides que les autres parties de la Marine qui sont incomparablement plus simples. Il falloit non-seulement que les diverse Théories sur le mouvement dont elle dépend, & dont l'époque est assez recente, fussent portées plus loin, il étoit encore nécessaire que l'Analyse même & les methods géométriques qui devoient servir à réfoudre les grandes difficultés qui lui sont propres, parvinrent elles-mêmes à un degré de perfection qu'il ni a pas longtemps qu'elles ont acquis."

This witnesses the intrinsic physical and mathematical difficulties connected with the development of the subject. It is not casual that previous development was due to the best mechanician-mathematician of the ancient Greece (although he flourished in Magna-Grecia, present Italy...).

The work was completed by the Rev. Moseley (Moseley 1850) introducing the concept of dynamic stability in 1850: "Whence it follows that the work necessary to incline a floating body through any given angle is equal to that necessary to raise it bodily through a height equal to the difference of the vertical displacements of its centre of gravity and that of its immersed part, so that other things being the same, that ship is the most stable the product of whose weight by this difference is the greatest."

Quoting Barnes (Barnes 1861): "The first general theorem for the determination of the measure of a ship's stability was given by M. Bouguer, in his *Traité du Navire*, about a century ago. This measure of a ship's stability, although only strictly true when the angle of inclination from the upright is extremely small, yet gives the relative stabilities of ships of the usual form for a tolerably large angle of inclination with sufficient exactness for all practical purposes. Bouguer's measure, in consequence of the simplicity of the calculations for obtaining the height of the metacentre and its close approximation to the correct results, is that which is in general use: but a naval architect should also be familiar with the mechanical principles upon which the stability of a ship depends, and be able to determine the exact stability of a ship of any form whatever, at any given finite angle of inclination."

Unfortunately, the idea of Bouguer didn't have real practical applications. Notwithstanding fierce debates, mostly in the frame of the Institution of Naval Architects, as a consequence of the sudden sinking of the monitor *Captain* (designed by Cole) having a



higher metacentric height but a smaller freeboard giving a smaller range of positive stability with respect to the Monarch (designed by Reed). White and John (White and John 1871) comment: "In 1867 calculations were made at the Admiralty of the stability of two or three low-sided vessels, and the results were embodied in a Paper read by Mr. Reed at the Meetings of this Institution in 1868. With this Paper most of the Members and Associates are doubtless familiar. It showed conclusively that instability would occur in such vessels at a very moderate angle of inclination, and illustrated the contrast, as regards stability and safety, existing between rigged ships with high freeboard and those with low freeboard. ... This paper did not succeed, however, in impressing members of the profession with the necessity for more complete calculations of stability, and the subject remained in comparative obscurity until the loss of the Captain forced it into painful prominence."

The reasons for the absence of transformation of Bouguer intuition in practical (stability) rules are well explained by Rahola in his doctoral thesis: "Even the most recent of the fundamental laws that determine the amount of stability for a vessel are already about 200 years old. Consequently, it would seem natural that the estimating of a vessel's stability and the determining of its minimum amount should have drawn attention very early. However, that is by no means the case. Only about a hundred years after forming the principles for the theory of stability one began to understand, by reason of a certain accident having occurred, the great importance the stability qualities of a vessel have for its seaworthiness and non-sinking qualities. This earlier under-valuation of the stability circumstances appears at first sight difficult to explain, particularly when one compares the fortunes of this question with those of its parallel question, the development of the problem of preventing the overloading of vessels. ... The slight interest roused for the amount of a vessel's stability can in a way be explained very simply. So long as the wind was

the propelling force for the ships, one was obliged, without studying the matter theoretically, generally to have a comparatively high freeboard for the hull. This brought about at the same time that the range of stability became great. The master of a sailing ship was also aware at every moment of the approximate amount of the stability, because when sailing he constantly happened to perform some kind of inclining experiment with his vessel, even if it was primitive. It was therefore easy for the master to avoid imperiling the stability of his ship, and whenever he was tempted to load an excessive deck-cargo or otherwise reduce the stability, he probably did so well aware of the risk he was causing his vessel. ... The construction of a diverging type of vessel led to a flagrant violation of the building rules for well tested sailing vessels.

4. THE BEGINNING OF THE MODERN AGE

This is situated in the '30s of last century and is substantially based on two papers. First of all, Pierrottet (Pierrottet 1935) laid the foundations of what later will be the weather criterion. During his presentation in front of the Royal Institution, the following debate, illuminating about the general conception of stability at that time, was recorded: "The CHAIRMAN: I do not wish in the least to detract from the good work that Professor Pierrottet has done. I think the Paper will be very useful to us, but I do hope it will be a long time before it is made the basis for new Board of Trade regulations by the Classification Societies. The number of losses from capsizing is so exceedingly small, even more tiny than he says, that it would be a very stiff to impose these regulations. After all, when you had imposed them, the skipper might upset them all by his loading of the ship. There is the difficulty. I hope Professor Pierrottet will not assume that I am pouring too much cold water on his scheme, for I think you will agree with me that he has devoted his energy, brains and ability to producing an interesting and, I



believe, a useful Paper, and that we ought to accord him a very hearty vote of thanks”

PIERROTET: “To Sir Archibal Denny I would say that I think the problem of stability is rather neglected by ship designers. I can see danger in his recommendations of empirical, rather than scientific methods. If the proportions of bridges across rivers were decided empirically, I am sure that sooner or later there would be many a disaster. The limits of the field over which empirical methods can safely be applied are very vague. It is my opinion, therefore, that no effort should be spared to study scientifically the stability of ships, and to ensure that designers do not neglect its consideration. I am rather doubtful, moreover, if this object can be attained without the application of binding regulations. I quite agree that at 50° inclination nothing would remain still on deck, but that is not the problem : when a ship is unfortunate enough to acquire a list of 50° , the problem is not so much of how to keep all the passengers safely on board, but rather to prevent her from capsizing. I should not be adverse, though, to reducing the proposed 50° to some smaller figure.”

Second came the PhD Thesis of Rahola (Rahola 1939). It is a too important contribution to be summarized here, but it is important to consider at least the following couple of sentences from the introduction: “The object of the present investigation is to find a procedure by means of which it may be possible to judge with adequate certainty the amount of the stability of a certain vessel which may come to navigate under the conditions prevailing on the lakes and the waters adjacent to our country, and to decide whether it is sufficient or not.” ... “With regard to stability circumstances we must clearly make a distinction between the determining and the judging of stability.”

Almost contemporarily, the first issue of the Principles of Naval Architecture (Vincent 1939), in line with the thinking of the time, considering that still paid more attention to

comfort that to safety from capsizing: “Suitable Metacentric Height. Metacentric height is one of the fundamental features of a design and should have such a value that it will meet the following requirements:

(a) Large enough in passenger ships to prevent capsizing or an excessive list in case of flooding a portion of the ship during an accident.

(b) Large enough to prevent listing to unpleasant or dangerous angles in case all passengers crowd to one side. This may require considerable GM in light displacement vessels, such as excursion steamers, carrying large numbers of passengers.

(c) Large enough to minimize the possibility of a serious list under pressure from strong beam winds.

(d) Small enough to prevent violent rolling in waves. As explained in Chapter I, Volume 2, an excessive GM results in unpleasant rolling that may even be dangerous should the period of roll approximately synchronize with that of the waves. The traveling public is inclined to avoid vessels known to roll badly. Several large ships that were unpopular because they rolled badly have undergone costly major alterations to improve the condition.”

And following: “Damaged stability considerations may occasionally require excessive metacentric heights. Recognizing this, several formulas have been devised to establish the maximum GM that need be provided in the interest of safety. In the light condition modern passenger vessels ordinarily have very little positive GM, often not over 1 per cent of the beam, and many of the older liners have negative GM when light. For all classes of vessels there is an advantage in having at least positive GM in this condition, as such a vessel does not require as careful handling as one that has a negative GM. A few authorities insist upon at least positive GM in the light condition. The above views on the



maximum GM acceptable for passenger vessels are those of the author (S. A. Vincent) but not those of all naval architects and others interested in shipping. Some believe that a higher load GM should be used, if necessary to give adequate stability in the flooded condition.”

It is worth Noting that at the time, no substantial progress was still made by SOLAS, still involved in the development of subdivision rules after Titanic’s sinking, in addressing the issue of stability. Finally, concerning dynamic stability, in spite of the tremendous work done, mostly published in the Proceedings of the Institution of Naval Architects (PNA 1988) following Moseley: “The dynamical stability of a ship at a given inclination is defined as the work done in heeling the vessel to that inclination. Dynamical stability is rarely calculated in practical merchant ship design work, but is used in investigations of the motion of a vessel among waves, the list due to firing guns and similar problems.”

The far-looking intuitions of Rahola and Pierrottet, not to speak of Bouguer and Moseley, had to wait long time, respectively 30 and 50 years, and the birth of IMCO (later IMO), before becoming international regulations. Only starting with the 1988 edition the Principles of Naval Architecture dedicates due attention to minimum standards of intact stability: “In Chapter II more attention is given to stability curves and to criteria for acceptable stability based on them.”

5. THE FIRST GENERATION INTACT STABILITY CRITERIA

Provisions concerning intact ship stability have been introduced at a late stage in international regulations of ship safety. The need of intact stability rules was indeed uncertain until SOLAS 1948, where it was stated, in the Recommendations contained in Annex D:

“The Conference examined the need and the practical possibility of adopting rules relative to the intact ship stability. Considering that the rules adopted relatively to the damage stability have an influence on the intact stability of the ship, the Conference believes that, before establishing additional rules concerning intact stability, further experience to establish the extent to which such rules are necessary is needed. The Conference recommends therefore to the Administrations to examine in more detail the intact ship stability and to exchange information on such subject.”.

We have not to forget that the adopted rules for damage stability practically consisted in: “In the case of symmetrical flooding the residual metacentric height shall be positive, except that, in special cases, the Administration may accept a negative metacentric height (upright) provided the resulting heel is not more than seven degrees.”

The first international intact ship stability rule was originated by a recommendation contained in the conclusions of SOLAS’60: “The Conference, having considered proposals made by certain governments to adopt as part of the present Convention regulations for intact stability, concluded that further study should be given to these proposals and to any other relevant material which may be submitted by international Governments.

The Conference therefore recommends that the Organization should, at a convenient opportunity, initiate studies on the basis of the information referred to above, of:

- a) intact stability of passenger ships;
- b) intact stability of cargo ships;
- c) intact stability of fishing vessels, and
- d) standards of stability information...”



As a result, the General Stability Criteria based on righting arm characteristics was adopted by IMCO in 1968 as Res. A.167. Following Kobyliński (Kobyliński 1975): “In 1962 IMCO started its work towards the development of stability criteria for fishing vessels for small passenger and cargo vessels of less than 100 metres in length. The work was completed in 1968 the criteria were introduced by IMCO as recommendations”

The Weather Criterion was adopted in 1985 as Res. A.562. Again, this rule originated as an answer to a recommendation given in the conclusions of SOLAS'74: “(IMO) Recommends that steps be taken to formulate improved international standards on intact stability of ships taking into account, inter alia, external forces affecting ships in a seaway which may lead to capsizing or to unacceptable angles of heel”.

Weather Criteria were already enforced in several countries including Japan (Yamagata 1959) and Australia. We just mention here that present weather criterion was obtained merging the Japanese standard, which still constitutes the backbone, with the Russian standard especially for the evaluation of roll-back angle and the effect of appendages on roll damping.

Both criteria were based on ideas, concepts and ship typologies/dimensions, existing long before their adoption.

6. THE “RENAISSANCE”

The renaissance of Ship Stability in general and Intact Ship Stability in particular can be identified with the mid '70s of past century due to the intuition of Prof. Kuo from Strathclyde University that there was a diffuse greater sensitivity to the subject. In 1975 he organized *The International Conference on Stability of Ships and Ocean Vehicles* which was an unprecedented event with many consequences. In addition to gathering the experts on the subject, he organized a Questionnaire which is

of great interest to understand the feeling of that time. Almost all contributions to the Conference and to the Questionnaire should be mentioned in this paper, which is out of possibility. It is however important to remind the answers to selected questions:

Existing criteria (IMO Res. A.167): only 29% of respondents felt that the existing stability criteria based on the use of the righting arm curve met practical needs. Almost 50% felt that the criteria were unsatisfactory;

Main priorities: the two main priorities for research were seen as: (a) the effects of waves, and (b) the development of fresh methods for relating motion characteristics to stability criteria;

Metacentric height: a large majority of respondents considered such knowledge to be very important whereas the remainder thought that it was not important as long as it had a positive value. Of the respondents to the question on minimum metacentric height 55% of all respondents opted for 300 mm or more.

Several critical paper were developed to the existing Stability Criteria (mostly to the so-called statistical one represented by Res. A. 167, but also to the Weather Criterion, Res. A. 562, although its being partly a physical approach). Among these, since the beginning, there was Kobiliński (Kobiliński 1975), calling for “rational criteria”: “At the time IMCO started its work towards elaborating international stability criteria several countries introduced stability criteria going beyond the requirements of 1960 SOLAS Convention, All national requirements and regulations were carefully analysed, but the main source of inspiration for the evaluation of IMCO-Criteria was an analysis of casualty records and a comparison of the various stability parameters for vessels which capsized with those which were found safe in service. From all the stability parameters which could be used as stability criteria, the ones chosen for further analysis were those which lead to the lowest



position of KG. This was decided on the basis of statistics. ... It should be underlined, however, that the approach was a pure statistical one. Its main drawback was that the available data constituted only a small population of vessels. In consequence, the statistical analysis was not satisfactory. During the discussions at IMCO, the view was expressed several times that in future more rational stability criteria are needed. Rational stability criteria are understood to be those that can take into account the physical phenomena occurring during the ship's service and all external forces exerted on them. The development of such rational criteria is a long-term task and for this reason simpler statistical approaches are first adopted at IMCO."

This objective was further-on proposed by Francescutto (Francescutto 1993): "As we have seen, too often we assist the attempt to circumvent the actual stability rules, whose inadequacy and arbitrariness, on the other hand, has been declared by different authorities. It is difficult to change mental habits, but it is possible to intervene in the rules, not only to strengthen them, but to change the approach to ship safety. The conclusion is that the only way to overcome the many difficulties lies in the development of a system for the time domain simulation of ship motions in a seaway, including a detailed description of the environment and taking into account the non-linearities present and the dynamic effect of liquids with free surface in tanks, or on board as a result of deck wetness or damage. This will be called the *Physical Approach* to the hydrodynamic aspects of ship safety. Of course, it is a long term program involving the solution of many aspects connected with non-linear dynamics of motions and with the development of the non-linear hydrodynamics necessary to deal with large amplitude, transient asymmetric motions. The reason for the use of such a system as part of the design process from the beginning is to improve ship safety. This allows a further step in a procedure that usually uses optimization taking into account resistance, propulsion and

seakeeping only. In this way, the hydrodynamic aspects of ship safety could be treated in a probabilistic way, as pertains to their very nature, overcoming the actual approach based on 'simple, certain, rules'. This could allow the introduction of the concept of 'safety performance' and the development of training tools for safety. It is not clear at this point if this approach leads to much more restrictive rules, but it is clear that the rules will be more realistic and defensible.";

Spyrou (Spyrou 1998): "Whilst one might think of many different methods for assessing the behaviour of a system, there is little doubt that the most reliable are those which are based on sufficient understanding of the system's key properties. For ship stability assessment however the application of this principle has been, so far at least, less than straightforward; because the behaviour of a ship in an extreme wave environment, where stability problems mostly arise, is often determined by very complex, hydrodynamic or ship dynamic, processes."; and by Spyrou and Papanikolaou (Spyrou and Papanikolaou 2000): "Is it possible to use in ship design the latest findings from the modern analyses of capsizes based on the theory of nonlinear dynamics? This is the question which we are attempting to address in the present paper. Our goal is the establishment of a rigorous scientific basis for quantitative assessment of dynamic stability which will cover all the known types of ship capsizes. Our approach will be comprised of two levels: The first refers to a very early stage of design where it is desirable to have simple analytical predictors of dynamic stability (or, for a certain standard of stability, of the required values of influential parameters such as damping), while our knowledge about the ship is still limited. The detailed account of a ship's form takes place at a second level where the stability analysis is performed with suitable numerical methods. It is remarked that the presented measures of stability could be relevant also for the operational side of the problem which however should be the subject of another publication. We think that a rational approach



about ship safety entails the best available scientific knowledge to be "infused" with the current practices of design, operation and rule setting. These notwithstanding, we are urged to note the profound lack of a proper methodological framework of ship stability assessment which would exploit the recent progress in understanding the dynamic origins of capsize and play the role of an interface between practice and research. The development of such a framework is nontrivial because the process of ship capsize is often determined by nonlinear phenomena and is not a simple task to develop scientifically sound and yet simple-to-understand and practical, quantitative measures of dynamic stability covering all possible types of capsize. Recent advances in the study of ship dynamics have allowed us to develop a two-level framework for a rigorous quantitative assessment of ship stability. This framework can be useful to a designer who wants to determine, along with other design considerations, a hull geometry and appendages that maximize safety against capsize."

It is worth noting that both call, in some way, for layered approach to stability regulations, an approach later-on adopted in the development of Second Generation Intact Stability Criteria.

7. THE SECOND GENERATION INTACT STABILITY CRITERIA

The revision process started in 2001 (Francescutto 2004, Francescutto 2007) with a critical analysis submitted by Italian delegation to IMO (IMO 2001, Francescutto et al. 2001) concerning the need of updating and tuning some coefficients of the Weather Criterion in view of its excessive weight in determining the limiting KG for ships with large values of B/d. This was considered a good opportunity to "shake" the ISC foundations putting them on a more physical basis through the development of new *performance based criteria* (PBC) originally intended to replace the old ones.

These last were indeed identified as a source of difficulties due to their partly or totally empirical character which originated a non-uniform distribution of safety among different ship typologies. At the same time, their structure rendered these criteria quite difficult to modify without a possible significant loss of safety level of covering of present world fleet. The first part of the long work undertaken in the revision of the IMO Intact Stability Code in 2001 with the establishment of an ad-hoc Working Group (WGIS) operating during the Sessions of the Sub-Committee on Stability and Load Lines and on Fishing Vessel Safety (SLF) and intersessionally between them, was completed in 2008.

This part of the WGIS activity was mostly devoted to restructuring the previous Intact Stability Code (IMO 1993) in several parts and making Part A of the new International Code on Intact Stability, 2008 (IS Code 2008) mandatory under the provisions of both SOLAS and ILLC Conventions. This action was partly a consequence of the development of an FSA study, made by the German Delegation at IMO (IMO 2003), proving the potential cost-effectiveness implied in this change of legal status. The Code was also subject to some polishing and clarification, elimination of some ambiguities. In addition explanatory notes to the 2008 IS Code have been issued mostly consisting in a review of history of intact stability leading to present regulatory situation. It is however noteworthy that explanatory notes also contain guidance for an alternative application of "criteria regarding righting lever curve properties", in particular the rule requiring the position of the maximum of GZ to be above 25 deg. The new Part A contains mandatory instruments for passenger and cargo ships, while Part B contains recommendations for other ship typologies. An originally planned "Part C" containing nomenclature, an historical part describing the origins and the developments of intact stability criteria and explanatory notes to the new International Intact Stability Code 2008, has been finalized as an MSC Circular



(MSC.1/Circ.1281). Although what is now Part A was previously made de-facto mandatory under umbrellas different from IMO (European Directives, Classification Societies rules, etc.), the fact that after its adoption by SOLAS/ILLC the Code will become mandatory erga-omnes, constitutes a big change, because no attenuation to its standards is acceptable unless the “equivalent level of safety” with existing regulations is proved to the satisfaction of Administrations. This in turn is made difficult by the lack of knowledge of the actual safety level of present regulations. There is in fact the strong feeling that they provide an unequal distribution of safety among different typologies and, even within the same typologies, to different ship size. As a result, the revision made necessary the request and subsequent implementation of some important changes in the two basic design criteria.

As to the Weather Criterion, an alternative way of assessment, completely or partially based on experiments on scale models in towing tank/wind tunnel, was approved, based on both the obsolescence of the existing Weather Criterion due to the variations in ship forms and loading, and to correct some inconsistencies in the original formulation.

Notwithstanding the importance of this work, the most important part of the initial scope of the revision, i.e. the formulation and implementation of a new generation intact stability criteria performance-based was still to a large extent lying on the carpet. The time flown was in any case important for proving the potential cost-effectiveness implied in the new criteria and for the maturation of some important concepts connected with the dangerous phenomena to be covered, the basic structure and dictionary, and the philosophy of application of the new criteria.

It was subsequently decided that the following five possible stability failures should be individually addressed (IMO 2007, IMO 2010, Bassler et al. 2009, Francescutto and Umeda 2010, Peters et al., 2011.):

- dead ship conditions;
- following/stern quartering seas associated with matters related to stability variation in waves, in particular reduced righting levers of a ship situated on a wave crest;
- parametric resonance, including consideration of matters related to large accelerations and loads on cargo and stability variation in waves;
- broaching including consideration of matters related to manoeuvrability and course keeping ability as they affect stability;
- excessive accelerations.

Moreover the new generation intact stability criteria should be structured in three levels:

- Vulnerability 1st level;
- Vulnerability 2nd level;
- Direct assessment.

Specific Operational Guidelines should be added as a sort of "fourth level", in the acknowledgement that not all dangerous situations can be avoided only by design prescriptions.

After an initial good starting, the development of the procedures for the assessment of all the identified failure modes, mostly for the first two levels assessment, slightly diverged in a number for alternatives. During the last meeting of the Working Group, at SDC 2 (IMO 2015) last February, however, several choices were made concerning the application, the resolving of the alternatives for some failure modes, the development of explanatory notes and the development of “ways-out”, in the form of operational limitations or operational guidelines (IMO 2013) at the different levels.



Work is in progress at inter-sessional level to arrive at next meeting of SDC 3 in 2016 with a polished text for all the identified failure modes, ready for thorough checks. It is encouraging that both the remaining failure modes for which alternatives were present are presently converging towards an agreed text.

8. REFERENCES

- PNA, 1988, "Principles of Naval Architecture - II Revision", Lewis, E. V., Vol. I, Stability and Strength, SNAME.
- Barnes, F. K., 1861, "On a New Method of Calculating the Statical and Dynamical Stabilities of a Ship", Trans. INA, Vol. II, pag. 163
- Bassler, C., Belenky, V., Bulian, G., Francescutto, A., Spyrou, K., and Umeda, N., 2009, "A review of available methods for application to second level vulnerability criteria", Proceedings of the 10th International Conference on Stability of ships and ocean vehicles - STAB 2009, Saint Petersburg, pp. 111–128.
- Bouguer, P., 1746, "Traité du Navire, de sa Construction et de ses Mouvements (Treatise of the Ship, its Construction and Movements)", Jombert, Paris.
- Francescutto, A., Umeda, N., 2010, "Current Status of New Generation Intact Stability Criteria Development", Proceedings 11th International Ship Stability Workshop, Wageningen, pp. 1-5.
- Francescutto, A., 2004, "Intact Ship Stability - The Way Ahead", Marine Technology, Vol. 41, pp. 31-37.
- Francescutto, A., 2007, "Intact Stability of Ships: Recent Developments and Trends", Proc. 10th International Symposium on Practical Design of Ships and Other Floating Structures – PRADS'07, Houston, Vol. 1, pp. 487-496.
- Francescutto, A., 1993, "Is it Really Impossible to Design Safe Ships?", Transactions Royal Institution of Naval Architects, Vol. 135, pp. 163-173.
- Francescutto, A., Papanikolaou, A. D., 2011, "Buoyancy, Stability and Subdivision: From Archimedes to SOLAS2009 and the Way Ahead", International Journal of Engineering for the Maritime Environment (Proceedings Institution of Mechanical Engineers, Part M), Vol. 225, pp. 17-32.
- Francescutto, A., Serra, A., Scarpa, S., 2001, "A Critical Analysis of Weather Criterion for Intact Stability of Large Passenger Vessels", Proceedings 20th International Conference on Offshore Mechanics and Arctic Engineering - OMAE'2001, Rio de Janeiro, Vol. 1, pp. 829-836.
- IMO, 1993, "Code of Intact Stability for all Ships Covered by IMO Instruments", Res. A. 749.
- IMO, 2001, "Weather criterion for large passenger ships", Submitted by Italy, SLF44/INF.6.
- IMO, 2003, "Revision of the Code on Intact Stability", MSC78/24/1, Submitted by Germany,.
- IMO, 2007, "Framework for the development of new generation criteria for intact stability, submitted by Japan, the Netherlands and the USA", IMO SLF50/4/4.
- IMO, 2010, "Development of new generation intact stability criteria – Report of the Working Group (Part 1)", SLF52/WP.1.
- IMO, 2013, "Development of Second Generation Intact Stability Criteria - Comments on present status of development of second generation intact



- stability criteria”, Submitted by Italy, SLF 55/3/7
- IMO, 2015, “Development of Second Generation Intact Stability Criteria - Development of Amendments To Part B of The 2008 IS Code on Towing, Lifting and Anchor Handling Operations - Report of the working group (Part 1)”, SDC 2/WP.4.
- IS Code, 2008, “International Code on Intact Stability, 2008”, IMO, London.
- Kobyliński, L., 1975, “Rational Stability Criteria and the Probability of Capsizing”, Proceedings (1st) International Conference on Stability of Ships and Ocean Vehicles, Kuo, C., Paper 1.4.
- Moseley, H., 1850, “On the Dynamical Stability and on the Oscillations of Floating Bodies”, Phil. Trans. of the Royal Society of London, Vol. 140, pp. 609-643.
- Nowacki, H. and Ferreiro, L. D., 2003, “Historical roots of the theory of hydrostatic stability of ships”, Proceedings of the 8th International Conference on Stability of Ships and Ocean Vehicles - STAB 2003, Madrid.
- Nowacki, H., 2001, “Archimedes and ship stability”, Proceedings of the Euro-Conference on Passenger ship design, operation and safety, Anissaras-Chersonissos, Crete, 2001.
- Pierrottet, E., 1935, “Standards of Stability for Ships”, Transactions Institution of Naval Architects, Vol. 77, pp. 208-222.
- Rahola, J., 1939, “The Judging of the Stability of Ships and the Determination of the Minimum Amount of Stability Especially Considering the Vessels Navigating Finnish Waters”, Ph.D. Thesis, Technical University of Finland, Helsinki.
- Russo, L., 2004, “The forgotten revolution: how science was born in 300 BC and why it had to be reborn”, Springer, Berlin.
- Spyrou, K. J., 1998, “Ship Capsize Assessment and Nonlinear Dynamics”, Proceedings 4th International Workshop on Theoretical Advances in Ship Stability and Practical Impact, St John's, Newfoundland, Canada.
- Spyrou, K. J., Papanikolaou, A. D., 2000, “Ship Design for Dynamic Stability”, Proceedings of the 7th International Marine Design Conference - IMDC2000, KS Min & J-J Kim, Kyongju, Korea, pp. 167-178.
- Vincent, S. A., 1939, “Transverse Stability”, Principles of Naval Architecture – Written by a Group of Authorities, Rossell, H. E. & Chapman, L. B., Vol. I, Chapter III, SNAME, pp. 99-137.
- Peters, W., Belenky, V., Bassler, C., Spyrou, K. Umeda, N., Bulian, G., Altmayer, B., 2011, “The Second Generation Intact Stability Criteria: An Overview of Development”, Transactions - The Society of Naval Architects and Marine Engineers, Vol. 119, pp. 225-264.
- White, W. H., John, W., “On the Calculation of the Stability of Ships, and some Matters of Interest Connected Therewith”, Transactions Institution of Naval Architects, Vol. XII, 1871, pp. 76-127.
- Yamagata, M., 1959, “Standard of stability adopted in Japan”, Transactions of Institution of Naval Architects, Vol. 101, pp. 417-443.

This page is intentionally left blank